# A Preliminary Mechanistic Evaluation of PCC Cross-Sections Using ISLAB2000 – A Parametric Study

Neeraj Buch, Ph.D.
Kaenvit Vongchusiri, M.S.

**Michigan State University**
**Department of Civil and Environmental Engineering**

Dennis Gilliland, Ph.D**.**

**Michigan State University**
**Department of Statistics and Probability**

Thomas Van Dam, Ph.D., P.E.

**Michigan Technological University**
**Department of Civil and Environmental Engineering**

***Final Report***
August 2004

**DISCLAIMER**

| | | |
|---|---|---|
| 1. Report No.<br>Research Report RC-1441 | 2. Government Accession No. | 3. MDOT Project Manager<br>Curtis Bleech, P.E. |
| 4. Title and Subtitle<br>A Preliminary Mechanistic Evaluation of PCC Cross-Sections Using ISLAB2000 – A Parametric Study | | 5. Report Date<br>August, 2004 |
| 7. Author(s) Neeraj Buch, Ph.D., Dennis Gilliland, Ph.D., Kaenvit Vongchusiri, M.S.Thomas Van Dam, Ph.D., P.E. | | 6. Performing Organization Code |
| 9. Performing Organization Name and Address<br>Michigan State University<br>3546 Engineering Building<br>East Lansing, MI 48824 | | 8. Performing Org Report No.<br>61-9522 |
| 12. Sponsoring Agency Name and Address<br>Michigan Department of Transportation<br>Construction and Technology Division<br>P.O. Box 30049<br>Lansing, MI 48909 | | 10. Work Unit No. (TRAIS)<br>11. Contract Number:<br>11(a). Authorization Number: |
| 15. Supplementary Notes | | 13. Type of Report & Period Covered<br>14. Sponsoring Agency Code |

16. Abstract

This report summarizes the impact of structural, environmental and loading factors on jointed concrete pavement responses. The report also highlights the sensitivity of pavement response to the interactions between these factors. As a part of the project, relevant issues that relate the implementation of pavement responses to engineering practice using the ISLAB2000 structural model are also discussed. To this end an experimental matrix was constructed based on the concept of complete factorial for all combinations of design inputs reflecting MDOT practice, climatic condition, and load configurations in Michigan. Several engineering principles and common knowledge were applied to modify the experimental matrix with the purpose of making the matrix more concise, but providing the same level of information. 43,092 combinations of parameters were identified for the preliminary parametric study. The ISLAB2000 structural model was used for the analysis. In addition to the analysis an interpolation scheme was developed to compute mechanistic responses for all combinations of the non-discrete inputs, not addressed in the final experimental matrix.

| | | | |
|---|---|---|---|
| 17. Key Words<br>Pavement response, finite element, axle configuration, lateral support | 18. Distribution Statement<br>No restrictions. This document is available to the public through the Michigan Department of Transportation. | | |
| 19. Security Classification (report)<br>Unclassified | 20. Security Classification (Page)<br>Unclassified | 21. No of Pages | 22. Price |

# TABLE OF CONTENTS

# TABLE OF CONTENTS
## (CONTINUED)



## Appendices

# LIST OF TABLES

# LIST OF FIGURES

# LIST OF FIGURES
## (CONTINUED)

# LIST OF FIGURES
## (CONTINUED)

# Executive Summary

The responses of rigid pavements are influenced by three major factors: (i) structural, (ii) loading, and (iii) environmental. However, the interaction between these factors cannot be directly addressed by the current AASHTO 1993 design method. This report summarizes the preliminary findings of a two-year project to study rigid pavement response due to the variations in the above mentioned factors. The report also highlights the sensitivity of pavement response to the interactions between these factors. As a part of the project, relevant issues that relate the implementation of pavement responses to engineering practice using the ISLAB2000 structural model are also discussed.

The primary objectives of this study were to i) evaluate the robustness and user friendliness of the ISLAB2000 software, ii) perform a preliminary parametric study on current and anticipated Michigan Department of Transportation (MDOT) rigid pavement cross-sections, using design inputs consistent with Michigan loading, climatic conditions, materials, subgrade support and construction parameters, and iii) prepare and conduct a technology transfer workshop for MDOT pavement designers to familiarize them with the ISLAB2000 program.

The analysis was based on a sample of 14 “approved” designs for projects that were either recently constructed or were programmed for construction in the near future. These designs provided input parameters like pavement cross-sections, material properties, traffic and environmental conditions. The final experimental matrix for the preliminary parametric study contained 43,092 combinations of inputs. Some findings based on a sample of 14 designs are summarized below:

- The ISLAB2000 program is robust and user friendly. The results from the ISLAB2000 structural model compare well with the Westergaard solutions (after considering the relevant assumptions) and other widely accepted FE structural models.

- The critical load location is influenced by joint spacing and truck or axle configuration. The fractional factorial analysis indicated that the critical load location is generally not influenced by slab thickness, base/subbase thickness, modulus of subgrade reaction, lateral support condition, and thermal gradient or thermal strain gradient.

- For a flat slab condition, when the slab thickness changes from 9 to 12 in. the resulting stress is reduced by approximately 35%. For a constant thermal gradient, pavements constructed with different slab thickness have different temperature differentials, and therefore, the pavement responses could not be compared.

- For a flat slab condition, pavement cross-sections with thicker base/subbase thickness (from 4 to 26 in.) resulted in about 5-30% lower stresses and as the slab thickness increases the impact of base/subbase thickness becomes less significant.

- Pavements constructed with 27 feet joint spacing resulted in about 33% higher longitudinal stresses as compared to pavements constructed with 15 feet joint spacing for curled slab

conditions at a thermal strain gradient value of $+10x10^{-6}$ $in.^{-1}$. The severity depends on the level of thermal curling or thermal strain gradient.

- For the load located along the wheel path (approximately 20” from the traffic stripe), pavements constructed with PCC shoulders resulted in the lowest stresses among the three lateral support conditions (12’ lane with tied PCC shoulders, 12’ lane with AC shoulders and 14’ lane with AC shoulders) that are considered in the study. Although the pavements were constructed with the same AC shoulder, the magnitudes of longitudinal stresses for pavements with 12-ft lane (standard lane) were higher than that for pavements with 14-ft lane (widened lane). As the wheel path shifted 2 ft towards the centerline for pavements with widened lane, a pseudo-interior loading condition was created, resulting in the reduction of stresses from edge loading. Pavements constructed with AC shoulders (12-ft lane with AC shoulder) resulted in about 13% and 9% higher longitudinal stress values than pavements constructed with PCC shoulder (12-ft lane with tied PCC shoulder) and widened lane (14-ft lane with untied AC shoulder), respectively.

- Lateral wander (or lateral placement) of traffic load resulted in higher edge stresses as the load moves from the wheel path towards lane/shoulder longitudinal joint (about 10% for tied PCC shoulder and 30% for AC shoulder).

- The experimental matrix only included three levels of non-discrete inputs (base/subbase thickness, modulus of subgrade reaction and thermal strain gradients), therefore the application of interpolation was employed to capture combinations of non-discrete inputs not included in the experimental matrix. In the validation process considering all axle types, the bias (average error), variance, and mean square of errors (MSE) of the best scheme (scheme 16) were 0.51 psi, 8.63 $psi^2$, and 8.89 $psi^2$, respectively, indicating that the interpolation scheme was highly accurate and precise in computing pavement response as compared with the results directly obtained from the ISLAB2000 program.

The pavement response plays a significant role in the mechanistic-empirical (M-E) design process; however, it is necessary to integrate the pavement response with several other components. For the M-E process to be implemental and reflect Michigan practice, the following issues need to be investigated:

1) The coefficient of thermal expansion (CTE) values for concrete mixes and also aggregate (as concrete making material) used in paving Michigan roads need to be determined and cataloged, since CTE plays a critical role in the thermal analysis of jointed concrete pavements. The slab movement and joint opening are also influenced by the CTE of concrete.

2) An extensive traffic database, e.g. WIM database, should be made available for the pavement network as hourly axle spectra is a key input for damage computations. The hourly axle spectra allow for calculation of pavement responses that account for daily and seasonal conditions of climate, roadbed and material. The axle repetitions from the axle spectra and the corresponding pavement responses are the inputs to the cumulative damage calculation.

3) Develop and calibrate transfer functions for key jointed concrete pavement distresses that reflect Michigan practice. The process involves statistical correlation of the cumulative damages to the measured distresses corresponding to the time periods to obtain a calibrated model that can be used for Michigan jointed concrete pavement design.

# Chapter I

# INTRODUCTION

## 1.1 Background

The design of rigid pavements in the State of Michigan has changed over time. For the most part, the design process is based on the AASHTO 1993 method, with modifications to reflect the Michigan Department of Transportation (MDOT)'s experience and observations of pavement performance. In general, the rigid pavement cross-sections are comprised of a concrete slab 230 to 280 mm (9 to 11 in.) thick, a 100 mm (4 in.) aggregate base (OGDC or otherwise), a separator layer (either a 100 mm (4 in.) dense graded or a geotextile interlayer) all on a 250 to 300 mm (10 to 12 in.) sand subbase. The final cross-section selection is based on various considerations including the following:

- Traffic volumes, commercial trucks and load;
- Roadbed soil, including frost susceptibility;
- Drainage;
- Initial and life cycle costs;
- Joint spacing;
- Load transfer and reinforcement; and
- Life cycle cost analysis.

Current practice is to select the final cross-section based on the guidelines presented in the 1986/1993 AASHTO Guide for the Design of Pavement Structures. However, this design practice is most highly correlated to pavement ride quality, but does not necessarily assure structural integrity, nor does it directly account for the effects of pavement type (JPCP versus JRCP), joint spacing, lane width, variation in material properties along a project, environmental impact and joint design (aggregate interlock versus dowel bars) on pavement design. Further, it does not effectively address the impact of the heavy, multi-axle "Michigan Truck" on the performance of rigid pavements.

Realizing that the only way to address the multiple factors influencing rigid pavement response is through a more mechanistic approach, MDOT and Minnesota Department of Transportation (MnDOT) jointly funded a study to enhance the ILLISLAB 2-D FEM rigid pavement analysis program (Tabatabaie and Barenberg, 1980). ILLISLAB is widely recognized as the most versatile state-of-the-practice rigid pavement analysis software available. Unfortunately, its application was highly limited because of the poor user interface and limitations on the complexity of the problems that it could evaluate. The enhancement entailed the complete rewriting of the code to remove inefficiencies, significantly improving the computational ability of the software. It also included the employment of a graphical user interface (GUI) both for inputting data and examining the output. The use of ISLAB2000 allows the user to assess pavement response due to temperature, cross-section, loading and construction variables.

## 1.2 Research Objectives

The objective of the project was to study the impact of various parameters and their interrelationship on mechanistic responses of jointed concrete pavement (JCP) using the ISLAB2000 structural model. The primary objective was achieved in the project by i) evaluating the ISLAB2000 software and provide feedback to the developers, ii) performing a preliminary parametric study on current and anticipated MDOT rigid pavement cross-sections, using design inputs consistent with Michigan loading, climatic conditions, materials, subgrade support and construction parameters, and iii) preparing and conducting a technology transfer workshop for MDOT pavement designers to familiarize them with the ISLAB2000 program.

## 1.3 Scope of Research

The research plan was divided into five tasks to achieve the research objectives and to provide a better understanding of each phase of this project and the connection among them.

**Task 1: Determine the robustness and friendliness of ISLAB2000**

Various scenarios will be systematically evaluated to establish the robustness of the software and the comparability of the analysis results to the Westergaard's closed form solutions. The results will be compared to known design examples illustrated in the textbook "Pavement Analysis and Design" (Huang, 1993). The user friendliness of the graphical user interface (GUI) will also be assessed.

**Task 2: Conduct the parametric study and sensitivity analysis**

A parametric study will be designed and conducted using statistically sound practices to evaluate the impact of the following variables on pavement performance:

- Pavement thickness;
- Slab geometry;
- Load transfer;
- Support conditions;
- Axle loading, configurations, and locations;
- Temperature gradient;
- Variable material characteristics; and
- Variable support conditions.

The ISLAB2000 program will be used to calculate response (stress, strain and deflection) of a sample of pavement cross-sections. This information will be evaluated to determine design features that impact pavement response.

**Task 3: Create an MDOT specific on-line help feature**

To increase the usefulness of the ISLAB2000 program, an MDOT specific on-line help feature will be created. Using this feature, the user will be able to find guidance in generating the various inputs on-line. Typical values for Michigan conditions will be presented, as well as background information to assist the user in making decisions. The full user manual will also be developed and included on the CD-ROM for an easy access, including a search feature to assist the user in finding desired information.

**Task 4: Conduct technology transfer workshop**

A full-day technology workshop will be developed and presented to MDOT pavement designers and researchers who are the anticipated users of the ISLAB2000 program. The workshop will include:

- An introduction to the theory behind the ISLAB2000 program and mechanistic design;
- A description of the various required inputs and how reasonable values for these inputs can be obtained;
- A demonstration of how to prepare a complete input file;
- A discussion of the results, including example of transfer functions that will enhance the meaningfulness of the output; and
- Hand-on exercises that will allow each participant to develop the input and analyze the output of the problems that are of concern to them.

Each workshop participant will be provided an ISLAB2000 user's guide and a participant's workbook for future reference, as well as a CD-ROM containing the ISLAB2000 program, example problems, and electronic copies of the ISLAB2000 user's guide, participant's workbook, and copies of the presentations used during the workshop.

**Task 5: Complete the final report**

At the conclusion of the study the PI will submit a draft copy (multiple copies will be submitted if the PM so requests) of the final report documenting the results of the study. It is expected that the PM will review the draft final report and provide feedback within one month after receiving the report. The PI will incorporate the changes and submit the final revised report within one month of receiving the comments. The final submission will consist of 50 double-sided bound copies and one copy single-sided unbound copy`. Furthermore, a CD containing the entire report will also be submitted.

## 1.4 Organization of Report

This report contains background information on the parametric study of mechanistic responses of JCP using ISLAB2000, a discussion of the analyses performed and the results obtained from the parametric study, and a summary of the conclusions and recommendations derived from this study. A more detailed breakdown of the contents of individual chapters is as follows. Chapter II includes: background on the robustness and accuracy of ISLAB2000 are determined, a summary of Westergaard Theory and a summary of finite element (FE) method used in ISLAB2000. Chapter III provides an overview of the data collection process and how the final experimental matrix for the parametric study is obtained. A detailed analysis process of the parametric study is given in Chapter IV. This chapter also includes documentation and interpretation of the analysis results. The application of 'Interpolation Scheme' in quantifying the magnitude of mechanistic response at the combinations of parameters that are not addressed in the experimental matrix and its validation including the goodness of fit are elaborated in Chapter V. In addition, example use of interpolation scheme and a catalog of mechanistic responses based on the use of this interpolation scheme are also included in this chapter. Chapter VI presents a demonstration of a future step to potentially implement the product of this project into a mechanistic-empirical design process with existing transfer functions. A summary of findings and recommendations for future research arising from the analyses performed in this study as well as a listing of future research needs related to mechanistic analysis and mechanistic-empirical design of JCP are contained in Chapter VII.

Thirteen appendices are also included in this report, which are listed as follows:

Appendix A: Review of the Kirchhoff plate theory
Appendix B: Comparison between ISLAB2000 results and Westergaard's solution
Appendix C: ISLAB2000 graphical results for the comparison with Westergaard's solution
Appendix D: Data collection
Appendix E: Validation of thermal strain gradient (the product $\alpha(\Delta T/D)$)
Appendix F: Documentation of pavement response
Appendix G: Impact of lateral placement on different lateral support conditions
Appendix H: Equivalent stress cross-sections
Appendix I: Catalog of pavement response
Appendix J: Hourly load spectra from WIM database
Appendix K: Hourly thermal gradient from EICM
Appendix L: Michigan ISLAB2000 (submitted in a CD)
Appendix M: Technology transfer package

# Chapter II

# ROBUSTNESS AND USER FRIENDLINESS OF ISLAB2000

The robustness and user friendliness of ISLAB2000 program are investigated in this chapter based on two approaches: i) comparison of published results with ISLAB2000 results and ii) comparison of results based on ISLAB2000 program with another FE program for JCP, called EverFE (Davids and Mahoney, 1999). Several types of problems from the textbook “Pavement Analysis and Design” (Huang, 1993) are used for the first approach, while selected MDOT designs are used for the second approach.

## 2.1 Review of Westergaard Theory

Mechanistic analysis of rigid pavement was first introduced in the 1920’s by Westergaard. Since then, mechanistic analysis has been a crucial part of the analysis and design of rigid pavement. The closed-form equations by Westergaard, however, rely on several assumptions (Westergaard, 1926) and they include:

- Infinite slab dimension,
- Full contact interface between slab and subgrade,
- Single layer (no base or subbase layers),
- Single slab (free edge boundary),
- Semi-infinite foundation,
- Single tire print,
- Circular or semi-circular loading area only,
- Dense liquid foundation (Winkler foundation).

The review of the Westergaard theory in this chapter includes information about the Winkler foundation, load cases considered in the Westergaard analysis and the Bradbury thermal curling stress formulation.

**Winkler foundation**

The Winkler foundation, also referred to as the Dense Liquid foundation (DL), has been traditionally used as a subgrade idealization in rigid pavement design and analysis. This idealization is based on assumptions that the subgrade cannot transfer shear stress and the slab is subjected to vertical reaction pressure equal to deflection times a constant k (modulus of subgrade reaction). In other words, the subgrade will deflect only under the area of applied load. According to McCullough (McCullough and Boedecker, 1968), the Winkler foundation model used in Westergaard’s theory is a dense liquid with a density equal to k times the deflection under the load, or a bed of spring with spring constant k as illustrated in Figure 2-1.

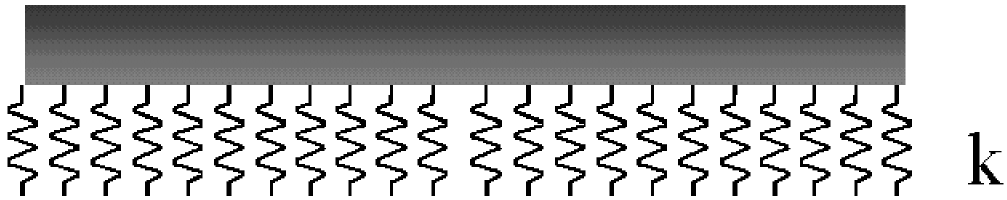


**Figure 2-1: Idealization of dense liquid foundation**

## Load Cases

In addition to the several assumptions and the dense liquid foundation, the Westergaard's closed from solutions are also limited to only three loading conditions: interior, edge, and corner (stress at the top of the slab).

## Interior loading condition (Load Case I)

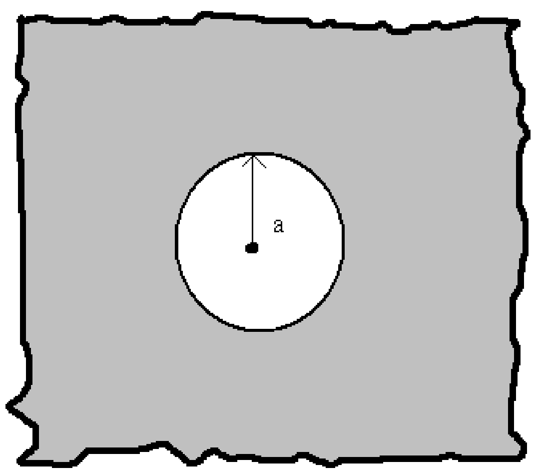


**Figure 2-2: Interior loading condition**

Interior loading condition is the case of a wheel load at a considerable distance from the edges. The loading stress equation was the earliest formula developed by Westergaard in 1926, (Westergaard, 1926) as illustrated in Figure 2-2. The stress at the bottom of the Portland Cement Concrete (PCC) slab due to a circular loaded area of radius "a" is computed as:

$$\sigma_i = \frac{3 \cdot (1+\mu) \cdot P}{2 \cdot \pi \cdot D^2} \cdot \left( \ln \frac{l}{b} + 0.6159 \right) \quad \text{(2-1)}$$

Where b = a when $a \geq 1.724 \cdot D$

= $\sqrt{1.6 \cdot a^2 + D^2} - 0.675 \cdot D$ when $a < 1.724 \cdot D$

$\ell$ = radius of relative stiffness

$$l = \sqrt[4]{\frac{E_c \cdot D^3}{12 \cdot (1-\mu^2) \cdot k}} \qquad (2\text{-}2)$$

D = concrete slab thickness, in.
$E_c$= modulus of elasticity of concrete slab, psi
k = elastic modulus of subgrade support, psi/in.
μ = Poisson's ratio for concrete (0.15-0.20 as typical values)

For the same loading condition as shown in Figure 2-2, deflection of the PCC slab underneath the loading area can be calculated using the following equation.

$$\delta_i = \frac{P}{8 \cdot k \cdot l^2} \cdot \left\{ 1 + \frac{1}{2 \cdot \pi} \cdot \left[ \ln\left( \frac{a}{2 \cdot l} \right) - 0.673 \right] \cdot \left( \frac{a}{l} \right)^2 \right\} \qquad (2\text{-}3)$$

**Edge loading condition (Load Case II)**

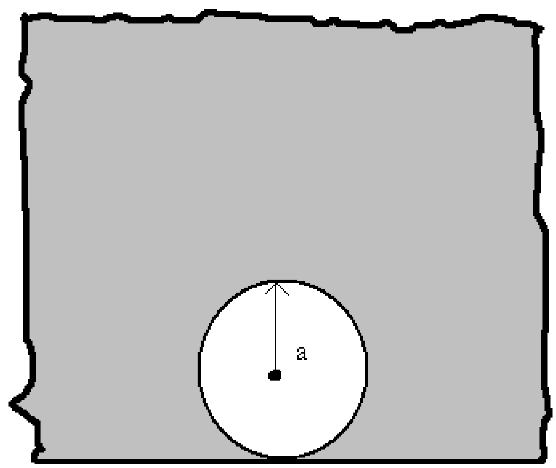


**Figure 2-3: Edge loading condition**

As illustrated in Figure 2-3, edge loading condition is the case in which the wheel load is at the edge, but at a considerable distance from any corner. Westergaard presented the edge loading stress equation in 1926 (Westergaard, 1926). This loading condition is important in that it results in the most critical stress at bottom of PCC slab of all three loading condition according to Westergaard. The stress and deflection formulation is as follows:

$$\sigma_e = \frac{3 \cdot (1+\mu) \cdot P}{\pi \cdot (3+\mu) \cdot D^2} \cdot \left[ \ln\left( \frac{E_c \cdot D^3}{100 \cdot k \cdot a^4} \right) + 1.84 - \frac{4 \cdot \mu}{3} + \frac{1-\mu}{2} + \frac{1.18 \cdot (1+2 \cdot \mu) \cdot a}{l} \right] \qquad (2\text{-}4)$$

$$\delta_e = \frac{\sqrt{2+1.2 \cdot \mu} \cdot P}{\sqrt{E_c \cdot D^3 \cdot k}} \cdot \left[ 1 - \frac{(0.76+0.4 \cdot \mu) \cdot a}{l} \right] \qquad (2\text{-}5)$$

**Corner loading condition (Load Case III)**

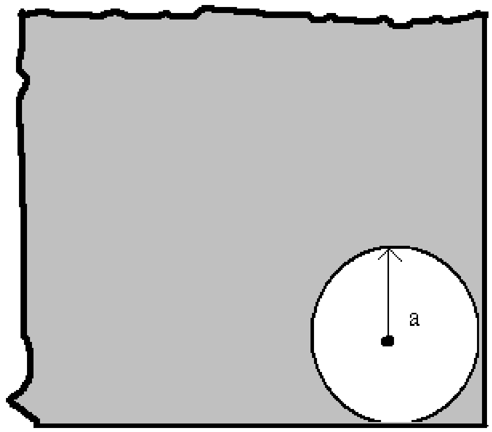


**Figure 2-4: Corner loading condition**

Corner loading condition is the case in which the wheel load is at a corner of the slab. Even though an equation for determining stress due to the corner loading condition was developed by Goldbeck (1919) and Older (1924) earlier, Westergaard was the first to discover that the maximum stress due to corner loading condition is not at the slab corner, but is at a distance of $2.38\sqrt{al}$ from the corner. Westergaard also included this correction into his formulas for determining stress and deflection in 1926 as shown below, respectively.

$$\sigma_c = \frac{3 \cdot P}{D^2} \cdot \left[ 1 - \left( \frac{a \cdot \sqrt{2}}{l} \right)^{0.6} \right] \quad (2\text{-}6)$$

$$\delta_c = \frac{P}{k \cdot l^2} \cdot \left[ 1.1 - 0.88 \cdot \left( \frac{a \cdot \sqrt{2}}{l} \right) \right] \quad (2\text{-}7)$$

The corner loading condition according to Westergaard's produces the most critical deflection of all three Westergaard loading conditions. It should also be noted that the maximum stress due to this loading condition is located at the top of PCC slab (not bottom as edge and interior loading conditions).

Among the three loading conditions by Westergaard, the corner loading condition is the most obscure. It should be noted that fully contacted interface between layers is one of the assumptions used in Westergaard's formulations and this assumption is not realistic because it leads to underestimation of stresses and deflections at top of PCC layer. In other words, the incapability of simulating the lack of support in Westergaard's formulation causes the variation between Westergaard's and FE solutions for corner loading condition, at which the lack of support has a significant impact on stresses and deflections. Stress and deflection equations for the corner loading condition based on the FE method were suggested as shown below (Ioannides et al, 1985).

$$\sigma_c = \left(\frac{3 \cdot P}{h^2}\right) \cdot \left[1.0 - \left(\frac{c}{l}\right)^{0.72}\right] \tag{2-8}$$

$$\delta_c = \left(\frac{P}{k \cdot l^2}\right) \cdot \left[1.205 - 0.69 \cdot \left(\frac{c}{l}\right)\right] \tag{2-9}$$

Results based on equations recommended by Ioannides et al (1985) were also compared with ISLAB2000 results.

**Dual tires simulation**

Since all Westergaard's loading stress equations for a single tire print are circular loading area based. It is necessary to convert dual tires into a single circular loading area. Equation 2-10 allows for the conversion from dual tires to a single tire (Huang, 1993).

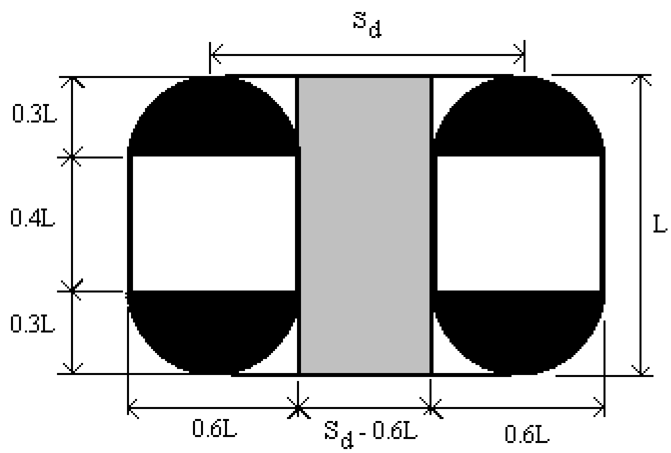


**Figure 2-5: Dual tires simulation represented by a circular loading area**

$$a = \sqrt{\frac{0.8521 \cdot P_d}{q \cdot \pi} + \frac{S_d}{\pi} \cdot \left(\frac{P_d}{0.5227 \cdot q}\right)^{\frac{1}{2}}} \tag{2-10}$$

Where $P_d$ = load on one tire
$q$ = contact pressure (one tire)
$S_d$ = dual spacing (center to center)

**Curling stress formulation**

The environmental effects on rigid pavements can be accounted for in terms of temperature differential between top and bottom layers of PCC. Positive temperature gradient (top layer is warmer than bottom layer) contributes to downward curling, whereas negative temperature gradient (bottom layer is warmer than top layer) contributes to upward curling. This is illustrated in the Figure 2-6.

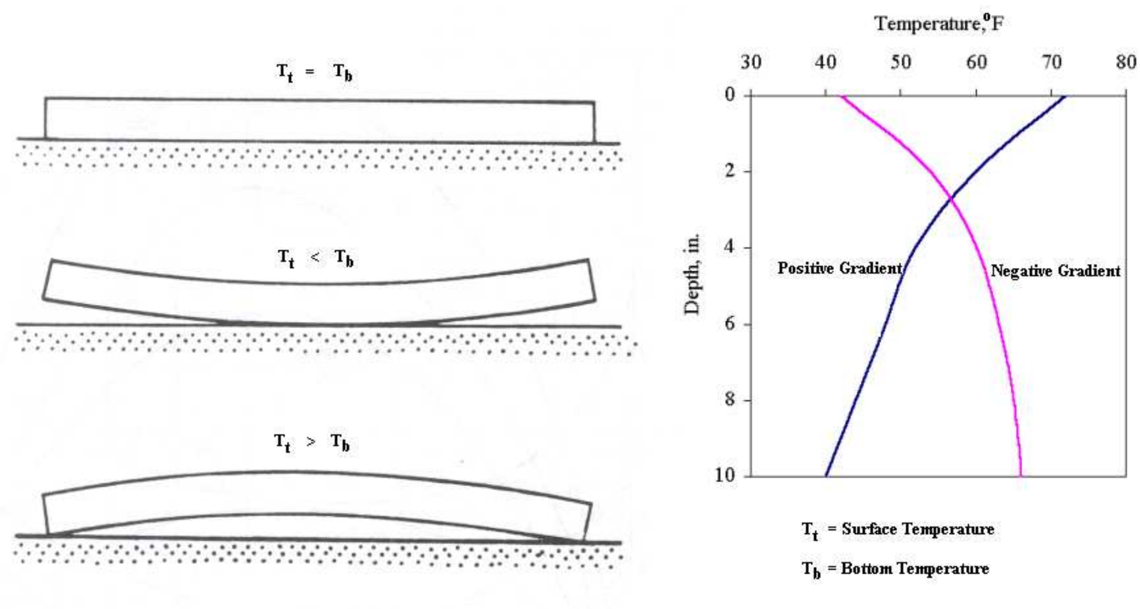


**Figure 2-6: Effect of temperature gradient on slab curling**

For upward curling, the top layer of PCC contracts while the bottom layer expands with respect to the neutral axis; however, the concrete slab weight will try to move the corners of slab down. Negative moment due to slab weight will cause tension at top of PCC layer and compression at bottom of PCC layer. In contrast, for downward curling, top of PCC layer expands while bottom of PCC layer contracts with respect to the neutral axis; corners of slab will move down but slab center will lift up. Consequently, slab weight will try to move its center down and this causes tension at bottom and compression at top of PCC layer. The following are the curling stress equations by Bradbury.

$$\sigma_{ix} = \frac{E_c \cdot \alpha_t \cdot \Delta t}{2 \cdot (1 - \mu^2)} \cdot (C_x + \mu \cdot C_y) \qquad (2\text{-}11)$$

$$\sigma_{iy} = \frac{E_c \cdot \alpha_t \cdot \Delta t}{2 \cdot (1 - \mu^2)} \cdot (C_y + \mu \cdot C_x) \qquad (2\text{-}12)$$

$$\sigma_e = \frac{C \cdot E_c \cdot \alpha_t \cdot \Delta t}{2} \qquad (2\text{-}13)$$

Where
$\sigma_{ix}$ = interior curling stress in x-direction
$\sigma_{iy}$ = interior curling stress in y-direction
$\sigma_e$ = edge curling stress (can be used for x and y-direction)
$\alpha_t$ = coefficient of thermal expansion
$\Delta t$ = temperature differential
$C_x$, $C_y$ = finite slab correction factor in x and y-direction

From slab dimension and radius of relative stiffness, finite slab correction factors for both x and y-direction can be approximated using the following chart.

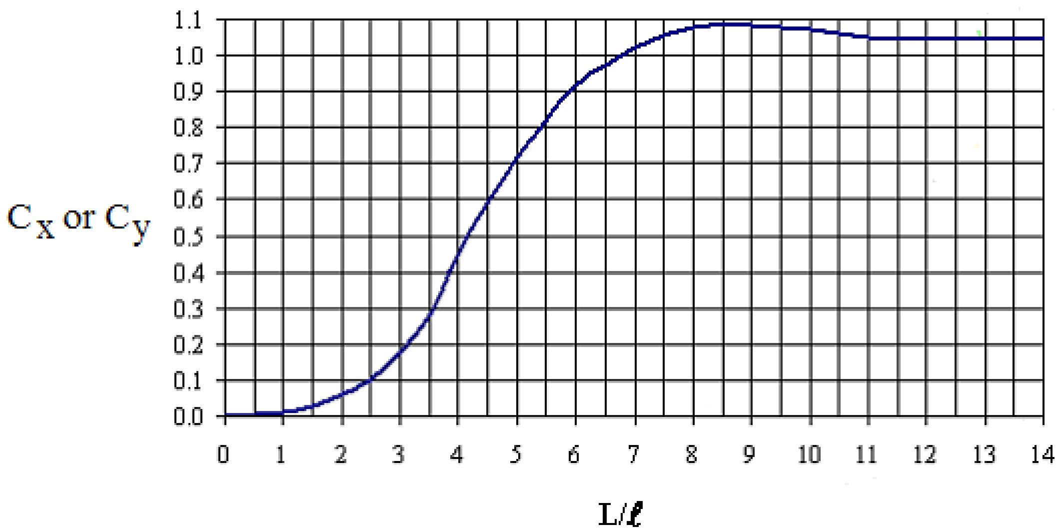


**Figure 2-7: Finite slab stress correction factors (Huang, 1993)**

## 2.2 Review of FE Method

Kirchhoff plate theory, which is the theory behind ISLAB2000 FE model, is reviewed, including the Winkler foundation in FE, element discretization, and FE global system. The details of the Kirchhoff plate theory can be found in Appendix A.

## 2.3 Comparison of Published Results with ISLAB2000 Results

Several examples and problems in chapter 4 (Stresses and Deflections in Rigid Pavements) of the textbook "Pavement Analysis and Design" by Yang H. Huang were solved using ISLAB2000. The software was used to simulate traffic loads, temperature gradients, pavement features such as PCC thickness, joint spacing, and subgrade soils as listed in the textbook. The results obtained from the ISLAB2000 model and Westergaard solutions were compared. It has to be noted that in order to simulate problems using ISLAB2000, two assumptions need to be made: slab size requirements to simulate infinite slab behavior and square load contact area to simulate circular load contact area as indicated in Westergaard's theory.

The following are slab size requirements for Westergaard responses based on the FE method, (Ioannides et al, 1985), in terms of $L/\ell$ when L is least slab dimension and $\ell$ is radius of relative stiffness.

**Table 2-1: Required L/l ratio for FE solutions to satisfy Westergaard's assumptions (Ioannides et al, 1985)**

| Response | Load Placement | | |
|---|---|---|---|
| | Interior | Edge | Corner |
| Maximum Deflection | 8.0 | 8.0 | 5.0 |
| Maximum Bending Stress | 3.5 | 5.0 | 4.0 |

The problems can be categorized into three groups:

1. curling (temperature) stress only,
2. corner, interior, and edge stresses and deflections due to wheel load(s),
3. combined temperature and loading stresses.

Each problem was divided into two parts: the textbook solution, and the ISLAB2000 solution (FE solution). The textbook solution consists of the problem statement, an illustration of the problem, and solution based on Westergaard's equations, while the FE solution consists of the summary of inputs, illustration of the mesh and loading used in problem, followed by a short explanation if necessary, and numerical and graphical outputs in Appendices B and C, respectively. Out of the nine problems selected from the textbook, four problems were solved for four mesh sizes (3, 6, 12, and 24 in.) using ISLAB2000. The difference of the results based on 3 in. and 6 in. mesh sizes was found to be negligible. Therefore, the other five problems were solved only for three mesh sizes (6, 12, and 24 in.). It should also be noted that the mesh aspect ratio of 1 (square mesh) was used for all the problems.

## 2.4 Summary Comparison of Published Results with ISLAB2000 Results

In summary, the variations between the published results based on the Westergaard solutions and the ISLAB2000 results are shown in Table 2-2. The results suggest that responses obtained from the ISLAB2000 program and from the Westergaard theory are comparable with the exception of the corner loading condition. Relatively large variations were observed for corner stress and deflection results. However, the difference in the results between the two approaches has been reported, (Ioannides et al, 1985). After applying the equations suggested by Ioannides et al (1985), the ISLAB2000 results and the results based on the closed form solutions appear to be more comparable. Table 2-3 summarizes the overall percent variation between the closed form and the ISLAB2000 results.

**Table 2-2: Summary of results and percent variation of the results**

| Problem | Response Type | Textbook Results | Unit | FE Results ISLAB2000 with Various Mesh Sizes | | | | Percent Variation ISLAB2000 with Various Mesh Sizes | | | |
|---|---|---|---|---|---|---|---|---|---|---|---|
| | | | | 24" | 12" | 6" | 3" | 24" | 12" | 6" | 3" |
| 1 | Int. Stress | 238.0 | psi | 231.6 | 230.1 | 230.3 | 230.5 | 2.69 | 3.31 | 3.25 | 3.14 |
| | Edg. Stress | 214.0 | psi | 219.0 | 220.1 | 220.3 | 219.8 | 2.35 | 2.87 | 2.95 | 2.72 |
| 2 | Cor. Stress | 186.6 | psi | 198.4 | 197.9 | 195.8 | 195.8 | 6.32 | 6.06 | 4.93 | 4.93 |
| | Cor. Stress* | 190.2 | psi | 198.4 | 197.9 | 195.8 | 195.8 | 4.29 | 4.03 | 2.93 | 2.93 |
| 3 | Int. Stress | 143.7 | psi | 140.6 | 159.0 | 151.9 | 144.2 | 2.16 | 10.65 | 5.69 | 0.35 |
| 4 | Edg. Stress | 279.4 | psi | 285.9 | 306.5 | 294.9 | 287.2 | 2.33 | 9.70 | 5.54 | 2.79 |
| 5 | Cor. Stress | 166.8 | psi | 182.3 | 178.1 | 177.6 | - | 9.29 | 6.77 | 6.47 | - |
| | Int. Stress | 130.8 | psi | 135.5 | 144.2 | 132.8 | - | 3.59 | 10.24 | 1.54 | - |
| | Edg. Stress | 244.2 | psi | 263.8 | 267.6 | 255.2 | - | 8.03 | 9.58 | 4.50 | - |
| 6 | Int. Stress | 282.4 | psi | 296.6 | 296.3 | 296.2 | - | 5.03 | 4.92 | 4.89 | - |
| | Edg. Stress | 240.0 | psi | 244.2 | 244.9 | 245.4 | - | 1.74 | 2.05 | 2.23 | - |
| | Pt. A | 211.4 | psi | 197.3 | 195.3 | 194.8 | - | 6.69 | 7.62 | 7.87 | - |
| | Pt. B | 198.0 | psi | 197.8 | 196.3 | 196.0 | - | 0.09 | 0.86 | 1.04 | - |
| | Pt. C | 57.6 | psi | 50.4 | 49.9 | 49.7 | - | 12.55 | 13.42 | 13.65 | - |
| 7 | Cor. Stress | 172.8 | psi | 171.1 | 166.5 | 164.5 | - | 0.98 | 3.65 | 4.80 | - |
| 8 | Int. Stress | 139.7 | psi | 137.6 | 134.1 | 123.3 | - | 1.50 | 4.01 | 11.74 | - |
| 9 | Edg. Stress | 252.5 | psi | 247.7 | 237.9 | 227.4 | - | 1.90 | 5.78 | 9.94 | - |
| 2 | Cor. Defl. | 0.0502 | in. | 0.0562 | 0.0563 | 0.0563 | 0.0563 | 11.95 | 12.15 | 12.15 | 12.15 |
| | Cor. Defl.* | 0.0560 | in. | 0.0562 | 0.0563 | 0.0563 | 0.0563 | 0.36 | 0.54 | 0.54 | 0.54 |
| 3 | Int. Defl. | 0.0067 | in. | 0.0068 | 0.0069 | 0.0069 | 0.0069 | 1.94 | 3.28 | 2.99 | 2.84 |
| 4 | Edg. Defl. | 0.0207 | in. | 0.0211 | 0.0212 | 0.0212 | 0.0212 | 2.08 | 2.32 | 2.42 | 2.42 |

* Remarks: the comparison is based on Ioannides's approach

**Table 2-3: Overall variation between Westergaard and FE solutions**

| Response Type and Location | Variation (%) |
|---|---|
| Interior Loading Stress | 3.84 |
| Interior Loading Deflection | 2.99 |
| Edge Loading Stress | 4.09 |
| Edge Loading Deflection | 2.42 |
| Corner Loading Stress* | 2.93 |
| Corner Loading Deflection* | 0.54 |

* Remarks: the comparison is based on Ioannides's approach

## 2.5 Summary Comparison of Practical Engineering Results based on ISLAB2000 and EverFE

The capability of the ISLAB2000 program to provide comparable results with the closed form solutions has been demonstrated in the previous section; however, the load configurations and the structural conditions in the closed form solutions are not realistic. It is also important to ensure that the ISLAB2000 is also able to provide accurate results for practical engineering problems. To achieve this, the ISLAB2000 program and EverFE program are used to analyze selected MDOT designs. The comparability of the results based on these two FE programs is investigated through following engineering problems:

**Problem 1**: A pavement system with 11.8-in. PCC slab, 15.7-in. aggregate base, 99-psi/in. roadbed, 315-in. joint spacing, 12-ft lane, and tied PCC shoulder is given (an MDOT design on I-75 (C.S. 82191 & 82194 and J.N. 45699) submitted on June 12, 2001 as the second design alternative). Analyze this pavement system for longitudinal stress at the bottom of the slab under the impact of 18-kips single axle edge loading using the ISLAB2000 and EverFE program.

Solution: The same mesh size (12 in. by 12 in.) is used for both ISLAB2000 and EverFE program. The results obtained from the ISLAB2000 and EverFE program are 87.1 psi and 97.4 psi, respectively. Figures 2-10 and 2-11 illustrate the graphical results obtained from both programs. It can be seen that the peak stress magnitudes and locations obtained from these models are comparable.

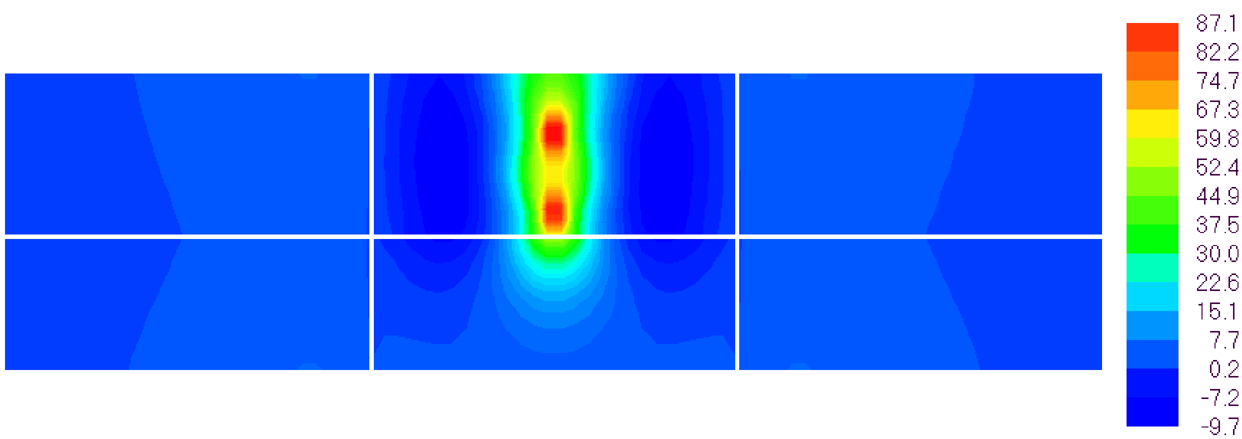


**Figure 2-10: Longitudinal stress at the bottom of the slab from ISLAB2000 for Problem 1**

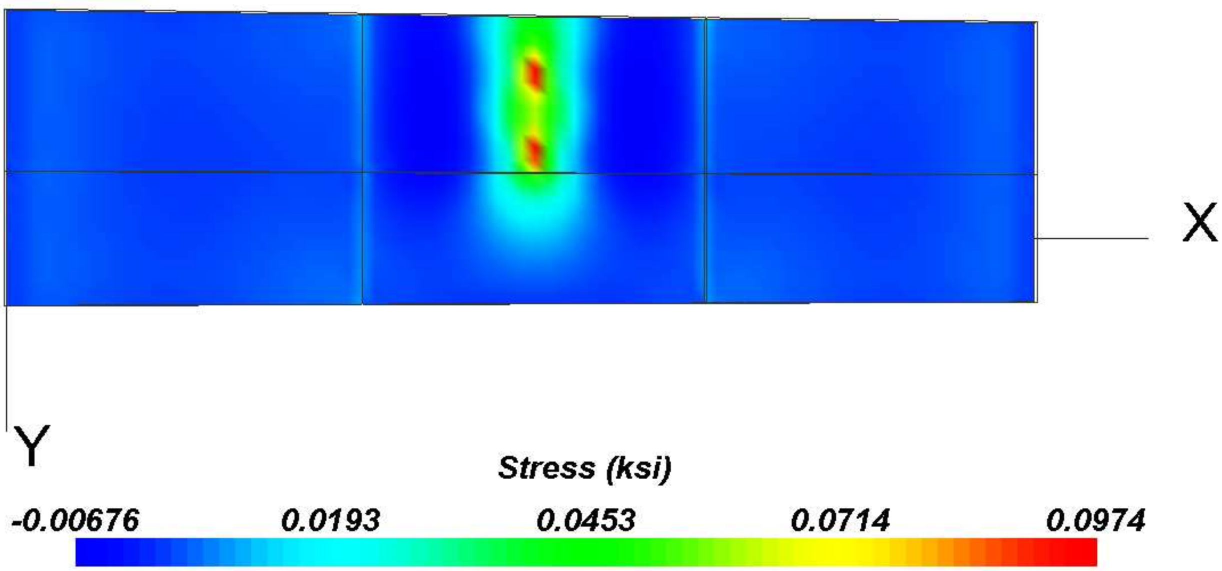


**Figure 2-11: Longitudinal stress at the bottom of the slab from EverFE for Problem 1**

**Problem 2**: A pavement system with 11.0-in. PCC slab, 3.9-in. aggregate base, 169-psi/in. roadbed, 177-in. joint spacing, 14-ft lane, and untied AC shoulder is given (an MDOT design on M-39 (C.S. 82192 and J.N. 45702) submitted on July 5, 2000 as the second design alternative). Analyze this pavement system for longitudinal stress at the bottom of the slab under the impact of 18-kips single axle edge loading using the ISLAB2000 and EverFE program.

Solution: The same mesh size (12 in. by 12 in.) is used for both ISLAB2000 and EverFE program. The results obtained from the ISLAB2000 and EverFE program are 97.1 psi and 104 psi, respectively. Figures 2-12 and 2-13 illustrate the graphical results obtained from both programs. It can be seen that the peak stress magnitudes and locations obtained from these models are comparable.

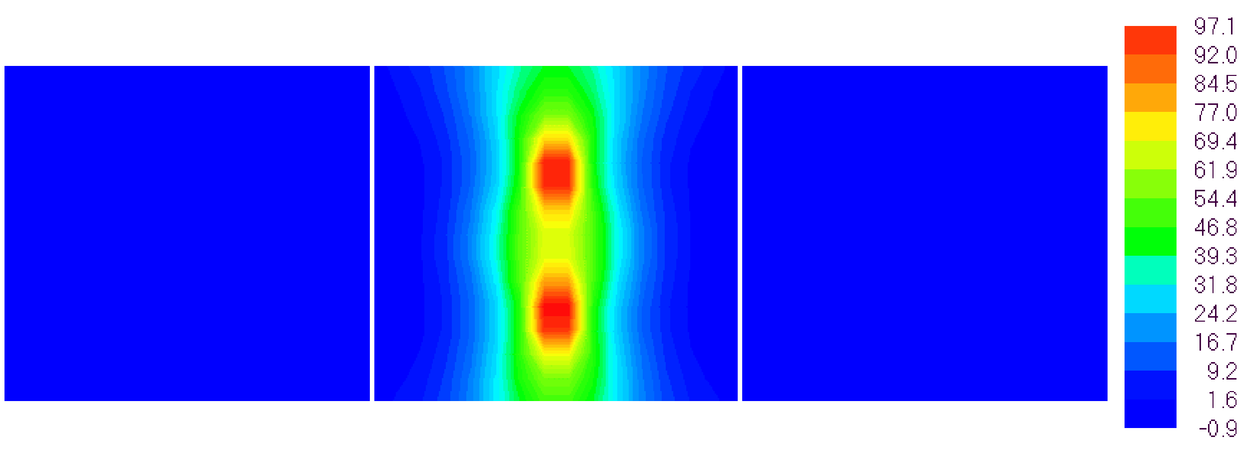


**Figure 2-12: Longitudinal stress at the bottom of the slab from ISLAB2000 for Problem 2**

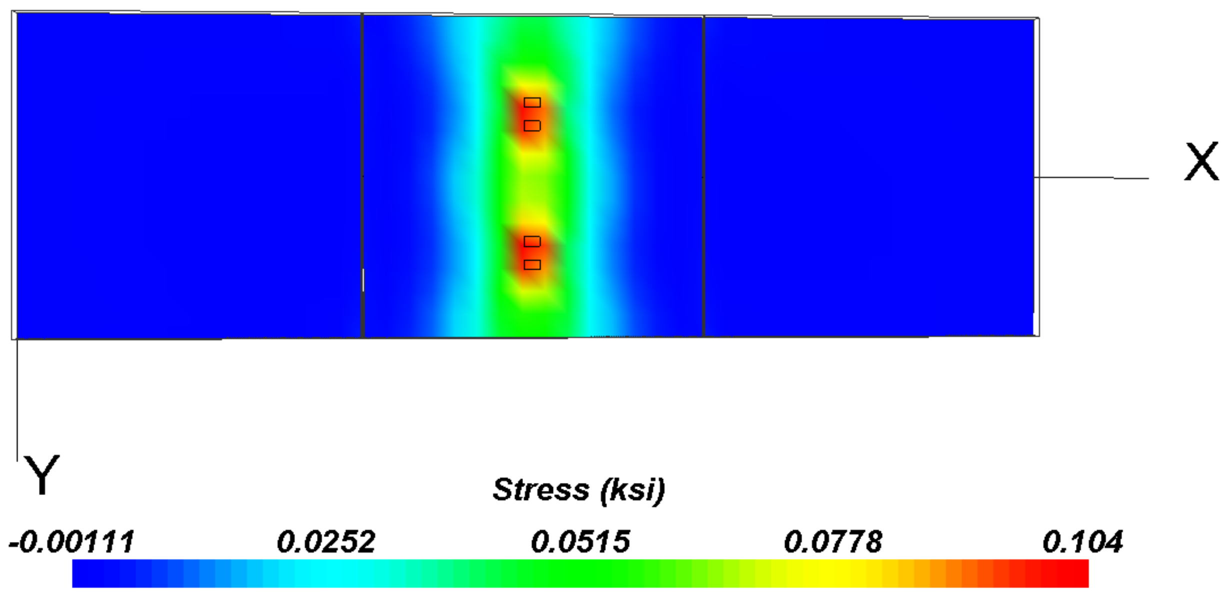


**Figure 2-13: Longitudinal stress at the bottom of the slab from EverFE for Problem 2**

It should be noted that unlike ISLAB2000, EverFE is not capable of modeling slabs with more than one material in the same system. Therefore, the untied AC shoulder is modeled by having no shoulder for both analyses.

**Problem 3**: Repeat Problem 1, but also consider a positive thermal gradient of 4 $^{o}$F/in.

Solution: The same mesh size (12 in. by 12 in.) is used for both ISLAB2000 and EverFE program. The results obtained from the ISLAB2000 and EverFE program are 557.5 psi and 571 psi, respectively. Figures 2-14 and 2-15 illustrate the graphical results obtained from both programs. It can be seen that the peak stress magnitudes and locations obtained from these models are comparable.

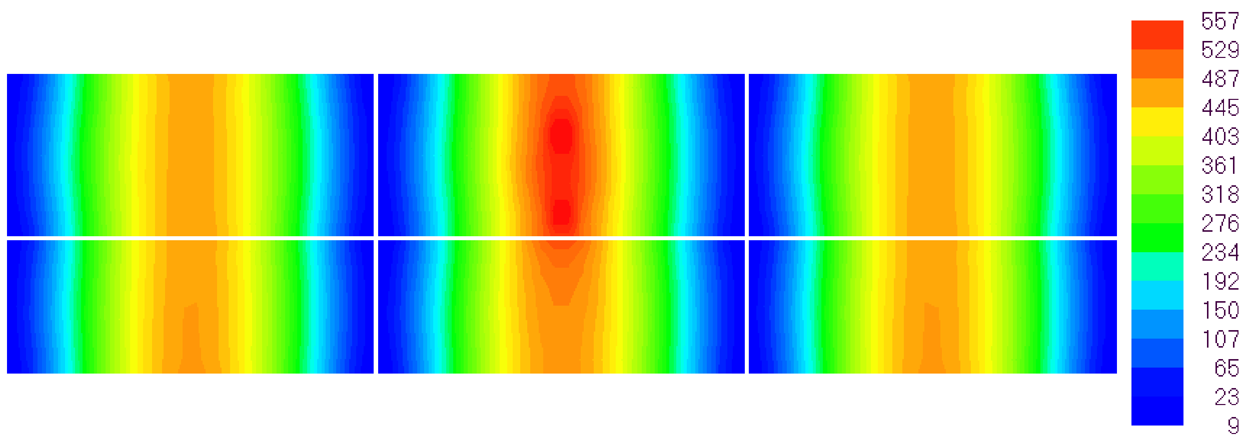


**Figure 2-14: Longitudinal stress at the bottom of the slab from ISLAB2000 for Problem 3**

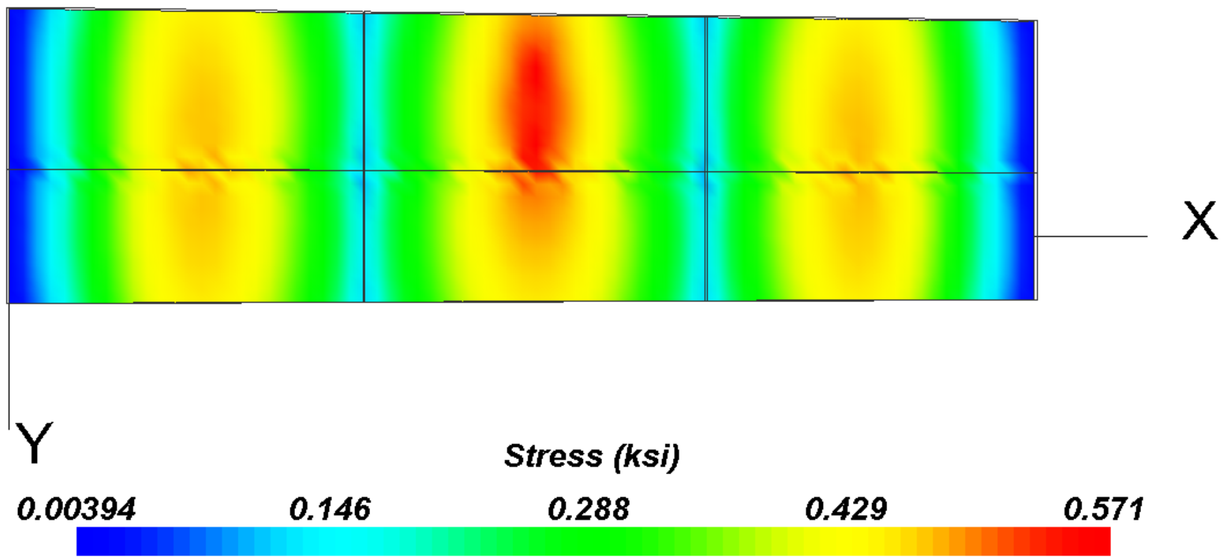


**Figure 2-15: Longitudinal stress at the bottom of the slab from EverFE for Problem 3**

It is important to note that due to their difference in structural models in that the ISLAB2000 program is a 2-D FE program, while the EverFE program is a 3-D FE program, the results obtained from these programs are not expected to perfectly match. However, according to these three practical engineering problems, the ISLAB2000 appears to provide similar results, when compared with results obtained from EverFE, which is another independent analysis approach. Therefore, this proves that the ISLAB2000 program is capable of providing reasonable analysis results for practical engineering problems.

# Chapter III

# EXPERIMENTAL MATRIX

An experimental matrix was constructed based on the concept of complete factorial for all combinations of design inputs reflecting MDOT practice, climatic condition, and load configurations in Michigan. Several engineering principles and common knowledge were applied to modify the experimental matrix with the purpose of making the experimental matrix more concise, but providing the same level of information. An overview of the process is illustrated in Figure 3-1.

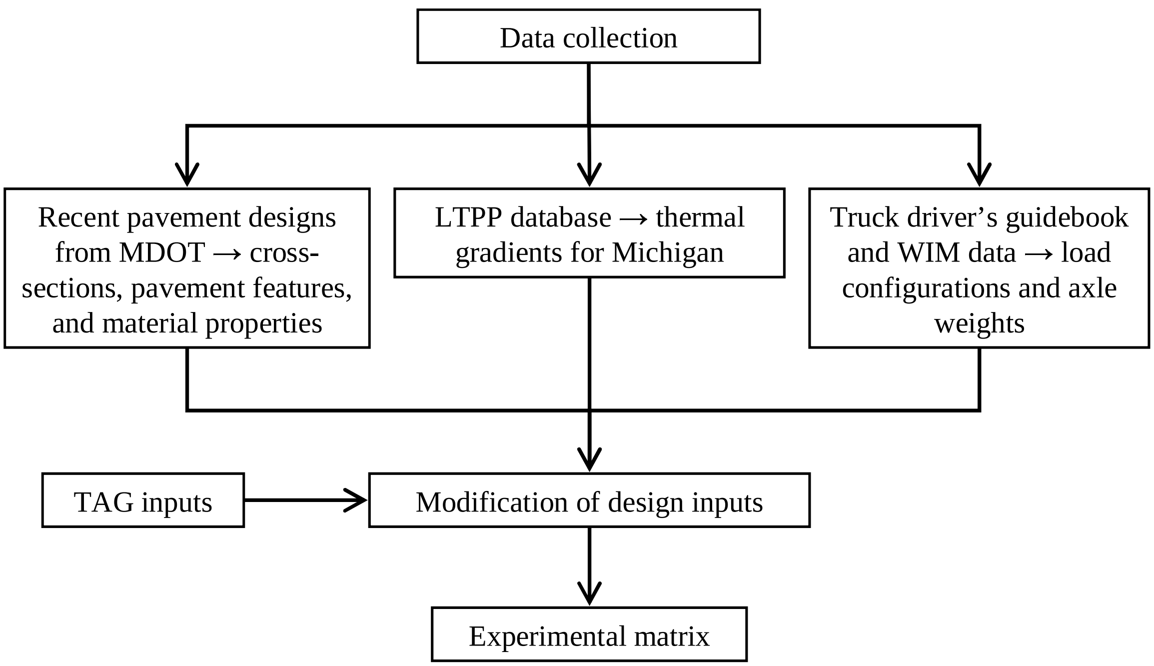


**Figure 3-1: An overview of the process of development of experimental matrix for parametric study**

## 3.1 Data Collection

The MDOT Technology Advisory Group (TAG) provided 14 "approved" designs for projects that were either recently constructed or were programmed for construction in the near future. These designs provided the structural parameters used for Michigan rigid pavements, e.g., cross-sections, pavement features, material properties, and etc. The ranges of inputs obtained from the MDOT designs are summarized in Table 3-1. Additional details are summarized in Appendix D.

**Table 3-1: Summary of design parameters from the 14 MDOT designs**

| Inputs | Min. | Max. |
|---|---|---|
| PCC thickness | 240 mm (9.5 in.) | 300 mm (12.0 in.) |
| Base thickness | 100 mm (4.0 in.) | 400 mm (16.0 in.) |
| Subbase thickness | No subbase | 300 mm (12.0 in.) |
| Joint spacing | 4.5 m (177 in.) | 8.0 m (315 in.) |
| Lane width | 3.6 m (12 ft) | 4.2 m (14 ft) |
| Lateral support condition | PCC shoulder, AC shoulder Widened lane | |
| Joint design | Doweled (1.25 in. diameter at 12 in. spacing center to center) | |
| $E_{pcc}$ | $29x10^6$ kPa ($4.2x10^6$ psi) | |
| Modulus of subgrade reaction | 24 kPa/mm (90 psi/in.) | 60 kPa/mm (220 psi/in.) |

In addition to the above mentioned input parameters, the analytical model required the following additional parameters (i) coefficient of thermal expansion (CTE) of the concrete, (ii) thermal gradients, (iii) axle and truck configurations, (iv) Poisson's ratio and unit weight. Based on the review of the literature (Klieger and Lamond, 1994), LTPP database, Truck driver's guidebook for Michigan (Michigan Center for Truck Safety, 2001), and conversations with the TAG, ranges for these additional input parameters were established and are summarized in Table 3-2.

**Table 3-2: Ranges of input parameters obtained from other sources**

| Input variables | Ranges |
|---|---|
| Concrete unit weight | 0.0087 lb/in.$^3$ |
| Concrete Poisson's ratio | 0.15 - 0.20 |
| Aggregate base unit weight | 0.0061 lb/in.$^3$ |
| Aggregate base Poisson's ratio | 0.35 |
| Thermal gradient | -4 - +4 $^oF$/in. |
| Coefficient of thermal expansion | $3x10^{-6}$ - 9 x $10^{-6}$ in./in./$^oF$ |
| Location of stress | Top and bottom |
| Load configuration | Single axle, tandem axle,… Multi-axle (8), MI-1, MI-2,… MI-20 |

## 3.2 Preparation of Experimental Matrix

An important first step in data analysis is to ensure that the project objectives can be accomplished within the limitations of time and funds. If every combination of input parameters is to be considered, the complete factorial experimental matrix would result in millions of FE runs. Hence, the experimental matrix size must be reduced, while the final product still serves the primary objectives. The preparation of the final matrix was achieved by carrying out the following strategies: combining variables, considering only frequently seen load configurations, and adjusting increments for non-discrete inputs.

**Combining Variables**

Two variables are combined into one variable to reduce the number of input combinations in the experimental matrix based on an assumption that the mechanistic response computed considering the combined variable would be the same or approximately the same as that computed considering the two variables, separately. The variables to be combined are base thickness and subbase thickness, which are combined into base/subbase thickness, and CTE ($\alpha$) and thermal gradient ($\Delta T/D$), which are combined into thermal strain gradient.

Figure 3-2 illustrates how base thickness and subbase thickness can be combined. It is assumed that the two layers have an unbonded interface, one elastic modulus represents the combined layer, and the Poisson's ratios of the two layers are approximately the same (Khazanovich and Yu, 2001). Sensitivity study of the accuracy of the combined base/subbase thickness was conducted for the 14 MDOT designs by comparing the mechanistic responses computed based on the two-layer system (PCC and combined base/subbase layers on the top of subgrade) and that based on the three-layer system (PCC, base and subbase layers on the top of subgrade). In this sensitivity study, for the three-layer system approach, an unbonded interface condition and Totski interface model (ERES Consultants, 1999) were considered between base and subbase layers and between PCC and base layers, respectively. An unbonded interface condition was considered for the two-layer system approach. It was found that the difference in the magnitudes of stresses between the two approaches is less than 4%. The results from the sensitivity study are illustrated in Figure 3-3 as compared with the results based on no subbase for the 14 MDOT design.

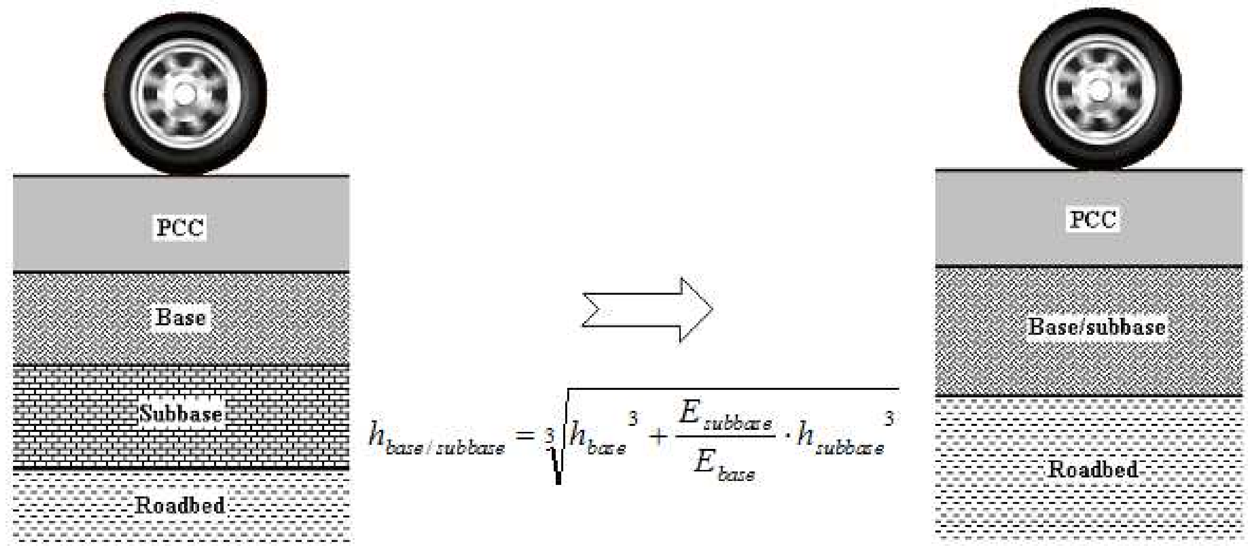


**Figure 3-2: Combining base and subbase layers**

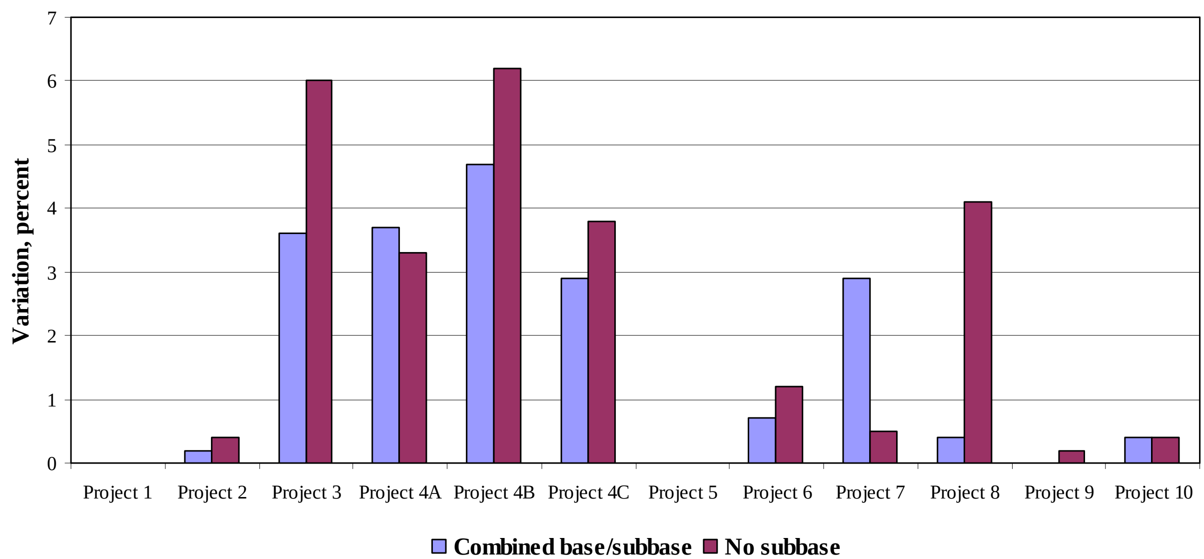


**Figure 3-3: Comparison of variation in results for combined base/subbase and no subbase approaches**

*Remarks: there is no subbase layer for projects 1 and 5

The CTE and thermal gradient are simultaneously accounted for in terms of the product of the two variables, $\alpha(\Delta T/D)$ or thermal strain gradient. Figure 3-4 illustrates the sensitivity plots to validate this assumption. The sensitivity study was conducted for nine cases by comparing the mechanistic responses computed based on two analysis approaches. Analysis approach 1 consists of varying CTE, while keeping thermal gradient constant. Analysis approach 2 consists of keeping CTE constant, while varying thermal gradient.

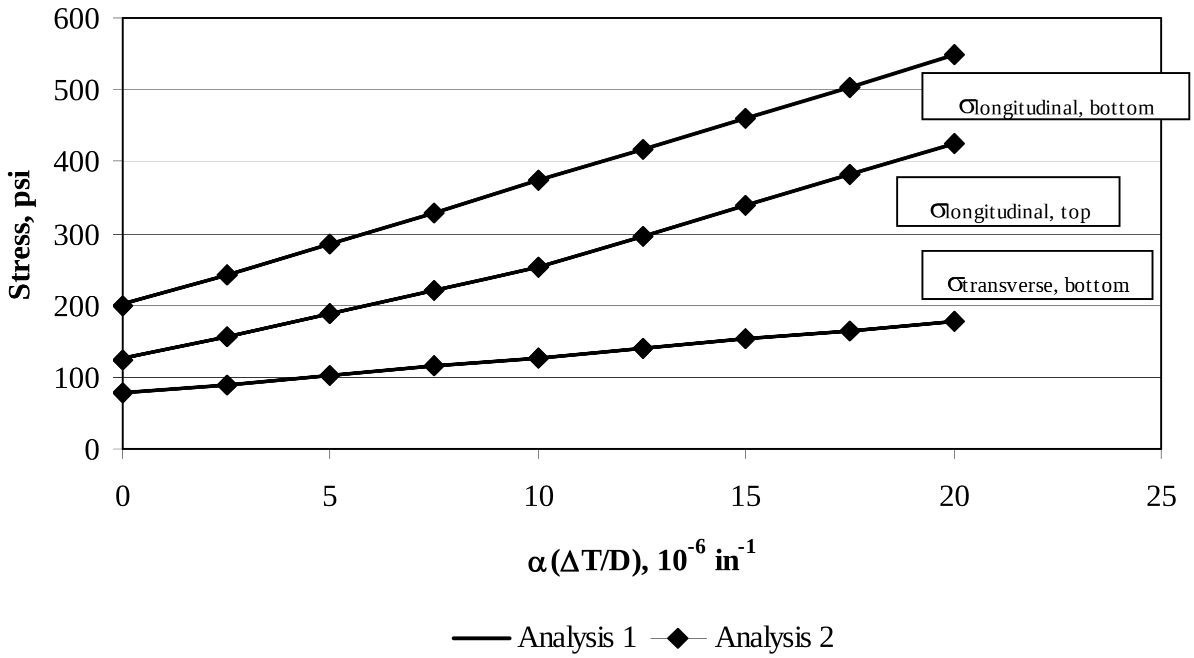


**Figure 3-4: Combining CTE and thermal gradient**

* Analysis 1: Constant temperature gradient (+2 $^{o}$F/in.) with variation of CTE ($0.1x10^{-6}$ to $10x10^{-6}$ in./in./$^{o}$F)
Analysis 2: Constant CTE ($5x10^{-6}$ in./in./$^{o}$F) with variation of temperature gradient (0 to +4 $^{o}$F/in.)

** PCC shoulder, 10-in. PCC thickness, 16-in. base/subbase thickness, 100-psi/in. k-value, single axle loading, 177-in. joint spacing

It was found that the mechanistic responses computed based on the two approaches are identical. A statistical experiment to illustrate the validity of combining CTE and thermal gradient was conducted by repeating this process for eight more combinations of pavement parameters selected based on a fractional factorial (Appendix E). It should be noted that pavements with different slab thickness with the same thermal strain gradient is not valid for comparison since the pavements are subjected to different temperature differentials. Comparison of pavement responses under a curled slab condition, therefore, should only be made within the same slab thickness.

**Considering Only Frequently Seen Load Configurations**

Several axle and truck configurations are contained in the Truck driver's guidebook for Michigan (Michigan Center for Truck Safety, 2001). Based on the TAG's recommendations, certain axle and truck configurations, not existent or not frequently seen, could presumably be omitted. Only 8 axle configurations and 11 truck configurations are selected for the experimental matrix. Figures 3-5 (a) and (b) illustrate the axle and truck configurations included in the parametric study.

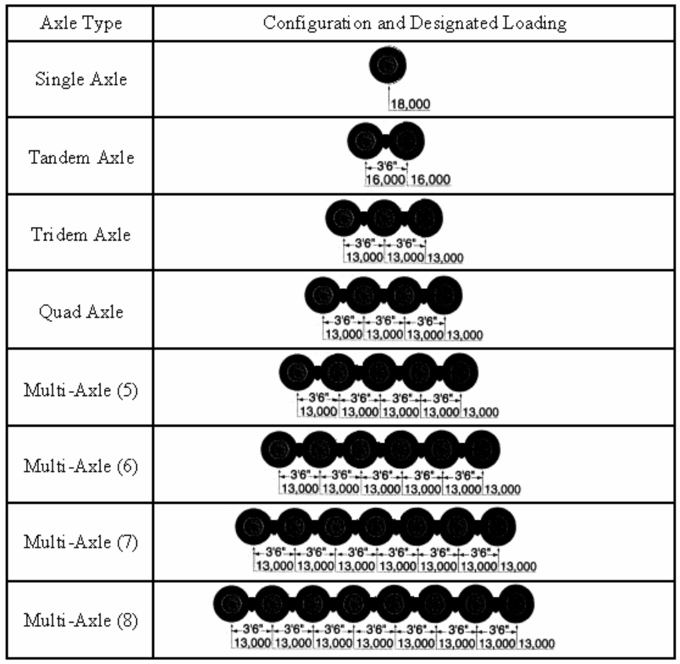


**(a) Axle configurations**

**Figure 3-5: Load configurations considered in the study**

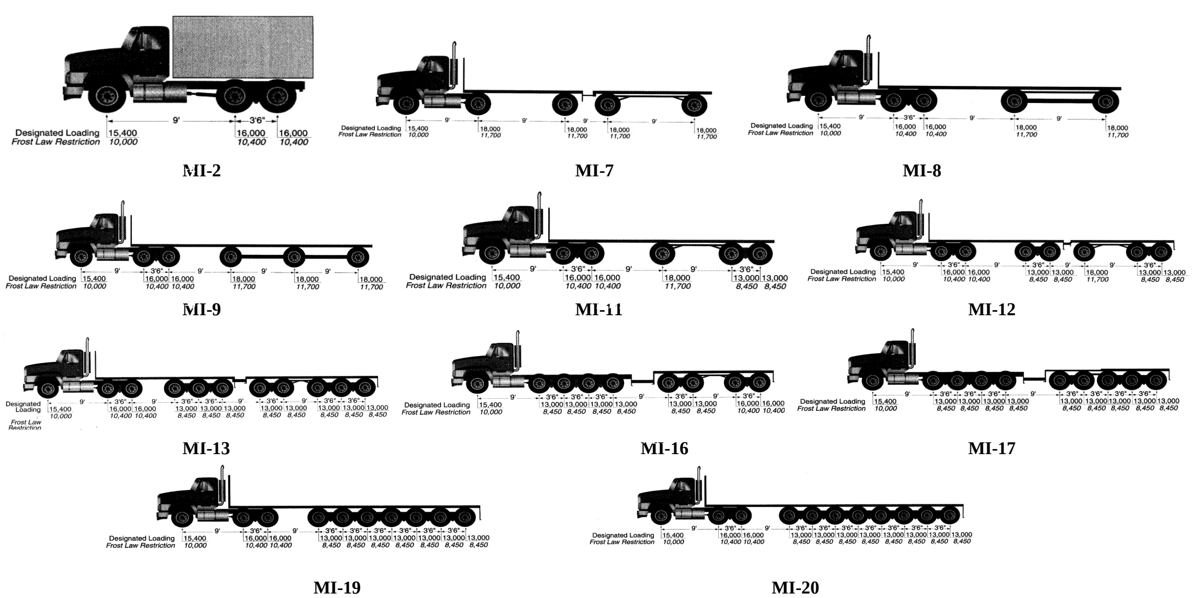


**(b) Truck configurations**

**Figure 3-5: Load configurations considered in the study (continued)**

## Adjusting Increments for Non-Discrete Inputs

Input increments need to be carefully considered for non-discrete variables, in this case, these included base/subbase thickness, modulus of subgrade reaction (k-value), and thermal strain gradient. The finer increments can better capture trends of the mechanistic responses, but will also result in increased number of FE runs. Therefore, it is crucial to capture trends of the mechanistic responses with large increments of input parameters as possible. Five values of each non-discrete variable were used in the sensitivity study of input increments. Based on this "mini analysis", it was determined that response trends could be adequately captured by using three values for each non-discrete variable. These values for the base/subbase thickness, k-value, and thermal strain gradient are 4, 16, 26 in., 30, 100, 200 psi/in., and 0, ±10, $\pm 20 \times 10^{-6}$ $in.^{-1}$, respectively. It should be noted that positive thermal gradients are considered for analysis of stresses at the bottom of the PCC slab, while negative thermal gradients are considered for analysis of stresses at the top of the PCC slab, since the critical stress locations correspond with the types of thermal gradient. Figures 3-6 through 3-8 illustrate the trends of stresses with variations of base/subbase thickness, modulus of subgrade reaction, and thermal strain gradient, respectively. Note that if not specified, the parameters for these sensitivity plots are 10-in. PCC slab, 16-in. base/subbase, 100-psi/in. modulus of subgrade reaction, PCC shoulder, 177-in. joint spacing, 18-kips single axle, and thermal strain gradient of zero.

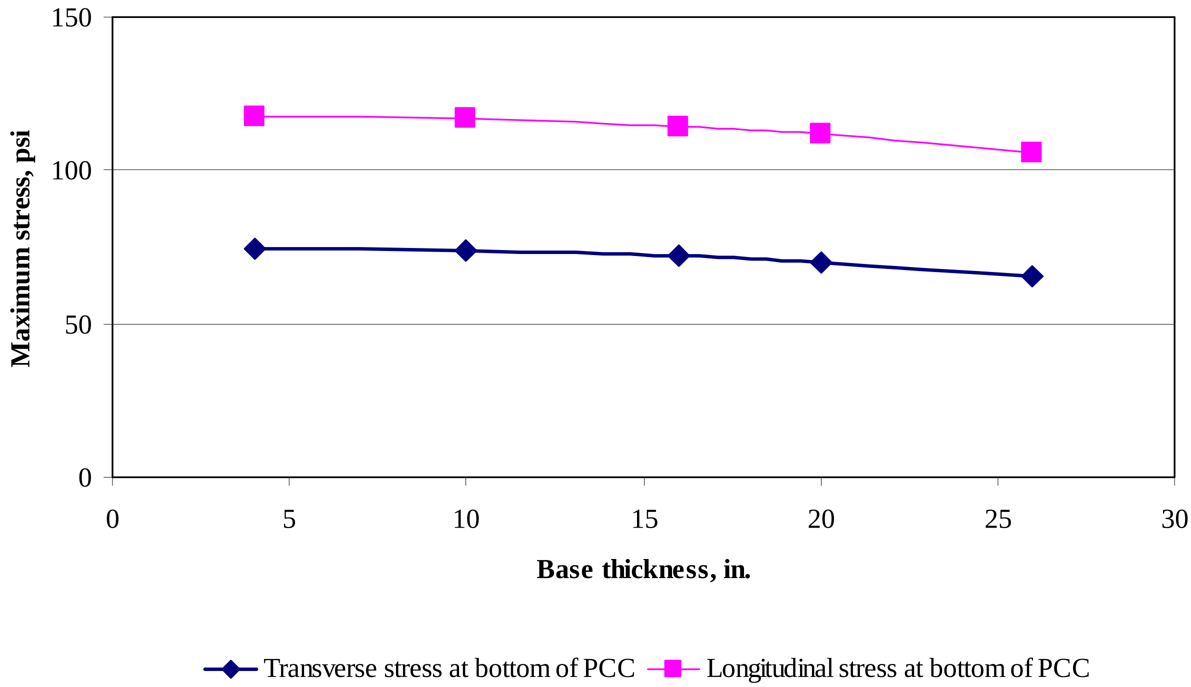


**Figure 3-6: Sensitivity trend due to the variation in base/subbase thickness**

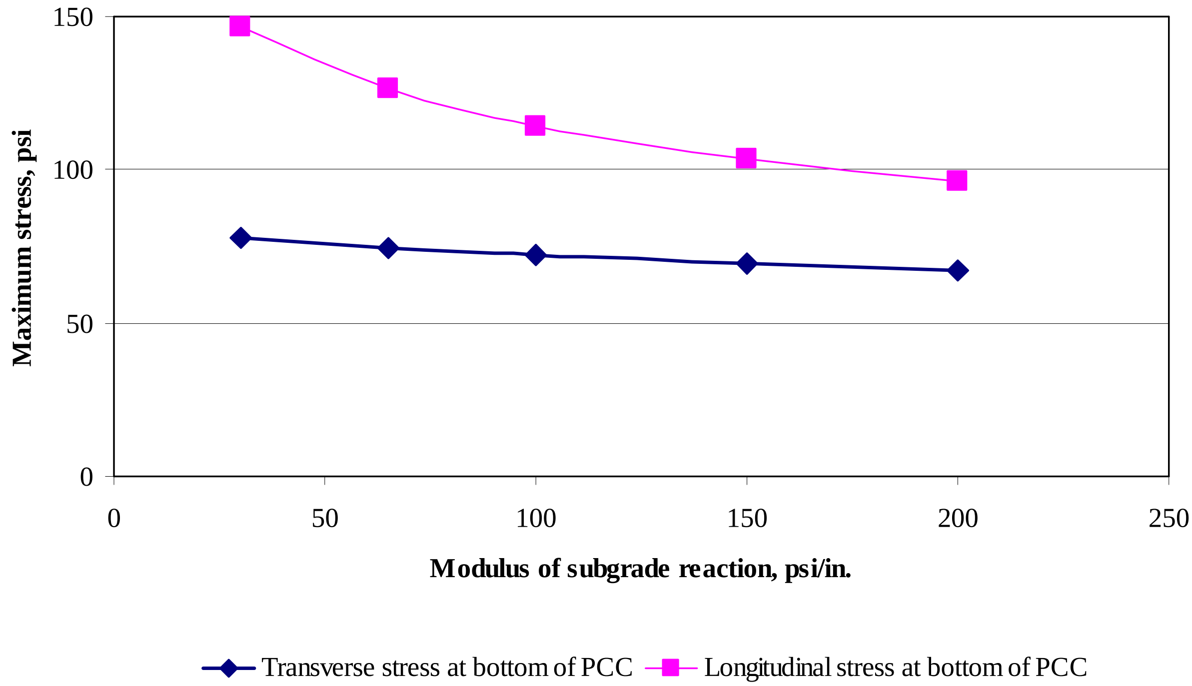


**Figure 3-7: Sensitivity trend due to the variation in modulus of subgrade reaction**

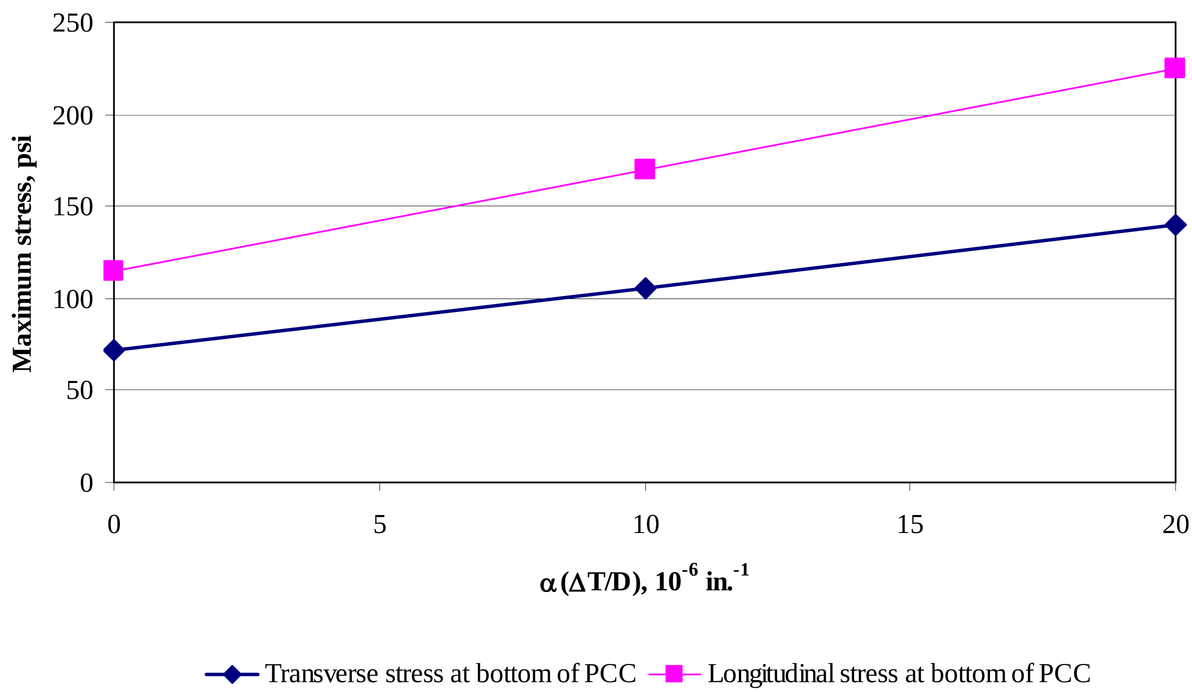


**Figure 3-8: Sensitivity trend due to the variation in thermal strain gradient**

## 3.3 Final Experimental Matrix

In addition to the above mentioned strategies, locations of stresses (at the bottom and the top of the PCC slab) are also effectively selected to reduce the number of runs. For positive thermal gradients, only stresses at the bottom of the PCC slab are considered, while stresses at the top of the PCC slab are considered for negative thermal gradients. The experimental matrix size has been reduced to 43,092 FE runs as illustrated in Table 3-3. It should be noted that all possible input parameters for all discrete variables and three levels of each non-discrete variable are addressed in this final experimental matrix. However, the combinations of non-discrete variables that are not addressed in this final experimental matrix are still of interest and will be obtained through the interpolation scheme, which is to be discussed later.

**Table 3-3: Final experimental matrix**

| Input variables | Number of cases |
|---|---|
| PCC slab thickness | 7 (6, 7,… 12 in.) |
| Base/subbase thickness | 3 (4, 16, 26 in.) |
| Modulus of subgrade reaction | 3 (30, ,100, 200 psi/in.) |
| Slab length (joint spacing) | 2 |
| Joint design | 1 |
| Shoulder type | 3 |
| $\alpha.\Delta T/D$ | 3 (0, ±10, ±20x10$^{-6}$ in$^{-1}$) |
| Location of stress | 2 |
| Load configuration | 19 |
| Total combinations | 43,092 |

# Chapter IV

# PARAMETRIC STUDY

Based on a complete factorial of 43,092 combinations of parameters identified in the previous chapter, a preliminary parametric study is conducted by performing a series of FE analyses using the ISLAB2000 program. The results obtained from this parametric study are included in this chapter. The parametric study will be presented in four parts: structural model, analysis process, documentation of analysis results and interpretation of analysis results.

## 4.1 Structural Model

The pavement system for this analysis typically comprises of three to six PCC slabs, depending on the length of the load configuration. This is to ensure that the first and last PCC slabs are unloaded as recommended in Report 1-26 (NCHRP, 1990) to analyze the pavement system with extended slabs in order to reflect realistic boundary conditions that all the slabs are bounded by two slabs on both directions. Two lane widths (12 and 14 ft) and two shoulder types (untied AC and tied PCC) are considered. The study focuses on the analysis of the mechanistic responses in the outer lane (the truck lane), which is traditionally the design lane. Two joint spacings (177 and 315 in.) are considered. The structural model with two traffic lanes was not found to result in different pavement response in the outer wheel path as compared to the results obtained from the structural model with one traffic lane. Therefore, the second traffic lane is not included in the structural model to reduce the structure size and consequently analysis time. The wheel path considered in this study is 20 in. from center of outer wheel to the traffic stripe, similar to the pavement model used by Darter et al, 1994. Mesh size of 12x12 in. is used as a standard mesh size. This mesh size was found to achieve both satisfactory convergence and reasonable runtime. Figure 4-1 illustrates the typical slab structure layout as modeled using ISLAB2000.

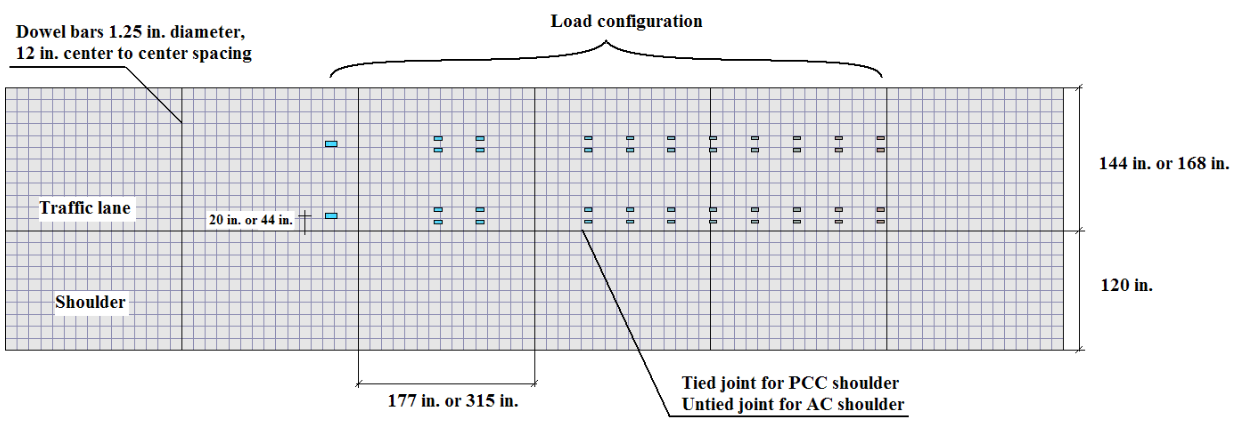


**Figure 4-1: Overview of structural model**

## 4.2 Analysis Process

The flow chart in Figure 4-2 illustrates the required components for the FE analysis. It can be seen that all structural and environmental factors have been addressed in the final experimental matrix. However, the critical load location needs to be derived first before the creation of the stress catalog. The critical load location is defined by the load location along the wheel path that results in the most critical mechanistic response, the highest value of the maximum responses for each load location.

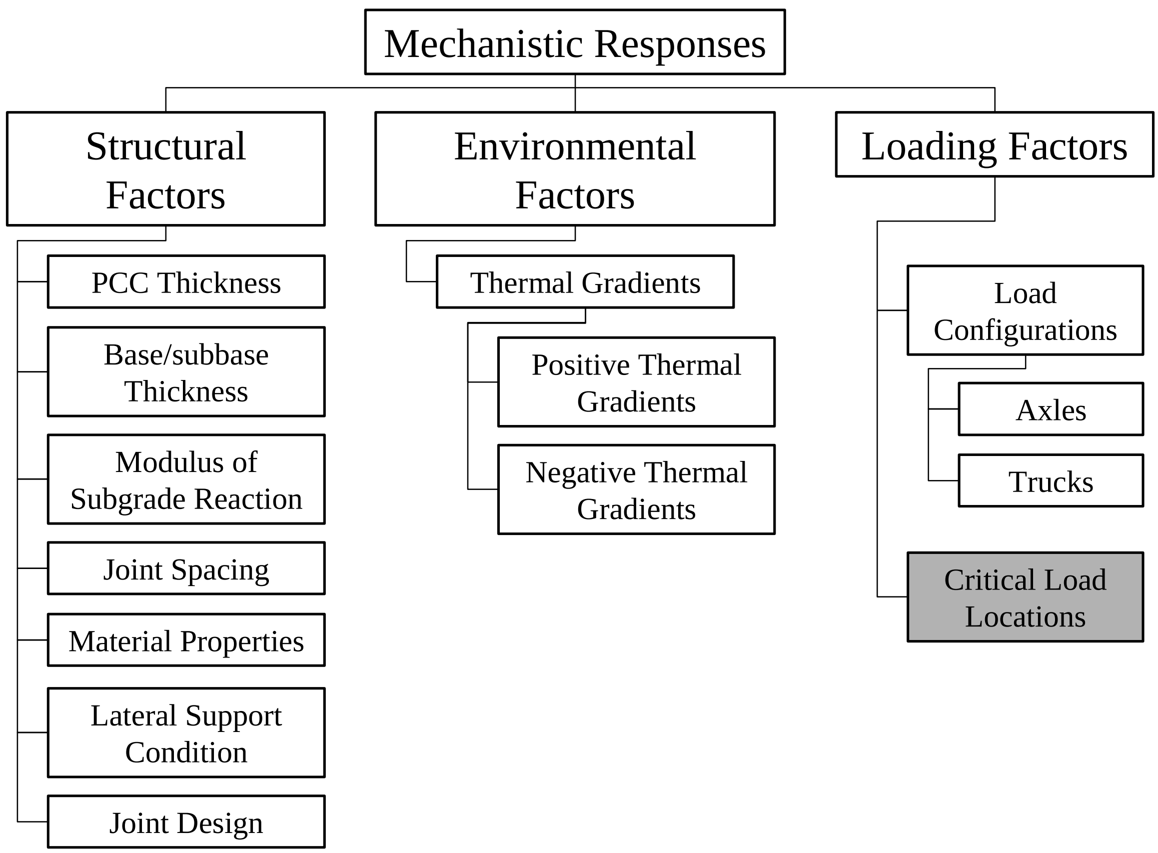


**Figure 4-2: Required components for the analytical tool**

### Procedure of determining critical load location

The procedure for determining critical load location is illustrated in Figure 4-3. The procedure involves the computation of stresses at every load location along the wheel path along the slab length for a given set of conditions. The load location that results in the most critical (maximum) stress will be considered as the critical load location.

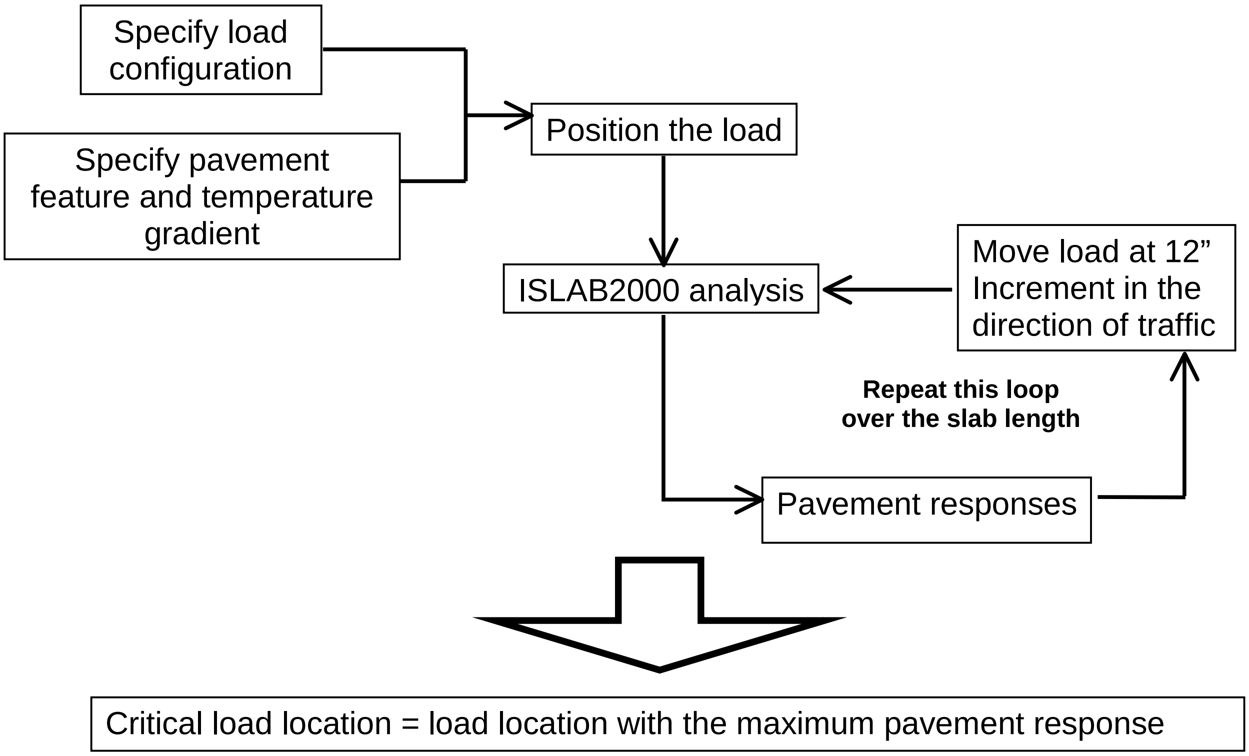


**Figure 4-3: Procedure of determining critical load location**

**Assumptions and validation process**

The procedure for determining critical load location is a time consuming process and is impractical to be performed for all possible combinations of input parameters in the final experimental matrix. It was assumed that variations in the following variables do not affect critical load locations:

- PCC thickness,
- Base/subbase thickness,
- k-value,
- Lateral support condition and
- Thermal strain gradient.

Validation of these assumptions was conducted to show that the critical load location is constant with the variation of the five non-influential variables. The fractional factorial design of $\frac{1}{3^3} \cdot 3^5 = 9$ is the method used to study the impact of variables within a practical size of validation matrix. The validation matrix used for all trucks and axles is summarized in Figure 4-4 (a). Note that fractional factorial design is a statistical method that allows for fractionation of a complete experimental factorial, while still balancing the fraction.

| | Validation#1 | Validation#2 | Validation#3 | Validation#4 | Validation#5 | Validation#6 | Validation#7 | Validation#8 | Validation#9 |
|---|---|---|---|---|---|---|---|---|---|
| Shoulder Type | PCC | AC | Widened Lane | PCC | AC | Widened Lane | PCC | AC | Widened Lane |
| PCC thickness, in. | 10" | 10" | 10" | 12" | 12" | 12" | 8" | 8" | 8" |
| Base/subbase thickness, in. | 16" | 26" | 4" | 26" | 4" | 16" | 4" | 16" | 26" |
| k-value, psi/in. | 100 | 30 | 200 | 200 | 100 | 30 | 30 | 200 | 100 |
| $\alpha.\Delta T/D$, x$10^{-6}$ in$^{-1}$ | 10 | 5 | 15 | 10 | 5 | 15 | 10 | 5 | 15 |
| Location increment, in. | 12 | 24 | 24 | 24 | 24 | 24 | 24 | 24 | 24 |

**(a) Validation matrix**

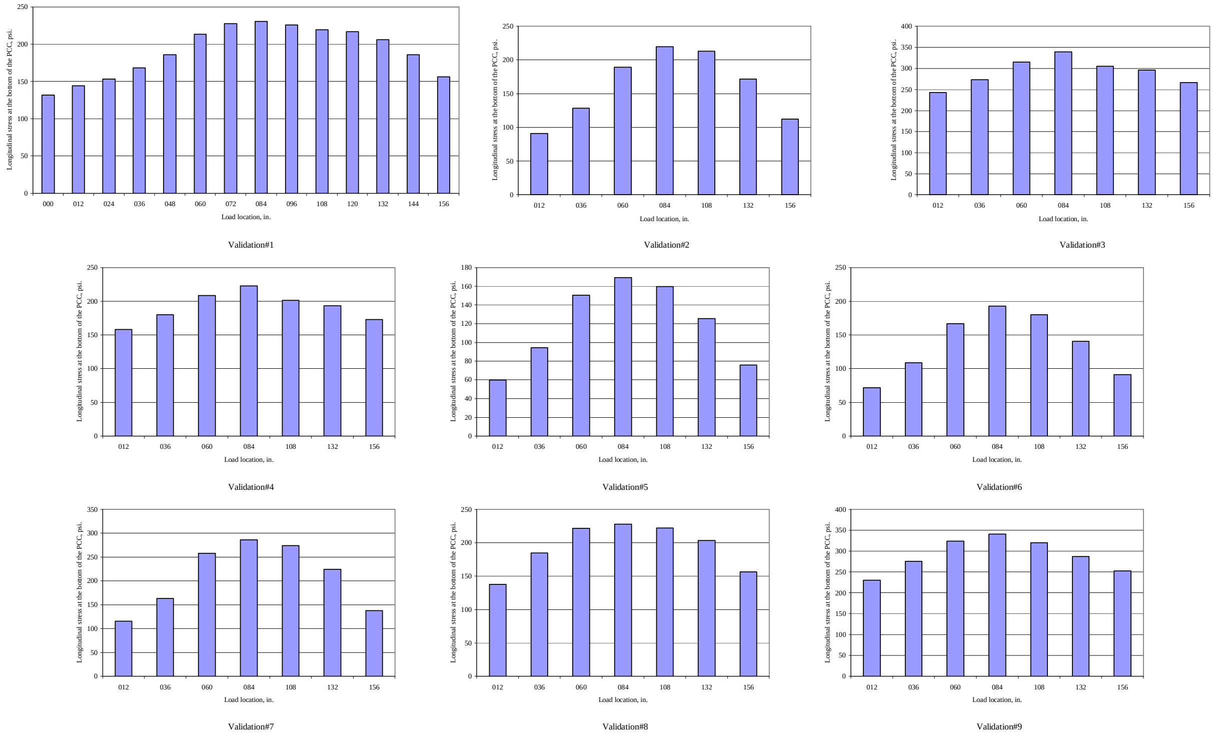


**(b) Example validation and determination (bottom stresses, MI-16, 177-in. joint spacing)**

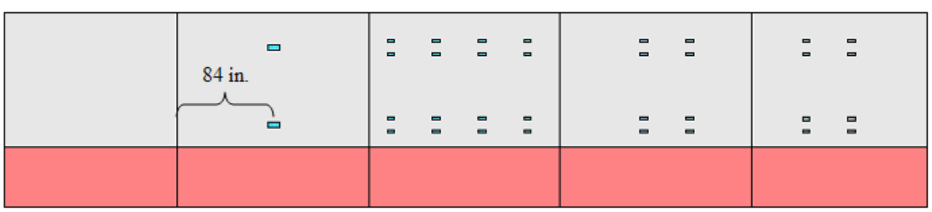


**(c) Physical meaning of determined critical load location**

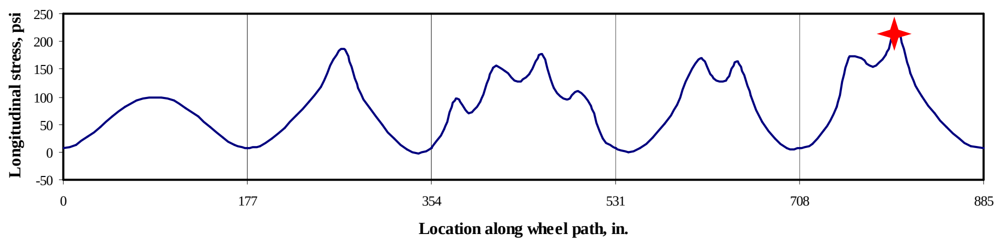


**(d) Longitudinal stress profile and location of critical stress at critical load location for validation case 1**

**Figure 4-4: Validation and determination of critical load location**

Figure 4-4 (b) illustrates an example of the assumption validation process used in the determination of the critical load location for bottom stresses for MI-16 on 177-in. joint spacing pavements. Stresses were computed for load locations along the wheel path for the nine validation cases as identified in Figure 4-4 (a). From the analysis results in Figure 4-4 (b), the non-influential variables were found to impact the stress magnitude; however, the non-influential variables did not significantly impact critical load location. For this example, the critical load location was approximately 84 in. for all the nine cases irrespective of the variation of the non-influential factors. Figure 4-4 (c) illustrates the physical meaning of the computed critical location in Figure 4-4 (b). An example stress profile for validation case 1 and the corresponding critical stress location are illustrated in Figure 4-4 (d). More example illustrations can be seen in Figures 4-5 and 4-6.


**Figure 4-5: Example validation and determination (bottom stresses, MI-9, 177-in. joint spacing)**


**Figure 4-6: Example validation and determination (bottom stresses, MI-20, 177-in. joint spacing)**

**Table 4-1: Summary of critical load locations**

| Load configuration | For critical stress at the bottom of the PCC | | For critical stress at the top of the PCC | |
|---|---|---|---|---|
| | 177 in. joint spacing | 315 in. joint spacing | 177 in. joint spacing | 315 in. joint spacing |
| Single axle | axle center at the midslab | axle center at the midslab | axle at the joint | axle at the joint |
| Tandem axle | axle center at the midslab | axle center at the midslab | 1st set of two wheels at the joint | 1st set of two wheels at the joint |
| Tridem axle | axle center at the midslab | axle center at the midslab | 1st set of two wheels at the joint | 3rd set of two wheels at the joint |
| Quad axle | axle center at the midslab | axle center at the midslab | 1st set of two wheels at the joint | 4th set of two wheels at the joint |
| Multi-axle 5 | axle center at the midslab | axle center at the midslab | 1st set of two wheels at the joint | 5th set of two wheels at the joint |
| Multi-axle 6 | axle center at the midslab | axle center at the midslab | 1st set of two wheels at the joint | 6th set of two wheels at the joint |
| Multi-axle 7 | axle center at the midslab | axle center at the midslab | 1st set of two wheels at the joint | 7th set of two wheels at the joint |
| Multi-axle 8 | axle center at the midslab | axle center at the midslab | 1st set of two wheels at the joint | 8th set of two wheels at the joint |
| MI-2 | 108 in. from the joint | 48 in. from the joint | 24 in. from the joint | 240 in. from the joint |
| MI-7 | at the joint | 36 in. from the joint | 96 in. from the joint | 192 in. from the joint |
| MI-8 | 60 in. from the joint | 96 in. from the joint | 60 in. from the joint | 264 in. from the joint |
| MI-9 | 132 in. from the joint | at the joint | 60 in. from the joint | 264 in. from the joint |
| MI-11 | 144 in. from the joint | 36 in. from the joint | 60 in. from the joint | 264 in. from the joint |
| MI-12 | 144 in. from the joint | 48 in. from the joint | 48 in. from the joint | 264 in. from the joint |
| MI-13 | 144 in. from the joint | 156 in. from the joint | 48 in. from the joint | 264 in. from the joint |
| MI-16 | 84 in. from the joint | 252 in. from the joint | 156 in. from the joint | 180 in. from the joint |
| MI-17 | 72 in. from the joint | 156 in. from the joint | 144 in. from the joint | 180 in. from the joint |
| MI-19 | 144 in. from the joint | 36 in. from the joint | 48 in. from the joint | 276 in. from the joint |
| MI-20 | 144 in. from the joint | 36 in. from the joint | 48 in. from the joint | 252 in. from the joint |

It is important to note that this process needs to be repeated for every axle and truck configuration, joint spacing, and stress location (top and bottom of the PCC slab) as these factors are considered influential in affecting critical load locations. Critical load locations for all eight axle configurations and 11 truck configurations are summarized in Table 4-1. Critical load locations for axle configurations were found to be in the vicinity of the middle of the slab and the transverse joint for stresses at the bottom and top of the PCC slab, respectively. However, no typical location was found for critical load locations for truck configurations due to the complex combinations of the axles and axle spacings within truck configurations.

## 4.3 Documentation of Analysis Results

Impact of structural factors, environmental factors, loading factors, and interaction between these factors on three types of mechanistic responses: longitudinal stress at the bottom of the PCC slab, transverse stress at the bottom of the PCC slab, and longitudinal stress at the top of the PCC slab is investigated.

**Impact of structural factors**

Figures 4-7 (a) through (f) are example illustrations of the impact of structural features on the longitudinal stress at the bottom of the PCC slab under various conditions as stated in the figures. Note that these figures represent MI-16 loading (see Figure 4-7 (c) for configuration), 16-in. base/subbase, 100-psi/in. k-value, PCC shoulder, and 177-in. joint spacing unless identified otherwise. All the figures show that PCC thickness has a significant impact in reducing stresses. In addition, the figures show that the changes in stresses due to changes in base/subbase thickness, k-value, and lateral support condition appear to be less relevant as the PCC slab becomes thicker. Also, joint spacing does not appear to have significant impact on edge stresses. Impact of lateral support condition will be discussed in detail later. Figures 4-7 (d) and (f) show an interaction of k-value and joint spacing with thermal gradients, which is to be discussed later. Although the magnitude of longitudinal stress at the bottom of the PCC slab were found to vary with combinations of input parameters, similar trends were observed in sensitivity plots over the entire experimental matrix. Similar trends were observed for the transverse stress at the bottom of the PCC slab with the exception of the impact of joint spacing, which was found to have no significant impact on the transverse stresses, even under the influence of a thermal gradient. An example critical location of stress is illustrated in Figure 4-7 (g).

The impact of structural features on longitudinal stress at the top of the PCC slab is illustrated in Figures 4-8 (a) through 4-8 (f). Note that these figures represent MI-16 loading (see Figure 3-4 (b) for configuration), 16-in. base/subbase, 100-psi/in. k-value, PCC shoulder, and 177-in. joint spacing the same conditions as previous parts unless identified otherwise. It can be seen in these figures that the magnitudes of longitudinal stresses at the top of the PCC slab are lower than the longitudinal stresses at the bottom of the PCC slab illustrated in the previous part. However, the trends observed for these stresses are similar. It should be noted that negative thermal gradients are considered in Figures 4-8 (d) and 4-8 (f), since the critical location of stresses is at the top of the PCC slab in these figures. An example critical location of stress is illustrated in Figure 4-8 (g).

**Impact of loading factors**

Figures 4-7 (h) and 4-8 (h) are example illustrations of the impact of the load configurations (axles and trucks) on the magnitude and normalized magnitude (by total weight of the configuration) of longitudinal stresses at the bottom and top of the PCC slab, respectively. In order to compare the contribution of each axle type (carrying different weight) on loading stress, it is necessary to express the stress as psi/kip. It can be seen that the normalized stress magnitudes are lower as the axle configurations have more load carrying wheels, implying that at the same stress level, a multi-axle can carry heavier loads than a single or tandem axle. However, the impact of truck configurations is not shown in these figures because each truck configuration makes various numbers of passes at the point of interest on the pavement slab. For example, the truck type MI-16 (see Figure 3-4 (b)) will result in four peaks of stresses corresponding to one single axle (driving axle), one quad axle, and two tandem axles. Hence, normalization based on total weight is not valid. The normalization should be based on the number of passes made by each axle group.

Impact of load lateral placement on mechanistic responses is presented in Figure 4-9 (a). Stresses were calculated for several load locations across the lane width. It was found that the PCC shoulder resulted in the lowest stresses among the three lateral support conditions considered in the study for the load located along the wheel path. It was found that the magnitudes of longitudinal stresses for AC shoulder (12-ft lane with AC shoulder) were higher than that for widened lane (also AC shoulder but with 14-ft lane). This could be attributed to the fact that a widened lane (14 ft.) creates a pseudo-interior loading condition (the wheel path shifted 2 ft towards the centerline, resulting in the reduction of stresses from edge loading). An example sensitivity plot of temperature-induced stresses in Figure 4-9 (b) illustrates that lateral support condition does not have a significant impact on temperature-induced stress in longitudinal direction. A series of sensitivity plots of the impact of lateral load placement on stresses for different lateral support conditions are presented in Appendix G.

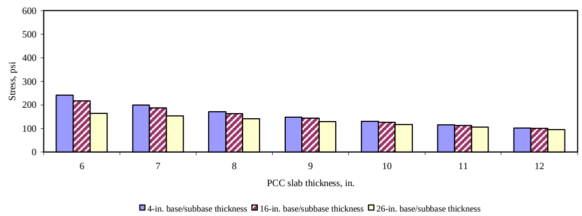


(a) Impact of base/subbase thickness, $\alpha(\Delta T/D) = 0\text{x}10^{-6}$ in.$^{-1}$

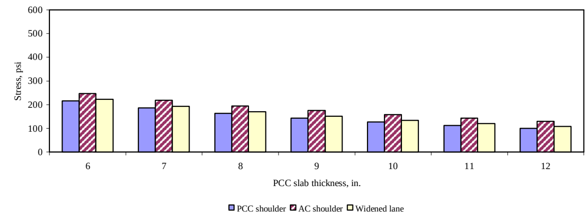


(b) Impact of lateral support condition, $\alpha(\Delta T/D) = 0\text{x}10^{-6}$ in.$^{-1}$

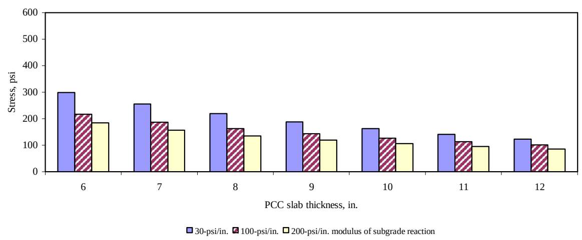


(c) Impact of modulus of subgrade reaction, $\alpha(\Delta T/D) = 0\text{x}10^{-6}$ in.$^{-1}$

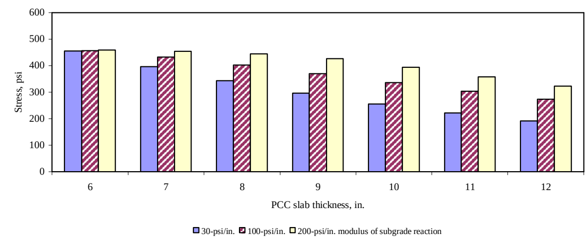


(d) Impact of modulus of subgrade reaction, $\alpha(\Delta T/D) = +20\text{x}10^{-6}$ in.$^{-1}$

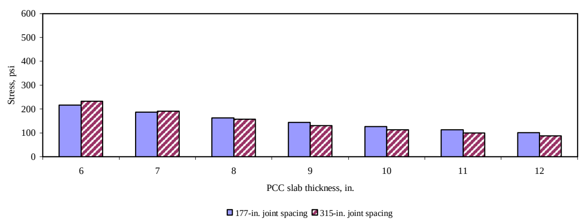


(e) Impact of joint spacing, $\alpha(\Delta T/D) = 0\text{x}10^{-6}$ in.$^{-1}$

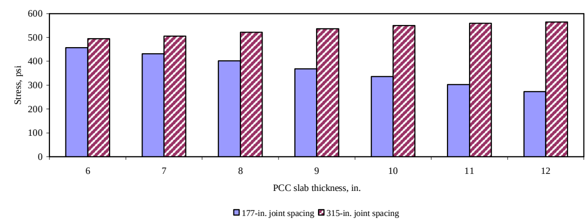


(f) Impact of joint spacing, $\alpha(\Delta T/D) = +20\text{x}10^{-6}$ in.$^{-1}$

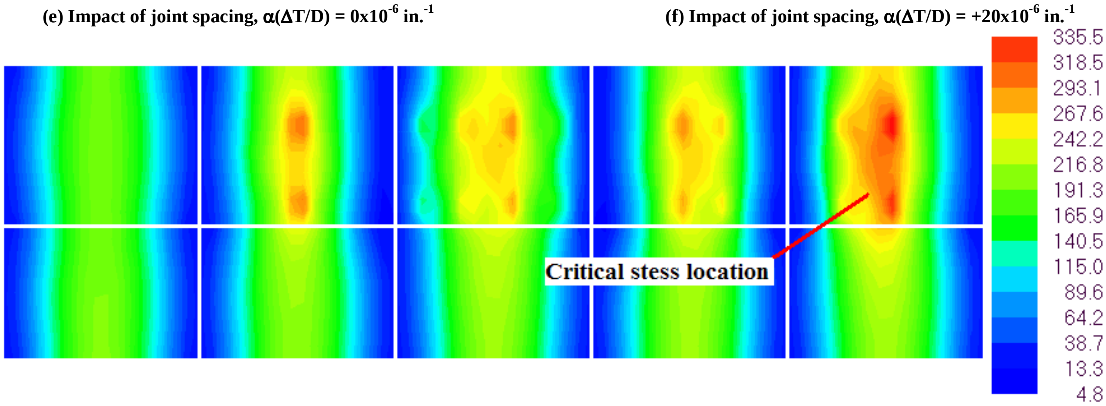


(g) Stress contour for 10-in. PCC slab, thermal strain gradient = $+20\text{x}10^{-6}$ in.$^{-1}$

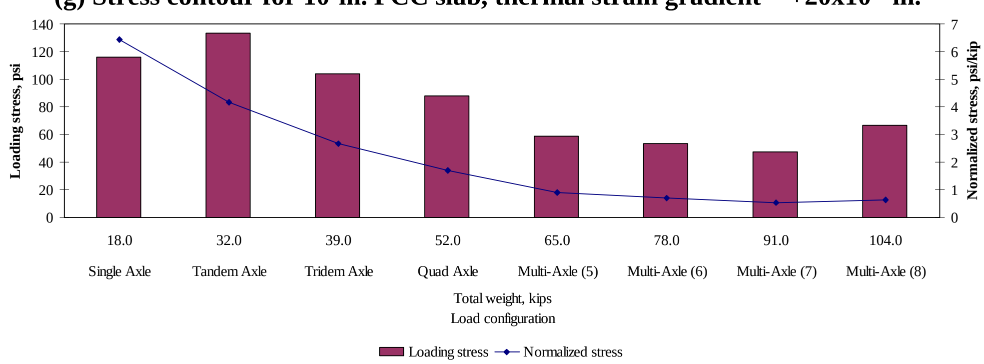


(h) 10-in. PCC slab, thermal strain gradient = $0\text{x}10^{-6}$ in.$^{-1}$

**Figure 4-7: Example sensitivity plots of longitudinal stresses at the bottom of the PCC slab**

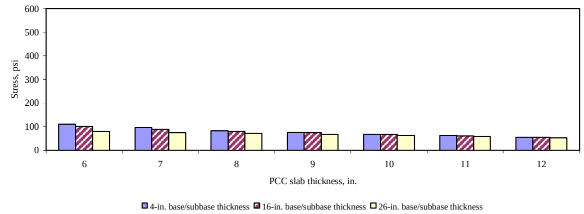


**(a) Impact of base/subbase thickness, α(ΔT/D) = 0x10$^{-6}$ in.$^{-1}$**

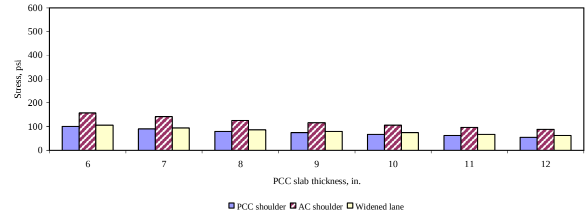


**(b) Impact of lateral support condition, α(ΔT/D) = 0x10$^{-6}$ in.$^{-1}$**

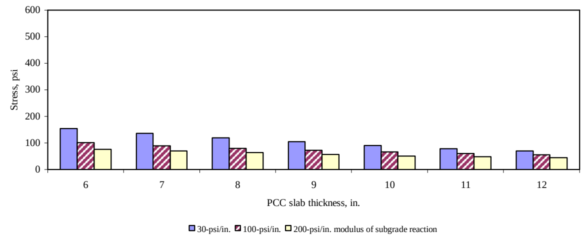


**(c) Impact of modulus of subgrade reaction, α(ΔT/D) = 0x10$^{-6}$ in.$^{-1}$**

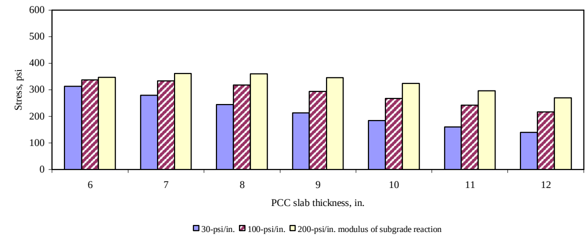


**(d) Impact of modulus of subgrade reaction, α(ΔT/D) = -20x10$^{-6}$ in.$^{-1}$**

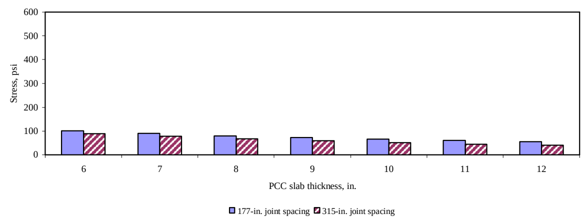


**(e) Impact of joint spacing, α(ΔT/D) = 0x10$^{-6}$ in.$^{-1}$**

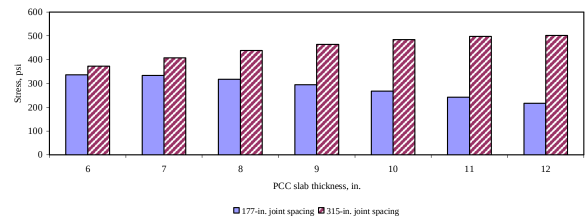


**(f) Impact of joint spacing, α(ΔT/D) = -20x10$^{-6}$ in.$^{-1}$**

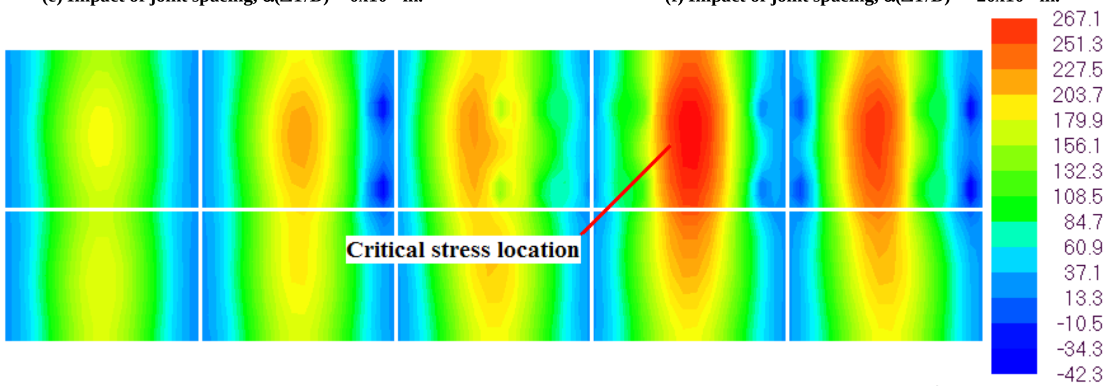


**(g) Stress contour for 10-in. PCC slab, thermal strain gradient = -20x10$^{-6}$ in.$^{-1}$**

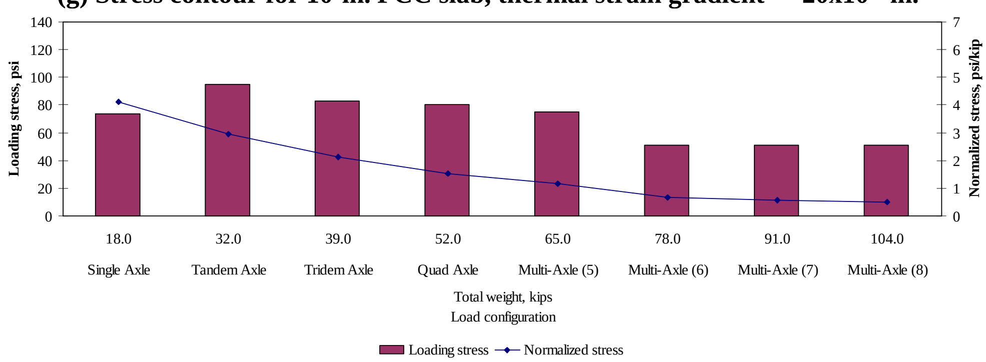


**(h) 10-in. PCC slab, thermal strain gradient = 0x10$^{-6}$ in.$^{-1}$**

**Figure 4-8: Example sensitivity plots of longitudinal stresses at the top of the PCC slab**

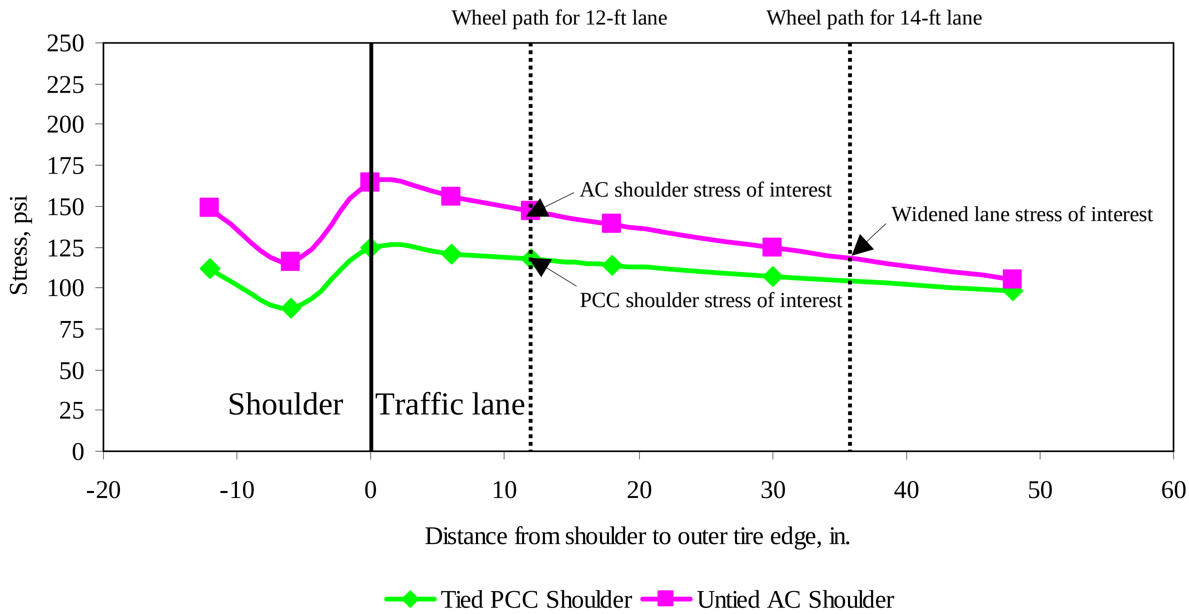


**(a) Effect of load lateral placement on different lateral support conditions**

Remarks: Longitudinal stresses at the bottom of the PCC slab, 10-in. PCC thickness, 16-in. base/subbase thickness, 100-psi/in. k-value, single axle, zero thermal gradient)

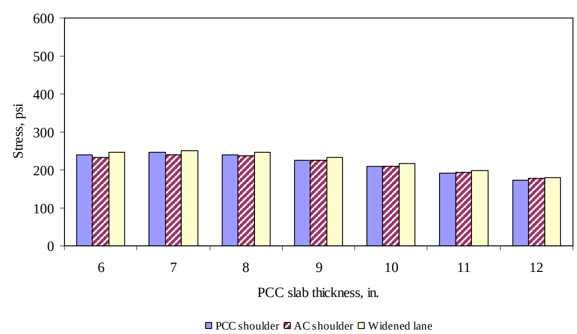


**(b) Longitudinal temperature stress at the bottom of the PCC slab**

**Figure 4-9: Impact of lateral support condition**

## Impact of environmental factors

Environmental factors in this study are accounted in terms of thermal strain gradient (the product of CTE with positive or negative thermal gradients). As illustrated in Figures 4-10 (a) and (b), a positive gradient causes a downward curling of the slab, while a negative gradient causes an upward curling of the slab. The increase in magnitude of thermal gradient results in the increase in the magnitude of stresses, when positive and negative thermal gradients are considered in computation of stresses at the bottom and top of the PCC slab, respectively. As observed in the previous section (Figures 4-7 (d) and 4-8 (d)), the magnitude of the longitudinal stress appears to be impacted by the interaction between the thermal strain gradients, k-value and pavement thickness. This interactive trend is supported by the curling stress equations by Bradbury (Huang, 1993), where thermal curling stress is a function of finite slab correction factor. This factor generally increases with the increase in the ratio of joint spacing (for longitudinal stresses) to radius of relative stiffness.

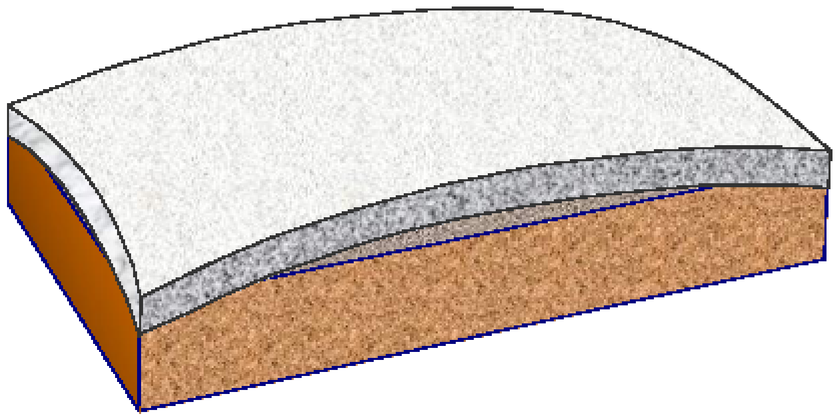

**(a) Downward curling of slab due to a positive thermal gradient**

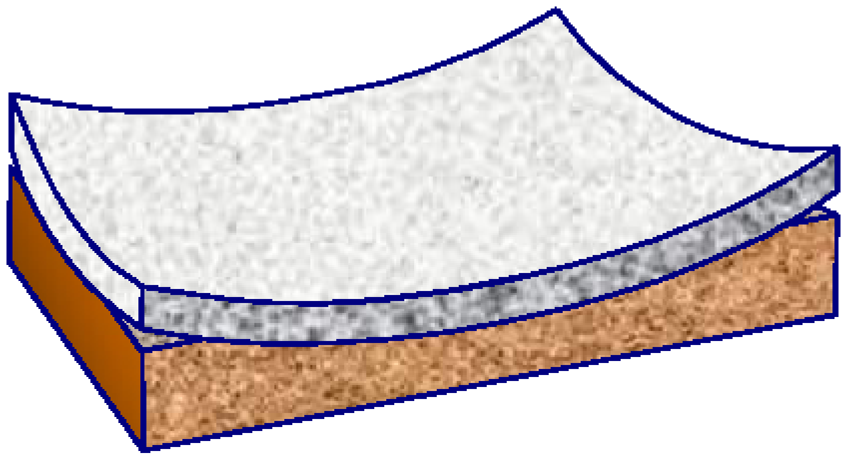

**(b) Upward curling of slab due to a negative thermal gradient**

**Figure 4-10: Slab curling due to different types of thermal gradients (Yu et al, 2004)**

Boundary support condition along the longitudinal joints of the slabs is characterized through AGG factor in ISLAB2000 program. It is crucial that an appropriate value of AGG factor is selected to represent the load transfer mechanism. The AGG factor can be empirically estimated as follows (Crovetti, 1994):

$$AGG = \left( \frac{\frac{1}{LTE} - 0.01}{0.012} \right)^{-\frac{1}{0.849}} \cdot k \cdot l \qquad (4\text{-}1)$$

Where AGG = AGG factor
LTE = Load transfer efficiency, percent
$\ell$ = Radius of relative stiffness, in
k = Modulus of subgrade reaction

The radius of relative stiffness is defined as follows:

$$l = \sqrt[4]{\frac{E \cdot h^3}{12(1-\mu^2) \cdot k}} \qquad (4\text{-}2)$$

Where $\ell$ = Radius of relative stiffness, in
E = Elastic modulus of layer 1
h = Thickness of layer 1
$\mu$ = Poisson's ratio for layer 1
k = Modulus of subgrade reaction

In general, the typical values of LTE for tied PCC shoulder and untied AC shoulder vary from 25-90 % and 0-40 %, respectively. Based on equation 4-1, the ranges of AGG/k$\ell$ were calculated as 0-0.77 and 0.34-16.5 for tied PCC shoulder and untied AC shoulder, respectively. Based on the inputs in the parametric study, the range of k$\ell$ varies from 1188 to 8286 psi. A sensitivity study of the effect of AGG factor on magnitude of edge stresses is conducted for ranges of AGG factor from 5 to 7,000 psi (AC shoulder and widened lane) and from 300 to 2,500,000 psi (PCC shoulder). Based on these results, the AGG factors of 1,000,000 psi and 1,000 psi are selected for tied PCC shoulder and untied AC shoulder for the parametric study, respectively. Note that this sensitivity study is conducted for 177-in. joint spacing and 18-kips single axle at flat slab condition. Several sensitivity plots are generated as illustrated in Figures 4-11 (a) through 4-11 (c). It can be seen that the stress magnitude is not significantly sensitive to AGG factor for PCC shoulder and widened lane, while for AC shoulder the variation in stress magnitude could be up to 10% from stress magnitude computed based on the selected AGG factor (1,000 psi).

A complete documentation of interaction between all design parameters in the parametric study can be seen in Appendix F. Summary of the interaction is summarized in Table 4-2.

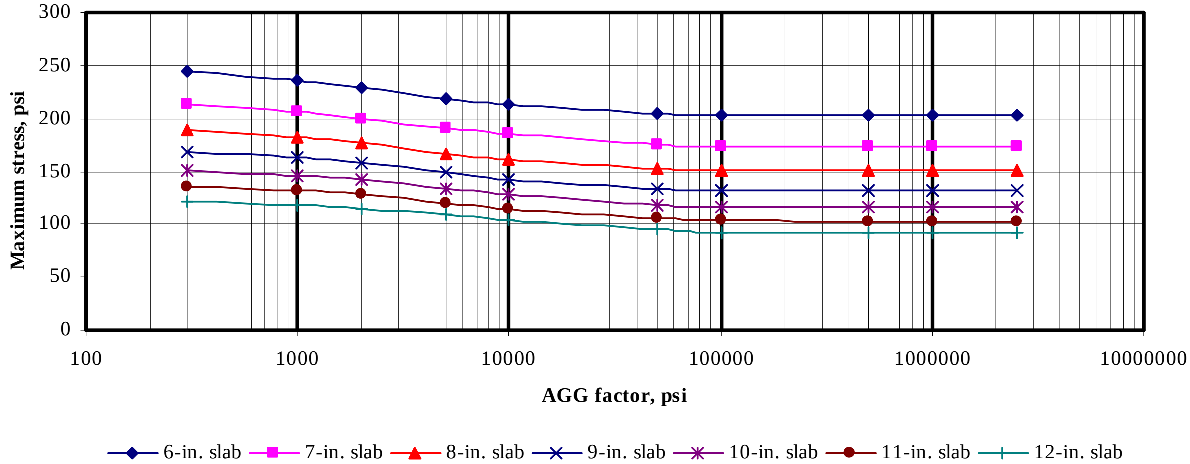


**(a) PCC shoulder**

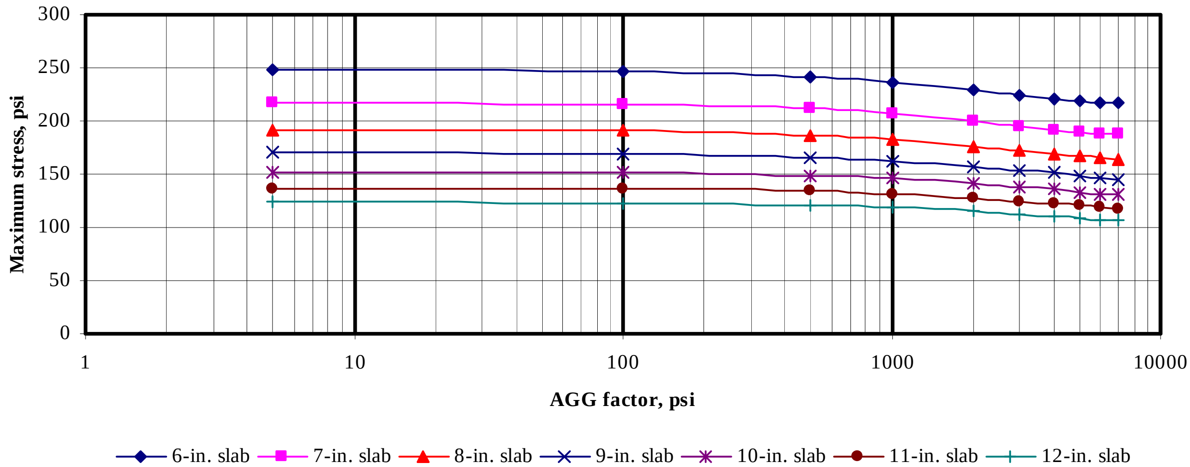


**(b) AC shoulder**

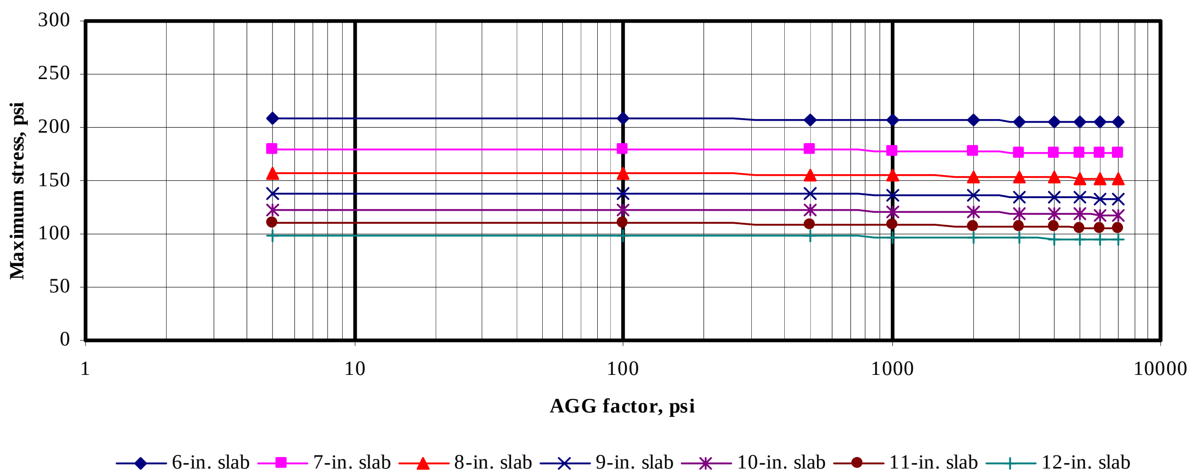


**(c) Widened lane**

**Figure 4-11: Effect of longitudinal joint AGG factor on stress magnitude**

**Table 4-2: Summary of interaction between parameters on stresses**

| Parameters | Slab condition | Response type | Effects of parameters |
|---|---|---|---|
| PCC thickness versus base/subbase thickness | Flat slab | Longitudinal at bottom of PCC | Thicker base/subbase thickness results in lower stress, but smaller magnitude of stress reduction was observed with thicker PCC |
| | | Longitudinal at top of PCC | Same as that for longitudinal stress at bottom of PCC |
| | | Transverse at bottom of PCC | Same as that for longitudinal stress at bottom of PCC |
| | Curled slab | Longitudinal at bottom of PCC | With higher temperature differential (thicker PCC), thicker base/subbase thickness results in higher stress magnitude |
| | | Longitudinal at top of PCC | Same as that for longitudinal stress at bottom of PCC |
| | | Transverse at bottom of PCC | Same as that for longitudinal stress at bottom of PCC |
| PCC thickness versus modulus of subgrade reaction | Flat slab | Longitudinal at bottom of PCC | Higher value of modulus of subgrade reaction results in lower stress value. There is no significant interaction between these parameters observed. |
| | | Longitudinal at top of PCC | Same as that for longitudinal stress at bottom of PCC |
| | | Transverse at bottom of PCC | Same as that for longitudinal stress at bottom of PCC |
| | Curled slab | Longitudinal at bottom of PCC | Higher value of modulus of subgrade reaction results in higher stress value. Change in stress due to modulus of subgrade reaction is larger as temperature differential increases (PCC thickness increases), and eventually the change in stress will remain constant. |
| | | Longitudinal at top of PCC | Same as that for longitudinal stress at bottom of PCC |
| | | Transverse at bottom of PCC | Same as that for longitudinal stress at bottom of PCC |
| PCC thickness versus lateral support condition | Flat slab | Longitudinal at bottom of PCC | Higher stress value is observed in pavement with AC shoulder. There is no significant interaction between these parameters observed. |
| | | Longitudinal at top of PCC | Same as that for longitudinal stress at bottom of PCC |
| | | Transverse at bottom of PCC | The magnitude of stress are about the same for all three lateral support conditions. There is no significant interaction between these parameters observed. |
| | Curled slab | Longitudinal at bottom of PCC | Higher stress value is observed in pavement with AC shoulder. There is no significant interaction between these parameters observed. |
| | | Longitudinal at top of PCC | Same as that for longitudinal stress at bottom of PCC |
| | | Transverse at bottom of PCC | Higher stress value is observed in pavement with Widened lane. There is no significant interaction between these parameters observed. |

**Table 4-2: Summary of interaction between parameters on stresses (continued)**

| Parameters | Slab condition | Response type | Effects of parameters |
|---|---|---|---|
| Product of CTE with thermal gradient versus base/subbase thickness | 177-in. joint spacing, curled slab | Longitudinal at bottom of PCC | Increase in product of CTE with thermal gradient linearly results in increase in stress magnitude. Interaction between these parameters is observed that increase in stress magnitude due to increase in product of CTE with thermal gradient is more intense with thicker base/subbase |
| | | Longitudinal at top of PCC | Same as that for longitudinal stress at bottom of PCC |
| | | Transverse at bottom of PCC | Same as that for longitudinal stress at bottom of PCC |
| | 315-in. joint spacing, curled slab | Longitudinal at bottom of PCC | Increase in product of CTE with thermal gradient linearly results in increase in stress magnitude. However, the interaction observed for 177-in. joint spacing is not observed for this 315-in. joint spacing. |
| | | Longitudinal at top of PCC | Increase in product of CTE with thermal gradient linearly results in increase in stress magnitude. However, the interaction observed for 177-in. joint spacing is not observed for this 315-in. joint spacing. |
| | | Transverse at bottom of PCC | Same as that for 177-in. joint spacing |
| Product of CTE with thermal gradient versus base/subbase thickness | 177-in. joint spacing, curled slab | Longitudinal at bottom of PCC | Increase in product of CTE with thermal gradient linearly results in increase in stress magnitude. Interaction between these parameters is observed that increase in stress magnitude due to increase in product of CTE with thermal gradient is more intense with higher value of moduluf of subgrade reaction |
| | | Longitudinal at top of PCC | Same as that for longitudinal stress at bottom of PCC |
| | | Transverse at bottom of PCC | Same as that for longitudinal stress at bottom of PCC |
| | 315-in. joint spacing, curled slab | Longitudinal at bottom of PCC | Increase in product of CTE with thermal gradient linearly results in increase in stress magnitude. However, the interaction observed for this 315-in. joint spacing is not as intense as that for 177-in. joint spacing. |
| | | Longitudinal at top of PCC | Increase in product of CTE with thermal gradient linearly results in increase in stress magnitude. However, the interaction observed for this 315-in. joint spacing is not as intense as that for 177-in. joint spacing. |
| | | Transverse at bottom of PCC | Same as that for 177-in. joint spacing |
| Product of CTE with thermal gradient versus joint spacing | Curled slab | Longitudinal at bottom of PCC | Increase in product of CTE with thermal gradient linearly results in increase in stress magnitude. Interaction between these parameters is observed that increase in stress magnitude due to increase in product of CTE with thermal gradient is more intense with longer joint spacing. |
| | | Longitudinal at top of PCC | Same as that for longitudinal stress at bottom of PCC |
| | | Transverse at bottom of PCC | Increase in product of CTE with thermal gradient linearly results in increase in stress magnitude. Joint spacing has no significant impact on stress magnitude. |

## 4.4 Possible Application of Analysis Results

Although pavements experience a wide variety of stress magnitudes, the preliminary results obtained from the parametric study can be used to obtain pavement cross-sections that will likely have the same stress level. Through the application of the interpolation scheme (to be discussed in the Chapter 5), several pavement design alternatives with the same level of loading stress can be obtained. For example, three cross-sections in Figure 4-12 have different design parameters, but they experience the same level of stress. This application offers the pavement engineers more design alternatives with the same behavior (response) from the mechanistic standpoint. An extensive set of equivalent stress cross-sections is presented in Appendix H.

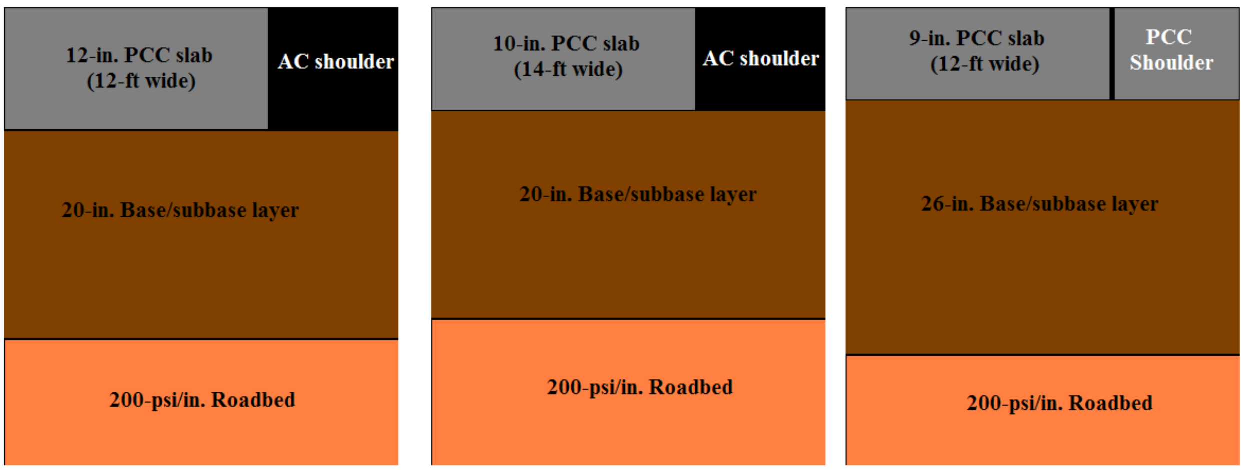


**Figure 4-12: Example illustrations of equivalent stress sections**
**(100 psi stress level under 18-kips single axle)**

# Chapter V

# INTERPOLATION SCHEME

Interpolation scheme is a statistical procedure used to approximate unknown values (non-nodal points) in the vicinity of known values (nodal points). Interpolation scheme in this project is used because it is required to obtain mechanistic responses for all the combinations of the non-discrete inputs, not addressed in the final experimental matrix. The experimental matrix includes all possibilities of all the discrete design inputs: PCC thickness, joint spacing, lateral support condition, and load configuration. However, only three values were specified for each of these non-discrete inputs in the final experimental matrix:

- k-value (30 psi/in., 100 psi/in., 200 psi/in.),
- Base/subbase thickness (4 in., 16 in., 26 in.),
- Thermal strain gradients (0 in.$^{-1}$, ±10x10$^{-6}$ in.$^{-1}$, ±20x10$^{-6}$ in.$^{-1}$).

Since the interpolation process in this study is used to approximate the results that are not directly analyzed by the FE model across ranges of the three non-discrete input parameters: modulus of subgrade reaction, base/subbase thickness, thermal strain gradient, this interpolation scheme is a three-dimensional process.

## 5.1 Least-Squares Criteria

The statistical method least-square approximation, proposed by the German mathematician Carl Friedrich Gauss in 1795, is applied to develop and evaluate interpolation schemes in this study. In general, the method is unbiased and algebraically provides an approximation to a dependent (response) variable *Y* that has the lowest variance. This research study focuses on three response variables: longitudinal stress at the top of the PCC, longitudinal stress at the bottom of the PCC, and transverse stress at the bottom of the PCC. With a linear model, coefficients $\beta_j$ for the least-squares solution satisfy the normal equations:

$$\frac{\partial\left(\sum_{i=1}^{n} e_i^2\right)}{\partial \beta_j} = 0 \text{ , } j = 0, 1, 2, \ldots, m \qquad (5\text{-}1)$$

where $Y_i$ is the value of variable *Y* at point *i*, $y_i = \beta_0 + \beta_1 \cdot x_i^1 + \beta_2 \cdot x_i^2 + \beta_3 \cdot x_i^3 + \ldots + \beta_m \cdot x_i^m$ is the predicted value at point *i*, $e_i = Y_i - y_i$ is error of the predicted value, and $x_i^1, x_i^2, x_i^3, \ldots x_i^m$ are independent (predictor) variables evaluated at point *i*, *i* = 1, 2, …, *n*.

The matrix formulation of the solution in the nonsingular case is:

$$y_i = \beta_0 + \beta_1 \cdot x_i^1 + \beta_2 \cdot x_i^2 + \beta_3 \cdot x_i^3 + \ldots + \beta_m \cdot x_i^m = \overline{x}_i \cdot \overline{\beta} \qquad (5\text{-}2)$$

$$\bar{x}_i = \{1 \quad x_i^1 \quad x_i^2 \quad \dots \quad x_i^m\} \tag{5-3}$$

$$\bar{\beta} = \begin{Bmatrix} \beta_0 \\ \beta_1 \\ \beta_2 \\ \vdots \\ \beta_m \end{Bmatrix} = \left[X^T \cdot X\right]^{-1} \cdot X^T \cdot \bar{Y} \tag{5-4}$$

$$X = \begin{Bmatrix} \bar{x}_1 \\ \bar{x}_2 \\ \bar{x}_3 \\ \vdots \\ \bar{x}_n \end{Bmatrix} = \begin{Bmatrix} 1 & x_1^1 & x_1^2 & \cdots & x_1^m \\ 1 & x_2^1 & x_2^2 & \cdots & x_2^m \\ 1 & x_3^1 & x_3^2 & \dots & x_3^m \\ \vdots & \vdots & \vdots & & \vdots \\ 1 & x_n^1 & x_n^2 & \cdots & x_n^m \end{Bmatrix} \tag{5-5}$$

$$\bar{Y} = \begin{Bmatrix} Y_1 \\ Y_2 \\ Y_3 \\ \vdots \\ Y_n \end{Bmatrix} \tag{5-6}$$

The matrix formulation of the least-squares criteria is used to describe the interpolation process which will be discussed later.

## 5.2 Development of Interpolation Scheme

First, a sensitivity study was conducted to investigate the impact of the three non-discrete input parameters. The impact of modulus of subgrade reaction and base/subbase thickness on the magnitude of stresses were found to be highly non-linear as the change in the slope of the relationship was observed. On the other hand, initial trials showed the impact of thermal strain gradient to have little curvature. Therefore, the interpolation process is divided into two steps: (i) two-dimensional interpolation based on known anchor results obtained from the FE model across ranges of base/subbase thickness and modulus of subgrade reaction at each level of thermal strain gradient, and (ii) one-dimensional interpolation based on the interpolated results from step 1 across range of thermal strain gradient. The interpolation is illustrated in Figure 5-1. Using the least-squares criteria, several interpolation schemes were developed and compared as discussed later. The prototype of the interpolation scheme is explained below in matrix form.

**<u>Step 1</u>:**

$$\sigma(H^*, k^*, \alpha_i) = \bar{X}^* \cdot \hat{\beta} \tag{5-7}$$

Where $\sigma(H^*, k^*, \alpha_i)$ is mechanistic response for the target combination of base/subbase thickness and modulus of subgrade reaction at level $\alpha_i$ of thermal strain gradient

$\overline{X}*$ is the vector of predictor variables

$$\overline{X}* = \left\{ 1 \quad H* \quad H*^2 \quad \ln(k*) \quad H*\cdot\ln(k*) \quad H*^2\cdot\ln(k*) \quad \frac{1}{k*} \quad \frac{H*}{k*} \quad \frac{H*^2}{k*} \right\} \tag{5-8}$$

Where H* is target base/subbase thickness
k* is target modulus of subgrade reaction
$\alpha_1$ is anchor value 0 in.$^{-1}$ of thermal strain gradient
$\alpha_2$ is anchor value ±10x10$^{-6}$ in.$^{-1}$ of thermal strain gradient
$\alpha_3$ is anchor value ±20x10$^{-6}$ in.$^{-1}$ of thermal strain gradient
$\hat{\beta}$ is least-squares coefficient vector

$$\hat{\beta} = \begin{Bmatrix} \beta_0 \\ \beta_1 \\ \beta_2 \\ \beta_3 \\ \beta_4 \\ \beta_5 \\ \beta_6 \\ \beta_7 \\ \beta_8 \end{Bmatrix} = \left[X^T \cdot X\right]^{-1} \cdot X^T \cdot \hat{\sigma} \tag{5-9}$$

$$X = \begin{Bmatrix} \overline{X}(H_1,k_1) \\ \overline{X}(H_1,k_2) \\ \overline{X}(H_1,k_3) \\ \overline{X}(H_2,k_1) \\ \overline{X}(H_2,k_2) \\ \overline{X}(H_2,k_3) \\ \overline{X}(H_3,k_1) \\ \overline{X}(H_3,k_2) \\ \overline{X}(H_3,k_3) \end{Bmatrix} = \begin{bmatrix}
1 & H_1 & H_1^2 & \ln(k_1) & H_1\cdot\ln(k_1) & H_1^2\cdot\ln(k_1) & \frac{1}{k_1} & \frac{H_1}{k_1} & \frac{H_1^2}{k_1} \\
1 & H_1 & H_1^2 & \ln(k_2) & H_1\cdot\ln(k_2) & H_1^2\cdot\ln(k_2) & \frac{1}{k_2} & \frac{H_1}{k_2} & \frac{H_1^2}{k_2} \\
1 & H_1 & H_1^2 & \ln(k_3) & H_1\cdot\ln(k_3) & H_1^2\cdot\ln(k_3) & \frac{1}{k_3} & \frac{H_1}{k_3} & \frac{H_1^2}{k_3} \\
1 & H_2 & H_2^2 & \ln(k_1) & H_2\cdot\ln(k_1) & H_2^2\cdot\ln(k_1) & \frac{1}{k_1} & \frac{H_2}{k_1} & \frac{H_2^2}{k_1} \\
1 & H_2 & H_2^2 & \ln(k_2) & H_2\cdot\ln(k_2) & H_2^2\cdot\ln(k_2) & \frac{1}{k_2} & \frac{H_2}{k_2} & \frac{H_2^2}{k_2} \\
1 & H_2 & H_2^2 & \ln(k_3) & H_2\cdot\ln(k_3) & H_2^2\cdot\ln(k_3) & \frac{1}{k_3} & \frac{H_2}{k_3} & \frac{H_2^2}{k_3} \\
1 & H_3 & H_3^2 & \ln(k_1) & H_3\cdot\ln(k_1) & H_3^2\cdot\ln(k_1) & \frac{1}{k_1} & \frac{H_3}{k_1} & \frac{H_3^2}{k_1} \\
1 & H_3 & H_3^2 & \ln(k_2) & H_3\cdot\ln(k_2) & H_3^2\cdot\ln(k_2) & \frac{1}{k_2} & \frac{H_3}{k_2} & \frac{H_3^2}{k_2} \\
1 & H_3 & H_3^2 & \ln(k_3) & H_3\cdot\ln(k_3) & H_3^2\cdot\ln(k_3) & \frac{1}{k_3} & \frac{H_3}{k_3} & \frac{H_3^2}{k_3}
\end{bmatrix} \tag{5-10}$$

Where $H_1$ is anchor value base/subbase thickness of 4 in.
$H_2$ is anchor value base/subbase thickness of 16 in.
$H_3$ is anchor value base/subbase thickness of 26 in.
$k_1$ is anchor value modulus of subgrade reaction of 30 psi/in.
$k_2$ is anchor value modulus of subgrade reaction of 100 psi/in.

$k_3$ is anchor value modulus of subgrade reaction of 200 psi/in.

$$\hat{\sigma} = \begin{Bmatrix} \sigma_{11} \\ \sigma_{12} \\ \sigma_{13} \\ \sigma_{21} \\ \sigma_{22} \\ \sigma_{23} \\ \sigma_{31} \\ \sigma_{32} \\ \sigma_{33} \end{Bmatrix} \tag{5-11}$$

Where $\sigma_{ij}$ is known anchor value stress from FE analysis at $H_i$ and $k_j$

**<u>Step 2</u>:**

$$\sigma(H^*, k^*, \alpha^*) = \overline{\alpha}^* \cdot \hat{\gamma} \tag{5-12}$$

Where $\sigma(H^*, k^*, \alpha^*)$ is mechanistic response for the target combination of base/subbase thickness, modulus of subgrade reaction, and product of $\alpha(\Delta T/D)$
$\overline{\alpha}^*$ is the vector of predictor variables based on $\alpha(\Delta T/D)$

$$\overline{\alpha}^* = \{1 \quad \alpha^* \quad \alpha^{*2}\} \tag{5-13}$$

$$\hat{\gamma} = \begin{Bmatrix} \gamma_0 \\ \gamma_1 \\ \gamma_2 \end{Bmatrix} = \begin{bmatrix} 1 & \alpha_1 & \alpha_1^2 \\ 1 & \alpha_2 & \alpha_2^2 \\ 1 & \alpha_3 & \alpha_3^2 \end{bmatrix}^{-1} \cdot \begin{Bmatrix} \sigma(H^*, k^*, \alpha_1) \\ \sigma(H^*, k^*, \alpha_2) \\ \sigma(H^*, k^*, \alpha_3) \end{Bmatrix} \tag{5-14}$$

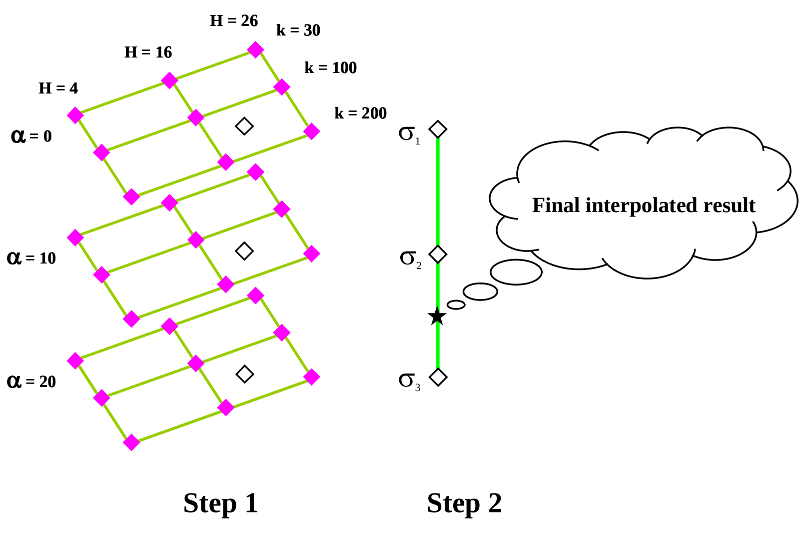


**Figure 5-1: Interpolation process**

Several interpolation schemes were developed following this prototype with different terms used in the prediction vectors (8) in step 1 and (13) in step 2. Examples of prediction vectors used in some of the schemes developed in this study are given in Table 5-1. It should be noted that the natural logarithm of modulus of subgrade reaction and the interaction terms with base/subbase thickness in the prediction matrices for schemes 15 and 16 are similar to terms suggested in the Westergaard's closed form stress equations (Huang, 1993). A significant drop in error due to the use of these terms was observed. Comparing the interpolated results with FE results at non-nodal points validates these two interpolation schemes. Also note that the solutions to the normal equations for schemes 15 and 16 produce perfect fits at the nine nodal points corresponding to each level of the product $\alpha(\Delta T/D)$. Several more schemes have also been investigated. Most of these schemes that contain high order interaction term(s) in "step 1", e.g. $H^{*2}k^{*2}$, $H^*k^{*3}$, $H^{*3}k^*$, were found to result in low predictive power.

**Table 5-1: Example prediction matrices**

| Scheme No. | Prediction Matrix for Step 1 | Prediction Matrix for Step 2 |
|---|---|---|
| Scheme 5 | $\{1 \quad (H^*) \quad (k^*) \quad (H^*)^2 \quad (k^*)^2 \quad (H^*k^*)\}$ | $\{1 \quad \alpha^*\}$ |
| Scheme 6 | $\{1 \quad (H^*) \quad (k^*) \quad (H^*)^2 \quad (k^*)^2 \quad (H^*k^*) \quad (H^*/k^*)^{0.5}\}$ | $\{1 \quad \alpha^*\}$ |
| Scheme 9 | $\{1 \quad (H^*) \quad (k^*) \quad (H^*)^2 \quad (k^*)^2 \quad (H^*k^*) \quad (H^{*2}k^*)\}$ | $\{1 \quad \alpha^*\}$ |
| Scheme 10 | $\{1 \quad (H^*) \quad (k^*) \quad (H^*)^2 \quad (k^*)^2 \quad (H^*k^*) \quad (H^*k^{*2})\}$ | $\{1 \quad \alpha^*\}$ |
| Scheme 15 | $\{1 \quad (H^*) \quad (H^*)^2 \quad (\ln k^*) \quad (H^* \ln k^*) \quad (H^{*2} \ln k^*) \quad (1/k^*) \quad (H^*/k^*) \quad (H^{*2}/k^*)\}$ | $\{1 \quad \alpha^*\}$ |
| Scheme 16 | $\{1 \quad (H^*) \quad (H^*)^2 \quad (\ln k^*) \quad (H^* \ln k^*) \quad (H^{*2} \ln k^*) \quad (1/k^*) \quad (H^*/k^*) \quad (H^{*2}/k^*)\}$ | $\{1 \quad \alpha^* \quad \alpha^{*2}\}$ |

## 5.3 Validation and Goodness of Fit

The validation process is illustrated in Figures 5-2 and 5-3. This process involves obtaining FE results at non-nodal points that were not used in developing interpolation schemes. Error is defined as the difference between the interpolated result and the FE result directly obtained from the ISLAB2000.

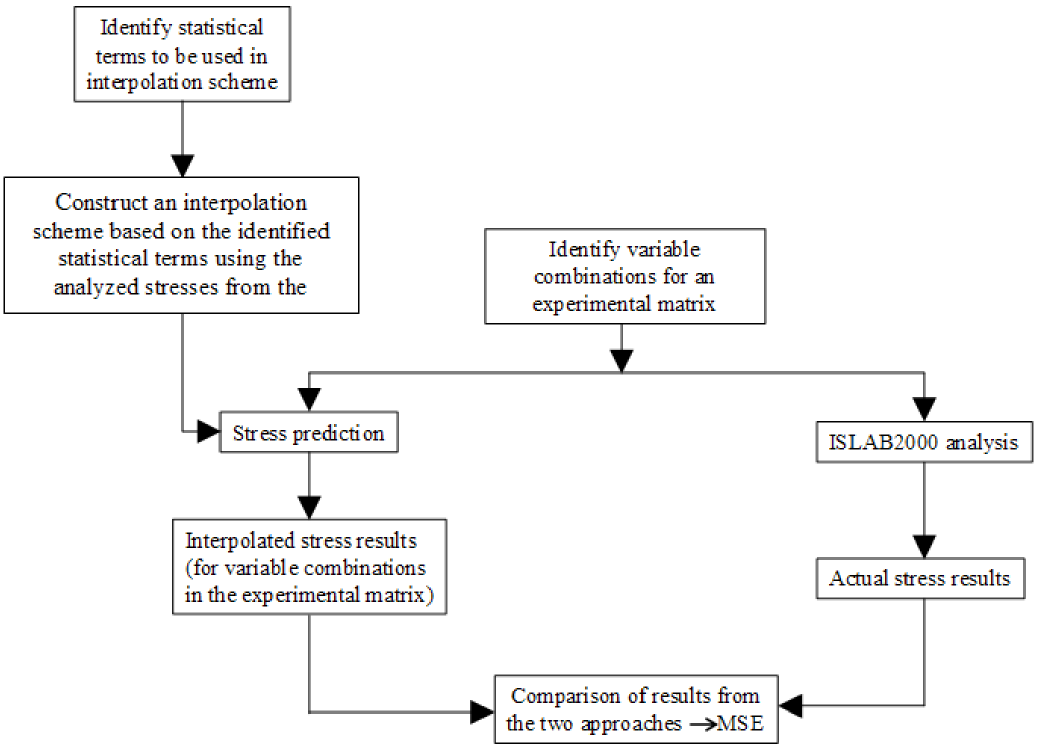


**Figure 5-2: Validation procedure**

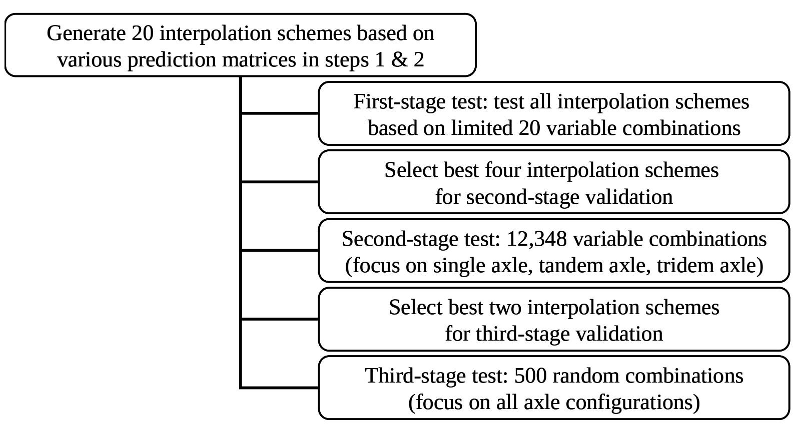


**Figure 5-3: Overview of validation process**

More than 12,000 non-nodal FE results have been obtained and used to validate and select from interpolation schemes. The three stages of the validation process are as follow:

**<u>Validation Stage 1</u>:** In the first stage, all interpolation schemes that were developed are validated with a limited number of non-nodal points. The validation matrix covers 20 non-nodal points with variations of all three non-discrete variables for a fixed combination of discrete variables (10-in. PCC thickness, 16-in. base/subbase thickness, 177-in. joint spacing, PCC shoulder, and single axle edge loading). Non-nodal points at the middle in between the anchor values are considered in this validation stage. These non-nodal points are believed to result in large magnitudes of errors since they are far from the anchor values. Mean square of errors (MSE), bias, and variance are the measures of the goodness of fit of the interpolation schemes considered in this study, which will be discussed later. These values were calculated for the errors (difference between the FE results and interpolated results) obtained from the validation process. Figures 5-4 (a) through (e) illustrate the validation results at the first stage for six most promising interpolation schemes. The comparison between FE and interpolated results illustrated in Figure 5-4 (a) suggests that all these schemes have high predictive power. However, based on MSE, bias, and variance in Figures 5-4 (b) through (e), schemes 5, 6, 15, and 16 appear to be the best four performing interpolation schemes, and consequently are selected for the next stage of validation.

**<u>Validation Stage 2</u>:** The validation matrix for this stage consists of 12,348 non-nodal points. The experimental matrix of "validation stage 2" is a complete factorial of all discrete variable and five values of each of the three non-discrete variables (including two mid points). The process focuses on single, tandem, and tridem axles for all non-discrete and discrete variables. The middle points between nodal points are also used for this validation stage. The validation results are illustrated in Figures 5-5 (a) through (e). Based on the validation results, the two best performing schemes are 15 and 16.

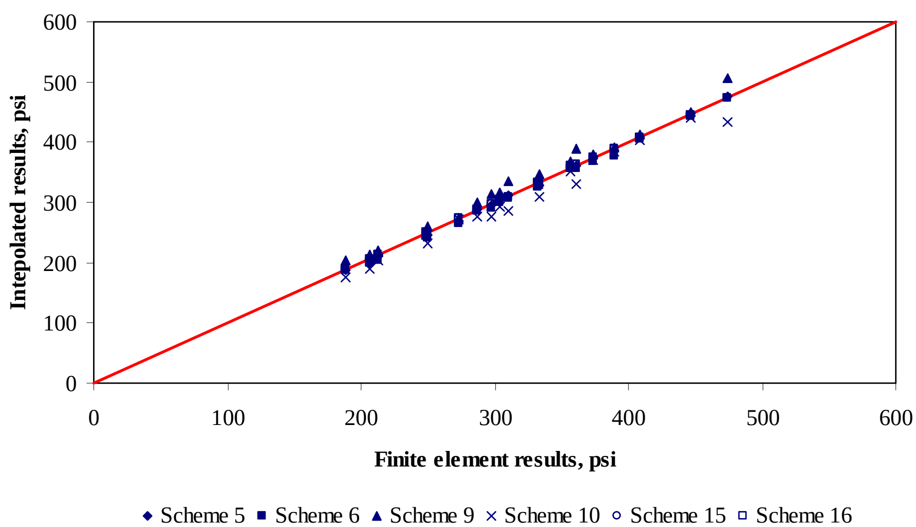


**(a) Comparison between FE and interpolated results**

**Figure 5-4: Validation results – stage 1**

| Goodness of Fit | Scheme 5 | Scheme 6 | Scheme 9 | Scheme 10 | Scheme 15 | Scheme 16 |
|---|---|---|---|---|---|---|
| MSE, $psi^2$ | 6.34 | 32.29 | 202.31 | 267.70 | 1.24 | 1.22 |
| Variance, $psi^2$ | 6.23 | 13.64 | 69.31 | 120.71 | 1.08 | 1.07 |
| Absolute Bias, psi | 0.33 | 4.32 | 11.53 | 12.12 | 0.40 | 0.39 |

**(b) Summary of goodness of fit**

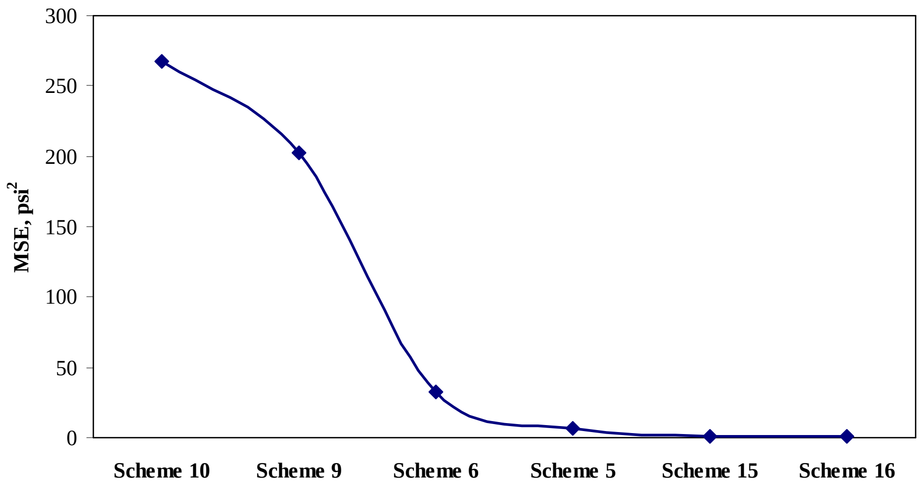


**(c) Comparison of MSE**

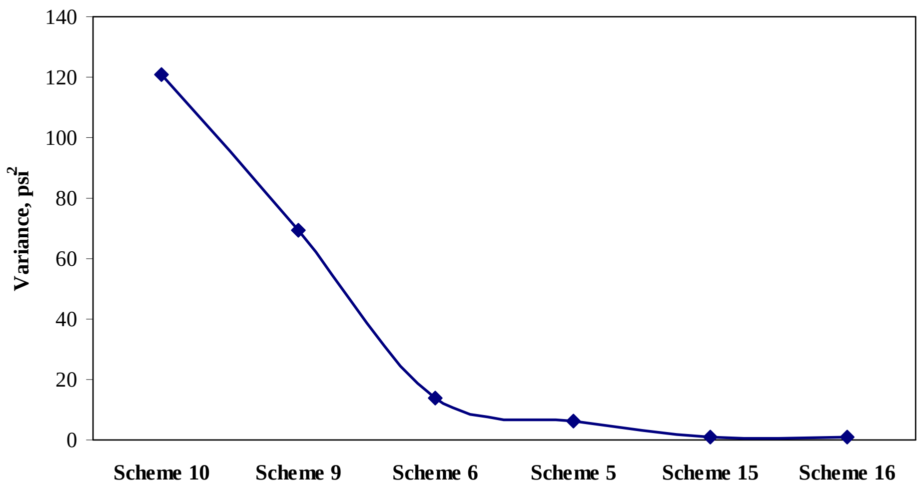


**(d) Comparison of variance**

**Figure 5-4: Validation results – stage 1 (continued)**

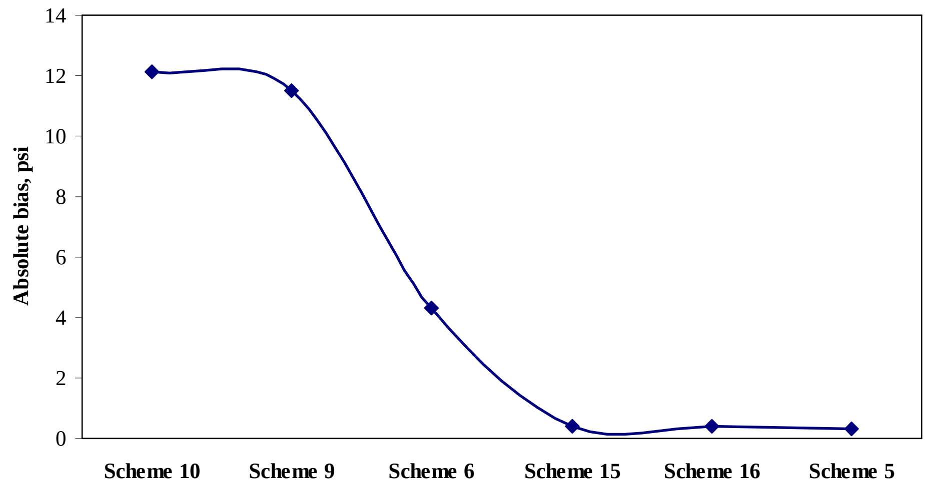


**(e) Comparison of absolute value of bias**

**Figure 5-4: Validation results – stage 1 (continued)**

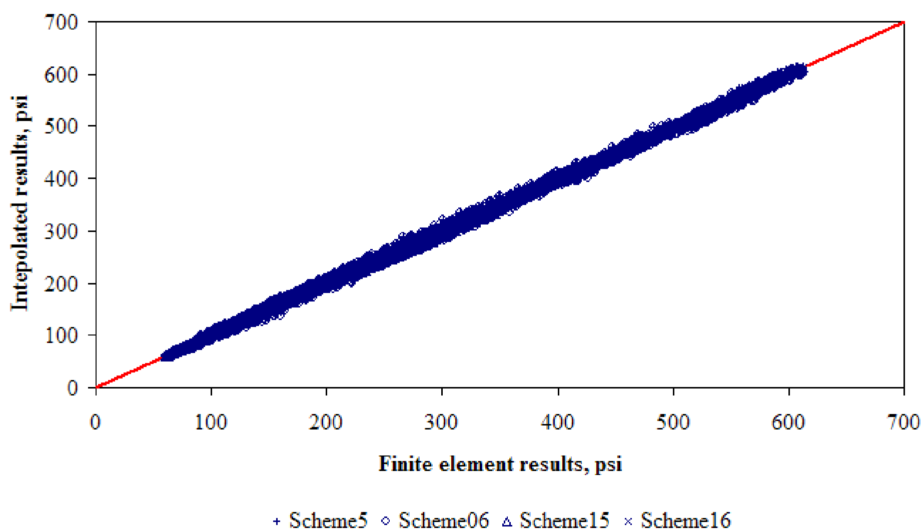


**(a) Comparison between FE and interpolated results**

| Goodness of Fit | Scheme 5 | Scheme 6 | Scheme 15 | Scheme 16 |
|---|---|---|---|---|
| MSE, psi$^2$ | 16.47 | 41.43 | 4.15 | 3.11 |
| Variance, psi$^2$ | 16.40 | 28.39 | 4.14 | 3.11 |
| Absolute Bias, psi | 0.25 | 3.61 | 0.11 | 0.01 |

**(b) Summary of goodness of fit**

**Figure 5-5: Validation results – stage 2**

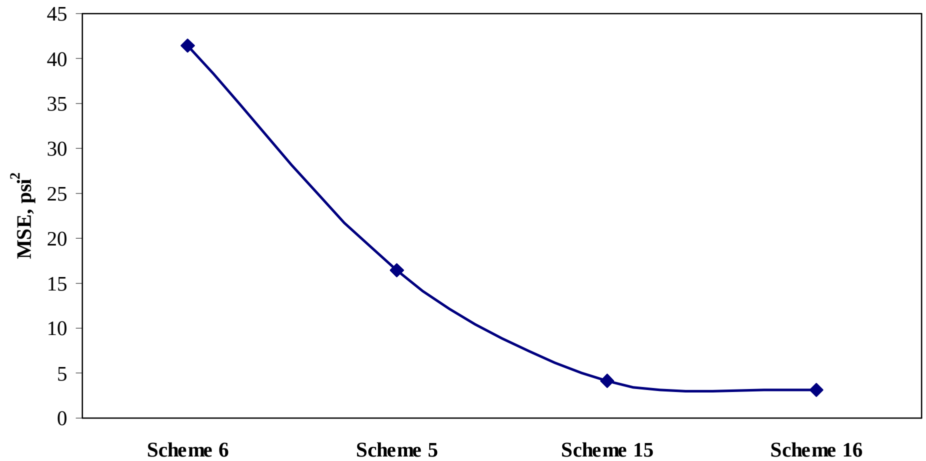


**(c) Comparison of MSE**

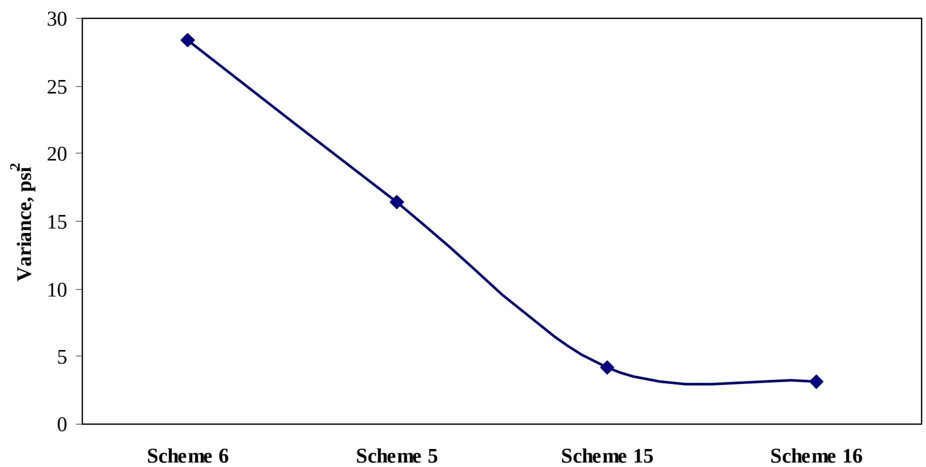


**(d) Comparison of variance**

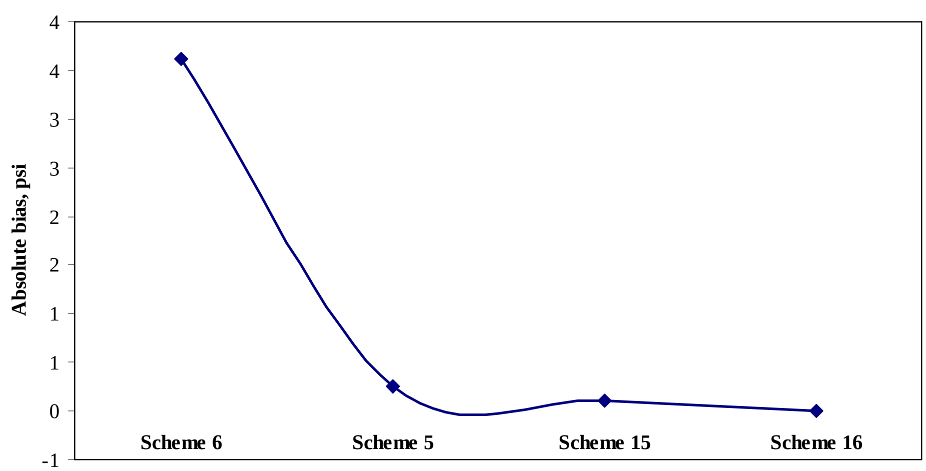


**(e) Comparison of absolute value of bias**

**Figure 5-5: Validation results – stage 2 (continued)**

**<u>Validation Stage 3</u>:** Instead of using the middle points between nodal points in the validation process, this validation stage considers non-nodal points that are randomly selected. This validation stage is based on 300 cases for single through tridem axles and 200 cases for quad through multi-axle (8). The validation results illustrated in Figures 5-6 (a) and (b) and Table 5-2 suggest that scheme 16 is the best performing interpolation scheme. It should be noted that the only difference between schemes 15 and 16 is the prediction matrix in step 2. The values of MSE, bias, and variance obtained from this validation stage were found to be larger than those obtained from the other stages. Since the values for all three non-discrete variables are randomly selected, this validation stage should produce a more realistic result compared to the other stages.

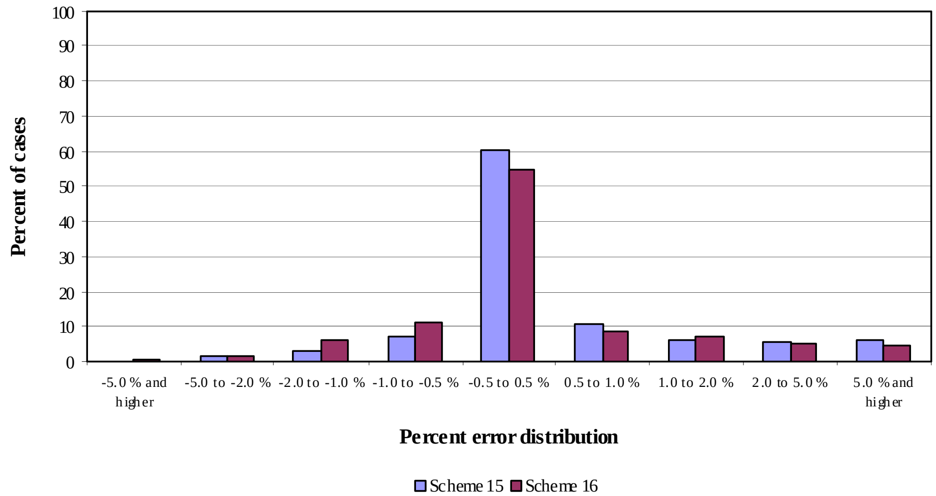


**(a) Example error distribution**

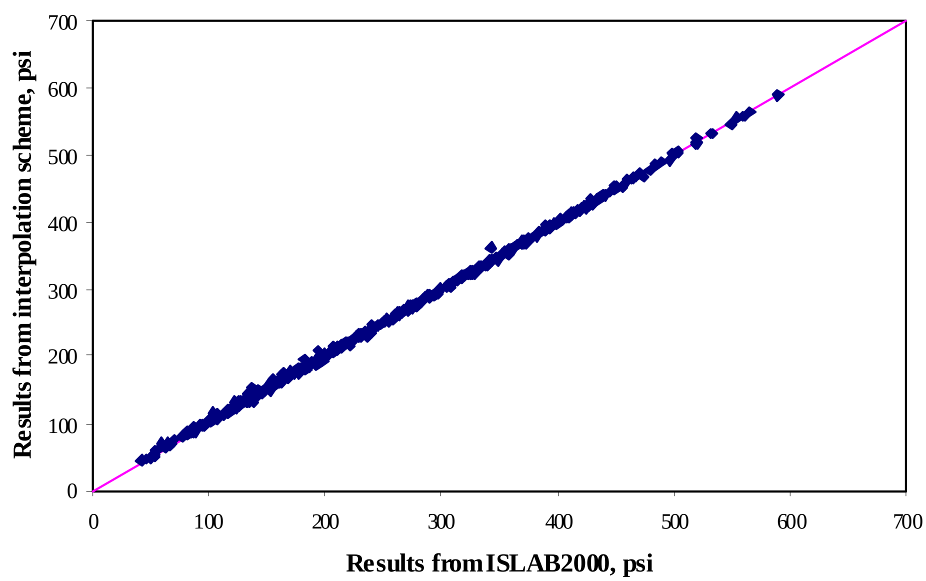


**(b) Comparison between actual and interpolated results**

**Figure 5-6: Validation results – stage 3 (single axle through multi-axle (8))**

**Table 5-2: Comparison of MSE, bias, and variance**

| Cases No. | Statistic Results | Longitudinal stress at bottom | | Transverse stress at bottom | |
|---|---|---|---|---|---|
| | | Scheme15 | Scheme16 | Scheme15 | Scheme16 |
| 1-500 | MSE, psi$^2$ | 11.51 | 8.89 | 16.40 | 15.93 |
| | Bias, psi | 1.02 | 0.51 | -0.89 | -1.21 |
| | Variance, psi$^2$ | 10.46 | 8.63 | 15.61 | 14.47 |
| 1-300 | MSE, psi$^2$ | 3.90 | 3.38 | 9.70 | 8.77 |
| | Bias, psi | 0.16 | 0.02 | -0.36 | -0.59 |
| | Variance, psi$^2$ | 3.87 | 3.38 | 9.57 | 8.41 |
| 301-500 | MSE, psi$^2$ | 22.93 | 17.15 | 26.46 | 26.67 |
| | Bias, psi | 2.32 | 1.25 | -1.68 | -2.13 |
| | Variance, psi$^2$ | 17.53 | 15.60 | 23.63 | 22.14 |

MSE, which is given by the average of the squared errors (differences between actual and interpolated values), is an overall measure of goodness of fit. MSE represents the overall measure of goodness of fit, estimated by the average of square of errors (difference between actual and interpolated values). The MSE can be decomposed into two parts: square of bias and variance. Bias is the average value of errors, while variance is the average of squared deviation of errors from average error. Based on the results from validation stage 3, scheme 16 was found to be most promising. Figures 5-6 (a) and (b) provide for a comparison between actual and interpolated values based on these schemes. These figures suggest that the interpolation schemes can be a reliable alternative for approximating mechanistic responses. Table 5-2 also shows that the interpolated results for single through tridem axles are exceptionally accurate and precise. The biases and variances associated with the longitudinal stress at the bottom of the PCC slab for scheme 16 are 0.0 psi and 3.38 psi$^2$, respectively. Overall maximum absolute biases based on this scheme are 0.6 psi and 2.1 psi for single through tridem axles and quad through multi-axle (8), respectively.

As the validation process has been completed, the interpolation scheme is used to generate a catalog of stresses by assigning a series of sets of design inputs that are not addressed in the experimental matrix into the interpolation scheme. The catalog of stresses can be found in Appendix I.

## 5.4 Example Use of Interpolation Scheme

Interpolation schemes can simply be implemented by carrying out the mathematical expressions as described earlier. For example, the longitudinal stress is estimated at the bottom of the PCC slab. The pavement cross-section includes a 275-mm (11-in.) PCC slab, 500-mm (20-in.) base/subbase thickness, 40.7-kPa/mm (150-psi/in.) k-value, 8.0-m (27-ft) joint spacing, tied PCC shoulder, thermal strain gradient of $6x10^{-7}$ mm$^{-1}$ ($15x10^{-6}$ in.$^{-1}$), 142-kN (32-kips) tandem axle.

**Step 1:** Interpolation in 2-D space across the ranges of base/subbase thickness and k-value

Prediction vector was computed based on H* and k* at the target point (equation 5-8)

$$\overline{X}* = \left\{1 \quad 500 \quad 500^2 \quad \ln(40.7) \quad 500 \cdot \ln(40.7) \quad 500^2 \cdot \ln(40.7) \quad \frac{1}{40.7} \quad \frac{500}{40.7} \quad \frac{500^2}{40.7}\right\}$$

A nine by nine matrix was computed based on $H_i$ and $k_j$ at nodal points (equation 5-10)

$$X = \begin{bmatrix} \overline{X}(100,8.13) \\ \overline{X}(100,27.1) \\ \overline{X}(100,54.2) \\ \overline{X}(400,8.13) \\ \overline{X}(400,27.1) \\ \overline{X}(400,54.2) \\ \overline{X}(650,8.13) \\ \overline{X}(650,27.1) \\ \overline{X}(650,54.2) \end{bmatrix} = \begin{bmatrix} 1 & 100 & 10000 & 2.10 & 210 & 20956 & 0.1230 & 12.30 & 1230 \\ 1 & 100 & 10000 & 3.30 & 330 & 32995 & 0.0369 & 3.69 & 369 \\ 1 & 100 & 10000 & 3.99 & 399 & 39927 & 0.0185 & 1.85 & 185 \\ 1 & 400 & 160000 & 2.10 & 838 & 335290 & 0.1230 & 49.20 & 19680 \\ 1 & 400 & 160000 & 3.30 & 1320 & 527925 & 0.0369 & 14.76 & 5904 \\ 1 & 400 & 160000 & 3.99 & 1597 & 638829 & 0.0185 & 7.38 & 2952 \\ 1 & 650 & 422500 & 2.10 & 1362 & 885374 & 0.1230 & 79.95 & 51968 \\ 1 & 650 & 422500 & 3.30 & 2145 & 1394053 & 0.0369 & 23.99 & 15590 \\ 1 & 650 & 422500 & 3.99 & 2595 & 1686908 & 0.0185 & 11.99 & 7795 \end{bmatrix}$$

Anchor stresses were obtained from FE analysis at $H_i$ and $k_j$ for $\alpha$=0, 4 and 8x10$^{-7}$ mm$^{-1}$ (equation 5-11)

$$\hat{\sigma}_{\alpha=0} = \begin{Bmatrix} 1092.6 \\ 752.2 \\ 619.3 \\ 1074.0 \\ 738.9 \\ 608.0 \\ 1017.1 \\ 698.3 \\ 573.7 \end{Bmatrix} kPa \qquad \hat{\sigma}_{\alpha=4} = \begin{Bmatrix} 2192.8 \\ 2312.6 \\ 2320.8 \\ 2182.2 \\ 2298.5 \\ 2305.9 \\ 2150.9 \\ 2255.9 \\ 2266.8 \end{Bmatrix} kPa \qquad \hat{\sigma}_{\alpha=8} = \begin{Bmatrix} 3293.1 \\ 3857.2 \\ 3989.4 \\ 3290.4 \\ 3857.1 \\ 4035.2 \\ 3284.7 \\ 3813.5 \\ 3969.3 \end{Bmatrix} kPa$$

Then, stresses at target H* and k* corresponding to the three levels of $\alpha$ were computed (equations 5-7 and 5-9)

$$\sigma(500,40.7,0) = \overline{X}* \cdot \left[\left[X^T \cdot X\right]^{-1} \cdot X^T \cdot \hat{\sigma}_{\alpha=0}\right] = 647.5 \quad kPa$$
$$\sigma(500,40.7,4) = \overline{X}* \cdot \left[\left[X^T \cdot X\right]^{-1} \cdot X^T \cdot \hat{\sigma}_{\alpha=4}\right] = 2292.5 \quad kPa$$
$$\sigma(500,40.7,8) = \overline{X}* \cdot \left[\left[X^T \cdot X\right]^{-1} \cdot X^T \cdot \hat{\sigma}_{\alpha=8}\right] = 3954.2 \quad kPa$$

**Step 2:** Interpolation in 1-D across the range of thermal strain gradient

Prediction vector was computed based on $\alpha$* at the target point (equation 5-13)

$$\overline{\alpha}* = \{1 \quad 6 \quad 6^2\}$$

A least-squares coefficient vector was computed based on $\alpha_i$ at nodal points and computed stresses obtained from step 1 (equation 5-14)

$$\hat{\gamma} = \begin{bmatrix} 1 & 0 & 0 \\ 1 & 4 & 16 \\ 1 & 8 & 64 \end{bmatrix}^{-1} \cdot \begin{Bmatrix} 647.5 \\ 2292.5 \\ 3954.2 \end{Bmatrix} = \begin{Bmatrix} 647.5 \\ 409.1 \\ 0.526 \end{Bmatrix}$$

Then, the target stress at H*, k* and α* was computed (equation 5-12)

$$\sigma(H^*, k^*, \alpha^*) = \{1 \quad 6 \quad 36\} \cdot \begin{Bmatrix} 647.5 \\ 409.1 \\ 0.526 \end{Bmatrix} = 3121.2 \quad kPa$$

The stress computed using interpolation scheme is 3121.2 kPa (452.353 psi), while the result directly obtained from FE analysis is 3121.8 kPa (452.436 psi). The error of interpolated result in this example is 0.6 kPa (0.1 psi) or 0.02%.

# Chapter VI

# POTENTIAL IMPLEMENTATION OF STUDY RESULTS

The mechanistic responses obtained from the parametric study not only provide an opportunity to study the interaction between structural, environmental and loading factors on the mechanistic responses as discussed in previous chapters but also can be directly applied to mechanistic-empirical design process of JCP. This chapter reviews the mechanistic-empirical design procedure for JCP and also illustrates how mechanistic responses are used in the process.

## 6.1 Mechanistic-Empirical Design Concept

The concept of mechanistic-empirical design process is to relate mechanistic responses to certain pavement performance that are considered in design. For each type of performance (e.g. fatigue cracking), the design process is based on damage calculated using mechanistic responses (e.g. longitudinal stresses at bottom of the slab) and accumulated over the entire analysis period as a function of pavement structural features, material properties, axle weights, axle configurations, and thermal gradients that the pavement actually experience. The damage calculation is done using the Miner's hypothesis as shown in (6-1):

$$Damage = \sum_{i}\sum_{j}\sum_{k}\sum_{l}\sum_{m}\sum_{n}\frac{n_{ijklmn}}{N_{ijklmn}}, \qquad (6\text{-}1)$$

where: $n_{ijklmn}$ = Applied number of load repetitions at condition i, j, k, l, m, n
$N_{ijklmn}$ = Allowable number of load repetitions at condition i, j, k, l, m, n
i = Age (year)
j = Season (winter, spring, summer, and fall)
k = Axle configuration (single axle, tandem axle, tridem axle, and etc.)
l = Load level (kips)
m = Thermal gradient ($^{o}$F/in.)
n = Traffic path

With the application of interpolation scheme as discussed in the previous chapter, mechanistic responses can be computed based on the information for each load repetition at the condition i, j, k, l, m, n. The damage calculation also requires additional data from three sources: material models, hourly axle spectra from WIM (Weigh-in-Motion) database, and hourly thermal gradient generated using EICM (Enhanced Integrated Climatic Model). The computed mechanistic responses, then, are used to calculate the allowable number of load repetitions, $N_{ijklmn}$. Figure 6-1 illustrates a schematic overview of the damage calculation as a part of the mechanistic-empirical design process.

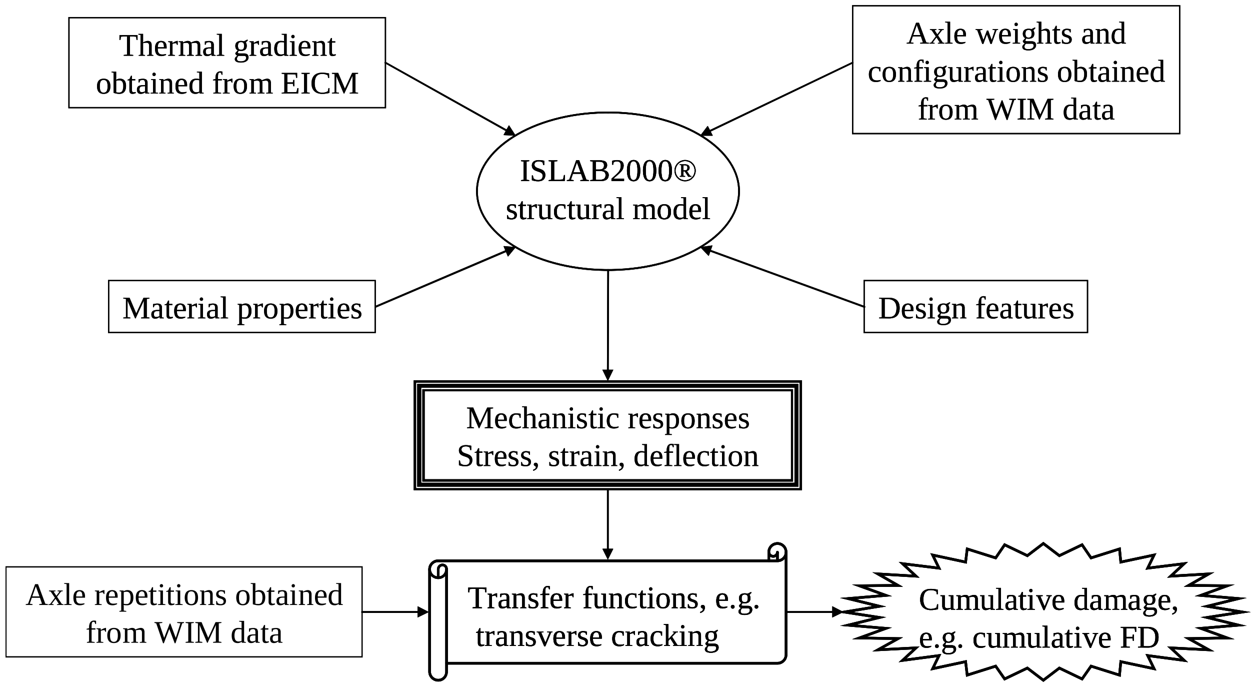


**Figure 6-1: Schematic illustration of damage calculation process**

The allowable repetitions, $N_{ijklmn}$, can be obtained by computing mechanistic response at the condition i, j, k, l, m and n and inputting the computed response into performance transfer functions. For fatigue cracking, the input to the transfer function is the ratio of tensile stress to 28-day modulus of rupture, R. Several researchers have suggested equations for fatigue transfer function of plain concrete as follows:

1) Vesic and Sexana (1970): $N = 225{,}000 \times R^{-4}$ (6-2)

2) Portland Cement Association (1975): $Log_{10} N = 11.78 - 12.11 \times R$ (6-3)

3) Zero-Maintenance Project (1977): $Log_{10} N = 17.61 - 17.61 \times R$ (6-4)

4) Khazanovich and Yu (2001): $Log_{10} N = 2.13 \cdot R^{-1.2}$ (6-5)

5) NCHRP 1-37 A (2004): $Log_{10} N = 2 \cdot R^{-1.22} + 0.4371$ (6-6)

Figures 6-2 and 6-3 show the comparison of allowable repetitions and fatigue damage calculated based on these transfer functions at varying values of the R-ratio. It appears that the allowable repetitions and fatigue damage calculated based on the fatigue transfer function suggested in NCHRP 1-37A (Rao et al, 2004) are more conservative than the other models for the range of the R-ratio between 0.60 and 0.85. For the R-ratio greater than 0.85, the results obtained from the Portland Cement Association model are the most conservative.

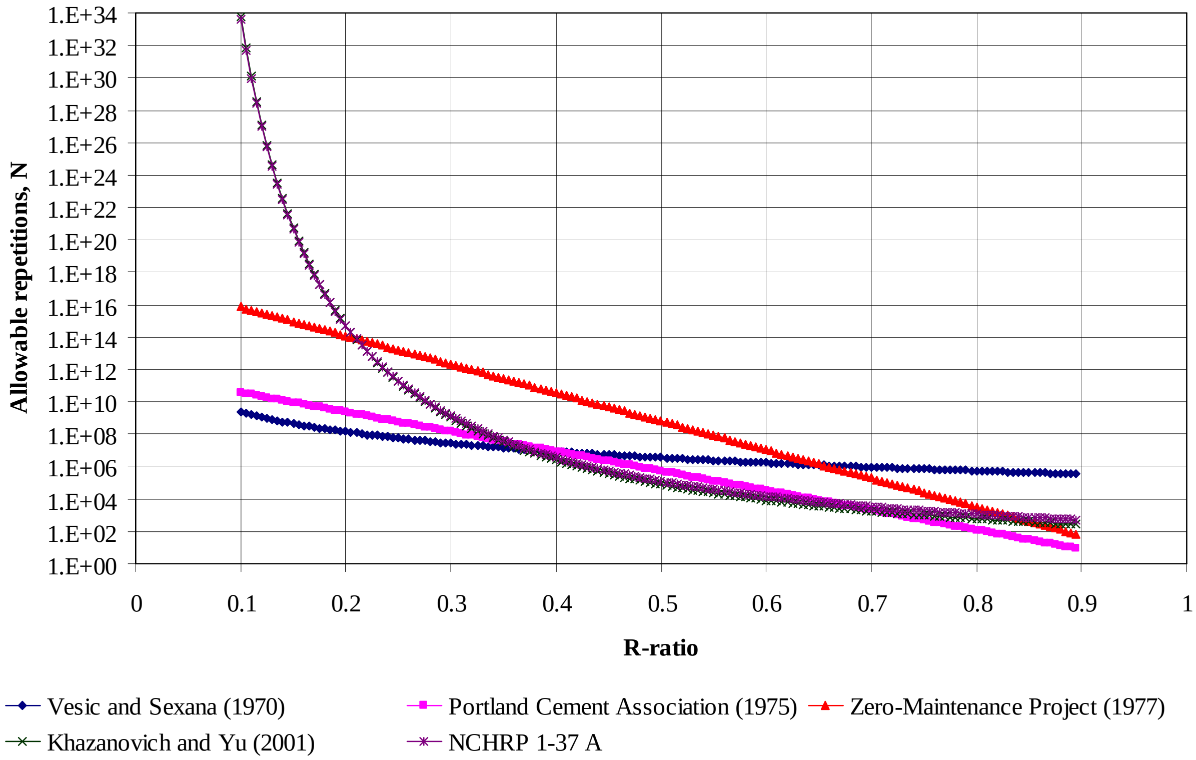


**Figure 6-2: Comparison of allowable repetitions based on different fatigue transfer functions**

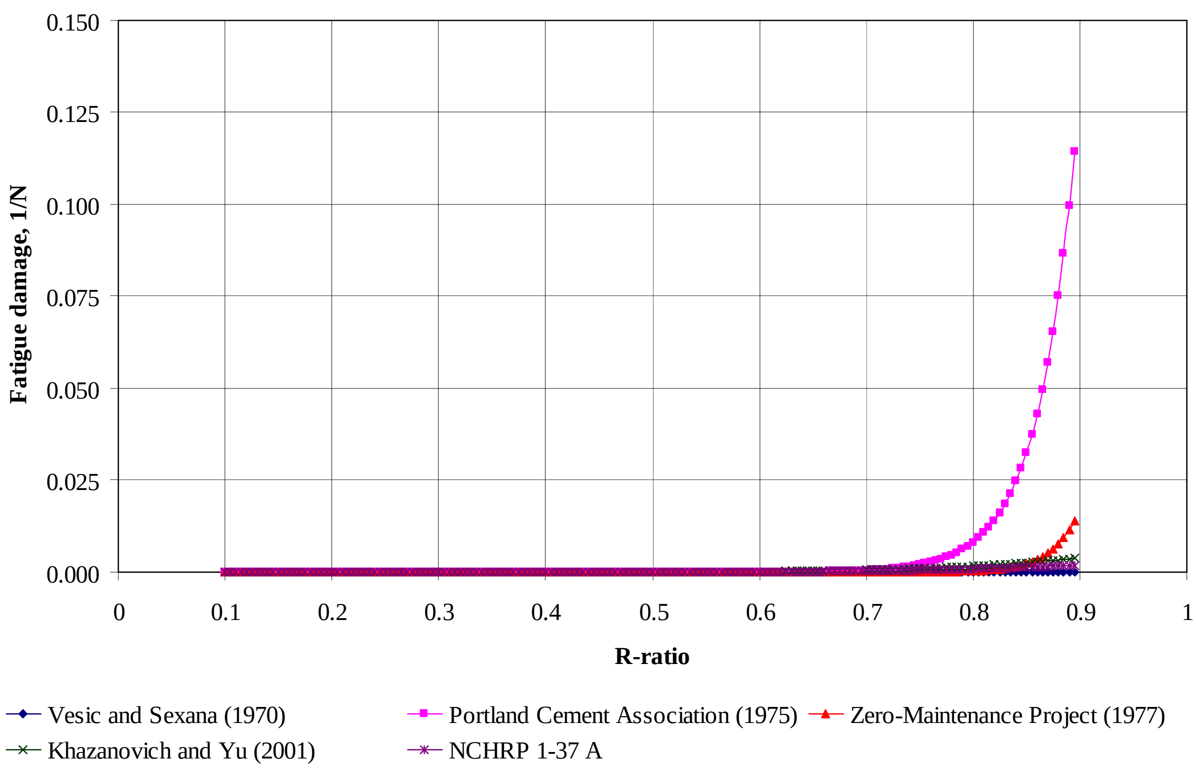


**Figure 6-3: Comparison of fatigue damage based on different fatigue transfer functions**

## 6.2 Weigh-in-Motion (WIM) Data Synthesis

As a part of the demonstration of the fatigue damage calculation, WIM data are synthesized for the Michigan SPS-2 sections (US-23 Northbound) from 1998 to 2000. The hourly traffic spectra are generated for each month and each axle type on 3-hour basis. Figures 6-4 and 6-5 are examples of the load spectra. The rest of load spectra are available in Appendix J.

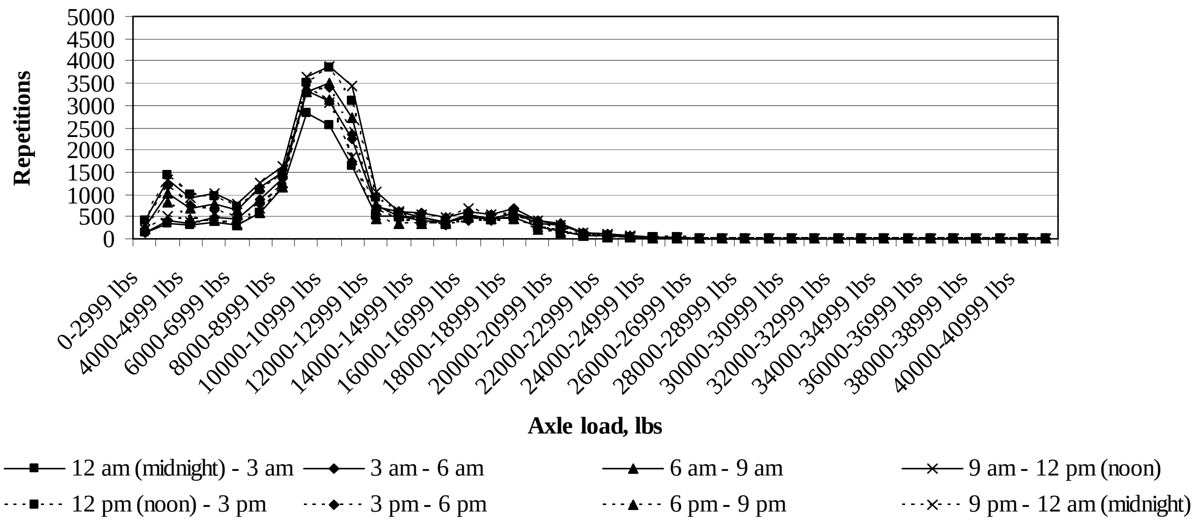


**Figure 6-4: Load spectrum from SPS2 sections for single axle in July, 1998**

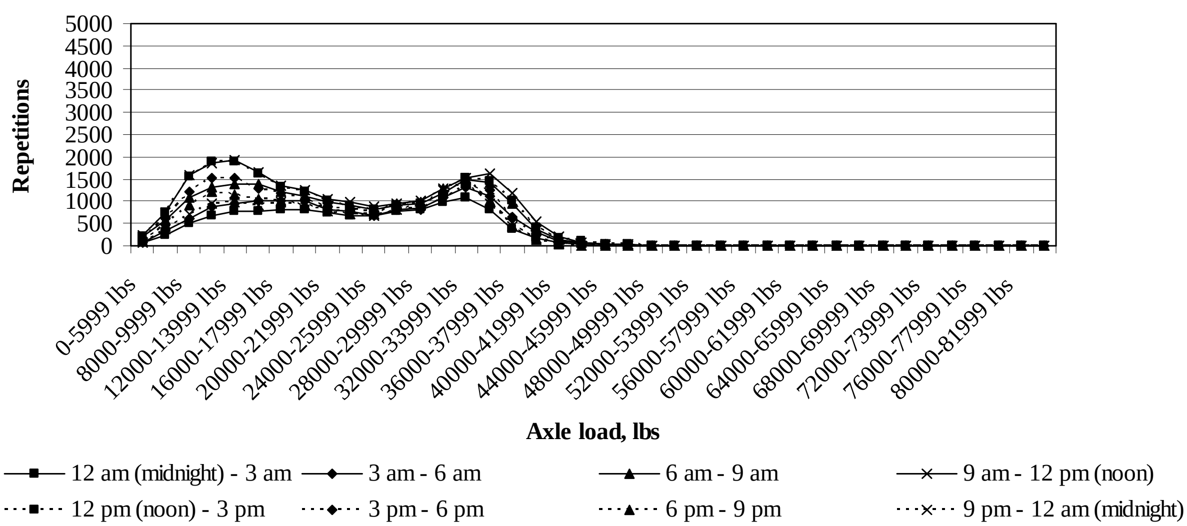


**Figure 6-5: Load spectrum from SPS2 sections for tandem axle in July, 1998**

The axle repetitions obtained of the WIM database are summarized in Tables 6-1 through 6-8 for each axle configuration. These tables show that the combination of single axle, tandem axle and tridem axle are majority number of repetitions for the SPS-2 sections.

**Table 6-1: Summary of single axle load repetitions from SPS-2 section**

| Load range, lbs | Time interval | | | | | | | | | |
|---|---|---|---|---|---|---|---|---|---|---|
| | 7/98-9/98 | 10/98-12/98 | 1/99-3/99 | 4/99-6/99 | 7/99-9/99 | 10/99-12/99 | 1/00-3/00 | 4/00-6/00 | 7/00-9/00 | 10/00-12/00 |
| 0-4999 | 73,897 | 32,139 | 34,057 | 66,686 | 64,857 | 49,400 | 34,017 | 52,423 | 68,877 | 58,896 |
| 5000-7999 | 60,122 | 30,905 | 34,364 | 58,049 | 58,986 | 52,168 | 46,874 | 42,322 | 58,098 | 55,975 |
| 8000-10999 | 214,552 | 127,964 | 141,516 | 225,246 | 208,159 | 206,808 | 142,597 | 153,711 | 219,733 | 208,158 |
| 11000-13999 | 99,780 | 55,168 | 65,935 | 106,207 | 100,406 | 91,723 | 69,660 | 72,201 | 93,886 | 94,095 |
| 14000-16999 | 44,970 | 27,668 | 30,027 | 48,737 | 43,026 | 38,696 | 38,084 | 29,325 | 38,642 | 34,699 |
| 17000-19999 | 30,322 | 16,948 | 19,744 | 32,313 | 31,365 | 30,560 | 29,086 | 23,056 | 32,010 | 26,885 |
| 20000-22999 | 9,427 | 4,683 | 6,560 | 9,720 | 9,756 | 9,254 | 6,412 | 6,144 | 9,188 | 7,113 |
| 23000-25999 | 2,018 | 1,100 | 1,467 | 2,264 | 2,334 | 1,744 | 1,106 | 991 | 1,471 | 1,172 |
| 26000-28999 | 594 | 307 | 488 | 561 | 628 | 496 | 276 | 221 | 300 | 275 |
| 29000-31999 | 133 | 68 | 149 | 158 | 148 | 116 | 73 | 53 | 60 | 54 |
| 32000-34999 | 36 | 20 | 46 | 34 | 29 | 26 | 18 | 12 | 20 | 11 |
| 35000-37999 | 5 | 4 | 16 | 9 | 13 | 5 | 4 | 4 | 10 | 3 |
| 38000-40999 | 4 | 1 | 4 | 2 | 2 | 3 | 0 | 1 | 0 | 0 |
| >41000 | 1 | 0 | 4 | 1 | 4 | 0 | 0 | 0 | 0 | 0 |

**Table 6-2: Summary of tandem axle load repetitions from SPS-2 section**

| Load range, lbs | Time interval | | | | | | | | | |
|---|---|---|---|---|---|---|---|---|---|---|
| | 7/98-9/98 | 10/98-12/98 | 1/99-3/99 | 4/99-6/99 | 7/99-9/99 | 10/99-12/99 | 1/00-3/00 | 4/00-6/00 | 7/00-9/00 | 10/00-12/00 |
| 0-9999 | 65,457 | 55,233 | 39,411 | 52,386 | 54,205 | 53,444 | 31,429 | 24,211 | 44,844 | 38,954 |
| 10000-15999 | 113,470 | 97,841 | 62,729 | 100,599 | 99,644 | 98,989 | 79,753 | 70,261 | 101,550 | 102,054 |
| 16000-21999 | 81,779 | 72,875 | 50,835 | 82,935 | 75,736 | 74,204 | 67,743 | 61,949 | 81,472 | 83,218 |
| 22000-27999 | 73,319 | 64,717 | 47,237 | 74,352 | 64,502 | 60,455 | 53,444 | 49,981 | 64,713 | 65,338 |
| 28000-33999 | 98,301 | 91,484 | 65,400 | 105,950 | 95,230 | 89,498 | 77,218 | 73,024 | 96,309 | 91,395 |
| 34000-39999 | 41,867 | 35,275 | 27,330 | 44,421 | 48,277 | 48,201 | 41,889 | 33,371 | 49,251 | 43,921 |
| 40000-45999 | 7,619 | 4,633 | 3,391 | 5,619 | 6,485 | 4,388 | 2,907 | 2,161 | 3,776 | 3,129 |
| 46000-51999 | 695 | 399 | 377 | 505 | 626 | 399 | 287 | 210 | 330 | 339 |
| 52000-57999 | 105 | 64 | 83 | 78 | 95 | 62 | 53 | 35 | 55 | 52 |
| 58000-63999 | 27 | 22 | 14 | 19 | 18 | 17 | 16 | 8 | 11 | 5 |
| 64000-69999 | 6 | 4 | 4 | 8 | 2 | 5 | 2 | 2 | 1 | 1 |
| 70000-75999 | 1 | 0 | 1 | 0 | 1 | 0 | 0 | 0 | 0 | 0 |
| 76000-81999 | 1 | 0 | 0 | 0 | 0 | 0 | 0 | 0 | 0 | 0 |
| >82000 | 0 | 0 | 0 | 0 | 0 | 0 | 0 | 0 | 0 | 0 |

**Table 6-3: Summary of tridem axle load repetitions from SPS-2 section**

| Load range, lbs | Time interval | | | | | | | | | |
|---|---|---|---|---|---|---|---|---|---|---|
| | 7/98-9/98 | 10/98-12/98 | 1/99-3/99 | 4/99-6/99 | 7/99-9/99 | 10/99-12/99 | 1/00-3/00 | 4/00-6/00 | 7/00-9/00 | 10/00-12/00 |
| 0-17999 | 7,305 | 4,891 | 1,547 | 3,049 | 3,495 | 4,312 | 2,237 | 2,188 | 2,906 | 3,486 |
| 18000-26999 | 1,340 | 727 | 475 | 799 | 798 | 684 | 654 | 610 | 686 | 631 |
| 27000-35999 | 1,507 | 1,394 | 992 | 1,438 | 1,059 | 1,317 | 1,074 | 1,200 | 1,374 | 1,596 |
| 36000-44999 | 4,833 | 5,160 | 2,889 | 6,679 | 5,588 | 5,483 | 3,817 | 5,352 | 7,466 | 7,245 |
| 45000-53999 | 4,194 | 4,160 | 1,924 | 3,894 | 4,224 | 3,469 | 1,605 | 1,735 | 3,662 | 2,825 |
| 54000-62999 | 695 | 587 | 244 | 465 | 487 | 443 | 206 | 251 | 439 | 343 |
| 63000-71999 | 84 | 53 | 38 | 57 | 72 | 53 | 28 | 32 | 92 | 47 |
| 72000-80999 | 10 | 8 | 5 | 8 | 11 | 12 | 1 | 7 | 10 | 4 |
| 81000-89999 | 1 | 2 | 5 | 3 | 4 | 2 | 1 | 1 | 3 | 2 |
| 90000-98999 | 3 | 0 | 0 | 0 | 0 | 0 | 0 | 4 | 3 | 0 |
| >99000 | 0 | 0 | 1 | 0 | 0 | 0 | 0 | 1 | 1 | 0 |

**Table 6-4: Summary of quad axle load repetitions from SPS-2 section**

| Load range, lbs | Time interval | | | | | | | | | |
|---|---|---|---|---|---|---|---|---|---|---|
| | 7/98-9/98 | 10/98-12/98 | 1/99-3/99 | 4/99-6/99 | 7/99-9/99 | 10/99-12/99 | 1/00-3/00 | 4/00-6/00 | 7/00-9/00 | 10/00-12/00 |
| 0-23999 | 848 | 678 | 379 | 453 | 535 | 767 | 325 | 316 | 493 | 413 |
| 24000-35999 | 442 | 323 | 239 | 499 | 448 | 407 | 438 | 382 | 460 | 371 |
| 36000-47999 | 631 | 701 | 436 | 761 | 877 | 728 | 477 | 403 | 685 | 703 |
| 48000-59999 | 2,497 | 2,837 | 1,454 | 3,437 | 3,790 | 3,071 | 1,691 | 2,534 | 3,692 | 3,105 |
| 60000-71999 | 1,309 | 1,160 | 486 | 1,020 | 1,218 | 1,030 | 673 | 916 | 2,050 | 1,506 |
| 72000-83999 | 89 | 62 | 38 | 115 | 82 | 45 | 22 | 66 | 157 | 94 |
| 84000-95999 | 3 | 1 | 7 | 6 | 6 | 4 | 2 | 3 | 12 | 11 |
| 96000-107999 | 2 | 1 | 1 | 5 | 1 | 7 | 0 | 0 | 1 | 1 |
| 108000-119999 | 0 | 4 | 0 | 0 | 1 | 0 | 0 | 0 | 1 | 0 |
| 120000-131999 | 0 | 0 | 0 | 0 | 0 | 0 | 0 | 0 | 0 | 0 |
| >132000 | 0 | 0 | 0 | 0 | 0 | 0 | 0 | 0 | 0 | 0 |

**Table 6-5: Summary of multi-axle (5) load repetitions from SPS-2 section**

| Load range, lbs | Time interval | | | | | | | | | |
|---|---|---|---|---|---|---|---|---|---|---|
| | 7/98-9/98 | 10/98-12/98 | 1/99-3/99 | 4/99-6/99 | 7/99-9/99 | 10/99-12/99 | 1/00-3/00 | 4/00-6/00 | 7/00-9/00 | 10/00-12/00 |
| 0-29999 | 634 | 316 | 221 | 306 | 337 | 473 | 237 | 238 | 283 | 273 |
| 30000-44999 | 62 | 19 | 45 | 41 | 39 | 71 | 41 | 23 | 40 | 23 |
| 45000-59999 | 73 | 79 | 68 | 158 | 99 | 160 | 75 | 97 | 96 | 135 |
| 60000-74999 | 686 | 779 | 386 | 1,142 | 1,207 | 983 | 513 | 710 | 1,053 | 1,018 |
| 75000-89999 | 267 | 199 | 137 | 242 | 409 | 175 | 86 | 123 | 223 | 113 |
| 90000-104999 | 17 | 18 | 16 | 14 | 12 | 11 | 5 | 3 | 7 | 8 |
| 105000-119999 | 3 | 3 | 4 | 8 | 2 | 1 | 0 | 1 | 2 | 0 |
| 120000-134999 | 0 | 0 | 0 | 0 | 0 | 0 | 0 | 0 | 0 | 0 |
| 135000-149999 | 0 | 0 | 0 | 0 | 0 | 0 | 0 | 0 | 0 | 0 |
| 150000-164999 | 0 | 0 | 0 | 0 | 0 | 0 | 0 | 0 | 0 | 0 |
| >165000 | 0 | 0 | 0 | 0 | 0 | 0 | 0 | 0 | 0 | 0 |

**Table 6-6: Summary of multi-axle (6) load repetitions from SPS-2 section**

| Load range, lbs | Time interval | | | | | | | | | |
|---|---|---|---|---|---|---|---|---|---|---|
| | 7/98-9/98 | 10/98-12/98 | 1/99-3/99 | 4/99-6/99 | 7/99-9/99 | 10/99-12/99 | 1/00-3/00 | 4/00-6/00 | 7/00-9/00 | 10/00-12/00 |
| 0-35999 | 79 | 5 | 2 | 1 | 11 | 23 | 8 | 2 | 7 | 2 |
| 36000-53999 | 58 | 10 | 88 | 29 | 15 | 23 | 40 | 19 | 33 | 16 |
| 54000-71999 | 139 | 114 | 147 | 163 | 200 | 131 | 79 | 96 | 170 | 103 |
| 72000-89999 | 666 | 833 | 450 | 657 | 898 | 660 | 415 | 825 | 1,110 | 810 |
| 90000-107999 | 345 | 152 | 84 | 135 | 181 | 175 | 51 | 191 | 332 | 107 |
| 108000-125999 | 4 | 2 | 0 | 0 | 7 | 13 | 1 | 0 | 1 | 2 |
| 126000-143999 | 0 | 0 | 0 | 0 | 0 | 1 | 0 | 0 | 0 | 0 |
| 144000-161999 | 0 | 0 | 0 | 0 | 0 | 0 | 0 | 0 | 0 | 0 |
| 162000-179999 | 0 | 0 | 0 | 0 | 0 | 0 | 0 | 0 | 0 | 0 |
| 180000-197999 | 0 | 0 | 0 | 0 | 0 | 0 | 0 | 0 | 0 | 0 |
| >198000 | 0 | 0 | 0 | 0 | 0 | 0 | 0 | 0 | 0 | 0 |

**Table 6-7: Summary of multi-axle (7) load repetitions from SPS-2 section**

| Load range, lbs | Time interval | | | | | | | | | |
|---|---|---|---|---|---|---|---|---|---|---|
| | 7/98-9/98 | 10/98-12/98 | 1/99-3/99 | 4/99-6/99 | 7/99-9/99 | 10/99-12/99 | 1/00-3/00 | 4/00-6/00 | 7/00-9/00 | 10/00-12/00 |
| 0-41999 | 4 | 6 | 2 | 4 | 4 | 6 | 6 | 1 | 4 | 4 |
| 42000-62999 | 23 | 6 | 9 | 21 | 29 | 18 | 23 | 13 | 31 | 21 |
| 63000-83999 | 128 | 104 | 62 | 115 | 77 | 81 | 93 | 118 | 197 | 155 |
| 84000-104999 | 249 | 100 | 46 | 147 | 211 | 168 | 140 | 139 | 308 | 394 |
| 105000-125999 | 25 | 21 | 6 | 5 | 15 | 9 | 6 | 6 | 16 | 20 |
| 126000-146999 | 0 | 0 | 0 | 0 | 1 | 0 | 0 | 0 | 1 | 0 |
| 147000-167999 | 0 | 0 | 0 | 0 | 0 | 0 | 0 | 0 | 0 | 0 |
| 168000-188999 | 0 | 0 | 0 | 0 | 0 | 0 | 0 | 0 | 0 | 0 |
| 189000-209999 | 0 | 0 | 0 | 0 | 0 | 0 | 0 | 0 | 0 | 0 |
| 210000-230999 | 0 | 0 | 0 | 0 | 0 | 0 | 0 | 0 | 0 | 0 |
| >231000 | 0 | 0 | 0 | 0 | 0 | 0 | 0 | 0 | 0 | 0 |

**Table 6-8: Summary of multi-axle (8) load repetitions from SPS-2 section**

| Load range, lbs | Time interval | | | | | | | | | |
|---|---|---|---|---|---|---|---|---|---|---|
| | 7/98-9/98 | 10/98-12/98 | 1/99-3/99 | 4/99-6/99 | 7/99-9/99 | 10/99-12/99 | 1/00-3/00 | 4/00-6/00 | 7/00-9/00 | 10/00-12/00 |
| 0-47999 | 10 | 4 | 4 | 5 | 10 | 2 | 12 | 4 | 6 | 2 |
| 48000-71999 | 35 | 20 | 18 | 53 | 43 | 42 | 42 | 24 | 30 | 39 |
| 72000-95999 | 295 | 355 | 195 | 331 | 277 | 330 | 293 | 293 | 416 | 419 |
| 96000-119999 | 248 | 251 | 174 | 406 | 337 | 381 | 199 | 331 | 391 | 252 |
| 120000-143999 | 8 | 11 | 9 | 8 | 11 | 2 | 3 | 8 | 17 | 6 |
| 144000-167999 | 0 | 2 | 0 | 0 | 0 | 0 | 0 | 0 | 0 | 0 |
| 168000-191999 | 0 | 0 | 0 | 0 | 0 | 0 | 0 | 0 | 0 | 0 |
| 192000-215999 | 0 | 0 | 0 | 0 | 0 | 0 | 0 | 0 | 0 | 0 |
| 216000-239999 | 0 | 0 | 0 | 0 | 0 | 0 | 0 | 0 | 0 | 0 |
| 240000-263999 | 0 | 0 | 0 | 0 | 0 | 0 | 0 | 0 | 0 | 0 |
| >264000 | 0 | 0 | 0 | 0 | 0 | 0 | 0 | 0 | 0 | 0 |

## 6.3 Hourly Thermal Gradients

As a part of fatigue damage calculation, hourly thermal gradients are generated through the use of Enhanced Integrated Climatic Model (EICM). The hourly thermal gradients are obtained for four dense-graded aggregate base (DGAB) SPS-2 sections (26-0213 through 26-0216). The details of these sections are as shown in Table 6.9 below:

**Table 6-9: Design features and material properties for the SPS-2 sections**

| Description | 26-0213 | 26-0214 | 26-0215 | 26-0216 |
|---|---|---|---|---|
| PCC thickness, in. | 8 | 8.1 | 10.7 | 11.1 |
| Base thickness, in. | 6.1 | 5.8 | 6.2 | 5.9 |
| Joint spacing, ft | 15 | 15 | 15 | 15 |
| Lateral support condition | Widened lane | AC shoulder | AC shoulder | Widened lane |
| One-year modulus of rupture*, psi | 915 | 1000 | 915 | 1000** |
| Design 14-day modulus of rupture, psi | 550 | 900 | 550 | 900 |
| k-value, psi/in. | See Table 6-10 | | | |

Remark: * Obtained from "SPS-2 Construction Report" (Soil and Materials Engineering, Inc., 1995)
** Assumed equal to the modulus of rupture of section 26-0214, since this information is not available in the construction report

**Table 6-10: Seasonal backcalculated k-value obtained from LTPP database (FHWA, 2001)**

| Month | 26-0213 | 26-0214 | 26-0215 | 26-0216 |
|---|---|---|---|---|
| January | 248 | 300 | 254 | 267 |
| February | 203 | 215 | 244 | 221 |
| March | 203 | 215 | 244 | 221 |
| April | 203 | 215 | 244 | 221 |
| May | 158 | 130 | 235 | 174 |
| June | 158 | 130 | 235 | 174 |
| July | 158 | 130 | 235 | 174 |
| August | 203 | 215 | 244 | 221 |
| September | 203 | 215 | 244 | 221 |
| October | 203 | 215 | 244 | 221 |
| November | 248 | 300 | 254 | 267 |
| December | 248 | 300 | 254 | 267 |

Figure 6-6 illustrates an example of hourly thermal gradient distribution obtained from EICM. The rest of hourly thermal gradient distributions are also available in Appendix K.

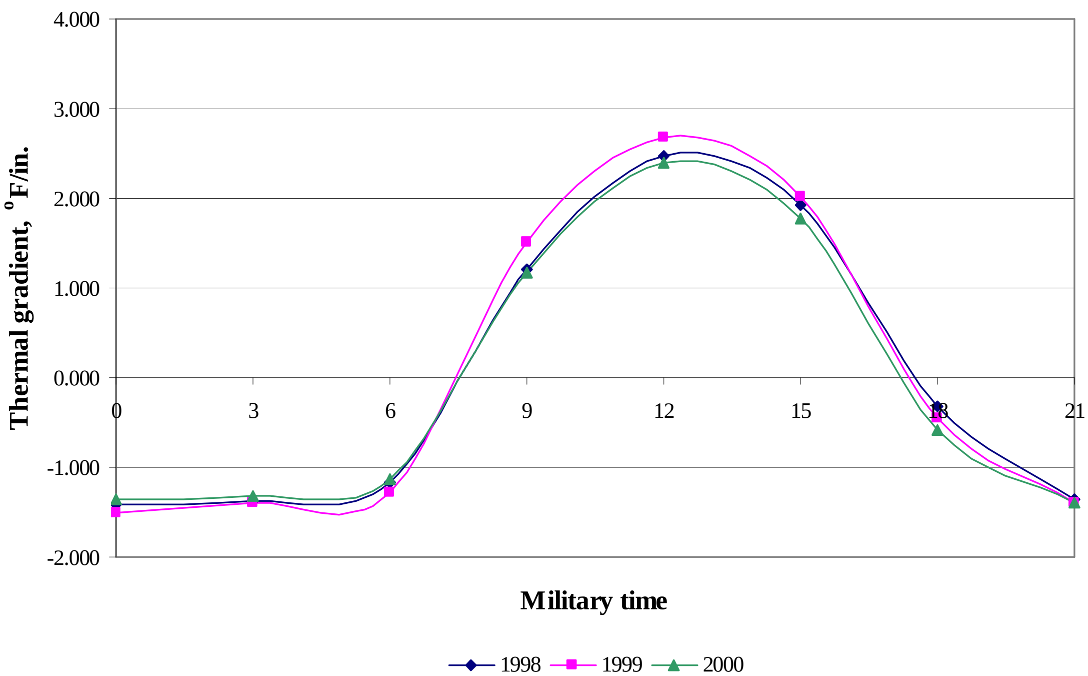


**Figure 6-6: Hourly thermal gradients generated by EICM for 8-in. sections in September**

## 6.4 Mechanistic-Empirical Procedure for JCP - Example

Mechanistic-empirical design procedure for JCP relies on relationship between cumulative damage and level of distress. For example, fatigue damage could be calculated using the NCHRP 1-37 A transfer function (Equation 6-6) based on the magnitude of longitudinal stress at the bottom of the slab corresponding to axle type, axle weight, seasonal k-value and hourly thermal gradient for each axle repetition over the analysis period, which could be obtained from the catalog of stresses. This results in the allowable number of load repetitions at a specified condition, N, in the Miner's hypothesis (Equation 6-1). Along with the number of axle repetitions, n, which could be obtained through the WIM database or any available traffic database, cumulative damage could be calculated. The schematic of the process is shown in Figure 6-7.

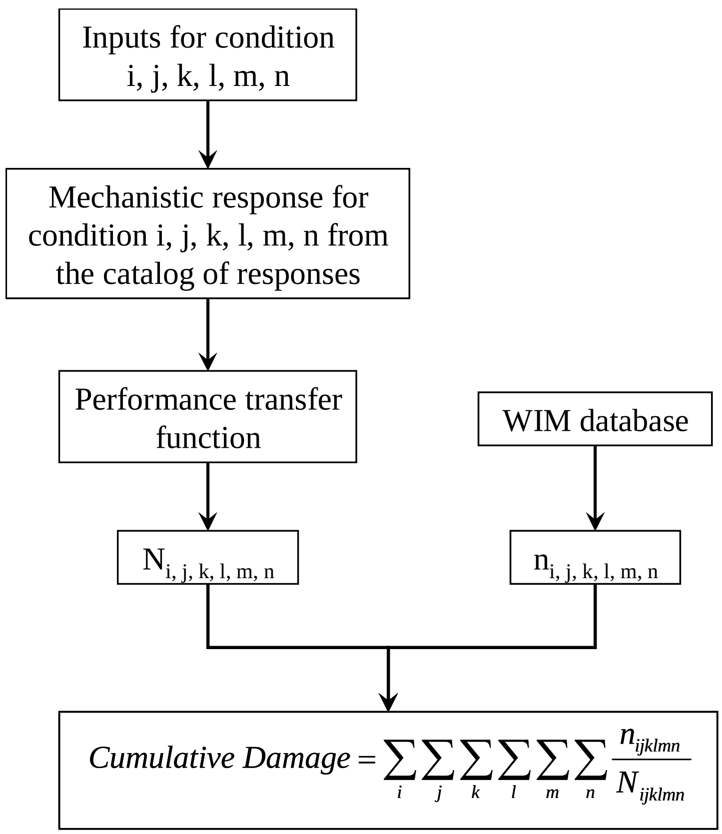


**Figure 6-7: Cumulative damage calculation process**

The next step is to plot the computed cumulative damage against distress (e.g. cracking). It is widely believed that a cumulative damage of 1.0 relates to a failed pavement. On a plot of cumulative damage versus distress, the cumulative damage of 1.0 may not match with the cracking threshold established by the agency; hence the performance curve needs to be calibrated. The calibration process is illustrated in Figure 6-8. For example, Figures 6-9 and 6-10 illustrate an example characteristic fatigue curve before and after calibration process for 50% slabs cracked considered as the rehabilitation distress level.

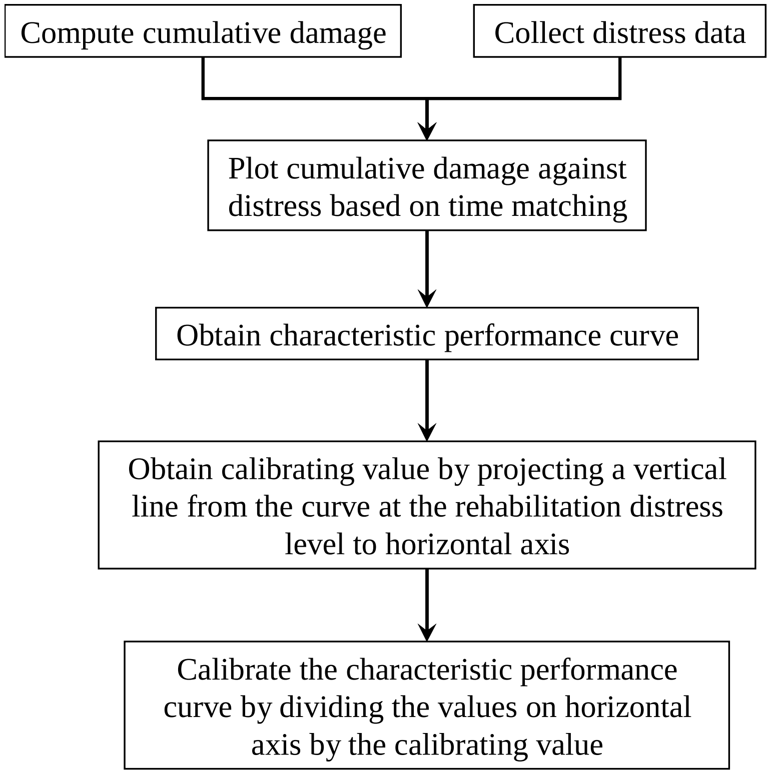


**Figure 6-8: Calibration process for the relationship between cumulative damage and distress**

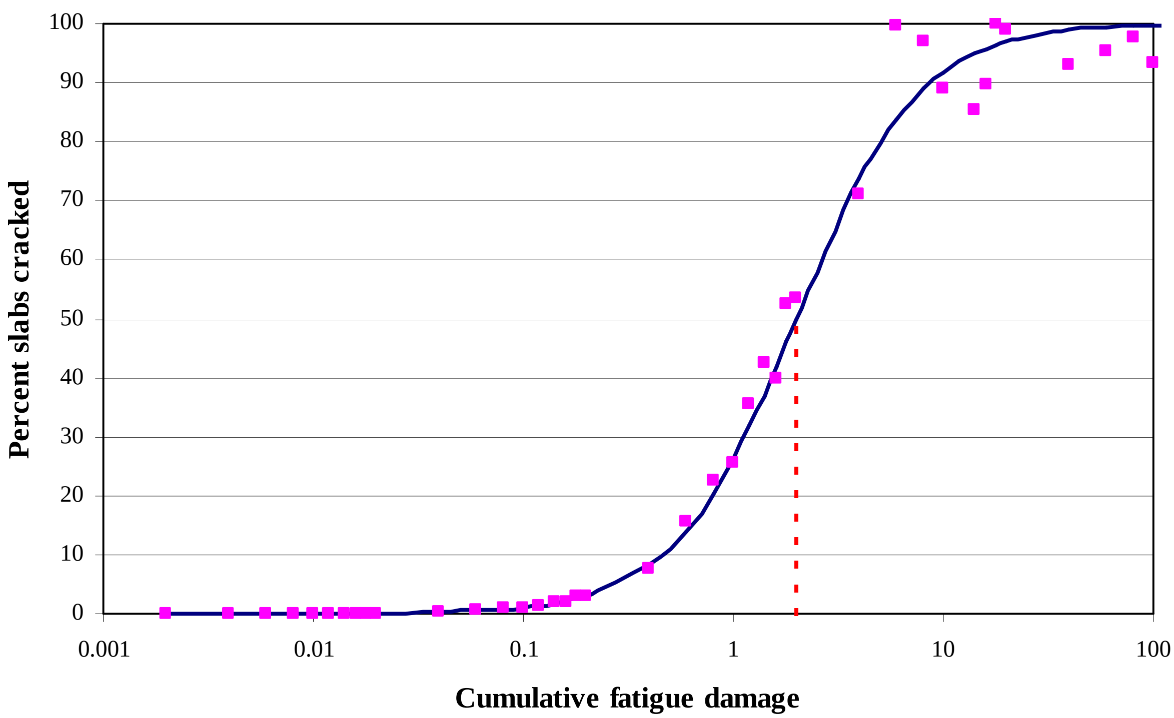


**Figure 6-9: Example characteristic fatigue curve before calibration process**

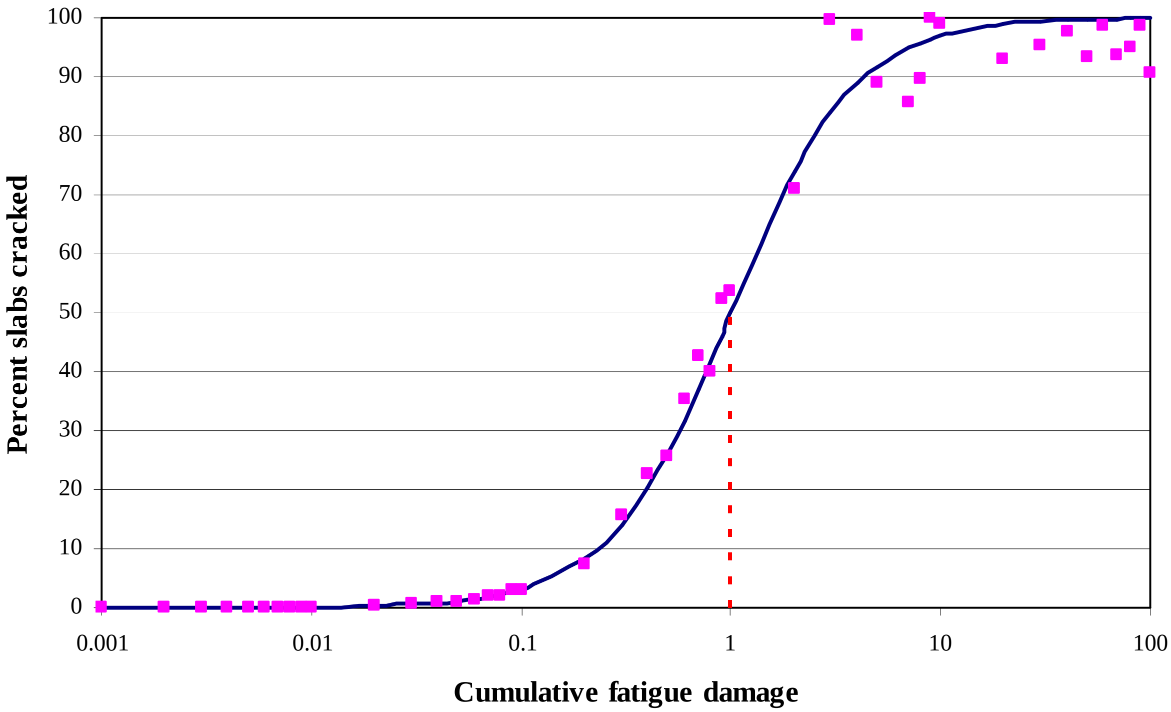


**Figure 6-10: Example characteristic fatigue curve after calibration process**

The design process for faulting and spalling are also based on cumulative damage concept. However, the relationship between cumulative damage and these distresses is expressed in different forms from cracking. Based on NCHRP 1-37 A (Khazanovich et al, 2004), the design process for faulting and spalling could be summarized as follows:

### Design of Faulting

$$Fault_m = \sum_{i=1}^{m} \Delta Fault_i \qquad (6\text{-}7)$$

$$\Delta Fault_i = C_{34} \times \left(FAULTMAX_{i-1} - Fault_{i-1}\right)^2 \times DE_i \qquad (6\text{-}8)$$

$$FAULTMAX_i = FAULTMAX_0 + C_7 \times \sum_{j=1}^{m} DE_j \times \log\left(1 + C_5 \times 5.0^{EROD}\right)^{C_6} \qquad (6\text{-}9)$$

$$FAULTMAX_0 = C_{12} \times \delta_{curling} \times \left[\log\left(1 + C_5 \times 5.0^{EROD}\right) \times \log\left(\frac{P_{200} \times WetDays}{P_s}\right)\right]^{C_6} \qquad (6\text{-}10)$$

Where:
$Fault_m$ = mean joint faulting at the end of month m, in.
$\Delta Fault_i$ = incremental change (monthly) in mean transverse joint faulting during month i, in.
$FAULTMAX_i$ = maximum mean transverse joint faulting for month i, in.
$FAULTMAX_0$ = initial maximum mean transverse joint faulting, in.
EROD = base/subbase erodibility factor

DE = differential elastic deformation energy

$$DE = \frac{1}{2} \cdot k \cdot \left(W_L + W_{UL}\right) \cdot \left(W_L - W_{UL}\right)$$

k = modulus of subgrade reaction, kPa/mm
$W_L$ = deflection of loaded slab, mm
$W_{UL}$ = deflection of unloaded slab, mm
$\delta_{curling}$ = maximum mean monthly slab corner upward deflection PCC due to temperature curling and moisture warping
$P_s$ = overburden on subgrade, lb.
$P_{200}$ = percent subgrade material passing #200 sieve
WetDays = average annual number of wet days (greater than 0.1 in. rainfall)
$C_1$ through $C_7$ and $C_{12}$, $C_{34}$ are calibration constants:

$C_{12} = C_1 + C_2 * FR^{0.25}$

$C_{34} = C_3 + C_4 * FR^{0.25}$

$C_1 = 1.29$, $C_2 = 1.1$, $C_3 = 0.0001725$, $C_4 = 0.0008$, $C_5 = 250$, $C_6 = 0.4$, $C_7 = 1.2$

FR = base freezing index defined as percentage of time the top base temperature is below freezing (32 $^oF$) temperature

**Design of Spalling**

$$SPALL = \left[\frac{AGE}{AGE + 0.01}\right] \cdot \left[\frac{100}{1 + 1.005^{(-12*AGE + SCF)}}\right] \quad (6\text{-}11)$$

Where:
SPALL = percentage joints spalled (medium- and high-severities)
AGE = pavement age since construction, years
SCF = scaling factor based on site-, design-, and climate-related variables

$$SCF = -1400 + 350 \cdot AIR\% \cdot (0.5 + PREFORM) + 3.4 \cdot f'_c \cdot 0.4 - 0.2\left(FTCYC \cdot AGE\right) + 43 \cdot h_{PCC} - 536 \cdot WC\_Ratio$$

AIR% = PCC air content, percent
PREFORM = 1 if preformed sealant is present; 0 if not
$f'_c$ = PCC compressive strength, psi
FTCYC = average annual number of freeze-thaw cycles
$h_{PCC}$ = PCC slab thickness, in.
WC_Ratio = PCC water/cement ratio

Seven illustrative examples to demonstrate the calculation process for fatigue damage, faulting damage and spalling damage are presented. Relevant inputs and details, including calculation results for these examples are summarized in Table 6-11.

**Table 6-11: Summary of illustrative examples**

| Example | Type of Damage | | | Inputs | Results | Remarks |
|---|---|---|---|---|---|---|
| | Fatigue | Faulting | Spalling | | | |
| 1 | X | | | 10-in. slab thickness, 16-in. aggregate base, 100-psi/in. roadbed, 177-in. joint spacing, 12-ft lane with tied PCC shoulder, positive thermal gradient of 2 $^oF$/in., i) 18-kips single axle, 32-kips tandem axle and 39-kips tridem axle | Allowable number of axle repetitions: 3.81 million for single axle, 0.83 million for tandem axle and 8.24 million for tridem axle | Fatigue damage due to different axle configurations |
| 2 | X | | | Same as Example 1 but with i) 12-ft lane with untied AC shoulder and ii) 14-ft lane with untied AC shoulder and only under 39-kips tridem axle | Allowable number of axle repetitions: 0.87 million for 12 ft lane with untied AC shoulder and 3.07 million for 14-ft lane with untied AC shoulder | Fatigue damage due to different lateral support conditions |
| 3 | X | | | Same as Example 1 but with 8, 9, 11 and 12-in. slab thickness and only under 32-kips tandem axle | Allowable number of axle repetitions: 0.056 million for 8 in. slab, 0.193 million for 9-in. slab, 4.60 million for 11-in. slab and 32.53 million for 12-in. slab | Fatigue damage due to different slab thickness |
| 4 | | X | | Same as Example 1 but consider typical traffic spectra and climatic conditions in Michigan | Predicted faulting at the end of 20-years period: 0.1671 in. | Transverse joint faulting damage calculation |
| 5 | | X | | Same as Example 4 but with i) 1.5-in. dowel dia. at 12 in. spacing, ii) 1.25-in. dowel dia. at 18 in. spacing, iii) 1.5-in. dowel dia. at 18 in. spacing | Predicted faulting at the end of 20-years period: 0.0935 in. for 1.5-in. dowel dia. at 12 in. spacing, 0.1682 in. for 1.25-in. dowel dia. at 18 in. spacing, 0.0941 in. for 1.5-in. dowel dia. at 18 in. spacing | Transverse joint faulting damage due to different joint designs |
| 6 | | X | | Same as Example 4 but with lean concrete base (LCB) and asphalt treated base (ATB) | Predicted faulting at the end of 20-years period: 0.1066 in. for LCB and 0.1280 in. for ATB | Transverse joint faulting damage due to different base types |
| 7 | | | X | 3% air content, no preformed sealant, 2,000-psi concrete compressive strength, average freeze thaw cycles per year of 250, 8-in. slab and 0.45 water/cement ratio | Predicted percent slabs spalled at the end of 20-years period: 3% | Transverse joint spalling damage |

**<u>Illustrative Example 1</u>** (fatigue damage due to different axle configurations)

Analyze the number of load repetitions of 18-kips single axle, 32-kips tandem axle, and 39-kips tridem axle that could be carried at daytime thermal gradient of 2 $^oF$/in. by a pavement system with the following features:

- 10-in. slab thickness,
- 16-in. aggregate base,
- 100-psi/in. roadbed soil,

- 177-in. joint spacing,
- 12-ft lane,
- tied PCC shoulder,
- and 1.25-in. dowel diameter at 12 in. center to center spacing.

Note that the concrete coefficient of thermal expansion and 28-day modulus of rupture were found to be 5 in./in./$^{o}$F and 550 psi, respectively.

From the catalog of stresses in Appendix I, the magnitudes of the longitudinal stresses at the bottom of the PCC slab are:

| | | |
|---|---|---|
| For 18-kips single axle: | 219.2 | psi |
| For 32-kips tandem axle: | 230.3 | psi |
| For 39-kips tridem axle: | 198.0 | psi |

The stress ratios for the three axle configurations are calculated as follows:

For 18-kips single axle: $R_{\text{18-kips single axle}} = \dfrac{219.2}{550} = 0.399$

For 32-kips tandem axle: $R_{\text{32-kips tandem axle}} = \dfrac{230.3}{550} = 0.419$

For 39-kips tridem axle: $R_{\text{39-kips tridem axle}} = \dfrac{198.0}{550} = 0.360$

Considering the performance transfer function in equation (6-6), the number of load repetitions of 18-kips single axle, 32-kips tandem axle and 39-kips tridem axle that could be carried for the given conditions could be analyzed as follows:

Recall that $Log_{10} N = 2 \cdot R^{-1.22} + 0.4371$ or $N = 10^{\left[2 \cdot R^{-1.22} + 0.4371\right]}$

For 18-kips single axle: $N_{\text{18-kips single axle}} = 10^{\left[2 \cdot (0.399)^{-1.22} + 0.4371\right]} = 3.81$ *million cycles*

For 32-kips tandem axle: $N_{\text{32-kips tandem axle}} = 10^{\left[2 \cdot (0.419)^{-1.22} + 0.4371\right]} = 1.67$ *million cycles*

For 39-kips tridem axle: $N_{\text{39-kips tridem axle)}} = 10^{\left[2 \cdot (0.360)^{-1.22} + 0.4371\right]} = 24.71$ *million cycles*

However, the number of repetitions needed to account for the number of repetitions within each axle group. For example, each tandem and tridem axle results in peak stress level two and three times, respectively. The number of repetitions for each axle could be adjusted as follows:

Adjusted number of repetitions, $N_{adjusted} = \dfrac{N}{\text{number of repetitions within each axle}}$

For 18-kips single axle: $N_{\text{18-kips single axle}} = \dfrac{3.81}{1} = 3.81$ *million cycles*

For 32-kips tandem axle: $N_{\text{32-kips tandem axle}} = \frac{1.67}{2} = 0.83 \quad \textit{million cycles}$

For 39-kips tridem axle: $N_{\text{39-kips tridem axle)}} = \frac{24.71}{3} = 8.24 \quad \textit{million cycles}$

Figure 6-11 illustrates the number of allowable repetitions and the weight of each axle. It can be seen that the pavement could carry more repetitions of 39-kips tridem axle, when compared with the others. The more number of wheels in an axle reduce the level of stress and consequently increase the number of allowable repetition.

With the use of WIM database, the actual number of load repetitions, n, could be additionally applied to the allowable number of repetitions, N, to compute the damage, n/N. Then, the summation of the damage over conditions, i, j, k, l, m, and n will provide cumulative damage as described in Figure 6-7. With availability of pavement performance data (percent slabs cracked for this case), the cumulative damage could be plotted against the performance data. After that, calibration process is required to match the cumulative damage of one with the rehabilitation distress level, illustrated in Figure 6-8.

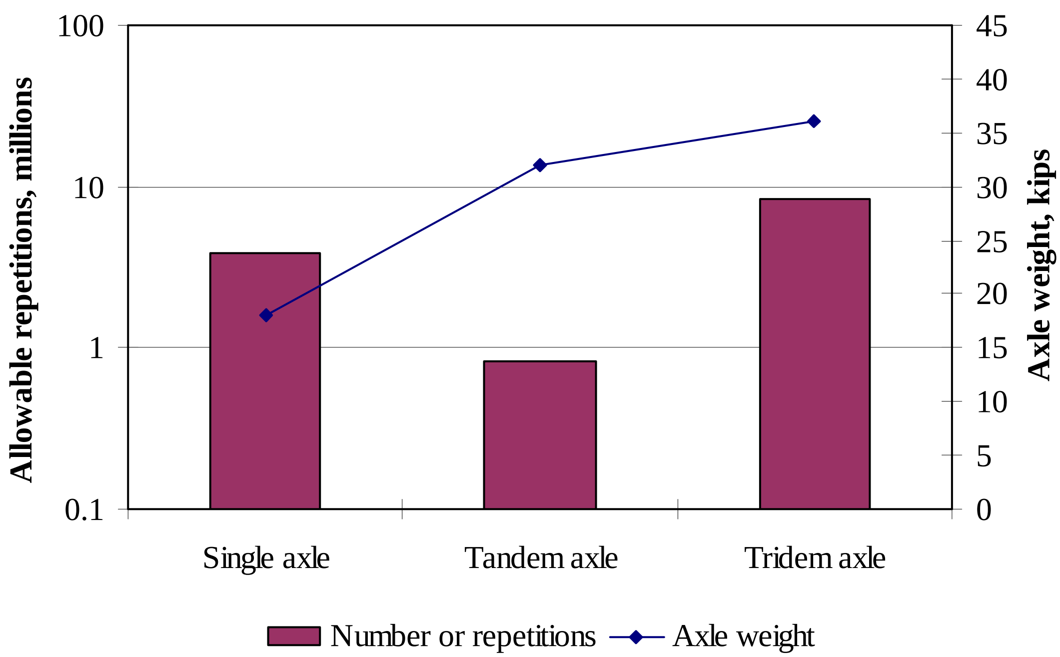


**Figure 6-11: Comparison of results for Example 1**

**<u>Illustrative Example 2</u>** (fatigue damage due to different lateral support conditions)

Analyze the number of load repetitions of 39-kips tridem axle that could be carried at daytime thermal gradient of 2 $^{o}$F/in. by pavement systems in Example 1 but with 12-ft lane with untied AC shoulder and 14-ft lane with untied AC shoulder.

From the catalog of stresses in Appendix I, the magnitudes of the longitudinal stresses at the bottom of the PCC slab are:

For 12-ft lane with untied AC shoulder: 224.1 psi
For 14-ft lane with untied AC shoulder: 208.6 psi

The stress ratios for the two lateral support conditions are calculated as follows:

For 12-ft lane with untied AC shoulder: $R_{\text{12-ft lane with united AC shoulder}} = \dfrac{224.1}{550} = 0.407$

For 14-ft lane with untied AC shoulder: $R_{\text{14-ft lane with untied AC shoulder}} = \dfrac{208.6}{550} = 0.379$

Considering the performance transfer function in equation (6-6), the number of load repetitions of 39-kips tridem axle that could be carried for the given conditions could be analyzed as follows:

Recall that $Log_{10} N = 2 \cdot R^{-1.22} + 0.4371$ or $N = 10^{\left[2 \cdot R^{-1.22} + 0.4371\right]}$

For 12-ft lane with untied AC shoulder:

$N_{\text{12-ft lane with united AC shoulder}} = 10^{\left[2 \cdot (0.407)^{-1.22} + 0.4371\right]} = 2.62 \quad \textit{million cycles}$

For 14-ft lane with untied AC shoulder:

$N_{\text{14-ft lane with united AC shoulder}} = 10^{\left[2 \cdot (0.379)^{-1.22} + 0.4371\right]} = 9.21 \quad \textit{million cycles}$

However, the number of repetitions needed to account for the number of repetitions within each axle group. The number of repetitions for each axle could be adjusted as follows:

Adjusted number of repetitions, $N_{adjusted} = \dfrac{N}{\text{number of repetitions within each axle}}$

For 12-ft lane with untied AC shoulder:

$N_{\text{12-ft lane with united AC shoulder}} = \dfrac{2.62}{3} = 0.87 \quad \textit{million cycles}$

For 14-ft lane with untied AC shoulder:

$N_{\text{14-ft lane with united AC shoulder}} = \dfrac{9.21}{3} = 3.07 \quad \textit{million cycles}$

Figure 6-12 illustrates the number of allowable repetitions for each lateral support condition, including the 12-ft lane with tied PCC shoulder from Example 1. It can be seen that the pavement with 12-ft lane with tied PCC shoulder could carry more repetitions of 39-kips tridem axle, when compared with the others. For the untied AC shoulder pavements, the 14-ft lane pavement could carry more load repetitions than the 12-ft pavement. The two-foot shifting of the wheel path away from the edge creates the pseudo-interior loading condition for the 14-ft lane pavement and consequently reduces the level of stress.

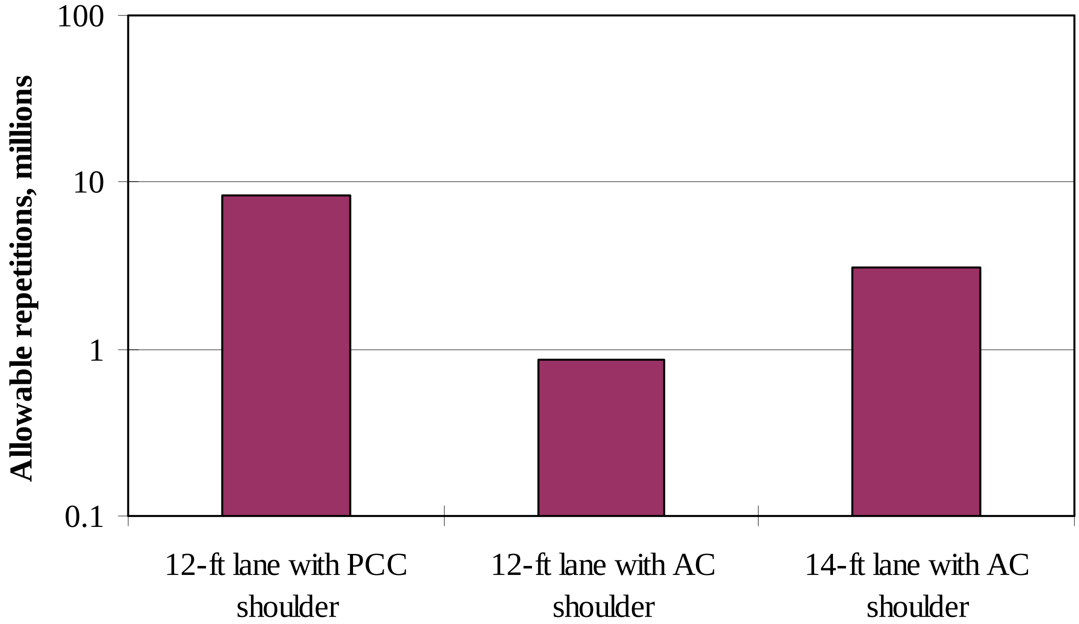


**Figure 6-12: Comparison of results for Example 2**

**<u>Illustrative Example 3</u>** (fatigue damage due to different slab thickness)

Analyze the number of load repetitions of 32-kips tandem axle that could be carried at daytime thermal gradient of 2 $^{o}$F/in. by pavement systems in Example 1 but with 8, 9, 11, and 12-in. PCC slab.

From the catalog of stresses in Appendix I, the magnitudes of the longitudinal stresses at the bottom of the PCC slab are:

For 8-in. slab: 277.2 psi
For 9-in. slab: 253.3 psi
For 11-in. slab: 208.6 psi
For 12-in. slab: 188.7 psi

The stress ratios for the four slab thicknesses are calculated as follows:

For 8-in. slab: $R_{8\text{-in.}} = \dfrac{277.2}{550} = 0.504$

For 9-in. slab: $R_{9\text{-in.}} = \dfrac{253.3}{550} = 0.461$

For 11-in. slab: $R_{11\text{-in.}} = \dfrac{208.6}{550} = 0.379$

$$\text{For 12-in. slab: } R_{12\text{-in.}} = \frac{188.7}{550} = 0.343$$

Considering the performance transfer function in equation (6-6), the number of load repetitions of 39-kips tridem axle that could be carried for the given conditions could be analyzed as follows:

$$\text{Recall that } Log_{10} N = 2 \cdot R^{-1.22} + 0.4371 \text{ or } N = 10^{\left[2 \cdot R^{-1.22} + 0.4371\right]}$$
$$\text{For 8-in. slab: } N_{8\text{-in.}} = 10^{\left[2 \cdot (0.504)^{-1.22} + 0.4371\right]} = 0.112 \quad \textit{million cycles}$$
$$\text{For 9-in. slab: } N_{9\text{-in.}} = 10^{\left[2 \cdot (0.461)^{-1.22} + 0.4371\right]} = 0.387 \quad \textit{million cycles}$$
$$\text{For 11-in. slab: } N_{11\text{-in.}} = 10^{\left[2 \cdot (0.379)^{-1.22} + 0.4371\right]} = 9.21 \quad \textit{million cycles}$$
$$\text{For 12-in. slab: } N_{12\text{-in.}} = 10^{\left[2 \cdot (0.343)^{-1.22} + 0.4371\right]} = 65.05 \quad \textit{million cycles}$$

However, the number of repetitions needed to account for the number of repetitions within each axle group. The number of repetitions for each axle could be adjusted as follows:

$$\text{Adjusted number of repetitions, } N_{adjusted} = \frac{N}{\text{number of repetitions within each axle}}$$
$$\text{For 8-in. slab: } N_{8\text{-in.}} = \frac{0.112}{2} = 0.056 \quad \textit{million cycles}$$
$$\text{For 9-in. slab: } N_{9\text{-in.}} = \frac{0.387}{2} = 0.193 \quad \textit{million cycles}$$
$$\text{For 11-in. slab: } N_{11\text{-in.}} = \frac{9.21}{2} = 4.60 \quad \textit{million cycles}$$
$$\text{For 12-in. slab: } N_{12\text{-in.}} = \frac{65.05}{2} = 32.53 \quad \textit{million cycles}$$

Figure 6-13 illustrates the number of allowable repetitions for each slab thickness, including the 10-in. slab from Example 1. The number of allowable load repetitions is very sensitive to the slab thickness. It can be seen that load carrying capacity of the pavement is logarithmically related to the slab thickness as a linear relationship could be observed on a semi-logarithmic plot.

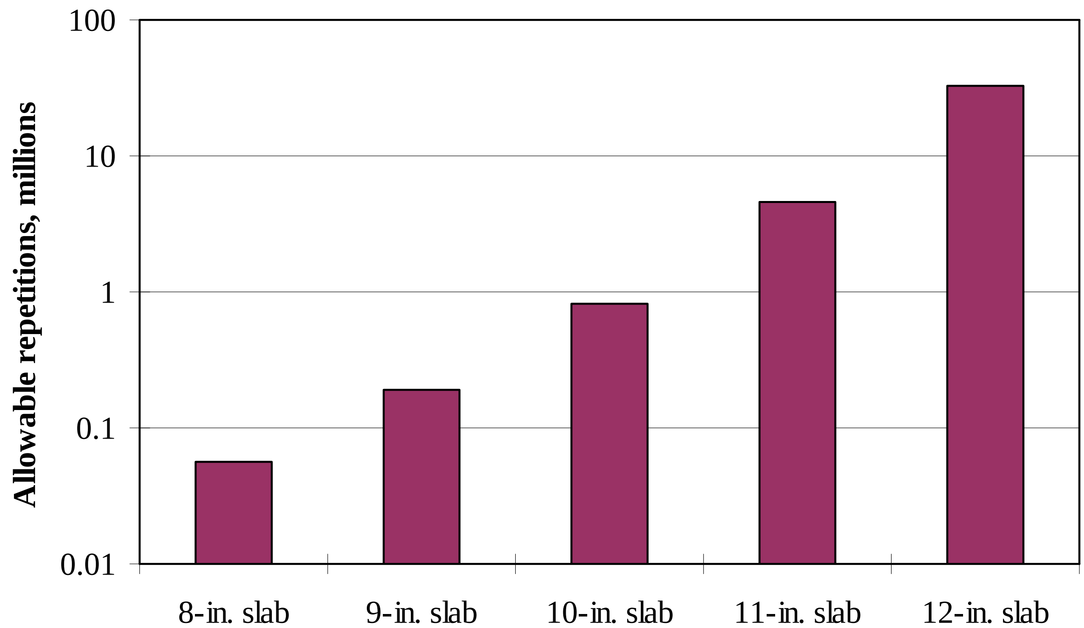


**Figure 6-13: Comparison of results for Example 3**

**Illustrative Example 4** (faulting damage)

Analyze the joint faulting of pavement systems in Example 1 at the end of a design period of 20 years.

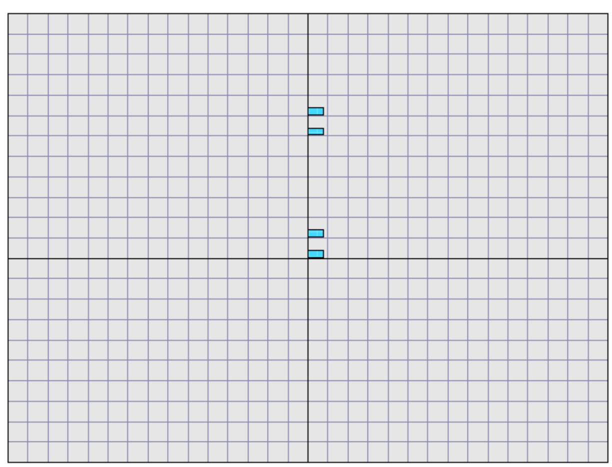

**Figure 6-14: Overview of analysis of joint faulting for Example 4**

The analysis joint faulting damage involves the calculation of differential elastic deformation energy, which is a function of slab corner deflections obtained from FE analysis with loading at the transverse joint, e.g. 18-kips single axle as shown in Figure 6-14.

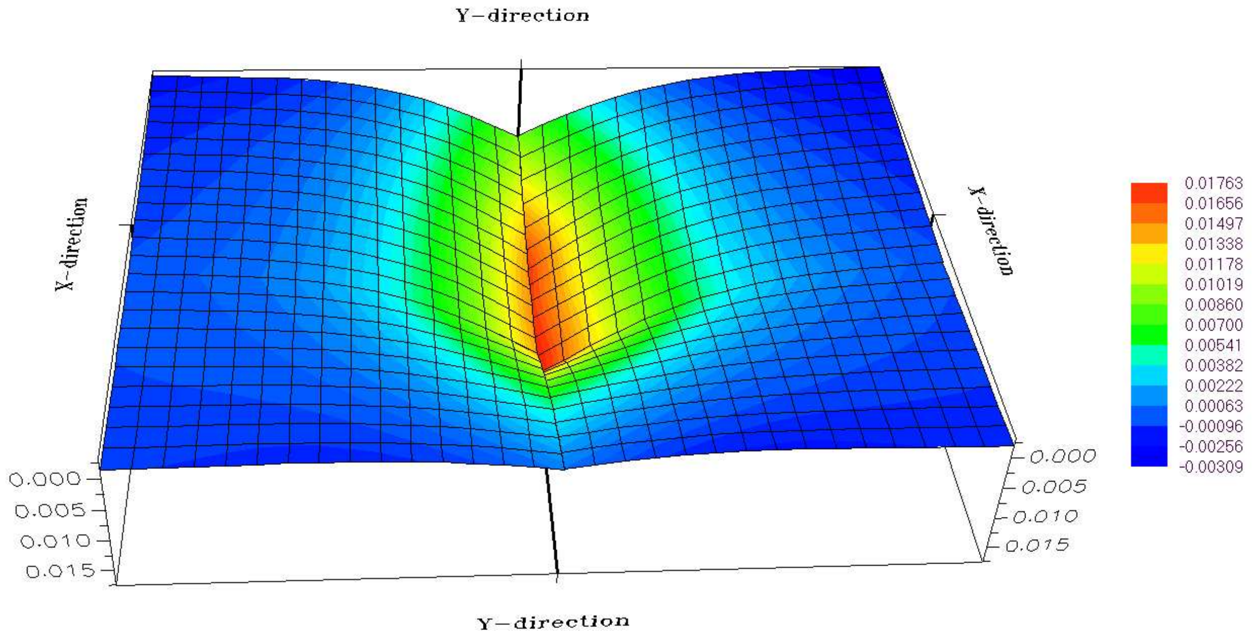


**Figure 6-15: Slab deflection results for Example 4**

From the results shown in Figure 6-15, the slab deflections on both loaded and unloaded sides at the corners of the slabs could be obtained as follows:

Unloaded deflection, $W_{UL} = 0.013797\ in. = 0.35044\ mm$

Loaded deflection, $W_L = 0.017627\ in. = 0.44773\ mm$

For the given modulus of subgrade reaction (100 psi/in. or 27.145 kPa/mm), the differential elastic deformation energy could be calculated as follows:

Differential elastic deformation energy, $DE = \frac{1}{2} \cdot k \cdot (W_L + W_{UL}) \cdot (W_L - W_{UL})$

$$DE = \frac{1}{2} \cdot (27.145) \cdot (0.44773 + 0.35044) \cdot (0.44773 - 0.35044) = 1.053871\ kPa \cdot mm$$

If a typical load spectrum and a typical climatic condition for Michigan are assumed for this example, the faulting calculation could be conducted using Equations 6-7 through 6-10. It should be noted that an erodibility index of 3 (erosion resistant) is assumed for this example.

The predicted faulting is illustrated in Figure 6-16. The predicted faulting is 0.1671 in. at the end of the design period.

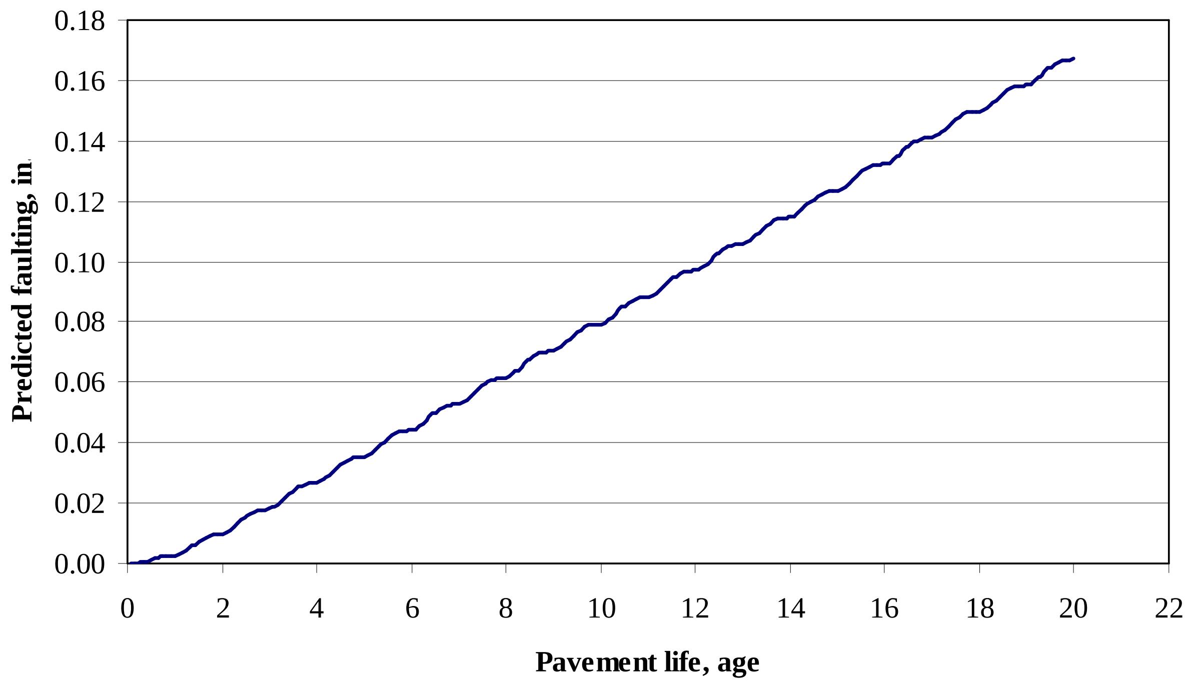


**Figure 6-16: Predicted faulting for Example 4**

<u>**Illustrative Example 5**</u> (faulting damage due to different joint designs)

Repeat Example 4 but with three of the following transverse joint designs:

- 1.5-in. dowel diameter at 12 in. center to center spacing,
- 1.25-in. dowel diameter at 18 in. center to center spacing and
- 1.5-in. dowel diameter at 18 in. center to center spacing.

Figure 6-17 illustrates the differential elastic deformation energy for the three joint designs as well as the joint design from Example 4 at the end of the design period of 20 years. It can be seen that the increase in the dowel diameter size result in a decrease in the differential elastic deformation energy, while dowel spacing has only slight impact on the differential elastic deformation energy. The predicted faulting is illustrated in Figure 6-18.

It is important to note that the variation in the joint design directly affects the slab deflections on both loaded and unloaded sides and consequently the differential elastic deformation energy. As illustrated in Figure 6-19, the decrease in the differential elastic deformation energy results in reduced faulting magnitudes.

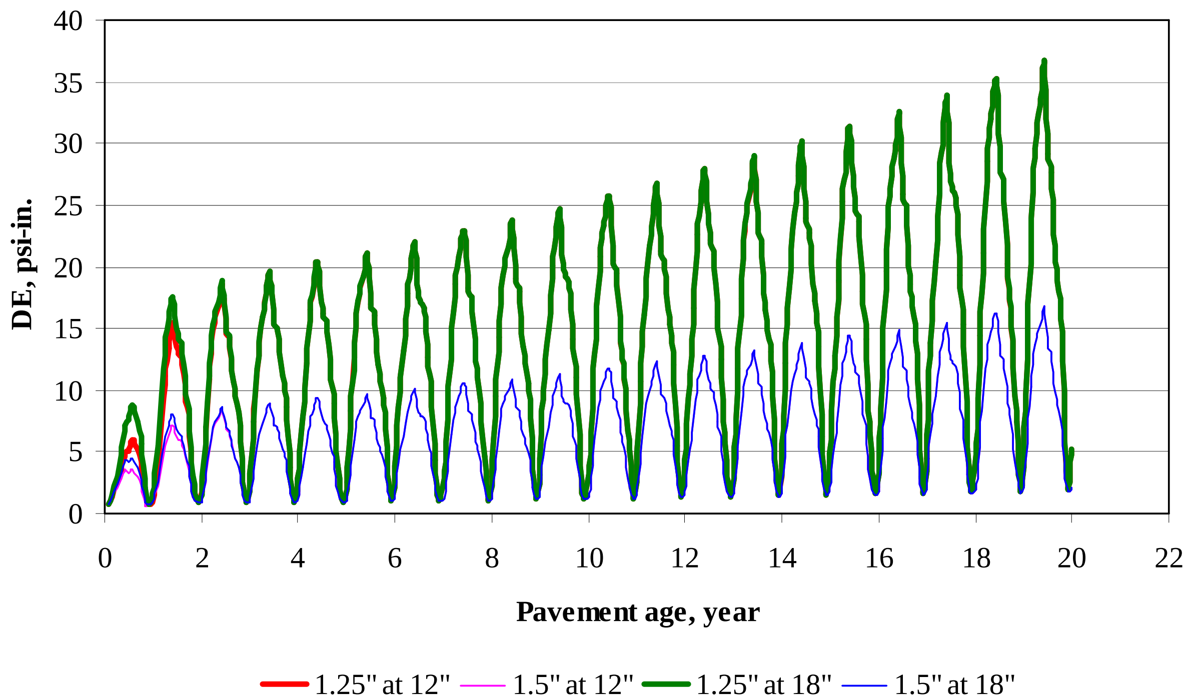


**Figure 6-17: Differential elastic deformation energy for Example 5**

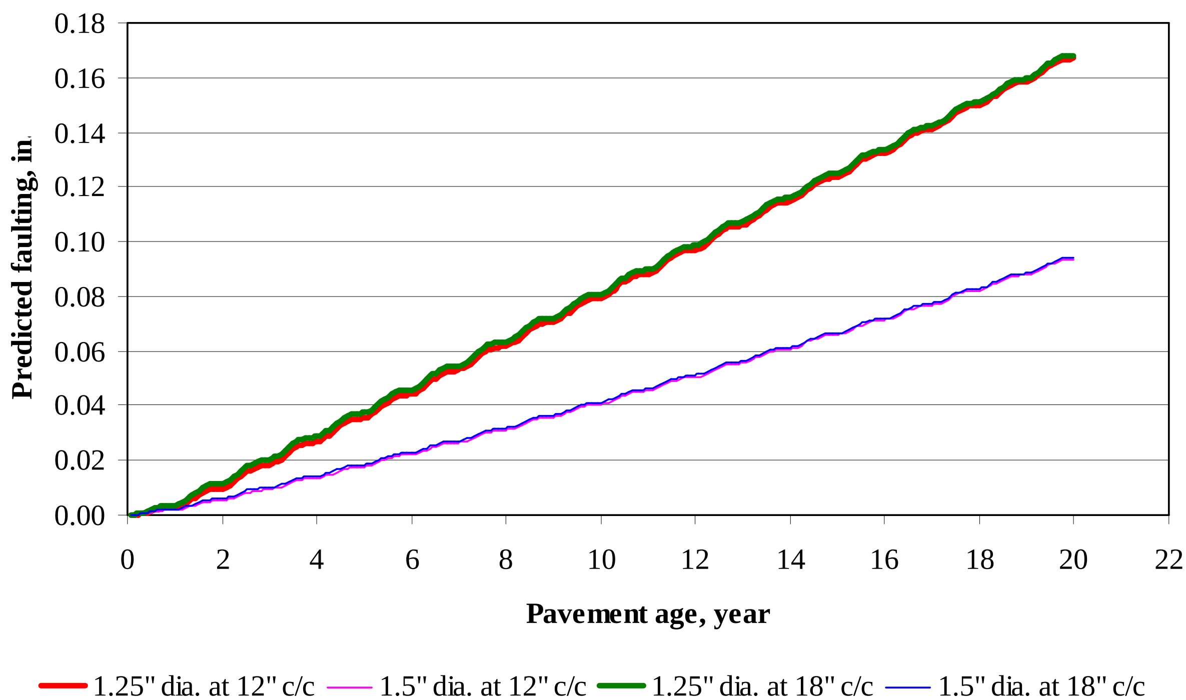


**Figure 6-18: Predicted faultings for Example 5**

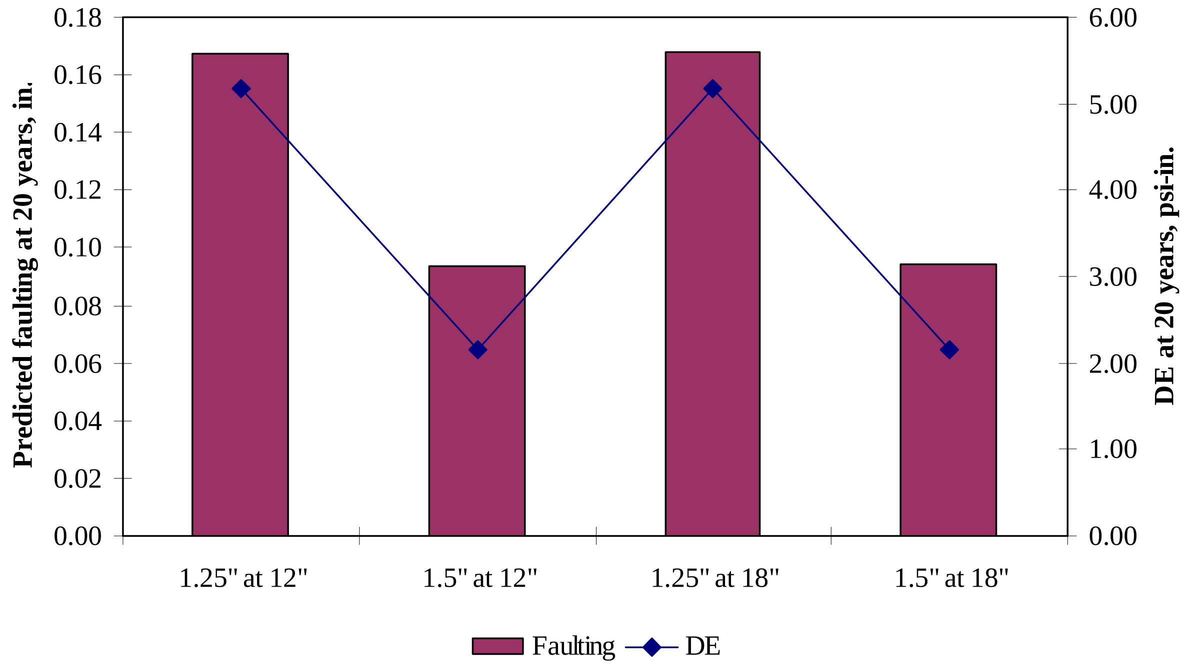


**Figure 6-19: Predicted faultings and differential elastic deformation energy at the end of 20 years**

**<u>Illustrative Example 6</u>** (faulting damage due to different base types)

Repeat Example 4 but with lean concrete base (elastic modulus of 2,000,000 psi, Poisson's ratio of 0.15 and erodibility index of 1 or "extremely resistant") and asphalt treated base (elastic modulus of 300,000 psi, Poisson's ratio of 0.30 and erodibility index of 2 or "very erosion resistant"). Then, also compare the results with Example 4, which is an aggregate base section.

Figure 6-20 illustrates the differential elastic deformation energy for the three base types. The differential elastic deformation energies for all base types were observed to be approximately equal. However, differential elastic deformation energy is not only a function of slab deflections, but also a function of modulus of subgrade reaction. In this case, the three pavement systems have different values of modulus of subgrade reaction. Therefore, the ratio of differential elastic deformation energy to modulus of subgrade reaction, DE/k, is illustrated in Figure 6-21 to eliminate the impact of modulus of subgrade reaction and focus on the slab deflections.

Predicted faulting for the three pavement systems is illustrated in Figure 6-22. It can be seen in Figure 6-23 that the level of the predicted faulting at the end of 20 years of design period corresponds to the ratio DE/k.

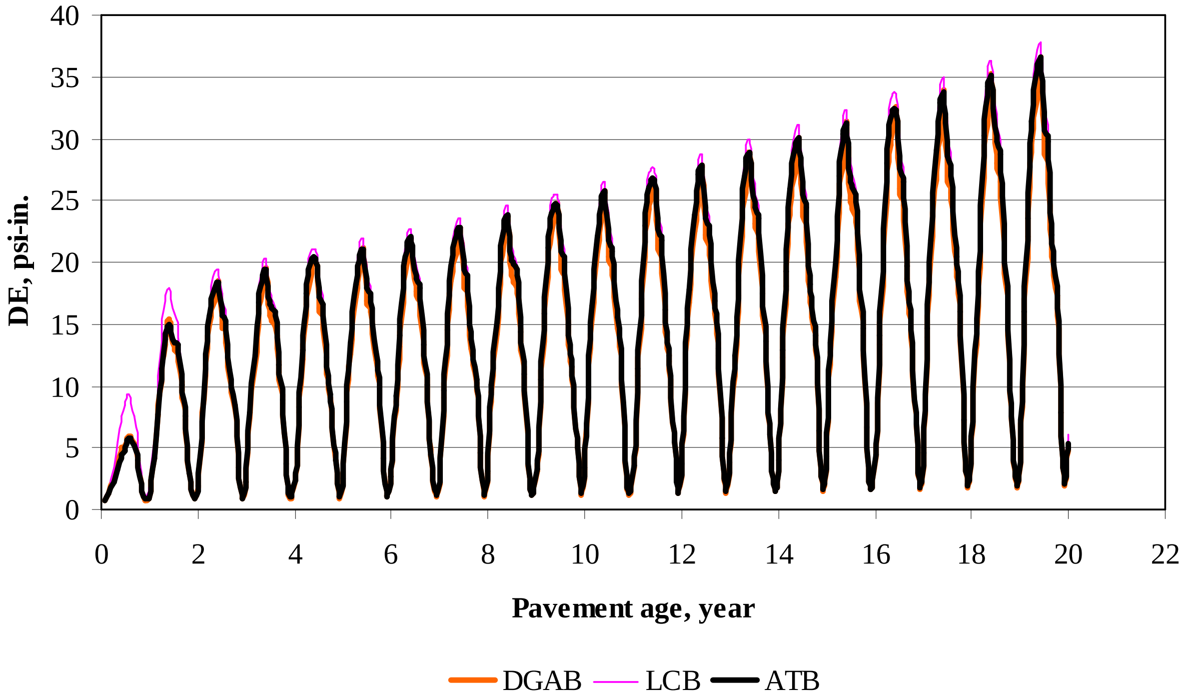


**Figure 6-20: Differential elastic deformation energy for Example 6**

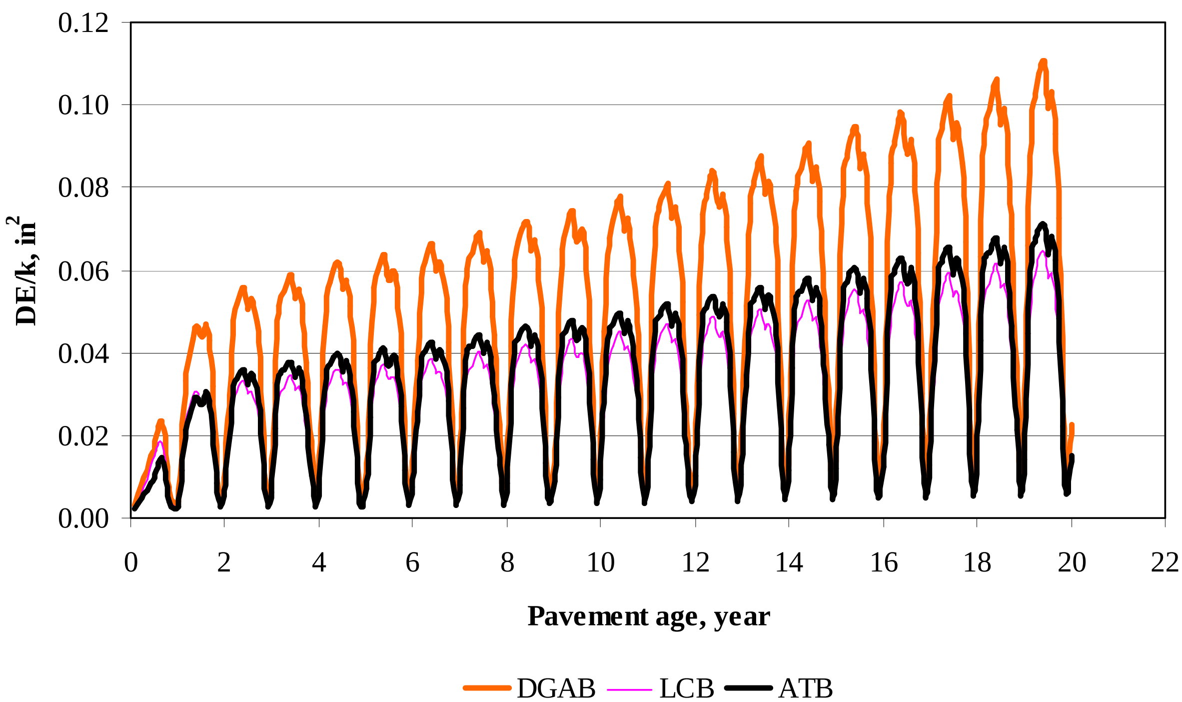


**Figure 6-21: Ratio DE/k for Example 6**

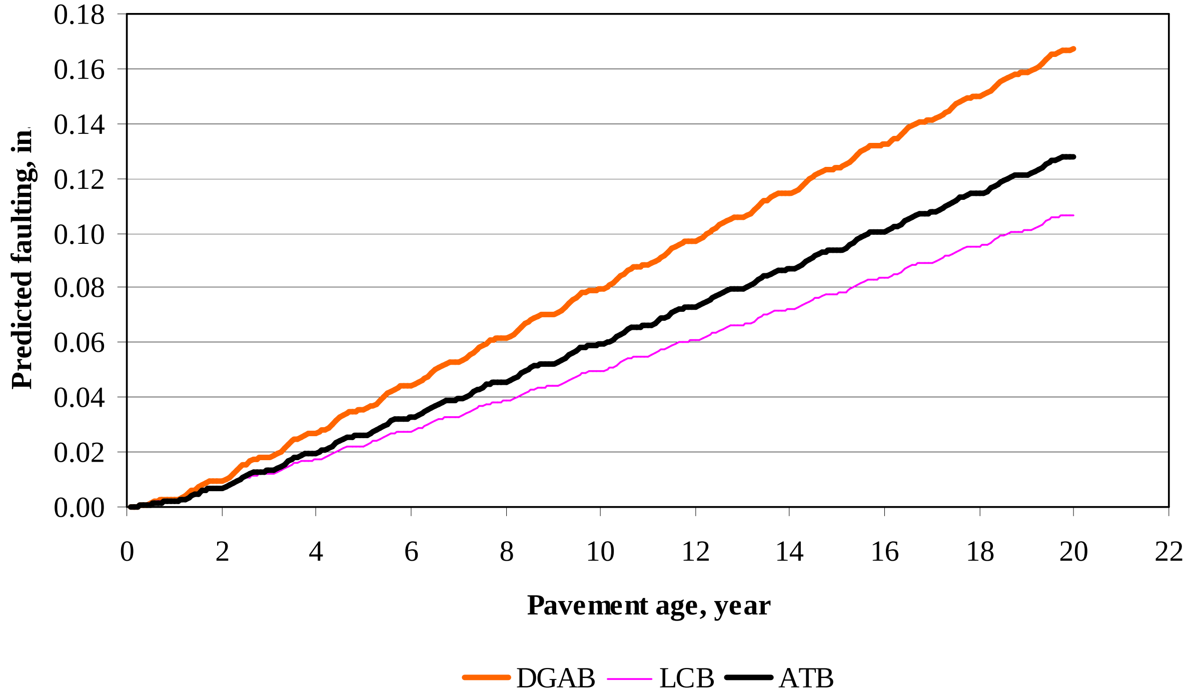


**Figure 6-18: Predicted faultings for Example 6**

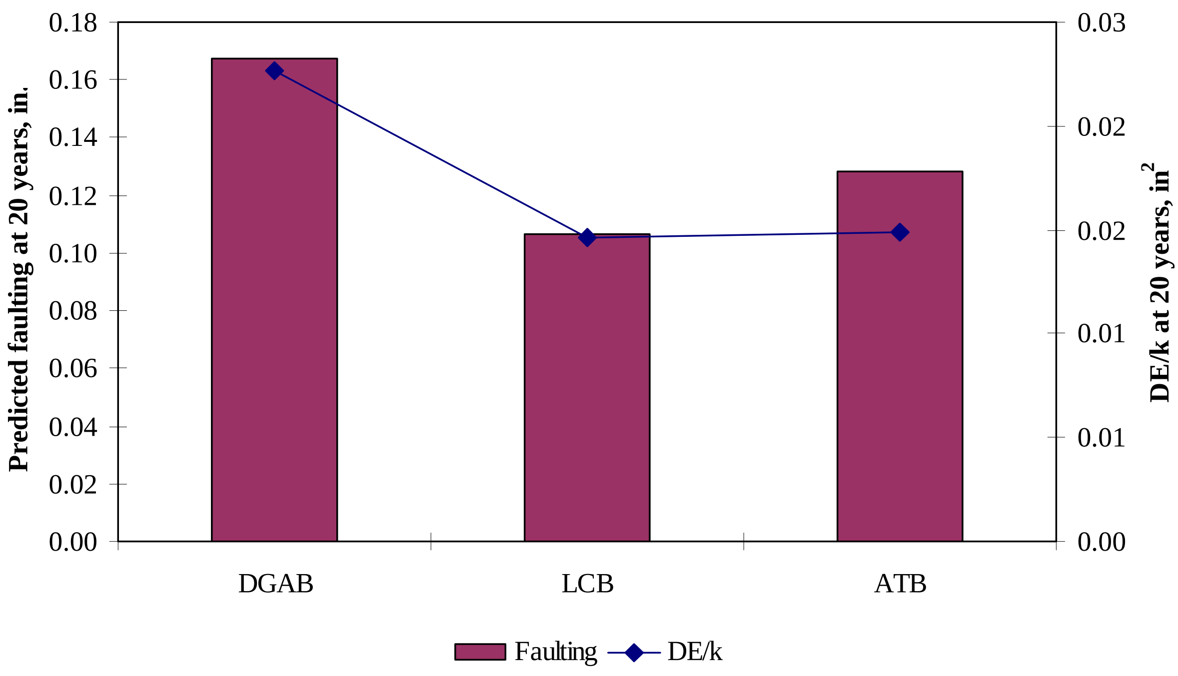


**Figure 6-19: Predicted faultings and ratio DE/k at the end of 20 years**

**Illustrative Example 7** (spalling damage)

Analyze percentage of joints spalled at the end of 20 years of design period for a pavement system with 3% air content, no preformed sealant, 2,000-psi compressive strength, an average of 250 freeze thaw cycles per year, 8-in. slab, and 0.45 water/cement ratio.

Scaling factor can be computed based on the given information as follows:

$$\begin{aligned} SCF &= -1400 + 350 \cdot AIR\% \cdot (0.5 + PREFORM) + 3.4 \cdot f'_c \cdot 0.4 \\ &\quad - 0.2\left(FTCYC \cdot AGE\right) + 43 \cdot h_{PCC} - 536 \cdot WC\_Ratio \\ SCF &= -1400 + 350 \cdot \left(3\right) \cdot (0.5 + 0) + 3.4 \cdot \left(2{,}000\right) \cdot 0.4 \\ &\quad - 0.2\left(250 \cdot 20\right) + 43 \cdot 8 - 536 \cdot \left(0.45\right) \\ &= 947.8 \end{aligned}$$

Percentage joints spalled can be compute as follow:

$$SPALL = \left[\frac{AGE}{AGE + 0.01}\right] \cdot \left[\frac{100}{1 + 1.005^{\left(-12 * AGE + SCF\right)}}\right]$$

$$SPALL = \left[\frac{20}{20 + 0.01}\right] \cdot \left[\frac{100}{1 + 1.005^{\left(-12 * 20 + 947.8\right)}}\right] = 3\%$$

# Chapter VII

# SUMMARY OF FINDINGS AND RECOMMENDATIONS FOR FUTURE RESEARCH

## 7.1 Summary of Findings

The primary objective of this research study was to conduct a preliminary parametric study to investigate the impact of the interaction between structural, environmental, and load factors on pavement responses using ISLAB2000 structural model. This was accomplished through performing structural analysis of 43,092 input combinations and the use of interpolation scheme. The secondary objective is to develop a technology transfer package that will introduce the rigid pavement analysis tools to the MDOT pavement engineers, demonstrate the versatility of the rigid pavement analysis tool and summarize a variety of pavement design scenarios in a workbook for the MDOT pavement engineers. An elaborate tutorial for the use of ISLAB2000 program and several step-by-step examples were included in the technology transfer package to fulfill this objective. The package should enable engineers to apply the ISLAB2000 program to analyze JCP systems. In addition, several MDOT designs were selected as practice problems, for which the key answers were also provided.

The analysis results of this study lead to several findings, which can be categorized into three groups: robustness and user friendliness of the ISLAB2000 program, parametric study results and interpolation scheme.

**Findings Related to Robustness and User Friendliness of the ISLAB2000 Program**

- The ISLAB2000 program is robust and user friendly. The results from the ISLAB2000 structural model compare well with the Westergaard solutions (after considering the relevant assumptions) and other widely accepted FE structural models.

- The variations of stresses and deflections obtained from the ISLAB2000 structural model, when using mesh size of 12 in., were found to be about 4% and 3%, respectively.

**Findings Related to Parametric Study Results**

- The critical load location is influenced by joint spacing and truck or axle configuration. The fractional factorial analysis indicated that the critical load location is not influenced by slab thickness, base/subbase thickness, modulus of subgrade reaction, lateral support condition, and thermal gradient or thermal strain gradient.

- For a flat slab condition, when the slab thickness changes from 9 to 12 in. the resulting stress is reduced by approximately in about 35% lower stresses. For a constant thermal gradient, pavements constructed with different slab thickness have different temperature differentials, and therefore, the pavement responses could not be compared.

- For a flat slab condition, pavement cross-sections with thicker base/subbase thickness (from 4 to 26 in.) resulted in about 5-30% lower stresses and as the slab thickness increases the impact of base/subbase thickness becomes less significant.

- Pavements constructed with 27 feet joint spacing resulted in about 33% higher longitudinal stresses as compared to pavements constructed with 15 feet joint spacing for curled slab conditions at a thermal strain gradient value of $+10\text{x}10^{-6}$ $\text{in.}^{-1}$. The severity depends on the level of thermal curling or thermal strain gradient.

- For the load located along the wheel path (approximately 20" from the traffic stripe), pavements constructed with PCC shoulders resulted in the lowest stresses among the three lateral support conditions (12' lane with tied PCC shoulders, 12' lane with AC shoulders and 14' lane with AC shoulders) that are considered in the study. Although the pavements were constructed with the same AC shoulder, the magnitudes of longitudinal stresses for pavements with 12-ft lane (standard lane) were higher than that for pavements with 14-ft lane (widened lane). As the wheel path shifted 2 ft towards the centerline for pavements with widened lane, a pseudo-interior loading condition was created, resulting in the reduction of stresses from edge loading. Pavements constructed with AC shoulders (12-ft lane with AC shoulder) resulted in about 13% and 9% higher longitudinal stress values than pavements constructed with PCC shoulder (12-ft lane with tied PCC shoulder) and widened lane (14-ft lane with untied AC shoulder), respectively.

- Lateral wander (or lateral placement) of traffic load resulted in about 10% and 30% higher edge stresses as the load moves from the wheel path towards longitudinal joint (lane/shoulder joint) for tied PCC shoulder and AC shoulder, respectively.

**Findings Related to Interpolation Scheme**

- In the validation process considering all axle types, the bias (average error), variance, and mean square of errors (MSE) of the best scheme (scheme 16) were 0.51 psi, 8.63 $\text{psi}^2$, and 8.89 $\text{psi}^2$, respectively, indicating that the interpolation scheme was highly accurate and precise in computing pavement response as compared with the results directly obtained from the ISLAB2000 program.

- If only single, tandem and tridem axles were considered, the bias, variance and MSE of the best scheme were found to be 0.02 psi, 3.38 $\text{psi}^2$, and 3.38 $\text{psi}^2$, respectively.

## 7.2 Recommendations for Future Research

This research study focuses on pavement responses and several factors that affect them. Although pavement response plays a significant role in the mechanistic-empirical design process, it is necessary to integrate the pavement response with several other components in order for it to become practical. Pavement responses need to be used an inputs to transfer function, which relate responses to performance. However, the transfer function coefficients need to be localized and therefore it is important to ensure the constants reflect climatic and loading conditions in Michigan. Calibration process also needs to take place to ensure MDOT policies are met in the calculation process. The following research topics are recommended:

1) The CTE values for concrete mixes and also aggregate (as concrete making material) used in paving Michigan roads need to be determined and cataloged, since CTE plays a critical role in the thermal analysis of jointed concrete pavements. The slab movement and joint opening are also influenced by the CTE of concrete.

2) An extensive traffic database, e.g. WIM database, should be made available for the pavement network as hourly axle spectra is a key input for damage computations. The hourly axle spectra allow for calculation of pavement responses that account for daily and seasonal conditions of climate, roadbed and material. The axle repetitions from the axle spectra and the corresponding pavement responses are the inputs to the cumulative damage calculation.

3) Develop and calibrate transfer functions for key jointed concrete pavement distresses that reflect Michigan practice. The process involves statistical correlation of the cumulative damages to the measured distresses corresponding to the time periods to obtain a calibrated model that can be used for Michigan jointed concrete pavement design.

# REFERENCES

American Association of State Highway and Transportation Officials (AASHTO). AASHTO Guide for Design of Pavement Structures. Washington, DC, USA, 1993.

Armaghani, J.M; Larsen, T.J; Smith, L.L. Temperature Response of Concrete Pavements. Transportation Research Record 1121, TRB, National Research Council, Washington, DC, USA, 1987, pp. 23-33.

Channakeshava, C.; Barzegar, F.; Voyiadjis, G.Z. Nonlinear FE analysis of plain concrete pavements with doweled joints. Journal of Transportation Engineering, v 119, n 5, American Society of Civil Engineers, New York, NY, USA, 1993, pp. 763-781.

Crovetti, J. A.; Darter, M. I. Void detection for jointed concrete pavements. Transportation Research Record 1041, TRB, National Research Council, Washington, DC, USA, 1985, pp. 59-68.

Darter, M.I; Hall, K.T; Kuo, C. Support Under Concrete Pavements. University of Illinois, Urbana-Champaign, Illinois, USA, 1994.

Darter, M; Khazanovich, L; Snyder, M; Rao, S; Hallin, J. Development and Calibration of a Mechanic Design Procedure for Jointed Plain Concrete Pavements. 7$^{th}$ International Conference on Concrete Pavements, Orlando, FL, USA, 2001.

Davids, W.G.; Mahoney, J.P. Experimental verification of rigid pavement joint load transfer modeling with EverFe. Transportation Research Record 1684, TRB, National Research Council, Washington, DC, USA, 1999, pp. 81-89.

Huang, Y.H. Pavement Analysis and Design. Prentice-Hall, Englewood, NJ, USA, 1993.

Ioannides, A.M.; Thompson, M.R.; Barenberg, E.J. Westergaard solutions reconsidered. Transportation Research Record 1043, TRB, National Research Council, Washington, DC, USA, 1985, pp. 13-23.

Khazanovich, L.; Yu, H.T. Modeling of jointed plain concrete pavement fatigue cracking in PaveSpec 3.0. Transportation Research Record 1778, TRB, National Research Council, Washington, DC, USA, 2001, pp. 33-42.

Khazanovich, L; Darter, M.I.; Yu, T. Mechanistic-empirical for transverse joint faulting prediction. Presented at the 83$^{rd}$ Annual Meeting of the TRB, Washington, DC, USA, 2004.

Michigan Center for Truck Safety. Truck driver's guidebook, 6$^{th}$ edition. Michigan Center for Truck Safety, Lansing, MI, USA, 2001.

Mirambell, E. Temperature and Stress Distributions in Plain Concrete Pavements Under Thermal and Mechanical Loads. 2nd International Workshop on the Theoretical Design of Concrete Pavements, Siquenza, Spain, 1990.

NCHRP. Calibrated Mechanistic Structural Analysis Precedures for Pavement. NCHRP 1-26, Vol. 1, Final Report; Vol. 2, Appendices, University of Illinois, Urbana-Champaign, Illinois, USA, 1990.

Oh, B.H. Cumulative damage theory of concrete under variable-amplitude fatigue loadings. ACI Materials Journal, v 88, n 1, American Concrete Institute, Detroit, MI, USA, 1991, pp. 41-48.

Rao, C; Barenberg, E.J; Snyder, M.B; Schmidt, S. Effects of Temperature and Moisture on the Response of Jointed Concrete Pavements. 7th International Conference on Concrete Pavements, Orlando, FL, USA, 2001.

Rao, C; Selezneva, O; Darter, M.I. Calibration of a mechanistic empirical performance model for CRCP punchouts. Presented at the 83rd Annual Meeting of the TRB, Washington, DC, USA, 2004.

Strategic Highway Research Program. Specific pavement studies experimental design and research plan for experiment SPS-2 strategic study of structural factors for rigid pavements. National Research Council, Washington, DC, USA, 1990.

Tabatabaie, A.M.; Barenberg, E.J. Structural analysis of concrete pavements systems. Journal of Transportation Engineering, v 106, n 5, American Society of Civil Engineers, New York, NY, USA, 1980, pp. 493-506.

Tayabji, S.D.; Colley, B.E. Improved rigid pavement joints. Transportation Research Record 930, TRB, National Research Council, Washington, DC, USA, 1983, pp. 69-78.

Ullidtz, P. Pavement Analysis. Elsevier, New York, NY, USA, 1987.

Westergaard, H.M. Stresses in concrete pavements computed by theoretical analysis. Public Road, v 7, 1926, pp. 25-35.

Yu, T.; Khazanovich, L.; Darter, M.I. Consideration of JPCP curling and warping in the 2002 Design Guide. Presented at the 83rd Annual Meeting of the TRB, Washington, DC, USA, 2004.

# Appendix A

**Review of Kirchhoff Plate Theory**

**Kirchhoff plate theory and FE**

Rigid pavement can be idealized using Kirchhoff theory, which is applicable to thin plates (Cook et al, 1989; Reddy, 1993). In other words, since rigid pavement thickness is very lesser than other two dimensions, transverse shear deformation is insignificant and can be neglected. With this important statement, all stress-strain relations that involved transverse shear deformation are vanished and what remains is the plane stress-strain relation that is shown below in form of matrices (for an isotropic material).

$$\begin{Bmatrix} \sigma_x \\ \sigma_y \\ \tau_{xy} \end{Bmatrix} = \begin{bmatrix} E' & E'' & 0 \\ E'' & E' & 0 \\ 0 & 0 & G \end{bmatrix} \cdot \left( \begin{Bmatrix} \varepsilon_x \\ \varepsilon_y \\ \gamma_{xy} \end{Bmatrix} - \begin{Bmatrix} \alpha \cdot T \\ \alpha \cdot T \\ 0 \end{Bmatrix} \right) \qquad \text{(A-12)}$$

When α = coefficient of thermal expansion of concrete
μ = Poisson’s ratio of concrete
T = temperature differential between top and bottom of concrete

$$E' = \frac{E''}{\mu} = \frac{E}{1-\mu^2} \qquad \text{(A-13)}$$

$$G = \frac{E}{2 \cdot (1+\mu)} \qquad \text{(A-14)}$$

Based on stress-strain relations as written in matrix form above, stiffness matrix of concrete slab $[K_p]$ may be derived using the following formula.

$$[K_p] = \int_A [B]^T \cdot [D_k] \cdot [B] \, dA \qquad \text{(A-15)}$$

When [B] = strain-displacement matrix (will be discussed later)
A = area boundary of an element

$$[D_k] = \begin{bmatrix} D & \mu \cdot D & 0 \\ \mu \cdot D & D & 0 \\ 0 & 0 & \frac{(1-\mu) \cdot D}{2} \end{bmatrix} \qquad \text{(A-16)}$$

D = flexural rigidity

$$D = \frac{E \cdot t^3}{12 \cdot (1-\mu^2)} \qquad \text{(A-17)}$$

When t = slab thickness

## Winkler foundation and FE

Theoretically, rigid pavement, which is actually a slab on grade, can be approximately considered as one elastic structure supported by a foundation model called Winkler foundation. There are a great many other foundation models available for rigid pavement foundation idealization; however, Winkler foundation is traditionally used and considered as the most effective model. Details of characteristics, advantages, and disadvantages of Winkler foundation will not be discussed at this time. Another name of Winkler foundation is "Dense Liquid" foundation because this foundation simulates the behavior of subgrade or original soil under concrete slab by providing a vertical resistant pressure equal to βw when w is vertical deflection and β is the Winkler foundation modulus (modulus of subgrade reaction). Stiffness matrix of foundation is written below in matrix form.

$$[K_f] = \int_A \beta \cdot [N]^T \cdot [N]\, dA \qquad \text{(A-18)}$$

When [N] = interpolation functions matrix (will be discussed later)
A = area boundary of an element

## Discretization into FE and interpolation functions

Since rigid pavement has rectangular geometry, the pavement can be discretized using rectangular linear FE with three degrees of freedom at each node: one vertical displacement, and two horizontal rotations as shown in FigureA-8. In other words, one FE contains twelve degrees of freedom and this means each element has 12x12 stiffness matrix and 12x1 force vector and 12x1 displacement vector.

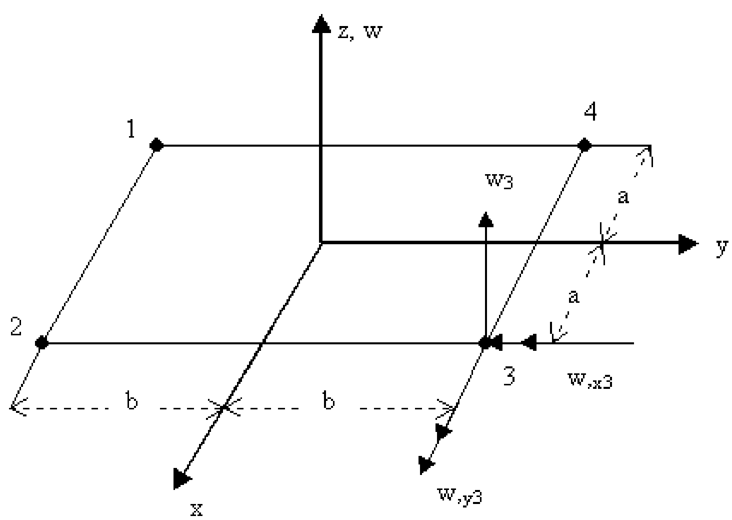


**Figure A-8: Twelve-d.o.f. rectangular Kirchhoff plate element with typical d.o.f. shown at node 3**

Since Kirchhoff plate elements provide interelement continuity of vertical displacements and rotations in x and y directions, the elements can be considered $C^1$ elements; therefore, interpolation functions for $C^0$ elements like Lagrange's interpolation formula may not be applied. Hermitian interpolation function, one of interpolation functions $C^1$ elements, can be used for this situation (thin plate elements). For an element that has four nodes: 1, 2, 3, and 4, Hermitian interpolation functions can be derived using following formulae.

$$\begin{aligned} w &= N_1 \cdot w_1 + N_{x1} \cdot \theta_{x1} + N_{y1} \cdot \theta_{y1} + N_2 \cdot w_2 + N_{x2} \cdot \theta_{x2} + N_{y2} \cdot \theta_{y2} \\ &+ N_3 \cdot w_3 + N_{x3} \cdot \theta_{x3} + N_{y3} \cdot \theta_{y3} + N_4 \cdot w_4 + N_{x4} \cdot \theta_{x4} + N_{y4} \cdot \theta_{y4} \end{aligned} \tag{A-19}$$

When

$$\begin{bmatrix} N_1 & N_{x1} & N_{y1} \end{bmatrix} = \frac{1}{16} \cdot X_1 Y_1 [X_1 Y_1 - X_2 Y_2 + 2X_1 Y_2 + 2Y_1 Y_2 \quad 2bY_1 Y_2 \quad -2aX_1 X_2] \tag{A-20-1}$$

$$\begin{bmatrix} N_2 & N_{x2} & N_{y2} \end{bmatrix} = \frac{1}{16} \cdot X_2 Y_1 [X_2 Y_1 - X_1 Y_2 + 2X_1 Y_2 + 2Y_1 Y_2 \quad 2bY_1 Y_2 \quad 2aX_1 X_2] \tag{A-20-2}$$

$$\begin{bmatrix} N_3 & N_{x3} & N_{y3} \end{bmatrix} = \frac{1}{16} \cdot X_2 Y_2 [X_2 Y_2 - X_1 Y_1 + 2X_1 Y_2 + 2Y_1 Y_2 \quad -2bY_1 Y_2 \quad 2aX_1 X_2] \tag{A-20-3}$$

$$\begin{bmatrix} N_4 & N_{x4} & N_{y4} \end{bmatrix} = \frac{1}{16} \cdot X_1 Y_2 [X_1 Y_2 - X_2 Y_1 + 2X_1 Y_2 + 2Y_1 Y_2 \quad -2bY_1 Y_2 \quad -2aX_1 X_2] \tag{A-20-4}$$

When $X_1 = 1 - \dfrac{x}{a}$ (A-21-1)

$$X_2 = 1 + \frac{x}{a} \tag{A-21-2}$$

$$Y_1 = 1 - \frac{y}{b} \tag{A-21-3}$$

$$Y_2 = 1 + \frac{y}{b} \tag{A-21-4}$$

Now the interpolation functions can be written in matrix form 1x12 as shown below.

$$[N] = [N_1 \;\; N_{x1} \;\; N_{y1} \;\; N_2 \;\; N_{x2} \;\; N_{y2} \;\; N_3 \;\; N_{x3} \;\; N_{y3} \; N_4 \;\; N_{x4} \;\; N_{y4}] \tag{A-22}$$

Strain-displacement matrix [B] can also be written in matrix form 3x12 as shown below.

$$[B] = -\begin{bmatrix} \dfrac{\partial^2 N_1}{\partial x^2} & \dfrac{\partial^2 N_{x1}}{\partial x^2} & \dfrac{\partial^2 N_{y1}}{\partial x^2} & \cdots & \dfrac{\partial^2 N_{y4}}{\partial x^2} \\ \dfrac{\partial^2 N_1}{\partial y^2} & \dfrac{\partial^2 N_{x1}}{\partial y^2} & \dfrac{\partial^2 N_{y1}}{\partial y^2} & \cdots & \dfrac{\partial^2 N_{y4}}{\partial y^2} \\ 2 \cdot \dfrac{\partial^2 N_1}{\partial x \partial y} & 2 \cdot \dfrac{\partial^2 N_{x1}}{\partial x \partial y} & 2 \cdot \dfrac{\partial^2 N_{y1}}{\partial x \partial y} & \cdots & 2 \cdot \dfrac{\partial^2 N_{y4}}{\partial x \partial y} \end{bmatrix} \tag{A-23}$$

**FE of one element**

From previous part, stiffness matrix of each element [$K_e$] (12x12) can be derived as shown below.

$$[K_p] \cdot \{u_p\} + [K_f] \cdot \{u_f\} = \{r_e\} \tag{A-24-1}$$

but $\{u_p\} = \{u_f\} = \{u_e\}$ (A-24-2)

$$[K_e] \cdot \{u_e\} = \{r_e\} \quad \text{(A-24-3)}$$

$$[K_e] = [K_p] + [K_f] \quad \text{(A-24-4)}$$

When $\{u_p\}$ = slab displacement vector
$\{u_f\}$ = foundation displacement vector
$\{u_e\}$ = element displacement vector (12x1)

$$\{u_e\} = \begin{Bmatrix} w_1 \\ \theta_{x1} \\ \theta_{y1} \\ w_2 \\ \theta_{x2} \\ \theta_{y2} \\ w_3 \\ \theta_{x3} \\ \theta_{y3} \\ w_4 \\ \theta_{x4} \\ \theta_{y4} \end{Bmatrix} \quad \text{(A-25)}$$

$\{r_e\}$ = element force vector (12x1)

$$\{r_e\} = \int_A [B]^T \cdot [D_K] \cdot \{\kappa_o\} \, dA \quad \text{(A-26)}$$

$$\text{When} \quad \{\kappa_o\} = \begin{bmatrix} \frac{\alpha \cdot T}{t} & \frac{\alpha \cdot T}{t} & 0 \end{bmatrix}^T \quad \text{(A-27)}$$

**Global system**

Global stiffness matrix and force matrix can be computed based on element stiffness matrix and element force matrix. The concept of generating element stiffness matrix and element force vector into global stiffness matrix and global force vector is exactly the same as the concept of using Boolean matrix that is applicable for $C^0$ elements but the method is slightly different. This is because each node of a Kirchhoff element has 3 degrees of freedom. This means the element stiffness matrix, which is actually 12x12, can be considered as 4x4 and the element force vector, which is actually 12x1, can be considered 4x1 in order to generate them into global system as shown below.

$$[K_e] = \begin{bmatrix} K_{11(3x3)} & K_{12(3x3)} & K_{13(3x3)} & K_{14(3x3)} \\ K_{21(3x3)} & K_{22(3x3)} & K_{23(3x3)} & K_{24(3x3)} \\ K_{31(3x3)} & K_{32(3x3)} & K_{33(3x3)} & K_{34(3x3)} \\ K_{41(3x3)} & K_{42(3x3)} & K_{43(3x3)} & K_{44(3x3)} \end{bmatrix} \tag{A-28}$$

$$\{r_e\} = \begin{Bmatrix} r_{1(3x1)} \\ r_{2(3x1)} \\ r_{3(3x1)} \\ r_{4(3x1)} \end{Bmatrix} \tag{A-29}$$

Once global stiffness matrix and global force vector are derived, displacement vector of global system can be computed.

$$\{U\}_{3N\times1} = [KG]^{-1}_{3N\times3N} \cdot \{F\}_{3N\times1} \tag{A-30}$$

When {U} = global displacement vector
[KG] = global stiffness matrix
{F} = global force vector
N = number of nodes in global system

# Appendix B

## Comparison between ISLAB2000 Results and Westergaard's Solution

**Comparison between ISLAB2000 results and Westergaard's solution**

Each problem was divided into two parts: the textbook solution (Huang, 1993), and the ISLAB2000 solution (FE solution). The textbook solution consists of the problem statement, an illustration of the problem, and solution based on Westergaard's equations, while the finite element (FE) solution consists of the summary of inputs, illustration of the mesh and loading used in problem, followed by a short explanation if necessary, and numerical graphical outputs.

**Problem 1** (Example 4.1 page 172 in the textbook)

**Textbook solution**

| | | | | |
|---|---|---|---|---|
| Given: | Concrete elastic modulus | = | $4*10^6$ | psi |
| | Concrete Poisson ratio | = | 0.15 | |
| | Slab length | = | 25 | ft |
| | Slab width | = | 12 | ft |
| | Slab thickness | = | 8 | in. |
| | Temperature differential | = | 20 | $^oF$ |
| | k-value | = | 200 | psi/in. |
| | $\alpha_t$ | = | $5*10^{-6}$ | in./in./ $^oF$ |

Find: (a) The maximum curling stress in the interior of the slab
(b) The maximum curling stress at the edge of the slab

Problem illustration:

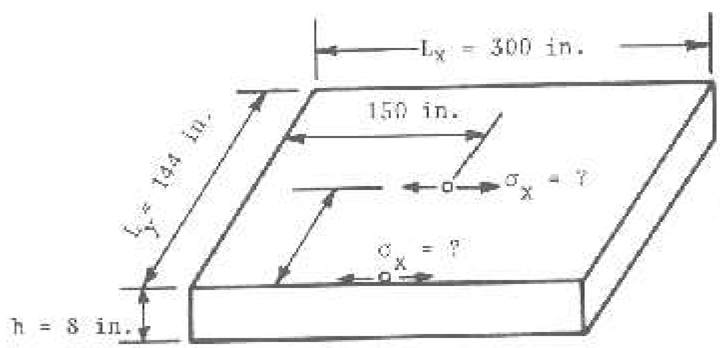


**Figure B-1: Problem illustration (Figure 4.5 in the textbook)**

Solutions (based on Westergaard's equations):

(a) The maximum curling stress in the interior of the slab = 238 psi (1641 kPa)
(b) The maximum curling stress at the edge of the slab = 214 psi (1476 kPa)

**FE solution**

Summary of inputs: All pavement features and temperature gradients used in this part are the same as indicated in the textbook solution. For the finite element model, fine mesh size (6"), medium mesh size (12"), coarse mesh size (24"), and manual mesh size (3") with mesh aspect ratio of one were chosen. It should be noted that these are the mesh configurations used for the rest of the analysis using ISLAB2000 in this report unless otherwise indicated. An illustration of the fine mesh size, which is a default in the software, is shown below.

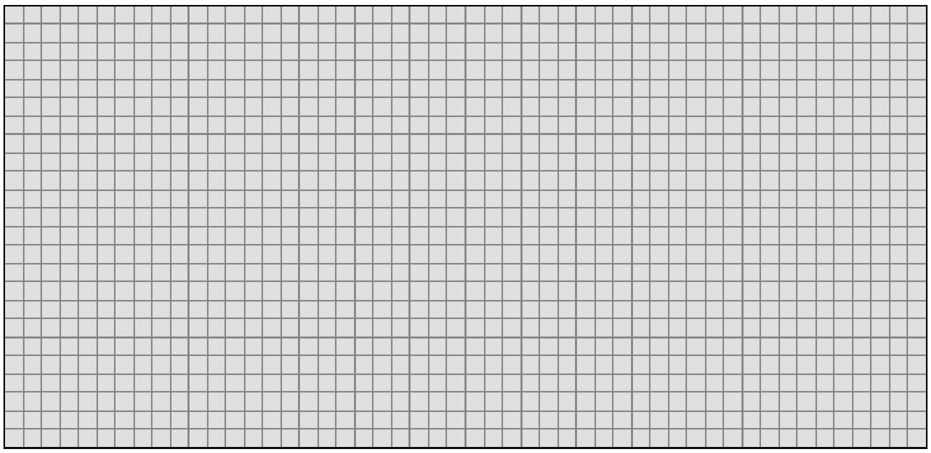

**Figure B-2: Mesh used for finite element model in ISLAB2000**

Numerical outputs:

For fine mesh:
- The maximum stress in the interior of the slab = 230.3 psi (1588 kPa)
- The maximum stress at the edge of the slab = 220.3 psi (1519 kPa)

For medium mesh:
- The maximum stress in the interior of the slab = 230.1 psi (1587 kPa)
- The maximum stress at the edge of the slab = 220.1 psi (1518 kPa)

For coarse mesh:
- The maximum stress in the interior of the slab = 231.6 psi (1597 kPa)
- The maximum stress at the edge of the slab = 219.0 psi (1510 kPa)

For manual mesh:
- The maximum stress in the interior of the slab = 230.5 psi (1589 kPa)
- The maximum stress at the edge of the slab = 219.8 psi (1516 kPa)

**Result comparison:**

**Table B-1: Maximum curling stress in the interior of the slab comparison**

| Approach | Maximum Curling Stress | | Difference (%) |
|---|---|---|---|
| | (psi) | (kPa) | |
| Westergaard's | 238.0 | 1641 | 0.00 |
| ISLAB2000 (24" mesh size) | 231.6 | 1597 | 2.69 |
| ISLAB2000 (12" mesh size) | 230.1 | 1587 | 3.31 |
| ISLAB2000 (6" mesh size) | 230.3 | 1588 | 3.25 |
| ISLAB2000 (3" mesh size) | 230.5 | 1590 | 3.14 |

**Table B-2: Maximum curling stress at the edge of the slab comparison**

| Approach | Maximum Curling Stress | | Difference (%) |
|---|---|---|---|
| | (psi) | (kPa) | |
| Westergaard's | 214.0 | 1476 | 0.00 |
| ISLAB2000 (24" mesh size) | 219.0 | 1510 | 2.35 |
| ISLAB2000 (12" mesh size) | 220.1 | 1518 | 2.87 |
| ISLAB2000 (6" mesh size) | 220.3 | 1519 | 2.95 |
| ISLAB2000 (3" mesh size) | 219.8 | 1516 | 2.72 |

**Problem 2** (Example 4.2 page 176 in the textbook)

**Textbook solution**

Given: Concrete elastic modulus = $4*10^6$ psi
Concrete Poisson ratio = 0.15
Slab thickness = 10 in.
k-value = 100 psi/in.
Tire contact radius = 6 in.
Wheel load = 10,000 lb

Find: (a) The maximum stress due to corner loading
(b) The maximum deflection due to corner loading

Problem illustration:

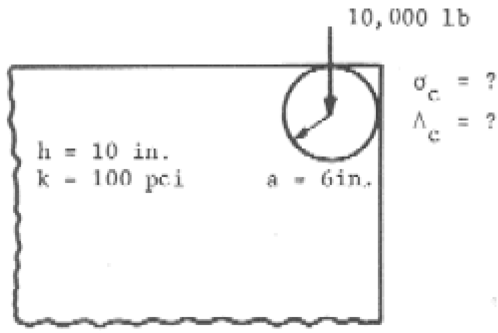


**Figure B-3: Problem illustration (Figure 4.7 in the textbook)**

Solutions (based on Westergaard's equations):

(a) The maximum stress due to corner loading = 186.6 psi (1287 kPa)
(b) The maximum deflection due to corner loading = 0.0502 in. (1275 microns)

**FE solution**

Summary of inputs: All pavement features used in this part are the same as indicated in the textbook solution. However, the circular tire contact area as illustrated in the problem is not an option in ISLAB2000. As a result, a square tire contact area with the same tire contact pressure and wheel load was used instead. The tire contact pressure will be used again in problems 3 and 4. The tire pressure is computed as follows.

$$\text{Tire contact pressure, } q = \frac{P}{\pi \cdot a^2} = \frac{10{,}000}{\pi \cdot 6^2} = 88.42 \quad psi \qquad \text{(A-1)}$$

Figures A4 and A5 represent the mesh used in the analysis.

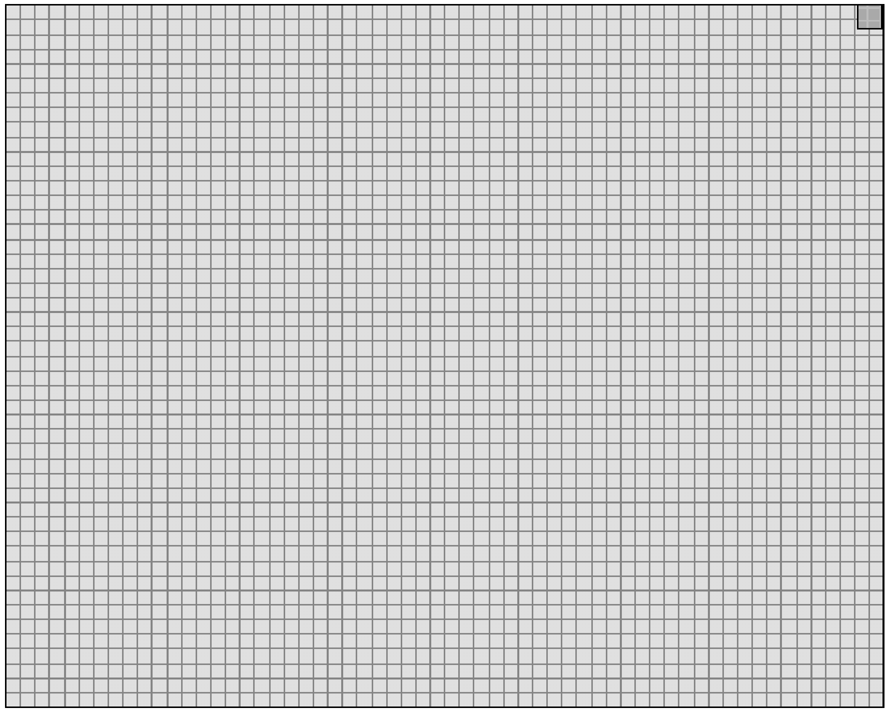

**Figure B-4: Mesh used for finite element model in ISLAB2000**

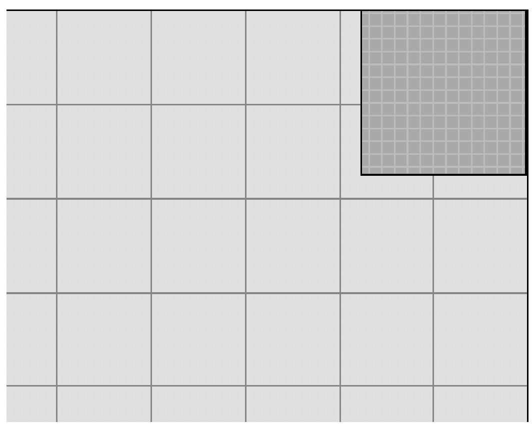

**Figure B-5: Equivalent square contact area used in ISLAB2000**

Numerical outputs:

<u>For fine mesh</u>:

| | | |
|---|---|---|
| The maximum stress due to corner loading | = 195.8 | psi (1350 kPa) |
| The maximum deflection due to corner loading | = 0.0563 | in. (1430 microns) |

<u>For medium mesh</u>:

| | | |
|---|---|---|
| The maximum stress due to corner loading | = 197.9 | psi (1365 kPa) |
| The maximum deflection due to corner loading | = 0.0563 | in. (1430 microns) |

<u>For coarse mesh</u>:

| | | |
|---|---|---|
| The maximum stress due to corner loading | = 198.4 | psi (1368 kPa) |
| The maximum deflection due to corner loading | = 0.0562 | in. (1427 microns) |

For manual mesh:

The maximum stress due to corner loading = 195.8 psi (1350 kPa)
The maximum deflection due to corner loading = 0.0563 in. (1430 microns)

**Result comparison:**

**Table B-3: Stress result comparison**

| Approach | Maximum Curling Stress | | Difference (%) |
|---|---|---|---|
| | (psi) | (kPa) | |
| Westergaard's | 186.6 | 1287 | 0.00 |
| ISLAB2000 (24" mesh size) | 198.4 | 1368 | 6.32 |
| ISLAB2000 (12" mesh size) | 197.9 | 1365 | 6.06 |
| ISLAB2000 (6" mesh size) | 195.8 | 1350 | 4.93 |
| ISLAB2000 (3" mesh size) | 195.8 | 1350 | 4.93 |

**Table B-4: Deflection result comparison**

| Approach | Maximum Deflection | | Difference (%) |
|---|---|---|---|
| | (in.) | (microns) | |
| Westergaard's | 0.0502 | 1275 | 0.00 |
| ISLAB2000 (24" mesh size) | 0.0562 | 1427 | 11.95 |
| ISLAB2000 (12" mesh size) | 0.0563 | 1430 | 12.15 |
| ISLAB2000 (6" mesh size) | 0.0563 | 1430 | 12.15 |
| ISLAB2000 (3" mesh size) | 0.0563 | 1430 | 12.15 |

**Table B-5: Stress result comparison**

| Approach | Maximum Curling Stress | | Difference (%) |
|---|---|---|---|
| | (psi) | (kPa) | |
| Ioannides's | 190.2 | 1311 | 0.00 |
| ISLAB2000 (24" mesh size) | 198.4 | 1368 | 4.31 |
| ISLAB2000 (12" mesh size) | 197.9 | 1365 | 4.05 |
| ISLAB2000 (6" mesh size) | 195.8 | 1350 | 2.94 |
| ISLAB2000 (3" mesh size) | 195.8 | 1350 | 2.94 |

**Table B-6: Deflection result comparison**

| Approach | Maximum Deflection | | Difference (%) |
|---|---|---|---|
| | (in.) | (microns) | |
| Ioannides's | 0.0560 | 1422 | 0.00 |
| ISLAB2000 (24" mesh size) | 0.0562 | 1427 | 0.36 |
| ISLAB2000 (12" mesh size) | 0.0563 | 1430 | 0.54 |
| ISLAB2000 (6" mesh size) | 0.0563 | 1430 | 0.54 |
| ISLAB2000 (3" mesh size) | 0.0563 | 1430 | 0.54 |

**Problem 3** (Example 4.3 page 177 in the textbook)

**Textbook solution**

Given: Concrete elastic modulus = $4*10^6$ psi
Concrete Poisson ratio = 0.15
Slab thickness = 10 in.
k-value = 100 psi/in.
Tire contact radius = 6 in.
Wheel load = 10,000 lb

Find: (a) The maximum stress due to interior loading
(b) The maximum deflection due to interior loading

Problem illustration:

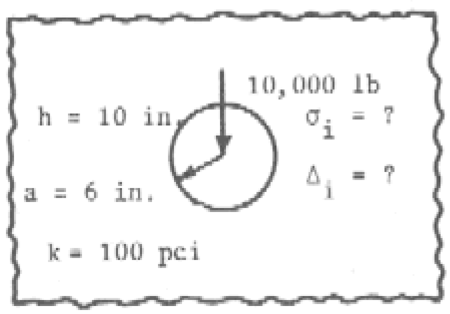


**Figure B-6: Problem illustration (Figure 4.8 in the textbook)**

Solutions (based on Westergaard's equations):

(a) The maximum stress due to interior loading = 143.7 psi (991 kPa)
(b) The maximum deflection due to interior loading = 0.00670 in. (170 microns)

**FE solution**

Figures A7 and A8 represent the mesh used in the analysis.

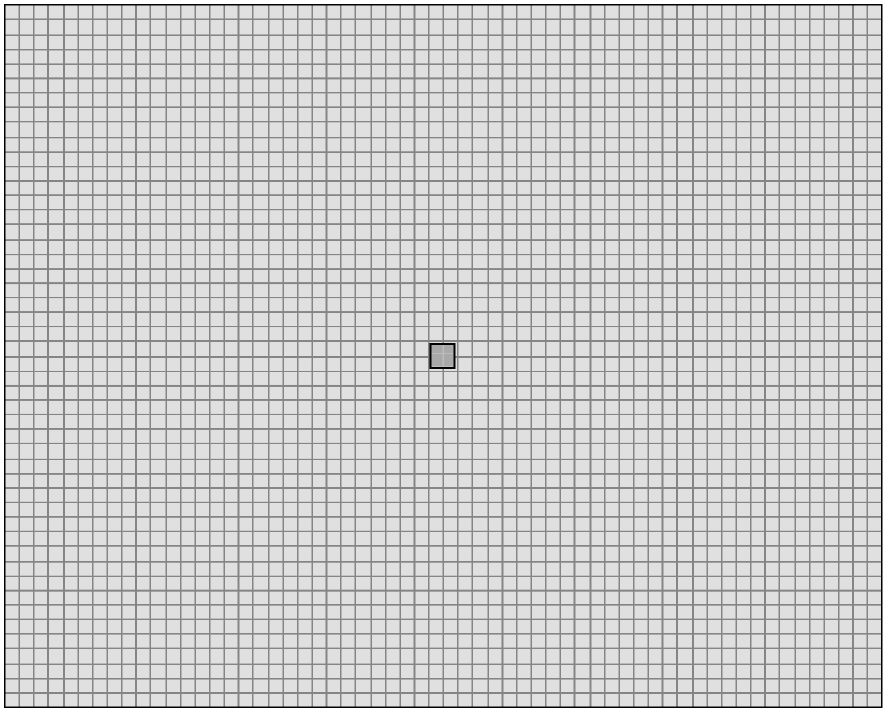

**Figure B-7: Mesh used for finite element model in ISLAB2000**

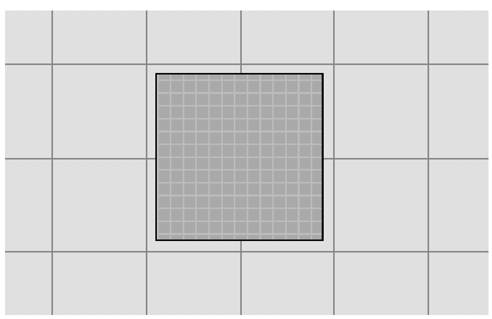

**Figure B-8: Equivalent square contact area used in ISLAB2000**

Numerical outputs:

For fine mesh:
- The maximum stress due to interior loading = 151.9 psi (1047 kPa)
- The maximum deflection due to interior loading = 0.00690 in. (175 microns)

For medium mesh:
- The maximum stress due to interior loading = 159.0 psi (1096 kPa)
- The maximum deflection due to interior loading = 0.00692 in. (176 microns)

For coarse mesh:

The maximum stress due to interior loading = 140.6 psi (969 kPa)
The maximum deflection due to interior loading = 0.00683 in. (173 microns)

For manual mesh:

The maximum stress due to interior loading = 144.2 psi (994 kPa)
The maximum deflection due to interior loading = 0.00689 in. (175 microns)

**Result comparison:**

**Table B-7: Stress result comparison**

| Approach | Maximum Deflection | | Difference (%) |
|---|---|---|---|
| | (in.) | (microns) | |
| Westergaard's | 0.00670 | 170 | 0.00 |
| ISLAB2000 (24" mesh size) | 0.00683 | 173 | 1.94 |
| ISLAB2000 (12" mesh size) | 0.00692 | 176 | 3.28 |
| ISLAB2000 (6" mesh size) | 0.00690 | 175 | 2.99 |
| ISLAB2000 (3" mesh size) | 0.00689 | 175 | 2.84 |

**Table B-8: Deflection result comparison**

| Approach | Maximum Curling Stress | | Difference (%) |
|---|---|---|---|
| | (psi) | (kPa) | |
| Westergaard's | 143.7 | 991 | 0.00 |
| ISLAB2000 (24" mesh size) | 140.6 | 969 | 2.16 |
| ISLAB2000 (12" mesh size) | 159.0 | 1096 | 10.65 |
| ISLAB2000 (6" mesh size) | 151.9 | 1047 | 5.69 |
| ISLAB2000 (3" mesh size) | 144.2 | 994 | 0.35 |

**Problem 4** (Example 4.4 page 178 in the textbook)

**Textbook solution**

Given: Concrete elastic modulus = $4*10^6$ psi
Concrete Poisson ratio = 0.15
Slab thickness = 10 in.
k-value = 100 psi/in.
Tire contact radius = 6 in.
Wheel load = 10,000 lb

Find: (a) The maximum stress due to edge loading
(b) The maximum deflection due to edge loading

Problem illustration:

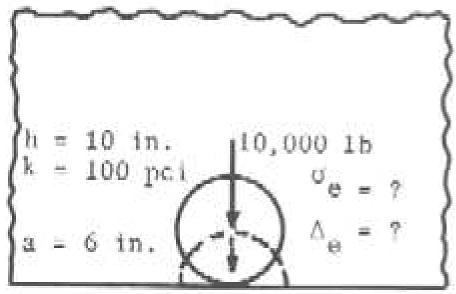


**Figure B-9: Problem illustration (Figure 4.9 in the textbook)**

Solutions (based on Westergaard's equations):

(a) The maximum stress due to edge loading = 279.4 psi (1926 kPa)
(b) The maximum deflection due to edge loading = 0.0207 in. (526 microns)

**FE solution**

Figures A10 and A11 represent the mesh used in the analysis.

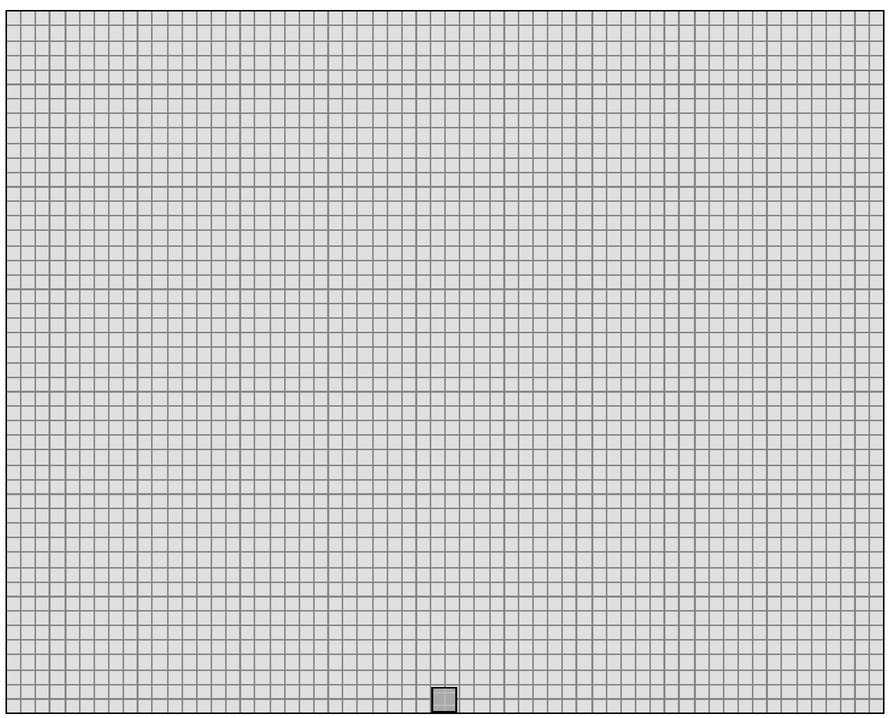

**Figure B-10: Mesh used for finite element model in ISLAB2000**

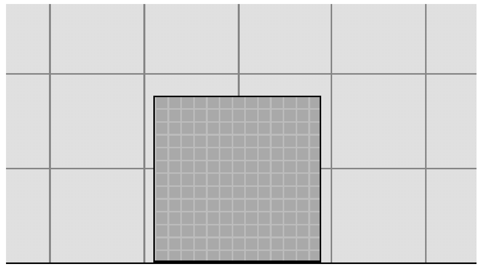

**Figure B-11: Equivalent square contact area used in ISLAB2000**

Numerical outputs:

For fine mesh:
The maximum stress due to edge loading = 294.9 psi (2033 kPa)
The maximum deflection due to edge loading = 0.0212 in. (538 microns)
For medium mesh:
The maximum stress due to edge loading = 306.5 psi (2113 kPa)
The maximum deflection due to edge loading = 0.0212 in. (538 microns)
For coarse mesh:
The maximum stress due to edge loading = 285.9 psi (1971 kPa)
The maximum deflection due to edge loading = 0.0211 in. (537 microns)
For manual mesh:
The maximum stress due to edge loading = 287.2 psi (1980 kPa)
The maximum deflection due to edge loading = 0.0212 in. (538 microns)

**Result comparison:**

**Table B-9: Stress result comparison**

| Approach | Maximum Curling Stress | | Difference (%) |
|---|---|---|---|
| | (psi) | (kPa) | |
| Westergaard's | 279.4 | 1926 | 0.00 |
| ISLAB2000 (24" mesh size) | 285.9 | 1971 | 2.33 |
| ISLAB2000 (12" mesh size) | 306.5 | 2113 | 9.70 |
| ISLAB2000 (6" mesh size) | 294.9 | 2033 | 5.54 |
| ISLAB2000 (3" mesh size) | 287.2 | 1980 | 2.79 |

**Table B-10: Deflection result comparison**

| Approach | Maximum Deflection | | Difference (%) |
|---|---|---|---|
| | (in.) | (microns) | |
| Westergaard's | 0.0207 | 526 | 0.00 |
| ISLAB2000 (24" mesh size) | 0.0211 | 537 | 2.08 |
| ISLAB2000 (12" mesh size) | 0.0212 | 538 | 2.32 |
| ISLAB2000 (6" mesh size) | 0.0212 | 538 | 2.42 |
| ISLAB2000 (3" mesh size) | 0.0212 | 538 | 2.42 |

**Problem 5** (Example 4.5 page 180 in the textbook)

**Textbook solution**

Given: Concrete elastic modulus = $4*10^6$ psi
Concrete Poisson ratio = 0.15
Slab thickness = 10 in.
k-value = 100 psi/in.
Dual tire spacing = 14 in.
Tire contact pressure = 88.42 psi
Wheel load = 10,000 lb (5,000 lb each)

Find: (a) The maximum stress due to corner loading
(b) The maximum stress due to interior loading
(c) The maximum stress due to edge loading

Problem illustration:

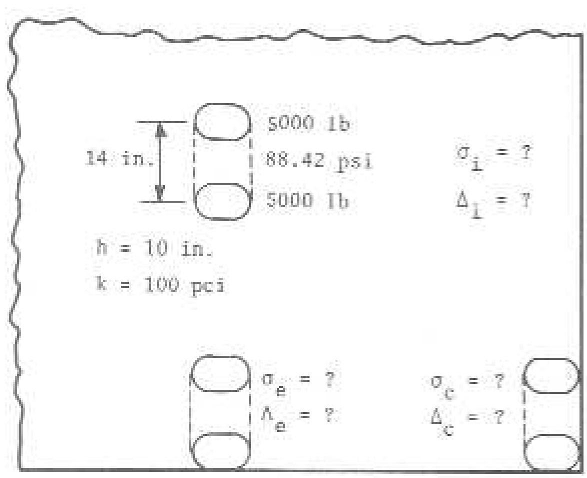


**Figure B-12: Problem illustration (Figure 4.11 in the textbook)**

Solutions (based on Westergaard's equations):

(a) The maximum stress due to corner loading = 166.8 psi (1150 kPa)
(b) The maximum stress due to interior loading = 130.8 psi (902 kPa)
(c) The maximum stress due to edge loading = 244.2 psi (1684 kPa)

**FE solution**

Summary of inputs: All pavement features used in this part are the same as indicated in the textbook solution. However, the circular tire contact area as illustrated in the problem was not the option in ISLAB2000. As a result, a square tire contact area with the same tire contact pressure and wheel load was used instead. The tire pressure was computed as follows.

Radius of contact area,

$$a = \sqrt{\frac{0.8521 \cdot P_d}{q \cdot \pi} + \frac{S_d}{\pi} \cdot \left( \frac{P_d}{0.5227 \cdot q} \right)^{1/2}} \quad \text{(A-2, Eq. 4.31 in the textbook)}$$

$$= \sqrt{\frac{0.8521 \times 5000}{88.42} + \frac{14}{\pi} \cdot \left( \frac{5000}{0.5227 \times 88.42} \right)^{1/2}} = 7.85 \quad in.$$

Tire contact pressure, $q = \dfrac{P}{\pi \cdot a^2} = \dfrac{10{,}000}{\pi \cdot 7.85^2} = 51.65 \quad psi$

A fine mesh size (6") with an aspect ratio of one was used for this analysis and is illustrated in Figures A13-A18.

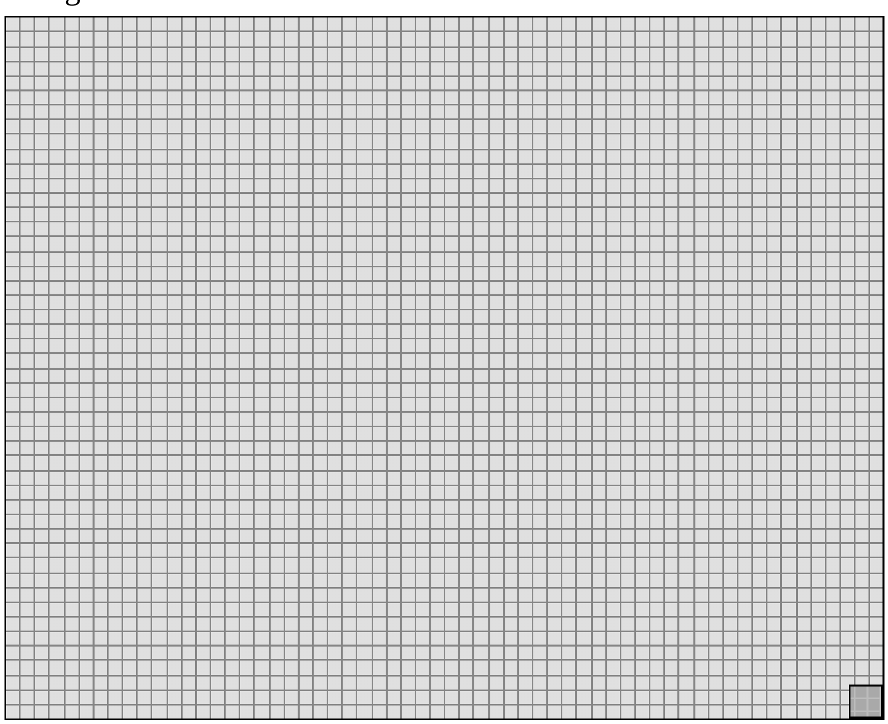

**Figure B-13: Mesh used for finite element model for corner loading in ISLAB2000**

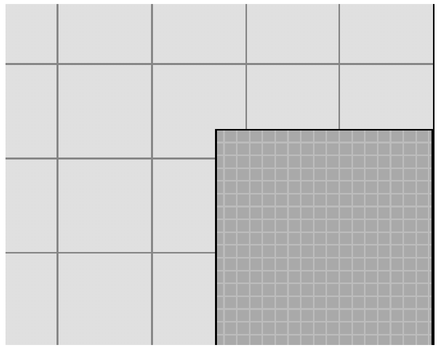

**Figure B-14: Equivalent square contact area used for corner loading in ISLAB2000**

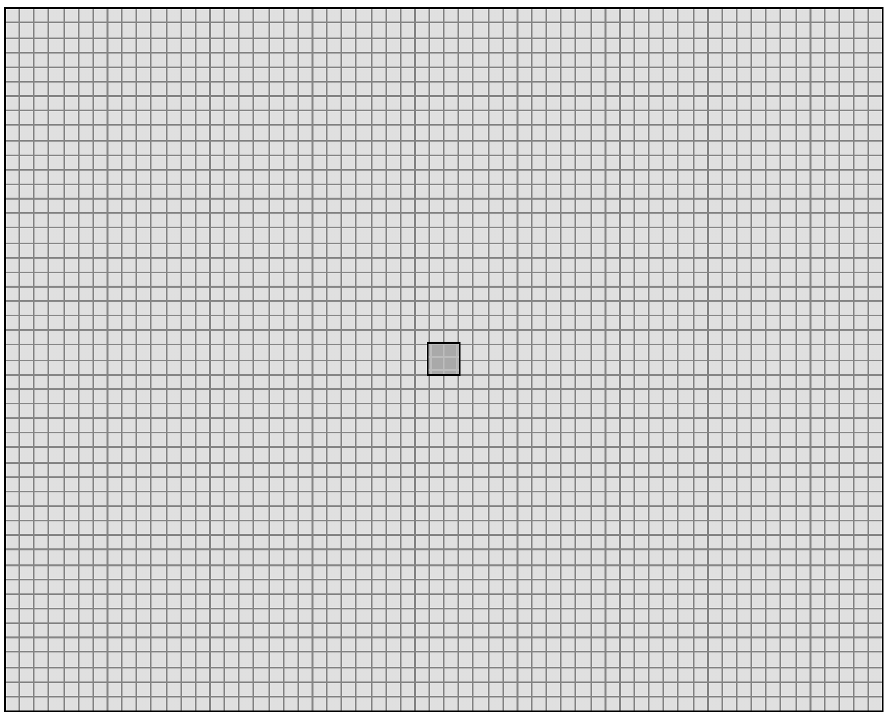

**Figure B-15: Mesh used for finite element model for interior loading in ISLAB2000**

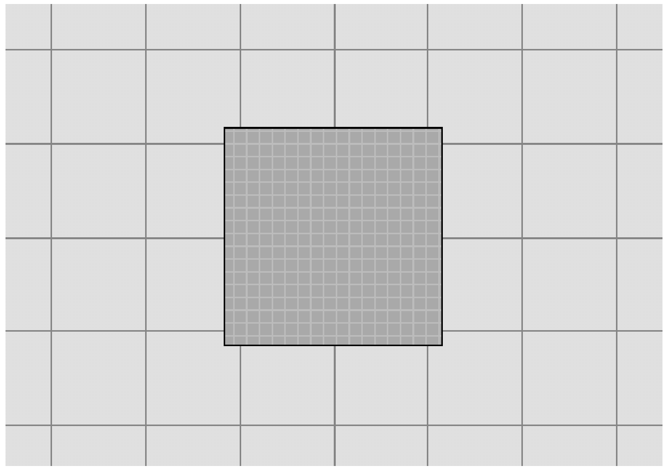

**Figure B-16: Equivalent square contact area used for interior loading in ISLAB2000**

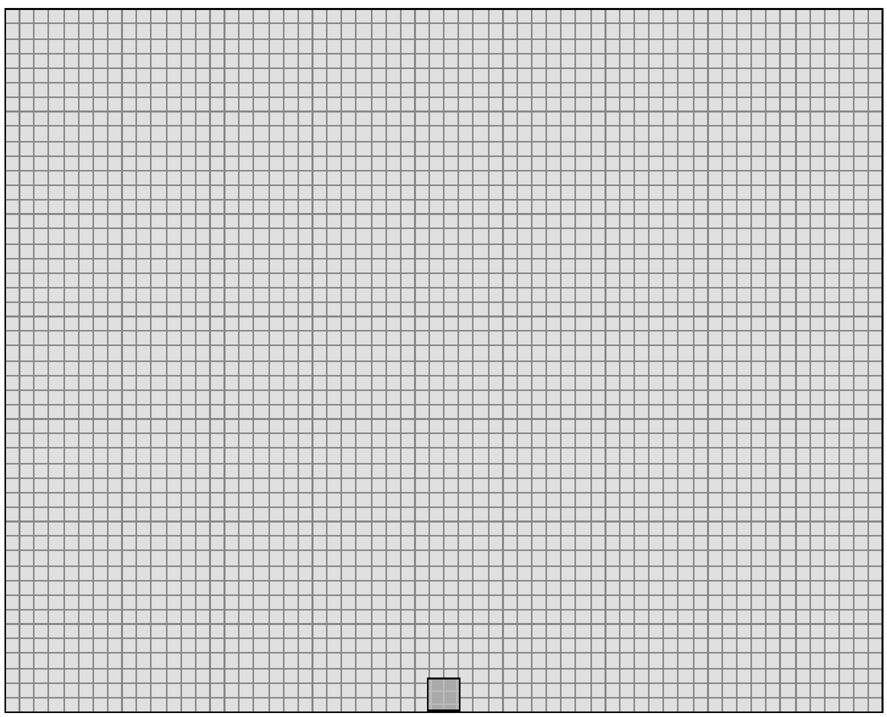

**Figure B-17: Mesh used for finite element model for edge loading in ISLAB2000**

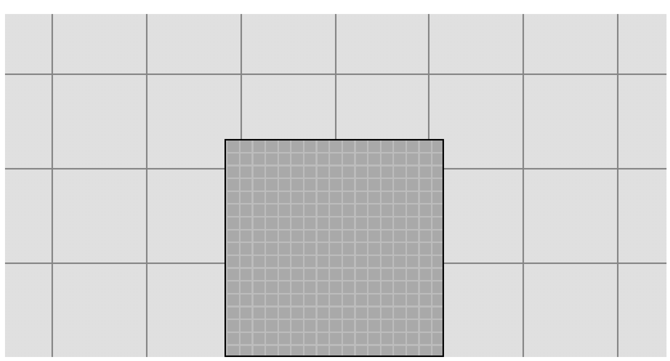

**Figure B-18: Equivalent square contact area used for edge loading in ISLAB2000**

Numerical outputs:

For fine mesh:
The maximum stress due to corner loading = 177.6 psi (1225 kPa)
The maximum stress due to interior loading = 132.8 psi (916 kPa)
The maximum stress due to edge loading = 255.2 psi (1760 kPa)
For medium mesh:
The maximum stress due to corner loading = 178.1 psi (1228 kPa)
The maximum stress due to interior loading = 144.2 psi (994 kPa)
The maximum stress due to edge loading = 267.6 psi (1845 kPa)
For coarse mesh:
The maximum stress due to corner loading = 182.3 psi (1257 kPa)
The maximum stress due to interior loading = 135.5 psi (934 kPa)
The maximum stress due to edge loading = 263.8 psi (1819 kPa)

**Result comparison:**

**Table B-11: Stress result comparison for corner loading**

| Approach | Maximum Curling Stress | | Difference (%) |
|---|---|---|---|
| | (psi) | (kPa) | |
| Westergaard's | 166.8 | 1150 | 0.00 |
| ISLAB2000 (24" mesh size) | 182.3 | 1257 | 9.29 |
| ISLAB2000 (12" mesh size) | 178.1 | 1228 | 6.77 |
| ISLAB2000 (6" mesh size) | 177.6 | 1225 | 6.47 |

**Table B-12: Stress result comparison for interior loading**

| Approach | Maximum Curling Stress | | Difference (%) |
|---|---|---|---|
| | (psi) | (kPa) | |
| Westergaard's | 130.8 | 902 | 0.00 |
| ISLAB2000 (24" mesh size) | 135.5 | 934 | 3.59 |
| ISLAB2000 (12" mesh size) | 144.2 | 994 | 10.24 |
| ISLAB2000 (6" mesh size) | 132.8 | 916 | 1.54 |

**Table B-13: Stress result comparison for edge loading**

| Approach | Maximum Curling Stress | | Difference (%) |
|---|---|---|---|
| | (psi) | (kPa) | |
| Westergaard's | 244.2 | 1684 | 0.00 |
| ISLAB2000 (24" mesh size) | 263.8 | 1819 | 8.03 |
| ISLAB2000 (12" mesh size) | 267.6 | 1845 | 9.58 |
| ISLAB2000 (6" mesh size) | 255.2 | 1760 | 4.50 |

**Problem 6** (Problem 4-1 page 203 in the textbook)

**Textbook solution**

| | | | | |
|---|---|---|---|---|
| Given: Concrete elastic modulus | = | $4*10^6$ | psi | |
| Concrete Poisson ratio | = | 0.15 | | |
| Slab length | = | 20 | ft | (for part b.) |
| Slab width | = | 12 | ft | (for part b.) |
| Slab thickness | = | 8 | in. | |
| Temperature differential | = | 24 | $^oF$ | |
| k-value | = | 50 | psi/in. | |
| $\alpha_t$ | = | $5*10^{-6}$ | in./in./ $^oF$ | |

Find: a) for an infinite slab

The maximum curling stress in the interior of the slab

The maximum curling stress at the edge of the slab

b) for a finite slab

The maximum curling stress at points A, B, and C in the Figure P4.1

Problem illustration:

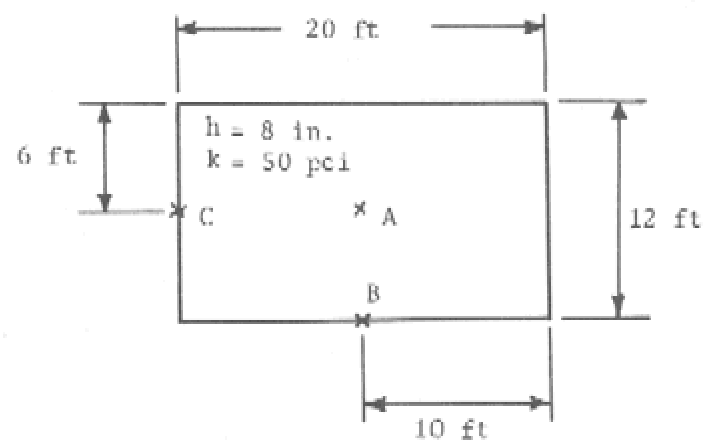


**Figure B-19: Problem illustration (Figure P4.1 in the textbook)**

Solutions (based on Westergaard's equations):

(a) for an infinite slab

The maximum curling stress in the interior of the slab= 282.4 psi (1947 kPa)

The maximum curling stress at the edge of the slab = 240.0 psi (1655 kPa)

(b) for a finite slab

The maximum curling stress at points A = 211.4 psi (1458 kPa)

The maximum curling stress at points B = 198.0 psi (1365 kPa)

The maximum curling stress at points C = 57.6 psi (397 kPa)

**FE solution**

Summary of inputs: All pavement features and temperature gradient used in this part are the same as indicated in the textbook solution. The slab dimension of 48' by 60' was used to represent the infinite slab. A fine mesh with an aspect ratio of one was chosen and is illustrated in Figures A20 and A21.

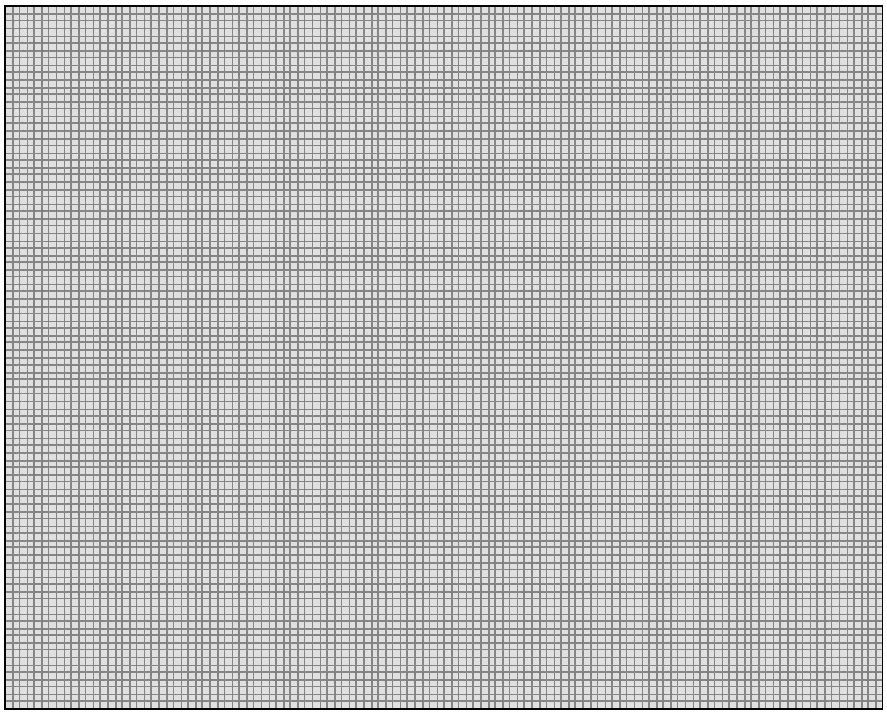

**Figure B-20: Mesh used for finite element model for an infinite slab in ISLAB2000**

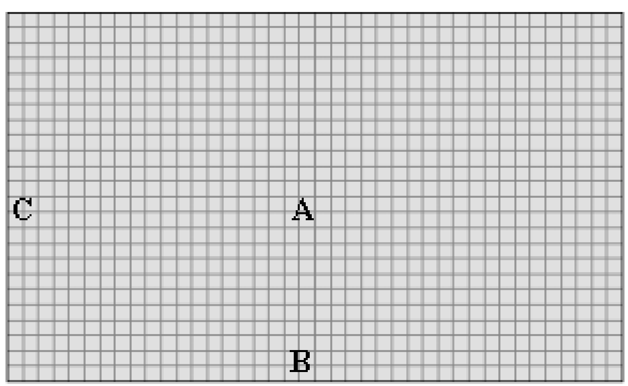


**Figure B-21: Mesh used for finite element model for a finite slab in ISLAB2000**

Numerical outputs:

I. For an infinite slab

For fine mesh:

The maximum curling stress in the interior of the slab = 296.2 psi (2042 kPa)
The maximum curling stress at the edge of the slab = 245.3 psi (1692 kPa)

For medium mesh:

The maximum curling stress in the interior of the slab = 296.3 psi (2043 kPa)
The maximum curling stress at the edge of the slab = 244.9 psi (1689 kPa)

For coarse mesh:

The maximum curling stress in the interior of the slab = 296.6 psi (2045 kPa)
The maximum curling stress at the edge of the slab = 244.2 psi (1684 kPa)

II. For a finite slab

For fine mesh:

The maximum curling stress at points A = 194.8 psi (1343 kPa)
The maximum curling stress at points B = 196.0 psi (1351 kPa)
The maximum curling stress at points C = 49.7 psi (343 kPa)

For medium mesh:

The maximum curling stress at points A = 195.3 psi (1347 kPa)
The maximum curling stress at points B = 196.3 psi (1353 kPa)
The maximum curling stress at points C = 49.9 psi (344 kPa)

For coarse mesh:

The maximum curling stress at points A = 197.3 psi (1360 kPa)
The maximum curling stress at points B = 197.8 psi (1364 kPa)
The maximum curling stress at points C = 50.4 psi (347 kPa)

## Result comparison:

**Table B-14: The maximum curling stress comparison in the interior of an infinite slab**

| Approach | Maximum Curling Stress | | Difference (%) |
|---|---|---|---|
| | (psi) | (kPa) | |
| Westergaard's | 282.4 | 1947 | 0.00 |
| ISLAB2000 (24" mesh size) | 296.6 | 2045 | 5.03 |
| ISLAB2000 (12" mesh size) | 296.3 | 2043 | 4.92 |
| ISLAB2000 (6" mesh size) | 296.2 | 2042 | 4.89 |

**Table B-15: The maximum curling stress comparison at the edge of an infinite slab**

| Approach | Maximum Curling Stress | | Difference (%) |
|---|---|---|---|
| | (psi) | (kPa) | |
| Westergaard's | 240.0 | 1655 | 0.00 |
| ISLAB2000 (24" mesh size) | 244.2 | 1684 | 1.74 |
| ISLAB2000 (12" mesh size) | 244.9 | 1689 | 2.05 |
| ISLAB2000 (6" mesh size) | 245.4 | 1692 | 2.23 |

**Table B-16: The maximum curling stress comparison at points A of a finite slab**

| Approach | Maximum Curling Stress | | Difference (%) |
|---|---|---|---|
| | (psi) | (kPa) | |
| Westergaard's | 211.4 | 1458 | 0.00 |
| ISLAB2000 (24" mesh size) | 197.3 | 1360 | 6.69 |
| ISLAB2000 (12" mesh size) | 195.3 | 1347 | 7.62 |
| ISLAB2000 (6" mesh size) | 194.8 | 1343 | 7.87 |

**Table B-17: The maximum curling stress comparison at points B of a finite slab**

| Approach | Maximum Curling Stress | | Difference (%) |
|---|---|---|---|
| | (psi) | (kPa) | |
| Westergaard's | 198.0 | 1365 | 0.00 |
| ISLAB2000 (24" mesh size) | 197.8 | 1364 | 0.09 |
| ISLAB2000 (12" mesh size) | 196.3 | 1353 | 0.86 |
| ISLAB2000 (6" mesh size) | 196.0 | 1351 | 1.04 |

**Table B-18: The maximum curling stress comparison at points C of a finite slab**

| Approach | Maximum Curling Stress | | Difference (%) |
|---|---|---|---|
| | (psi) | (kPa) | |
| Westergaard's | 57.6 | 397 | 0.00 |
| ISLAB2000 (24" mesh size) | 50.4 | 347 | 12.55 |
| ISLAB2000 (12" mesh size) | 49.9 | 344 | 13.42 |
| ISLAB2000 (6" mesh size) | 49.7 | 343 | 13.65 |

**Problem 7** (Problem 4-2 page 204 in the textbook)

**Textbook solution**

| | | | | |
|---|---|---|---|---|
| Given: | Concrete elastic modulus | = | $4*10^6$ | psi |
| | Concrete Poisson ratio | = | 0.15 | |
| | Slab thickness | = | 10 | in. |
| | k-value | = | 200 | psi/in. |
| | Tire contact pressure | = | 80 | psi |
| | Wheel load | = | 12,000 | lb (6,000 lb each) |
| | Dual tire spacing | = | 14 | in. |

Find: (a) The maximum stress due to corner loading

Problem illustration:

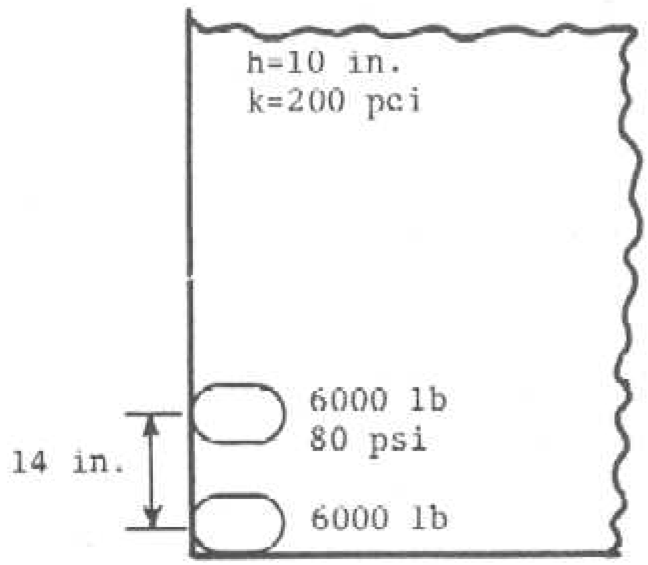


**Figure B-22: Problem illustration (Figure P4.2 in the textbook)**

Solutions (based on Westergaard's equations):

(a) The maximum stress due to corner loading = 172.8 psi (1191 kPa)

**FE solution**

Summary of inputs: All pavement features used in this part are the same as indicated in the textbook solution. However, the circular tire contact area as illustrated in the problem was not the option in ISLAB2000. As a result, a square tire contact area with the same tire contact pressure and wheel load was used instead. It should be noted that this tire contact pressure will also be used in problem 8 and 9. The tire pressure was computed as follows.

Radius of contact area,

$$a = \sqrt{\frac{0.8521 \cdot P_d}{q \cdot \pi} + \frac{S_d}{\pi} \cdot \left(\frac{P_d}{0.5227 \cdot q}\right)^{1/2}} \quad \text{(A-2, Eq. 4.31 in the textbook)}$$

$$= \sqrt{\frac{0.8521 \times 6000}{80} + \frac{14}{\pi} \cdot \left(\frac{6000}{0.5227 \times 80}\right)^{1/2}} = 10.83 \quad in.$$

Tire contact pressure, $q = \frac{P}{\pi \cdot a^2} = \frac{12{,}000}{\pi \cdot 10.83^2} = 32.57 \quad psi$

Figures A23 and A24 represent the mesh used in the analysis.

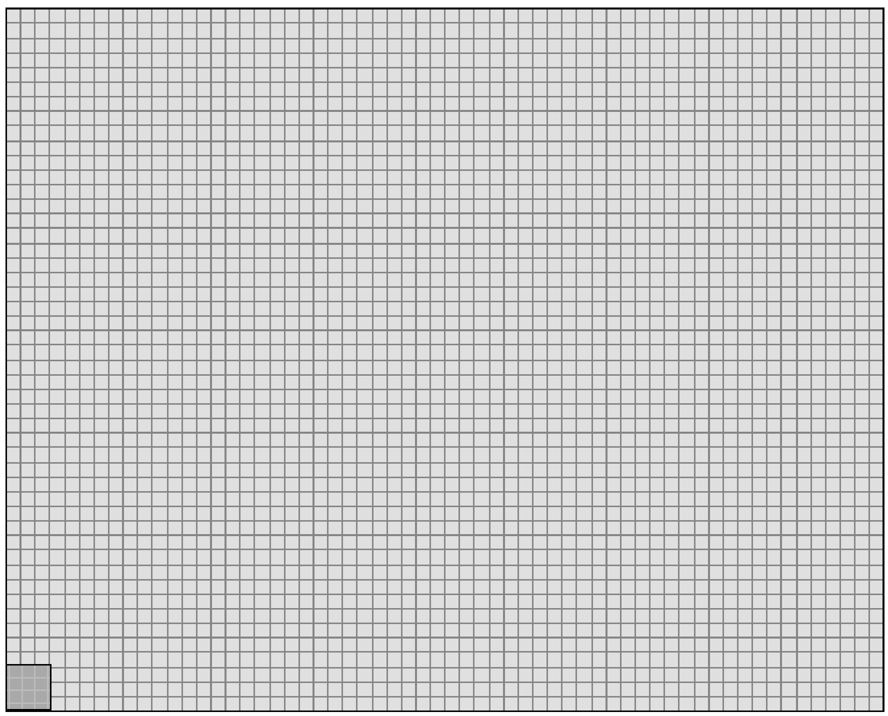

**Figure B-23: Mesh used for finite element model in ISLAB2000**

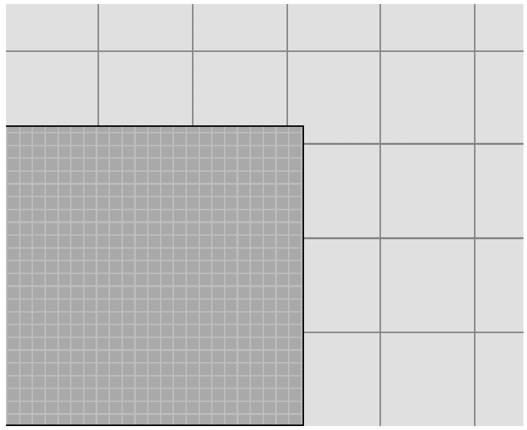

**Figure B-24: Equivalent square contact area used in ISLAB2000**

Numerical outputs:

For fine mesh:
The maximum stress due to corner loading = 164.5 psi (1134 kPa)
For medium mesh:
The maximum stress due to corner loading = 166.5 psi (1148 kPa)
For coarse mesh:
The maximum stress due to corner loading = 171.1 psi (1180 kPa)

## Result comparison:

**Table B-19: Stress result comparison for corner loading**

| Approach | Maximum Curling Stress | | Difference (%) |
|---|---|---|---|
| | (psi) | (kPa) | |
| Westergaard's | 172.8 | 1191 | 0.00 |
| ISLAB2000 (24" mesh size) | 171.1 | 1180 | 0.98 |
| ISLAB2000 (12" mesh size) | 166.5 | 1148 | 3.65 |
| ISLAB2000 (6" mesh size) | 164.5 | 1134 | 4.80 |

**Problem 8** (Problem 4-3 page 204 in the textbook)

**Textbook solution**

| | | | | |
|---|---|---|---|---|
| Given: | Concrete elastic modulus | = | $4*10^6$ | psi |
| | Concrete Poisson ratio | = | 0.15 | |
| | Slab thickness | = | 10 | in. |
| | k-value | = | 200 | psi/in. |
| | Tire contact pressure | = | 80 | psi |
| | Wheel load | = | 12,000 | lb (6,000 lb each) |
| | Dual tire spacing | = | 14 | in. |

Find: (a) The maximum stress due to interior loading

Problem illustration:

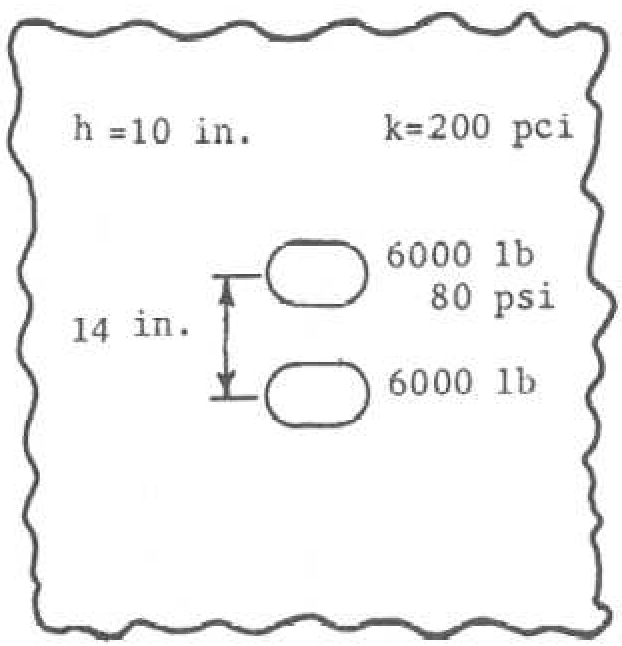


**Figure B-25: Problem illustration (Figure P4.3 in the textbook)**

Solutions (based on Westergaard's equations):

(a) The maximum stress due to interior loading = 139.7 psi (963 kPa)

**FE solution**

Figures A26 and A27 represent the mesh used in the analysis.

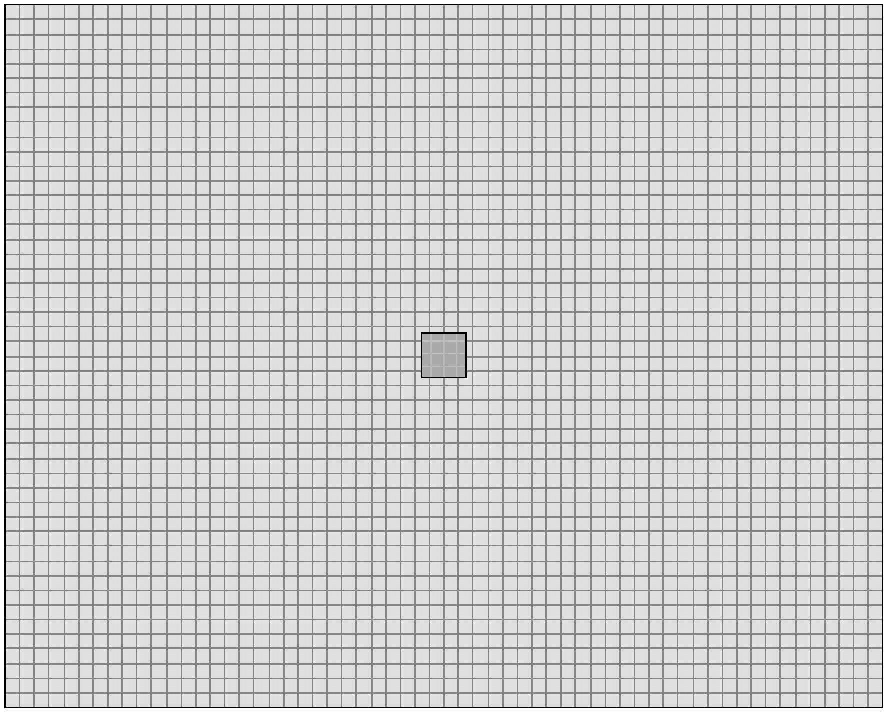
**Figure B-26: Mesh used for finite element model in ISLAB2000**

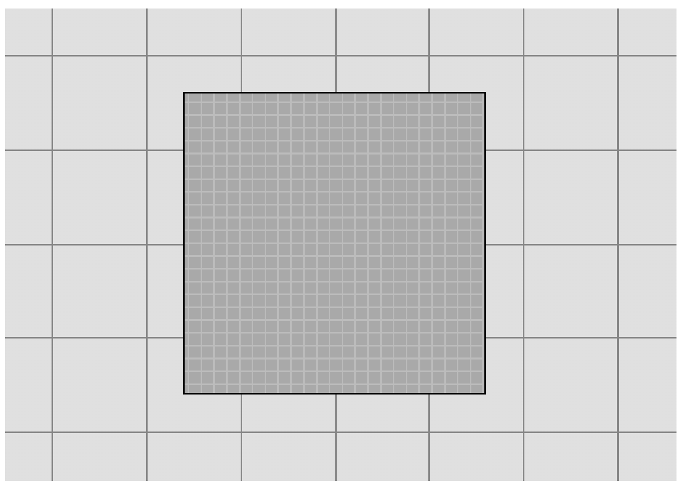
**Figure B-27: Equivalent square contact area used in ISLAB2000**

Numerical outputs:

For fine mesh:
The maximum stress due to interior loading = 123.3 psi (850 kPa)
For medium mesh:
The maximum stress due to interior loading = 134.1 psi (925 kPa)
For coarse mesh:
The maximum stress due to interior loading = 137.6 psi (949 kPa)

**Result comparison:**

**Table B-20: Stress result comparison for interior loading**

| Approach | Maximum Curling Stress | | Difference (%) |
|---|---|---|---|
| | (psi) | (kPa) | |
| Westergaard's | 139.7 | 963 | 0.00 |
| ISLAB2000 (24" mesh size) | 137.6 | 949 | 1.50 |
| ISLAB2000 (12" mesh size) | 134.1 | 925 | 4.01 |
| ISLAB2000 (6" mesh size) | 123.3 | 850 | 11.74 |

**Problem 9** (Problem 4-4 page 204 in the textbook)

**Textbook solution**

Given: Concrete elastic modulus = $4*10^6$ psi
Concrete Poisson ratio = 0.15
Slab thickness = 10 in.
k-value = 200 psi/in.
Tire contact pressure = 80 psi
Wheel load = 12,000 lb (6,000 lb each)
Dual tire spacing = 14 in.

Find: (a) The maximum stress due to edge loading

Problem illustration:

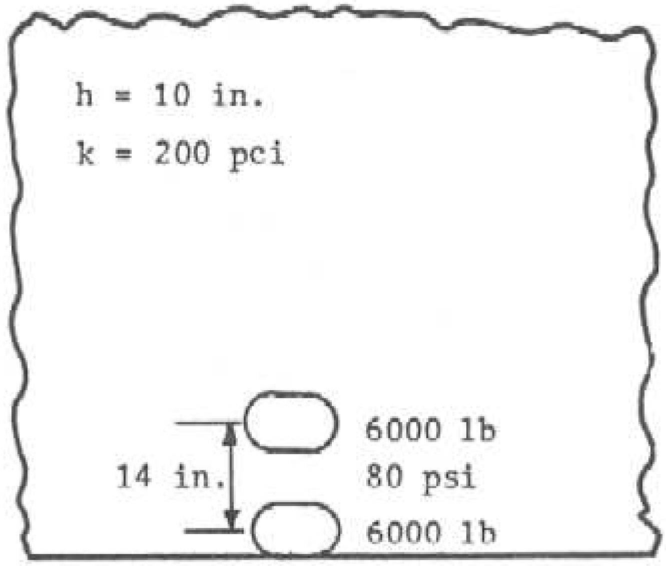


**Figure B-28: Problem illustration (Figure P4.4 in the textbook)**

Solutions (based on Westergaard's equations):

(a) The maximum stress due to edge loading = 252.5 psi (1741 kPa)

## FE solution

Figures A29 and A30 represent the mesh used in the analysis.

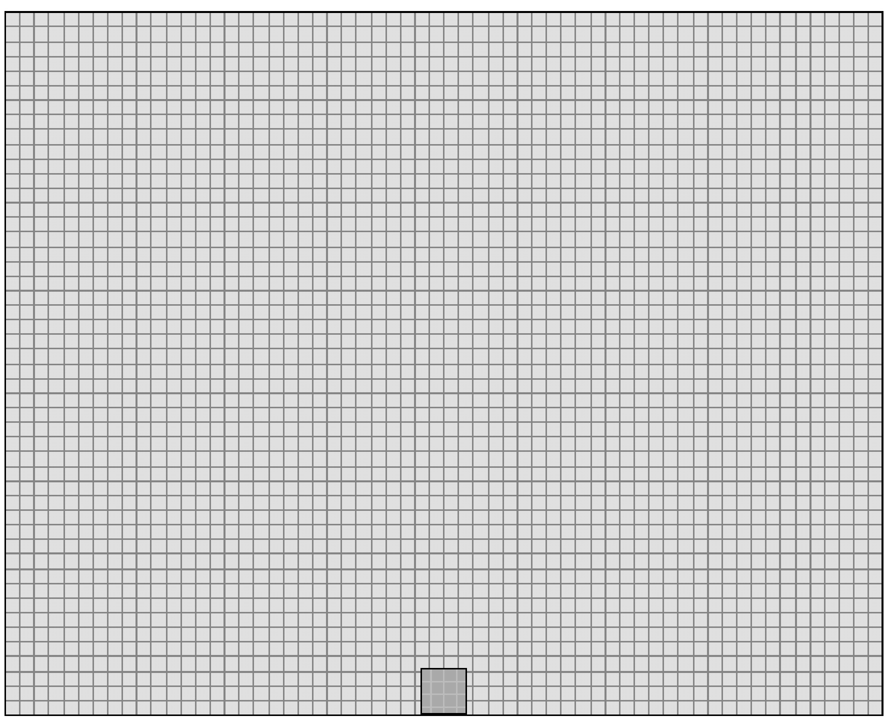

**Figure B-29: Mesh used for finite element model in ISLAB2000**

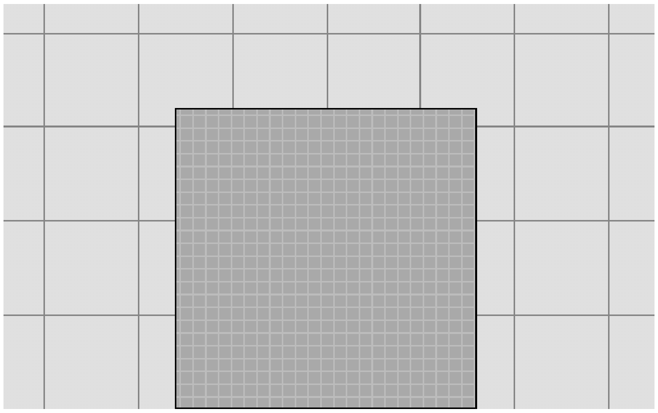

**Figure B-30: Equivalent square contact area used in ISLAB2000**

Numerical outputs:

For fine mesh:

The maximum stress due to edge loading = 227.4 psi (1568 kPa)

For medium mesh:

The maximum stress due to edge loading = 237.9 psi (1640 kPa)

For coarse mesh:

The maximum stress due to edge loading = 247.7 psi (1708 kPa)

**Result comparison:**

**Table B-21: Stress result comparison for edge loading**

| Approach | Maximum Curling Stress | | Difference (%) |
|---|---|---|---|
| | (psi) | (kPa) | |
| Westergaard's | 252.5 | 1741 | 0.00 |
| ISLAB2000 (24" mesh size) | 247.7 | 1708 | 1.90 |
| ISLAB2000 (12" mesh size) | 237.9 | 1640 | 5.78 |
| ISLAB2000 (6" mesh size) | 227.4 | 1568 | 9.94 |

# Appendix C

## ISLAB2000 Graphical Results for the Comparison with Westergaard’s Solution

**Problem 1** (Example 4.1 page 172 in the textbook)

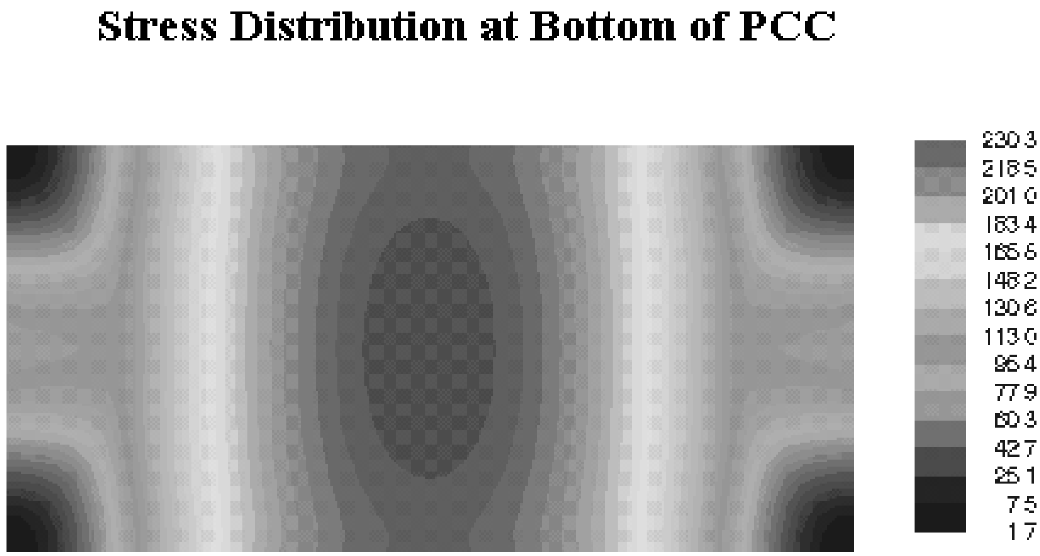


**Figure C-1: Graphical stress results using ISLAB2000 (fine mesh)**

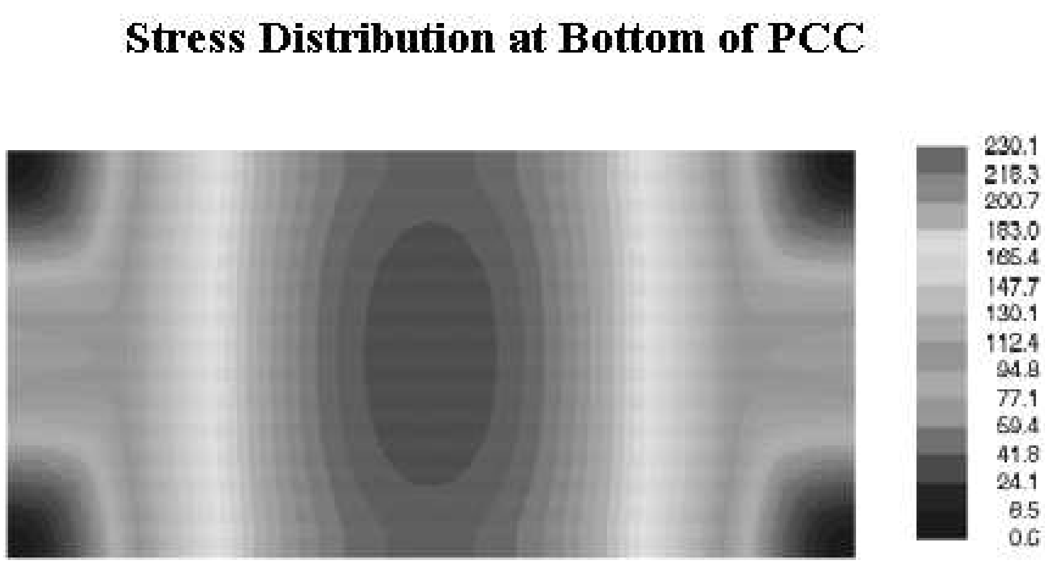


**Figure C-2: Graphical stress results using ISLAB2000 (medium mesh)**

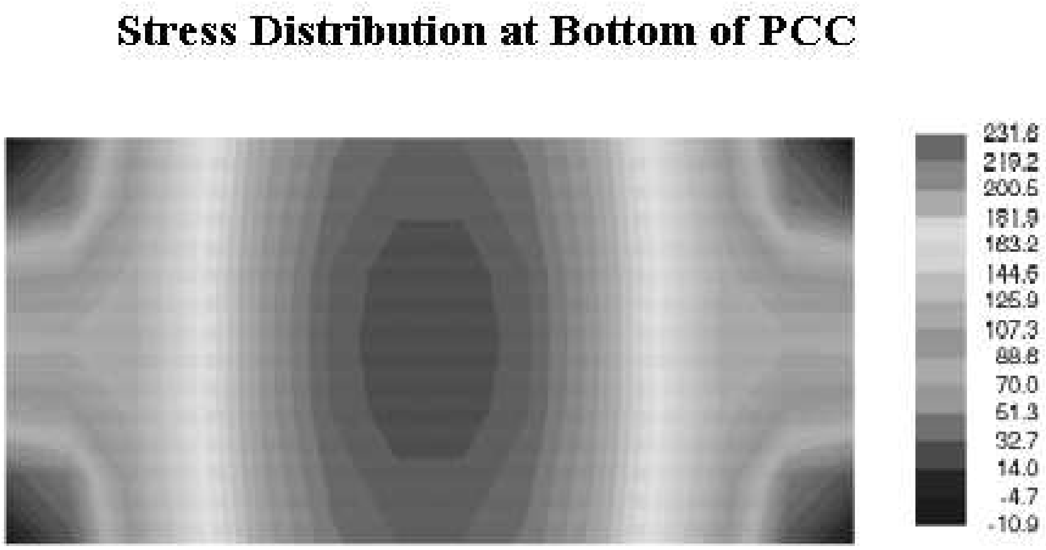


**Figure C-3: Graphical stress results using ISLAB2000 (coarse mesh)**

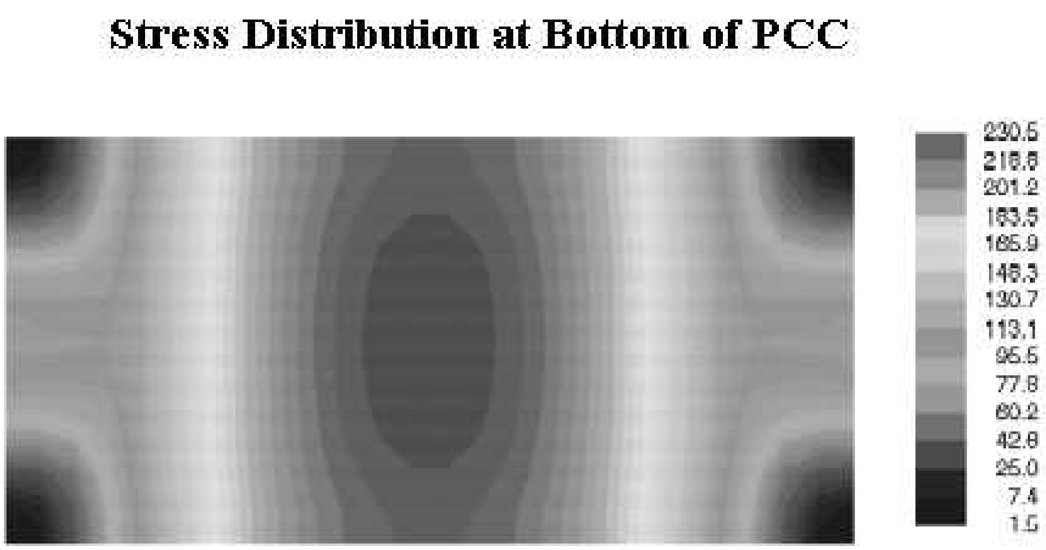


**Figure C-4: Graphical stress results using ISLAB2000 (manual mesh)**

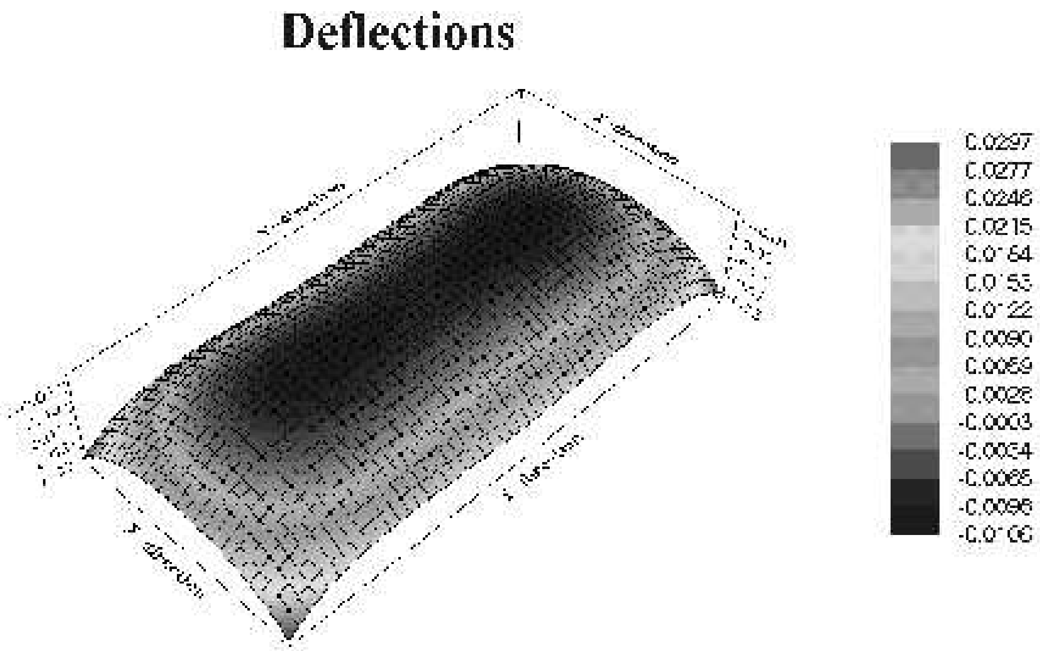


**Figure C-7: Graphical deflection results using ISLAB2000 (fine mesh)**

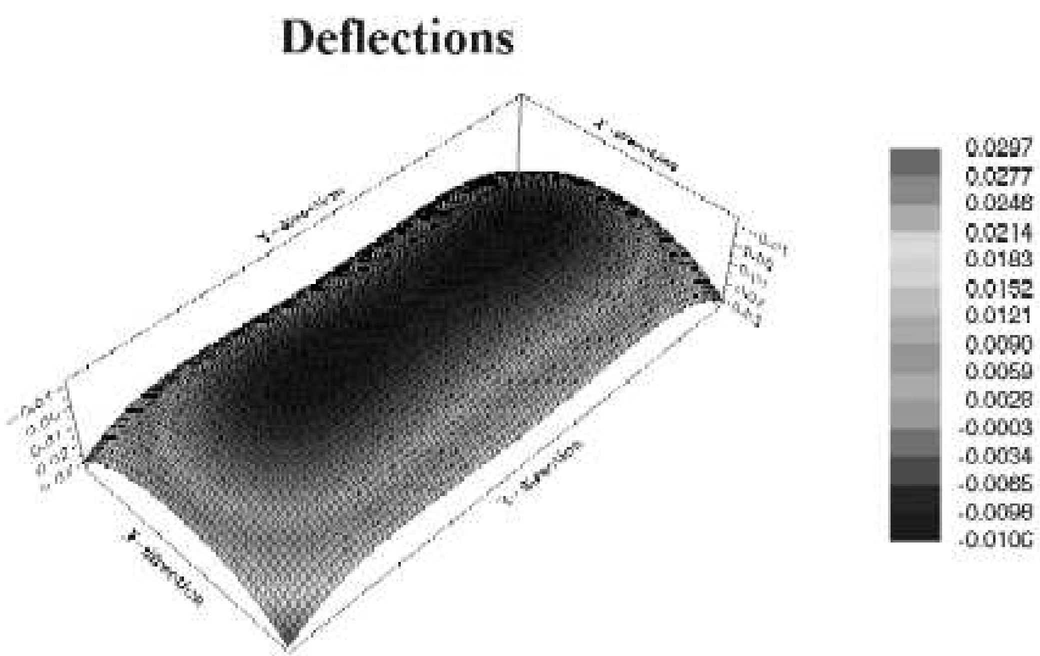


**Figure C-8: Graphical deflection results using ISLAB2000 (medium mesh)**

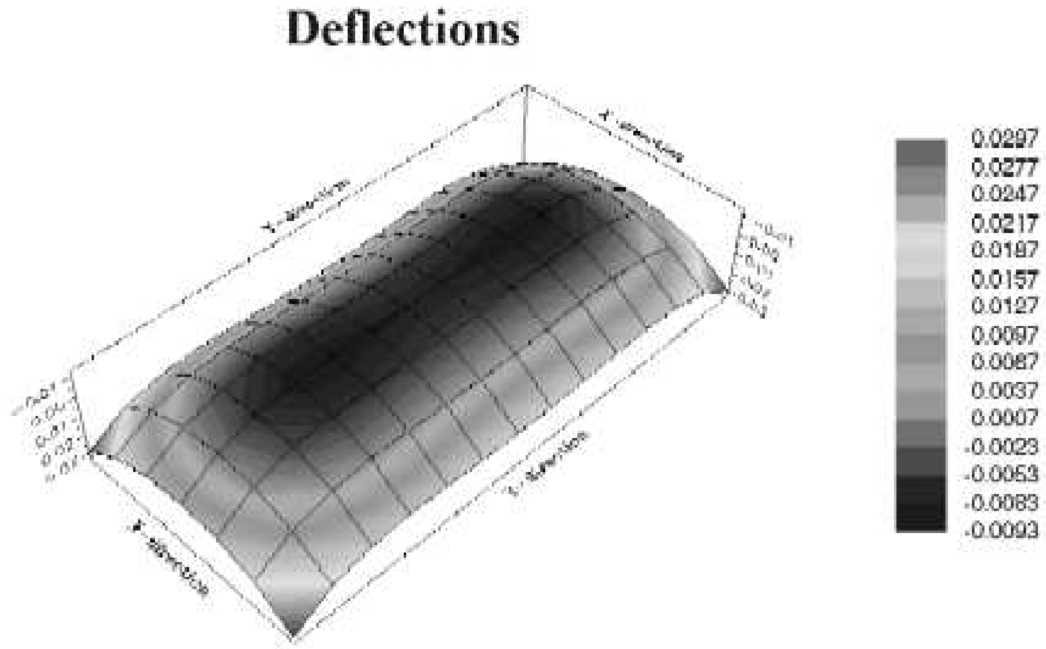


**Figure C-9: Graphical deflection results using ISLAB2000 (coarse mesh)**

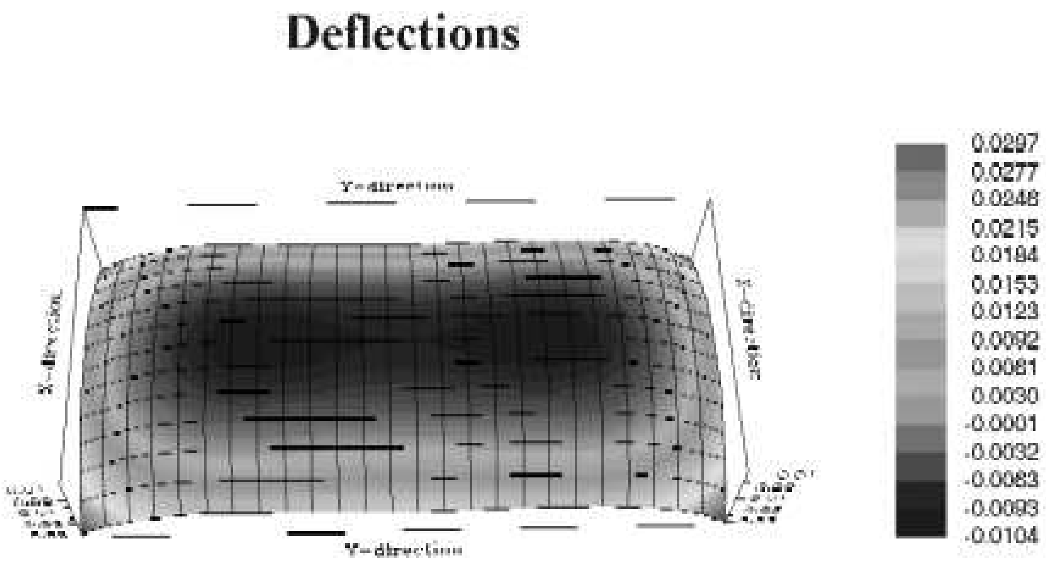


**Figure C-10: Graphical deflection results using ISLAB2000 (manual mesh)**

**Problem 2** (Example 4.2 page 176 in the textbook)

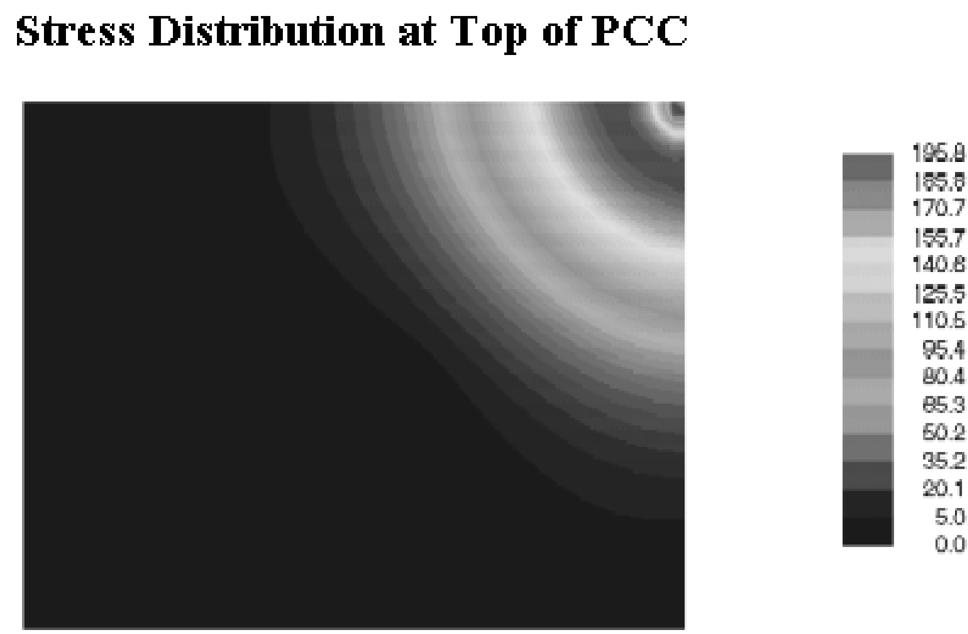


**Figure C-13: Graphical stress results using ISLAB2000 (fine mesh)**

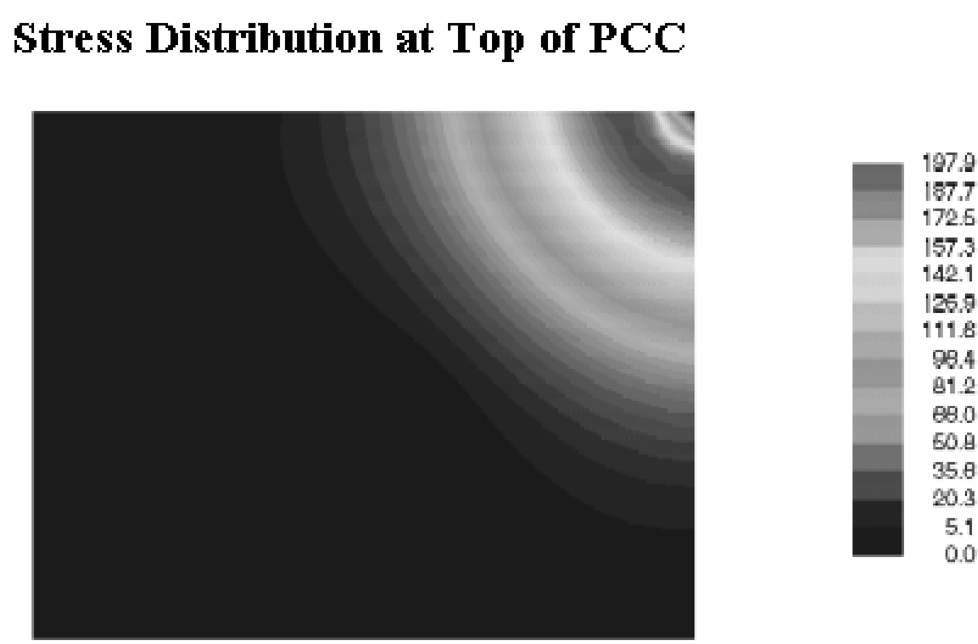


**Figure C-14: Graphical stress results using ISLAB2000 (medium mesh)**

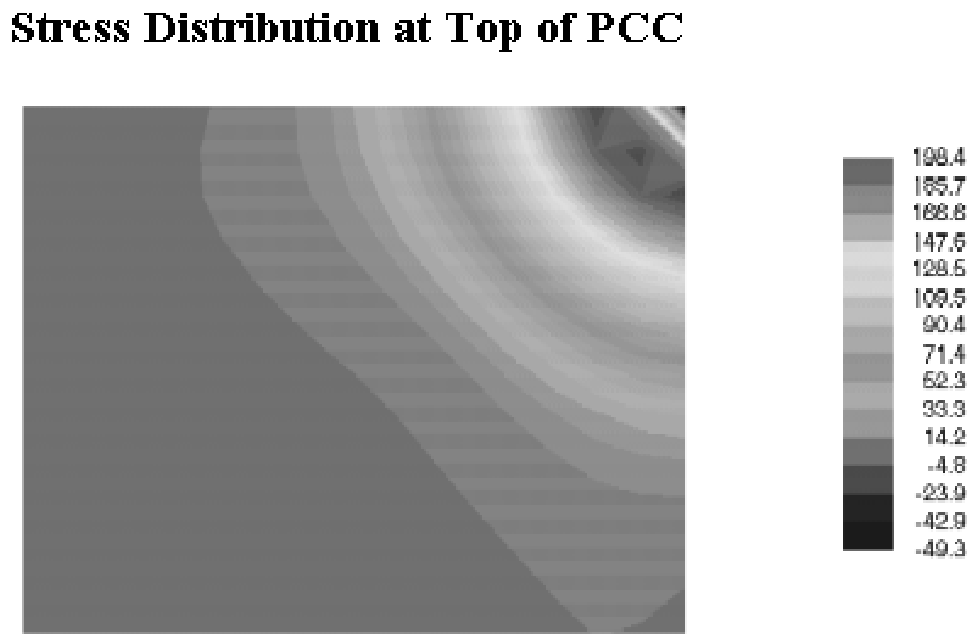


**Figure C-15: Graphical stress results using ISLAB2000 (coarse mesh)**

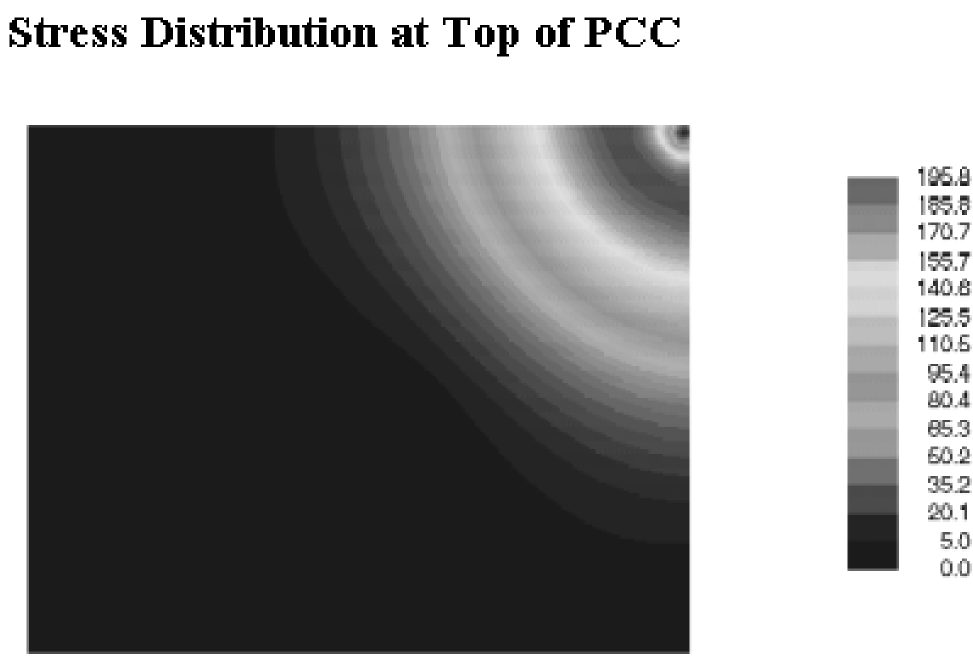


**Figure C-16: Graphical stress results using ISLAB2000 (manual mesh)**

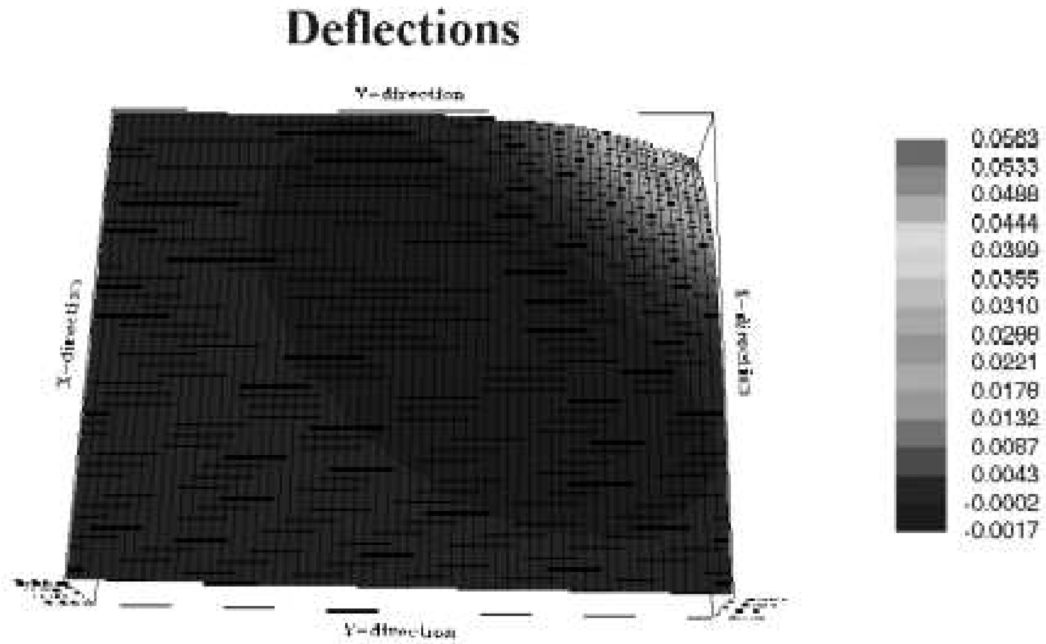


**Figure C-19: Graphical deflection results using ISLAB2000 (fine mesh)**

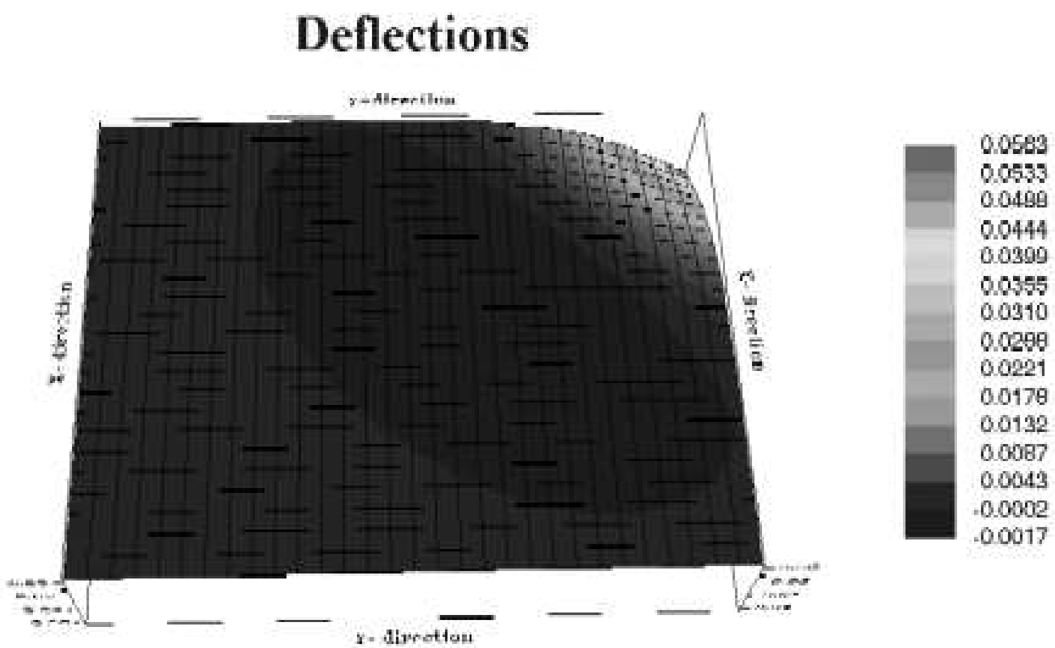


**Figure C-20: Graphical deflection results using ISLAB2000 (medium mesh)**

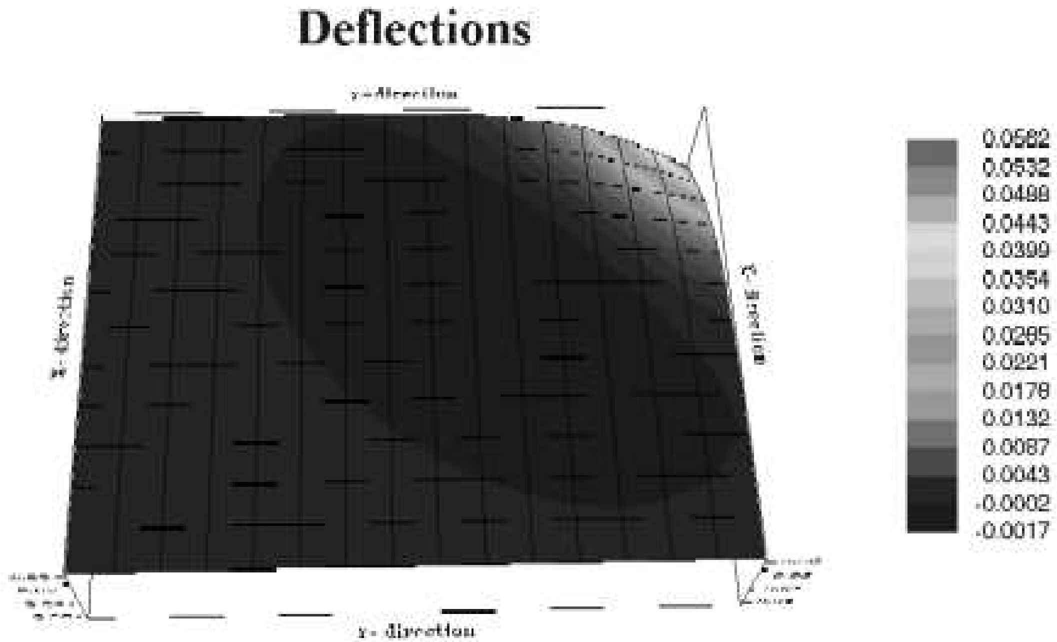


**Figure C-21:Graphical deflection results using ISLAB2000 (coarse mesh)**

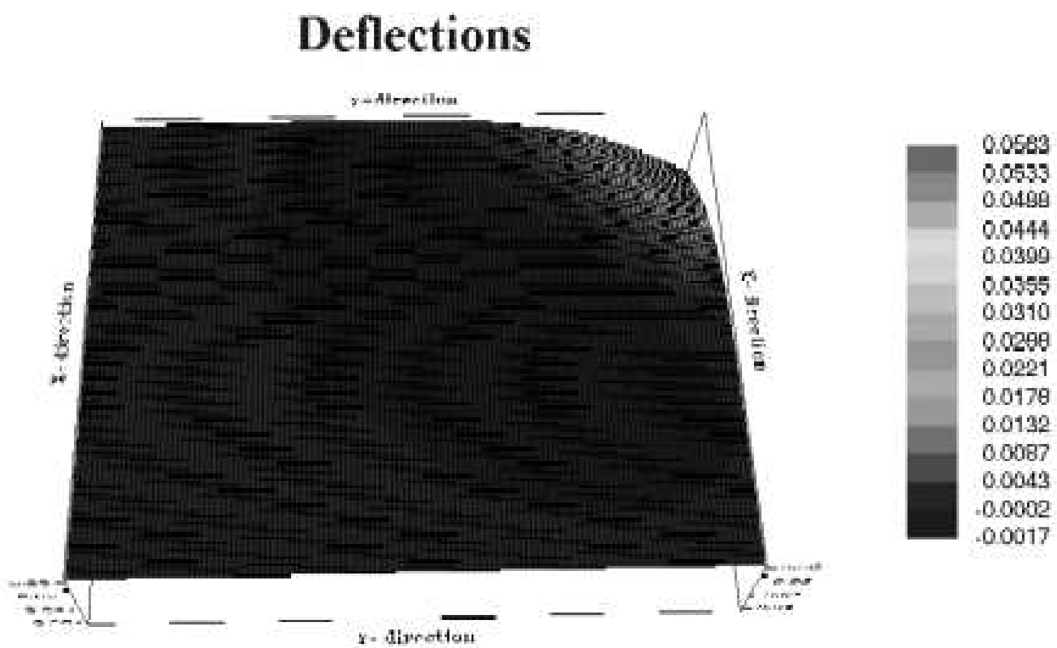


**Figure C-22: Graphical deflection results using ISLAB2000 (manual mesh)**

**Problem 3** (Example 4.3 page 177 in the textbook)

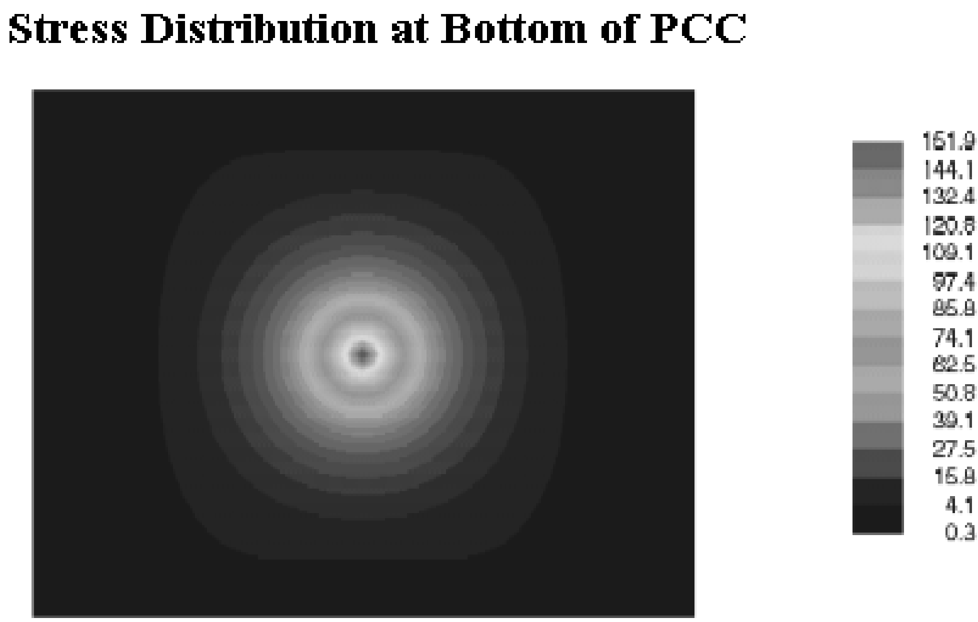


**Figure C-25: Graphical stress results using ISLAB2000 (fine mesh)**

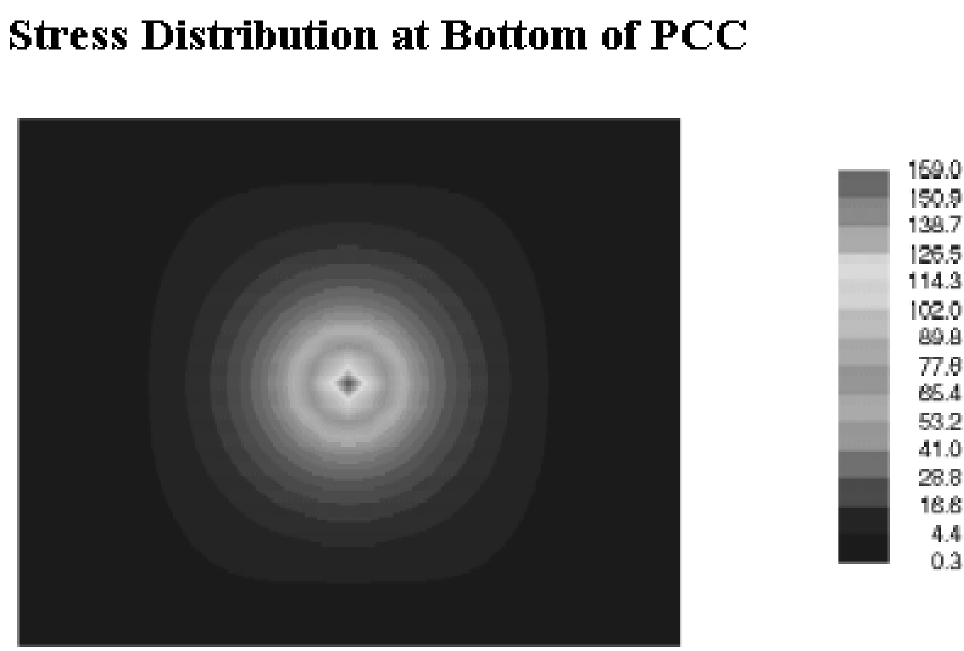


**Figure C-26: Graphical stress results using ISLAB2000 (medium mesh)**

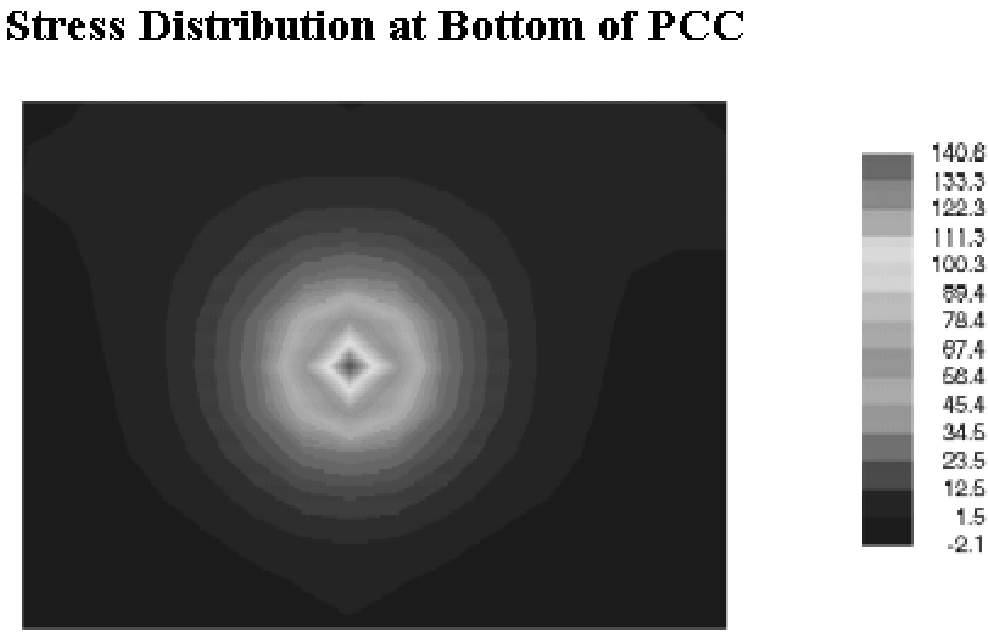


**Figure C-27: Graphical stress results using ISLAB2000 (coarse mesh)**

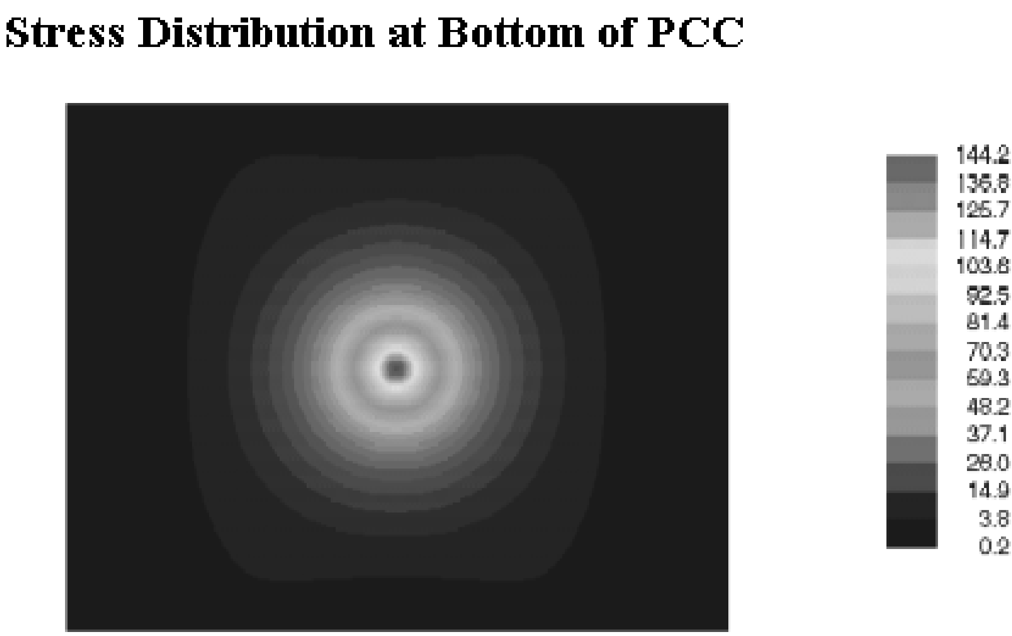


**Figure C-28: Graphical stress results using ISLAB2000 (manual mesh)**

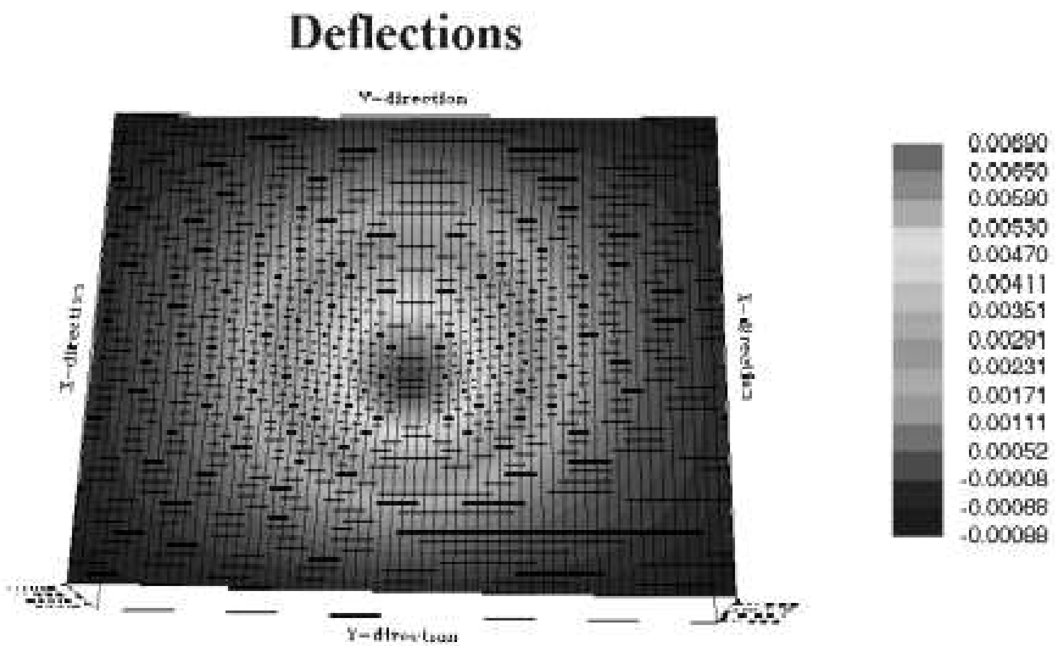


**Figure C-31: Graphical deflection results using ISLAB2000 (fine mesh)**

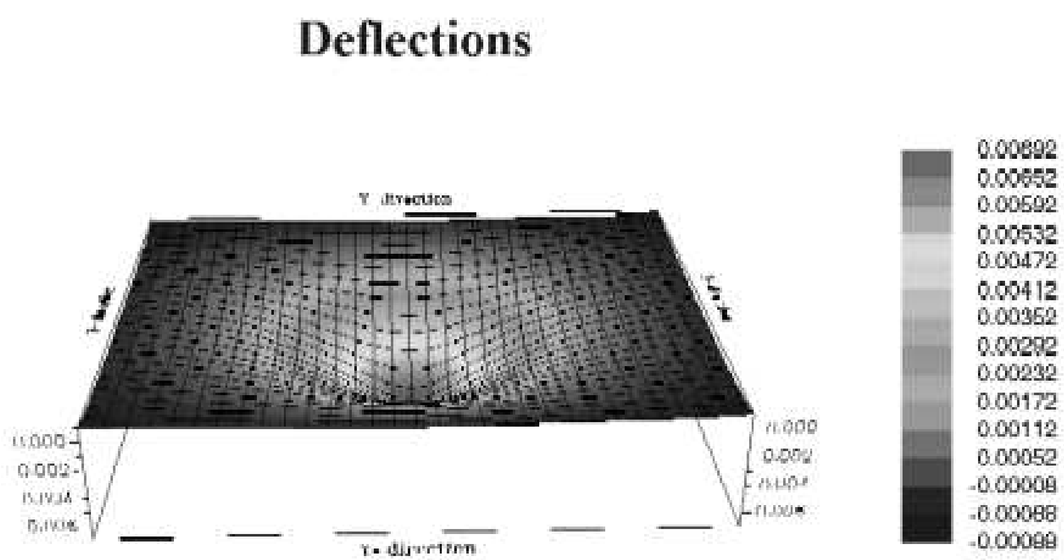


**Figure C-32: Graphical deflection results using ISLAB2000 (medium mesh)**

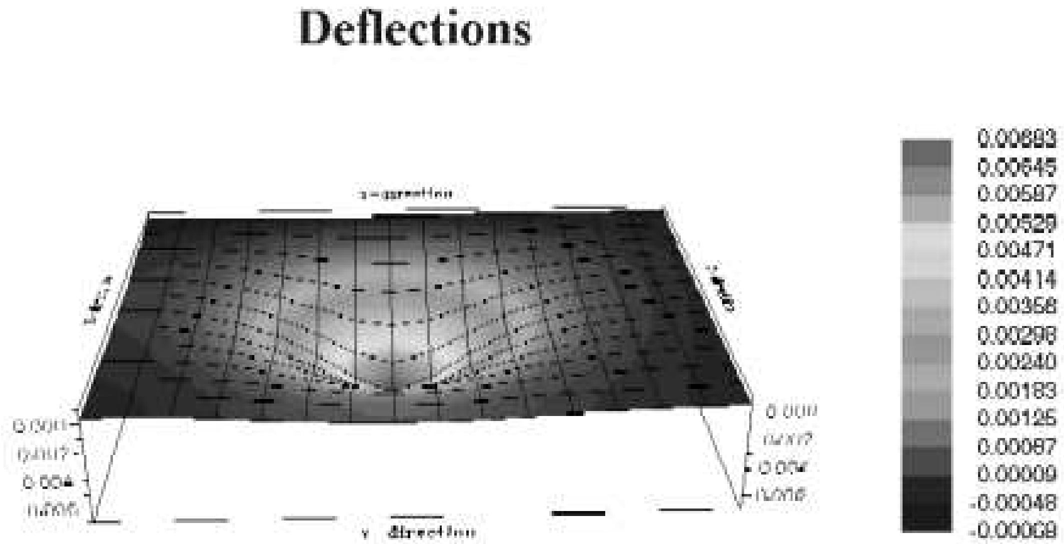


**Figure C-33: Graphical deflection results using ISLAB2000 (coarse mesh)**

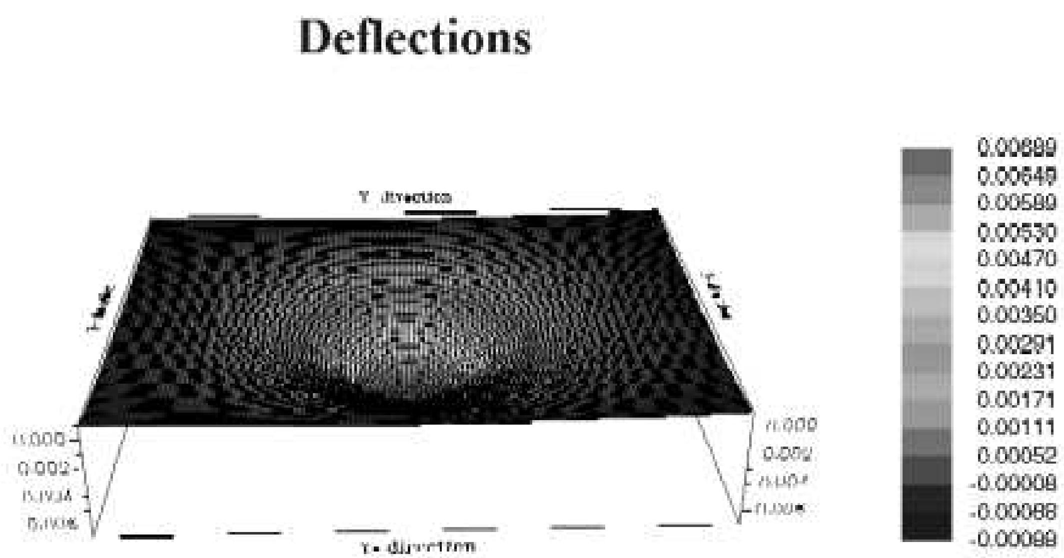


**Figure C-34: Graphical deflection results using ISLAB2000 (manual mesh)**

**Problem 4** (Example 4.4 page 178 in the textbook)

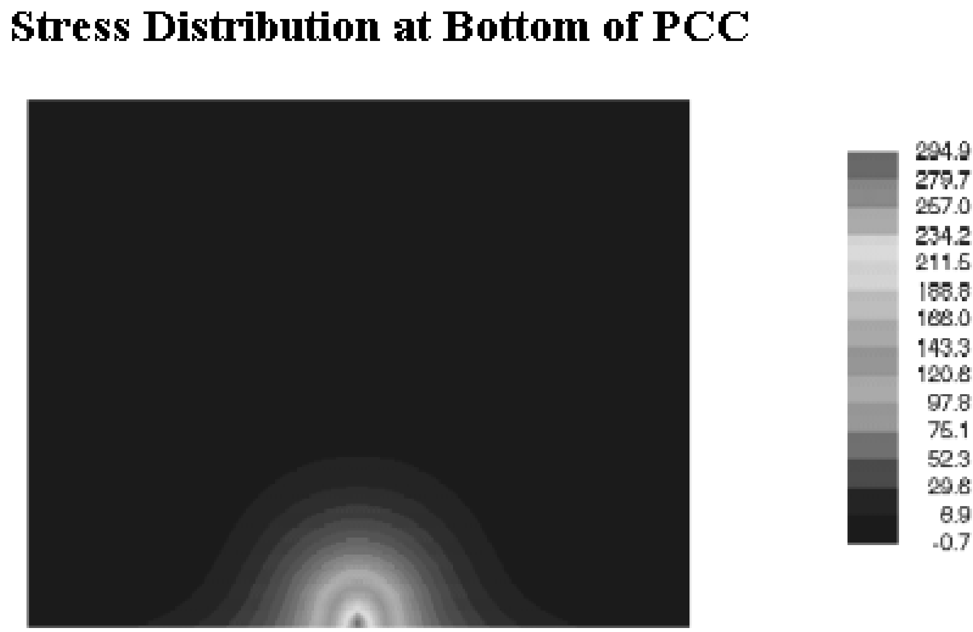


**Figure C-37: Graphical stress results using ISLAB2000 (fine mesh)**

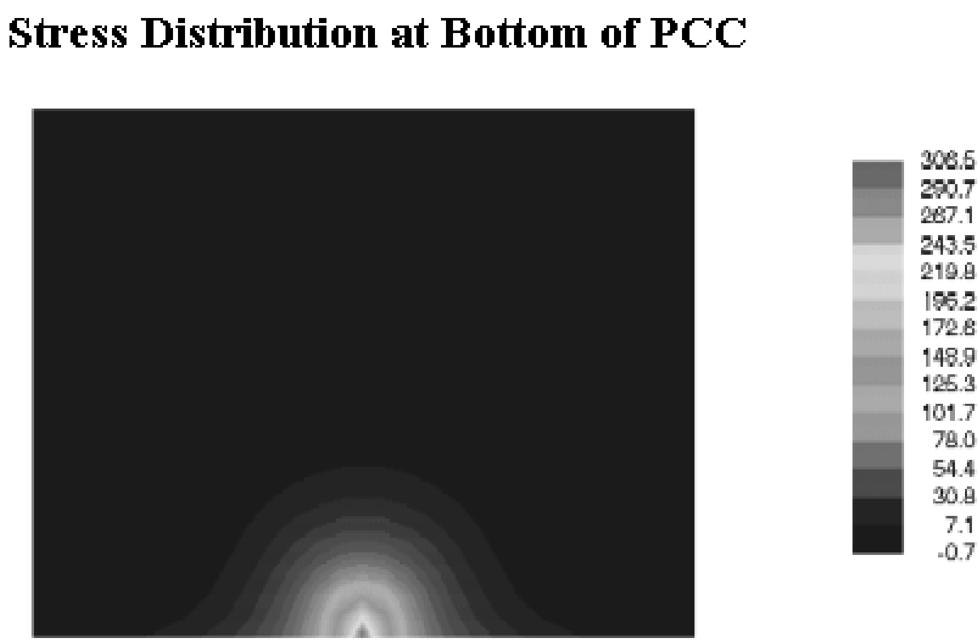


**Figure C-38: Graphical stress results using ISLAB2000 (medium mesh)**

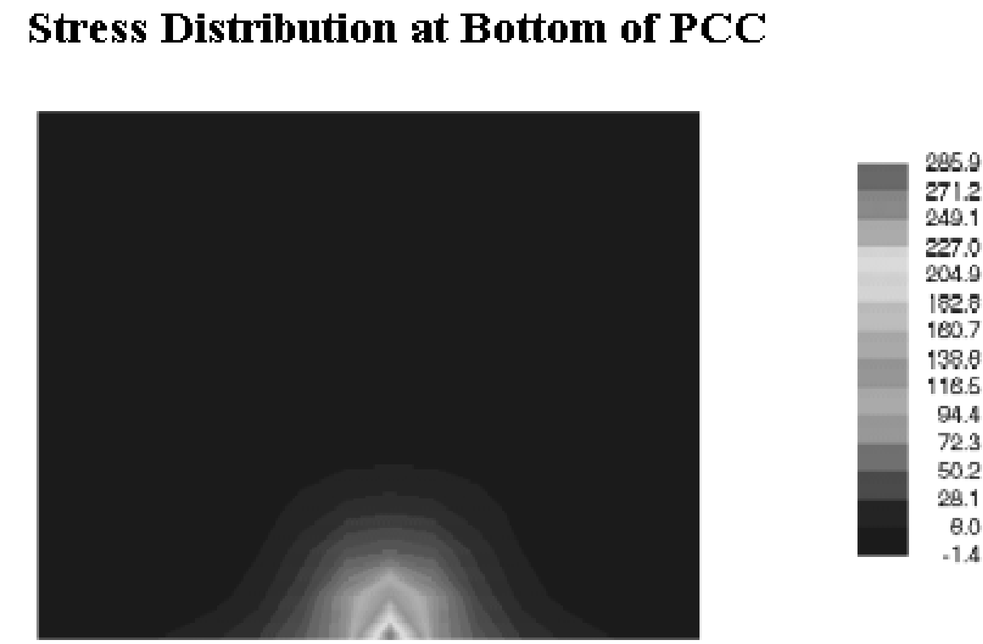


**Figure C-39: Graphical stress results using ISLAB2000 (coarse mesh)**

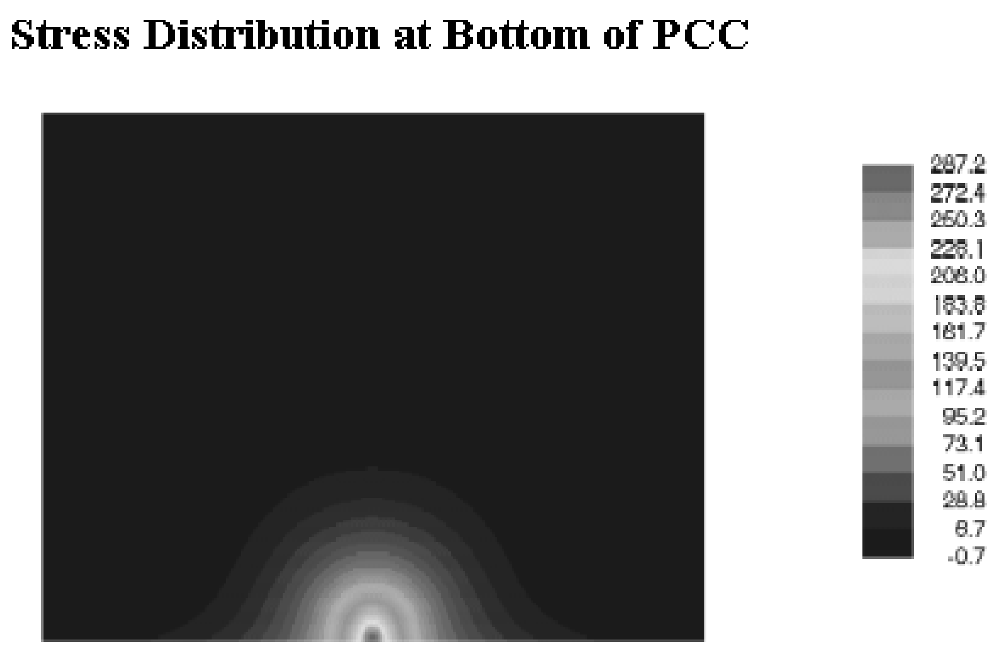


**Figure C-40: Graphical stress results using ISLAB2000 (manual mesh)**

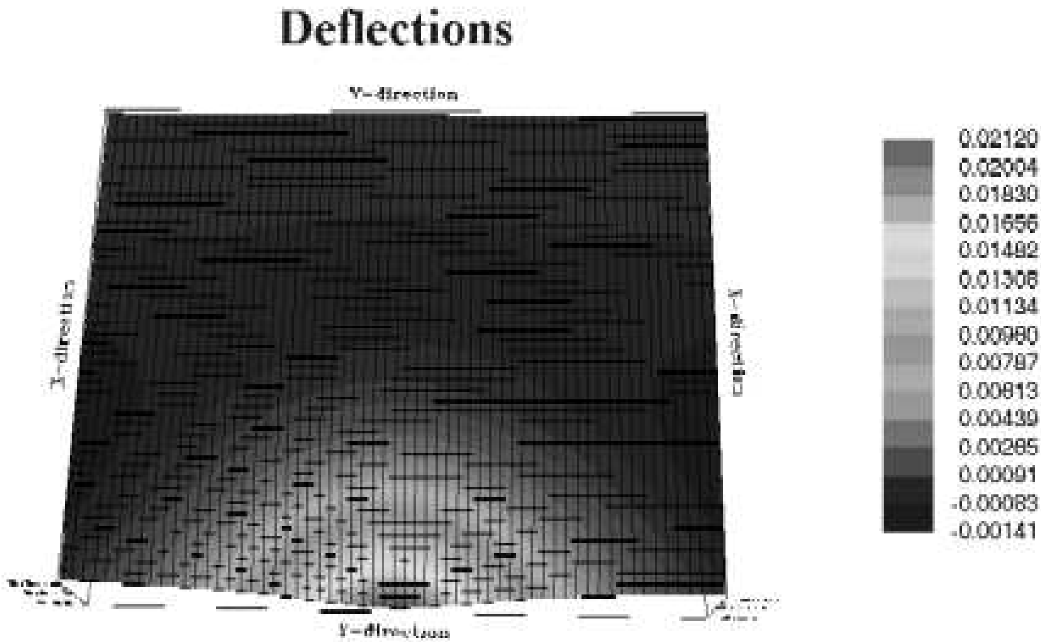


**Figure C-43: Graphical deflection results using ISLAB2000 (fine mesh)**

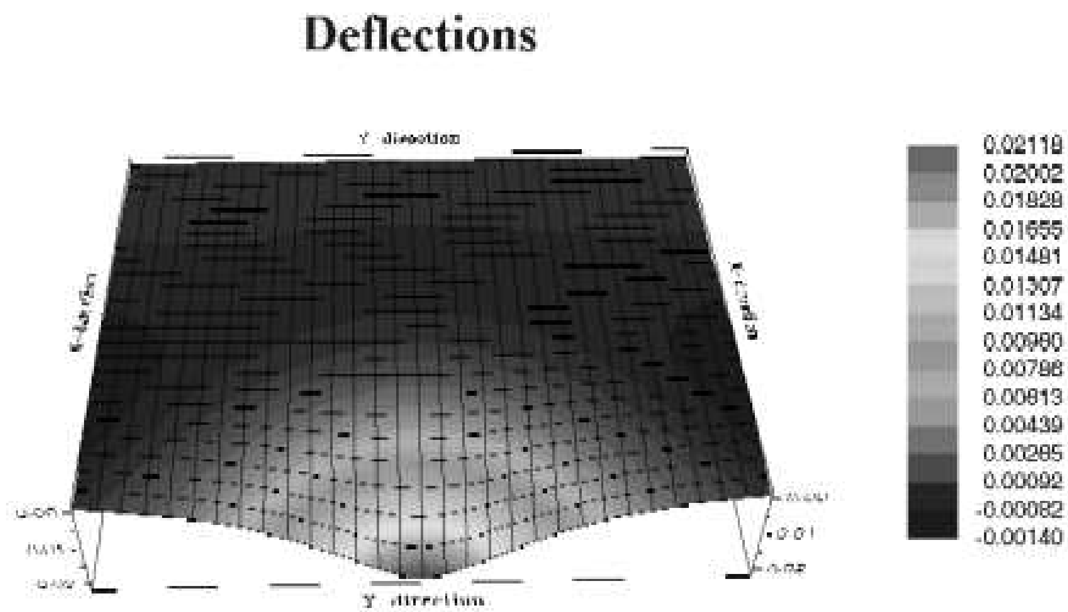


**Figure C-44: Graphical deflection results using ISLAB2000 (medium mesh)**

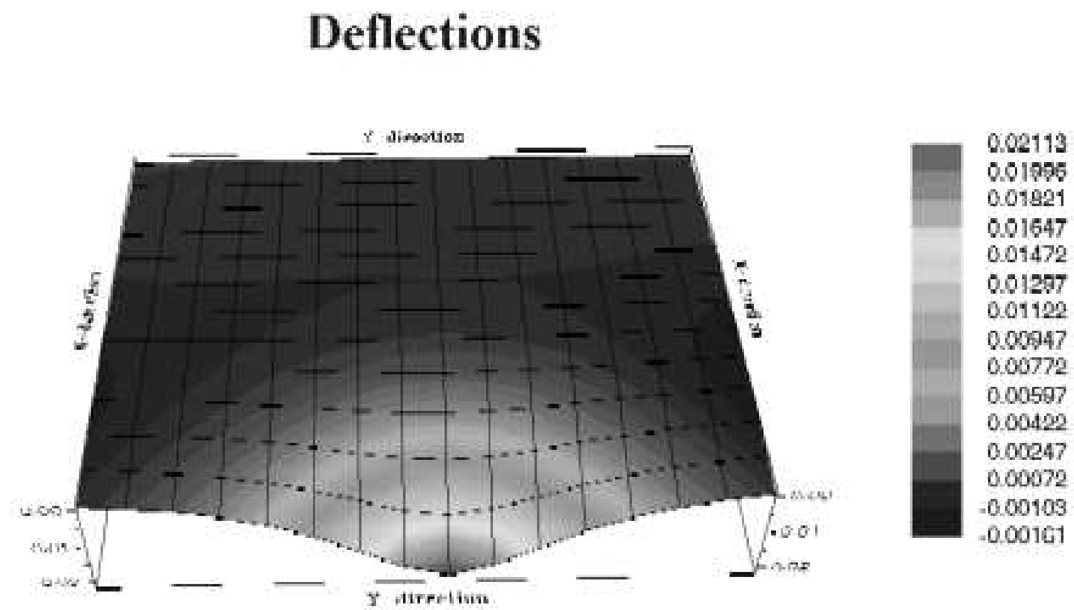


**Figure C-45: Graphical deflection results using ISLAB2000 (coarse mesh)**

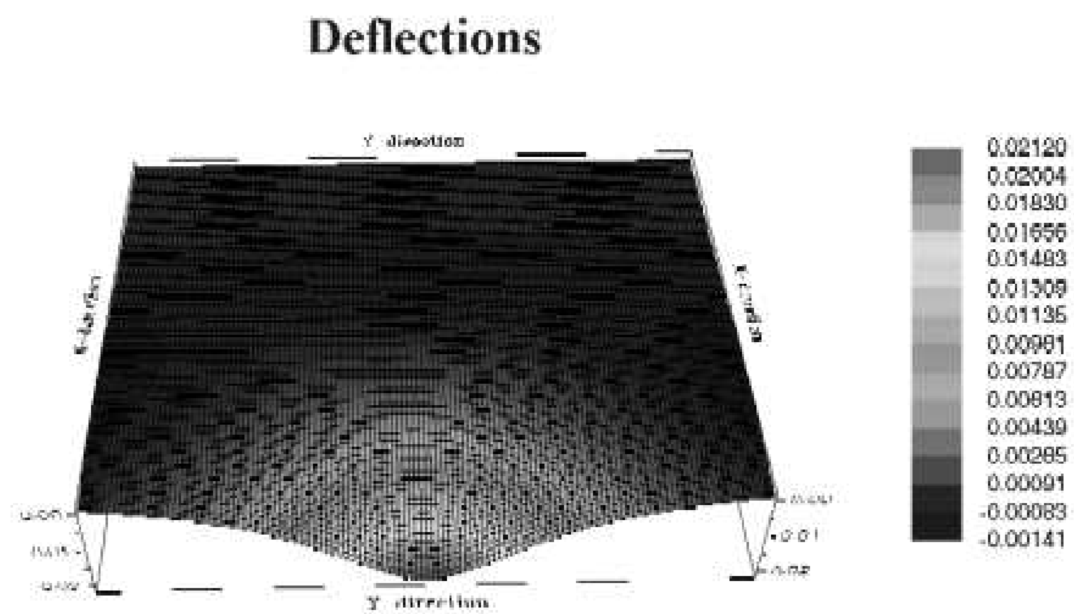


**Figure C-46: Graphical deflection results using ISLAB2000 (manual mesh)**

**Problem 5** (Example 4.5 page 180 in the textbook)

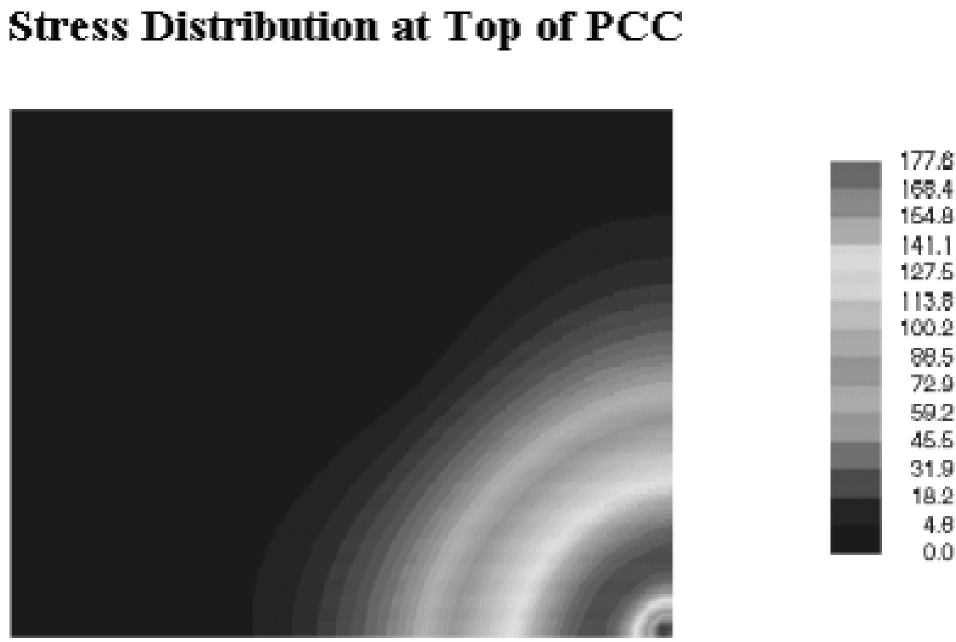


**Figure C-49: Graphical stress results using ISLAB2000 (fine mesh)**

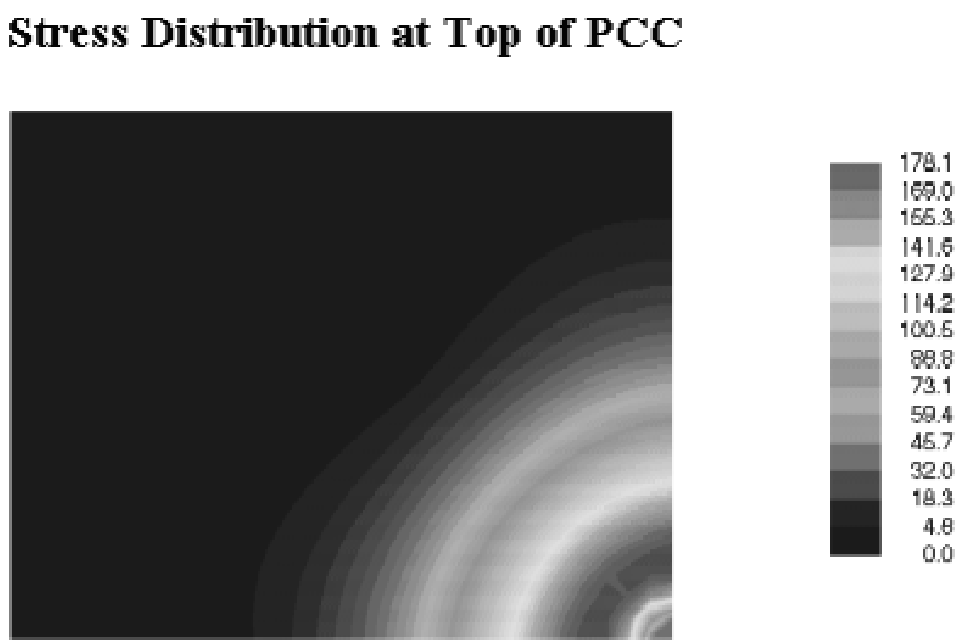


**Figure C-50: Graphical stress results using ISLAB2000 (medium mesh)**

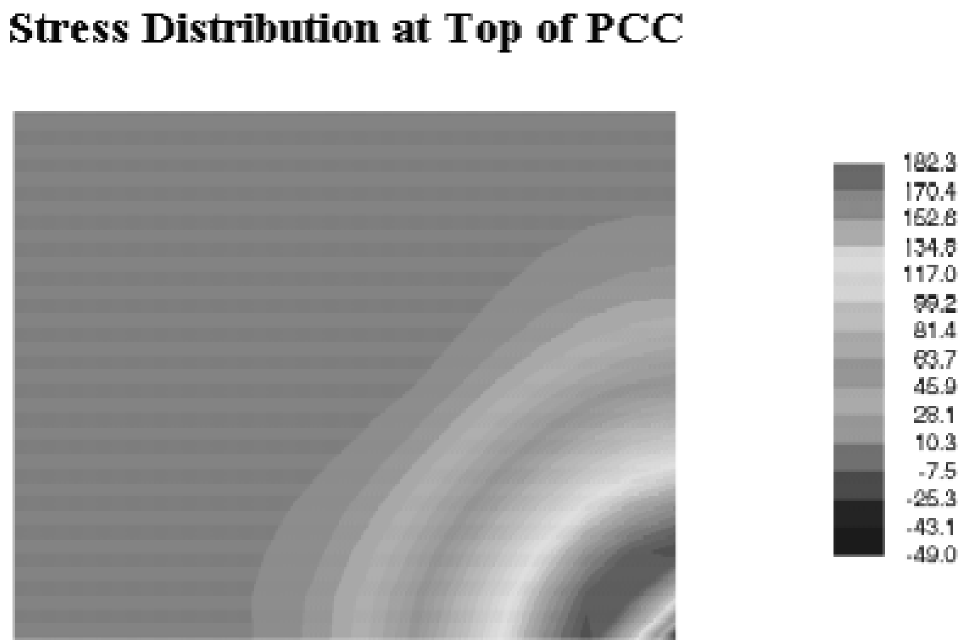


**Figure C-51: Graphical stress results using ISLAB2000 (coarse mesh)**

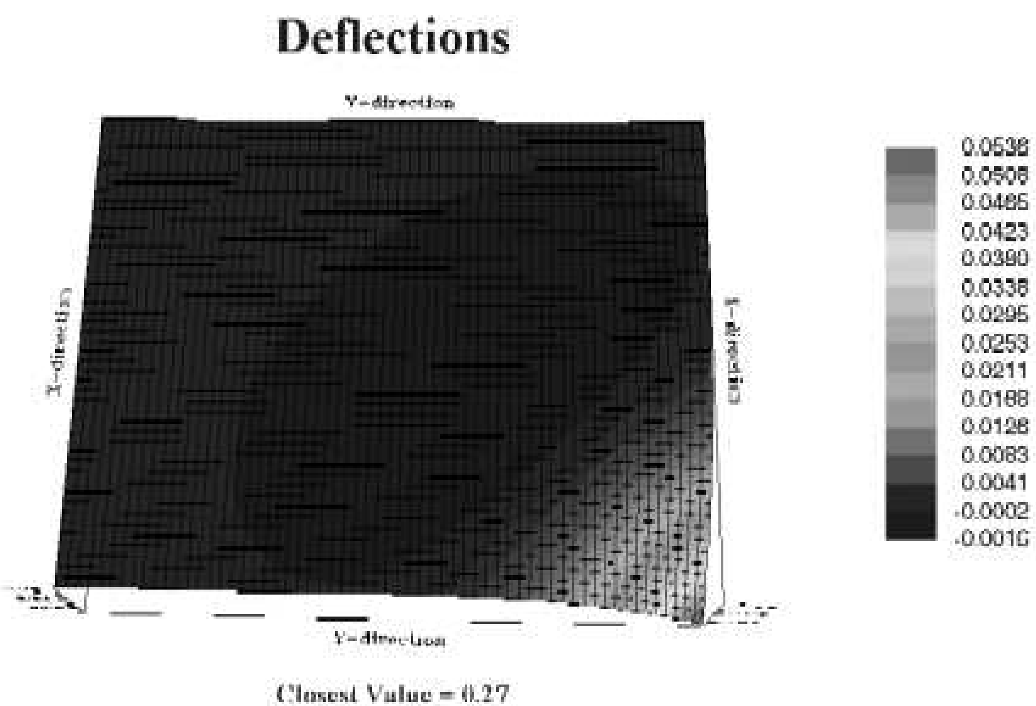


**Figure C-54: Graphical deflection results using ISLAB2000 (fine mesh)**

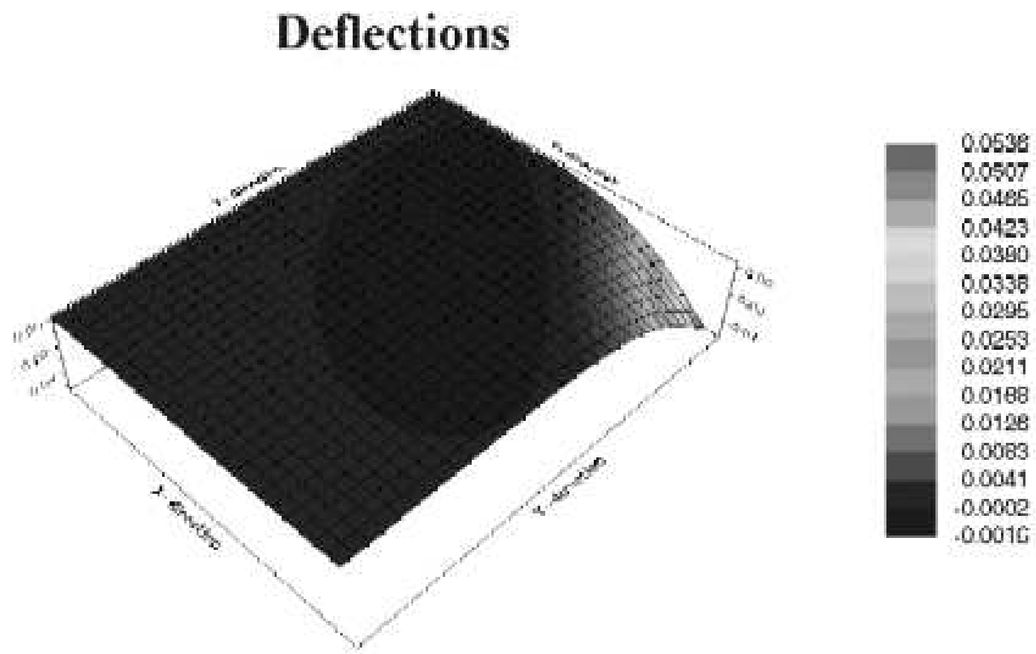


**Figure C-55: Graphical deflection results using ISLAB2000 (medium mesh)**

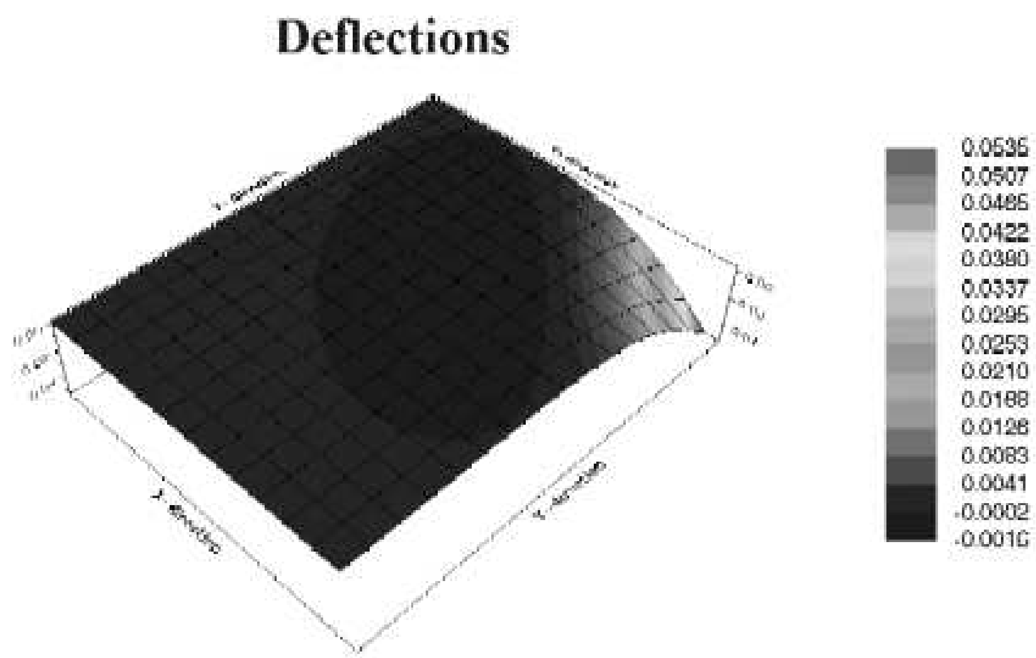


**Figure C-56: Graphical deflection results using ISLAB2000 (coarse mesh)**

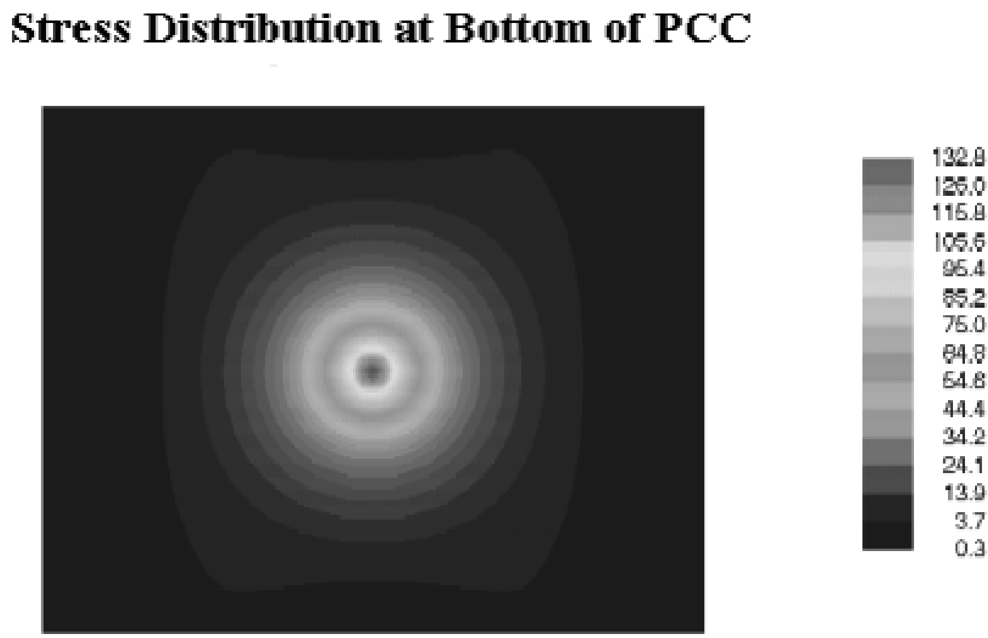


**Figure C-59: Graphical stress results using ISLAB2000 (fine mesh)**

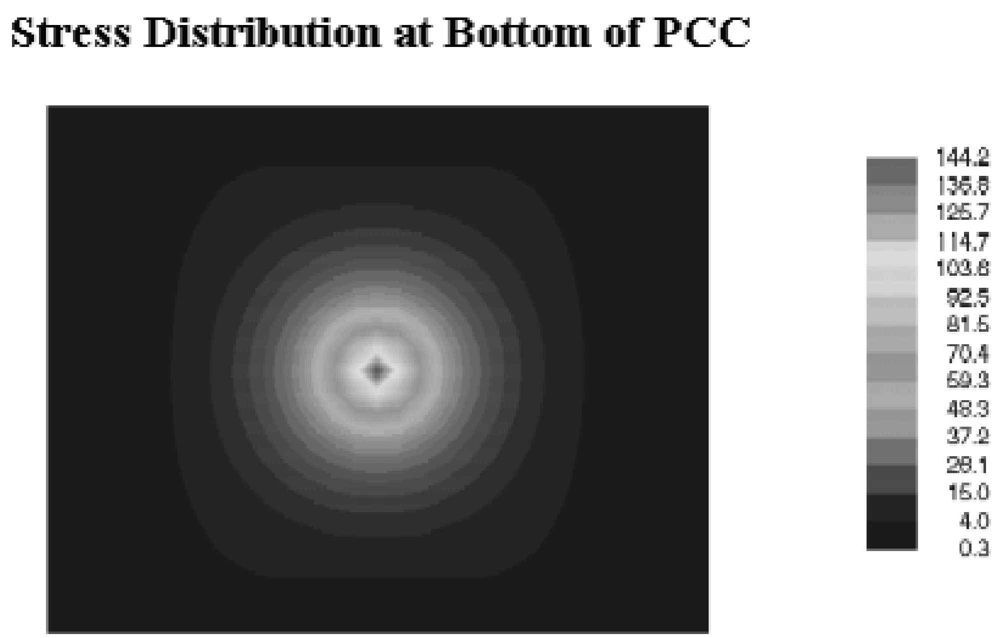


**Figure C-60: Graphical stress results using ISLAB2000 (medium mesh)**

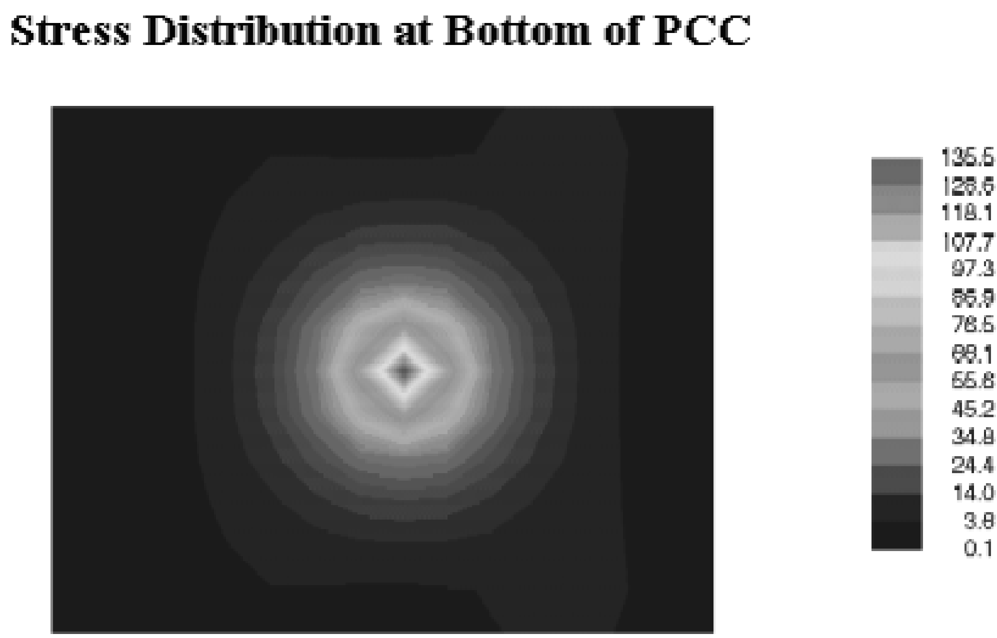


**Figure C-61: Graphical stress results using ISLAB2000 (coarse mesh)**

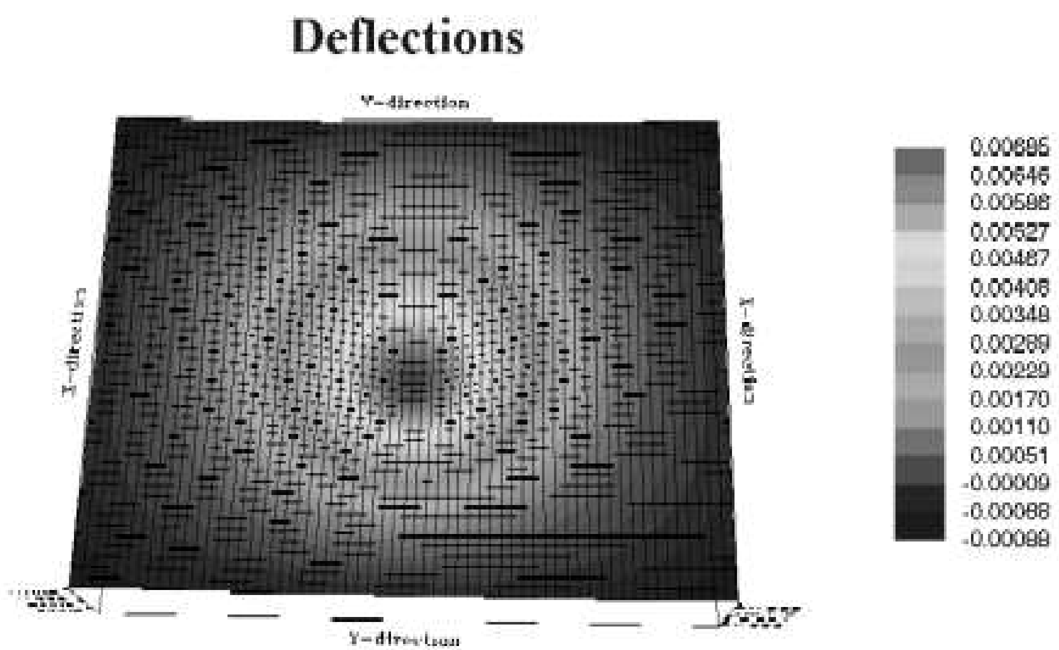


**Figure C-64: Graphical deflection results using ISLAB2000 (fine mesh)**

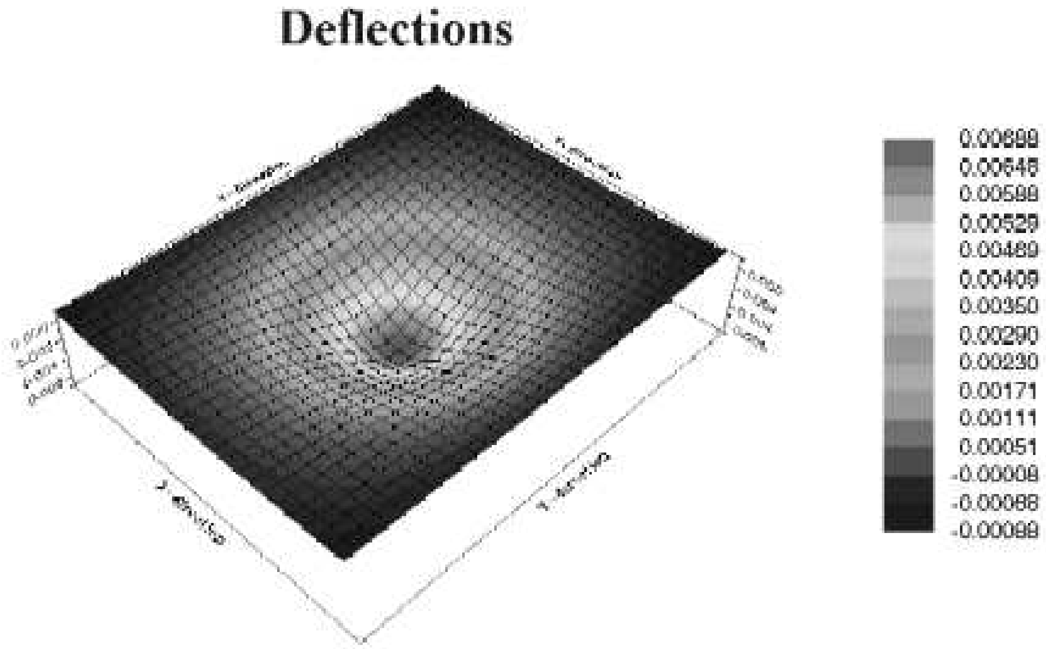


**Figure C-65: Graphical deflection results using ISLAB2000 (medium mesh)**

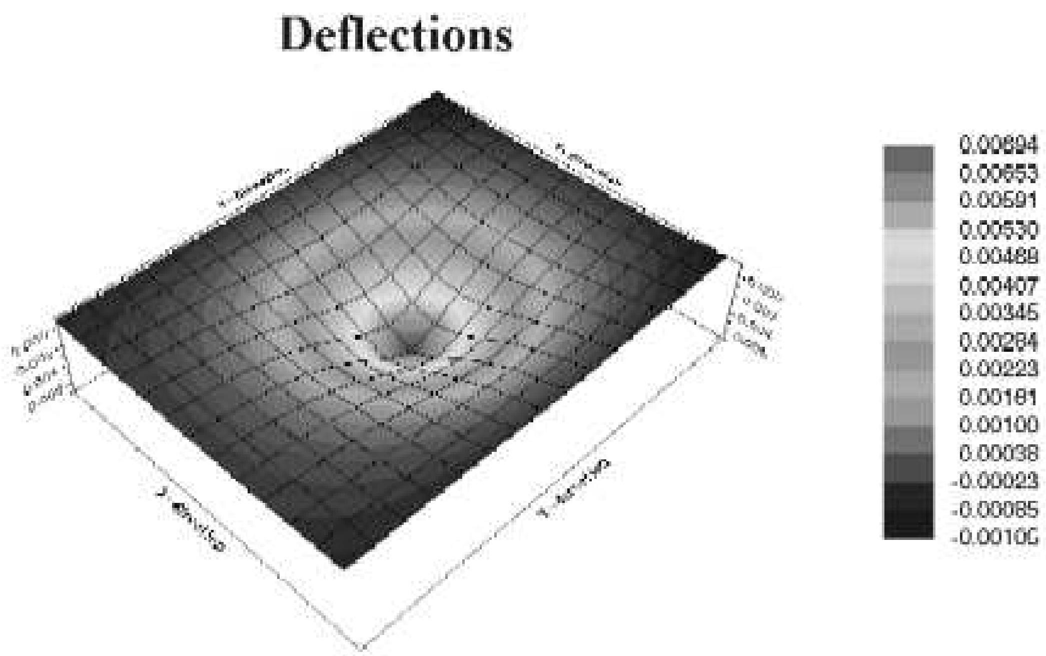


**Figure C-66: Graphical deflection results using ISLAB2000 (coarse mesh)**

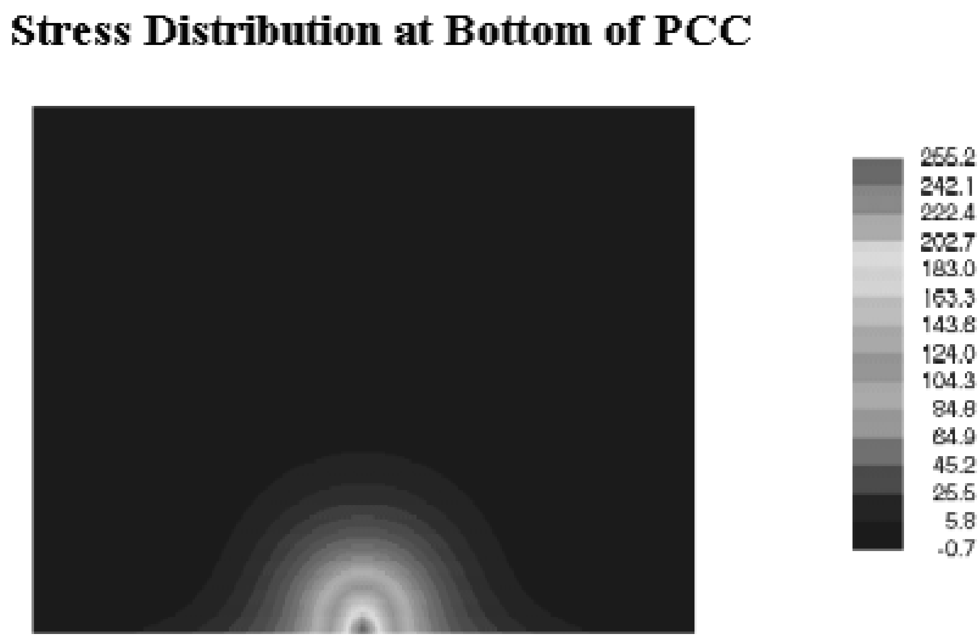


**Figure C-69: Graphical stress results using ISLAB2000 (fine mesh)**

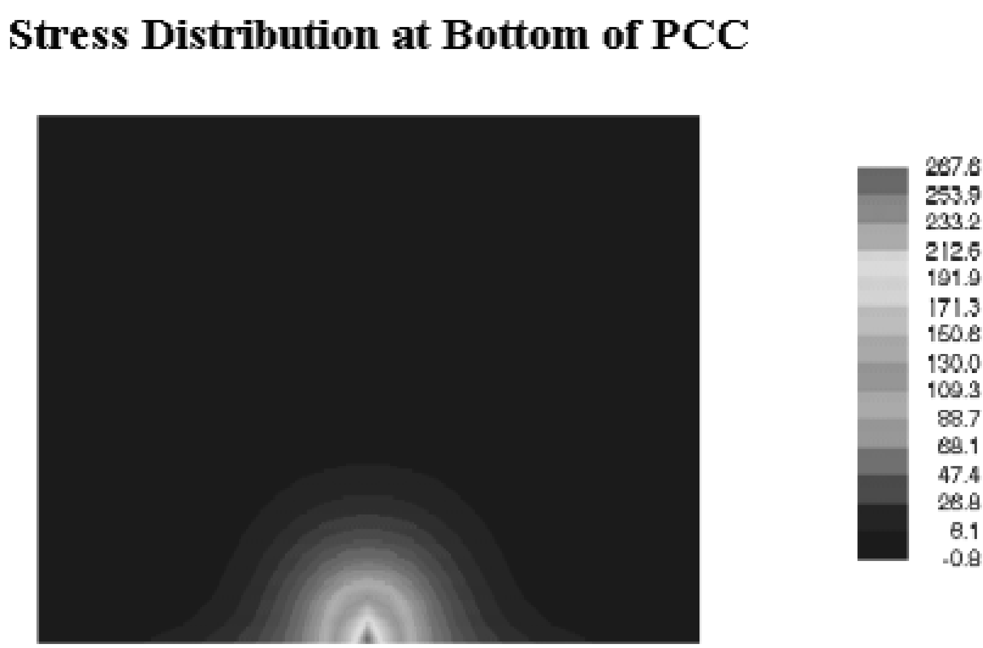


**Figure C-70: Graphical stress results using ISLAB2000 (medium mesh)**

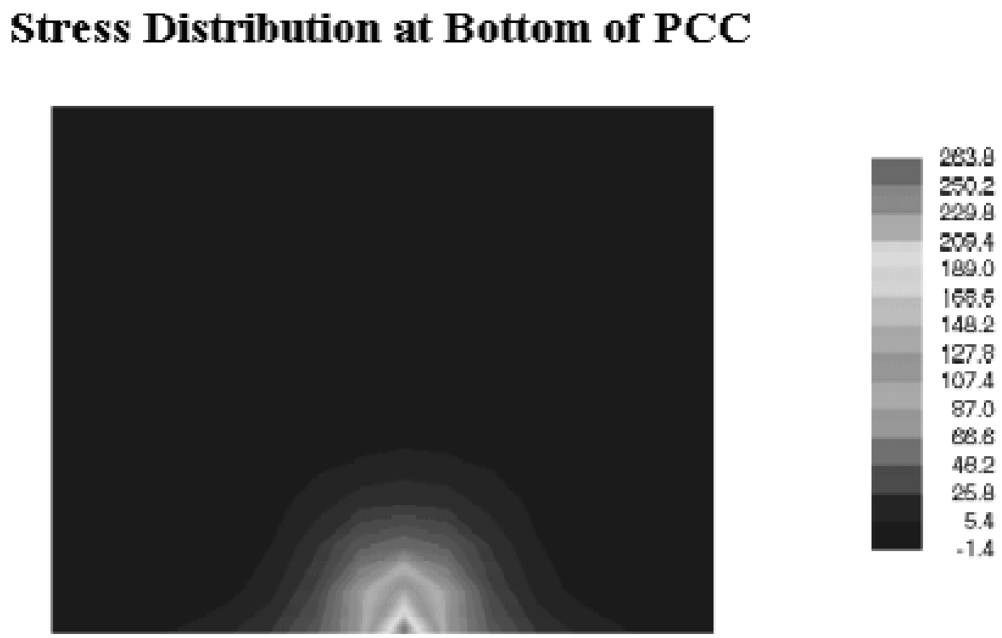


**Figure C-71: Graphical stress results using ISLAB2000 (coarse mesh)**

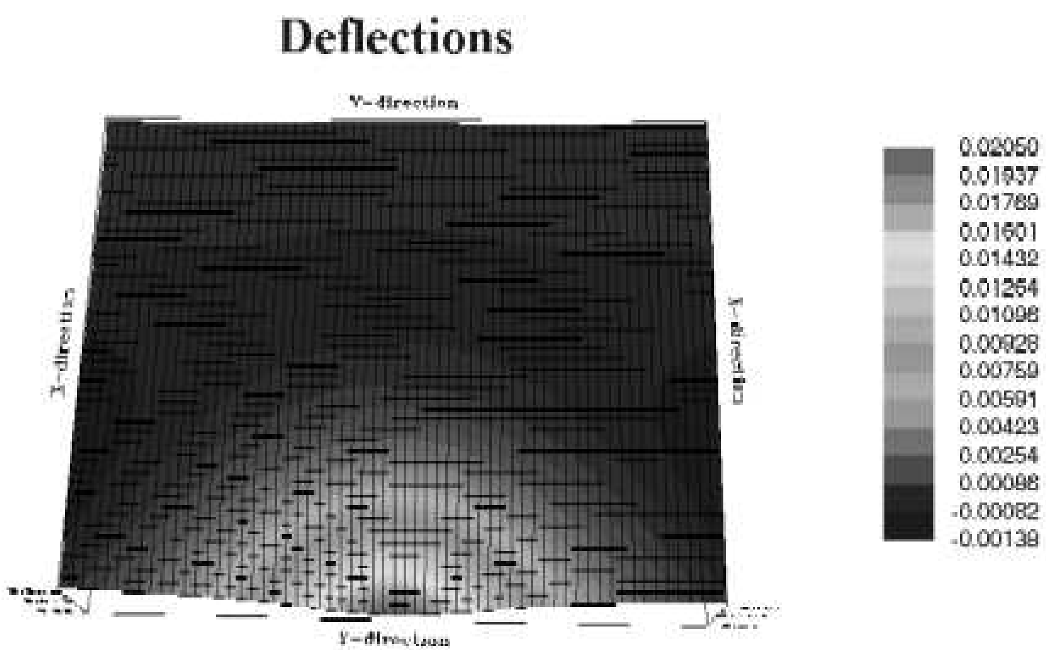


**Figure C-74: Graphical deflection results using ISLAB2000 (fine mesh)**

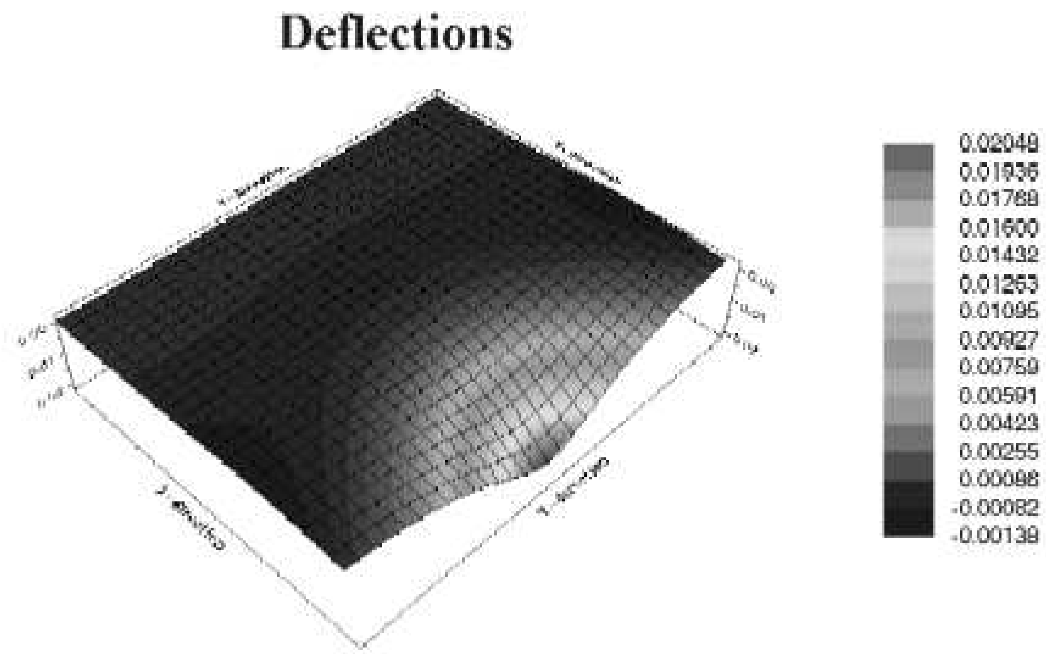


**Figure C-75: Graphical deflection results using ISLAB2000 (medium mesh)**

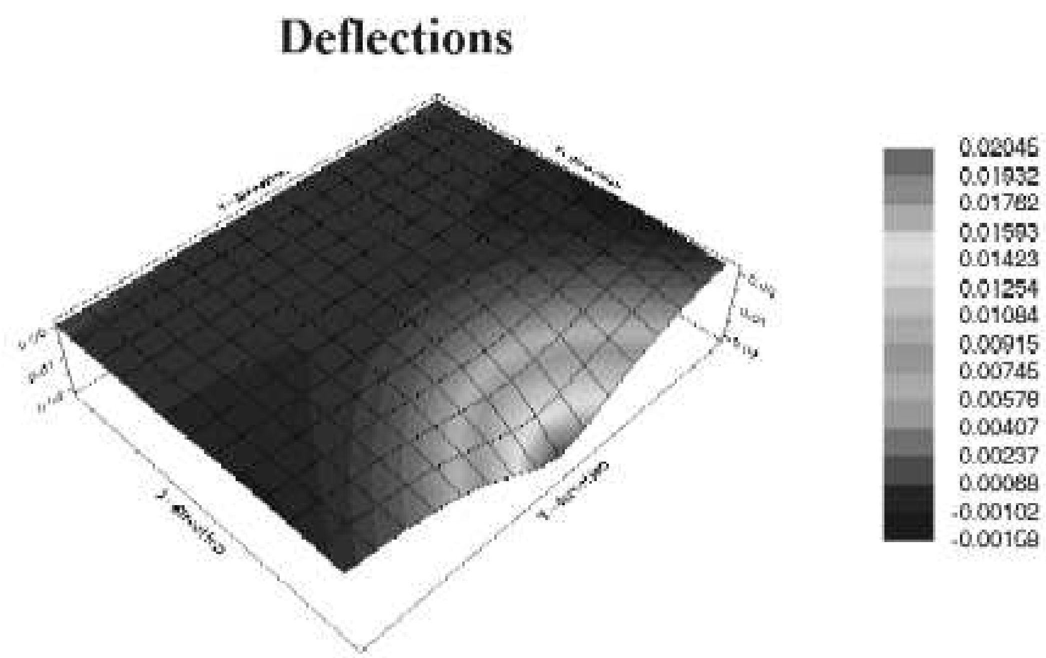


**Figure C-76: Graphical deflection results using ISLAB2000 (coarse mesh)**

**Problem 6** (Problem 4-1 page 203 in the textbook)

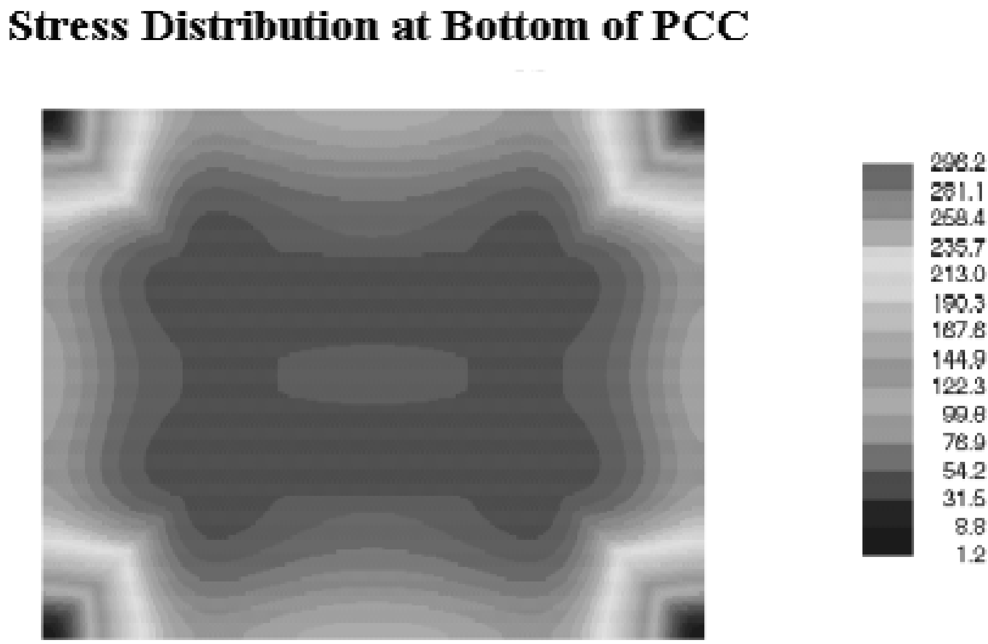


**Figure C-79: Graphical stress results using ISLAB2000 (fine mesh)**

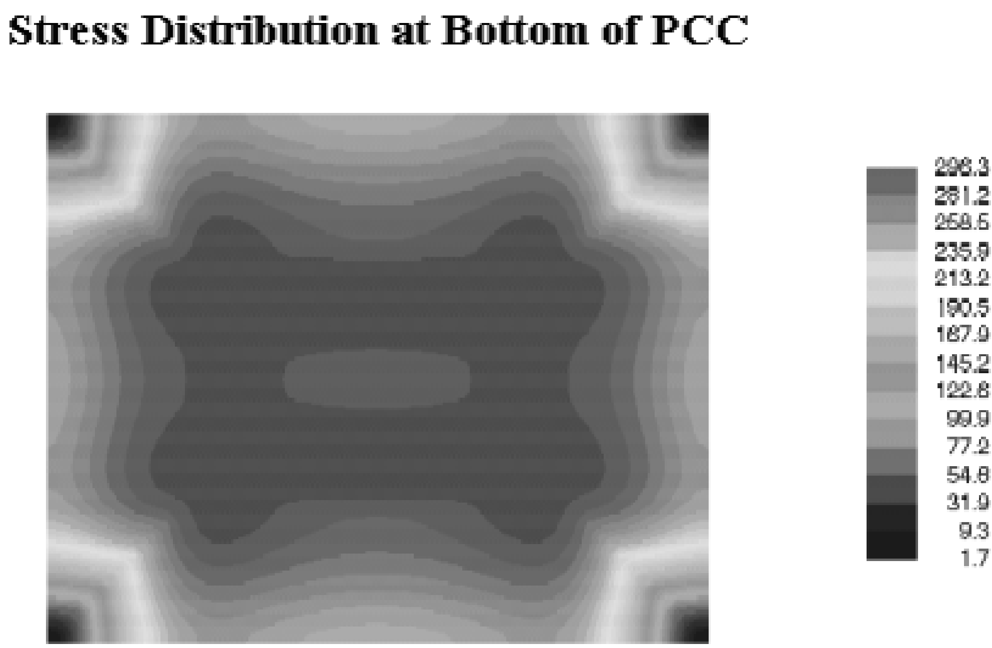


**Figure C-80: Graphical stress results using ISLAB2000 (medium mesh)**

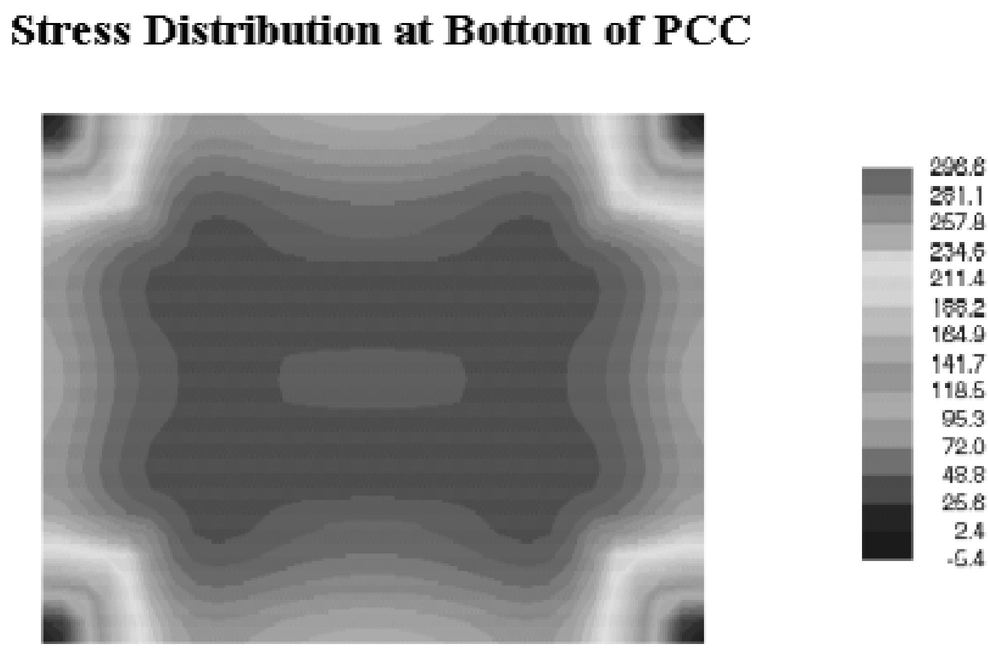


**Figure C-81: Graphical stress results using ISLAB2000 (coarse mesh)**

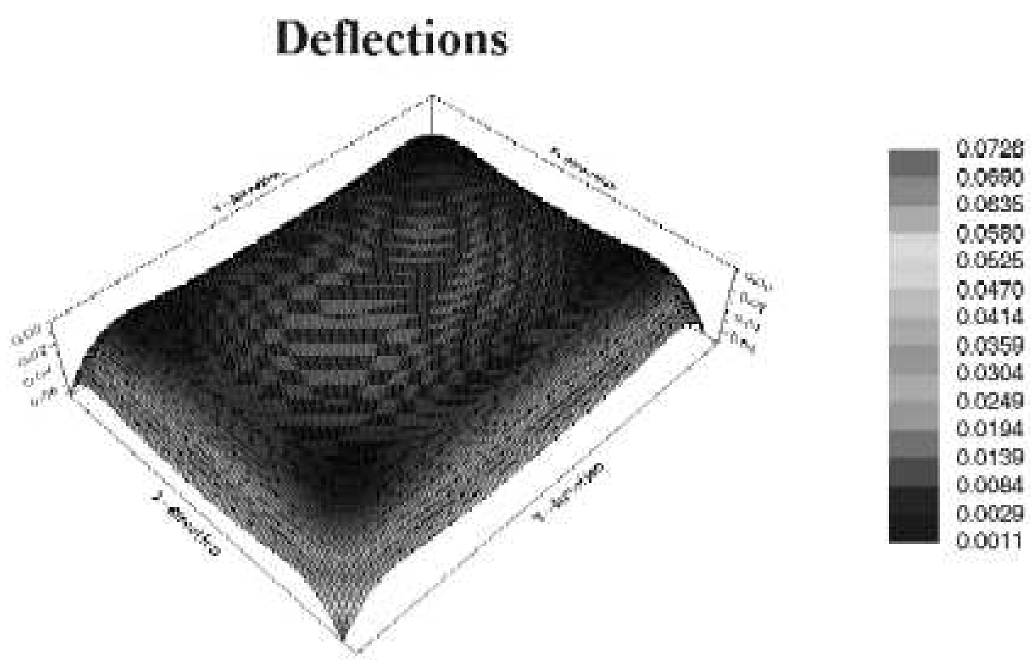


**Figure C-84: Graphical deflection results using ISLAB2000 (fine mesh)**

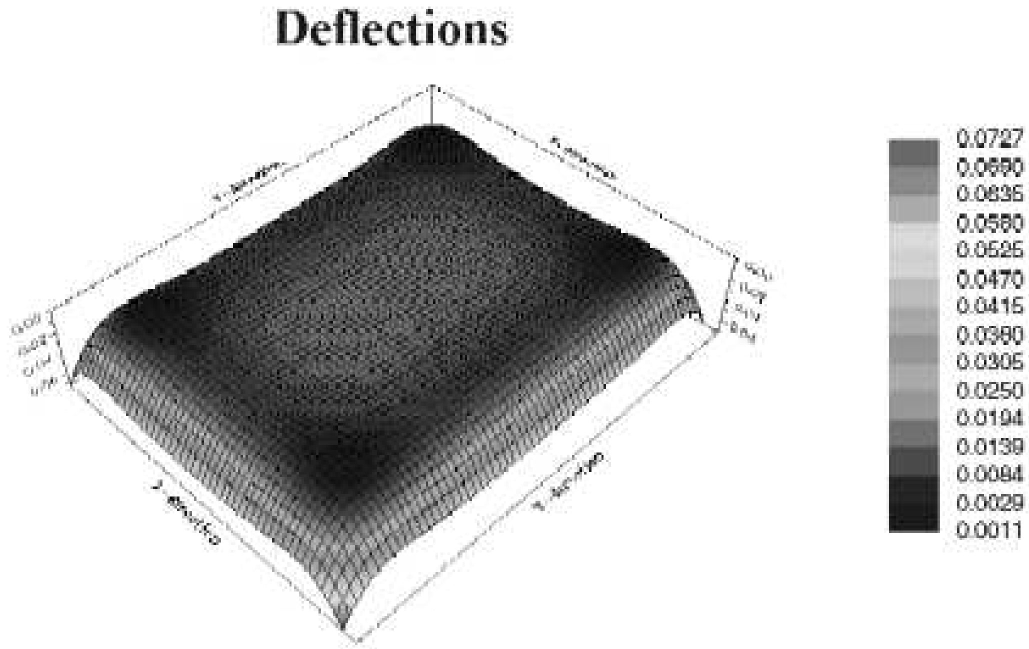


**Figure C-85: Graphical deflection results using ISLAB2000 (medium mesh)**

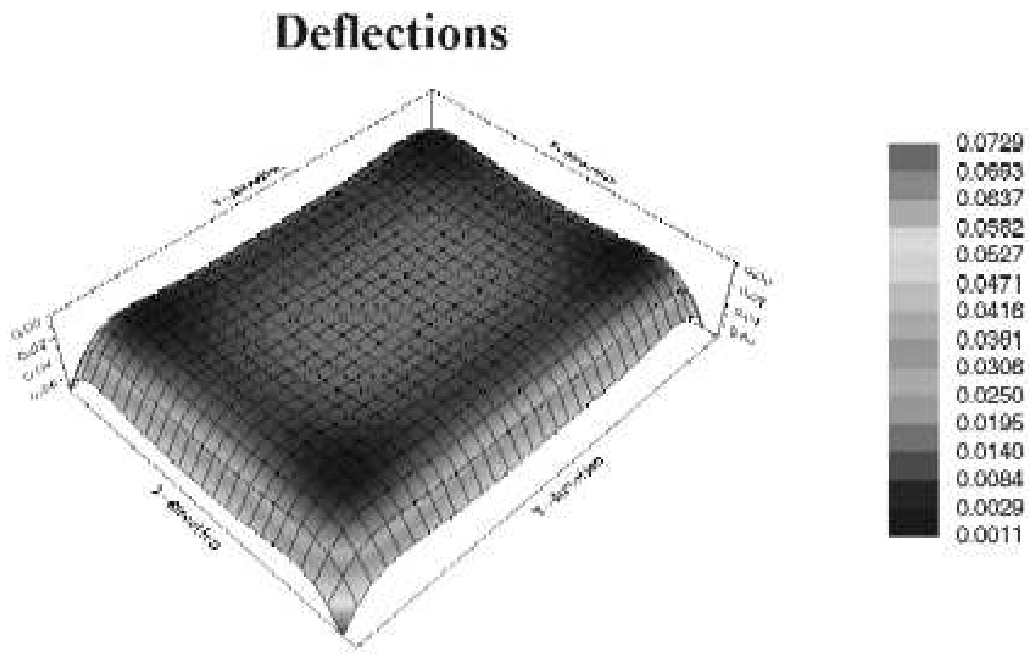


**Figure C-86: Graphical deflection results using ISLAB2000 (coarse mesh)**

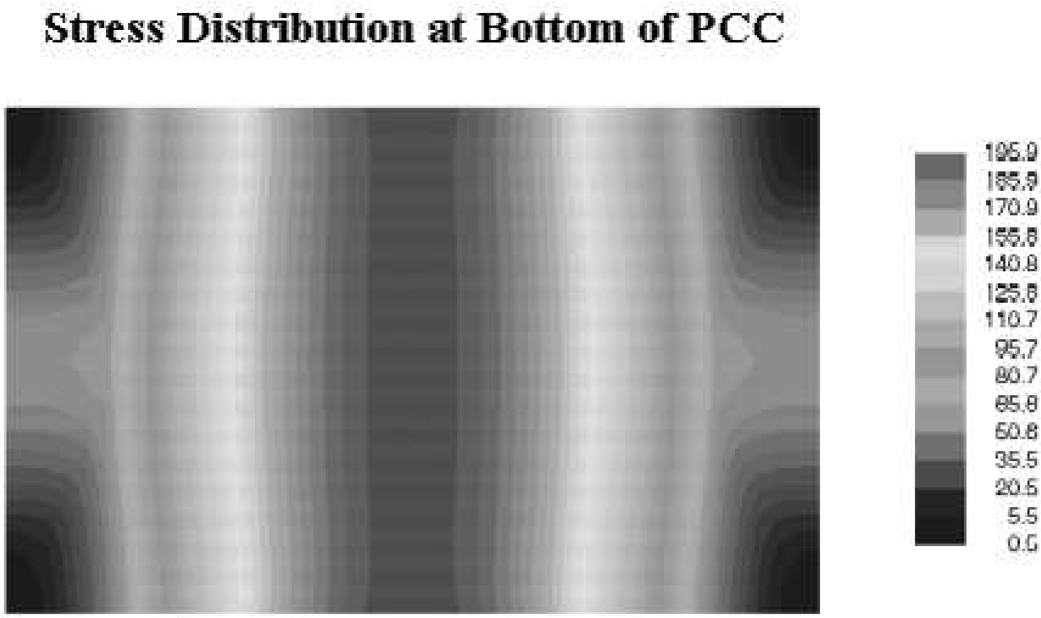


**Figure C-89: Graphical stress results using ISLAB2000 (fine mesh)**

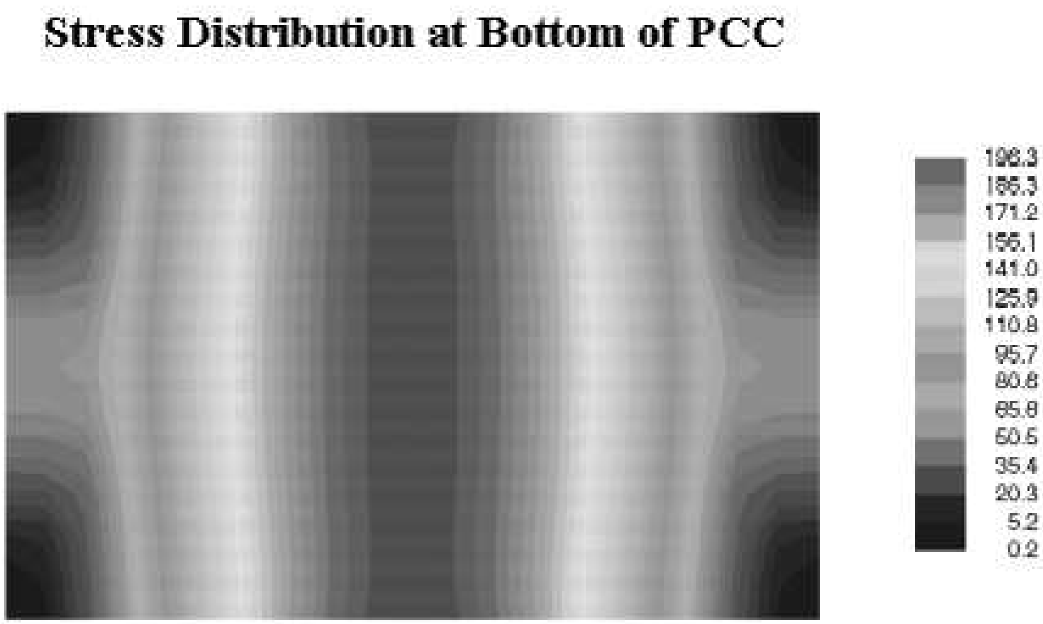


**Figure C-90: Graphical stress results using ISLAB2000 (medium mesh)**

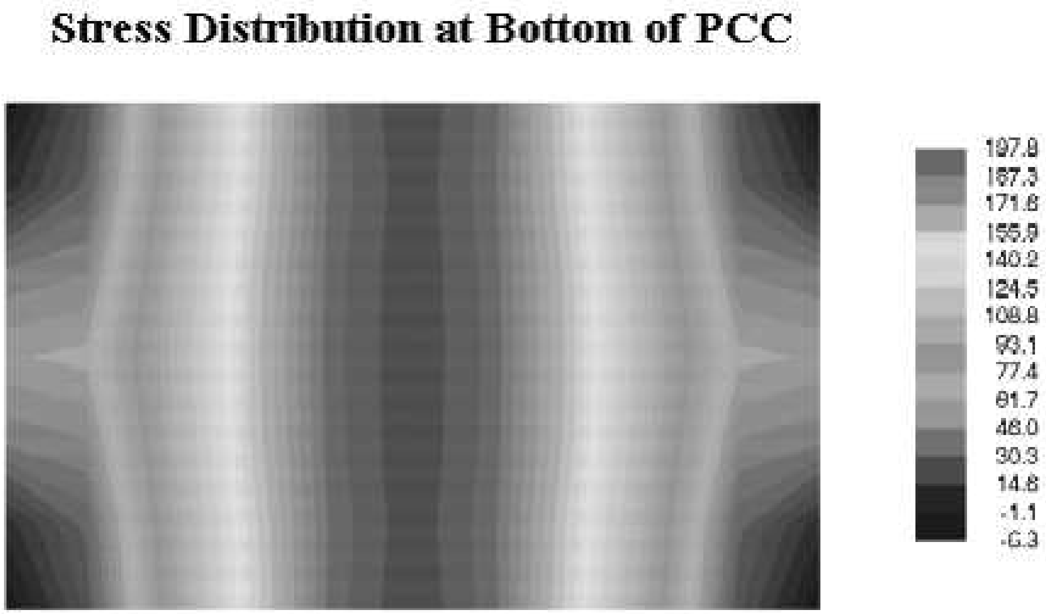


**Figure C-91: Graphical stress results using ISLAB2000 (coarse mesh)**

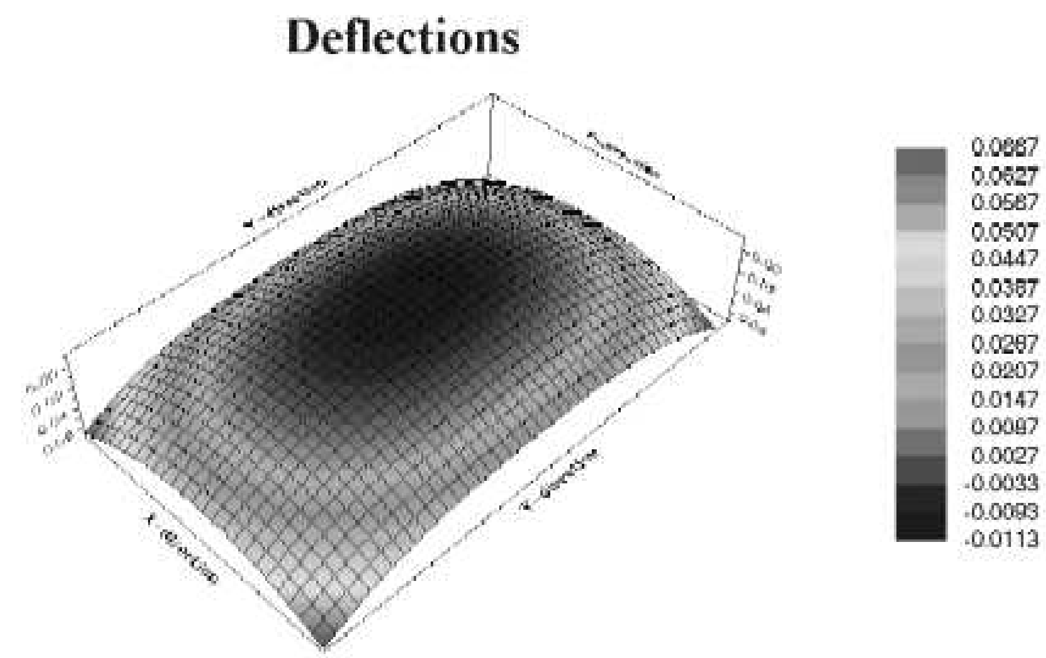


**Figure C-94: Graphical deflection results using ISLAB2000 (fine mesh)**

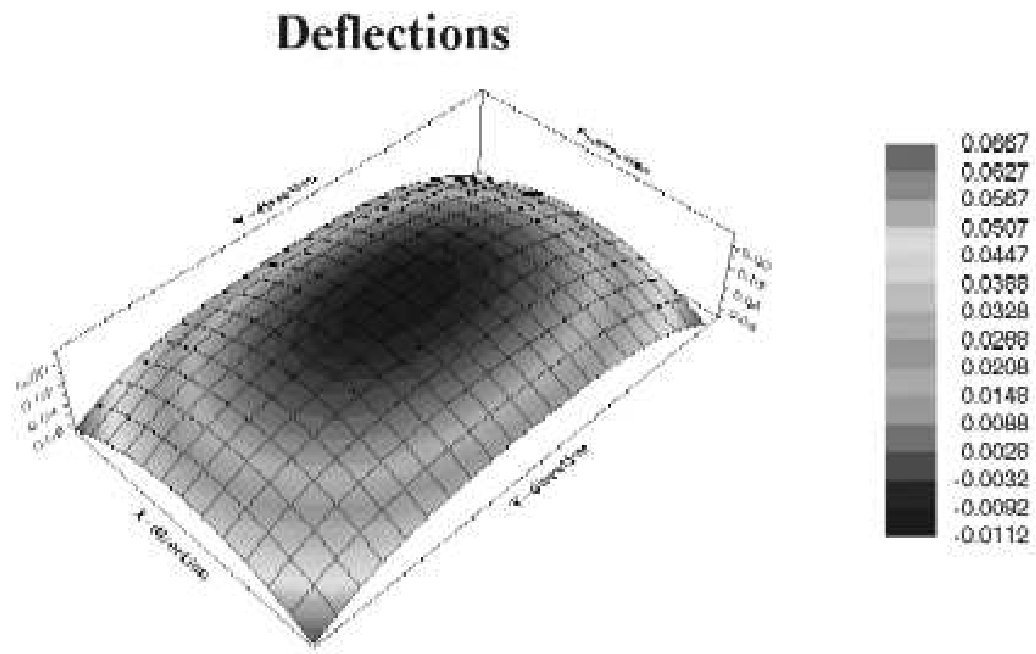


**Figure C-95: Graphical deflection results using ISLAB2000 (medium mesh)**

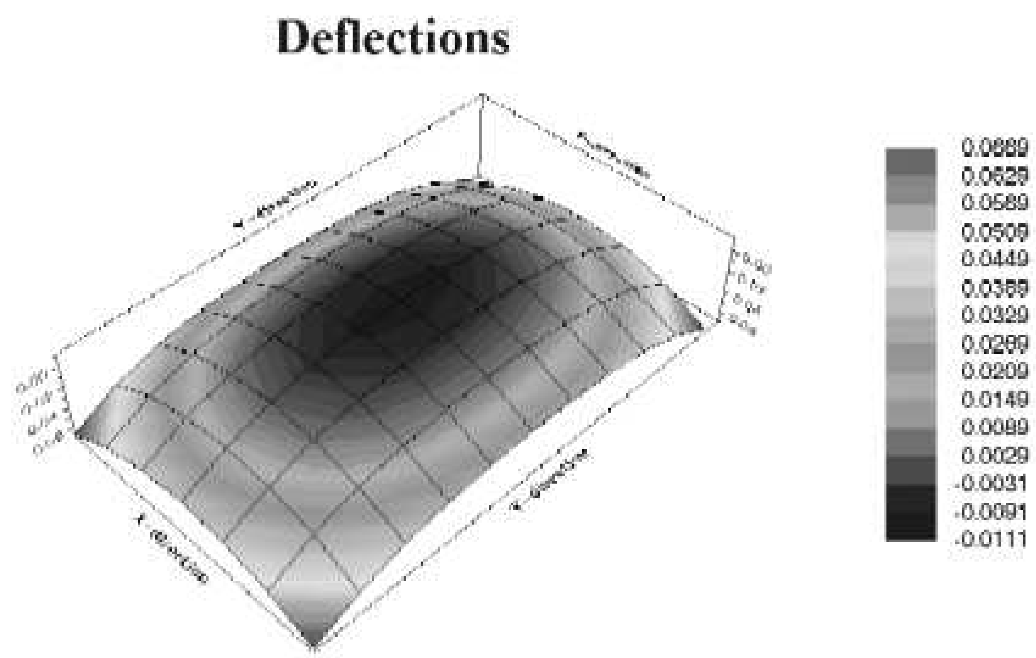


**Figure C-96: Graphical deflection results using ISLAB2000 (coarse mesh)**

**Problem 7** (Problem 4-2 page 204 in the textbook)

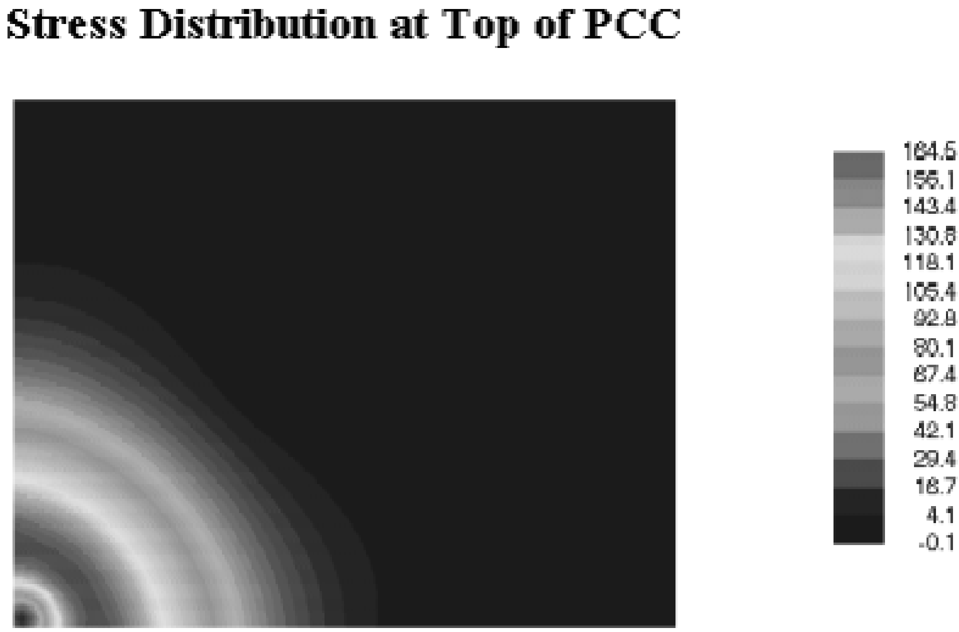


**Figure C-99: Graphical stress results using ISLAB2000 (fine mesh)**

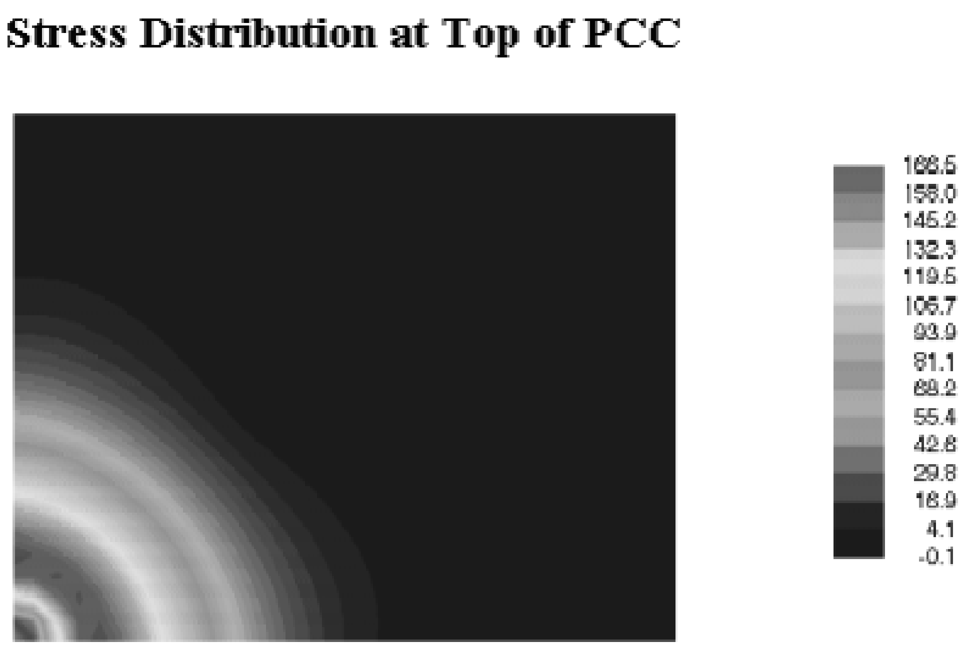


**Figure C-100: Graphical stress results using ISLAB2000 (medium mesh)**

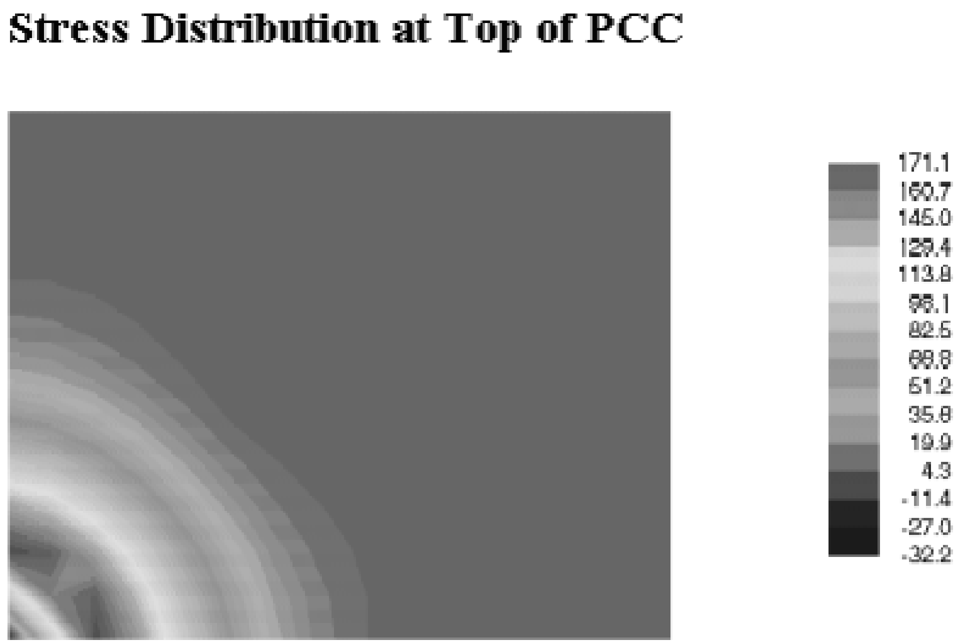


**Figure C-101: Graphical stress results using ISLAB2000 (coarse mesh)**

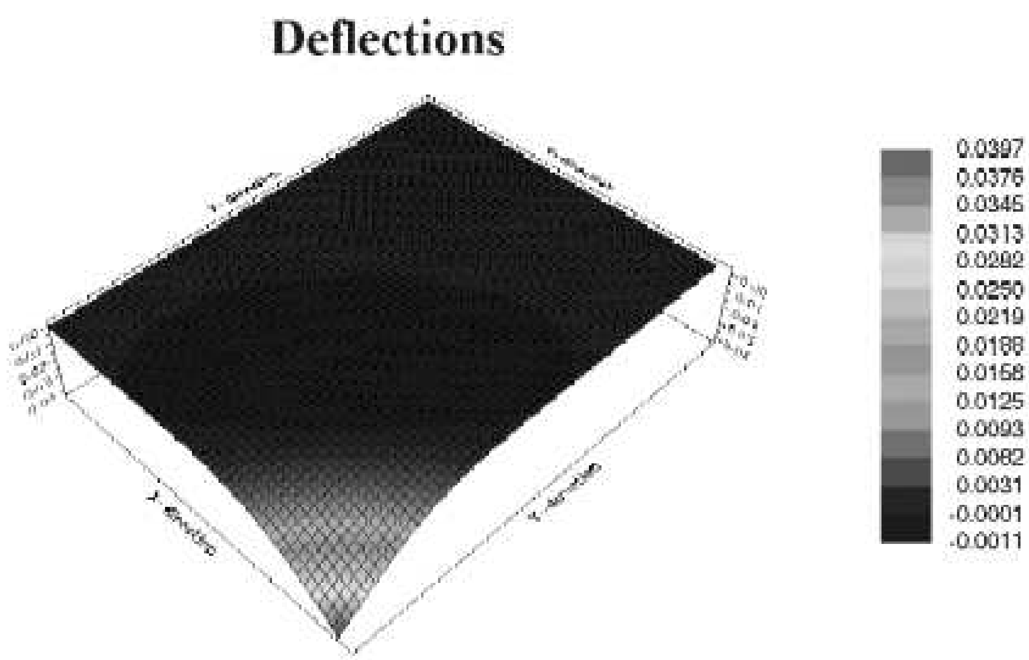


**Figure C-104: Graphical deflection results using ISLAB2000 (fine mesh)**

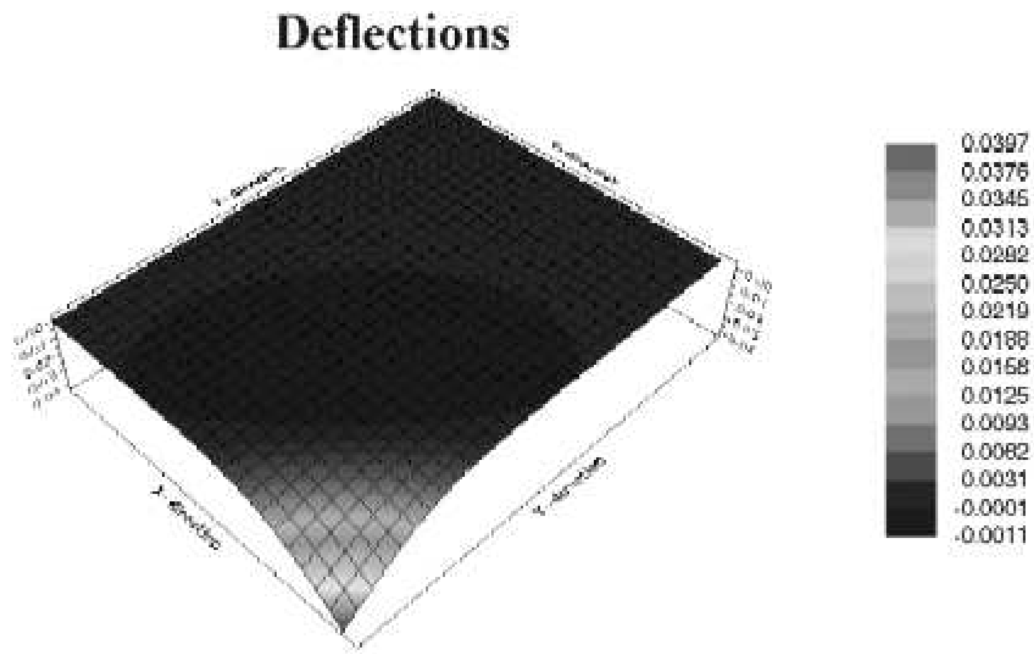


**Figure C-105: Graphical deflection results using ISLAB2000 (medium mesh)**

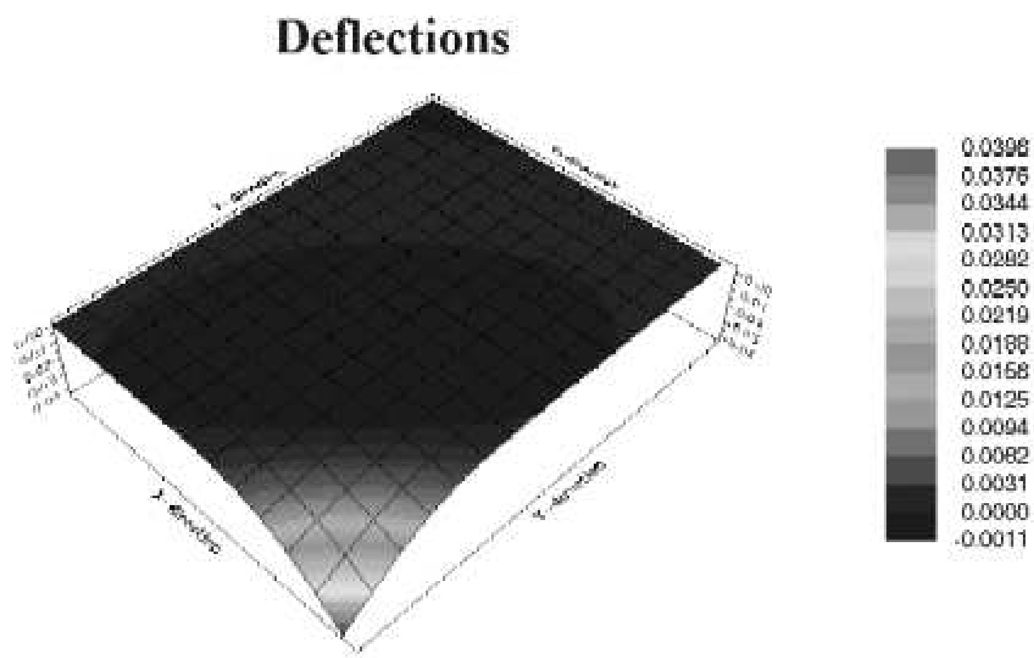


**Figure C-106: Graphical deflection results using ISLAB2000 (coarse mesh)**

**Problem 8** (Problem 4-3 page 204 in the textbook)

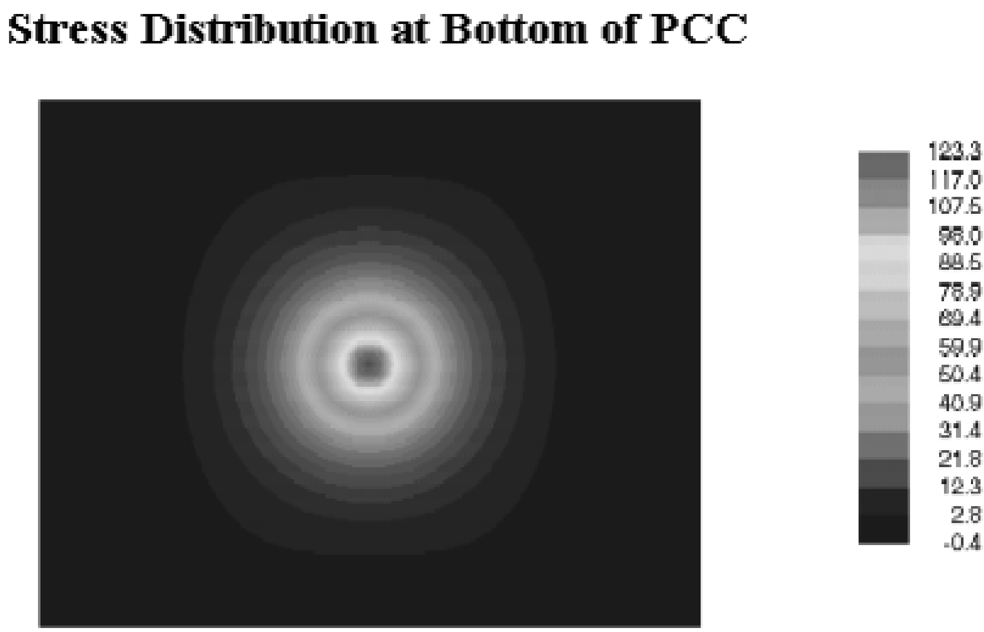


**Figure C-109: Graphical stress results using ISLAB2000 (fine mesh)**

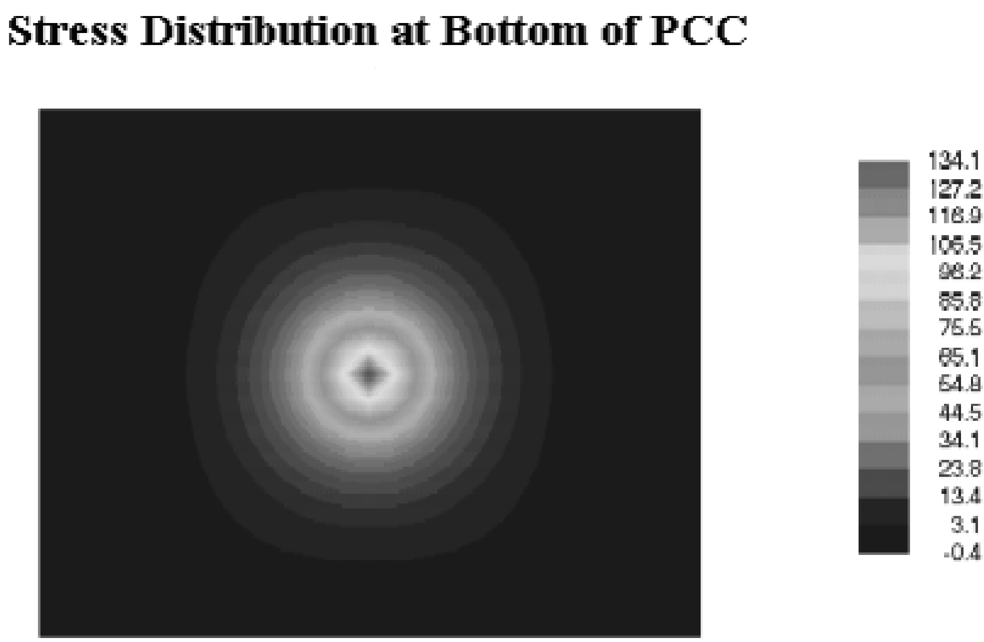


**Figure C-110: Graphical stress results using ISLAB2000 (medium mesh)**

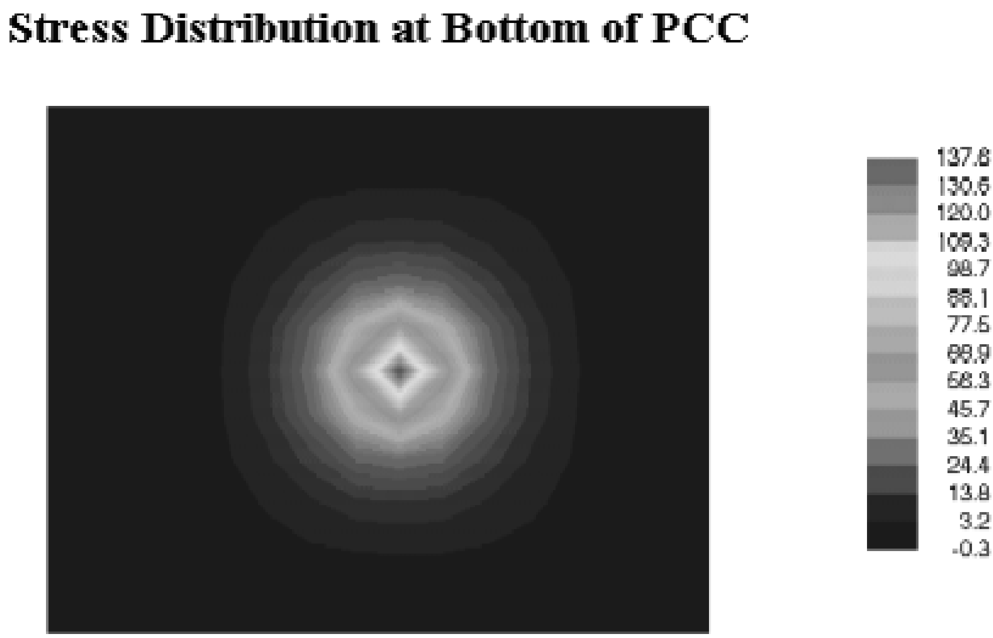


**Figure C-111: Graphical stress results using ISLAB2000 (coarse mesh)**

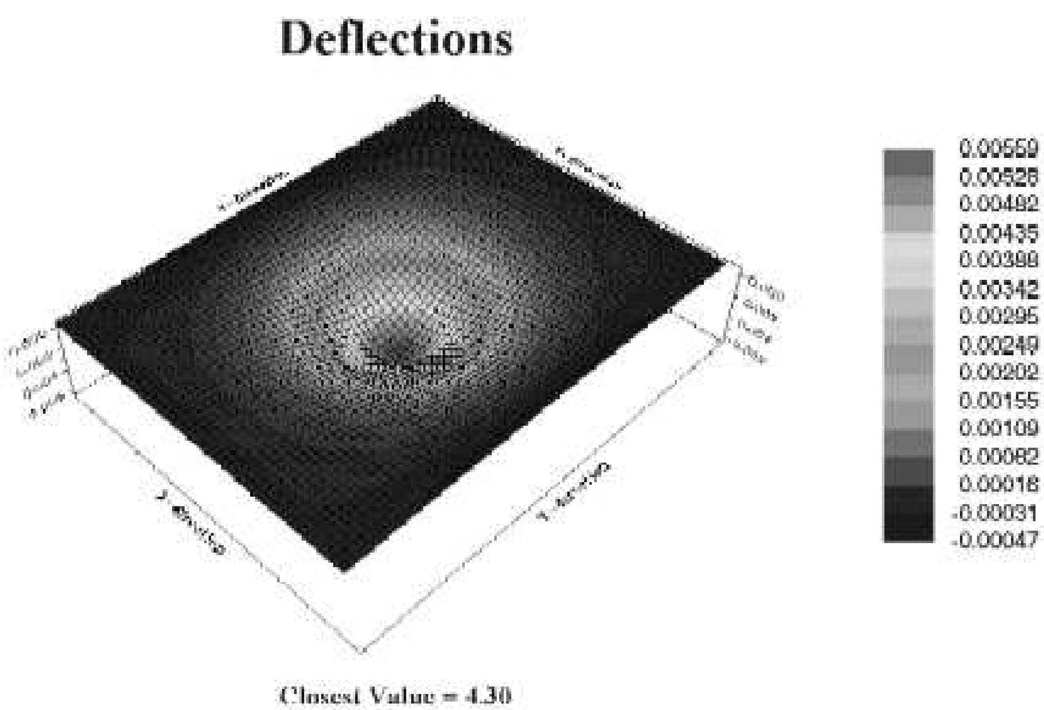


**Figure C-114: Graphical deflection results using ISLAB2000 (fine mesh)**

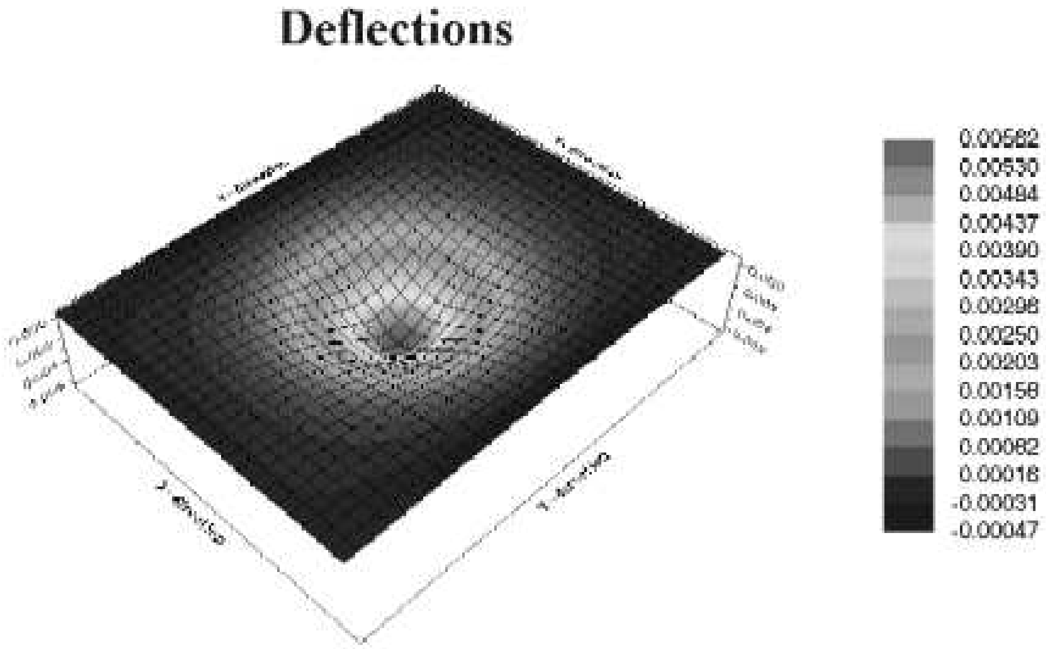


**Figure C-115: Graphical deflection results using ISLAB2000 (medium mesh)**

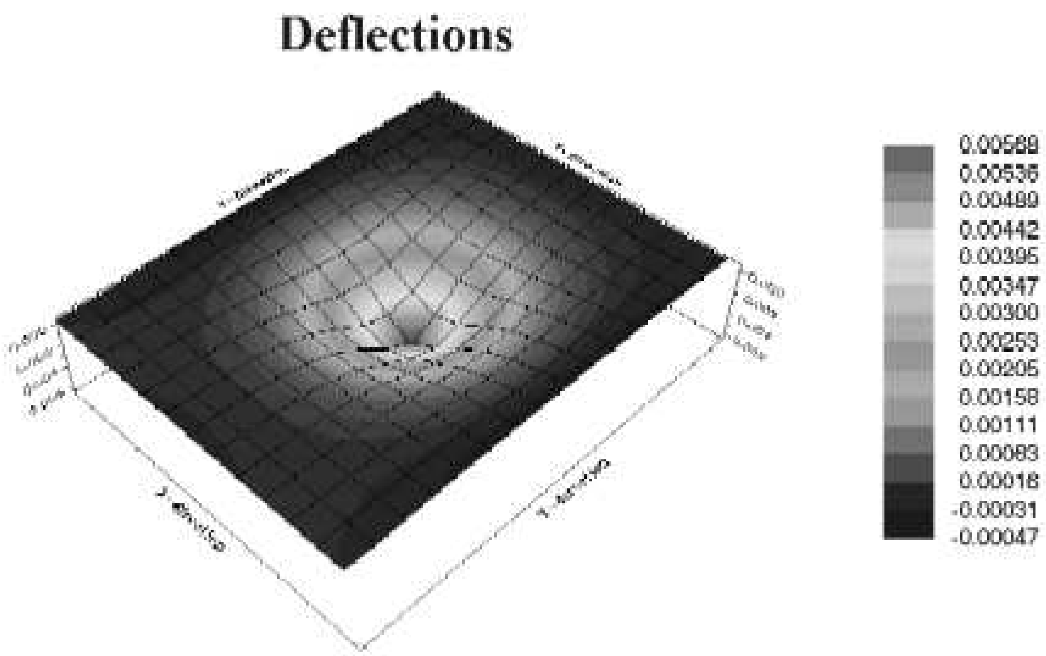


**Figure C-116: Graphical deflection results using ISLAB2000 (coarse mesh)**

**Problem 9** (Problem 4-4 page 204 in the textbook)

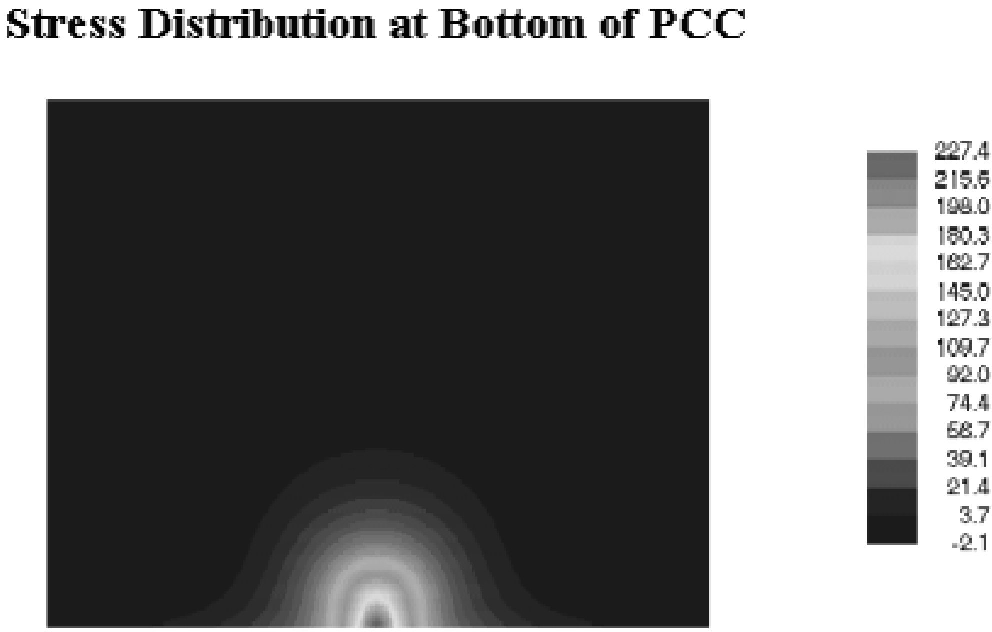


**Figure C-119: Graphical stress results using ISLAB2000 (fine mesh)**

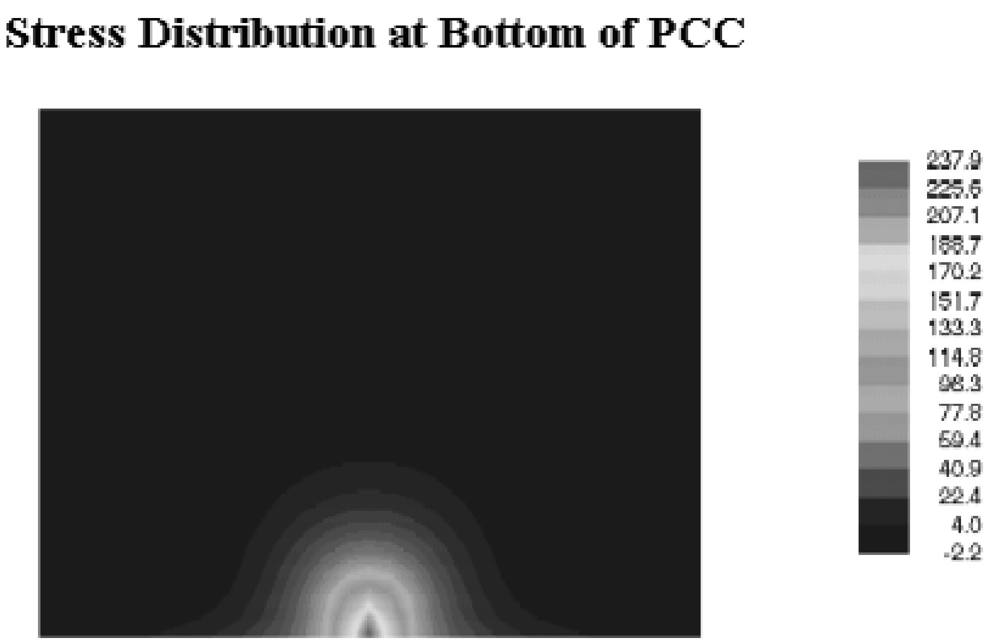


**Figure C-120: Graphical stress results using ISLAB2000 (medium mesh)**

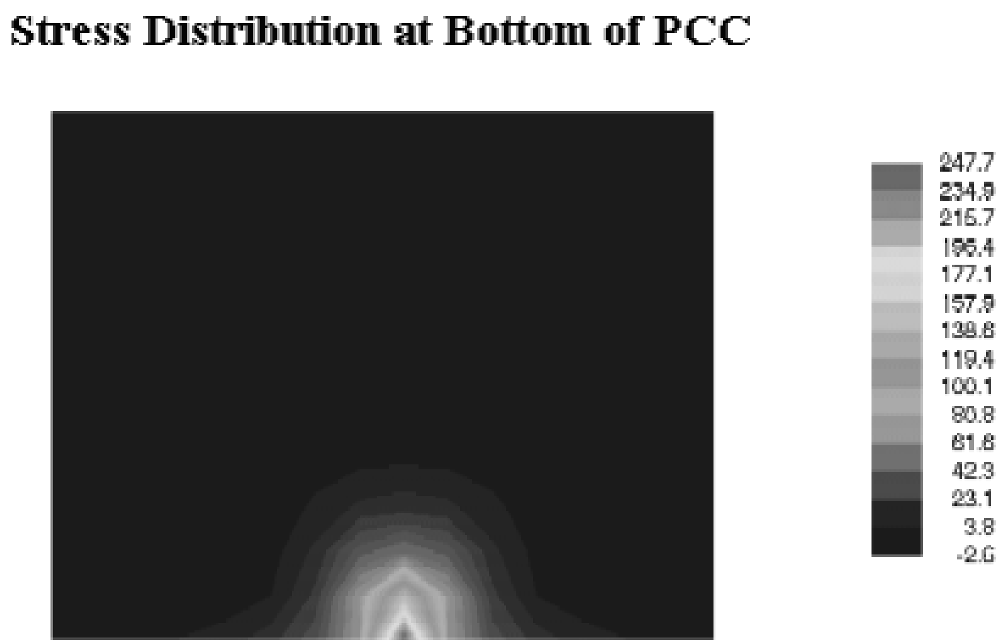


**Figure C-121: Graphical stress results using ISLAB2000 (coarse mesh)**

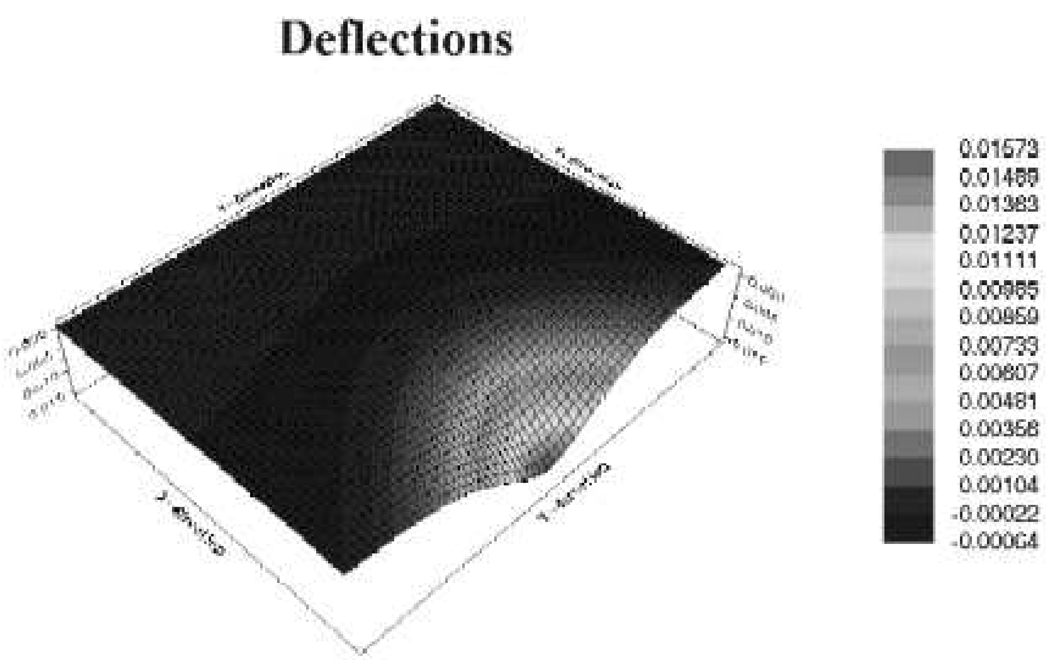


**Figure C-124: Graphical deflection results using ISLAB2000 (fine mesh)**

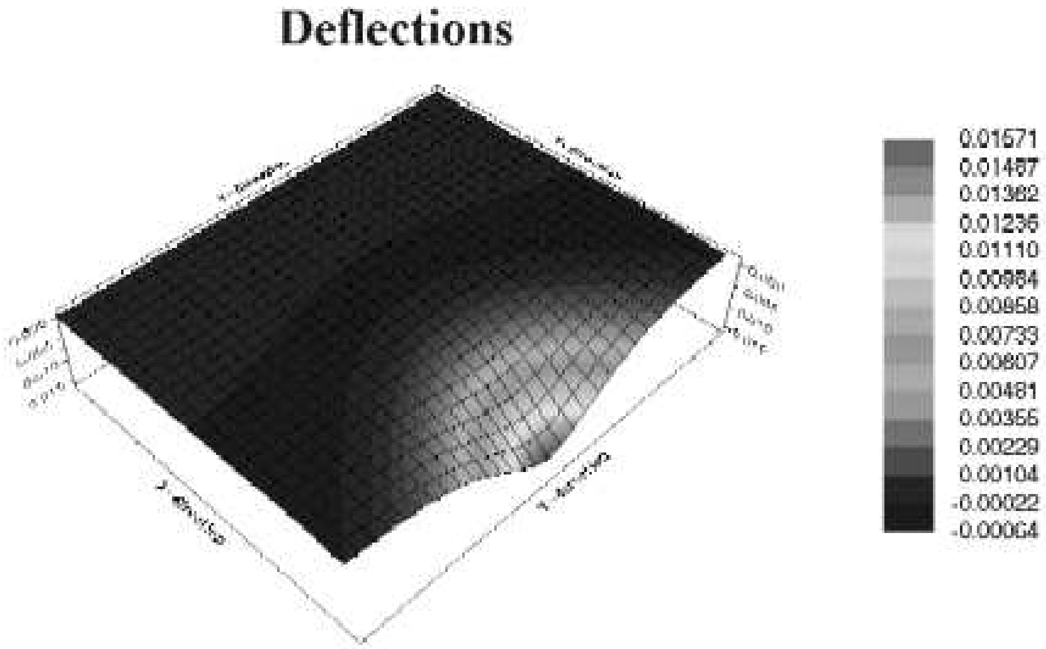


**Figure C-125: Graphical deflection results using ISLAB2000 (medium mesh)**

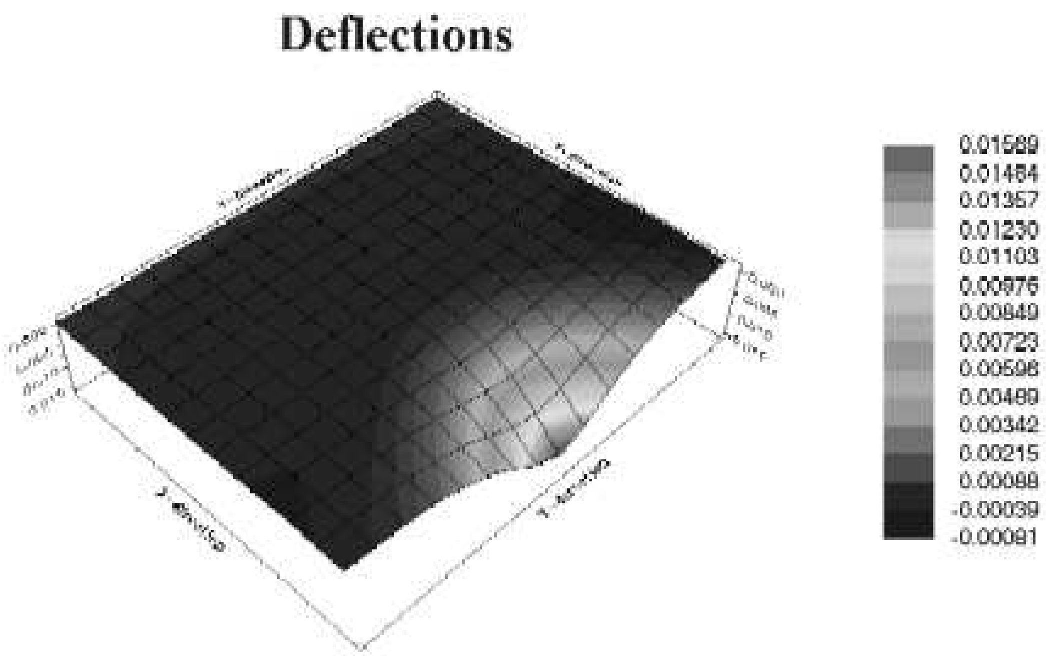


**Figure C-126: Graphical deflection results using ISLAB2000 (coarse mesh)**

# Appendix D

# Data Collection

**Table D-1: Descriptions of projects**

| Project No. | Alternative No. | Route | Pavement Type | C.S. | J.N. | Submitted Date |
|---|---|---|---|---|---|---|
| 1 | 2 | I-75 | JRCP | 82191 & 82194 | 45699 | 12-Jun-01 |
| 2 | 2A | I-96 | JRCP | 23152 | 45640 | 20-Mar-01 |
| | 2B | | JRCP | | | |
| | 2C | | JRCP | | | |
| 3 | 2 | I-69 | JPCP | 12033 & 12034 | 49921 | 16-Apr-01 |
| 4 | 2A | US-127 | JPCP | 38111 | 43497 | 27-Nov-00 |
| | 2B | | JPCP | | | |
| | 2C | | JPCP | | | |
| 5 | 2 | M-39 | JPCP | 82192 | 45702 | 5-Jul-00 |
| 6 | 2 | US-127 | JRCP | 82011 & 82061 | 45688 | 20-Mar-00 |
| 7 | 2 | US-24 | JRCP | 63031 | 45714 | 1-Nov-99 |
| 8 | 2 | I-96 | JPCP | 41024 | 51908 | 30-Aug-99 |
| 9 | 2 | I-496 | JRCP | 33045 | 51396 | 19-Jul-00 |
| 10 | 2 | I-75 | JRCP | 09034 & 09035 | 46575 | 1-Apr-00 |

**Table D-2: Summary of pavement data from MDOT**

| Proj. No. | Date | Route | Alt. No. | Pavement Type | PCC Thickness (mm) | | | Base Thickness (mm) | | |
|---|---|---|---|---|---|---|---|---|---|---|
| | | | | | Mainline | Outside Shoulder | Inside Shoulder | Mainline | Outside Shoulder | Inside Shoulder |
| 1 | 12-Jun-01 | I-75 | 2 | JRCP | 300 | 300 | 220 | 400 | 400 | 480 |
| 2 | 20-Mar-01 | I-96 | 2A | JRCP | 280 | AC | AC | 100 | NA | NA |
| | | | 2B | JRCP | 280 | AC | AC | 100 | NA | NA |
| | | | 2C | JRCP | 280 | AC | AC | 100 | NA | NA |
| 3 | 16-Apr-01 | I-69 | 2 | JPCP | 280 | AC | AC | 100 | NA | NA |
| 4 | 27-Nov-00 | US-127 | 2A | JPCP | 240 | AC | AC | 100 | NA | NA |
| | | | 2B | JPCP | 240 | AC | AC | 100 | NA | NA |
| | | | 2C | JPCP | 240 | AC | AC | 100 | NA | NA |
| 5 | 5-Jul-00 | M-39 | 2 | JPCP | 260 | Valley Gutter | Valley Gutter | 400 | NA | NA |
| 6 | 20-Mar-00 | US-127 | 2 | JRCP | 280 | 280 | 220 | 100 | 100 | 160 |
| 7 | 1-Nov-99 | US-24 | 2 | JRCP | 240 | Valley Gutter | Valley Gutter | 100 | NA | NA |
| 8 | 30-Aug-99 | I-96 | 2 | JPCP | 260 | AC | AC | 100 | NA | NA |
| 9 | 19-Jul-00 | I-496 | 2 | JRCP | 260 | 260 | 220 | 100 | 100 | 140 |
| 10 | 1-Apr-00 | I-75 | 2 | JRCP | 260 | 260 | 220 | 100 | 100 | 140 |

**Table D-2 (continued): Summary of pavement data from MDOT**

| Proj. No. | Date | Route | Alt. | Subbase1 | | Subbase2 | | MR of soils | Jt. Spa | Width (m) | DARWin Inputs | | | |
|---|---|---|---|---|---|---|---|---|---|---|---|---|---|---|
| | | | No. | Thickness | Type | Thickness | Type | (kPa) | (m) | Inner shoulder/lanes/outer shoulder | Sc (kPa) | E (kPa) | k-value (kPa/mm) | J |
| 1 | 12-Jun-01 | I-75 | 2 | NA | NA | NA | NA | 20,684 | 8 | 2.4/3.6/3.6/3.6/3.0 | 4,620 | 28,958,000 | 27 | 2.7 |
| 2 | 20-Mar-01 | I-96 | 2A | 300 | Sand | NA | NA | 22,260 | 8 | 3.0(AC)/3.6/3.6/3.6/3.0(AC) | 4,620 | 28,958,000 | 35 | 2.7 |
| | | | 2B | 46 | Sand | 254 | Ex. Subbase | 22,260 | 8 | 3.0(AC)/3.6/3.6/3.6/3.0(AC) | 4,620 | 28,958,000 | 35 | 2.7 |
| | | | 2C | 300 | Sand | NA | NA | 22,260 | 8 | 3.0(AC)/3.6/3.6/3.6/3.0(AC) | 4,620 | 28,958,000 | 35 | 2.7 |
| 3 | 16-Apr-01 | I-69 | 2 | 300 | Sand | NA | NA | 26,890 | 4.5 | 1.2(FSO)/3.6/4.2/2.4(FSO) | 4,620 | 28,958,000 | 46 | 2.7 |
| 4 | 27-Nov-00 | US-127 | 2A | 305 | Ex. Subbase | NA | NA | 31,000 | 4.5 | 1.2(FSO)/3.6/4.2/2.4(FSO) | 4,620 | 28,958,000 | 43 | 2.7 |
| | | | 2B | 182 | Sand | 305 | Ex. Subbase | 31,000 | 4.5 | 1.2(FSO)/3.6/4.2/2.4(FSO) | 4,620 | 28,958,000 | 43 | 2.7 |
| | | | 2C | 300 | Sand | NA | NA | 31,000 | 4.5 | 1.2(FSO)/3.6/4.2/2.4(FSO) | 4,620 | 28,958,000 | 43 | 2.7 |
| 5 | 5-Jul-00 | M-39 | 2 | NA | NA | NA | NA | 24,475 | 4.5 | NA/3.6/3.6/3.6/NA | 4,620 | 28,958,000 | 60 | 2.7 |
| 6 | 20-Mar-00 | US-127 | 2 | 300 | Sand | NA | NA | 20,680 | 8 | 1.5/3.6/3.6/3.0 | 4,620 | 28,958,000 | 35 | 2.7 |
| 7 | 1-Nov-99 | US-24 | 2 | 300 | Sand | 452 | Ex. Subbase | 20,684 | 8 | 3.658/3.658/3.658/3.658 | 4,620 | 28,958,000 | 38 | 2.7 |
| 8 | 30-Aug-99 | I-96 | 2 | 280 | Ex. Sand | NA | NA | 26,200 | 4.5 | 1.2(AC)/3.6/3.6/3.0(AC) | 4,620 | 28,958,000 | 43 | 2.7 |
| 9 | 19-Jul-00 | I-496 | 2 | 219 | Ex. Subbase | NA | NA | 20,684 | 8 | 2.4/3.6/3.6/3.6/3.0 | 4,620 | 28,958,000 | 24 | 2.7 |
| 10 | 1-Apr-00 | I-75 | 2 | 300 | Sand | NA | NA | 27,500 | 8 | 2.4/3.6/3.6/3.6/3.6 | 4,620 | 28,958,000 | 41 | 2.7 |

**Table D-3: Source of input**

| Inputs | MDOT | Other sources |
|---|---|---|
| Slab width (outer), in | ✔ | |
| Slab width (next to outer), in | ✔ | |
| Outer shoulder width (if PCC), in | ✔ | |
| Outer shoulder width (if AC), in | ✔ | |
| Joint spacing, in. | ✔ | |
| PCC thickness, in | ✔ | |
| PCC elastic modulus, psi | ✔ | |
| PCC CTE, in./in./°F | | ✔ |
| PCC unit weight, lb/in$^3$ | | ✔ |
| PCC Poisson's ratio | | ✔ |
| AC elastic modulus (AC shoulder), psi | | ✔ |
| Interface condition | | ✔ |
| Base thickness, in | ✔ | |
| Base elastic modulus, psi | | ✔ |
| Base CTE, in./in./°F | | ✔ |
| Base unit weight, lb/in$^3$ | | ✔ |
| Base Poisson's ratio | | ✔ |
| Subbase thickness, in | ✔ | |
| Subbase elastic modulus, psi | | ✔ |
| Subbase CTE, in./in./°F | | ✔ |
| Subbase unit weight, lb/in$^3$ | | ✔ |
| Subbase Poisson's ratio | | ✔ |
| k-value, psi/in | ✔ | |
| Dowel bar diameter, in. | ✔ | |
| Dowel bar spacing, in. | ✔ | |
| LTE lane/lane (AGG), psi | | ✔ |
| LTE lane/shoulder (AGG), psi | | ✔ |
| Total | 12 | 15 |

**Table D-4: Additional inputs used in ISLAB2000 analysis**

| Inputs | Possible Range | | Selected Value | Reason for Selection |
|---|---|---|---|---|
| | Min. | Max. | | |
| PCC CTE, in./in./$^oF$ | $3.3x10^{-6}$ | $6.7x10^{-6}$ | $5.0x10^{-6}$ | typical value |
| PCC unit weight, lb/in$^3$ | 0.070 | 0.104 | 0.087 | typical value (150 pcf) |
| PCC Poisson's ratio | 0.15 | 0.20 | 0.15 | typical value |
| AC elastic modulus (AC shoulder), psi | 300,000 | 600,000 | 300,000 | conservative value |
| Interface condition | unbonded | bonded | unbonded | untreated granular base |
| Base elastic modulus, psi | 15,000 | 45,000 | 30,000 | typical value |
| Base CTE, in./in./$^oF$ | $3.0x10^{-6}$ | $6.0x10^{-6}$ | $3.0x10^{-6}$ | typical value for limestone |
| Base unit weight, lb/in$^3$ | 0.049 | 0.070 | 0.061 | typical value (105 pcf) |
| Base Poisson's ratio | 0.30 | 0.40 | 0.35 | typical value |
| Subbase elastic modulus, psi | 10,000 | 25,000 | 15,000 | typical value for sand |
| Subbase CTE, in./in./$^oF$ | $3.0x10^{-6}$ | $6.0x10^{-6}$ | $3.0x10^{-6}$ | typical value for sand |
| Subbase unit weight, lb/in$^3$ | 0.049 | 0.070 | 0.061 | typical value (105 pcf) |
| Subbase Poisson's ratio | 0.30 | 0.45 | 0.35 | typical value |
| LTE lane/lane (AGG), psi | 1,000 | 1,000,000 | 1,000,000 | high aggregate interlock |
| LTE lane/shoulder (AGG), psi | 1,000 | 1,000,000 | 1,000 (AC shoulder) | low aggregate interlock |
| | | | 1,000,000 (PCC shoulder) | high aggregate interlock |

## Table D-5: Summary of inputs used in ISLAB2000 analysis

| Group | Subgroup | Inputs | 1/2 | 2/2A | 2/2B | 2/2C | 3/2 | 4/2A | 4/2B |
|---|---|---|---|---|---|---|---|---|---|
| | | Slab width (outer), in | 142 | 142 | 142 | 142 | 165 | 165 | 165 |
| | | Slab width (next to outer), in | 142 | 142 | 142 | 142 | 142 | 142 | 142 |
| | | Outer shoulder width (if PCC), in | 118 | 0 | 0 | 0 | 0 | 0 | 0 |
| | | Outer shoulder width (if AC), in | 0 | 118 | 118 | 118 | 94 | 94 | 94 |
| | | Joint spacing, in. | 315 | 315 | 315 | 315 | 177 | 177 | 177 |
| | | PCC thickness, in | 12 | 11 | 11 | 11 | 11 | 9 | 9 |
| | | PCC elastic modulus, psi | 4.2x10$^{6}$ | 4.2x10$^{6}$ | 4.2x10$^{6}$ | 4.2x10$^{6}$ | 4.2x10$^{6}$ | 4.2x10$^{6}$ | 4.2x10$^{6}$ |
| | | PCC CTE, in./in./$^{o}$F | 5.0x10$^{-6}$ | 5.0x10$^{-6}$ | 5.0x10$^{-6}$ | 5.0x10$^{-6}$ | 5.0x10$^{-6}$ | 5.0x10$^{-6}$ | 5.0x10$^{-6}$ |
| | | PCC unit weight, lb/in$^{2}$ | 0.087 | 0.087 | 0.087 | 0.087 | 0.087 | 0.087 | 0.087 |
| | | PCC Poisson's ratio | 0.15 | 0.15 | 0.15 | 0.15 | 0.15 | 0.15 | 0.15 |
| | | AC elastic modulus (for AC shoulder), psi | 0 | 300,000 | 300,000 | 300,000 | 300,000 | 300,000 | 300,000 |
| | | Interface condition | unbonded | unbonded | unbonded | unbonded | unbonded | unbonded | unbonded |
| Most realistic simulation | | Base thickness, in | 15.75 | 3.94 | 3.94 | 3.94 | 3.94 | 3.94 | 3.94 |
| | | Base elastic modulus, psi | 30,000 | 30,000 | 30,000 | 30,000 | 30,000 | 30,000 | 30,000 |
| | | Base CTE, in./in./$^{o}$F | 2.0x10$^{-6}$ | 2.0x10$^{-6}$ | 2.0x10$^{-6}$ | 2.0x10$^{-6}$ | 2.0x10$^{-6}$ | 2.0x10$^{-6}$ | 2.0x10$^{-6}$ |
| | | Base unit weight, lb/in$^{3}$ | 0.061 | 0.061 | 0.061 | 0.061 | 0.061 | 0.061 | 0.061 |
| | | Base Poisson't ratio | 0.35 | 0.35 | 0.35 | 0.35 | 0.35 | 0.35 | 0.35 |
| | | Subbase thickness, in | 0.0 | 11.8 | 11.8 | 11.8 | 11.8 | 12.0 | 19.2 |
| | | Subbase elastic modulus, psi | 15,000 | 15,000 | 15,000 | 15,000 | 15,000 | 15,000 | 15,000 |
| | | Subbase CTE, in./in./$^{o}$F | 2.0x10$^{-6}$ | 2.0x10$^{-6}$ | 2.0x10$^{-6}$ | 2.0x10$^{-6}$ | 2.0x10$^{-6}$ | 2.0x10$^{-6}$ | 2.0x10$^{-6}$ |
| | | Subbase unit weight, lb/in$^{3}$ | 0.061 | 0.061 | 0.061 | 0.061 | 0.061 | 0.061 | 0.061 |
| | | Subbase Poisson's ratio | 0.35 | 0.35 | 0.35 | 0.35 | 0.35 | 0.35 | 0.35 |
| Simplified simulation | Combined base/subbase | Base/subbase thickness, in | 15.75 | 9.60 | 9.60 | 9.60 | 9.60 | 9.75 | 15.31 |
| | | Base/subbase elastic modulus, psi | 30,000 | 30,000 | 30,000 | 30,000 | 30,000 | 30,000 | 30,000 |
| | | Base/subbase CTE, in./in./$^{o}$F | 2.0x10$^{-6}$ | 2.0x10$^{-6}$ | 2.0x10$^{-6}$ | 2.0x10$^{-6}$ | 2.0x10$^{-6}$ | 2.0x10$^{-6}$ | 2.0x10$^{-6}$ |
| | | Base/subbase unit weight, lb/in3 | 0.061 | 0.061 | 0.061 | 0.061 | 0.061 | 0.061 | 0.061 |
| | | Base/subbase Poisson's ratio | 0.35 | 0.35 | 0.35 | 0.35 | 0.35 | 0.35 | 0.35 |
| | No subbase layer | Base thickness, in | 15.75 | 3.94 | 3.94 | 3.94 | 3.94 | 3.94 | 3.94 |
| | | Base elastic modulus, psi | 30,000 | 30,000 | 30,000 | 30,000 | 30,000 | 30,000 | 30,000 |
| | | Base CTE, in./in./$^{o}$F | 2.0x10$^{-6}$ | 2.0x10$^{-6}$ | 2.0x10$^{-6}$ | 2.0x10$^{-6}$ | 2.0x10$^{-6}$ | 2.0x10$^{-6}$ | 2.0x10$^{-6}$ |
| | | Base unit weight, lb/in$^{3}$ | 0.061 | 0.061 | 0.061 | 0.061 | 0.061 | 0.061 | 0.061 |
| | | Base Poisson't ratio | 0.35 | 0.35 | 0.35 | 0.35 | 0.35 | 0.35 | 0.35 |
| | | Subbase layer | No | No | No | No | No | No | No |
| | | k-value, psi/in | 99.5 | 128.9 | 128.9 | 128.9 | 169.5 | 158.4 | 158.4 |
| | | Dowel bar diameter, in. | 1.25 | 1.25 | 1.25 | 1.25 | 1.25 | 1.25 | 1.25 |
| | | Dowel bar spacing, in. | 12 | 12 | 12 | 12 | 12 | 12 | 12 |
| | | Dowel bar in shoulder | No | No | No | No | No | No | No |
| | | LTE lane/lane (AGG), psi | 1x10$^{6}$ | 1x10$^{6}$ | 1x10$^{6}$ | 1x10$^{6}$ | 1x10$^{6}$ | 1x10$^{6}$ | 1x10$^{6}$ |
| | | LTE lane/shoulder (AGG), psi | 1x10$^{6}$ | 1,000 | 1,000 | 1,000 | 1,000 | 1,000 | 1,000 |

**Table D-5: Summary of inputs used in ISLAB2000 analysis (continued)**

| | | Inputs | 4/2C | 5/2 | 6/2 | 7/2 | 8/2 | 9/2 | 10/2 |
|---|---|---|---|---|---|---|---|---|---|
| | | Slab width (outer), in | 165 | 142 | 142 | 144 | 142 | 142 | 142 |
| | | Slab width (next to outer), in | 142 | 142 | 142 | 144 | 142 | 142 | 142 |
| | | Outer shoulder width (if PCC), in | 0 | 12 | 118 | 12 | 0 | 118 | 142 |
| | | Outer shoulder width (if AC), in | 94 | 0 | 0 | 0 | 118 | 0 | 0 |
| | | Joint spacing, in. | 177 | 177 | 315 | 315 | 177 | 315 | 315 |
| | | PCC thickness, in | 9 | 10 | 11 | 9 | 10 | 10 | 10 |
| | | PCC elastic modulus, psi | $4.2x10^6$ | $4.2x10^6$ | $4.2x10^6$ | $4.2x10^6$ | $4.2x10^6$ | $4.2x10^6$ | $4.2x10^6$ |
| | | PCC CTE, in./in./$^o$F | $5.0x10^{-6}$ | $5.0x10^{-6}$ | $5.0x10^{-6}$ | $5.0x10^{-6}$ | $5.0x10^{-6}$ | $5.0x10^{-6}$ | $5.0x10^{-6}$ |
| | | PCC unit weight, lb/in$^2$ | 0.087 | 0.087 | 0.087 | 0.087 | 0.087 | 0.087 | 0.087 |
| | | PCC Poisson's ratio | 0.15 | 0.15 | 0.15 | 0.15 | 0.15 | 0.15 | 0.15 |
| | | AC elastic modulus (for AC shoulder), psi | 300,000 | 0 | 0 | 0 | 300,000 | 0 | 0 |
| | | Interface condition | unbonded | unbonded | unbonded | unbonded | unbonded | unbonded | unbonded |
| Most realistic simulation | | Base thickness, in | 3.94 | 15.75 | 3.94 | 3.94 | 3.94 | 3.94 | 3.94 |
| | | Base elastic modulus, psi | 30,000 | 30,000 | 30,000 | 30,000 | 30,000 | 30,000 | 30,000 |
| | | Base CTE, in./in./$^o$F | $2.0x10^{-6}$ | $2.0x10^{-6}$ | $2.0x10^{-6}$ | $2.0x10^{-6}$ | $2.0x10^{-6}$ | $2.0x10^{-6}$ | $2.0x10^{-6}$ |
| | | Base unit weight, lb/in$^3$ | 0.061 | 0.061 | 0.061 | 0.061 | 0.061 | 0.061 | 0.061 |
| | | Base Poisson't ratio | 0.35 | 0.35 | 0.35 | 0.35 | 0.35 | 0.35 | 0.35 |
| | | Subbase thickness, in | 11.8 | 0.0 | 11.8 | 29.6 | 11.0 | 8.6 | 11.8 |
| | | Subbase elastic modulus, psi | 15,000 | 15,000 | 15,000 | 15,000 | 15,000 | 15,000 | 15,000 |
| | | Subbase CTE, in./in./$^o$F | $2.0x10^{-6}$ | $2.0x10^{-6}$ | $2.0x10^{-6}$ | $2.0x10^{-6}$ | $2.0x10^{-6}$ | $2.0x10^{-6}$ | $2.0x10^{-6}$ |
| | | Subbase unit weight, lb/in$^3$ | 0.061 | 0.061 | 0.061 | 0.061 | 0.061 | 0.061 | 0.061 |
| | | Subbase Poisson's ratio | 0.35 | 0.35 | 0.35 | 0.35 | 0.35 | 0.35 | 0.35 |
| Simplified simulation | Combined base/subbase | Base/subbase thickness, in | 9.60 | 15.75 | 9.60 | 23.54 | 9.01 | 7.25 | 9.60 |
| | | Base/subbase elastic modulus, psi | 30,000 | 30,000 | 30,000 | 30,000 | 30,000 | 30,000 | 30,000 |
| | | Base/subbase CTE, in./in./$^o$F | $2.0x10^{-6}$ | $2.0x10^{-6}$ | $2.0x10^{-6}$ | $2.0x10^{-6}$ | $2.0x10^{-6}$ | $2.0x10^{-6}$ | $2.0x10^{-6}$ |
| | | Base/subbase unit weight, lb/in3 | 0.061 | 0.061 | 0.061 | 0.061 | 0.061 | 0.061 | 0.061 |
| | | Base/subbase Poisson's ratio | 0.35 | 0.35 | 0.35 | 0.35 | 0.35 | 0.35 | 0.35 |
| | No subbase layer | Base thickness, in | 3.94 | 15.75 | 3.94 | 3.94 | 3.94 | 3.94 | 3.94 |
| | | Base elastic modulus, psi | 30,000 | 30,000 | 30,000 | 30,000 | 30,000 | 30,000 | 30,000 |
| | | Base CTE, in./in./$^o$F | $2.0x10^{-6}$ | $2.0x10^{-6}$ | $2.0x10^{-6}$ | $2.0x10^{-6}$ | $2.0x10^{-6}$ | $2.0x10^{-6}$ | $2.0x10^{-6}$ |
| | | Base unit weight, lb/in$^3$ | 0.061 | 0.061 | 0.061 | 0.061 | 0.061 | 0.061 | 0.061 |
| | | Base Poisson't ratio | 0.35 | 0.35 | 0.35 | 0.35 | 0.35 | 0.35 | 0.35 |
| | | Subbase layer | No | No | No | No | No | No | No |
| | | k-value, psi/in | 158.4 | 221.0 | 128.9 | 140.0 | 158.4 | 88.4 | 151.0 |
| | | Dowel bar diameter, in. | 1.25 | 1.25 | 1.25 | 1.25 | 1.25 | 1.25 | 1.25 |
| | | Dowel bar spacing, in. | 12 | 12 | 12 | 12 | 12 | 12 | 12 |
| | | Dowel bar in shoulder | No | No | No | No | No | No | No |
| | | LTE lane/lane (AGG), psi | $1x10^6$ | $1x10^6$ | $1x10^6$ | $1x10^6$ | $1x10^6$ | $1x10^6$ | $1x10^6$ |
| | | LTE lane/shoulder (AGG), psi | 1,000 | $1x10^6$ | $1x10^6$ | $1x10^6$ | 1,000 | $1x10^6$ | $1x10^6$ |

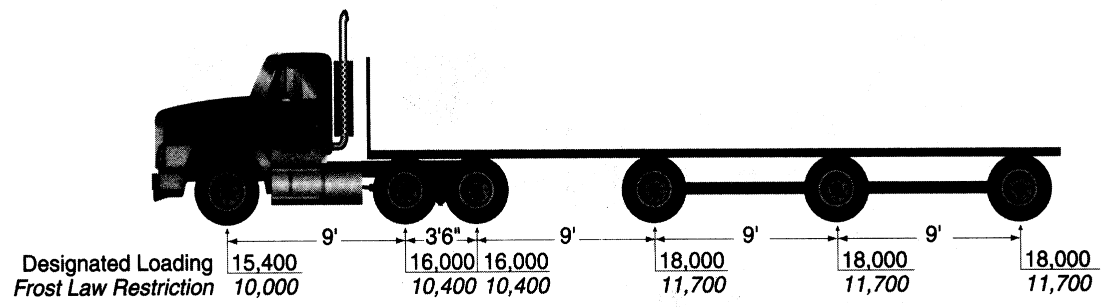


**Figure D-1: Example of truck configuration (MI-9)**

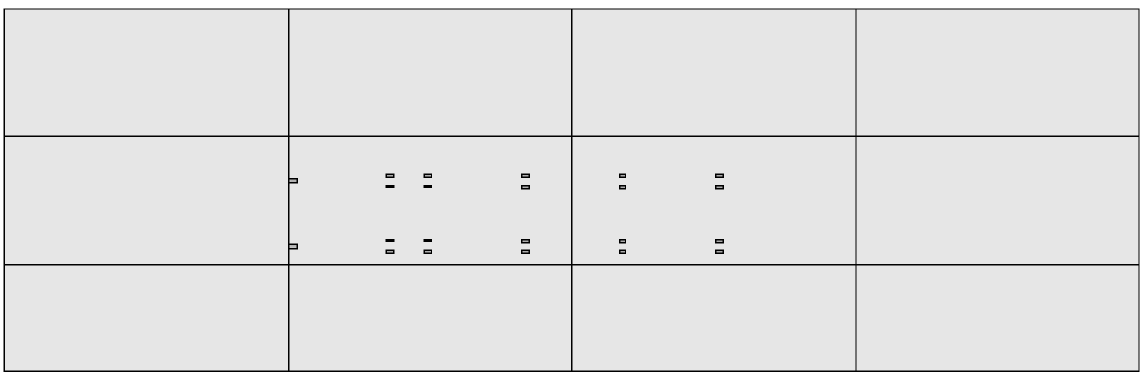

**Figure D-2: Example of pavement feature with PCC/AC shoulder in ISLAB2000 analysis**

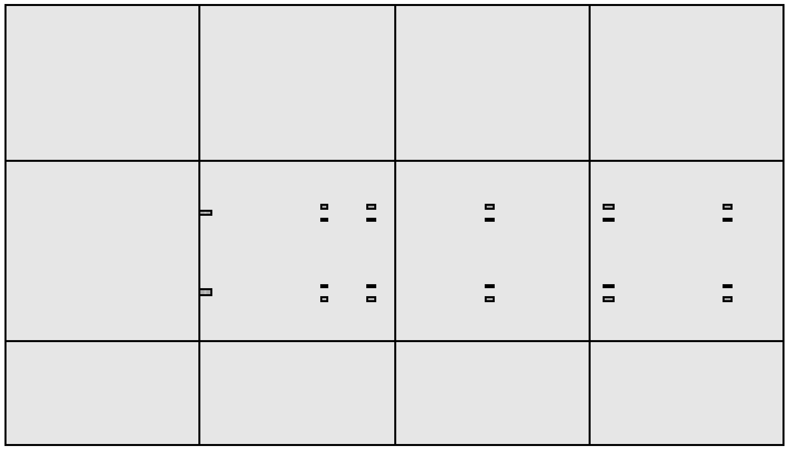

**Figure D-3: Example of pavement feature with widened lane in ISLAB2000 analysis**

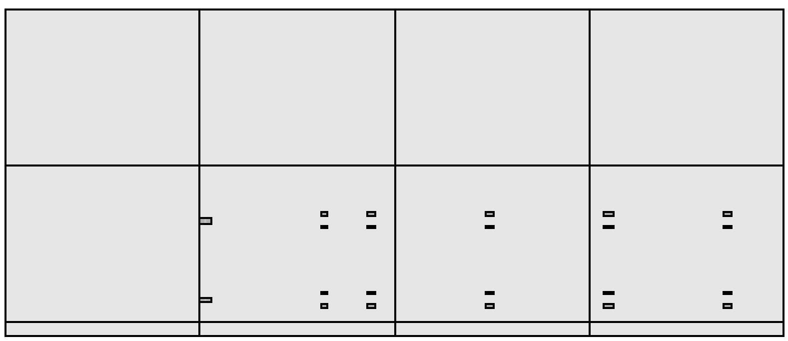

**Figure D-4: Example of pavement feature with valley gutter in ISLAB2000 analysis**

# Appendix E

## Validation of the Product $\alpha(\Delta T/D)$

**Table E- 1: Experimental matrix**

| | Validation#1 | Validation#2 | Validation#3 | Validation#4 | Validation#5 | Validation#6 | Validation#7 | Validation#8 | Validation#9 |
|---|---|---|---|---|---|---|---|---|---|
| Shoulder Type | PCC | AC | Widened Lane | PCC | AC | Widened Lane | PCC | AC | Widened Lane |
| PCC thickness, in. | 10" | 10" | 10" | 12" | 12" | 12" | 8" | 8" | 8" |
| Base/subbase thickness, in. | 16" | 26" | 4" | 26" | 4" | 16" | 4" | 16" | 26" |
| k-value, psi/in. | 100 | 30 | 200 | 200 | 100 | 30 | 30 | 200 | 100 |
| Loading type | Single Axle | Tandem Axle | Multi-Axle (8) | Tandem Axle | Multi-Axle (8) | Single Axle | Multi-Axle (8) | Single Axle | Tandem Axle |
| Joint spacing, in. | 177 | 315 | 315 | 177 | 177 | 315 | 315 | 177 | 177 |

**Table E- 2: Validation#1**

| $\alpha(\Delta T/D)$ ($10^{-6}$ in.$^{-1}$) | Analysis 1 | | | | | Analysis 2 | | | | |
|---|---|---|---|---|---|---|---|---|---|---|
| | Gradient (°F/in.) | CTE ($10^{-6}$ in./in./°F) | $\sigma_{long,bottom}$ (psi) | $\sigma_{trans,bottom}$ (psi) | $\sigma_{long,top}$ (psi) | Gradient (°F/in.) | CTE ($10^{-6}$ in./in./°F) | $\sigma_{long,bottom}$ (psi) | $\sigma_{trans,bottom}$ (psi) | $\sigma_{long,top}$ (psi) |
| 0.0 | +2 or -2 | 0.10 | 118.2 | 76.0 | 75.6 | 0 | 5.00 | 116.1 | 74.8 | 74.0 |
| 2.5 | +2 or -2 | 1.25 | 141.9 | 89.4 | 94.5 | +0.5 or -0.5 | 5.00 | 141.9 | 89.4 | 94.5 |
| 5.0 | +2 or -2 | 2.50 | 167.7 | 104.0 | 115.1 | +1 or -1 | 5.00 | 167.7 | 104.0 | 115.1 |
| 7.5 | +2 or -2 | 3.75 | 193.4 | 118.6 | 135.6 | +1.5 or -1.5 | 5.00 | 193.4 | 118.6 | 135.6 |
| 10.0 | +2 or -2 | 5.00 | 219.2 | 133.2 | 156.2 | +2 or -2 | 5.00 | 219.2 | 133.2 | 156.2 |
| 12.5 | +2 or -2 | 6.25 | 245.2 | 149.7 | 177.3 | +2.5 or -2.5 | 5.00 | 245.2 | 149.7 | 177.3 |
| 15.0 | +2 or -2 | 7.50 | 271.2 | 166.3 | 198.3 | +3 or -3 | 5.00 | 271.2 | 166.3 | 198.3 |
| 17.5 | +2 or -2 | 8.75 | 297.2 | 182.8 | 219.4 | +3.5 or -3.5 | 5.00 | 297.2 | 182.8 | 219.4 |
| 20.0 | +2 or -2 | 10.00 | 323.2 | 199.3 | 240.4 | +4 or -4 | 5.00 | 323.2 | 199.3 | 240.4 |

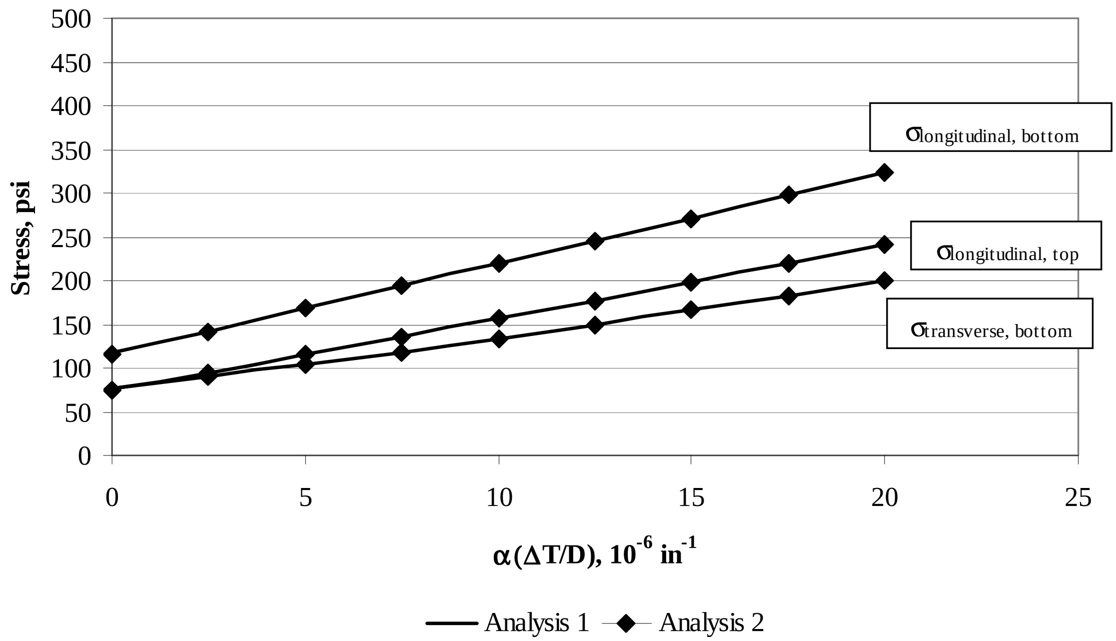


**Figure E- 1: Plot of validation#1**

Analysis 1: Constant temperature gradient (+2 °F/in.) with variation of CTE ($0.1 \times 10^{-6}$ to $10 \times 10^{-6}$ in./in./°F)

Analysis 2: Constant CTE ($5 \times 10^{-6}$ in./in./°F) with variation of temperature gradient (0 to +4 °F/in.)

- Shoulder type: PCC
- PCC thickness: 10”
- Base/subbase thickness: 16”
- k-value: 100 psi/in.
- Loading type: single axle
- Joint spacing: 177”

**Table E- 3: Validation#2**

| α(ΔT/D) ($10^{-6}$ in.$^{-1}$) | Analysis 1 | | | | | Analysis 2 | | | | |
|---|---|---|---|---|---|---|---|---|---|---|
| | Gradient (°F/in.) | CTE ($10^{-6}$ in./in./°F) | $\sigma_{long,bottom}$ (psi) | $\sigma_{trans,bottom}$ (psi) | $\sigma_{long,top}$ (psi) | Gradient (°F/in.) | CTE ($10^{-6}$ in./in./°F) | $\sigma_{long,bottom}$ (psi) | $\sigma_{trans,bottom}$ (psi) | $\sigma_{long,top}$ (psi) |
| 0.0 | +2 or -2 | 0.10 | 201.6 | 78.0 | 125.3 | 0 | 5.00 | 198.1 | 77.0 | 122.7 |
| 2.5 | +2 or -2 | 1.25 | 241.8 | 89.6 | 155.4 | +0.5 or -0.5 | 5.00 | 241.8 | 89.6 | 155.4 |
| 5.0 | +2 or -2 | 2.50 | 285.6 | 102.2 | 188.1 | +1 or -1 | 5.00 | 285.6 | 102.2 | 188.1 |
| 7.5 | +2 or -2 | 3.75 | 329.3 | 114.7 | 220.7 | +1.5 or -1.5 | 5.00 | 329.3 | 114.7 | 220.7 |
| 10.0 | +2 or -2 | 5.00 | 373.0 | 127.3 | 253.4 | +2 or -2 | 5.00 | 373.0 | 127.3 | 253.4 |
| 12.5 | +2 or -2 | 6.25 | 416.8 | 139.9 | 296.6 | +2.5 or -2.5 | 5.00 | 416.8 | 139.9 | 296.6 |
| 15.0 | +2 or -2 | 7.50 | 460.5 | 152.4 | 339.7 | +3 or -3 | 5.00 | 460.5 | 152.4 | 339.7 |
| 17.5 | +2 or -2 | 8.75 | 504.3 | 165.0 | 382.9 | +3.5 or -3.5 | 5.00 | 504.3 | 165.0 | 382.9 |
| 20.0 | +2 or -2 | 10.00 | 548.0 | 177.5 | 426.0 | +4 or -4 | 5.00 | 548.0 | 177.5 | 426.0 |

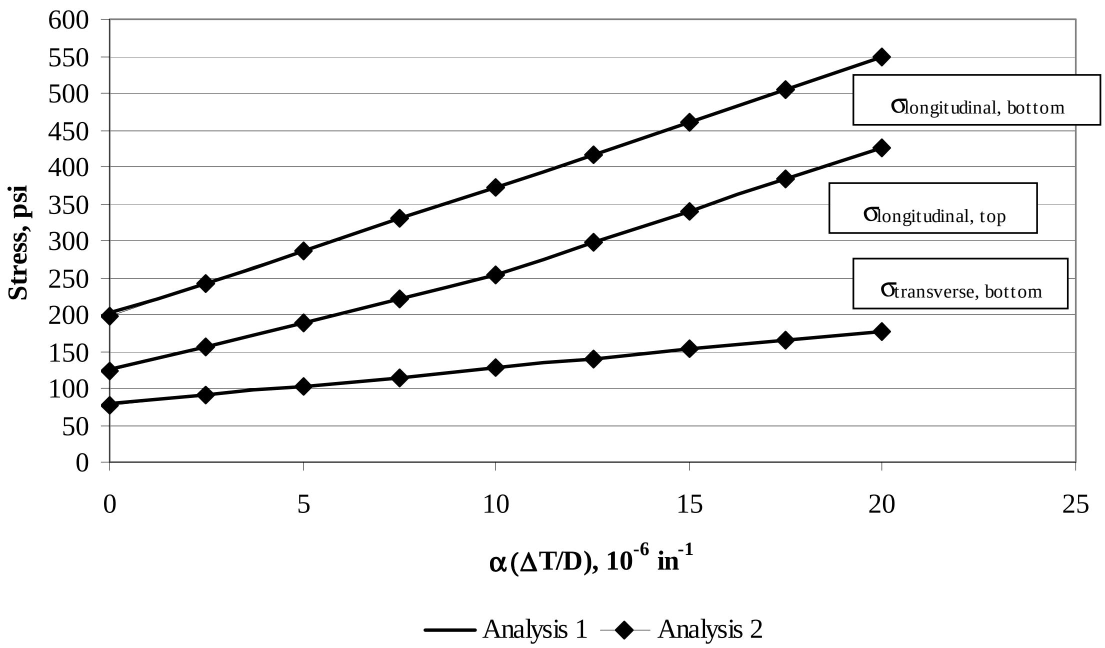


**Figure E- 2: Plot of validation#2**

Analysis 1: Constant temperature gradient (+2 °F/in.) with variation of CTE ($0.1 \times 10^{-6}$ to $10 \times 10^{-6}$ in./in./°F)

Analysis 2: Constant CTE ($5 \times 10^{-6}$ in./in./°F) with variation of temperature gradient (0 to +4 °F/in.)

- Shoulder type: AC
- PCC thickness: 10”
- Base/subbase thickness: 26”
- k-value: 30 psi/in.
- Loading type: tandem axle
- Joint spacing 315”

**Table E- 4: Validation#3**

| $\alpha(\Delta T/D)$ ($10^{-6}$ in.$^{-1}$) | Analysis 1 | | | | | Analysis 2 | | | | |
|---|---|---|---|---|---|---|---|---|---|---|
| | Gradient (°F/in.) | CTE ($10^{-6}$ in./in./°F) | $\sigma_{long,bottom}$ (psi) | $\sigma_{trans,bottom}$ (psi) | $\sigma_{long,top}$ (psi) | Gradient (°F/in.) | CTE ($10^{-6}$ in./in./°F) | $\sigma_{long,bottom}$ (psi) | $\sigma_{trans,bottom}$ (psi) | $\sigma_{long,top}$ (psi) |
| 0.0 | +2 or -2 | 0.10 | 57.2 | 88.8 | 29.5 | 0 | 5.00 | 52.8 | 86.4 | 24.8 |
| 2.5 | +2 or -2 | 1.25 | 107.8 | 116.7 | 84.1 | +0.5 or -0.5 | 5.00 | 107.8 | 116.7 | 84.1 |
| 5.0 | +2 or -2 | 2.50 | 162.9 | 147.0 | 143.4 | +1 or -1 | 5.00 | 162.9 | 147.0 | 143.4 |
| 7.5 | +2 or -2 | 3.75 | 217.9 | 177.3 | 202.7 | +1.5 or -1.5 | 5.00 | 217.9 | 177.3 | 202.7 |
| 10.0 | +2 or -2 | 5.00 | 272.9 | 207.6 | 262.0 | +2 or -2 | 5.00 | 272.9 | 207.6 | 262.0 |
| 12.5 | +2 or -2 | 6.25 | 331.3 | 240.2 | 316.3 | +2.5 or -2.5 | 5.00 | 331.3 | 240.2 | 316.3 |
| 15.0 | +2 or -2 | 7.50 | 389.7 | 272.9 | 370.7 | +3 or -3 | 5.00 | 389.7 | 272.9 | 370.7 |
| 17.5 | +2 or -2 | 8.75 | 448.0 | 305.5 | 425.0 | +3.5 or -3.5 | 5.00 | 448.0 | 305.5 | 425.0 |
| 20.0 | +2 or -2 | 10.00 | 506.4 | 338.1 | 479.3 | +4 or -4 | 5.00 | 506.4 | 338.1 | 479.3 |

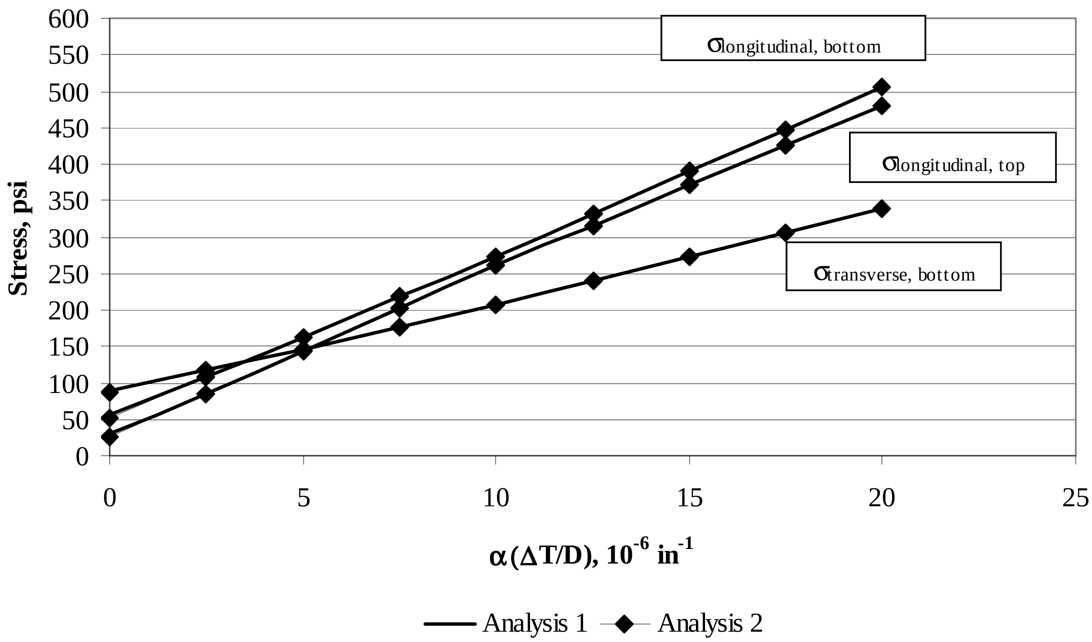


**Figure E- 3: Plot of validation#3**

Analysis 1: Constant temperature gradient (+2 °F/in.) with variation of CTE ($0.1 \times 10^{-6}$ to $10 \times 10^{-6}$ in./in./°F)

Analysis 2: Constant CTE ($5 \times 10^{-6}$ in./in./°F) with variation of temperature gradient (0 to +4 °F/in.)

- Shoulder type: Widened lane
- PCC thickness: 10”
- Base/subbase thickness: 4”
- k-value: 200 psi/in.
- Loading type: Multi-axle (8)
- Joint spacing 315”

**Table E- 5: Validation#4**

| α(ΔT/D) ($10^{-6}$ in.$^{-1}$) | Analysis 1 | | | | | Analysis 2 | | | | |
|---|---|---|---|---|---|---|---|---|---|---|
| | Gradient ($^{o}$F/in.) | CTE ($10^{-6}$ in./in./$^{o}$F) | $\sigma_{long,bottom}$ (psi) | $\sigma_{trans,bottom}$ (psi) | $\sigma_{long,top}$ (psi) | Gradient ($^{o}$F/in.) | CTE ($10^{-6}$ in./in./$^{o}$F) | $\sigma_{long,bottom}$ (psi) | $\sigma_{trans,bottom}$ (psi) | $\sigma_{long,top}$ (psi) |
| 0.0 | +2 or -2 | 0.10 | 88.1 | 60.4 | 64.9 | 0 | 5.00 | 85.5 | 58.6 | 62.5 |
| 2.5 | +2 or -2 | 1.25 | 118.4 | 81.1 | 91.9 | +0.5 or -0.5 | 5.00 | 118.4 | 81.1 | 91.9 |
| 5.0 | +2 or -2 | 2.50 | 151.4 | 103.5 | 121.2 | +1 or -1 | 5.00 | 151.4 | 103.5 | 121.2 |
| 7.5 | +2 or -2 | 3.75 | 184.3 | 126.0 | 150.6 | +1.5 or -1.5 | 5.00 | 184.3 | 126.0 | 150.6 |
| 10.0 | +2 or -2 | 5.00 | 217.2 | 148.4 | 179.9 | +2 or -2 | 5.00 | 217.2 | 148.4 | 179.9 |
| 12.5 | +2 or -2 | 6.25 | 248.6 | 169.6 | 206.8 | +2.5 or -2.5 | 5.00 | 248.6 | 169.6 | 206.8 |
| 15.0 | +2 or -2 | 7.50 | 280.1 | 190.8 | 233.7 | +3 or -3 | 5.00 | 280.1 | 190.8 | 233.7 |
| 17.5 | +2 or -2 | 8.75 | 311.5 | 211.9 | 260.6 | +3.5 or -3.5 | 5.00 | 311.5 | 211.9 | 260.6 |
| 20.0 | +2 or -2 | 10.00 | 342.9 | 233.1 | 287.5 | +4 or -4 | 5.00 | 342.9 | 233.1 | 287.5 |

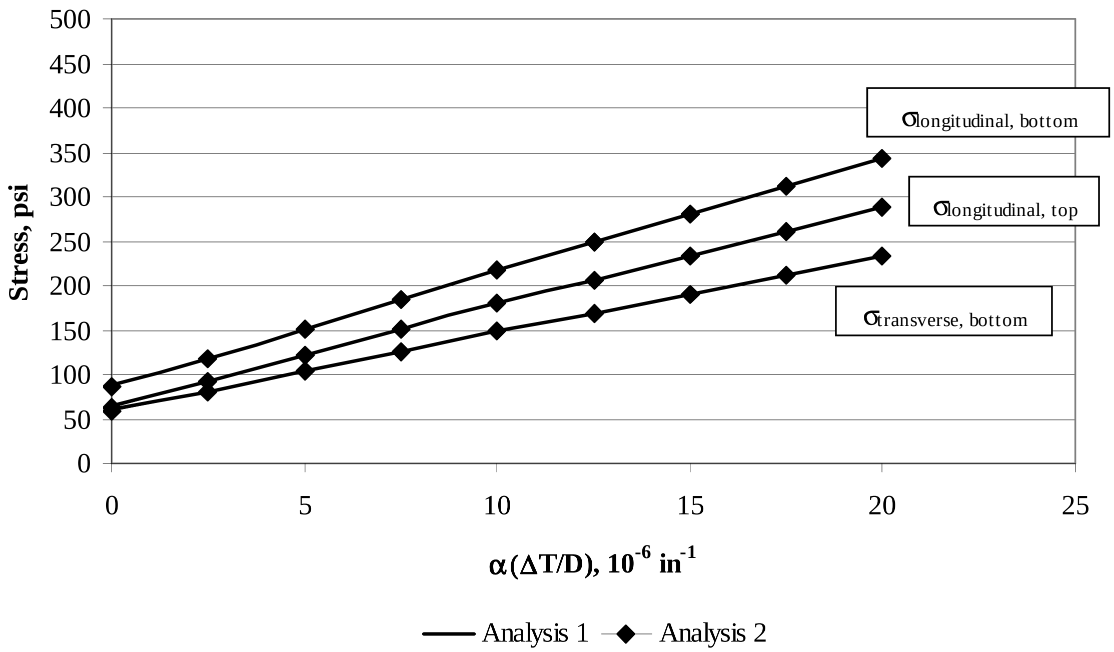


**Figure E- 4: Plot of validation#4**

Analysis 1: Constant temperature gradient (+2 $^{o}$F/in.) with variation of CTE (0.1x10$^{-6}$ to 10x10$^{-6}$ in./in./$^{o}$F)

Analysis 2: Constant CTE (5x10$^{-6}$ in./in./$^{o}$F) with variation of temperature gradient (0 to +4 $^{o}$F/in.)

- Shoulder type: PCC
- PCC thickness: 12”
- Base/subbase thickness: 26”
- k-value: 200 psi/in.
- Loading type: tandem axle
- Joint spacing 177”

**Table E- 6: Validation#5**

| $\alpha(\Delta T/D)$ ($10^{-6}$ in.$^{-1}$) | Analysis 1 | | | | | Analysis 2 | | | | |
|---|---|---|---|---|---|---|---|---|---|---|
| | Gradient (°F/in.) | CTE ($10^{-6}$ in./in./°F) | $\sigma_{long,bottom}$ (psi) | $\sigma_{trans,bottom}$ (psi) | $\sigma_{long,top}$ (psi) | Gradient (°F/in.) | CTE ($10^{-6}$ in./in./°F) | $\sigma_{long,bottom}$ (psi) | $\sigma_{trans,bottom}$ (psi) | $\sigma_{long,top}$ (psi) |
| 0.0 | +2 or -2 | 0.10 | 52.9 | 56.6 | 66.4 | 0 | 5.00 | 51.6 | 55.8 | 65.0 |
| 2.5 | +2 or -2 | 1.25 | 68.4 | 65.7 | 82.5 | +0.5 or -0.5 | 5.00 | 68.4 | 65.7 | 82.5 |
| 5.0 | +2 or -2 | 2.50 | 85.1 | 75.6 | 100.1 | +1 or -1 | 5.00 | 85.1 | 75.6 | 100.1 |
| 7.5 | +2 or -2 | 3.75 | 101.9 | 85.4 | 117.6 | +1.5 or -1.5 | 5.00 | 101.9 | 85.4 | 117.6 |
| 10.0 | +2 or -2 | 5.00 | 118.6 | 95.3 | 135.2 | +2 or -2 | 5.00 | 118.6 | 95.3 | 135.2 |
| 12.5 | +2 or -2 | 6.25 | 133.3 | 106.6 | 147.8 | +2.5 or -2.5 | 5.00 | 133.3 | 106.6 | 147.8 |
| 15.0 | +2 or -2 | 7.50 | 148.0 | 118.0 | 160.3 | +3 or -3 | 5.00 | 148.0 | 118.0 | 160.3 |
| 17.5 | +2 or -2 | 8.75 | 162.6 | 129.3 | 172.9 | +3.5 or -3.5 | 5.00 | 162.6 | 129.3 | 172.9 |
| 20.0 | +2 or -2 | 10.00 | 177.3 | 140.6 | 185.4 | +4 or -4 | 5.00 | 177.3 | 140.6 | 185.4 |

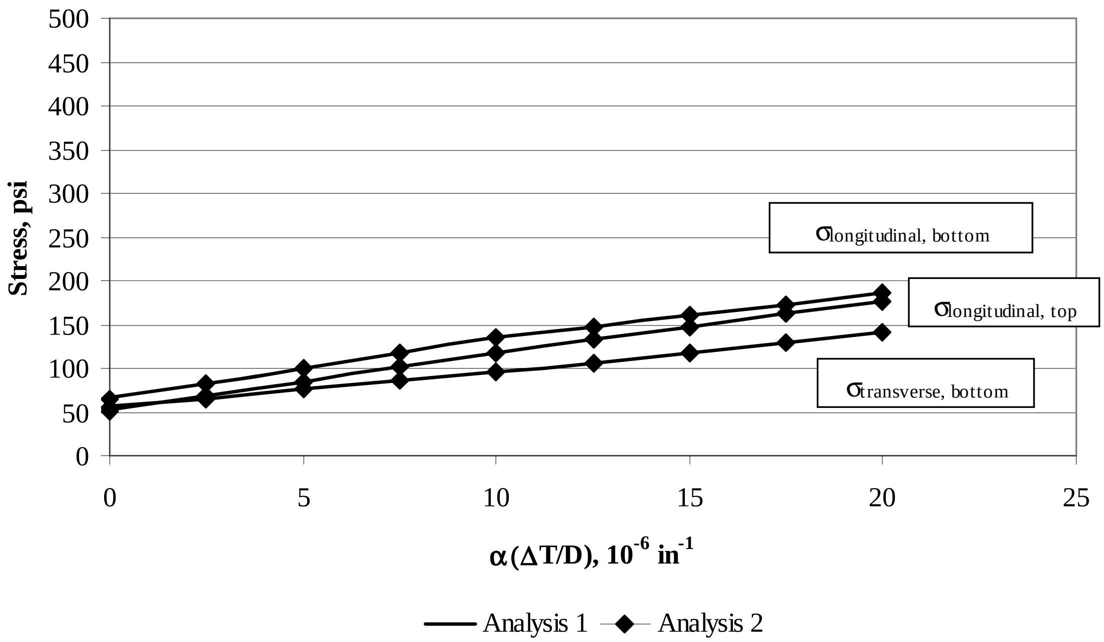


**Figure E- 5: Plot of validation#5**

Analysis 1: Constant temperature gradient (+2 °F/in.) with variation of CTE ($0.1 \times 10^{-6}$ to $10 \times 10^{-6}$ in./in./°F)

Analysis 2: Constant CTE ($5 \times 10^{-6}$ in./in./°F) with variation of temperature gradient (0 to +4 °F/in.)

- Shoulder type: AC
- PCC thickness: 12”
- Base/subbase thickness: 4”
- k-value: 100 psi/in.
- Loading type: Multi-axle (8)
- Joint spacing 177”

**Table E- 7: Validation#6**

| $\alpha(\Delta T/D)$ ($10^{-6}$ in.$^{-1}$) | Analysis 1 | | | | | Analysis 2 | | | | |
|---|---|---|---|---|---|---|---|---|---|---|
| | Gradient (°F/in.) | CTE ($10^{-6}$ in./in./°F) | $\sigma_{long,bottom}$ (psi) | $\sigma_{trans,bottom}$ (psi) | $\sigma_{long,top}$ (psi) | Gradient (°F/in.) | CTE ($10^{-6}$ in./in./°F) | $\sigma_{long,bottom}$ (psi) | $\sigma_{trans,bottom}$ (psi) | $\sigma_{long,top}$ (psi) |
| 0.0 | +2 or -2 | 0.10 | 124.1 | 63.0 | 64.3 | 0 | 5.00 | 120.7 | 62.3 | 61.3 |
| 2.5 | +2 or -2 | 1.25 | 162.9 | 70.5 | 98.5 | +0.5 or -0.5 | 5.00 | 162.9 | 70.5 | 98.5 |
| 5.0 | +2 or -2 | 2.50 | 205.1 | 78.7 | 135.8 | +1 or -1 | 5.00 | 205.1 | 78.7 | 135.8 |
| 7.5 | +2 or -2 | 3.75 | 247.2 | 86.8 | 173.0 | +1.5 or -1.5 | 5.00 | 247.2 | 86.8 | 173.0 |
| 10.0 | +2 or -2 | 5.00 | 289.4 | 95.0 | 210.2 | +2 or -2 | 5.00 | 289.4 | 95.0 | 210.2 |
| 12.5 | +2 or -2 | 6.25 | 331.6 | 103.2 | 252.6 | +2.5 or -2.5 | 5.00 | 331.6 | 103.2 | 252.6 |
| 15.0 | +2 or -2 | 7.50 | 373.8 | 111.3 | 295.0 | +3 or -3 | 5.00 | 373.8 | 111.3 | 295.0 |
| 17.5 | +2 or -2 | 8.75 | 416.0 | 119.5 | 337.3 | +3.5 or -3.5 | 5.00 | 416.0 | 119.5 | 337.3 |
| 20.0 | +2 or -2 | 10.00 | 458.2 | 127.6 | 379.7 | +4 or -4 | 5.00 | 458.2 | 127.6 | 379.7 |

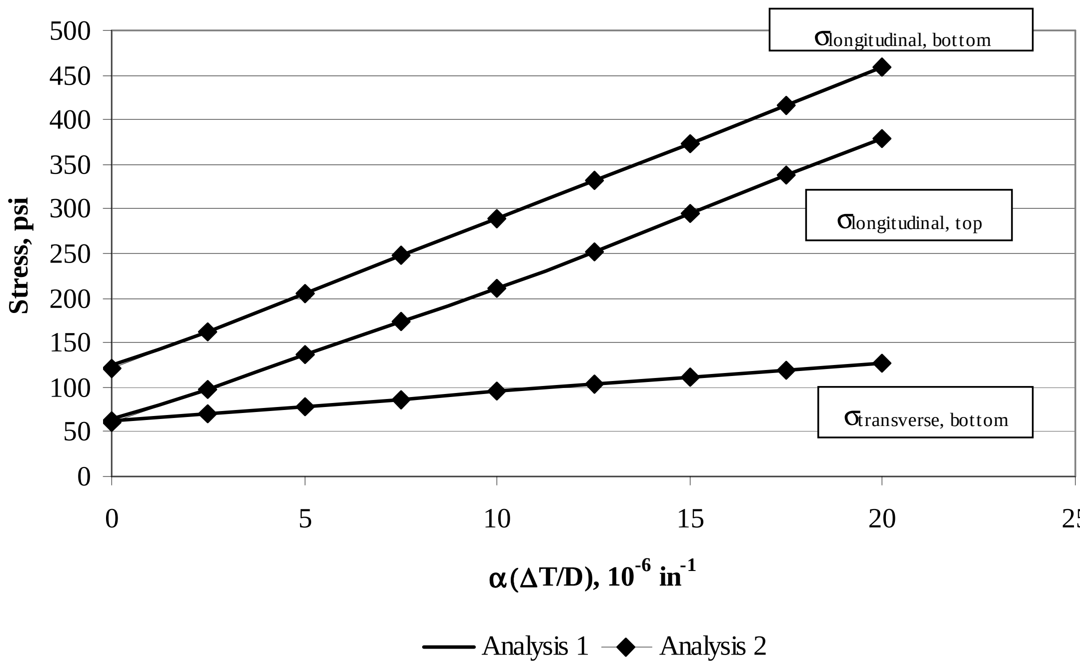


**Figure E- 6: Plot of validation#6**

Analysis 1: Constant temperature gradient (+2 °F/in.) with variation of CTE (0.1x$10^{-6}$ to 10x$10^{-6}$ in./in./°F)

Analysis 2: Constant CTE (5x$10^{-6}$ in./in./°F) with variation of temperature gradient (0 to +4 °F/in.)

- Shoulder type: Widened lane
- PCC thickness: 12”
- Base/subbase thickness: 16”
- k-value: 30 psi/in.
- Loading type: single axle
- Joint spacing 315”

**Table E- 8: Validation#7**

| $\alpha(\Delta T/D)$ ($10^{-6}$ in.$^{-1}$) | Analysis 1 | | | | | Analysis 2 | | | | |
|---|---|---|---|---|---|---|---|---|---|---|
| | Gradient ($^oF$/in.) | CTE ($10^{-6}$ in./in./$^oF$) | $\sigma_{long,bottom}$ (psi) | $\sigma_{trans,bottom}$ (psi) | $\sigma_{long,top}$ (psi) | Gradient ($^oF$/in.) | CTE ($10^{-6}$ in./in./$^oF$) | $\sigma_{long,bottom}$ (psi) | $\sigma_{trans,bottom}$ (psi) | $\sigma_{long,top}$ (psi) |
| 0.0 | +2 or -2 | 0.10 | 113.9 | 158.4 | 68.9 | 0 | 5.00 | 111.2 | 157.8 | 65.7 |
| 2.5 | +2 or -2 | 1.25 | 144.7 | 165.2 | 105.8 | +0.5 or -0.5 | 5.00 | 144.7 | 165.2 | 105.8 |
| 5.0 | +2 or -2 | 2.50 | 178.2 | 172.6 | 145.9 | +1 or -1 | 5.00 | 178.2 | 172.6 | 145.9 |
| 7.5 | +2 or -2 | 3.75 | 211.7 | 179.9 | 185.9 | +1.5 or -1.5 | 5.00 | 211.7 | 179.9 | 185.9 |
| 10.0 | +2 or -2 | 5.00 | 245.2 | 187.3 | 226.0 | +2 or -2 | 5.00 | 245.2 | 187.3 | 226.0 |
| 12.5 | +2 or -2 | 6.25 | 284.4 | 196.0 | 264.8 | +2.5 or -2.5 | 5.00 | 284.4 | 196.0 | 264.8 |
| 15.0 | +2 or -2 | 7.50 | 323.6 | 204.7 | 303.6 | +3 or -3 | 5.00 | 323.6 | 204.7 | 303.6 |
| 17.5 | +2 or -2 | 8.75 | 362.7 | 213.4 | 342.3 | +3.5 or -3.5 | 5.00 | 362.7 | 213.4 | 342.3 |
| 20.0 | +2 or -2 | 10.00 | 401.9 | 222.1 | 381.1 | +4 or -4 | 5.00 | 401.9 | 222.1 | 381.1 |

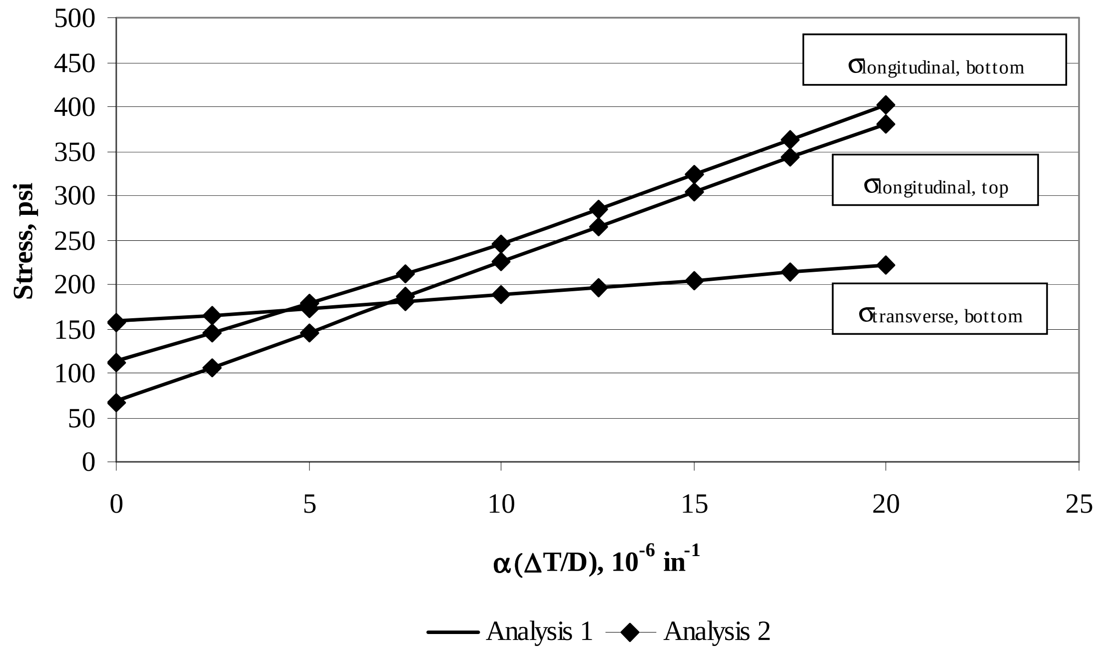


**Figure E- 7: Plot of validation#7**

Analysis 1: Constant temperature gradient (+2 $^oF$/in.) with variation of CTE ($0.1x10^{-6}$ to $10x10^{-6}$ in./in./$^oF$)

Analysis 2: Constant CTE ($5x10^{-6}$ in./in./$^oF$) with variation of temperature gradient (0 to +4 $^oF$/in.)

- Shoulder type: PCC
- PCC thickness: 8”
- Base/subbase thickness: 4”
- k-value: 30 psi/in.
- Loading type: Multi-axle (8)
- Joint spacing 315”

**Table E- 9: Validation#8**

| $\alpha(\Delta T/D)$ ($10^{-6}$ in.$^{-1}$) | Analysis 1 | | | | | Analysis 2 | | | | |
|---|---|---|---|---|---|---|---|---|---|---|
| | Gradient (°F/in.) | CTE ($10^{-6}$ in./in./°F) | $\sigma_{long,bottom}$ (psi) | $\sigma_{trans,bottom}$ (psi) | $\sigma_{long,top}$ (psi) | Gradient (°F/in.) | CTE ($10^{-6}$ in./in./°F) | $\sigma_{long,bottom}$ (psi) | $\sigma_{trans,bottom}$ (psi) | $\sigma_{long,top}$ (psi) |
| 0.0 | +2 or -2 | 0.10 | 154.8 | 96.5 | 87.1 | 0 | 5.00 | 151.9 | 94.4 | 84.9 |
| 2.5 | +2 or -2 | 1.25 | 188.7 | 120.4 | 112.1 | +0.5 or -0.5 | 5.00 | 188.7 | 120.4 | 112.1 |
| 5.0 | +2 or -2 | 2.50 | 225.4 | 146.4 | 139.4 | +1 or -1 | 5.00 | 225.4 | 146.4 | 139.4 |
| 7.5 | +2 or -2 | 3.75 | 262.2 | 172.4 | 166.6 | +1.5 or -1.5 | 5.00 | 262.2 | 172.4 | 166.6 |
| 10.0 | +2 or -2 | 5.00 | 298.9 | 198.4 | 193.8 | +2 or -2 | 5.00 | 298.9 | 198.4 | 193.8 |
| 12.5 | +2 or -2 | 6.25 | 335.5 | 227.6 | 228.0 | +2.5 or -2.5 | 5.00 | 335.5 | 227.6 | 228.0 |
| 15.0 | +2 or -2 | 7.50 | 372.1 | 256.8 | 262.3 | +3 or -3 | 5.00 | 372.1 | 256.8 | 262.3 |
| 17.5 | +2 or -2 | 8.75 | 408.7 | 286.0 | 296.5 | +3.5 or -3.5 | 5.00 | 408.7 | 286.0 | 296.5 |
| 20.0 | +2 or -2 | 10.00 | 445.3 | 315.2 | 330.7 | +4 or -4 | 5.00 | 445.3 | 315.2 | 330.7 |

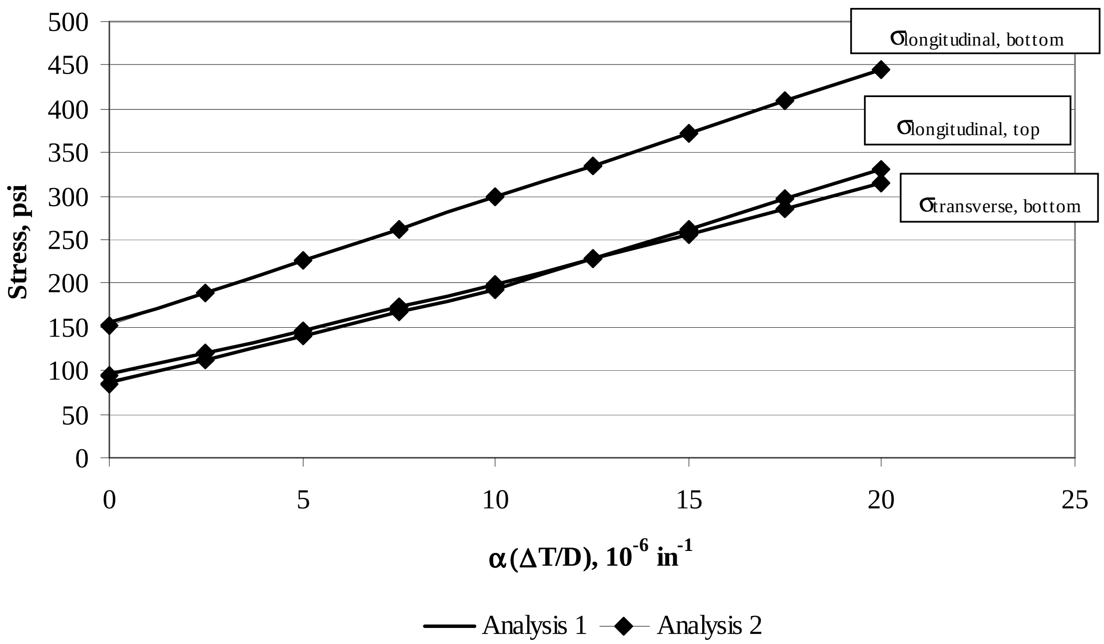


**Figure E- 8: Plot of validation#8**

Analysis 1: Constant temperature gradient (+2 °F/in.) with variation of CTE ($0.1\times10^{-6}$ to $10\times10^{-6}$ in./in./°F)

Analysis 2: Constant CTE ($5\times10^{-6}$ in./in./°F) with variation of temperature gradient (0 to +4 °F/in.)

- Shoulder type: AC
- PCC thickness: 8”
- Base/subbase thickness: 16”
- k-value: 200 psi/in.
- Loading type: single axle
- Joint spacing 177”

**Table E- 10: Validation#9**

| $\alpha(\Delta T/D)$ ($10^{-6}$ in.$^{-1}$) | Analysis 1 | | | | | Analysis 2 | | | | |
|---|---|---|---|---|---|---|---|---|---|---|
| | Gradient (°F/in.) | CTE ($10^{-6}$ in./in./°F) | $\sigma_{long,bottom}$ (psi) | $\sigma_{trans,bottom}$ (psi) | $\sigma_{long,top}$ (psi) | Gradient (°F/in.) | CTE ($10^{-6}$ in./in./°F) | $\sigma_{long,bottom}$ (psi) | $\sigma_{trans,bottom}$ (psi) | $\sigma_{long,top}$ (psi) |
| 0.0 | +2 or -2 | 0.10 | 153.8 | 108.4 | 79.3 | 0 | 5.00 | 151.4 | 106.3 | 77.1 |
| 2.5 | +2 or -2 | 1.25 | 181.9 | 132.2 | 105.1 | +0.5 or -0.5 | 5.00 | 181.9 | 132.2 | 105.1 |
| 5.0 | +2 or -2 | 2.50 | 212.4 | 158.2 | 133.1 | +1 or -1 | 5.00 | 212.4 | 158.2 | 133.1 |
| 7.5 | +2 or -2 | 3.75 | 242.8 | 184.1 | 161.2 | +1.5 or -1.5 | 5.00 | 242.8 | 184.1 | 161.2 |
| 10.0 | +2 or -2 | 5.00 | 273.3 | 210.0 | 189.2 | +2 or -2 | 5.00 | 273.3 | 210.0 | 189.2 |
| 12.5 | +2 or -2 | 6.25 | 303.8 | 237.2 | 220.0 | +2.5 or -2.5 | 5.00 | 303.8 | 237.2 | 220.0 |
| 15.0 | +2 or -2 | 7.50 | 334.3 | 264.4 | 250.8 | +3 or -3 | 5.00 | 334.3 | 264.4 | 250.8 |
| 17.5 | +2 or -2 | 8.75 | 364.8 | 291.6 | 281.5 | +3.5 or -3.5 | 5.00 | 364.8 | 291.6 | 281.5 |
| 20.0 | +2 or -2 | 10.00 | 395.3 | 318.8 | 312.3 | +4 or -4 | 5.00 | 395.3 | 318.8 | 312.3 |

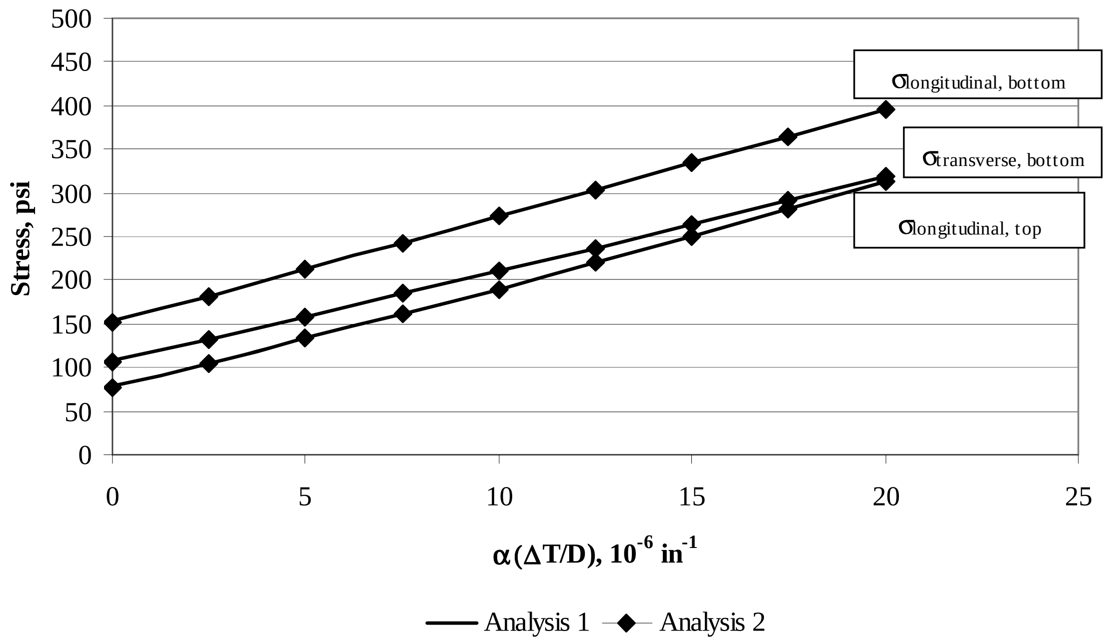


**Figure E- 9: Plot of validation#9**

Analysis 1: Constant temperature gradient (+2 °F/in.) with variation of CTE ($0.1 \times 10^{-6}$ to $10 \times 10^{-6}$ in./in./°F)

Analysis 2: Constant CTE ($5 \times 10^{-6}$ in./in./°F) with variation of temperature gradient (0 to +4 °F/in.)

- Shoulder type: Widened lane
- PCC thickness: 8”
- Base/subbase thickness: 26”
- k-value: 100 psi/in.
- Loading type: tandem axle
- Joint spacing 177”

# Appendix F

## Documentation of Pavement Responses

**Sub Appendix F-1**

**Documentation of Pavement Responses for**


**18-kips Single Axle**

Figures F-1-1 through F-1-12 illustrate the impact of PCC thickness and base/subbase thickness on stresses (100-psi/in. modulus of subgrade reaction and PCC shoulder)

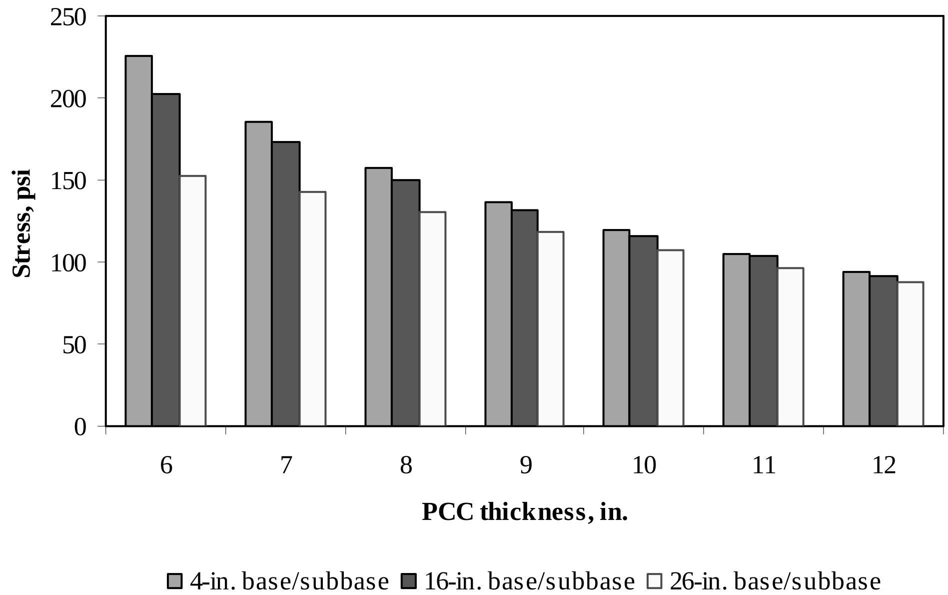


**Figure F-1-1: Impact of PCC thickness and base/subbase thickness on longitudinal stress at bottom of the Slab (177-in. joint spacing and $\alpha(\Delta T/D)$ of 0 in.$^{-1}$)**

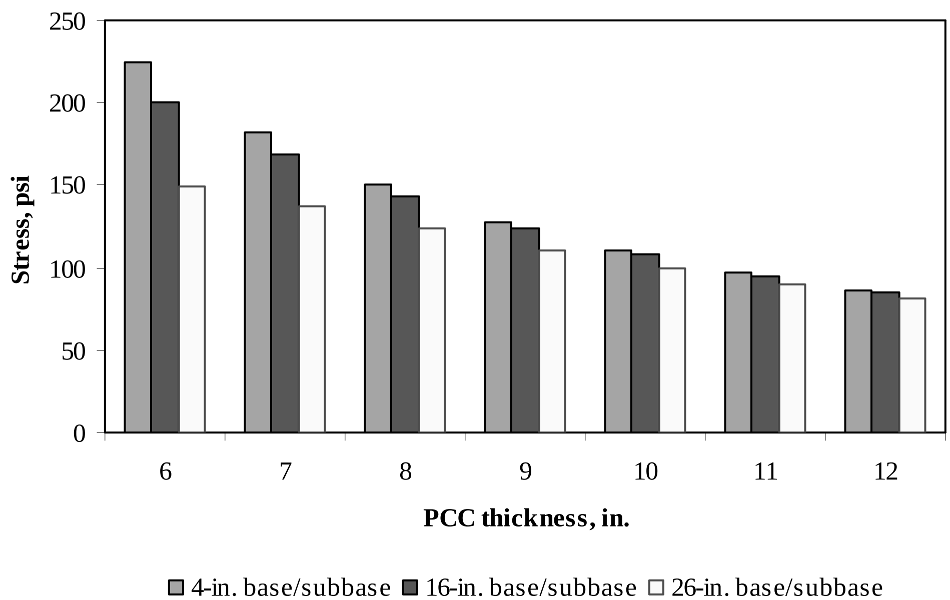


**Figure F-1-2: Impact of PCC thickness and base/subbase thickness on longitudinal stress at bottom of the Slab (315-in. joint spacing and $\alpha(\Delta T/D)$ of 0 in.$^{-1}$)**

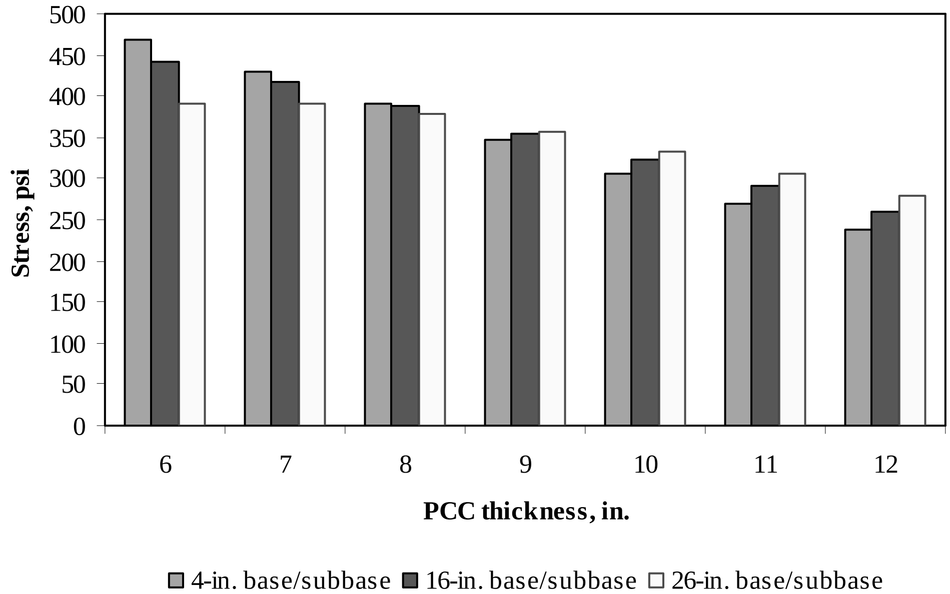


**Figure F-1-3: Impact of PCC thickness and base/subbase thickness on longitudinal stress at bottom of the Slab (177-in. joint spacing and $\alpha(\Delta T/D)$ of $20x10^{-6}$ in.$^{-1}$)**

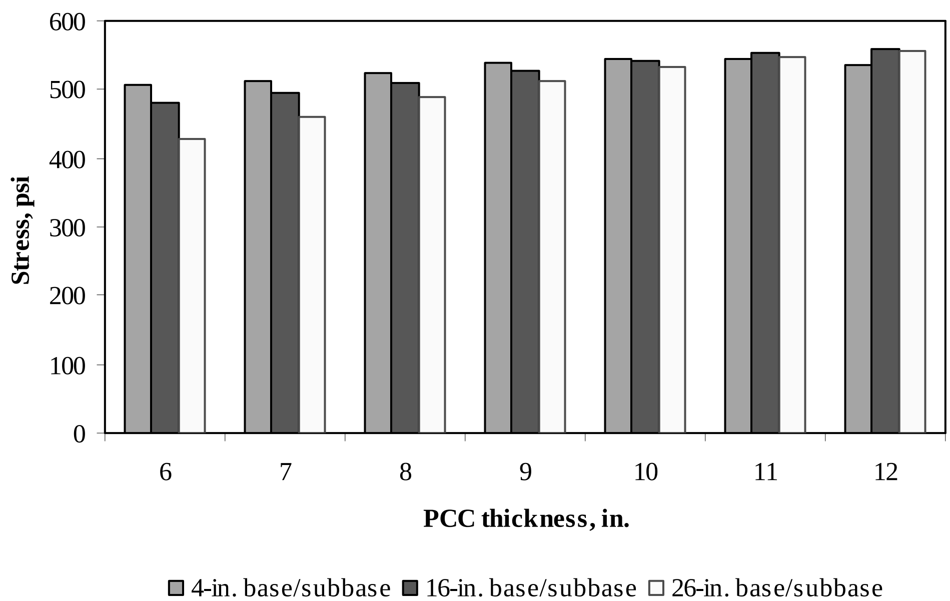


**Figure F-1-4: Impact of PCC thickness and base/subbase thickness on longitudinal stress at bottom of the Slab (315-in. joint spacing and $\alpha(\Delta T/D)$ of $20x10^{-6}$ in.$^{-1}$)**

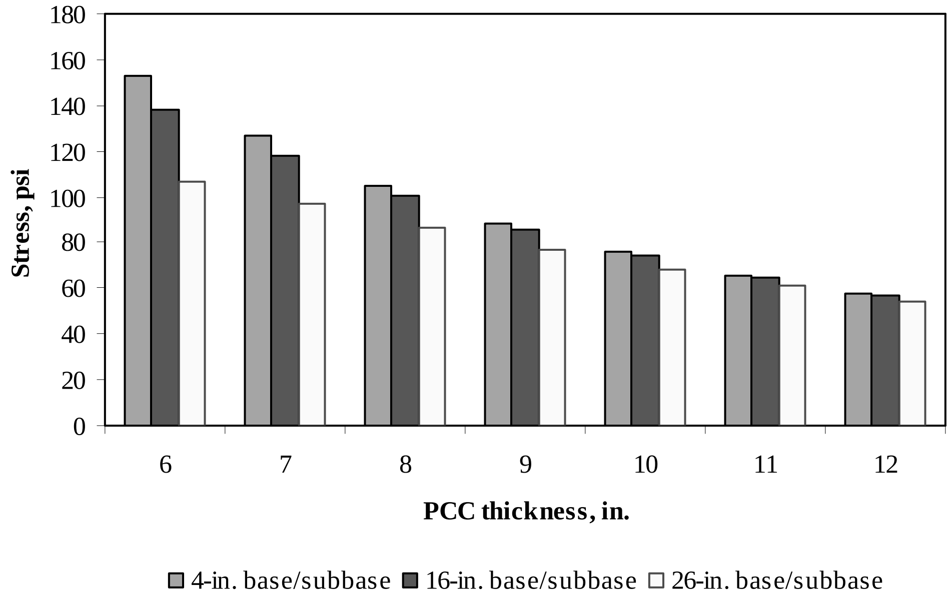


**Figure F-1-5: Impact of PCC thickness and base/subbase thickness on longitudinal stress at top of the Slab (177-in. joint spacing and $\alpha(\Delta T/D)$ of 0 in.$^{-1}$)**

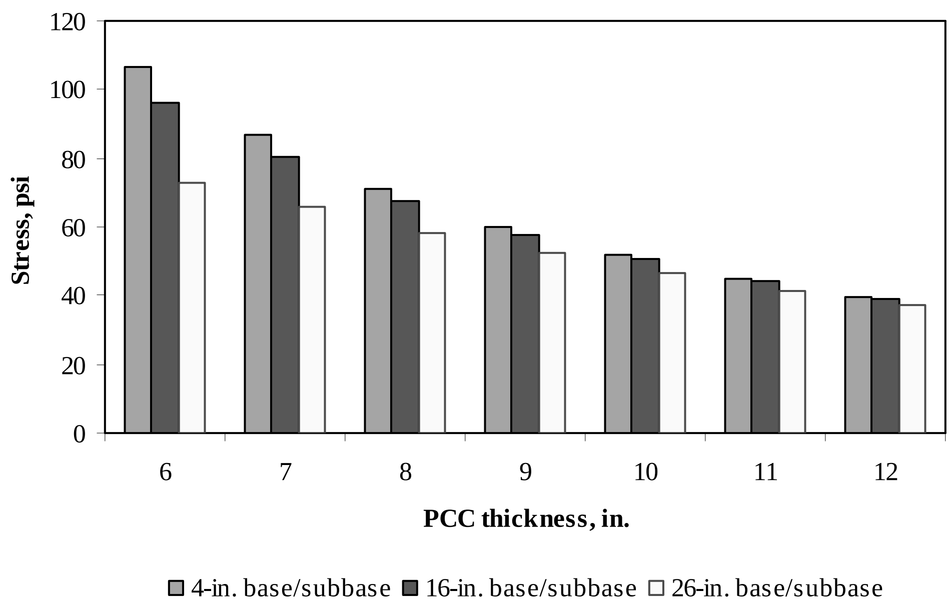


**Figure F-1-6: Impact of PCC thickness and base/subbase thickness on longitudinal stress at top of the Slab (315-in. joint spacing and $\alpha(\Delta T/D)$ of 0 in.$^{-1}$)**

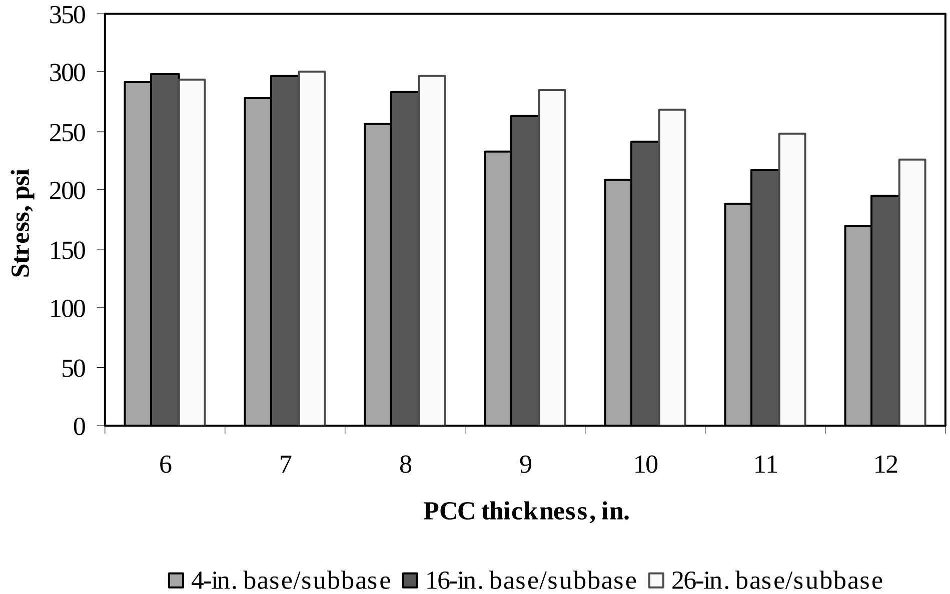


**Figure F-1-7: Impact of PCC thickness and base/subbase thickness on longitudinal stress at top of the Slab (177-in. joint spacing and $\alpha(\Delta T/D)$ of $-20x10^{-6}$ in.$^{-1}$)**

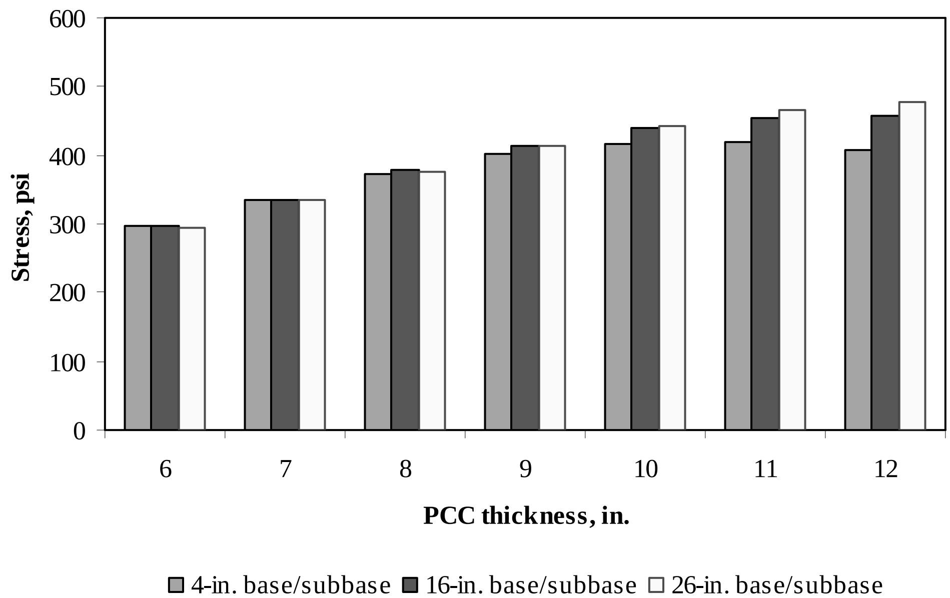


**Figure F-1-8: Impact of PCC thickness and base/subbase thickness on longitudinal stress at top of the Slab (315-in. joint spacing and $\alpha(\Delta T/D)$ of $-20x10^{-6}$ in.$^{-1}$)**

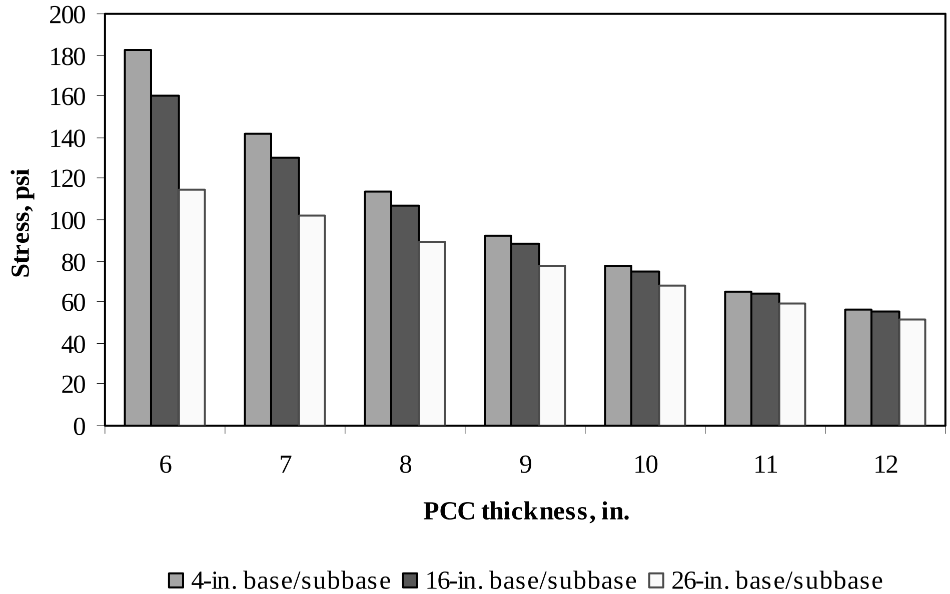


**Figure F-1-9: Impact of PCC thickness and base/subbase thickness on transverse stress at bottom of the Slab (177-in. joint spacing and $\alpha(\Delta T/D)$ of 0 in.$^{-1}$)**

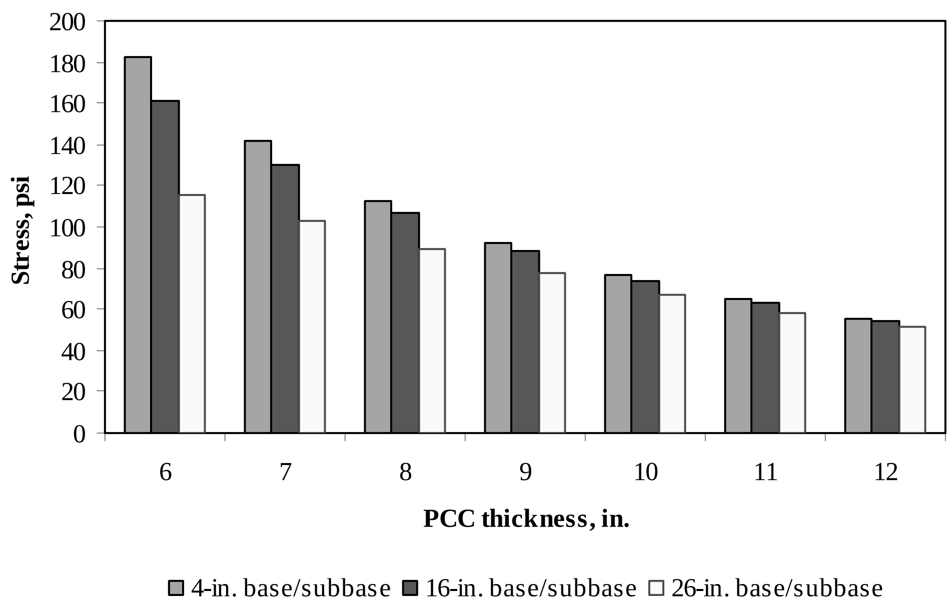


**Figure F-1-10: Impact of PCC thickness and base/subbase thickness on transverse stress at bottom of the Slab (315-in. joint spacing and $\alpha(\Delta T/D)$ of 0 in.$^{-1}$)**

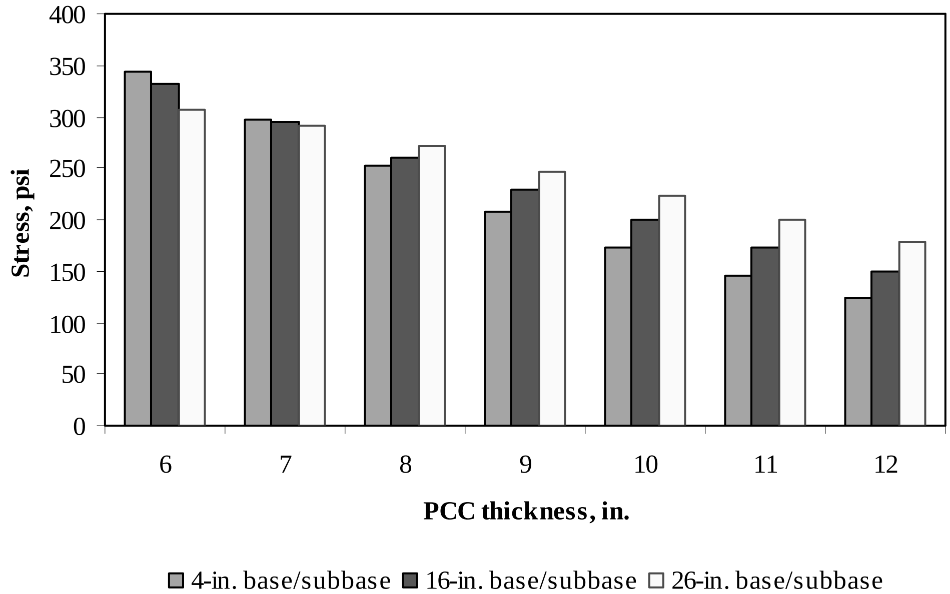


**Figure F-1-11: Impact of PCC thickness and base/subbase thickness on transverse stress at bottom of the Slab (177-in. joint spacing and $\alpha(\Delta T/D)$ of $20 \times 10^{-6}$ in.$^{-1}$)**

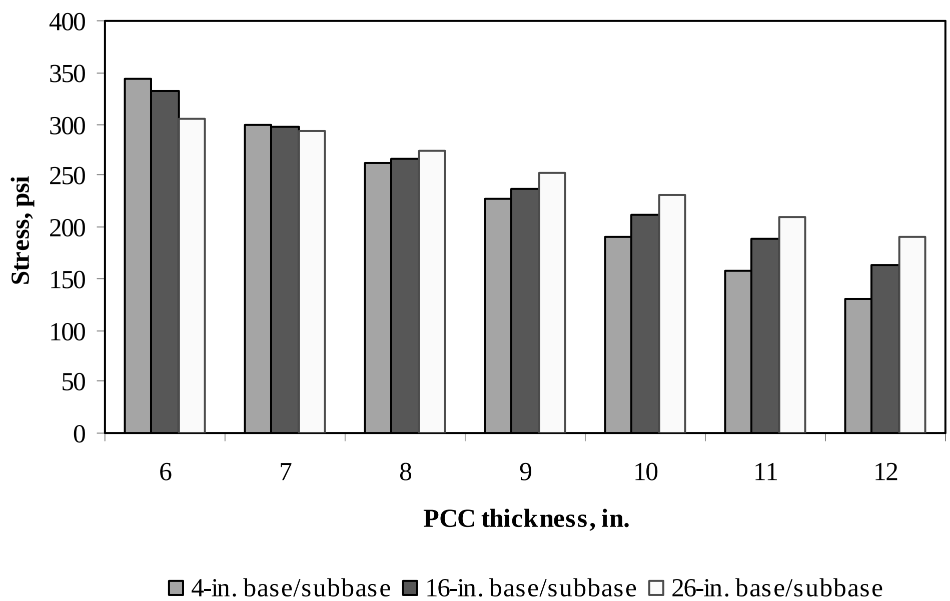


**Figure F-1-12: Impact of PCC thickness and base/subbase thickness on transverse stress at bottom of the Slab (315-in. joint spacing and $\alpha(\Delta T/D)$ of $20 \times 10^{-6}$ in.$^{-1}$)**

Figures F-1-13 through F-1-24 illustrate the impact of PCC thickness and modulus of subgrade reaction on stresses (16-in. base/subbase thickness and PCC shoulder)

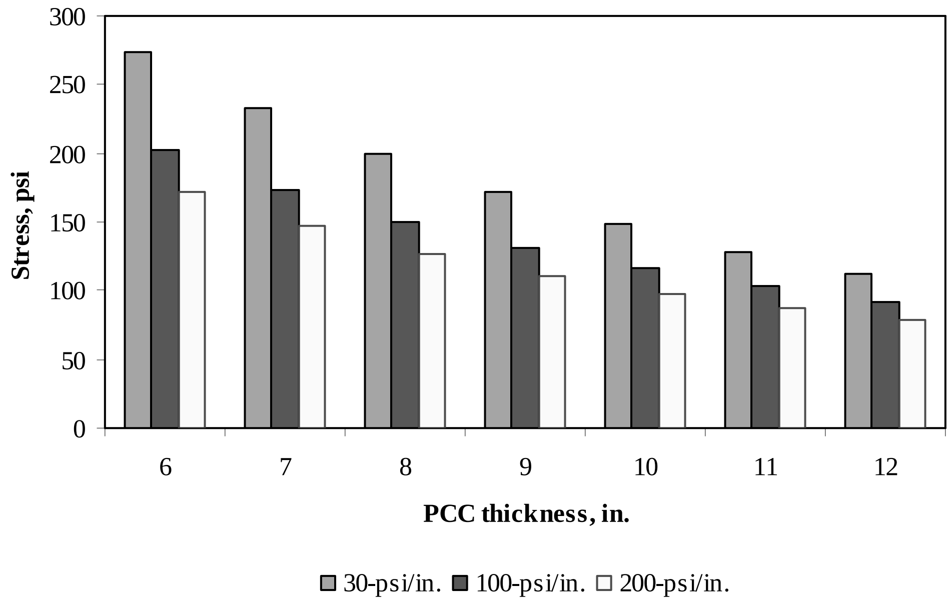


**Figure F-1-13: Impact of PCC thickness and modulus of subgrade reaction on longitudinal stress at bottom of the slab (177-in. joint spacing and $\alpha(\Delta T/D)$ of 0 in.$^{-1}$)**

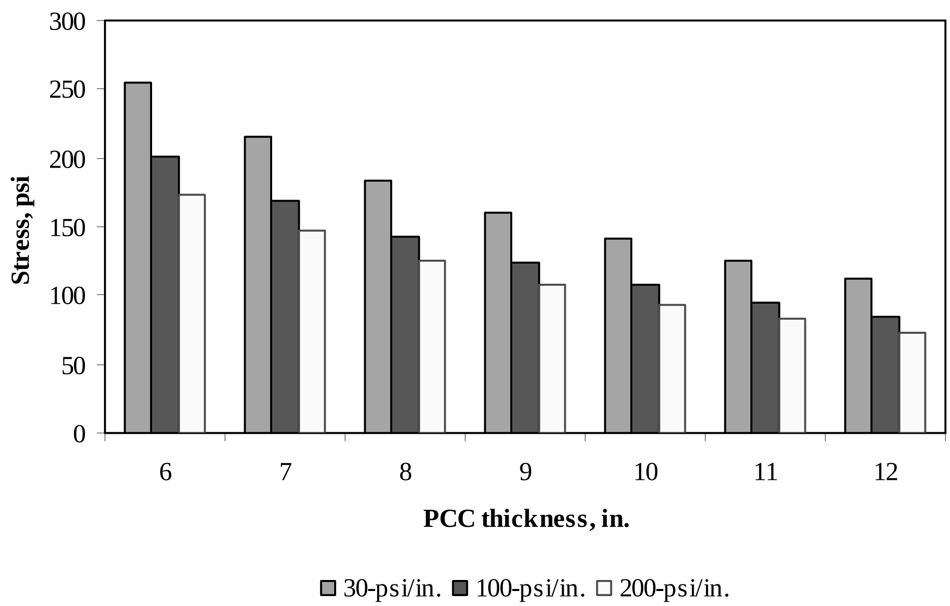


**Figure F-1-14: Impact of PCC thickness and modulus of subgrade reaction on longitudinal stress at bottom of the slab (315-in. joint spacing and $\alpha(\Delta T/D)$ of 0 in.$^{-1}$)**

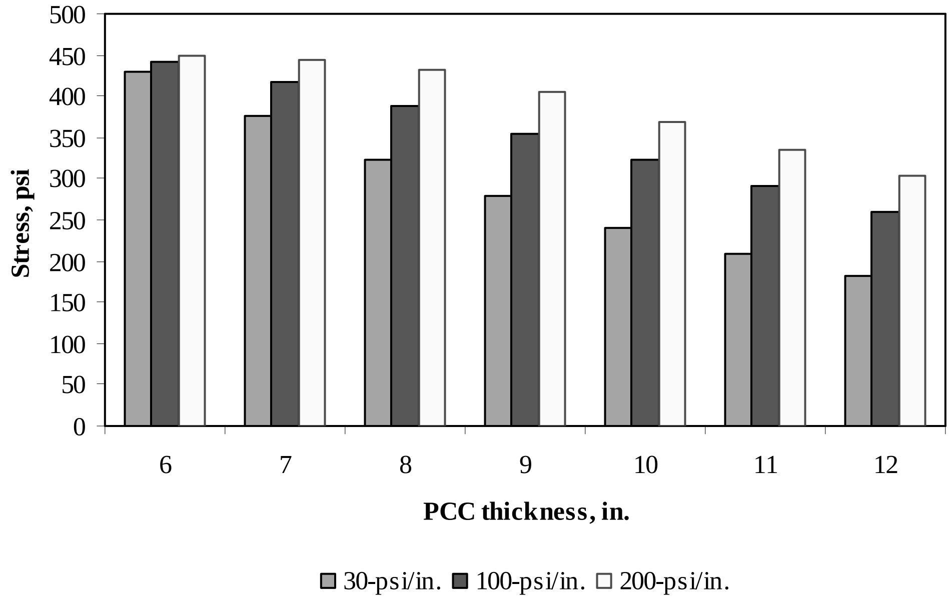


**Figure F-1-15: Impact of PCC thickness and modulus of subgrade reaction on longitudinal stress at bottom of the slab (177-in. joint spacing and $\alpha(\Delta T/D)$ of $20x10^{-6}$ in.$^{-1}$)**

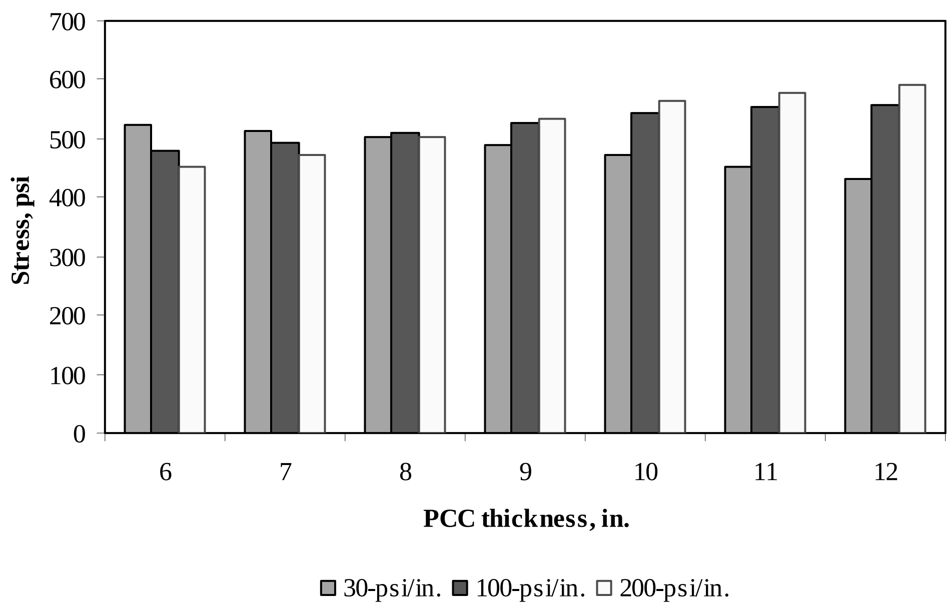


**Figure F-1-16: Impact of PCC thickness and modulus of subgrade reaction on longitudinal stress at bottom of the slab (315-in. joint spacing and $\alpha(\Delta T/D)$ of $20x10^{-6}$ in.$^{-1}$)**

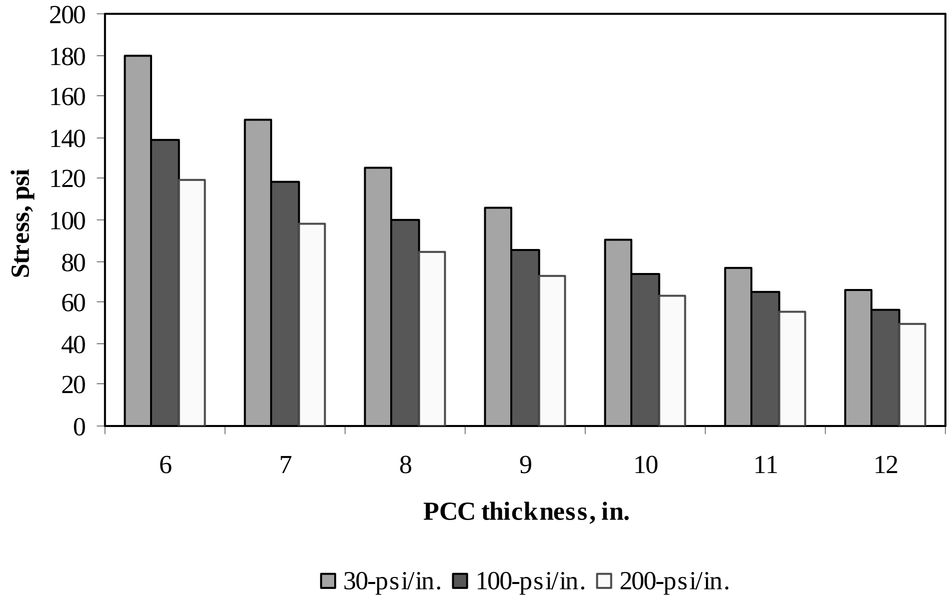


**Figure F-1-17: Impact of PCC thickness and modulus of subgrade reaction on longitudinal stress at top of the Slab (177-in. joint spacing and $\alpha(\Delta T/D)$ of 0 in.$^{-1}$)**

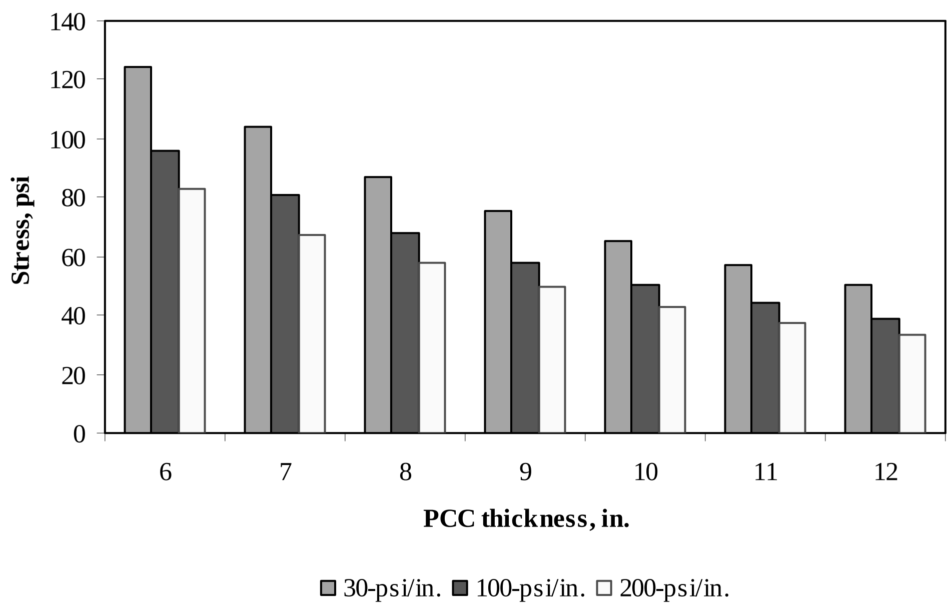


**Figure F-1-18: Impact of PCC thickness and modulus of subgrade reaction on longitudinal stress at top of the Slab (315-in. joint spacing and $\alpha(\Delta T/D)$ of 0 in.$^{-1}$)**

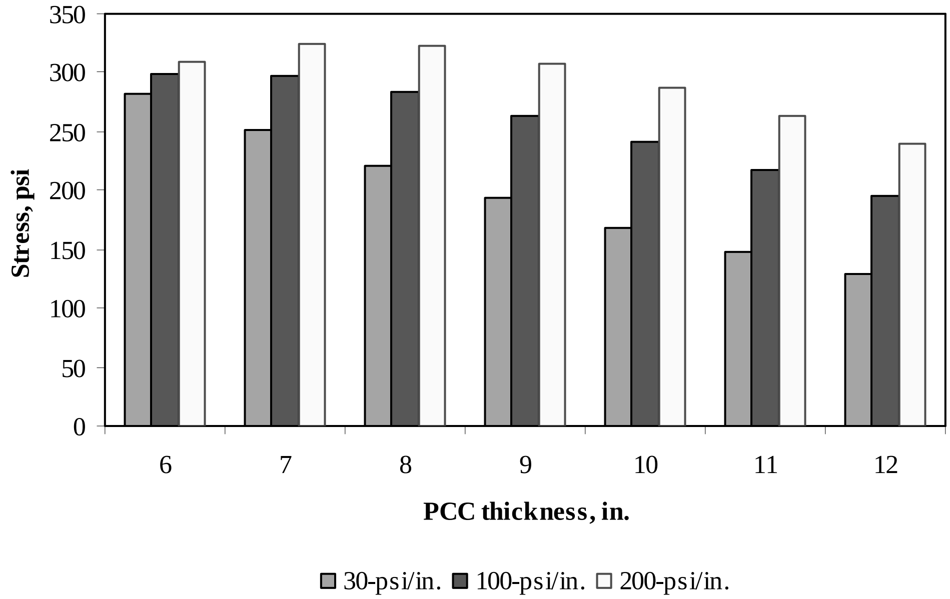


**Figure F-1-19: Impact of PCC thickness and modulus of subgrade reaction on longitudinal stress at top of the Slab (177-in. joint spacing and $\alpha(\Delta T/D)$ of $-20x10^{-6}$ in.$^{-1}$)**

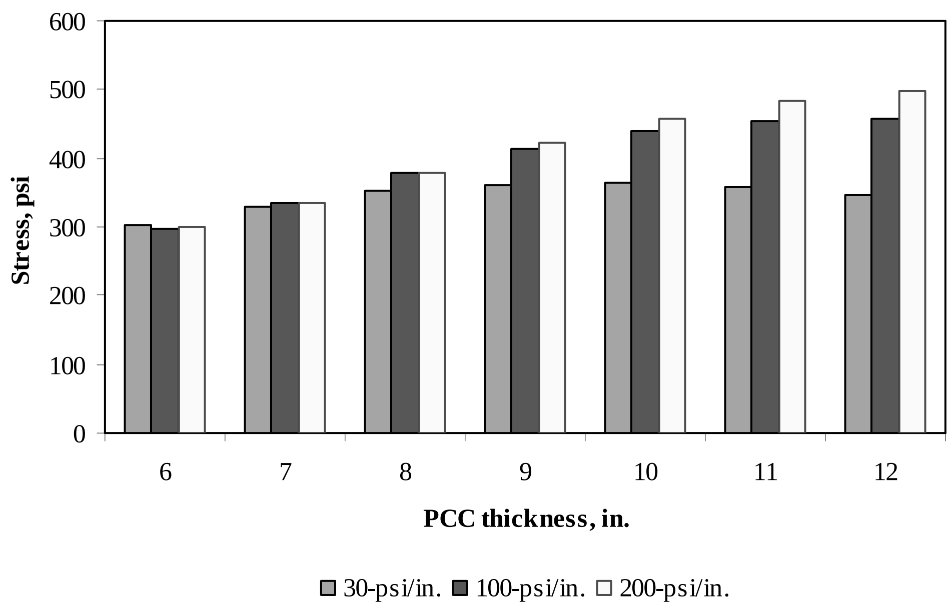


**Figure F-1-20: Impact of PCC thickness and modulus of subgrade reaction on longitudinal stress at top of the Slab (315-in. joint spacing and $\alpha(\Delta T/D)$ of $-20x10^{-6}$ in.$^{-1}$)**

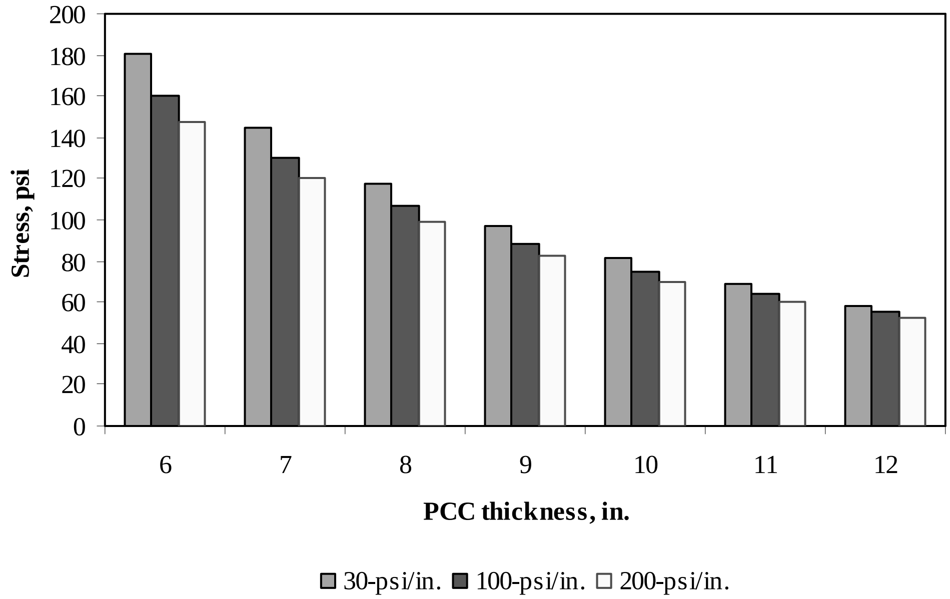


**Figure F-1-21: Impact of PCC thickness and modulus of subgrade reaction on transverse stress at bottom of the Slab (177-in. joint spacing and $\alpha(\Delta T/D)$ of 0 in.$^{-1}$)**

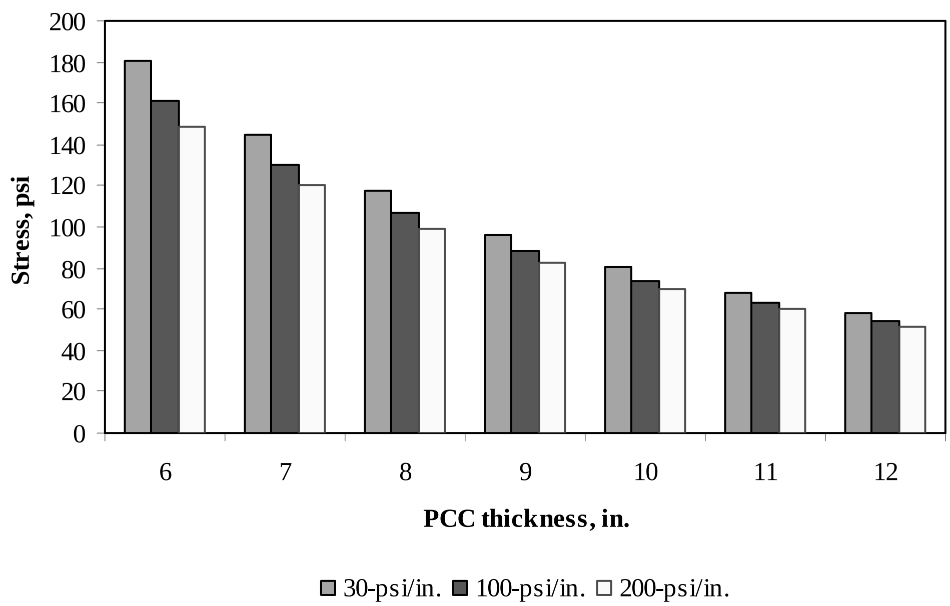


**Figure F-1-22: Impact of PCC thickness and modulus of subgrade reaction on transverse stress at bottom of the Slab (315-in. joint spacing and $\alpha(\Delta T/D)$ of 0 in.$^{-1}$)**

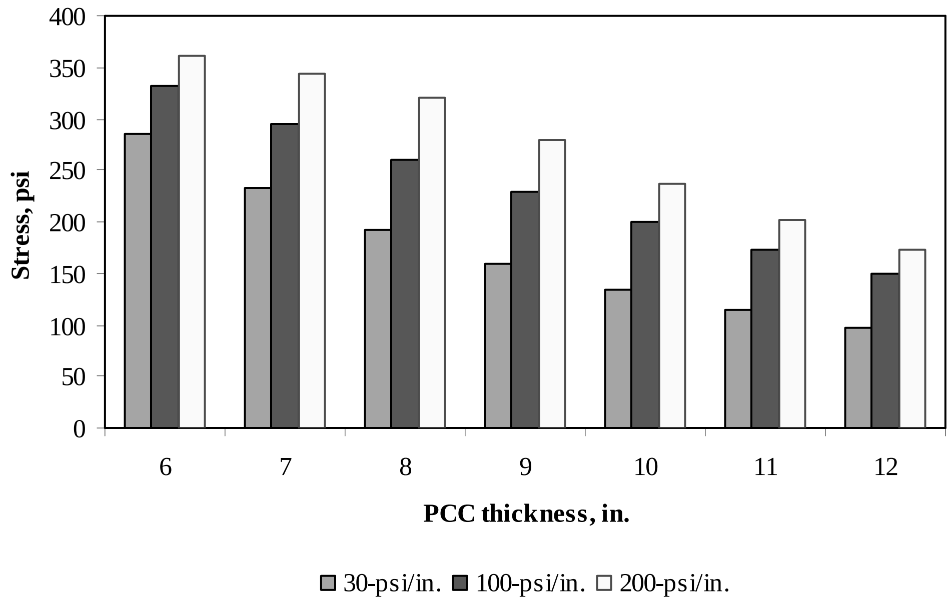


**Figure F-1-23: Impact of PCC thickness and modulus of subgrade reaction on transverse stress at bottom of the Slab (177-in. joint spacing and $\alpha(\Delta T/D)$ of $20x10^{-6}$ in.$^{-1}$)**

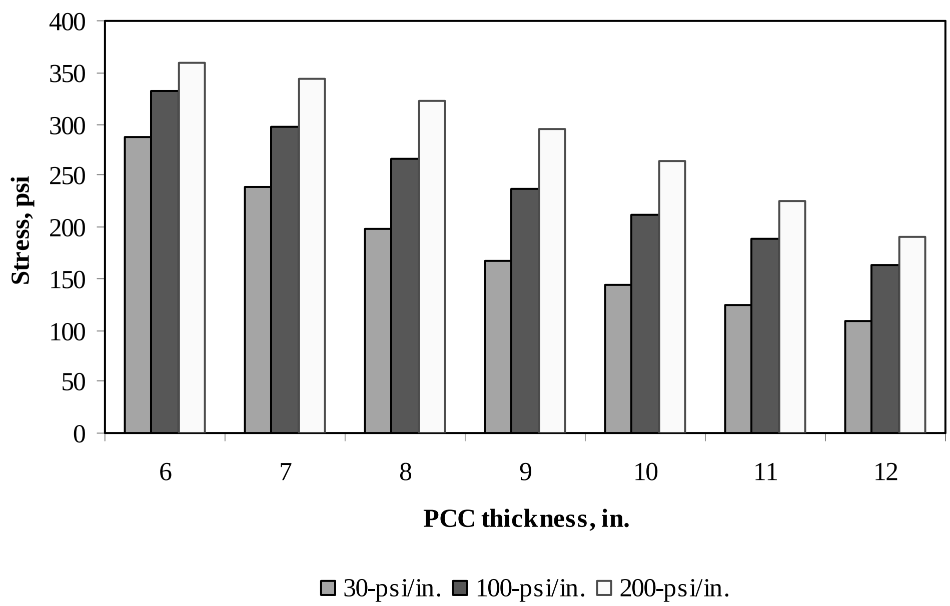


**Figure F-1-24: Impact of PCC thickness and modulus of subgrade reaction on transverse stress at bottom of the Slab (315-in. joint spacing and $\alpha(\Delta T/D)$ of $20x10^{-6}$ in.$^{-1}$)**

Figures F-1-25 through F-1-36 illustrate the impact of PCC thickness and lateral support condition on stresses (16-in. base/subbase and 100-psi/in. modulus of subgrade reaction)

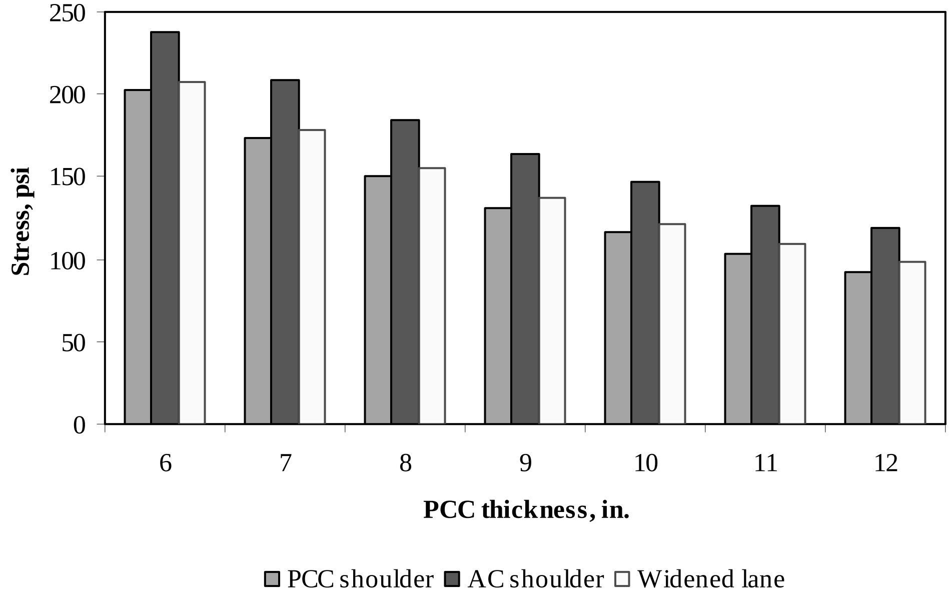


**Figure F-1-25: Impact of PCC thickness and lateral support condition on longitudinal stress at bottom of the Slab (177-in. joint spacing and $\alpha(\Delta T/D)$ of 0 in.$^{-1}$)**

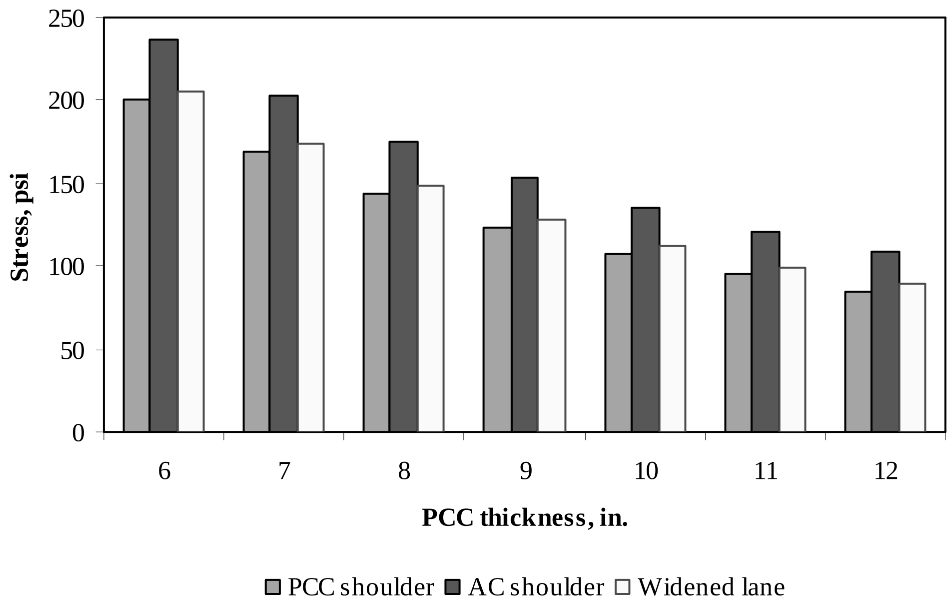


**Figure F-1-26: Impact of PCC thickness and lateral support condition on longitudinal stress at bottom of the Slab (315-in. joint spacing and $\alpha(\Delta T/D)$ of 0 in.$^{-1}$)**

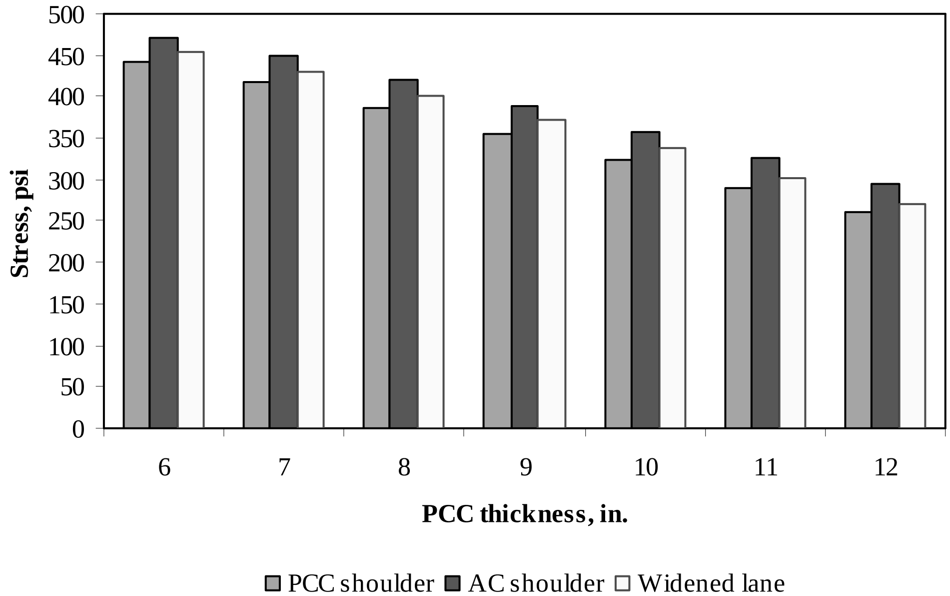


**Figure F-1-27: Impact of PCC thickness and lateral support condition on longitudinal stress at bottom of the Slab (177-in. joint spacing and $\alpha(\Delta T/D)$ of $20x10^{-6}$ in.$^{-1}$)**

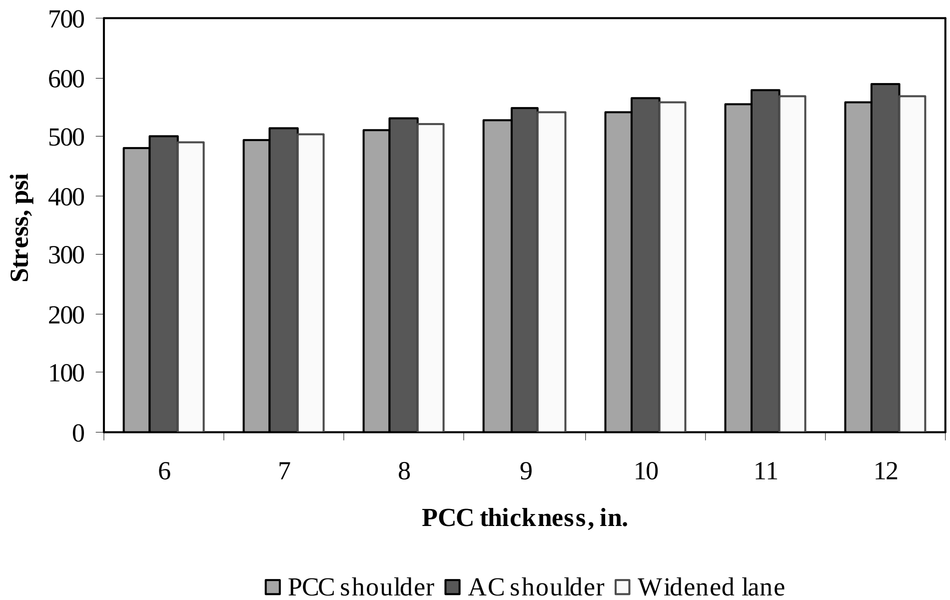


**Figure F-1-28: Impact of PCC thickness and lateral support condition on longitudinal stress at bottom of the Slab (315-in. joint spacing and $\alpha(\Delta T/D)$ of $20x10^{-6}$ in.$^{-1}$)**

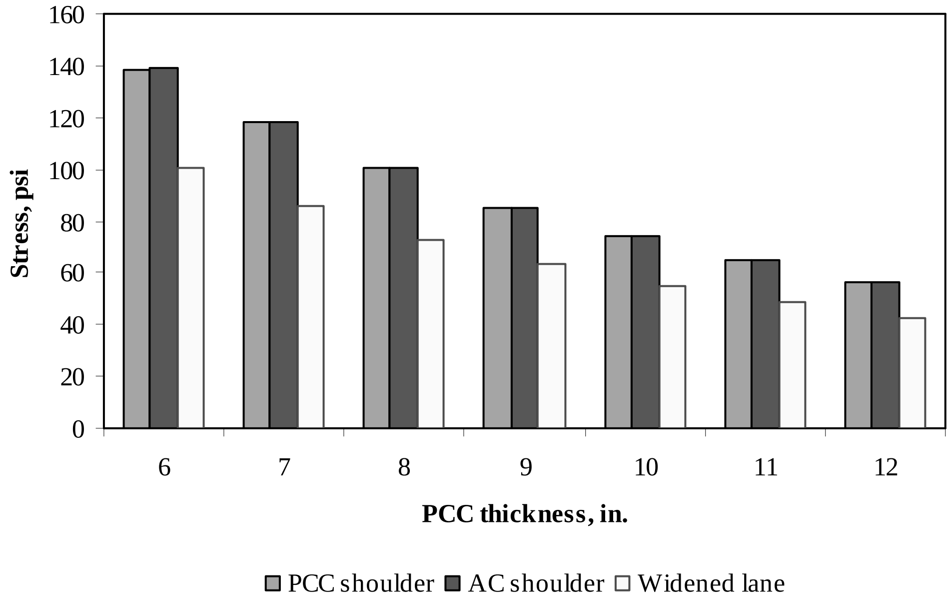


**Figure F-1-29: Impact of PCC thickness and lateral support condition on longitudinal stress at top of the Slab (177-in. joint spacing and $\alpha(\Delta T/D)$ of 0 in.$^{-1}$)**

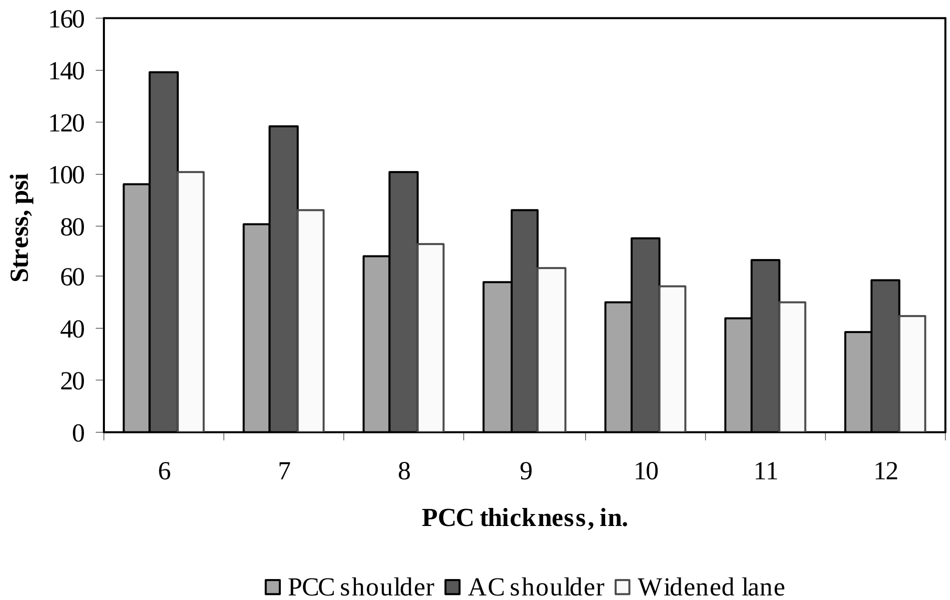


**Figure F-1-30: Impact of PCC thickness and lateral support condition on longitudinal stress at top of the Slab (315-in. joint spacing and $\alpha(\Delta T/D)$ of 0 in.$^{-1}$)**

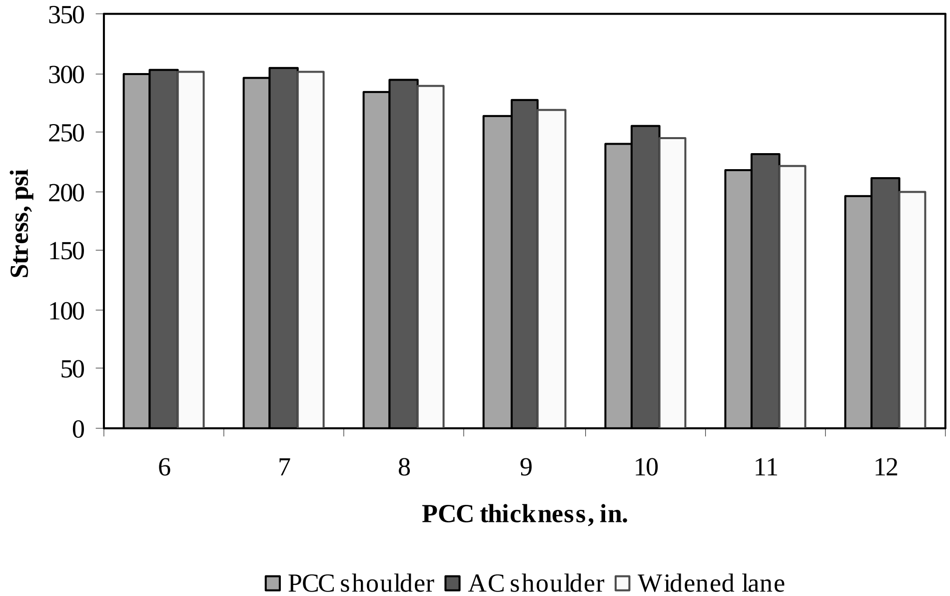


**Figure F-1-31: Impact of PCC thickness and lateral support condition on longitudinal stress at top of the Slab (177-in. joint spacing and $\alpha(\Delta T/D)$ of $-20 x 10^{-6}$ in.$^{-1}$)**

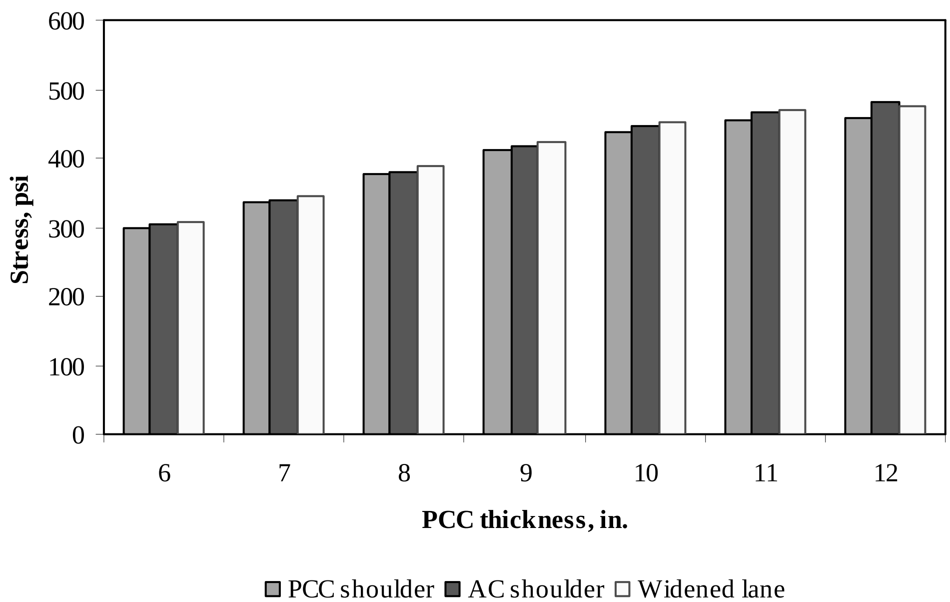


**Figure F-1-32: Impact of PCC thickness and lateral support condition on longitudinal stress at top of the Slab (315-in. joint spacing and $\alpha(\Delta T/D)$ of $-20 x 10^{-6}$ in.$^{-1}$)**

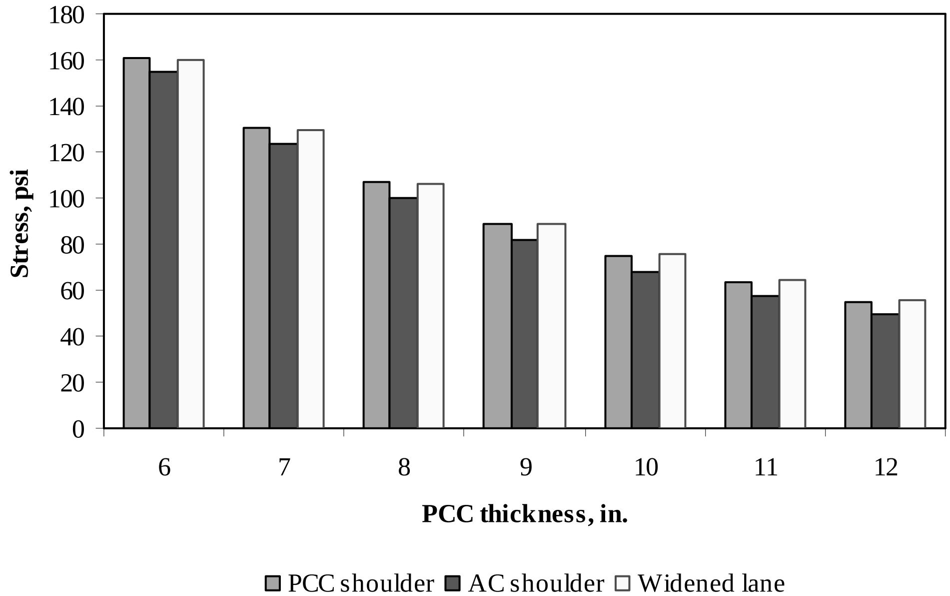


**Figure F-1-33: Impact of PCC thickness and lateral support condition on transverse stress at bottom of the Slab (177-in. joint spacing and $\alpha(\Delta T/D)$ of 0 in.$^{-1}$)**

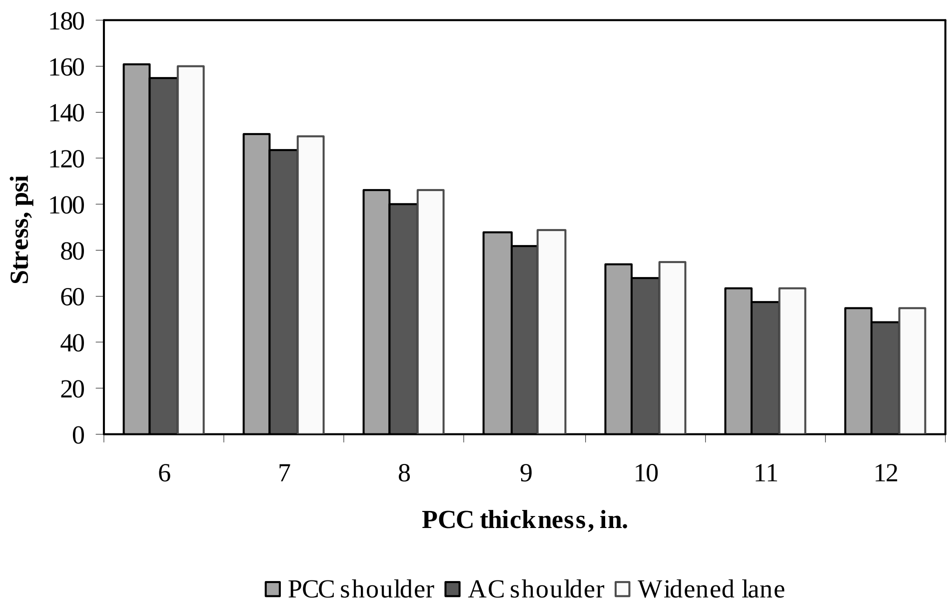


**Figure F-1-34: Impact of PCC thickness and lateral support condition on transverse stress at bottom of the Slab (315-in. joint spacing and $\alpha(\Delta T/D)$ of 0 in.$^{-1}$)**

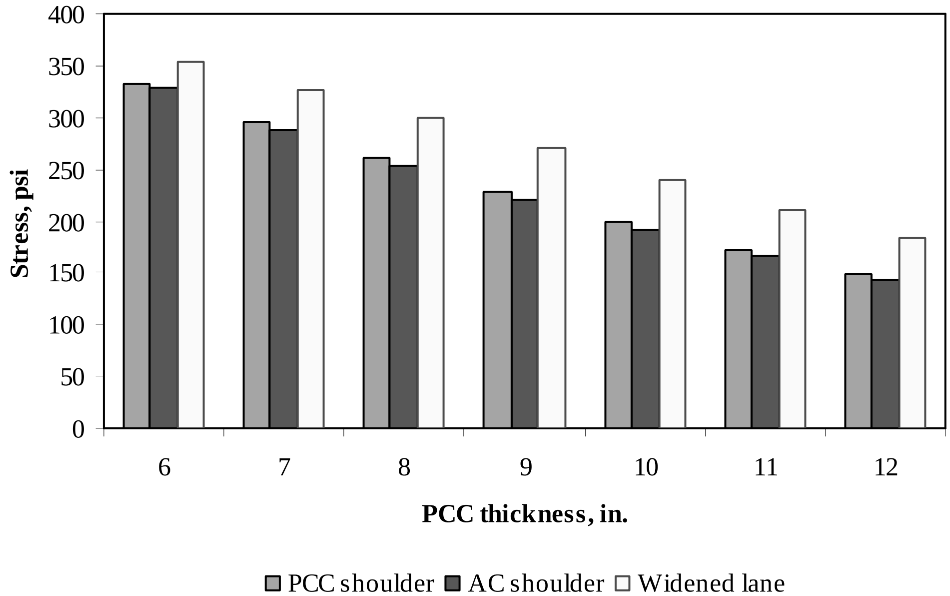


**Figure F-1-35: Impact of PCC thickness and lateral support condition on transverse stress at bottom of the Slab (177-in. joint spacing and $\alpha(\Delta T/D)$ of $20 x 10^{-6}$ in.$^{-1}$)**

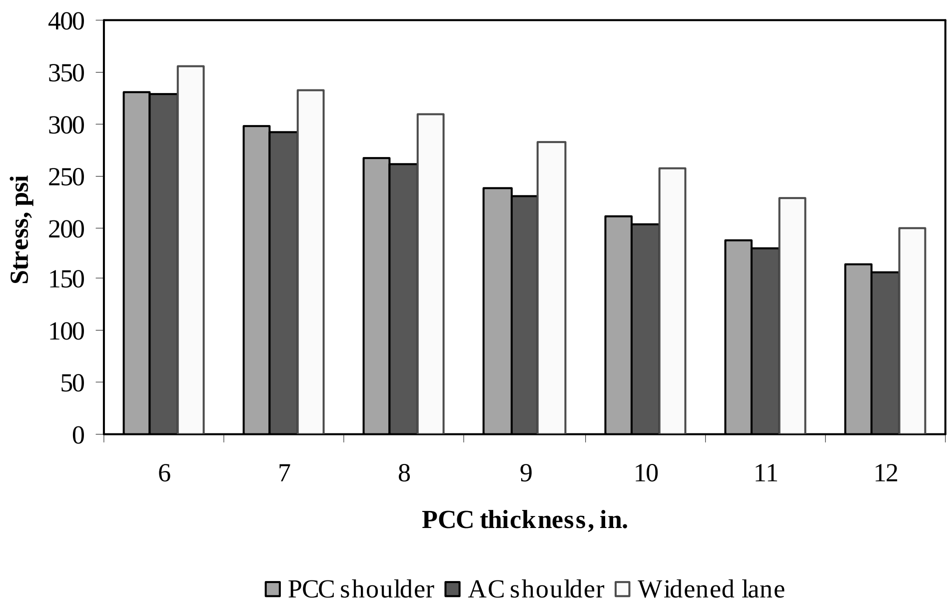


**Figure F-1-36: Impact of PCC thickness and lateral support condition on transverse stress at bottom of the Slab (315-in. joint spacing and $\alpha(\Delta T/D)$ of $20 x 10^{-6}$ in.$^{-1}$)**

Figures F-1-37 through F-1-42 illustrate the impact of base/subbase thickness and product $\alpha(\Delta T/D)$ on stresses (10-in. PCC thickness, 100-psi/in. modulus of subgrade reaction and PCC shoulder)

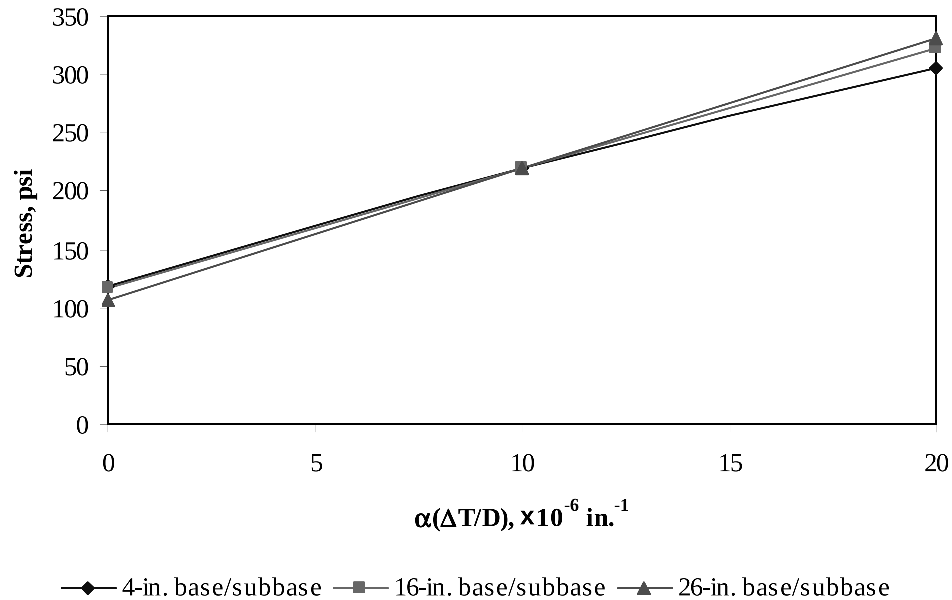


**Figure F-1-37: Impact of base/subbase thickness and product $\alpha(\Delta T/D)$ on longitudinal stress at bottom of the slab (177-in. joint spacing)**

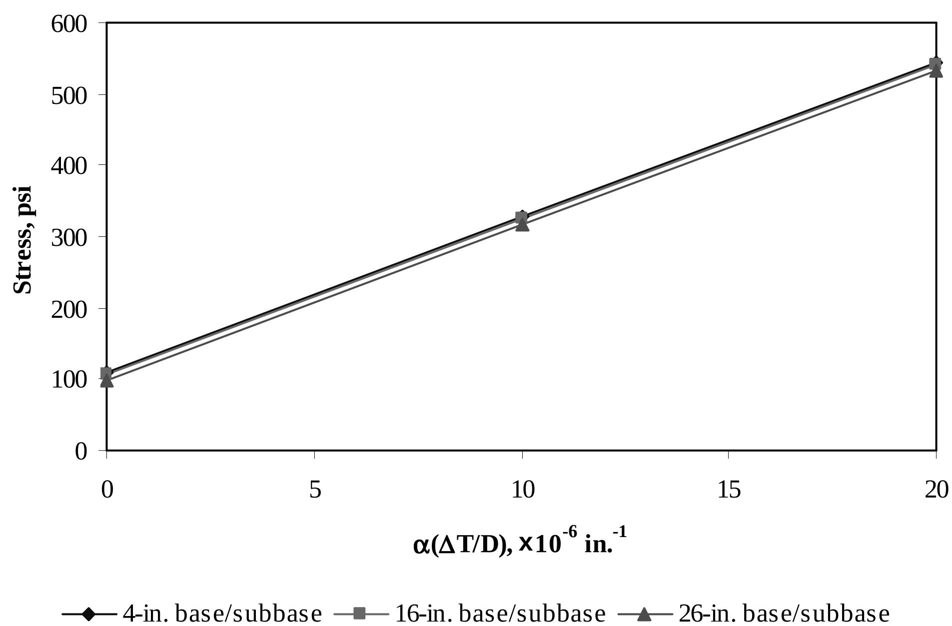


**Figure F-1-38: Impact of base/subbase thickness and product $\alpha(\Delta T/D)$ on longitudinal stress at bottom of the slab (315-in. joint spacing)**

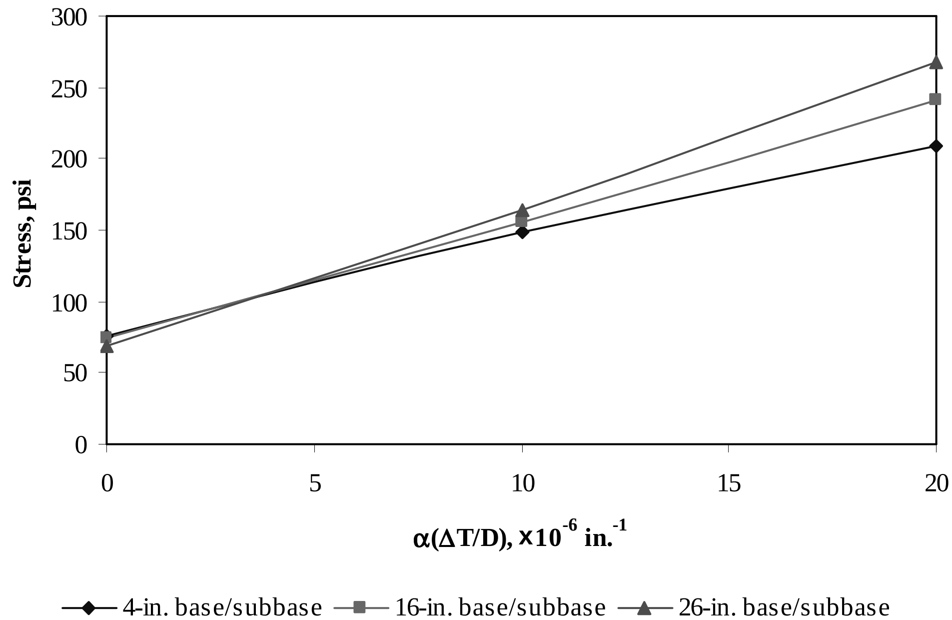


**Figure F-1-39: Impact of base/subbase thickness and product α(ΔT/D) on longitudinal stress at top of the slab (177-in. joint spacing)**

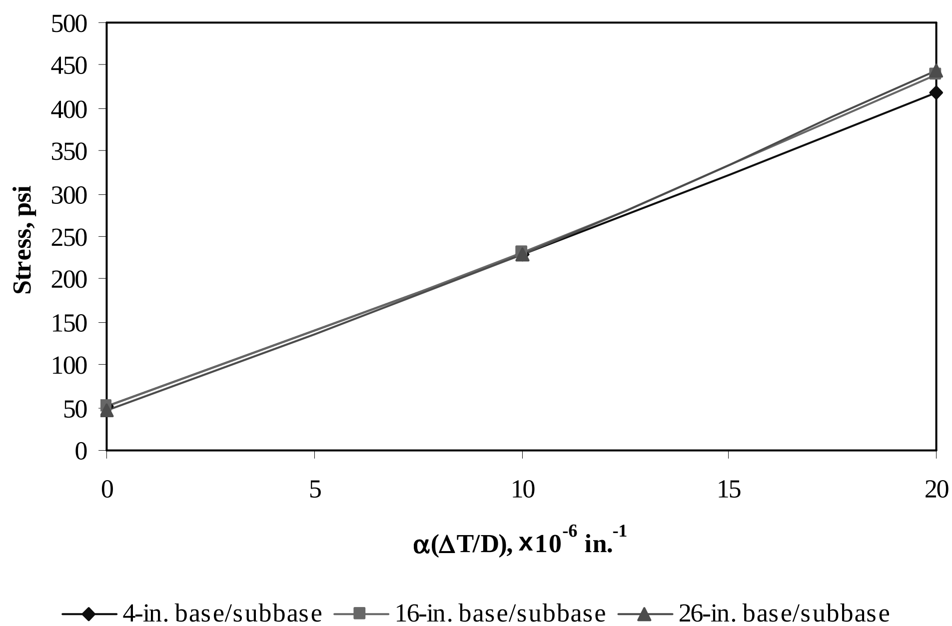


**Figure F-1-40: Impact of base/subbase thickness and product α(ΔT/D) on longitudinal stress at top of the slab (315-in. joint spacing)**

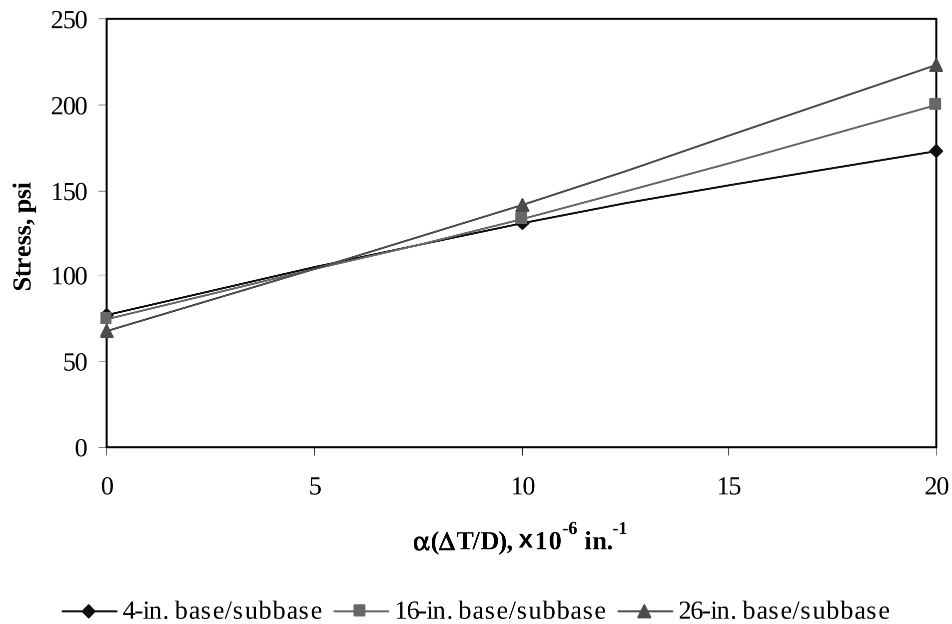


**Figure F-1-41: Impact of base/subbase thickness and product α(ΔT/D) on transverse stress at bottom of the slab (177-in. joint spacing)**

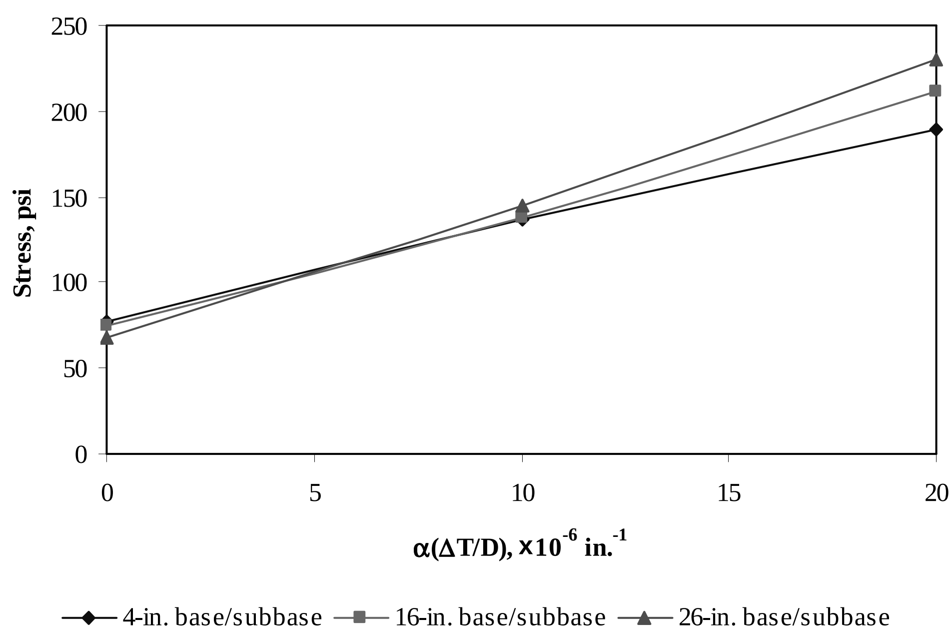


**Figure F-1-42: Impact of base/subbase thickness and product α(ΔT/D) on transverse stress at bottom of the slab (315-in. joint spacing)**

Figures F-1-43 through F-1-48 illustrate the impact of modulus of subgrade reaction and product α(ΔT/D) on stresses (10-in. PCC thickness, 16-in. base/subbase thickness and PCC shoulder)

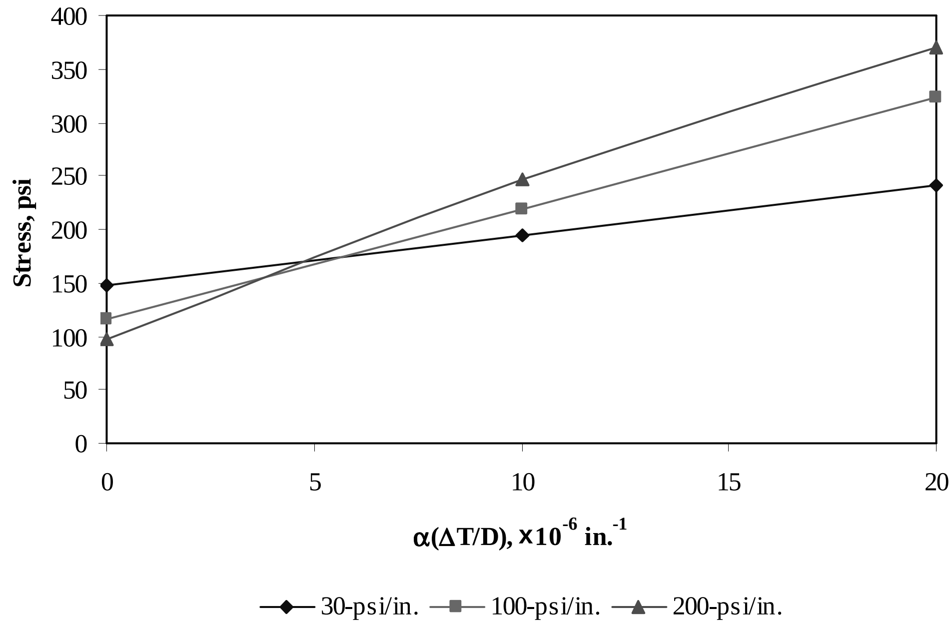


**Figure F-1-43: Impact of modulus of subgrade reaction and product α(ΔT/D) on longitudinal stress at bottom of the slab (177-in. joint spacing)**

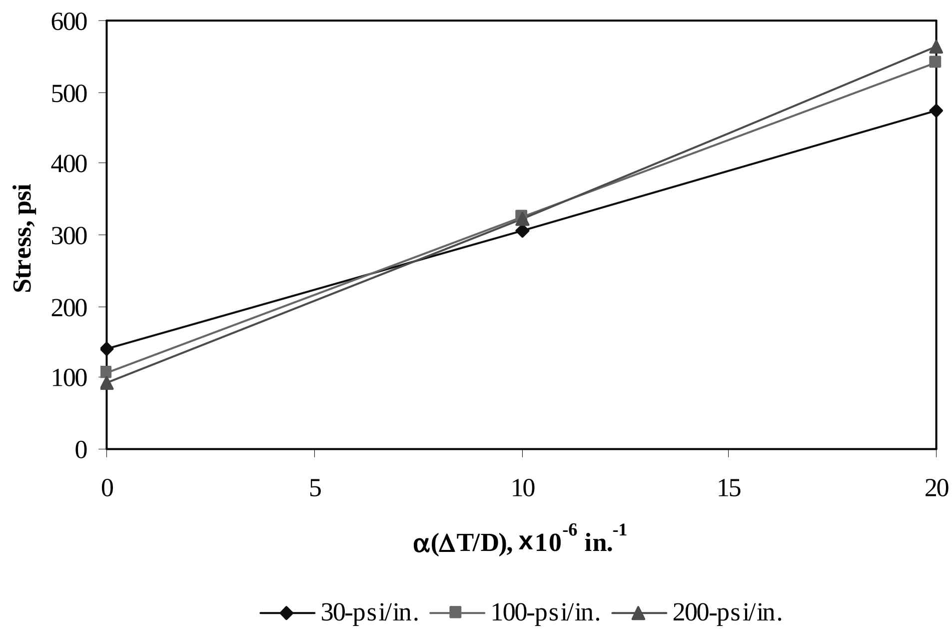


**Figure F-1-44: Impact of modulus of subgrade reaction and product α(ΔT/D) on longitudinal stress at bottom of the slab (315-in. joint spacing)**

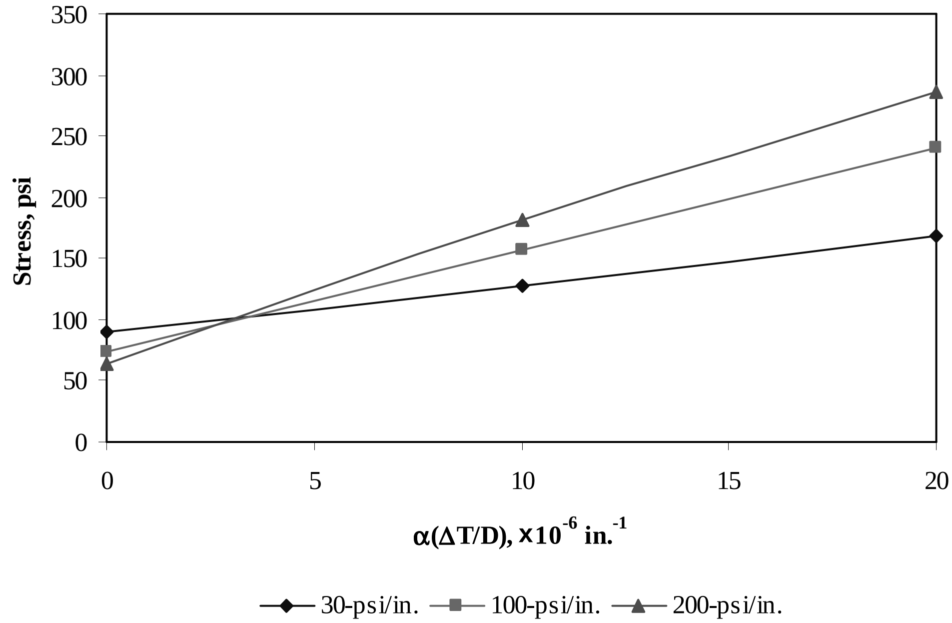


**Figure F-1-45: Impact of modulus of subgrade reaction and product $\alpha(\Delta T/D)$ on longitudinal stress at top of the slab (177-in. joint spacing)**

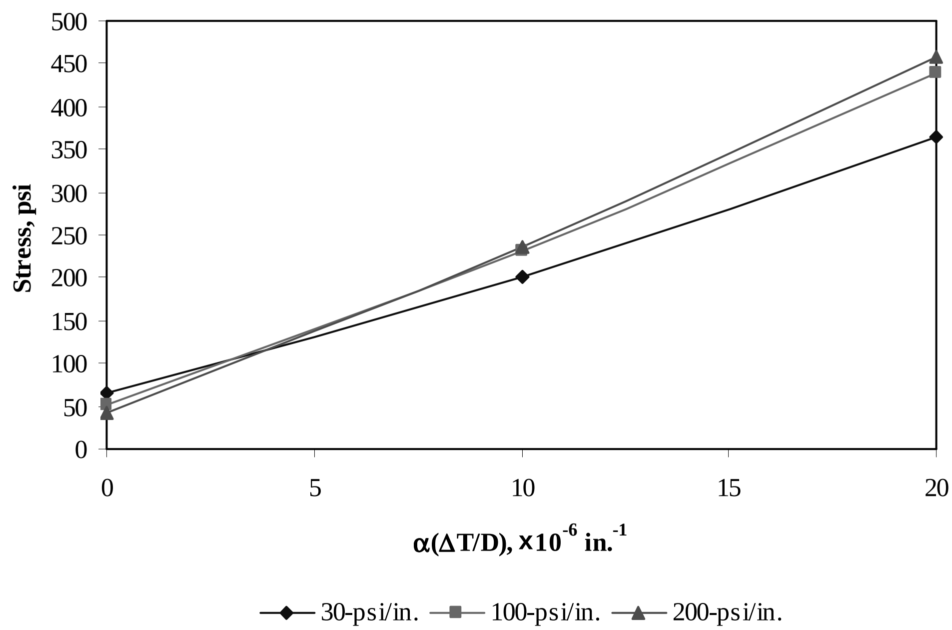


**Figure F-1-46: Impact of modulus of subgrade reaction and product $\alpha(\Delta T/D)$ on longitudinal stress at top of the slab (315-in. joint spacing)**

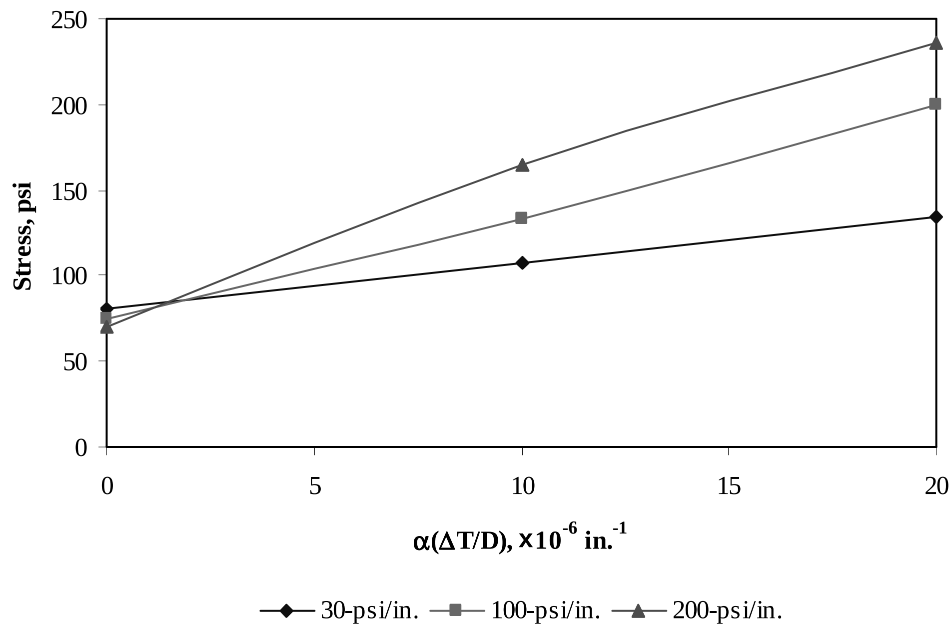


**Figure F-1-47: Impact of modulus of subgrade reaction and product α(ΔT/D) on transverse stress at bottom of the slab (177-in. joint spacing)**

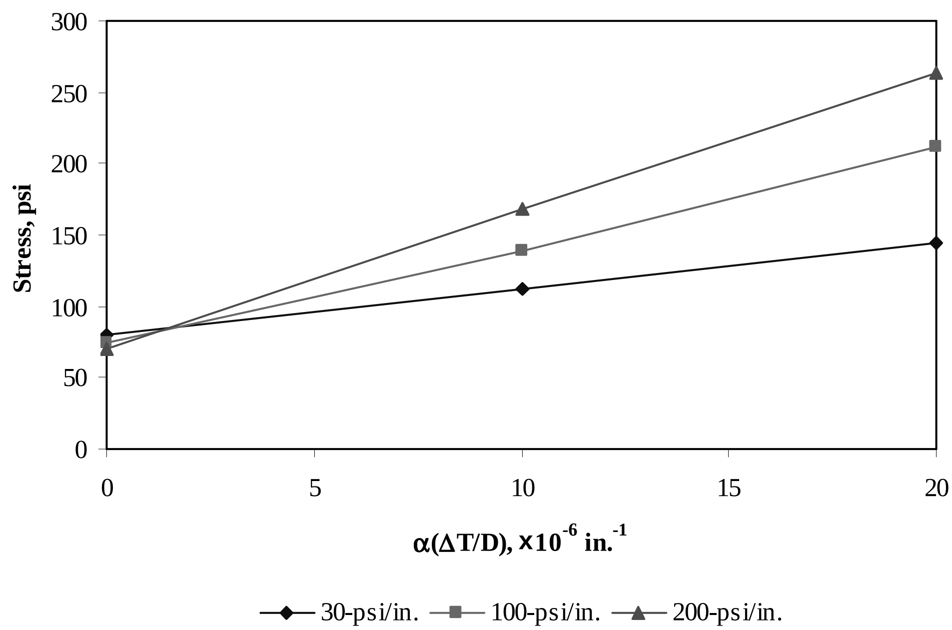


**Figure F-1-48: Impact of modulus of subgrade reaction and product α(ΔT/D) on transverse stress at bottom of the slab (315-in. joint spacing)**

Figures F-1-49 through F-1-51 illustrate the impact of joint spacing and product $\alpha(\Delta T/D)$ on stresses (10-in. PCC thickness, 16-in. base/subbase thickness, 100-psi/in. modulus of subgrade reaction and PCC shoulder)

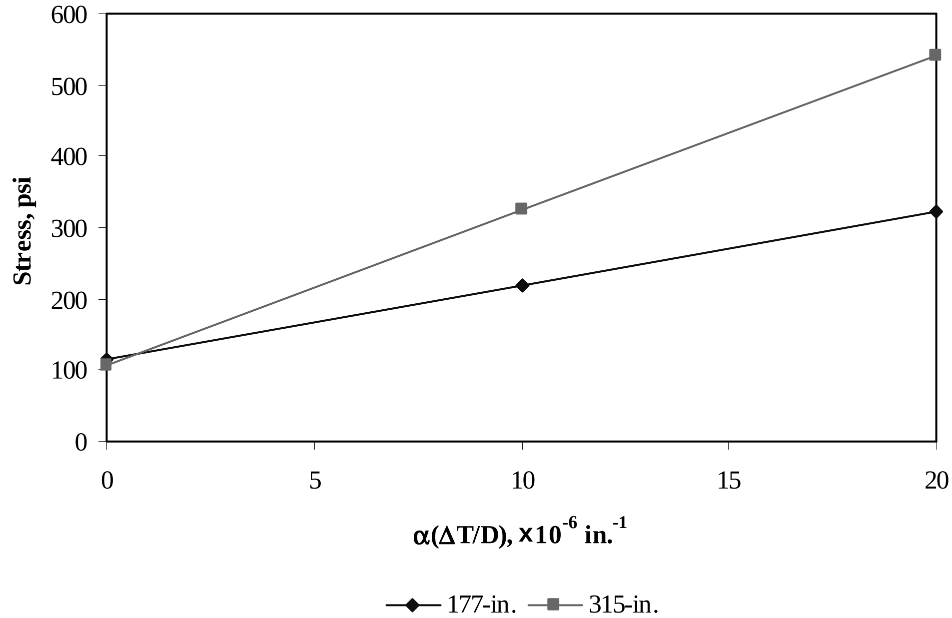


**Figure F-1-49: Impact of joint spacing and product $\alpha(\Delta T/D)$ on longitudinal stress at bottom of the slab**

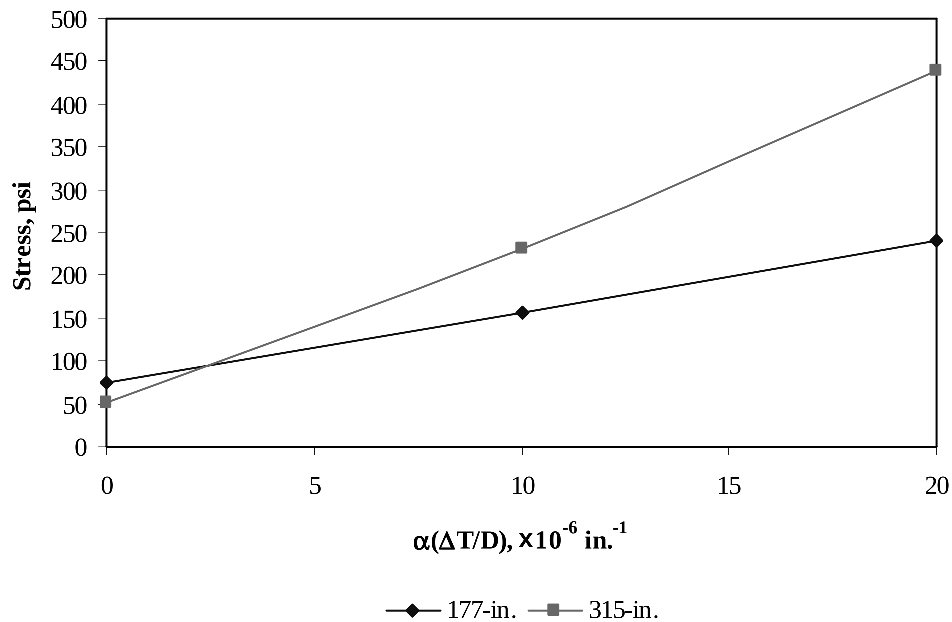


**Figure F-1-50: Impact of joint spacing and product $\alpha(\Delta T/D)$ on longitudinal stress at top of the slab**

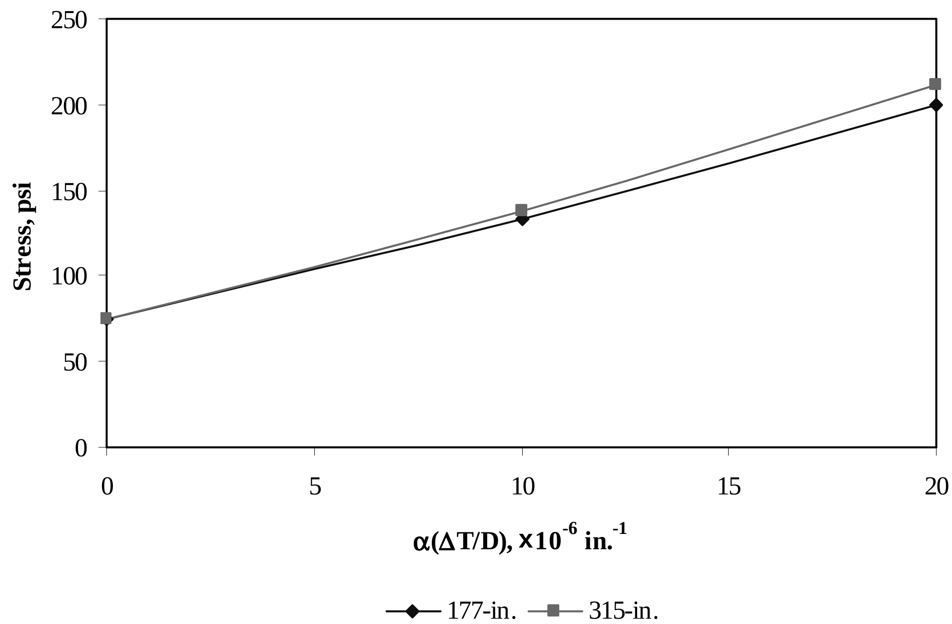


**Figure F-1-51: Impact of joint spacing and product $\alpha(\Delta T/D)$ on transverse stress at bottom of the slab**

**Sub Appendix F-2**

**Documentation of Pavement Responses for**


**32-kips Tandem Axle**

Figures F-2-1 through F-2-12 illustrate the impact of PCC thickness and base/subbase thickness on stresses (100-psi/in. modulus of subgrade reaction and PCC shoulder)

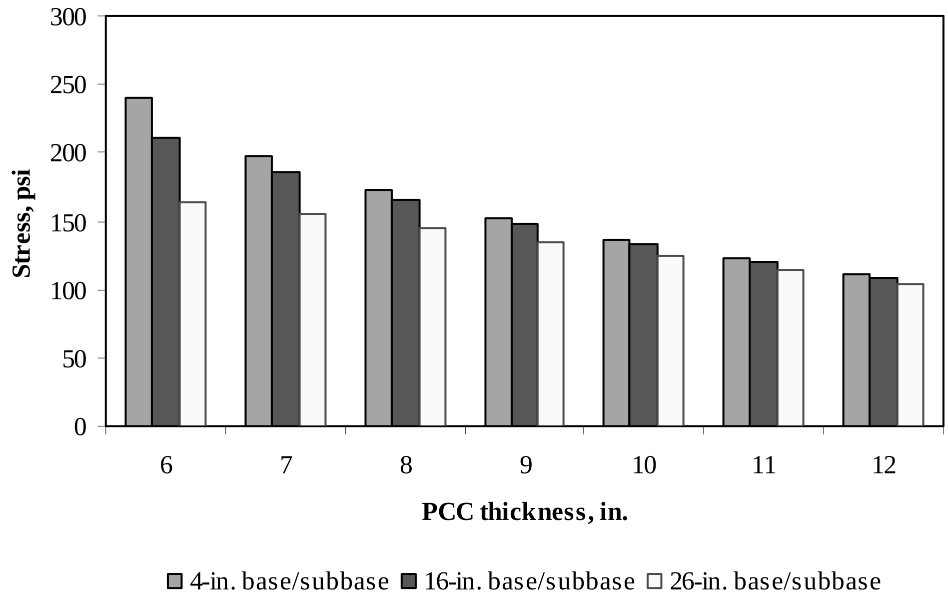


**Figure F-2-1: Impact of PCC thickness and base/subbase thickness on longitudinal stress at bottom of the Slab (177-in. joint spacing and $\alpha(\Delta T/D)$ of 0 in.$^{-1}$)**

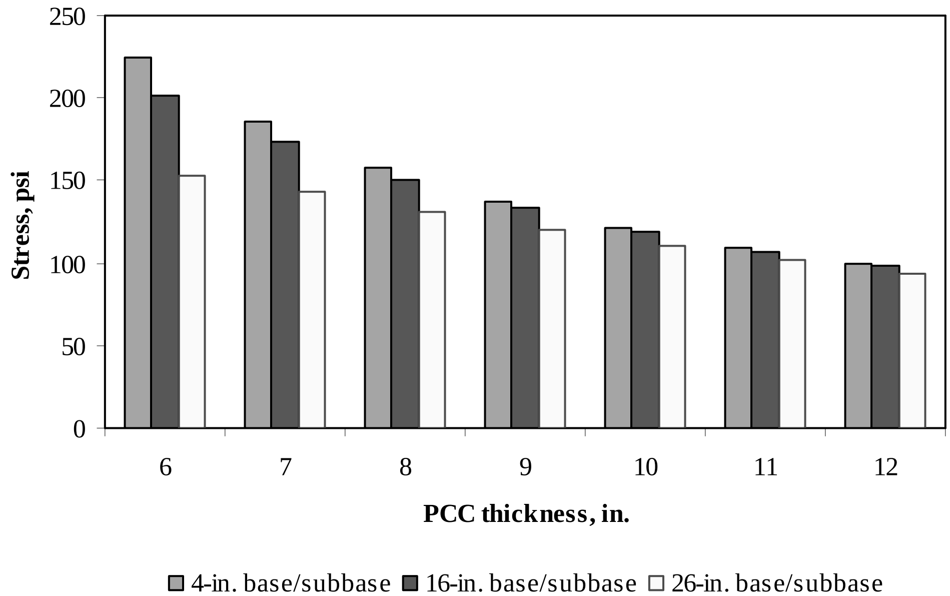


**Figure F-2-2: Impact of PCC thickness and base/subbase thickness on longitudinal stress at bottom of the Slab (315-in. joint spacing and $\alpha(\Delta T/D)$ of 0 in.$^{-1}$)**

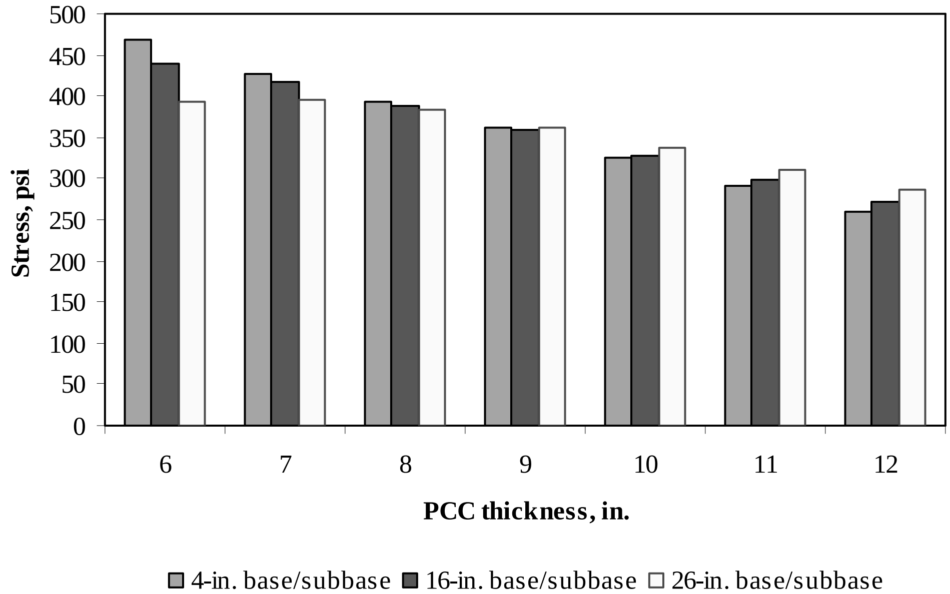


**Figure F-2-3: Impact of PCC thickness and base/subbase thickness on longitudinal stress at bottom of the Slab (177-in. joint spacing and $\alpha(\Delta T/D)$ of $20x10^{-6}$ in.$^{-1}$)**

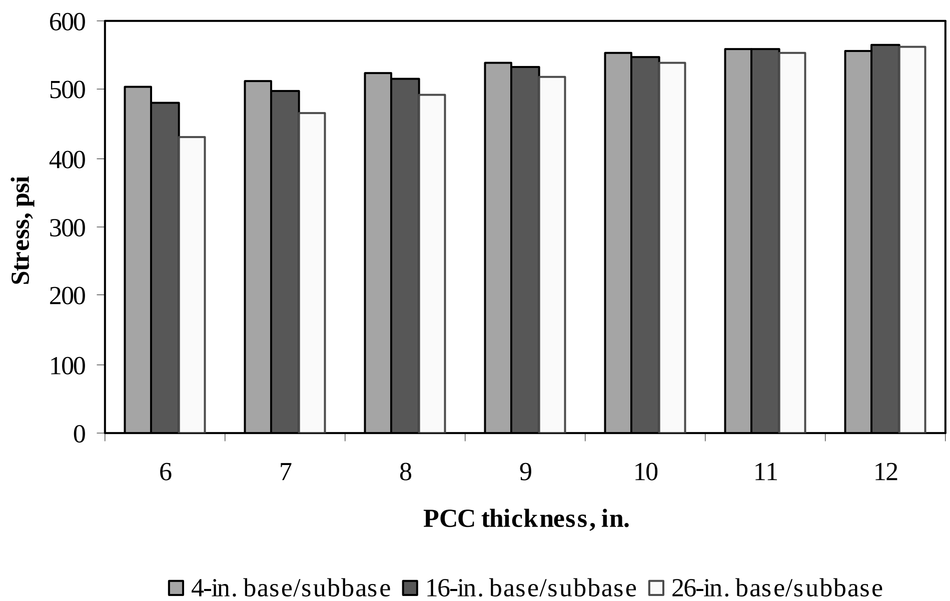


**Figure F-2-4: Impact of PCC thickness and base/subbase thickness on longitudinal stress at bottom of the Slab (315-in. joint spacing and $\alpha(\Delta T/D)$ of $20x10^{-6}$ in.$^{-1}$)**

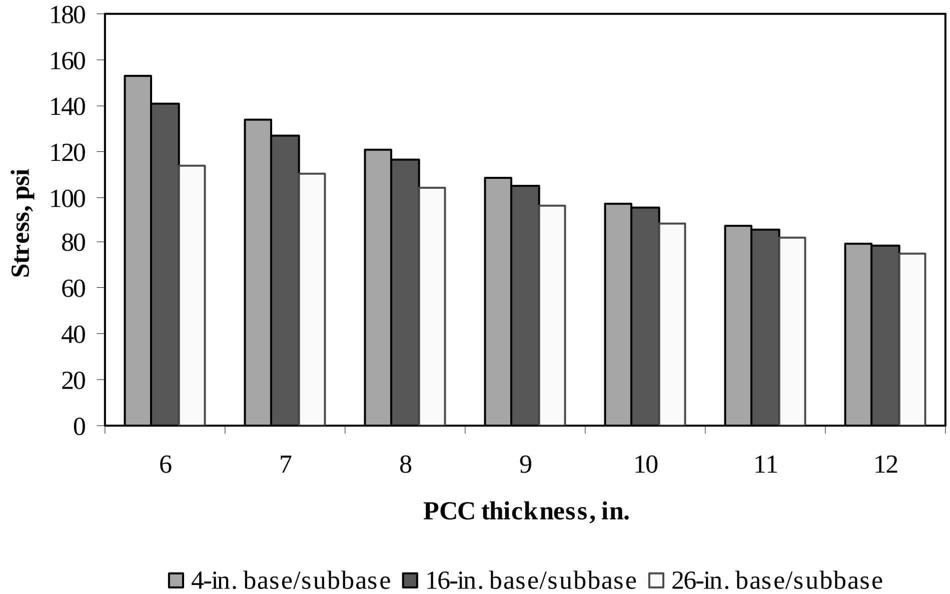


**Figure F-2-5: Impact of PCC thickness and base/subbase thickness on longitudinal stress at top of the Slab (177-in. joint spacing and α(ΔT/D) of 0 in.$^{-1}$)**

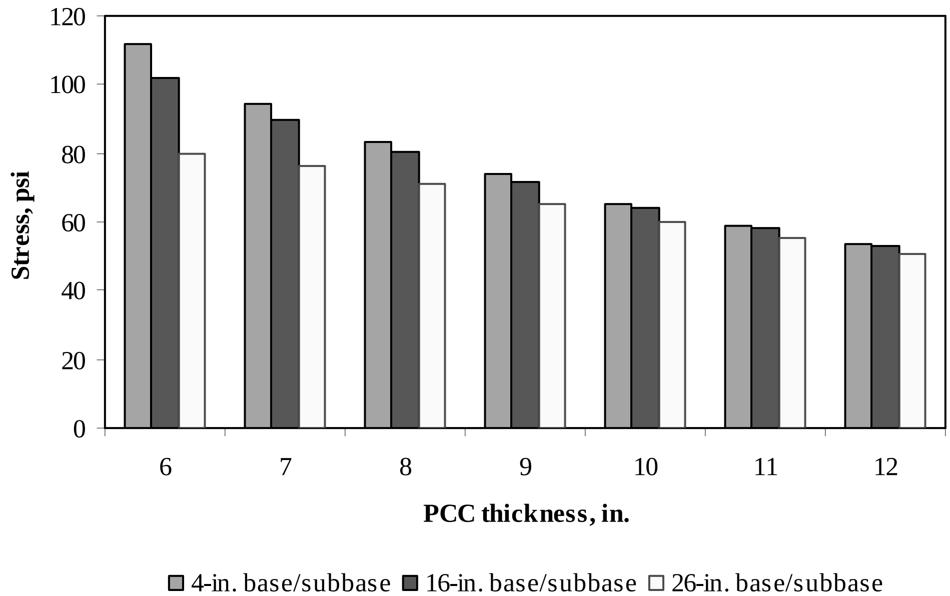


**Figure F-2-6: Impact of PCC thickness and base/subbase thickness on longitudinal stress at top of the Slab (315-in. joint spacing and α(ΔT/D) of 0 in.$^{-1}$)**

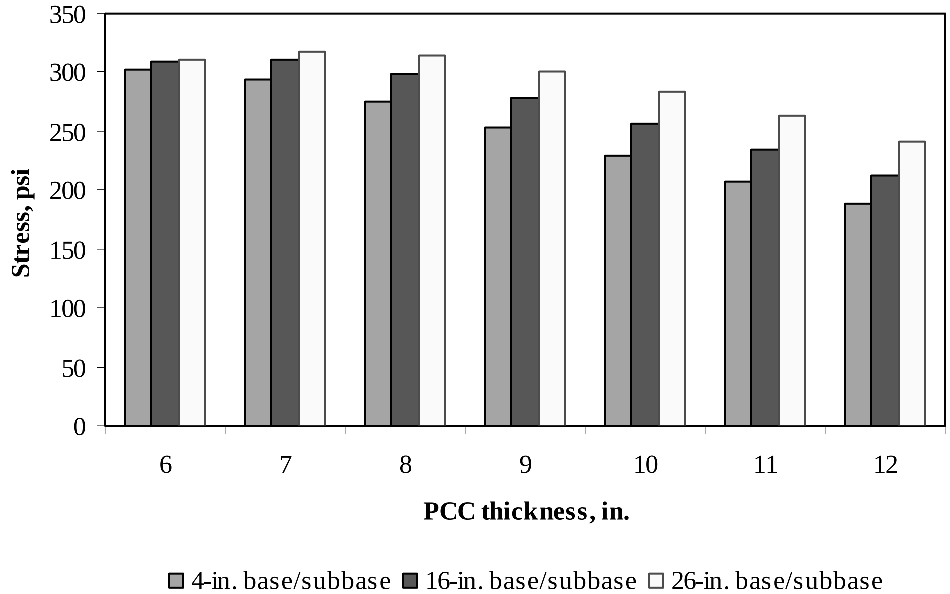


**Figure F-2-7: Impact of PCC thickness and base/subbase thickness on longitudinal stress at top of the Slab (177-in. joint spacing and $\alpha(\Delta T/D)$ of $-20x10^{-6}$ in.$^{-1}$)**

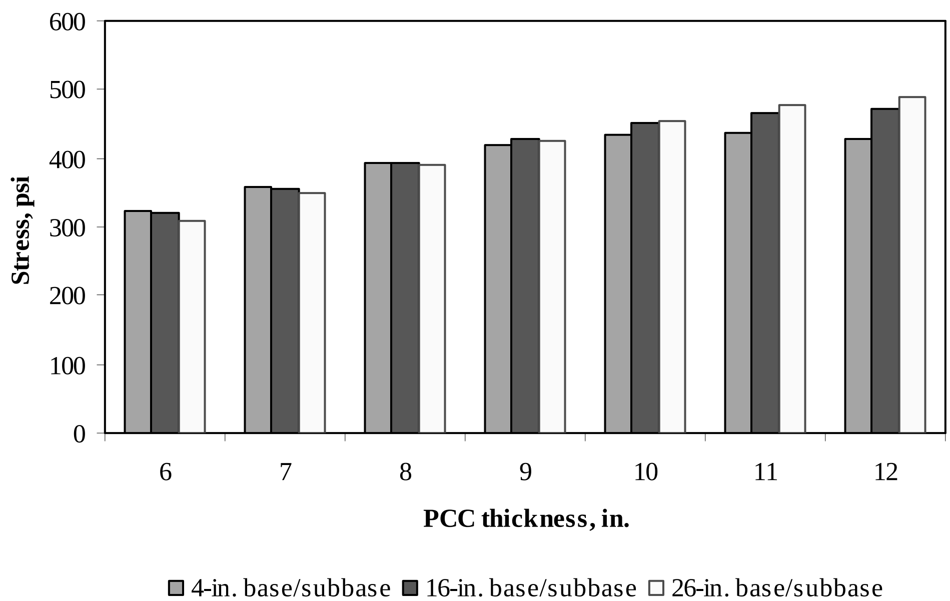


**Figure F-2-8: Impact of PCC thickness and base/subbase thickness on longitudinal stress at top of the Slab (315-in. joint spacing and $\alpha(\Delta T/D)$ of $-20x10^{-6}$ in.$^{-1}$)**

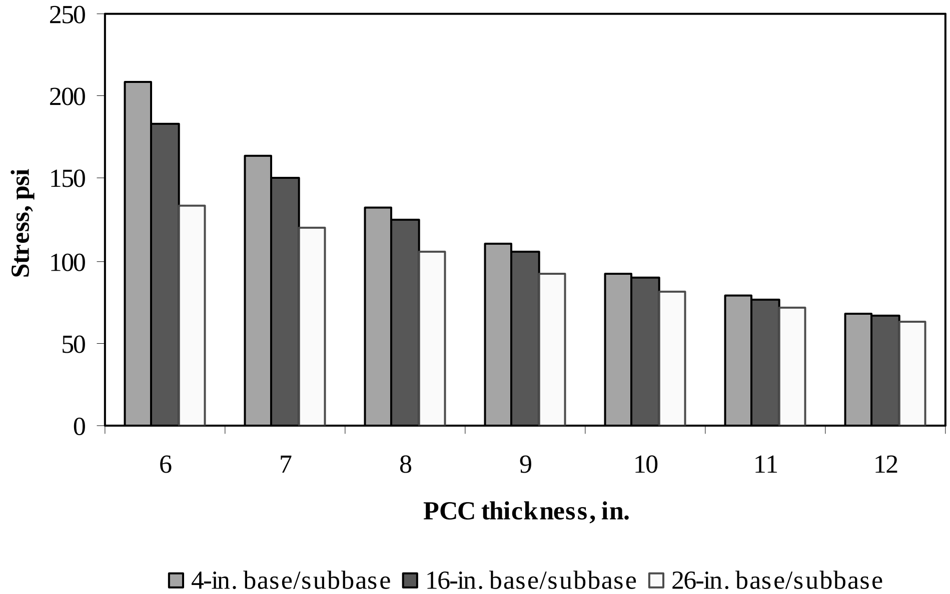


**Figure F-2-9: Impact of PCC thickness and base/subbase thickness on transverse stress at bottom of the Slab (177-in. joint spacing and $\alpha(\Delta T/D)$ of 0 in.$^{-1}$)**

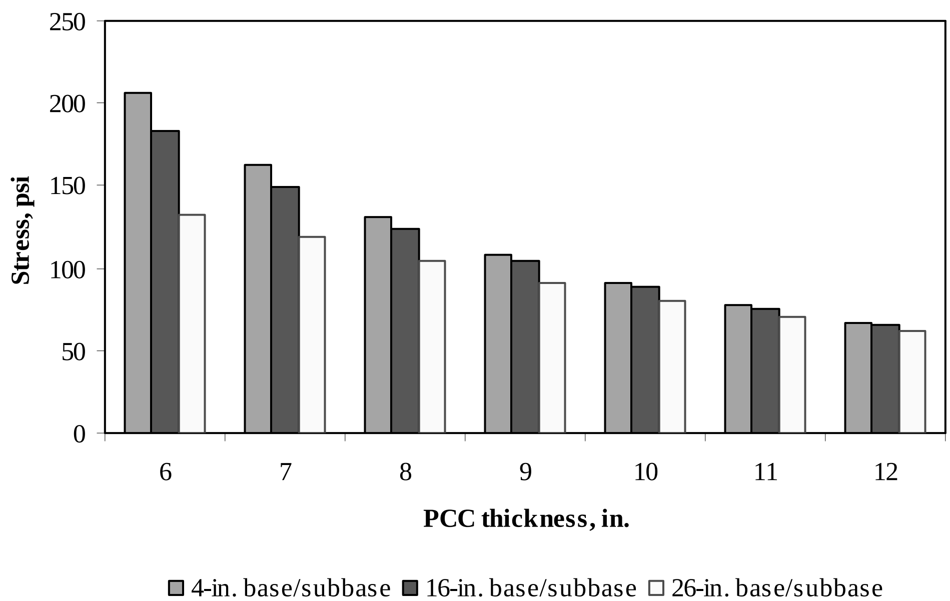


**Figure F-2-10: Impact of PCC thickness and base/subbase thickness on transverse stress at bottom of the Slab (315-in. joint spacing and $\alpha(\Delta T/D)$ of 0 in.$^{-1}$)**

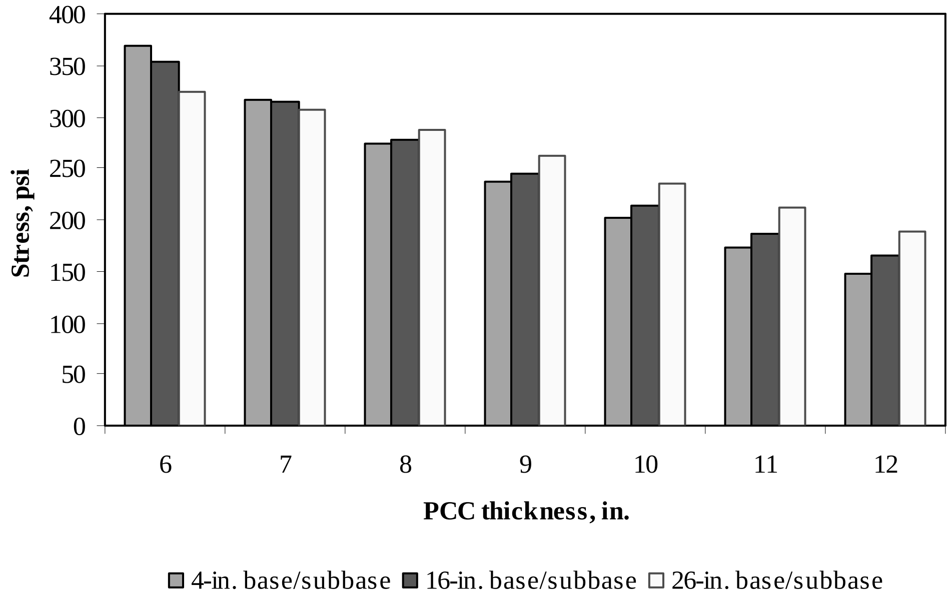


**Figure F-2-11: Impact of PCC thickness and base/subbase thickness on transverse stress at bottom of the Slab (177-in. joint spacing and $\alpha(\Delta T/D)$ of $20x10^{-6}$ in.$^{-1}$)**

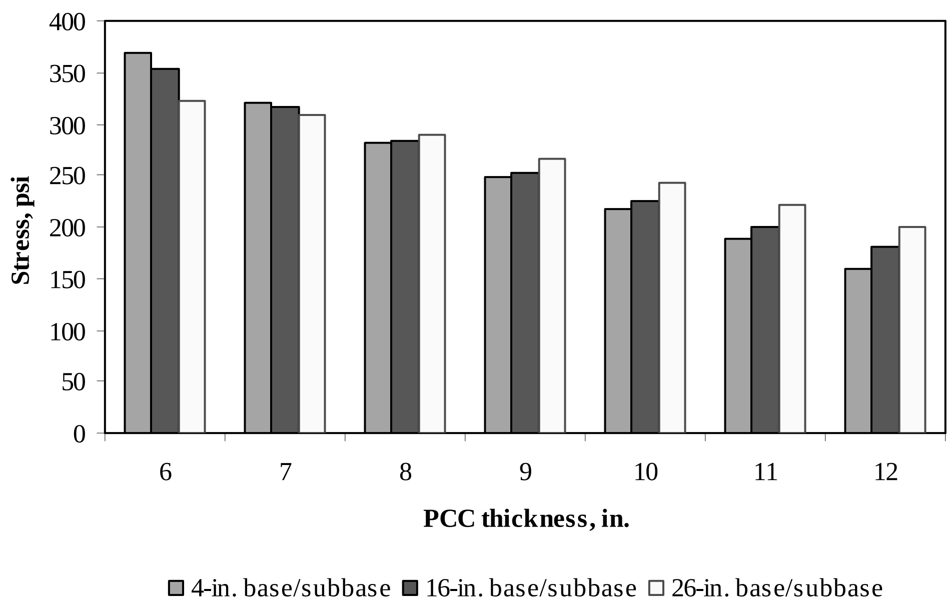


**Figure F-2-12: Impact of PCC thickness and base/subbase thickness on transverse stress at bottom of the Slab (315-in. joint spacing and $\alpha(\Delta T/D)$ of $20x10^{-6}$ in.$^{-1}$)**

Figures F-2-13 through F-2-24 illustrate the impact of PCC thickness and modulus of subgrade reaction on stresses (16-in. base/subbase thickness and PCC shoulder)

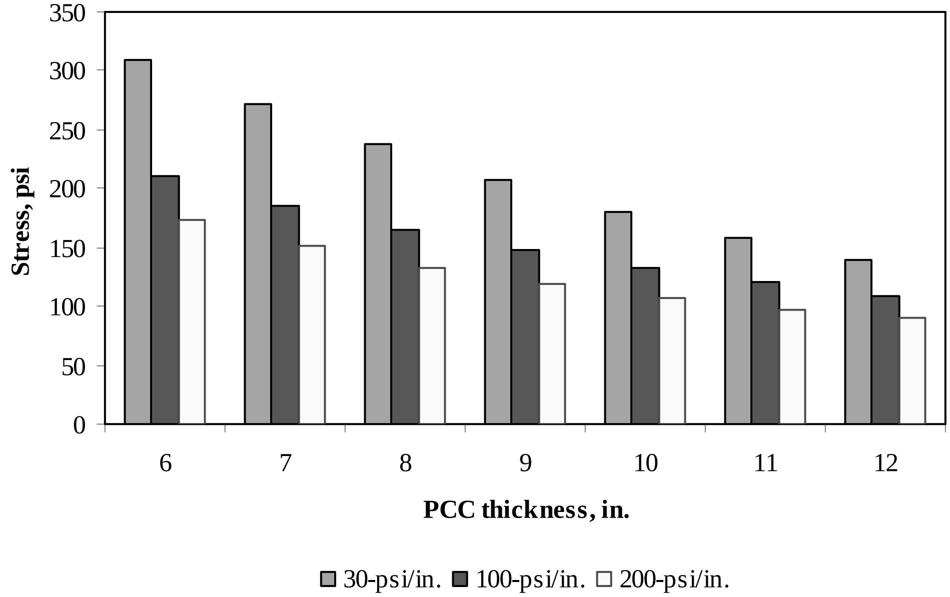


**Figure F-2-13: Impact of PCC thickness and modulus of subgrade reaction on longitudinal stress at bottom of the slab (177-in. joint spacing and $\alpha(\Delta T/D)$ of 0 $in.^{-1}$)**

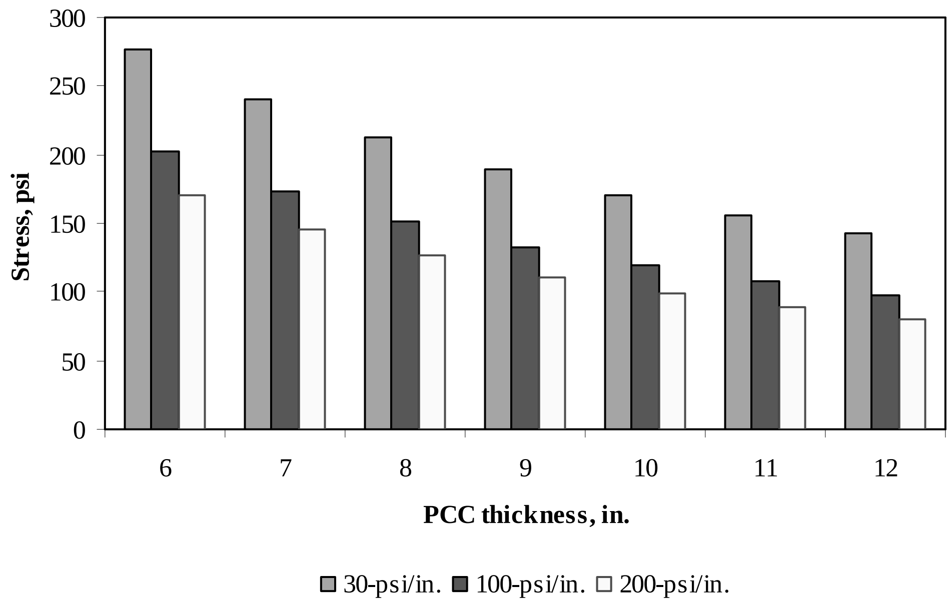


**Figure F-2-14: Impact of PCC thickness and modulus of subgrade reaction on longitudinal stress at bottom of the slab (315-in. joint spacing and $\alpha(\Delta T/D)$ of 0 $in.^{-1}$)**

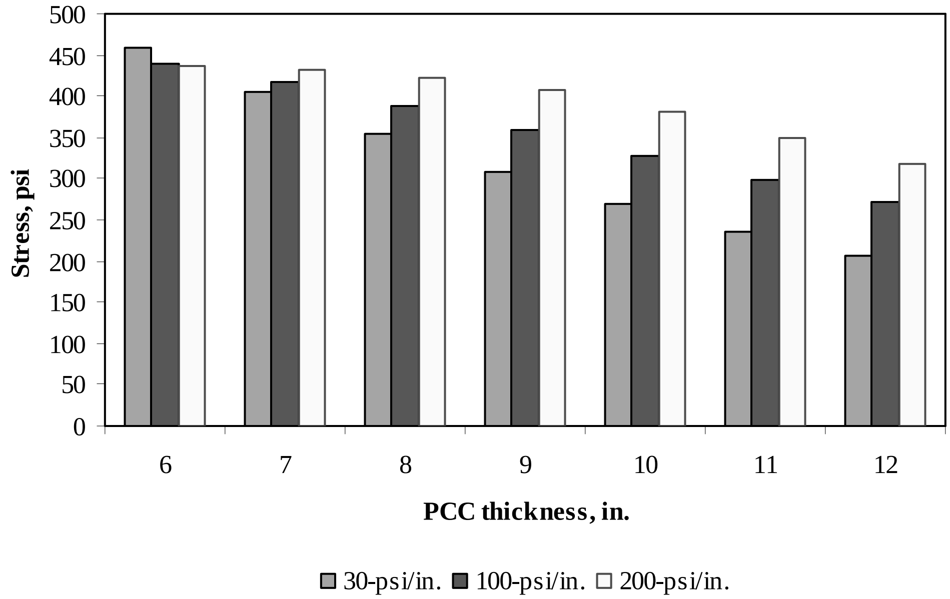


**Figure F-2-15: Impact of PCC thickness and modulus of subgrade reaction on longitudinal stress at bottom of the slab (177-in. joint spacing and $\alpha(\Delta T/D)$ of $20x10^{-6}$ in.$^{-1}$)**

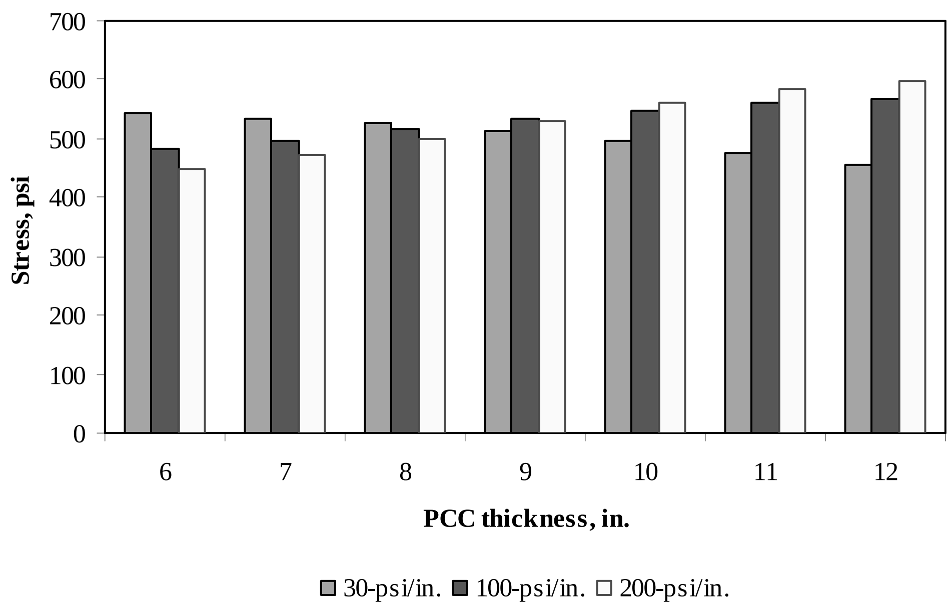


**Figure F-2-16: Impact of PCC thickness and modulus of subgrade reaction on longitudinal stress at bottom of the slab (315-in. joint spacing and $\alpha(\Delta T/D)$ of $20x10^{-6}$ in.$^{-1}$)**

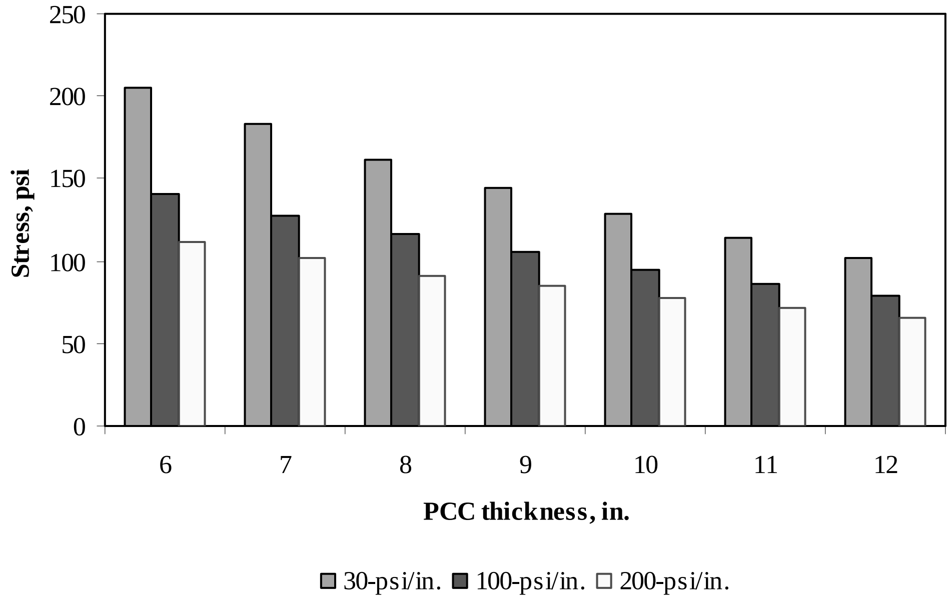


**Figure F-2-17: Impact of PCC thickness and modulus of subgrade reaction on longitudinal stress at top of the Slab (177-in. joint spacing and $\alpha(\Delta T/D)$ of 0 in.$^{-1}$)**

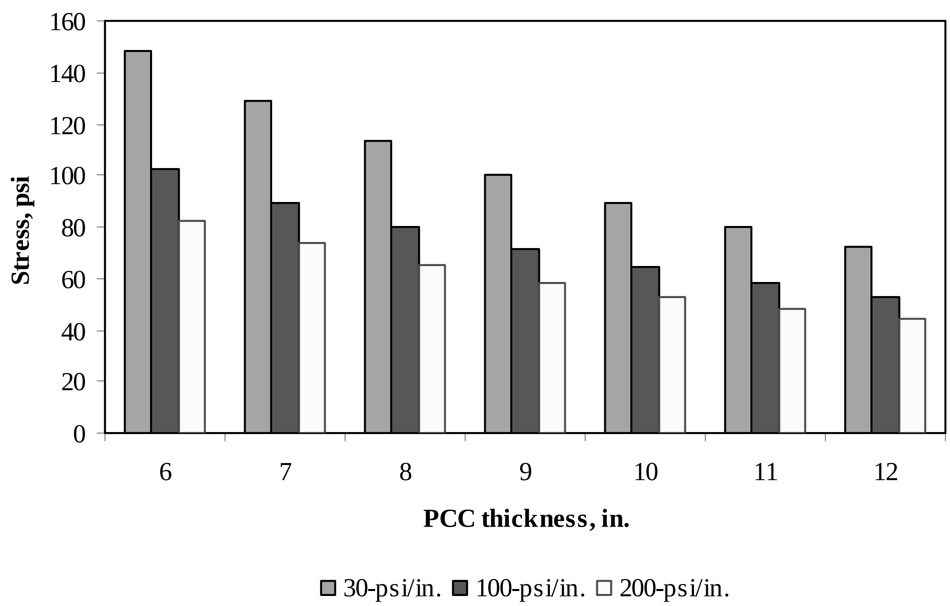


**Figure F-2-18: Impact of PCC thickness and modulus of subgrade reaction on longitudinal stress at top of the Slab (315-in. joint spacing and $\alpha(\Delta T/D)$ of 0 in.$^{-1}$)**

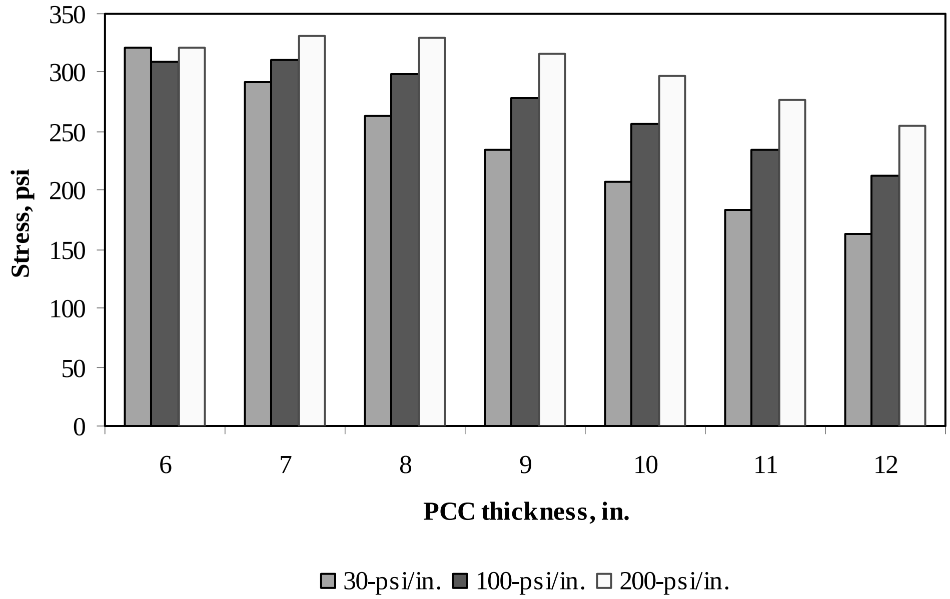


**Figure F-2-19: Impact of PCC thickness and modulus of subgrade reaction on longitudinal stress at top of the Slab (177-in. joint spacing and $\alpha(\Delta T/D)$ of $-20 \times 10^{-6}$ in.$^{-1}$)**

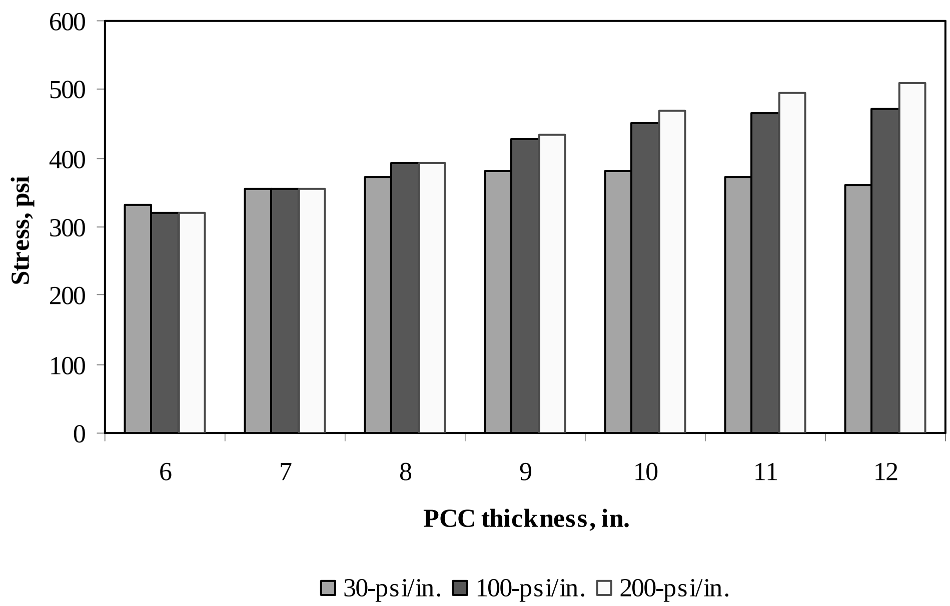


**Figure F-2-20: Impact of PCC thickness and modulus of subgrade reaction on longitudinal stress at top of the Slab (315-in. joint spacing and $\alpha(\Delta T/D)$ of $-20 \times 10^{-6}$ in.$^{-1}$)**

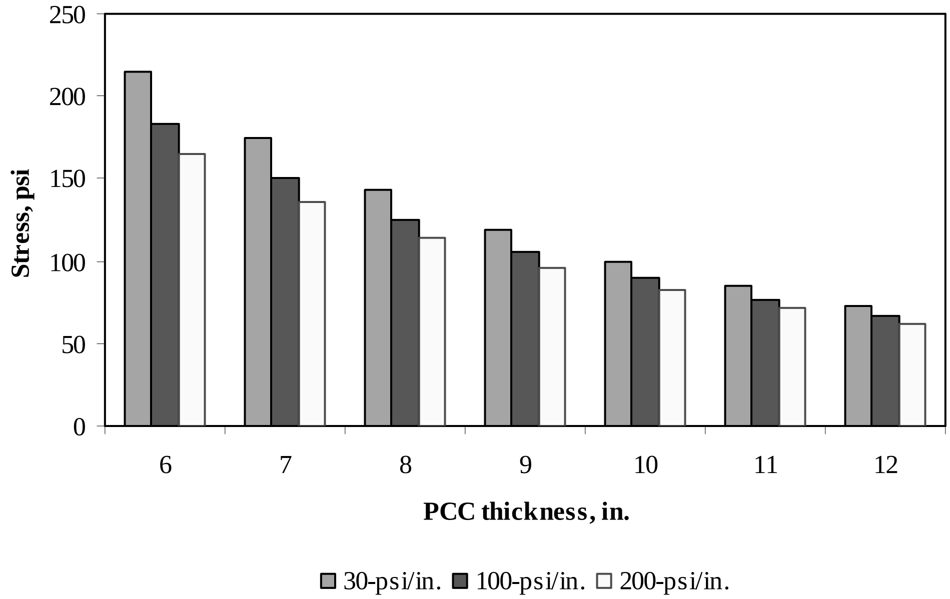


**Figure F-2-21: Impact of PCC thickness and modulus of subgrade reaction on transverse stress at bottom of the Slab (177-in. joint spacing and $\alpha(\Delta T/D)$ of 0 in.$^{-1}$)**

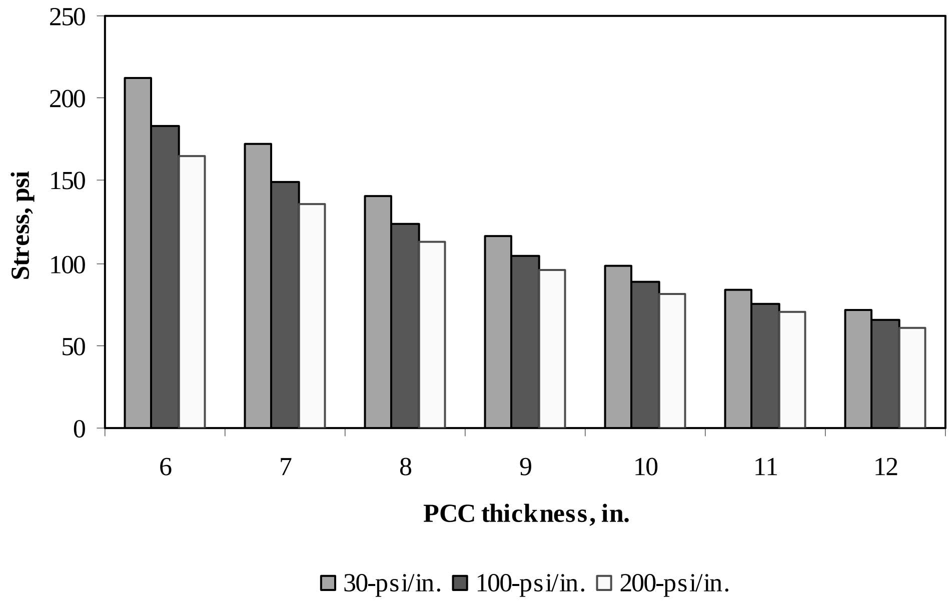


**Figure F-2-22: Impact of PCC thickness and modulus of subgrade reaction on transverse stress at bottom of the Slab (315-in. joint spacing and $\alpha(\Delta T/D)$ of 0 in.$^{-1}$)**

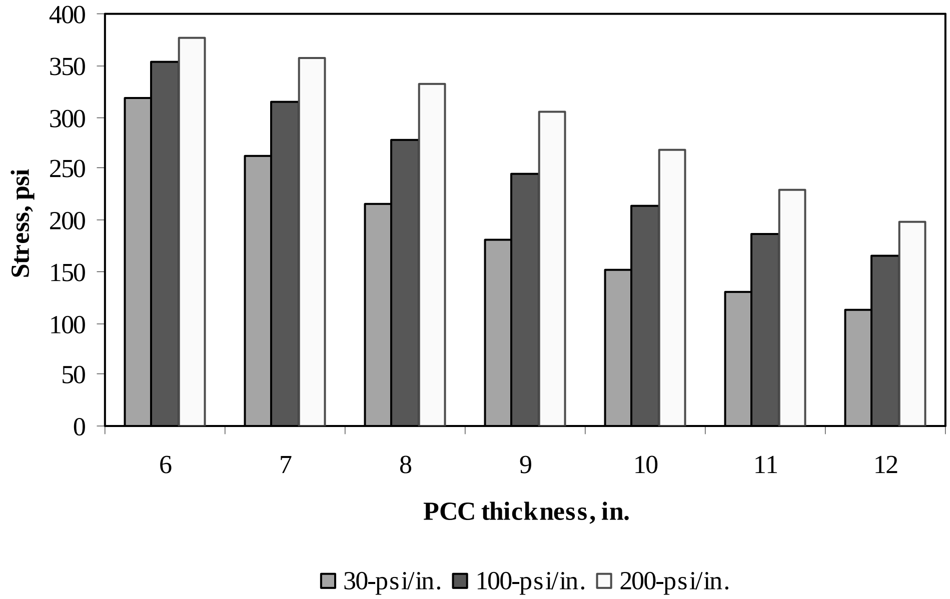


**Figure F-2-23: Impact of PCC thickness and modulus of subgrade reaction on transverse stress at bottom of the Slab (177-in. joint spacing and $\alpha(\Delta T/D)$ of $20x10^{-6}$ in.$^{-1}$)**

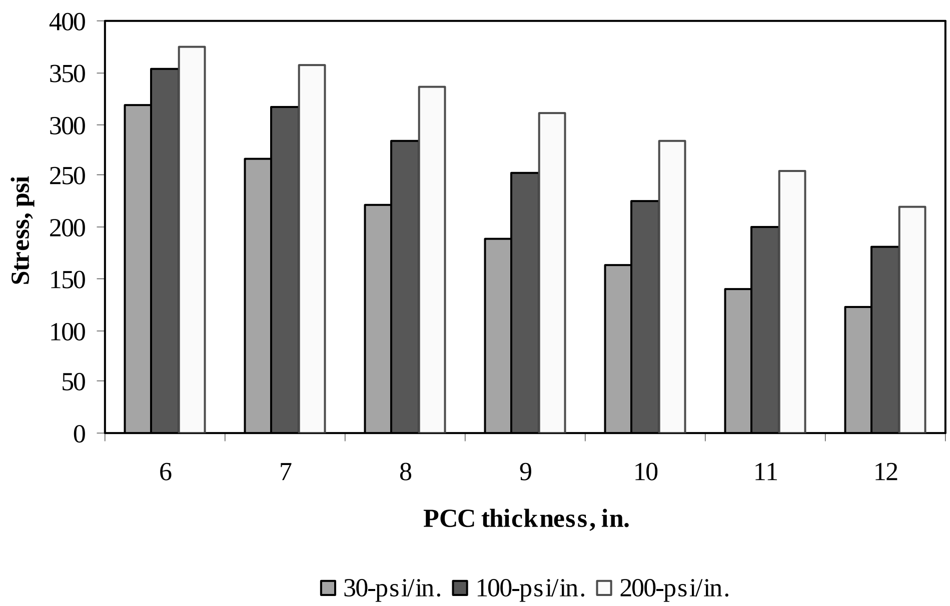


**Figure F-2-24: Impact of PCC thickness and modulus of subgrade reaction on transverse stress at bottom of the Slab (315-in. joint spacing and $\alpha(\Delta T/D)$ of $20x10^{-6}$ in.$^{-1}$)**

Figures F-2-25 through F-2-36 illustrate the impact of PCC thickness and lateral support condition on stresses (16-in. base/subbase and 100-psi/in. modulus of subgrade reaction)

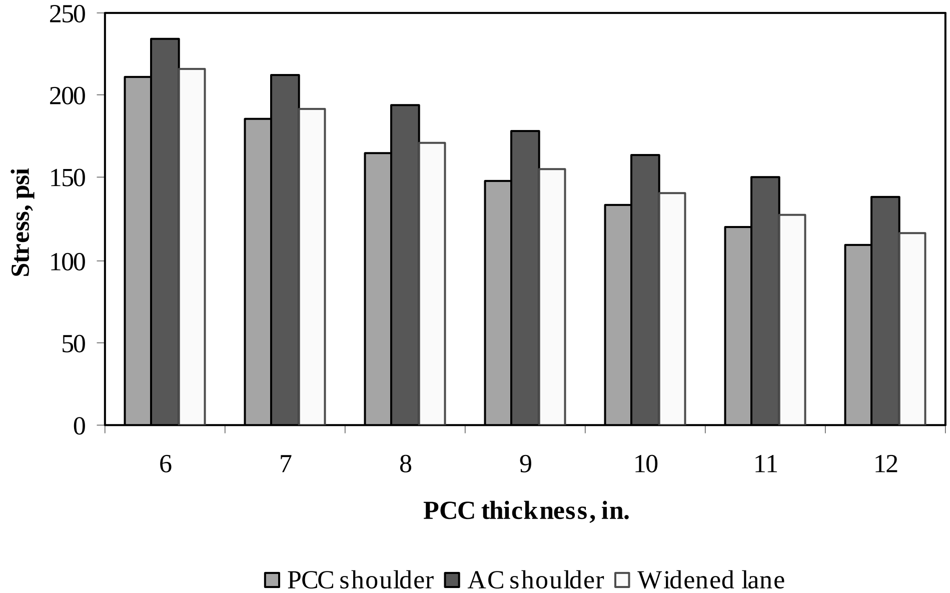


**Figure F-2-25: Impact of PCC thickness and lateral support condition on longitudinal stress at bottom of the Slab (177-in. joint spacing and $\alpha(\Delta T/D)$ of 0 in.$^{-1}$)**

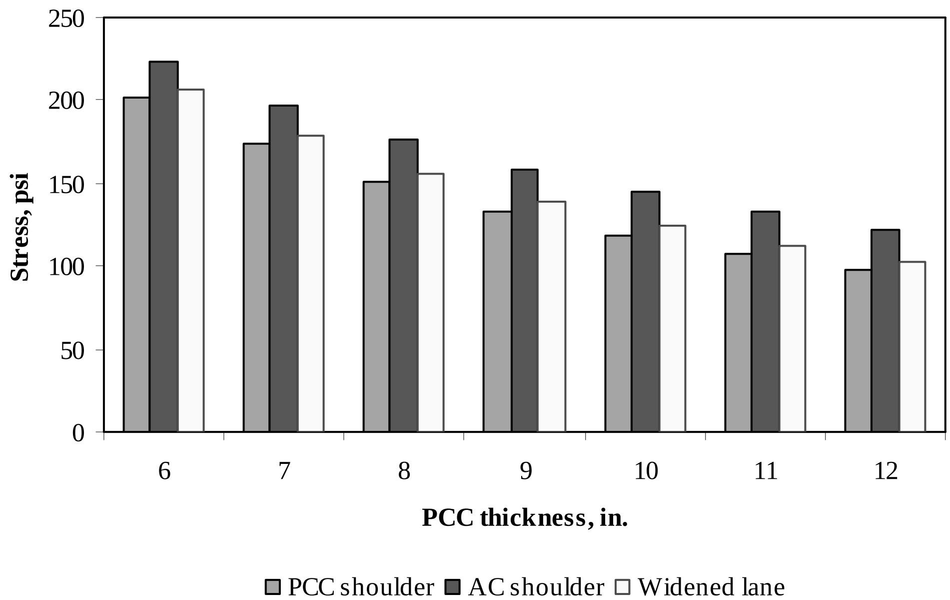


**Figure F-2-26: Impact of PCC thickness and lateral support condition on longitudinal stress at bottom of the Slab (315-in. joint spacing and $\alpha(\Delta T/D)$ of 0 in.$^{-1}$)**

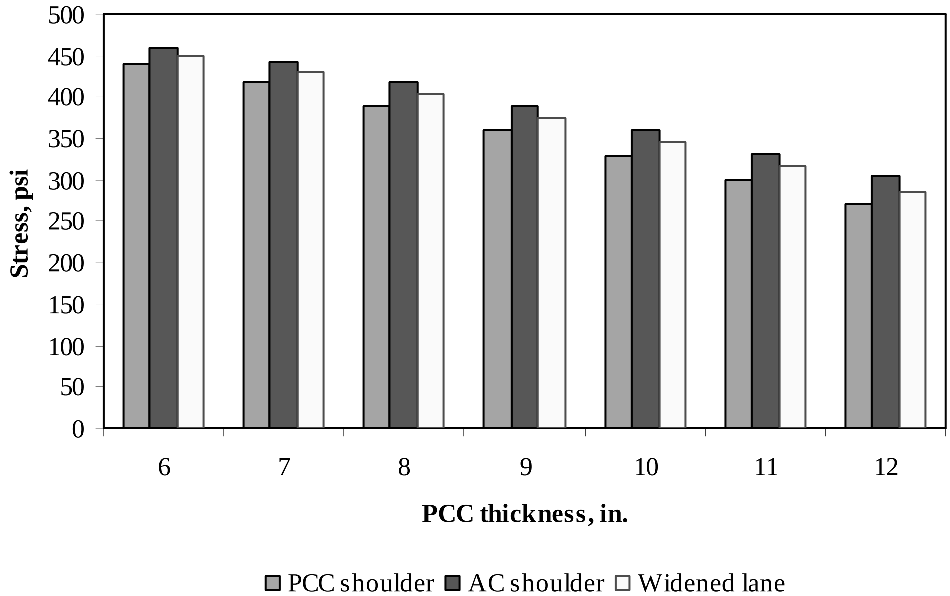


**Figure F-2-27: Impact of PCC thickness and lateral support condition on longitudinal stress at bottom of the Slab (177-in. joint spacing and $\alpha(\Delta T/D)$ of $20x10^{-6}$ in.$^{-1}$)**

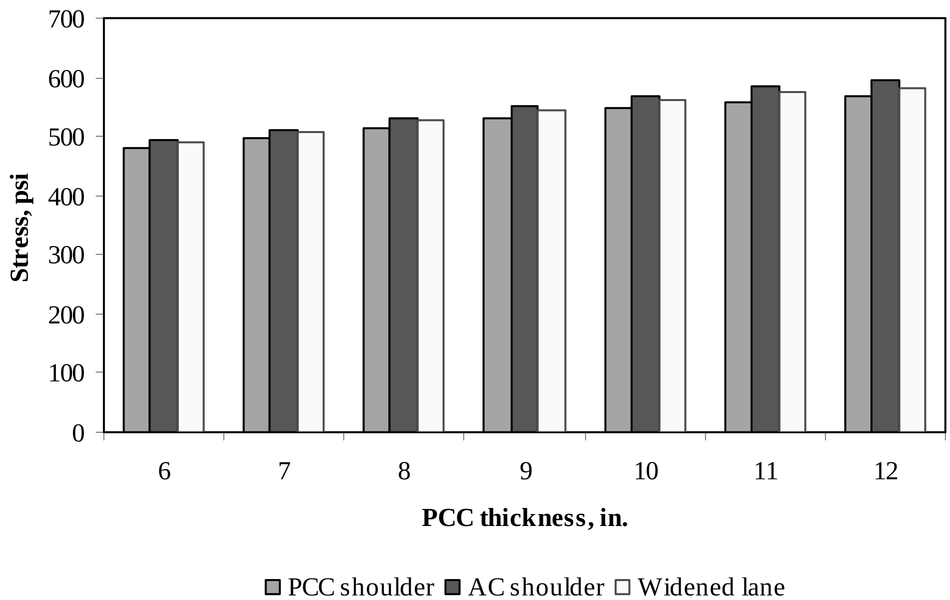


**Figure F-2-28: Impact of PCC thickness and lateral support condition on longitudinal stress at bottom of the Slab (315-in. joint spacing and $\alpha(\Delta T/D)$ of $20x10^{-6}$ in.$^{-1}$)**

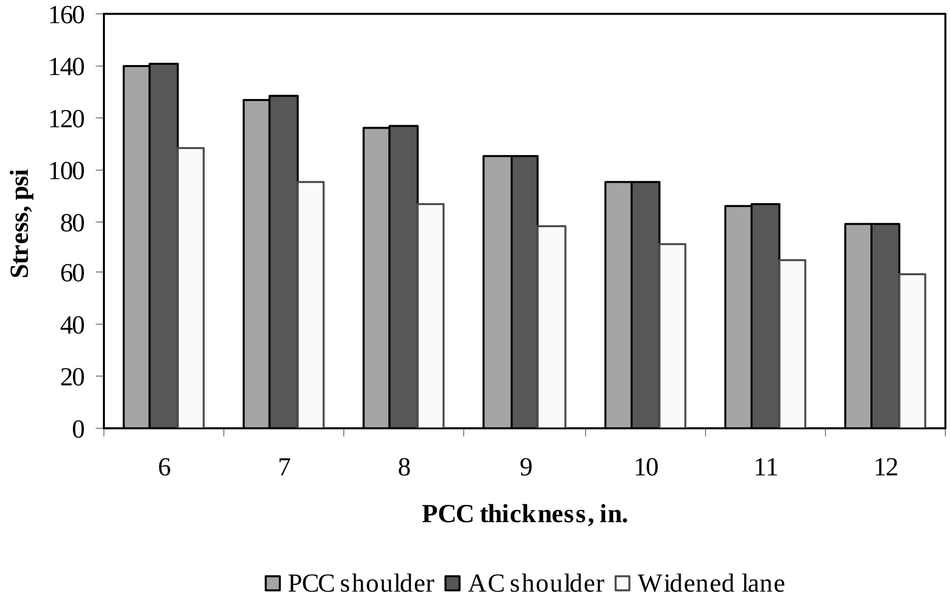


**Figure F-2-29: Impact of PCC thickness and lateral support condition on longitudinal stress at top of the Slab (177-in. joint spacing and $\alpha(\Delta T/D)$ of 0 in.$^{-1}$)**

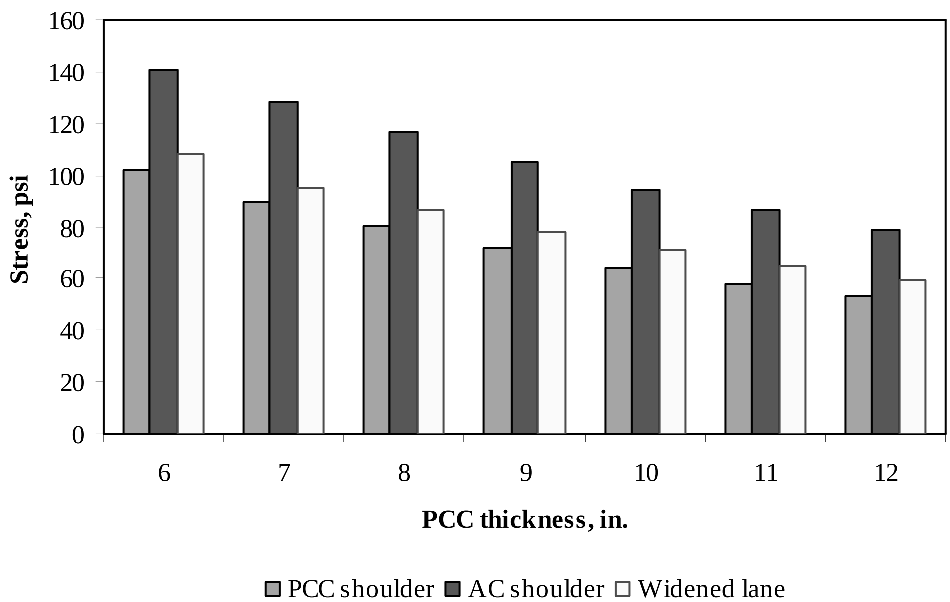


**Figure F-2-30: Impact of PCC thickness and lateral support condition on longitudinal stress at top of the Slab (315-in. joint spacing and $\alpha(\Delta T/D)$ of 0 in.$^{-1}$)**

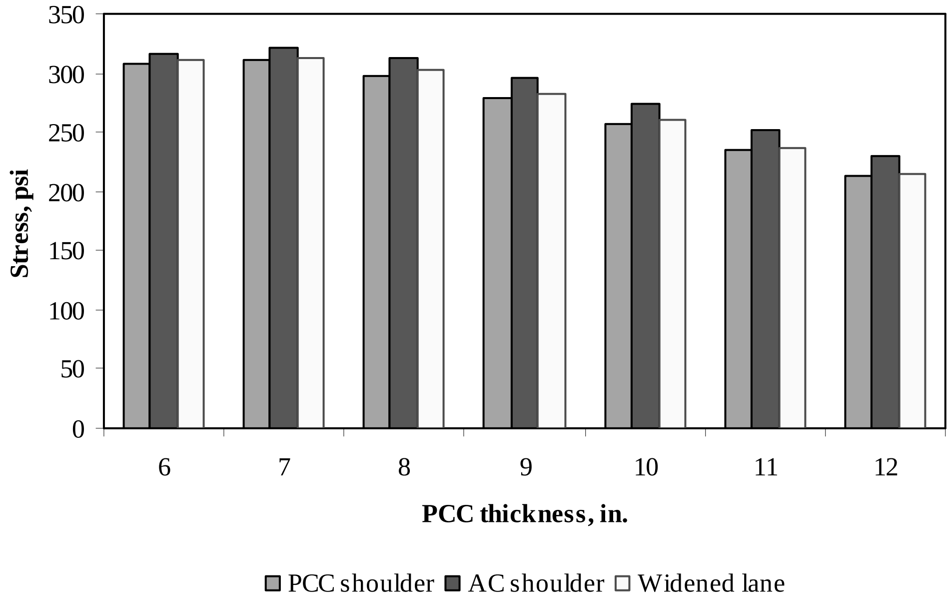


**Figure F-2-31: Impact of PCC thickness and lateral support condition on longitudinal stress at top of the Slab (177-in. joint spacing and $\alpha(\Delta T/D)$ of $-20x10^{-6}$ in.$^{-1}$)**

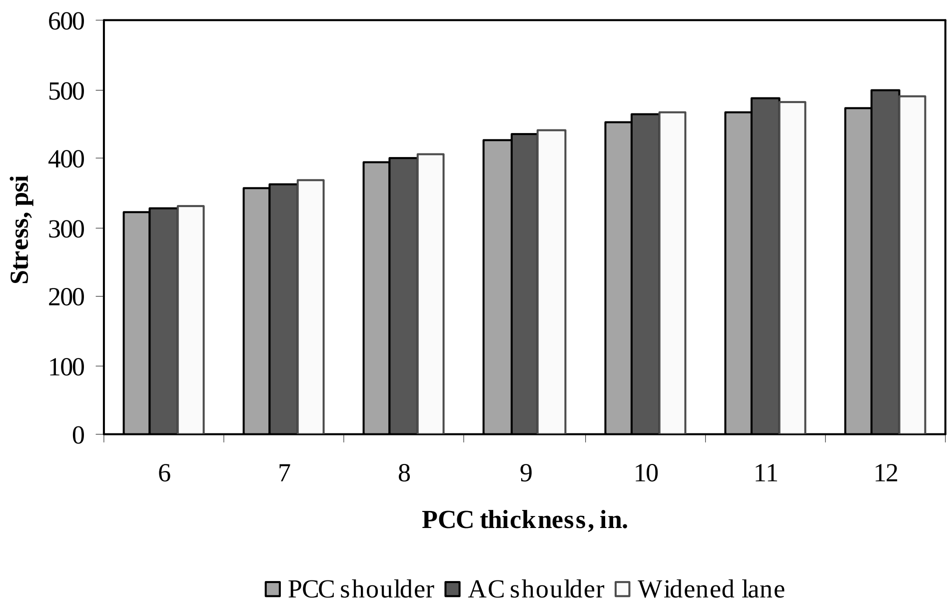


**Figure F-2-32: Impact of PCC thickness and lateral support condition on longitudinal stress at top of the Slab (315-in. joint spacing and $\alpha(\Delta T/D)$ of $-20x10^{-6}$ in.$^{-1}$)**

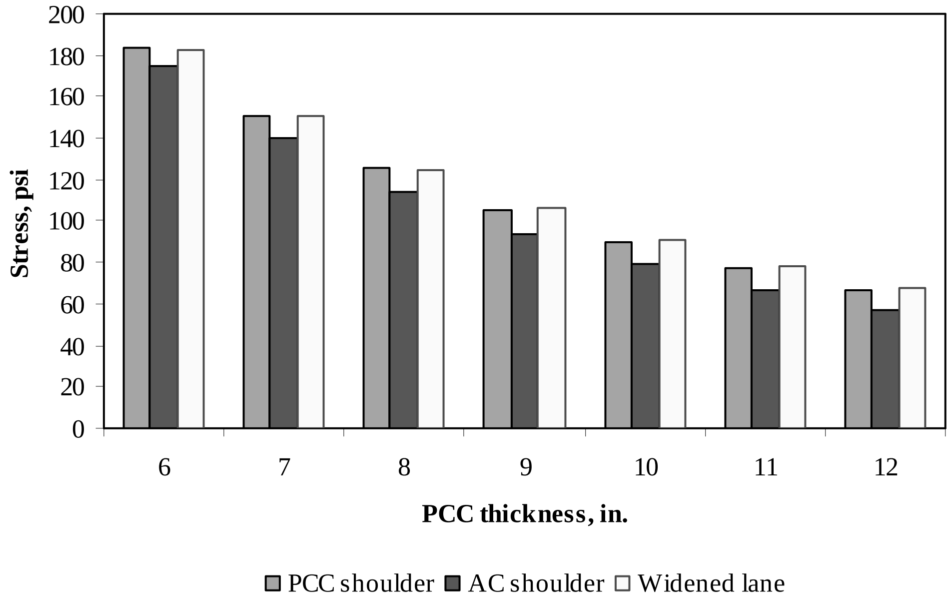


**Figure F-2-33: Impact of PCC thickness and lateral support condition on transverse stress at bottom of the Slab (177-in. joint spacing and $\alpha(\Delta T/D)$ of 0 in.$^{-1}$)**

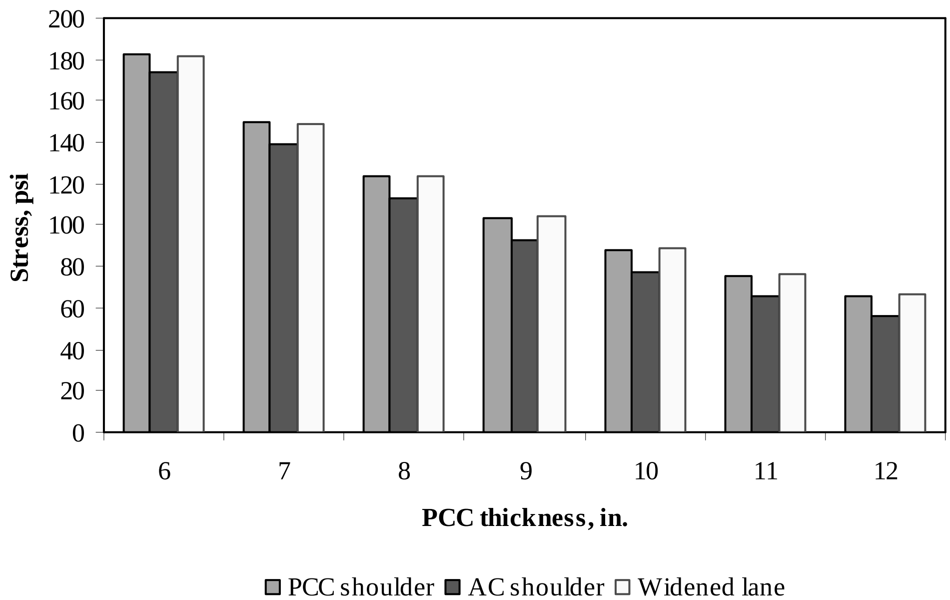


**Figure F-2-34: Impact of PCC thickness and lateral support condition on transverse stress at bottom of the Slab (315-in. joint spacing and $\alpha(\Delta T/D)$ of 0 in.$^{-1}$)**

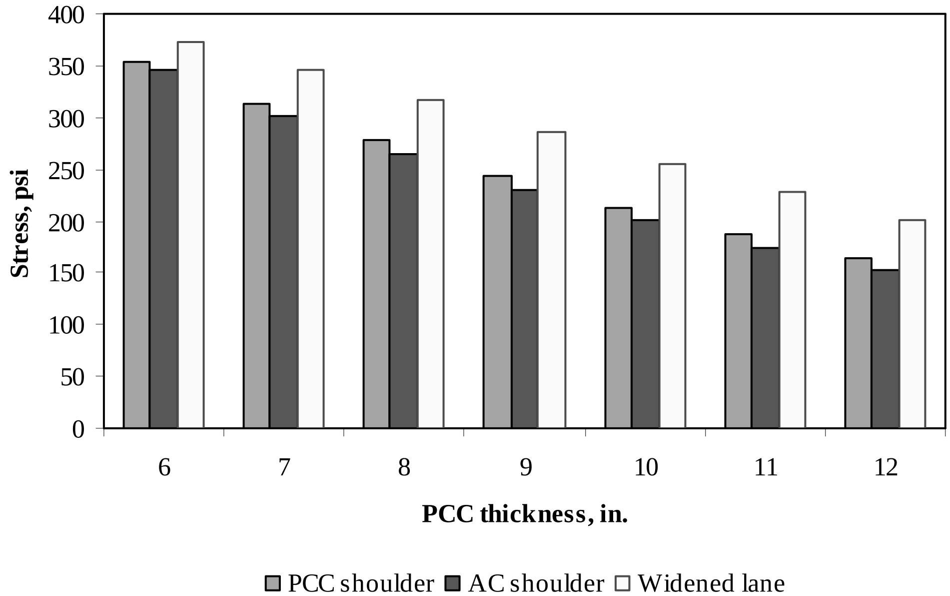


**Figure F-2-35: Impact of PCC thickness and lateral support condition on transverse stress at bottom of the Slab (177-in. joint spacing and $\alpha(\Delta T/D)$ of $20 \times 10^{-6}$ in.$^{-1}$)**

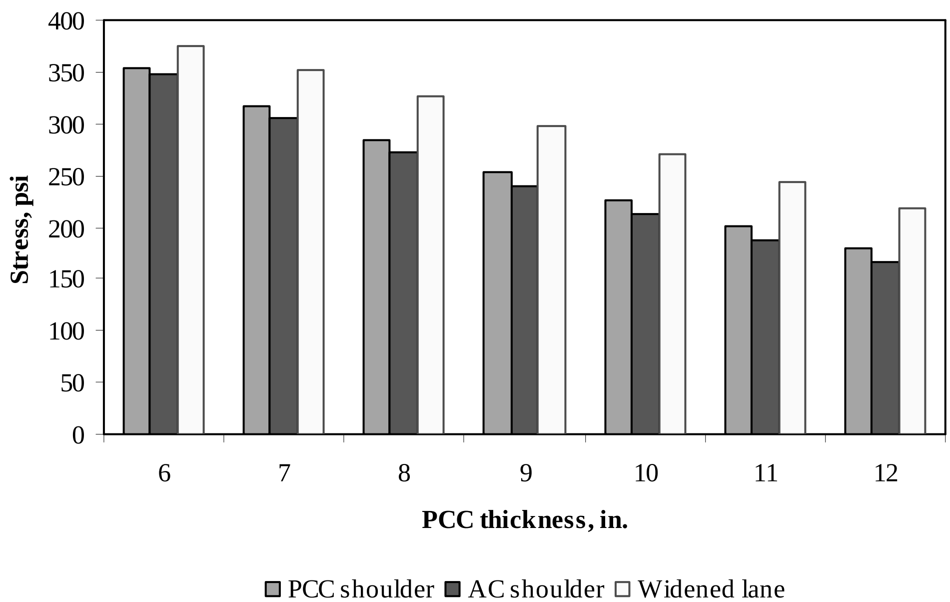


**Figure F-2-36: Impact of PCC thickness and lateral support condition on transverse stress at bottom of the Slab (315-in. joint spacing and $\alpha(\Delta T/D)$ of $20 \times 10^{-6}$ in.$^{-1}$)**

Figures F-2-37 through F-2-42 illustrate the impact of base/subbase thickness and product α(ΔT/D) on stresses (10-in. PCC thickness, 100-psi/in. modulus of subgrade reaction and PCC shoulder)

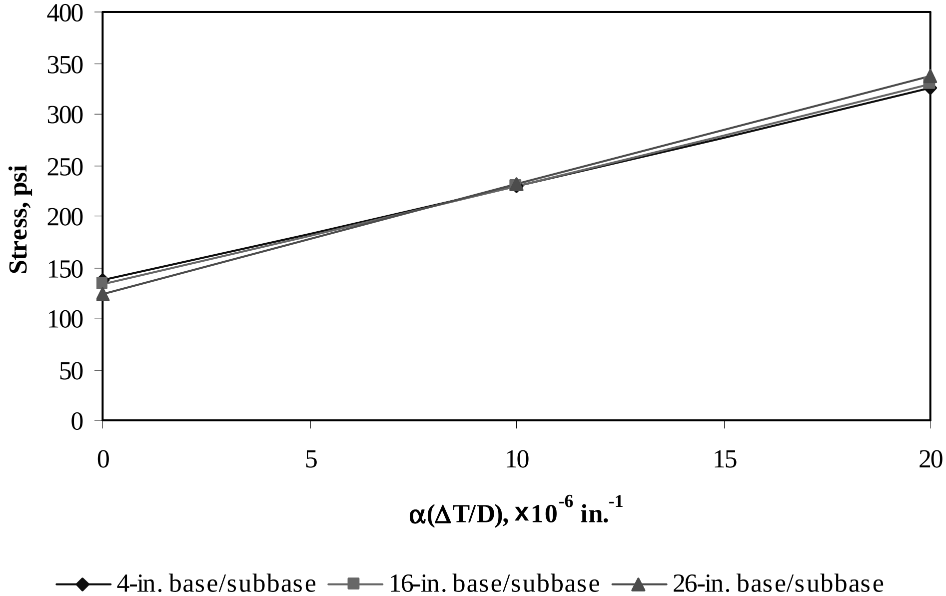


**Figure F-2-37: Impact of base/subbase thickness and product α(ΔT/D) on longitudinal stress at bottom of the slab (177-in. joint spacing)**

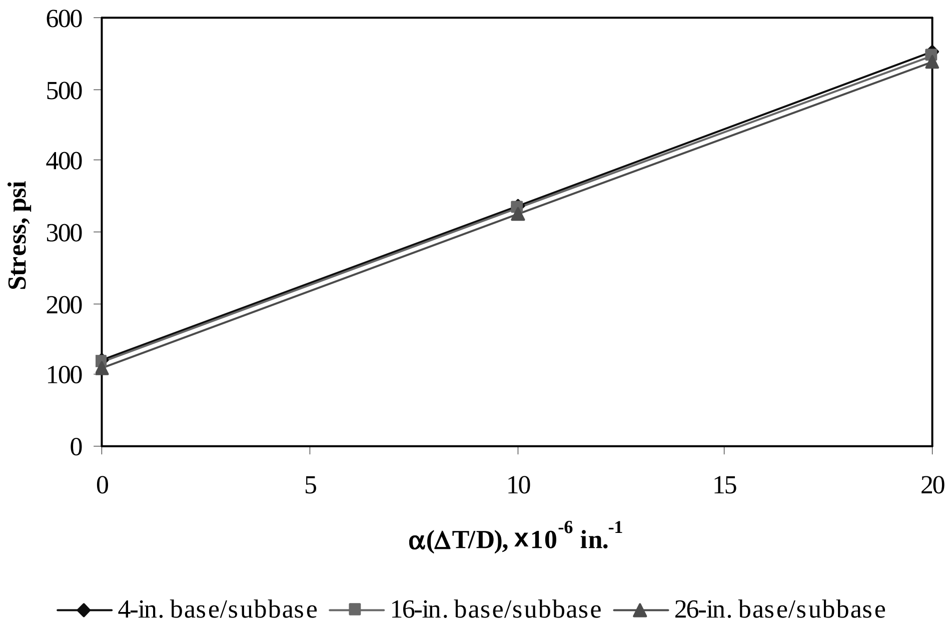


**Figure F-2-38: Impact of base/subbase thickness and product α(ΔT/D) on longitudinal stress at bottom of the slab (315-in. joint spacing)**

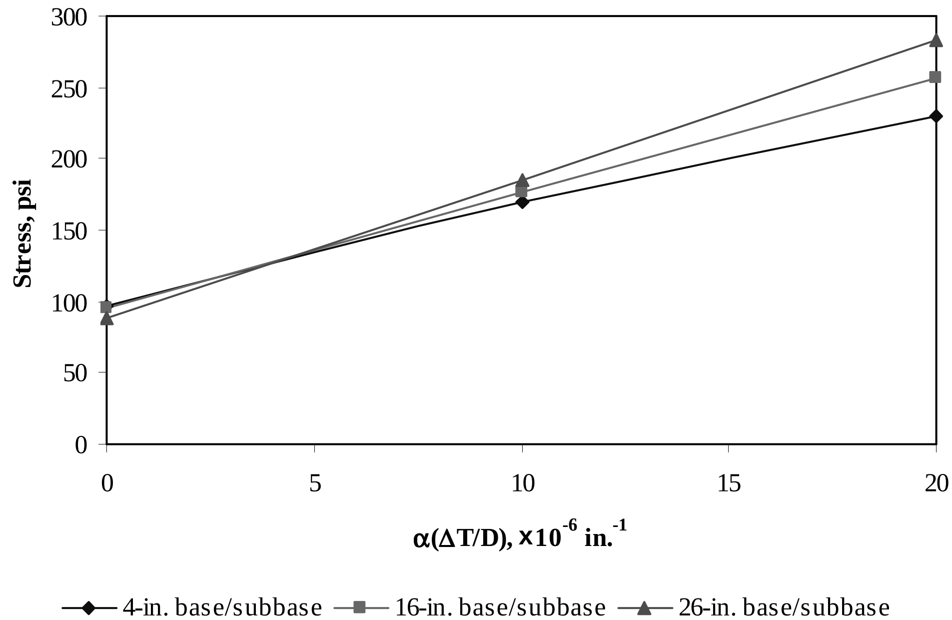


**Figure F-2-39: Impact of base/subbase thickness and product α(ΔT/D) on longitudinal stress at top of the slab (177-in. joint spacing)**

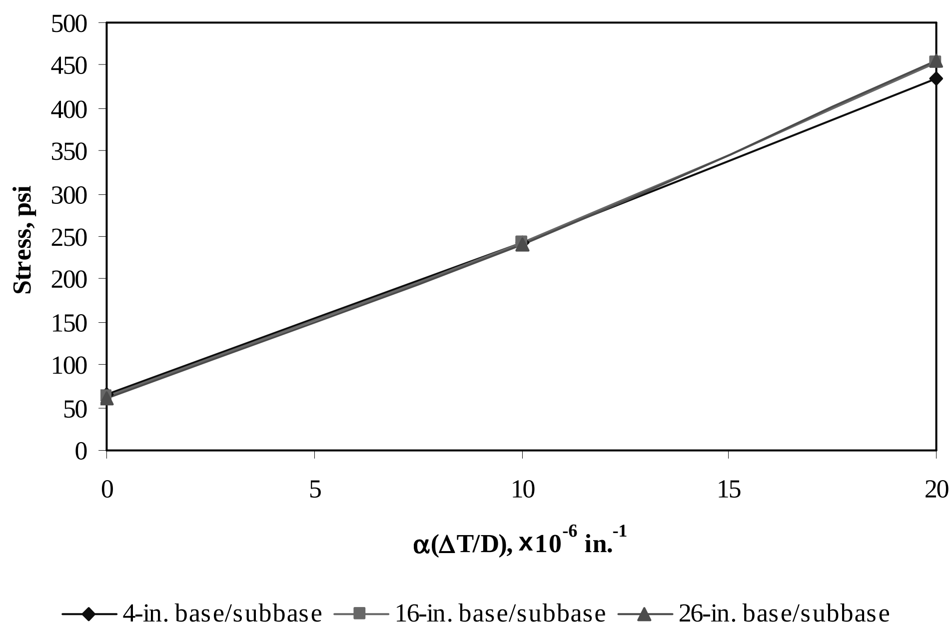


**Figure F-2-40: Impact of base/subbase thickness and product α(ΔT/D) on longitudinal stress at top of the slab (315-in. joint spacing)**

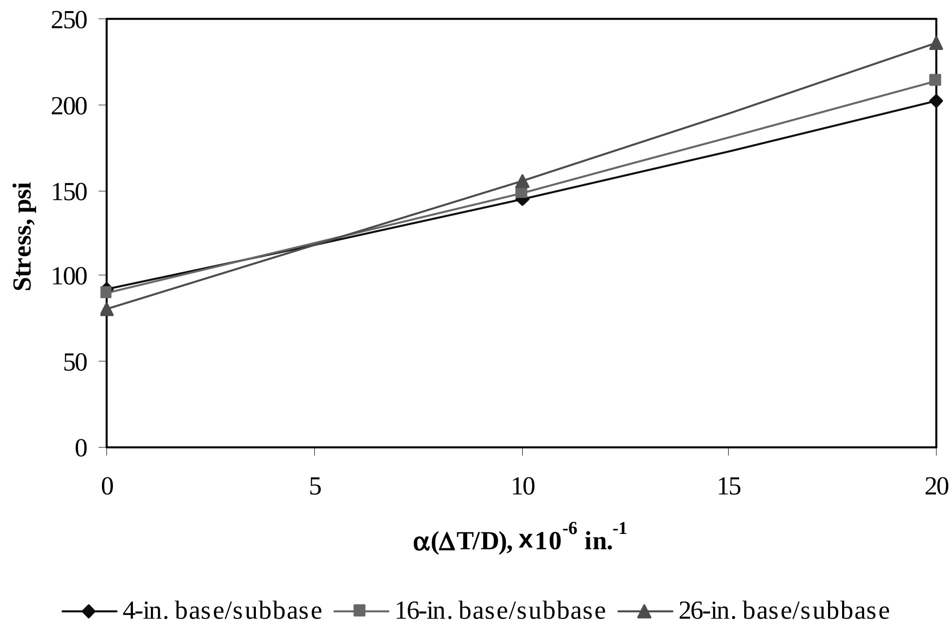


**Figure F-2-41: Impact of base/subbase thickness and product α(ΔT/D) on transverse stress at bottom of the slab (177-in. joint spacing)**

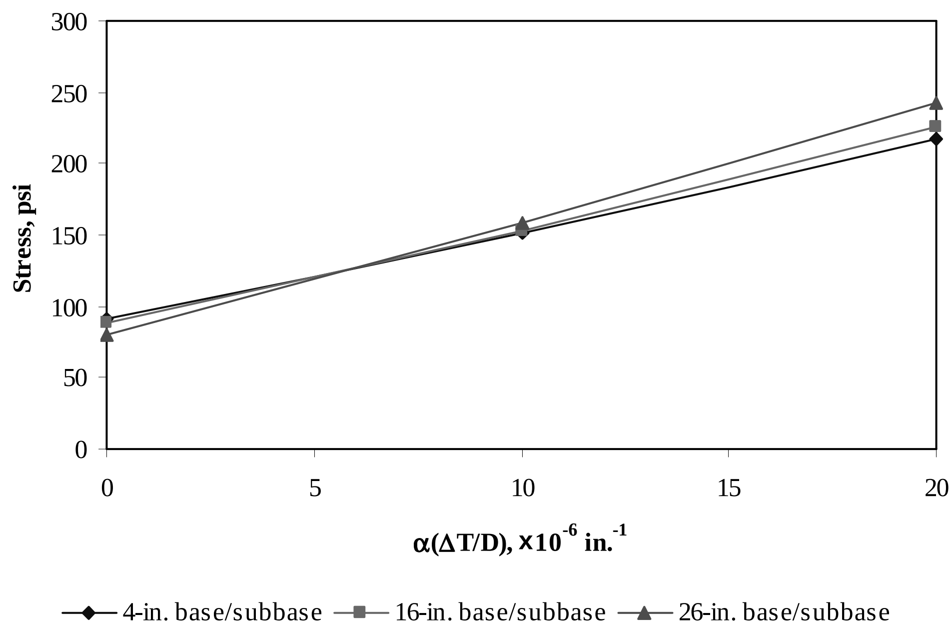


**Figure F-2-42: Impact of base/subbase thickness and product α(ΔT/D) on transverse stress at bottom of the slab (315-in. joint spacing)**

Figures F-2-43 through F-2-48 illustrate the impact of modulus of subgrade reaction and product α(ΔT/D) on stresses (10-in. PCC thickness, 16-in. base/subbase thickness and PCC shoulder)

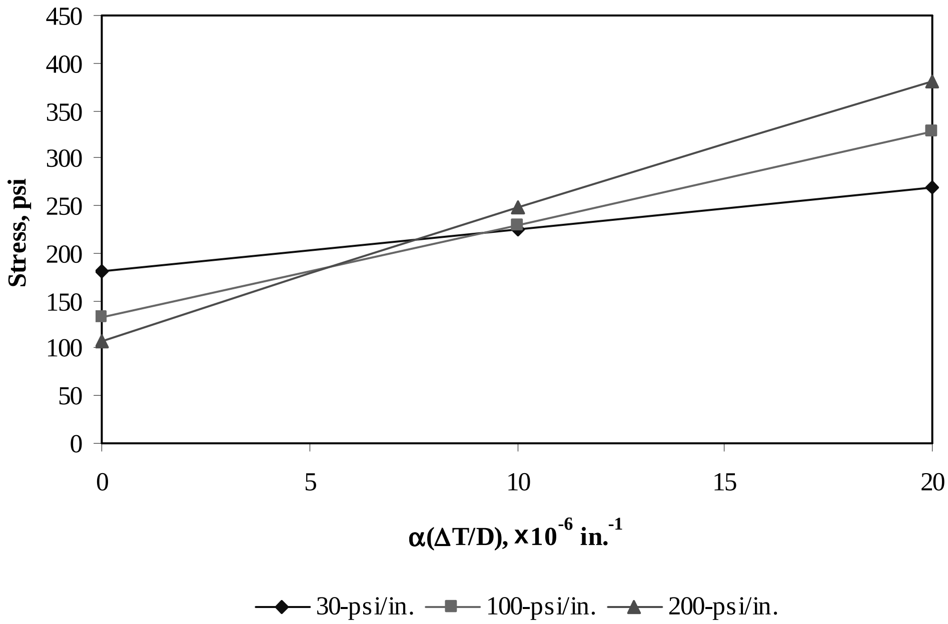


**Figure F-2-43: Impact of modulus of subgrade reaction and product α(ΔT/D) on longitudinal stress at bottom of the slab (177-in. joint spacing)**

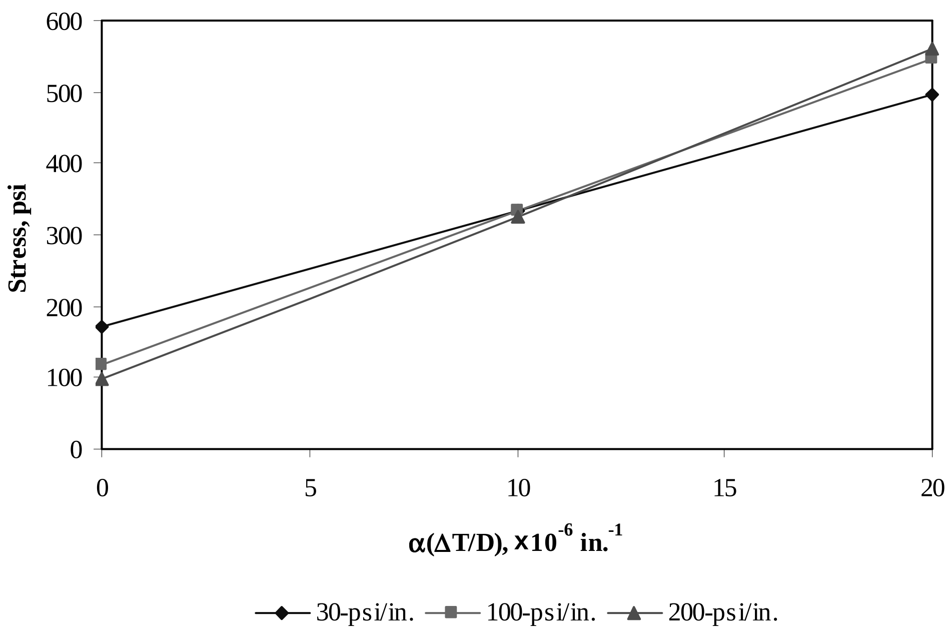


**Figure F-2-44: Impact of modulus of subgrade reaction and product α(ΔT/D) on longitudinal stress at bottom of the slab (315-in. joint spacing)**

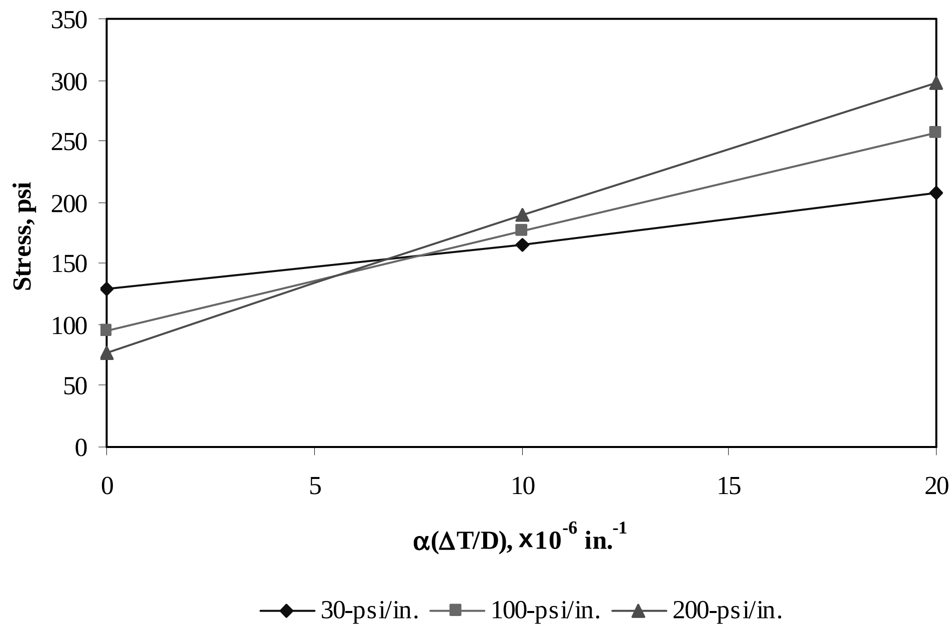


**Figure F-2-45: Impact of modulus of subgrade reaction and product α(ΔT/D) on longitudinal stress at top of the slab (177-in. joint spacing)**

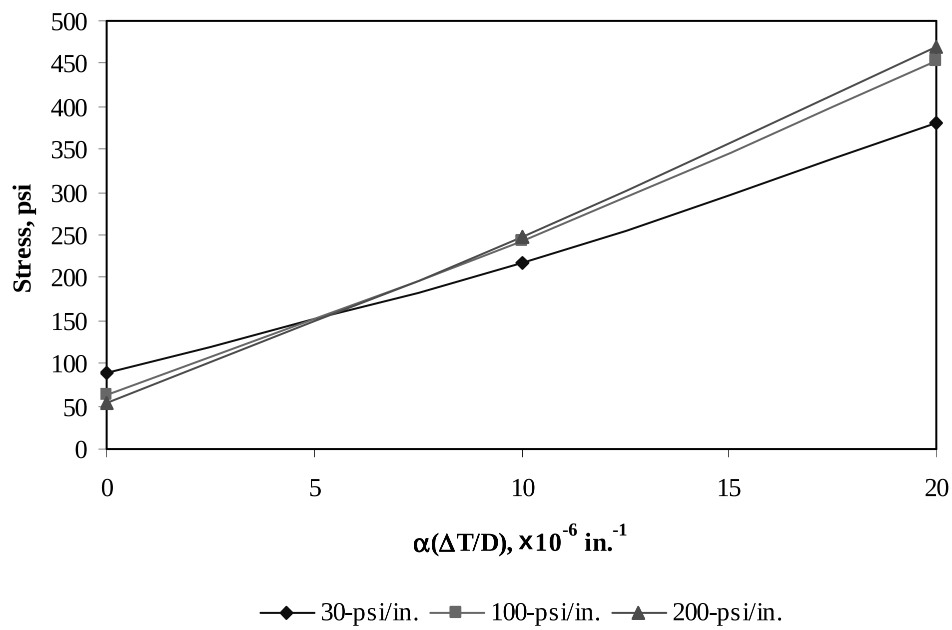


**Figure F-2-46: Impact of modulus of subgrade reaction and product α(ΔT/D) on longitudinal stress at top of the slab (315-in. joint spacing)**

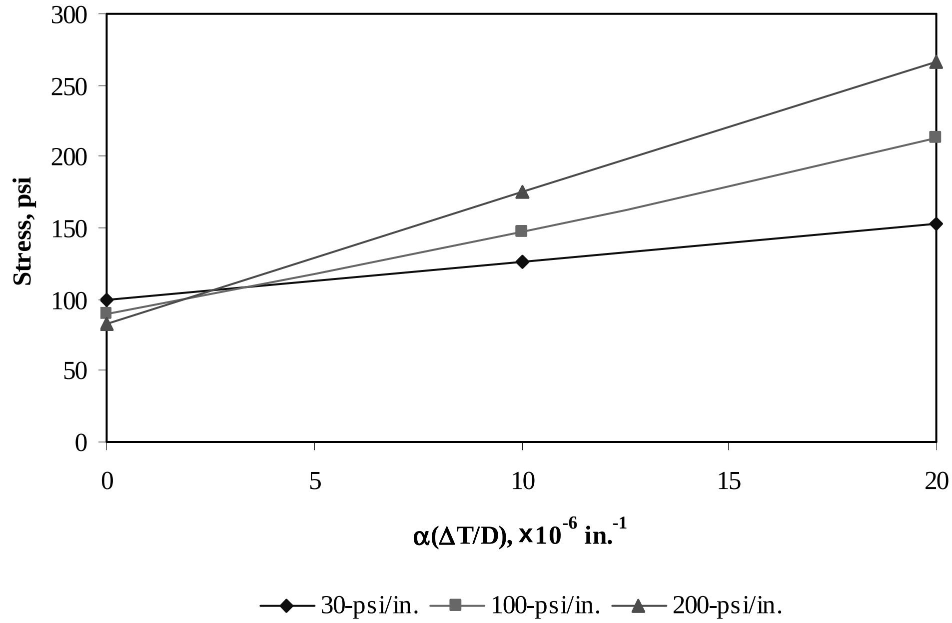


**Figure F-2-47: Impact of modulus of subgrade reaction and product α(ΔT/D) on transverse stress at bottom of the slab (177-in. joint spacing)**

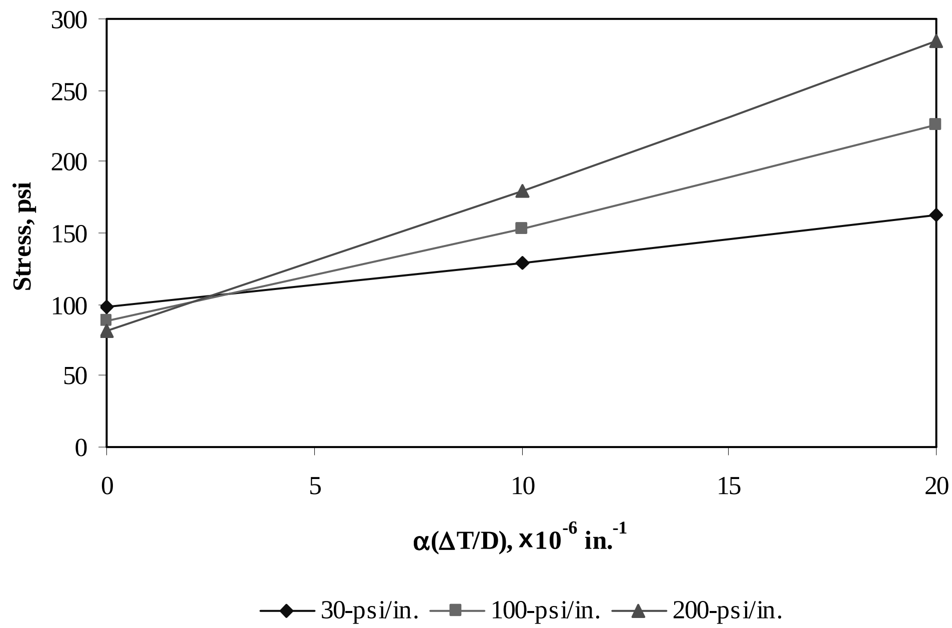


**Figure F-2-48: Impact of modulus of subgrade reaction and product α(ΔT/D) on transverse stress at bottom of the slab (315-in. joint spacing)**

Figures F-2-49 through F-2-51 illustrate the impact of joint spacing and product α(ΔT/D) on stresses (10-in. PCC thickness, 16-in. base/subbase thickness, 100-psi/in. modulus of subgrade reaction and PCC shoulder)

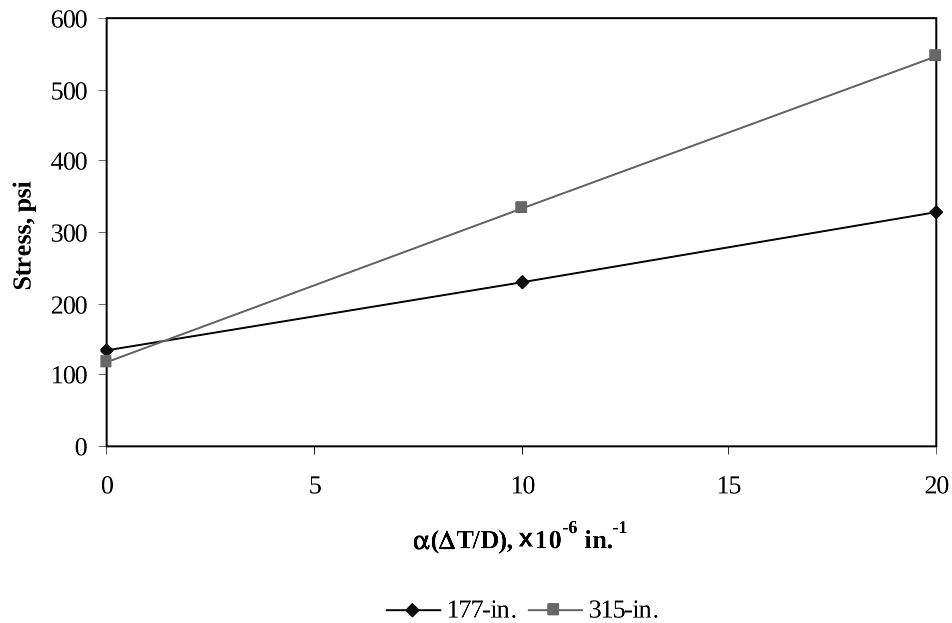


**Figure F-2-49: Impact of joint spacing and product α(ΔT/D) on longitudinal stress at bottom of the slab**

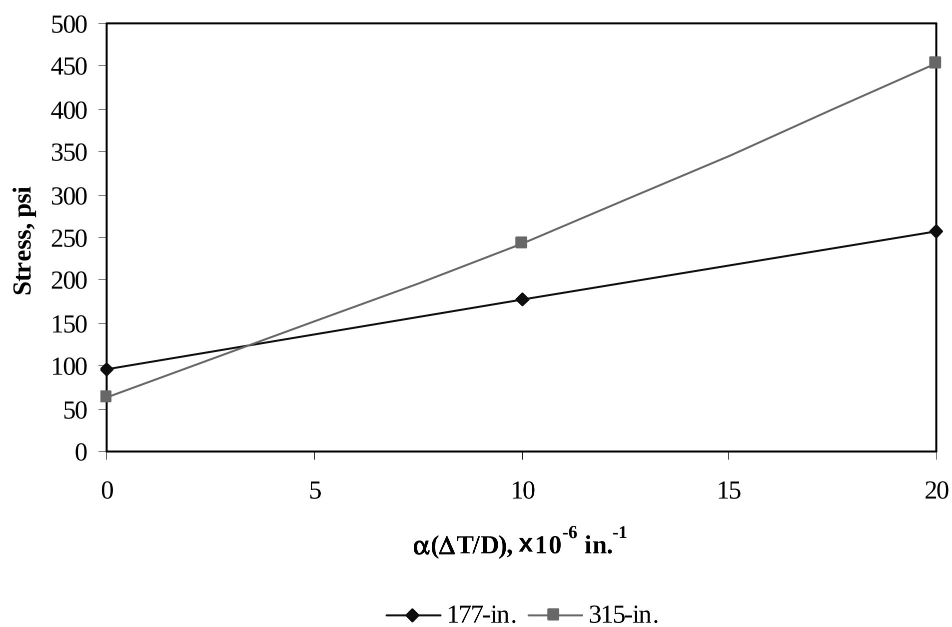


**Figure F-2-50: Impact of joint spacing and product α(ΔT/D) on longitudinal stress at top of the slab**

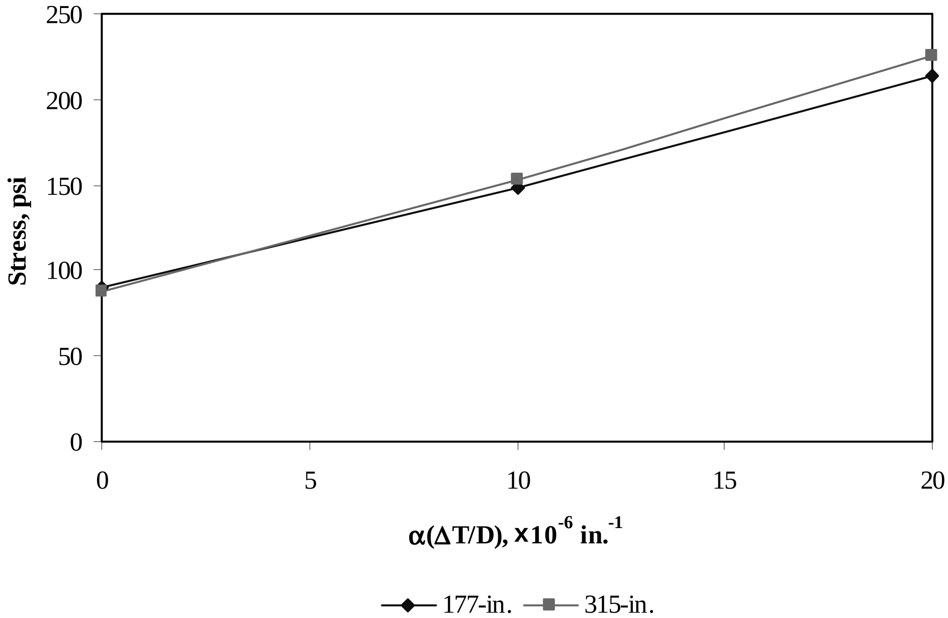


**Figure F-2-51: Impact of joint spacing and product α(ΔT/D) on transverse stress at bottom of the slab**

**Sub Appendix F-3**

**Documentation of Pavement Responses for**

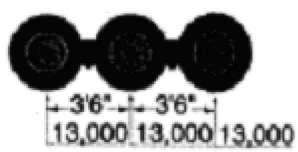


**39-kips Tridem Axle**

Figures F-3-1 through F-3-12 illustrate the impact of PCC thickness and base/subbase thickness on stresses (100-psi/in. modulus of subgrade reaction and PCC shoulder)

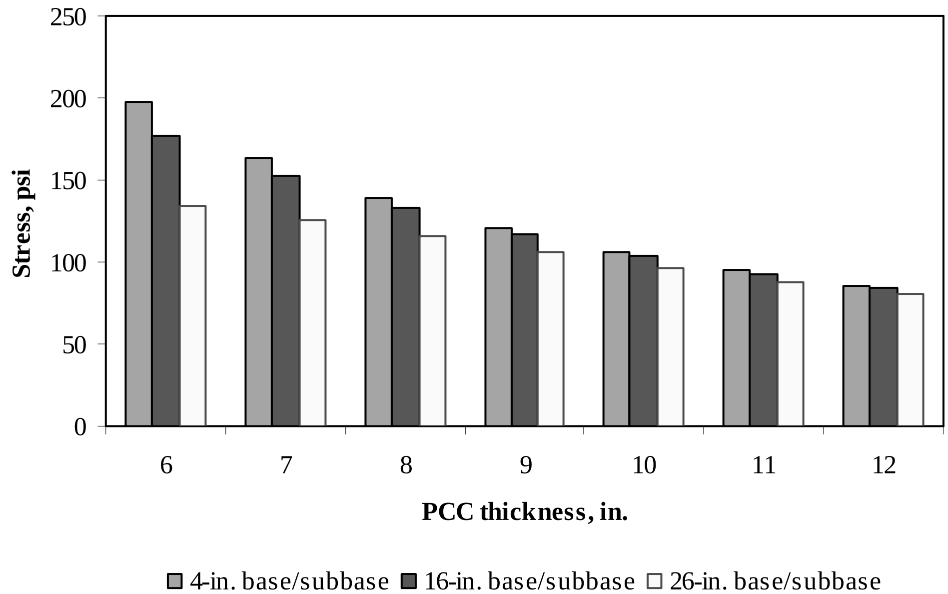


**Figure F-3-1: Impact of PCC thickness and base/subbase thickness on longitudinal stress at bottom of the Slab (177-in. joint spacing and $\alpha(\Delta T/D)$ of 0 in.$^{-1}$)**

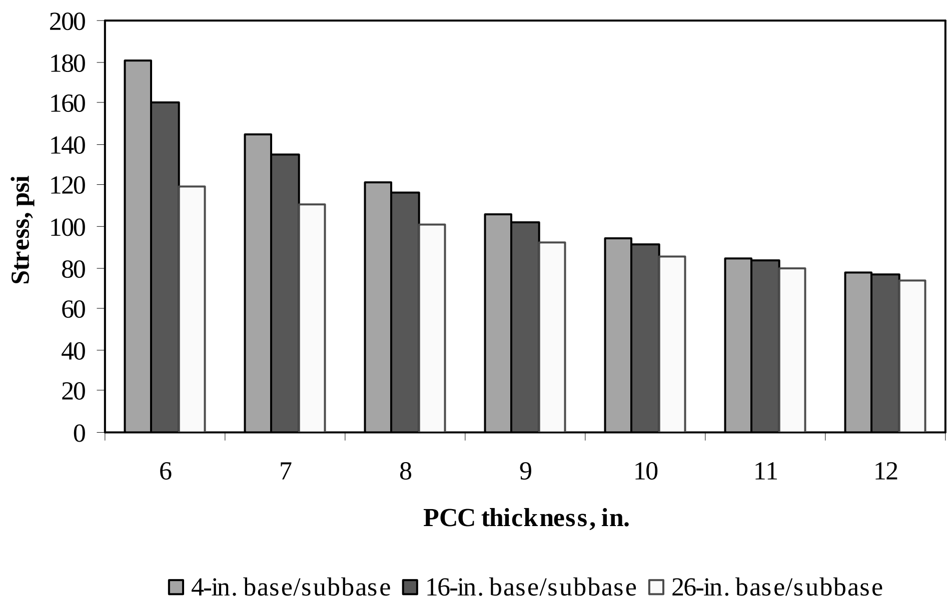


**Figure F-3-2: Impact of PCC thickness and base/subbase thickness on longitudinal stress at bottom of the Slab (315-in. joint spacing and $\alpha(\Delta T/D)$ of 0 in.$^{-1}$)**

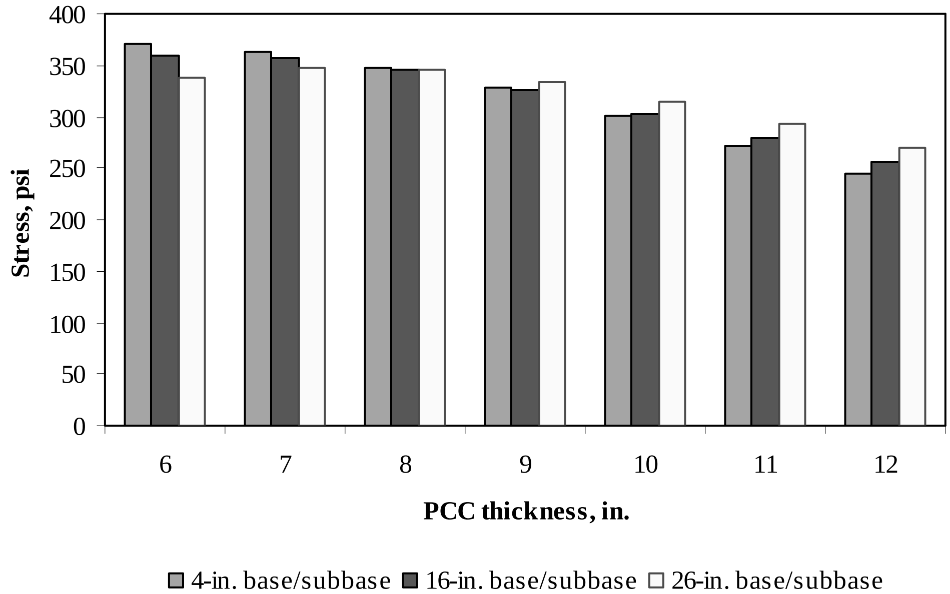


**Figure F-3-3: Impact of PCC thickness and base/subbase thickness on longitudinal stress at bottom of the Slab (177-in. joint spacing and $\alpha(\Delta T/D)$ of $20x10^{-6}$ in.$^{-1}$)**

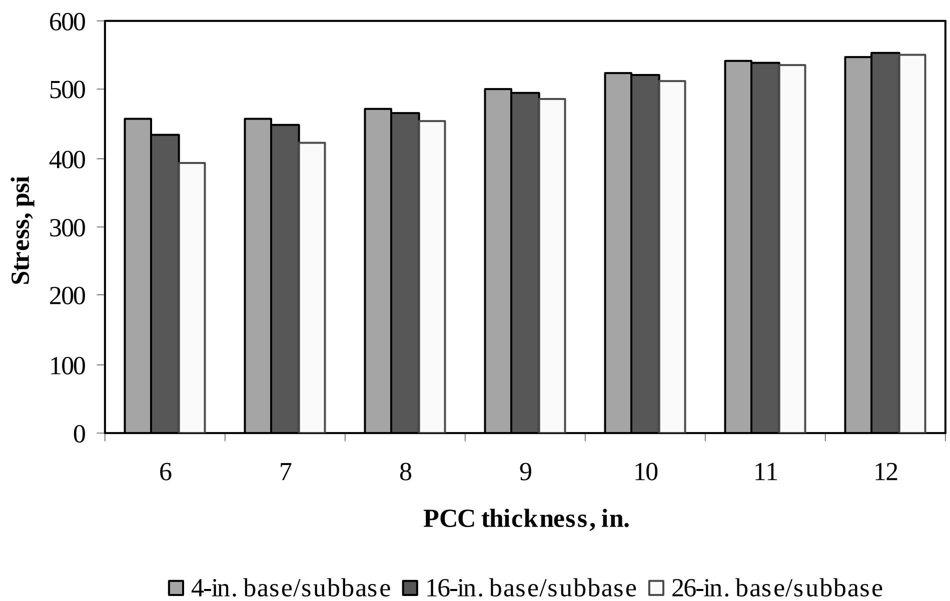


**Figure F-3-4: Impact of PCC thickness and base/subbase thickness on longitudinal stress at bottom of the Slab (315-in. joint spacing and $\alpha(\Delta T/D)$ of $20x10^{-6}$ in.$^{-1}$)**

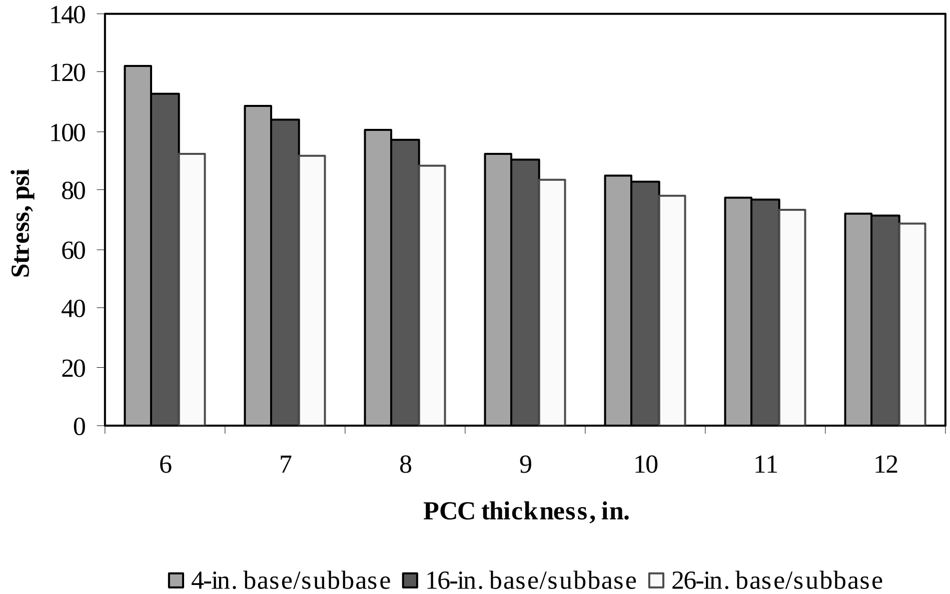


**Figure F-3-5: Impact of PCC thickness and base/subbase thickness on longitudinal stress at top of the Slab (177-in. joint spacing and $\alpha(\Delta T/D)$ of 0 in.$^{-1}$)**

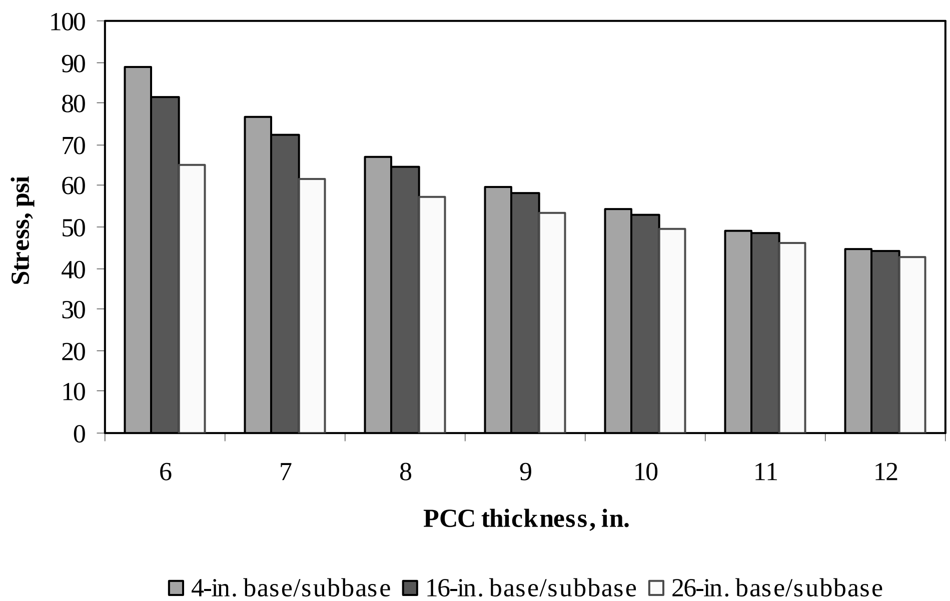


**Figure F-3-6: Impact of PCC thickness and base/subbase thickness on longitudinal stress at top of the Slab (315-in. joint spacing and $\alpha(\Delta T/D)$ of 0 in.$^{-1}$)**

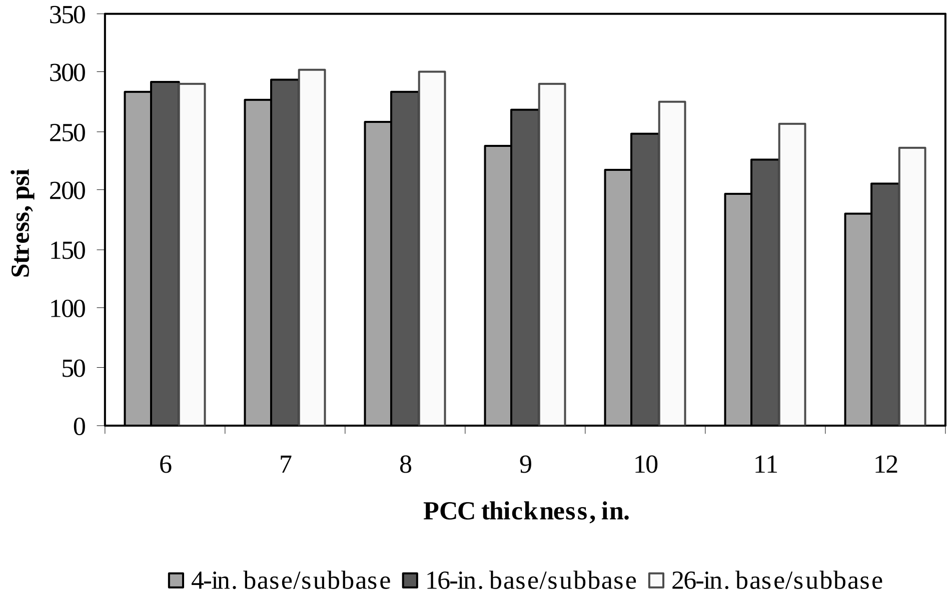


**Figure F-3-7: Impact of PCC thickness and base/subbase thickness on longitudinal stress at top of the Slab (177-in. joint spacing and $\alpha(\Delta T/D)$ of -20x10$^{-6}$ in.$^{-1}$)**

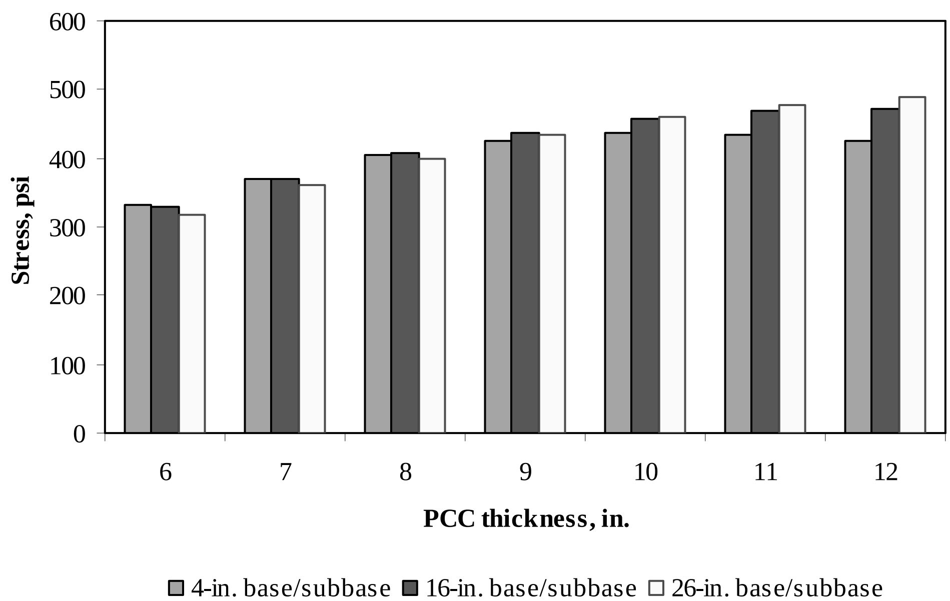


**Figure F-3-8: Impact of PCC thickness and base/subbase thickness on longitudinal stress at top of the Slab (315-in. joint spacing and $\alpha(\Delta T/D)$ of -20x10$^{-6}$ in.$^{-1}$)**

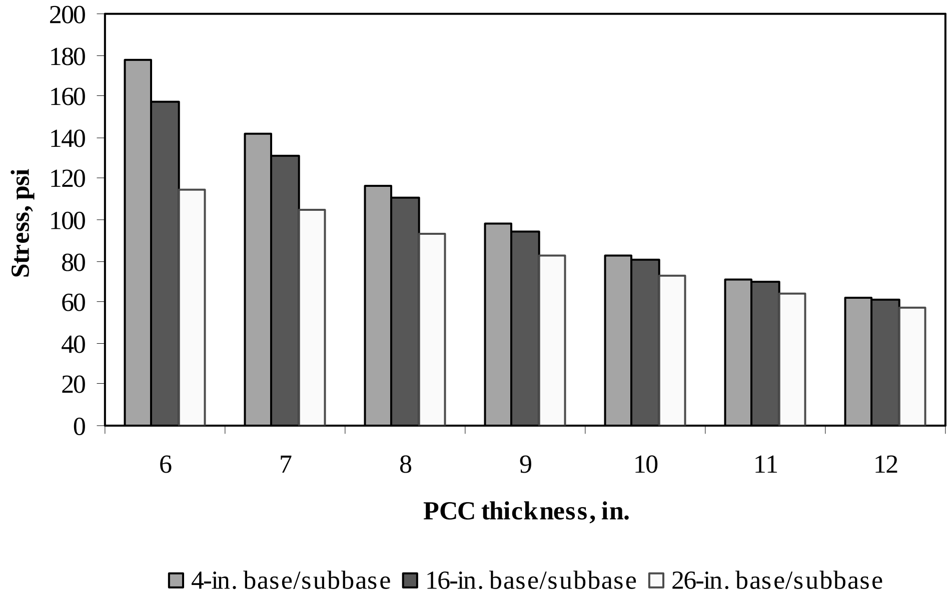


**Figure F-3-9: Impact of PCC thickness and base/subbase thickness on transverse stress at bottom of the Slab (177-in. joint spacing and $\alpha(\Delta T/D)$ of 0 in.$^{-1}$)**

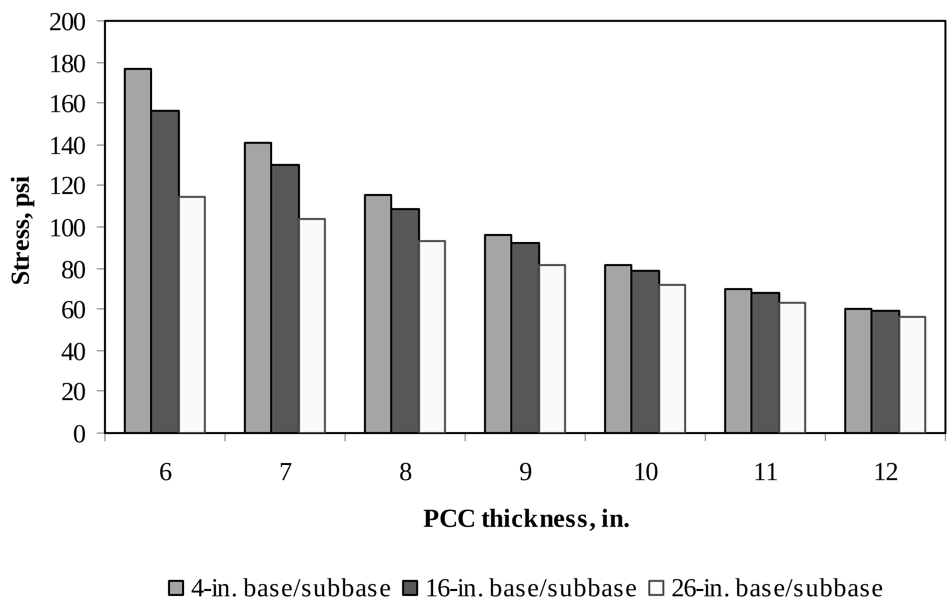


**Figure F-3-10: Impact of PCC thickness and base/subbase thickness on transverse stress at bottom of the Slab (315-in. joint spacing and $\alpha(\Delta T/D)$ of 0 in.$^{-1}$)**

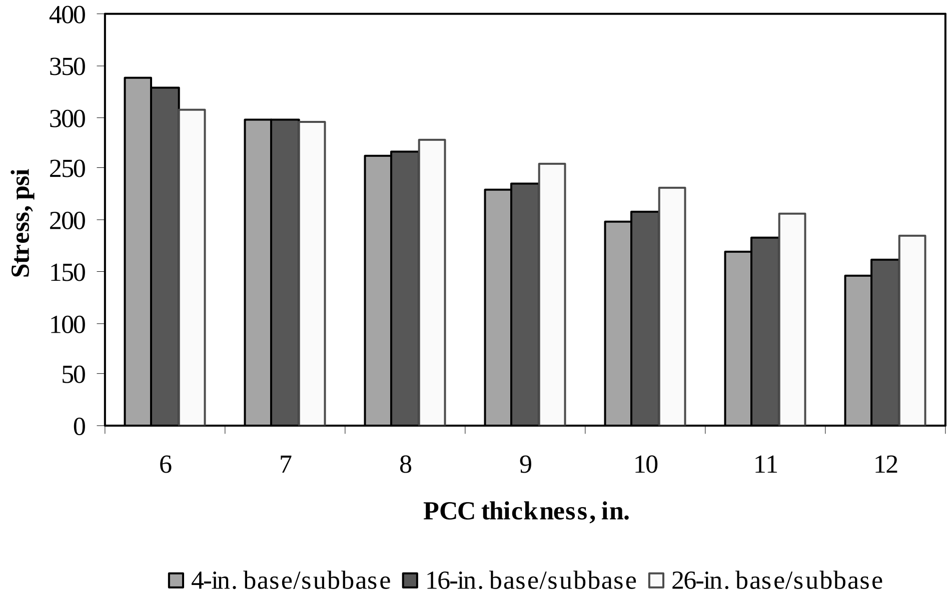


**Figure F-3-11: Impact of PCC thickness and base/subbase thickness on transverse stress at bottom of the Slab (177-in. joint spacing and $\alpha(\Delta T/D)$ of $20x10^{-6}$ in.$^{-1}$)**

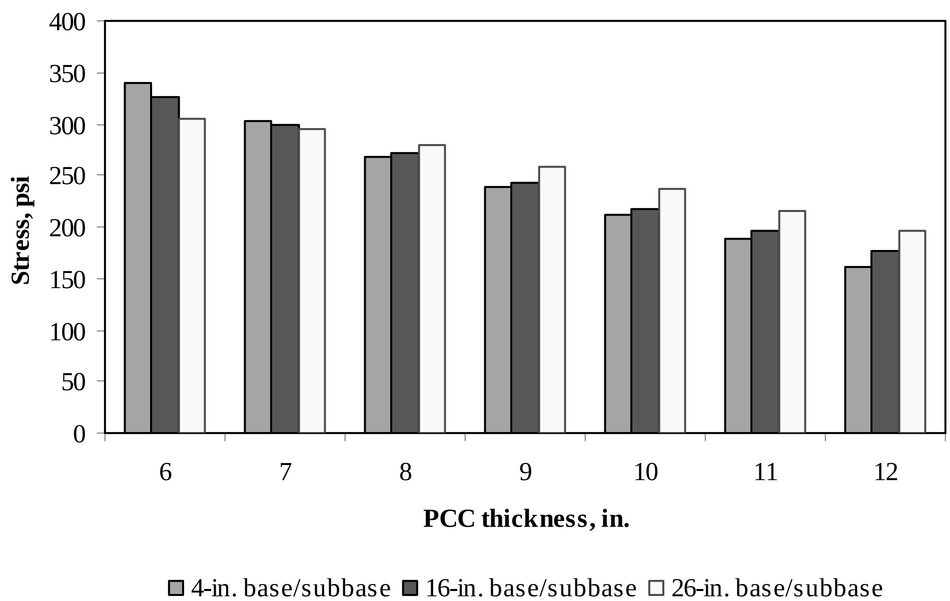


**Figure F-3-12: Impact of PCC thickness and base/subbase thickness on transverse stress at bottom of the Slab (315-in. joint spacing and $\alpha(\Delta T/D)$ of $20x10^{-6}$ in.$^{-1}$)**

Figures F-3-13 through F-3-24 illustrate the impact of PCC thickness and modulus of subgrade reaction on stresses (16-in. base/subbase thickness and PCC shoulder)

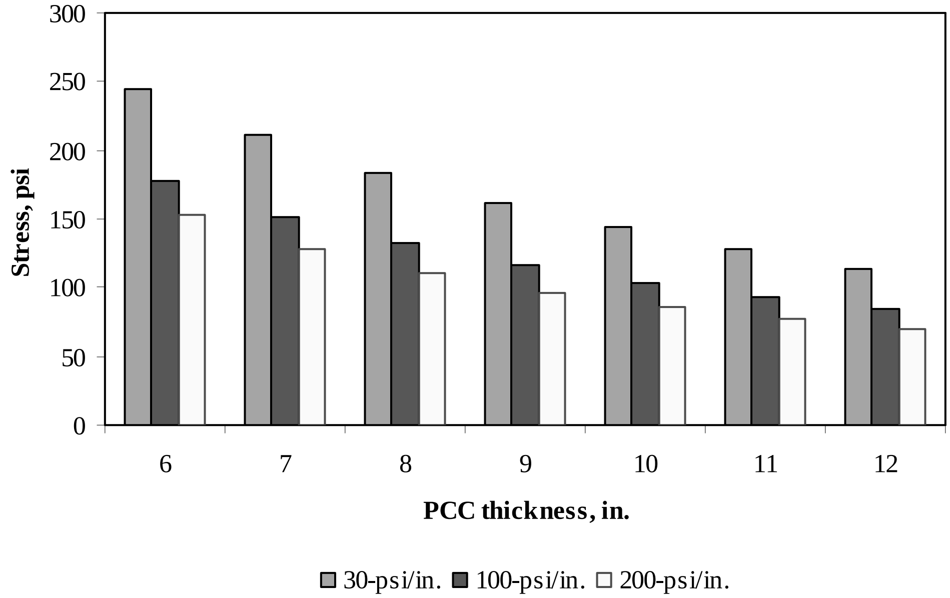


**Figure F-3-13: Impact of PCC thickness and modulus of subgrade reaction on longitudinal stress at bottom of the slab (177-in. joint spacing and $\alpha(\Delta T/D)$ of 0 in.$^{-1}$)**

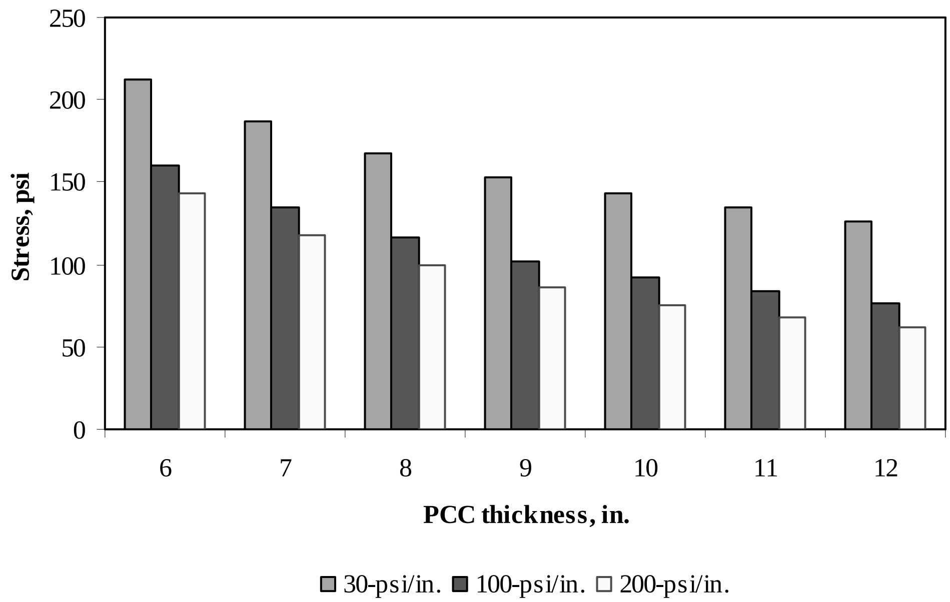


**Figure F-3-14: Impact of PCC thickness and modulus of subgrade reaction on longitudinal stress at bottom of the slab (315-in. joint spacing and $\alpha(\Delta T/D)$ of 0 in.$^{-1}$)**

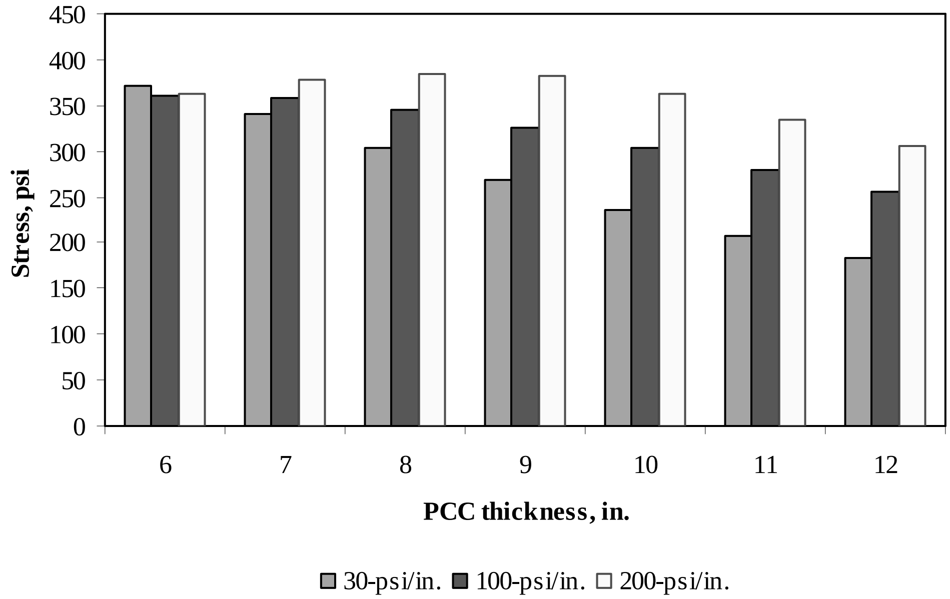


**Figure F-3-15: Impact of PCC thickness and modulus of subgrade reaction on longitudinal stress at bottom of the slab (177-in. joint spacing and $\alpha(\Delta T/D)$ of $20x10^{-6}$ in.$^{-1}$)**

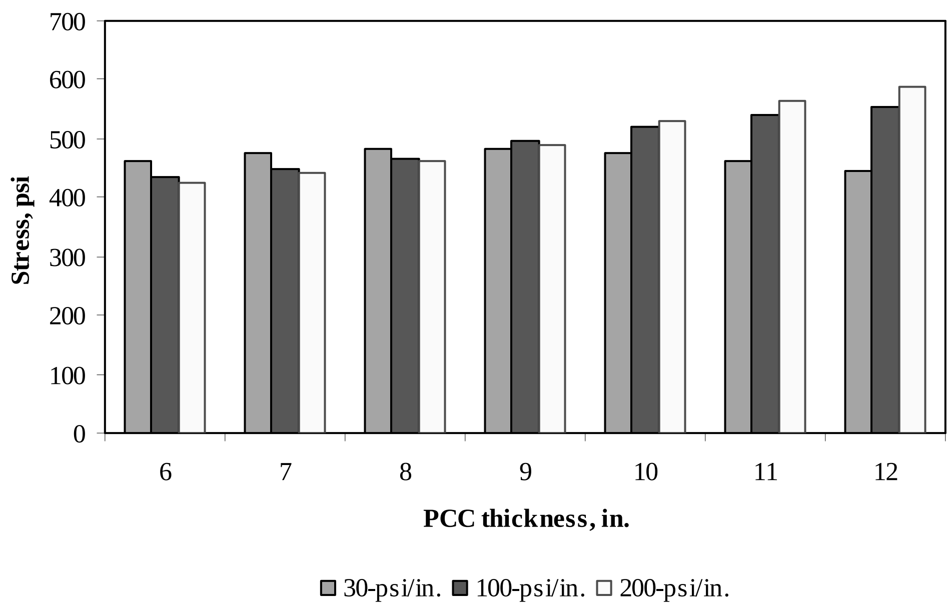


**Figure F-3-16: Impact of PCC thickness and modulus of subgrade reaction on longitudinal stress at bottom of the slab (315-in. joint spacing and $\alpha(\Delta T/D)$ of $20x10^{-6}$ in.$^{-1}$)**

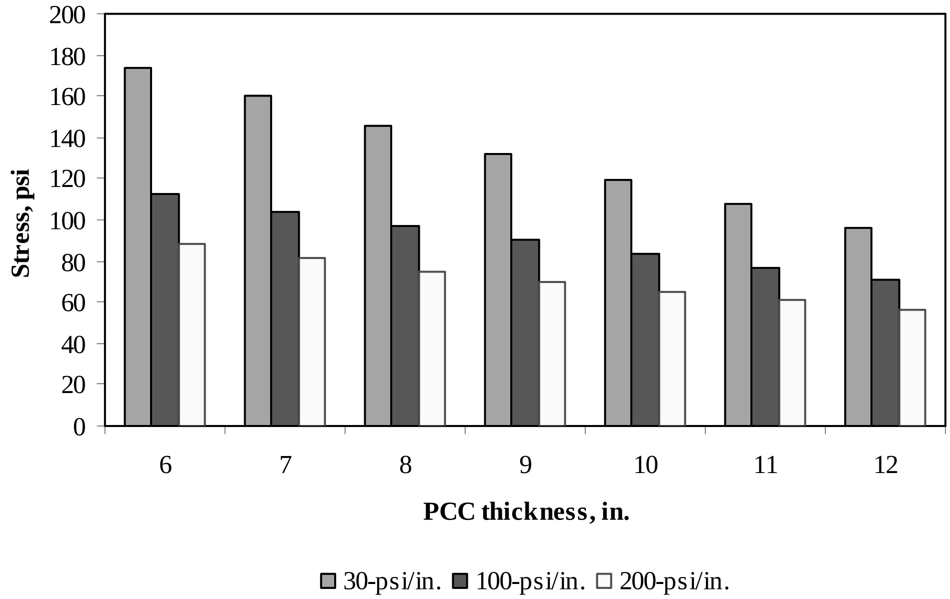


**Figure F-3-17: Impact of PCC thickness and modulus of subgrade reaction on longitudinal stress at top of the Slab (177-in. joint spacing and $\alpha(\Delta T/D)$ of 0 $in.^{-1}$)**

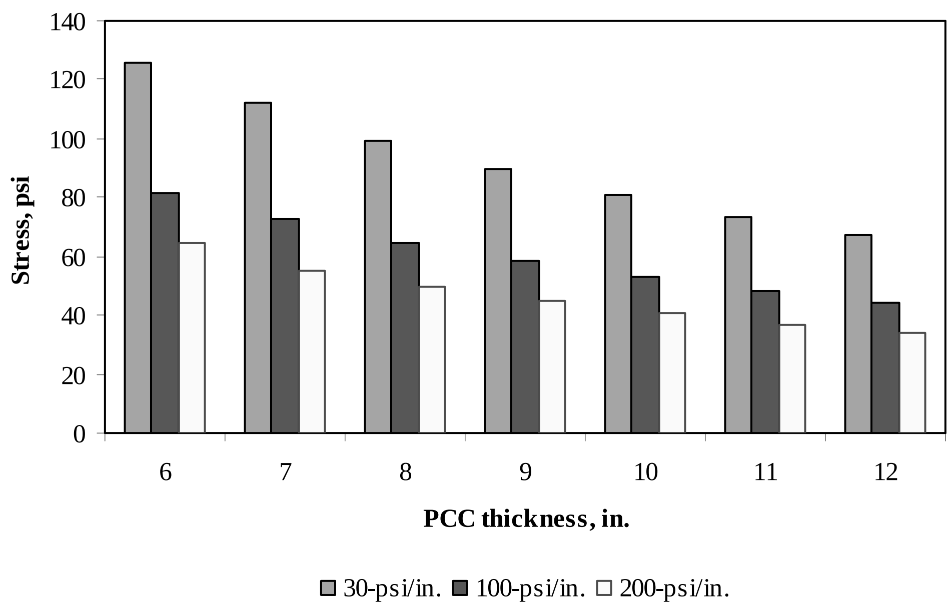


**Figure F-3-18: Impact of PCC thickness and modulus of subgrade reaction on longitudinal stress at top of the Slab (315-in. joint spacing and $\alpha(\Delta T/D)$ of 0 $in.^{-1}$)**

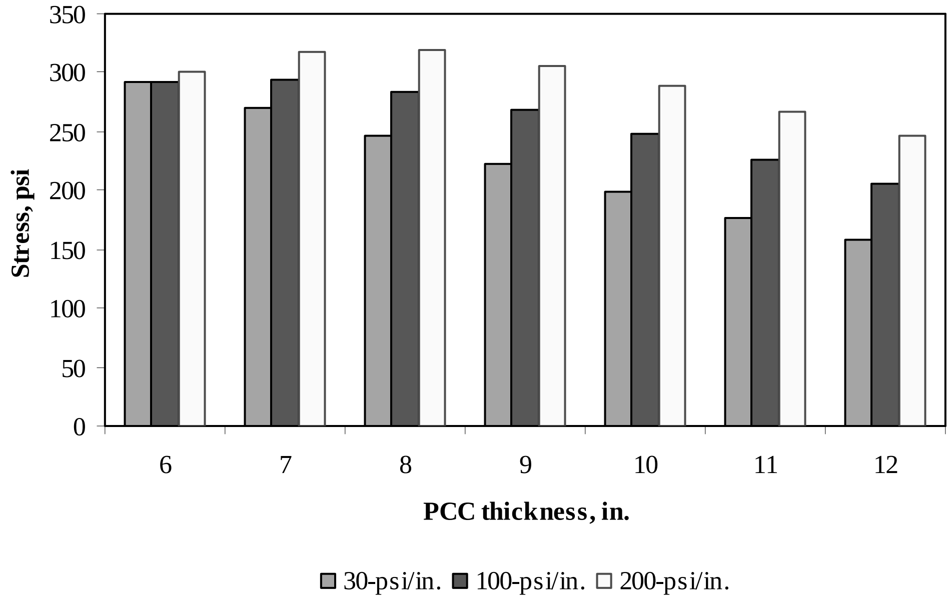


**Figure F-3-19: Impact of PCC thickness and modulus of subgrade reaction on longitudinal stress at top of the Slab (177-in. joint spacing and $\alpha(\Delta T/D)$ of $-20x10^{-6}$ in.$^{-1}$)**

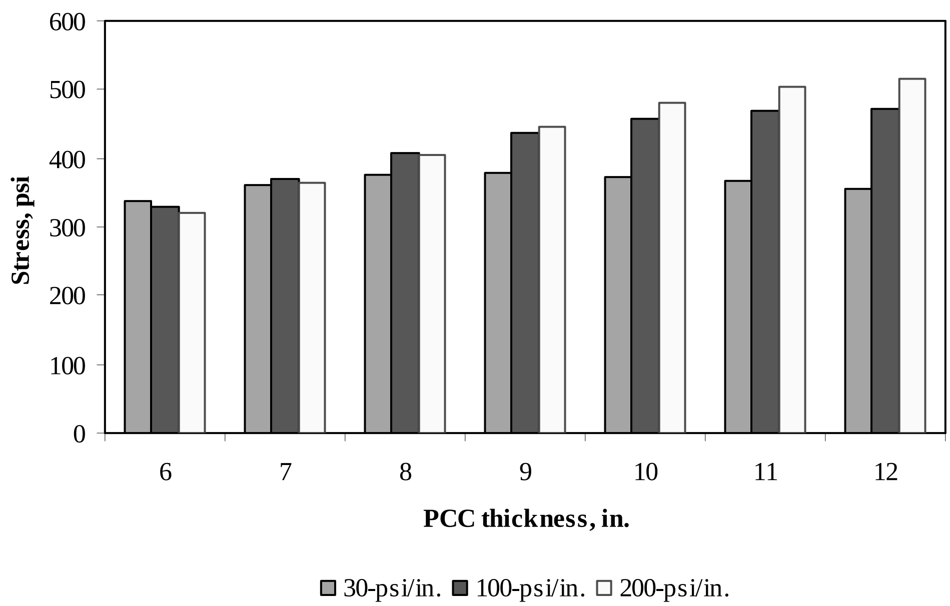


**Figure F-3-20: Impact of PCC thickness and modulus of subgrade reaction on longitudinal stress at top of the Slab (315-in. joint spacing and $\alpha(\Delta T/D)$ of $-20x10^{-6}$ in.$^{-1}$)**

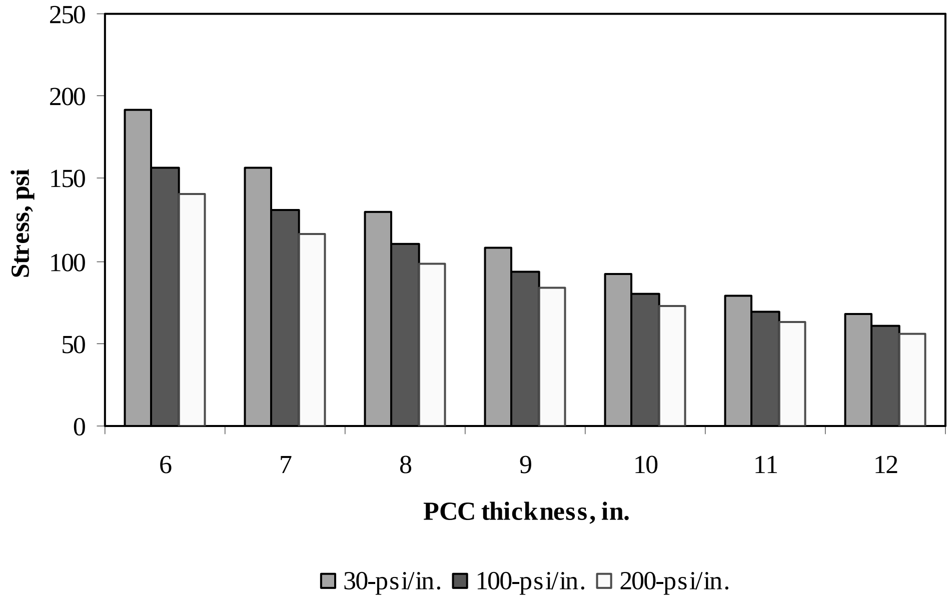


**Figure F-3-21: Impact of PCC thickness and modulus of subgrade reaction on transverse stress at bottom of the Slab (177-in. joint spacing and $\alpha(\Delta T/D)$ of 0 in.$^{-1}$)**

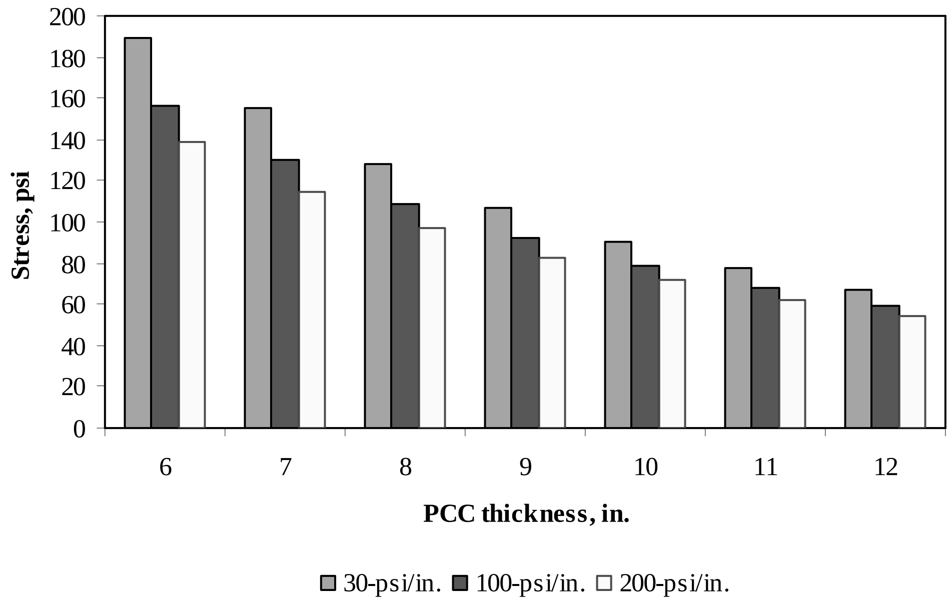


**Figure F-3-22: Impact of PCC thickness and modulus of subgrade reaction on transverse stress at bottom of the Slab (315-in. joint spacing and $\alpha(\Delta T/D)$ of 0 in.$^{-1}$)**

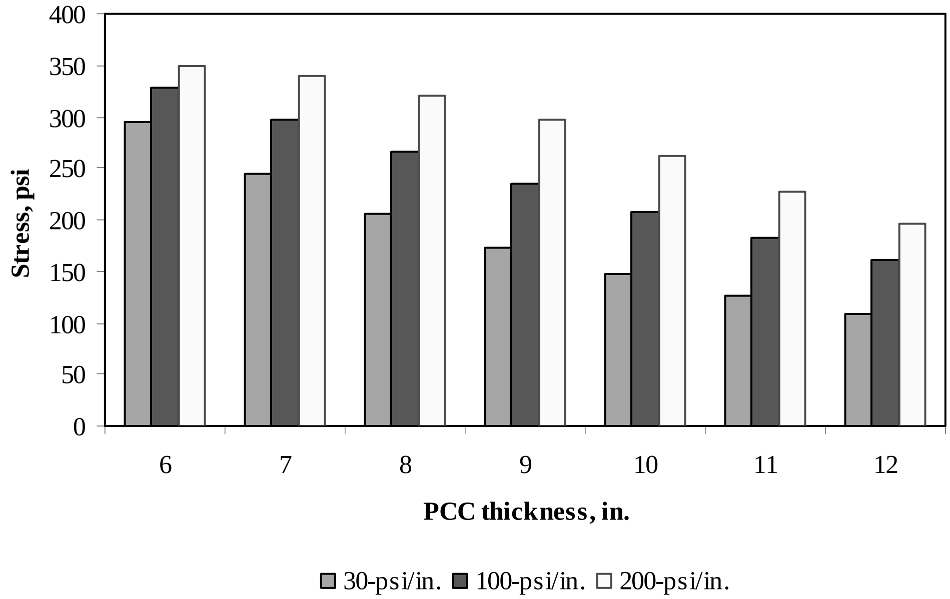


**Figure F-3-23: Impact of PCC thickness and modulus of subgrade reaction on transverse stress at bottom of the Slab (177-in. joint spacing and $\alpha(\Delta T/D)$ of $20x10^{-6}$ in.$^{-1}$)**

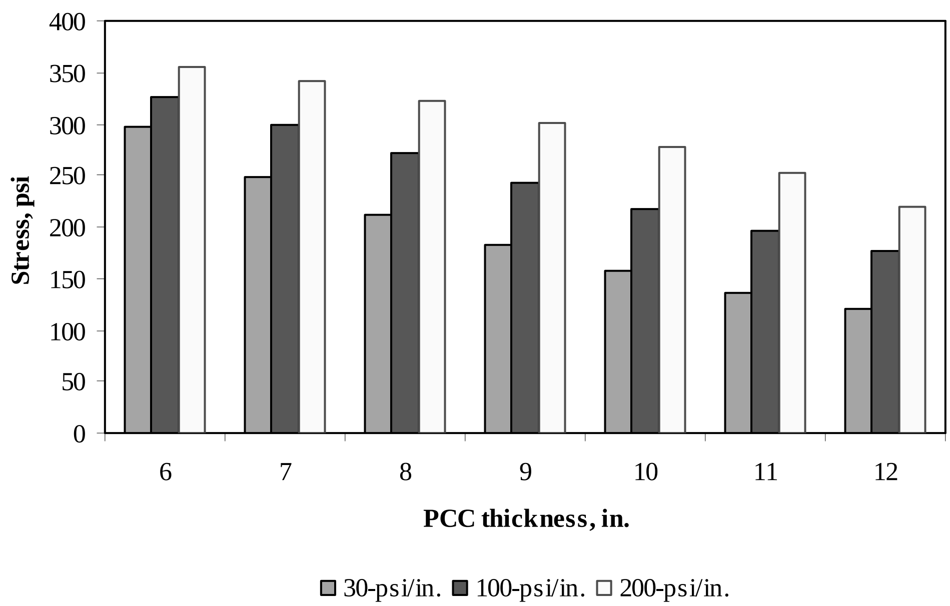


**Figure F-3-24: Impact of PCC thickness and modulus of subgrade reaction on transverse stress at bottom of the Slab (315-in. joint spacing and $\alpha(\Delta T/D)$ of $20x10^{-6}$ in.$^{-1}$)**

Figures F-3-25 through F-3-36 illustrate the impact of PCC thickness and lateral support condition on stresses (16-in. base/subbase and 100-psi/in. modulus of subgrade reaction)

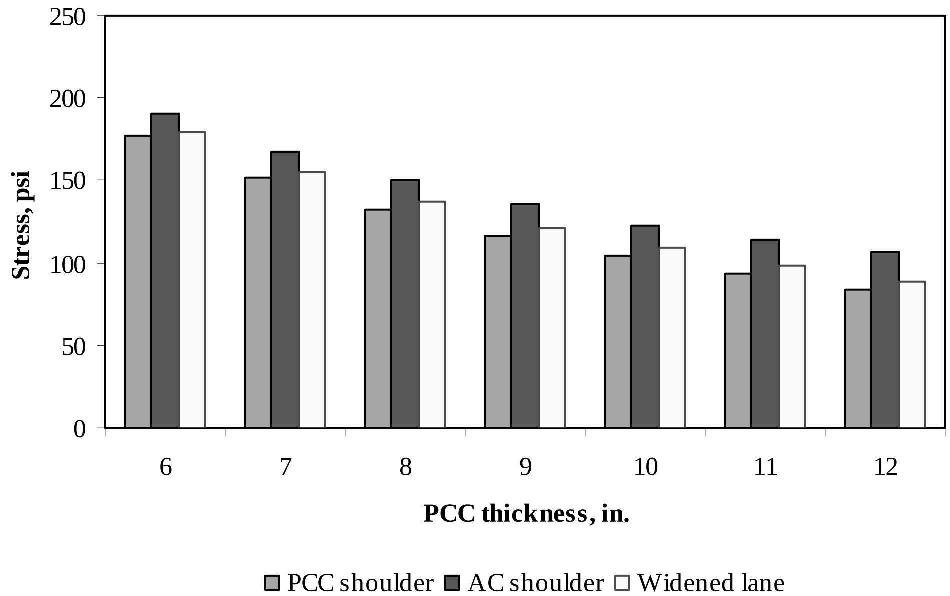


**Figure F-3-25: Impact of PCC thickness and lateral support condition on longitudinal stress at bottom of the Slab (177-in. joint spacing and $\alpha(\Delta T/D)$ of 0 in.$^{-1}$)**

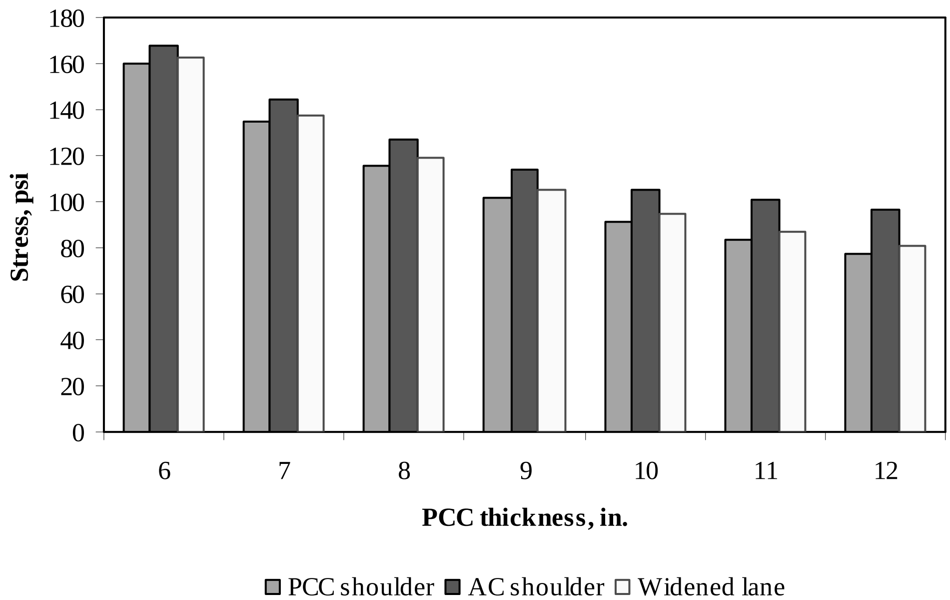


**Figure F-3-26: Impact of PCC thickness and lateral support condition on longitudinal stress at bottom of the Slab (315-in. joint spacing and $\alpha(\Delta T/D)$ of 0 in.$^{-1}$)**

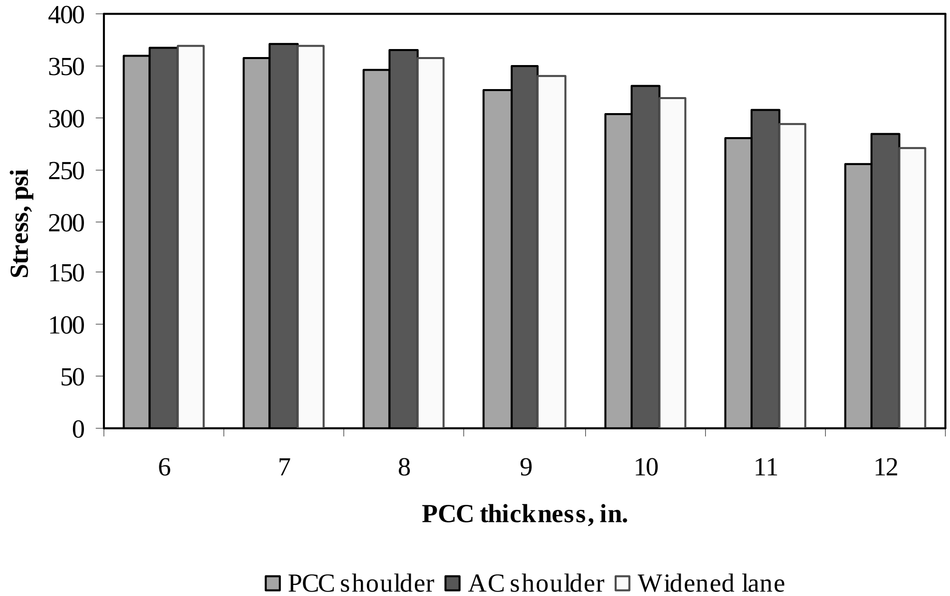


**Figure F-3-27: Impact of PCC thickness and lateral support condition on longitudinal stress at bottom of the Slab (177-in. joint spacing and $\alpha(\Delta T/D)$ of $20x10^{-6}$ in.$^{-1}$)**

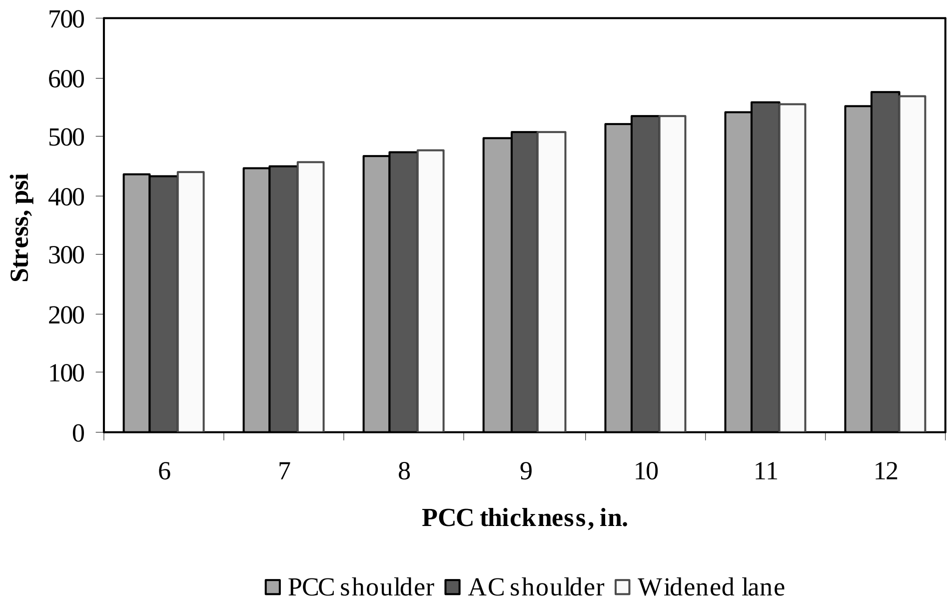


**Figure F-3-28: Impact of PCC thickness and lateral support condition on longitudinal stress at bottom of the Slab (315-in. joint spacing and $\alpha(\Delta T/D)$ of $20x10^{-6}$ in.$^{-1}$)**

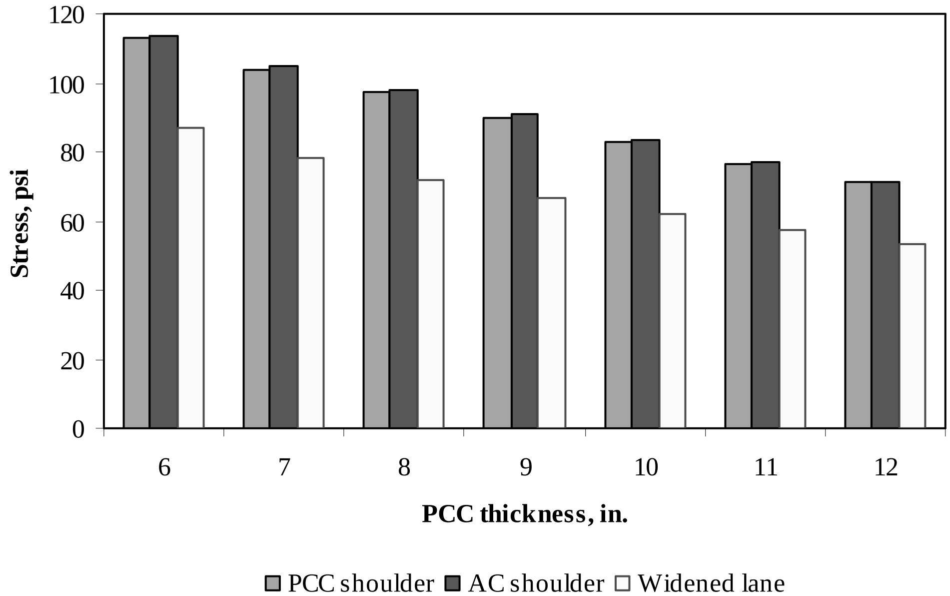


**Figure F-3-29: Impact of PCC thickness and lateral support condition on longitudinal stress at top of the Slab (177-in. joint spacing and $\alpha(\Delta T/D)$ of 0 in.$^{-1}$)**

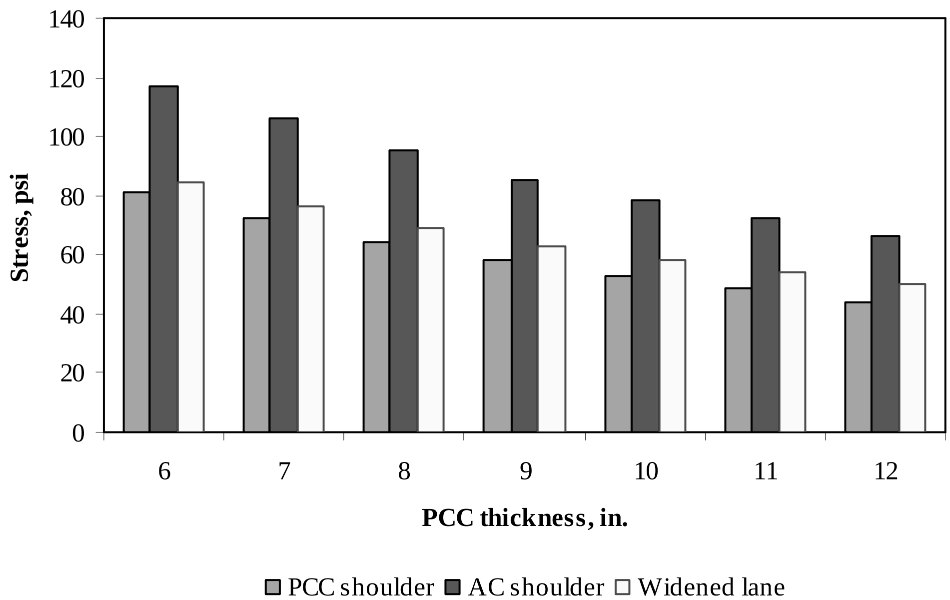


**Figure F-3-30: Impact of PCC thickness and lateral support condition on longitudinal stress at top of the Slab (315-in. joint spacing and $\alpha(\Delta T/D)$ of 0 in.$^{-1}$)**

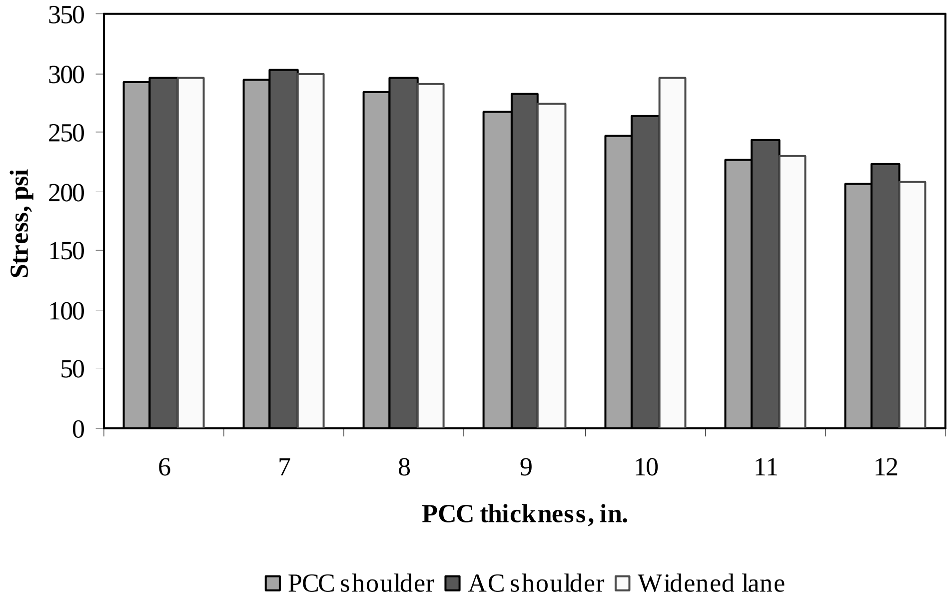


**Figure F-3-31: Impact of PCC thickness and lateral support condition on longitudinal stress at top of the Slab (177-in. joint spacing and $\alpha(\Delta T/D)$ of -20x$10^{-6}$ in.$^{-1}$)**

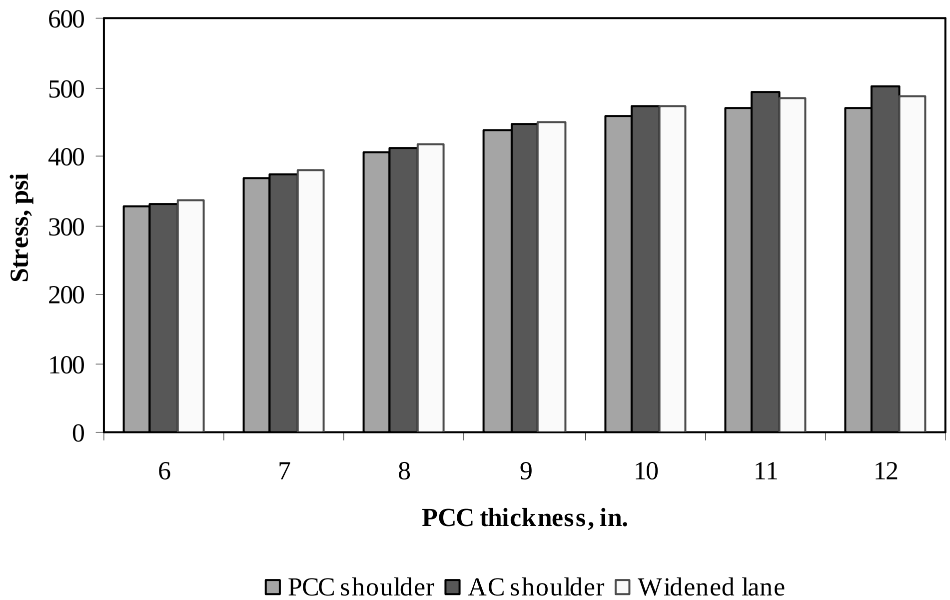


**Figure F-3-32: Impact of PCC thickness and lateral support condition on longitudinal stress at top of the Slab (315-in. joint spacing and $\alpha(\Delta T/D)$ of -20x$10^{-6}$ in.$^{-1}$)**

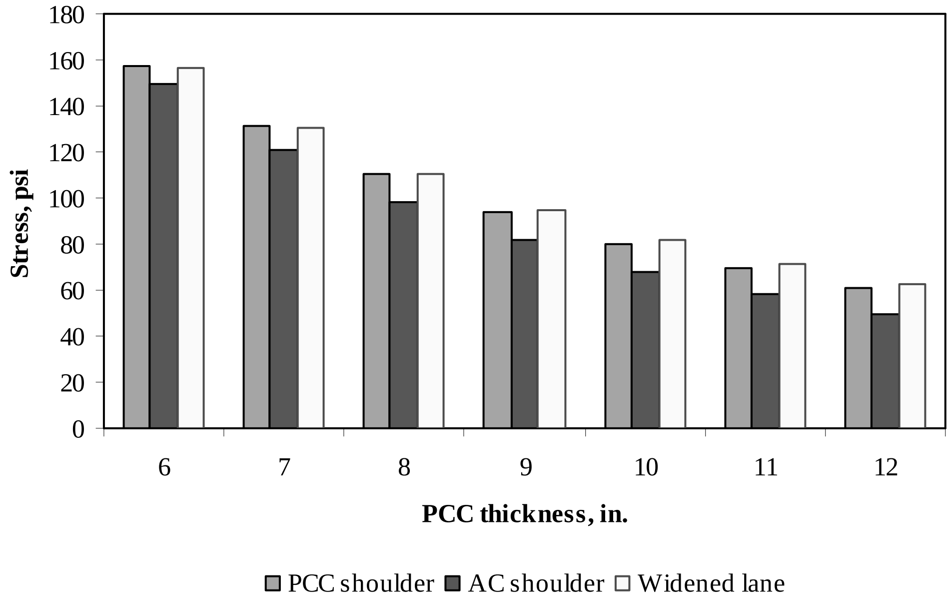


**Figure F-3-33: Impact of PCC thickness and lateral support condition on transverse stress at bottom of the Slab (177-in. joint spacing and $\alpha(\Delta T/D)$ of 0 in.$^{-1}$)**

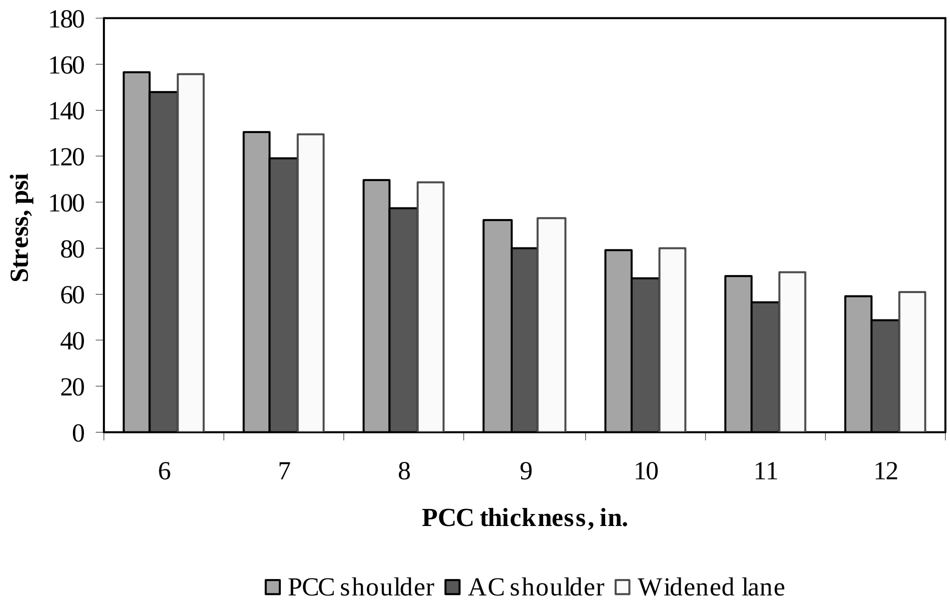


**Figure F-3-34: Impact of PCC thickness and lateral support condition on transverse stress at bottom of the Slab (315-in. joint spacing and $\alpha(\Delta T/D)$ of 0 in.$^{-1}$)**

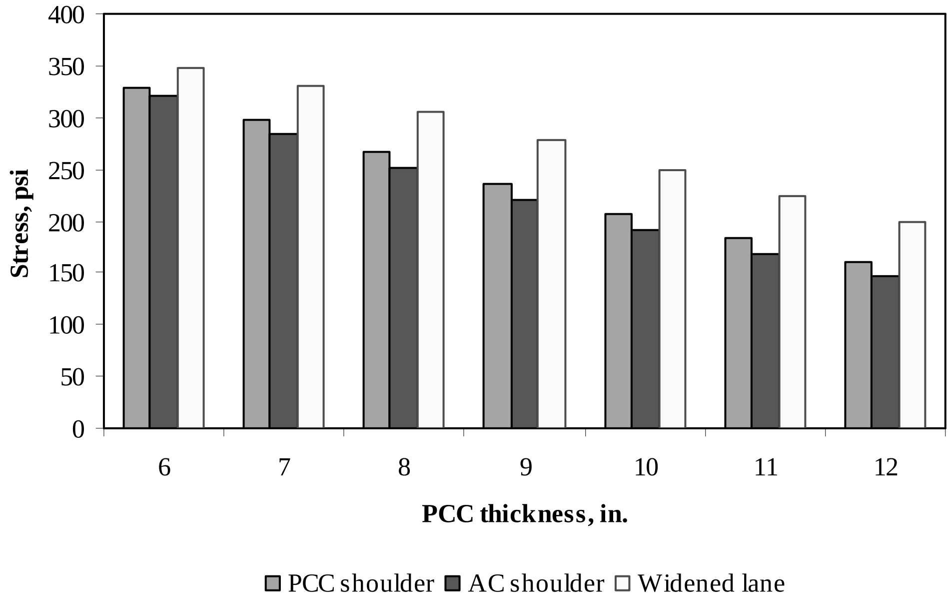


**Figure F-3-35: Impact of PCC thickness and lateral support condition on transverse stress at bottom of the Slab (177-in. joint spacing and $\alpha(\Delta T/D)$ of $20x10^{-6}$ in.$^{-1}$)**

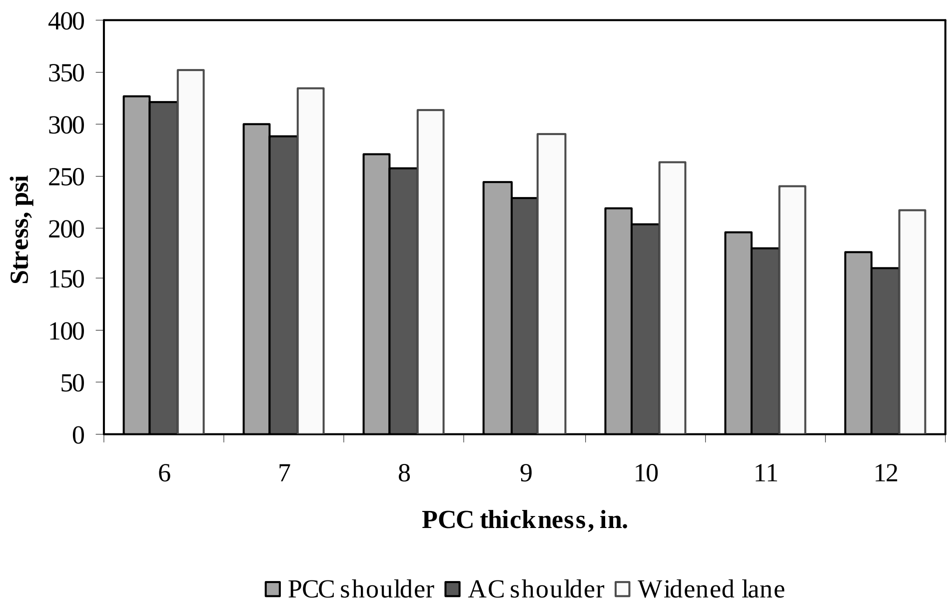


**Figure F-3-36: Impact of PCC thickness and lateral support condition on transverse stress at bottom of the Slab (315-in. joint spacing and $\alpha(\Delta T/D)$ of $20x10^{-6}$ in.$^{-1}$)**

Figures F-3-37 through F-3-42 illustrate the impact of base/subbase thickness and product α(ΔT/D) on stresses (10-in. PCC thickness, 100-psi/in. modulus of subgrade reaction and PCC shoulder)

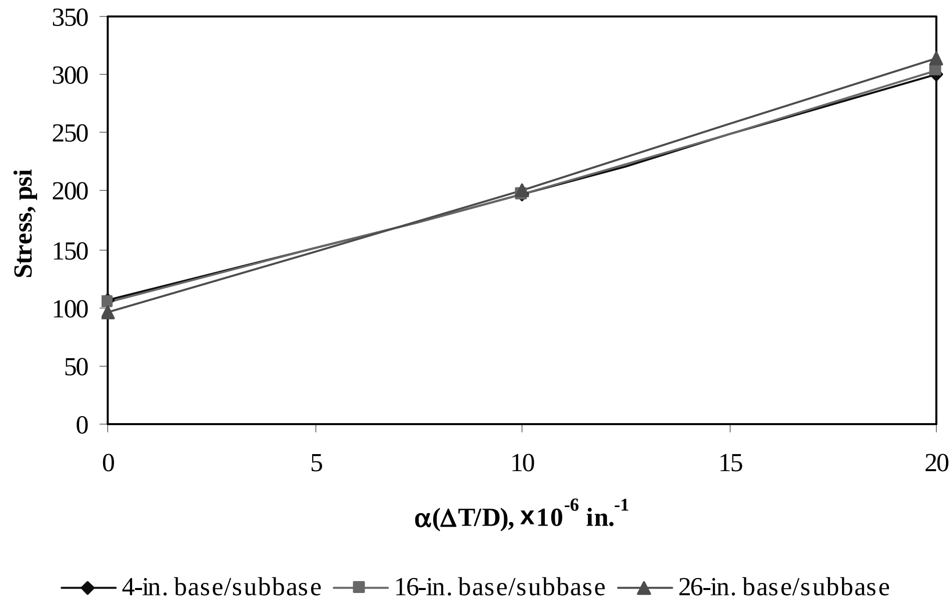


**Figure F-3-37: Impact of base/subbase thickness and product α(ΔT/D) on longitudinal stress at bottom of the slab (177-in. joint spacing)**

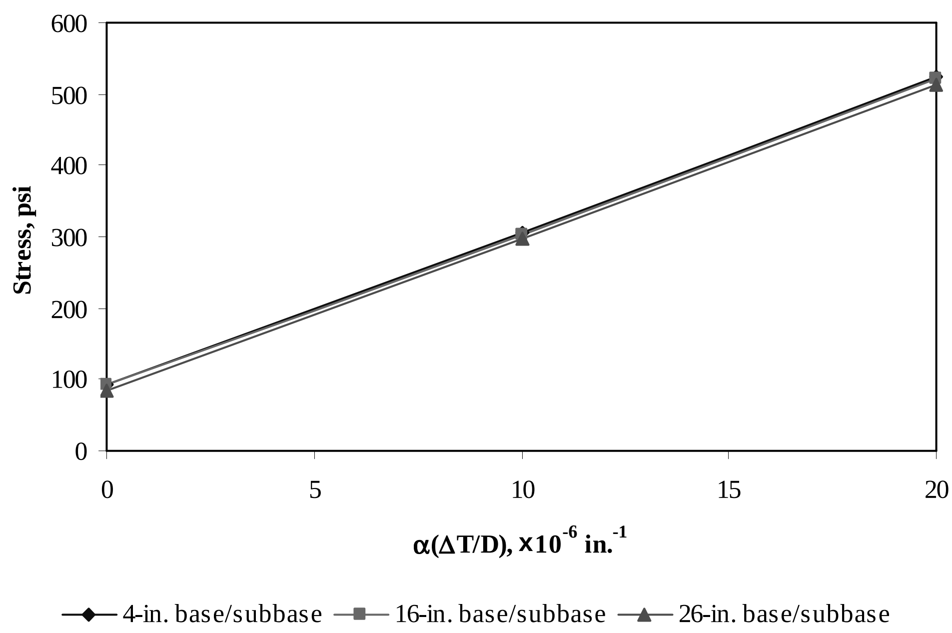


**Figure F-3-38: Impact of base/subbase thickness and product α(ΔT/D) on longitudinal stress at bottom of the slab (315-in. joint spacing)**

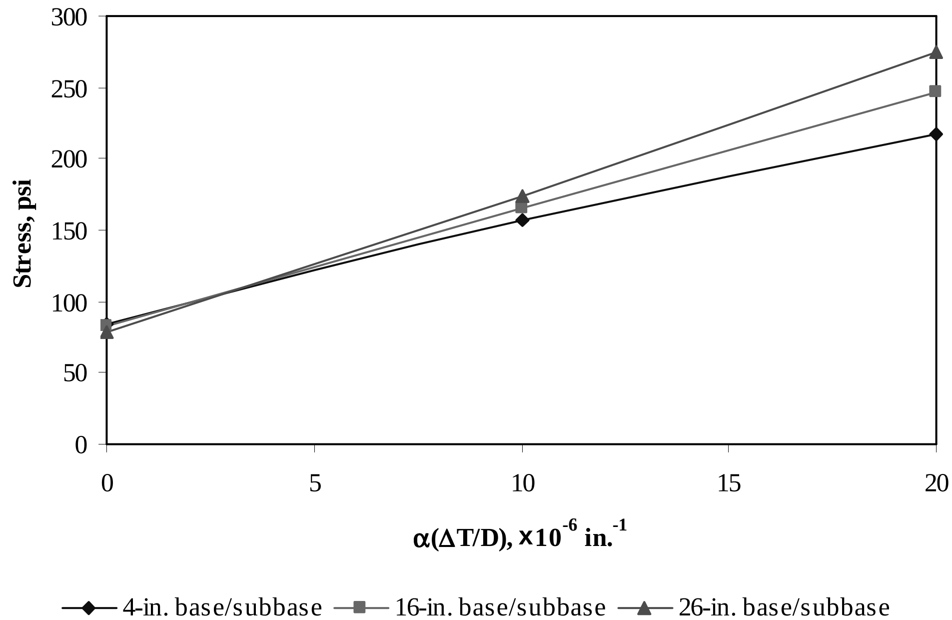


**Figure F-3-39: Impact of base/subbase thickness and product α(ΔT/D) on longitudinal stress at top of the slab (177-in. joint spacing)**

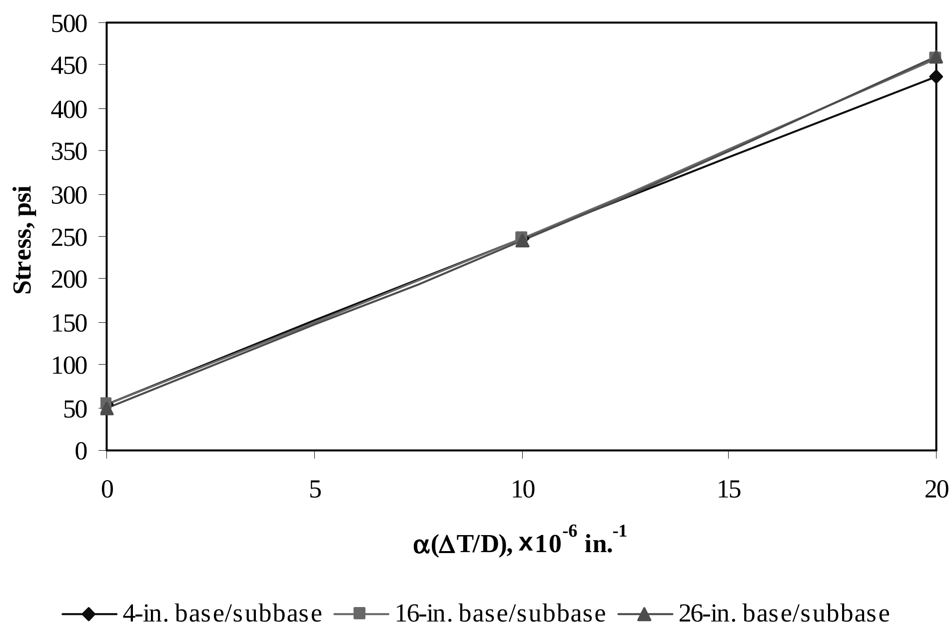


**Figure F-3-40: Impact of base/subbase thickness and product α(ΔT/D) on longitudinal stress at top of the slab (315-in. joint spacing)**

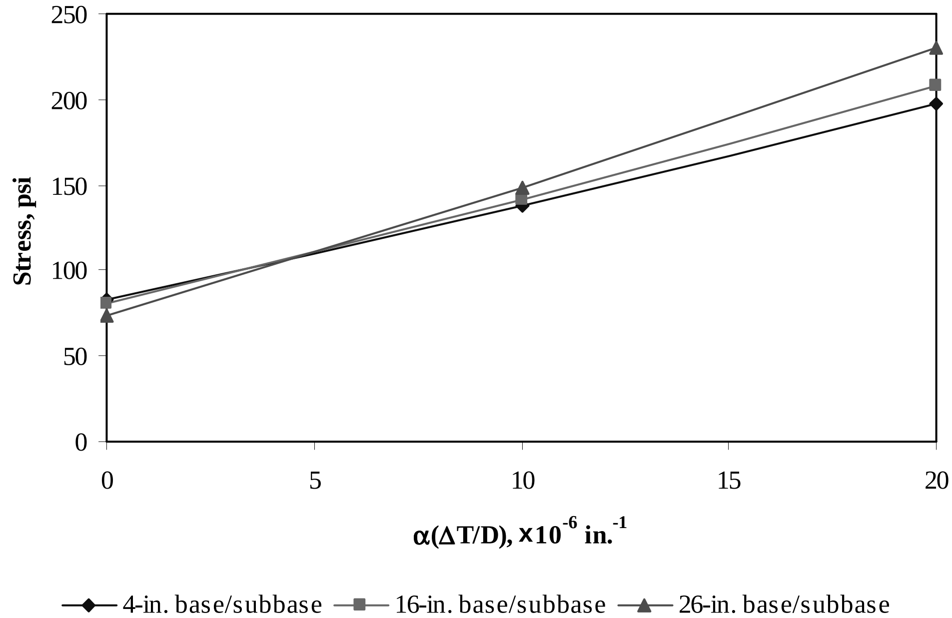


**Figure F-3-41: Impact of base/subbase thickness and product α(ΔT/D) on transverse stress at bottom of the slab (177-in. joint spacing)**

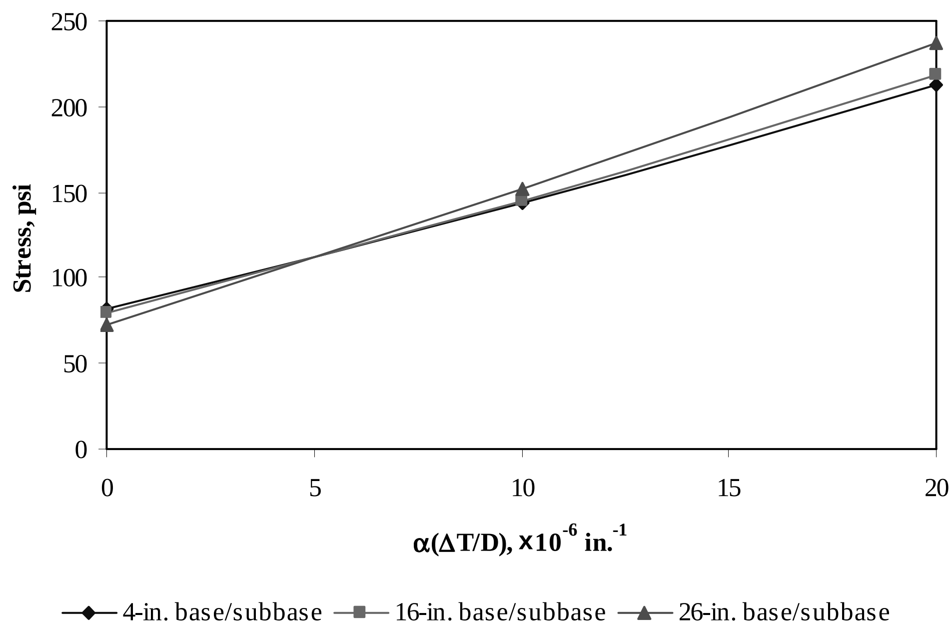


**Figure F-3-42: Impact of base/subbase thickness and product α(ΔT/D) on transverse stress at bottom of the slab (315-in. joint spacing)**

Figures F-3-43 through F-3-48 illustrate the impact of modulus of subgrade reaction and product α(ΔT/D) on stresses (10-in. PCC thickness, 16-in. base/subbase thickness and PCC shoulder)

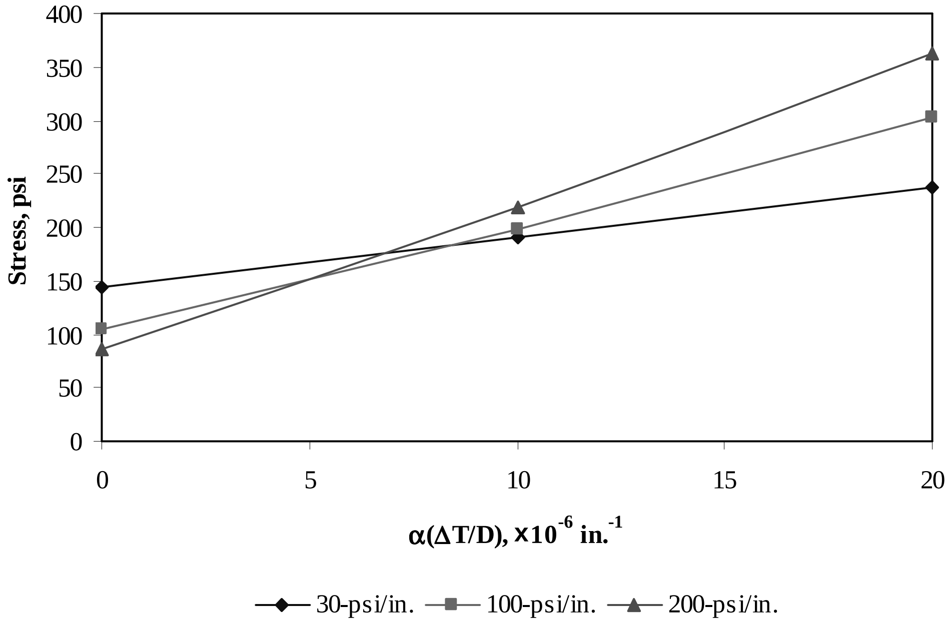


**Figure F-3-43: Impact of modulus of subgrade reaction and product α(ΔT/D) on longitudinal stress at bottom of the slab (177-in. joint spacing)**

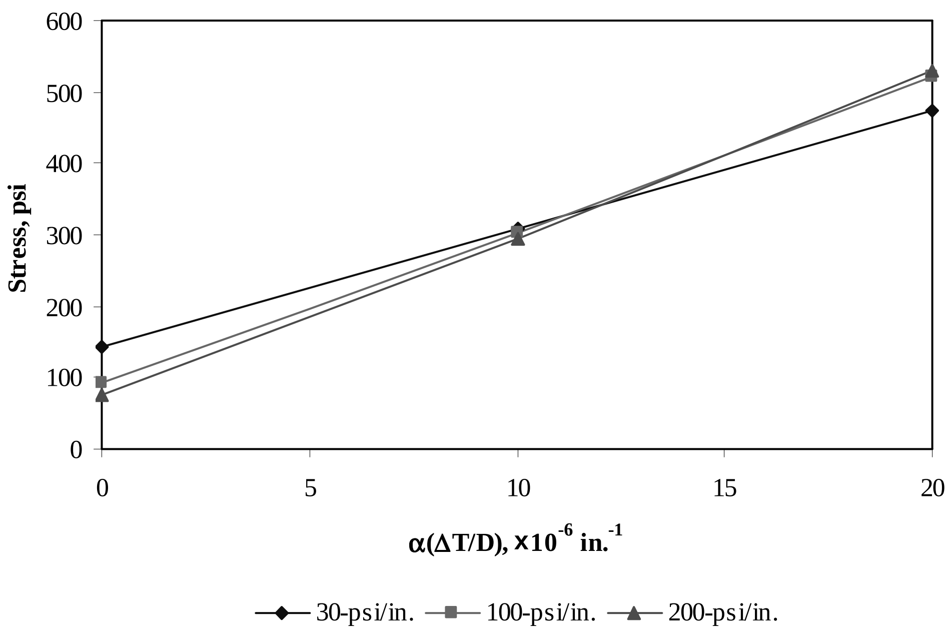


**Figure F-3-44: Impact of modulus of subgrade reaction and product α(ΔT/D) on longitudinal stress at bottom of the slab (315-in. joint spacing)**

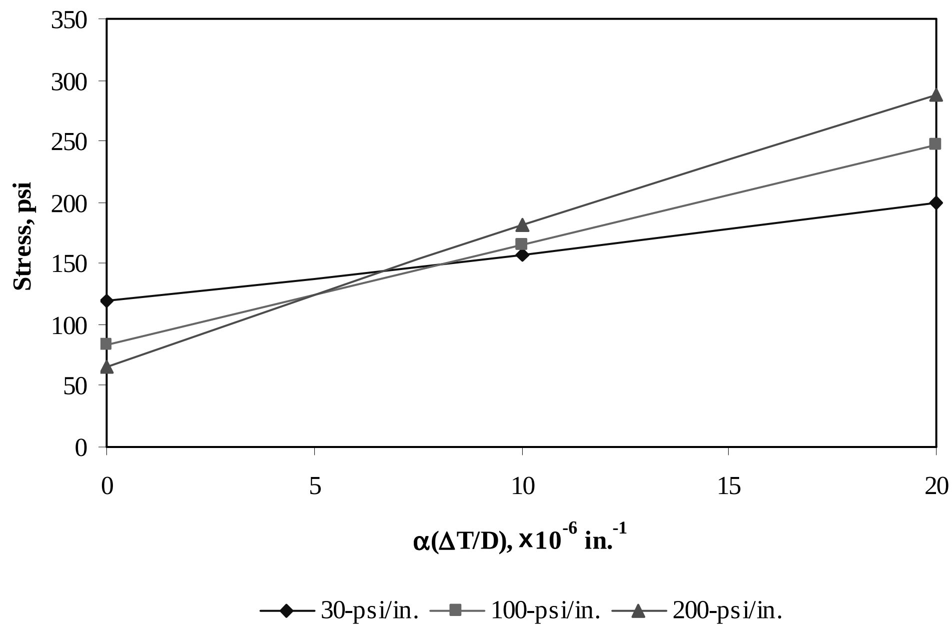


**Figure F-3-45: Impact of modulus of subgrade reaction and product α(ΔT/D) on longitudinal stress at top of the slab (177-in. joint spacing)**

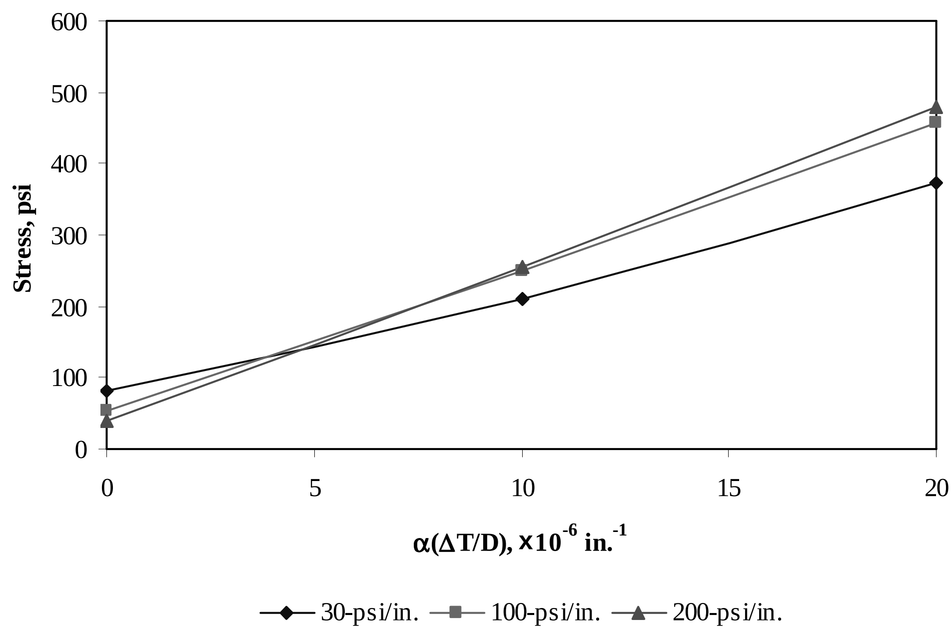


**Figure F-3-46: Impact of modulus of subgrade reaction and product α(ΔT/D) on longitudinal stress at top of the slab (315-in. joint spacing)**

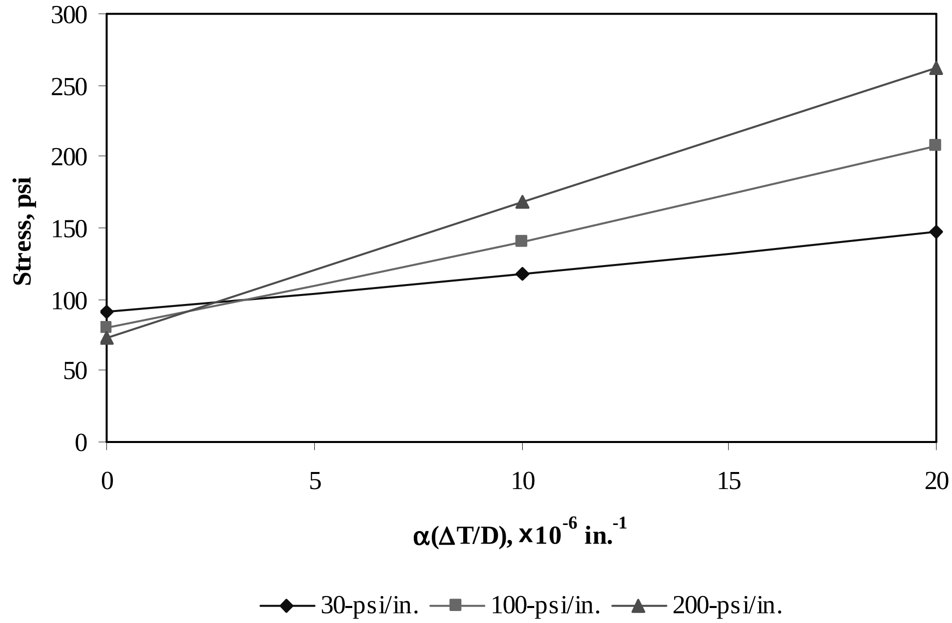


**Figure F-3-47: Impact of modulus of subgrade reaction and product α(ΔT/D) on transverse stress at bottom of the slab (177-in. joint spacing)**

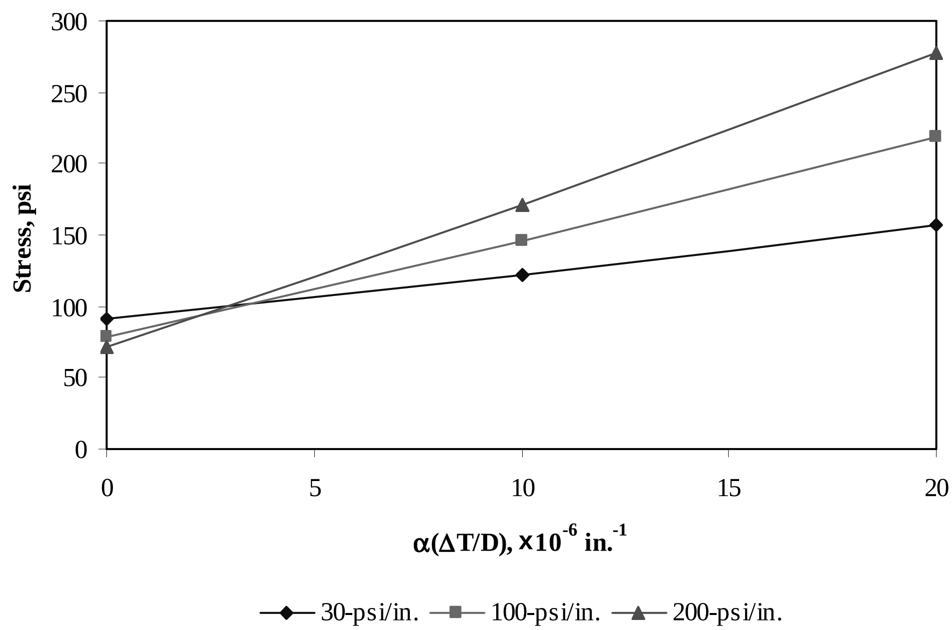


**Figure F-3-48: Impact of modulus of subgrade reaction and product α(ΔT/D) on transverse stress at bottom of the slab (315-in. joint spacing)**

Figures F-3-49 through F-3-51 illustrate the impact of joint spacing and product α(ΔT/D) on stresses (10-in. PCC thickness, 16-in. base/subbase thickness, 100-psi/in. modulus of subgrade reaction and PCC shoulder)

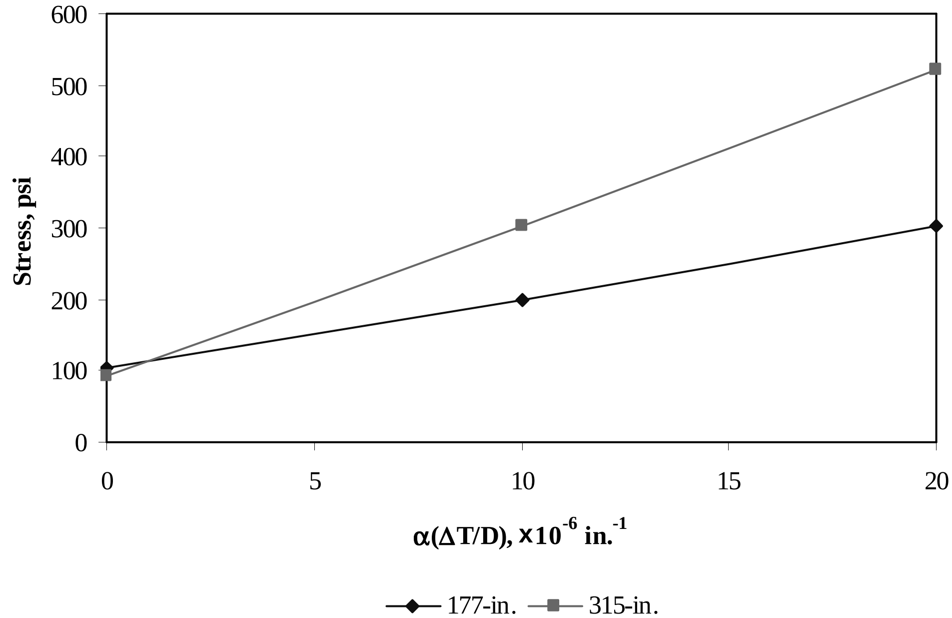


**Figure F-3-49: Impact of joint spacing and product α(ΔT/D) on longitudinal stress at bottom of the slab**

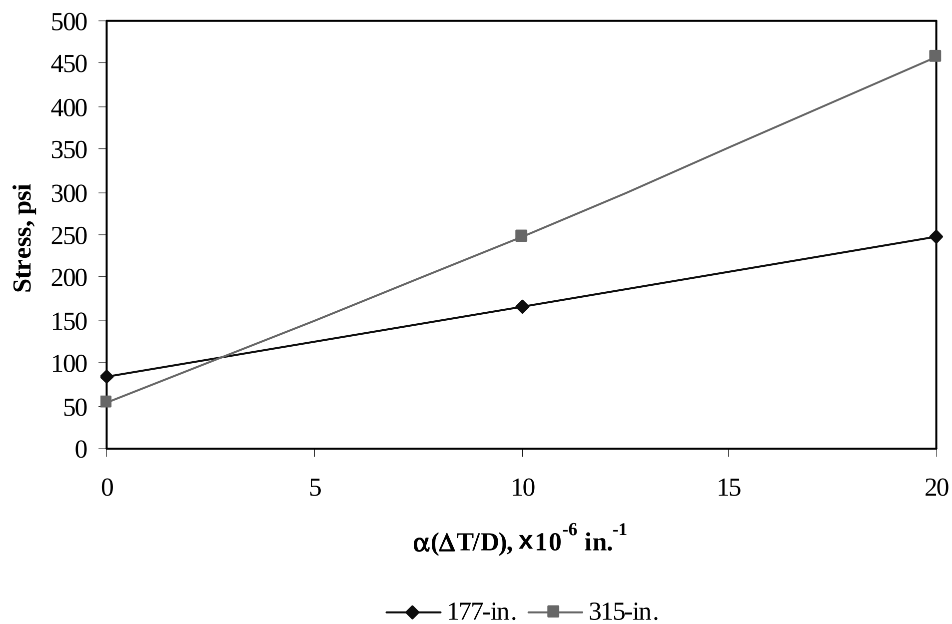


**Figure F-3-50: Impact of joint spacing and product α(ΔT/D) on longitudinal stress at top of the slab**

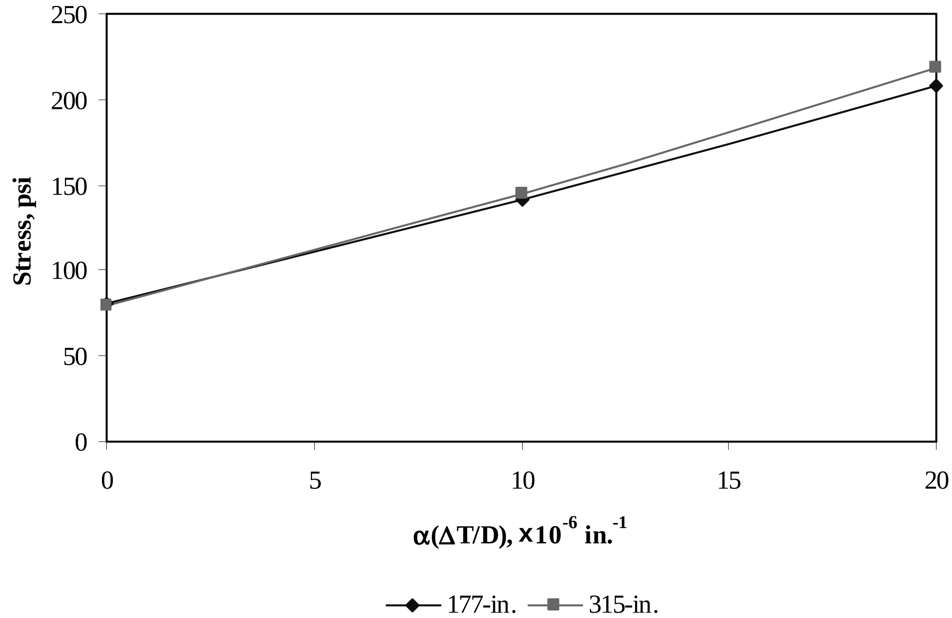


**Figure F-3-51: Impact of joint spacing and product α(ΔT/D) on transverse stress at bottom of the slab**

**Sub Appendix F-4**

**Documentation of Pavement Responses for**


**52-kips Quad Axle**

Figures F-4-1 through F-4-12 illustrate the impact of PCC thickness and base/subbase thickness on stresses (100-psi/in. modulus of subgrade reaction and PCC shoulder)

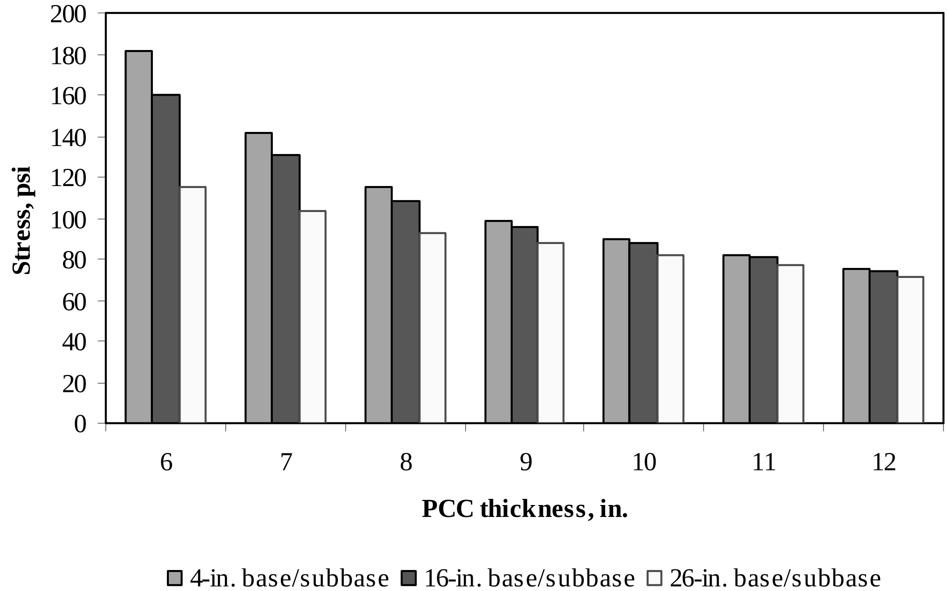


**Figure F-4-1: Impact of PCC thickness and base/subbase thickness on longitudinal stress at bottom of the Slab (177-in. joint spacing and $\alpha(\Delta T/D)$ of 0 in.$^{-1}$)**

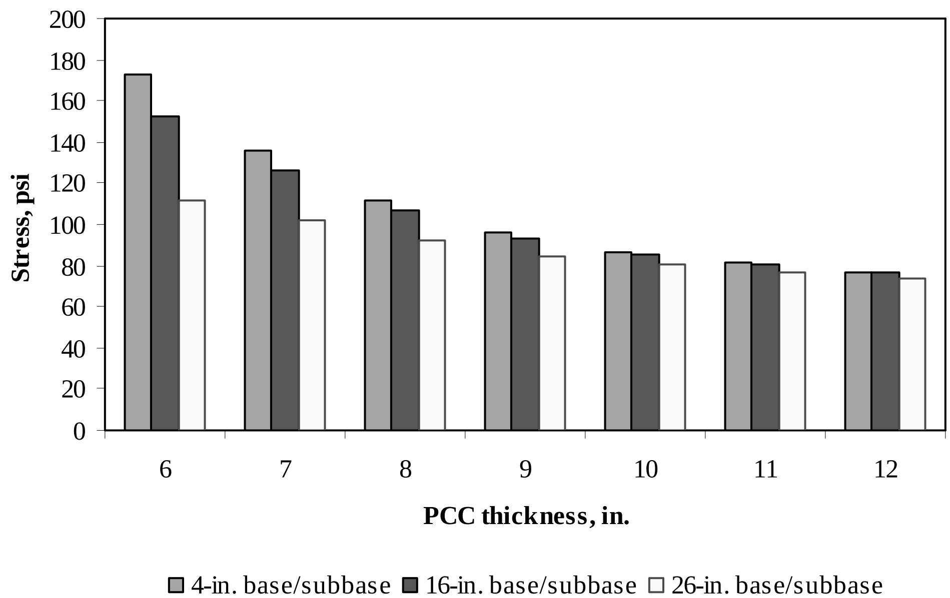


**Figure F-4-2: Impact of PCC thickness and base/subbase thickness on longitudinal stress at bottom of the Slab (315-in. joint spacing and $\alpha(\Delta T/D)$ of 0 in.$^{-1}$)**

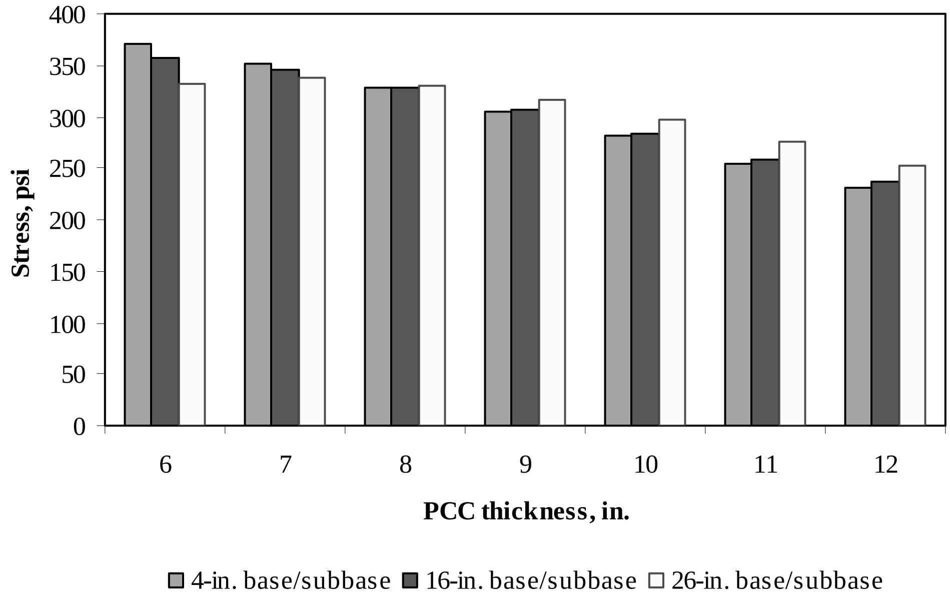


**Figure F-4-3: Impact of PCC thickness and base/subbase thickness on longitudinal stress at bottom of the Slab (177-in. joint spacing and $\alpha(\Delta T/D)$ of $20x10^{-6}$ in.$^{-1}$)**

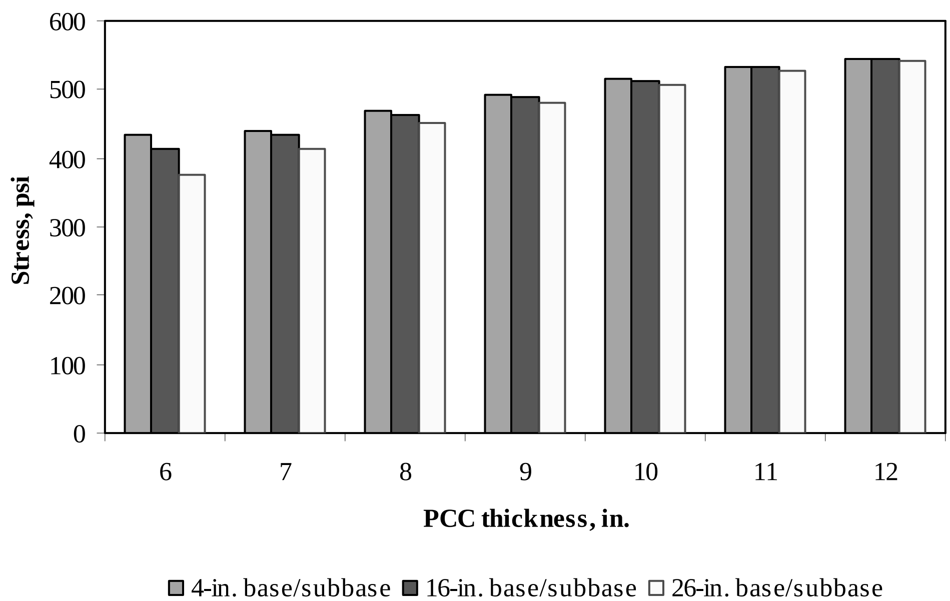


**Figure F-4-4: Impact of PCC thickness and base/subbase thickness on longitudinal stress at bottom of the Slab (315-in. joint spacing and $\alpha(\Delta T/D)$ of $20x10^{-6}$ in.$^{-1}$)**

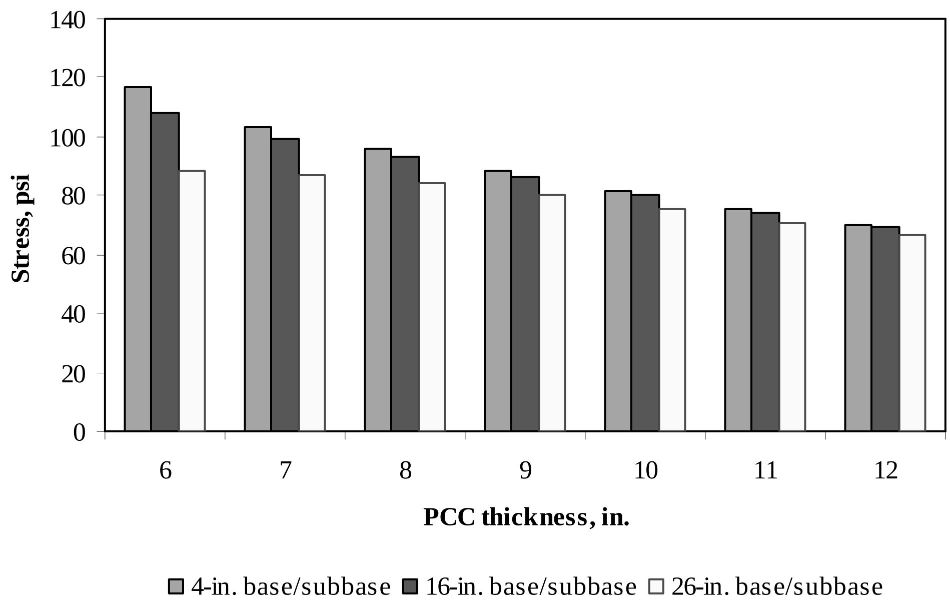


**Figure F-4-5: Impact of PCC thickness and base/subbase thickness on longitudinal stress at top of the Slab (177-in. joint spacing and $\alpha(\Delta T/D)$ of 0 in.$^{-1}$)**

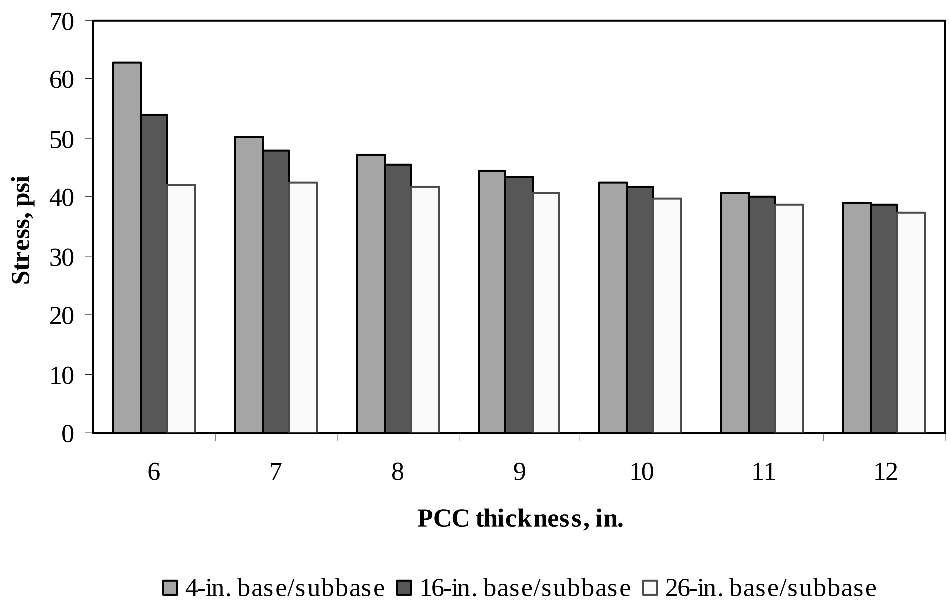


**Figure F-4-6: Impact of PCC thickness and base/subbase thickness on longitudinal stress at top of the Slab (315-in. joint spacing and $\alpha(\Delta T/D)$ of 0 in.$^{-1}$)**

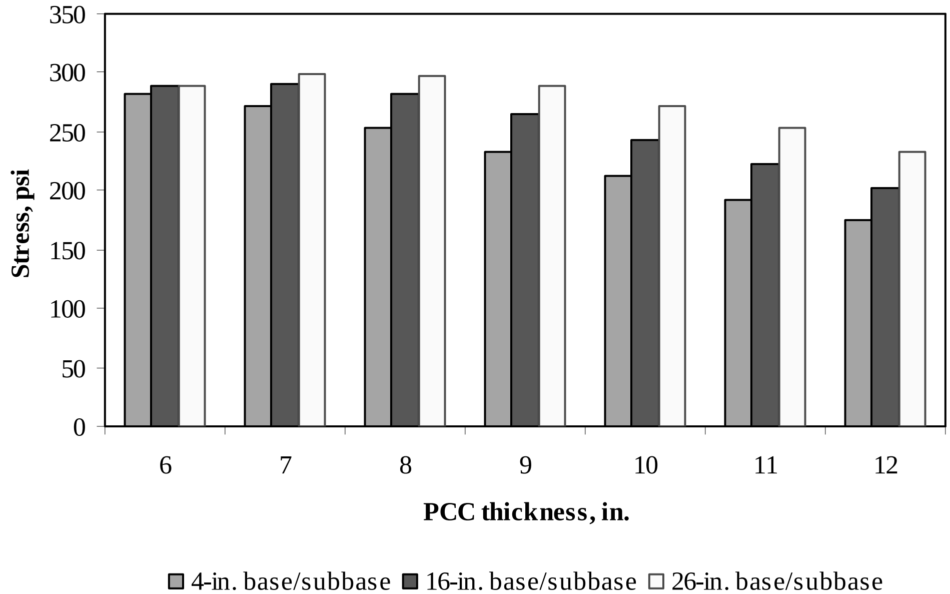


**Figure F-4-7: Impact of PCC thickness and base/subbase thickness on longitudinal stress at top of the Slab (177-in. joint spacing and $\alpha(\Delta T/D)$ of $-20x10^{-6}$ in.$^{-1}$)**

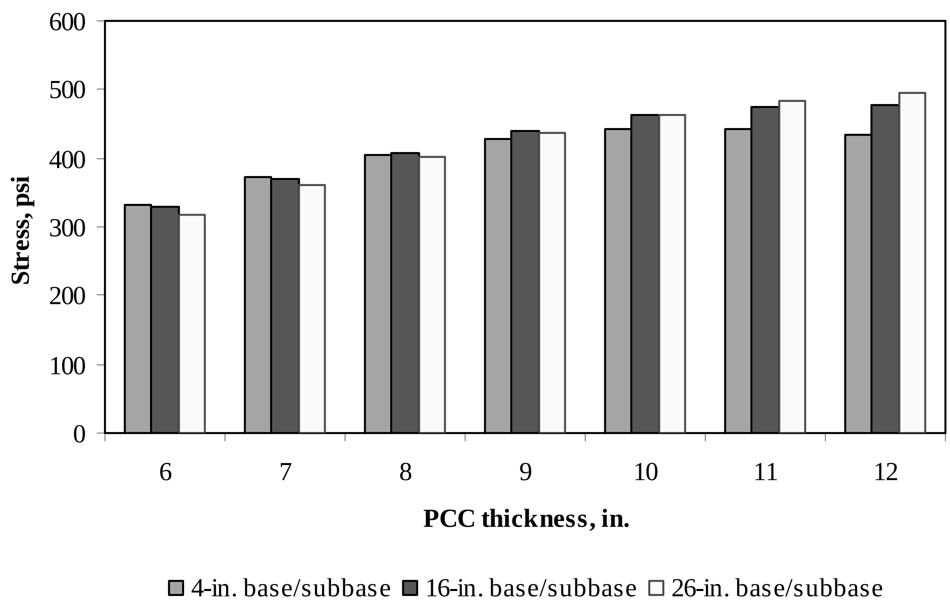


**Figure F-4-8: Impact of PCC thickness and base/subbase thickness on longitudinal stress at top of the Slab (315-in. joint spacing and $\alpha(\Delta T/D)$ of $-20x10^{-6}$ in.$^{-1}$)**

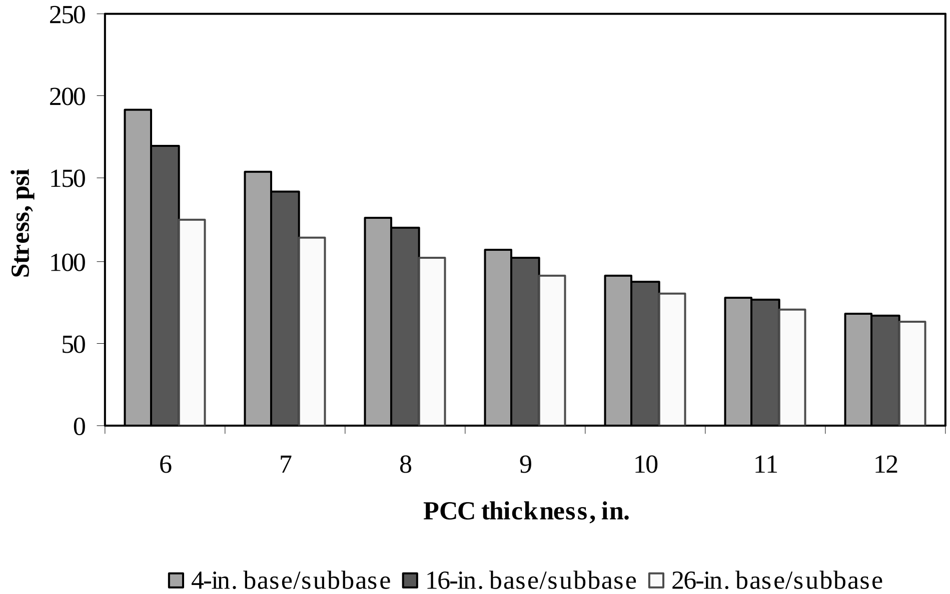


**Figure F-4-9: Impact of PCC thickness and base/subbase thickness on transverse stress at bottom of the Slab (177-in. joint spacing and α(ΔT/D) of 0 in.$^{-1}$)**

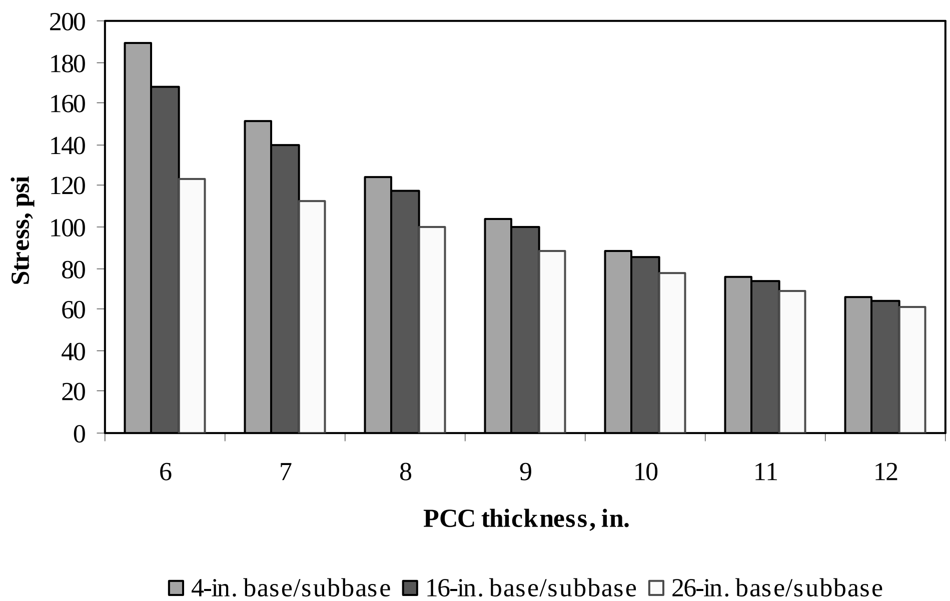


**Figure F-4-10: Impact of PCC thickness and base/subbase thickness on transverse stress at bottom of the Slab (315-in. joint spacing and α(ΔT/D) of 0 in.$^{-1}$)**

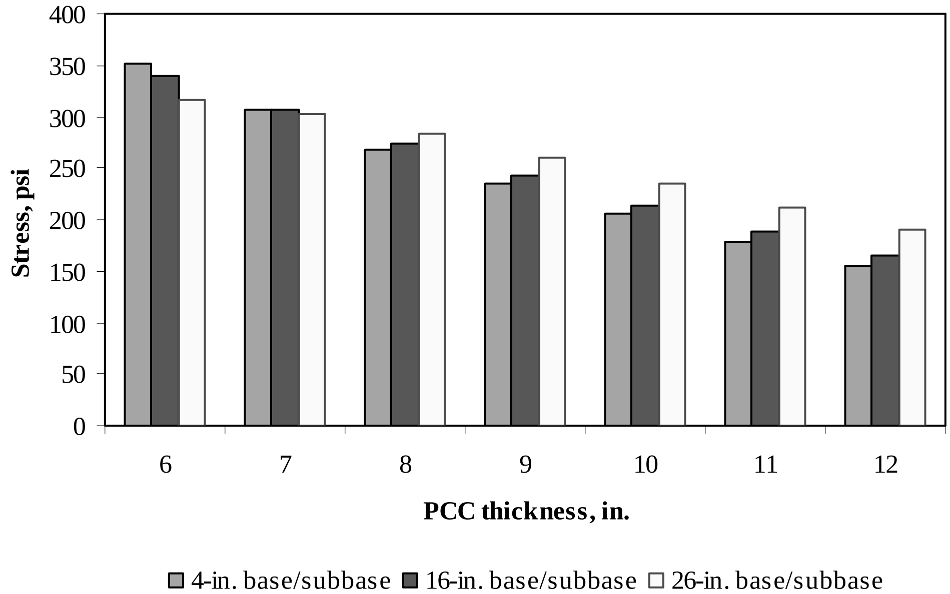


**Figure F-4-11: Impact of PCC thickness and ba se/subbase thickness on transverse stress at bottom of the Slab (177-in. joint spacing and $\alpha(\Delta T/D)$ of $20x10^{-6}$ in.$^{-1}$)**

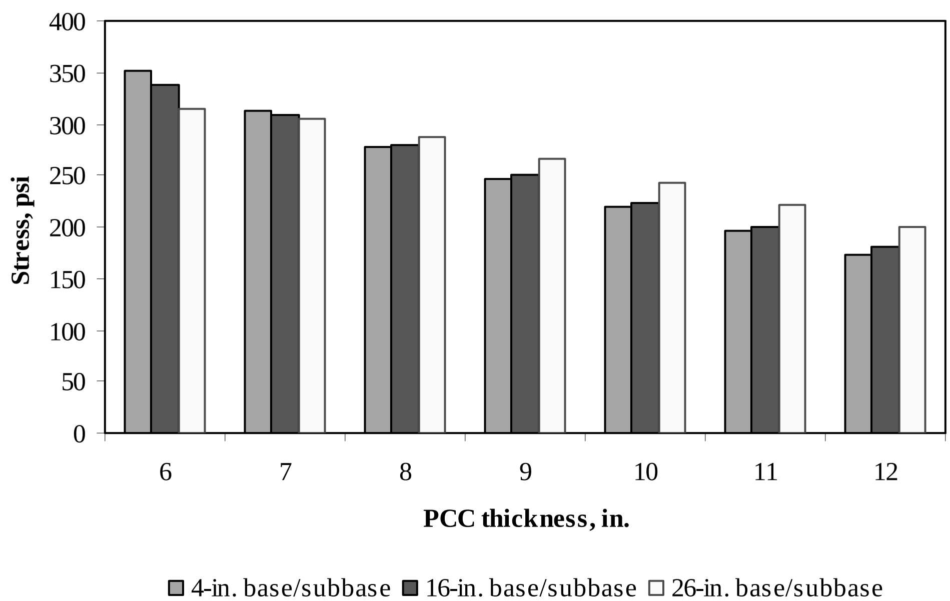


**Figure F-4-12: Impact of PCC thickness and base/subbase thickness on transverse stress at bottom of the Slab (315-in. joint spacing and $\alpha(\Delta T/D)$ of $20x10^{-6}$ in.$^{-1}$)**

Figures F-4-13 through F-4-24 illustrate the impact of PCC thickness and modulus of subgrade reaction on stresses (16-in. base/subbase thickness and PCC shoulder)

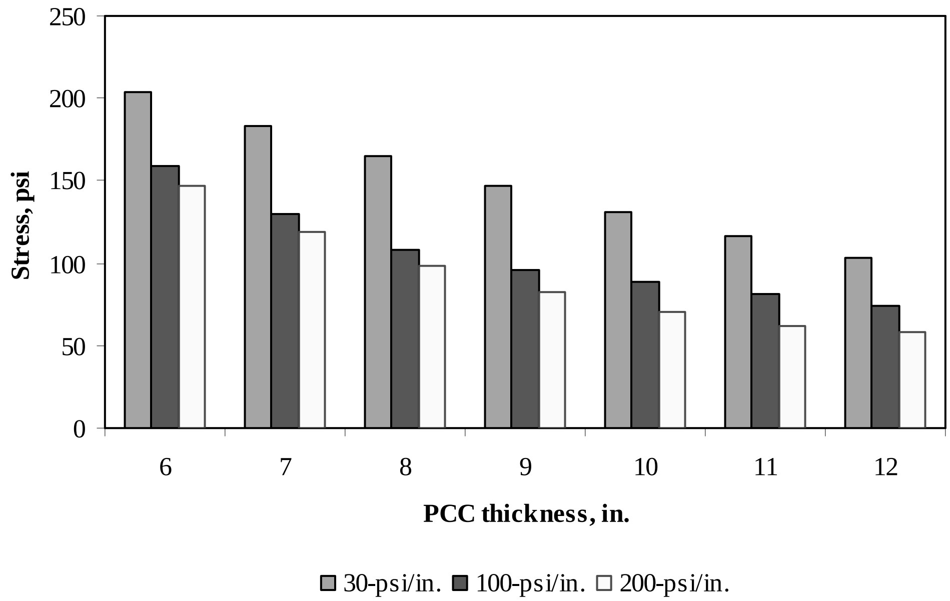


**Figure F-4-13: Impact of PCC thickness and modulus of subgrade reaction on longitudinal stress at bottom of the slab (177-in. joint spacing and $\alpha(\Delta T/D)$ of 0 in.$^{-1}$)**

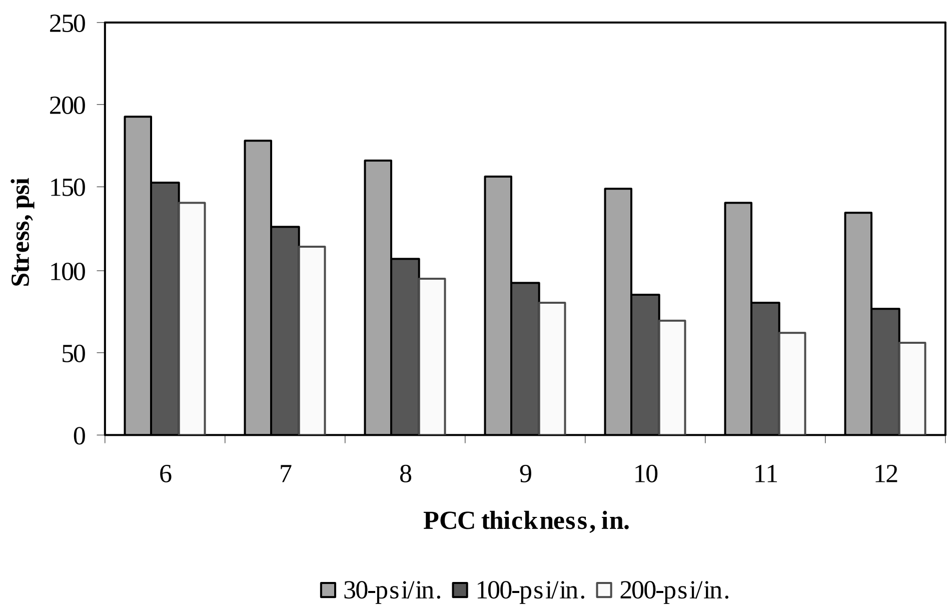


**Figure F-4-14: Impact of PCC thickness and modulus of subgrade reaction on longitudinal stress at bottom of the slab (315-in. joint spacing and $\alpha(\Delta T/D)$ of 0 in.$^{-1}$)**

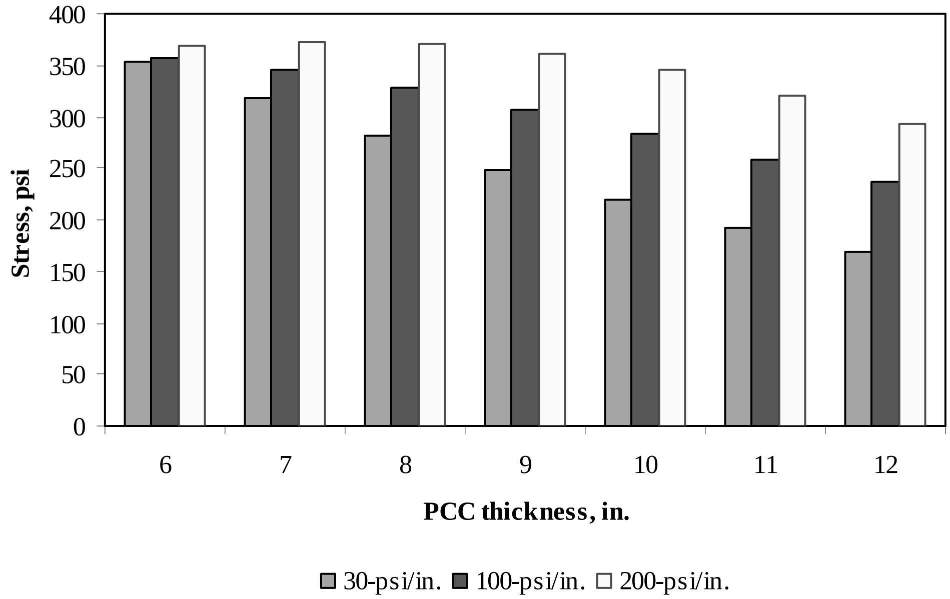


**Figure F-4-15: Impact of PCC thickness and modulus of subgrade reaction on longitudinal stress at bottom of the slab (177-in. joint spacing and $\alpha(\Delta T/D)$ of $20x10^{-6}$ in.$^{-1}$)**

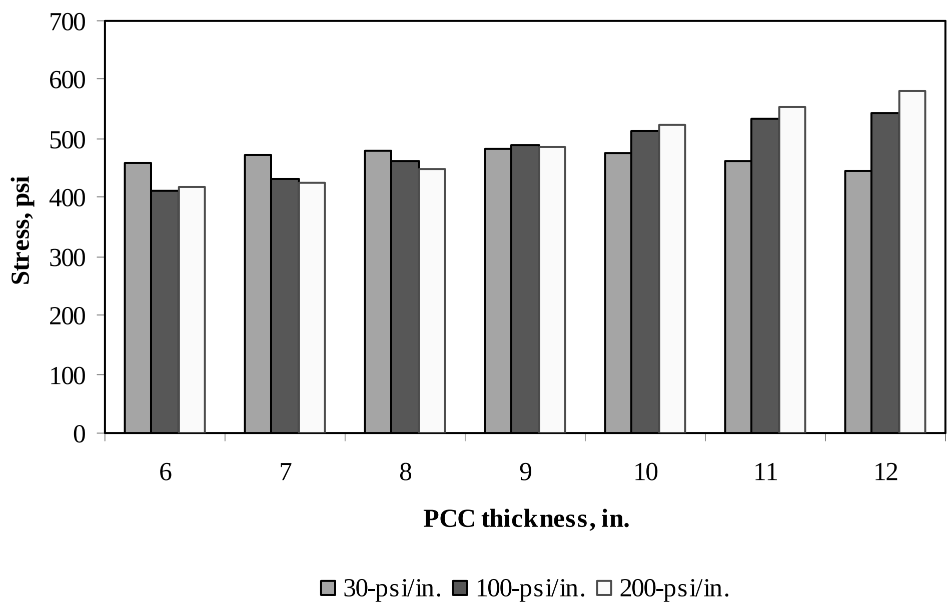


**Figure F-4-16: Impact of PCC thickness and modulus of subgrade reaction on longitudinal stress at bottom of the slab (315-in. joint spacing and $\alpha(\Delta T/D)$ of $20x10^{-6}$ in.$^{-1}$)**

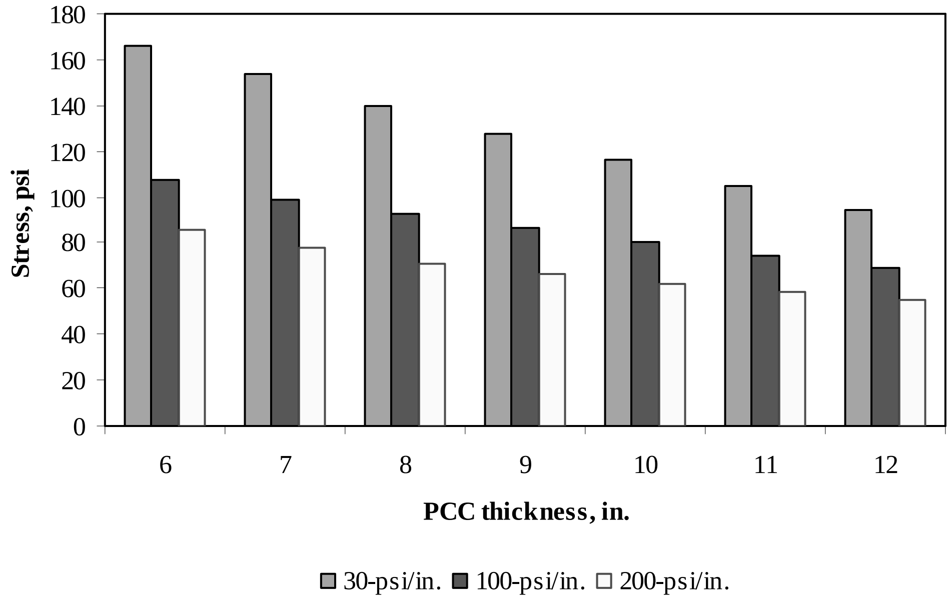


**Figure F-4-17: Impact of PCC thickness and modulus of subgrade reaction on longitudinal stress at top of the Slab (177-in. joint spacing and $\alpha(\Delta T/D)$ of 0 in.$^{-1}$)**

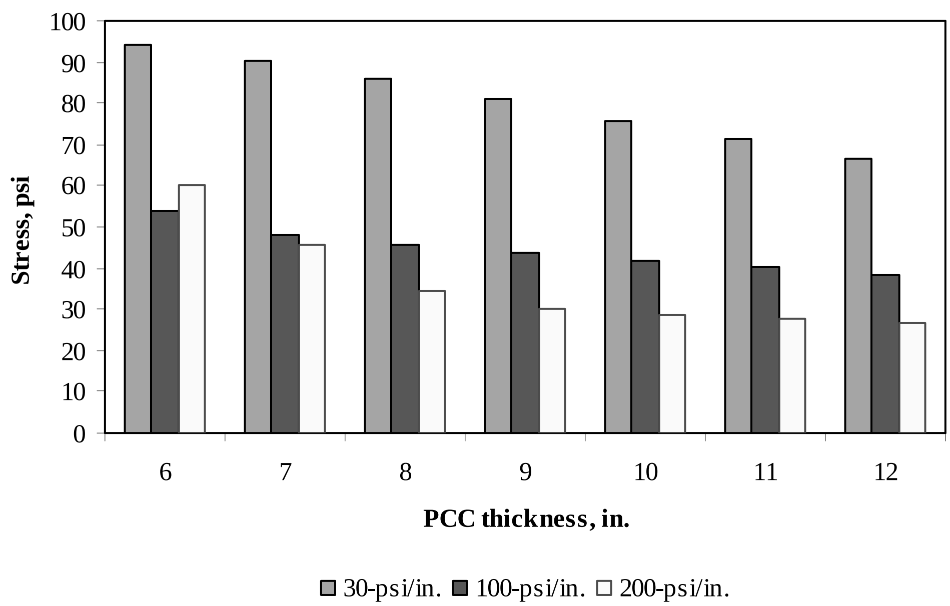


**Figure F-4-18: Impact of PCC thickness and modulus of subgrade reaction on longitudinal stress at top of the Slab (315-in. joint spacing and $\alpha(\Delta T/D)$ of 0 in.$^{-1}$)**

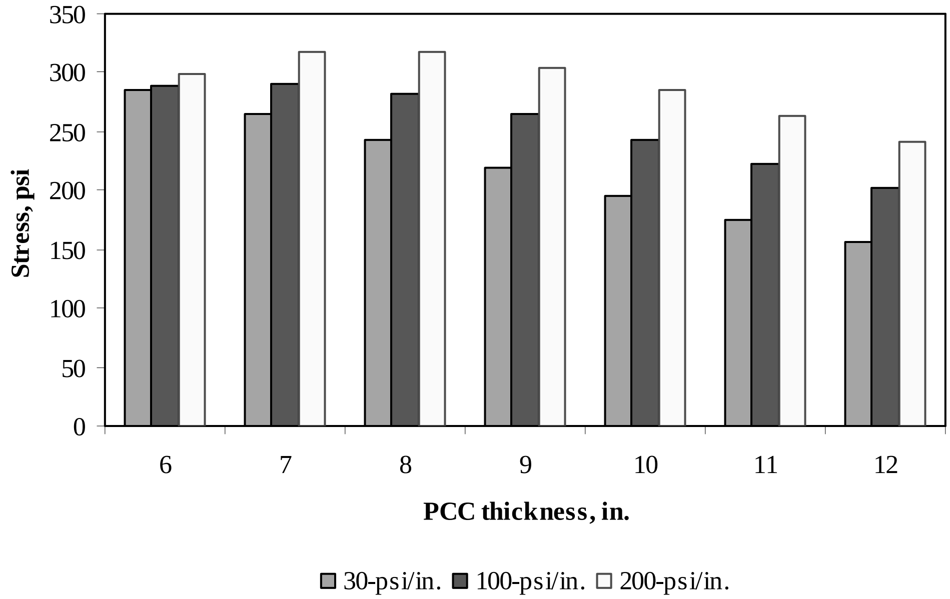


**Figure F-4-19: Impact of PCC thickness and modulus of subgrade reaction on longitudinal stress at top of the Slab (177-in. joint spacing and $\alpha(\Delta T/D)$ of $-20x10^{-6}$ in.$^{-1}$)**

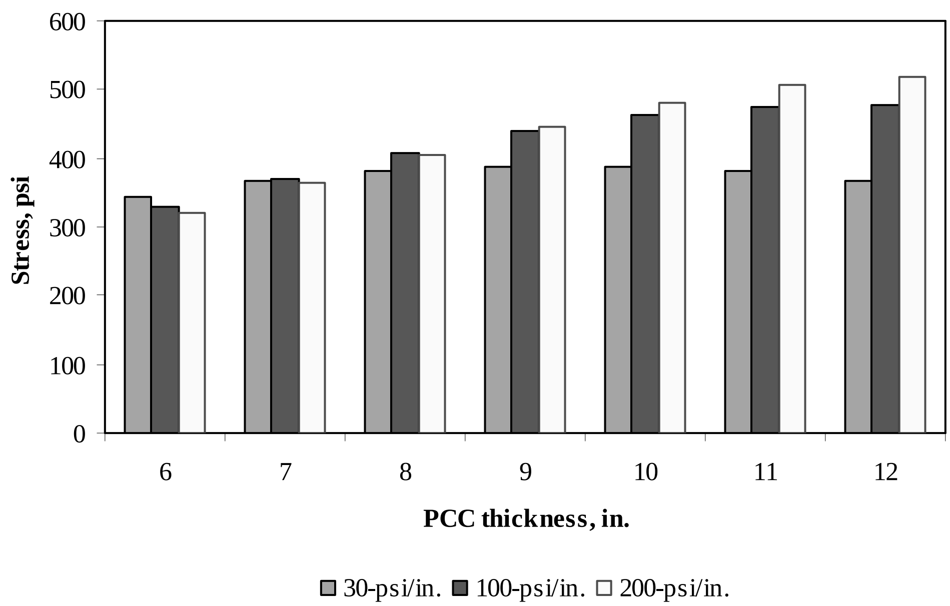


**Figure F-4-20: Impact of PCC thickness and modulus of subgrade reaction on longitudinal stress at top of the Slab (315-in. joint spacing and $\alpha(\Delta T/D)$ of $-20x10^{-6}$ in.$^{-1}$)**

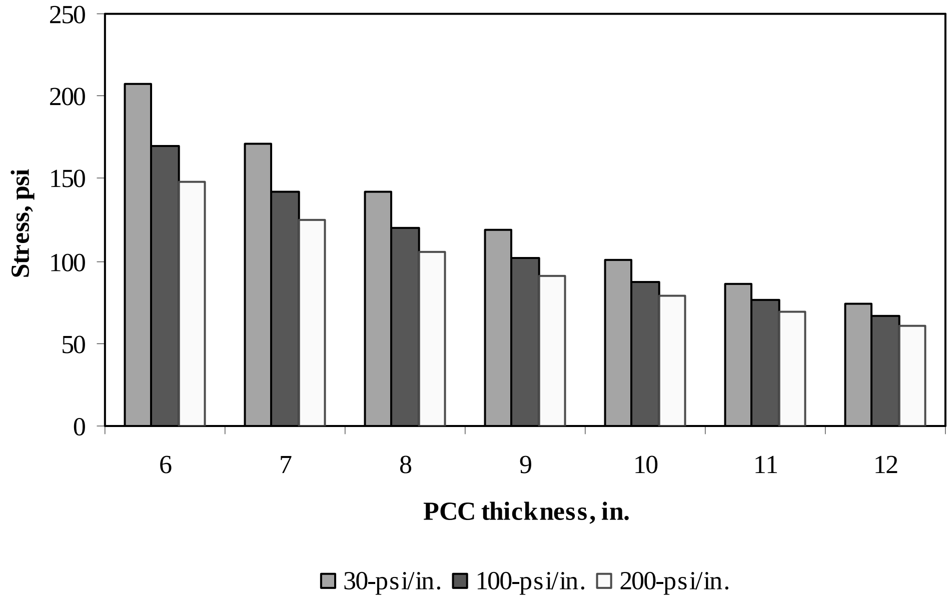


**Figure F-4-21: Impact of PCC thickness and modulus of subgrade reaction on transverse stress at bottom of the Slab (177-in. joint spacing and $\alpha(\Delta T/D)$ of 0 in.$^{-1}$)**

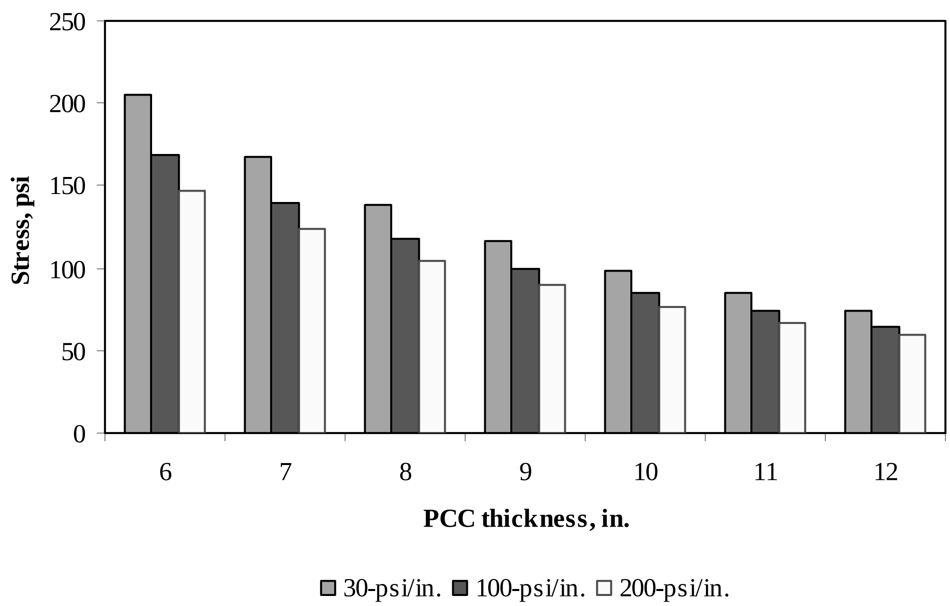


**Figure F-4-22: Impact of PCC thickness and modulus of subgrade reaction on transverse stress at bottom of the Slab (315-in. joint spacing and $\alpha(\Delta T/D)$ of 0 in.$^{-1}$)**

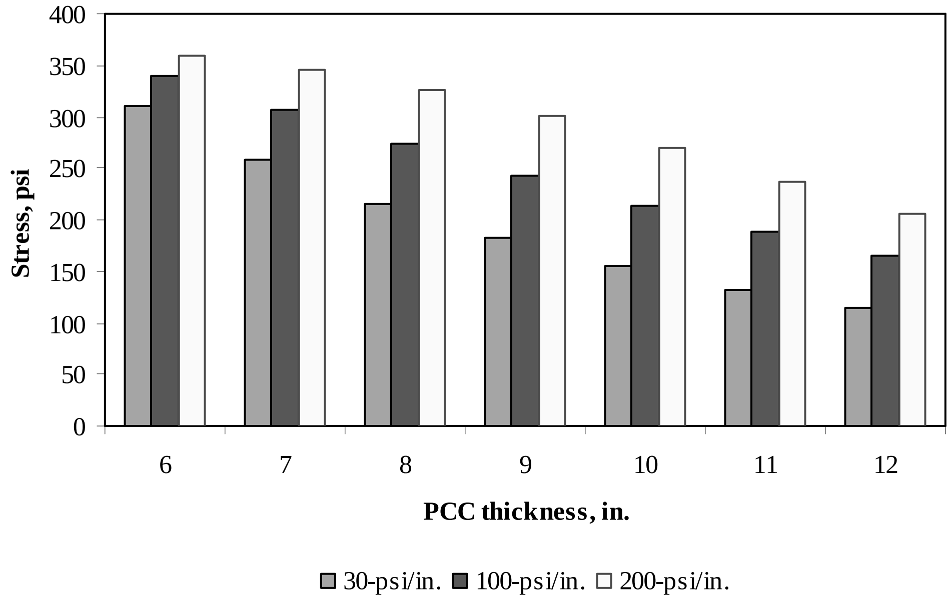


**Figure F-4-23: Impact of PCC thickness and modulus of subgrade reaction on transverse stress at bottom of the Slab (177-in. joint spacing and $\alpha(\Delta T/D)$ of $20x10^{-6}$ $in.^{-1}$)**

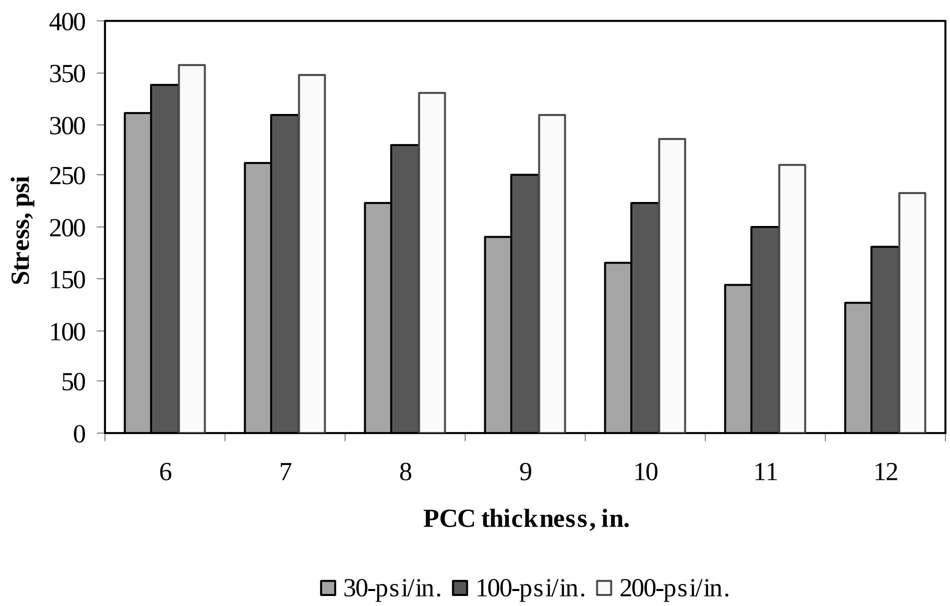


**Figure F-4-24: Impact of PCC thickness and modulus of subgrade reaction on transverse stress at bottom of the Slab (315-in. joint spacing and $\alpha(\Delta T/D)$ of $20x10^{-6}$ $in.^{-1}$)**

Figures F-4-25 through F-4-36 illustrate the impact of PCC thickness and lateral support condition on stresses (16-in. base/subbase and 100-psi/in. modulus of subgrade reaction)

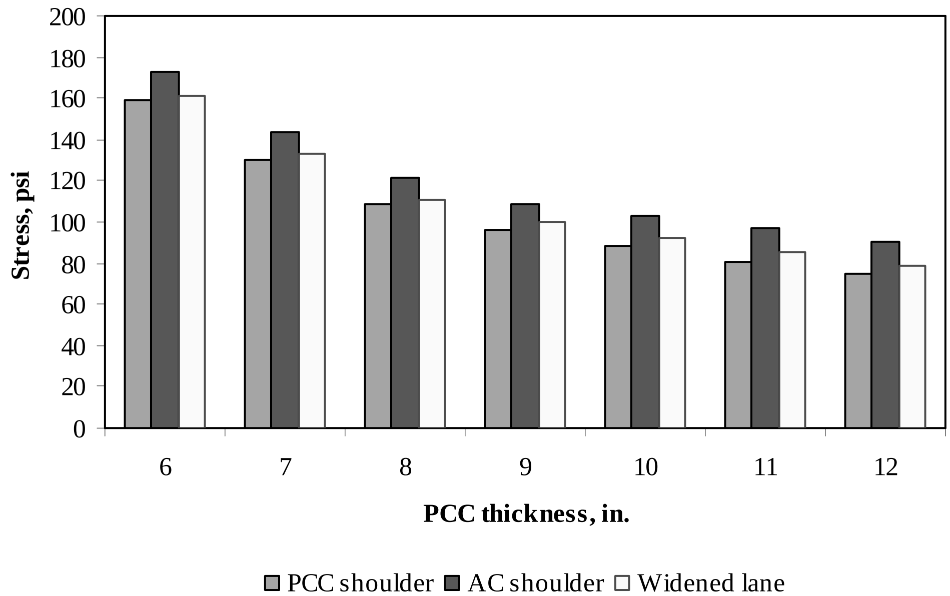


**Figure F-4-25: Impact of PCC thickness and lateral support condition on longitudinal stress at bottom of the Slab (177-in. joint spacing and $\alpha(\Delta T/D)$ of 0 in.$^{-1}$)**

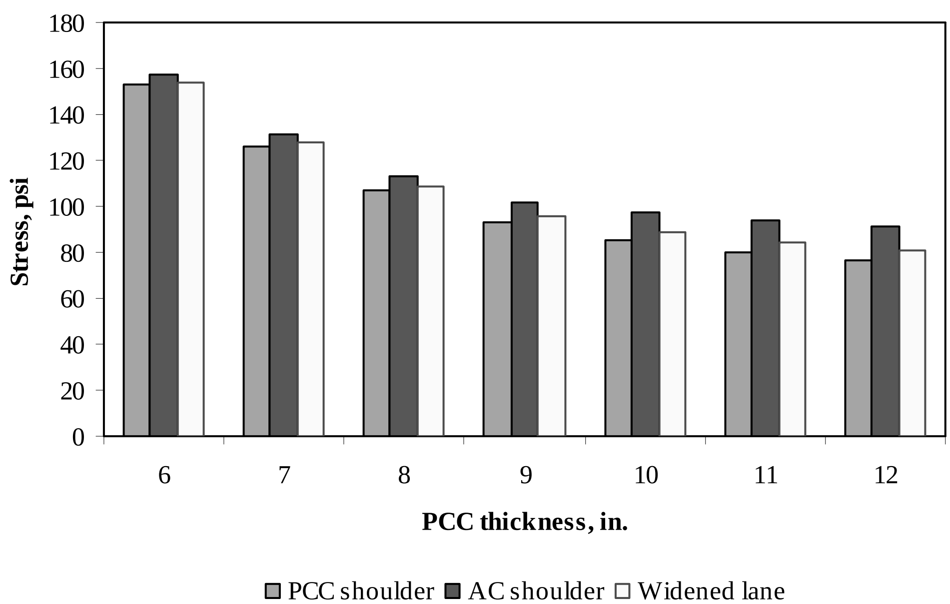


**Figure F-4-26: Impact of PCC thickness and lateral support condition on longitudinal stress at bottom of the Slab (315-in. joint spacing and $\alpha(\Delta T/D)$ of 0 in.$^{-1}$)**

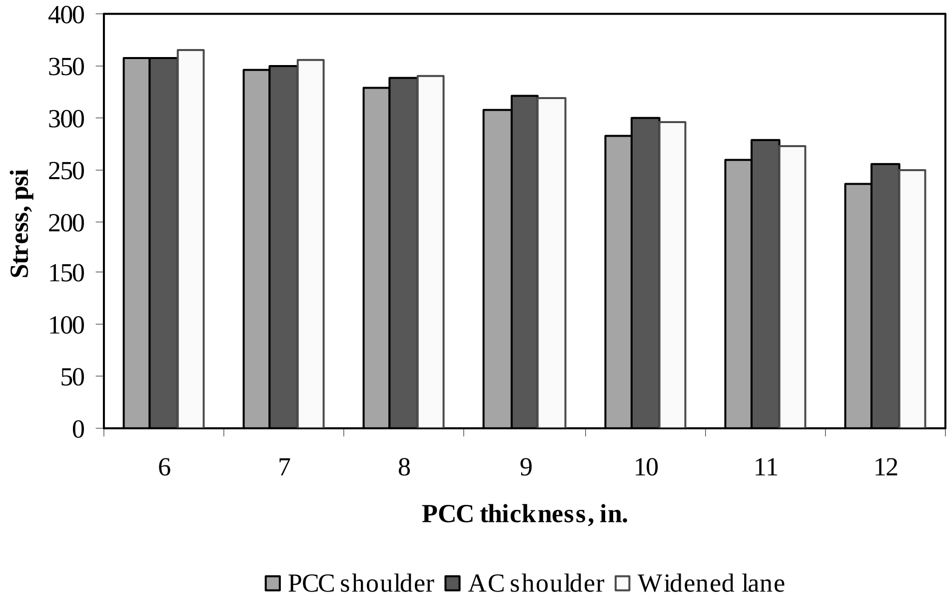


**Figure F-4-27: Impact of PCC thickness and lateral support condition on longitudinal stress at bottom of the Slab (177-in. joint spacing and $\alpha(\Delta T/D)$ of 20x10$^{-6}$ in.$^{-1}$)**

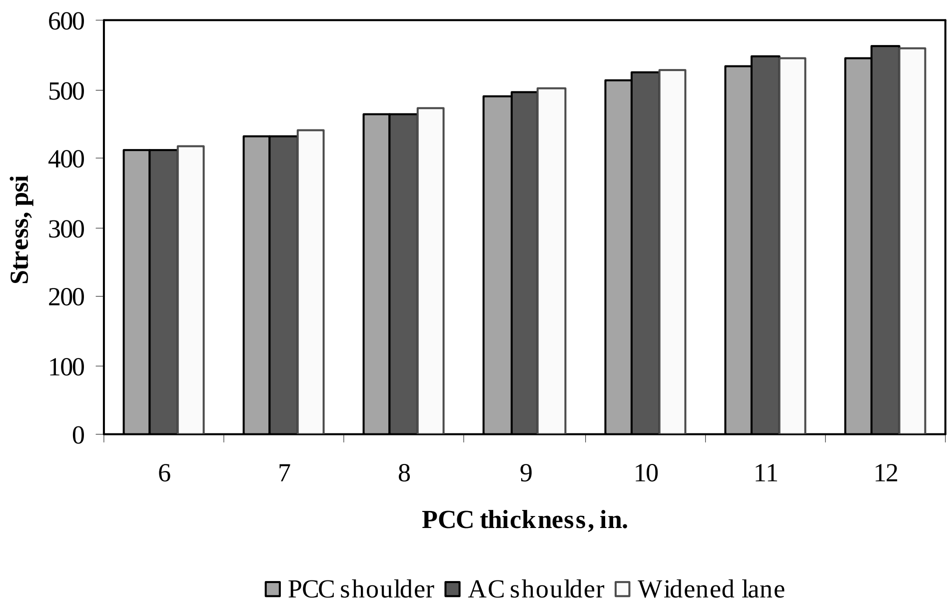


**Figure F-4-28: Impact of PCC thickness and lateral support condition on longitudinal stress at bottom of the Slab (315-in. joint spacing and $\alpha(\Delta T/D)$ of 20x10$^{-6}$ in.$^{-1}$)**

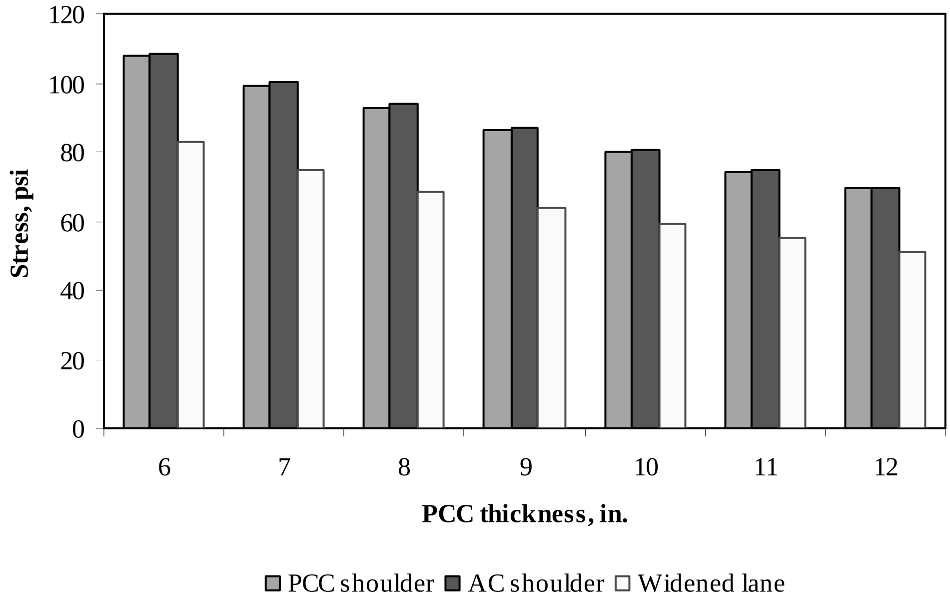


**Figure F-4-29: Impact of PCC thickness and lateral support condition on longitudinal stress at top of the Slab (177-in. joint spacing and $\alpha(\Delta T/D)$ of 0 in.$^{-1}$)**

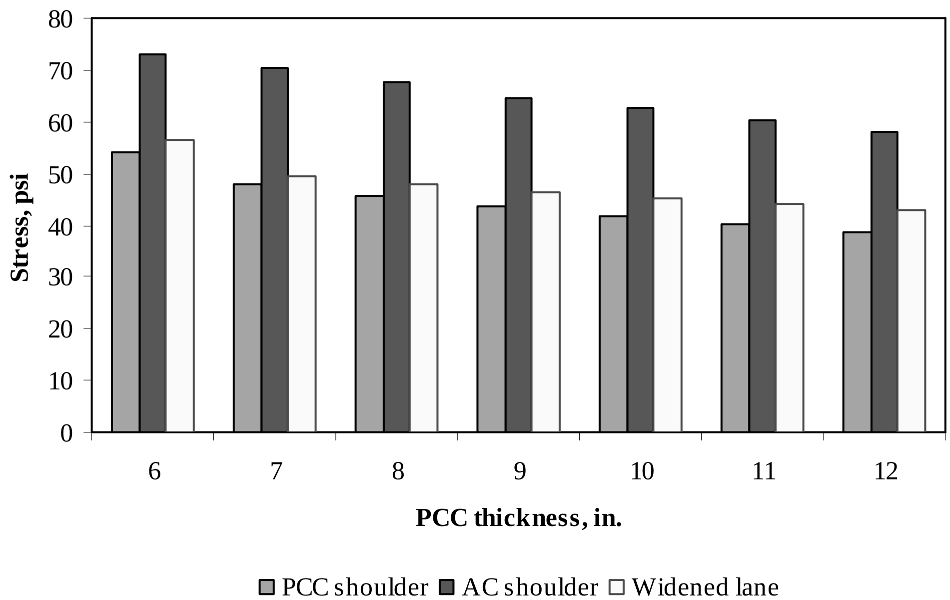


**Figure F-4-30: Impact of PCC thickness and lateral support condition on longitudinal stress at top of the Slab (315-in. joint spacing and $\alpha(\Delta T/D)$ of 0 in.$^{-1}$)**

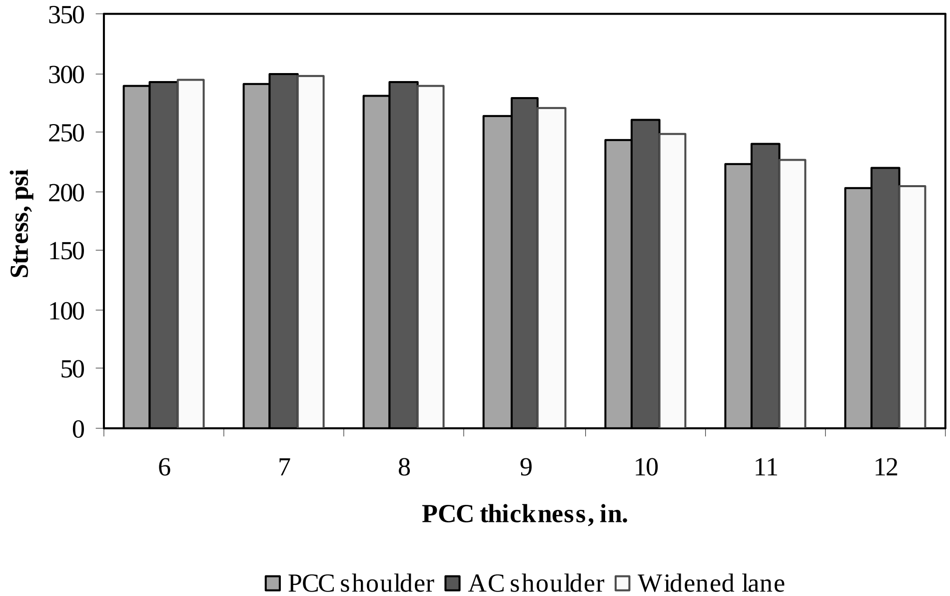


**Figure F-4-31: Impact of PCC thickness and lateral support condition on longitudinal stress at top of the Slab (177-in. joint spacing and $\alpha(\Delta T/D)$ of $-20x10^{-6}$ in.$^{-1}$)**

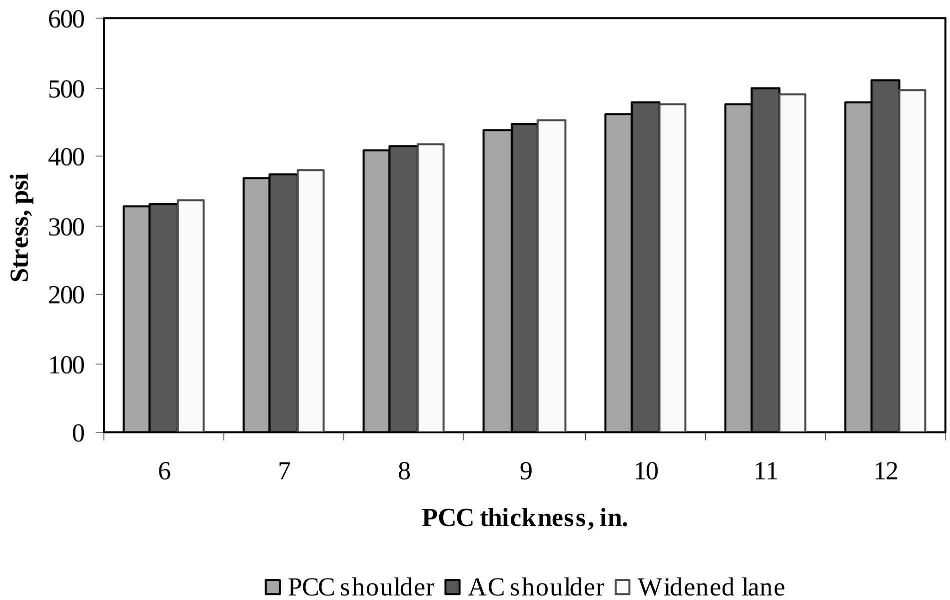


**Figure F-4-32: Impact of PCC thickness and lateral support condition on longitudinal stress at top of the Slab (315-in. joint spacing and $\alpha(\Delta T/D)$ of $-20x10^{-6}$ in.$^{-1}$)**

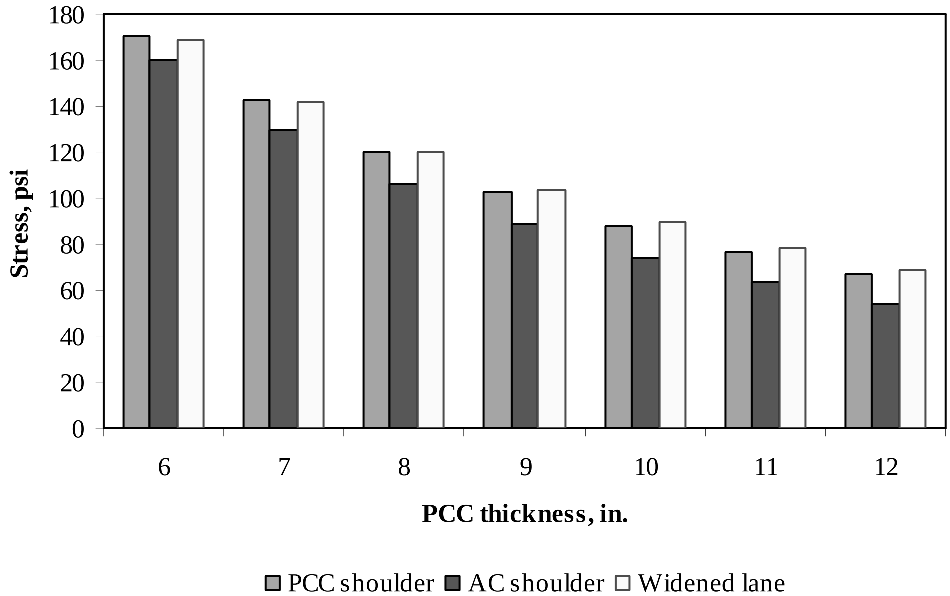


**Figure F-4-33: Impact of PCC thickness and lateral support condition on transverse stress at bottom of the Slab (177-in. joint spacing and $\alpha(\Delta T/D)$ of 0 in.$^{-1}$)**

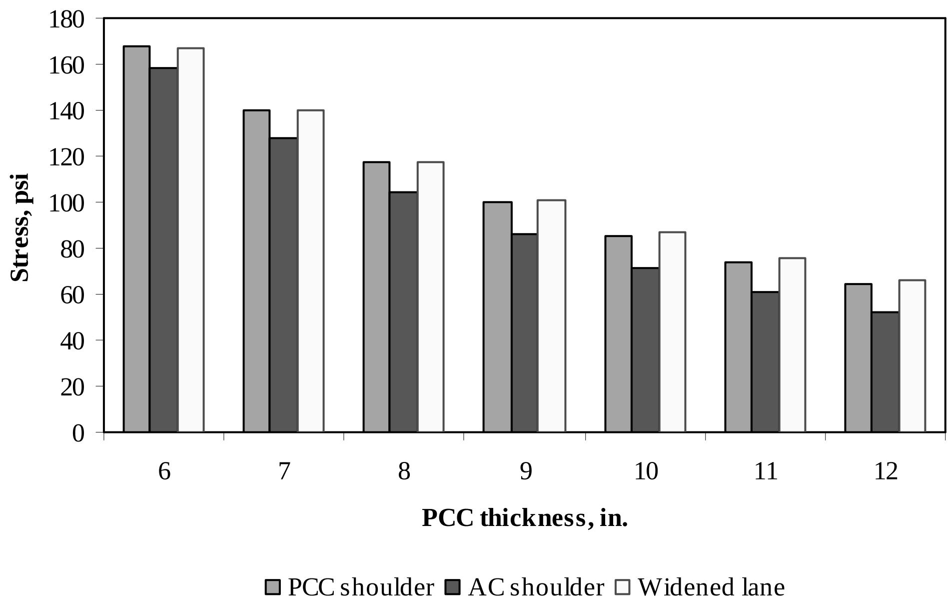


**Figure F-4-34: Impact of PCC thickness and lateral support condition on transverse stress at bottom of the Slab (315-in. joint spacing and $\alpha(\Delta T/D)$ of 0 in.$^{-1}$)**

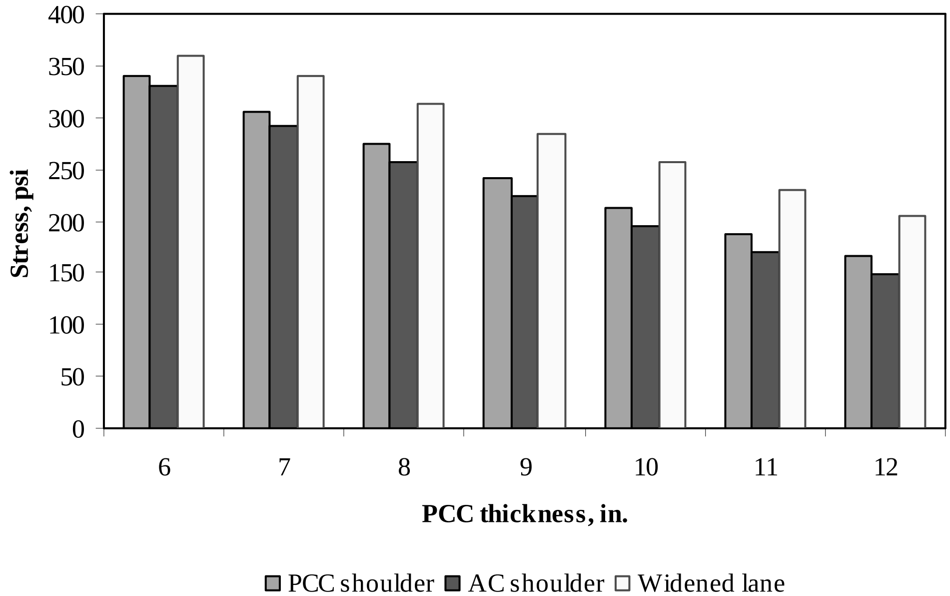


**Figure F-4-35: Impact of PCC thickness and lateral support condition on transverse stress at bottom of the Slab (177-in. joint spacing and $\alpha(\Delta T/D)$ of $20x10^{-6}$ in.$^{-1}$)**

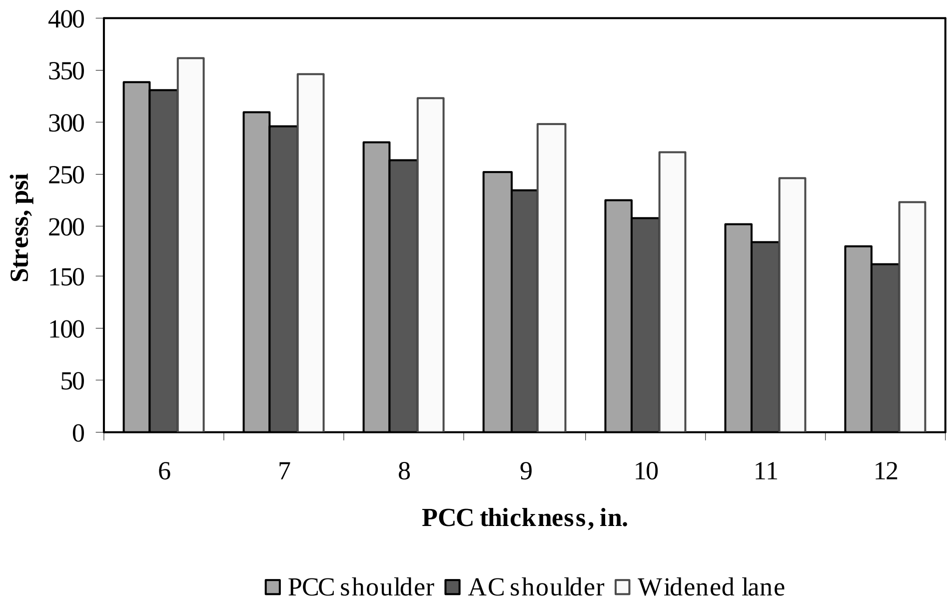


**Figure F-4-36: Impact of PCC thickness and lateral support condition on transverse stress at bottom of the Slab (315-in. joint spacing and $\alpha(\Delta T/D)$ of $20x10^{-6}$ in.$^{-1}$)**

Figures F-4-37 through F-4-42 illustrate the impact of base/subbase thickness and product α(ΔT/D) on stresses (10-in. PCC thickness, 100-psi/in. modulus of subgrade reaction and PCC shoulder)

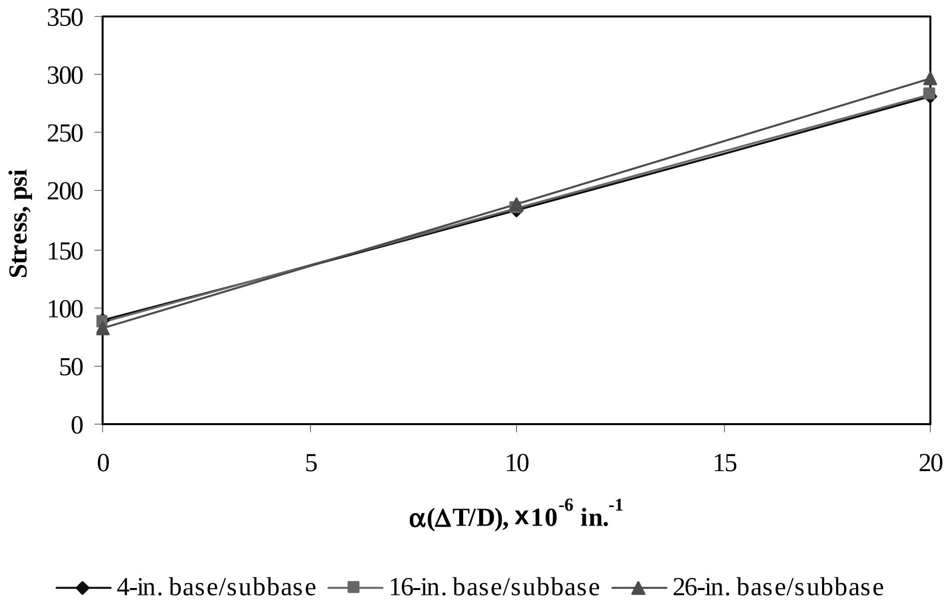


**Figure F-4-37: Impact of base/subbase thickness and product α(ΔT/D) on longitudinal stress at bottom of the slab (177-in. joint spacing)**

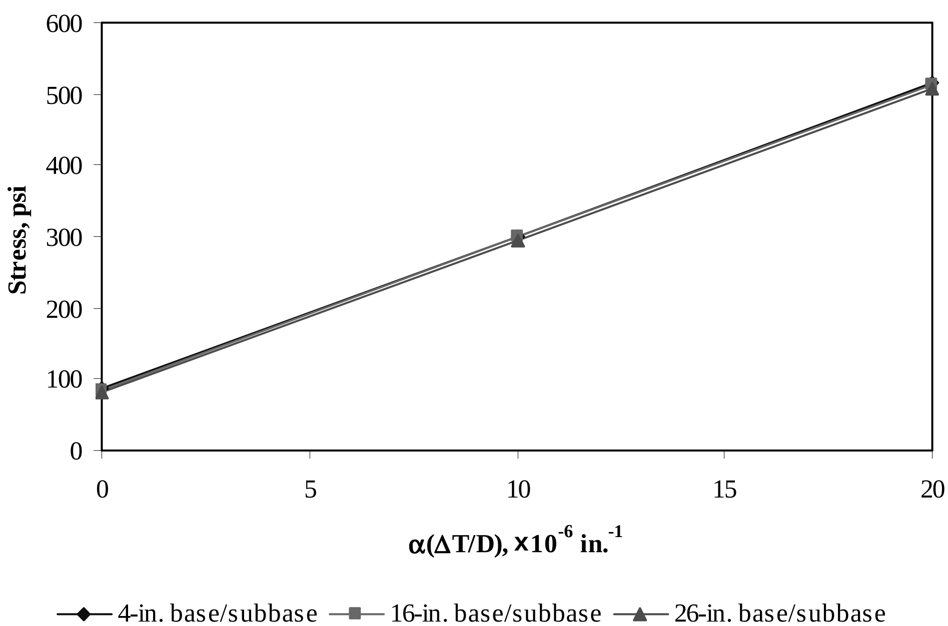


**Figure F-4-38: Impact of base/subbase thickness and product α(ΔT/D) on longitudinal stress at bottom of the slab (315-in. joint spacing)**

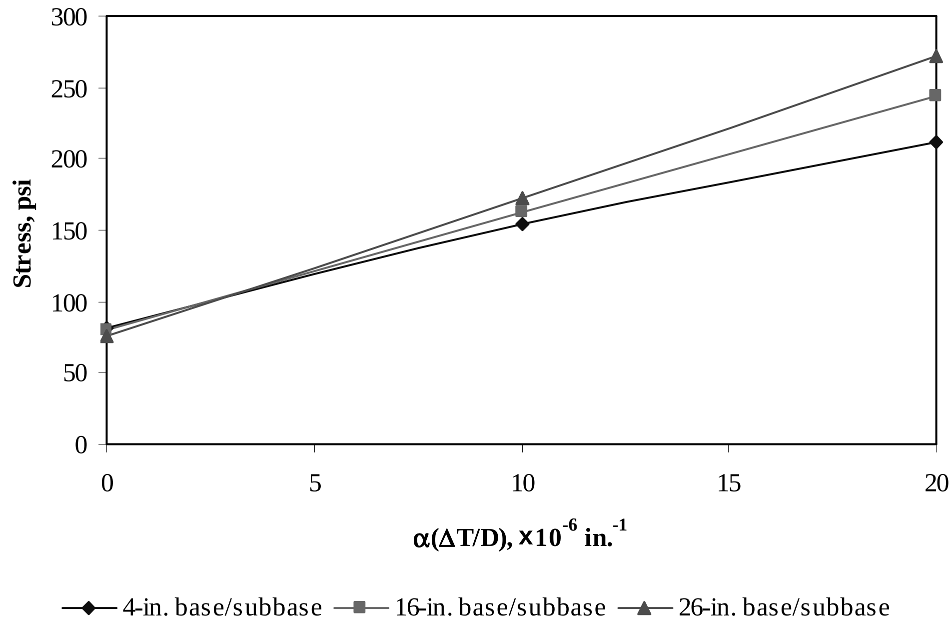


**Figure F-4-39: Impact of base/subbase thickness and product α(ΔT/D) on longitudinal stress at top of the slab (177-in. joint spacing)**

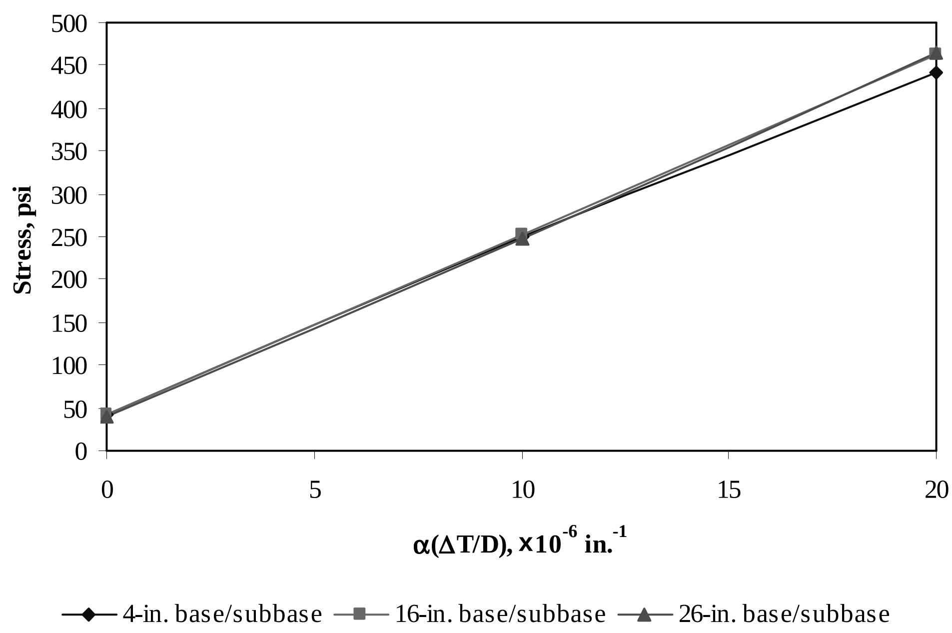


**Figure F-4-40: Impact of base/subbase thickness and product α(ΔT/D) on longitudinal stress at top of the slab (315-in. joint spacing)**

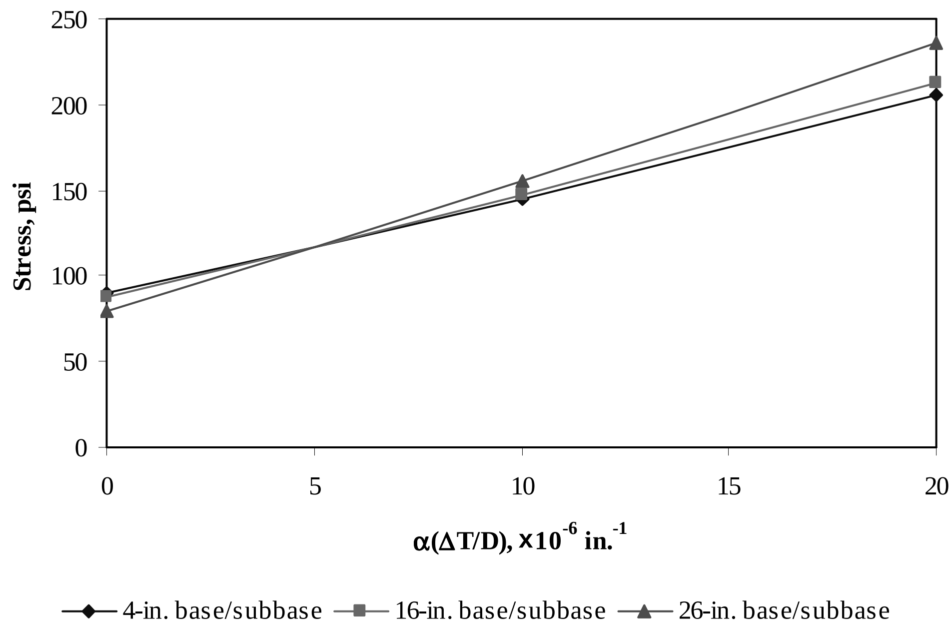


**Figure F-4-41: Impact of base/subbase thickness and product α(ΔT/D) on transverse stress at bottom of the slab (177-in. joint spacing)**

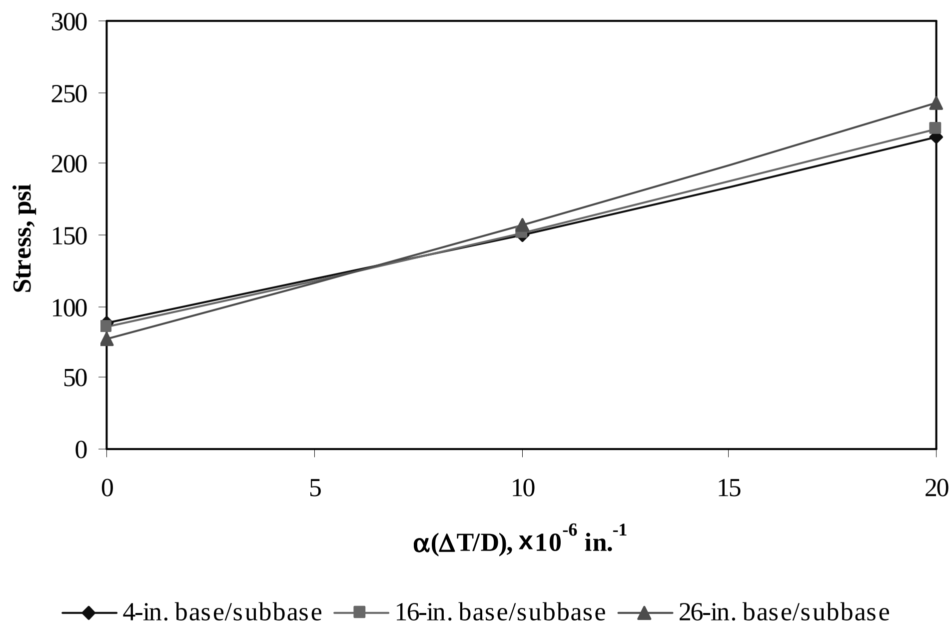


**Figure F-4-42: Impact of base/subbase thickness and product α(ΔT/D) on transverse stress at bottom of the slab (315-in. joint spacing)**

Figures F-4-43 through F-4-48 illustrate the impact of modulus of subgrade reaction and product α(ΔT/D) on stresses (10-in. PCC thickness, 16-in. base/subbase thickness and PCC shoulder)

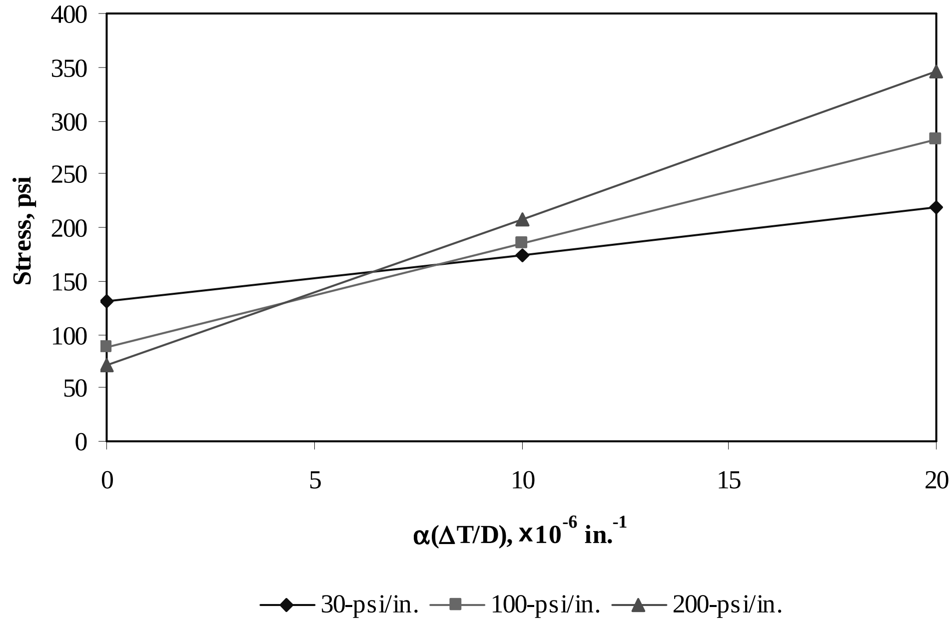


**Figure F-4-43: Impact of modulus of subgrade reaction and product α(ΔT/D) on longitudinal stress at bottom of the slab (177-in. joint spacing)**

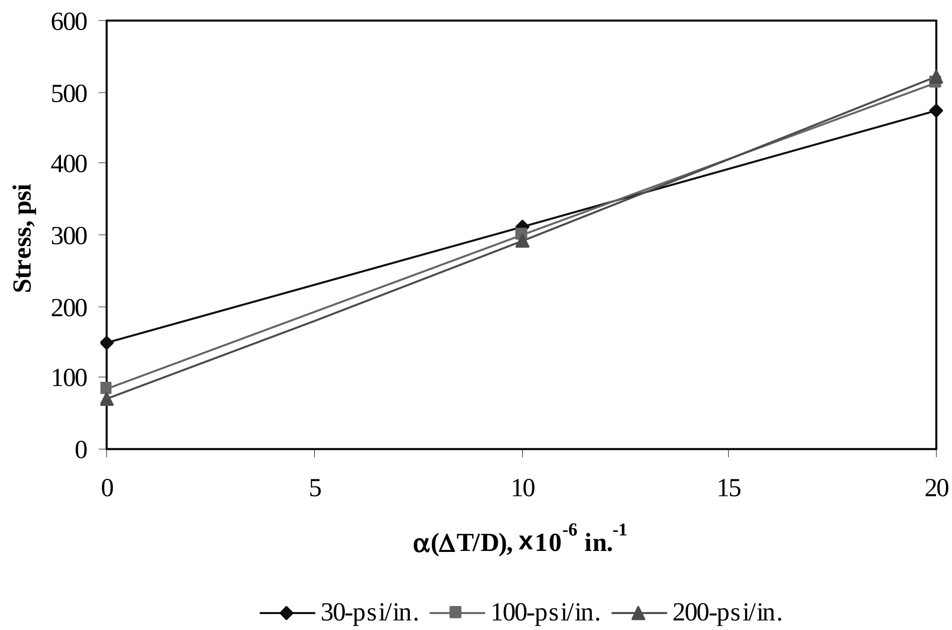


**Figure F-4-44: Impact of modulus of subgrade reaction and product α(ΔT/D) on longitudinal stress at bottom of the slab (315-in. joint spacing)**

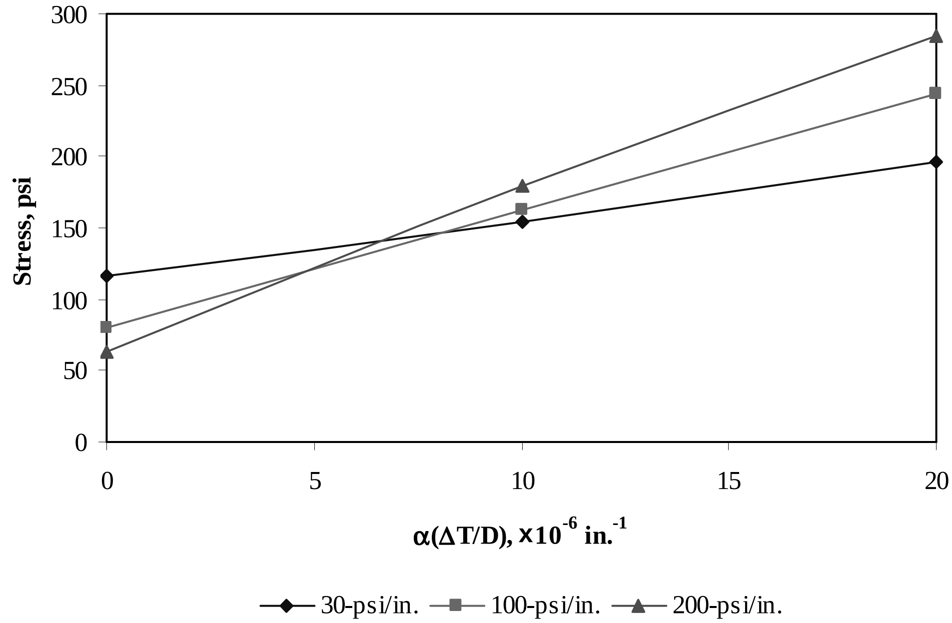


**Figure F-4-45: Impact of modulus of subgrade reaction and product $\alpha(\Delta T/D)$ on longitudinal stress at top of the slab (177-in. joint spacing)**

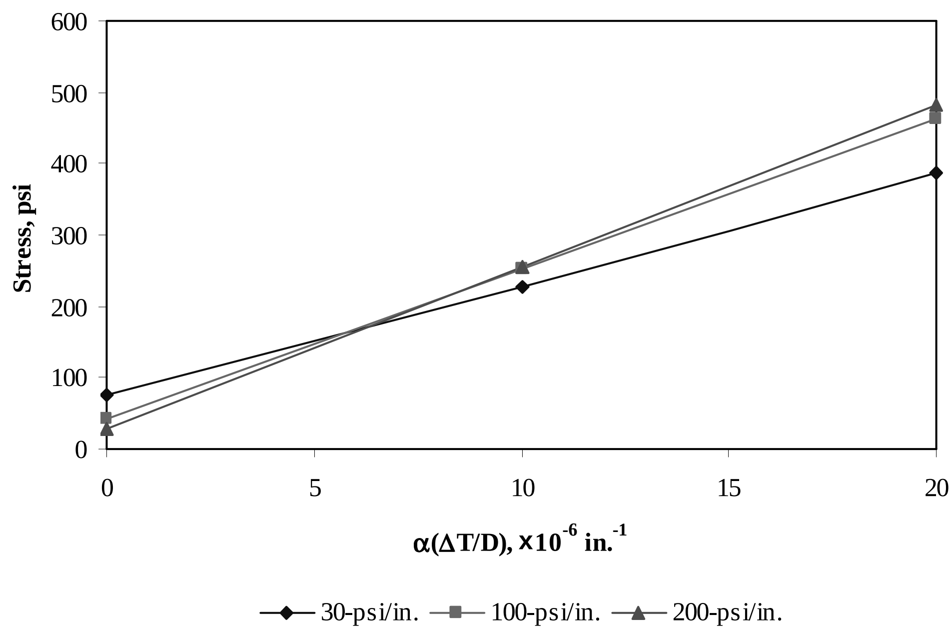


**Figure F-4-46: Impact of modulus of subgrade reaction and product $\alpha(\Delta T/D)$ on longitudinal stress at top of the slab (315-in. joint spacing)**

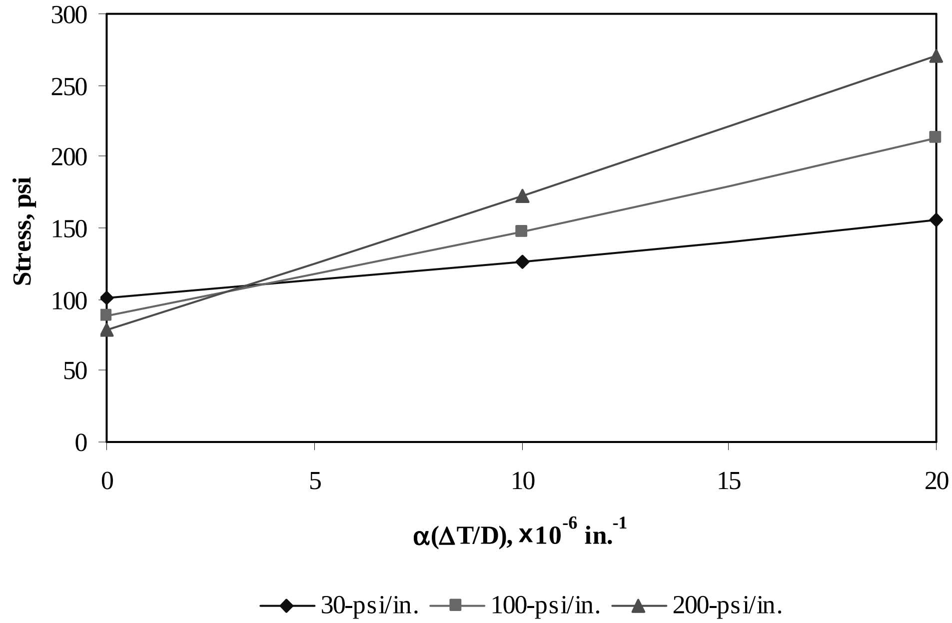


**Figure F-4-47: Impact of modulus of subgrade reaction and product α(ΔT/D) on transverse stress at bottom of the slab (177-in. joint spacing)**

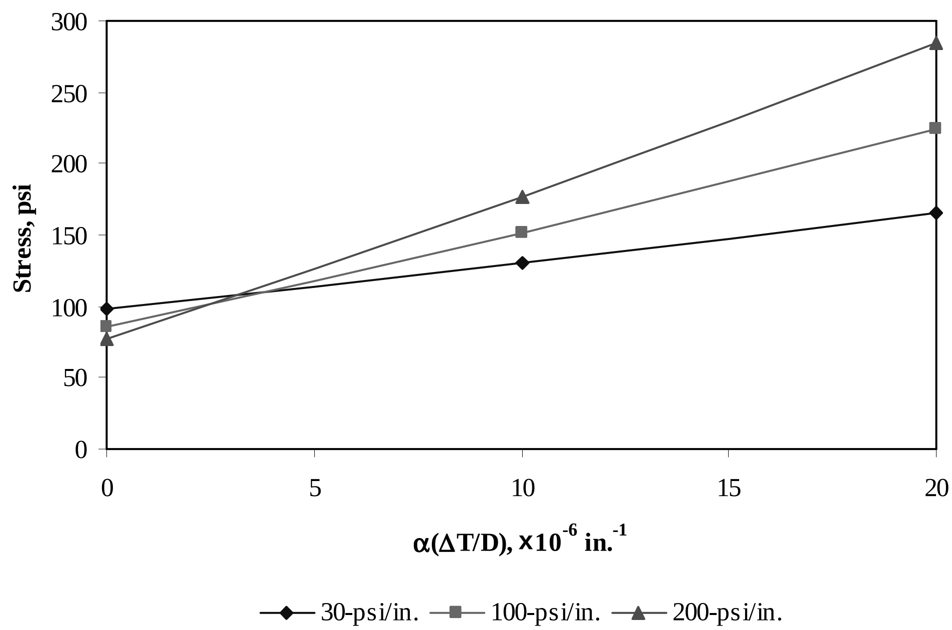


**Figure F-4-48: Impact of modulus of subgrade reaction and product α(ΔT/D) on transverse stress at bottom of the slab (315-in. joint spacing)**

Figures F-4-49 through F-4-51 illustrate the impact of joint spacing and product $\alpha(\Delta T/D)$ on stresses (10-in. PCC thickness, 16-in. base/subbase thickness, 100-psi/in. modulus of subgrade reaction and PCC shoulder)

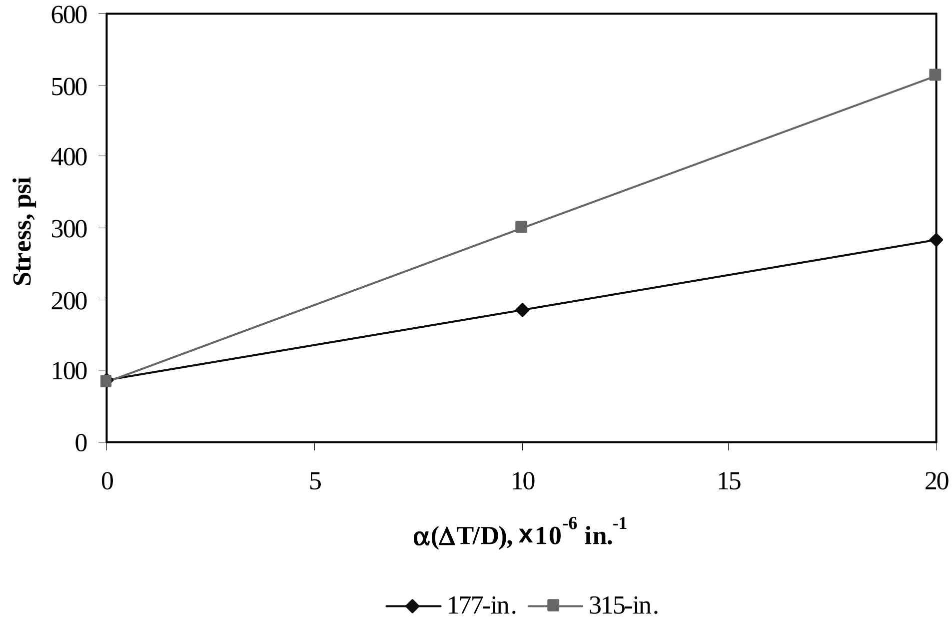


**Figure F-4-49: Impact of joint spacing and product $\alpha(\Delta T/D)$ on longitudinal stress at bottom of the slab**

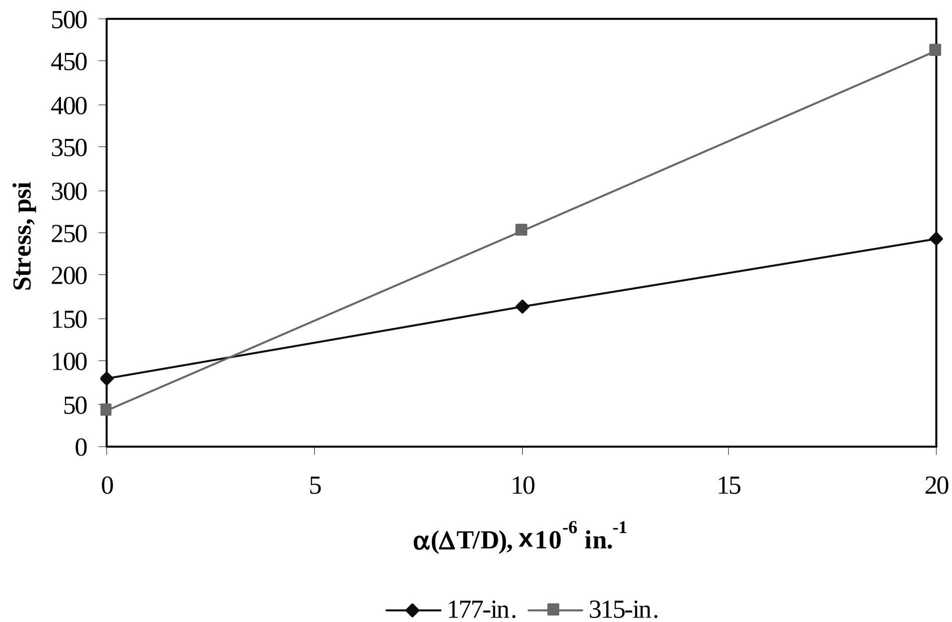


**Figure F-4-50: Impact of joint spacing and product $\alpha(\Delta T/D)$ on longitudinal stress at top of the slab**

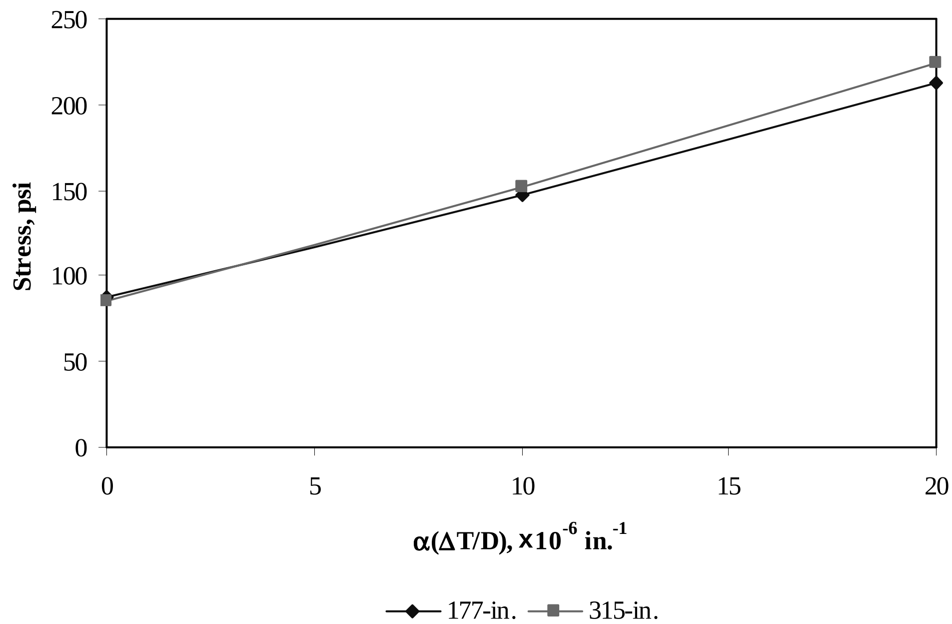


**Figure F-4-51: Impact of joint spacing and product α(ΔT/D) on transverse stress at bottom of the slab**

**Sub Appendix F-5**

**Documentation of Pavement Responses for**


**65-kips Multi-axle (5)**

Figures F-5-1 through F-5-12 illustrate the impact of PCC thickness and base/subbase thickness on stresses (100-psi/in. modulus of subgrade reaction and PCC shoulder)

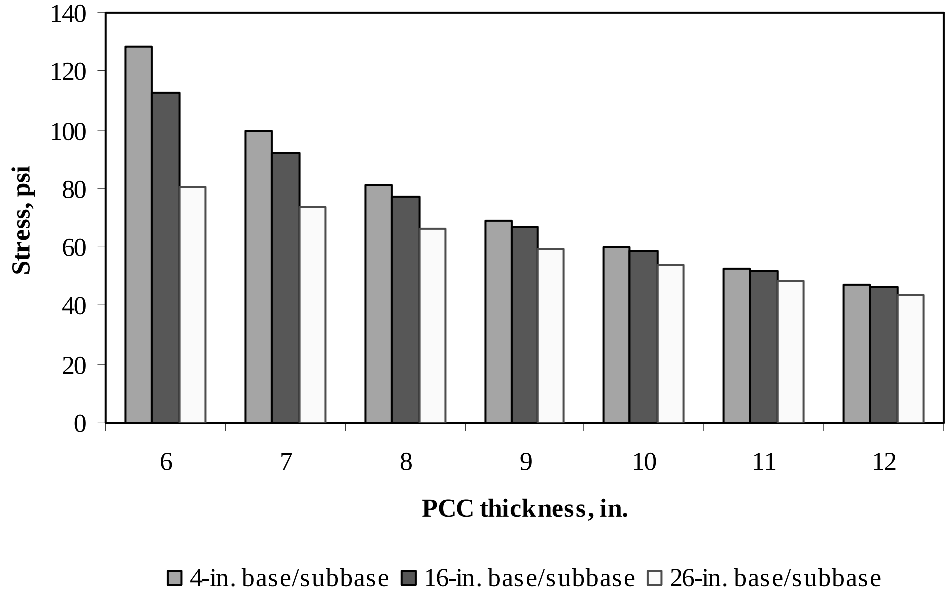


**Figure F-5-1: Impact of PCC thickness and base/subbase thickness on longitudinal stress at bottom of the Slab (177-in. joint spacing and $\alpha(\Delta T/D)$ of 0 $in.^{-1}$)**

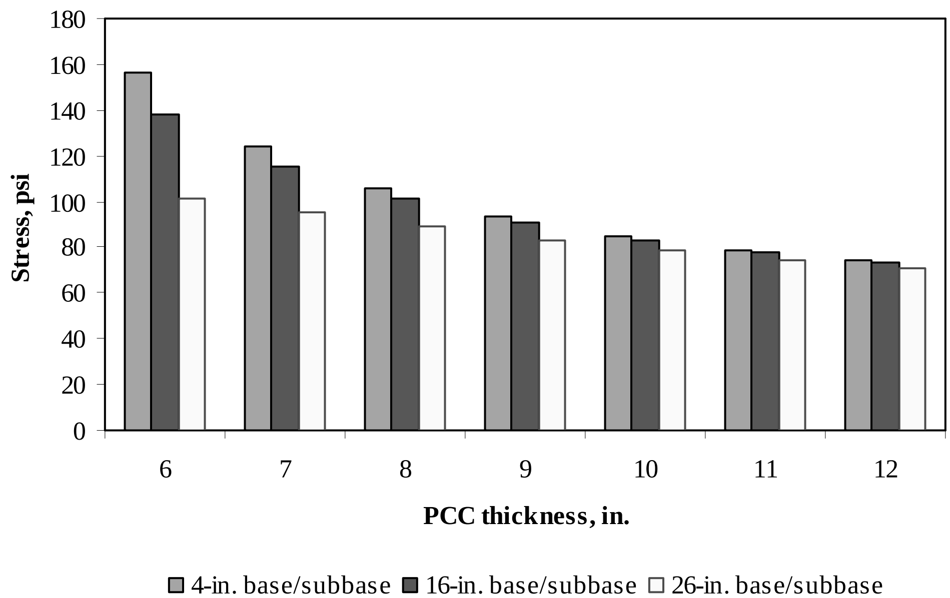


**Figure F-5-2: Impact of PCC thickness and base/subbase thickness on longitudinal stress at bottom of the Slab (315-in. joint spacing and $\alpha(\Delta T/D)$ of 0 $in.^{-1}$)**

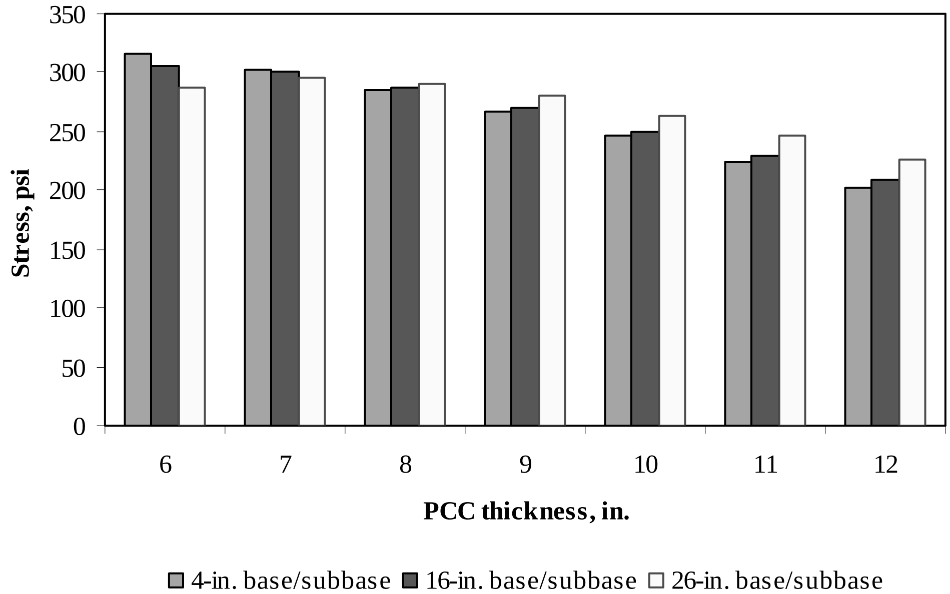


**Figure F-5-3: Impact of PCC thickness and base/subbase thickness on longitudinal stress at bottom of the Slab (177-in. joint spacing and $\alpha(\Delta T/D)$ of $20x10^{-6}$ in.$^{-1}$)**

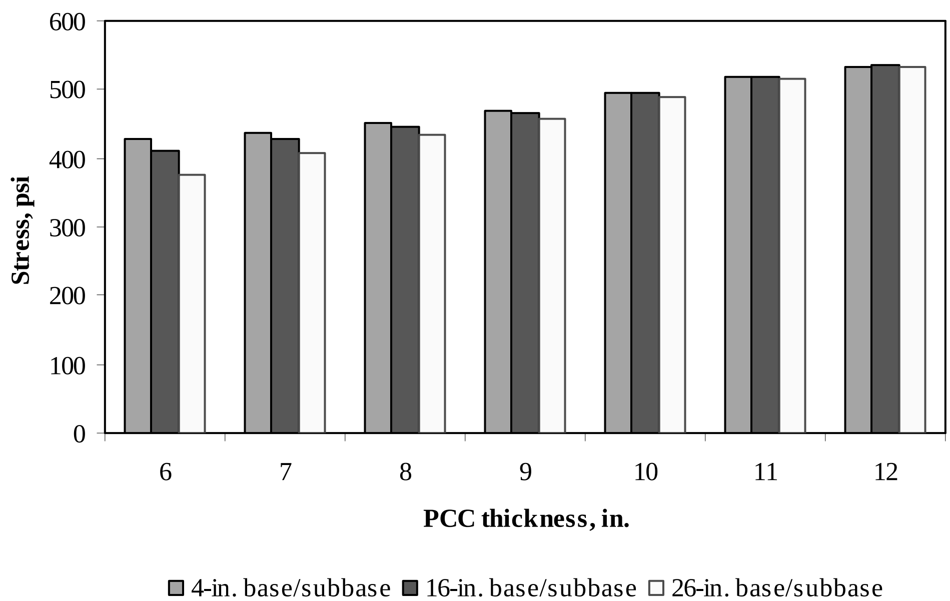


**Figure F-5-4: Impact of PCC thickness and base/subbase thickness on longitudinal stress at bottom of the Slab (315-in. joint spacing and $\alpha(\Delta T/D)$ of $20x10^{-6}$ in.$^{-1}$)**

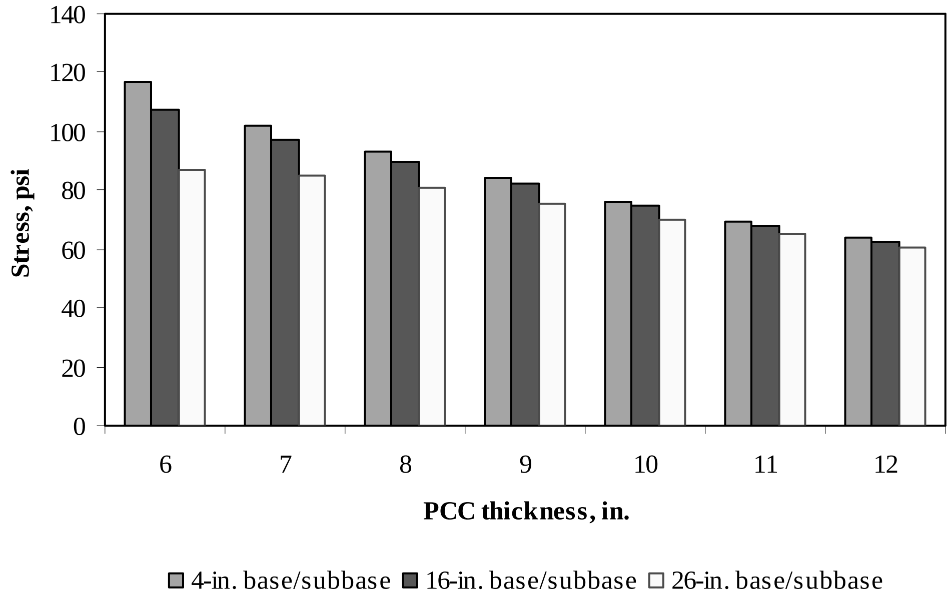


**Figure F-5-5: Impact of PCC thickness and base/subbase thickness on longitudinal stress at top of the Slab (177-in. joint spacing and α(ΔT/D) of 0 in.$^{-1}$)**

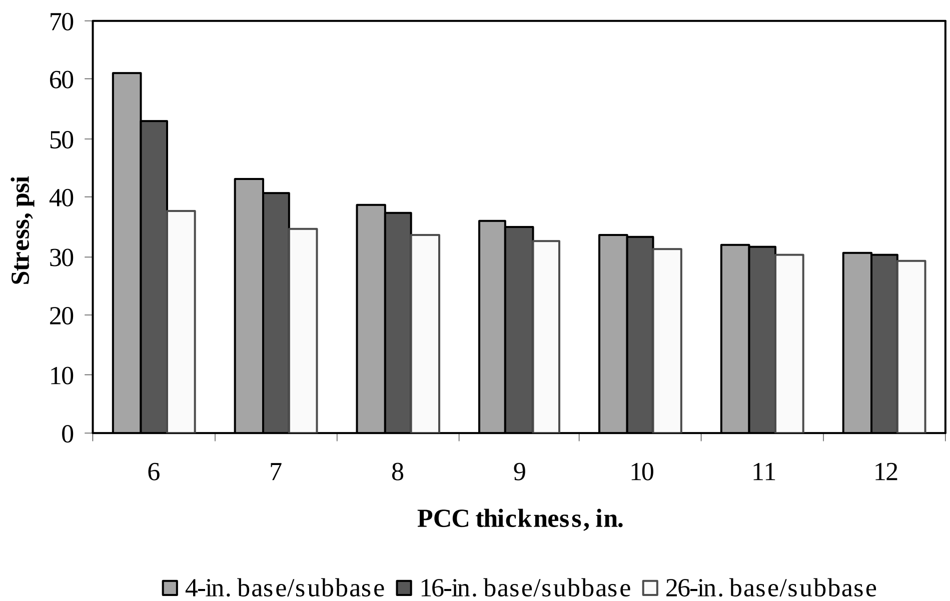


**Figure F-5-6: Impact of PCC thickness and base/subbase thickness on longitudinal stress at top of the Slab (315-in. joint spacing and α(ΔT/D) of 0 in.$^{-1}$)**

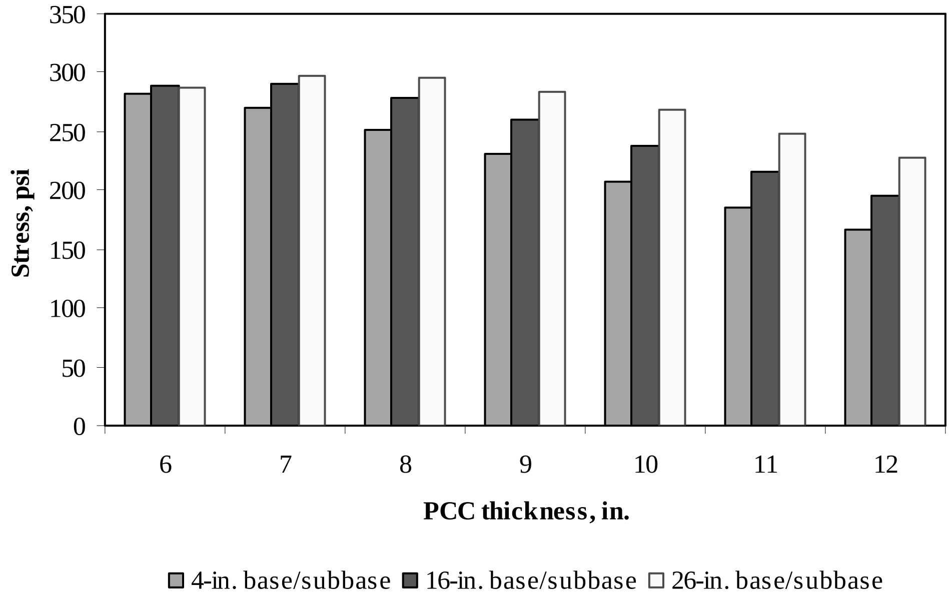


**Figure F-5-7: Impact of PCC thickness and base/subbase thickness on longitudinal stress at top of the Slab (177-in. joint spacing and $\alpha(\Delta T/D)$ of $-20 \times 10^{-6}$ in.$^{-1}$)**

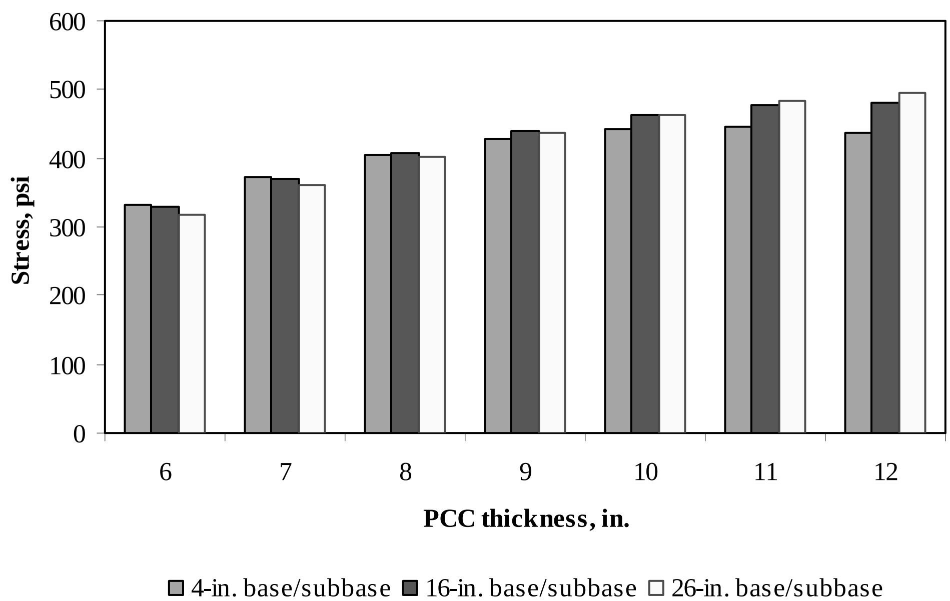


**Figure F-5-8: Impact of PCC thickness and base/subbase thickness on longitudinal stress at top of the Slab (315-in. joint spacing and $\alpha(\Delta T/D)$ of $-20 \times 10^{-6}$ in.$^{-1}$)**

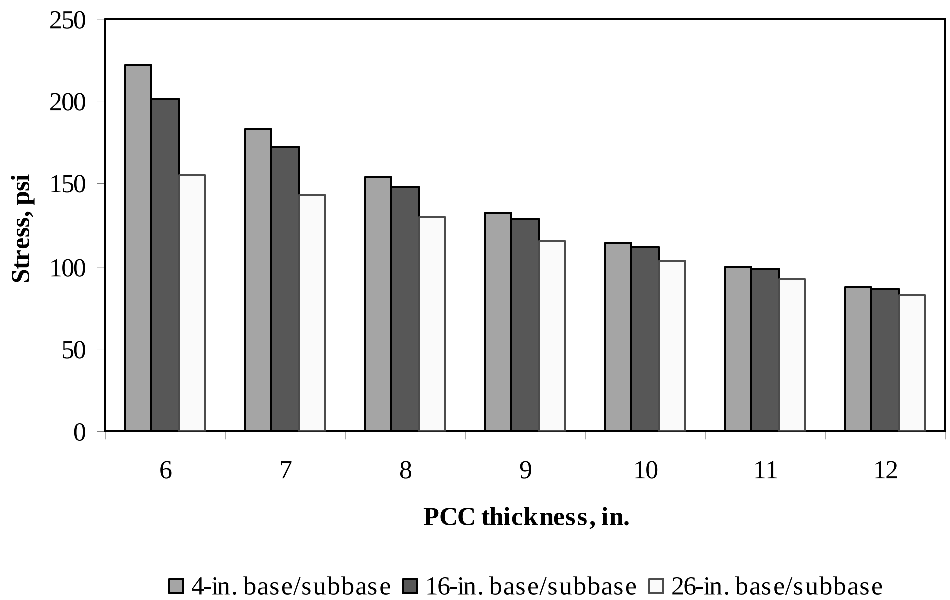


**Figure F-5-9: Impact of PCC thickness and base/subbase thickness on transverse stress at bottom of the Slab (177-in. joint spacing and $\alpha(\Delta T/D)$ of 0 in.$^{-1}$)**

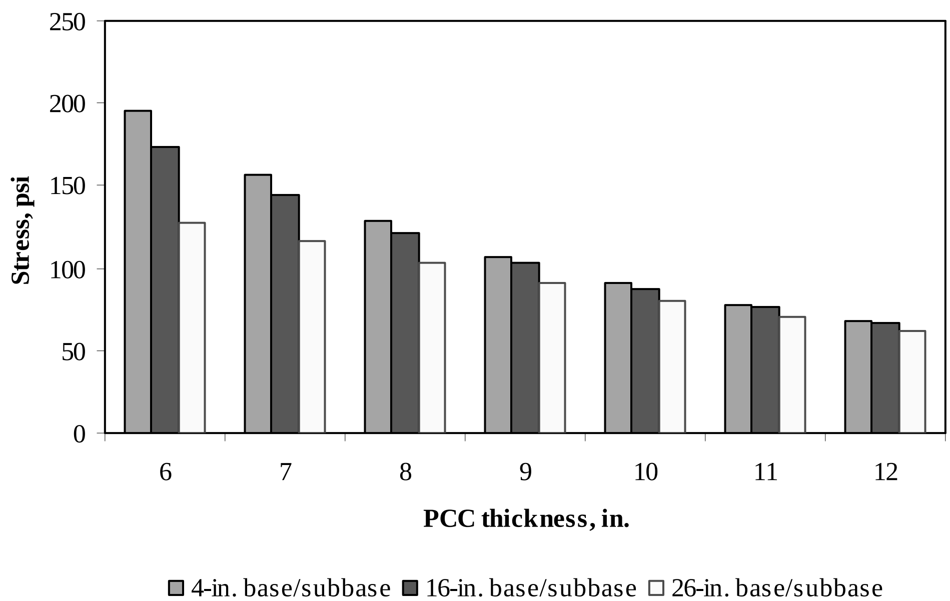


**Figure F-5-10: Impact of PCC thickness and base/subbase thickness on transverse stress at bottom of the Slab (315-in. joint spacing and $\alpha(\Delta T/D)$ of 0 in.$^{-1}$)**

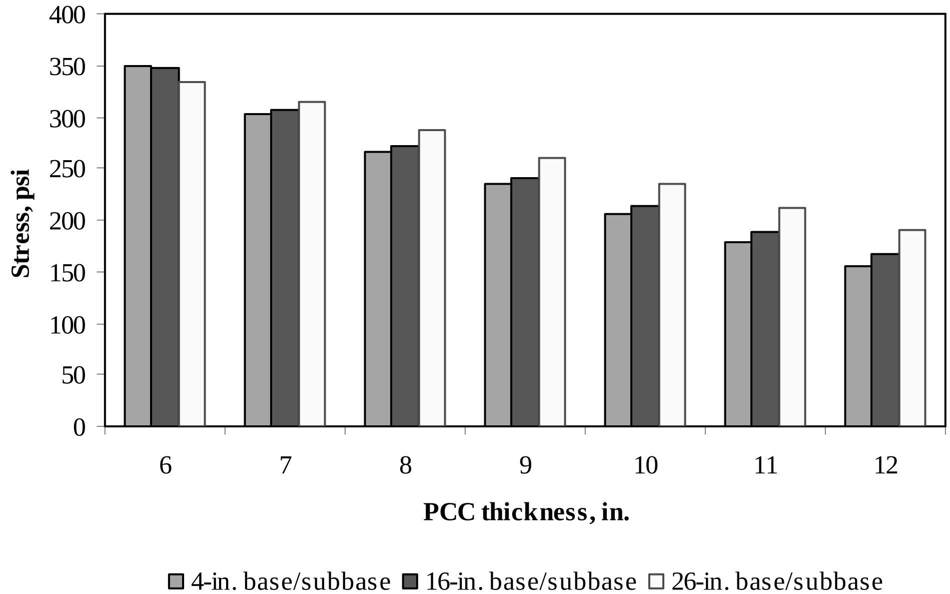


**Figure F-5-11: Impact of PCC thickness and base/subbase thickness on transverse stress at bottom of the Slab (177-in. joint spacing and α(ΔT/D) of 20x10$^{-6}$ in.$^{-1}$)**

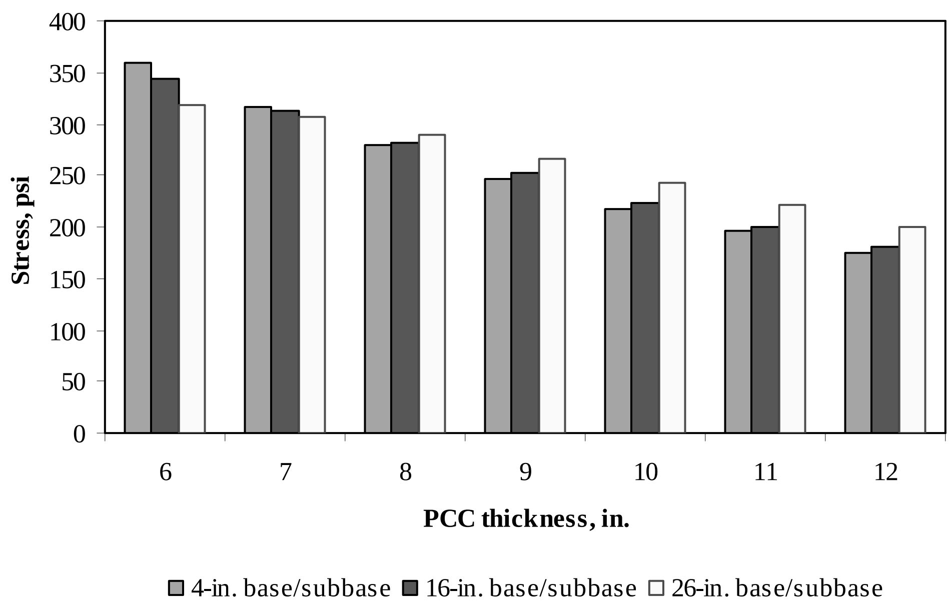


**Figure F-5-12: Impact of PCC thickness and base/subbase thickness on transverse stress at bottom of the Slab (315-in. joint spacing and α(ΔT/D) of 20x10$^{-6}$ in.$^{-1}$)**

Figures F-5-13 through F-5-24 illustrate the impact of PCC thickness and modulus of subgrade reaction on stresses (16-in. base/subbase thickness and PCC shoulder)

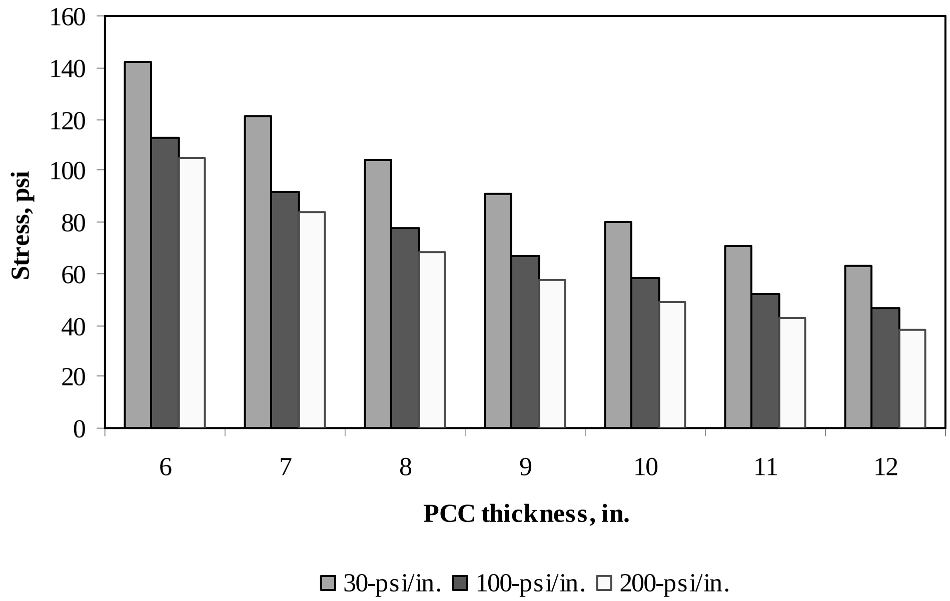


**Figure F-5-13: Impact of PCC thickness and modulus of subgrade reaction on longitudinal stress at bottom of the slab (177-in. joint spacing and $\alpha(\Delta T/D)$ of 0 in.$^{-1}$)**

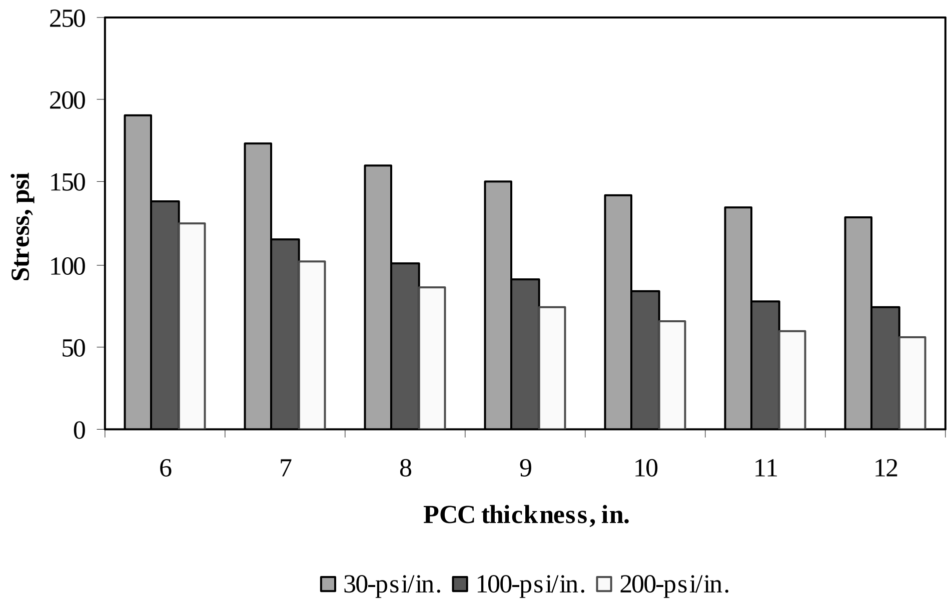


**Figure F-5-14: Impact of PCC thickness and modulus of subgrade reaction on longitudinal stress at bottom of the slab (315-in. joint spacing and $\alpha(\Delta T/D)$ of 0 in.$^{-1}$)**

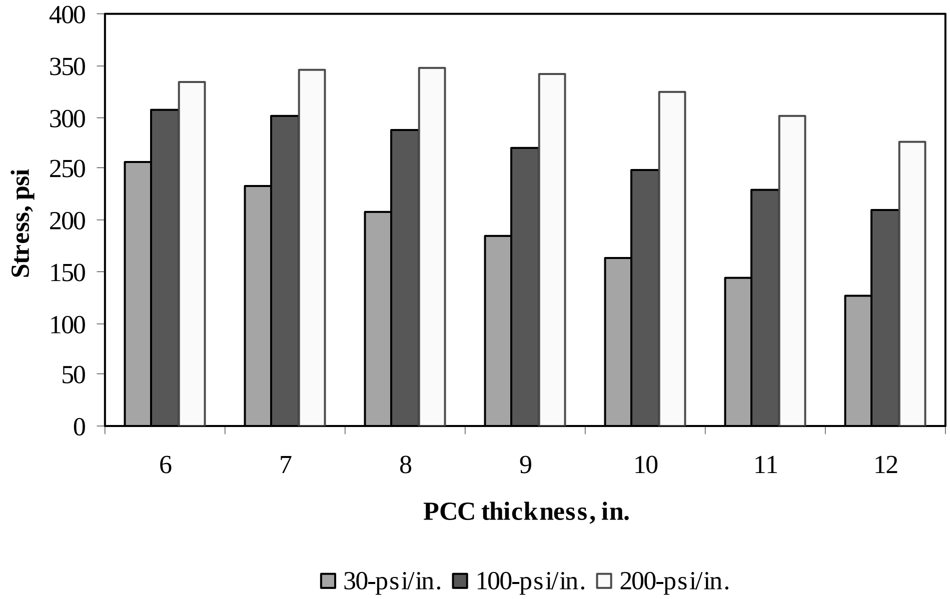


**Figure F-5-15: Impact of PCC thickness and modulus of subgrade reaction on longitudinal stress at bottom of the slab (177-in. joint spacing and $\alpha(\Delta T/D)$ of $20x10^{-6}$ in.$^{-1}$)**

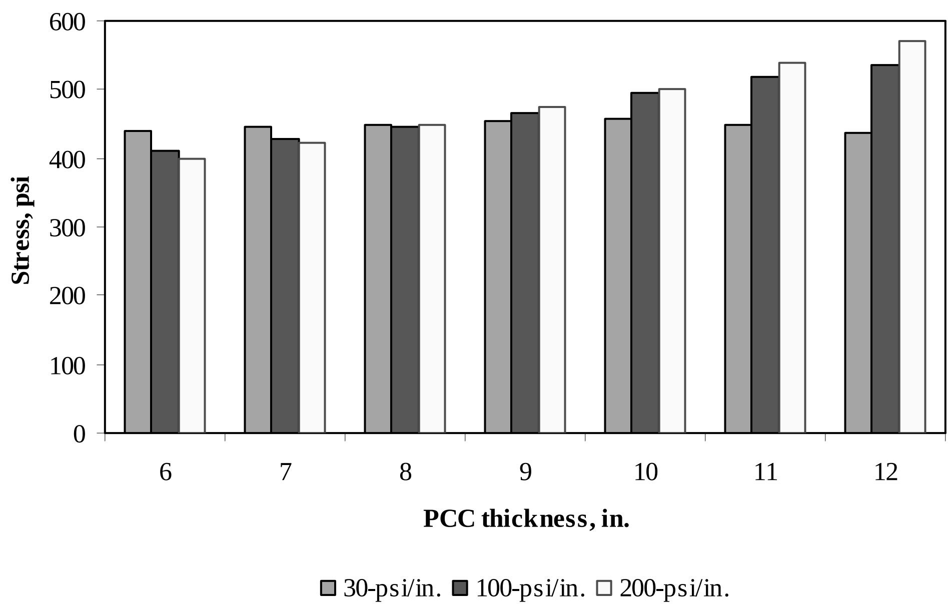


**Figure F-5-16: Impact of PCC thickness and modulus of subgrade reaction on longitudinal stress at bottom of the slab (315-in. joint spacing and $\alpha(\Delta T/D)$ of $20x10^{-6}$ in.$^{-1}$)**

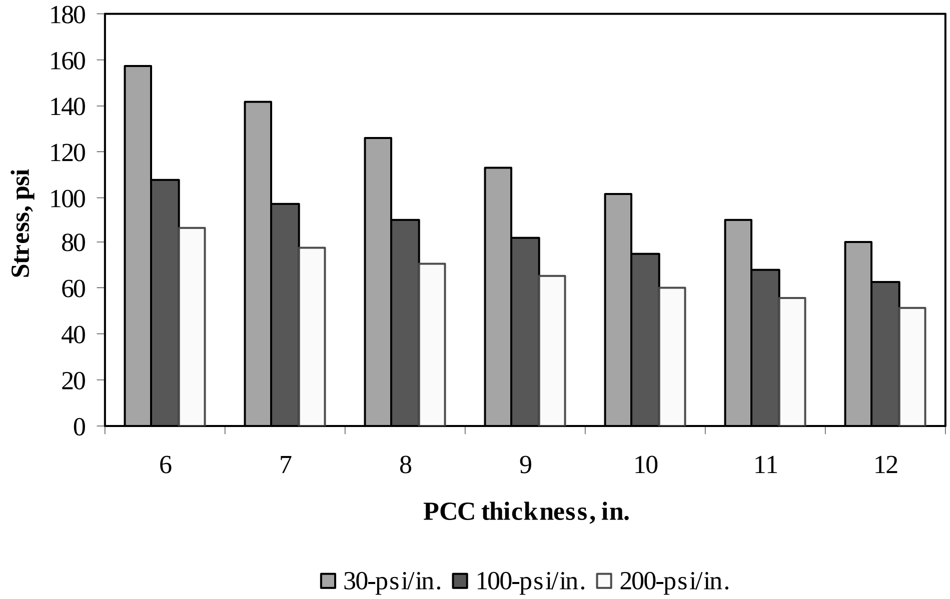


**Figure F-5-17: Impact of PCC thickness and modulus of subgrade reaction on longitudinal stress at top of the Slab (177-in. joint spacing and $\alpha(\Delta T/D)$ of 0 in.$^{-1}$)**

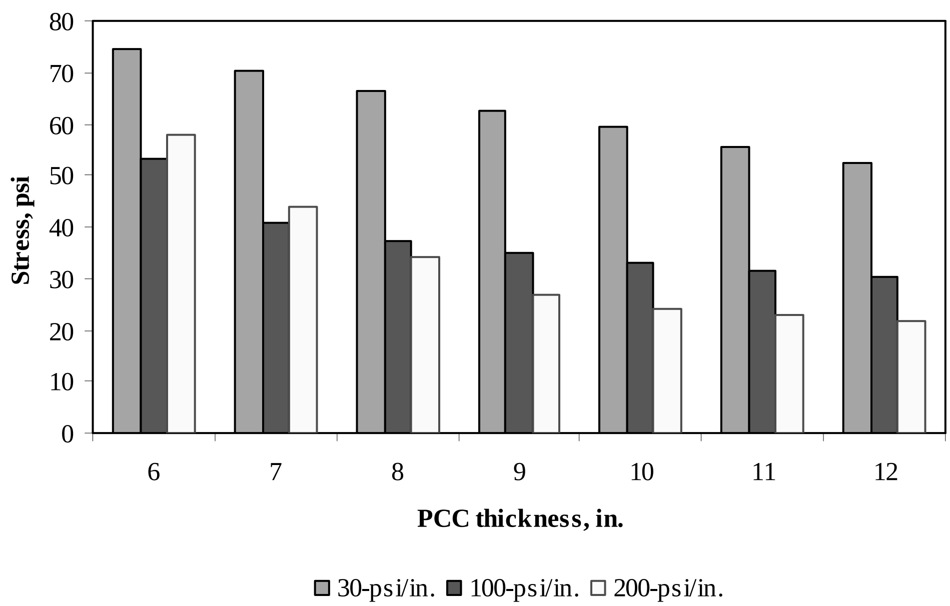


**Figure F-5-18: Impact of PCC thickness and modulus of subgrade reaction on longitudinal stress at top of the Slab (315-in. joint spacing and $\alpha(\Delta T/D)$ of 0 in.$^{-1}$)**

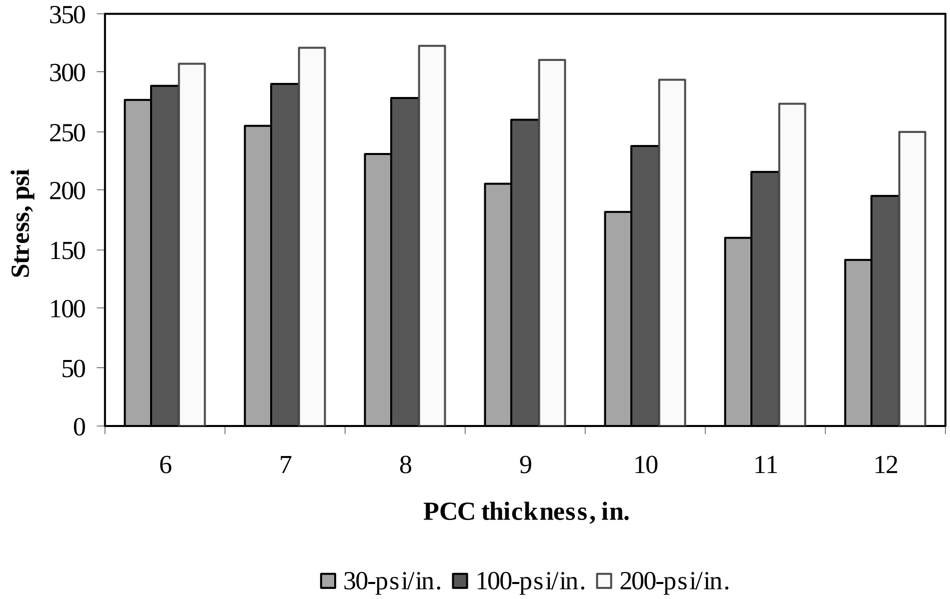


**Figure F-5-19: Impact of PCC thickness and modulus of subgrade reaction on longitudinal stress at top of the Slab (177-in. joint spacing and $\alpha(\Delta T/D)$ of $-20x10^{-6}$ in.$^{-1}$)**

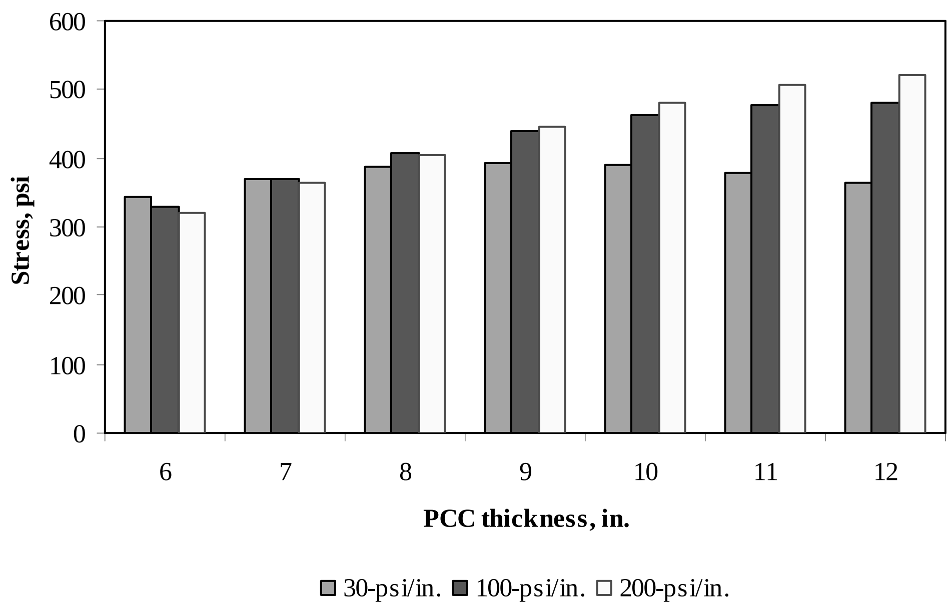


**Figure F-5-20: Impact of PCC thickness and modulus of subgrade reaction on longitudinal stress at top of the Slab (315-in. joint spacing and $\alpha(\Delta T/D)$ of $-20x10^{-6}$ in.$^{-1}$)**

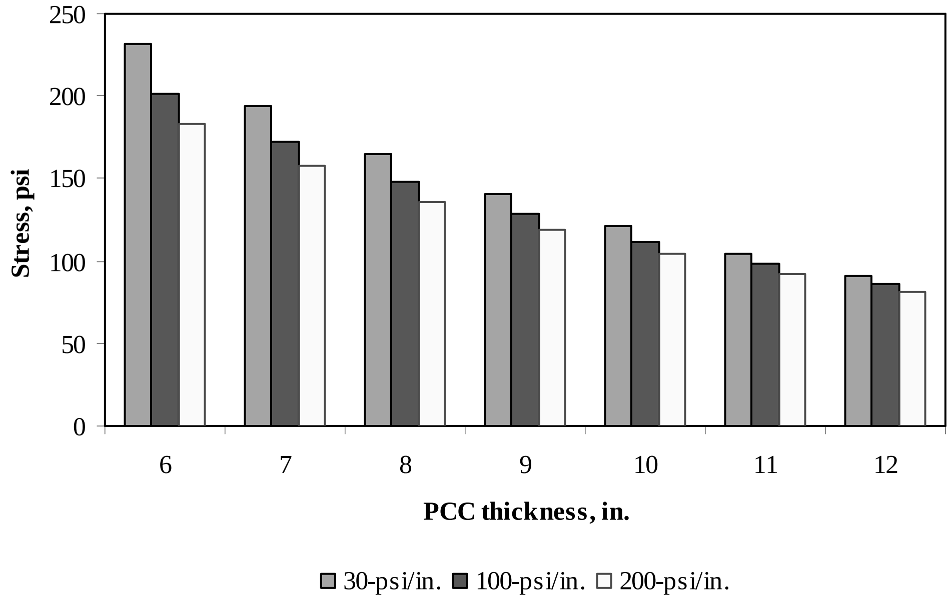


**Figure F-5-21: Impact of PCC thickness and modulus of subgrade reaction on transverse stress at bottom of the Slab (177-in. joint spacing and $\alpha(\Delta T/D)$ of 0 in.$^{-1}$)**

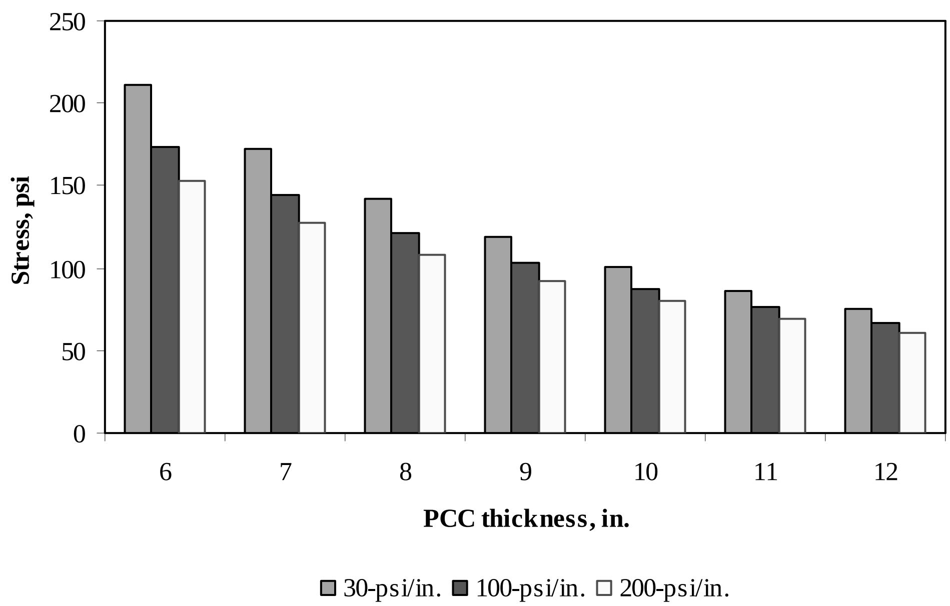


**Figure F-5-22: Impact of PCC thickness and modulus of subgrade reaction on transverse stress at bottom of the Slab (315-in. joint spacing and $\alpha(\Delta T/D)$ of 0 in.$^{-1}$)**

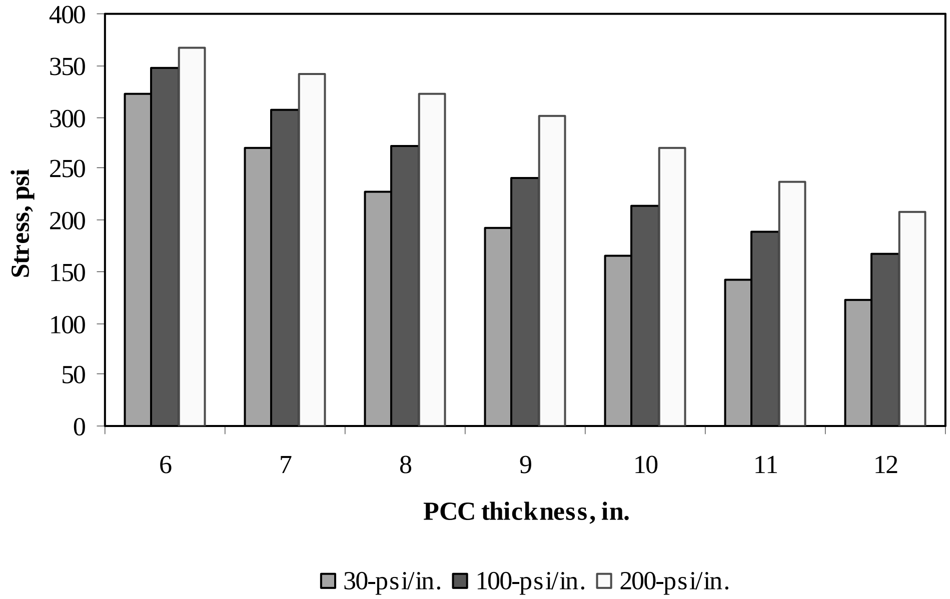


**Figure F-5-23: Impact of PCC thickness and modulus of subgrade reaction on transverse stress at bottom of the Slab (177-in. joint spacing and $\alpha(\Delta T/D)$ of $20x10^{-6}$ in.$^{-1}$)**

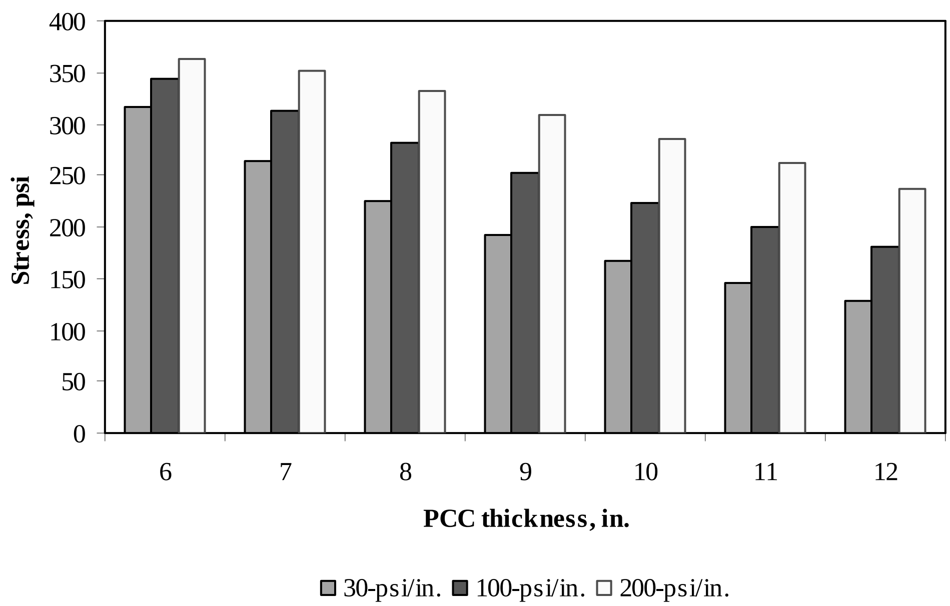


**Figure F-5-24: Impact of PCC thickness and modulus of subgrade reaction on transverse stress at bottom of the Slab (315-in. joint spacing and $\alpha(\Delta T/D)$ of $20x10^{-6}$ in.$^{-1}$)**

Figures F-5-25 through F-5-36 illustrate the impact of PCC thickness and lateral support condition on stresses (16-in. base/subbase and 100-psi/in. modulus of subgrade reaction)

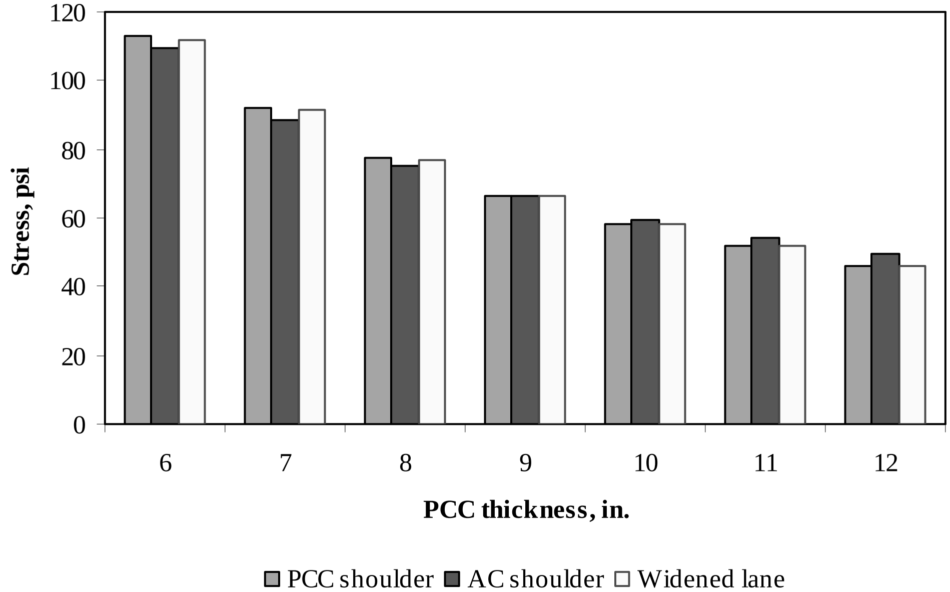


**Figure F-5-25: Impact of PCC thickness and lateral support condition on longitudinal stress at bottom of the Slab (177-in. joint spacing and $\alpha(\Delta T/D)$ of 0 in.$^{-1}$)**

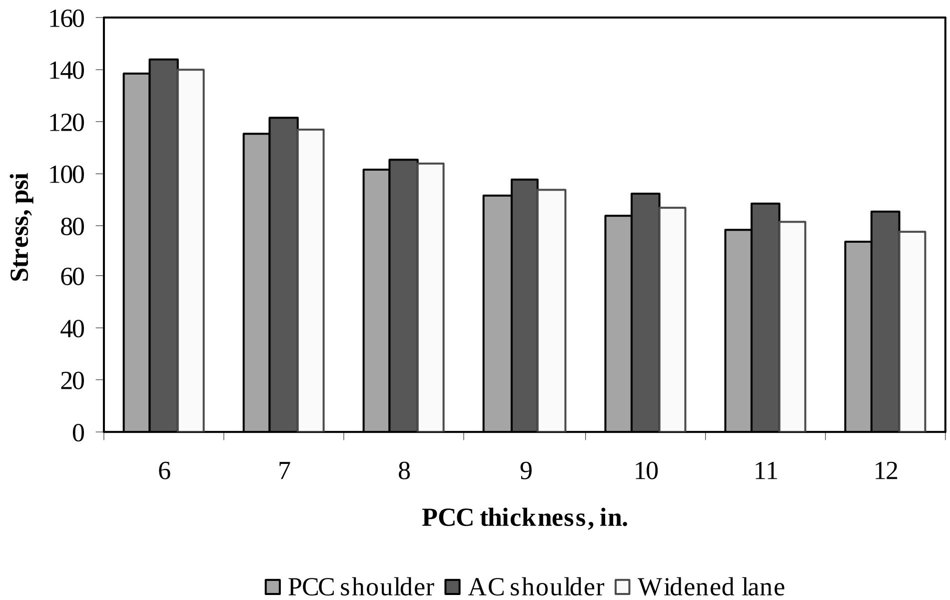


**Figure F-5-26: Impact of PCC thickness and lateral support condition on longitudinal stress at bottom of the Slab (315-in. joint spacing and $\alpha(\Delta T/D)$ of 0 in.$^{-1}$)**

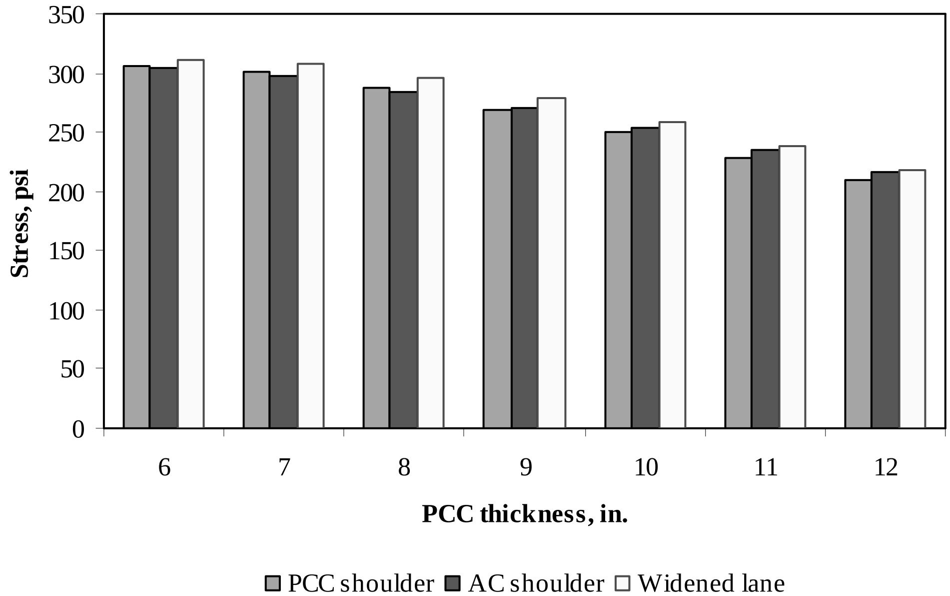


**Figure F-5-27: Impact of PCC thickness and lateral support condition on longitudinal stress at bottom of the Slab (177-in. joint spacing and $\alpha(\Delta T/D)$ of 20x10$^{-6}$ in.$^{-1}$)**

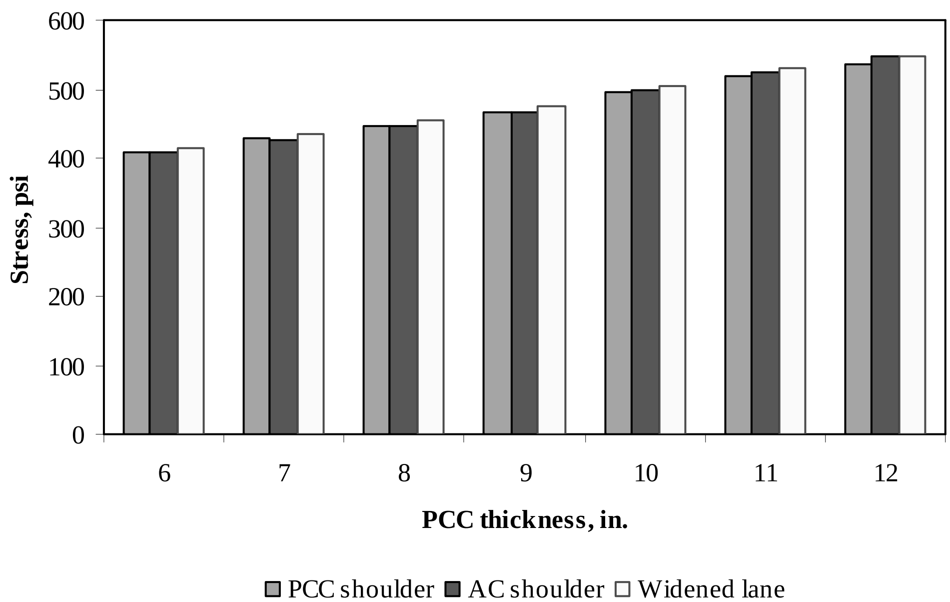


**Figure F-5-28: Impact of PCC thickness and lateral support condition on longitudinal stress at bottom of the Slab (315-in. joint spacing and $\alpha(\Delta T/D)$ of 20x10$^{-6}$ in.$^{-1}$)**

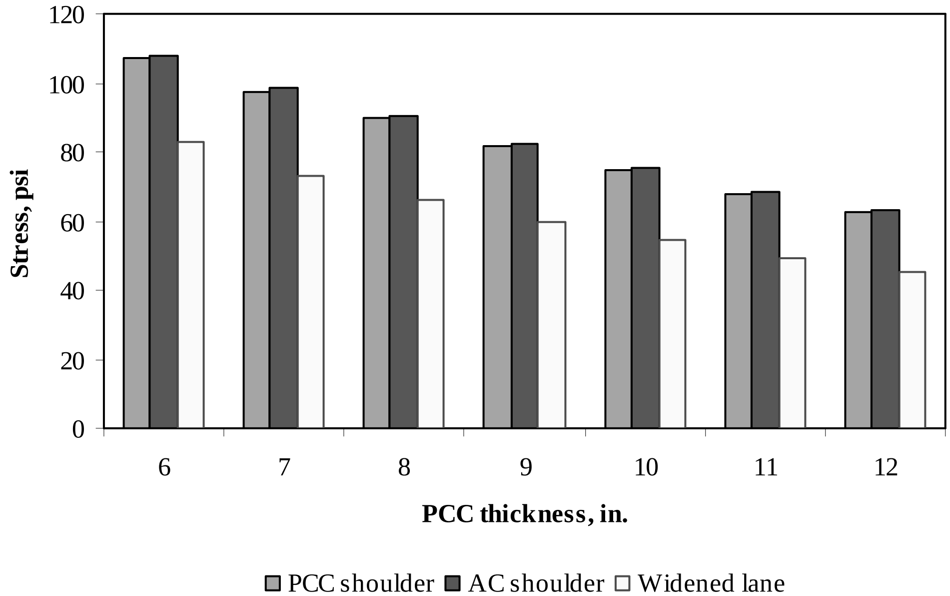


**Figure F-5-29: Impact of PCC thickness and lateral support condition on longitudinal stress at top of the Slab (177-in. joint spacing and $\alpha(\Delta T/D)$ of 0 in.$^{-1}$)**

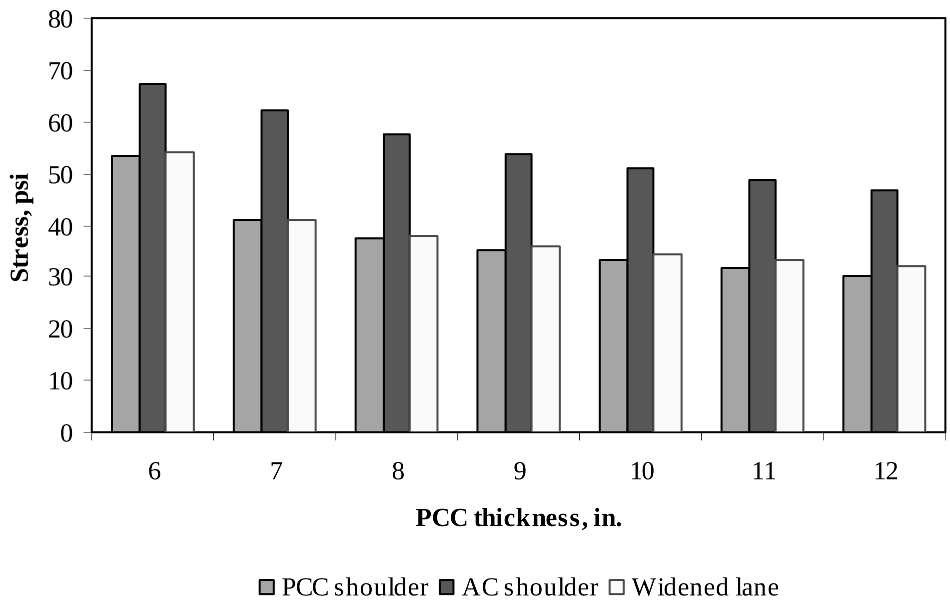


**Figure F-5-30: Impact of PCC thickness and lateral support condition on longitudinal stress at top of the Slab (315-in. joint spacing and $\alpha(\Delta T/D)$ of 0 in.$^{-1}$)**

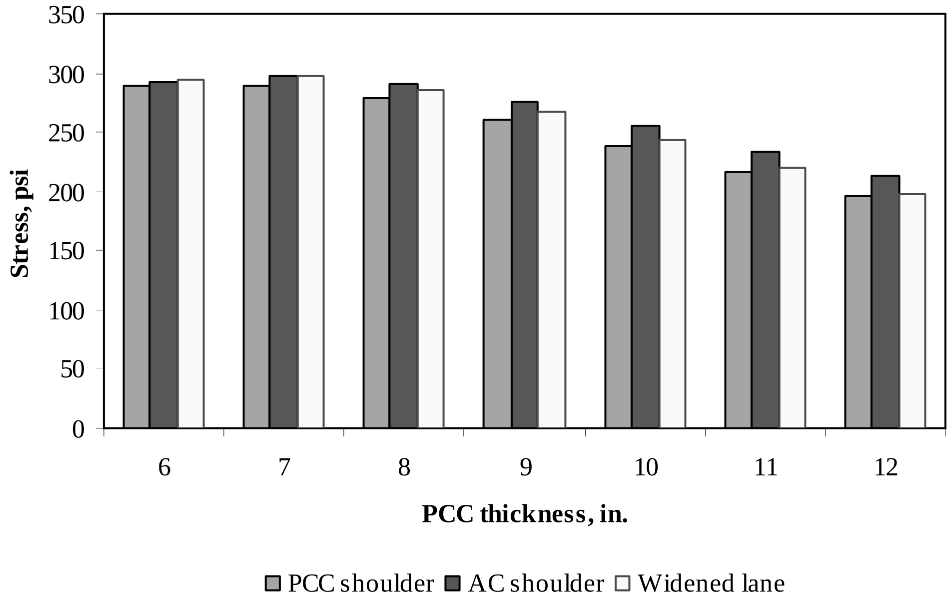


**Figure F-5-31: Impact of PCC thickness and lateral support condition on longitudinal stress at top of the Slab (177-in. joint spacing and $\alpha(\Delta T/D)$ of -20x$10^{-6}$ in.$^{-1}$)**

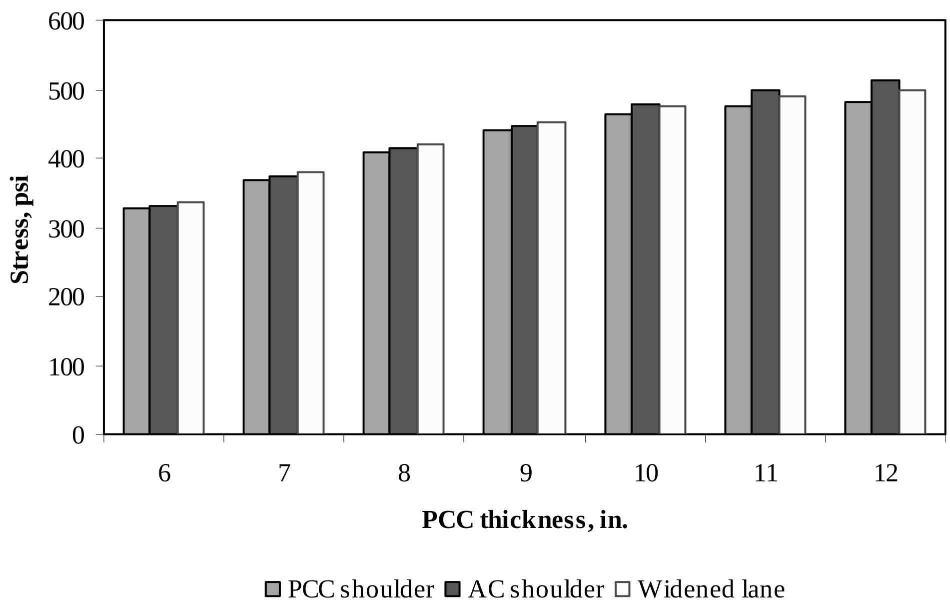


**Figure F-5-32: Impact of PCC thickness and lateral support condition on longitudinal stress at top of the Slab (315-in. joint spacing and $\alpha(\Delta T/D)$ of -20x$10^{-6}$ in.$^{-1}$)**

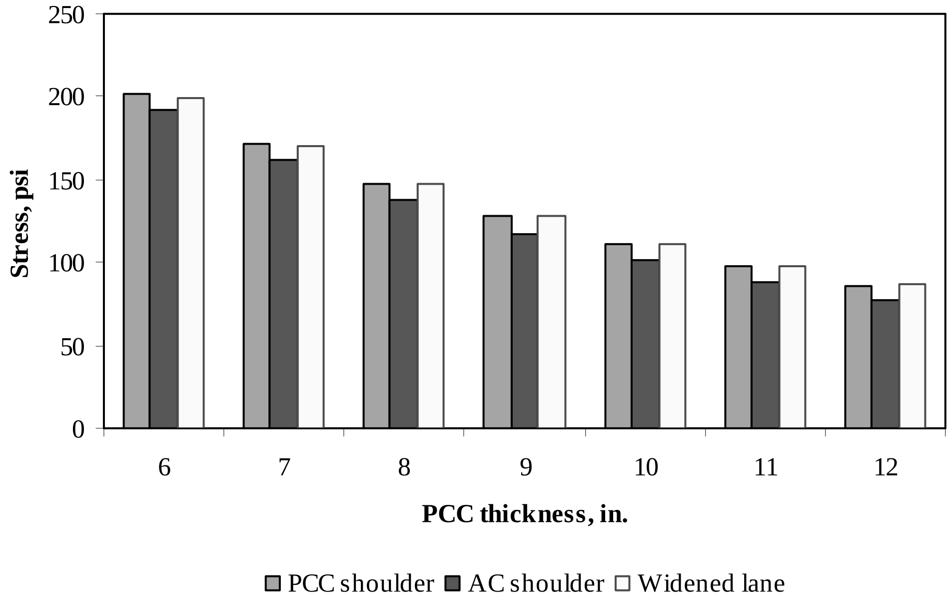


**Figure F-5-33: Impact of PCC thickness and lateral support condition on transverse stress at bottom of the Slab (177-in. joint spacing and $\alpha(\Delta T/D)$ of 0 in.$^{-1}$)**

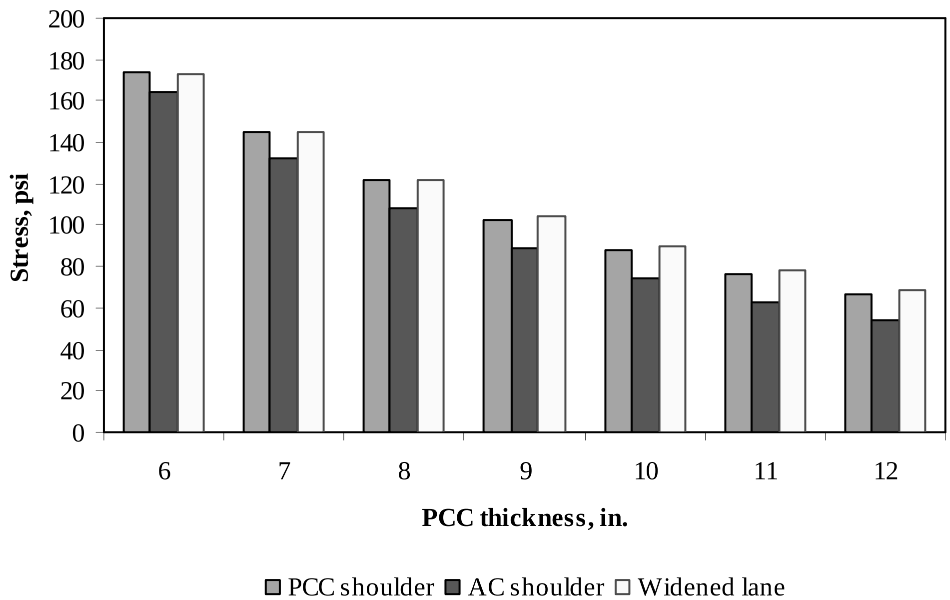


**Figure F-5-34: Impact of PCC thickness and lateral support condition on transverse stress at bottom of the Slab (315-in. joint spacing and $\alpha(\Delta T/D)$ of 0 in.$^{-1}$)**

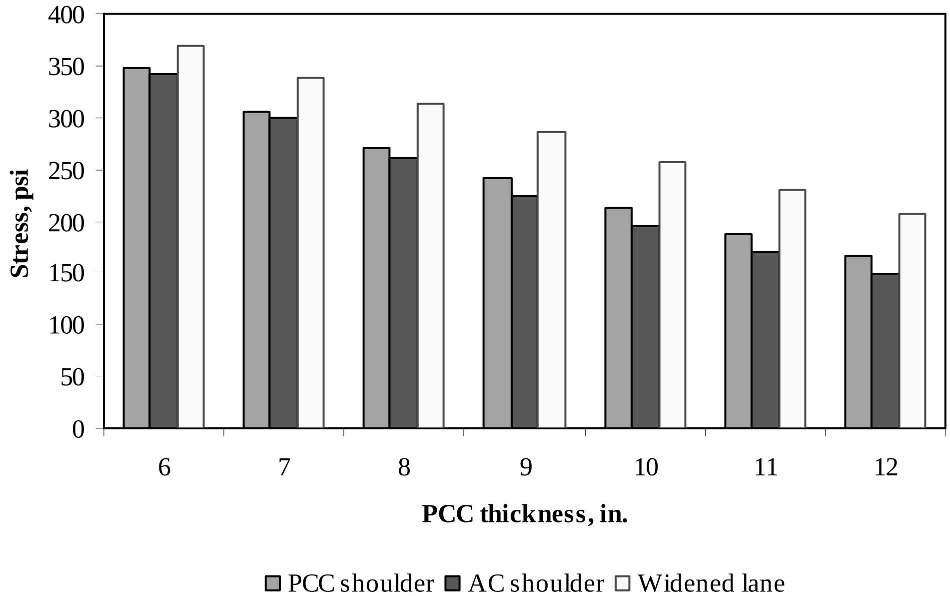


**Figure F-5-35: Impact of PCC thickness and lateral support condition on transverse stress at bottom of the Slab (177-in. joint spacing and $\alpha(\Delta T/D)$ of 20x$10^{-6}$ in.$^{-1}$)**

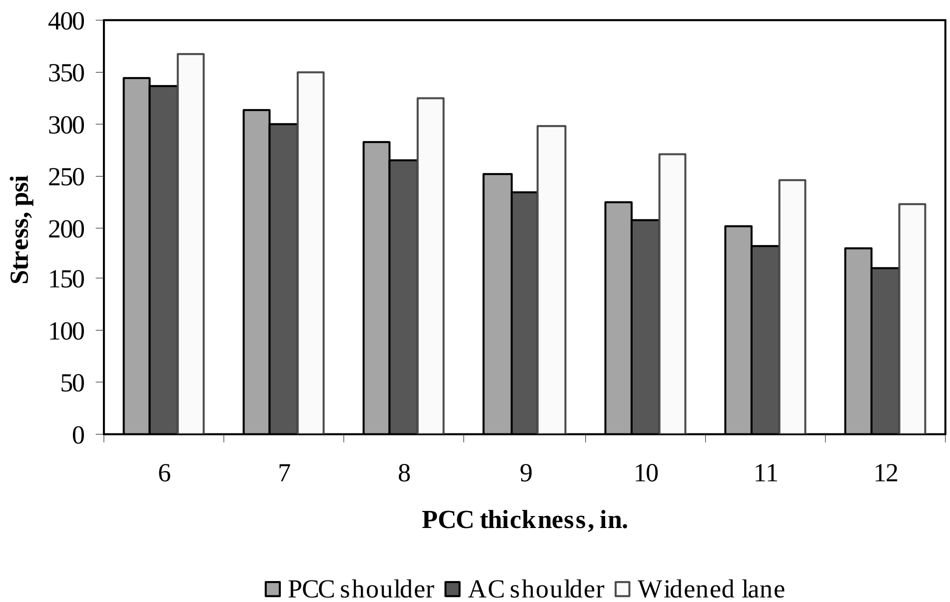


**Figure F-5-36: Impact of PCC thickness and lateral support condition on transverse stress at bottom of the Slab (315-in. joint spacing and $\alpha(\Delta T/D)$ of 20x$10^{-6}$ in.$^{-1}$)**

Figures F-5-37 through F-5-42 illustrate the impact of base/subbase thickness and product α(ΔT/D) on stresses (10-in. PCC thickness, 100-psi/in. modulus of subgrade reaction and PCC shoulder)

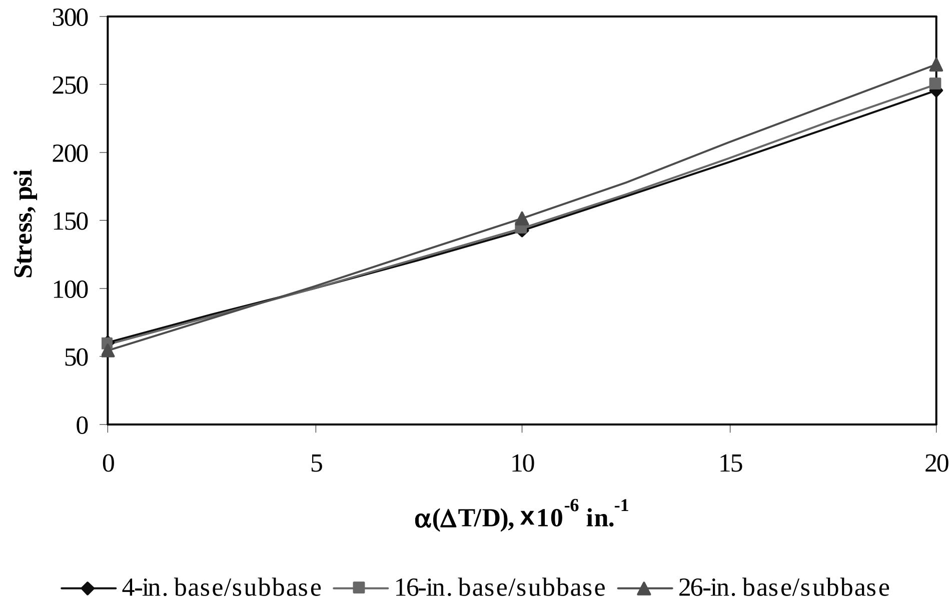


**Figure F-5-37: Impact of base/subbase thickness and product α(ΔT/D) on longitudinal stress at bottom of the slab (177-in. joint spacing)**

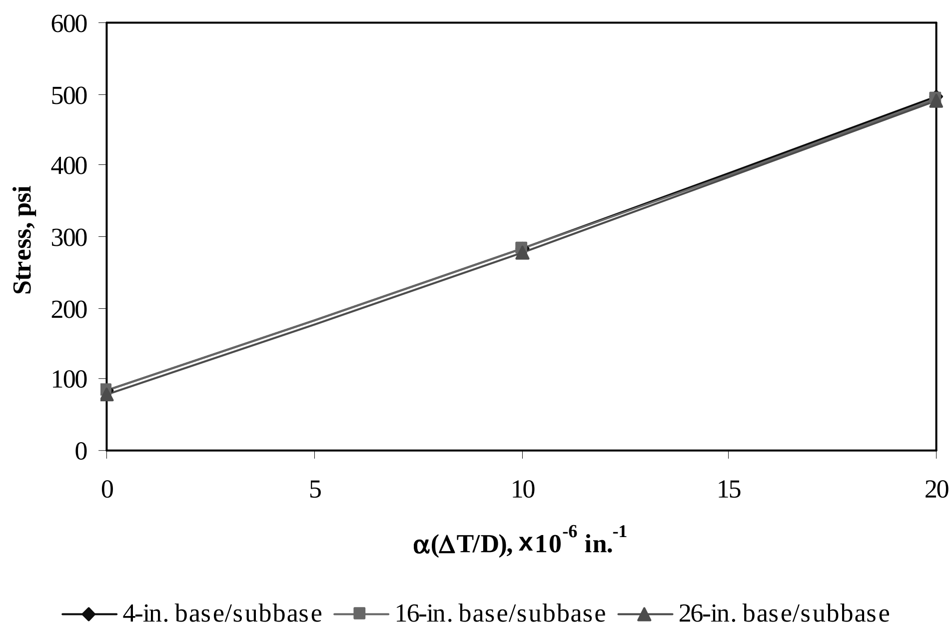


**Figure F-5-38: Impact of base/subbase thickness and product α(ΔT/D) on longitudinal stress at bottom of the slab (315-in. joint spacing)**

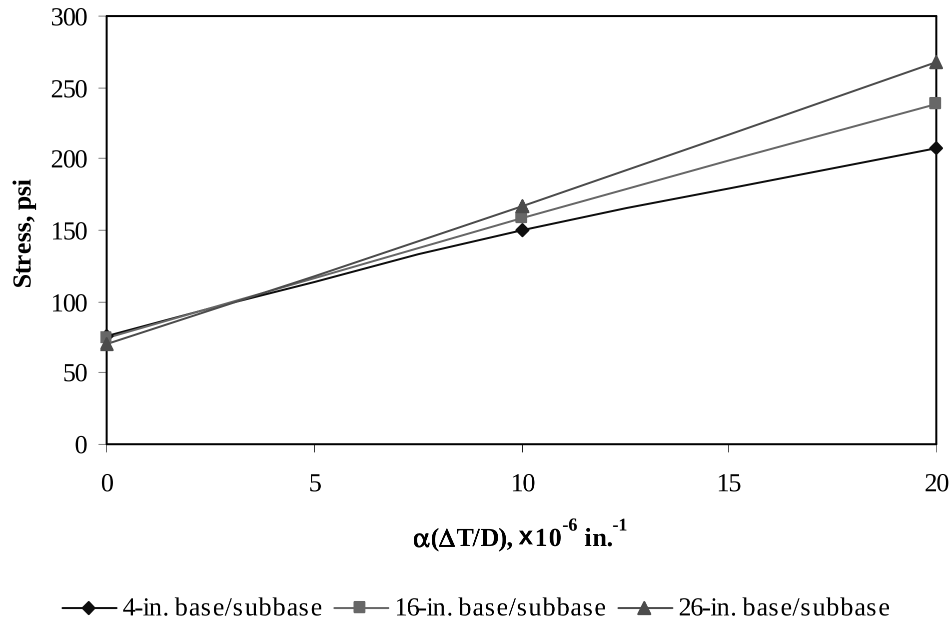


**Figure F-5-39: Impact of base/subbase thickness and product α(ΔT/D) on longitudinal stress at top of the slab (177-in. joint spacing)**

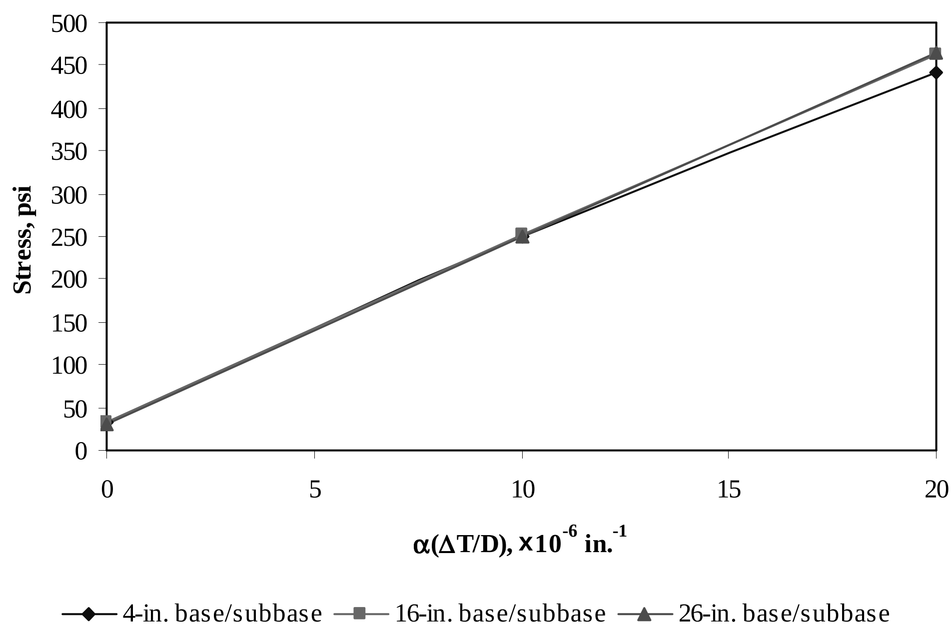


**Figure F-5-40: Impact of base/subbase thickness and product α(ΔT/D) on longitudinal stress at top of the slab (315-in. joint spacing)**

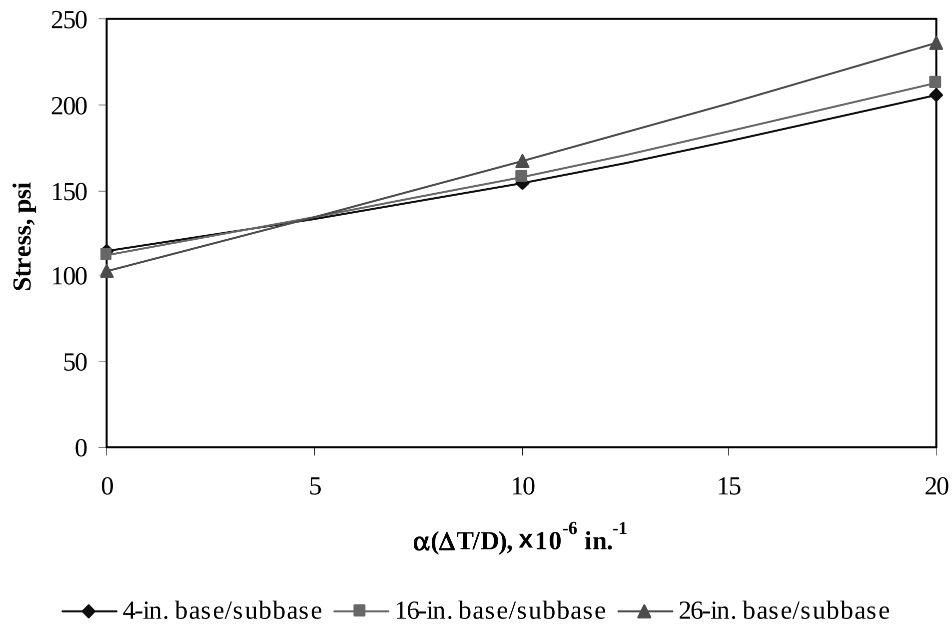


**Figure F-5-41: Impact of base/subbase thickness and product α(ΔT/D) on transverse stress at bottom of the slab (177-in. joint spacing)**

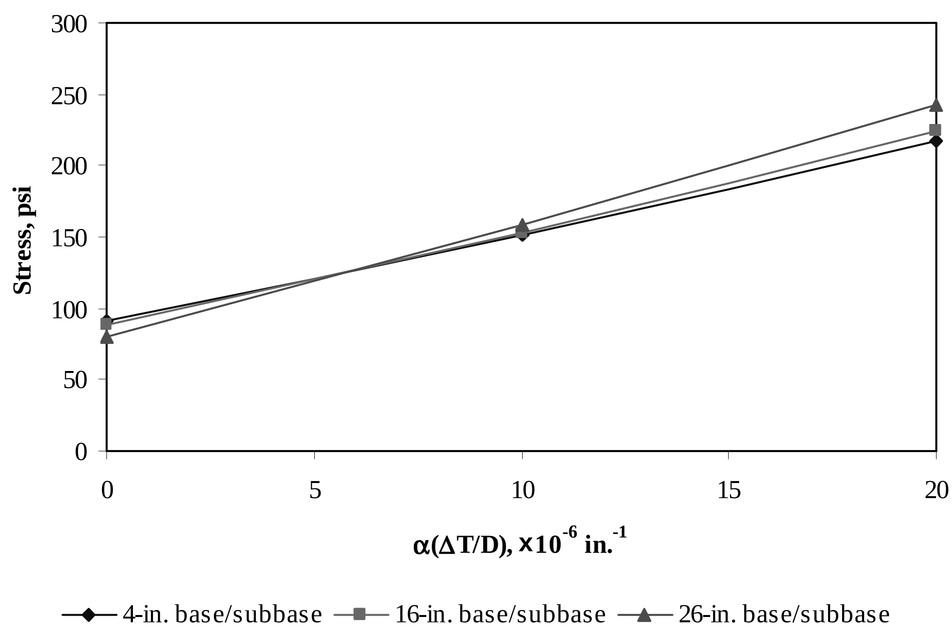


**Figure F-5-42: Impact of base/subbase thickness and product α(ΔT/D) on transverse stress at bottom of the slab (315-in. joint spacing)**

Figures F-5-43 through F-5-48 illustrate the impact of modulus of subgrade reaction and product α(ΔT/D) on stresses (10-in. PCC thickness, 16-in. base/subbase thickness and PCC shoulder)

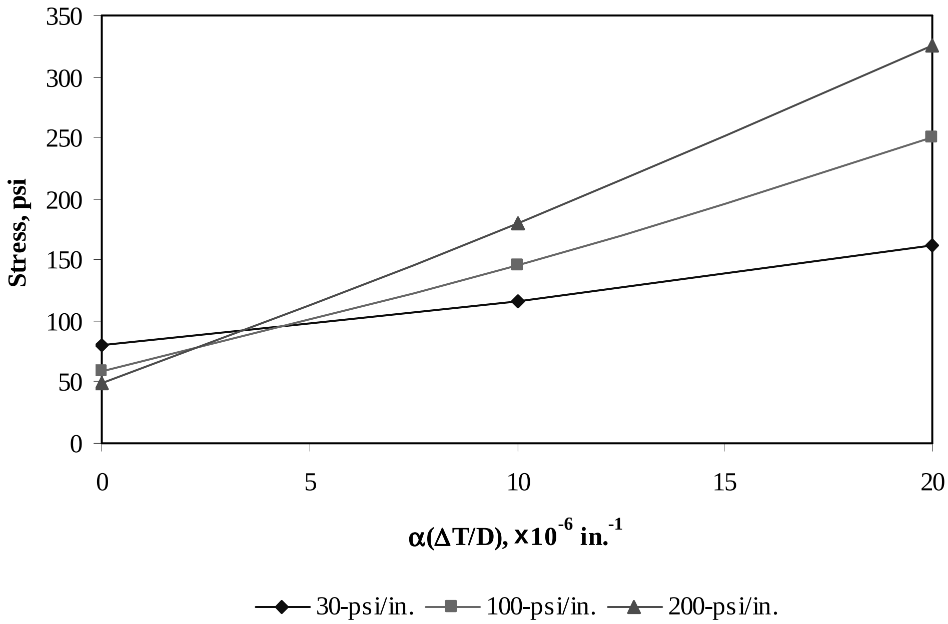


**Figure F-5-43: Impact of modulus of subgrade reaction and product α(ΔT/D) on longitudinal stress at bottom of the slab (177-in. joint spacing)**

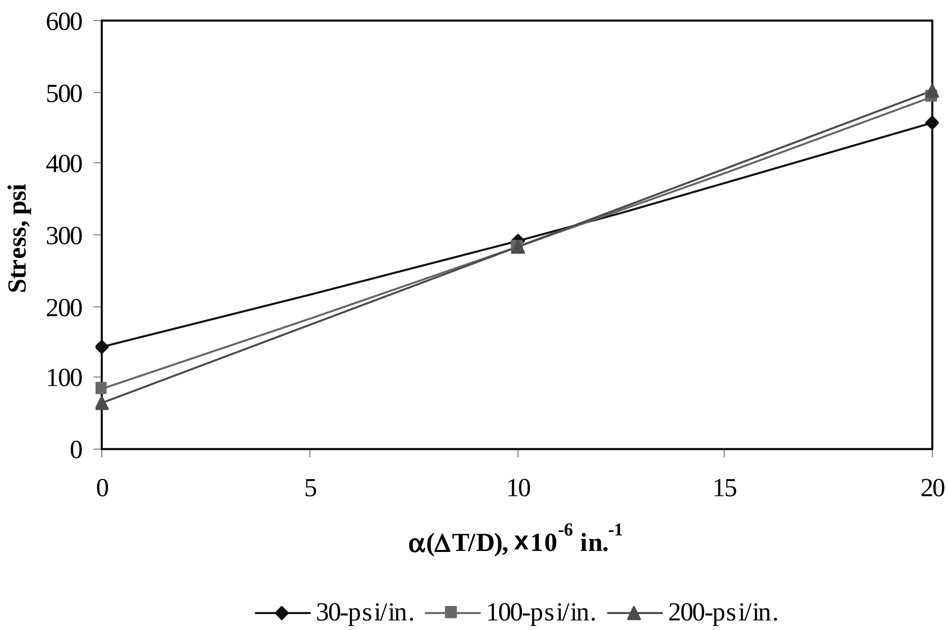


**Figure F-5-44: Impact of modulus of subgrade reaction and product α(ΔT/D) on longitudinal stress at bottom of the slab (315-in. joint spacing)**

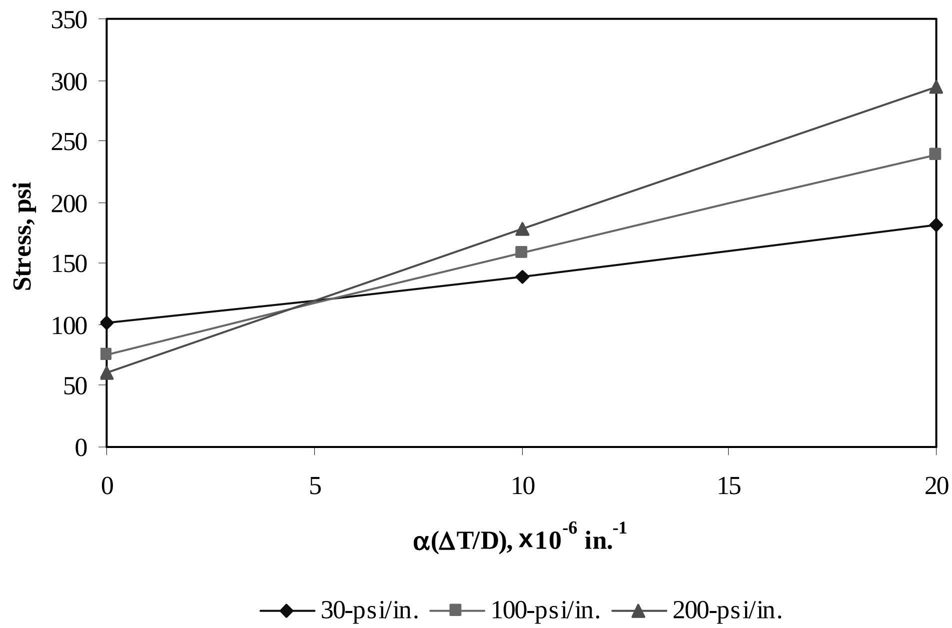


**Figure F-5-45: Impact of modulus of subgrade reaction and product α(ΔT/D) on longitudinal stress at top of the slab (177-in. joint spacing)**

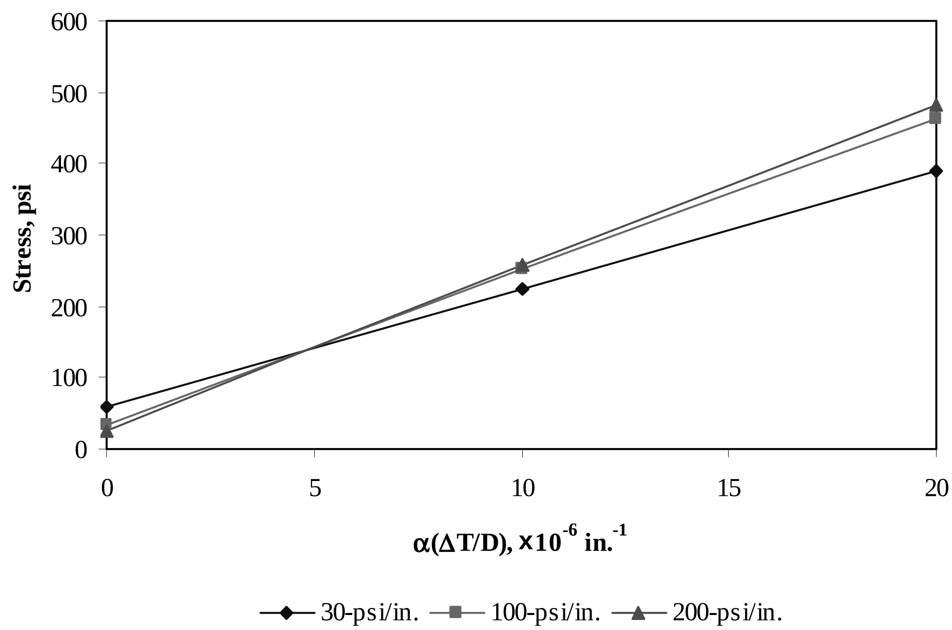


**Figure F-5-46: Impact of modulus of subgrade reaction and product α(ΔT/D) on longitudinal stress at top of the slab (315-in. joint spacing)**

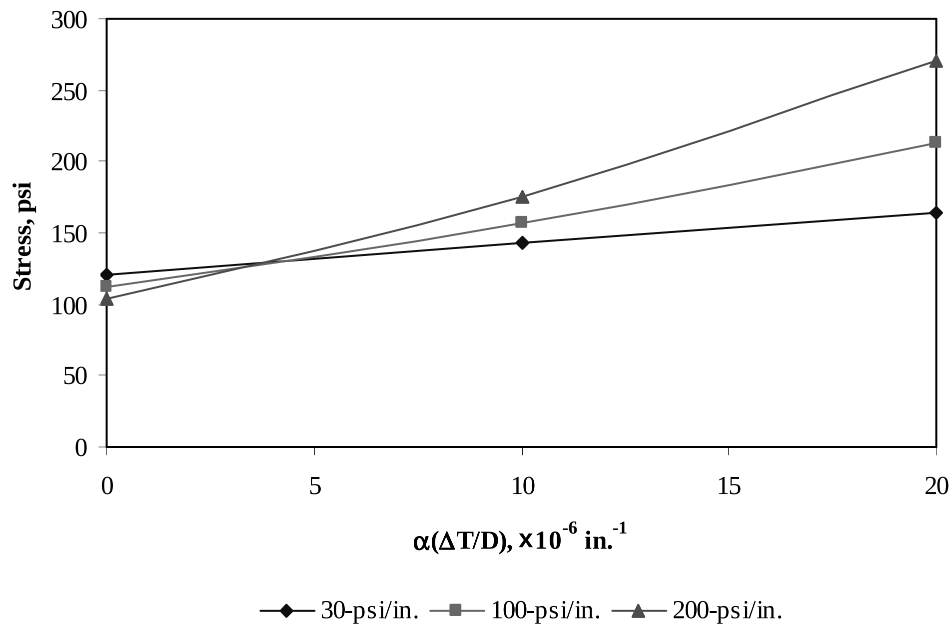


**Figure F-5-47: Impact of modulus of subgrade reaction and product α(ΔT/D) on transverse stress at bottom of the slab (177-in. joint spacing)**

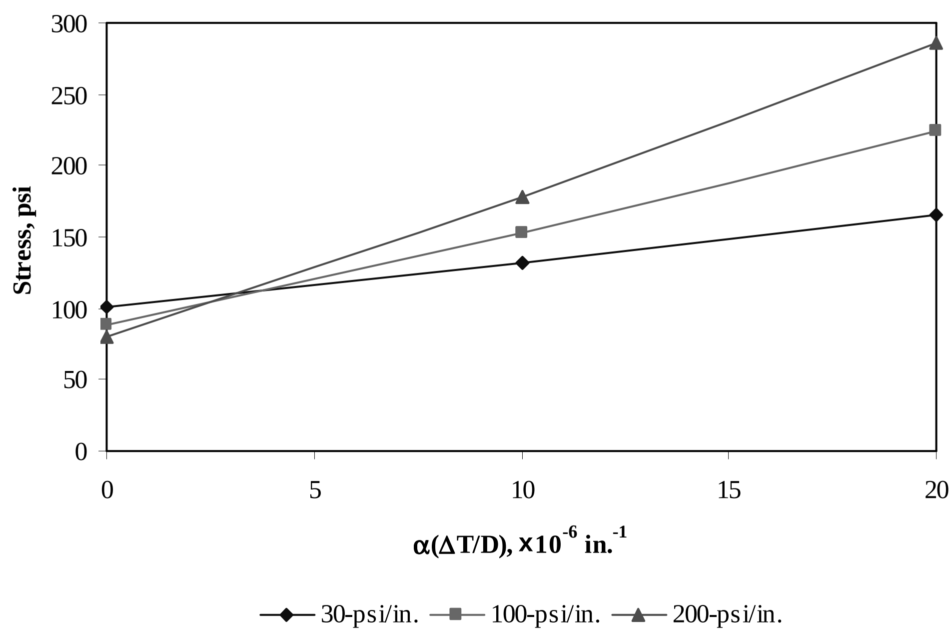


**Figure F-5-48: Impact of modulus of subgrade reaction and product α(ΔT/D) on transverse stress at bottom of the slab (315-in. joint spacing)**

Figures F-5-49 through F-5-51 illustrate the impact of joint spacing and product α(ΔT/D) on stresses (10-in. PCC thickness, 16-in. base/subbase thickness, 100-psi/in. modulus of subgrade reaction and PCC shoulder)

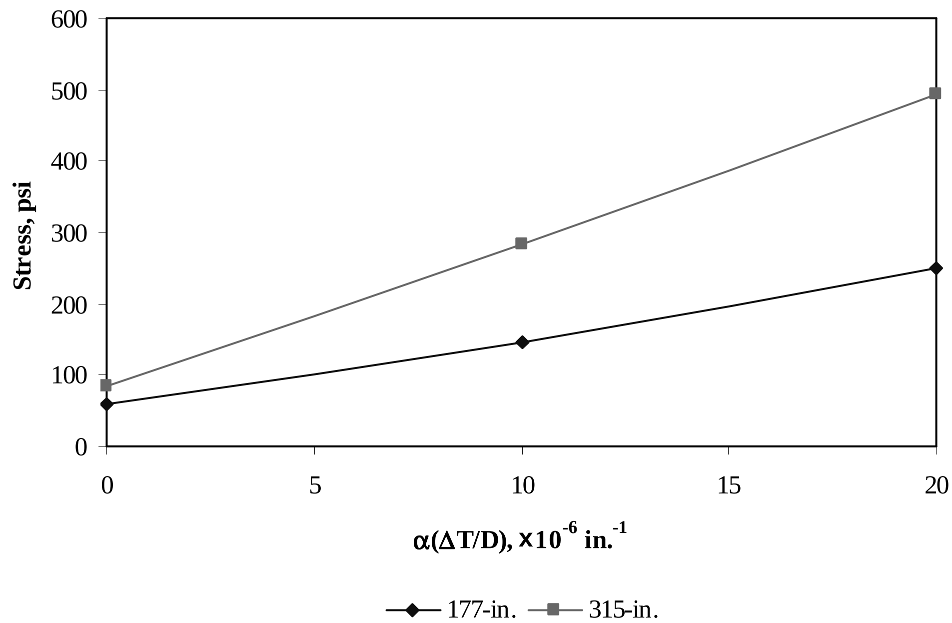


**Figure F-5-49: Impact of joint spacing and product α(ΔT/D) on longitudinal stress at bottom of the slab**

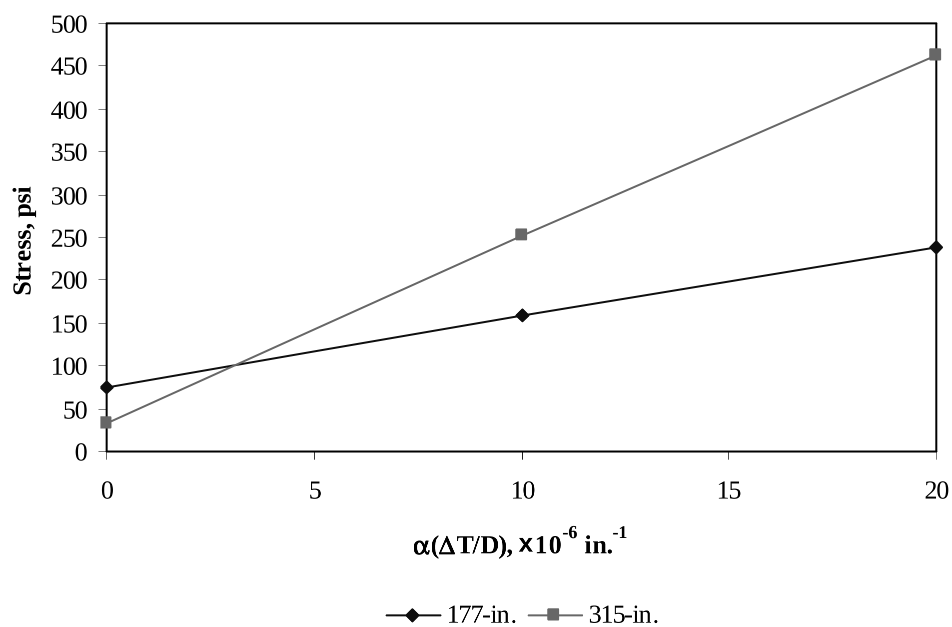


**Figure F-5-50: Impact of joint spacing and product α(ΔT/D) on longitudinal stress at top of the slab**

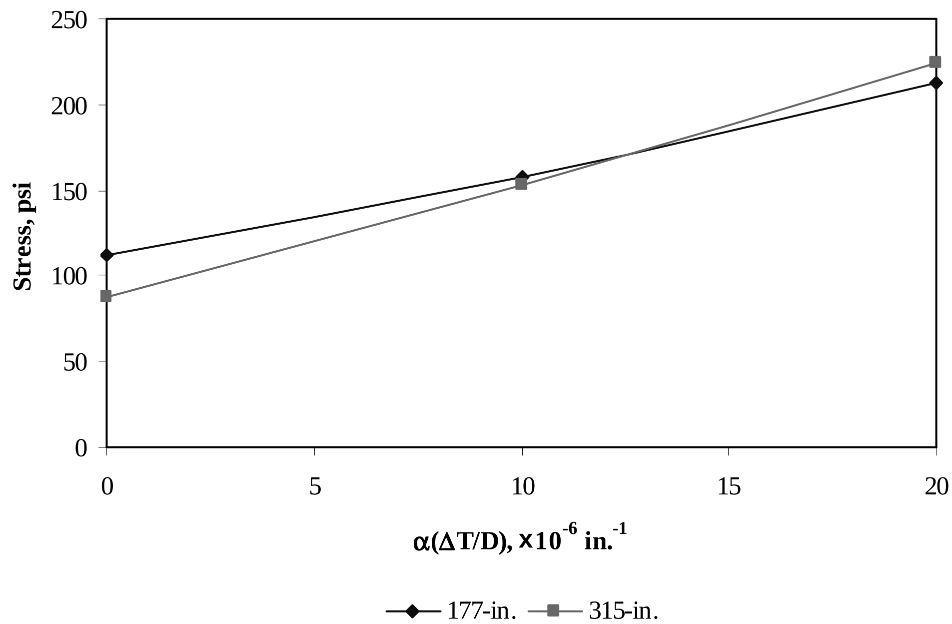


**Figure F-5-51: Impact of joint spacing and product α(ΔT/D) on transverse stress at bottom of the slab**

**Sub Appendix F-6**

**Documentation of Pavement Responses for**

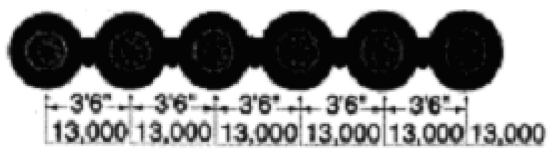


**78-kips Multi-axle (6)**

Figures F-6-1 through F-6-12 illustrate the impact of PCC thickness and base/subbase thickness on stresses (100-psi/in. modulus of subgrade reaction and PCC shoulder)

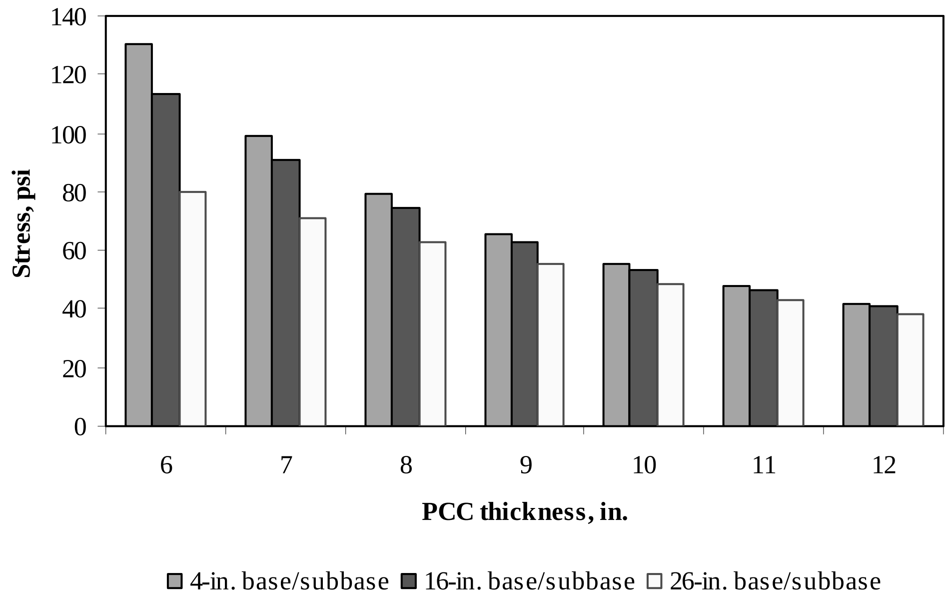


**Figure F-6-1: Impact of PCC thickness and base/subbase thickness on longitudinal stress at bottom of the Slab (177-in. joint spacing and $\alpha(\Delta T/D)$ of 0 in.$^{-1}$)**

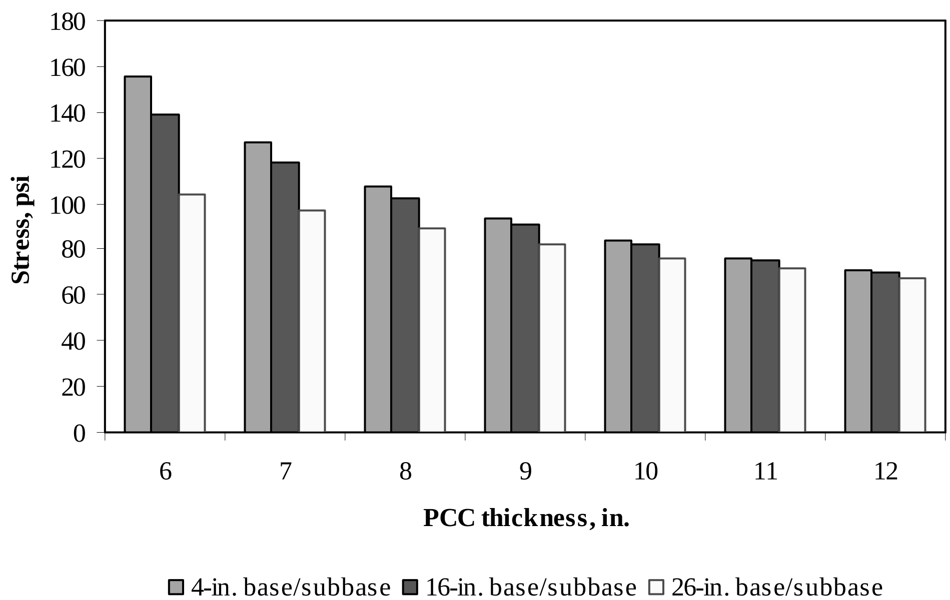


**Figure F-6-2: Impact of PCC thickness and base/subbase thickness on longitudinal stress at bottom of the Slab (315-in. joint spacing and $\alpha(\Delta T/D)$ of 0 in.$^{-1}$)**

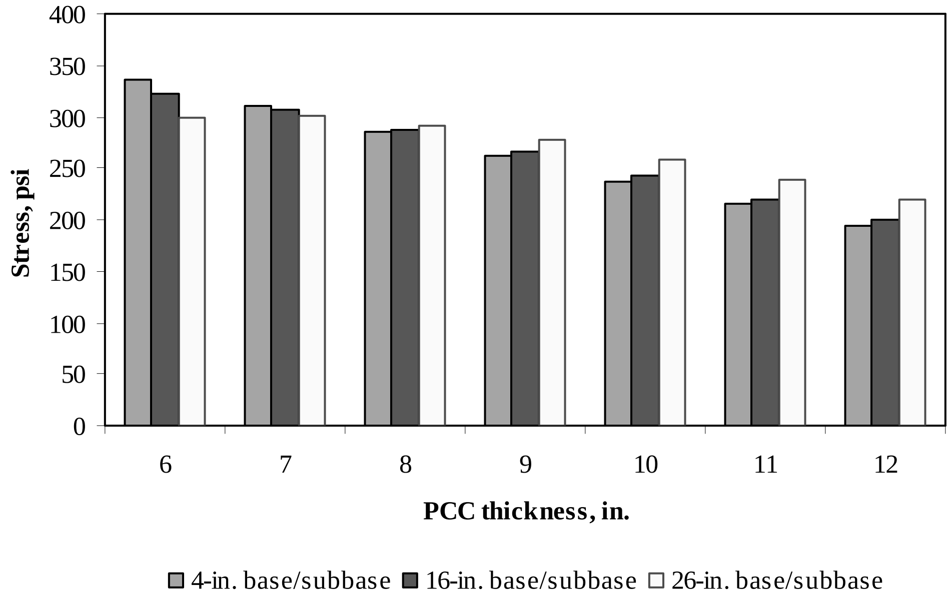


**Figure F-6-3: Impact of PCC thickness and base/subbase thickness on longitudinal stress at bottom of the Slab (177-in. joint spacing and $\alpha(\Delta T/D)$ of $20x10^{-6}$ in.$^{-1}$)**

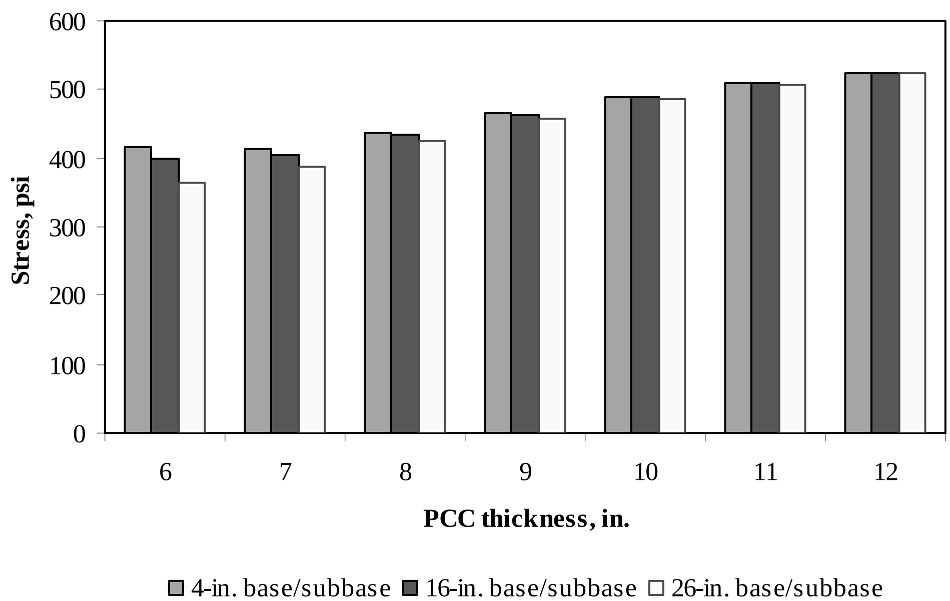


**Figure F-6-4: Impact of PCC thickness and base/subbase thickness on longitudinal stress at bottom of the Slab (315-in. joint spacing and $\alpha(\Delta T/D)$ of $20x10^{-6}$ in.$^{-1}$)**

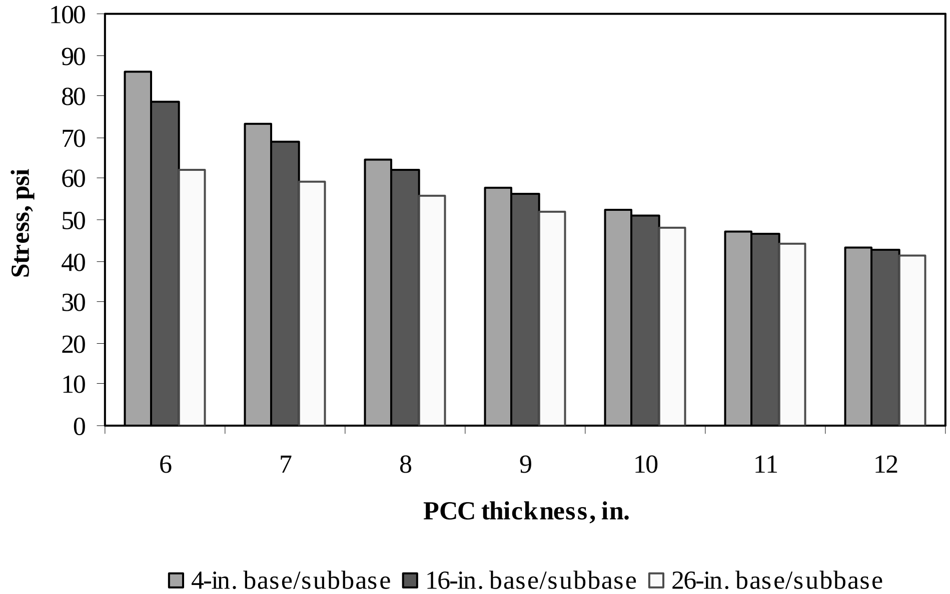


**Figure F-6-5: Impact of PCC thickness and base/subbase thickness on longitudinal stress at top of the Slab (177-in. joint spacing and $\alpha(\Delta T/D)$ of 0 in.$^{-1}$)**

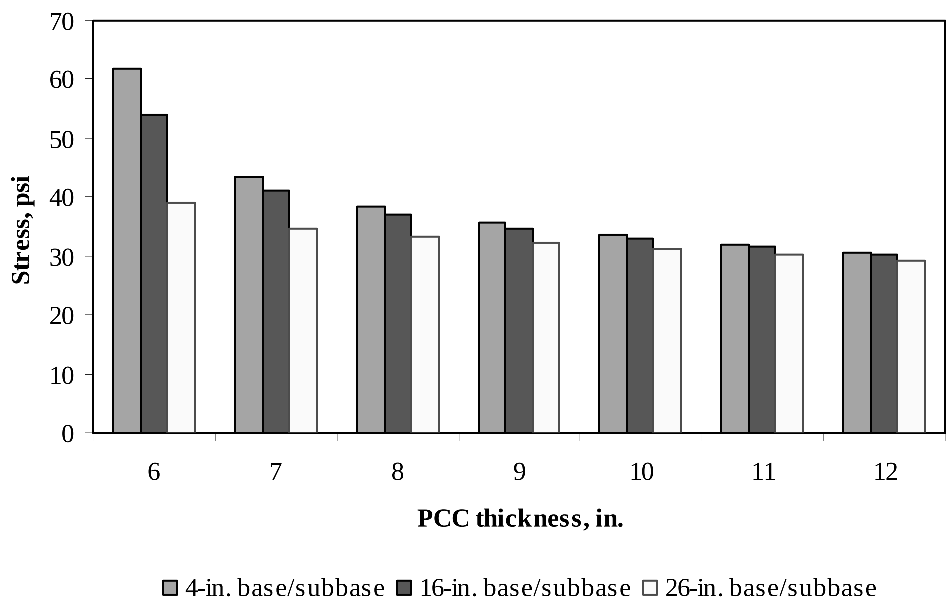


**Figure F-6-6: Impact of PCC thickness and base/subbase thickness on longitudinal stress at top of the Slab (315-in. joint spacing and $\alpha(\Delta T/D)$ of 0 in.$^{-1}$)**

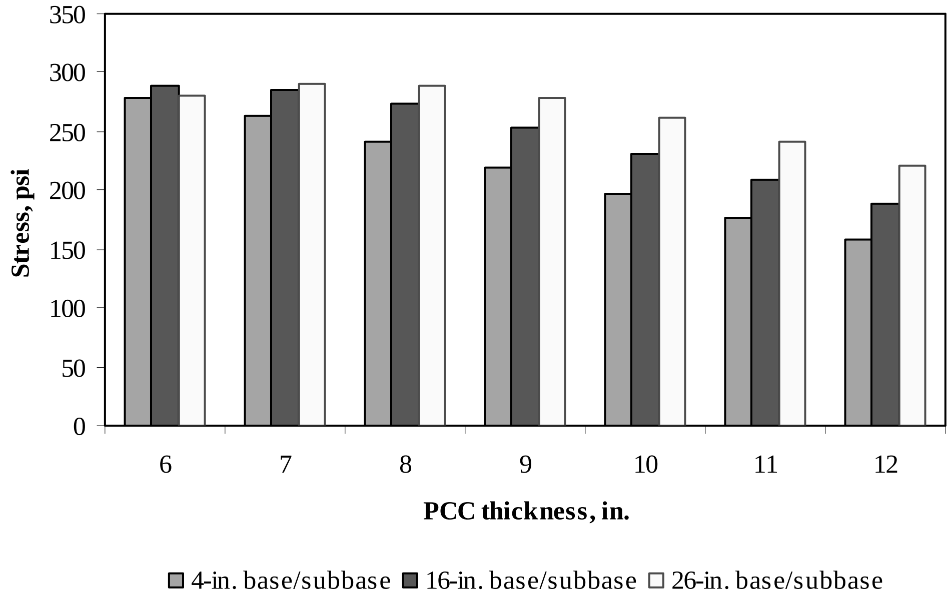


**Figure F-6-7: Impact of PCC thickness and base/subbase thickness on longitudinal stress at top of the Slab (177-in. joint spacing and $\alpha(\Delta T/D)$ of $-20\times10^{-6}$ in.$^{-1}$)**

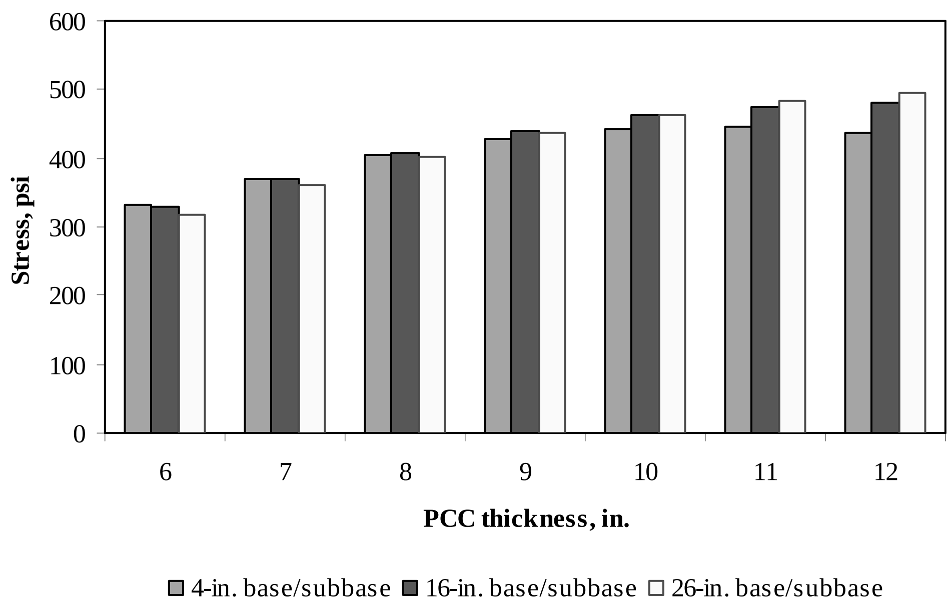


**Figure F-6-8: Impact of PCC thickness and base/subbase thickness on longitudinal stress at top of the Slab (315-in. joint spacing and $\alpha(\Delta T/D)$ of $-20\times10^{-6}$ in.$^{-1}$)**

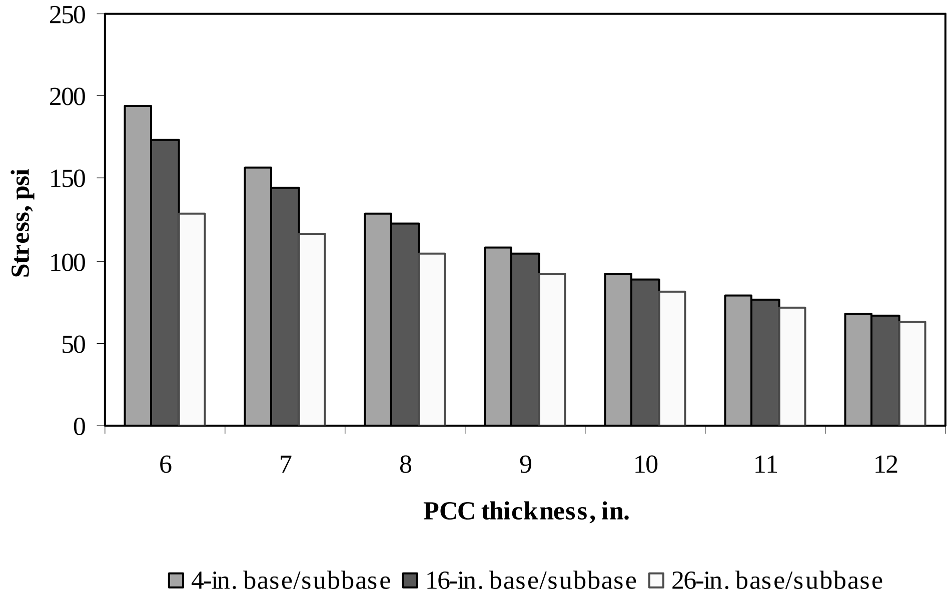


**Figure F-6-9: Impact of PCC thickness and base/subbase thickness on transverse stress at bottom of the Slab (177-in. joint spacing and $\alpha(\Delta T/D)$ of 0 in.$^{-1}$)**

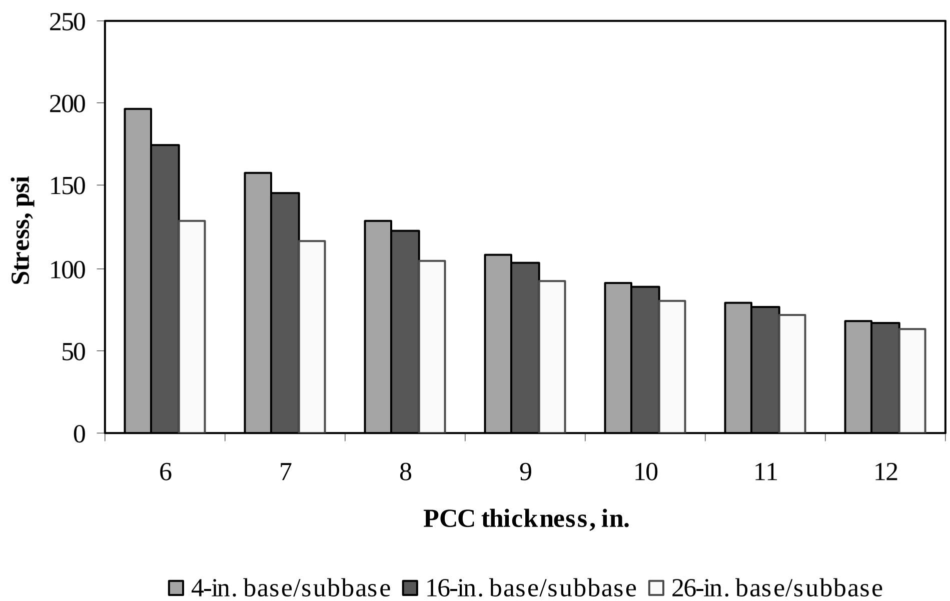


**Figure F-6-10: Impact of PCC thickness and base/subbase thickness on transverse stress at bottom of the Slab (315-in. joint spacing and $\alpha(\Delta T/D)$ of 0 in.$^{-1}$)**

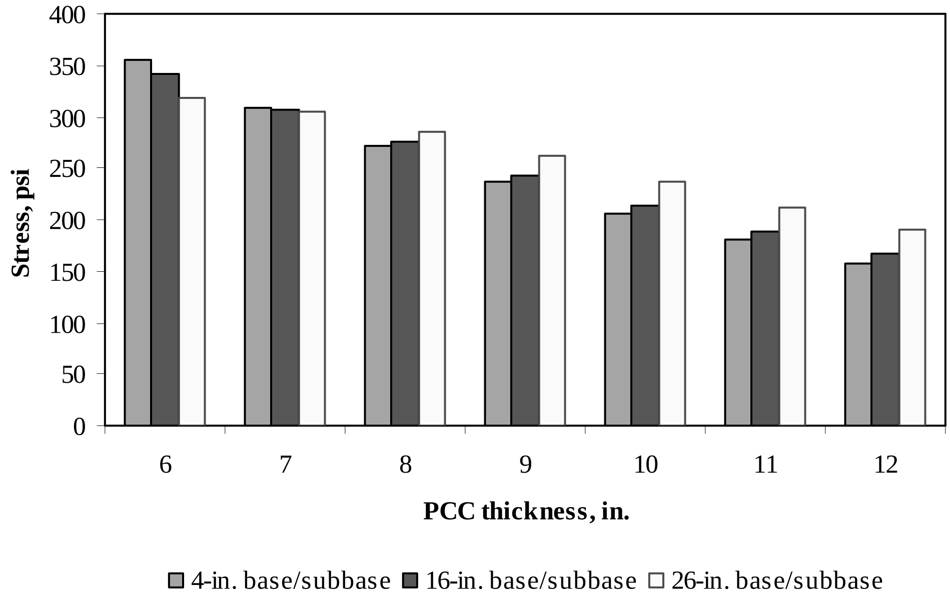


**Figure F-6-11: Impact of PCC thickness and base/subbase thickness on transverse stress at bottom of the Slab (177-in. joint spacing and $\alpha(\Delta T/D)$ of $20 \times 10^{-6}$ in.$^{-1}$)**

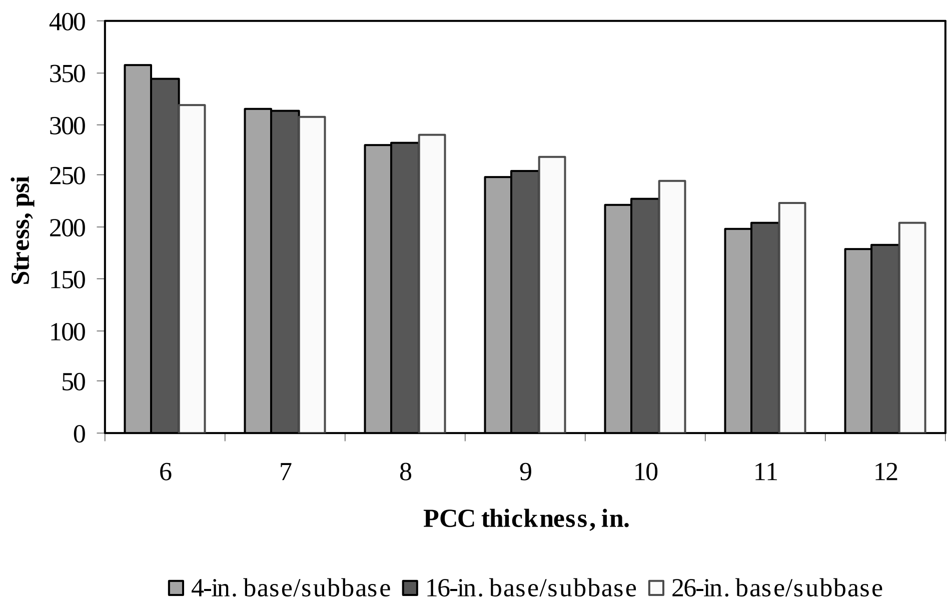


**Figure F-6-12: Impact of PCC thickness and base/subbase thickness on transverse stress at bottom of the Slab (315-in. joint spacing and $\alpha(\Delta T/D)$ of $20 \times 10^{-6}$ in.$^{-1}$)**

Figures F-6-13 through F-6-24 illustrate the impact of PCC thickness and modulus of subgrade reaction on stresses (16-in. base/subbase thickness and PCC shoulder)

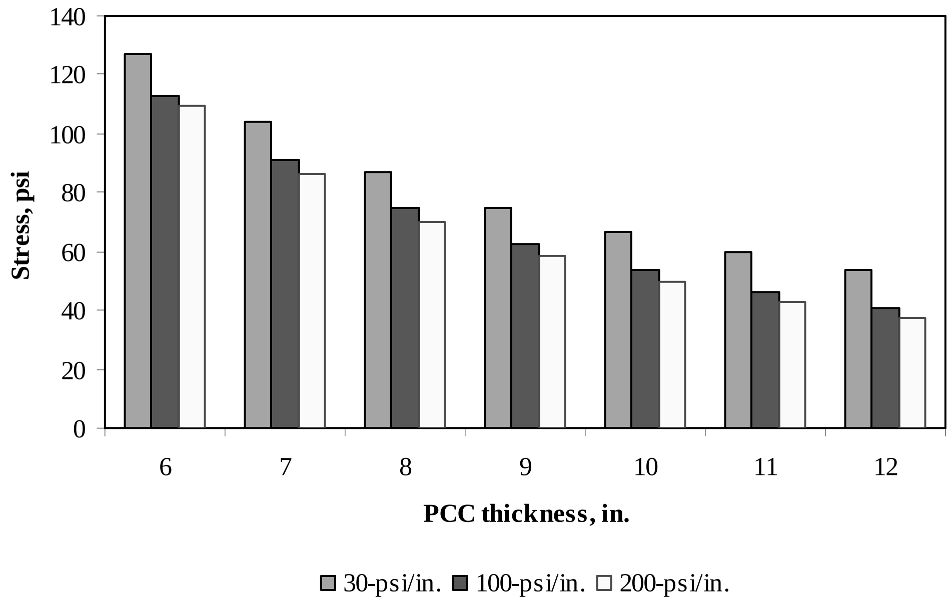


**Figure F-6-13: Impact of PCC thickness and modulus of subgrade reaction on longitudinal stress at bottom of the slab (177-in. joint spacing and $\alpha(\Delta T/D)$ of 0 in.$^{-1}$)**

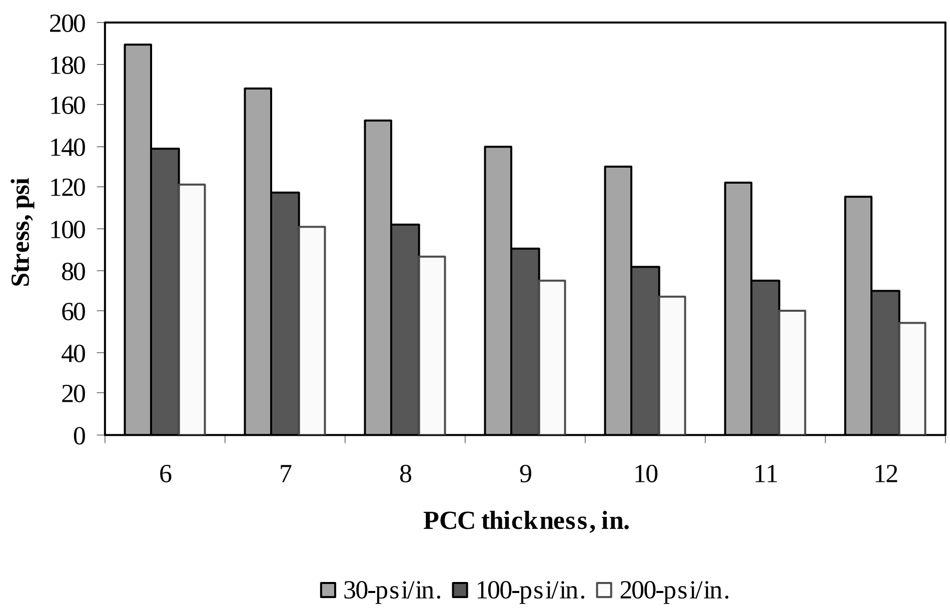


**Figure F-6-14: Impact of PCC thickness and modulus of subgrade reaction on longitudinal stress at bottom of the slab (315-in. joint spacing and $\alpha(\Delta T/D)$ of 0 in.$^{-1}$)**

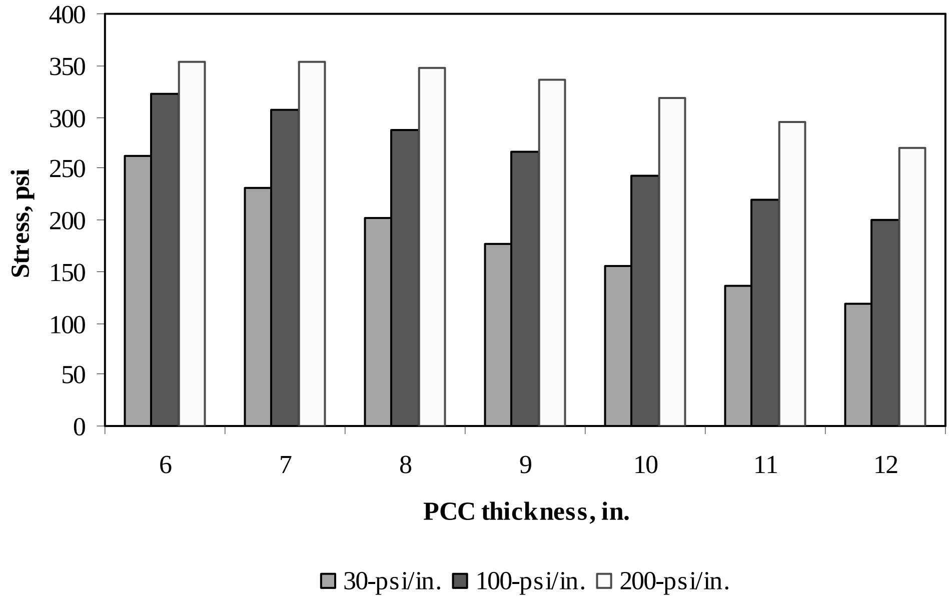


**Figure F-6-15: Impact of PCC thickness and modulus of subgrade reaction on longitudinal stress at bottom of the slab (177-in. joint spacing and $\alpha(\Delta T/D)$ of 20x10$^{-6}$ in.$^{-1}$)**

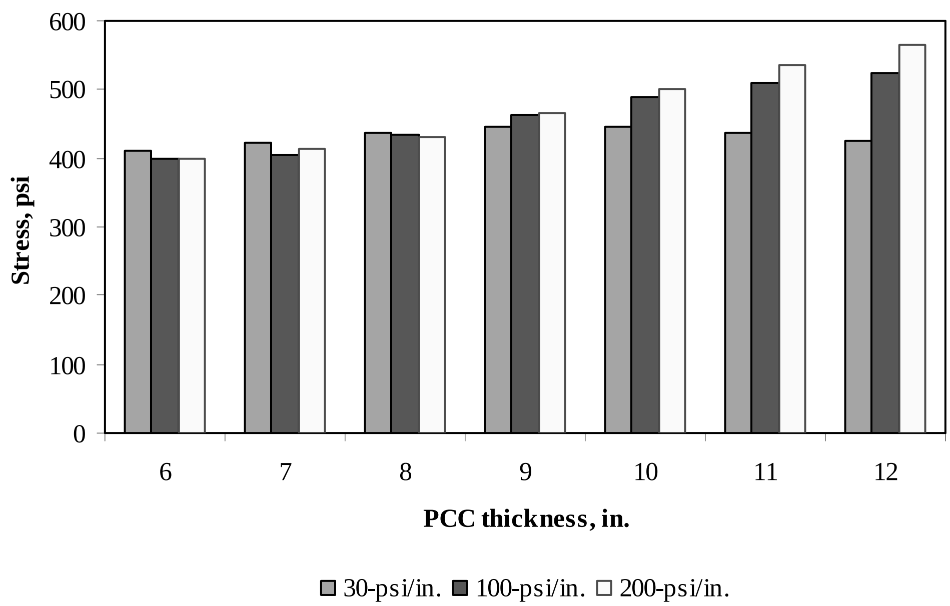


**Figure F-6-16: Impact of PCC thickness and modulus of subgrade reaction on longitudinal stress at bottom of the slab (315-in. joint spacing and $\alpha(\Delta T/D)$ of 20x10$^{-6}$ in.$^{-1}$)**

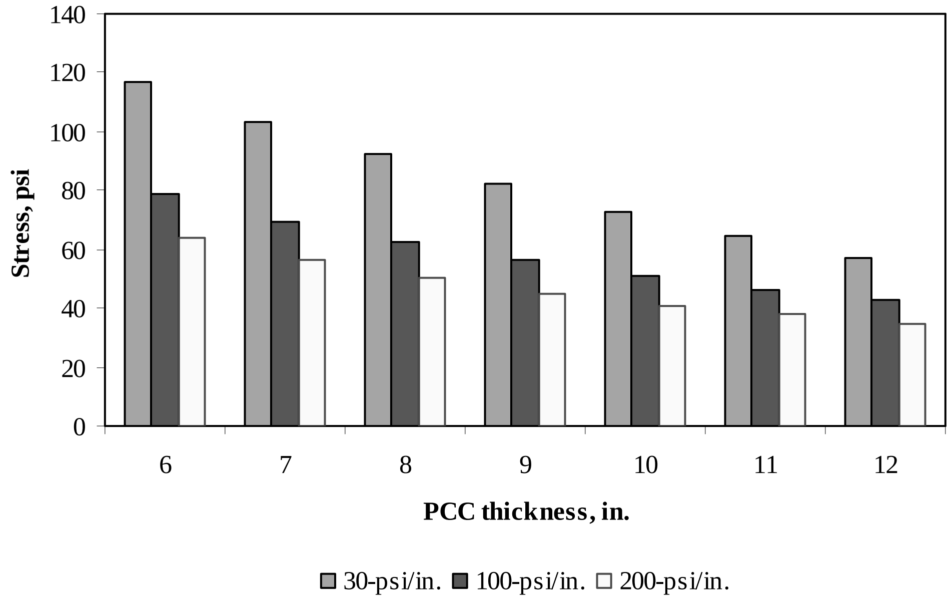


**Figure F-6-17: Impact of PCC thickness and modulus of subgrade reaction on longitudinal stress at top of the Slab (177-in. joint spacing and $\alpha(\Delta T/D)$ of 0 in.$^{-1}$)**

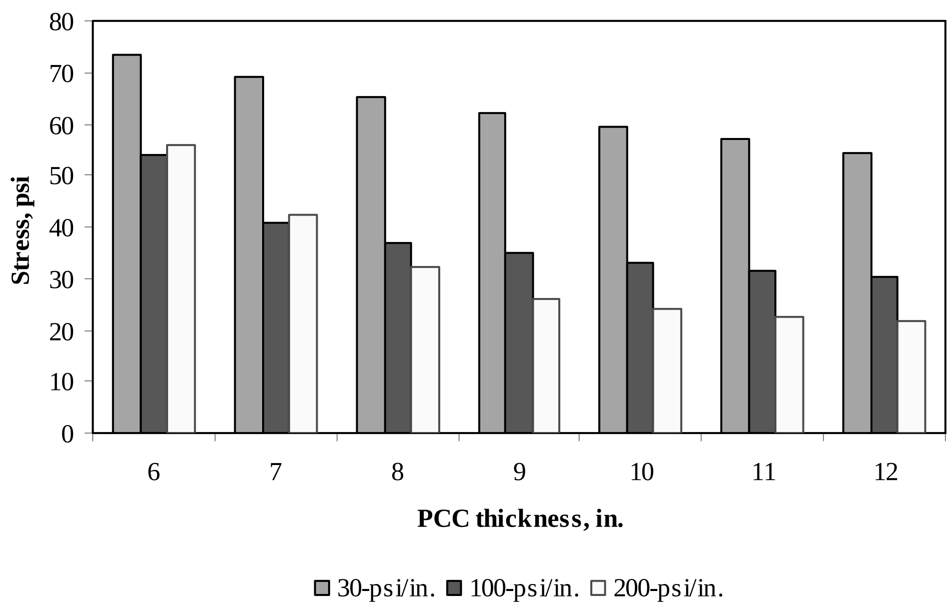


**Figure F-6-18: Impact of PCC thickness and modulus of subgrade reaction on longitudinal stress at top of the Slab (315-in. joint spacing and $\alpha(\Delta T/D)$ of 0 in.$^{-1}$)**

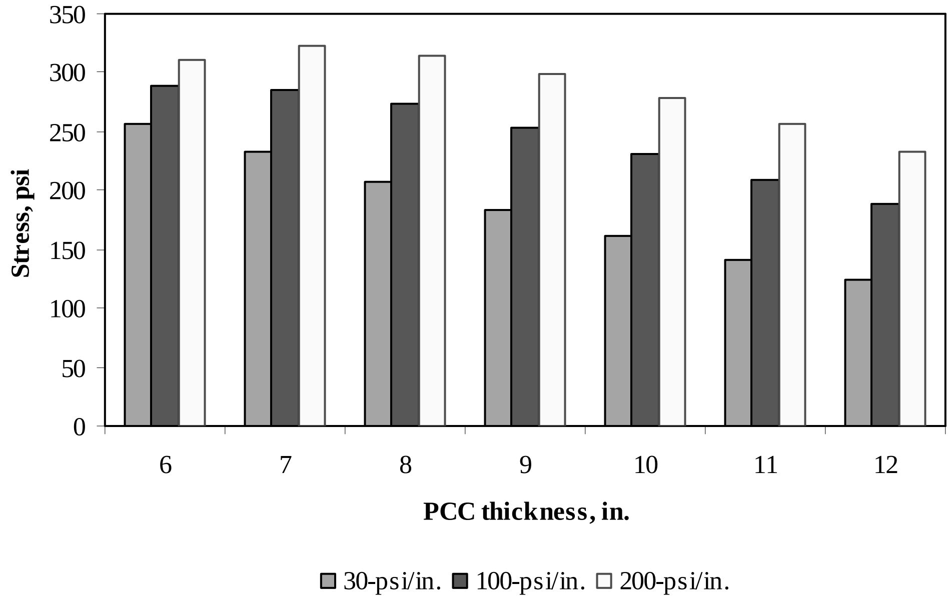


**Figure F-6-19: Impact of PCC thickness and modulus of subgrade reaction on longitudinal stress at top of the Slab (177-in. joint spacing and $\alpha(\Delta T/D)$ of $-20x10^{-6}$ in.$^{-1}$)**

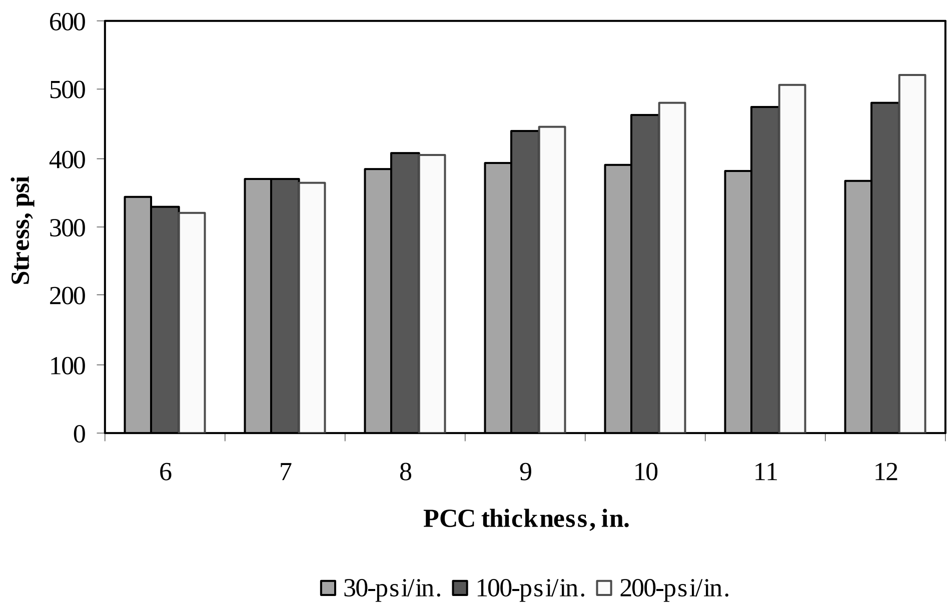


**Figure F-6-20: Impact of PCC thickness and modulus of subgrade reaction on longitudinal stress at top of the Slab (315-in. joint spacing and $\alpha(\Delta T/D)$ of $-20x10^{-6}$ in.$^{-1}$)**

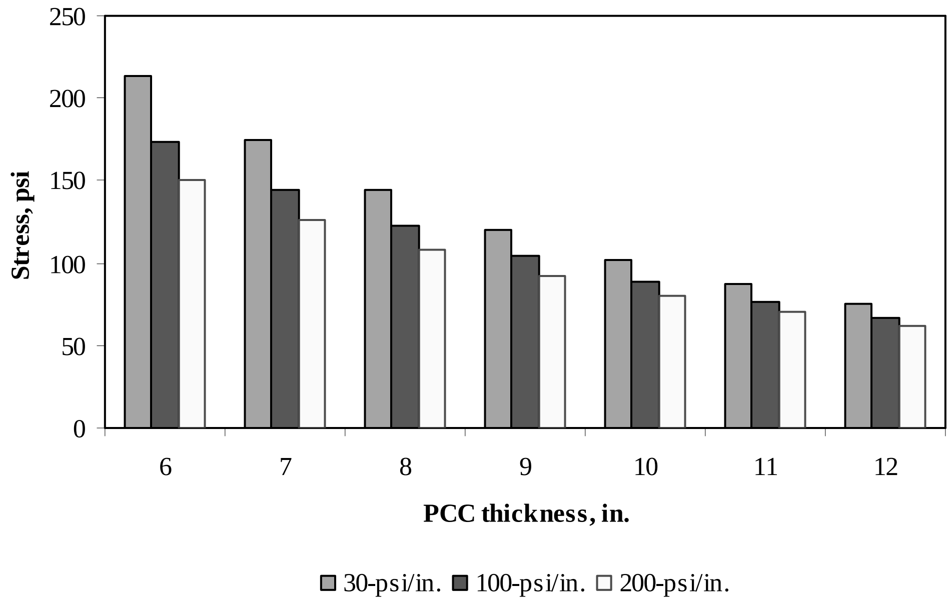


**Figure F-6-21: Impact of PCC thickness and modulus of subgrade reaction on transverse stress at bottom of the Slab (177-in. joint spacing and $\alpha(\Delta T/D)$ of 0 in.$^{-1}$)**

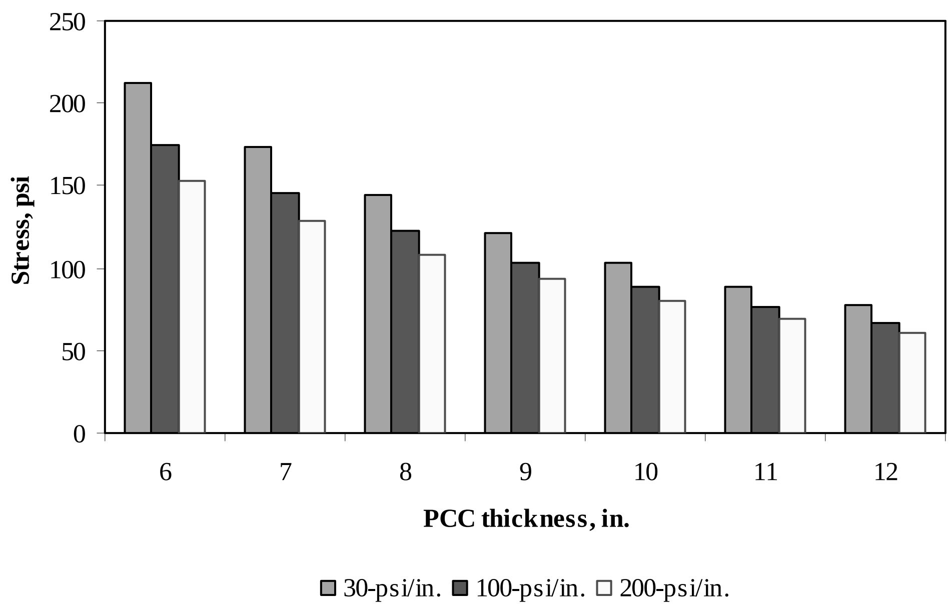


**Figure F-6-22: Impact of PCC thickness and modulus of subgrade reaction on transverse stress at bottom of the Slab (315-in. joint spacing and $\alpha(\Delta T/D)$ of 0 in.$^{-1}$)**

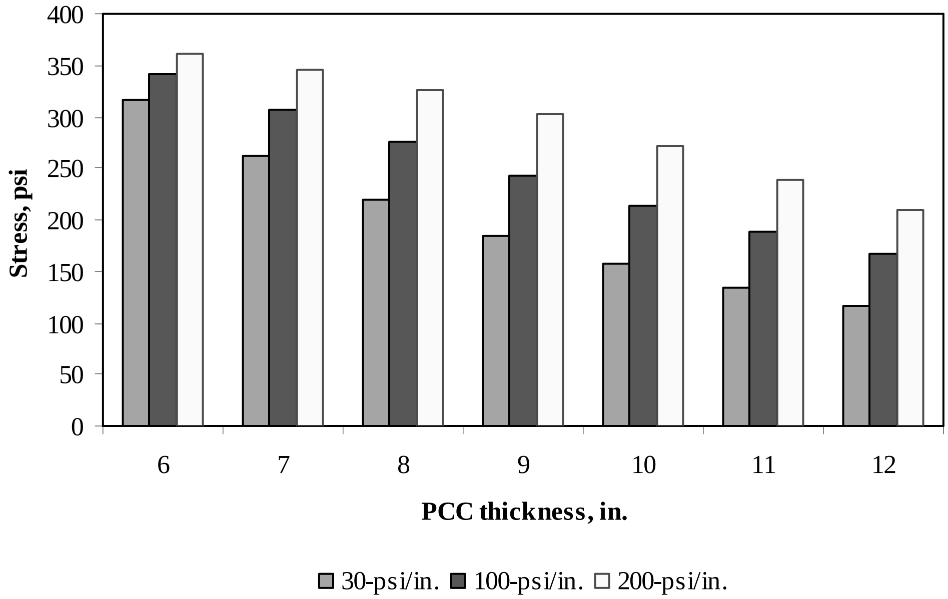


**Figure F-6-23: Impact of PCC thickness and modulus of subgrade reaction on transverse stress at bottom of the Slab (177-in. joint spacing and $\alpha(\Delta T/D)$ of $20x10^{-6}$ in.$^{-1}$)**

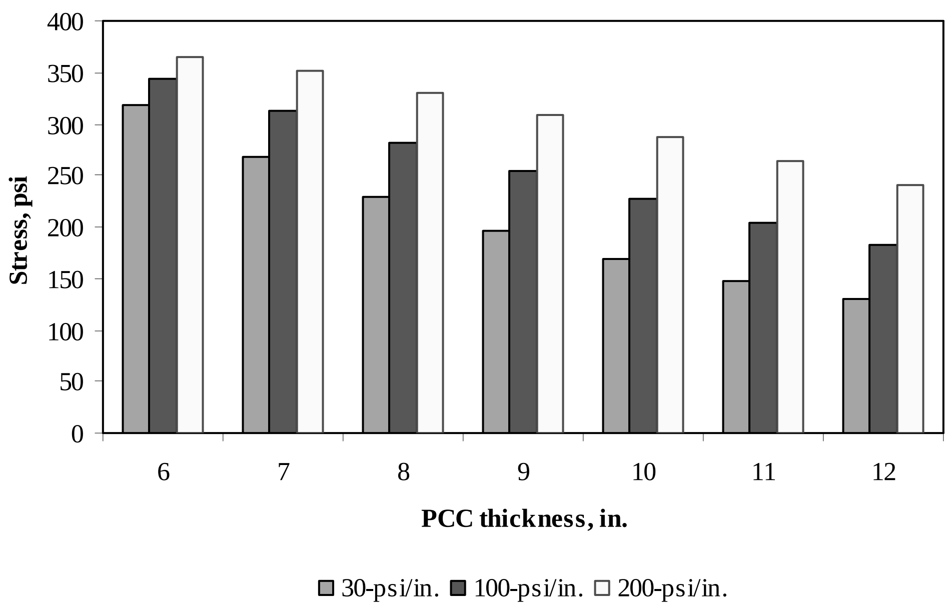


**Figure F-6-24: Impact of PCC thickness and modulus of subgrade reaction on transverse stress at bottom of the Slab (315-in. joint spacing and $\alpha(\Delta T/D)$ of $20x10^{-6}$ in.$^{-1}$)**

Figures F-6-25 through F-6-36 illustrate the impact of PCC thickness and lateral support condition on stresses (16-in. base/subbase and 100-psi/in. modulus of subgrade reaction)

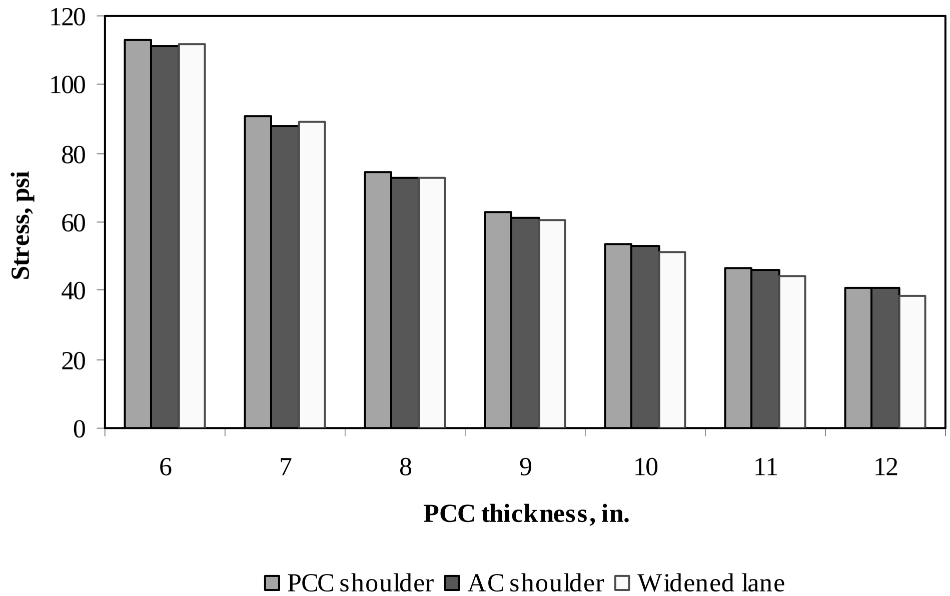


**Figure F-6-25: Impact of PCC thickness and lateral support condition on longitudinal stress at bottom of the Slab (177-in. joint spacing and $\alpha(\Delta T/D)$ of 0 in.$^{-1}$)**

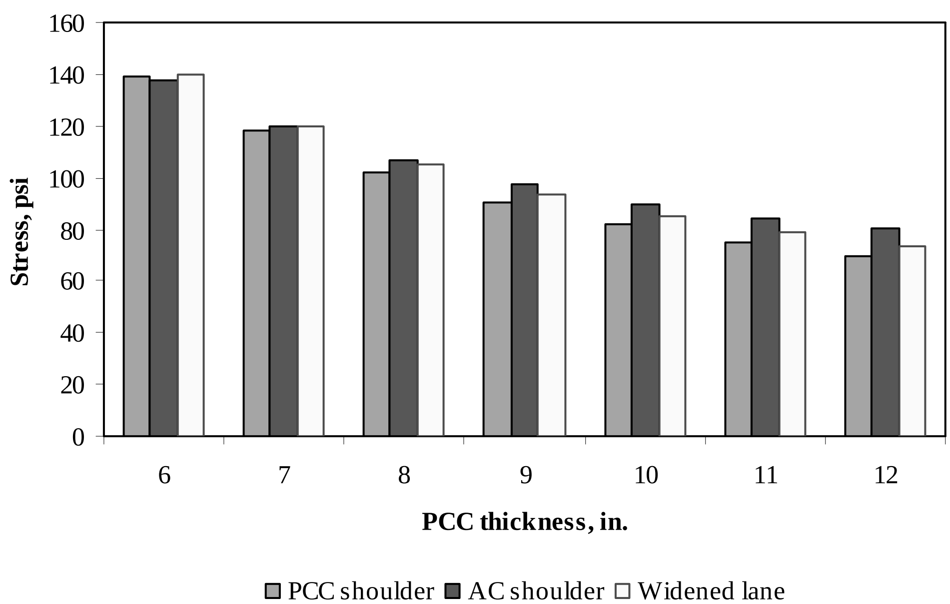


**Figure F-6-26: Impact of PCC thickness and lateral support condition on longitudinal stress at bottom of the Slab (315-in. joint spacing and $\alpha(\Delta T/D)$ of 0 in.$^{-1}$)**

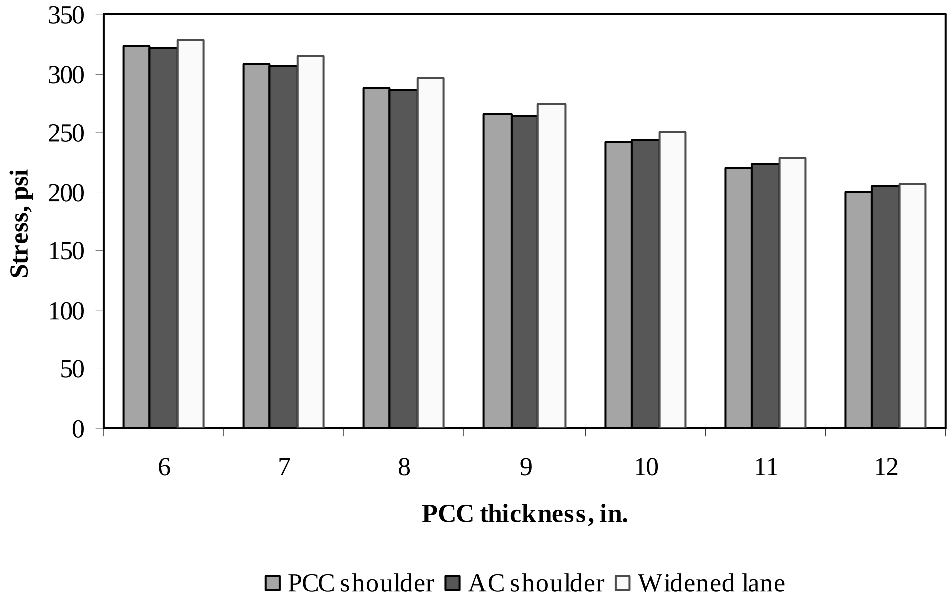


**Figure F-6-27: Impact of PCC thickness and lateral support condition on longitudinal stress at bottom of the Slab (177-in. joint spacing and $\alpha(\Delta T/D)$ of $20x10^{-6}$ in.$^{-1}$)**

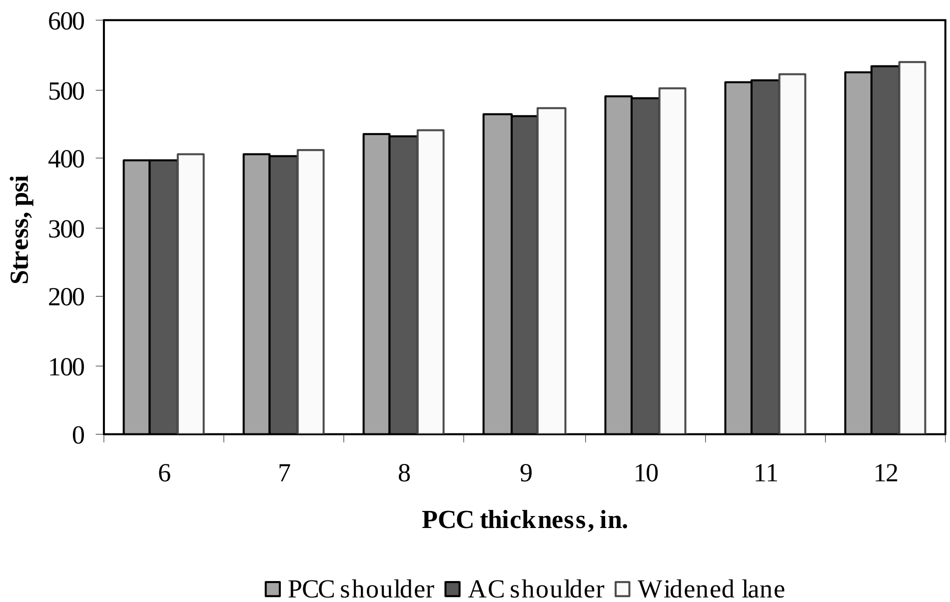


**Figure F-6-28: Impact of PCC thickness and lateral support condition on longitudinal stress at bottom of the Slab (315-in. joint spacing and $\alpha(\Delta T/D)$ of $20x10^{-6}$ in.$^{-1}$)**

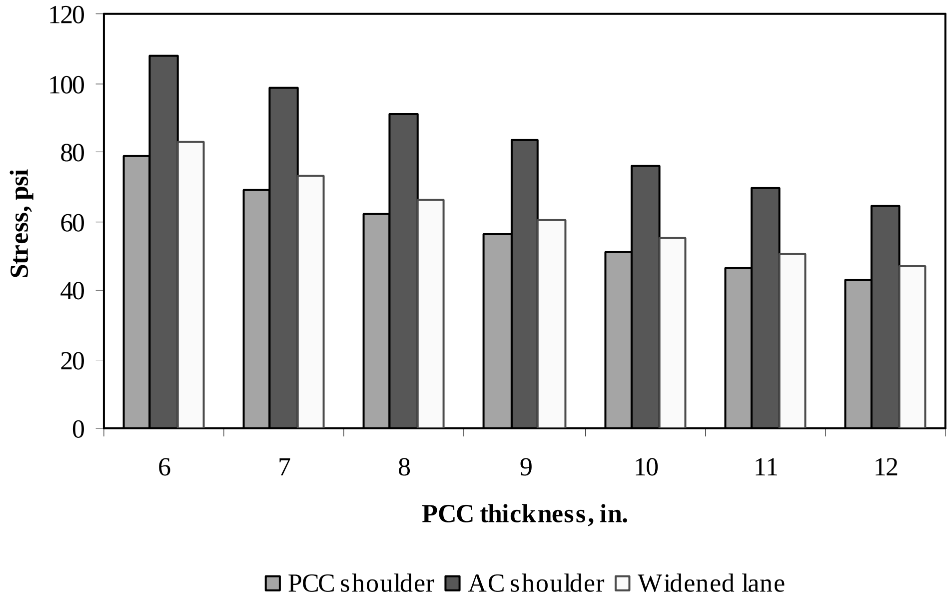


**Figure F-6-29: Impact of PCC thickness and lateral support condition on longitudinal stress at top of the Slab (177-in. joint spacing and $\alpha(\Delta T/D)$ of 0 in.$^{-1}$)**

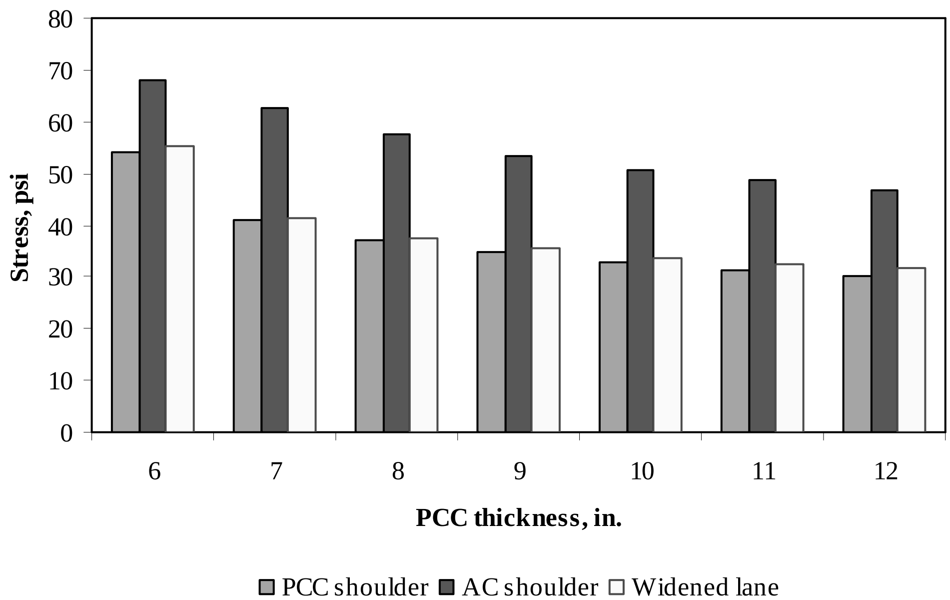


**Figure F-6-30: Impact of PCC thickness and lateral support condition on longitudinal stress at top of the Slab (315-in. joint spacing and $\alpha(\Delta T/D)$ of 0 in.$^{-1}$)**

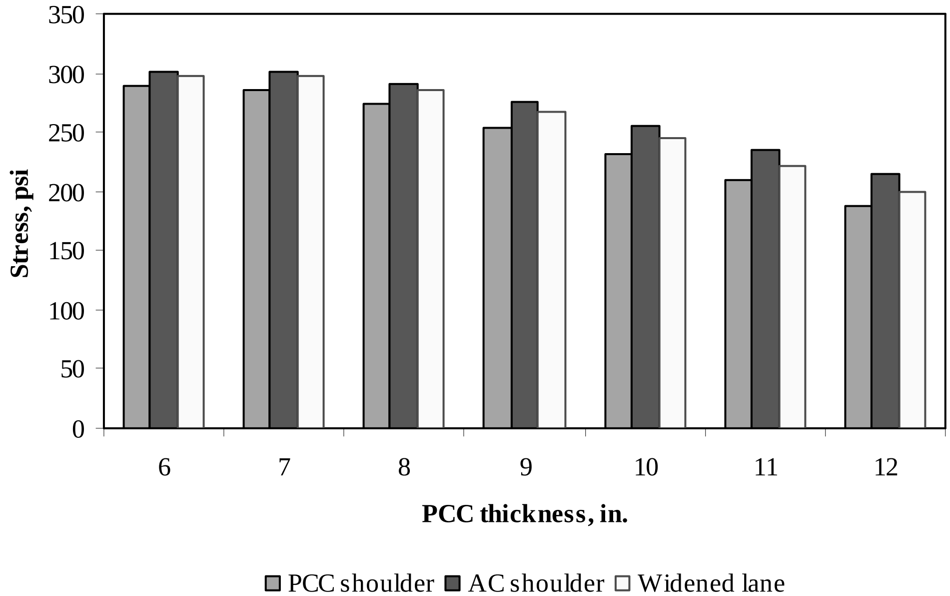


**Figure F-6-31: Impact of PCC thickness and lateral support condition on longitudinal stress at top of the Slab (177-in. joint spacing and $\alpha(\Delta T/D)$ of -20x10$^{-6}$ in.$^{-1}$)**

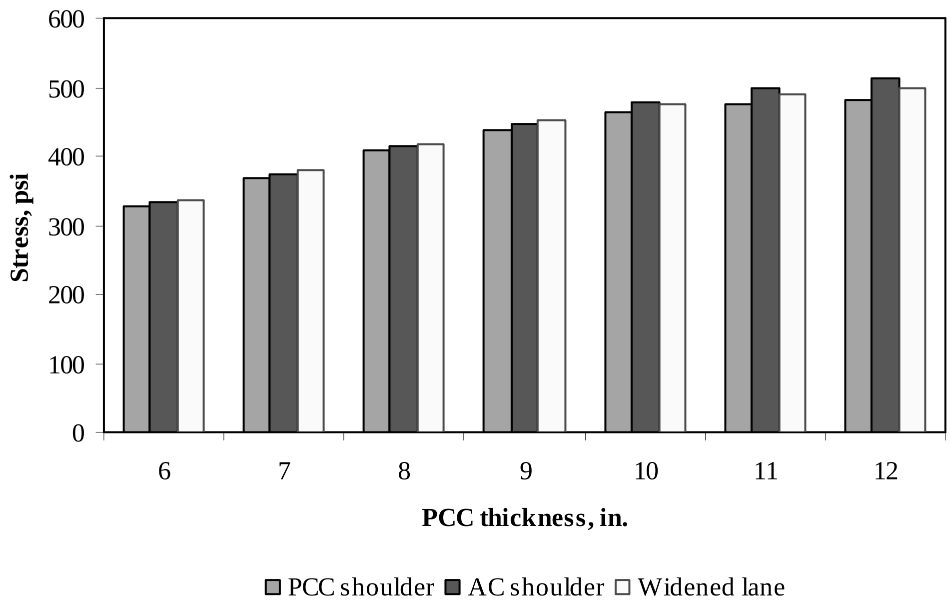


**Figure F-6-32: Impact of PCC thickness and lateral support condition on longitudinal stress at top of the Slab (315-in. joint spacing and $\alpha(\Delta T/D)$ of -20x10$^{-6}$ in.$^{-1}$)**

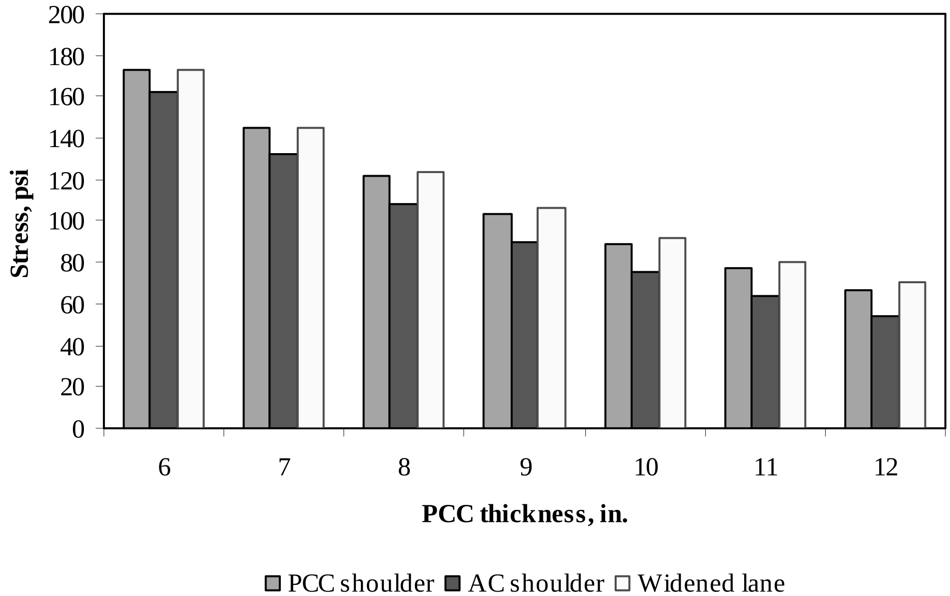


**Figure F-6-33: Impact of PCC thickness and lateral support condition on transverse stress at bottom of the Slab (177-in. joint spacing and α(ΔT/D) of 0 in.$^{-1}$)**

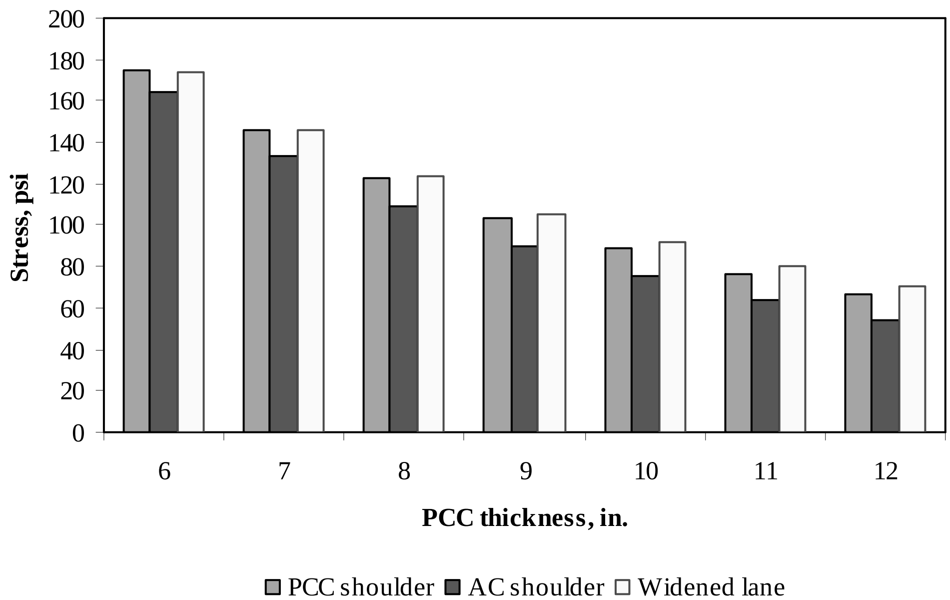


**Figure F-6-34: Impact of PCC thickness and lateral support condition on transverse stress at bottom of the Slab (315-in. joint spacing and α(ΔT/D) of 0 in.$^{-1}$)**

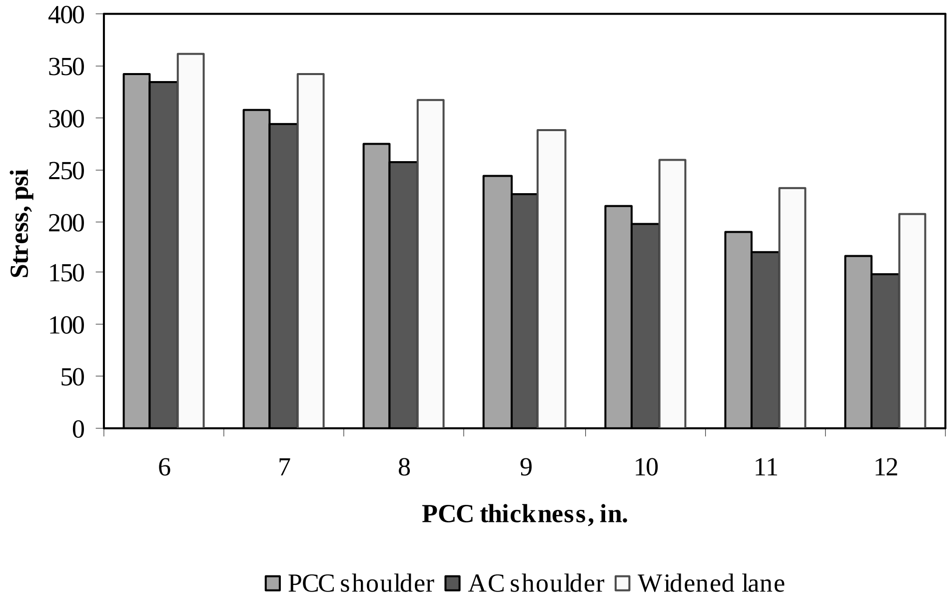


**Figure F-6-35: Impact of PCC thickness and lateral support condition on transverse stress at bottom of the Slab (177-in. joint spacing and $\alpha(\Delta T/D)$ of $20x10^{-6}$ in.$^{-1}$)**

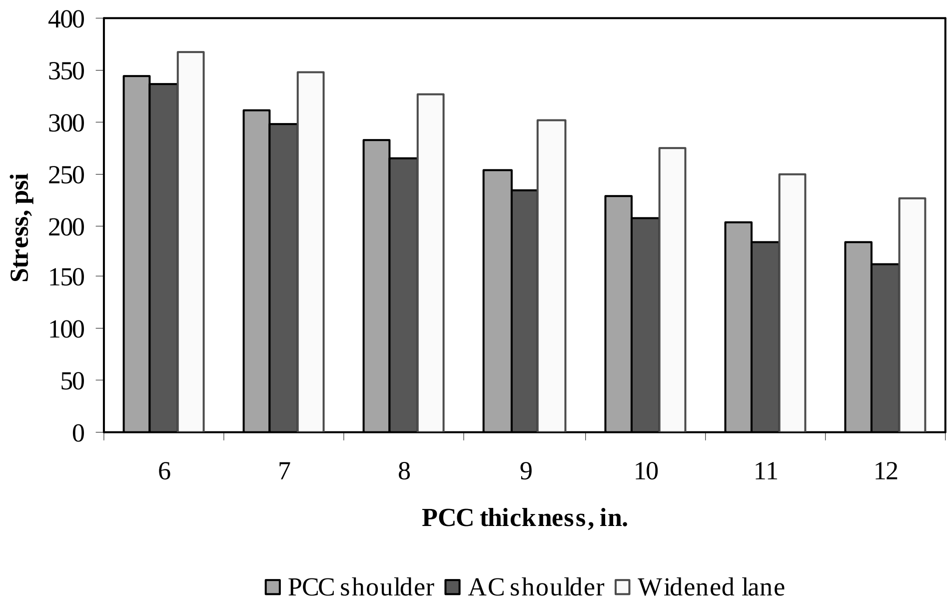


**Figure F-6-36: Impact of PCC thickness and lateral support condition on transverse stress at bottom of the Slab (315-in. joint spacing and $\alpha(\Delta T/D)$ of $20x10^{-6}$ in.$^{-1}$)**

Figures F-6-37 through F-6-42 illustrate the impact of base/subbase thickness and product $\alpha(\Delta T/D)$ on stresses (10-in. PCC thickness, 100-psi/in. modulus of subgrade reaction and PCC shoulder)

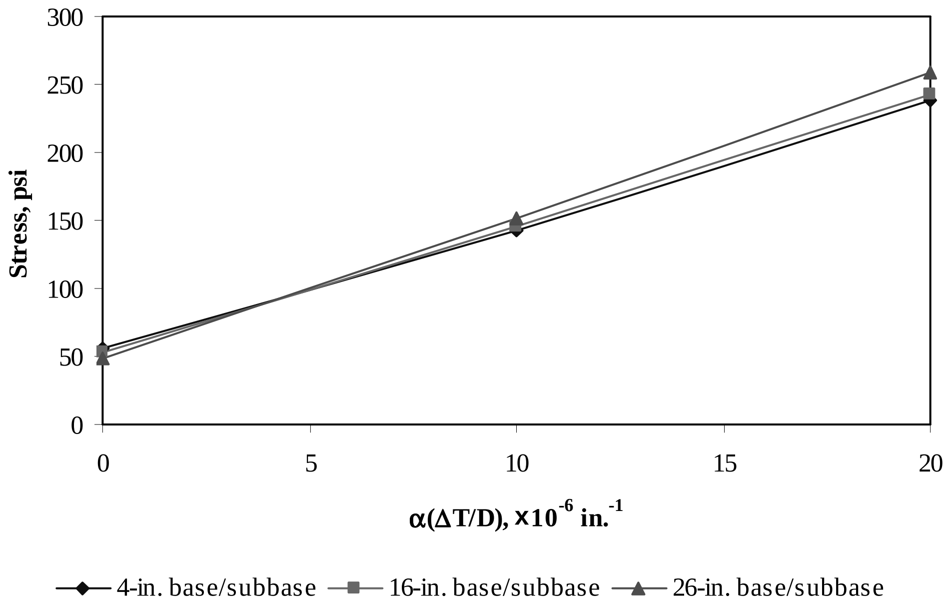


**Figure F-6-37: Impact of base/subbase thickness and product $\alpha(\Delta T/D)$ on longitudinal stress at bottom of the slab (177-in. joint spacing)**

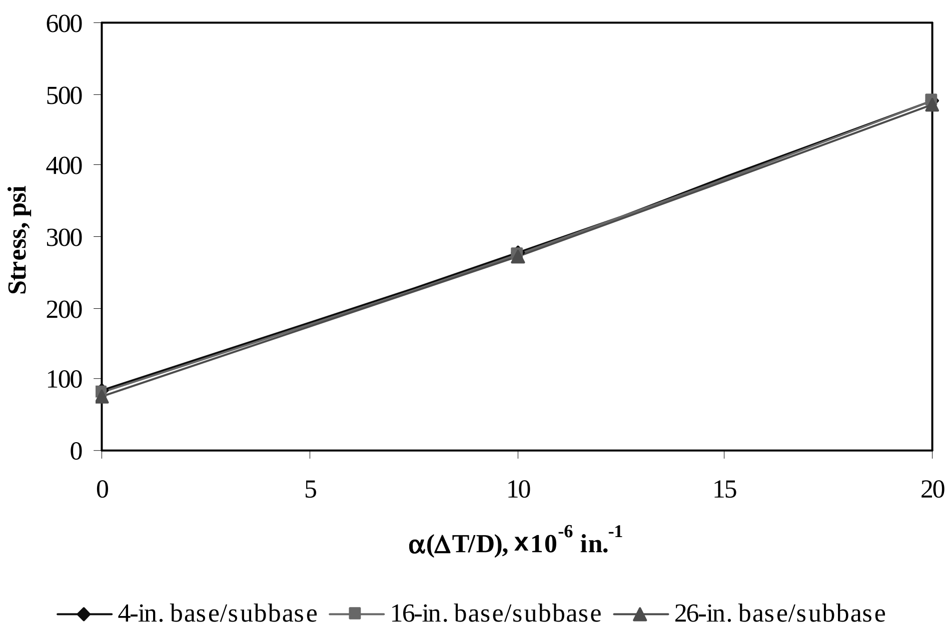


**Figure F-6-38: Impact of base/subbase thickness and product $\alpha(\Delta T/D)$ on longitudinal stress at bottom of the slab (315-in. joint spacing)**

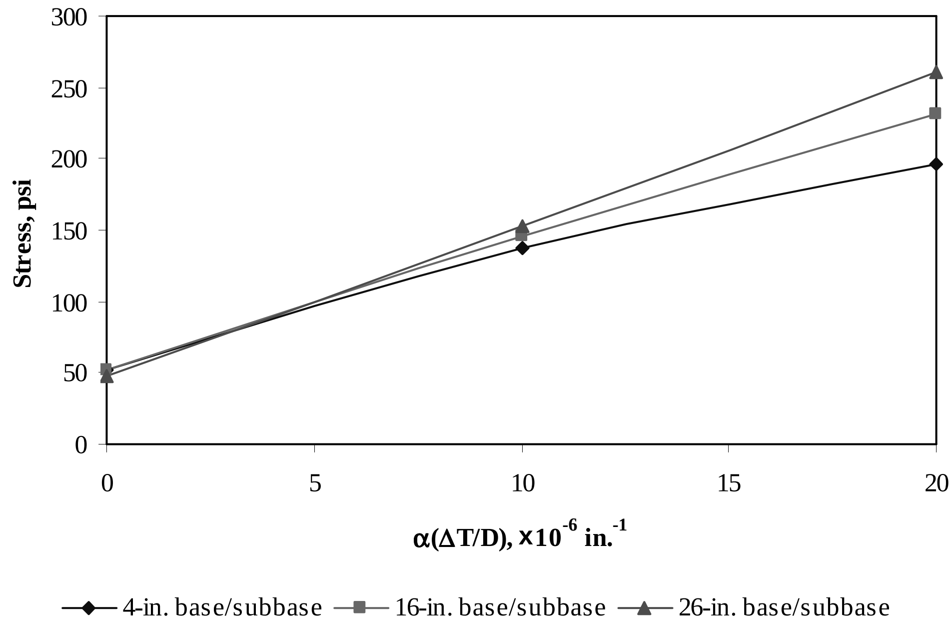


**Figure F-6-39: Impact of base/subbase thickness and product α(ΔT/D) on longitudinal stress at top of the slab (177-in. joint spacing)**

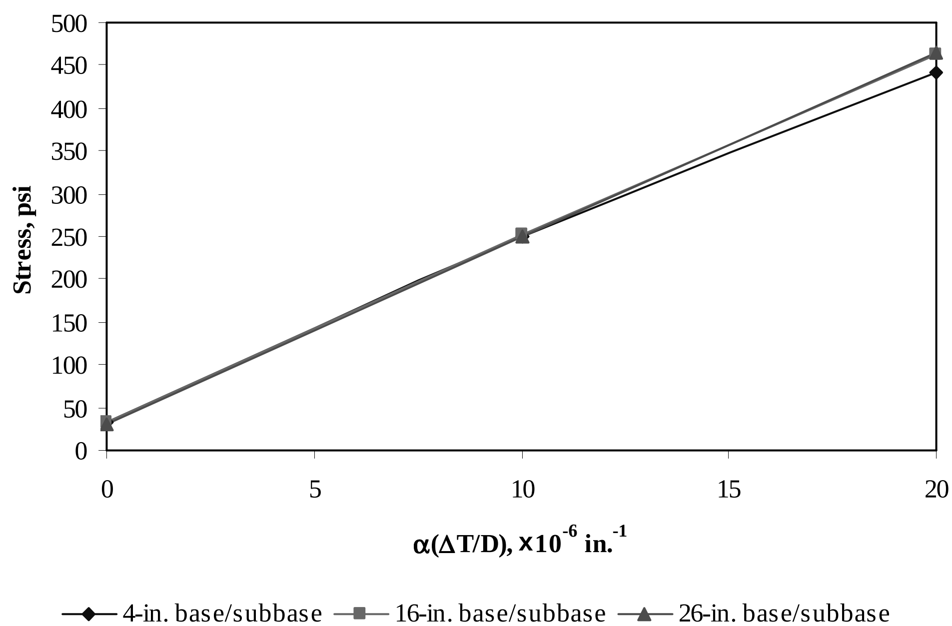


**Figure F-6-40: Impact of base/subbase thickness and product α(ΔT/D) on longitudinal stress at top of the slab (315-in. joint spacing)**

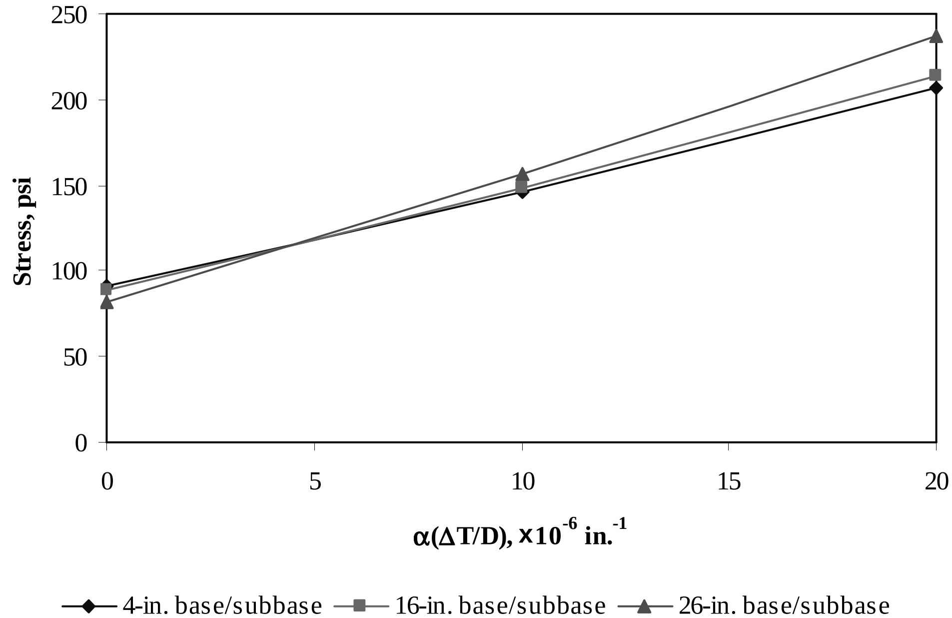


**Figure F-6-41: Impact of base/subbase thickness and product α(ΔT/D) on transverse stress at bottom of the slab (177-in. joint spacing)**

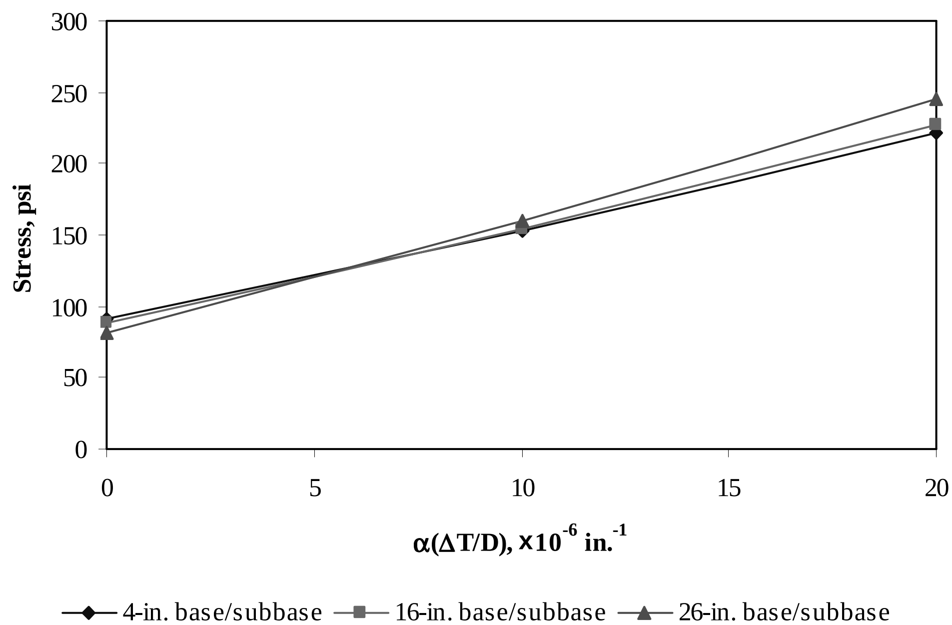


**Figure F-6-42: Impact of base/subbase thickness and product α(ΔT/D) on transverse stress at bottom of the slab (315-in. joint spacing)**

Figures F-6-43 through F-6-48 illustrate the impact of modulus of subgrade reaction and product α(ΔT/D) on stresses (10-in. PCC thickness, 16-in. base/subbase thickness and PCC shoulder)

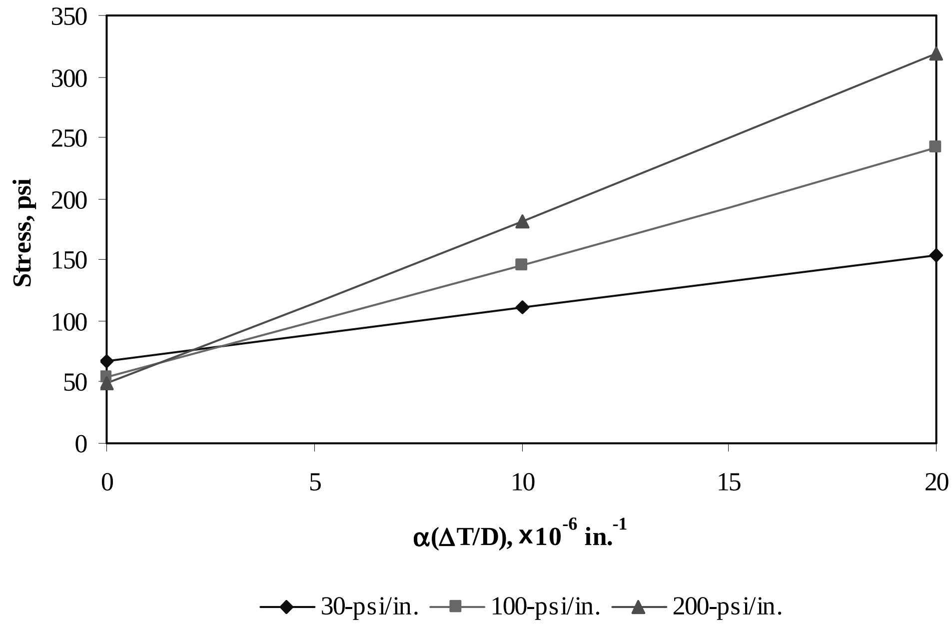


**Figure F-6-43: Impact of modulus of subgrade reaction and product α(ΔT/D) on longitudinal stress at bottom of the slab (177-in. joint spacing)**

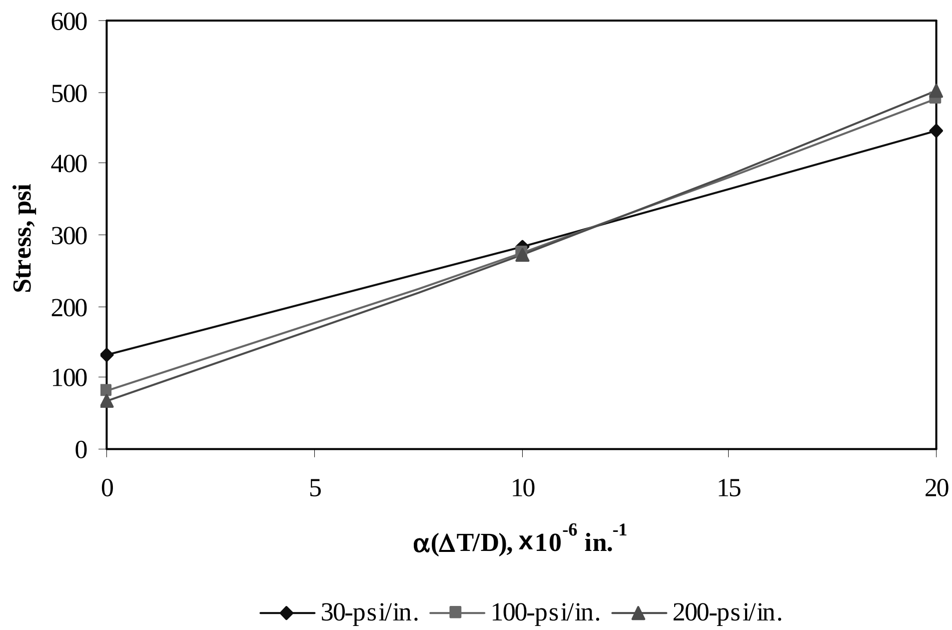


**Figure F-6-44: Impact of modulus of subgrade reaction and product α(ΔT/D) on longitudinal stress at bottom of the slab (315-in. joint spacing)**

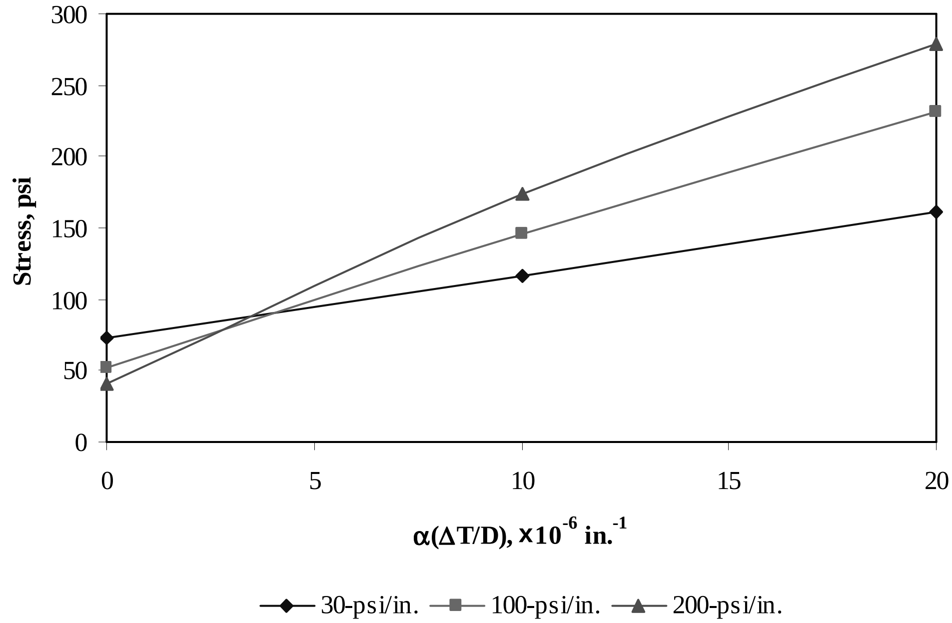


**Figure F-6-45: Impact of modulus of subgrade reaction and product α(ΔT/D) on longitudinal stress at top of the slab (177-in. joint spacing)**

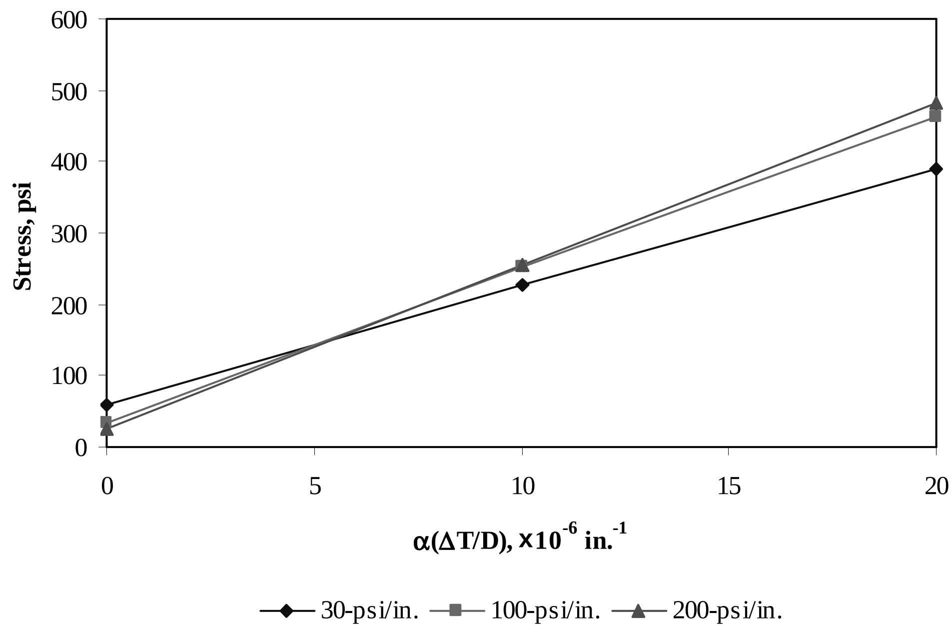


**Figure F-6-46: Impact of modulus of subgrade reaction and product α(ΔT/D) on longitudinal stress at top of the slab (315-in. joint spacing)**

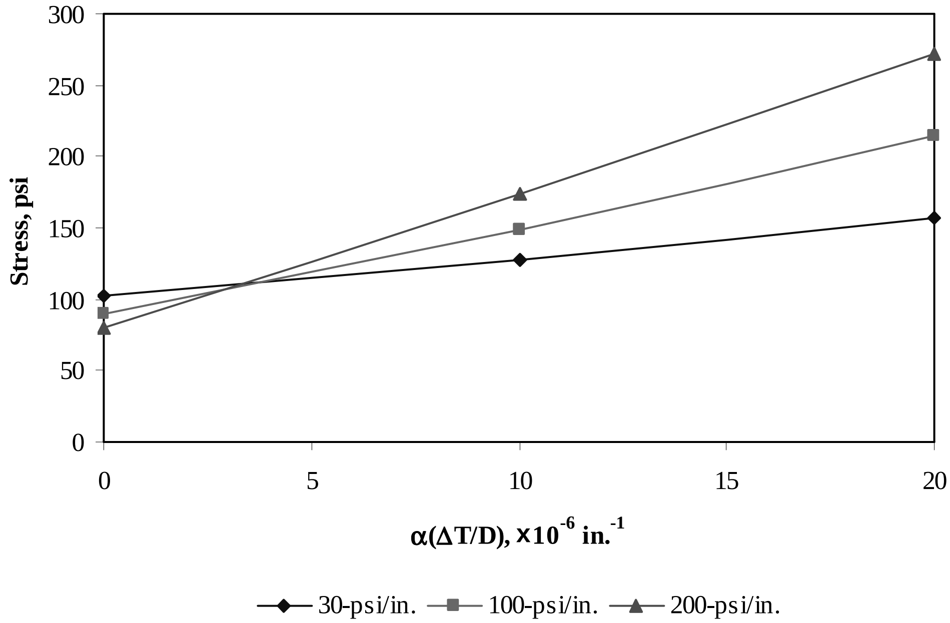


**Figure F-6-47: Impact of modulus of subgrade reaction and product α(ΔT/D) on transverse stress at bottom of the slab (177-in. joint spacing)**

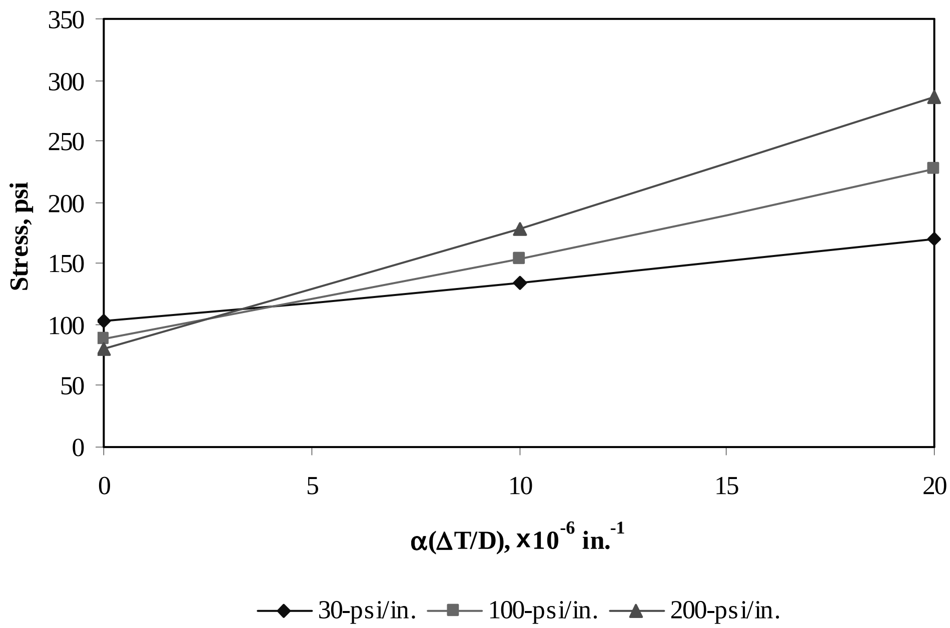


**Figure F-6-48: Impact of modulus of subgrade reaction and product α(ΔT/D) on transverse stress at bottom of the slab (315-in. joint spacing)**

Figures F-6-49 through F-6-51 illustrate the impact of joint spacing and product α(ΔT/D) on stresses (10-in. PCC thickness, 16-in. base/subbase thickness, 100-psi/in. modulus of subgrade reaction and PCC shoulder)

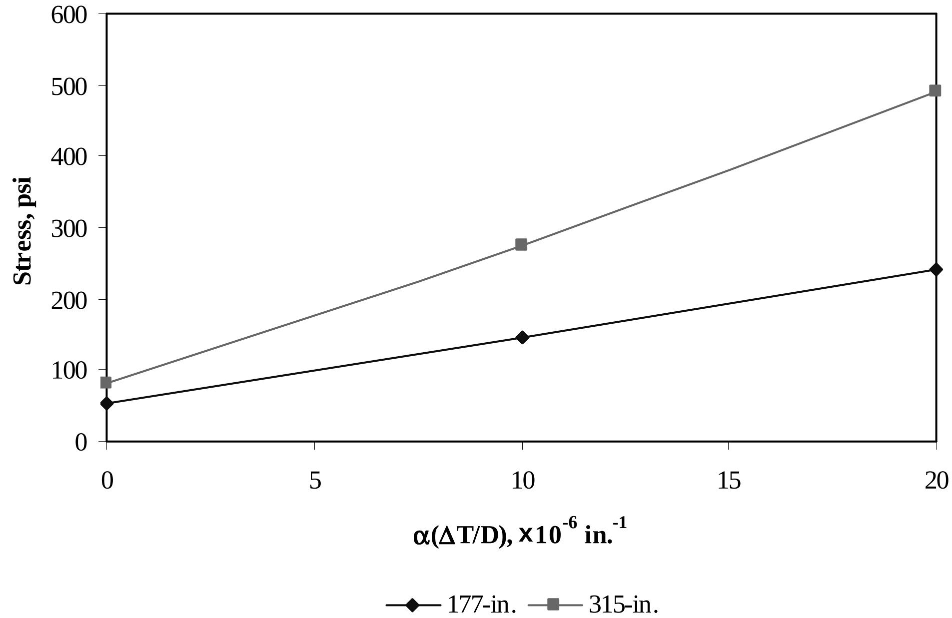


**Figure F-6-49: Impact of joint spacing and product α(ΔT/D) on longitudinal stress at bottom of the slab**

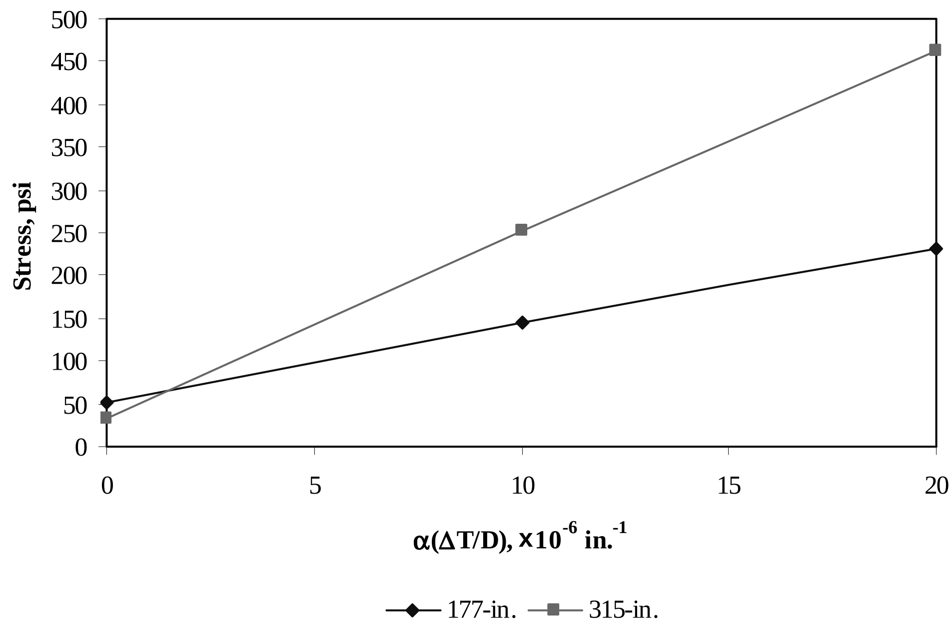


**Figure F-6-50: Impact of joint spacing and product α(ΔT/D) on longitudinal stress at top of the slab**

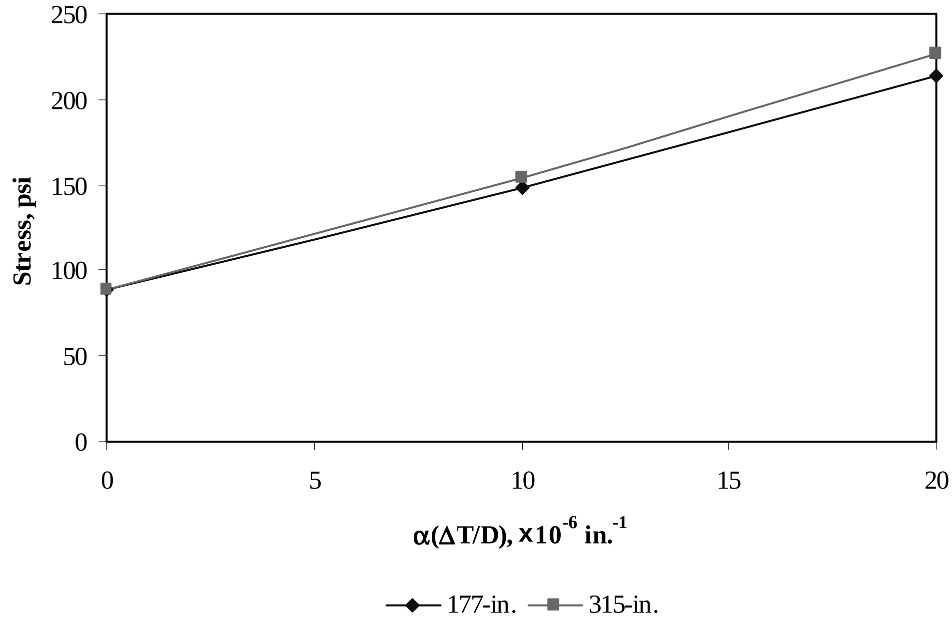


**Figure F-6-51: Impact of joint spacing and product $\alpha(\Delta T/D)$ on transverse stress at bottom of the slab**

**Sub Appendix F-7**

**Documentation of Pavement Responses for**


**91-kips Multi-axle (7)**

Figures F-7-1 through F-7-12 illustrate the impact of PCC thickness and base/subbase thickness on stresses (100-psi/in. modulus of subgrade reaction and PCC shoulder)

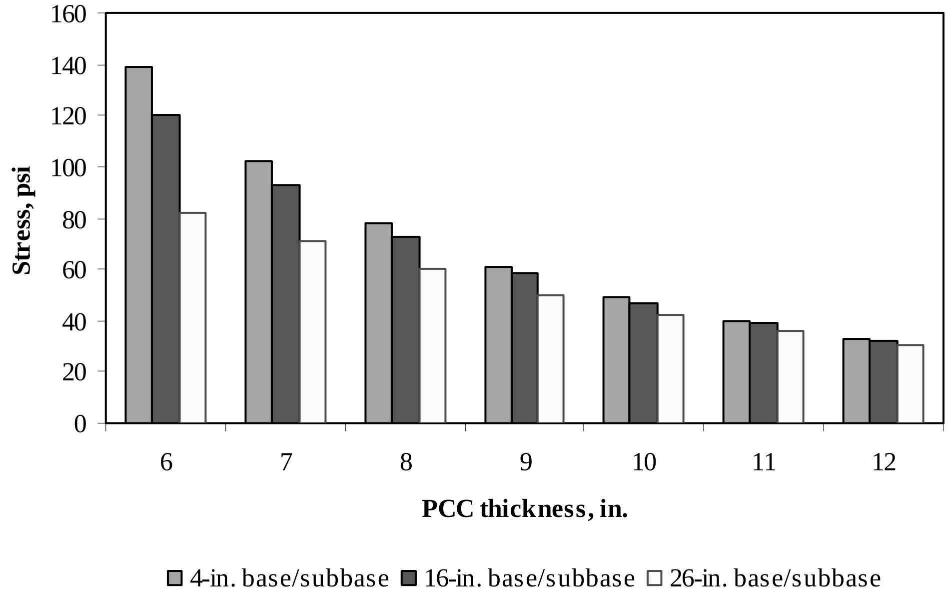


**Figure F-7-1: Impact of PCC thickness and base/subbase thickness on longitudinal stress at bottom of the Slab (177-in. joint spacing and $\alpha(\Delta T/D)$ of 0 in.$^{-1}$)**

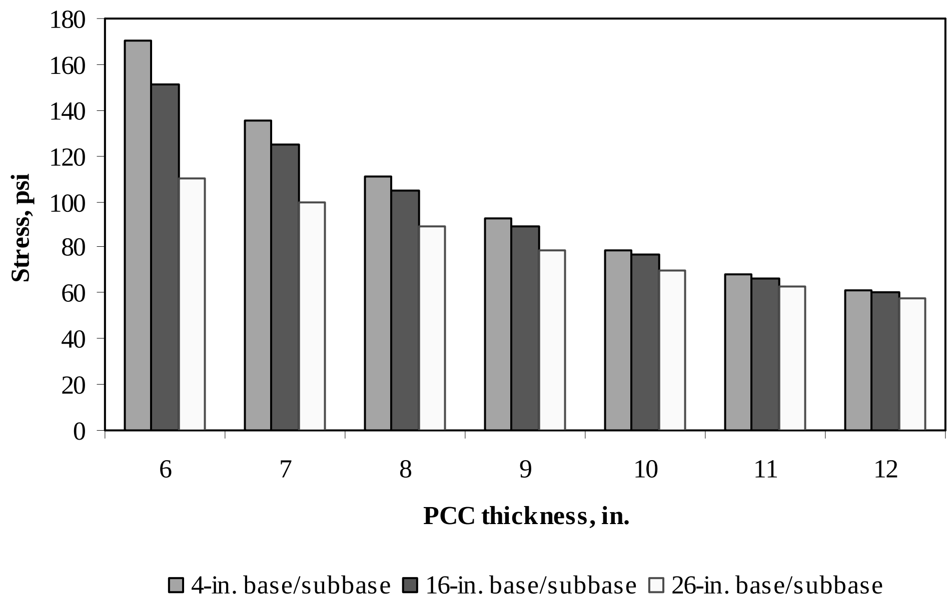


**Figure F-7-2: Impact of PCC thickness and base/subbase thickness on longitudinal stress at bottom of the Slab (315-in. joint spacing and $\alpha(\Delta T/D)$ of 0 in.$^{-1}$)**

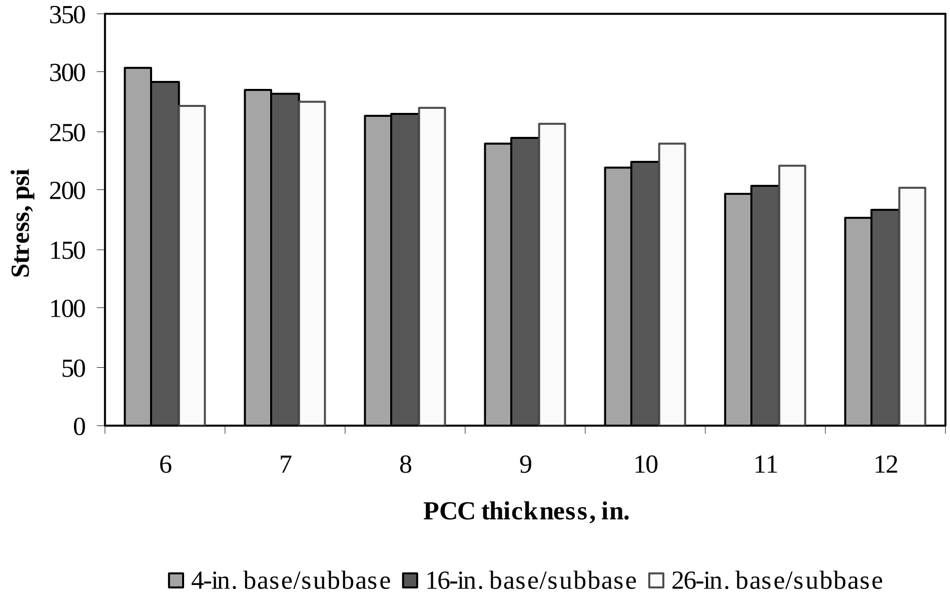


**Figure F-7-3: Impact of PCC thickness and base/subbase thickness on longitudinal stress at bottom of the Slab (177-in. joint spacing and $\alpha(\Delta T/D)$ of $20x10^{-6}$ in.$^{-1}$)**

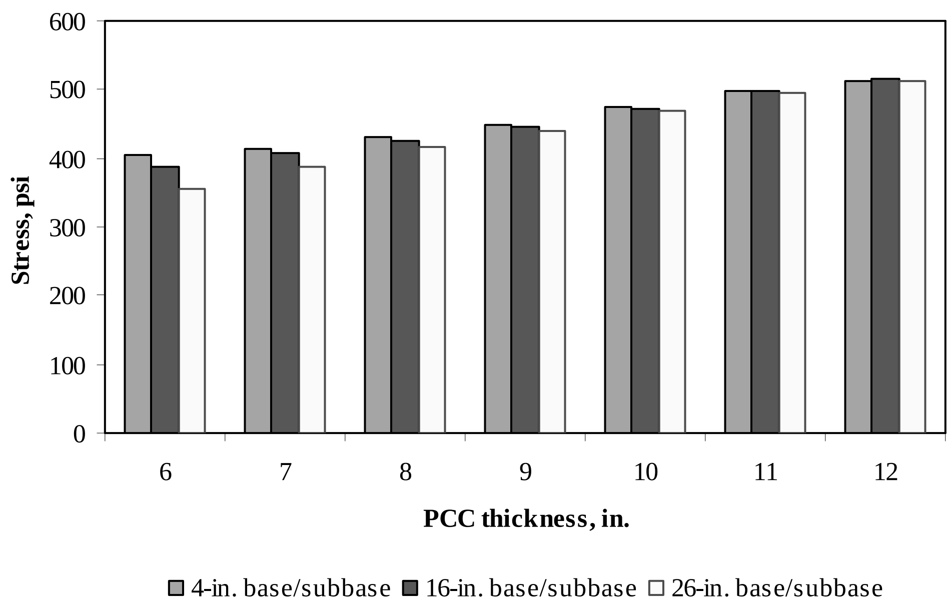


**Figure F-7-4: Impact of PCC thickness and base/subbase thickness on longitudinal stress at bottom of the Slab (315-in. joint spacing and $\alpha(\Delta T/D)$ of $20x10^{-6}$ in.$^{-1}$)**

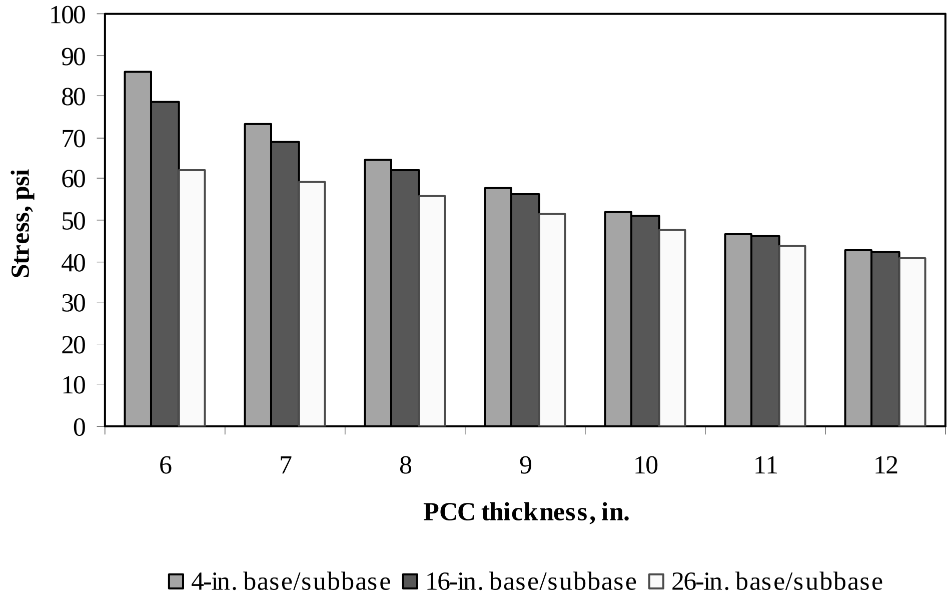


**Figure F-7-5: Impact of PCC thickness and base/subbase thickness on longitudinal stress at top of the Slab (177-in. joint spacing and $\alpha(\Delta T/D)$ of 0 in.$^{-1}$)**

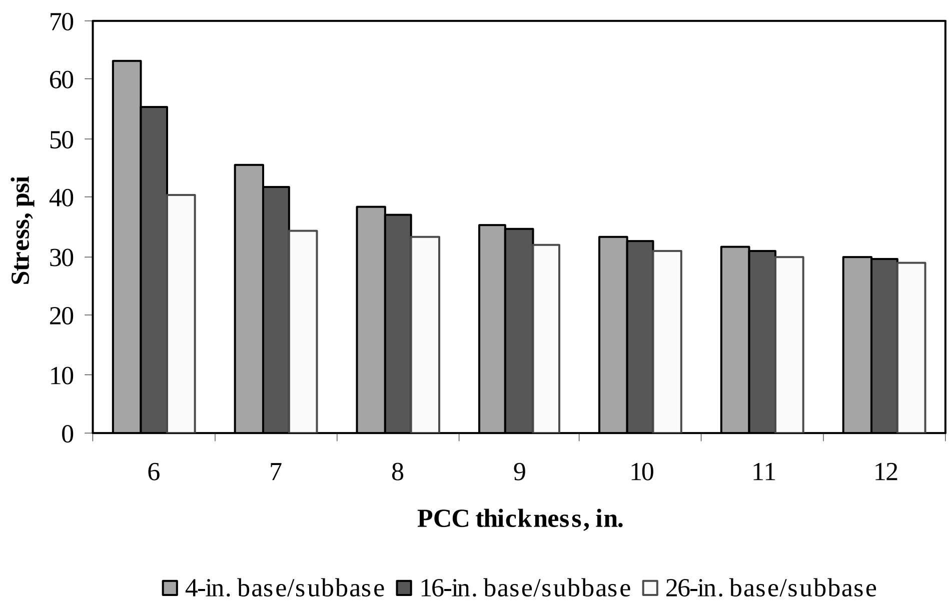


**Figure F-7-6: Impact of PCC thickness and base/subbase thickness on longitudinal stress at top of the Slab (315-in. joint spacing and $\alpha(\Delta T/D)$ of 0 in.$^{-1}$)**

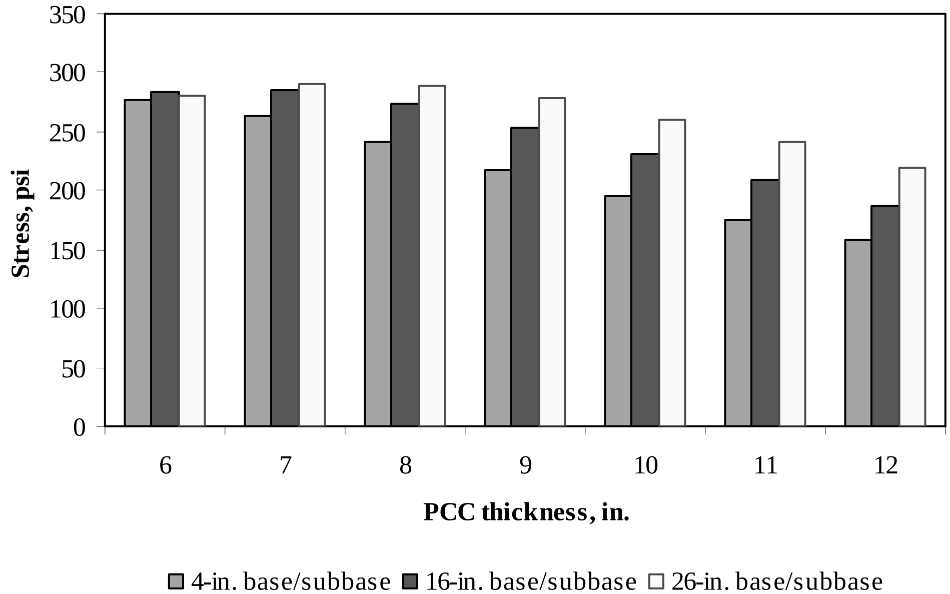


**Figure F-7-7: Impact of PCC thickness and base/subbase thickness on longitudinal stress at top of the Slab (177-in. joint spacing and $\alpha(\Delta T/D)$ of $-20x10^{-6}$ in.$^{-1}$)**

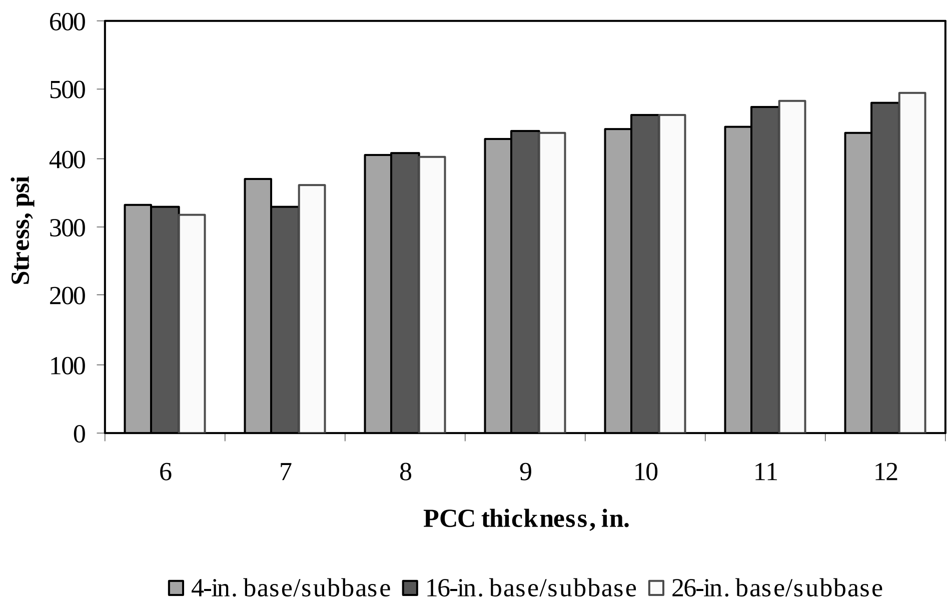


**Figure F-7-8: Impact of PCC thickness and base/subbase thickness on longitudinal stress at top of the Slab (315-in. joint spacing and $\alpha(\Delta T/D)$ of $-20x10^{-6}$ in.$^{-1}$)**

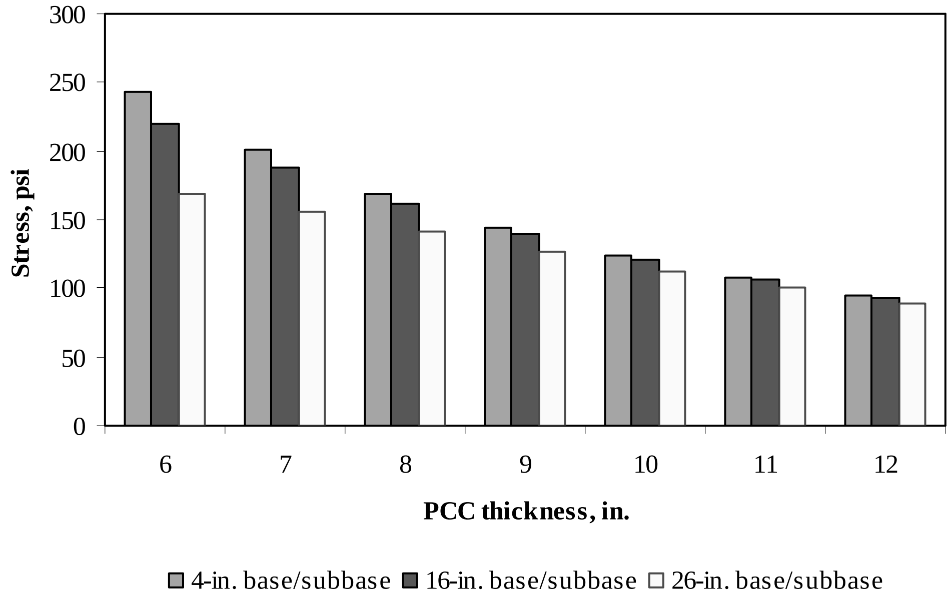


**Figure F-7-9: Impact of PCC thickness and base/subbase thickness on transverse stress at bottom of the Slab (177-in. joint spacing and $\alpha(\Delta T/D)$ of 0 in.$^{-1}$)**

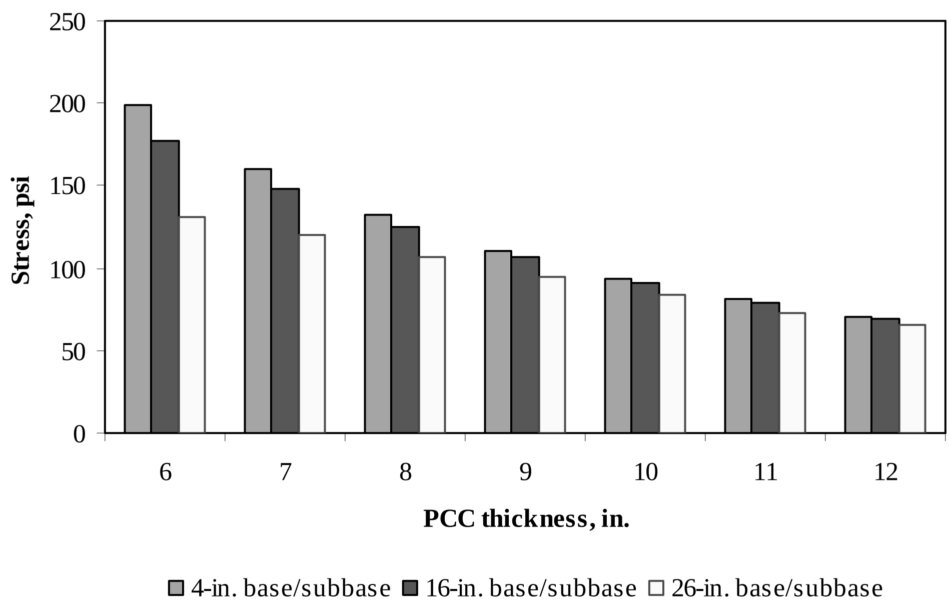


**Figure F-7-10: Impact of PCC thickness and base/subbase thickness on transverse stress at bottom of the Slab (315-in. joint spacing and $\alpha(\Delta T/D)$ of 0 in.$^{-1}$)**

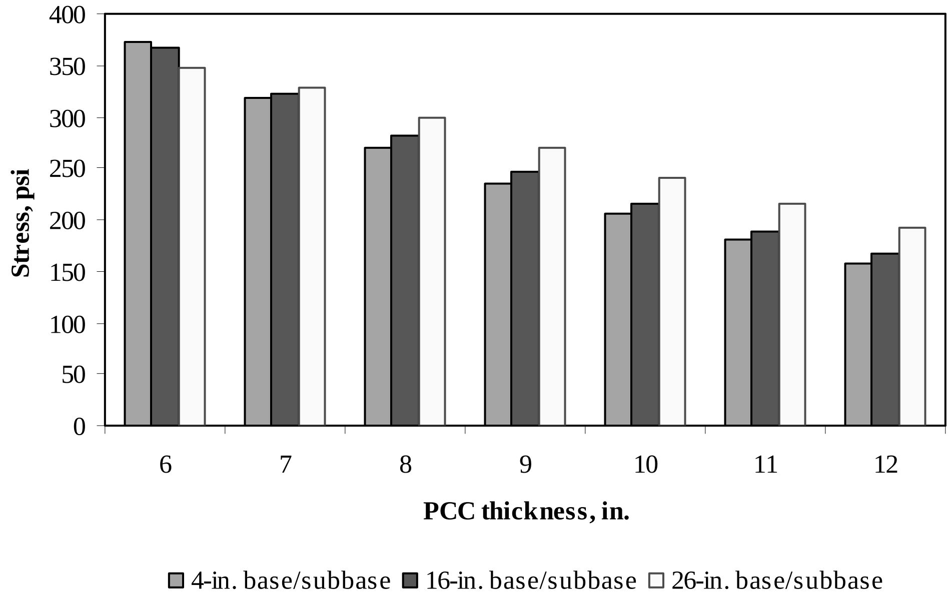


**Figure F-7-11: Impact of PCC thickness and base/subbase thickness on transverse stress at bottom of the Slab (177-in. joint spacing and $\alpha(\Delta T/D)$ of 20x10$^{-6}$ in.$^{-1}$)**

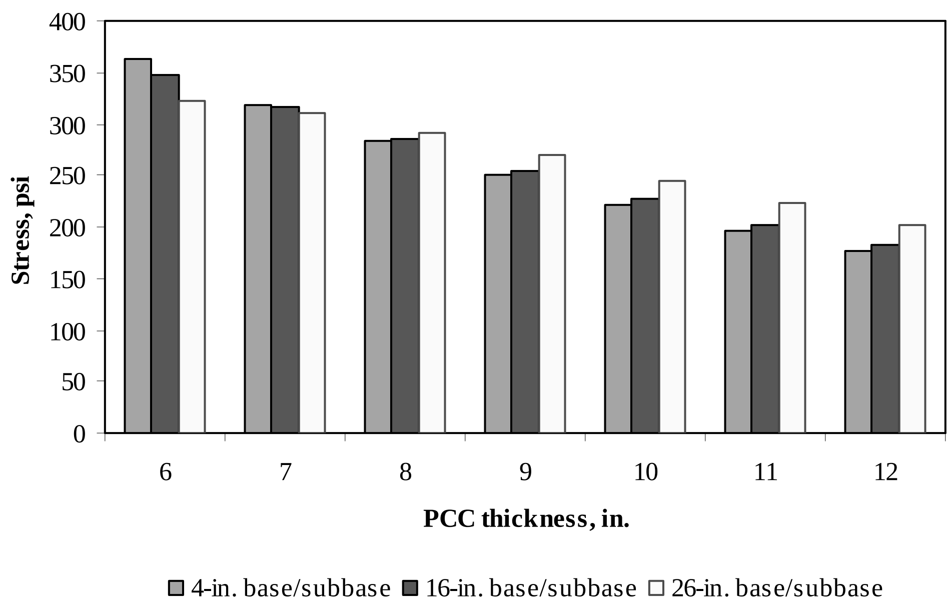


**Figure F-7-12: Impact of PCC thickness and base/subbase thickness on transverse stress at bottom of the Slab (315-in. joint spacing and $\alpha(\Delta T/D)$ of 20x10$^{-6}$ in.$^{-1}$)**

Figures F-7-13 through F-7-24 illustrate the impact of PCC thickness and modulus of subgrade reaction on stresses (16-in. base/subbase thickness and PCC shoulder)

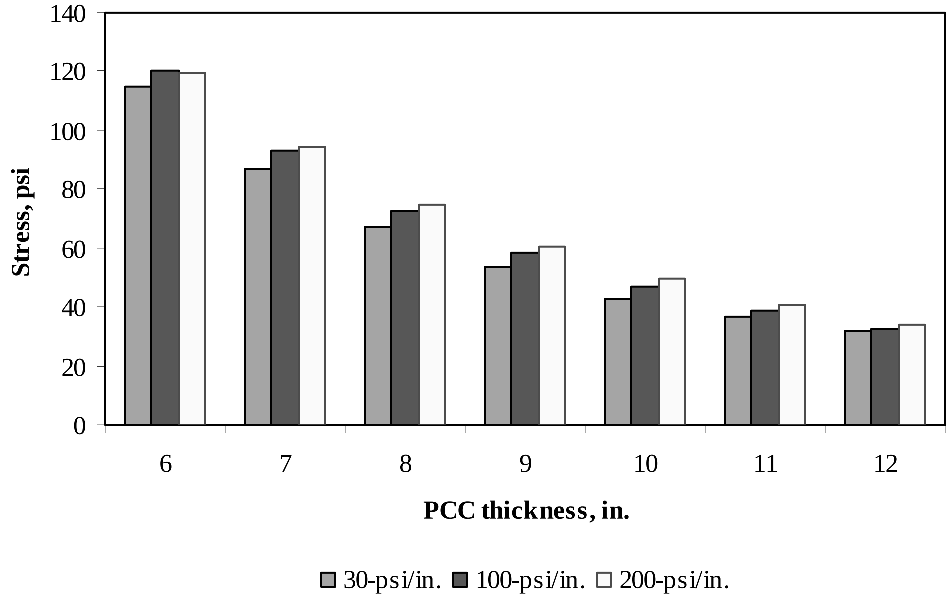


**Figure F-7-13: Impact of PCC thickness and modulus of subgrade reaction on longitudinal stress at bottom of the slab (177-in. joint spacing and $\alpha(\Delta T/D)$ of 0 in.$^{-1}$)**

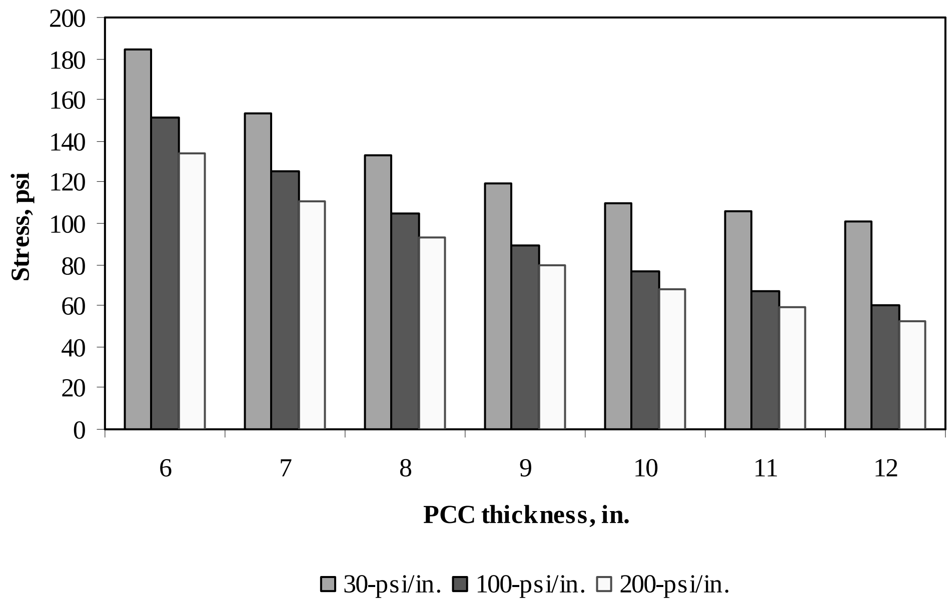


**Figure F-7-14: Impact of PCC thickness and modulus of subgrade reaction on longitudinal stress at bottom of the slab (315-in. joint spacing and $\alpha(\Delta T/D)$ of 0 in.$^{-1}$)**

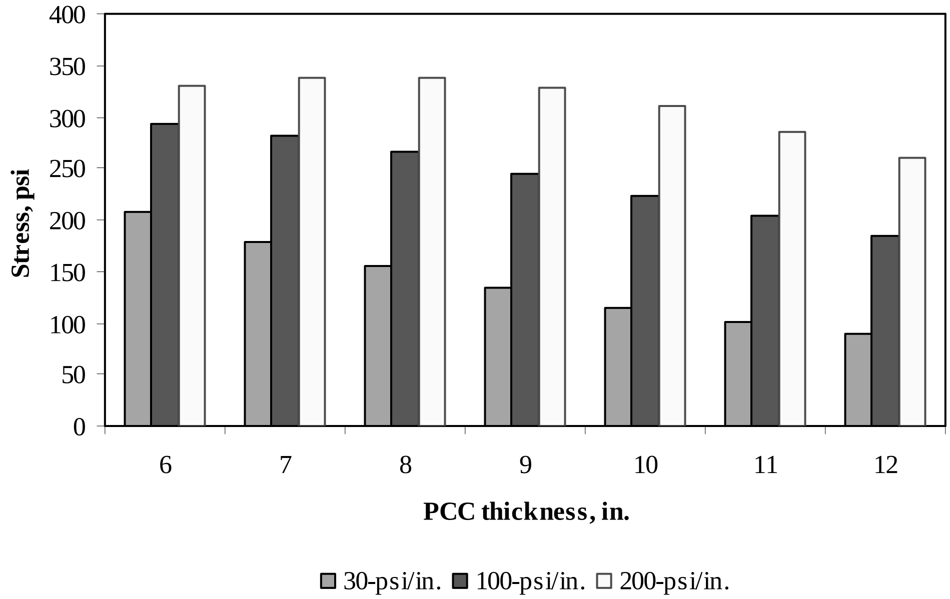


**Figure F-7-15: Impact of PCC thickness and modulus of subgrade reaction on longitudinal stress at bottom of the slab (177-in. joint spacing and $\alpha(\Delta T/D)$ of $20x10^{-6}$ in.$^{-1}$)**

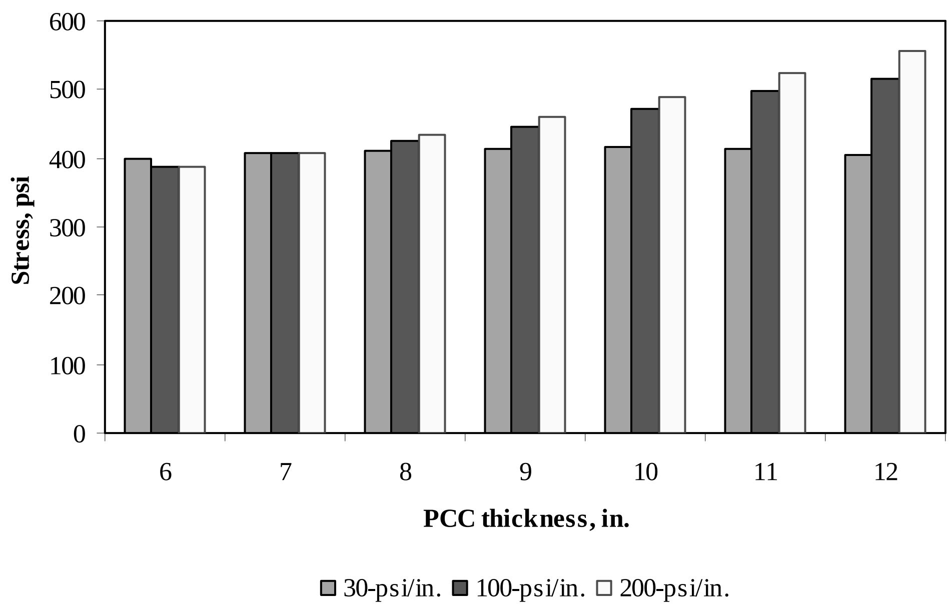


**Figure F-7-16: Impact of PCC thickness and modulus of subgrade reaction on longitudinal stress at bottom of the slab (315-in. joint spacing and $\alpha(\Delta T/D)$ of $20x10^{-6}$ in.$^{-1}$)**

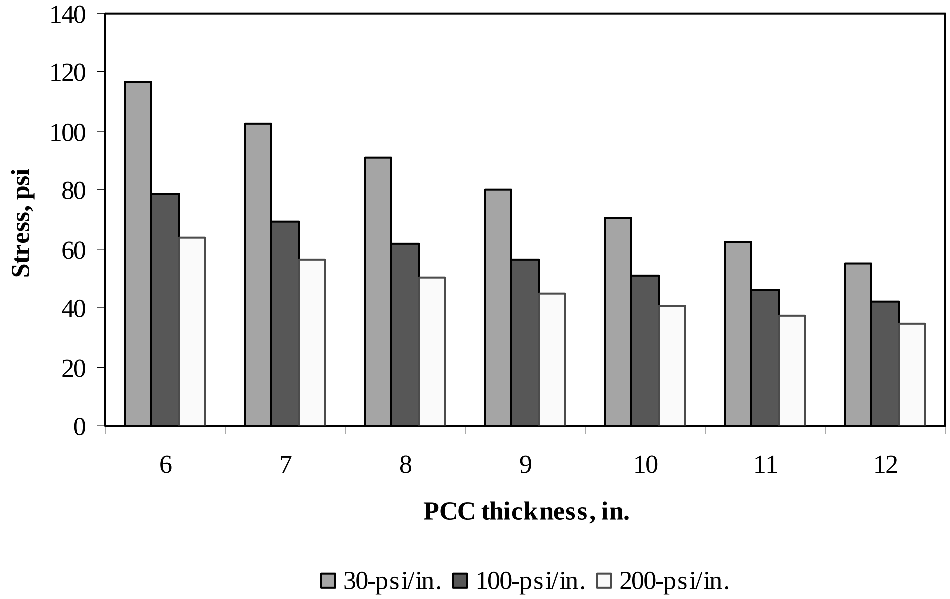


**Figure F-7-17: Impact of PCC thickness and modulus of subgrade reaction on longitudinal stress at top of the Slab (177-in. joint spacing and α(ΔT/D) of 0 $in.^{-1}$)**

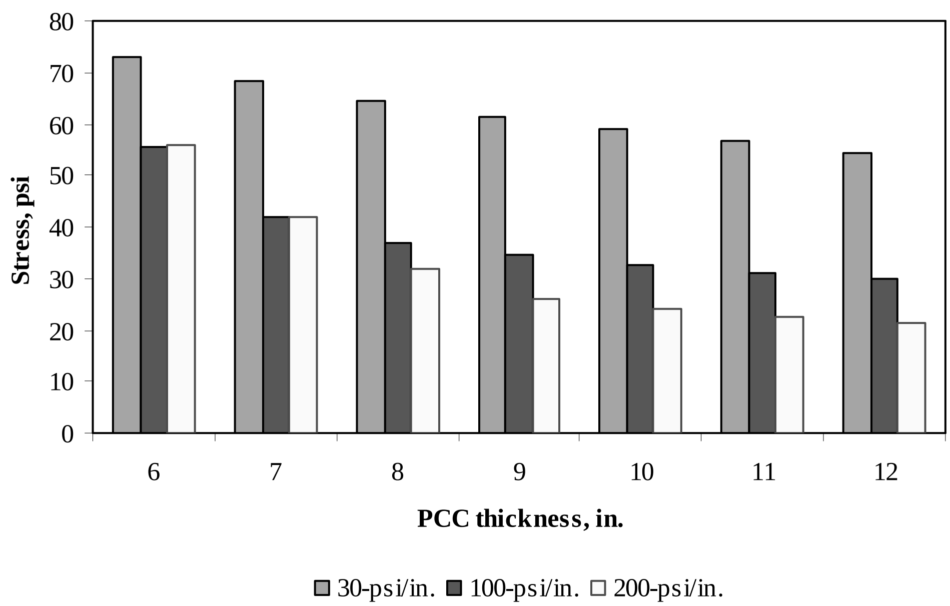


**Figure F-7-18: Impact of PCC thickness and modulus of subgrade reaction on longitudinal stress at top of the Slab (315-in. joint spacing and α(ΔT/D) of 0 $in.^{-1}$)**

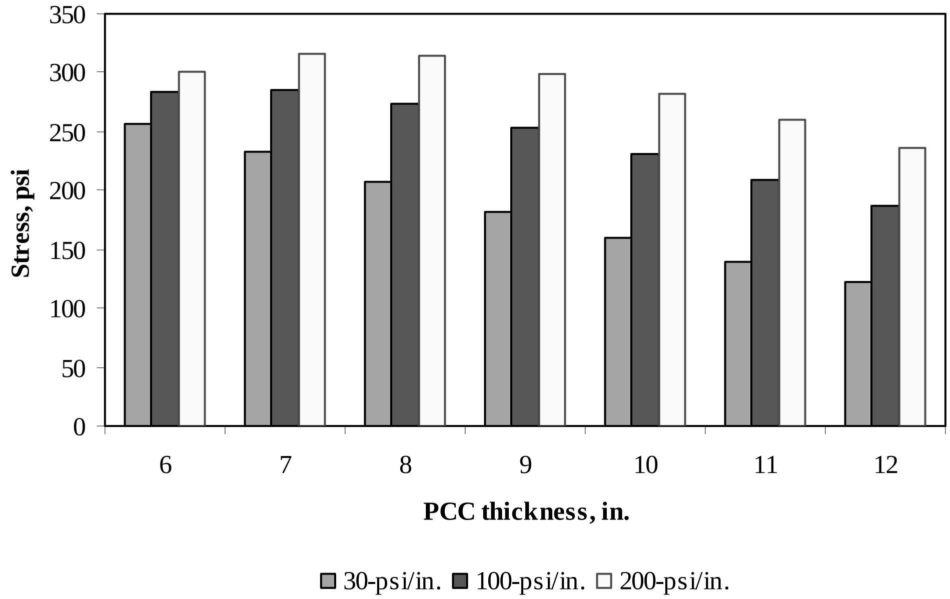


**Figure F-7-19: Impact of PCC thickness and modulus of subgrade reaction on longitudinal stress at top of the Slab (177-in. joint spacing and $\alpha(\Delta T/D)$ of $-20x10^{-6}$ in.$^{-1}$)**

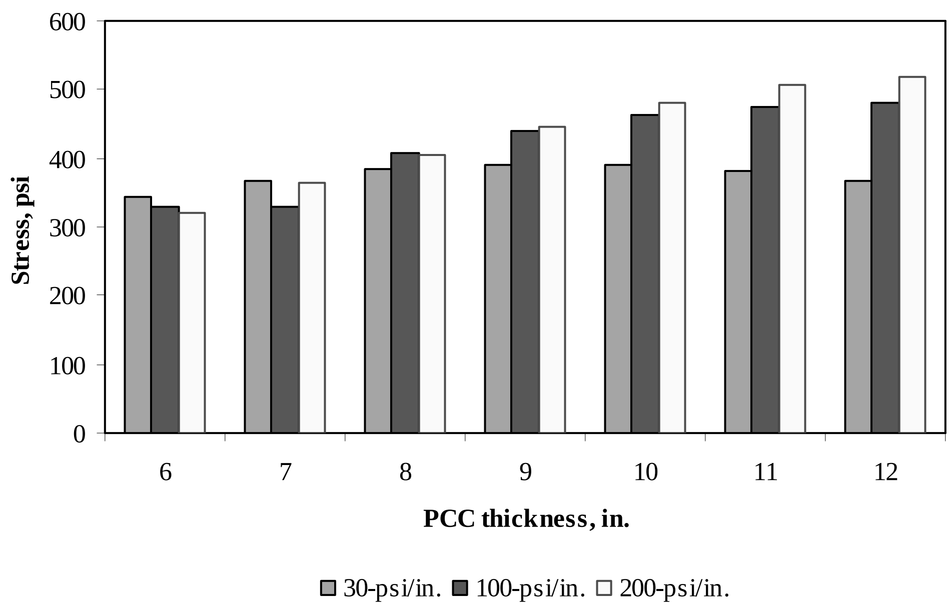


**Figure F-7-20: Impact of PCC thickness and modulus of subgrade reaction on longitudinal stress at top of the Slab (315-in. joint spacing and $\alpha(\Delta T/D)$ of $-20x10^{-6}$ in.$^{-1}$)**

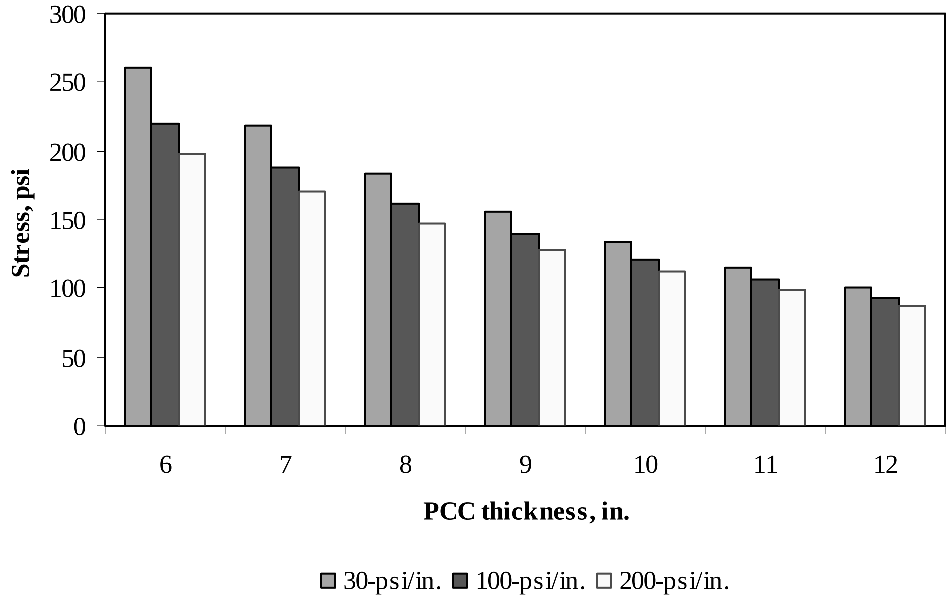


**Figure F-7-21: Impact of PCC thickness and modulus of subgrade reaction on transverse stress at bottom of the Slab (177-in. joint spacing and $\alpha(\Delta T/D)$ of 0 $in.^{-1}$)**

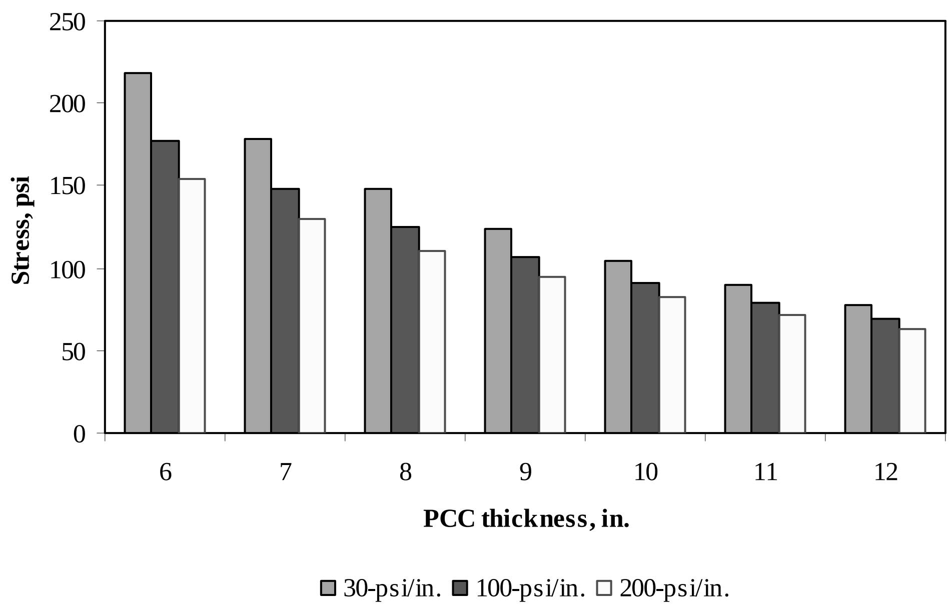


**Figure F-7-22: Impact of PCC thickness and modulus of subgrade reaction on transverse stress at bottom of the Slab (315-in. joint spacing and $\alpha(\Delta T/D)$ of 0 $in.^{-1}$)**

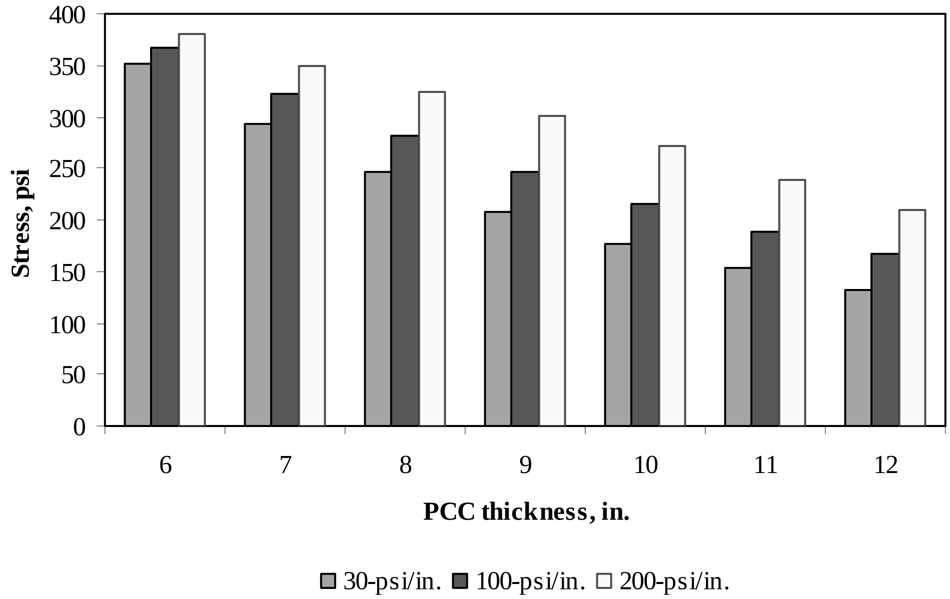


**Figure F-7-23: Impact of PCC thickness and modulus of subgrade reaction on transverse stress at bottom of the Slab (177-in. joint spacing and $\alpha(\Delta T/D)$ of $20x10^{-6}$ in.$^{-1}$)**

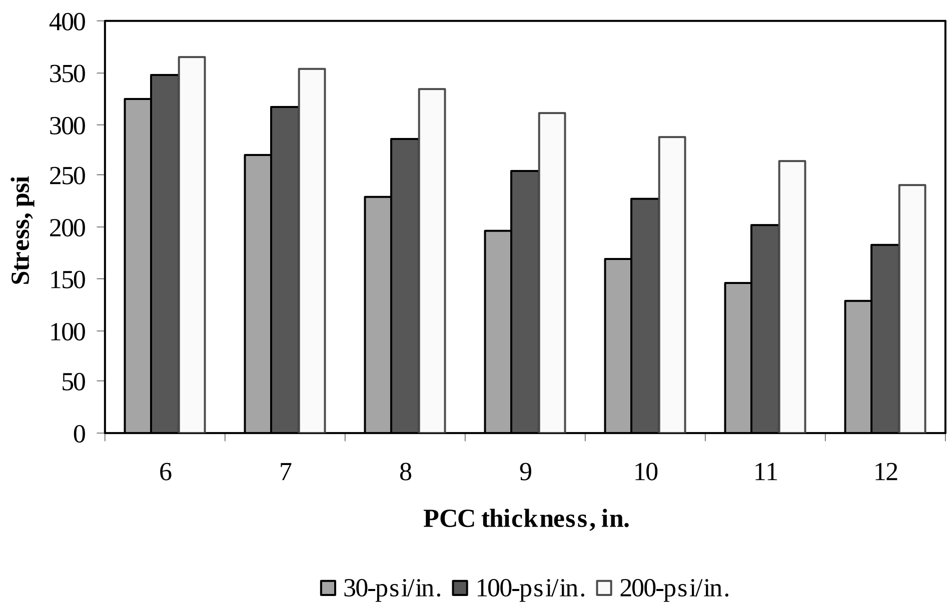


**Figure F-7-24: Impact of PCC thickness and modulus of subgrade reaction on transverse stress at bottom of the Slab (315-in. joint spacing and $\alpha(\Delta T/D)$ of $20x10^{-6}$ in.$^{-1}$)**

Figures F-7-25 through F-7-36 illustrate the impact of PCC thickness and lateral support condition on stresses (16-in. base/subbase and 100-psi/in. modulus of subgrade reaction)

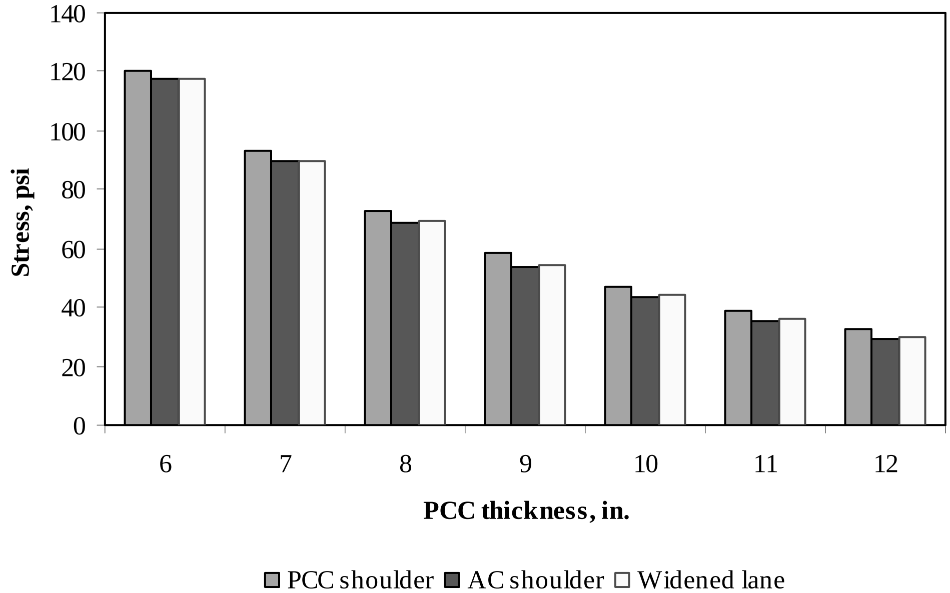


**Figure F-7-25: Impact of PCC thickness and lateral support condition on longitudinal stress at bottom of the Slab (177-in. joint spacing and $\alpha(\Delta T/D)$ of 0 in.$^{-1}$)**

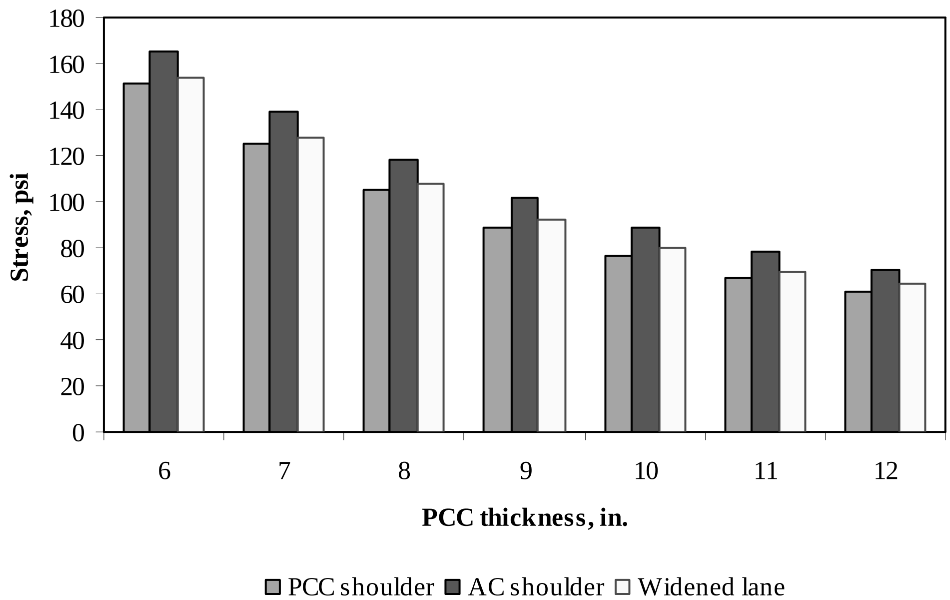


**Figure F-7-26: Impact of PCC thickness and lateral support condition on longitudinal stress at bottom of the Slab (315-in. joint spacing and $\alpha(\Delta T/D)$ of 0 in.$^{-1}$)**

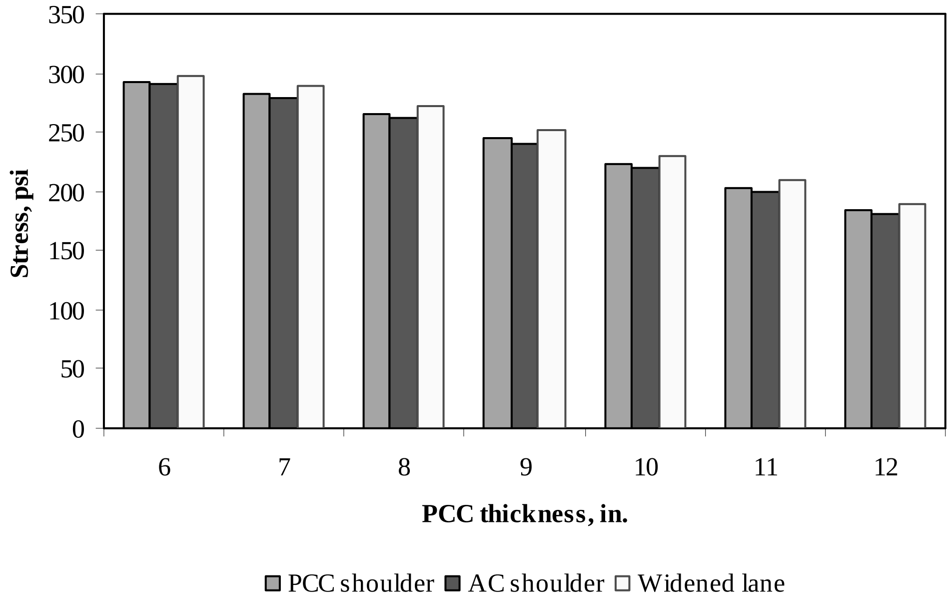


**Figure F-7-27: Impact of PCC thickness and lateral support condition on longitudinal stress at bottom of the Slab (177-in. joint spacing and $\alpha(\Delta T/D)$ of $20x10^{-6}$ in.$^{-1}$)**

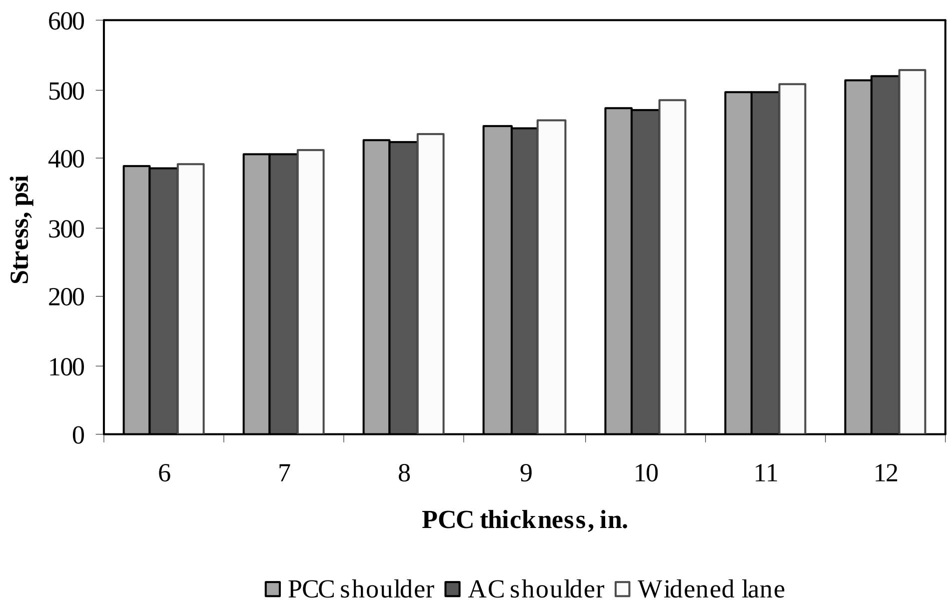


**Figure F-7-28: Impact of PCC thickness and lateral support condition on longitudinal stress at bottom of the Slab (315-in. joint spacing and $\alpha(\Delta T/D)$ of $20x10^{-6}$ in.$^{-1}$)**

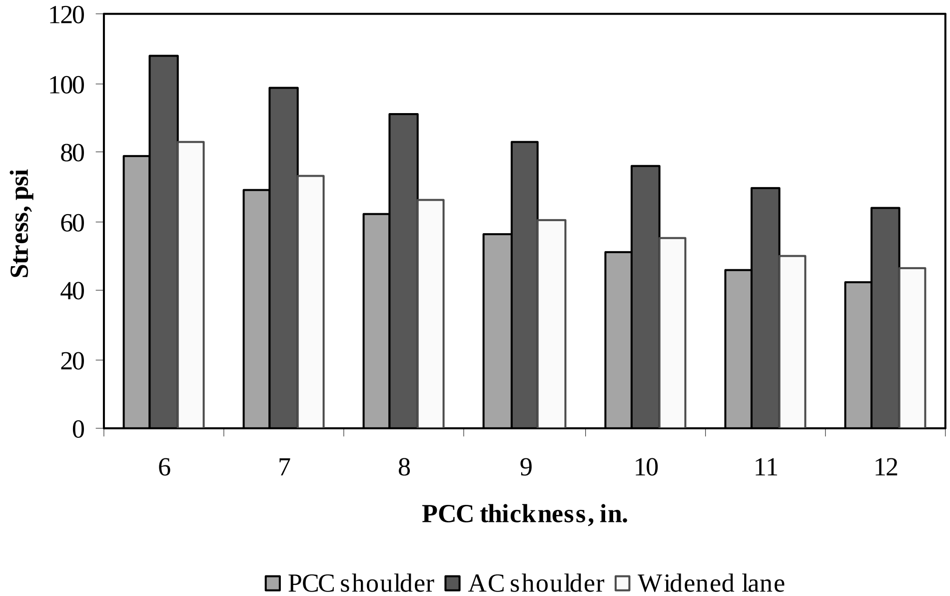


**Figure F-7-29: Impact of PCC thickness and lateral support condition on longitudinal stress at top of the Slab (177-in. joint spacing and $\alpha(\Delta T/D)$ of 0 in.$^{-1}$)**

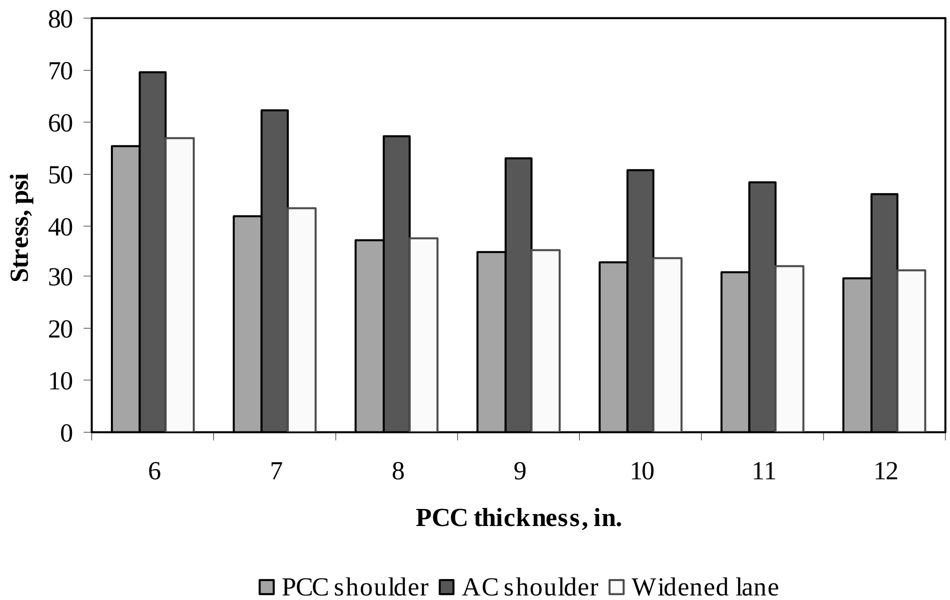


**Figure F-7-30: Impact of PCC thickness and lateral support condition on longitudinal stress at top of the Slab (315-in. joint spacing and $\alpha(\Delta T/D)$ of 0 in.$^{-1}$)**

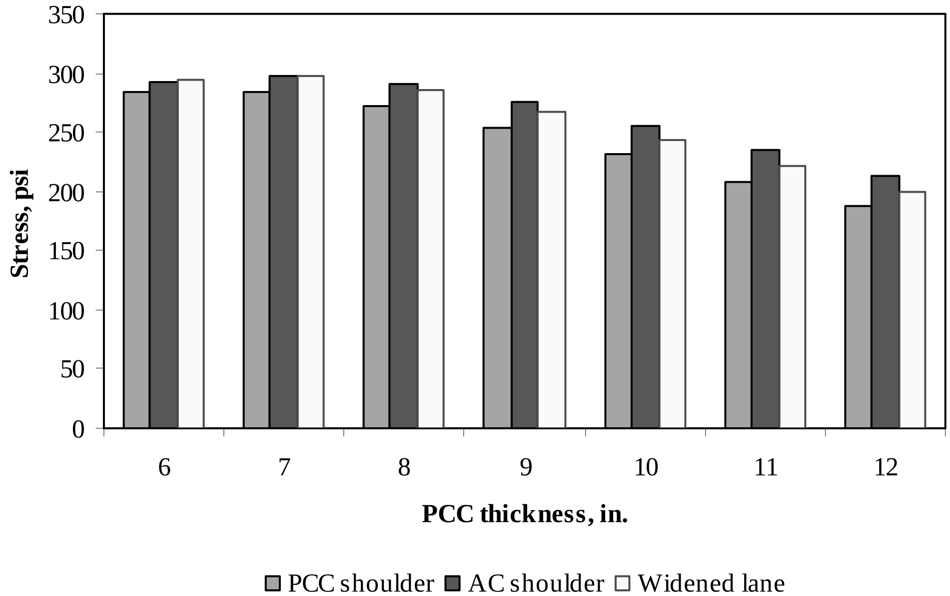


**Figure F-7-31: Impact of PCC thickness and lateral support condition on longitudinal stress at top of the Slab (177-in. joint spacing and $\alpha(\Delta T/D)$ of $-20 \times 10^{-6}$ in.$^{-1}$)**

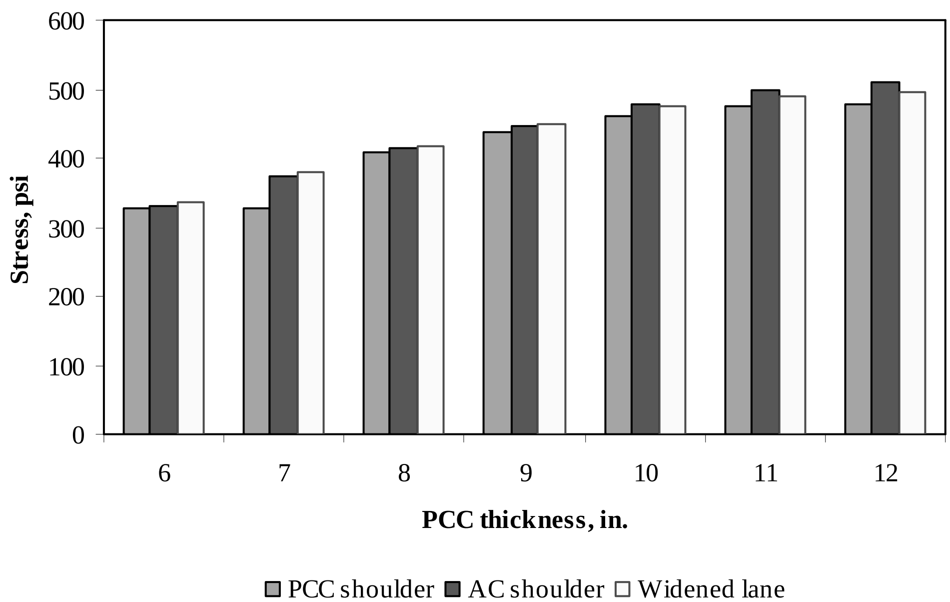


**Figure F-7-32: Impact of PCC thickness and lateral support condition on longitudinal stress at top of the Slab (315-in. joint spacing and $\alpha(\Delta T/D)$ of $-20 \times 10^{-6}$ in.$^{-1}$)**

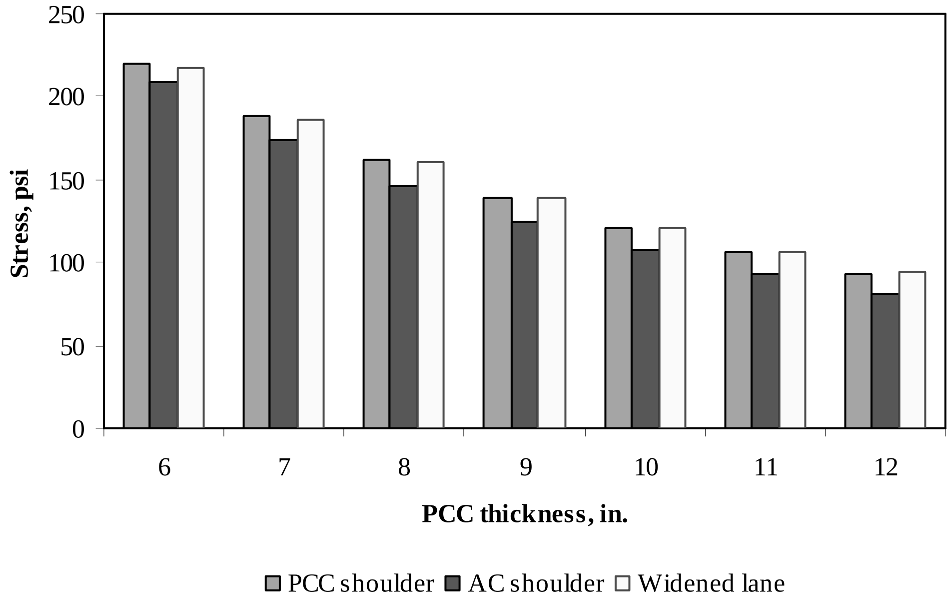


**Figure F-7-33: Impact of PCC thickness and lateral support condition on transverse stress at bottom of the Slab (177-in. joint spacing and α(ΔT/D) of 0 in.$^{-1}$)**

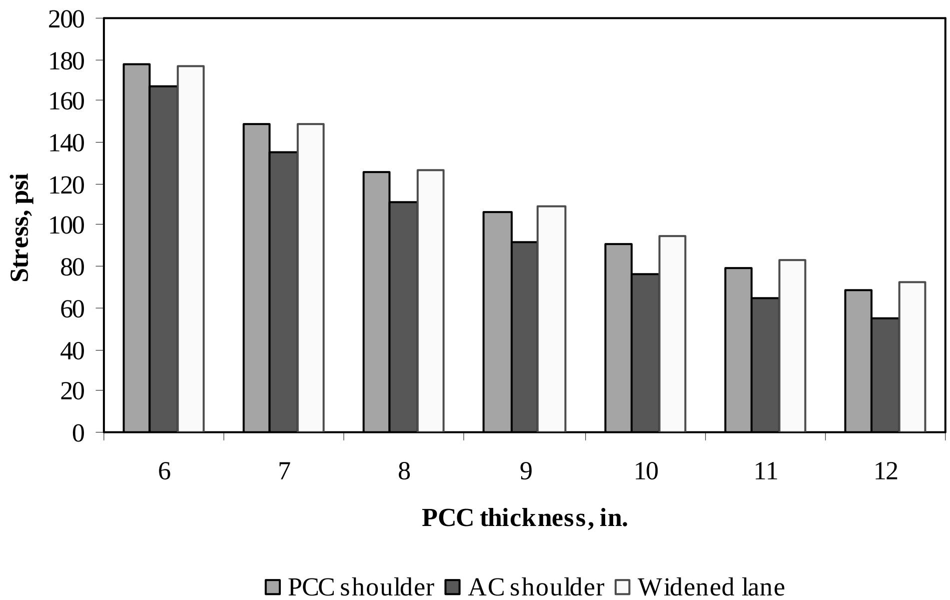


**Figure F-7-34: Impact of PCC thickness and lateral support condition on transverse stress at bottom of the Slab (315-in. joint spacing and α(ΔT/D) of 0 in.$^{-1}$)**

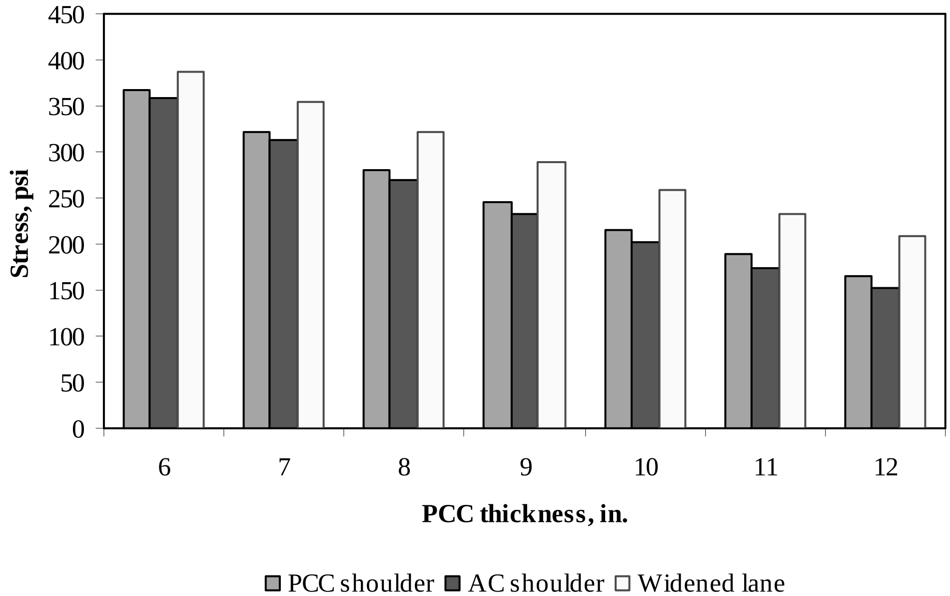


**Figure F-7-35: Impact of PCC thickness and lateral support condition on transverse stress at bottom of the Slab (177-in. joint spacing and $\alpha(\Delta T/D)$ of $20x10^{-6}$ in.$^{-1}$)**

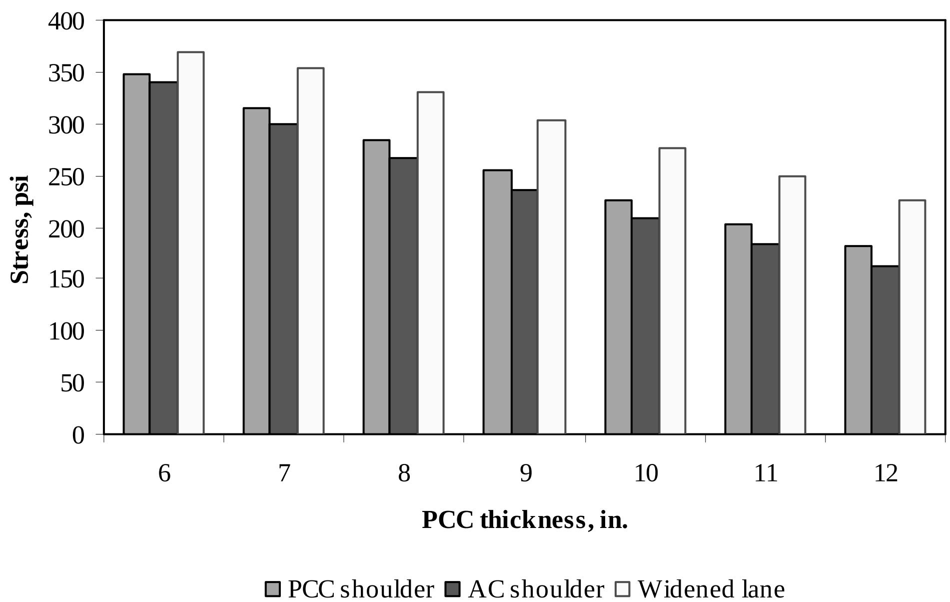


**Figure F-7-36: Impact of PCC thickness and lateral support condition on transverse stress at bottom of the Slab (315-in. joint spacing and $\alpha(\Delta T/D)$ of $20x10^{-6}$ in.$^{-1}$)**

Figures F-7-37 through F-7-42 illustrate the impact of base/subbase thickness and product α(ΔT/D) on stresses (10-in. PCC thickness, 100-psi/in. modulus of subgrade reaction and PCC shoulder)

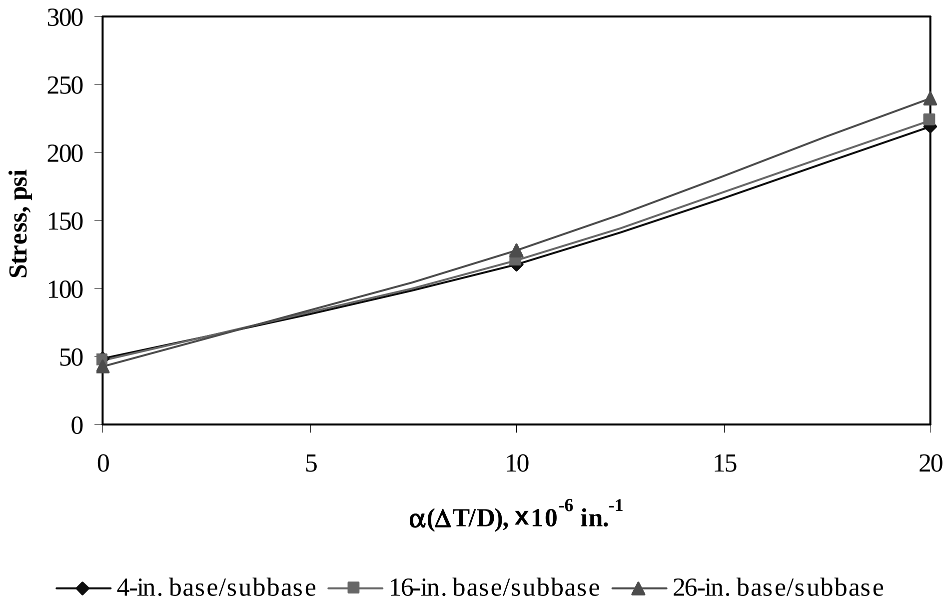


**Figure F-7-37: Impact of base/subbase thickness and product α(ΔT/D) on longitudinal stress at bottom of the slab (177-in. joint spacing)**

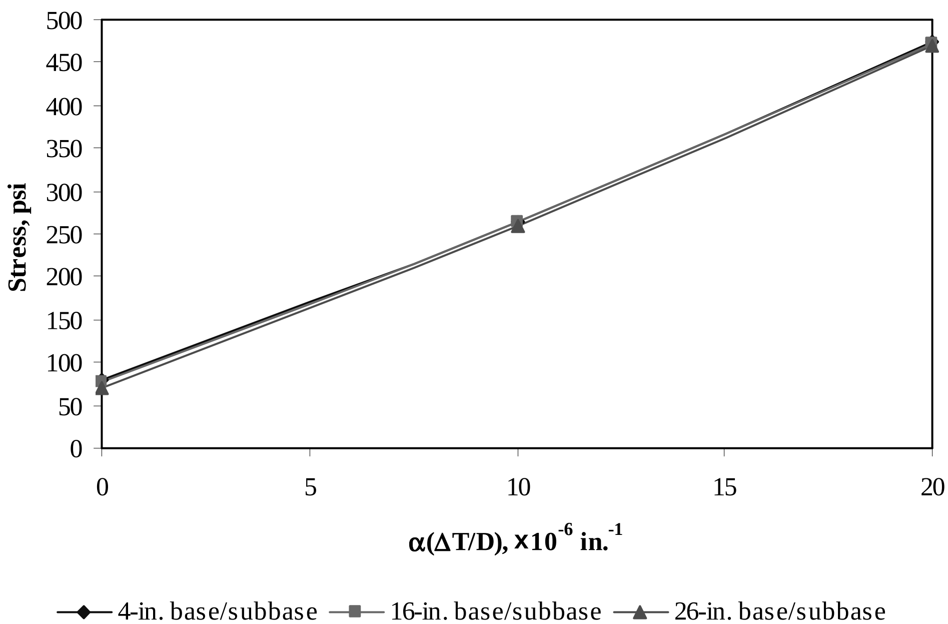


**Figure F-7-38: Impact of base/subbase thickness and product α(ΔT/D) on longitudinal stress at bottom of the slab (315-in. joint spacing)**

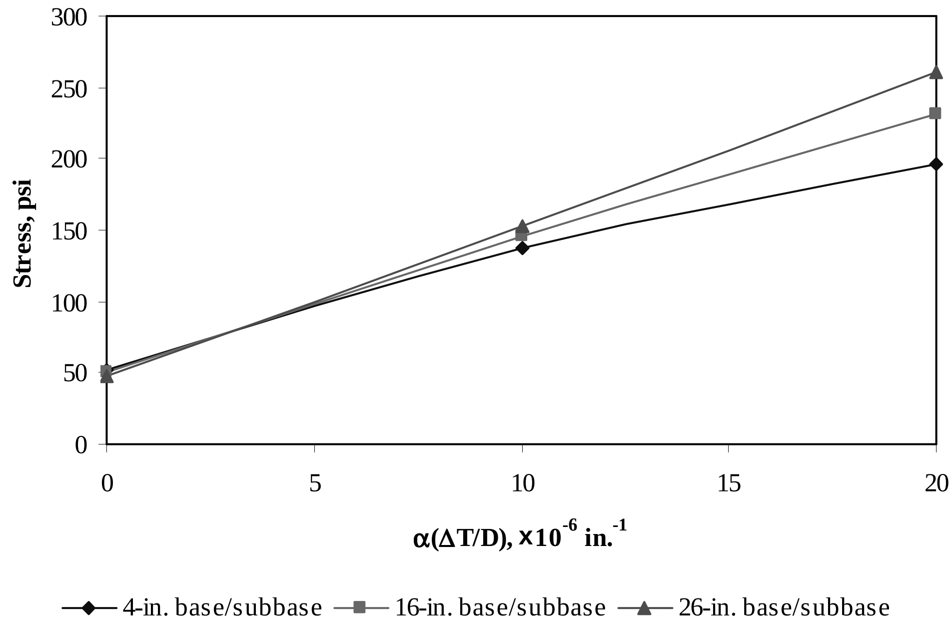


**Figure F-7-39: Impact of base/subbase thickness and product α(ΔT/D) on longitudinal stress at top of the slab (177-in. joint spacing)**

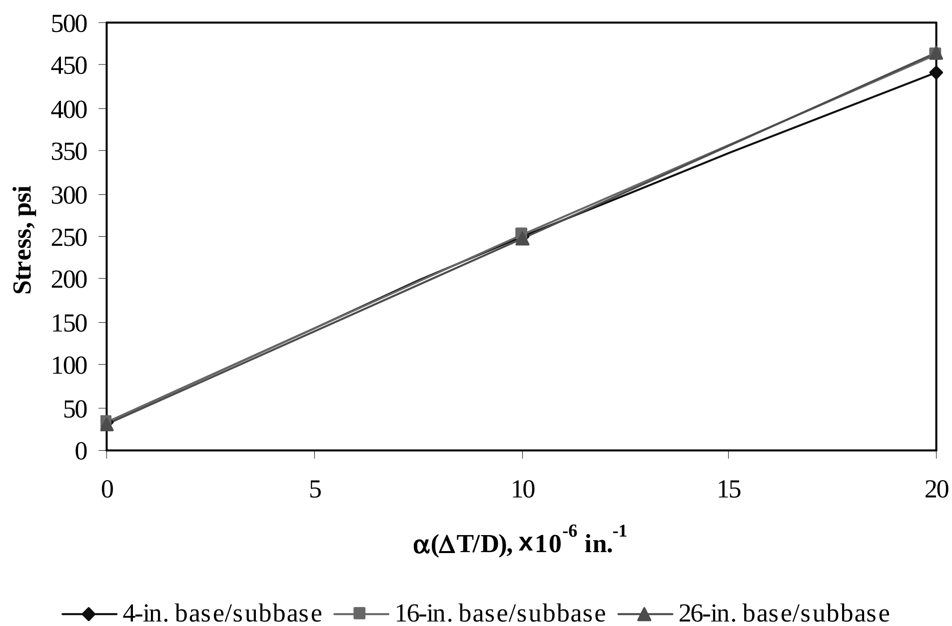


**Figure F-7-40: Impact of base/subbase thickness and product α(ΔT/D) on longitudinal stress at top of the slab (315-in. joint spacing)**

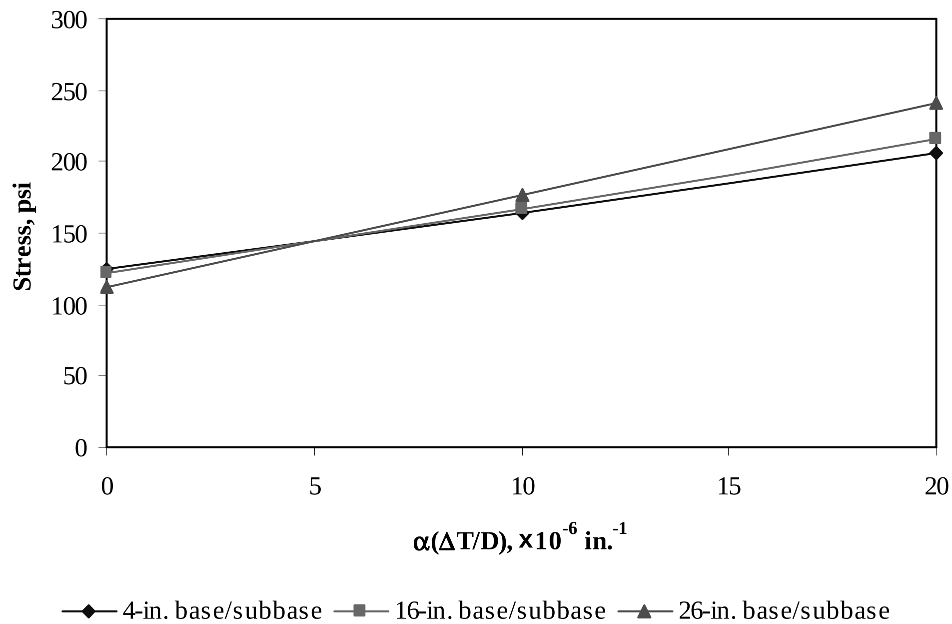


**Figure F-7-41: Impact of base/subbase thickness and product $\alpha(\Delta T/D)$ on transverse stress at bottom of the slab (177-in. joint spacing)**

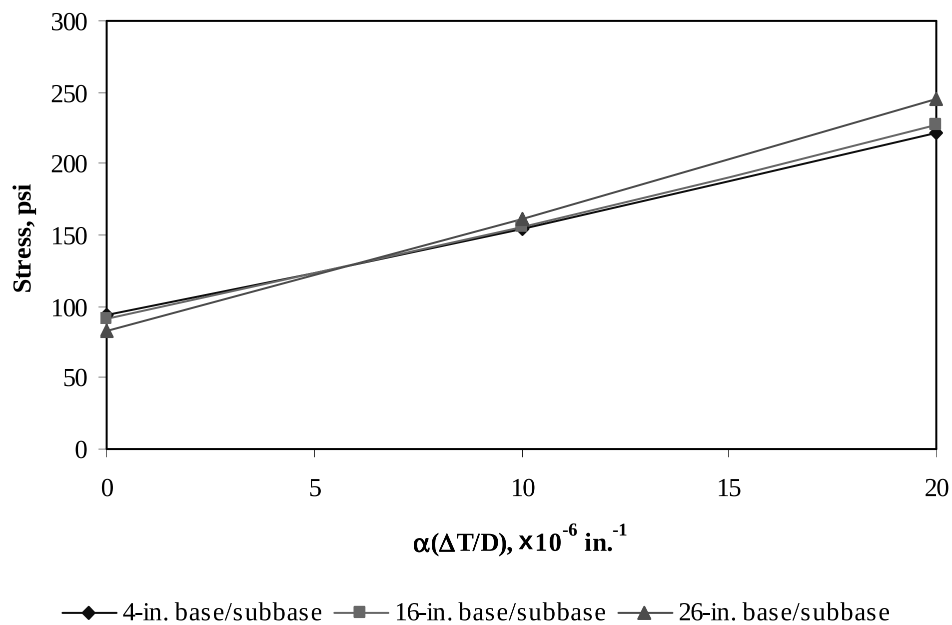


**Figure F-7-42: Impact of base/subbase thickness and product $\alpha(\Delta T/D)$ on transverse stress at bottom of the slab (315-in. joint spacing)**

Figures F-7-43 through F-7-48 illustrate the impact of modulus of subgrade reaction and product α(ΔT/D) on stresses (10-in. PCC thickness, 16-in. base/subbase thickness and PCC shoulder)

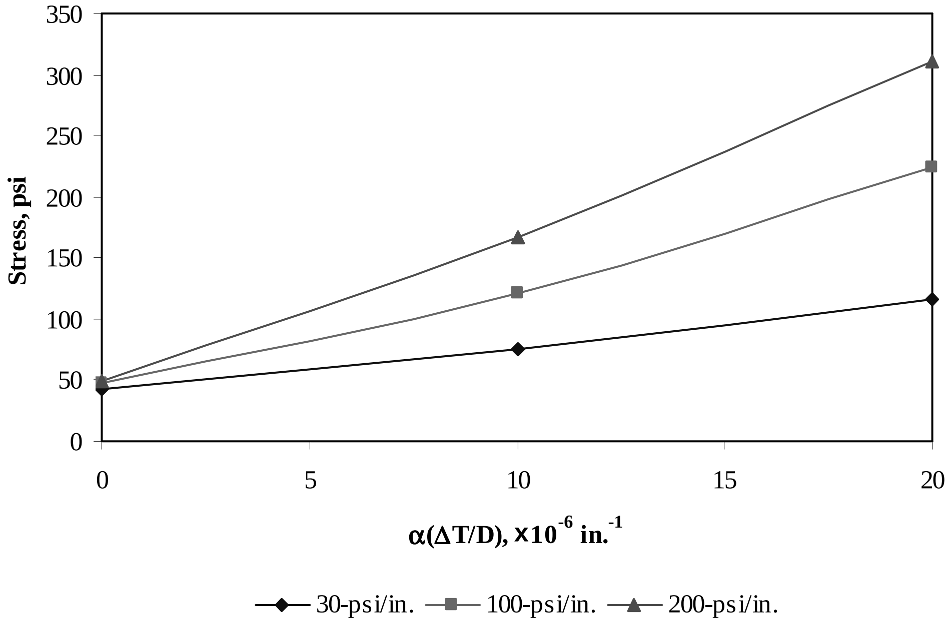


**Figure F-7-43: Impact of modulus of subgrade reaction and product α(ΔT/D) on longitudinal stress at bottom of the slab (177-in. joint spacing)**

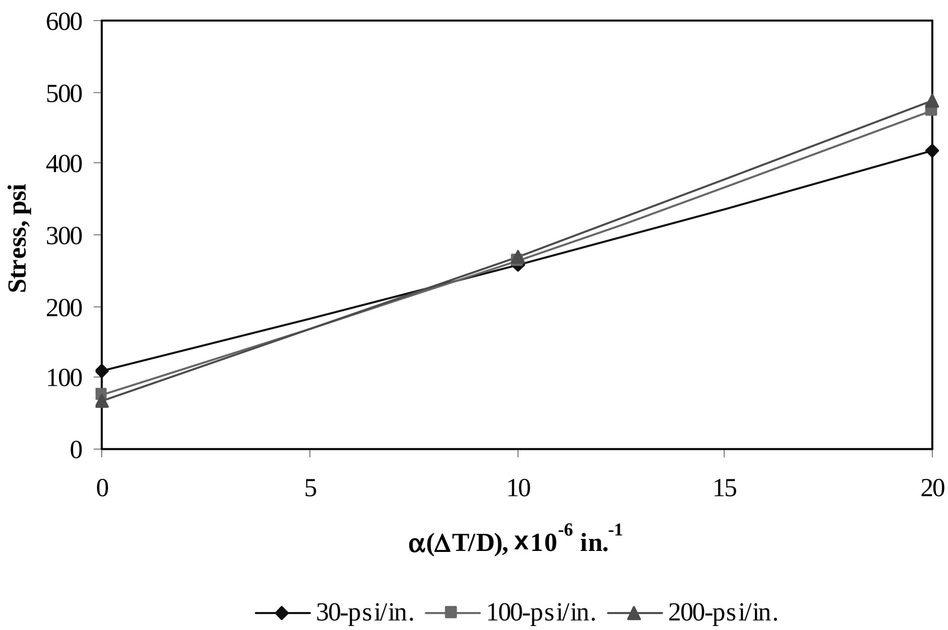


**Figure F-7-44: Impact of modulus of subgrade reaction and product α(ΔT/D) on longitudinal stress at bottom of the slab (315-in. joint spacing)**

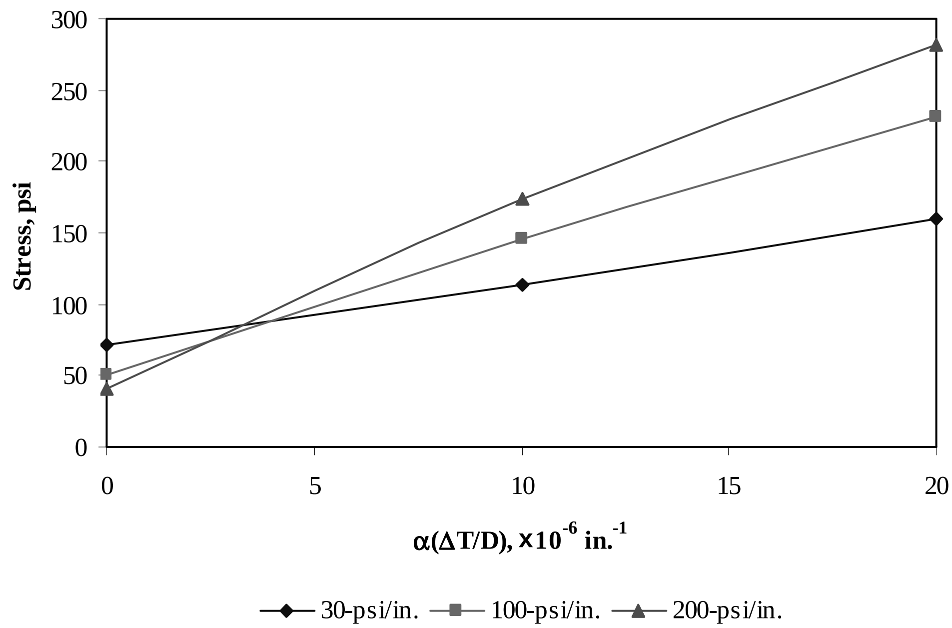


**Figure F-7-45: Impact of modulus of subgrade reaction and product α(ΔT/D) on longitudinal stress at top of the slab (177-in. joint spacing)**

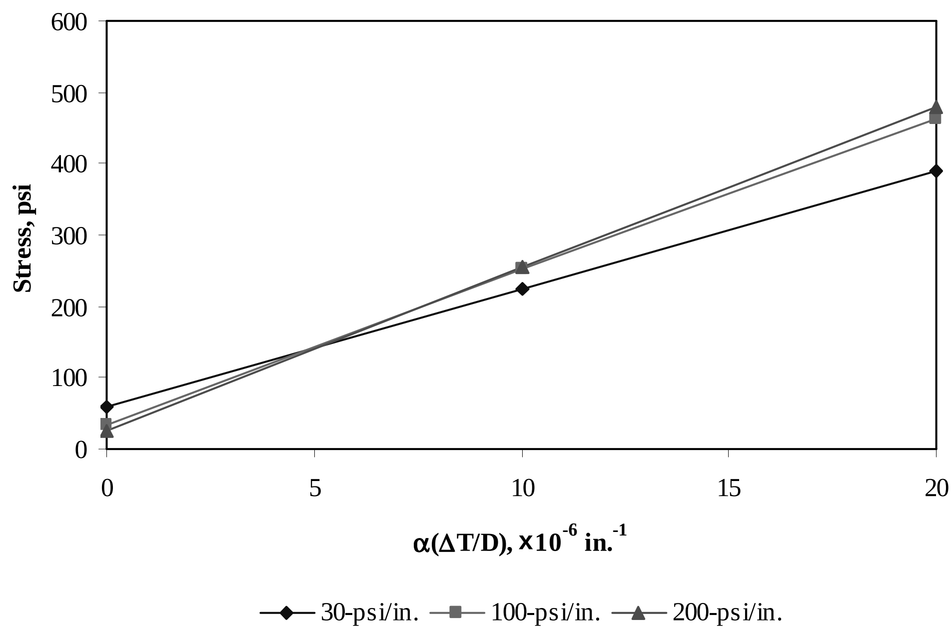


**Figure F-7-46: Impact of modulus of subgrade reaction and product α(ΔT/D) on longitudinal stress at top of the slab (315-in. joint spacing)**

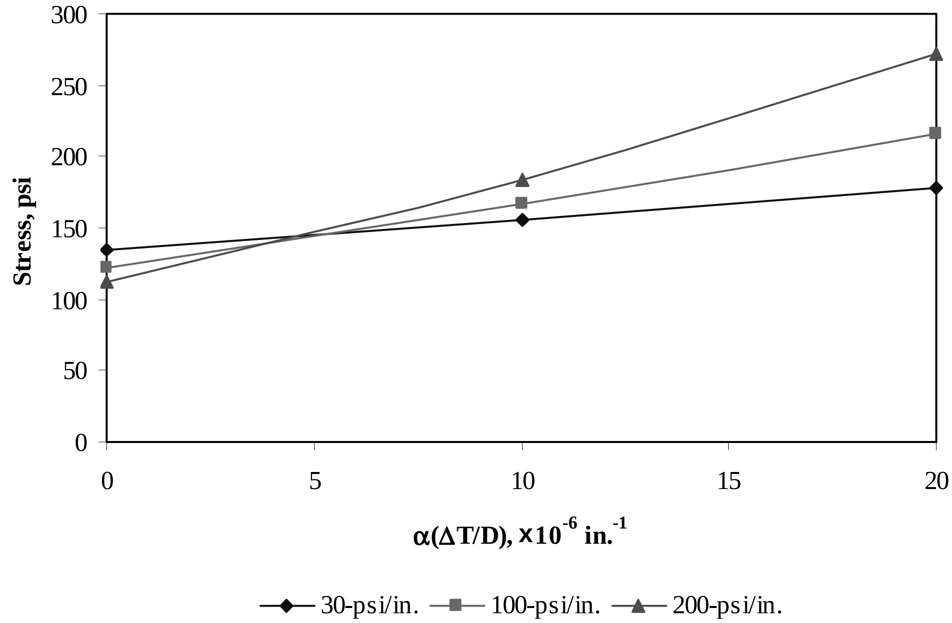


**Figure F-7-47: Impact of modulus of subgrade reaction and product $\alpha(\Delta T/D)$ on transverse stress at bottom of the slab (177-in. joint spacing)**

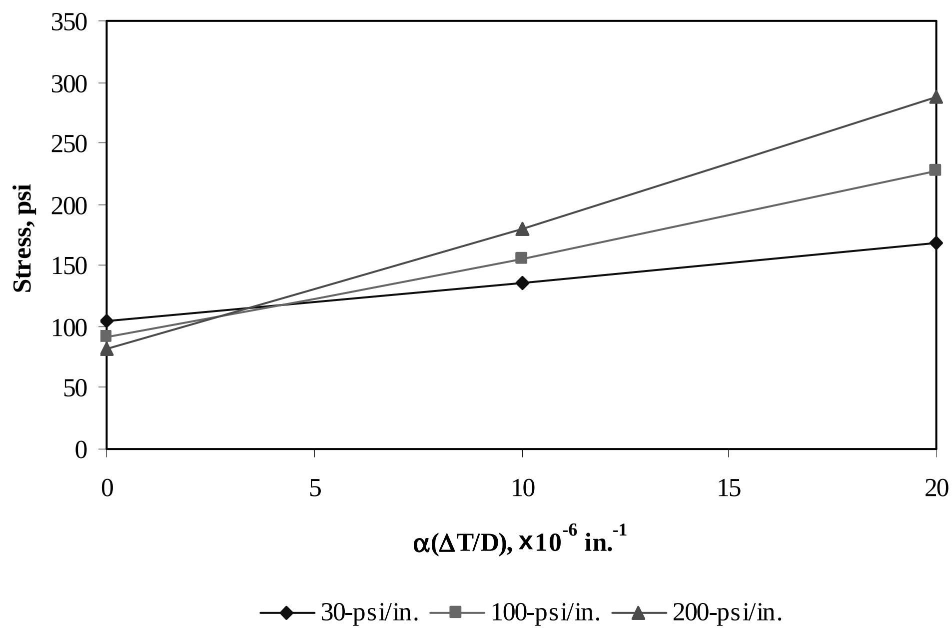


**Figure F-7-48: Impact of modulus of subgrade reaction and product $\alpha(\Delta T/D)$ on transverse stress at bottom of the slab (315-in. joint spacing)**

Figures F-7-49 through F-7-51 illustrate the impact of joint spacing and product α(ΔT/D) on stresses (10-in. PCC thickness, 16-in. base/subbase thickness, 100-psi/in. modulus of subgrade reaction and PCC shoulder)

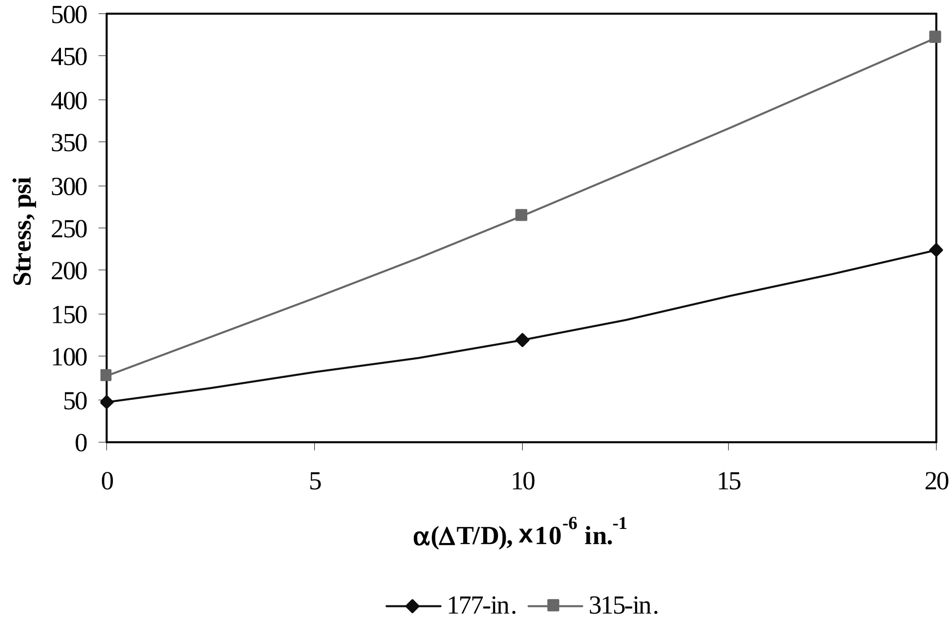


**Figure F-7-49: Impact of joint spacing and product α(ΔT/D) on longitudinal stress at bottom of the slab**

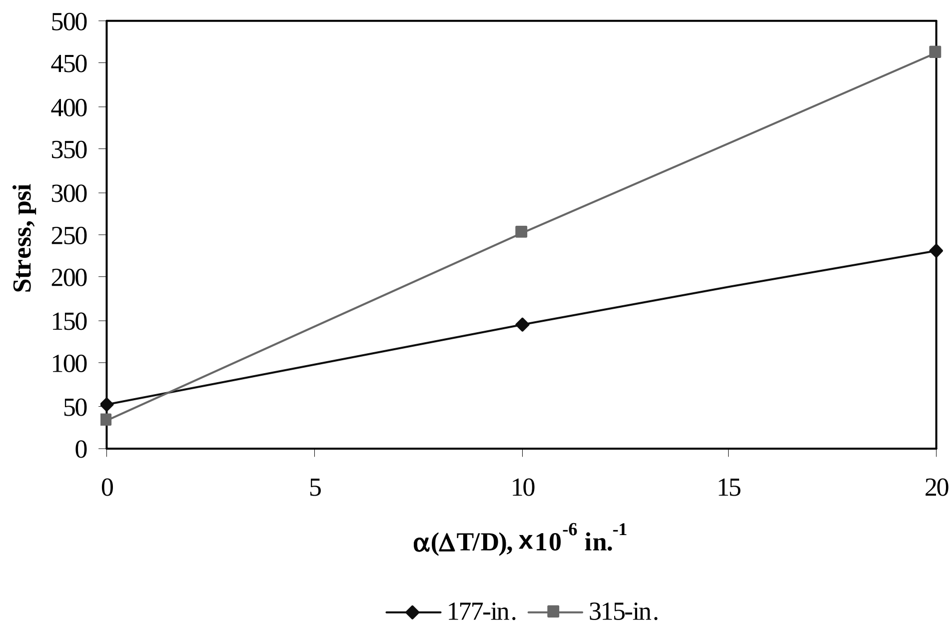


**Figure F-7-50: Impact of joint spacing and product α(ΔT/D) on longitudinal stress at top of the slab**

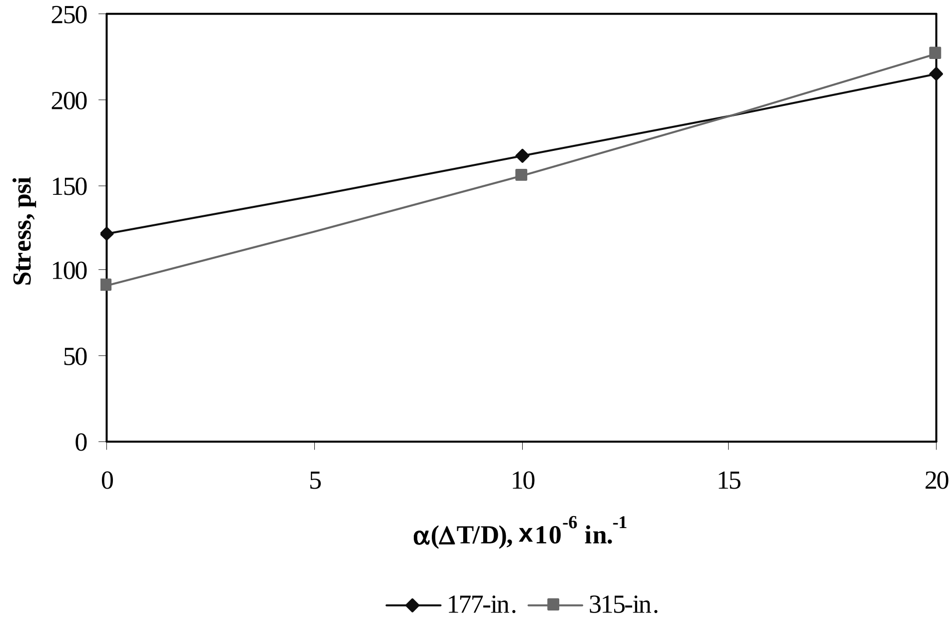


**Figure F-7-51: Impact of joint spacing and product α(ΔT/D) on transverse stress at bottom of the slab**

**Sub Appendix F-8**

**Documentation of Pavement Responses for**


**104-kips Multi-axle (8)**

Figures F-8-1 through F-8-12 illustrate the impact of PCC thickness and base/subbase thickness on stresses (100-psi/in. modulus of subgrade reaction and PCC shoulder)

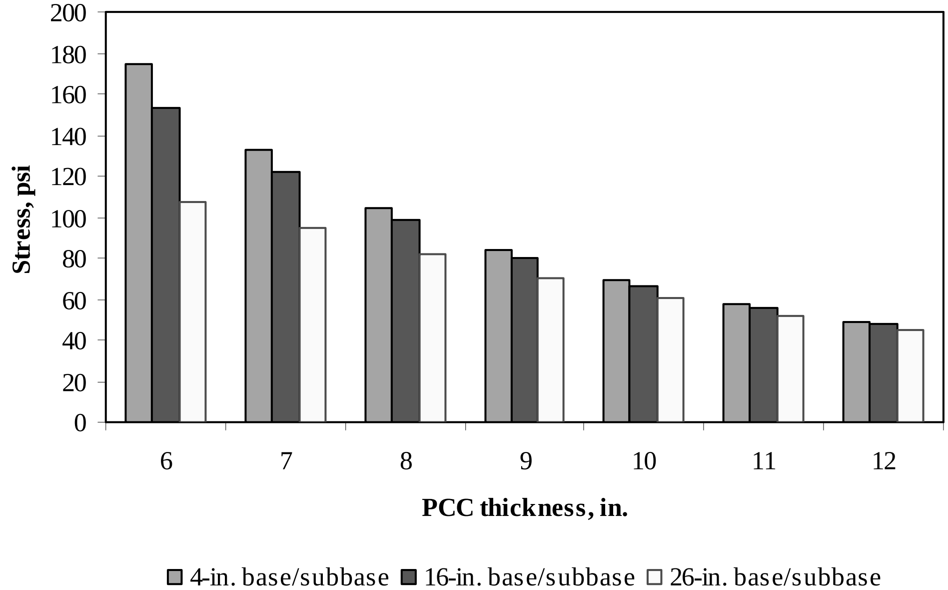


**Figure F-8-1: Impact of PCC thickness and base/subbase thickness on longitudinal stress at bottom of the Slab (177-in. joint spacing and $\alpha(\Delta T/D)$ of 0 in.$^{-1}$)**

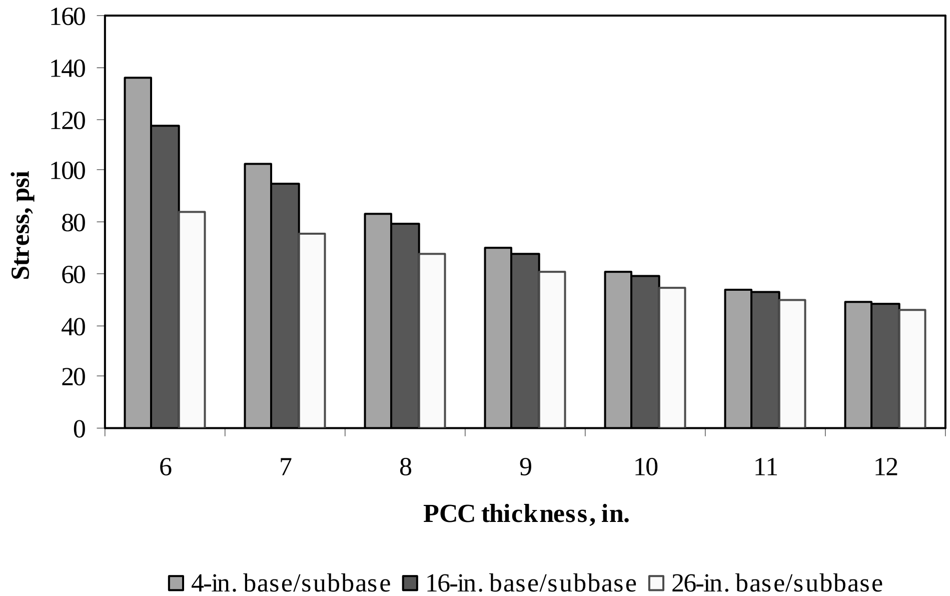


**Figure F-8-2: Impact of PCC thickness and base/subbase thickness on longitudinal stress at bottom of the Slab (315-in. joint spacing and $\alpha(\Delta T/D)$ of 0 in.$^{-1}$)**

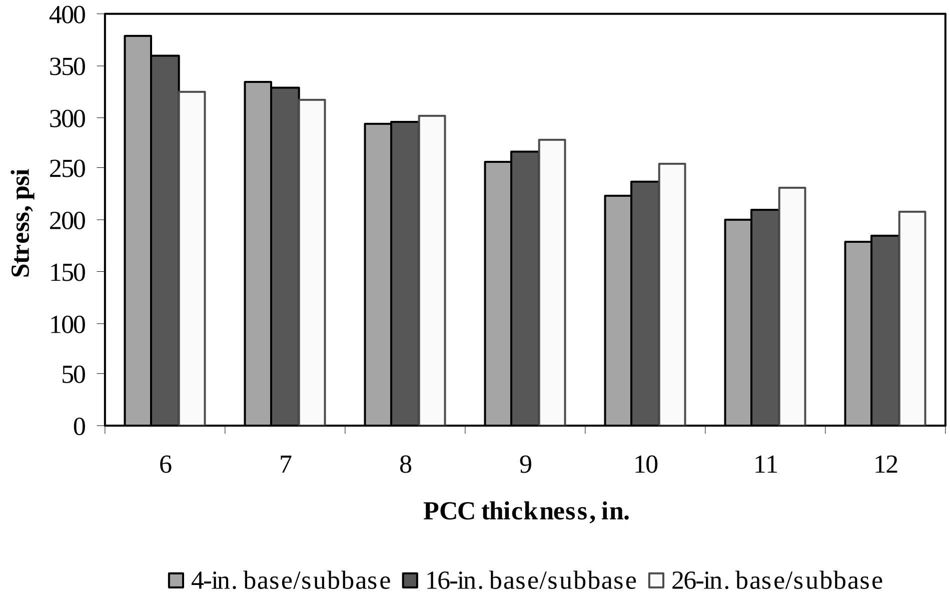


**Figure F-8-3: Impact of PCC thickness and base/subbase thickness on longitudinal stress at bottom of the Slab (177-in. joint spacing and $\alpha(\Delta T/D)$ of $20 \times 10^{-6}$ in.$^{-1}$)**

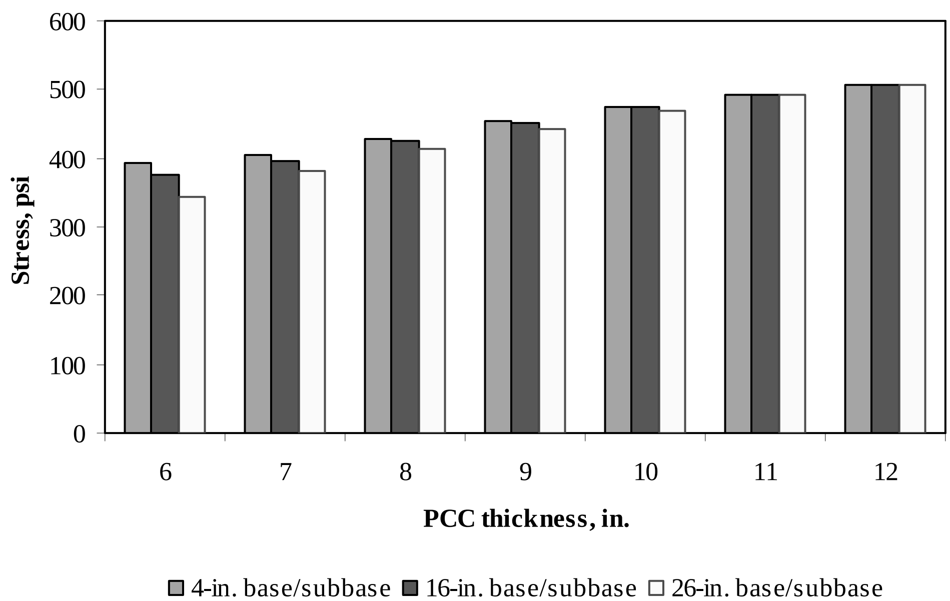


**Figure F-8-4: Impact of PCC thickness and base/subbase thickness on longitudinal stress at bottom of the Slab (315-in. joint spacing and $\alpha(\Delta T/D)$ of $20 \times 10^{-6}$ in.$^{-1}$)**

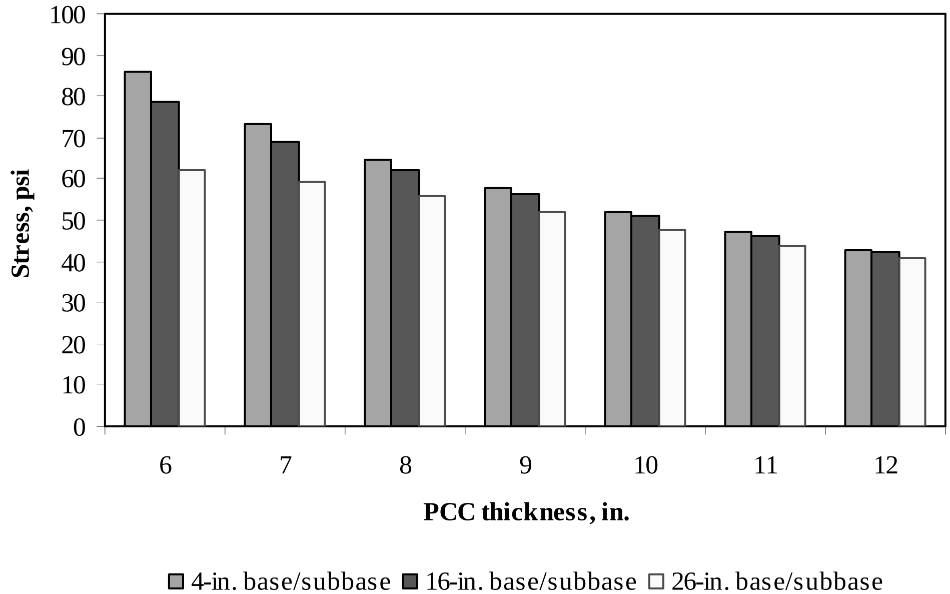


**Figure F-8-5: Impact of PCC thickness and base/subbase thickness on longitudinal stress at top of the Slab (177-in. joint spacing and $\alpha(\Delta T/D)$ of 0 in.$^{-1}$)**

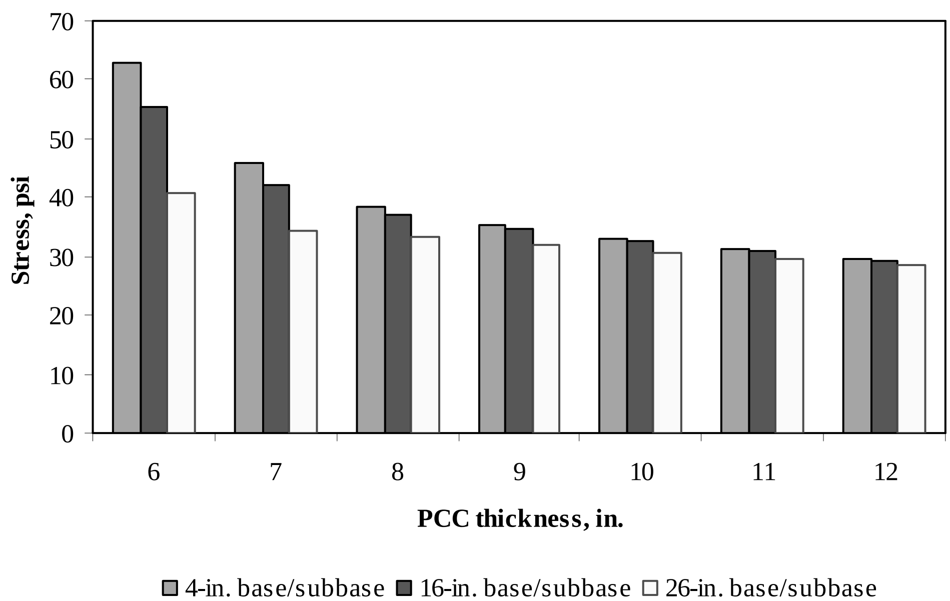


**Figure F-8-6: Impact of PCC thickness and base/subbase thickness on longitudinal stress at top of the Slab (315-in. joint spacing and $\alpha(\Delta T/D)$ of 0 in.$^{-1}$)**

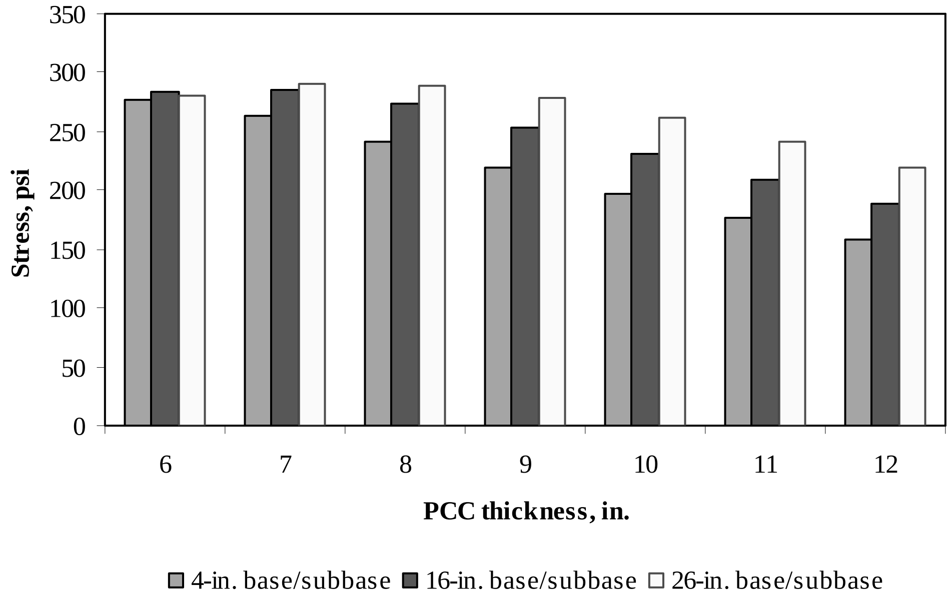


**Figure F-8-7: Impact of PCC thickness and base/subbase thickness on longitudinal stress at top of the Slab (177-in. joint spacing and $\alpha(\Delta T/D)$ of -20x10$^{-6}$ in.$^{-1}$)**

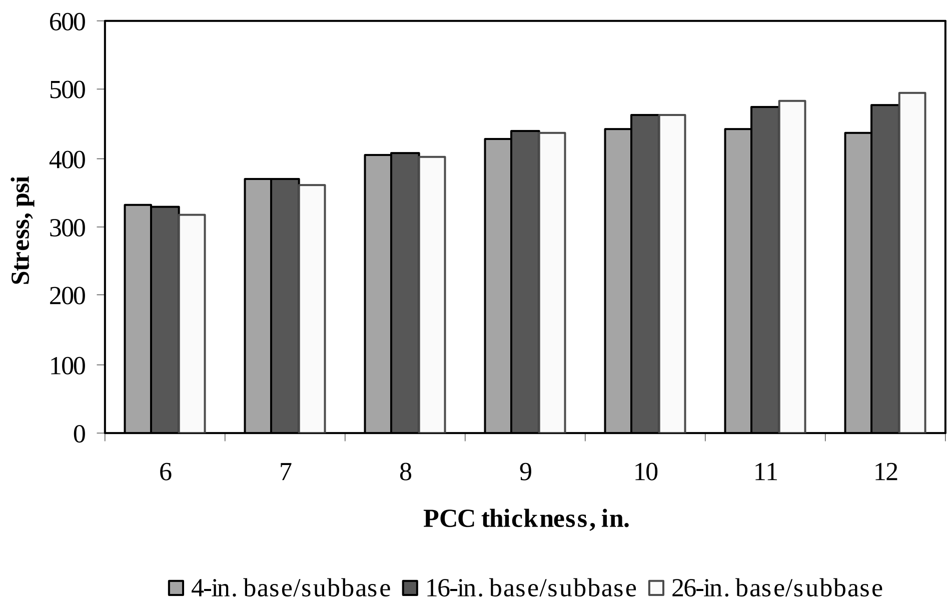


**Figure F-8-8: Impact of PCC thickness and base/subbase thickness on longitudinal stress at top of the Slab (315-in. joint spacing and $\alpha(\Delta T/D)$ of -20x10$^{-6}$ in.$^{-1}$)**

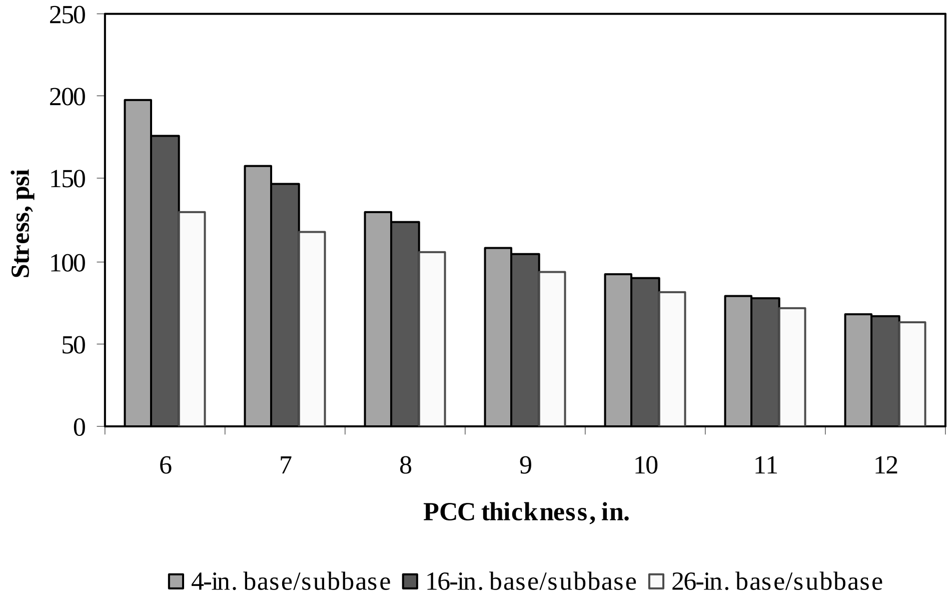


**Figure F-8-9: Impact of PCC thickness and base/subbase thickness on transverse stress at bottom of the Slab (177-in. joint spacing and $\alpha(\Delta T/D)$ of 0 in.$^{-1}$)**

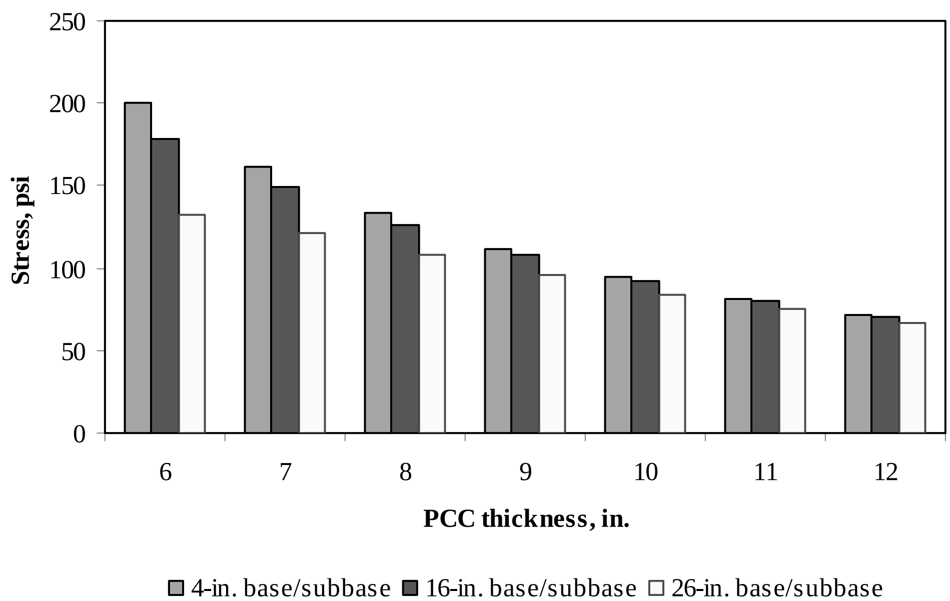


**Figure F-8-10: Impact of PCC thickness and base/subbase thickness on transverse stress at bottom of the Slab (315-in. joint spacing and $\alpha(\Delta T/D)$ of 0 in.$^{-1}$)**

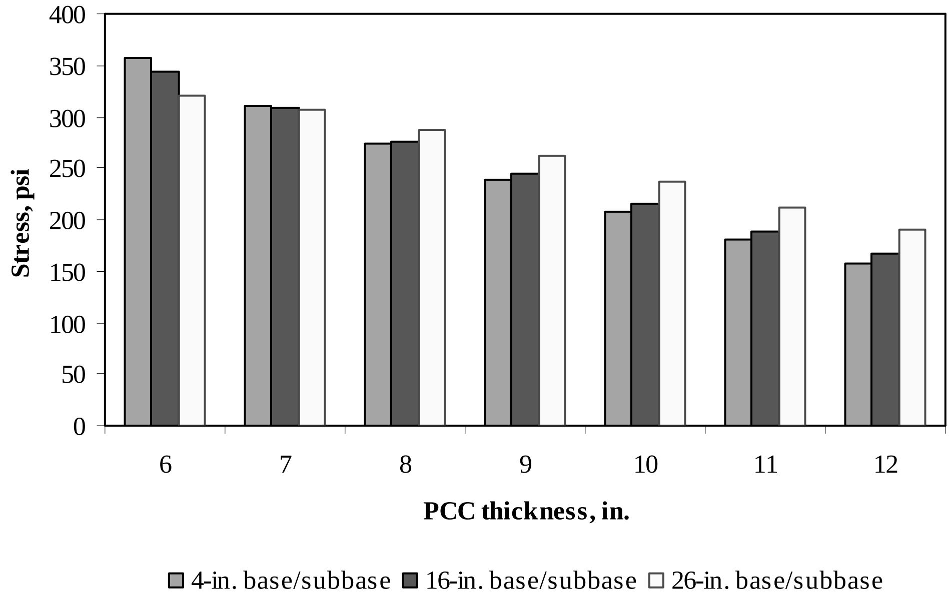


**Figure F-8-11: Impact of PCC thickness and base/subbase thickness on transverse stress at bottom of the Slab (177-in. joint spacing and $\alpha(\Delta T/D)$ of $20x10^{-6}$ in.$^{-1}$)**

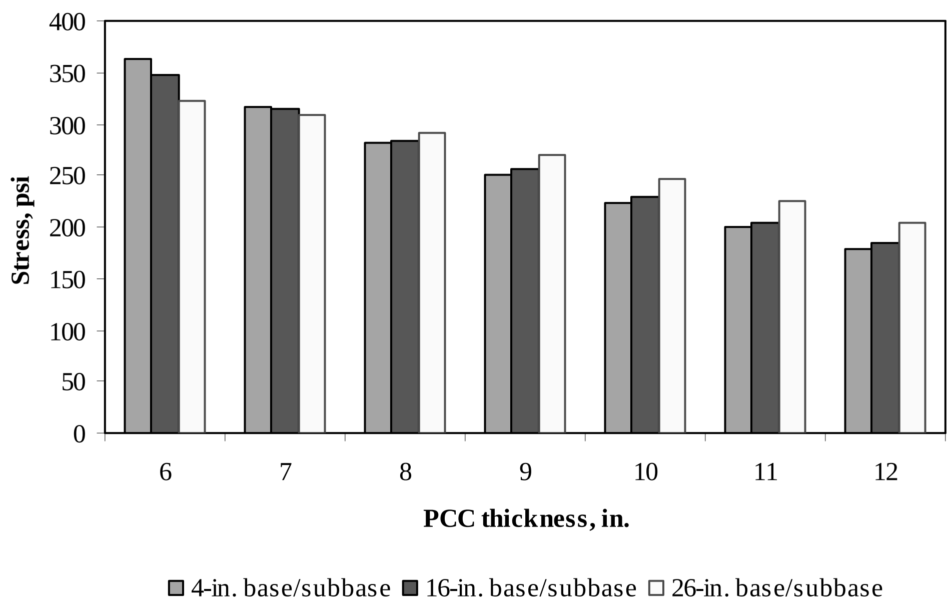


**Figure F-8-12: Impact of PCC thickness and base/subbase thickness on transverse stress at bottom of the Slab (315-in. joint spacing and $\alpha(\Delta T/D)$ of $20x10^{-6}$ in.$^{-1}$)**

Figures F-8-13 through F-8-24 illustrate the impact of PCC thickness and modulus of subgrade reaction on stresses (16-in. base/subbase thickness and PCC shoulder)

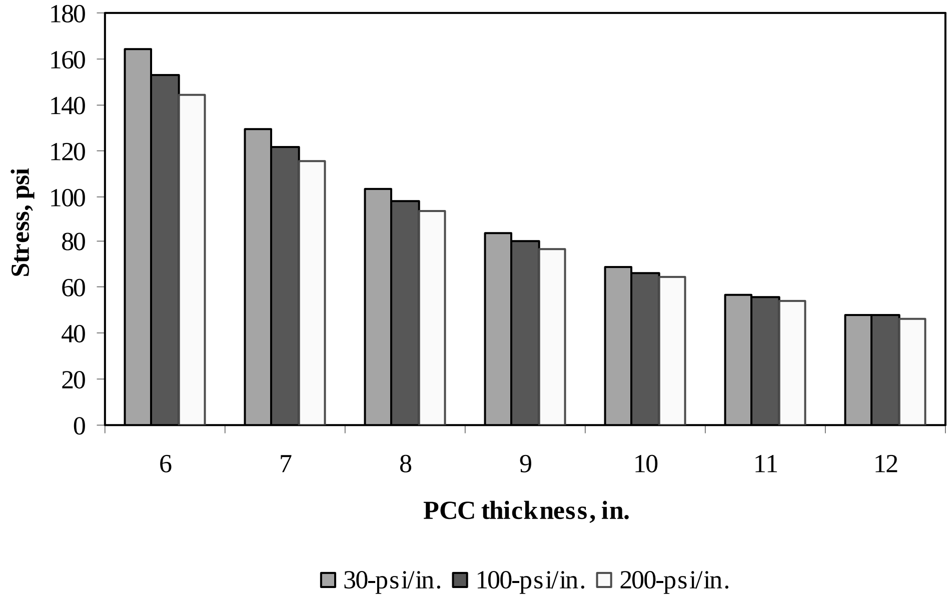


**Figure F-8-13: Impact of PCC thickness and modulus of subgrade reaction on longitudinal stress at bottom of the slab (177-in. joint spacing and $\alpha(\Delta T/D)$ of 0 in.$^{-1}$)**

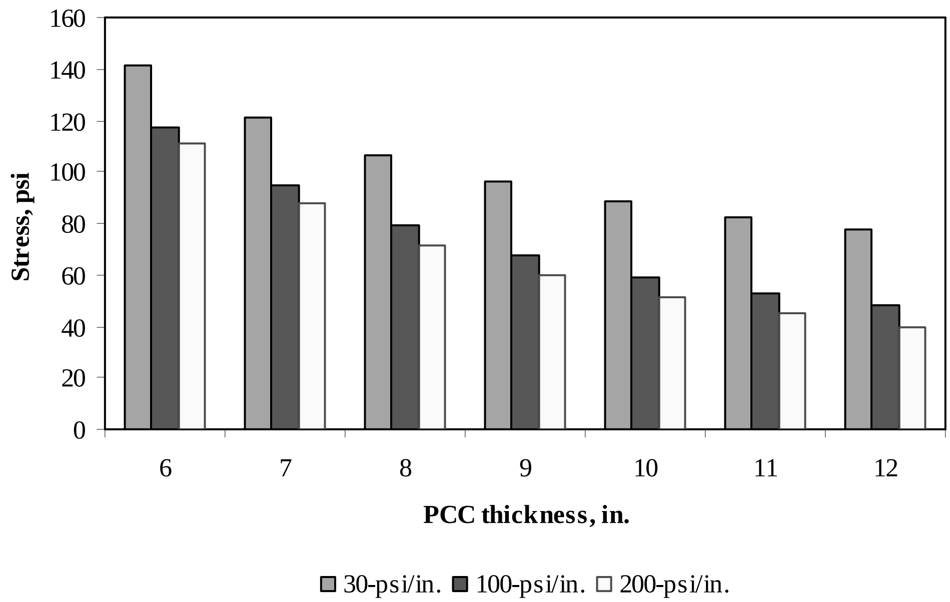


**Figure F-8-14: Impact of PCC thickness and modulus of subgrade reaction on longitudinal stress at bottom of the slab (315-in. joint spacing and $\alpha(\Delta T/D)$ of 0 in.$^{-1}$)**

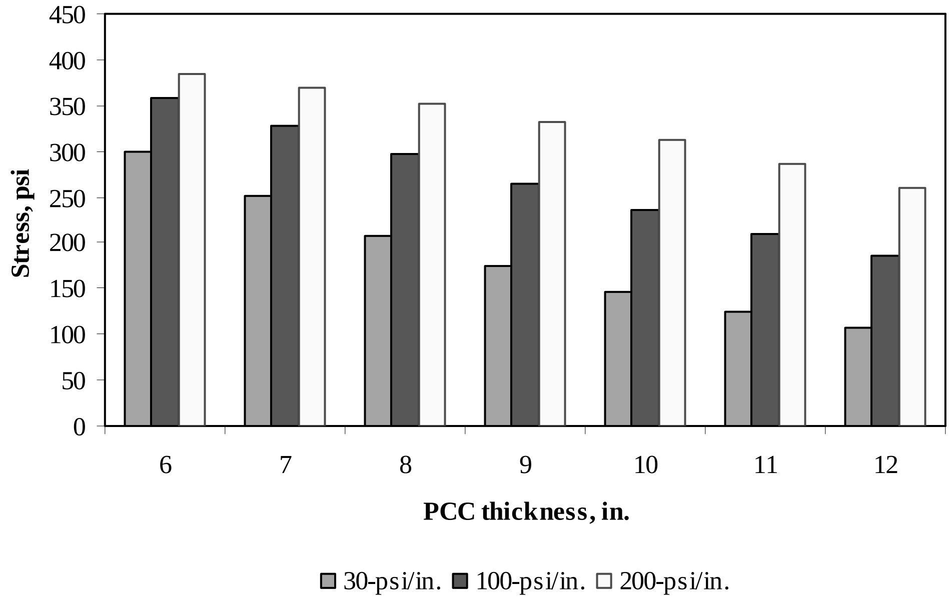


**Figure F-8-15: Impact of PCC thickness and modulus of subgrade reaction on longitudinal stress at bottom of the slab (177-in. joint spacing and $\alpha(\Delta T/D)$ of $20x10^{-6}$ in.$^{-1}$)**

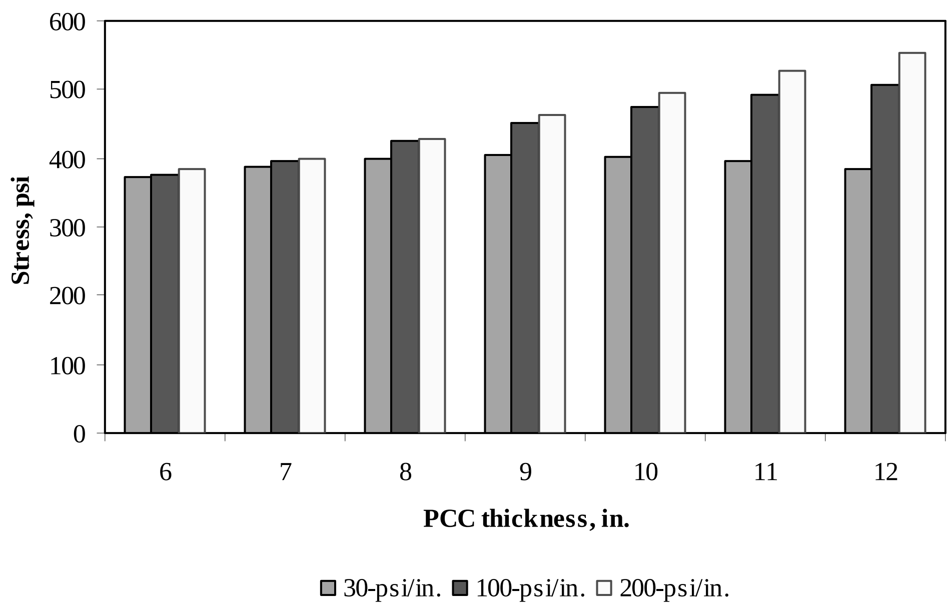


**Figure F-8-16: Impact of PCC thickness and modulus of subgrade reaction on longitudinal stress at bottom of the slab (315-in. joint spacing and $\alpha(\Delta T/D)$ of $20x10^{-6}$ in.$^{-1}$)**

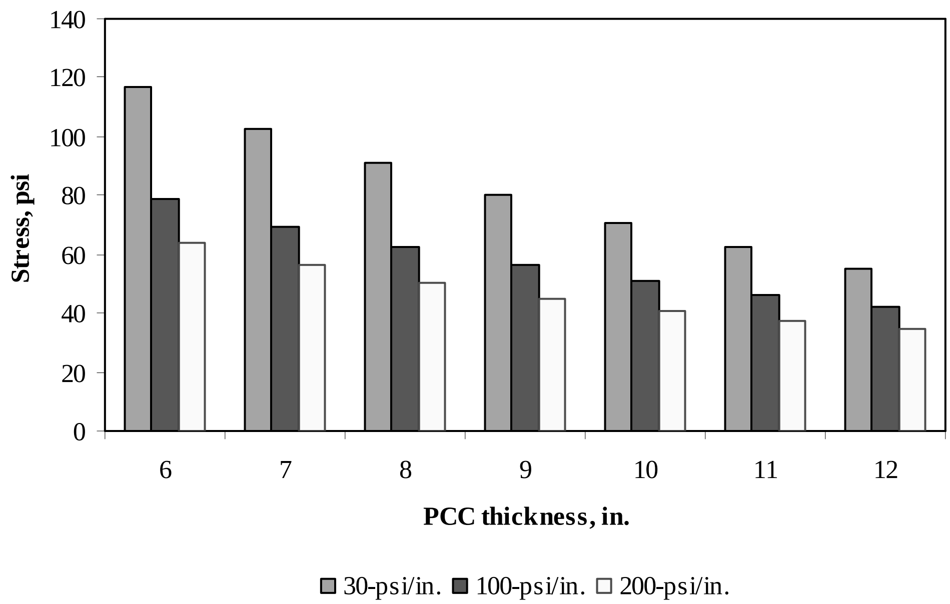


**Figure F-8-17: Impact of PCC thickness and modulus of subgrade reaction on longitudinal stress at top of the Slab (177-in. joint spacing and $\alpha(\Delta T/D)$ of 0 in.$^{-1}$)**

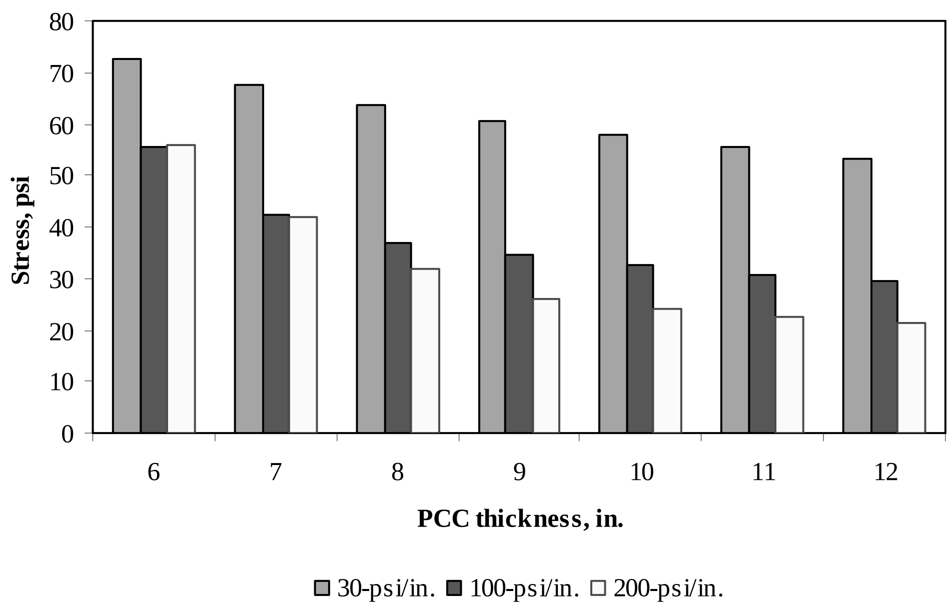


**Figure F-8-18: Impact of PCC thickness and modulus of subgrade reaction on longitudinal stress at top of the Slab (315-in. joint spacing and $\alpha(\Delta T/D)$ of 0 in.$^{-1}$)**

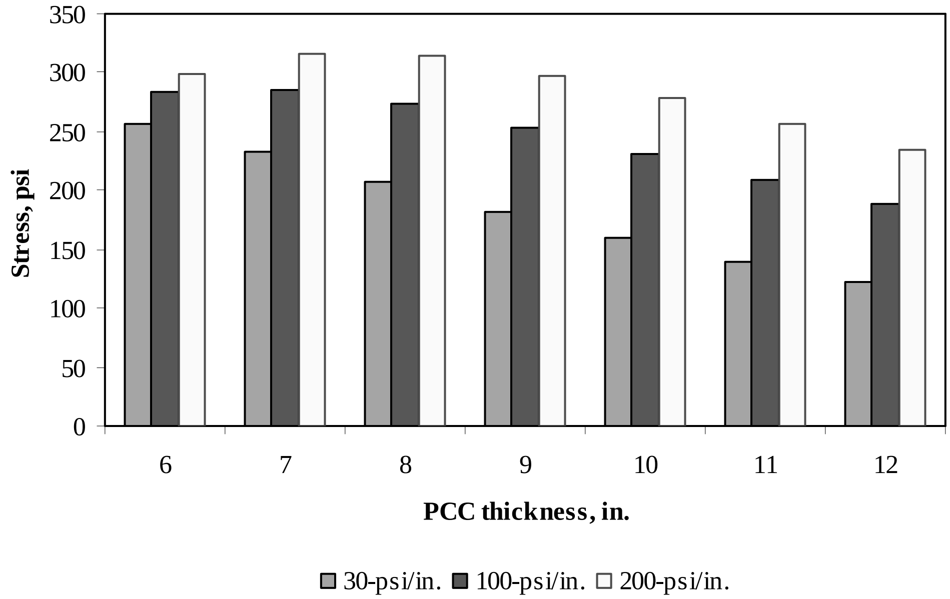


**Figure F-8-19: Impact of PCC thickness and modulus of subgrade reaction on longitudinal stress at top of the Slab (177-in. joint spacing and $\alpha(\Delta T/D)$ of $-20x10^{-6}$ in.$^{-1}$)**

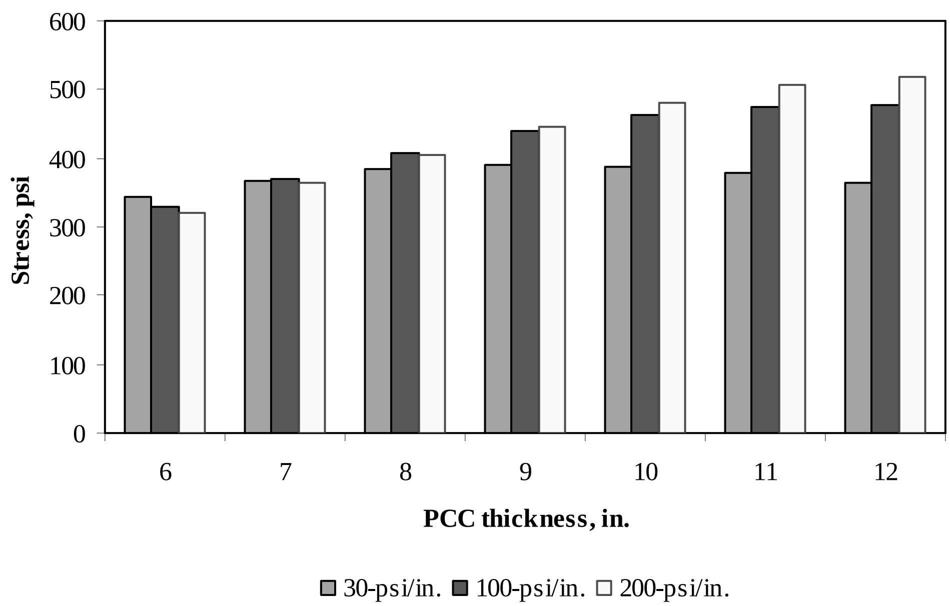


**Figure F-8-20: Impact of PCC thickness and modulus of subgrade reaction on longitudinal stress at top of the Slab (315-in. joint spacing and $\alpha(\Delta T/D)$ of $-20x10^{-6}$ in.$^{-1}$)**

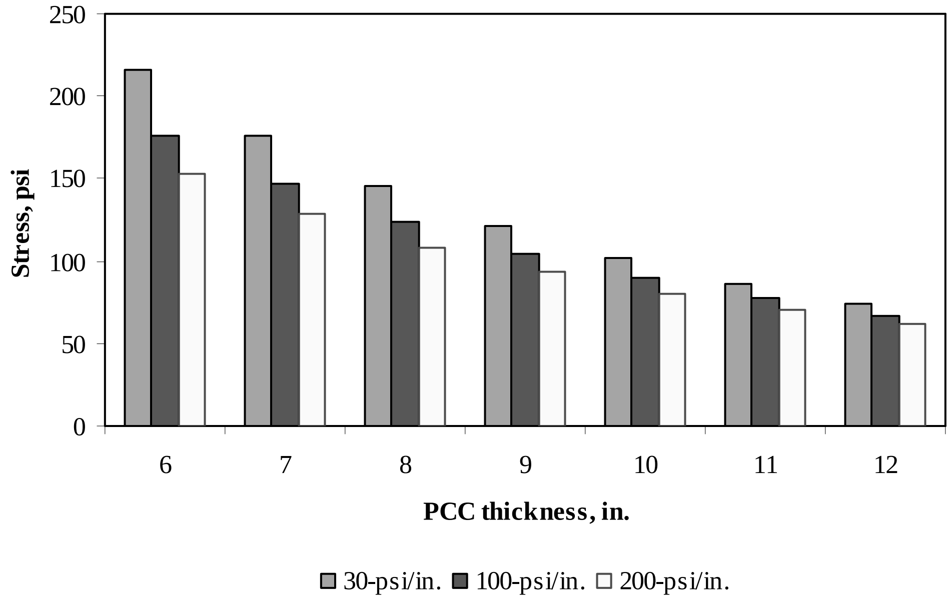


**Figure F-8-21: Impact of PCC thickness and modulus of subgrade reaction on transverse stress at bottom of the Slab (177-in. joint spacing and $\alpha(\Delta T/D)$ of 0 in.$^{-1}$)**

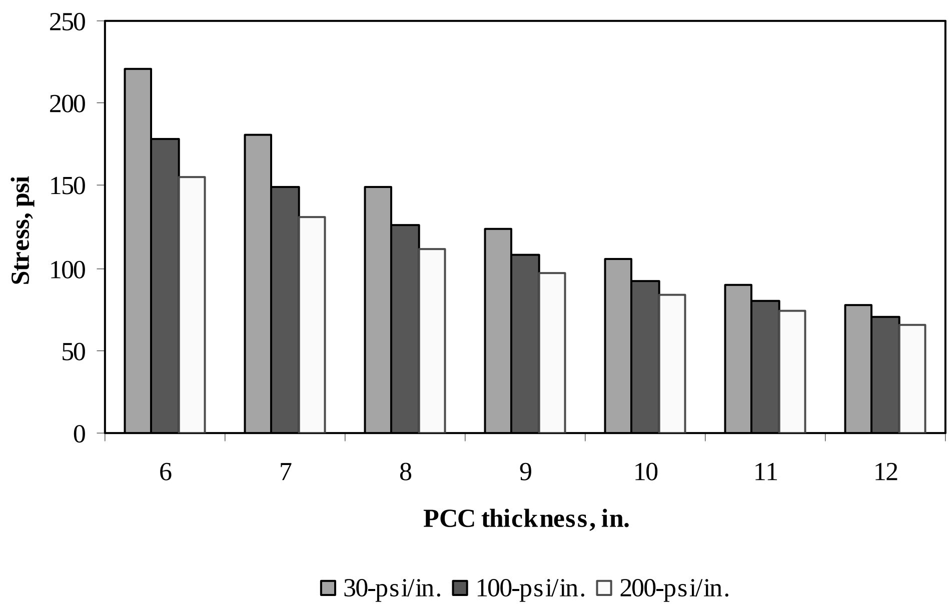


**Figure F-8-22: Impact of PCC thickness and modulus of subgrade reaction on transverse stress at bottom of the Slab (315-in. joint spacing and $\alpha(\Delta T/D)$ of 0 in.$^{-1}$)**

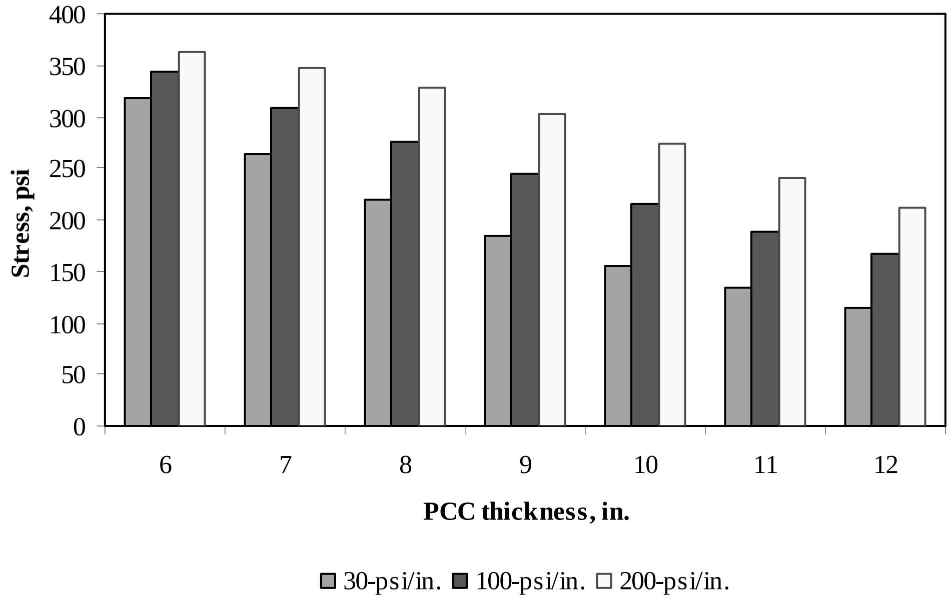


**Figure F-8-23: Impact of PCC thickness and modulus of subgrade reaction on transverse stress at bottom of the Slab (177-in. joint spacing and $\alpha(\Delta T/D)$ of 20x10$^{-6}$ in.$^{-1}$)**

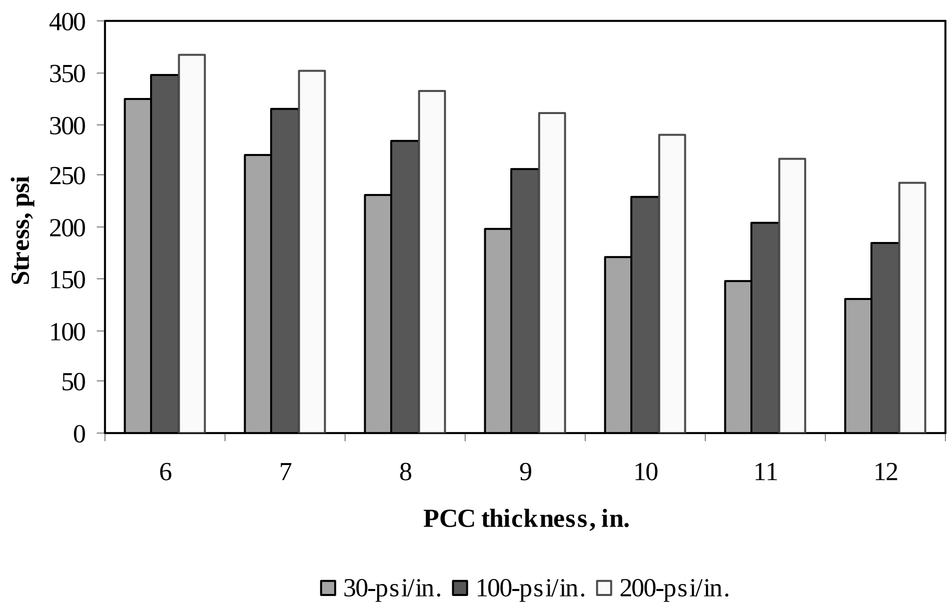


**Figure F-8-24: Impact of PCC thickness and modulus of subgrade reaction on transverse stress at bottom of the Slab (315-in. joint spacing and $\alpha(\Delta T/D)$ of 20x10$^{-6}$ in.$^{-1}$)**

Figures F-8-25 through F-8-36 illustrate the impact of PCC thickness and lateral support condition on stresses (16-in. base/subbase and 100-psi/in. modulus of subgrade reaction)

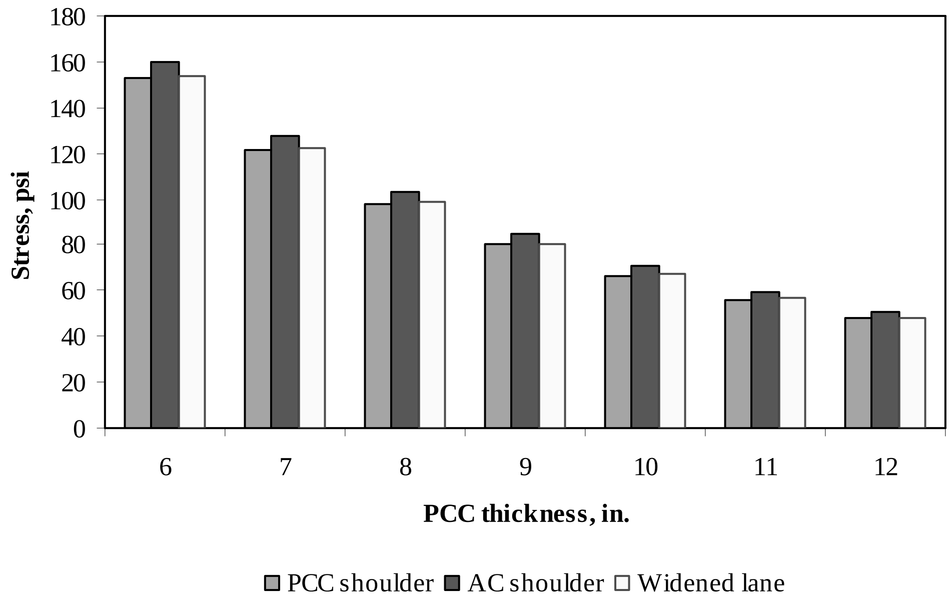


**Figure F-8-25: Impact of PCC thickness and lateral support condition on longitudinal stress at bottom of the Slab (177-in. joint spacing and $\alpha(\Delta T/D)$ of 0 in.$^{-1}$)**

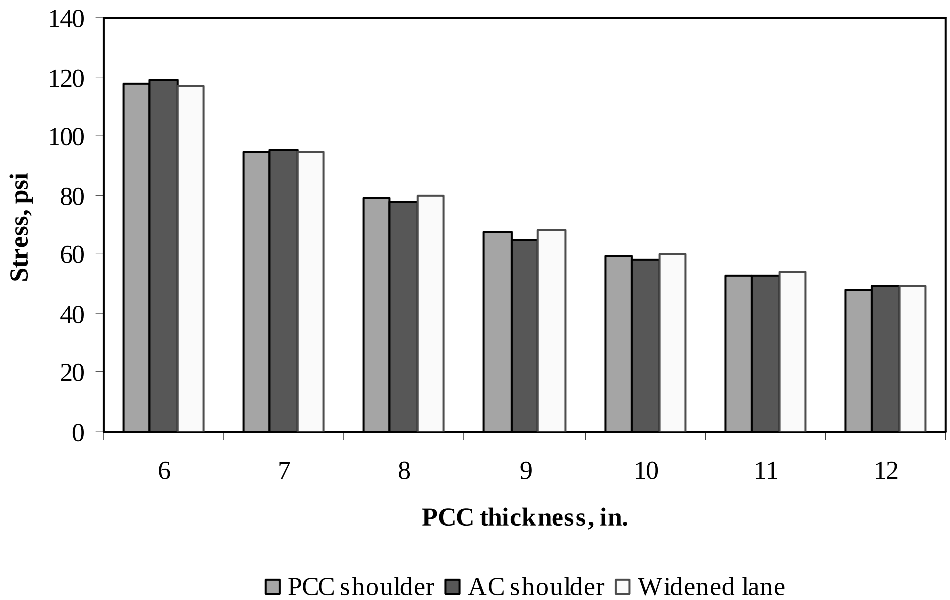


**Figure F-8-26: Impact of PCC thickness and lateral support condition on longitudinal stress at bottom of the Slab (315-in. joint spacing and $\alpha(\Delta T/D)$ of 0 in.$^{-1}$)**

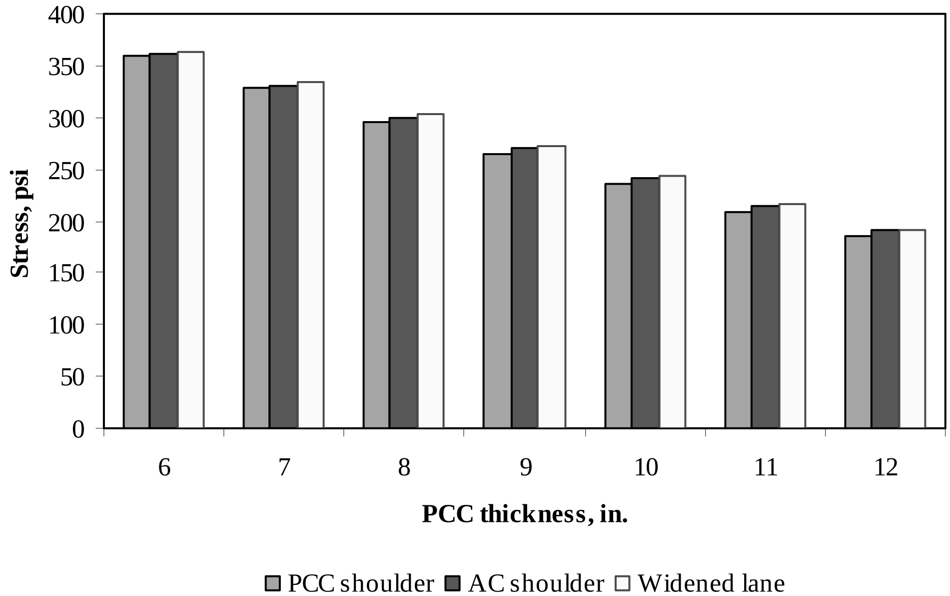


**Figure F-8-27: Impact of PCC thickness and lateral support condition on longitudinal stress at bottom of the Slab (177-in. joint spacing and $\alpha(\Delta T/D)$ of $20\text{x}10^{-6}$ in.$^{-1}$)**

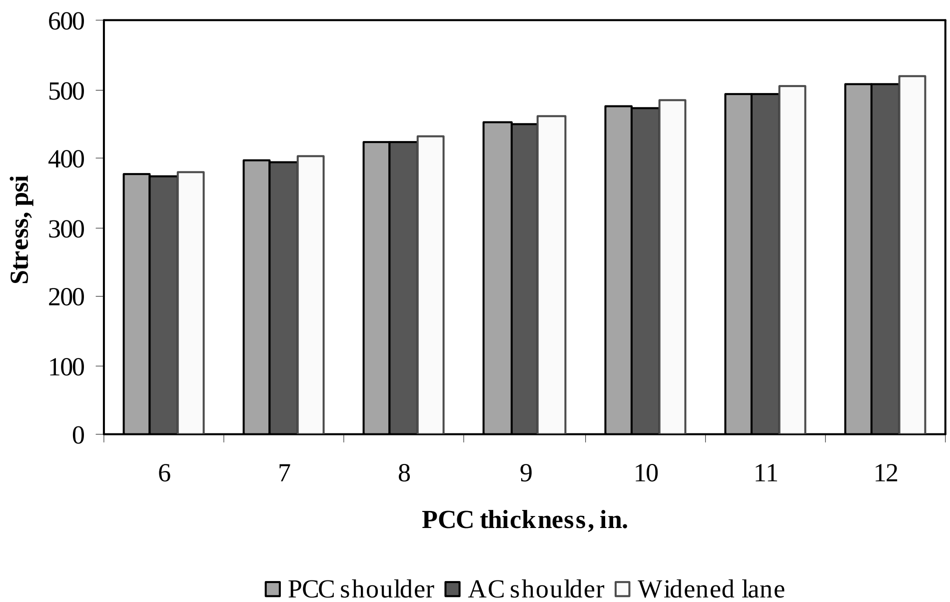


**Figure F-8-28: Impact of PCC thickness and lateral support condition on longitudinal stress at bottom of the Slab (315-in. joint spacing and $\alpha(\Delta T/D)$ of $20\text{x}10^{-6}$ in.$^{-1}$)**

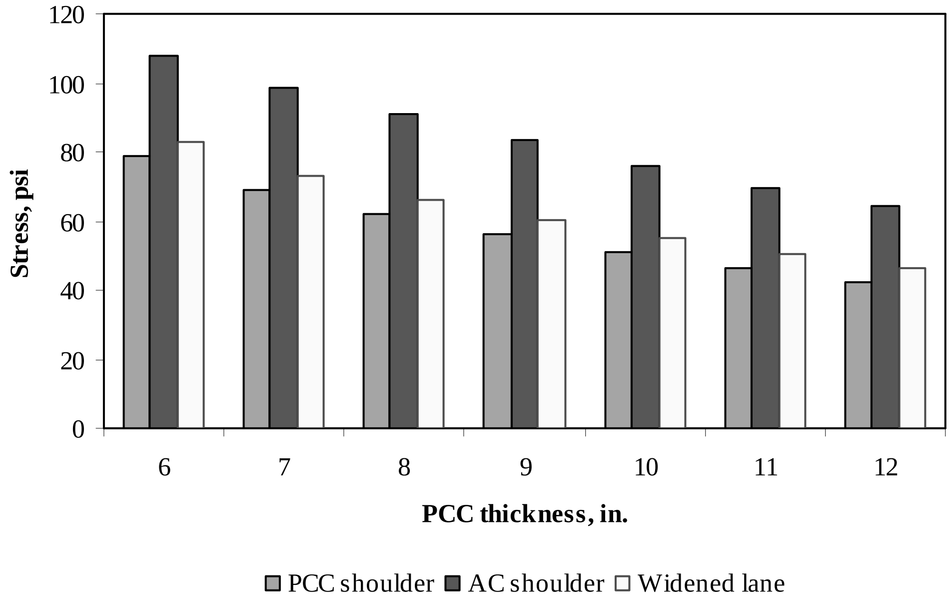


**Figure F-8-29: Impact of PCC thickness and lateral support condition on longitudinal stress at top of the Slab (177-in. joint spacing and $\alpha(\Delta T/D)$ of 0 in.$^{-1}$)**

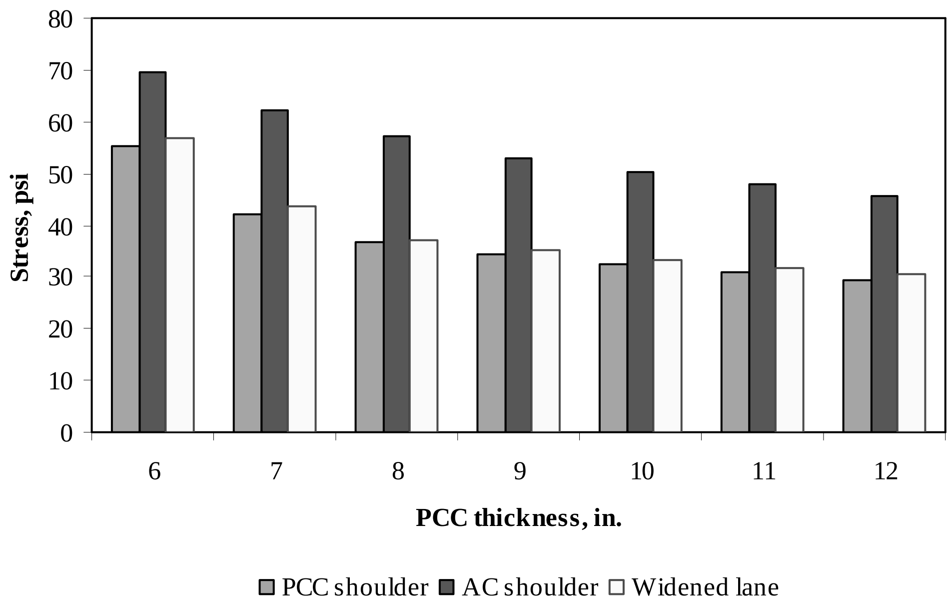


**Figure F-8-30: Impact of PCC thickness and lateral support condition on longitudinal stress at top of the Slab (315-in. joint spacing and $\alpha(\Delta T/D)$ of 0 in.$^{-1}$)**

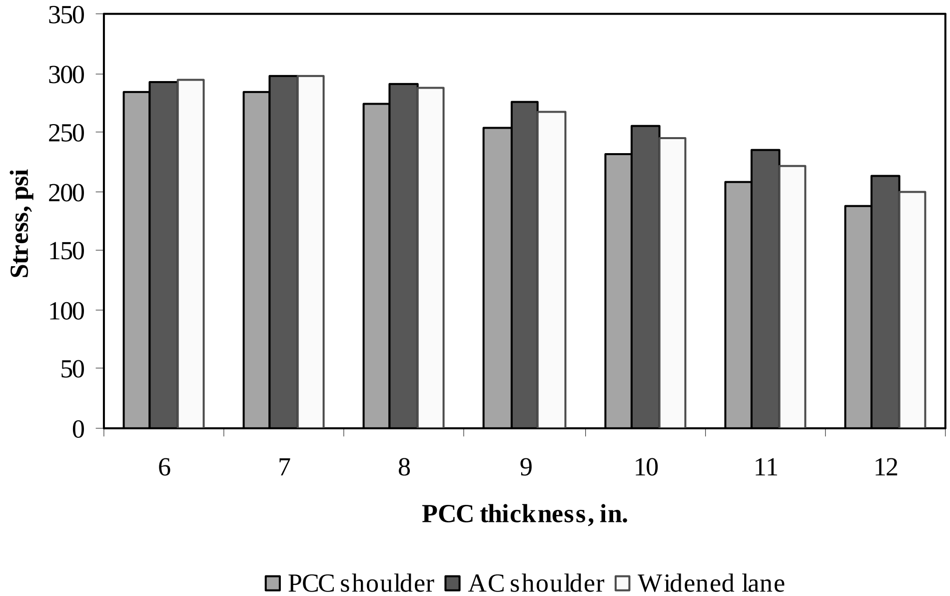


**Figure F-8-31: Impact of PCC thickness and lateral support condition on longitudinal stress at top of the Slab (177-in. joint spacing and $\alpha(\Delta T/D)$ of -20x$10^{-6}$ in.$^{-1}$)**

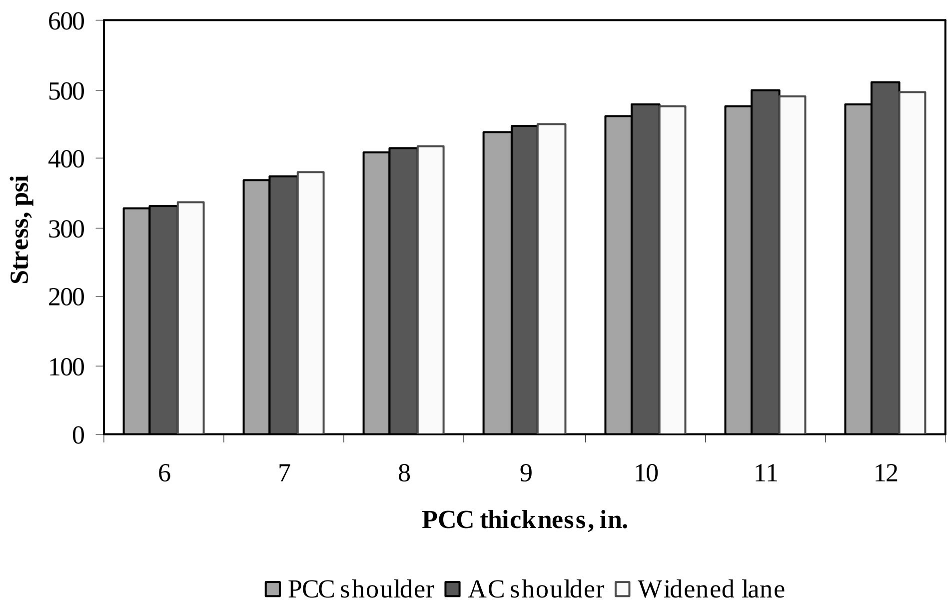


**Figure F-8-32: Impact of PCC thickness and lateral support condition on longitudinal stress at top of the Slab (315-in. joint spacing and $\alpha(\Delta T/D)$ of -20x$10^{-6}$ in.$^{-1}$)**

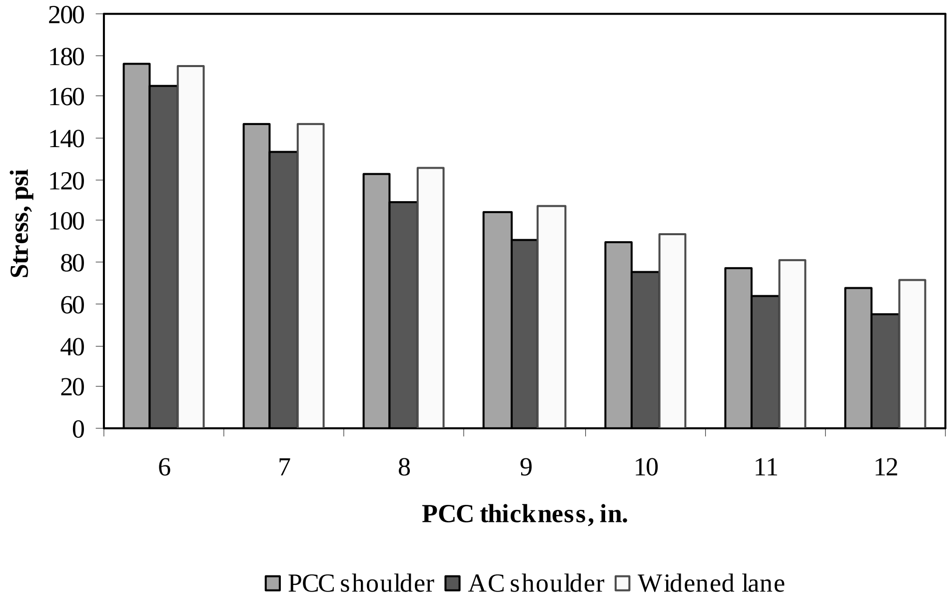


**Figure F-8-33: Impact of PCC thickness and lateral support condition on transverse stress at bottom of the Slab (177-in. joint spacing and $\alpha(\Delta T/D)$ of 0 in.$^{-1}$)**

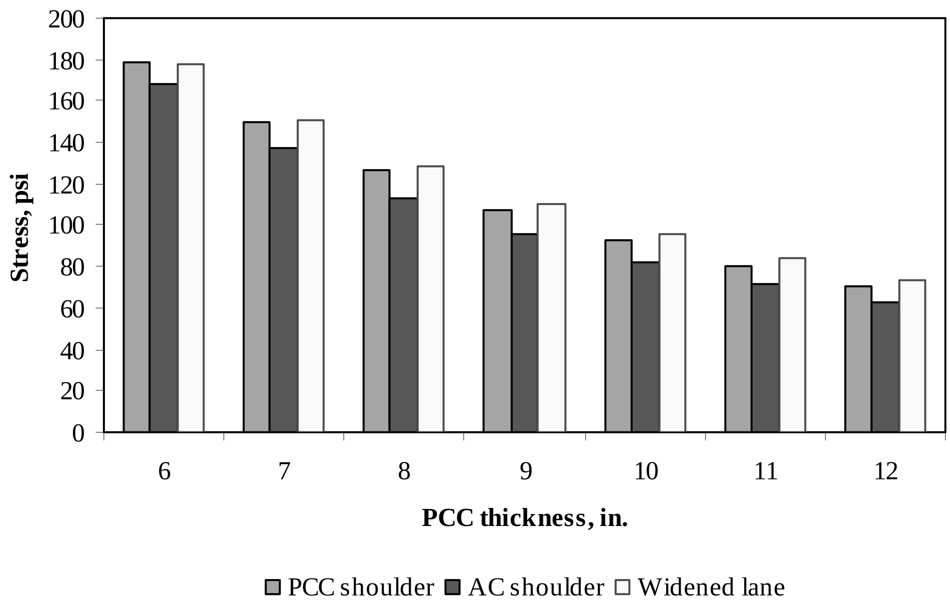


**Figure F-8-34: Impact of PCC thickness and lateral support condition on transverse stress at bottom of the Slab (315-in. joint spacing and $\alpha(\Delta T/D)$ of 0 in.$^{-1}$)**

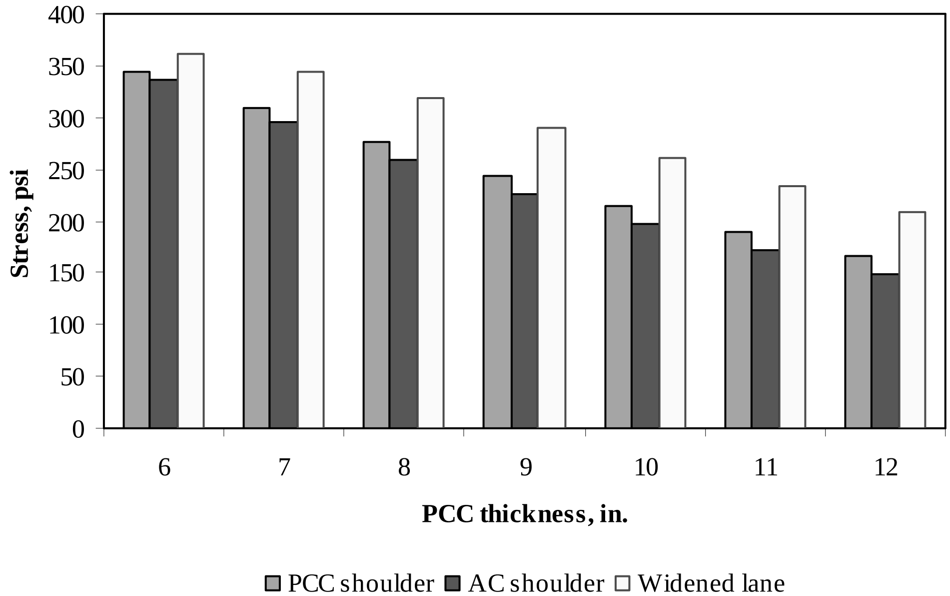


**Figure F-8-35: Impact of PCC thickness and lateral support condition on transverse stress at bottom of the Slab (177-in. joint spacing and $\alpha(\Delta T/D)$ of $20x10^{-6}$ in.$^{-1}$)**

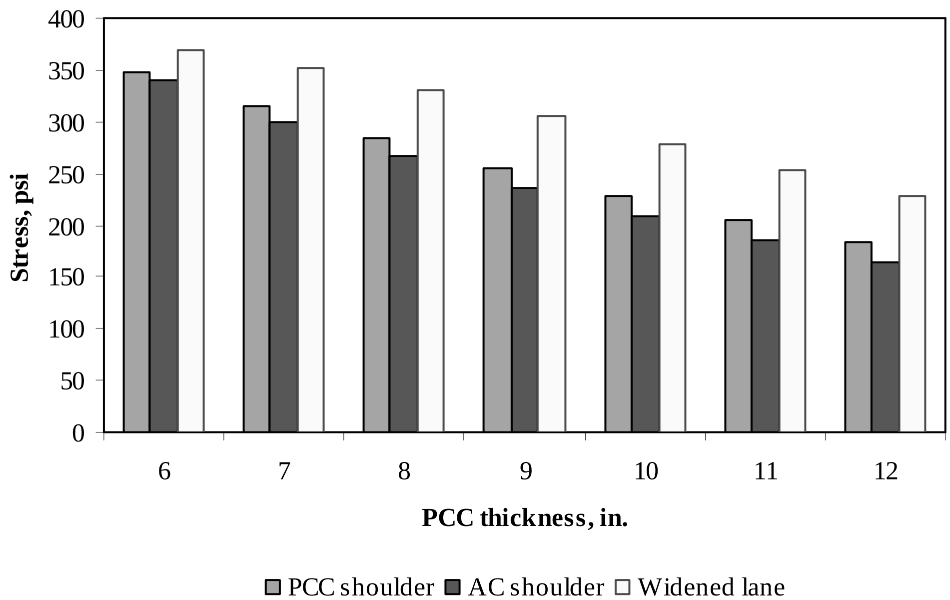


**Figure F-8-36: Impact of PCC thickness and lateral support condition on transverse stress at bottom of the Slab (315-in. joint spacing and $\alpha(\Delta T/D)$ of $20x10^{-6}$ in.$^{-1}$)**

Figures F-8-37 through F-8-42 illustrate the impact of base/subbase thickness and product α(ΔT/D) on stresses (10-in. PCC thickness, 100-psi/in. modulus of subgrade reaction and PCC shoulder)

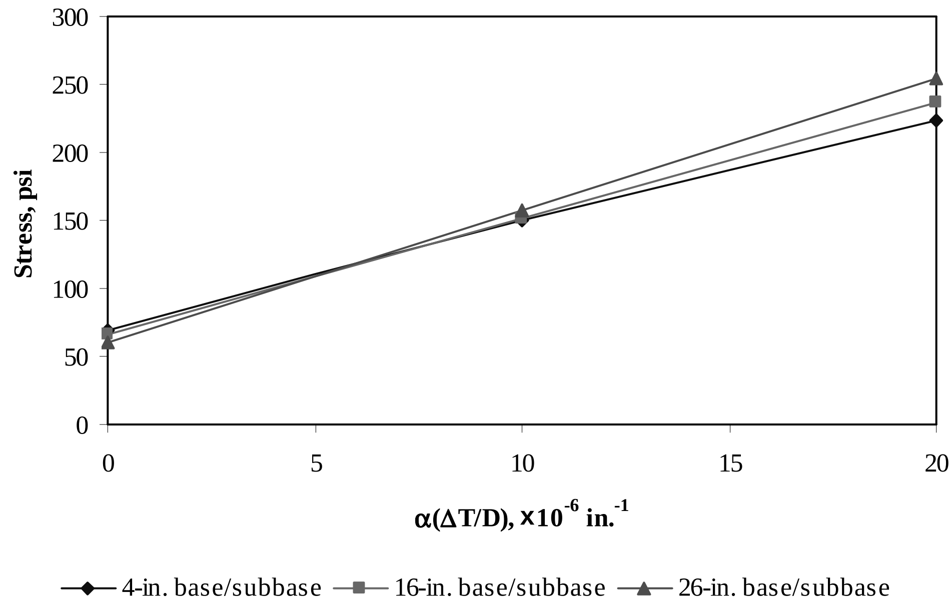


**Figure F-8-37: Impact of base/subbase thickness and product α(ΔT/D) on longitudinal stress at bottom of the slab (177-in. joint spacing)**

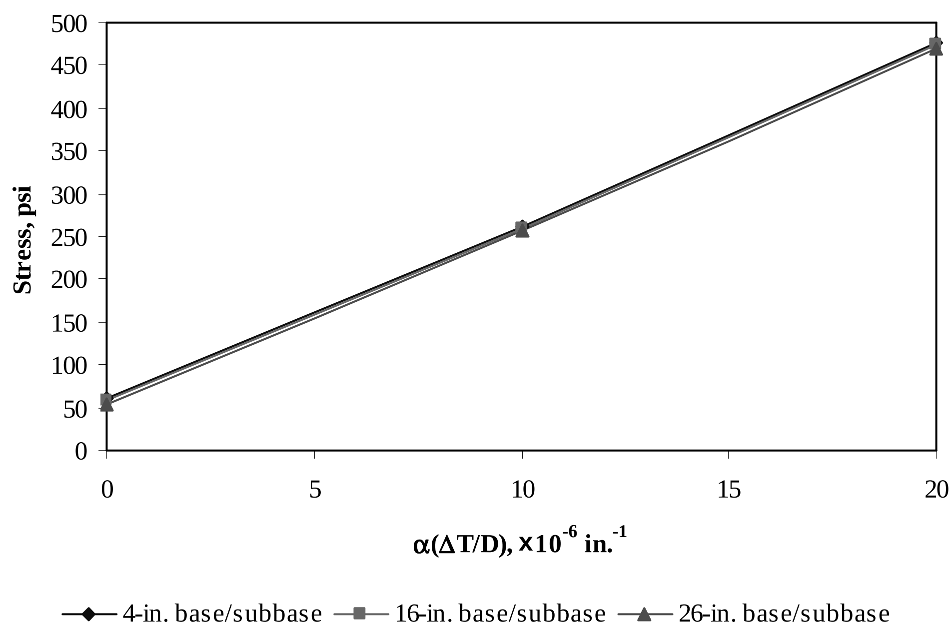


**Figure F-8-38: Impact of base/subbase thickness and product α(ΔT/D) on longitudinal stress at bottom of the slab (315-in. joint spacing)**

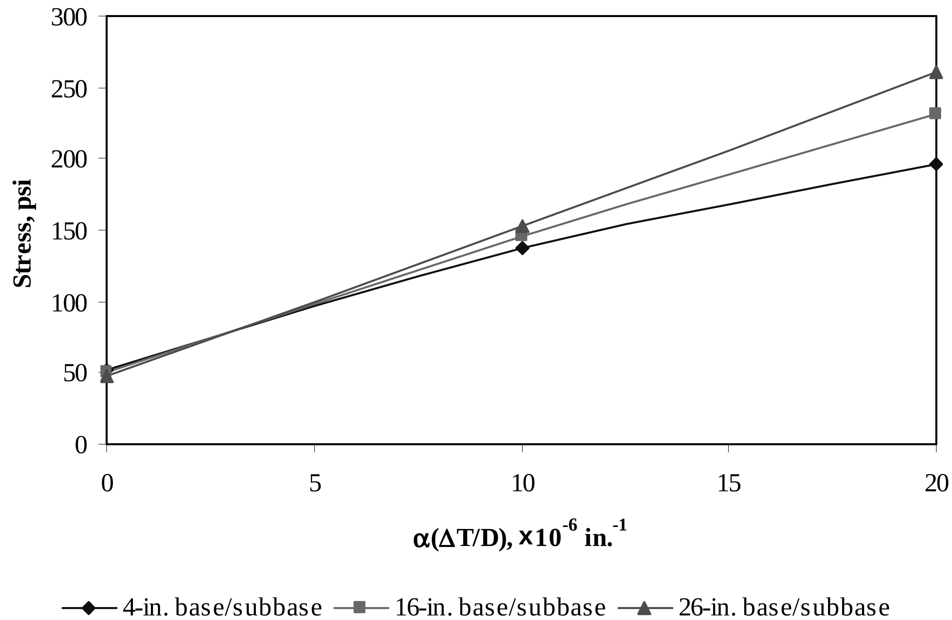


**Figure F-8-39: Impact of base/subbase thickness and product α(ΔT/D) on longitudinal stress at top of the slab (177-in. joint spacing)**

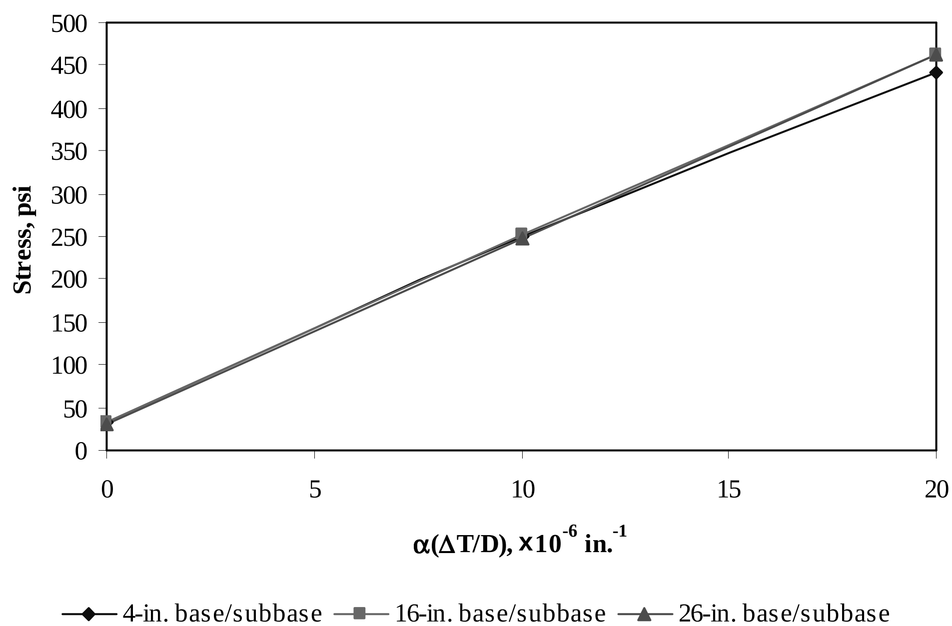


**Figure F-8-40: Impact of base/subbase thickness and product α(ΔT/D) on longitudinal stress at top of the slab (315-in. joint spacing)**

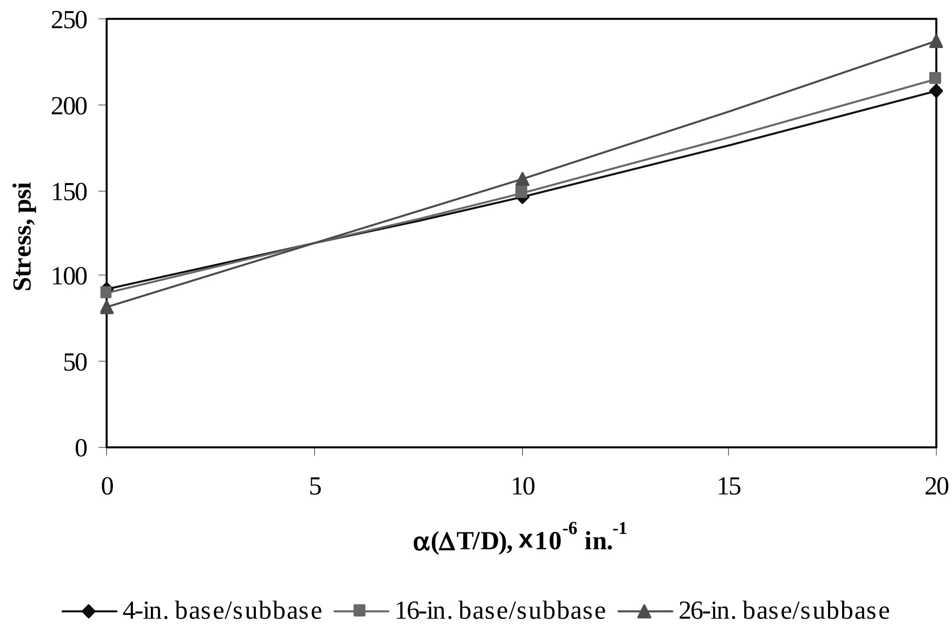


**Figure F-8-41: Impact of base/subbase thickness and product α(ΔT/D) on transverse stress at bottom of the slab (177-in. joint spacing)**

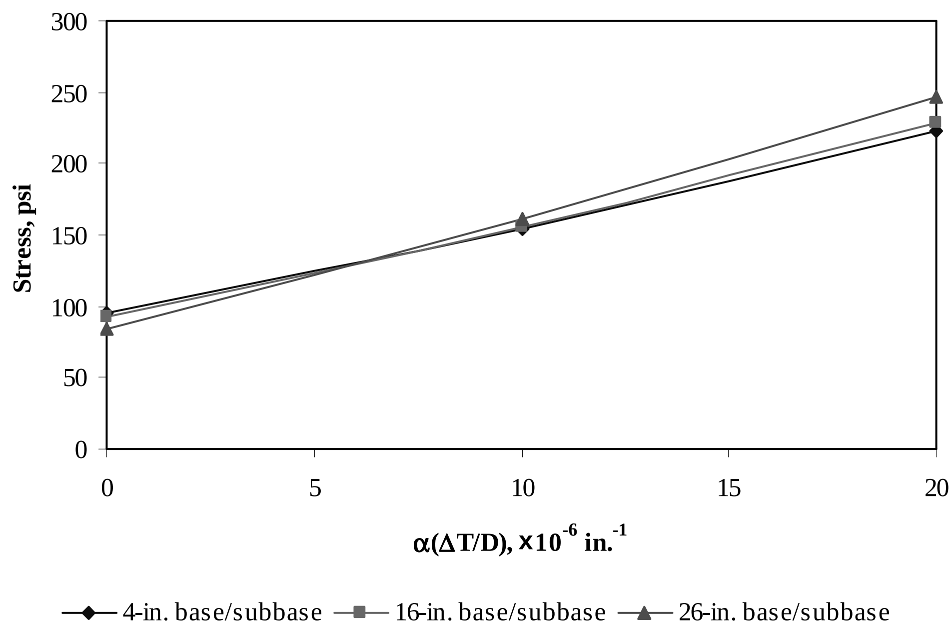


**Figure F-8-42: Impact of base/subbase thickness and product α(ΔT/D) on transverse stress at bottom of the slab (315-in. joint spacing)**

Figures F-8-43 through F-8-48 illustrate the impact of modulus of subgrade reaction and product α(ΔT/D) on stresses (10-in. PCC thickness, 16-in. base/subbase thickness and PCC shoulder)

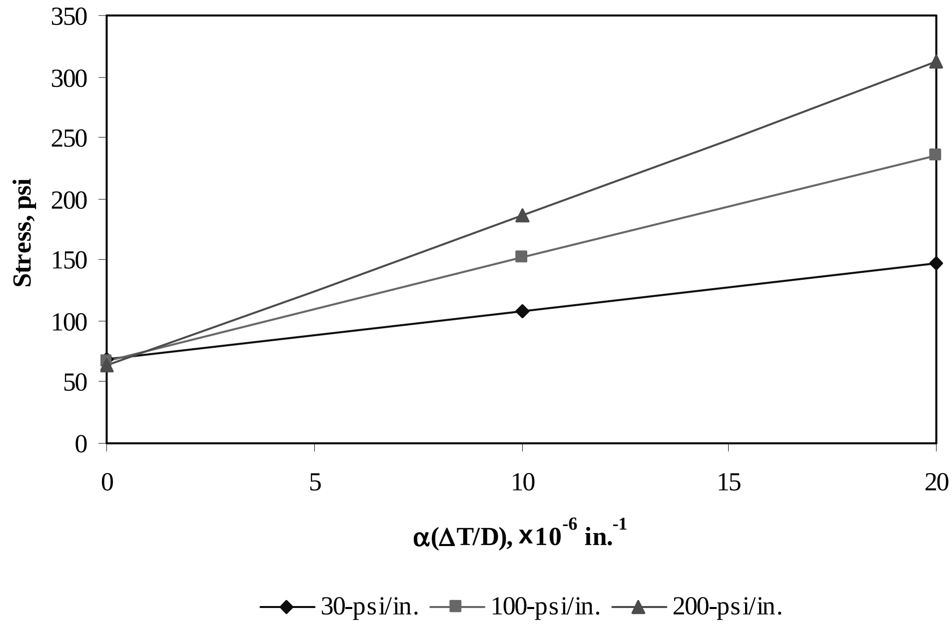


**Figure F-8-43: Impact of modulus of subgrade reaction and product α(ΔT/D) on longitudinal stress at bottom of the slab (177-in. joint spacing)**

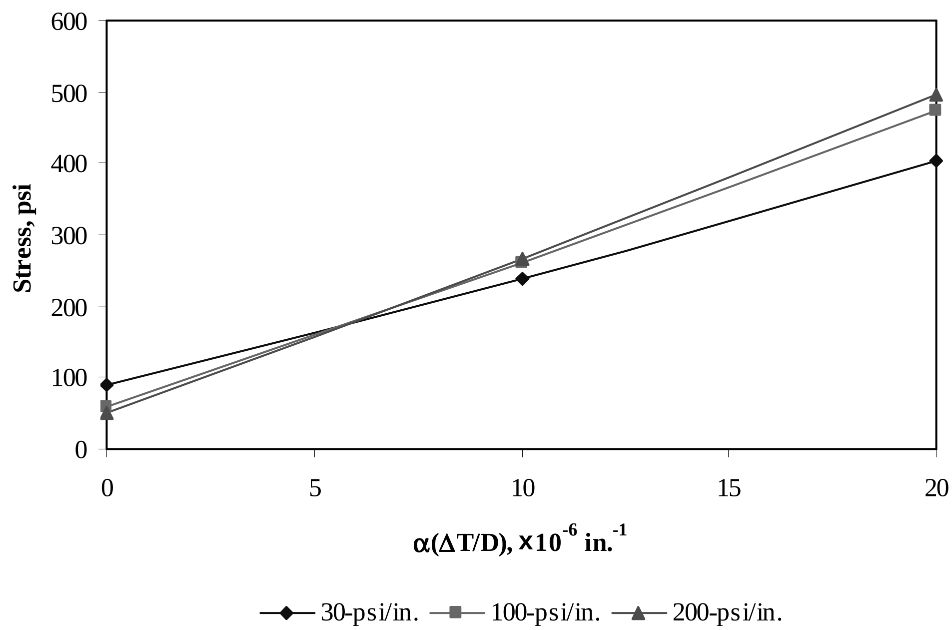


**Figure F-8-44: Impact of modulus of subgrade reaction and product α(ΔT/D) on longitudinal stress at bottom of the slab (315-in. joint spacing)**

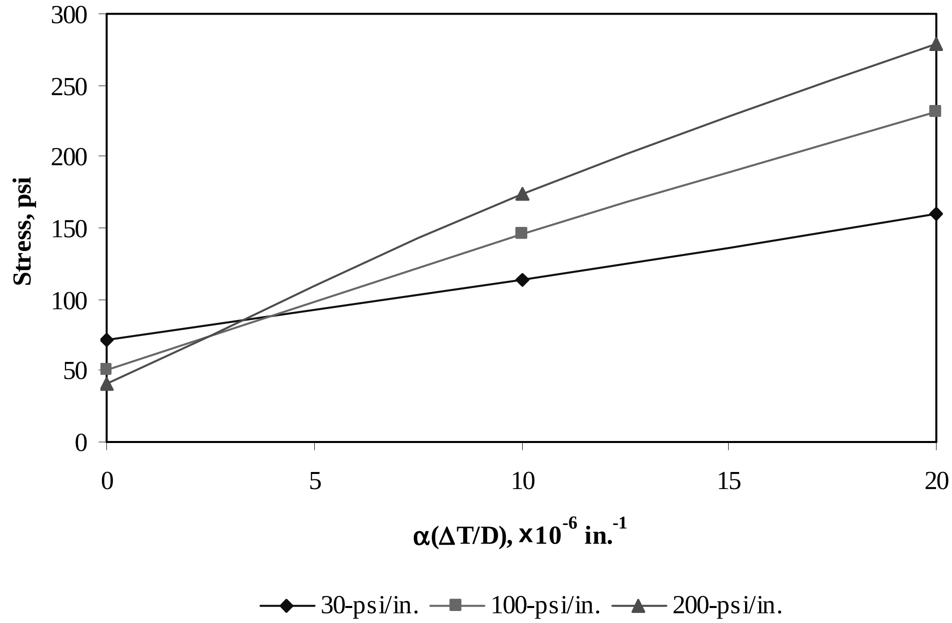


**Figure F-8-45: Impact of modulus of subgrade reaction and product α(ΔT/D) on longitudinal stress at top of the slab (177-in. joint spacing)**

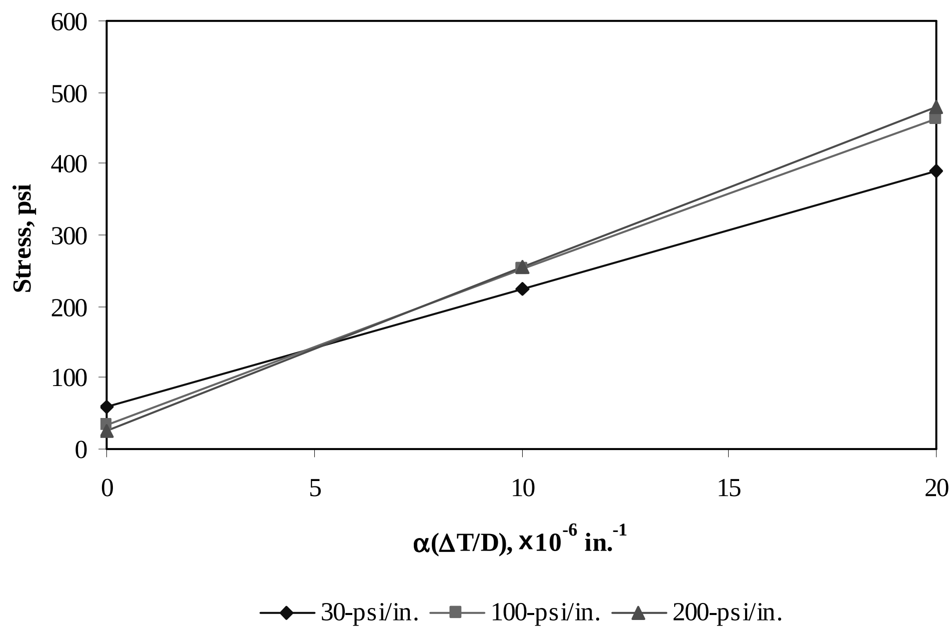


**Figure F-8-46: Impact of modulus of subgrade reaction and product α(ΔT/D) on longitudinal stress at top of the slab (315-in. joint spacing)**

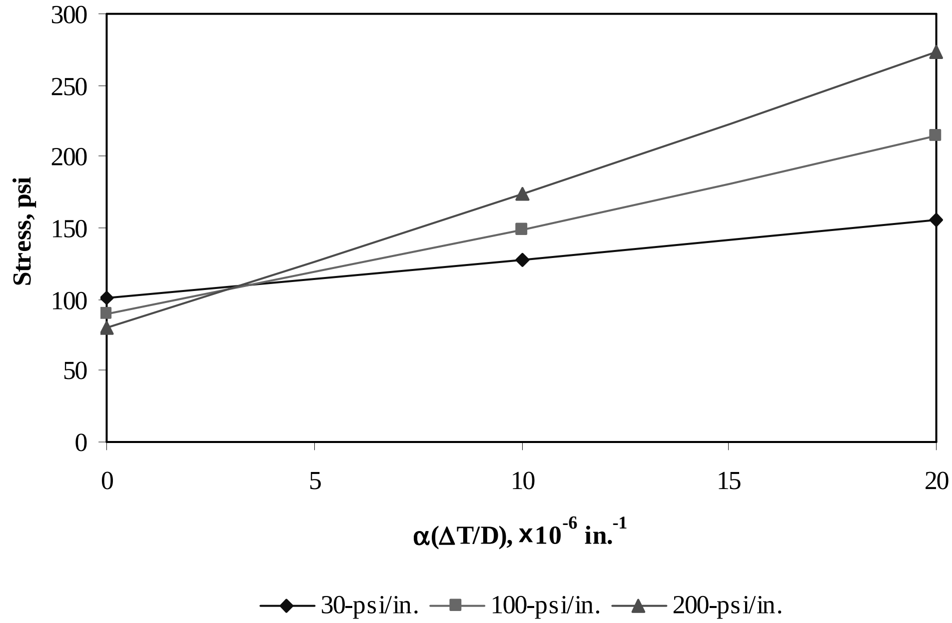


**Figure F-8-47: Impact of modulus of subgrade reaction and product α(ΔT/D) on transverse stress at bottom of the slab (177-in. joint spacing)**

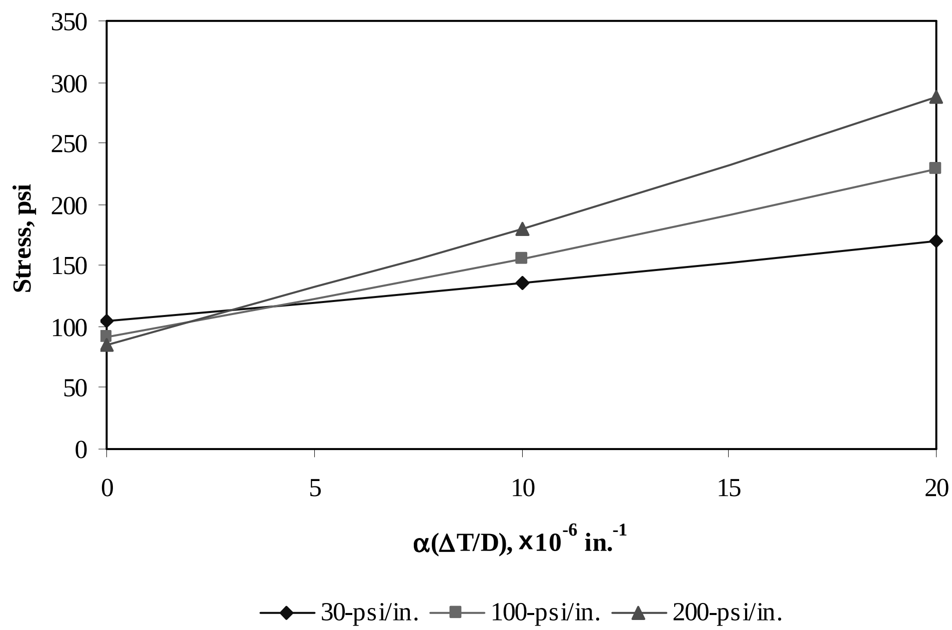


**Figure F-8-48: Impact of modulus of subgrade reaction and product α(ΔT/D) on transverse stress at bottom of the slab (315-in. joint spacing)**

Figures F-8-49 through F-8-51 illustrate the impact of joint spacing and product α(ΔT/D) on stresses (10-in. PCC thickness, 16-in. base/subbase thickness, 100-psi/in. modulus of subgrade reaction and PCC shoulder)

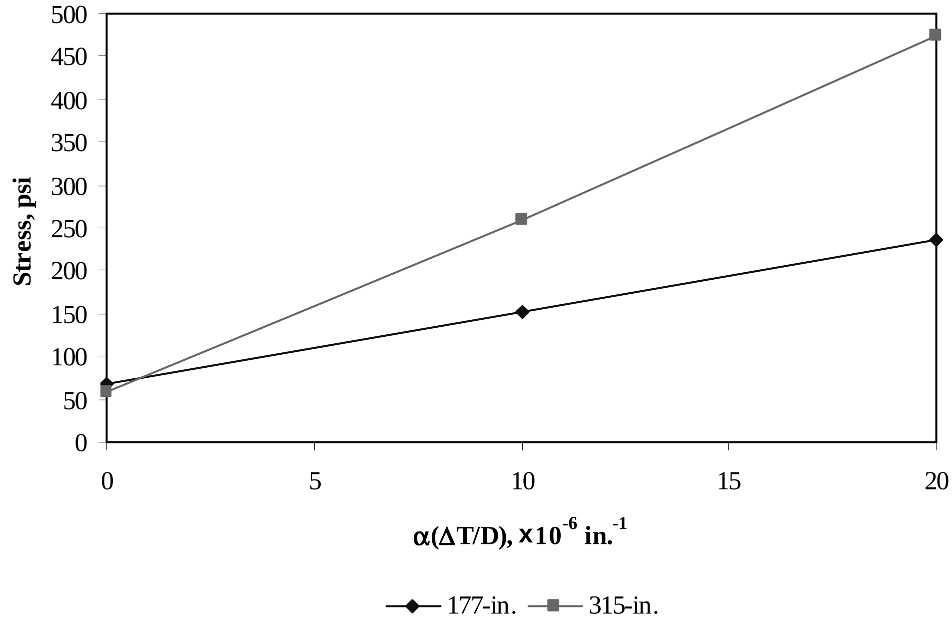


**Figure F-8-49: Impact of joint spacing and product α(ΔT/D) on longitudinal stress at bottom of the slab**

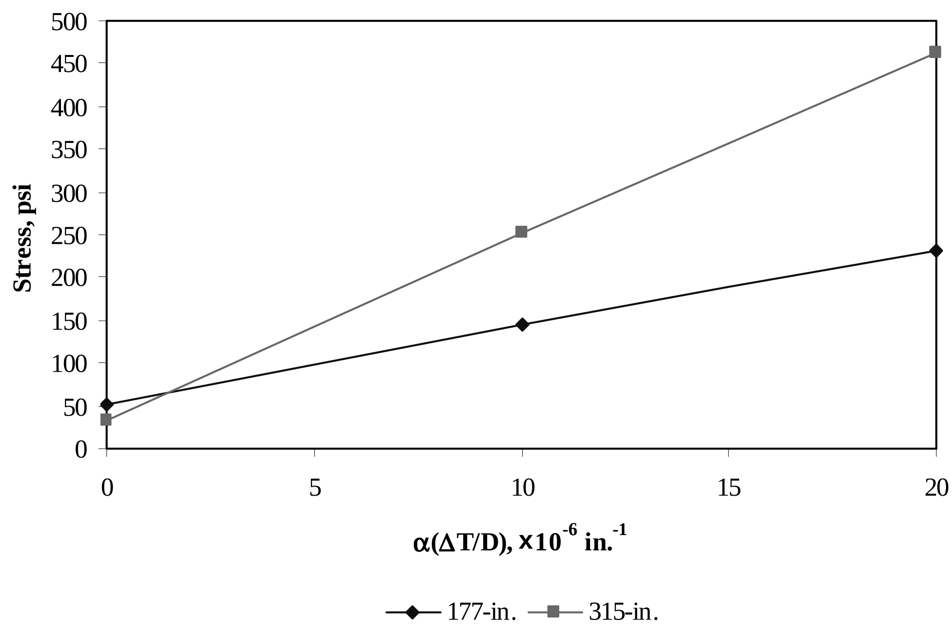


**Figure F-8-50: Impact of joint spacing and product α(ΔT/D) on longitudinal stress at top of the slab**

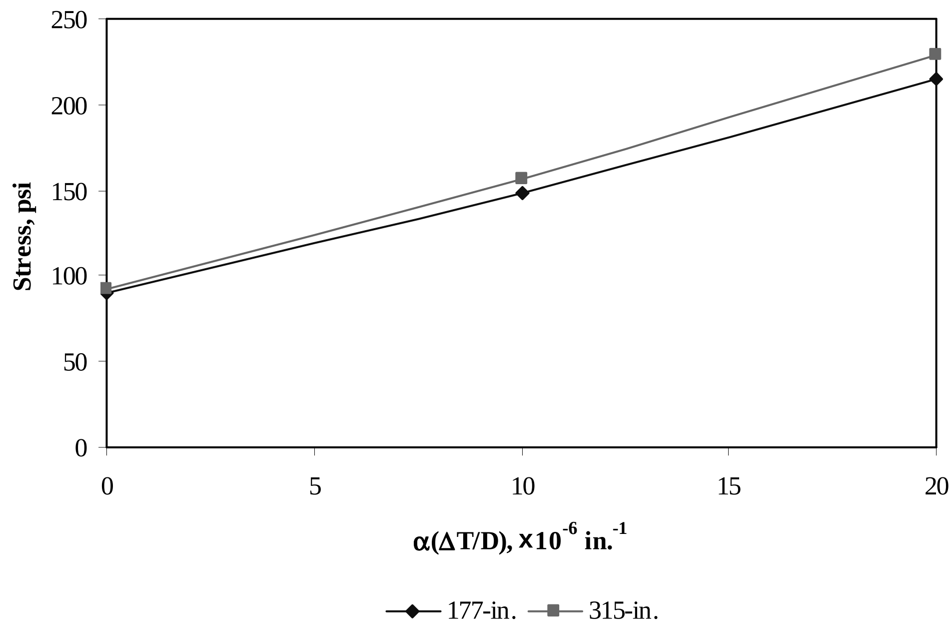


**Figure F-8-51: Impact of joint spacing and product $\alpha(\Delta T/D)$ on transverse stress at bottom of the slab**

**Sub Appendix F-9**

**Documentation of Pavement Responses for**

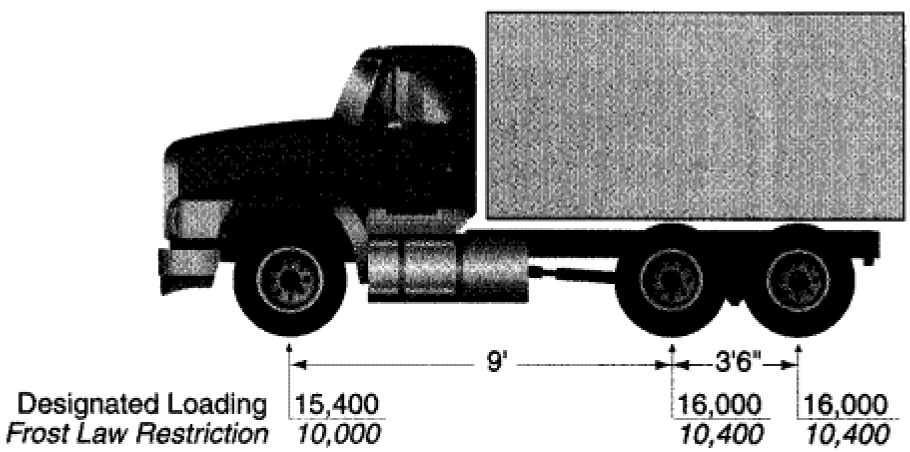


**MI-2**

Figures F-9-1 through F-9-12 illustrate the impact of PCC thickness and base/subbase thickness on stresses (100-psi/in. modulus of subgrade reaction and PCC shoulder)

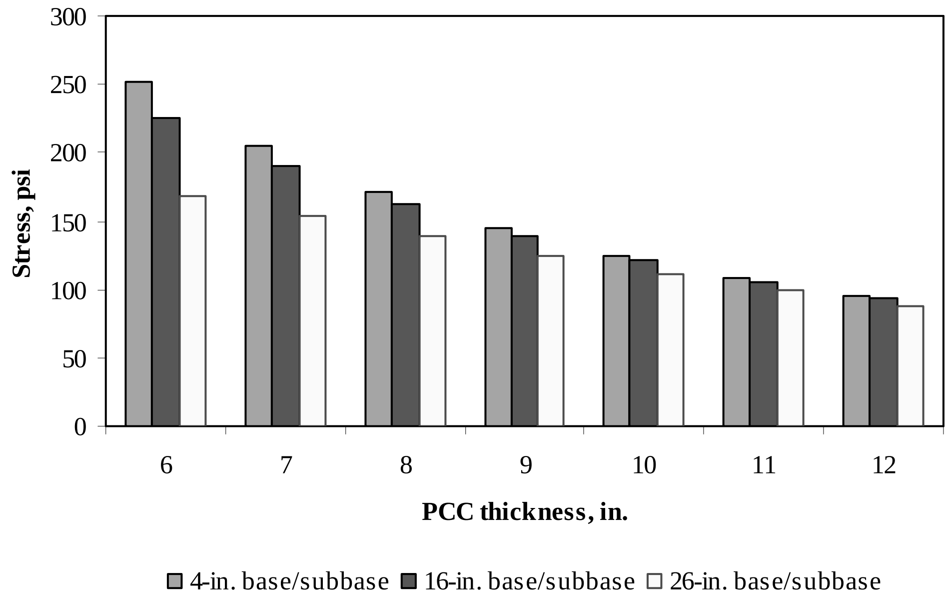


**Figure F-9-1: Impact of PCC thickness and base/subbase thickness on longitudinal stress at bottom of the Slab (177-in. joint spacing and $\alpha(\Delta T/D)$ of 0 in.$^{-1}$)**

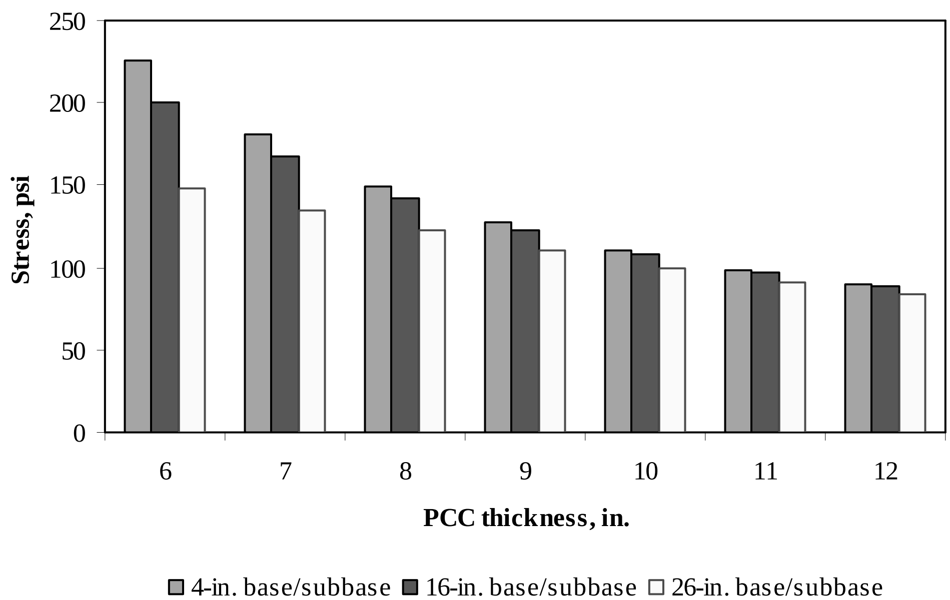


**Figure F-9-2: Impact of PCC thickness and base/subbase thickness on longitudinal stress at bottom of the Slab (315-in. joint spacing and $\alpha(\Delta T/D)$ of 0 in.$^{-1}$)**

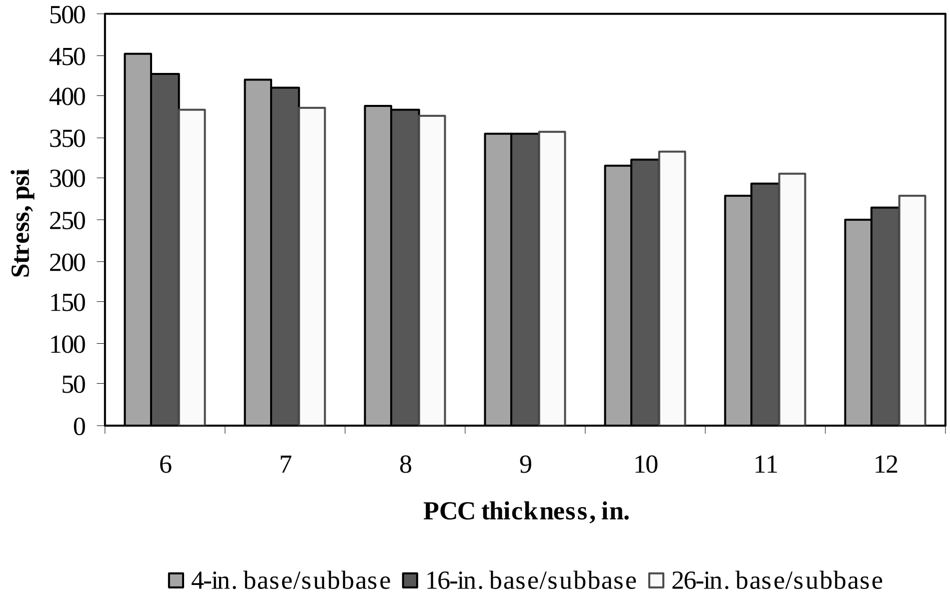


**Figure F-9-3: Impact of PCC thickness and base/subbase thickness on longitudinal stress at bottom of the Slab (177-in. joint spacing and $\alpha(\Delta T/D)$ of $20x10^{-6}$ in.$^{-1}$)**

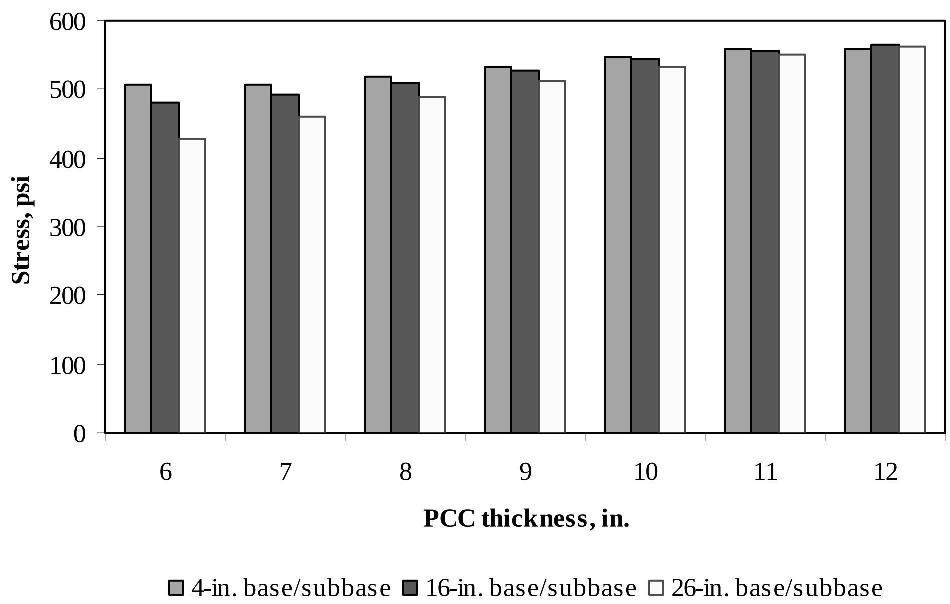


**Figure F-9-4: Impact of PCC thickness and base/subbase thickness on longitudinal stress at bottom of the Slab (315-in. joint spacing and $\alpha(\Delta T/D)$ of $20x10^{-6}$ in.$^{-1}$)**

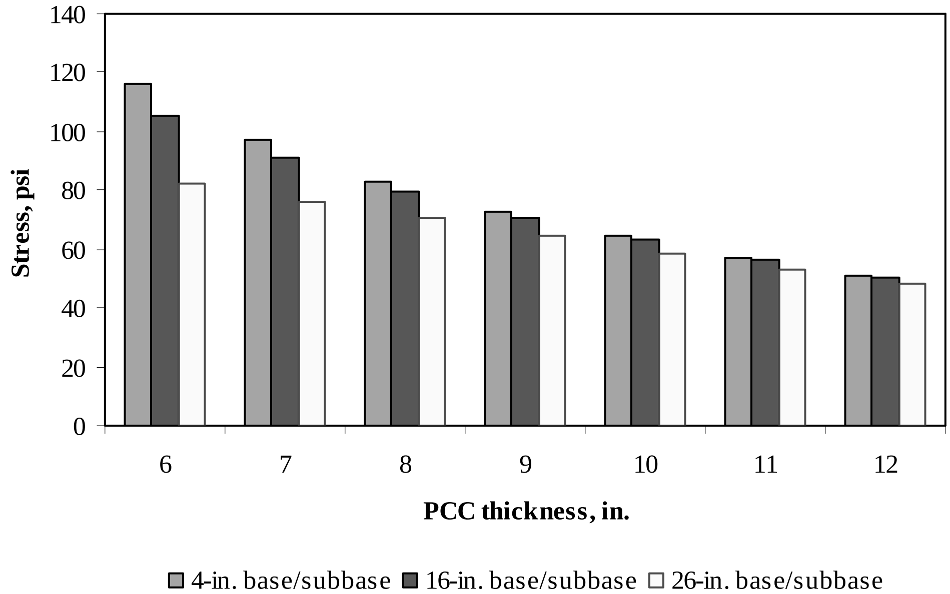


**Figure F-9-5: Impact of PCC thickness and base/subbase thickness on longitudinal stress at top of the Slab (177-in. joint spacing and $\alpha(\Delta T/D)$ of 0 in.$^{-1}$)**

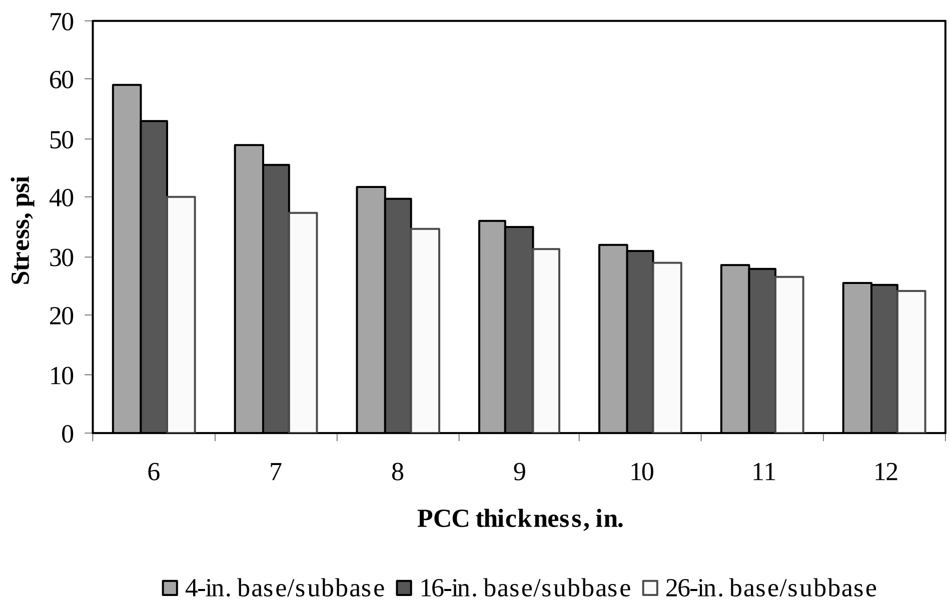


**Figure F-9-6: Impact of PCC thickness and base/subbase thickness on longitudinal stress at top of the Slab (315-in. joint spacing and $\alpha(\Delta T/D)$ of 0 in.$^{-1}$)**

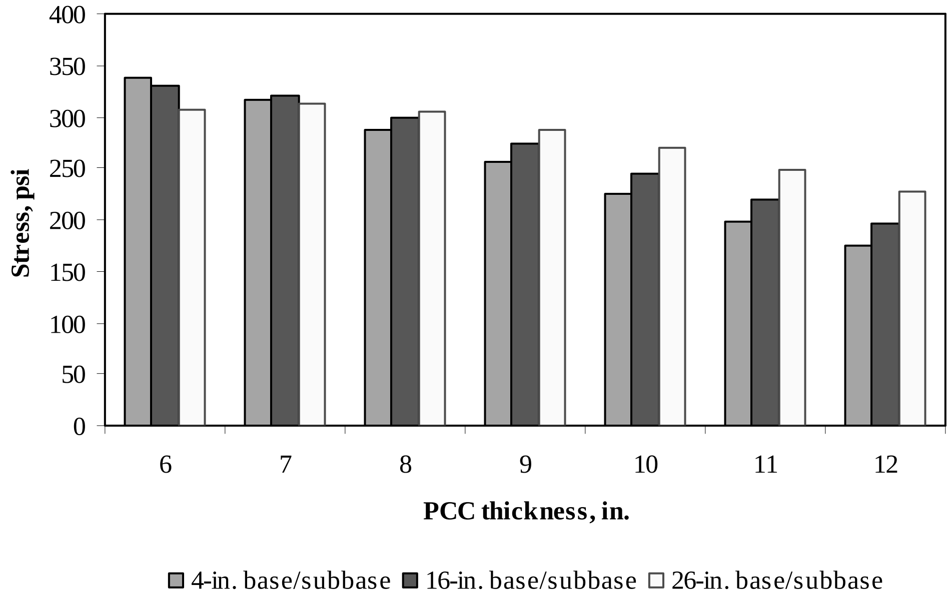


**Figure F-9-7: Impact of PCC thickness and base/subbase thickness on longitudinal stress at top of the Slab (177-in. joint spacing and $\alpha(\Delta T/D)$ of $-20x10^{-6}$ in.$^{-1}$)**

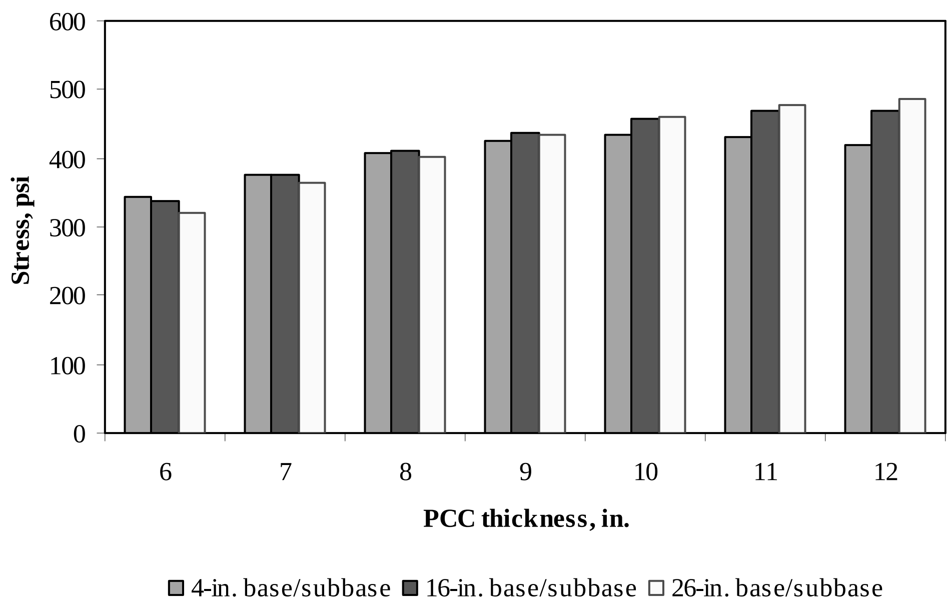


**Figure F-9-8: Impact of PCC thickness and base/subbase thickness on longitudinal stress at top of the Slab (315-in. joint spacing and $\alpha(\Delta T/D)$ of $-20x10^{-6}$ in.$^{-1}$)**

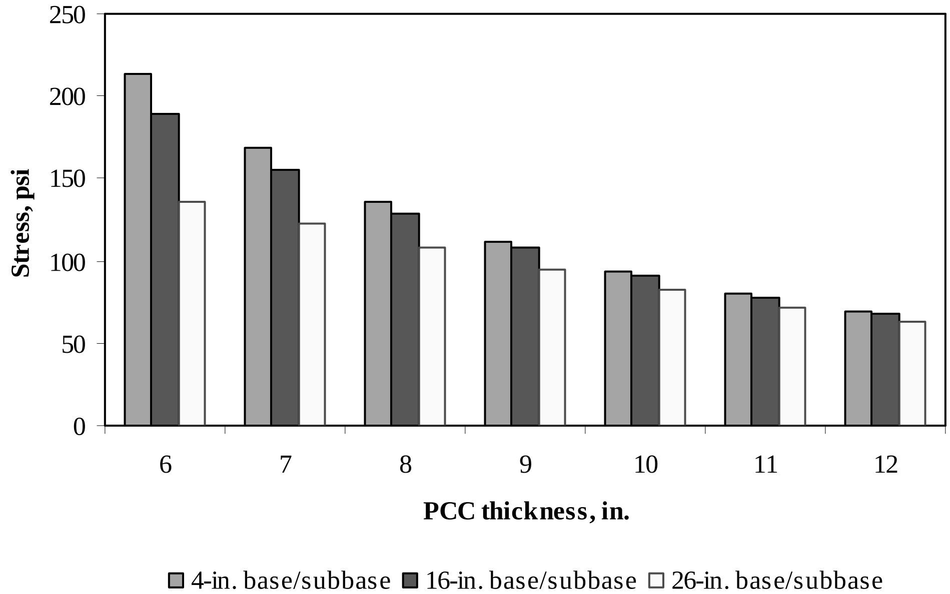


**Figure F-9-9: Impact of PCC thickness and base/subbase thickness on transverse stress at bottom of the Slab (177-in. joint spacing and $\alpha(\Delta T/D)$ of 0 in.$^{-1}$)**

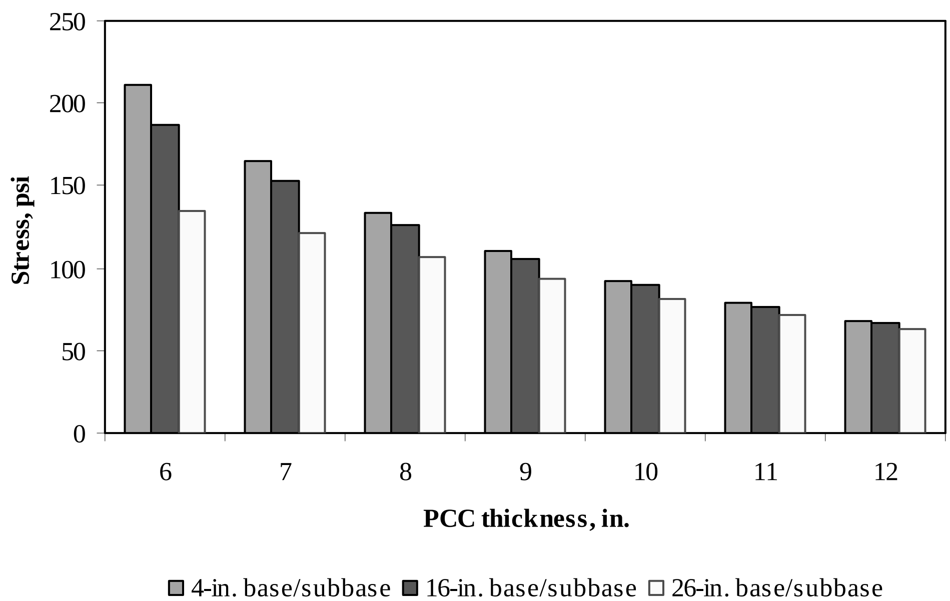


**Figure F-9-10: Impact of PCC thickness and base/subbase thickness on transverse stress at bottom of the Slab (315-in. joint spacing and $\alpha(\Delta T/D)$ of 0 in.$^{-1}$)**

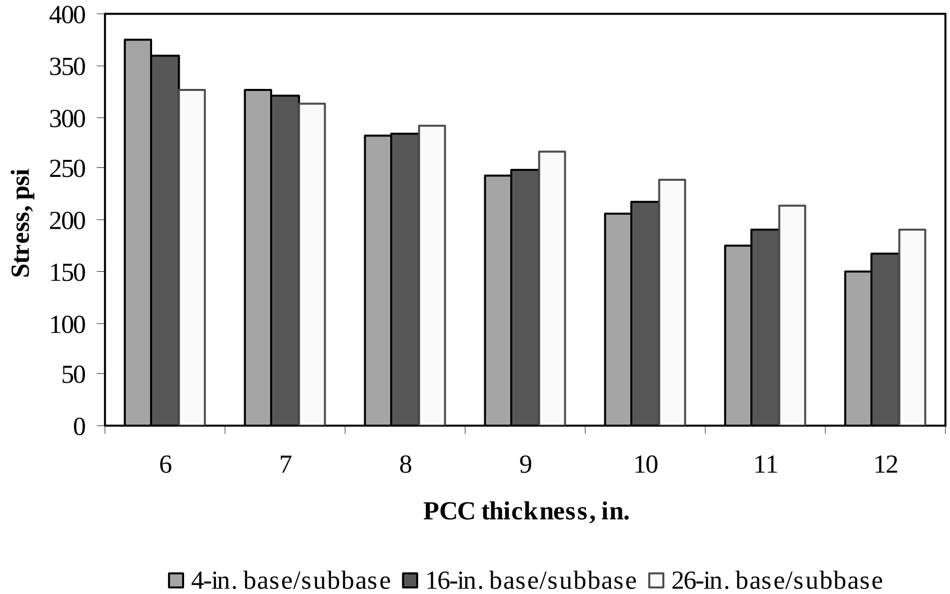


**Figure F-9-11: Impact of PCC thickness and base/subbase thickness on transverse stress at bottom of the Slab (177-in. joint spacing and $\alpha(\Delta T/D)$ of $20x10^{-6}$ in.$^{-1}$)**

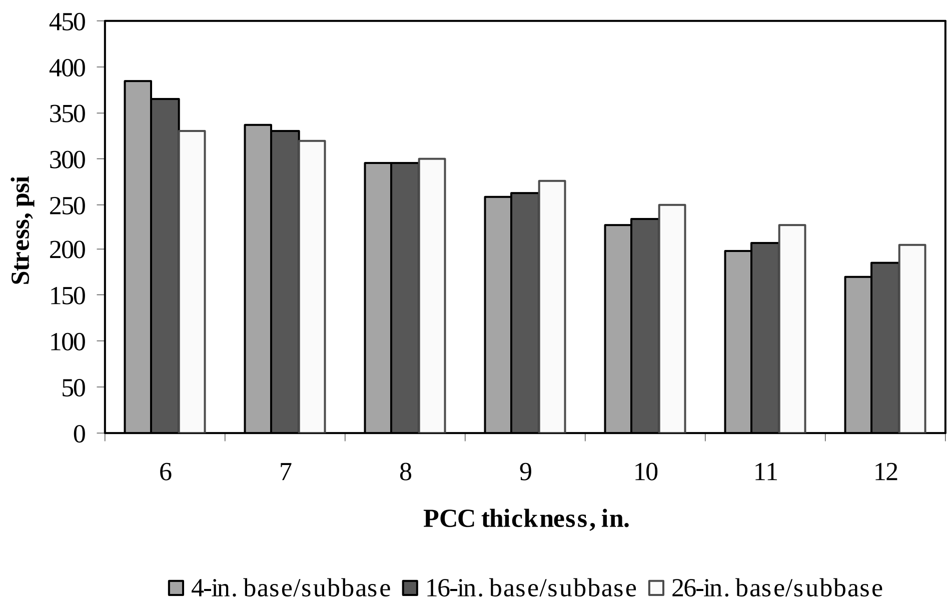


**Figure F-9-12: Impact of PCC thickness and base/subbase thickness on transverse stress at bottom of the Slab (315-in. joint spacing and $\alpha(\Delta T/D)$ of $20x10^{-6}$ in.$^{-1}$)**

Figures F-9-13 through F-9-24 illustrate the impact of PCC thickness and modulus of subgrade reaction on stresses (16-in. base/subbase thickness and PCC shoulder)

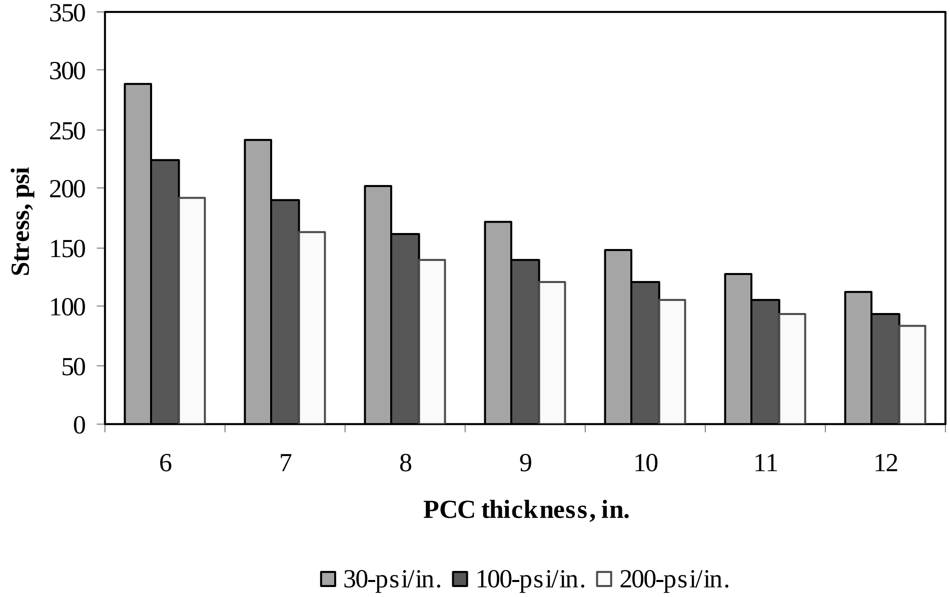


**Figure F-9-13: Impact of PCC thickness and modulus of subgrade reaction on longitudinal stress at bottom of the slab (177-in. joint spacing and $\alpha(\Delta T/D)$ of 0 in.$^{-1}$)**

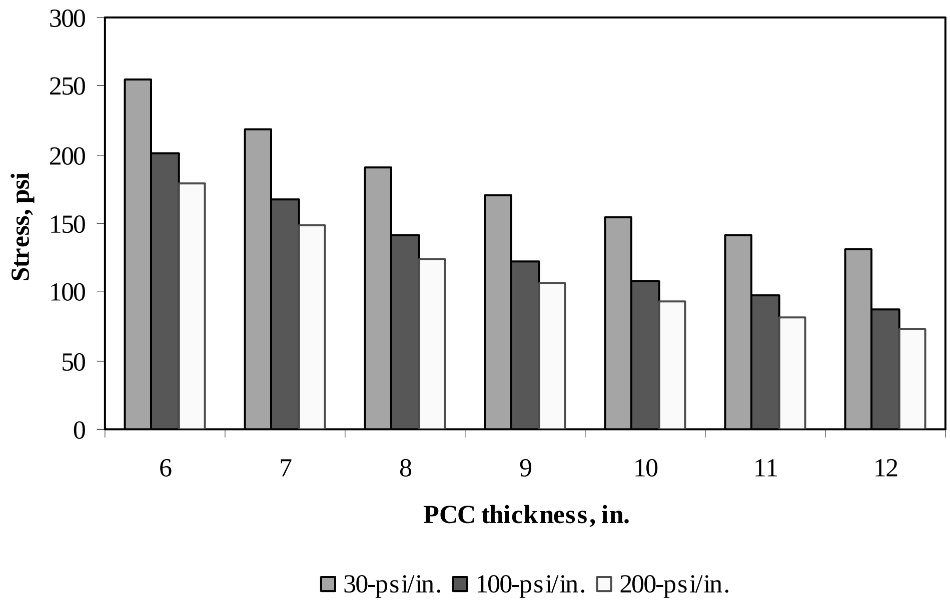


**Figure F-9-14: Impact of PCC thickness and modulus of subgrade reaction on longitudinal stress at bottom of the slab (315-in. joint spacing and $\alpha(\Delta T/D)$ of 0 in.$^{-1}$)**

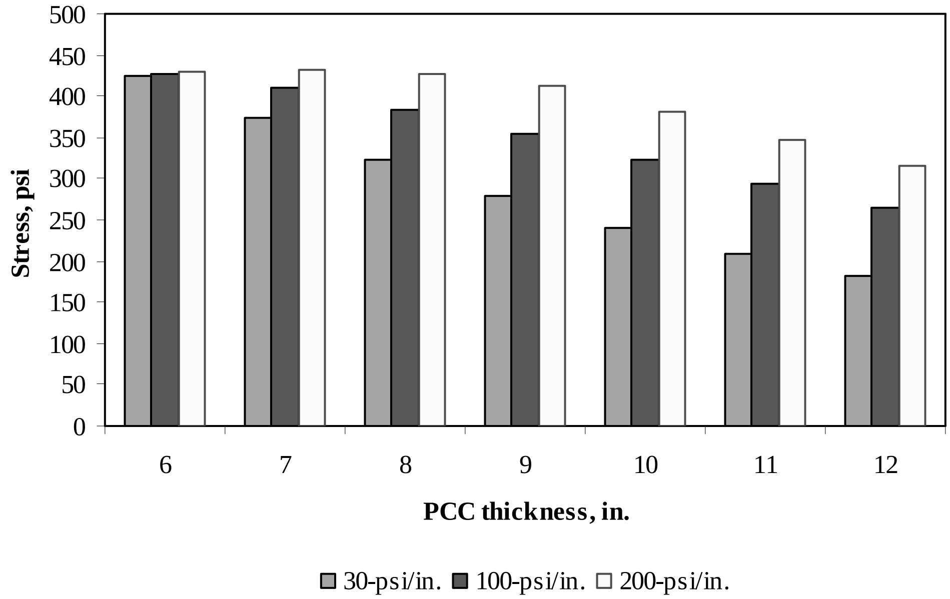


**Figure F-9-15: Impact of PCC thickness and modulus of subgrade reaction on longitudinal stress at bottom of the slab (177-in. joint spacing and $\alpha(\Delta T/D)$ of $20\text{x}10^{-6}$ in.$^{-1}$)**

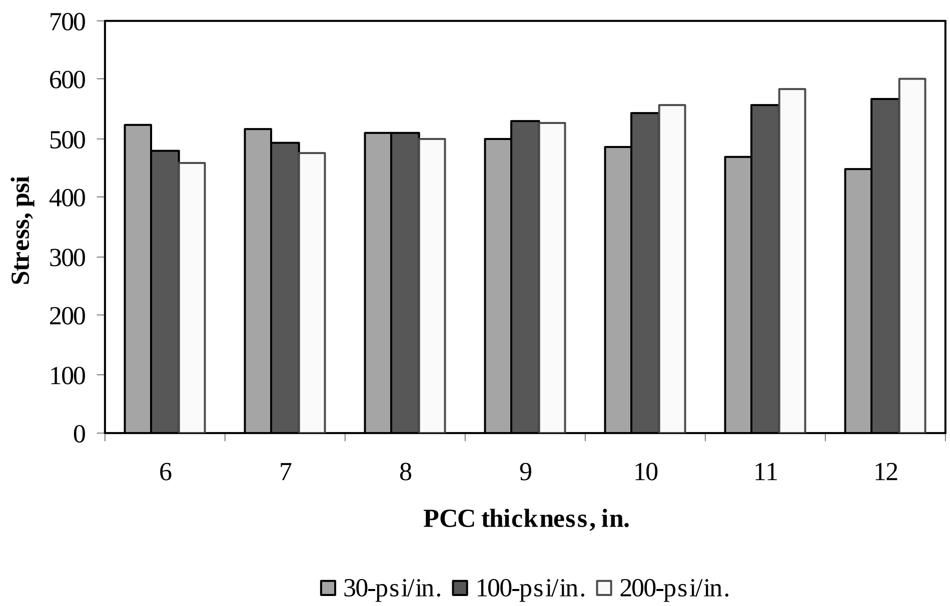


**Figure F-9-16: Impact of PCC thickness and modulus of subgrade reaction on longitudinal stress at bottom of the slab (315-in. joint spacing and $\alpha(\Delta T/D)$ of $20\text{x}10^{-6}$ in.$^{-1}$)**

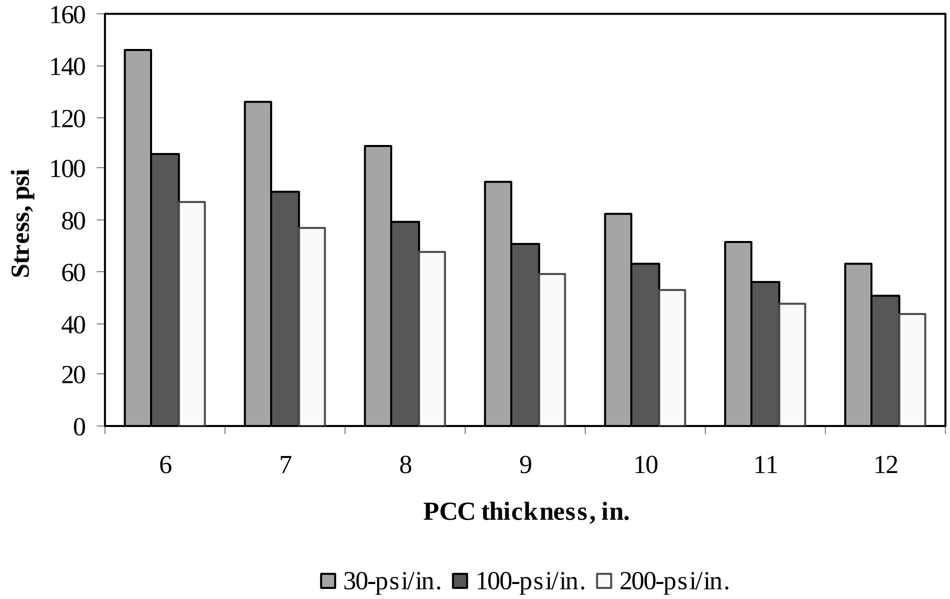


**Figure F-9-17: Impact of PCC thickness and modulus of subgrade reaction on longitudinal stress at top of the Slab (177-in. joint spacing and $\alpha(\Delta T/D)$ of 0 in.$^{-1}$)**

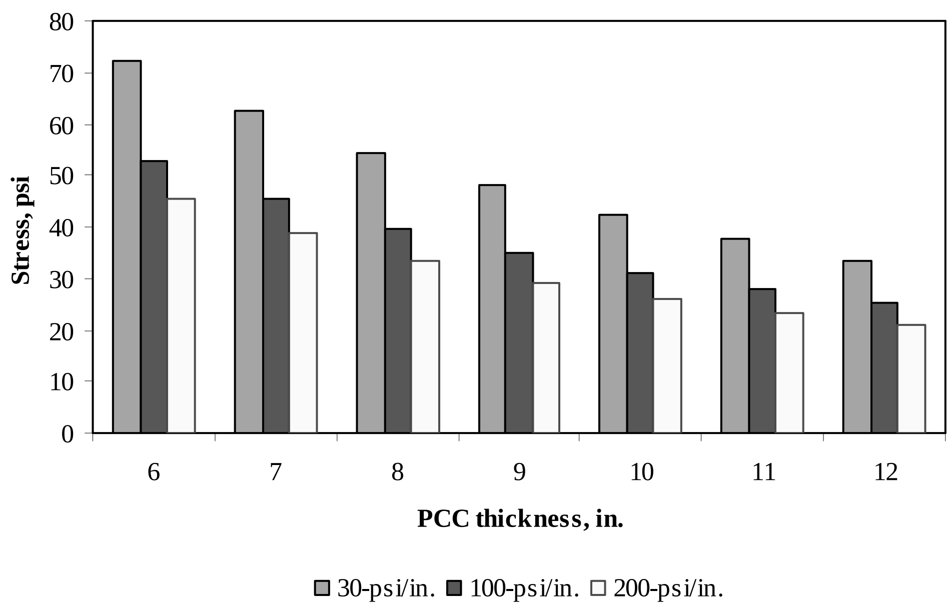


**Figure F-9-18: Impact of PCC thickness and modulus of subgrade reaction on longitudinal stress at top of the Slab (315-in. joint spacing and $\alpha(\Delta T/D)$ of 0 in.$^{-1}$)**

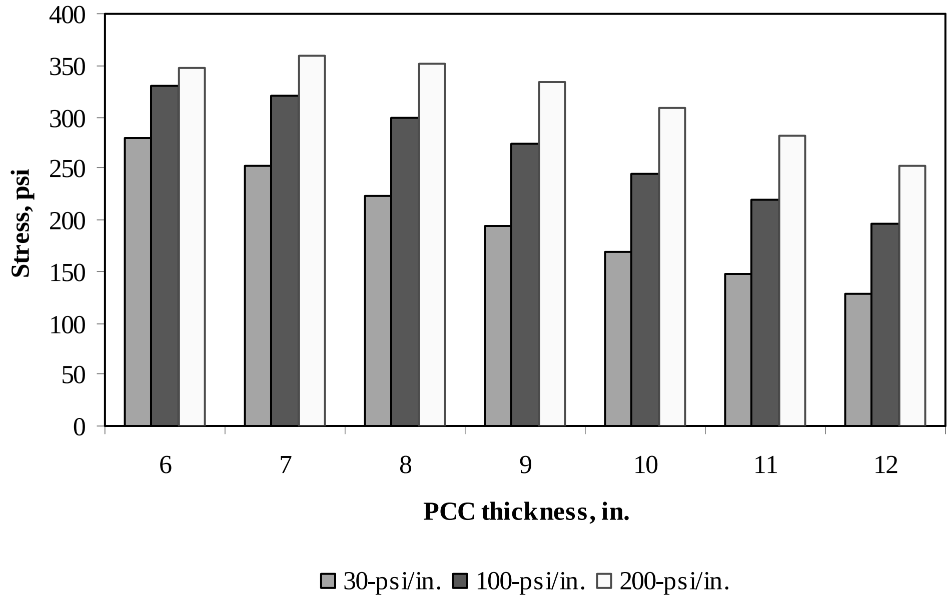


**Figure F-9-19: Impact of PCC thickness and modulus of subgrade reaction on longitudinal stress at top of the Slab (177-in. joint spacing and $\alpha(\Delta T/D)$ of $-20x10^{-6}$ in.$^{-1}$)**

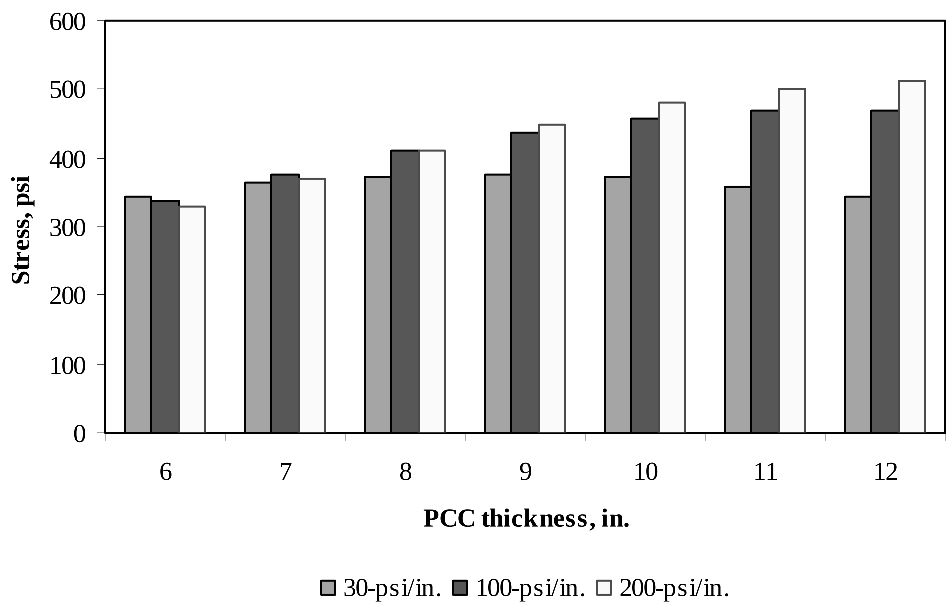


**Figure F-9-20: Impact of PCC thickness and modulus of subgrade reaction on longitudinal stress at top of the Slab (315-in. joint spacing and $\alpha(\Delta T/D)$ of $-20x10^{-6}$ in.$^{-1}$)**

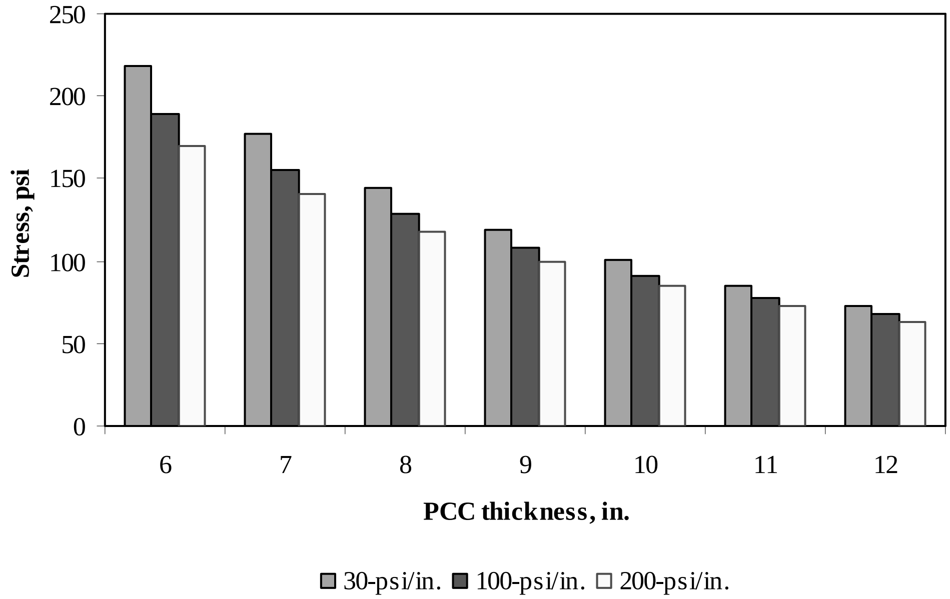


**Figure F-9-21: Impact of PCC thickness and modulus of subgrade reaction on transverse stress at bottom of the Slab (177-in. joint spacing and $\alpha(\Delta T/D)$ of 0 in.$^{-1}$)**

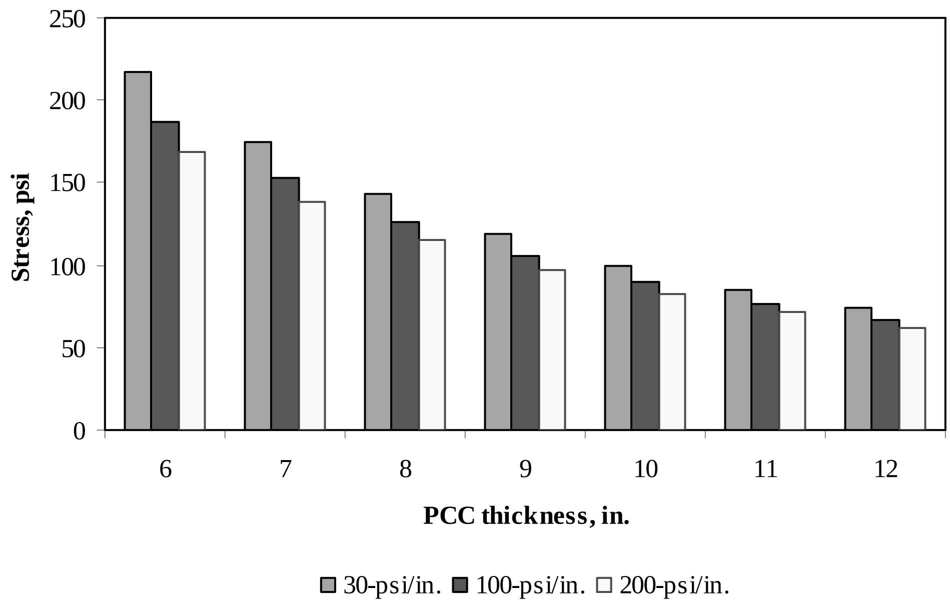


**Figure F-9-22: Impact of PCC thickness and modulus of subgrade reaction on transverse stress at bottom of the Slab (315-in. joint spacing and $\alpha(\Delta T/D)$ of 0 in.$^{-1}$)**

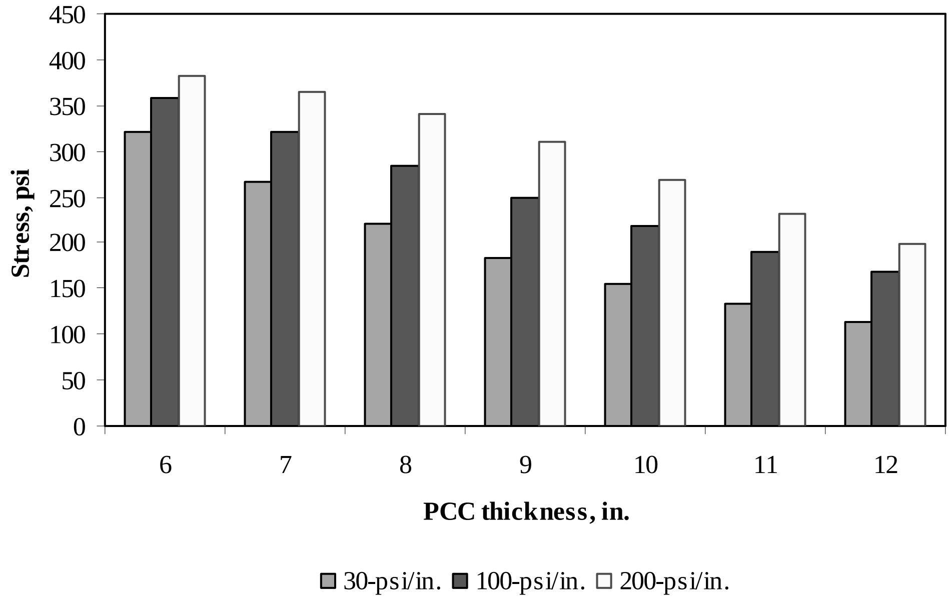


**Figure F-9-23: Impact of PCC thickness and modulus of subgrade reaction on transverse stress at bottom of the Slab (177-in. joint spacing and $\alpha(\Delta T/D)$ of $20 \times 10^{-6}$ in.$^{-1}$)**

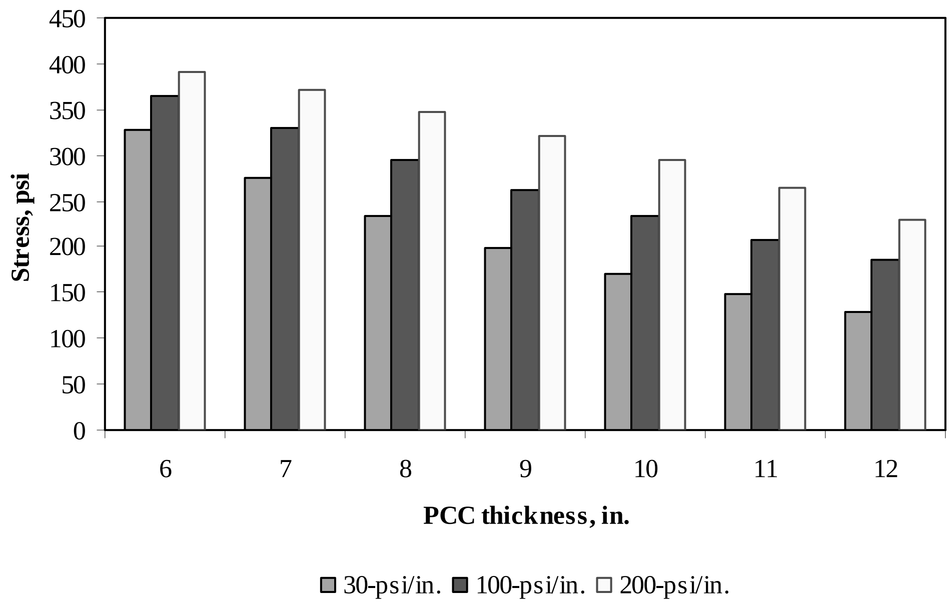


**Figure F-9-24: Impact of PCC thickness and modulus of subgrade reaction on transverse stress at bottom of the Slab (315-in. joint spacing and $\alpha(\Delta T/D)$ of $20 \times 10^{-6}$ in.$^{-1}$)**

Figures F-9-25 through F-9-36 illustrate the impact of PCC thickness and lateral support condition on stresses (16-in. base/subbase and 100-psi/in. modulus of subgrade reaction)

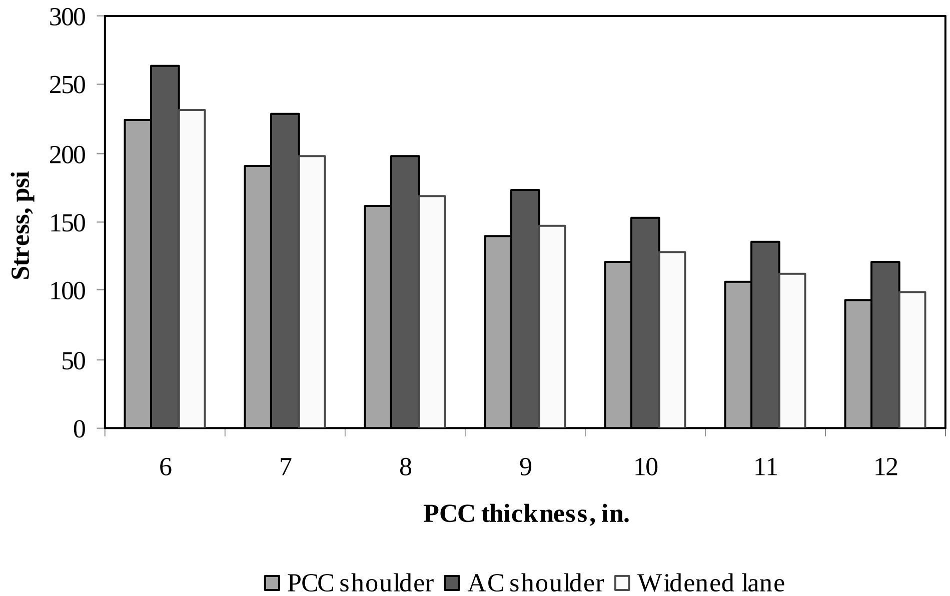


**Figure F-9-25: Impact of PCC thickness and lateral support condition on longitudinal stress at bottom of the Slab (177-in. joint spacing and $\alpha(\Delta T/D)$ of 0 in.$^{-1}$)**

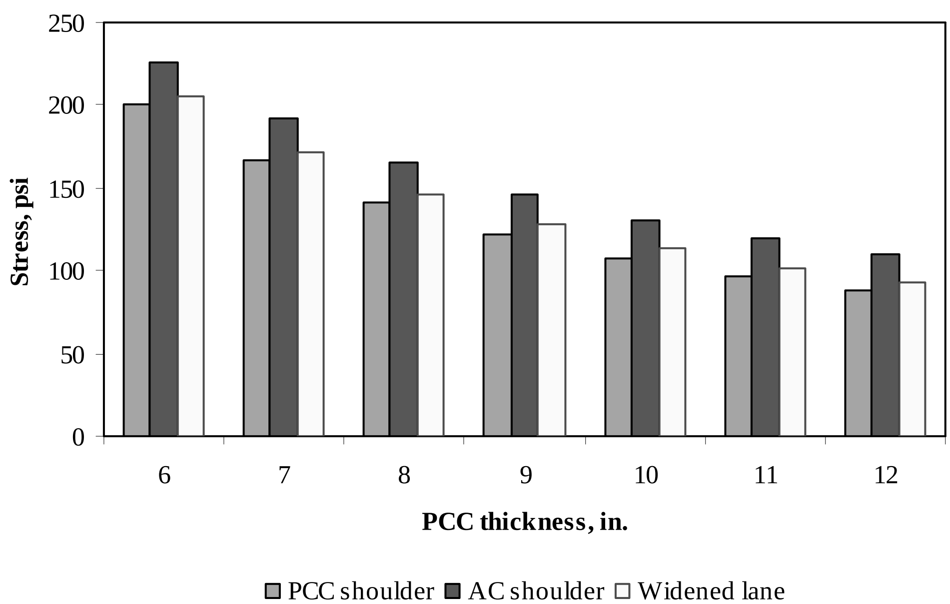


**Figure F-9-26: Impact of PCC thickness and lateral support condition on longitudinal stress at bottom of the Slab (315-in. joint spacing and $\alpha(\Delta T/D)$ of 0 in.$^{-1}$)**

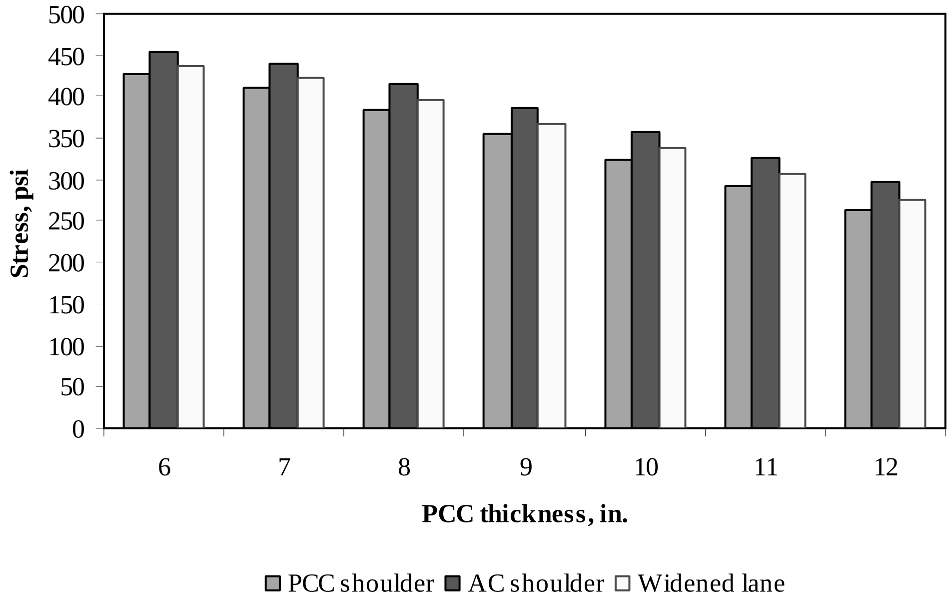


**Figure F-9-27: Impact of PCC thickness and lateral support condition on longitudinal stress at bottom of the Slab (177-in. joint spacing and $\alpha(\Delta T/D)$ of 20x10$^{-6}$ in.$^{-1}$)**

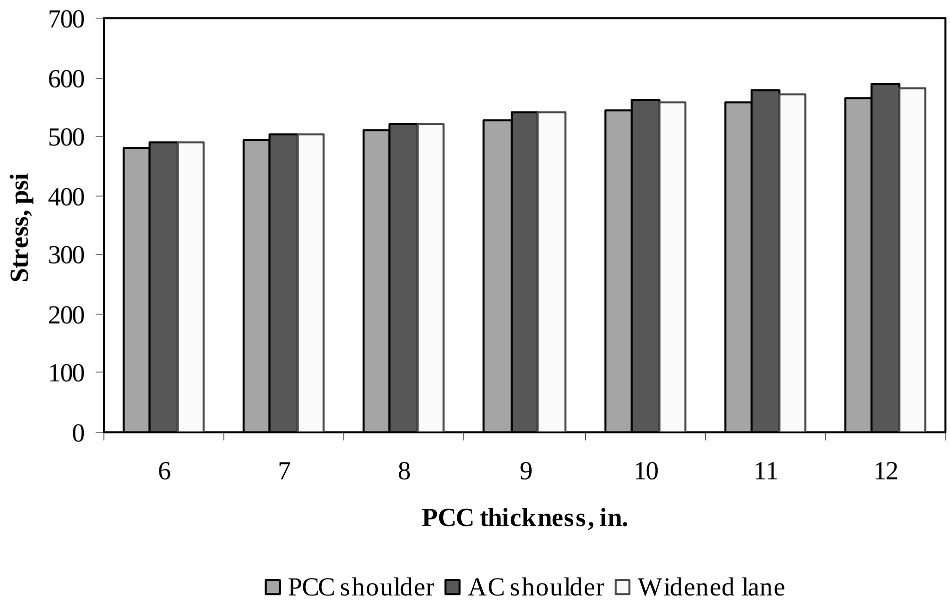


**Figure F-9-28: Impact of PCC thickness and lateral support condition on longitudinal stress at bottom of the Slab (315-in. joint spacing and $\alpha(\Delta T/D)$ of 20x10$^{-6}$ in.$^{-1}$)**

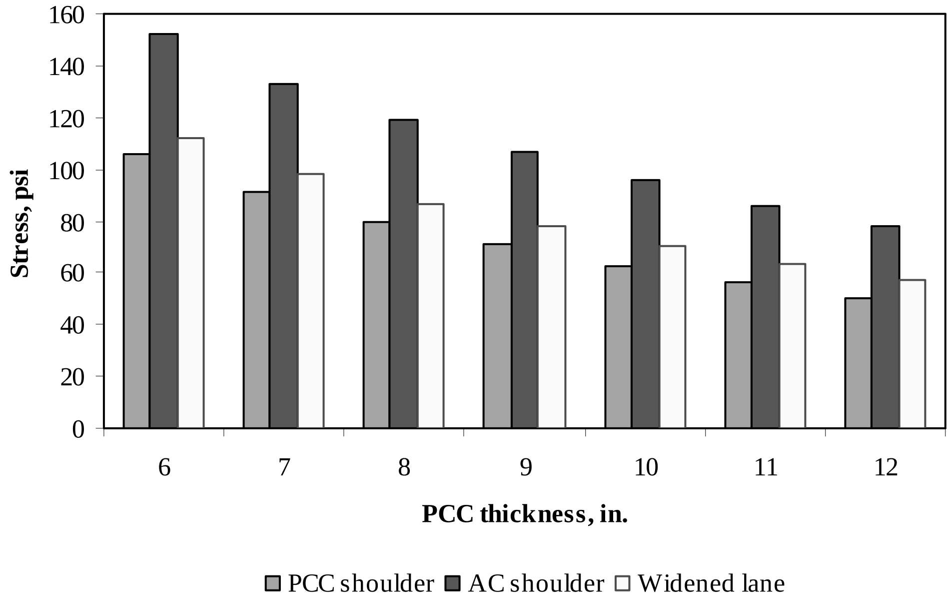


**Figure F-9-29: Impact of PCC thickness and lateral support condition on longitudinal stress at top of the Slab (177-in. joint spacing and $\alpha(\Delta T/D)$ of 0 in.$^{-1}$)**

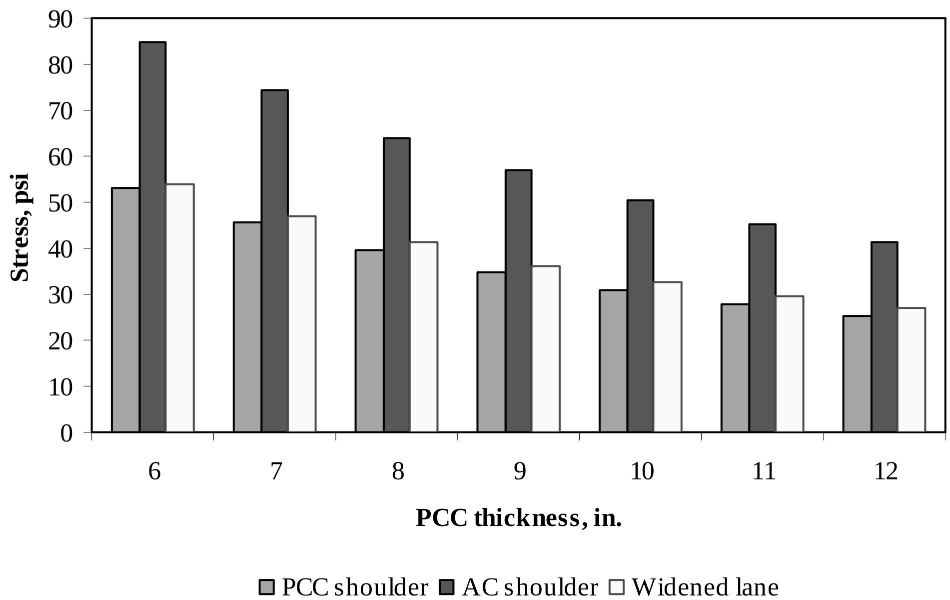


**Figure F-9-30: Impact of PCC thickness and lateral support condition on longitudinal stress at top of the Slab (315-in. joint spacing and $\alpha(\Delta T/D)$ of 0 in.$^{-1}$)**

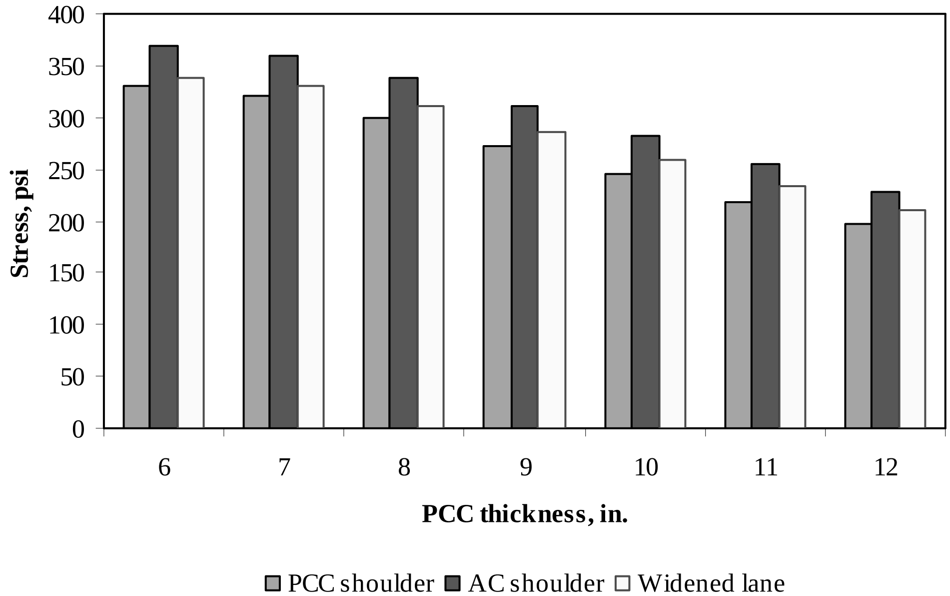


**Figure F-9-31: Impact of PCC thickness and lateral support condition on longitudinal stress at top of the Slab (177-in. joint spacing and $\alpha(\Delta T/D)$ of $-20x10^{-6}$ in.$^{-1}$)**

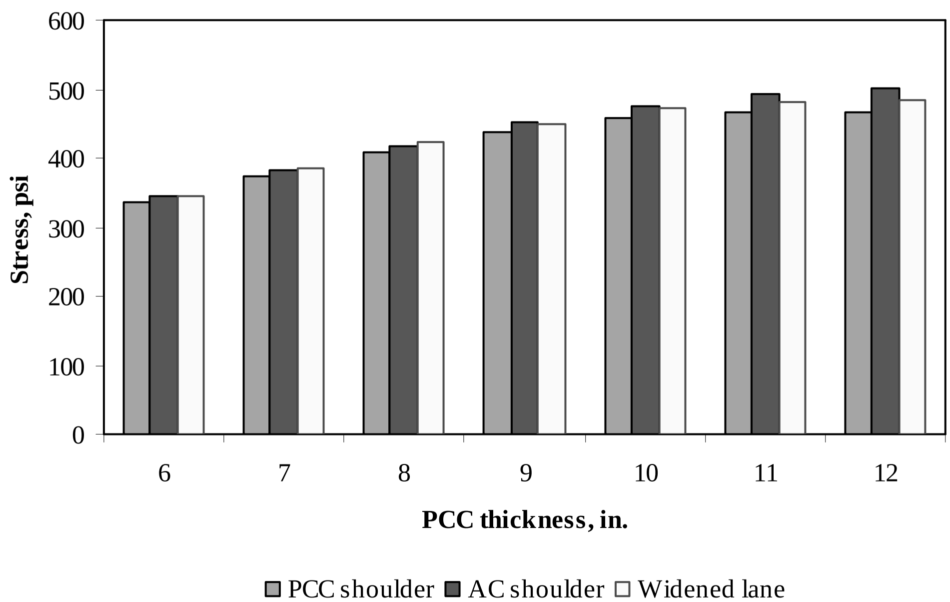


**Figure F-9-32: Impact of PCC thickness and lateral support condition on longitudinal stress at top of the Slab (315-in. joint spacing and $\alpha(\Delta T/D)$ of $-20x10^{-6}$ in.$^{-1}$)**

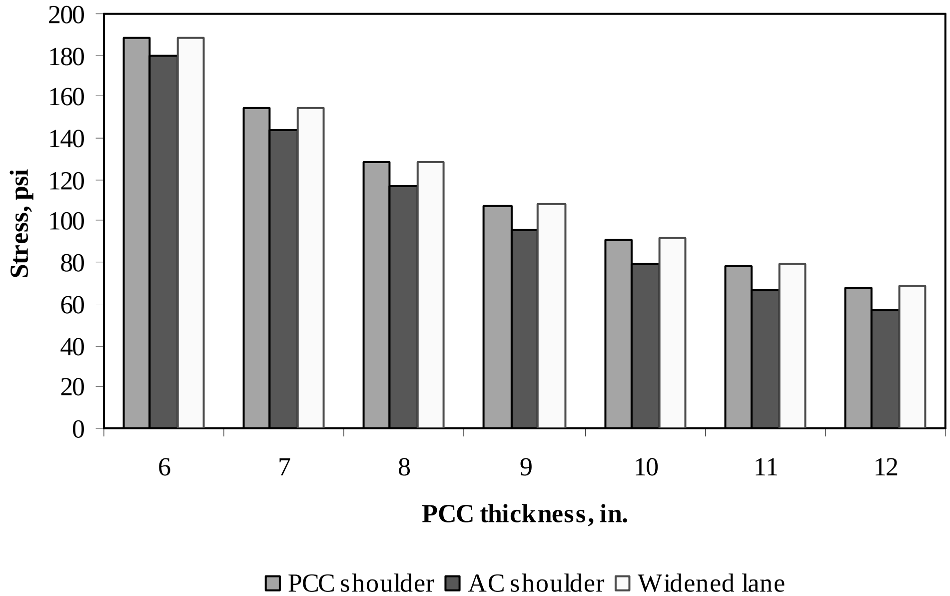


**Figure F-9-33: Impact of PCC thickness and lateral support condition on transverse stress at bottom of the Slab (177-in. joint spacing and $\alpha(\Delta T/D)$ of 0 in.$^{-1}$)**

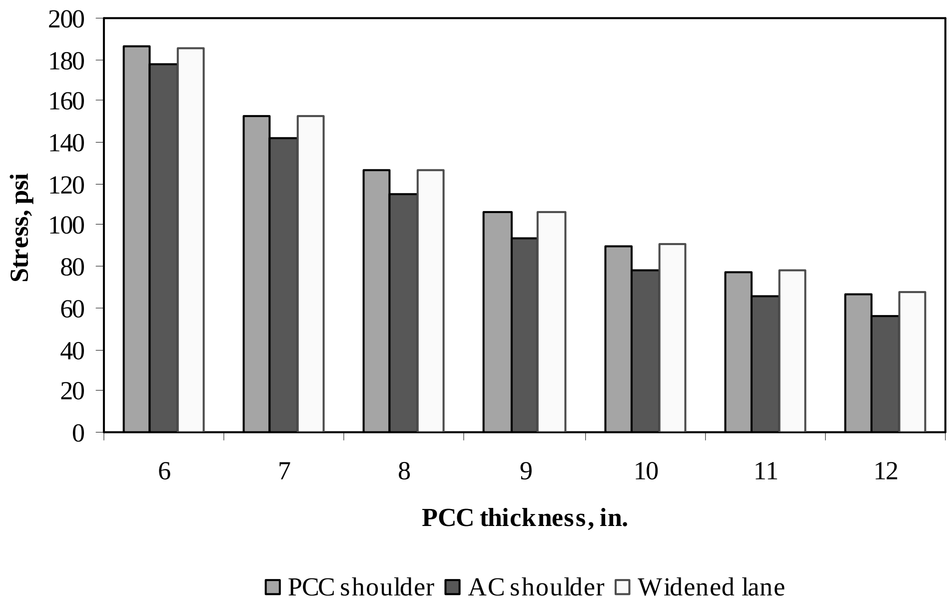


**Figure F-9-34: Impact of PCC thickness and lateral support condition on transverse stress at bottom of the Slab (315-in. joint spacing and $\alpha(\Delta T/D)$ of 0 in.$^{-1}$)**

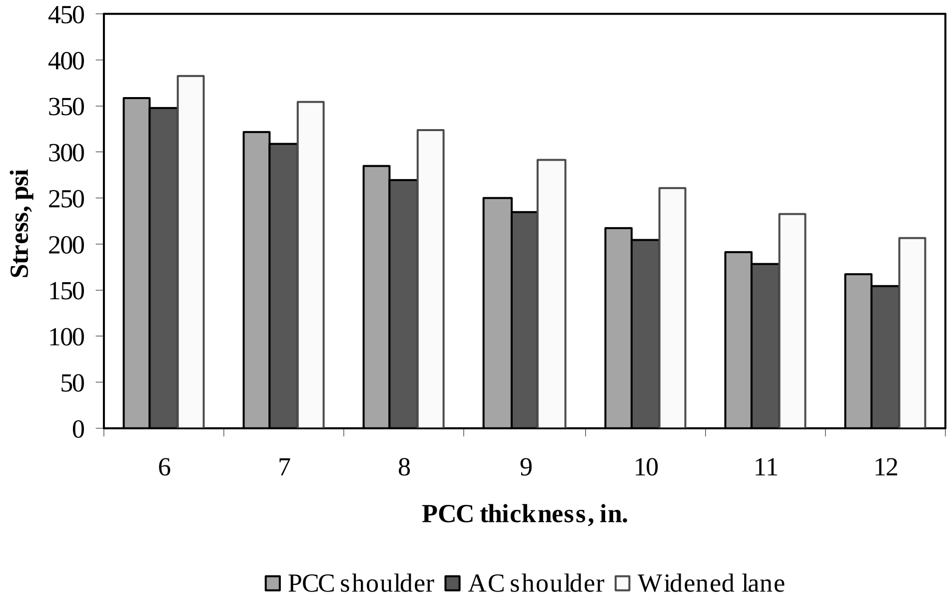


**Figure F-9-35: Impact of PCC thickness and lateral support condition on transverse stress at bottom of the Slab (177-in. joint spacing and $\alpha(\Delta T/D)$ of $20x10^{-6}$ in.$^{-1}$)**

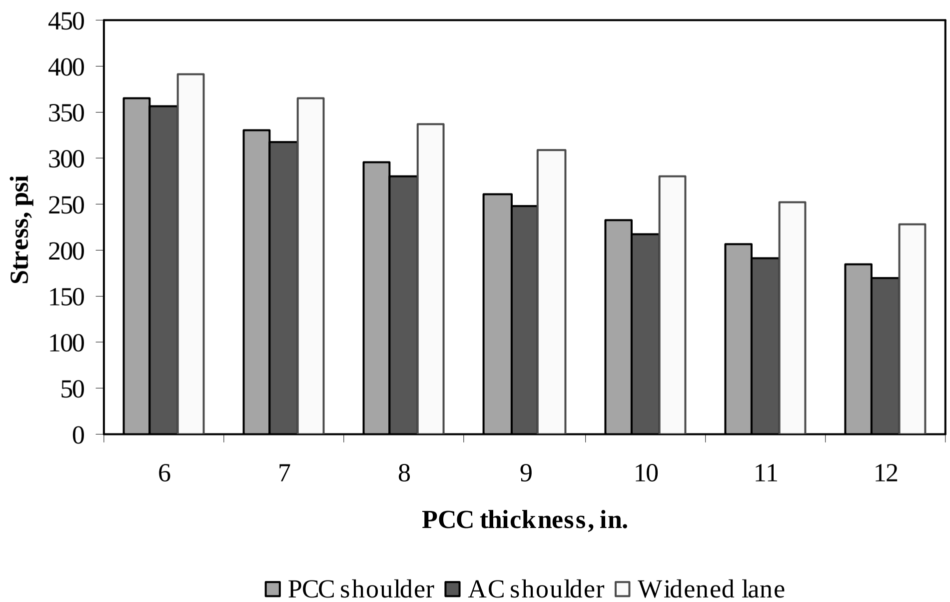


**Figure F-9-36: Impact of PCC thickness and lateral support condition on transverse stress at bottom of the Slab (315-in. joint spacing and $\alpha(\Delta T/D)$ of $20x10^{-6}$ in.$^{-1}$)**

Figures F-9-37 through F-9-42 illustrate the impact of base/subbase thickness and product α(ΔT/D) on stresses (10-in. PCC thickness, 100-psi/in. modulus of subgrade reaction and PCC shoulder)

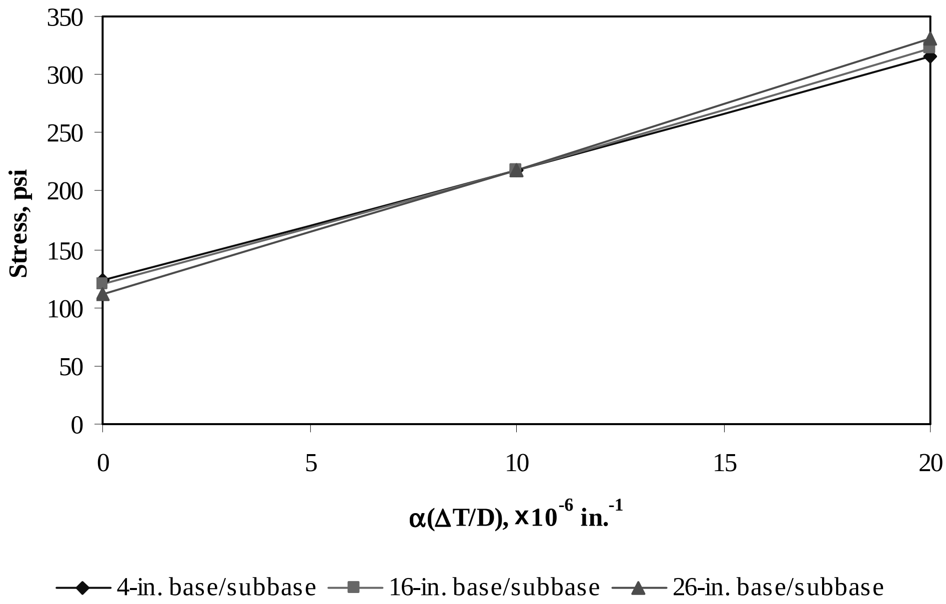


**Figure F-9-37: Impact of base/subbase thickness and product α(ΔT/D) on longitudinal stress at bottom of the slab (177-in. joint spacing)**

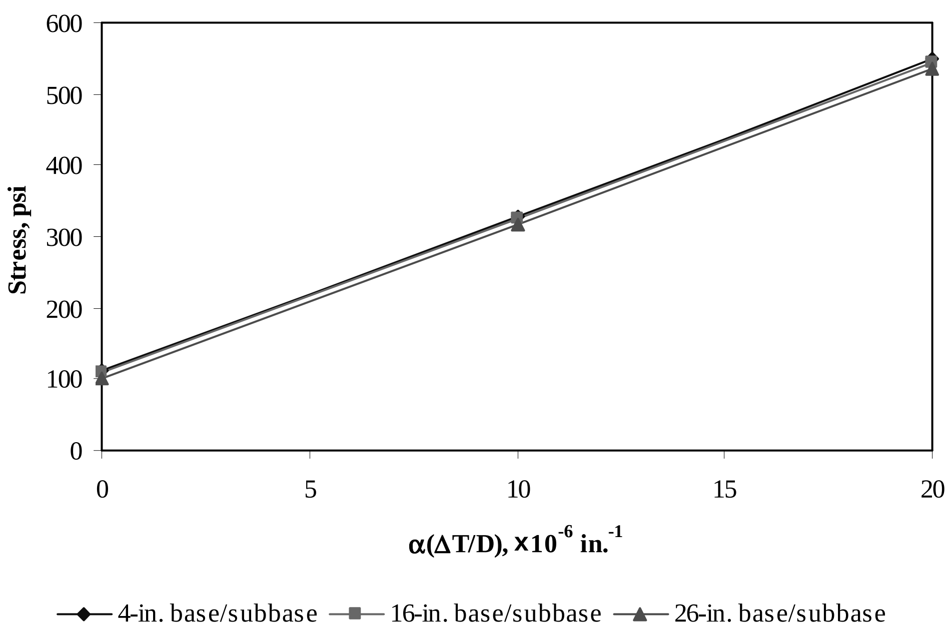


**Figure F-9-38: Impact of base/subbase thickness and product α(ΔT/D) on longitudinal stress at bottom of the slab (315-in. joint spacing)**

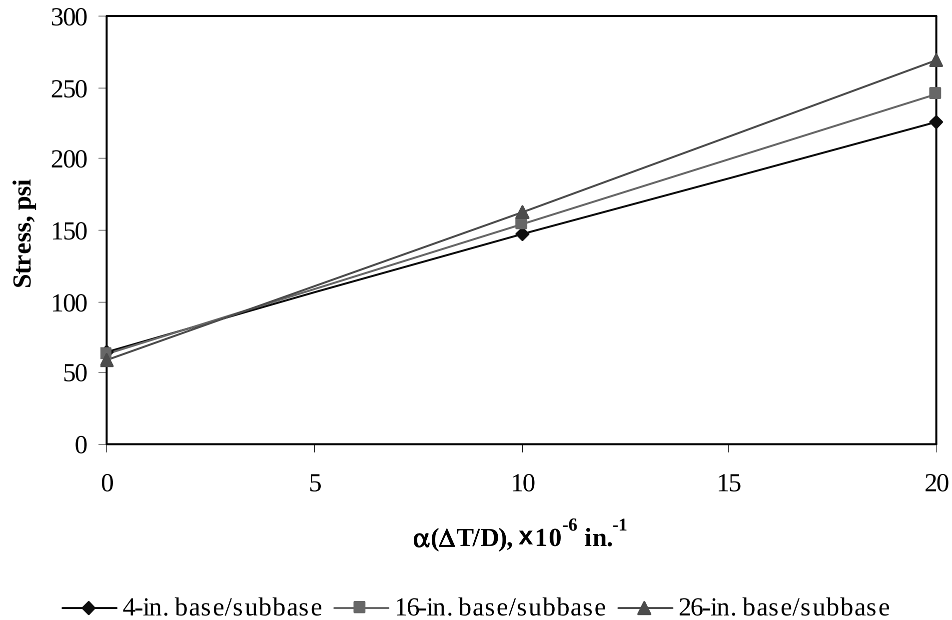


**Figure F-9-39: Impact of base/subbase thickness and product α(ΔT/D) on longitudinal stress at top of the slab (177-in. joint spacing)**

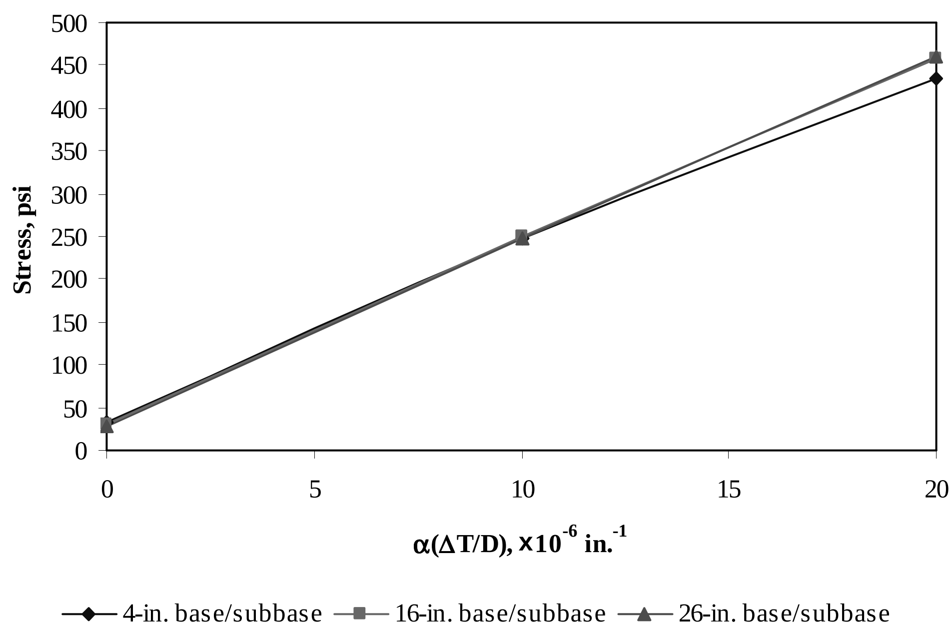


**Figure F-9-40: Impact of base/subbase thickness and product α(ΔT/D) on longitudinal stress at top of the slab (315-in. joint spacing)**

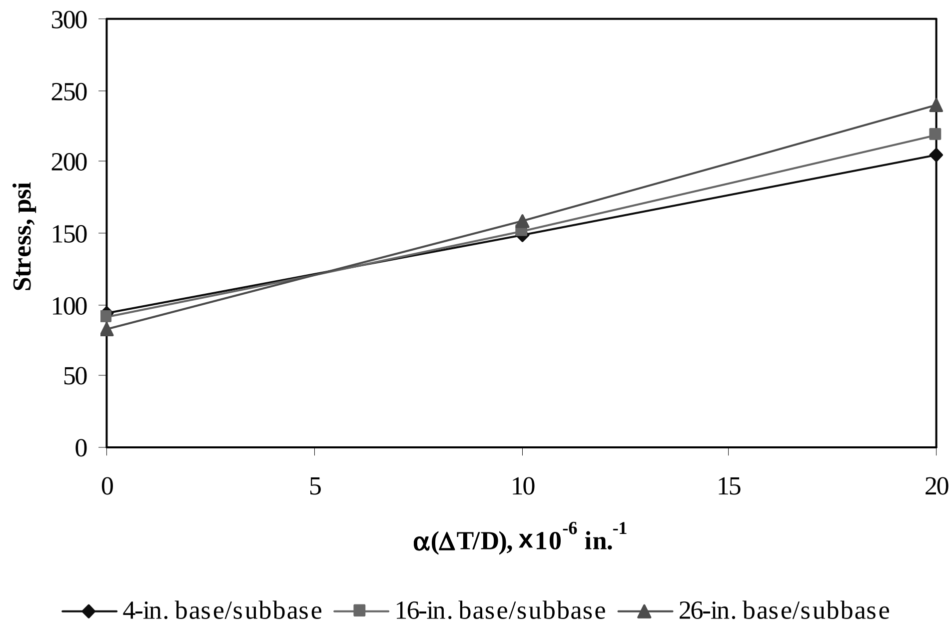


**Figure F-9-41: Impact of base/subbase thickness and product α(ΔT/D) on transverse stress at bottom of the slab (177-in. joint spacing)**

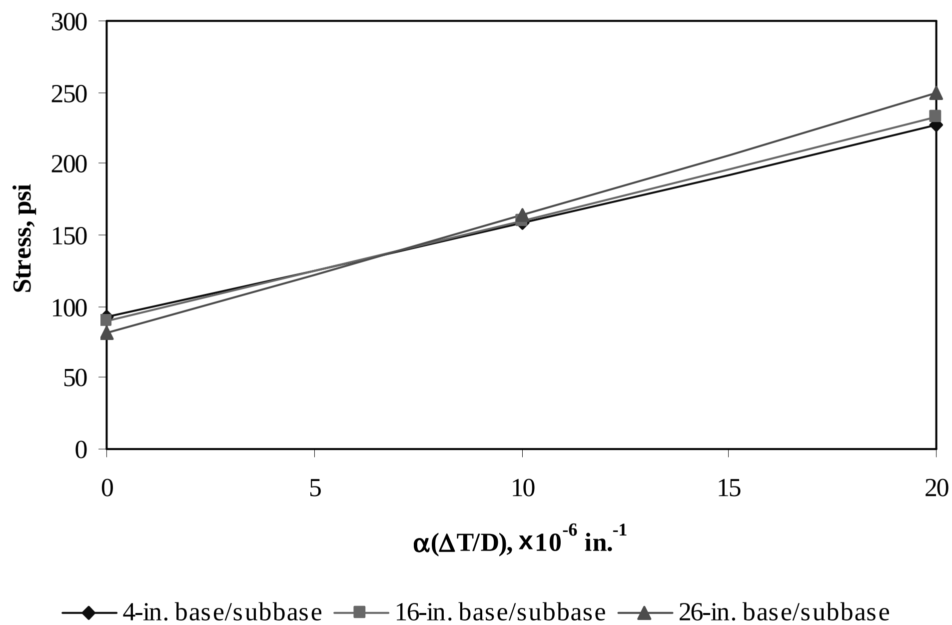


**Figure F-9-42: Impact of base/subbase thickness and product α(ΔT/D) on transverse stress at bottom of the slab (315-in. joint spacing)**

Figures F-9-43 through F-9-48 illustrate the impact of modulus of subgrade reaction and product α(ΔT/D) on stresses (10-in. PCC thickness, 16-in. base/subbase thickness and PCC shoulder)

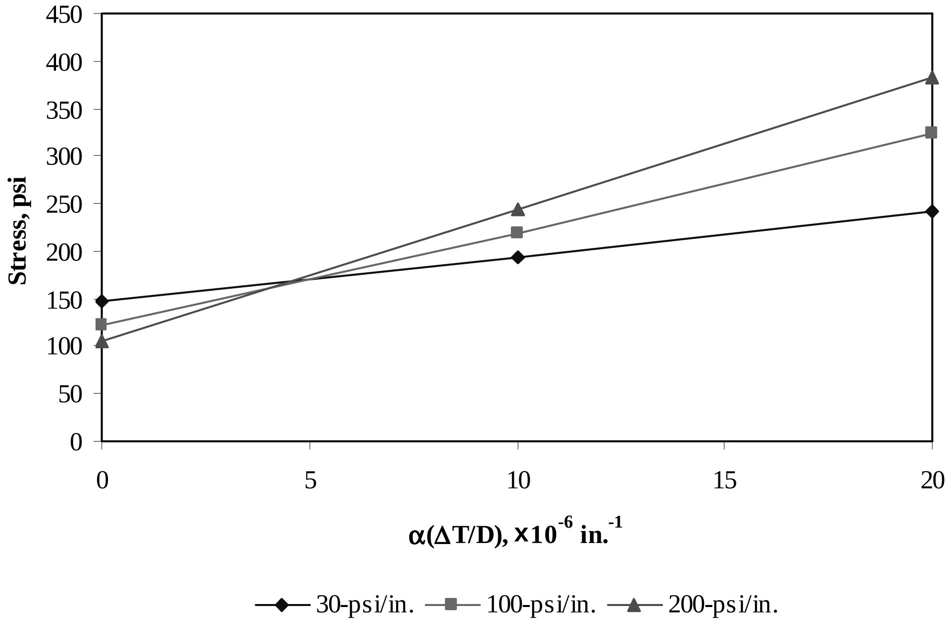


**Figure F-9-43: Impact of modulus of subgrade reaction and product α(ΔT/D) on longitudinal stress at bottom of the slab (177-in. joint spacing)**

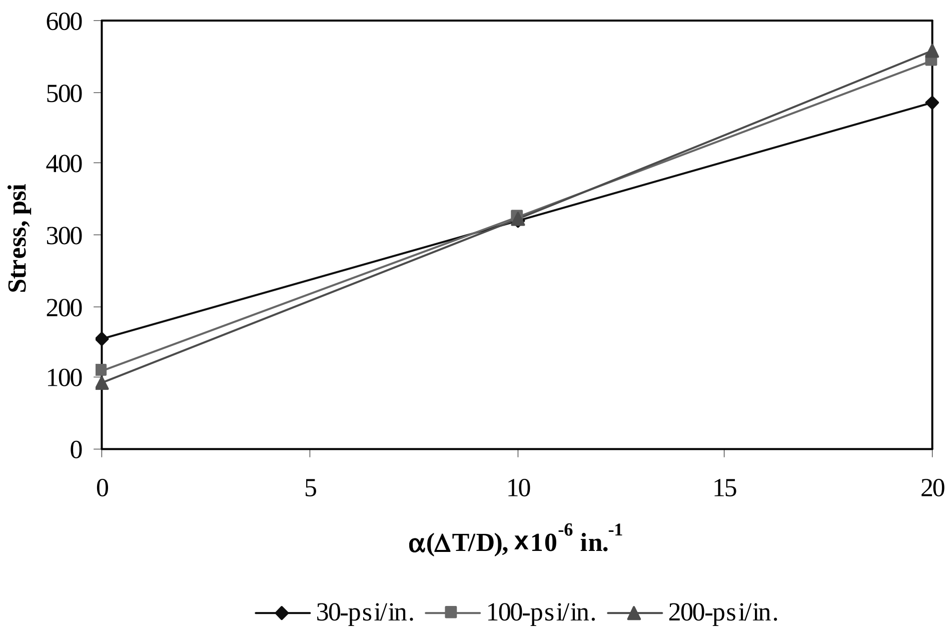


**Figure F-9-44: Impact of modulus of subgrade reaction and product α(ΔT/D) on longitudinal stress at bottom of the slab (315-in. joint spacing)**

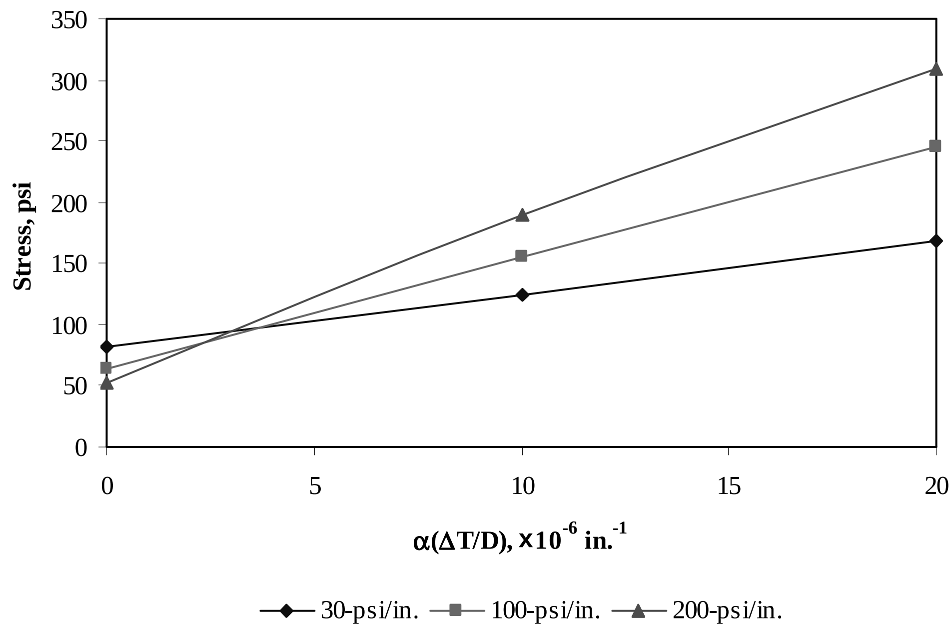


**Figure F-9-45: Impact of modulus of subgrade reaction and product α(ΔT/D) on longitudinal stress at top of the slab (177-in. joint spacing)**

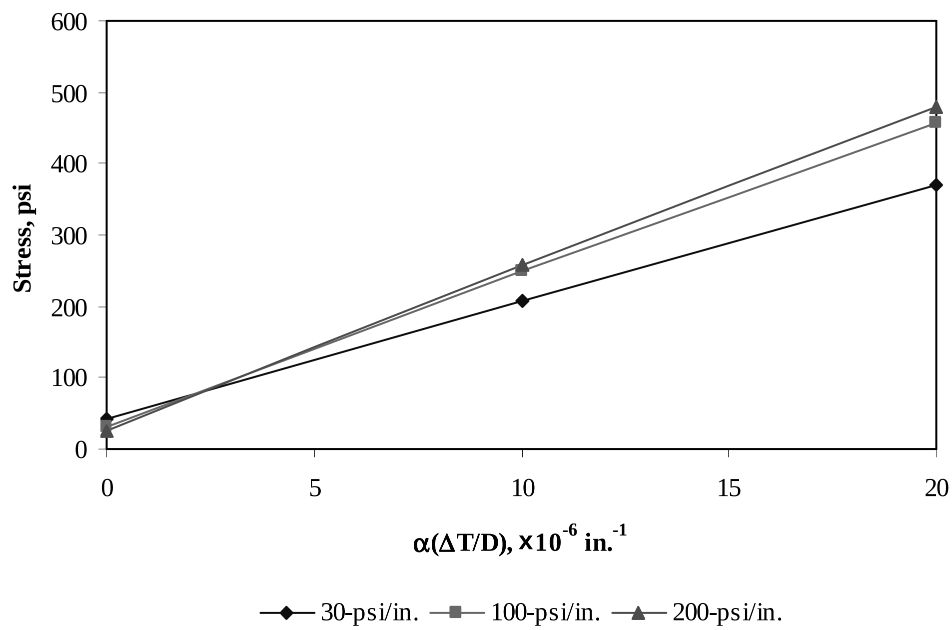


**Figure F-9-46: Impact of modulus of subgrade reaction and product α(ΔT/D) on longitudinal stress at top of the slab (315-in. joint spacing)**

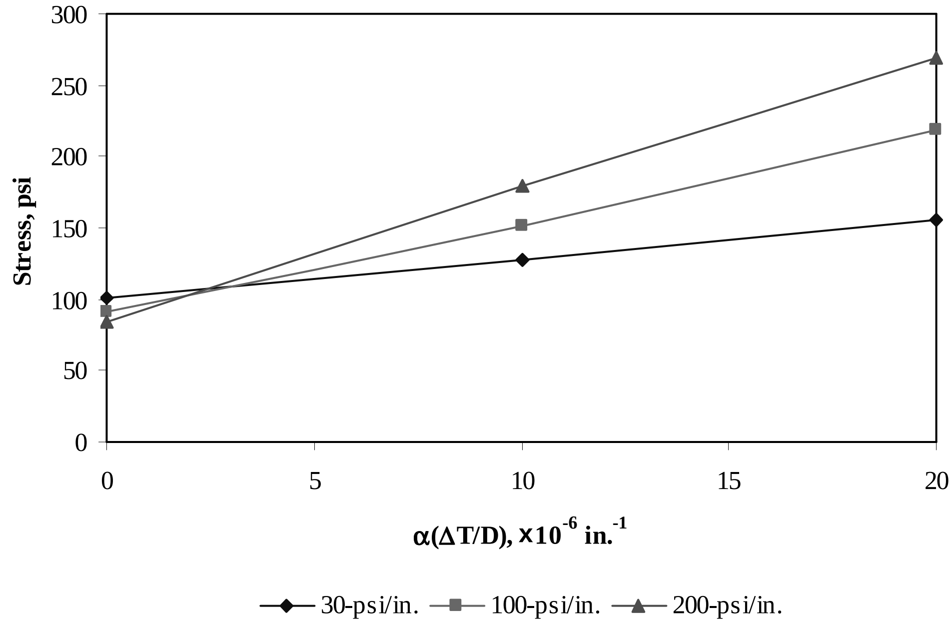


**Figure F-9-47: Impact of modulus of subgrade reaction and product α(ΔT/D) on transverse stress at bottom of the slab (177-in. joint spacing)**

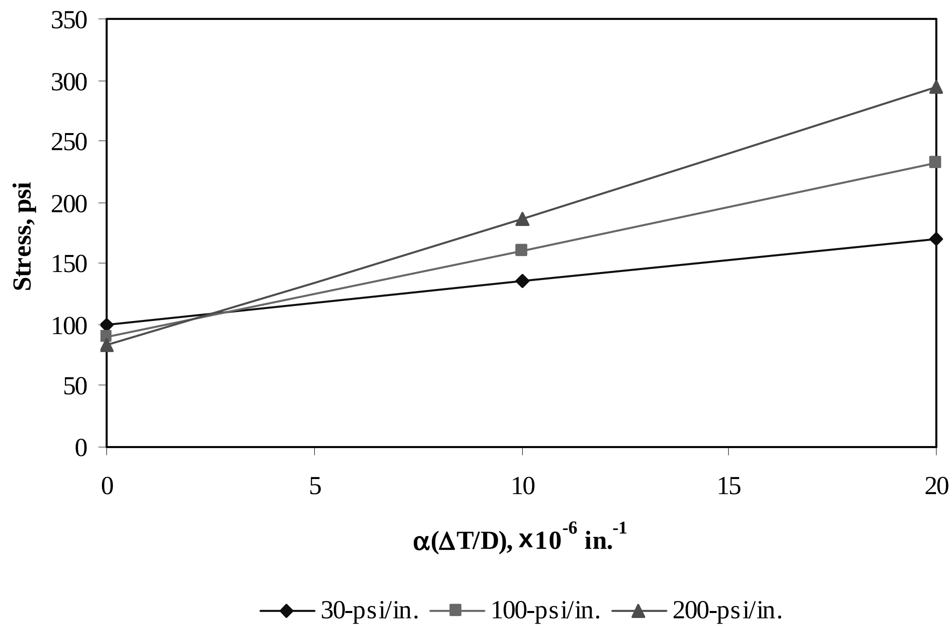


**Figure F-9-48: Impact of modulus of subgrade reaction and product α(ΔT/D) on transverse stress at bottom of the slab (315-in. joint spacing)**

Figures F-9-49 through F-9-51 illustrate the impact of joint spacing and product α(ΔT/D) on stresses (10-in. PCC thickness, 16-in. base/subbase thickness, 100-psi/in. modulus of subgrade reaction and PCC shoulder)

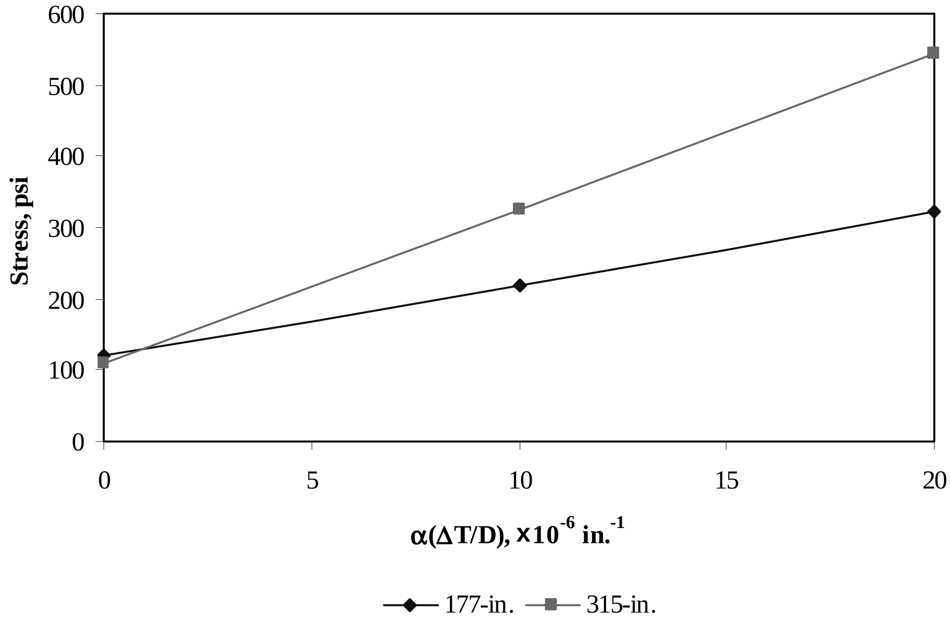


**Figure F-9-49: Impact of joint spacing and product α(ΔT/D) on longitudinal stress at bottom of the slab**

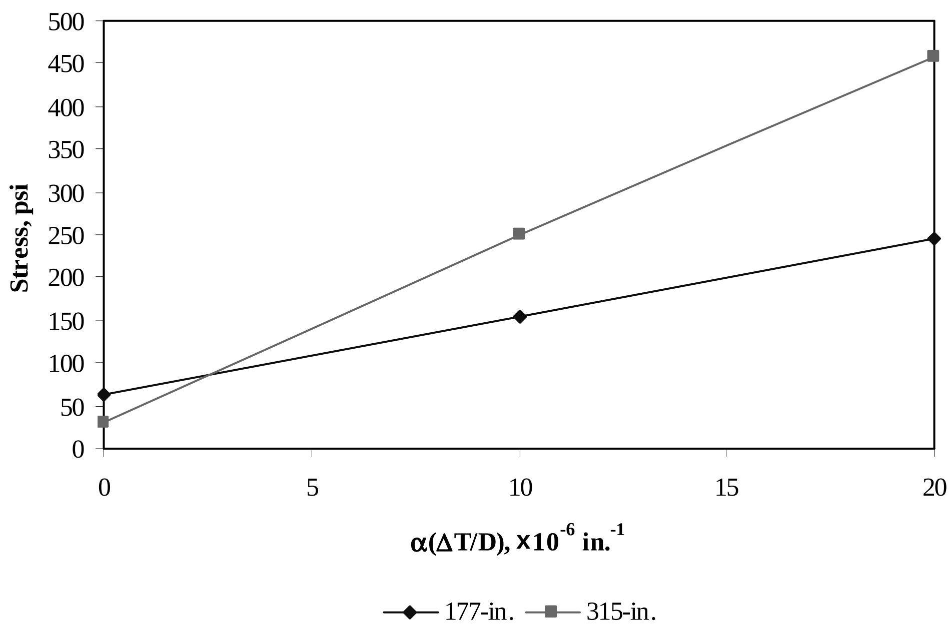


**Figure F-9-50: Impact of joint spacing and product α(ΔT/D) on longitudinal stress at top of the slab**

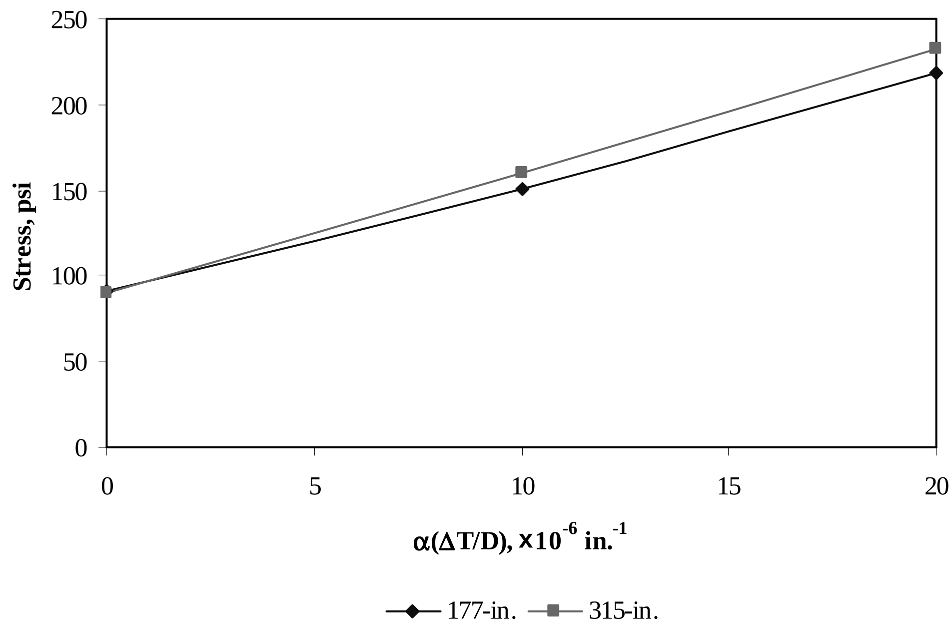


**Figure F-9-51: Impact of joint spacing and product $\alpha(\Delta T/D)$ on transverse stress at bottom of the slab**

**Sub Appendix F-10**

**Documentation of Pavement Responses for**

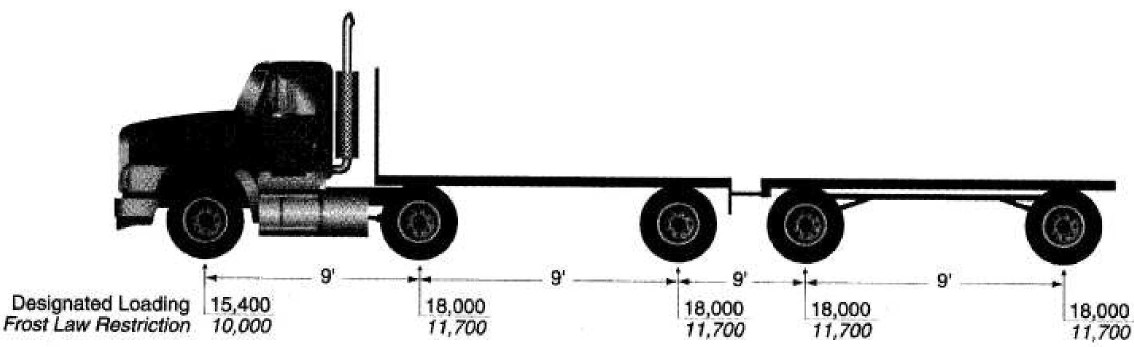


**MI-7**

Figures F-10-1 through F-10-12 illustrate the impact of PCC thickness and base/subbase thickness on stresses (100-psi/in. modulus of subgrade reaction and PCC shoulder)

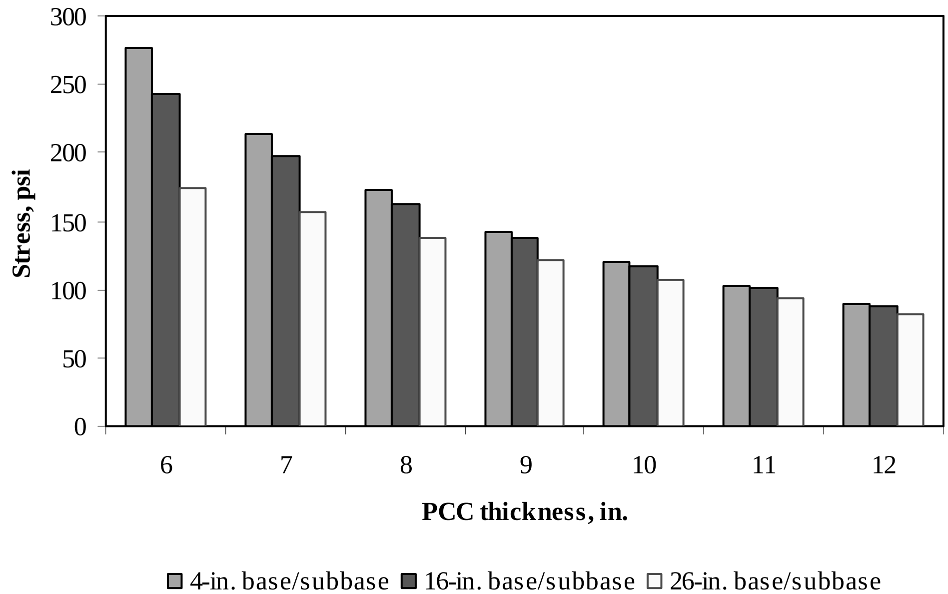


**Figure F-10-1: Impact of PCC thickness and base/subbase thickness on longitudinal stress at bottom of the Slab (177-in. joint spacing and $\alpha(\Delta T/D)$ of 0 in.$^{-1}$)**

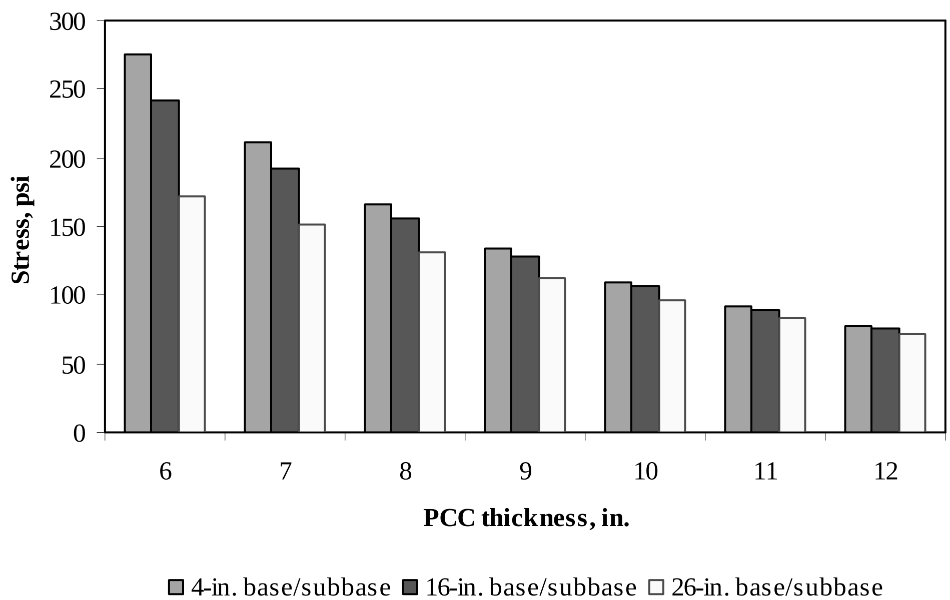


**Figure F-10-2: Impact of PCC thickness and base/subbase thickness on longitudinal stress at bottom of the Slab (315-in. joint spacing and $\alpha(\Delta T/D)$ of 0 in.$^{-1}$)**

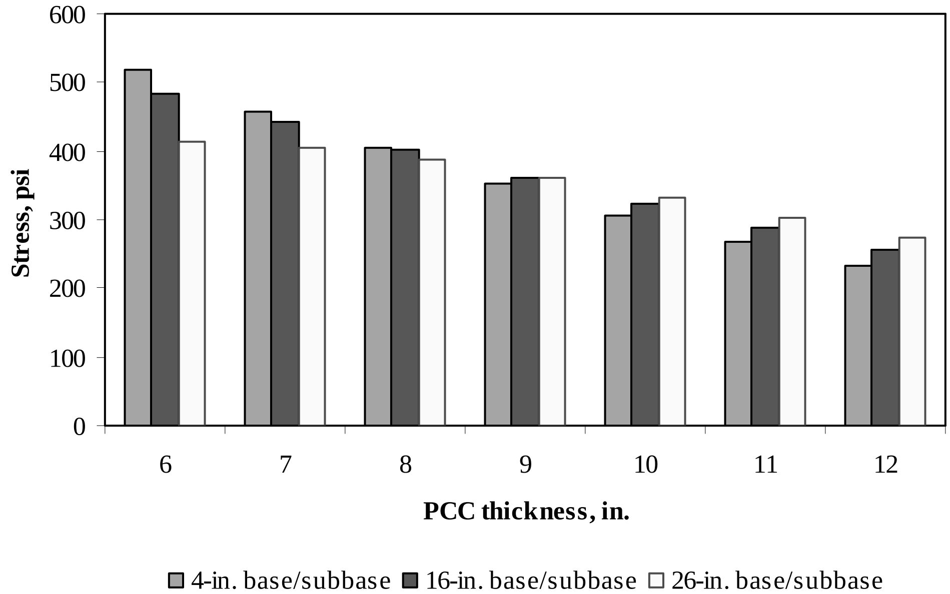


**Figure F-10-3: Impact of PCC thickness and base/subbase thickness on longitudinal stress at bottom of the Slab (177-in. joint spacing and $\alpha(\Delta T/D)$ of $20x10^{-6}$ in.$^{-1}$)**

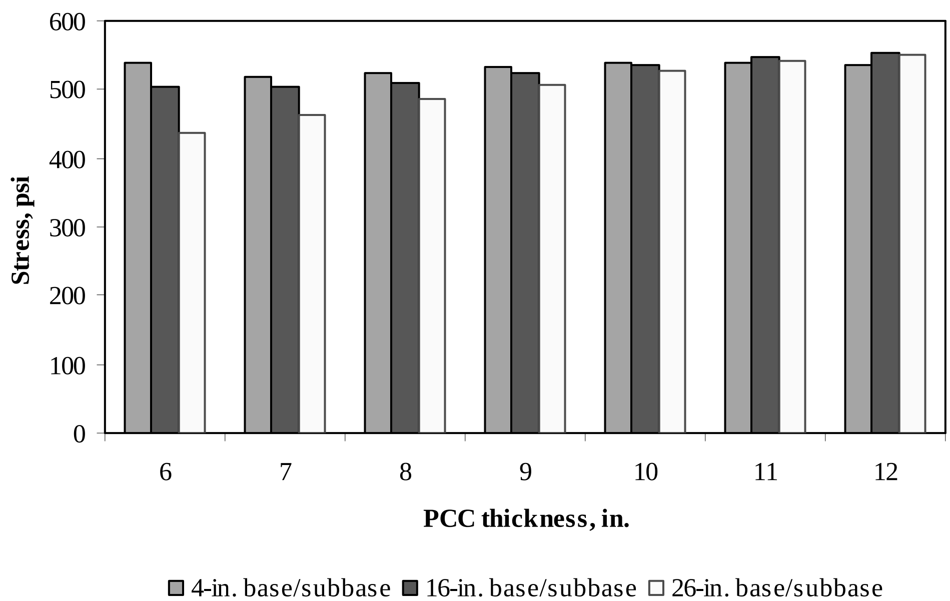


**Figure F-10-4: Impact of PCC thickness and base/subbase thickness on longitudinal stress at bottom of the Slab (315-in. joint spacing and $\alpha(\Delta T/D)$ of $20x10^{-6}$ in.$^{-1}$)**

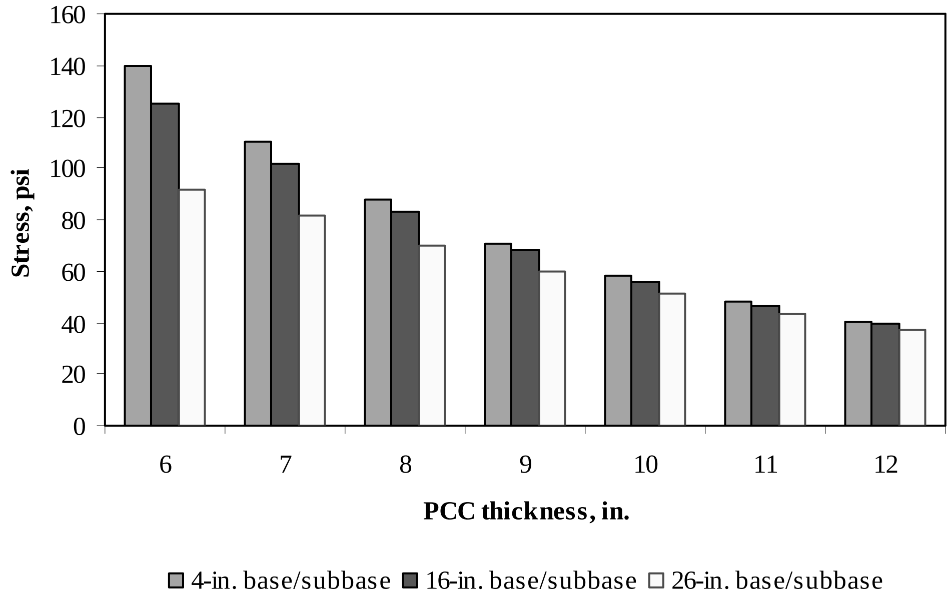


**Figure F-10-5: Impact of PCC thickness and base/subbase thickness on longitudinal stress at top of the Slab (177-in. joint spacing and $\alpha(\Delta T/D)$ of 0 in.$^{-1}$)**

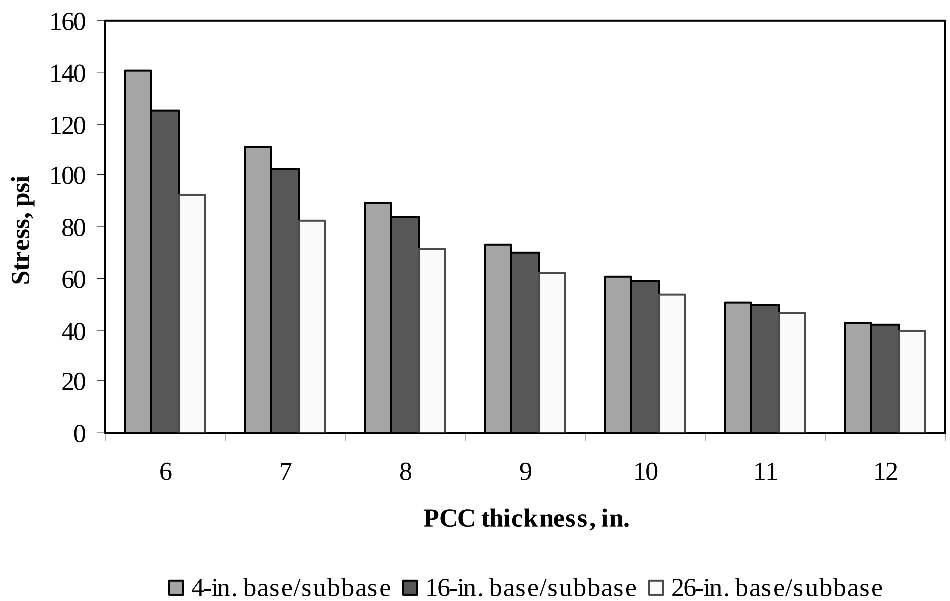


**Figure F-10-6: Impact of PCC thickness and base/subbase thickness on longitudinal stress at top of the Slab (315-in. joint spacing and $\alpha(\Delta T/D)$ of 0 in.$^{-1}$)**

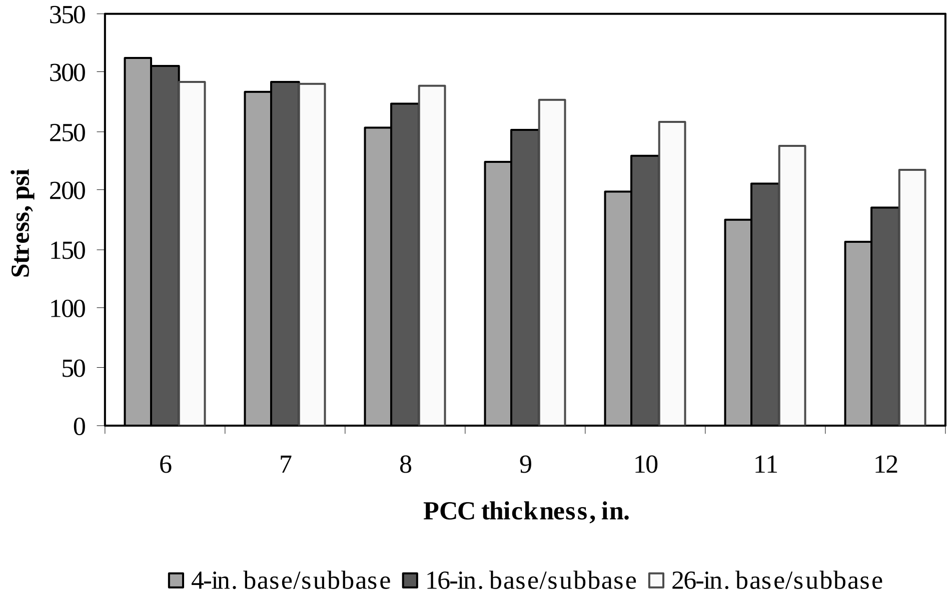


**Figure F-10-7: Impact of PCC thickness and base/subbase thickness on longitudinal stress at top of the Slab (177-in. joint spacing and $\alpha(\Delta T/D)$ of $-20 \times 10^{-6}$ in.$^{-1}$)**

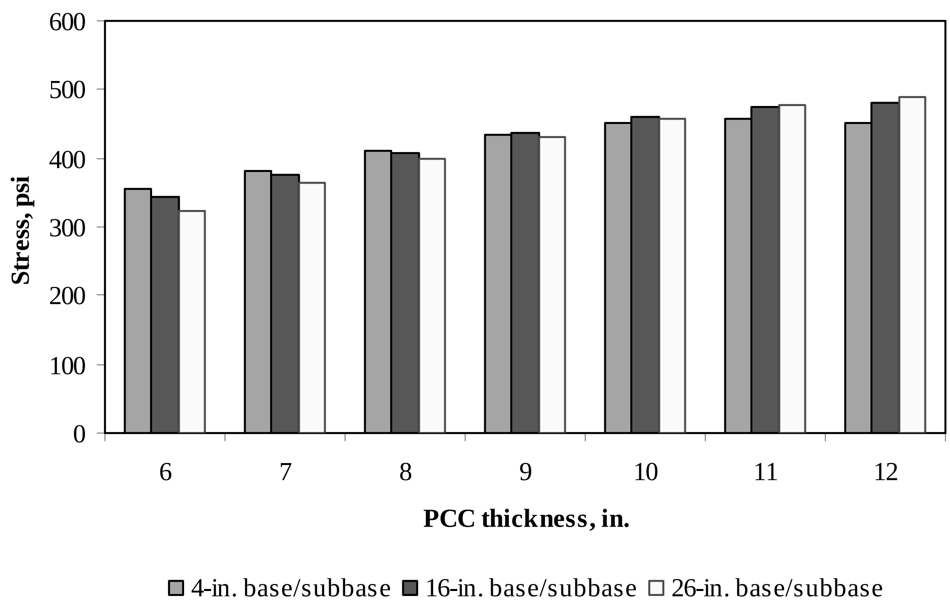


**Figure F-10-8: Impact of PCC thickness and base/subbase thickness on longitudinal stress at top of the Slab (315-in. joint spacing and $\alpha(\Delta T/D)$ of $-20 \times 10^{-6}$ in.$^{-1}$)**

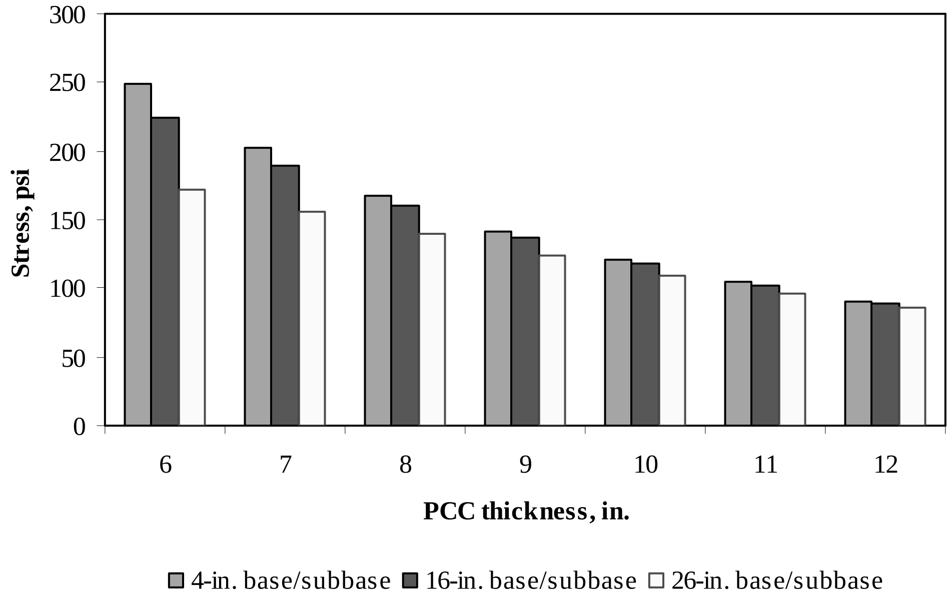


**Figure F-10-9: Impact of PCC thickness and base/subbase thickness on transverse stress at bottom of the Slab (177-in. joint spacing and $\alpha(\Delta T/D)$ of 0 in.$^{-1}$)**

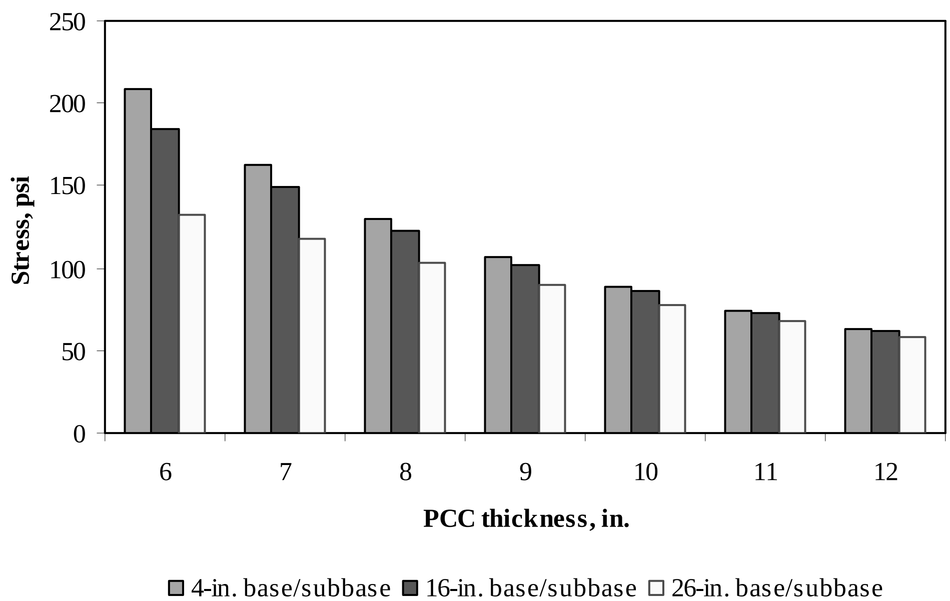


**Figure F-10-10: Impact of PCC thickness and base/subbase thickness on transverse stress at bottom of the Slab (315-in. joint spacing and $\alpha(\Delta T/D)$ of 0 in.$^{-1}$)**

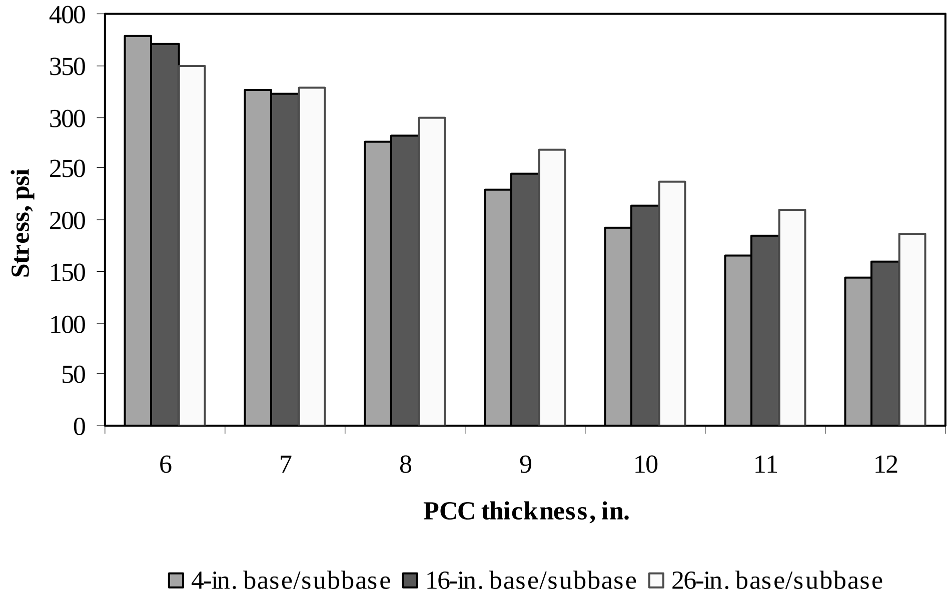


**Figure F-10-11: Impact of PCC thickness and base/subbase thickness on transverse stress at bottom of the Slab (177-in. joint spacing and $\alpha(\Delta T/D)$ of 20x10$^{-6}$ in.$^{-1}$)**

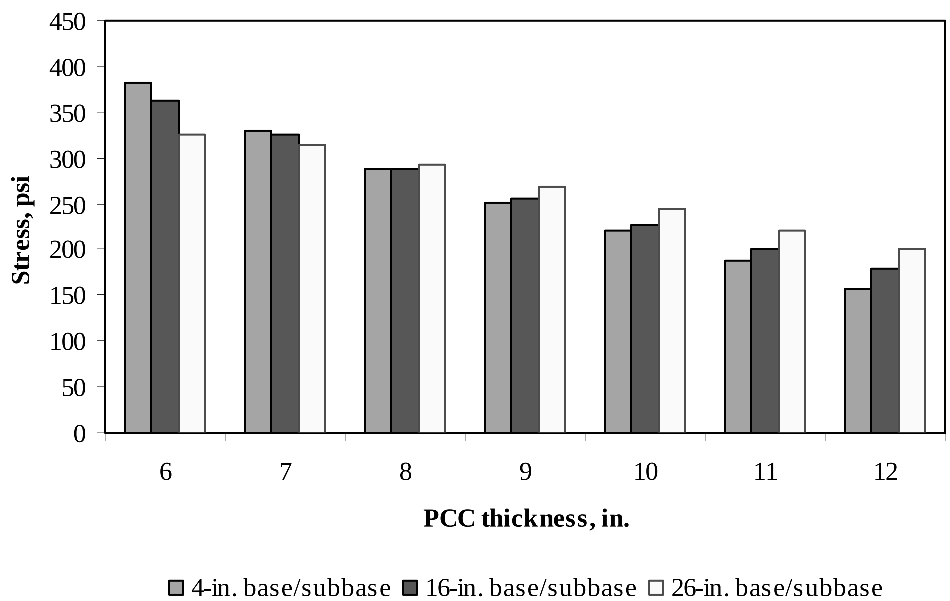


**Figure F-10-12: Impact of PCC thickness and base/subbase thickness on transverse stress at bottom of the Slab (315-in. joint spacing and $\alpha(\Delta T/D)$ of 20x10$^{-6}$ in.$^{-1}$)**

Figures F-10-13 through F-10-24 illustrate the impact of PCC thickness and modulus of subgrade reaction on stresses (16-in. base/subbase thickness and PCC shoulder)

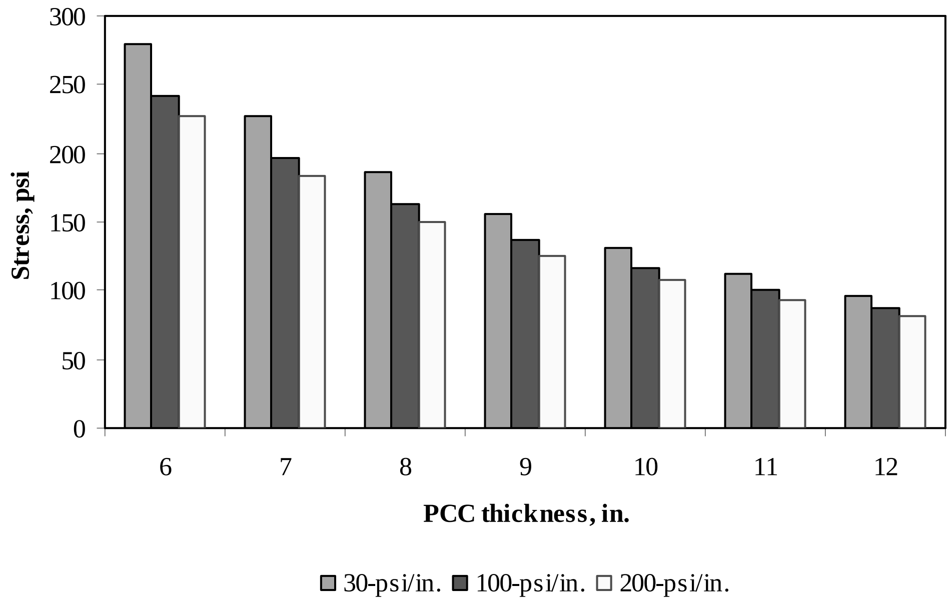


**Figure F-10-13: Impact of PCC thickness and modulus of subgrade reaction on longitudinal stress at bottom of the slab (177-in. joint spacing and $\alpha(\Delta T/D)$ of 0 in.$^{-1}$)**

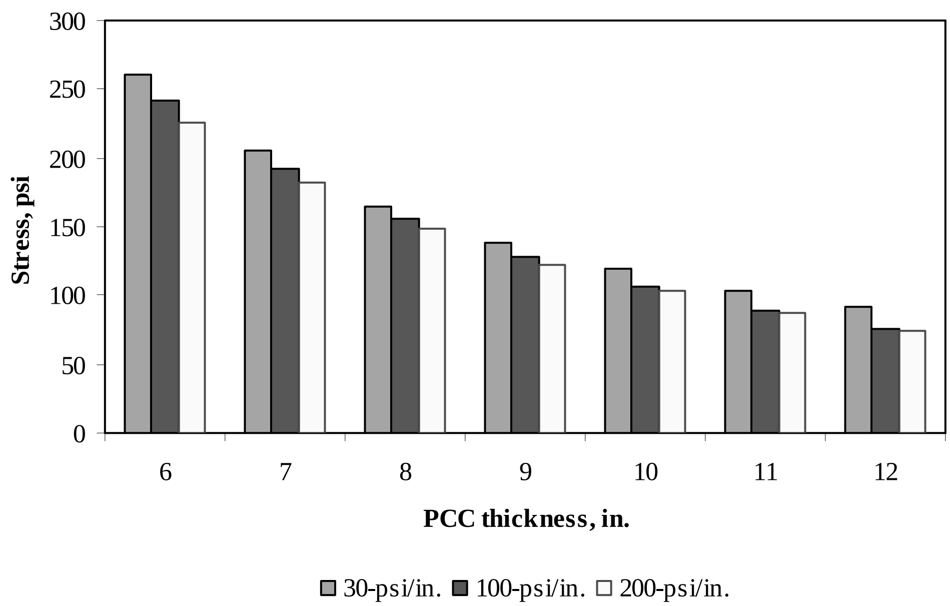


**Figure F-10-14: Impact of PCC thickness and modulus of subgrade reaction on longitudinal stress at bottom of the slab (315-in. joint spacing and $\alpha(\Delta T/D)$ of 0 in.$^{-1}$)**

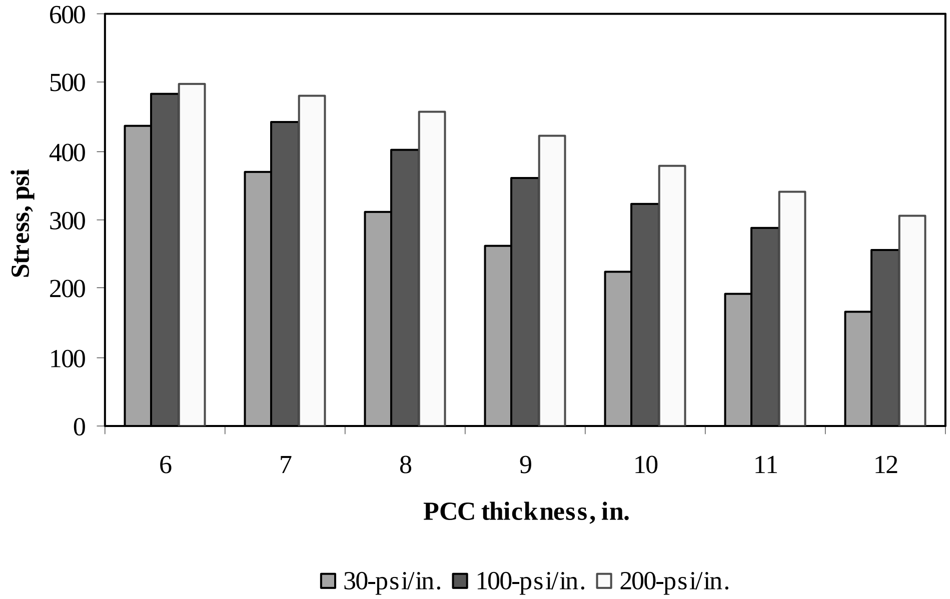


**Figure F-10-15: Impact of PCC thickness and modulus of subgrade reaction on longitudinal stress at bottom of the slab (177-in. joint spacing and $\alpha(\Delta T/D)$ of $20x10^{-6}$ in.$^{-1}$)**

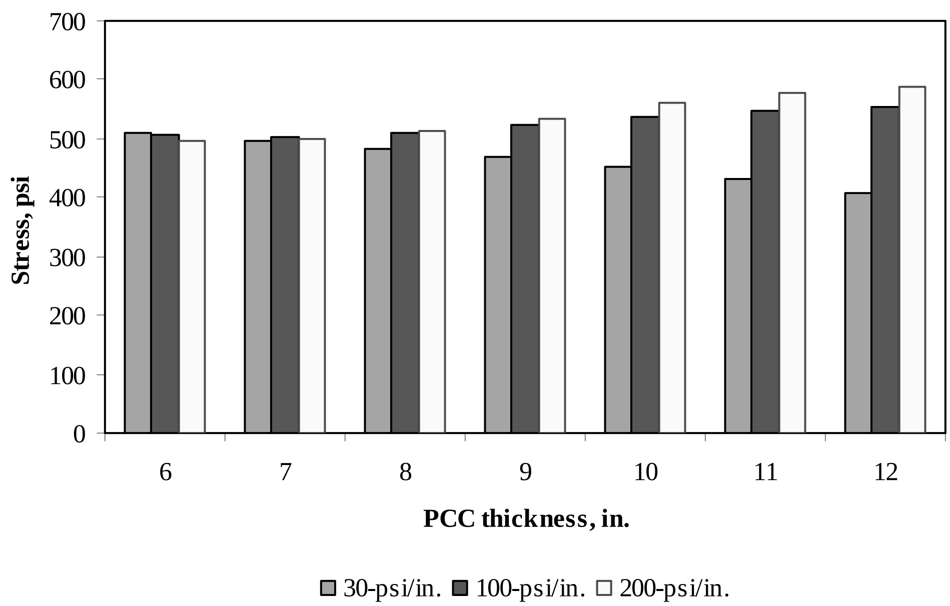


**Figure F-10-16: Impact of PCC thickness and modulus of subgrade reaction on longitudinal stress at bottom of the slab (315-in. joint spacing and $\alpha(\Delta T/D)$ of $20x10^{-6}$ in.$^{-1}$)**

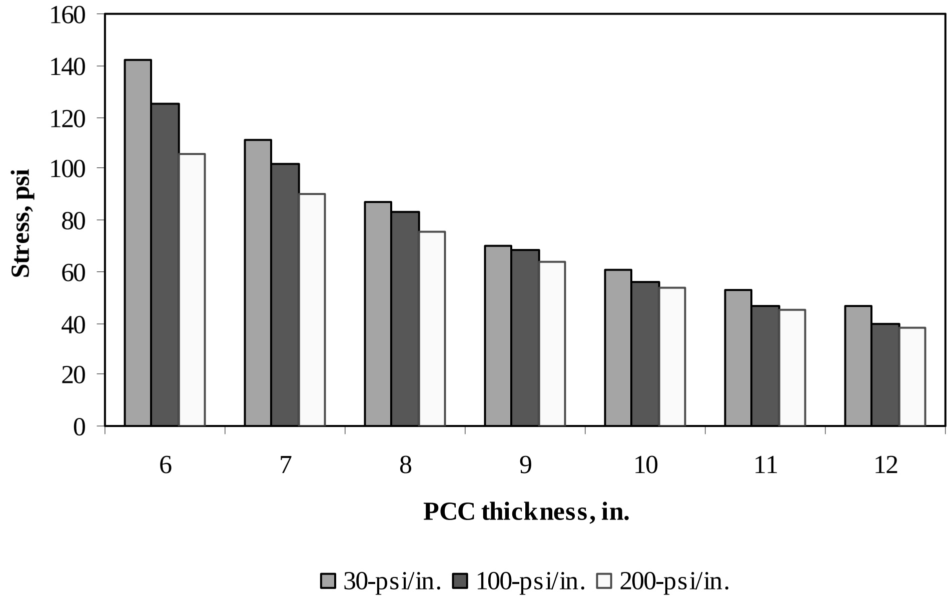


**Figure F-10-17: Impact of PCC thickness and modulus of subgrade reaction on longitudinal stress at top of the Slab (177-in. joint spacing and $\alpha(\Delta T/D)$ of 0 in.$^{-1}$)**

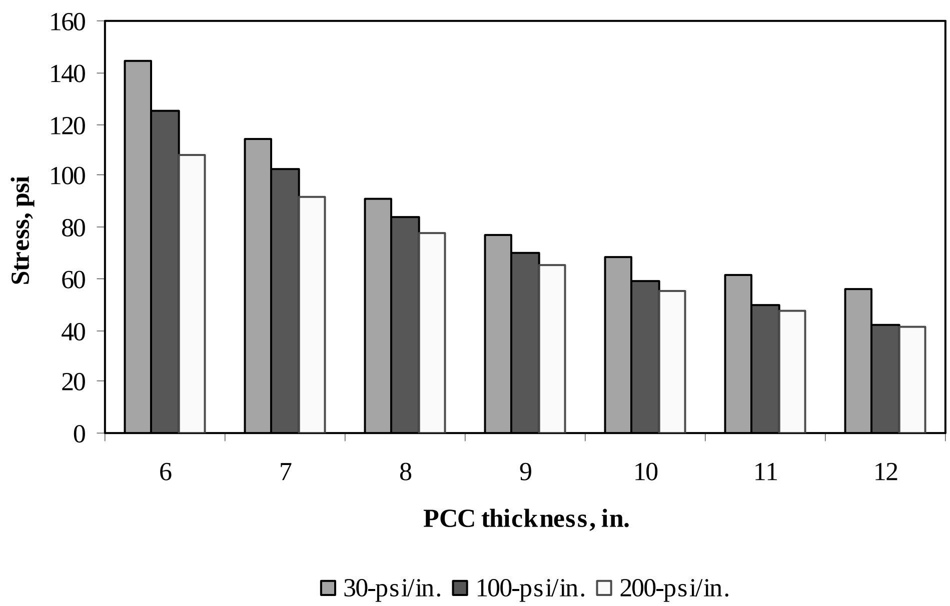


**Figure F-10-18: Impact of PCC thickness and modulus of subgrade reaction on longitudinal stress at top of the Slab (315-in. joint spacing and $\alpha(\Delta T/D)$ of 0 in.$^{-1}$)**

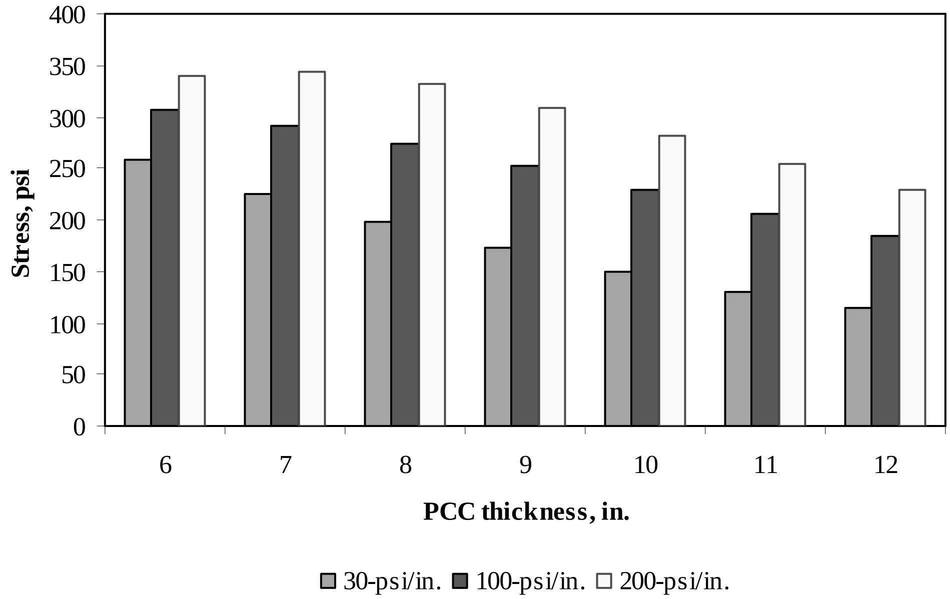


**Figure F-10-19: Impact of PCC thickness and modulus of subgrade reaction on longitudinal stress at top of the Slab (177-in. joint spacing and $\alpha(\Delta T/D)$ of $-20x10^{-6}$ in.$^{-1}$)**

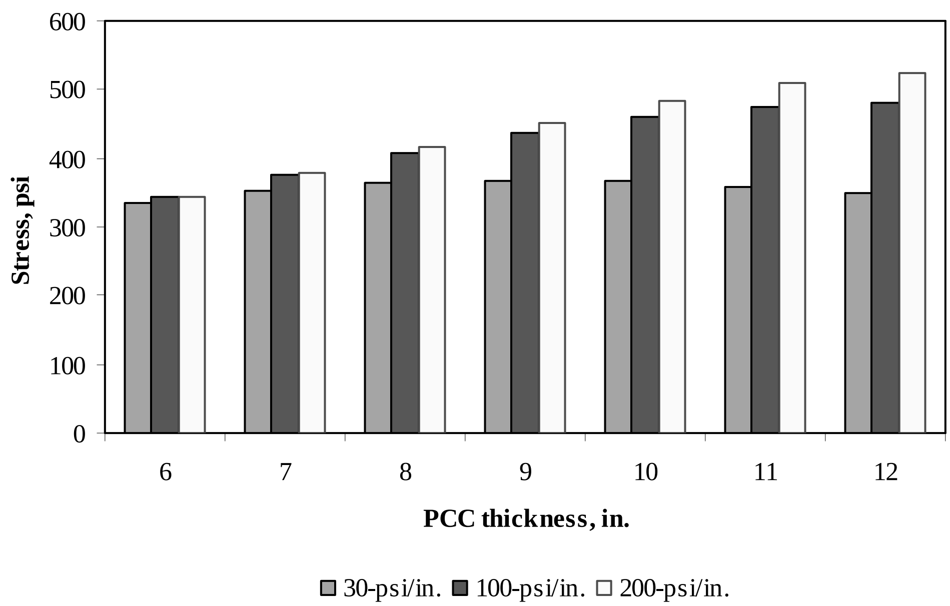


**Figure F-10-20: Impact of PCC thickness and modulus of subgrade reaction on longitudinal stress at top of the Slab (315-in. joint spacing and $\alpha(\Delta T/D)$ of $-20x10^{-6}$ in.$^{-1}$)**

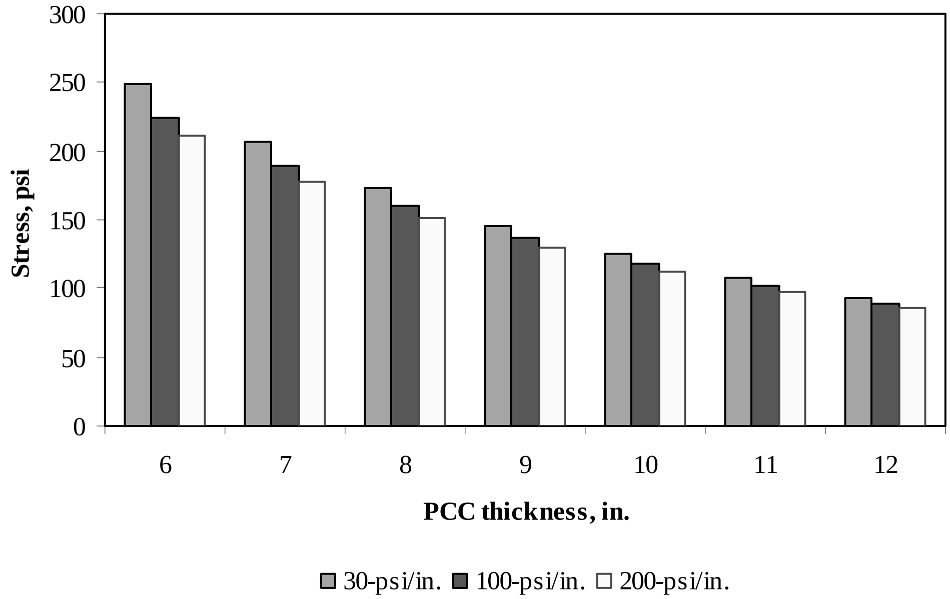


**Figure F-10-21: Impact of PCC thickness and modulus of subgrade reaction on transverse stress at bottom of the Slab (177-in. joint spacing and $\alpha(\Delta T/D)$ of 0 in.$^{-1}$)**

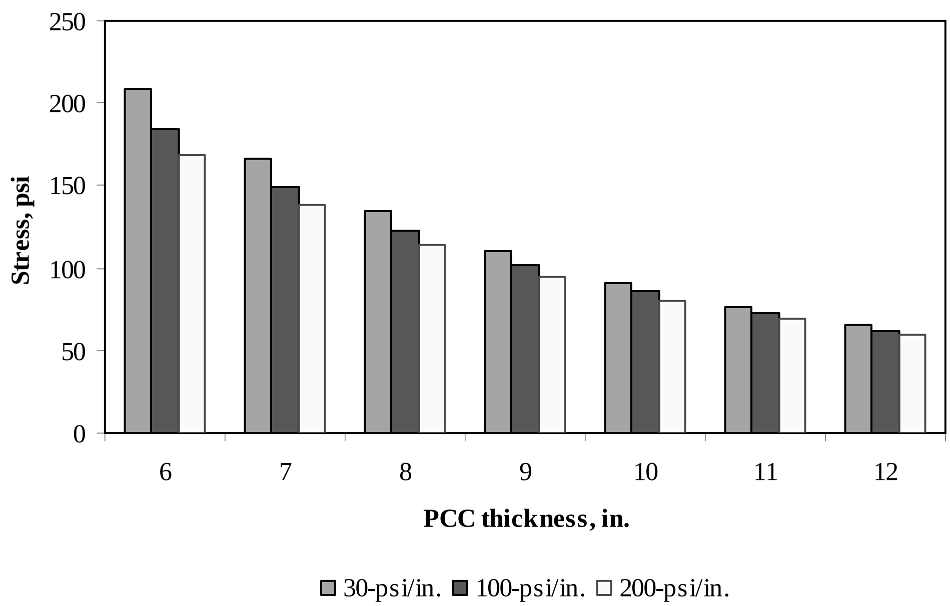


**Figure F-10-22: Impact of PCC thickness and modulus of subgrade reaction on transverse stress at bottom of the Slab (315-in. joint spacing and $\alpha(\Delta T/D)$ of 0 in.$^{-1}$)**

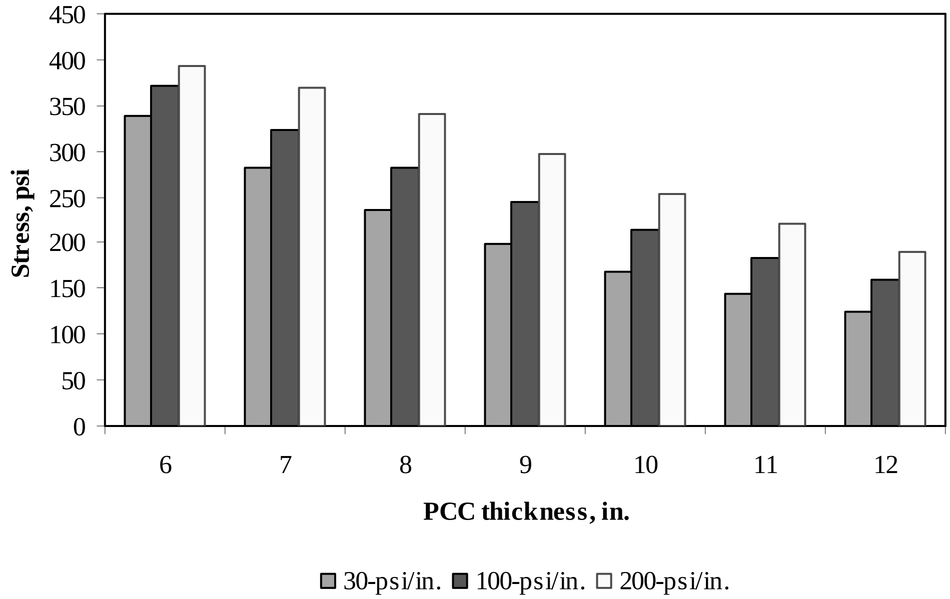


**Figure F-10-23: Impact of PCC thickness and modulus of subgrade reaction on transverse stress at bottom of the Slab (177-in. joint spacing and $\alpha(\Delta T/D)$ of $20\text{x}10^{-6}$ in.$^{-1}$)**

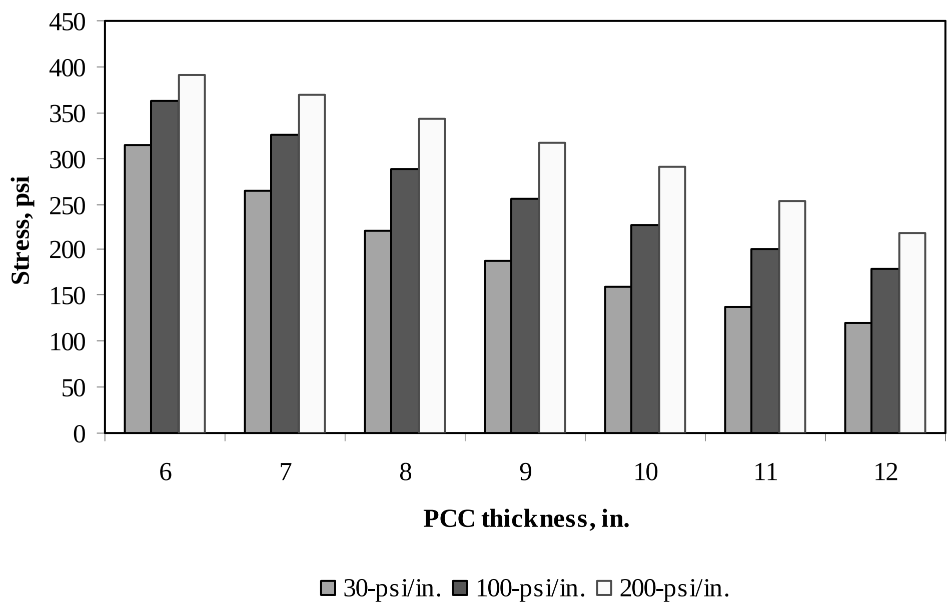


**Figure F-10-24: Impact of PCC thickness and modulus of subgrade reaction on transverse stress at bottom of the Slab (315-in. joint spacing and $\alpha(\Delta T/D)$ of $20\text{x}10^{-6}$ in.$^{-1}$)**

Figures F-10-25 through F-10-36 illustrate the impact of PCC thickness and lateral support condition on stresses (16-in. base/subbase and 100-psi/in. modulus of subgrade reaction)

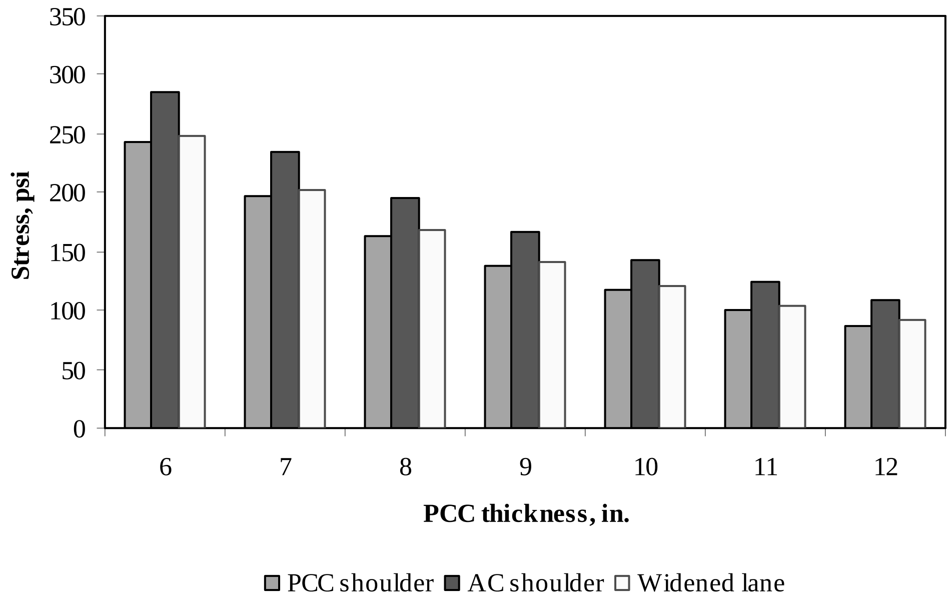


**Figure F-10-25: Impact of PCC thickness and lateral support condition on longitudinal stress at bottom of the Slab (177-in. joint spacing and $\alpha(\Delta T/D)$ of 0 in.$^{-1}$)**

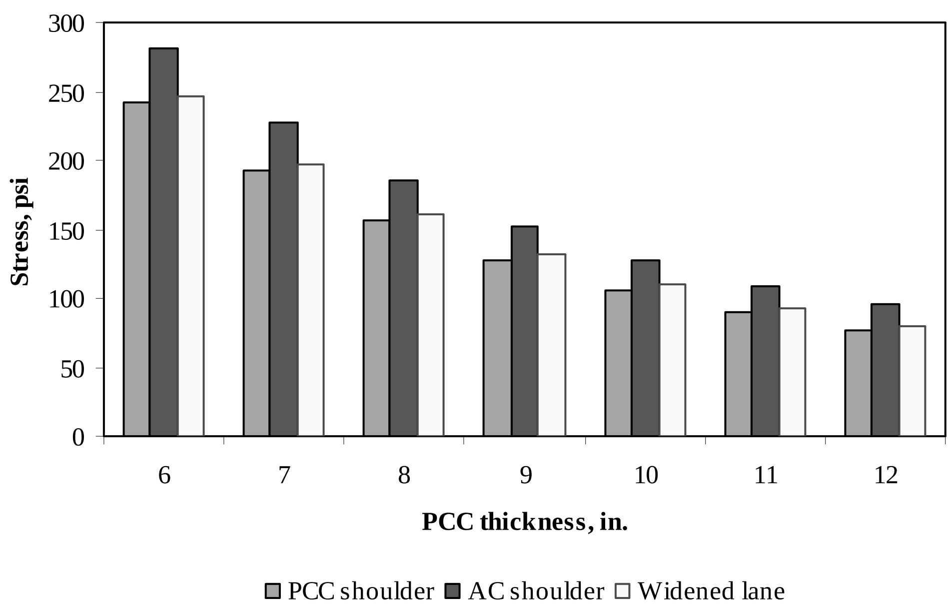


**Figure F-10-26: Impact of PCC thickness and lateral support condition on longitudinal stress at bottom of the Slab (315-in. joint spacing and $\alpha(\Delta T/D)$ of 0 in.$^{-1}$)**

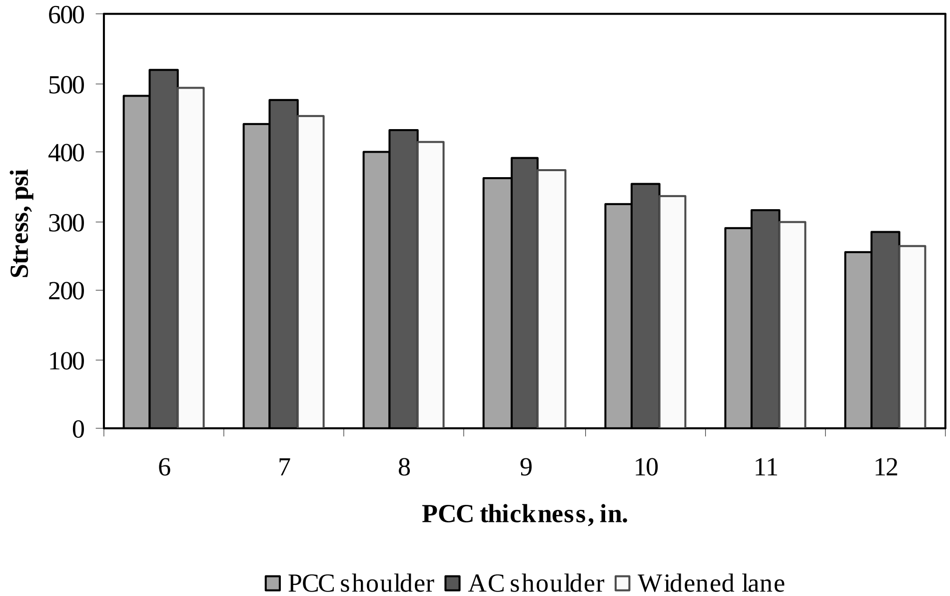


**Figure F-10-27: Impact of PCC thickness and lateral support condition on longitudinal stress at bottom of the Slab (177-in. joint spacing and $\alpha(\Delta T/D)$ of $20x10^{-6}$ in.$^{-1}$)**

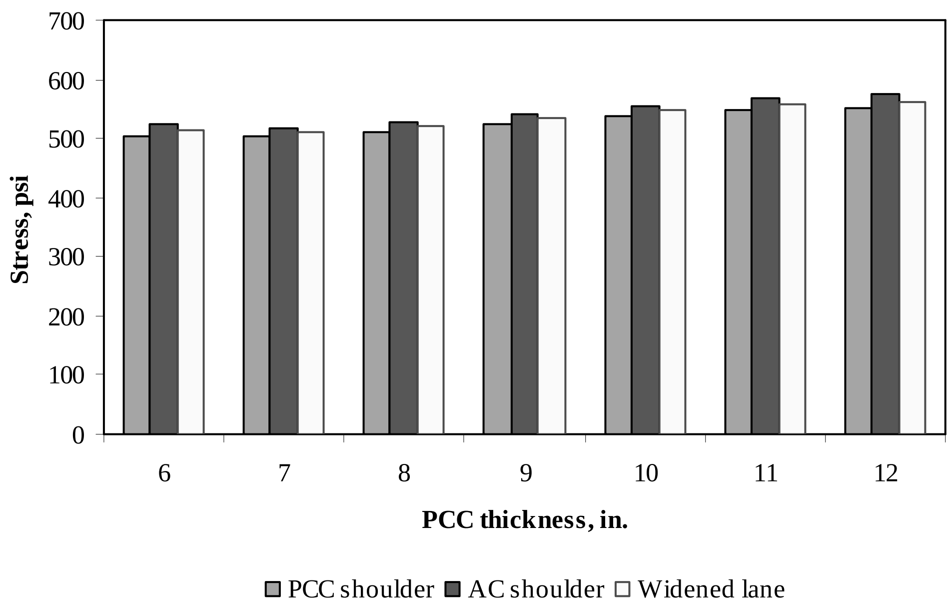


**Figure F-10-28: Impact of PCC thickness and lateral support condition on longitudinal stress at bottom of the Slab (315-in. joint spacing and $\alpha(\Delta T/D)$ of $20x10^{-6}$ in.$^{-1}$)**

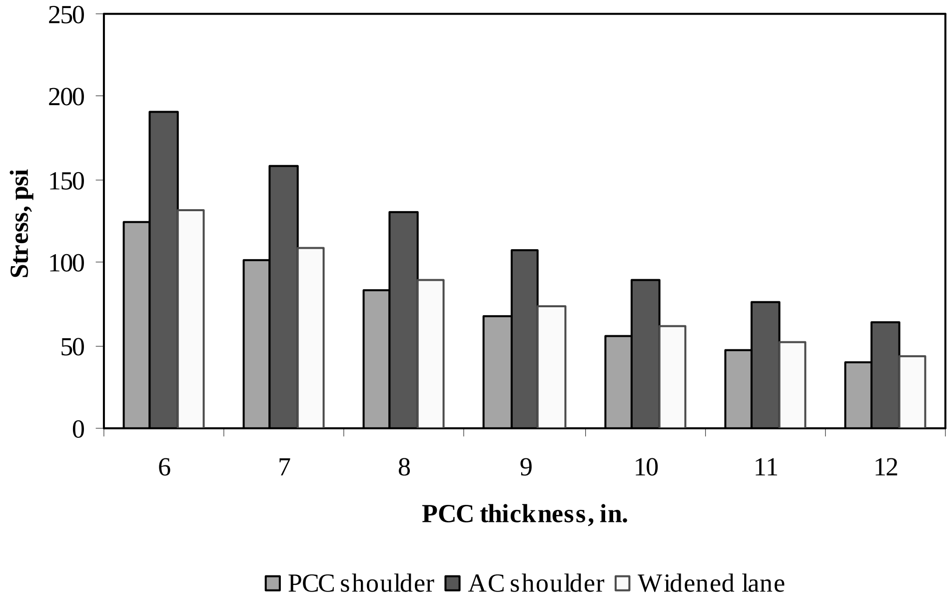


**Figure F-10-29: Impact of PCC thickness and lateral support condition on longitudinal stress at top of the Slab (177-in. joint spacing and $\alpha(\Delta T/D)$ of 0 in.$^{-1}$)**

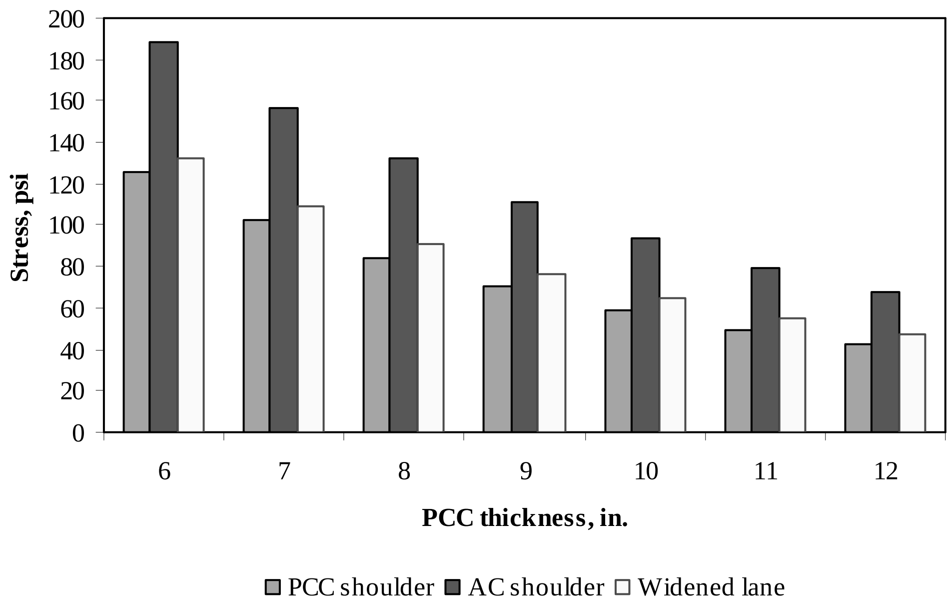


**Figure F-10-30: Impact of PCC thickness and lateral support condition on longitudinal stress at top of the Slab (315-in. joint spacing and $\alpha(\Delta T/D)$ of 0 in.$^{-1}$)**

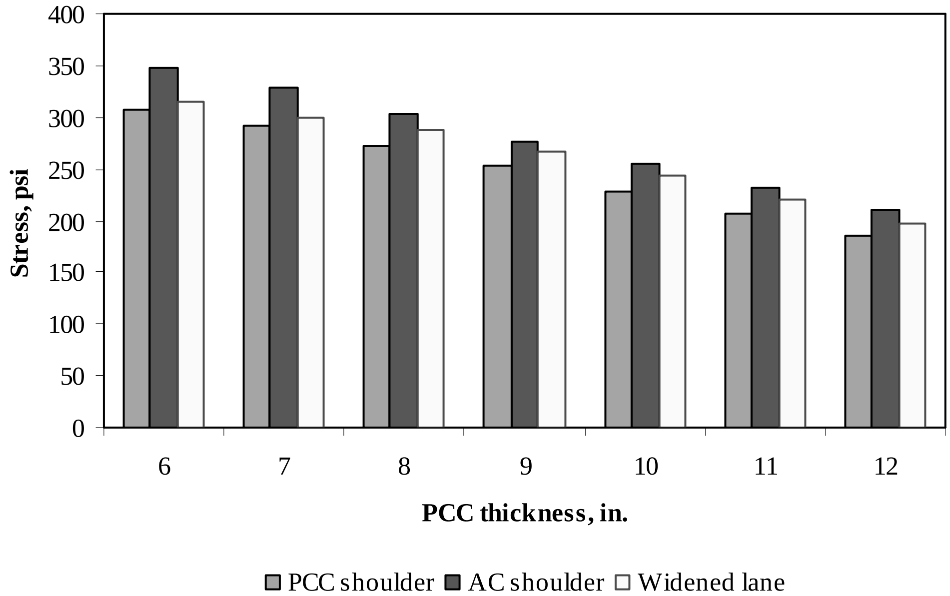


**Figure F-10-31: Impact of PCC thickness and lateral support condition on longitudinal stress at top of the Slab (177-in. joint spacing and $\alpha(\Delta T/D)$ of $-20x10^{-6}$ in.$^{-1}$)**

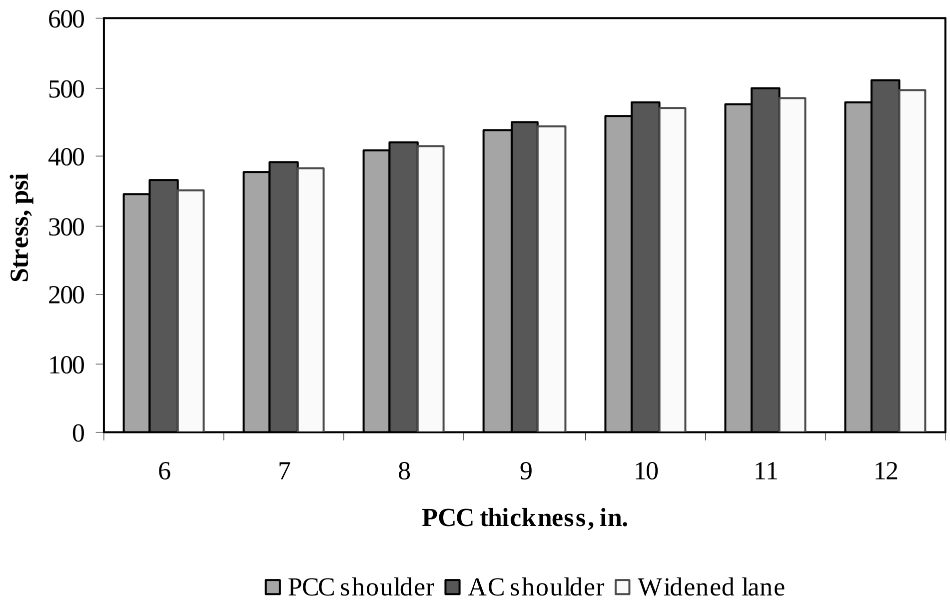


**Figure F-10-32: Impact of PCC thickness and lateral support condition on longitudinal stress at top of the Slab (315-in. joint spacing and $\alpha(\Delta T/D)$ of $-20x10^{-6}$ in.$^{-1}$)**

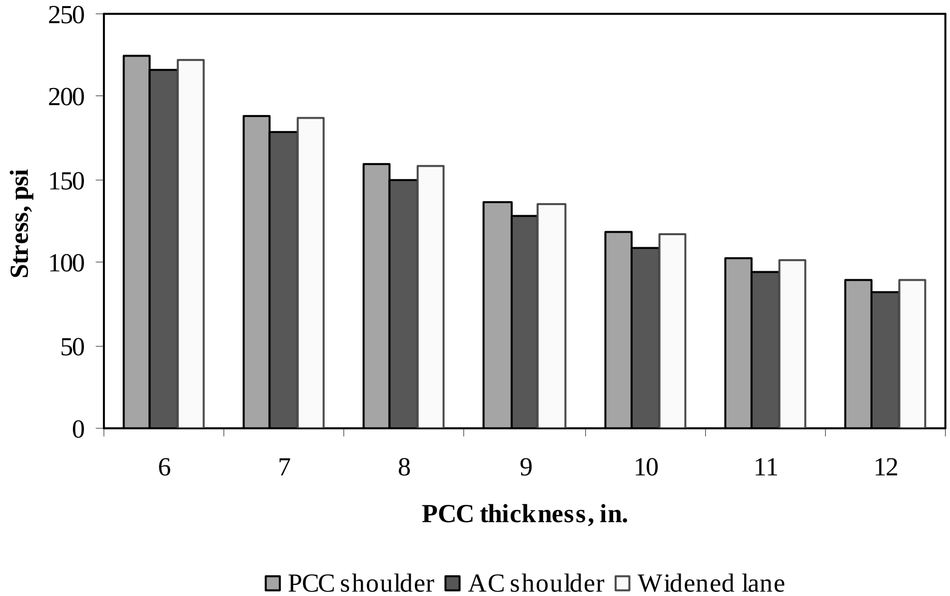


**Figure F-10-33: Impact of PCC thickness and lateral support condition on transverse stress at bottom of the Slab (177-in. joint spacing and $\alpha(\Delta T/D)$ of 0 in.$^{-1}$)**

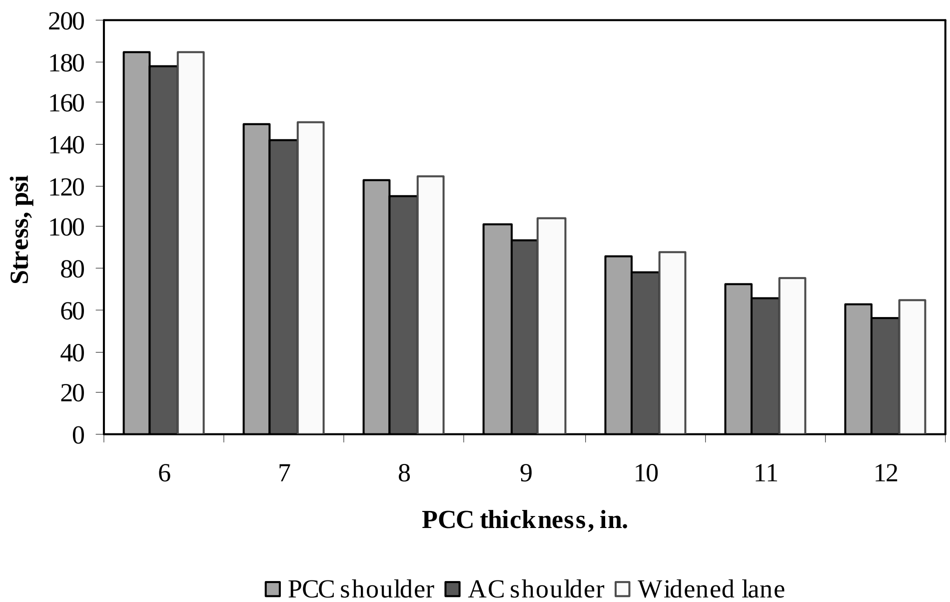


**Figure F-10-34: Impact of PCC thickness and lateral support condition on transverse stress at bottom of the Slab (315-in. joint spacing and $\alpha(\Delta T/D)$ of 0 in.$^{-1}$)**

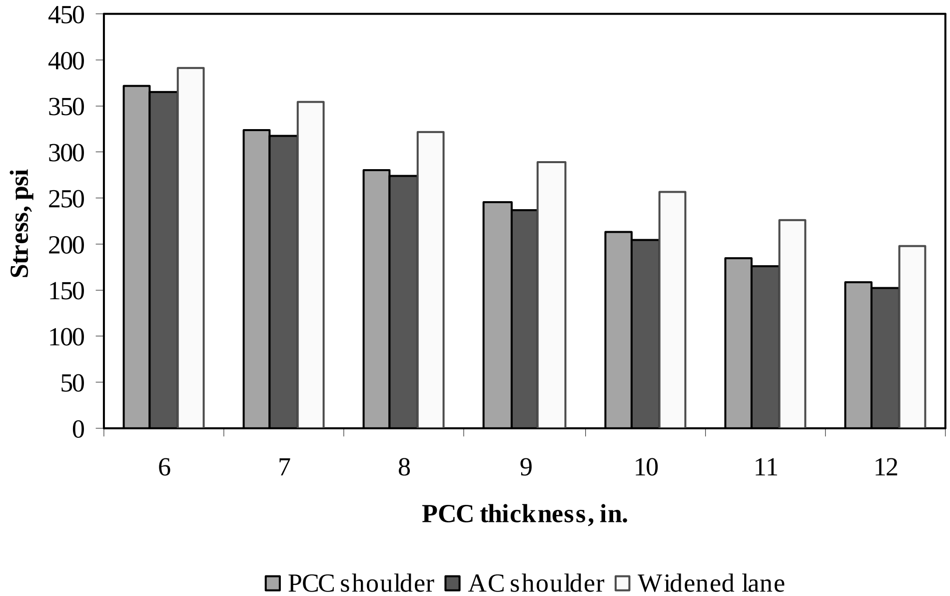


**Figure F-10-35: Impact of PCC thickness and lateral support condition on transverse stress at bottom of the Slab (177-in. joint spacing and $\alpha(\Delta T/D)$ of $20\text{x}10^{-6}$ in.$^{-1}$)**

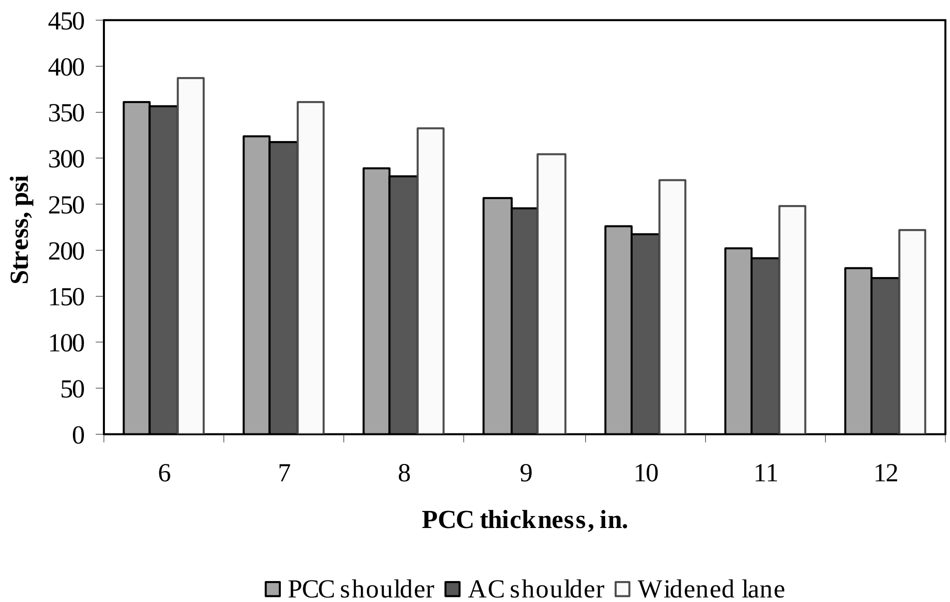


**Figure F-10-36: Impact of PCC thickness and lateral support condition on transverse stress at bottom of the Slab (315-in. joint spacing and $\alpha(\Delta T/D)$ of $20\text{x}10^{-6}$ in.$^{-1}$)**

Figures F-10-37 through F-10-42 illustrate the impact of base/subbase thickness and product α(ΔT/D) on stresses (10-in. PCC thickness, 100-psi/in. modulus of subgrade reaction and PCC shoulder)

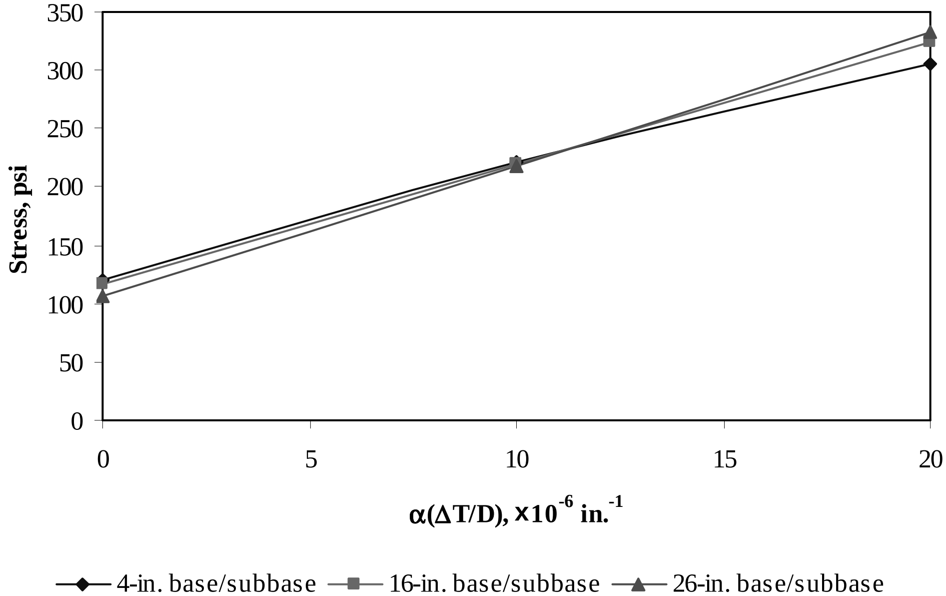


**Figure F-10-37: Impact of base/subbase thickness and product α(ΔT/D) on longitudinal stress at bottom of the slab (177-in. joint spacing)**

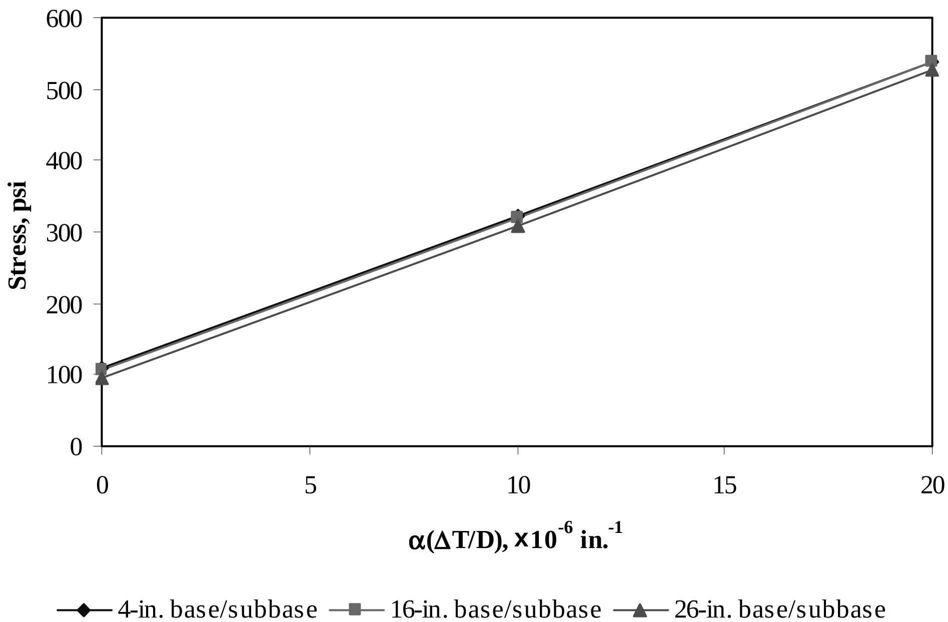


**Figure F-10-38: Impact of base/subbase thickness and product α(ΔT/D) on longitudinal stress at bottom of the slab (315-in. joint spacing)**

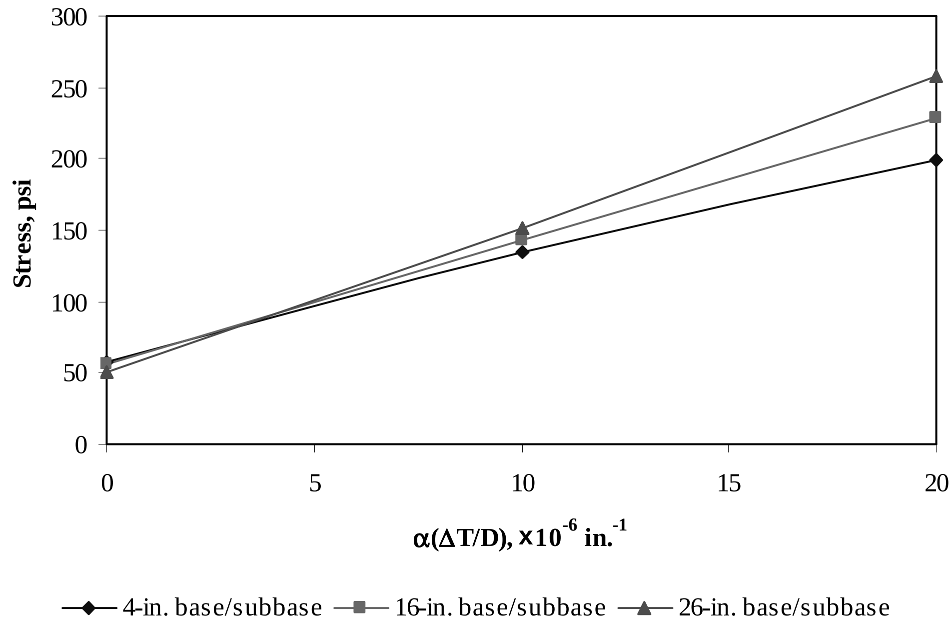


**Figure F-10-39: Impact of base/subbase thickness and product α(ΔT/D) on longitudinal stress at top of the slab (177-in. joint spacing)**

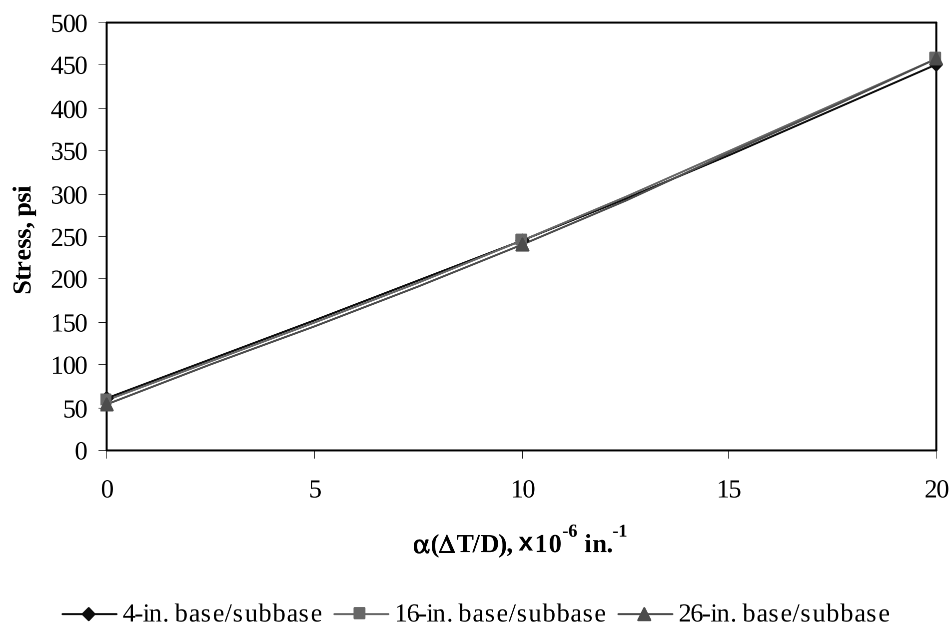


**Figure F-10-40: Impact of base/subbase thickness and product α(ΔT/D) on longitudinal stress at top of the slab (315-in. joint spacing)**

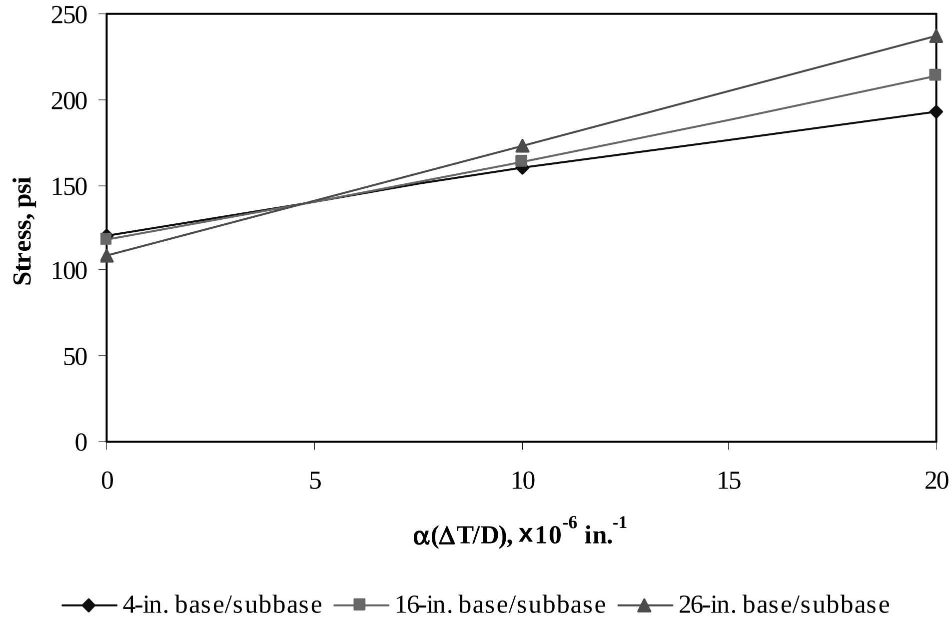


**Figure F-10-41: Impact of base/subbase thickness and product α(ΔT/D) on transverse stress at bottom of the slab (177-in. joint spacing)**

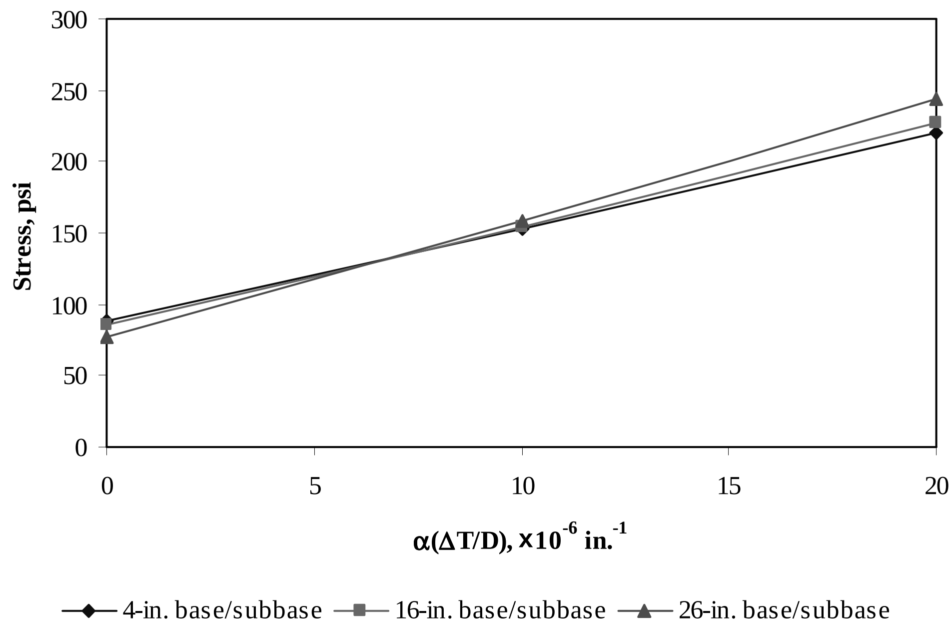


**Figure F-10-42: Impact of base/subbase thickness and product α(ΔT/D) on transverse stress at bottom of the slab (315-in. joint spacing)**

Figures F-10-43 through F-10-48 illustrate the impact of modulus of subgrade reaction and product α(ΔT/D) on stresses (10-in. PCC thickness, 16-in. base/subbase thickness and PCC shoulder)

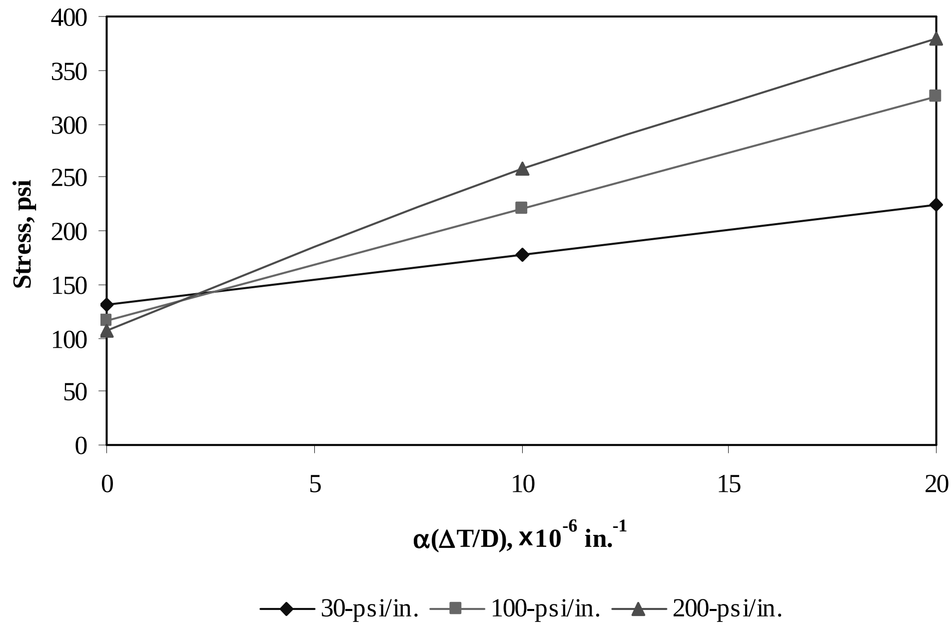


**Figure F-10-43: Impact of modulus of subgrade reaction and product α(ΔT/D) on longitudinal stress at bottom of the slab (177-in. joint spacing)**

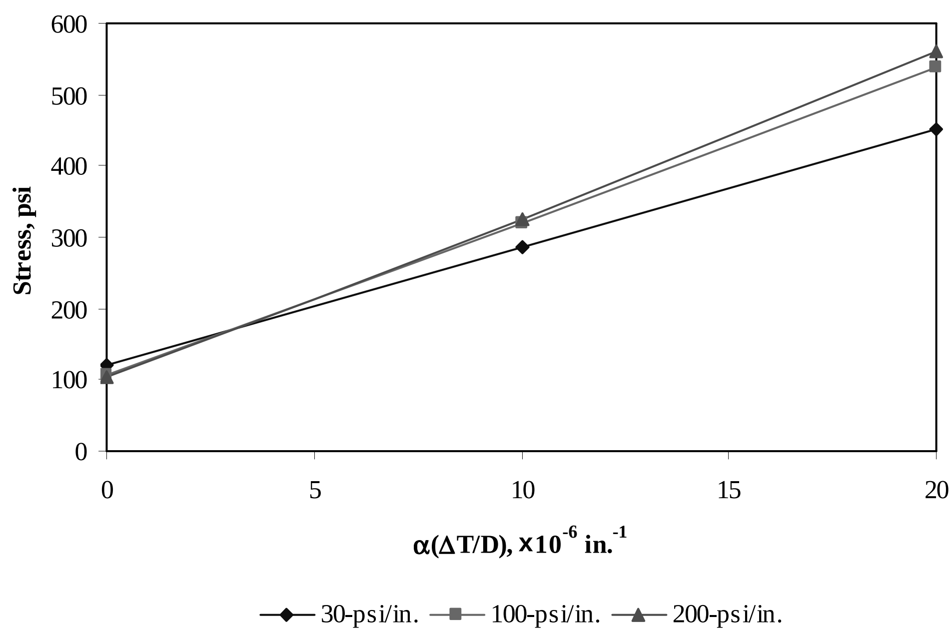


**Figure F-10-44: Impact of modulus of subgrade reaction and product α(ΔT/D) on longitudinal stress at bottom of the slab (315-in. joint spacing)**

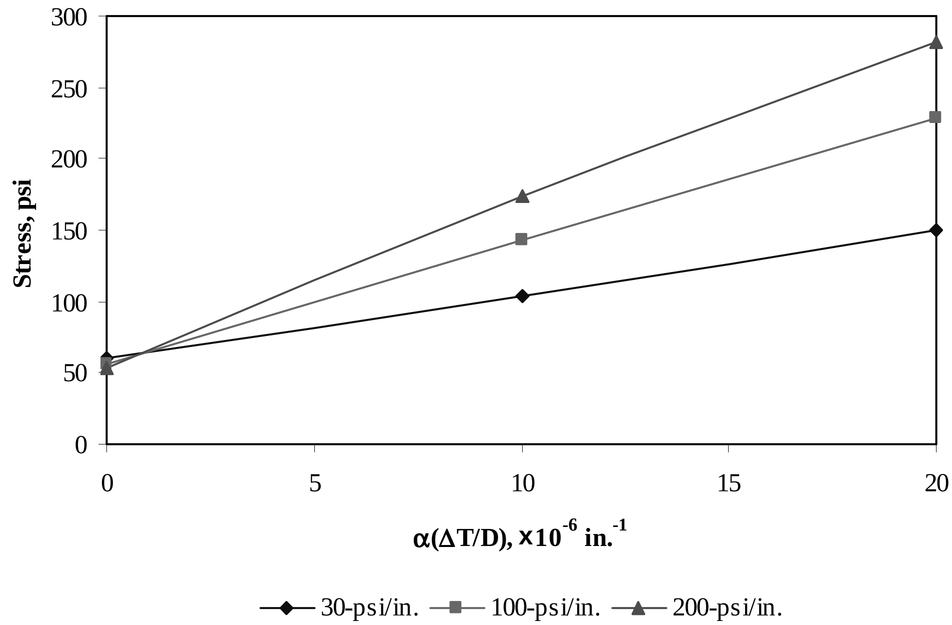


**Figure F-10-45: Impact of modulus of subgrade reaction and product α(ΔT/D) on longitudinal stress at top of the slab (177-in. joint spacing)**

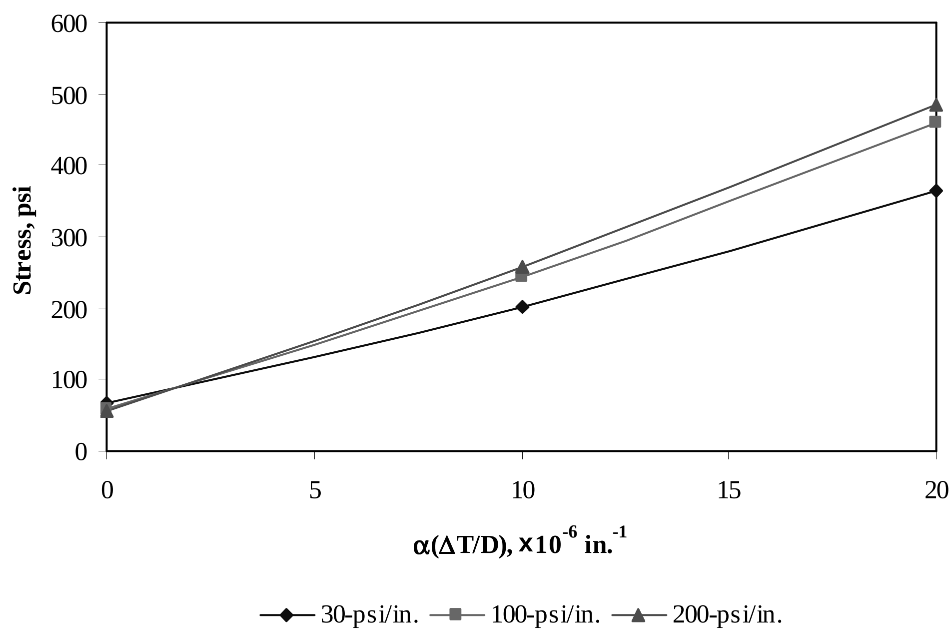


**Figure F-10-46: Impact of modulus of subgrade reaction and product α(ΔT/D) on longitudinal stress at top of the slab (315-in. joint spacing)**

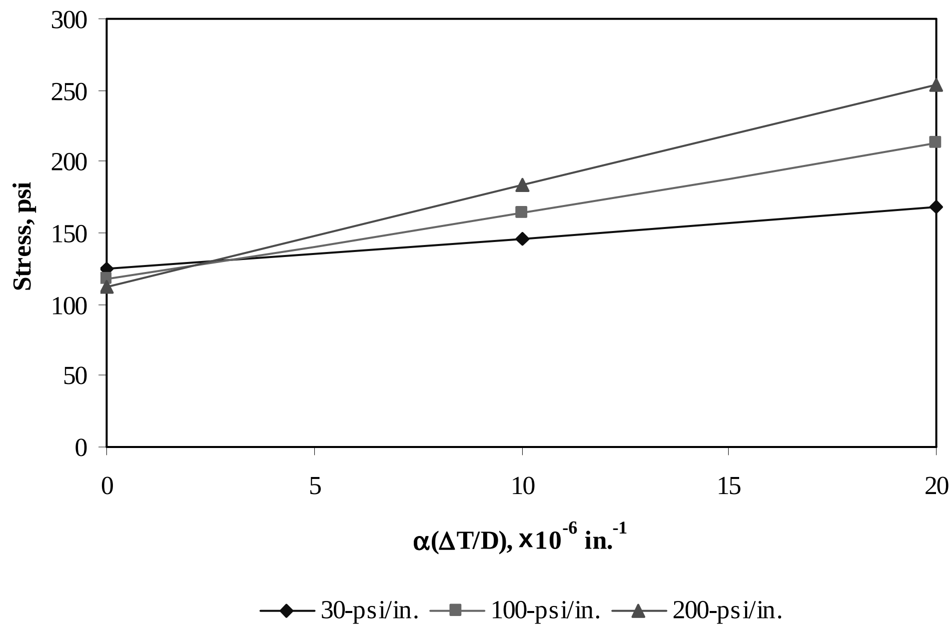


**Figure F-10-47: Impact of modulus of subgrade reaction and product $\alpha(\Delta T/D)$ on transverse stress at bottom of the slab (177-in. joint spacing)**

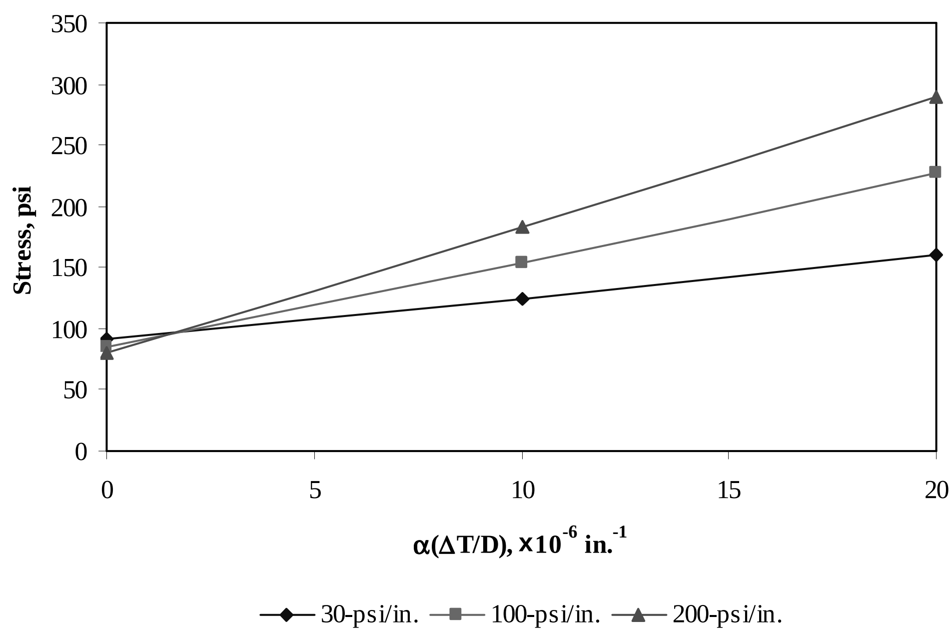


**Figure F-10-48: Impact of modulus of subgrade reaction and product $\alpha(\Delta T/D)$ on transverse stress at bottom of the slab (315-in. joint spacing)**

Figures F-10-49 through F-10-51 illustrate the impact of joint spacing and product α(ΔT/D) on stresses (10-in. PCC thickness, 16-in. base/subbase thickness, 100-psi/in. modulus of subgrade reaction and PCC shoulder)

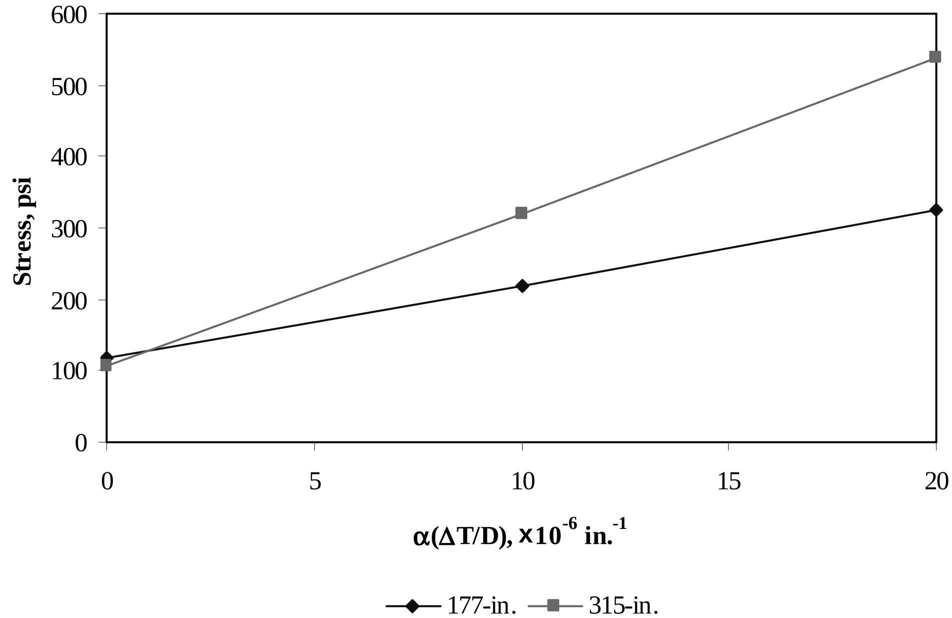


**Figure F-10-49: Impact of joint spacing and product α(ΔT/D) on longitudinal stress at bottom of the slab**

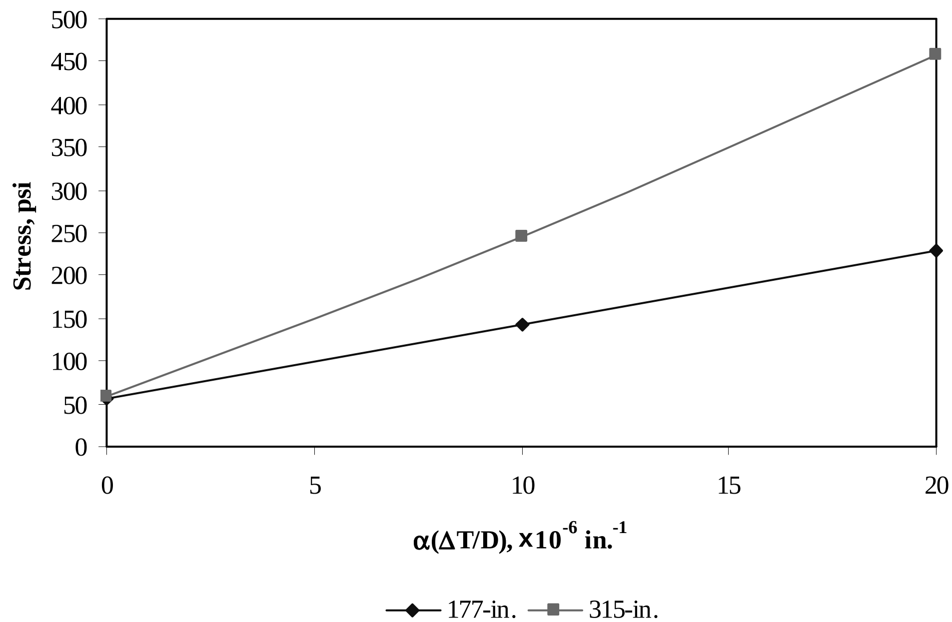


**Figure F-10-50: Impact of joint spacing and product α(ΔT/D) on longitudinal stress at top of the slab**

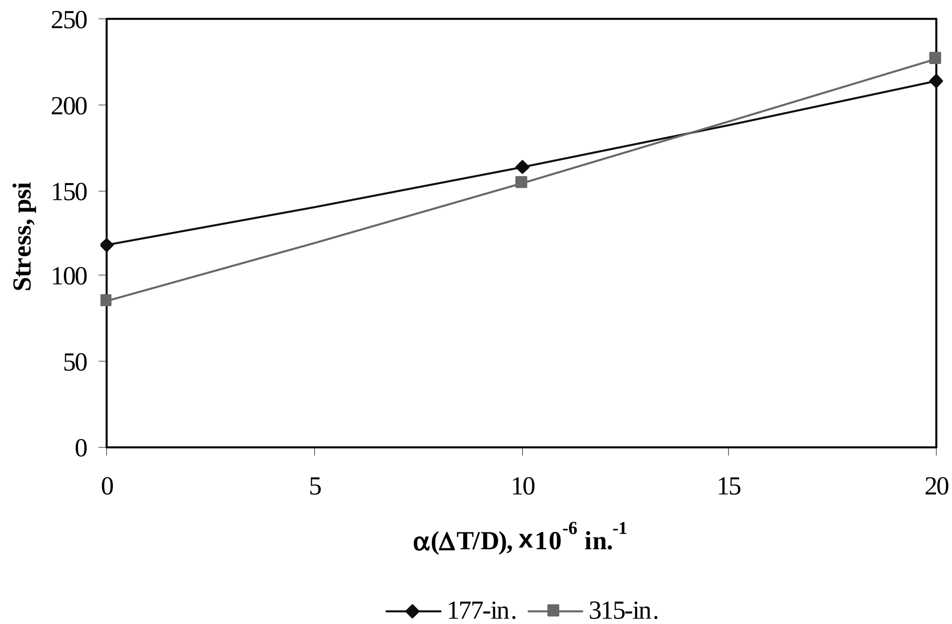


**Figure F-10-51: Impact of joint spacing and product α(ΔT/D) on transverse stress at bottom of the slab**

**Sub Appendix F-11**

**Documentation of Pavement Responses for**

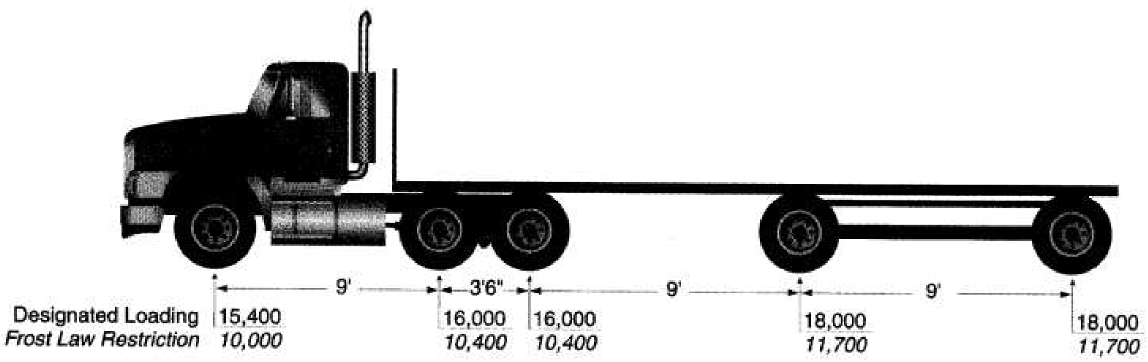


**MI-8**

Figures F-11-1 through F-11-12 illustrate the impact of PCC thickness and base/subbase thickness on stresses (100-psi/in. modulus of subgrade reaction and PCC shoulder)

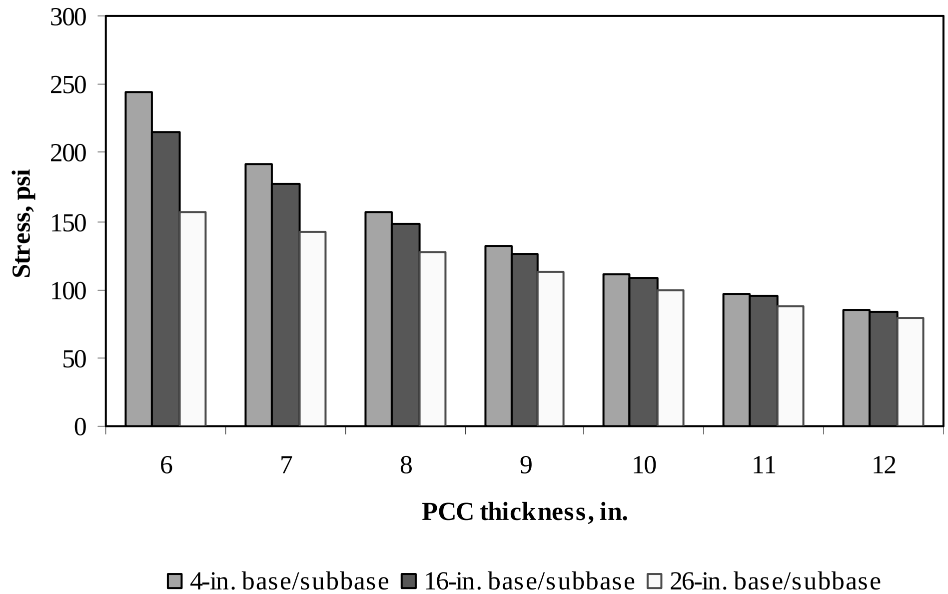


**Figure F-11-1: Impact of PCC thickness and base/subbase thickness on longitudinal stress at bottom of the Slab (177-in. joint spacing and $\alpha(\Delta T/D)$ of 0 in.$^{-1}$)**

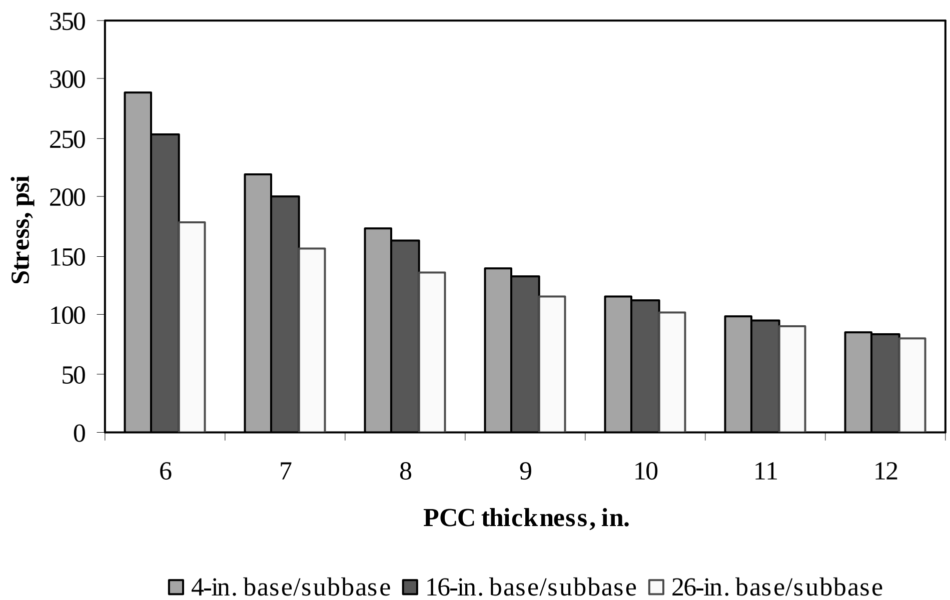


**Figure F-11-2: Impact of PCC thickness and base/subbase thickness on longitudinal stress at bottom of the Slab (315-in. joint spacing and $\alpha(\Delta T/D)$ of 0 in.$^{-1}$)**

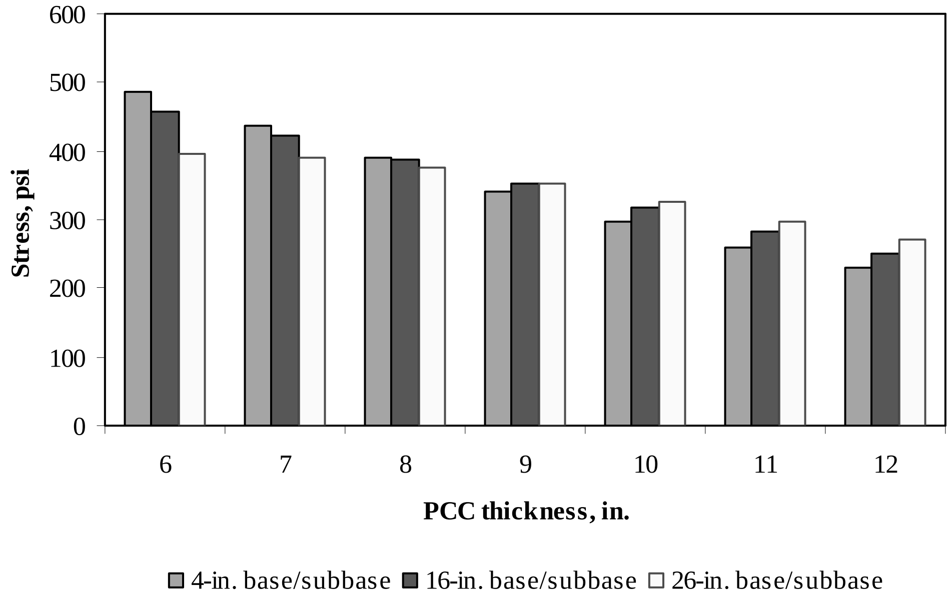


**Figure F-11-3: Impact of PCC thickness and base/subbase thickness on longitudinal stress at bottom of the Slab (177-in. joint spacing and $\alpha(\Delta T/D)$ of 20x10$^{-6}$ in.$^{-1}$)**

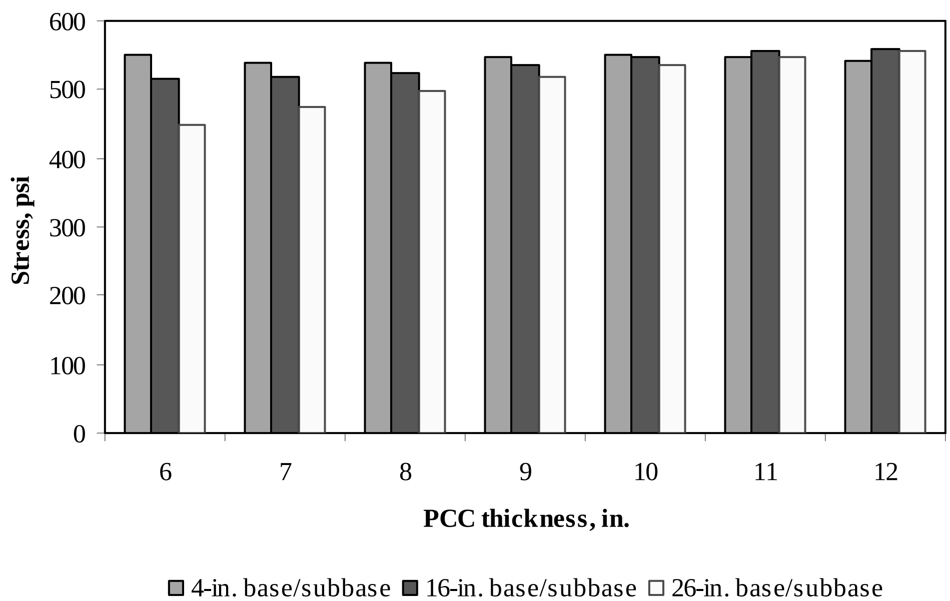


**Figure F-11-4: Impact of PCC thickness and base/subbase thickness on longitudinal stress at bottom of the Slab (315-in. joint spacing and $\alpha(\Delta T/D)$ of 20x10$^{-6}$ in.$^{-1}$)**

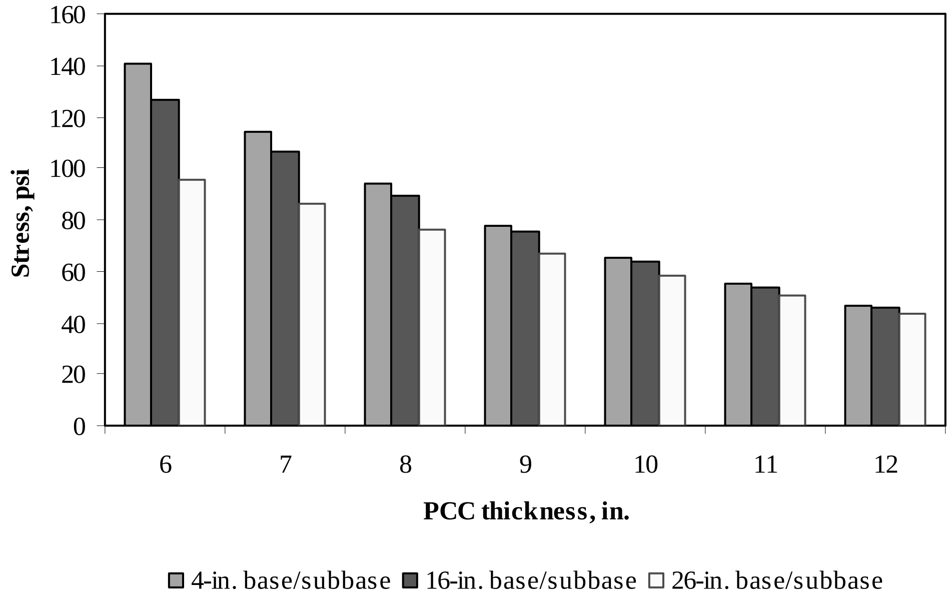


**Figure F-11-5: Impact of PCC thickness and base/subbase thickness on longitudinal stress at top of the Slab (177-in. joint spacing and $\alpha(\Delta T/D)$ of 0 in.$^{-1}$)**

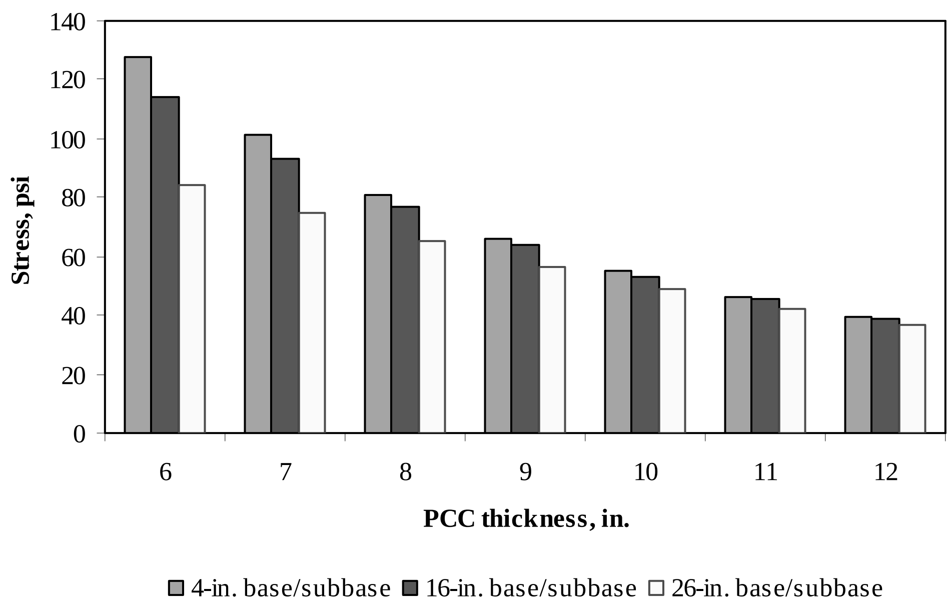


**Figure F-11-6: Impact of PCC thickness and base/subbase thickness on longitudinal stress at top of the Slab (315-in. joint spacing and $\alpha(\Delta T/D)$ of 0 in.$^{-1}$)**

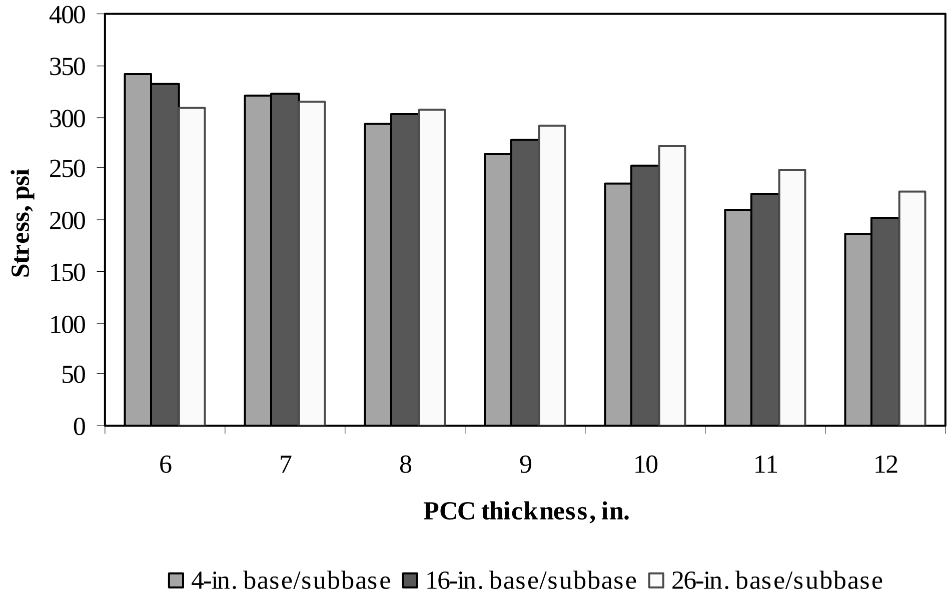


**Figure F-11-7: Impact of PCC thickness and base/subbase thickness on longitudinal stress at top of the Slab (177-in. joint spacing and $\alpha(\Delta T/D)$ of $-20\times10^{-6}$ in.$^{-1}$)**

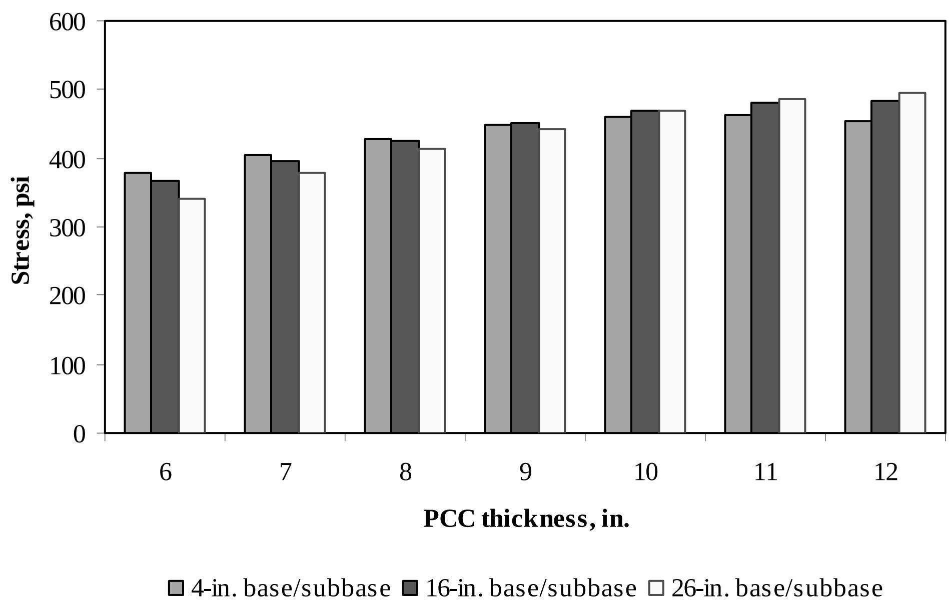


**Figure F-11-8: Impact of PCC thickness and base/subbase thickness on longitudinal stress at top of the Slab (315-in. joint spacing and $\alpha(\Delta T/D)$ of $-20\times10^{-6}$ in.$^{-1}$)**

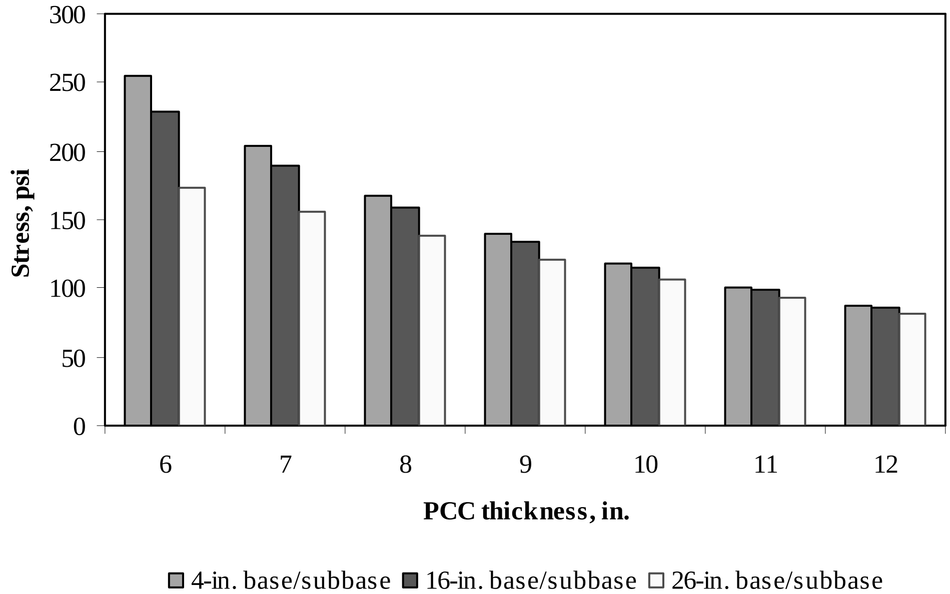


**Figure F-11-9: Impact of PCC thickness and base/subbase thickness on transverse stress at bottom of the Slab (177-in. joint spacing and α(ΔT/D) of 0 in.$^{-1}$)**

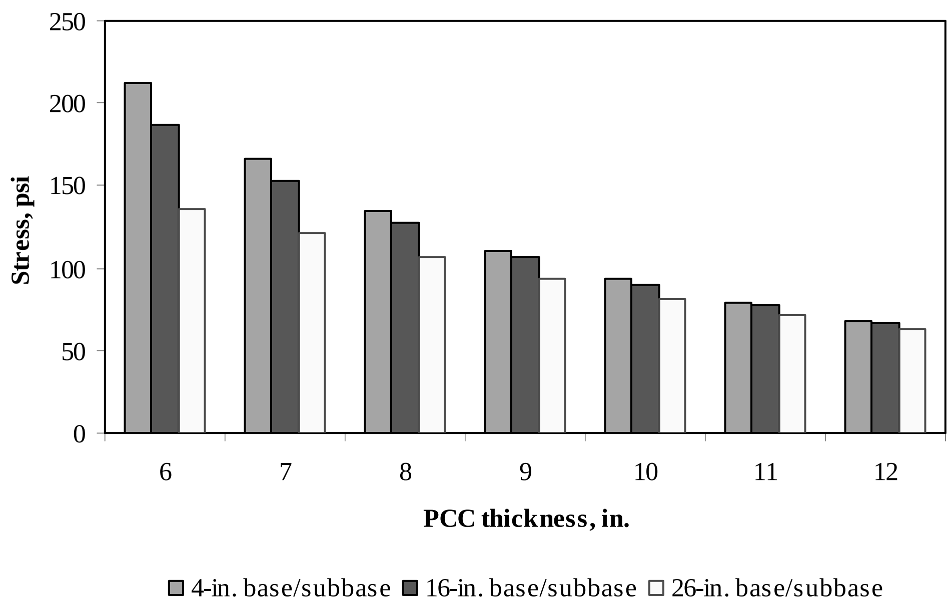


**Figure F-11-10: Impact of PCC thickness and base/subbase thickness on transverse stress at bottom of the Slab (315-in. joint spacing and α(ΔT/D) of 0 in.$^{-1}$)**

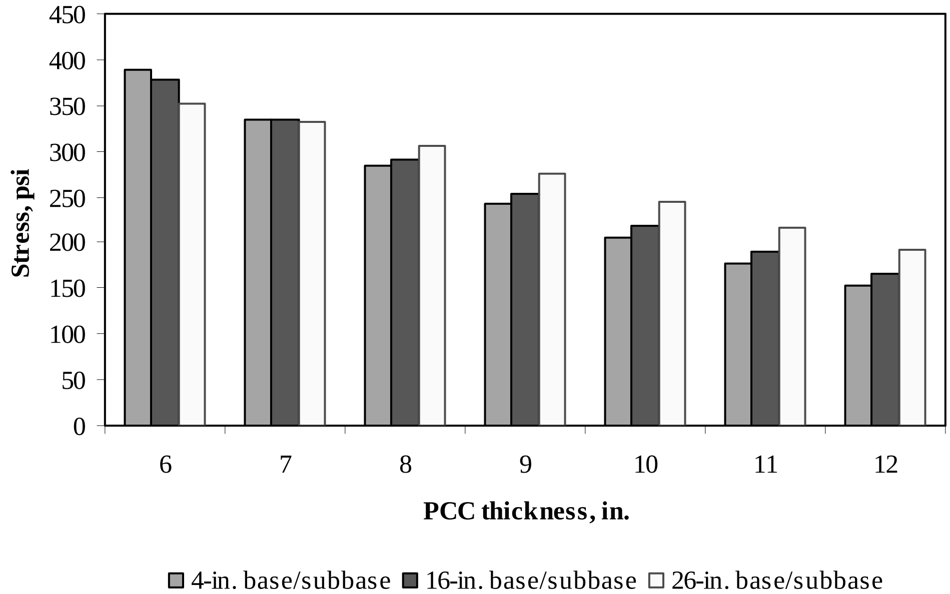


**Figure F-11-11: Impact of PCC thickness and base/subbase thickness on transverse stress at bottom of the Slab (177-in. joint spacing and $\alpha(\Delta T/D)$ of $20x10^{-6}$ in.$^{-1}$)**

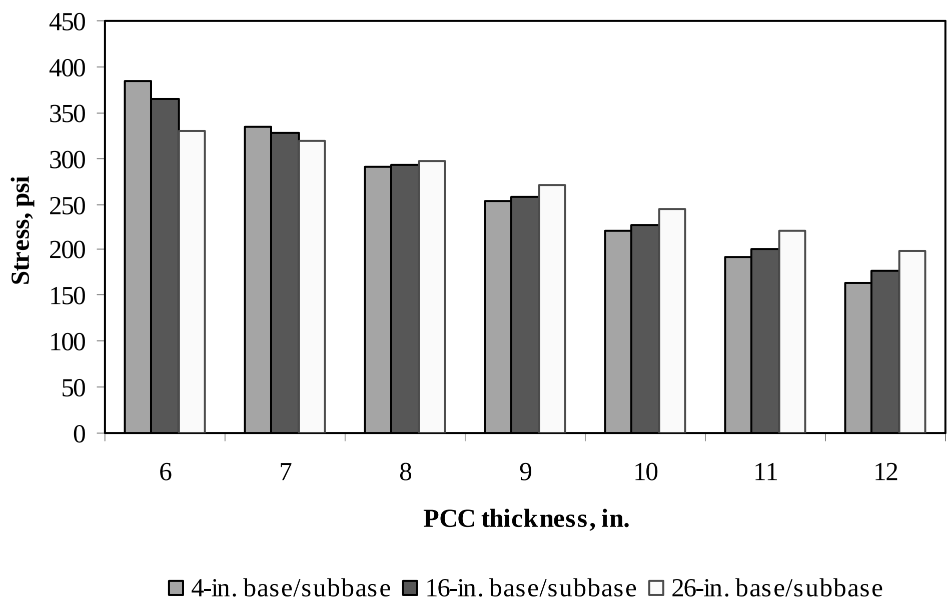


**Figure F-11-12: Impact of PCC thickness and base/subbase thickness on transverse stress at bottom of the Slab (315-in. joint spacing and $\alpha(\Delta T/D)$ of $20x10^{-6}$ in.$^{-1}$)**

Figures F-11-13 through F-11-24 illustrate the impact of PCC thickness and modulus of subgrade reaction on stresses (16-in. base/subbase thickness and PCC shoulder)

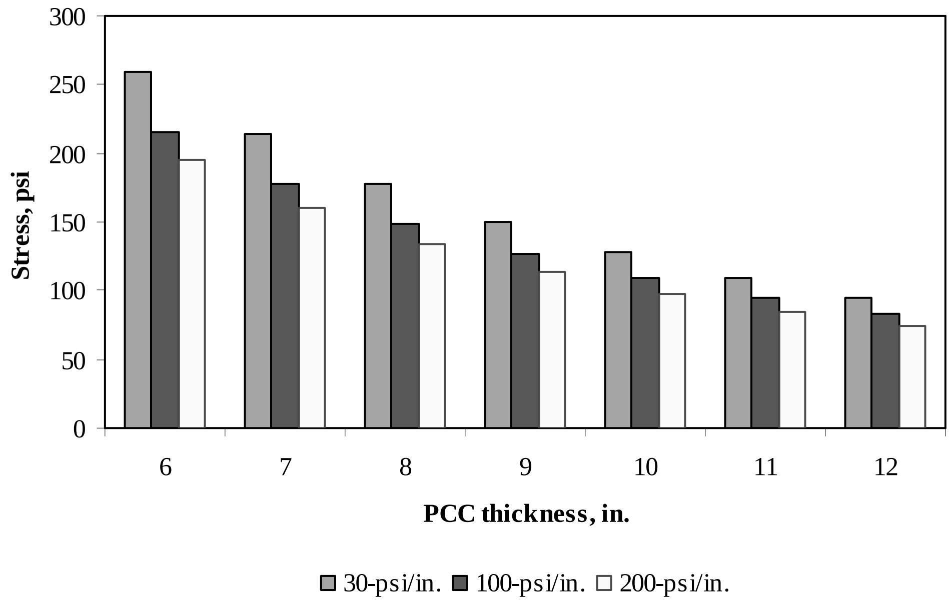


**Figure F-11-13: Impact of PCC thickness and modulus of subgrade reaction on longitudinal stress at bottom of the slab (177-in. joint spacing and $\alpha(\Delta T/D)$ of 0 in.$^{-1}$)**

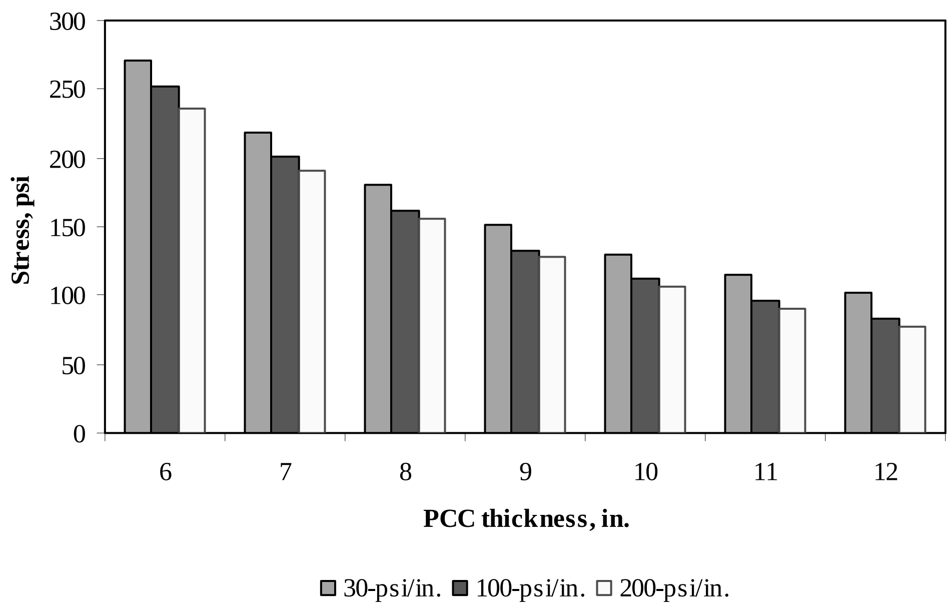


**Figure F-11-14: Impact of PCC thickness and modulus of subgrade reaction on longitudinal stress at bottom of the slab (315-in. joint spacing and $\alpha(\Delta T/D)$ of 0 in.$^{-1}$)**

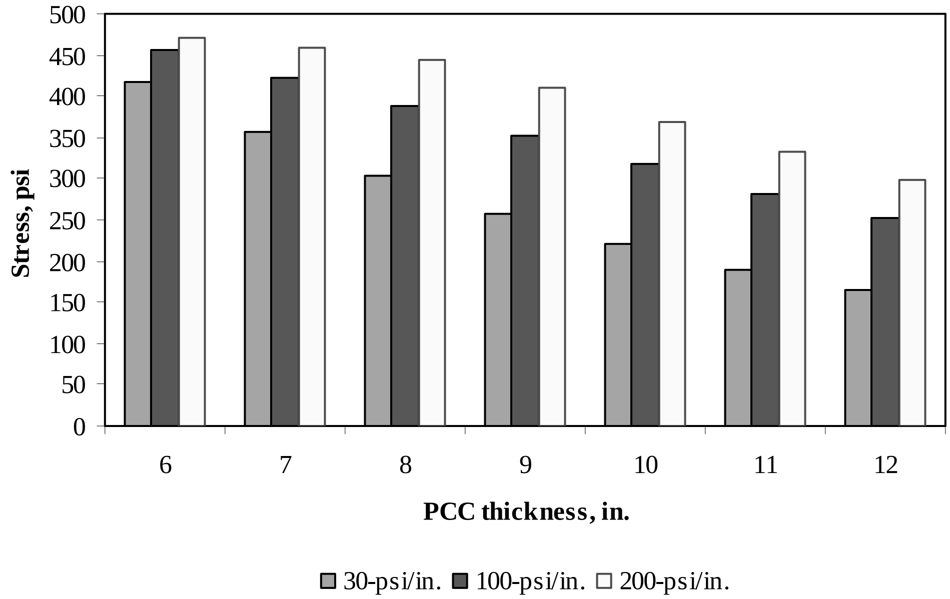


**Figure F-11-15: Impact of PCC thickness and modulus of subgrade reaction on longitudinal stress at bottom of the slab (177-in. joint spacing and $\alpha(\Delta T/D)$ of $20x10^{-6}$ in.$^{-1}$)**

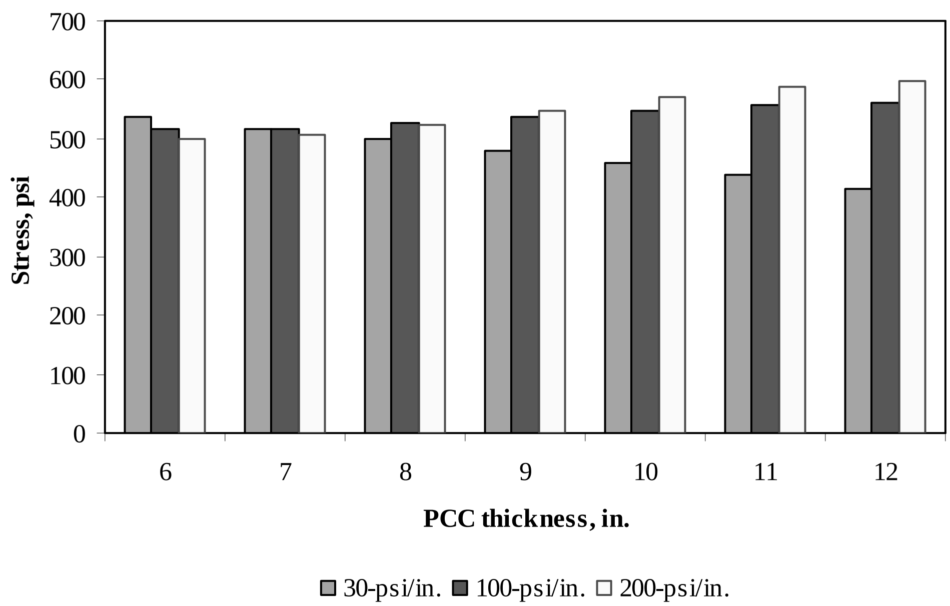


**Figure F-11-16: Impact of PCC thickness and modulus of subgrade reaction on longitudinal stress at bottom of the slab (315-in. joint spacing and $\alpha(\Delta T/D)$ of $20x10^{-6}$ in.$^{-1}$)**

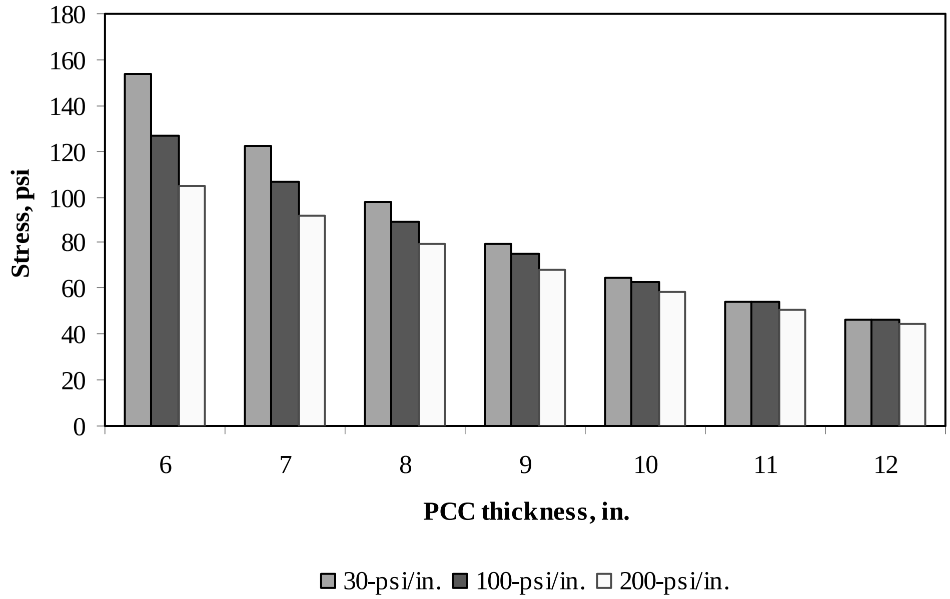


**Figure F-11-17: Impact of PCC thickness and modulus of subgrade reaction on longitudinal stress at top of the Slab (177-in. joint spacing and $\alpha(\Delta T/D)$ of 0 in.$^{-1}$)**

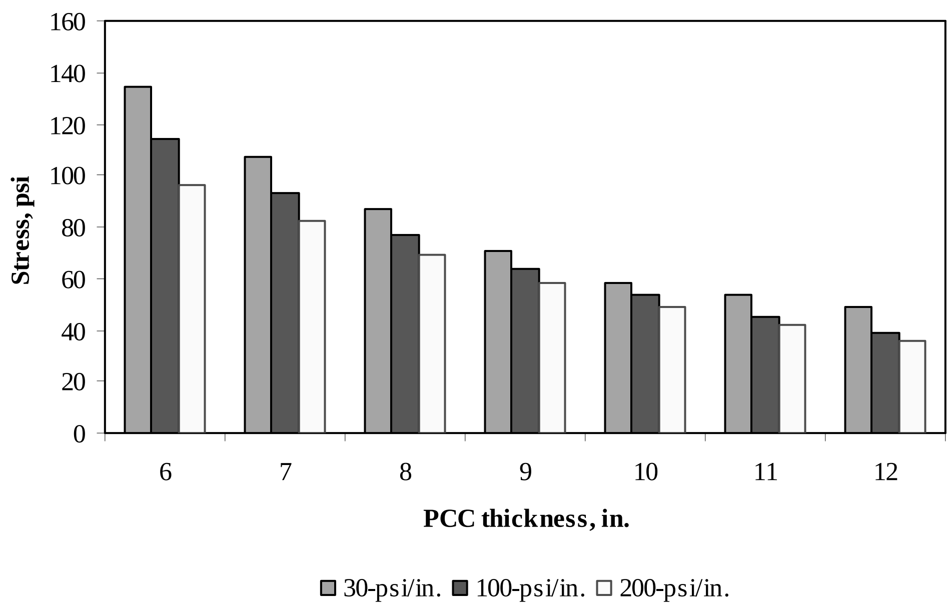


**Figure F-11-18: Impact of PCC thickness and modulus of subgrade reaction on longitudinal stress at top of the Slab (315-in. joint spacing and $\alpha(\Delta T/D)$ of 0 in.$^{-1}$)**

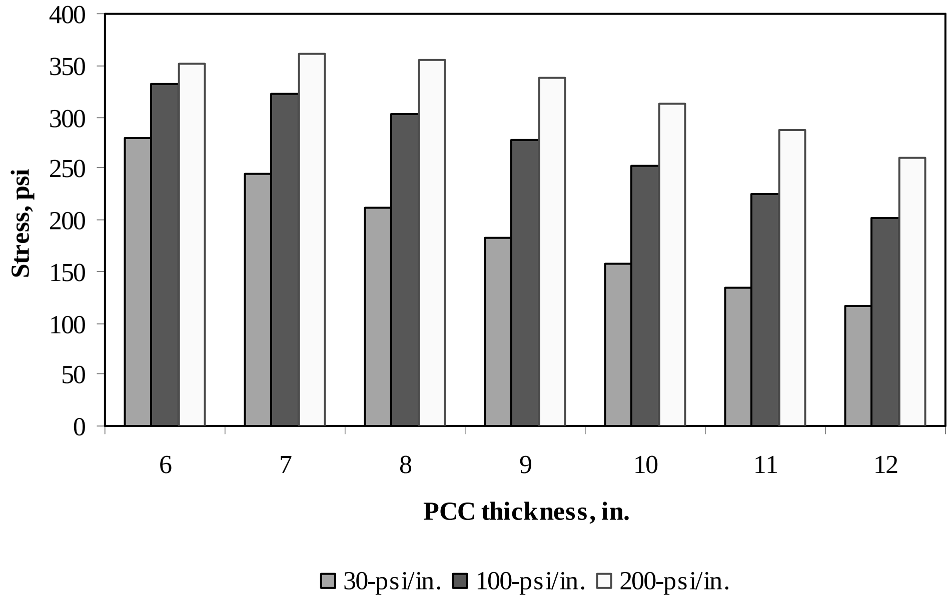


**Figure F-11-19: Impact of PCC thickness and modulus of subgrade reaction on longitudinal stress at top of the Slab (177-in. joint spacing and $\alpha(\Delta T/D)$ of $-20 \times 10^{-6}$ in.$^{-1}$)**

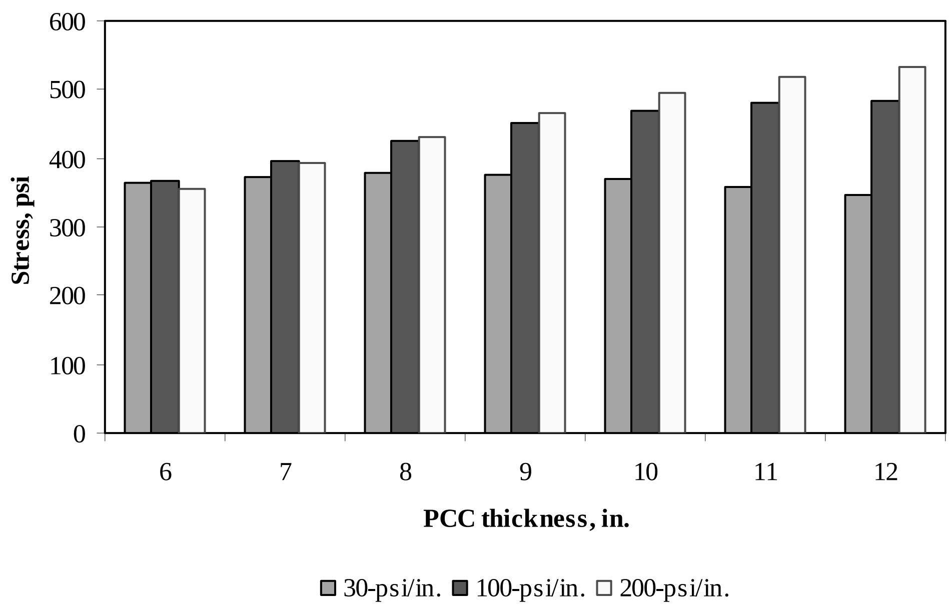


**Figure F-11-20: Impact of PCC thickness and modulus of subgrade reaction on longitudinal stress at top of the Slab (315-in. joint spacing and $\alpha(\Delta T/D)$ of $-20 \times 10^{-6}$ in.$^{-1}$)**

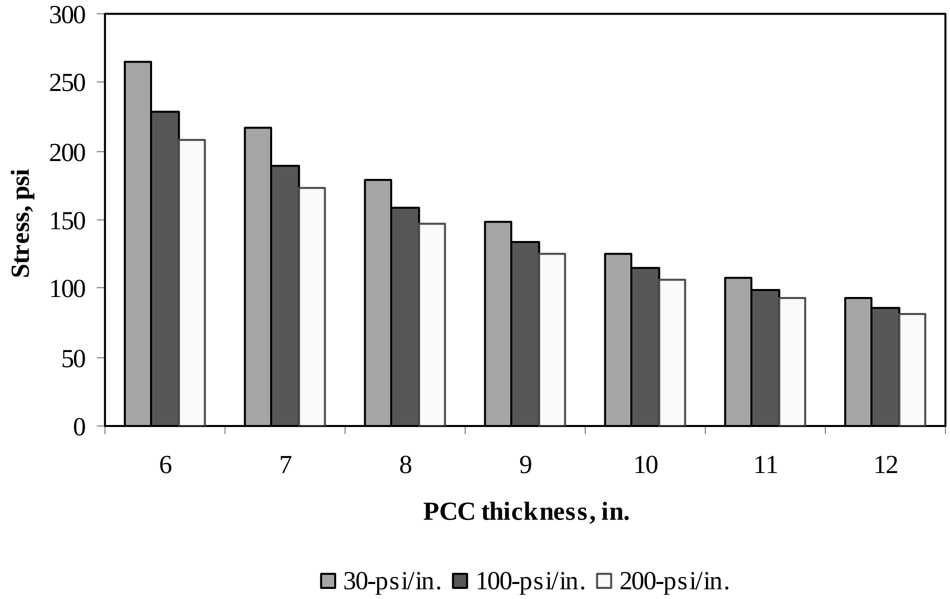


**Figure F-11-21: Impact of PCC thickness and modulus of subgrade reaction on transverse stress at bottom of the Slab (177-in. joint spacing and $\alpha(\Delta T/D)$ of 0 in.$^{-1}$)**

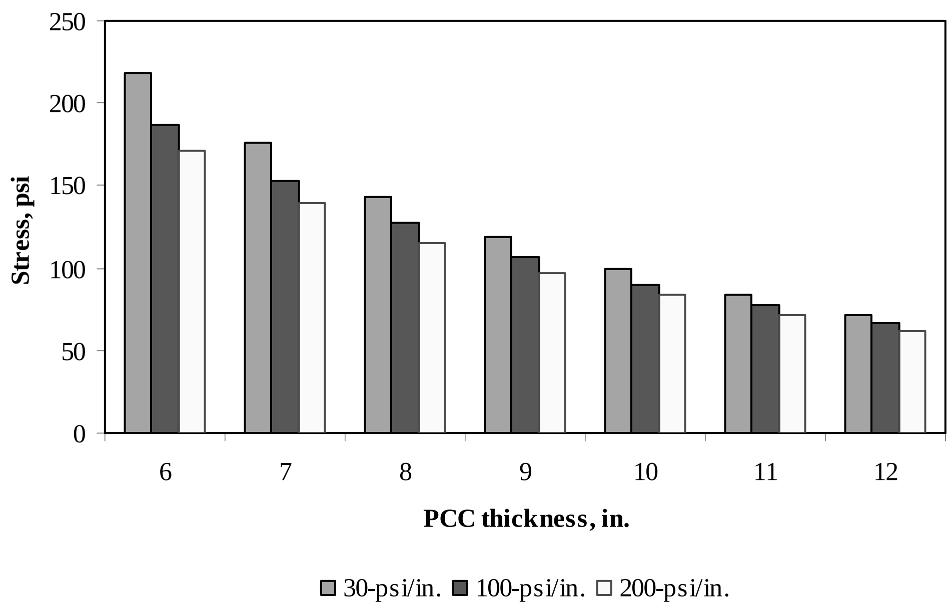


**Figure F-11-22: Impact of PCC thickness and modulus of subgrade reaction on transverse stress at bottom of the Slab (315-in. joint spacing and $\alpha(\Delta T/D)$ of 0 in.$^{-1}$)**

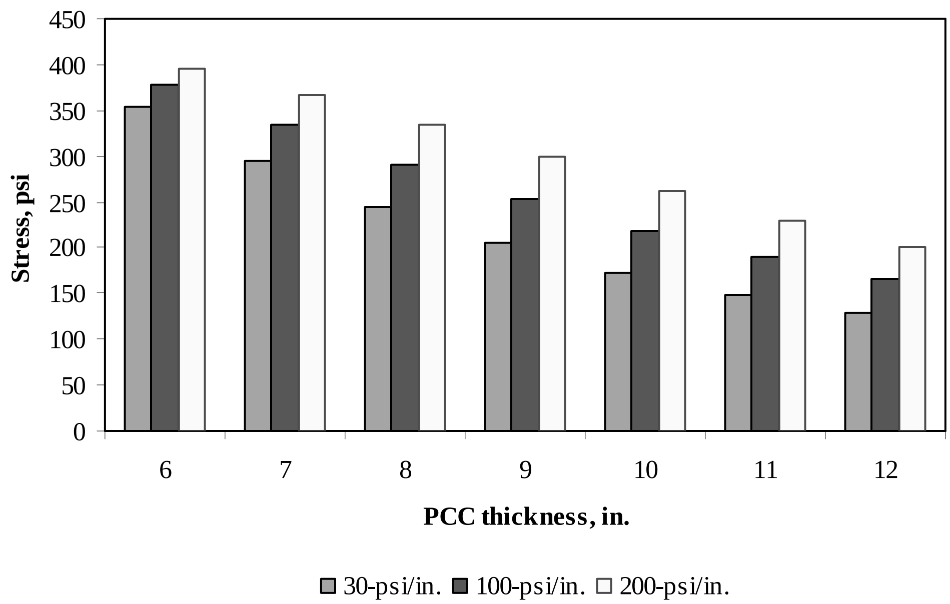


**Figure F-11-23: Impact of PCC thickness and modulus of subgrade reaction on transverse stress at bottom of the Slab (177-in. joint spacing and $\alpha(\Delta T/D)$ of $20x10^{-6}$ $in.^{-1}$)**

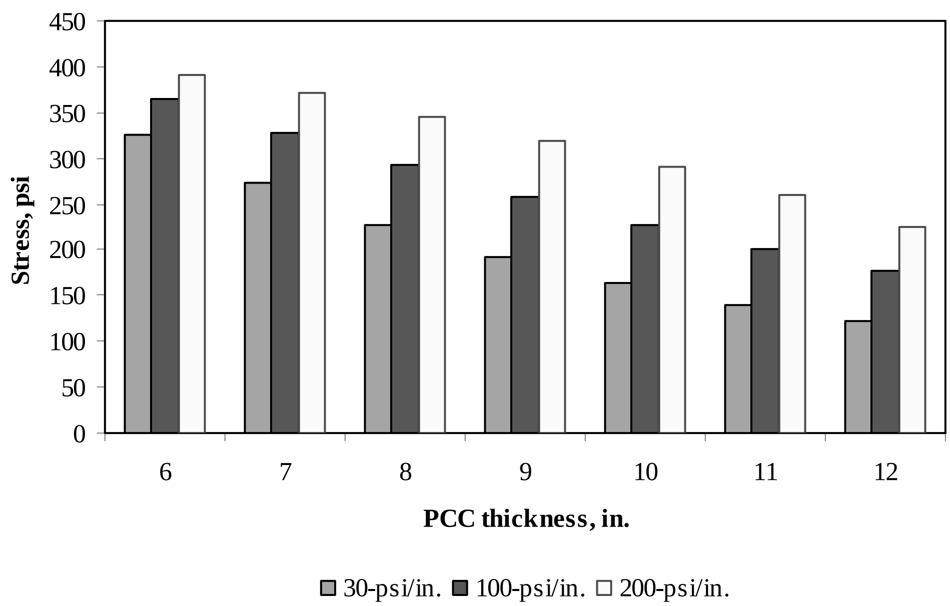


**Figure F-11-24: Impact of PCC thickness and modulus of subgrade reaction on transverse stress at bottom of the Slab (315-in. joint spacing and $\alpha(\Delta T/D)$ of $20x10^{-6}$ $in.^{-1}$)**

Figures F-11-25 through F-11-36 illustrate the impact of PCC thickness and lateral support condition on stresses (16-in. base/subbase and 100-psi/in. modulus of subgrade reaction)

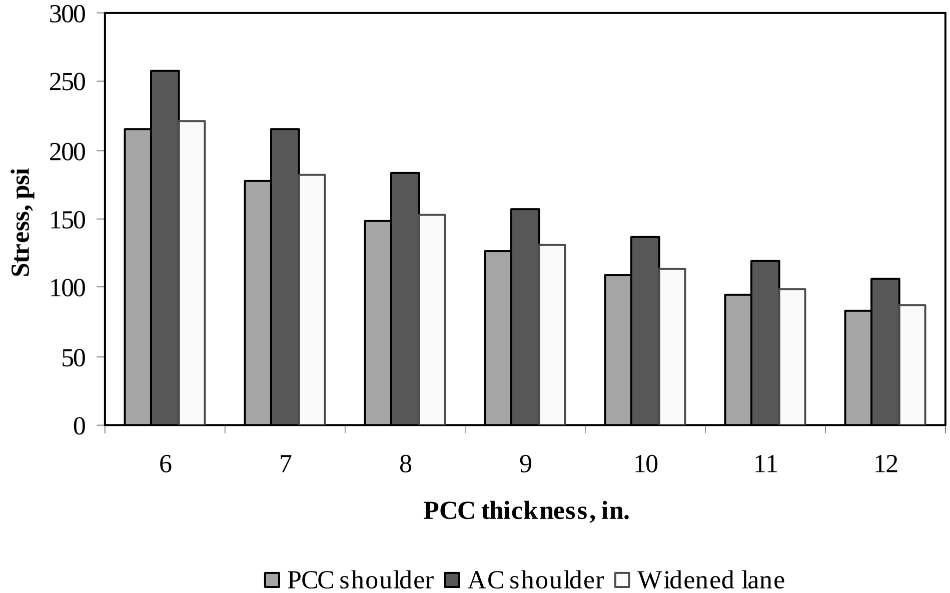


**Figure F-11-25: Impact of PCC thickness and lateral support condition on longitudinal stress at bottom of the Slab (177-in. joint spacing and $\alpha(\Delta T/D)$ of 0 in.$^{-1}$)**

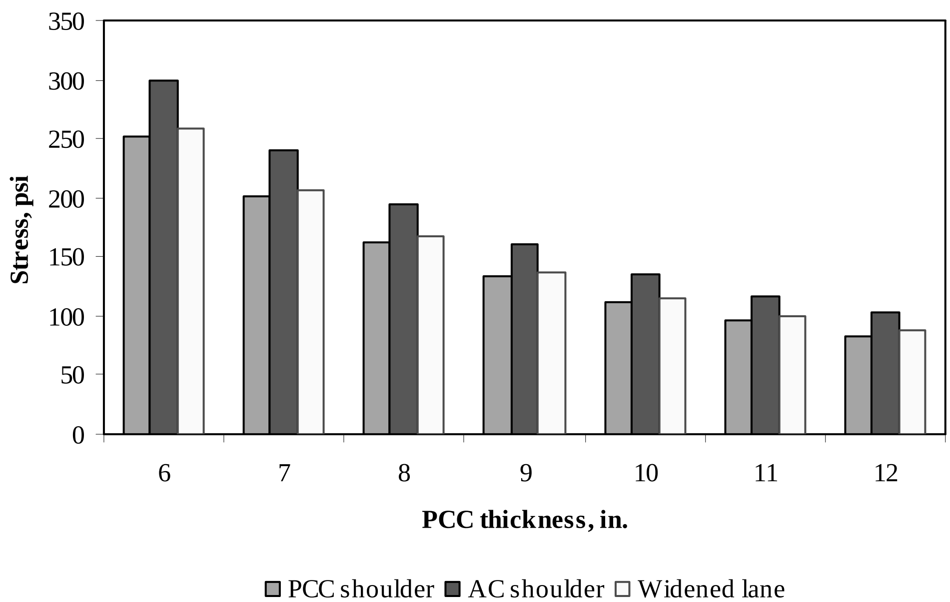


**Figure F-11-26: Impact of PCC thickness and lateral support condition on longitudinal stress at bottom of the Slab (315-in. joint spacing and $\alpha(\Delta T/D)$ of 0 in.$^{-1}$)**

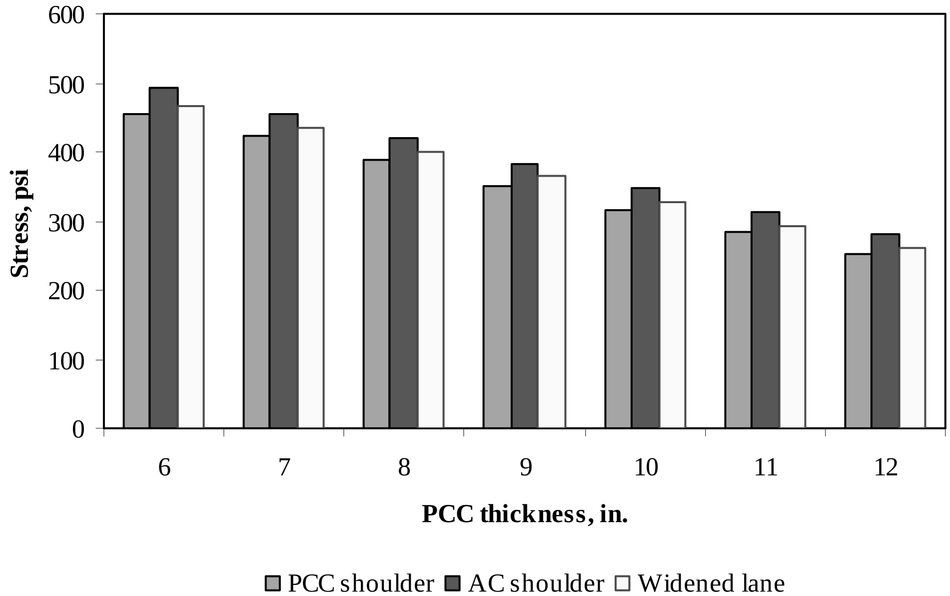


**Figure F-11-27: Impact of PCC thickness and lateral support condition on longitudinal stress at bottom of the Slab (177-in. joint spacing and α(ΔT/D) of $20x10^{-6}$ in.$^{-1}$)**

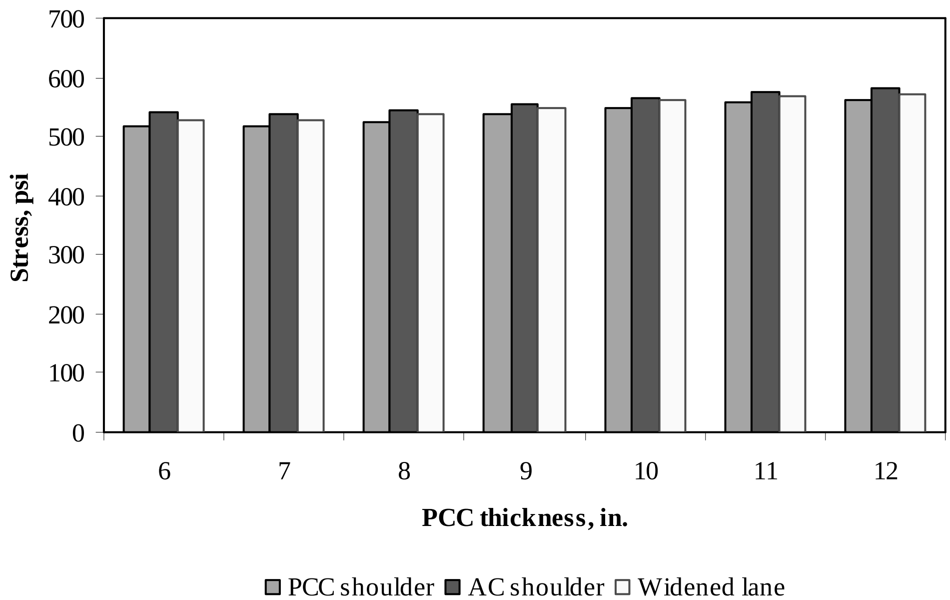


**Figure F-11-28: Impact of PCC thickness and lateral support condition on longitudinal stress at bottom of the Slab (315-in. joint spacing and α(ΔT/D) of $20x10^{-6}$ in.$^{-1}$)**

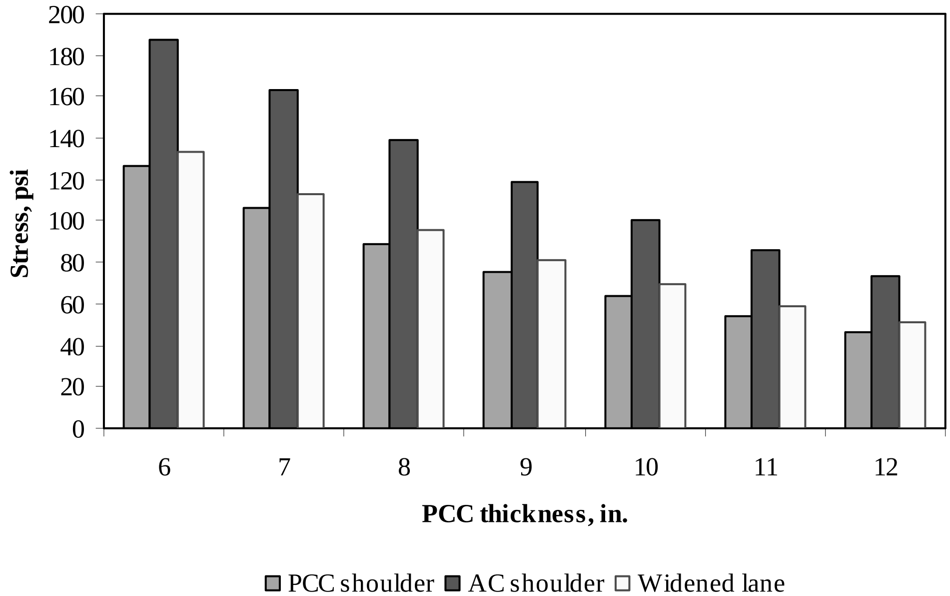


**Figure F-11-29: Impact of PCC thickness and lateral support condition on longitudinal stress at top of the Slab (177-in. joint spacing and $\alpha(\Delta T/D)$ of 0 $in.^{-1}$)**

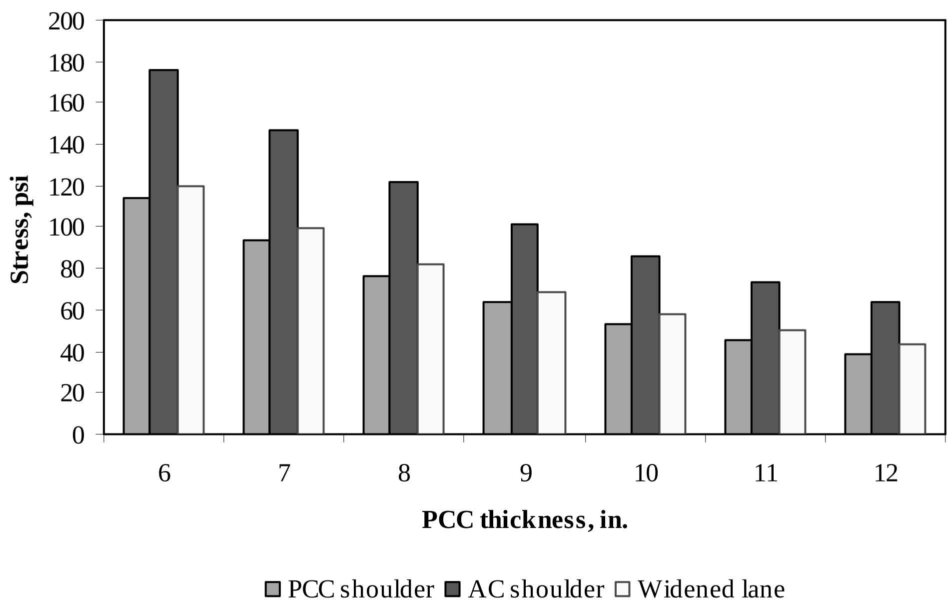


**Figure F-11-30: Impact of PCC thickness and lateral support condition on longitudinal stress at top of the Slab (315-in. joint spacing and $\alpha(\Delta T/D)$ of 0 $in.^{-1}$)**

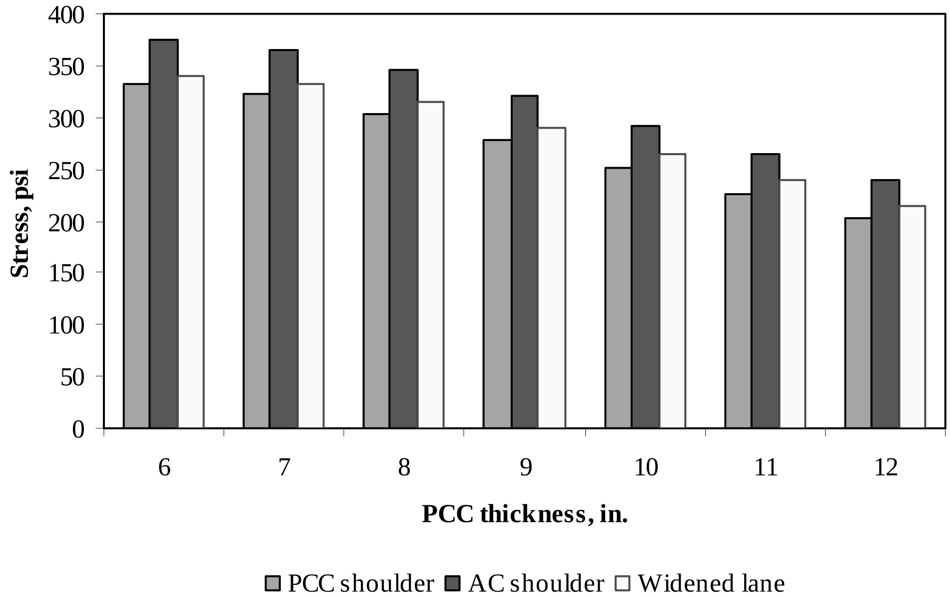


**Figure F-11-31: Impact of PCC thickness and lateral support condition on longitudinal stress at top of the Slab (177-in. joint spacing and $\alpha(\Delta T/D)$ of $-20x10^{-6}$ in.$^{-1}$)**

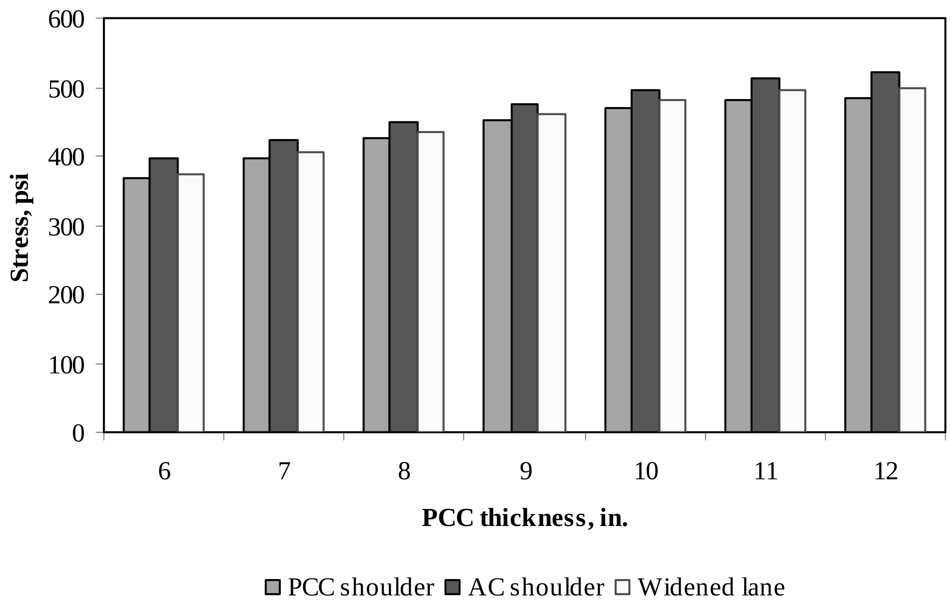


**Figure F-11-32: Impact of PCC thickness and lateral support condition on longitudinal stress at top of the Slab (315-in. joint spacing and $\alpha(\Delta T/D)$ of $-20x10^{-6}$ in.$^{-1}$)**

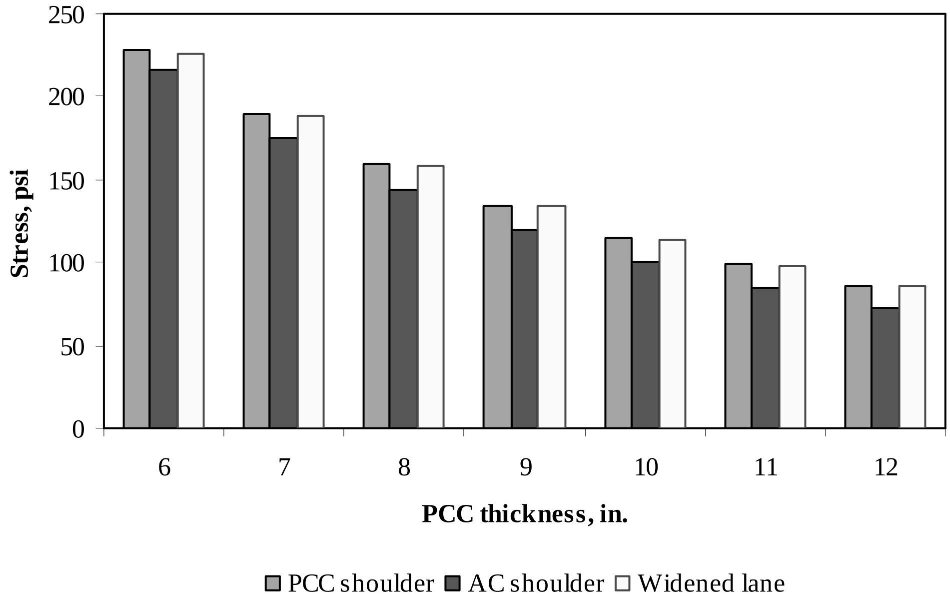


**Figure F-11-33: Impact of PCC thickness and lateral support condition on transverse stress at bottom of the Slab (177-in. joint spacing and α(ΔT/D) of 0 in.$^{-1}$)**

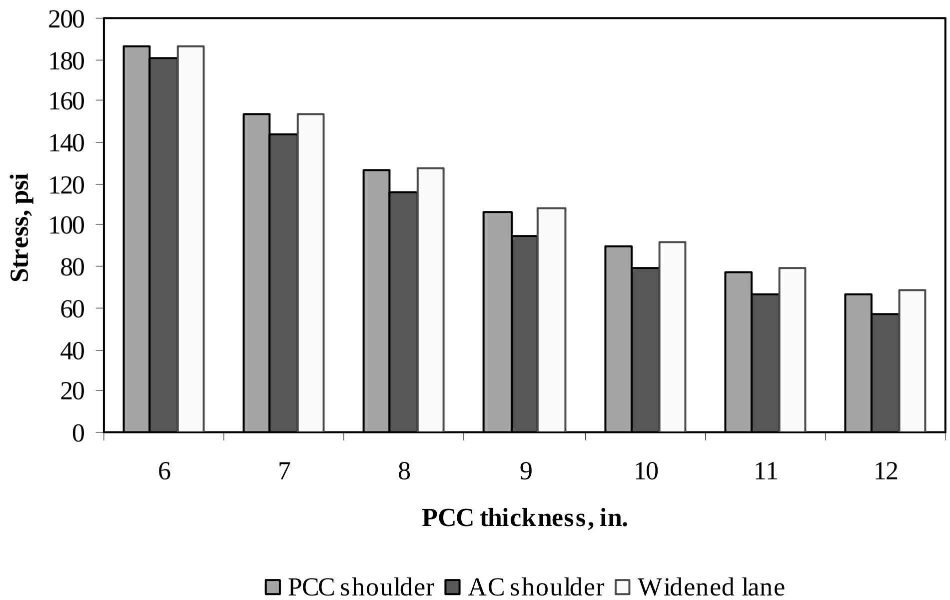


**Figure F-11-34: Impact of PCC thickness and lateral support condition on transverse stress at bottom of the Slab (315-in. joint spacing and α(ΔT/D) of 0 in.$^{-1}$)**

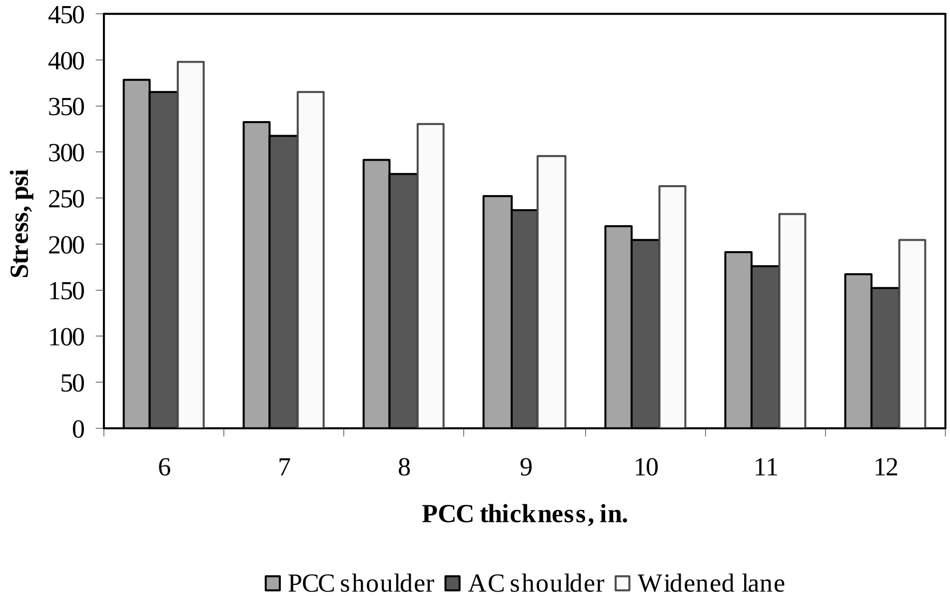


**Figure F-11-35: Impact of PCC thickness and lateral support condition on transverse stress at bottom of the Slab (177-in. joint spacing and $\alpha(\Delta T/D)$ of $20 x 10^{-6}$ in.$^{-1}$)**

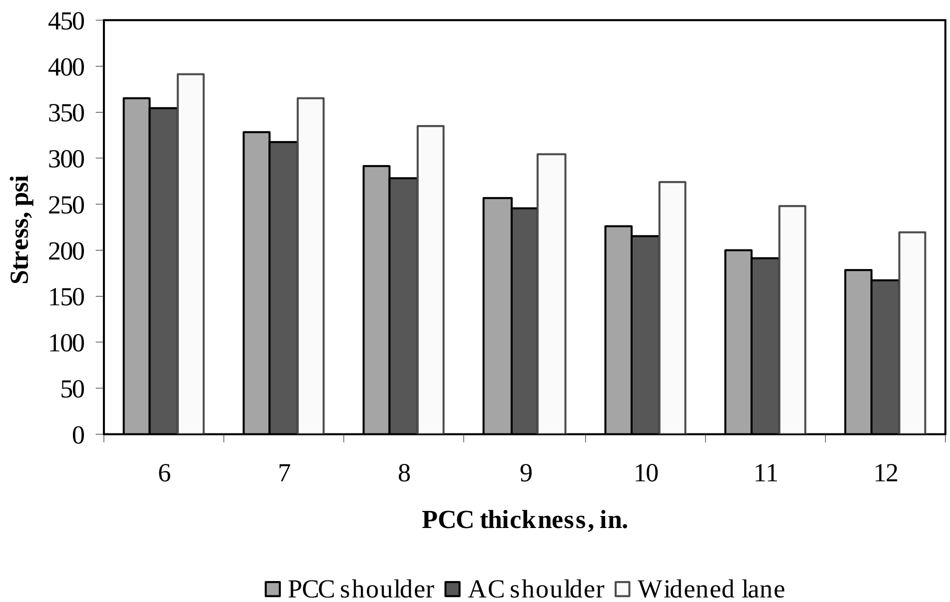


**Figure F-11-36: Impact of PCC thickness and lateral support condition on transverse stress at bottom of the Slab (315-in. joint spacing and $\alpha(\Delta T/D)$ of $20 x 10^{-6}$ in.$^{-1}$)**

Figures F-11-37 through F-11-42 illustrate the impact of base/subbase thickness and product α(ΔT/D) on stresses (10-in. PCC thickness, 100-psi/in. modulus of subgrade reaction and PCC shoulder)

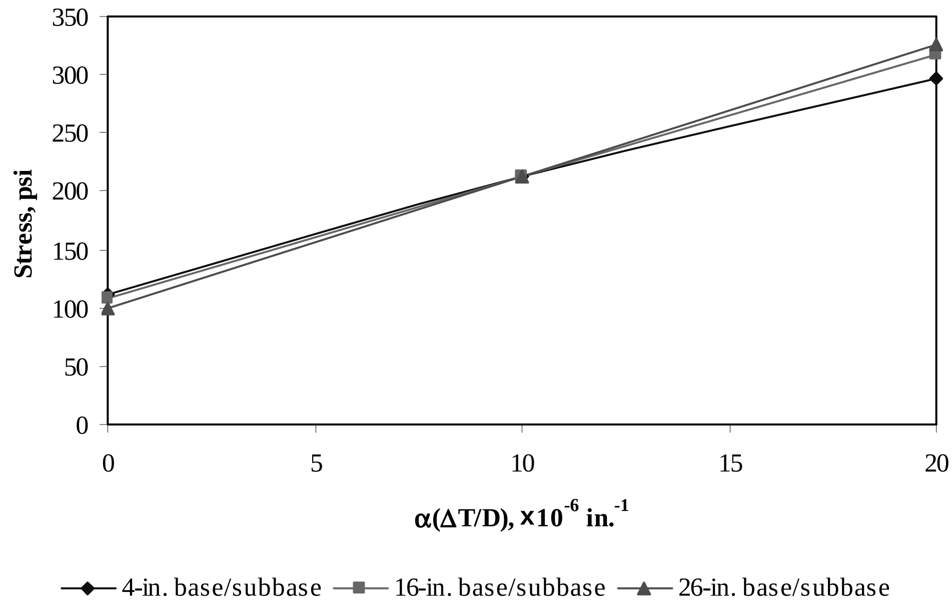


**Figure F-11-37: Impact of base/subbase thickness and product α(ΔT/D) on longitudinal stress at bottom of the slab (177-in. joint spacing)**

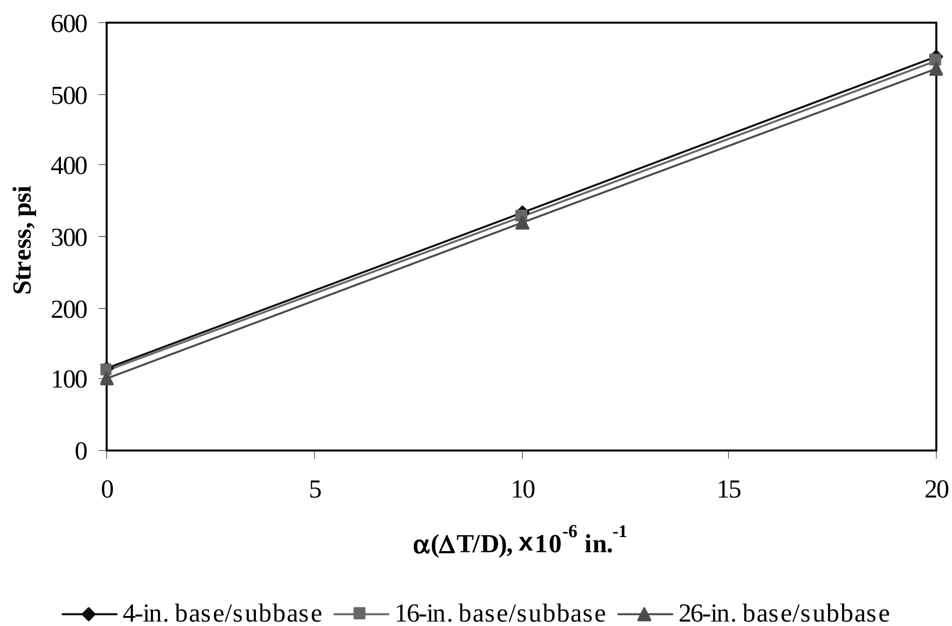


**Figure F-11-38: Impact of base/subbase thickness and product α(ΔT/D) on longitudinal stress at bottom of the slab (315-in. joint spacing)**

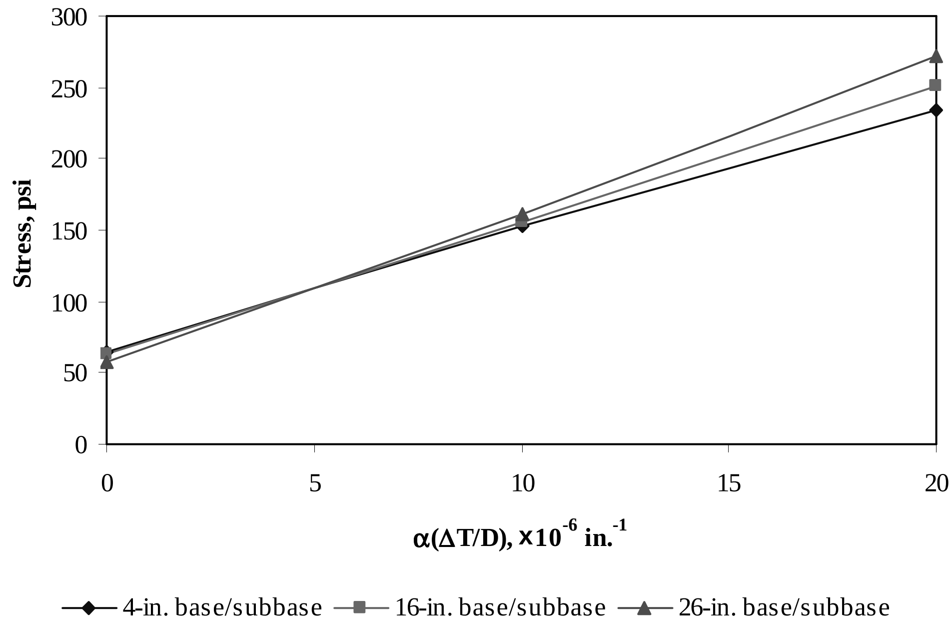


**Figure F-11-39: Impact of base/subbase thickness and product α(ΔT/D) on longitudinal stress at top of the slab (177-in. joint spacing)**

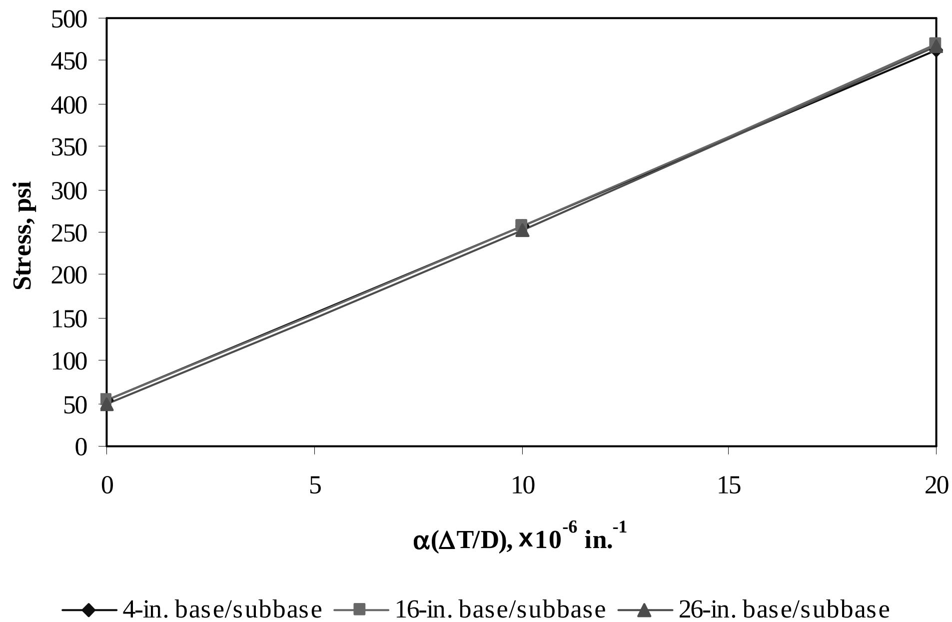


**Figure F-11-40: Impact of base/subbase thickness and product α(ΔT/D) on longitudinal stress at top of the slab (315-in. joint spacing)**

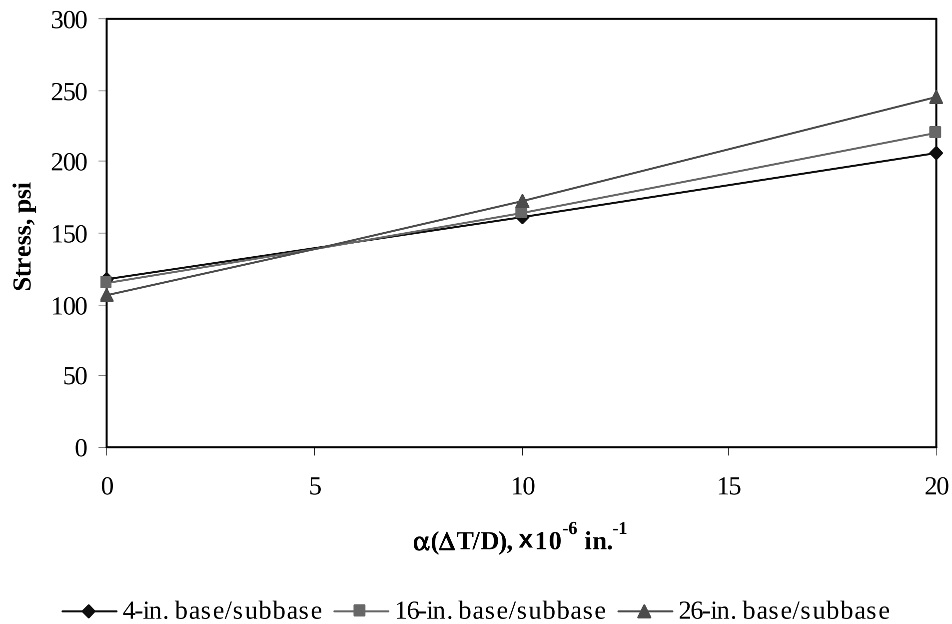


**Figure F-11-41: Impact of base/subbase thickness and product α(ΔT/D) on transverse stress at bottom of the slab (177-in. joint spacing)**

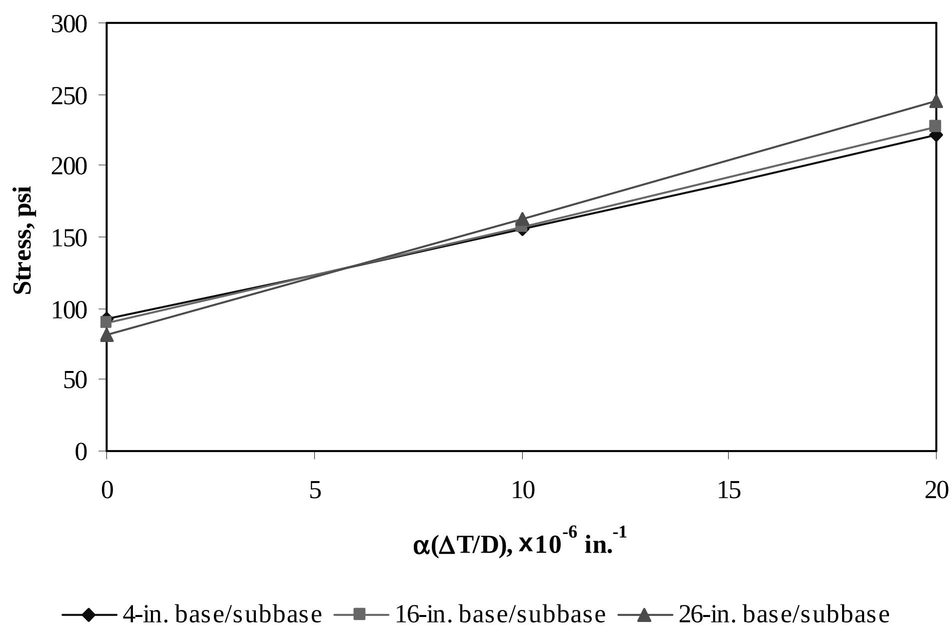


**Figure F-11-42: Impact of base/subbase thickness and product α(ΔT/D) on transverse stress at bottom of the slab (315-in. joint spacing)**

Figures F-11-43 through F-11-48 illustrate the impact of modulus of subgrade reaction and product α(ΔT/D) on stresses (10-in. PCC thickness, 16-in. base/subbase thickness and PCC shoulder)

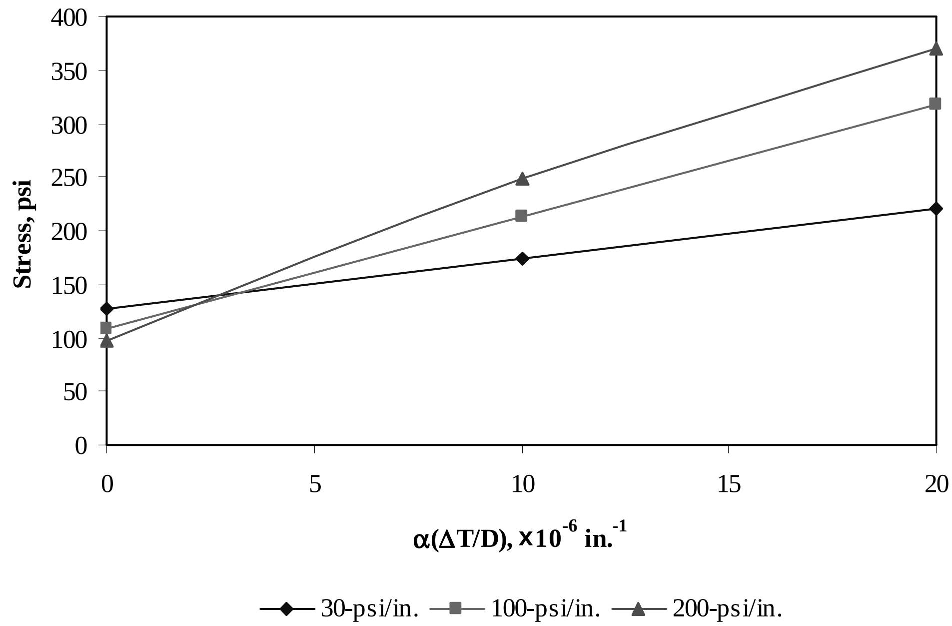


**Figure F-11-43: Impact of modulus of subgrade reaction and product α(ΔT/D) on longitudinal stress at bottom of the slab (177-in. joint spacing)**

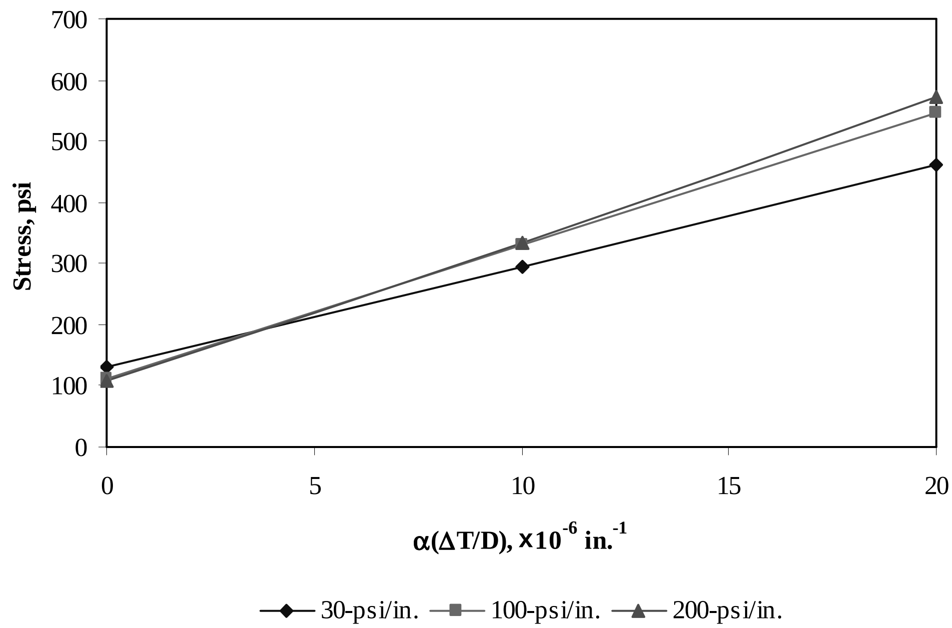


**Figure F-11-44: Impact of modulus of subgrade reaction and product α(ΔT/D) on longitudinal stress at bottom of the slab (315-in. joint spacing)**

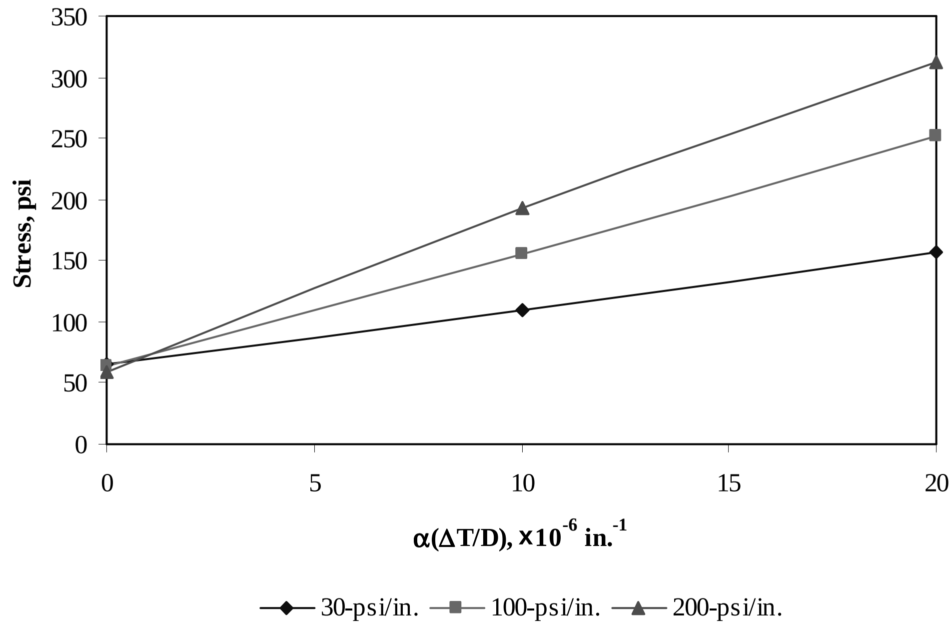


**Figure F-11-45: Impact of modulus of subgrade reaction and product α(ΔT/D) on longitudinal stress at top of the slab (177-in. joint spacing)**

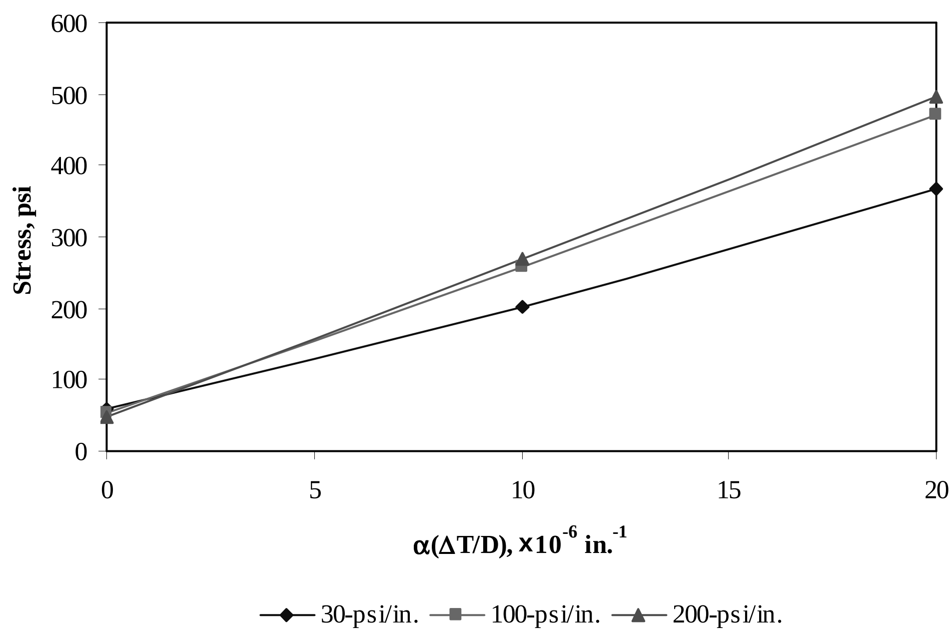


**Figure F-11-46: Impact of modulus of subgrade reaction and product α(ΔT/D) on longitudinal stress at top of the slab (315-in. joint spacing)**

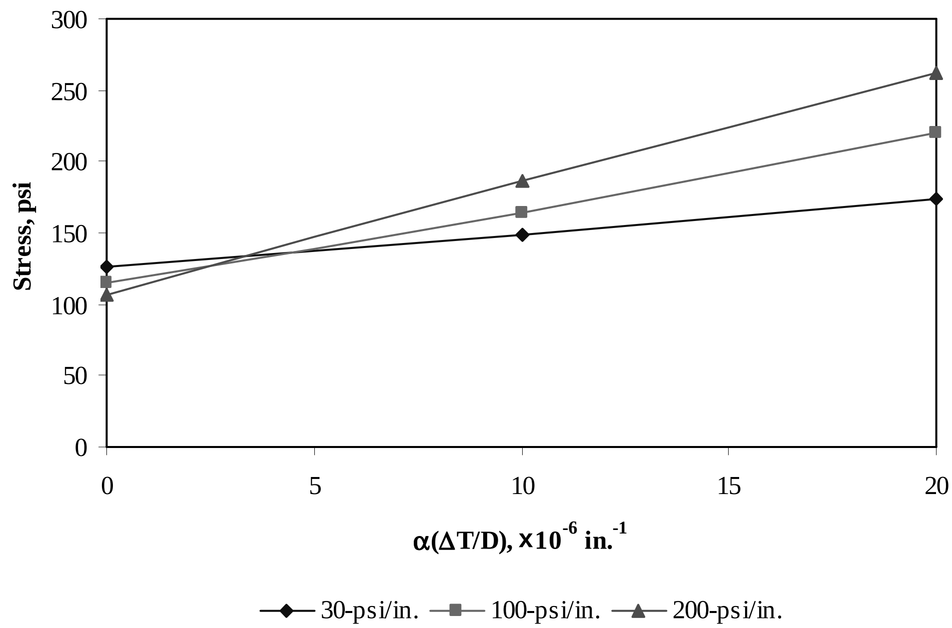


**Figure F-11-47: Impact of modulus of subgrade reaction and product α(ΔT/D) on transverse stress at bottom of the slab (177-in. joint spacing)**

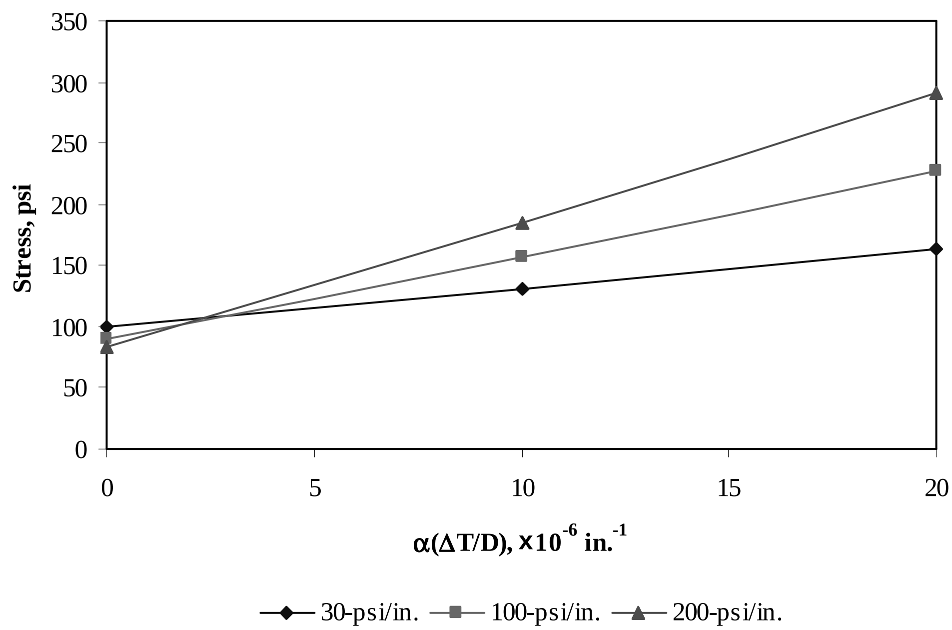


**Figure F-11-48: Impact of modulus of subgrade reaction and product α(ΔT/D) on transverse stress at bottom of the slab (315-in. joint spacing)**

Figures F-11-49 through F-11-51 illustrate the impact of joint spacing and product α(ΔT/D) on stresses (10-in. PCC thickness, 16-in. base/subbase thickness, 100-psi/in. modulus of subgrade reaction and PCC shoulder)

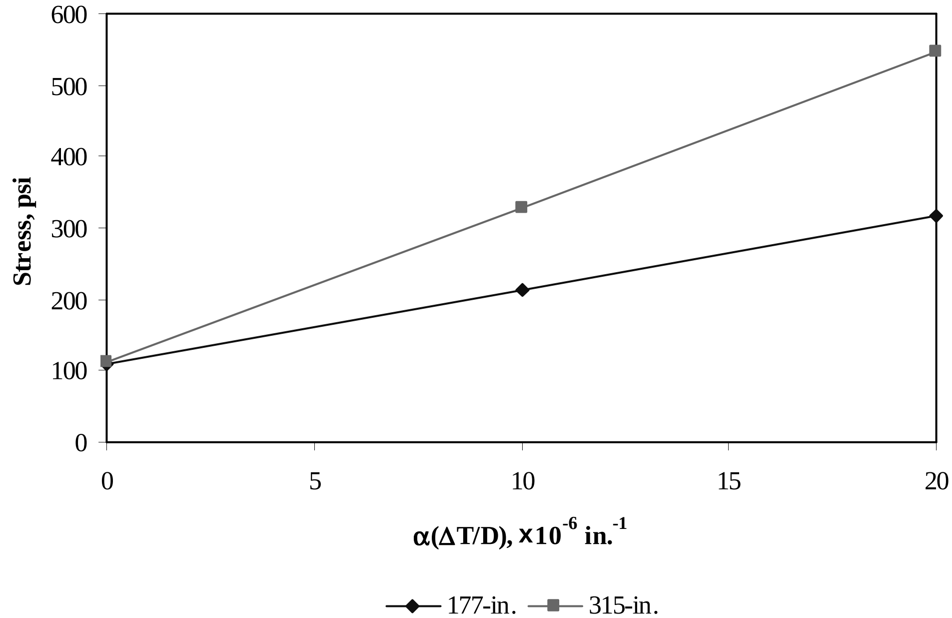


**Figure F-11-49: Impact of joint spacing and product α(ΔT/D) on longitudinal stress at bottom of the slab**

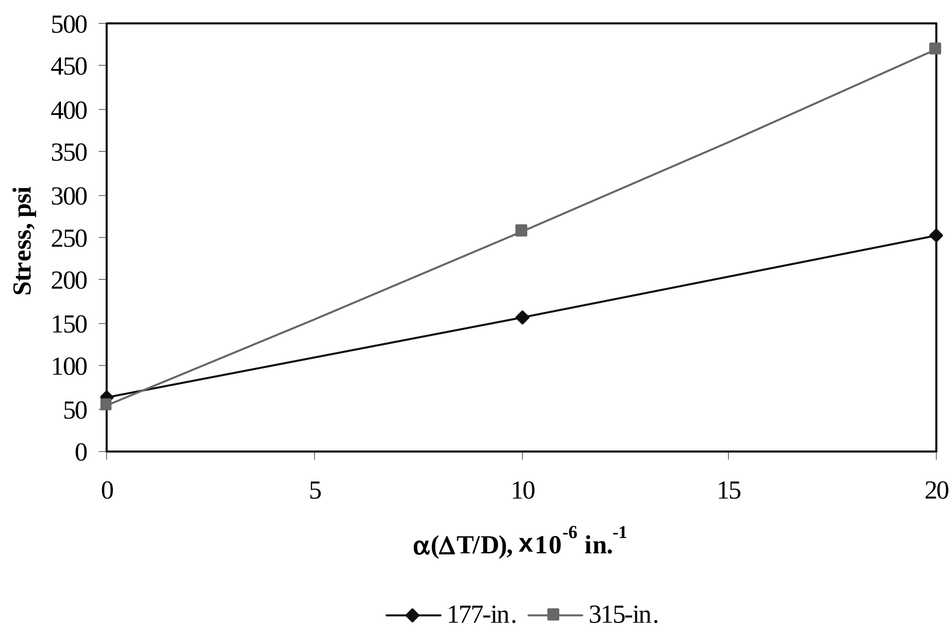


**Figure F-11-50: Impact of joint spacing and product α(ΔT/D) on longitudinal stress at top of the slab**

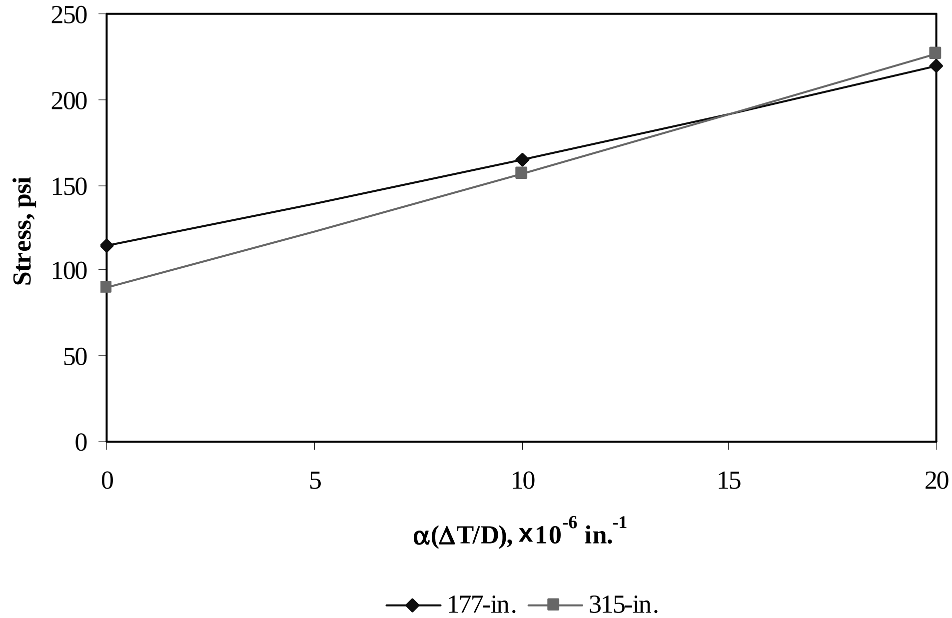


**Figure F-11-51: Impact of joint spacing and product $\alpha(\Delta T/D)$ on transverse stress at bottom of the slab**

**Sub Appendix F-12**

**Documentation of Pavement Responses for**

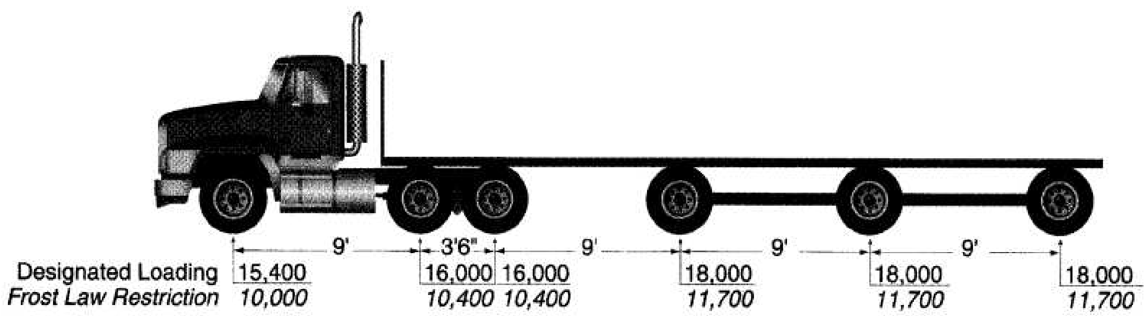


**MI-9**

Figures F-12-1 through F-12-12 illustrate the impact of PCC thickness and base/subbase thickness on stresses (100-psi/in. modulus of subgrade reaction and PCC shoulder)

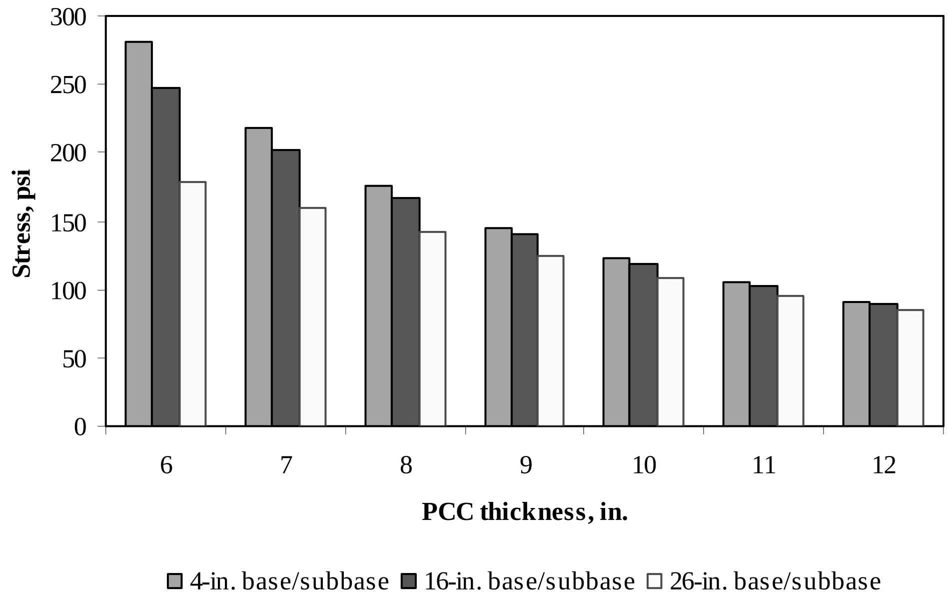


**Figure F-12-1: Impact of PCC thickness and base/subbase thickness on longitudinal stress at bottom of the Slab (177-in. joint spacing and $\alpha(\Delta T/D)$ of 0 in.$^{-1}$)**

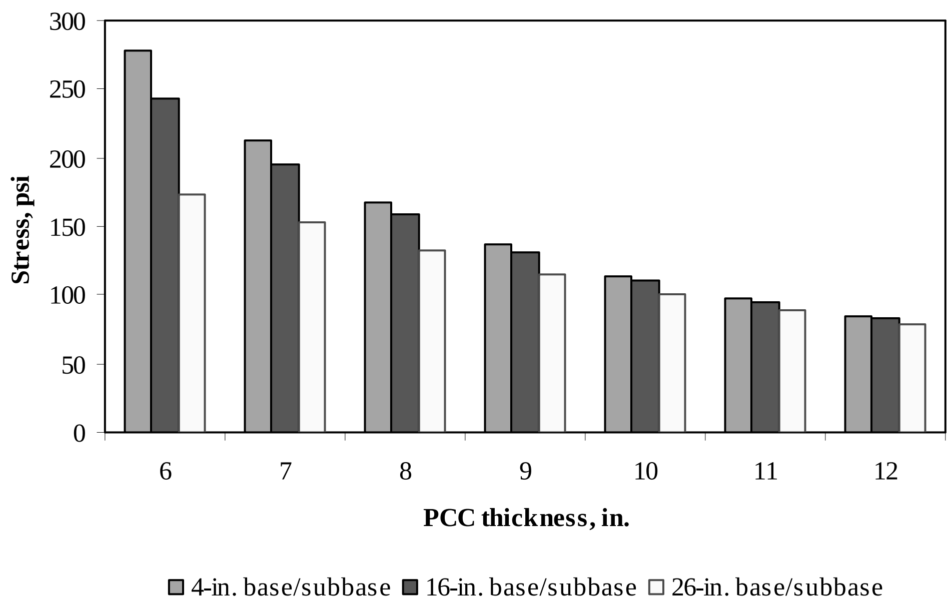


**Figure F-12-2: Impact of PCC thickness and base/subbase thickness on longitudinal stress at bottom of the Slab (315-in. joint spacing and $\alpha(\Delta T/D)$ of 0 in.$^{-1}$)**

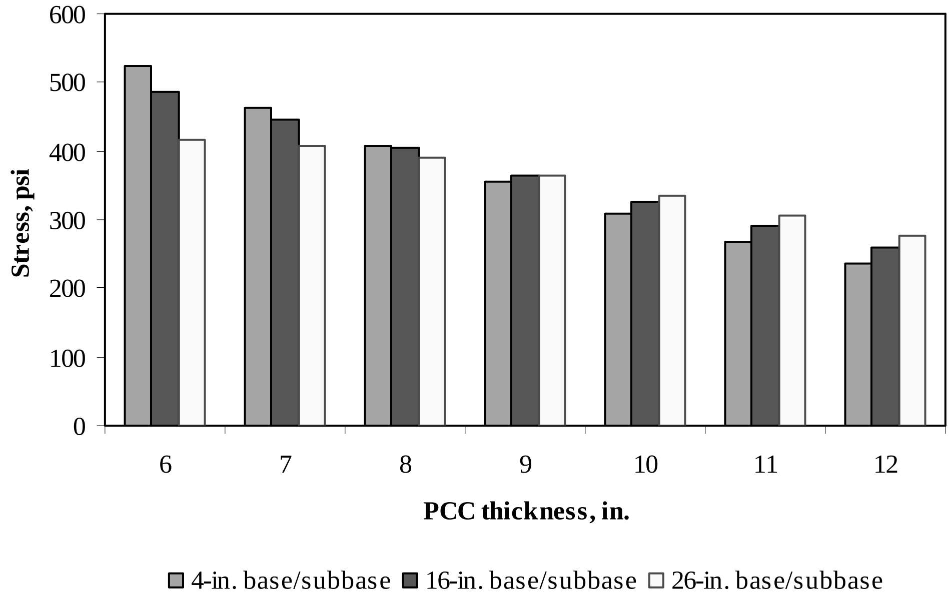


**Figure F-12-3: Impact of PCC thickness and base/subbase thickness on longitudinal stress at bottom of the Slab (177-in. joint spacing and $\alpha(\Delta T/D)$ of $20 x 10^{-6}$ in.$^{-1}$)**

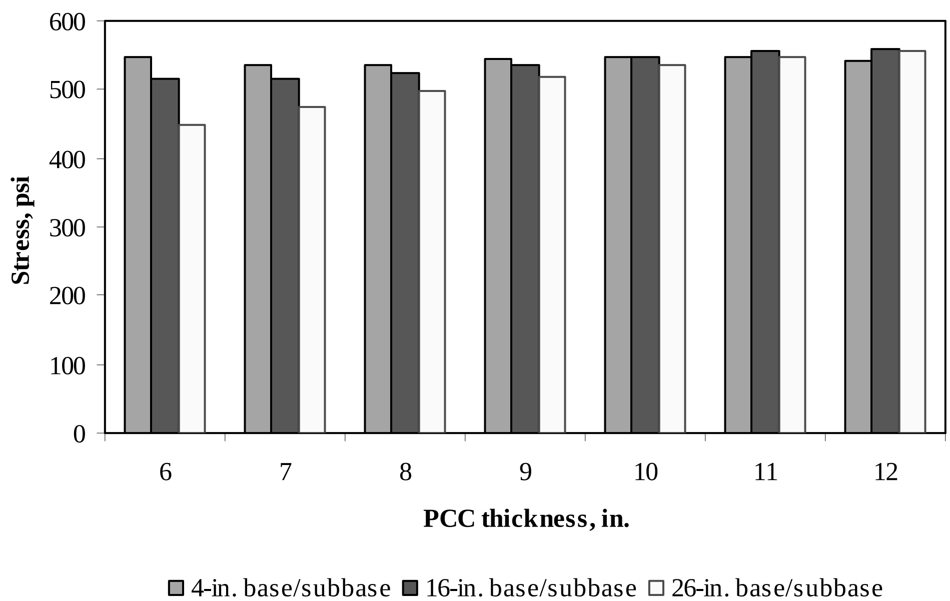


**Figure F-12-4: Impact of PCC thickness and base/subbase thickness on longitudinal stress at bottom of the Slab (315-in. joint spacing and $\alpha(\Delta T/D)$ of $20 x 10^{-6}$ in.$^{-1}$)**

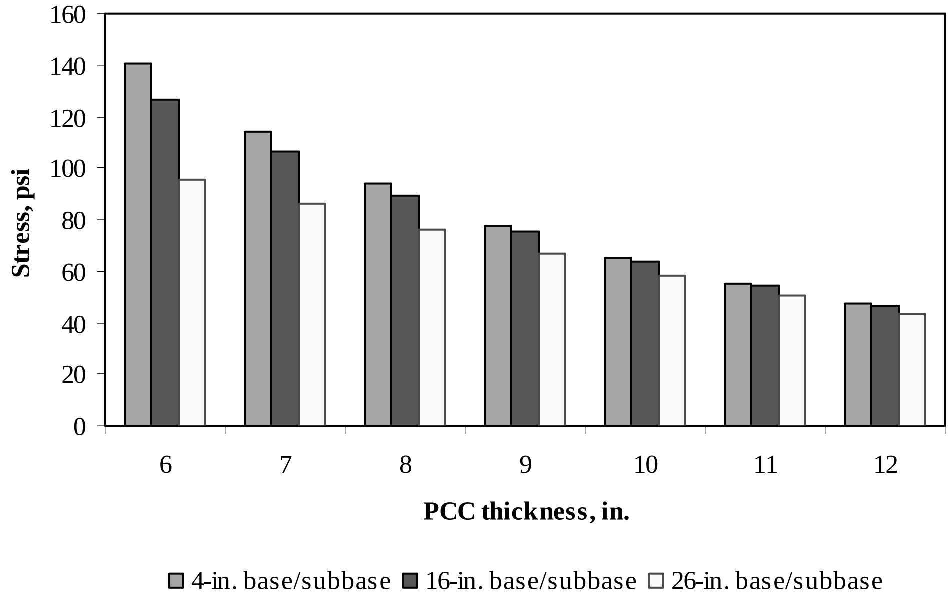


**Figure F-12-5: Impact of PCC thickness and base/subbase thickness on longitudinal stress at top of the Slab (177-in. joint spacing and $\alpha(\Delta T/D)$ of 0 in.$^{-1}$)**

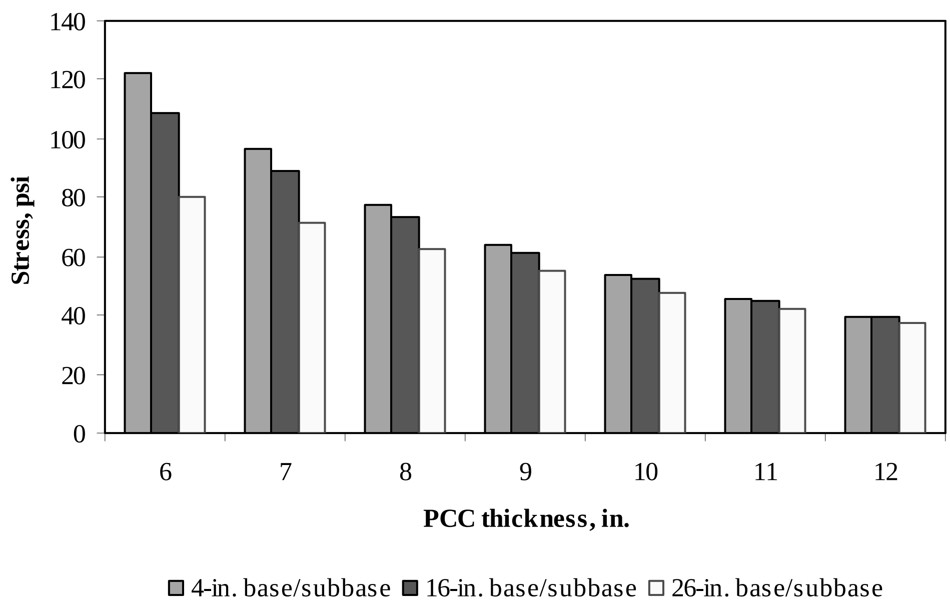


**Figure F-12-6: Impact of PCC thickness and base/subbase thickness on longitudinal stress at top of the Slab (315-in. joint spacing and $\alpha(\Delta T/D)$ of 0 in.$^{-1}$)**

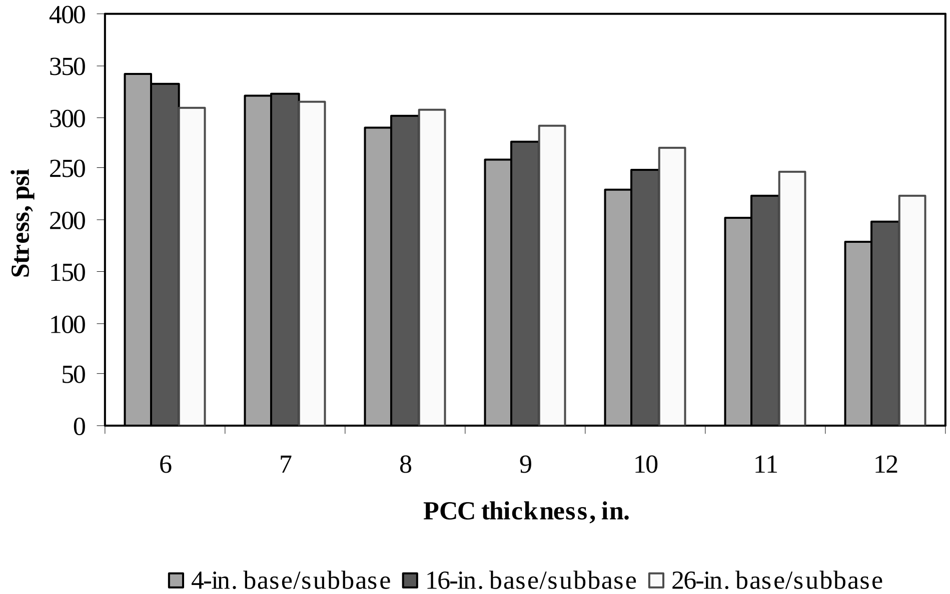


**Figure F-12-7: Impact of PCC thickness and base/subbase thickness on longitudinal stress at top of the Slab (177-in. joint spacing and $\alpha(\Delta T/D)$ of -20x$10^{-6}$ in.$^{-1}$)**

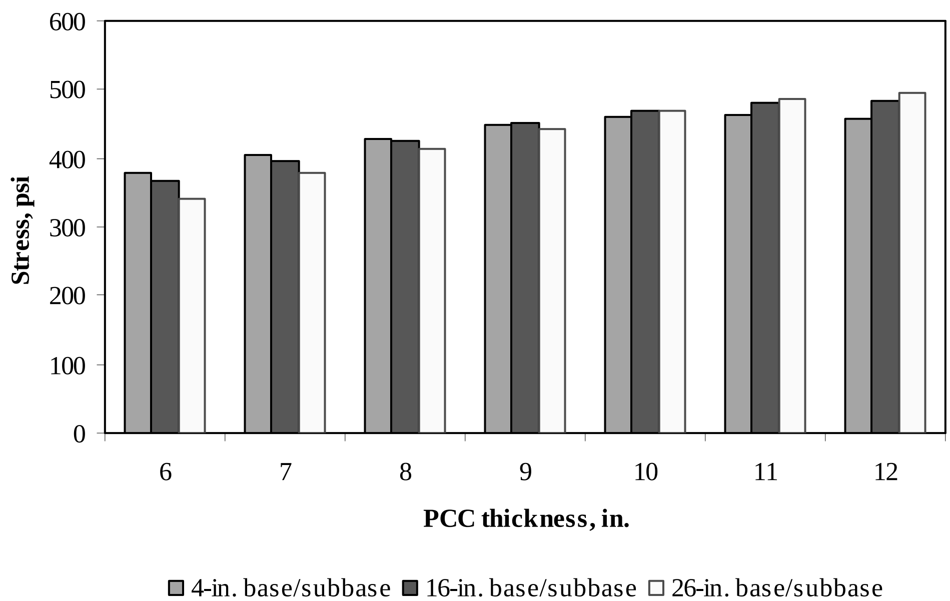


**Figure F-12-8: Impact of PCC thickness and base/subbase thickness on longitudinal stress at top of the Slab (315-in. joint spacing and $\alpha(\Delta T/D)$ of -20x$10^{-6}$ in.$^{-1}$)**

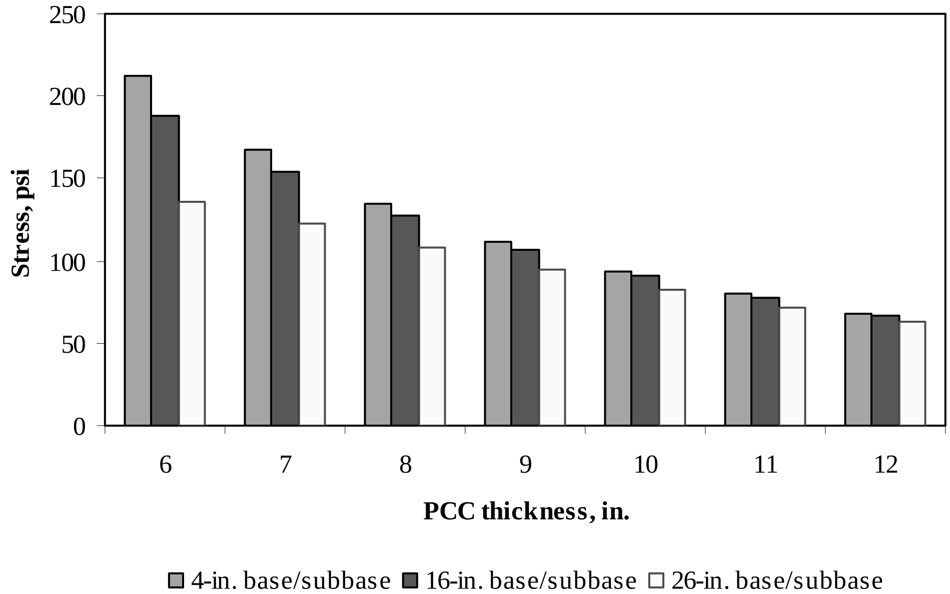


**Figure F-12-9: Impact of PCC thickness and base/subbase thickness on transverse stress at bottom of the Slab (177-in. joint spacing and $\alpha(\Delta T/D)$ of 0 in.$^{-1}$)**

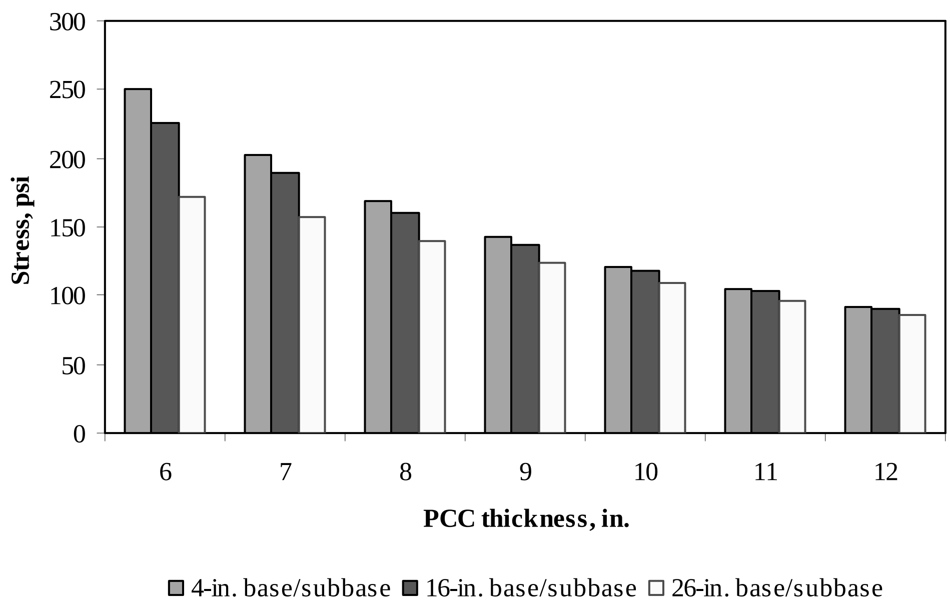


**Figure F-12-10: Impact of PCC thickness and base/subbase thickness on transverse stress at bottom of the Slab (315-in. joint spacing and $\alpha(\Delta T/D)$ of 0 in.$^{-1}$)**

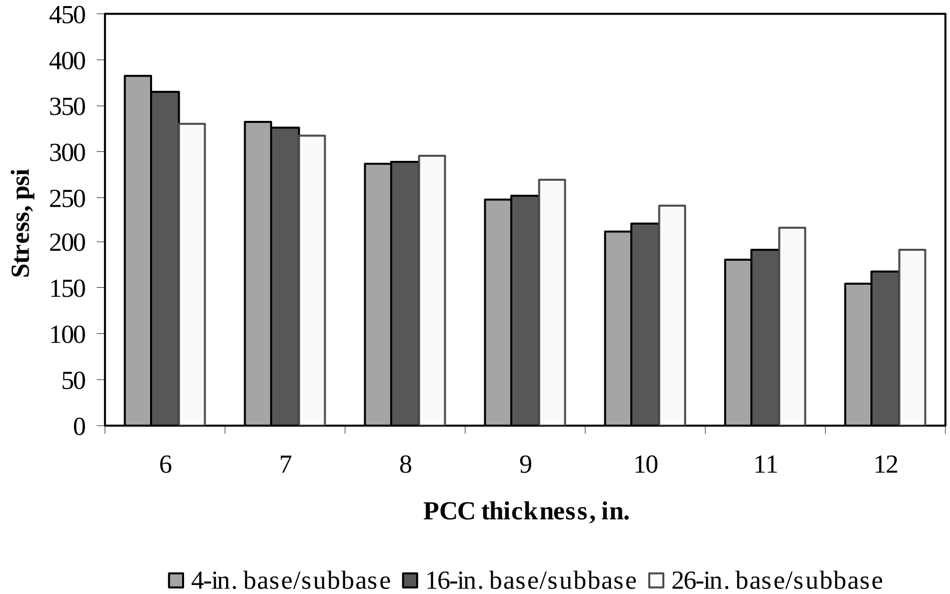


**Figure F-12-11: Impact of PCC thickness and base/subbase thickness on transverse stress at bottom of the Slab (177-in. joint spacing and $\alpha(\Delta T/D)$ of $20x10^{-6}$ in.$^{-1}$)**

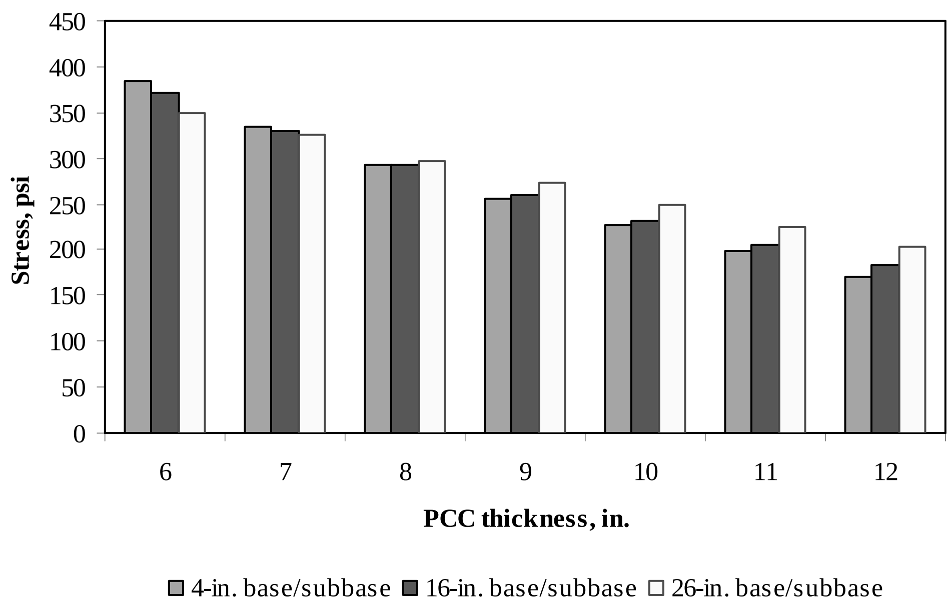


**Figure F-12-12: Impact of PCC thickness and base/subbase thickness on transverse stress at bottom of the Slab (315-in. joint spacing and $\alpha(\Delta T/D)$ of $20x10^{-6}$ in.$^{-1}$)**

Figures F-12-13 through F-12-24 illustrate the impact of PCC thickness and modulus of subgrade reaction on stresses (16-in. base/subbase thickness and PCC shoulder)

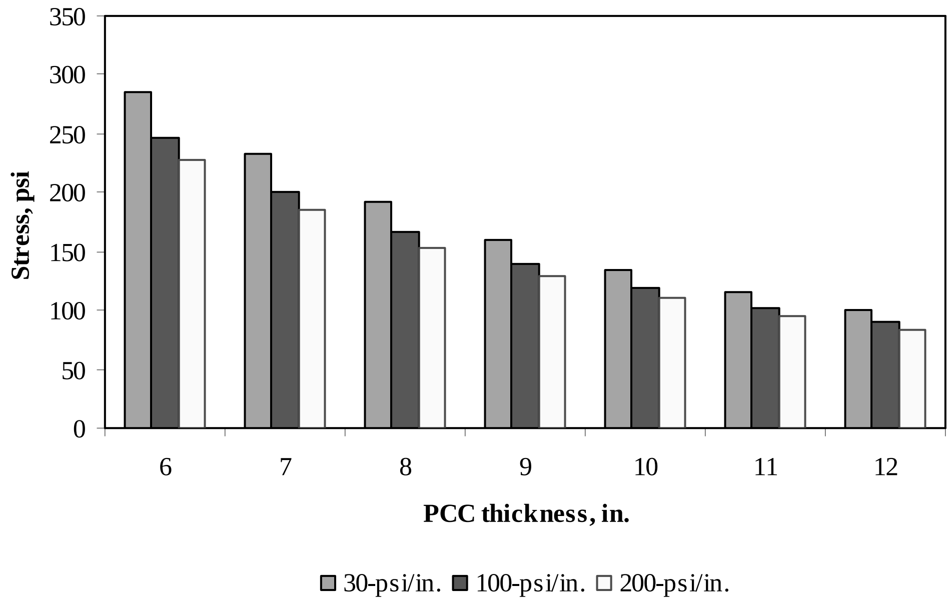


**Figure F-12-13: Impact of PCC thickness and modulus of subgrade reaction on longitudinal stress at bottom of the slab (177-in. joint spacing and $\alpha(\Delta T/D)$ of 0 in.$^{-1}$)**

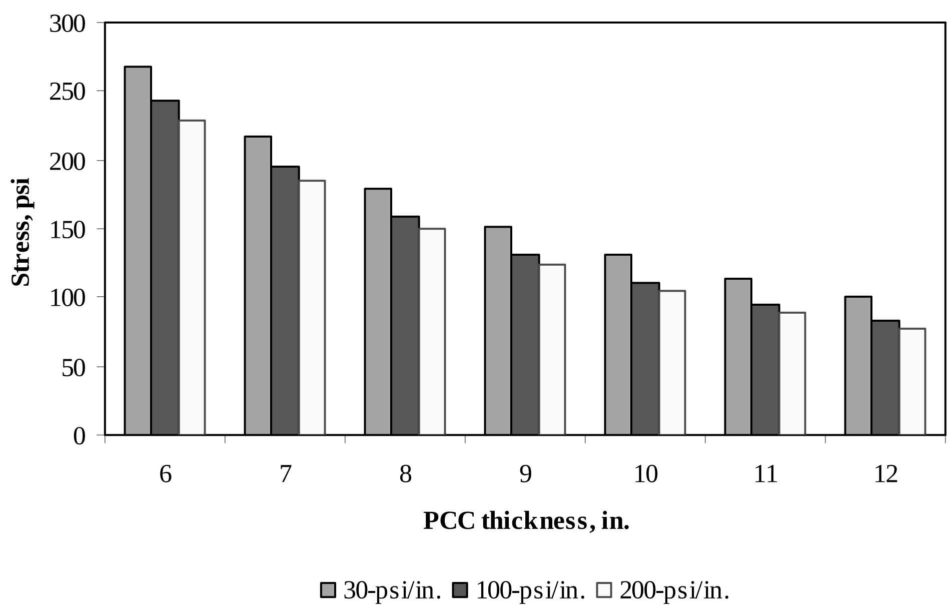


**Figure F-12-14: Impact of PCC thickness and modulus of subgrade reaction on longitudinal stress at bottom of the slab (315-in. joint spacing and $\alpha(\Delta T/D)$ of 0 in.$^{-1}$)**

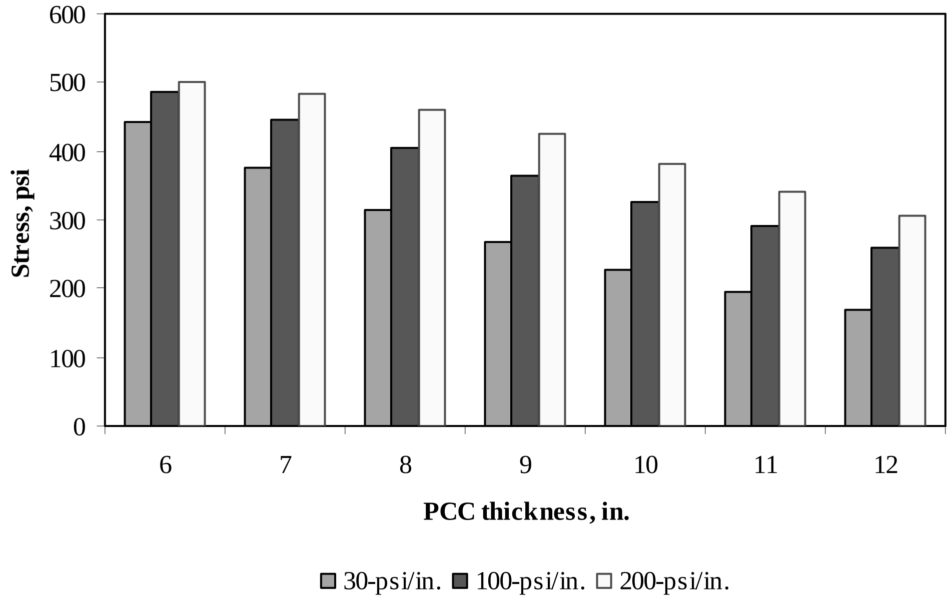


**Figure F-12-15: Impact of PCC thickness and modulus of subgrade reaction on longitudinal stress at bottom of the slab (177-in. joint spacing and $\alpha(\Delta T/D)$ of $20 x 10^{-6}$ in.$^{-1}$)**

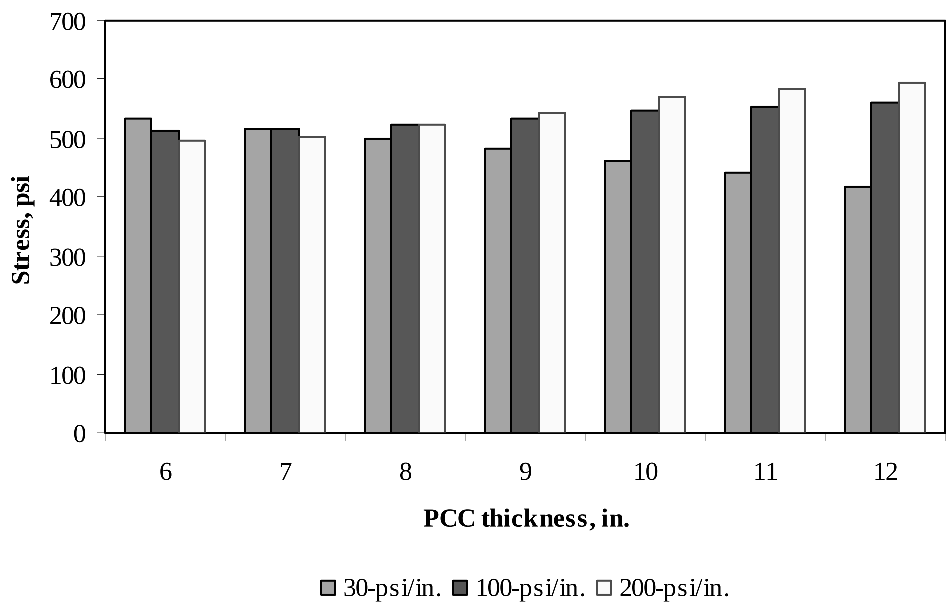


**Figure F-12-16: Impact of PCC thickness and modulus of subgrade reaction on longitudinal stress at bottom of the slab (315-in. joint spacing and $\alpha(\Delta T/D)$ of $20 x 10^{-6}$ in.$^{-1}$)**

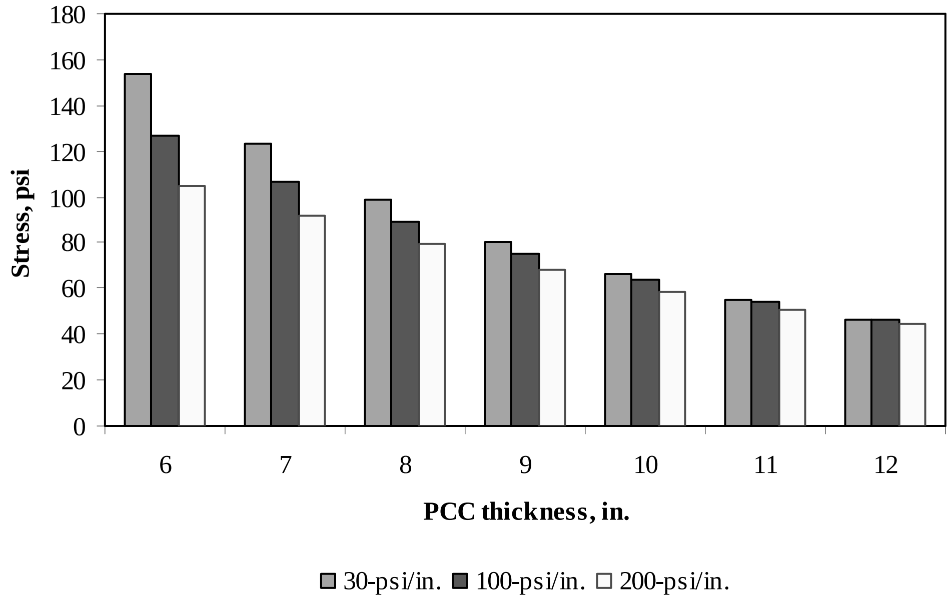


**Figure F-12-17: Impact of PCC thickness and modulus of subgrade reaction on longitudinal stress at top of the Slab (177-in. joint spacing and $\alpha(\Delta T/D)$ of 0 in.$^{-1}$)**

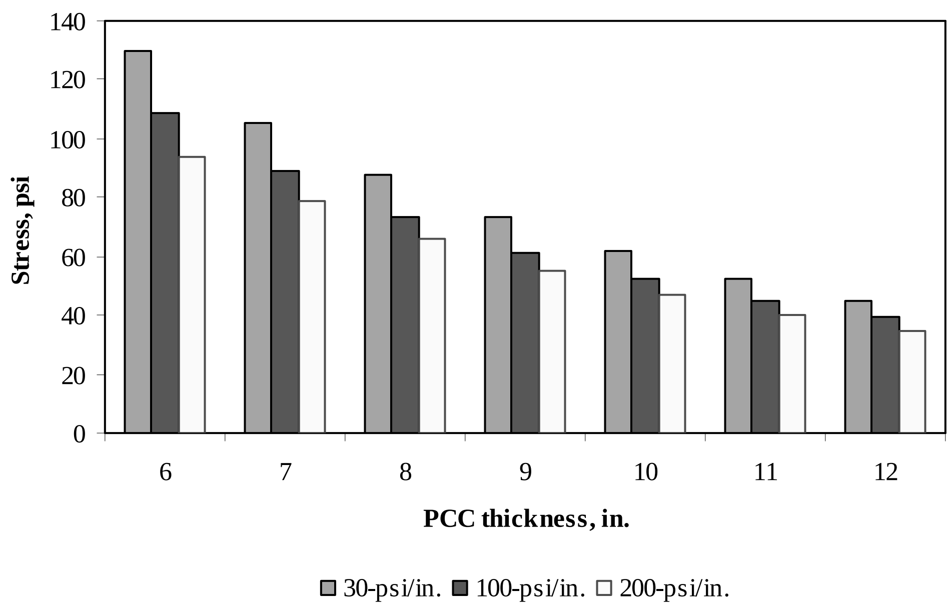


**Figure F-12-18: Impact of PCC thickness and modulus of subgrade reaction on longitudinal stress at top of the Slab (315-in. joint spacing and $\alpha(\Delta T/D)$ of 0 in.$^{-1}$)**

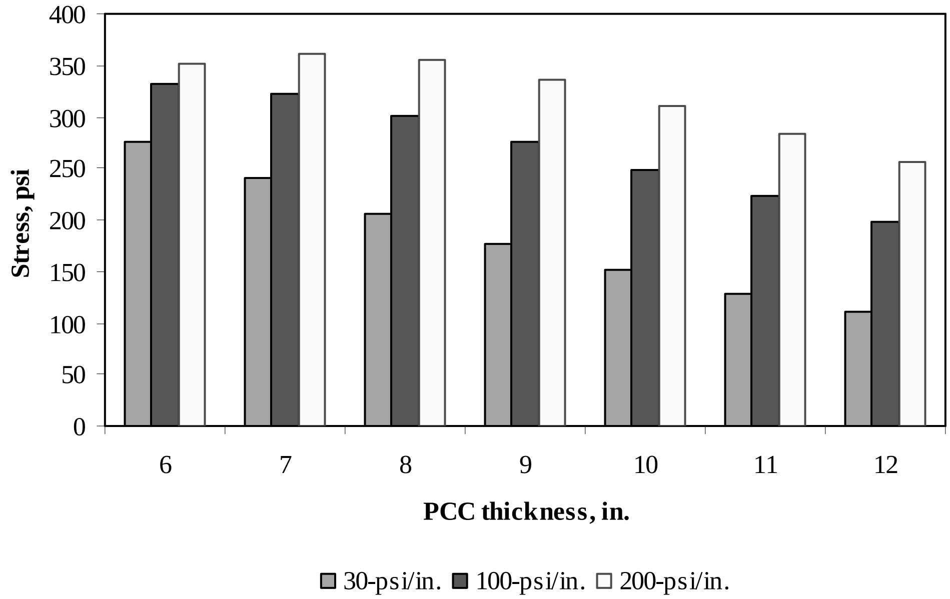


**Figure F-12-19: Impact of PCC thickness and modulus of subgrade reaction on longitudinal stress at top of the Slab (177-in. joint spacing and $\alpha(\Delta T/D)$ of $-20x10^{-6}$ in.$^{-1}$)**

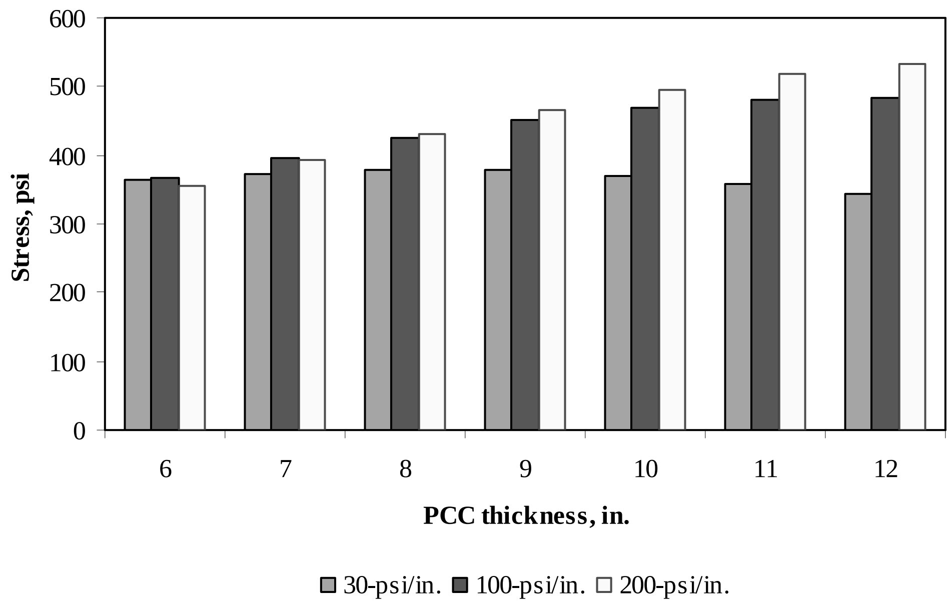


**Figure F-12-20: Impact of PCC thickness and modulus of subgrade reaction on longitudinal stress at top of the Slab (315-in. joint spacing and $\alpha(\Delta T/D)$ of $-20x10^{-6}$ in.$^{-1}$)**

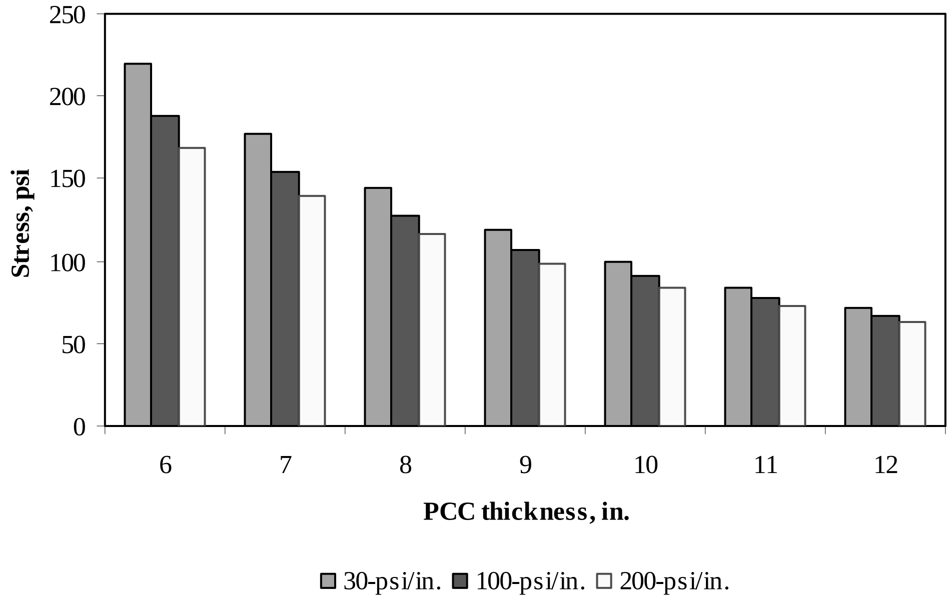


**Figure F-12-21: Impact of PCC thickness and modulus of subgrade reaction on transverse stress at bottom of the Slab (177-in. joint spacing and $\alpha(\Delta T/D)$ of 0 in.$^{-1}$)**

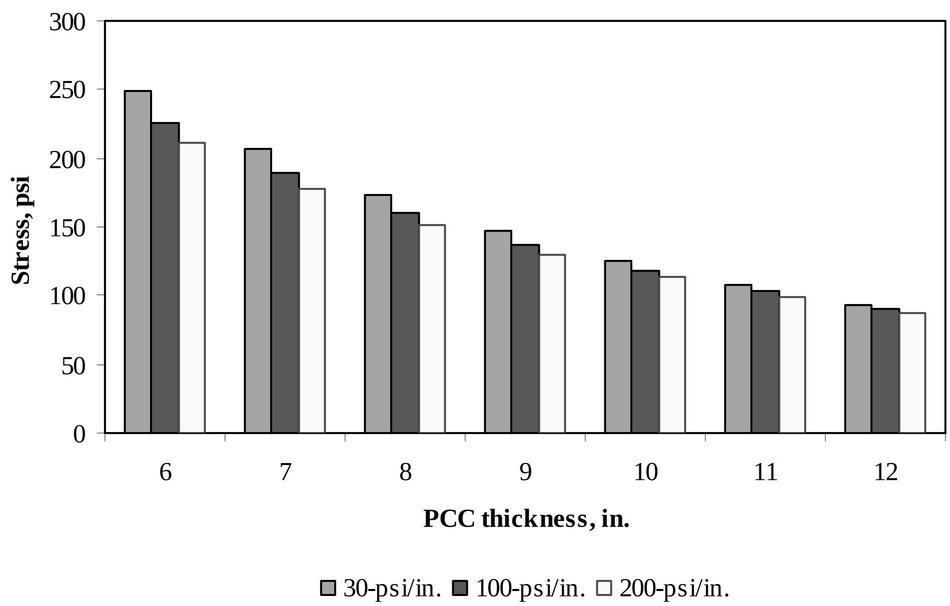


**Figure F-12-22: Impact of PCC thickness and modulus of subgrade reaction on transverse stress at bottom of the Slab (315-in. joint spacing and $\alpha(\Delta T/D)$ of 0 in.$^{-1}$)**

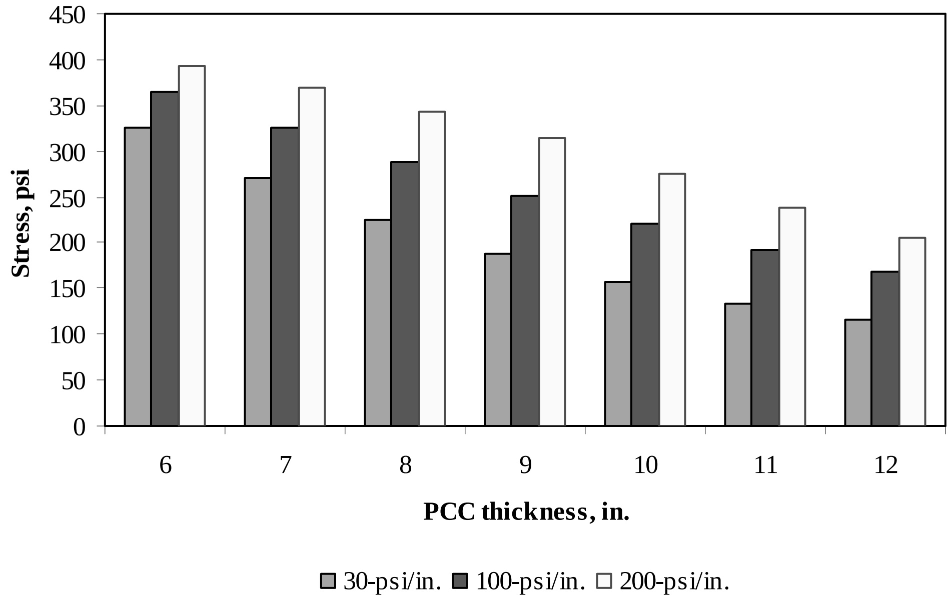


**Figure F-12-23: Impact of PCC thickness and modulus of subgrade reaction on transverse stress at bottom of the Slab (177-in. joint spacing and $\alpha(\Delta T/D)$ of $20x10^{-6}$ in.$^{-1}$)**

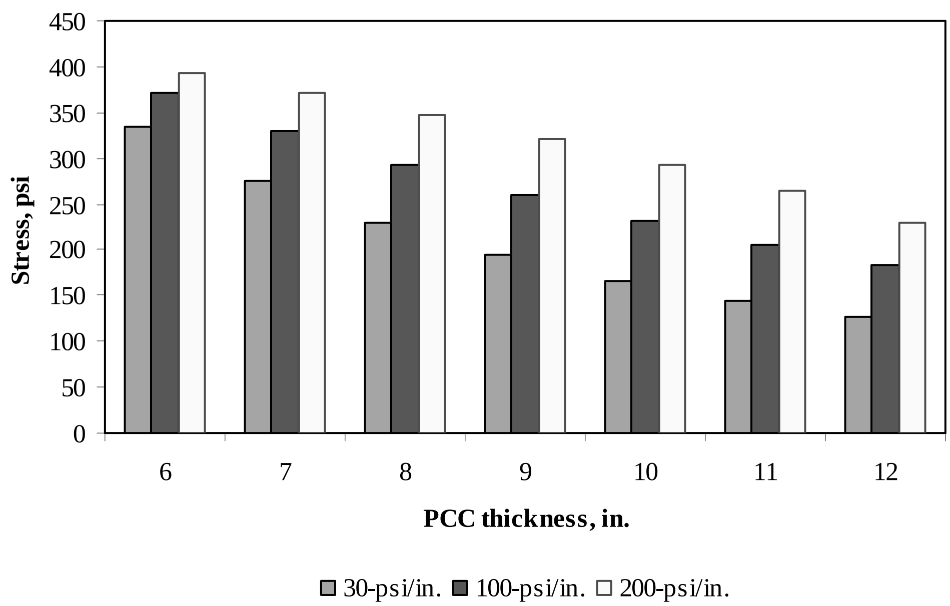


**Figure F-12-24: Impact of PCC thickness and modulus of subgrade reaction on transverse stress at bottom of the Slab (315-in. joint spacing and $\alpha(\Delta T/D)$ of $20x10^{-6}$ in.$^{-1}$)**

Figures F-12-25 through F-12-36 illustrate the impact of PCC thickness and lateral support condition on stresses (16-in. base/subbase and 100-psi/in. modulus of subgrade reaction)

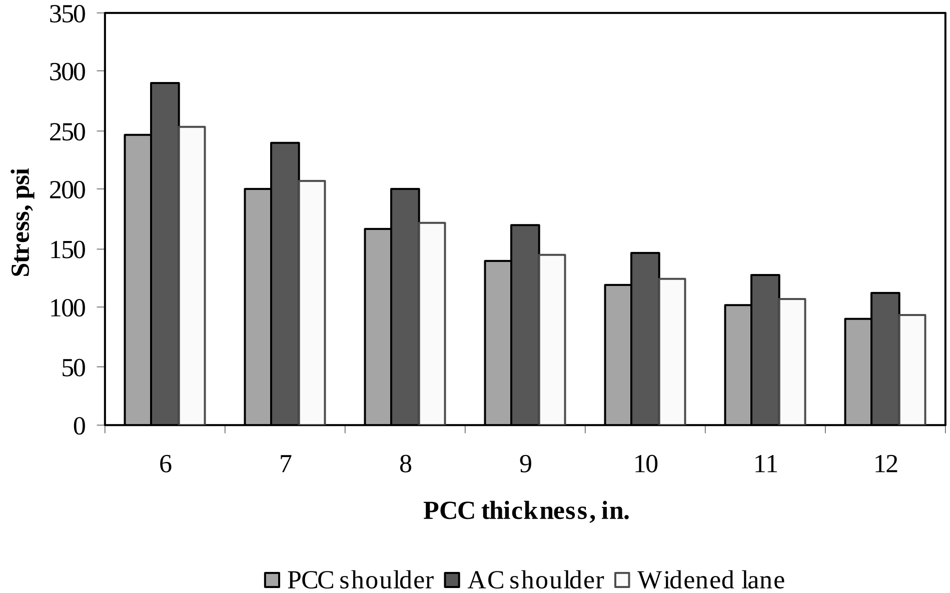


**Figure F-12-25: Impact of PCC thickness and lateral support condition on longitudinal stress at bottom of the Slab (177-in. joint spacing and α(ΔT/D) of 0 in.$^{-1}$)**

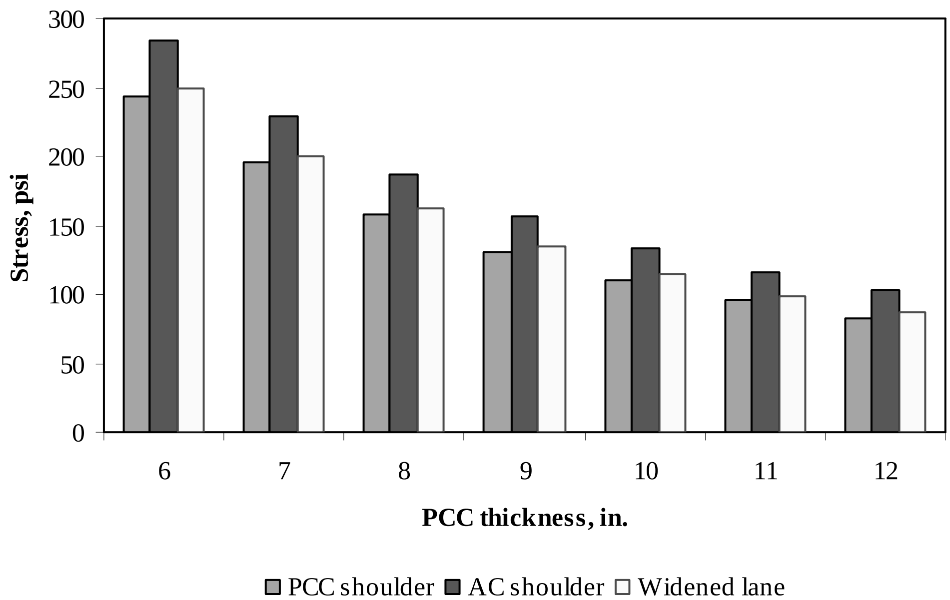


**Figure F-12-26: Impact of PCC thickness and lateral support condition on longitudinal stress at bottom of the Slab (315-in. joint spacing and α(ΔT/D) of 0 in.$^{-1}$)**

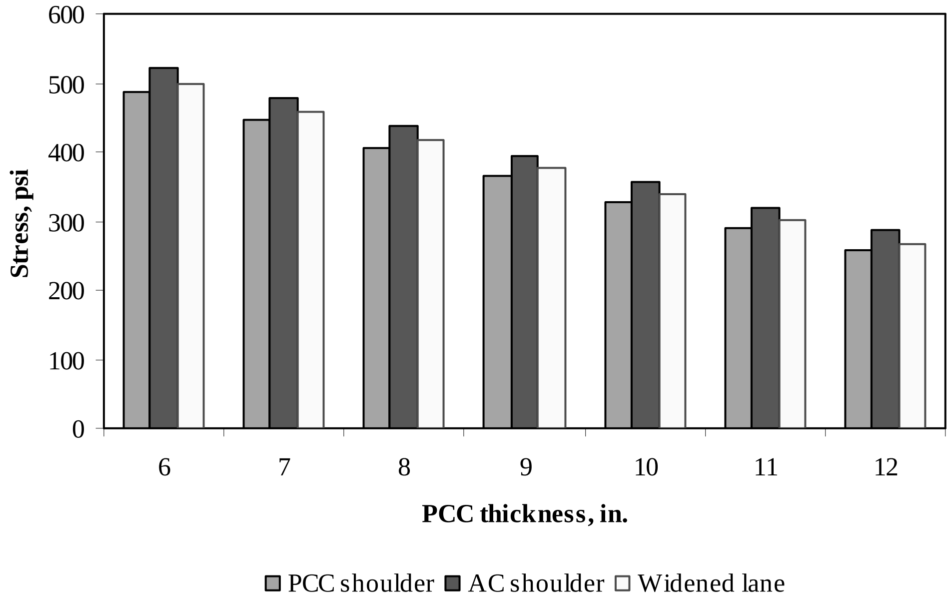


**Figure F-12-27: Impact of PCC thickness and lateral support condition on longitudinal stress at bottom of the Slab (177-in. joint spacing and $\alpha(\Delta T/D)$ of $20x10^{-6}$ in.$^{-1}$)**

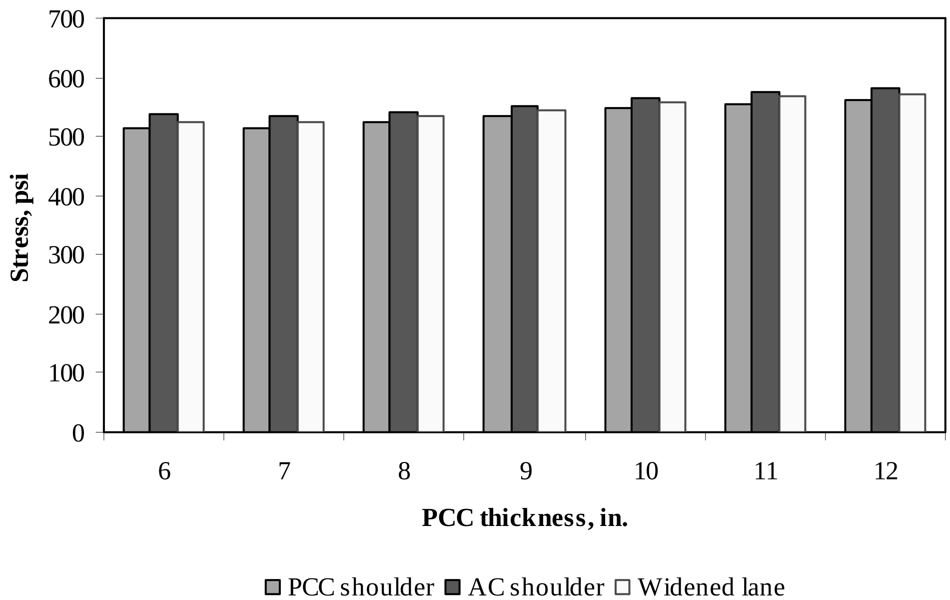


**Figure F-12-28: Impact of PCC thickness and lateral support condition on longitudinal stress at bottom of the Slab (315-in. joint spacing and $\alpha(\Delta T/D)$ of $20x10^{-6}$ in.$^{-1}$)**

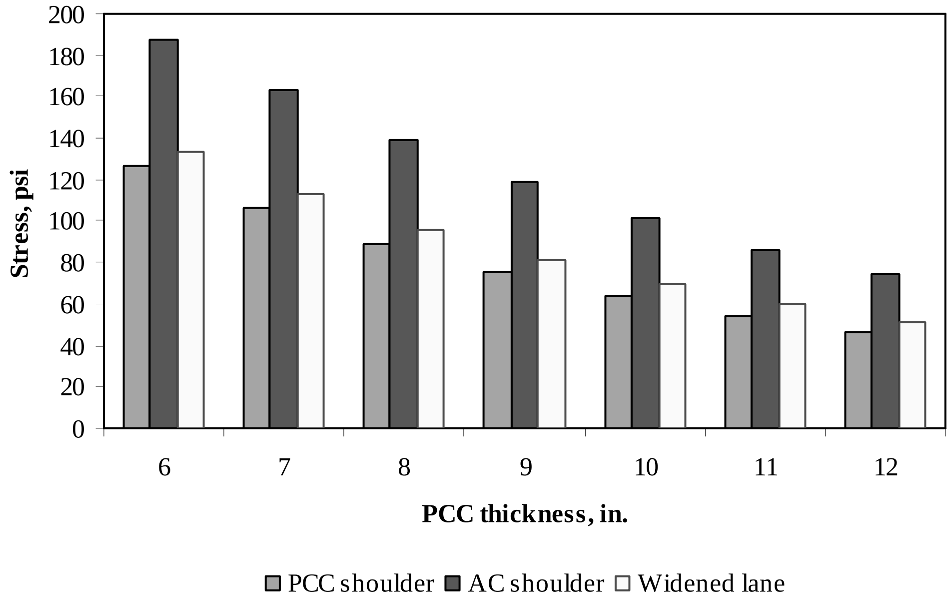


**Figure F-12-29: Impact of PCC thickness and lateral support condition on longitudinal stress at top of the Slab (177-in. joint spacing and $\alpha(\Delta T/D)$ of 0 in.$^{-1}$)**

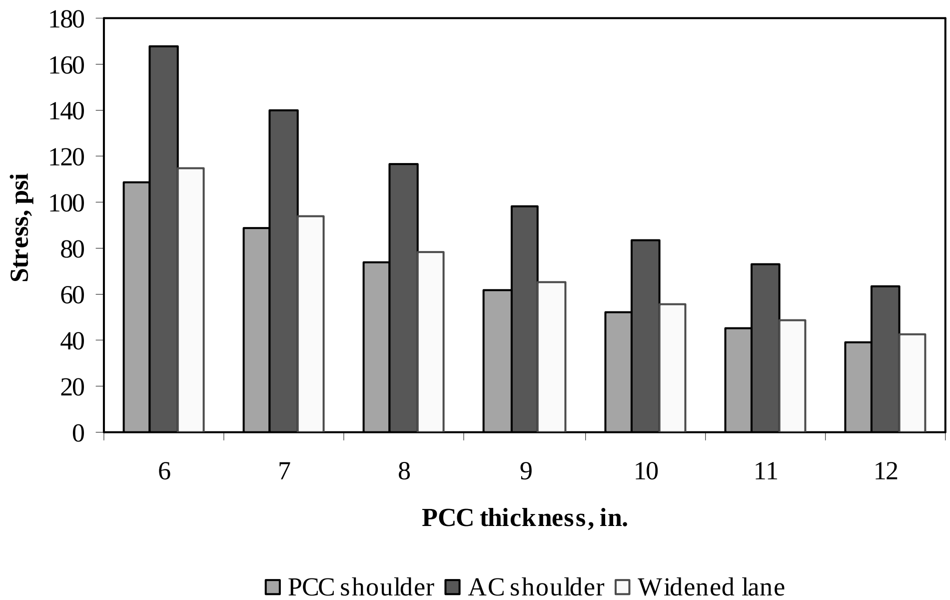


**Figure F-12-30: Impact of PCC thickness and lateral support condition on longitudinal stress at top of the Slab (315-in. joint spacing and $\alpha(\Delta T/D)$ of 0 in.$^{-1}$)**

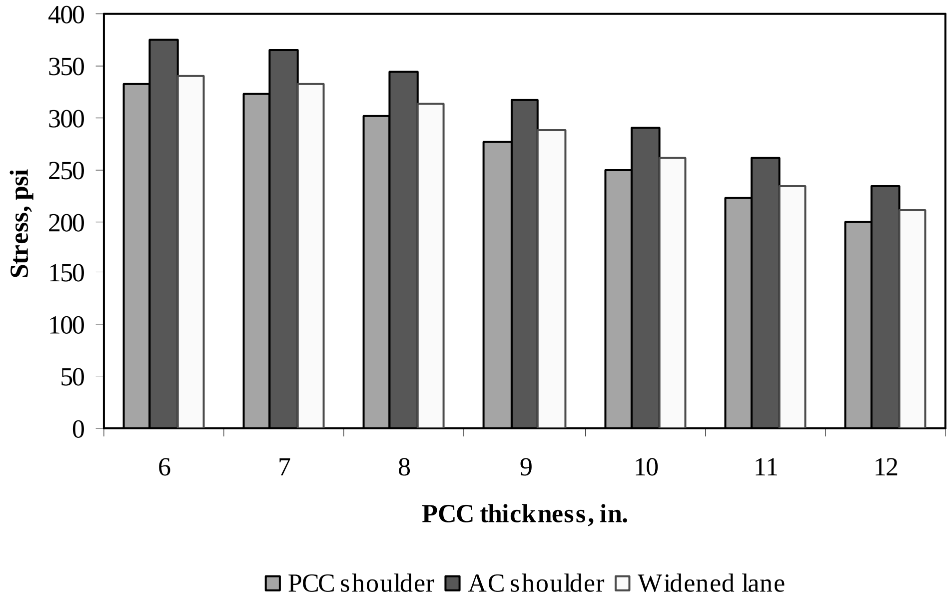


**Figure F-12-31: Impact of PCC thickness and lateral support condition on longitudinal stress at top of the Slab (177-in. joint spacing and $\alpha(\Delta T/D)$ of $-20x10^{-6}$ in.$^{-1}$)**

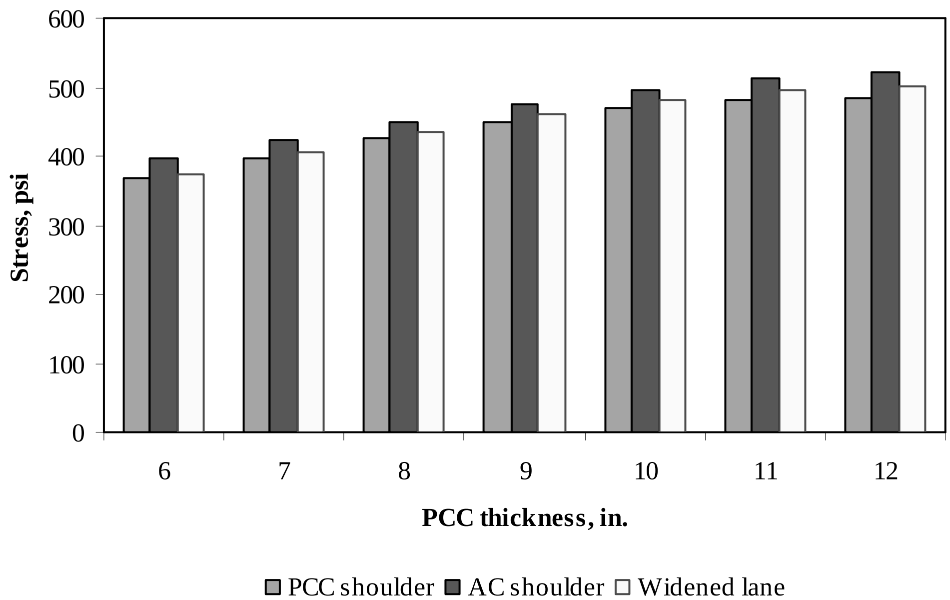


**Figure F-12-32: Impact of PCC thickness and lateral support condition on longitudinal stress at top of the Slab (315-in. joint spacing and $\alpha(\Delta T/D)$ of $-20x10^{-6}$ in.$^{-1}$)**

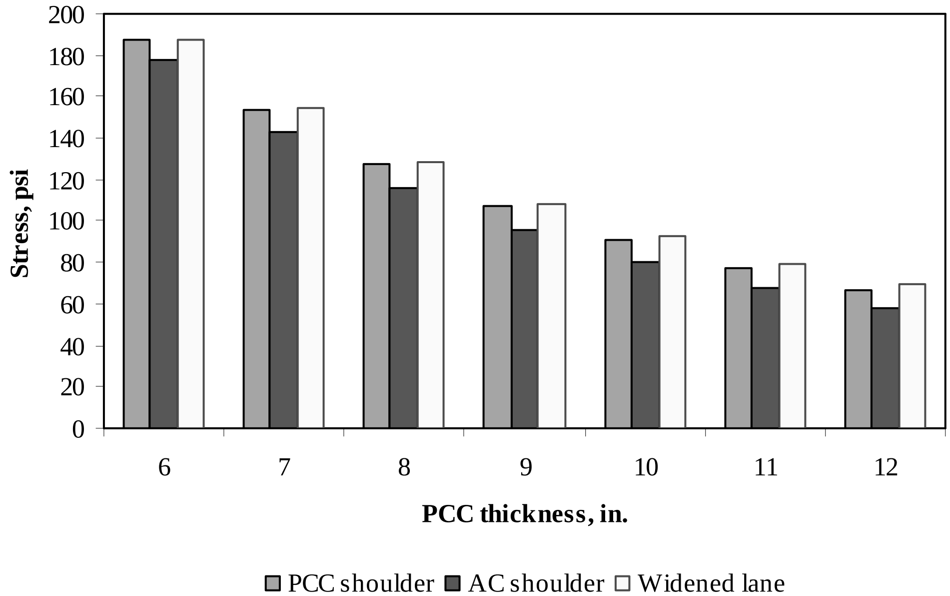


**Figure F-12-33: Impact of PCC thickness and lateral support condition on transverse stress at bottom of the Slab (177-in. joint spacing and $\alpha(\Delta T/D)$ of 0 in.$^{-1}$)**

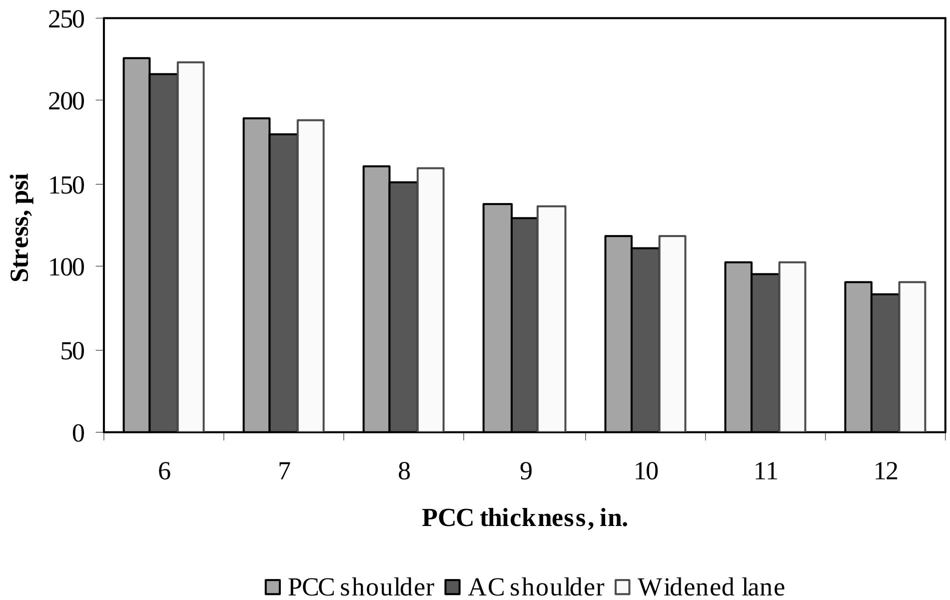


**Figure F-12-34: Impact of PCC thickness and lateral support condition on transverse stress at bottom of the Slab (315-in. joint spacing and $\alpha(\Delta T/D)$ of 0 in.$^{-1}$)**

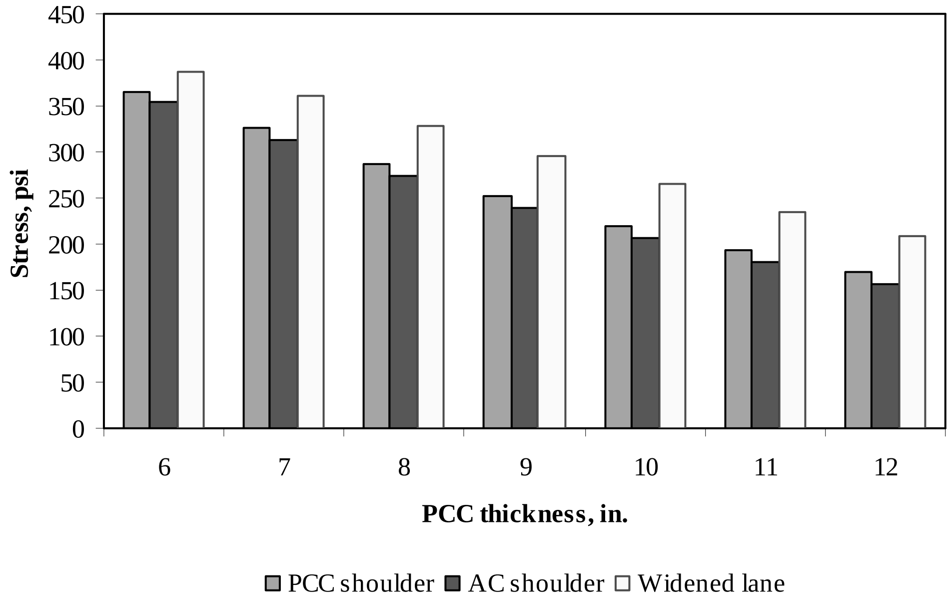


**Figure F-12-35: Impact of PCC thickness and lateral support condition on transverse stress at bottom of the Slab (177-in. joint spacing and $\alpha(\Delta T/D)$ of $20x10^{-6}$ in.$^{-1}$)**

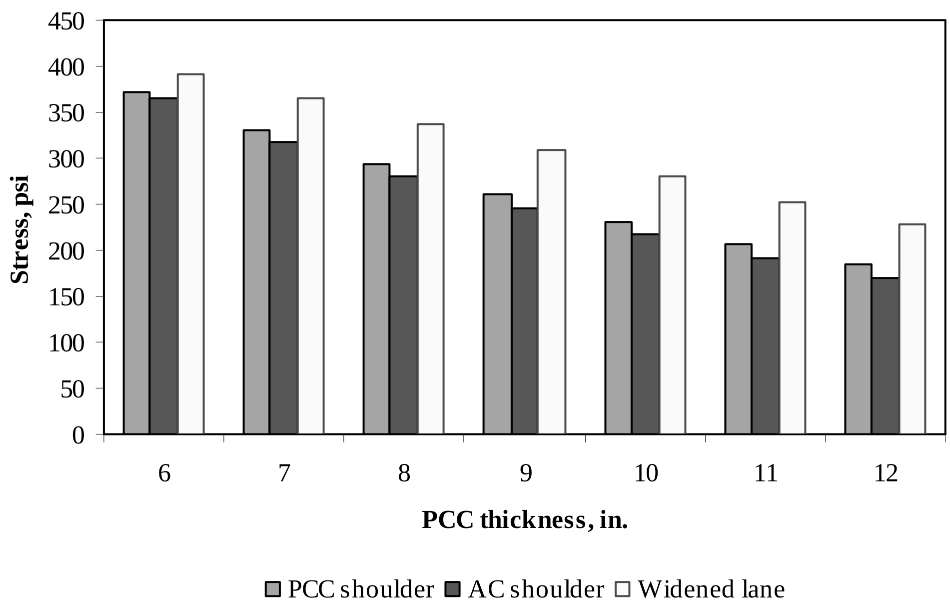


**Figure F-12-36: Impact of PCC thickness and lateral support condition on transverse stress at bottom of the Slab (315-in. joint spacing and $\alpha(\Delta T/D)$ of $20x10^{-6}$ in.$^{-1}$)**

Figures F-12-37 through F-12-42 illustrate the impact of base/subbase thickness and product α(ΔT/D) on stresses (10-in. PCC thickness, 100-psi/in. modulus of subgrade reaction and PCC shoulder)

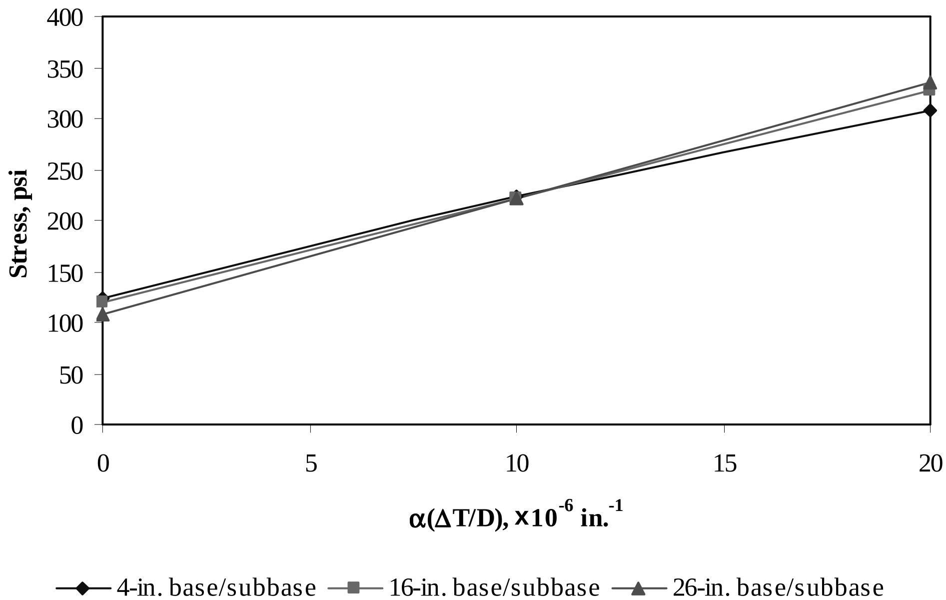


**Figure F-12-37: Impact of base/subbase thickness and product α(ΔT/D) on longitudinal stress at bottom of the slab (177-in. joint spacing)**

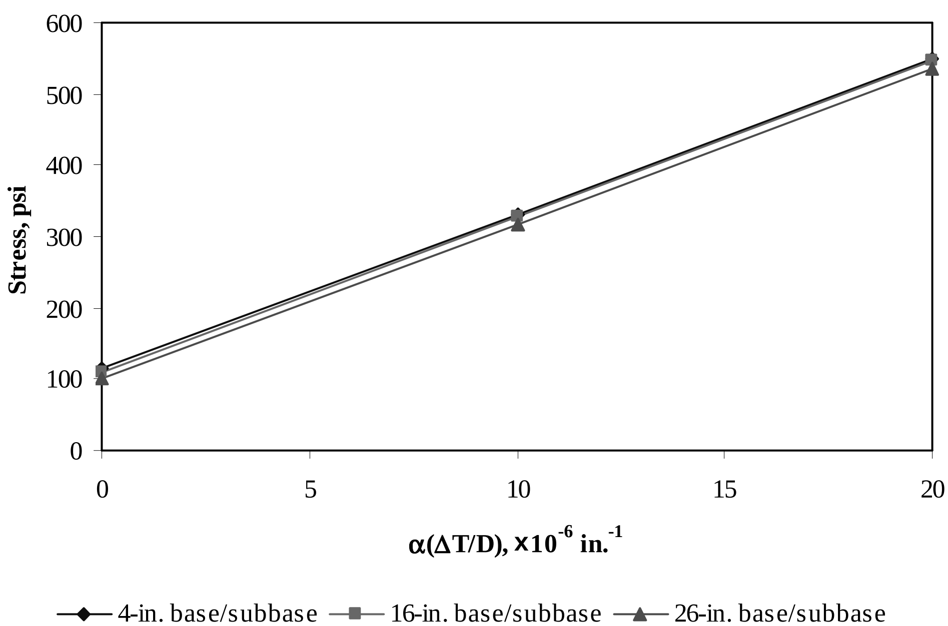


**Figure F-12-38: Impact of base/subbase thickness and product α(ΔT/D) on longitudinal stress at bottom of the slab (315-in. joint spacing)**

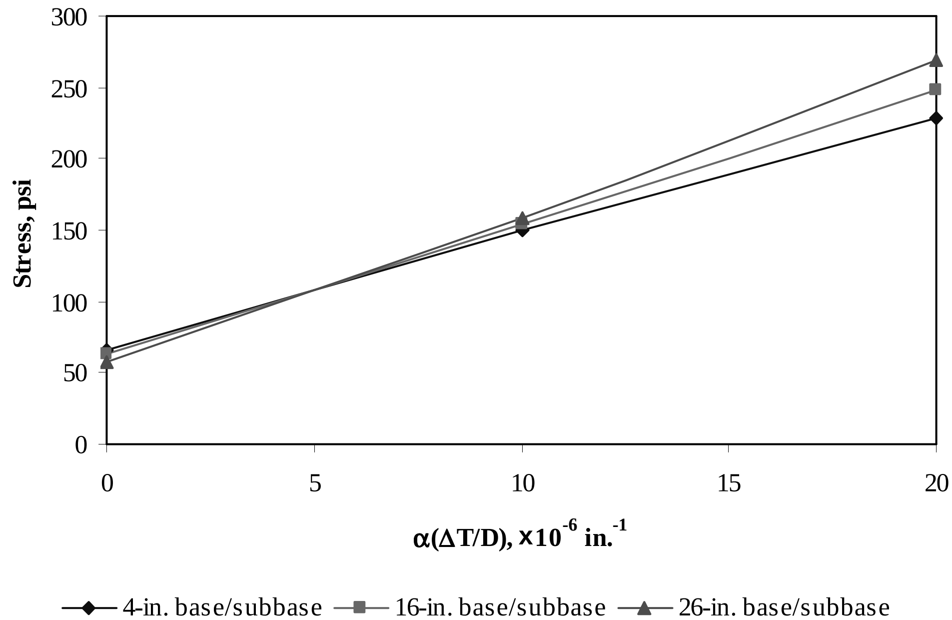


**Figure F-12-39: Impact of base/subbase thickness and product α(ΔT/D) on longitudinal stress at top of the slab (177-in. joint spacing)**

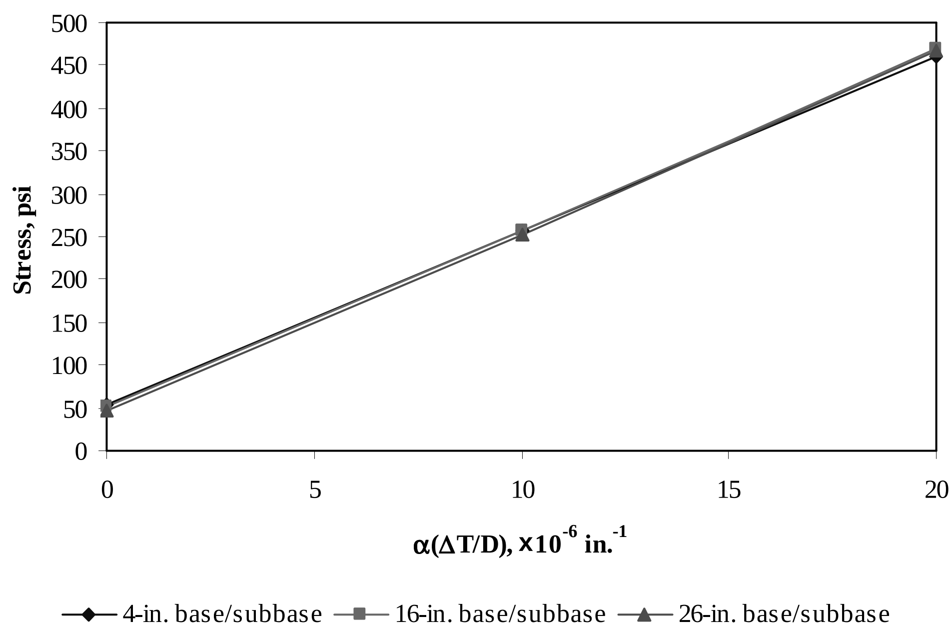


**Figure F-12-40: Impact of base/subbase thickness and product α(ΔT/D) on longitudinal stress at top of the slab (315-in. joint spacing)**

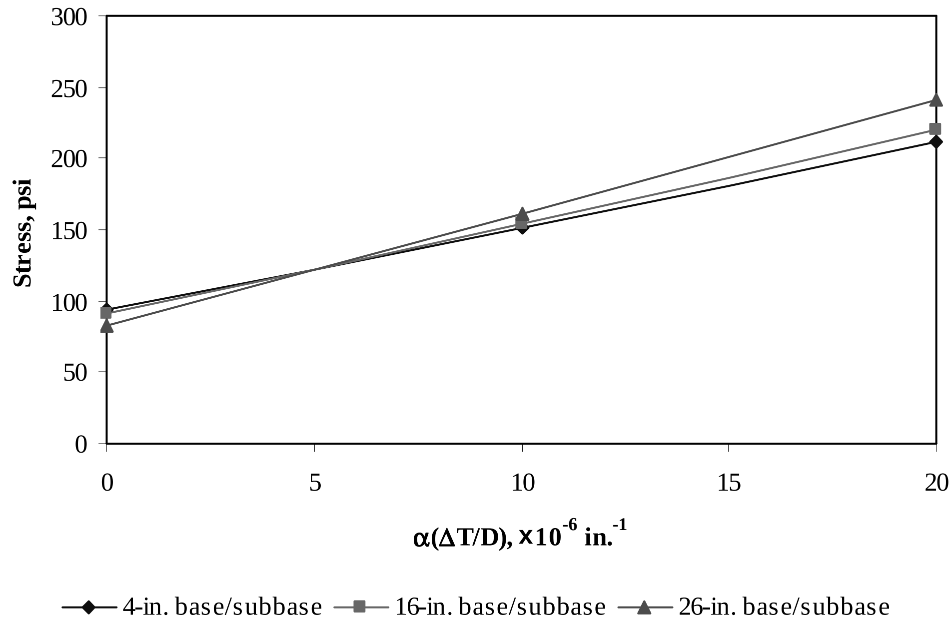


**Figure F-12-41: Impact of base/subbase thickness and product α(ΔT/D) on transverse stress at bottom of the slab (177-in. joint spacing)**

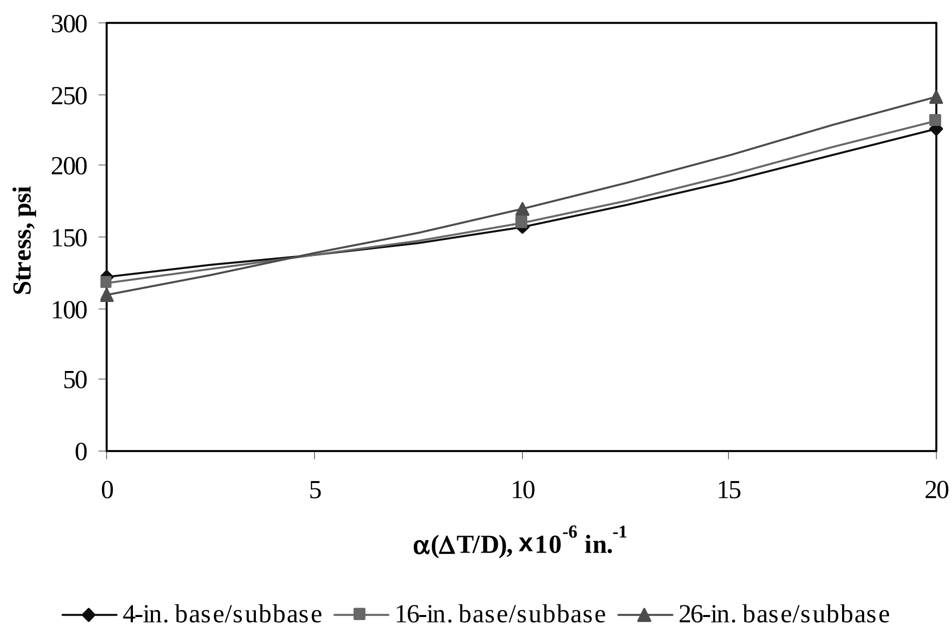


**Figure F-12-42: Impact of base/subbase thickness and product α(ΔT/D) on transverse stress at bottom of the slab (315-in. joint spacing)**

Figures F-12-43 through F-12-48 illustrate the impact of modulus of subgrade reaction and product α(ΔT/D) on stresses (10-in. PCC thickness, 16-in. base/subbase thickness and PCC shoulder)

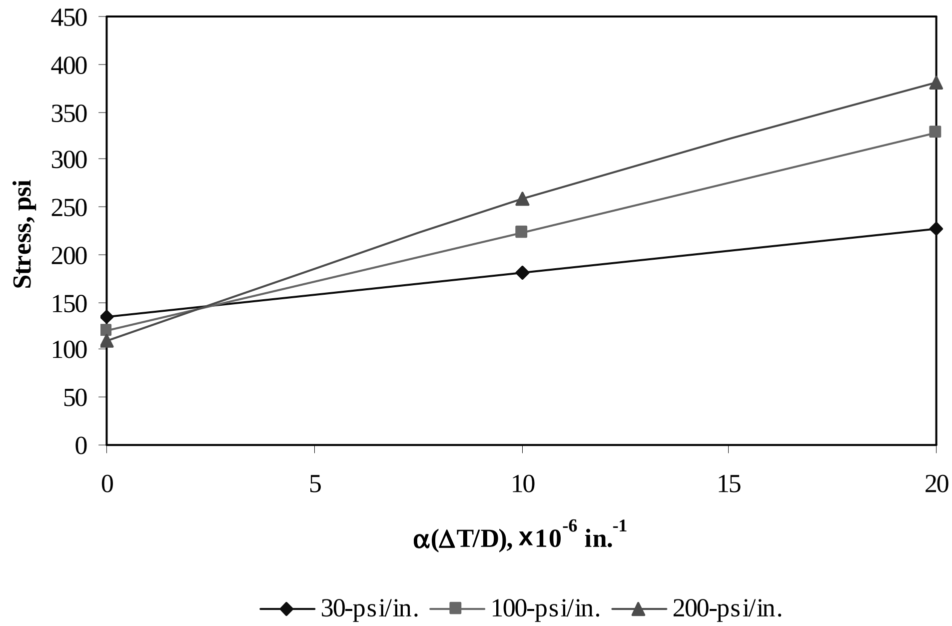


**Figure F-12-43: Impact of modulus of subgrade reaction and product α(ΔT/D) on longitudinal stress at bottom of the slab (177-in. joint spacing)**

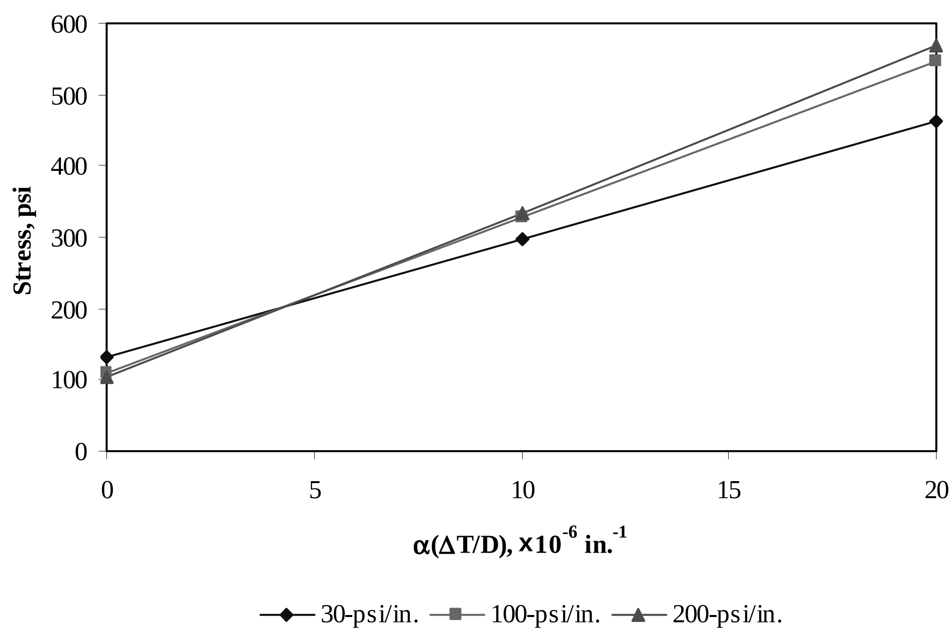


**Figure F-12-44: Impact of modulus of subgrade reaction and product α(ΔT/D) on longitudinal stress at bottom of the slab (315-in. joint spacing)**

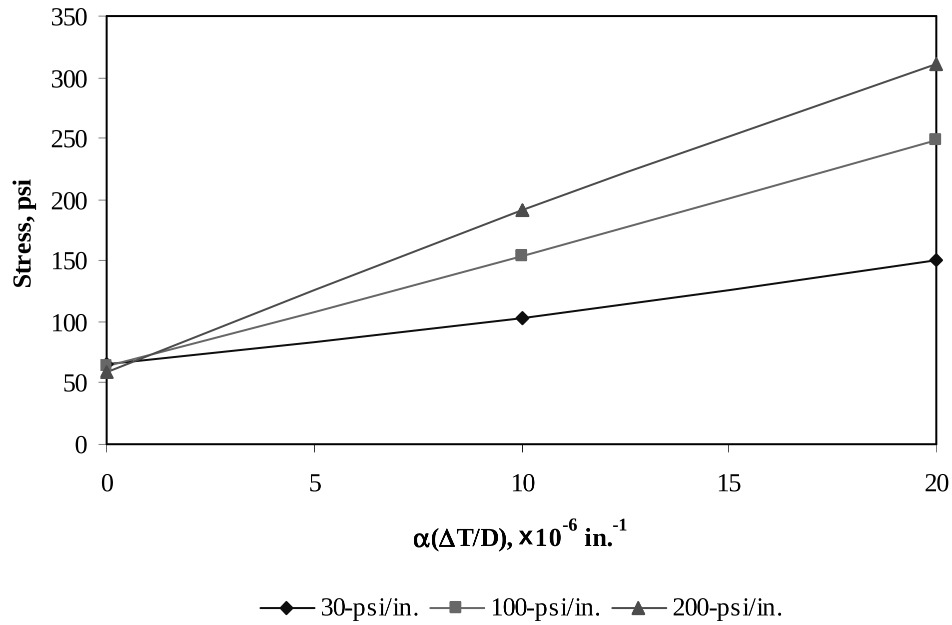


**Figure F-12-45: Impact of modulus of subgrade reaction and product α(ΔT/D) on longitudinal stress at top of the slab (177-in. joint spacing)**

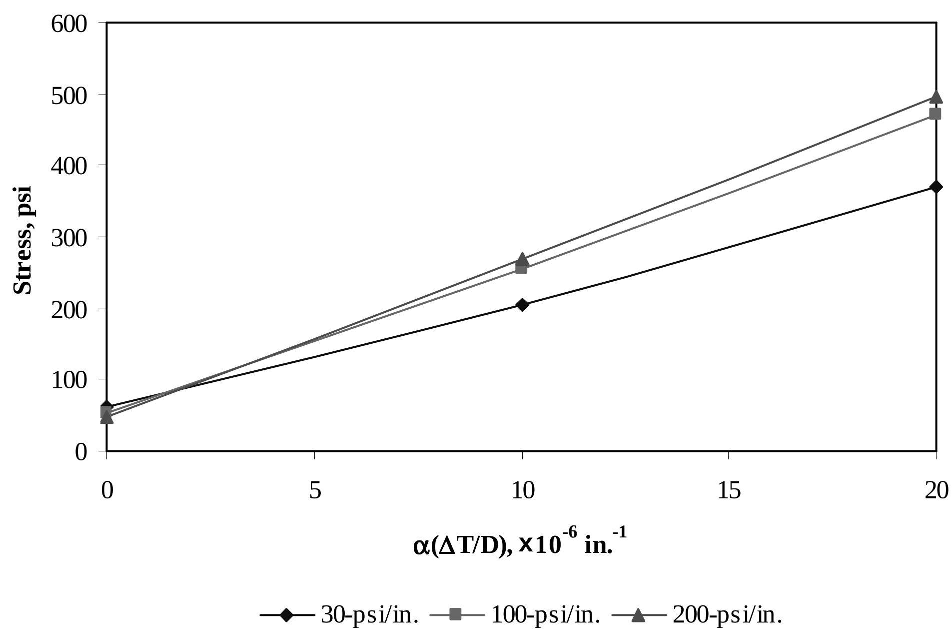


**Figure F-12-46: Impact of modulus of subgrade reaction and product α(ΔT/D) on longitudinal stress at top of the slab (315-in. joint spacing)**

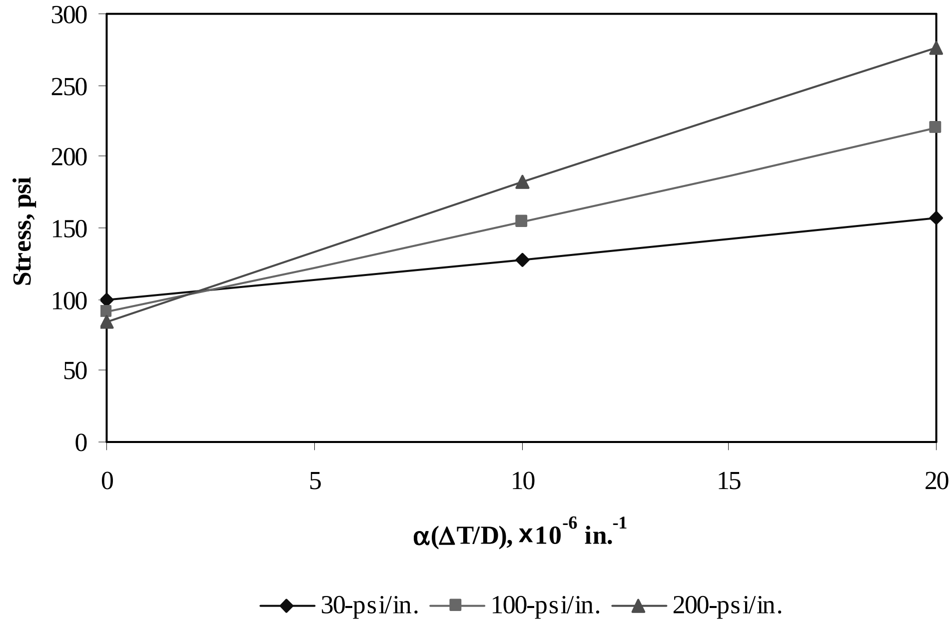


**Figure F-12-47: Impact of modulus of subgrade reaction and product α(ΔT/D) on transverse stress at bottom of the slab (177-in. joint spacing)**

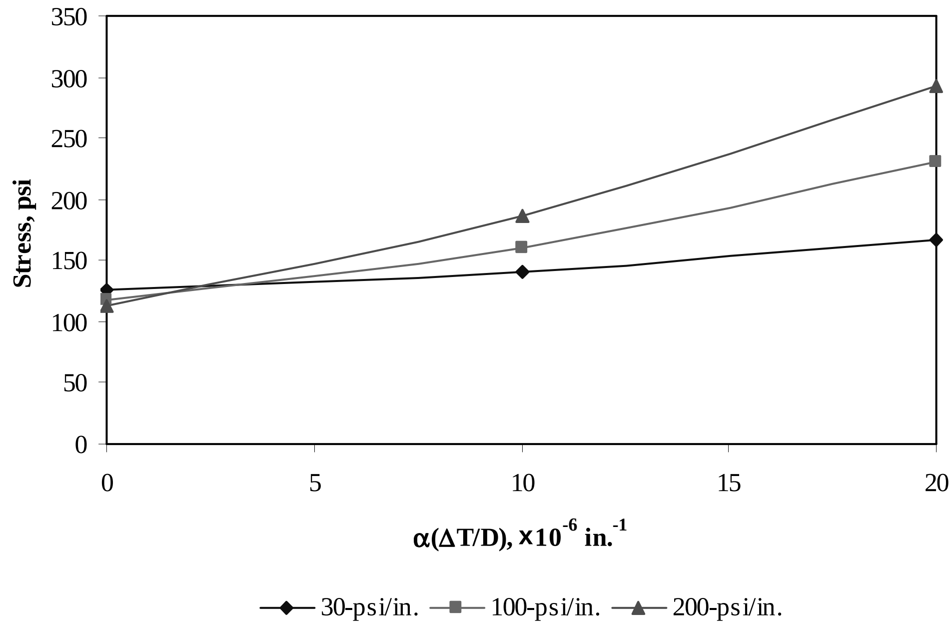


**Figure F-12-48: Impact of modulus of subgrade reaction and product α(ΔT/D) on transverse stress at bottom of the slab (315-in. joint spacing)**

Figures F-12-49 through F-12-51 illustrate the impact of joint spacing and product α(ΔT/D) on stresses (10-in. PCC thickness, 16-in. base/subbase thickness, 100-psi/in. modulus of subgrade reaction and PCC shoulder)

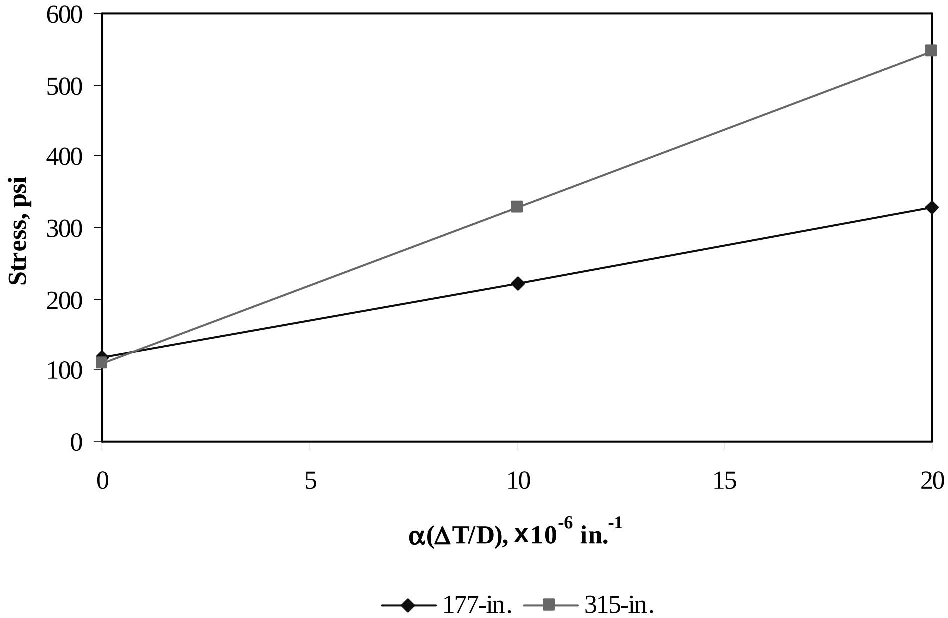


**Figure F-12-49: Impact of joint spacing and product α(ΔT/D) on longitudinal stress at bottom of the slab**

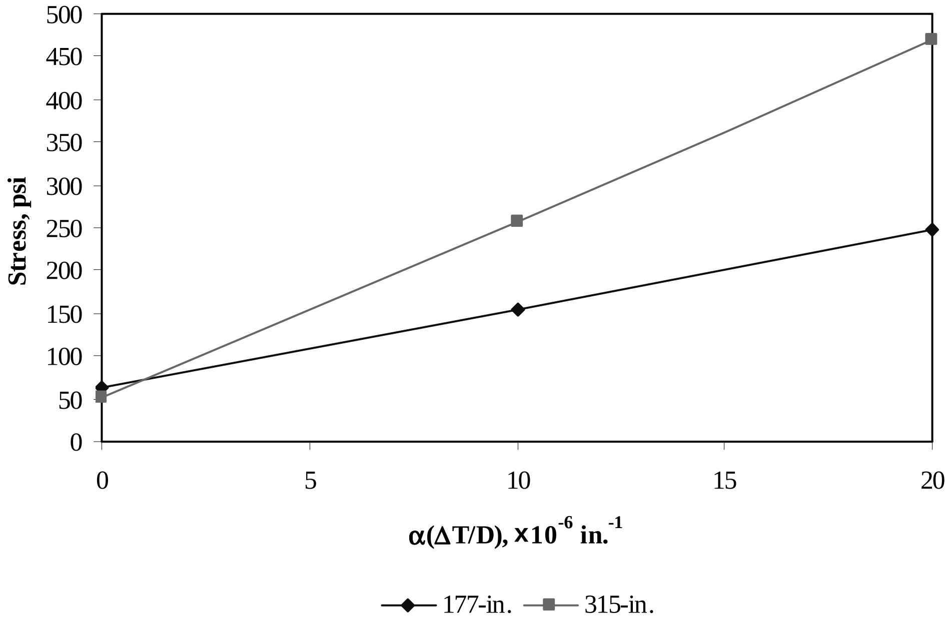


**Figure F-12-50: Impact of joint spacing and product α(ΔT/D) on longitudinal stress at top of the slab**

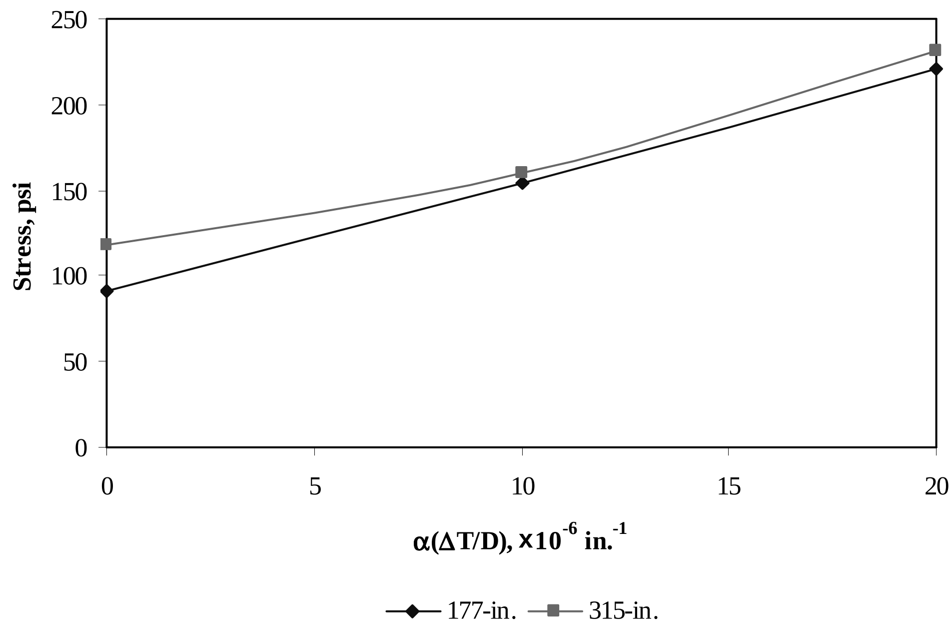


**Figure F-12-51: Impact of joint spacing and product α(ΔT/D) on transverse stress at bottom of the slab**

**Sub Appendix F-13**

**Documentation of Pavement Responses for**

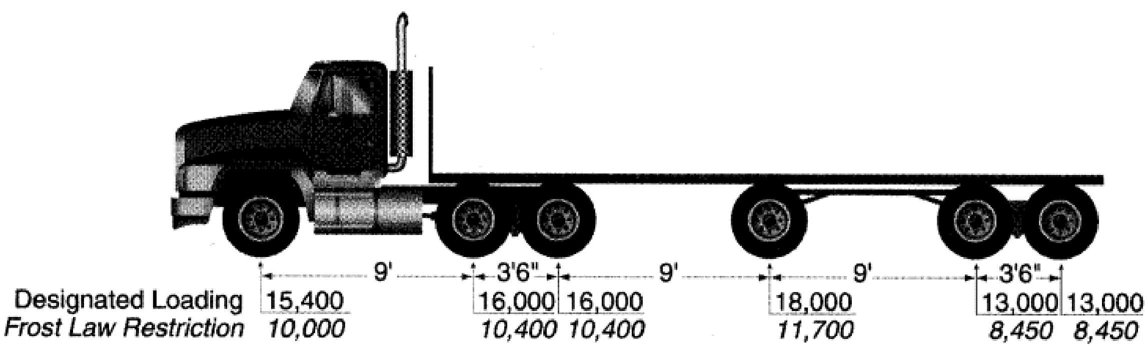


**MI-11**

Figures F-13-1 through F-13-12 illustrate the impact of PCC thickness and base/subbase thickness on stresses (100-psi/in. modulus of subgrade reaction and PCC shoulder)

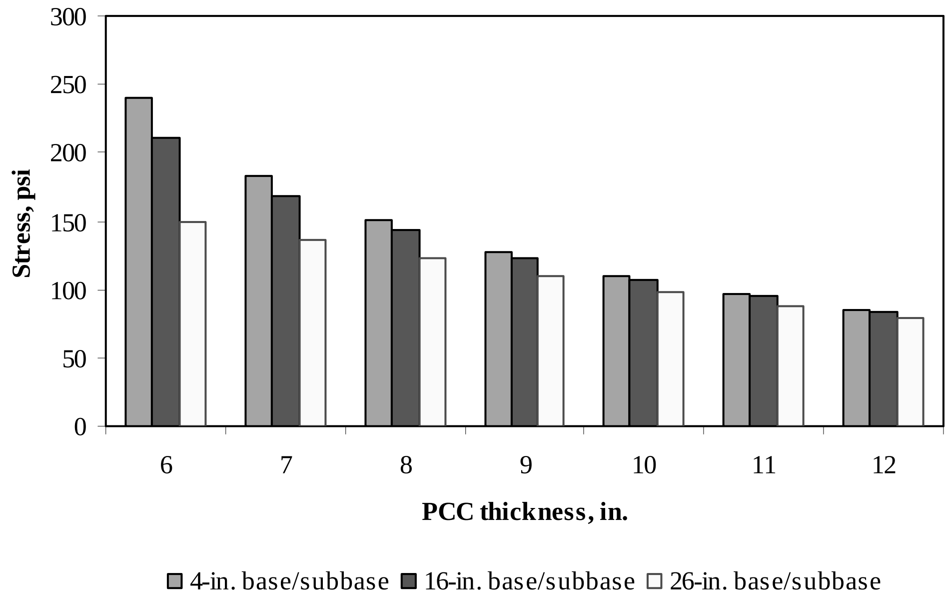


**Figure F-13-1: Impact of PCC thickness and base/subbase thickness on longitudinal stress at bottom of the Slab (177-in. joint spacing and $\alpha(\Delta T/D)$ of 0 in.$^{-1}$)**

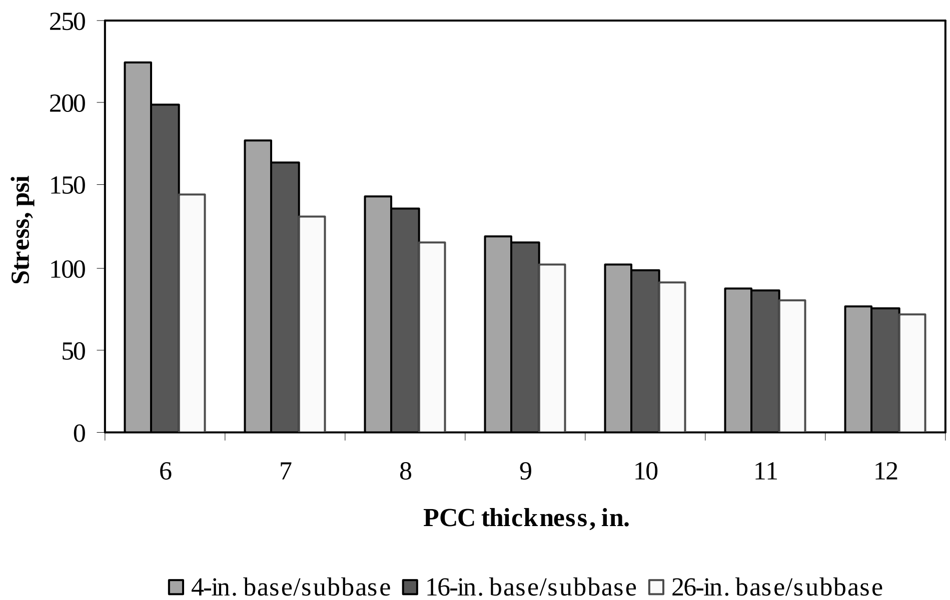


**Figure F-13-2: Impact of PCC thickness and base/subbase thickness on longitudinal stress at bottom of the Slab (315-in. joint spacing and $\alpha(\Delta T/D)$ of 0 in.$^{-1}$)**

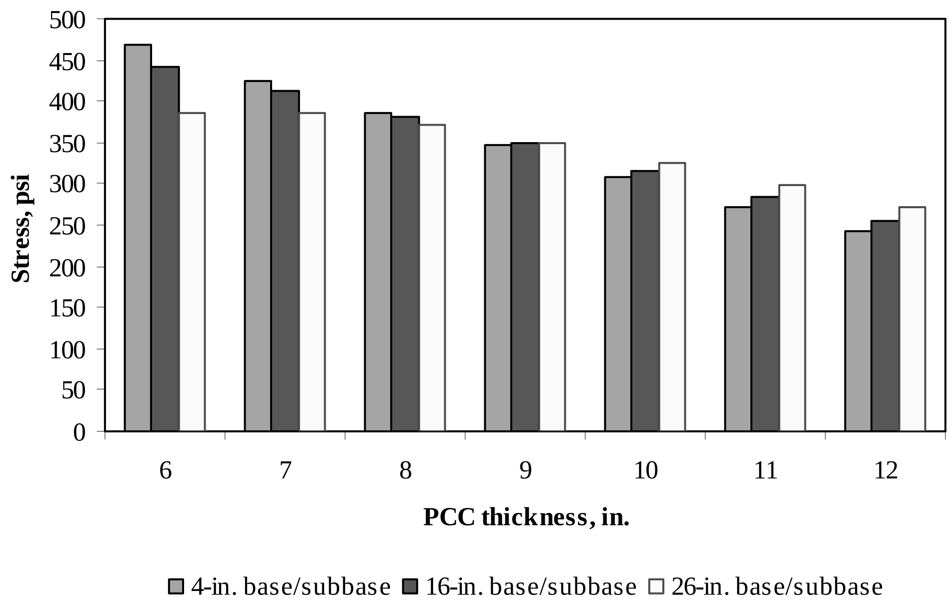


**Figure F-13-3: Impact of PCC thickness and base/subbase thickness on longitudinal stress at bottom of the Slab (177-in. joint spacing and $\alpha(\Delta T/D)$ of $20x10^{-6}$ in.$^{-1}$)**

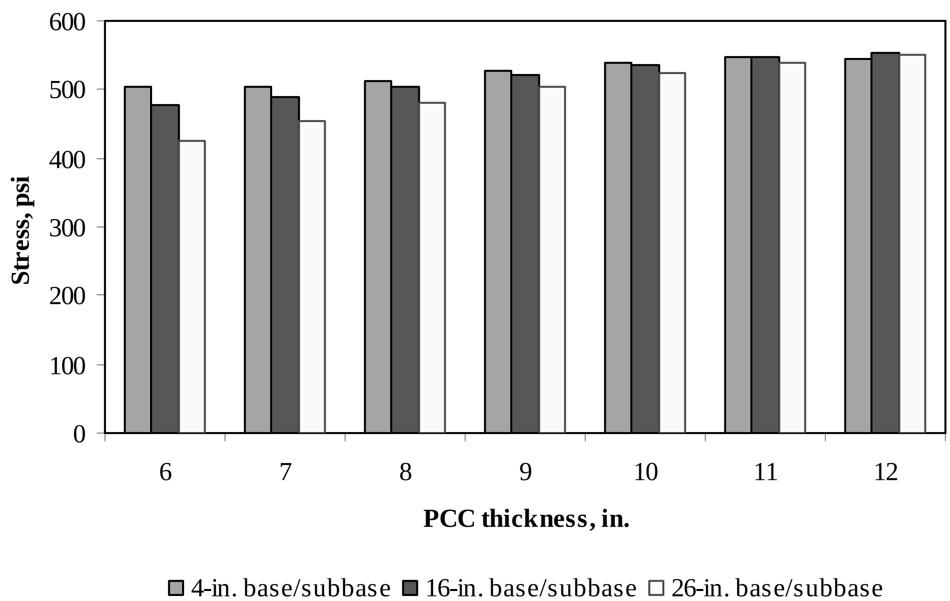


**Figure F-13-4: Impact of PCC thickness and base/subbase thickness on longitudinal stress at bottom of the Slab (315-in. joint spacing and $\alpha(\Delta T/D)$ of $20x10^{-6}$ in.$^{-1}$)**

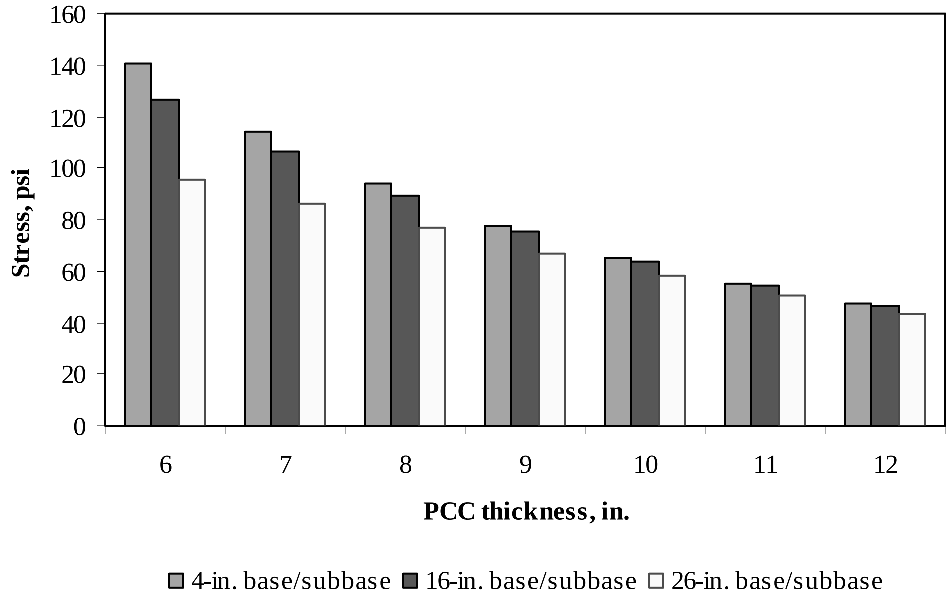


**Figure F-13-5: Impact of PCC thickness and base/subbase thickness on longitudinal stress at top of the Slab (177-in. joint spacing and $\alpha(\Delta T/D)$ of 0 $in.^{-1}$)**

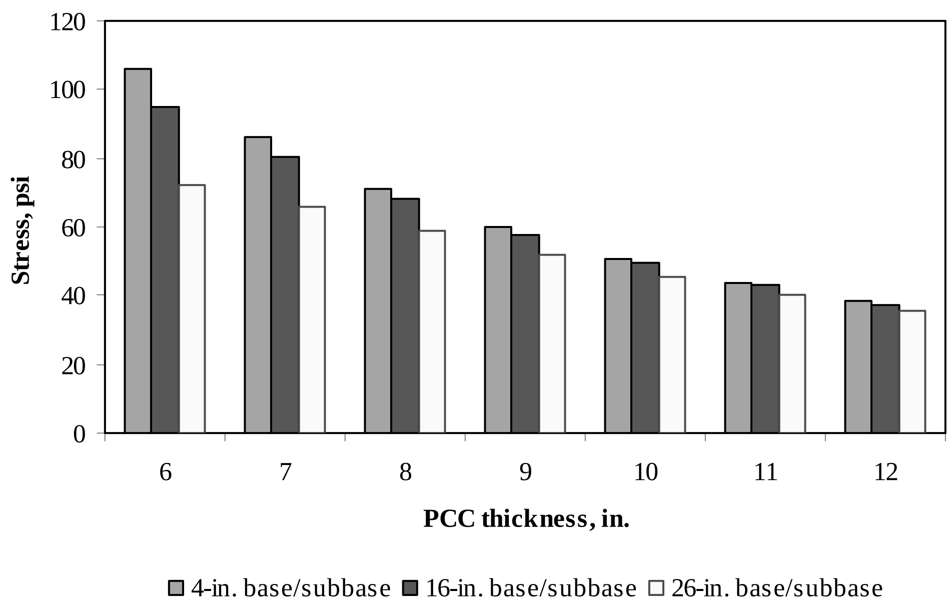


**Figure F-13-6: Impact of PCC thickness and base/subbase thickness on longitudinal stress at top of the Slab (315-in. joint spacing and $\alpha(\Delta T/D)$ of 0 $in.^{-1}$)**

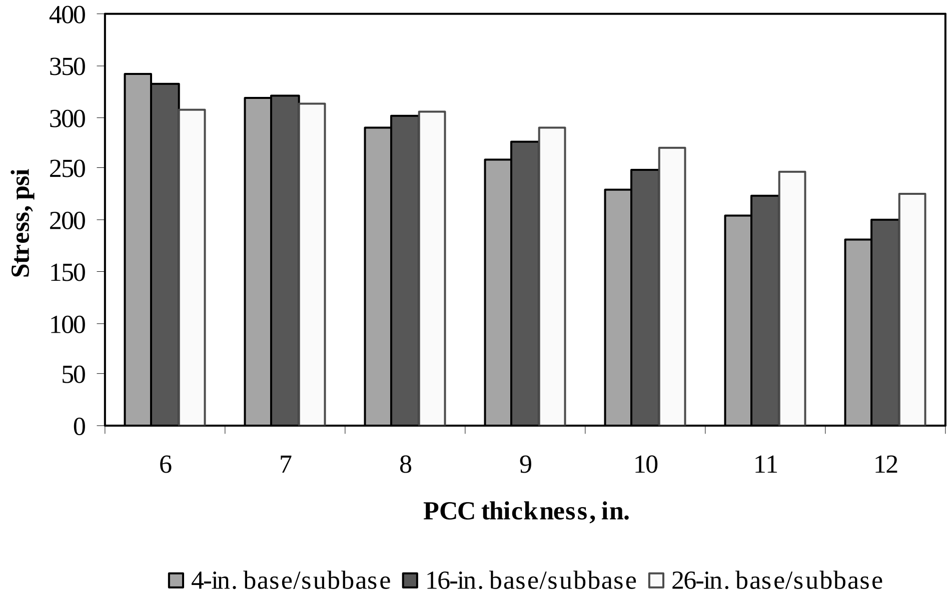


**Figure F-13-7: Impact of PCC thickness and base/subbase thickness on longitudinal stress at top of the Slab (177-in. joint spacing and $\alpha(\Delta T/D)$ of $-20 \times 10^{-6}$ in.$^{-1}$)**

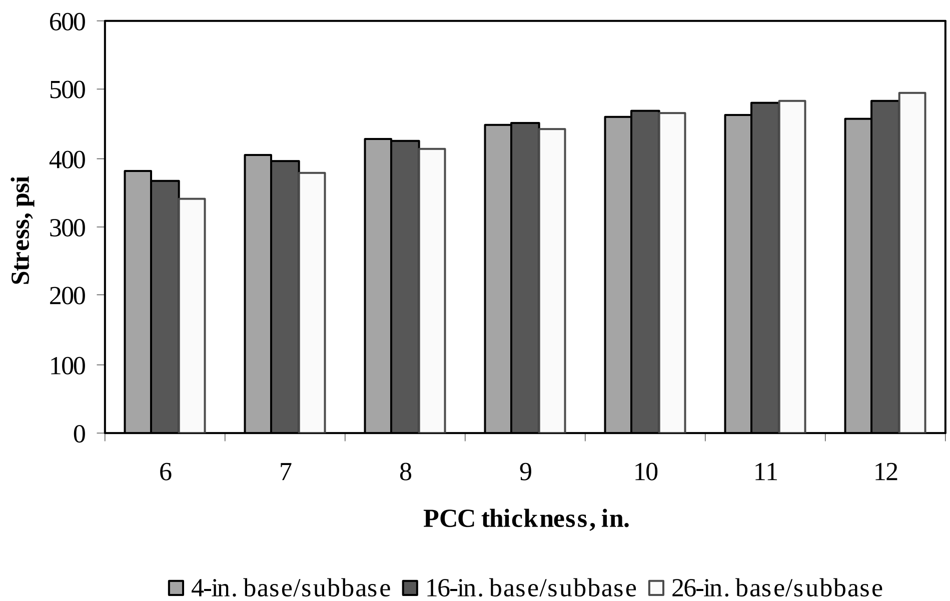


**Figure F-13-8: Impact of PCC thickness and base/subbase thickness on longitudinal stress at top of the Slab (315-in. joint spacing and $\alpha(\Delta T/D)$ of $-20 \times 10^{-6}$ in.$^{-1}$)**

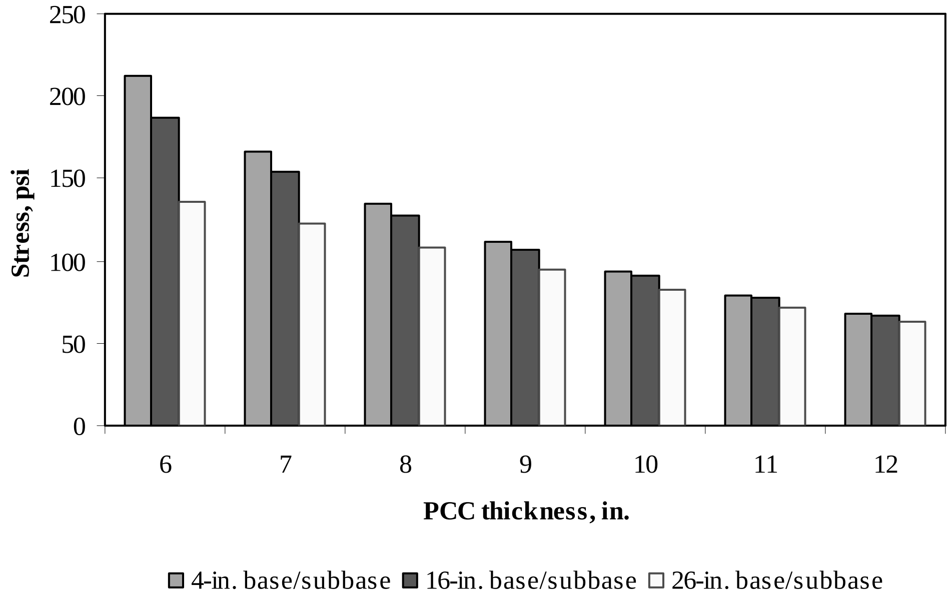


**Figure F-13-9: Impact of PCC thickness and base/subbase thickness on transverse stress at bottom of the Slab (177-in. joint spacing and $\alpha(\Delta T/D)$ of 0 in.$^{-1}$)**

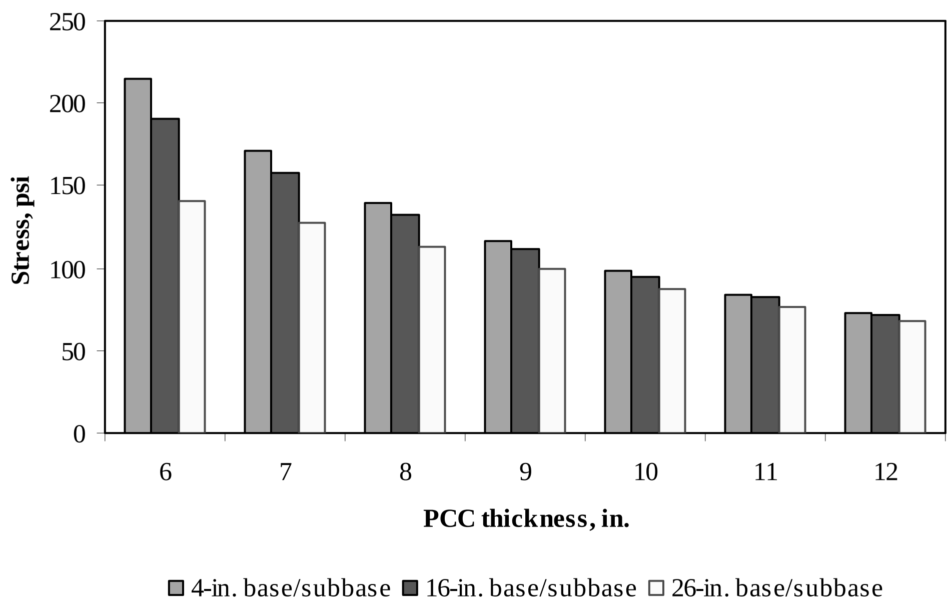


**Figure F-13-10: Impact of PCC thickness and base/subbase thickness on transverse stress at bottom of the Slab (315-in. joint spacing and $\alpha(\Delta T/D)$ of 0 in.$^{-1}$)**

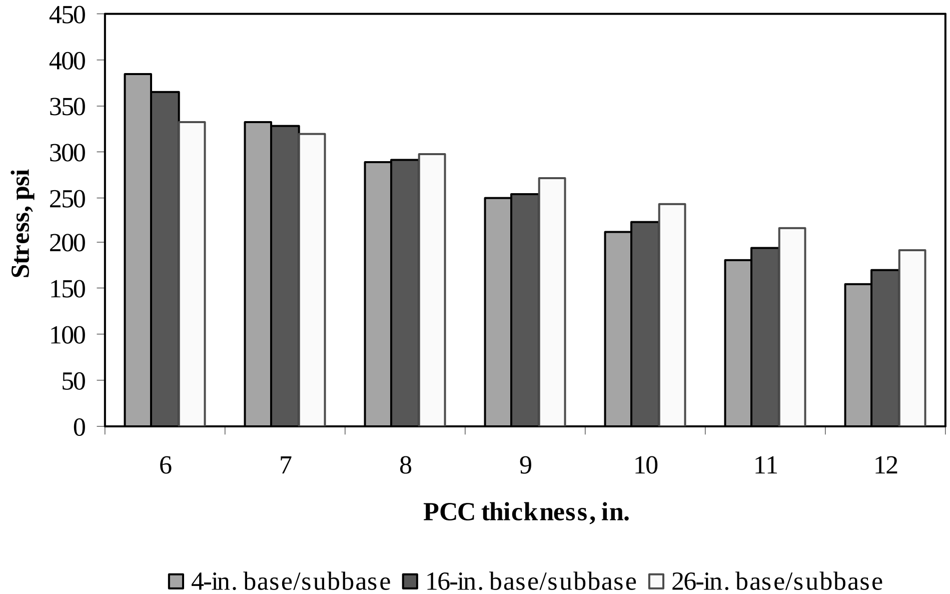


**Figure F-13-11: Impact of PCC thickness and base/subbase thickness on transverse stress at bottom of the Slab (177-in. joint spacing and $\alpha(\Delta T/D)$ of $20x10^{-6}$ in.$^{-1}$)**

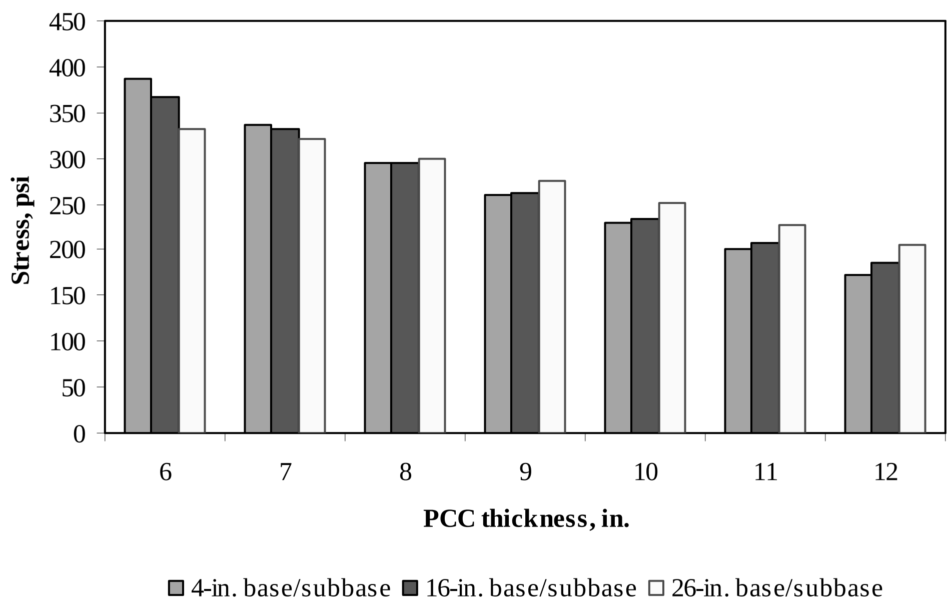


**Figure F-13-12: Impact of PCC thickness and base/subbase thickness on transverse stress at bottom of the Slab (315-in. joint spacing and $\alpha(\Delta T/D)$ of $20x10^{-6}$ in.$^{-1}$)**

Figures F-13-13 through F-13-24 illustrate the impact of PCC thickness and modulus of subgrade reaction on stresses (16-in. base/subbase thickness and PCC shoulder)

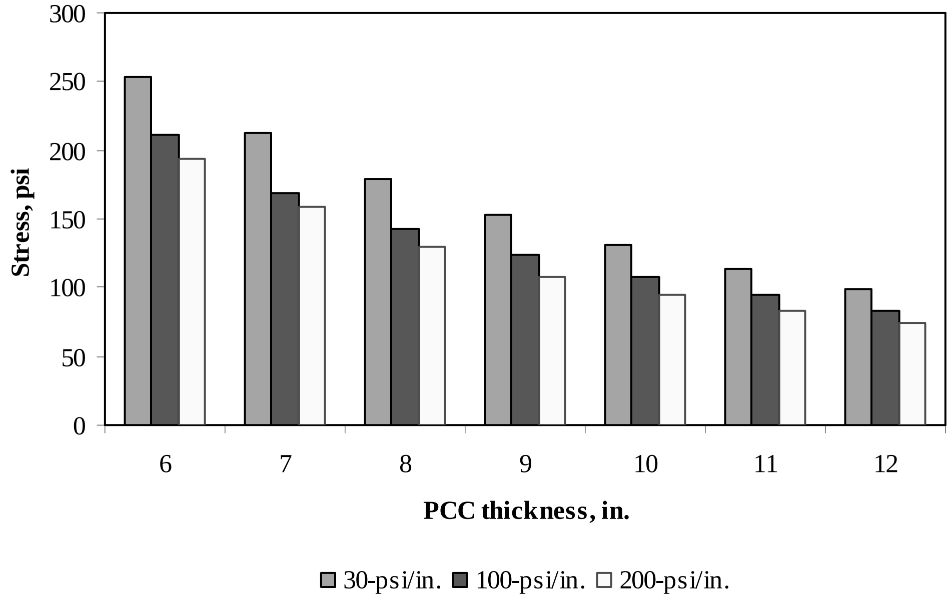


**Figure F-13-13: Impact of PCC thickness and modulus of subgrade reaction on longitudinal stress at bottom of the slab (177-in. joint spacing and $\alpha(\Delta T/D)$ of 0 in.$^{-1}$)**

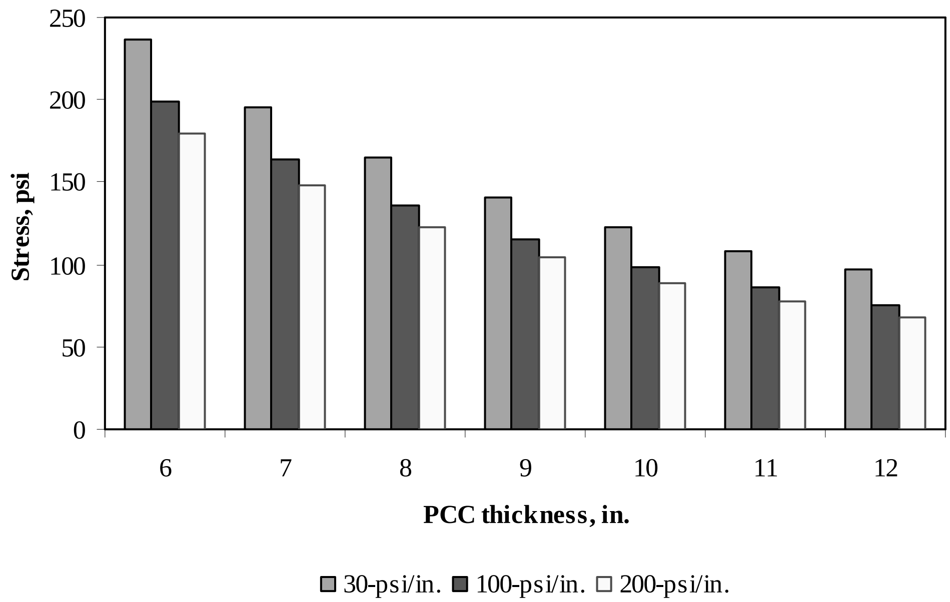


**Figure F-13-14: Impact of PCC thickness and modulus of subgrade reaction on longitudinal stress at bottom of the slab (315-in. joint spacing and $\alpha(\Delta T/D)$ of 0 in.$^{-1}$)**

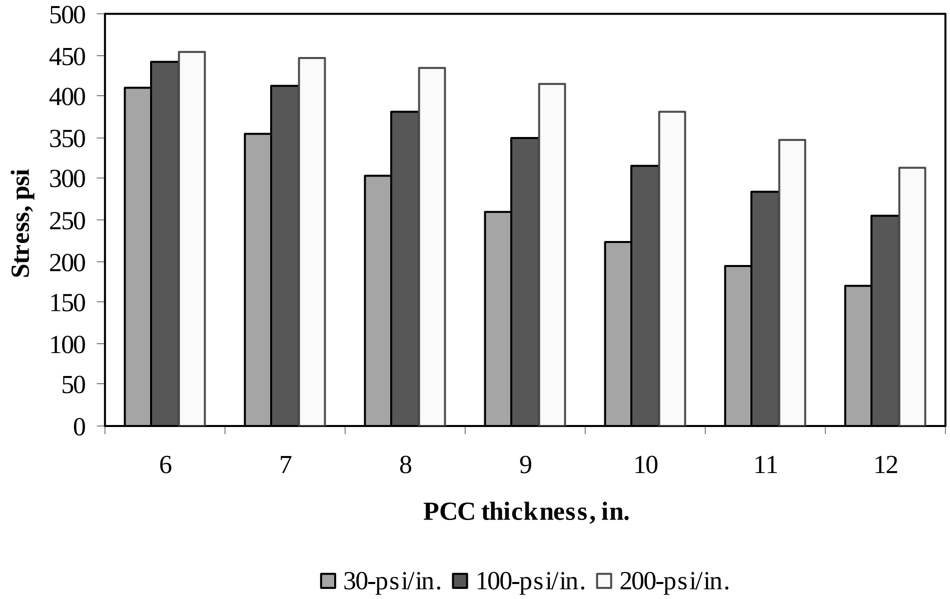


**Figure F-13-15: Impact of PCC thickness and modulus of subgrade reaction on longitudinal stress at bottom of the slab (177-in. joint spacing and $\alpha(\Delta T/D)$ of $20x10^{-6}$ in.$^{-1}$)**

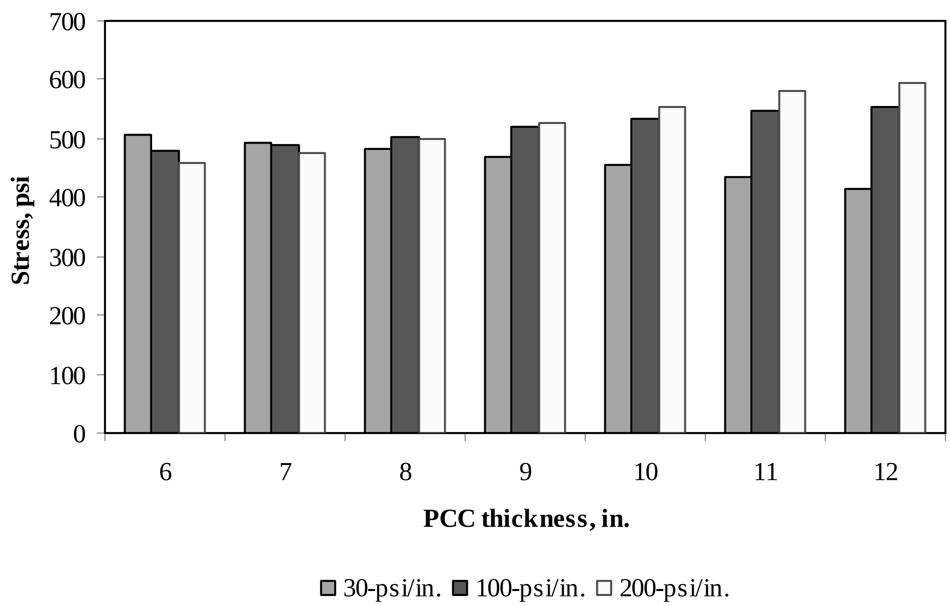


**Figure F-13-16: Impact of PCC thickness and modulus of subgrade reaction on longitudinal stress at bottom of the slab (315-in. joint spacing and $\alpha(\Delta T/D)$ of $20x10^{-6}$ in.$^{-1}$)**

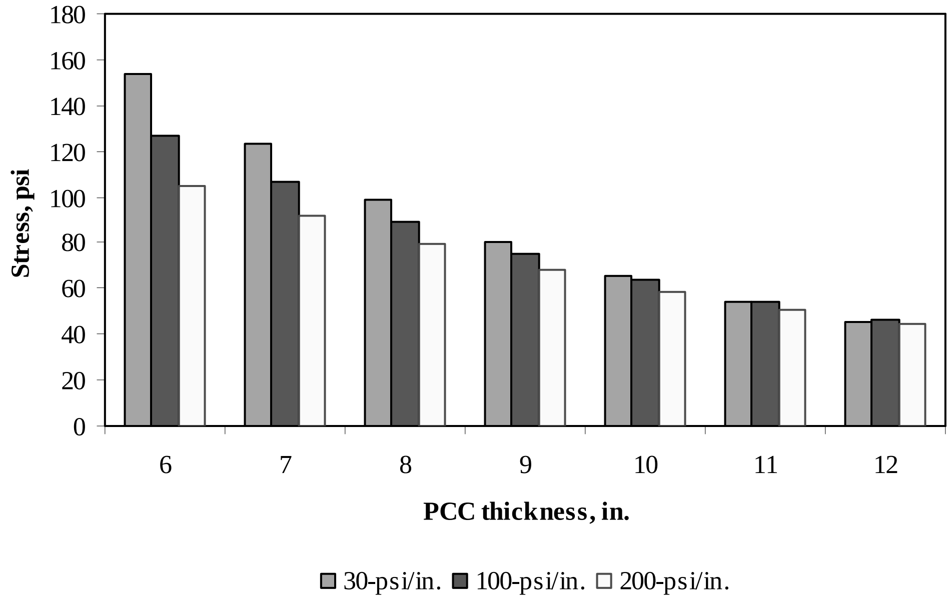


**Figure F-13-17: Impact of PCC thickness and modulus of subgrade reaction on longitudinal stress at top of the Slab (177-in. joint spacing and $\alpha(\Delta T/D)$ of 0 in.$^{-1}$)**

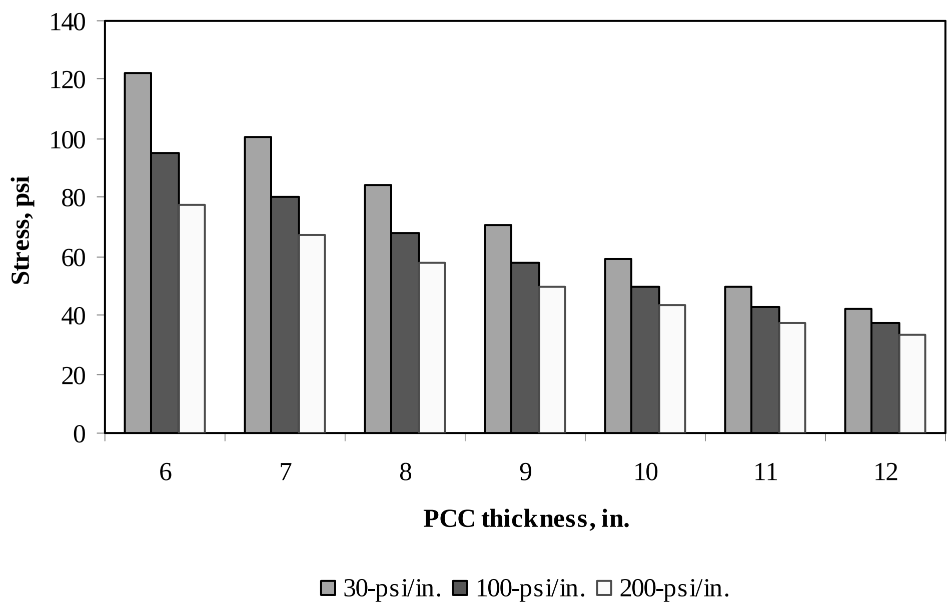


**Figure F-13-18: Impact of PCC thickness and modulus of subgrade reaction on longitudinal stress at top of the Slab (315-in. joint spacing and $\alpha(\Delta T/D)$ of 0 in.$^{-1}$)**

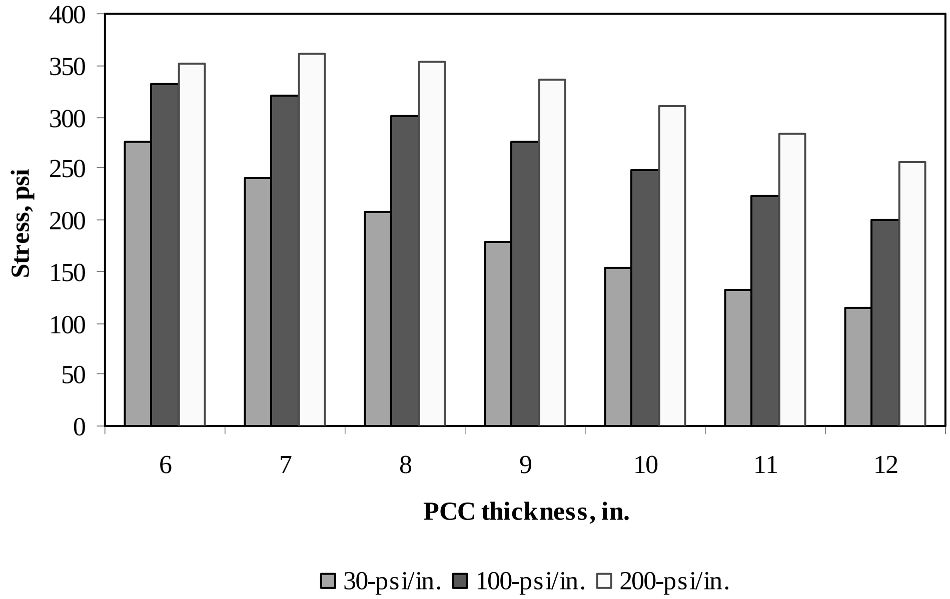


**Figure F-13-19: Impact of PCC thickness and modulus of subgrade reaction on longitudinal stress at top of the Slab (177-in. joint spacing and $\alpha(\Delta T/D)$ of $-20x10^{-6}$ in.$^{-1}$)**

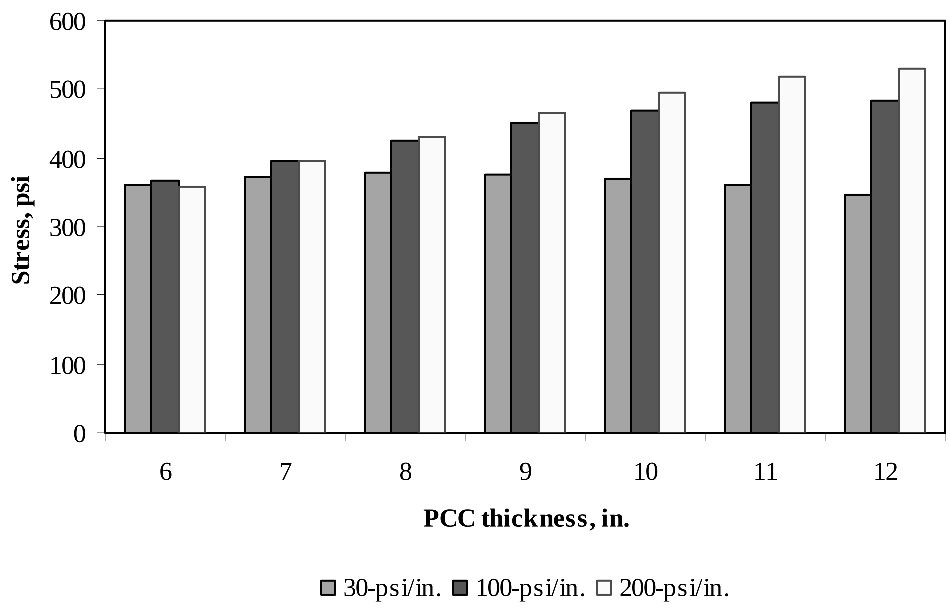


**Figure F-13-20: Impact of PCC thickness and modulus of subgrade reaction on longitudinal stress at top of the Slab (315-in. joint spacing and $\alpha(\Delta T/D)$ of $-20x10^{-6}$ in.$^{-1}$)**

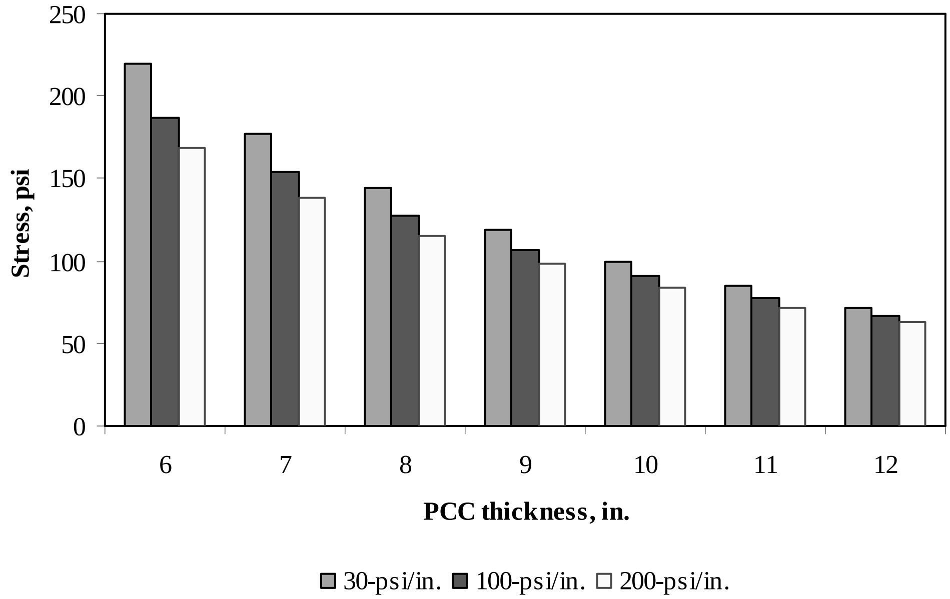


**Figure F-13-21: Impact of PCC thickness and modulus of subgrade reaction on transverse stress at bottom of the Slab (177-in. joint spacing and $\alpha(\Delta T/D)$ of 0 in.$^{-1}$)**

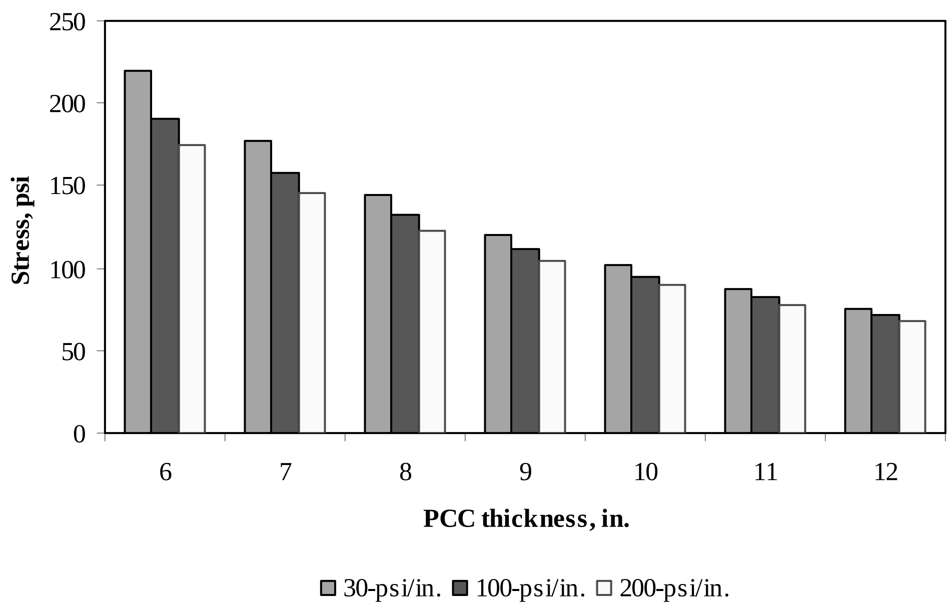


**Figure F-13-22: Impact of PCC thickness and modulus of subgrade reaction on transverse stress at bottom of the Slab (315-in. joint spacing and $\alpha(\Delta T/D)$ of 0 in.$^{-1}$)**

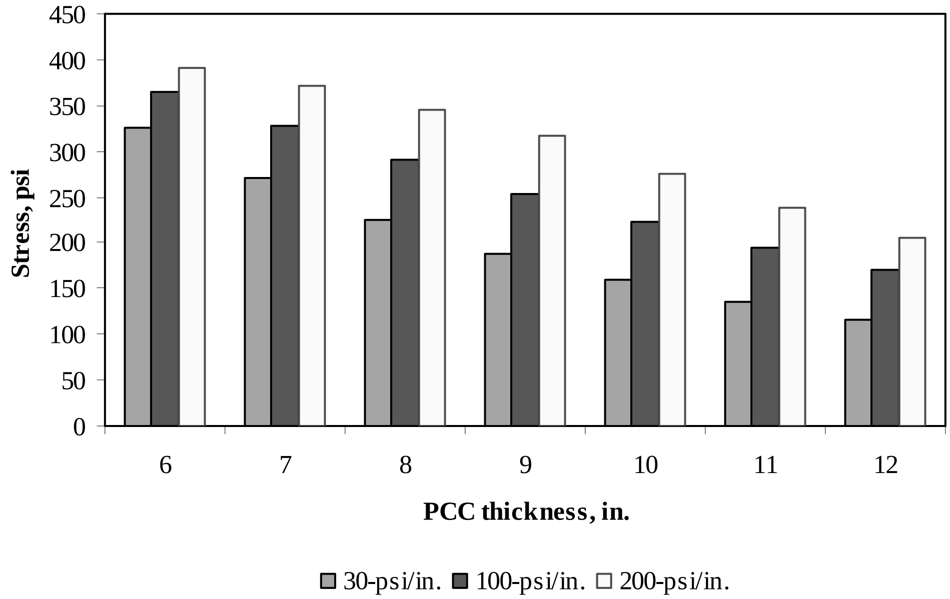


**Figure F-13-23: Impact of PCC thickness and modulus of subgrade reaction on transverse stress at bottom of the Slab (177-in. joint spacing and $\alpha(\Delta T/D)$ of $20x10^{-6}$ $in.^{-1}$)**

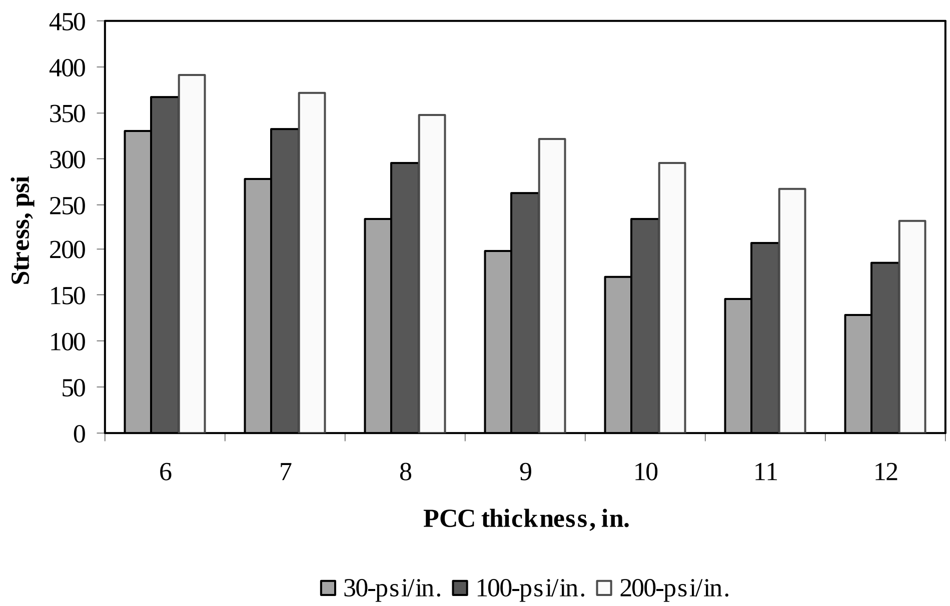


**Figure F-13-24: Impact of PCC thickness and modulus of subgrade reaction on transverse stress at bottom of the Slab (315-in. joint spacing and $\alpha(\Delta T/D)$ of $20x10^{-6}$ $in.^{-1}$)**

Figures F-13-25 through F-13-36 illustrate the impact of PCC thickness and lateral support condition on stresses (16-in. base/subbase and 100-psi/in. modulus of subgrade reaction)

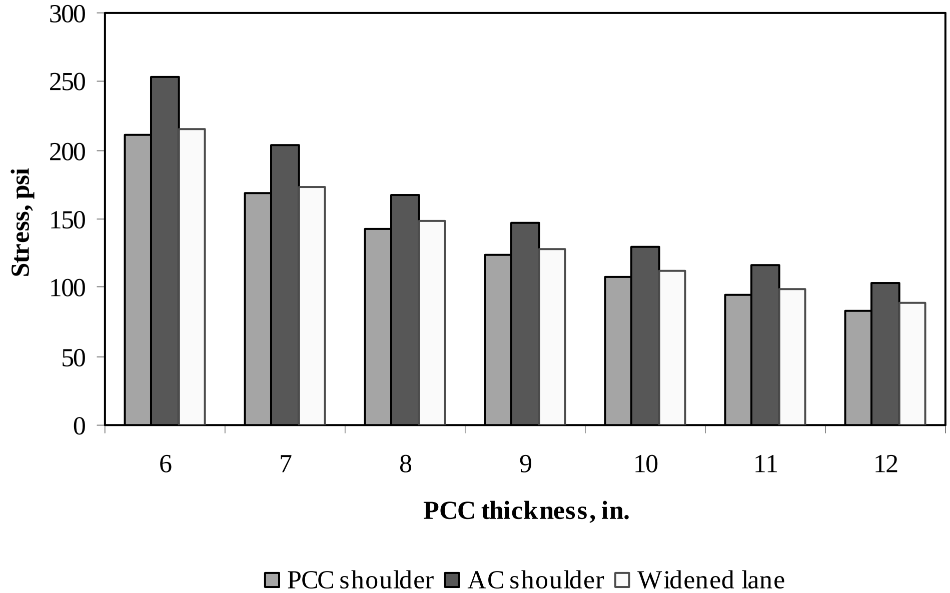


**Figure F-13-25: Impact of PCC thickness and lateral support condition on longitudinal stress at bottom of the Slab (177-in. joint spacing and α(ΔT/D) of 0 in.$^{-1}$)**

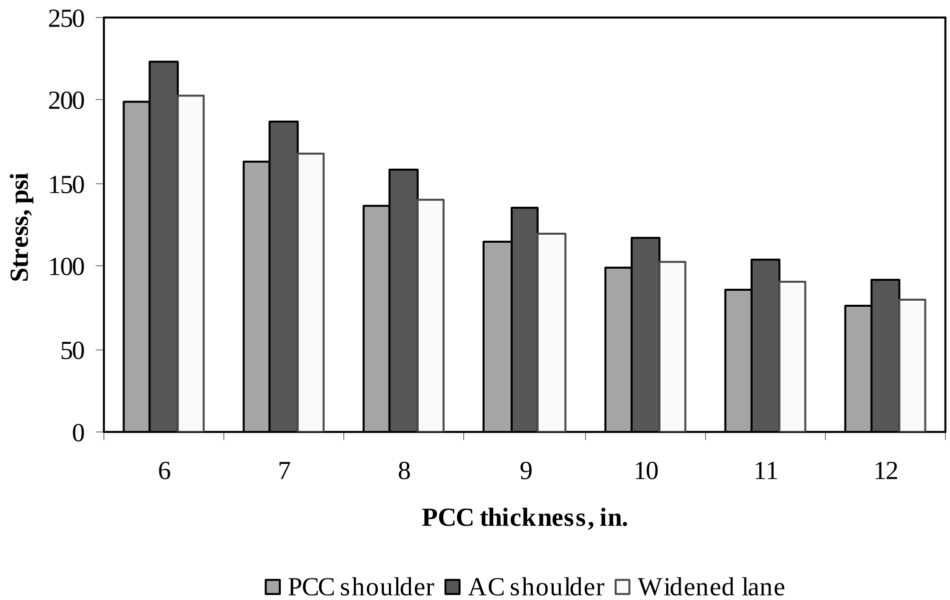


**Figure F-13-26: Impact of PCC thickness and lateral support condition on longitudinal stress at bottom of the Slab (315-in. joint spacing and α(ΔT/D) of 0 in.$^{-1}$)**

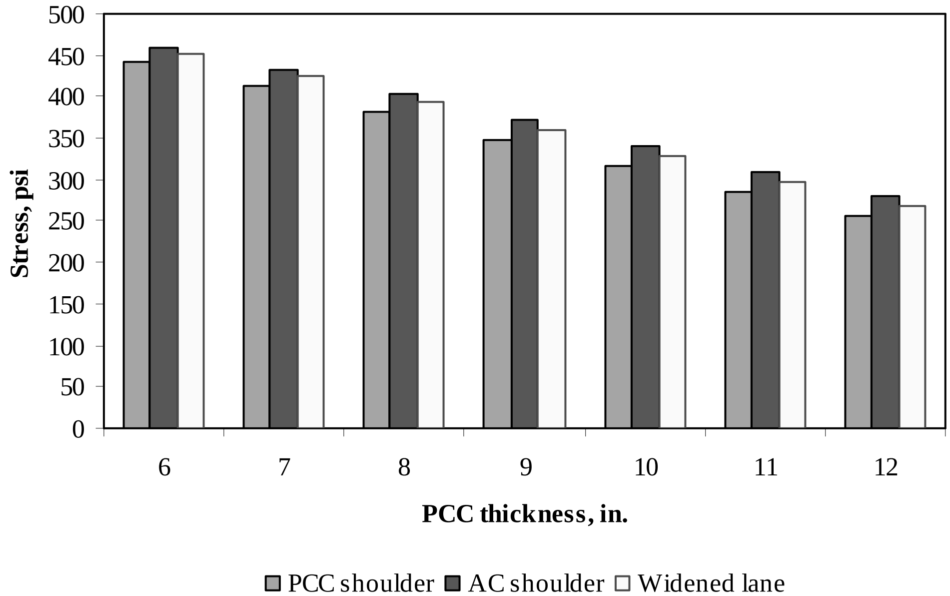


**Figure F-13-27: Impact of PCC thickness and lateral support condition on longitudinal stress at bottom of the Slab (177-in. joint spacing and $\alpha(\Delta T/D)$ of $20\text{x}10^{-6}$ in.$^{-1}$)**

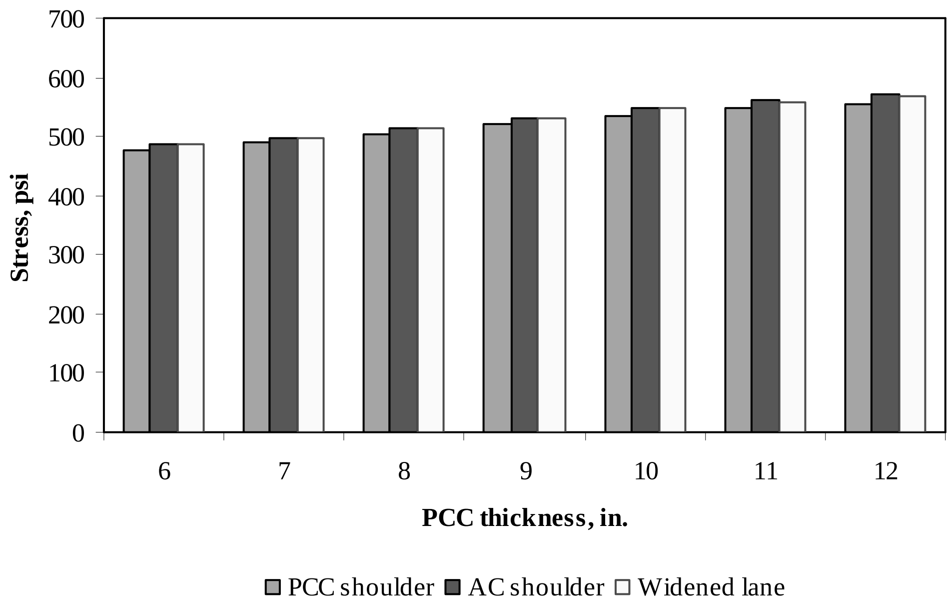


**Figure F-13-28: Impact of PCC thickness and lateral support condition on longitudinal stress at bottom of the Slab (315-in. joint spacing and $\alpha(\Delta T/D)$ of $20\text{x}10^{-6}$ in.$^{-1}$)**

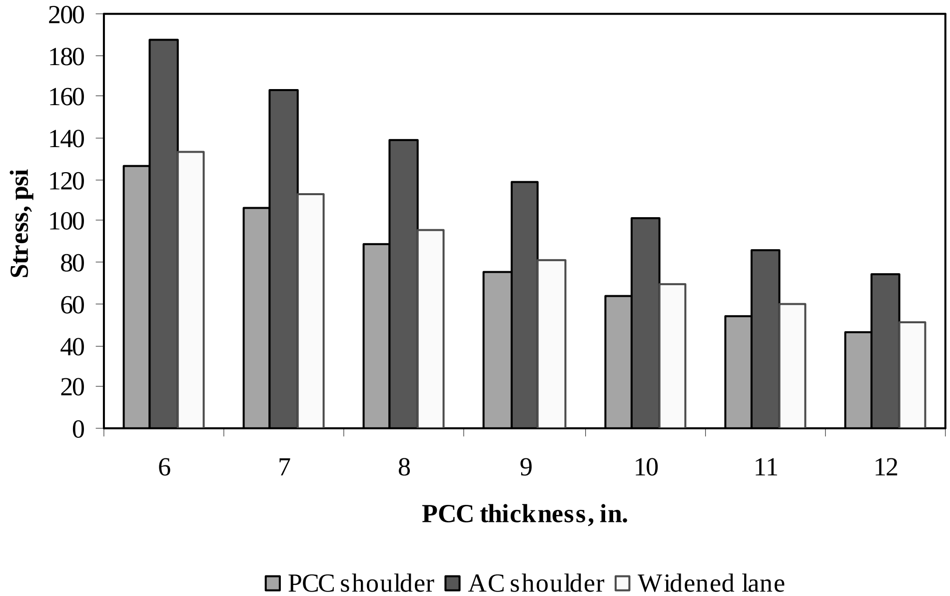


**Figure F-13-29: Impact of PCC thickness and lateral support condition on longitudinal stress at top of the Slab (177-in. joint spacing and $\alpha(\Delta T/D)$ of 0 in.$^{-1}$)**

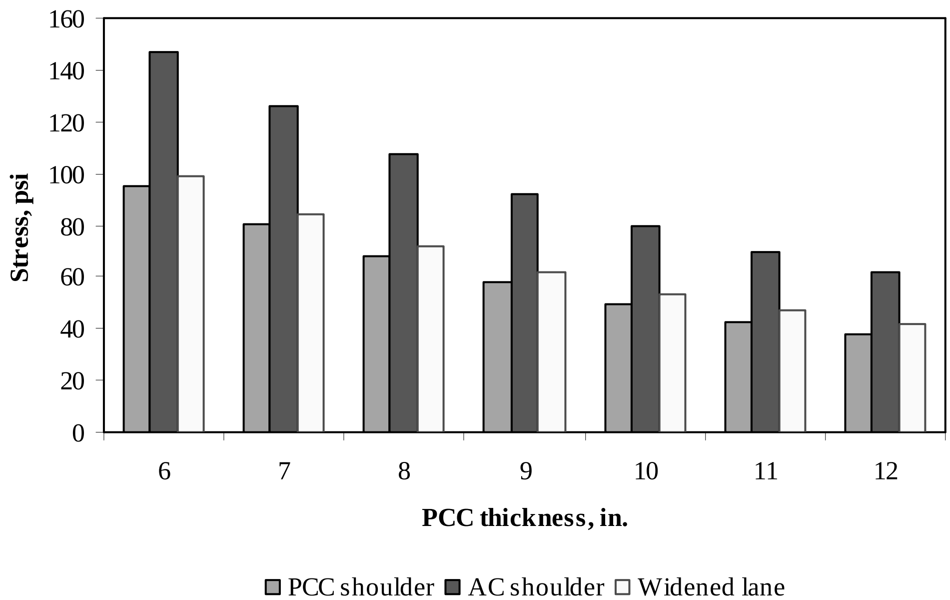


**Figure F-13-30: Impact of PCC thickness and lateral support condition on longitudinal stress at top of the Slab (315-in. joint spacing and $\alpha(\Delta T/D)$ of 0 in.$^{-1}$)**

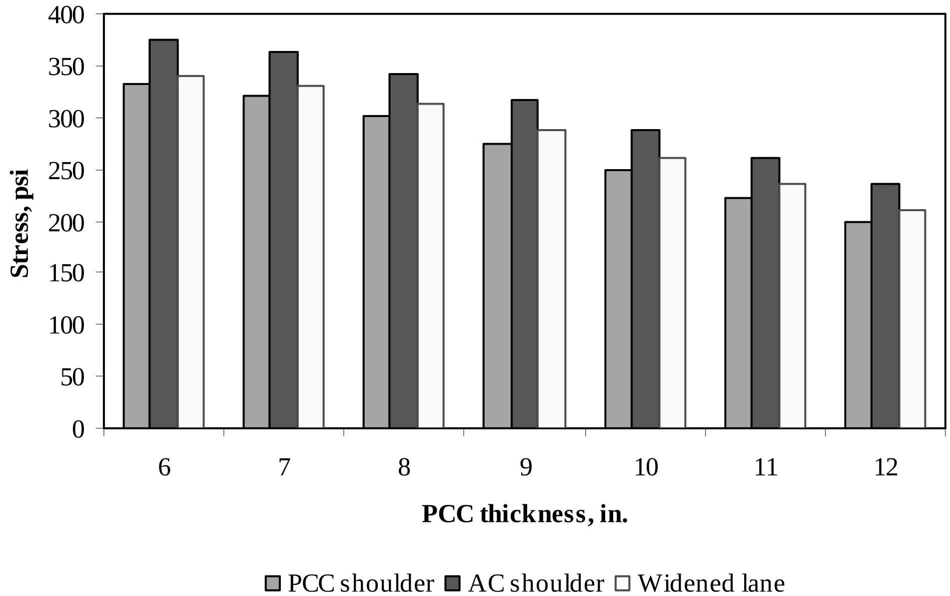


**Figure F-13-31: Impact of PCC thickness and lateral support condition on longitudinal stress at top of the Slab (177-in. joint spacing and $\alpha(\Delta T/D)$ of $-20x10^{-6}$ in.$^{-1}$)**

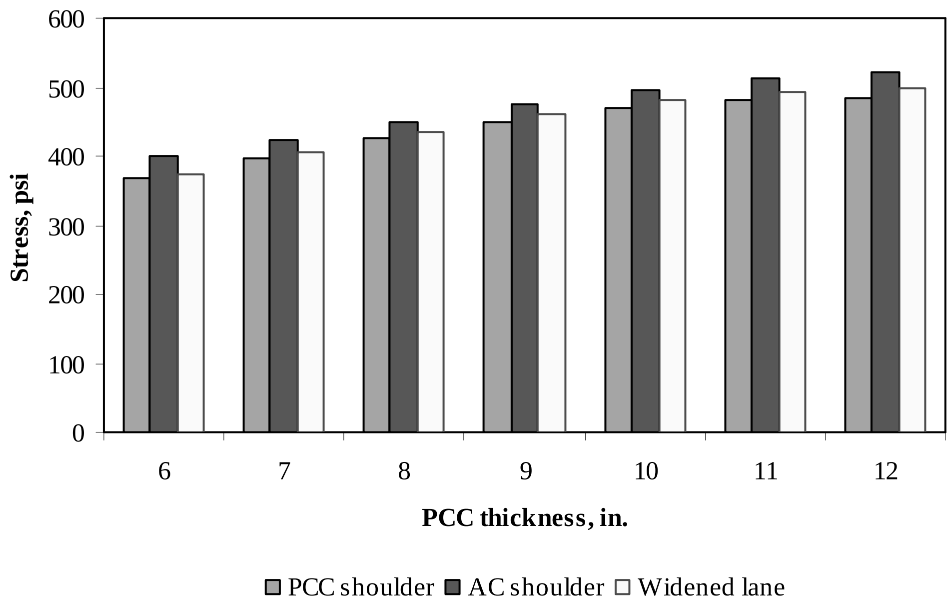


**Figure F-13-32: Impact of PCC thickness and lateral support condition on longitudinal stress at top of the Slab (315-in. joint spacing and $\alpha(\Delta T/D)$ of $-20x10^{-6}$ in.$^{-1}$)**

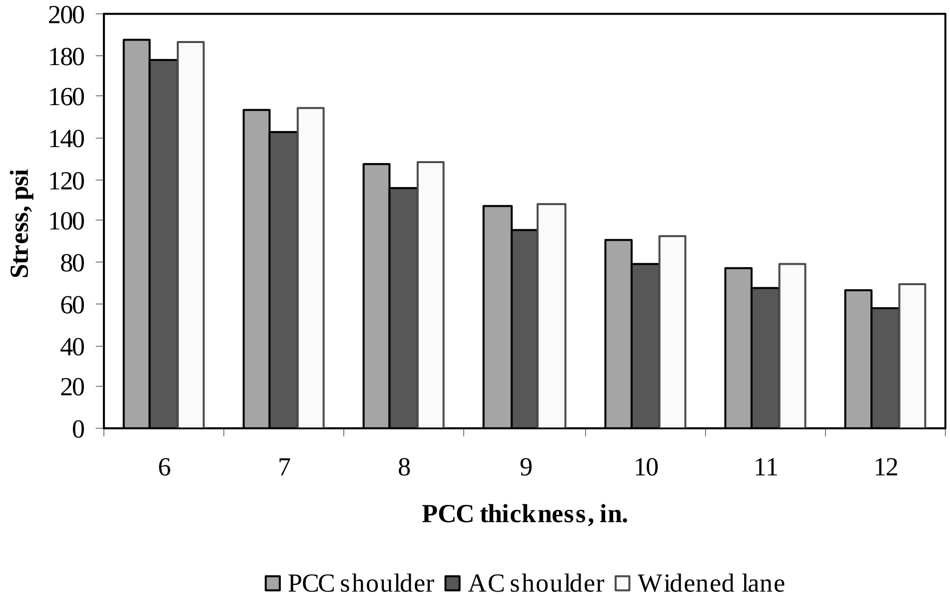


**Figure F-13-33: Impact of PCC thickness and lateral support condition on transverse stress at bottom of the Slab (177-in. joint spacing and $\alpha(\Delta T/D)$ of 0 in.$^{-1}$)**

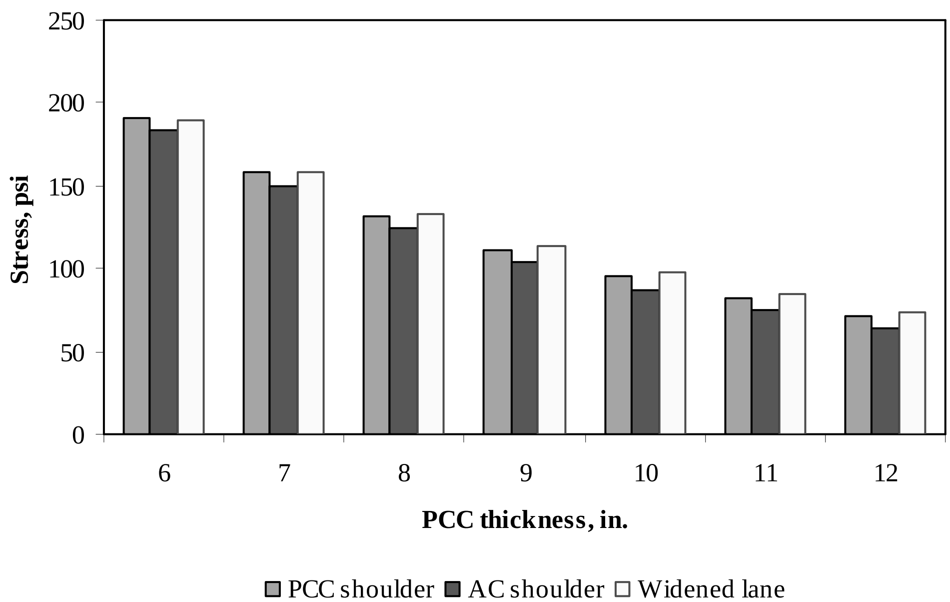


**Figure F-13-34: Impact of PCC thickness and lateral support condition on transverse stress at bottom of the Slab (315-in. joint spacing and $\alpha(\Delta T/D)$ of 0 in.$^{-1}$)**

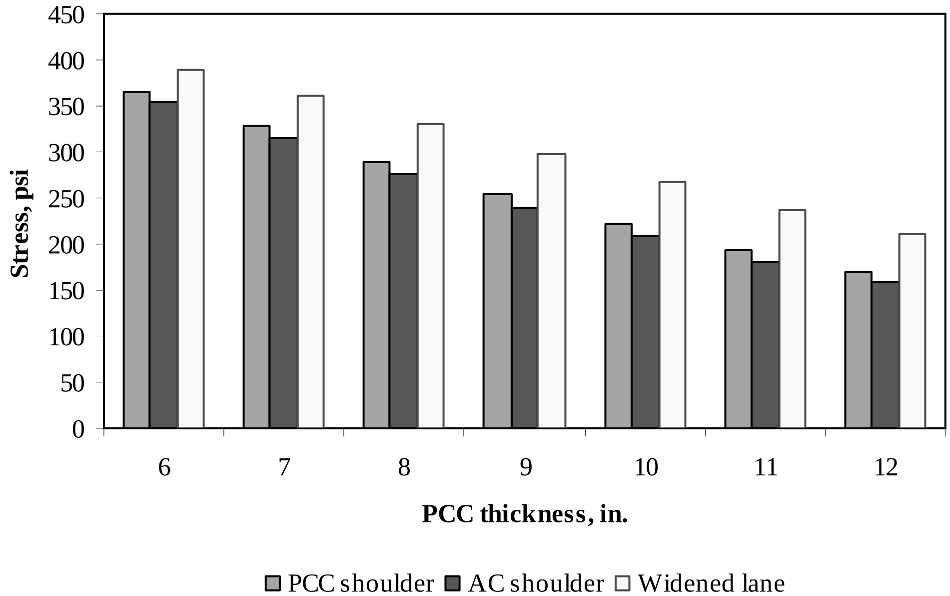


**Figure F-13-35: Impact of PCC thickness and lateral support condition on transverse stress at bottom of the Slab (177-in. joint spacing and $\alpha(\Delta T/D)$ of $20x10^{-6}$ in.$^{-1}$)**

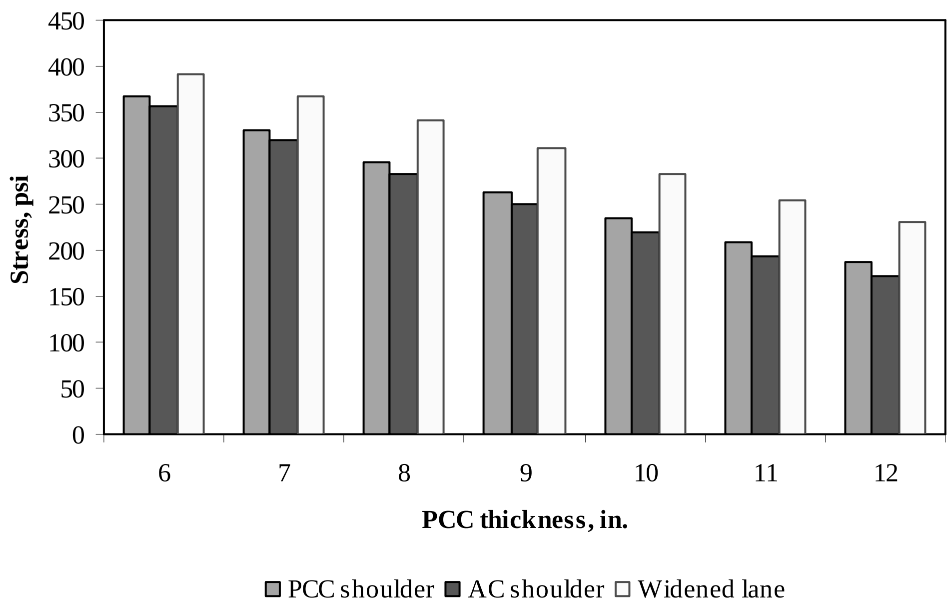


**Figure F-13-36: Impact of PCC thickness and lateral support condition on transverse stress at bottom of the Slab (315-in. joint spacing and $\alpha(\Delta T/D)$ of $20x10^{-6}$ in.$^{-1}$)**

Figures F-13-37 through F-13-42 illustrate the impact of base/subbase thickness and product $\alpha(\Delta T/D)$ on stresses (10-in. PCC thickness, 100-psi/in. modulus of subgrade reaction and PCC shoulder)

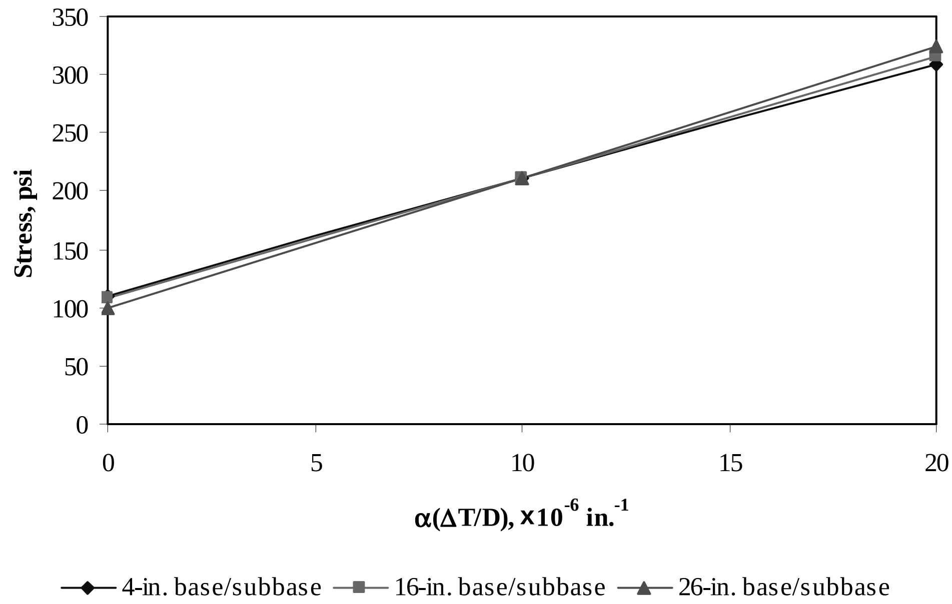


**Figure F-13-37: Impact of base/subbase thickness and product $\alpha(\Delta T/D)$ on longitudinal stress at bottom of the slab (177-in. joint spacing)**

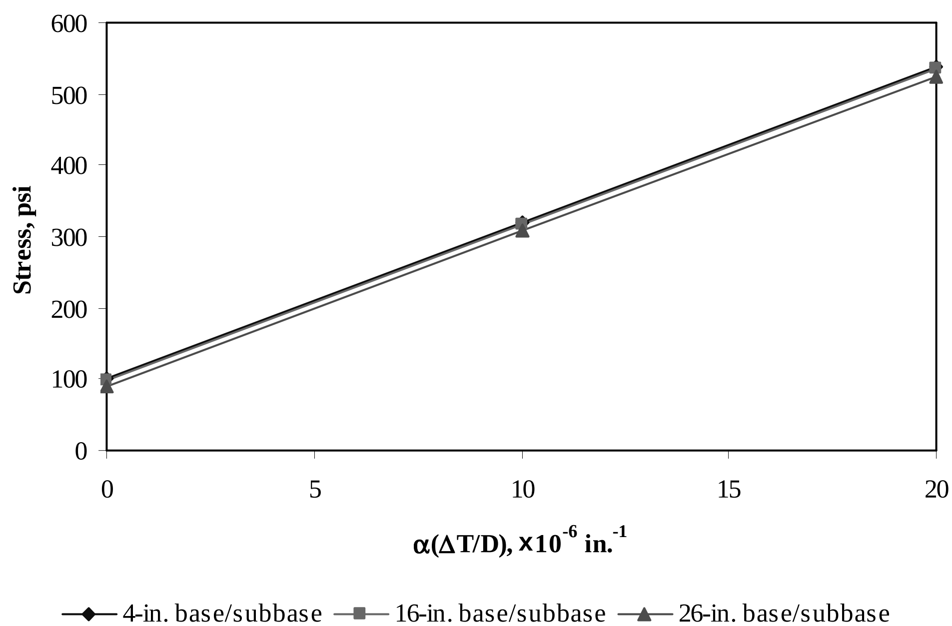


**Figure F-13-38: Impact of base/subbase thickness and product $\alpha(\Delta T/D)$ on longitudinal stress at bottom of the slab (315-in. joint spacing)**

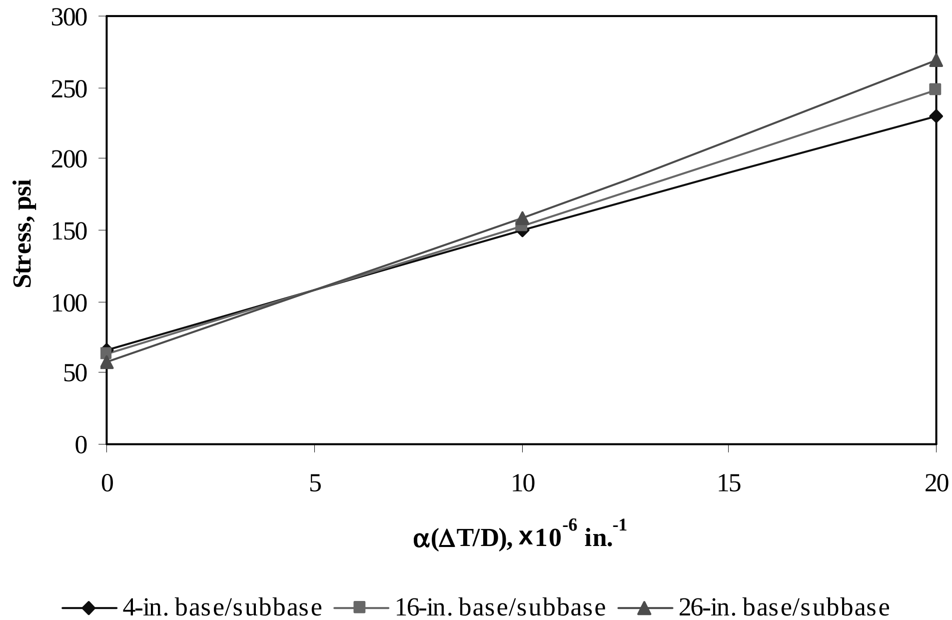


**Figure F-13-39: Impact of base/subbase thickness and product α(ΔT/D) on longitudinal stress at top of the slab (177-in. joint spacing)**

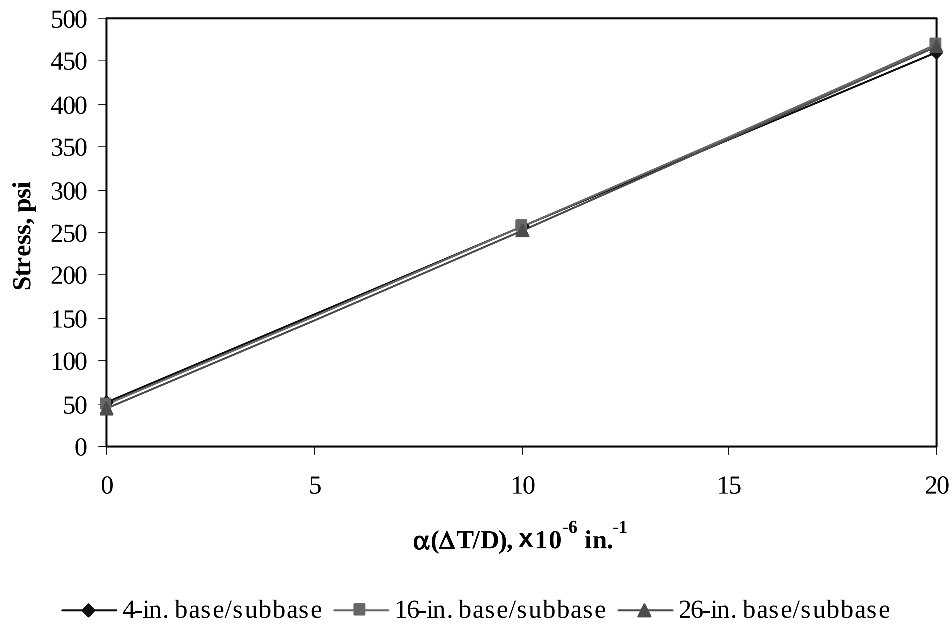


**Figure F-13-40: Impact of base/subbase thickness and product α(ΔT/D) on longitudinal stress at top of the slab (315-in. joint spacing)**

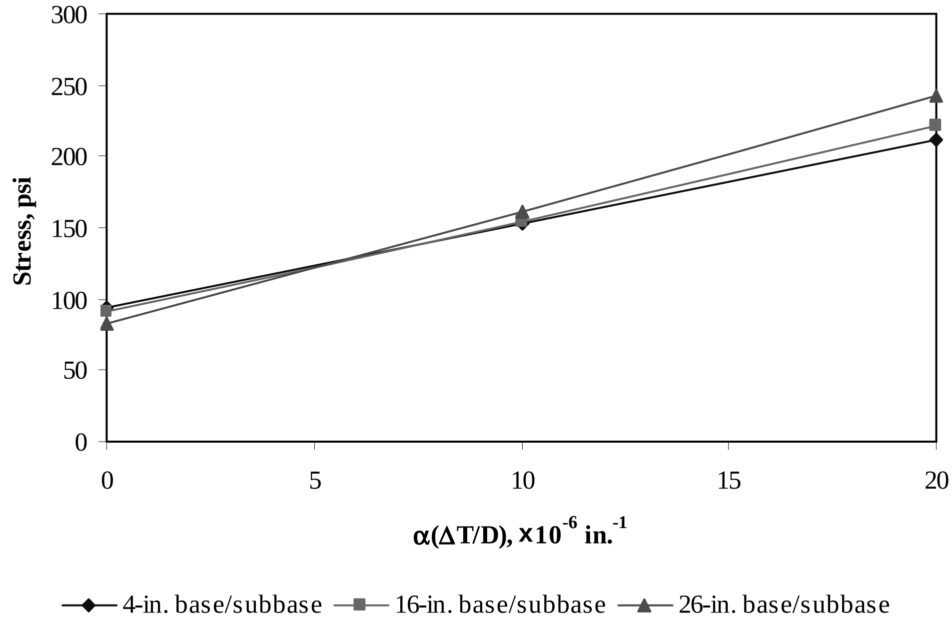


**Figure F-13-41: Impact of base/subbase thickness and product α(ΔT/D) on transverse stress at bottom of the slab (177-in. joint spacing)**

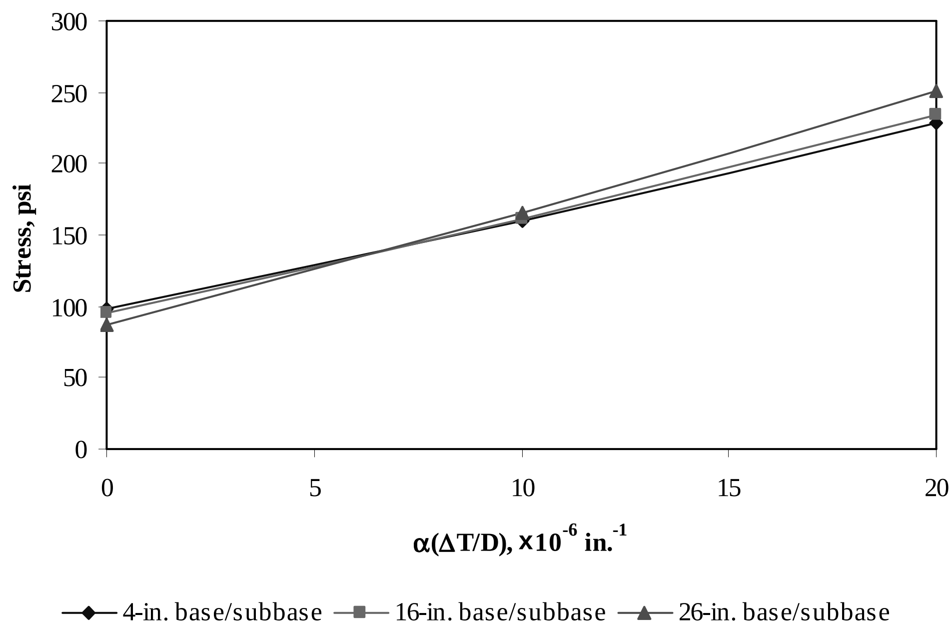


**Figure F-13-42: Impact of base/subbase thickness and product α(ΔT/D) on transverse stress at bottom of the slab (315-in. joint spacing)**

Figures F-13-43 through F-13-48 illustrate the impact of modulus of subgrade reaction and product α(ΔT/D) on stresses (10-in. PCC thickness, 16-in. base/subbase thickness and PCC shoulder)

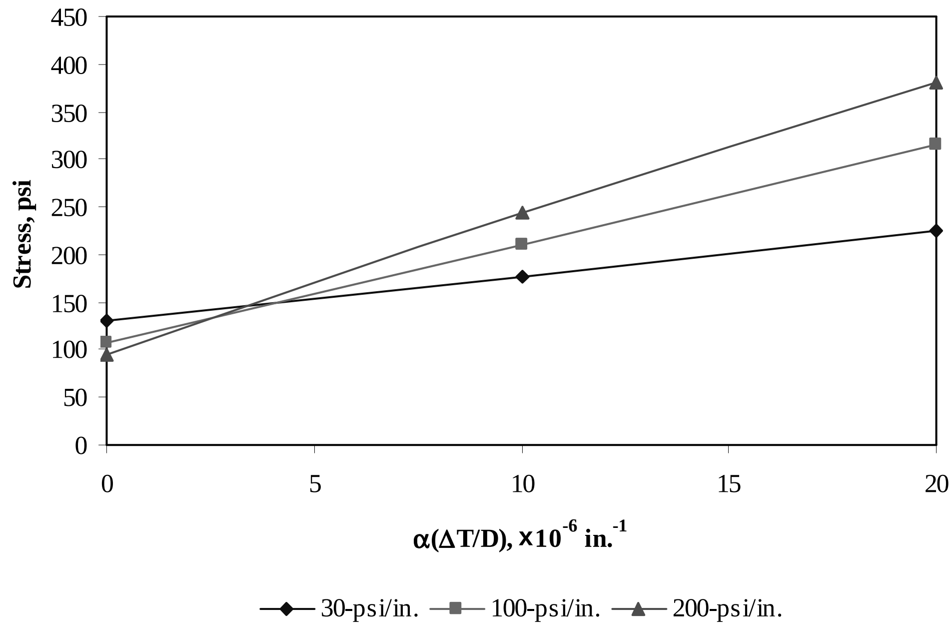


**Figure F-13-43: Impact of modulus of subgrade reaction and product α(ΔT/D) on longitudinal stress at bottom of the slab (177-in. joint spacing)**

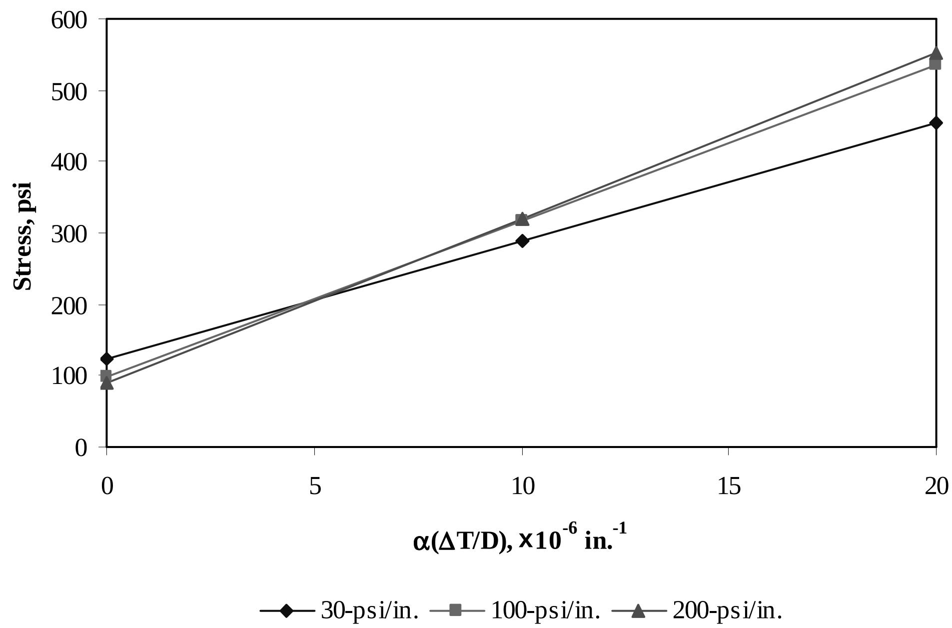


**Figure F-13-44: Impact of modulus of subgrade reaction and product α(ΔT/D) on longitudinal stress at bottom of the slab (315-in. joint spacing)**

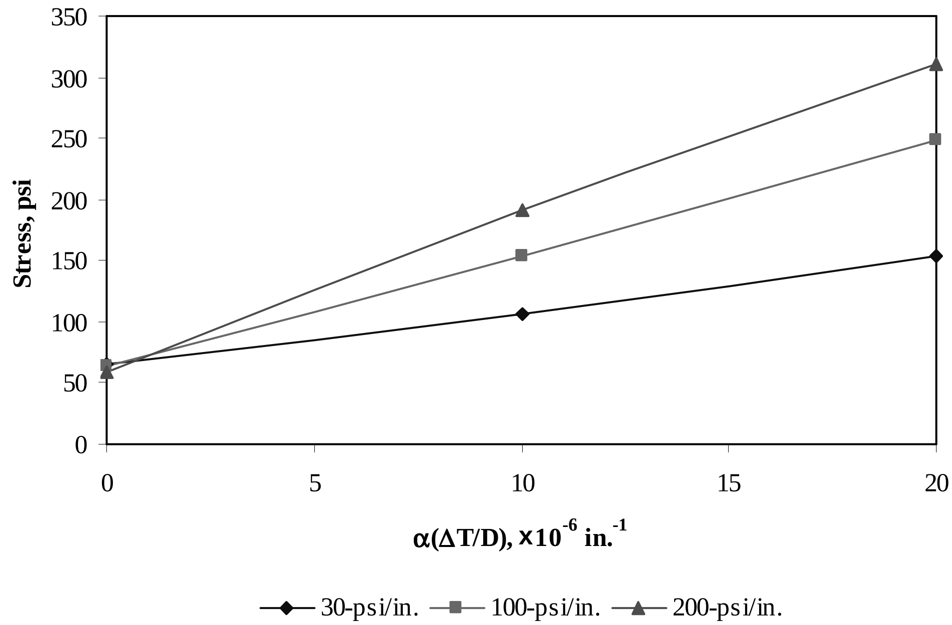


**Figure F-13-45: Impact of modulus of subgrade reaction and product α(ΔT/D) on longitudinal stress at top of the slab (177-in. joint spacing)**

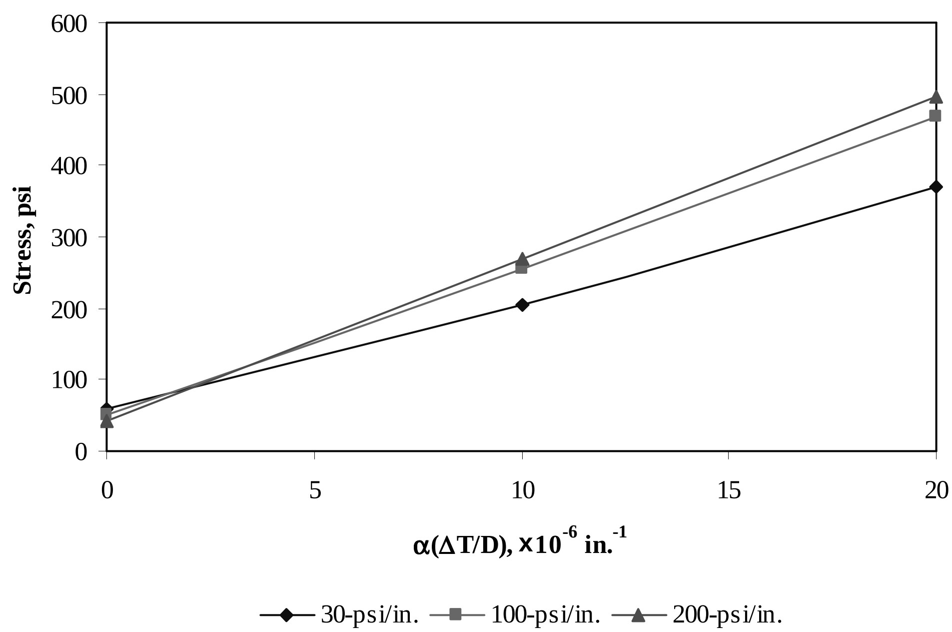


**Figure F-13-46: Impact of modulus of subgrade reaction and product α(ΔT/D) on longitudinal stress at top of the slab (315-in. joint spacing)**

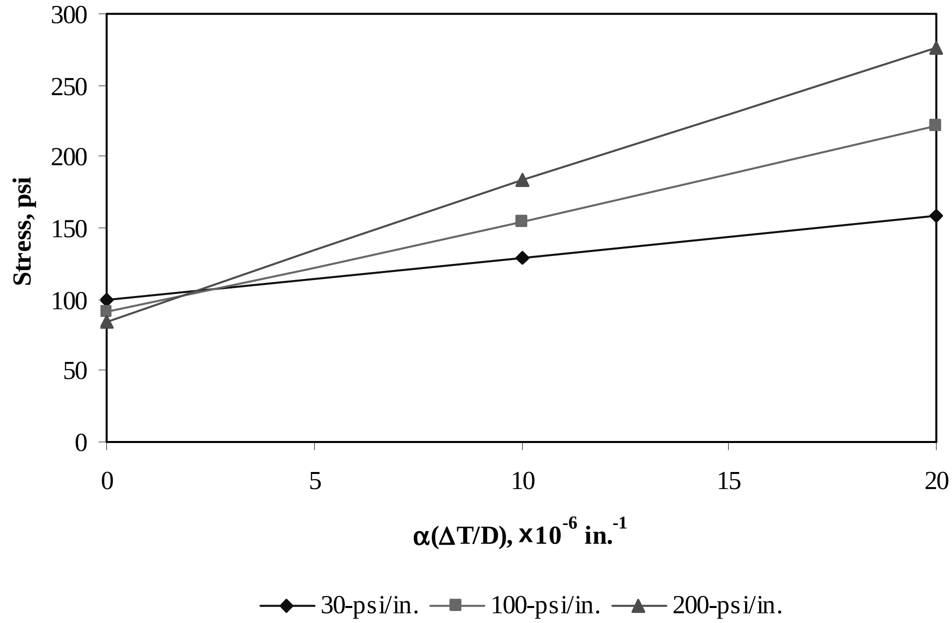


**Figure F-13-47: Impact of modulus of subgrade reaction and product α(ΔT/D) on transverse stress at bottom of the slab (177-in. joint spacing)**

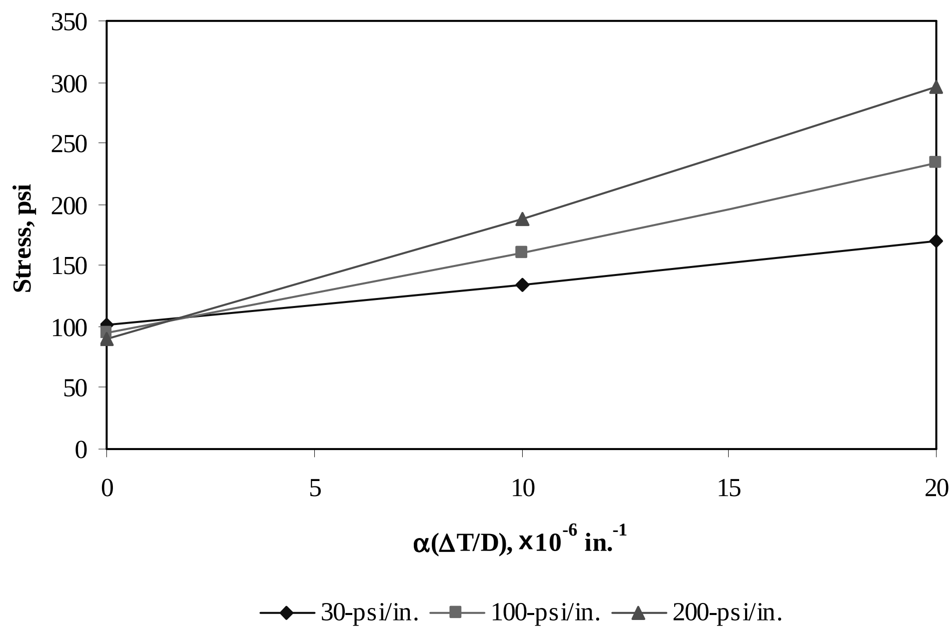


**Figure F-13-48: Impact of modulus of subgrade reaction and product α(ΔT/D) on transverse stress at bottom of the slab (315-in. joint spacing)**

Figures F-13-49 through F-13-51 illustrate the impact of joint spacing and product $\alpha(\Delta T/D)$ on stresses (10-in. PCC thickness, 16-in. base/subbase thickness, 100-psi/in. modulus of subgrade reaction and PCC shoulder)

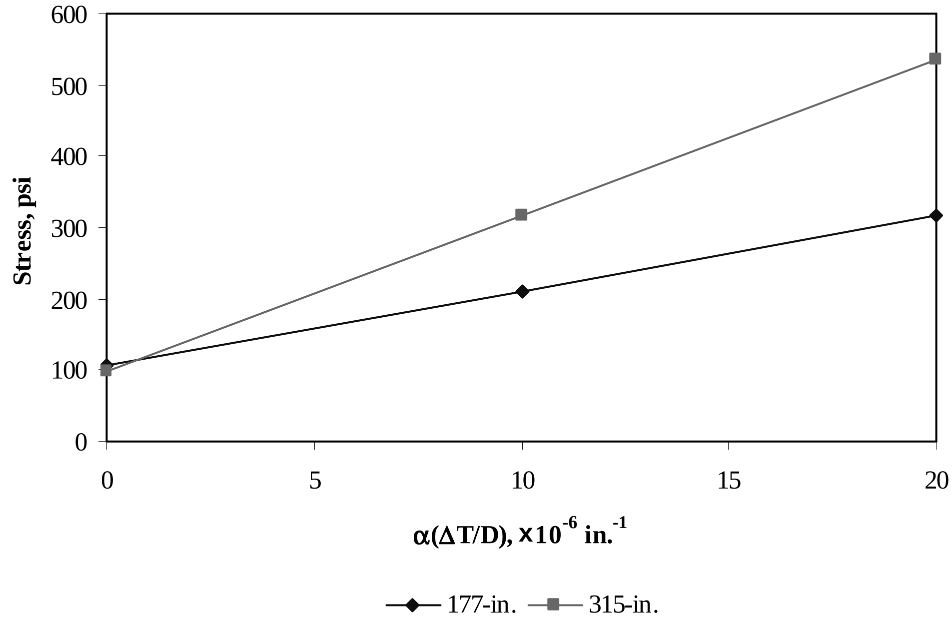


**Figure F-13-49: Impact of joint spacing and product $\alpha(\Delta T/D)$ on longitudinal stress at bottom of the slab**

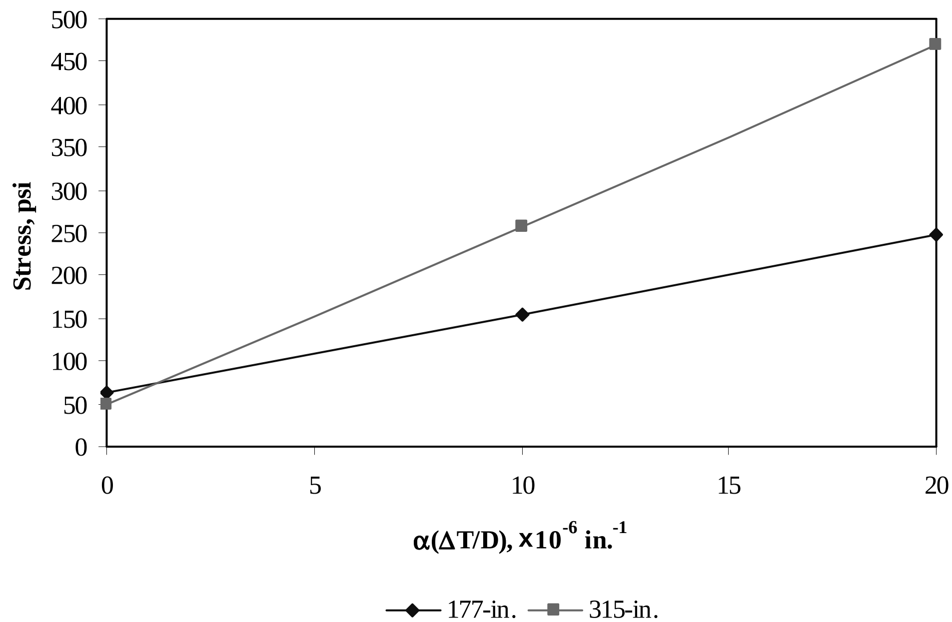


**Figure F-13-50: Impact of joint spacing and product $\alpha(\Delta T/D)$ on longitudinal stress at top of the slab**

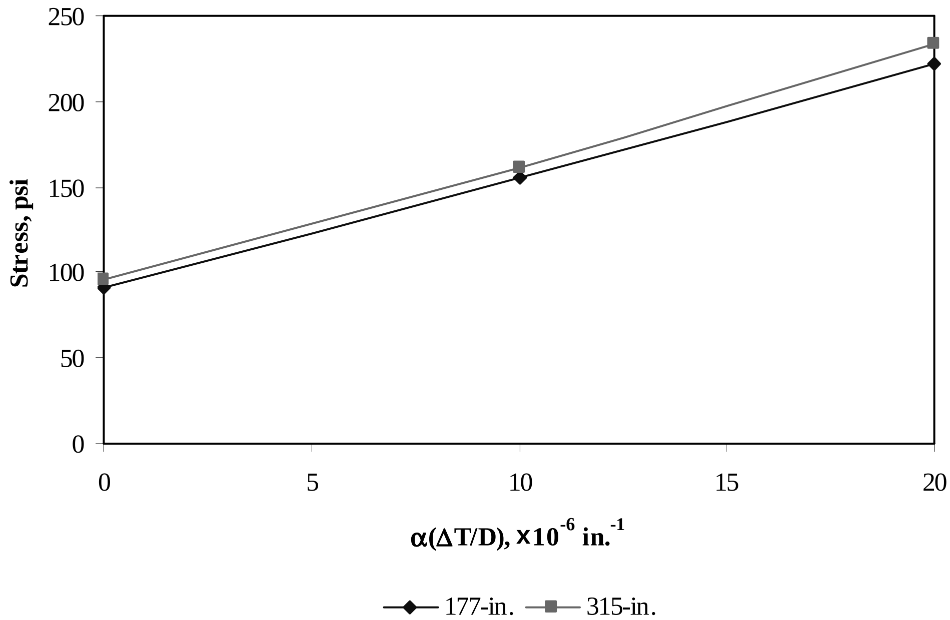


**Figure F-13-51: Impact of joint spacing and product α(ΔT/D) on transverse stress at bottom of the slab**

**Sub Appendix F-14**

**Documentation of Pavement Responses for**

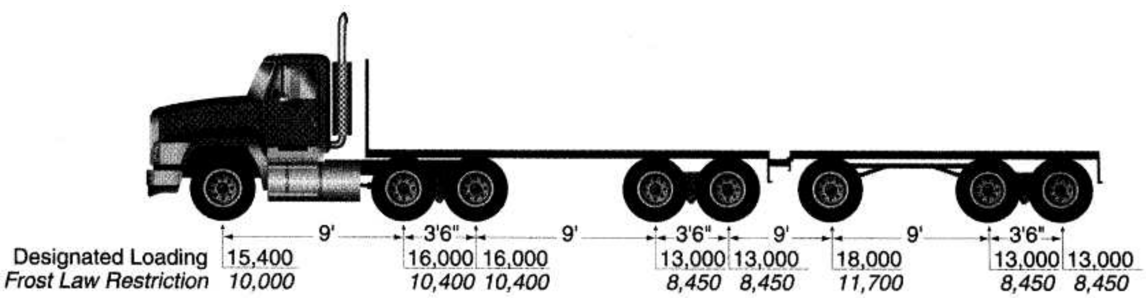


**MI-12**

Figures F-14-1 through F-14-12 illustrate the impact of PCC thickness and base/subbase thickness on stresses (100-psi/in. modulus of subgrade reaction and PCC shoulder)

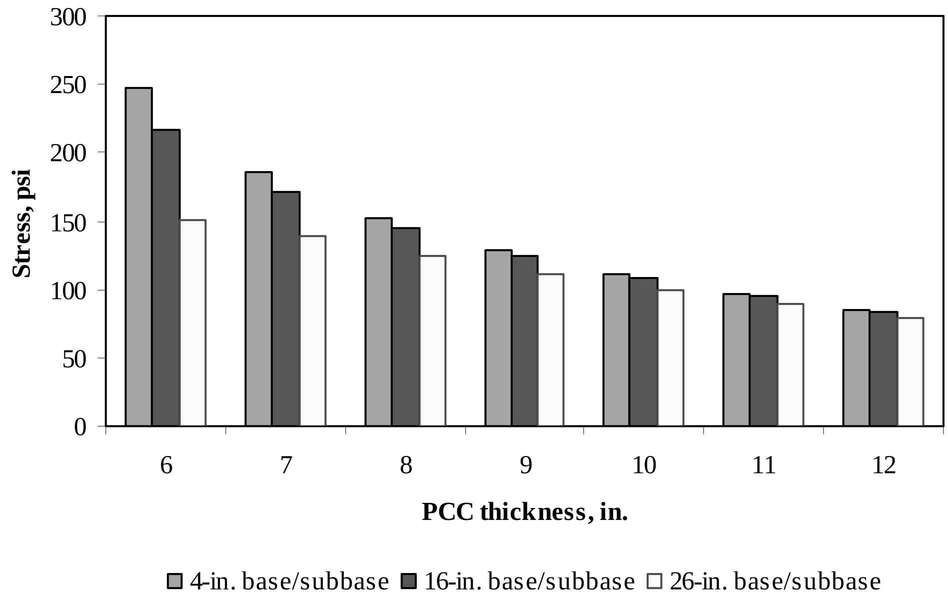


**Figure F-14-1: Impact of PCC thickness and base/subbase thickness on longitudinal stress at bottom of the Slab (177-in. joint spacing and $\alpha(\Delta T/D)$ of 0 in.$^{-1}$)**

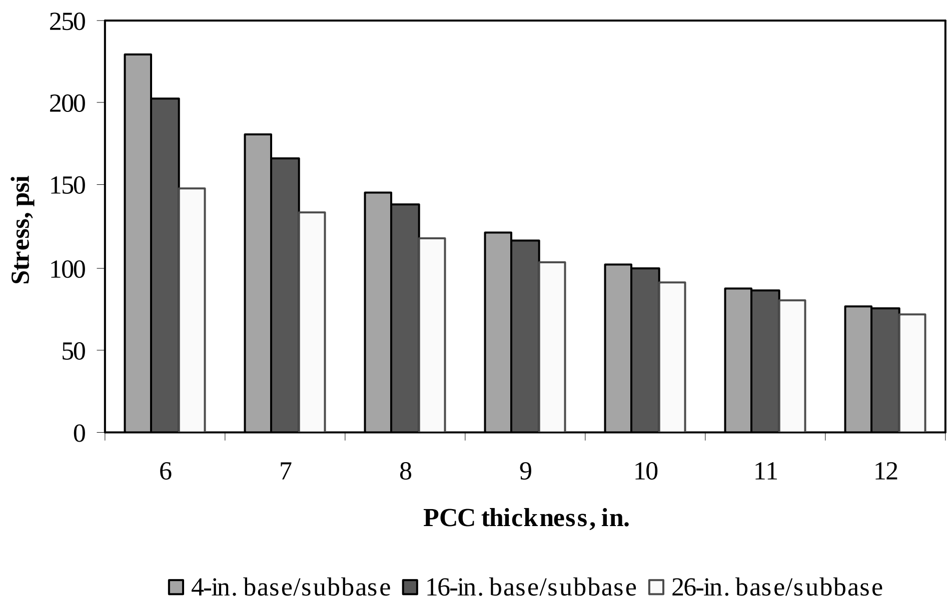


**Figure F-14-2: Impact of PCC thickness and base/subbase thickness on longitudinal stress at bottom of the Slab (315-in. joint spacing and $\alpha(\Delta T/D)$ of 0 in.$^{-1}$)**

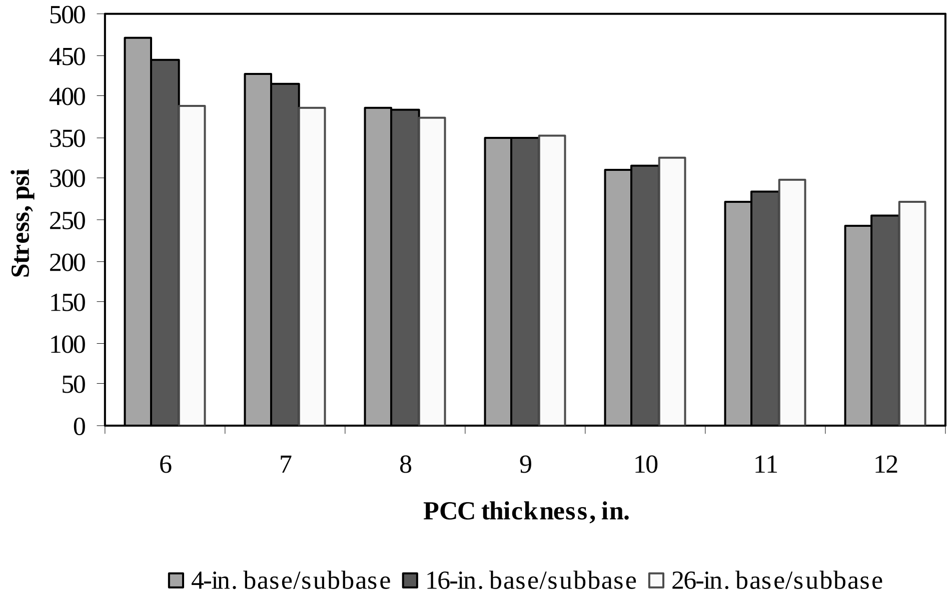


**Figure F-14-3: Impact of PCC thickness and base/subbase thickness on longitudinal stress at bottom of the Slab (177-in. joint spacing and $\alpha(\Delta T/D)$ of $20x10^{-6}$ in.$^{-1}$)**

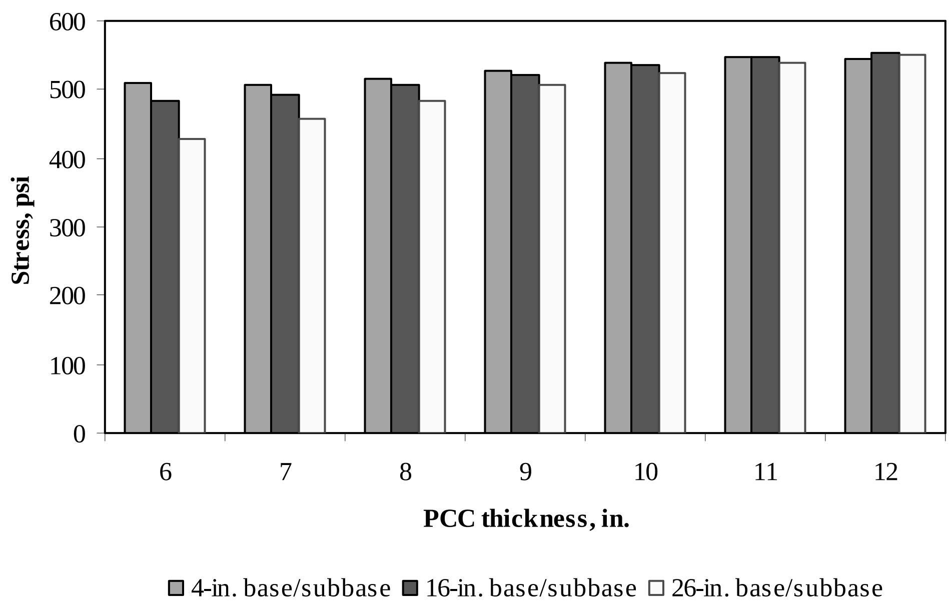


**Figure F-14-4: Impact of PCC thickness and base/subbase thickness on longitudinal stress at bottom of the Slab (315-in. joint spacing and $\alpha(\Delta T/D)$ of $20x10^{-6}$ in.$^{-1}$)**

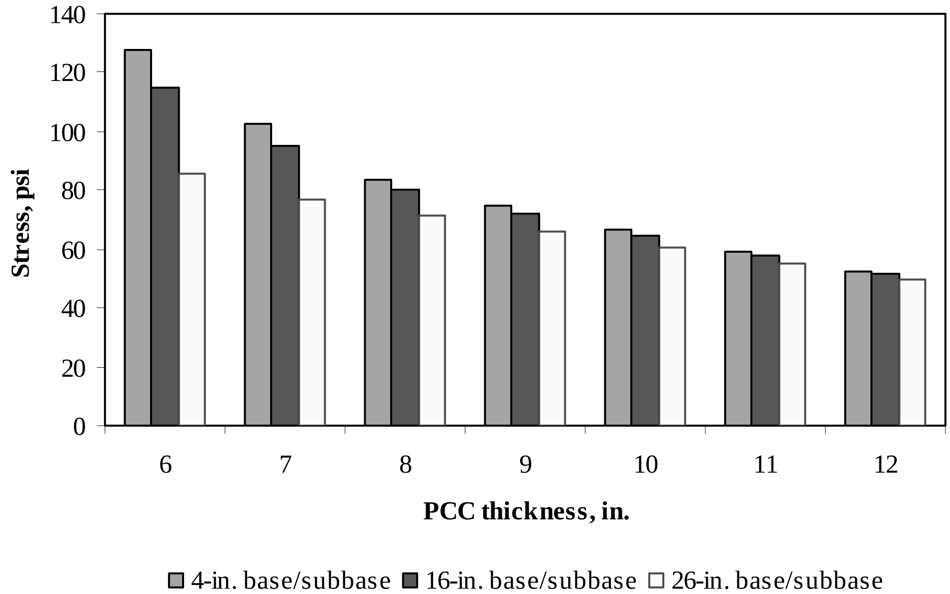


**Figure F-14-5: Impact of PCC thickness and base/subbase thickness on longitudinal stress at top of the Slab (177-in. joint spacing and $\alpha(\Delta T/D)$ of 0 in.$^{-1}$)**

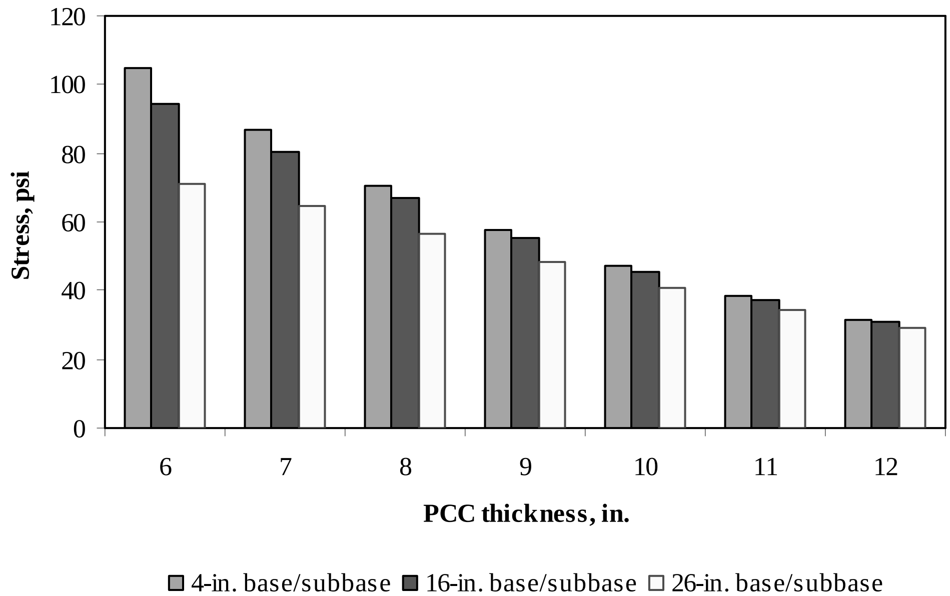


**Figure F-14-6: Impact of PCC thickness and base/subbase thickness on longitudinal stress at top of the Slab (315-in. joint spacing and $\alpha(\Delta T/D)$ of 0 in.$^{-1}$)**

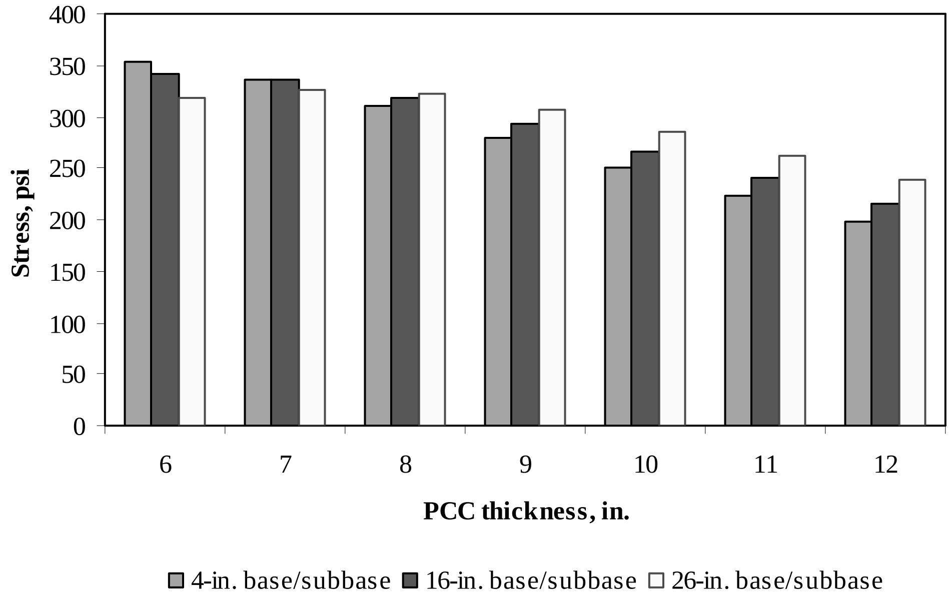


**Figure F-14-7: Impact of PCC thickness and base/subbase thickness on longitudinal stress at top of the Slab (177-in. joint spacing and $\alpha(\Delta T/D)$ of $-20 \times 10^{-6}$ in.$^{-1}$)**

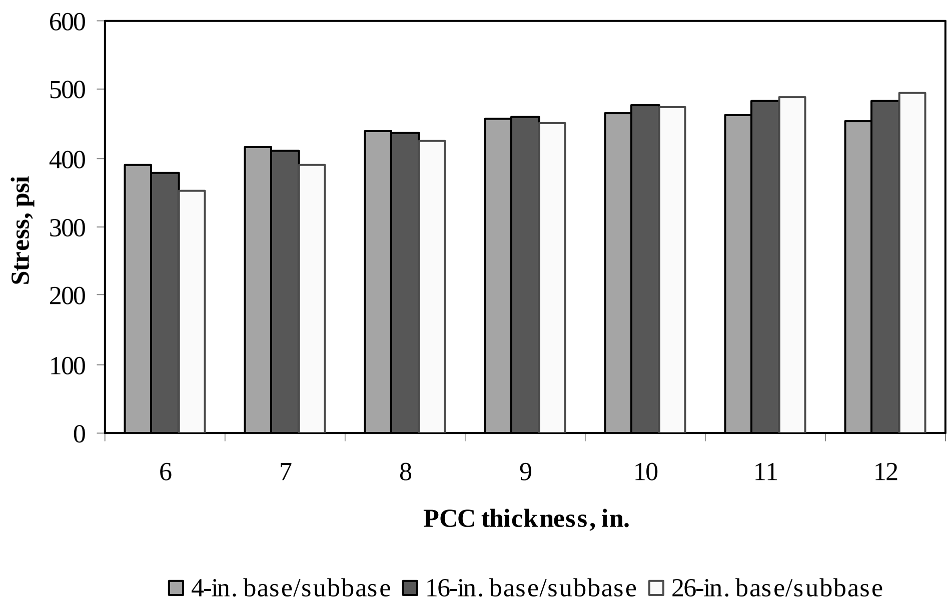


**Figure F-14-8: Impact of PCC thickness and base/subbase thickness on longitudinal stress at top of the Slab (315-in. joint spacing and $\alpha(\Delta T/D)$ of $-20 \times 10^{-6}$ in.$^{-1}$)**

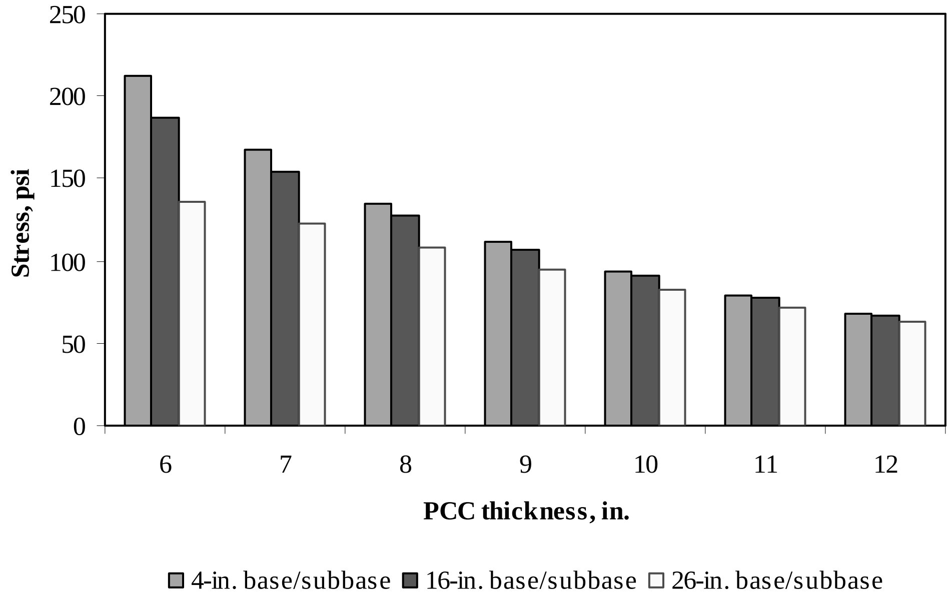


**Figure F-14-9: Impact of PCC thickness and base/subbase thickness on transverse stress at bottom of the Slab (177-in. joint spacing and α(ΔT/D) of 0 in.$^{-1}$)**

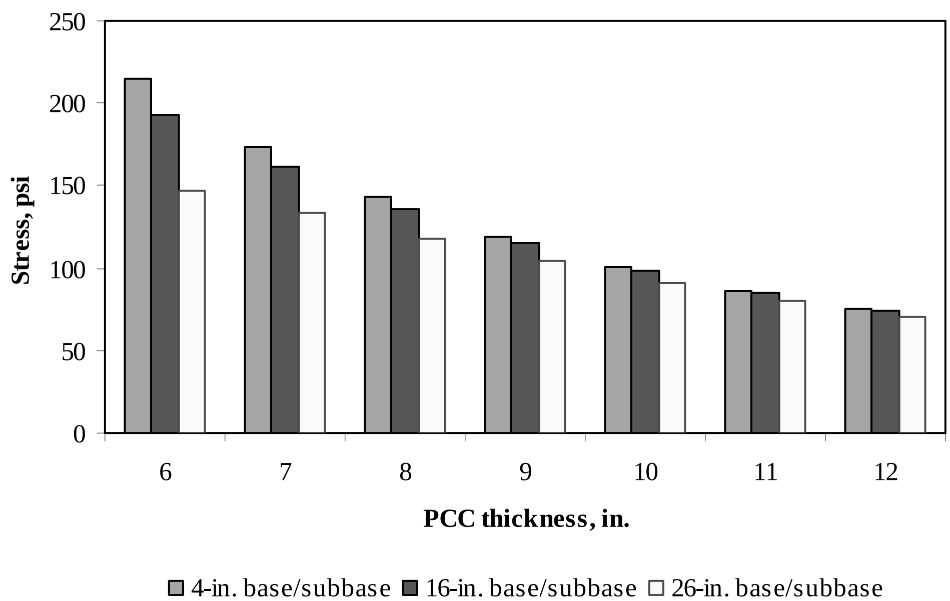


**Figure F-14-10: Impact of PCC thickness and base/subbase thickness on transverse stress at bottom of the Slab (315-in. joint spacing and α(ΔT/D) of 0 in.$^{-1}$)**

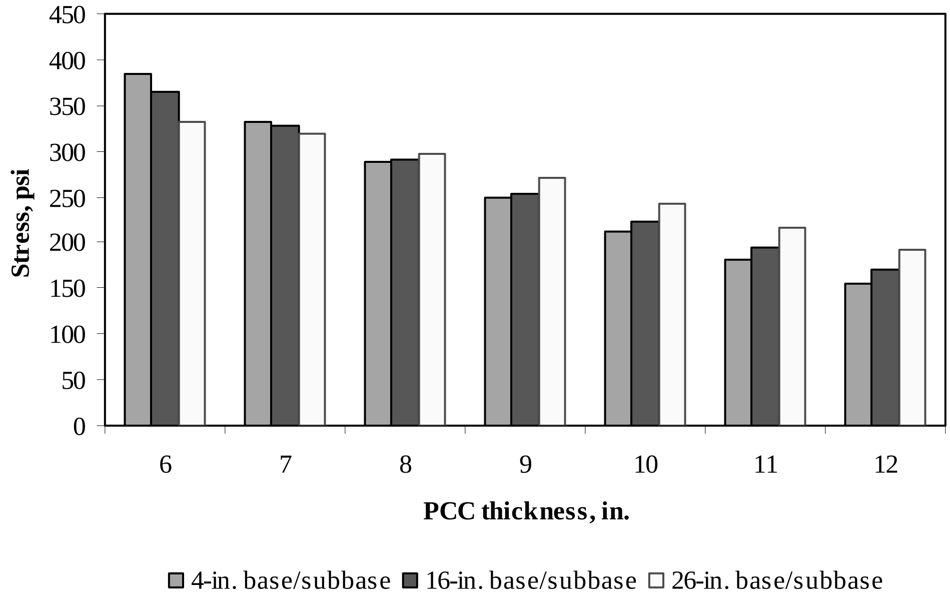


**Figure F-14-11: Impact of PCC thickness and base/subbase thickness on transverse stress at bottom of the Slab (177-in. joint spacing and $\alpha(\Delta T/D)$ of 20x10$^{-6}$ in.$^{-1}$)**

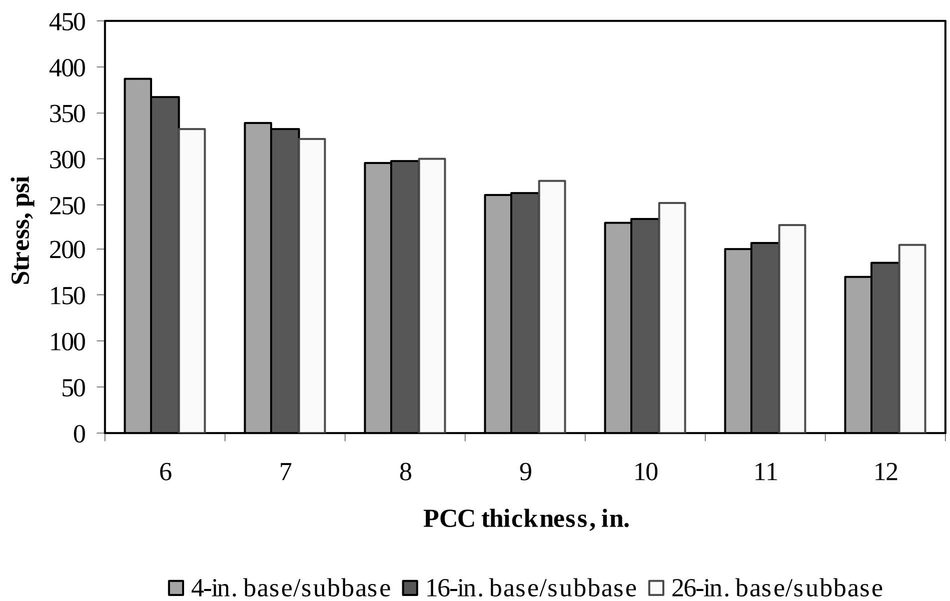


**Figure F-14-12: Impact of PCC thickness and base/subbase thickness on transverse stress at bottom of the Slab (315-in. joint spacing and $\alpha(\Delta T/D)$ of 20x10$^{-6}$ in.$^{-1}$)**

Figures F-14-13 through F-14-24 illustrate the impact of PCC thickness and modulus of subgrade reaction on stresses (16-in. base/subbase thickness and PCC shoulder)

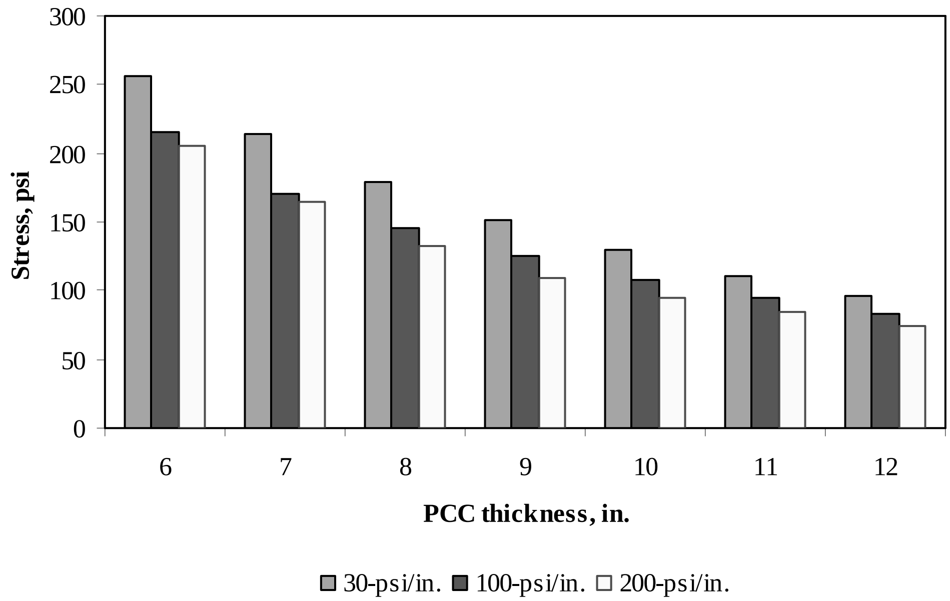


**Figure F-14-13: Impact of PCC thickness and modulus of subgrade reaction on longitudinal stress at bottom of the slab (177-in. joint spacing and $\alpha(\Delta T/D)$ of 0 in.$^{-1}$)**

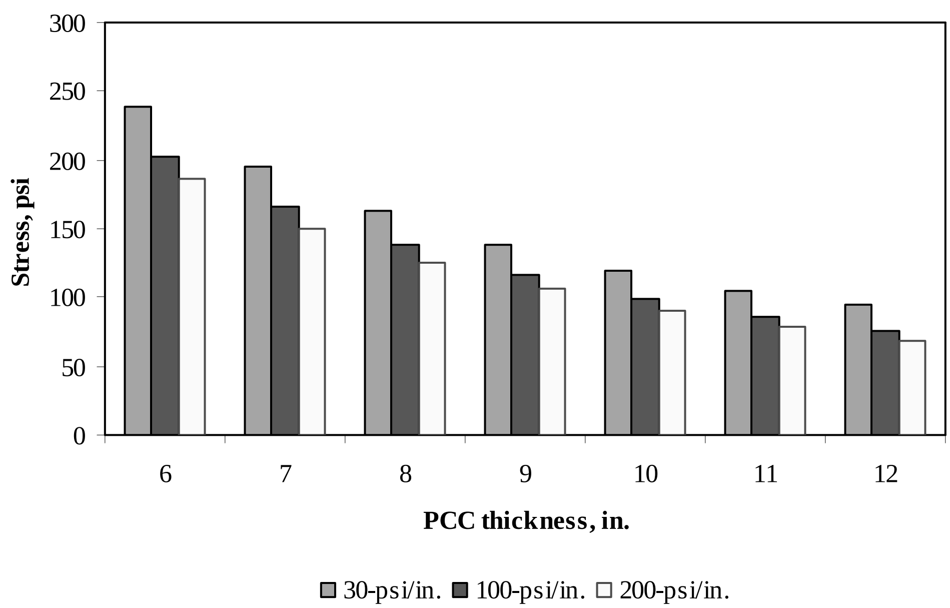


**Figure F-14-14: Impact of PCC thickness and modulus of subgrade reaction on longitudinal stress at bottom of the slab (315-in. joint spacing and $\alpha(\Delta T/D)$ of 0 in.$^{-1}$)**

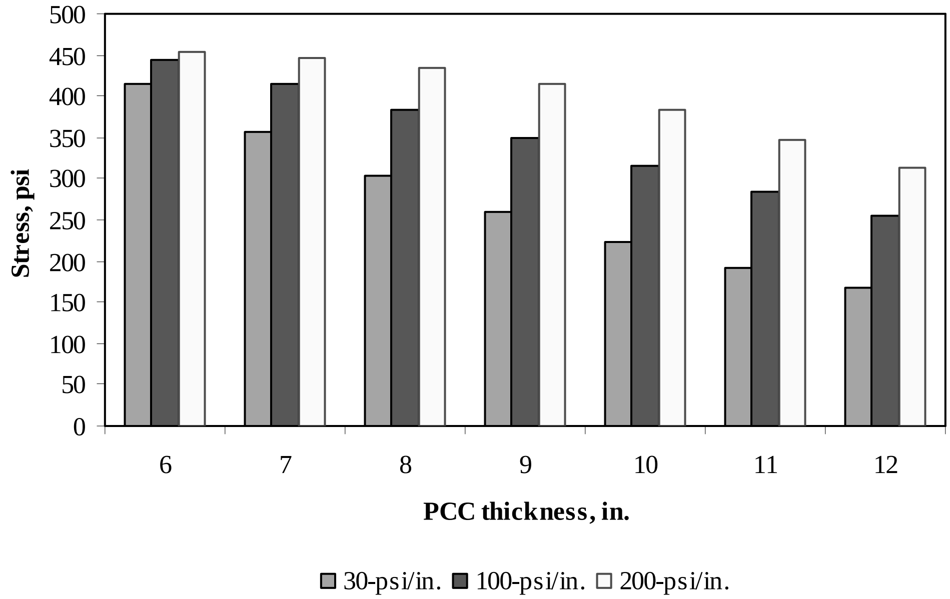


**Figure F-14-15: Impact of PCC thickness and modulus of subgrade reaction on longitudinal stress at bottom of the slab (177-in. joint spacing and $\alpha(\Delta T/D)$ of $20x10^{-6}$ in.$^{-1}$)**

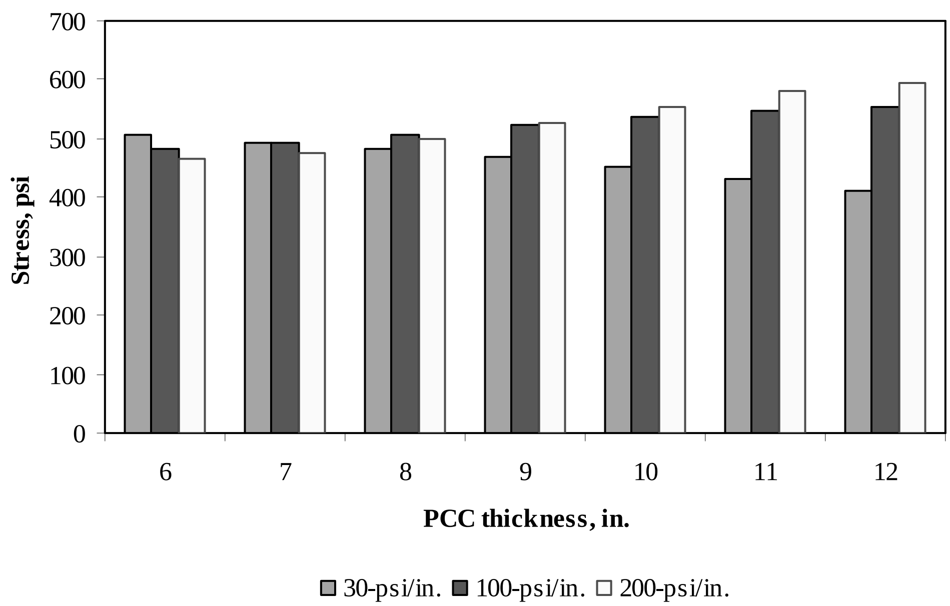


**Figure F-14-16: Impact of PCC thickness and modulus of subgrade reaction on longitudinal stress at bottom of the slab (315-in. joint spacing and $\alpha(\Delta T/D)$ of $20x10^{-6}$ in.$^{-1}$)**

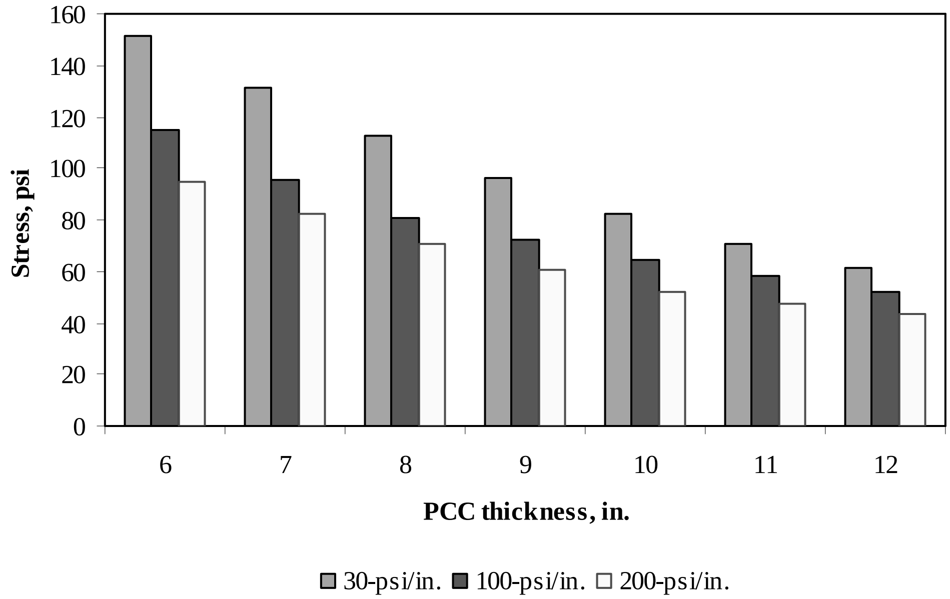


**Figure F-14-17: Impact of PCC thickness and modulus of subgrade reaction on longitudinal stress at top of the Slab (177-in. joint spacing and $\alpha(\Delta T/D)$ of 0 in.$^{-1}$)**

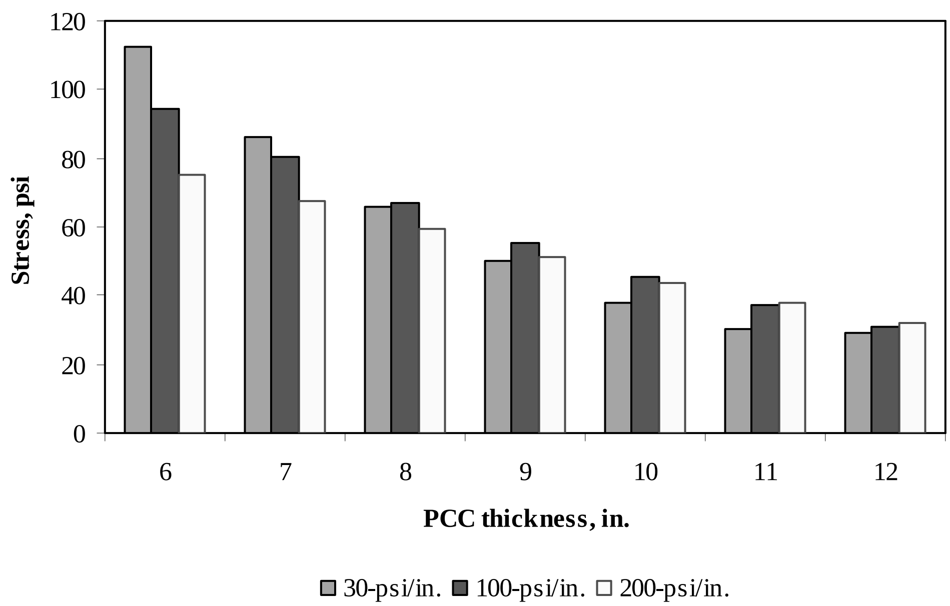


**Figure F-14-18: Impact of PCC thickness and modulus of subgrade reaction on longitudinal stress at top of the Slab (315-in. joint spacing and $\alpha(\Delta T/D)$ of 0 in.$^{-1}$)**

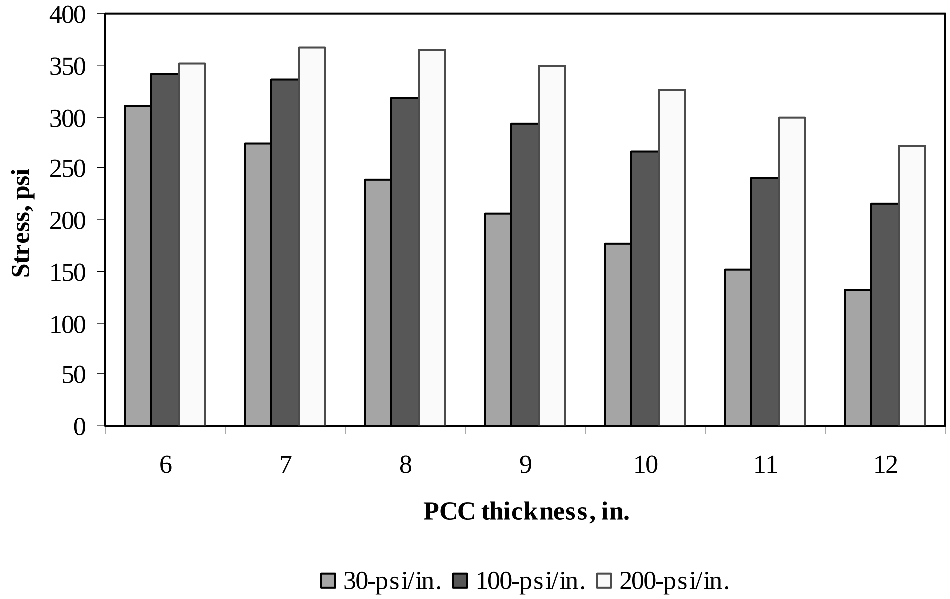


**Figure F-14-19: Impact of PCC thickness and modulus of subgrade reaction on longitudinal stress at top of the Slab (177-in. joint spacing and $\alpha(\Delta T/D)$ of $-20x10^{-6}$ in.$^{-1}$)**

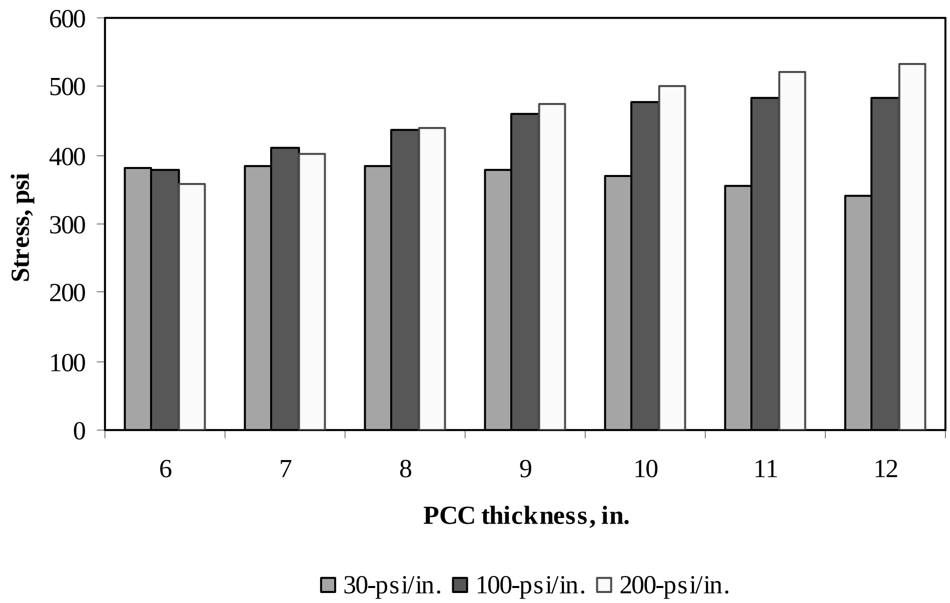


**Figure F-14-20: Impact of PCC thickness and modulus of subgrade reaction on longitudinal stress at top of the Slab (315-in. joint spacing and $\alpha(\Delta T/D)$ of $-20x10^{-6}$ in.$^{-1}$)**

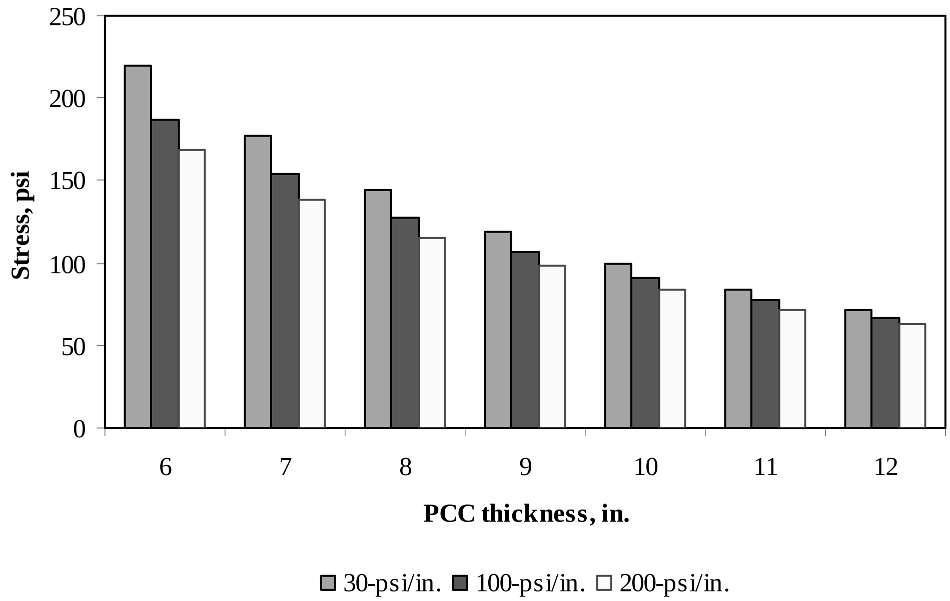


**Figure F-14-21: Impact of PCC thickness and modulus of subgrade reaction on transverse stress at bottom of the Slab (177-in. joint spacing and $\alpha(\Delta T/D)$ of 0 in.$^{-1}$)**

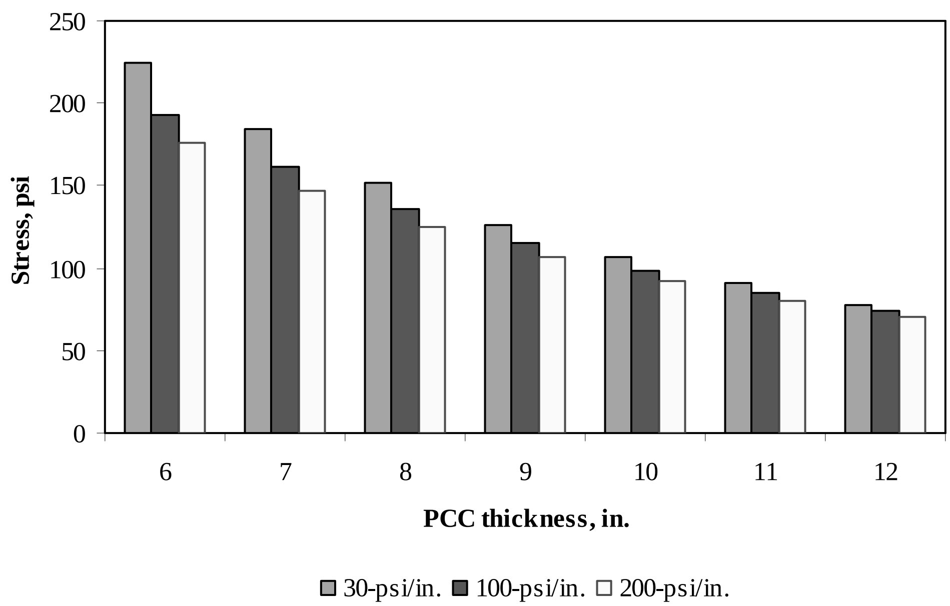


**Figure F-14-22: Impact of PCC thickness and modulus of subgrade reaction on transverse stress at bottom of the Slab (315-in. joint spacing and $\alpha(\Delta T/D)$ of 0 in.$^{-1}$)**

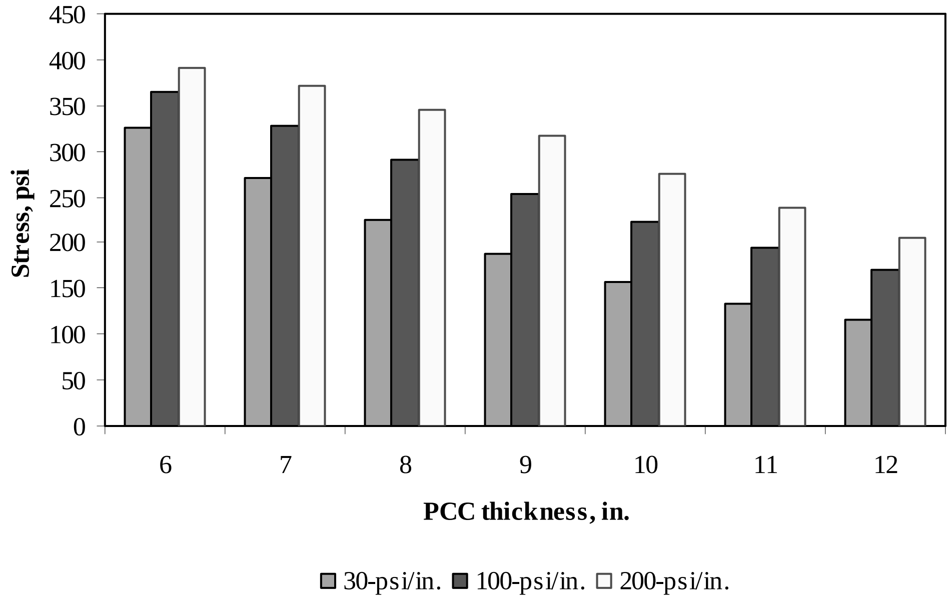


**Figure F-14-23: Impact of PCC thickness and modulus of subgrade reaction on transverse stress at bottom of the Slab (177-in. joint spacing and $\alpha(\Delta T/D)$ of $20x10^{-6}$ in.$^{-1}$)**

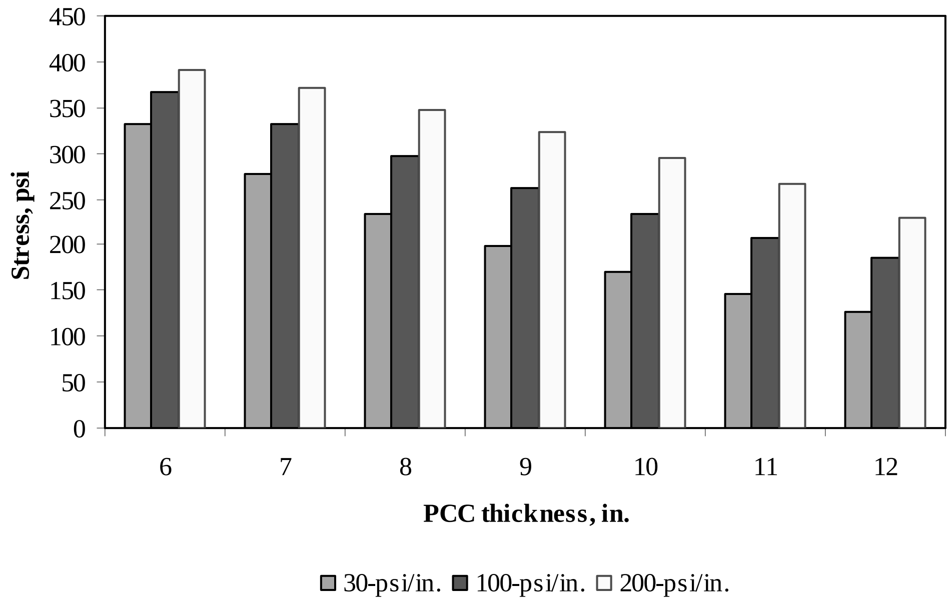


**Figure F-14-24: Impact of PCC thickness and modulus of subgrade reaction on transverse stress at bottom of the Slab (315-in. joint spacing and $\alpha(\Delta T/D)$ of $20x10^{-6}$ in.$^{-1}$)**

Figures F-14-25 through F-14-36 illustrate the impact of PCC thickness and lateral support condition on stresses (16-in. base/subbase and 100-psi/in. modulus of subgrade reaction)

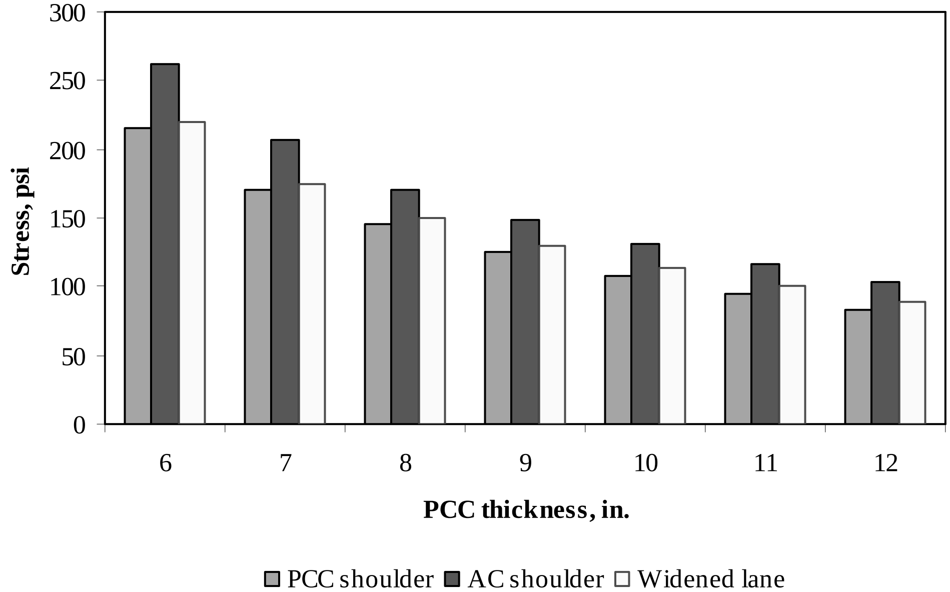


**Figure F-14-25: Impact of PCC thickness and lateral support condition on longitudinal stress at bottom of the Slab (177-in. joint spacing and α(ΔT/D) of 0 in.$^{-1}$)**

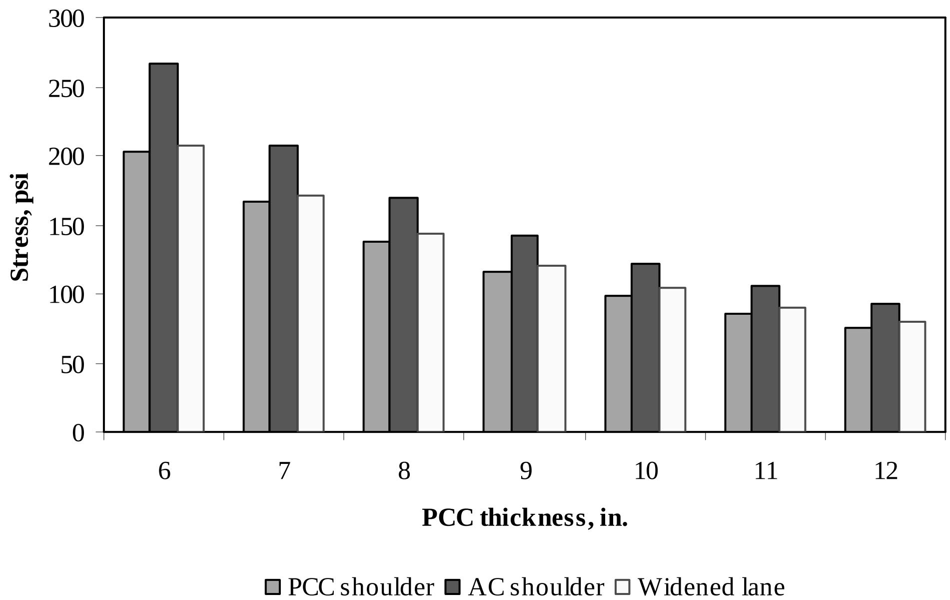


**Figure F-14-26: Impact of PCC thickness and lateral support condition on longitudinal stress at bottom of the Slab (315-in. joint spacing and α(ΔT/D) of 0 in.$^{-1}$)**

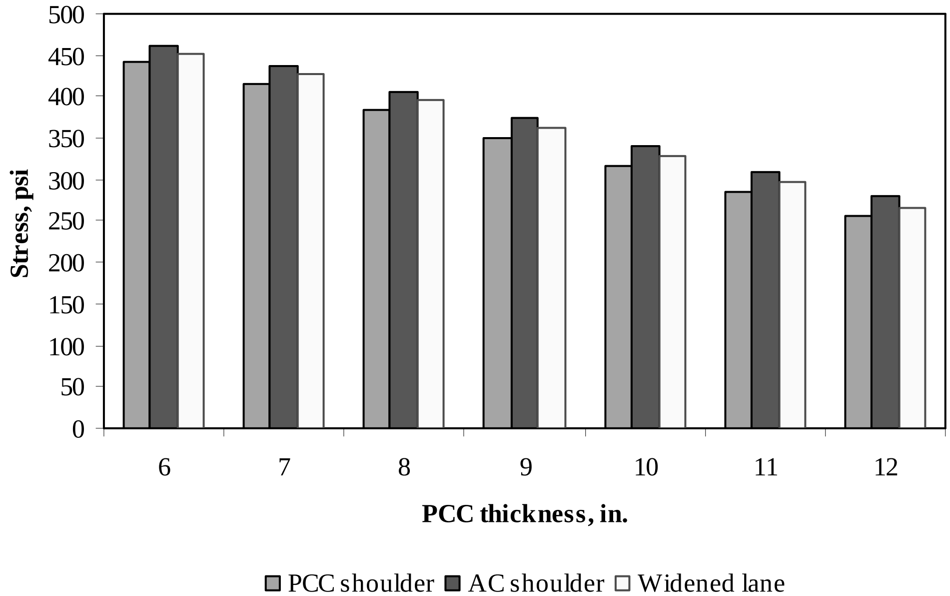


**Figure F-14-27: Impact of PCC thickness and lateral support condition on longitudinal stress at bottom of the Slab (177-in. joint spacing and $\alpha(\Delta T/D)$ of $20\times10^{-6}$ in.$^{-1}$)**

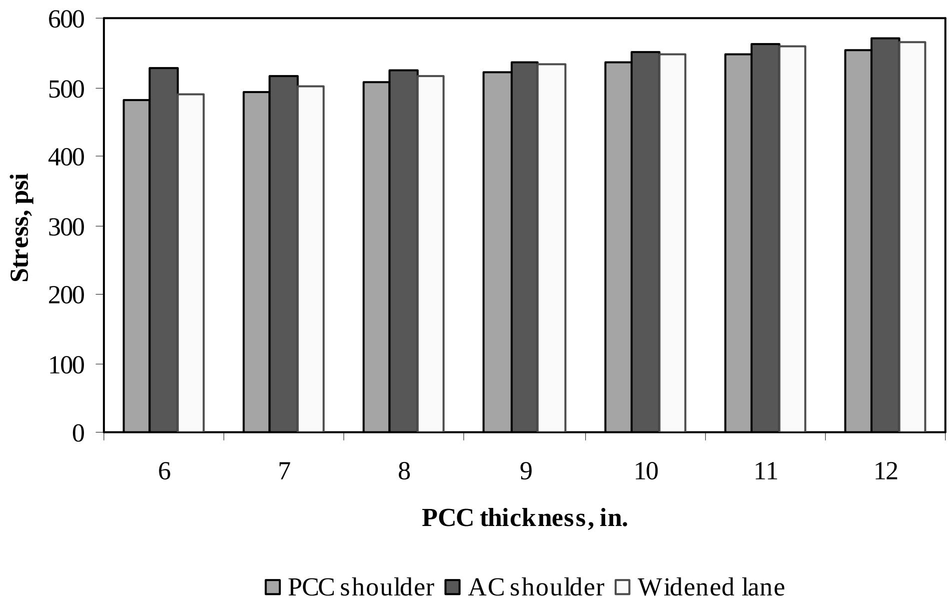


**Figure F-14-28: Impact of PCC thickness and lateral support condition on longitudinal stress at bottom of the Slab (315-in. joint spacing and $\alpha(\Delta T/D)$ of $20\times10^{-6}$ in.$^{-1}$)**

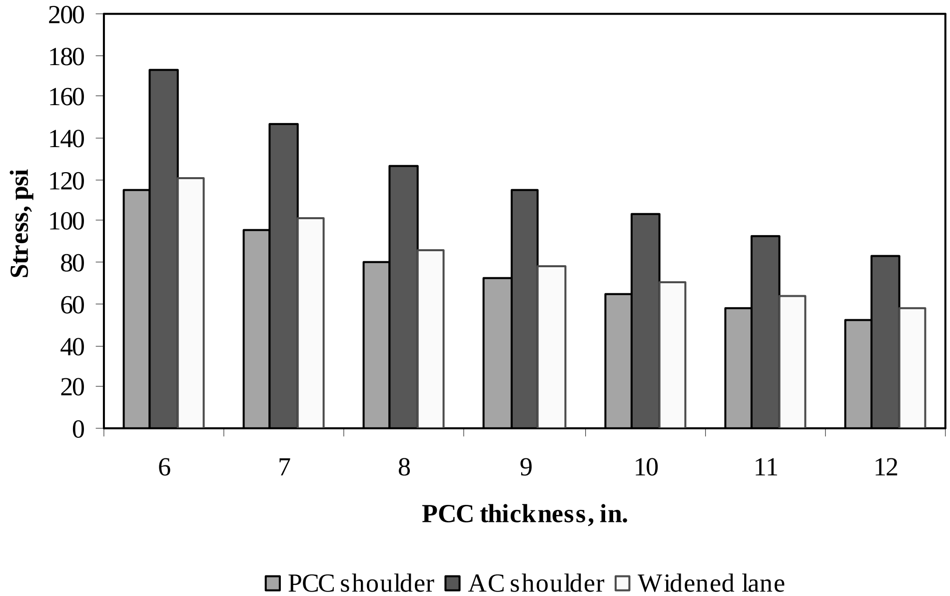


**Figure F-14-29: Impact of PCC thickness and lateral support condition on longitudinal stress at top of the Slab (177-in. joint spacing and $\alpha(\Delta T/D)$ of 0 in.$^{-1}$)**

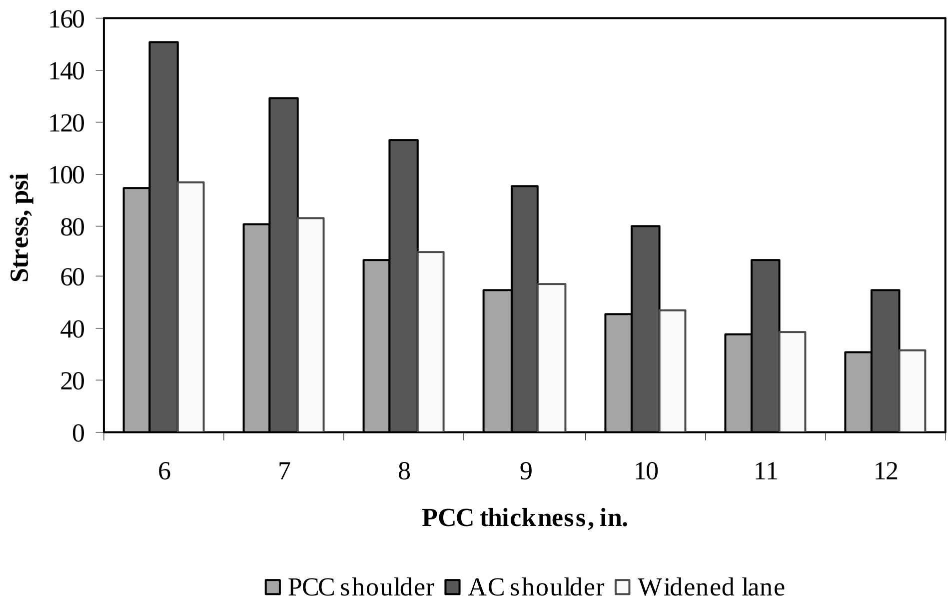


**Figure F-14-30: Impact of PCC thickness and lateral support condition on longitudinal stress at top of the Slab (315-in. joint spacing and $\alpha(\Delta T/D)$ of 0 in.$^{-1}$)**

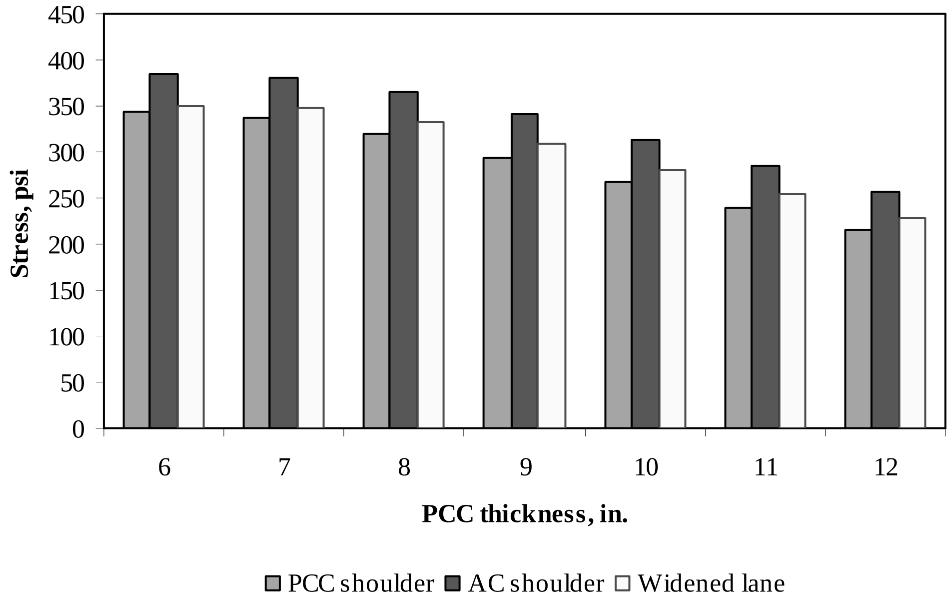


**Figure F-14-31: Impact of PCC thickness and lateral support condition on longitudinal stress at top of the Slab (177-in. joint spacing and $\alpha(\Delta T/D)$ of $-20 \times 10^{-6}$ in.$^{-1}$)**

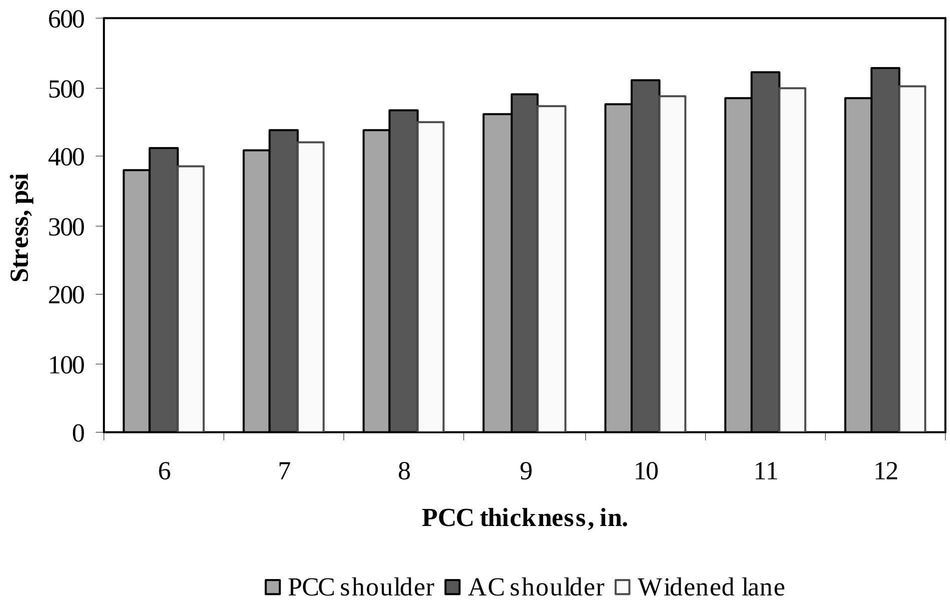


**Figure F-14-32: Impact of PCC thickness and lateral support condition on longitudinal stress at top of the Slab (315-in. joint spacing and $\alpha(\Delta T/D)$ of $-20 \times 10^{-6}$ in.$^{-1}$)**

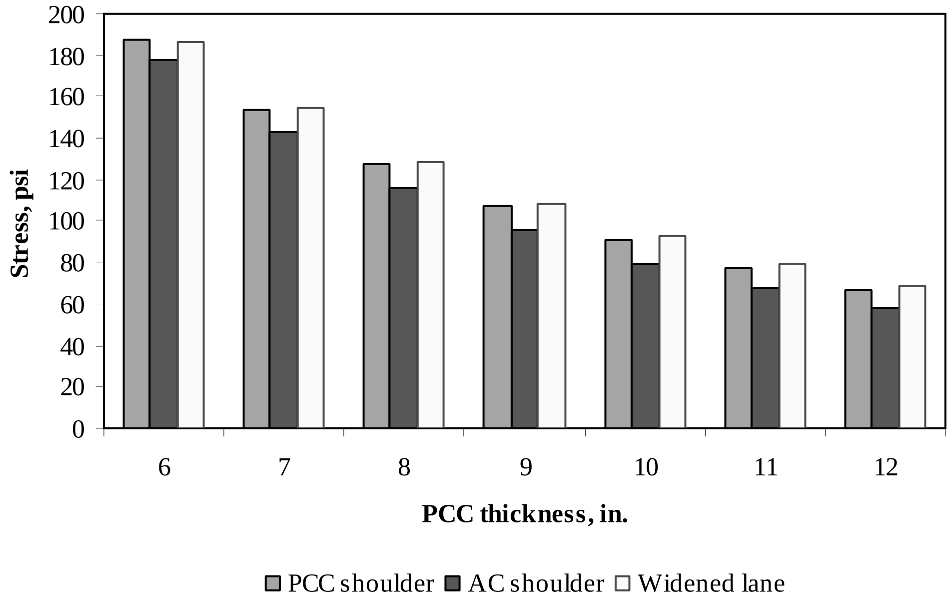


**Figure F-14-33: Impact of PCC thickness and lateral support condition on transverse stress at bottom of the Slab (177-in. joint spacing and $\alpha(\Delta T/D)$ of 0 in.$^{-1}$)**

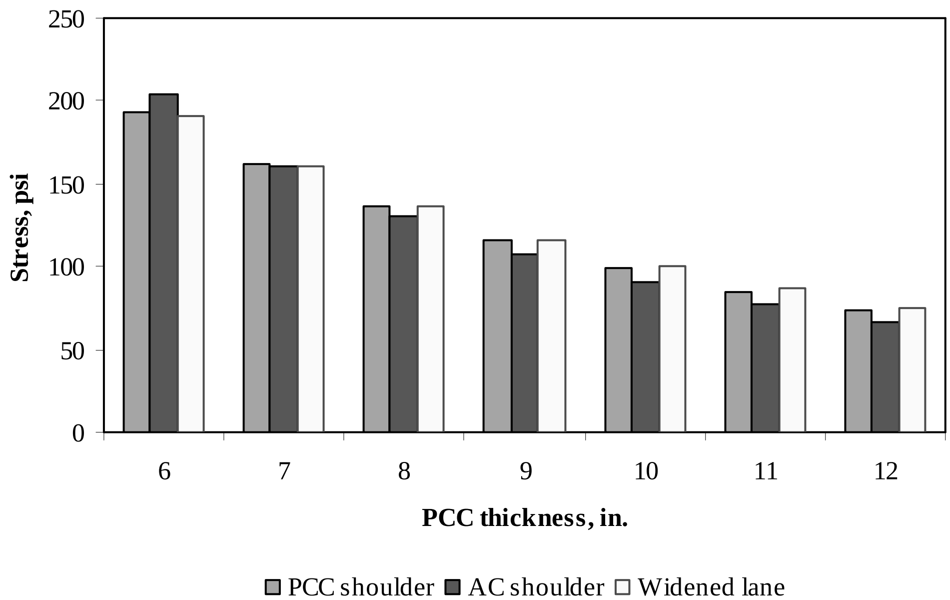


**Figure F-14-34: Impact of PCC thickness and lateral support condition on transverse stress at bottom of the Slab (315-in. joint spacing and $\alpha(\Delta T/D)$ of 0 in.$^{-1}$)**

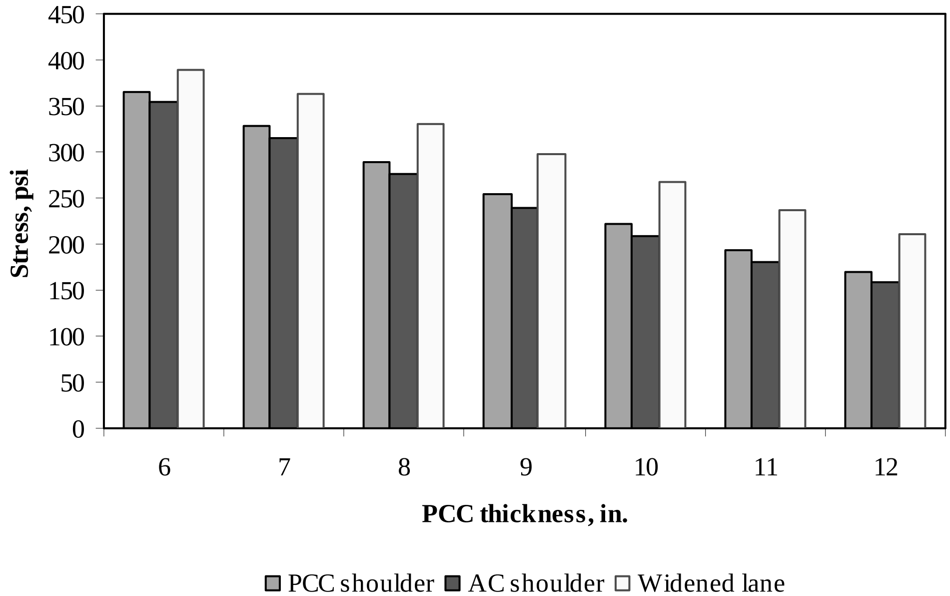


**Figure F-14-35: Impact of PCC thickness and lateral support condition on transverse stress at bottom of the Slab (177-in. joint spacing and $\alpha(\Delta T/D)$ of $20x10^{-6}$ in.$^{-1}$)**

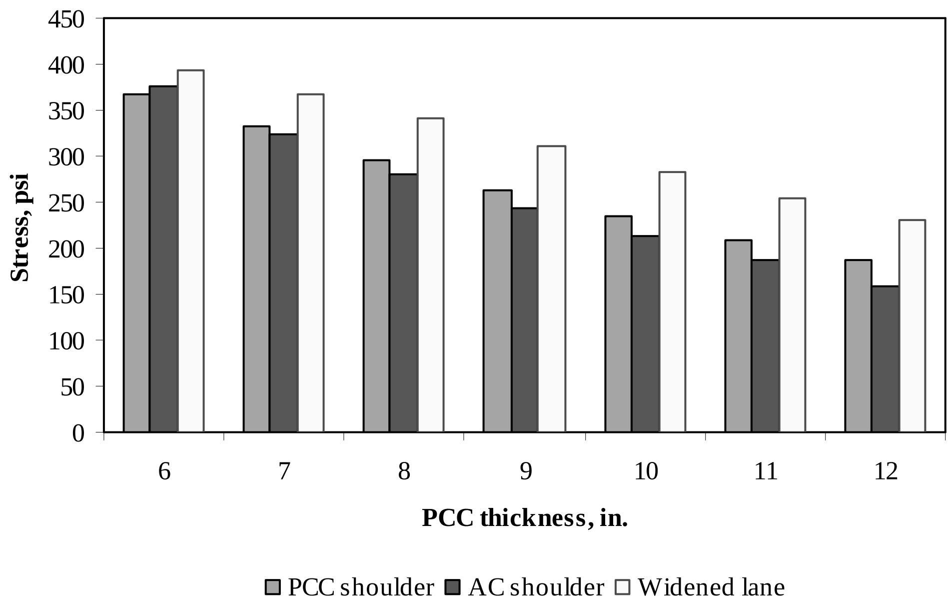


**Figure F-14-36: Impact of PCC thickness and lateral support condition on transverse stress at bottom of the Slab (315-in. joint spacing and $\alpha(\Delta T/D)$ of $20x10^{-6}$ in.$^{-1}$)**

Figures F-14-37 through F-14-42 illustrate the impact of base/subbase thickness and product α(ΔT/D) on stresses (10-in. PCC thickness, 100-psi/in. modulus of subgrade reaction and PCC shoulder)

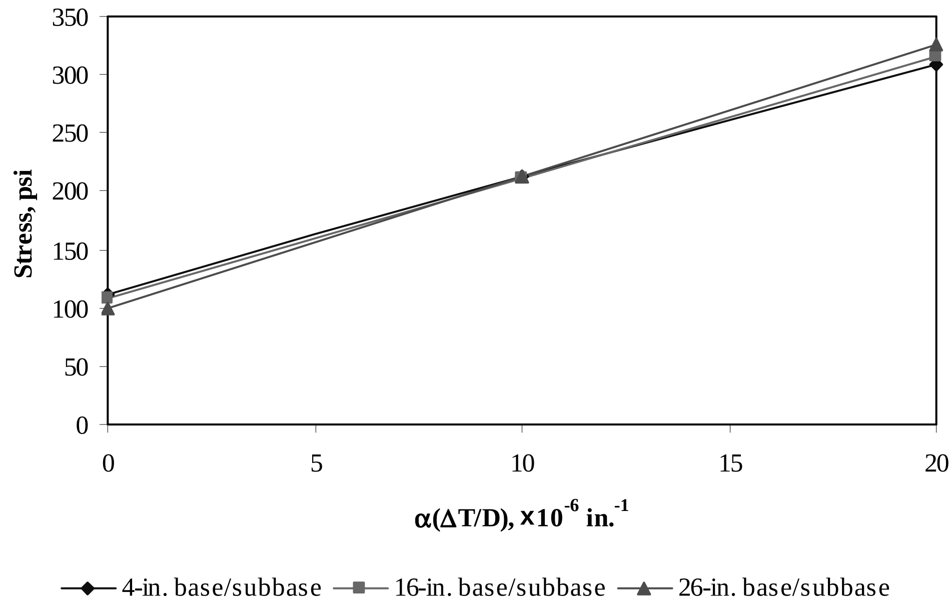


**Figure F-14-37: Impact of base/subbase thickness and product α(ΔT/D) on longitudinal stress at bottom of the slab (177-in. joint spacing)**

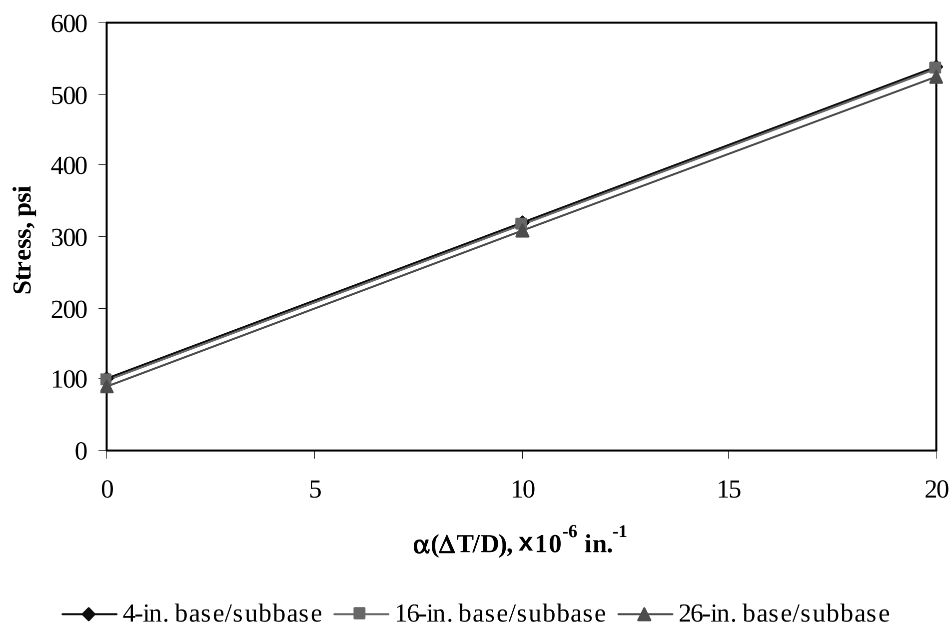


**Figure F-14-38: Impact of base/subbase thickness and product α(ΔT/D) on longitudinal stress at bottom of the slab (315-in. joint spacing)**

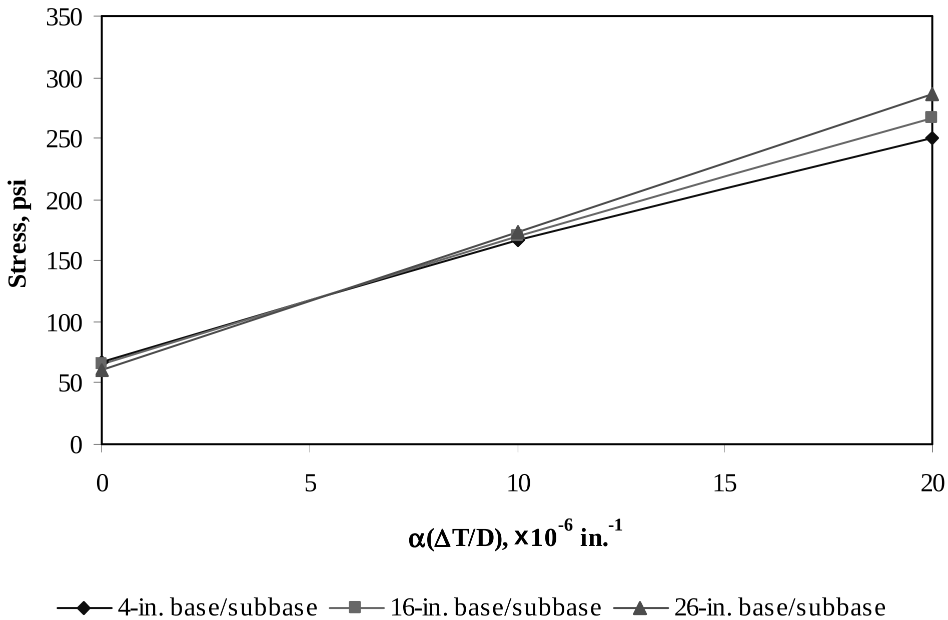


**Figure F-14-39: Impact of base/subbase thickness and product α(ΔT/D) on longitudinal stress at top of the slab (177-in. joint spacing)**

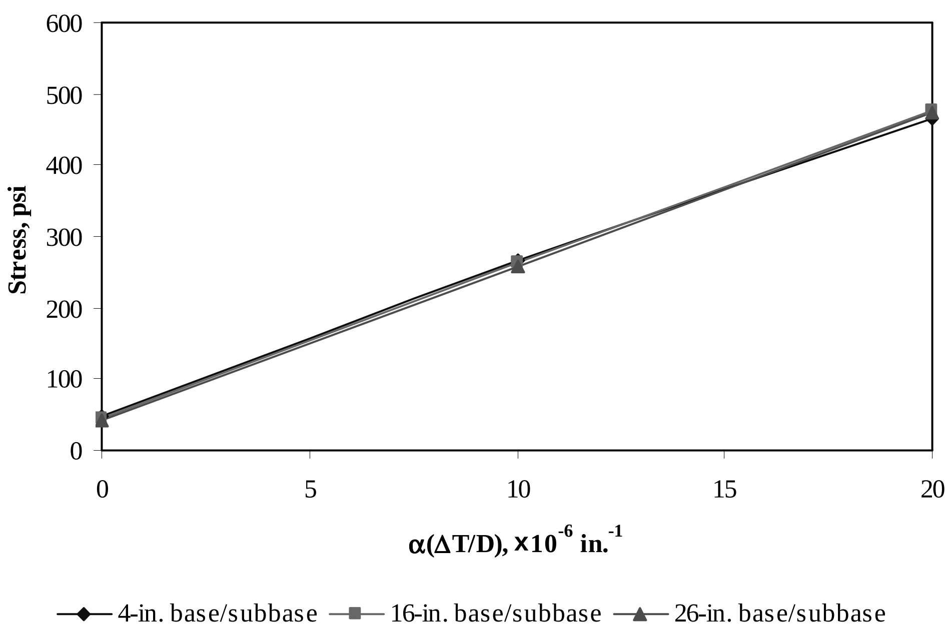


**Figure F-14-40: Impact of base/subbase thickness and product α(ΔT/D) on longitudinal stress at top of the slab (315-in. joint spacing)**

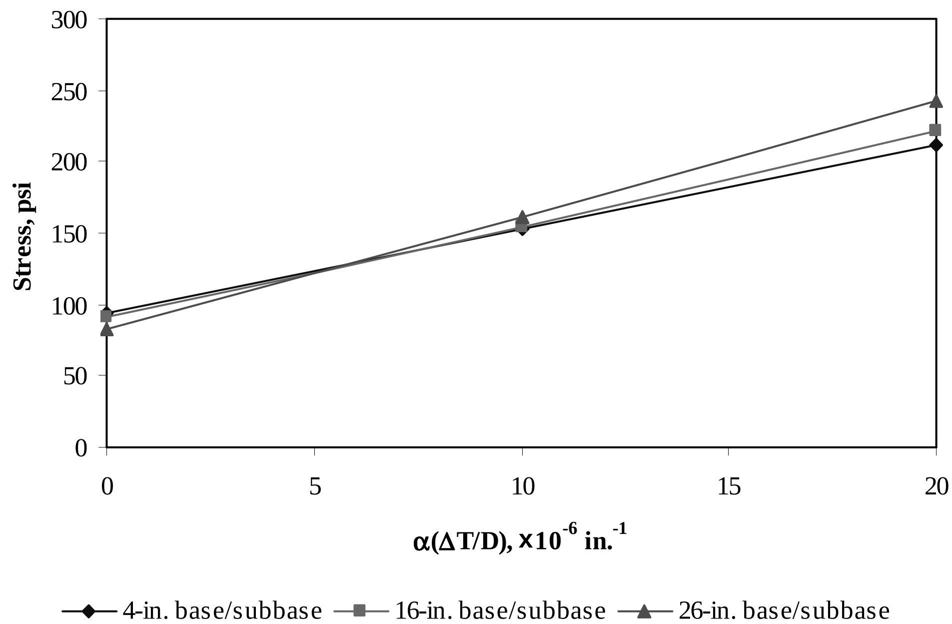


**Figure F-14-41: Impact of base/subbase thickness and product α(ΔT/D) on transverse stress at bottom of the slab (177-in. joint spacing)**

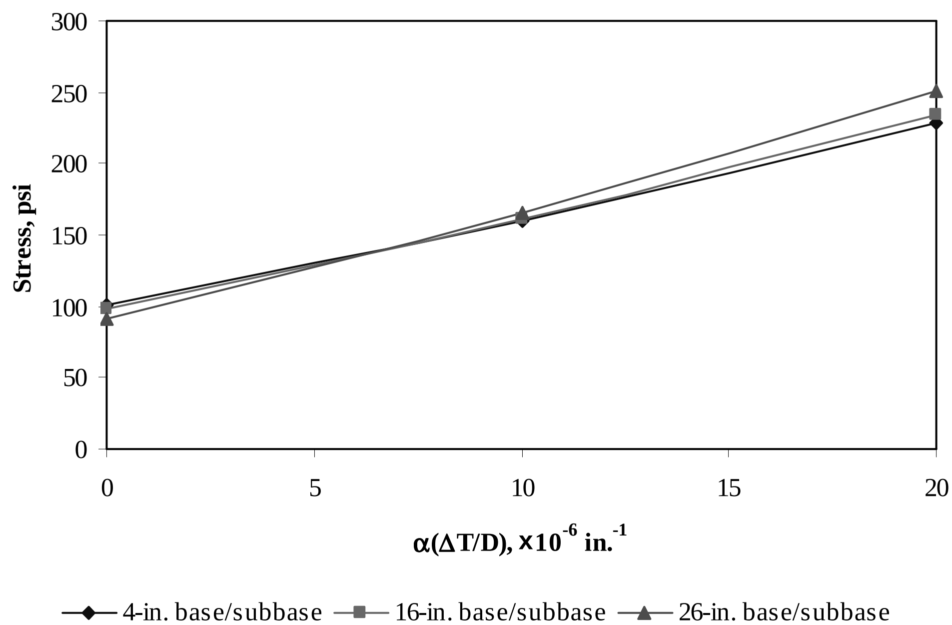


**Figure F-14-42: Impact of base/subbase thickness and product α(ΔT/D) on transverse stress at bottom of the slab (315-in. joint spacing)**

Figures F-14-43 through F-14-48 illustrate the impact of modulus of subgrade reaction and product α(ΔT/D) on stresses (10-in. PCC thickness, 16-in. base/subbase thickness and PCC shoulder)

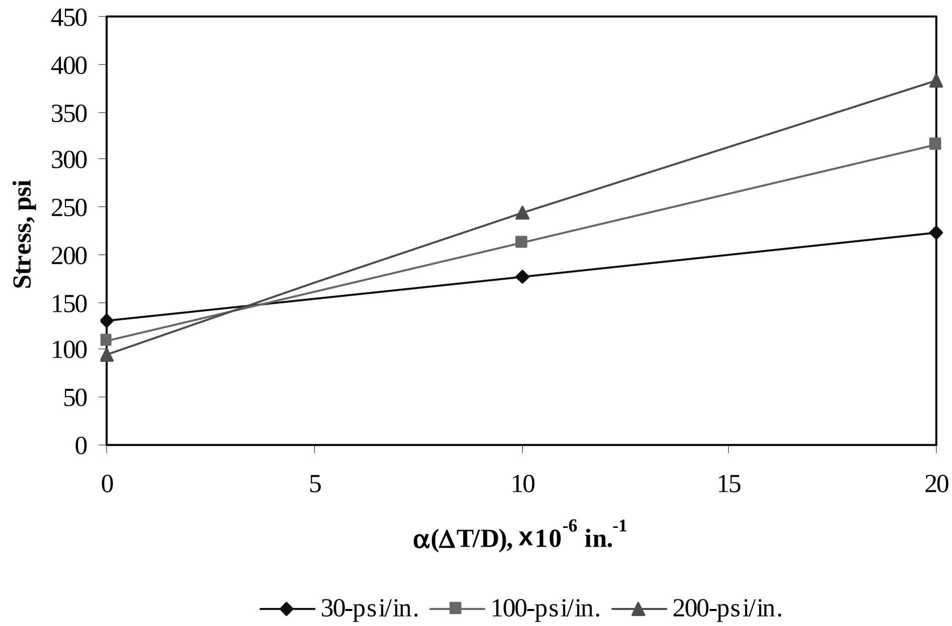


**Figure F-14-43: Impact of modulus of subgrade reaction and product α(ΔT/D) on longitudinal stress at bottom of the slab (177-in. joint spacing)**

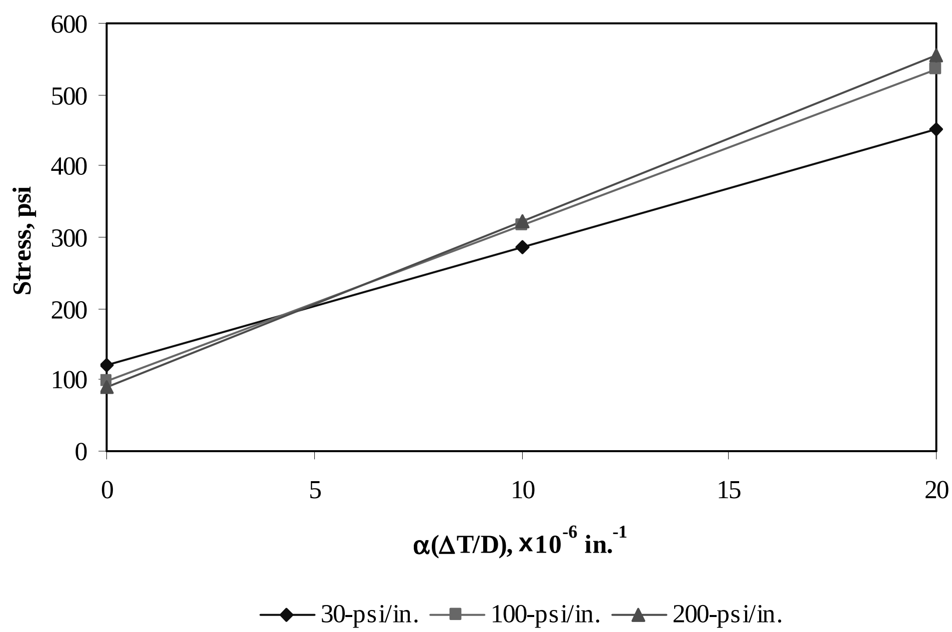


**Figure F-14-44: Impact of modulus of subgrade reaction and product α(ΔT/D) on longitudinal stress at bottom of the slab (315-in. joint spacing)**

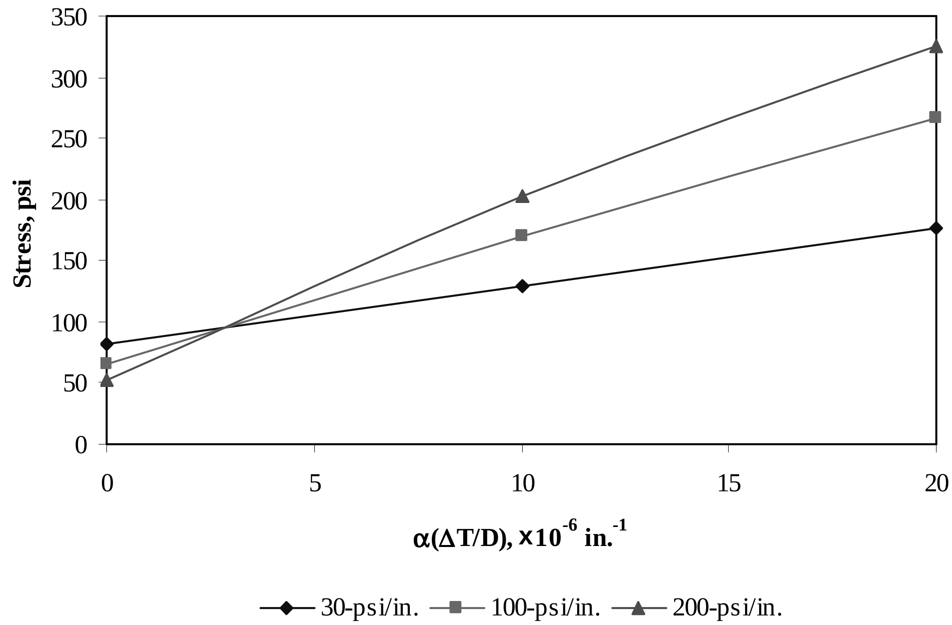


**Figure F-14-45: Impact of modulus of subgrade reaction and product α(ΔT/D) on longitudinal stress at top of the slab (177-in. joint spacing)**

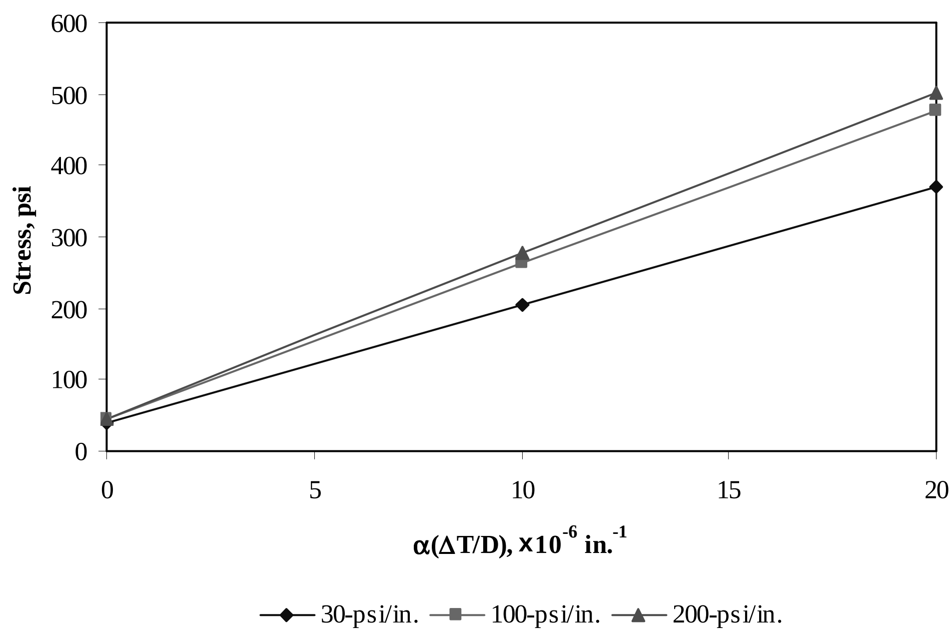


**Figure F-14-46: Impact of modulus of subgrade reaction and product α(ΔT/D) on longitudinal stress at top of the slab (315-in. joint spacing)**

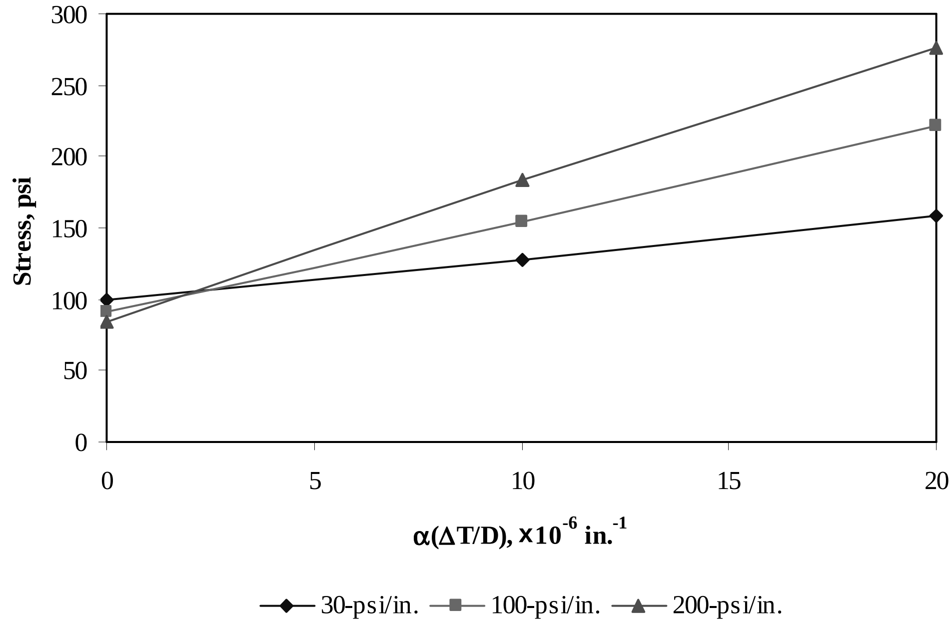


**Figure F-14-47: Impact of modulus of subgrade reaction and product α(ΔT/D) on transverse stress at bottom of the slab (177-in. joint spacing)**

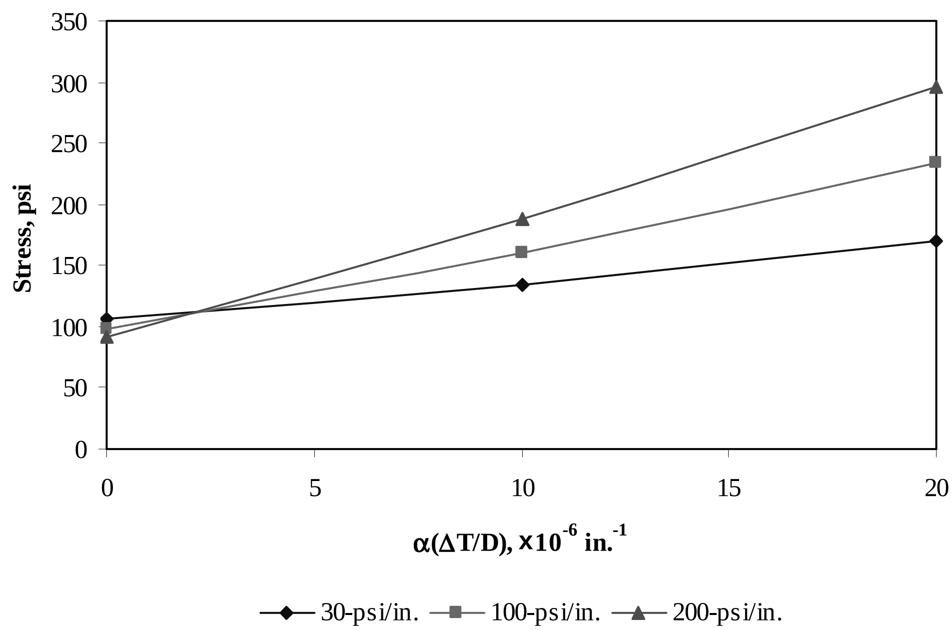


**Figure F-14-48: Impact of modulus of subgrade reaction and product α(ΔT/D) on transverse stress at bottom of the slab (315-in. joint spacing)**

Figures F-14-49 through F-14-51 illustrate the impact of joint spacing and product α(ΔT/D) on stresses (10-in. PCC thickness, 16-in. base/subbase thickness, 100-psi/in. modulus of subgrade reaction and PCC shoulder)

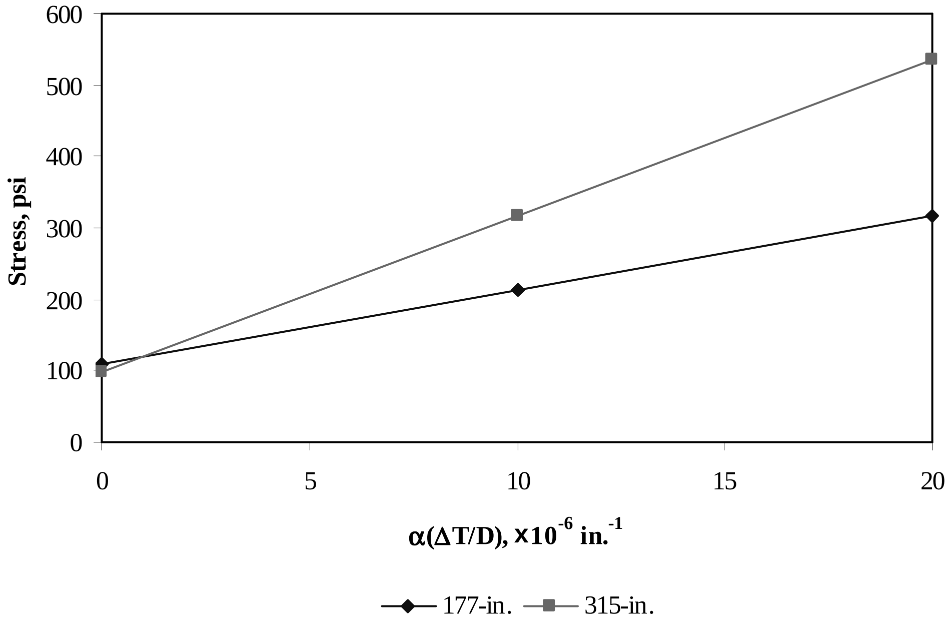


**Figure F-14-49: Impact of joint spacing and product α(ΔT/D) on longitudinal stress at bottom of the slab**

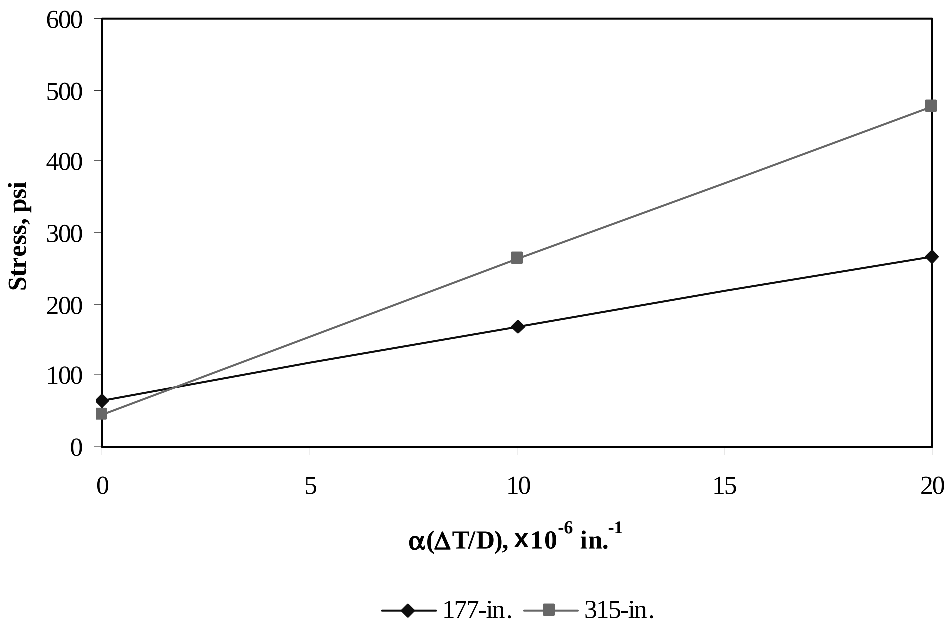


**Figure F-14-50: Impact of joint spacing and product α(ΔT/D) on longitudinal stress at top of the slab**

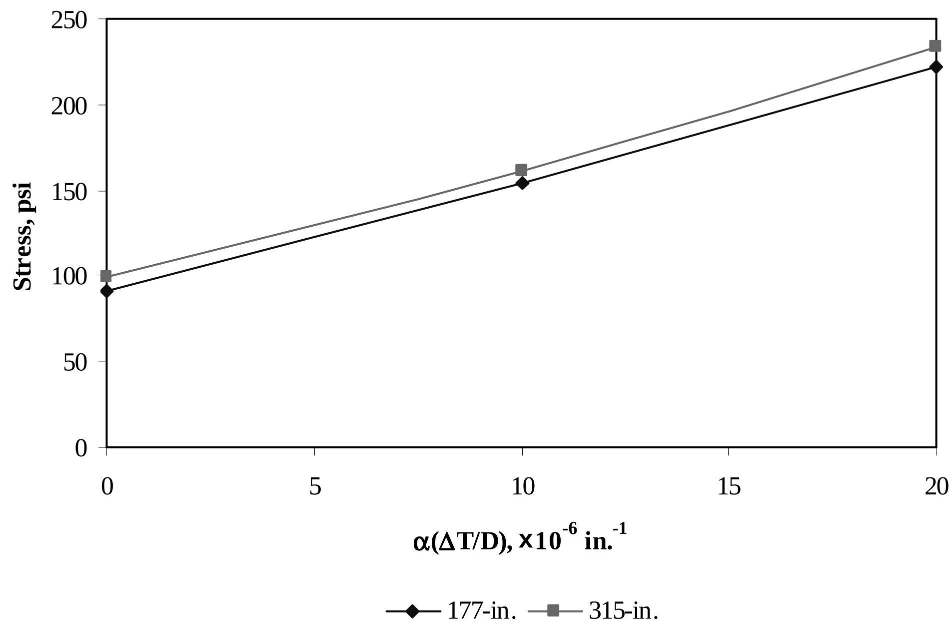


**Figure F-14-51: Impact of joint spacing and product α(ΔT/D) on transverse stress at bottom of the slab**

**Sub Appendix F-15**

**Documentation of Pavement Responses for**

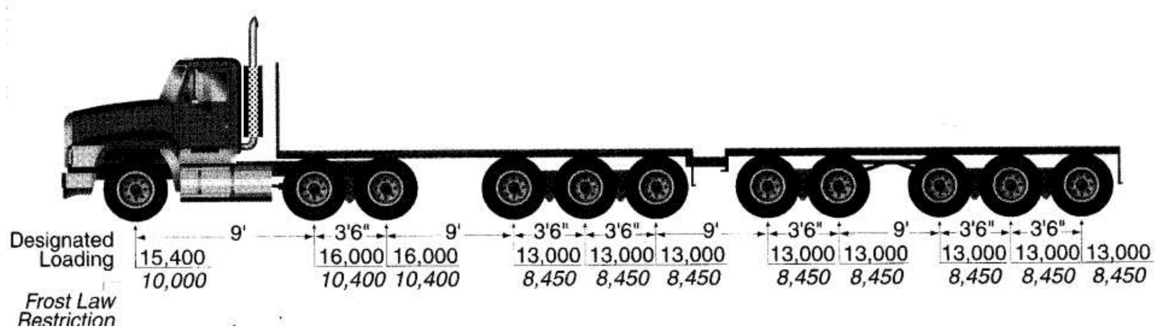


**MI-13**

Figures F-15-1 through F-15-12 illustrate the impact of PCC thickness and base/subbase thickness on stresses (100-psi/in. modulus of subgrade reaction and PCC shoulder)

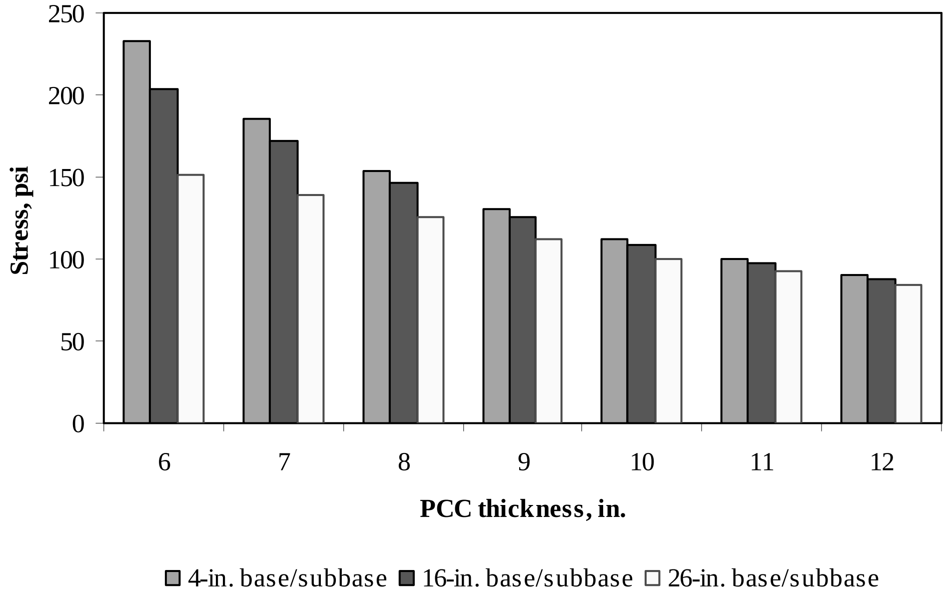


**Figure F-15-1: Impact of PCC thickness and base/subbase thickness on longitudinal stress at bottom of the Slab (177-in. joint spacing and $\alpha(\Delta T/D)$ of 0 in.$^{-1}$)**

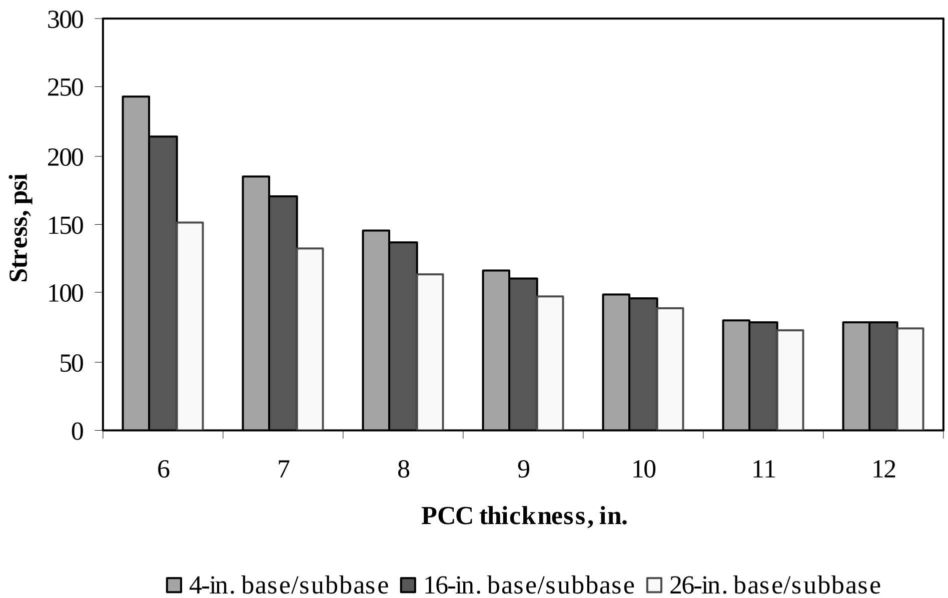


**Figure F-15-2: Impact of PCC thickness and base/subbase thickness on longitudinal stress at bottom of the Slab (315-in. joint spacing and $\alpha(\Delta T/D)$ of 0 in.$^{-1}$)**

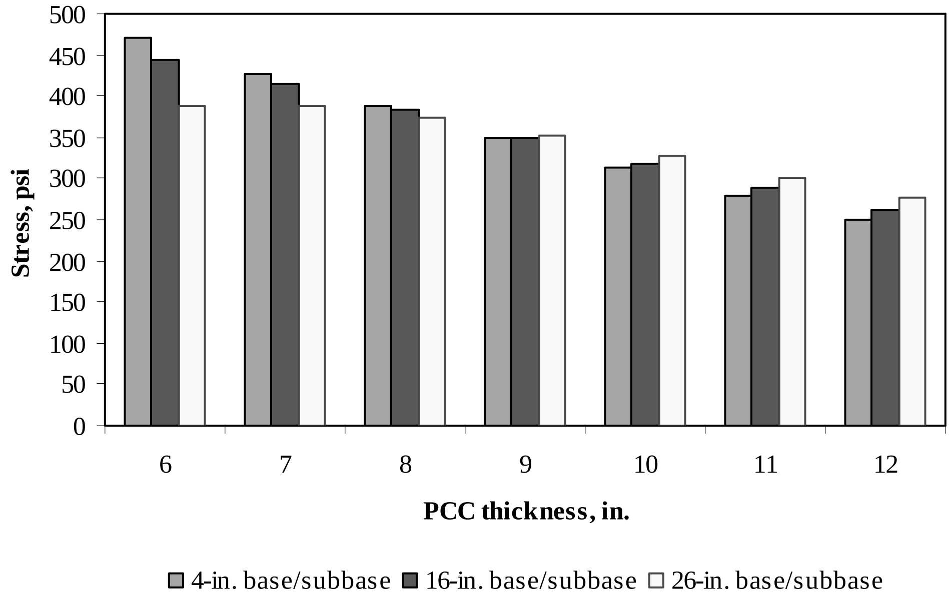


**Figure F-15-3: Impact of PCC thickness and base/subbase thickness on longitudinal stress at bottom of the Slab (177-in. joint spacing and $\alpha(\Delta T/D)$ of $20 x 10^{-6}$ in.$^{-1}$)**

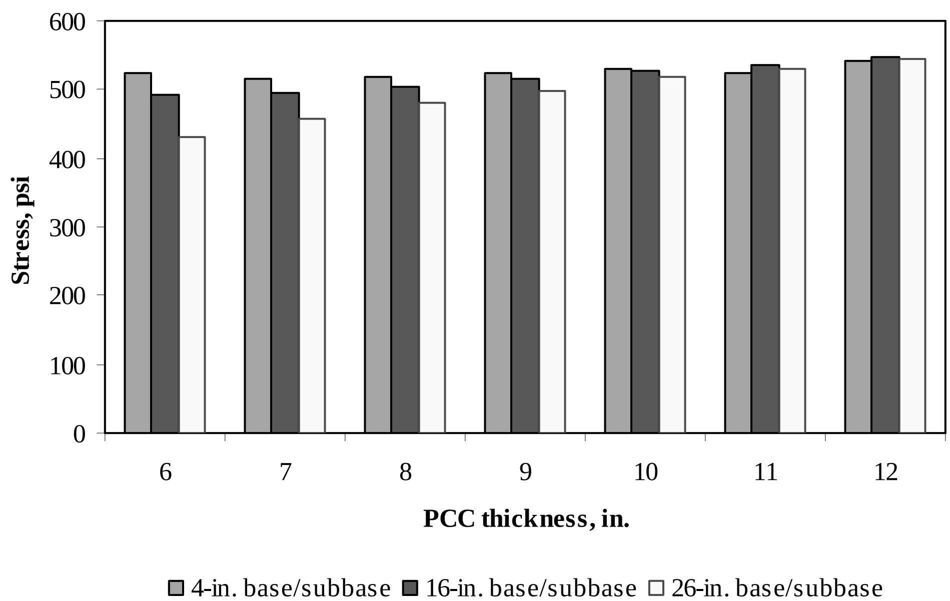


**Figure F-15-4: Impact of PCC thickness and base/subbase thickness on longitudinal stress at bottom of the Slab (315-in. joint spacing and $\alpha(\Delta T/D)$ of $20 x 10^{-6}$ in.$^{-1}$)**

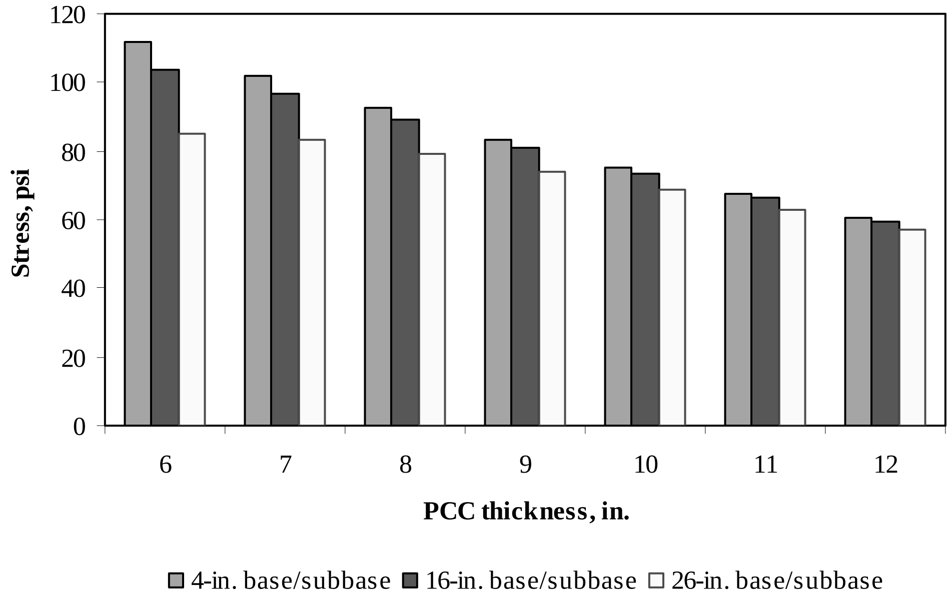


**Figure F-15-5: Impact of PCC thickness and base/subbase thickness on longitudinal stress at top of the Slab (177-in. joint spacing and $\alpha(\Delta T/D)$ of 0 in.$^{-1}$)**

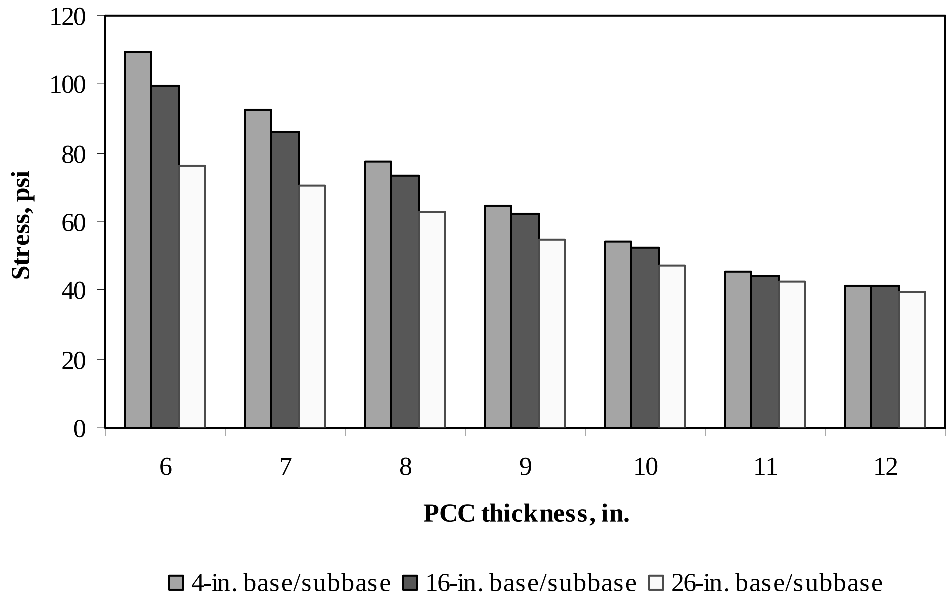


**Figure F-15-6: Impact of PCC thickness and base/subbase thickness on longitudinal stress at top of the Slab (315-in. joint spacing and $\alpha(\Delta T/D)$ of 0 in.$^{-1}$)**

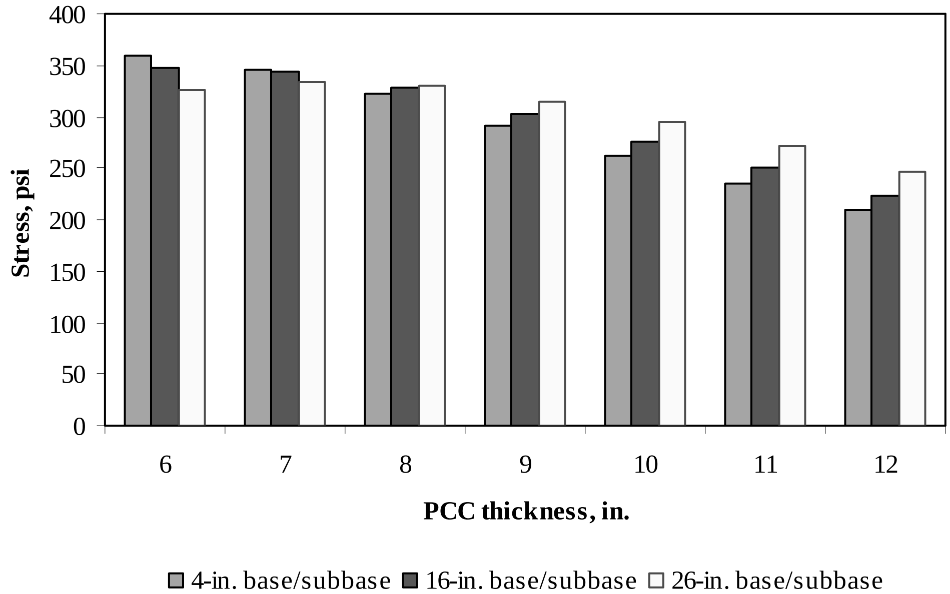


**Figure F-15-7: Impact of PCC thickness and base/subbase thickness on longitudinal stress at top of the Slab (177-in. joint spacing and $\alpha(\Delta T/D)$ of $-20x10^{-6}$ in.$^{-1}$)**

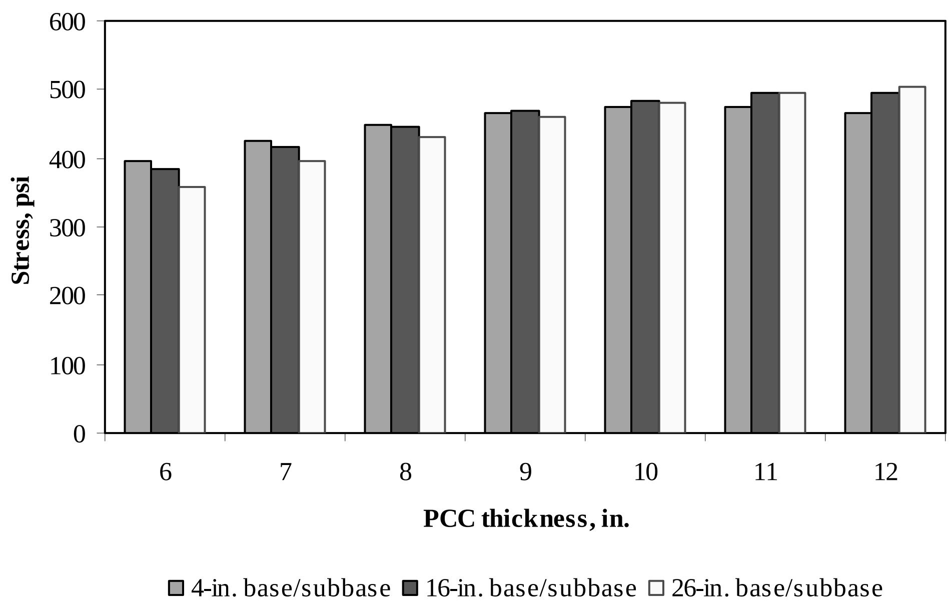


**Figure F-15-8: Impact of PCC thickness and base/subbase thickness on longitudinal stress at top of the Slab (315-in. joint spacing and $\alpha(\Delta T/D)$ of $-20x10^{-6}$ in.$^{-1}$)**

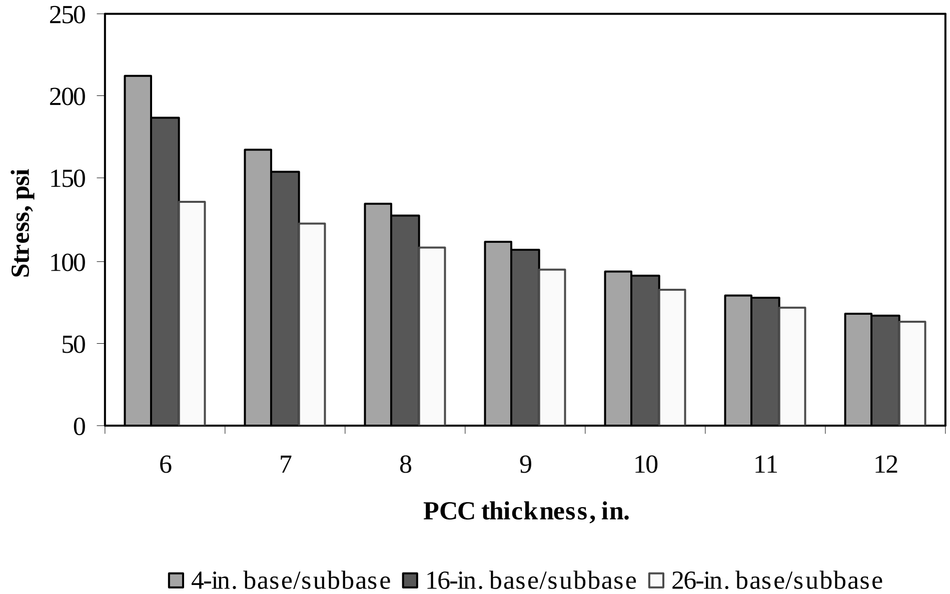


**Figure F-15-9: Impact of PCC thickness and base/subbase thickness on transverse stress at bottom of the Slab (177-in. joint spacing and $\alpha(\Delta T/D)$ of 0 in.$^{-1}$)**

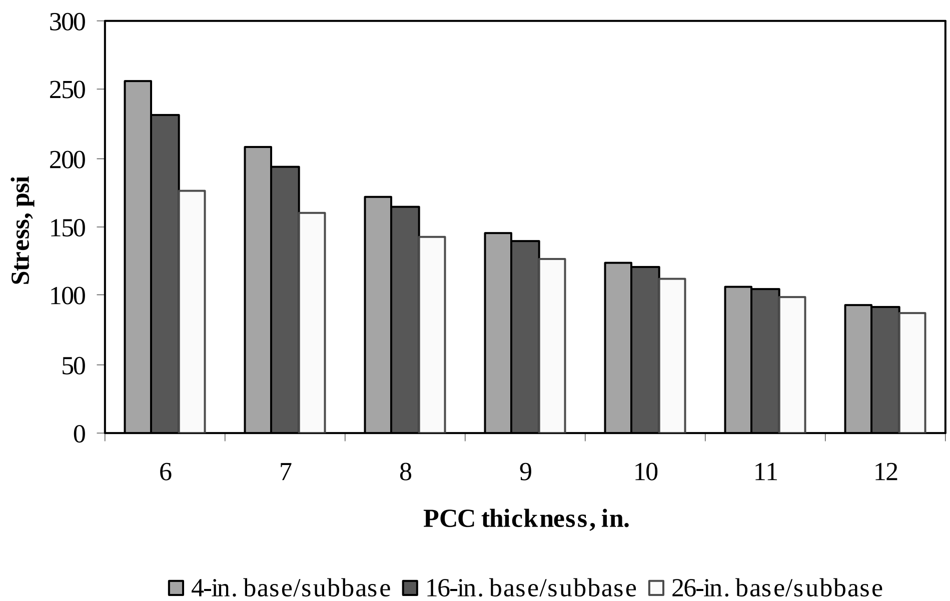


**Figure F-15-10: Impact of PCC thickness and base/subbase thickness on transverse stress at bottom of the Slab (315-in. joint spacing and $\alpha(\Delta T/D)$ of 0 in.$^{-1}$)**

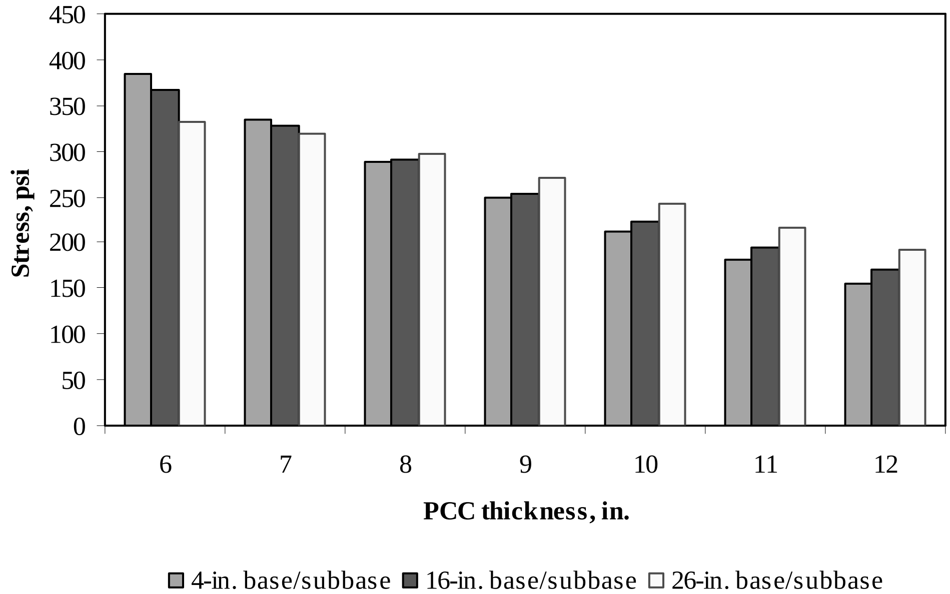


**Figure F-15-11: Impact of PCC thickness and base/subbase thickness on transverse stress at bottom of the Slab (177-in. joint spacing and $\alpha(\Delta T/D)$ of $20x10^{-6}$ in.$^{-1}$)**

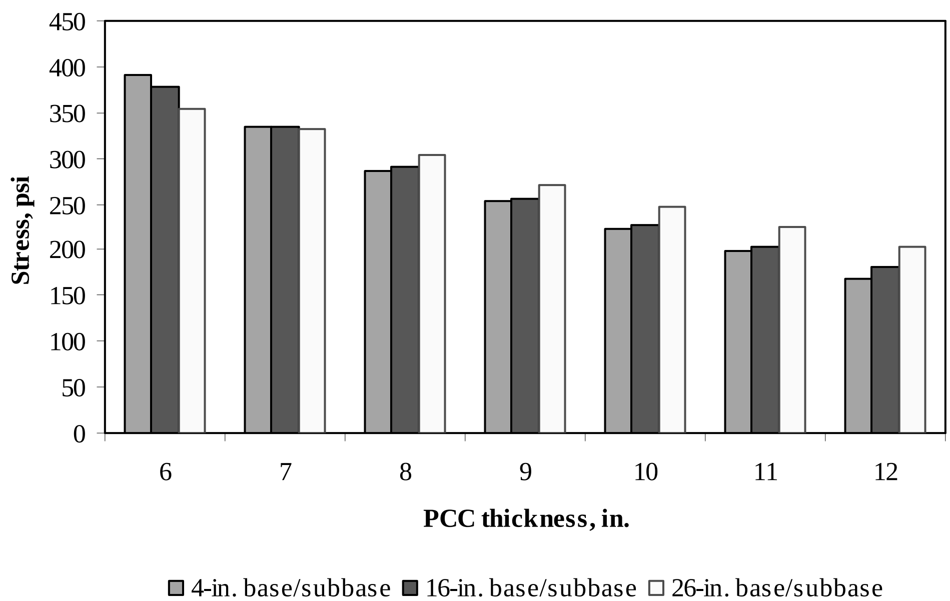


**Figure F-15-12: Impact of PCC thickness and base/subbase thickness on transverse stress at bottom of the Slab (315-in. joint spacing and $\alpha(\Delta T/D)$ of $20x10^{-6}$ in.$^{-1}$)**

Figures F-15-13 through F-15-24 illustrate the impact of PCC thickness and modulus of subgrade reaction on stresses (16-in. base/subbase thickness and PCC shoulder)

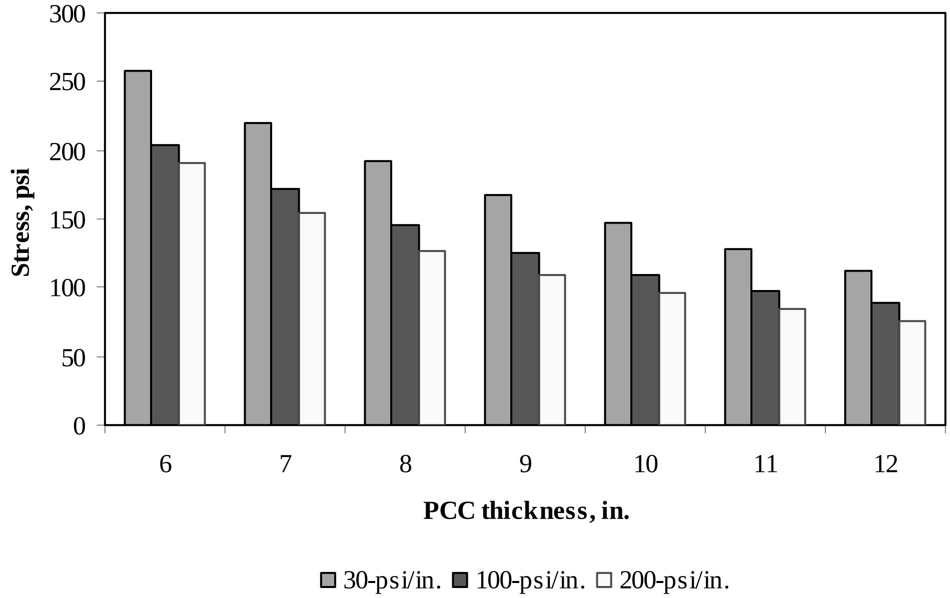


**Figure F-15-13: Impact of PCC thickness and modulus of subgrade reaction on longitudinal stress at bottom of the slab (177-in. joint spacing and $\alpha(\Delta T/D)$ of 0 in.$^{-1}$)**

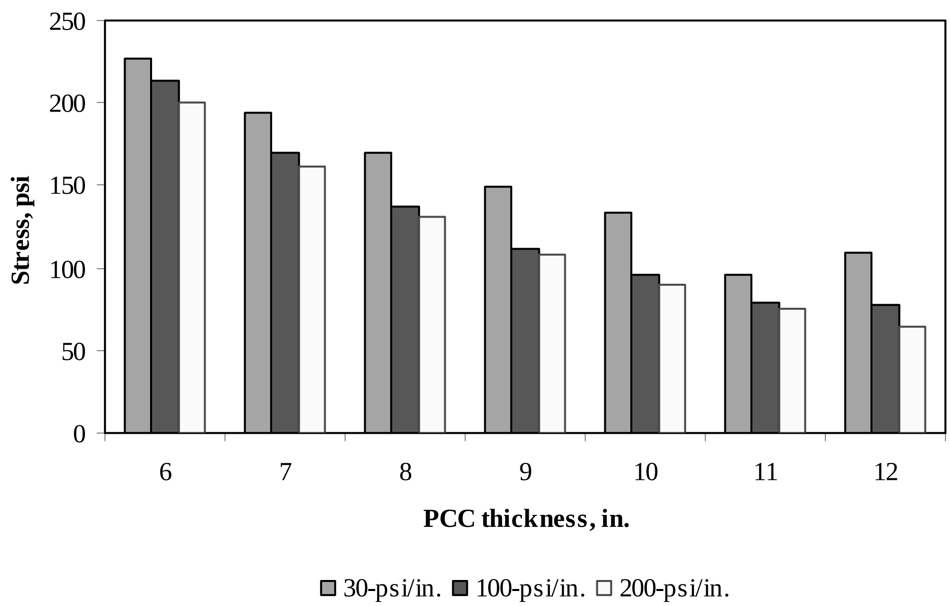


**Figure F-15-14: Impact of PCC thickness and modulus of subgrade reaction on longitudinal stress at bottom of the slab (315-in. joint spacing and $\alpha(\Delta T/D)$ of 0 in.$^{-1}$)**

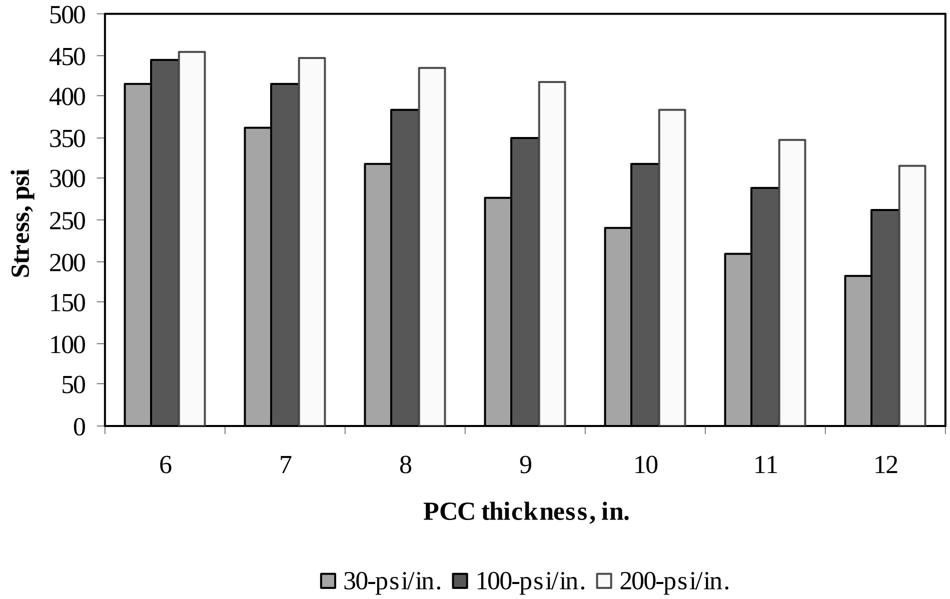


**Figure F-15-15: Impact of PCC thickness and modulus of subgrade reaction on longitudinal stress at bottom of the slab (177-in. joint spacing and $\alpha(\Delta T/D)$ of $20x10^{-6}$ in.$^{-1}$)**

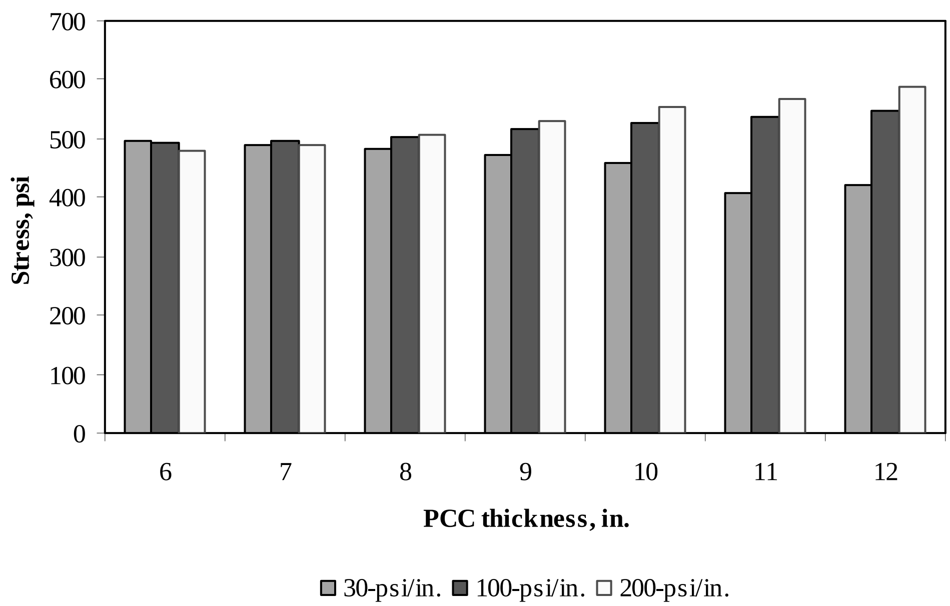


**Figure F-15-16: Impact of PCC thickness and modulus of subgrade reaction on longitudinal stress at bottom of the slab (315-in. joint spacing and $\alpha(\Delta T/D)$ of $20x10^{-6}$ in.$^{-1}$)**

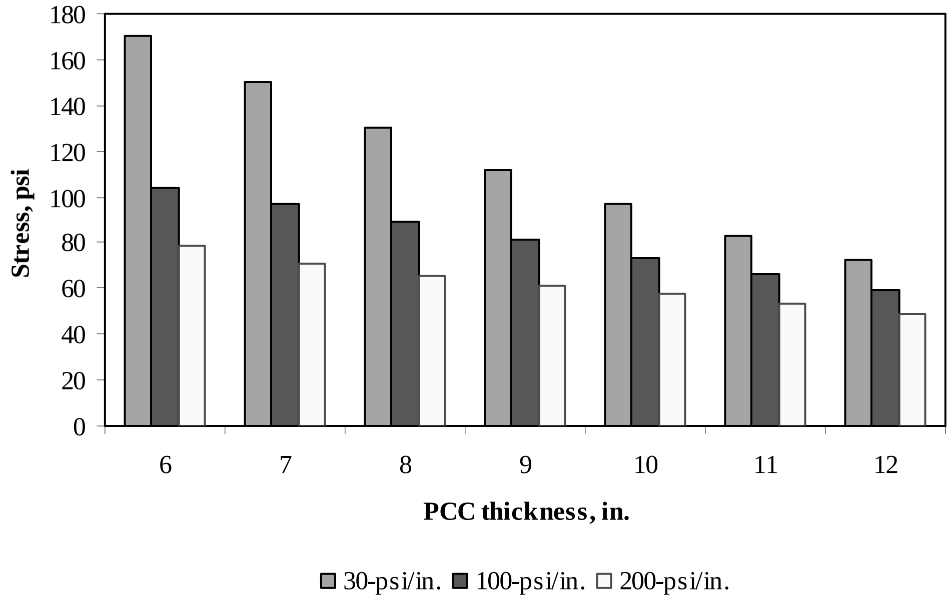


**Figure F-15-17: Impact of PCC thickness and modulus of subgrade reaction on longitudinal stress at top of the Slab (177-in. joint spacing and $\alpha(\Delta T/D)$ of 0 in.$^{-1}$)**

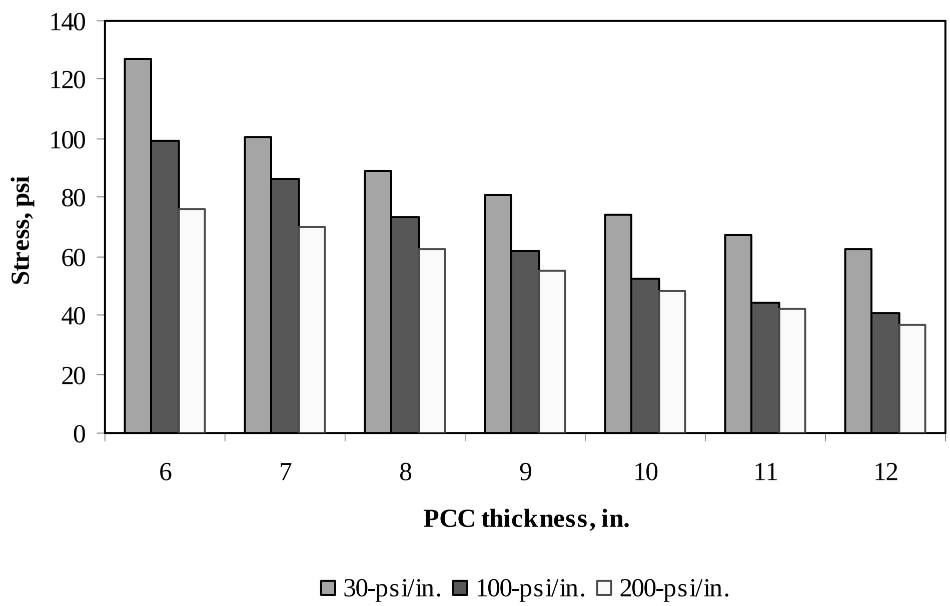


**Figure F-15-18: Impact of PCC thickness and modulus of subgrade reaction on longitudinal stress at top of the Slab (315-in. joint spacing and $\alpha(\Delta T/D)$ of 0 in.$^{-1}$)**

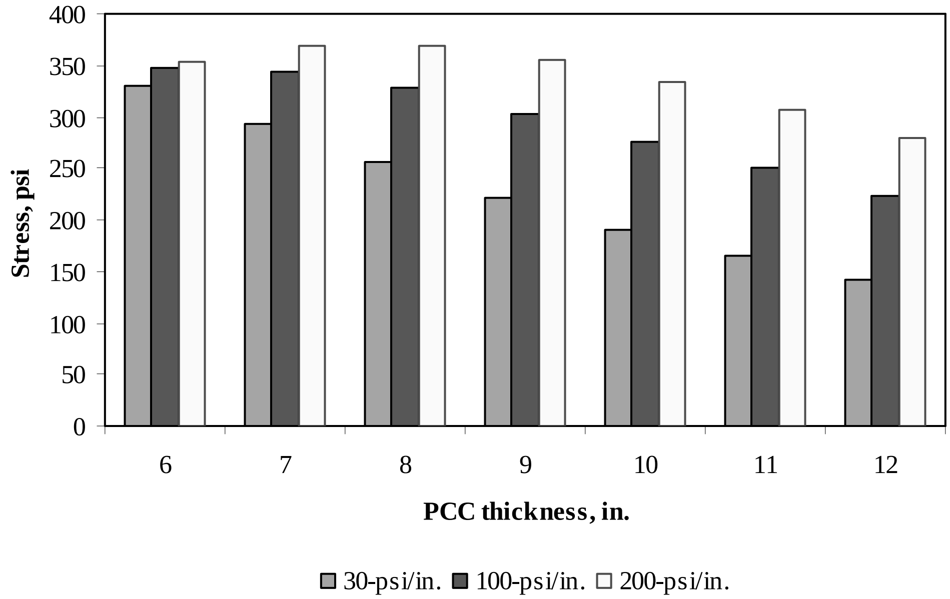


**Figure F-15-19: Impact of PCC thickness and modulus of subgrade reaction on longitudinal stress at top of the Slab (177-in. joint spacing and $\alpha(\Delta T/D)$ of $-20 \times 10^{-6}$ in.$^{-1}$)**

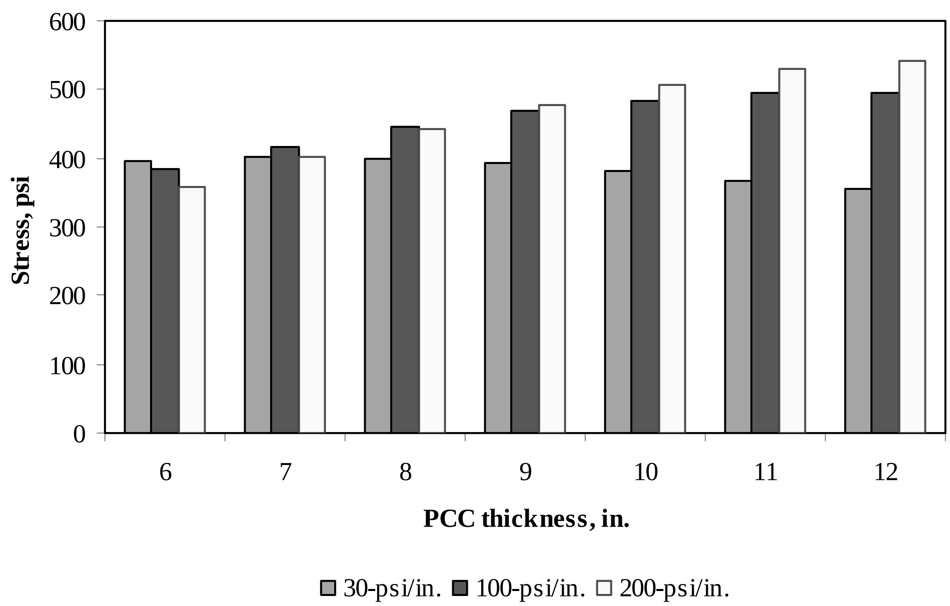


**Figure F-15-20: Impact of PCC thickness and modulus of subgrade reaction on longitudinal stress at top of the Slab (315-in. joint spacing and $\alpha(\Delta T/D)$ of $-20 \times 10^{-6}$ in.$^{-1}$)**

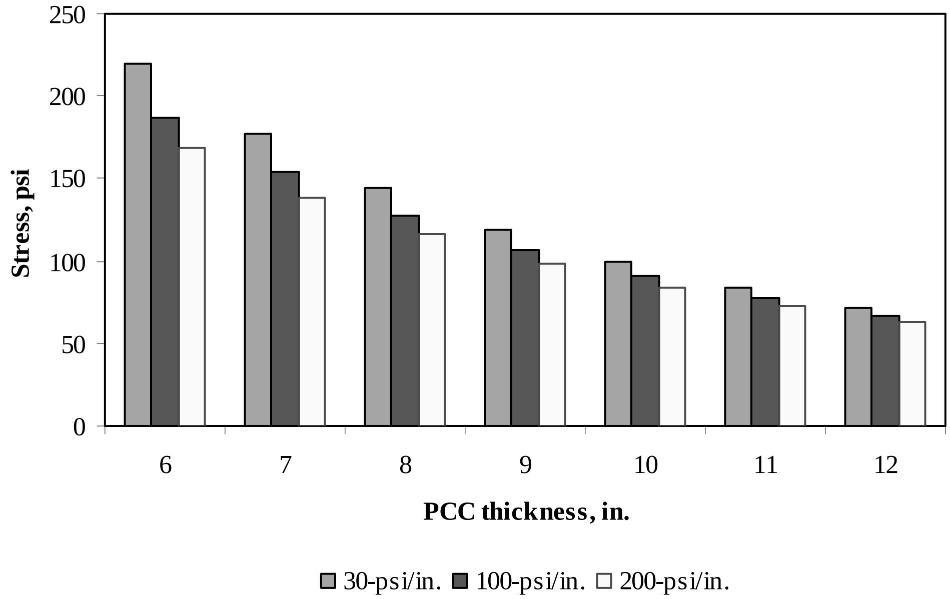


**Figure F-15-21: Impact of PCC thickness and modulus of subgrade reaction on transverse stress at bottom of the Slab (177-in. joint spacing and $\alpha(\Delta T/D)$ of 0 in.$^{-1}$)**

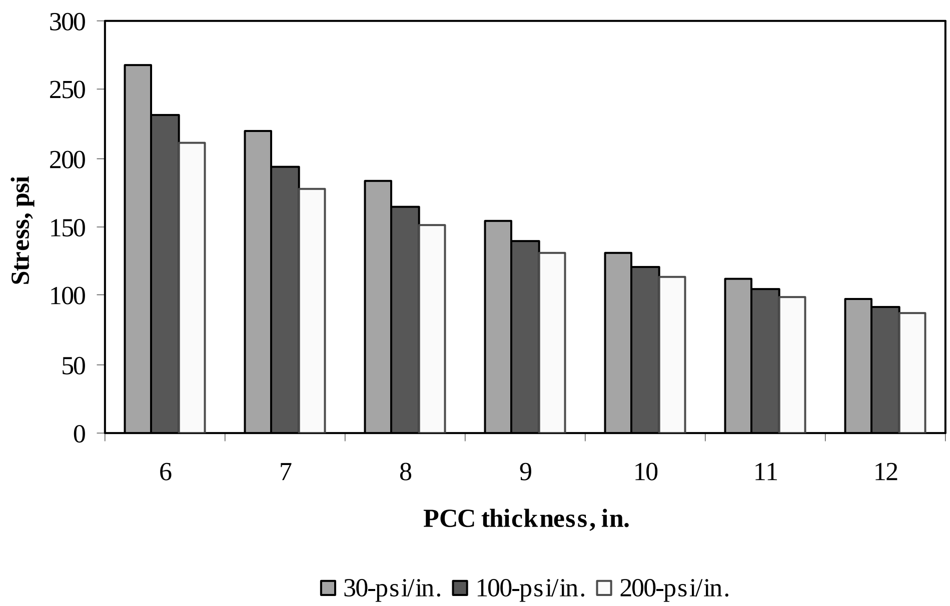


**Figure F-15-22: Impact of PCC thickness and modulus of subgrade reaction on transverse stress at bottom of the Slab (315-in. joint spacing and $\alpha(\Delta T/D)$ of 0 in.$^{-1}$)**

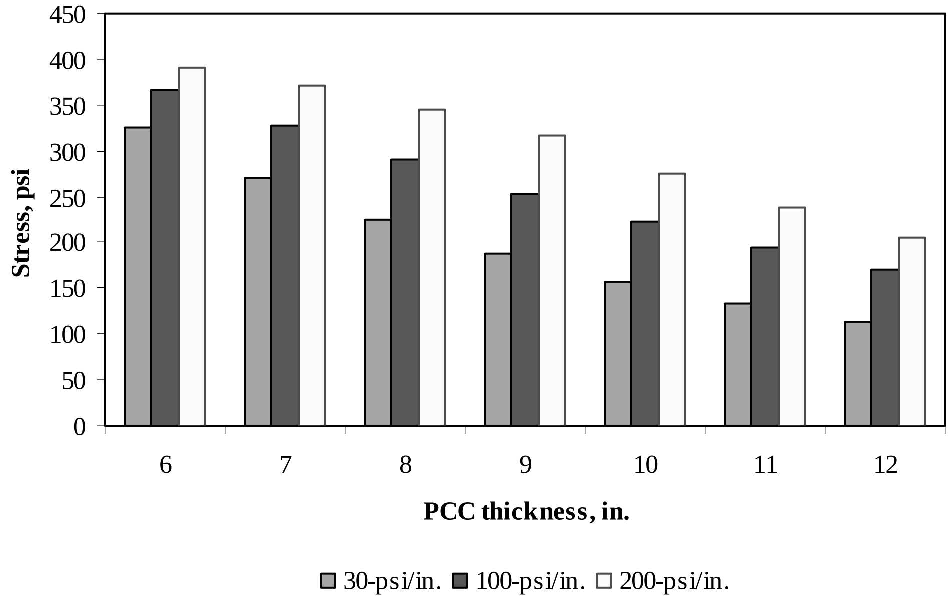


**Figure F-15-23: Impact of PCC thickness and modulus of subgrade reaction on transverse stress at bottom of the Slab (177-in. joint spacing and $\alpha(\Delta T/D)$ of $20x10^{-6}$ in.$^{-1}$)**

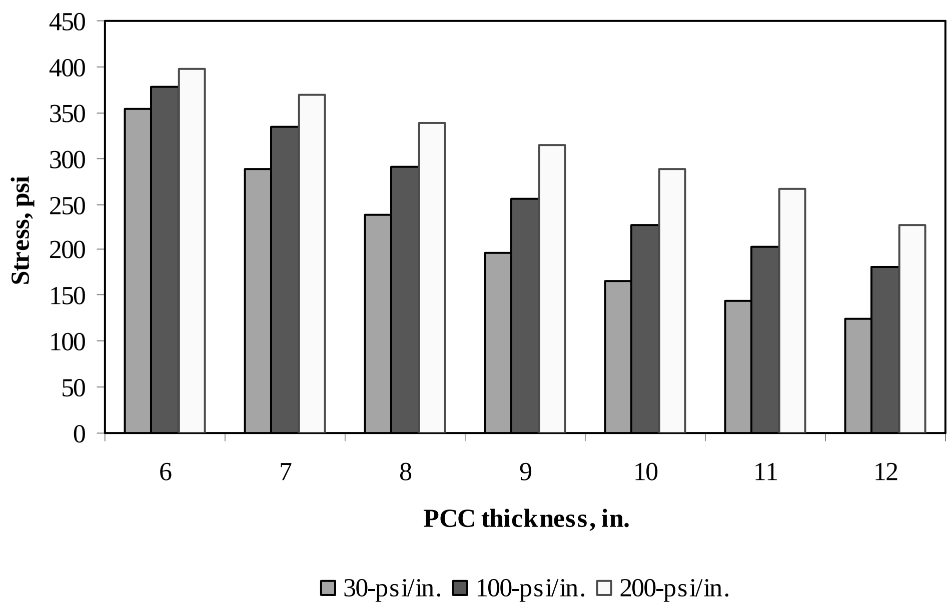


**Figure F-15-24: Impact of PCC thickness and modulus of subgrade reaction on transverse stress at bottom of the Slab (315-in. joint spacing and $\alpha(\Delta T/D)$ of $20x10^{-6}$ in.$^{-1}$)**

Figures F-15-25 through F-15-36 illustrate the impact of PCC thickness and lateral support condition on stresses (16-in. base/subbase and 100-psi/in. modulus of subgrade reaction)

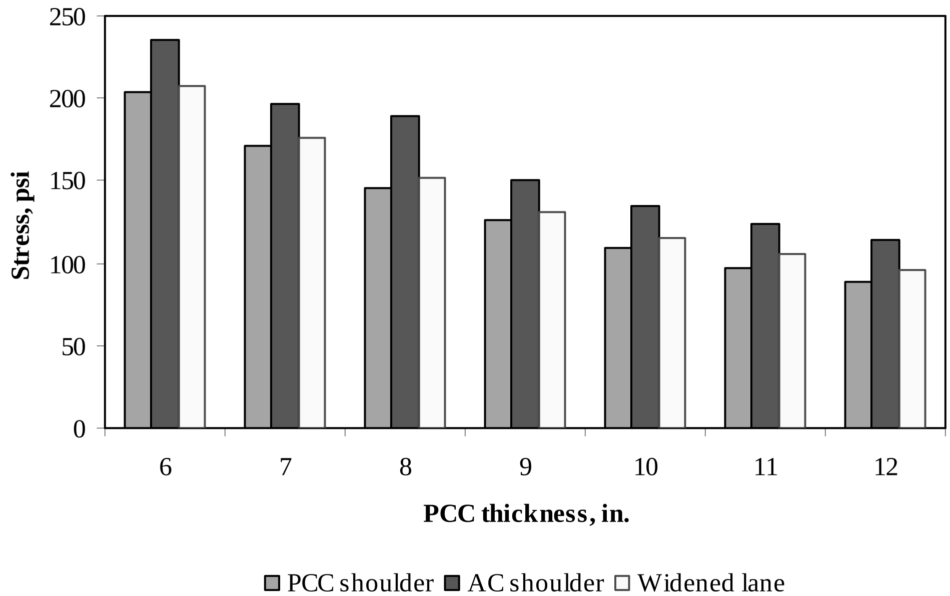


**Figure F-15-25: Impact of PCC thickness and lateral support condition on longitudinal stress at bottom of the Slab (177-in. joint spacing and $\alpha(\Delta T/D)$ of 0 in.$^{-1}$)**

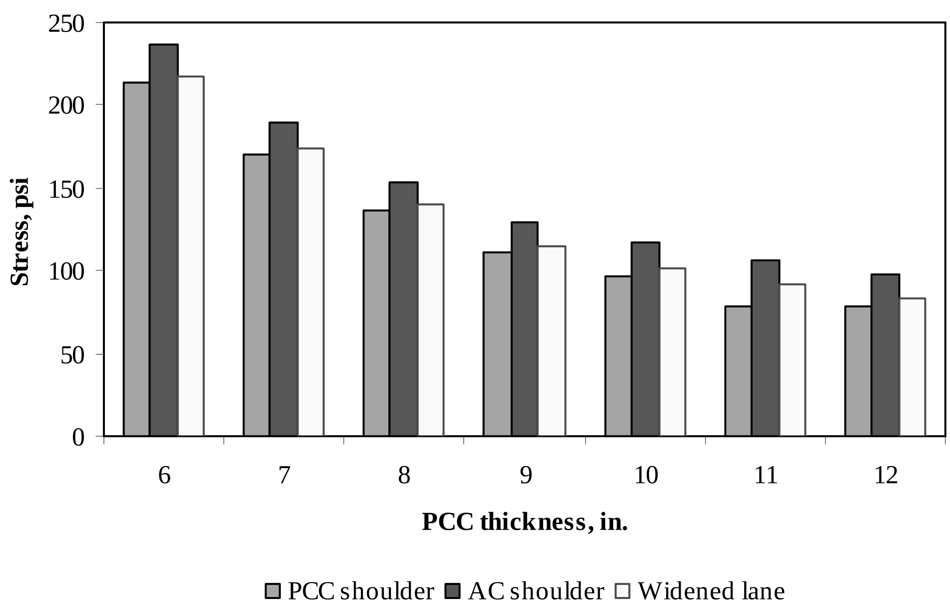


**Figure F-15-26: Impact of PCC thickness and lateral support condition on longitudinal stress at bottom of the Slab (315-in. joint spacing and $\alpha(\Delta T/D)$ of 0 in.$^{-1}$)**

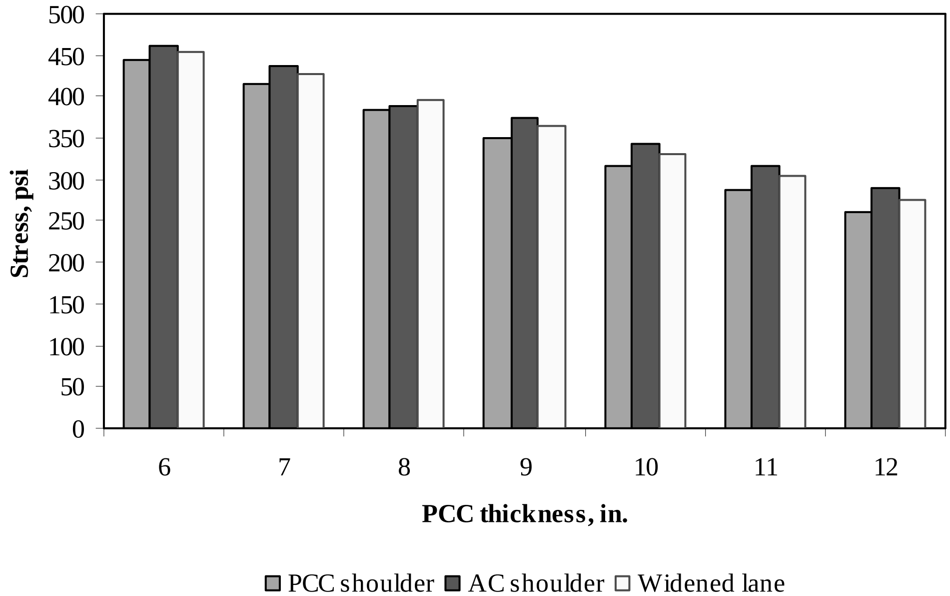


**Figure F-15-27: Impact of PCC thickness and lateral support condition on longitudinal stress at bottom of the Slab (177-in. joint spacing and $\alpha(\Delta T/D)$ of $20x10^{-6}$ in.$^{-1}$)**

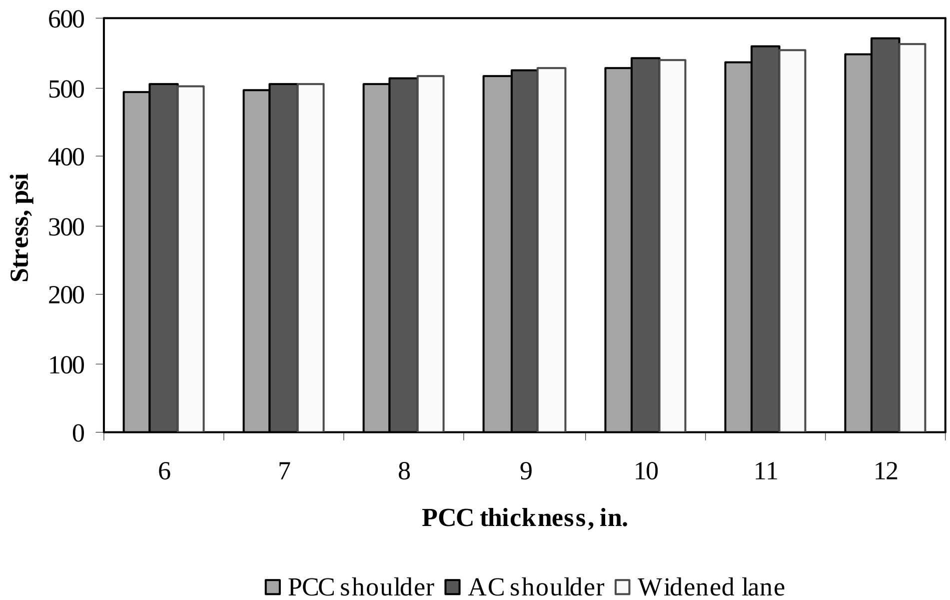


**Figure F-15-28: Impact of PCC thickness and lateral support condition on longitudinal stress at bottom of the Slab (315-in. joint spacing and $\alpha(\Delta T/D)$ of $20x10^{-6}$ in.$^{-1}$)**

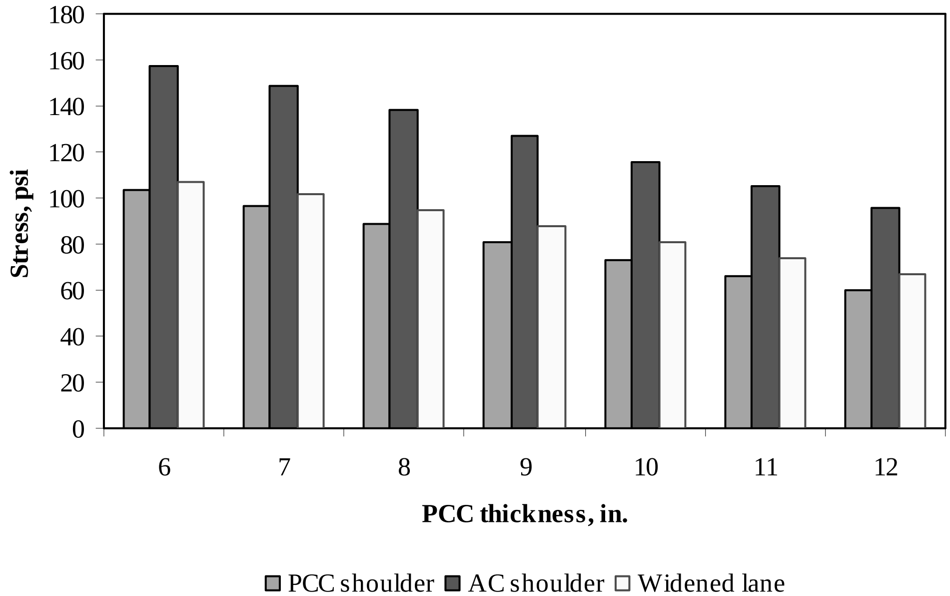


**Figure F-15-29: Impact of PCC thickness and lateral support condition on longitudinal stress at top of the Slab (177-in. joint spacing and α(ΔT/D) of 0 in.$^{-1}$)**

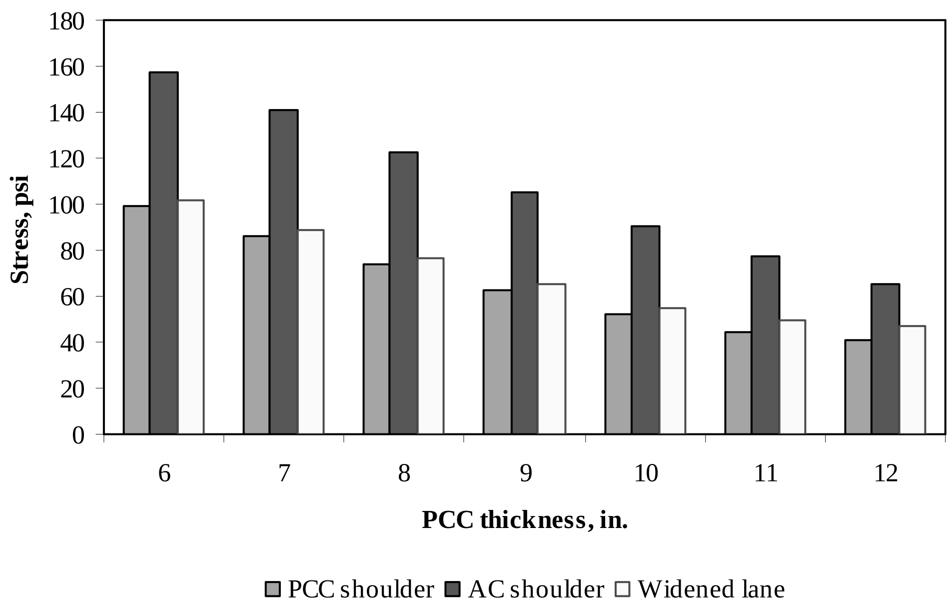


**Figure F-15-30: Impact of PCC thickness and lateral support condition on longitudinal stress at top of the Slab (315-in. joint spacing and α(ΔT/D) of 0 in.$^{-1}$)**

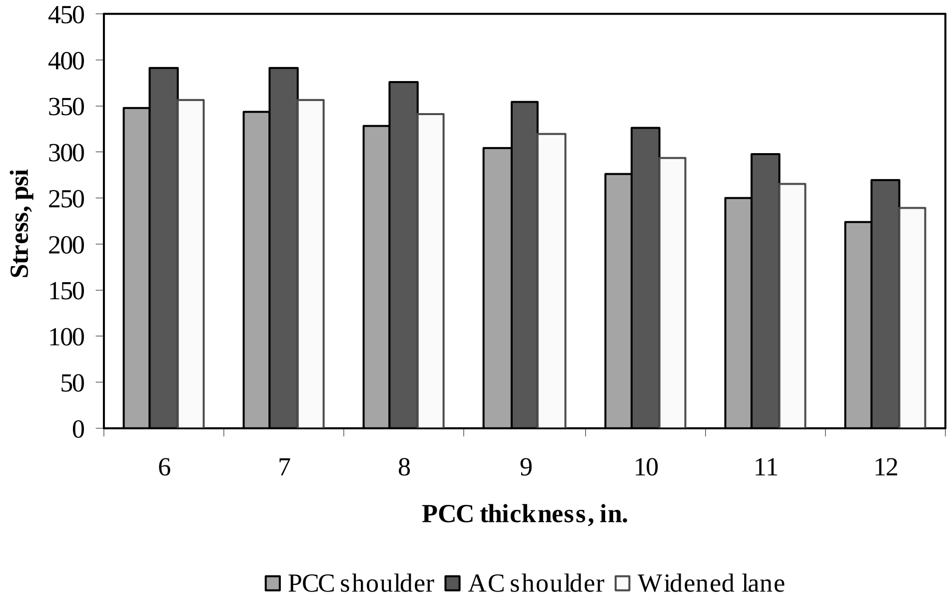


**Figure F-15-31: Impact of PCC thickness and lateral support condition on longitudinal stress at top of the Slab (177-in. joint spacing and $\alpha(\Delta T/D)$ of $-20x10^{-6}$ in.$^{-1}$)**

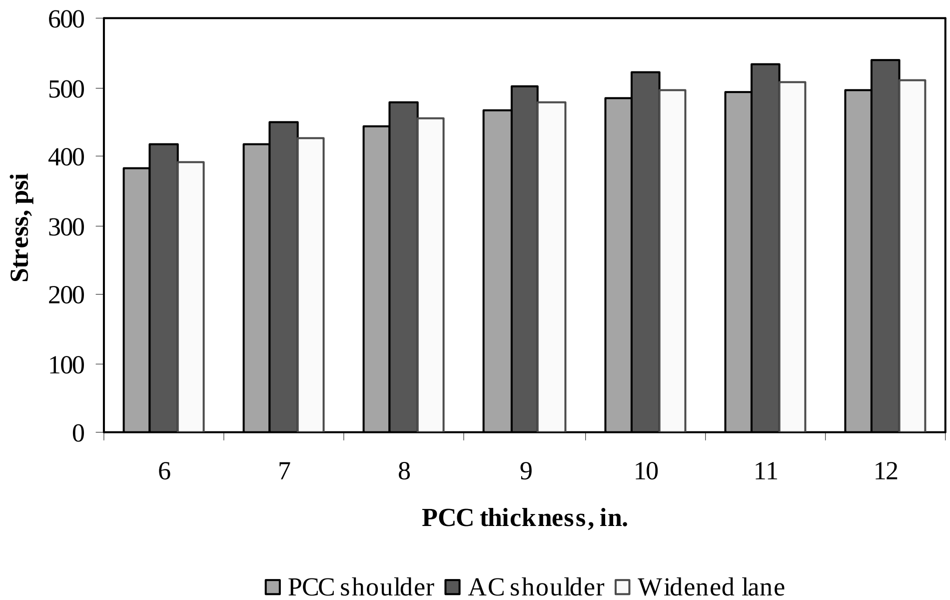


**Figure F-15-32: Impact of PCC thickness and lateral support condition on longitudinal stress at top of the Slab (315-in. joint spacing and $\alpha(\Delta T/D)$ of $-20x10^{-6}$ in.$^{-1}$)**

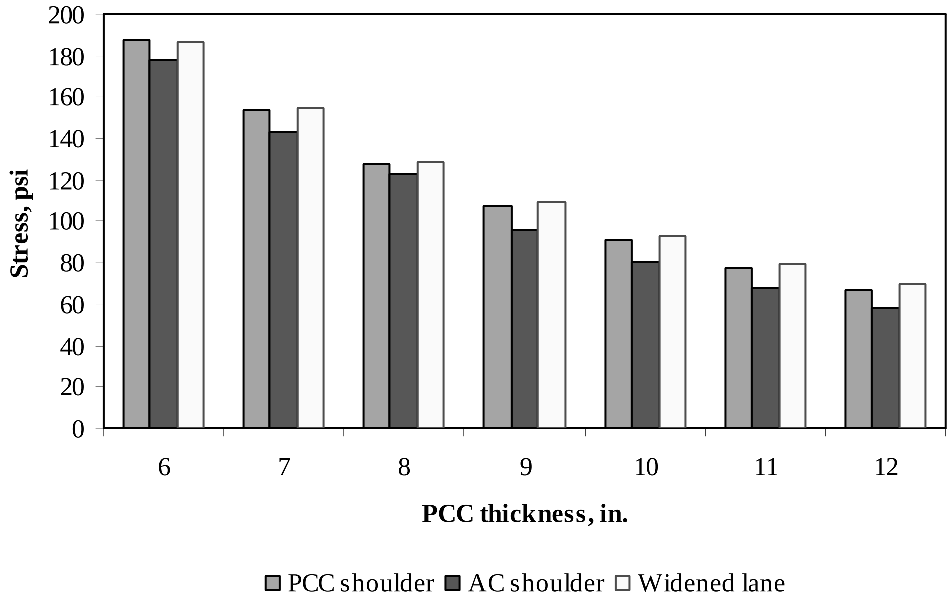


**Figure F-15-33: Impact of PCC thickness and lateral support condition on transverse stress at bottom of the Slab (177-in. joint spacing and $\alpha(\Delta T/D)$ of 0 in.$^{-1}$)**

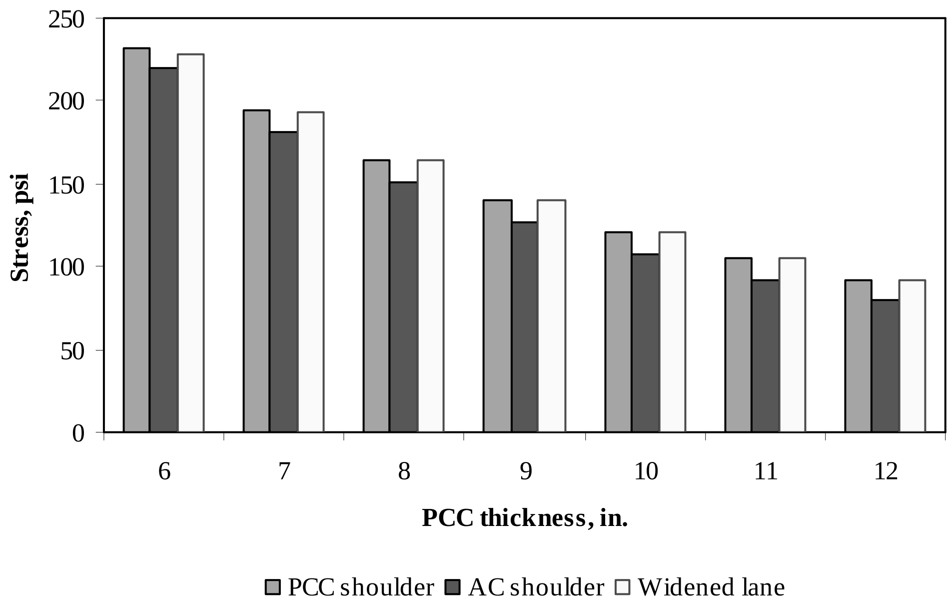


**Figure F-15-34: Impact of PCC thickness and lateral support condition on transverse stress at bottom of the Slab (315-in. joint spacing and $\alpha(\Delta T/D)$ of 0 in.$^{-1}$)**

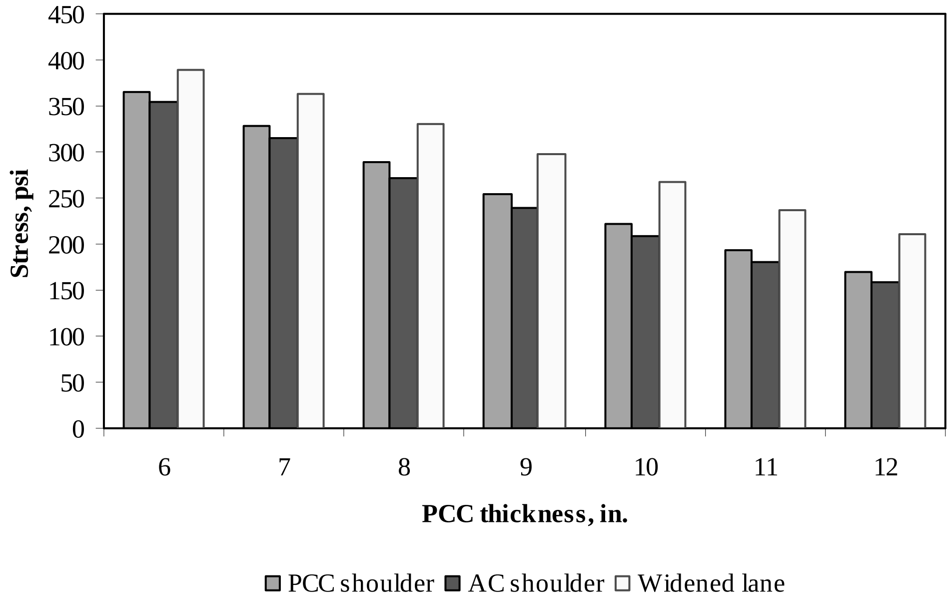


**Figure F-15-35: Impact of PCC thickness and lateral support condition on transverse stress at bottom of the Slab (177-in. joint spacing and $\alpha(\Delta T/D)$ of $20x10^{-6}$ in.$^{-1}$)**

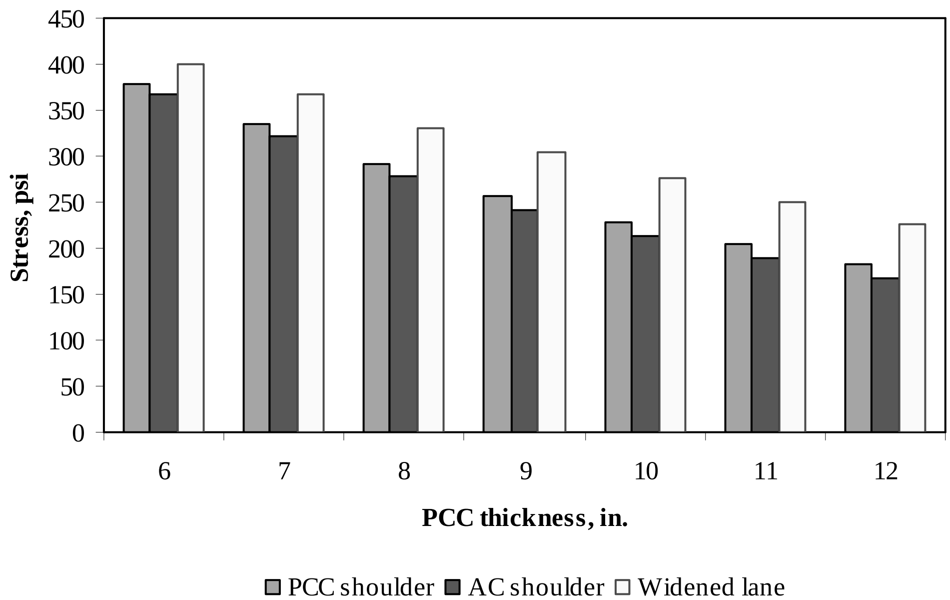


**Figure F-15-36: Impact of PCC thickness and lateral support condition on transverse stress at bottom of the Slab (315-in. joint spacing and $\alpha(\Delta T/D)$ of $20x10^{-6}$ in.$^{-1}$)**

Figures F-15-37 through F-15-42 illustrate the impact of base/subbase thickness and product α(ΔT/D) on stresses (10-in. PCC thickness, 100-psi/in. modulus of subgrade reaction and PCC shoulder)

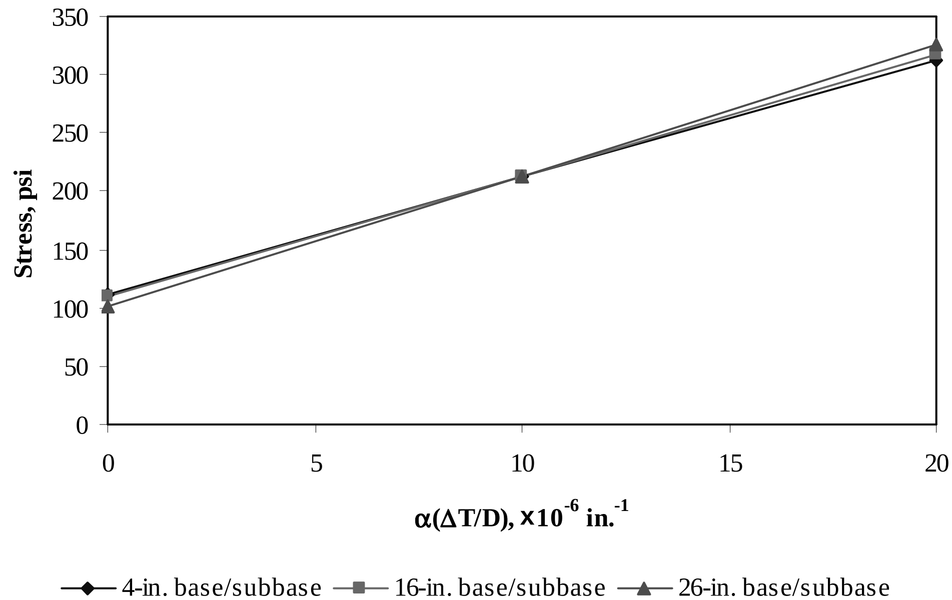


**Figure F-15-37: Impact of base/subbase thickness and product α(ΔT/D) on longitudinal stress at bottom of the slab (177-in. joint spacing)**

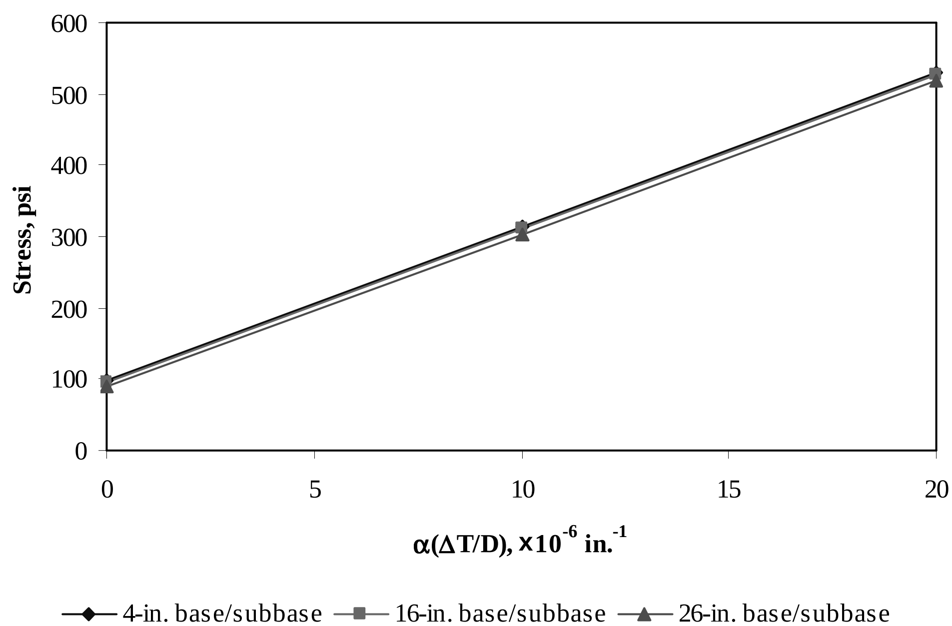


**Figure F-15-38: Impact of base/subbase thickness and product α(ΔT/D) on longitudinal stress at bottom of the slab (315-in. joint spacing)**

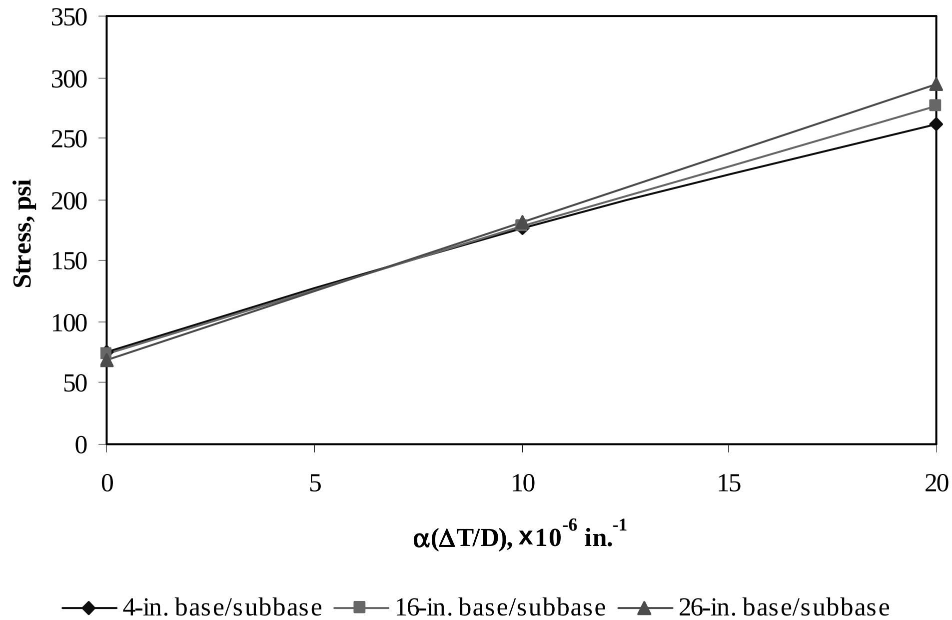


**Figure F-15-39: Impact of base/subbase thickness and product α(ΔT/D) on longitudinal stress at top of the slab (177-in. joint spacing)**

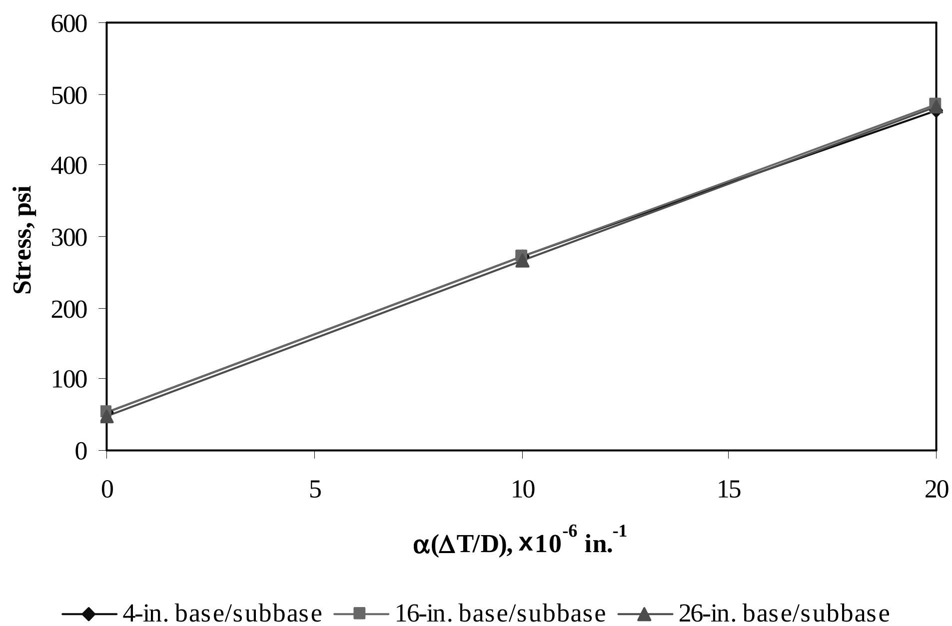


**Figure F-15-40: Impact of base/subbase thickness and product α(ΔT/D) on longitudinal stress at top of the slab (315-in. joint spacing)**

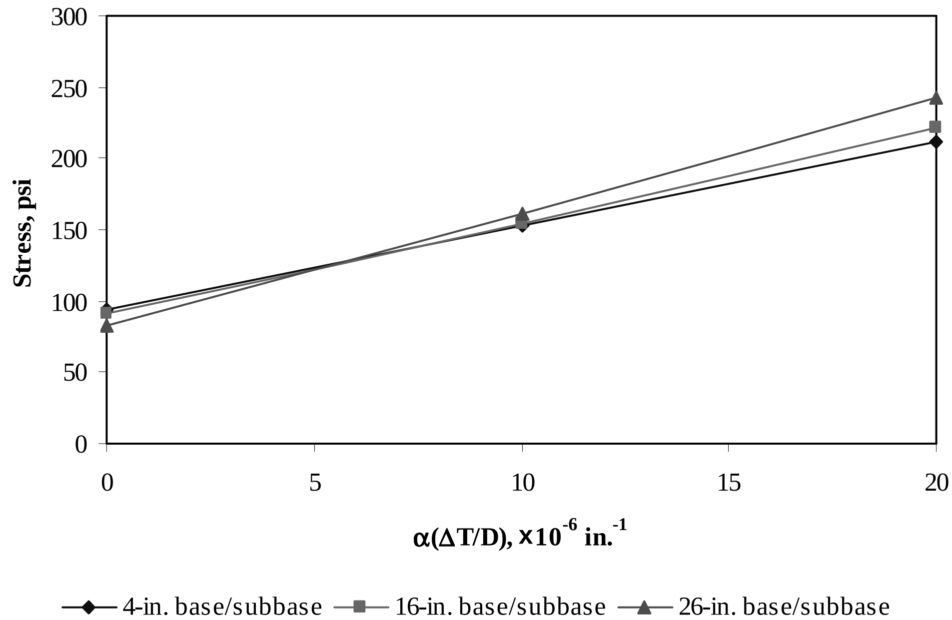


**Figure F-15-41: Impact of base/subbase thickness and product α(ΔT/D) on transverse stress at bottom of the slab (177-in. joint spacing)**

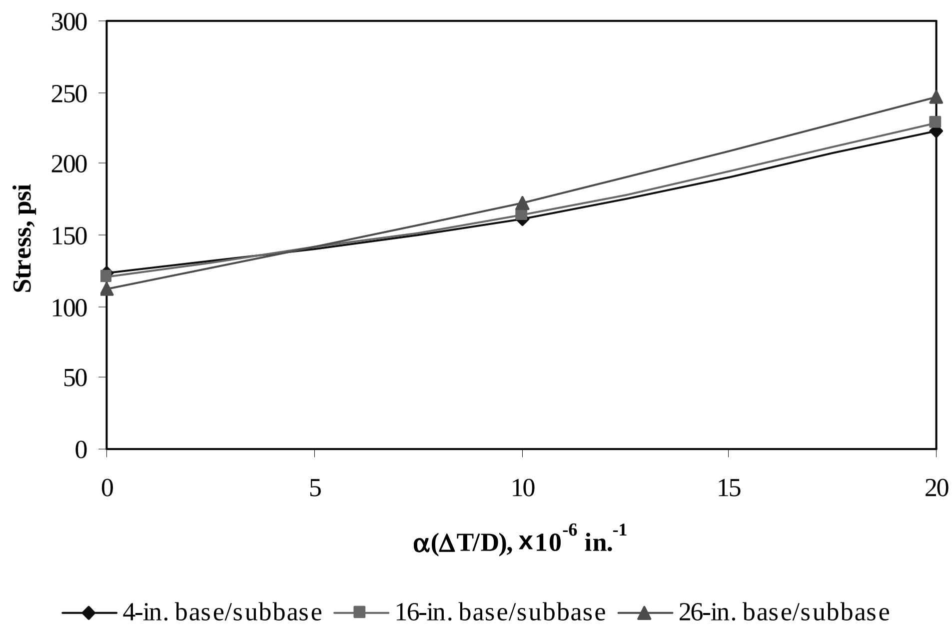


**Figure F-15-42: Impact of base/subbase thickness and product α(ΔT/D) on transverse stress at bottom of the slab (315-in. joint spacing)**

Figures F-15-43 through F-15-48 illustrate the impact of modulus of subgrade reaction and product α(ΔT/D) on stresses (10-in. PCC thickness, 16-in. base/subbase thickness and PCC shoulder)

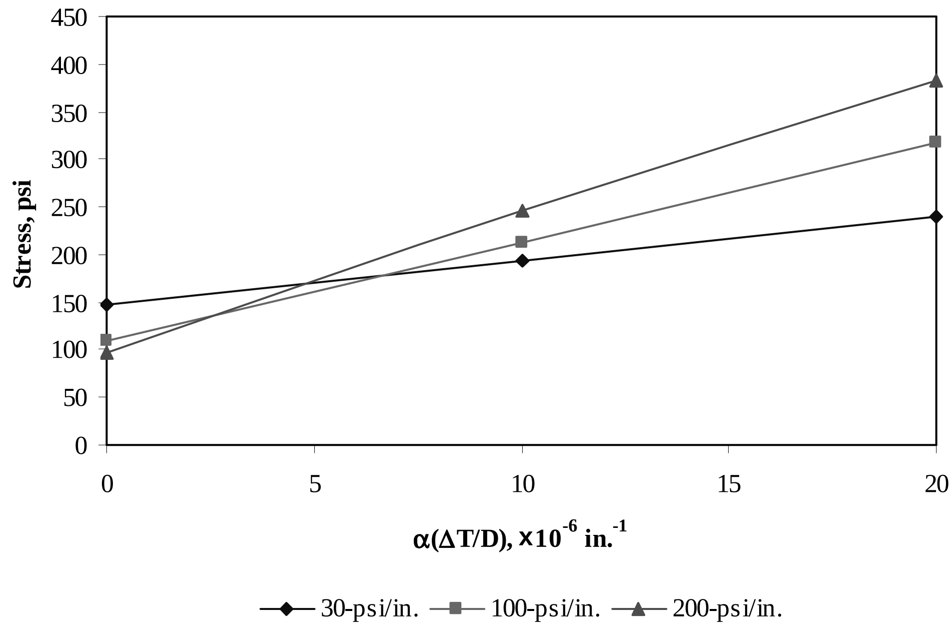


**Figure F-15-43: Impact of modulus of subgrade reaction and product α(ΔT/D) on longitudinal stress at bottom of the slab (177-in. joint spacing)**

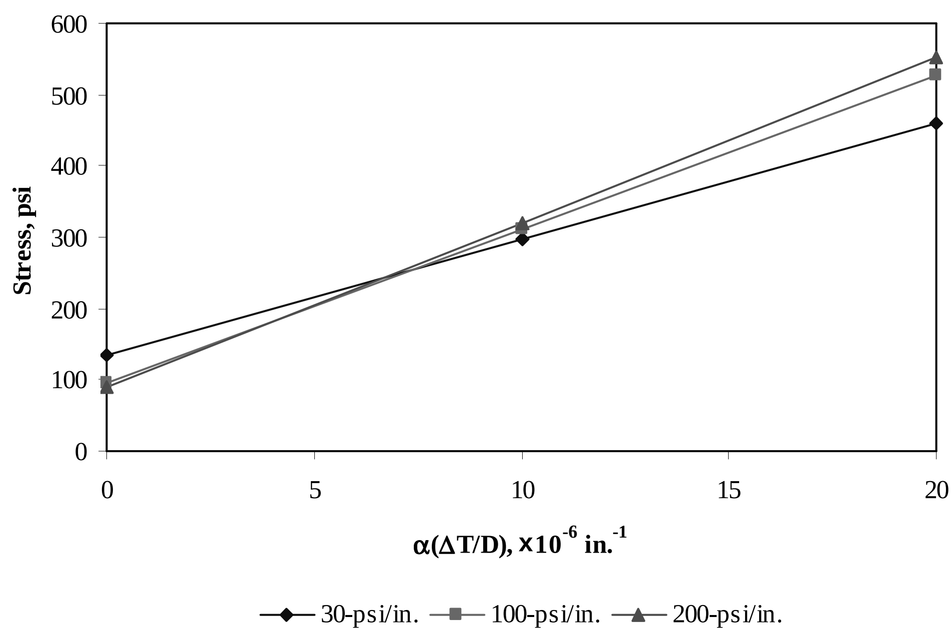


**Figure F-15-44: Impact of modulus of subgrade reaction and product α(ΔT/D) on longitudinal stress at bottom of the slab (315-in. joint spacing)**

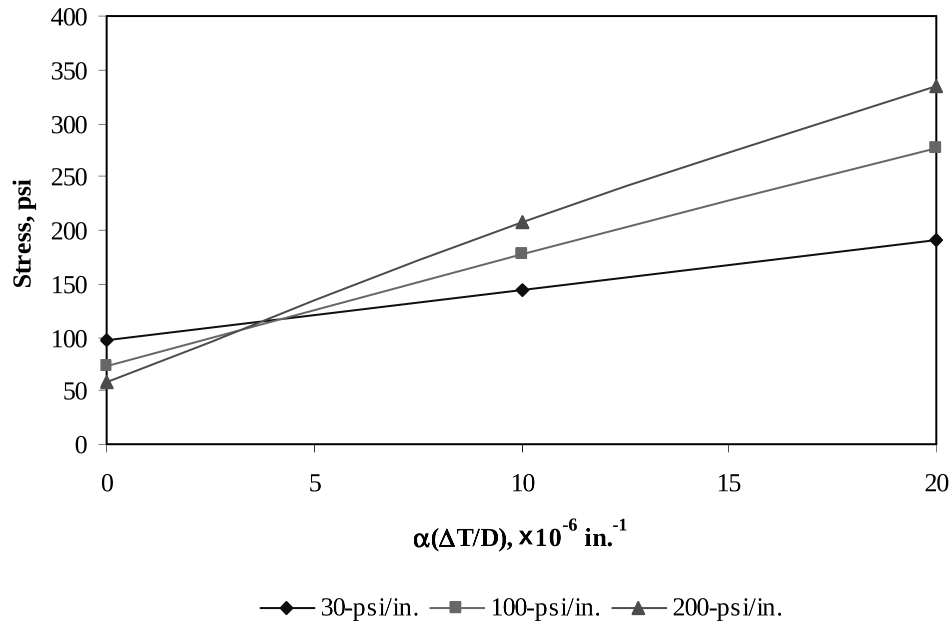


**Figure F-15-45: Impact of modulus of subgrade reaction and product α(ΔT/D) on longitudinal stress at top of the slab (177-in. joint spacing)**

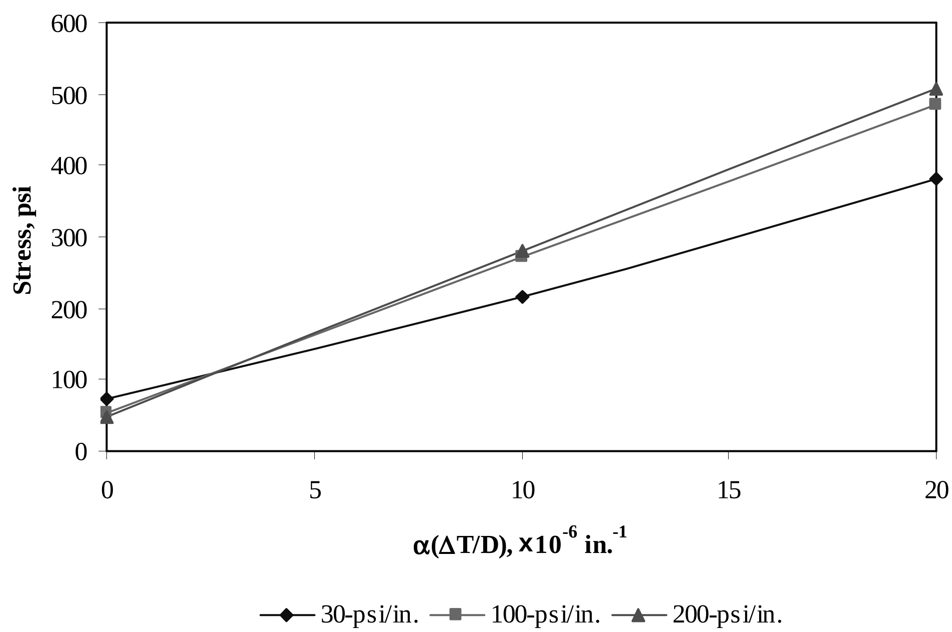


**Figure F-15-46: Impact of modulus of subgrade reaction and product α(ΔT/D) on longitudinal stress at top of the slab (315-in. joint spacing)**

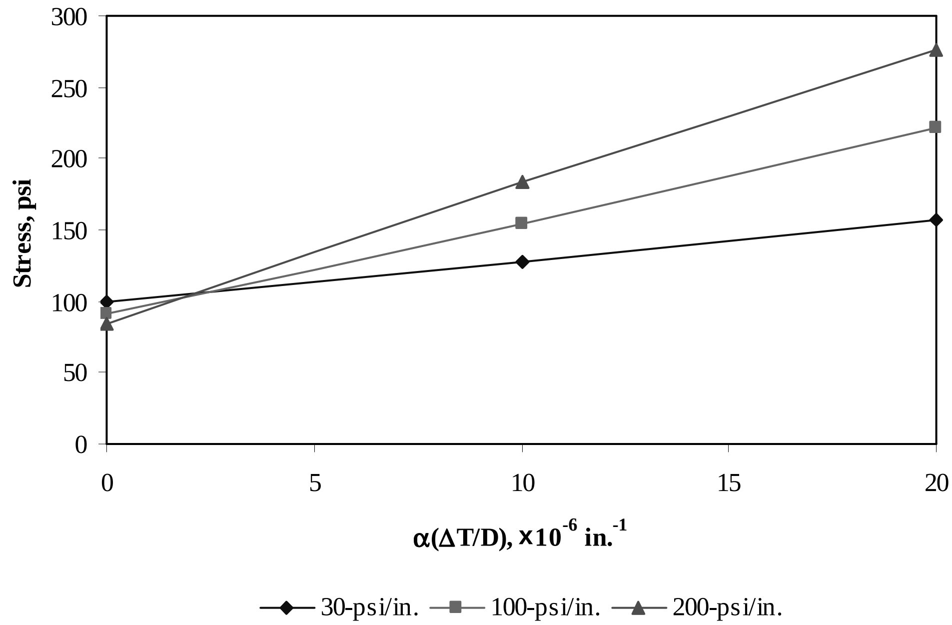


**Figure F-15-47: Impact of modulus of subgrade reaction and product α(ΔT/D) on transverse stress at bottom of the slab (177-in. joint spacing)**

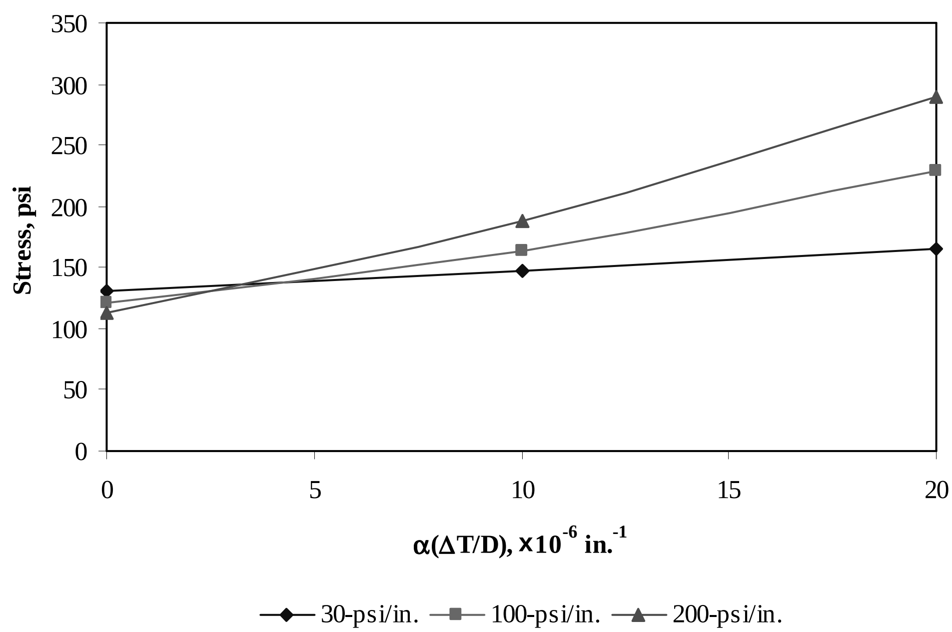


**Figure F-15-48: Impact of modulus of subgrade reaction and product α(ΔT/D) on transverse stress at bottom of the slab (315-in. joint spacing)**

Figures F-15-49 through F-15-51 illustrate the impact of joint spacing and product $\alpha(\Delta T/D)$ on stresses (10-in. PCC thickness, 16-in. base/subbase thickness, 100-psi/in. modulus of subgrade reaction and PCC shoulder)

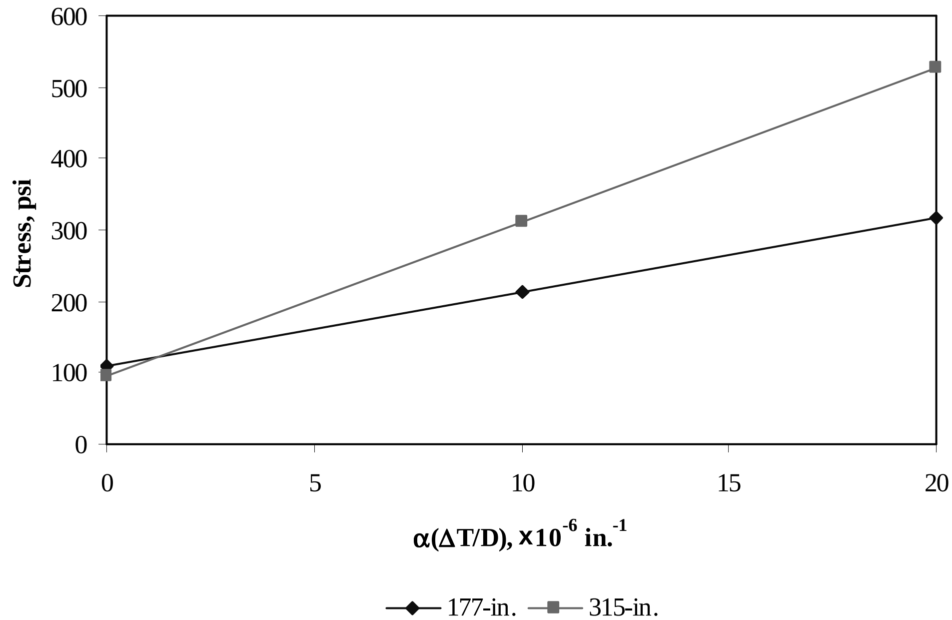


**Figure F-15-49: Impact of joint spacing and product $\alpha(\Delta T/D)$ on longitudinal stress at bottom of the slab**

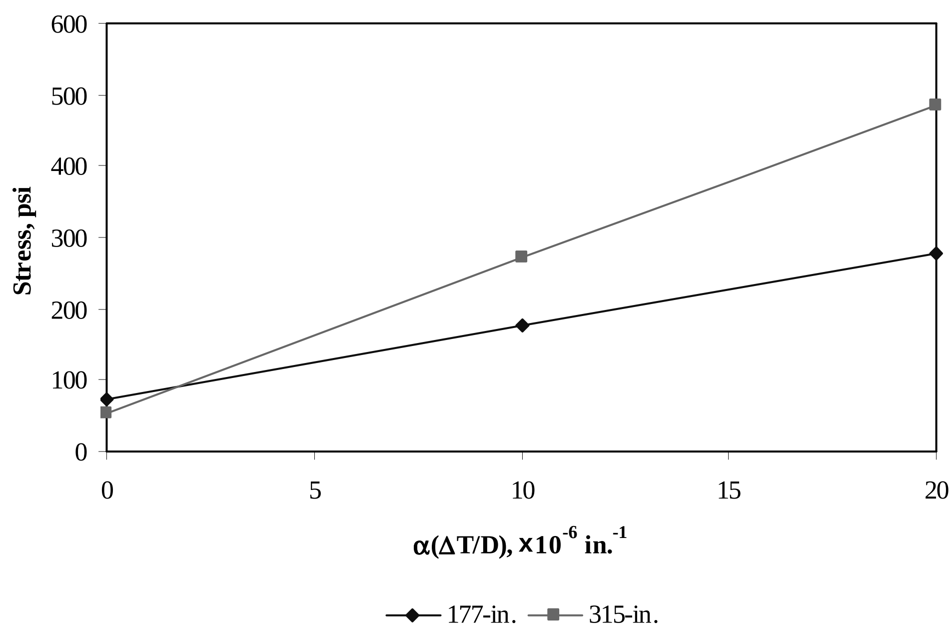


**Figure F-15-50: Impact of joint spacing and product $\alpha(\Delta T/D)$ on longitudinal stress at top of the slab**

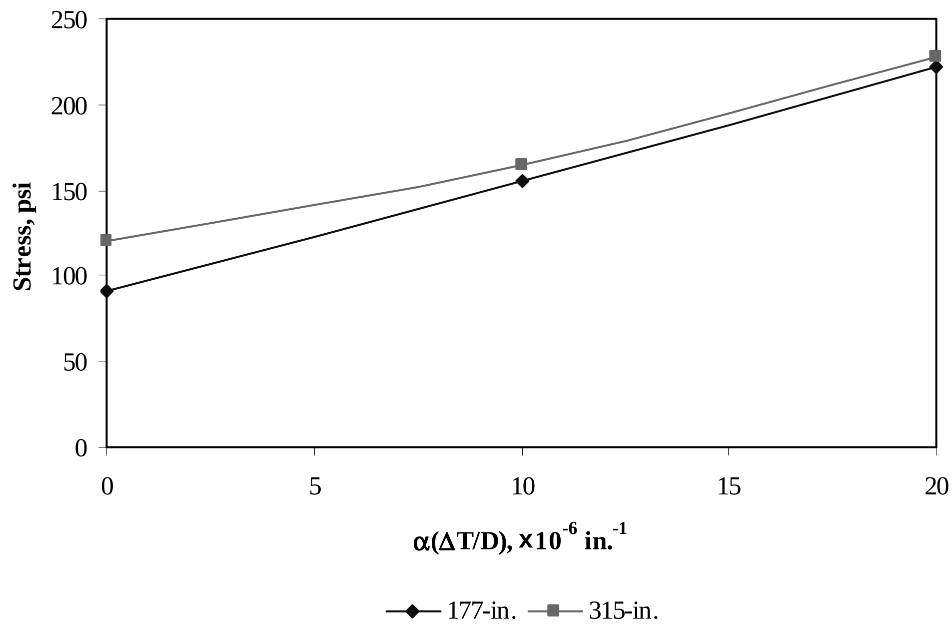


**Figure F-15-51: Impact of joint spacing and product α(ΔT/D) on transverse stress at bottom of the slab**

**Sub Appendix F-16**

**Documentation of Pavement Responses for**

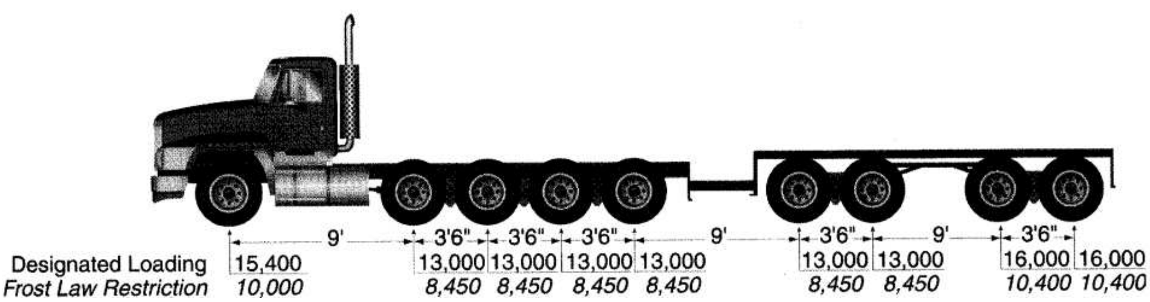


**MI-16**

Figures F-16-1 through F-16-12 illustrate the impact of PCC thickness and base/subbase thickness on stresses (100-psi/in. modulus of subgrade reaction and PCC shoulder)

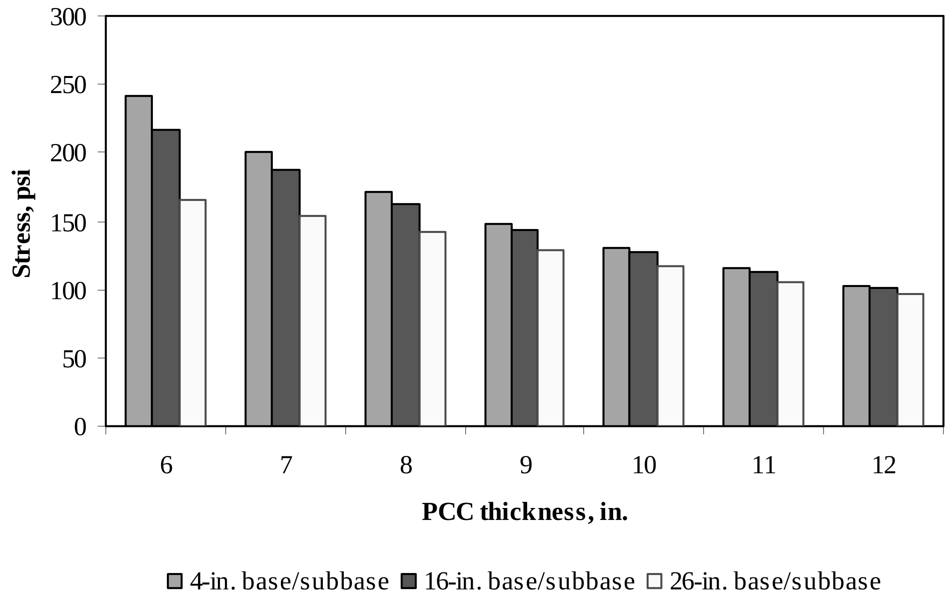


**Figure F-16-1: Impact of PCC thickness and base/subbase thickness on longitudinal stress at bottom of the Slab (177-in. joint spacing and $\alpha(\Delta T/D)$ of 0 in.$^{-1}$)**

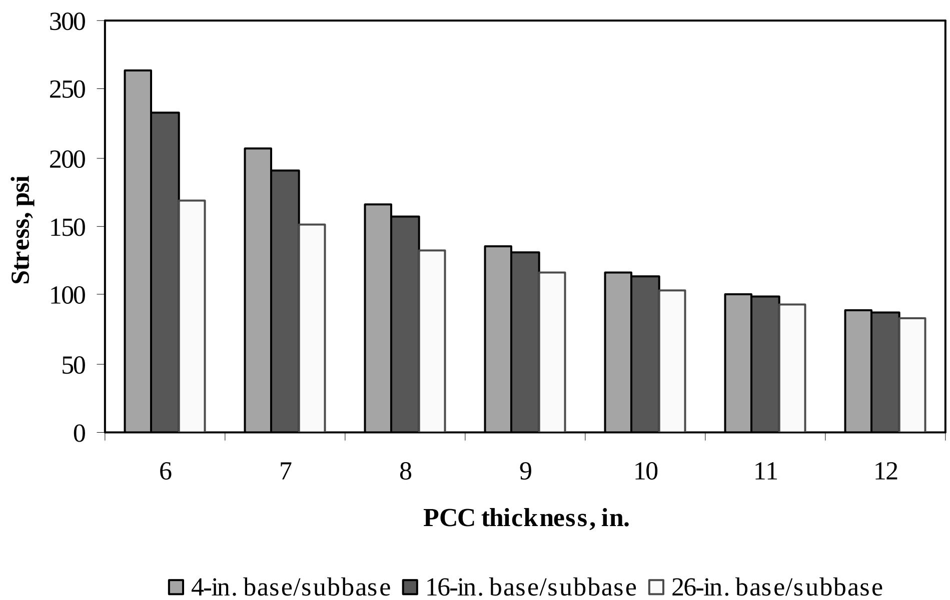


**Figure F-16-2: Impact of PCC thickness and base/subbase thickness on longitudinal stress at bottom of the Slab (315-in. joint spacing and $\alpha(\Delta T/D)$ of 0 in.$^{-1}$)**

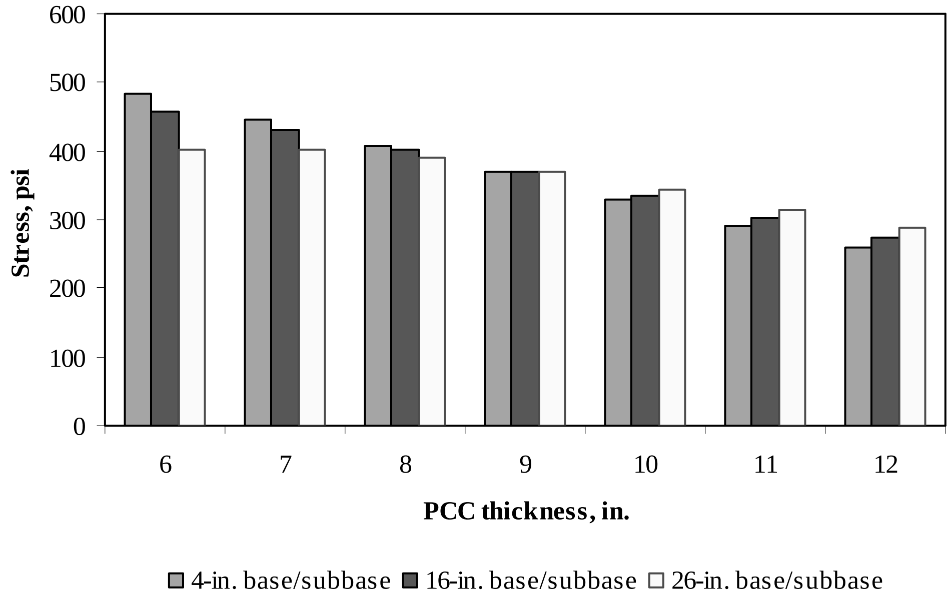


**Figure F-16-3: Impact of PCC thickness and base/subbase thickness on longitudinal stress at bottom of the Slab (177-in. joint spacing and $\alpha(\Delta T/D)$ of $20x10^{-6}$ in.$^{-1}$)**

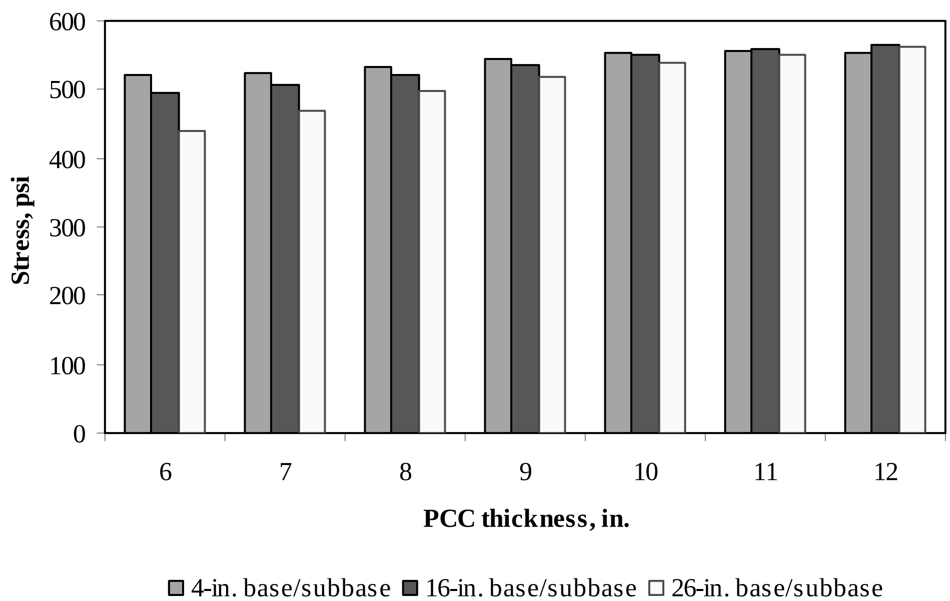


**Figure F-16-4: Impact of PCC thickness and base/subbase thickness on longitudinal stress at bottom of the Slab (315-in. joint spacing and $\alpha(\Delta T/D)$ of $20x10^{-6}$ in.$^{-1}$)**

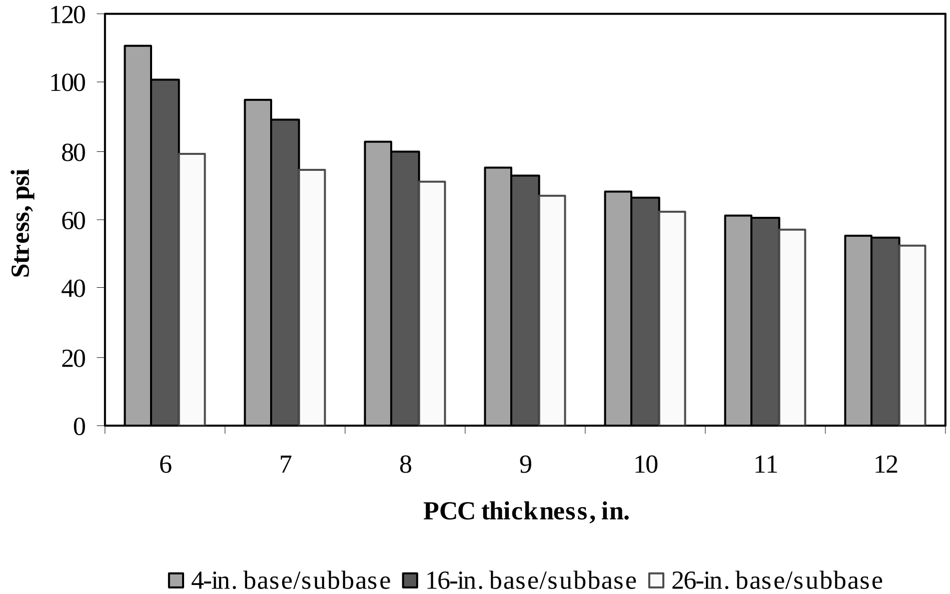


**Figure F-16-5: Impact of PCC thickness and base/subbase thickness on longitudinal stress at top of the Slab (177-in. joint spacing and $\alpha(\Delta T/D)$ of 0 in.$^{-1}$)**

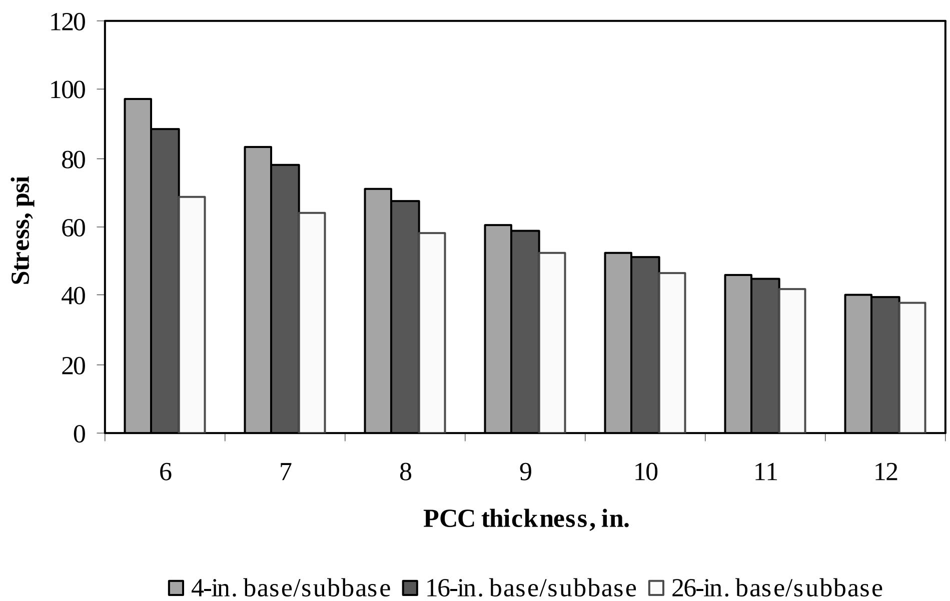


**Figure F-16-6: Impact of PCC thickness and base/subbase thickness on longitudinal stress at top of the Slab (315-in. joint spacing and $\alpha(\Delta T/D)$ of 0 in.$^{-1}$)**

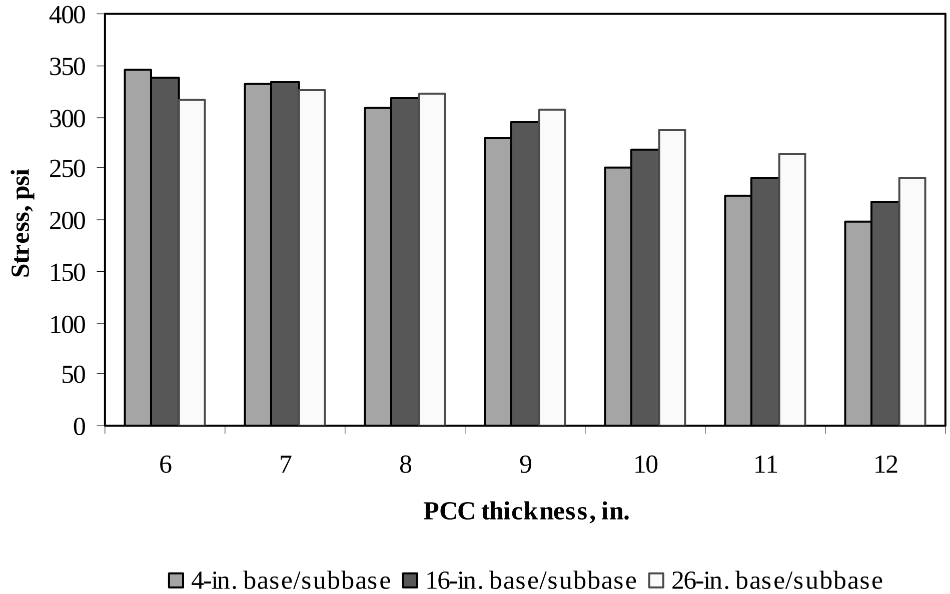


**Figure F-16-7: Impact of PCC thickness and base/subbase thickness on longitudinal stress at top of the Slab (177-in. joint spacing and $\alpha(\Delta T/D)$ of $-20x10^{-6}$ in.$^{-1}$)**

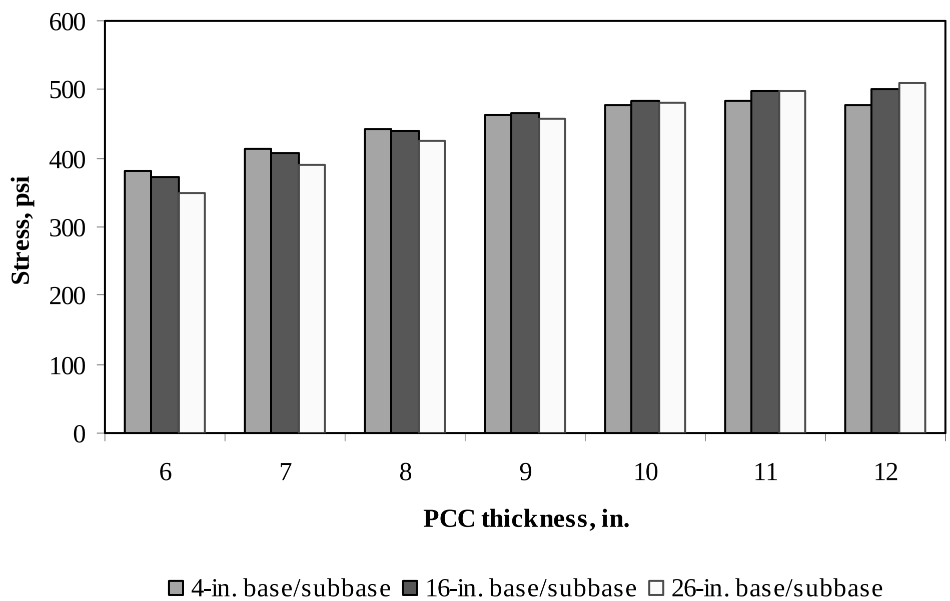


**Figure F-16-8: Impact of PCC thickness and base/subbase thickness on longitudinal stress at top of the Slab (315-in. joint spacing and $\alpha(\Delta T/D)$ of $-20x10^{-6}$ in.$^{-1}$)**

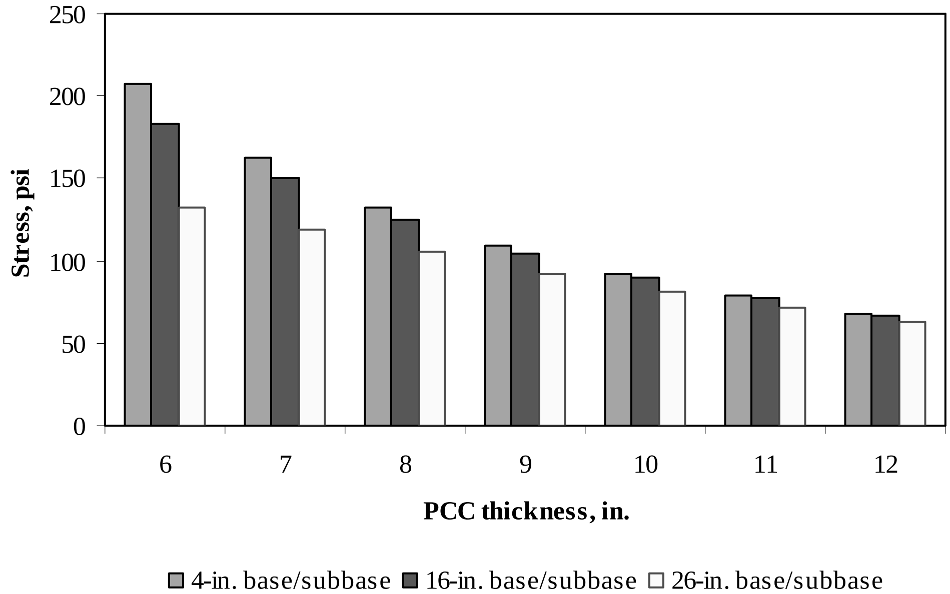


**Figure F-16-9: Impact of PCC thickness and base/subbase thickness on transverse stress at bottom of the Slab (177-in. joint spacing and α(ΔT/D) of 0 in.$^{-1}$)**

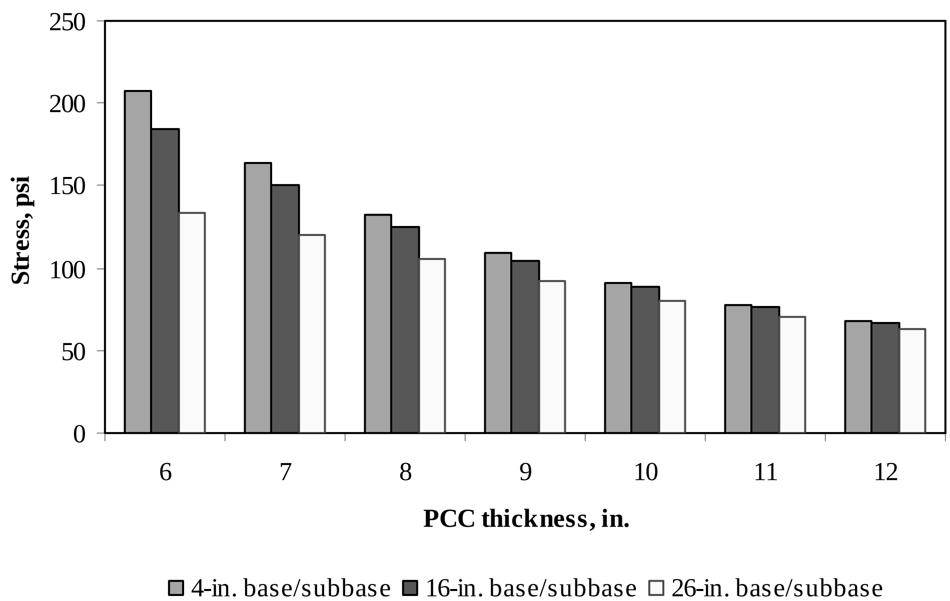


**Figure F-16-10: Impact of PCC thickness and base/subbase thickness on transverse stress at bottom of the Slab (315-in. joint spacing and α(ΔT/D) of 0 in.$^{-1}$)**

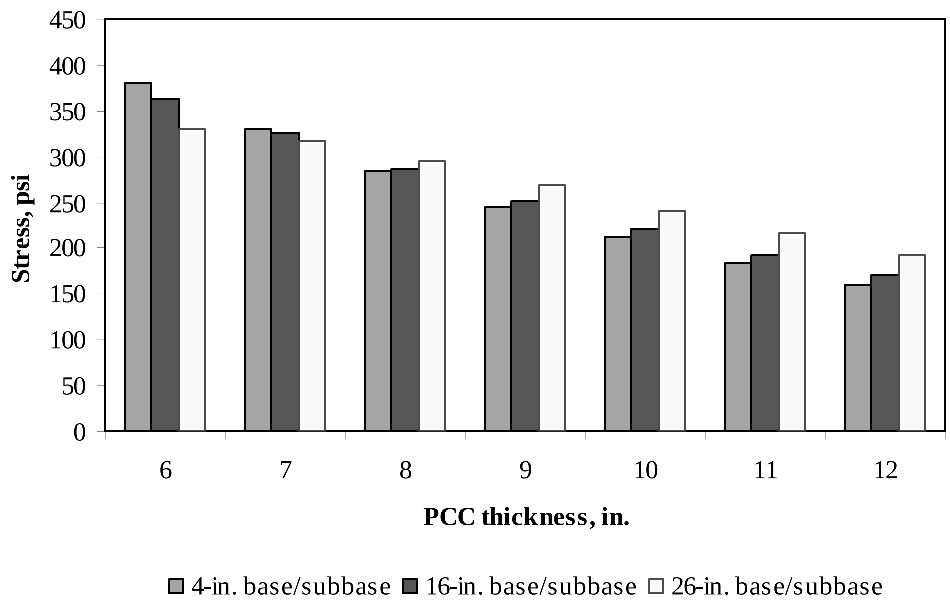


**Figure F-16-11: Impact of PCC thickness and base/subbase thickness on transverse stress at bottom of the Slab (177-in. joint spacing and $\alpha(\Delta T/D)$ of $20x10^{-6}$ in.$^{-1}$)**

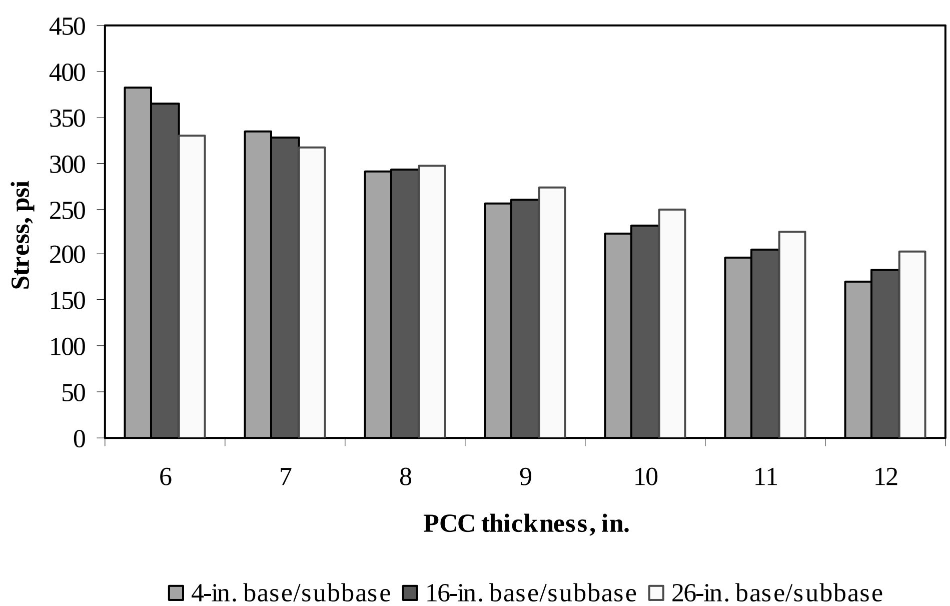


**Figure F-16-12: Impact of PCC thickness and base/subbase thickness on transverse stress at bottom of the Slab (315-in. joint spacing and $\alpha(\Delta T/D)$ of $20x10^{-6}$ in.$^{-1}$)**

Figures F-16-13 through F-16-24 illustrate the impact of PCC thickness and modulus of subgrade reaction on stresses (16-in. base/subbase thickness and PCC shoulder)

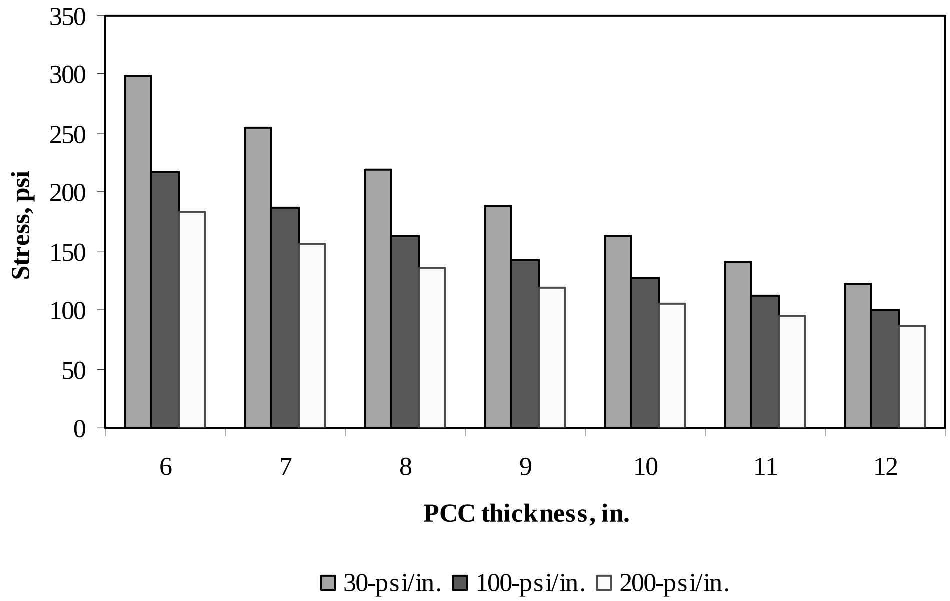


**Figure F-16-13: Impact of PCC thickness and modulus of subgrade reaction on longitudinal stress at bottom of the slab (177-in. joint spacing and $\alpha(\Delta T/D)$ of 0 in.$^{-1}$)**

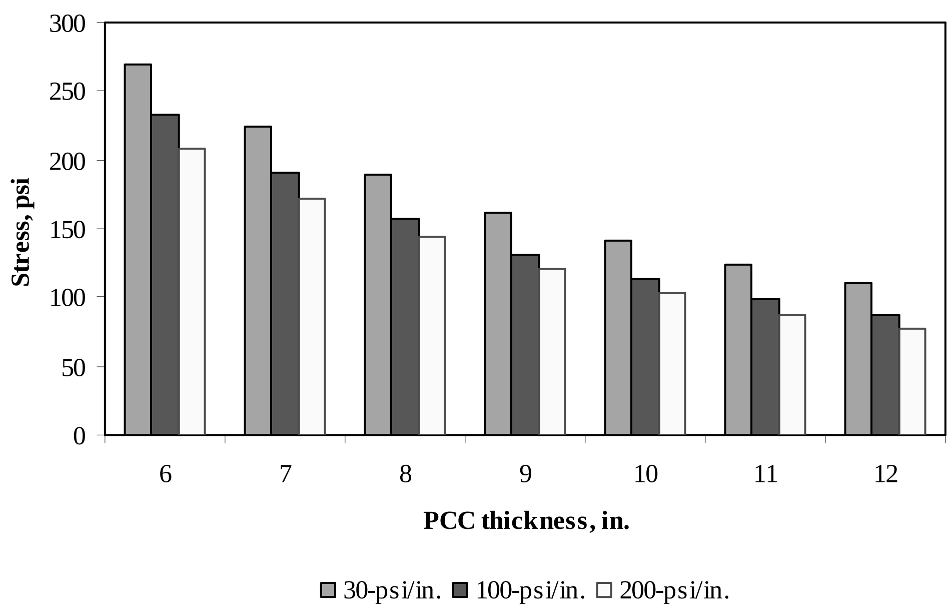


**Figure F-16-14: Impact of PCC thickness and modulus of subgrade reaction on longitudinal stress at bottom of the slab (315-in. joint spacing and $\alpha(\Delta T/D)$ of 0 in.$^{-1}$)**

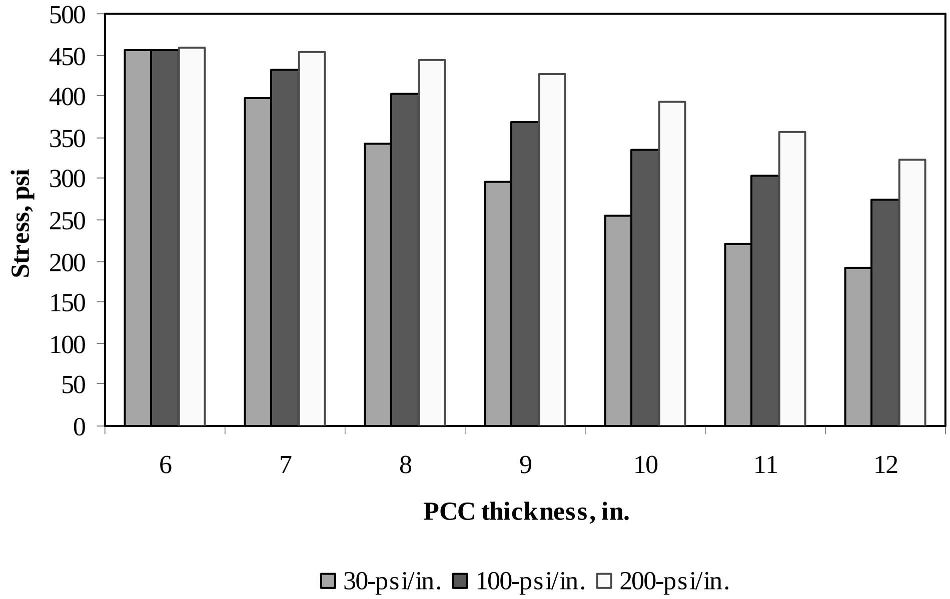


**Figure F-16-15: Impact of PCC thickness and modulus of subgrade reaction on longitudinal stress at bottom of the slab (177-in. joint spacing and $\alpha(\Delta T/D)$ of $20 x 10^{-6}$ in.$^{-1}$)**

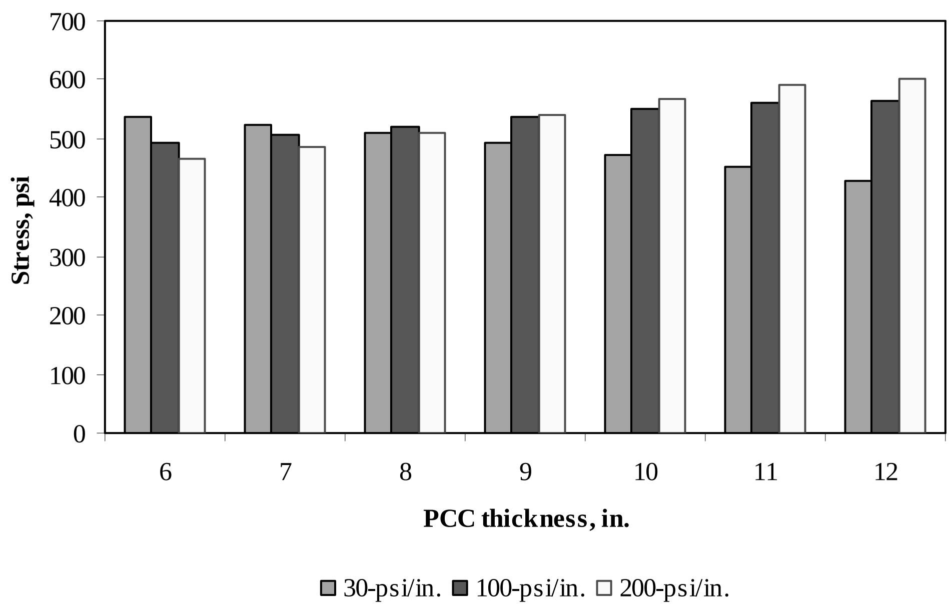


**Figure F-16-16: Impact of PCC thickness and modulus of subgrade reaction on longitudinal stress at bottom of the slab (315-in. joint spacing and $\alpha(\Delta T/D)$ of $20 x 10^{-6}$ in.$^{-1}$)**

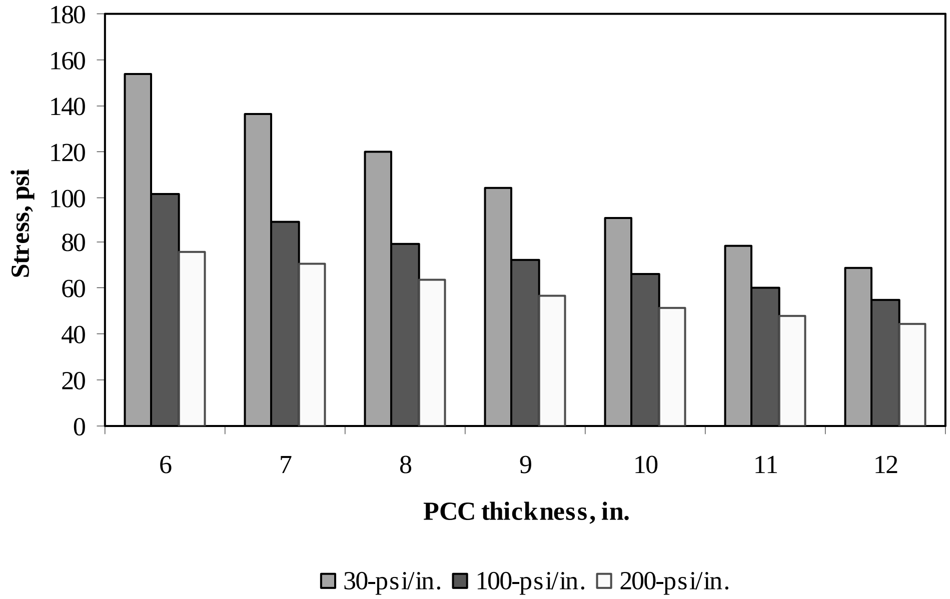


**Figure F-16-17: Impact of PCC thickness and modulus of subgrade reaction on longitudinal stress at top of the Slab (177-in. joint spacing and $\alpha(\Delta T/D)$ of 0 $in.^{-1}$)**

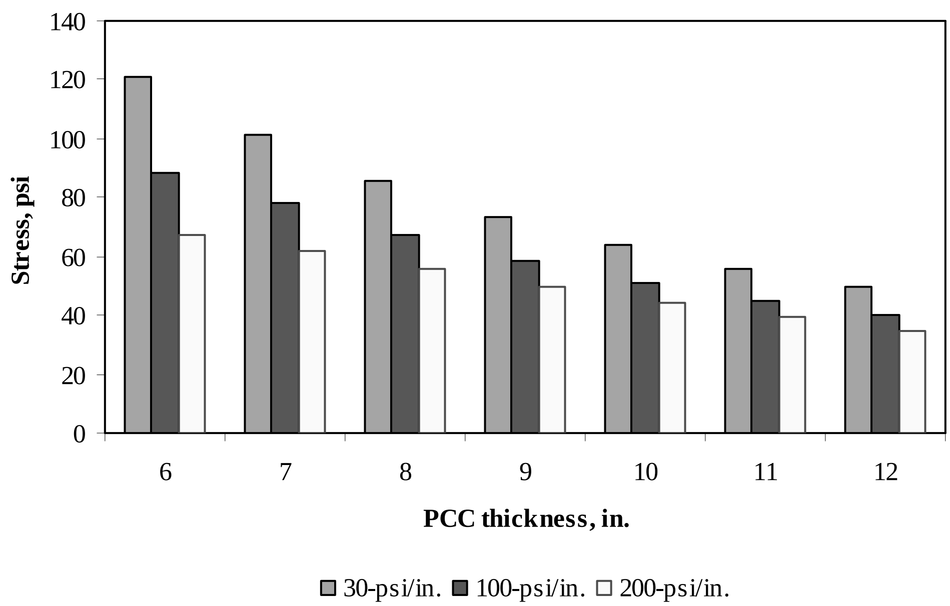


**Figure F-16-18: Impact of PCC thickness and modulus of subgrade reaction on longitudinal stress at top of the Slab (315-in. joint spacing and $\alpha(\Delta T/D)$ of 0 $in.^{-1}$)**

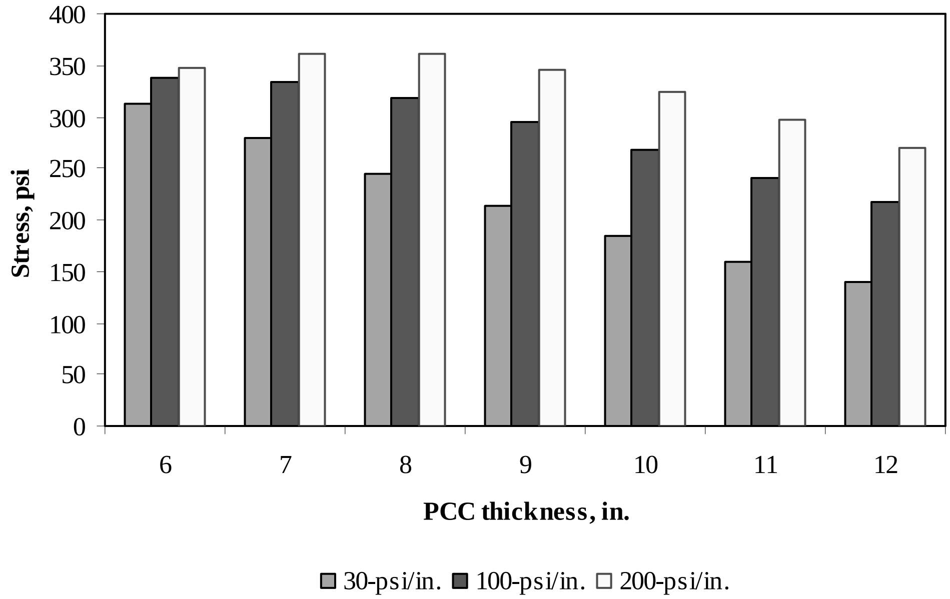


**Figure F-16-19: Impact of PCC thickness and modulus of subgrade reaction on longitudinal stress at top of the Slab (177-in. joint spacing and $\alpha(\Delta T/D)$ of $-20x10^{-6}$ in.$^{-1}$)**

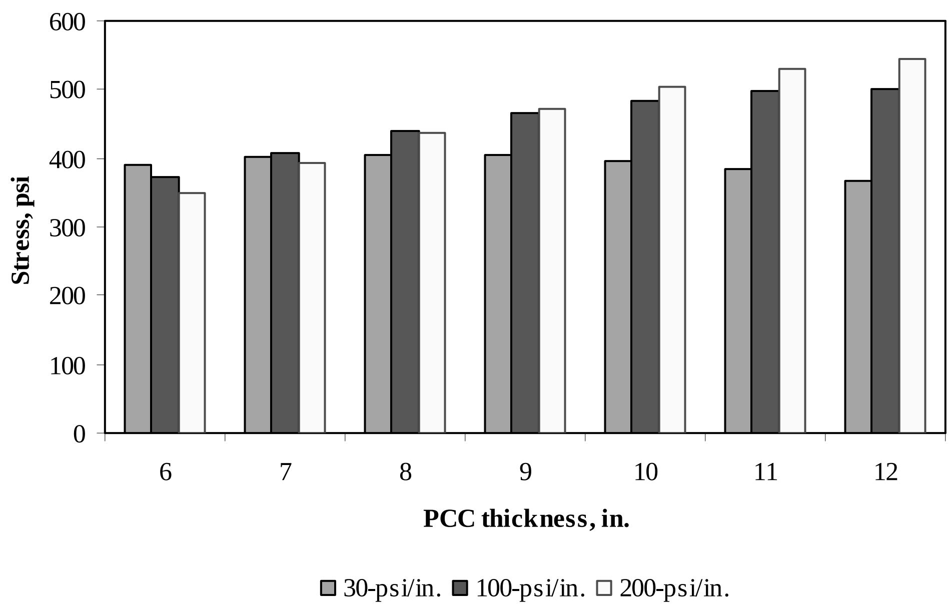


**Figure F-16-20: Impact of PCC thickness and modulus of subgrade reaction on longitudinal stress at top of the Slab (315-in. joint spacing and $\alpha(\Delta T/D)$ of $-20x10^{-6}$ in.$^{-1}$)**

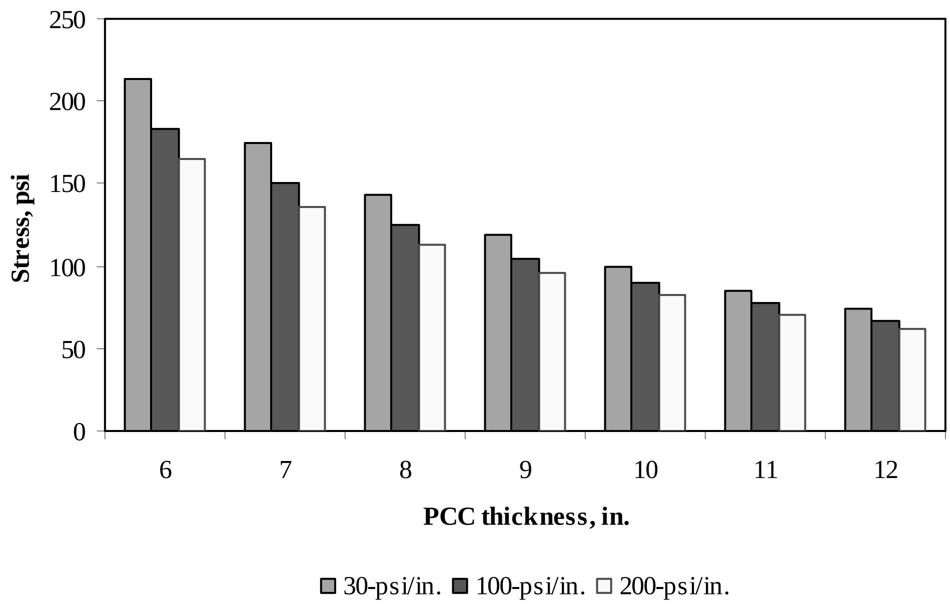


**Figure F-16-21: Impact of PCC thickness and modulus of subgrade reaction on transverse stress at bottom of the Slab (177-in. joint spacing and $\alpha(\Delta T/D)$ of 0 in.$^{-1}$)**

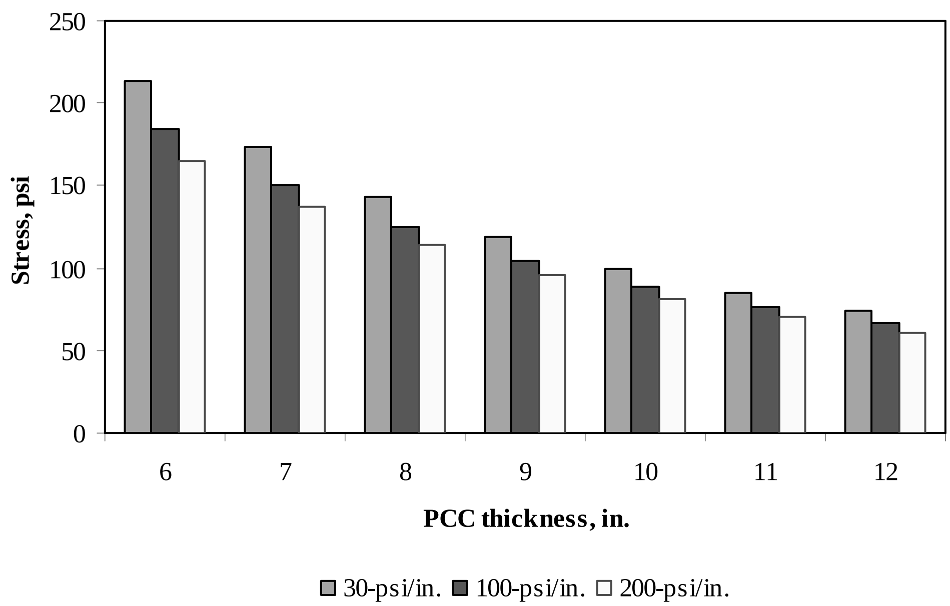


**Figure F-16-22: Impact of PCC thickness and modulus of subgrade reaction on transverse stress at bottom of the Slab (315-in. joint spacing and $\alpha(\Delta T/D)$ of 0 in.$^{-1}$)**

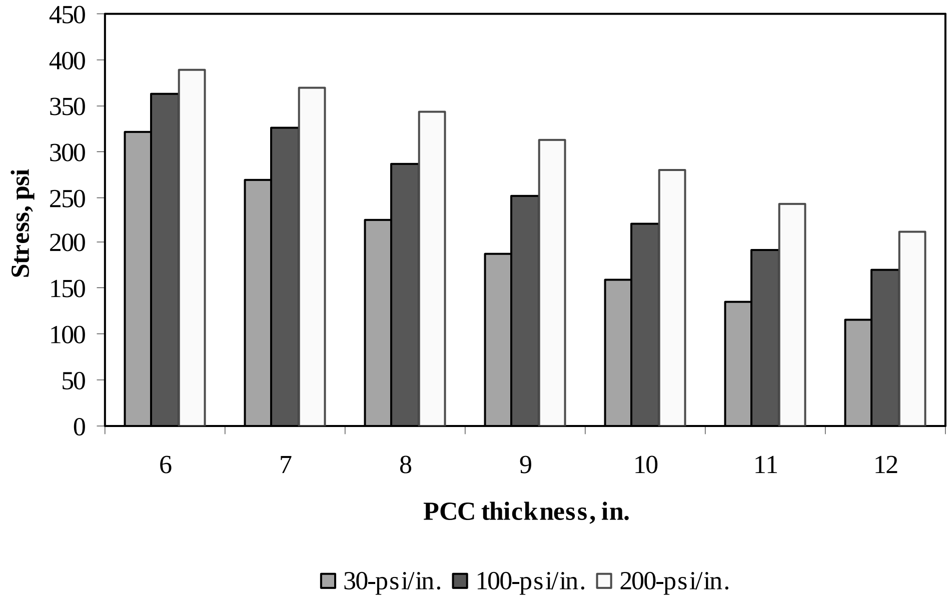


**Figure F-16-23: Impact of PCC thickness and modulus of subgrade reaction on transverse stress at bottom of the Slab (177-in. joint spacing and $\alpha(\Delta T/D)$ of $20x10^{-6}$ in.$^{-1}$)**

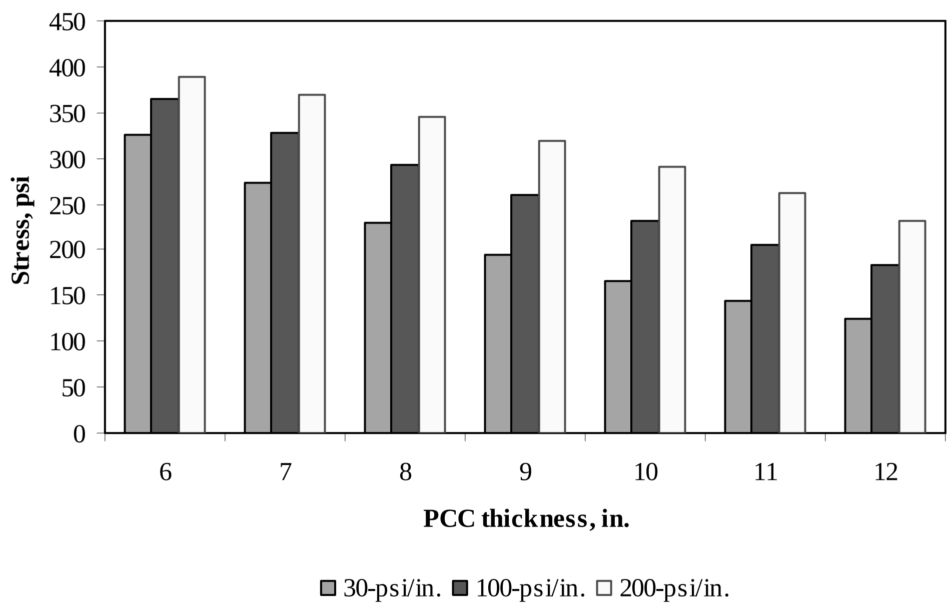


**Figure F-16-24: Impact of PCC thickness and modulus of subgrade reaction on transverse stress at bottom of the Slab (315-in. joint spacing and $\alpha(\Delta T/D)$ of $20x10^{-6}$ in.$^{-1}$)**

Figures F-16-25 through F-16-36 illustrate the impact of PCC thickness and lateral support condition on stresses (16-in. base/subbase and 100-psi/in. modulus of subgrade reaction)

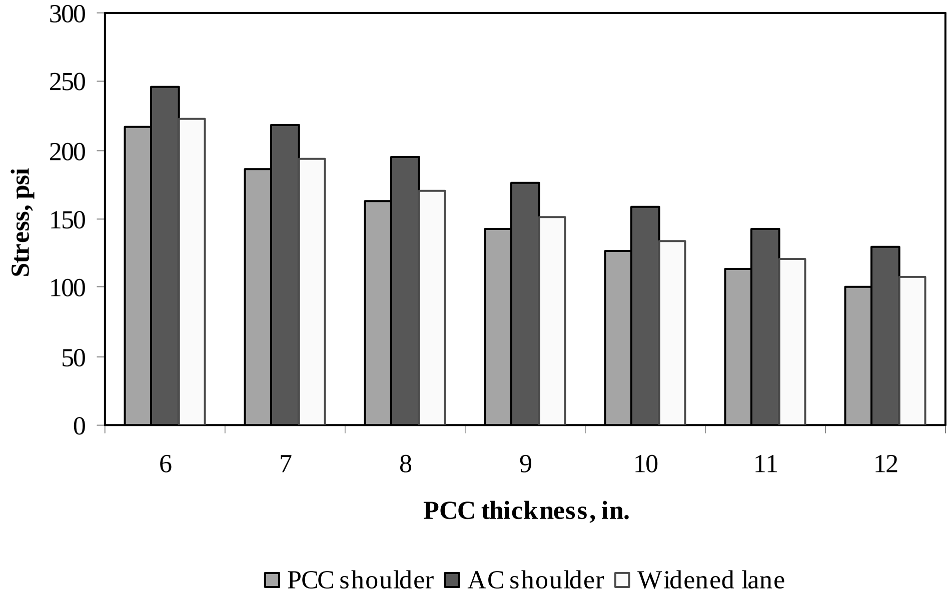


**Figure F-16-25: Impact of PCC thickness and lateral support condition on longitudinal stress at bottom of the Slab (177-in. joint spacing and α(ΔT/D) of 0 in.$^{-1}$)**

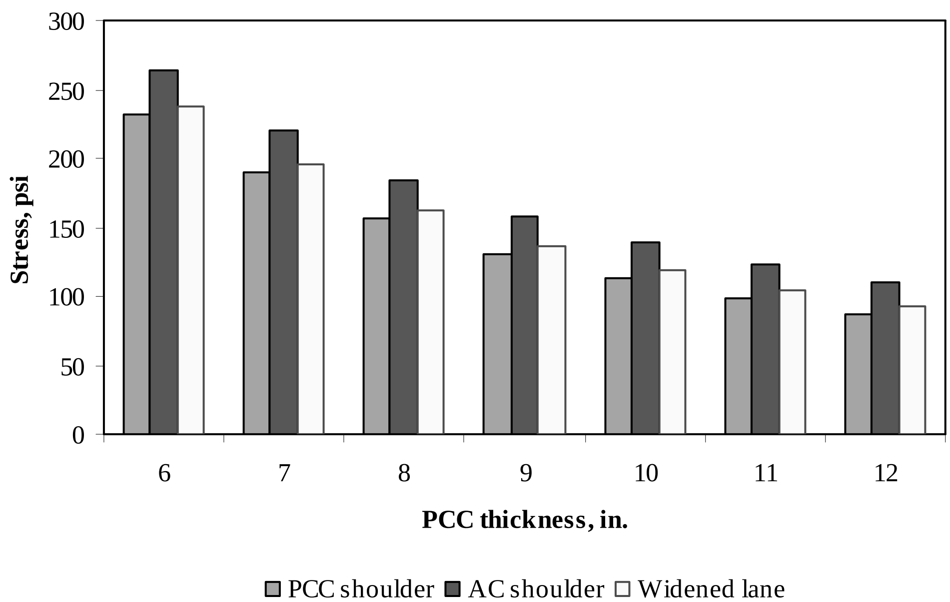


**Figure F-16-26: Impact of PCC thickness and lateral support condition on longitudinal stress at bottom of the Slab (315-in. joint spacing and α(ΔT/D) of 0 in.$^{-1}$)**

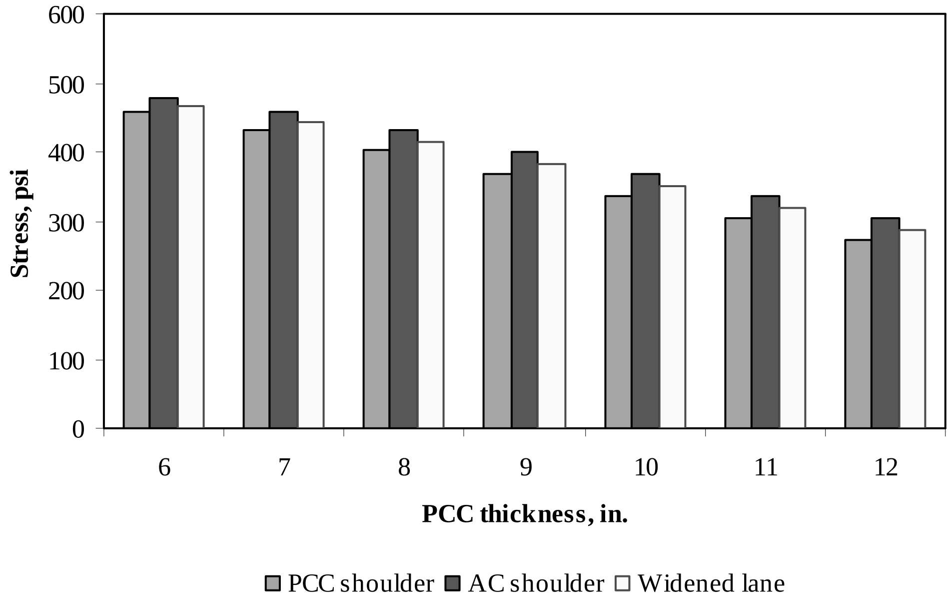


**Figure F-16-27: Impact of PCC thickness and lateral support condition on longitudinal stress at bottom of the Slab (177-in. joint spacing and $\alpha(\Delta T/D)$ of $20 \times 10^{-6}$ in.$^{-1}$)**

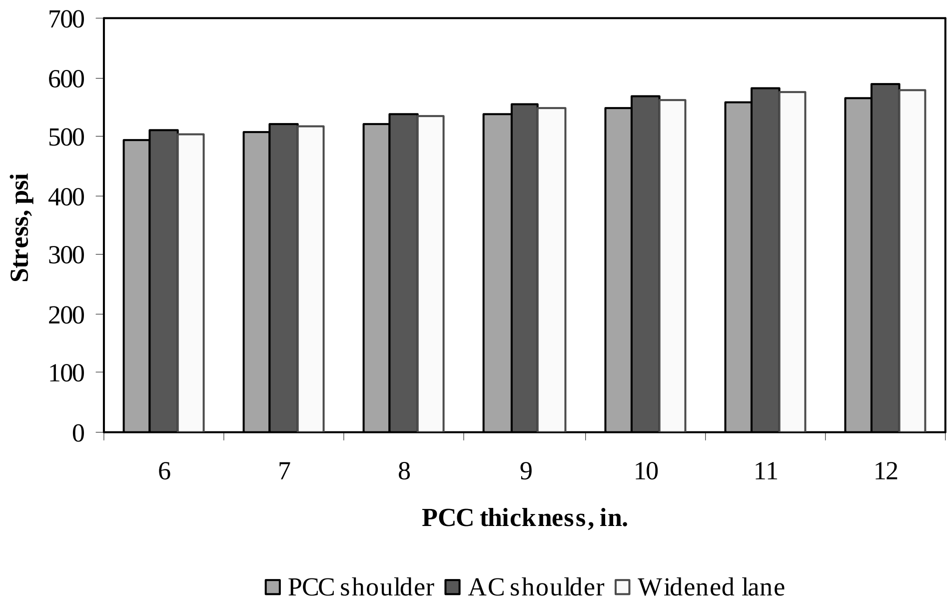


**Figure F-16-28: Impact of PCC thickness and lateral support condition on longitudinal stress at bottom of the Slab (315-in. joint spacing and $\alpha(\Delta T/D)$ of $20 \times 10^{-6}$ in.$^{-1}$)**

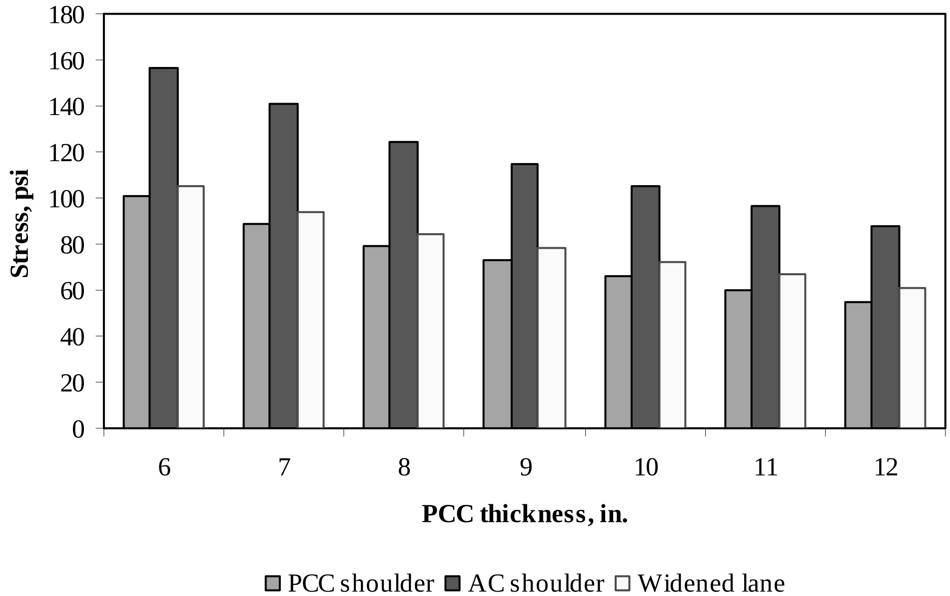


**Figure F-16-29: Impact of PCC thickness and lateral support condition on longitudinal stress at top of the Slab (177-in. joint spacing and $\alpha(\Delta T/D)$ of 0 in.$^{-1}$)**

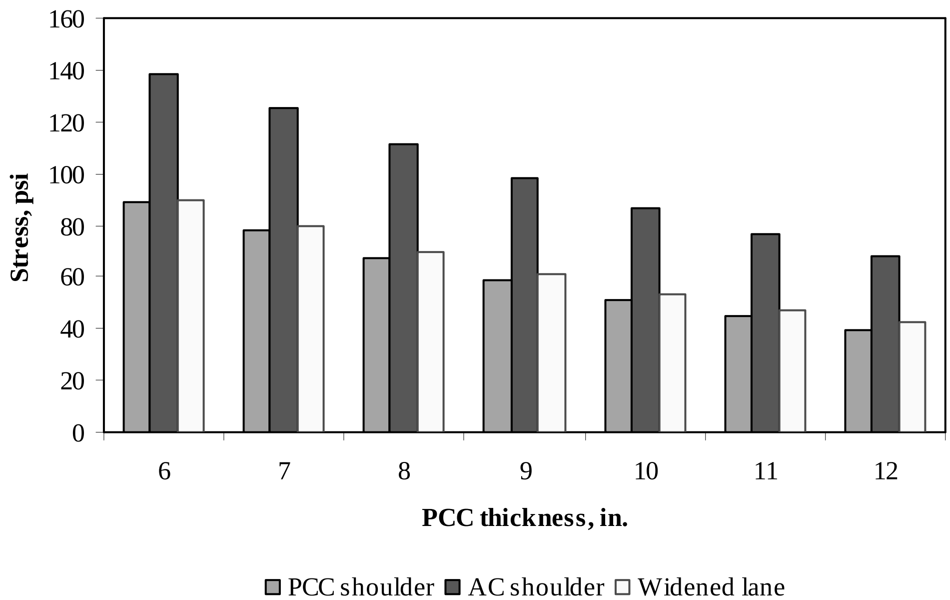


**Figure F-16-30: Impact of PCC thickness and lateral support condition on longitudinal stress at top of the Slab (315-in. joint spacing and $\alpha(\Delta T/D)$ of 0 in.$^{-1}$)**

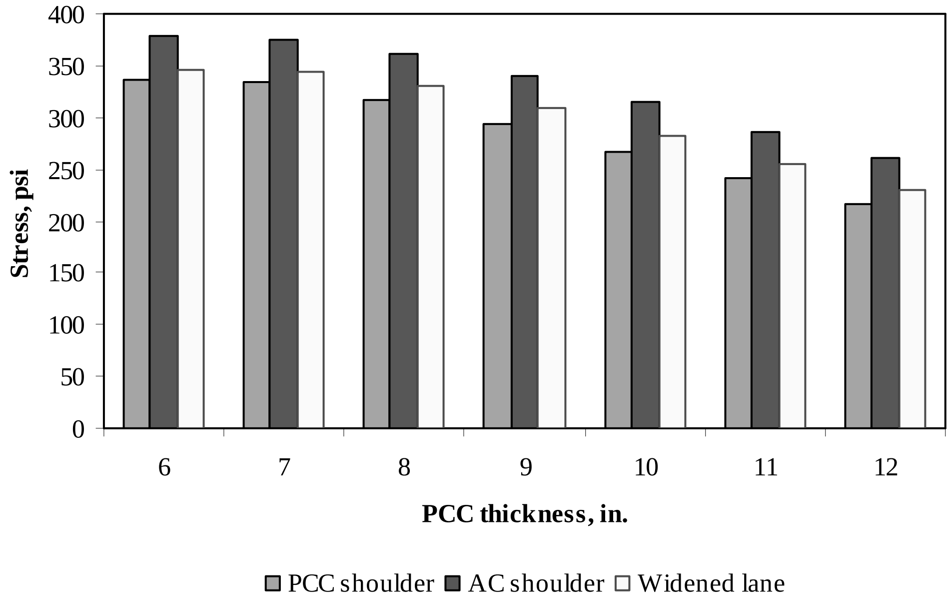


**Figure F-16-31: Impact of PCC thickness and lateral support condition on longitudinal stress at top of the Slab (177-in. joint spacing and α(ΔT/D) of $-20x10^{-6}$ in.$^{-1}$)**

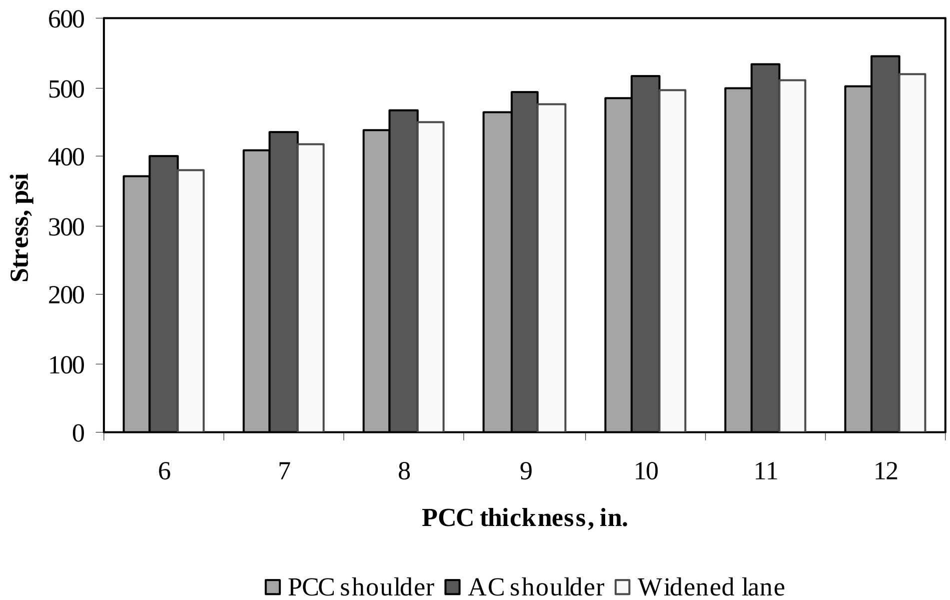


**Figure F-16-32: Impact of PCC thickness and lateral support condition on longitudinal stress at top of the Slab (315-in. joint spacing and α(ΔT/D) of $-20x10^{-6}$ in.$^{-1}$)**

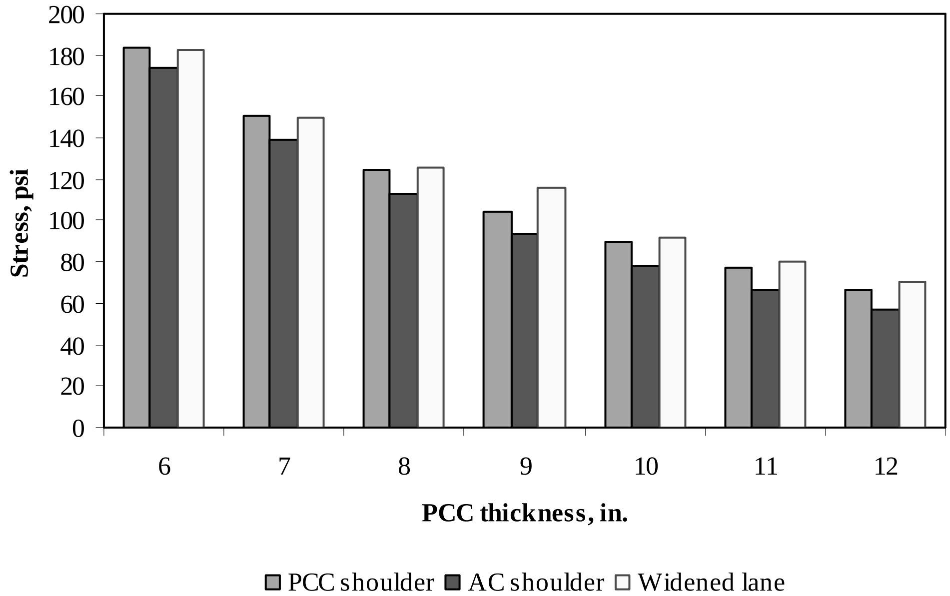


**Figure F-16-33: Impact of PCC thickness and lateral support condition on transverse stress at bottom of the Slab (177-in. joint spacing and $\alpha(\Delta T/D)$ of 0 in.$^{-1}$)**

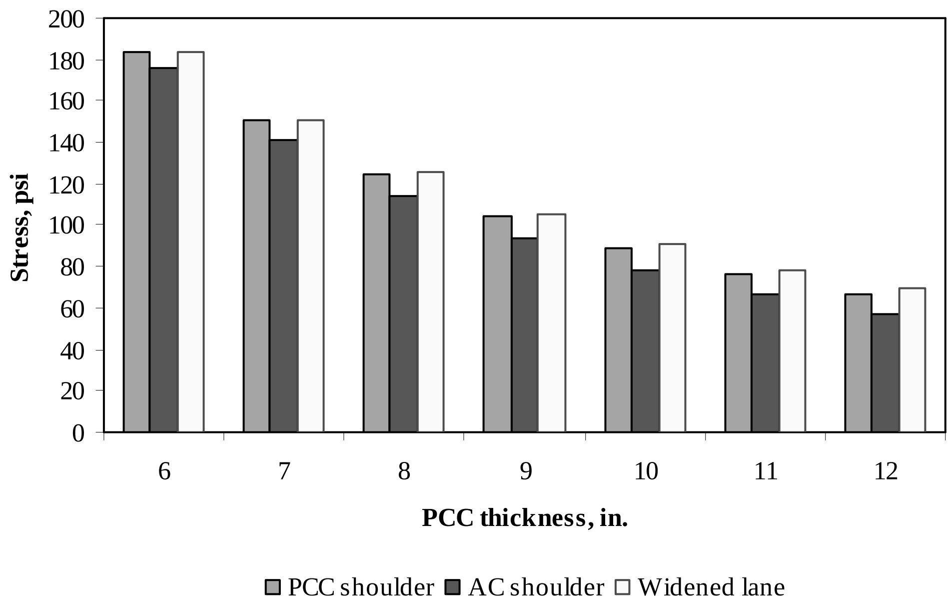


**Figure F-16-34: Impact of PCC thickness and lateral support condition on transverse stress at bottom of the Slab (315-in. joint spacing and $\alpha(\Delta T/D)$ of 0 in.$^{-1}$)**

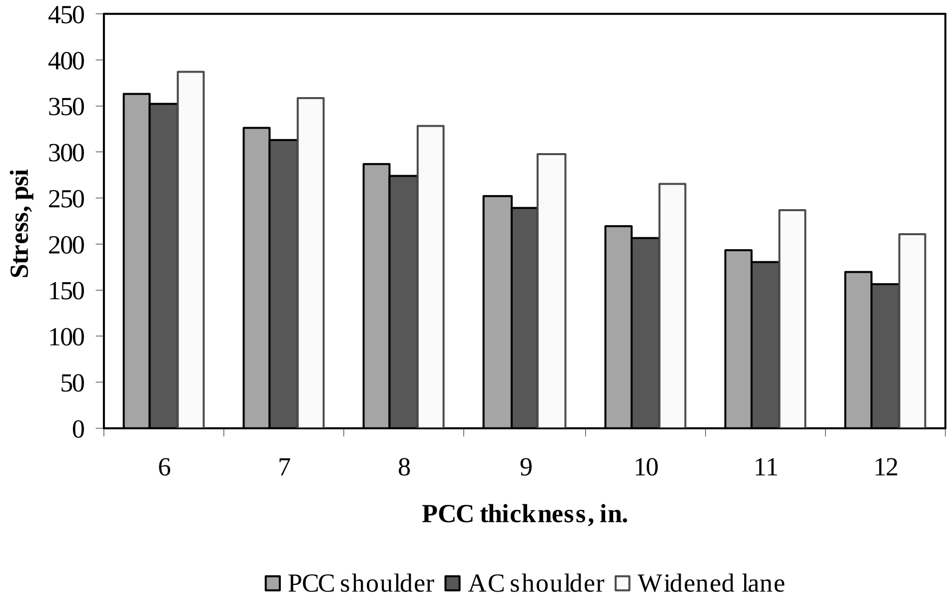


**Figure F-16-35: Impact of PCC thickness and lateral support condition on transverse stress at bottom of the Slab (177-in. joint spacing and $\alpha(\Delta T/D)$ of 20x10$^{-6}$ in.$^{-1}$)**

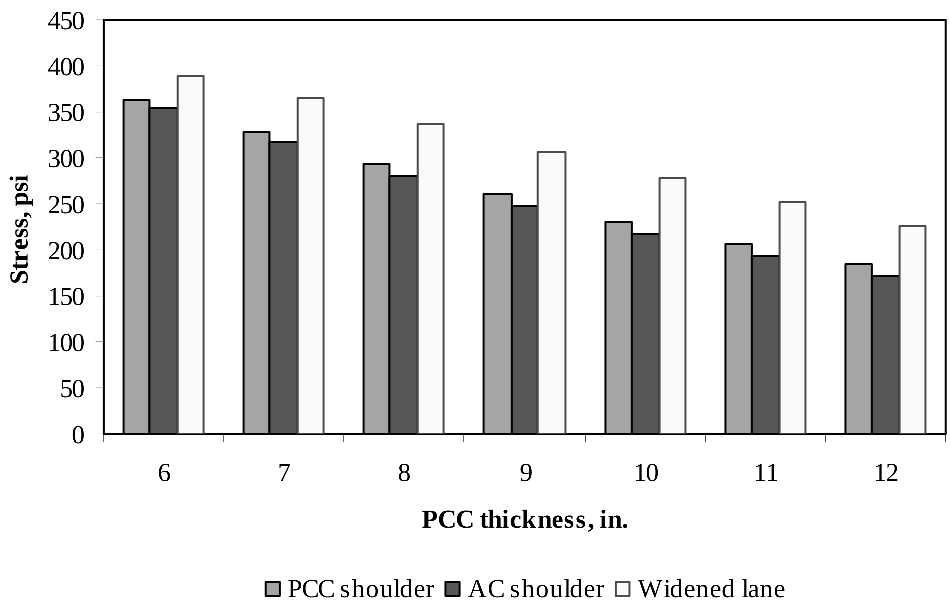


**Figure F-16-36: Impact of PCC thickness and lateral support condition on transverse stress at bottom of the Slab (315-in. joint spacing and $\alpha(\Delta T/D)$ of 20x10$^{-6}$ in.$^{-1}$)**

Figures F-16-37 through F-16-42 illustrate the impact of base/subbase thickness and product α(ΔT/D) on stresses (10-in. PCC thickness, 100-psi/in. modulus of subgrade reaction and PCC shoulder)

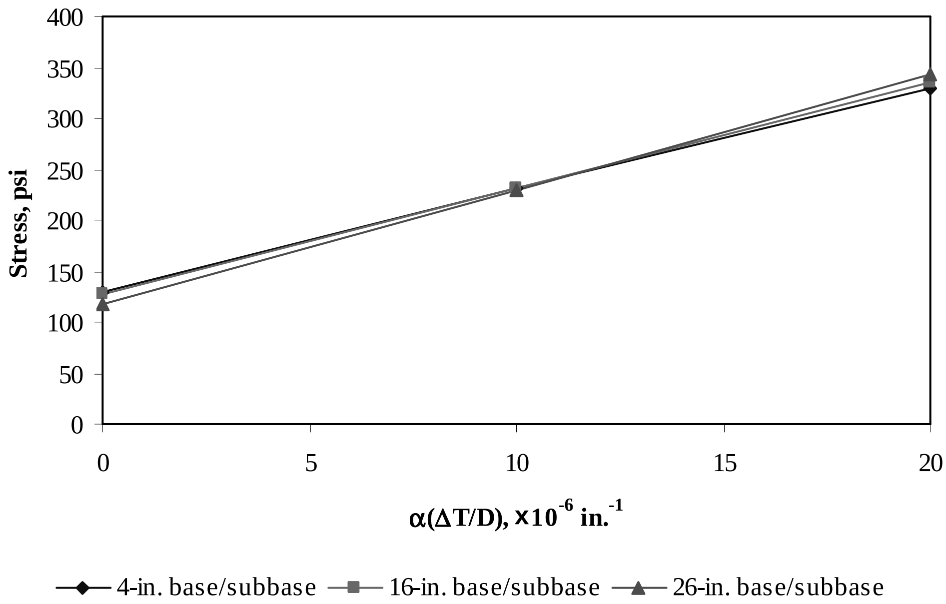


**Figure F-16-37: Impact of base/subbase thickness and product α(ΔT/D) on longitudinal stress at bottom of the slab (177-in. joint spacing)**

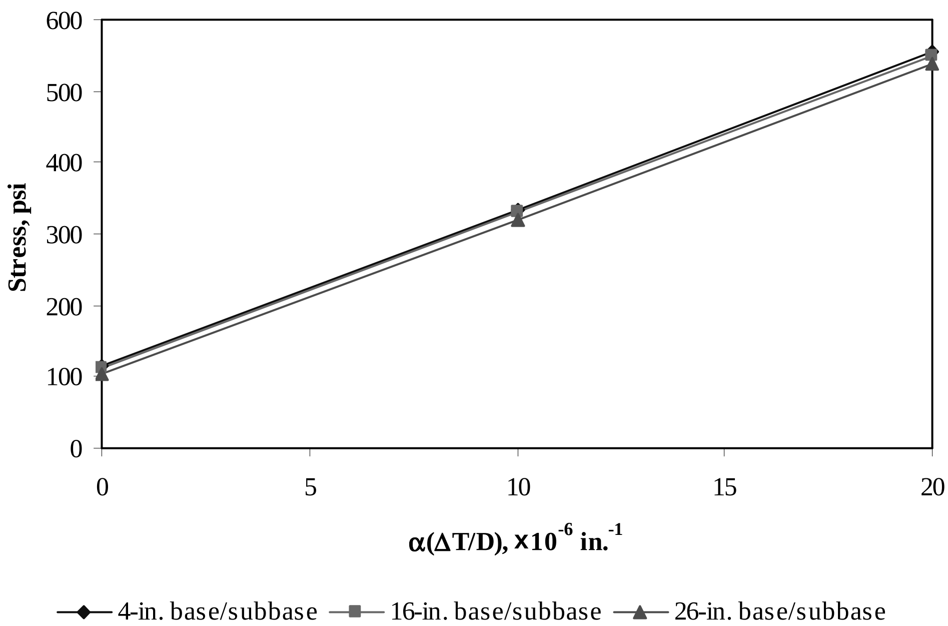


**Figure F-16-38: Impact of base/subbase thickness and product α(ΔT/D) on longitudinal stress at bottom of the slab (315-in. joint spacing)**

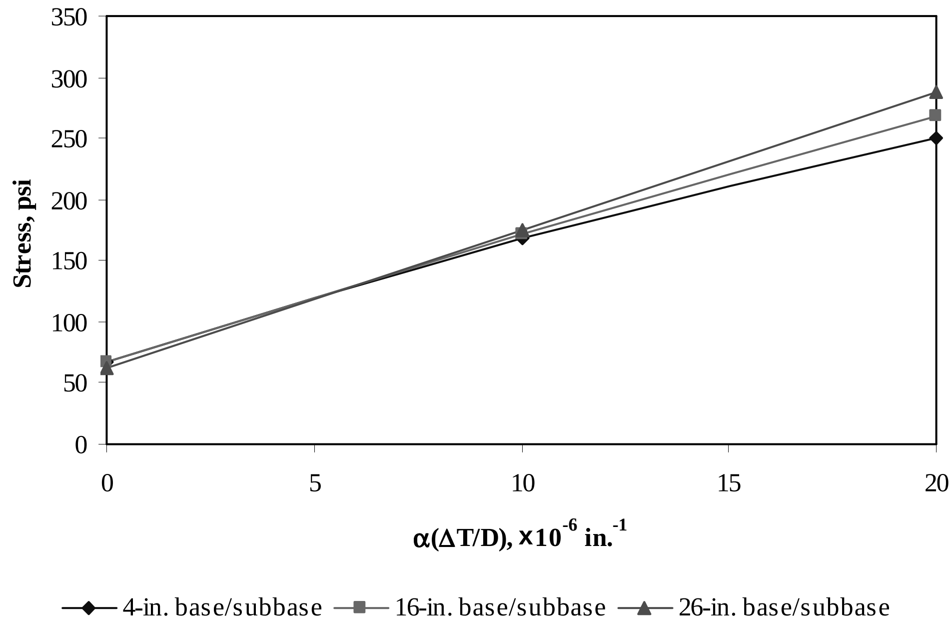


**Figure F-16-39: Impact of base/subbase thickness and product α(ΔT/D) on longitudinal stress at top of the slab (177-in. joint spacing)**

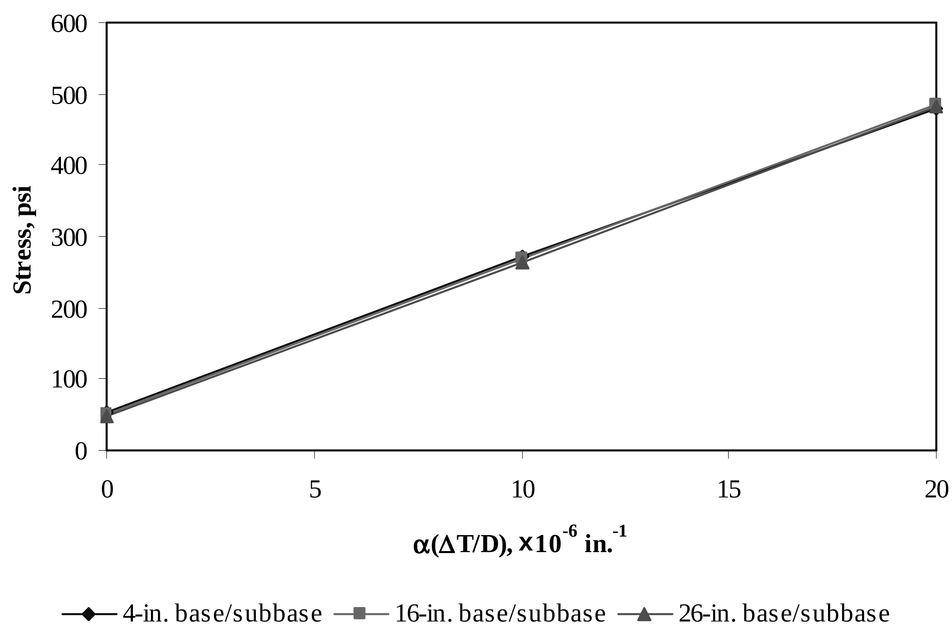


**Figure F-16-40: Impact of base/subbase thickness and product α(ΔT/D) on longitudinal stress at top of the slab (315-in. joint spacing)**

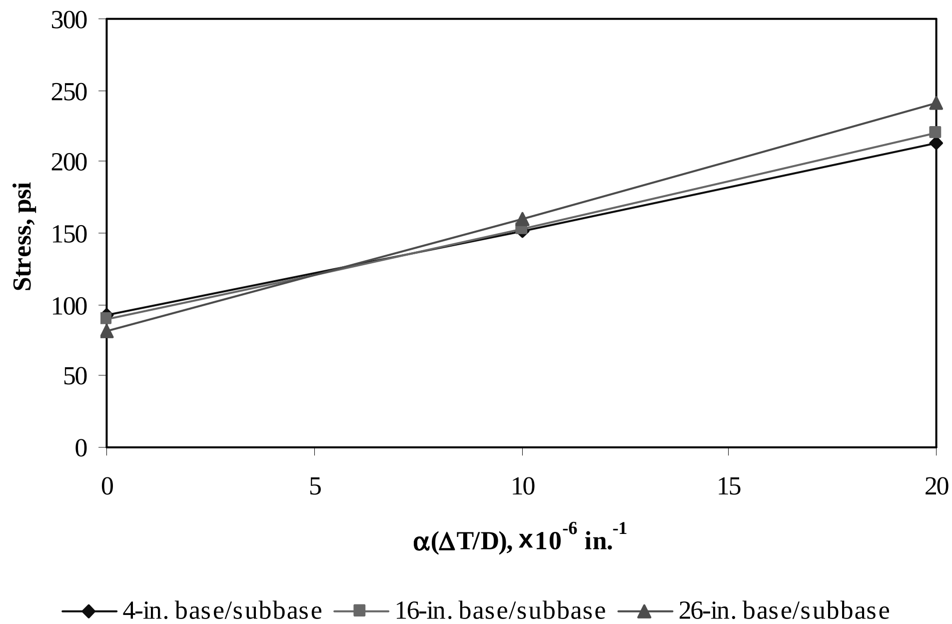


**Figure F-16-41: Impact of base/subbase thickness and product α(ΔT/D) on transverse stress at bottom of the slab (177-in. joint spacing)**

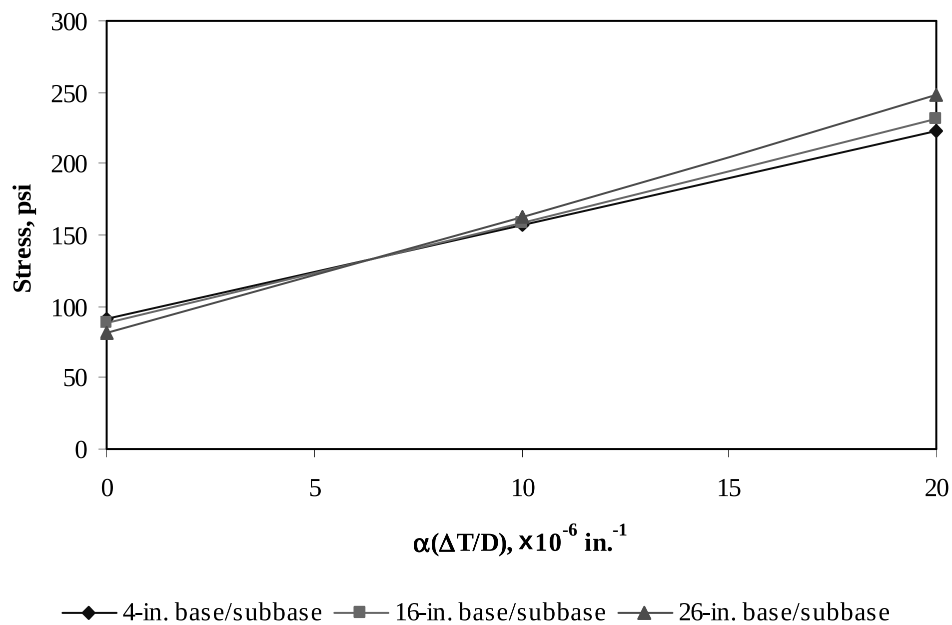


**Figure F-16-42: Impact of base/subbase thickness and product α(ΔT/D) on transverse stress at bottom of the slab (315-in. joint spacing)**

Figures F-16-43 through F-16-48 illustrate the impact of modulus of subgrade reaction and product α(ΔT/D) on stresses (10-in. PCC thickness, 16-in. base/subbase thickness and PCC shoulder)

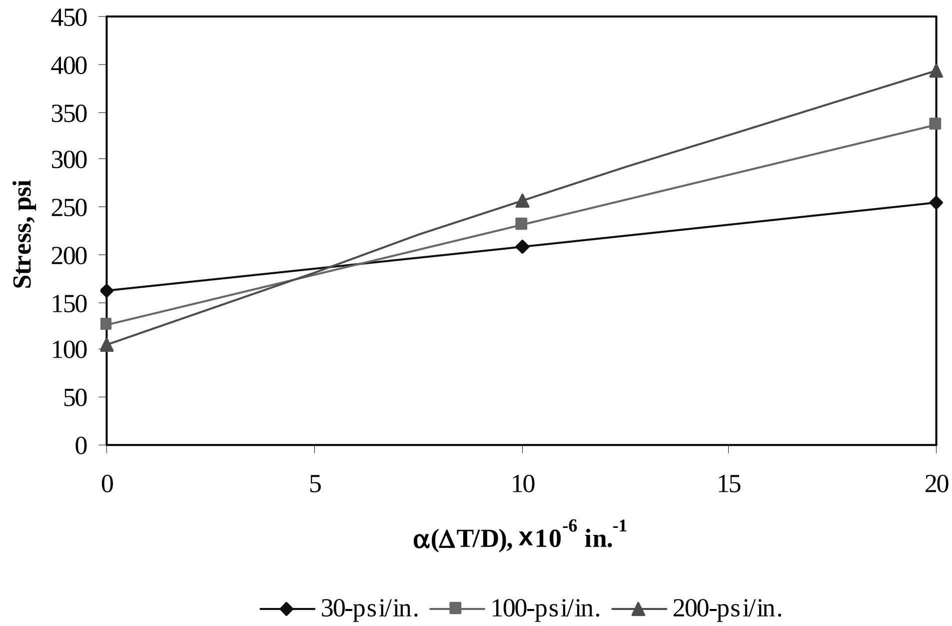


**Figure F-16-43: Impact of modulus of subgrade reaction and product α(ΔT/D) on longitudinal stress at bottom of the slab (177-in. joint spacing)**

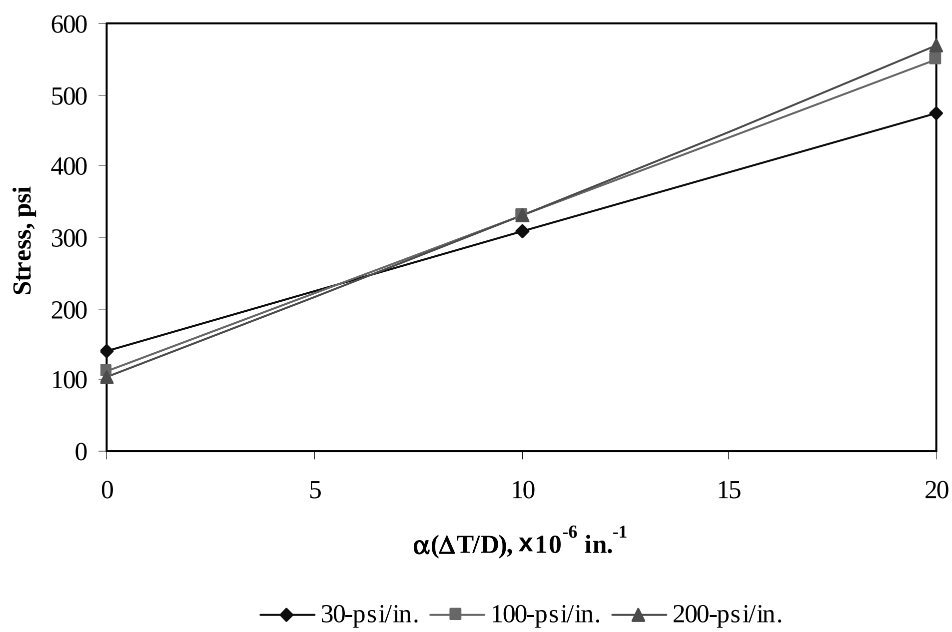


**Figure F-16-44: Impact of modulus of subgrade reaction and product α(ΔT/D) on longitudinal stress at bottom of the slab (315-in. joint spacing)**

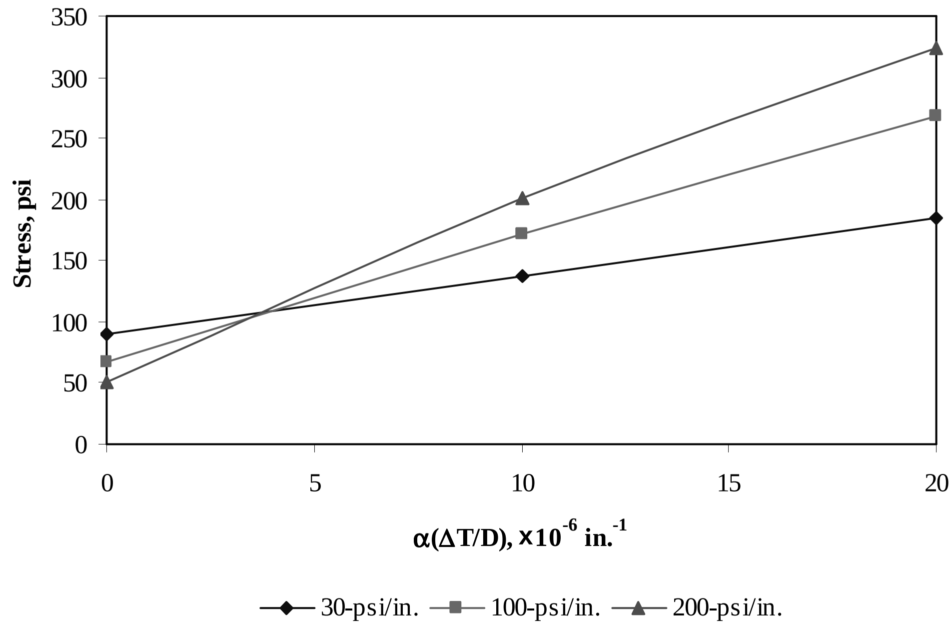


**Figure F-16-45: Impact of modulus of subgrade reaction and product α(ΔT/D) on longitudinal stress at top of the slab (177-in. joint spacing)**

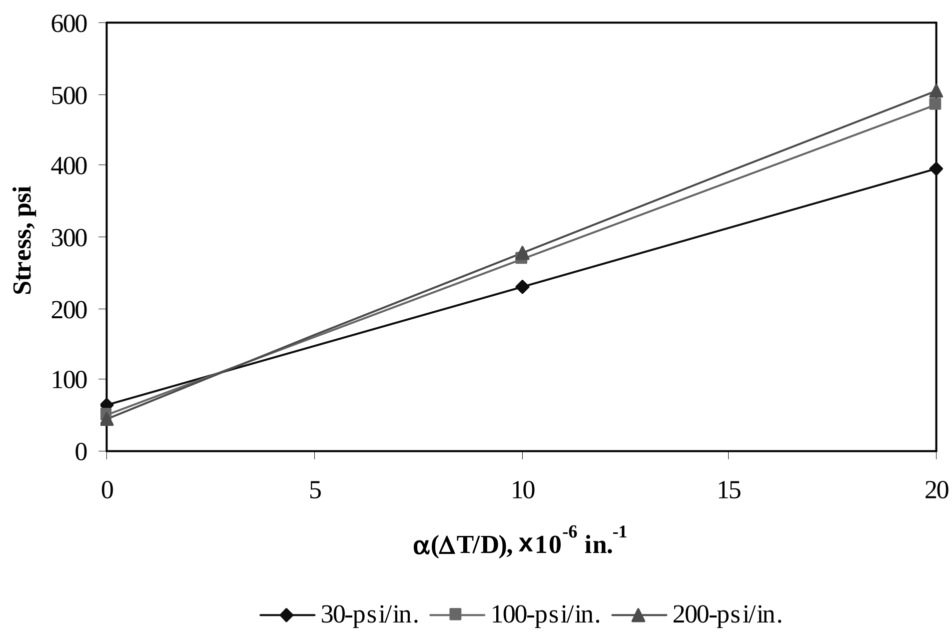


**Figure F-16-46: Impact of modulus of subgrade reaction and product α(ΔT/D) on longitudinal stress at top of the slab (315-in. joint spacing)**

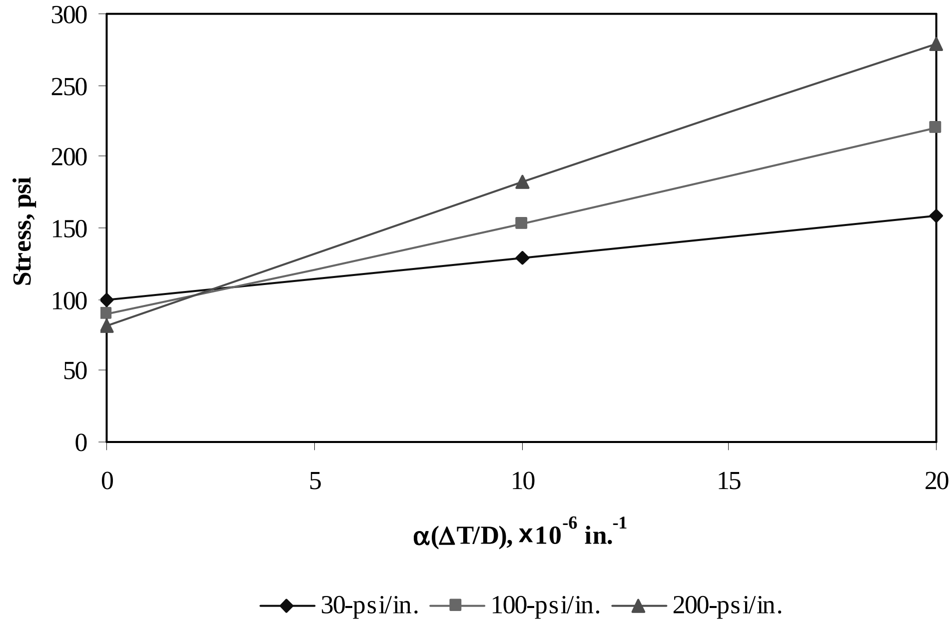


**Figure F-16-47: Impact of modulus of subgrade reaction and product α(ΔT/D) on transverse stress at bottom of the slab (177-in. joint spacing)**

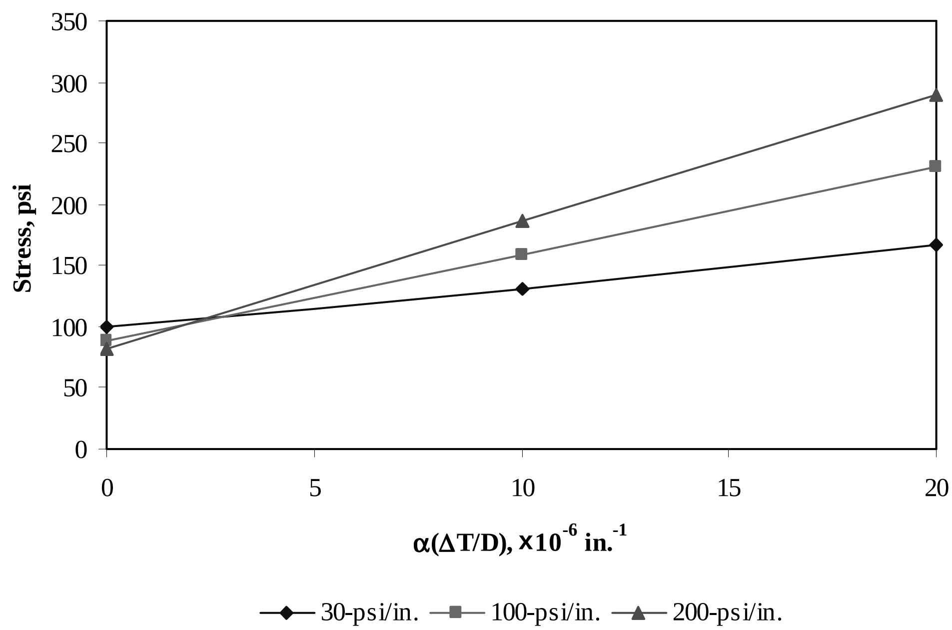


**Figure F-16-48: Impact of modulus of subgrade reaction and product α(ΔT/D) on transverse stress at bottom of the slab (315-in. joint spacing)**

Figures F-16-49 through F-16-51 illustrate the impact of joint spacing and product α(ΔT/D) on stresses (10-in. PCC thickness, 16-in. base/subbase thickness, 100-psi/in. modulus of subgrade reaction and PCC shoulder)

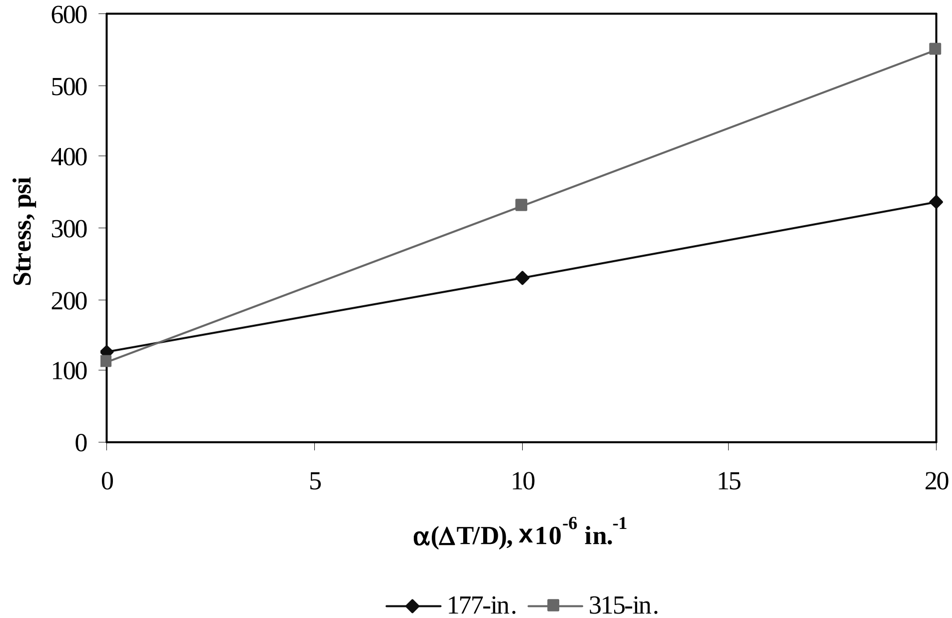


**Figure F-16-49: Impact of joint spacing and product α(ΔT/D) on longitudinal stress at bottom of the slab**

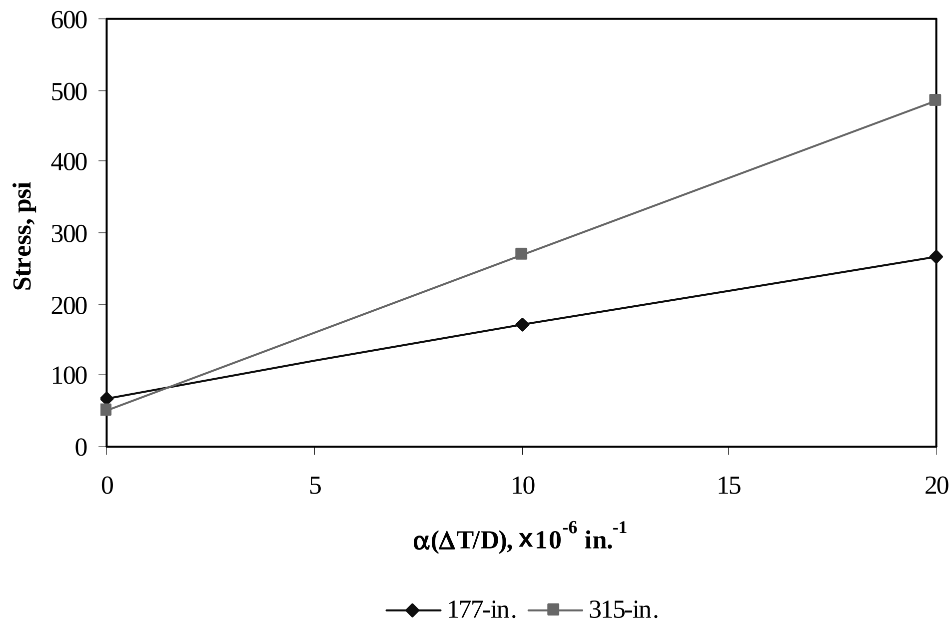


**Figure F-16-50: Impact of joint spacing and product α(ΔT/D) on longitudinal stress at top of the slab**

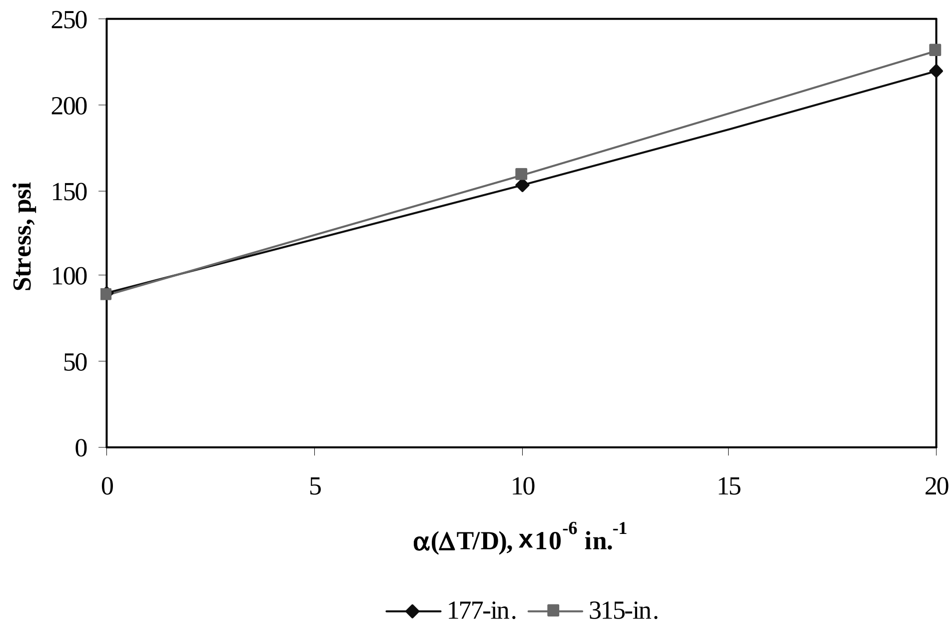


**Figure F-16-51: Impact of joint spacing and product $\alpha(\Delta T/D)$ on transverse stress at bottom of the slab**

**Sub Appendix F-17**

**Documentation of Pavement Responses for**

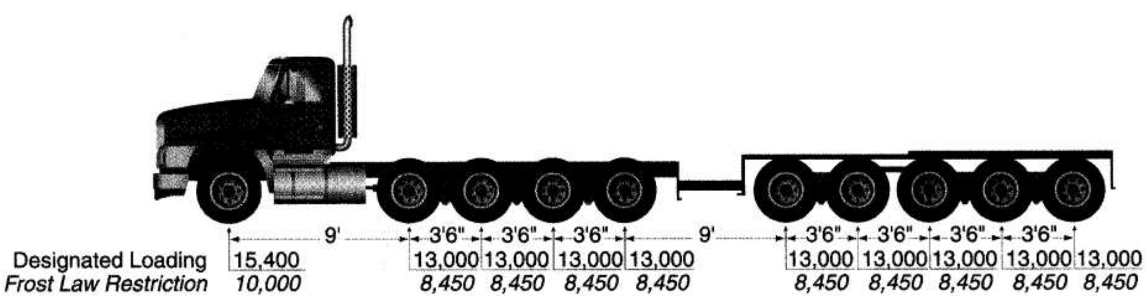


**MI-17**

Figures F-17-1 through F-17-12 illustrate the impact of PCC thickness and base/subbase thickness on stresses (100-psi/in. modulus of subgrade reaction and PCC shoulder)

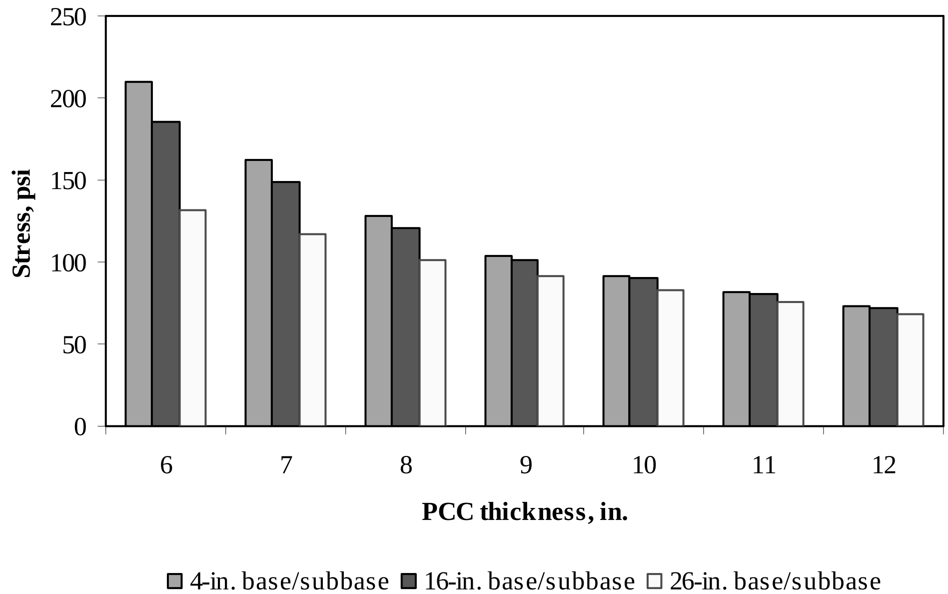


**Figure F-17-1: Impact of PCC thickness and base/subbase thickness on longitudinal stress at bottom of the Slab (177-in. joint spacing and α(ΔT/D) of 0 in.$^{-1}$)**

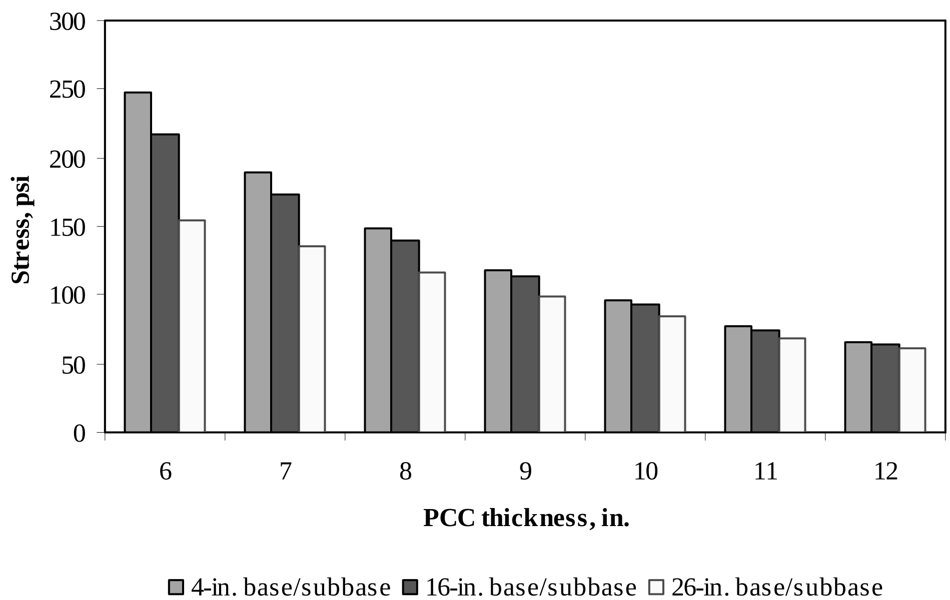


**Figure F-17-2: Impact of PCC thickness and base/subbase thickness on longitudinal stress at bottom of the Slab (315-in. joint spacing and α(ΔT/D) of 0 in.$^{-1}$)**

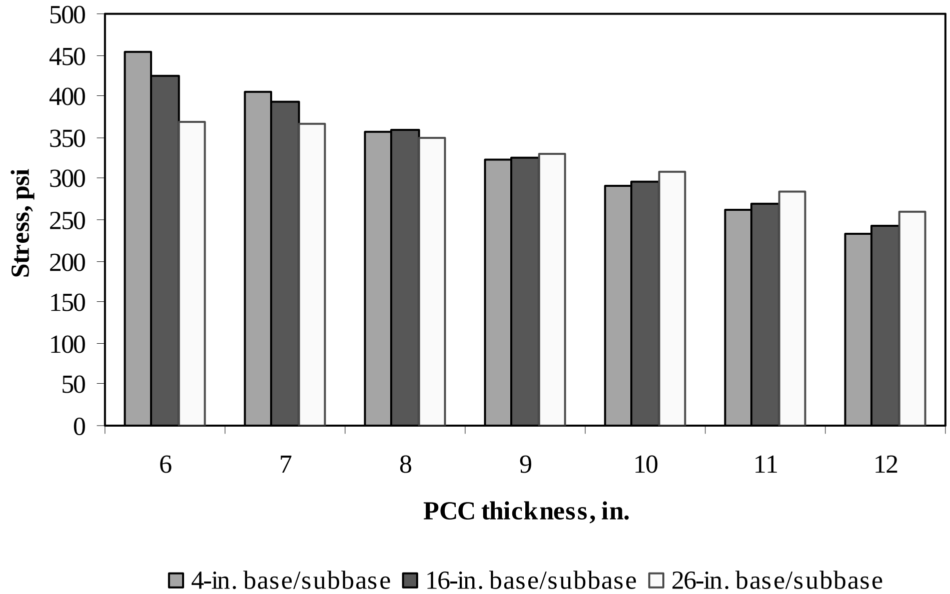


**Figure F-17-3: Impact of PCC thickness and base/subbase thickness on longitudinal stress at bottom of the Slab (177-in. joint spacing and $\alpha(\Delta T/D)$ of $20x10^{-6}$ in.$^{-1}$)**

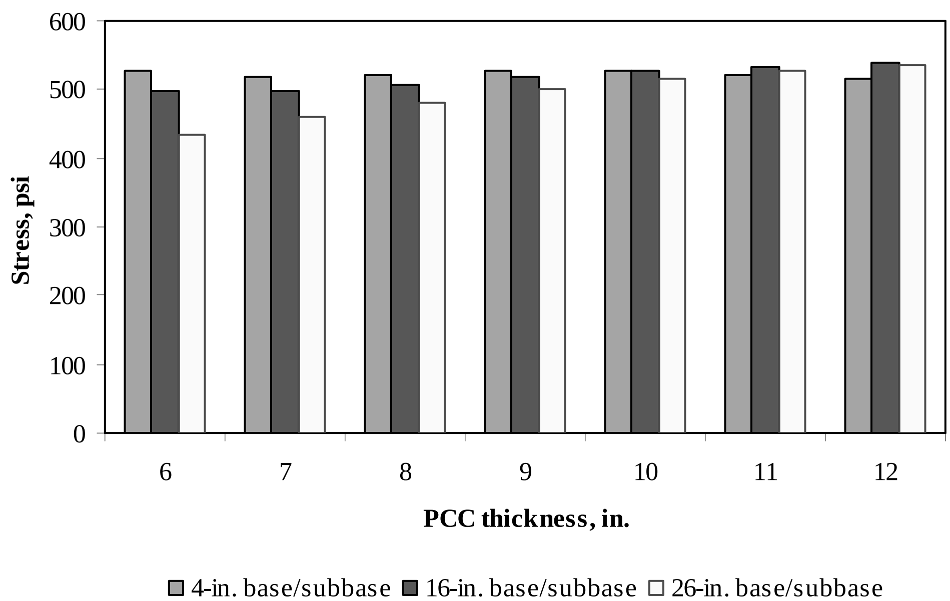


**Figure F-17-4: Impact of PCC thickness and base/subbase thickness on longitudinal stress at bottom of the Slab (315-in. joint spacing and $\alpha(\Delta T/D)$ of $20x10^{-6}$ in.$^{-1}$)**

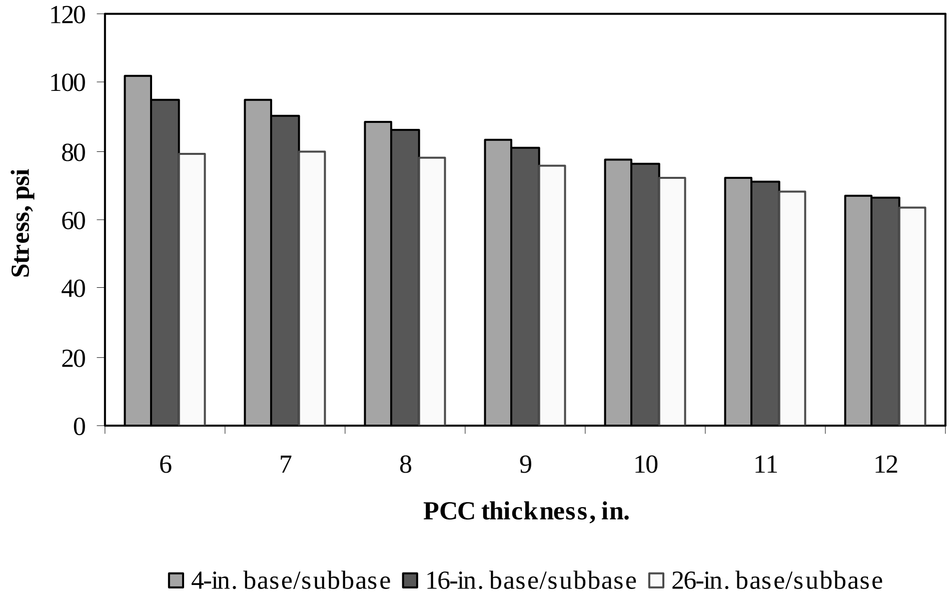


**Figure F-17-5: Impact of PCC thickness and base/subbase thickness on longitudinal stress at top of the Slab (177-in. joint spacing and $\alpha(\Delta T/D)$ of 0 in.$^{-1}$)**

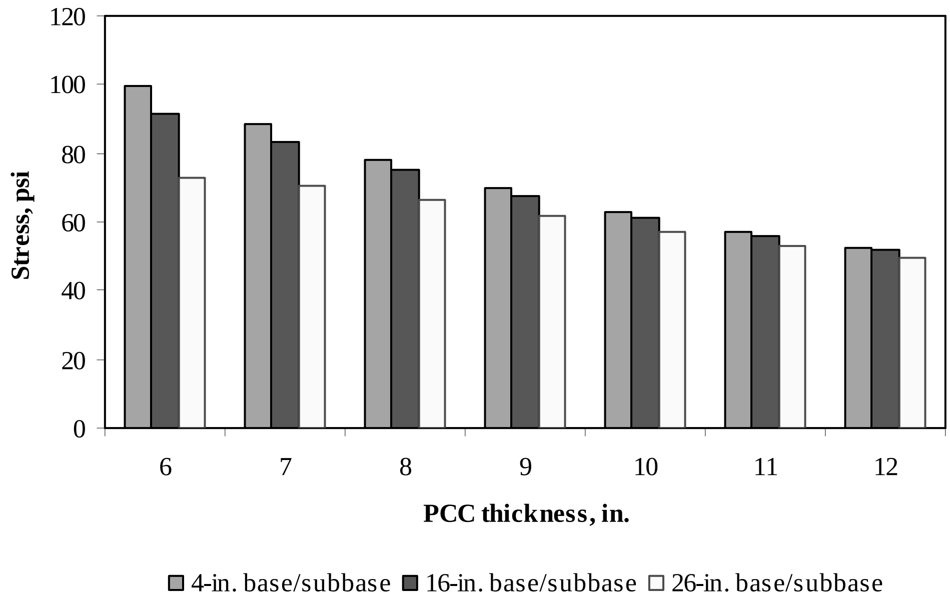


**Figure F-17-6: Impact of PCC thickness and base/subbase thickness on longitudinal stress at top of the Slab (315-in. joint spacing and $\alpha(\Delta T/D)$ of 0 in.$^{-1}$)**

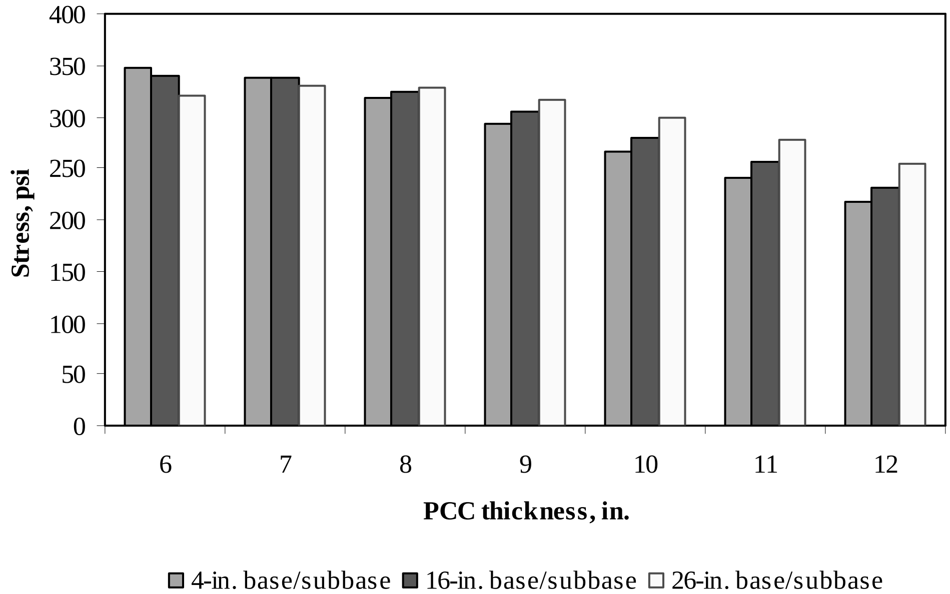


**Figure F-17-7: Impact of PCC thickness and base/subbase thickness on longitudinal stress at top of the Slab (177-in. joint spacing and $\alpha(\Delta T/D)$ of -20x10$^{-6}$ in.$^{-1}$)**

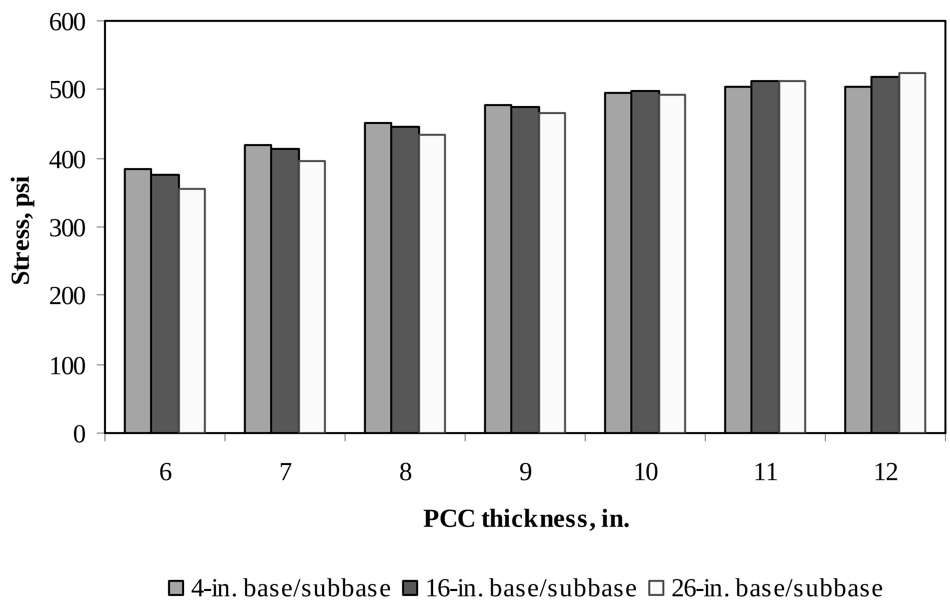


**Figure F-17-8: Impact of PCC thickness and base/subbase thickness on longitudinal stress at top of the Slab (315-in. joint spacing and $\alpha(\Delta T/D)$ of -20x10$^{-6}$ in.$^{-1}$)**

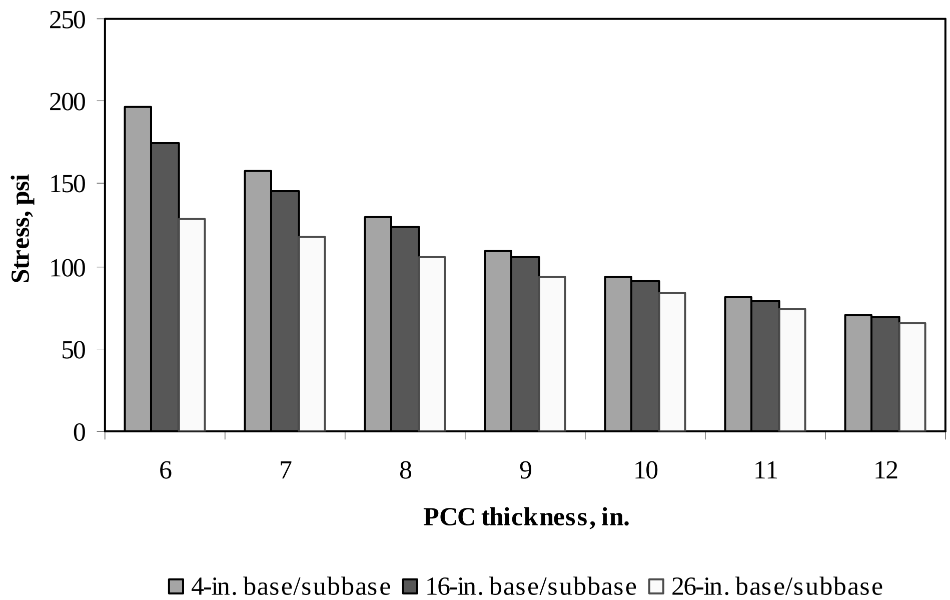


**Figure F-17-9: Impact of PCC thickness and base/subbase thickness on transverse stress at bottom of the Slab (177-in. joint spacing and $\alpha(\Delta T/D)$ of 0 in.$^{-1}$)**

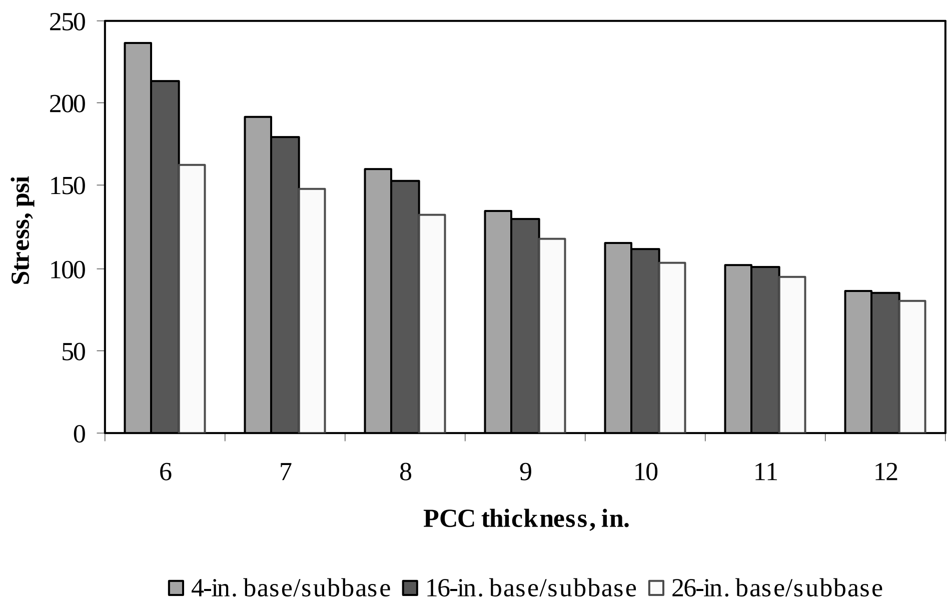


**Figure F-17-10: Impact of PCC thickness and base/subbase thickness on transverse stress at bottom of the Slab (315-in. joint spacing and $\alpha(\Delta T/D)$ of 0 in.$^{-1}$)**

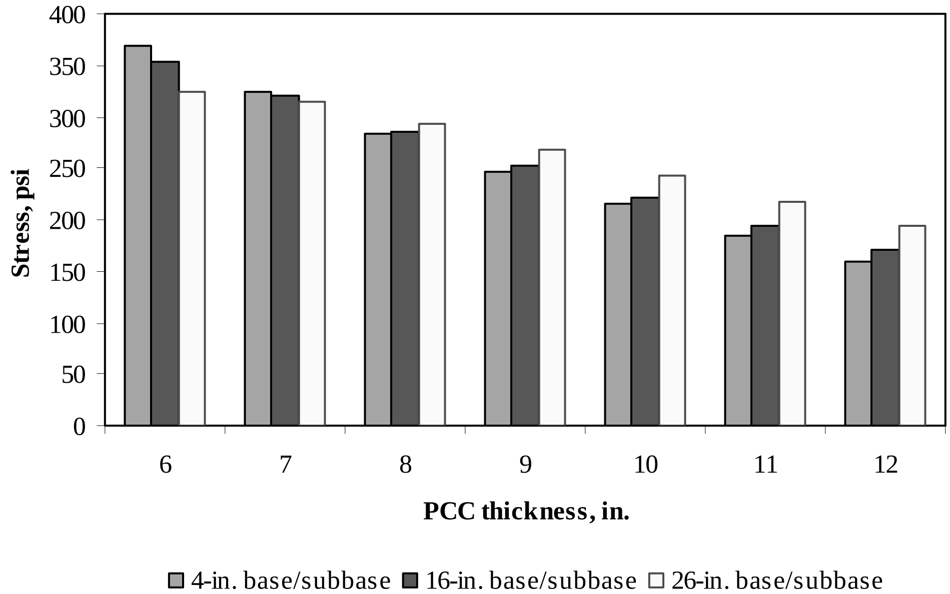


**Figure F-17-11: Impact of PCC thickness and base/subbase thickness on transverse stress at bottom of the Slab (177-in. joint spacing and $\alpha(\Delta T/D)$ of $20 x 10^{-6}$ in.$^{-1}$)**

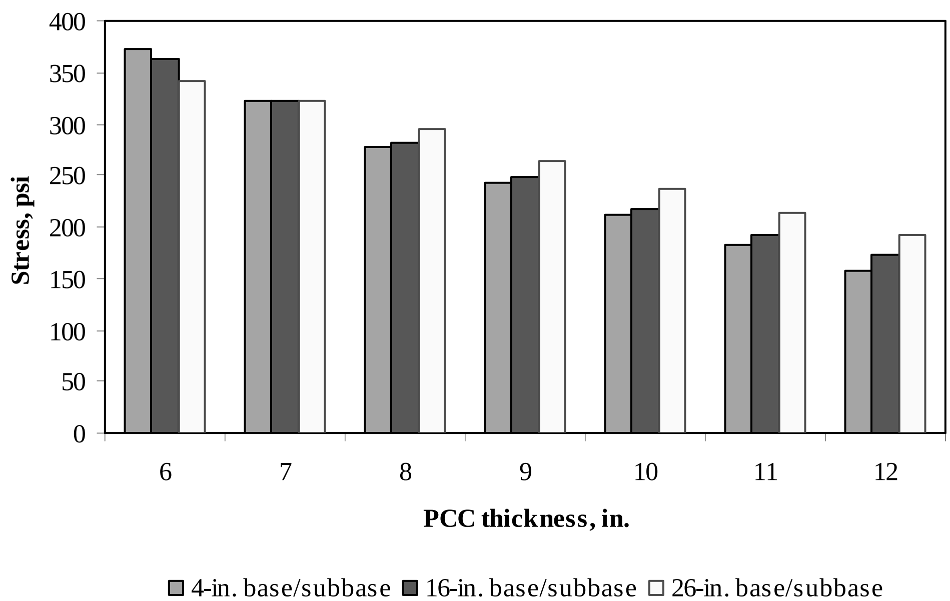


**Figure F-17-12: Impact of PCC thickness and base/subbase thickness on transverse stress at bottom of the Slab (315-in. joint spacing and $\alpha(\Delta T/D)$ of $20 x 10^{-6}$ in.$^{-1}$)**

Figures F-17-13 through F-17-24 illustrate the impact of PCC thickness and modulus of subgrade reaction on stresses (16-in. base/subbase thickness and PCC shoulder)

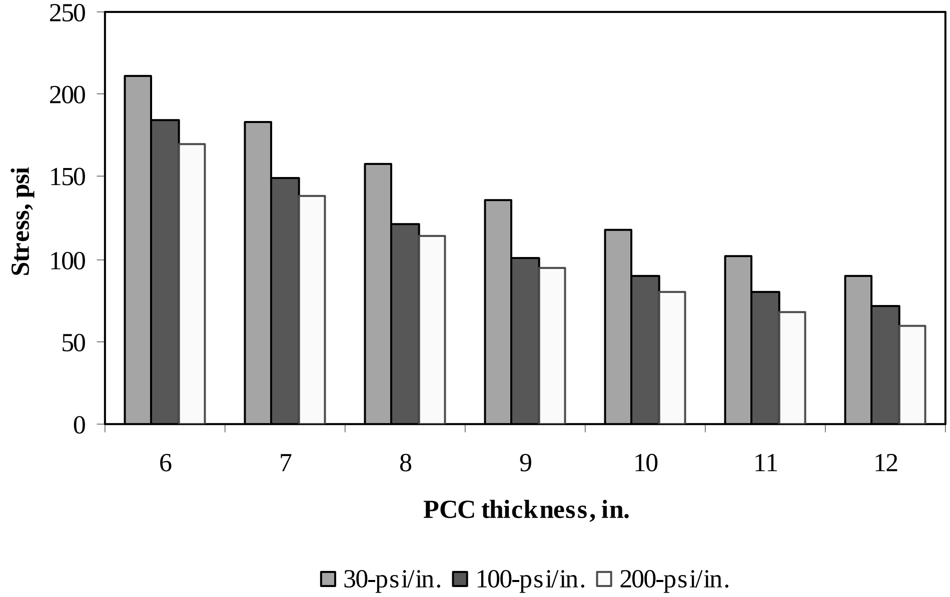


**Figure F-17-13: Impact of PCC thickness and modulus of subgrade reaction on longitudinal stress at bottom of the slab (177-in. joint spacing and $\alpha(\Delta T/D)$ of 0 in.$^{-1}$)**

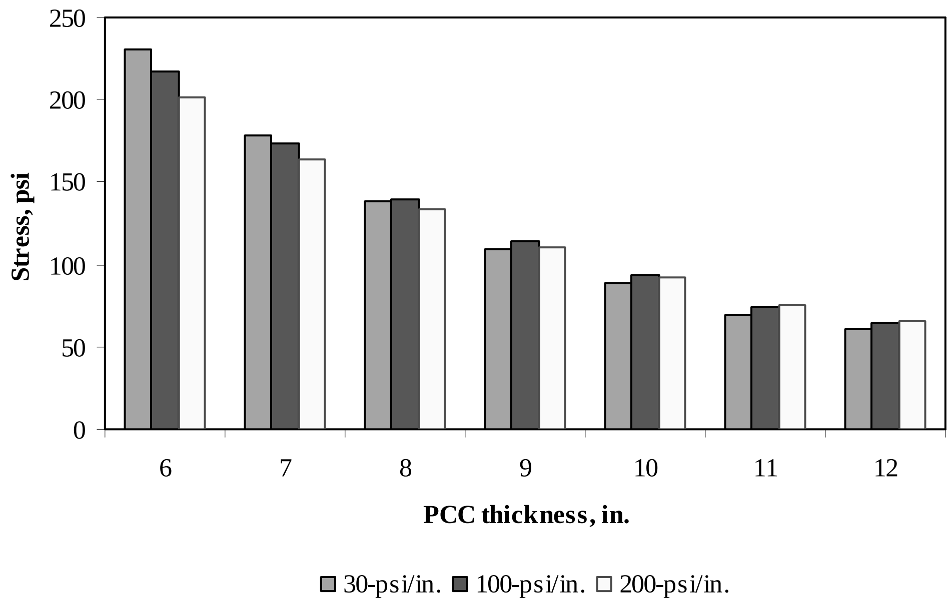


**Figure F-17-14: Impact of PCC thickness and modulus of subgrade reaction on longitudinal stress at bottom of the slab (315-in. joint spacing and $\alpha(\Delta T/D)$ of 0 in.$^{-1}$)**

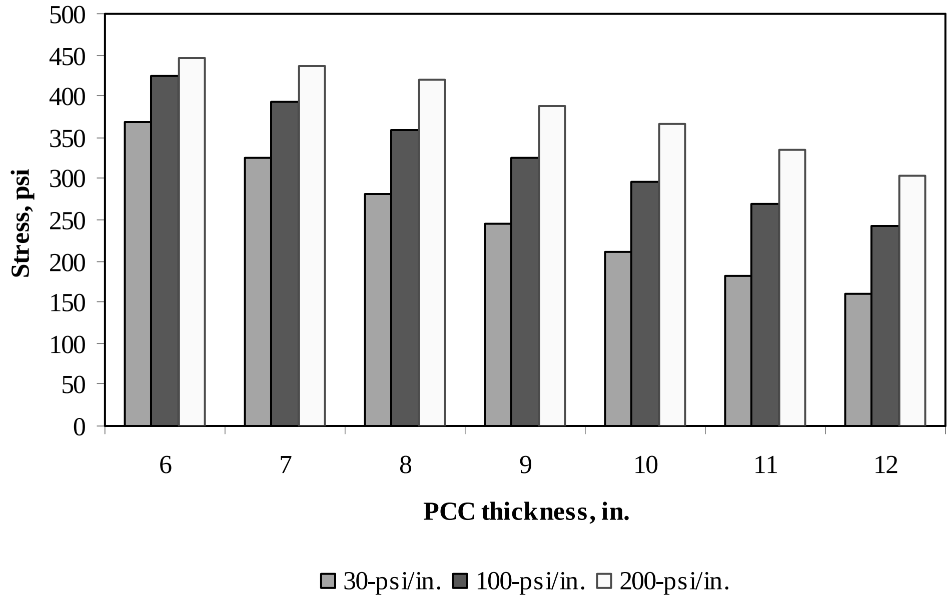


**Figure F-17-15: Impact of PCC thickness and modulus of subgrade reaction on longitudinal stress at bottom of the slab (177-in. joint spacing and $\alpha(\Delta T/D)$ of $20x10^{-6}$ in.$^{-1}$)**

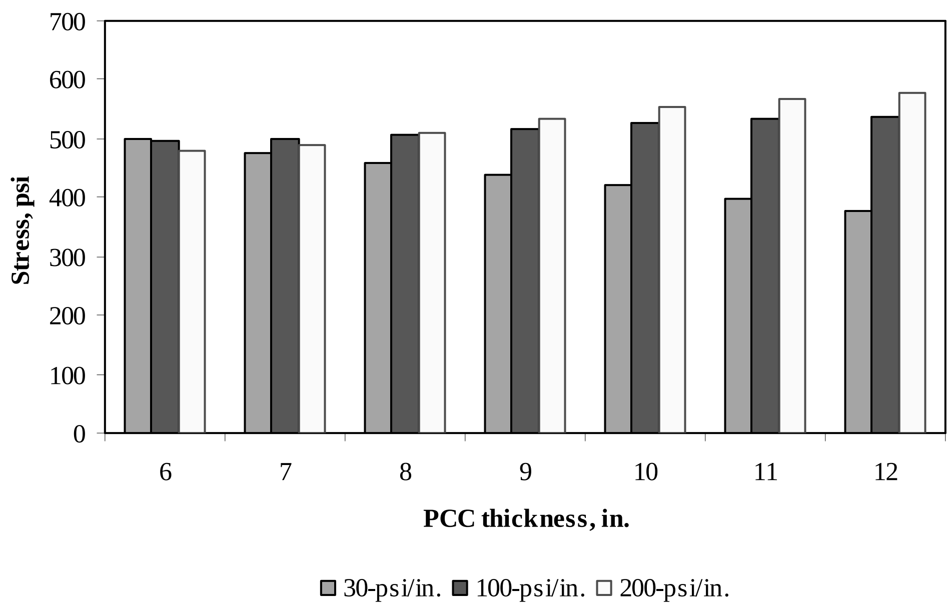


**Figure F-17-16: Impact of PCC thickness and modulus of subgrade reaction on longitudinal stress at bottom of the slab (315-in. joint spacing and $\alpha(\Delta T/D)$ of $20x10^{-6}$ in.$^{-1}$)**

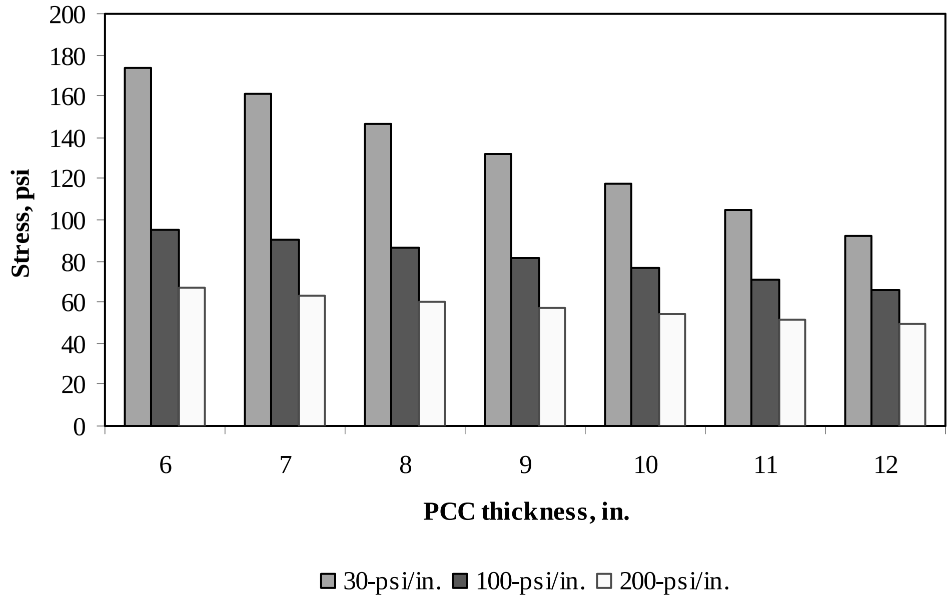


**Figure F-17-17: Impact of PCC thickness and modulus of subgrade reaction on longitudinal stress at top of the Slab (177-in. joint spacing and $\alpha(\Delta T/D)$ of 0 $in.^{-1}$)**

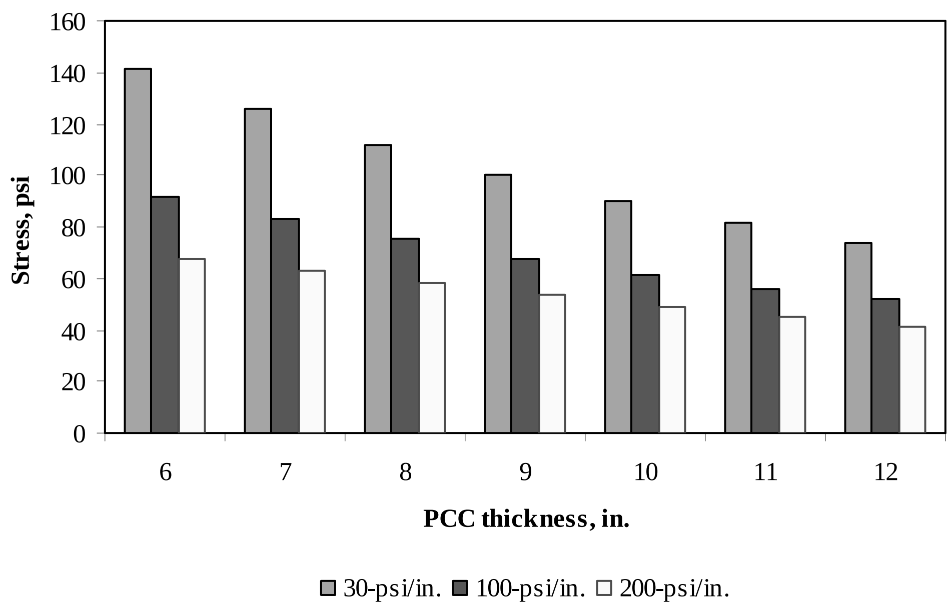


**Figure F-17-18: Impact of PCC thickness and modulus of subgrade reaction on longitudinal stress at top of the Slab (315-in. joint spacing and $\alpha(\Delta T/D)$ of 0 $in.^{-1}$)**

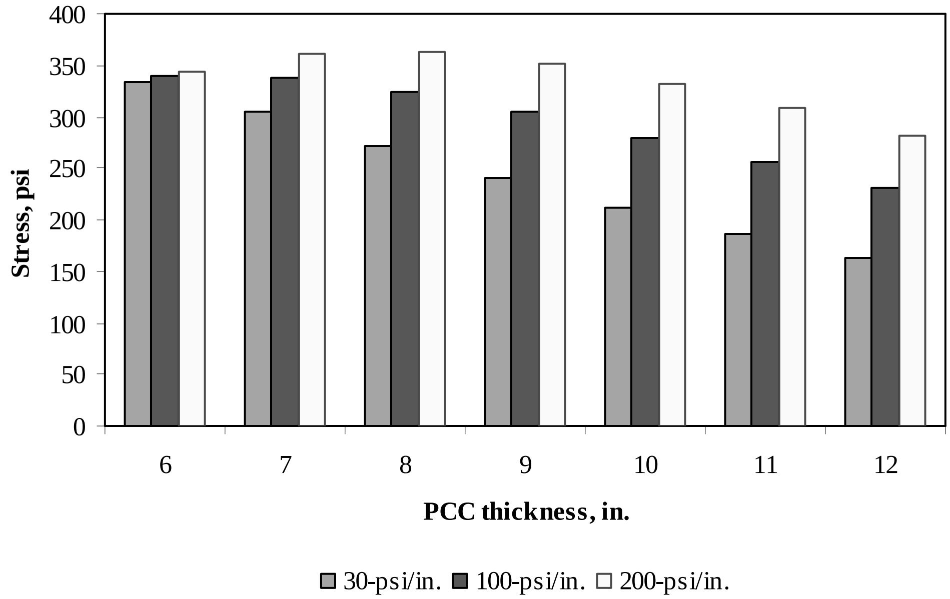


**Figure F-17-19: Impact of PCC thickness and modulus of subgrade reaction on longitudinal stress at top of the Slab (177-in. joint spacing and α(ΔT/D) of $-20x10^{-6}$ in.$^{-1}$)**

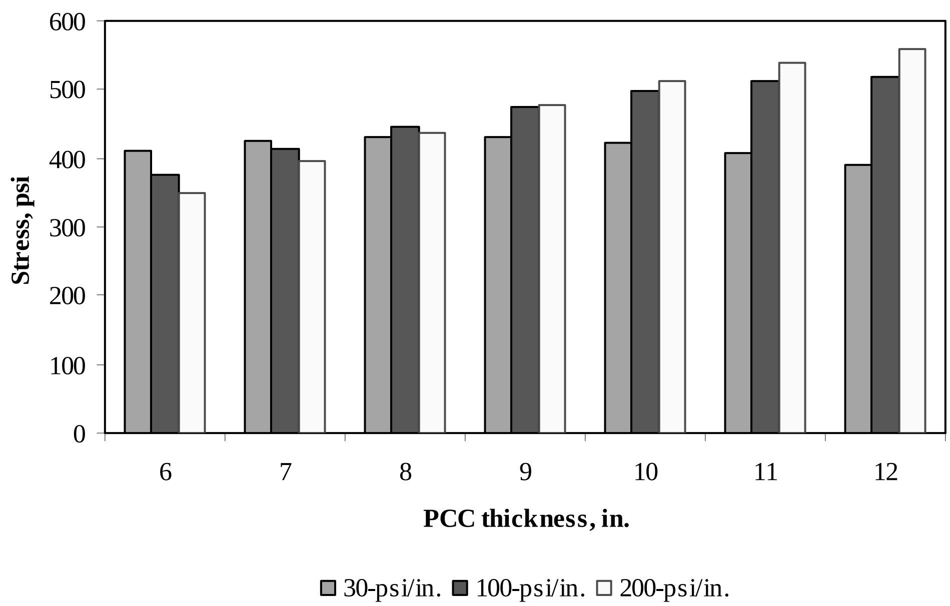


**Figure F-17-20: Impact of PCC thickness and modulus of subgrade reaction on longitudinal stress at top of the Slab (315-in. joint spacing and α(ΔT/D) of $-20x10^{-6}$ in.$^{-1}$)**

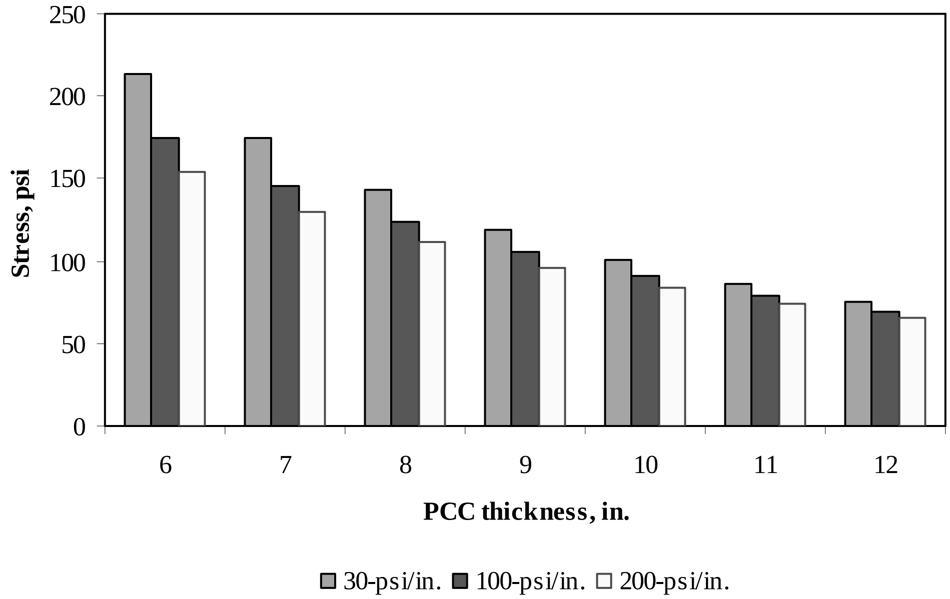


**Figure F-17-21: Impact of PCC thickness and modulus of subgrade reaction on transverse stress at bottom of the Slab (177-in. joint spacing and $\alpha(\Delta T/D)$ of 0 in.$^{-1}$)**

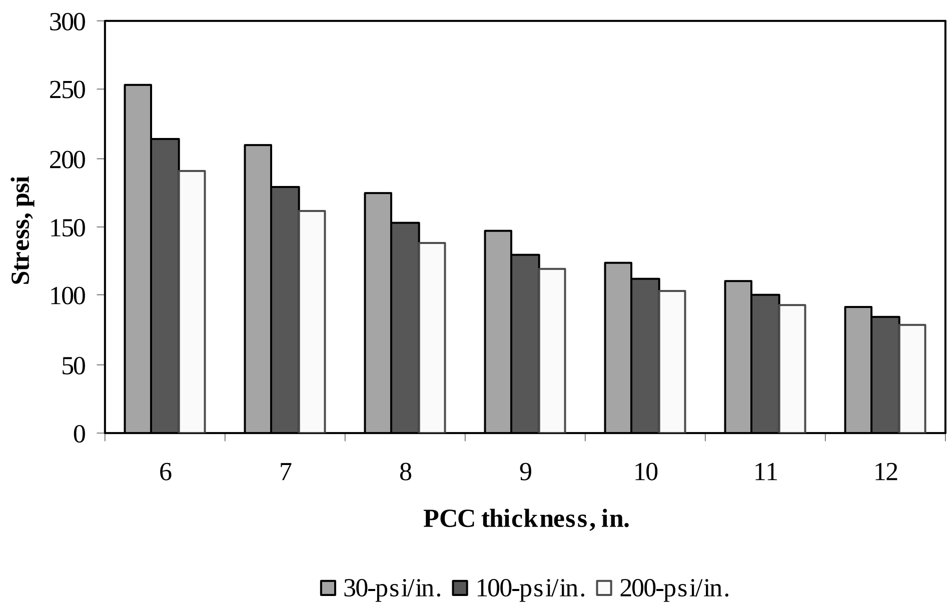


**Figure F-17-22: Impact of PCC thickness and modulus of subgrade reaction on transverse stress at bottom of the Slab (315-in. joint spacing and $\alpha(\Delta T/D)$ of 0 in.$^{-1}$)**

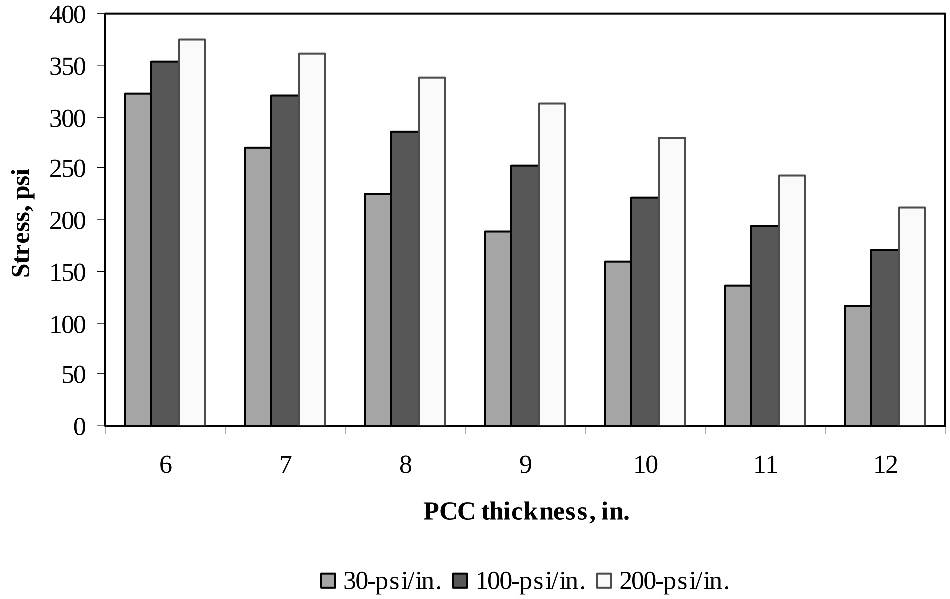


**Figure F-17-23: Impact of PCC thickness and modulus of subgrade reaction on transverse stress at bottom of the Slab (177-in. joint spacing and $\alpha(\Delta T/D)$ of $20x10^{-6}$ in.$^{-1}$)**

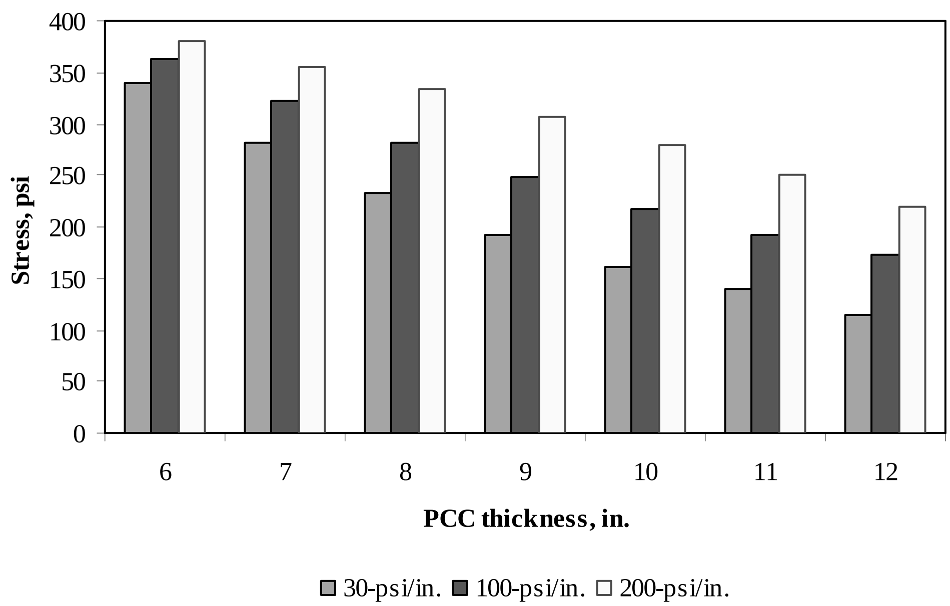


**Figure F-17-24: Impact of PCC thickness and modulus of subgrade reaction on transverse stress at bottom of the Slab (315-in. joint spacing and $\alpha(\Delta T/D)$ of $20x10^{-6}$ in.$^{-1}$)**

Figures F-17-25 through F-17-36 illustrate the impact of PCC thickness and lateral support condition on stresses (16-in. base/subbase and 100-psi/in. modulus of subgrade reaction)

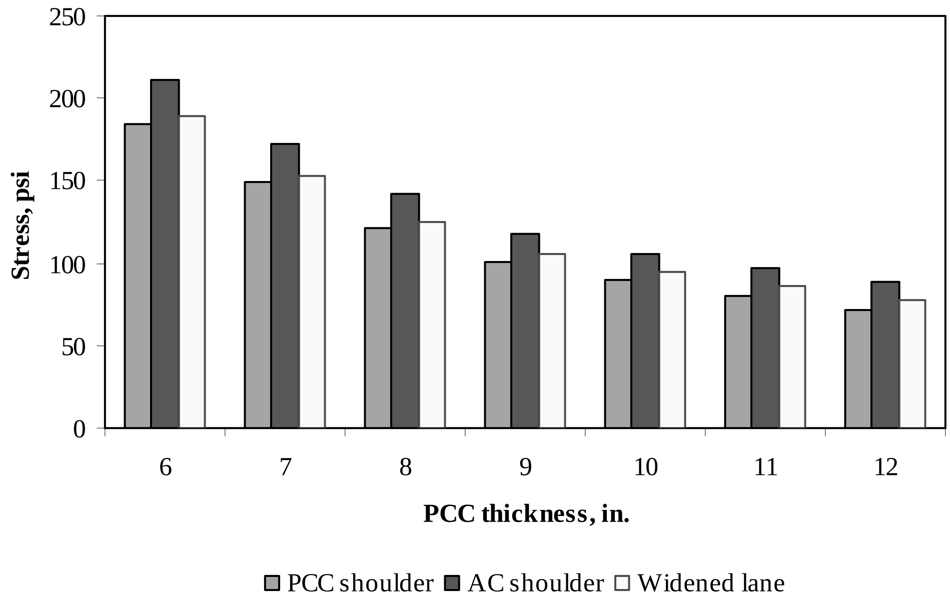


**Figure F-17-25: Impact of PCC thickness and lateral support condition on longitudinal stress at bottom of the Slab (177-in. joint spacing and $\alpha(\Delta T/D)$ of 0 in.$^{-1}$)**

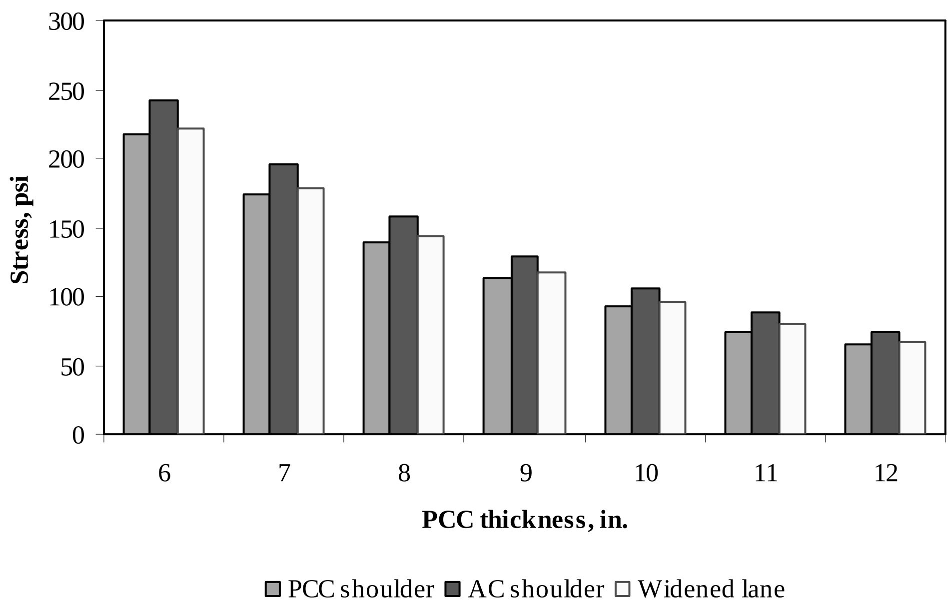


**Figure F-17-26: Impact of PCC thickness and lateral support condition on longitudinal stress at bottom of the Slab (315-in. joint spacing and $\alpha(\Delta T/D)$ of 0 in.$^{-1}$)**

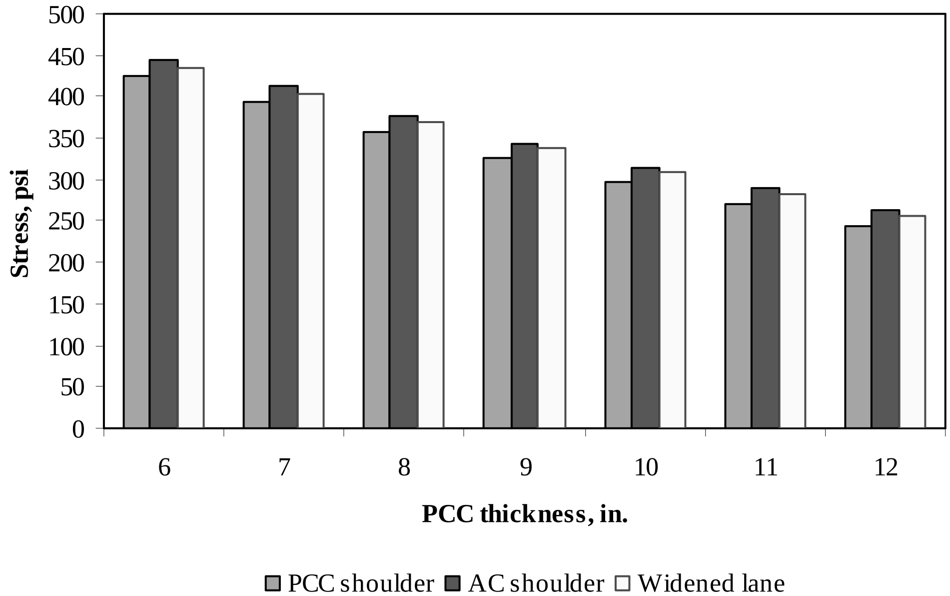


**Figure F-17-27: Impact of PCC thickness and lateral support condition on longitudinal stress at bottom of the Slab (177-in. joint spacing and $\alpha(\Delta T/D)$ of $20x10^{-6}$ in.$^{-1}$)**

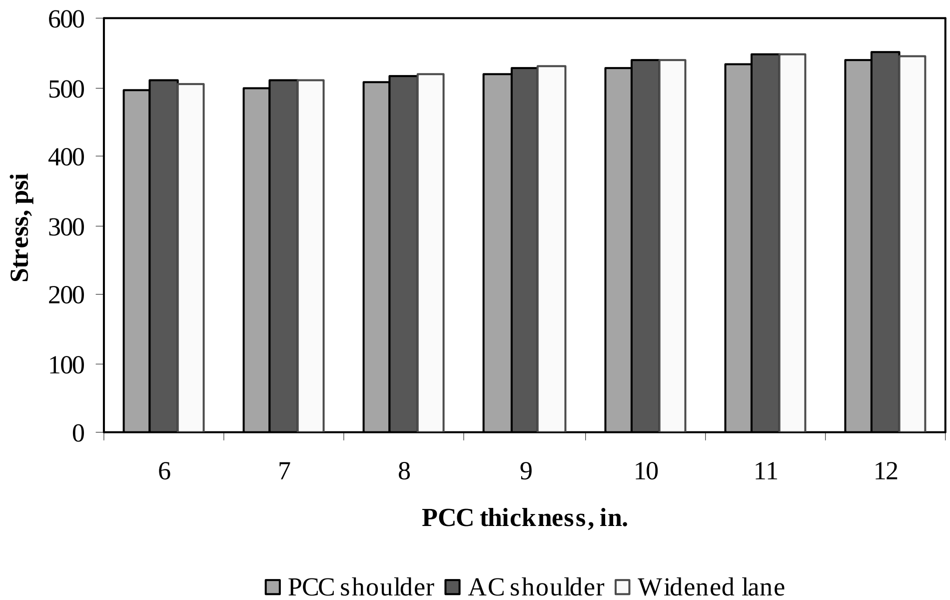


**Figure F-17-28: Impact of PCC thickness and lateral support condition on longitudinal stress at bottom of the Slab (315-in. joint spacing and $\alpha(\Delta T/D)$ of $20x10^{-6}$ in.$^{-1}$)**

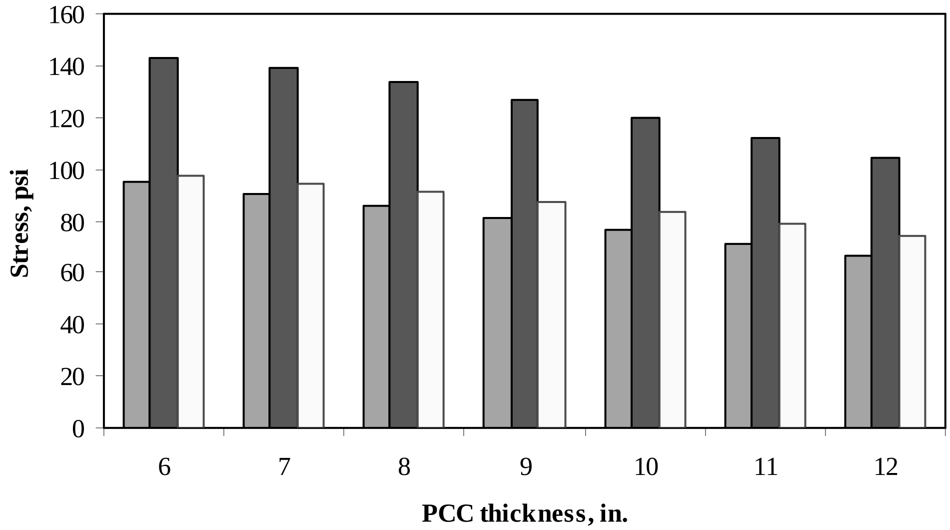


PCC shoulder ■ AC shoulder □ Widened lane

**Figure F-17-29: Impact of PCC thickness and lateral support condition on longitudinal stress at top of the Slab (177-in. joint spacing and α(ΔT/D) of 0 in.$^{-1}$)**

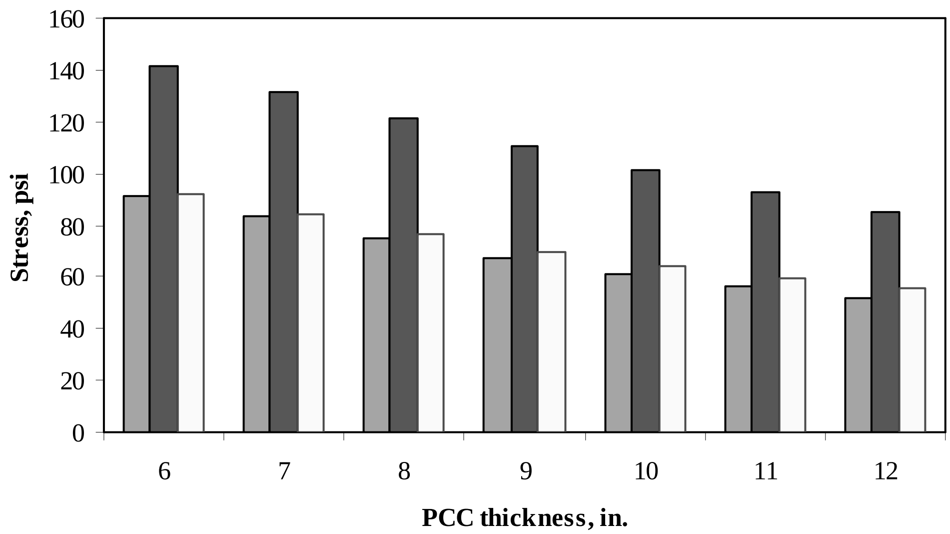


PCC shoulder ■ AC shoulder □ Widened lane

**Figure F-17-30: Impact of PCC thickness and lateral support condition on longitudinal stress at top of the Slab (315-in. joint spacing and α(ΔT/D) of 0 in.$^{-1}$)**

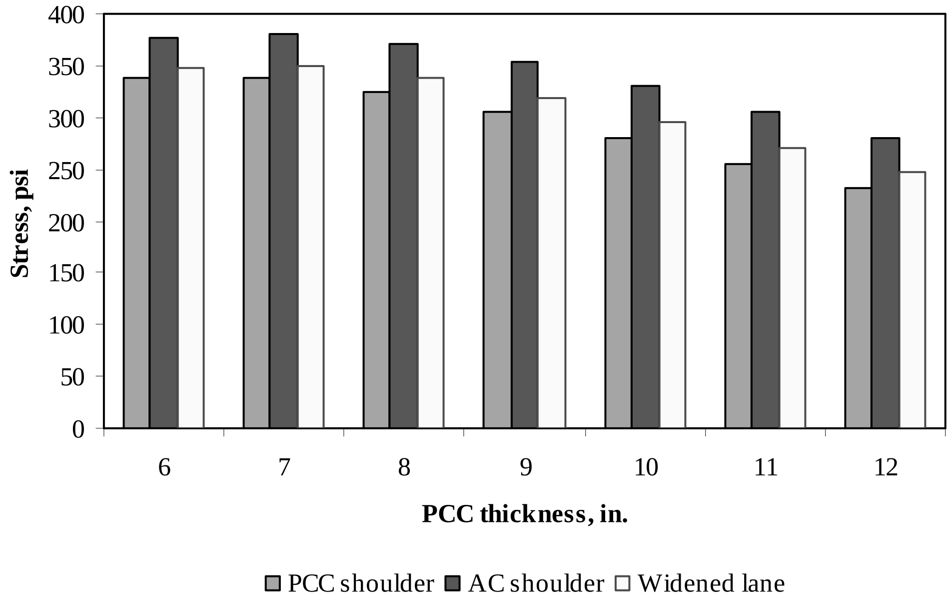


**Figure F-17-31: Impact of PCC thickness and lateral support condition on longitudinal stress at top of the Slab (177-in. joint spacing and $\alpha(\Delta T/D)$ of $-20x10^{-6}$ in.$^{-1}$)**

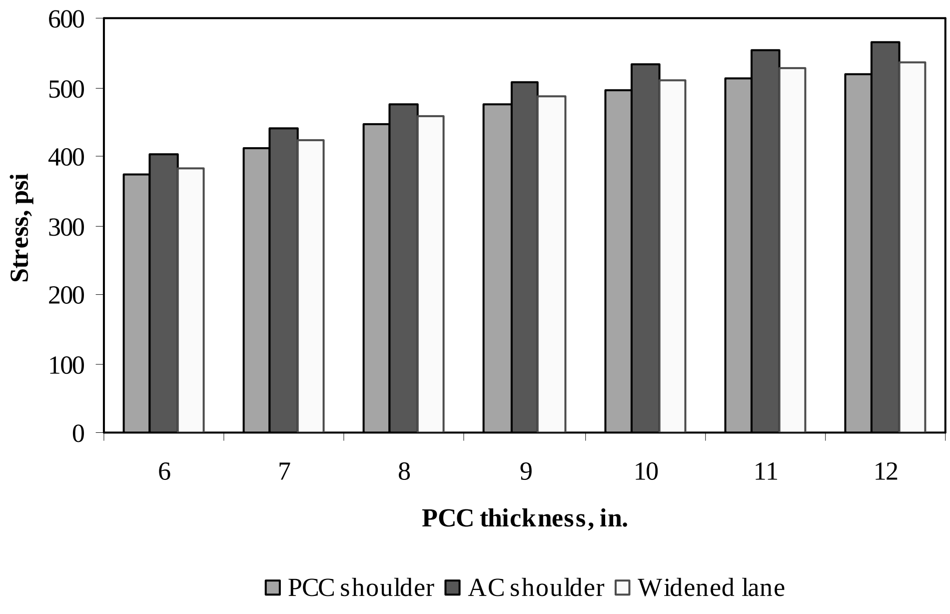


**Figure F-17-32: Impact of PCC thickness and lateral support condition on longitudinal stress at top of the Slab (315-in. joint spacing and $\alpha(\Delta T/D)$ of $-20x10^{-6}$ in.$^{-1}$)**

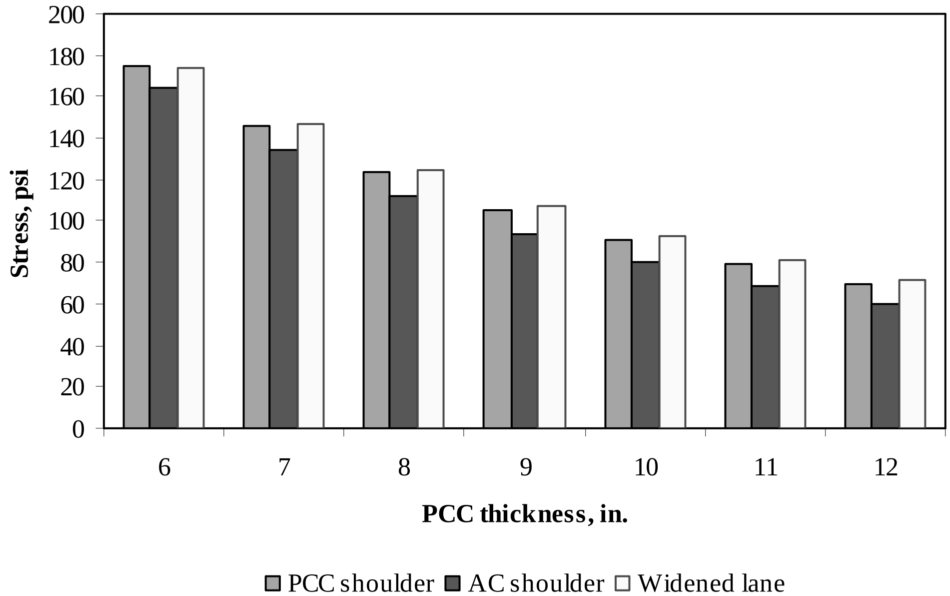


**Figure F-17-33: Impact of PCC thickness and lateral support condition on transverse stress at bottom of the Slab (177-in. joint spacing and $\alpha(\Delta T/D)$ of 0 in.$^{-1}$)**

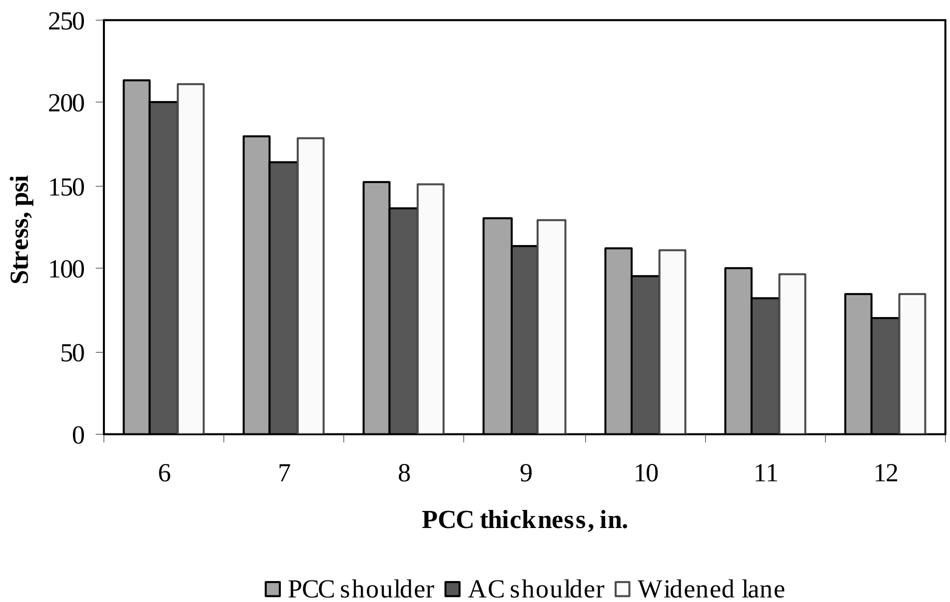


**Figure F-17-34: Impact of PCC thickness and lateral support condition on transverse stress at bottom of the Slab (315-in. joint spacing and $\alpha(\Delta T/D)$ of 0 in.$^{-1}$)**

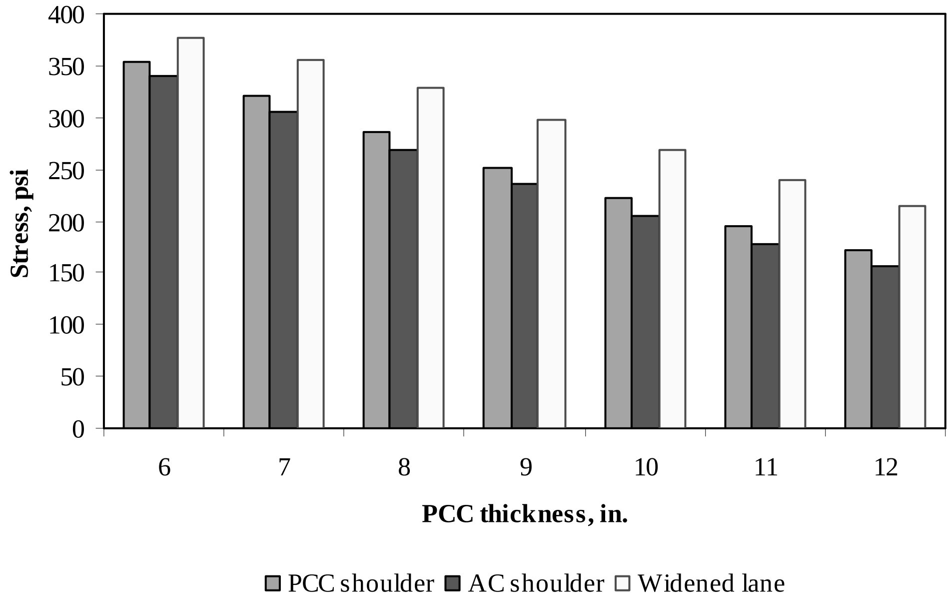


**Figure F-17-35: Impact of PCC thickness and lateral support condition on transverse stress at bottom of the Slab (177-in. joint spacing and $\alpha(\Delta T/D)$ of $20x10^{-6}$ in.$^{-1}$)**

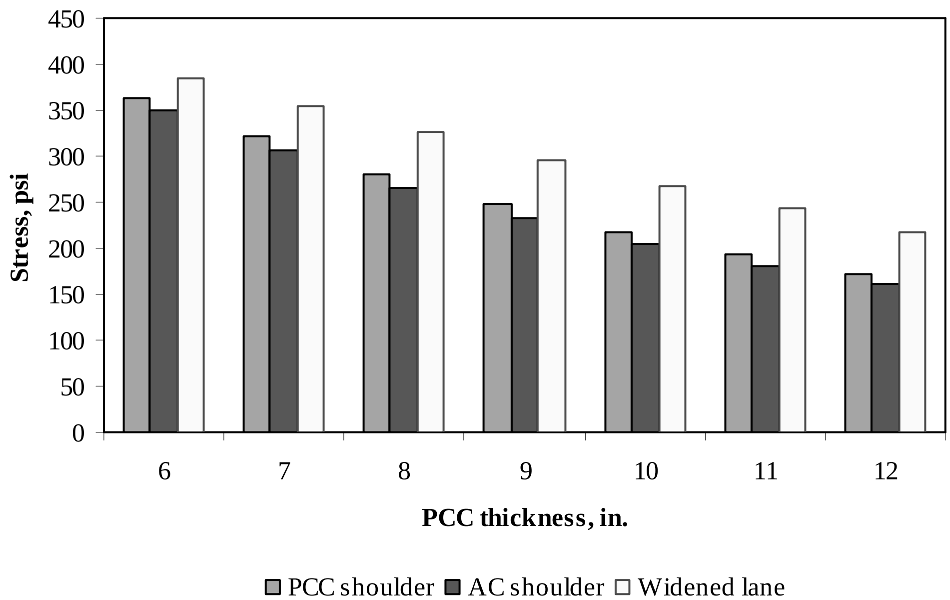


**Figure F-17-36: Impact of PCC thickness and lateral support condition on transverse stress at bottom of the Slab (315-in. joint spacing and $\alpha(\Delta T/D)$ of $20x10^{-6}$ in.$^{-1}$)**

Figures F-17-37 through F-17-42 illustrate the impact of base/subbase thickness and product α(ΔT/D) on stresses (10-in. PCC thickness, 100-psi/in. modulus of subgrade reaction and PCC shoulder)

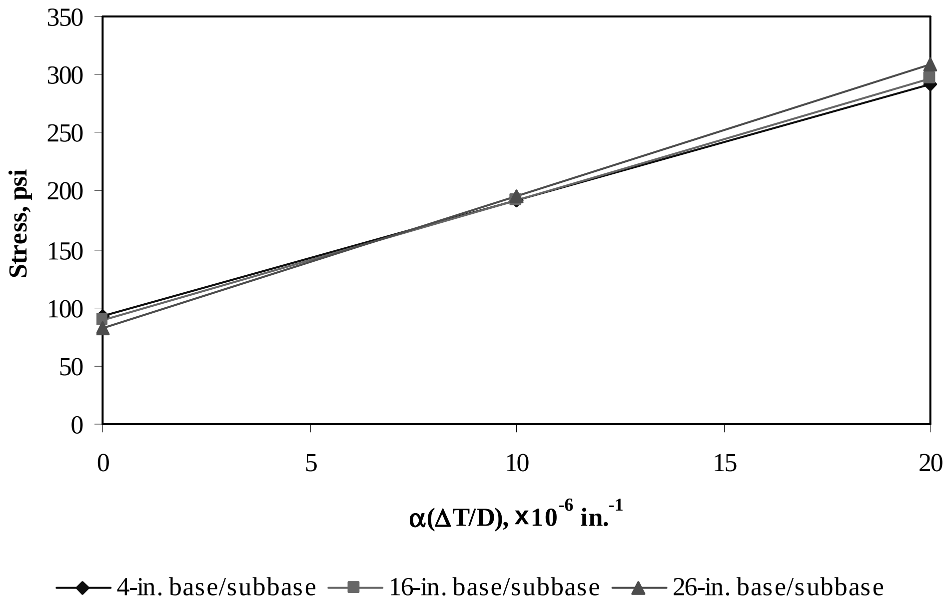


**Figure F-17-37: Impact of base/subbase thickness and product α(ΔT/D) on longitudinal stress at bottom of the slab (177-in. joint spacing)**

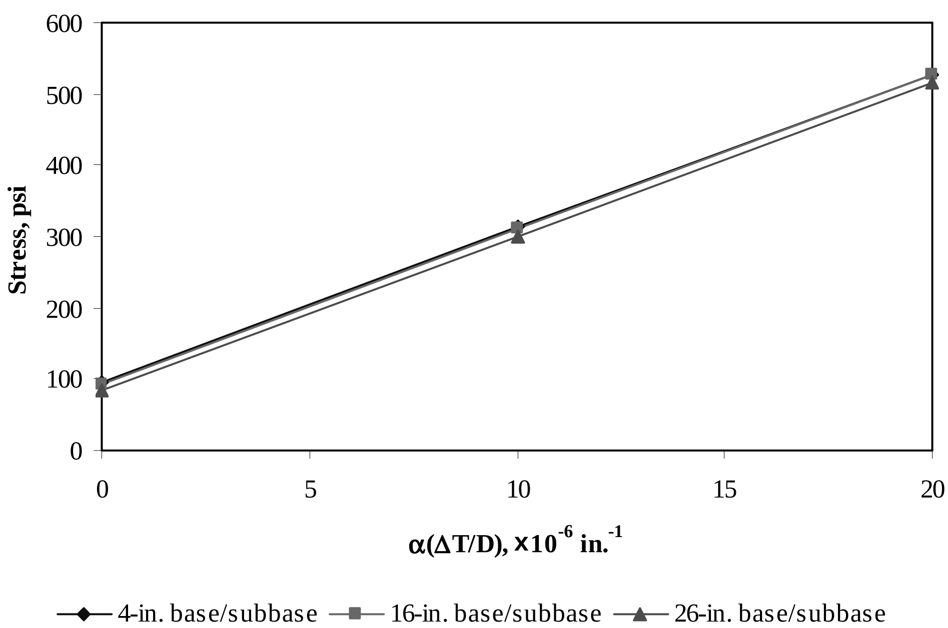


**Figure F-17-38: Impact of base/subbase thickness and product α(ΔT/D) on longitudinal stress at bottom of the slab (315-in. joint spacing)**

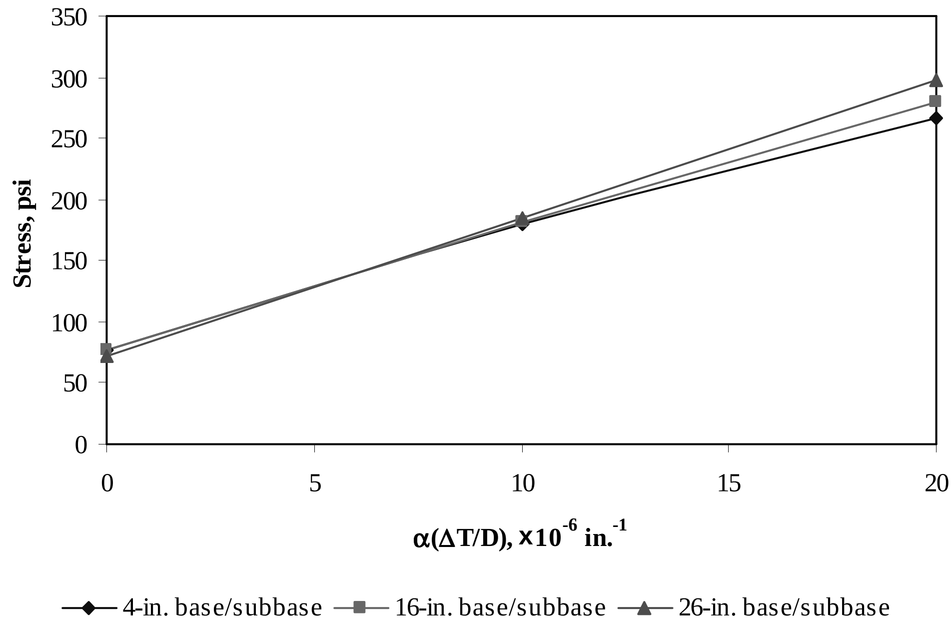


**Figure F-17-39: Impact of base/subbase thickness and product α(ΔT/D) on longitudinal stress at top of the slab (177-in. joint spacing)**

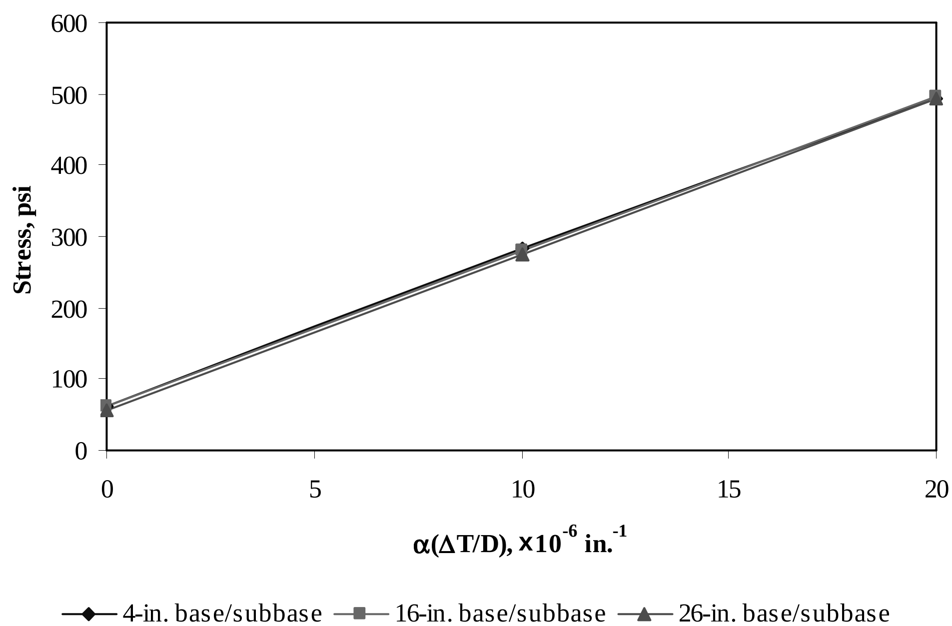


**Figure F-17-40: Impact of base/subbase thickness and product α(ΔT/D) on longitudinal stress at top of the slab (315-in. joint spacing)**

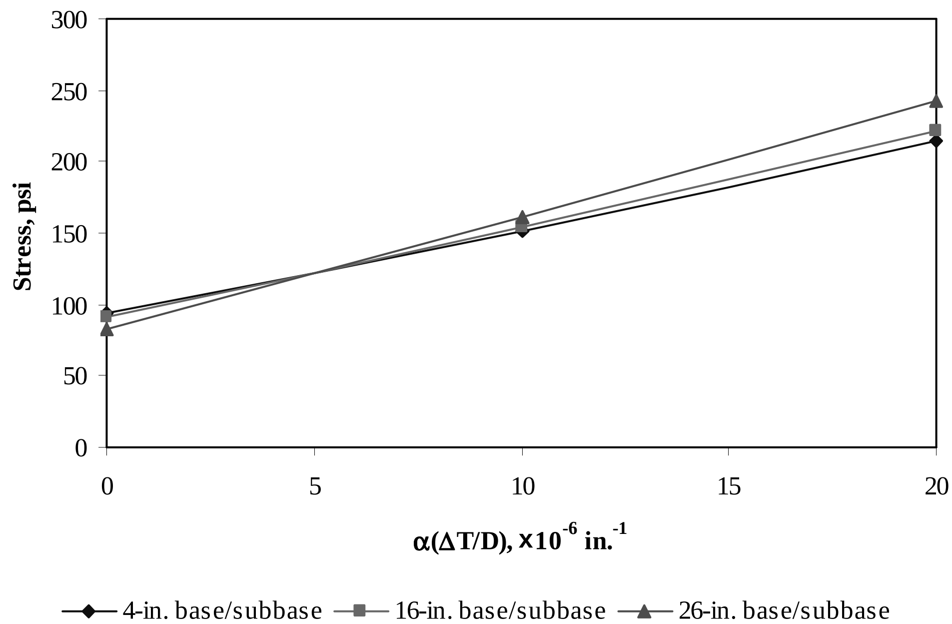


**Figure F-17-41: Impact of base/subbase thickness and product α(ΔT/D) on transverse stress at bottom of the slab (177-in. joint spacing)**

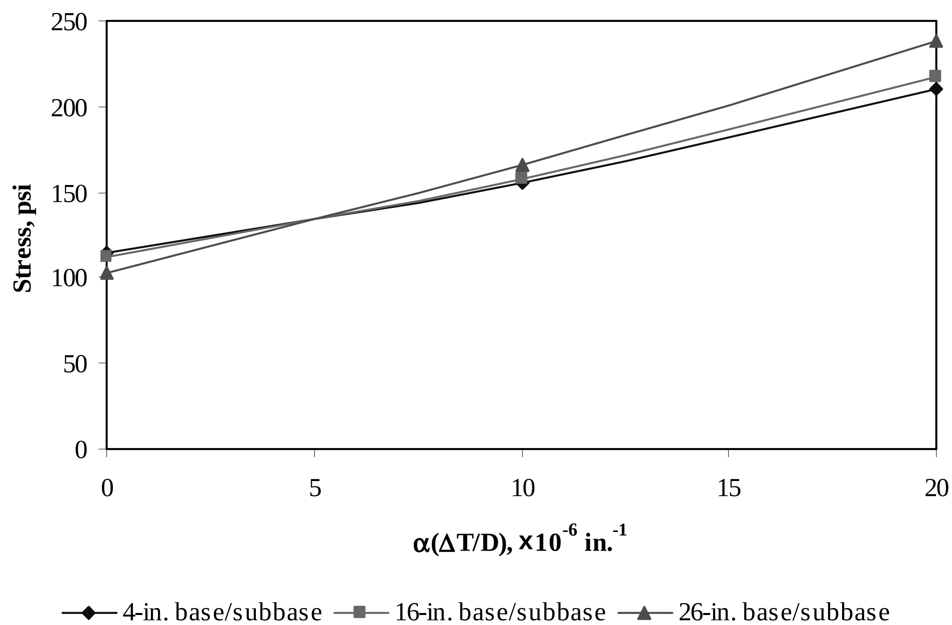


**Figure F-17-42: Impact of base/subbase thickness and product α(ΔT/D) on transverse stress at bottom of the slab (315-in. joint spacing)**

Figures F-17-43 through F-17-48 illustrate the impact of modulus of subgrade reaction and product α(ΔT/D) on stresses (10-in. PCC thickness, 16-in. base/subbase thickness and PCC shoulder)

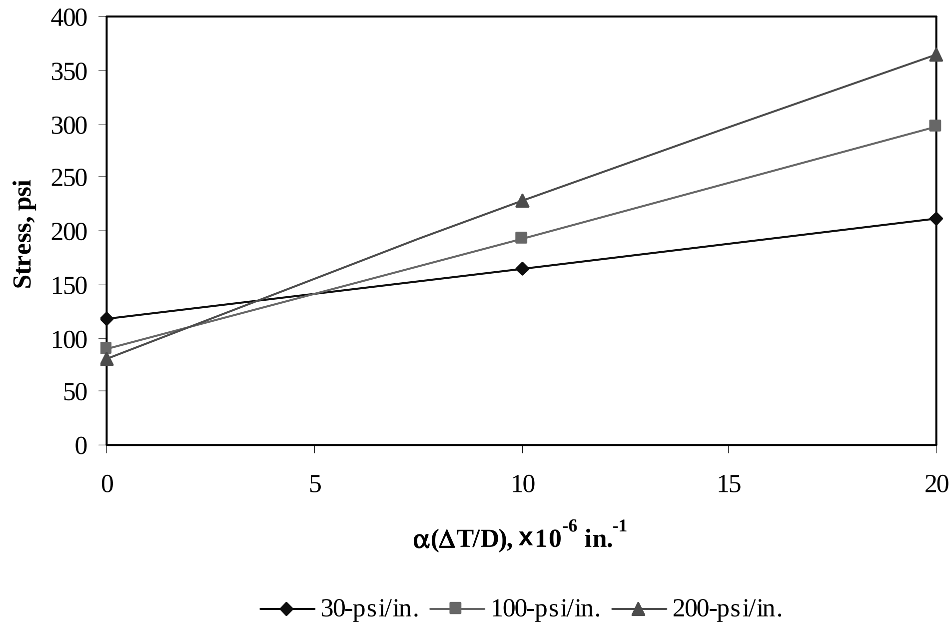


**Figure F-17-43: Impact of modulus of subgrade reaction and product α(ΔT/D) on longitudinal stress at bottom of the slab (177-in. joint spacing)**

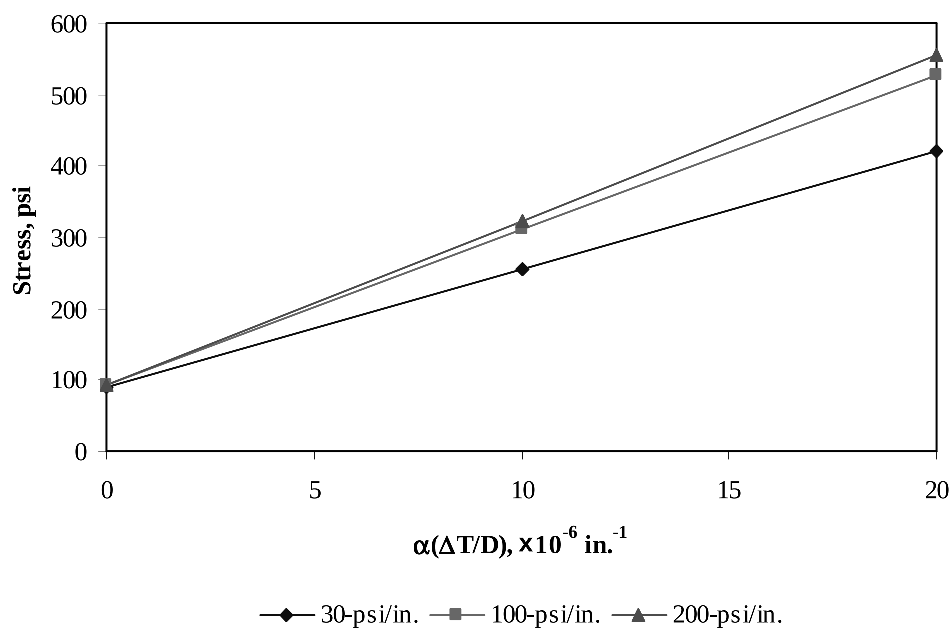


**Figure F-17-44: Impact of modulus of subgrade reaction and product α(ΔT/D) on longitudinal stress at bottom of the slab (315-in. joint spacing)**

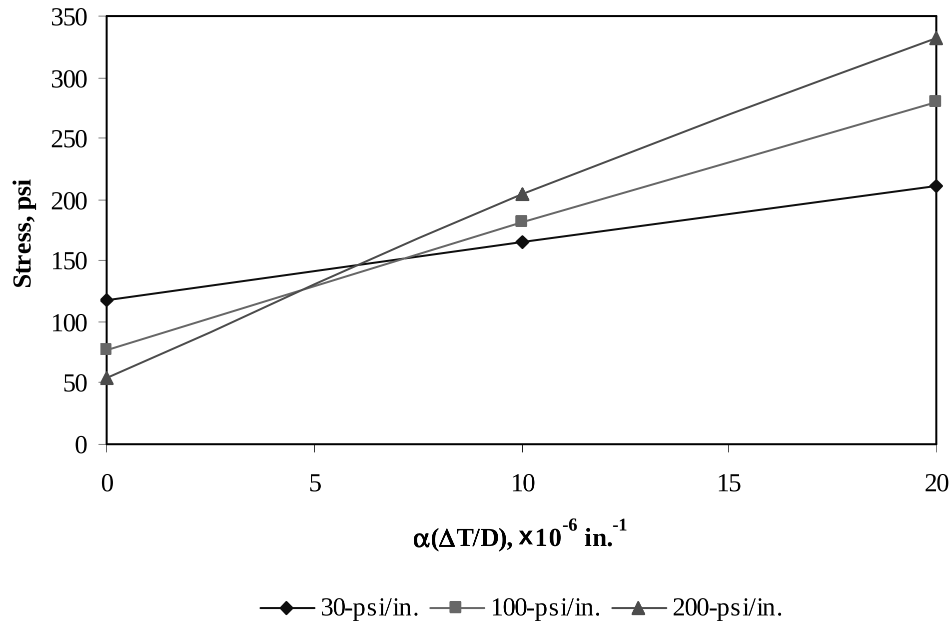


**Figure F-17-45: Impact of modulus of subgrade reaction and product α(ΔT/D) on longitudinal stress at top of the slab (177-in. joint spacing)**

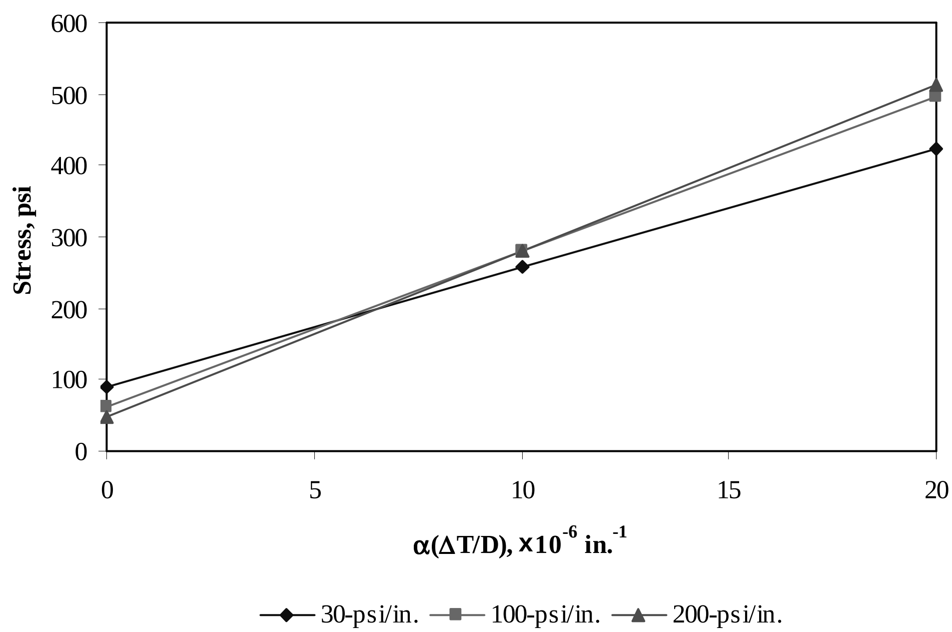


**Figure F-17-46: Impact of modulus of subgrade reaction and product α(ΔT/D) on longitudinal stress at top of the slab (315-in. joint spacing)**

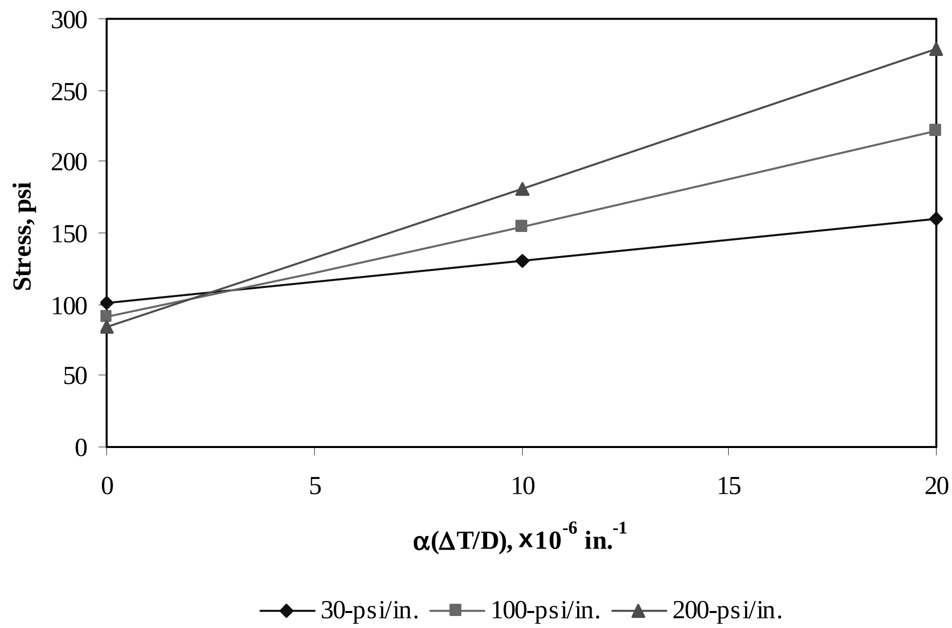


**Figure F-17-47: Impact of modulus of subgrade reaction and product α(ΔT/D) on transverse stress at bottom of the slab (177-in. joint spacing)**

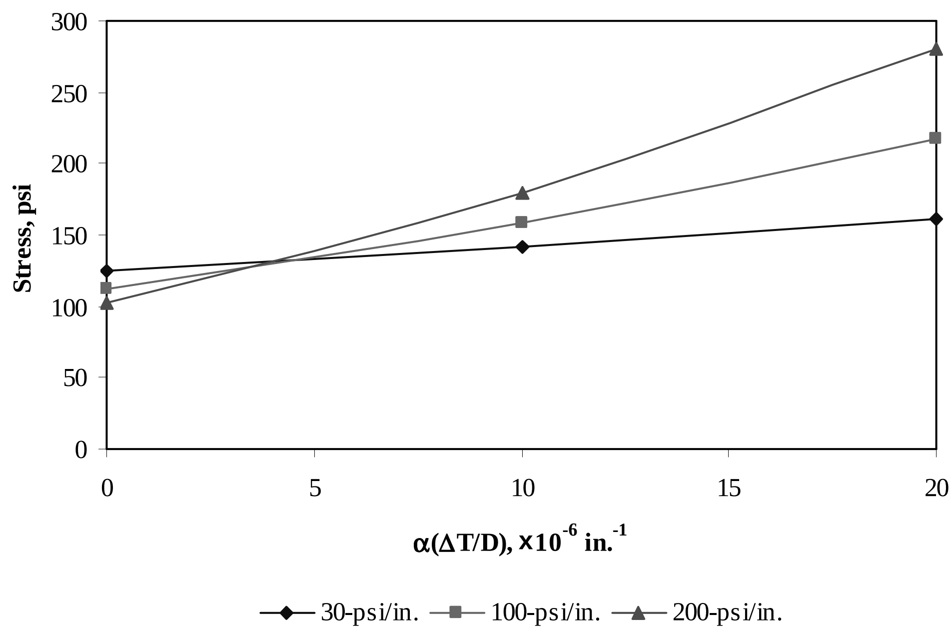


**Figure F-17-48: Impact of modulus of subgrade reaction and product α(ΔT/D) on transverse stress at bottom of the slab (315-in. joint spacing)**

Figures F-17-49 through F-17-51 illustrate the impact of joint spacing and product α(ΔT/D) on stresses (10-in. PCC thickness, 16-in. base/subbase thickness, 100-psi/in. modulus of subgrade reaction and PCC shoulder)

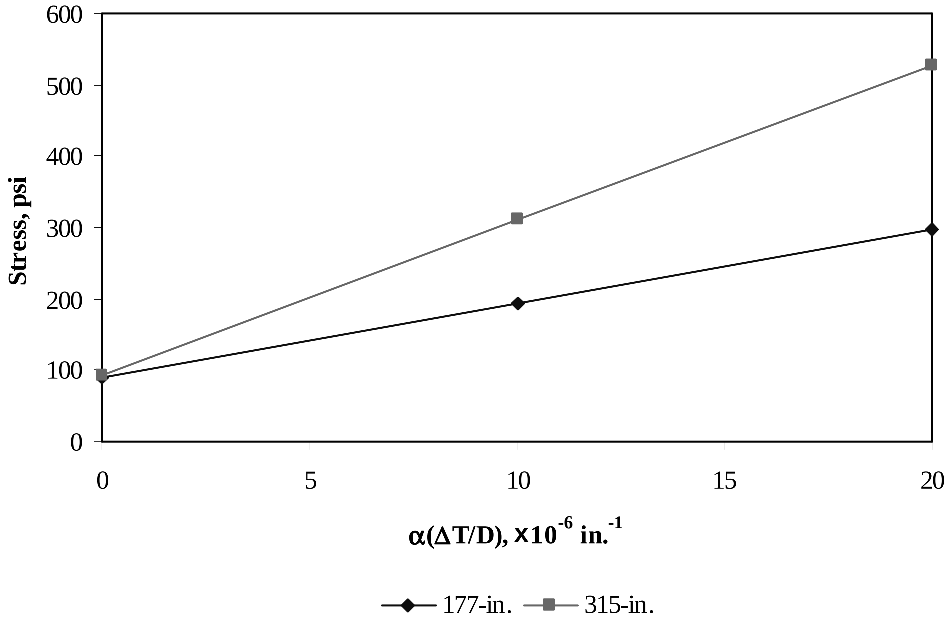


**Figure F-17-49: Impact of joint spacing and product α(ΔT/D) on longitudinal stress at bottom of the slab**

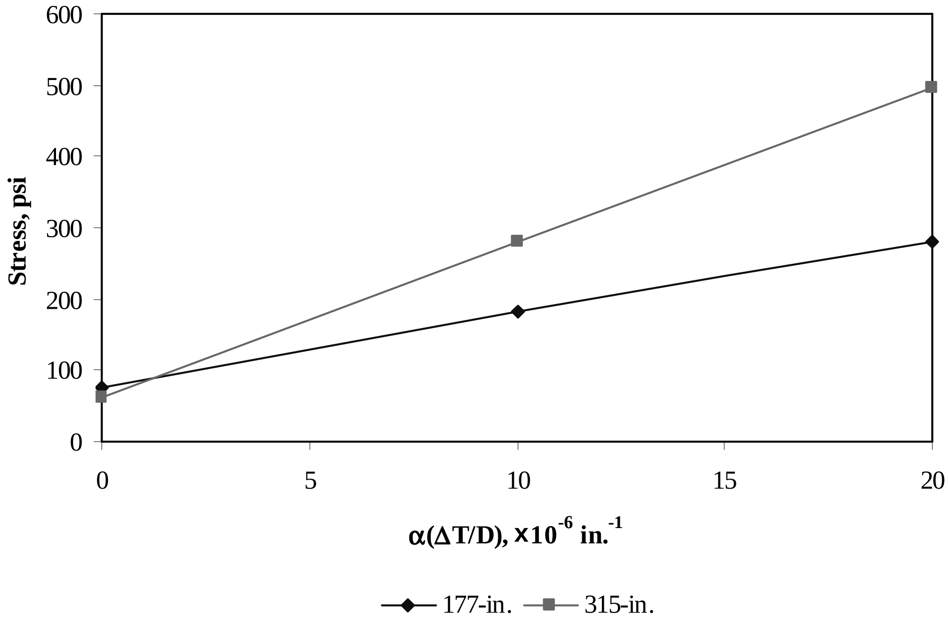


**Figure F-17-50: Impact of joint spacing and product α(ΔT/D) on longitudinal stress at top of the slab**

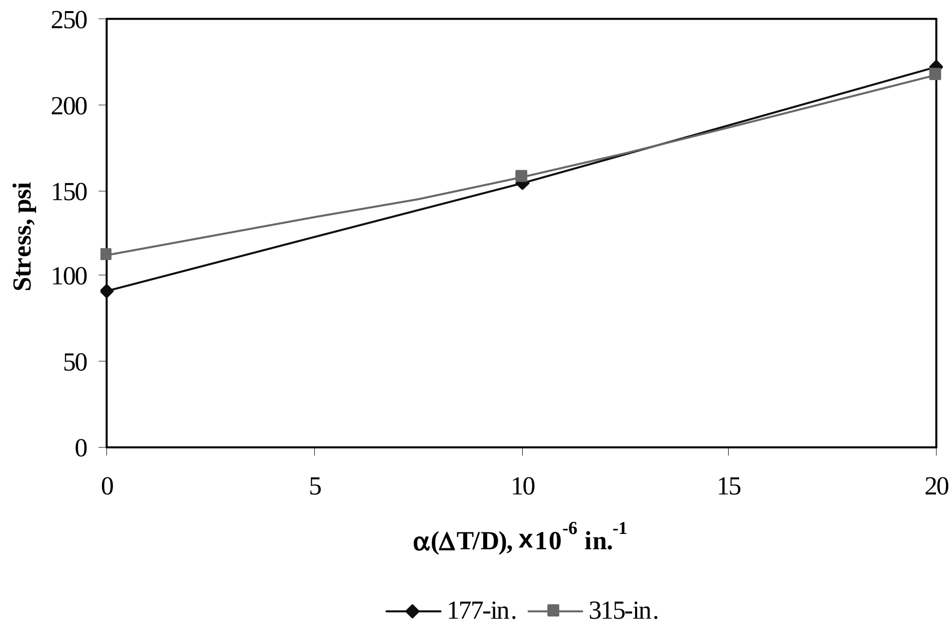


**Figure F-17-51: Impact of joint spacing and product $\alpha(\Delta T/D)$ on transverse stress at bottom of the slab**

**Sub Appendix F-18**

**Documentation of Pavement Responses for**

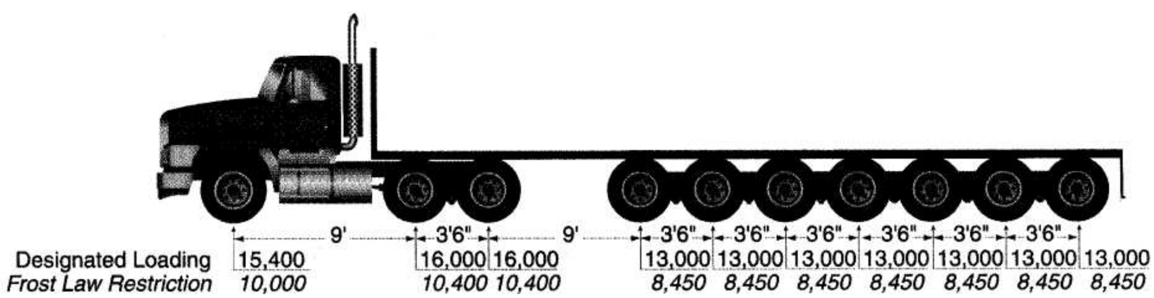


**MI-19**

Figures F-18-1 through F-18-12 illustrate the impact of PCC thickness and base/subbase thickness on stresses (100-psi/in. modulus of subgrade reaction and PCC shoulder)

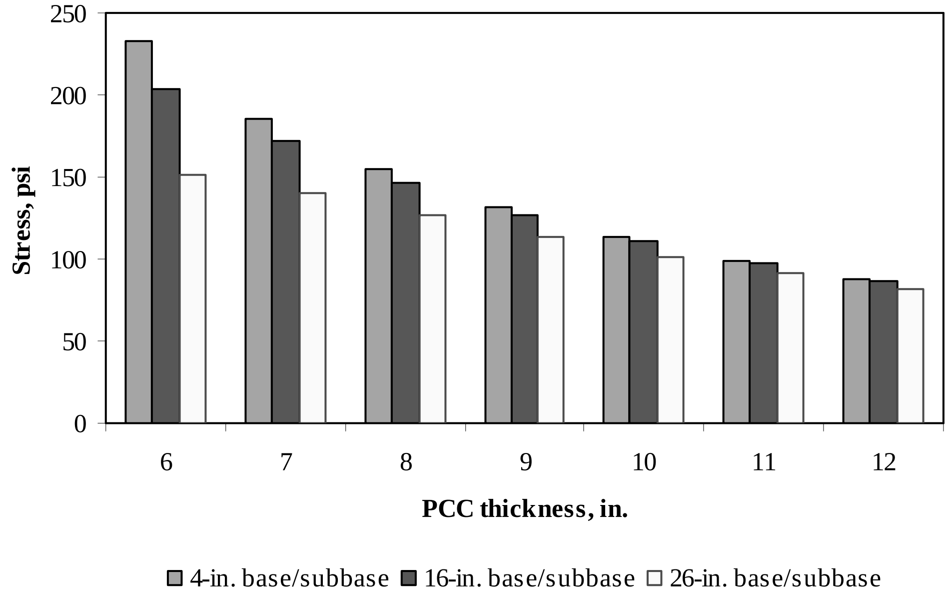


**Figure F-18-1: Impact of PCC thickness and base/subbase thickness on longitudinal stress at bottom of the Slab (177-in. joint spacing and $\alpha(\Delta T/D)$ of 0 in.$^{-1}$)**

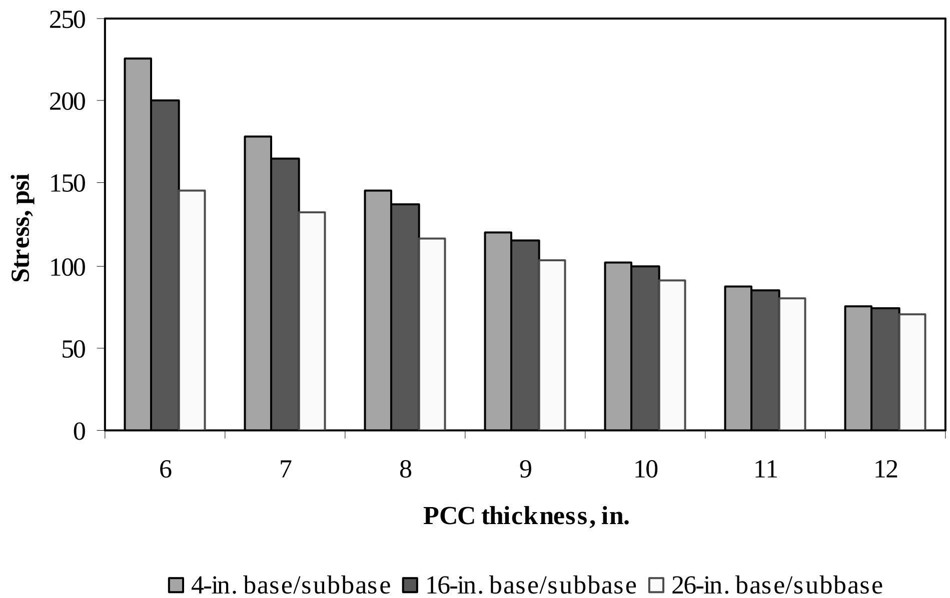


**Figure F-18-2: Impact of PCC thickness and base/subbase thickness on longitudinal stress at bottom of the Slab (315-in. joint spacing and $\alpha(\Delta T/D)$ of 0 in.$^{-1}$)**

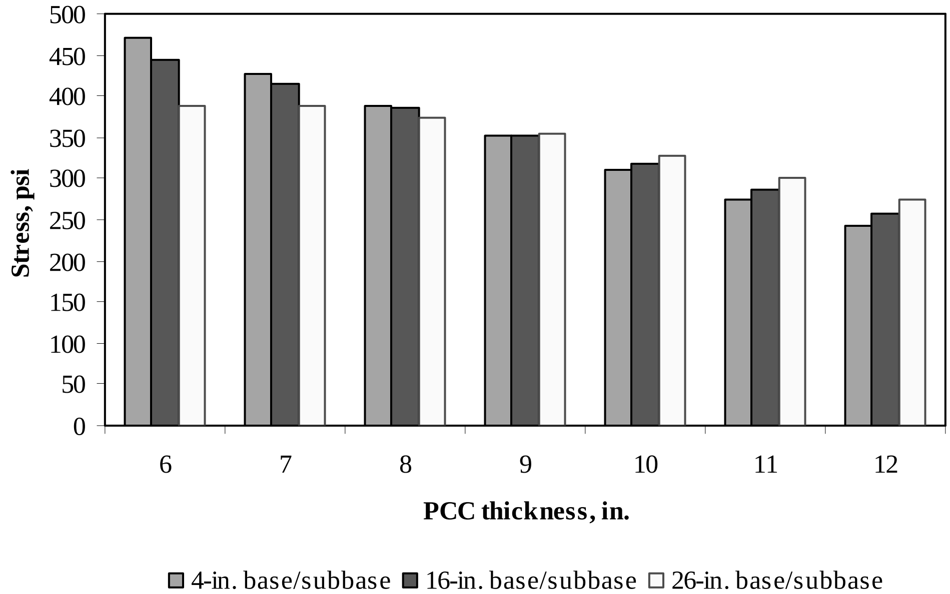


**Figure F-18-3: Impact of PCC thickness and base/subbase thickness on longitudinal stress at bottom of the Slab (177-in. joint spacing and $\alpha(\Delta T/D)$ of 20x$10^{-6}$ in.$^{-1}$)**

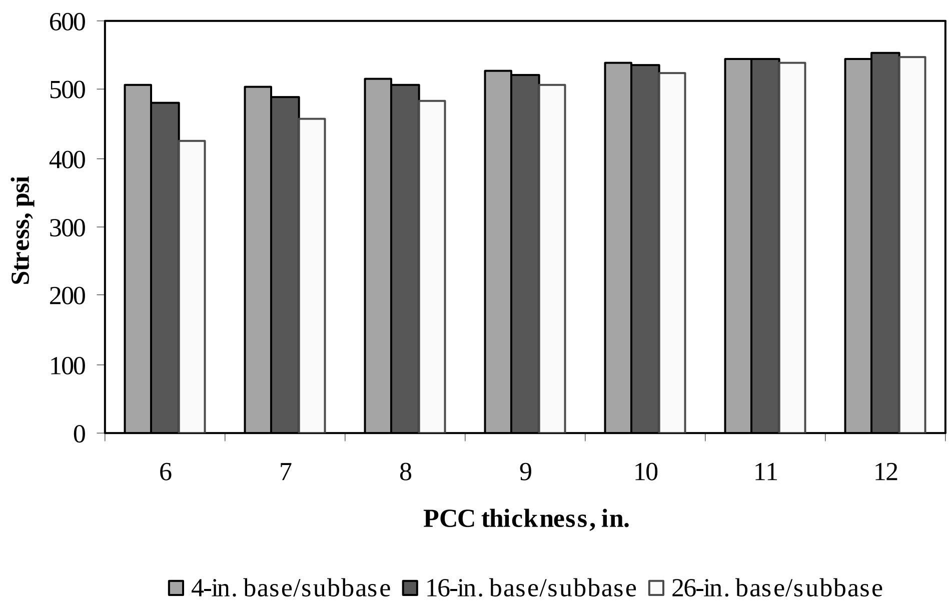


**Figure F-18-4: Impact of PCC thickness and base/subbase thickness on longitudinal stress at bottom of the Slab (315-in. joint spacing and $\alpha(\Delta T/D)$ of 20x$10^{-6}$ in.$^{-1}$)**

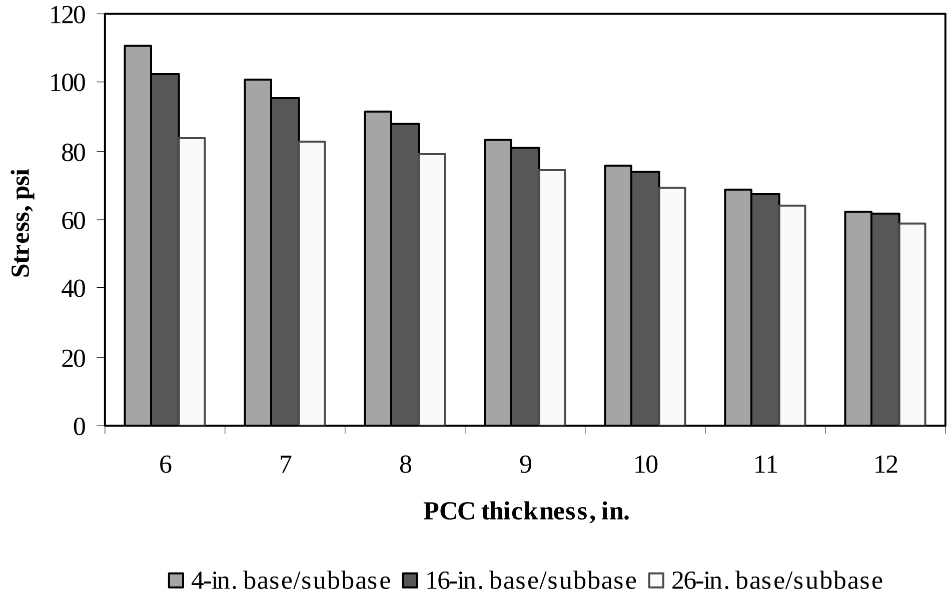


**Figure F-18-5: Impact of PCC thickness and base/subbase thickness on longitudinal stress at top of the Slab (177-in. joint spacing and $\alpha(\Delta T/D)$ of 0 in.$^{-1}$)**

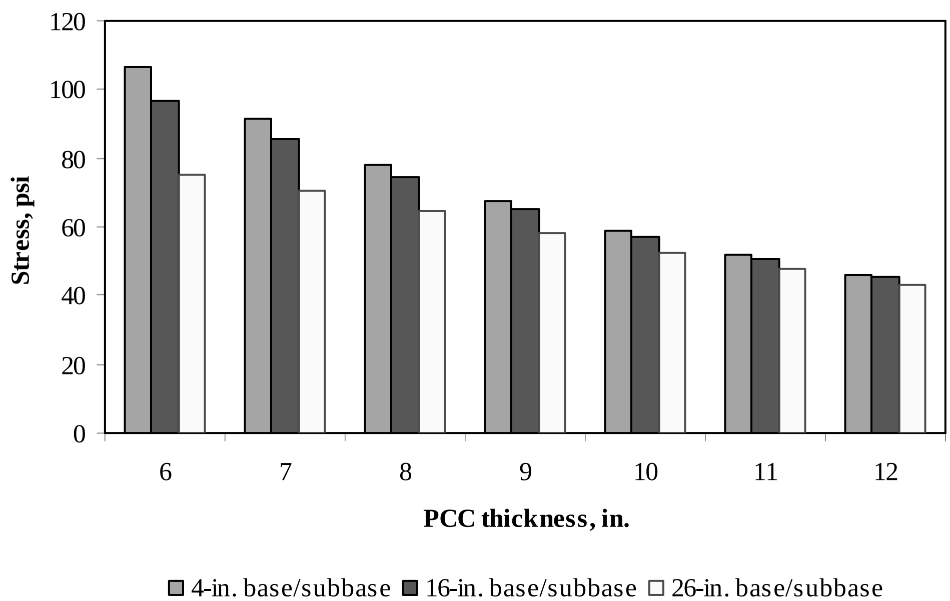


**Figure F-18-6: Impact of PCC thickness and base/subbase thickness on longitudinal stress at top of the Slab (315-in. joint spacing and $\alpha(\Delta T/D)$ of 0 in.$^{-1}$)**

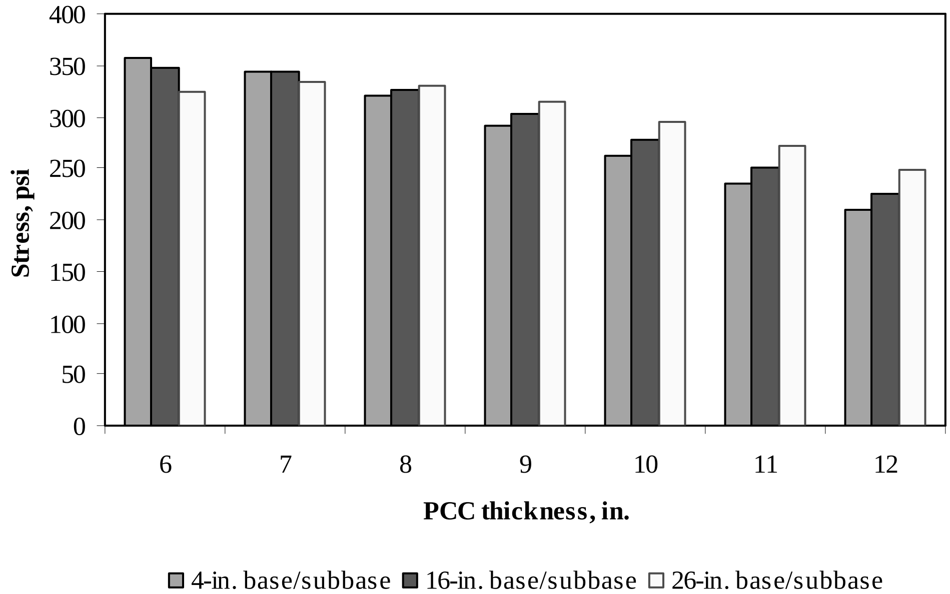


**Figure F-18-7: Impact of PCC thickness and base/subbase thickness on longitudinal stress at top of the Slab (177-in. joint spacing and $\alpha(\Delta T/D)$ of $-20x10^{-6}$ in.$^{-1}$)**

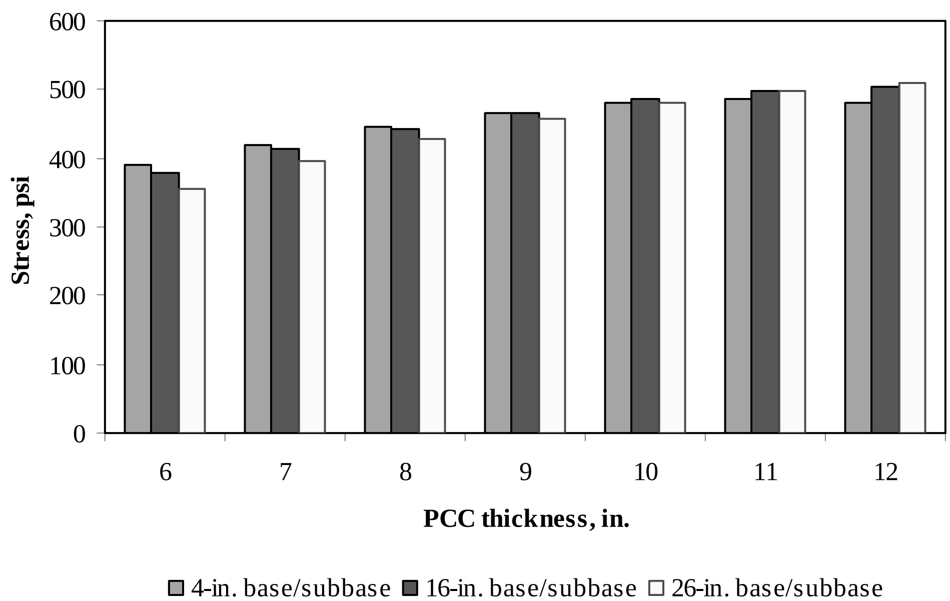


**Figure F-18-8: Impact of PCC thickness and base/subbase thickness on longitudinal stress at top of the Slab (315-in. joint spacing and $\alpha(\Delta T/D)$ of $-20x10^{-6}$ in.$^{-1}$)**

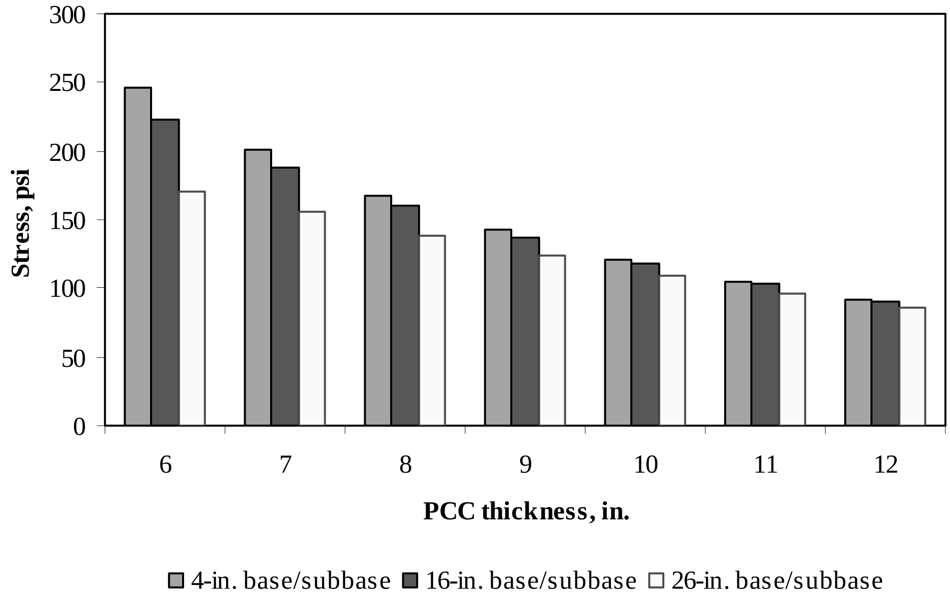


**Figure F-18-9: Impact of PCC thickness and base/subbase thickness on transverse stress at bottom of the Slab (177-in. joint spacing and $\alpha(\Delta T/D)$ of 0 in.$^{-1}$)**

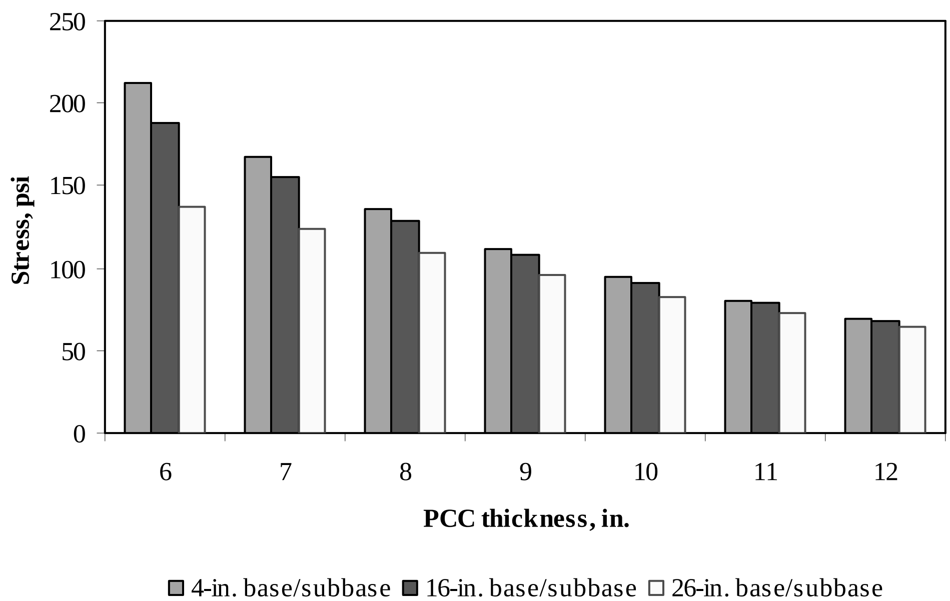


**Figure F-18-10: Impact of PCC thickness and base/subbase thickness on transverse stress at bottom of the Slab (315-in. joint spacing and $\alpha(\Delta T/D)$ of 0 in.$^{-1}$)**

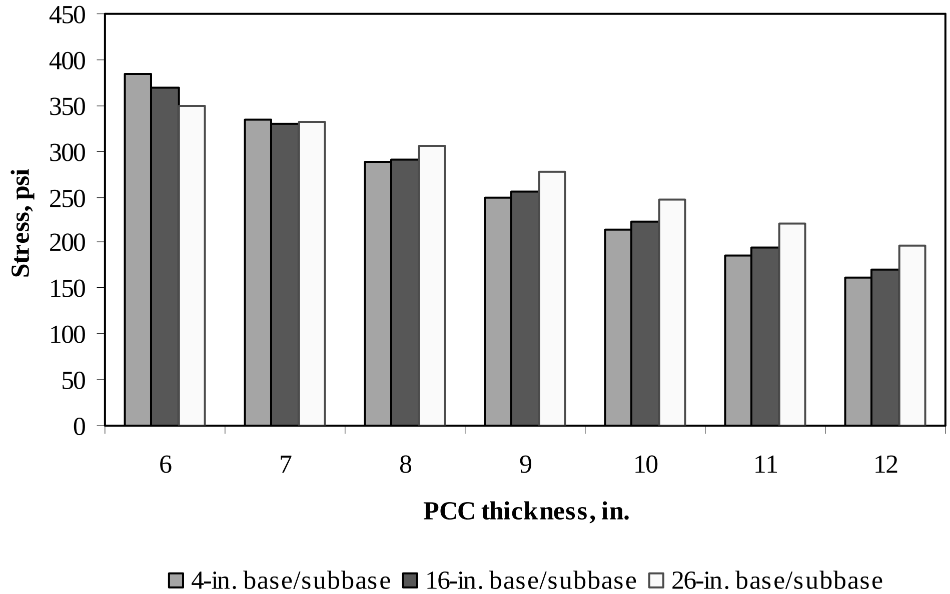


**Figure F-18-11: Impact of PCC thickness and base/subbase thickness on transverse stress at bottom of the Slab (177-in. joint spacing and $\alpha(\Delta T/D)$ of $20x10^{-6}$ in.$^{-1}$)**

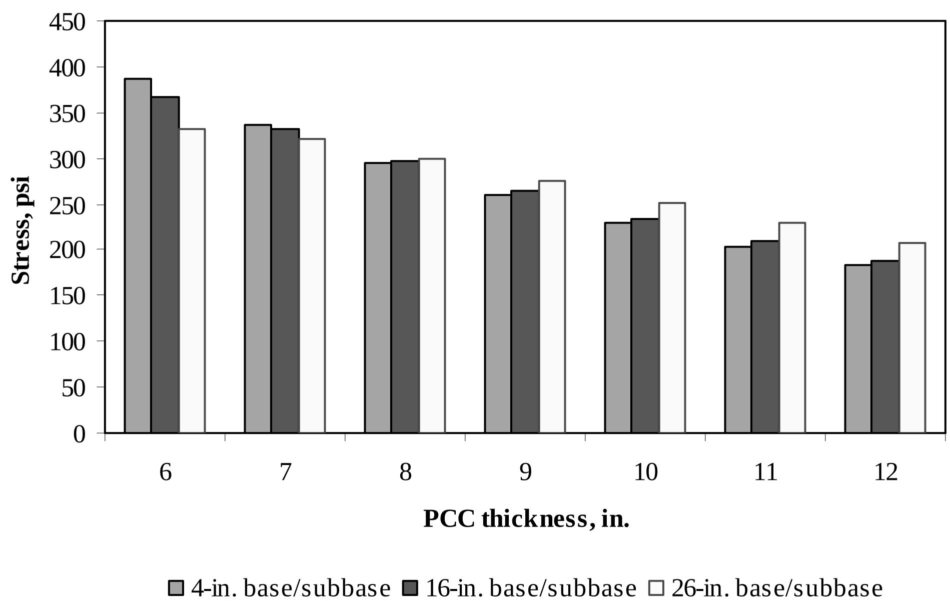


**Figure F-18-12: Impact of PCC thickness and base/subbase thickness on transverse stress at bottom of the Slab (315-in. joint spacing and $\alpha(\Delta T/D)$ of $20x10^{-6}$ in.$^{-1}$)**

Figures F-18-13 through F-18-24 illustrate the impact of PCC thickness and modulus of subgrade reaction on stresses (16-in. base/subbase thickness and PCC shoulder)

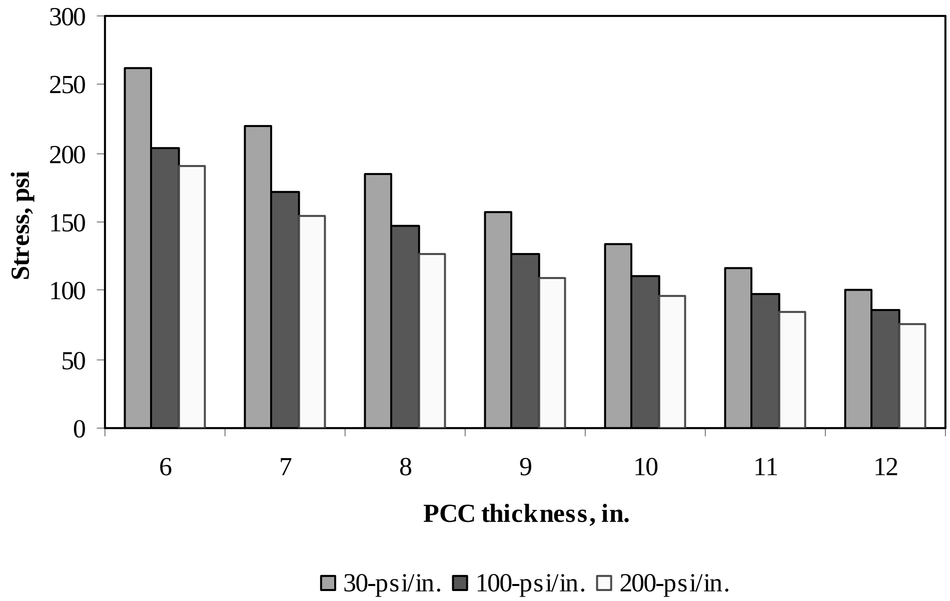


**Figure F-18-13: Impact of PCC thickness and modulus of subgrade reaction on longitudinal stress at bottom of the slab (177-in. joint spacing and $\alpha(\Delta T/D)$ of 0 in.$^{-1}$)**

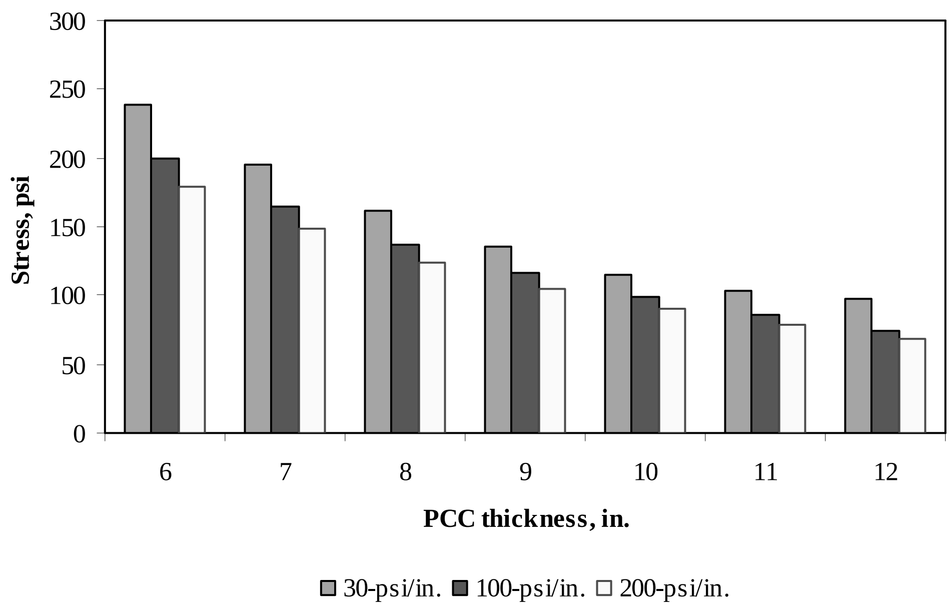


**Figure F-18-14: Impact of PCC thickness and modulus of subgrade reaction on longitudinal stress at bottom of the slab (315-in. joint spacing and $\alpha(\Delta T/D)$ of 0 in.$^{-1}$)**

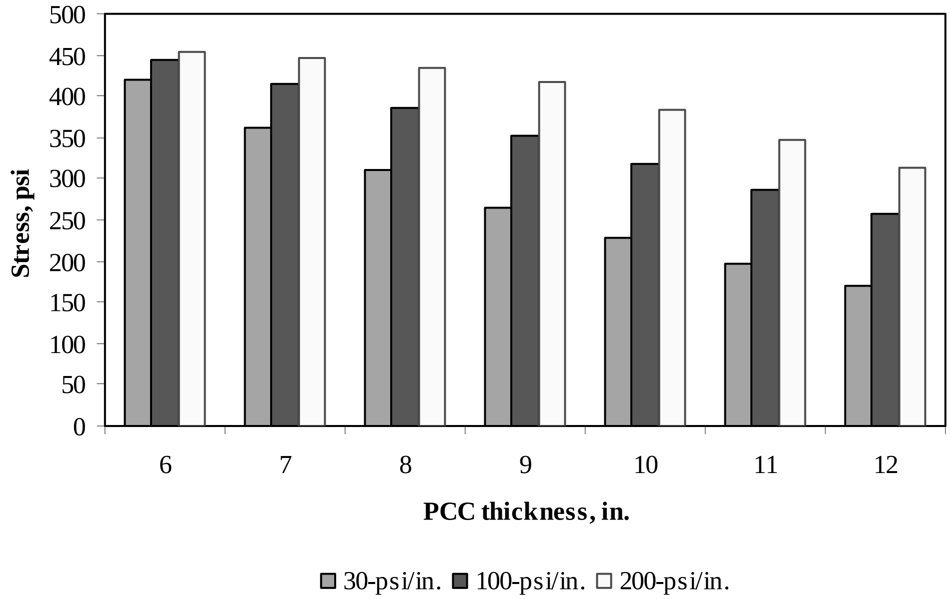


**Figure F-18-15: Impact of PCC thickness and modulus of subgrade reaction on longitudinal stress at bottom of the slab (177-in. joint spacing and $\alpha(\Delta T/D)$ of $20x10^{-6}$ in.$^{-1}$)**

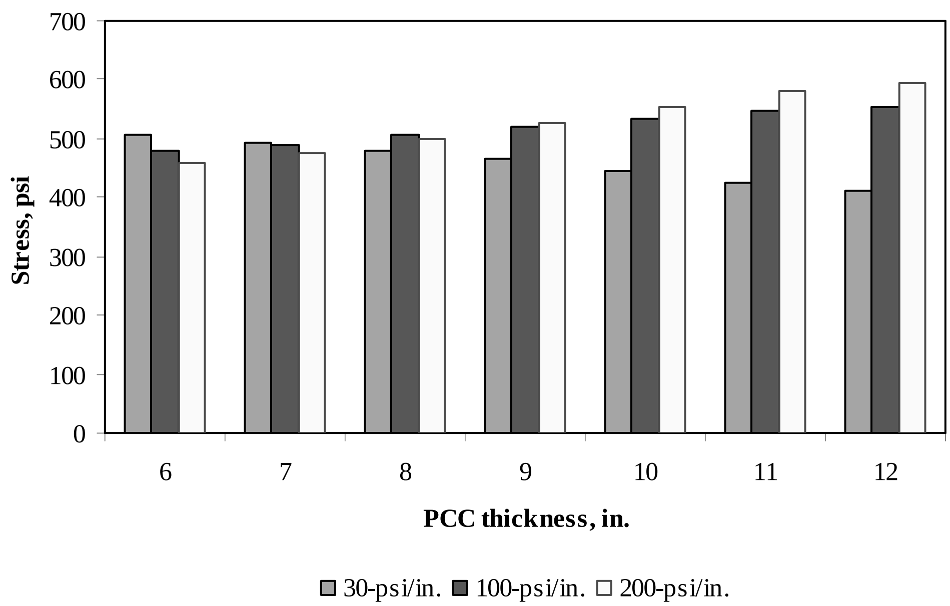


**Figure F-18-16: Impact of PCC thickness and modulus of subgrade reaction on longitudinal stress at bottom of the slab (315-in. joint spacing and $\alpha(\Delta T/D)$ of $20x10^{-6}$ in.$^{-1}$)**

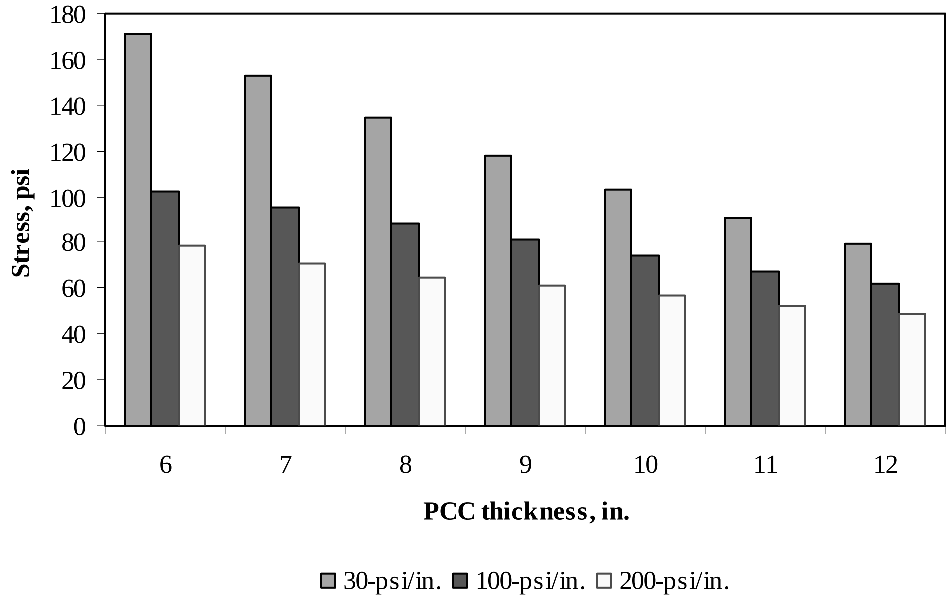


**Figure F-18-17: Impact of PCC thickness and modulus of subgrade reaction on longitudinal stress at top of the Slab (177-in. joint spacing and $\alpha(\Delta T/D)$ of 0 in.$^{-1}$)**

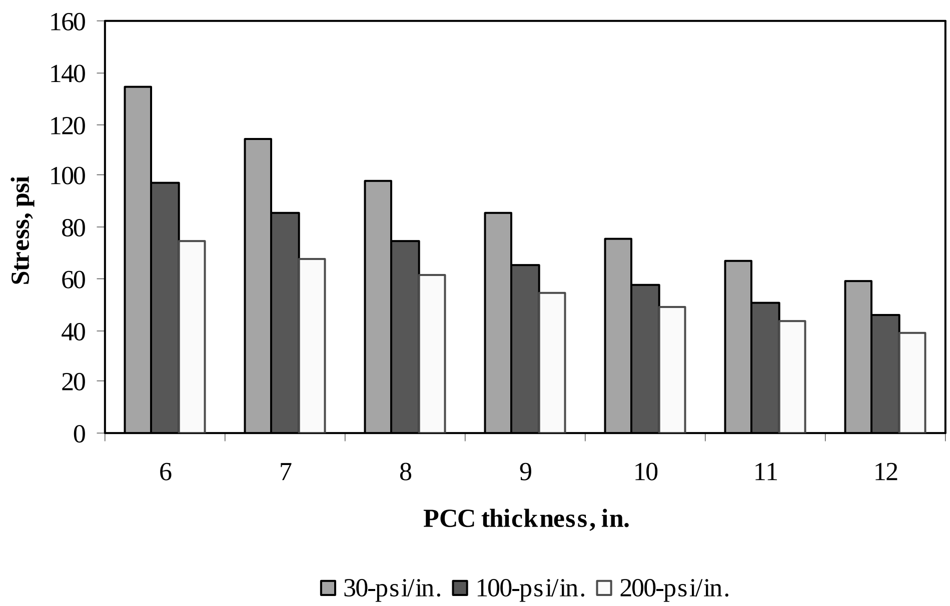


**Figure F-18-18: Impact of PCC thickness and modulus of subgrade reaction on longitudinal stress at top of the Slab (315-in. joint spacing and $\alpha(\Delta T/D)$ of 0 in.$^{-1}$)**

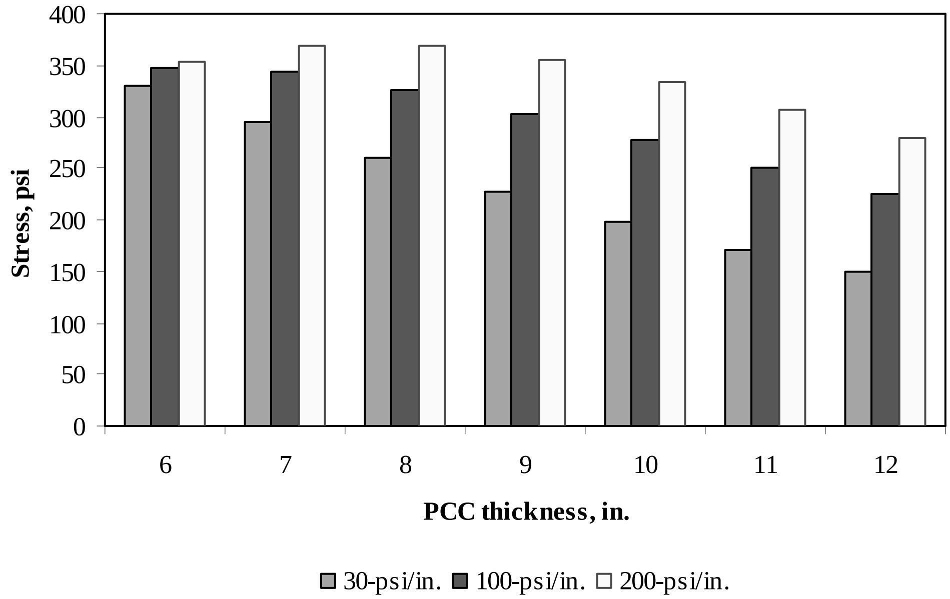


**Figure F-18-19: Impact of PCC thickness and modulus of subgrade reaction on longitudinal stress at top of the Slab (177-in. joint spacing and $\alpha(\Delta T/D)$ of $-20x10^{-6}$ in.$^{-1}$)**

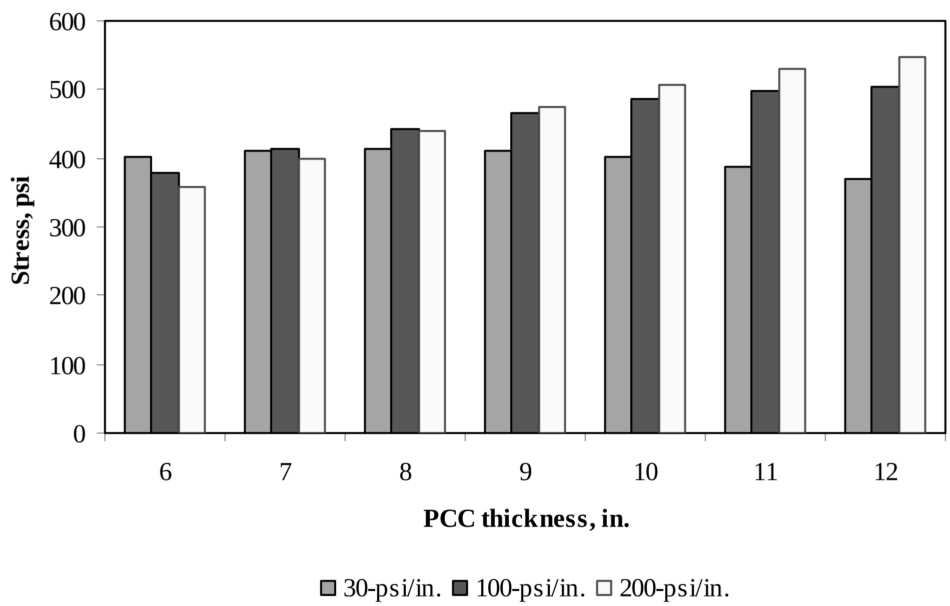


**Figure F-18-20: Impact of PCC thickness and modulus of subgrade reaction on longitudinal stress at top of the Slab (315-in. joint spacing and $\alpha(\Delta T/D)$ of $-20x10^{-6}$ in.$^{-1}$)**

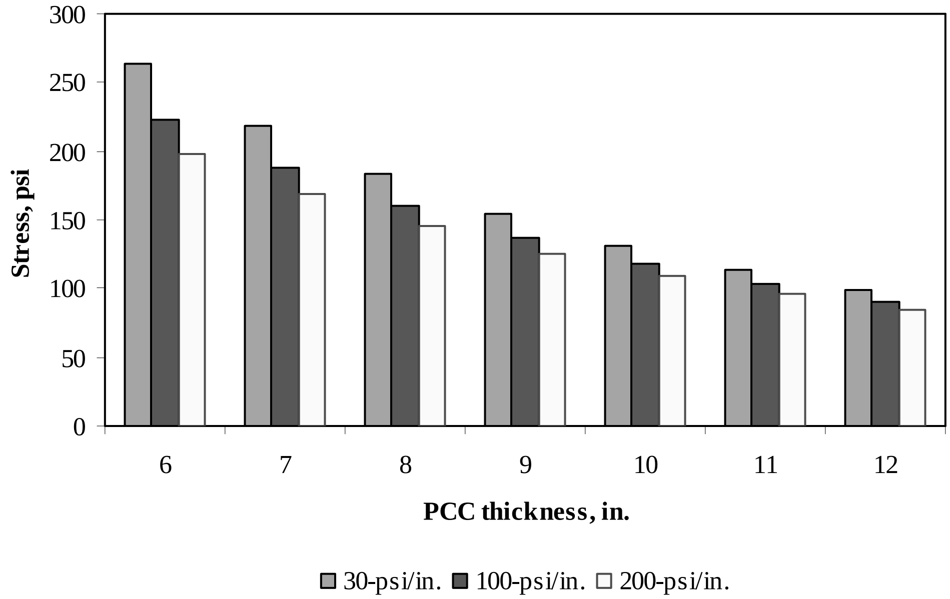


**Figure F-18-21: Impact of PCC thickness and modulus of subgrade reaction on transverse stress at bottom of the Slab (177-in. joint spacing and $\alpha(\Delta T/D)$ of 0 $in.^{-1}$)**

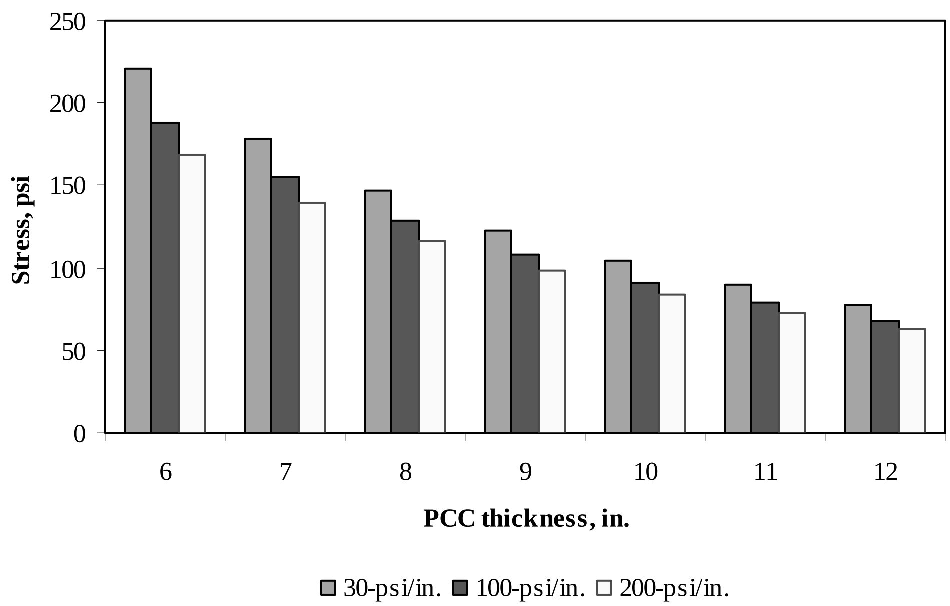


**Figure F-18-22: Impact of PCC thickness and modulus of subgrade reaction on transverse stress at bottom of the Slab (315-in. joint spacing and $\alpha(\Delta T/D)$ of 0 $in.^{-1}$)**

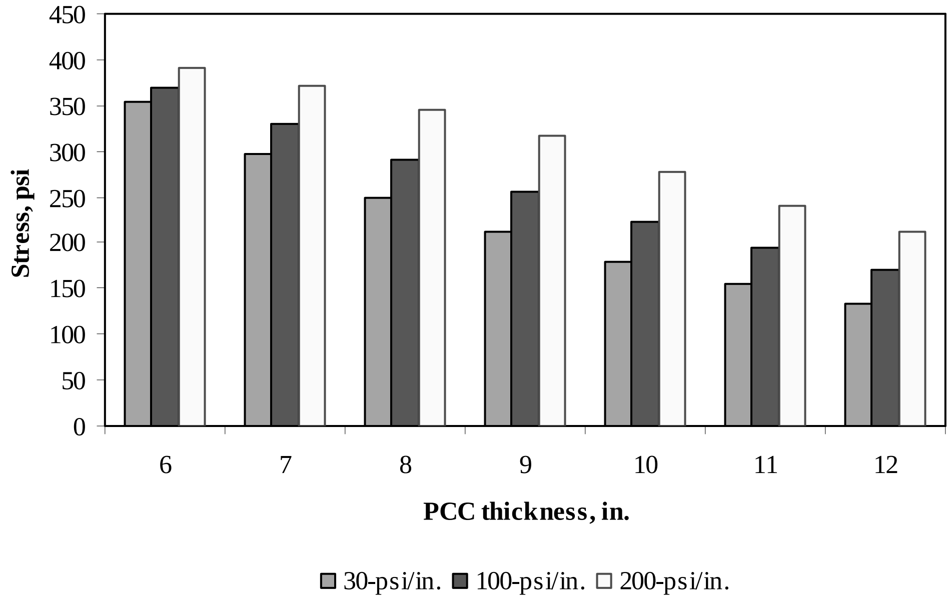


**Figure F-18-23: Impact of PCC thickness and modulus of subgrade reaction on transverse stress at bottom of the Slab (177-in. joint spacing and $\alpha(\Delta T/D)$ of $20x10^{-6}$ $in.^{-1}$)**

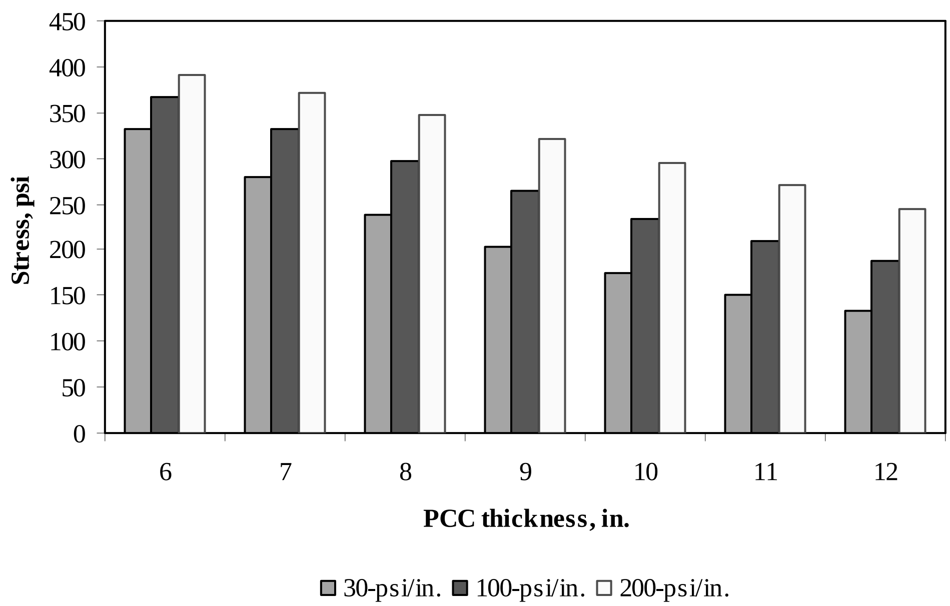


**Figure F-18-24: Impact of PCC thickness and modulus of subgrade reaction on transverse stress at bottom of the Slab (315-in. joint spacing and $\alpha(\Delta T/D)$ of $20x10^{-6}$ $in.^{-1}$)**

Figures F-18-25 through F-18-36 illustrate the impact of PCC thickness and lateral support condition on stresses (16-in. base/subbase and 100-psi/in. modulus of subgrade reaction)

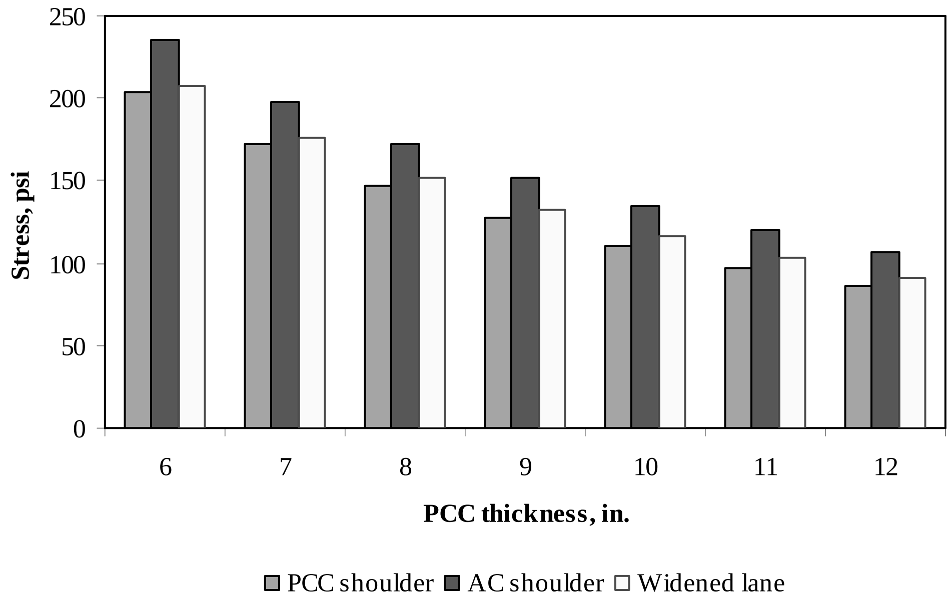


**Figure F-18-25: Impact of PCC thickness and lateral support condition on longitudinal stress at bottom of the Slab (177-in. joint spacing and $\alpha(\Delta T/D)$ of 0 in.$^{-1}$)**

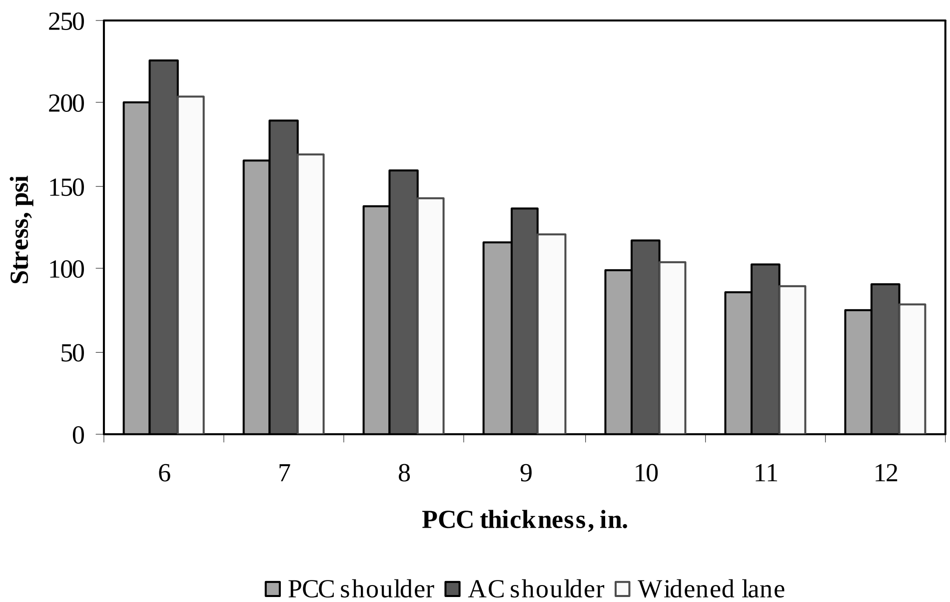


**Figure F-18-26: Impact of PCC thickness and lateral support condition on longitudinal stress at bottom of the Slab (315-in. joint spacing and $\alpha(\Delta T/D)$ of 0 in.$^{-1}$)**

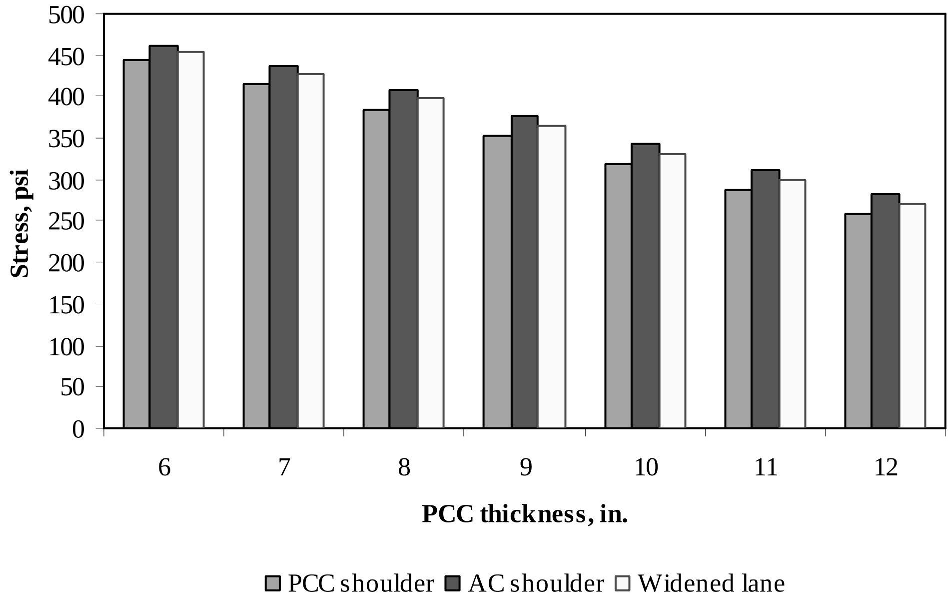


**Figure F-18-27: Impact of PCC thickness and lateral support condition on longitudinal stress at bottom of the Slab (177-in. joint spacing and $\alpha(\Delta T/D)$ of $20 x 10^{-6}$ in.$^{-1}$)**

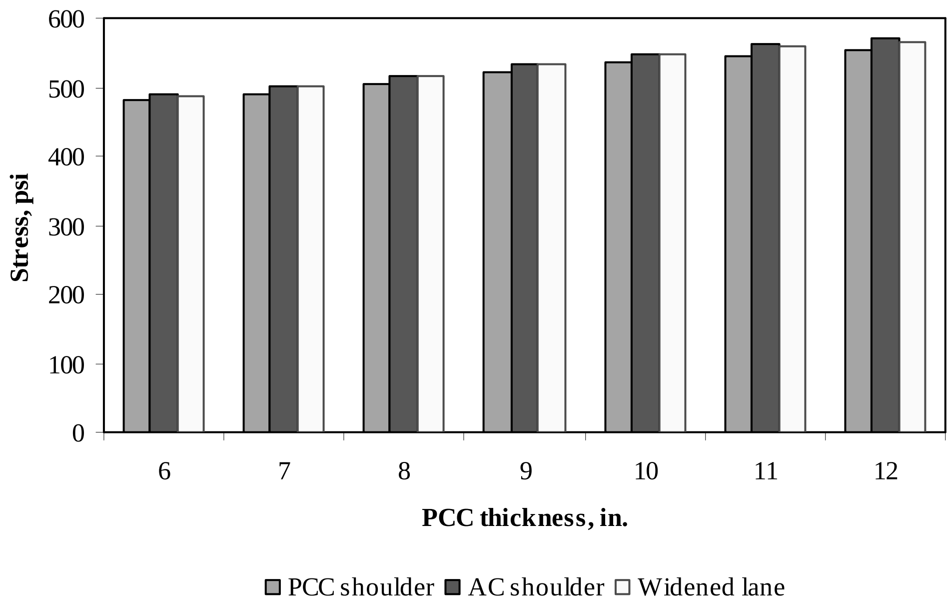


**Figure F-18-28: Impact of PCC thickness and lateral support condition on longitudinal stress at bottom of the Slab (315-in. joint spacing and $\alpha(\Delta T/D)$ of $20 x 10^{-6}$ in.$^{-1}$)**

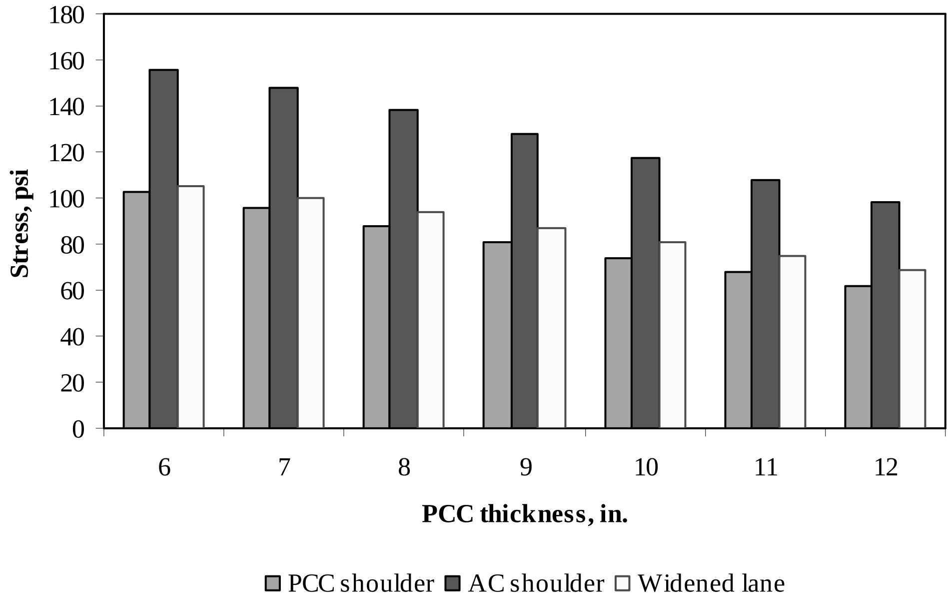


**Figure F-18-29: Impact of PCC thickness and lateral support condition on longitudinal stress at top of the Slab (177-in. joint spacing and $\alpha(\Delta T/D)$ of 0 in.$^{-1}$)**

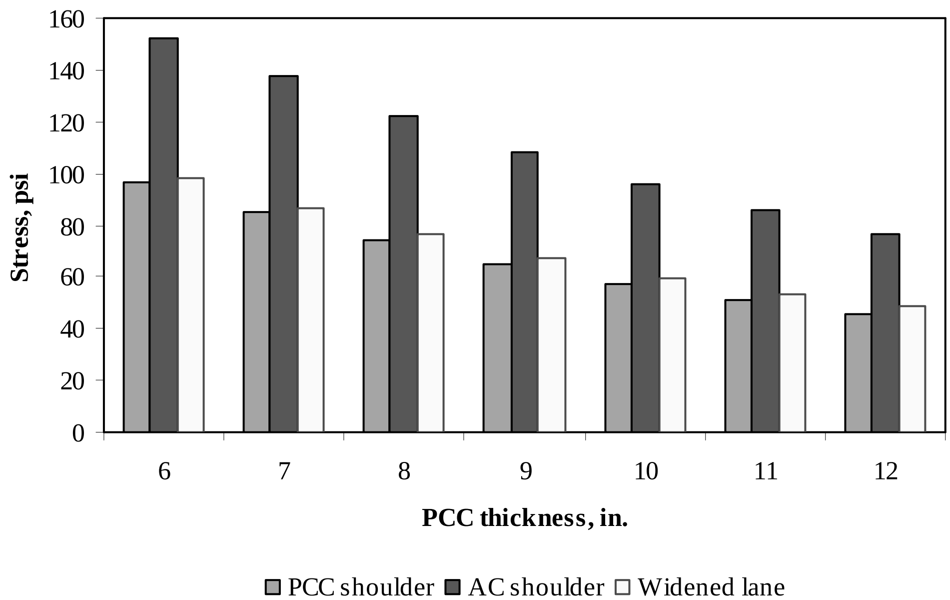


**Figure F-18-30: Impact of PCC thickness and lateral support condition on longitudinal stress at top of the Slab (315-in. joint spacing and $\alpha(\Delta T/D)$ of 0 in.$^{-1}$)**

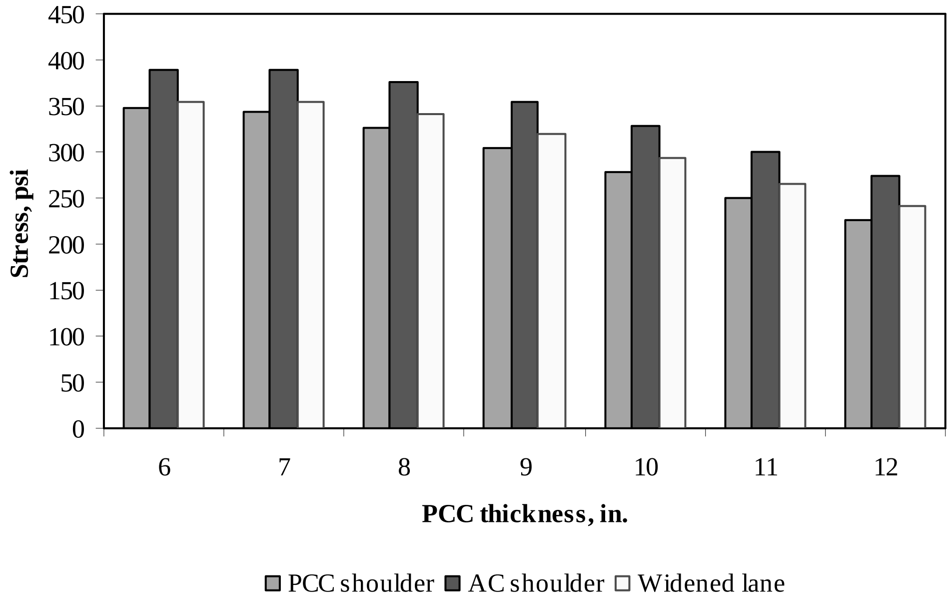


**Figure F-18-31: Impact of PCC thickness and lateral support condition on longitudinal stress at top of the Slab (177-in. joint spacing and $\alpha(\Delta T/D)$ of $-20\text{x}10^{-6}$ in.$^{-1}$)**

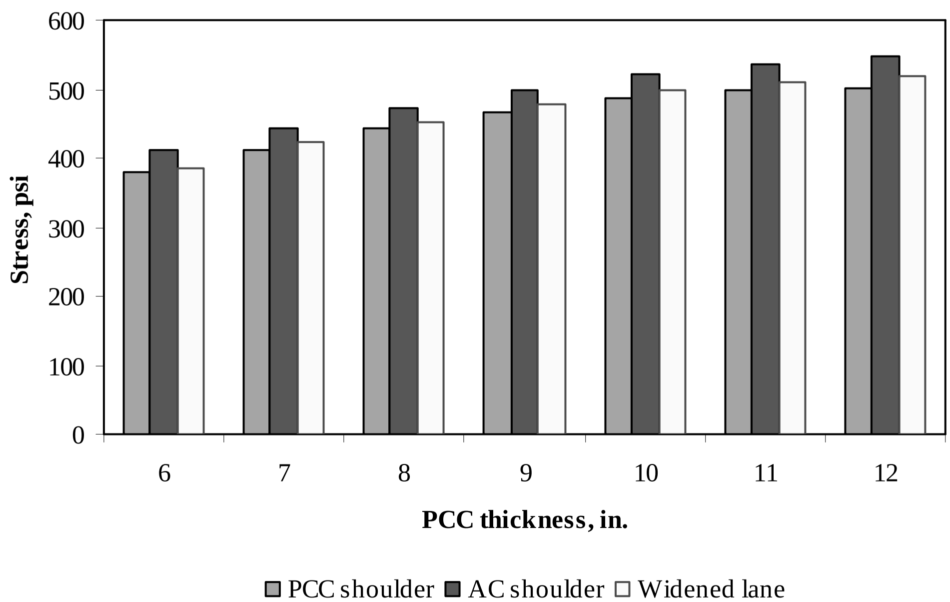


**Figure F-18-32: Impact of PCC thickness and lateral support condition on longitudinal stress at top of the Slab (315-in. joint spacing and $\alpha(\Delta T/D)$ of $-20\text{x}10^{-6}$ in.$^{-1}$)**

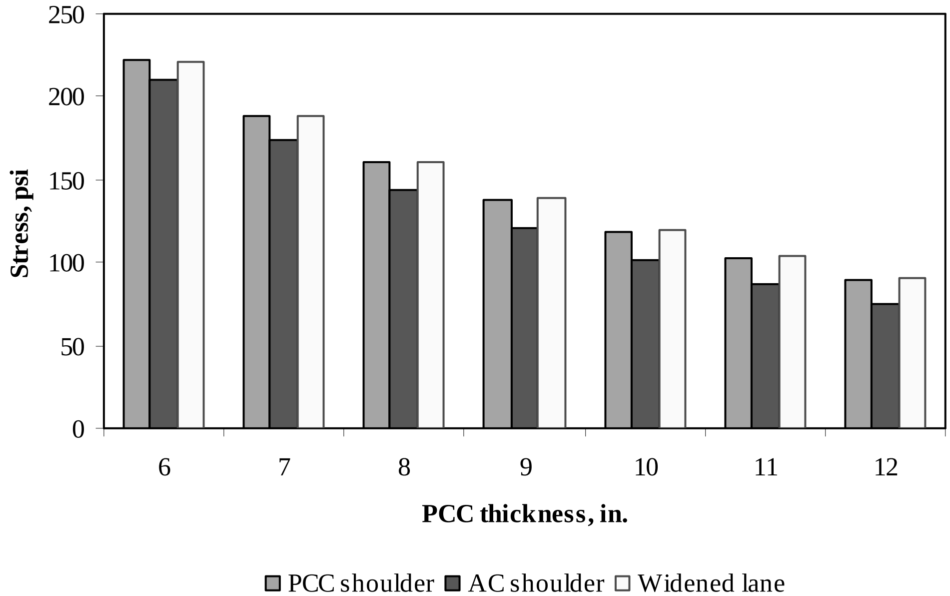


**Figure F-18-33: Impact of PCC thickness and lateral support condition on transverse stress at bottom of the Slab (177-in. joint spacing and $\alpha(\Delta T/D)$ of 0 in.$^{-1}$)**

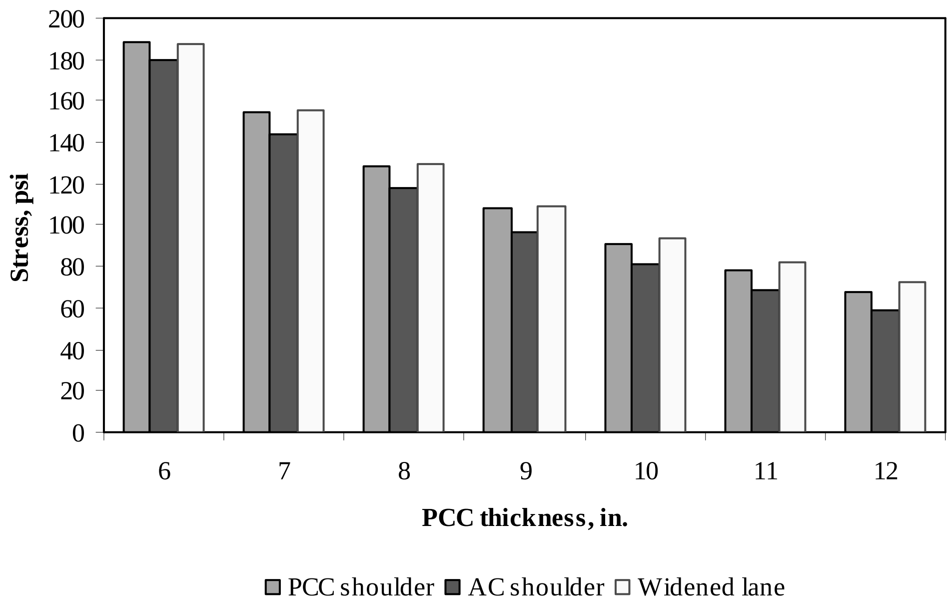


**Figure F-18-34: Impact of PCC thickness and lateral support condition on transverse stress at bottom of the Slab (315-in. joint spacing and $\alpha(\Delta T/D)$ of 0 in.$^{-1}$)**

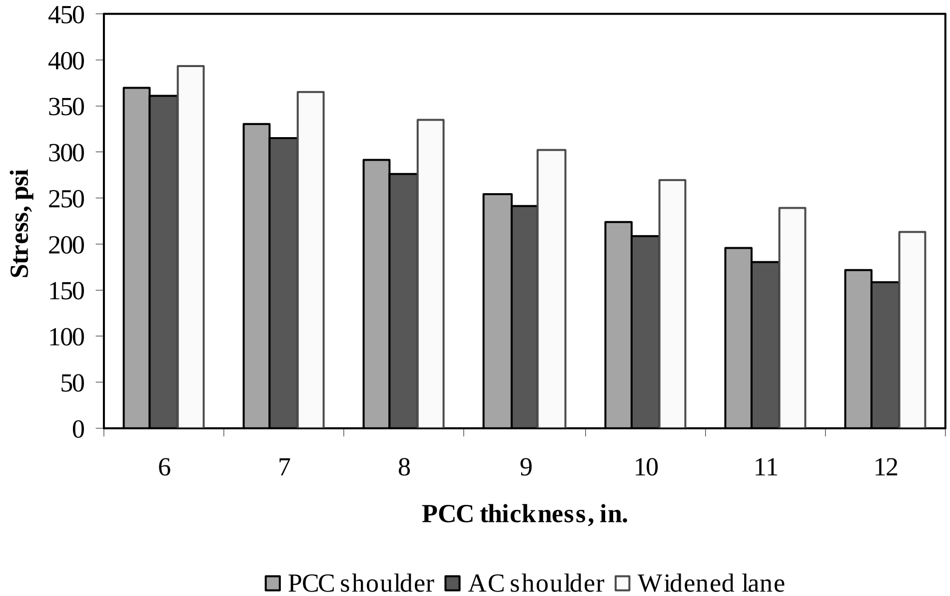


**Figure F-18-35: Impact of PCC thickness and lateral support condition on transverse stress at bottom of the Slab (177-in. joint spacing and $\alpha(\Delta T/D)$ of $20x10^{-6}$ in.$^{-1}$)**

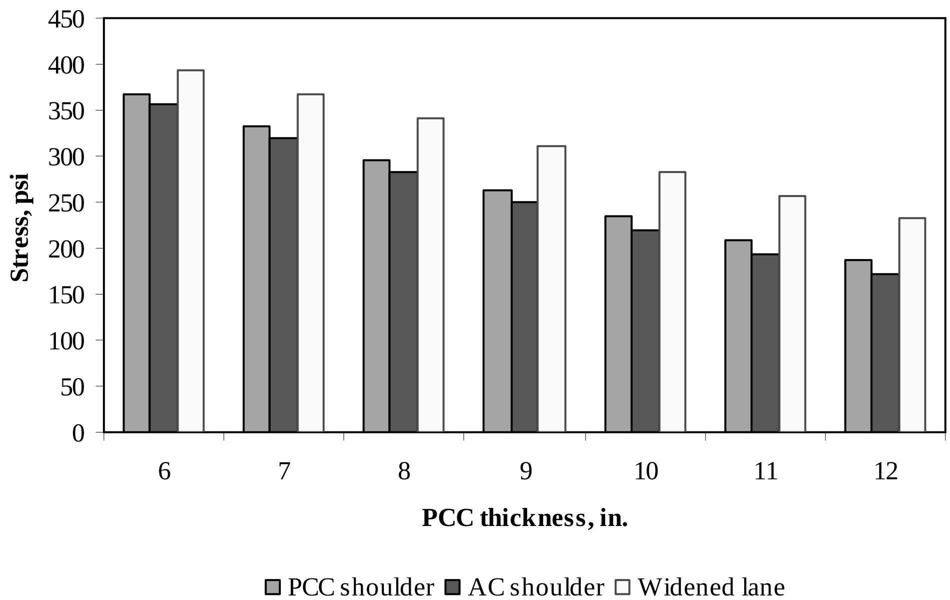


**Figure F-18-36: Impact of PCC thickness and lateral support condition on transverse stress at bottom of the Slab (315-in. joint spacing and $\alpha(\Delta T/D)$ of $20x10^{-6}$ in.$^{-1}$)**

Figures F-18-37 through F-18-42 illustrate the impact of base/subbase thickness and product α(ΔT/D) on stresses (10-in. PCC thickness, 100-psi/in. modulus of subgrade reaction and PCC shoulder)

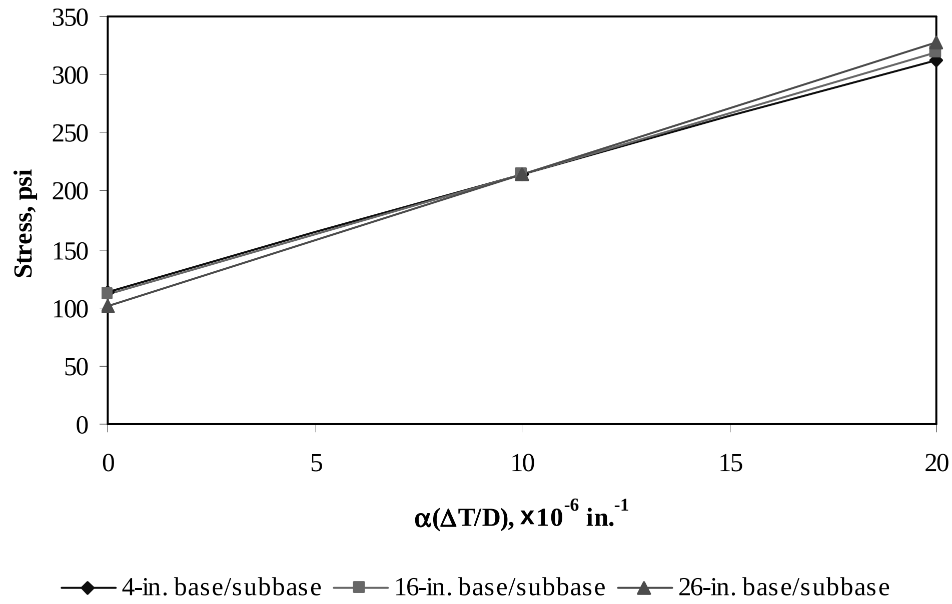


**Figure F-18-37: Impact of base/subbase thickness and product α(ΔT/D) on longitudinal stress at bottom of the slab (177-in. joint spacing)**

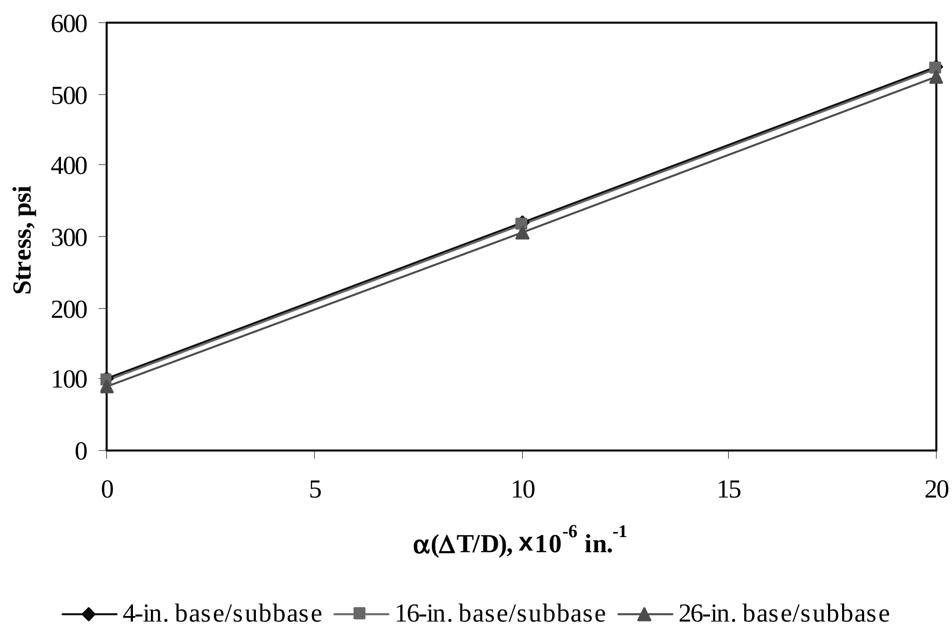


**Figure F-18-38: Impact of base/subbase thickness and product α(ΔT/D) on longitudinal stress at bottom of the slab (315-in. joint spacing)**

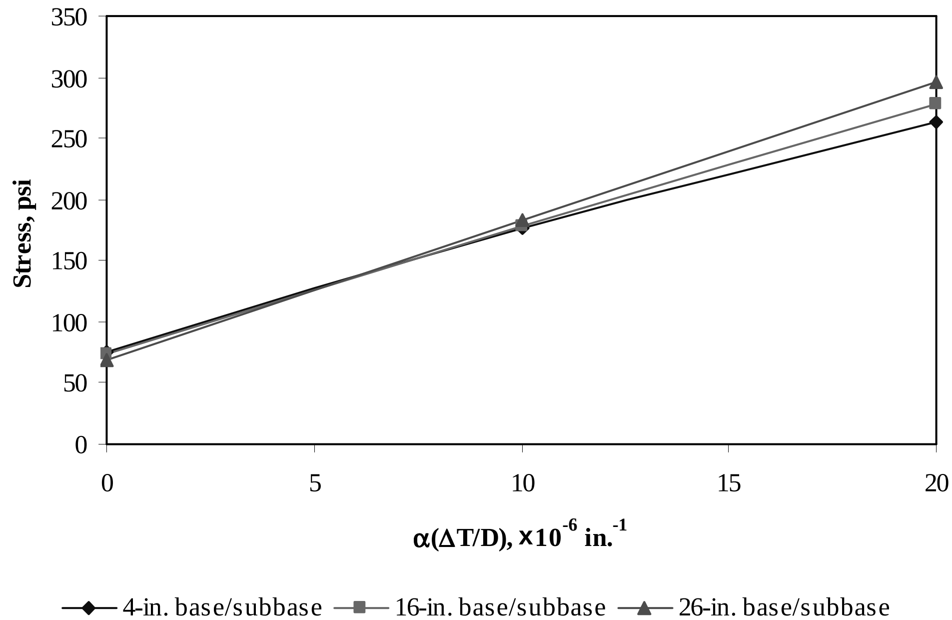


**Figure F-18-39: Impact of base/subbase thickness and product α(ΔT/D) on longitudinal stress at top of the slab (177-in. joint spacing)**

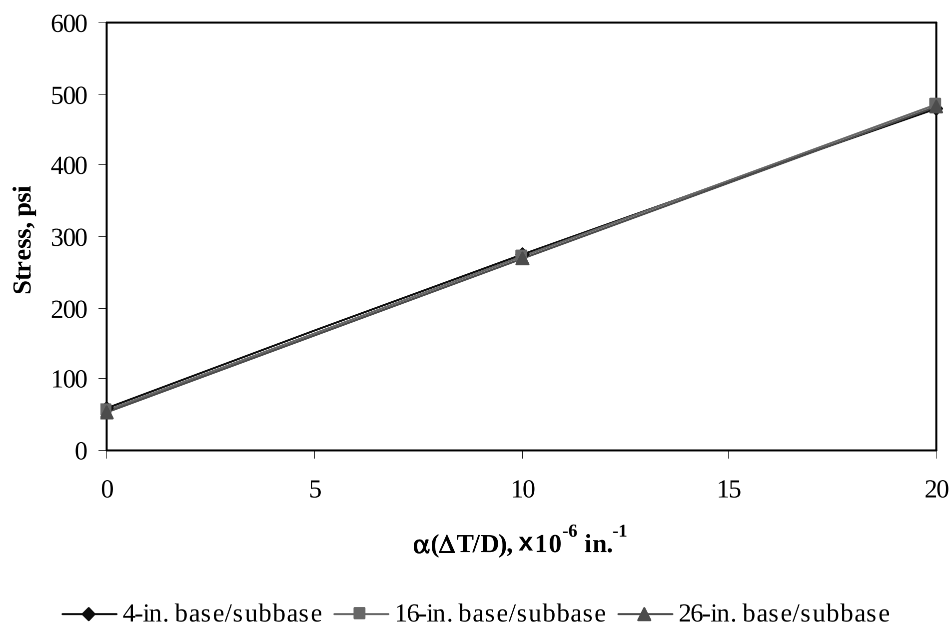


**Figure F-18-40: Impact of base/subbase thickness and product α(ΔT/D) on longitudinal stress at top of the slab (315-in. joint spacing)**

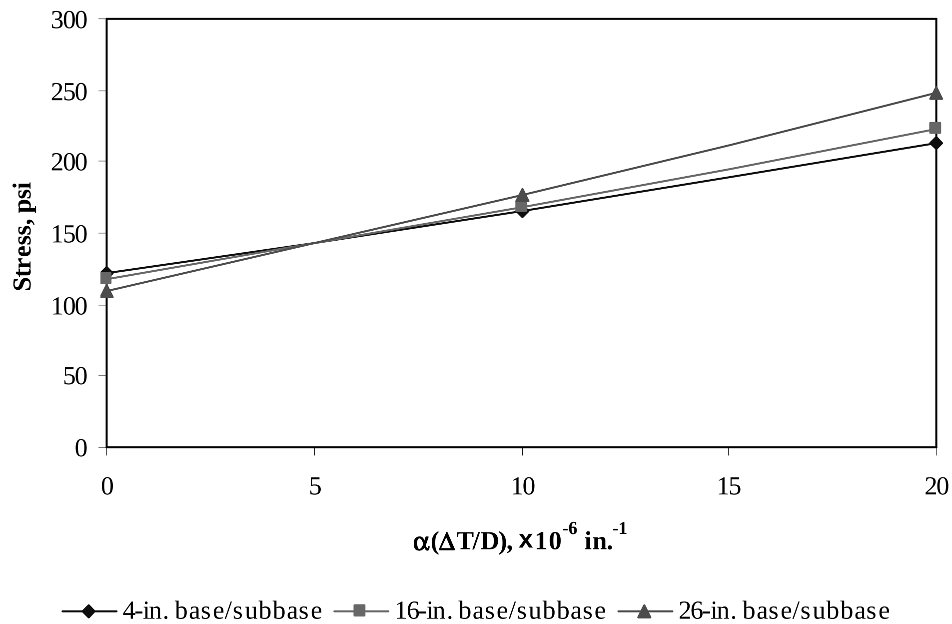


**Figure F-18-41: Impact of base/subbase thickness and product α(ΔT/D) on transverse stress at bottom of the slab (177-in. joint spacing)**

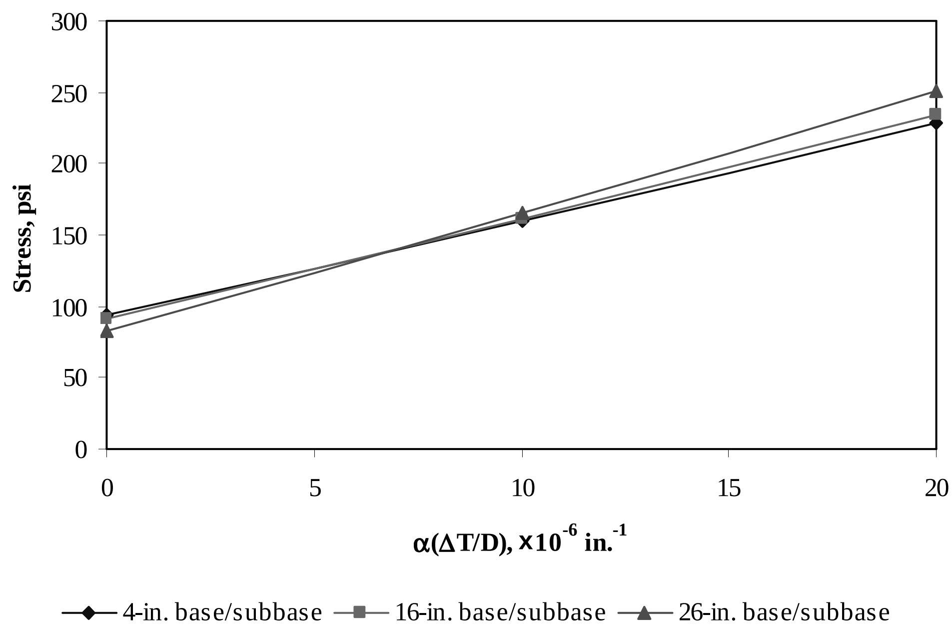


**Figure F-18-42: Impact of base/subbase thickness and product α(ΔT/D) on transverse stress at bottom of the slab (315-in. joint spacing)**

Figures F-18-43 through F-18-48 illustrate the impact of modulus of subgrade reaction and product α(ΔT/D) on stresses (10-in. PCC thickness, 16-in. base/subbase thickness and PCC shoulder)

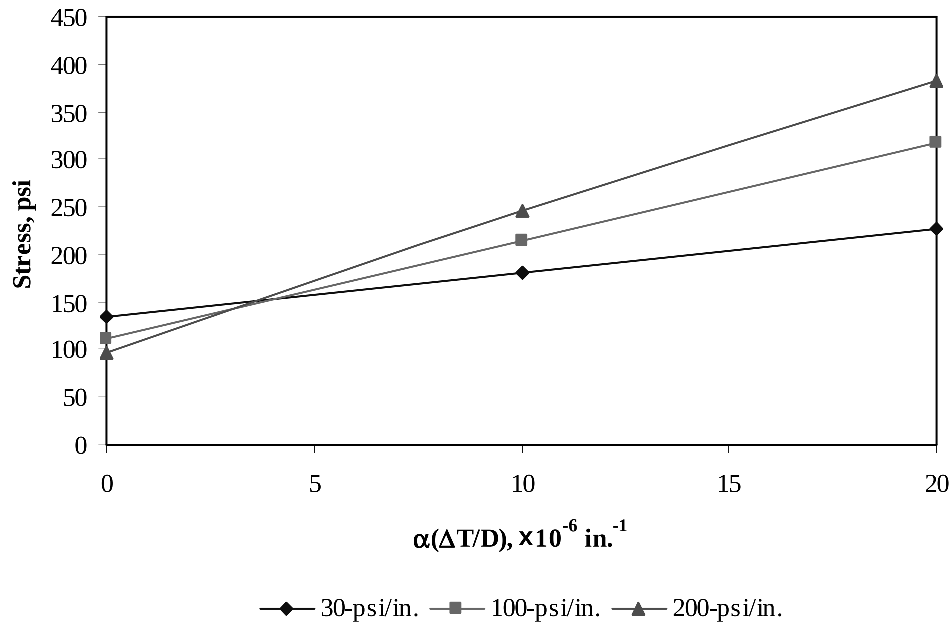


**Figure F-18-43: Impact of modulus of subgrade reaction and product α(ΔT/D) on longitudinal stress at bottom of the slab (177-in. joint spacing)**

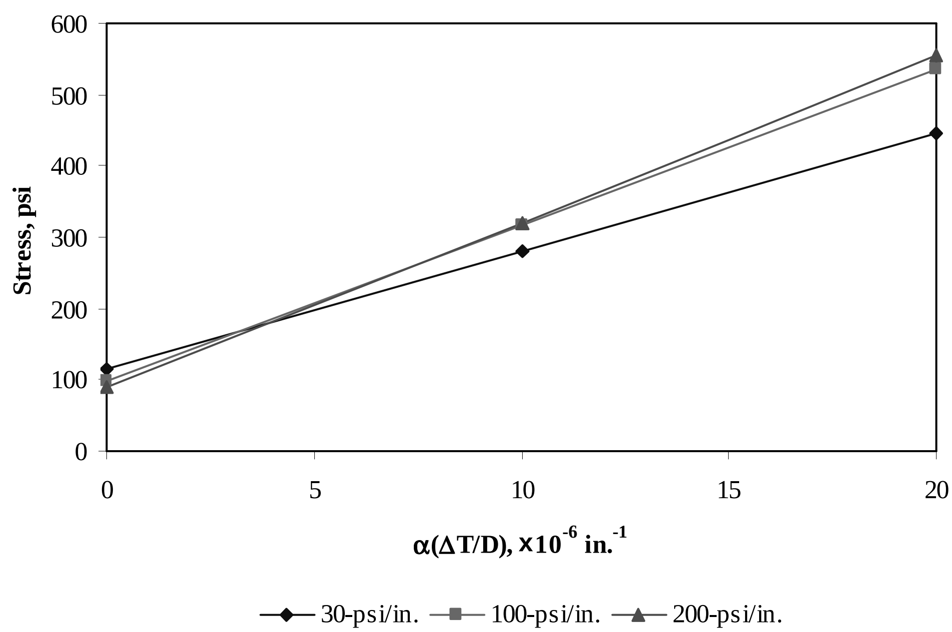


**Figure F-18-44: Impact of modulus of subgrade reaction and product α(ΔT/D) on longitudinal stress at bottom of the slab (315-in. joint spacing)**

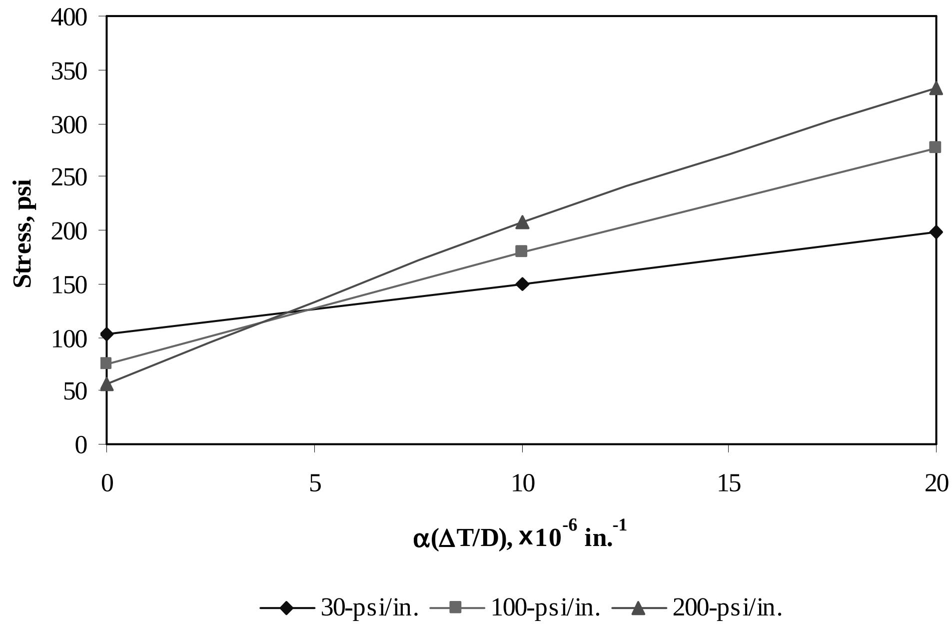


**Figure F-18-45: Impact of modulus of subgrade reaction and product α(ΔT/D) on longitudinal stress at top of the slab (177-in. joint spacing)**

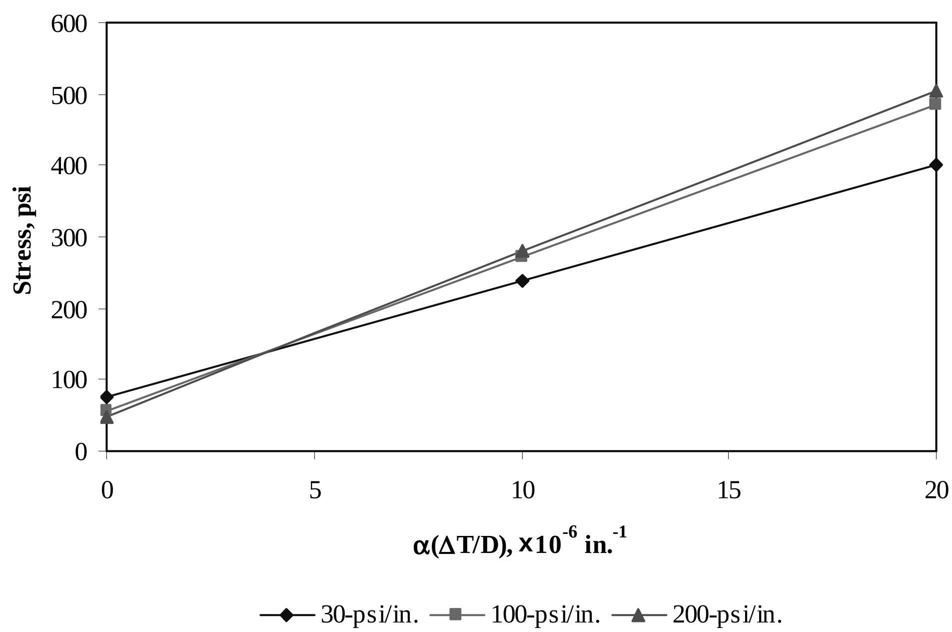


**Figure F-18-46: Impact of modulus of subgrade reaction and product α(ΔT/D) on longitudinal stress at top of the slab (315-in. joint spacing)**

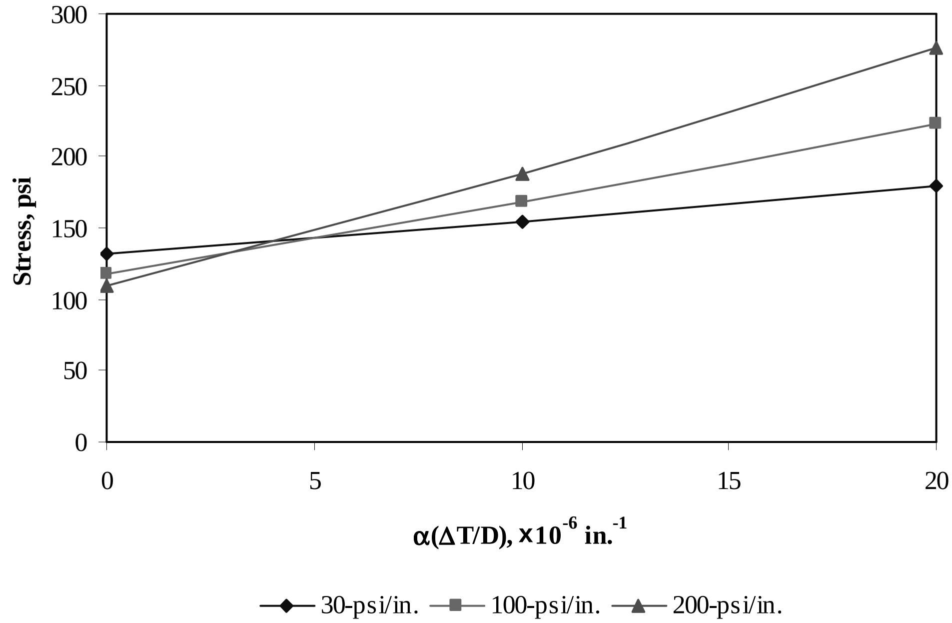


**Figure F-18-47: Impact of modulus of subgrade reaction and product α(ΔT/D) on transverse stress at bottom of the slab (177-in. joint spacing)**

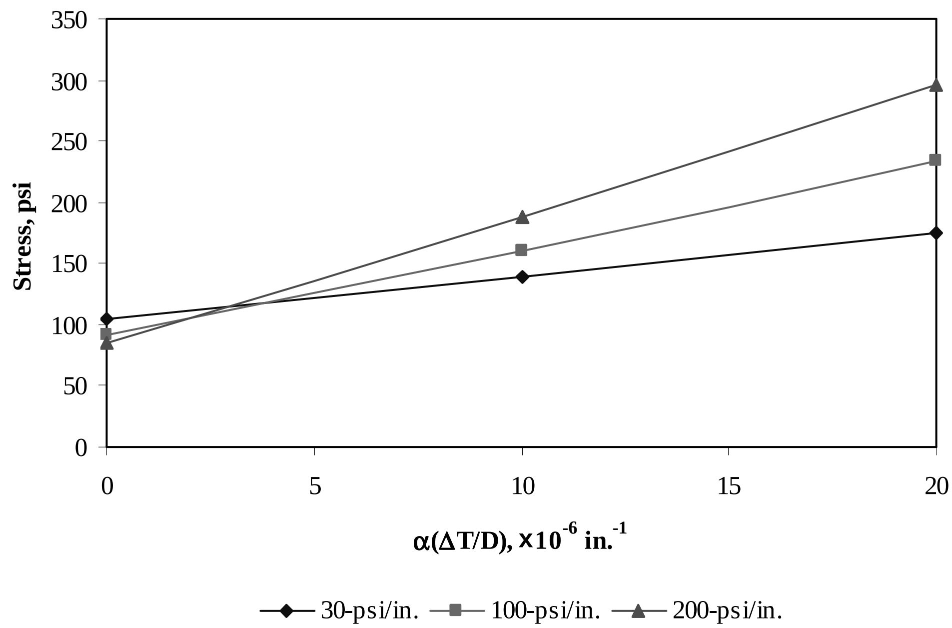


**Figure F-18-48: Impact of modulus of subgrade reaction and product α(ΔT/D) on transverse stress at bottom of the slab (315-in. joint spacing)**

Figures F-18-49 through F-18-51 illustrate the impact of joint spacing and product $\alpha(\Delta T/D)$ on stresses (10-in. PCC thickness, 16-in. base/subbase thickness, 100-psi/in. modulus of subgrade reaction and PCC shoulder)

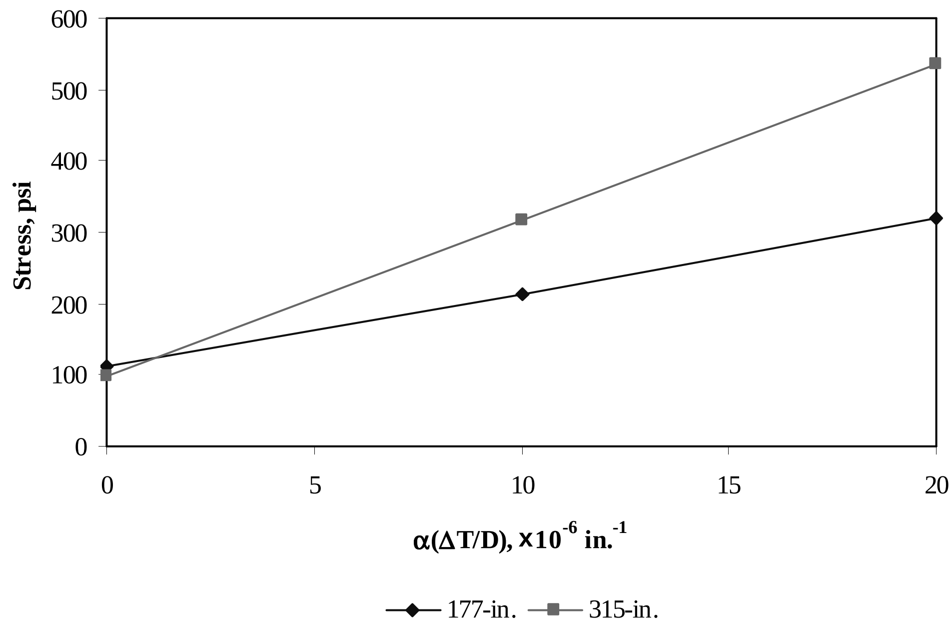


**Figure F-18-49: Impact of joint spacing and product $\alpha(\Delta T/D)$ on longitudinal stress at bottom of the slab**

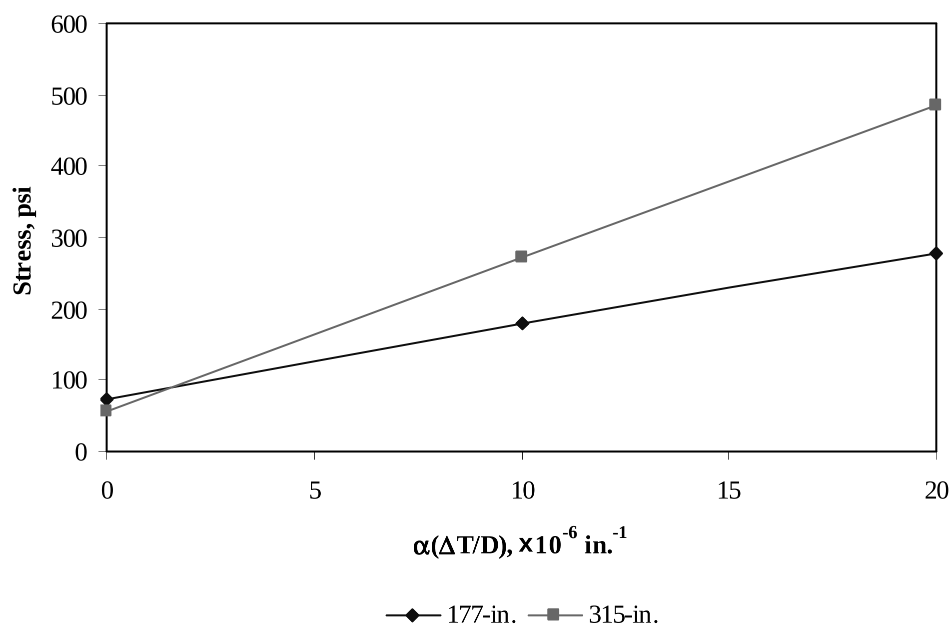


**Figure F-18-50: Impact of joint spacing and product $\alpha(\Delta T/D)$ on longitudinal stress at top of the slab**

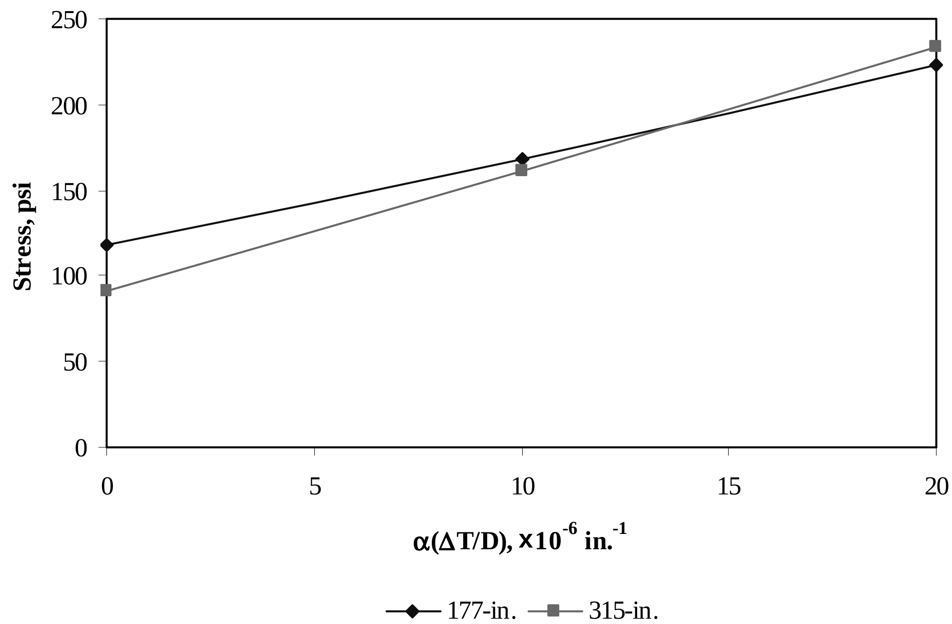


**Figure F-18-51: Impact of joint spacing and product α(ΔT/D) on transverse stress at bottom of the slab**

**Sub Appendix F-19**

**Documentation of Pavement Responses for**

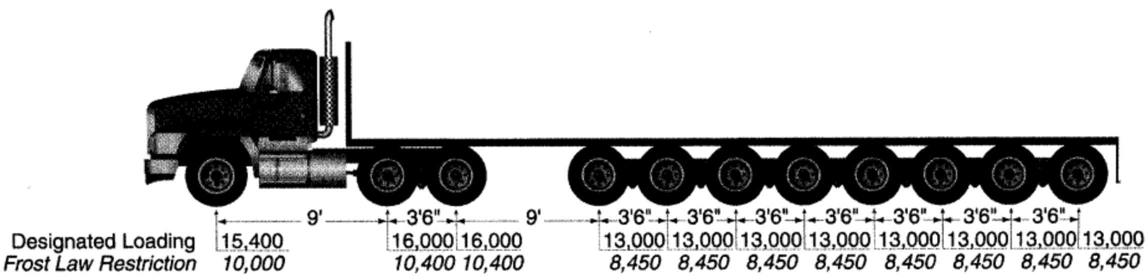


**MI-20**

Figures F-19-1 through F-19-12 illustrate the impact of PCC thickness and base/subbase thickness on stresses (100-psi/in. modulus of subgrade reaction and PCC shoulder)

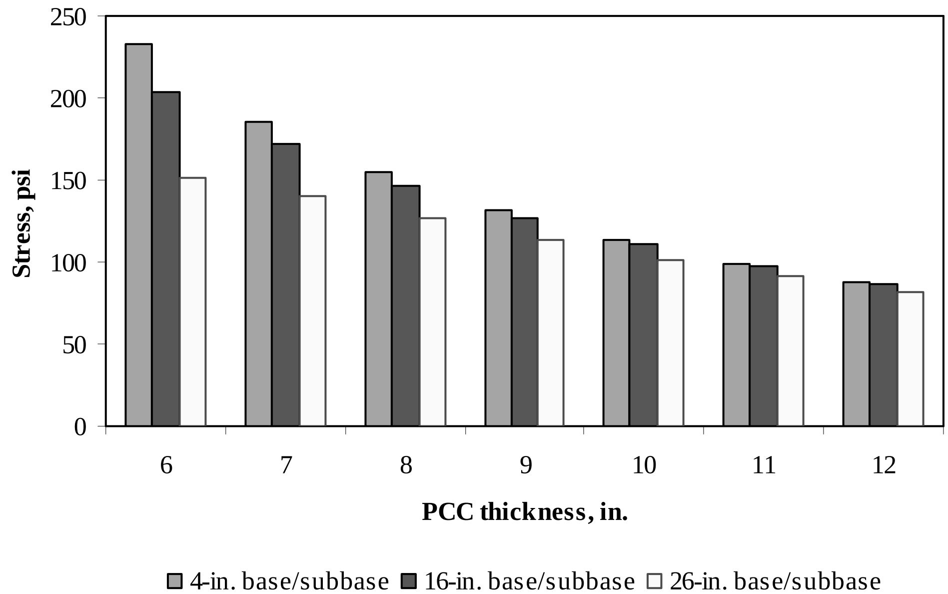


**Figure F-19-1: Impact of PCC thickness and base/subbase thickness on longitudinal stress at bottom of the Slab (177-in. joint spacing and $\alpha(\Delta T/D)$ of 0 in.$^{-1}$)**

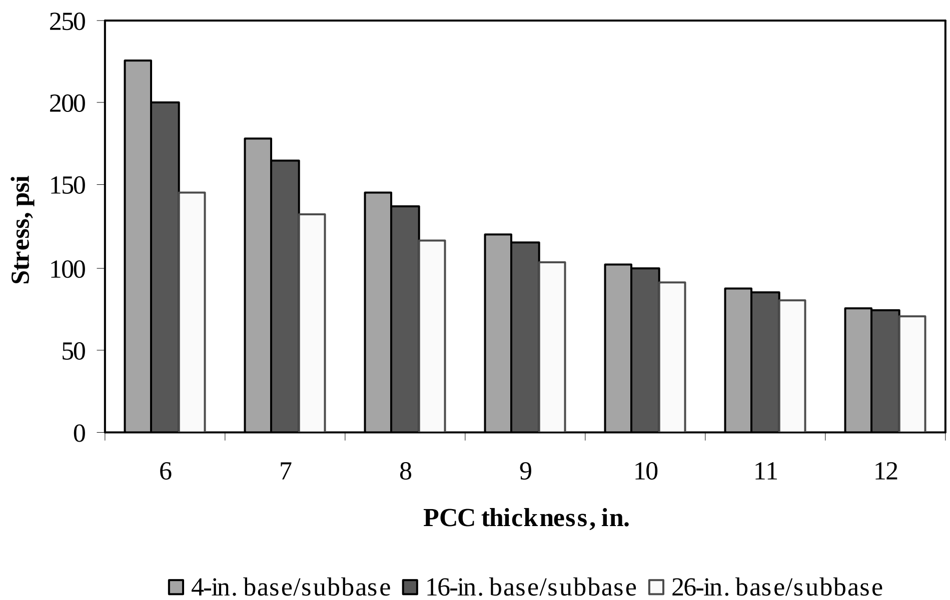


**Figure F-19-2: Impact of PCC thickness and base/subbase thickness on longitudinal stress at bottom of the Slab (315-in. joint spacing and $\alpha(\Delta T/D)$ of 0 in.$^{-1}$)**

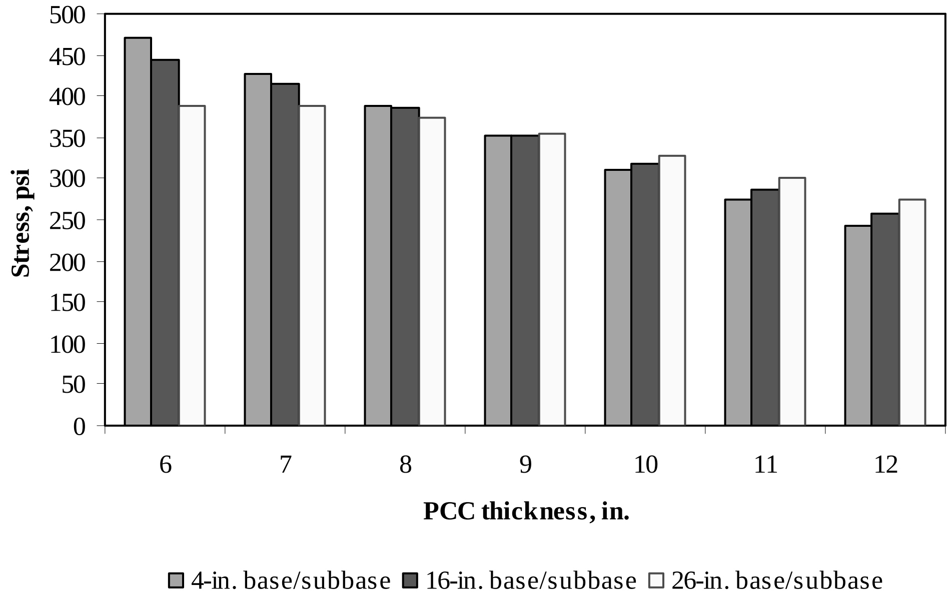


**Figure F-19-3: Impact of PCC thickness and base/subbase thickness on longitudinal stress at bottom of the Slab (177-in. joint spacing and $\alpha(\Delta T/D)$ of $20x10^{-6}$ in.$^{-1}$)**

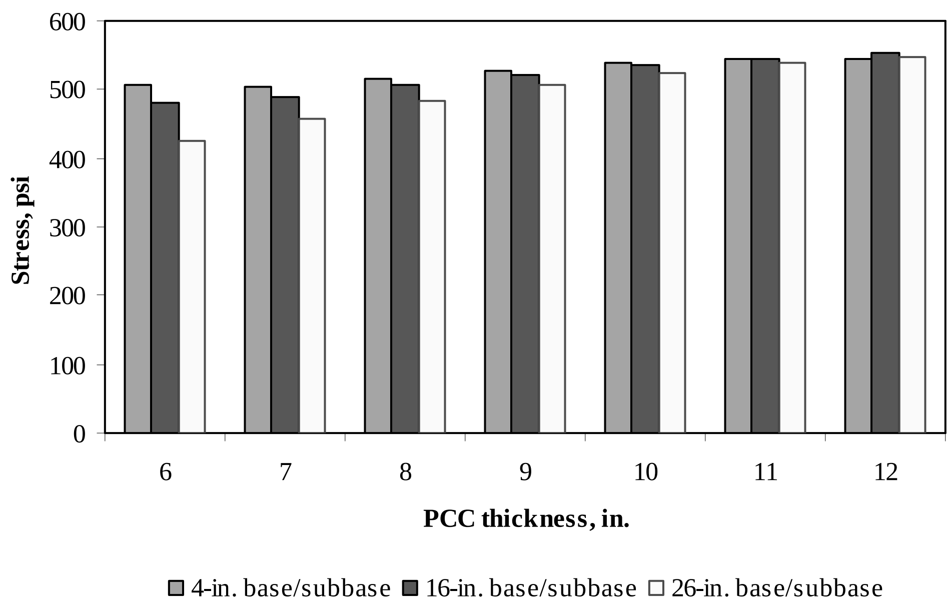


**Figure F-19-4: Impact of PCC thickness and base/subbase thickness on longitudinal stress at bottom of the Slab (315-in. joint spacing and $\alpha(\Delta T/D)$ of $20x10^{-6}$ in.$^{-1}$)**

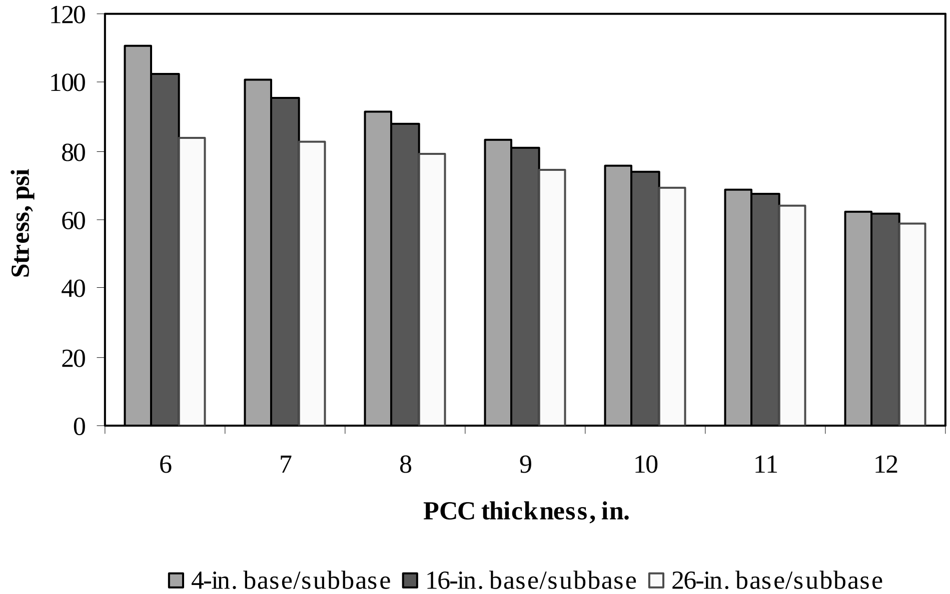


**Figure F-19-5: Impact of PCC thickness and base/subbase thickness on longitudinal stress at top of the Slab (177-in. joint spacing and $\alpha(\Delta T/D)$ of 0 in.$^{-1}$)**

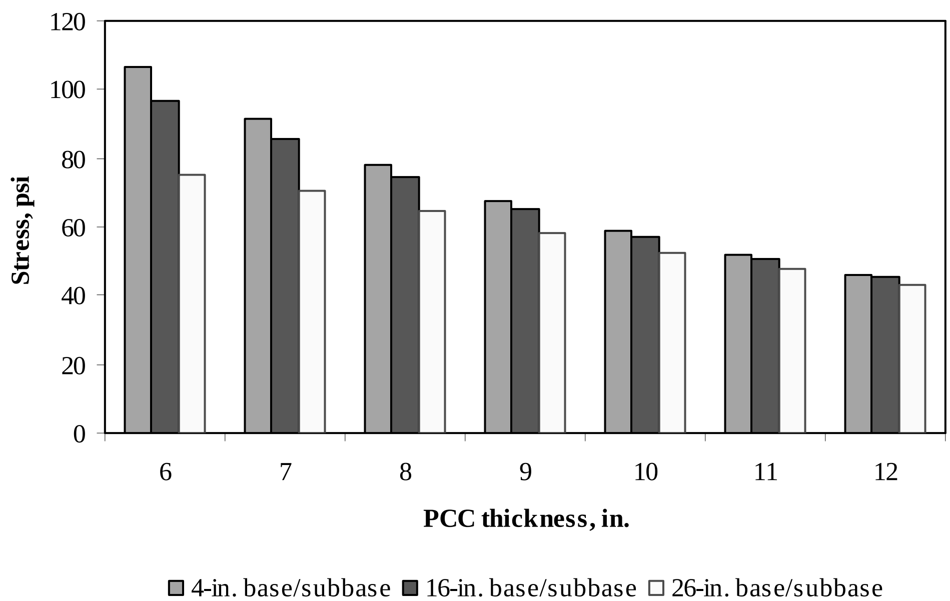


**Figure F-19-6: Impact of PCC thickness and base/subbase thickness on longitudinal stress at top of the Slab (315-in. joint spacing and $\alpha(\Delta T/D)$ of 0 in.$^{-1}$)**

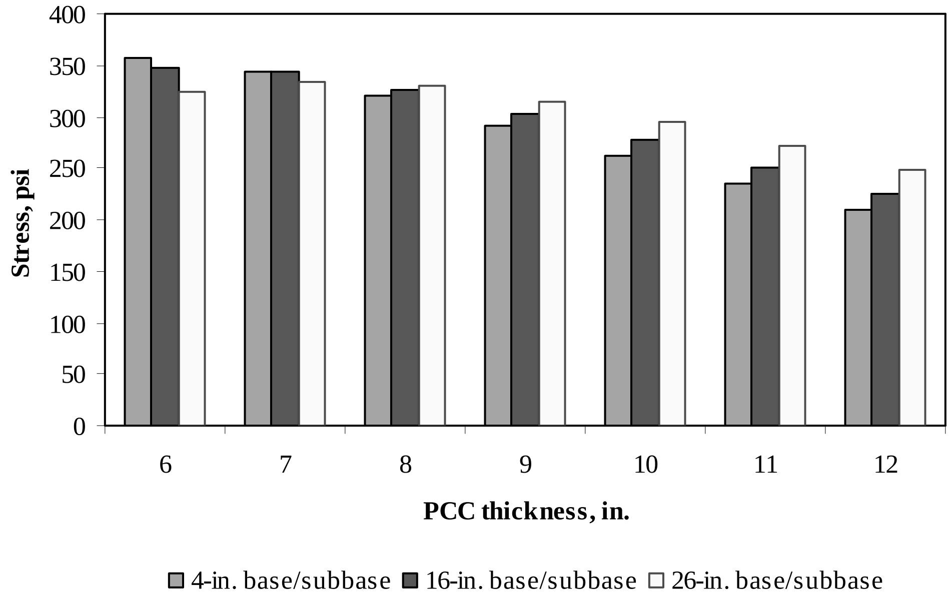


**Figure F-19-7: Impact of PCC thickness and base/subbase thickness on longitudinal stress at top of the Slab (177-in. joint spacing and $\alpha(\Delta T/D)$ of $-20x10^{-6}$ in.$^{-1}$)**

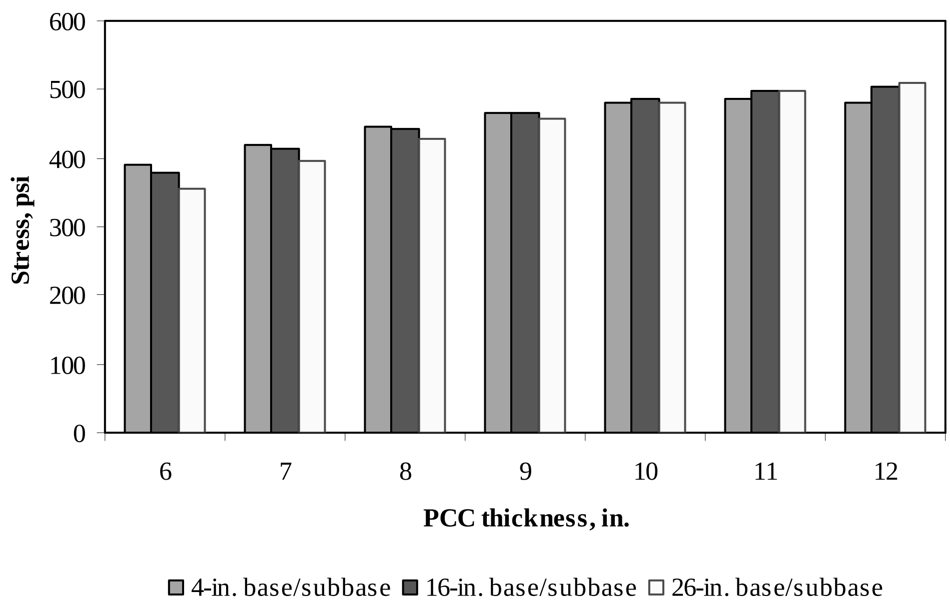


**Figure F-19-8: Impact of PCC thickness and base/subbase thickness on longitudinal stress at top of the Slab (315-in. joint spacing and $\alpha(\Delta T/D)$ of $-20x10^{-6}$ in.$^{-1}$)**

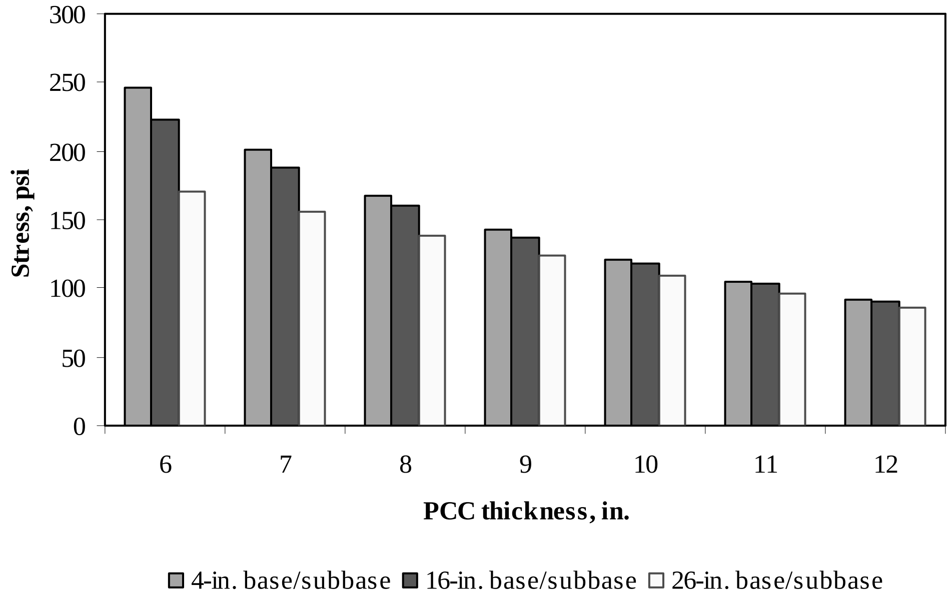


**Figure F-19-9: Impact of PCC thickness and base/subbase thickness on transverse stress at bottom of the Slab (177-in. joint spacing and $\alpha(\Delta T/D)$ of 0 in.$^{-1}$)**

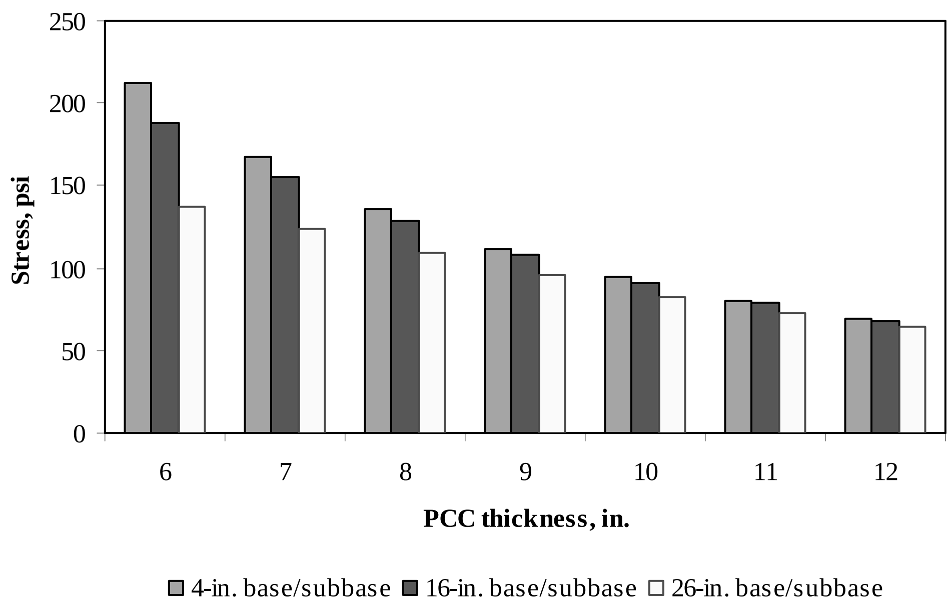


**Figure F-19-10: Impact of PCC thickness and base/subbase thickness on transverse stress at bottom of the Slab (315-in. joint spacing and $\alpha(\Delta T/D)$ of 0 in.$^{-1}$)**

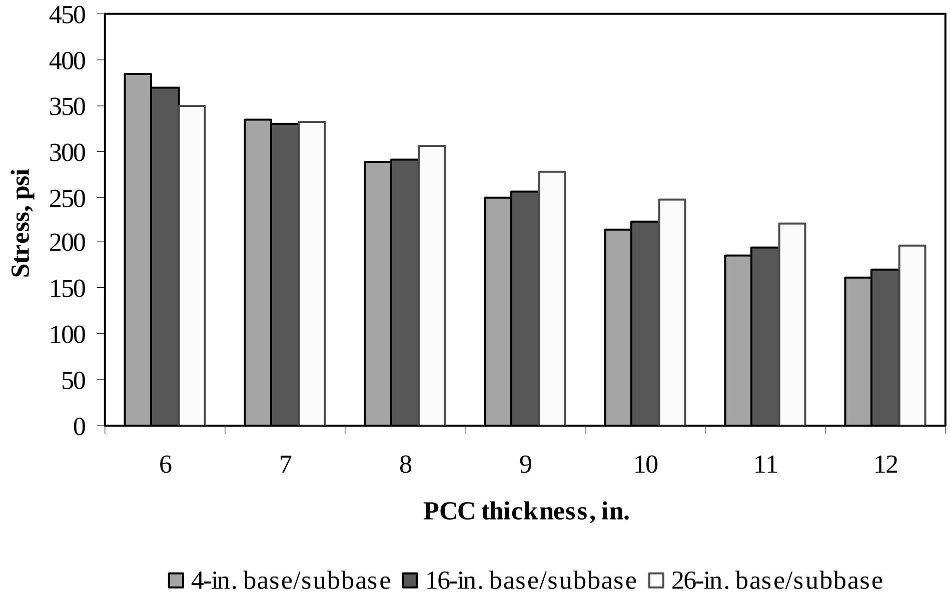


**Figure F-19-11: Impact of PCC thickness and base/subbase thickness on transverse stress at bottom of the Slab (177-in. joint spacing and $\alpha(\Delta T/D)$ of $20x10^{-6}$ in.$^{-1}$)**

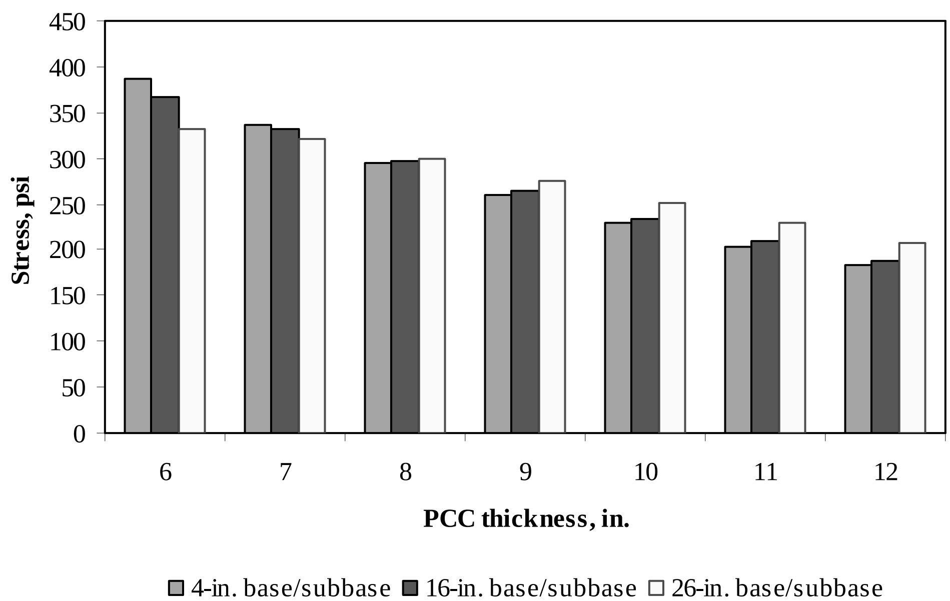


**Figure F-19-12: Impact of PCC thickness and base/subbase thickness on transverse stress at bottom of the Slab (315-in. joint spacing and $\alpha(\Delta T/D)$ of $20x10^{-6}$ in.$^{-1}$)**

Figures F-19-13 through F-19-24 illustrate the impact of PCC thickness and modulus of subgrade reaction on stresses (16-in. base/subbase thickness and PCC shoulder)

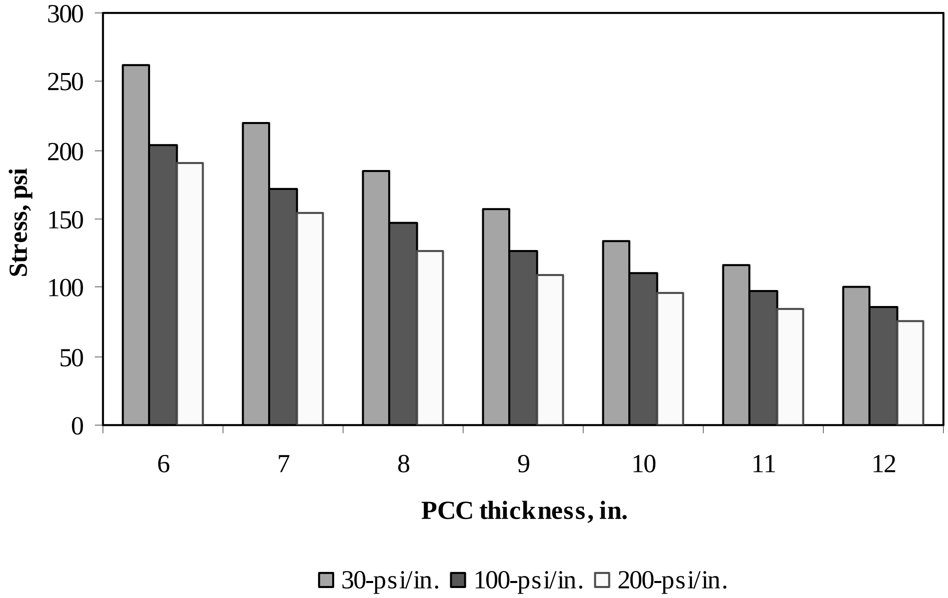


**Figure F-19-13: Impact of PCC thickness and modulus of subgrade reaction on longitudinal stress at bottom of the slab (177-in. joint spacing and $\alpha(\Delta T/D)$ of 0 in.$^{-1}$)**

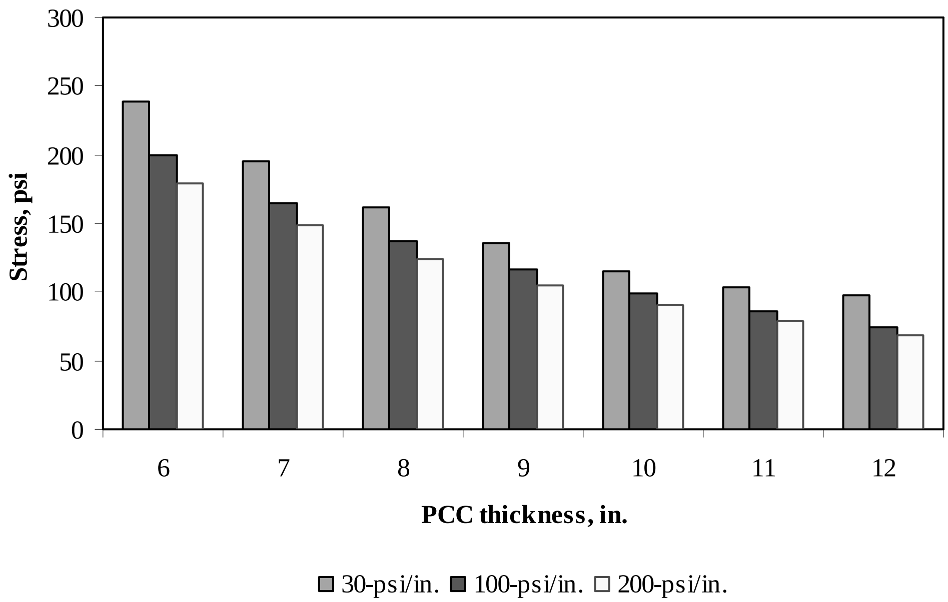


**Figure F-19-14: Impact of PCC thickness and modulus of subgrade reaction on longitudinal stress at bottom of the slab (315-in. joint spacing and $\alpha(\Delta T/D)$ of 0 in.$^{-1}$)**

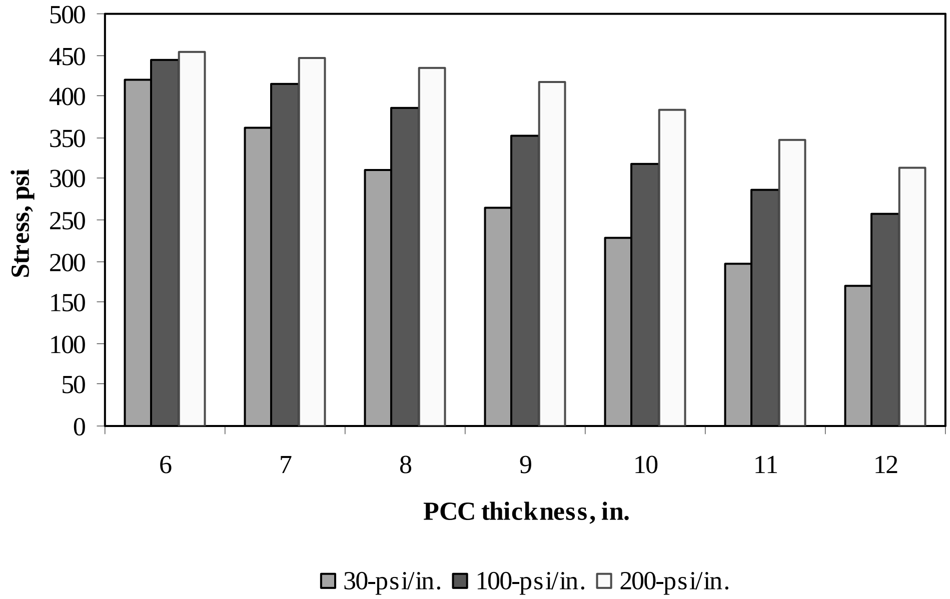


**Figure F-19-15: Impact of PCC thickness and modulus of subgrade reaction on longitudinal stress at bottom of the slab (177-in. joint spacing and $\alpha(\Delta T/D)$ of $20 \times 10^{-6}$ in.$^{-1}$)**

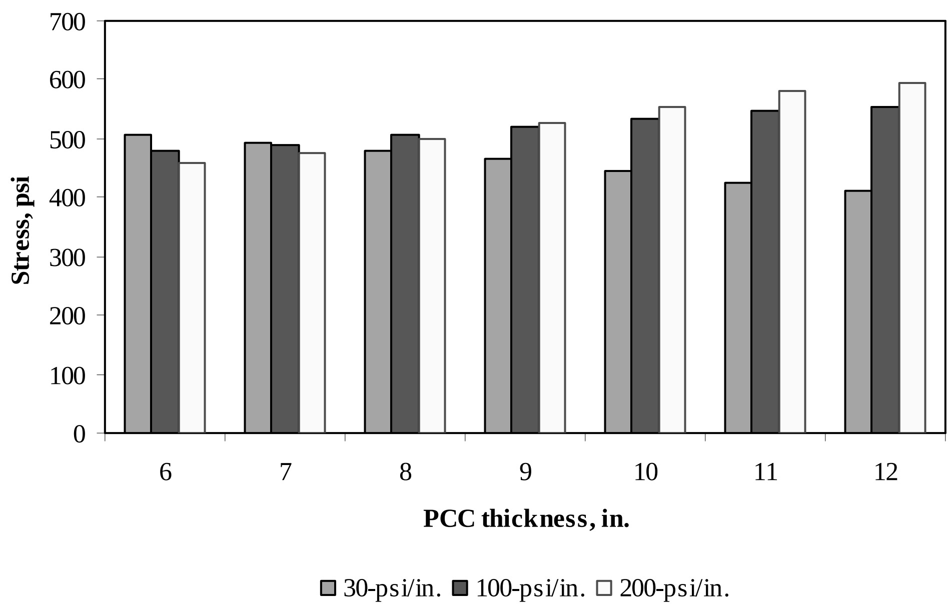


**Figure F-19-16: Impact of PCC thickness and modulus of subgrade reaction on longitudinal stress at bottom of the slab (315-in. joint spacing and $\alpha(\Delta T/D)$ of $20 \times 10^{-6}$ in.$^{-1}$)**

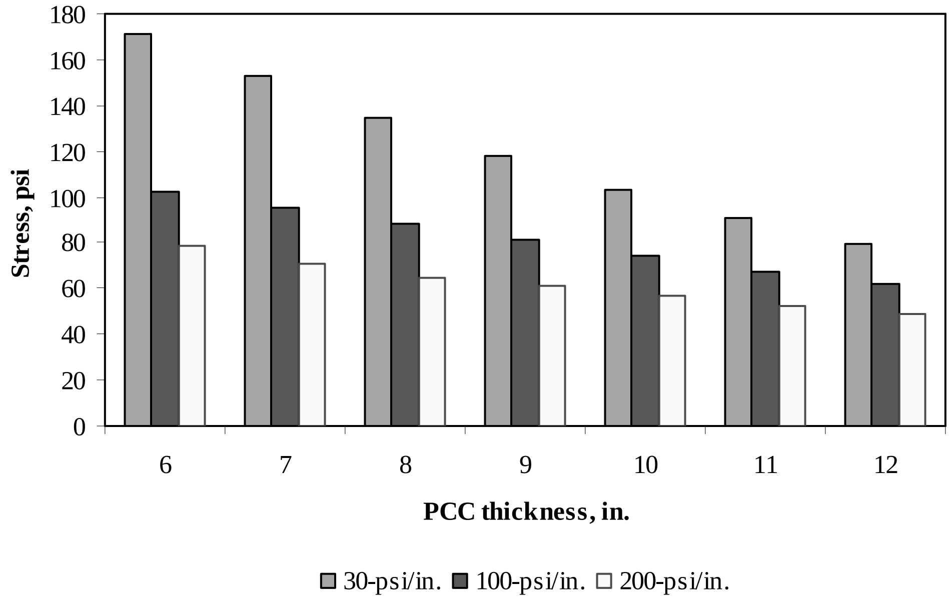


**Figure F-19-17: Impact of PCC thickness and modulus of subgrade reaction on longitudinal stress at top of the Slab (177-in. joint spacing and $\alpha(\Delta T/D)$ of 0 in.$^{-1}$)**

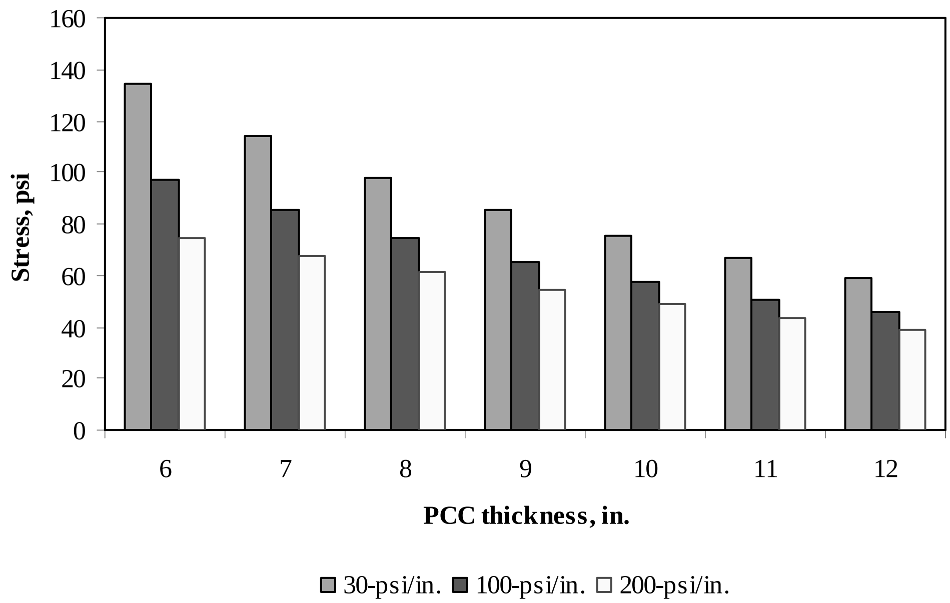


**Figure F-19-19: Impact of PCC thickness and modulus of subgrade reaction on longitudinal stress at top of the Slab (315-in. joint spacing and $\alpha(\Delta T/D)$ of 0 in.$^{-1}$)**

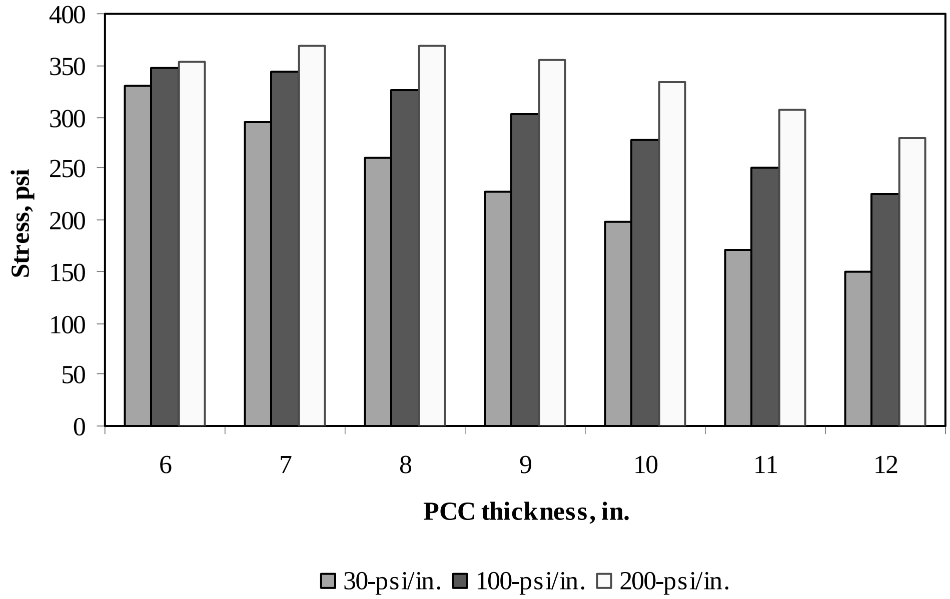


**Figure F-19-19: Impact of PCC thickness and modulus of subgrade reaction on longitudinal stress at top of the Slab (177-in. joint spacing and $\alpha(\Delta T/D)$ of $-20 \times 10^{-6}$ in.$^{-1}$)**

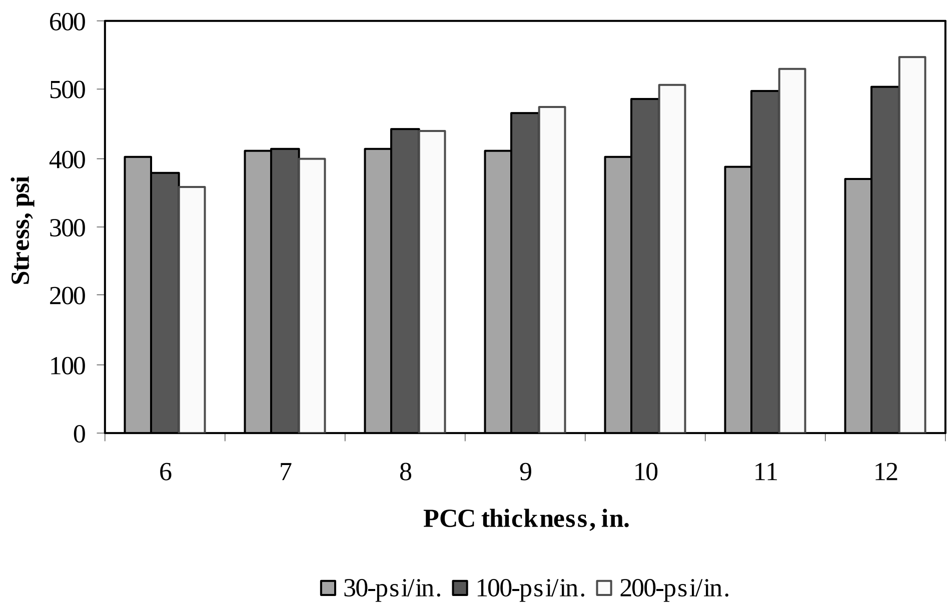


**Figure F-19-20: Impact of PCC thickness and modulus of subgrade reaction on longitudinal stress at top of the Slab (315-in. joint spacing and $\alpha(\Delta T/D)$ of $-20 \times 10^{-6}$ in.$^{-1}$)**

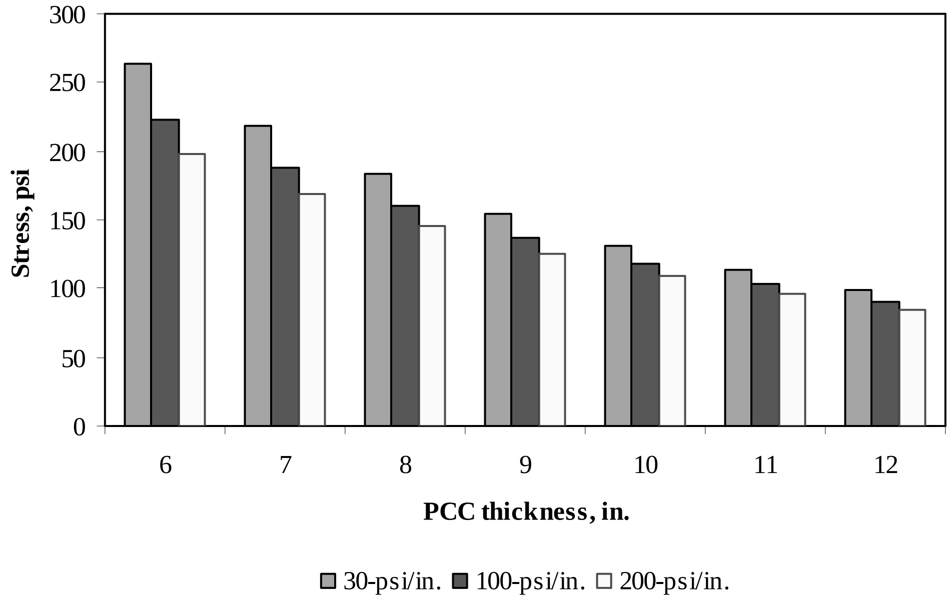


**Figure F-19-21: Impact of PCC thickness and modulus of subgrade reaction on transverse stress at bottom of the Slab (177-in. joint spacing and $\alpha(\Delta T/D)$ of 0 $in.^{-1}$)**

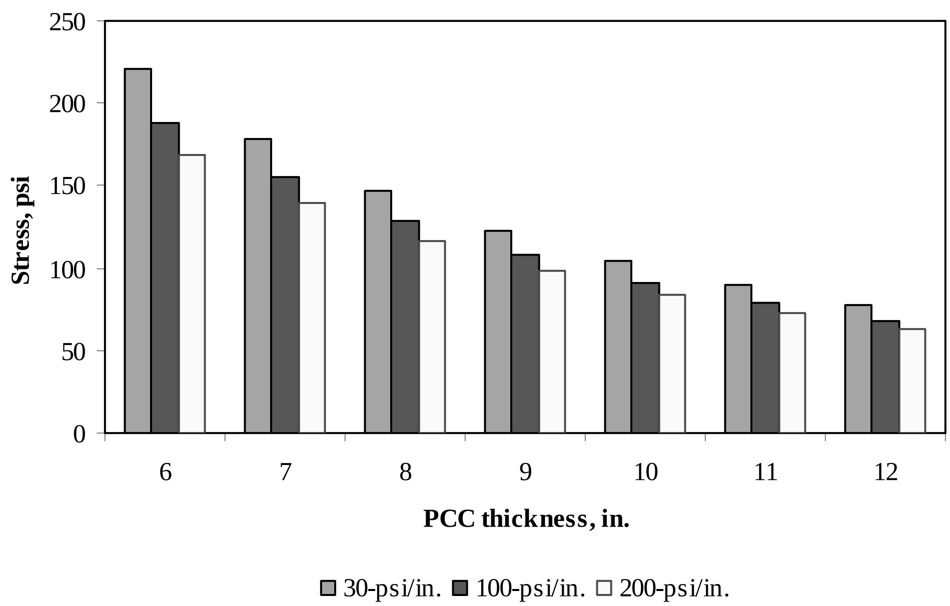


**Figure F-19-22: Impact of PCC thickness and modulus of subgrade reaction on transverse stress at bottom of the Slab (315-in. joint spacing and $\alpha(\Delta T/D)$ of 0 $in.^{-1}$)**

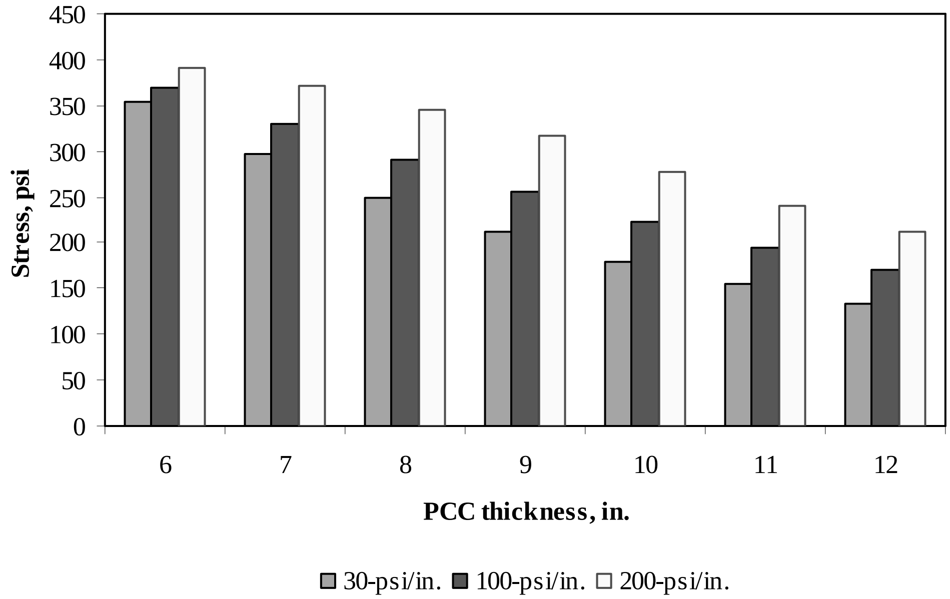


**Figure F-19-23: Impact of PCC thickness and modulus of subgrade reaction on transverse stress at bottom of the Slab (177-in. joint spacing and $\alpha(\Delta T/D)$ of $20 \times 10^{-6}$ in.$^{-1}$)**

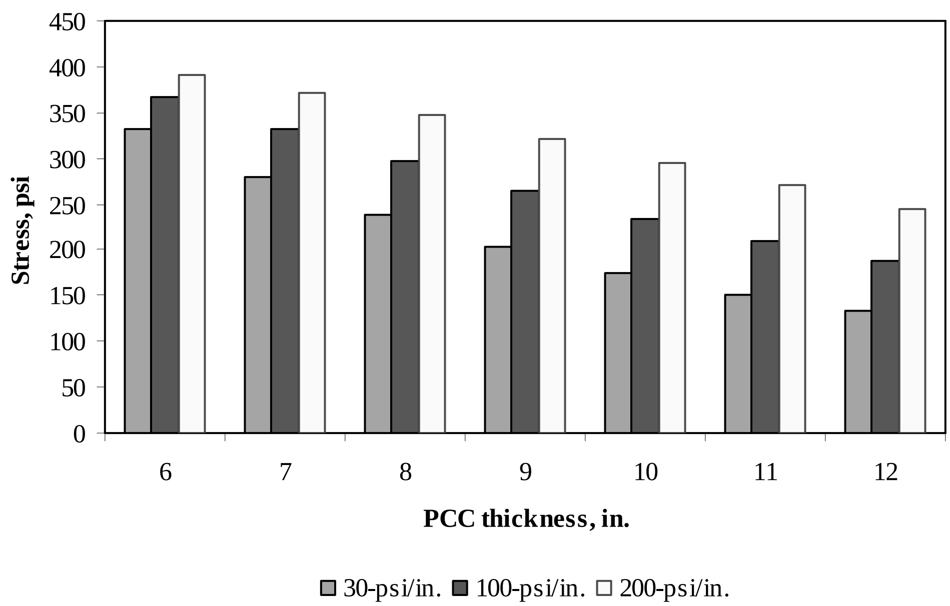


**Figure F-19-24: Impact of PCC thickness and modulus of subgrade reaction on transverse stress at bottom of the Slab (315-in. joint spacing and $\alpha(\Delta T/D)$ of $20 \times 10^{-6}$ in.$^{-1}$)**

Figures F-19-25 through F-19-36 illustrate the impact of PCC thickness and lateral support condition on stresses (16-in. base/subbase and 100-psi/in. modulus of subgrade reaction)

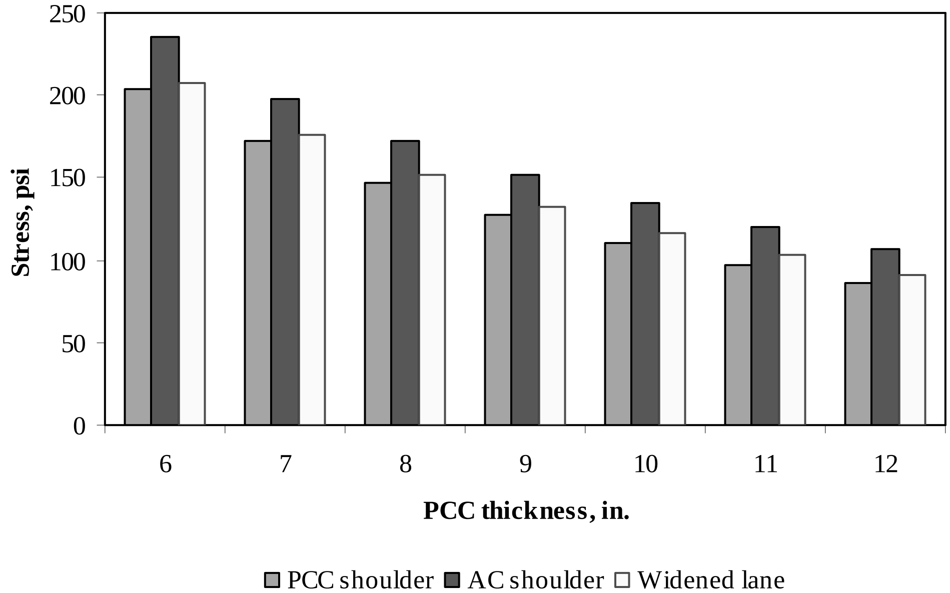


**Figure F-19-25: Impact of PCC thickness and lateral support condition on longitudinal stress at bottom of the Slab (177-in. joint spacing and $\alpha(\Delta T/D)$ of 0 in.$^{-1}$)**

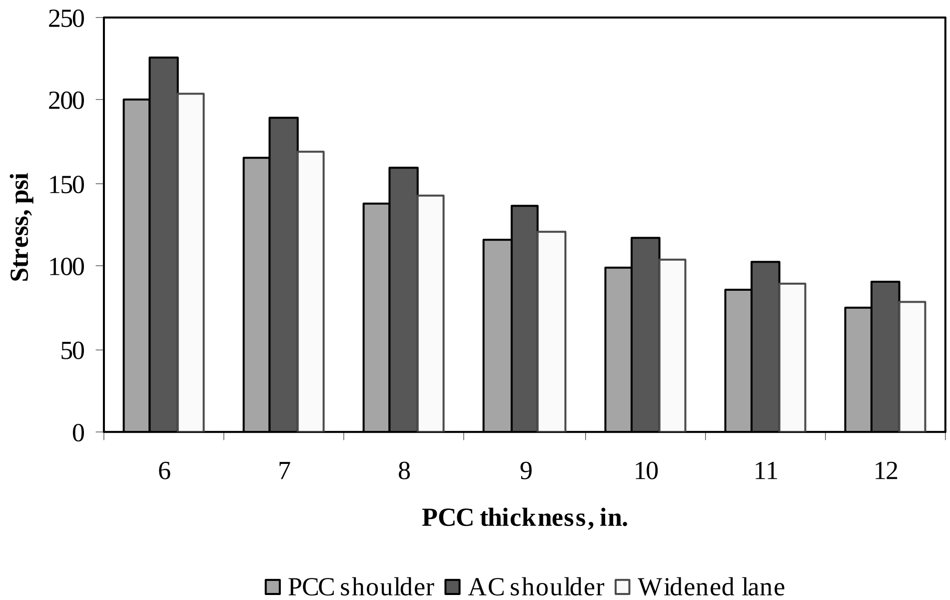


**Figure F-19-26: Impact of PCC thickness and lateral support condition on longitudinal stress at bottom of the Slab (315-in. joint spacing and $\alpha(\Delta T/D)$ of 0 in.$^{-1}$)**

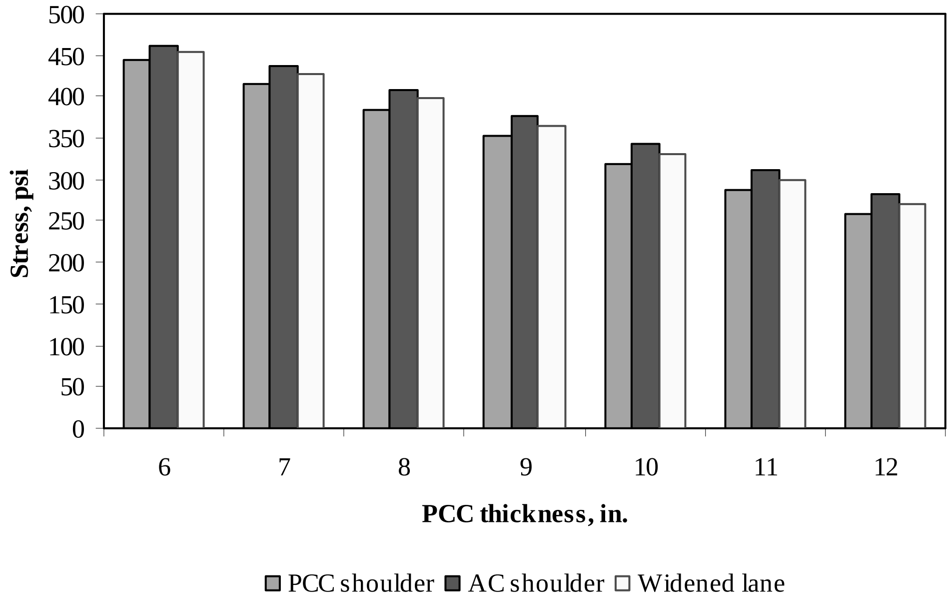


**Figure F-19-27: Impact of PCC thickness and lateral support condition on longitudinal stress at bottom of the Slab (177-in. joint spacing and $\alpha(\Delta T/D)$ of $20x10^{-6}$ in.$^{-1}$)**

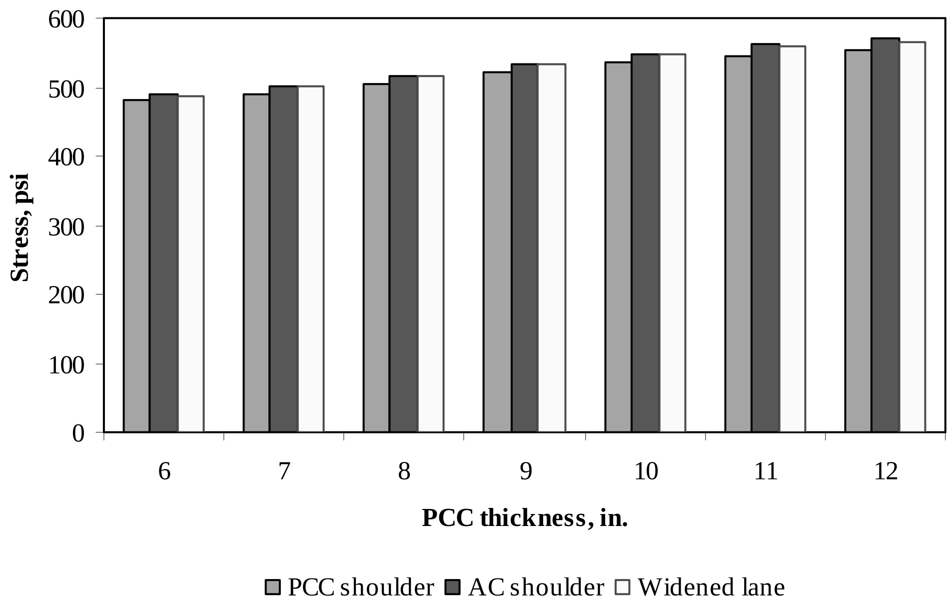


**Figure F-19-28: Impact of PCC thickness and lateral support condition on longitudinal stress at bottom of the Slab (315-in. joint spacing and $\alpha(\Delta T/D)$ of $20x10^{-6}$ in.$^{-1}$)**

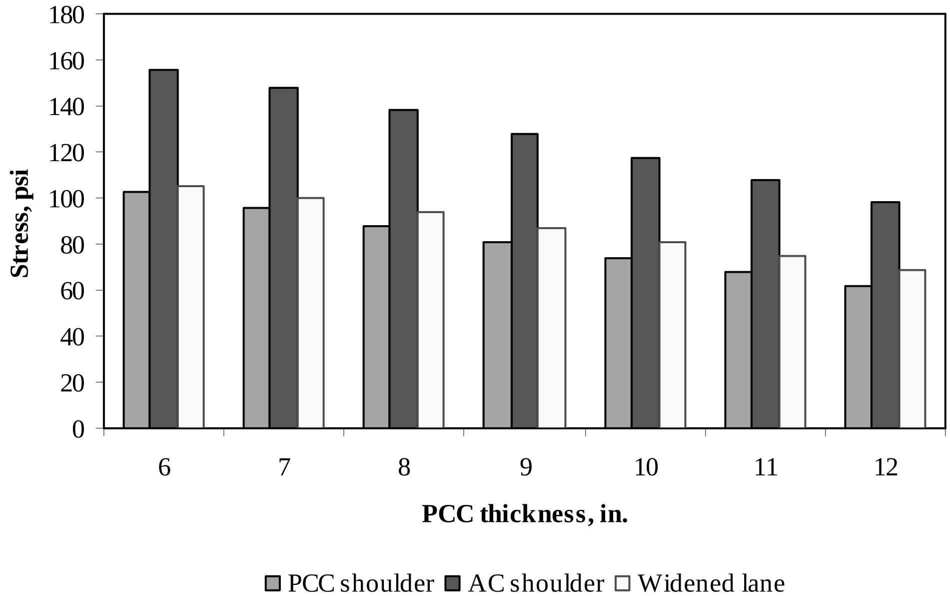


**Figure F-19-29: Impact of PCC thickness and lateral support condition on longitudinal stress at top of the Slab (177-in. joint spacing and $\alpha(\Delta T/D)$ of 0 in.$^{-1}$)**

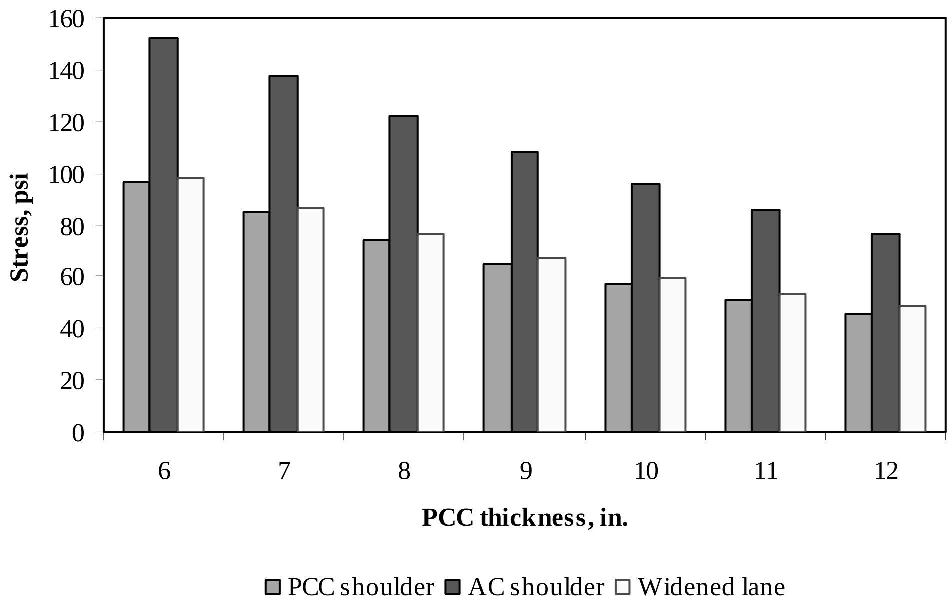


**Figure F-19-30: Impact of PCC thickness and lateral support condition on longitudinal stress at top of the Slab (315-in. joint spacing and $\alpha(\Delta T/D)$ of 0 in.$^{-1}$)**

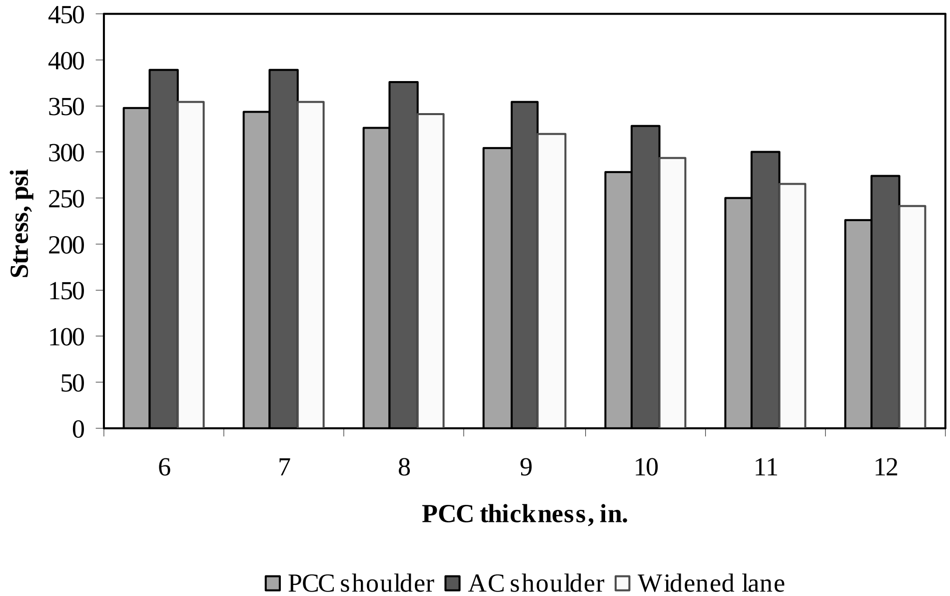


**Figure F-19-31: Impact of PCC thickness and lateral support condition on longitudinal stress at top of the Slab (177-in. joint spacing and $\alpha(\Delta T/D)$ of $-20x10^{-6}$ in.$^{-1}$)**

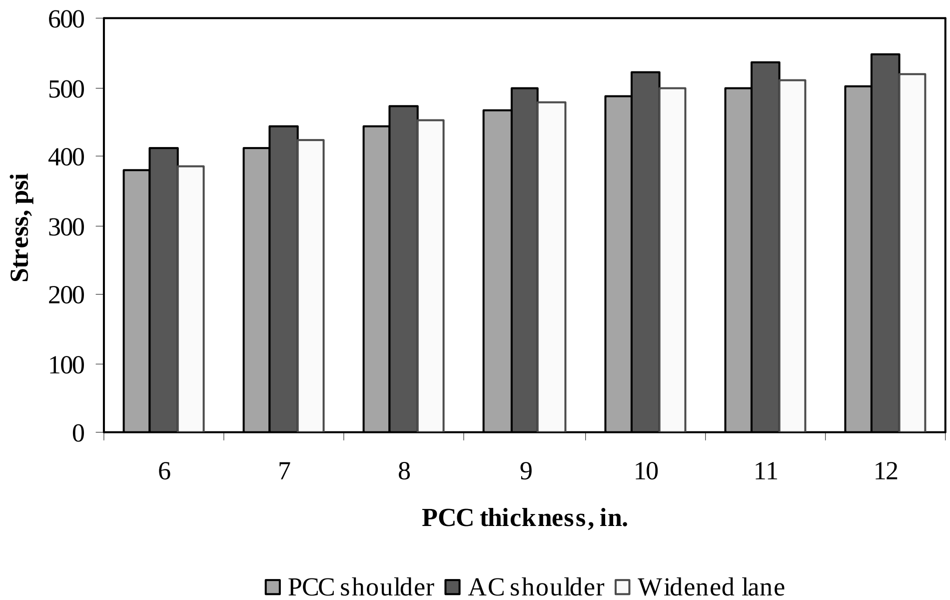


**Figure F-19-32: Impact of PCC thickness and lateral support condition on longitudinal stress at top of the Slab (315-in. joint spacing and $\alpha(\Delta T/D)$ of $-20x10^{-6}$ in.$^{-1}$)**

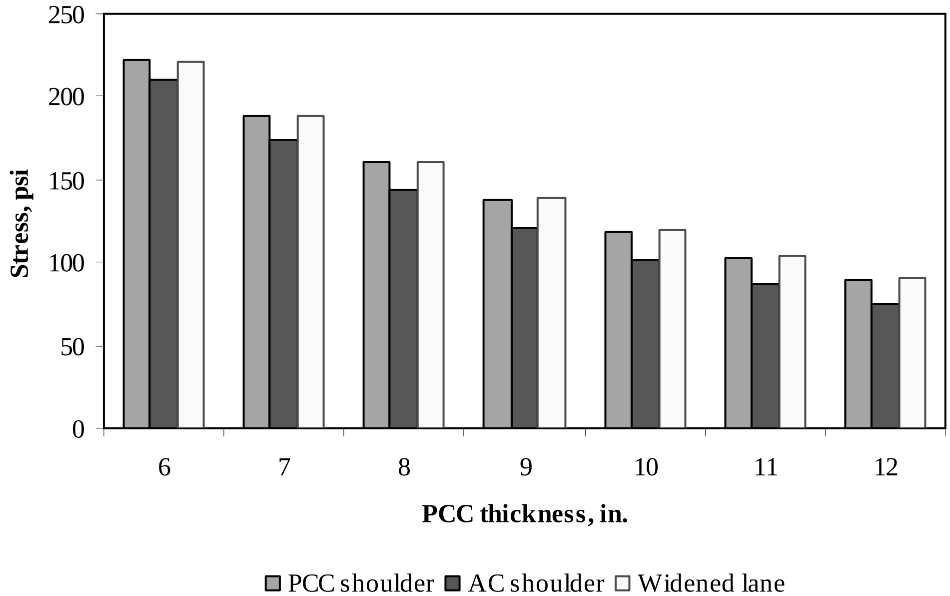


**Figure F-19-33: Impact of PCC thickness and lateral support condition on transverse stress at bottom of the Slab (177-in. joint spacing and $\alpha(\Delta T/D)$ of 0 in.$^{-1}$)**

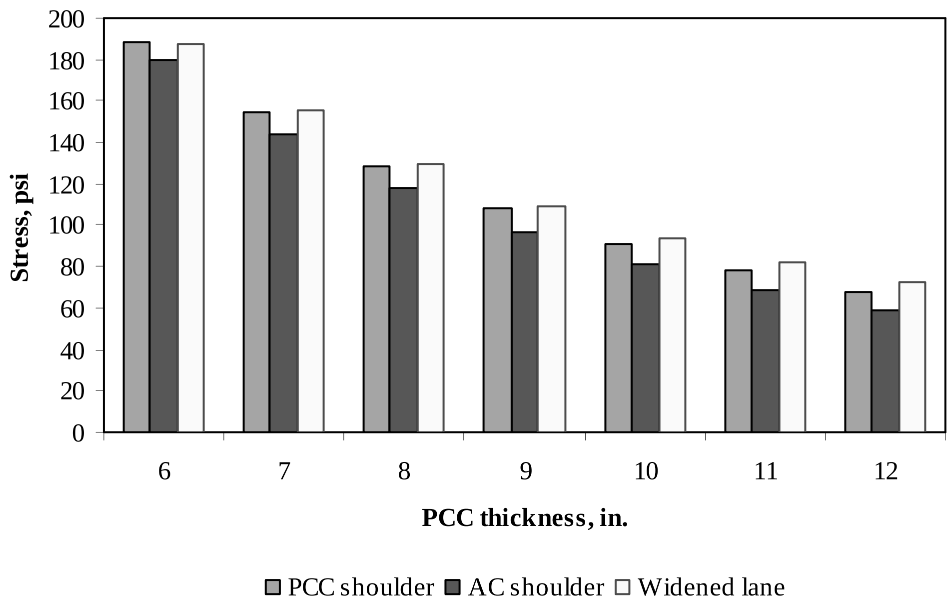


**Figure F-19-34: Impact of PCC thickness and lateral support condition on transverse stress at bottom of the Slab (315-in. joint spacing and $\alpha(\Delta T/D)$ of 0 in.$^{-1}$)**

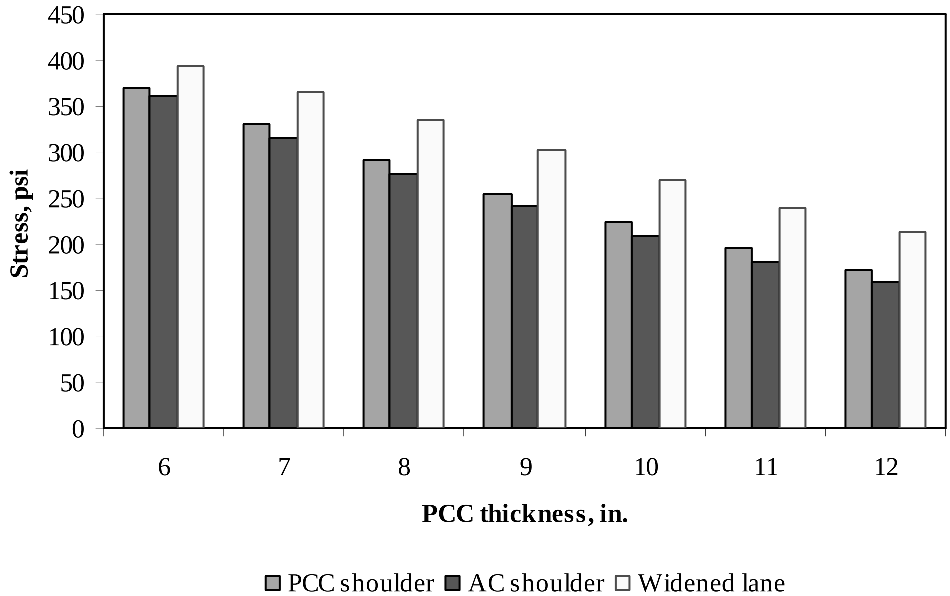


**Figure F-19-35: Impact of PCC thickness and lateral support condition on transverse stress at bottom of the Slab (177-in. joint spacing and $\alpha(\Delta T/D)$ of $20x10^{-6}$ $in.^{-1}$)**

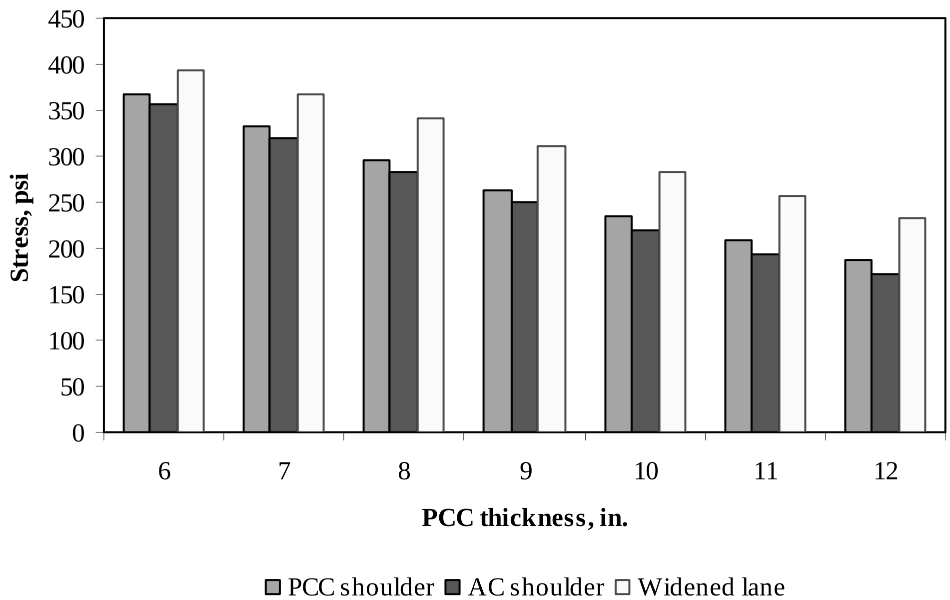


**Figure F-19-36: Impact of PCC thickness and lateral support condition on transverse stress at bottom of the Slab (315-in. joint spacing and $\alpha(\Delta T/D)$ of $20x10^{-6}$ $in.^{-1}$)**

Figures F-19-37 through F-19-42 illustrate the impact of base/subbase thickness and product α(ΔT/D) on stresses (10-in. PCC thickness, 100-psi/in. modulus of subgrade reaction and PCC shoulder)

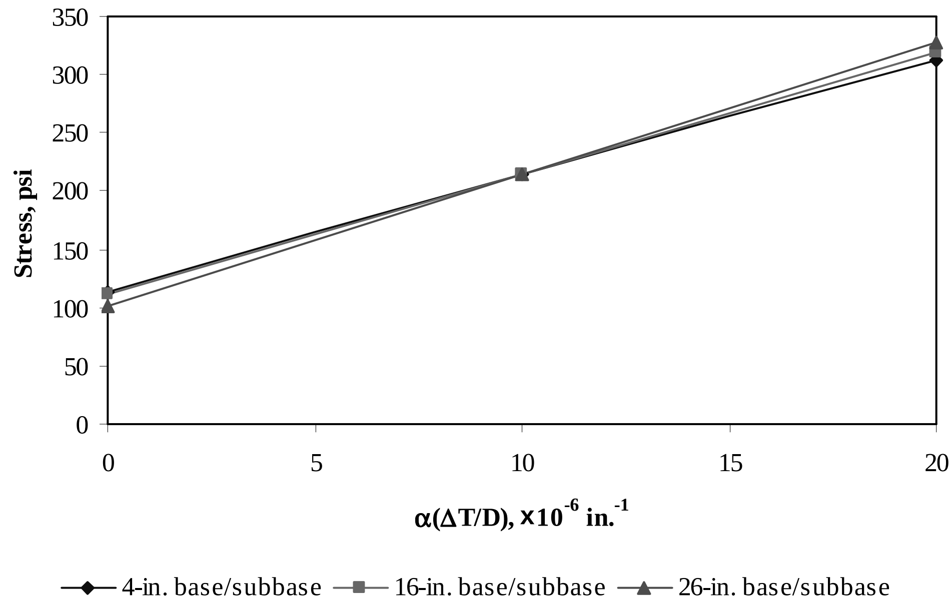


**Figure F-19-37: Impact of base/subbase thickness and product α(ΔT/D) on longitudinal stress at bottom of the slab (177-in. joint spacing)**

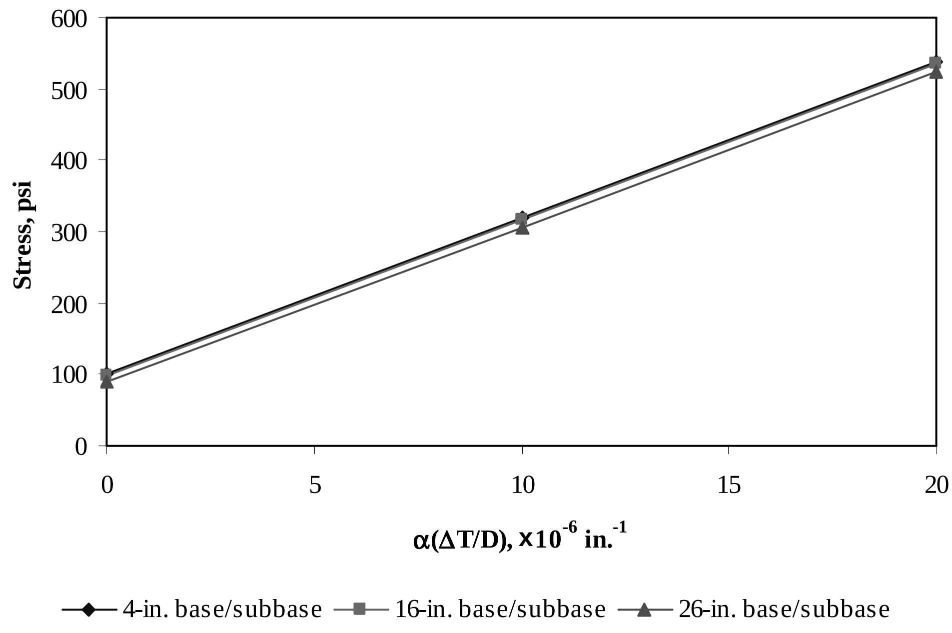


**Figure F-19-38: Impact of base/subbase thickness and product α(ΔT/D) on longitudinal stress at bottom of the slab (315-in. joint spacing)**

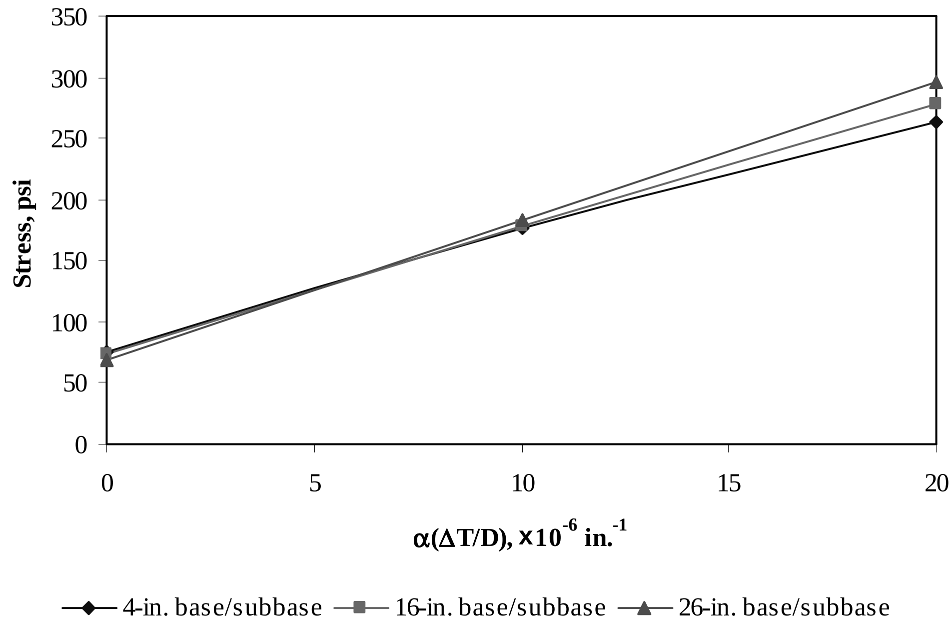


**Figure F-19-39: Impact of base/subbase thickness and product α(ΔT/D) on longitudinal stress at top of the slab (177-in. joint spacing)**

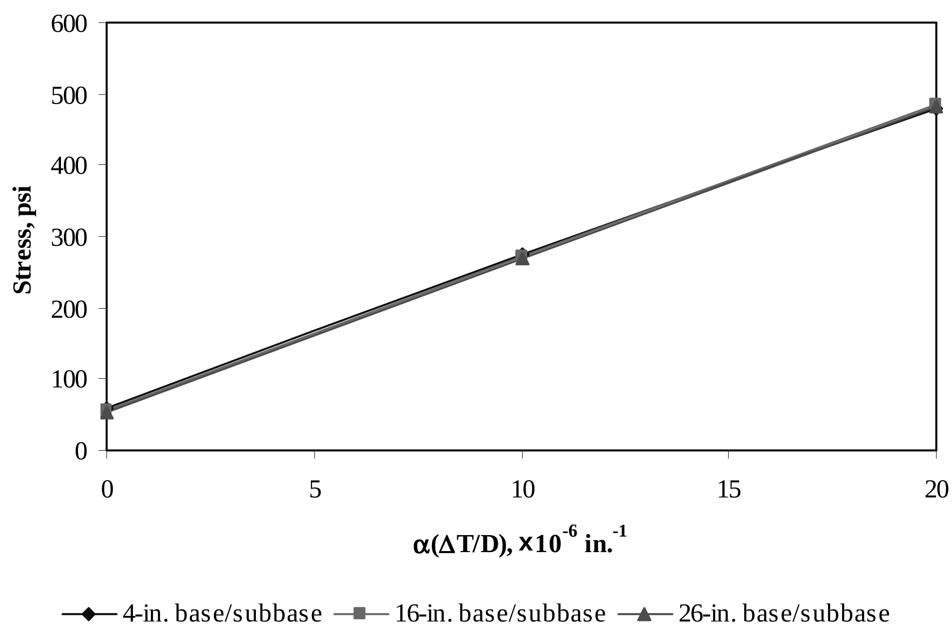


**Figure F-19-40: Impact of base/subbase thickness and product α(ΔT/D) on longitudinal stress at top of the slab (315-in. joint spacing)**

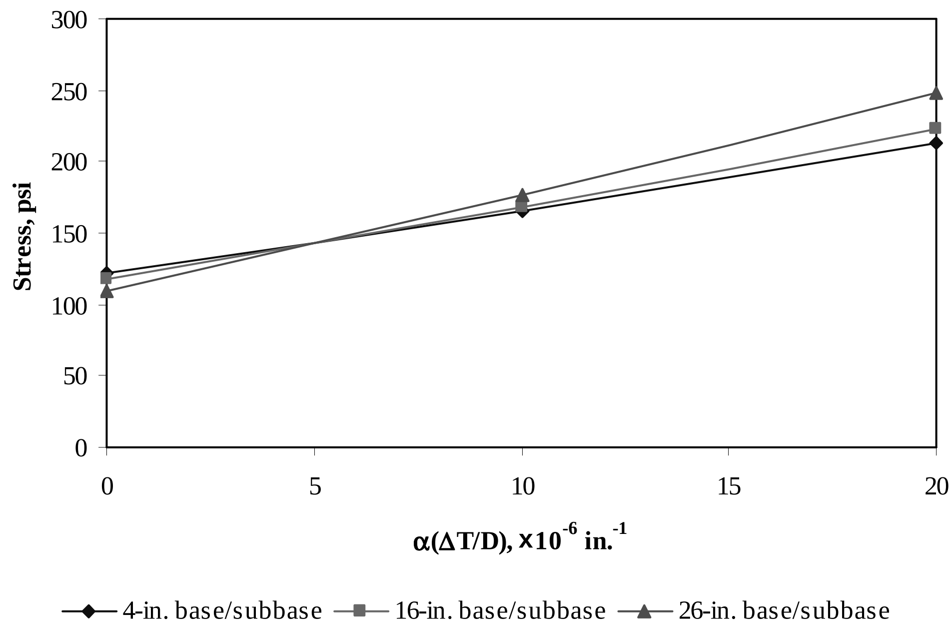


**Figure F-19-41: Impact of base/subbase thickness and product α(ΔT/D) on transverse stress at bottom of the slab (177-in. joint spacing)**

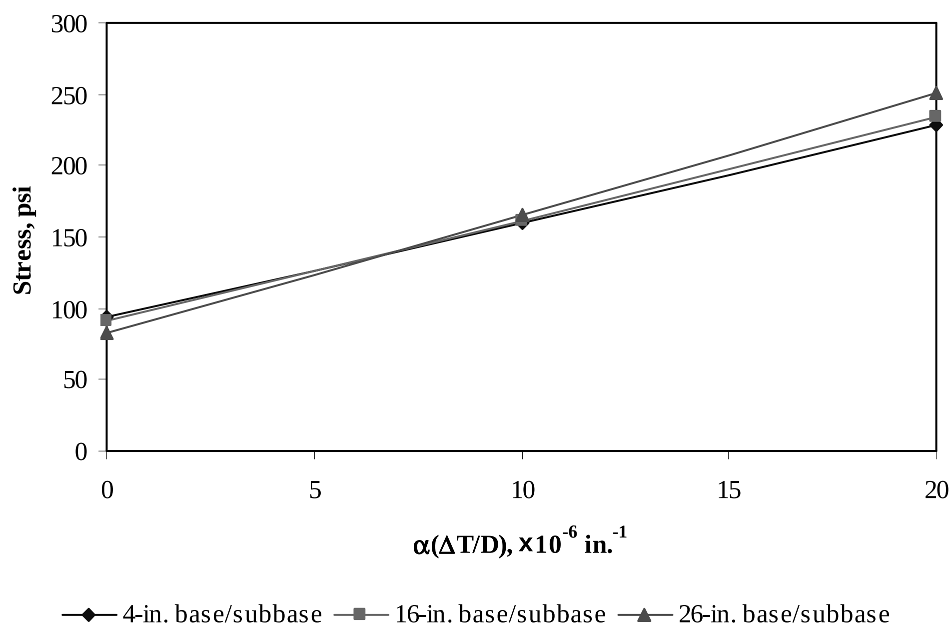


**Figure F-19-42: Impact of base/subbase thickness and product α(ΔT/D) on transverse stress at bottom of the slab (315-in. joint spacing)**

Figures F-19-43 through F-19-48 illustrate the impact of modulus of subgrade reaction and product α(ΔT/D) on stresses (10-in. PCC thickness, 16-in. base/subbase thickness and PCC shoulder)

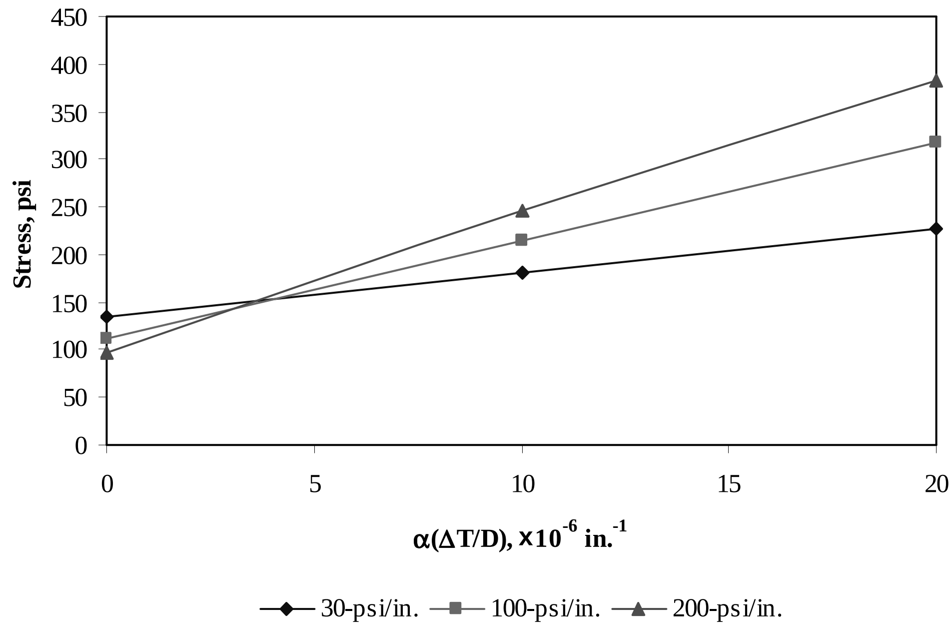


**Figure F-19-43: Impact of modulus of subgrade reaction and product α(ΔT/D) on longitudinal stress at bottom of the slab (177-in. joint spacing)**

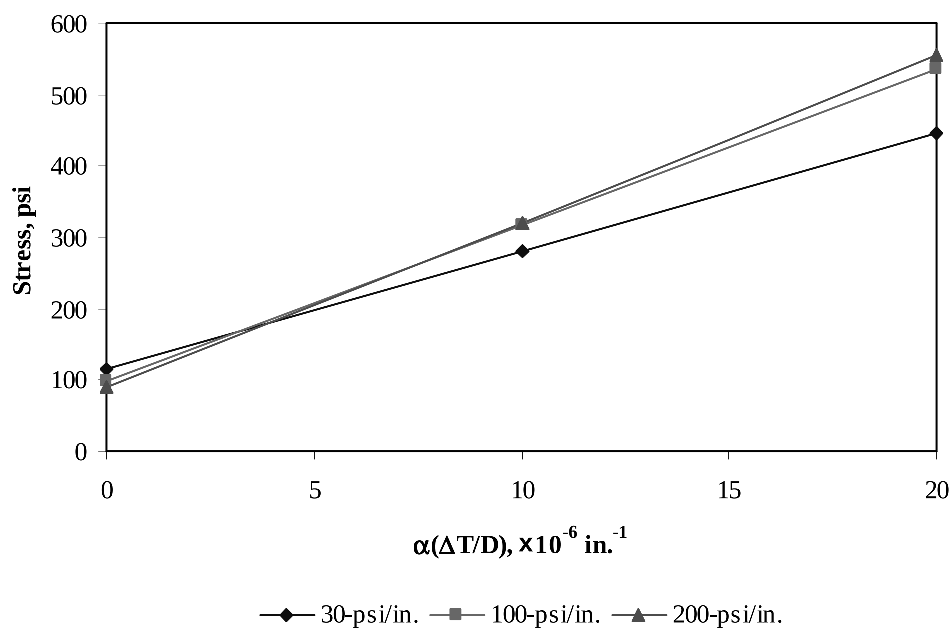


**Figure F-19-44: Impact of modulus of subgrade reaction and product α(ΔT/D) on longitudinal stress at bottom of the slab (315-in. joint spacing)**

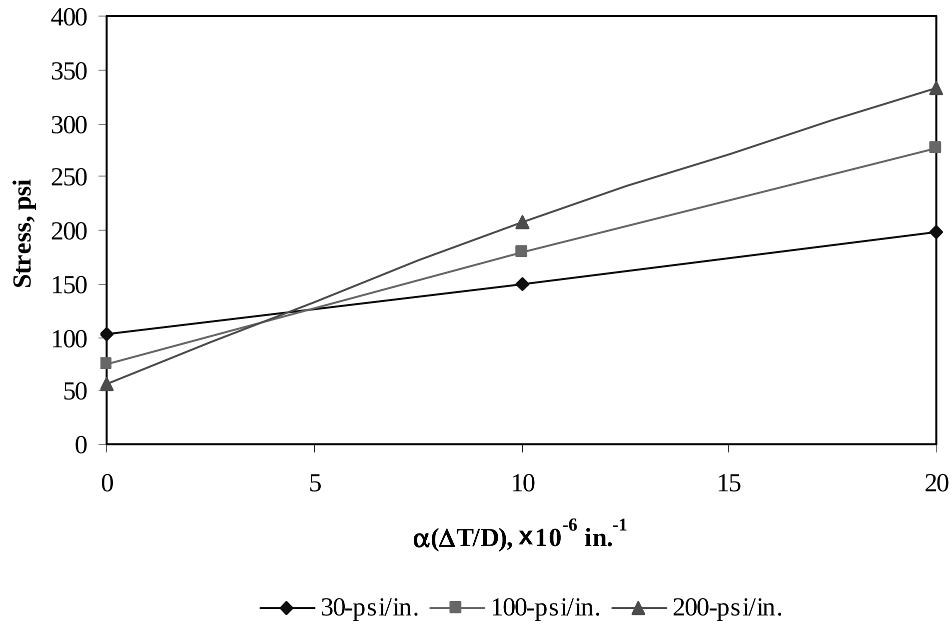


**Figure F-19-45: Impact of modulus of subgrade reaction and product α(ΔT/D) on longitudinal stress at top of the slab (177-in. joint spacing)**

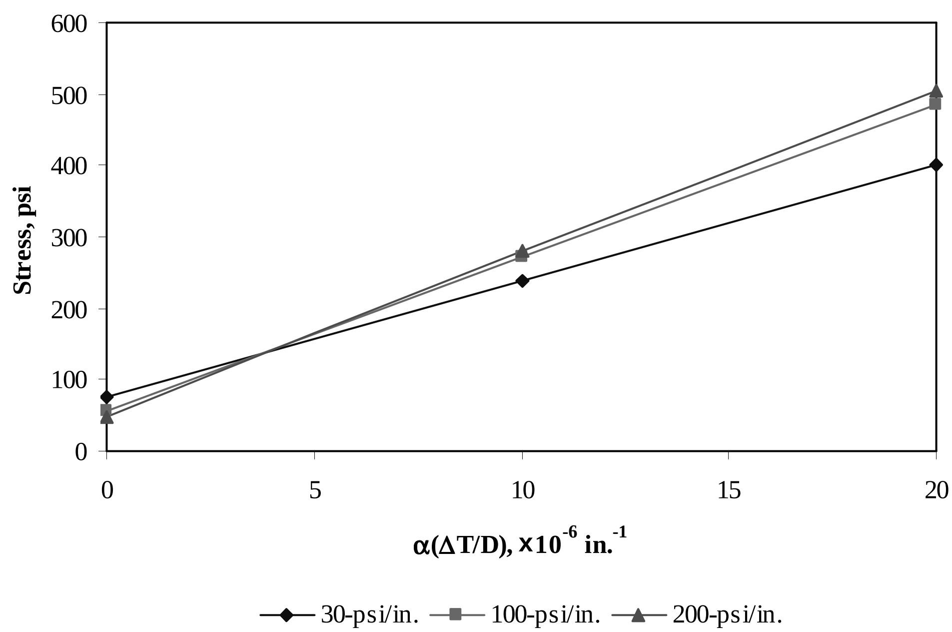


**Figure F-19-46: Impact of modulus of subgrade reaction and product α(ΔT/D) on longitudinal stress at top of the slab (315-in. joint spacing)**

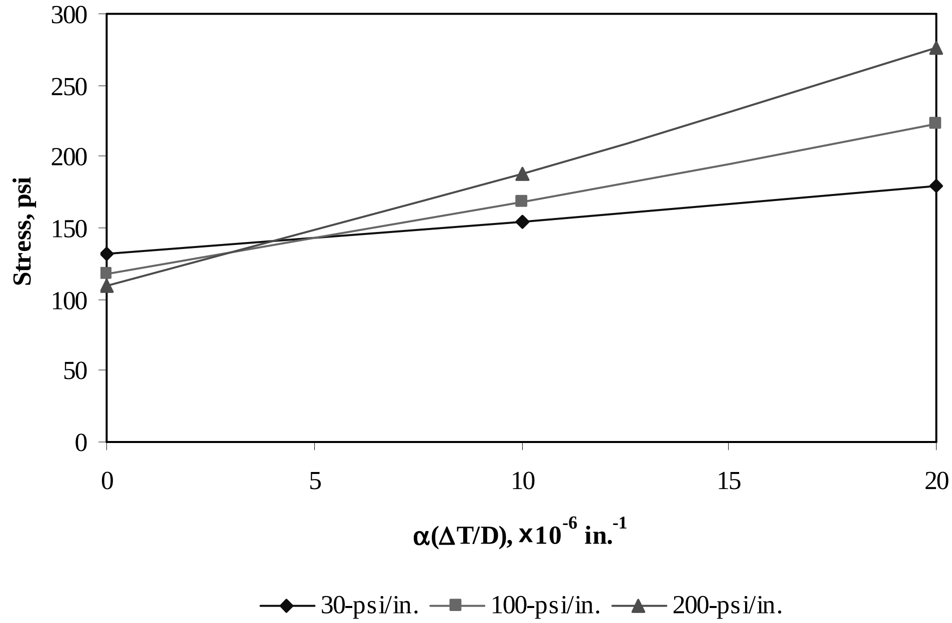


**Figure F-19-47: Impact of modulus of subgrade reaction and product α(ΔT/D) on transverse stress at bottom of the slab (177-in. joint spacing)**

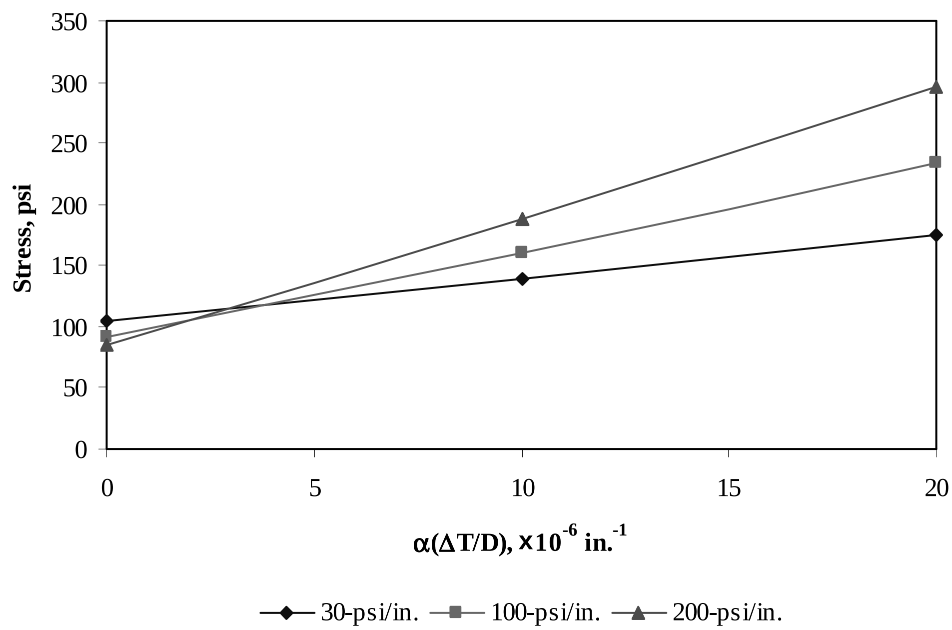


**Figure F-19-48: Impact of modulus of subgrade reaction and product α(ΔT/D) on transverse stress at bottom of the slab (315-in. joint spacing)**

Figures F-19-49 through F-19-51 illustrate the impact of joint spacing and product $\alpha(\Delta T/D)$ on stresses (10-in. PCC thickness, 16-in. base/subbase thickness, 100-psi/in. modulus of subgrade reaction and PCC shoulder)

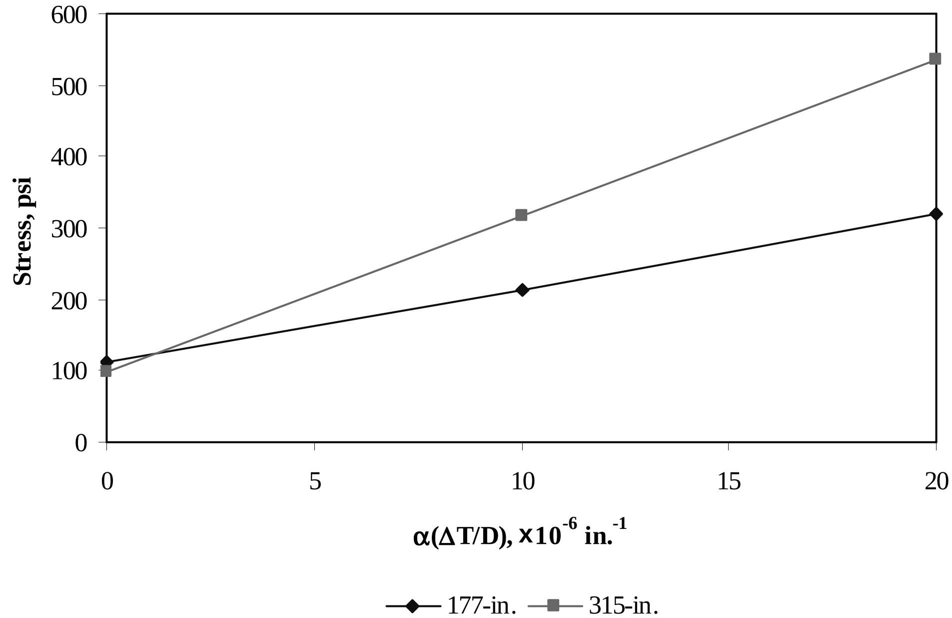


**Figure F-19-49: Impact of joint spacing and product $\alpha(\Delta T/D)$ on longitudinal stress at bottom of the slab**

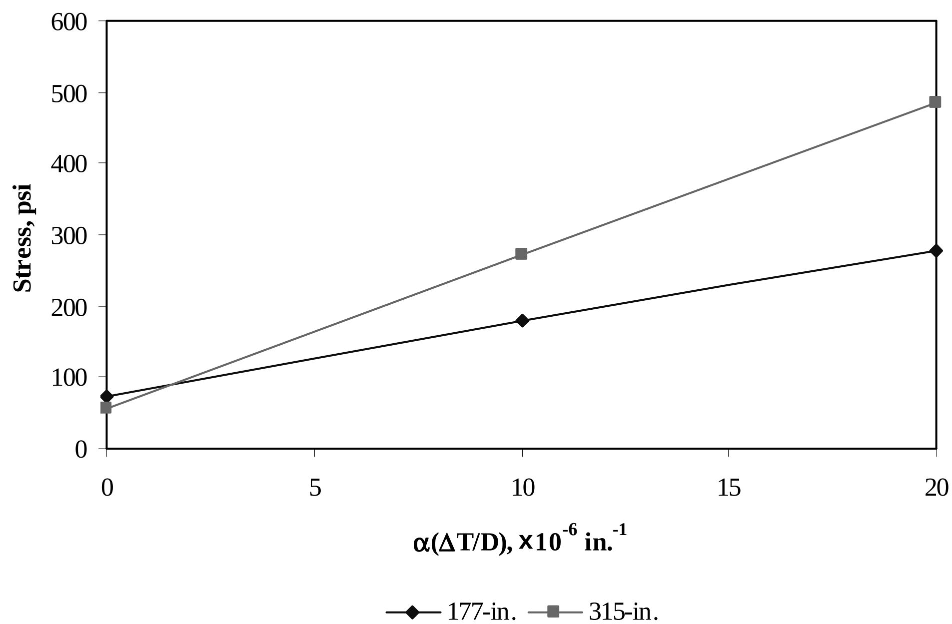


**Figure F-19-50: Impact of joint spacing and product $\alpha(\Delta T/D)$ on longitudinal stress at top of the slab**

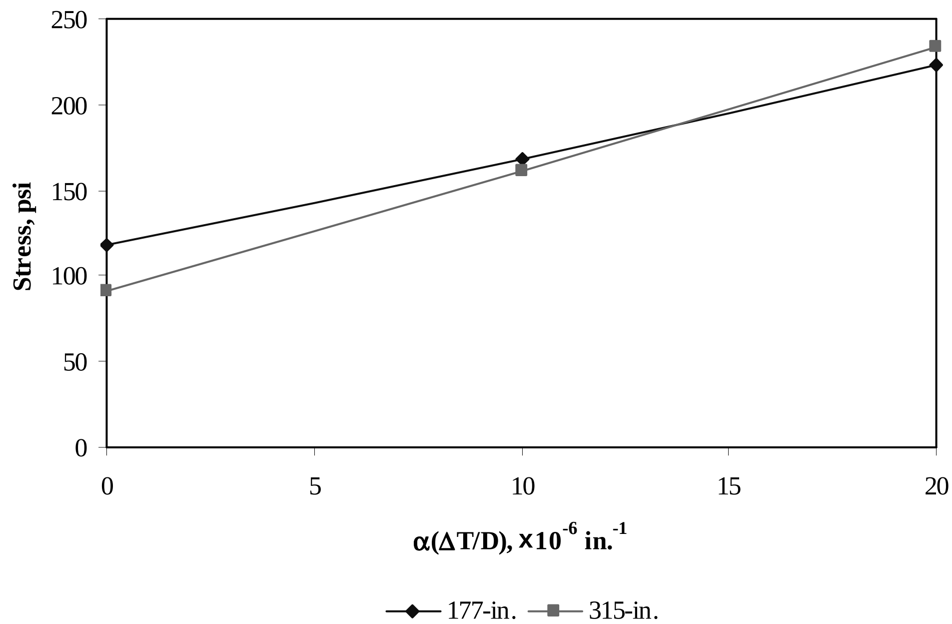


**Figure F-19-51: Impact of joint spacing and product α(ΔT/D) on transverse stress at bottom of the slab**

# Appendix G

# Impact of Lateral Placement on Different Lateral Support Conditions

**Table G-1: Experimental matrix for lateral placement study**

| Stress type | $\alpha(\Delta T/D)$, $10^{-6}$ in.$^{-1}$ | 177-in. joint spacing | | | 315-in. joint spacing | | |
|---|---|---|---|---|---|---|---|
| | | 12-ft wide lane with tied PCC shoulder | 12-ft wide lane with untied AC shoulder | 14-ft wide lane with untied AC shoulder | 12-ft wide lane with tied PCC shoulder | 12-ft wide lane with untied AC shoulder | 14-ft wide lane with untied AC shoulder |
| Longitudinal stress at the bottom of the PCC slab | 0 | ✔ | ✔ | ✔ | ✔ | ✔ | ✔ |
| | 10 | ✔ | ✔ | ✔ | ✔ | ✔ | ✔ |
| | 20 | ✔ | ✔ | ✔ | ✔ | ✔ | ✔ |
| Longitudinal stress at the top of the PCC slab | 0 | ✔ | ✔ | ✔ | ✔ | ✔ | ✔ |
| | -10 | ✔ | ✔ | ✔ | ✔ | ✔ | ✔ |
| | -20 | ✔ | ✔ | ✔ | ✔ | ✔ | ✔ |

Remarks:

1) Each condition contains seven lateral placements: 0, 6, 12, 18, 24, 36, and 48 in.

2) Each condition contains three types of axles: single, tandem, and tridem.

3) Load positions are edge and corner loading conditions for analysis of stress at the bottom and the top of the PCC slab, respectively.

4) All the analyses are conducted for 10-in. PCC slab, 16-in. base/subbase, 100-psi/in. subgrade.

Figures G-1 through G-3 are illustrations of relationship between lateral placement and maximum longitudinal stress at the bottom of the PCC slab for 177-in. joint spacing and $\alpha(\Delta T/D)$ of $0x10^{-6}$ in.$^{-1}$ for various lateral support conditions

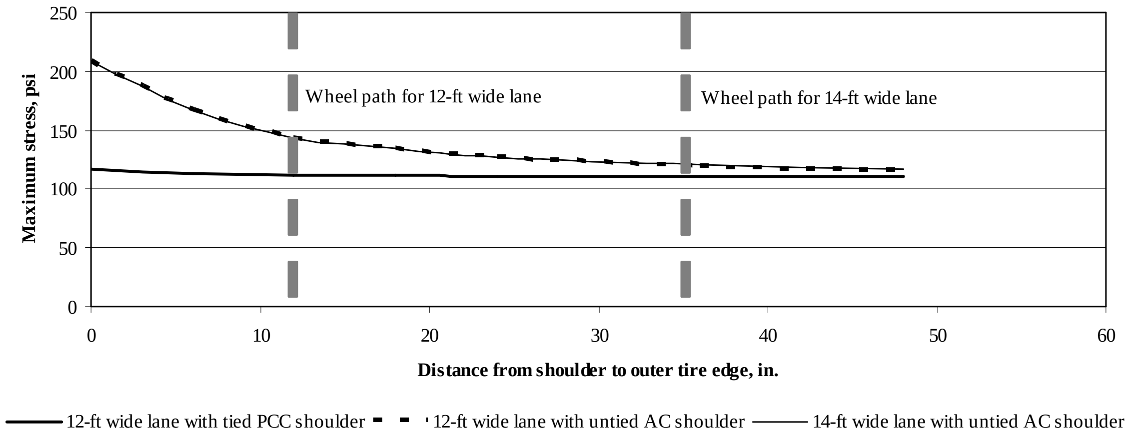


**Figure G-1: Illustration for single axle**

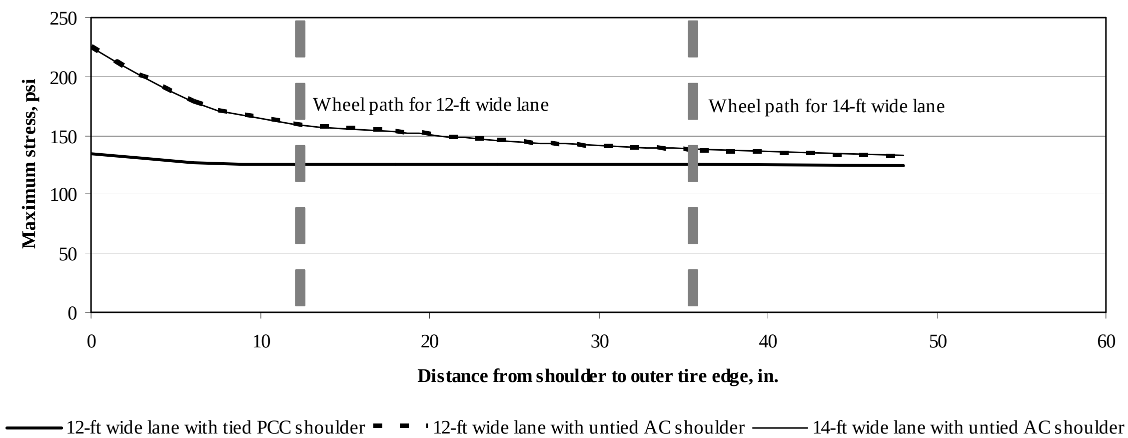


**Figure G-2: Illustration for tandem axle**

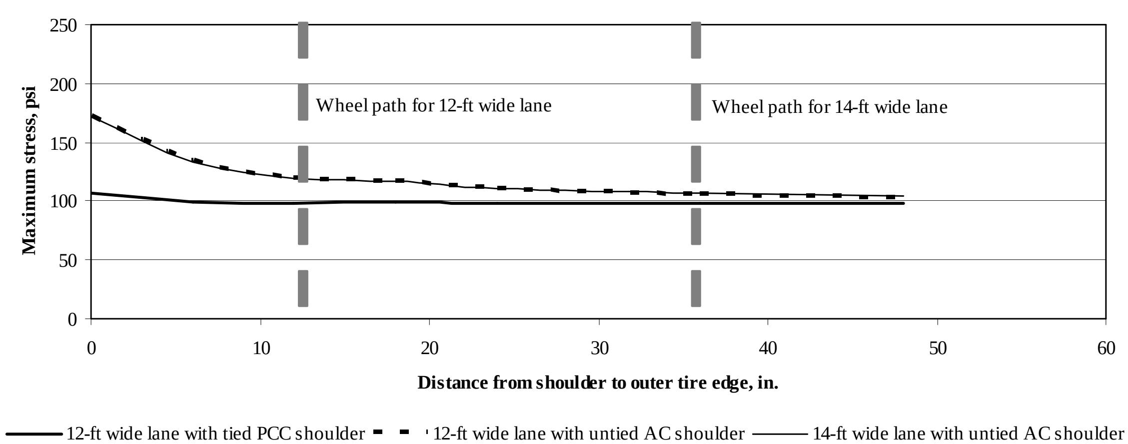


**Figure G-3: Illustration for tridem axle**

Figures G-4 through G-6 are illustrations of relationship between lateral placement and maximum longitudinal stress at the bottom of the PCC slab for 315-in. joint spacing and $\alpha(\Delta T/D)$ of $0x10^{-6}$ in.$^{-1}$ for various lateral support conditions

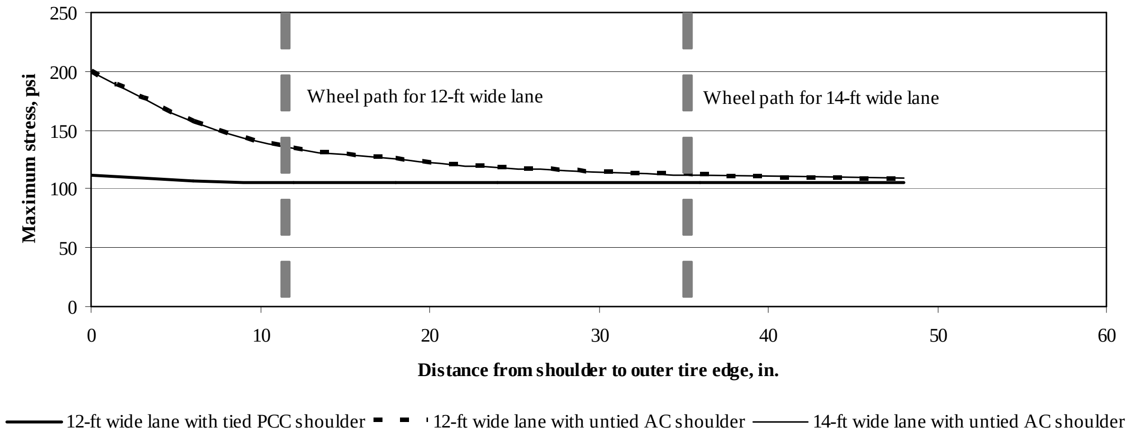


**Figure G-4: Illustration for single axle**

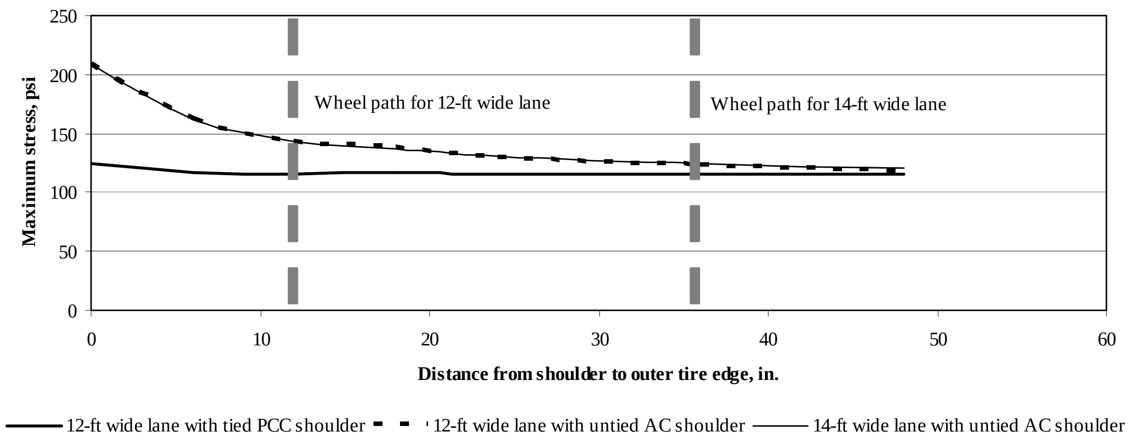


**Figure G-5: Illustration for tandem axle**

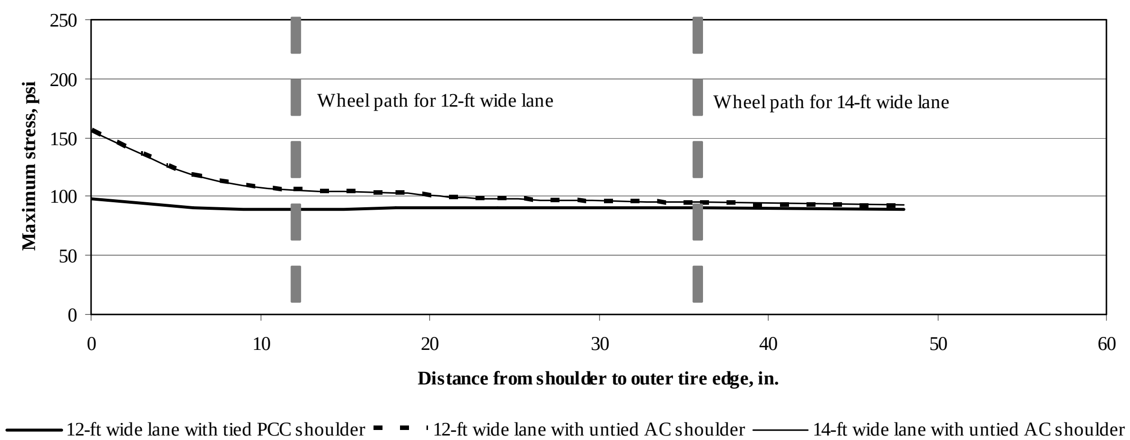


**Figure G-6: Illustration for tridem axle**

Figures G-7 through G-9 are illustrations of relationship between lateral placement and maximum longitudinal stress at the bottom of the PCC slab for 177-in. joint spacing and $\alpha(\Delta T/D)$ of $10x10^{-6}$ in.$^{-1}$ for various lateral support conditions

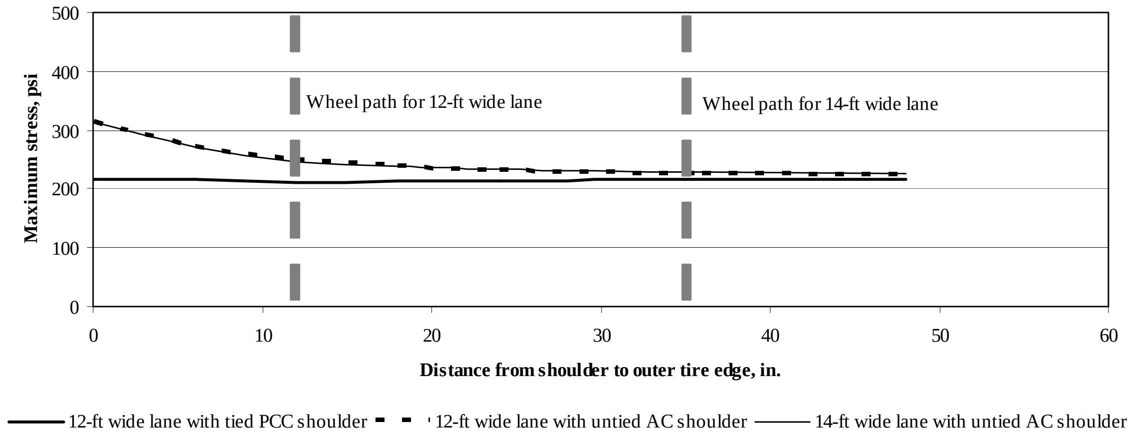


**Figure G-7: Illustration for single axle**

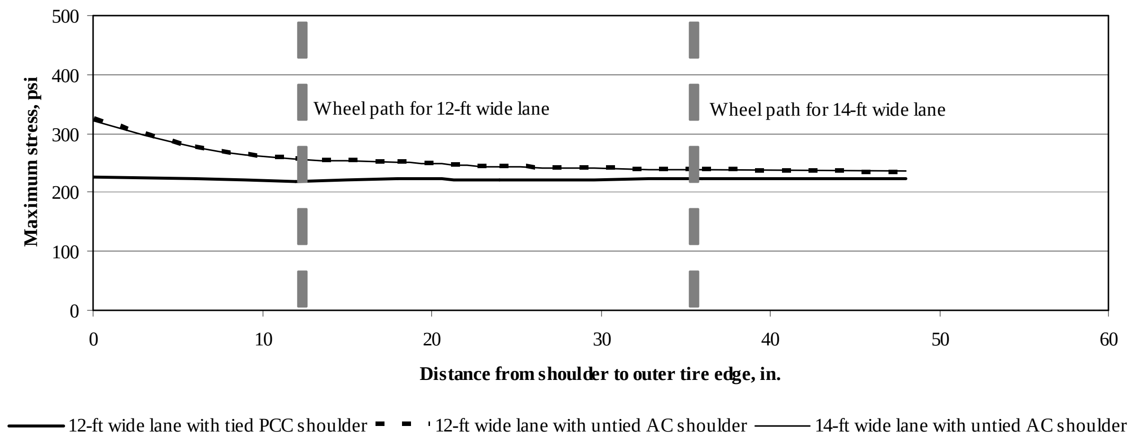


**Figure G-8: Illustration for tandem axle**

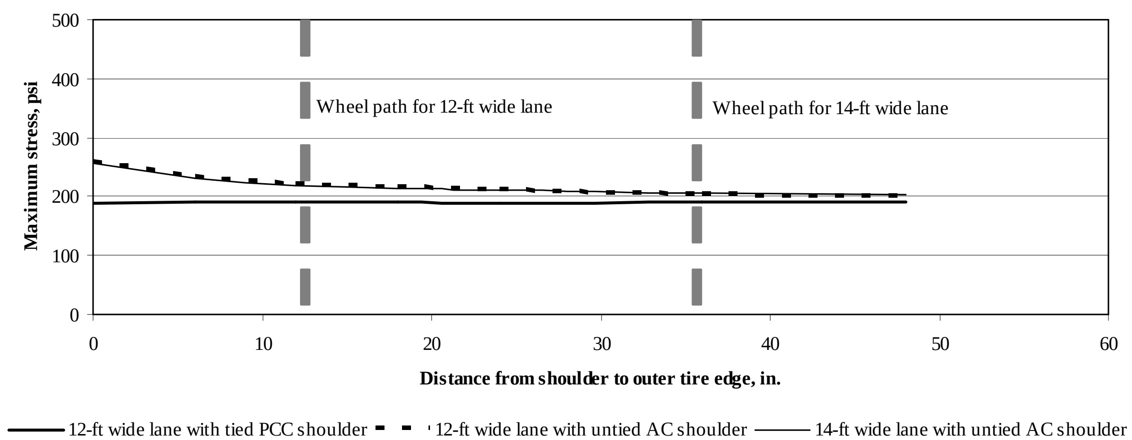


**Figure G-9: Illustration for tridem axle**

Figures G-10 through G-12 are illustrations of relationship between lateral placement and maximum longitudinal stress at the bottom of the PCC slab for 315-in. joint spacing and $\alpha(\Delta T/D)$ of $10x10^{-6}$ in.$^{-1}$ for various lateral support conditions

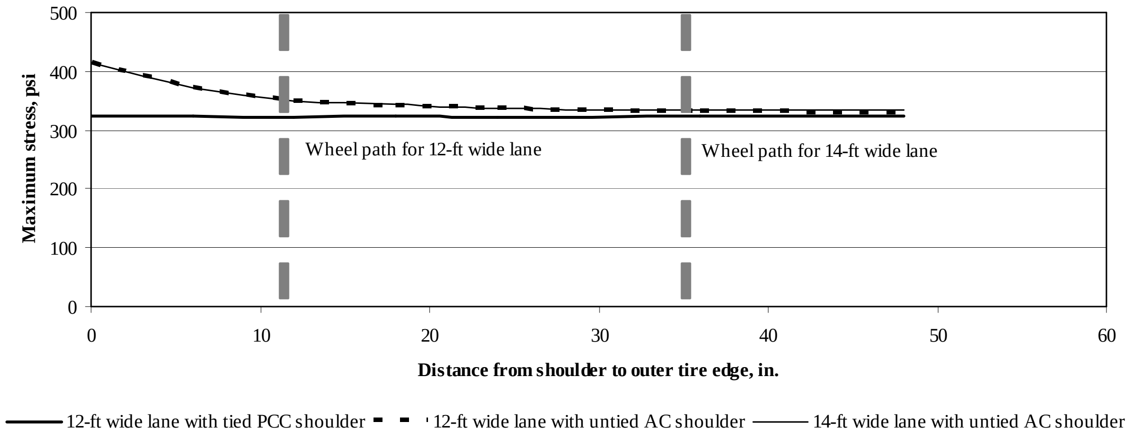


**Figure G-10: Illustration for single axle**

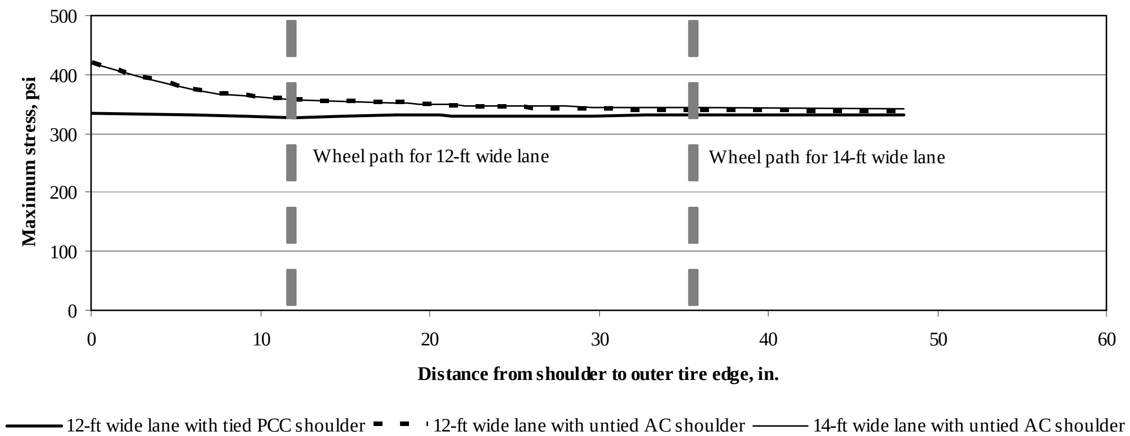


**Figure G-11: Illustration for tandem axle**

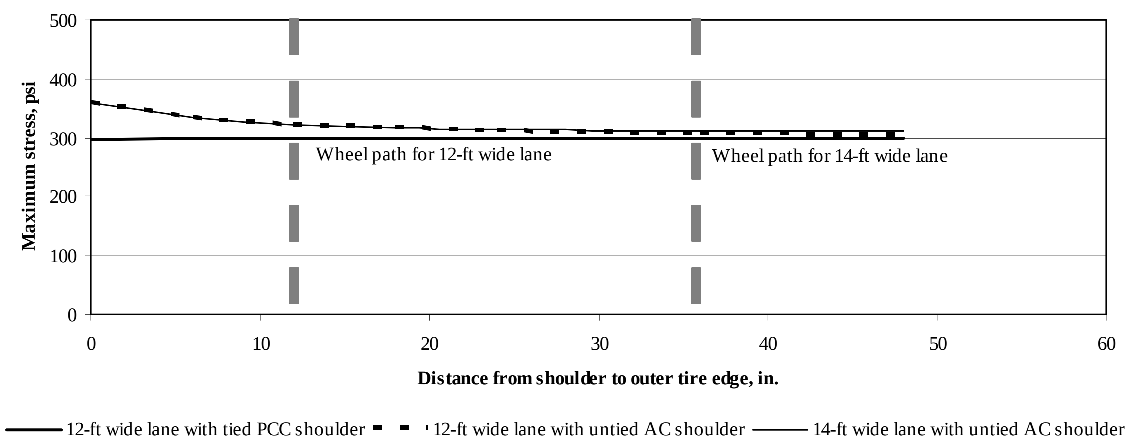


**Figure G-12: Illustration for tridem axle**

Figures G-13 through G-15 are illustrations of relationship between lateral placement and maximum longitudinal stress at the bottom of the PCC slab for 177-in. joint spacing and $\alpha(\Delta T/D)$ of $20 \times 10^{-6}$ in.$^{-1}$ for various lateral support conditions

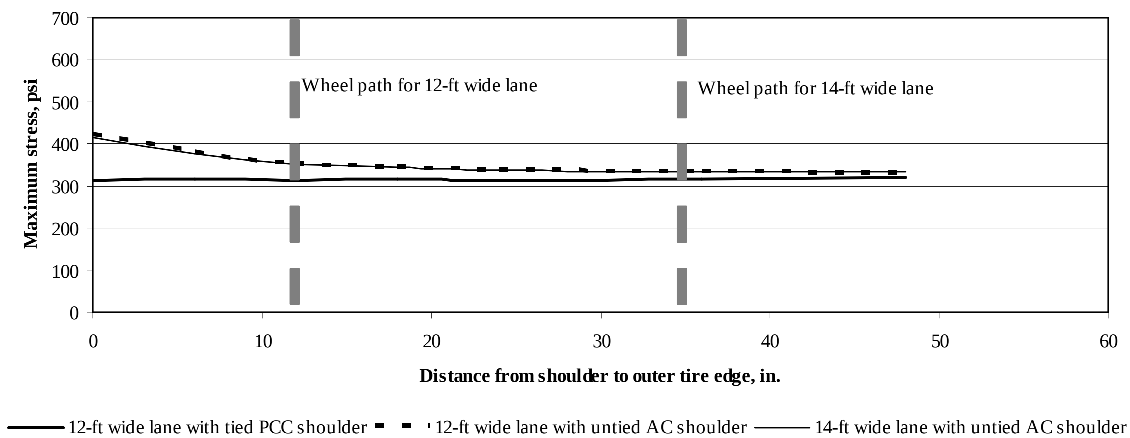


**Figure G-13: Illustration for single axle**

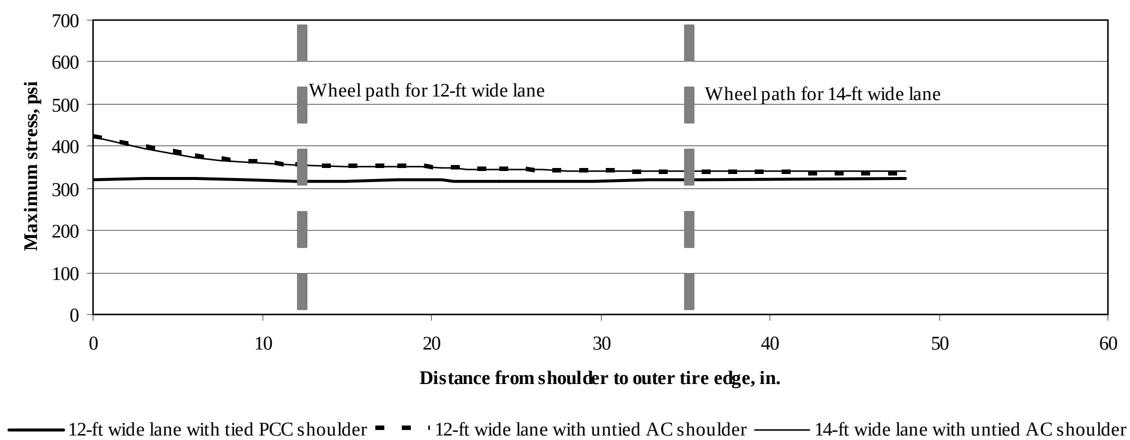


**Figure G-14: Illustration for tandem axle**

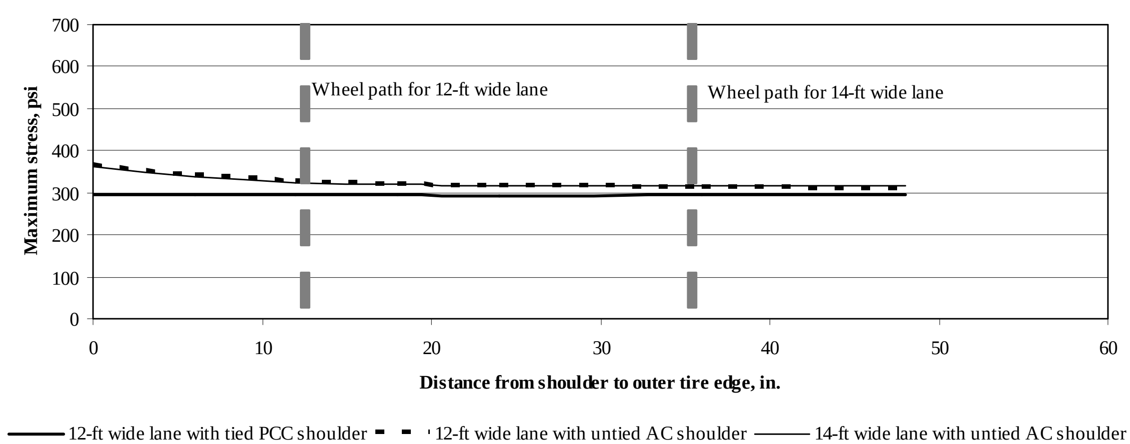


**Figure G-15: Illustration for tridem axle**

Figures G-16 through G-18 are illustrations of relationship between lateral placement and maximum longitudinal stress at the bottom of the PCC slab for 315-in. joint spacing and $\alpha(\Delta T/D)$ of $20 \times 10^{-6}$ in.$^{-1}$ for various lateral support conditions

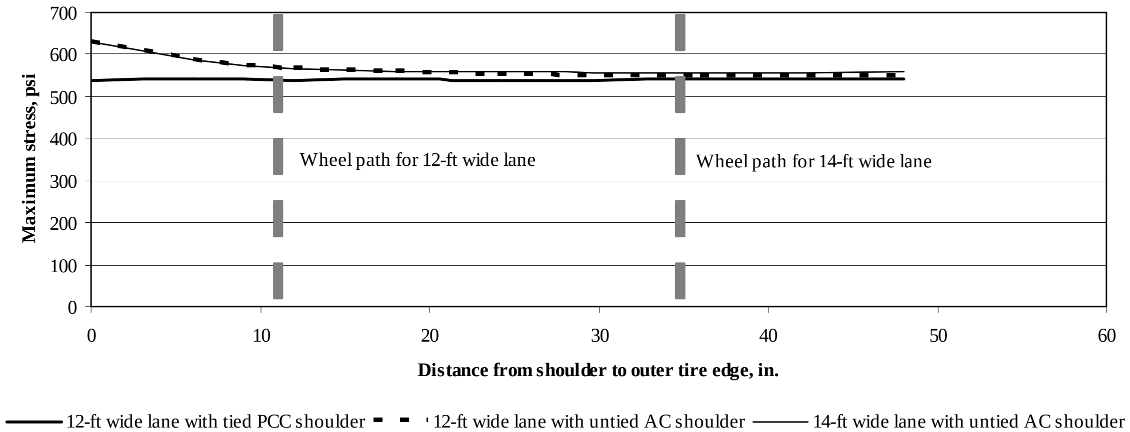


**Figure G-16: Illustration for single axle**

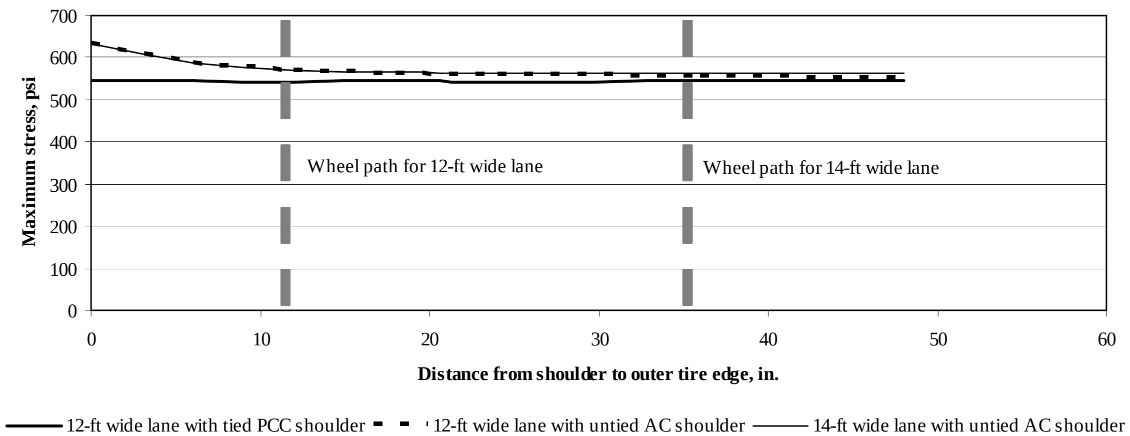


**Figure G-17: Illustration for tandem axle**

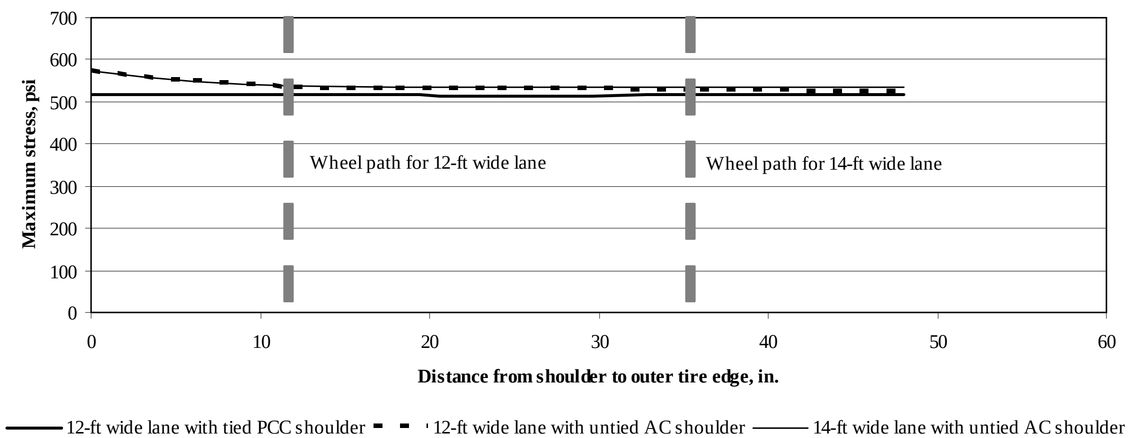


**Figure G-18: Illustration for tridem axle**

Figures G-19 through G-21 are illustrations of relationship between lateral placement and maximum longitudinal stress at the top of the PCC slab for 177-in. joint spacing and $\alpha(\Delta T/D)$ of $0x10^{-6}$ in.$^{-1}$ for various lateral support conditions

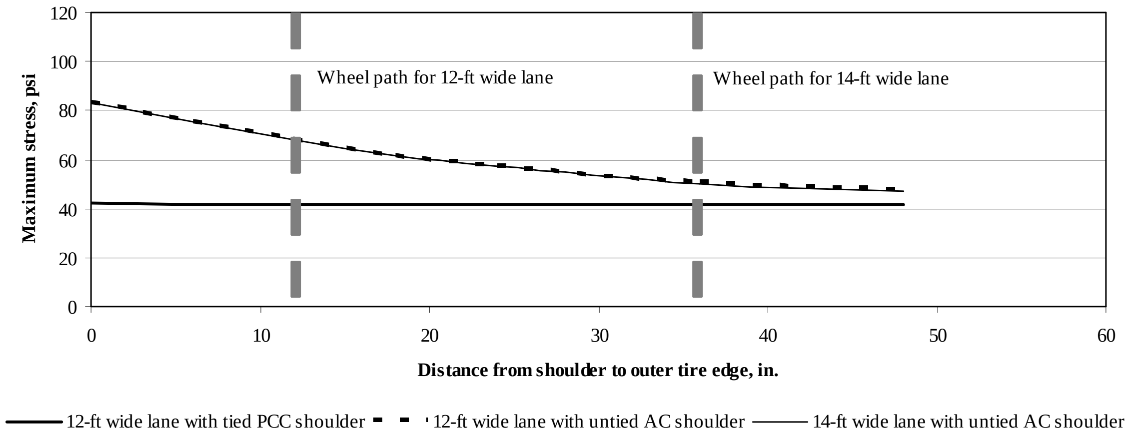


**Figure G-19: Illustration for single axle**

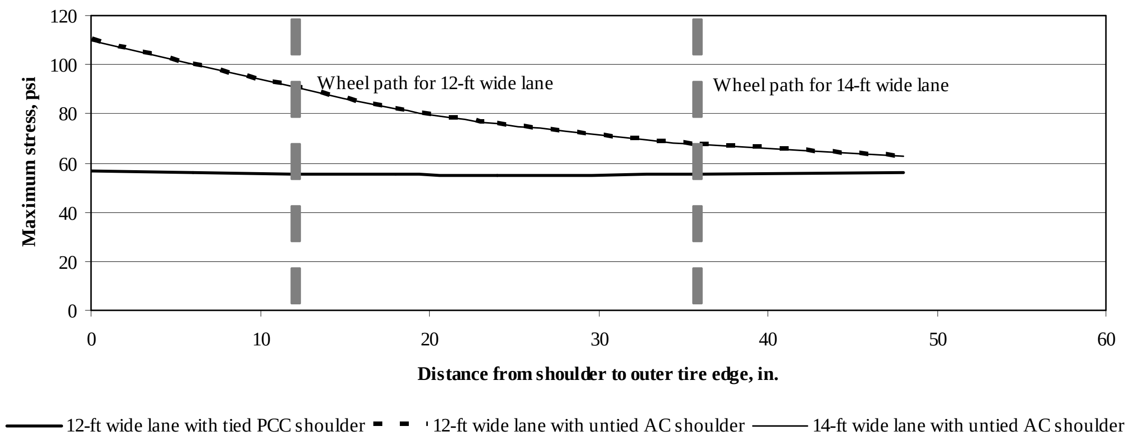


**Figure G-20: Illustration for tandem axle**

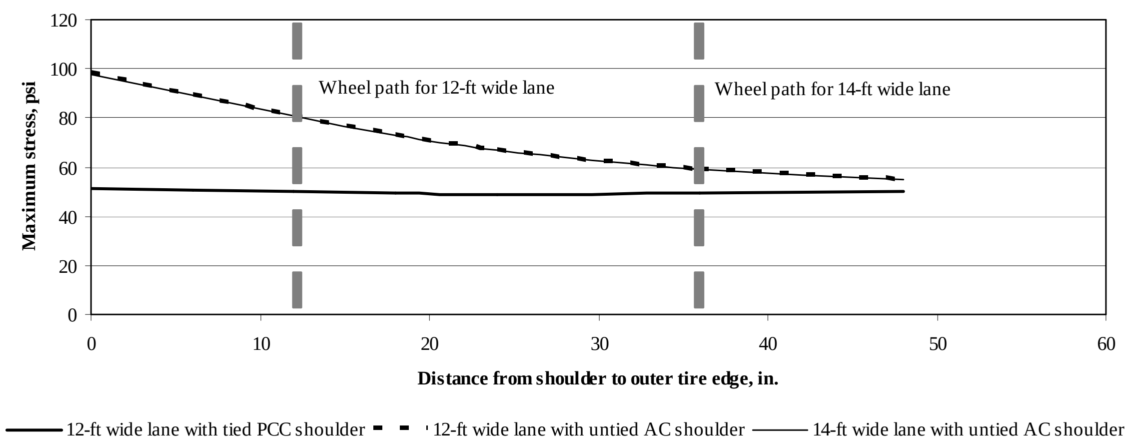


**Figure G-21: Illustration for tridem axle**

Figures G-22 through G-24 are illustrations of relationship between lateral placement and maximum longitudinal stress at the top of the PCC slab for 315-in. joint spacing and $\alpha(\Delta T/D)$ of $0x10^{-6}$ in.$^{-1}$ for various lateral support conditions

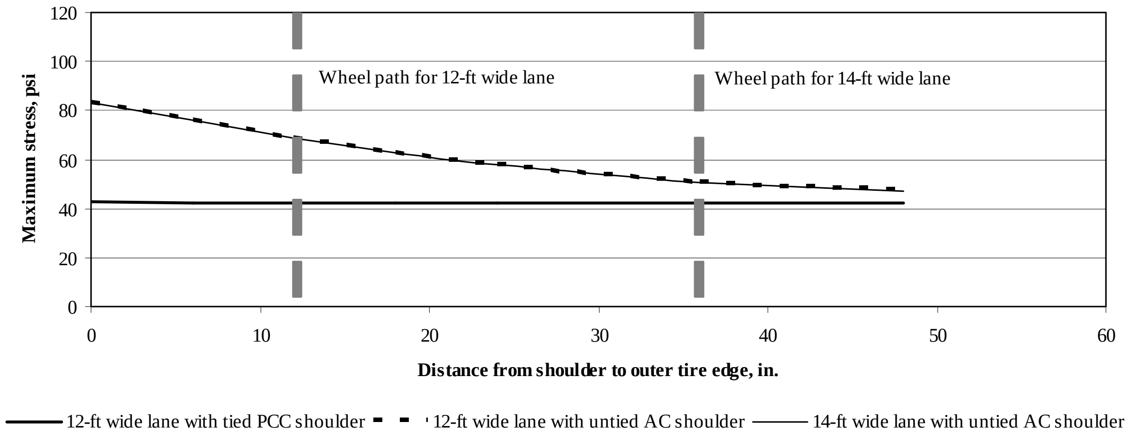


**Figure G-22: Illustration for single axle**

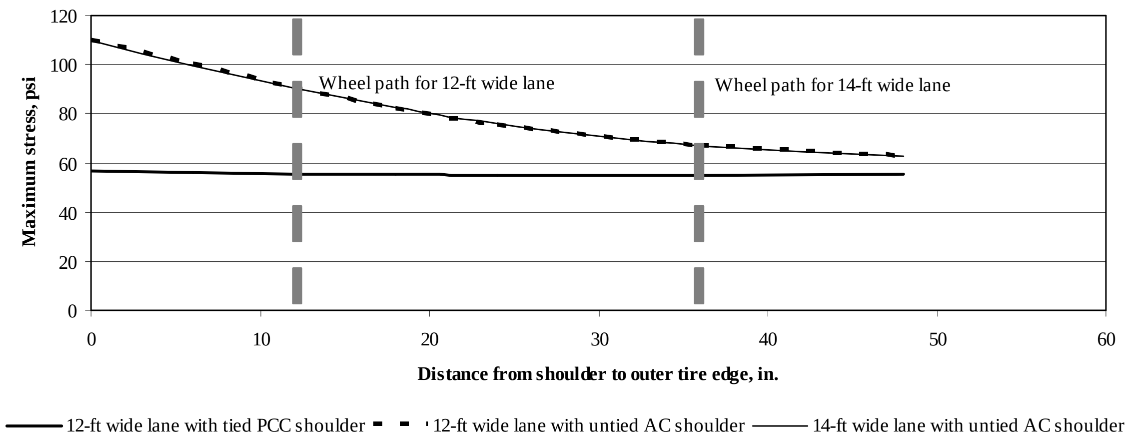


**Figure G-23: Illustration for tandem axle**

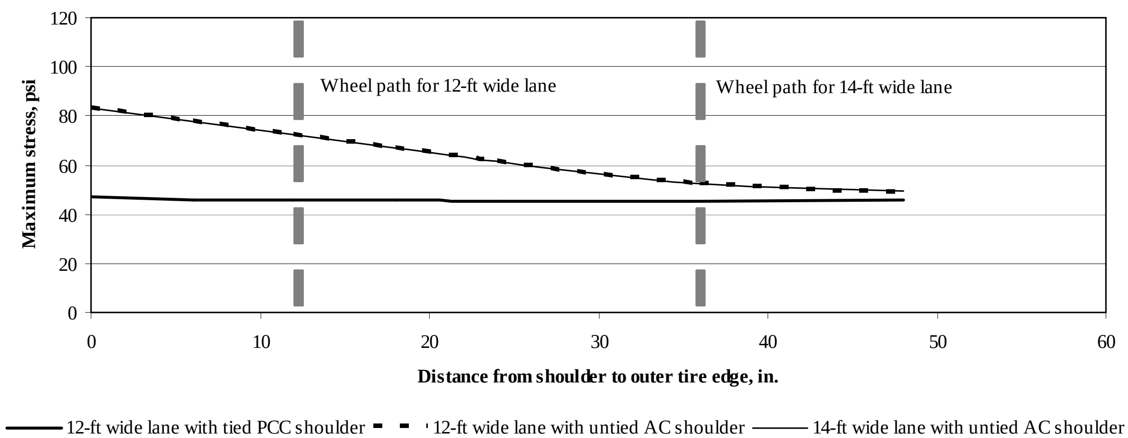


**Figure G-24: Illustration for tridem axle**

Figures G-25 through G-27 are illustrations of relationship between lateral placement and maximum longitudinal stress at the top of the PCC slab for 177-in. joint spacing and $\alpha(\Delta T/D)$ of $-10x10^{-6}$ in.$^{-1}$ for various lateral support conditions

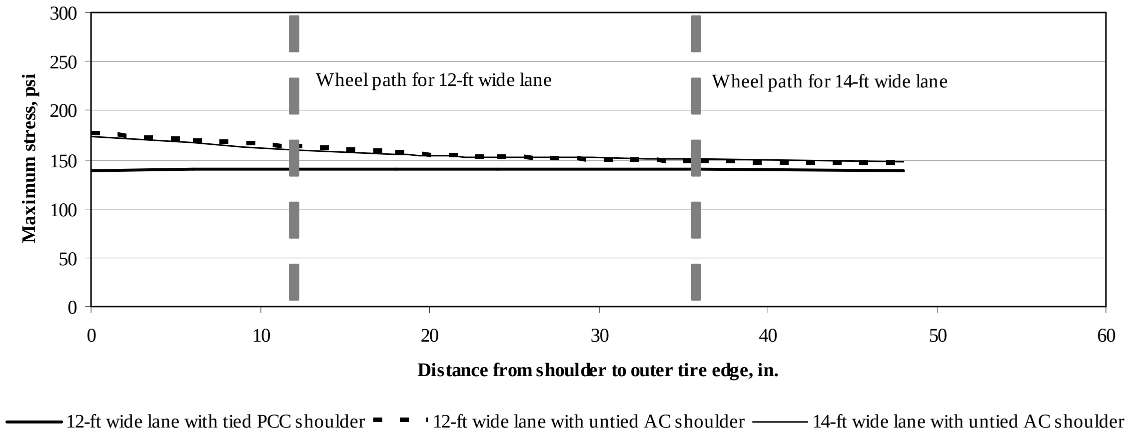


**Figure G-25: Illustration for single axle**

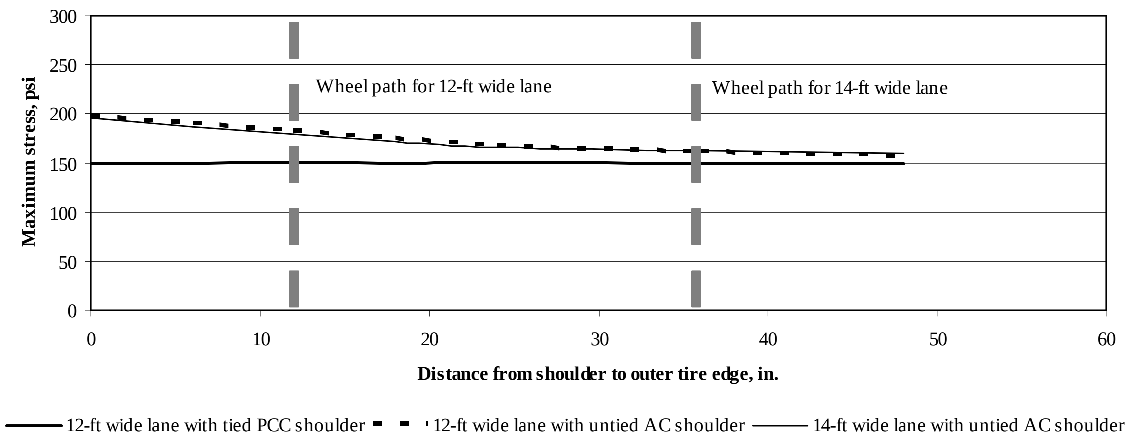


**Figure G-26: Illustration for tandem axle**

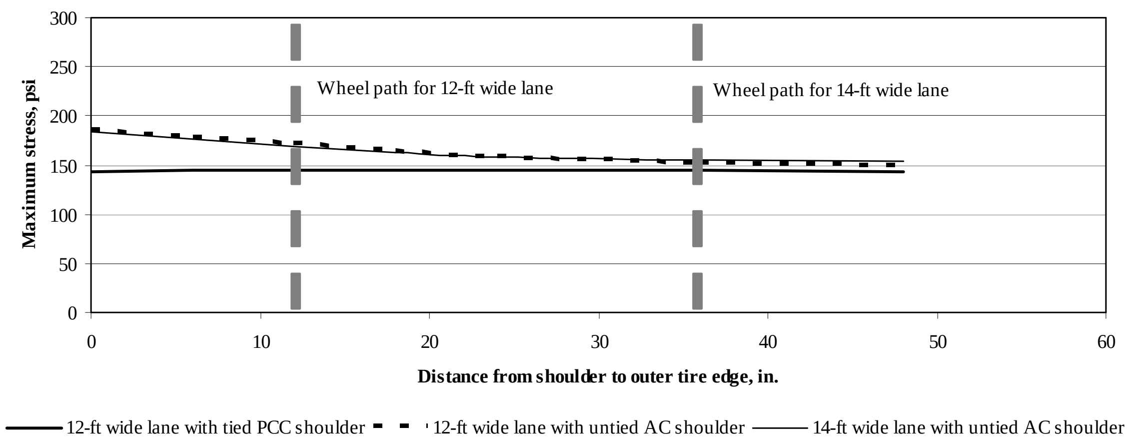


**Figure G-27: Illustration for tridem axle**

Figures G-28 through G-30 are illustrations of relationship between lateral placement and maximum longitudinal stress at the top of the PCC slab for 315-in. joint spacing and $\alpha(\Delta T/D)$ of $-10\times10^{-6}$ in.$^{-1}$ for various lateral support conditions

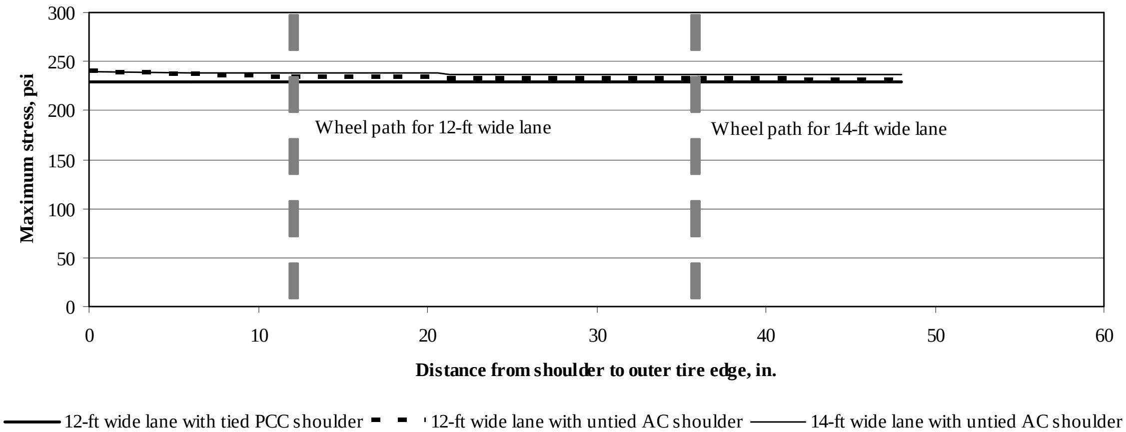


**Figure G-28: Illustration for single axle**

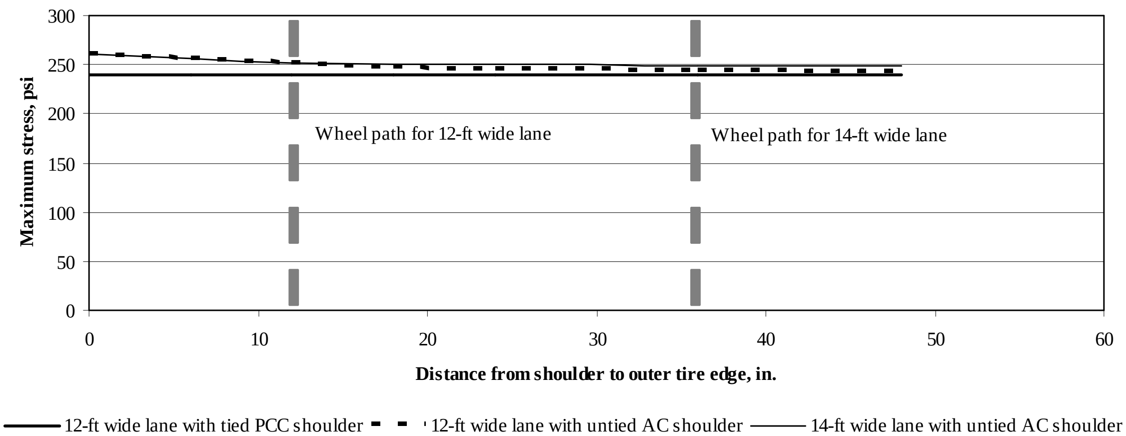


**Figure G-29: Illustration for tandem axle**

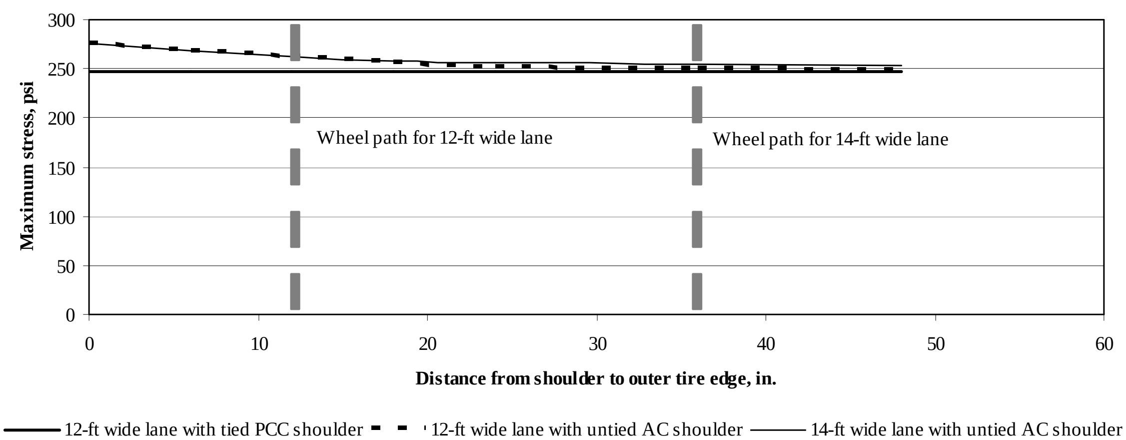


**Figure G-30: Illustration for tridem axle**

Figures G-31 through G-33 are illustrations of relationship between lateral placement and maximum longitudinal stress at the top of the PCC slab for 177-in. joint spacing and $\alpha(\Delta T/D)$ of $-20x10^{-6}$ in.$^{-1}$ for various lateral support conditions

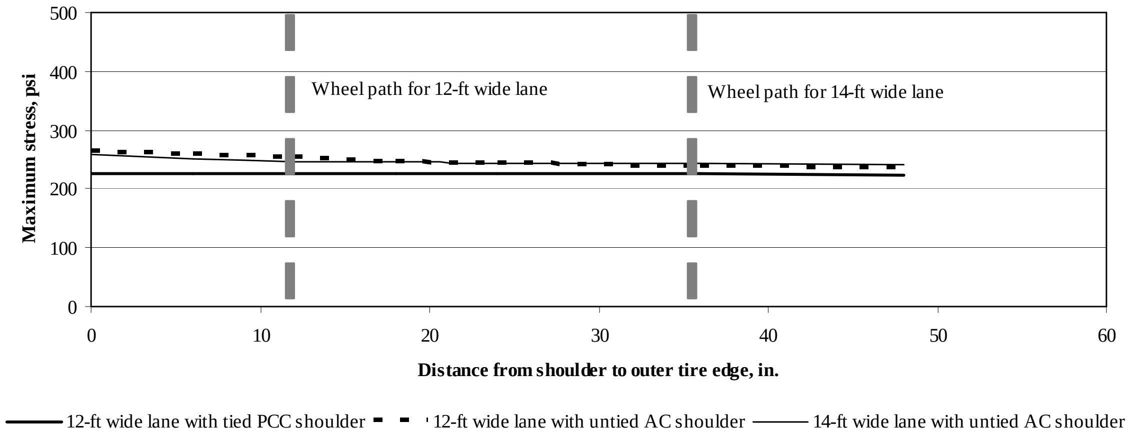


**Figure G-31: Illustration for single axle**

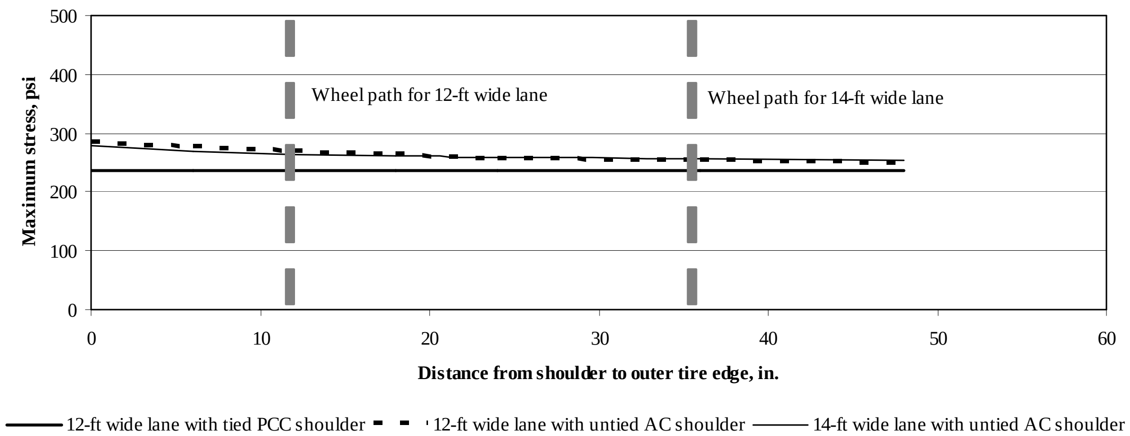


**Figure G-32: Illustration for tandem axle**

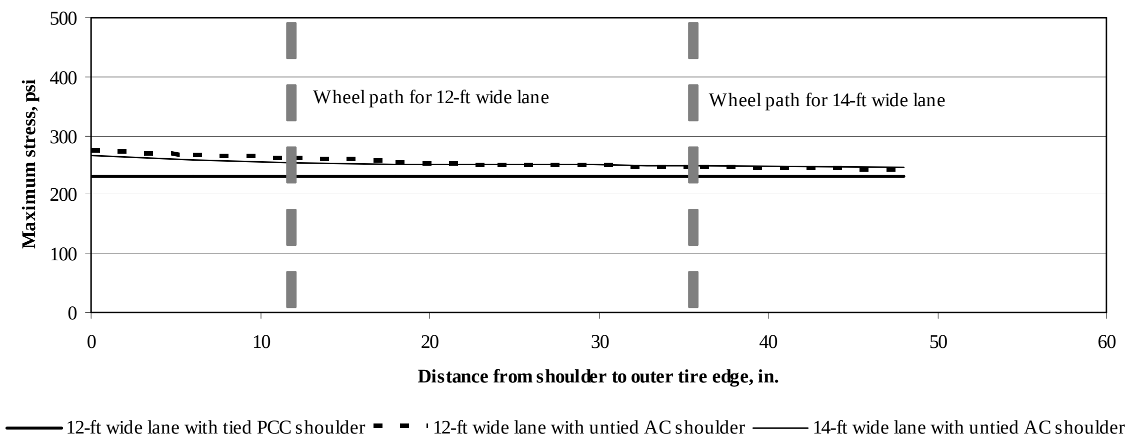


**Figure G-33: Illustration for tridem axle**

Figures G-34 through G-36 are illustrations of relationship between lateral placement and maximum longitudinal stress at the top of the PCC slab for 315-in. joint spacing and $\alpha(\Delta T/D)$ of $-20 \times 10^{-6}$ in.$^{-1}$ for various lateral support conditions

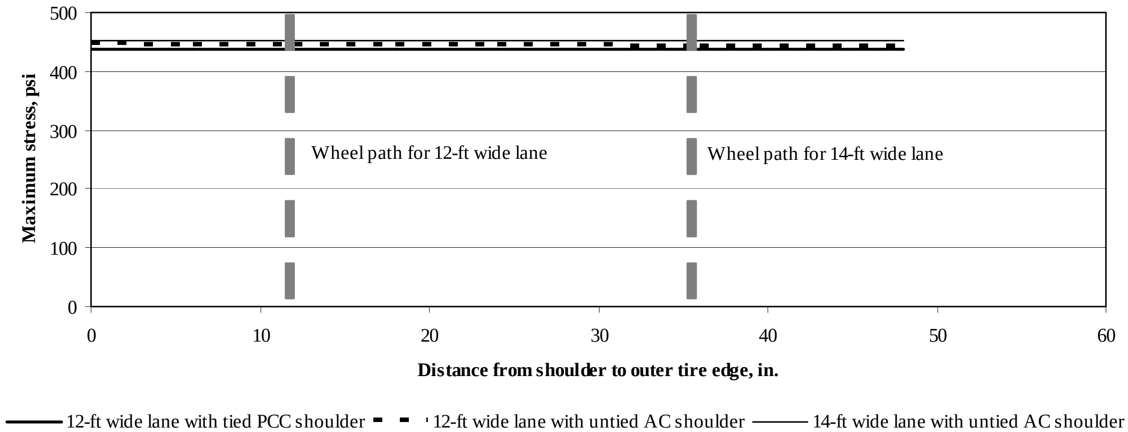


**Figure G-34: Illustration for single axle**

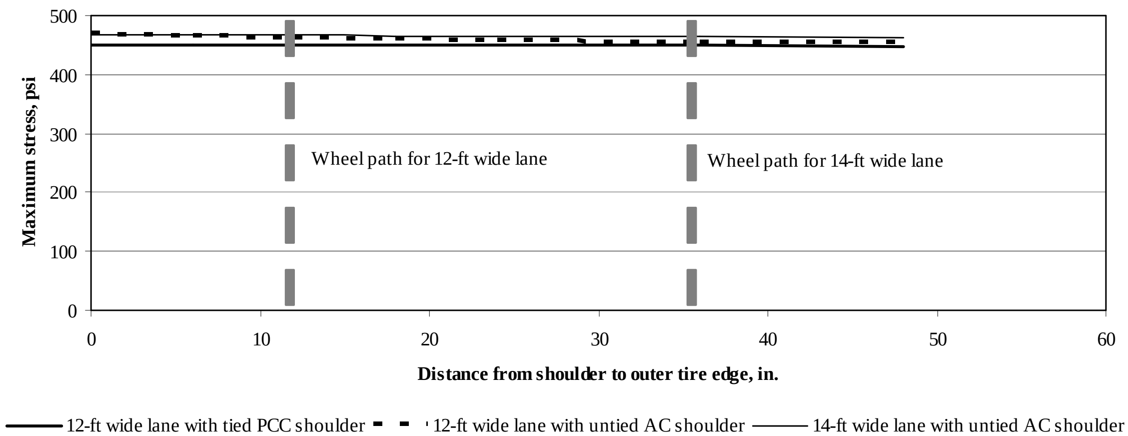


**Figure G-35: Illustration for tandem axle**

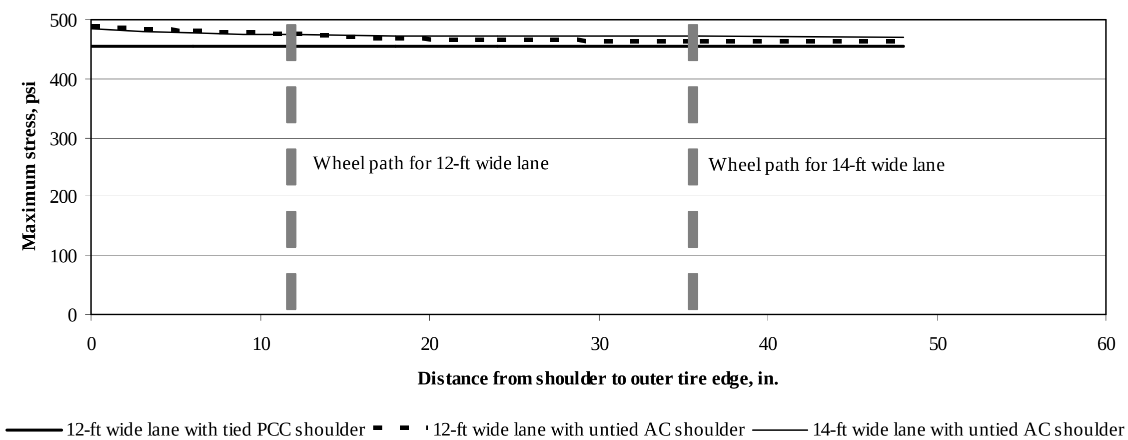


**Figure G-36: Illustration for tridem axle**

**Table G-2: Regression analysis for stress ratio PCC shoulder to AC shoulder (177-in. joint spacing and single axle edge loading)**

The regression equation is
PCC/AC = 0.860 - 0.0111 Dpcc +0.000483 k-value + 0.00439 AlphaGrad

| Predictor | Coef | SE Coef | T | P |
|---|---|---|---|---|
| Constant | 0.859752 | 0.009442 | 91.06 | 0.000 |
| Dpcc | -0.0111190 | 0.0009397 | -11.83 | 0.000 |
| k-value | 0.00048316 | 0.00002694 | 17.93 | 0.000 |
| AlphaGra | 0.0043865 | 0.0002302 | 19.06 | 0.000 |

S = 0.02584 R-Sq = 81.7% R-Sq(adj) = 81.4%

Analysis of Variance

| Source | DF | SS | MS | F | P |
|---|---|---|---|---|---|
| Regression | 3 | 0.55063 | 0.18354 | 274.92 | 0.000 |
| Residual Error | 185 | 0.12351 | 0.00067 | | |
| Total | 188 | 0.67414 | | | |

| Source | DF | Seq SS |
|---|---|---|
| Dpcc | 1 | 0.09347 |
| k-value | 1 | 0.21472 |
| AlphaGra | 1 | 0.24244 |

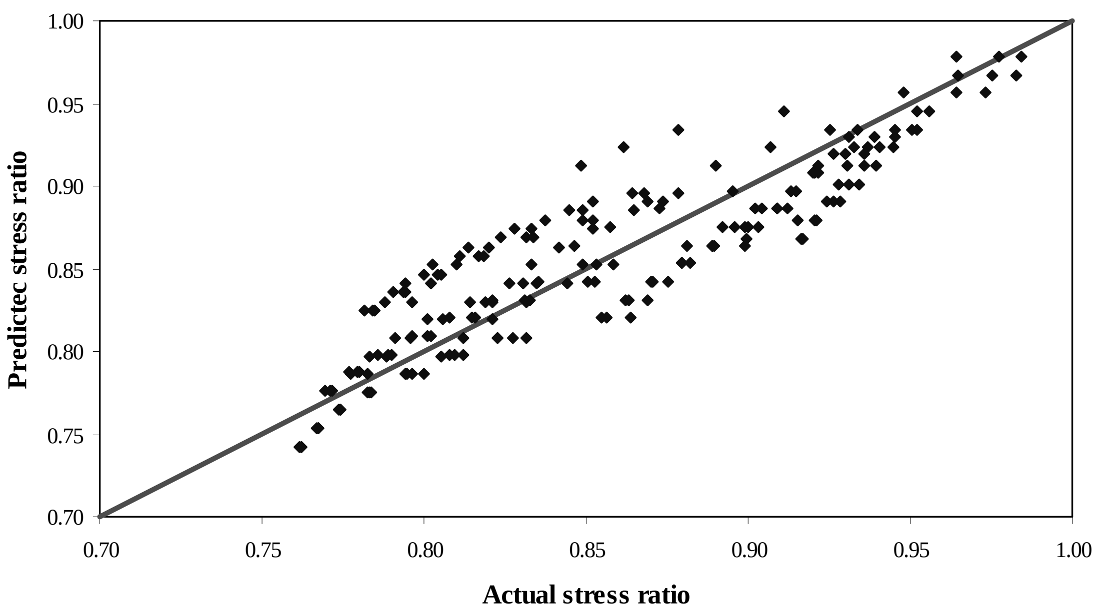


**Figure G-37: Comparison between predicted and actual stress ratio PCC shoulder to AC shoulder (177-in. joint spacing and single axle)**

**Table G-3: Regression analysis for stress ratio widened lane to AC shoulder (177-in. joint spacing and single axle edge loading)**

```
The regression equation is
Widened Lane/AC = 0.880 - 0.00761 Dpcc +0.000339 k-value + 0.00444 AlphaGrad
```

| Predictor | Coef | SE Coef | T | P |
|---|---|---|---|---|
| Constant | 0.879577 | 0.008856 | 99.32 | 0.000 |
| Dpcc | -0.0076058 | 0.0008815 | -8.63 | 0.000 |
| k-value | 0.00033932 | 0.00002527 | 13.43 | 0.000 |
| AlphaGra | 0.0044429 | 0.0002159 | 20.58 | 0.000 |

```
S = 0.02424     R-Sq = 78.6%     R-Sq(adj) = 78.2%

Analysis of Variance
```

| Source | DF | SS | MS | F | P |
|---|---|---|---|---|---|
| Regression | 3 | 0.39835 | 0.13278 | 226.06 | 0.000 |
| Residual Error | 185 | 0.10867 | 0.00059 | | |
| Total | 188 | 0.50702 | | | |

| Source | DF | Seq SS |
|---|---|---|
| Dpcc | 1 | 0.04373 |
| k-value | 1 | 0.10591 |
| AlphaGra | 1 | 0.24871 |

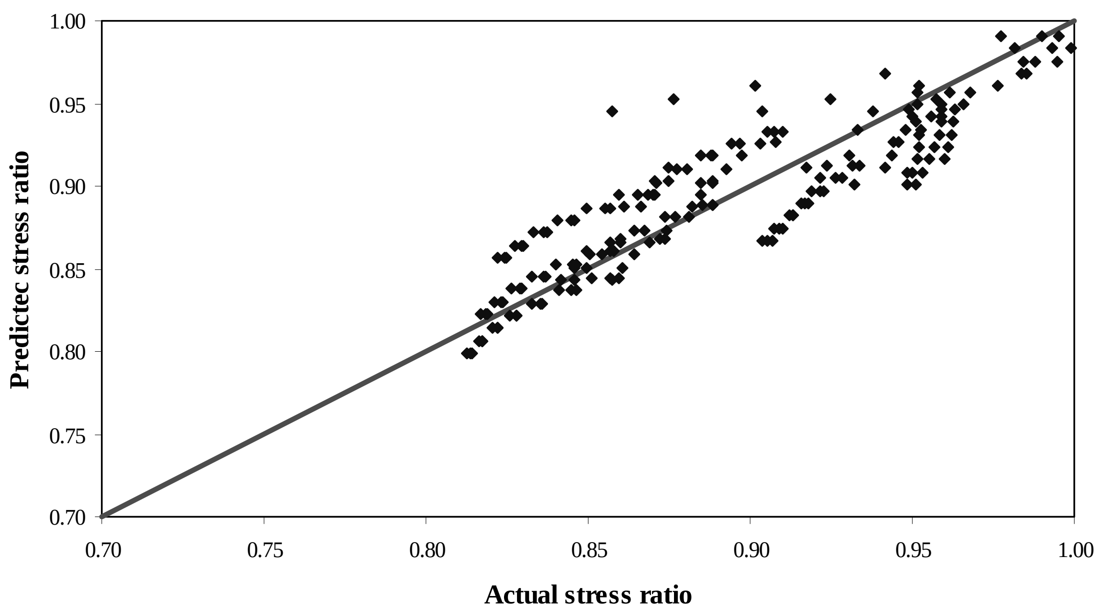


**Figure G-38: Comparison between predicted and actual stress ratio widened lane to AC shoulder (177-in. joint spacing and single axle)**

**Table G-4: Regression analysis for stress ratio PCC shoulder to AC shoulder (315-in. joint spacing and single axle edge loading)**

The regression equation is
PCC/AC = 0.827 - 0.00514 Dpcc +0.000367 k-value + 0.00691 AlphaGrad

| Predictor | Coef | SE Coef | T | P |
|---|---|---|---|---|
| Constant | 0.827158 | 0.009493 | 87.13 | 0.000 |
| Dpcc | -0.0051362 | 0.0009449 | -5.44 | 0.000 |
| k-value | 0.00036729 | 0.00002709 | 13.56 | 0.000 |
| AlphaGra | 0.0069079 | 0.0002314 | 29.85 | 0.000 |

S = 0.02598 R-Sq = 85.7% R-Sq(adj) = 85.4%

Analysis of Variance

| Source | DF | SS | MS | F | P |
|---|---|---|---|---|---|
| Regression | 3 | 0.74529 | 0.24843 | 368.08 | 0.000 |
| Residual Error | 185 | 0.12486 | 0.00067 | | |
| Total | 188 | 0.87015 | | | |

| Source | DF | Seq SS |
|---|---|---|
| Dpcc | 1 | 0.01994 |
| k-value | 1 | 0.12408 |
| AlphaGra | 1 | 0.60127 |

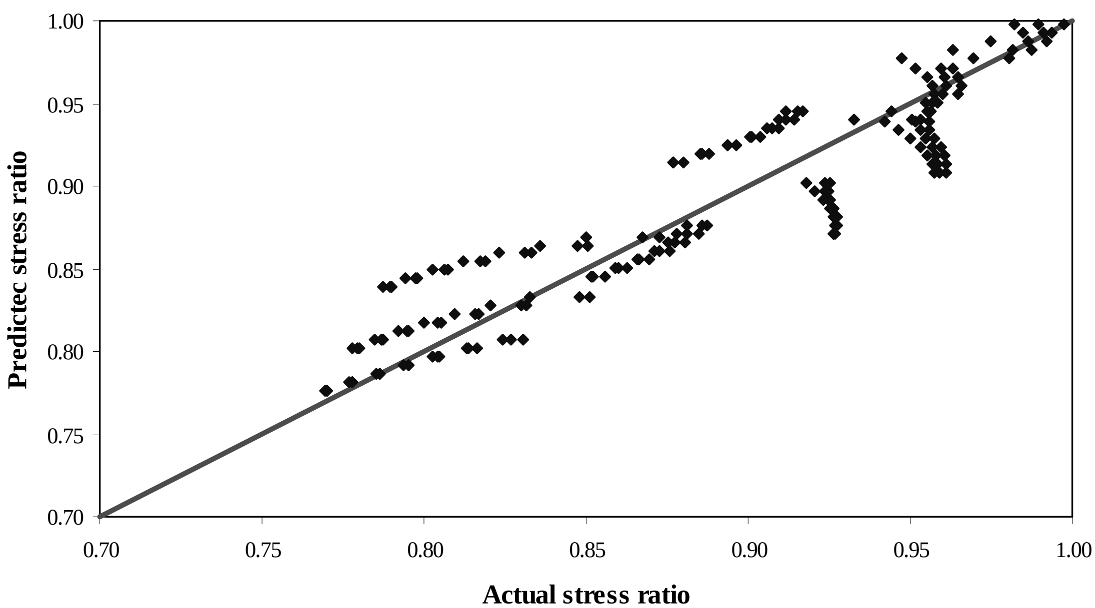


**Figure G-39: Comparison between predicted and actual stress ratio PCC shoulder to AC shoulder (315-in. joint spacing and single axle)**

**Table G-5: Regression analysis for stress ratio widened lane to AC shoulder (315-in. joint spacing and single axle edge loading)**

The regression equation is
Widened Lane/AC = 0.848 - 0.00252 Dpcc +0.000256 k-value + 0.00650 AlphaGrad

| Predictor | Coef | SE Coef | T | P |
|---|---|---|---|---|
| Constant | 0.847724 | 0.008801 | 96.32 | 0.000 |
| Dpcc | -0.0025212 | 0.0008760 | -2.88 | 0.004 |
| k-value | 0.00025563 | 0.00002511 | 10.18 | 0.000 |
| AlphaGra | 0.0064984 | 0.0002146 | 30.29 | 0.000 |

S = 0.02409     R-Sq = 84.8%     R-Sq(adj) = 84.5%

Analysis of Variance

| Source | DF | SS | MS | F | P |
|---|---|---|---|---|---|
| Regression | 3 | 0.59700 | 0.19900 | 343.03 | 0.000 |
| Residual Error | 185 | 0.10732 | 0.00058 | | |
| Total | 188 | 0.70432 | | | |

| Source | DF | Seq SS |
|---|---|---|
| Dpcc | 1 | 0.00481 |
| k-value | 1 | 0.06011 |
| AlphaGra | 1 | 0.53209 |

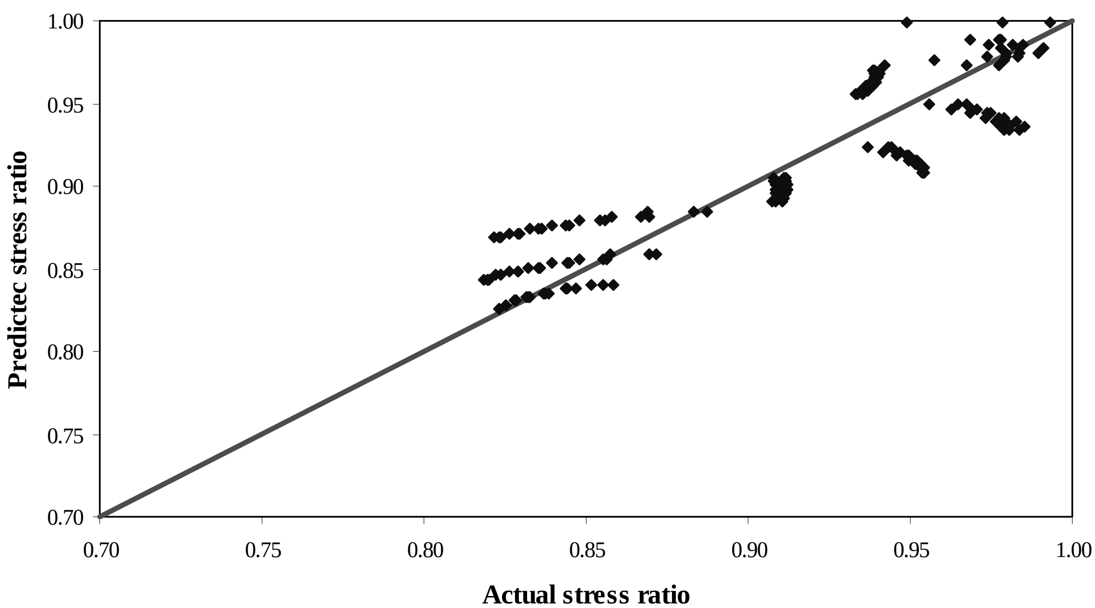


**Figure G-40: Comparison between predicted and actual stress ratio widened lane to AC shoulder (315-in. joint spacing and single axle)**

**Table G-6: Regression analysis for stress ratio PCC shoulder to AC shoulder (177-in. joint spacing and tandem axle edge loading)**

```
The regression equation is
PCC/AC = 0.915 - 0.0149 Dpcc +0.000563 k-value + 0.00354 AlphaGrad
```

| Predictor | Coef | SE Coef | T | P |
|---|---|---|---|---|
| Constant | 0.915068 | 0.008003 | 114.34 | 0.000 |
| Dpcc | -0.0149193 | 0.0007965 | -18.73 | 0.000 |
| k-value | 0.00056274 | 0.00002284 | 24.64 | 0.000 |
| AlphaGra | 0.0035389 | 0.0001951 | 18.14 | 0.000 |

```
S = 0.02190     R-Sq = 87.4%     R-Sq(adj) = 87.2%
```

Analysis of Variance

| Source | DF | SS | MS | F | P |
|---|---|---|---|---|---|
| Regression | 3 | 0.61735 | 0.20578 | 429.03 | 0.000 |
| Residual Error | 185 | 0.08874 | 0.00048 | | |
| Total | 188 | 0.70609 | | | |

| Source | DF | Seq SS |
|---|---|---|
| Dpcc | 1 | 0.16827 |
| k-value | 1 | 0.29128 |
| AlphaGra | 1 | 0.15780 |

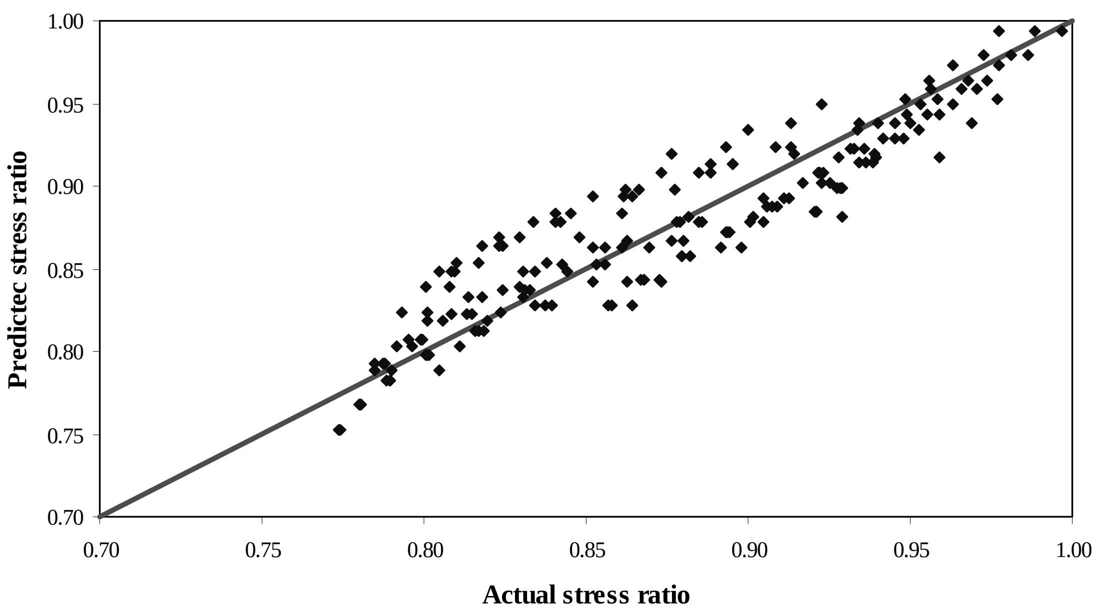


**Figure G-41: Comparison between predicted and actual stress ratio PCC shoulder to AC shoulder (177-in. joint spacing and tandem axle)**

**Table G-7: Regression analysis for stress ratio widened lane to AC shoulder (177-in. joint spacing and tandem axle edge loading)**

```
The regression equation is
Widened Lane/AC = 0.922 - 0.00989 Dpcc +0.000422 k-value + 0.00363 AlphaGrad
```

| Predictor | Coef | SE Coef | T | P |
|---|---|---|---|---|
| Constant | 0.921743 | 0.006767 | 136.21 | 0.000 |
| Dpcc | -0.0098915 | 0.0006735 | -14.69 | 0.000 |
| k-value | 0.00042194 | 0.00001931 | 21.85 | 0.000 |
| AlphaGra | 0.0036286 | 0.0001650 | 21.99 | 0.000 |

S = 0.01852  R-Sq = 86.4%  R-Sq(adj) = 86.2%

Analysis of Variance

| Source | DF | SS | MS | F | P |
|---|---|---|---|---|---|
| Regression | 3 | 0.40362 | 0.13454 | 392.29 | 0.000 |
| Residual Error | 185 | 0.06345 | 0.00034 | | |
| Total | 188 | 0.46707 | | | |

| Source | DF | Seq SS |
|---|---|---|
| Dpcc | 1 | 0.07397 |
| k-value | 1 | 0.16375 |
| AlphaGra | 1 | 0.16590 |

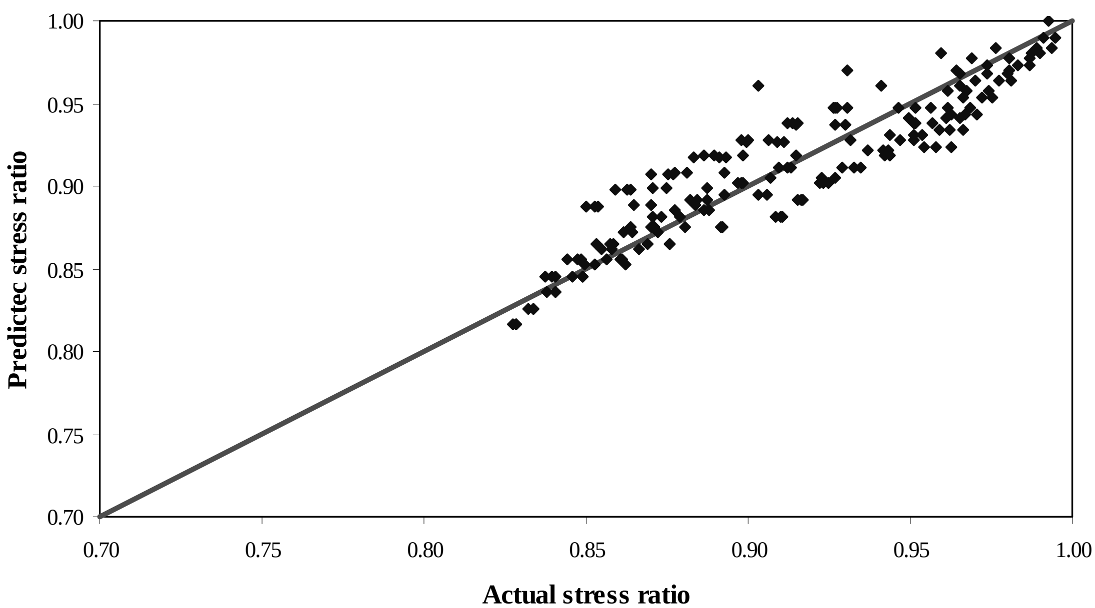


**Figure G-42: Comparison between predicted and actual stress ratio widened lane to AC shoulder (177-in. joint spacing and tandem axle)**

**Table G-8: Regression analysis for stress ratio PCC shoulder to AC shoulder (315-in. joint spacing and tandem axle edge loading)**

```
The regression equation is
PCC/AC = 0.889 - 0.00915 Dpcc +0.000427 k-value + 0.00547 AlphaGrad
```

| Predictor | Coef | SE Coef | T | P |
|---|---|---|---|---|
| Constant | 0.888734 | 0.008344 | 106.52 | 0.000 |
| Dpcc | -0.0091548 | 0.0008304 | -11.02 | 0.000 |
| k-value | 0.00042660 | 0.00002381 | 17.92 | 0.000 |
| AlphaGra | 0.0054675 | 0.0002034 | 26.88 | 0.000 |

S = 0.02283     R-Sq = 86.3%     R-Sq(adj) = 86.1%

Analysis of Variance

| Source | DF | SS | MS | F | P |
|---|---|---|---|---|---|
| Regression | 3 | 0.60741 | 0.20247 | 388.35 | 0.000 |
| Residual Error | 185 | 0.09645 | 0.00052 | | |
| Total | 188 | 0.70386 | | | |

| Source | DF | Seq SS |
|---|---|---|
| Dpcc | 1 | 0.06336 |
| k-value | 1 | 0.16739 |
| AlphaGra | 1 | 0.37665 |

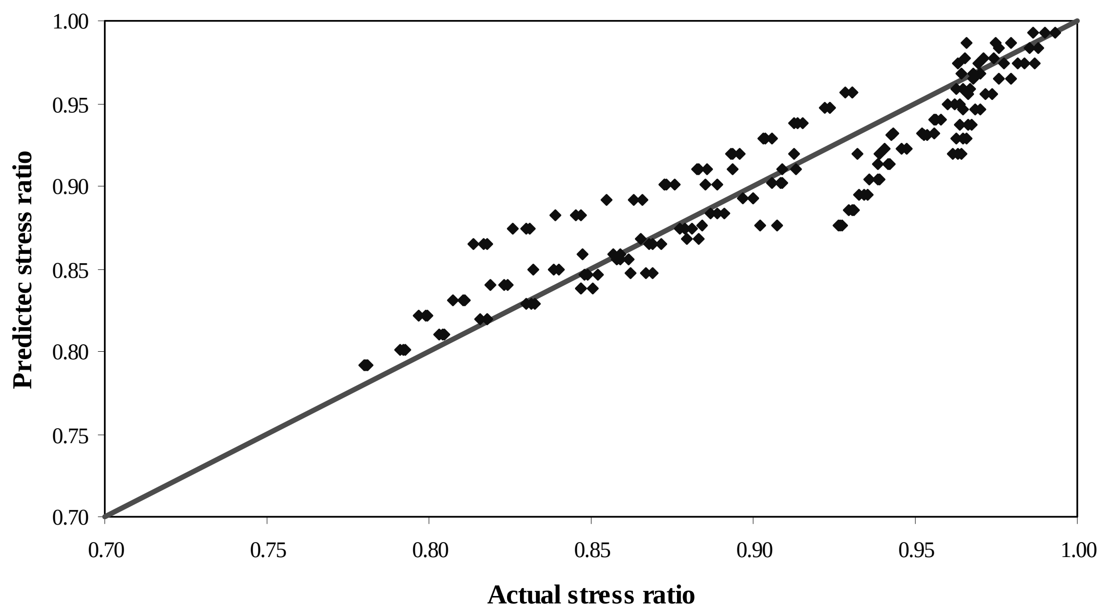


**Figure G-43: Comparison between predicted and actual stress ratio PCC shoulder to AC shoulder (315-in. joint spacing and tandem axle)**

**Table G-9: Regression analysis for stress ratio widened lane to AC shoulder (315-in. joint spacing and tandem axle edge loading)**

```
The regression equation is
Widened Lane/AC = 0.905 - 0.00581 Dpcc +0.000308 k-value + 0.00506 AlphaGrad
```

| Predictor | Coef | SE Coef | T | P |
|---|---|---|---|---|
| Constant | 0.905088 | 0.007328 | 123.51 | 0.000 |
| Dpcc | -0.0058122 | 0.0007293 | -7.97 | 0.000 |
| k-value | 0.00030774 | 0.00002091 | 14.72 | 0.000 |
| AlphaGra | 0.0050603 | 0.0001787 | 28.32 | 0.000 |

S = 0.02005     R-Sq = 85.4%     R-Sq(adj) = 85.2%

Analysis of Variance

| Source | DF | SS | MS | F | P |
|---|---|---|---|---|---|
| Regression | 3 | 0.43529 | 0.14510 | 360.80 | 0.000 |
| Residual Error | 185 | 0.07440 | 0.00040 | | |
| Total | 188 | 0.50969 | | | |

| Source | DF | Seq SS |
|---|---|---|
| Dpcc | 1 | 0.02554 |
| k-value | 1 | 0.08711 |
| AlphaGra | 1 | 0.32265 |

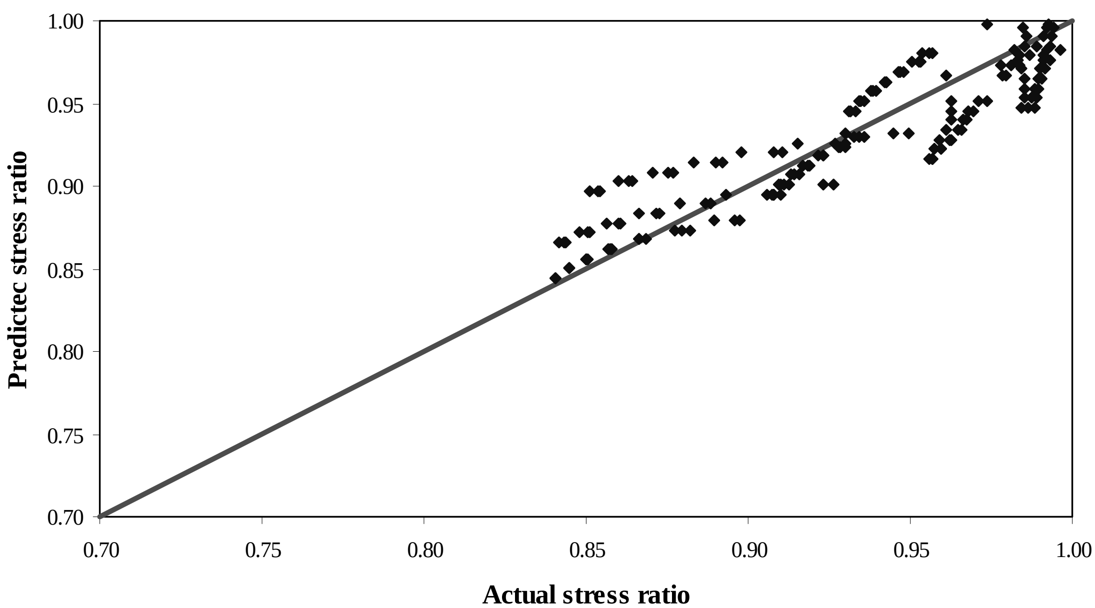


**Figure G-44: Comparison between predicted and actual stress ratio widened lane to AC shoulder (315-in. joint spacing and tandem axle)**

**Table G-10: Regression analysis for stress ratio PCC shoulder to AC shoulder (177-in. joint spacing and tridem axle edge loading)**

```
The regression equation is
PCC/AC = 0.932 - 0.0168 Dpcc +0.000696 k-value + 0.00304 AlphaGrad
```

| Predictor | Coef | SE Coef | T | P |
|---|---|---|---|---|
| Constant | 0.931984 | 0.008292 | 112.40 | 0.000 |
| Dpcc | -0.0167646 | 0.0008253 | -20.31 | 0.000 |
| k-value | 0.00069601 | 0.00002366 | 29.42 | 0.000 |
| AlphaGra | 0.0030373 | 0.0002022 | 15.02 | 0.000 |

```
S = 0.02269     R-Sq = 89.0%     R-Sq(adj) = 88.9%
```

Analysis of Variance

| Source | DF | SS | MS | F | P |
|---|---|---|---|---|---|
| Regression | 3 | 0.77429 | 0.25810 | 501.24 | 0.000 |
| Residual Error | 185 | 0.09526 | 0.00051 | | |
| Total | 188 | 0.86955 | | | |

| Source | DF | Seq SS |
|---|---|---|
| Dpcc | 1 | 0.21247 |
| k-value | 1 | 0.44558 |
| AlphaGra | 1 | 0.11624 |

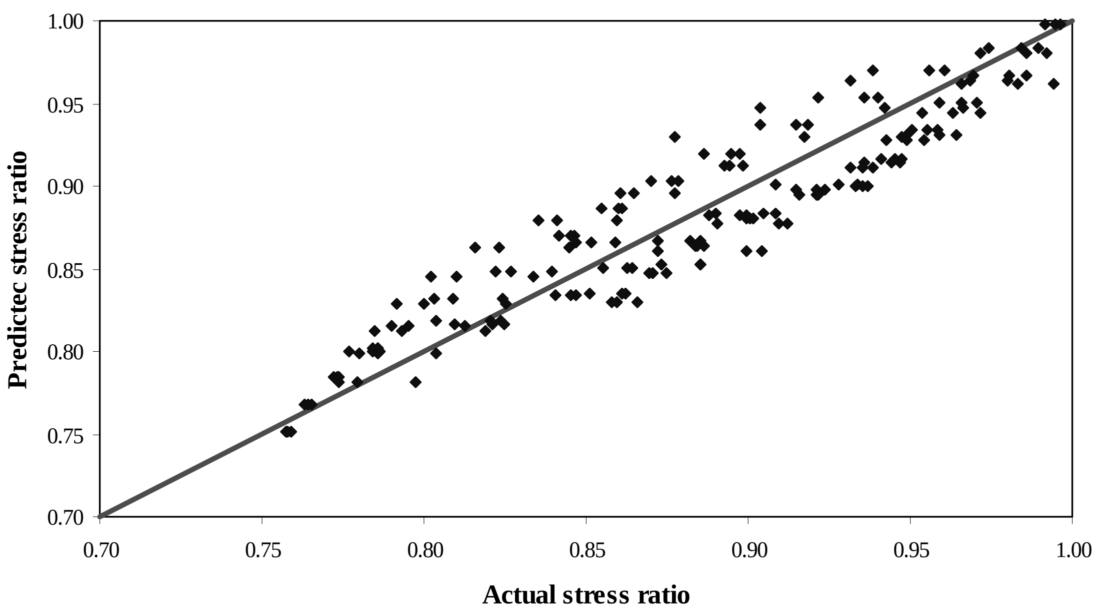


**Figure G-45: Comparison between predicted and actual stress ratio PCC shoulder to AC shoulder (177-in. joint spacing and tridem axle)**

**Table G-11: Regression analysis for stress ratio widened to AC shoulder (177-in. joint spacing and tridem axle edge loading)**

```
The regression equation is
Widened Lane/AC = 0.942 - 0.0120 Dpcc +0.000532 k-value + 0.00335 AlphaGrad
```

| Predictor | Coef | SE Coef | T | P |
|---|---|---|---|---|
| Constant | 0.941706 | 0.007279 | 129.38 | 0.000 |
| Dpcc | -0.0120106 | 0.0007245 | -16.58 | 0.000 |
| k-value | 0.00053182 | 0.00002077 | 25.61 | 0.000 |
| AlphaGra | 0.0033476 | 0.0001775 | 18.86 | 0.000 |

S = 0.01992 R-Sq = 87.4% R-Sq(adj) = 87.2%

Analysis of Variance

| Source | DF | SS | MS | F | P |
|---|---|---|---|---|---|
| Regression | 3 | 0.51041 | 0.17014 | 428.80 | 0.000 |
| Residual Error | 185 | 0.07340 | 0.00040 | | |
| Total | 188 | 0.58381 | | | |

| Source | DF | Seq SS |
|---|---|---|
| Dpcc | 1 | 0.10906 |
| k-value | 1 | 0.26015 |
| AlphaGra | 1 | 0.14120 |

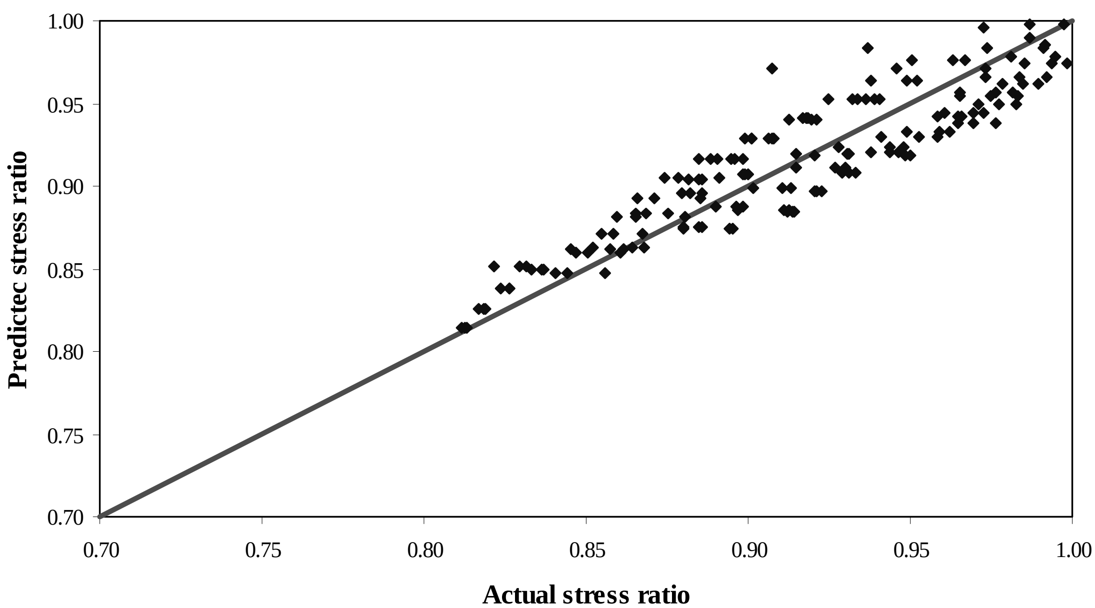


**Figure G-46: Comparison between predicted and actual stress ratio widened lane to AC shoulder (177-in. joint spacing and tridem axle)**

**Table G-12: Regression analysis for stress ratio PCC shoulder to AC shoulder (315-in. joint spacing and tridem axle edge loading)**

```
The regression equation is
PCC/AC = 0.943 - 0.0132 Dpcc +0.000560 k-value + 0.00418 AlphaGrad
```

| Predictor | Coef | SE Coef | T | P |
|---|---|---|---|---|
| Constant | 0.943019 | 0.008972 | 105.11 | 0.000 |
| Dpcc | -0.0131825 | 0.0008930 | -14.76 | 0.000 |
| k-value | 0.00055957 | 0.00002560 | 21.86 | 0.000 |
| AlphaGra | 0.0041833 | 0.0002187 | 19.13 | 0.000 |

S = 0.02455 R-Sq = 85.2% R-Sq(adj) = 84.9%

Analysis of Variance

| Source | DF | SS | MS | F | P |
|---|---|---|---|---|---|
| Regression | 3 | 0.63988 | 0.21329 | 353.81 | 0.000 |
| Residual Error | 185 | 0.11153 | 0.00060 | | |
| Total | 188 | 0.75141 | | | |

| Source | DF | Seq SS |
|---|---|---|
| Dpcc | 1 | 0.13138 |
| k-value | 1 | 0.28800 |
| AlphaGra | 1 | 0.22050 |

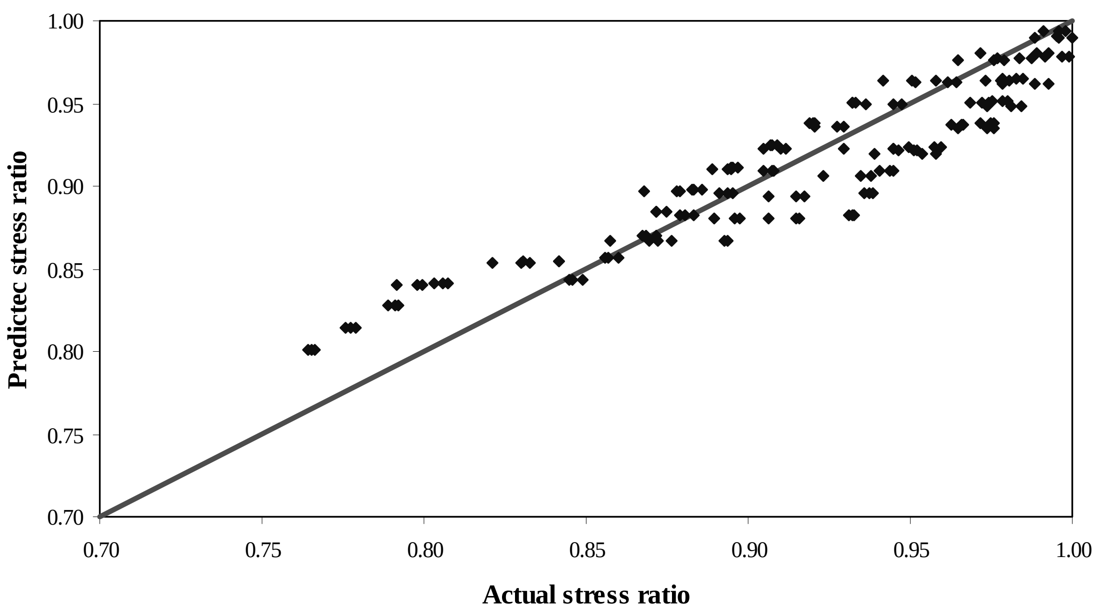


**Figure G-47: Comparison between predicted and actual stress ratio PCC shoulder to AC shoulder (315-in. joint spacing and tridem axle)**

**Table G-13: Regression analysis for stress ratio widened lane to AC shoulder (315-in. joint spacing and tridem axle edge loading)**

```
The regression equation is
Widened Lane/AC = 0.953 - 0.00909 Dpcc +0.000407 k-value + 0.00397 AlphaGrad
```

| Predictor | Coef | SE Coef | T | P |
|---|---|---|---|---|
| Constant | 0.952682 | 0.007765 | 122.69 | 0.000 |
| Dpcc | -0.0090886 | 0.0007728 | -11.76 | 0.000 |
| k-value | 0.00040699 | 0.00002216 | 18.37 | 0.000 |
| AlphaGra | 0.0039659 | 0.0001893 | 20.95 | 0.000 |

S = 0.02125 R-Sq = 83.2% R-Sq(adj) = 82.9%

Analysis of Variance

| Source | DF | SS | MS | F | P |
|---|---|---|---|---|---|
| Regression | 3 | 0.41298 | 0.13766 | 304.87 | 0.000 |
| Residual Error | 185 | 0.08353 | 0.00045 | | |
| Total | 188 | 0.49651 | | | |

| Source | DF | Seq SS |
|---|---|---|
| Dpcc | 1 | 0.06245 |
| k-value | 1 | 0.15236 |
| AlphaGra | 1 | 0.19817 |

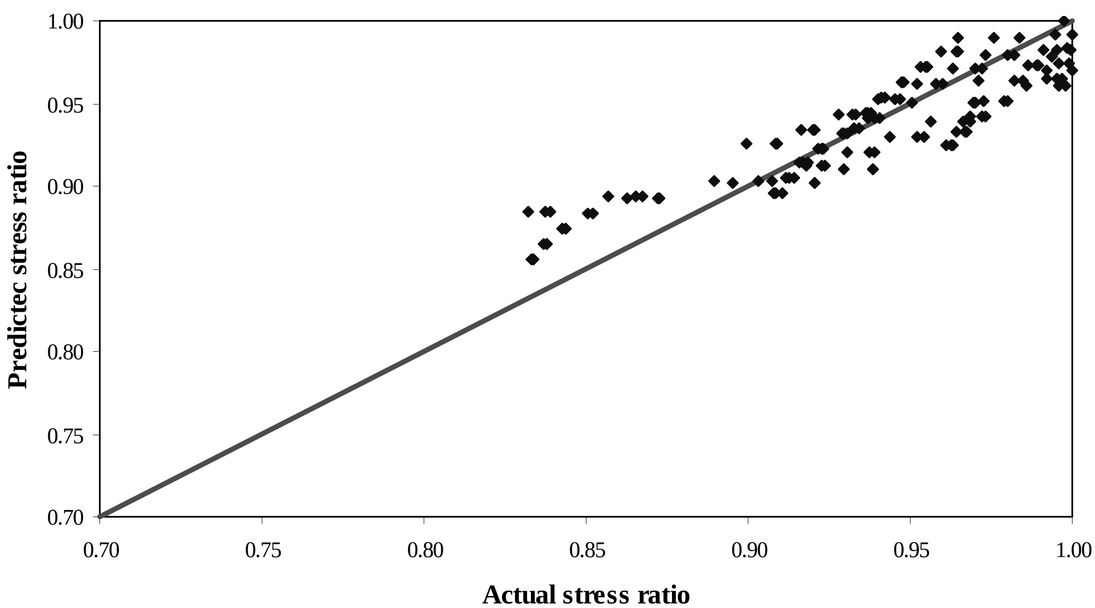


**Figure G-48: Comparison between predicted and actual stress ratio widened lane to AC shoulder (315-in. joint spacing and tridem axle)**

# Appendix H

# Equivalent Stress Cross-Sections

**Table H-1: Cross-sections with longitudinal stress of 75 psi under 18-kips single axle loading**

| Joint Spacing (in.) | Lateral Support Condition | Slab Thk. (in.) | Base/Subbase Thk. (in.) | k-value (psi/in.) | Long. Bot. Stress (psi) |
|---|---|---|---|---|---|
| 177 | 12-ft lane with tied PCC shoulder | 12 | 26 | 200 | 75.0 |
| 315 | 12-ft lane with tied PCC shoulder | 11 | 26 | 200 | 77.4 |
| 315 | 12-ft lane with tied PCC shoulder | 12 | 4 | 200 | 74.6 |
| 315 | 12-ft lane with tied PCC shoulder | 12 | 10 | 200 | 74.3 |
| 315 | 12-ft lane with tied PCC shoulder | 12 | 16 | 200 | 73.4 |
| 315 | 12-ft lane with tied PCC shoulder | 12 | 20 | 150 | 76.8 |
| 315 | 12-ft lane with tied PCC shoulder | 12 | 26 | 150 | 74.2 |
| 315 | 14-ft lane with AC shoulder | 12 | 10 | 200 | 77.5 |
| 315 | 14-ft lane with AC shoulder | 12 | 16 | 200 | 76.6 |
| 315 | 14-ft lane with AC shoulder | 12 | 20 | 200 | 75.5 |
| 315 | 14-ft lane with AC shoulder | 12 | 26 | 200 | 72.9 |

**Table H-2: Cross-sections with longitudinal stress of 100 psi under 18-kips single axle loading**

| Joint Spacing (in.) | Lateral Support Condition | Slab Thk. (in.) | Base/Subbase Thk. (in.) | k-value (psi/in.) | Long. Bot. Stress (psi) |
|---|---|---|---|---|---|
| 177 | 12-ft lane with tied PCC shoulder | 9 | 26 | 200 | 99.6 |
| 177 | 12-ft lane with tied PCC shoulder | 10 | 4 | 200 | 100.3 |
| 177 | 12-ft lane with tied PCC shoulder | 10 | 10 | 200 | 99.7 |
| 177 | 12-ft lane with tied PCC shoulder | 10 | 16 | 200 | 97.8 |
| 177 | 12-ft lane with tied PCC shoulder | 11 | 20 | 100 | 101.2 |
| 177 | 12-ft lane with tied PCC shoulder | 12 | 4 | 65 | 101.7 |
| 177 | 12-ft lane with tied PCC shoulder | 12 | 10 | 65 | 101.3 |
| 177 | 12-ft lane with tied PCC shoulder | 12 | 16 | 65 | 100.1 |
| 177 | 12-ft lane with tied PCC shoulder | 12 | 20 | 65 | 98.6 |
| 177 | 12-ft lane with AC shoulder | 12 | 4 | 200 | 101.7 |
| 177 | 12-ft lane with AC shoulder | 12 | 10 | 200 | 101.4 |
| 177 | 12-ft lane with AC shoulder | 12 | 16 | 200 | 100.3 |
| 177 | 12-ft lane with AC shoulder | 12 | 20 | 200 | 99.0 |
| 177 | 14-ft lane with AC shoulder | 10 | 16 | 200 | 101.7 |
| 177 | 14-ft lane with AC shoulder | 10 | 20 | 200 | 99.4 |
| 177 | 14-ft lane with AC shoulder | 10 | 26 | 150 | 101.6 |
| 177 | 14-ft lane with AC shoulder | 11 | 4 | 150 | 100.4 |
| 177 | 14-ft lane with AC shoulder | 11 | 10 | 150 | 99.9 |
| 177 | 14-ft lane with AC shoulder | 11 | 16 | 150 | 98.5 |
| 177 | 14-ft lane with AC shoulder | 11 | 26 | 100 | 102.4 |
| 177 | 14-ft lane with AC shoulder | 12 | 4 | 100 | 99.3 |
| 177 | 14-ft lane with AC shoulder | 12 | 10 | 100 | 98.9 |
| 177 | 14-ft lane with AC shoulder | 12 | 16 | 100 | 97.7 |
| 177 | 14-ft lane with AC shoulder | 12 | 26 | 65 | 101.3 |
| 315 | 12-ft lane with tied PCC shoulder | 9 | 26 | 150 | 101.8 |
| 315 | 12-ft lane with tied PCC shoulder | 10 | 4 | 150 | 101.8 |
| 315 | 12-ft lane with tied PCC shoulder | 10 | 10 | 150 | 101.2 |
| 315 | 12-ft lane with tied PCC shoulder | 10 | 16 | 150 | 99.1 |
| 315 | 12-ft lane with tied PCC shoulder | 10 | 26 | 100 | 99.2 |
| 315 | 12-ft lane with tied PCC shoulder | 11 | 26 | 65 | 98.3 |
| 315 | 12-ft lane with AC shoulder | 11 | 20 | 200 | 101.6 |
| 315 | 12-ft lane with AC shoulder | 12 | 4 | 150 | 100.8 |
| 315 | 12-ft lane with AC shoulder | 12 | 10 | 150 | 100.4 |
| 315 | 12-ft lane with AC shoulder | 12 | 16 | 150 | 99.3 |
| 315 | 12-ft lane with AC shoulder | 12 | 20 | 150 | 97.9 |
| 315 | 14-ft lane with AC shoulder | 9 | 26 | 200 | 99.4 |
| 315 | 14-ft lane with AC shoulder | 10 | 4 | 200 | 99.5 |
| 315 | 14-ft lane with AC shoulder | 10 | 10 | 200 | 98.9 |
| 315 | 14-ft lane with AC shoulder | 10 | 20 | 150 | 100.5 |
| 315 | 14-ft lane with AC shoulder | 11 | 4 | 100 | 101.6 |
| 315 | 14-ft lane with AC shoulder | 11 | 10 | 100 | 101.1 |
| 315 | 14-ft lane with AC shoulder | 11 | 16 | 100 | 99.6 |
| 315 | 14-ft lane with AC shoulder | 11 | 20 | 100 | 97.8 |
| 315 | 14-ft lane with AC shoulder | 12 | 4 | 65 | 100.6 |
| 315 | 14-ft lane with AC shoulder | 12 | 10 | 65 | 100.2 |
| 315 | 14-ft lane with AC shoulder | 12 | 16 | 65 | 99.1 |
| 315 | 14-ft lane with AC shoulder | 12 | 20 | 65 | 97.7 |

**Table H-3: Cross-sections with longitudinal stress of 125 psi under 18-kips single axle loading**

| Joint Spacing (in.) | Lateral Support Condition | Slab Thk. (in.) | Base/Subbase Thk. (in.) | k-value (psi/in.) | Long. Bot. Stress (psi) |
|---|---|---|---|---|---|
| 177 | 12-ft lane with tied PCC shoulder | 8 | 16 | 200 | 126.3 |
| 177 | 12-ft lane with tied PCC shoulder | 9 | 4 | 150 | 122.9 |
| 177 | 12-ft lane with tied PCC shoulder | 9 | 20 | 100 | 127.4 |
| 177 | 12-ft lane with tied PCC shoulder | 10 | 20 | 65 | 124.9 |
| 177 | 12-ft lane with tied PCC shoulder | 11 | 20 | 30 | 126.1 |
| 177 | 12-ft lane with AC shoulder | 9 | 26 | 200 | 122.8 |
| 177 | 12-ft lane with AC shoulder | 10 | 4 | 200 | 124.5 |
| 177 | 12-ft lane with AC shoulder | 10 | 10 | 200 | 123.8 |
| 177 | 12-ft lane with AC shoulder | 10 | 26 | 150 | 122.5 |
| 177 | 12-ft lane with AC shoulder | 11 | 26 | 100 | 124.7 |
| 177 | 12-ft lane with AC shoulder | 12 | 26 | 65 | 124.4 |
| 177 | 14-ft lane with AC shoulder | 7 | 26 | 200 | 123.2 |
| 177 | 14-ft lane with AC shoulder | 8 | 20 | 200 | 124.5 |
| 177 | 14-ft lane with AC shoulder | 9 | 10 | 150 | 126.5 |
| 177 | 14-ft lane with AC shoulder | 9 | 16 | 150 | 123.3 |
| 177 | 14-ft lane with AC shoulder | 9 | 26 | 100 | 123.8 |
| 177 | 14-ft lane with AC shoulder | 10 | 4 | 100 | 125.0 |
| 177 | 14-ft lane with AC shoulder | 10 | 10 | 100 | 124.3 |
| 177 | 14-ft lane with AC shoulder | 10 | 26 | 65 | 124.5 |
| 315 | 12-ft lane with tied PCC shoulder | 7 | 26 | 150 | 126.0 |
| 315 | 12-ft lane with tied PCC shoulder | 8 | 16 | 200 | 124.6 |
| 315 | 12-ft lane with tied PCC shoulder | 8 | 20 | 150 | 126.1 |
| 315 | 12-ft lane with tied PCC shoulder | 8 | 26 | 100 | 123.2 |
| 315 | 12-ft lane with tied PCC shoulder | 9 | 10 | 100 | 126.9 |
| 315 | 12-ft lane with tied PCC shoulder | 9 | 16 | 100 | 123.4 |
| 315 | 12-ft lane with tied PCC shoulder | 11 | 10 | 30 | 127.3 |
| 315 | 12-ft lane with tied PCC shoulder | 11 | 16 | 30 | 125.4 |
| 315 | 12-ft lane with tied PCC shoulder | 11 | 20 | 30 | 123.2 |
| 315 | 12-ft lane with AC shoulder | 9 | 20 | 200 | 127.2 |
| 315 | 12-ft lane with AC shoulder | 9 | 26 | 150 | 126.3 |
| 315 | 12-ft lane with AC shoulder | 10 | 4 | 150 | 127.0 |
| 315 | 12-ft lane with AC shoulder | 10 | 10 | 150 | 126.2 |
| 315 | 12-ft lane with AC shoulder | 10 | 16 | 150 | 123.8 |
| 315 | 12-ft lane with AC shoulder | 10 | 26 | 100 | 125.2 |
| 315 | 12-ft lane with AC shoulder | 11 | 4 | 100 | 123.3 |
| 315 | 12-ft lane with AC shoulder | 11 | 10 | 100 | 122.8 |
| 315 | 12-ft lane with AC shoulder | 11 | 26 | 65 | 125.9 |
| 315 | 12-ft lane with AC shoulder | 12 | 4 | 65 | 122.7 |
| 315 | 14-ft lane with AC shoulder | 9 | 20 | 100 | 124.0 |
| 315 | 14-ft lane with AC shoulder | 9 | 26 | 65 | 126.0 |
| 315 | 14-ft lane with AC shoulder | 10 | 4 | 65 | 126.7 |
| 315 | 14-ft lane with AC shoulder | 10 | 10 | 65 | 126.0 |
| 315 | 14-ft lane with AC shoulder | 10 | 16 | 65 | 123.5 |
| 315 | 14-ft lane with AC shoulder | 11 | 26 | 30 | 125.3 |
| 315 | 14-ft lane with AC shoulder | 12 | 4 | 30 | 122.6 |

**Table H-4: Cross-sections with longitudinal stress of 150 psi under 18-kips single axle loading**

| Joint Spacing (in.) | Lateral Support Condition | Slab Thk. (in.) | Base/Subbase Thk. (in.) | k-value (psi/in.) | Long. Bot. Stress (psi) |
|---|---|---|---|---|---|
| 177 | 12-ft lane with tied PCC shoulder | 8 | 16 | 100 | 150.1 |
| 177 | 12-ft lane with tied PCC shoulder | 9 | 4 | 65 | 151.0 |
| 177 | 12-ft lane with tied PCC shoulder | 9 | 10 | 65 | 149.8 |
| 177 | 12-ft lane with tied PCC shoulder | 10 | 4 | 30 | 152.5 |
| 177 | 12-ft lane with tied PCC shoulder | 10 | 10 | 30 | 151.5 |
| 177 | 12-ft lane with tied PCC shoulder | 10 | 16 | 30 | 148.2 |
| 177 | 12-ft lane with AC shoulder | 6 | 26 | 200 | 151.9 |
| 177 | 12-ft lane with AC shoulder | 8 | 16 | 200 | 151.9 |
| 177 | 12-ft lane with AC shoulder | 9 | 4 | 150 | 151.5 |
| 177 | 12-ft lane with AC shoulder | 9 | 10 | 150 | 150.4 |
| 177 | 12-ft lane with AC shoulder | 9 | 26 | 100 | 148.7 |
| 177 | 12-ft lane with AC shoulder | 10 | 4 | 100 | 150.8 |
| 177 | 12-ft lane with AC shoulder | 10 | 10 | 100 | 149.9 |
| 177 | 12-ft lane with AC shoulder | 10 | 26 | 65 | 151.3 |
| 177 | 12-ft lane with AC shoulder | 11 | 4 | 65 | 149.2 |
| 177 | 12-ft lane with AC shoulder | 11 | 10 | 65 | 148.5 |
| 177 | 12-ft lane with AC shoulder | 12 | 4 | 30 | 150.5 |
| 177 | 12-ft lane with AC shoulder | 12 | 10 | 30 | 149.8 |
| 177 | 12-ft lane with AC shoulder | 12 | 16 | 30 | 147.8 |
| 177 | 14-ft lane with AC shoulder | 7 | 16 | 200 | 150.0 |
| 177 | 14-ft lane with AC shoulder | 7 | 20 | 150 | 151.4 |
| 177 | 14-ft lane with AC shoulder | 8 | 20 | 100 | 149.2 |
| 177 | 14-ft lane with AC shoulder | 8 | 26 | 65 | 151.3 |
| 177 | 14-ft lane with AC shoulder | 9 | 20 | 65 | 148.2 |
| 315 | 12-ft lane with tied PCC shoulder | 6 | 26 | 100 | 148.9 |
| 315 | 12-ft lane with tied PCC shoulder | 7 | 26 | 65 | 148.9 |
| 315 | 12-ft lane with tied PCC shoulder | 8 | 4 | 100 | 150.8 |
| 315 | 12-ft lane with tied PCC shoulder | 8 | 10 | 100 | 149.0 |
| 315 | 12-ft lane with tied PCC shoulder | 8 | 20 | 65 | 149.2 |
| 315 | 12-ft lane with AC shoulder | 6 | 26 | 200 | 152.2 |
| 315 | 12-ft lane with AC shoulder | 7 | 26 | 150 | 152.1 |
| 315 | 12-ft lane with AC shoulder | 8 | 16 | 200 | 150.0 |
| 315 | 12-ft lane with AC shoulder | 8 | 26 | 100 | 152.2 |
| 315 | 12-ft lane with AC shoulder | 9 | 20 | 100 | 148.6 |
| 315 | 12-ft lane with AC shoulder | 9 | 26 | 65 | 151.8 |
| 315 | 12-ft lane with AC shoulder | 10 | 10 | 65 | 152.3 |
| 315 | 12-ft lane with AC shoulder | 10 | 16 | 65 | 149.3 |
| 315 | 12-ft lane with AC shoulder | 11 | 26 | 30 | 151.9 |
| 315 | 12-ft lane with AC shoulder | 12 | 4 | 30 | 149.0 |
| 315 | 12-ft lane with AC shoulder | 12 | 10 | 30 | 148.5 |
| 315 | 14-ft lane with AC shoulder | 7 | 16 | 200 | 149.8 |
| 315 | 14-ft lane with AC shoulder | 7 | 20 | 150 | 149.3 |
| 315 | 14-ft lane with AC shoulder | 8 | 16 | 100 | 148.3 |
| 315 | 14-ft lane with AC shoulder | 9 | 26 | 30 | 150.4 |
| 315 | 14-ft lane with AC shoulder | 10 | 4 | 30 | 152.3 |
| 315 | 14-ft lane with AC shoulder | 10 | 10 | 30 | 151.4 |
| 315 | 14-ft lane with AC shoulder | 10 | 16 | 30 | 148.4 |

**Table H-5: Cross-sections with longitudinal stress of 175 psi under 18-kips single axle loading**

| Joint Spacing (in.) | Lateral Support Condition | Slab Thk. (in.) | Base/Subbase Thk. (in.) | k-value (psi/in.) | Long. Bot. Stress (psi) |
|---|---|---|---|---|---|
| 177 | 12-ft lane with tied PCC shoulder | 6 | 16 | 200 | 172.6 |
| 177 | 12-ft lane with tied PCC shoulder | 7 | 16 | 100 | 173.3 |
| 177 | 12-ft lane with tied PCC shoulder | 8 | 4 | 65 | 175.5 |
| 177 | 12-ft lane with tied PCC shoulder | 8 | 10 | 65 | 173.5 |
| 177 | 12-ft lane with tied PCC shoulder | 9 | 10 | 30 | 176.6 |
| 177 | 12-ft lane with AC shoulder | 7 | 16 | 200 | 172.7 |
| 177 | 12-ft lane with AC shoulder | 7 | 20 | 150 | 175.9 |
| 177 | 12-ft lane with AC shoulder | 7 | 26 | 100 | 173.4 |
| 177 | 12-ft lane with AC shoulder | 8 | 20 | 100 | 176.8 |
| 177 | 12-ft lane with AC shoulder | 10 | 26 | 30 | 175.5 |
| 177 | 14-ft lane with AC shoulder | 6 | 16 | 200 | 175.7 |
| 177 | 14-ft lane with AC shoulder | 6 | 26 | 65 | 175.6 |
| 177 | 14-ft lane with AC shoulder | 7 | 4 | 150 | 172.8 |
| 177 | 14-ft lane with AC shoulder | 8 | 16 | 65 | 174.3 |
| 177 | 14-ft lane with AC shoulder | 9 | 20 | 30 | 175.1 |
| 315 | 12-ft lane with tied PCC shoulder | 6 | 16 | 200 | 173.7 |
| 315 | 12-ft lane with tied PCC shoulder | 7 | 26 | 30 | 175.0 |
| 315 | 12-ft lane with tied PCC shoulder | 8 | 20 | 30 | 175.8 |
| 315 | 12-ft lane with AC shoulder | 7 | 16 | 200 | 172.8 |
| 315 | 12-ft lane with AC shoulder | 7 | 20 | 150 | 173.8 |
| 315 | 12-ft lane with AC shoulder | 8 | 16 | 100 | 175.7 |
| 315 | 12-ft lane with AC shoulder | 9 | 4 | 65 | 174.9 |
| 315 | 12-ft lane with AC shoulder | 9 | 10 | 65 | 173.4 |
| 315 | 12-ft lane with AC shoulder | 10 | 20 | 30 | 174.9 |
| 315 | 14-ft lane with AC shoulder | 6 | 16 | 200 | 176.9 |
| 315 | 14-ft lane with AC shoulder | 7 | 16 | 100 | 173.7 |
| 315 | 14-ft lane with AC shoulder | 9 | 4 | 30 | 173.5 |

**Table H-6: Cross-sections with longitudinal stress of 200 psi under 18-kips single axle loading**

| Joint Spacing (in.) | Lateral Support Condition | Slab Thk. (in.) | Base/Subbase Thk. (in.) | k-value (psi/in.) | Long. Bot. Stress (psi) |
|---|---|---|---|---|---|
| 177 | 12-ft lane with tied PCC shoulder | 6 | 10 | 150 | 200.3 |
| 177 | 12-ft lane with tied PCC shoulder | 6 | 16 | 100 | 202.4 |
| 177 | 12-ft lane with tied PCC shoulder | 8 | 16 | 30 | 199.7 |
| 177 | 12-ft lane with AC shoulder | 6 | 16 | 200 | 198.6 |
| 177 | 12-ft lane with AC shoulder | 7 | 4 | 150 | 199.8 |
| 177 | 12-ft lane with AC shoulder | 8 | 20 | 65 | 198.6 |
| 177 | 14-ft lane with AC shoulder | 7 | 16 | 65 | 200.0 |
| 177 | 14-ft lane with AC shoulder | 7 | 26 | 30 | 197.9 |
| 177 | 14-ft lane with AC shoulder | 8 | 20 | 30 | 200.0 |
| 315 | 12-ft lane with tied PCC shoulder | 6 | 10 | 150 | 201.1 |
| 315 | 12-ft lane with tied PCC shoulder | 6 | 16 | 100 | 200.4 |
| 315 | 12-ft lane with tied PCC shoulder | 6 | 20 | 65 | 198.1 |
| 315 | 12-ft lane with tied PCC shoulder | 7 | 4 | 65 | 198.1 |
| 315 | 12-ft lane with tied PCC shoulder | 7 | 20 | 30 | 201.4 |
| 315 | 12-ft lane with AC shoulder | 6 | 16 | 200 | 200.3 |
| 315 | 12-ft lane with AC shoulder | 7 | 4 | 150 | 198.8 |
| 315 | 12-ft lane with AC shoulder | 8 | 10 | 65 | 200.6 |
| 315 | 12-ft lane with AC shoulder | 8 | 26 | 30 | 197.7 |
| 315 | 12-ft lane with AC shoulder | 9 | 16 | 30 | 201.1 |
| 315 | 14-ft lane with AC shoulder | 6 | 4 | 200 | 198.0 |
| 315 | 14-ft lane with AC shoulder | 7 | 10 | 65 | 201.1 |
| 315 | 14-ft lane with AC shoulder | 8 | 4 | 30 | 201.7 |
| 315 | 14-ft lane with AC shoulder | 8 | 10 | 30 | 199.3 |

**Table H-7: Cross-sections with longitudinal stress of 225 psi under 18-kips single axle loading**

| Joint Spacing (in.) | Lateral Support Condition | Slab Thk. (in.) | Base/Subbase Thk. (in.) | k-value (psi/in.) | Long. Bot. Stress (psi) |
|---|---|---|---|---|---|
| 177 | 12-ft lane with tied PCC shoulder | 6 | 4 | 100 | 226.0 |
| 177 | 12-ft lane with tied PCC shoulder | 6 | 16 | 65 | 225.0 |
| 177 | 12-ft lane with AC shoulder | 7 | 4 | 100 | 223.4 |
| 177 | 12-ft lane with AC shoulder | 9 | 10 | 30 | 225.8 |
| 177 | 14-ft lane with AC shoulder | 6 | 10 | 100 | 225.3 |
| 315 | 12-ft lane with tied PCC shoulder | 6 | 4 | 100 | 224.9 |
| 315 | 12-ft lane with AC shoulder | 6 | 4 | 200 | 223.2 |
| 315 | 12-ft lane with AC shoulder | 7 | 16 | 65 | 223.3 |
| 315 | 14-ft lane with AC shoulder | 6 | 10 | 100 | 224.0 |
| 315 | 14-ft lane with AC shoulder | 6 | 16 | 65 | 225.1 |
| 315 | 14-ft lane with AC shoulder | 7 | 16 | 30 | 223.2 |

**Table H-8: Cross-sections with longitudinal stress of 250 psi under 18-kips single axle loading**

| Joint Spacing (in.) | Lateral Support Condition | Slab Thk. (in.) | Base/Subbase Thk. (in.) | k-value (psi/in.) | Long. Bot. Stress (psi) |
|---|---|---|---|---|---|
| 177 | 12-ft lane with tied PCC shoulder | 6 | 4 | 65 | 250.9 |
| 177 | 12-ft lane with tied PCC shoulder | 6 | 20 | 30 | 248.8 |
| 177 | 12-ft lane with tied PCC shoulder | 7 | 4 | 30 | 250.8 |
| 177 | 12-ft lane with AC shoulder | 6 | 26 | 30 | 249.9 |
| 177 | 12-ft lane with AC shoulder | 7 | 4 | 65 | 251.8 |
| 177 | 12-ft lane with AC shoulder | 8 | 16 | 30 | 251.0 |
| 177 | 14-ft lane with AC shoulder | 6 | 10 | 65 | 251.3 |

**Table H-9: Cross-sections with longitudinal stress of 100 psi under 32-kips tandem axle loading**

| Joint Spacing (in.) | Lateral Support Condition | Slab Thk. (in.) | Base/Subbase Thk. (in.) | k-value (psi/in.) | Long. Bot. Stress (psi) |
|---|---|---|---|---|---|
| 177 | 12-ft lane with tied PCC shoulder | 10 | 26 | 200 | 99.7 |
| 177 | 12-ft lane with tied PCC shoulder | 11 | 4 | 200 | 99.2 |
| 177 | 12-ft lane with tied PCC shoulder | 11 | 10 | 200 | 98.8 |
| 177 | 12-ft lane with tied PCC shoulder | 11 | 26 | 150 | 100.8 |
| 177 | 12-ft lane with tied PCC shoulder | 12 | 4 | 150 | 98.6 |
| 177 | 12-ft lane with tied PCC shoulder | 12 | 10 | 150 | 98.2 |
| 177 | 14-ft lane with AC shoulder | 11 | 16 | 200 | 102.3 |
| 177 | 14-ft lane with AC shoulder | 11 | 20 | 200 | 100.7 |
| 177 | 14-ft lane with AC shoulder | 12 | 20 | 150 | 101.9 |
| 177 | 14-ft lane with AC shoulder | 12 | 26 | 150 | 98.8 |
| 315 | 12-ft lane with tied PCC shoulder | 9 | 26 | 200 | 99.8 |
| 315 | 12-ft lane with tied PCC shoulder | 10 | 4 | 200 | 100.6 |
| 315 | 12-ft lane with tied PCC shoulder | 10 | 10 | 200 | 100.0 |
| 315 | 12-ft lane with tied PCC shoulder | 10 | 16 | 200 | 98.1 |
| 315 | 12-ft lane with tied PCC shoulder | 10 | 26 | 150 | 98.3 |
| 315 | 12-ft lane with tied PCC shoulder | 11 | 26 | 100 | 101.2 |
| 315 | 12-ft lane with tied PCC shoulder | 12 | 4 | 100 | 99.0 |
| 315 | 12-ft lane with tied PCC shoulder | 12 | 10 | 100 | 98.7 |
| 315 | 12-ft lane with tied PCC shoulder | 12 | 16 | 100 | 97.7 |
| 315 | 12-ft lane with AC shoulder | 11 | 26 | 200 | 101.3 |
| 315 | 12-ft lane with AC shoulder | 12 | 4 | 200 | 99.6 |
| 315 | 12-ft lane with AC shoulder | 12 | 10 | 200 | 99.3 |
| 315 | 12-ft lane with AC shoulder | 12 | 16 | 200 | 98.3 |
| 315 | 14-ft lane with AC shoulder | 10 | 16 | 200 | 101.8 |
| 315 | 14-ft lane with AC shoulder | 10 | 20 | 200 | 99.5 |
| 315 | 14-ft lane with AC shoulder | 10 | 26 | 150 | 102.5 |
| 315 | 14-ft lane with AC shoulder | 11 | 4 | 150 | 101.5 |
| 315 | 14-ft lane with AC shoulder | 11 | 10 | 150 | 101.1 |
| 315 | 14-ft lane with AC shoulder | 11 | 16 | 150 | 99.7 |
| 315 | 14-ft lane with AC shoulder | 11 | 20 | 150 | 98.1 |
| 315 | 14-ft lane with AC shoulder | 12 | 20 | 100 | 101.9 |
| 315 | 14-ft lane with AC shoulder | 12 | 26 | 100 | 98.9 |

**Table H-10: Cross-sections with longitudinal stress of 125 psi under 32-kips tandem axle loading**

| Joint Spacing (in.) | Lateral Support Condition | Slab Thk. (in.) | Base/Subbase Thk. (in.) | k-value (psi/in.) | Long. Bot. Stress (psi) |
|---|---|---|---|---|---|
| 177 | 12-ft lane with tied PCC shoulder | 7 | 26 | 200 | 124.9 |
| 177 | 12-ft lane with tied PCC shoulder | 8 | 20 | 200 | 127.2 |
| 177 | 12-ft lane with tied PCC shoulder | 8 | 26 | 150 | 127.4 |
| 177 | 12-ft lane with tied PCC shoulder | 9 | 20 | 150 | 126.2 |
| 177 | 12-ft lane with tied PCC shoulder | 10 | 26 | 100 | 123.6 |
| 177 | 12-ft lane with tied PCC shoulder | 11 | 26 | 65 | 126.7 |
| 177 | 12-ft lane with tied PCC shoulder | 12 | 4 | 65 | 122.6 |
| 177 | 12-ft lane with AC shoulder | 9 | 26 | 200 | 127.3 |
| 177 | 12-ft lane with AC shoulder | 10 | 20 | 200 | 125.8 |
| 177 | 12-ft lane with AC shoulder | 11 | 26 | 150 | 125.6 |
| 177 | 12-ft lane with AC shoulder | 12 | 4 | 150 | 124.0 |
| 177 | 12-ft lane with AC shoulder | 12 | 10 | 150 | 123.6 |
| 177 | 14-ft lane with AC shoulder | 9 | 4 | 200 | 126.4 |
| 177 | 14-ft lane with AC shoulder | 9 | 10 | 200 | 125.5 |
| 177 | 14-ft lane with AC shoulder | 9 | 16 | 200 | 122.6 |
| 177 | 14-ft lane with AC shoulder | 9 | 26 | 150 | 123.3 |
| 177 | 14-ft lane with AC shoulder | 10 | 4 | 150 | 125.8 |
| 177 | 14-ft lane with AC shoulder | 10 | 10 | 150 | 125.2 |
| 177 | 14-ft lane with AC shoulder | 10 | 16 | 150 | 123.0 |
| 177 | 14-ft lane with AC shoulder | 11 | 20 | 100 | 125.5 |
| 177 | 14-ft lane with AC shoulder | 12 | 26 | 65 | 123.1 |
| 315 | 12-ft lane with tied PCC shoulder | 8 | 16 | 200 | 125.9 |
| 315 | 12-ft lane with tied PCC shoulder | 9 | 4 | 150 | 123.2 |
| 315 | 12-ft lane with tied PCC shoulder | 10 | 26 | 65 | 124.9 |
| 315 | 12-ft lane with tied PCC shoulder | 11 | 4 | 65 | 124.0 |
| 315 | 12-ft lane with tied PCC shoulder | 11 | 10 | 65 | 123.5 |
| 315 | 12-ft lane with AC shoulder | 8 | 26 | 200 | 126.2 |
| 315 | 12-ft lane with AC shoulder | 9 | 20 | 200 | 125.2 |
| 315 | 12-ft lane with AC shoulder | 10 | 20 | 150 | 125.1 |
| 315 | 12-ft lane with AC shoulder | 11 | 26 | 100 | 126.0 |
| 315 | 12-ft lane with AC shoulder | 12 | 4 | 100 | 124.4 |
| 315 | 12-ft lane with AC shoulder | 12 | 10 | 100 | 124.1 |
| 315 | 12-ft lane with AC shoulder | 12 | 16 | 100 | 122.8 |
| 315 | 14-ft lane with AC shoulder | 8 | 20 | 200 | 123.9 |
| 315 | 14-ft lane with AC shoulder | 9 | 10 | 150 | 126.6 |
| 315 | 14-ft lane with AC shoulder | 9 | 16 | 150 | 123.5 |
| 315 | 14-ft lane with AC shoulder | 9 | 26 | 100 | 125.3 |
| 315 | 14-ft lane with AC shoulder | 10 | 4 | 100 | 127.0 |
| 315 | 14-ft lane with AC shoulder | 10 | 10 | 100 | 126.3 |
| 315 | 14-ft lane with AC shoulder | 10 | 16 | 100 | 124.1 |
| 315 | 14-ft lane with AC shoulder | 11 | 20 | 65 | 126.7 |

**Table H-11: Cross-sections with longitudinal stress of 150 psi under 32-kips tandem axle loading**

| Joint Spacing (in.) | Lateral Support Condition | Slab Thk. (in.) | Base/Subbase Thk. (in.) | k-value (psi/in.) | Long. Bot. Stress (psi) |
|---|---|---|---|---|---|
| 177 | 12-ft lane with tied PCC shoulder | 7 | 16 | 200 | 150.1 |
| 177 | 12-ft lane with tied PCC shoulder | 8 | 4 | 150 | 151.3 |
| 177 | 12-ft lane with tied PCC shoulder | 8 | 10 | 150 | 149.8 |
| 177 | 12-ft lane with tied PCC shoulder | 9 | 10 | 100 | 151.4 |
| 177 | 12-ft lane with tied PCC shoulder | 9 | 16 | 100 | 147.9 |
| 177 | 12-ft lane with tied PCC shoulder | 10 | 16 | 65 | 150.6 |
| 177 | 12-ft lane with tied PCC shoulder | 11 | 26 | 30 | 148.1 |
| 177 | 12-ft lane with AC shoulder | 8 | 16 | 200 | 150.4 |
| 177 | 12-ft lane with AC shoulder | 8 | 26 | 150 | 149.3 |
| 177 | 12-ft lane with AC shoulder | 9 | 20 | 150 | 150.3 |
| 177 | 12-ft lane with AC shoulder | 11 | 16 | 100 | 151.3 |
| 177 | 12-ft lane with AC shoulder | 11 | 20 | 100 | 148.8 |
| 177 | 12-ft lane with AC shoulder | 12 | 26 | 65 | 148.4 |
| 177 | 14-ft lane with AC shoulder | 8 | 16 | 150 | 149.7 |
| 177 | 14-ft lane with AC shoulder | 8 | 26 | 100 | 151.3 |
| 177 | 14-ft lane with AC shoulder | 9 | 20 | 100 | 150.6 |
| 177 | 14-ft lane with AC shoulder | 10 | 26 | 65 | 147.9 |
| 177 | 14-ft lane with AC shoulder | 12 | 4 | 30 | 152.1 |
| 177 | 14-ft lane with AC shoulder | 12 | 10 | 30 | 151.4 |
| 177 | 14-ft lane with AC shoulder | 12 | 16 | 30 | 149.4 |
| 315 | 12-ft lane with tied PCC shoulder | 8 | 16 | 100 | 150.8 |
| 315 | 12-ft lane with tied PCC shoulder | 8 | 26 | 65 | 147.9 |
| 315 | 12-ft lane with tied PCC shoulder | 9 | 16 | 65 | 149.9 |
| 315 | 12-ft lane with AC shoulder | 7 | 20 | 200 | 151.6 |
| 315 | 12-ft lane with AC shoulder | 8 | 4 | 200 | 149.5 |
| 315 | 12-ft lane with AC shoulder | 8 | 10 | 200 | 147.9 |
| 315 | 12-ft lane with AC shoulder | 8 | 20 | 150 | 150.4 |
| 315 | 12-ft lane with AC shoulder | 10 | 4 | 100 | 148.2 |
| 315 | 12-ft lane with AC shoulder | 11 | 20 | 65 | 150.2 |
| 315 | 14-ft lane with AC shoulder | 7 | 16 | 200 | 148.2 |
| 315 | 14-ft lane with AC shoulder | 7 | 20 | 150 | 150.6 |
| 315 | 14-ft lane with AC shoulder | 7 | 26 | 100 | 147.6 |
| 315 | 14-ft lane with AC shoulder | 8 | 20 | 100 | 149.8 |
| 315 | 14-ft lane with AC shoulder | 9 | 20 | 65 | 152.1 |
| 315 | 14-ft lane with AC shoulder | 12 | 20 | 30 | 152.1 |

**Table H-12: Cross-sections with longitudinal stress of 175 psi under 32-kips tandem axle loading**

| Joint Spacing (in.) | Lateral Support Condition | Slab Thk. (in.) | Base/Subbase Thk. (in.) | k-value (psi/in.) | Long. Bot. Stress (psi) |
|---|---|---|---|---|---|
| 177 | 12-ft lane with tied PCC shoulder | 6 | 16 | 200 | 173.4 |
| 177 | 12-ft lane with tied PCC shoulder | 7 | 4 | 150 | 174.5 |
| 177 | 12-ft lane with tied PCC shoulder | 7 | 20 | 100 | 175.4 |
| 177 | 12-ft lane with tied PCC shoulder | 9 | 4 | 65 | 174.2 |
| 177 | 12-ft lane with tied PCC shoulder | 9 | 10 | 65 | 172.9 |
| 177 | 12-ft lane with tied PCC shoulder | 10 | 20 | 30 | 176.1 |
| 177 | 12-ft lane with AC shoulder | 7 | 4 | 200 | 175.9 |
| 177 | 12-ft lane with AC shoulder | 7 | 10 | 200 | 173.3 |
| 177 | 12-ft lane with AC shoulder | 7 | 20 | 150 | 173.8 |
| 177 | 12-ft lane with AC shoulder | 8 | 4 | 150 | 174.2 |
| 177 | 12-ft lane with AC shoulder | 8 | 10 | 150 | 172.6 |
| 177 | 12-ft lane with AC shoulder | 8 | 26 | 100 | 173.3 |
| 177 | 12-ft lane with AC shoulder | 9 | 20 | 100 | 174.2 |
| 177 | 12-ft lane with AC shoulder | 10 | 26 | 65 | 175.5 |
| 177 | 12-ft lane with AC shoulder | 11 | 4 | 65 | 174.9 |
| 177 | 12-ft lane with AC shoulder | 11 | 10 | 65 | 174.1 |
| 177 | 14-ft lane with AC shoulder | 6 | 16 | 200 | 175.7 |
| 177 | 14-ft lane with AC shoulder | 6 | 20 | 150 | 175.0 |
| 177 | 14-ft lane with AC shoulder | 7 | 10 | 150 | 176.0 |
| 177 | 14-ft lane with AC shoulder | 8 | 10 | 100 | 177.3 |
| 177 | 14-ft lane with AC shoulder | 8 | 26 | 65 | 173.9 |
| 177 | 14-ft lane with AC shoulder | 9 | 20 | 65 | 172.5 |
| 177 | 14-ft lane with AC shoulder | 10 | 26 | 30 | 176.5 |
| 177 | 14-ft lane with AC shoulder | 11 | 4 | 30 | 173.3 |
| 315 | 12-ft lane with tied PCC shoulder | 7 | 16 | 100 | 173.3 |
| 315 | 12-ft lane with tied PCC shoulder | 8 | 10 | 65 | 175.6 |
| 315 | 12-ft lane with tied PCC shoulder | 10 | 4 | 30 | 174.8 |
| 315 | 12-ft lane with tied PCC shoulder | 10 | 10 | 30 | 173.8 |
| 315 | 12-ft lane with AC shoulder | 6 | 26 | 100 | 173.7 |
| 315 | 12-ft lane with AC shoulder | 7 | 16 | 150 | 175.2 |
| 315 | 12-ft lane with AC shoulder | 8 | 16 | 100 | 177.0 |
| 315 | 12-ft lane with AC shoulder | 8 | 26 | 65 | 177.4 |
| 315 | 12-ft lane with AC shoulder | 9 | 20 | 65 | 176.8 |
| 315 | 12-ft lane with AC shoulder | 12 | 26 | 30 | 175.9 |
| 315 | 14-ft lane with AC shoulder | 6 | 26 | 65 | 176.6 |
| 315 | 14-ft lane with AC shoulder | 8 | 16 | 65 | 176.2 |
| 315 | 14-ft lane with AC shoulder | 10 | 20 | 30 | 177.1 |

**Table H-13: Cross-sections with longitudinal stress of 200 psi under 32-kips tandem axle loading**

| Joint Spacing (in.) | Lateral Support Condition | Slab Thk. (in.) | Base/Subbase Thk. (in.) | k-value (psi/in.) | Long. Bot. Stress (psi) |
|---|---|---|---|---|---|
| 177 | 12-ft lane with tied PCC shoulder | 7 | 4 | 100 | 197.9 |
| 177 | 12-ft lane with tied PCC shoulder | 7 | 20 | 65 | 201.5 |
| 177 | 12-ft lane with tied PCC shoulder | 8 | 4 | 65 | 197.9 |
| 177 | 12-ft lane with tied PCC shoulder | 9 | 20 | 30 | 199.9 |
| 177 | 12-ft lane with AC shoulder | 6 | 10 | 200 | 200.2 |
| 177 | 12-ft lane with AC shoulder | 7 | 20 | 100 | 201.7 |
| 177 | 12-ft lane with AC shoulder | 8 | 10 | 100 | 200.8 |
| 177 | 12-ft lane with AC shoulder | 8 | 26 | 65 | 201.2 |
| 177 | 12-ft lane with AC shoulder | 9 | 20 | 65 | 201.6 |
| 177 | 12-ft lane with AC shoulder | 11 | 20 | 30 | 200.0 |
| 177 | 14-ft lane with AC shoulder | 6 | 20 | 100 | 198.6 |
| 177 | 14-ft lane with AC shoulder | 7 | 10 | 100 | 200.9 |
| 177 | 14-ft lane with AC shoulder | 8 | 16 | 65 | 198.0 |
| 177 | 14-ft lane with AC shoulder | 10 | 4 | 30 | 198.2 |
| 315 | 12-ft lane with tied PCC shoulder | 6 | 10 | 150 | 197.7 |
| 315 | 12-ft lane with tied PCC shoulder | 6 | 16 | 100 | 201.5 |
| 315 | 12-ft lane with tied PCC shoulder | 7 | 26 | 30 | 199.7 |
| 315 | 12-ft lane with AC shoulder | 6 | 4 | 200 | 202.2 |
| 315 | 12-ft lane with AC shoulder | 6 | 16 | 150 | 198.4 |
| 315 | 12-ft lane with AC shoulder | 7 | 16 | 100 | 198.3 |
| 315 | 12-ft lane with AC shoulder | 8 | 16 | 65 | 201.7 |
| 315 | 12-ft lane with AC shoulder | 10 | 26 | 30 | 198.7 |
| 315 | 12-ft lane with AC shoulder | 11 | 4 | 30 | 201.2 |
| 315 | 12-ft lane with AC shoulder | 11 | 10 | 30 | 200.3 |
| 315 | 12-ft lane with AC shoulder | 11 | 16 | 30 | 197.5 |
| 315 | 14-ft lane with AC shoulder | 6 | 10 | 150 | 201.0 |
| 315 | 14-ft lane with AC shoulder | 7 | 16 | 65 | 200.9 |
| 315 | 14-ft lane with AC shoulder | 9 | 16 | 30 | 198.9 |

**Table H-14: Cross-sections with longitudinal stress of 225 psi under 32-kips tandem axle loading**

| Joint Spacing (in.) | Lateral Support Condition | Slab Thk. (in.) | Base/Subbase Thk. (in.) | k-value (psi/in.) | Long. Bot. Stress (psi) |
|---|---|---|---|---|---|
| 177 | 12-ft lane with tied PCC shoulder | 7 | 4 | 65 | 227.3 |
| 177 | 12-ft lane with tied PCC shoulder | 7 | 10 | 65 | 223.9 |
| 177 | 12-ft lane with tied PCC shoulder | 7 | 26 | 30 | 223.9 |
| 177 | 12-ft lane with tied PCC shoulder | 8 | 20 | 30 | 226.5 |
| 177 | 12-ft lane with AC shoulder | 6 | 4 | 150 | 224.7 |
| 177 | 12-ft lane with AC shoulder | 7 | 4 | 100 | 225.6 |
| 177 | 12-ft lane with AC shoulder | 8 | 16 | 65 | 227.3 |
| 177 | 12-ft lane with AC shoulder | 10 | 20 | 30 | 224.3 |
| 177 | 14-ft lane with AC shoulder | 9 | 10 | 30 | 225.5 |
| 315 | 12-ft lane with tied PCC shoulder | 6 | 4 | 100 | 224.5 |
| 315 | 12-ft lane with tied PCC shoulder | 6 | 16 | 65 | 225.1 |
| 315 | 12-ft lane with tied PCC shoulder | 7 | 20 | 30 | 226.6 |
| 315 | 12-ft lane with AC shoulder | 6 | 16 | 100 | 223.7 |
| 315 | 12-ft lane with AC shoulder | 7 | 16 | 65 | 225.6 |
| 315 | 12-ft lane with AC shoulder | 8 | 26 | 30 | 224.6 |
| 315 | 12-ft lane with AC shoulder | 9 | 20 | 30 | 225.7 |
| 315 | 14-ft lane with AC shoulder | 6 | 10 | 100 | 223.6 |

**Table H-15: Cross-sections with longitudinal stress of 250 psi under 32-kips tandem axle loading**

| Joint Spacing (in.) | Lateral Support Condition | Slab Thk. (in.) | Base/Subbase Thk. (in.) | k-value (psi/in.) | Long. Bot. Stress (psi) |
|---|---|---|---|---|---|
| 177 | 12-ft lane with tied PCC shoulder | 8 | 4 | 30 | 248.2 |
| 177 | 12-ft lane with AC shoulder | 6 | 10 | 100 | 251.5 |
| 177 | 12-ft lane with AC shoulder | 7 | 16 | 65 | 248.7 |
| 177 | 12-ft lane with AC shoulder | 9 | 20 | 30 | 250.8 |
| 177 | 14-ft lane with AC shoulder | 6 | 16 | 65 | 248.4 |
| 177 | 14-ft lane with AC shoulder | 8 | 16 | 30 | 249.4 |
| 315 | 12-ft lane with tied PCC shoulder | 6 | 4 | 65 | 250.6 |
| 315 | 12-ft lane with AC shoulder | 6 | 4 | 100 | 247.9 |
| 315 | 14-ft lane with AC shoulder | 6 | 10 | 65 | 251.0 |
| 315 | 14-ft lane with AC shoulder | 7 | 16 | 30 | 249.8 |

**Table H-16: Cross-sections with longitudinal stress of 75 psi under 39-kips tridem axle loading**

| Joint Spacing (in.) | Lateral Support Condition | Slab Thk. (in.) | Base/Subbase Thk. (in.) | k-value (psi/in.) | Long. Bot. Stress (psi) |
|---|---|---|---|---|---|
| 177 | 12-ft lane with tied PCC shoulder | 11 | 16 | 200 | 76.7 |
| 177 | 12-ft lane with tied PCC shoulder | 11 | 20 | 200 | 75.4 |
| 177 | 12-ft lane with tied PCC shoulder | 12 | 4 | 150 | 76.3 |
| 177 | 12-ft lane with tied PCC shoulder | 12 | 10 | 150 | 76.0 |
| 177 | 12-ft lane with tied PCC shoulder | 12 | 16 | 150 | 75.2 |
| 177 | 12-ft lane with tied PCC shoulder | 12 | 20 | 150 | 74.1 |
| 177 | 14-ft lane with AC shoulder | 11 | 26 | 200 | 75.6 |
| 177 | 14-ft lane with AC shoulder | 12 | 4 | 200 | 74.0 |
| 177 | 14-ft lane with AC shoulder | 12 | 10 | 200 | 73.7 |
| 177 | 14-ft lane with AC shoulder | 12 | 16 | 200 | 72.9 |
| 177 | 14-ft lane with AC shoulder | 12 | 26 | 150 | 75.7 |
| 315 | 12-ft lane with tied PCC shoulder | 9 | 26 | 200 | 76.8 |
| 315 | 12-ft lane with tied PCC shoulder | 10 | 4 | 200 | 77.1 |
| 315 | 12-ft lane with tied PCC shoulder | 10 | 10 | 200 | 76.6 |
| 315 | 12-ft lane with tied PCC shoulder | 10 | 16 | 200 | 75.2 |
| 315 | 12-ft lane with tied PCC shoulder | 10 | 20 | 200 | 73.5 |
| 315 | 12-ft lane with tied PCC shoulder | 10 | 26 | 150 | 75.2 |
| 315 | 12-ft lane with tied PCC shoulder | 11 | 4 | 150 | 74.4 |
| 315 | 12-ft lane with tied PCC shoulder | 11 | 10 | 150 | 74.1 |
| 315 | 12-ft lane with tied PCC shoulder | 11 | 16 | 150 | 73.1 |
| 315 | 12-ft lane with tied PCC shoulder | 12 | 10 | 100 | 77.4 |
| 315 | 12-ft lane with tied PCC shoulder | 12 | 16 | 100 | 76.7 |
| 315 | 12-ft lane with tied PCC shoulder | 12 | 20 | 100 | 75.8 |
| 315 | 12-ft lane with tied PCC shoulder | 12 | 26 | 100 | 73.6 |
| 315 | 12-ft lane with AC shoulder | 11 | 4 | 200 | 77.4 |
| 315 | 12-ft lane with AC shoulder | 11 | 10 | 200 | 77.1 |
| 315 | 12-ft lane with AC shoulder | 11 | 16 | 200 | 76.1 |
| 315 | 12-ft lane with AC shoulder | 11 | 20 | 200 | 74.9 |
| 315 | 14-ft lane with AC shoulder | 10 | 16 | 200 | 77.2 |
| 315 | 14-ft lane with AC shoulder | 10 | 20 | 200 | 75.4 |
| 315 | 14-ft lane with AC shoulder | 11 | 4 | 150 | 77.2 |
| 315 | 14-ft lane with AC shoulder | 11 | 10 | 150 | 76.9 |
| 315 | 14-ft lane with AC shoulder | 11 | 16 | 150 | 75.9 |
| 315 | 14-ft lane with AC shoulder | 11 | 20 | 150 | 74.6 |

**Table H-17: Cross-sections with longitudinal stress of 100 psi under 39-kips tridem axle loading**

| Joint Spacing (in.) | Lateral Support Condition | Slab Thk. (in.) | Base/Subbase Thk. (in.) | k-value (psi/in.) | Long. Bot. Stress (psi) |
|---|---|---|---|---|---|
| 177 | 12-ft lane with tied PCC shoulder | 9 | 4 | 200 | 99.4 |
| 177 | 12-ft lane with tied PCC shoulder | 9 | 10 | 200 | 98.6 |
| 177 | 12-ft lane with tied PCC shoulder | 9 | 20 | 150 | 100.7 |
| 177 | 12-ft lane with tied PCC shoulder | 10 | 20 | 100 | 101.2 |
| 177 | 12-ft lane with tied PCC shoulder | 11 | 20 | 65 | 101.4 |
| 177 | 12-ft lane with AC shoulder | 9 | 26 | 200 | 98.2 |
| 177 | 12-ft lane with AC shoulder | 10 | 4 | 200 | 100.1 |
| 177 | 12-ft lane with AC shoulder | 10 | 10 | 200 | 99.6 |
| 177 | 12-ft lane with AC shoulder | 10 | 16 | 200 | 97.9 |
| 177 | 12-ft lane with AC shoulder | 10 | 26 | 150 | 100.7 |
| 177 | 12-ft lane with AC shoulder | 11 | 4 | 150 | 100.7 |
| 177 | 12-ft lane with AC shoulder | 11 | 10 | 150 | 100.3 |
| 177 | 12-ft lane with AC shoulder | 11 | 16 | 150 | 99.0 |
| 177 | 14-ft lane with AC shoulder | 8 | 26 | 200 | 97.6 |
| 177 | 14-ft lane with AC shoulder | 9 | 4 | 200 | 102.3 |
| 177 | 14-ft lane with AC shoulder | 9 | 10 | 200 | 101.5 |
| 177 | 14-ft lane with AC shoulder | 9 | 16 | 200 | 99.0 |
| 177 | 14-ft lane with AC shoulder | 10 | 4 | 150 | 98.8 |
| 177 | 14-ft lane with AC shoulder | 10 | 10 | 150 | 98.2 |
| 177 | 14-ft lane with AC shoulder | 10 | 26 | 100 | 100.7 |
| 177 | 14-ft lane with AC shoulder | 11 | 4 | 100 | 99.9 |
| 177 | 14-ft lane with AC shoulder | 11 | 10 | 100 | 99.4 |
| 177 | 14-ft lane with AC shoulder | 11 | 16 | 100 | 98.0 |
| 177 | 14-ft lane with AC shoulder | 12 | 16 | 65 | 101.8 |
| 177 | 14-ft lane with AC shoulder | 12 | 20 | 65 | 100.4 |
| 315 | 12-ft lane with tied PCC shoulder | 7 | 26 | 150 | 100.1 |
| 315 | 12-ft lane with tied PCC shoulder | 8 | 16 | 200 | 98.9 |
| 315 | 12-ft lane with tied PCC shoulder | 8 | 20 | 150 | 100.3 |
| 315 | 12-ft lane with tied PCC shoulder | 8 | 26 | 100 | 100.4 |
| 315 | 12-ft lane with tied PCC shoulder | 9 | 16 | 100 | 101.6 |
| 315 | 12-ft lane with tied PCC shoulder | 9 | 20 | 100 | 98.6 |
| 315 | 12-ft lane with tied PCC shoulder | 10 | 26 | 65 | 98.1 |
| 315 | 12-ft lane with tied PCC shoulder | 11 | 4 | 65 | 98.1 |
| 315 | 12-ft lane with tied PCC shoulder | 11 | 10 | 65 | 97.8 |
| 315 | 12-ft lane with AC shoulder | 7 | 26 | 200 | 99.6 |
| 315 | 12-ft lane with AC shoulder | 8 | 20 | 200 | 100.4 |
| 315 | 12-ft lane with AC shoulder | 8 | 26 | 150 | 98.6 |
| 315 | 12-ft lane with AC shoulder | 9 | 16 | 150 | 100.3 |
| 315 | 12-ft lane with AC shoulder | 10 | 26 | 100 | 100.3 |
| 315 | 12-ft lane with AC shoulder | 11 | 10 | 100 | 102.4 |
| 315 | 12-ft lane with AC shoulder | 11 | 16 | 100 | 101.3 |
| 315 | 12-ft lane with AC shoulder | 11 | 20 | 100 | 100.0 |
| 315 | 12-ft lane with AC shoulder | 12 | 4 | 100 | 98.2 |
| 315 | 12-ft lane with AC shoulder | 12 | 10 | 100 | 98.0 |
| 315 | 14-ft lane with AC shoulder | 7 | 26 | 150 | 101.9 |
| 315 | 14-ft lane with AC shoulder | 8 | 16 | 200 | 100.5 |
| 315 | 14-ft lane with AC shoulder | 8 | 20 | 150 | 102.4 |
| 315 | 14-ft lane with AC shoulder | 9 | 20 | 100 | 101.9 |
| 315 | 14-ft lane with AC shoulder | 11 | 16 | 65 | 102.4 |
| 315 | 14-ft lane with AC shoulder | 11 | 20 | 65 | 101.1 |
| 315 | 14-ft lane with AC shoulder | 11 | 26 | 65 | 97.9 |
| 315 | 14-ft lane with AC shoulder | 12 | 4 | 65 | 98.7 |
| 315 | 14-ft lane with AC shoulder | 12 | 10 | 65 | 98.4 |
| 315 | 14-ft lane with AC shoulder | 12 | 16 | 65 | 97.6 |

**Table H-18: Cross-sections with longitudinal stress of 125 psi under 39-kips tridem axle loading**

| Joint Spacing (in.) | Lateral Support Condition | Slab Thk. (in.) | Base/Subbase Thk. (in.) | k-value (psi/in.) | Long. Bot. Stress (psi) |
|---|---|---|---|---|---|
| 177 | 12-ft lane with tied PCC shoulder | 7 | 26 | 100 | 124.5 |
| 177 | 12-ft lane with tied PCC shoulder | 8 | 4 | 150 | 123.8 |
| 177 | 12-ft lane with tied PCC shoulder | 8 | 20 | 100 | 126.2 |
| 177 | 12-ft lane with tied PCC shoulder | 9 | 20 | 65 | 126.9 |
| 177 | 12-ft lane with tied PCC shoulder | 11 | 16 | 30 | 127.4 |
| 177 | 12-ft lane with tied PCC shoulder | 11 | 20 | 30 | 125.0 |
| 177 | 12-ft lane with AC shoulder | 7 | 26 | 150 | 123.6 |
| 177 | 12-ft lane with AC shoulder | 8 | 4 | 200 | 125.8 |
| 177 | 12-ft lane with AC shoulder | 8 | 10 | 200 | 124.5 |
| 177 | 12-ft lane with AC shoulder | 8 | 20 | 150 | 126.3 |
| 177 | 12-ft lane with AC shoulder | 9 | 26 | 100 | 123.4 |
| 177 | 12-ft lane with AC shoulder | 10 | 4 | 100 | 126.2 |
| 177 | 12-ft lane with AC shoulder | 10 | 10 | 100 | 125.5 |
| 177 | 12-ft lane with AC shoulder | 10 | 16 | 100 | 123.3 |
| 177 | 12-ft lane with AC shoulder | 12 | 4 | 65 | 126.8 |
| 177 | 12-ft lane with AC shoulder | 12 | 10 | 65 | 126.3 |
| 177 | 12-ft lane with AC shoulder | 12 | 16 | 65 | 125.0 |
| 177 | 12-ft lane with AC shoulder | 12 | 20 | 65 | 123.4 |
| 177 | 14-ft lane with AC shoulder | 6 | 26 | 150 | 122.5 |
| 177 | 14-ft lane with AC shoulder | 8 | 4 | 150 | 127.1 |
| 177 | 14-ft lane with AC shoulder | 8 | 10 | 150 | 125.7 |
| 177 | 14-ft lane with AC shoulder | 9 | 4 | 100 | 125.2 |
| 177 | 14-ft lane with AC shoulder | 9 | 10 | 100 | 124.3 |
| 177 | 14-ft lane with AC shoulder | 9 | 26 | 65 | 123.8 |
| 177 | 14-ft lane with AC shoulder | 10 | 4 | 65 | 125.7 |
| 177 | 14-ft lane with AC shoulder | 10 | 10 | 65 | 124.9 |
| 177 | 14-ft lane with AC shoulder | 12 | 4 | 30 | 124.5 |
| 177 | 14-ft lane with AC shoulder | 12 | 10 | 30 | 124.0 |
| 315 | 12-ft lane with tied PCC shoulder | 7 | 4 | 200 | 126.7 |
| 315 | 12-ft lane with tied PCC shoulder | 7 | 10 | 200 | 124.3 |
| 315 | 12-ft lane with tied PCC shoulder | 7 | 16 | 150 | 123.4 |
| 315 | 12-ft lane with tied PCC shoulder | 7 | 20 | 100 | 125.7 |
| 315 | 12-ft lane with tied PCC shoulder | 7 | 26 | 65 | 122.6 |
| 315 | 12-ft lane with tied PCC shoulder | 8 | 20 | 65 | 124.5 |
| 315 | 12-ft lane with tied PCC shoulder | 12 | 4 | 30 | 127.3 |
| 315 | 12-ft lane with tied PCC shoulder | 12 | 10 | 30 | 127.0 |
| 315 | 12-ft lane with tied PCC shoulder | 12 | 16 | 30 | 125.8 |
| 315 | 12-ft lane with tied PCC shoulder | 12 | 20 | 30 | 124.5 |
| 315 | 12-ft lane with AC shoulder | 6 | 26 | 100 | 126.4 |
| 315 | 12-ft lane with AC shoulder | 8 | 16 | 100 | 126.5 |
| 315 | 12-ft lane with AC shoulder | 9 | 26 | 65 | 125.2 |
| 315 | 12-ft lane with AC shoulder | 10 | 20 | 65 | 126.5 |
| 315 | 12-ft lane with AC shoulder | 11 | 4 | 65 | 125.0 |
| 315 | 12-ft lane with AC shoulder | 11 | 10 | 65 | 124.5 |
| 315 | 12-ft lane with AC shoulder | 11 | 16 | 65 | 123.2 |
| 315 | 14-ft lane with AC shoulder | 7 | 10 | 200 | 125.4 |
| 315 | 14-ft lane with AC shoulder | 7 | 16 | 150 | 125.2 |
| 315 | 14-ft lane with AC shoulder | 7 | 26 | 65 | 126.2 |
| 315 | 14-ft lane with AC shoulder | 8 | 4 | 100 | 124.2 |
| 315 | 14-ft lane with AC shoulder | 8 | 10 | 100 | 122.8 |
| 315 | 14-ft lane with AC shoulder | 9 | 4 | 65 | 123.9 |
| 315 | 14-ft lane with AC shoulder | 9 | 10 | 65 | 123.0 |

**Table H-19: Cross-sections with longitudinal stress of 150 psi under 39-kips tridem axle loading**

| Joint Spacing (in.) | Lateral Support Condition | Slab Thk. (in.) | Base/Subbase Thk. (in.) | k-value (psi/in.) | Long. Bot. Stress (psi) |
|---|---|---|---|---|---|
| 177 | 12-ft lane with tied PCC shoulder | 6 | 16 | 200 | 151.8 |
| 177 | 12-ft lane with tied PCC shoulder | 6 | 26 | 65 | 149.3 |
| 177 | 12-ft lane with tied PCC shoulder | 7 | 16 | 100 | 151.1 |
| 177 | 12-ft lane with tied PCC shoulder | 8 | 16 | 65 | 148.5 |
| 177 | 12-ft lane with AC shoulder | 7 | 16 | 150 | 148.2 |
| 177 | 12-ft lane with AC shoulder | 8 | 16 | 100 | 149.8 |
| 177 | 12-ft lane with AC shoulder | 8 | 26 | 65 | 151.6 |
| 177 | 12-ft lane with AC shoulder | 9 | 20 | 65 | 150.9 |
| 177 | 12-ft lane with AC shoulder | 10 | 4 | 65 | 148.0 |
| 177 | 12-ft lane with AC shoulder | 12 | 16 | 30 | 151.3 |
| 177 | 12-ft lane with AC shoulder | 12 | 20 | 30 | 148.9 |
| 177 | 14-ft lane with AC shoulder | 6 | 20 | 150 | 148.1 |
| 177 | 14-ft lane with AC shoulder | 7 | 4 | 150 | 149.3 |
| 177 | 14-ft lane with AC shoulder | 8 | 20 | 65 | 148.2 |
| 177 | 14-ft lane with AC shoulder | 10 | 20 | 30 | 150.0 |
| 315 | 12-ft lane with tied PCC shoulder | 6 | 16 | 150 | 148.4 |
| 315 | 12-ft lane with tied PCC shoulder | 7 | 16 | 65 | 148.5 |
| 315 | 12-ft lane with tied PCC shoulder | 8 | 26 | 30 | 147.6 |
| 315 | 12-ft lane with tied PCC shoulder | 9 | 16 | 30 | 152.1 |
| 315 | 12-ft lane with tied PCC shoulder | 9 | 20 | 30 | 148.5 |
| 315 | 12-ft lane with AC shoulder | 6 | 20 | 100 | 152.3 |
| 315 | 12-ft lane with AC shoulder | 7 | 10 | 100 | 151.6 |
| 315 | 12-ft lane with AC shoulder | 8 | 4 | 65 | 151.5 |
| 315 | 12-ft lane with AC shoulder | 8 | 10 | 65 | 149.9 |
| 315 | 14-ft lane with AC shoulder | 6 | 16 | 150 | 149.7 |
| 315 | 14-ft lane with AC shoulder | 7 | 16 | 65 | 152.4 |
| 315 | 14-ft lane with AC shoulder | 9 | 26 | 30 | 149.0 |
| 315 | 14-ft lane with AC shoulder | 10 | 20 | 30 | 149.9 |

**Table H-20: Cross-sections with longitudinal stress of 175 psi under 39-kips tridem axle loading**

| Joint Spacing (in.) | Lateral Support Condition | Slab Thk. (in.) | Base/Subbase Thk. (in.) | k-value (psi/in.) | Long. Bot. Stress (psi) |
|---|---|---|---|---|---|
| 177 | 12-ft lane with tied PCC shoulder | 6 | 10 | 150 | 175.4 |
| 177 | 12-ft lane with tied PCC shoulder | 6 | 16 | 100 | 176.2 |
| 177 | 12-ft lane with tied PCC shoulder | 7 | 26 | 30 | 172.7 |
| 177 | 12-ft lane with tied PCC shoulder | 8 | 20 | 30 | 174.3 |
| 177 | 12-ft lane with AC shoulder | 6 | 10 | 200 | 173.1 |
| 177 | 12-ft lane with AC shoulder | 6 | 20 | 100 | 174.5 |
| 177 | 12-ft lane with AC shoulder | 7 | 10 | 100 | 176.1 |
| 177 | 12-ft lane with AC shoulder | 10 | 26 | 30 | 172.7 |
| 177 | 14-ft lane with AC shoulder | 6 | 10 | 150 | 177.4 |
| 177 | 14-ft lane with AC shoulder | 7 | 16 | 65 | 175.4 |
| 177 | 14-ft lane with AC shoulder | 9 | 10 | 30 | 176.3 |
| 315 | 12-ft lane with tied PCC shoulder | 6 | 10 | 100 | 174.1 |
| 315 | 12-ft lane with tied PCC shoulder | 6 | 16 | 65 | 174.0 |
| 315 | 12-ft lane with tied PCC shoulder | 7 | 20 | 30 | 175.9 |
| 315 | 12-ft lane with tied PCC shoulder | 8 | 4 | 30 | 173.7 |
| 315 | 12-ft lane with AC shoulder | 6 | 4 | 150 | 172.7 |
| 315 | 12-ft lane with AC shoulder | 7 | 4 | 65 | 173.6 |
| 315 | 12-ft lane with AC shoulder | 9 | 26 | 30 | 175.9 |
| 315 | 12-ft lane with AC shoulder | 11 | 4 | 30 | 176.7 |
| 315 | 12-ft lane with AC shoulder | 11 | 10 | 30 | 176.0 |
| 315 | 12-ft lane with AC shoulder | 11 | 16 | 30 | 173.8 |
| 315 | 14-ft lane with AC shoulder | 6 | 10 | 100 | 176.3 |
| 315 | 14-ft lane with AC shoulder | 8 | 16 | 30 | 173.2 |

**Table H-21: Cross-sections with longitudinal stress of 200 psi under 39-kips tridem axle loading**

| Joint Spacing (in.) | Lateral Support Condition | Slab Thk. (in.) | Base/Subbase Thk. (in.) | k-value (psi/in.) | Long. Bot. Stress (psi) |
|---|---|---|---|---|---|
| 177 | 12-ft lane with tied PCC shoulder | 7 | 20 | 30 | 197.6 |
| 177 | 12-ft lane with AC shoulder | 6 | 20 | 65 | 198.7 |
| 177 | 12-ft lane with AC shoulder | 7 | 10 | 65 | 202.0 |
| 177 | 12-ft lane with AC shoulder | 8 | 26 | 30 | 198.3 |
| 177 | 12-ft lane with AC shoulder | 9 | 20 | 30 | 200.1 |
| 177 | 14-ft lane with AC shoulder | 6 | 4 | 100 | 200.2 |
| 177 | 14-ft lane with AC shoulder | 6 | 16 | 65 | 201.2 |
| 177 | 14-ft lane with AC shoulder | 8 | 4 | 30 | 201.2 |
| 177 | 14-ft lane with AC shoulder | 8 | 10 | 30 | 198.8 |
| 315 | 12-ft lane with tied PCC shoulder | 7 | 4 | 30 | 198.3 |
| 315 | 12-ft lane with AC shoulder | 6 | 10 | 65 | 201.6 |
| 315 | 12-ft lane with AC shoulder | 7 | 20 | 30 | 200.7 |
| 315 | 12-ft lane with AC shoulder | 8 | 16 | 30 | 200.4 |
| 315 | 14-ft lane with AC shoulder | 6 | 4 | 65 | 198.5 |
| 315 | 14-ft lane with AC shoulder | 6 | 20 | 30 | 199.6 |
| 315 | 14-ft lane with AC shoulder | 7 | 10 | 30 | 201.8 |

**Table H-22: Cross-sections with longitudinal stress of 225 psi under 39-kips tridem axle loading**

| Joint Spacing (in.) | Lateral Support Condition | Slab Thk. (in.) | Base/Subbase Thk. (in.) | k-value (psi/in.) | Long. Bot. Stress (psi) |
|---|---|---|---|---|---|
| 177 | 12-ft lane with tied PCC shoulder | 7 | 4 | 30 | 225.5 |
| 177 | 12-ft lane with AC shoulder | 8 | 16 | 30 | 225.0 |
| 177 | 14-ft lane with AC shoulder | 6 | 4 | 65 | 223.9 |
| 315 | 12-ft lane with AC shoulder | 7 | 4 | 30 | 224.2 |

# Appendix J

# Hourly Load Spectra from WIM Database

# Appendix K

# Hourly Thermal Gradient from EICM

# Appendix L

# Technology Transfer Package

# A Preliminary Mechanistic Evaluation of PCC Cross-Sections Using ISLAB2000 – A Parametric Study

Neeraj Buch, Ph.D.

Kaenvit Vongchusiri, M.S.

**Michigan State University**

**Department of Civil and Environmental Engineering**

Thomas Van Dam, Ph.D., P.E.

**Michigan Technological University**

**Department of Civil and Environmental Engineering**

*Technology Transfer Workshop Package*

August, 2004

# Contents

# Part I: ISLAB2000 Tutorial

## Pavement Structure

The first step of modeling using ISLAB2000 is to identify the structural features and material properties of the pavement system. To do so, perform the following procedure.

### Step 1: Define Pavement Dimensions, Coordinate System, and FE Mesh Options

To input pavement dimensions, select **Geometry** from the main panel. The geometry panel appears (see Figure 1). In the **X-direction** section, click **Insert** to add shoulder and lane dimensions for the pavement system. In the **Y-direction** section, click **Insert** to add slab dimensions for the pavement system. Note that ISLAB2000 uses a rectangular coordinate system with X-direction in the transverse direction and Y-direction in the longitudinal direction, and the origin is at the left corner of the pavement system.

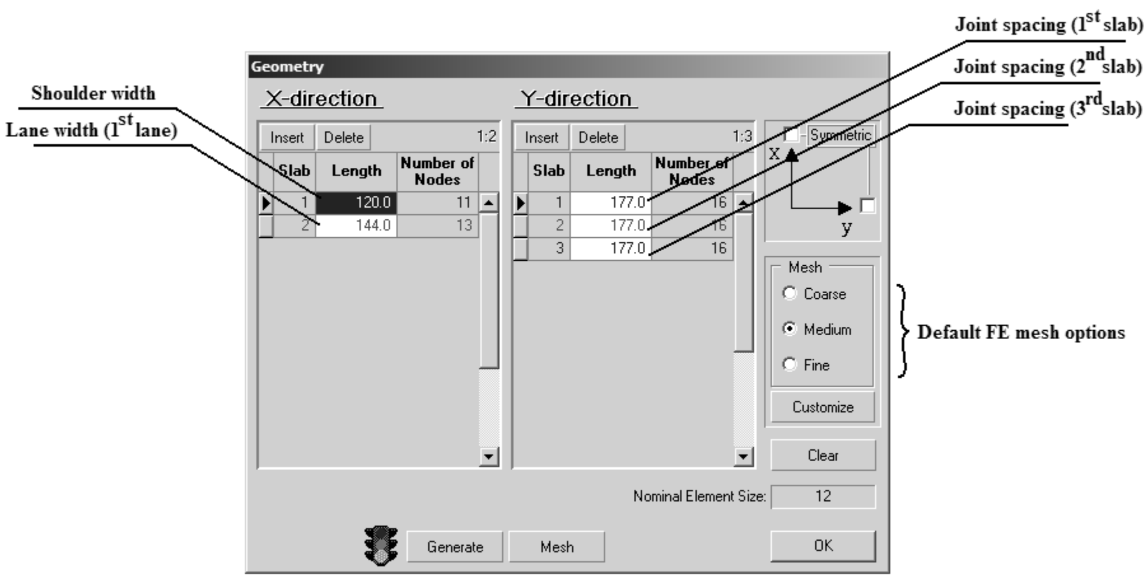


**Figure 1: Geometry Panel**

Three default finite element (FE) mesh options are available: coarse (24 in.), medium (12 in.), and fine (6 in.). To define FE mesh other than the defaults, click **Customize**, and then enter a new nominal element size.

After selecting mesh size, click **Generate** and then click **OK** to close the geometry panel and return to the main panel. Based on the inputs, the main panel displays the plan view of the pavement system as illustrated in Figure 2.

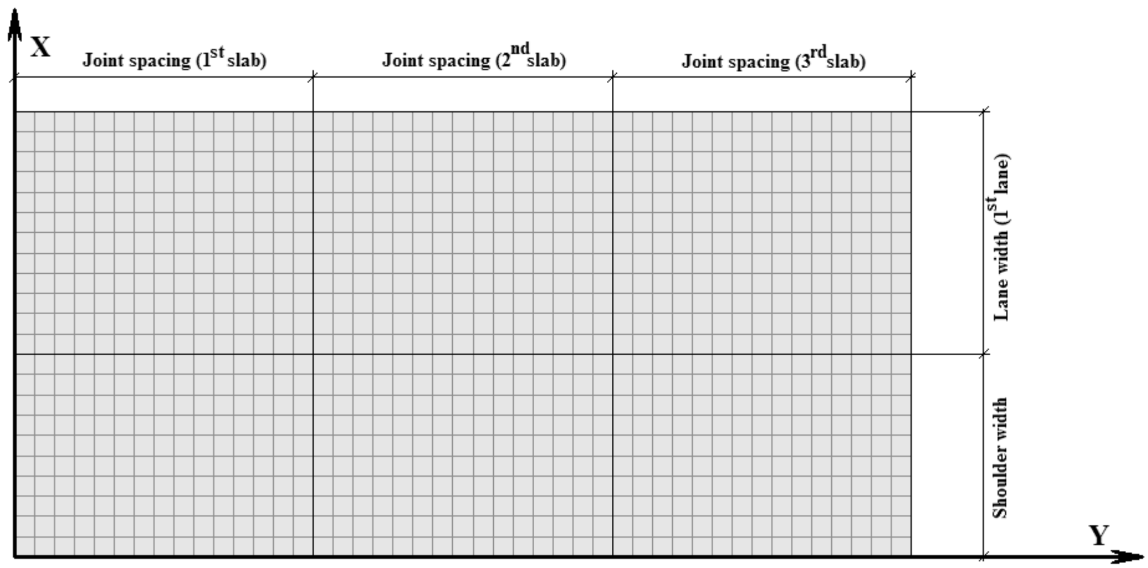


**Figure 2: Plan View of the Pavement System**

### Step 2: Define Layer Thickness and Typical Parameters for Material Properties

To define the thickness of layers and the design parameters, select **Layers** from the main panel. The layers panel appears (see Figure 3). Click **Add Layer** to enter the number of layers required for the design.

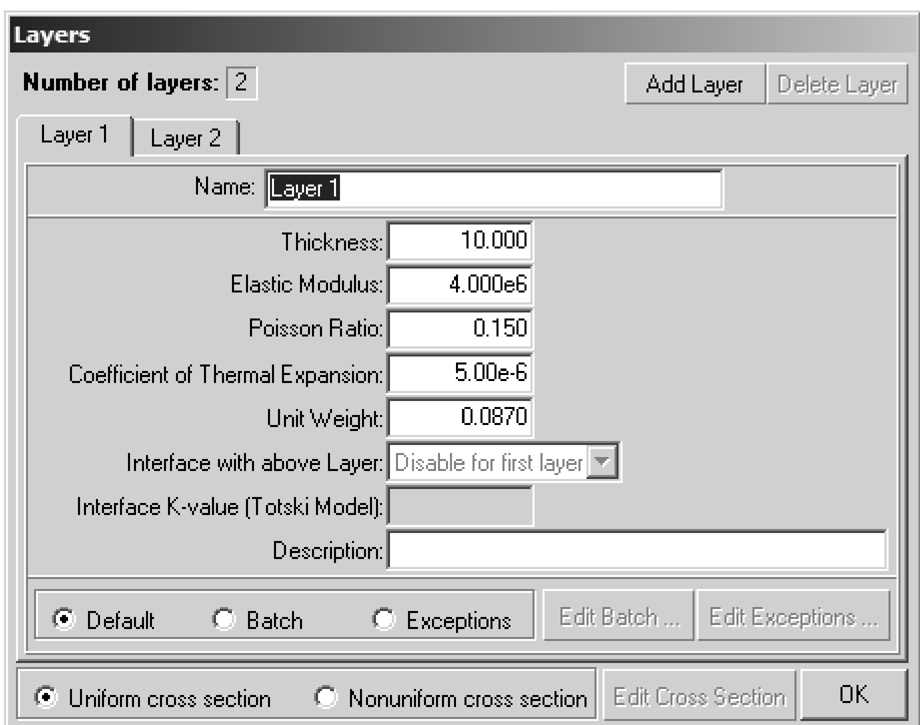


**Figure 3: Layers Panel**

After you enter the necessary layers you can enter the design parameters for each layer, including thickness (in.), elastic modulus (psi), Poisson's ratio, CTE (in./in./$^{o}$F), unit weight (lb/in.$^{3}$), and interface condition between two layers (only layers beneath PCC layer). Table 1 lists typical design parameter values.

| Layers | Design parameters | | | | |
|---|---|---|---|---|---|
| | Elastic modulus (psi) | Poisson's ratio | CTE (in./in./$^{o}$F) | Unit weight (lb/in.$^{3}$) | Interface condition |
| PCC slab | 4,000,000 | 0.15 | $5x10^{-6}$ | 0.087 | - |
| Aggregate base | 30,000 | 0.35 | $2x10^{-6}$ | 0.061 | Unbonded |
| Asphalt treated base | 300,000 | 0.35 | $2x10^{-6}$ | 0.061 | Bonded/unbonded |
| Lean concrete base | 2,000,000 | 0.20 | $4x10^{-6}$ | 0.087 | Bonded/unbonded |
| Sand subbase | 15,000 | 0.35 | $2x10^{-6}$ | 0.061 | Unbonded |

**Table 1: Typical values of design parameters for layers module**
(Sources: Huang (1993), Klieger and Lamond (1994))

## Step 3: Define Subgrade Model and Typical Parameters for Roadbed Soil

To define the design parameter for subgrade model, select **Subgrade** from the main panel. The subgrade panel appears (see Figure 4).

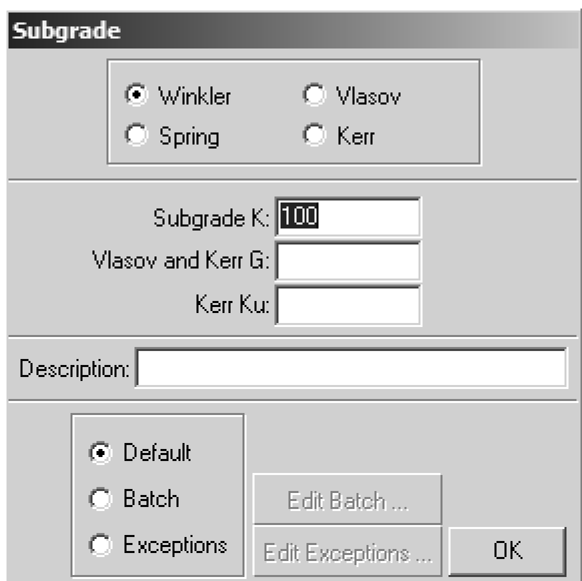


**Figure 4: Subgrade Panel**

Four subgrade models are available in ISLAB2000. In general, Winkler foundation is used in the design. Input for this subgrade model is **Subgrade K** (modulus of subgrade reaction, psi/in.).

## Step 4: Define Transverse and Longitudinal Joints and Typical Inputs for Joint Designs

To define design parameters for joint design, select **Joints** from the main panel. The joints panel appears (see Figure 5). **Joints in x-direction** and **Joints in y-direction** are longitudinal and transverse joints, respectively.

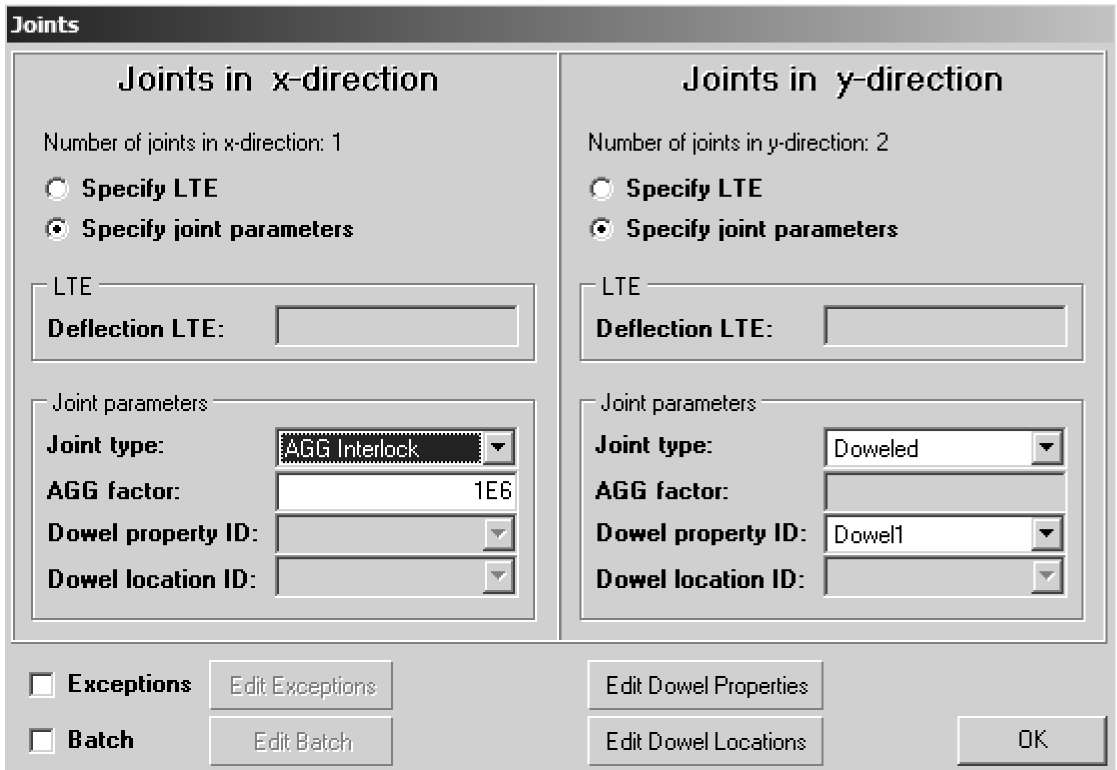


**Figure 5: Joints Panel**

For longitudinal joints, select **AGG Interlock** as the joint type. The value of the **AGG factor** parameter is dependent on the stiffness of the joint. For transverse joints, select **AGG Interlock** as the joint type for undoweled joints; select **Doweled** for the joint type for doweled joints. Example inputs for doweled joint are described in Example 8 of Part 2.

**NOTE**

For a pavement system with an area that differs from the rest of the pavement structure, select **Areas** from the main panel to define a special area. Example inputs for the area module are described in Examples 23 and 26 through 28 of Part 2.

## Vehicle Load

To define and position the load on the pavement, perform the following procedure.

### Step 1: Define the Axle Configuration Model and the Standard Configurations

Select **Load** from the main panel to open the load panel appears (see Figure 6).

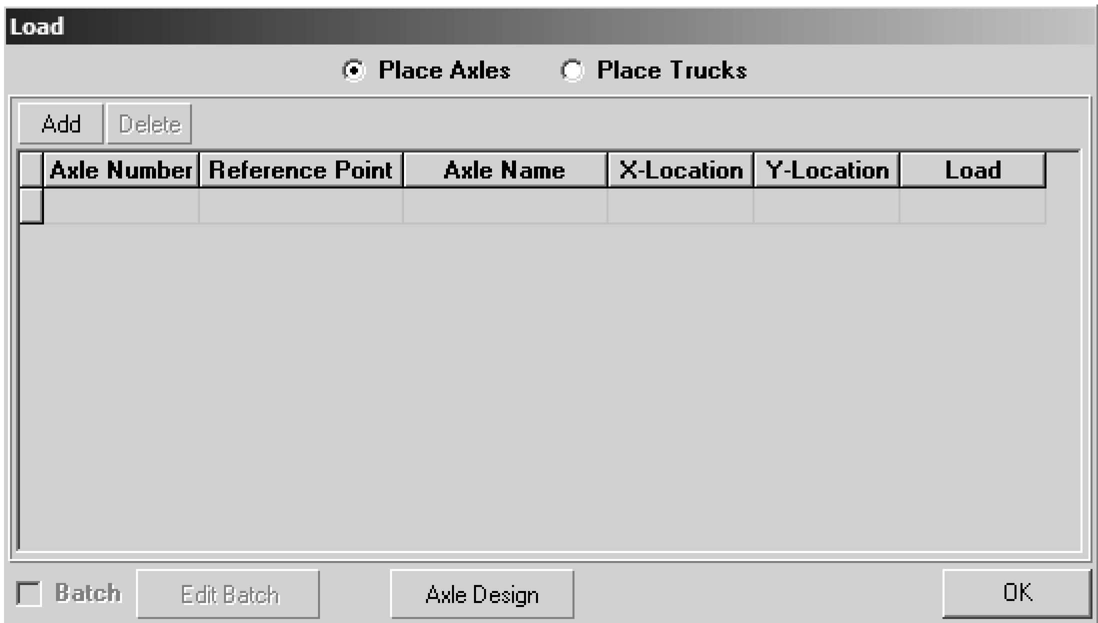


**Figure 6: Load Panel**

From the Load panel, select **Place Axles** and then click **Axle Design** to open the axle design panel (see Figure 7). ISLAB2000 is capable of modeling single, tandem, and tridem axles. Type an axle name into the **Axle Name** field, and then enter values for the data requested. If you do not have axle data specific to your application, use the standard inputs in Table 2.

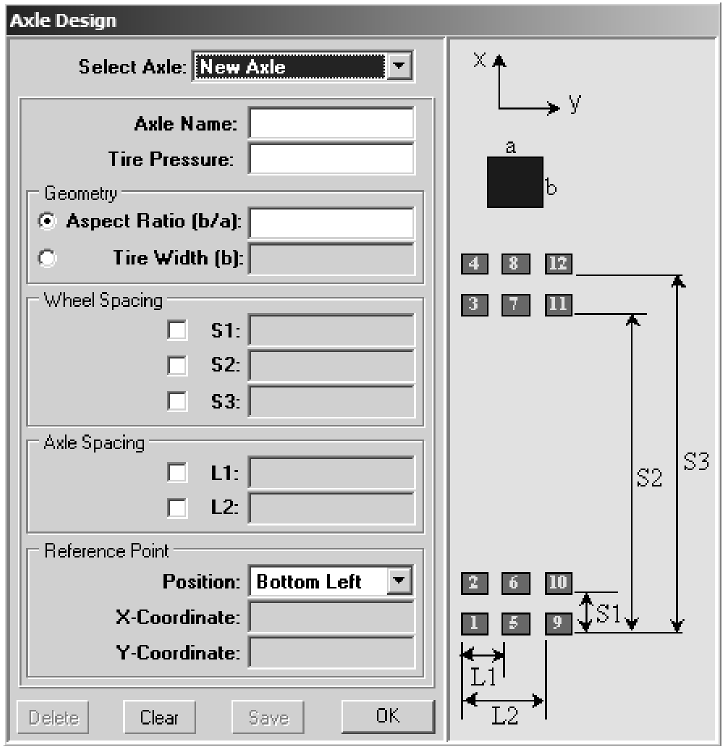


**Figure 7: Axle Design Panel**

| | Loading parameters | | | | | | |
|---|---|---|---|---|---|---|---|
| Axle and wheel type | Tire pressure (psi) | Tire aspect ratio | S1 (in.) | S2 (in.) | S3 (in.) | L1 (in.) | L2 (in.) |
| Single axle with single wheels | 60-120 | 0.5 | 72 | - | - | - | - |
| Single axle with dual wheels | 60-120 | 0.5 | 12 | 72 | 84 | - | - |
| Tandem axle with dual wheels | 60-120 | 0.5 | 12 | 72 | 84 | 42 | - |
| Tridem axle with dual wheels | 60-120 | 0.5 | 12 | 72 | 84 | 42 | 84 |

**Table 2: Standard Loading Parameters**
(Source: Truck Driver's Guidebook, 6th Edition)

**Bottom Left** is the default reference point. In Figure 7 this point corresponds to loading number 1.

### Step 2: Define the Truck Configuration Model

To model a truck loading, all axle components of the truck must already be defined. Select **Place Trucks** on the load panel, and then click **Truck Design**. The truck design panel appears (see Figure 8).

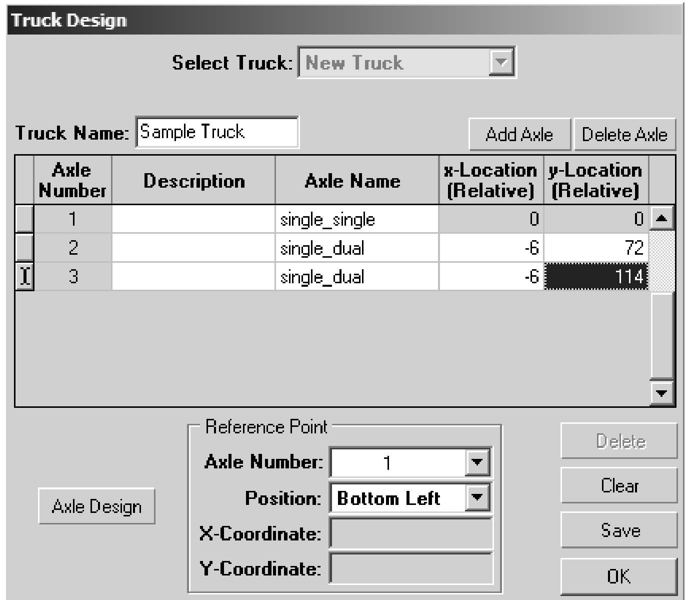


**Figure 8: Truck Design Panel**

Click **Add Axle** to add axles to the truck, and then select the axle name for each axle number corresponding to the axle type required for the truck. Next, enter x and y relative locations for each axle. Finally, select the reference axle of the truck. Axle number one is the default reference axle, but you can use other axles. The inputs used in Figure 8 result in a truck configuration as illustrated in Figure 9.

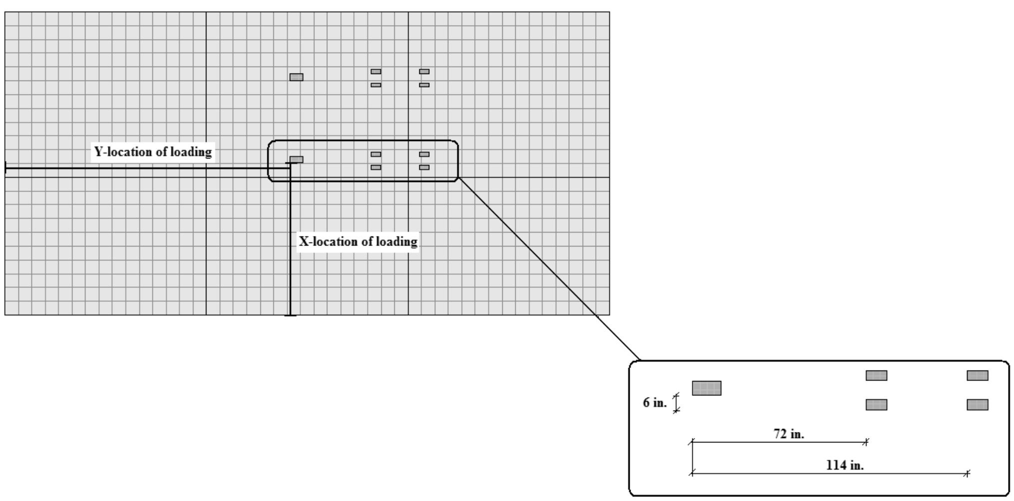


**Figure 9: Illustration of Truck Configuration and Load Location**

## Step 3: Define the Load Positioning System

After completing either axle design or truck design process, the load is to be positioned by identifying the X and Y locations for the axle or truck (see Figure 9).

## Layer Temperature

ISLAB2000 allows you to account for the impact of temperature through two options: *linear thermal gradients* and *non-linear temperature profile*.

- **Linear Thermal Gradient:** The linear thermal gradient is the temperature differential between the top and bottom of the PCC slab divided by the PCC thickness. To define a linear thermal gradient, select **Temperature** from the main panel. The layers temperature properties panel appears (see Figure 10). In the layers temperature properties panel, select the **Perform Temperature Analysis** check box, and then select **Linear** for the type of thermal gradient. In the **Difference** field, enter the temperature differential (in degrees Fahrenheit), which is equal to the thermal gradient multiplied by the PCC thickness.

  **NOTE**
  The positive thermal gradient or daytime gradient indicates that the top layer is warmer than the bottom layer, while negative thermal gradient or nighttime gradient indicates that the bottom layer is warmer than the top layer.

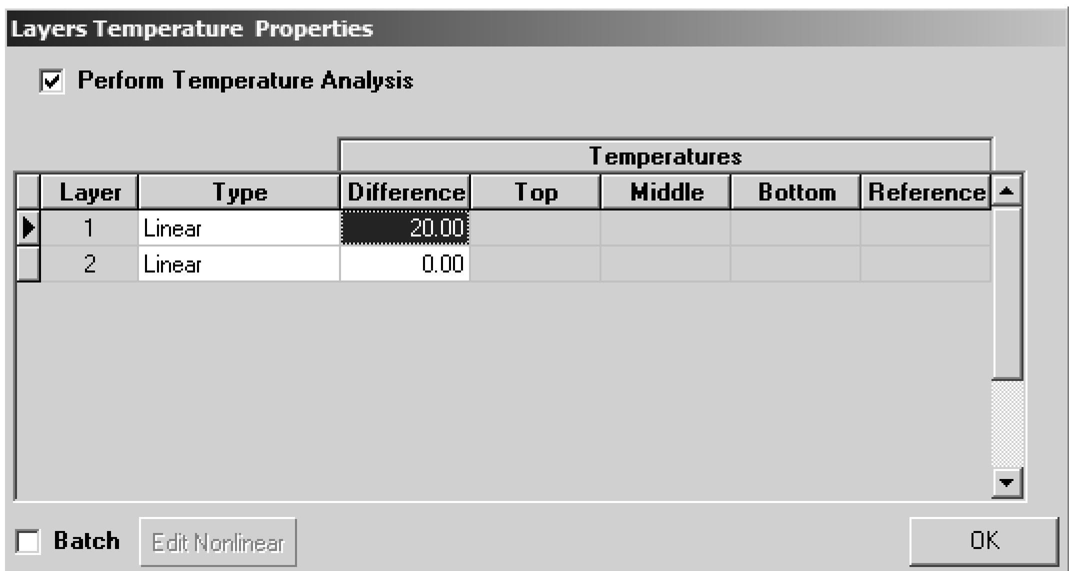


**Figure 10: Layers Temperature Properties Panel**

- **Non-linear Temperature Profile:** This option of temperature analysis requires temperatures from at least three different depths. First, select **Nonlinear** for the analysis type for layer 1 (see Figure 11), and then click on **Edit Nonlinear**.

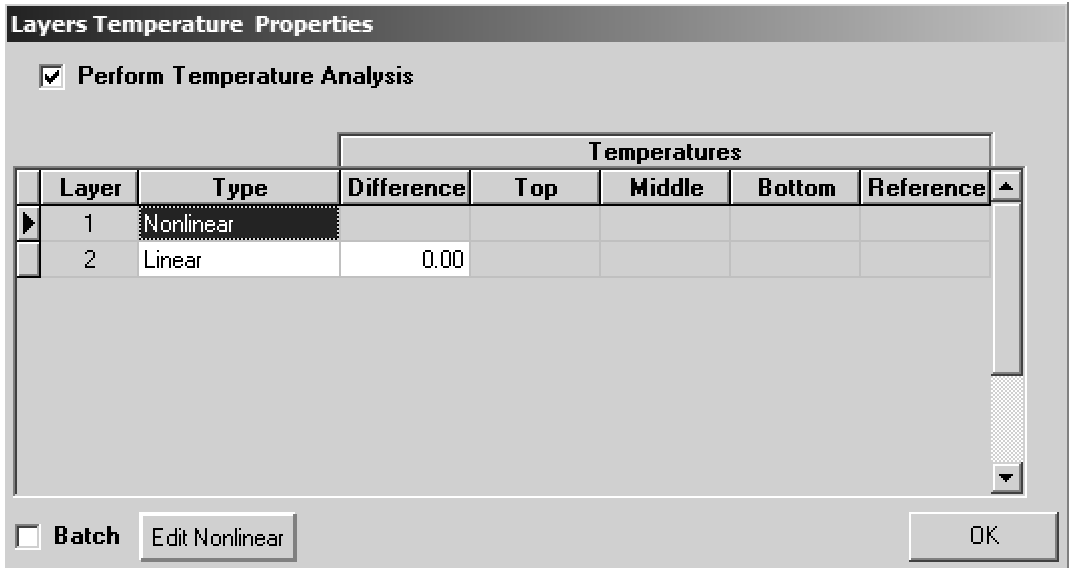


**Figure 11: Layers Temperature Properties Panel**

The edit nonlinear temperature distributions appear (see Figure 12). Type the temperature at each depth. If more temperature nodes are available, click **Insert Temperature Node** to add more temperatures.

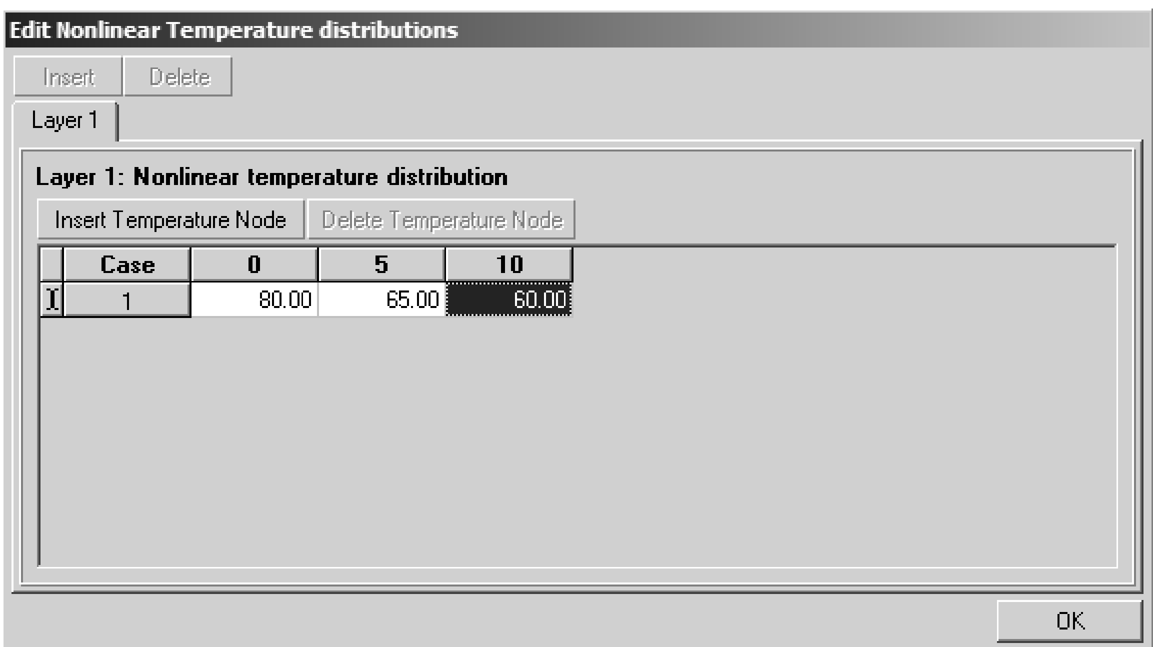


**Figure 12: Edit nonlinear temperature distributions panel**

# Batch Application

Through batch application, ISLAB2000 is capable of performing multiple analyses for structural conditions, loading levels, and temperature conditions. Batch application is available in three structural modules: Layers, Subgrade, and Joints.

- **Layers module:** Batch application allows for adding cases for each layer. The added cases could have thickness, elastic modulus, Poisson's ratio, CTE, unit weight, and also interface condition between two layers different from the original case. Figure 13 illustrates an example of batch application for the layers module.

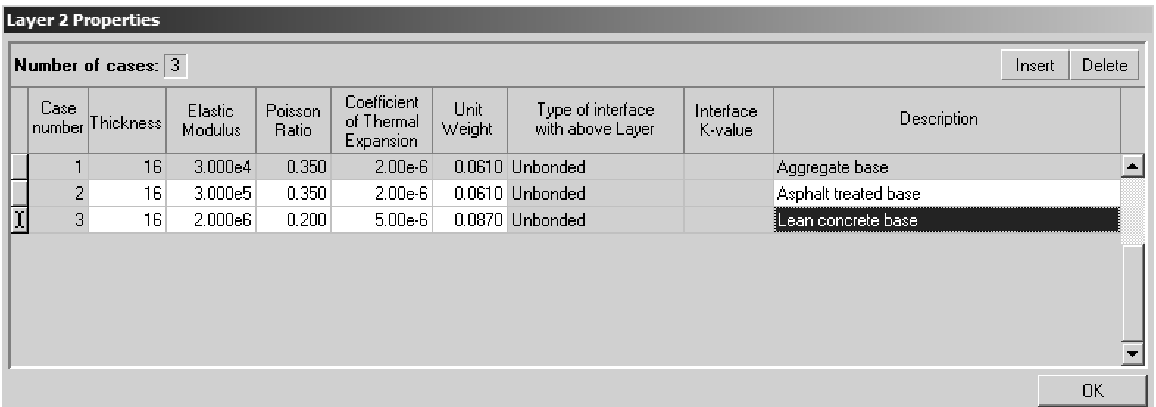

Layer 2 Properties

Number of cases: 3

| Case number | Thickness | Elastic Modulus | Poisson Ratio | Coefficient of Thermal Expansion | Unit Weight | Type of interface with above Layer | Interface K-value | Description |
|---|---|---|---|---|---|---|---|---|
| 1 | 16 | 3.000e4 | 0.350 | 2.00e-6 | 0.0610 | Unbonded | | Aggregate base |
| 2 | 16 | 3.000e5 | 0.350 | 2.00e-6 | 0.0610 | Unbonded | | Asphalt treated base |
| 3 | 16 | 2.000e6 | 0.200 | 5.00e-6 | 0.0870 | Unbonded | | Lean concrete base |



**Figure 13: Batch Application for Layers Module**

- **Multiple analyses for loading levels:** For the load module, batch application allows for analysis of several load levels at the same time. Figure 14 illustrates an example of batch application for the load module.

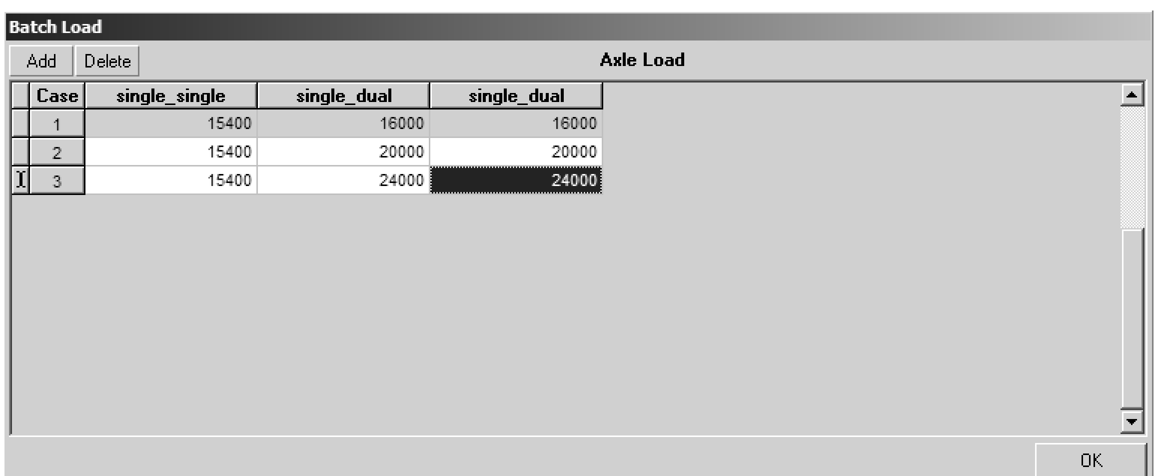

Batch Load

Axle Load

| Case | single_single | single_dual | single_dual |
|---|---|---|---|
| 1 | 15400 | 16000 | 16000 |
| 2 | 15400 | 20000 | 20000 |
| 3 | 15400 | 24000 | 24000 |



**Figure 14: Batch Application for Load Module**

- **Multiple analyses for temperature conditions:** Batch application allows for analysis of several temperature conditions at the same time. Figures 15 and 16 illustrate examples of batch application for linear thermal gradient and non-linear temperature profiles.

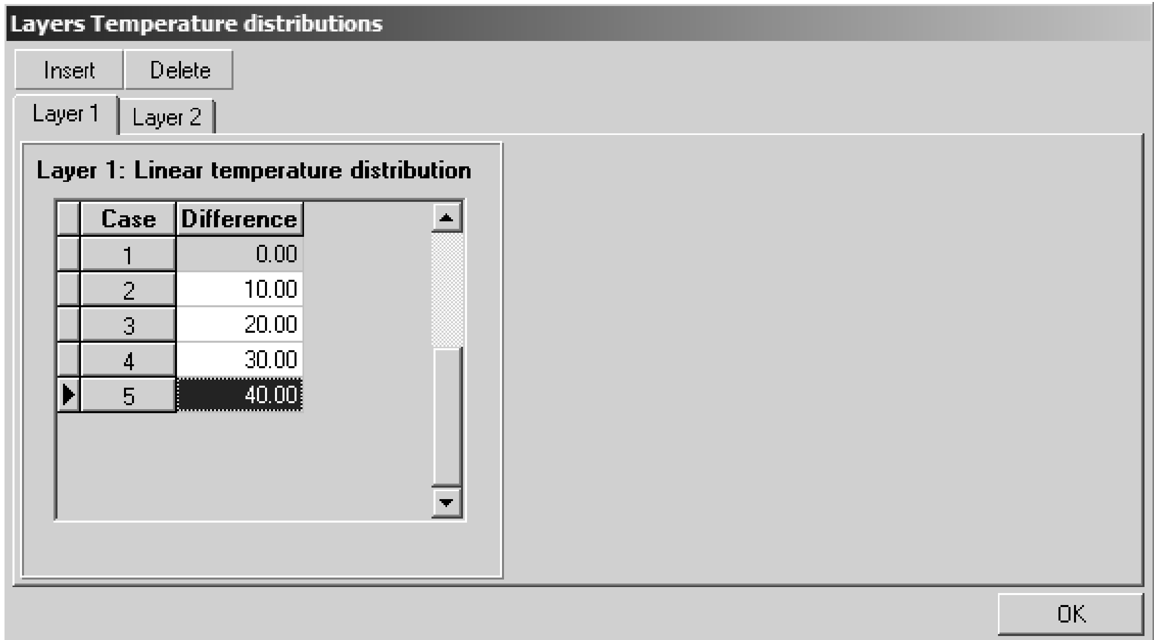


**Figure 15: Batch Application for Temperature Module (linear)**

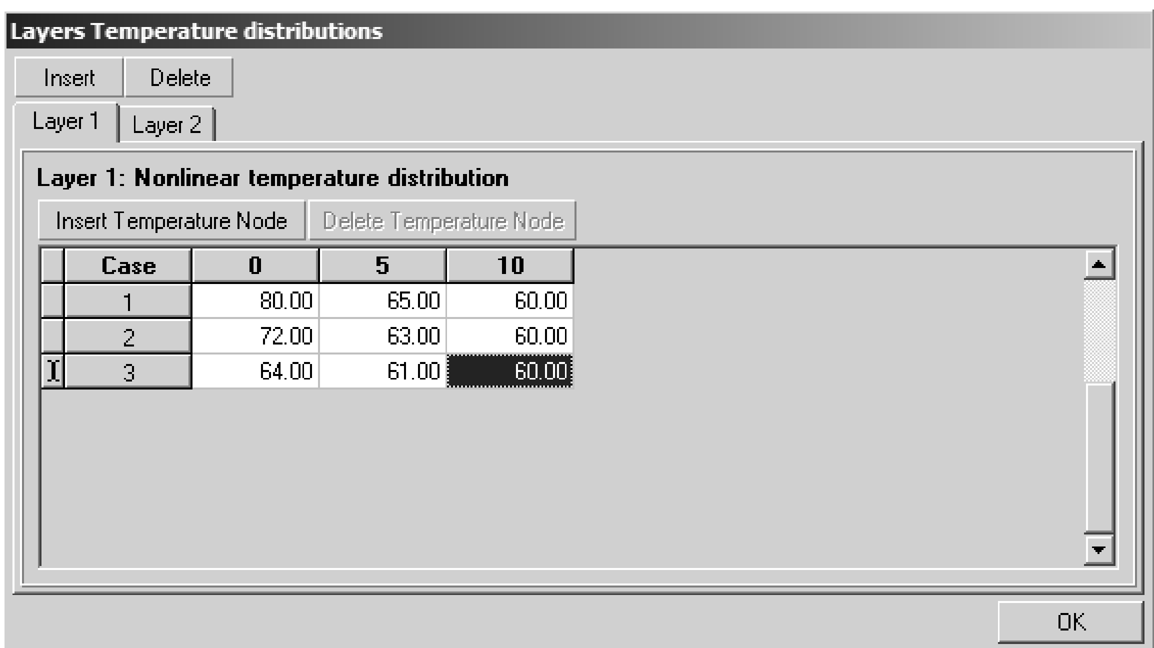


**Figure 16: Batch Application for Temperature Module (nonlinear)**

# Analysis Results

To generate results, first click **Generate Input Files** and then click **Run ISLAB2000** from the **Run** menu item. To view results in graphical form, click **View Analysis Results** from the **Run** menu item (see Figure 17).

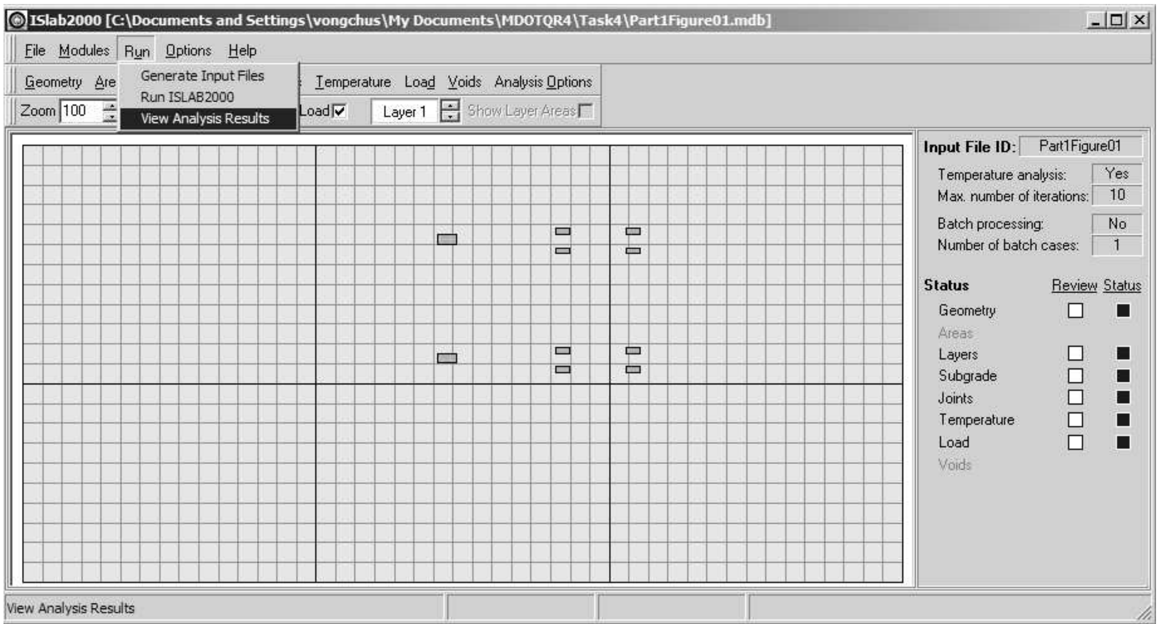


**Figure 17: View Analysis Results on Run Menu**

### Stresses and Deflection

Figures 18 and 19 shows typical graphical representations of stresses and deflection in ISLAB2000. As shown in the figure 18, the following types of stress contours are available for each layer and for top and bottom of the layer:

- X Stresses (transverse stresses)
- Y Stresses (longitudinal stresses)
- XY Stresses (shear stresses)
- Principal Stresses

Figure 19 shows a deflection contour based on the stresses shown in Figure 18. To view a deflection contour, select **Deflection** from the third pull down menu shown in Figure 17.

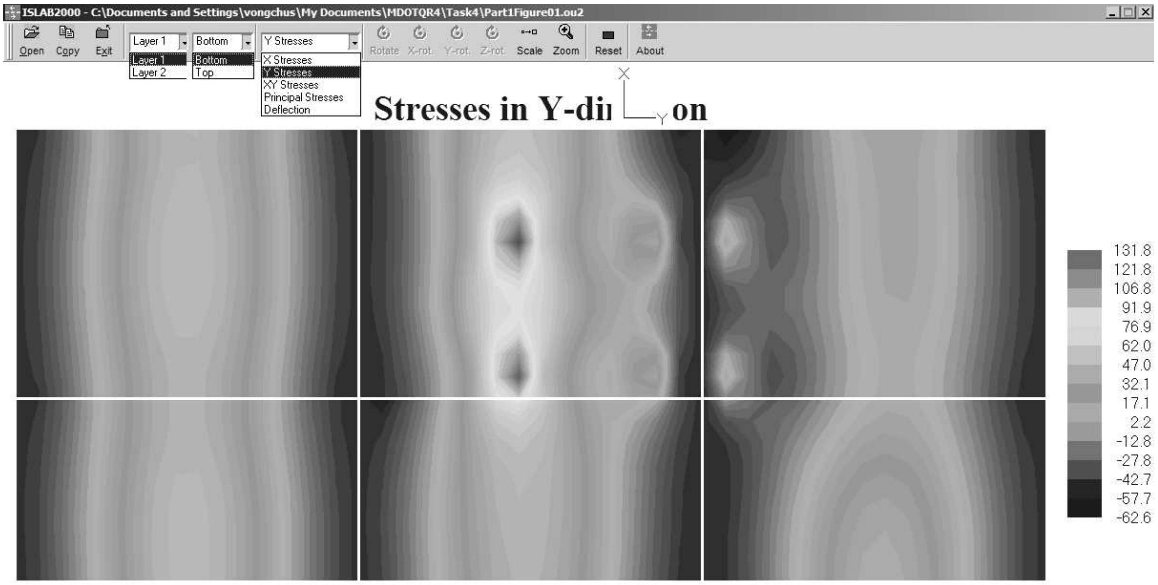


**Figure 18: Stress Contour Obtained from ISLAB2000**

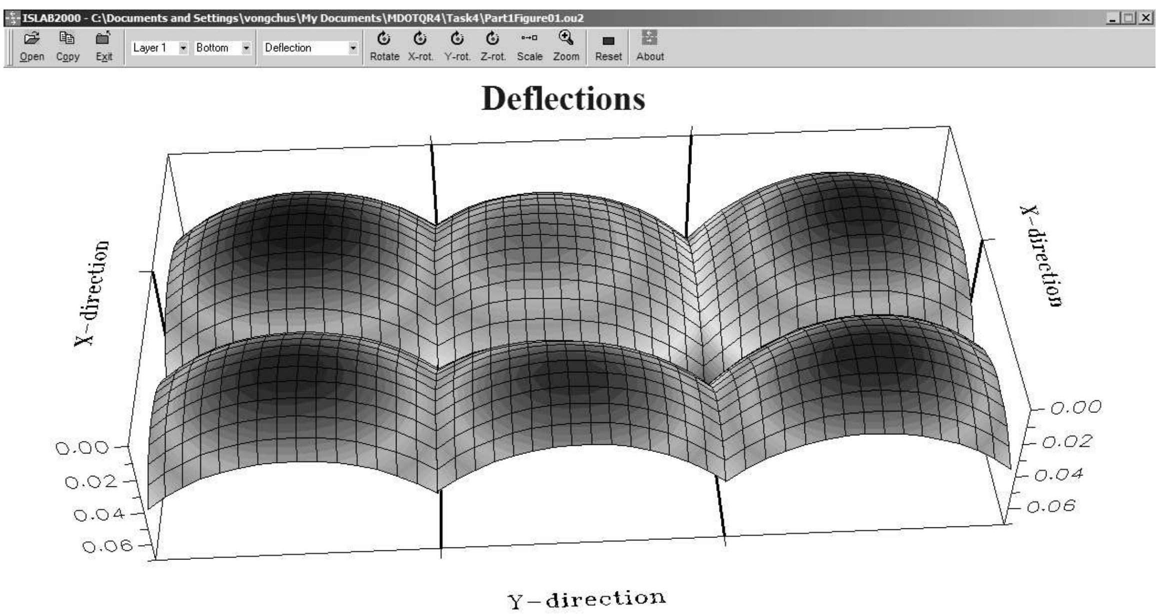


**Figure 19: Deflection Contour Obtained from ISLAB2000**

# Part II: Examples

## Example 1:
## Interior Loading of a Single Slab

### Problem statement

Determine the maximum deflection and maximum stress at the bottom of the PCC slab for Westergaard's interior loading condition.

### Given

| | | | |
|---|---|---|---|
| Concrete elastic modulus | = | $4 \times 10^6$ | psi |
| Concrete Poisson's ratio | = | 0.15 | |
| Slab thickness | = | 10 | in. |
| Slab dimension | = | 144 x 180 | $in^2$ |
| Mesh size | = | 12 x 12 | $in^2$ (medium) |
| k-value | = | 100 | psi/in. |
| Tire contact area | = | 7.5 x 15 | $in^2$ |
| Wheel load | = | 10,000 | lbs |

### Problem illustration

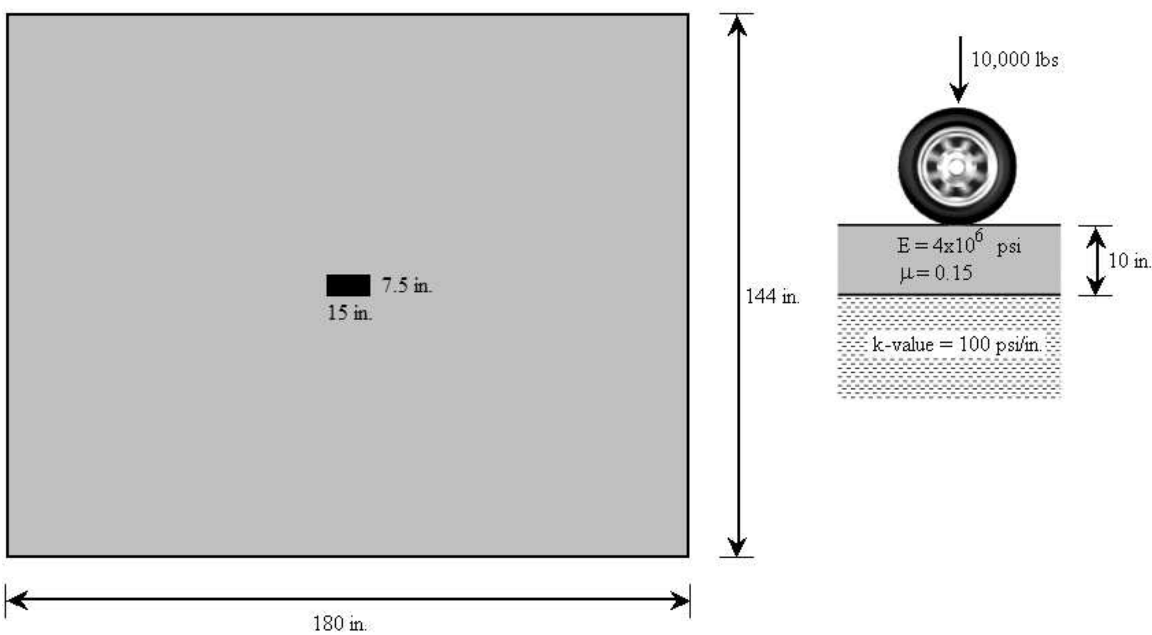


**Figure E1-1: Problem Ilustration**

# Solution

### Geometry Module

(see Figure E1-2)

Step 1: Click **Geometry** on the main panel to open the geometry panel.

Step 2: On the geometry panel, click **Insert** on the **X-direction** side, and then type the slab length, which is 144 in. for this example.

Step 3: Click **Insert** on the **Y-direction** side, and then type the slab length, which is 180 in. for this example.

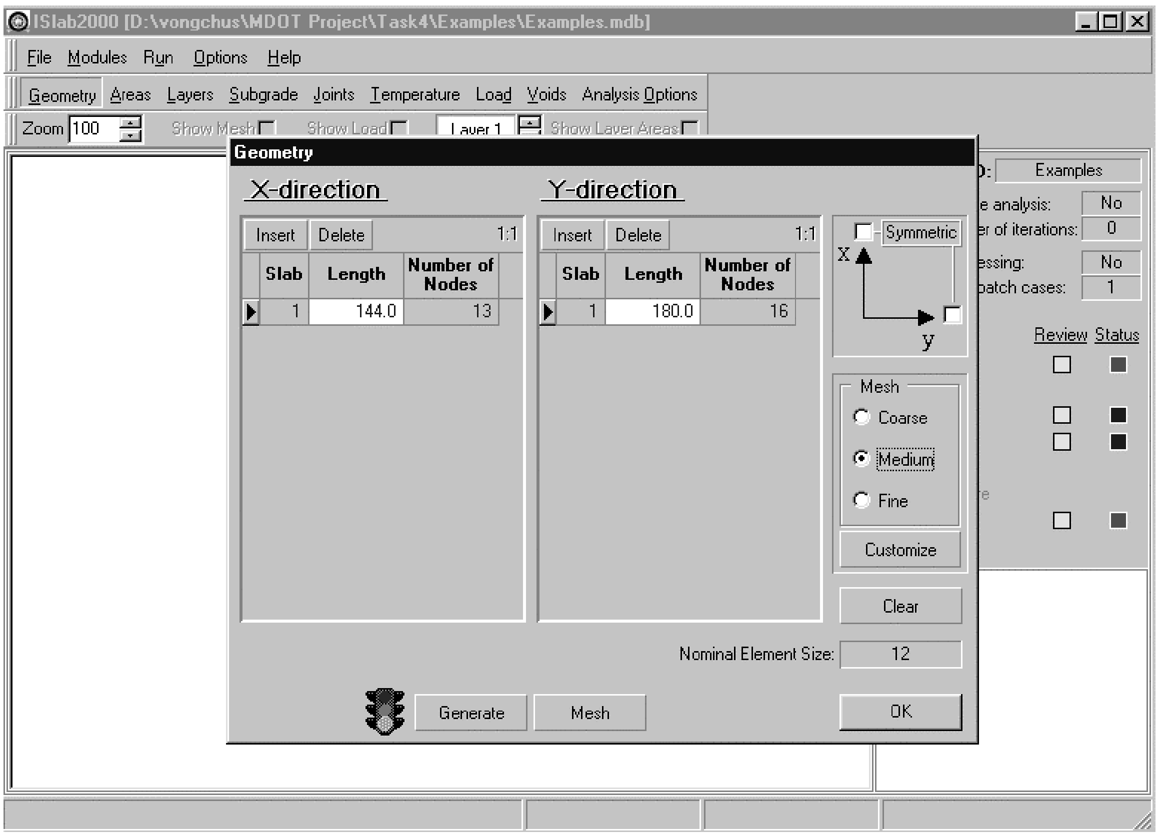


**Figure E1-2: Edit inputs for the geometry module**

Step 4: On the right side of the geometry panel, select the **Medium** radio button to select the medium mesh size.

Step 5: At the bottom of the panel, click **Generate** to generate the inputs to the input file, and then click **OK** to close the geometry panel.

## Layers Module

(see Figure E1-3)

Step 1: Click **Layers** on the main panel to open the layers panel.

Step 2: On the layers panel, type the inputs as identified in the problem statement.

Step 3: Click **OK** to close the layers panel.

## Subgrade Module

(see Figure E1-4)

Step 1: Click **Subgrade** on the main panel to open the subgrade panel.

Step 2: On the subgrade panel, type the inputs as identified in the problem statement.

Step 3: Click **OK** to close the subgrade panel.

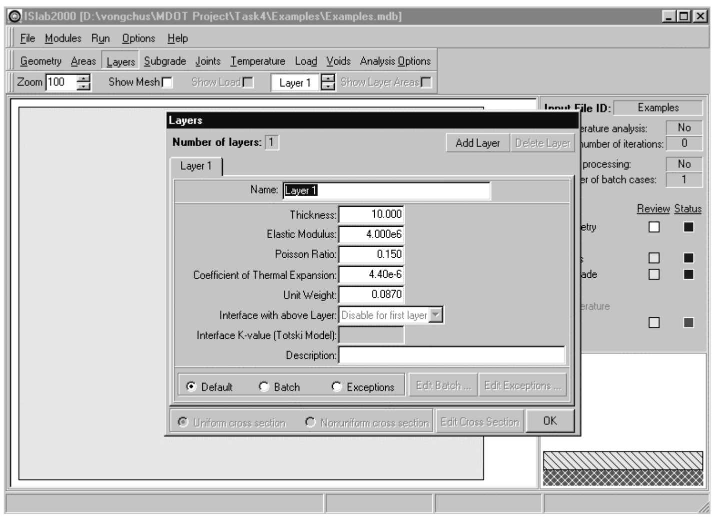


**Figure E1-3: Edit Inputs for the Layers Module**

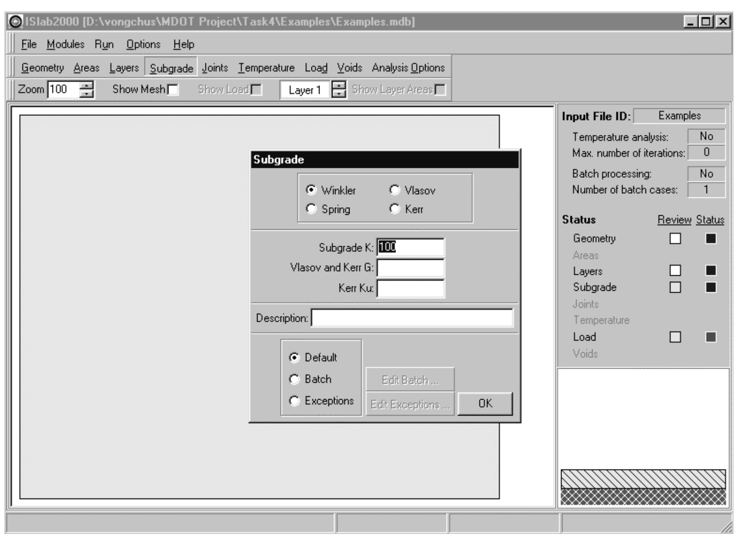


**Figure E1-4: Edit Inputs for the Subgrade Module**

## Load Module

(see Figures E1-5 and E1-6)

Step 1: Click **Load** on the main panel to open the load panel.

Step 2: On the load panel, click **Axle Design** to open the axle design panel.

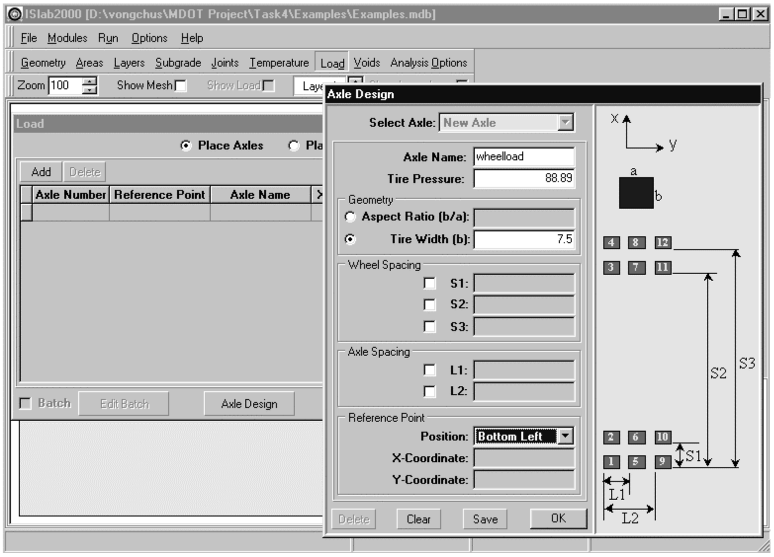

**Figure E1-5: Edit inputs for the load module**

Step 3: On the axle design panel, type "wheel load" in the **Axle Name** field to name the axle.

Step 4: Type the tire pressure in the **Tire Pressure** field. The tire pressure of the wheel load can be computed as shown below:

$$Tire\ Pressure = \frac{Wheel\ Load}{Contact\ Area} = \frac{10{,}000\ lbs}{7.5\ in. \times 15\ in.} = 88.89\ \ psi$$

Step 5: Type the tire width (7.5 in. for this example), in the **Tire Width** field.

Step 6: Select **Bottom Left** for the reference point position.

Step 7: Click **OK** to close the axle design panel.

Step 8: On the load panel (see Figure E1-6), click **Add** to add an axle.

Step 9: In the **Axle Name** field, select "wheel load."

Step 10: Enter an X-location and a Y-location to locate the wheel load. X-location and Y-location for interior loading conditions can be computed as shown below:

$$X - location = \frac{Slab\ width}{2} - \frac{wheel\ load\ width}{2}.$$

$$= \frac{144}{2} - \frac{7.5}{2} = 68.25\ in$$

$$Y - location = \frac{Slab\ length}{2} - \frac{wheel\ load\ length}{2}.$$

$$= \frac{180}{2} - \frac{15}{2} = 82.5\ in$$

Step 11: Enter the load for the wheel load, which is 10,000 lbs for this example.

Step 12: Click **OK** to close the load panel.

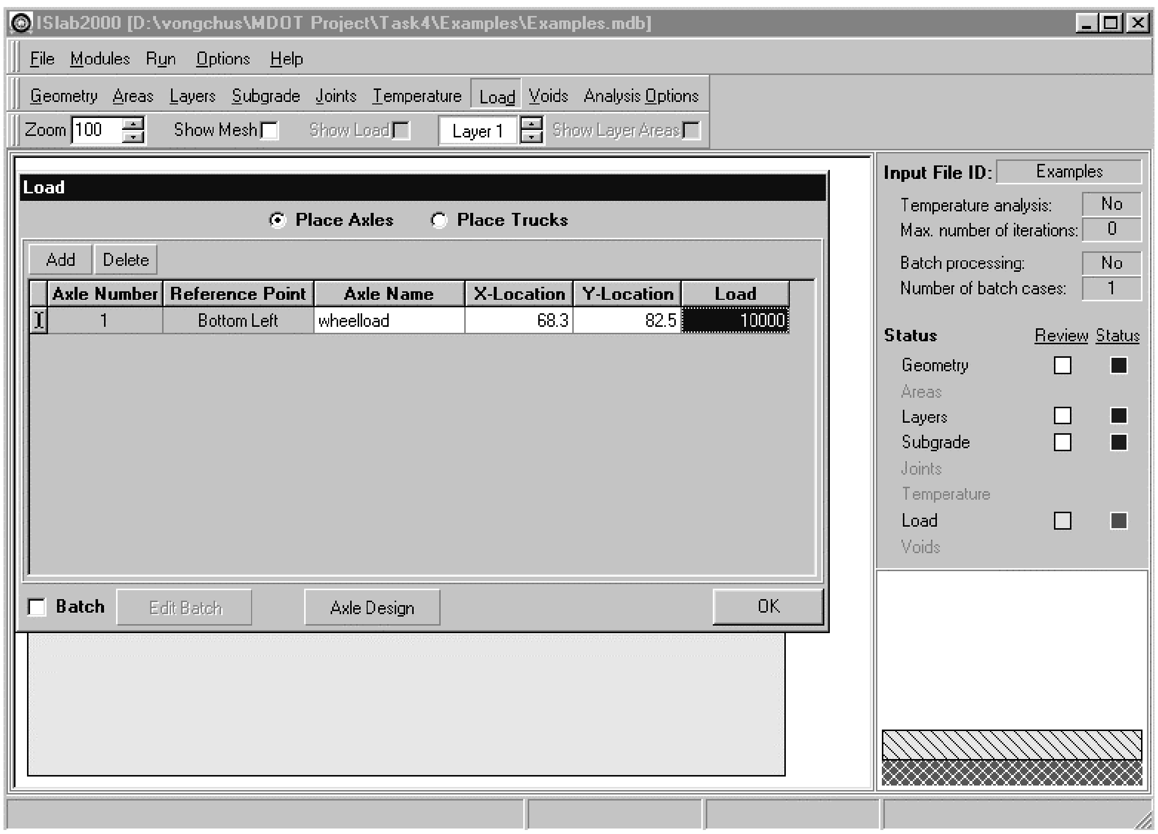


**Figure E1-6: Edit Inputs for the Load Module (continued)**

At this stage, all inputs are completed. If all the inputs are correct, the color of all status boxes will change from red to blue. The main panel should display the pavement structure, loading condition, and mesh as shown in Figure E1-7.

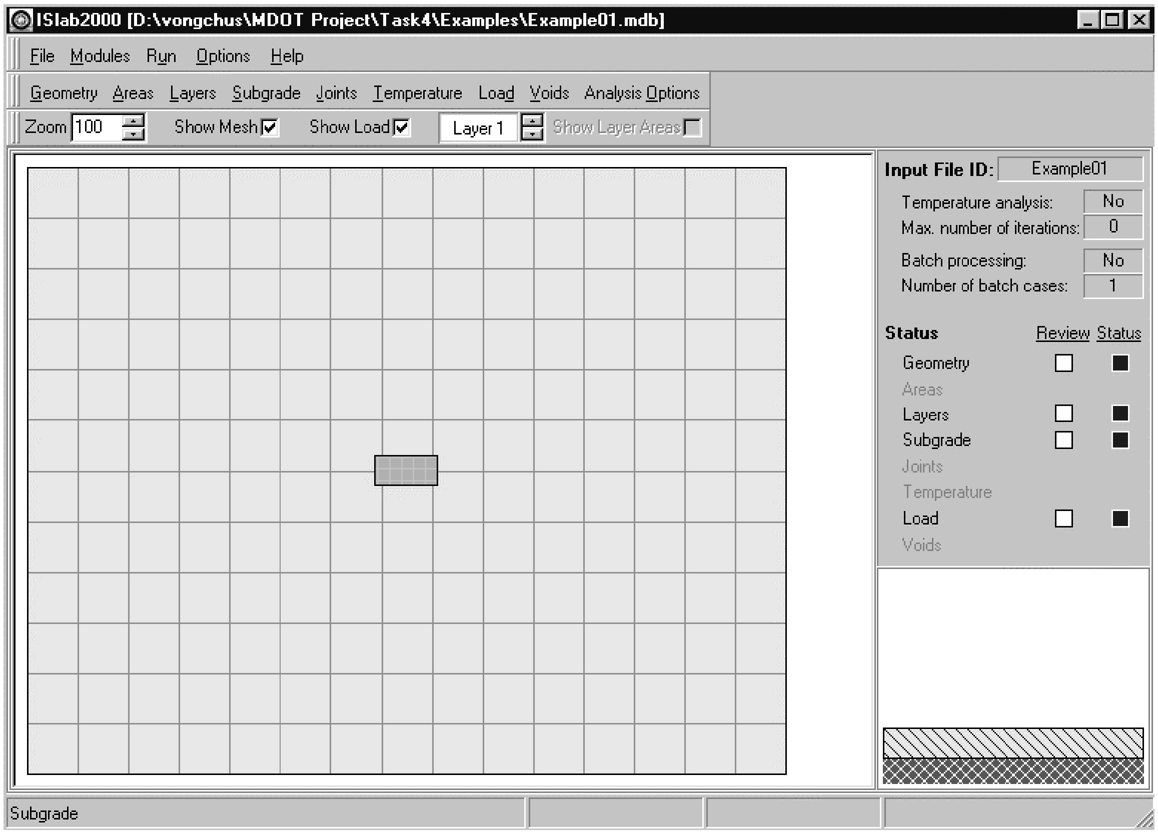


**Figure E1-7: Main Panel After the Completion of Inputs**

## *Analysis Results*

| | | |
|---|---|---|
| Maximum transverse stress at the bottom of the PCC slab (see Figure E1-8) | = | 140.6 psi |
| Maximum longitudinal stress at the bottom of the PCC slab (see Figure E1-9) | = | 123.4 psi |
| Maximum deflection of the PCC slab (see Figure E1-10) | = | 0.00796 in. |

**NOTE**
Positive and negative values of stress signify tensile and compressive stresses and positive value of deflection indicates deflection in downward direction.

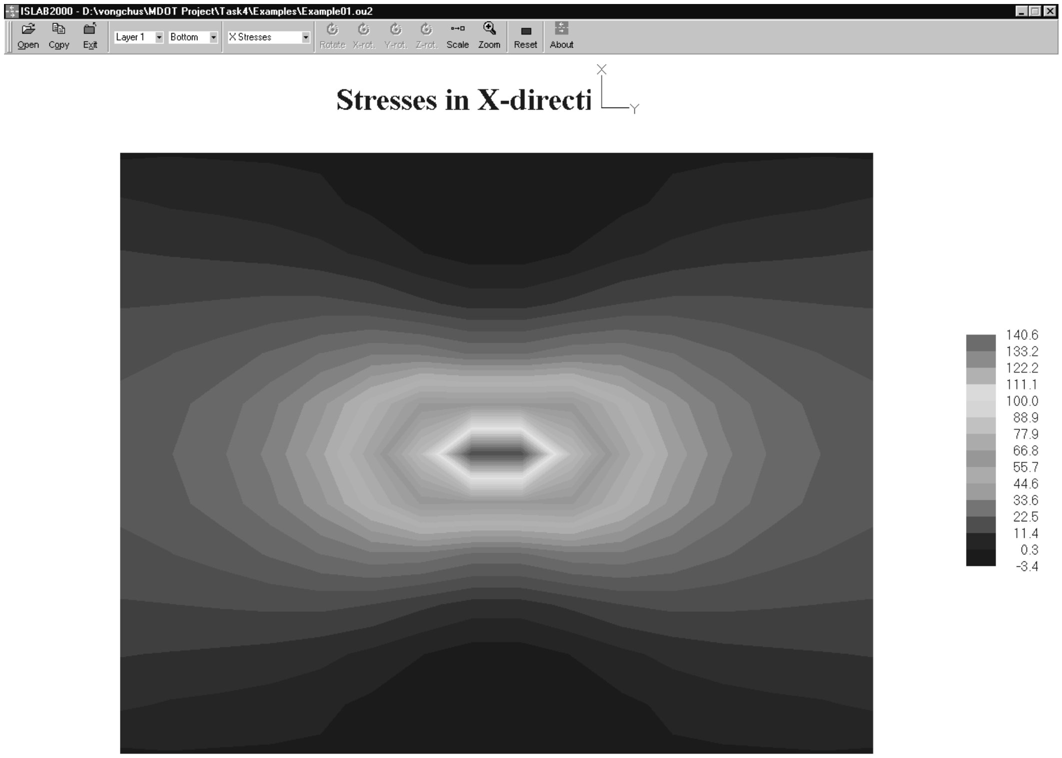


**Figure E1-8: Transverse Stress at the Bottom of the PCC Slab**

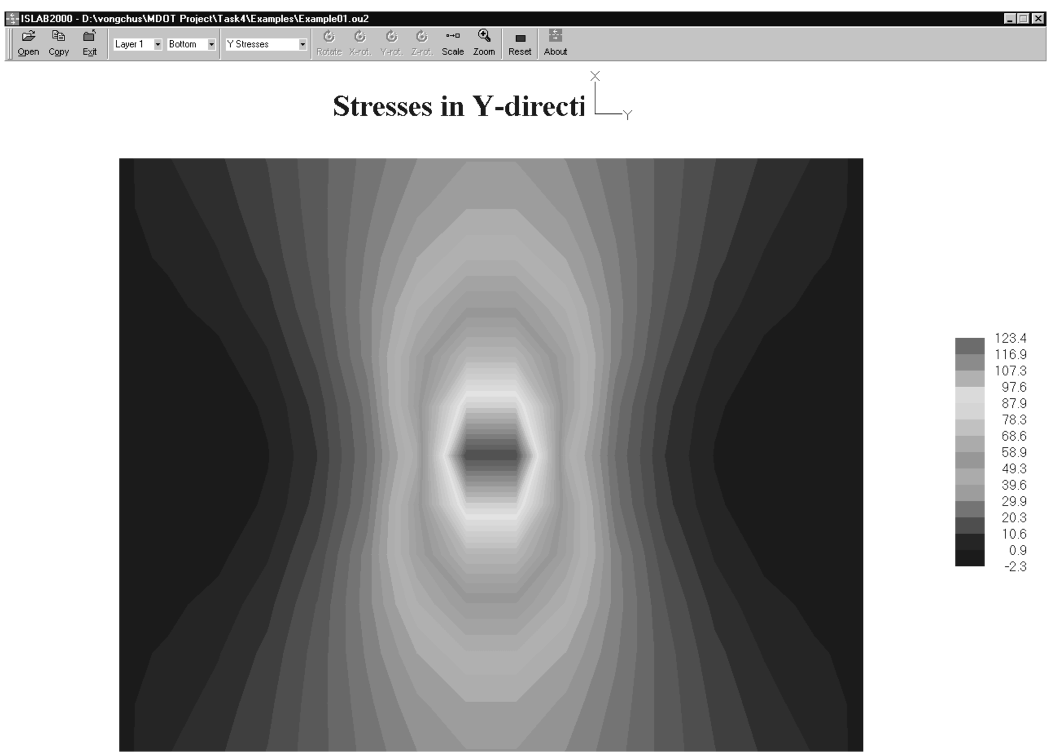


**Figure E1-9: Longitudinal Stress at the Bottom of the PCC Slab**

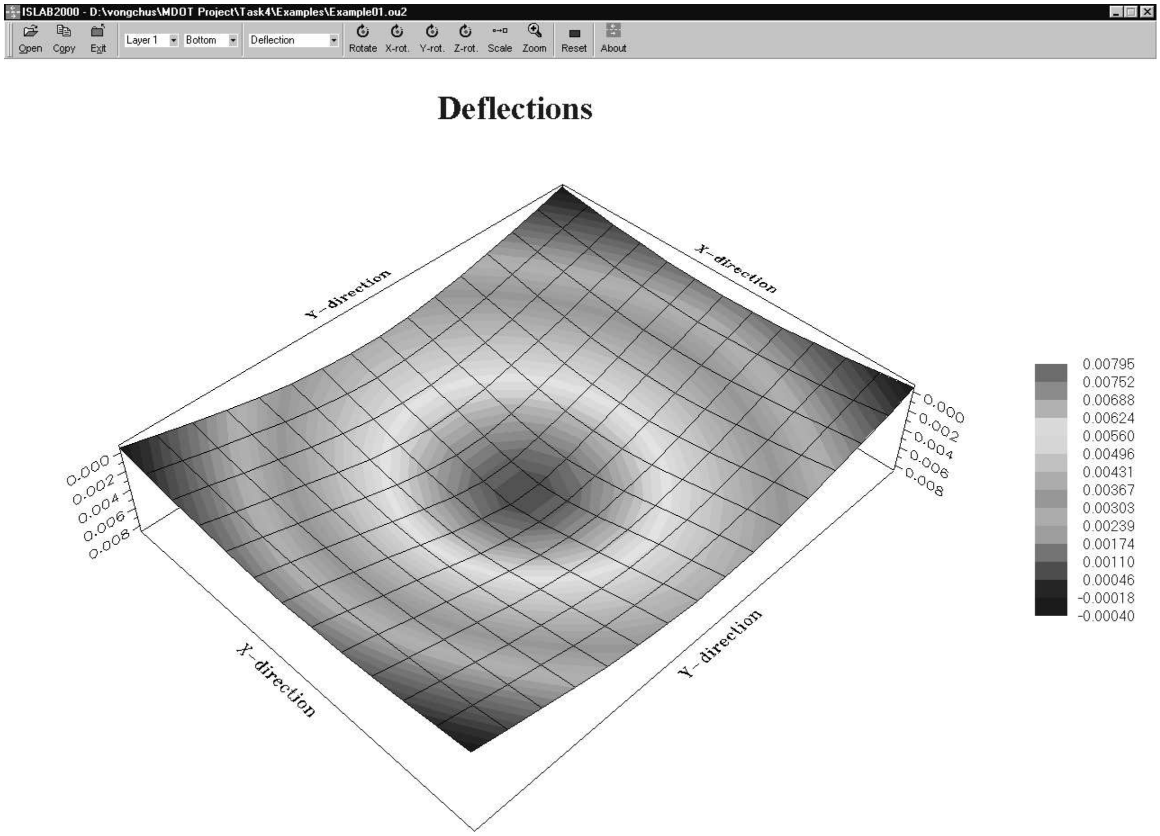


**Figure E1-10: Deflection of the PCC Slab**

# Example 2:
# Edge Loading of a Single Slab

### Problem Statement

Determine maximum deflection and stress for the PCC slab using Westergaard's edge loading condition.

### Given

| | | | |
|---|---|---|---|
| Concrete elastic modulus | = | $4 \times 10^6$ | psi |
| Concrete Poisson's ratio | = | 0.15 | |
| Slab thickness | = | 10 | in. |
| Slab dimension | = | 144 x 180 | $in^2$ |
| Mesh size | = | 12 x 12 | $in^2$ (medium) |
| k-value | = | 100 | psi/in. |
| Tire contact area | = | 7.5 x 15 | $in^2$ |
| Wheel load | = | 10,000 | lbs |

### Problem Illustration

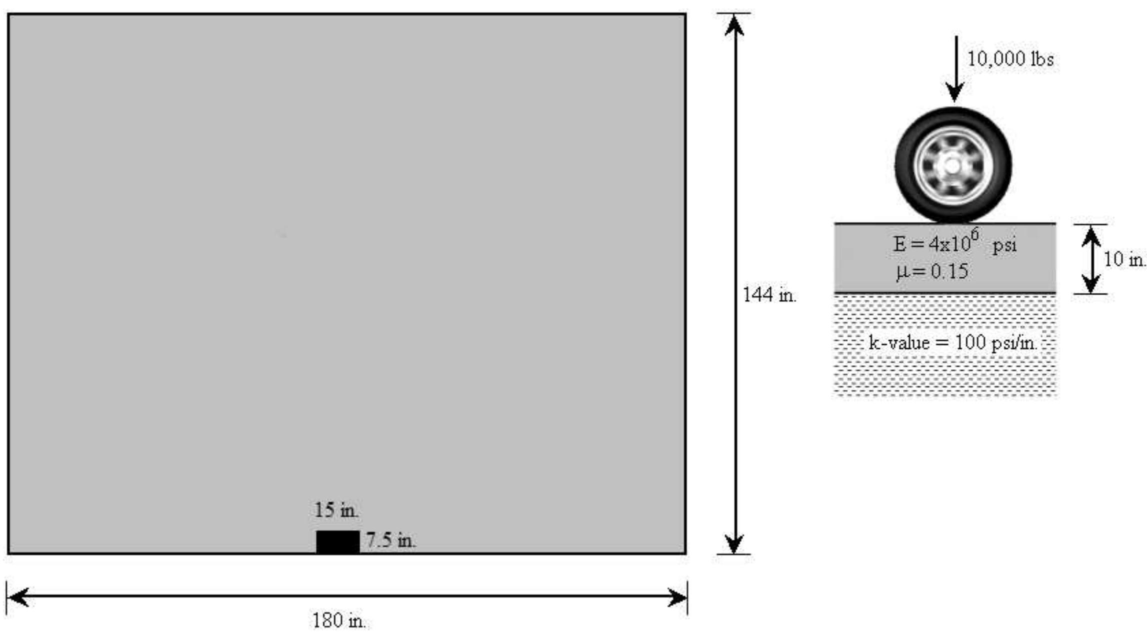


**Figure E2-1: Problem Illustration**

# Solution

### Geometry Module

Use this module from Example 1.

### Layers Module

Use this module from Example 1.

### Subgrade Module

Use this module from Example 1.

### Load Module

(see Figures E2-2)

Step 1: Follow steps 1 through 9 from the load module in Example 1.

Step 2: Enter an X-location and a Y-location to locate the wheel load. The X-location and Y-location for edge loading condition can be computed as shown below:

$$X - location = 0$$

$$Y - location = \frac{Slab\ length}{2} - \frac{wheel\ load\ length}{2}.$$

$$= \frac{180}{2} - \frac{15}{2} = 82.5\ in$$

Step 3: Type the load for the wheel load, which is 10,000 lbs for this example.

Step 4: Click **OK** to close the load panel.

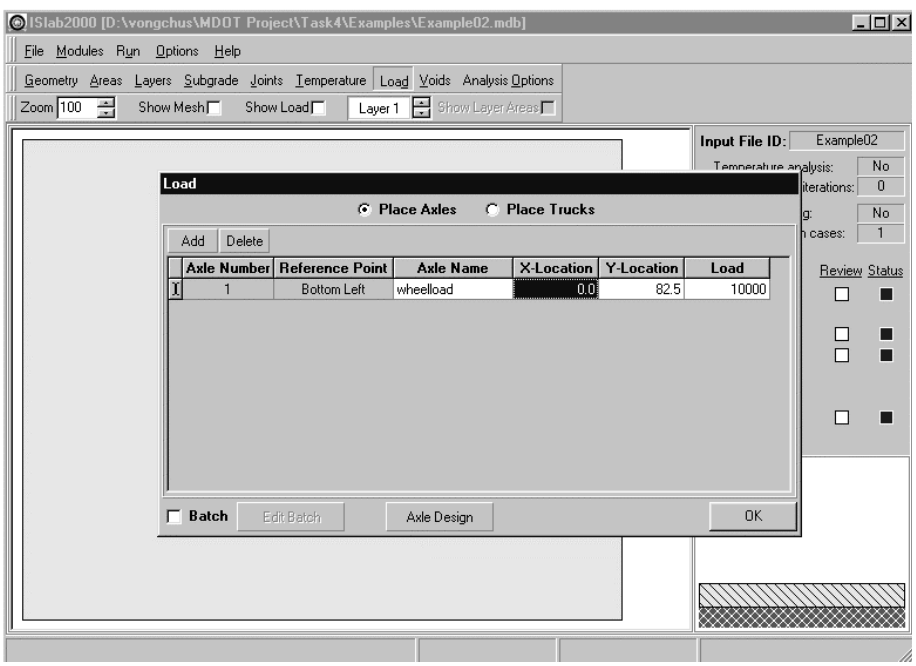


**Figure E2-2: Edit Inputs for the Load Module**

The main panel should display the pavement structure, loading condition, and meshing as shown in Figure E2-3.

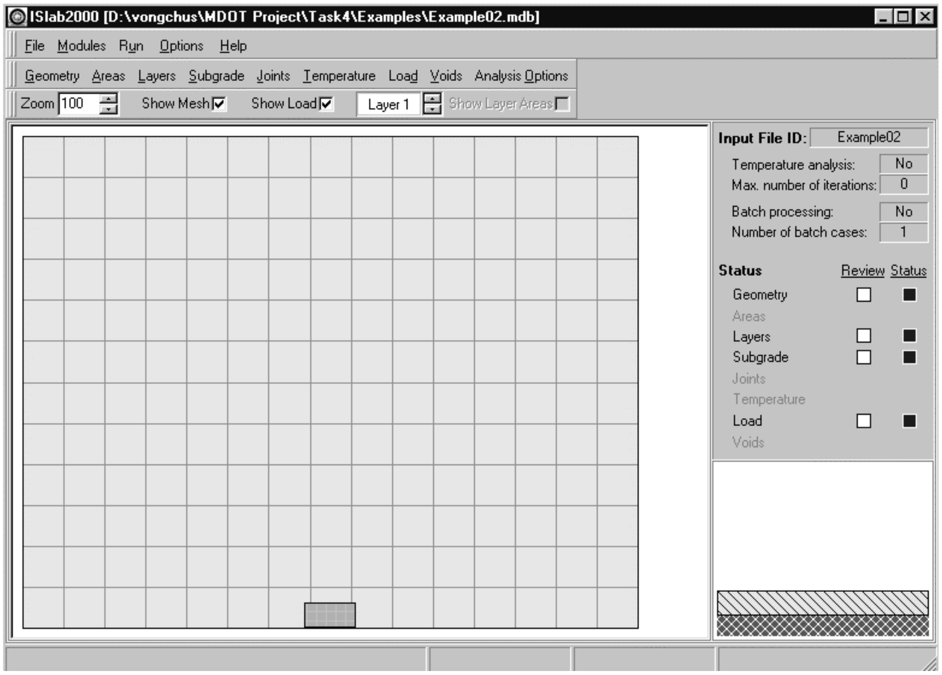


**Figure E2-3: Main Panel After the Completion of Inputs**

## *Analysis Results*

| | | |
|---|---|---|
| Maximum transverse stress at the bottom of the PCC slab (see Figure E2-4) | = | 37.4 psi |
| Maximum longitudinal stress at the bottom of the PCC slab (see Figure E2-5) | = | 245.5 psi |
| Maximum deflection of the PCC slab (see Figure E2-6) | = | 0.02514 in. |

**NOTE**
Positive and negative values of stress signify tensile and compressive stresses and positive value of deflection indicates deflection in downward direction.

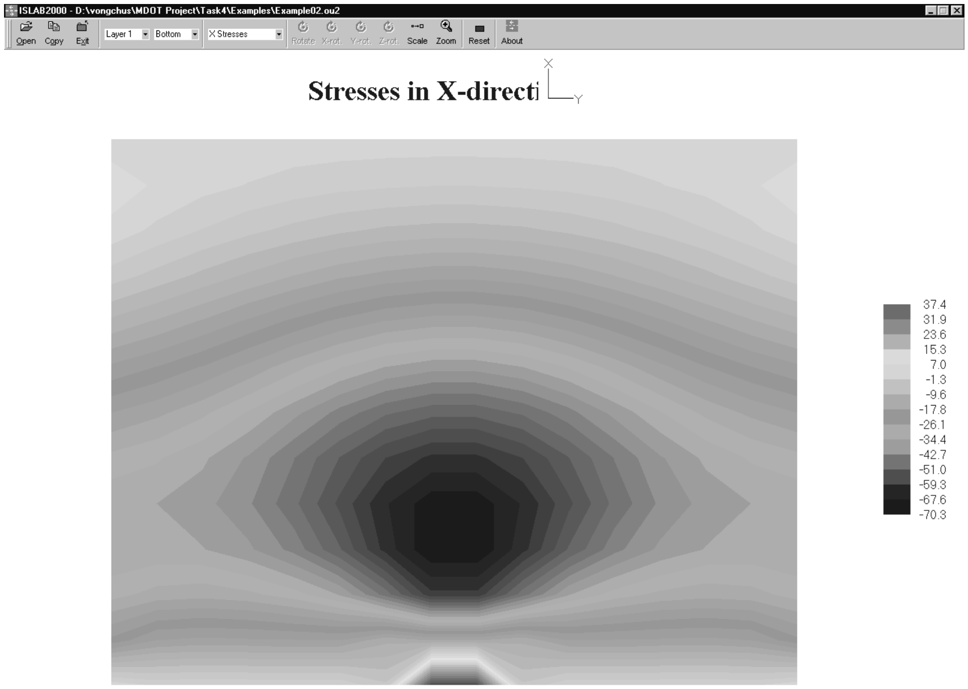


**Figure E2-4: Transverse Stress at the Bottom of the PCC Slab**

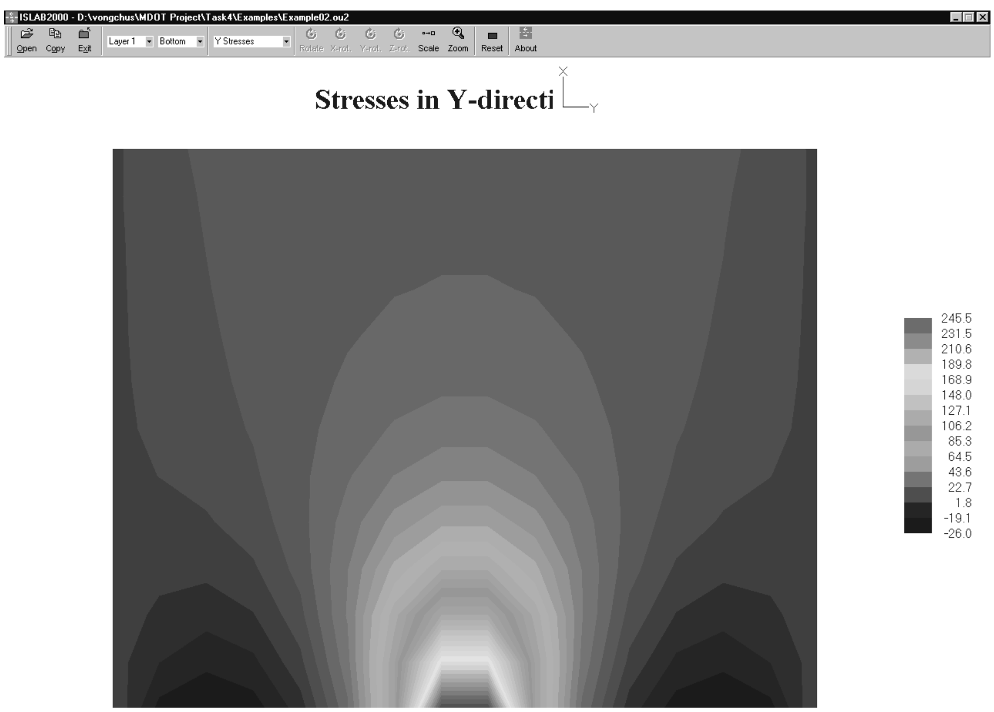


**Figure E2-5: Longitudinal Stress at the Bottom of the PCC Slab**

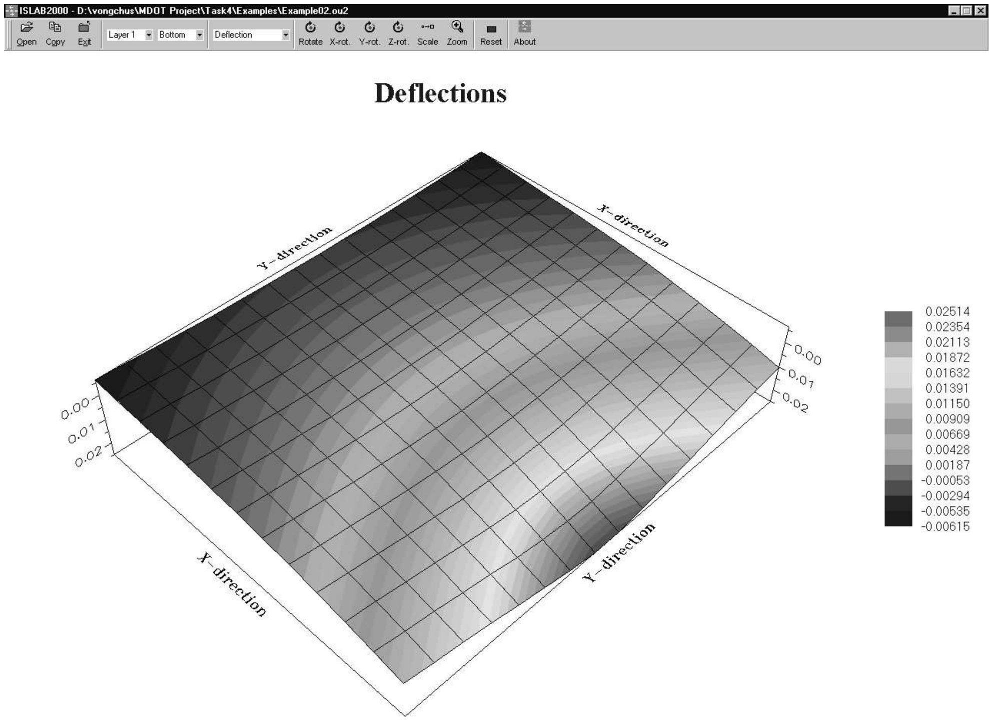


**Figure E2-6: Deflection of the PCC Slab**

# Example 3:
# Corner Loading of a Single Slab

### Problem Statement

Determine maximum deflection and stress at the top of the PCC slab for Westergaard's corner loading condition. Then, compare the results from interior and edge loading conditions in Examples 1 and 2.

### Given

| | | | |
|---|---|---|---|
| Concrete elastic modulus | = | $4 \times 10^6$ | psi |
| Concrete Poisson's ratio | = | 0.15 | |
| Slab thickness | = | 10 | in. |
| Slab dimension | = | 144 x 180 | $in^2$ |
| Mesh size | = | 12 x 12 | $in^2$ (medium) |
| k-value | = | 100 | psi/in. |
| Tire contact area | = | 7.5 x 15 | $in^2$ |
| Wheel load | = | 10,000 | lbs |

### Problem Illustration

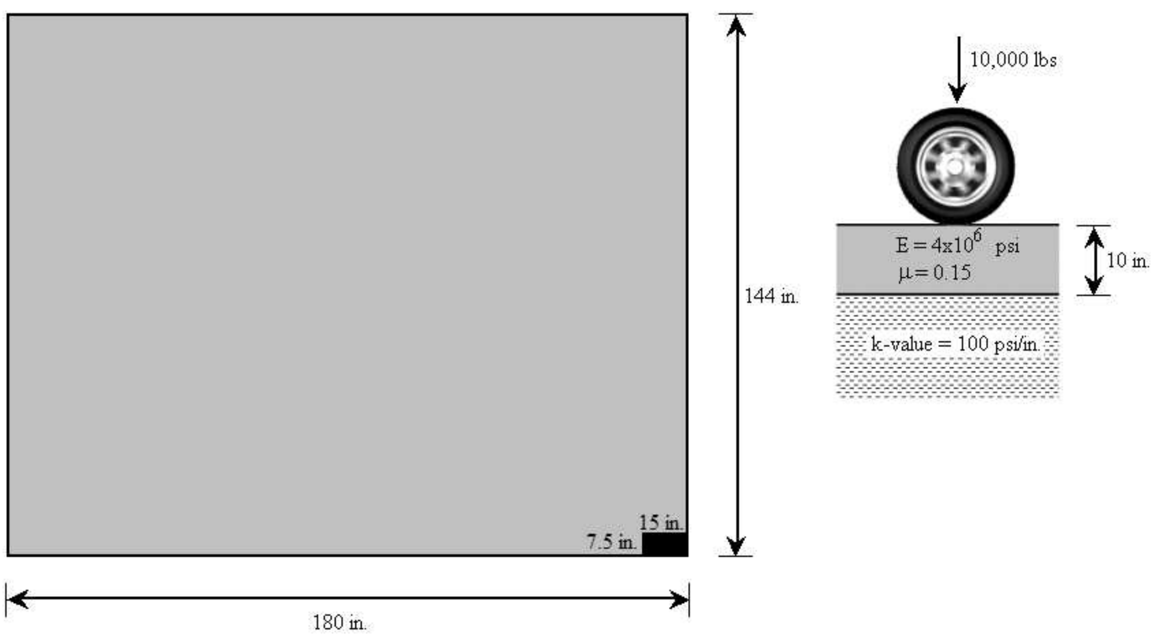


**Figure E3-1: Problem Illustration**

# Solution

### Geometry Module

Use this module from Example 1.

### Layers Module

Use this module from Example 1.

### Subgrade Module

Use this module from Example 1.

### Load Module

(see Figures E3-2)

Step 1: Follow steps 1 through 9 from the load module in Example 1.

Step 2: Type an X-location and a Y-location to locate the wheel load. The X-location and Y-location for corner loading condition can be computed as shown below:

$$X - location = 0$$

$$Y - location = Y - direction\ slab\ length - wheel\ load\ length.$$

$$= 180 - 15 = 165\ in$$

Step 3: Enter the load for the wheel load, which is 10,000 lbs for this example.

Step 4: Click **OK** to close the load panel.

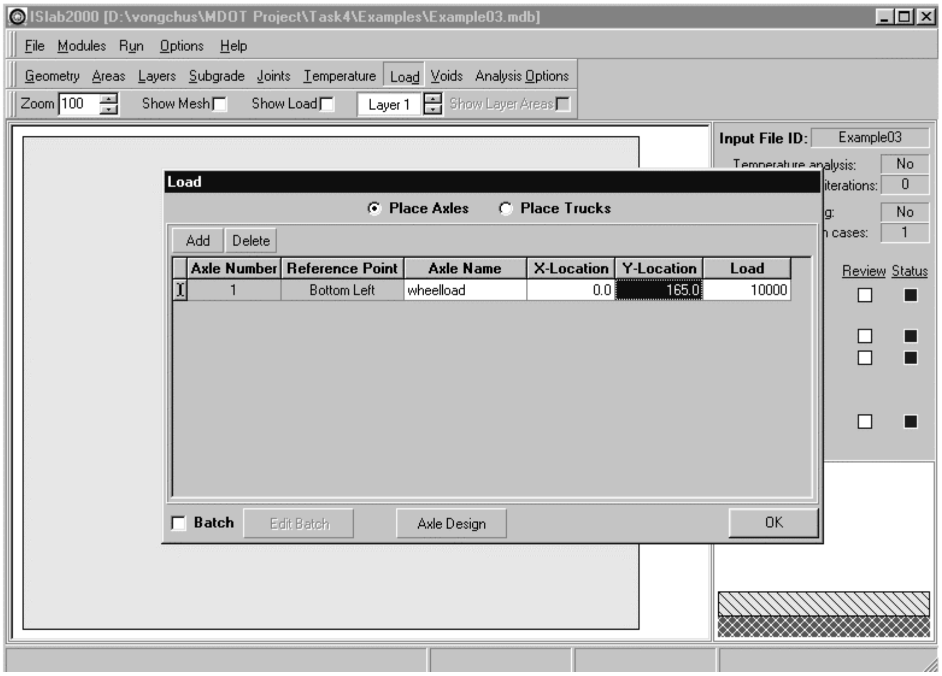


**Figure E3-2: Edit Inputs for the Load Module**

The main panel should display the pavement structure, loading condition, and meshing as shown in Figure E3-3.

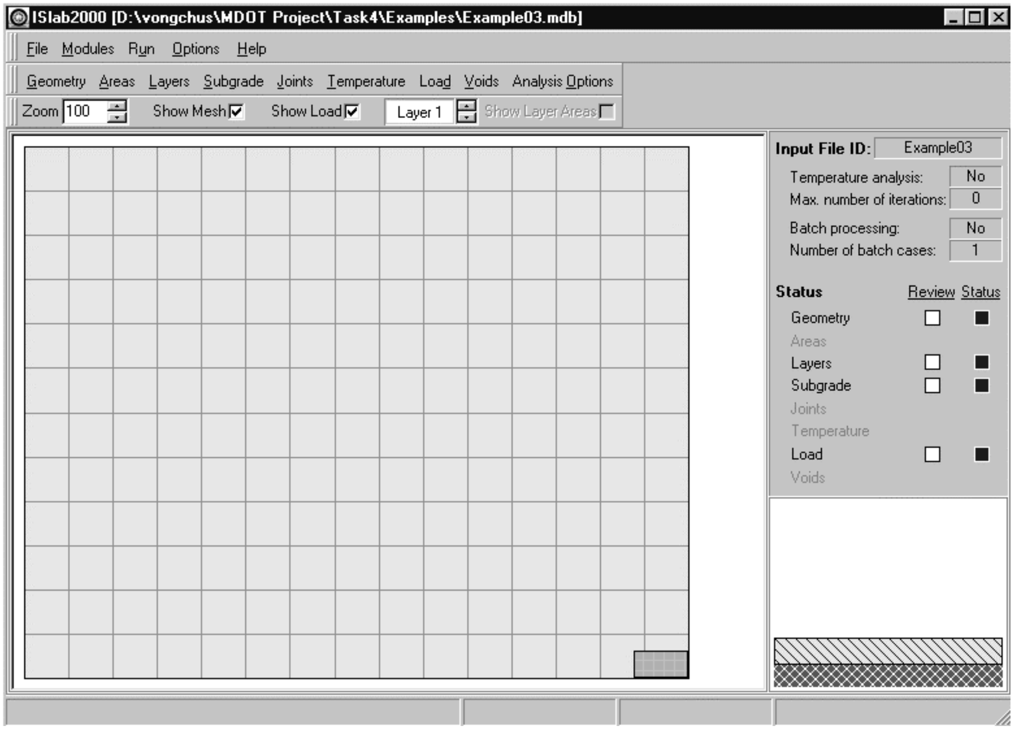


**Figure E3-3: Main Panel After the Completion of Inputs**

## *Analysis Results*

| | | |
|---|---|---|
| Maximum transverse stress at the top of the PCC slab (see Figure E3-4) | = | 137.3 psi |
| Maximum longitudinal stress at the top of the PCC slab (see Figure E3-5) | = | 131.1 psi |
| Maximum stress at the top of the PCC slab (see Figure E3-6) | = | 195.5 psi |
| Maximum deflection of the PCC slab (see Figure E3-7) | = | 0.0574 in. |

Comparison of stresses and deflections from the three loading conditions are illustrated in Figures E3-8 and E3-9.

**NOTE**
Positive and negative values of stress signify tensile and compressive stresses and positive value of deflection indicates deflection in downward direction.

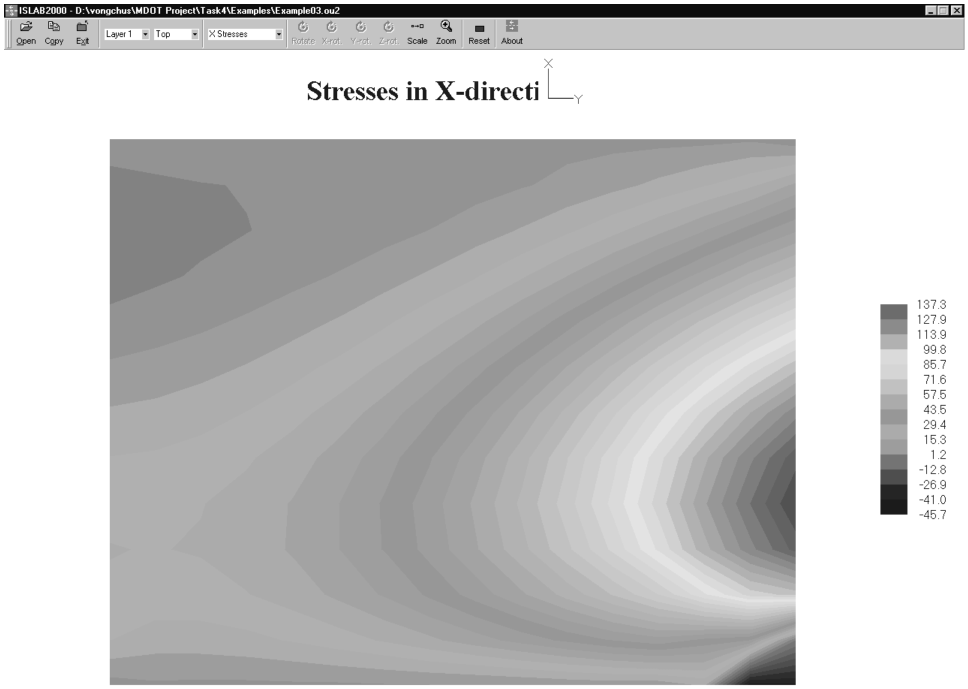


Figure E3-4: Transverse Stress at the Top of the PCC Slab

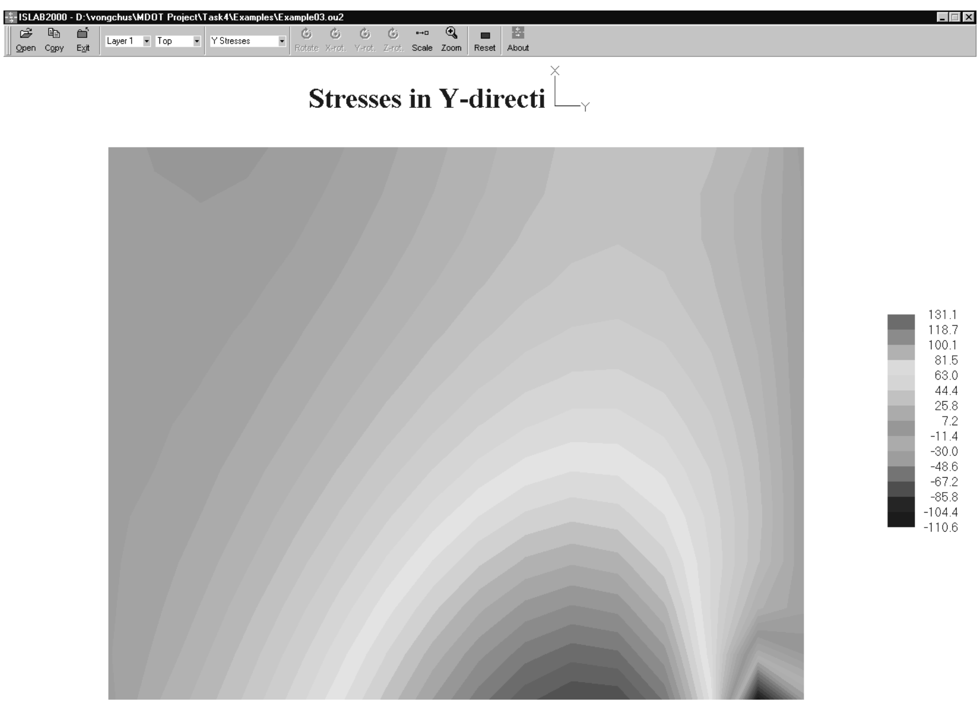


Figure E3-5: Longitudinal Stress at the Top of the PCC Slab

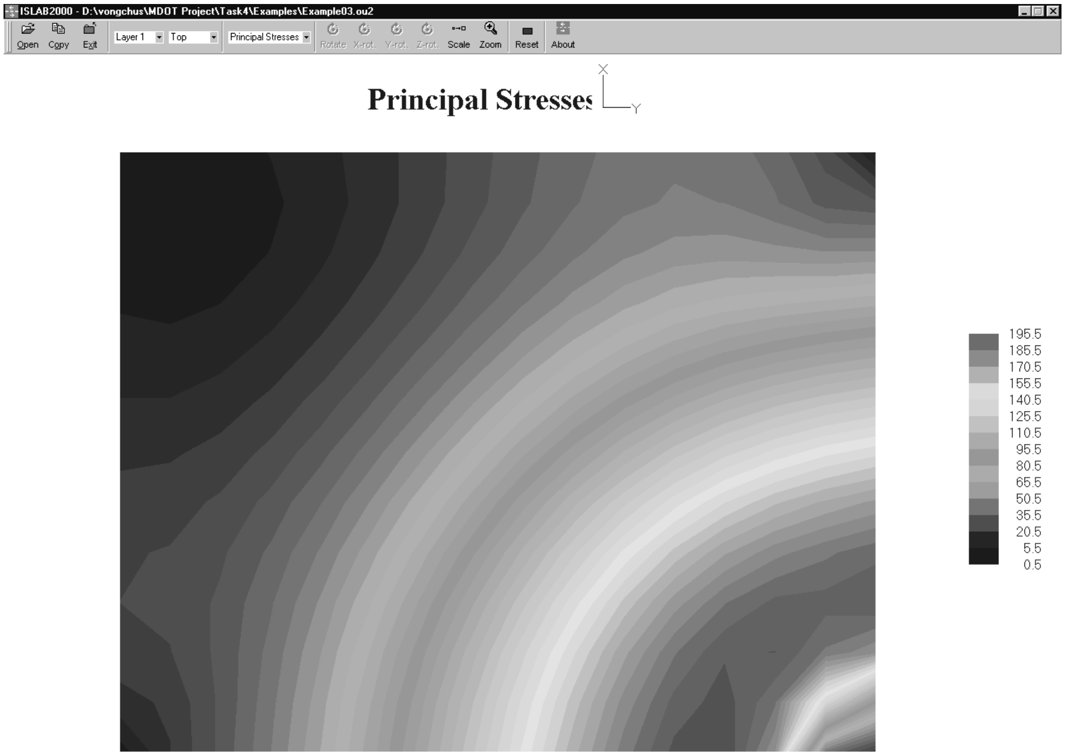


Figure E3-6: Principal Stress at the Top of the PCC Slab

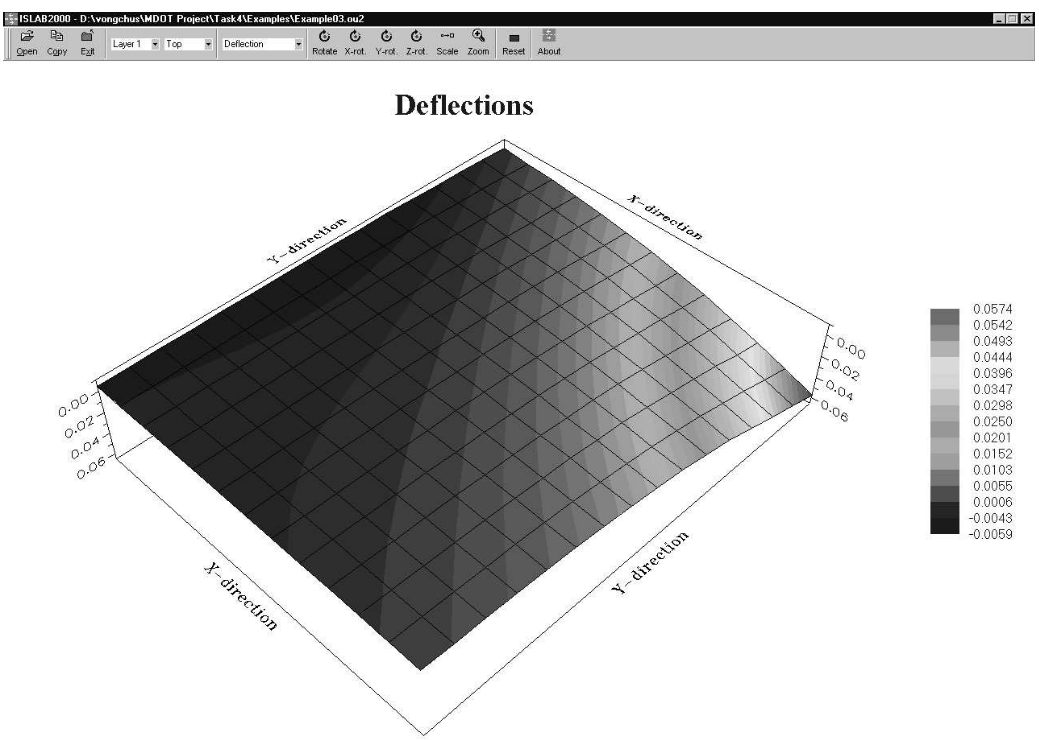


Figure E3-7: Deflection of the PCC Slab

| Loading condition | Maximum stress, psi | Maximum deflection, in. |
|---|---|---|
| Interior | 140.6 | 0.00796 |
| Edge | 245.5 | 0.02514 |
| Corner | 195.5 | 0.0574 |

**Table E3-1: Comparison of results between the three loading conditions**

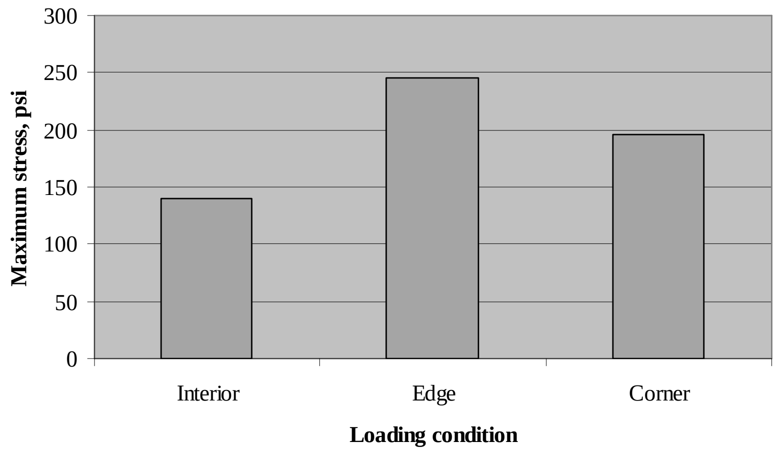


**Figure E3-8: Comparison of Maximum Stress from the Three Loading Conditions**

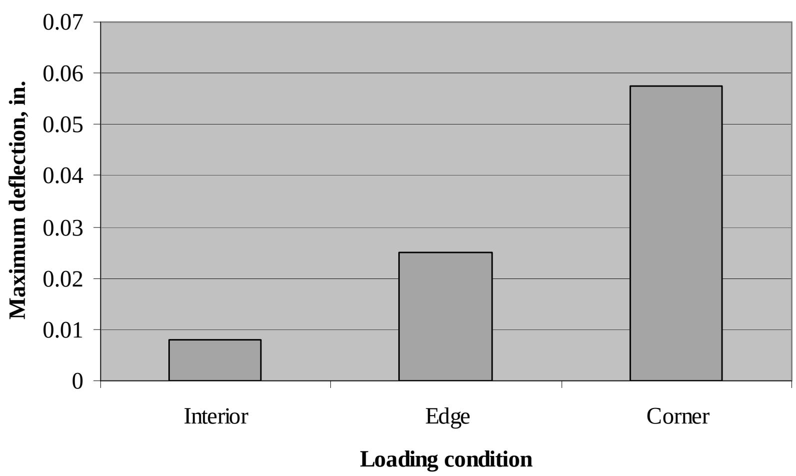


**Figure E3-9: Comparison of Maximum Deflection from the Three Loading Conditions**

# Example 4:
# Thermal Gradients on a Single Slab

### Problem Statement

Determine maximum deflection and stress at the top and bottom of the PCC slab due to temperature differentials, ΔT, of -20, -10, 0, +10, +20 $^oF$. Also, plot a graph to show relation between stresses and temperature differentials.

### Given

| | | | |
|---|---|---|---|
| Concrete elastic modulus | = | $4 \times 10^6$ | psi |
| Concrete Poisson's ratio | = | 0.15 | |
| Slab thickness | = | 10 | in. |
| Slab dimension | = | 144 x 180 | $in^2$ |
| Mesh size | = | 12 x 12 | $in^2$ (medium) |
| k-value | = | 100 | psi/in. |
| Coefficient of thermal exp., α | = | $4.4 \times 10^{-6}$ | in./in./$^oF$ |
| Temperature differential, ΔT | = | -20, -10, 0, +10, +20 | $^oF$ |

### Problem Illustration

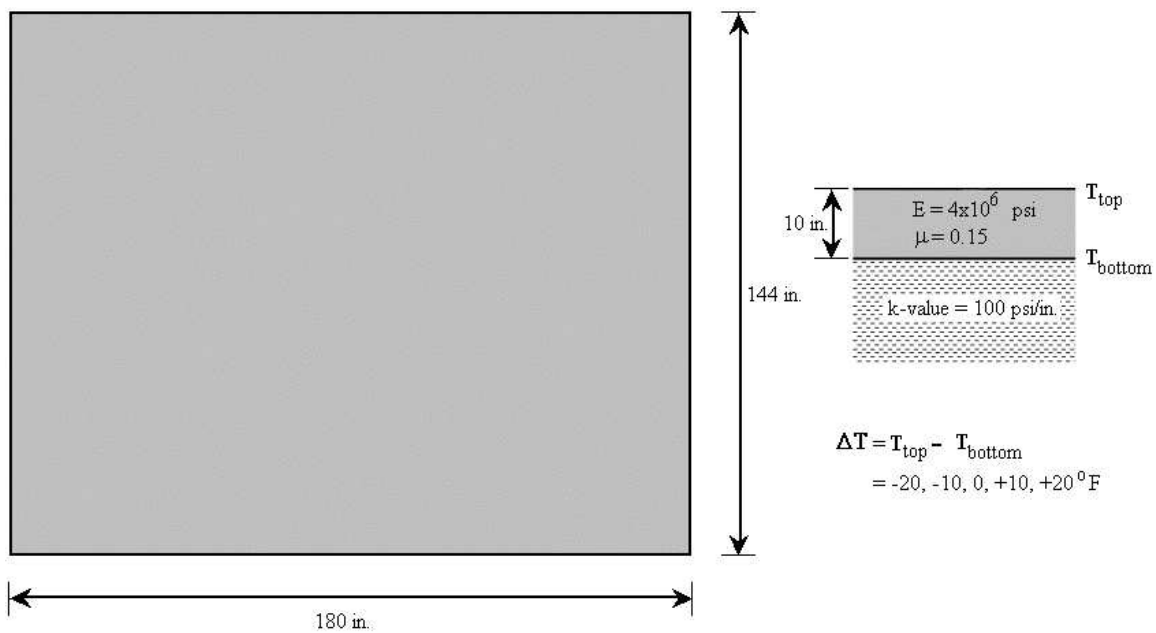


**Figure E4-1: Problem Illustration**

# Solution

### Geometry Module

Use this module from Example 1.

### Layers Module

Use this module from Example 1.

### Subgrade Module

Use this module from Example 1.

### Load Module

This module is not required for this example.

### Temperature Module

(see Figure E4-2)

Step 1: Click **Temperature** from the main panel to open the temperature panel.

Step 2: On the temperature panel, select the **Perform Temperature Analysis** and **Batch** check boxes.

Step 3: Enter the temperature differential of the first case in the **Difference** field, (-20 $^{o}$F for this problem).

Step 4: Click **Edit Batch** to open the layers temperature distributions panel.

Step 5: On the layers temperature distributions panel, click **Insert** four times to add four more cases of temperature differential. Then enter the other four temperature differentials as identified in the problem statement.

Step 6: Click **OK** to close the layers temperature distributions panel.

Step 7: Click **OK** layers temperature properties panel.

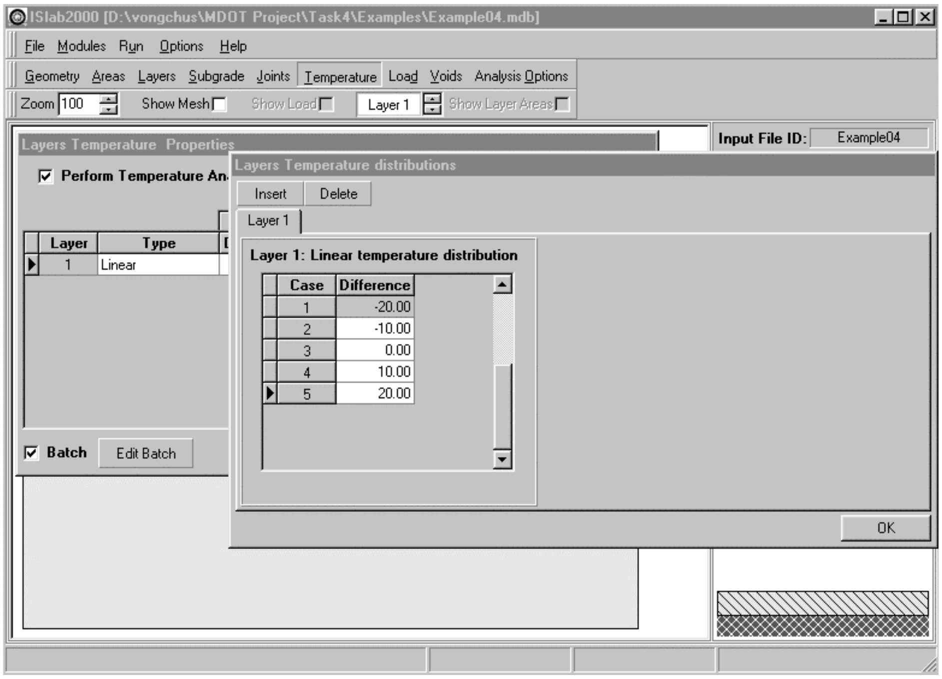


Figure E4-2: Edit Inputs for the Temperature Module

## Analysis Options Module

(see Figure E4-3)

Click **Analysis Options** to open the analysis options panel, and then select the **Batch Processing** checkbox. Click **OK** to close the analysis options panel.

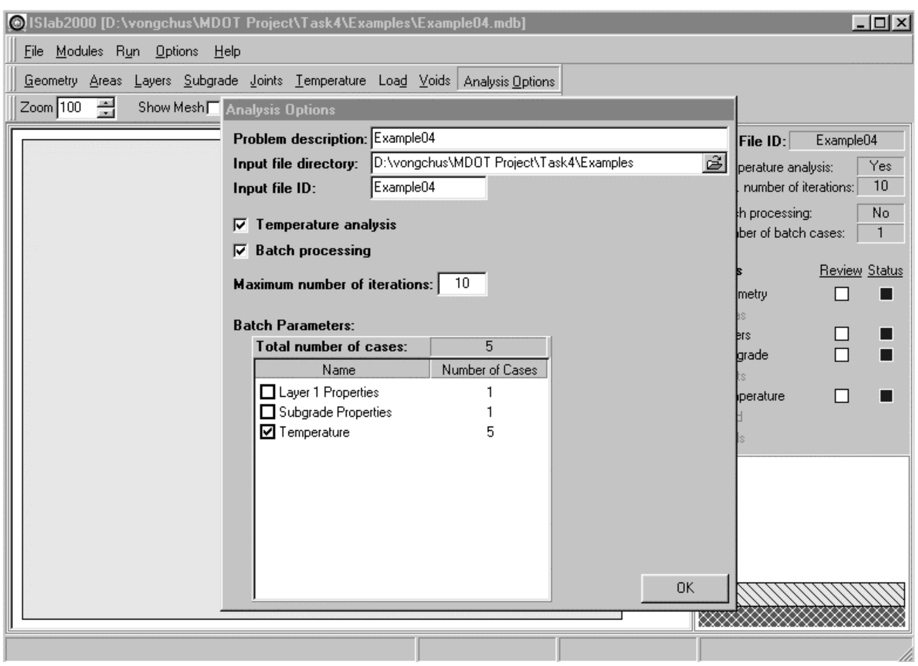


Figure E4-3: Analysis Option Module

The main panel displays the pavement structure, loading condition, and meshing as shown in Figure E4-4.

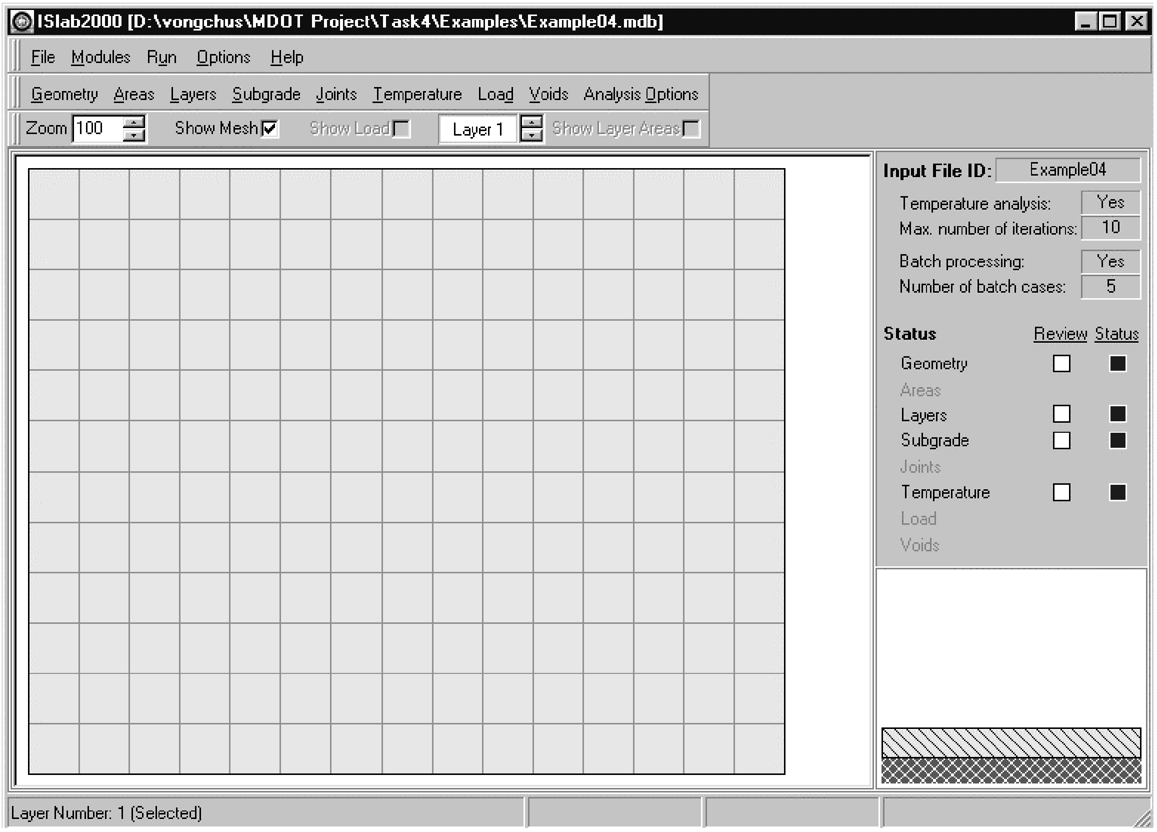


**Figure E4-4: Main Panel After the Completion of Inputs**

## *Analysis Results*

Table E4-1 summarizes the analysis results for all five temperature differentials. Stress and deflection contours from ISLAB2000 are also available in Figures E4-5 through E4-14. Figure E4-15 is the plot of relationship between stresses and temperature differentials.

| $\Delta T$, $^oF$ | Stress at the bottom of the PCC, psi | | Stress at the top of the PCC, psi | | Deflection, in. |
|---|---|---|---|---|---|
| | Transverse | Longitudinal | Transverse | Longitudinal | |
| -20 | -47.4 | -79.1 | 47.4 | 79.1 | 0.02163 |
| -10 | -27.2 | -45.9 | 27.2 | 45.9 | 0.01532 |
| 0 | 0.0 | 0.0 | 0.0 | 0.0 | 0.00870 |
| 10 | 27.6 | 46.5 | -27.6 | -46.5 | 0.02306 |
| 20 | 46.5 | 83.6 | -46.5 | -83.6 | 0.03739 |

**Table E4-1: Analysis Results**

**NOTE**

Positive and negative values of stress signify tensile and compressive stresses and positive value of deflection indicates deflection in downward direction.

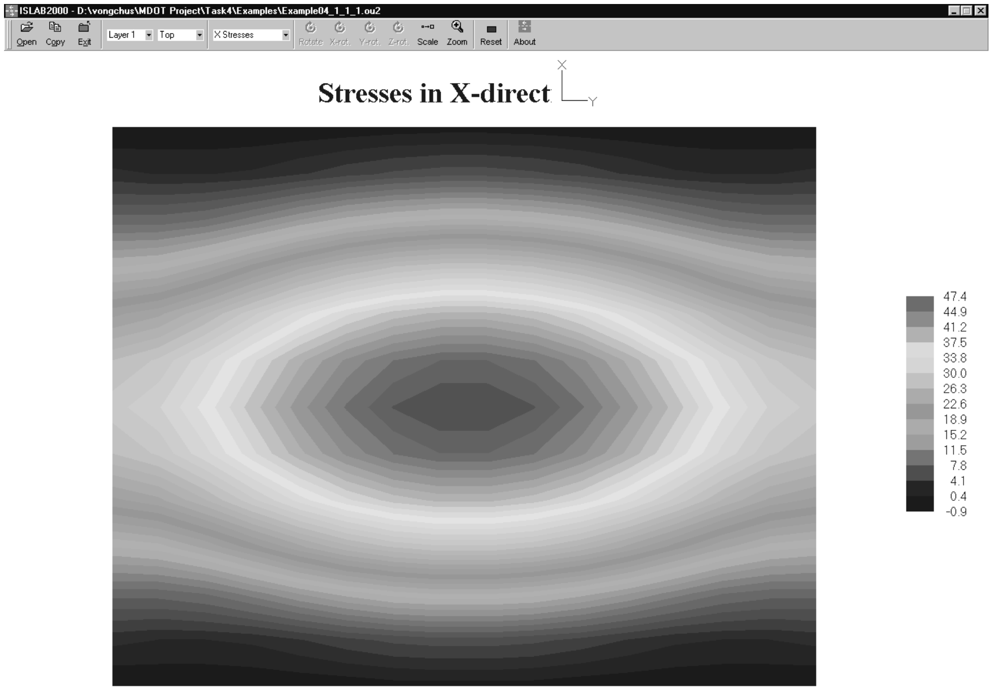


**Figure E4-5: Transverse Stress at the Top of the PCC Slab, ΔT = -20 °F**

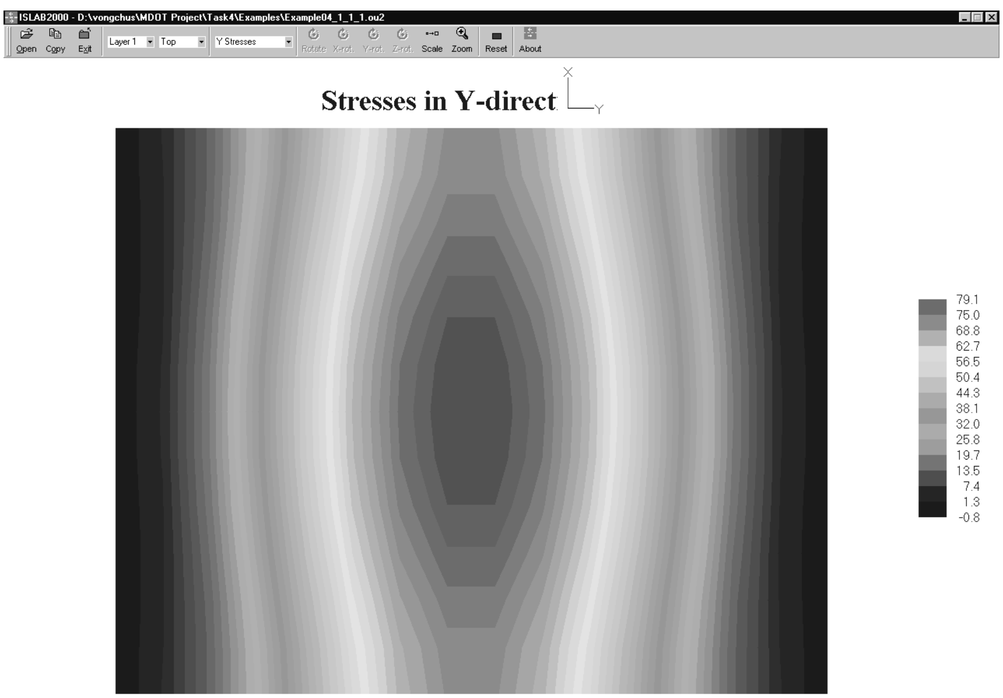


**Figure E4-6: Longitudinal Stress at the Top of the PCC Slab, ΔT = -20 °F**

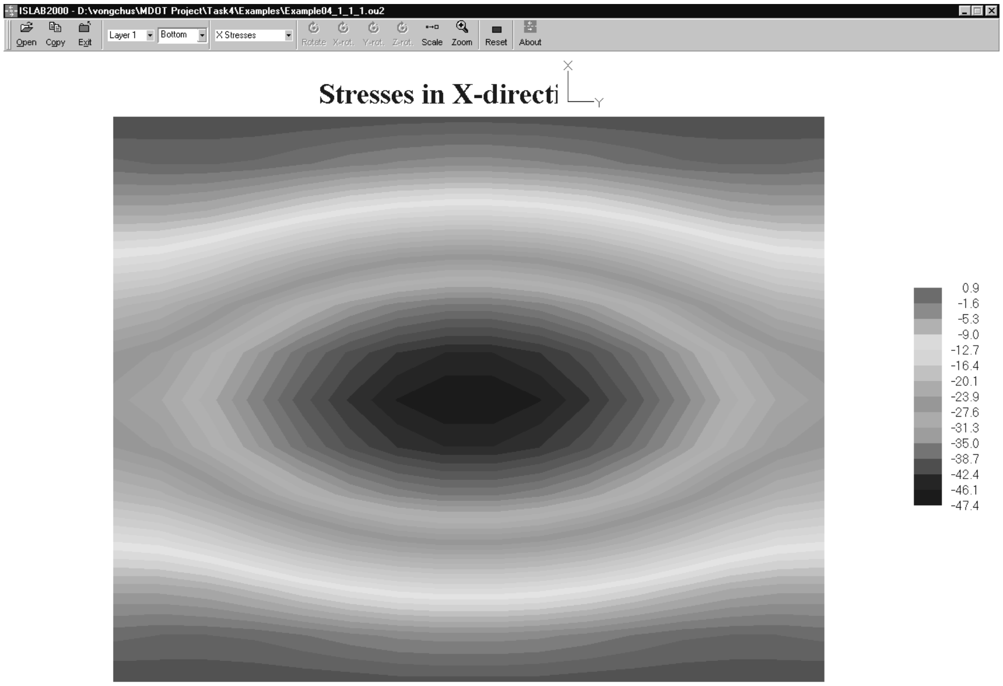


**Figure E4-7: Transverse Stress at the Bottom of the PCC Slab, ΔT = -20 °F**

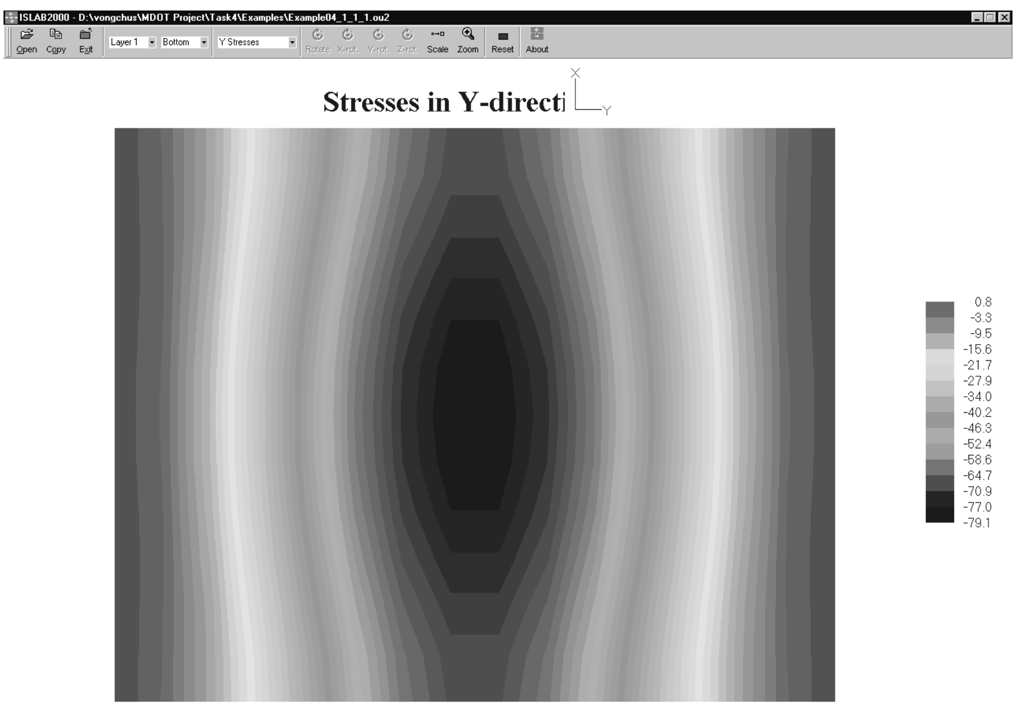


**Figure E4-8: Longitudinal Stress at the Bottom of the PCC Slab, ΔT = -20 °F**

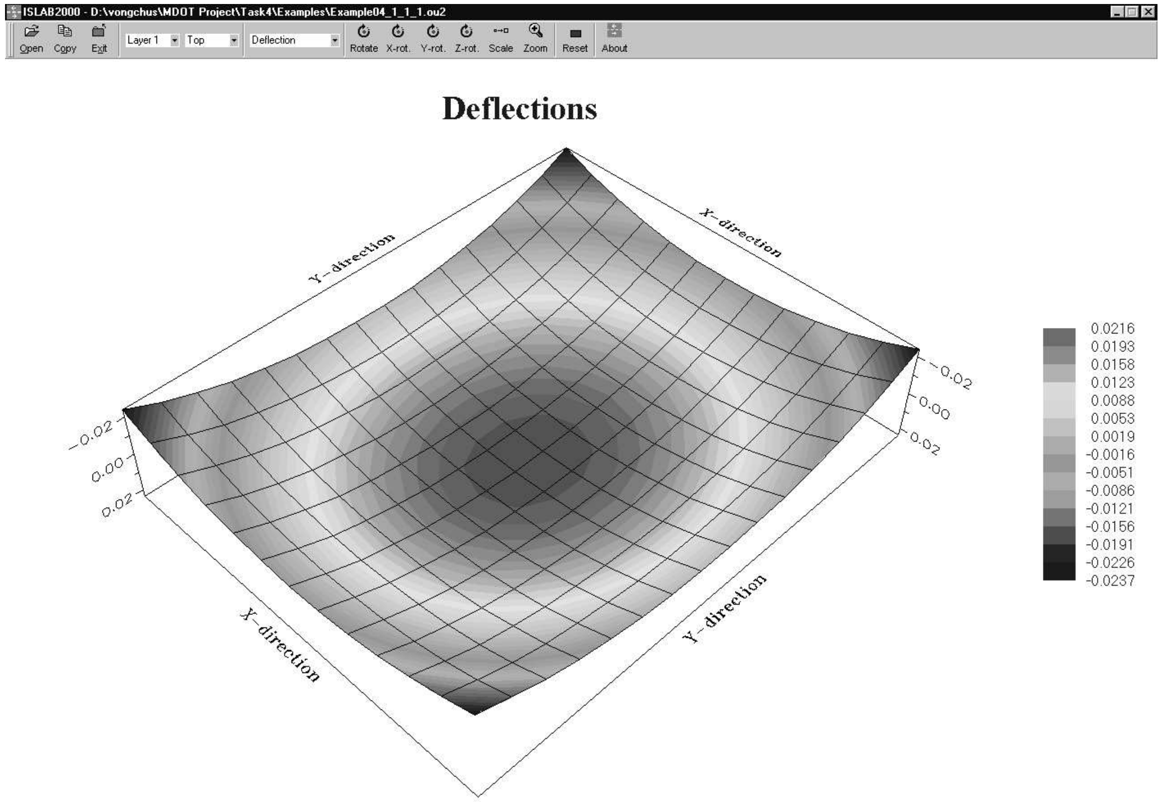


**Figure E4-9: Deflection of the PCC slab, ΔT = -20 °F**

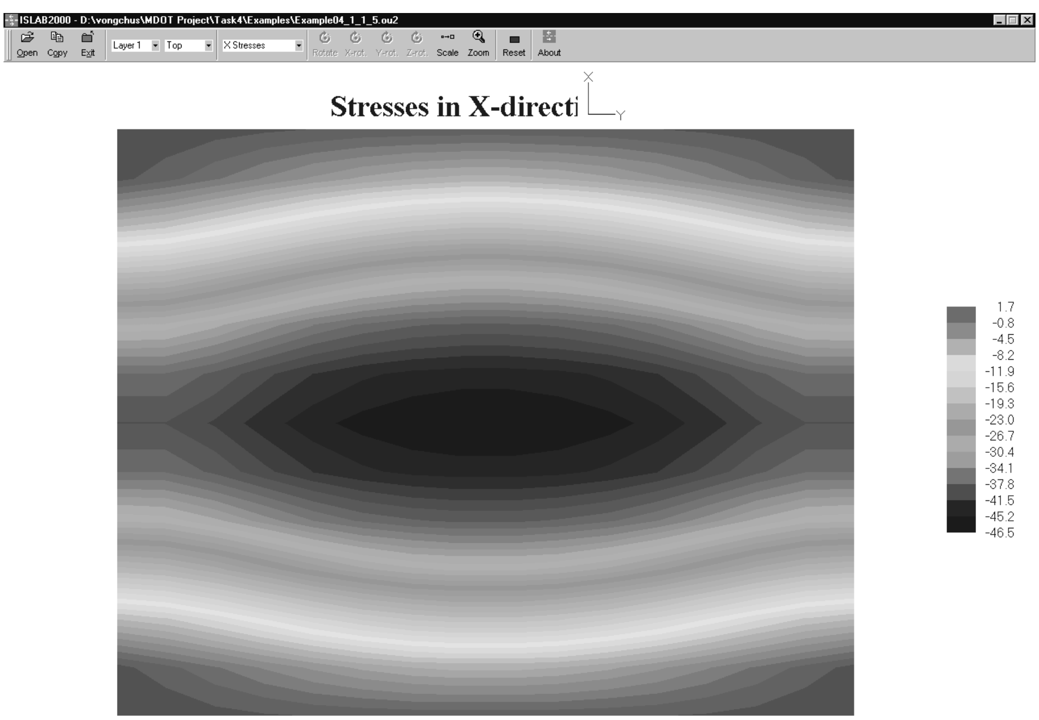


**Figure E4-10: Transverse stress at the top of the PCC slab, ΔT = +20 °F**

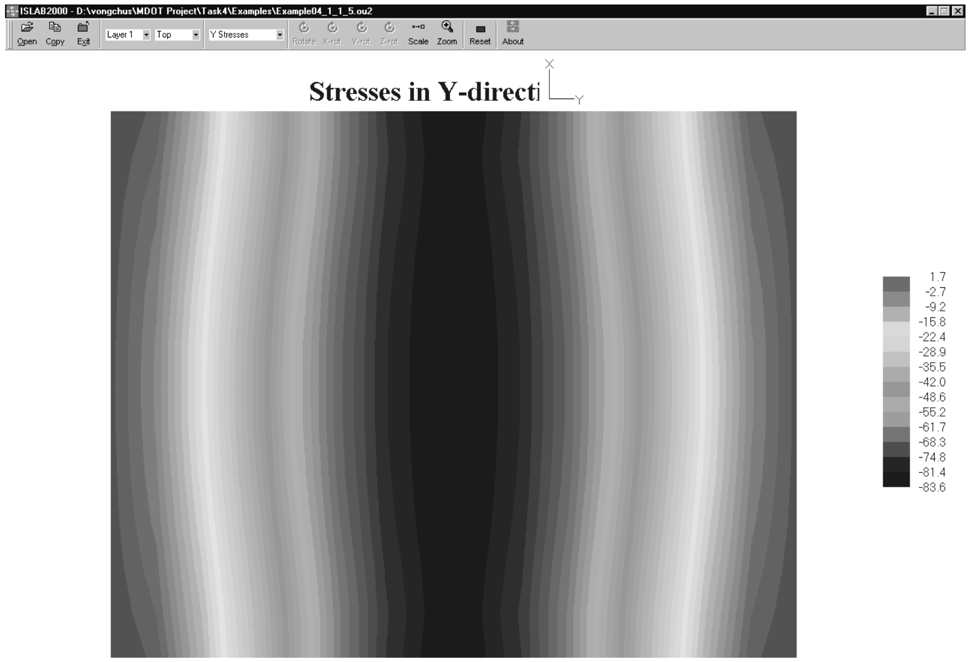


**Figure E4-11: Longitudinal stress at the top of the PCC slab, ∆T = +20 °F**

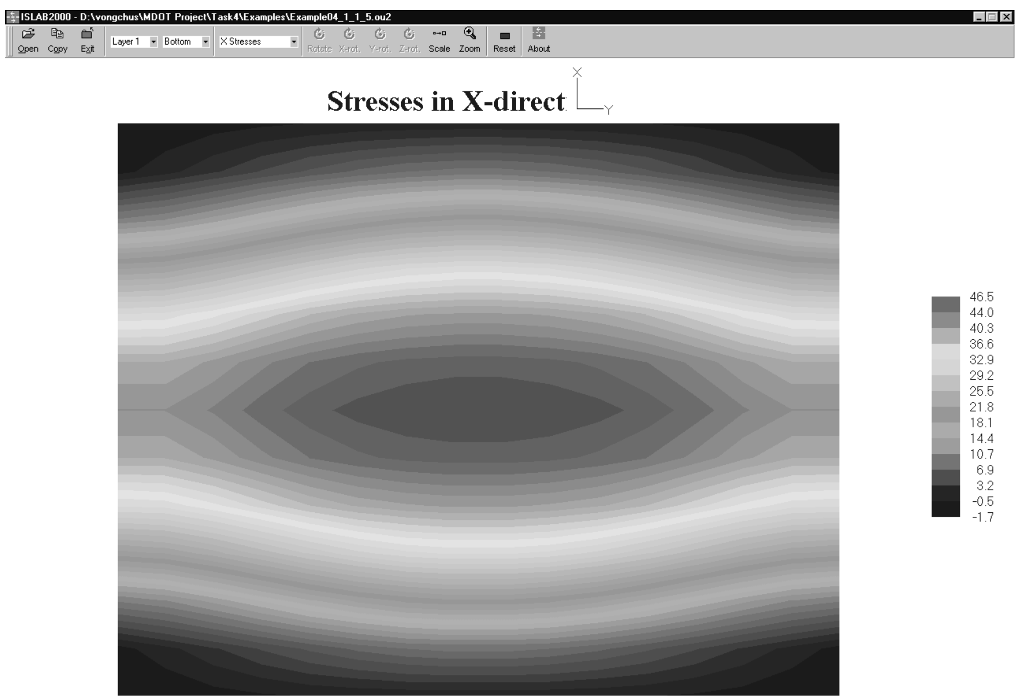


**Figure E4-12: Transverse stress at the bottom of the PCC slab, ∆T = +20 °F**


**Figure E4-13: Longitudinal Stress at the Bottom of the PCC Slab, $\Delta T$ = +20 °F**

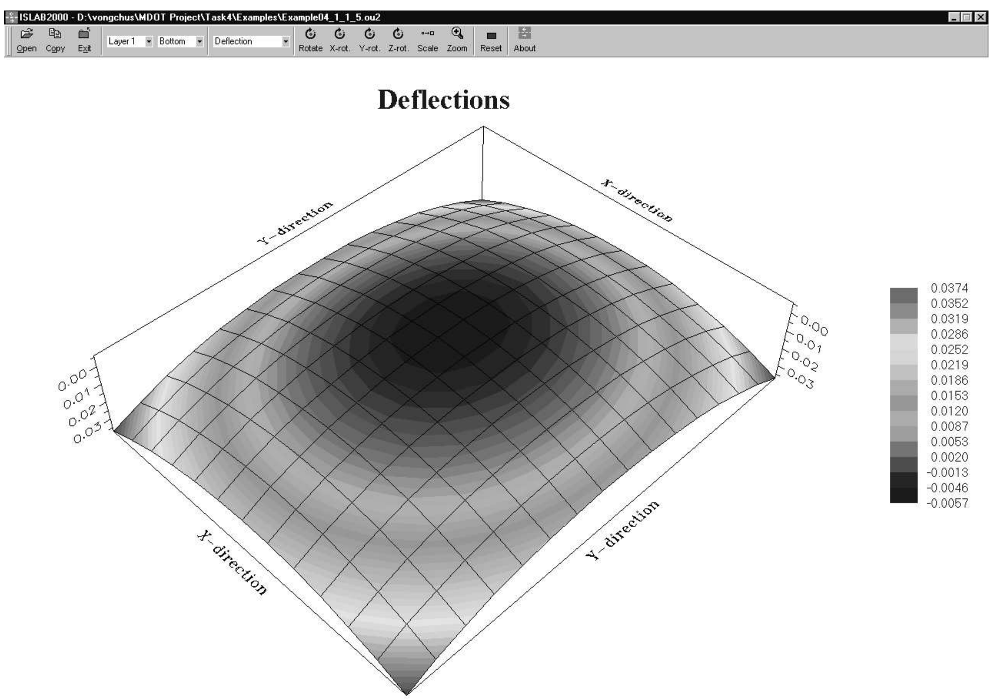


**Figure E4-14: Deflection of the PCC Slab, $\Delta T$ = +20 °F**

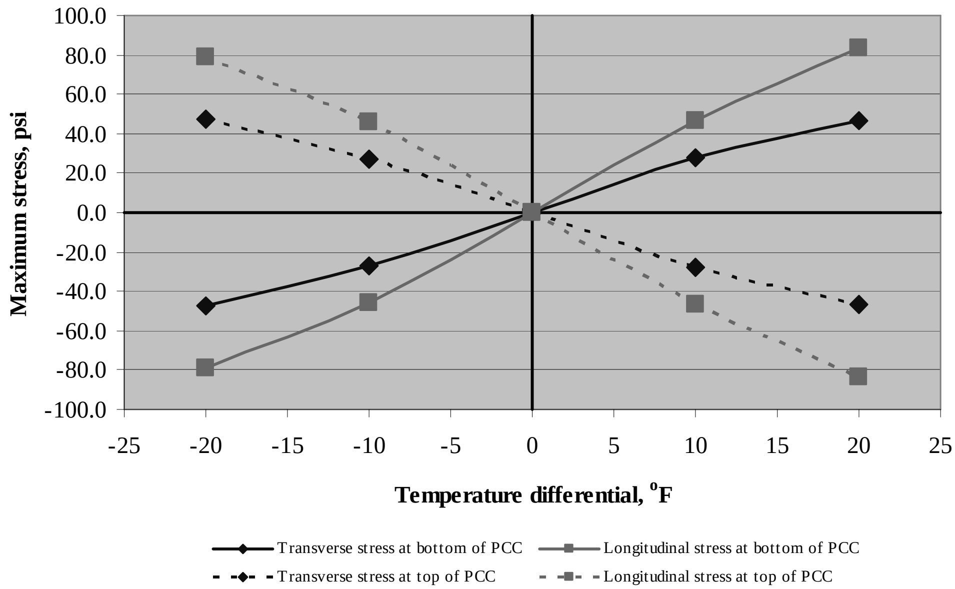


**Figure E4-15: Relationship Between Stresses and Temperature Differentials**

# Example 5:
# Interior Loading with Thermal Gradients on a Single Slab

## Problem Statement

Determine maximum deflection and stress at the bottom of the PCC slab for Westergaard's interior loading condition with temperature differentials, ΔT, of -20, -10, 0, +10, +20 °F.

## Given

| | | | |
|---|---|---|---|
| Concrete elastic modulus | = | $4 \times 10^6$ | psi |
| Concrete Poisson's ratio | = | 0.15 | |
| Slab thickness | = | 10 | in. |
| Slab dimension | = | 144 x 180 | $in^2$ |
| Mesh size | = | 12 x 12 | $in^2$ (medium) |
| k-value | = | 100 | psi/in. |
| Tire contact area | = | 7.5x15 | $in^2$ |
| Wheel load | = | 10,000 | lbs |
| Coefficient of thermal exp., α | = | $4.4 \times 10^{-6}$ | in./in./°F |
| Temperature differential, ΔT | = | -20, -10, 0, +10, +20 | °F |

## Problem Illustration

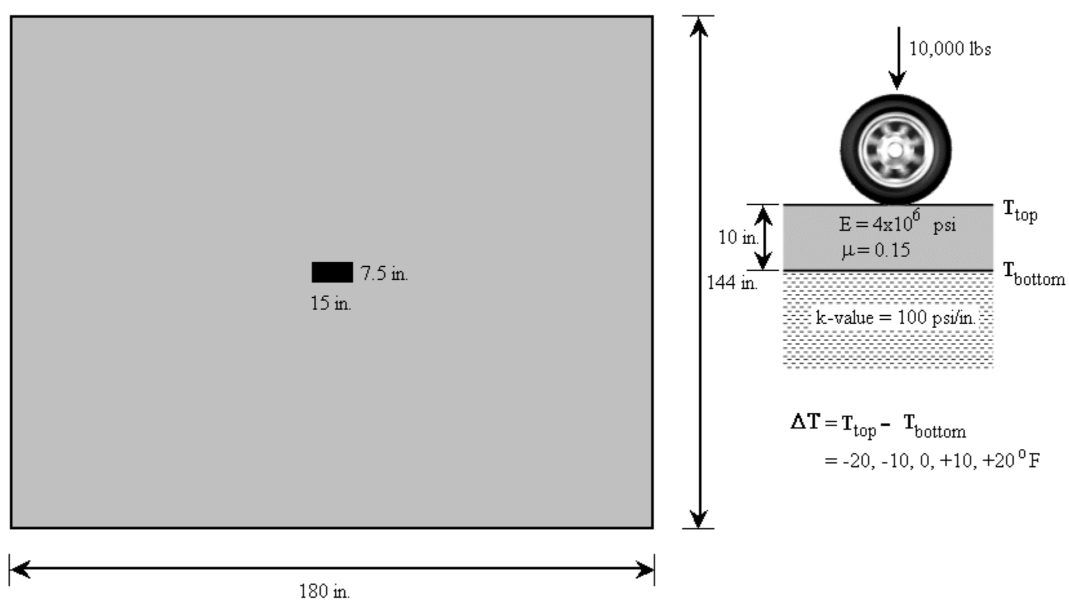


**Figure E5-1: Problem Illustration**

# Solution

### Geometry Module

Use this module from Example 1.

### Layers Module

Use this module from Example 1.

### Subgrade Module

Use this module from Example 1.

### Load Module

Use this module from Example 1.

### Temperature Module

Use this module from Example 4.

### Analysis options Module

Use this module from Example 4.

The main panel should display the pavement structure, loading condition, and meshing as shown in Example 1 (Figure E1-7.)

## *Analysis Results*

Table E5-1 summarizes the analysis results for all five temperature differentials. Stress and deflection contours from ISLAB2000 are also available in Figures E5-2 through E5-7. Figures E5-8 and E5-9 are the plots of relationship between stresses and temperature differentials and between deflections and temperature differentials, respectively.

| $\Delta T$, $^oF$ | Stress at the bottom of the PCC, psi | | Deflection, in. |
|---|---|---|---|
| | Transverse | Longitudinal | |
| -20 | 91.7 | 41.1 | 0.02971 |
| -10 | 113.5 | 77.5 | 0.01650 |
| 0 | 140.6 | 123.4 | 0.01480 |
| 10 | 168.2 | 169.8 | 0.01043 |
| 20 | 195.8 | 216.3 | 0.00607 |

**Table E5-1: Analysis Results**

**NOTE**
Positive and negative values of stress signify tensile and compressive stresses and positive value of deflection indicates deflection in downward direction.

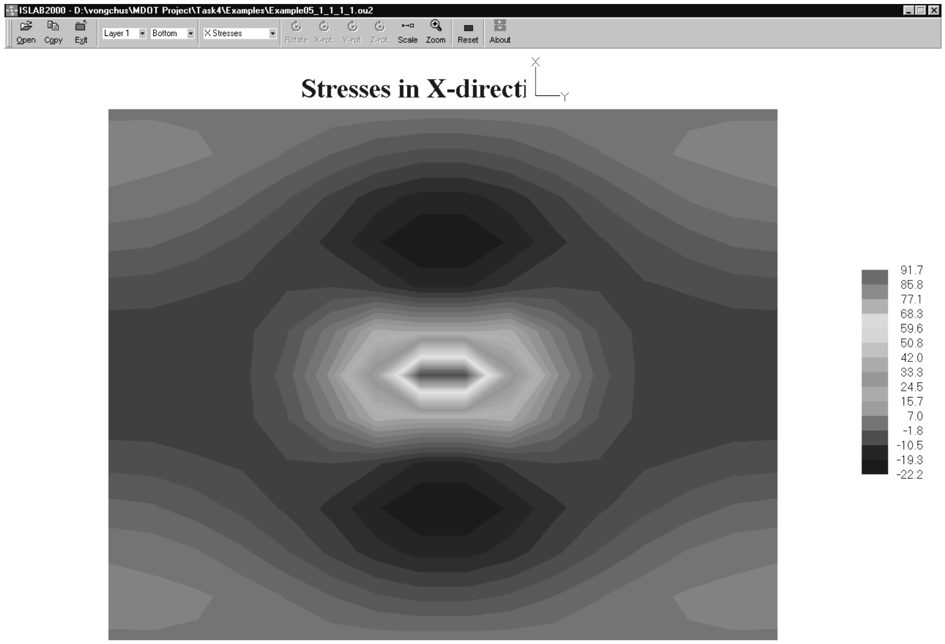


**Figure E5-2: Transverse Stress at the Bottom of the PCC Slab, ΔT = -20 $^{o}$F**

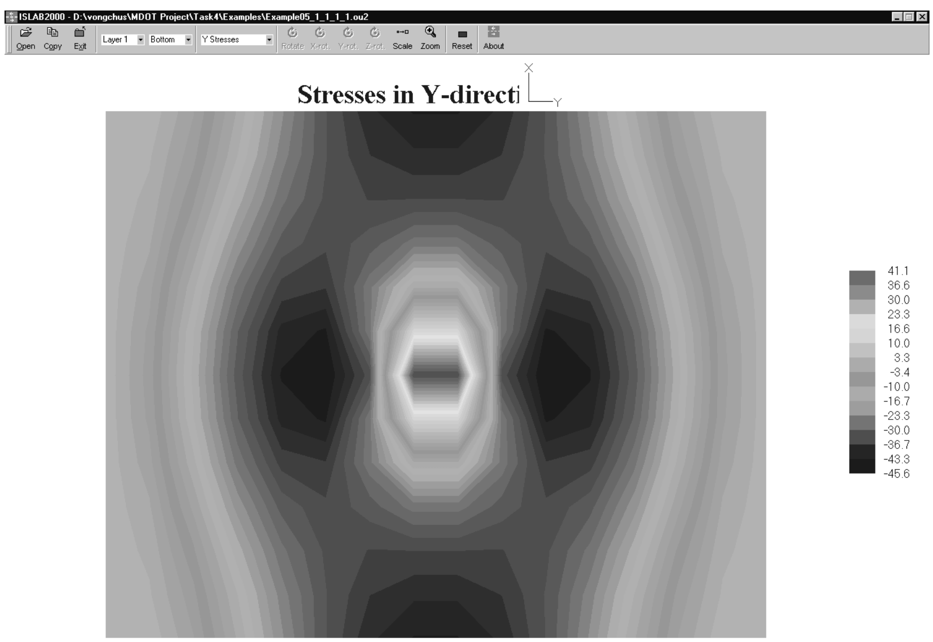


**Figure E5-3: Longitudinal Stress at the Bottom of the PCC Slab, ΔT = -20 $^{o}$F**

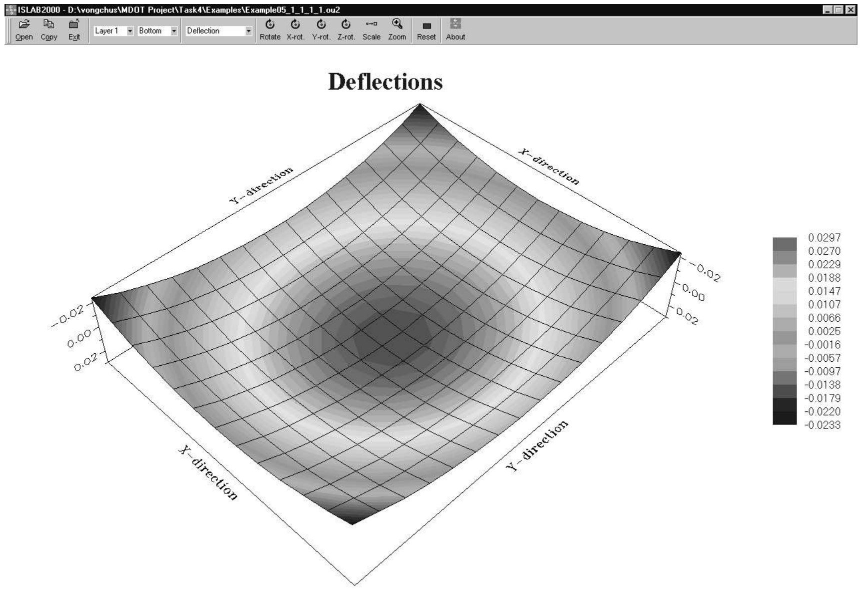


**Figure E5-4: Deflection of the PCC Slab, ΔT = -20 °F**

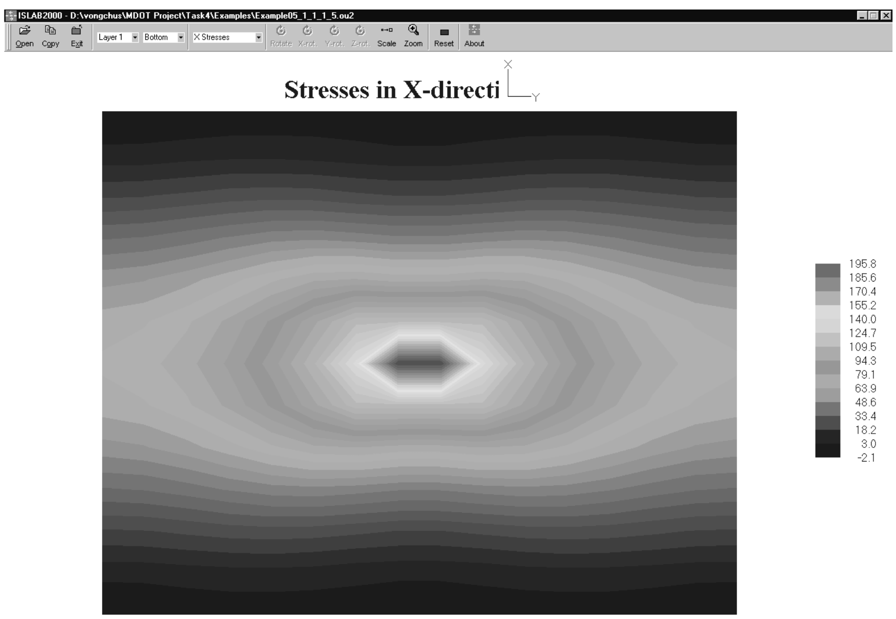


**Figure E5-5: Transverse Stress at the Bottom of the PCC Slab, ΔT = +20 °F**

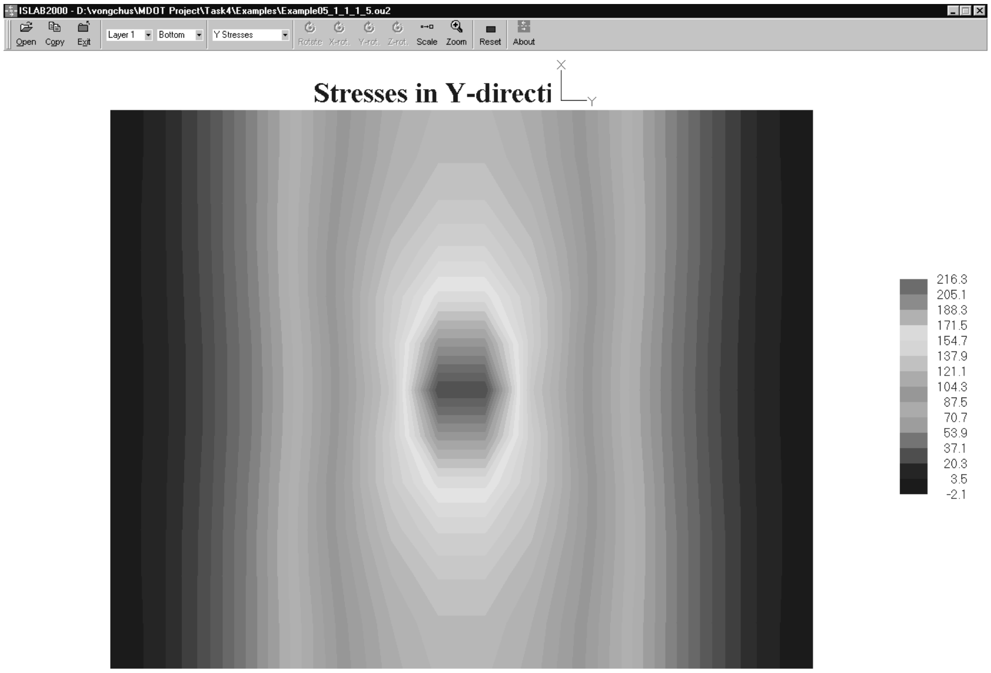


**Figure E5-6: Longitudinal Stress at the Bottom of the PCC Slab, ΔT = +20 °F**

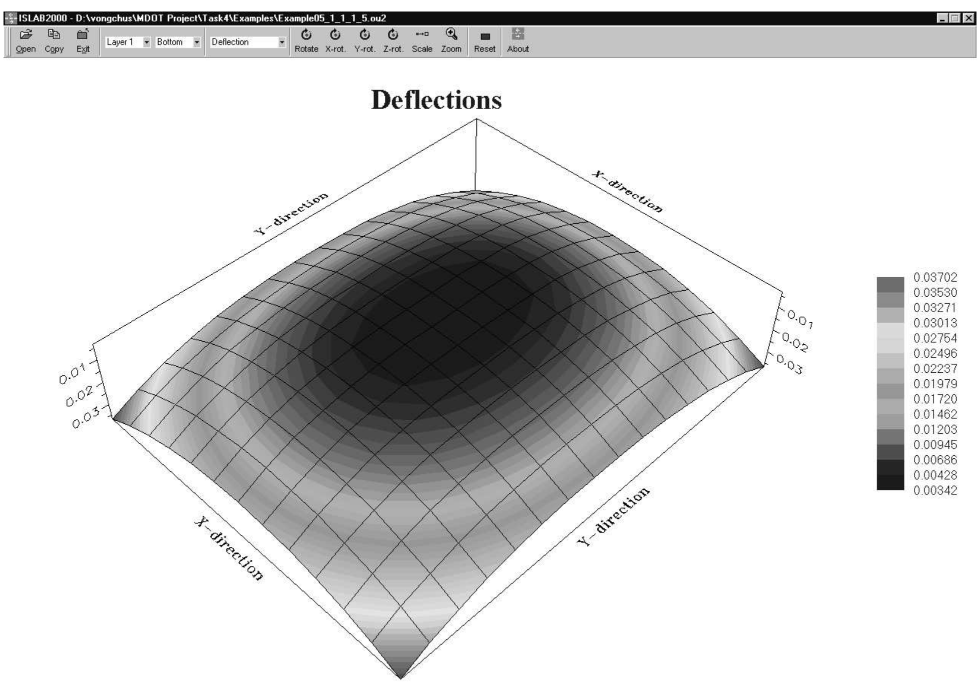


**Figure E5-7: Deflection of the PCC Slab, ΔT = +20 °F**

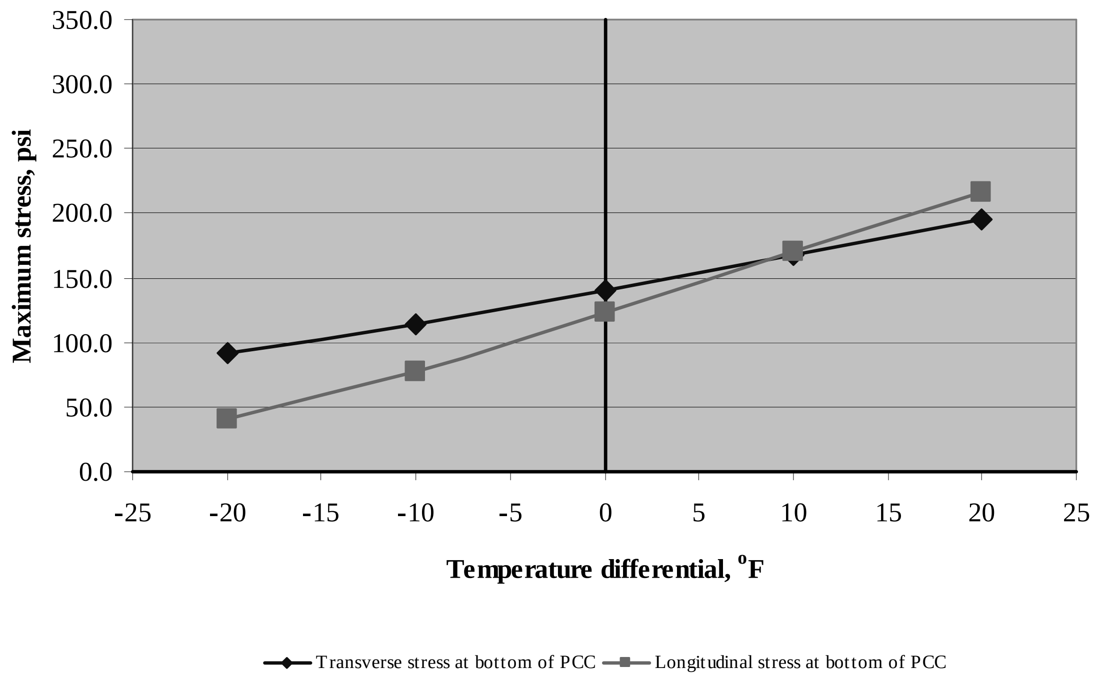


E5-8: Relationship Between Stresses and Temperature Differentials

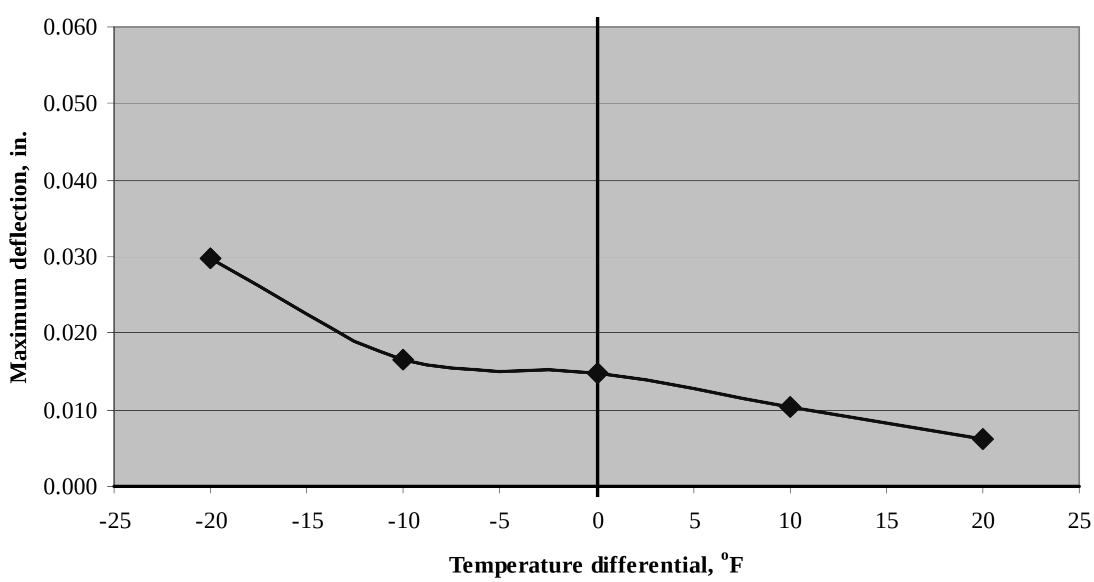


E5-9: Relationship Between Deflections and Temperature Differentials

# Example 6:
# Edge Loading with Thermal Gradients on a Single Slab

### Problem Statement

Determine maximum deflection and stress at the bottom of the PCC slab for Westergaard's edge loading condition with temperature differentials, ΔT, of -20, -10, 0, +10, +20 $^oF$.

### Given

| | | | |
|---|---|---|---|
| Concrete elastic modulus | = | 4 x $10^6$ | psi |
| Concrete Poisson's ratio | = | 0.15 | |
| Slab thickness | = | 10 | in. |
| Slab dimension | = | 144 x 180 | $in^2$ |
| Mesh size | = | 12 x 12 | $in^2$ (medium) |
| k-value | = | 100 | psi/in. |
| Tire contact area | = | 7.5 x 15 | $in^2$ |
| Wheel load | = | 10,000 | lbs |
| Coefficient of thermal exp., α | = | 4.4 x $10^{-6}$ | in./in./$^oF$ |
| Temperature differential, ΔT | = | -20, -10, 0, +10, +20 | $^oF$ |

### Problem Illustration

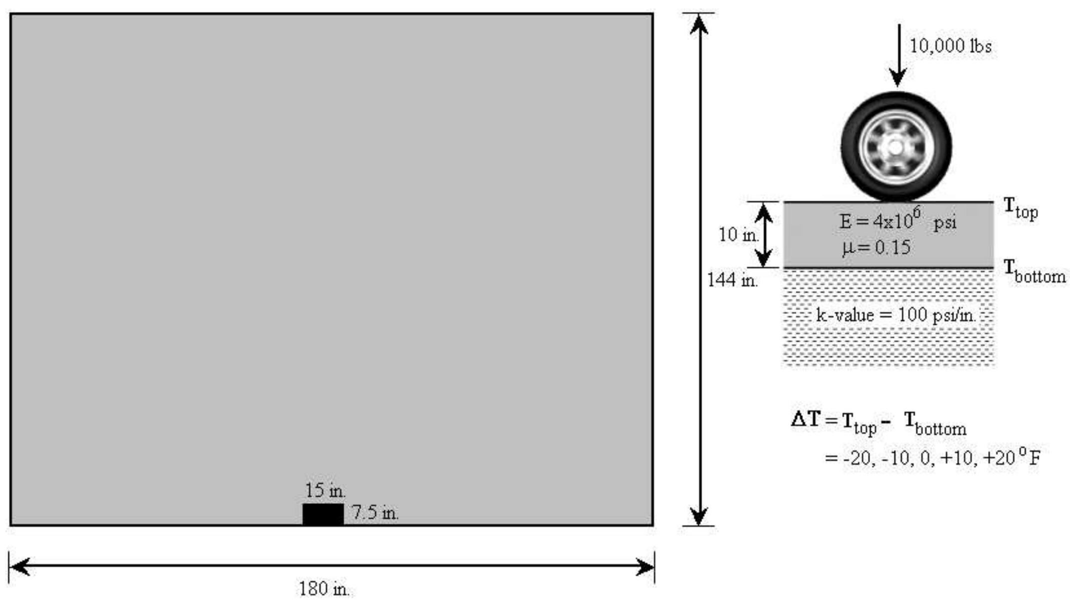


**Figure E6-1: Problem Illustration**

# Solution

### Geometry Module

Use this module from Example 1.

### Layers Module

Use this module from Example 1.

### Subgrade Module

Use this module from Example 1.

### Load Module

Use this module from Example 1.

### Temperature Module

Use this module from Example 4.

### Analysis Options Module

Use this module from Example 4.

The main panel should display the pavement structure, loading condition, and meshing as shown in Example 2 (Figure E2-3.)

## *Analysis Results*

Table E6-1 summarizes the analysis results for all five temperature differentials. Stress and deflection contours from ISLAB2000 are also available in Figures E6-2 through E6-7. Figures E6-8 and E6-9 are the plots of relationship between stresses and temperature differentials and between deflections and temperature differentials, respectively.

| $\Delta T$, $^{o}F$ | Stress at the bottom of the PCC, psi | | Deflection, in. |
|---|---|---|---|
| | Transverse | Longitudinal | |
| -20 | 37.4 | 165.4 | 0.03000 |
| -10 | 37.4 | 203.1 | 0.03130 |
| 0 | 37.4 | 245.5 | 0.03384 |
| 10 | 37.3 | 289.1 | 0.03685 |
| 20 | 37.3 | 332.1 | 0.03982 |

**Table E6-1: Analysis results**

**NOTE**
Positive and negative values of stress signify tensile and compressive stresses and positive value of deflection indicates deflection in downward direction.

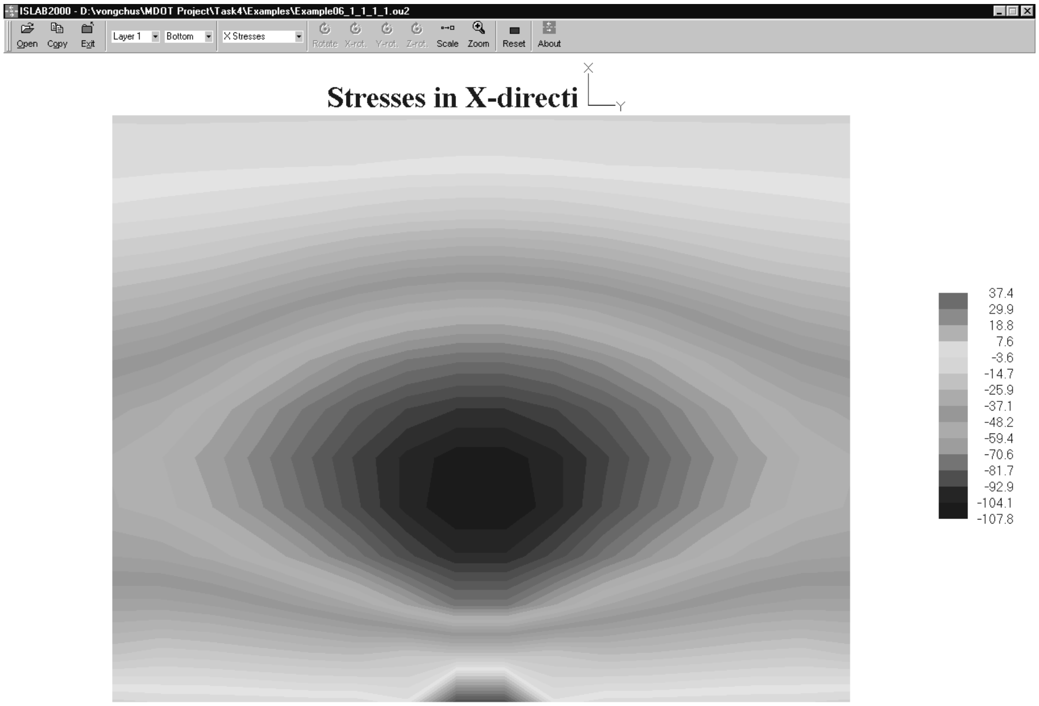


**Figure E6-2: Transverse Stress at the Bottom of the PCC Slab, ΔT = -20 °F**

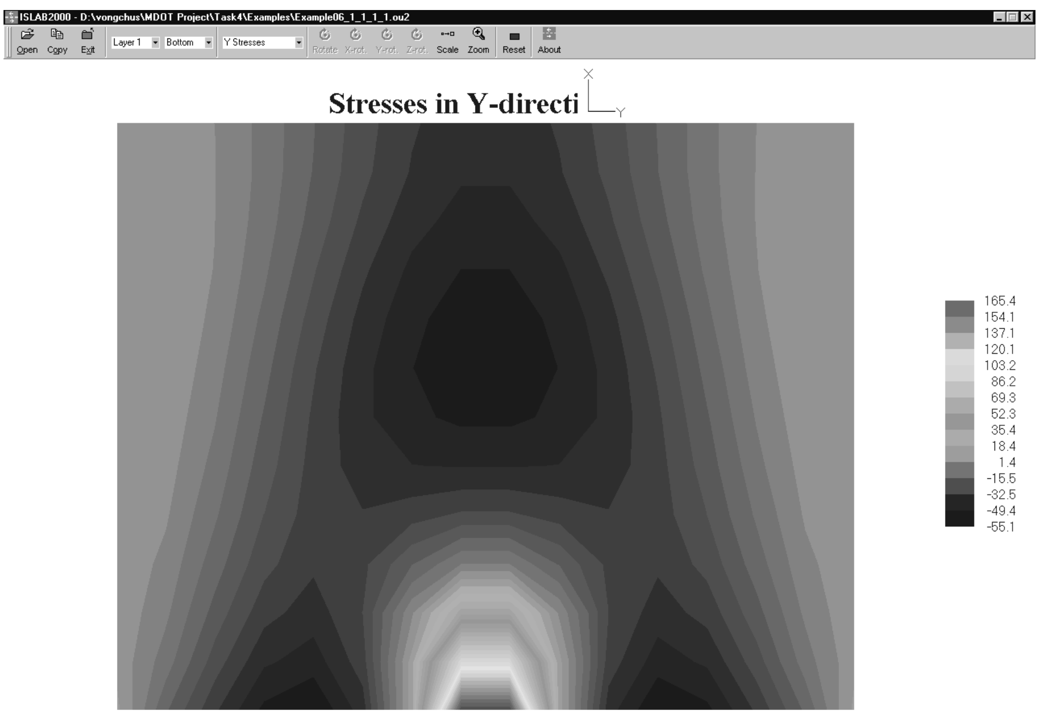


**Figure E6-3: Longitudinal Stress at the Bottom of the PCC Slab, ΔT = -20 °F**

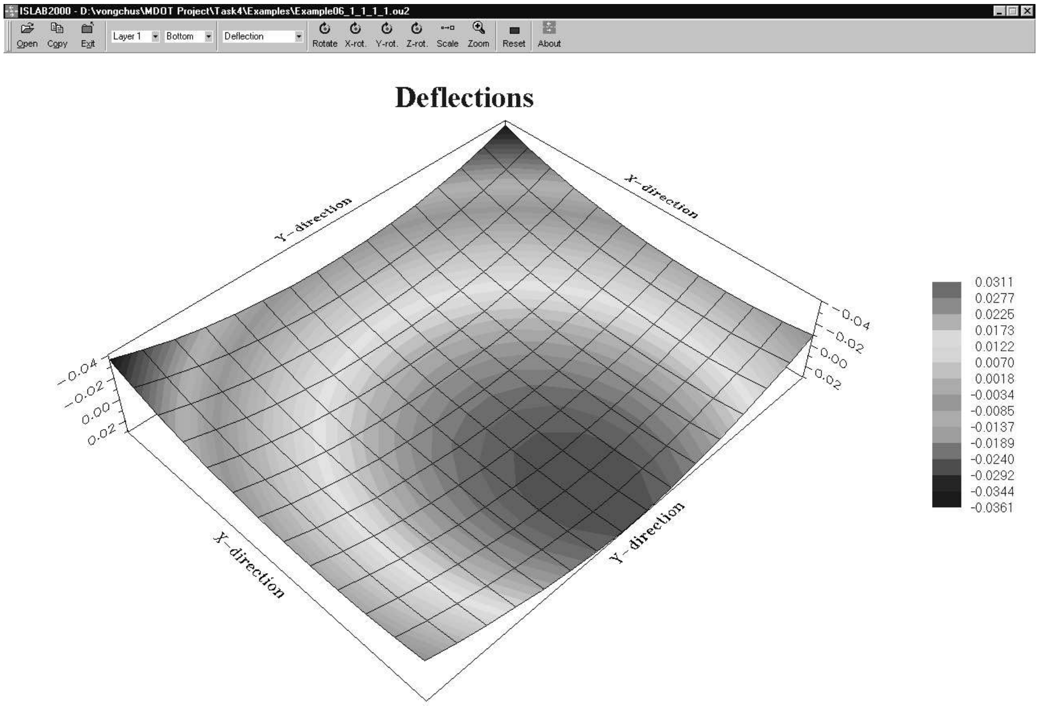


**Figure E6-4: Deflection of the PCC slab, ΔT = -20 °F**

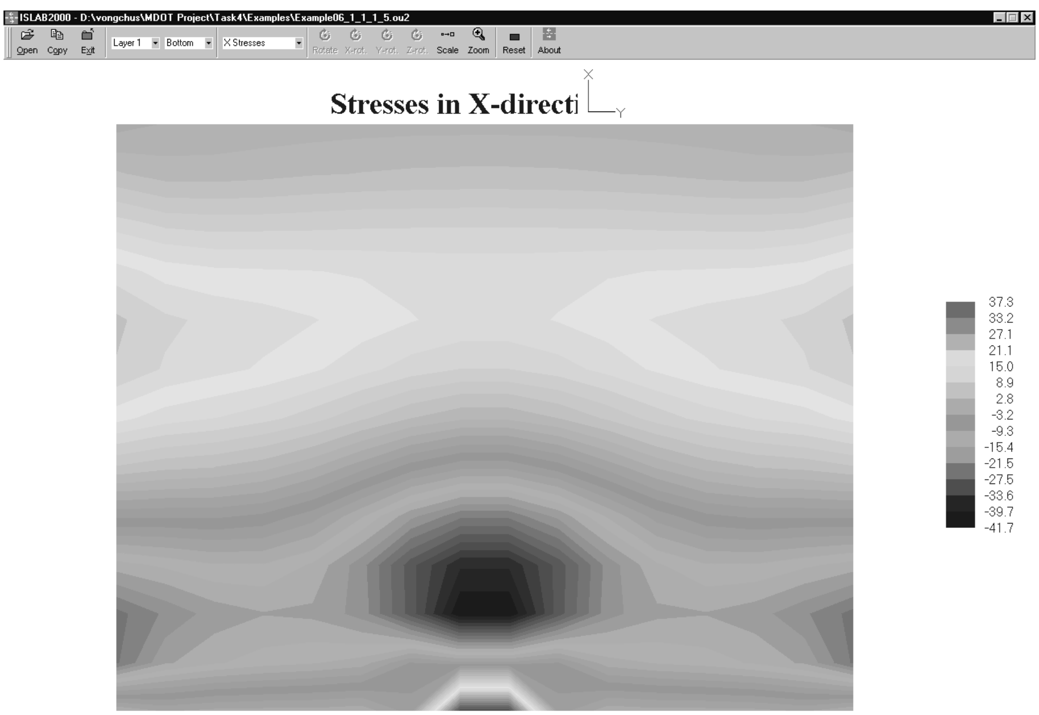


**Figure E6-5: Transverse Stress at the Bottom of the PCC Slab, ΔT = +20 °F**

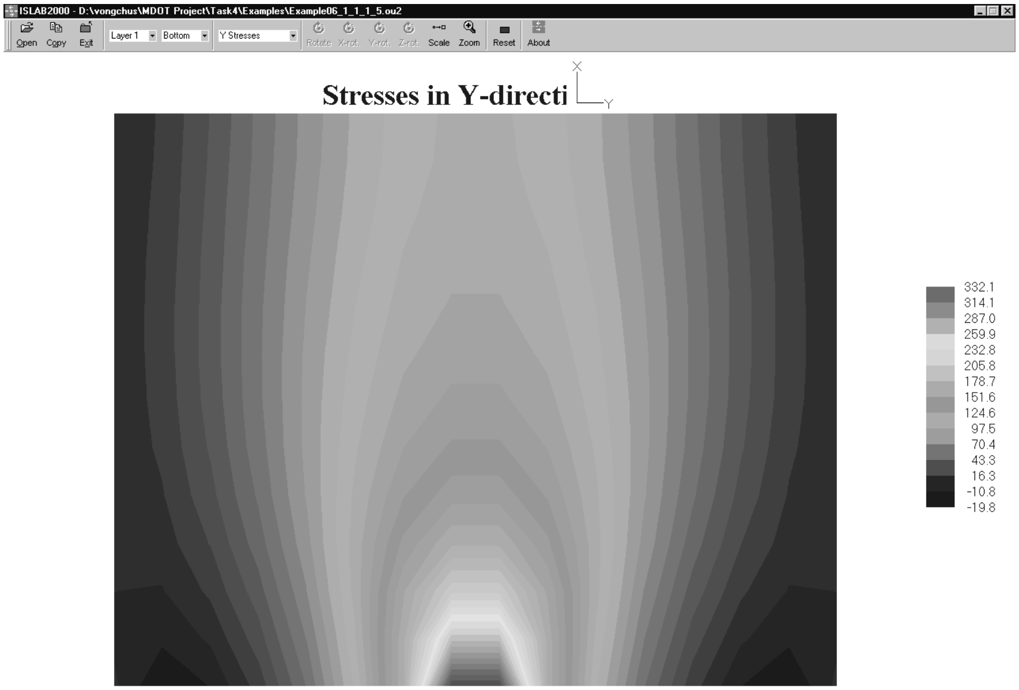


**Figure E6-6: Longitudinal Stress at the Bottom of the PCC Slab, ΔT = +20 °F**

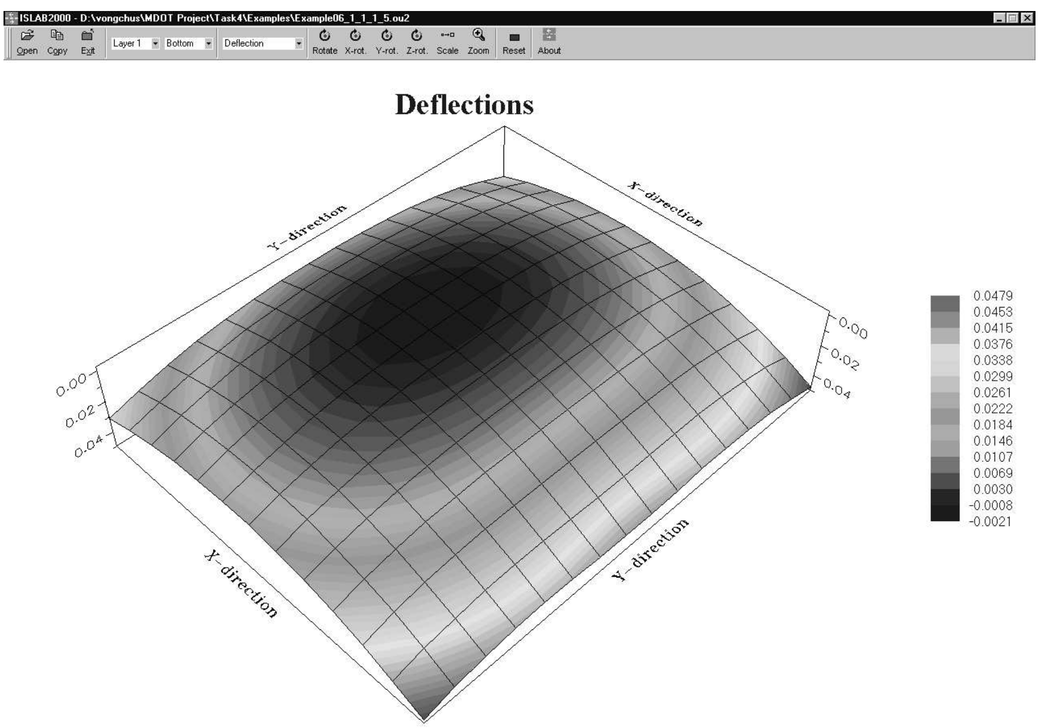


**Figure E6-7: Deflection of the PCC Slab, ΔT = +20 °F**

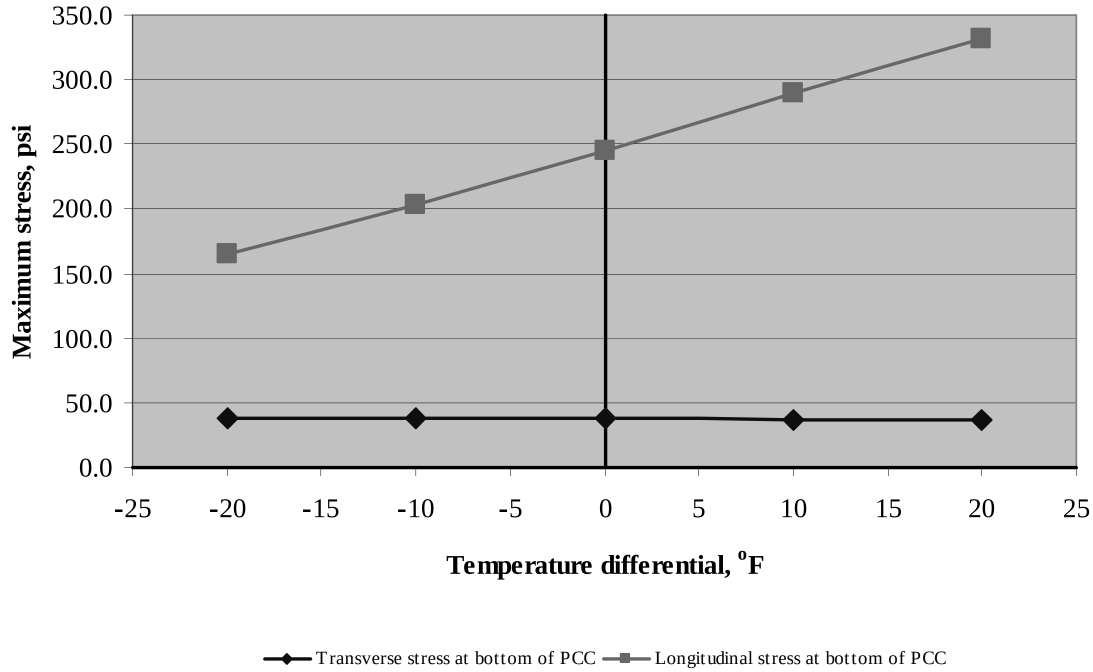


**E6-8: Relationship Between Stresses and Temperature Differentials**

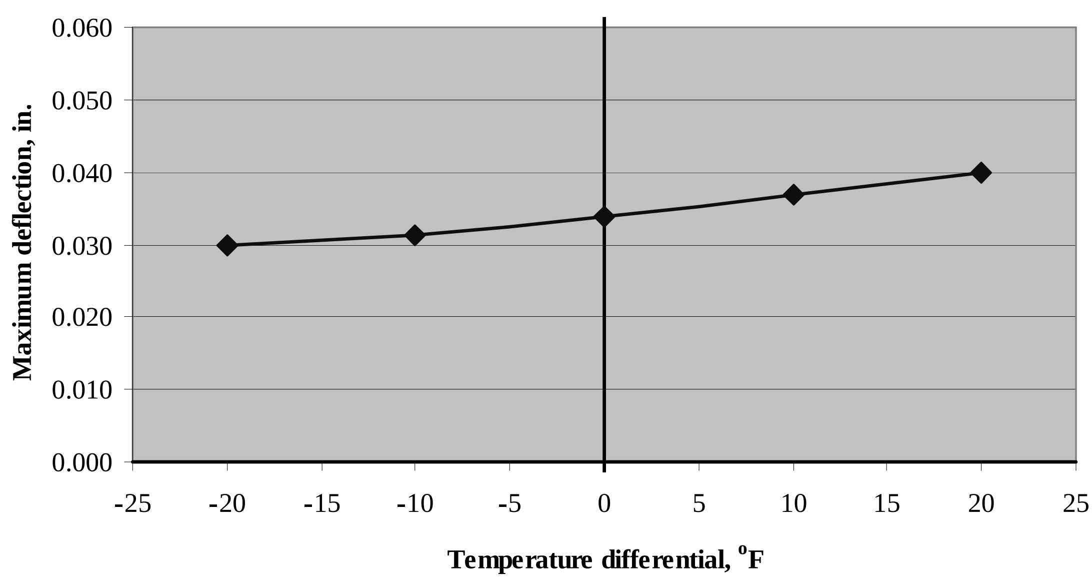


**E6-9: Relationship Between Deflections and Temperature Differentials**

# Example 7:
# Corner Loading with Thermal Gradients on a Single Slab

## Problem Statement

Determine maximum deflection and stress at the top of the PCC slab for Westergaard's corner loading condition with temperature differentials, $\Delta T$, of -20, -10, 0, +10, +20 $^oF$.

## Given

| | | | |
|---|---|---|---|
| Concrete elastic modulus | = | $4 \times 10^6$ | psi |
| Concrete Poisson's ratio | = | 0.15 | |
| Slab thickness | = | 10 | in. |
| Slab dimension | = | 144x180 | $in^2$ |
| Mesh size | = | 12x12 | $in^2$ (medium) |
| k-value | = | 100 | psi/in. |
| Tire contact area | = | 7.5x15 | $in^2$ |
| Wheel load | = | 10,000 | lbs |
| Coefficient of thermal exp., $\alpha$ | = | $4.4 \times 10^{-6}$ | in./in./$^oF$ |
| Temperature differential, $\Delta T$ | = | -20, -10, 0, +10, +20 | $^oF$ |

## Problem Illustration

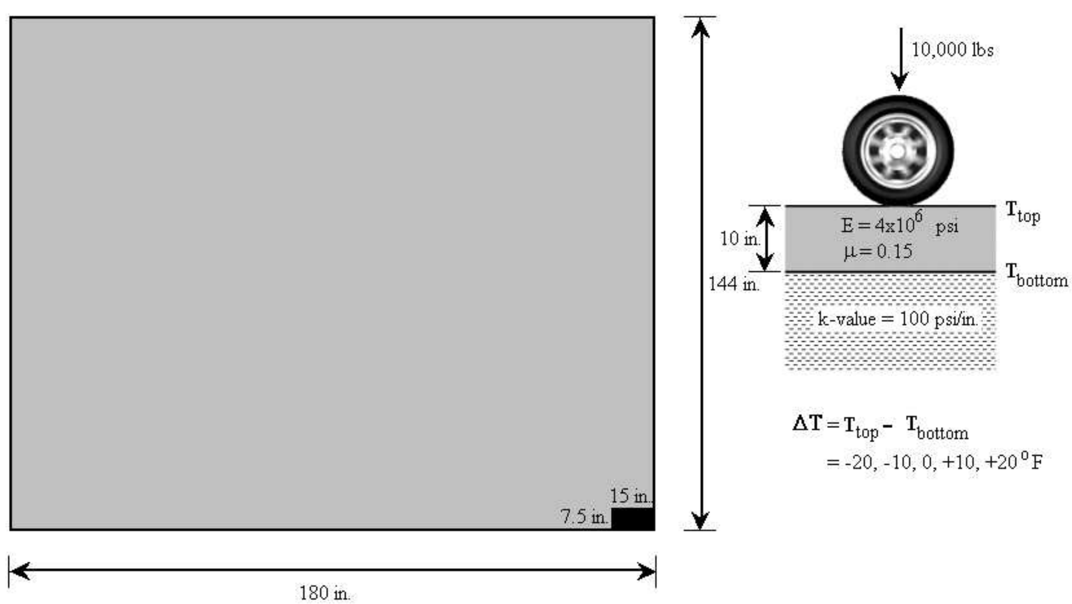


**Figure E7-1: Problem Illustration**

# Solution

### Geometry Module

Use this module from Example 1.

### Layers Module

Use this module from Example 1.

### Subgrade Module

Use this module from Example 1.

### Load Module

Use this module from Example 1.

### Temperature Module

Use this module from Example 4.

### Analysis Options Module

Use this module from Example 4.

The main panel should display the pavement structure, loading condition, and meshing as shown in Example 2 (Figure E2-3.)

## *Analysis Results*

Table E7-1 summarizes the analysis results for all five temperature differentials. Stress and deflection contours from ISLAB2000 are also available in Figures E7-2 through E7-5. Figures E7-6 and E7-7 are the plots of relationship between stresses and temperature differentials and between deflections and temperature differentials, respectively.

| $\Delta T$, $^oF$ | Corner stress, psi | Deflection, in. |
|---|---|---|
| -20 | 232.0 | 0.03923 |
| -10 | 213.5 | 0.05201 |
| 0 | 195.5 | 0.06614 |
| 10 | 182.5 | 0.08050 |
| 20 | 174.3 | 0.09524 |

**Table E7-1: Analysis Results**

**NOTE**
Positive and negative values of stress signify tensile and compressive stresses and positive value of deflection indicates deflection in downward direction.

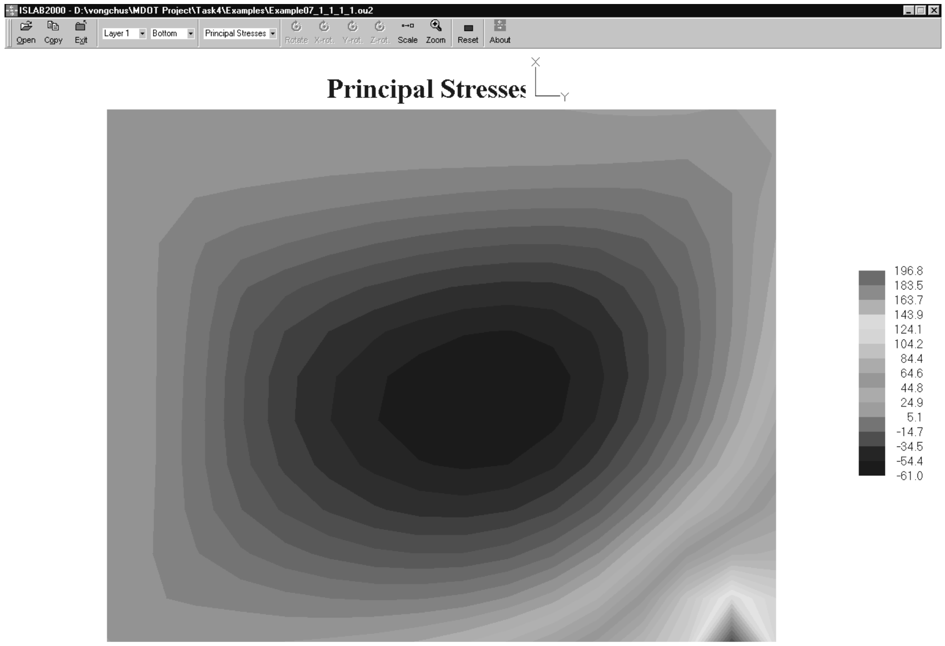


**Figure E7-2: Corner Stress at the Top of the PCC Slab, ΔT = -20 °F**

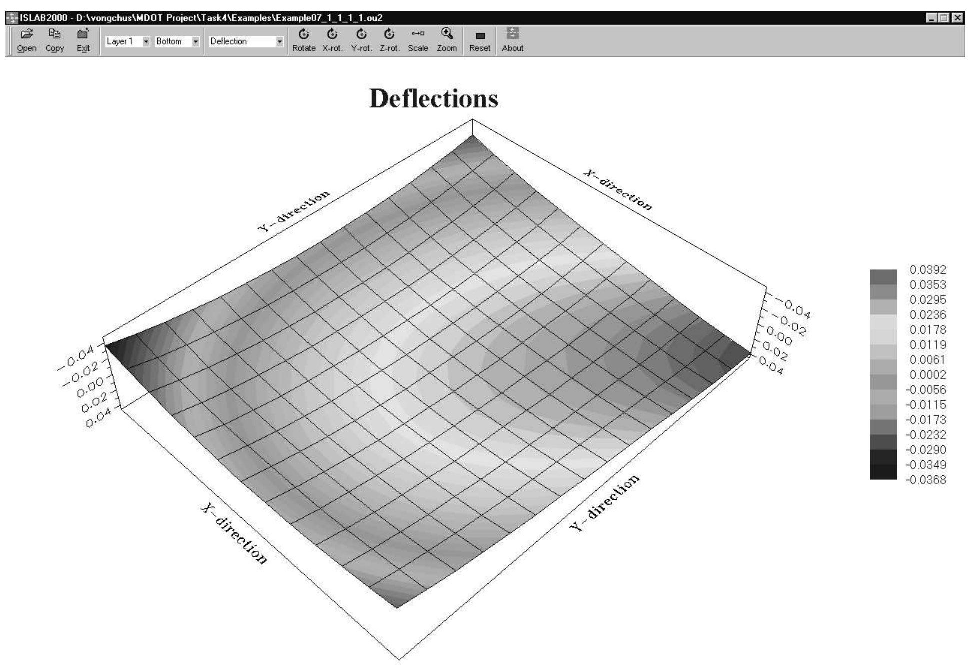


**Figure E7-3: Deflection of the PCC Slab, ΔT = -20 °F**

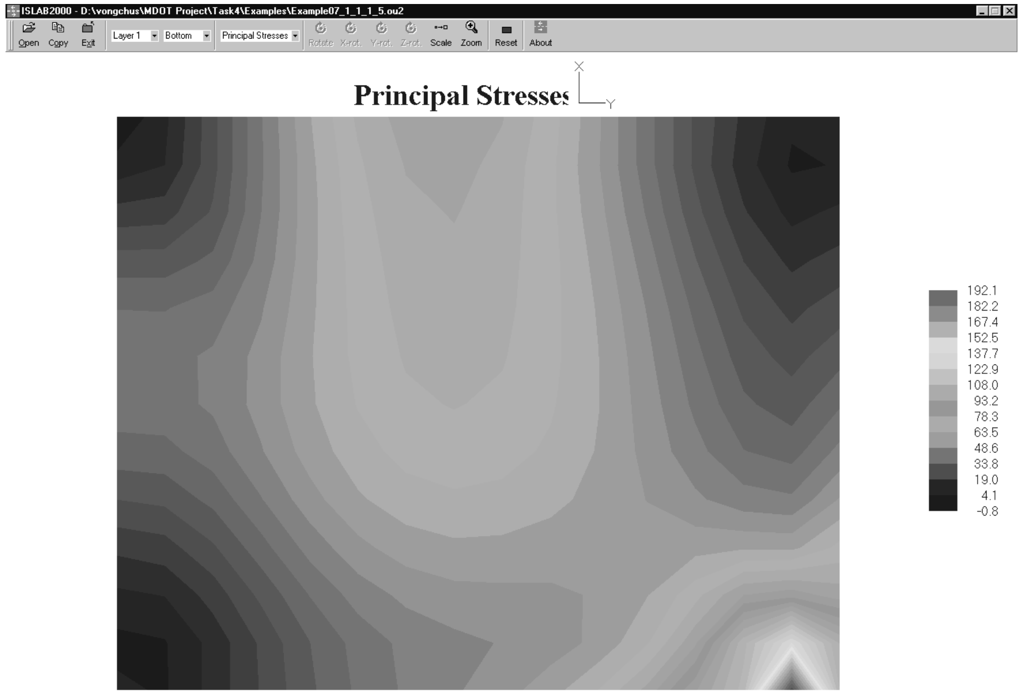


**Figure E7-4: Corner Stress at the Top of the PCC Slab, ΔT = +20 °F**

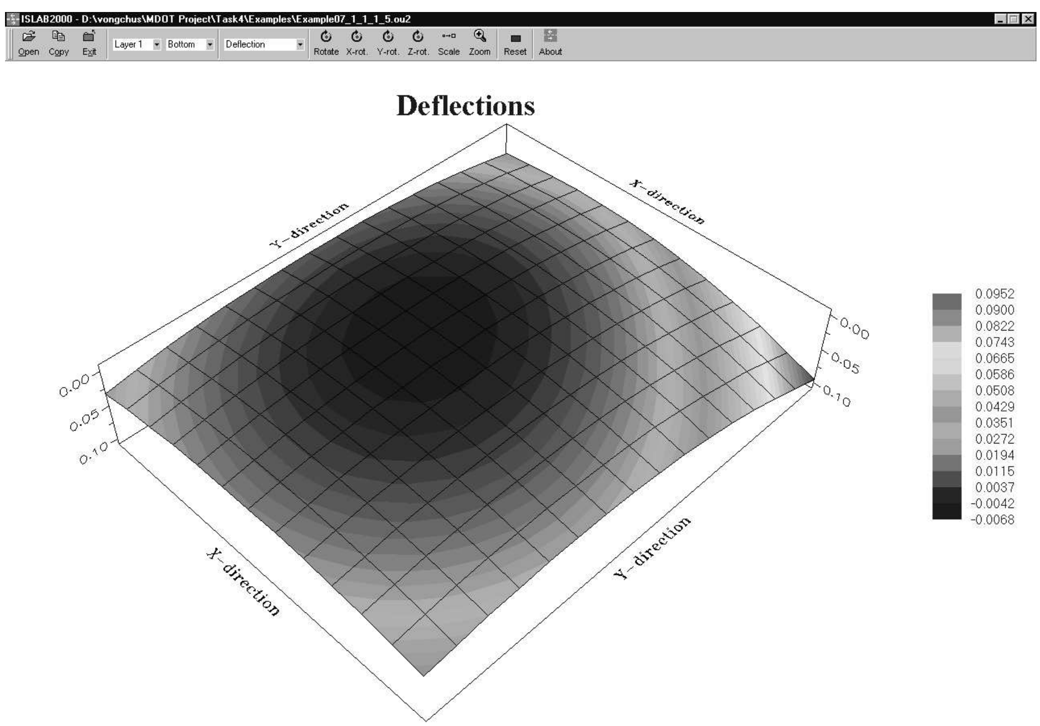


**Figure E7-5: Deflection of the PCC Slab, ΔT = +20 °F**

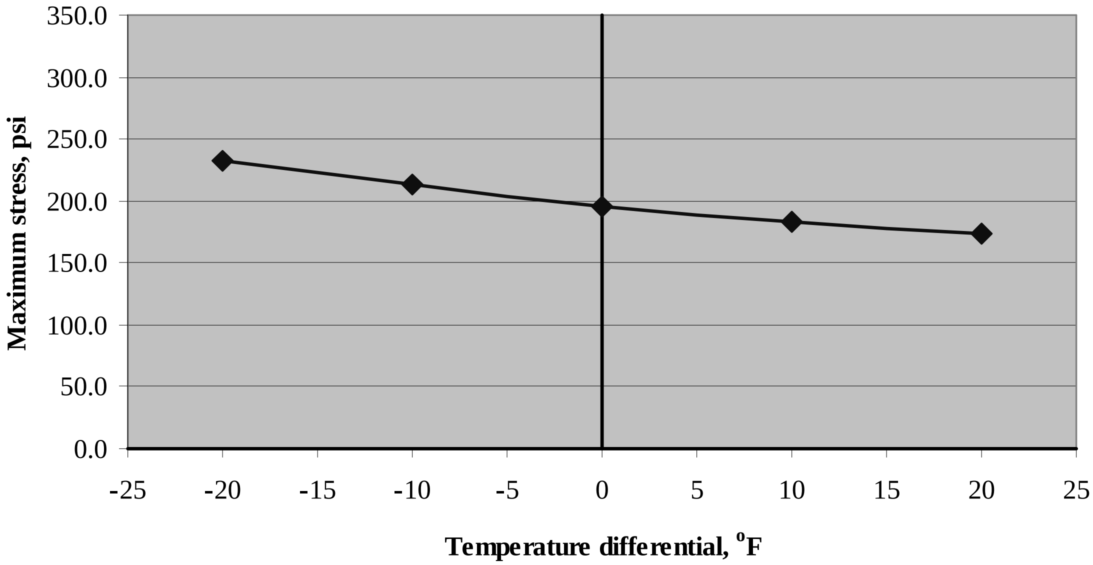


**E7-6: Relationship Between Stresses and Temperature Differentials**

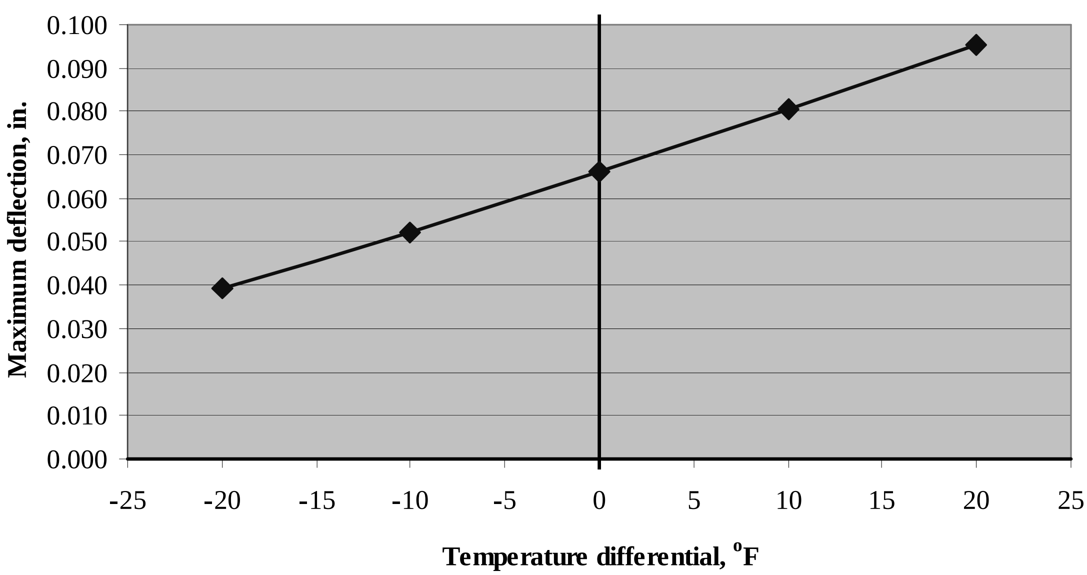


**E7-7: Relationship Between Deflections and Temperature Differentials**

# Example 8:
# Single Axle Edge Loading on a Pavement System

### Problem Statement

Determine maximum stresses at the bottom of the PCC slab for a pavement system and loading condition as illustrated in Figure E8-1.

### Given

| | | | |
|---|---|---|---|
| Concrete elastic modulus | = | $4 \times 10^6$ | psi |
| Concrete Poisson's ratio | = | 0.15 | |
| Slab thickness | = | 10 | in. |
| Base elastic modulus | = | $3 \times 10^4$ | psi |
| Base Poisson's ratio | = | 0.35 | |
| Base thickness | = | 16 | in. |
| Lane width | = | 144 | in. |
| Shoulder width | = | 120 | in. |
| Joint spacing | = | 180 | in. |
| Joint design | = | Dowel bars $\phi$ 1.25 in. @ 12 in. c/c | |
| AGG factor | = | $1 \times 10^6$ | psi |
| Mesh size | = | 12 x 12 | $in^2$ (medium) |
| k-value | = | 100 | psi/in. |
| Load configuration | = | standard single axle | |
| Axle weight | = | 18 | kips |
| Load location | = | edge loading | |
| Coefficient of thermal exp., $\alpha$ | = | $5 \times 10^{-6}$ | in./in./$^o$F |
| Temperature differential, $\Delta T$ | = | none | $^o$F |

### Problem Illustration:

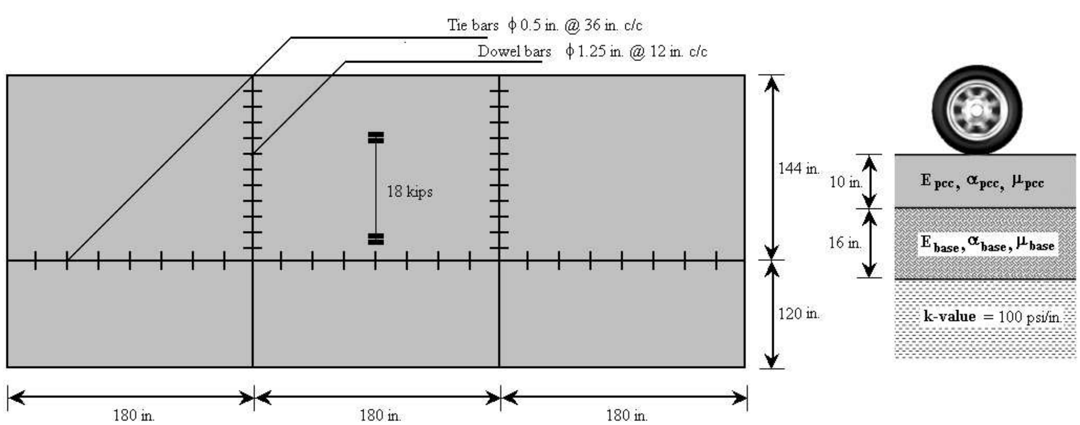


**Figure E8-1: Problem Illustration**

# Solution

## Geometry Module

(see Figure E8-2)

Step 1: Click **Geometry** on the main panel to open the geometry module.

Step 2: Click **Insert** twice on the **X-direction** side, and then enter 120 for the shoulder width and 144 for the lane width.

Step 3: Click **Insert** three times on the **Y-direction** side and then enter 180 for the joint spacing.

Step 4: On the geometry panel, select **Medium** to set the mesh size to medium.

Step 5: Click **Generate** to generate the inputs to the input file, and then click **OK** to close the geometry panel.

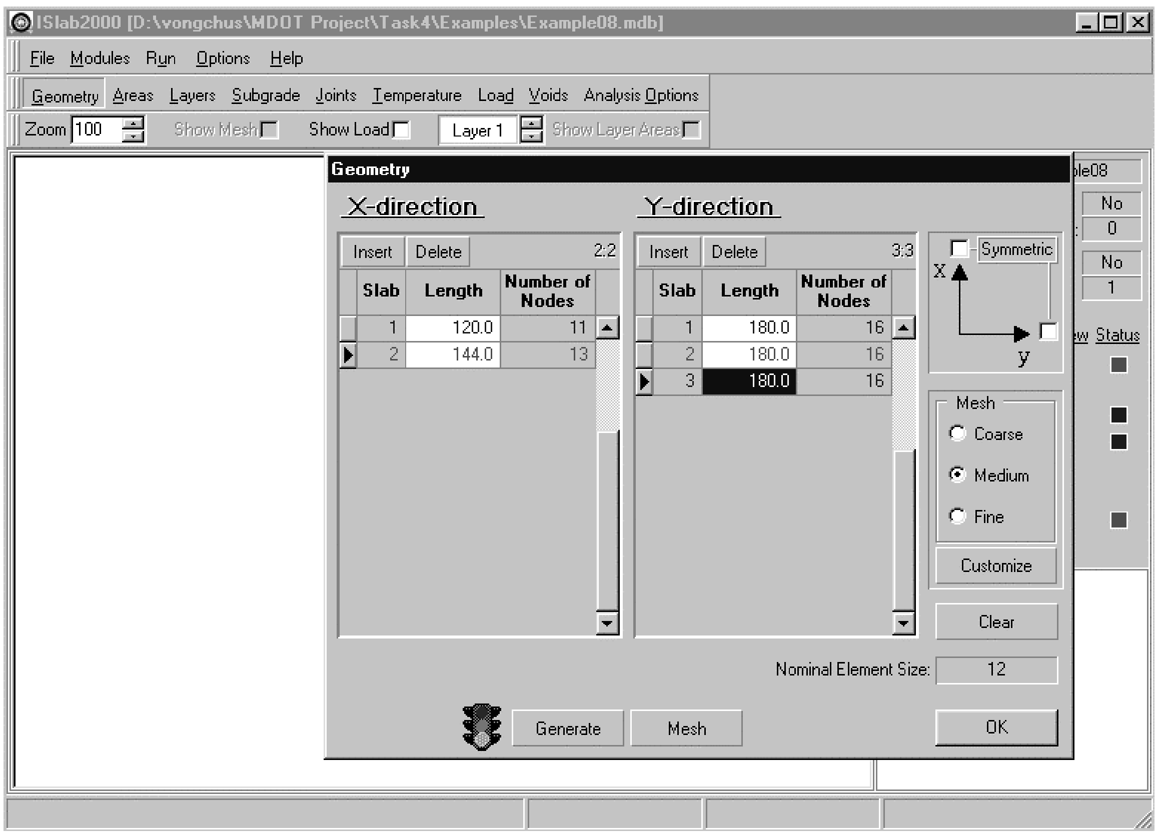


**Figure E8-2: Edit Inputs for the Geometry Module**

## Layers Module

(see Figures E8-3 and E8-4)

Step 1: Click **Layers** to open the layers panel.

Step 2: On the layers panel, type the inputs as identified in the problem statement for the PCC layer.

Step 3: Click **Add Layer** to open the add layer panel. Enter **2** in the **Layer number to add** field, and then click **OK** to close the add layer panel.

Step 4: On the layers panel, select **Layer 2**, and then type the inputs as identified in the problem statement for the base layer.

Step 5: Click **OK** to close the layers panel.

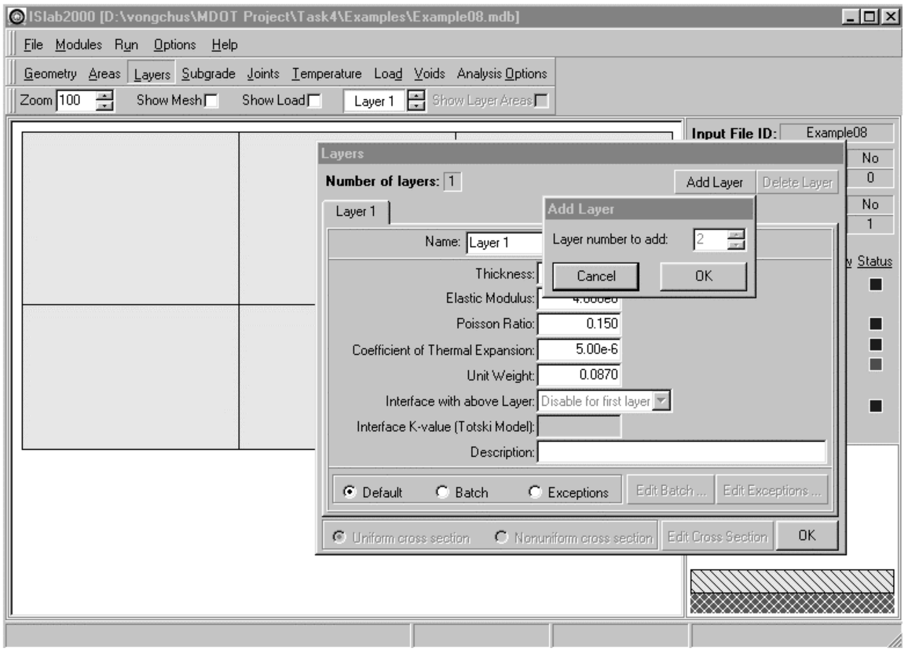


**Figure E8-3: Edit Inputs for the Layers Module**

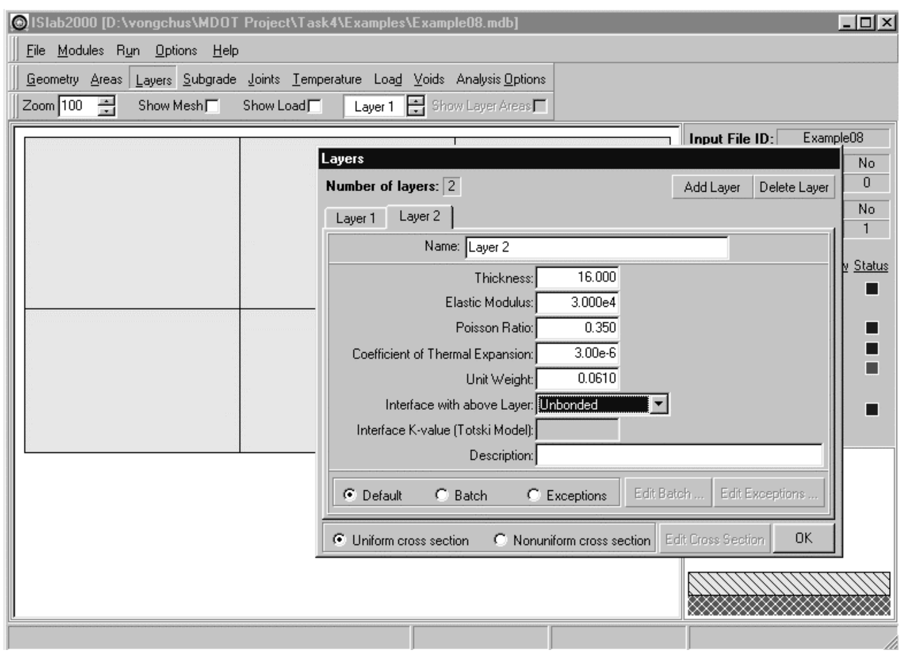


**Figure E8-4: Edit Inputs for the Layers Module (continued)**

## Subgrade Module

(see Figure E8-5)

Step 1: Click **Subgrade** to open the subgrade panel.

Step 2: Enter the inputs as identified in the problem statement.

Step 3: Click **OK** to close the subgrade panel.

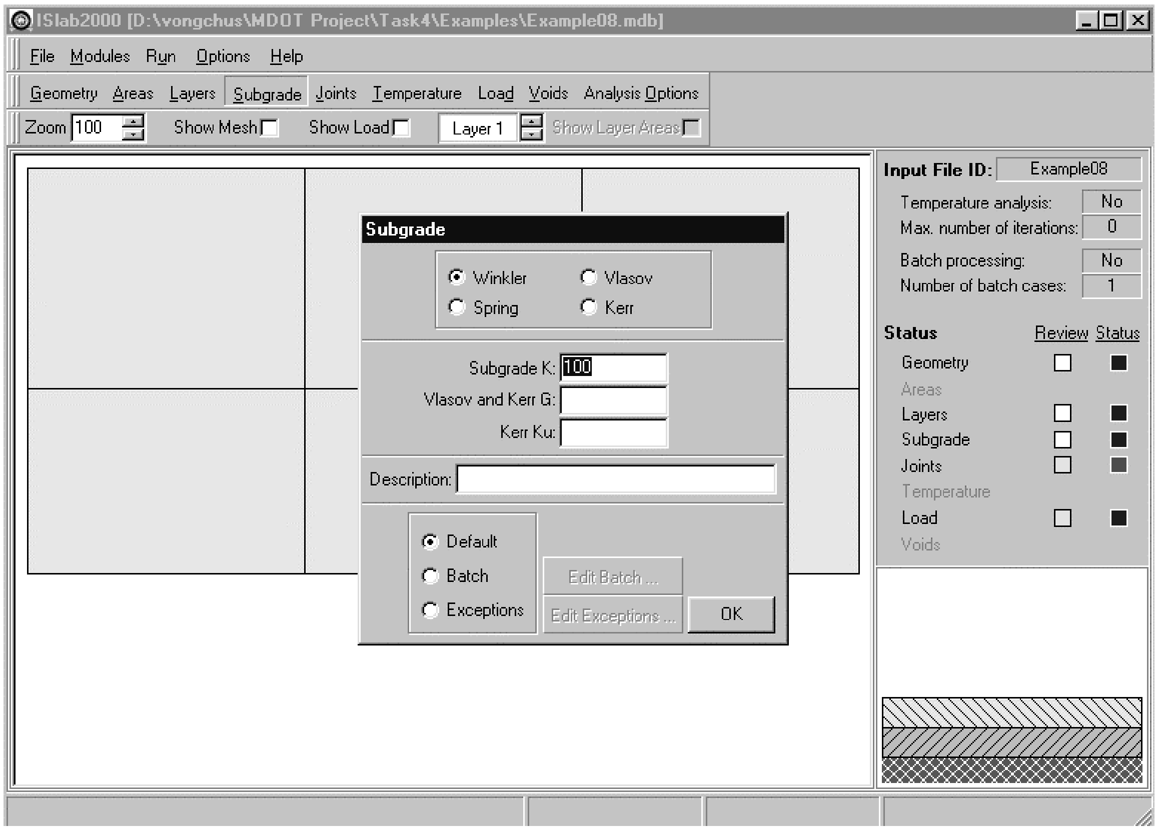


**Figure E8-5: Edit Inputs for the Subgrade Module**

## Joints Module

(see Figures E8-6 through E8-9)

Step 1: Click **Joints** to open the joints module.

Step 2: Under **Joints in x-direction**, select **Specify joint parameters**, select **AGG Interlock** in the **Joint type** field, and then enter 1 x $10^6$ (**1E6**) in the **AGG factor** field.

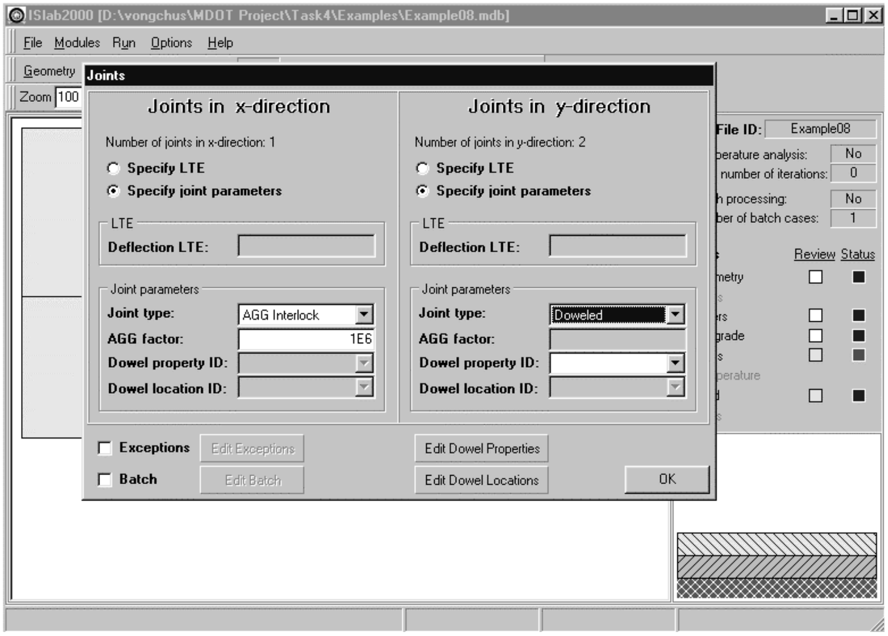


**Figure E8-6: Edit Inputs for the Joints Module**

Step 3: Under **Joints in y-direction**, select **Specify joint parameters**, select **Doweled** in the **Joint type** field, and then click **Edit Dowel Locations** to open the dowel locations panel (see Figure E8-7.)

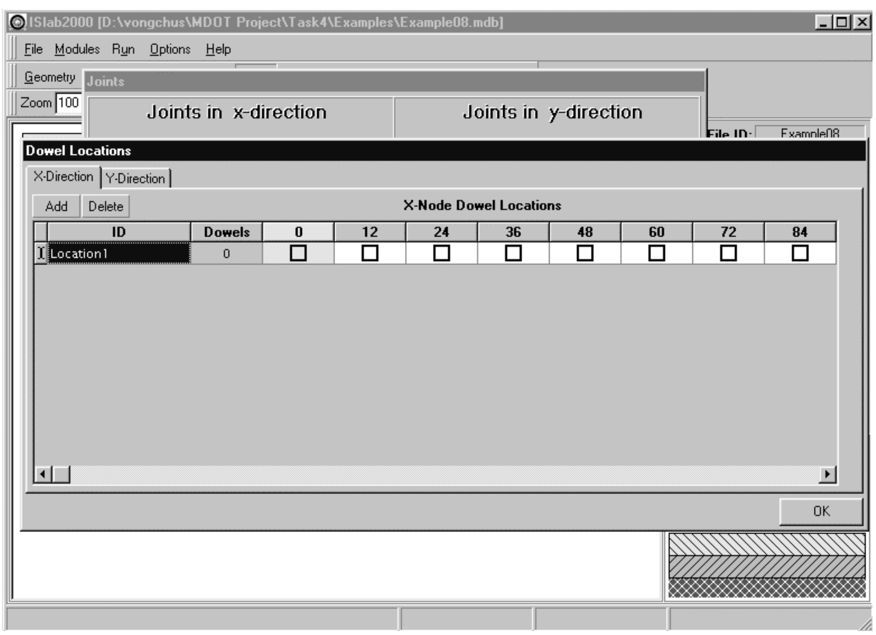


**Figure E8-7: Edit Inputs for the Joints Module (continued)**

Step 4: On the dowel locations panel, select the **X-Direction** tab, and then click **Add**. Enter “Location1” in the **ID** field, and then double click on the locations 132, 144… 252. Leave all the locations in the shoulder (locations 12, 24…108) blank (see Figure E8-8). Click **OK** to close the dowel location panel.

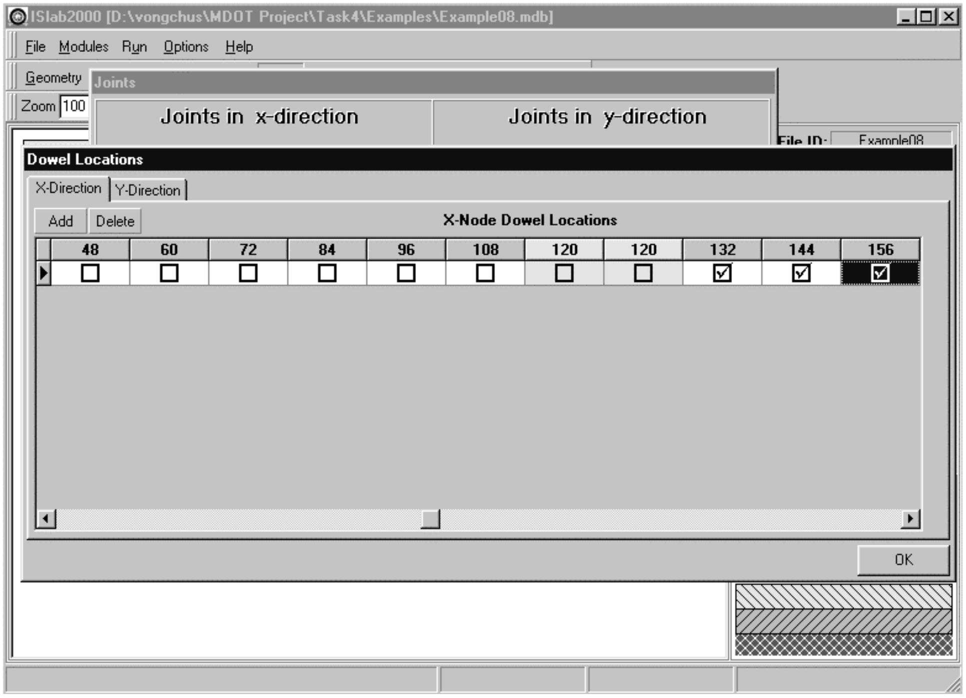


Figure E8-8: Edit Inputs for the Joints Module (continued)

Step 5: Select **Dowel1** in the **Dowel property ID** field, select **Location1** in the **Dowel location ID** field, and then click **OK** to close the joints panel (see Figure E8-9).

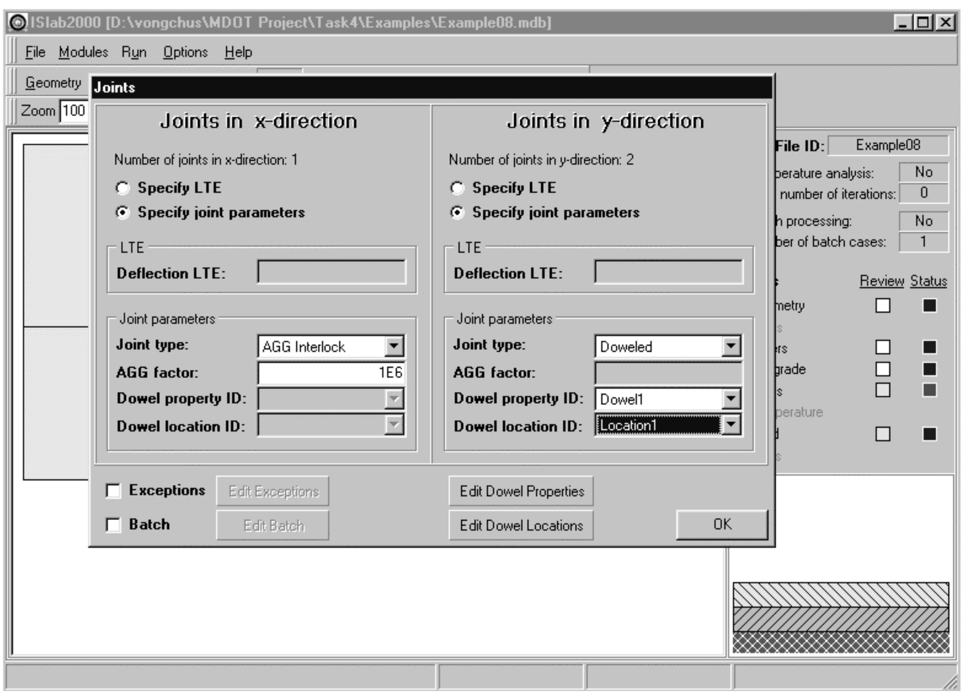


Figure E8-9: Edit Inputs for the Joints Module (continued)

## Load Module

(see Figure E8-10 and E8-11)

Step 1: Click **Load** to open the load panel.

Step 2: On the load panel, click **Axle Design** to open the axle design panel (see Figure E8-10.) Enter “Single Axle” in the **Axle Name** field.

Step 3: Type the tire pressure in the **Tire Pressure** field. The tire pressure of the wheel load can be computed as shown below (for more detail, see standard configuration of single axle):

$$Tire\ Pressure = \frac{Wheel\ Load}{Contact\ Area} = \frac{4{,}500\ lbs}{5\ in. \times 10\ in.} = 90\ psi$$

Step 4: Enter the tire width in the **Tire Width** field (5 in. for this example).

Step 5: Enter wheel spacing information as shown in Figure E8-10.

Step 6: Select **Bottom Left** for the reference point position.

Step 7: Click **OK** to close the axle design panel.

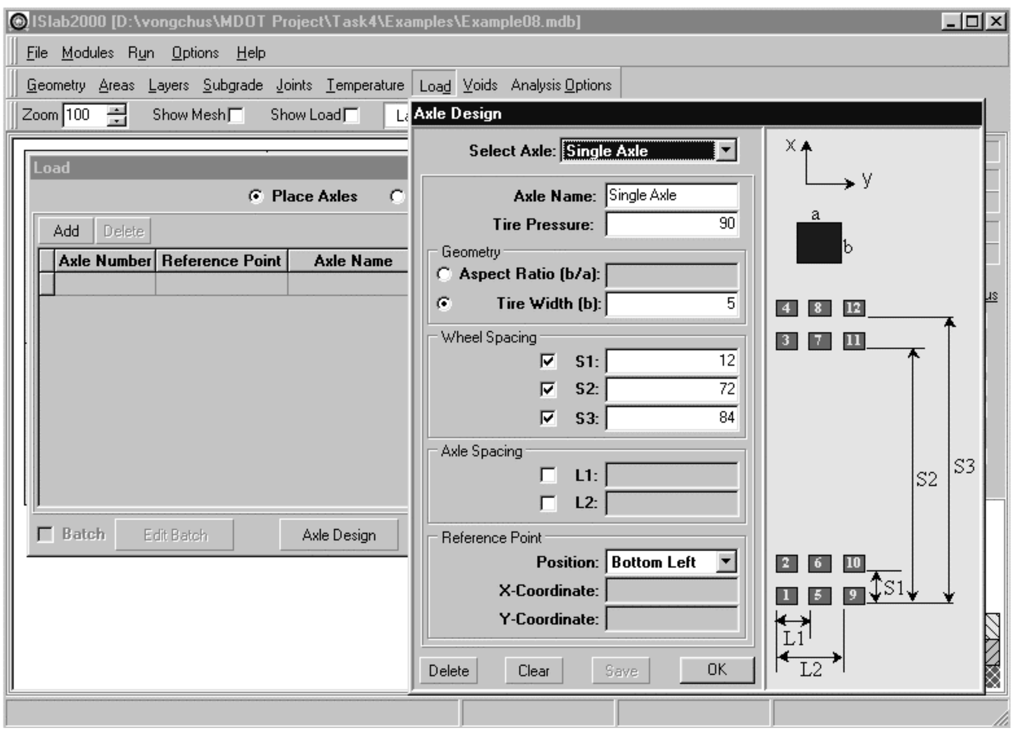


Figure E8-10: Edit Inputs for the Load Module

Step 8: On the load panel, click on **Add** to add an axle (see Figure E8-11).

Step 9: Select **Single Axle** in the **Axle Name** field.

Step 10: Enter an X-location and a Y-location to locate the wheel load. The X- and Y-location for an edge loading condition can be computed as shown below:

$$X - location = Shoulder\ width + Distance\ dual\ wheel\ center\ to\ shoulder$$
$$- Distance\ dual\ wheel\ center\ to\ reference\ point$$

$$= 120 + 20 - \left(\frac{5}{2} + \frac{12}{2}\right) = 131.5\ in$$

$$Y - location = Joint\ spacing + \frac{Joint\ spacing}{2} - \frac{wheel\ load\ length}{2}.$$

$$= 180 + \frac{180}{2} - \frac{10}{2} = 265\ in$$

Step 11: Enter the load for the single axle (18,000 lbs for this example).

Step 12: Click **OK** to close the load panel.

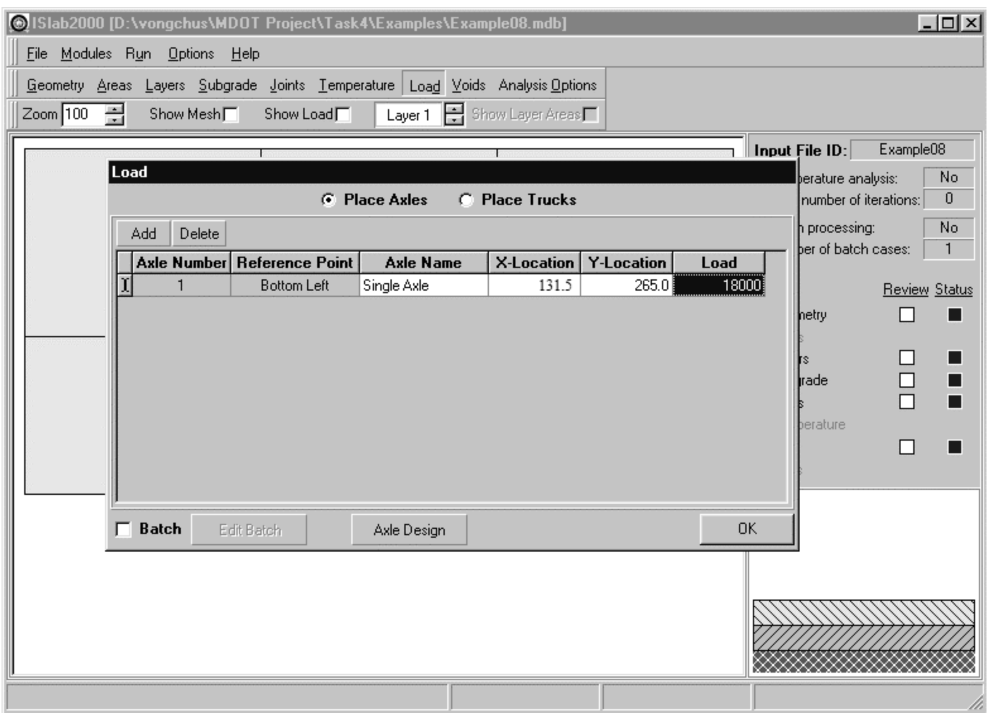


**Figure E8-11: Edit Inputs for the Load Module (continued)**

## Temperature Module

Temperature module is not required for this problem.

## Analysis Options Module

Use this module from Example 4.

The main panel should display the pavement structure, loading condition, and meshing as shown in Figure E8-12.

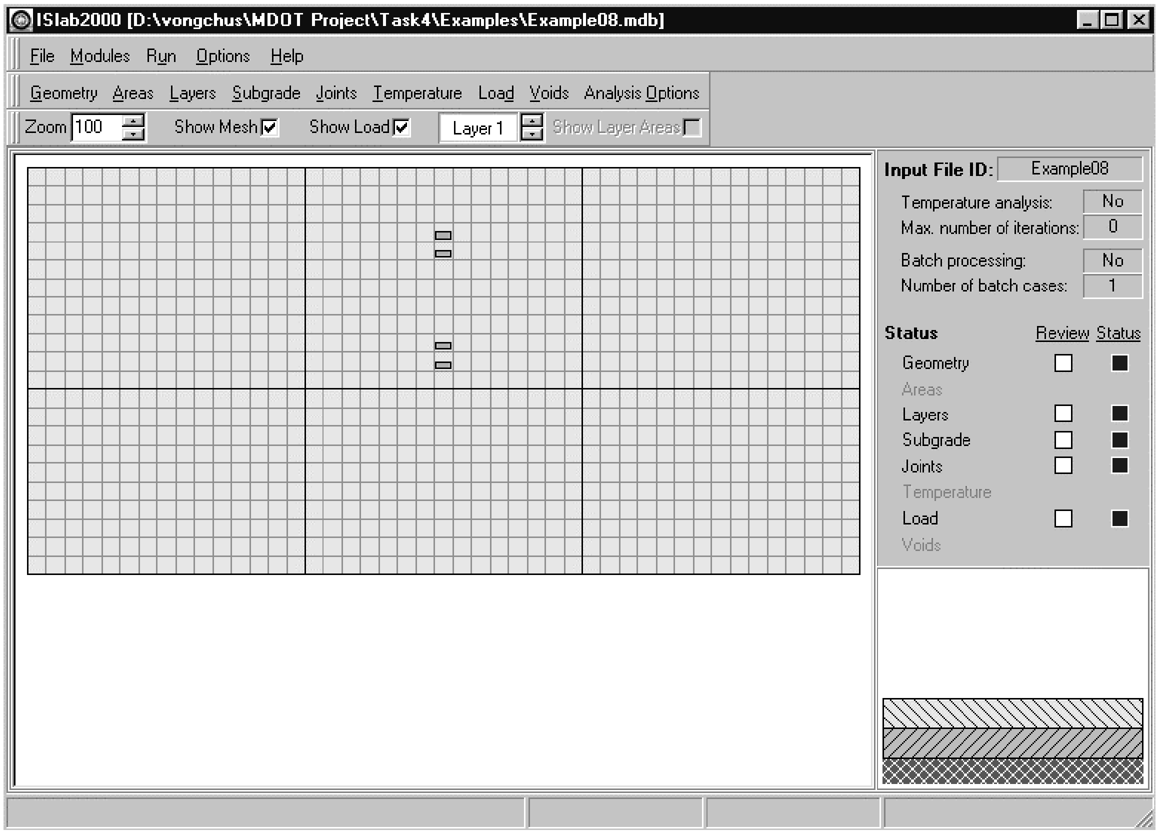


**Figure E8-12: Main Panel After the Completion of Inputs**

## *Analysis Results*

| | | |
|---|---|---|
| Maximum transverse stress at the bottom of the PCC slab (see Figure E8-13) | = | 72.1 psi |
| Maximum longitudinal stress at the bottom of the PCC slab (see Figure E8-14) | = | 114.5 psi |

**NOTE**
Positive and negative values of stress signify tensile and compressive stresses and positive value of deflection indicates deflection in downward direction.

Stress and deflection contours from ISLAB2000 are also shown in Figures E8-13 through E8-15.

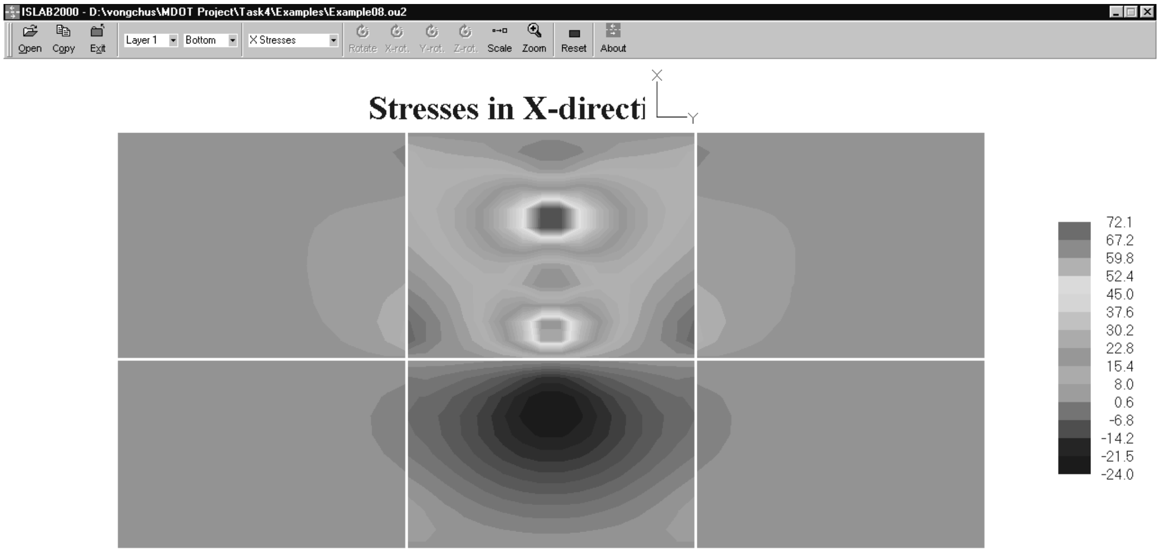


**Figure E8-13: Transverse Stress at the Bottom of the PCC Slab**

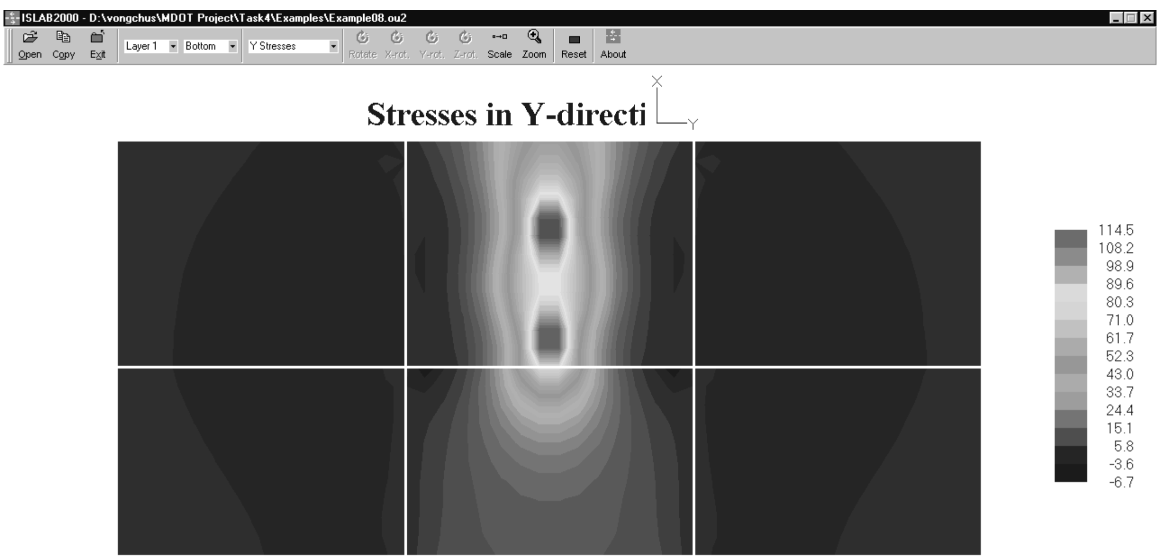


**Figure E8-14: Longitudinal Stress at the Bottom of the PCC Slab**

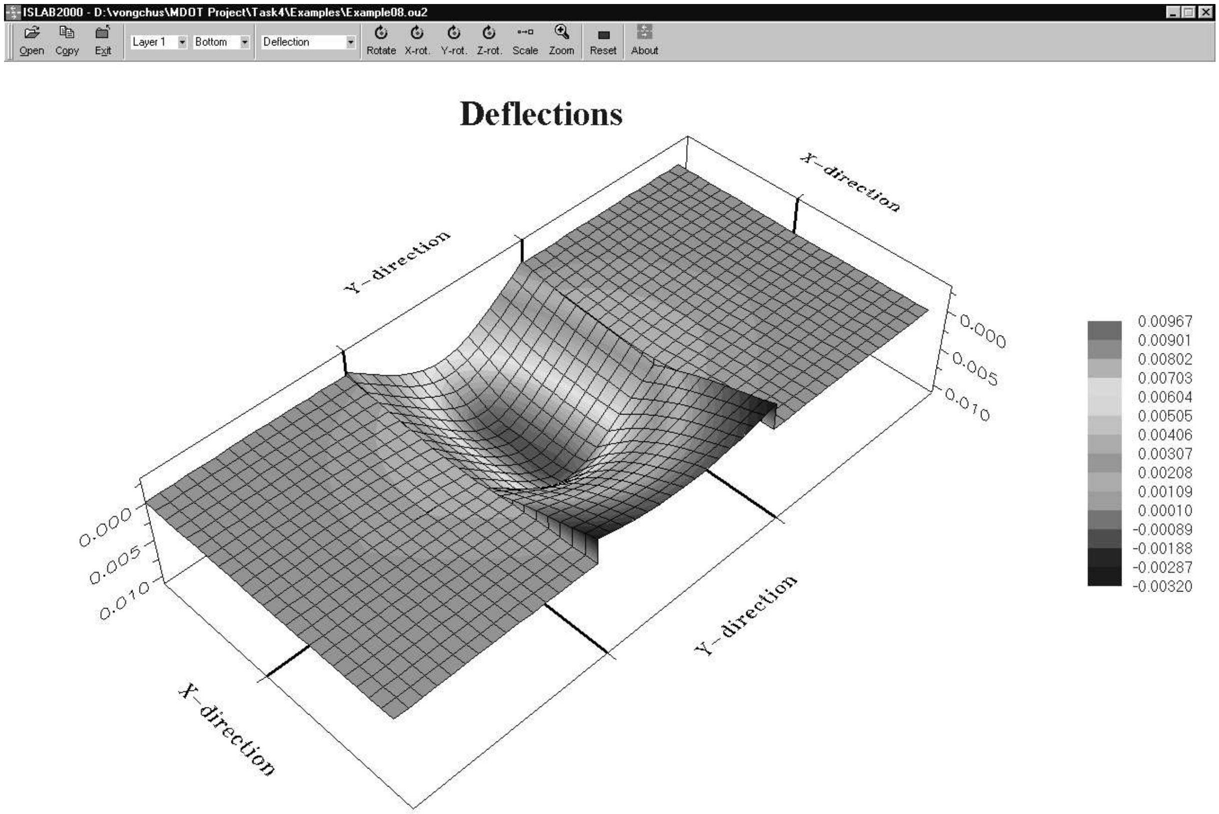


**Figure E8-15: Deflection of the PCC Slab**

# Example 9:
# Single Axle Edge Loading with Thermal Gradients

### Problem Statement

Determine maximum stresses at the bottom of the PCC slab for the pavement system and loading condition in Example 8 considering temperature differentials, ΔT, of 0, +10, +20 $^oF$.

### Given

| | | | |
|---|---|---|---|
| Temperature differential, ΔT | = | 0, +10, +20 | $^oF$ |

### Problem Illustration

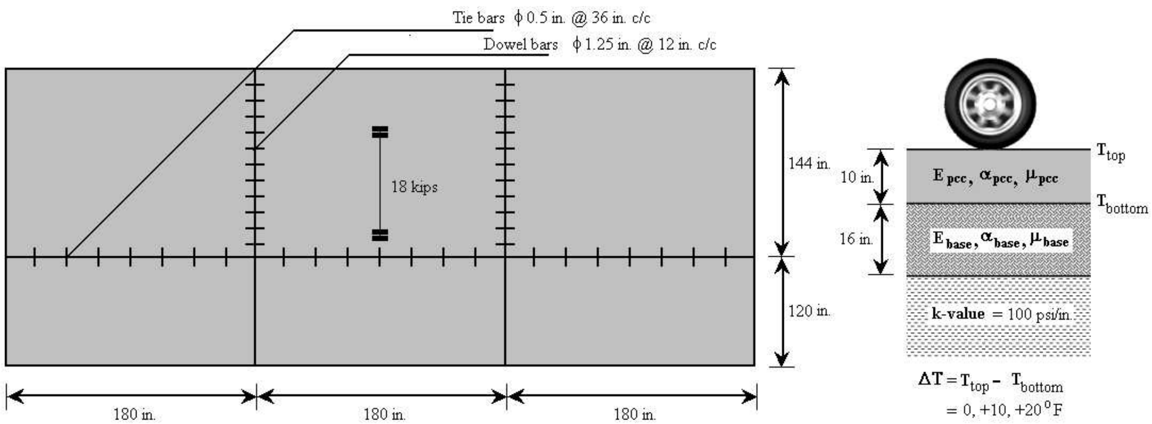


Figure E9-1: Problem Illustration

# Solution

## Geometry Module

Use this module from Example 8.

## Layers Module

Use this module from Example 8.

## Subgrade Module

Use this module from Example 8.

## Joints Module

Use this module from Example 8.

## Load Module

Use this module from Example 8.

## Temperature Module

(see Figures E9-2 and E9-3)

Step 1: Click **Temperature** to open the temperature panel.

Step 2: On the temperature module, select **Perform Temperature Analysis** and **Batch**.

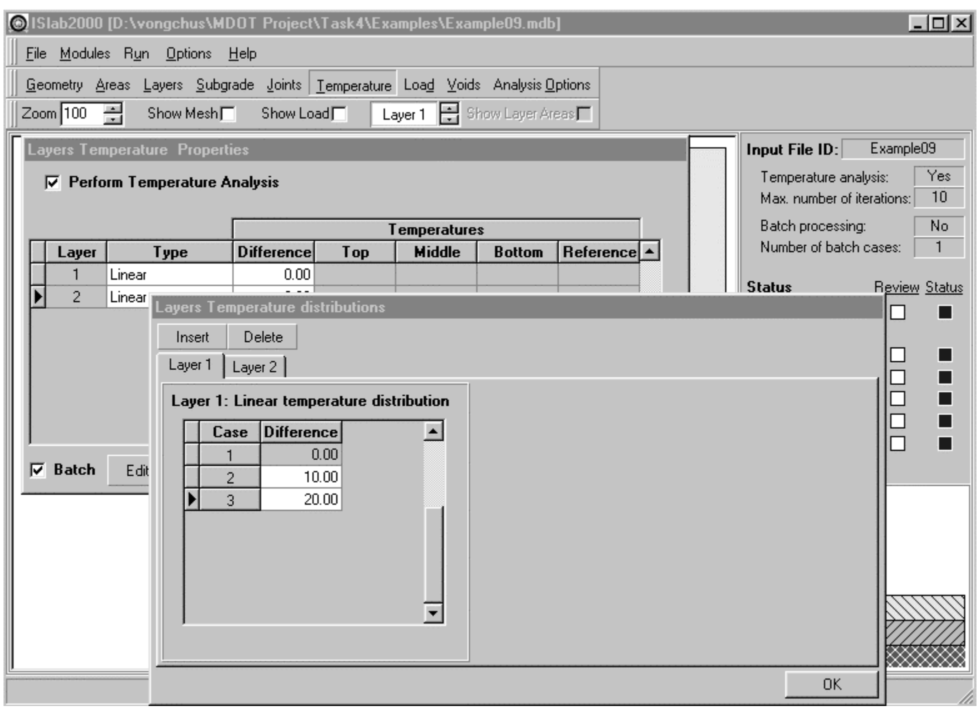


**Figure E9-2: Edit Inputs for the Temperature Module**

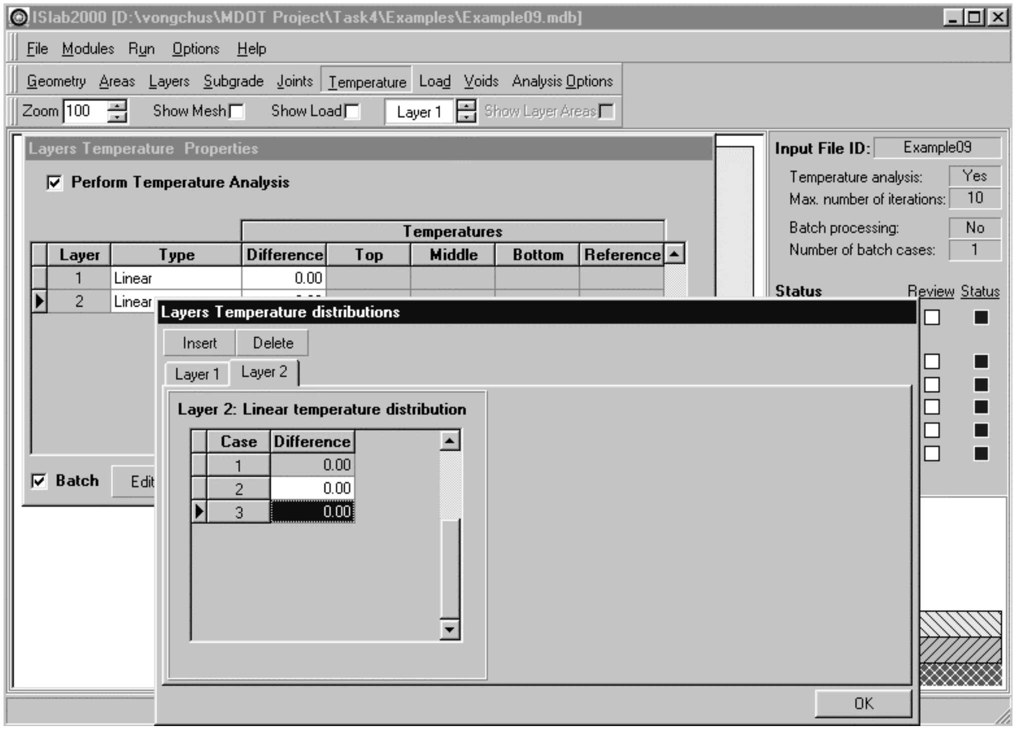


**Figure E9-3: Edit Inputs for the Temperature Module (continued)**

Step 3: In the **Difference** field, enter the temperature differential of the first case (0 $^{o}$F for this problem).

Step 4: Click **Edit Batch** to open the Layers temperature distributions panel.

Step 5: On the **Layer 1** tab of the layers temperature distributions panel, click **Insert** two times to add two more cases of temperature differential, and then, enter the other two temperature differentials as identified in the problem statement.

Step 6: On the **Layer 2** tab of the layers temperature distributions panel, enter zero (**0**) in the other two temperature differentials across the base layer.

Step 7: Click **OK** to close the layers temperature distributions panel.

Step 8: Click **OK** at the bottom right of the layers temperature properties panel. The panel will disappear.

## Analysis options module

Use this module from Example 4.

The main panel should display the pavement structure, loading condition, and meshing as shown in Example 8, Figure E8-12.

## *Analysis Results*

| ΔT, °F | Stress at the bottom of the PCC, psi | |
|---|---|---|
| | Transverse | Longitudinal |
| 0 | 72.1 | 114.5 |
| 10 | 105.9 | 169.5 |
| 20 | 139.7 | 224.5 |

**Table E9-1: Analysis Results**

> **NOTE**
> Positive and negative values of stress signify tensile and compressive stresses and positive value of deflection indicates deflection in downward direction.

Stress and deflection contours from ISLAB2000 are also available in Figures E9-4 through E9-6. Figure E9-10 illustrates relationship between maximum stresses and temperature differentials.

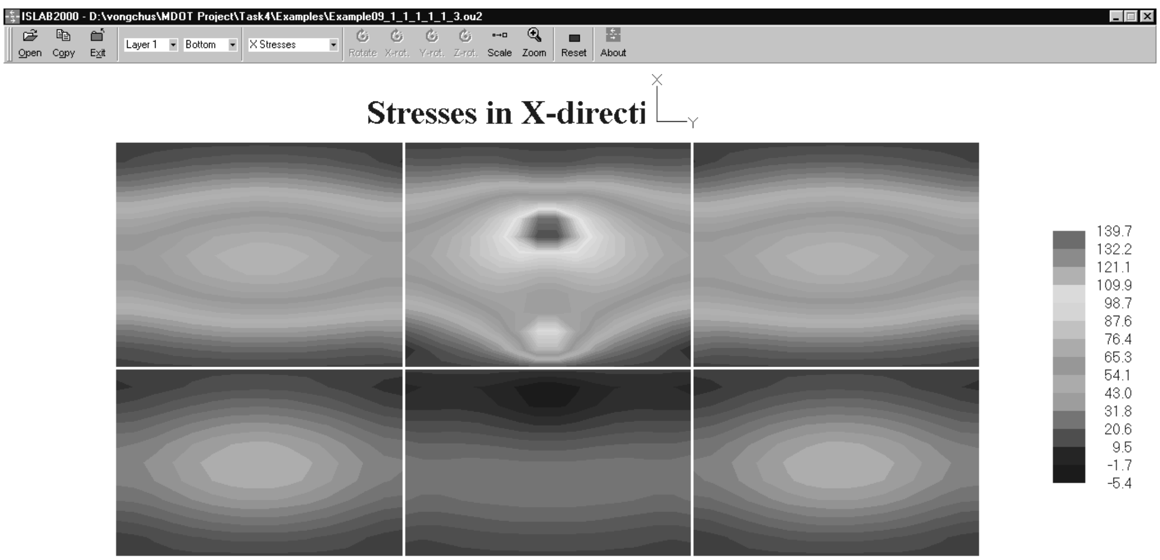


**Figure E9-4: Transverse Stress at the Bottom of the PCC Slab**

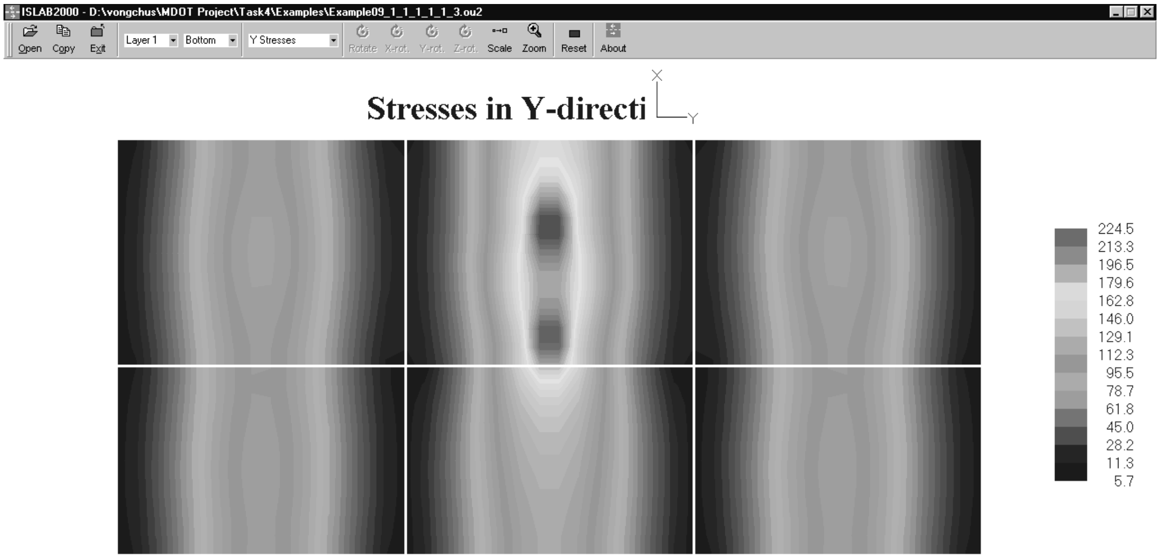


**Figure E9-5: Longitudinal Stress at the Bottom of the PCC Slab**

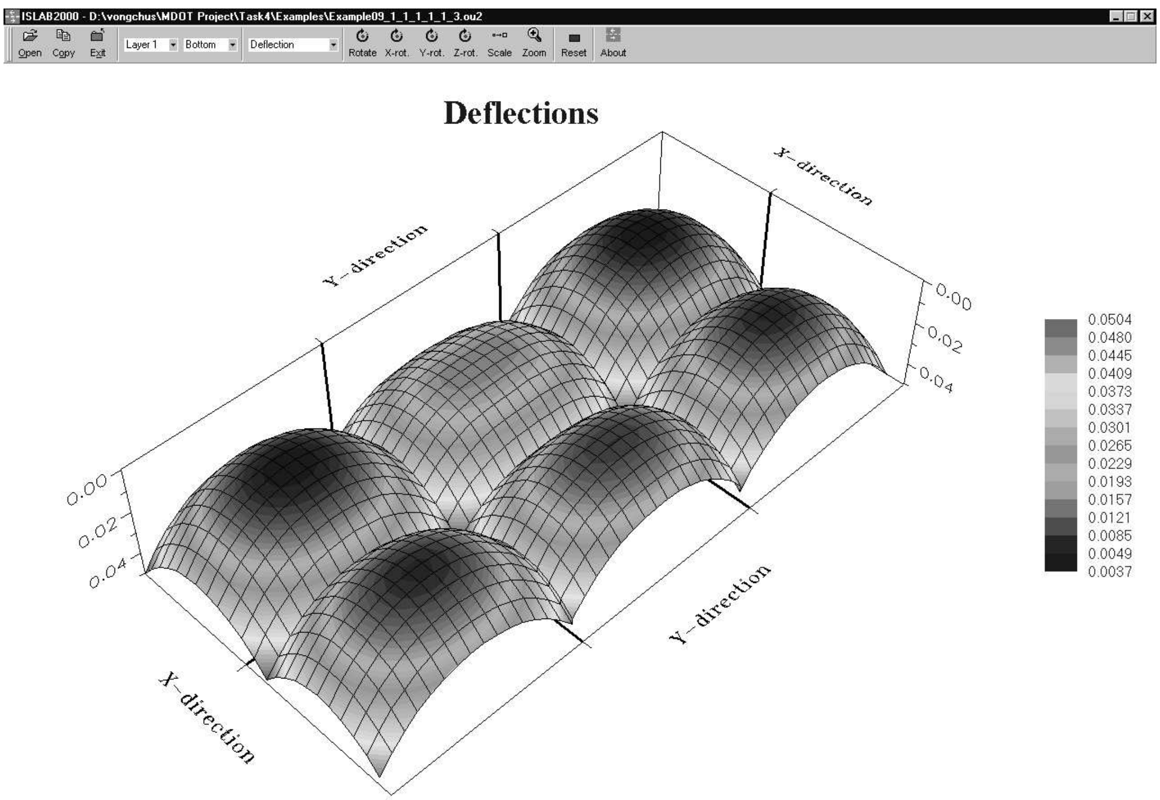


**Figure E9-6: Deflection of the PCC Slab**

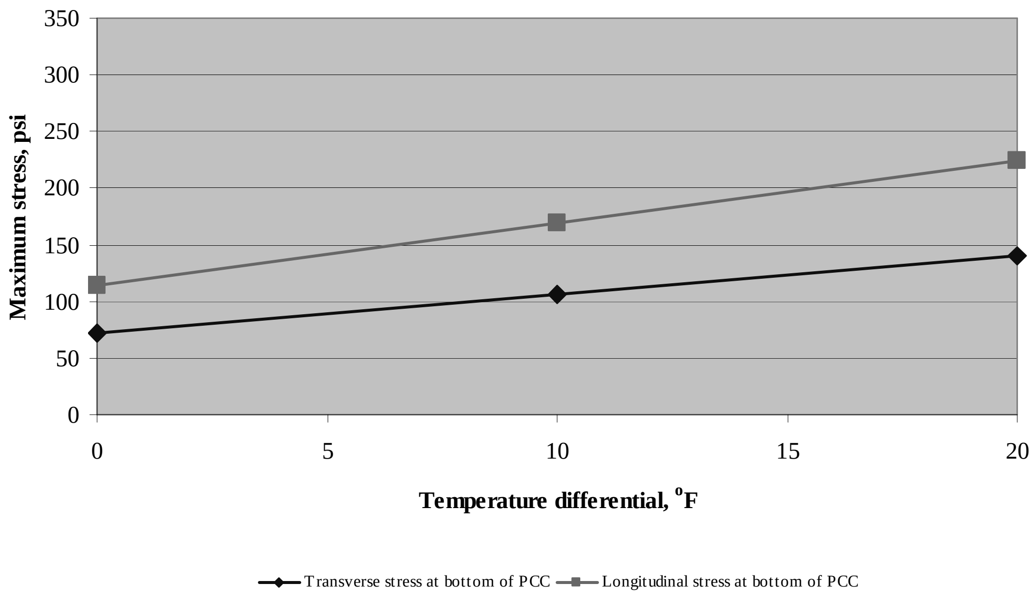


**E9-10: Relationship Between Stresses and Temperature Differentials**

# Example 10:
# Single Axle Corner Loading with Thermal Gradients

### Problem Statement

Determine maximum stresses at the top of the PCC slab for the pavement system in Example 8 but apply corner loading condition considering temperature differentials, ΔT, of -20, -10, and 0 $^oF$.

### Given

Temperature differential, ΔT = -20, -10, 0 $^oF$

### Problem Illustration

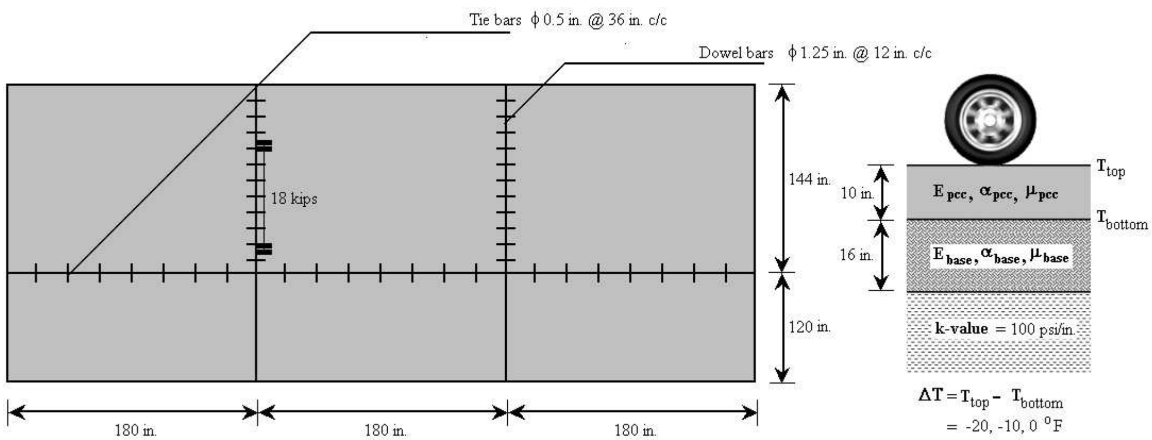


Figure E10-1: Problem Illustration

# Solution

### Geometry Module

Use this module from Example 8.

### Layers Module

Use this module from Example 8.

### Subgrade Module

Use this module from Example 8.

### Joints Module

Use this module from Example 8.

### Load Module (see Figure E10-2)

Step 1: Follow steps 1 through 7 from the Load Module in Example 8.

Step 2: On the load panel (see Figure E8-11), click **Add** to add an axle.

Step 3: Select **Single Axle** in the **Axle Name** field.

Step 4: Enter an X-location and Y-location to locate the wheel load. The X-location and Y-location for an edge loading condition can be computed as shown below:

$$X-location = Shoulder\ width + Distance\ dual\ wheel\ center\ to\ shoulder$$
$$- Distance\ dual\ wheel\ center\ to\ reference\ point$$

$$= 120 + 20 - \left(\frac{5}{2} + \frac{12}{2}\right) = 131.5\ in$$

$$Y-location = Joint\ spacing$$

$$= 180$$

Step 5: Enter the load for the single axle (18,000 lbs for this example).

Step 6: Click **OK** to close the load panel.

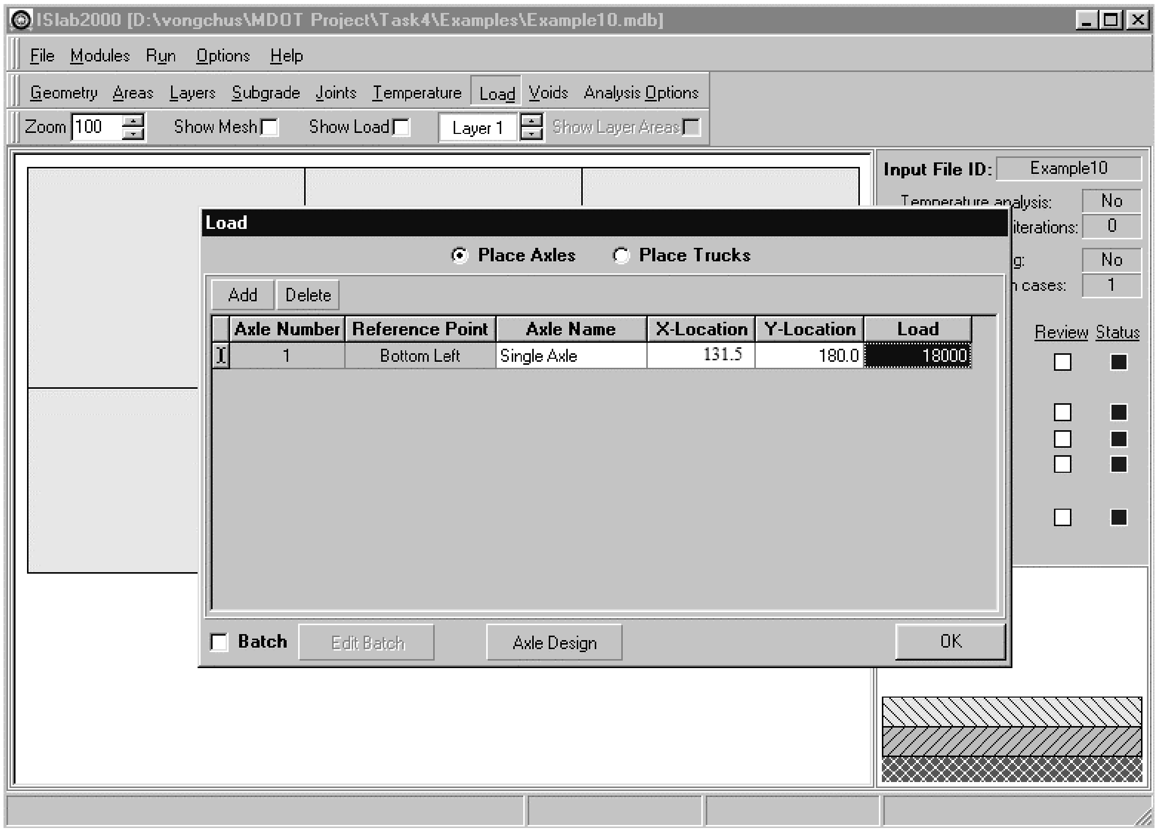


**Figure E10-2: Edit Inputs for the Load Module**

## Temperature Module

(see Figures E9-2 and E9-3)

Step 1: Click **Temperature** to open the temperature properties panel.

Step 2: On the temperature properties panel, select the **Perform Temperature Analysis** and **Batch** check boxes.

Step 3: Enter the temperature differential of the first case in the **Difference** field (-20 $^{o}$F for this example).

Step 4: Click **Edit Batch** to open the layers temperature distributions panel.

Step 5: On the **Layer 1** tab of the layers temperature distributions panel, click **Insert** two times to add two more cases of temperature differential, and then type the other two temperature differentials as identified in the problem statement.

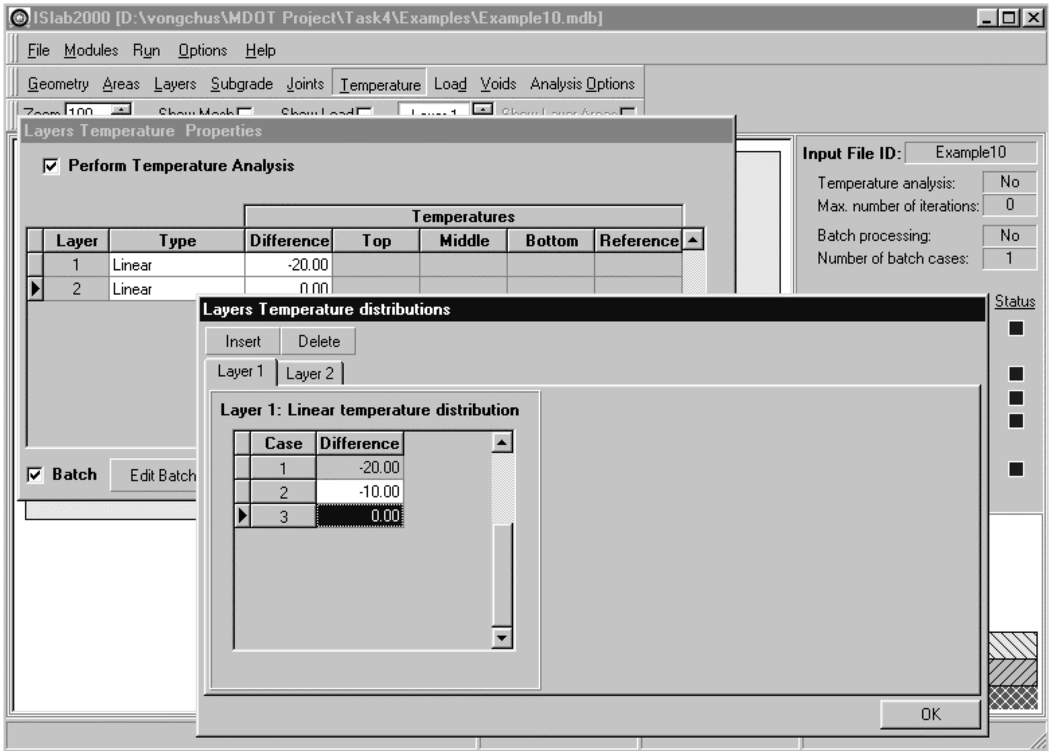


**Figure E10-3: Edit Inputs for the temperature module**

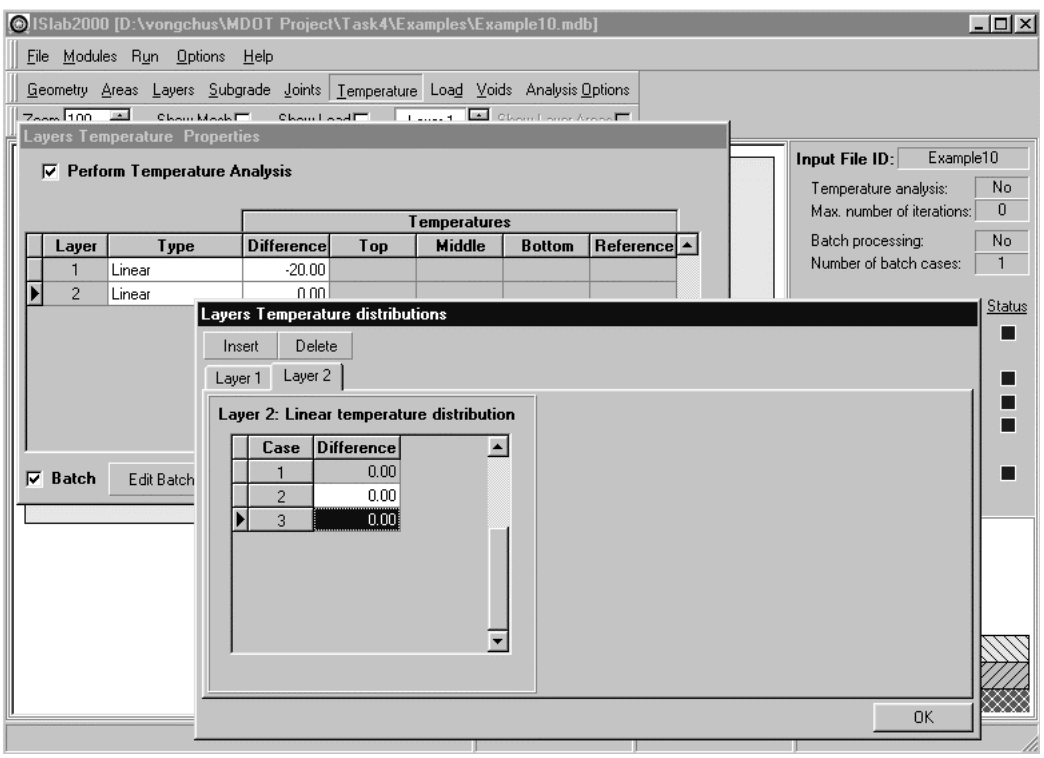


**Figure E10-4: Edit Inputs for the Temperature Module (continued)**

Step 6: On the **Layer 2** tab of the layers temperature distributions panel, enter zero (**0**) in the other two temperature differentials across the base layer.

Step 7: Click **OK** to close the layers temperature distributions panel.

Step 8: Click **OK** to close the layers temperature properties panel.

### Analysis Options Module

Use this module from Example 4.

The main panel should display the pavement structure, loading condition, and meshing as shown in Figure E10-5.

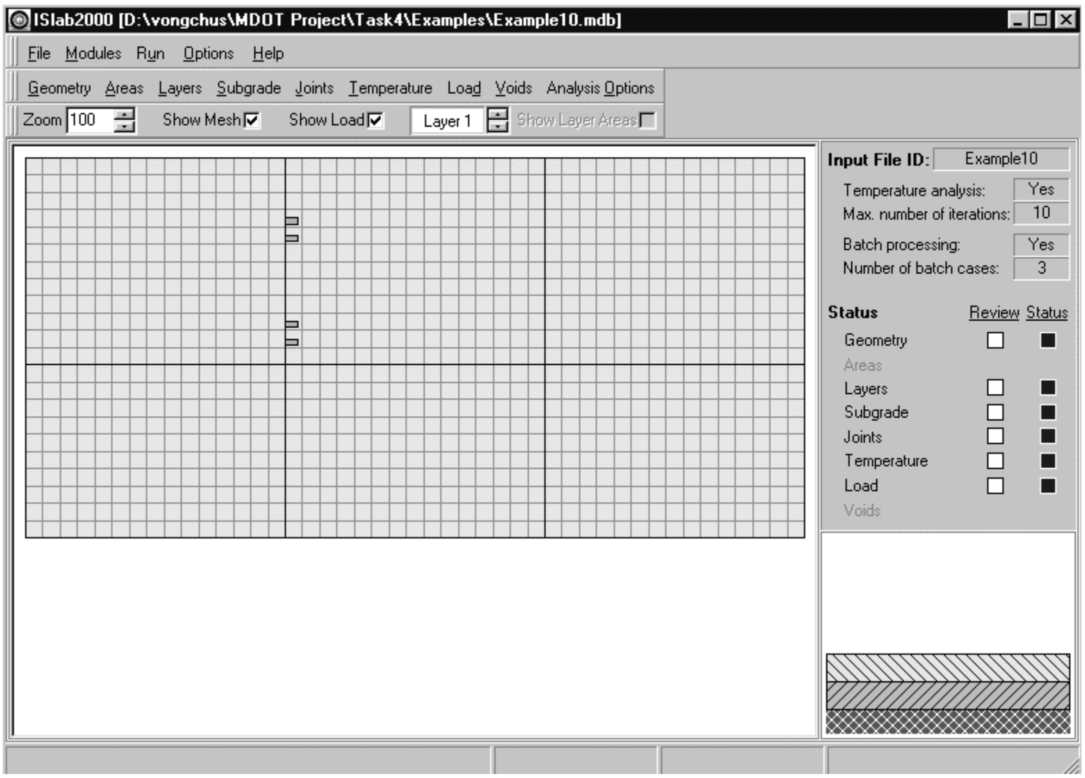


**Figure E10-5: Main Panel After the Completion of Inputs**

## *Analysis Results*

| ΔT, °F | Stress at the top of the PCC, psi | |
|---|---|---|
| | Transverse | Longitudinal |
| -20 | 87.9 | 148.4 |
| -10 | 63.2 | 95.2 |
| 0 | 38.9 | 47.5 |

**Table E10-1: Analysis Results**

**NOTE**

Positive and negative values of stress signify tensile and compressive stresses and positive value of deflection indicates deflection in downward direction.

Stress and deflection contours from ISLAB2000 are also available in Figures E10-6 through E10-8. Figure E10-9 illustrates relationship between maximum stresses and temperature differentials.

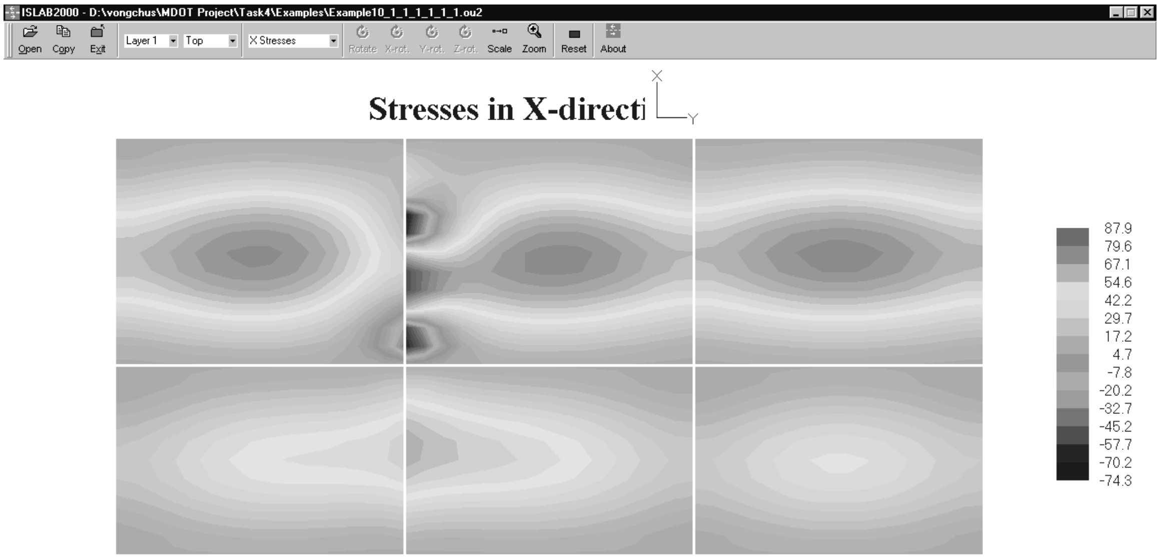


**Figure E10-6: Transverse Stress at the Top of the PCC Slab**

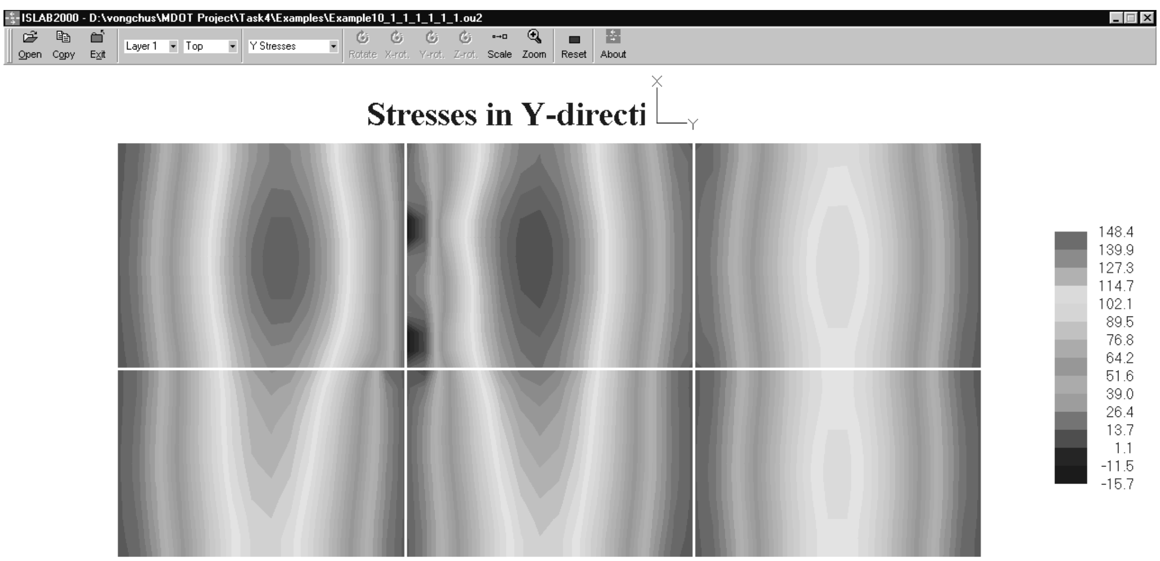


**Figure E10-7: Longitudinal Stress at the Top of the PCC Slab**

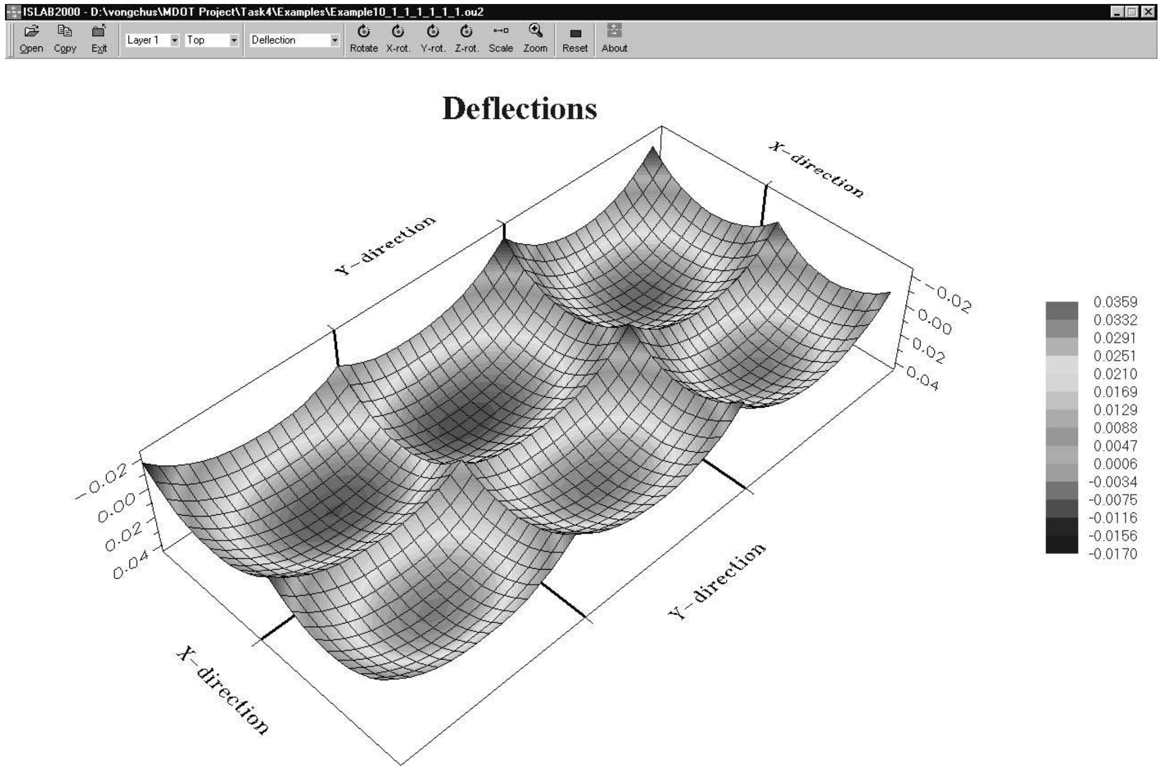


**Figure E10-8: Deflection of the PCC Slab**

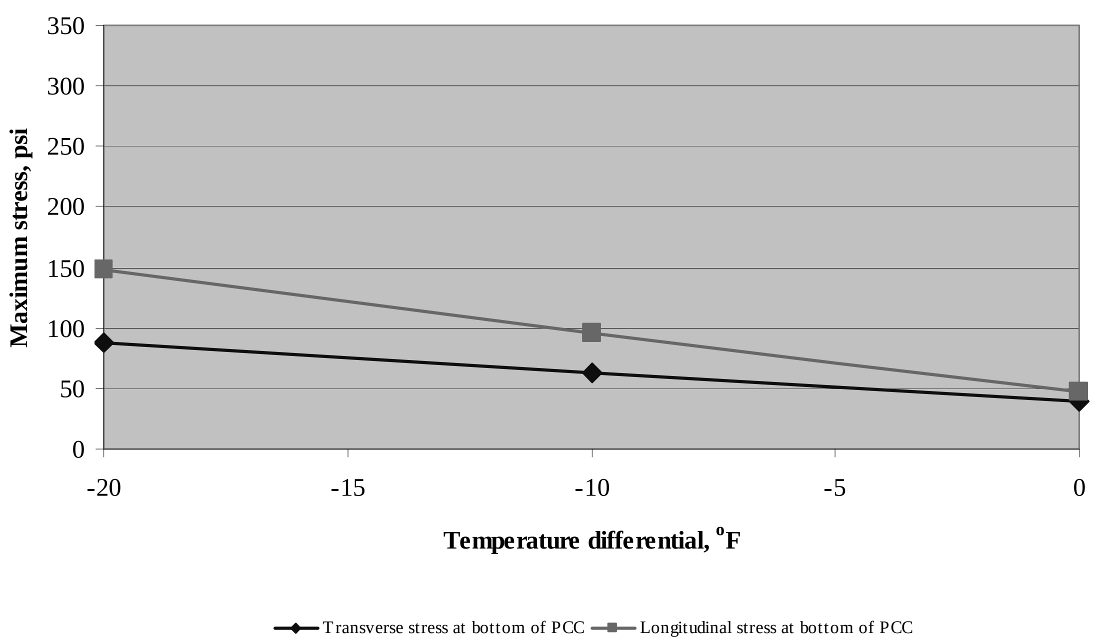


**E10-9: Relationship Between Stresses and Temperature Differentials**

# Example 11:
# Single Axle Edge Loading with Various PCC Edge Thicknesses

### Problem Statement

Determine maximum stresses at the bottom of the PCC slab for the pavement system and loading condition in Example 8 considering PCC thickness = 6, 8, 10, 12 in.

### Given

| | | | |
|---|---|---|---|
| PCC thickness | = | 6, 8, 10, 12 | in. |

### Problem Illustration

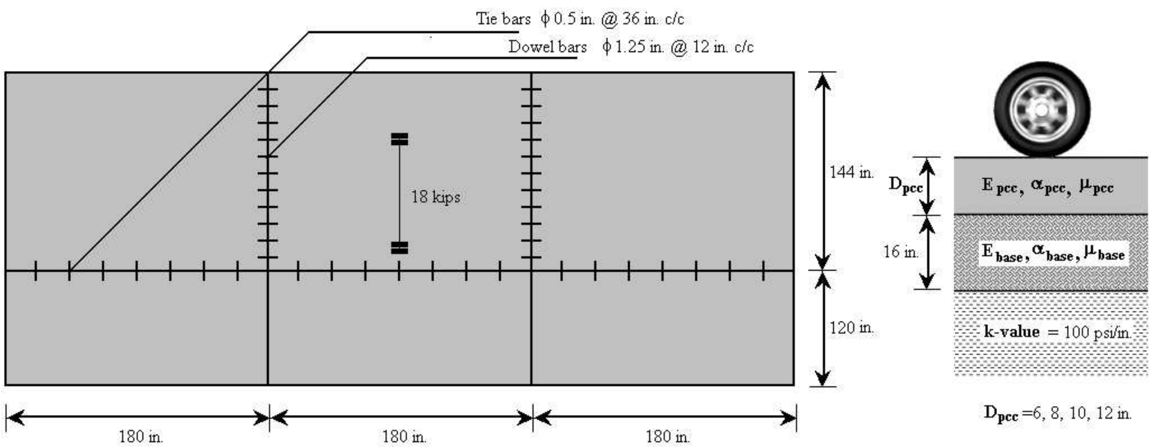


**Figure E11-1: Problem Illustration**

# Solution

### Geometry Module

Use this module from Example 8.

### Layers Module

(see Figures E11-2 and E11-3)

Step 1: Click **Layers** to open the layers panel.

Step 2: On the layers panel, enter the inputs as identified in the problem statement for the PCC layer.

Step 3: Click **Add Layer** to open the layer panel, enter **2** in the **Layer number to add** field, and then select **OK**.

Step 4: On the layers panel, select the **Layer 2** tab, and then enter the inputs as identified in the problem statement for the base layer.

Step 5: On the layers panel, select the **Layer 1** tab, select **Batch**, and then click **Edit Batch** to open the layer 1 properties panel (see Figure E11-2).

Step 6: On the layer 1 properties panel click **Insert** three times to add three additional cases, and then type the PCC thicknesses as identified in the problem statement. (see Figure E11-3)

Step 7: Click **OK** to close the layer 1 properties panel, and then click OK to close the layers panel.

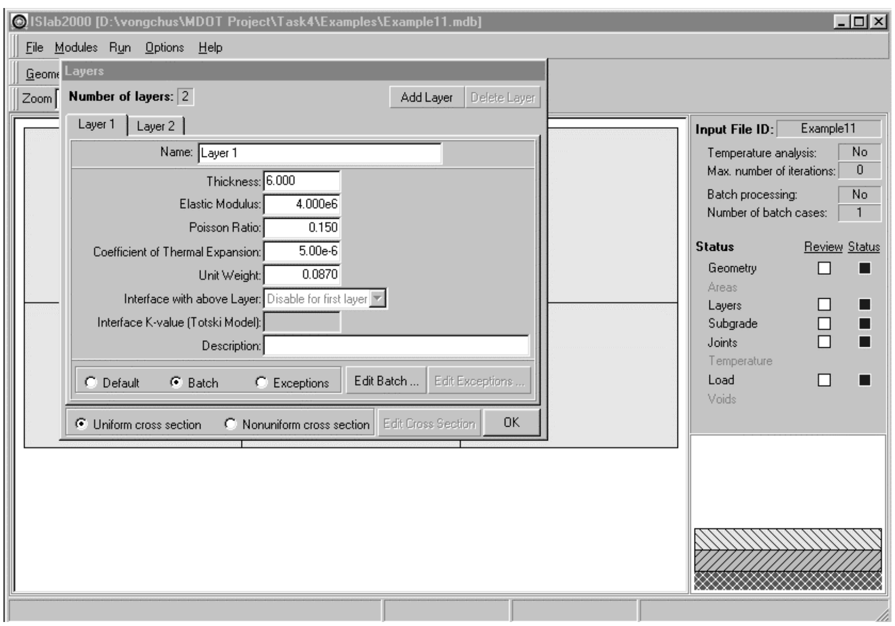


**Figure E11-2: Edit Inputs for the Layers Module**

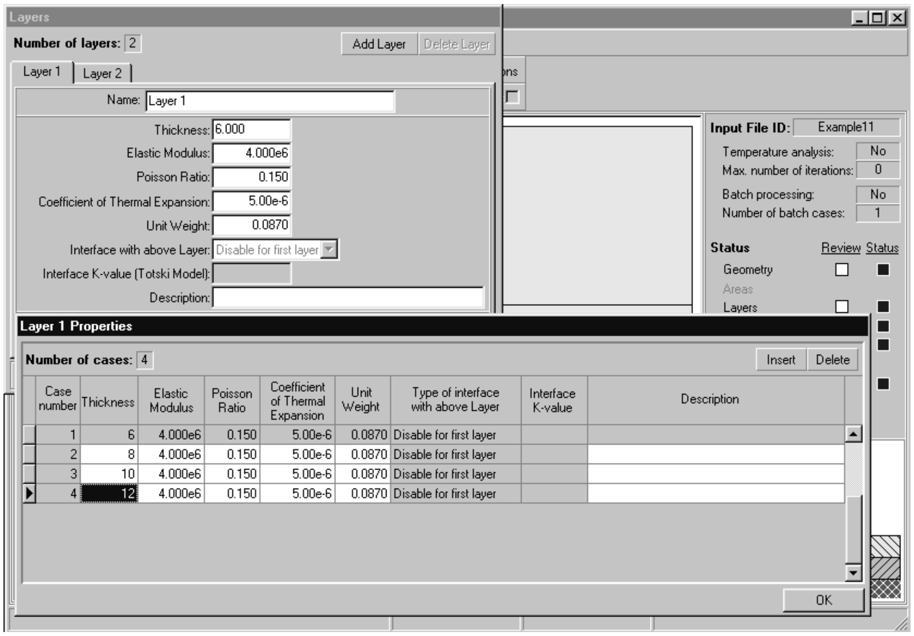


**Figure E11-3: Edit Inputs for the Layers Module (continued)**

## Subgrade Module

Use this module from Example 8.

## Joints Module

Use this module from Example 8.

## Load Module

Use this module from Example 8.

## Temperature Module

This module is not required for this problem.

## Analysis Options Module

Use this module from Example 4.

The main panel should display the pavement structure, loading condition, and meshing as shown in Example 8, Figure E8-12.

## *Analysis Results*

| PCC thickness, in. | Stress at the bottom of the PCC, psi | |
|---|---|---|
| | Transverse | Longitudinal |
| 6 | 151.8 | 199.3 |
| 8 | 102.3 | 148.0 |
| 10 | 72.1 | 114.5 |
| 12 | 52.8 | 90.9 |

**Table E11-1: Analysis Results**

**NOTE**

Positive and negative values of stress signify tensile and compressive stresses and positive value of deflection indicates deflection in downward direction.

Figure E11-4 illustrates relationship between maximum stresses and PCC thickness.

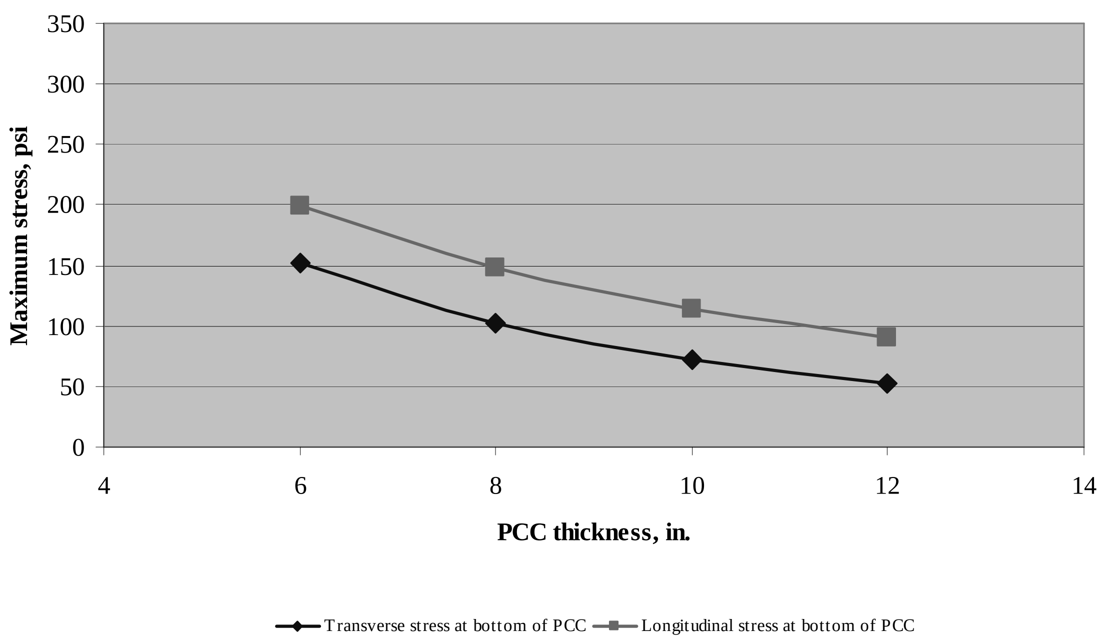


**Figure E11-4: Relationship Between Stresses and PCC Thickness**

# Example 12:
# Single Axle Edge Loading with Various Base Thicknesses

### Problem Statement

Determine maximum stresses at the bottom of the PCC slab for the pavement system and loading condition in Example 8 considering base thickness = 4, 10, 16, 20, 26 in.

### Given

| | | | |
|---|---|---|---|
| Base thickness | = | 4, 10, 16, 20, 26 | in. |

### Problem Illustration

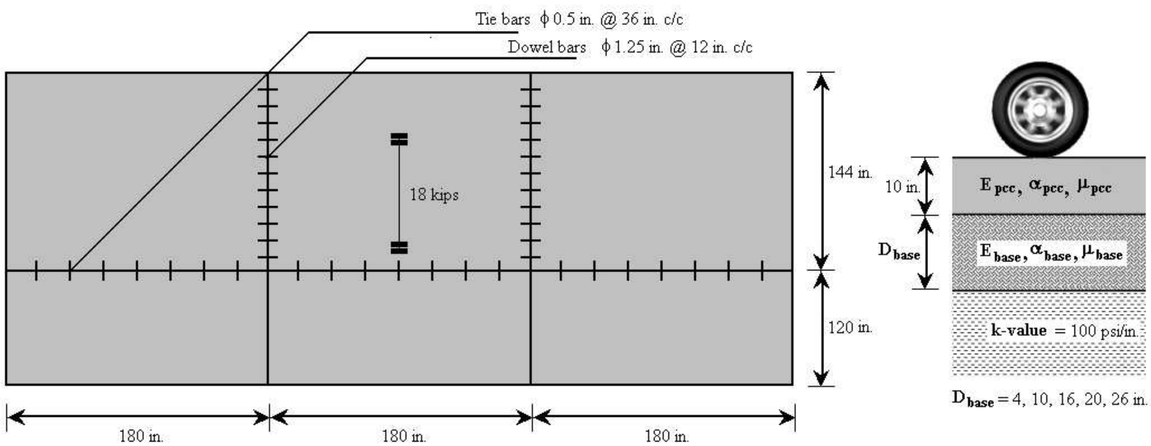


**Figure E12-1: Problem Illustration**

# Solution

### Geometry Module

Use this module from Example 8.

### Layers Module

(see Figures E12-2 and E12-3)

Step 1: Click **Layers** to open the layers panel.

Step 2: On the layers panel, enter the inputs as identified in the problem statement for the PCC layer.

Step 3: Click **Add Layer** to open the layer panel, enter **2** in the **Layer number to add** field, and then click **OK**.

Step 4: On the layers panel, select the **Layer 2** tab, and then type the inputs as identified in the problem statement for the base layer.

Step 5: Select **Batch** and then click **Edit Batch** to open the layer 2 properties panel (see Figure E12-2).

Step 6: Click **Insert** three times to add three additional cases, and then enter the base thicknesses as identified in the problem statement (see Figure E12-3).

Step 7: Click **OK** to close the layer 2 properties panel, and then click **OK** to close the layers panel.

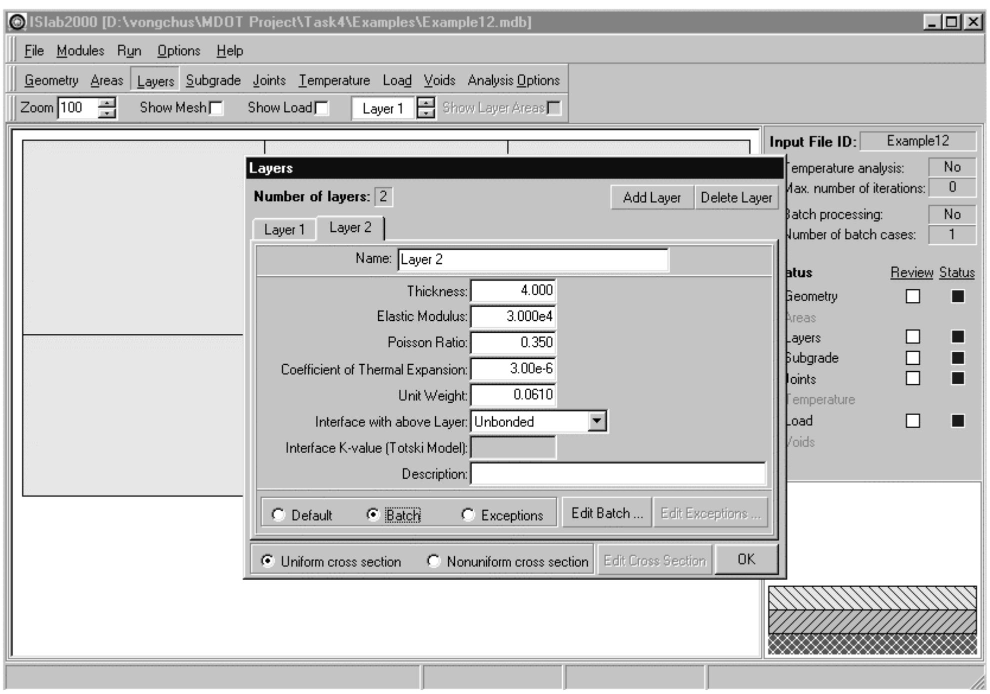


**Figure E12-2: Edit Inputs for the Layers Module**

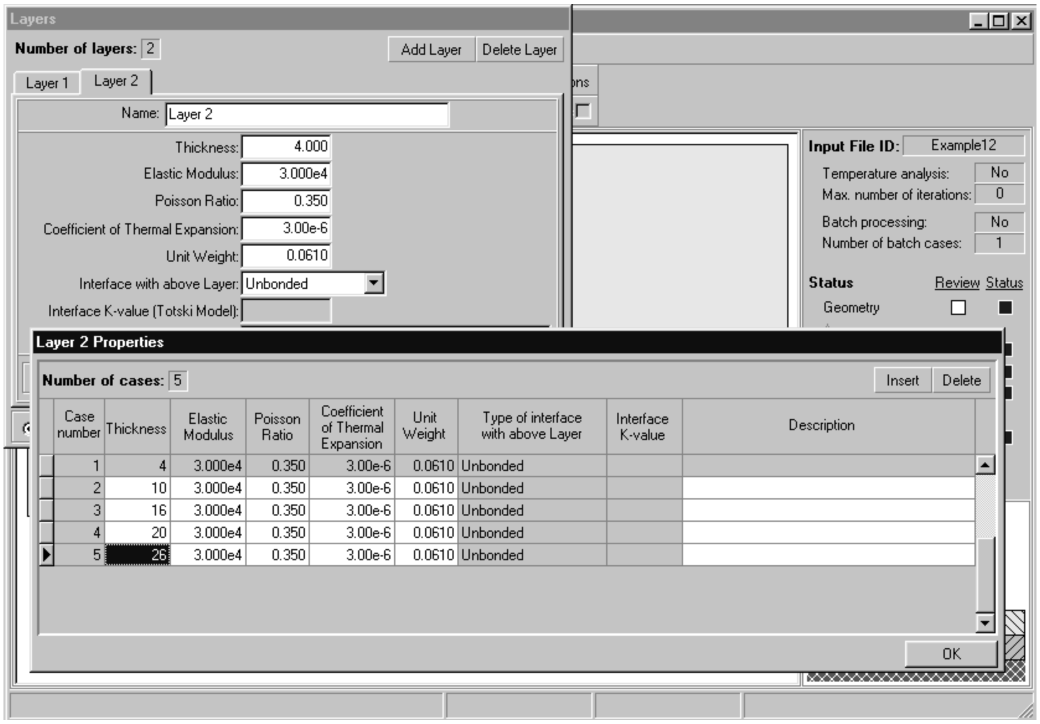


**Figure E12-3 Edit Inputs for the Layers Module (continued)**

## Subgrade Module

Use this module from Example 8.

## Joints Module

Use this module from Example 8.

## Load Module

Use this module from Example 8.

## Temperature Module

This module is not required for this problem.

## Analysis Options Module

Use this module from Example 4.

The main panel should display the pavement structure, loading condition, and meshing as shown in Example 8, Figure E8-12.

## *Analysis Results*

| Base thickness, in. | Stress at the bottom of the PCC, psi | |
|---|---|---|
| | Transverse | Longitudinal |
| 4 | 74.4 | 117.4 |
| 10 | 73.9 | 116.7 |
| 16 | 72.1 | 114.5 |
| 20 | 70.0 | 111.8 |
| 26 | 65.3 | 105.7 |

**Table E12-1: Analysis Results**

**NOTE**
Positive and negative values of stress signify tensile and compressive stresses and positive value of deflection indicates deflection in downward direction.

Figure E12-4 illustrates relationship between maximum stresses and base thickness.

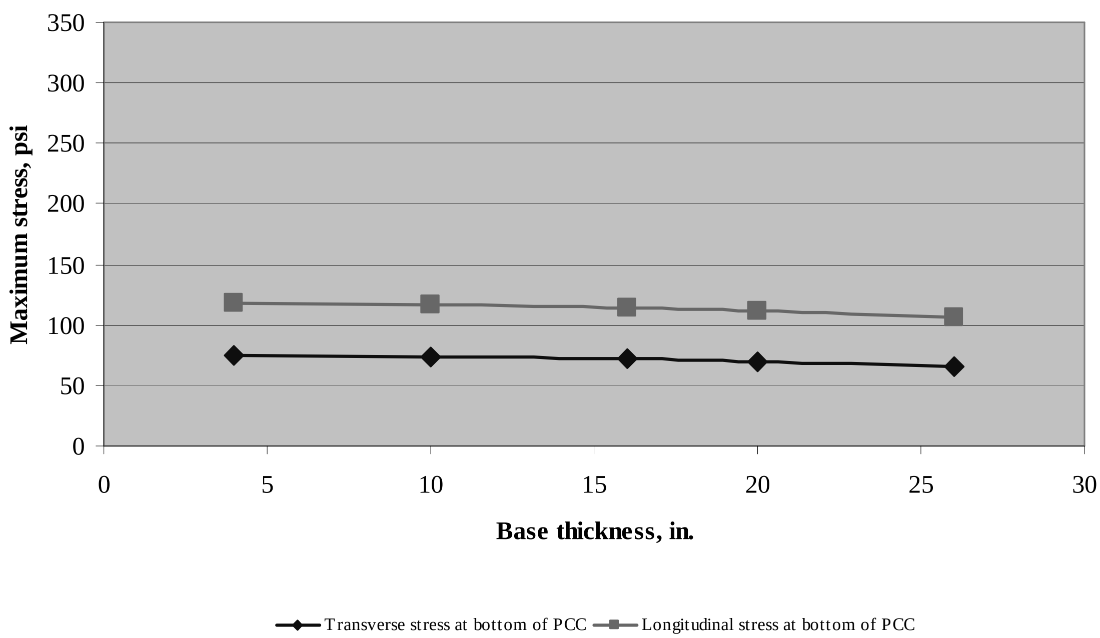


**Figure E12-4: Relationship Between Stresses and Temperature Differentials**

# Example 13:
# Single Axle Edge Loading with Various k-values

### Problem Statement

Determine maximum stresses at the bottom of the PCC slab for the pavement system and loading condition in Example 8 considering modulus of subgrade reaction, k-value, of 30, 65, 100, 150, 200 psi/in.

### Given

k-value = 30, 65, 100, 150, 200 psi/in.

### Problem Illustration

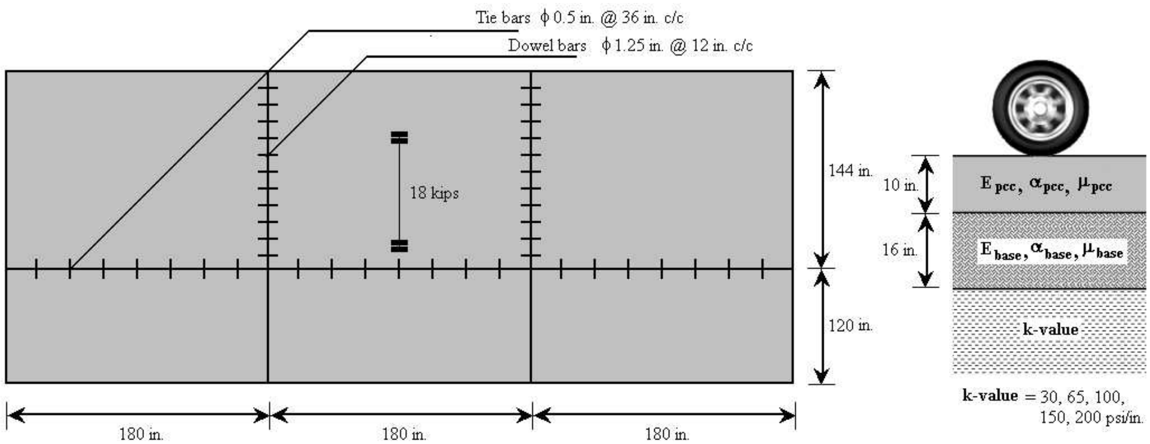


**Figure E13-1: Problem Illustration**

# Solution

### Geometry Module

Use this module from Example 8.

### Layers Module

Use this module from Example 8.

### Subgrade Module

(see Figures E13-2 and E13-3)

Step 1: Click **Layers** to open the layers panel.

Step 2: On the layers panel, enter the first input as identified in the problem statement.

Step 3: On the layers panel, select **Batch**, and then click **Edit Batch** to open the subgrade properties panel (see Figure E13-3).

Step 4: On the subgrade properties panel, click **Insert** four times to add four additional cases, and then type the k-value for each case as identified in the problem statement.

Step 5: Click **OK** to close the subgrade properties panel, and then click **OK** to close the Subgrade panel.

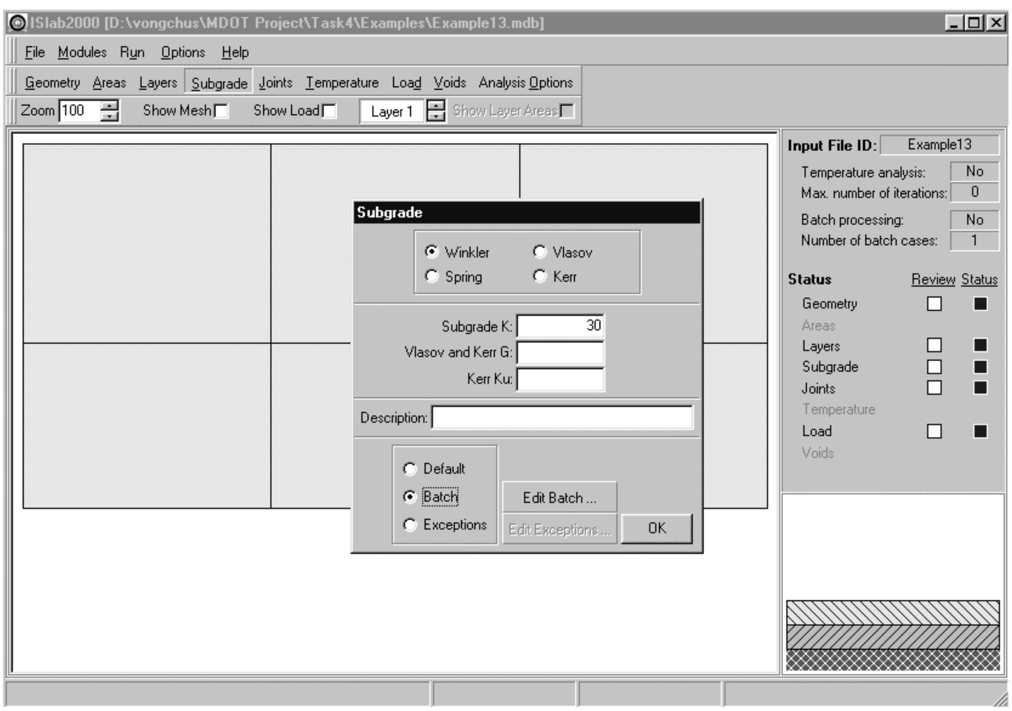


**Figure E13-2: Edit Inputs for the Subgrade Module**

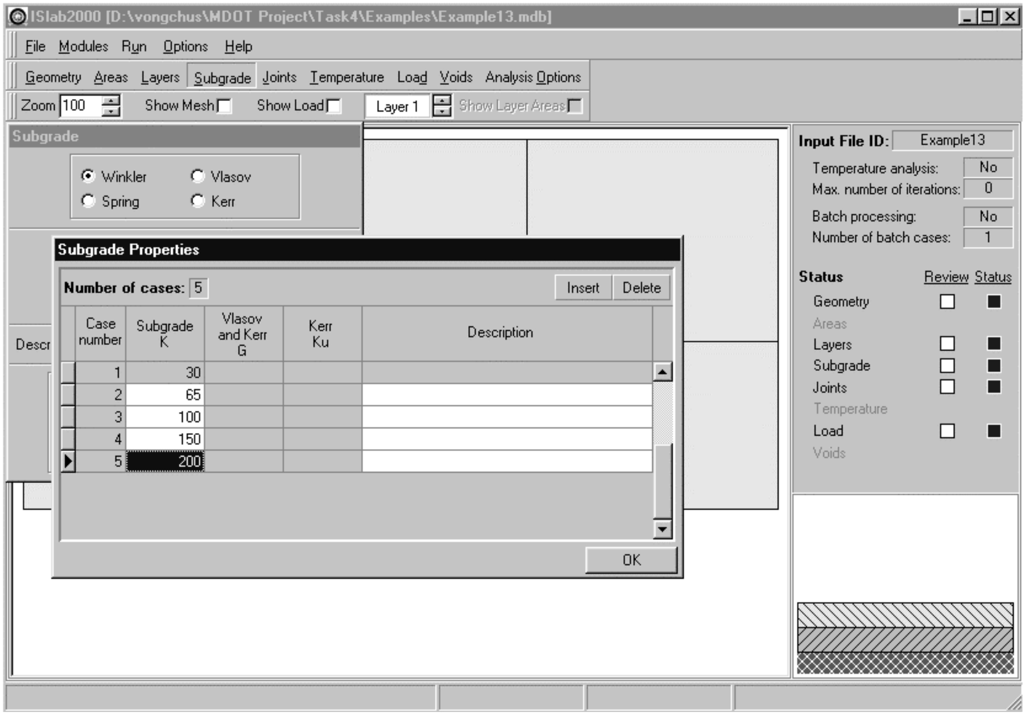


**Figure E13-3: Edit Inputs for the Subgrade Module (continued)**

## Joints Module

Use this module from Example 8.

## Load Module

Use this module from Example 8.

## Temperature Module

This module is not required for this problem.

## Analysis Options Module

Use this module from Example 4.

The main panel should display the pavement structure, loading condition, and meshing as shown in Example 8, Figure E8-12.

## *Analysis Results*

| k-value, psi/in. | Stress at the bottom of the PCC, psi | |
|---|---|---|
| | Transverse | Longitudinal |
| 30 | 77.6 | 146.6 |
| 65 | 74.5 | 126.3 |
| 100 | 72.1 | 114.5 |
| 150 | 69.4 | 103.7 |
| 200 | 67.2 | 96.5 |

**Table E13-1: Analysis Results**

**NOTE**
Positive and negative values of stress signify tensile and compressive stresses and positive value of deflection indicates deflection in downward direction.

Figure E13-4 illustrates relationship between maximum stresses and modulus of subgrade reaction.

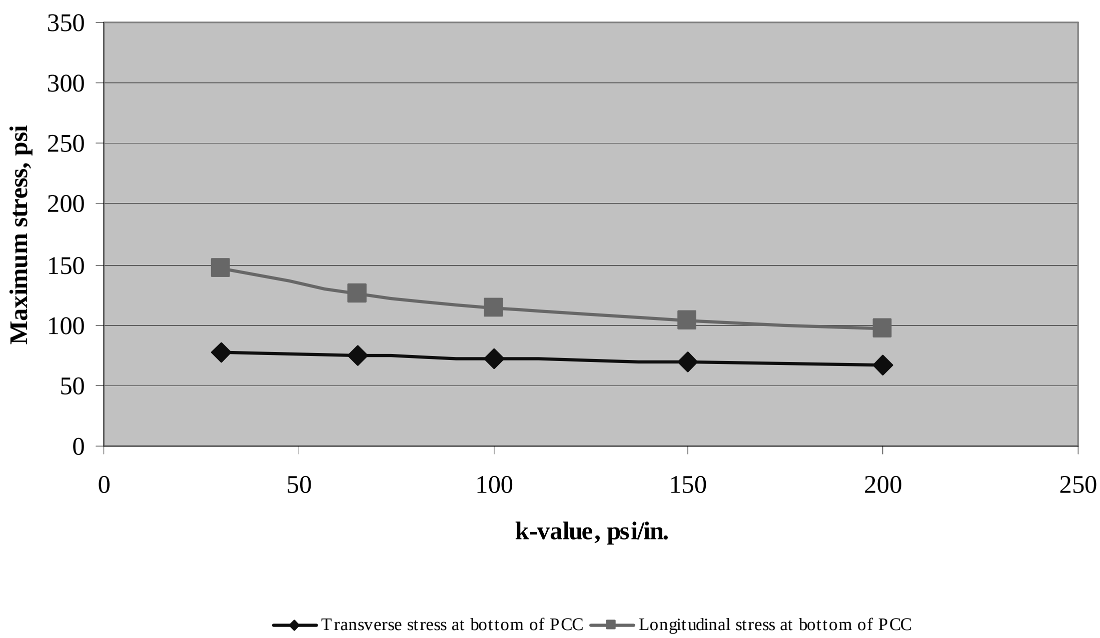


**Figure E13-4: Relationship Between Stresses and Modulus of Subgrade Reaction**

# Example 14:
# Single Axle Edge Loading with Various PCC Elastic Moduli

### Problem Statement

Determine maximum stresses at the bottom of the PCC slab for the pavement system and loading condition in Example 8 considering PCC elastic modulus, $E_{pcc}$, of 3, 4, 5, 6x$10^6$ psi

### Given

PCC elastic modulus, $E_{pcc}$ = 3, 4, 5, 6 x $10^6$ psi

### Problem Illustration

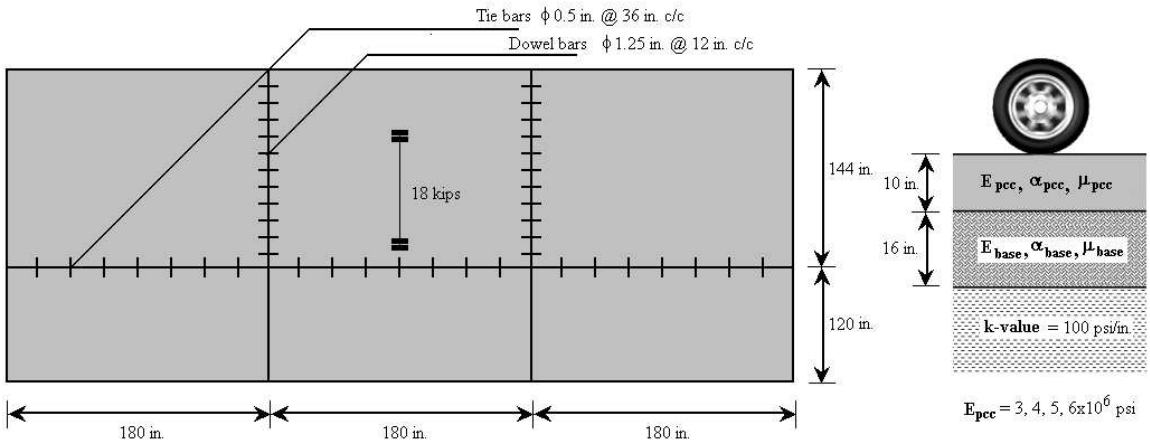


**Figure E14-1: Problem Illustration**

# Solution

### Geometry Module

Use this module from Example 8.

### Layers Module

(see Figures E14-2 and E14-3)

Step 1: Click **Layers** to open the layers panel.

Step 2: On the layers panel, enter the inputs as identified in the problem statement for the PCC layer.

Step 3: Click **Add Layer** to open the add layer panel, enter **2** in the **Layer number to add** field, and then click **OK** to close the add layer panel and add the layer.

Step 4: On the layers panel, select the **Layer 2** tab, and then type the inputs as identified in the problem statement for the base layer.

Step 5: On the layers panel, select the **Layer 1** tab, select **Batch**, and then click **Edit Batch** to open the layer 1 properties panel (see Figure E14-2).

Step 6: On the layer 1 properties panel, click **Insert** three times to add three additional cases, and then enter the PCC elastic modulus as identified in the problem statement (see Figure E14-3).

Step 7: Click **OK** to close the layer 1 properties panel, and then click **OK** to close the layers panel.

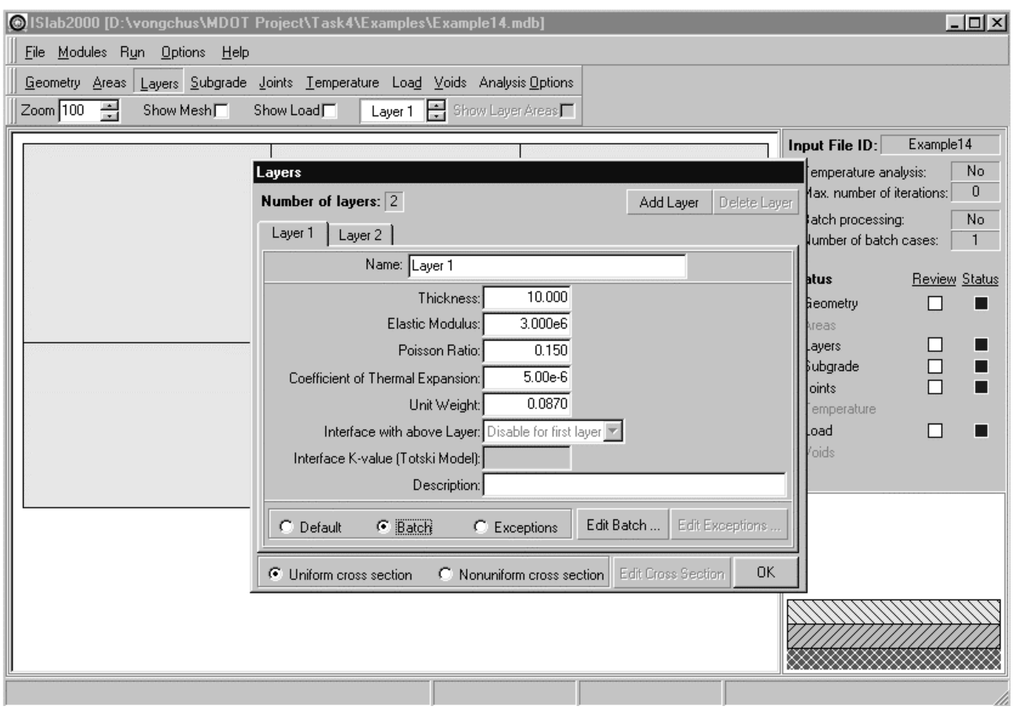


**Figure E14-2: Edit Inputs for the Layers Module**

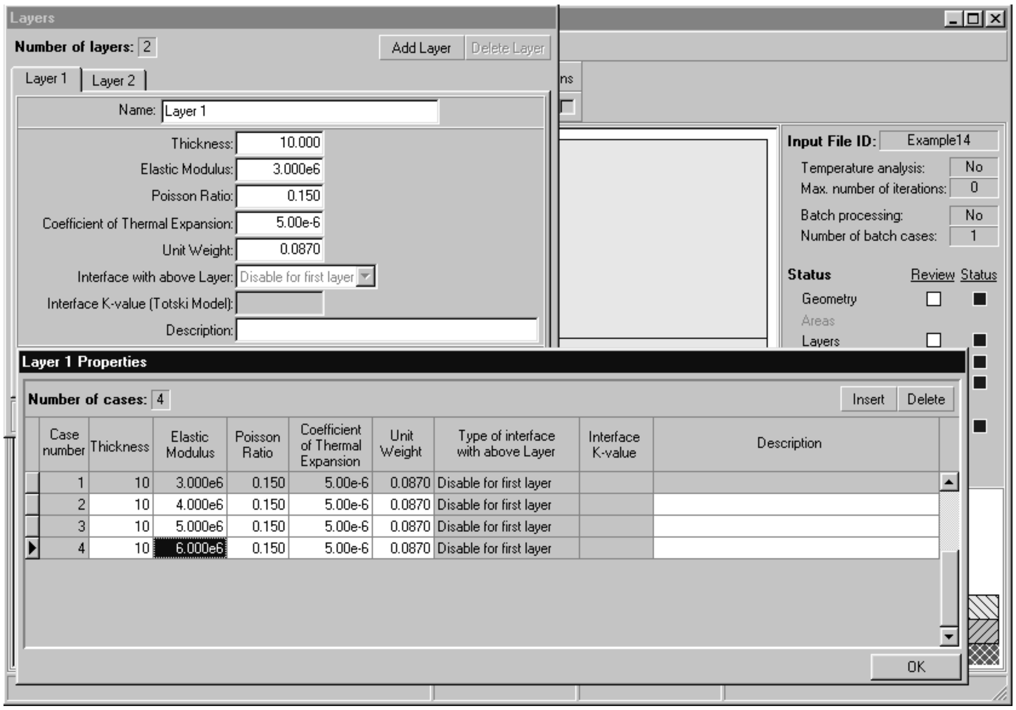


**Figure E14-3: Edit Inputs for the Layers Module (continued)**

### Subgrade Module

Use this module from Example 8.

### Joints Module

Use this module from Example 8.

### Load Module

Use this module from Example 8.

### Temperature Module

This module is not required for this problem.

### Analysis Options Module

Use this module from Example 4.

The main panel should display the pavement structure, loading condition, and meshing as shown in Example 8, Figure E8-12.

## *Analysis Results*

| $E_{pcc}$, x$10^6$ psi | Stress at the bottom of the PCC, psi | |
|---|---|---|
| | Transverse | Longitudinal |
| 3 | 69.5 | 105.8 |
| 4 | 72.1 | 114.5 |
| 5 | 73.9 | 121.2 |
| 6 | 75.1 | 126.7 |

**Table E14-1: Analysis Results**

**NOTE**
Positive and negative values of stress signify tensile and compressive stresses and positive value of deflection indicates deflection in downward direction.

Figure E14-4 illustrates relationship between maximum stresses and PCC elastic modulus.

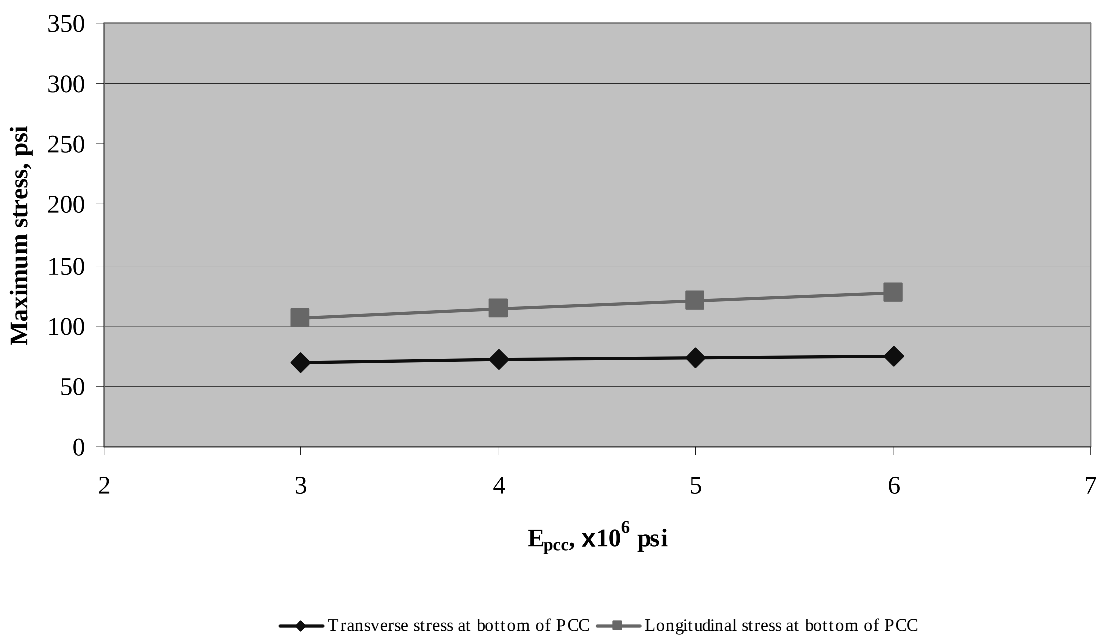


**Figure E14-9: Relationship Between Stresses and PCC Elastic Modulus**

# Example 15:
# Single Axle Edge Loading with Various Base Types

### Problem Statement

Determine maximum stresses at the bottom of the PCC slab for the pavement system and loading condition in Example 8 considering three different base types: dense-graded aggregate base (DAGB), permeable asphalt-treated base (PATB), lean concrete base (LCB)

### Given

$E_{DAGB}$ = $3 \times 10^4$ psi

$E_{PATB}$ = $3 \times 10^5$ psi

$E_{LCB}$ = $2 \times 10^6$ psi

$\mu_{DAGB}$ = 0.35

$\mu_{PATB}$ = 0.35

$\mu_{LCB}$ = 0.2

### Problem Illustration

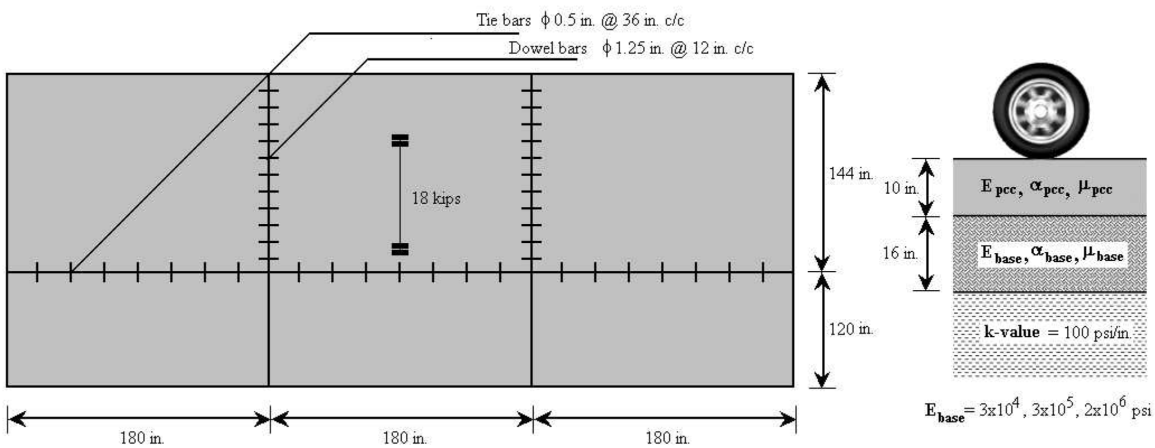


**Figure E15-1: Problem Illustration**

# Solution

## Geometry Module

Use this module from Example 8.

## Layers Module

(see Figures E15-2 and E15-3)

Step 1: Click **Layers** to open the layers panel.

Step 2: On the layers panel, enter the inputs as identified in the problem statement for the PCC layer.

Step 3: Click **Add Layer** to open the add layer panel, enter **2** in the **Layer number to add** field, and then click **OK** to close the add layer panel.

Step 4: On the layers panel, select the **Layer 2** tab, and then enter the inputs as identified in the problem statement for the base layer.

Step 5: Select **Batch**, and then click **Edit Batch** to open the layer 2 properties panel (see Figure E15-2).

Step 6: On the layer 2 properties panel, click **Insert** two times to add two additional cases, and then type the base elastic modulus and Poisson's ratio as identified in the problem statement (see Figure E15-3).

Step 7: Click **OK** to close the layer 2 properties panel, and then click **OK** to close the layers panel.

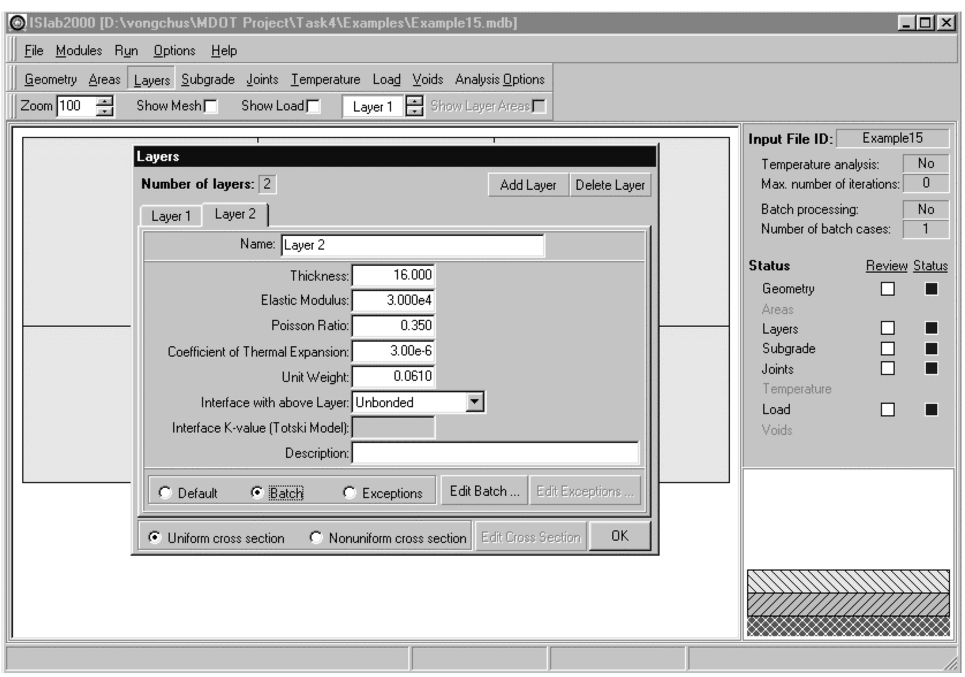


**Figure E15-2: Edit Inputs for the Layers Module**

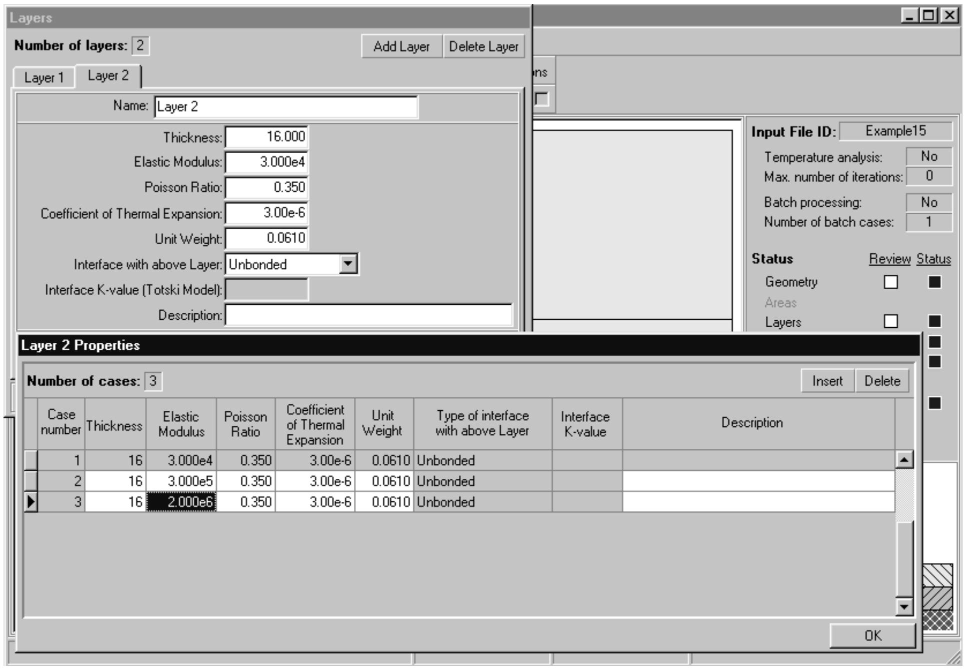


**Figure E15-3 Edit Inputs for the Layers Module (continued)**

### Subgrade Module

Use this module from Example 8.

### Joints Module

Use this module from Example 8.

### Load Module

Use this module from Example 8.

### Temperature Module

This module is not required for this problem.

### Analysis Options Module

Use this module from Example 4.

The main panel should display the pavement structure, loading condition, and meshing as shown in Example 8, Figure E8-12.

## *Analysis Results*

| Base type | Stress at the bottom of the PCC, psi | |
|---|---|---|
| | Transverse | Longitudinal |
| DAGB | 72.1 | 114.5 |
| PATB | 56.0 | 93.6 |
| LCB | 25.4 | 48.1 |

**Table E15-1: Analysis Results**

**NOTE**
Positive and negative values of stress signify tensile and compressive stresses and positive value of deflection indicates deflection in downward direction.

Figure E15-4 illustrates relationship between maximum stresses and base type.

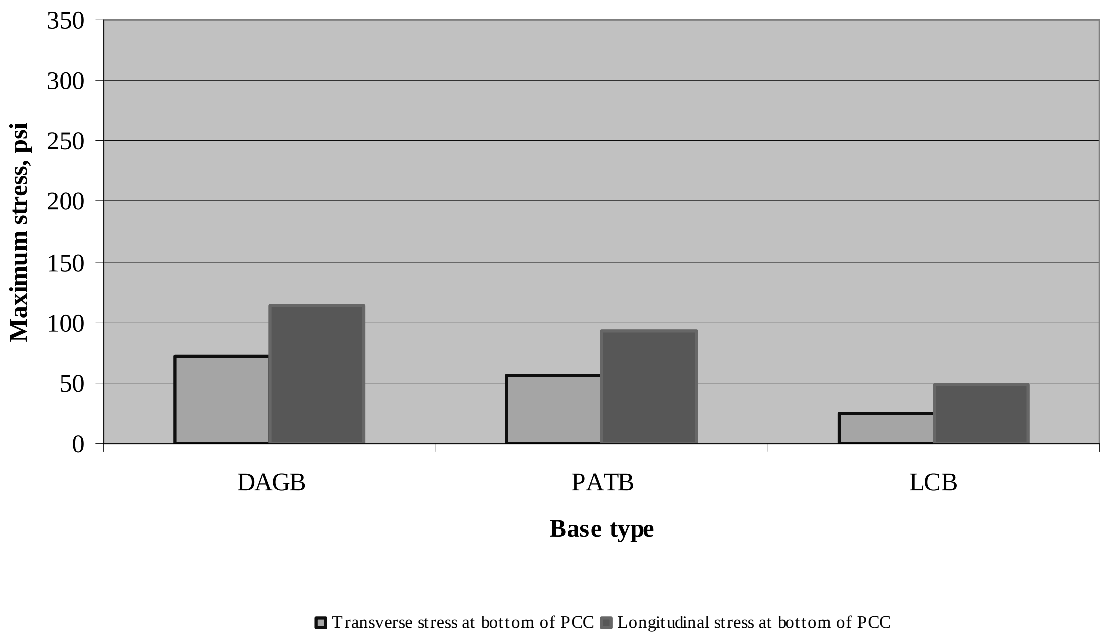


**E15-4: Relationship Between Stresses and Base Type**

# Example 16:
# Repeat Example 13 with a Thermal Gradient

### Problem Statement

Repeat Example 13 but at the same time, apply temperature differential, ΔT, of +20 $^{o}$F.

### Given

| | | | |
|---|---|---|---|
| Modulus of subgrade reaction, k-value | = | 30, 65, 100, 150, 200 | psi/in. |
| Temperature differential, ΔT | = | +20 | $^{o}$F. |

### Problem Illustration

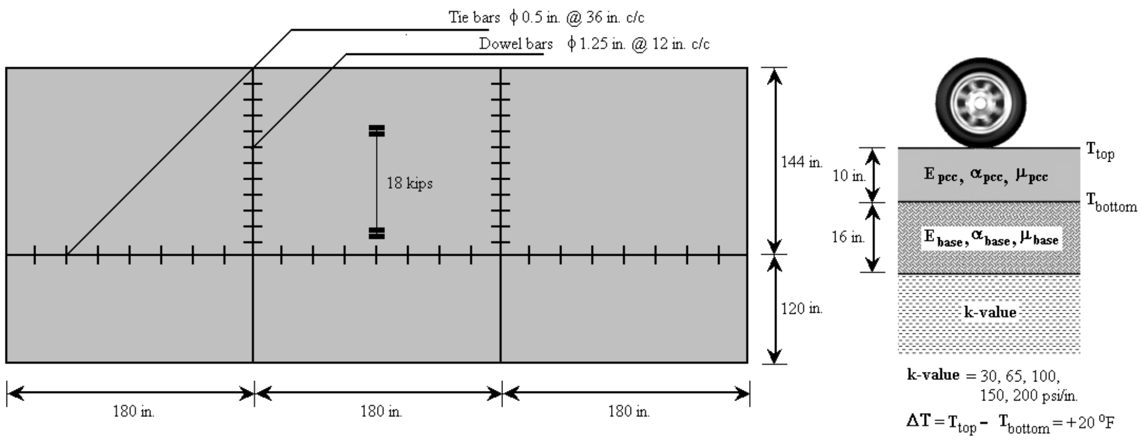


**Figure E16-1: Problem Illustration**

# Solution

### Geometry Module

Use this module from Example 8.

### Layers Module

Use this module from Example 8.

### Subgrade Module

Use this module from Example 13.

### Joints Module

Use this module from Example 8.

### Load Module

Use this module from Example 8.

### Temperature Module

(see Figure E16-2)

Step 1: Click **Temperature** to open the temperature properties panel.

Step 2: Select the **Perform Temperature Analysis** and the Batch check boxes.

Step 3: Enter the temperature differential of the first case in the **Difference** field (20 $^{o}$F for this problem).

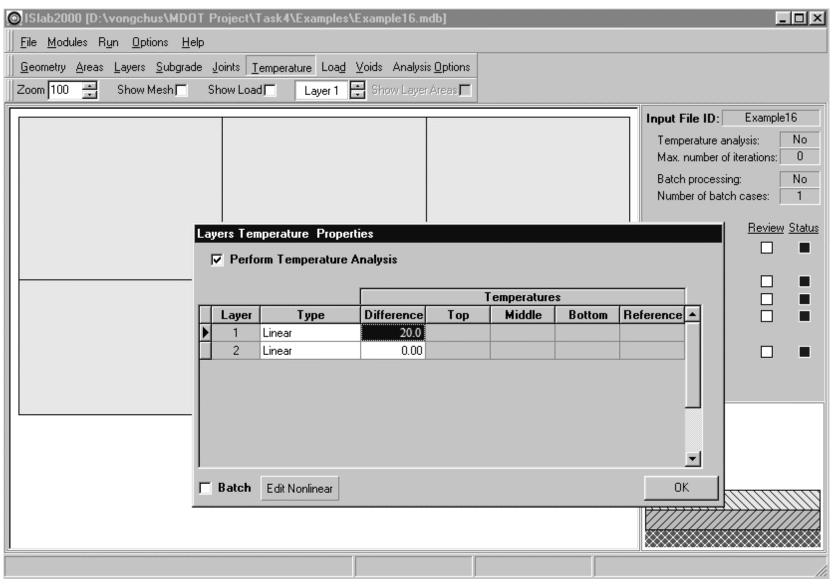


**Figure E16-2: Edit Inputs for the Temperature Module**

Step 4: Click **OK** to close the layers temperature properties panel.

### Analysis Options Module

Use this module from Example 4.

The main panel should display the pavement structure, loading condition, and meshing as shown in Example 8, Figure E8-12.

## *Analysis Results*

| k-value, psi/in. | Stress at the bottom of the PCC, psi | |
|---|---|---|
| | Transverse | Longitudinal |
| 30 | 107.7 | 198.8 |
| 65 | 124.9 | 211.5 |
| 100 | 139.7 | 224.5 |
| 150 | 157.3 | 240.1 |
| 200 | 171.7 | 252.4 |

**Table E16-1: Analysis Results**

**NOTE**
Positive and negative values of stress signify tensile and compressive stresses and positive value of deflection indicates deflection in downward direction.

Figure E16-3 illustrates relationship between maximum stresses and modulus of subgrade reaction.

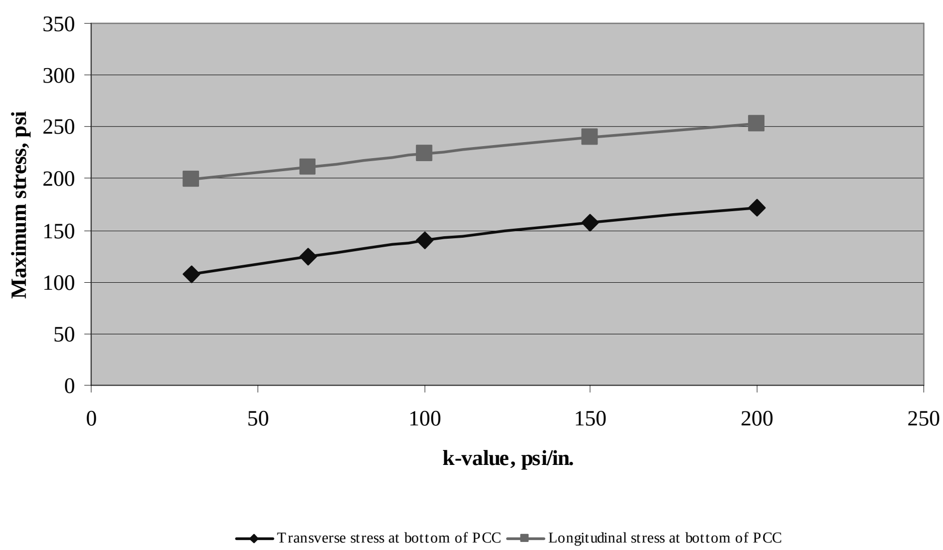


**Figure E16-3: Relationship between stresses and modulus of subgrade reaction**

# Example 17:
# Repeat Example 14 with a Thermal Gradient

### Problem Statement

Repeat Example 14 but at the same time, apply temperature differential, ΔT, of +20 °F.

### Given

| | | | |
|---|---|---|---|
| PCC elastic modulus, $E_{pcc}$ | = | 3, 4, 5, 6 x $10^6$ | psi |
| Temperature differential, ΔT | = | +20 | °F. |

### Problem Illustration

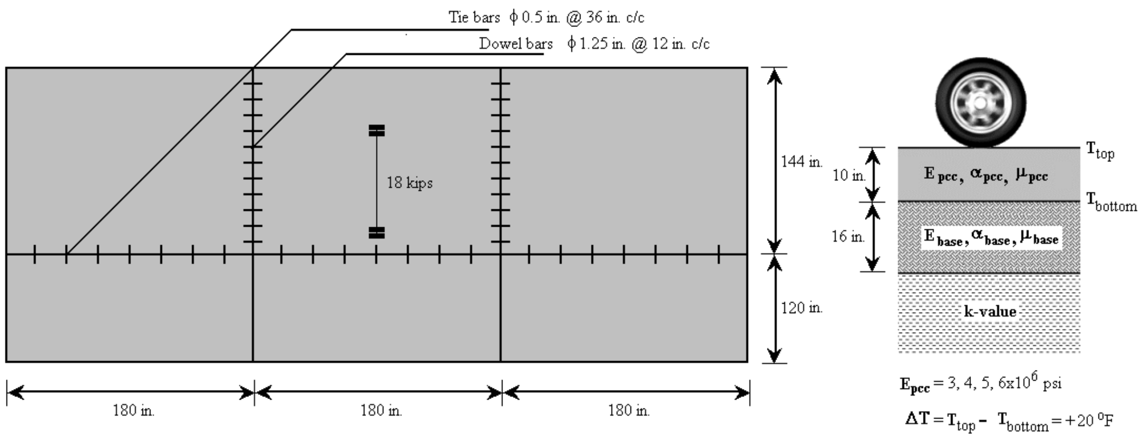


Figure E17-1: Problem Illustration

# Solution

### Geometry Module

Use this module from Example 8.

### Layers Module

Use this module from Example 14.

### Subgrade Module

Use this module from Example 8.

### Joints Module

Use this module from Example 8.

### Load Module

Use this module from Example 8.

### Temperature Module

Use this module from Example 16.

### Analysis Options Module

Use this module from Example 4.

The main panel should display the pavement structure, loading condition, and meshing as shown in Example 8, Figure E8-12.

## *Analysis Results*

| $E_{pcc}$, x$10^6$ psi | Stress at the bottom of the PCC, psi | |
|---|---|---|
| | Transverse | Longitudinal |
| 3 | 131.6 | 203.0 |
| 4 | 139.7 | 224.5 |
| 5 | 145.2 | 240.7 |
| 6 | 149.2 | 253.5 |

**Table E17-1: Analysis Results**

**NOTE**
Positive and negative values of stress signify tensile and compressive stresses and positive value of deflection indicates deflection in downward direction.

Figure E17-2 illustrates relationship between maximum stresses and PCC elastic modulus.

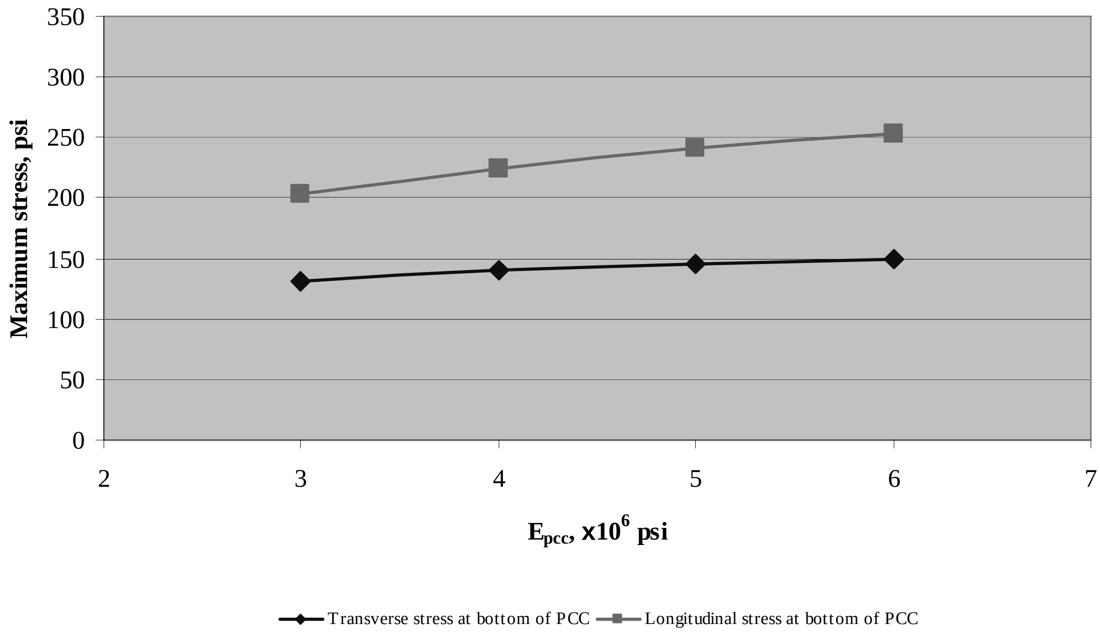


**Figure E17-2: Relationship Between Stresses and PCC Elastic Modulus**

# Example 18:
# Repeat Example 15 with a Thermal Gradient

### Problem Statement

Repeat Example 15 but at the same time, apply temperature differential, $\Delta T$, of +20 $^oF$.

### Given

$E_{DAGB}$ = $3 \times 10^4$ psi

$E_{PATB}$ = $3 \times 10^5$ psi

$E_{LCB}$ = $2 \times 10^6$ psi

$\mu_{DAGB}$ = 0.35

$\mu_{PATB}$ = 0.35

$\mu_{LCB}$ = 0.2

$\Delta T$ = +20 $^oF$.

### Problem Illustration

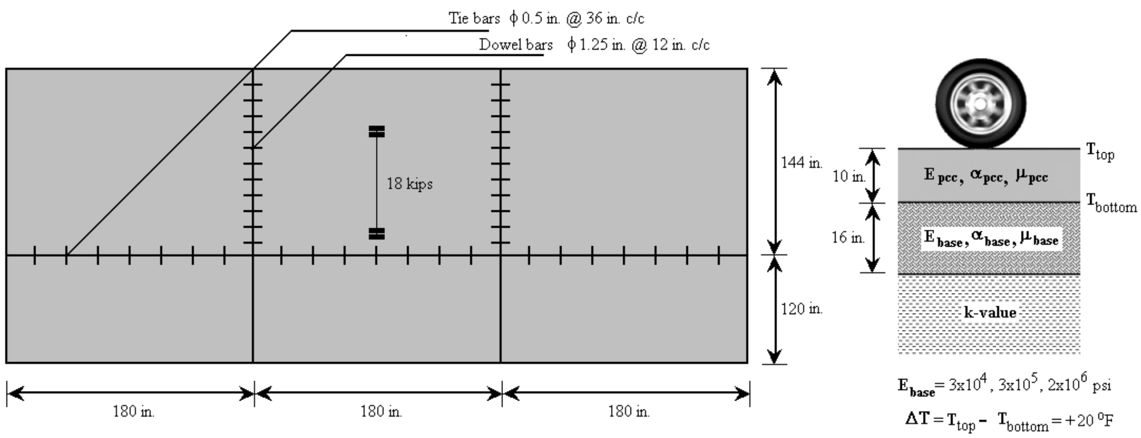


Figure E18-1: Problem Illustration

# Solution

### Geometry Module

Use this module from Example 8.

### Layers Module

Use this module from Example 15.

### Subgrade Module

Use this module from Example 8.

### Joints Module

Use this module from Example 8.

### Load Module

Use this module from Example 8.

### Temperature Module

Use this module from Example 16.

### Analysis Options Module

Use this module from Example 4.

The main panel should display the pavement structure, loading condition, and meshing as shown in Example 8, Figure E8-12.

## *Analysis Results*

| Base type | Stress at the bottom of the PCC, psi | |
|---|---|---|
| | Transverse | Longitudinal |
| DAGB | 139.7 | 224.5 |
| PATB | 157.5 | 223.7 |
| LCB | 194.0 | 223.9 |

**Table E18-1: Analysis Results**

**NOTE**
Positive and negative values of stress signify tensile and compressive stresses and positive value of deflection indicates deflection in downward direction.

Figure E18-3 illustrates relationship between maximum stresses and base type.

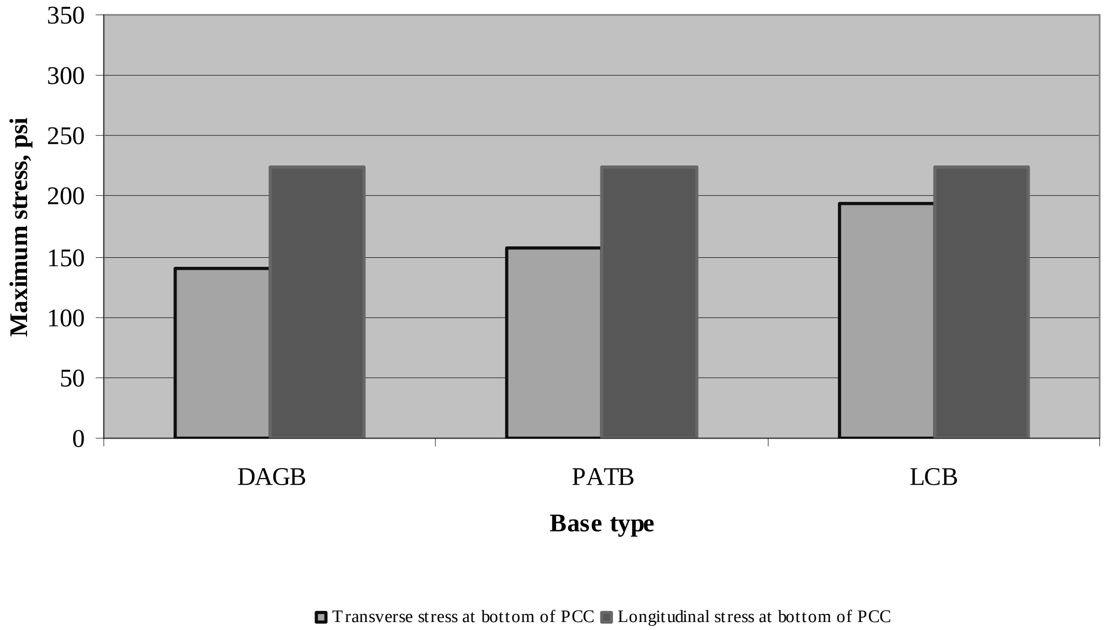


**Figure E18-3: Relationship Between Stresses and Base Type**

# Example 19:
# Single Axle Edge Loading with Various Load Levels

### Problem Statement

Repeat Example 8 but consider several axle weight levels for single axle: 10, 15, 18, 21, 25 kips

### Given

| | | | |
|---|---|---|---|
| Loading configuration | = | single axle | |
| Axle weight | = | 10, 15, 18, 21, 25 | kips |

### Problem Illustration

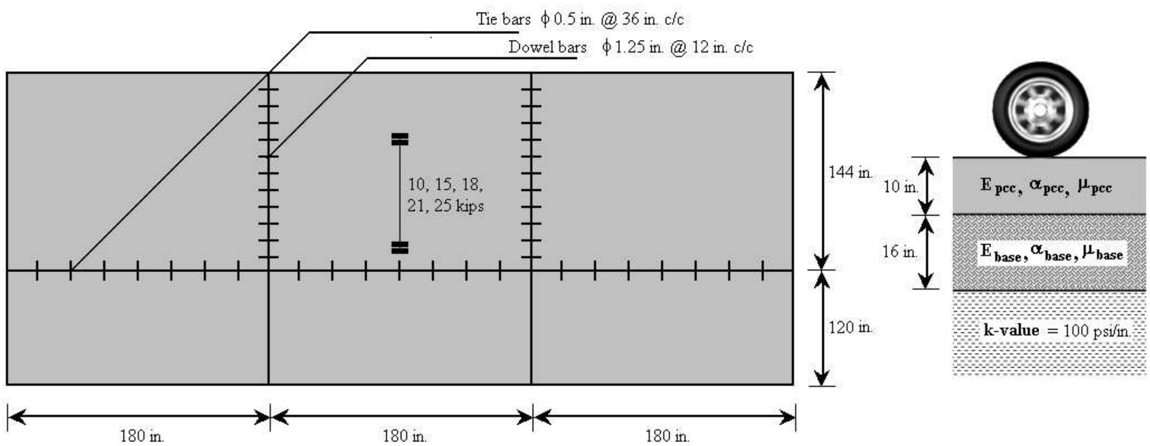


**Figure E19-1: Problem Illustration**

# Solution

### Geometry Module

Use this module from Example 8.

### Layers Module

Use this module from Example 8.

### Subgrade Module

Use this module from Example 8.

### Joints Module

Use this module from Example 8.

### Load Module

(see Figures E19-2 and E19-3)

Step 1: Follow steps 1 through 10 of Example 8.

Step 2: Enter the load for the first case of single axle (10,000 lbs for this example).

Step 3: Select **Batch** and then click **Edit Batch** to open the batch load panel (see Figure E19-2).

Step 4: Click **Add** four times, and then enter the other four axle weights.

Step 5: Click **OK** to close the batch load panel, and then click **OK** to close the Load panel.

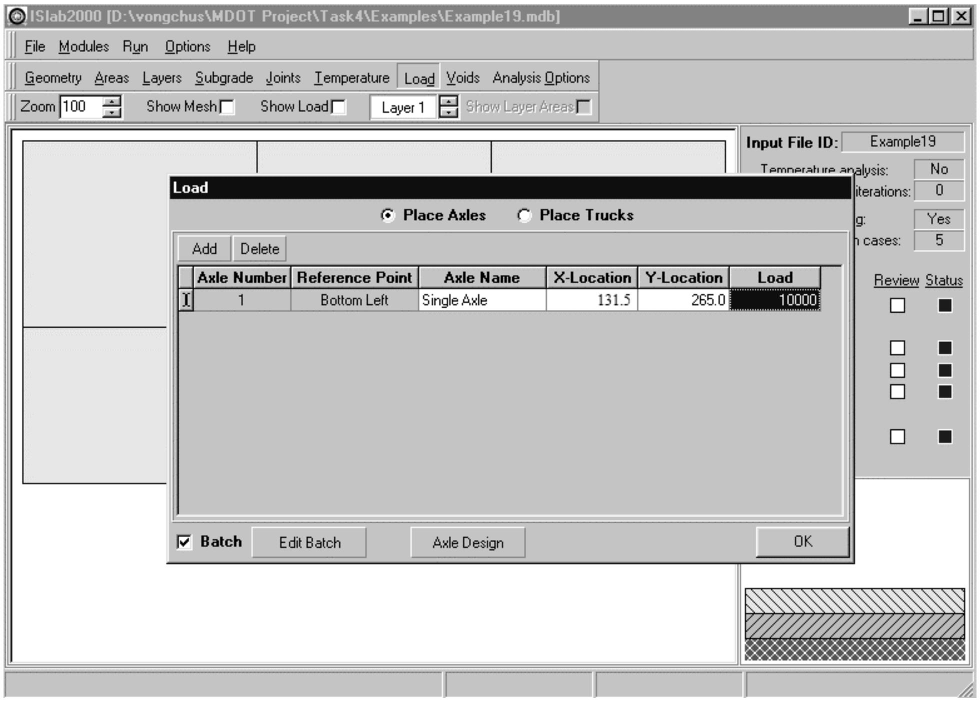


Figure E19-2: Edit Inputs for the Load Module

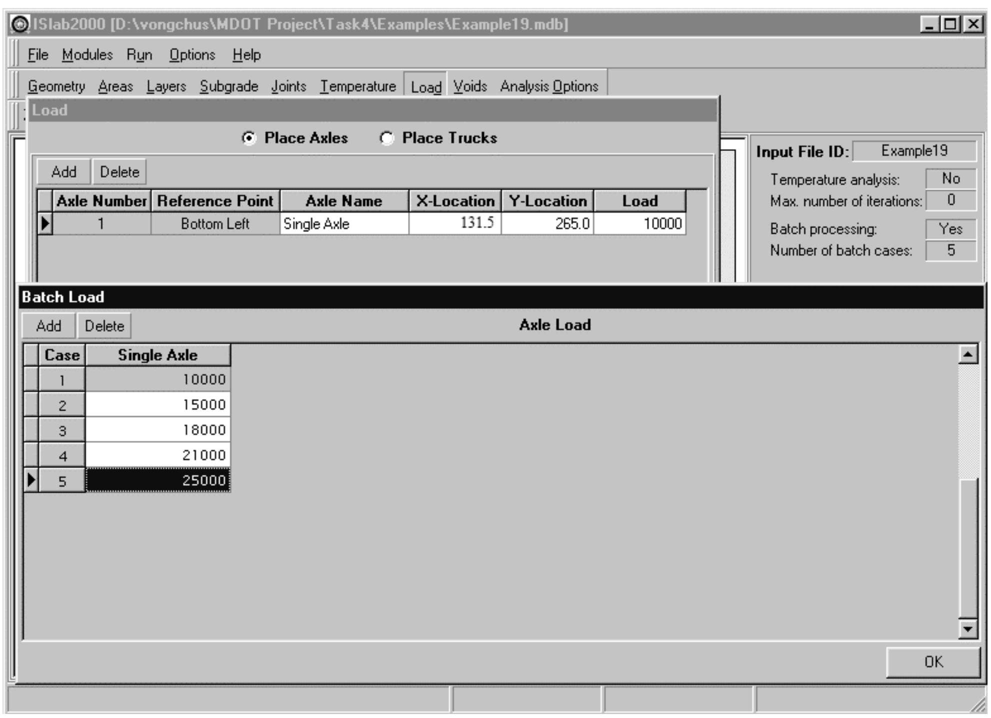


Figure E19-3: Edit Inputs for the Load Module (continued)

## Temperature Module

This module is not required for this problem.

### Analysis Options Module

Use this module from Example 4.

The main panel should display the pavement structure, loading condition, and meshing as shown in Example 8, Figure E8-12.

## *Analysis Results*

| Axle wt., kips | Stress at the bottom of the PCC, psi | |
|---|---|---|
| | Transverse | Longitudinal |
| 10 | 43.6 | 74.1 |
| 15 | 62.1 | 101.2 |
| 18 | 72.1 | 114.5 |
| 21 | 86.1 | 139.6 |
| 25 | 104.5 | 172.2 |

**Table E19-1: Analysis Results**

**NOTE**
Positive and negative values of stress signify tensile and compressive stresses and positive value of deflection indicates deflection in downward direction.

Figure E19-4 illustrates relationship between maximum stresses and axle weight.

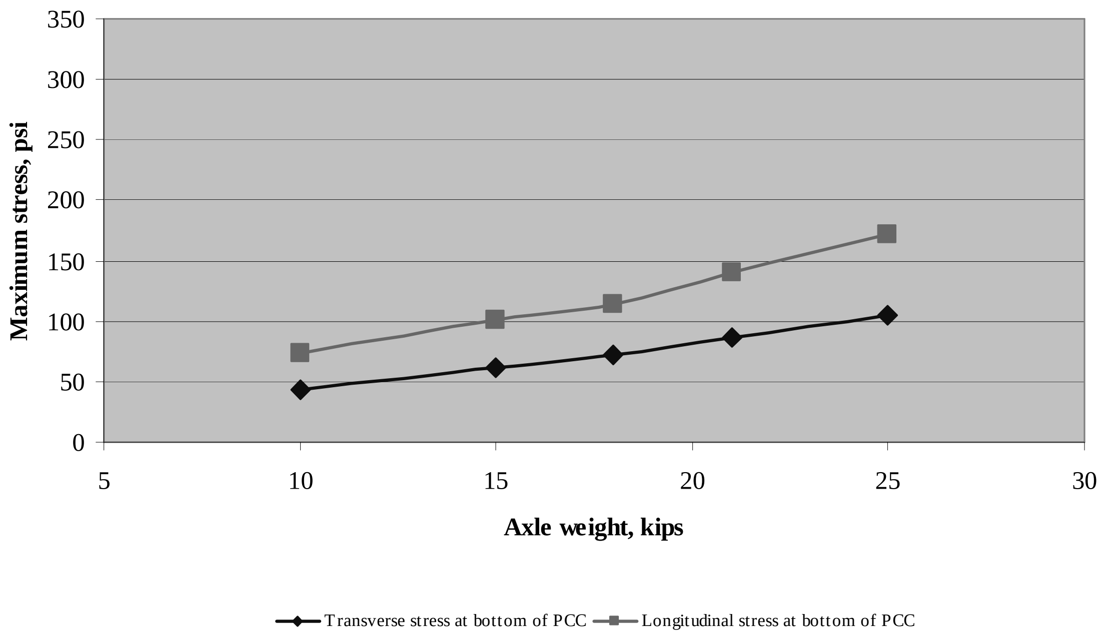


**Figure E19-4: Relationship Between Stresses and Axle Weight**

# Example 20:
# Tandem Axle Edge Loading with Various Load Levels

### Problem Statement

Repeat Example 8 but consider several axle weight levels for tandem axle: 21, 25, 32, 40 kips

### Given

| | | | |
|---|---|---|---|
| Loading configuration | = | tandem axle | |
| Axle weight | = | 21, 25, 32, 40 | kips |

### Problem Illustration

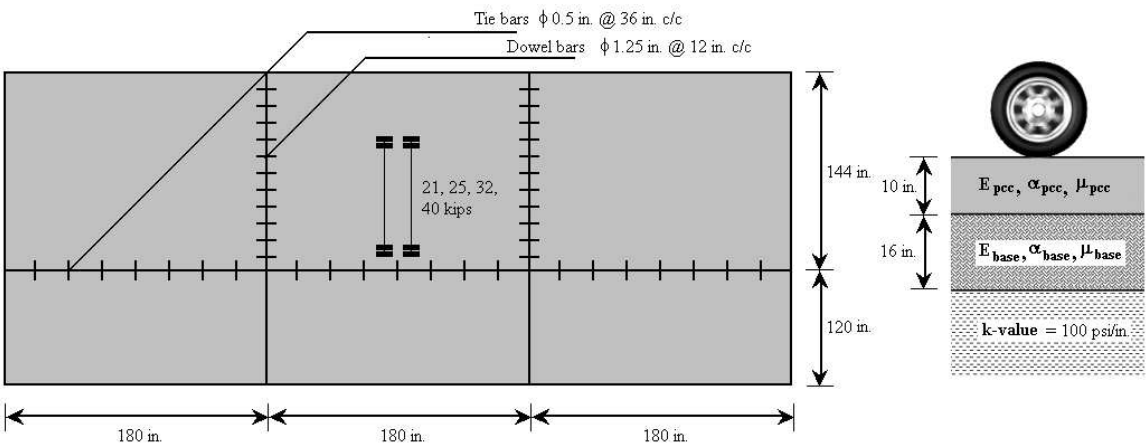


**Figure E20-1: Problem Illustration**

# Solution

### Geometry Module

Use this module from Example 8.

### Layers Module

Use this module from Example 8.

### Subgrade Module

Use this module from Example 8.

### Joints Module

Use this module from Example 8.

### Load Module

(see Figures E20-2 through E20-4)

Step 1: Click **Load** to open the load panel.

Step 2: Click **Axle Design** to open the axle design panel (see Figure E20-2), and then enter **Tandem Axle** in the **Axle Name** field.

Step 3: Enter the tire pressure in the **Tire Pressure** field. The tire pressure of the wheel load can be computed as shown below (for more detail, see standard configuration of tandem axle):

$$Tire\ Pressure = \frac{Wheel\ Load}{Contact\ Area} = \frac{4{,}000\ lbs}{5\ in. \times 10\ in.} = 80\ psi$$

Step 4: Enter the tire width in the **Tire Width** box (5 in. for this example).

Step 5: Enter wheel spacing information as shown in Figure E20-2.

Step 6: Select **Bottom Left** for the reference point position.

Step 7: Click **OK** to close the axle design panel.

Step 8: On the load panel, click **Add** to add a load (see Figure E20-3).

Step 9: In the **Axle Name** field, select **Tandem Axle**.

Step 10: Enter X-location and Y-location information to locate the wheel load. X-location and Y-location for an edge loading condition can be computed as shown below:

$$X - location = Shoulder\ width + Distance\ dual\ wheel\ center\ to\ shoulder - Distance\ dual\ wheel\ center\ to\ reference\ point$$

$$= 120 + 20 - \left(\frac{5}{2} + \frac{12}{2}\right) = 131.5\ in$$

$$Y - location = Joint\ spacing + \frac{Joint\ spacing}{2} - \frac{wheel\ load\ length}{2} - \frac{wheel\ spacing}{2}$$

$$= 180 + \frac{180}{2} - \frac{10}{2} - \frac{42}{2} = 244\ in$$

Step 11: Enter the load for the first case of tandem axle (21,000 lbs).

Step 12: Select **Batch** and then click **Edit Batch** to open the batch load panel (see Figure E20-4)

Step 13: Click **Add** three times to add three additional tandem axle cases, and then enter the other three axle weights.

Step 14: Click **OK** to close the batch load panel, and then click **OK** to close the load panel.

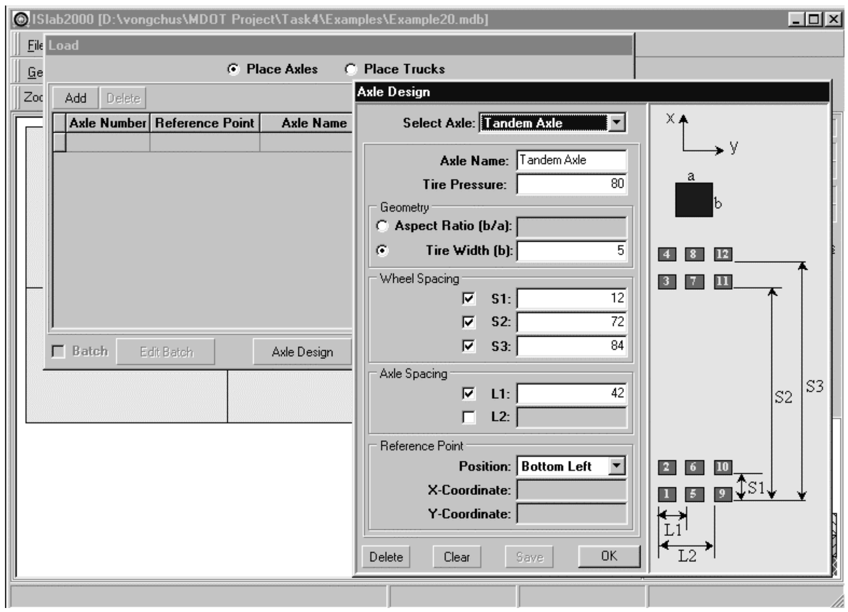


Figure E20-2: Edit Inputs for the Load Module

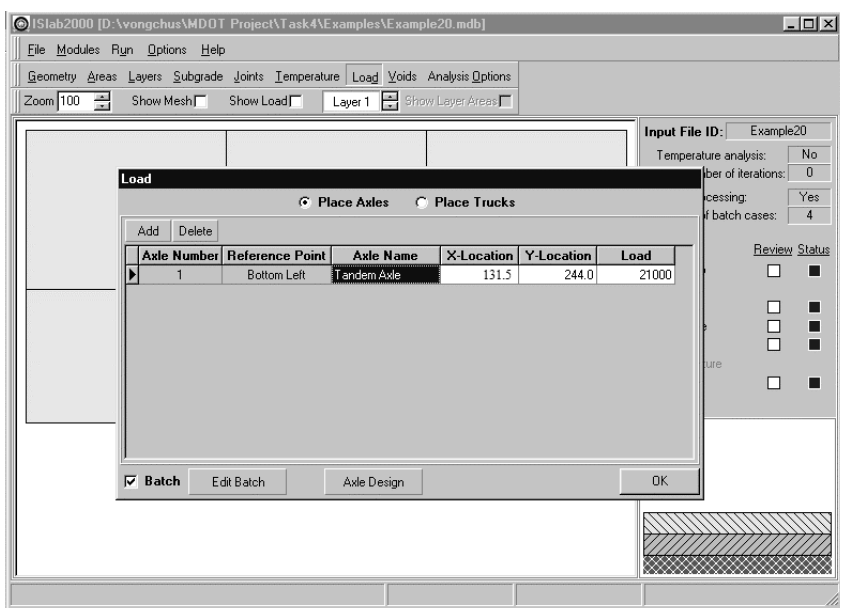


Figure E20-3: Edit Inputs for the Load Module (continued)

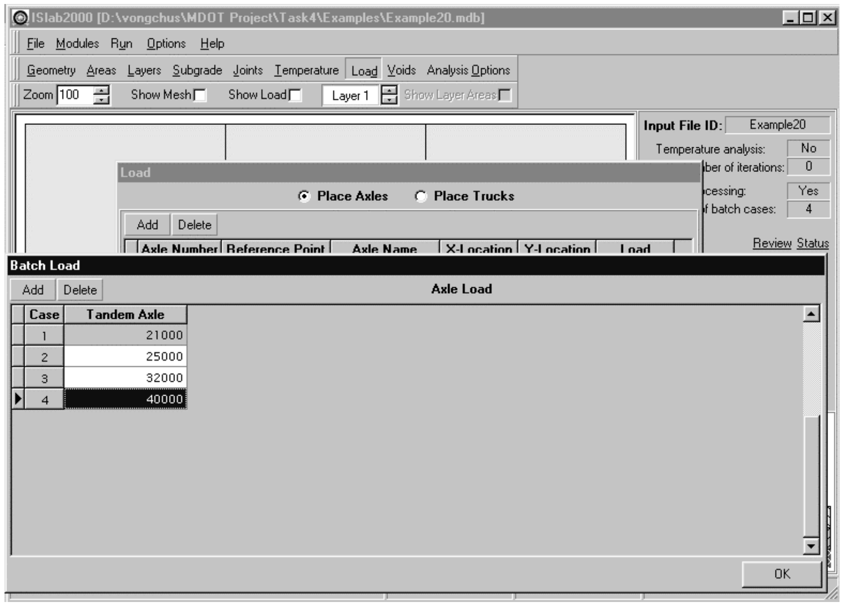


Figure E20-4: Edit Inputs for the Load Module (continued)

## Temperature Module

This module is not required for this problem.

## Analysis Options Module

Use this module from Example 4.

The main panel should display the pavement structure, loading condition, and meshing as shown in Figure E20-5.

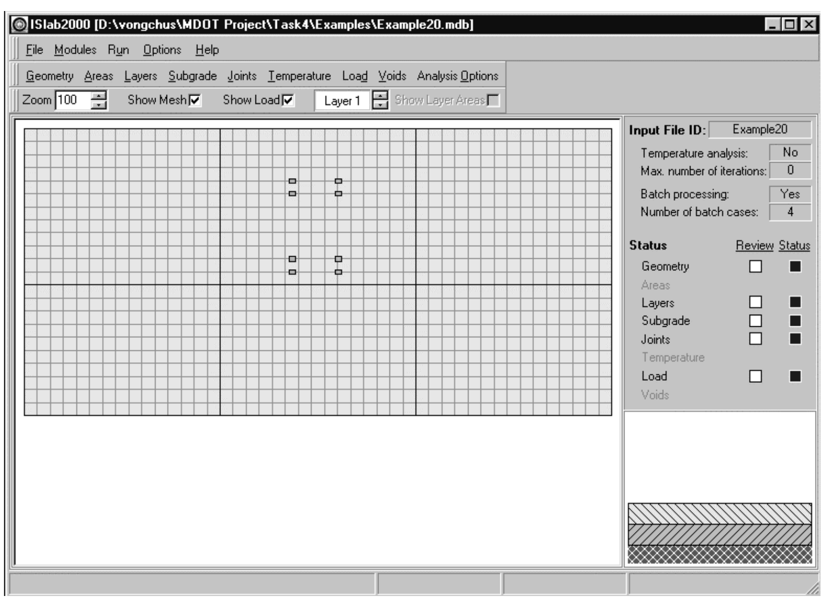


Figure E20-5: Main Panel After the Completion of Inputs

## *Analysis Results*

| Axle wt., kips | Stress at the bottom of the PCC, psi | |
|---|---|---|
| | Transverse | Longitudinal |
| 21 | 58.7 | 91.7 |
| 25 | 69.4 | 107.2 |
| 32 | 87.3 | 131.6 |
| 40 | 108.6 | 164.0 |

**Table E20-1: Analysis Results**

**NOTE**
Positive and negative values of stress signify tensile and compressive stresses and positive value of deflection indicates deflection in downward direction.

Stress and deflection contours from ISLAB2000 are also available in Figures E20-6 through E20-8.Figure E20-9 illustrates relationship between maximum stresses and axle weight.

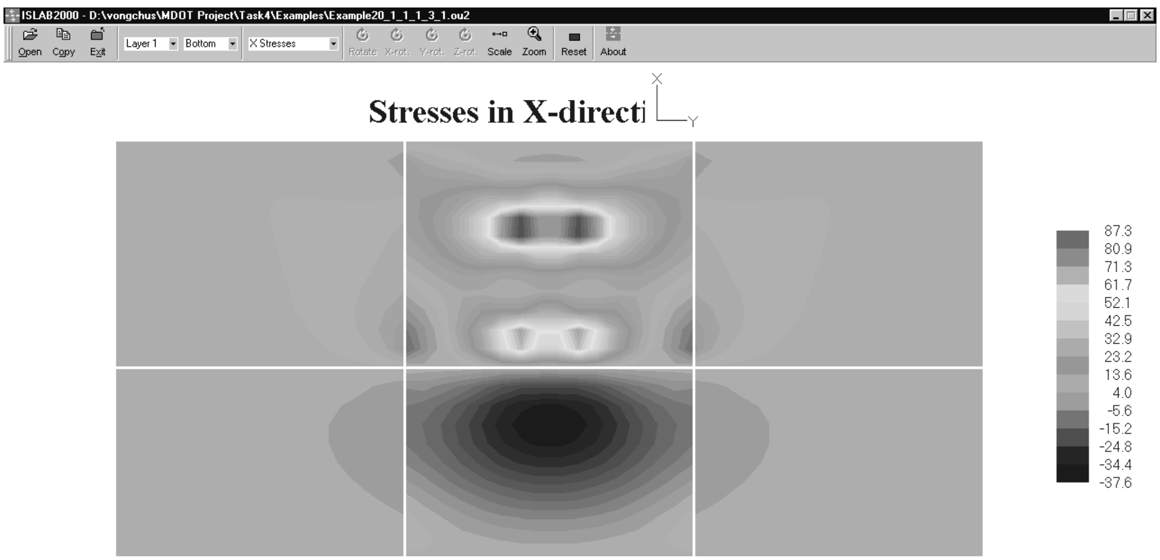


**Figure E20-6: Transverse Stress at the Bottom of the PCC Slab, 32-kips Axle Weight**

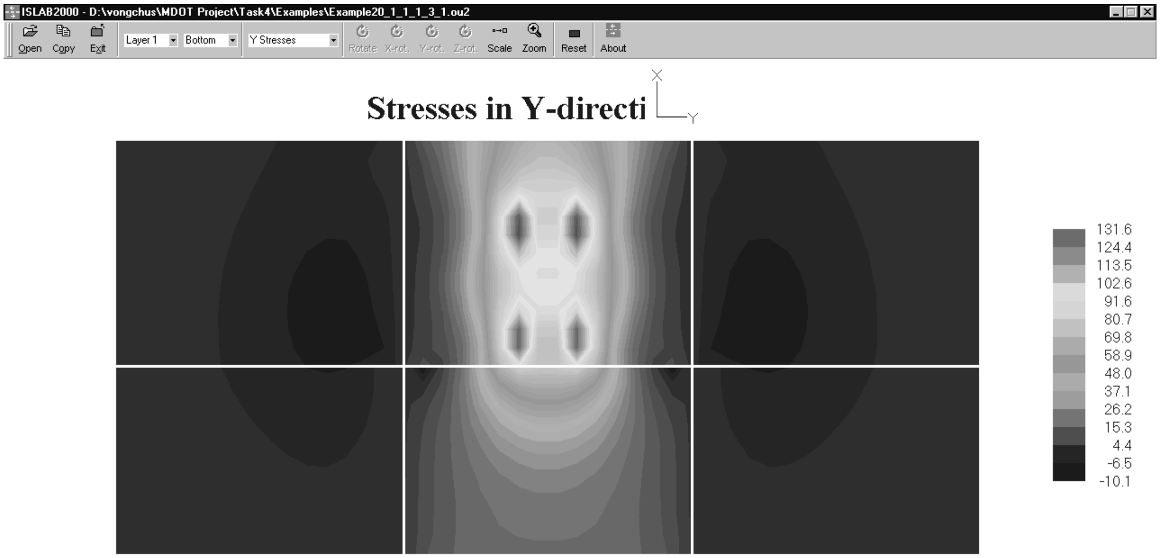


**Figure E20-7: Longitudinal Stress at the Bottom of the PCC From ISLAB2000, 32-kips Axle Weight**

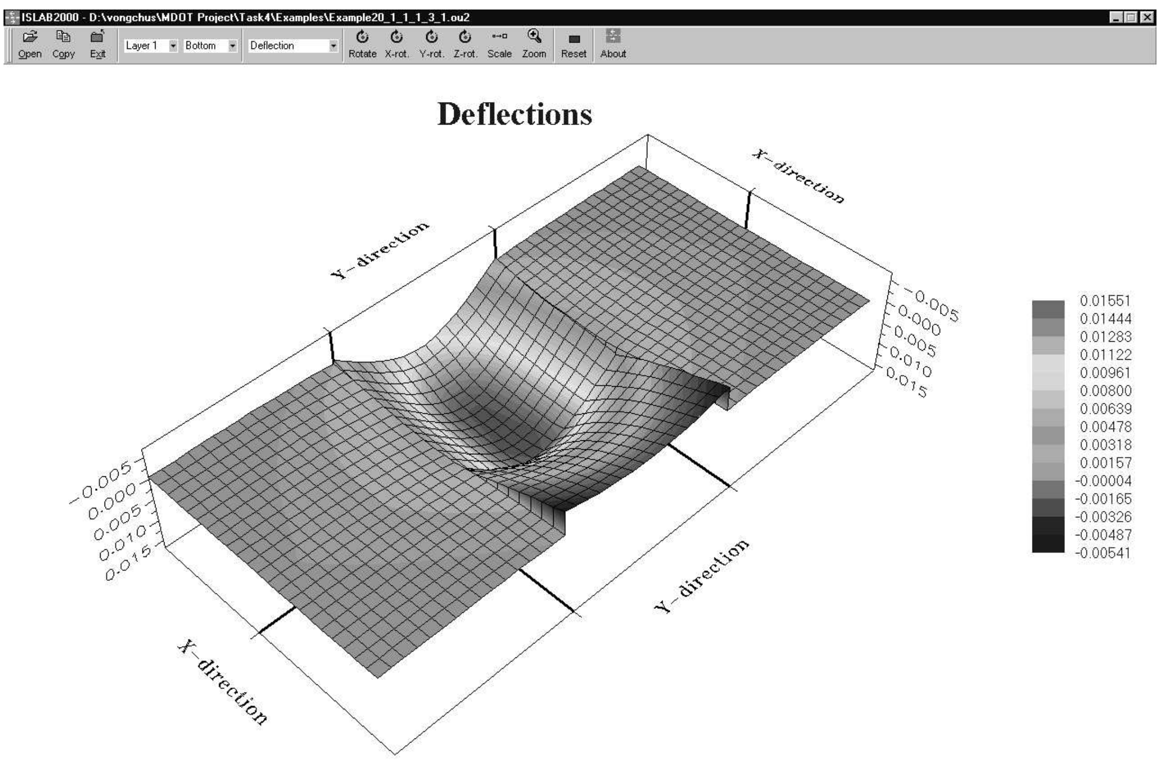


**Figure E20-8: Deflection of the PCC slab, 32-kips Axle Weight**

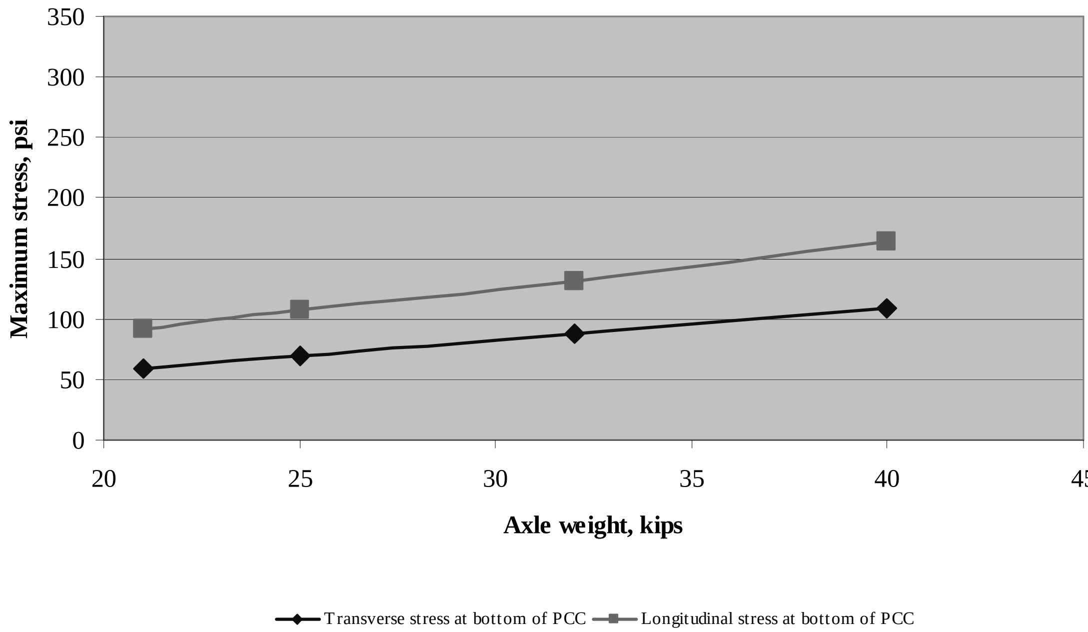


**Figure E20-9: Relationship Between Stresses and Axle Weight**

# Example 21:
# Tridem Axle Edge Loading with Various Load Levels

### Problem Statement

Repeat Example 8 but consider several axle weight levels for tridem axle: 21, 25, 32, 40 kips. Then, compare the results for 21 and 25 kips loading with the results from Examples 19 and 20.

### Given

| | | | |
|---|---|---|---|
| Loading configuration | = | tridem axle | |
| Axle weight | = | 21, 25, 32, 40 | kips |

### Problem Illustration

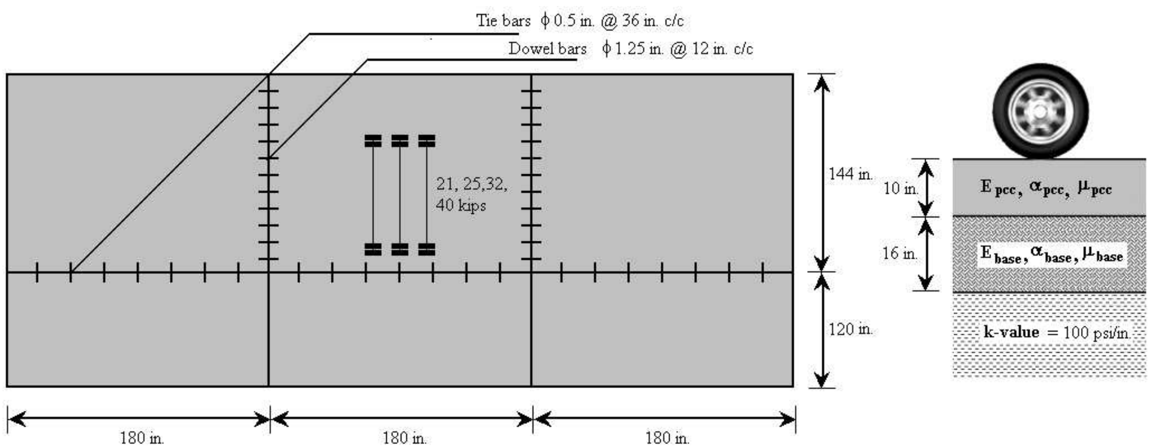


Figure E21-1: Problem Illustration

# Solution

### Geometry Module

Use this module from Example 8.

### Layers Module

Use this module from Example 8.

### Subgrade Module

Use this module from Example 8.

### Joints Module

Use this module from Example 8.

### Load Module

(see Figures E21-2 through E21-4)

Step 1: Click **Load** to open the load panel.

Step 2: On the load panel, click **Axle Design** to open the axle design panel (see Figure E21-2), and then enter **Tridem Axle** in the **Axle Name** field.

Step 3: Enter the tire pressure in the **Tire Pressure** field. The tire pressure of the wheel load can be computed as shown below (for more detail, see standard configuration of tridem axle):

$$Tire\ Pressure = \frac{Wheel\ Load}{Contact\ Area} = \frac{6{,}500\ lbs}{5\ in. \times 10\ in.} = 65\ psi$$

Step 4: Enter the tire width in the **Tire Width** box (5 in. for this example).

Step 5: Enter wheel spacing information as shown in Figure E21-2.

Step 6: Select **Bottom Left** for the reference point position.

Step 7: Click **OK** to close the axle design panel.

Step 8: On the load panel, click **Add** to add additional loads.

Step 9: In the Axle Name box, select **Tridem Axle**.

Step 10: Enter X-location and Y-location information to locate the wheel load. X-location and Y-location for edge loading condition can be computed as shown below:

$$X-location = Shoulder\ width + Distance\ dual\ wheel\ center\ to\ shoulder - Distance\ dual\ wheel\ center\ to\ reference\ point$$

$$= 120 + 20 - \left(\frac{5}{2} + \frac{12}{2}\right) = 131.5\ in$$

$$Y-location = Joint\ spacing + \frac{Joint\ spacing}{2} - \frac{wheel\ load\ length}{2} - wheel\ spacing$$

$$= 180 + \frac{180}{2} - \frac{10}{2} - 42 = 223\ in$$

Step 11: Enter the load for the first case of tridem axle (21,000 lbs).

Step 12: Select **Batch**, and then click **Edit Batch** (see Figure E21-3) to open the batch load panel (see Figure E21-4).

Step 13: Click **Add** three times to add three additional axles, and then enter the other three axle weights.

Step 14: Click **OK** to close the batch load panel, and then click OK to close the load panel.

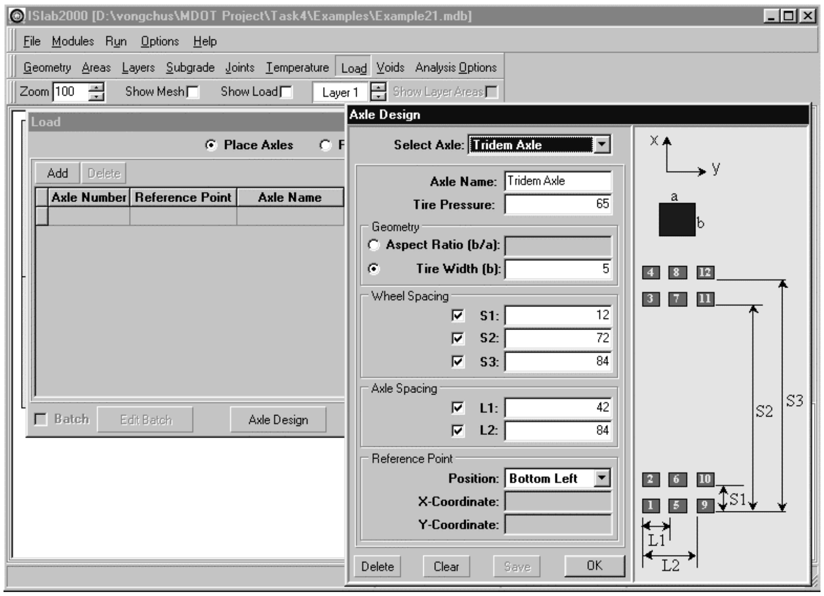


**Figure E21-2: Edit Inputs for the Load Module**

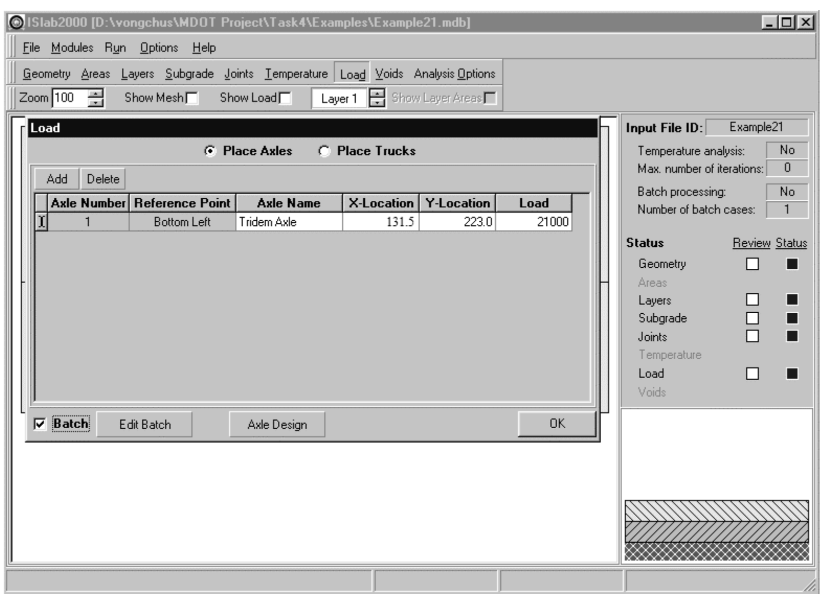


**Figure E21-3: Edit Inputs for the Load Module (continued)**

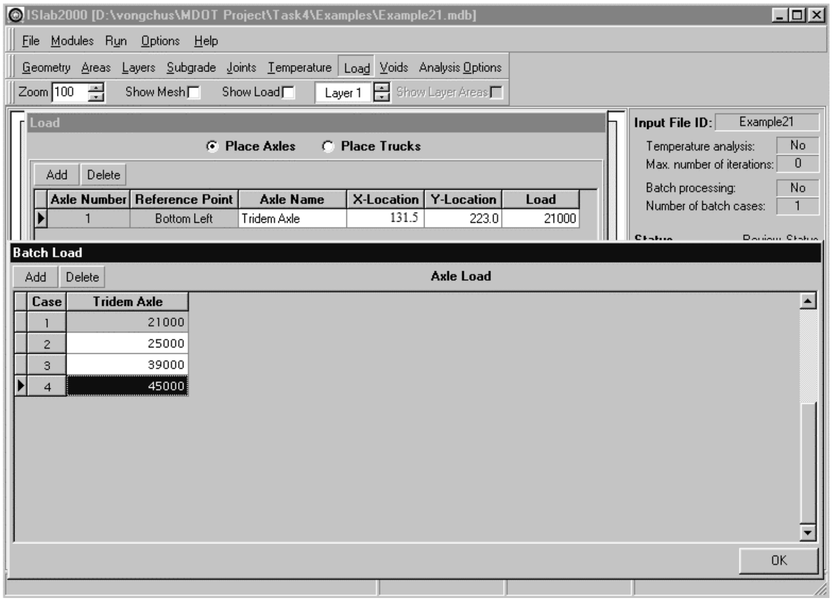


Figure E21-4: Edit Inputs for the Load Module (continued)

## Temperature Module

This module is not required for this problem.

## Analysis Options Module

Use this module from Example 4.

The main panel should display the pavement structure, loading condition, and meshing as shown in Figure E21-5.

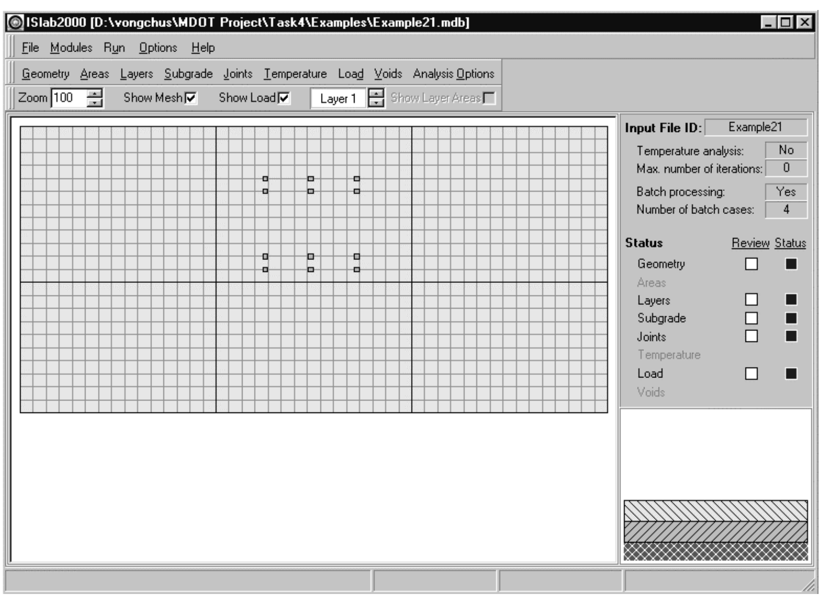


Figure E21-5: Main Panel After the Completion of Inputs

## *Analysis Results*

| Axle wt., kips | Stress at the bottom of the PCC, psi | |
|---|---|---|
| | Transverse | Longitudinal |
| 21 | 44.1 | 57.4 |
| 25 | 51.9 | 66.5 |
| 39 | 77.6 | 99.9 |
| 45 | 90.8 | 113.1 |

**Table E21-1: Analysis Results**

**NOTE**

Positive and negative values of stress signify tensile and compressive stresses and positive value of deflection indicates deflection in downward direction.

Stress and deflection contours from ISLAB2000 are also available in Figures E21-6 through E21-8. Figure E21-9 illustrates relationship between maximum stresses and axle weight. Figures E21-10 and E21-11 illustrate the comparison of the stresses between single, tandem, and tridem axle at the same level of loading.

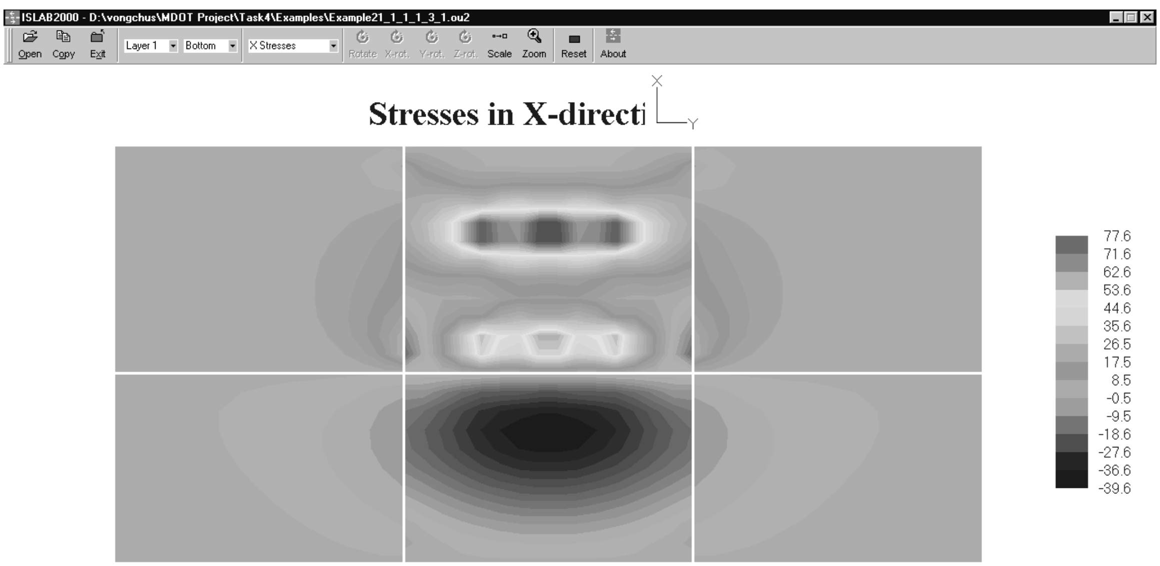


**Figure E21-6: Transverse Stress at the Bottom of the PCC Slab, 32-kips Axle Weight**

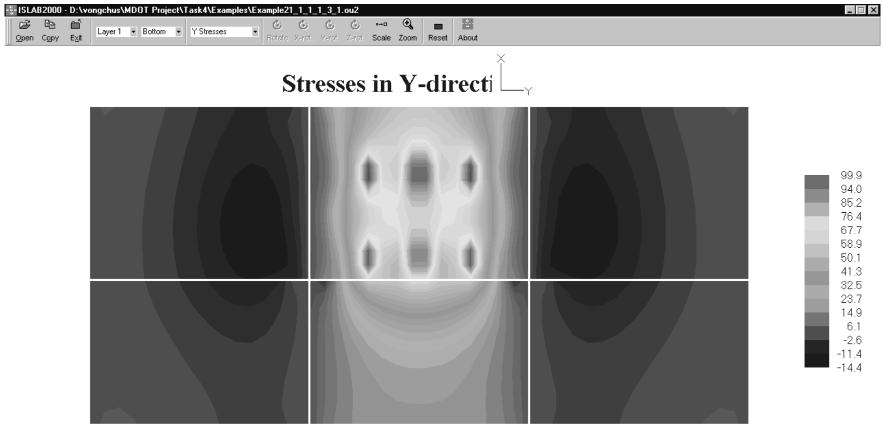


**Figure E21-7: Longitudinal Stress at the Bottom of the PCC From ISLAB2000, 32-kips Axle Weight**

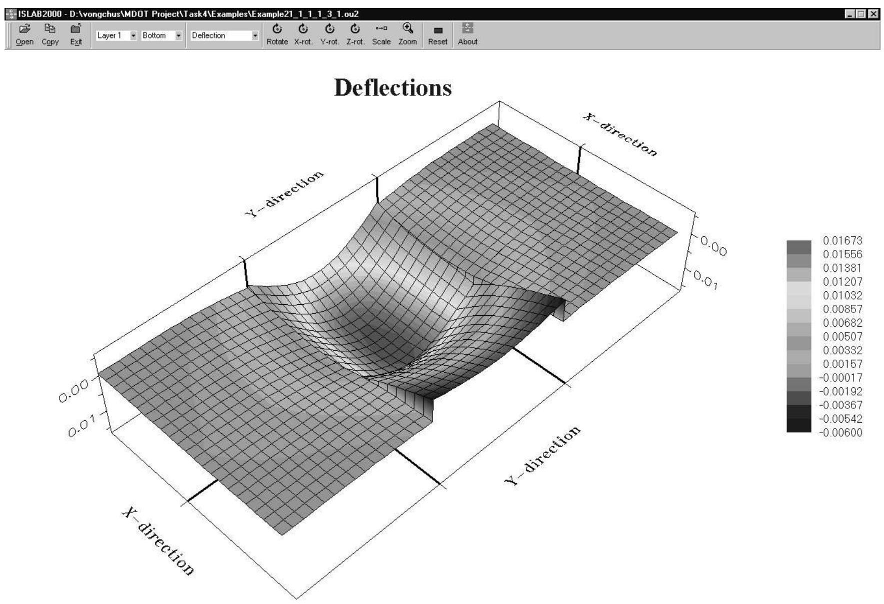


**Figure E21-8: Deflection of the PCC slab, 32-kips Axle Weight**

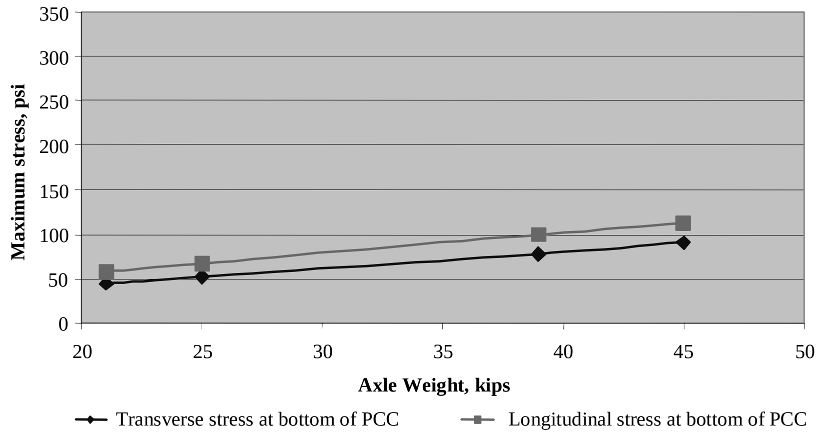


**Figure E21-9: Relationship Between Stresses and Axle Weight**

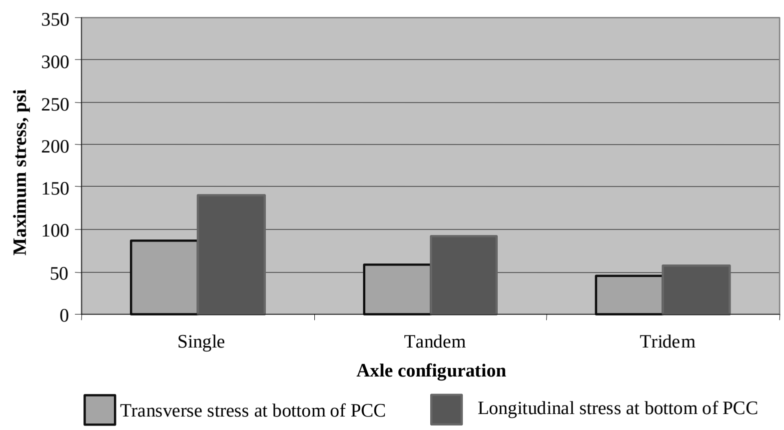


**Figure E21-10: Relationship Between Stresses and Axle Type, Axle Weight of 21 kips**

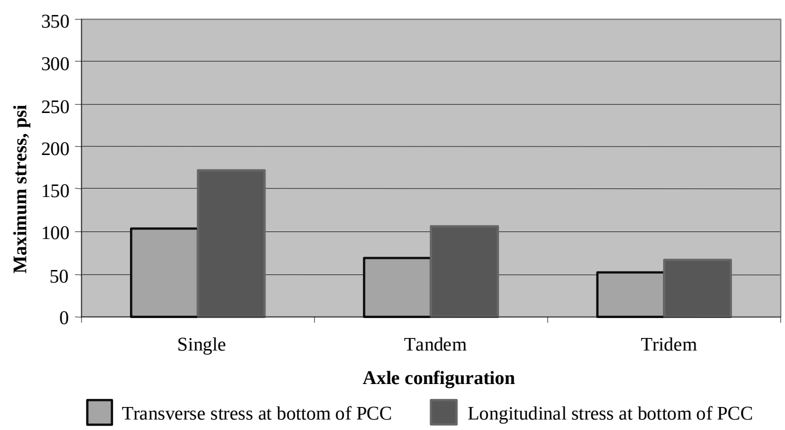


**Figure E21-11: Relationship Between Stresses and Axle Type, Axle Weight of 25 kips**

# Example 22:
# Single Axle Edge Loading with Various CTE Values

### Problem Statement

Repeat Example 8 but consider several PCC coefficient of thermal expansion, $\alpha_{pcc}$, of 3, 5, 7, 9x10$^{-6}$ in./in./$^{o}$F and at the same time, apply temperature differential, $\Delta$T, of +20 $^{o}$F. Then compare the results with the results from Example 9 by plotting a graph using the product $\alpha.\Delta T$ for X-axis.

### Given

| | | | |
|---|---|---|---|
| PCC coefficient of thermal expansion, $\alpha_{pcc}$ | = | 3, 5, 7, 9 x 10$^{-6}$ | in./in./$^{o}$F |
| Temperature differential, $\Delta$T | = | +20 | $^{o}$F. |

### Problem Illustration

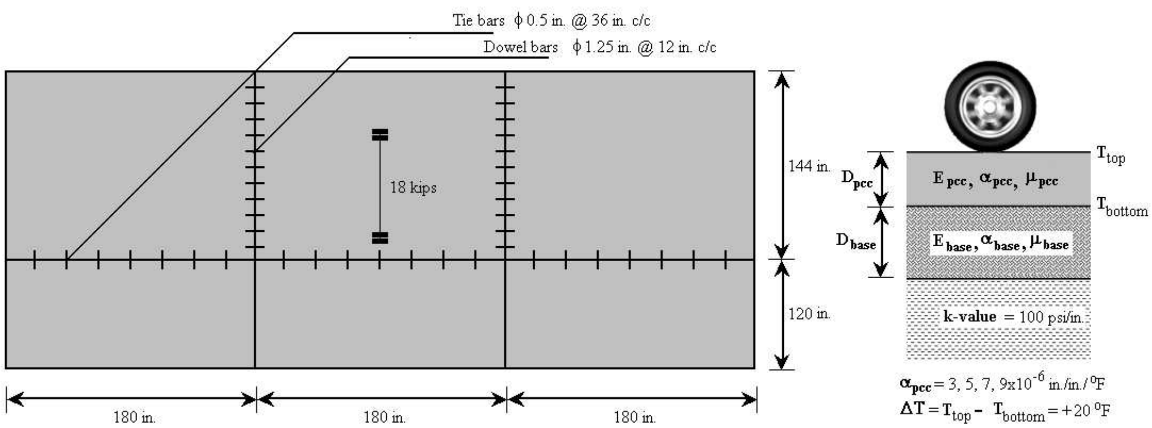


**Figure E22-1: Problem Illustration**

# Solution

### Geometry Module

Use this module from Example 8.

### Layers Module

Step 1: Follow steps 1 through 5 of this module in Example 14.

Step 2: Click **Insert** three times to add three additional cases, and then enter the PCC coefficient of thermal expansion as identified in the problem statement (see Figure E22-2).

Step 3: Click **OK** to close the layer 1 properties panel, and then click **OK** to close the layers panel.

### Subgrade Module

Use this module from Example 8.

### Joints Module

Use this module from Example 8.

### Load Module

Use this module from Example 8.

### Temperature Module

Use this module from Example 16.

### Analysis Options Module

Use this module from Example 4.

The main panel should display the pavement structure, loading condition, and meshing as shown in Example 8, Figure E8-12.

## *Analysis Results*

| $\alpha$, x$10^{-6}$ in./in./$^{o}$F | Stress at the bottom of the PCC, psi | |
|---|---|---|
| | Transverse | Longitudinal |
| 3 | 112.6 | 180.5 |
| 5 | 139.7 | 224.5 |
| 7 | 166.7 | 268.6 |
| 9 | 193.5 | 313.3 |

**Table E22-1: Analysis Results**

| $\alpha$, x$10^{-6}$ in./in./°F | ΔT, °F | $\alpha$.ΔT, x$10^{-6}$ | Stress at the bottom of the PCC, psi | |
|---|---|---|---|---|
| | | | Transverse | Longitudinal |
| From Example 9 | | | | |
| 5 | 0 | 0 | 72.1 | 114.5 |
| 5 | 10 | 50 | 105.9 | 169.5 |
| 5 | 20 | 100 | 139.7 | 224.5 |
| From Example 22 | | | | |
| 3 | 20 | 60 | 112.6 | 180.5 |
| 5 | 20 | 100 | 139.7 | 224.5 |
| 7 | 20 | 140 | 166.7 | 268.6 |
| 9 | 20 | 180 | 193.5 | 313.3 |

**Table E22-2: Comparison of Analysis Results**

**NOTE**

Positive and negative values of stress signify tensile and compressive stresses and positive value of deflection indicates deflection in downward direction.

Figure E22-3 illustrates relationship between maximum stresses and PCC coefficient of thermal expansion. Figure E22-4 illustrates relationship between maximum stresses and the product $\alpha$.ΔT from this example and Example 9.

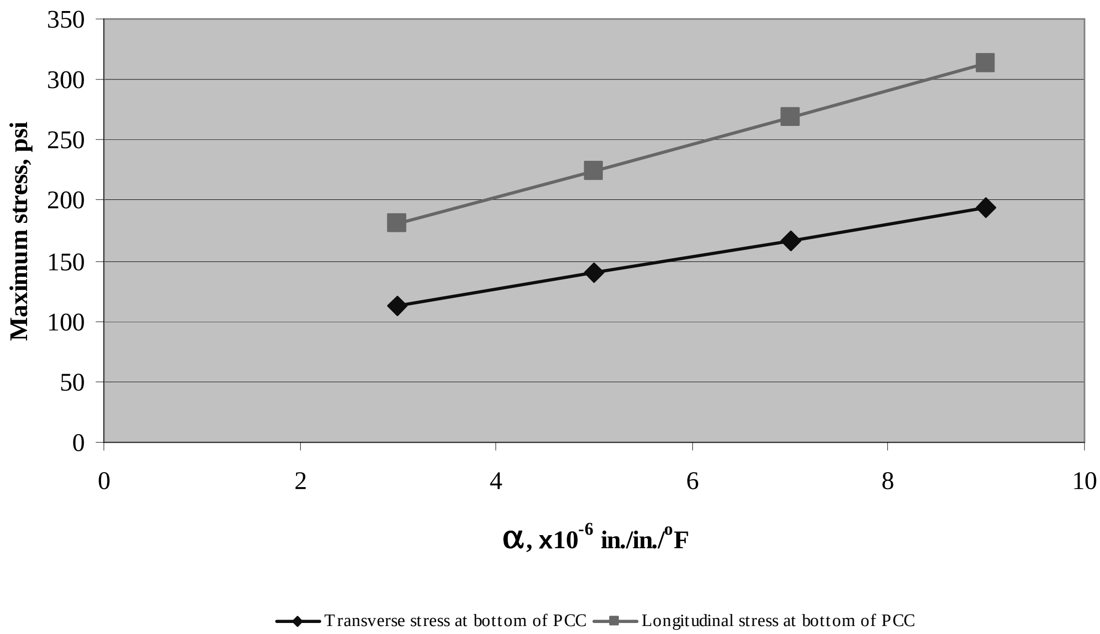


**Figure E22-3: Relationship Between Stresses and PCC Coefficient of Thermal Expansion**

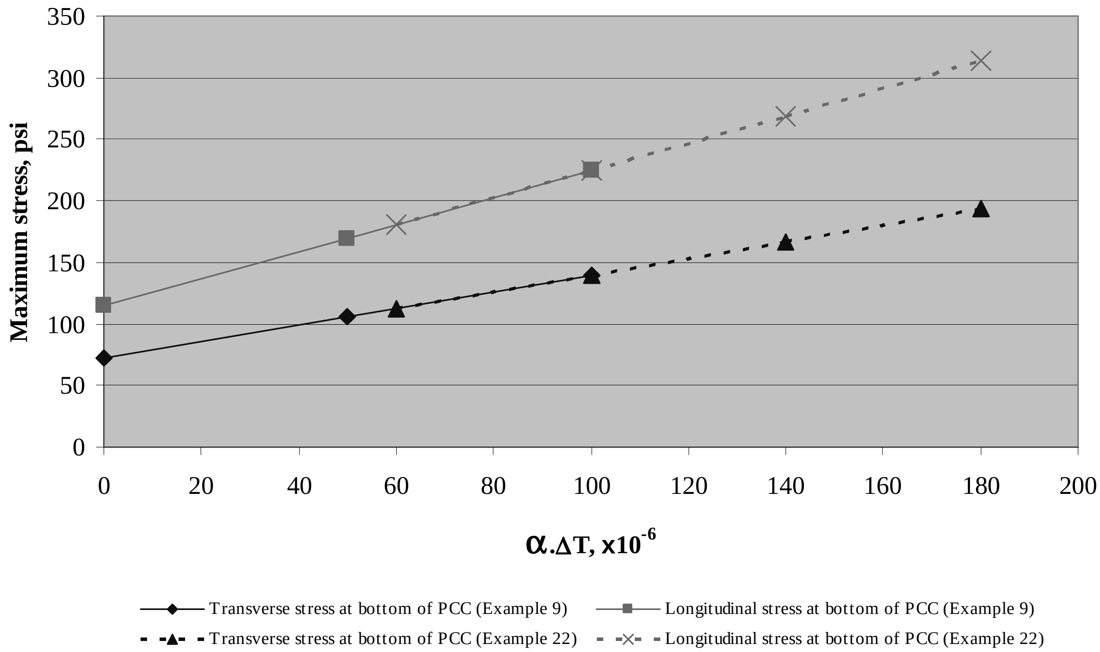


**Figure E22-4: Comparison of the Results from Example 9 and Example 22**

# Example 23:
# Single Axle Wander

### Problem Statement

Analyze three pavement systems: 1) 12-ft lane width with tied PCC shoulder (Example 8), 2) 12-ft lane width with untied AC shoulder, 3) 12-ft lane width with untied AC shoulder. Also consider lateral wanders of axle loading from shoulder toward the lane center: -12, -6, 0, 6, 12, 18, 30, 60 in. (distance from shoulder to outer edge of wheel load)

### Given

Lateral support condition = PCC shoulder, AC shoulder, widened lane

Lateral wanders = -12, -6, 0, 6, 12, 18, 30, 60 in.

### Problem Illustration

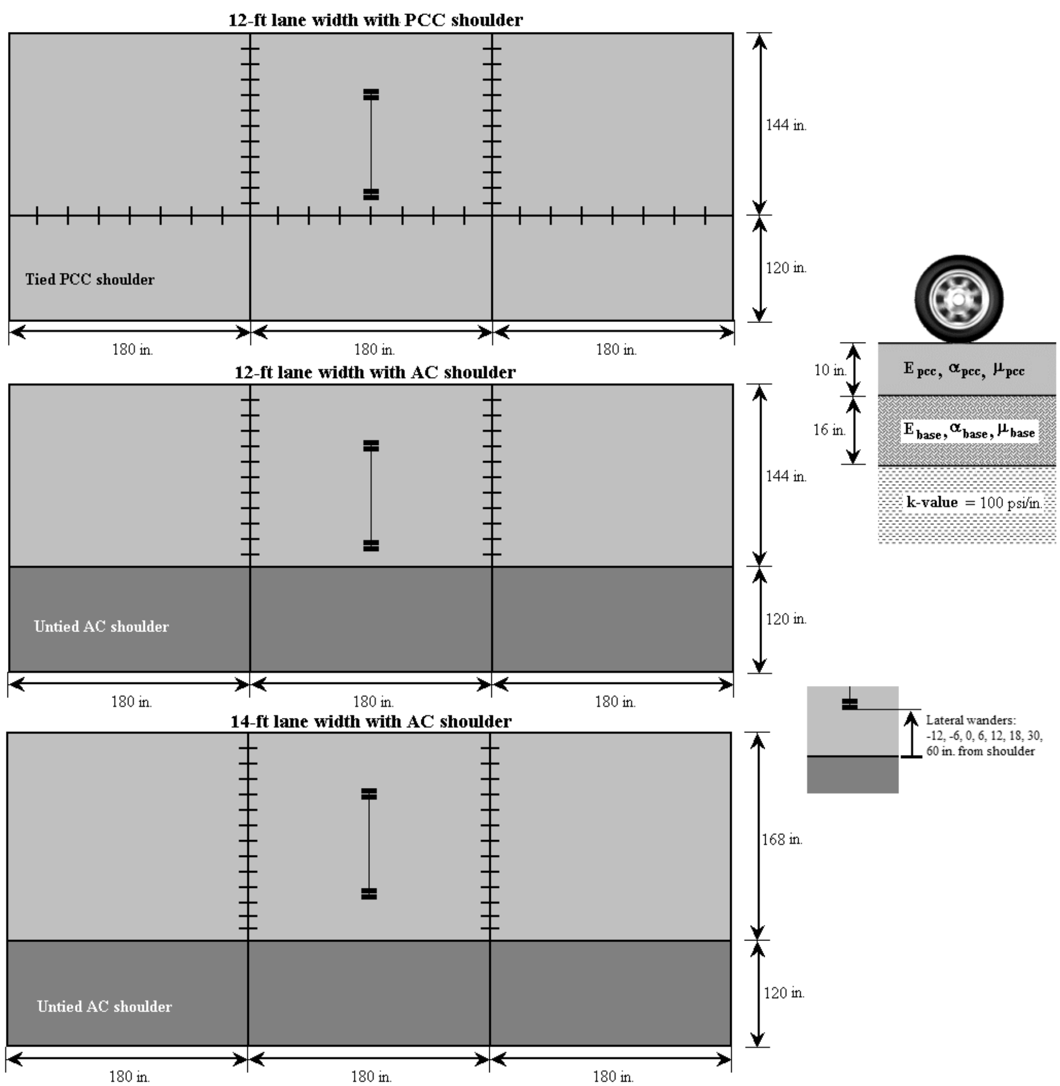


**Figure E23-1: Problem Illustration**

# Solution

### *Part 1: 12-ft lane width with tied PCC shoulder*

#### Geometry Module

Use this module from Example 8.

#### Layers Module

Use this module from Example 8.

#### Subgrade Module

Use this module from Example 8.

#### Joints Module

Use this module from Example 8.

#### Load Module

(see Figure E23-2)

Step 1: Follow steps 1 through 9 of this module in Example 8.

Step 2: Enter X-location and Y-location information to locate the wheel load. X-location and Y-location for an edge loading condition can be computed as shown below:

$$X - location = Shoulder\ width + + Lateral\ \ placement$$

$$= 120 + + Lateral\ \ placement$$

X-location inputs for all eleven lateral placements considered in this problem are summarized in Table E23-1.

$$Y - location = Joint\ spacing + \frac{Joint\ spacing}{2} - \frac{wheel\ load\ length}{2}.$$

$$= 180 + \frac{180}{2} - \frac{10}{2} = 265\ in$$

Step 3: Type the load for the single axle (18,000 lbs for this example).

Step 4: Click **OK** to close the load panel.

#### Temperature Module

This module is not required for this problem.

#### Analysis Options Module

This module is not required for this problem.

At this stage, all the steps for inputs are completed for the first of 11 lateral placements. If all the inputs are correct, the main panel should display the pavement structure, loading condition, and meshing as shown in Figure E23-3. For the next lateral placement, apply the X-location as the calculated value to be used shown in Table E23-1.

| Lateral placement (in.) | X-Location input |
|---|---|
| -12 | 108 |
| -6 | 114 |
| 0 | 120 |
| 6 | 126 |
| 12 | 132 |
| 18 | 138 |
| 30 | 150 |
| 48 | 168 |

**Table E23-1: X-location Input for each Lateral Placement**

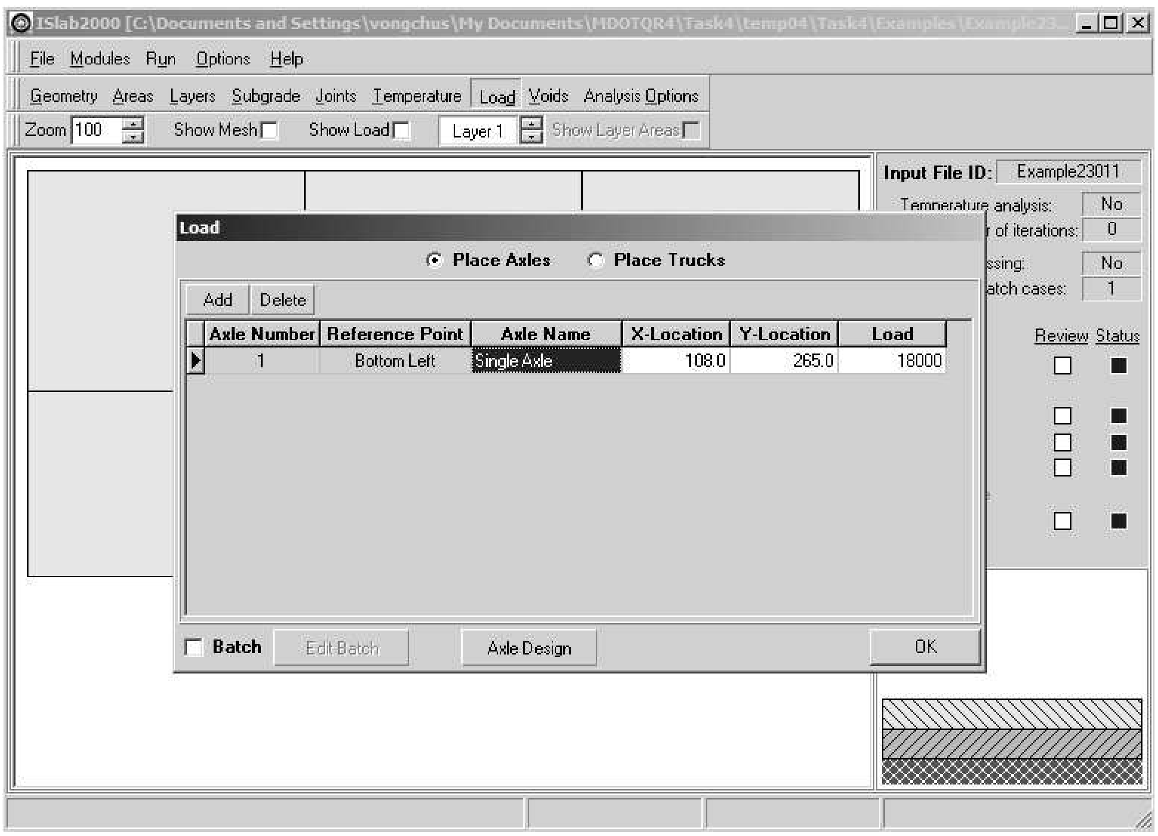


**Figure E23-2: Edit Inputs for the Load Module (12-ft lane width)**

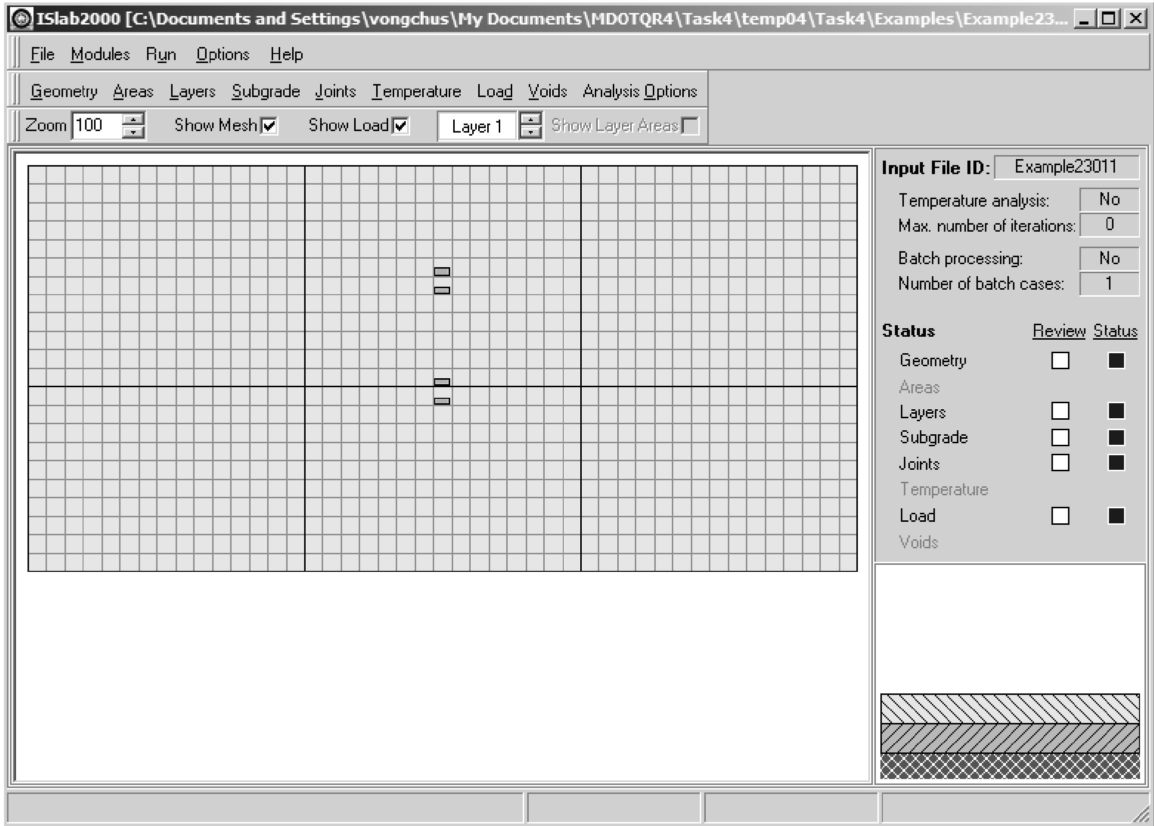


**Figure E23-3: Main Panel After the Completion of Inputs (12-ft lane width with PCC shoulder)**

### *Part 2: 12-ft lane width with untied AC shoulder*

### Geometry Module

Use this module from Example 8.

### Area Module

(see Figure E23-4)

Step 1: Click **Area** to open the area panel, click **Add** to add an area, and then enter **Shoulder** in the **Area Name** field.

Step 2: Select **Coordinates** in the **Coordinate Type** box.

Step 3: Enter the coordinate for the shoulder area as identified in the problem illustration.

Step 4: Click **OK** to close the area definition panel.

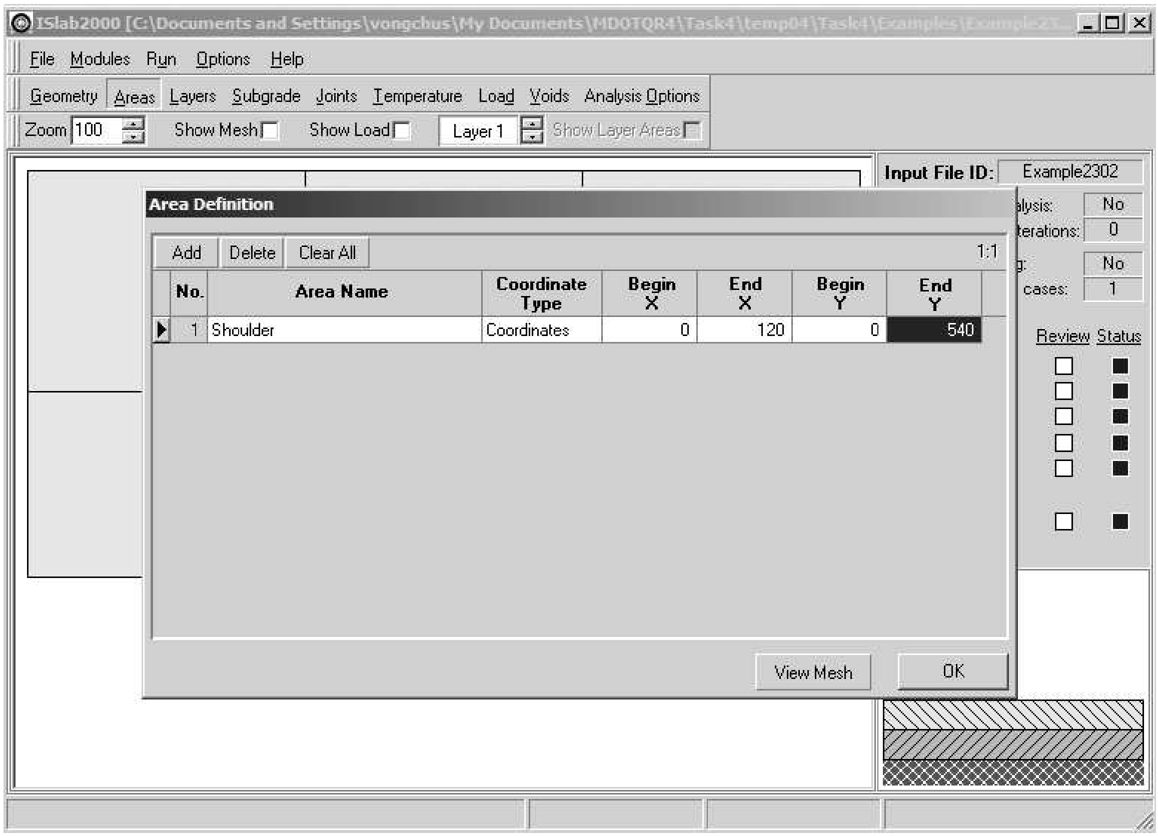


Figure E23-4: Edit Inputs for the Area Module

## Layers Module

(see Figures E23-5 and E23-6)

Step 1: Follow steps 1 through 4 of this module in Example 8.

Step 2: On Layer 1, select **Exception**, and then click **Edit Exception** to open the exception properties for layer 1 panel.

Step 3: Click **Insert** to add an additional area, and then select **Shoulder** in the **Area Name** box.

Step 4: Enter the material properties for AC shoulder as shown in Figure E23-6.

Step 5: Click **OK** to close the layers panel.

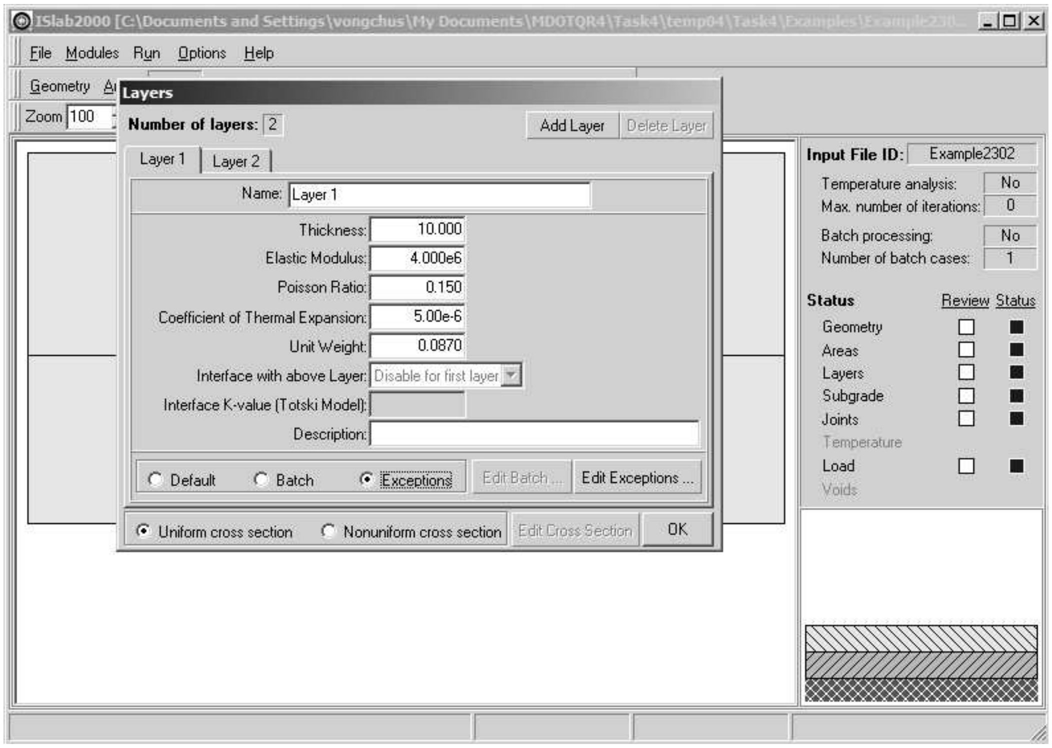


Figure E23-5: Edit Inputs for the Layers Module

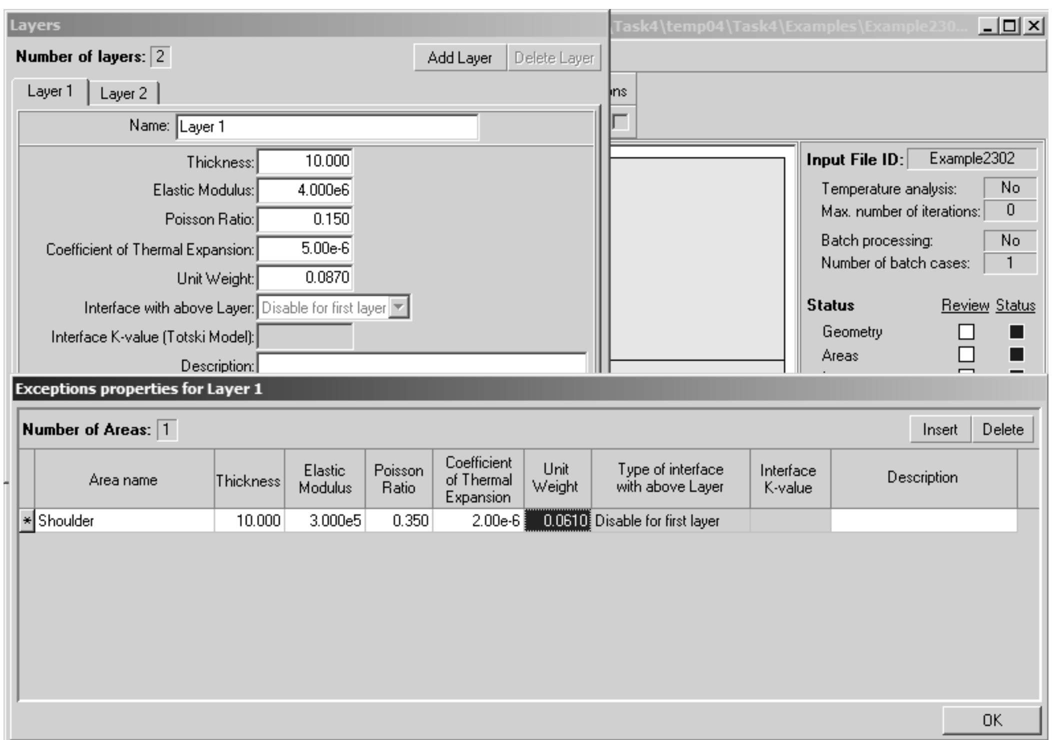


Figure E23-6: Edit Inputs for the Layers Module (continued)

### Subgrade Module

Use this module from Example 8.

### Joints Module

(see Figure E23-7)

Step 1: Click **Joints** to open the joints panel.

Step 2: In the **Joints in x-direction** section, select **Specify joint parameters**, select **AGG Interlock** in the **Joint type** field, and then enter the aggregate factor in the **AGG factor** field (assumed 1,000 psi.)

Step 3: Follow steps 3 through 5 of this module in Example 8.

### Load Module

Use this module from 12-ft lane width with PCC shoulder in this problem.

### Temperature Module

This module is not required for this problem.

### Analysis Options Module

This module is not required for this problem.

At this stage, all the steps for inputs are completed for the first of 11 lateral placements. If all the inputs are correct, the main panel should display the pavement structure, loading condition, and meshing as shown in Figure E23-8. For the next lateral placement, apply the X-location as the calculated value to be used shown in Table E23-1.

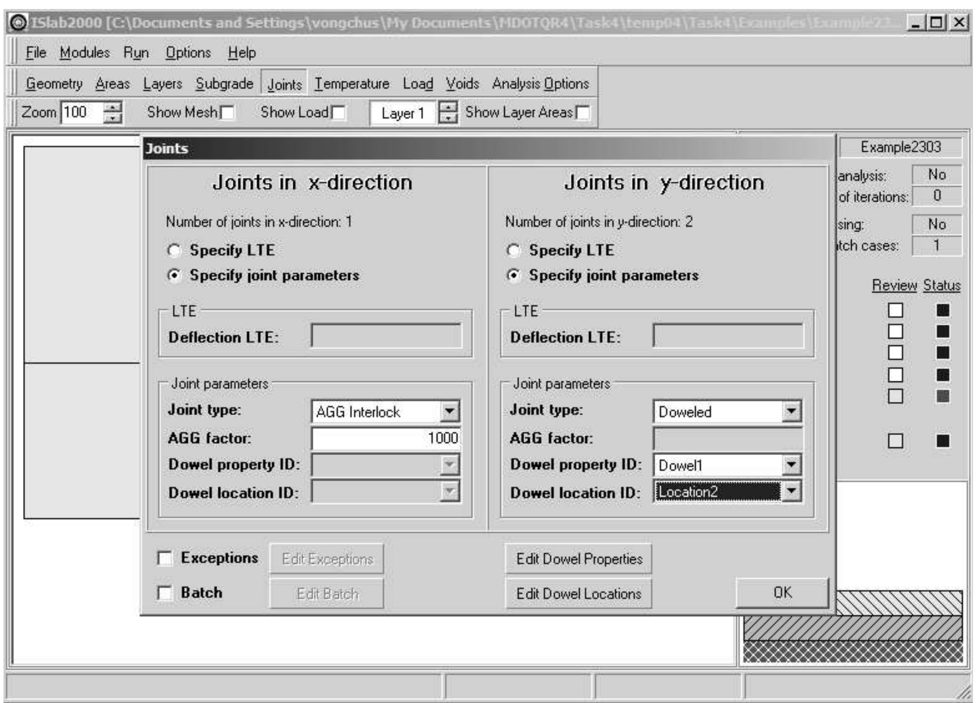


**Figure E23-7: Edit Inputs for the Joints Module (14-ft lane width with AC shoulder)**

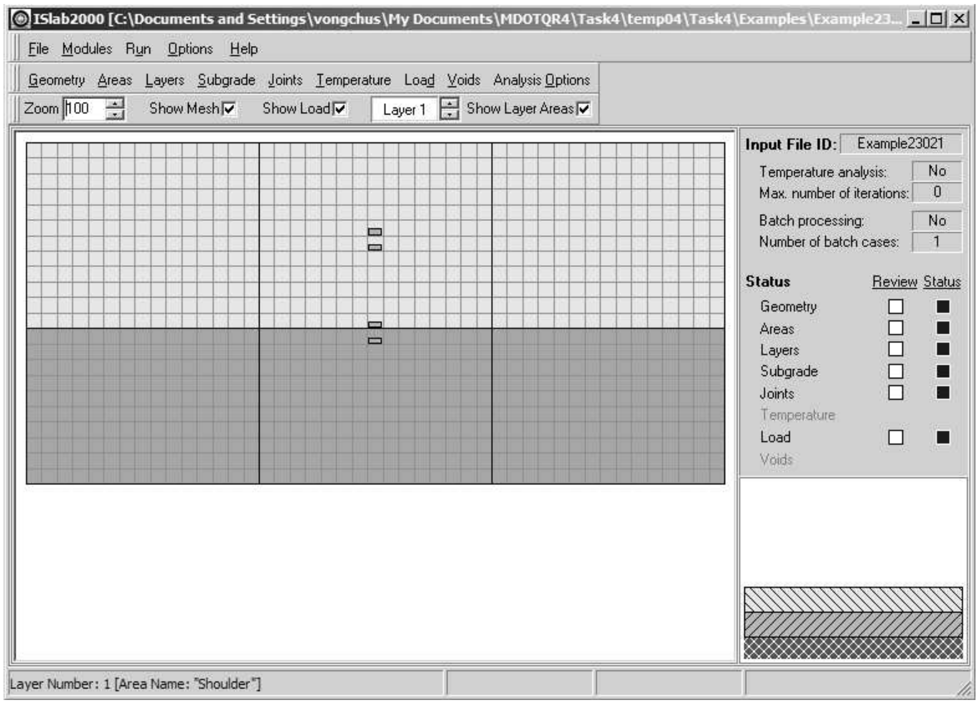


**Figure E23-8: Main Panel After the Completion of Inputs (12-ft lane width with AC shoulder)**

### *Part 3: 14-ft lane width with untied AC shoulder*

### Geometry module

(see Figure E23-9)

Step 1: Click **Geometry** to open the geometry panel.

Step 2: On the geometry panel, click **Insert** two times on the **X-direction** side to add additional slabs, and then enter the shoulder width (120 inches) and the lane width (168 inches).

Step 3: Follow steps 3 through 5 of this module in Example 8.

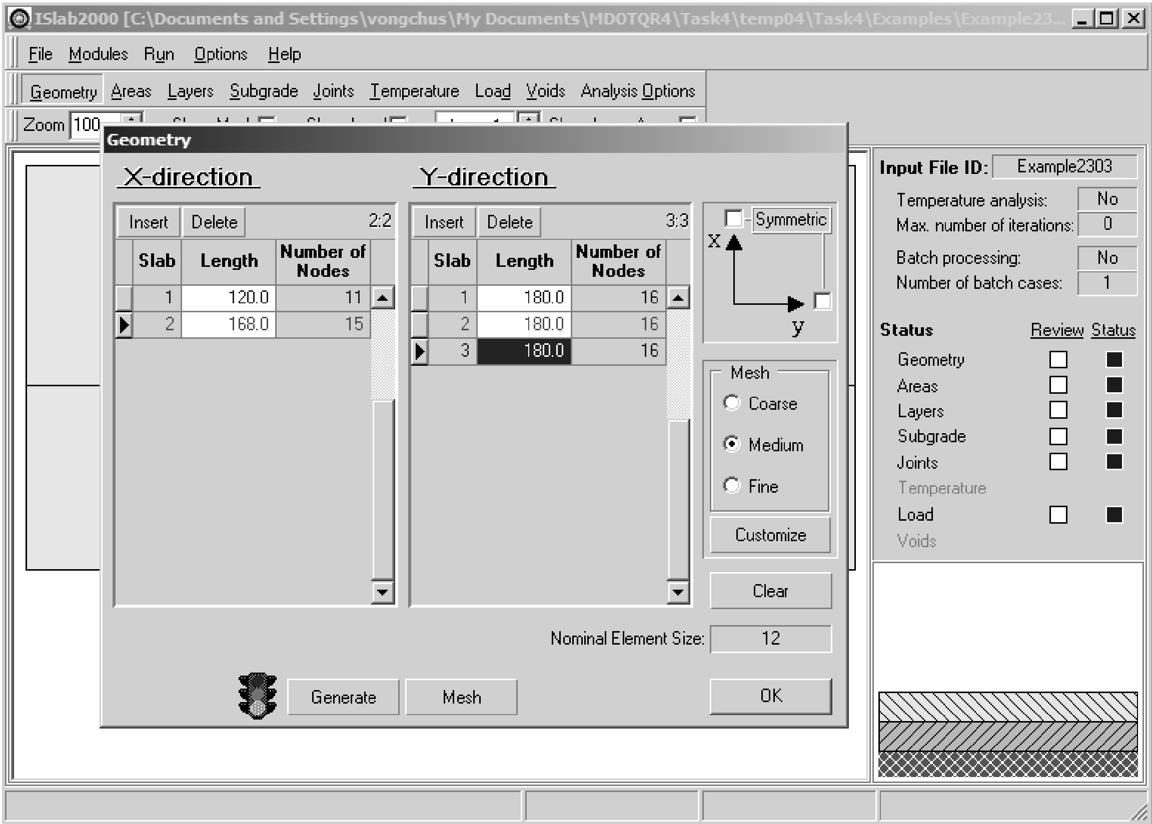


**Figure E23-9: Edit Inputs for the Geometry Module**

## Area Module

Use this module from 12-ft lane width with ACC shoulder in this problem.

## Layers Module

Use this module from 12-ft lane width with ACC shoulder in this problem.

## Subgrade Module

Use this module from Example 8.

## Joints Module

Use this module from 12-ft lane width with ACC shoulder in this problem.

## Load Module

(see Figure E23-10)

Step 1: Follow steps 1 through 9 of this module in Example 8.

Step 2: Enter X-location and Y-location information to locate the wheel load. X-location and Y-location for an edge loading condition can be computed as shown below:

$$X - location = Shoulder\ width + Lateral\ \ placement$$

$$= 120 + Lateral\ \ placement$$

X-location inputs for all eleven lateral placements considered in this problem are also summarized in Table E23-1.

$$Y - location = Joint\ spacing + \frac{Joint\ spacing}{2} - \frac{wheel\ load\ length}{2}.$$

$$= 180 + \frac{180}{2} - \frac{10}{2} = 265\ in$$

Step 3: Enter the load for the single axle (18,000 lbs for this example).

Step 4: Click **OK** to close the load panel.

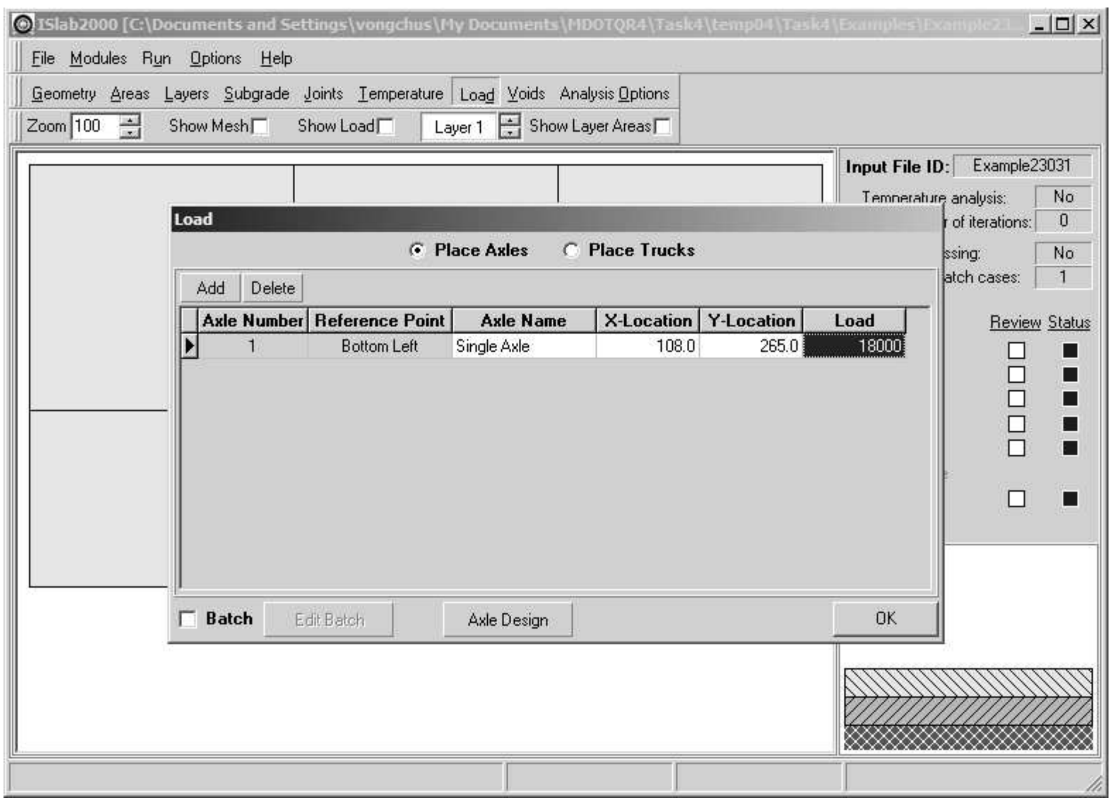


**Figure E23-10: Edit Inputs for the Load Module**

### Temperature Module

This module is not required for this problem.

### Analysis Options Module

This module is not required for this problem.

At this stage, all the steps for inputs are completed for the first of 11 lateral placements. If all the inputs are correct, the main panel should display the pavement structure, loading condition, and meshing as shown in Figure E23-11. For the next lateral placement, apply the X-location as the calculated value to be used shown in Table E23-1.

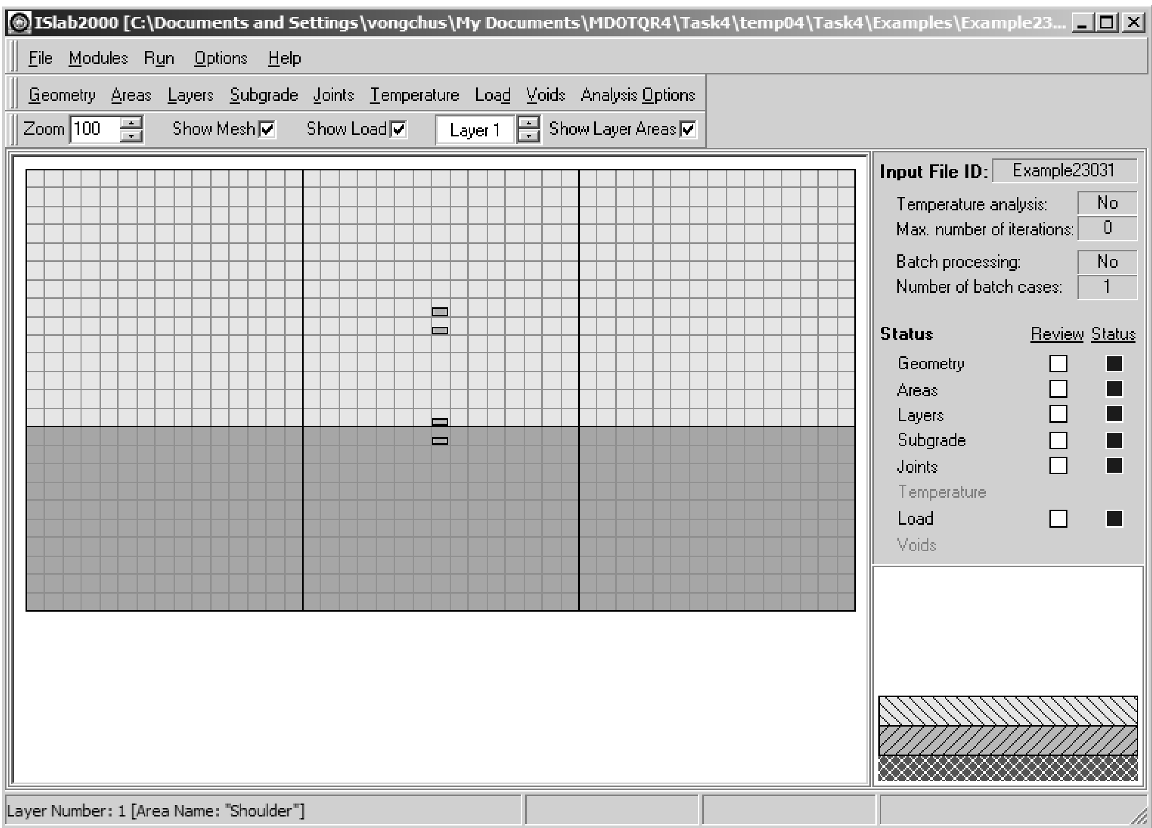


**Figure E23-11: Main Panel After the Completion of Inputs (14-ft lane width with AC shoulder)**

## *Analysis Results*

Table E23-2 summarizes maximum for all lateral placements and lateral support conditions. The relationship between maximum stress and lateral placement for each lateral support condition is illustrated in Figures E23-12 and E23-13 for transverse and longitudinal stress at the bottom of the PCC slab respectively.

**NOTE**
Positive and negative values of stress signify tensile and compressive stresses and positive value of deflection indicates deflection in downward direction.

| Lateral placement (in.) | Lateral support condition | | |
|---|---|---|---|
| | 12-ft lane width with PCC shoulder | 12-ft lane width with AC shoulder | 14-ft lane width with AC shoulder |
| Transverse stress at bottom of PCC | | | |
| -12 | 70.6 | 65.9 | 65.2 |
| -6 | 71.4 | 68.3 | 68.6 |
| 0 | 73.9 | 61.8 | 62.0 |
| 6 | 75.3 | 64.8 | 66.9 |
| 12 | 74.6 | 67.9 | 72.4 |
| 18 | 73.4 | 67.7 | 74.9 |
| 30 | 77.5 | 67.8 | 76.8 |
| 48 | 65.2 | 61.4 | 76.3 |
| Longitudinal stress at bottom of PCC | | | |
| -12 | 122.0 | 155.4 | 154.6 |
| -6 | 119.6 | 131.1 | 130.2 |
| 0 | 115.5 | 206.7 | 205.6 |
| 6 | 115.0 | 165.7 | 164.7 |
| 12 | 115.5 | 143.5 | 142.3 |
| 18 | 119.7 | 135.3 | 133.8 |
| 30 | 127.2 | 130.1 | 123.1 |
| 48 | 165.8 | 167.2 | 123.6 |

**Table E23-2: Analysis Results**

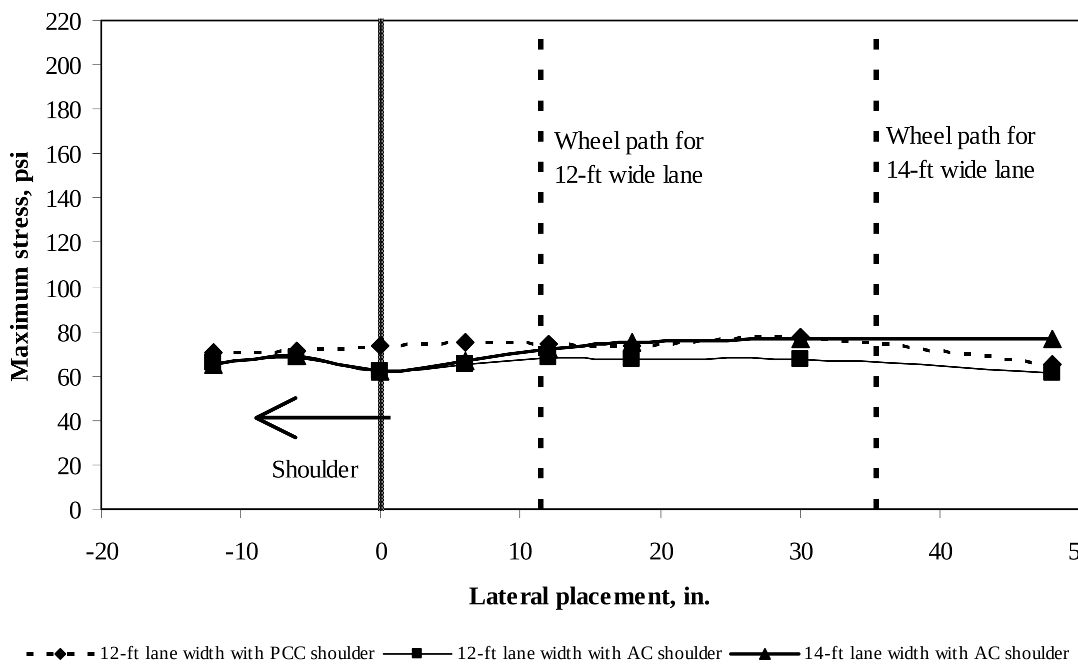


**Figure E23-12: Relationship between transverse stress at the bottom of the PCC slab and lateral placement for each lateral support condition**

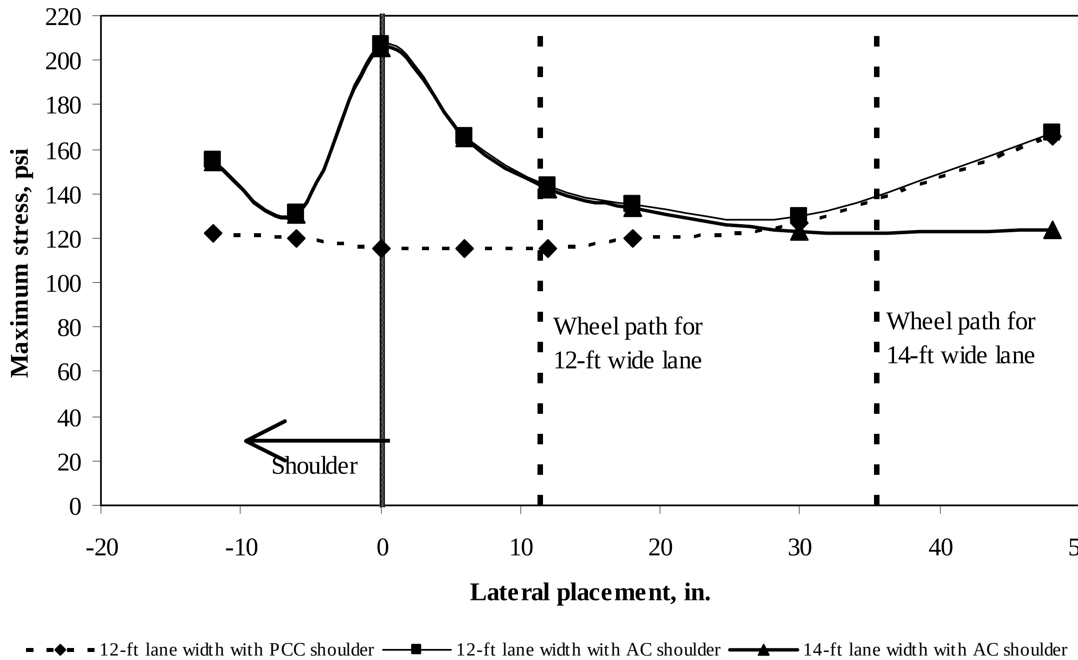


**Figure E23-13: Relationship between longitudinal stress at the bottom of the PCC slab and lateral placement for each lateral support condition**

# Example 24:
# Single Axle with Various Joint Spacing

### Problem Statement

Repeat Example 8 but consider joint spacing of 315 and 492 in. Then, compare the results with the results from Example 8.

### Given

| | | | |
|---|---|---|---|
| Joint spacing | = | 315, 492 | in. |

### Problem Illustration

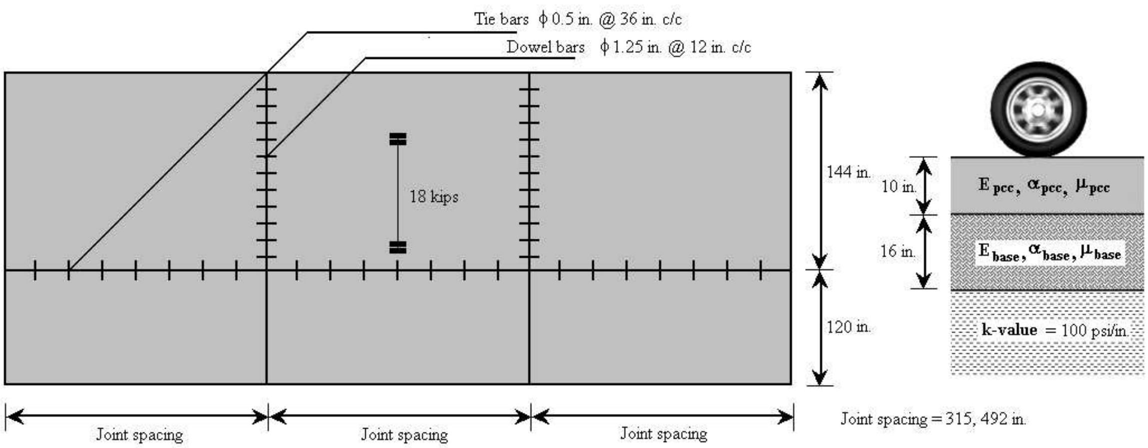


**Figure E24-1: Problem Illustration**

# Solution

### *Part 1: 315-in. joint spacing*

### Geometry Module

(see Figure E24-2)

Step 1: Follow steps 1 and 2 of this module in Example 8.

Step 2: Click **Insert** three times on the **Y-direction** side to add additional slabs, and then type the joint spacing (315 inches for this example).

Step 3: Follow steps 4 and 5 of this module in Example 8.

### Layers Module

Use this module from Example 8.

### Subgrade Module

Use this module from Example 8.

### Joints Module

Use this module from Example 8.

### Load Module

(see Figure E24-3)

Step 1: Follow steps 1 through 9 of this module in Example 8.

Step2: Enter X-location and Y-location to locate the wheel load. X-location and Y-location for edge loading condition can be computed as shown below:

$$X - location = Shoulder\ width + Distance\ dual\ wheel\ center\ to\ shoulder$$
$$- Distance\ dual\ wheel\ center\ to\ reference\ point$$

$$= 120 + 20 - \left(\frac{5}{2} + \frac{12}{2}\right) = 131.5\ in$$

$$Y - location = Joint\ spacing + \frac{Joint\ spacing}{2} - \frac{wheel\ load\ length}{2}.$$

$$= 315 + \frac{315}{2} - \frac{10}{2} = 467.5\ in$$

Step 3: Follow steps 11 and 12 of this module of Example 8.

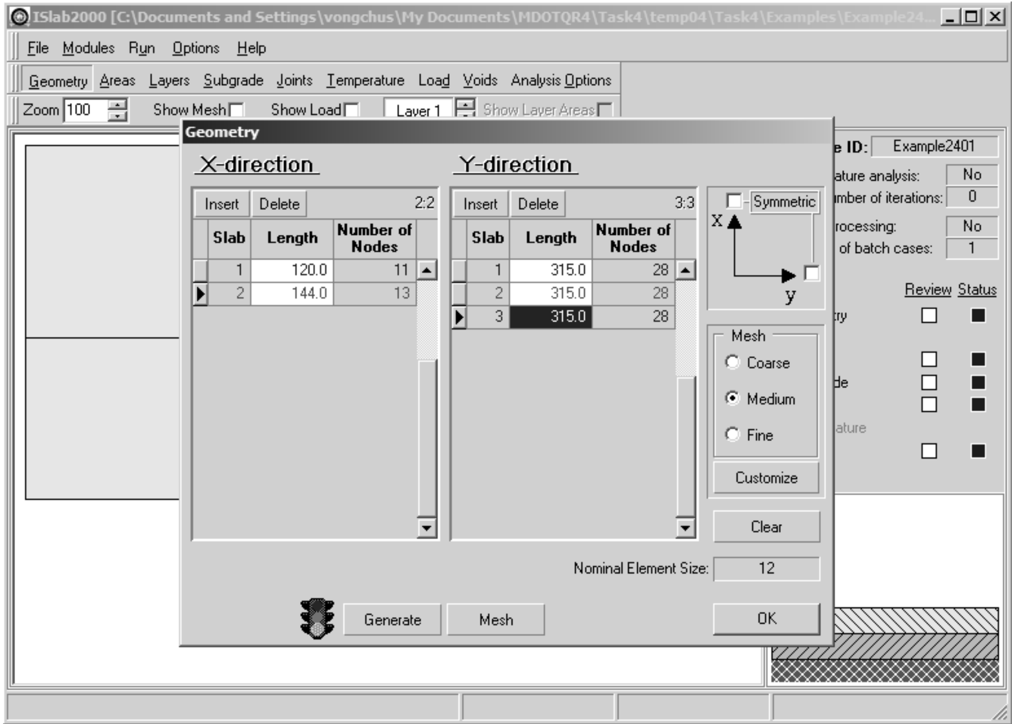

Figure E24-2: Edit Inputs for the Geometry Module

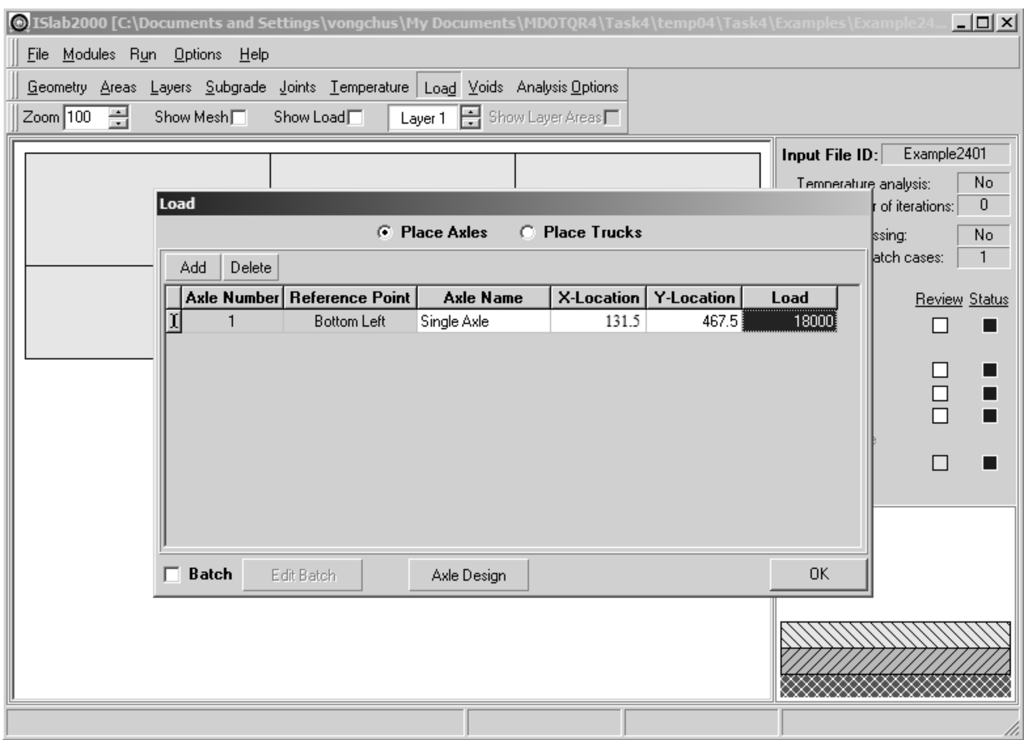

Figure E24-3: Edit Inputs for the Load Module

### Temperature Module

This module is not required for this problem.

### Analysis Options Module

This module is not required for this problem.

The main panel should display the pavement structure, loading condition, and meshing as shown in Figure E24-4.

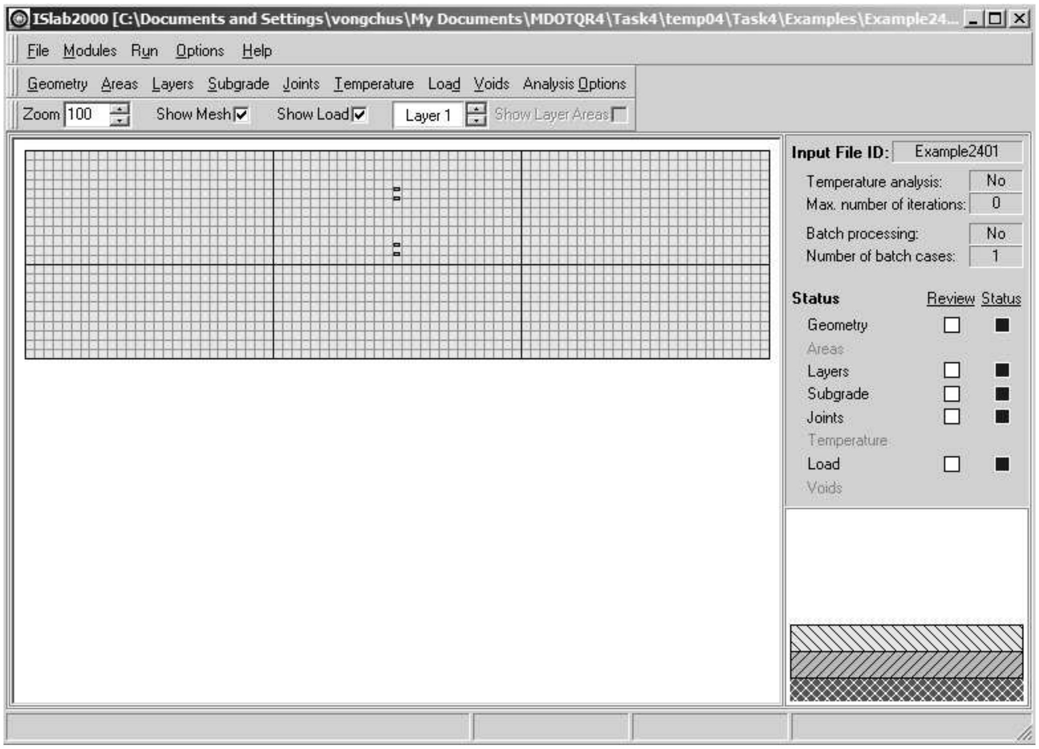


**Figure E24-4: Main Panel After the Completion of Inputs (315-in. joint spacing)**

### *Part 2: 492-in. joint spacing*

### Geometry Module

(see Figure E24-5)

Step 1: Follow steps 1 and 2 of this module in Example 8.

Step 2: Click **Insert** three times on the **Y-direction** side to add three additional slabs, and then enter the joint spacing (492 inches for this example).

Step 3: Follow steps 4 and 5 of this module in Example 8.

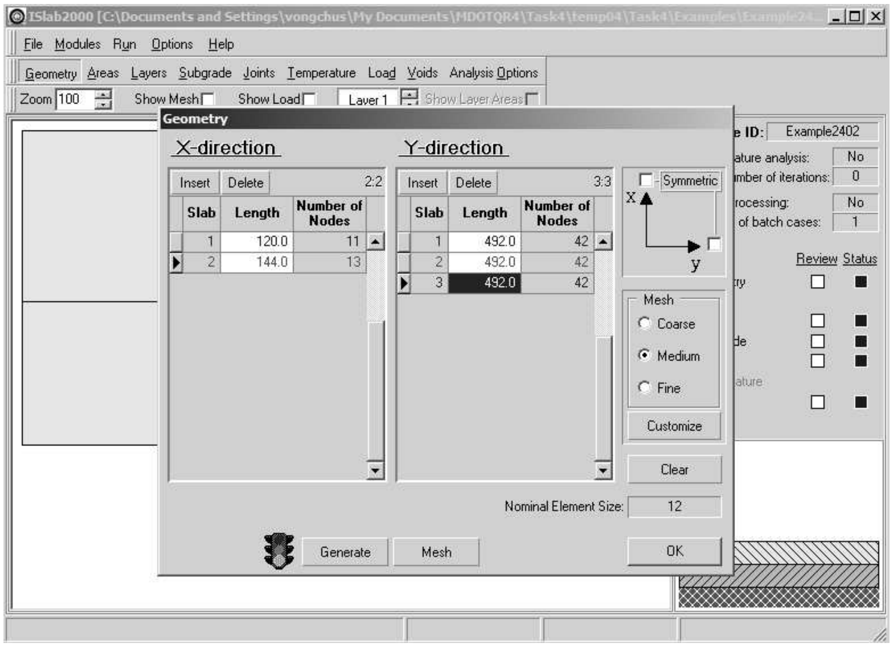


**Figure E24-5: Edit Inputs for the Geometry Module**

## Layers Module

Use this module from Example 8.

## Subgrade Module

Use this module from Example 8.

## Joints Module

Use this module from Example 8.

## Load Module

(see Figure E24-6)

Step 1: Follow steps 1 through 9 of this module in Example 8.

Step2: Type X-location and Y-location to locate the wheel load. X-location and Y-location for edge loading condition can be computed as shown below:

$$X-location = Shoulder\ width + Distance\ dual\ wheel\ center\ to\ shoulder - Distance\ dual\ wheel\ center\ to\ reference\ point$$

$$= 120 + 20 - \left(\frac{5}{2} + \frac{12}{2}\right) = 131.5\ in$$

$$Y-location = Joint\ spacing + \frac{Joint\ spacing}{2} - \frac{wheel\ load\ length}{2}.$$

$$= 315 + \frac{315}{2} - \frac{10}{2} = 467.5\ in$$

Step 3: Follow steps 11 and 12 of this module in Example 8.

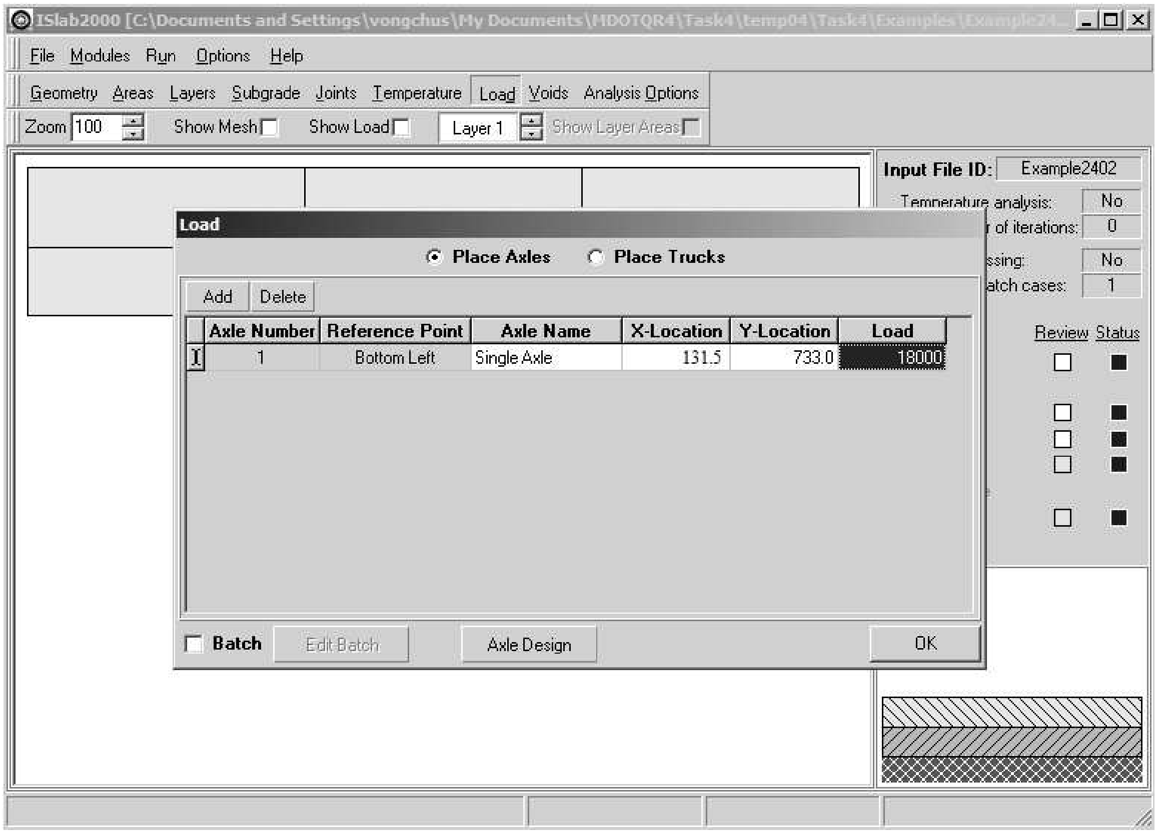


**Figure E24-6: Edit Inputs for the Load Module**

### Temperature Module

This module is not required for this problem.

### Analysis Options Module

This module is not required for this problem.

The main panel should display the pavement structure, loading condition, and meshing as shown in Figure E24-7.

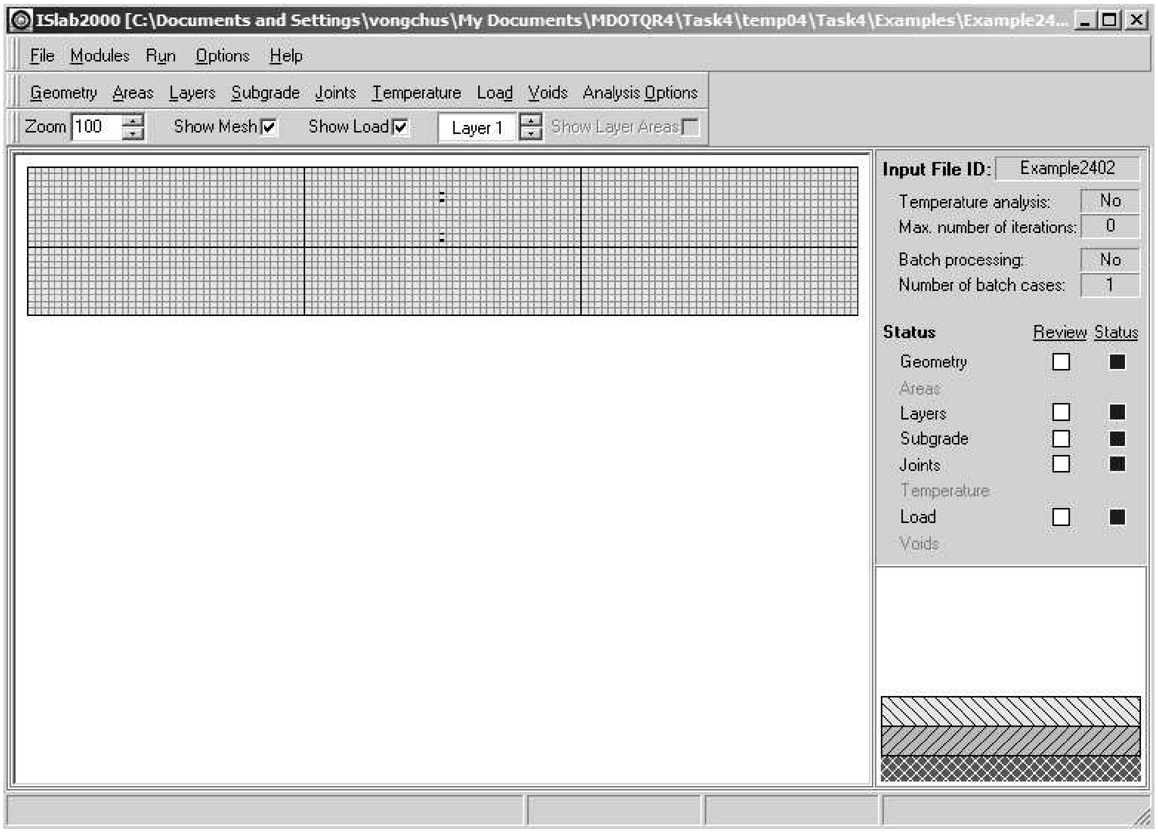


**Figure E24-7: Main Panel After the Completion of Inputs (492-in. joint spacing)**

## *Analysis Results*

| Joint spacing, in. | Stress at the bottom of the PCC, psi | |
|---|---|---|
| | Transverse | Longitudinal |
| 180 | 72.1 | 114.5 |
| 315 | 72.1 | 107.2 |
| 492 | 72.1 | 106.7 |

**Table E24-1: Analysis Results**

**NOTE**
Positive and negative values of stress signify tensile and compressive stresses and positive value of deflection indicates deflection in downward direction.

Stress and deflection contours from ISLAB2000 are also available in Figures E24-8 through E24-13. Figure E24-14 illustrates relationship between maximum stresses and joint spacing.

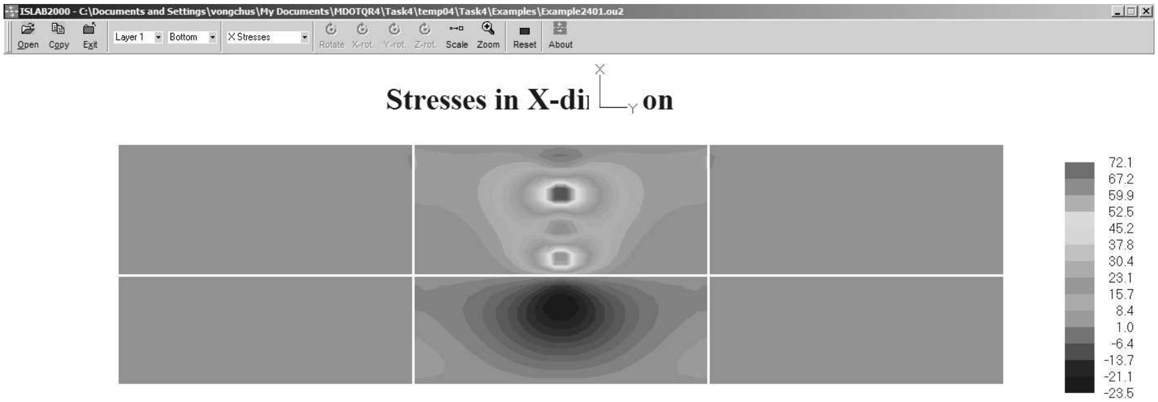


**Figure E24-8: Transverse Stress at the Bottom of the PCC Slab (315-ft joint spacing)**

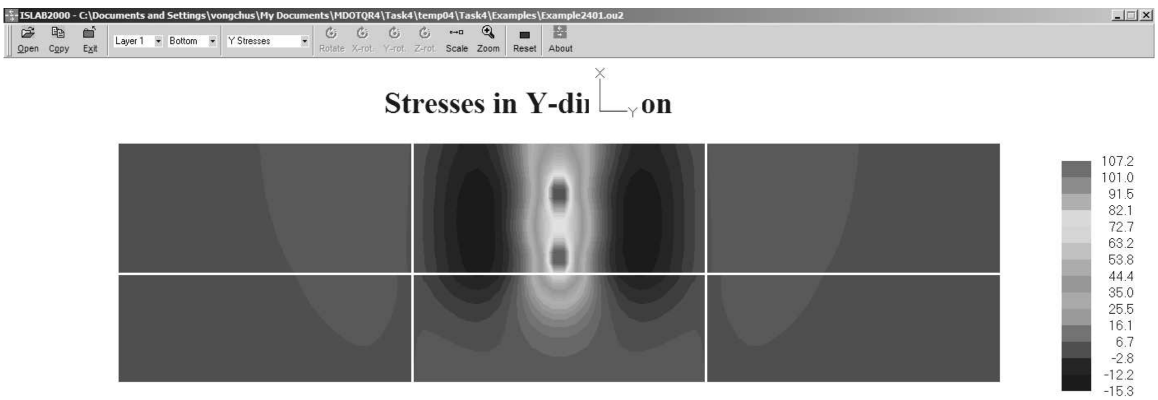


**Figure E24-9: Longitudinal Stress at the Bottom of the PCC Slab (315-ft joint spacing)**

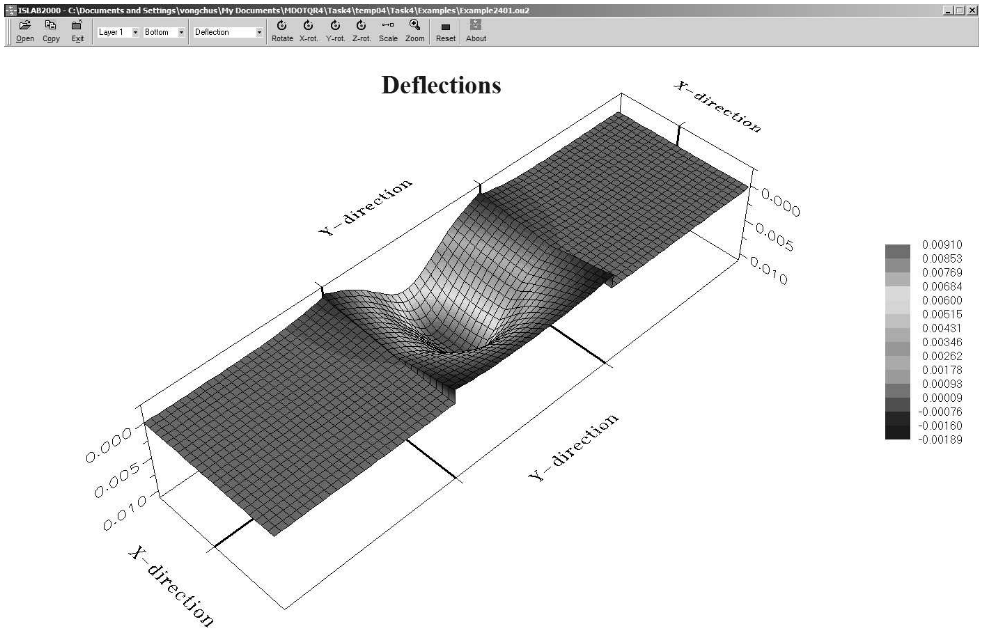


**Figure E24-10: Deflection of the PCC Slab (315-ft joint spacing)**

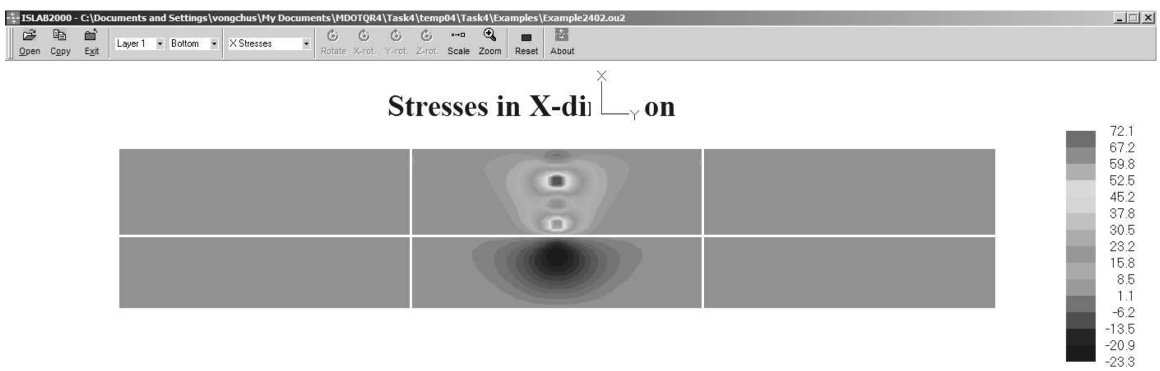


**Figure E24-11: Transverse Stress at the Bottom of the PCC Slab (492-ft joint spacing)**

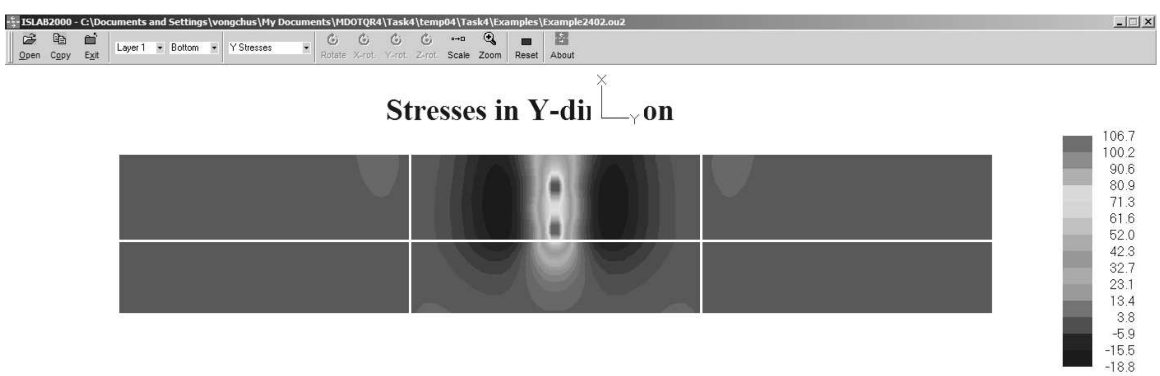


**Figure E24-12: Longitudinal Stress at the Bottom of the PCC Slab (492-ft joint spacing)**

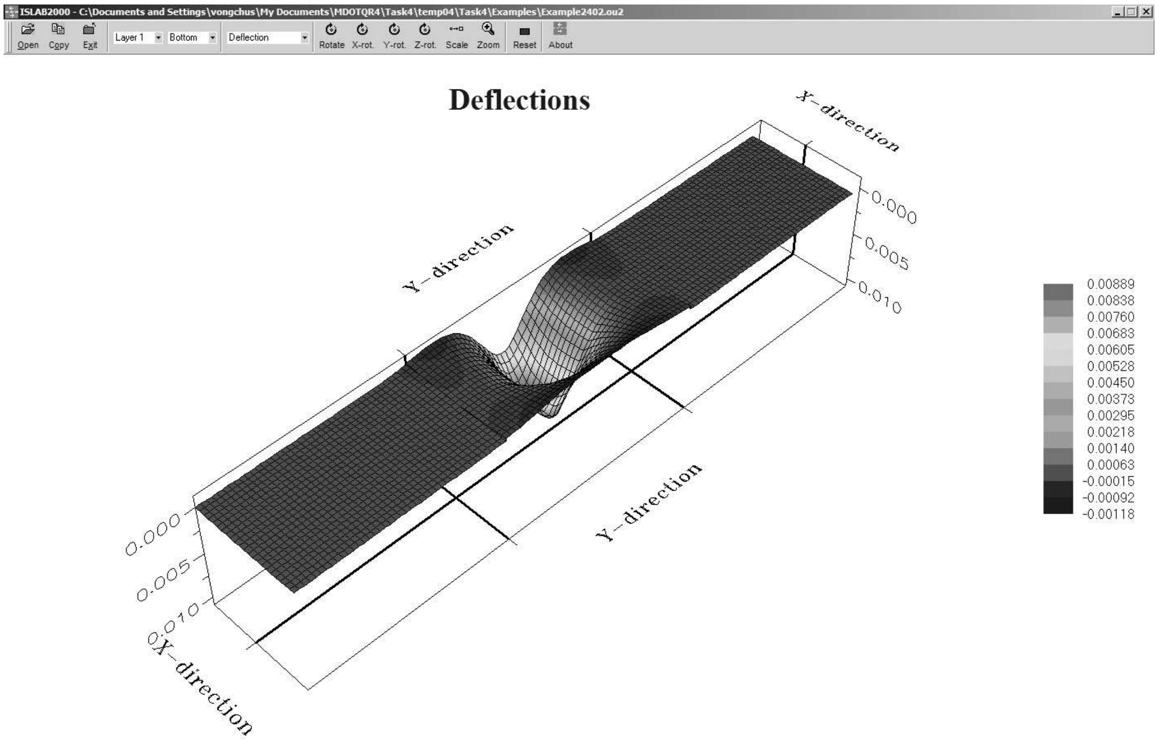


**Figure E24-13: Deflection of the PCC Slab (492-ft joint spacing)**

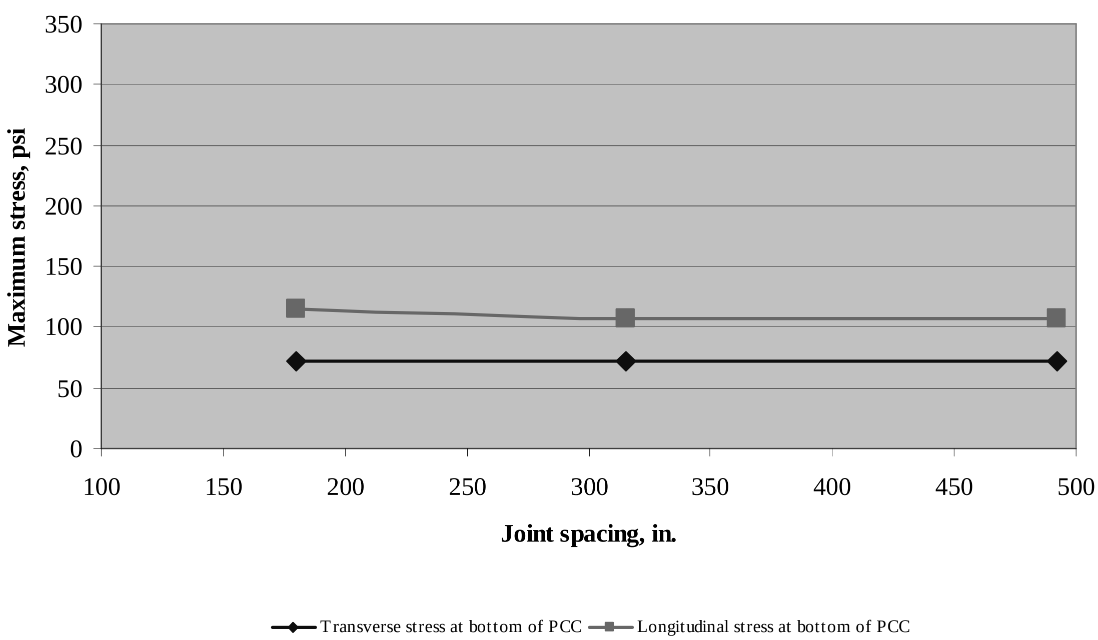


**Figure E24-14: Relationship Between Maximum Stresses and Joint Spacing**

# Example 25:
# Repeat Example 24 with a Thermal Gradient

## Problem Statement

Repeat Example 24 but also apply temperature differential, ΔT, of +20 $^{o}$F.

## Given

| | | | |
|---|---|---|---|
| Joint spacing | = | 315, 492 | in. |
| Temperature differential, ΔT | = | +20 | $^{o}$F. |

## Problem Illustration

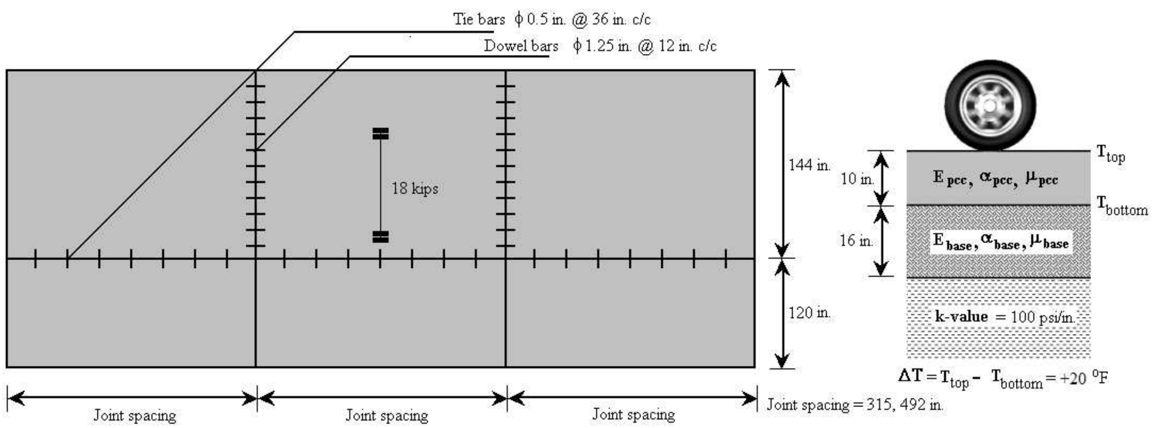


**Figure E25-1: Problem Illustration**

# Solution

### *PART 1: 315-in. joint spacing*

#### Geometry Module

Use this module from 315-ft joint spacing in Example 24.

#### Layers Module

Use this module from Example 8.

#### Subgrade Module

Use this module from Example 8.

#### Joints Module

Use this module from Example 8.

#### Load Module

Use this module from 315-ft joint spacing in Example 24.

#### Temperature Module

This module is not required for this problem.

#### Analysis Options Module

This module is not required for this problem.

The main panel should display the pavement structure, loading condition, and meshing as shown in Example 24, Figure E24-4.

### *PART 2: 492-in. joint spacing*

#### Geometry Module

Use this module from 492-ft joint spacing in Example 24.

#### Layers Module

Use this module from Example 8.

#### Subgrade Module

Use this module from Example 8.

#### Joints Module

Use this module from Example 8.

### Load Module

Use this module from 492-ft joint spacing in Example 24.

### Temperature Module

This module is not required for this problem.

### Analysis Options Module

This module is not required for this problem.

The main panel should display the pavement structure, loading condition, and meshing as shown in Example 24, Figure E24-7.

## *Analysis Results*

| Joint spacing, in. | Stress at the bottom of the PCC, psi | |
|---|---|---|
| | Transverse | Longitudinal |
| 180 | 139.7 | 224.5 |
| 315 | 145.0 | 325.8 |
| 492 | 140.2 | 326.2 |

**Table E25-1: Analysis Results**

**NOTE**
Positive and negative values of stress signify tensile and compressive stresses and positive value of deflection indicates deflection in downward direction.

Stress and deflection contours from ISLAB2000 are also available in Figures E25-2 through E25-7. Figure E25-8 illustrates relationship between maximum stresses and joint spacing.

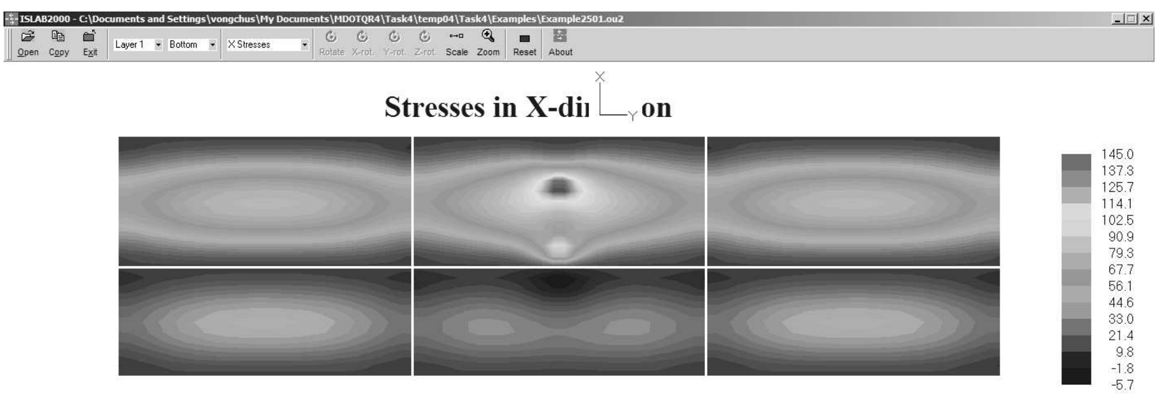


**Figure E25-2: Transverse Stress at the Bottom of the PCC Slab (315-ft joint spacing)**

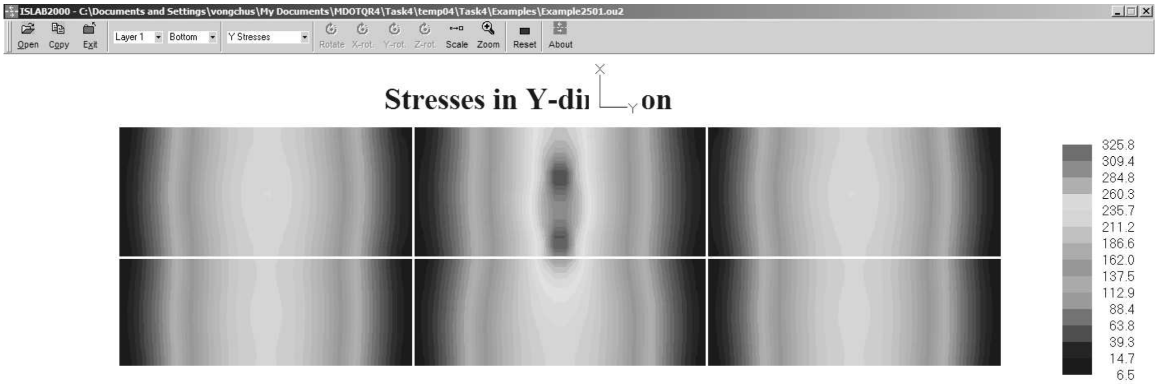


**Figure E25-3: Longitudinal Stress at the Bottom of the PCC Slab (315-ft joint spacing)**

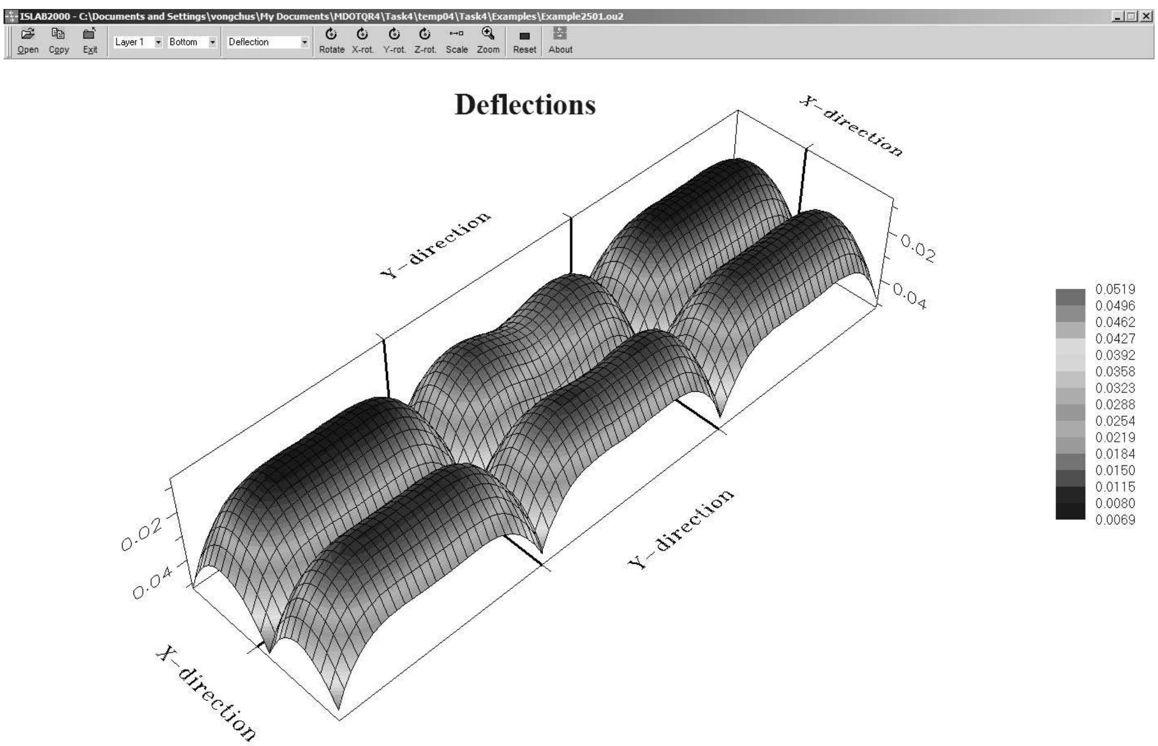


**Figure E25-4: Deflection of the PCC Slab (315-ft joint spacing)**

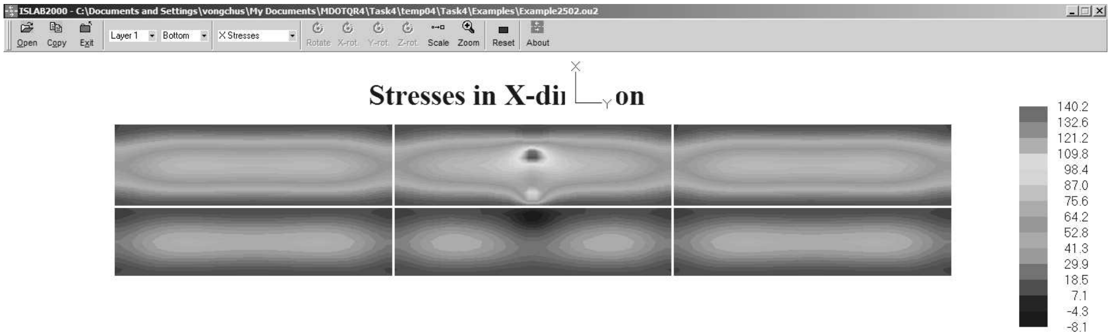


**Figure E25-5: Transverse Stress at the Bottom of the PCC Slab (492-ft joint spacing)**

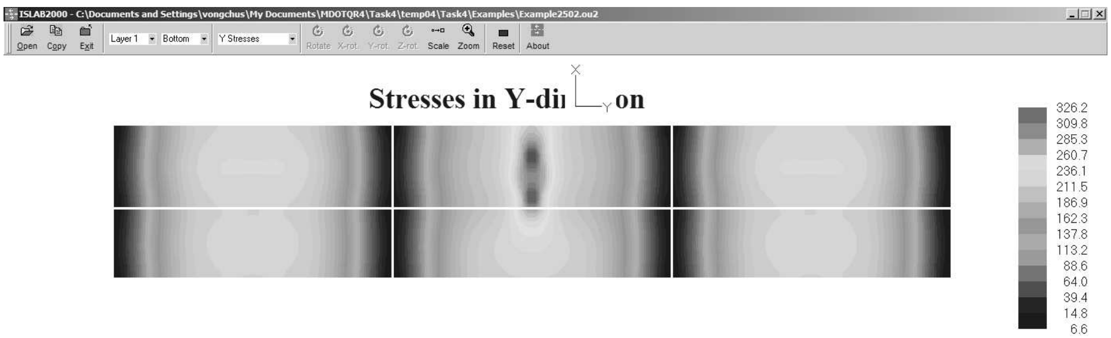


**Figure E25-6: Longitudinal Stress at the Bottom of the PCC Slab (492-ft joint spacing)**

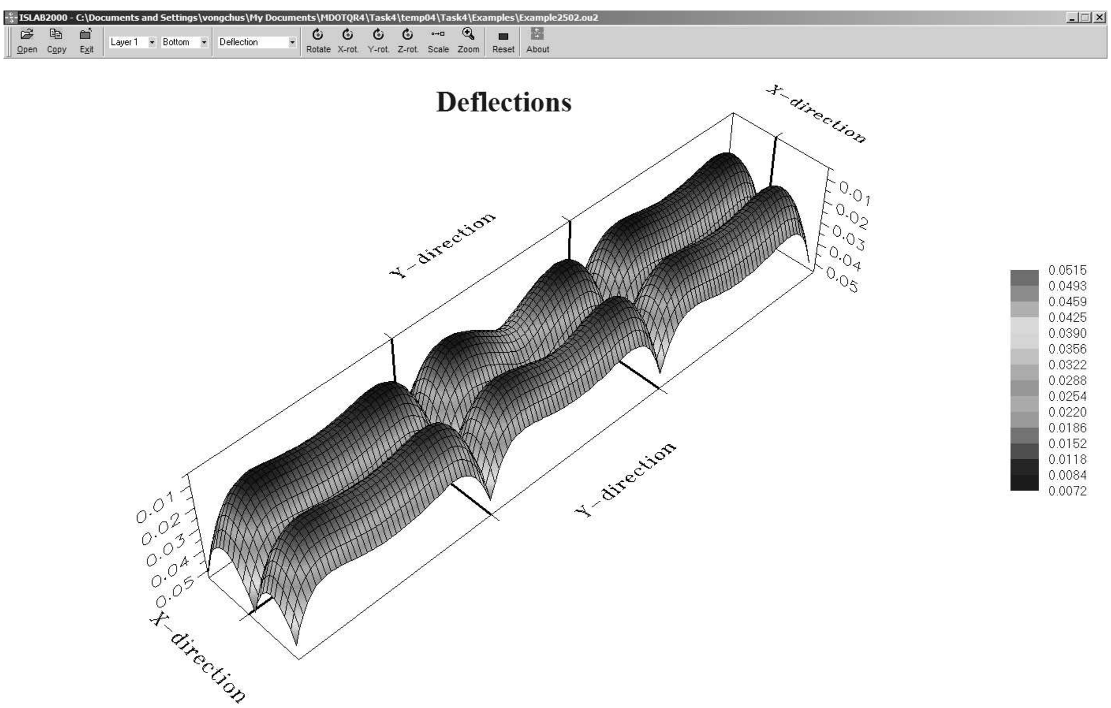


**Figure E25-7: Deflection of the PCC Slab (492-ft joint spacing)**

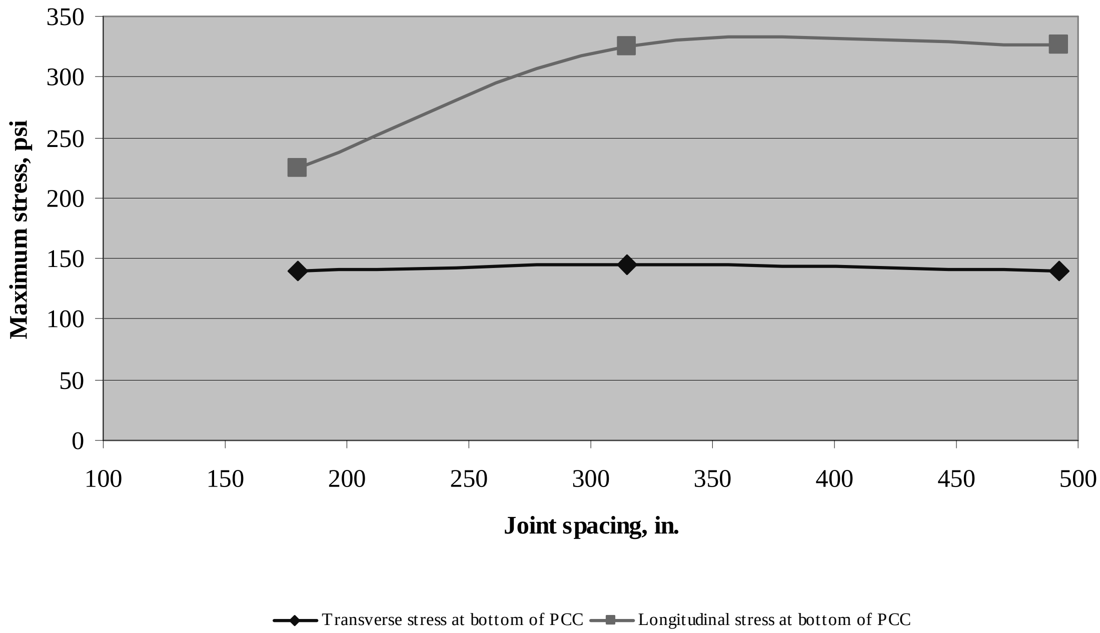


**Figure E25-8: Relationship Between Maximum Stresses and Joint Spacing**

# Example 26:
# Full-depth PCC Patch, 4 Feet Wide

### Problem Statement

Analyze the pavement system in Example 8, but also consider a 4-ft wide full-depth PCC patch in the middle of the lane.

### Given

| | | | |
|---|---|---|---|
| Patch elastic modulus | = | $3 \times 10^{6}$ | psi |
| Patch Poisson's ratio | = | 0.15 | |
| Patch coefficient of thermal exp | = | $7 \times 10^{-6}$ | in./in./$^{o}$F |

### Problem Illustration

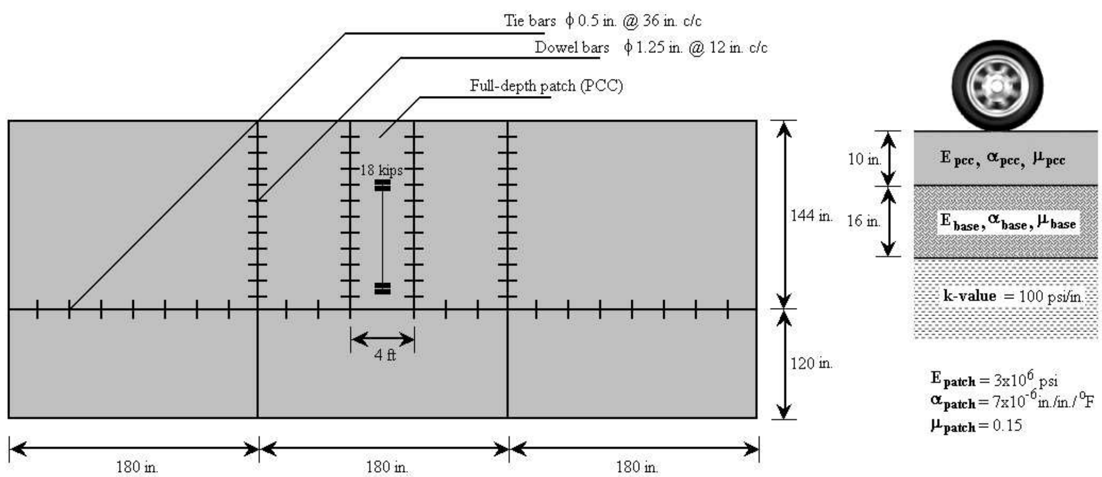


**Figure E26-1: Problem Illustration**

# Solution

### Geometry Module

(see Figure E26-2)

Step 1: Click **Geometry** to open the geometry panel.

Step 2: On the geometry panel, click **Insert** two times on the **X-direction** side to insert two additional slabs, and then enter the shoulder width (120 inches) and the lane width (144 inches) in the **Length** field for each slab.

Step 3: Click **Insert** five times on the **Y-direction** side to insert five additional slabs, and then enter the **180**, **66**, **48**, **66**, and **180** in the **Length** field for each slab.

Step 4: On the right side of the geometry panel, select **Medium** to set the mesh size.

Step 5: Click **Generate** to generate the inputs to the input file, and then click **OK** to close the geometry panel.

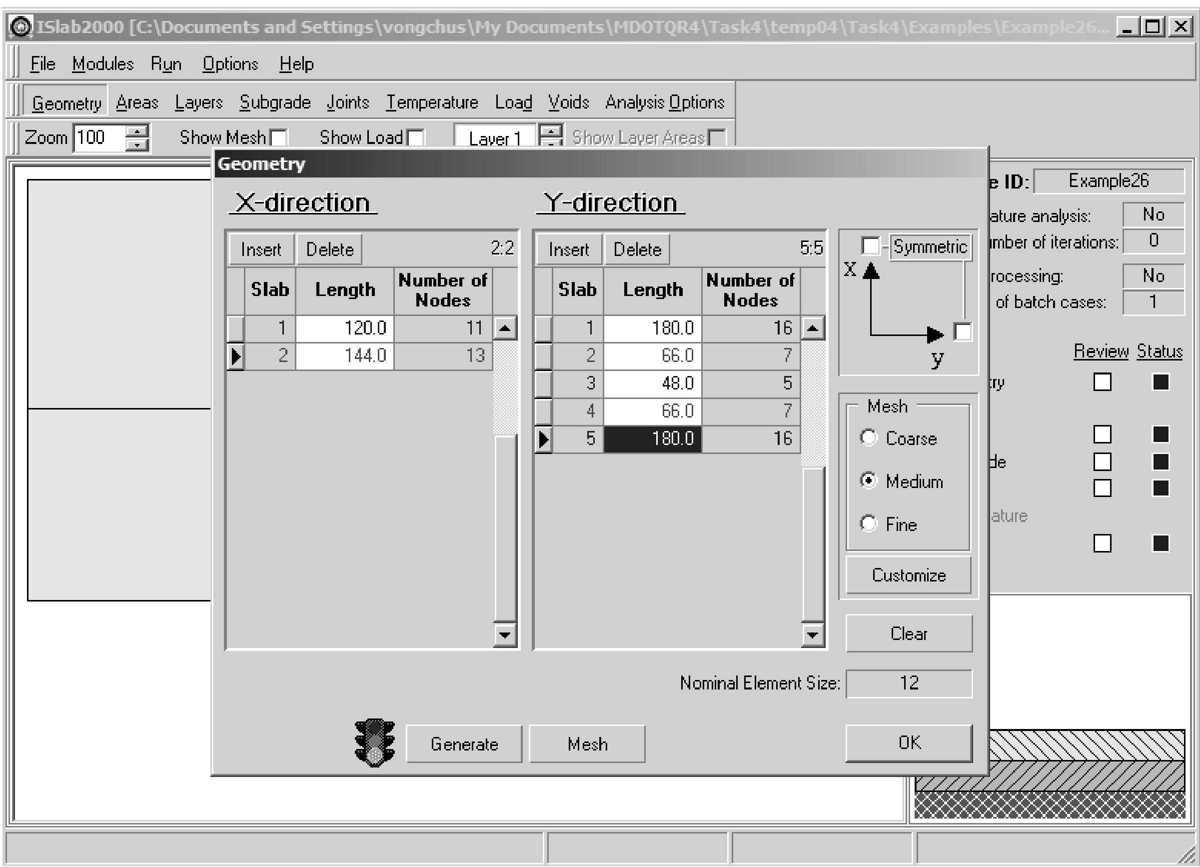


Figure E26-2: Edit Inputs for the Geometry Module

## Area Module

(see Figure E26-3)

Step 1: Click **Area** to open the area definition panel, and then click **Add** and enter **Patch** in the **Area Name** field.

Step 2: Select **Coordinates** in the **Coordinate Type** field.

Step 3: Enter the coordinate for the shoulder area as identified in the problem illustration.

Step 4: Click **OK** to close the area definition panel.

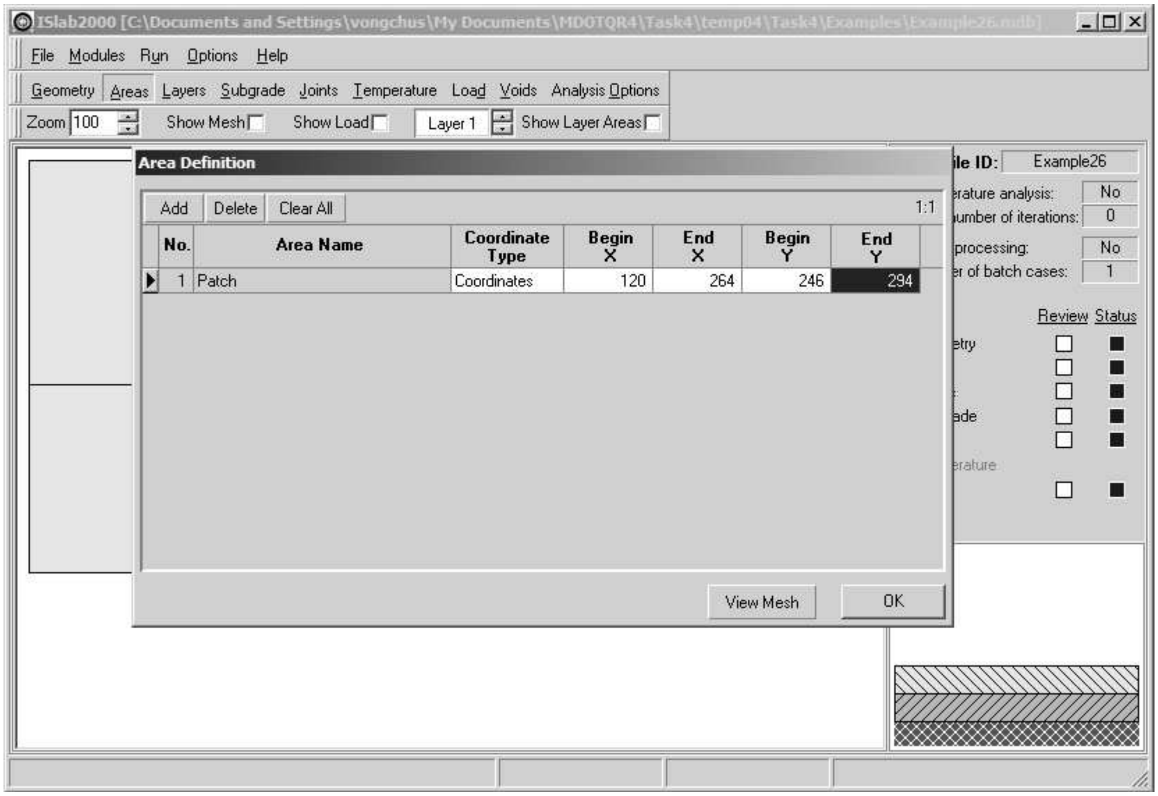


**Figure E26-3: Edit Inputs for the Area Module**

## Layers Module

(see Figure E26-4)

Step 1: Follow steps 1 through 4 of this module in Example 8.

Step 2: On Layer 1, select **Exception**, and then click **Edit Exception** to open the exception properties panel for layer 1.

Step 3: Click **Insert**, and then select **Patch** in the **Area Name** field.

Step 4: Enter the material properties for patch material as shown in Figure E26-4.

Step 5: Click **OK** to close the layers panel.

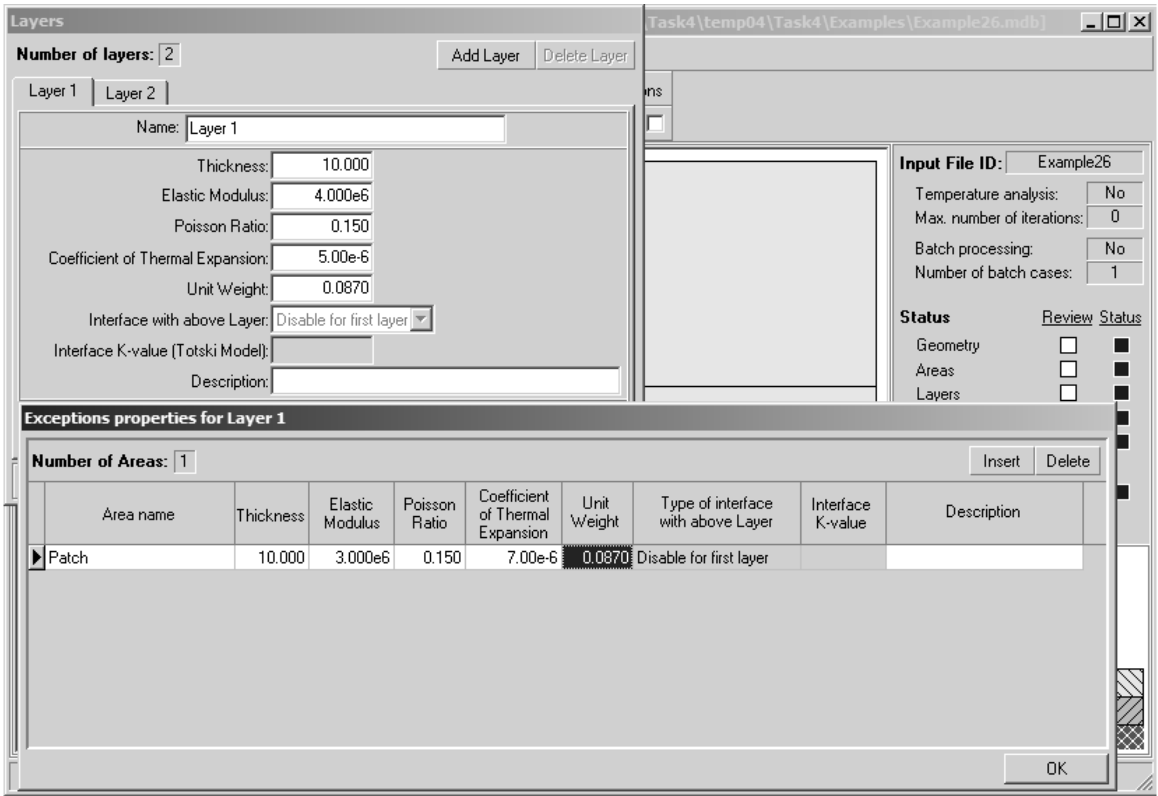


**Figure E26-4: Edit Inputs for the Layer Module**

## Subgrade Module

Use this module from Example 8.

## Joints Module

Use this module from Example 8.

## Load Module

Use this module from Example 8.

## Temperature Module

Temperature module is not required for this problem.

## Analysis Options Module

This module is not required for this problem.

The main panel should display the pavement structure, loading condition, and meshing as shown in Figure E26-5.

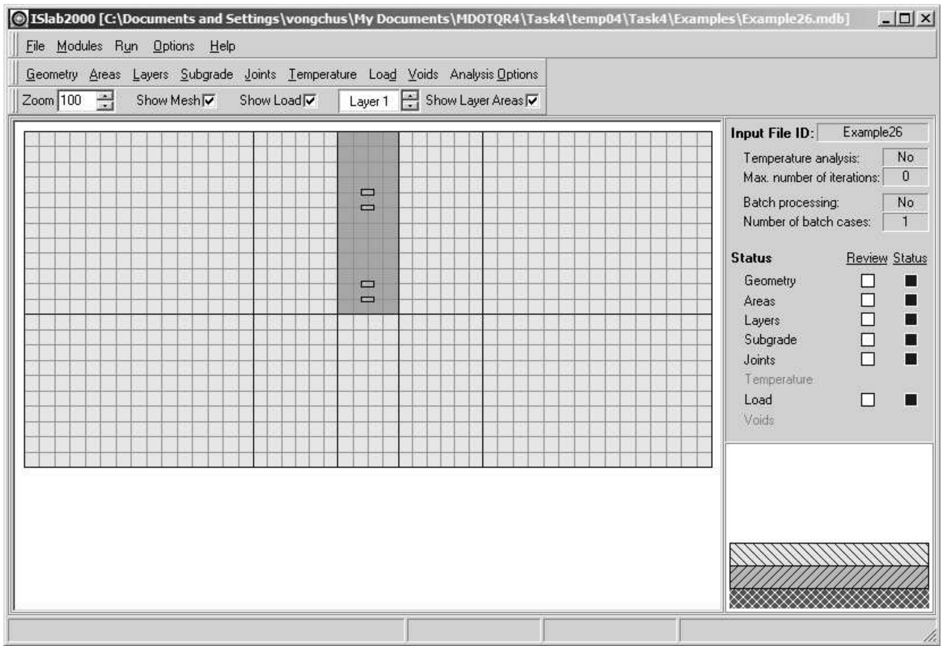


Figure E26-5: Main Panel After the Completion of Inputs

## *Analysis Results*

Maximum transverse stress at the bottom of the PCC slab = 87.6 psi (see Figure E26-6)

Maximum longitudinal stress at the bottom of the PCC slab = 91.5 psi (see Figure E26-7)

**NOTE**

Positive and negative values of stress signify tensile and compressive stresses and positive value of deflection indicates deflection in downward direction.

Stress and deflection contours from ISLAB2000 are also available in Figures E26-6 through E26-8.

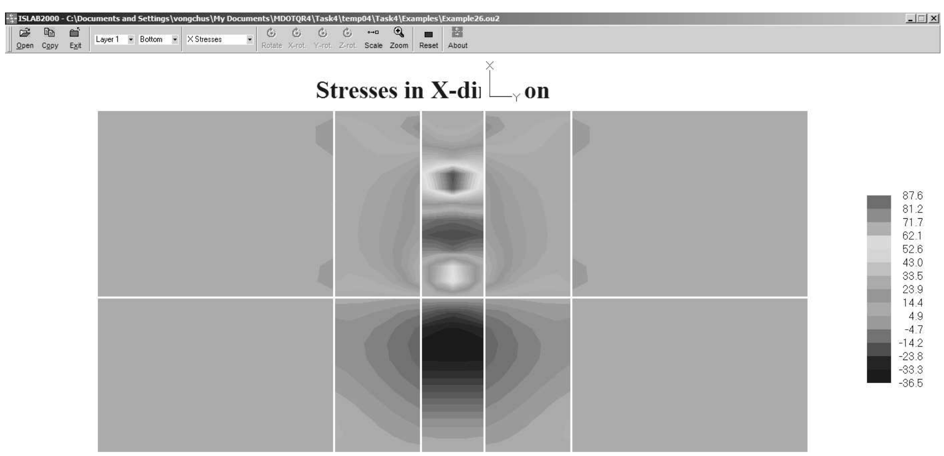


Figure E26-6: Transverse Stress at the Bottom of the PCC Slab

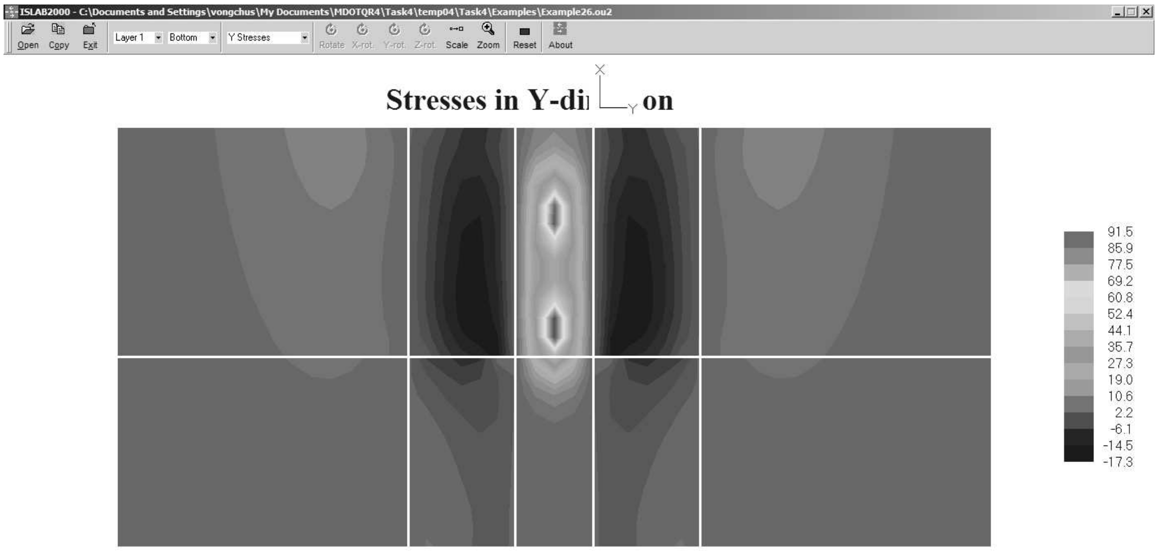


**Figure E26-7: Longitudinal Stress at the Bottom of the PCC Slab**

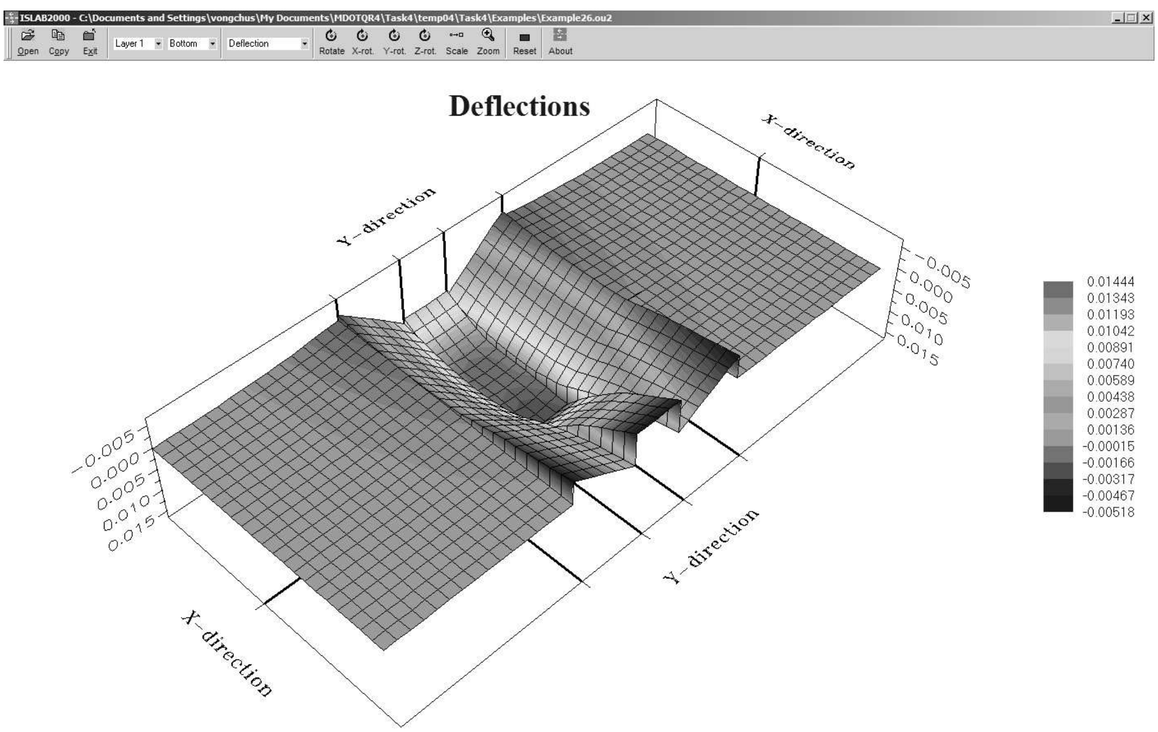


**Figure E26-8: Deflection of the PCC Slab**

# Example 27:
# Full Depth PCC Patch. 6 Feet Wide

## Problem Statement

Analyze a pavement system with a full-depth PCC patch similar to Example 26, but consider 315-in. joint spacing and a 6-ft wide full-depth PCC patch in the middle of the lane.

## Given

| | | | |
|---|---|---|---|
| Patch elastic modulus | = | $3 \times 10^6$ | psi |
| Patch Poisson's ratio | = | 0.15 | |
| Patch coefficient of thermal exp | = | $7 \times 10^{-6}$ | in./in./$^o$F |

## Problem Illustration

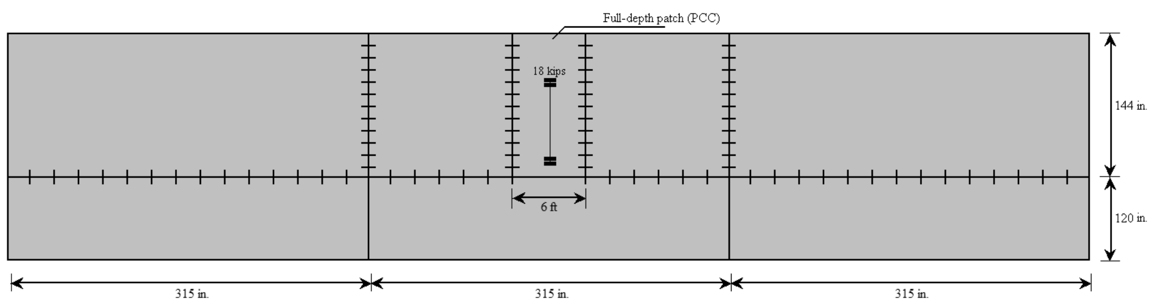


**Figure E27-1: Problem Illustration**

# Solution

### Geometry Module

(see Figure E27-2)

Step 1: Click **Geometry** to open the geometry panel.

Step 2: On the geometry panel, click **Insert** two times on the **X-direction** side to add two additional slabs, and then enter the shoulder width (120 inches) and the lane width (144 inches) in the length field for each slab.

Step 3: Click **Insert** five times on the **Y-direction** side to add five additional slabs, and then enter **315**, **121.5**, **72**, **121.5**, **315** in the **Length** field for each slab.

Step 4: On right hand side of the geometry panel, select **Medium** to set the mesh size.

Step 5: Click **Generate** to generate the inputs to the input file, and then click **OK** to close the geometry panel.

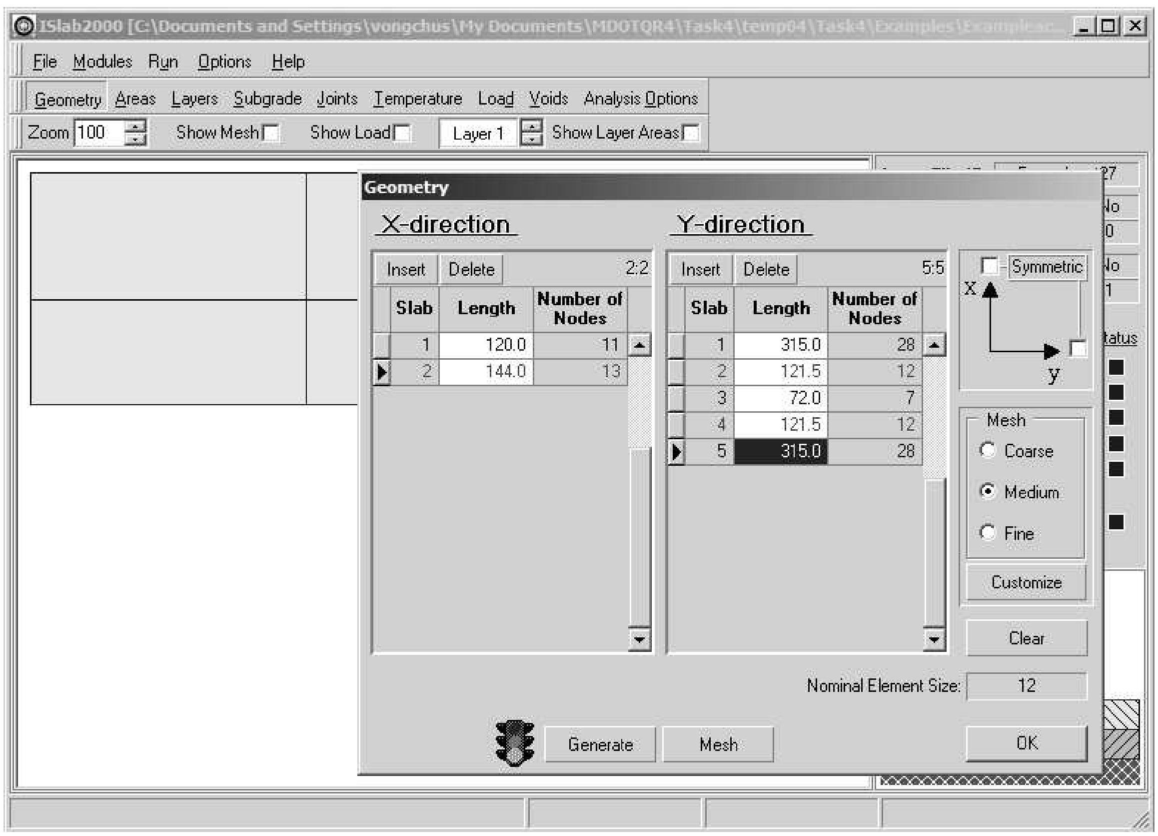


**Figure E27-2: Edit Inputs for the Geometry Module**

## Area Module

(see Figure E27-3)

Step 1: Click **Area** to open the area definition panel, and then click **Add** and enter **Patch** in the **Area Name** field.

Step 2: Select **Coordinates** in the **Coordinate type** field.

Step 3: Enter the coordinate for the shoulder area as identified in the problem illustration.

Step 4: Click **OK** to close the area definition panel.

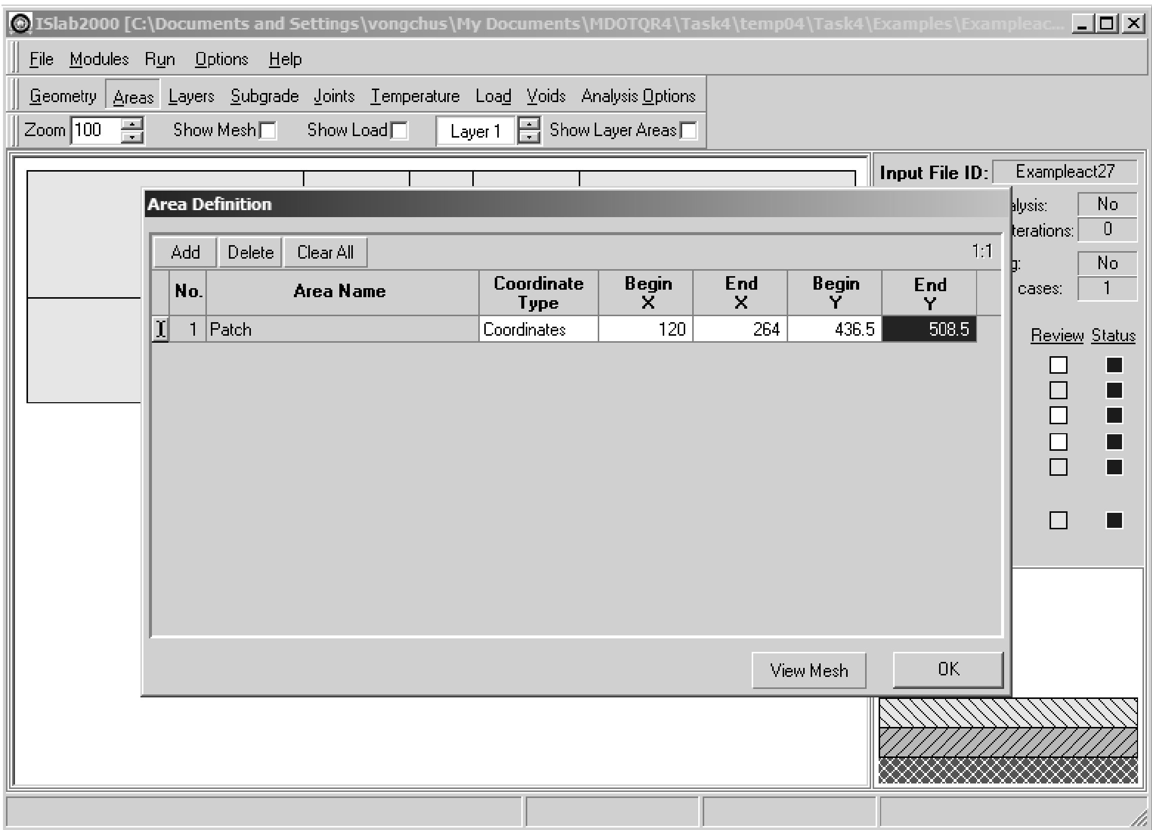


**Figure E27-3: Edit Inputs for the Area Module**

## Layers Module

(see Figure E27-4)

Step 1: Follow steps 1 through 4 of this module in Example 8.

Step 2: On Layer 1, select **Exception** and click **Edit Exception** to open the exception properties panel for layer 1.

Step 3: Click **Insert**, and then select **Patch** in the Are name field.

Step 4: Enter the material properties for patch material as shown in Figure E27-4.

Step 5: Click **OK** to close the layers panel.

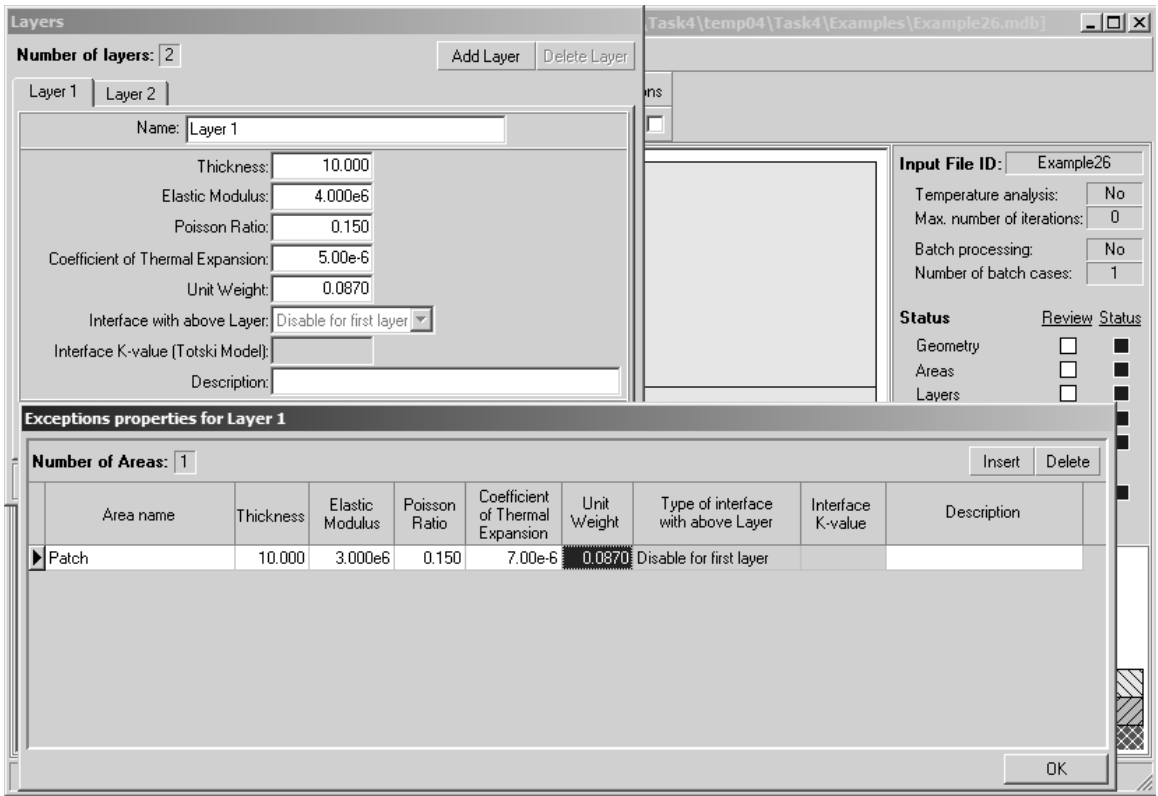


**Figure E27-4: Edit Inputs for the Layer Module**

## Subgrade Module

Use this module from Example 8.

## Joints Module

Use this module from Example 8.

## Load Module

Use this module from Example 8.

### Temperature Module

Temperature module is not required for this problem.

### Analysis Options Module

This module is not required for this problem.

The main panel should display the pavement structure, loading condition, and meshing as shown in Figure E27-5.

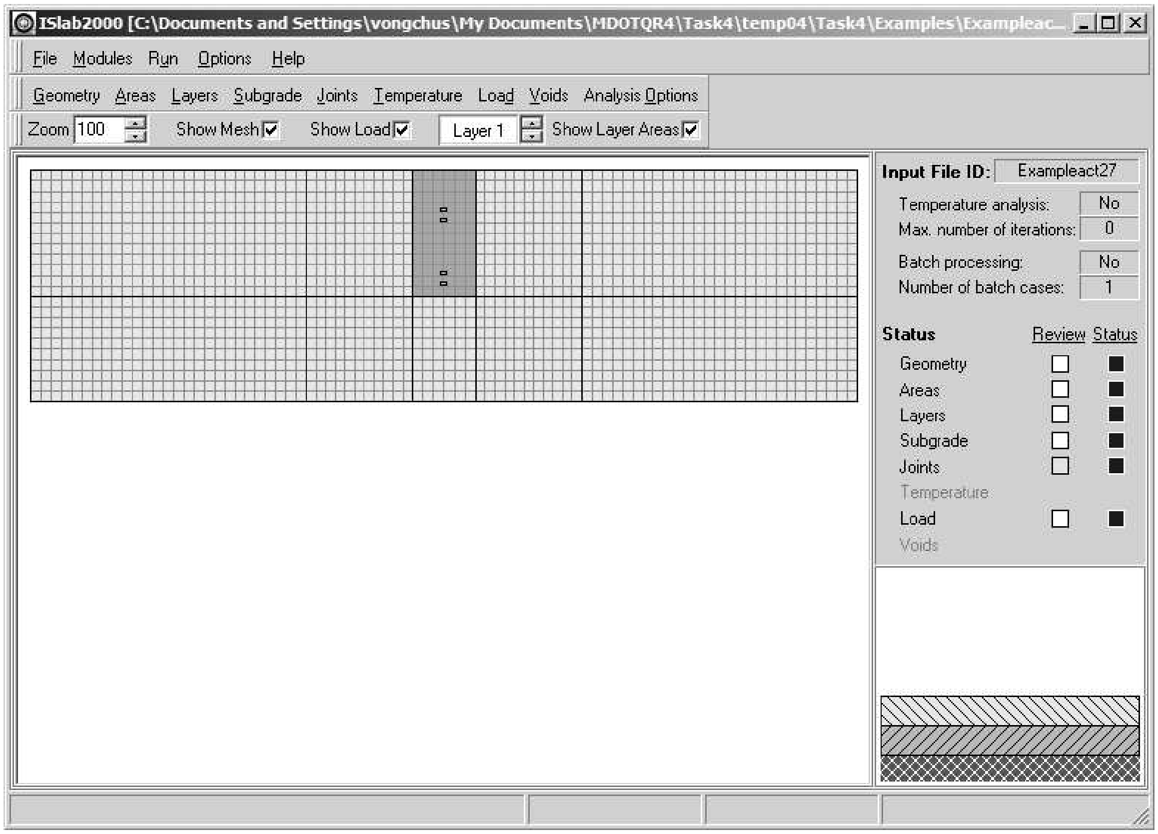


**Figure E27-5: Main Panel After the Completion of Inputs**

## *Analysis Results*

Maximum transverse stress at the bottom of the PCC slab = 83.7 psi (see Figure E27-6)

Maximum longitudinal stress at the bottom of the PCC slab = 114.3 psi (see Figure E27-7)

**NOTE**
Positive and negative values of stress signify tensile and compressive stresses and positive value of deflection indicates deflection in downward direction.

Stress and deflection contours from ISLAB2000 are also available in Figures E27-6 through E27-8.

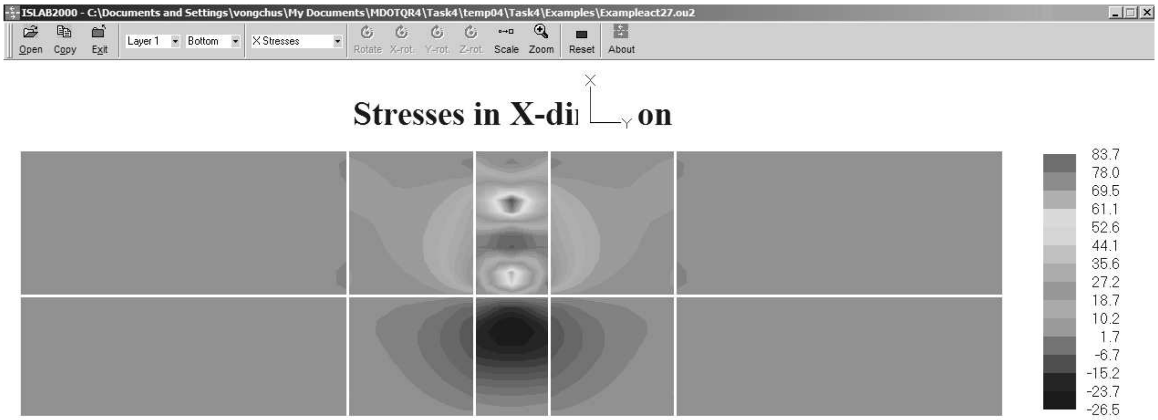


**Figure E27-6: Transverse Stress at the Bottom of the PCC Slab**

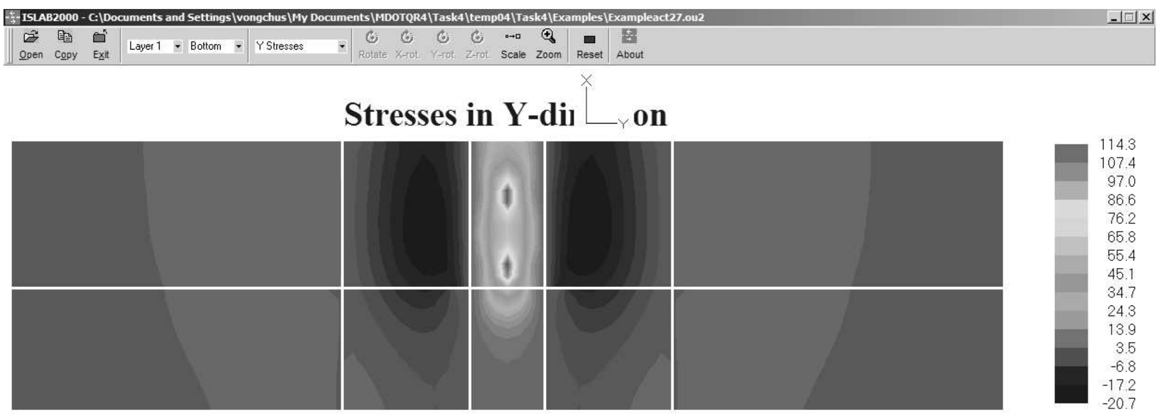


**Figure E27-7: Longitudinal Stress at the Bottom of the PCC Slab**

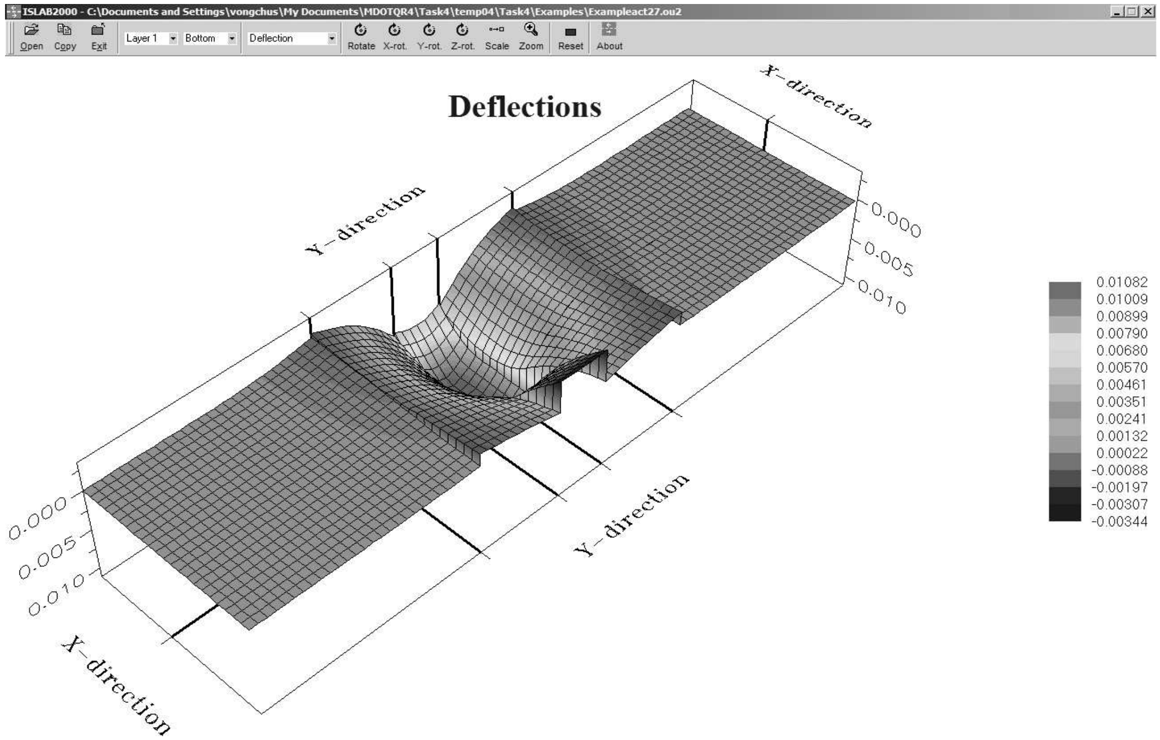


**Figure E27-8: Deflection of the PCC Slab**

# Example 28:
# Full-depth AC Patch

## Problem Statement

Analyze the pavement system in Example 8, but also consider a 4-ft wide full-depth AC patch at the middle of the lane.

## Given

| | | | |
|---|---|---|---|
| Patch elastic modulus | = | $3 \times 10^5$ | psi |
| Patch Poisson's ratio | = | 0.35 | |
| Patch coefficient of thermal exp | = | $2 \times 10^{-6}$ | in./in./$^o$F |

## Problem Illustration

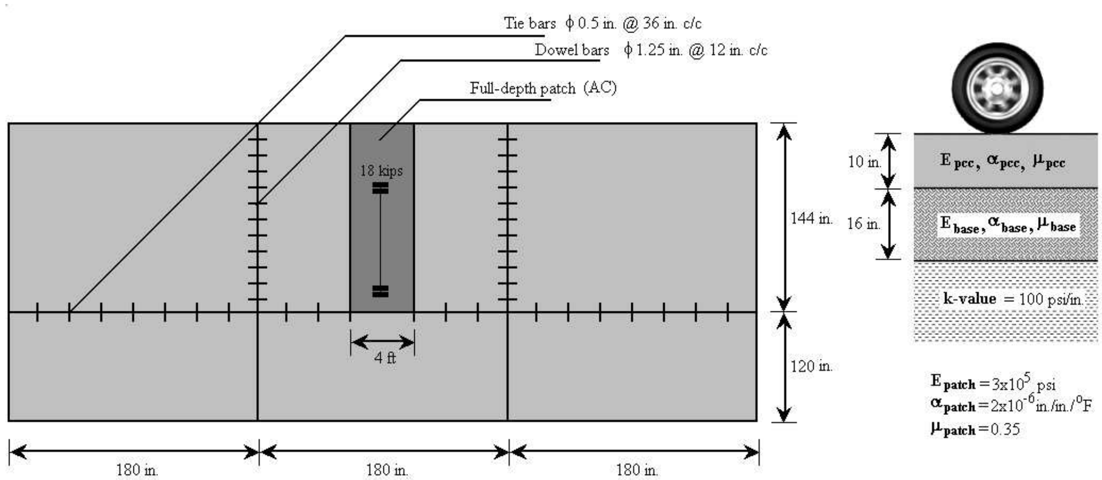


**Figure E28-1: Problem Illustration**

# Solution

### Geometry Module

Use this module from Example 26.

### Area Module

Use this module from Example 26.

### Layers Module

(see Figure E28-2)

Step 1: Follow steps 1 through 4 of this module in Example 8.

Step 2: On Layer 1, select **Exception**, and then click **Edit Exception** to open the exception properties panel for layer 1.

Step 3: Click **Insert**, and then select **Patch** in the area **Name** field.

Step 4: Enter the material properties for patch material as shown in Figure E28-2.

Step 5: Click **OK** to close the layers panel.

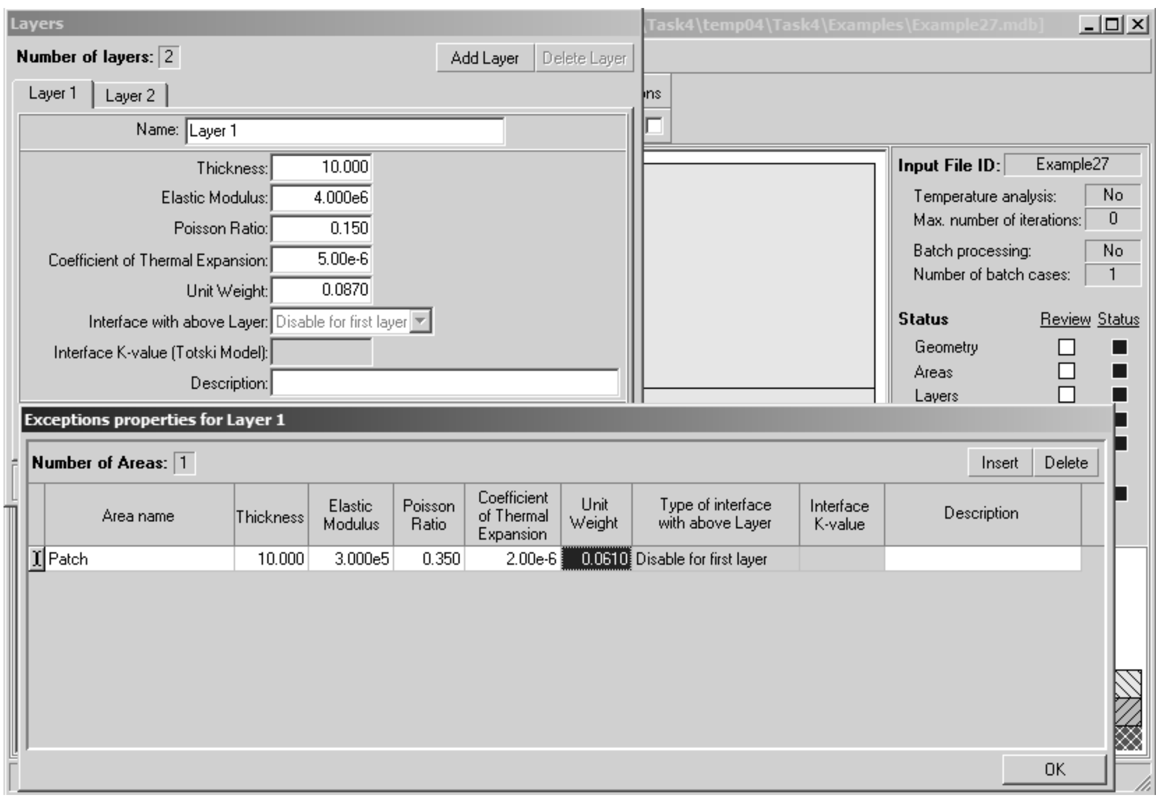


**Figure E28-2: Edit Inputs for the Layer Module**

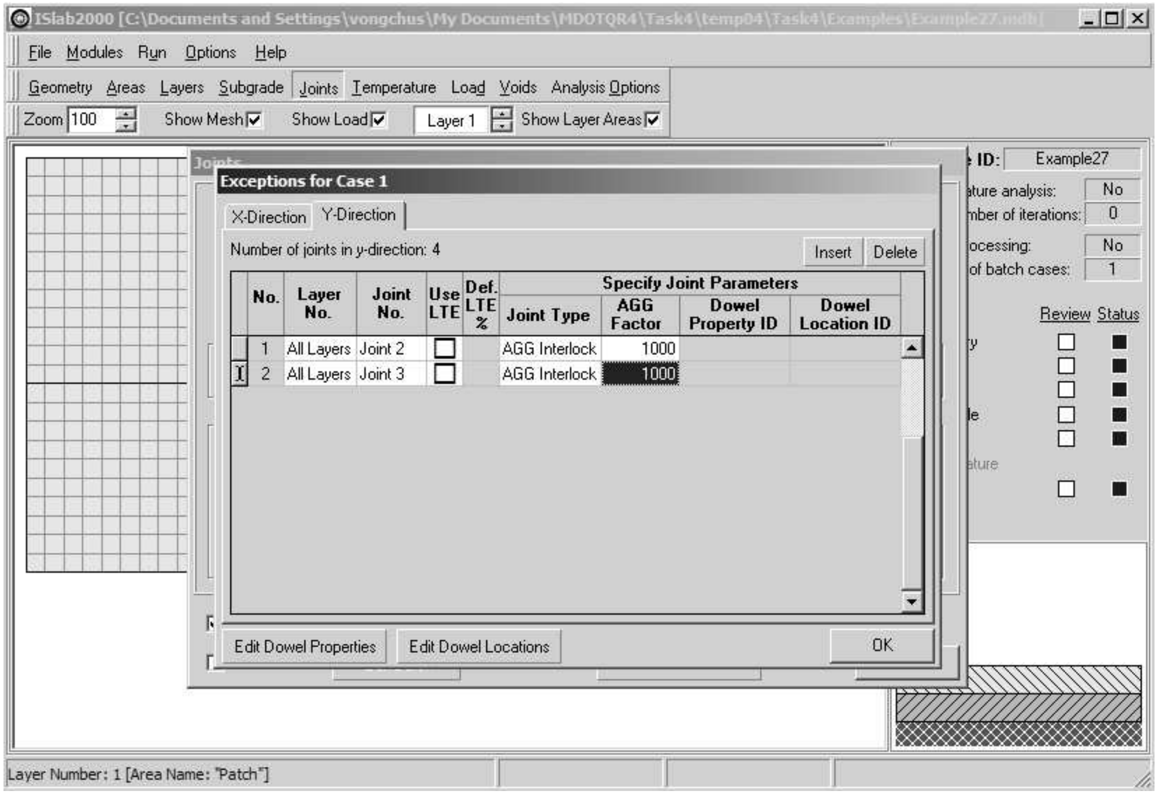


**Figure E28-3: Edit Inputs for the Joints Module**

### Subgrade Module

Use this module from Example 8.

### Joints Module

(see Figure E28-3)

Step 1: Follow steps 1 through 5 of this module in Example 8, but do not click on **OK** to close the joints panel.

Step 2: Select **Exceptions** and click Edit Exception to open the exception panel for case 1.

Step 3: Click **Insert** two times to add two additional joints. For No. 1, select **Joint 2**, **AGG Interlock,** and then enter **1000** for the AGG Factor. Do the same for No. 2 for Joint 3.

### Load Module

Use this module from Example 8.

### Temperature Module

Temperature module is not required for this problem.

### Analysis Options Module

This module is not required for this problem.

The main panel should display the pavement structure, loading condition, and meshing as shown in Example 26, Figure E26-5.

## *Analysis Results*

Maximum transverse stress at the bottom of the PCC slab = 64.5 psi (see Figure E28-4)

Maximum longitudinal stress at the bottom of the PCC slab = 64.8 psi (see Figure E28-5)

**NOTE**
Positive and negative values of stress signify tensile and compressive stresses and positive value of deflection indicates deflection in downward direction.

Stress and deflection contours from ISLAB2000 are also available in Figures E28-4 through E28-5.

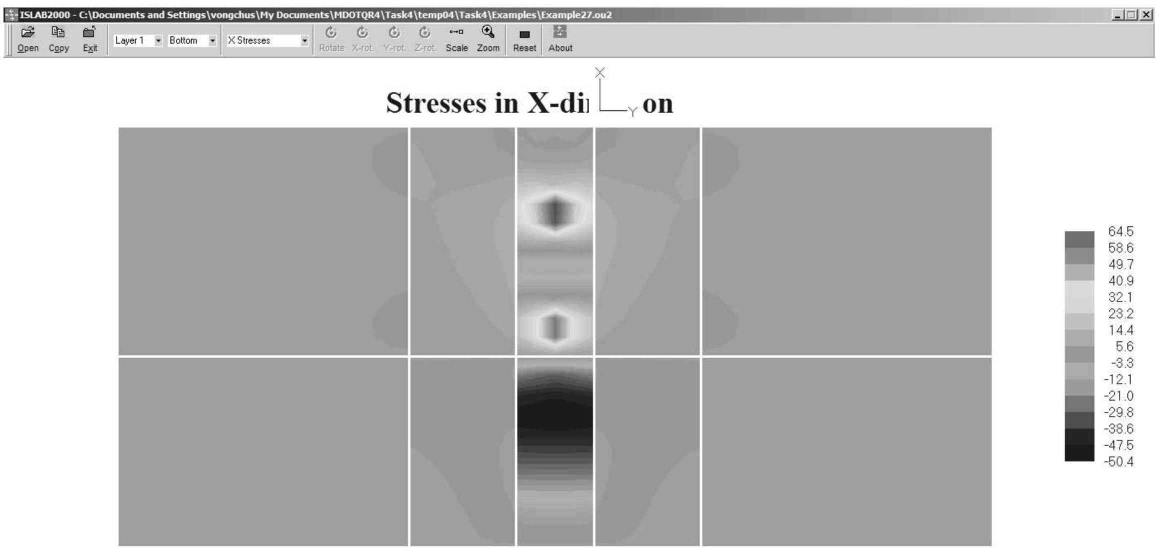


**Figure E28-4: Transverse Stress at the Bottom of the PCC Slab**

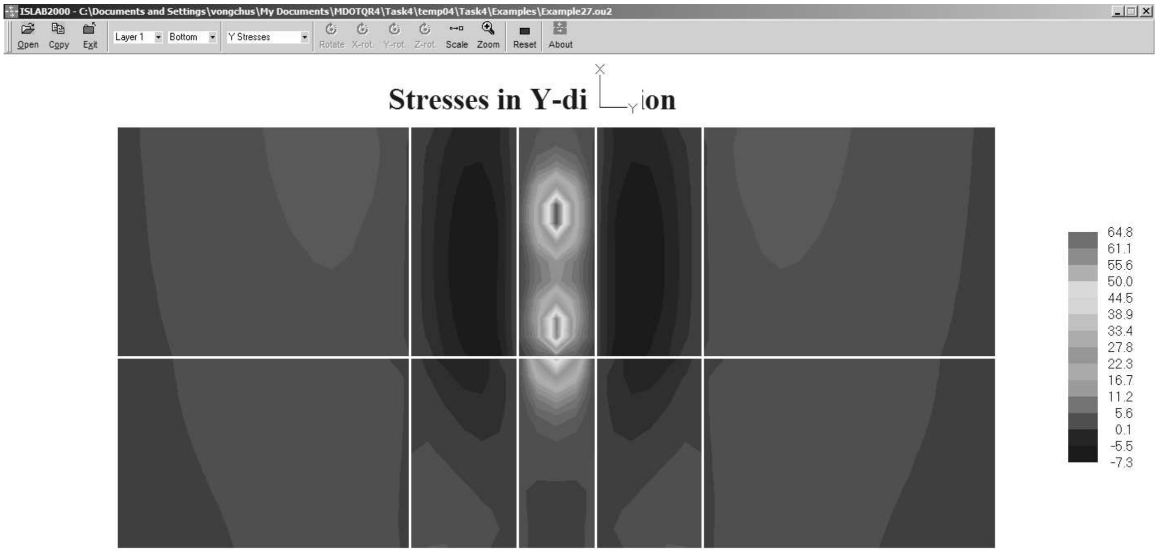


**Figure E28-5: Longitudinal Stress at the Bottom of the PCC Slab**

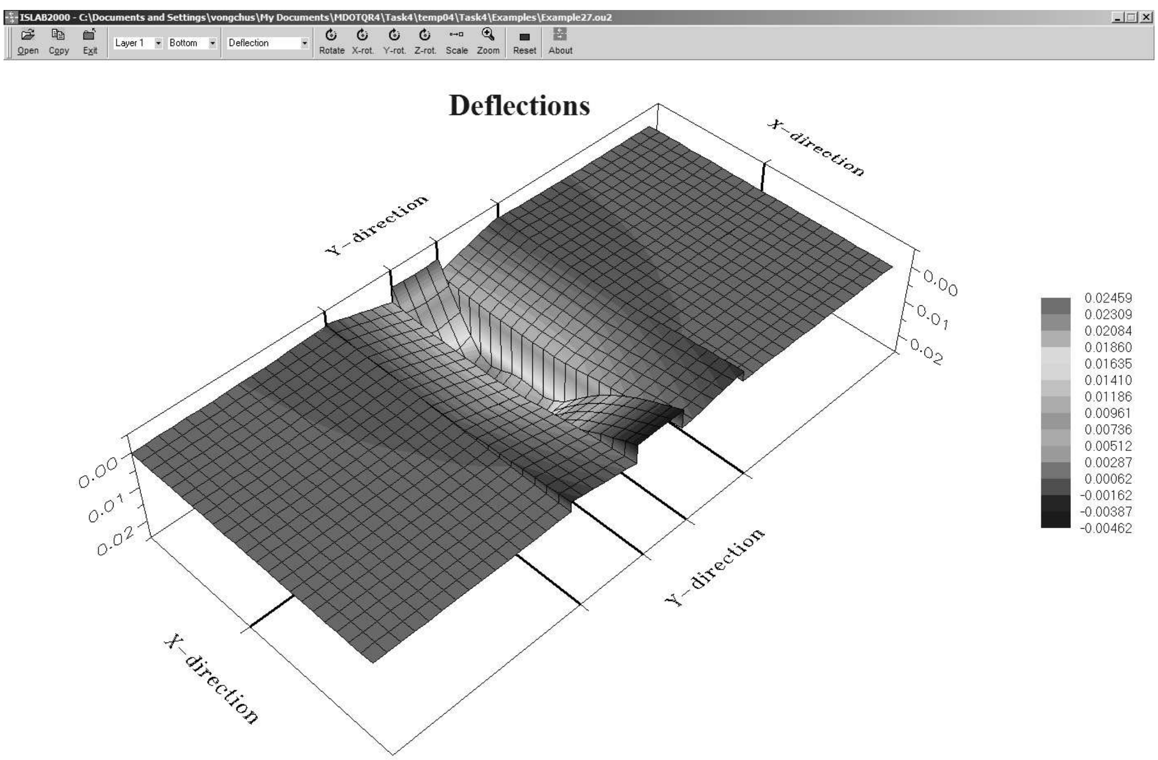


**Figure E28-6: Deflection of the PCC Slab**

# Example 29:
# Void at Slab Corner

### Problem Statement

Determine maximum tresses at the top of the PCC slab for the pavement system in Example 8, but also consider void potential at the slab corner as illustrated in Figure E29-1. Then, compare the results with the results from no void potential case, as in Example 10.

### Given

Void potential area = 2 x 2 $ft^2$

### Problem Illustration

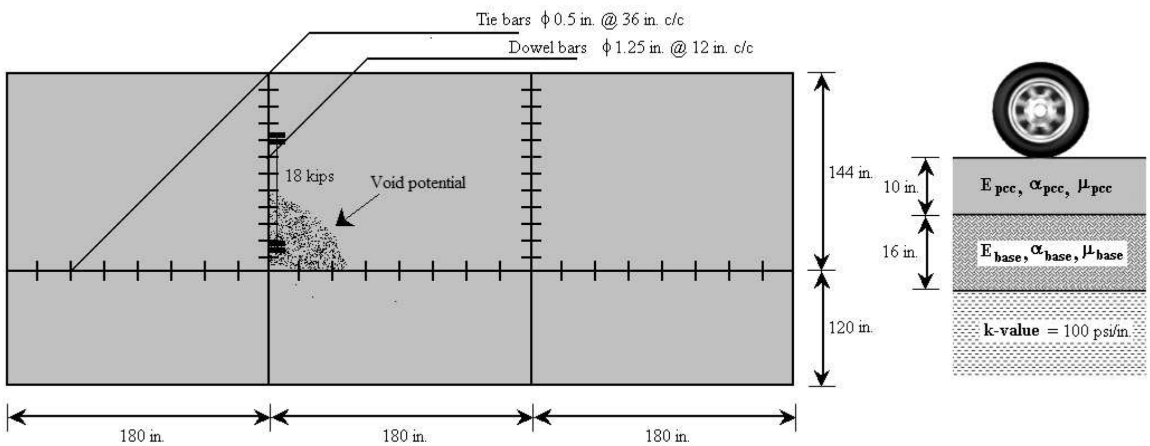


Figure E29-1: Problem Illustration

# Solution

### Geometry Module

Use this module from Example 8.

### Area Module

(see Figure E29-2)

Step 1: Click **Area** to open the area module, click on **Add** to open the area definition panel, and then enter **Void** in the **Area Name** field.

Step 2: Select **Coordinates** in the **Coordinate type** field.

Step 3: Enter the coordinate for the shoulder area as identified in the problem illustration.

Step 4: Click **OK** to close the area definition panel.

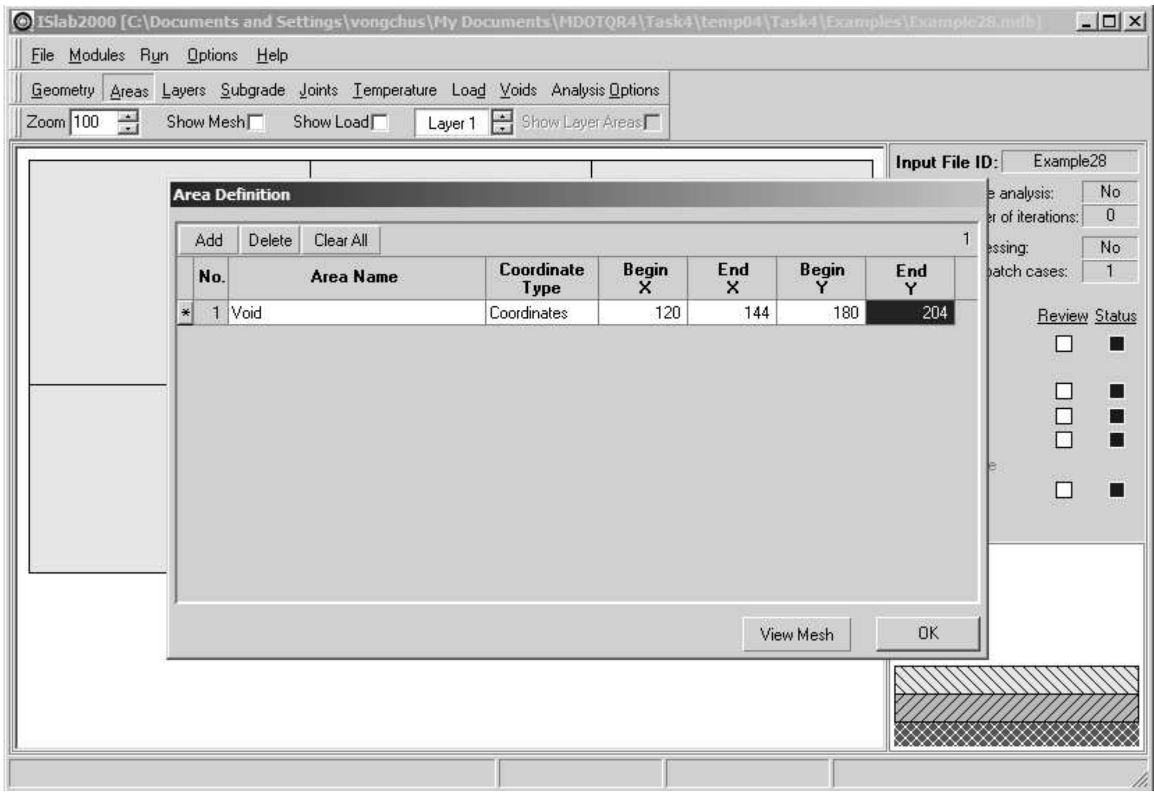


Figure E29-2: Edit Inputs for the Area Module

## Layers Module

Use this module from Example 8.

## Subgrade Module

(see Figure E29-3)

Step 1: Click **Layers** to open the layers panel.

Step 2: On the layers panel, enter the inputs as identified in the problem statement.

Step 3: Select **Exceptions**, click on **Edit Exception** to open the exceptions properties for subgrade panel, and then add the area **Void** and type 0.01 for k-value. Click **OK** to close the exceptions properties for subgrade panel

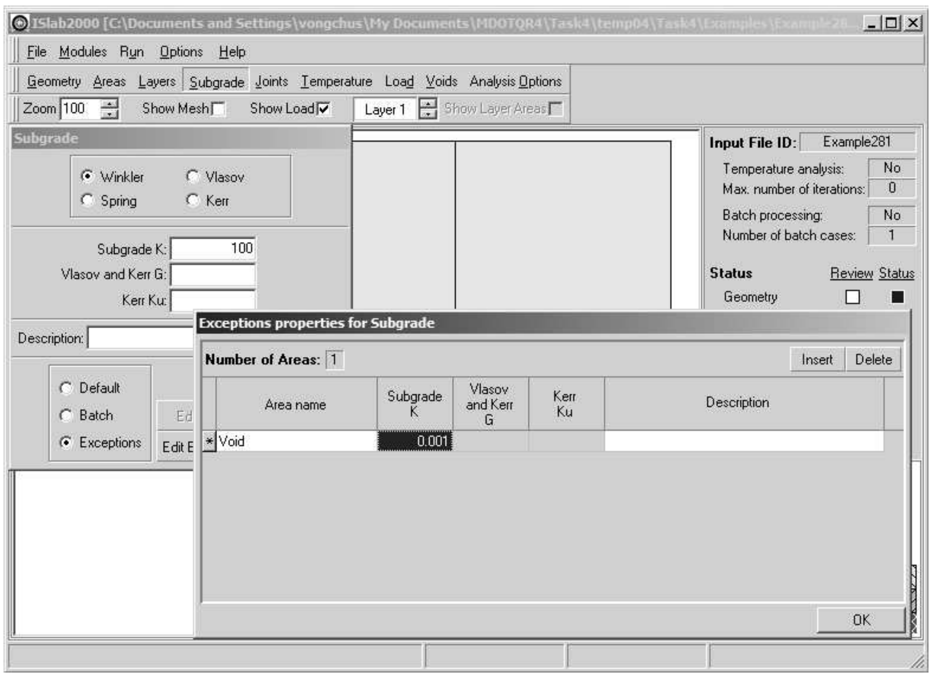


**Figure E29-3: Edit Inputs for the Subgrade Module**

## Joints Module

Use this module from Example 8.

## Load Module

Use this module from Example 10.

## Temperature Module

This module is not required for the problem.

## Analysis Options Module

This module is not required for this problem.

The main panel should display the pavement structure, loading condition, and meshing as shown in Figure E29-4.

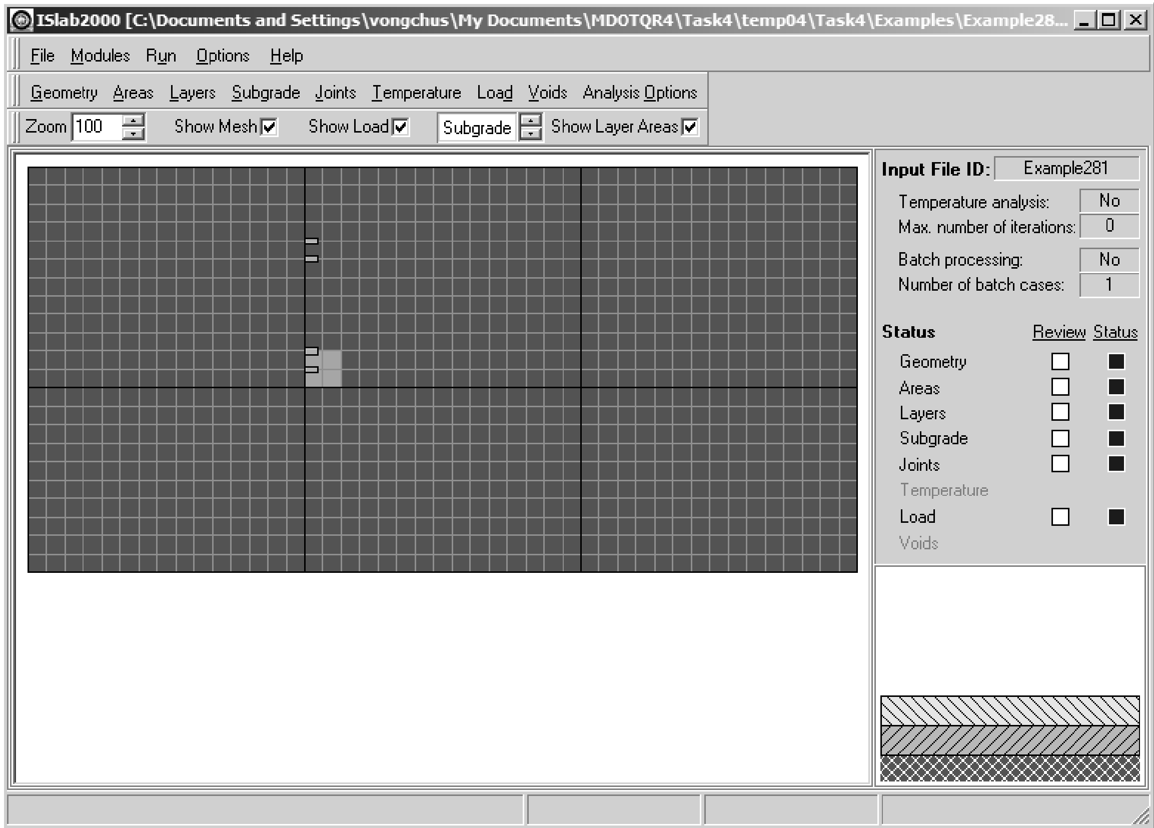


**Figure E29-4: Main Panel After the Completion of Inputs**

## *Analysis Results*

| Stress type | Without void potential (Example 10) | With void potential (Example 29) |
|---|---|---|
| Corner deflection | 0.03512 | 0.03935 |
| Transverse stress at top of PCC | 38.9 | 52.1 |
| Longitudinal stress at top of PCC | 47.5 | 51.8 |

**Table E29-1: Analysis Results**

**NOTE**

Positive and negative values of stress signify tensile and compressive stresses and positive value of deflection indicates deflection in downward direction.

ISLAB2000 stress and deflection contours are also available in Figures E29-5 through E29-7. Comparison of the results between with and without void potential is shown in Figure E29-8.

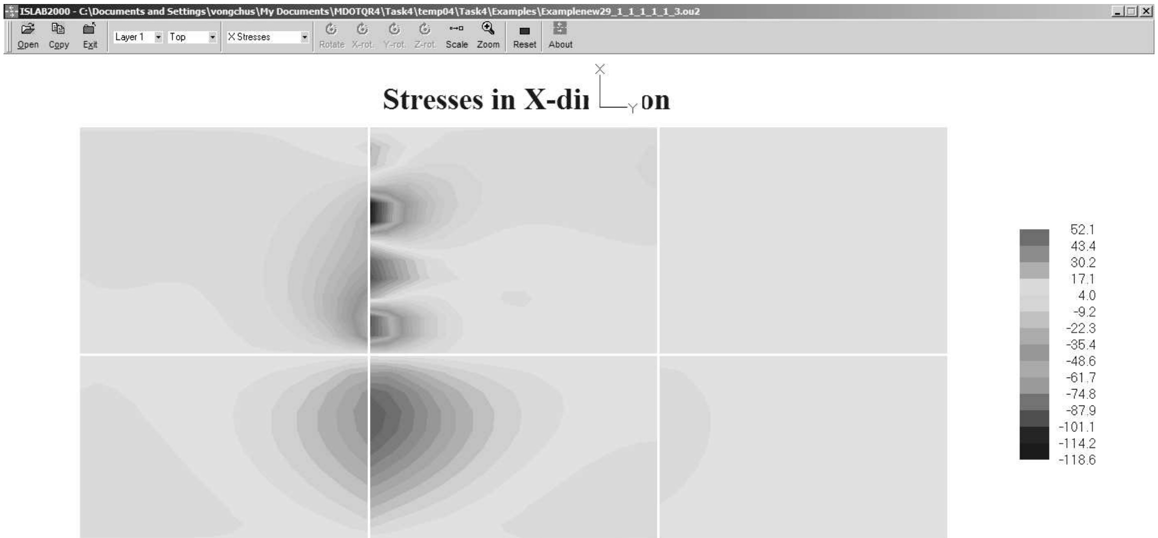


**Figure E29-5: Transverse Stress at the Top of the PCC Slab**

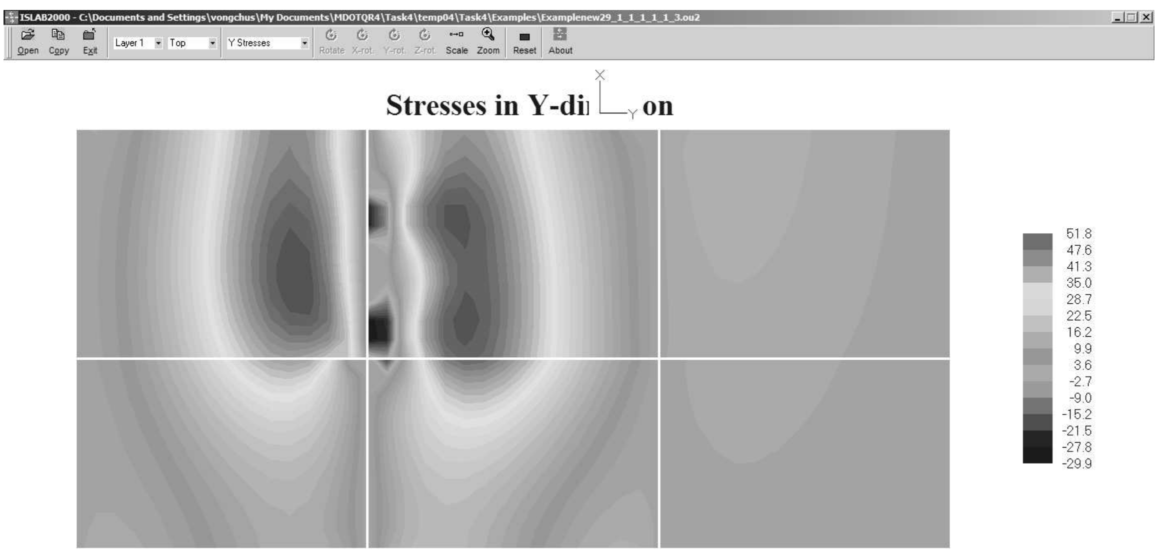


**Figure E29-6: Longitudinal Stress at the Top of the PCC Slab**

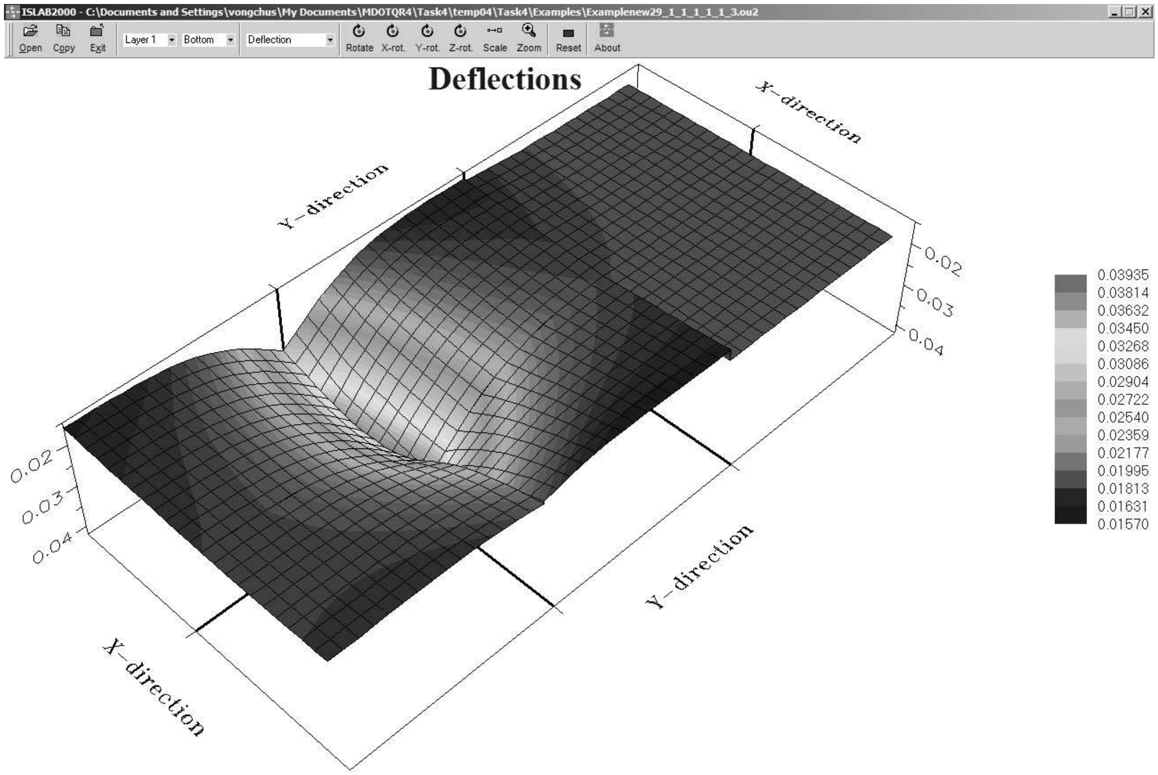


**Figure E29-7: Deflection of the PCC Slab**

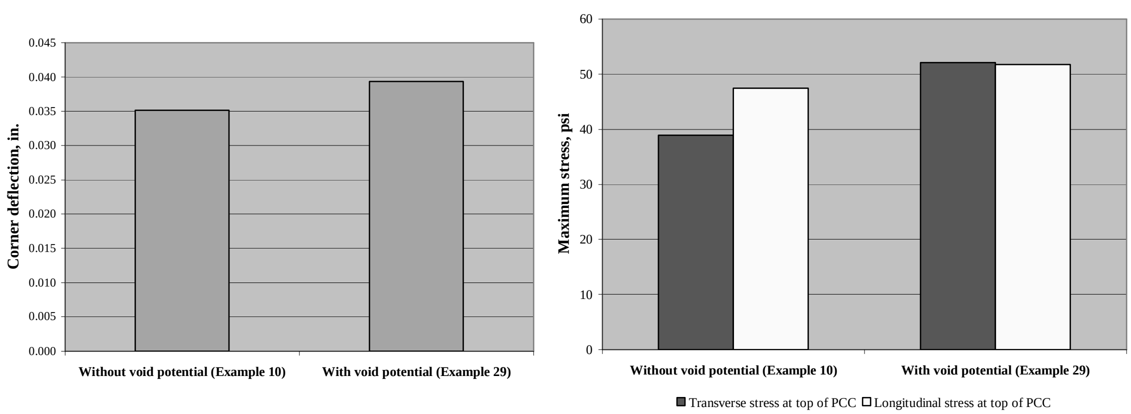


**Figure E29-8: Comparison of the Results Between with and Without Void Potential**

# Example 30: Three-layer System

### Problem Statement

Analyze the pavement system in Example 8, but consider a three-layer system (PCC, DAGB, sand subbase) instead of the two-layer system. Then, compare the analysis results with the results in Example 8.

### Given

| | | | |
|---|---|---|---|
| Sand sub base thickness | = | 20 | in. |

### Problem Illustration

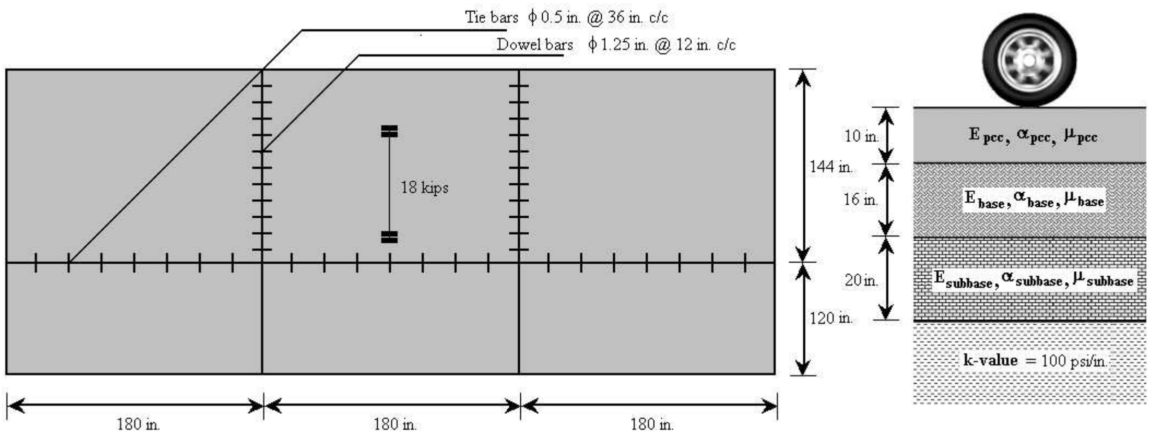


**Figure E30-1: Problem Illustration**

# Solution

### Geometry Module

Use this module from Example 8.

### Layers Module

(see Figures E30-2)

Step 1: Follow steps 1 through 4 of this module in Example 8.

Step 2: Add a third layer, and then enter the layer properties for sand subbase as illustrated in Figure E30-2.

Step 3: Click **OK** to close the layers panel.

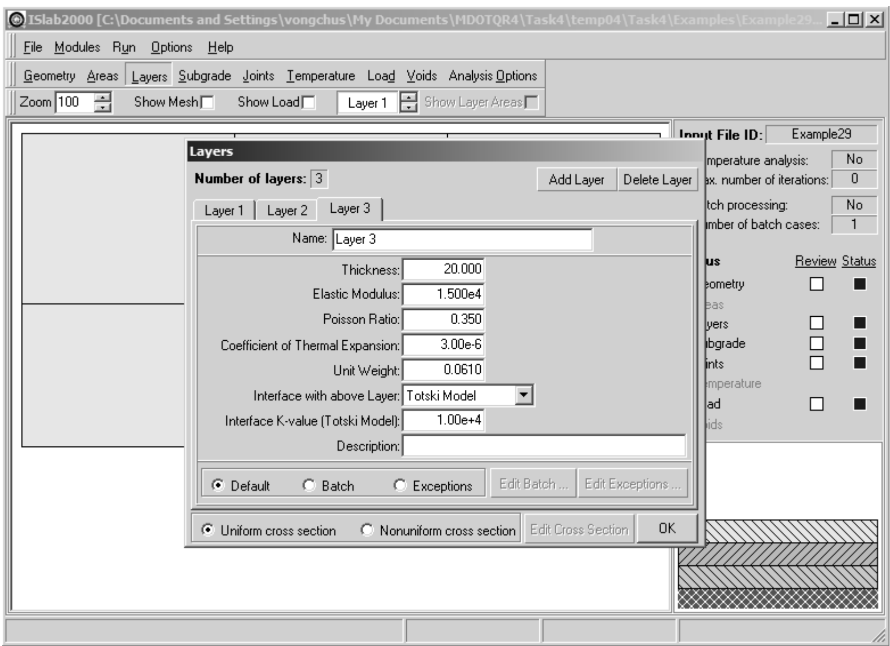


**Figure E30-2: Edit Inputs for the Layers Module**

### Subgrade Module

Use this module from Example 8.

### Joints Module

Use this module from Example 8.

### Load Module

Use this module from Example 8.

### Temperature Module

This module is not required for this problem.

The main panel should display the pavement structure, loading condition, and meshing as shown in Figure E30-3.

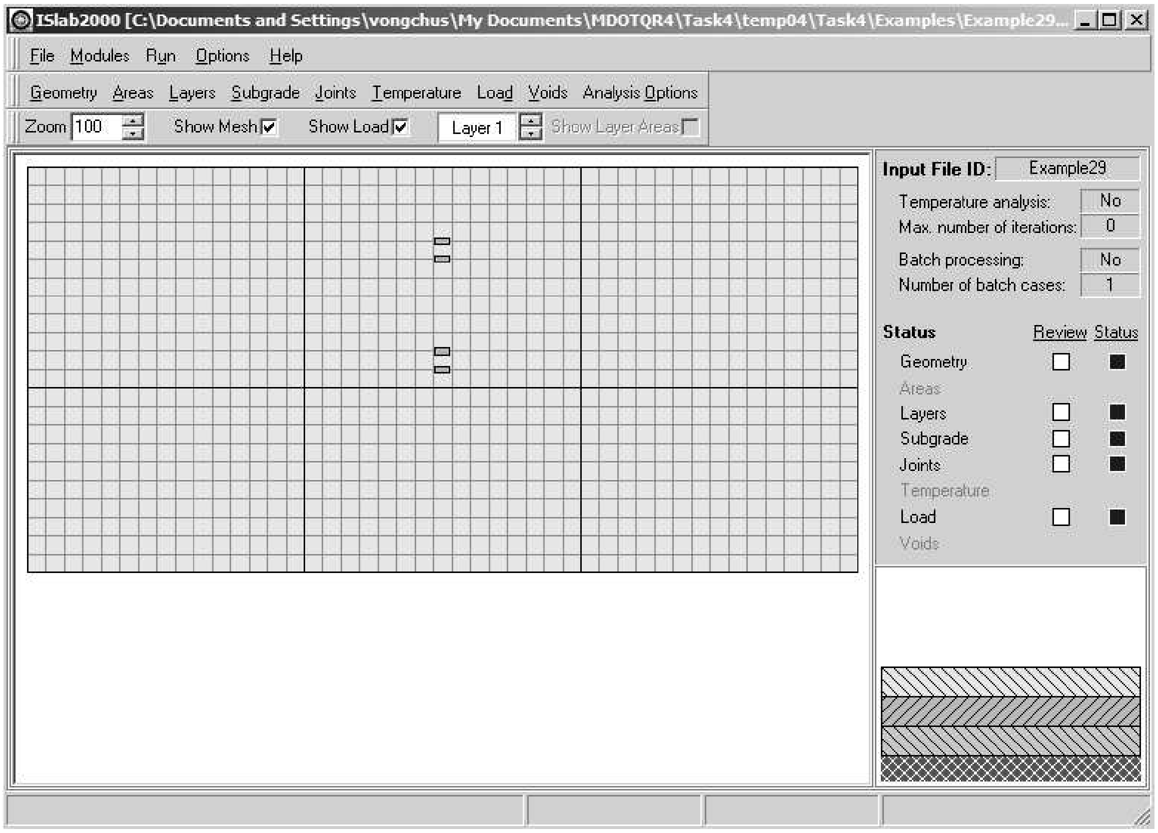


**Figure E30-3: Main Panel After Completion of Inputs**

## *Analysis Results*

| Pavement system | Transverse stress at bottom of PCC | Longitudinal stress at bottom of PCC |
|---|---|---|
| Two-layer (Example 8) | 72.1 | 114.5 |
| Three-layer (Example 30) | 70.3 | 112.1 |

**Table E30-1: Analysis Results**

**NOTE**
Positive and negative values of stress signify tensile and compressive stresses and positive value of deflection indicates deflection in downward direction.

Figure E30-4 illustrates relationship between maximum stresses and pavement system.

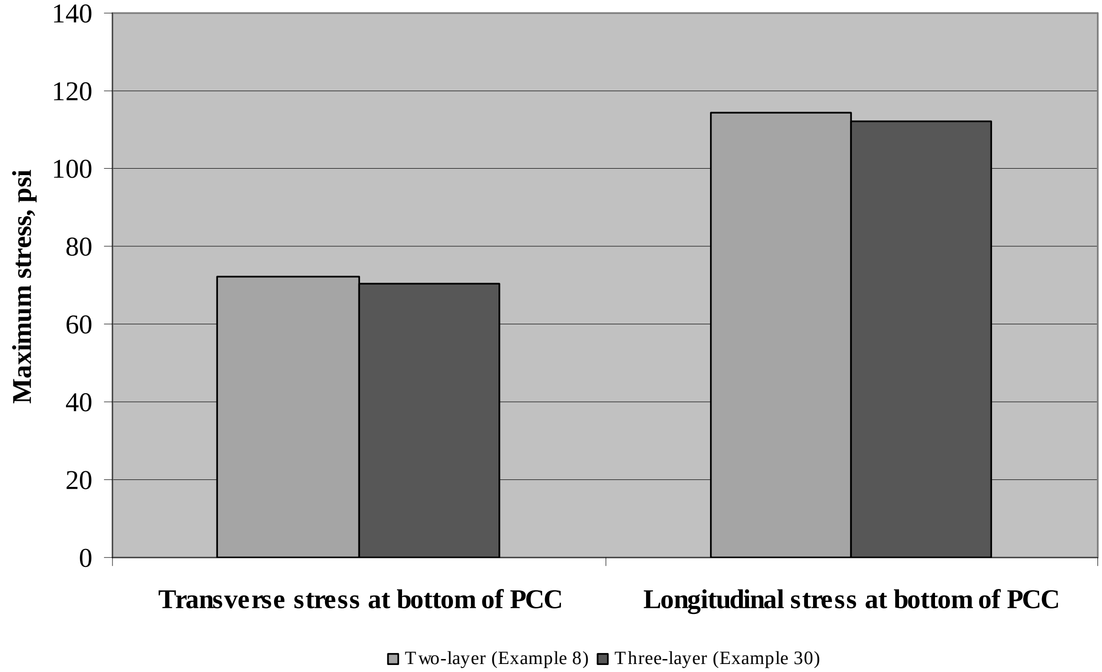


**E30-4: Relationship Between Stresses and Pavement System**

# Example 31: Non-linear Temperature Profiles

### Problem Statement

Analyze the pavement system in Example 9, but consider the two non-linear temperature profiles identified in Figure E31-1 instead of a linear temperature differential of +20 °F. Then, compare the analysis results with the results in Example 9.

### Problem Illustration

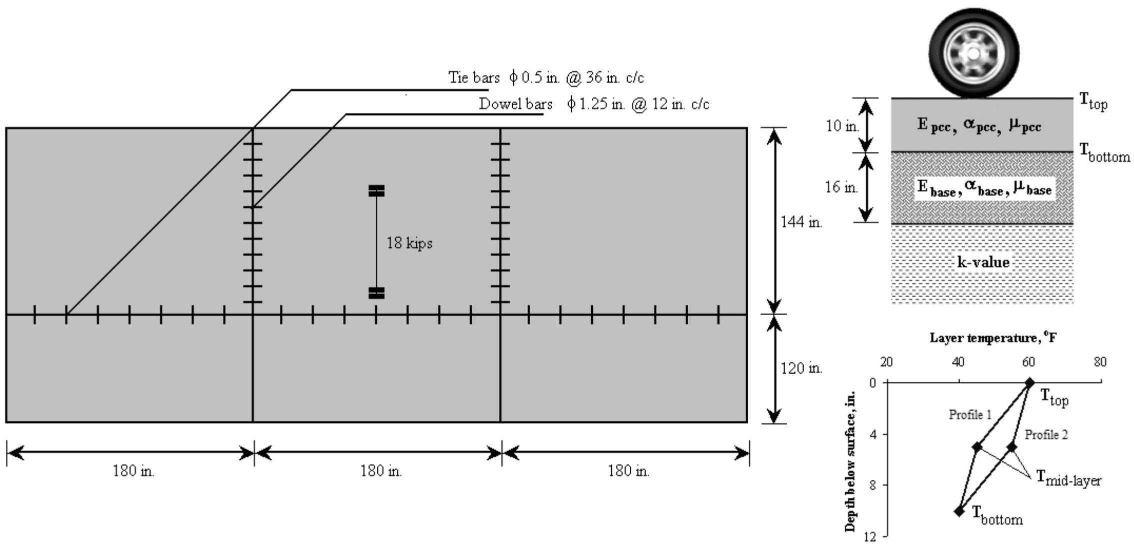


**Figure E31-1: Problem Illustration**

# Solution

### Geometry Module

Use this module from Example 8.

### Layers Module

Use this module from Example 8.

### Subgrade Module

Use this module from Example 8.

### Joints Module

Use this module from Example 8.

### Load Module

Use this module from Example 8.

### Temperature Module

(see Figures E31-2 and E31-3)

Step 1: Click **Temperature** to open the temperature properties panel.

Step 2: Select the **Perform Temperature Analysis** and the **Batch** check boxes.

Step 3: Select **Nonlinear** in the **Type** field for layer 1, select **Batch**, and then click **Edit Batch** to open the layers temperature distributions panel.

Step 4: On Layer 1, enter the identified layer temperatures for the two profiles as shown in Figure E31-2.

Step 5: On Layer 2, enter zero in the other temperature differential across the base layer (see Figure E31-3.)

Step 6: Click **OK** to close the layers temperature distributions panel.

Step 7: Click **OK** to close the layers temperature properties panel.

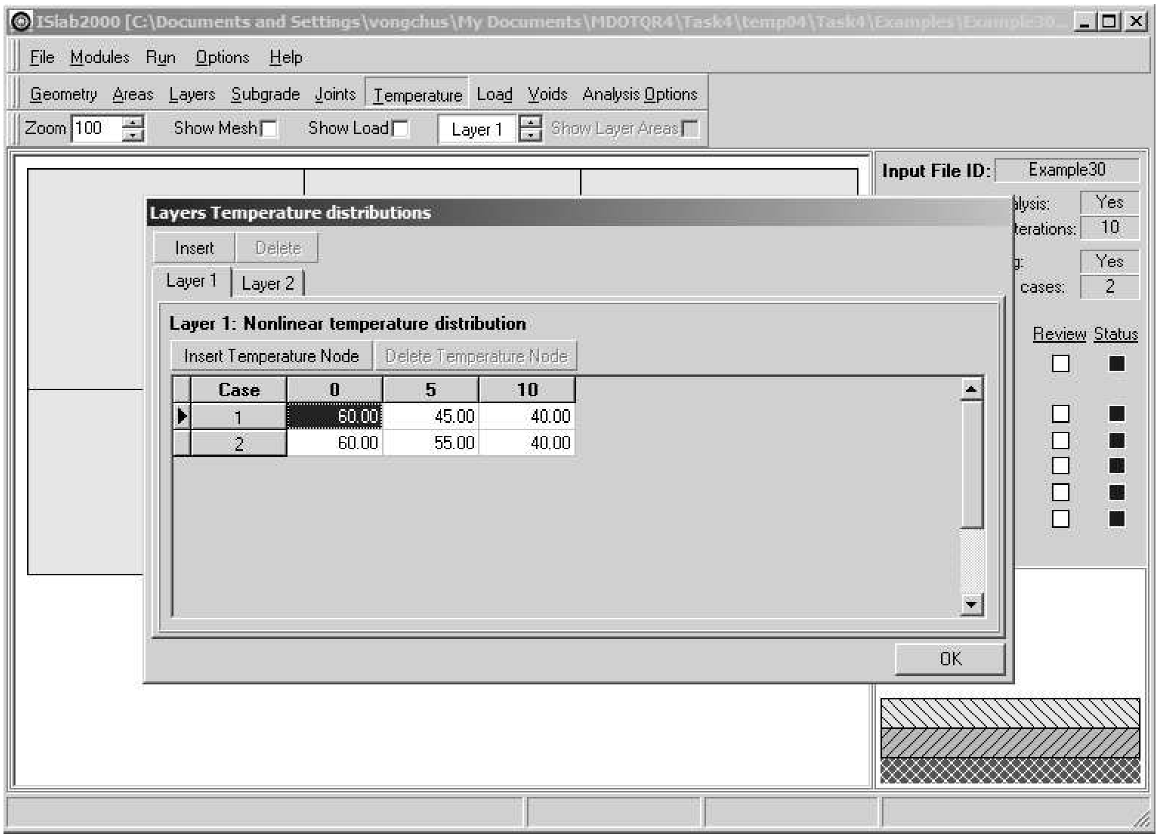


Figure 30-2: Edit Inputs for the Temperature Module

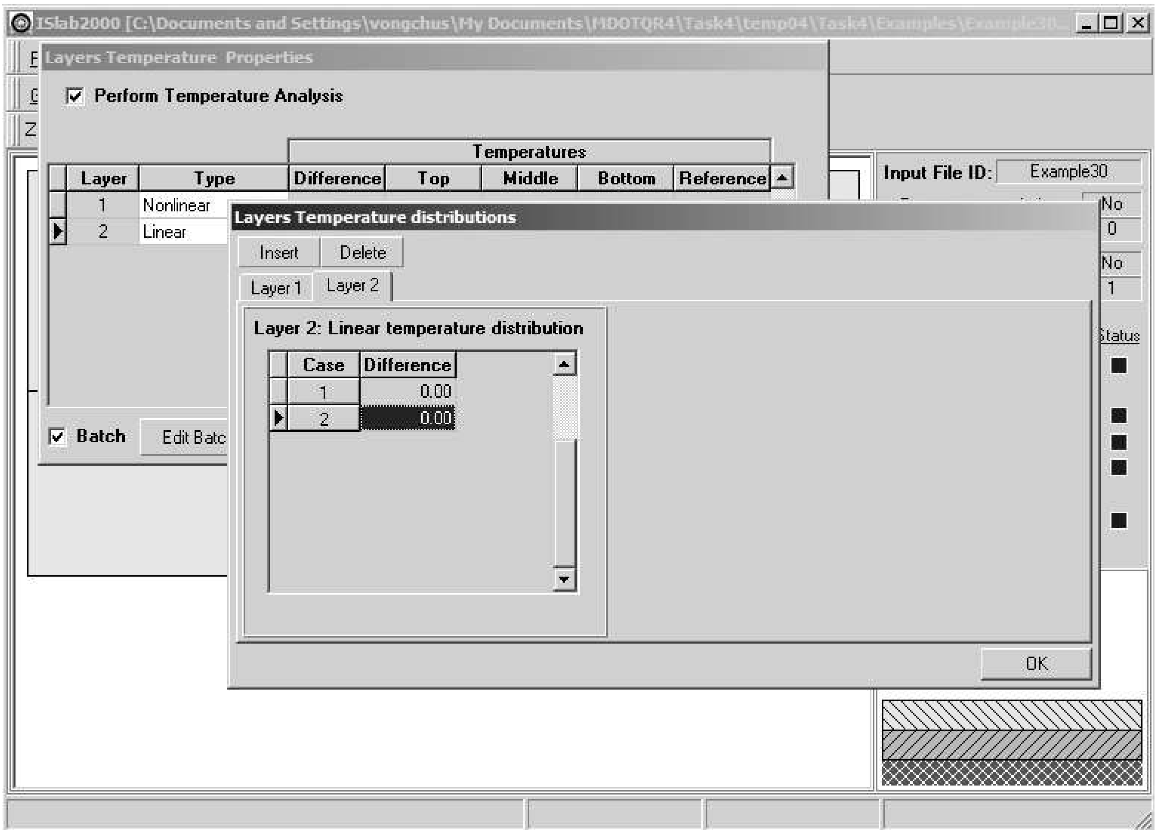


**Figure E31-3: Edit Inputs for the Temperature Module (continued)**

## Analysis Options Module

Use this module from Example 4.

The main panel should display the pavement structure, loading condition, and meshing as shown in Example 8, Figure E8-12.

## Analysis Results

| Temperature characteristic | Transverse stress at bottom of PCC | Longitudinal stress at bottom of PCC |
|---|---|---|
| Profile 1 | 80.9 | 165.4 |
| Profile 2 | 198.5 | 283.0 |
| Linear (Example 9) | 139.7 | 224.5 |

**Table E31-1: Analysis Results**

### NOTE

Positive and negative values of stress signify tensile and compressive stresses and positive value of deflection indicates deflection in downward direction.

Figure E31-4 illustrates relationship between maximum stresses and layer-temperature characteristic.

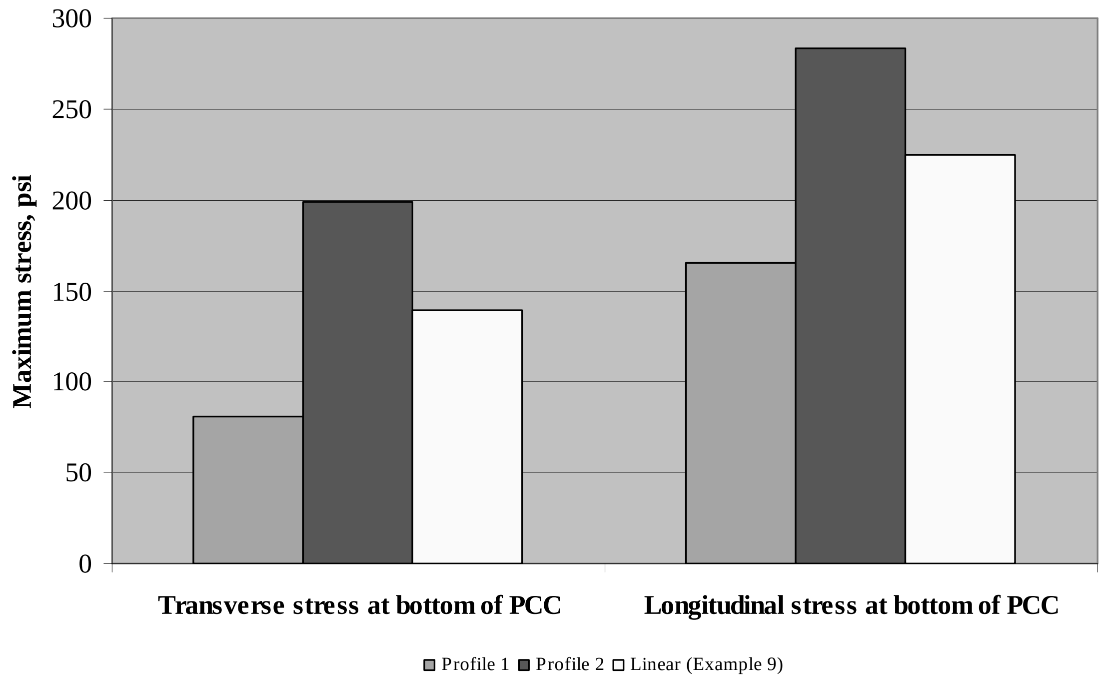


**E31-4: Relationship Between Stresses and Layer-temperature Characteristic**

# Part III: Practice with Actual MDOT Designs

## Problem Statement

Use ISLAB2000 to compute the following:

a) Maximum longitudinal stress at the bottom of the PCC slab under 18-kips single axle edge loading

b) Repeat part a) with a thermal gradient of +4 $^{o}$F/in.

c) Maximum longitudinal stress at the top of the PCC slab under 18-kips single axle corner loading

d) Repeat part c) with a thermal gradient of -4 $^{o}$F/in.

| Design No. | PCC thickness (in.) | Base thickness (in.) | k-value (psi/in.) | Joint spacing (in.) | Outer lane width (in.) | Shoulder width (in.) | Shoulder type | Joint design |
|---|---|---|---|---|---|---|---|---|
| 1 | 11.8 | 15.7 | 99 | 315 | 144 | 120 | PCC | Doweled 1.25 in. diameter at 12 in. center to center |
| 2 | 11.0 | 3.9 | 129 | 315 | 144 | 120 | AC | |
| 3 | 11.0 | 3.9 | 129 | 315 | 144 | 120 | AC | |
| 4 | 11.0 | 3.9 | 129 | 315 | 144 | 120 | AC | |
| 5 | 11.0 | 3.9 | 169 | 177 | 168 | 96 | AC | |
| 6 | 9.4 | 3.9 | 158 | 177 | 168 | 96 | AC | |
| 7 | 9.4 | 3.9 | 158 | 177 | 168 | 96 | AC | |
| 8 | 9.4 | 3.9 | 158 | 177 | 168 | 96 | AC | |
| 9 | 10.2 | 15.7 | 221 | 177 | 144 | - | Valley gutter | |
| 10 | 11.0 | 3.9 | 129 | 315 | 144 | 120 | PCC | |
| 11 | 9.4 | 3.9 | 140 | 315 | 144 | - | Valley gutter | |
| 12 | 10.2 | 3.9 | 158 | 177 | 144 | 120 | AC | |
| 13 | 10.2 | 3.9 | 88 | 315 | 144 | 120 | PCC | |
| 14 | 10.2 | 3.9 | 151 | 315 | 144 | 144 | PCC | |

**Table P1: Recent MDOT Rigid Pavement Designs**

# Answer Key

**Design No. 1**

a) 87.1 psi, b) 557.5 psi, c) 9.7 psi, d) 426.1 psi

**Design No. 2-4**

a) 115.6 psi, b) 573.5 psi, c) 21.5 psi, d) 383.8 psi

**Design No. 5**

a) 97.1 psi, b) 291.7 psi, c) 0.9 psi, d) 152.6 psi

**Design No. 6-8**

a) 119.2 psi, b) 372.3 psi, c) 2.4 psi, d) 191.0 psi

**Design No. 9**

a) 102.2 psi, b) 378.4 psi, c) 3.8 psi, d) 225.7 psi

**Design No. 10**

a) 92.0 psi, b) 551.6 psi, c) 13.2 psi, d) 384.9 psi

**Design No. 11**

a) 122.8 psi, b) 549.1 psi, c) 23.3 psi, d) 389.3 psi

**Design No. 12**

a) 129.5 psi, b) 349.7 psi, c) 4.7 psi, d) 153.3 psi

**Design No. 13**

a) 110.5 psi, b) 539.6 psi, c) 14.9 psi, d) 370.7 psi

**Design No. 14**

a) 98.9 psi, b) 553.0 psi, c) 15.7 psi, d) 394.4 psi

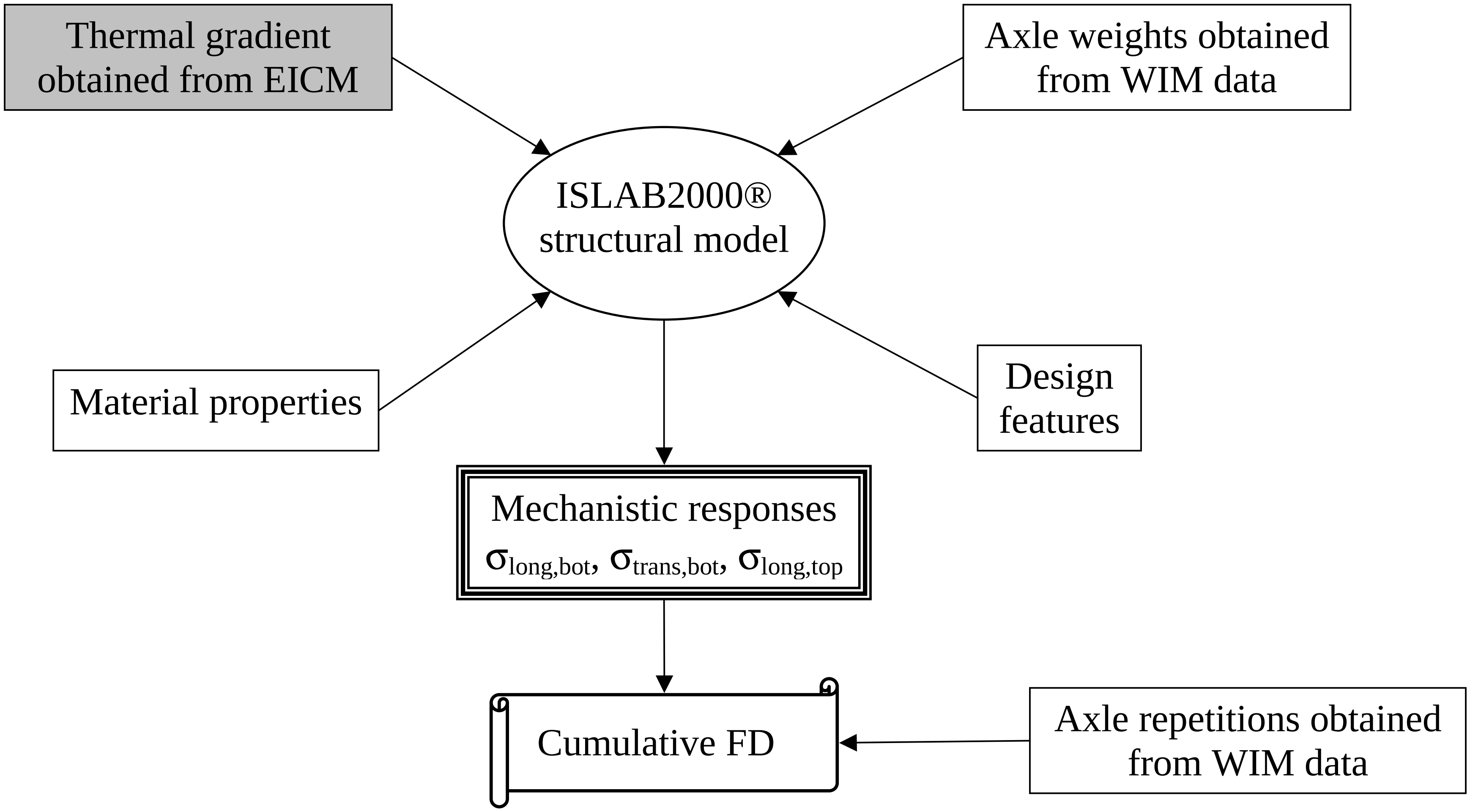


**Figure K-1: Role of thermal gradient from EICM in the design process**

**Table K-1: Thermal gradients generated by EICM for 8-in. sections (sections 26-0213, 26-0214)**

| Year | Month | 12 am - 3 am | 3 am - 6 am | 6 am - 9 am | 9 am - 12 pm | 12 pm - 3 pm | 3 pm - 6 pm | 6 pm - 9 pm | 9 pm - 12 am |
|---|---|---|---|---|---|---|---|---|---|
| 1998 | July | -1.398 | -1.386 | -0.257 | 2.280 | 2.962 | 2.169 | 0.354 | -1.316 |
| 1998 | August | -1.325 | -1.143 | -0.641 | 1.696 | 2.333 | 1.864 | -0.182 | -1.501 |
| 1998 | September | -1.418 | -1.382 | -1.167 | 1.205 | 2.476 | 1.924 | -0.328 | -1.361 |
| 1998 | October | -1.078 | -1.125 | -1.111 | 0.783 | 1.882 | 1.208 | -0.699 | -1.028 |
| 1998 | November | -0.812 | -0.786 | -0.678 | 0.311 | 1.427 | 0.815 | -0.518 | -0.742 |
| 1998 | December | -0.896 | -0.886 | -0.818 | 0.046 | 1.248 | 0.688 | -0.567 | -0.823 |
| 1999 | January | -0.720 | -0.839 | -0.852 | -0.224 | 0.703 | 0.361 | -0.702 | -0.786 |
| 1999 | February | -0.747 | -0.703 | -0.671 | 0.438 | 1.415 | 0.905 | -0.501 | -0.689 |
| 1999 | March | -0.926 | -1.017 | -0.937 | 1.154 | 2.065 | 1.802 | -0.400 | -0.841 |
| 1999 | April | -1.080 | -1.038 | -0.717 | 1.631 | 2.315 | 1.499 | -0.210 | -1.079 |
| 1999 | May | -1.374 | -1.309 | -0.269 | 2.110 | 2.796 | 1.827 | 0.003 | -1.381 |
| 1999 | June | -1.487 | -1.435 | -0.071 | 2.163 | 2.601 | 2.130 | 0.147 | -1.605 |
| 1999 | July | -1.591 | -1.494 | -0.278 | 2.189 | 2.618 | 2.217 | 0.187 | -1.514 |
| 1999 | August | -1.423 | -1.477 | -0.836 | 1.709 | 2.426 | 1.700 | -0.161 | -1.464 |
| 1999 | September | -1.511 | -1.403 | -1.288 | 1.502 | 2.674 | 2.010 | -0.459 | -1.404 |
| 1999 | October | -1.082 | -1.097 | -1.020 | 1.005 | 2.077 | 1.262 | -0.759 | -1.059 |
| 1999 | November | -0.883 | -0.941 | -0.904 | 0.268 | 1.555 | 1.014 | -0.610 | -0.804 |
| 1999 | December | -0.677 | -0.676 | -0.661 | 0.101 | 1.063 | 0.670 | -0.480 | -0.625 |
| 2000 | January | -0.898 | -1.039 | -1.036 | -0.283 | 0.856 | 0.368 | -0.813 | -0.898 |
| 2000 | February | -0.499 | -0.457 | -0.481 | 0.696 | 1.737 | 1.356 | -0.173 | -0.440 |
| 2000 | March | -0.930 | -0.980 | -0.903 | 1.101 | 2.303 | 1.551 | -0.462 | -0.978 |
| 2000 | April | -1.157 | -1.130 | -0.795 | 1.393 | 2.119 | 1.911 | -0.114 | -1.192 |
| 2000 | May | -1.349 | -1.184 | -0.286 | 1.876 | 2.589 | 1.725 | 0.045 | -1.370 |
| 2000 | June | -1.412 | -1.313 | -0.150 | 1.852 | 2.536 | 1.757 | 0.211 | -1.478 |
| 2000 | July | -1.538 | -1.363 | -0.295 | 1.790 | 2.598 | 2.040 | 0.076 | -1.510 |
| 2000 | August | -1.424 | -1.340 | -0.790 | 1.481 | 2.541 | 2.067 | 0.161 | -1.332 |
| 2000 | September | -1.362 | -1.312 | -1.135 | 1.168 | 2.395 | 1.773 | -0.583 | -1.402 |
| 2000 | October | -1.023 | -1.003 | -1.005 | 0.896 | 2.222 | 1.436 | -0.649 | -1.058 |
| 2000 | November | -0.895 | -0.849 | -0.807 | 0.213 | 1.191 | 0.744 | -0.635 | -0.806 |
| 2000 | December | -0.844 | -0.811 | -0.824 | -0.210 | 0.728 | 0.302 | -0.747 | -0.824 |

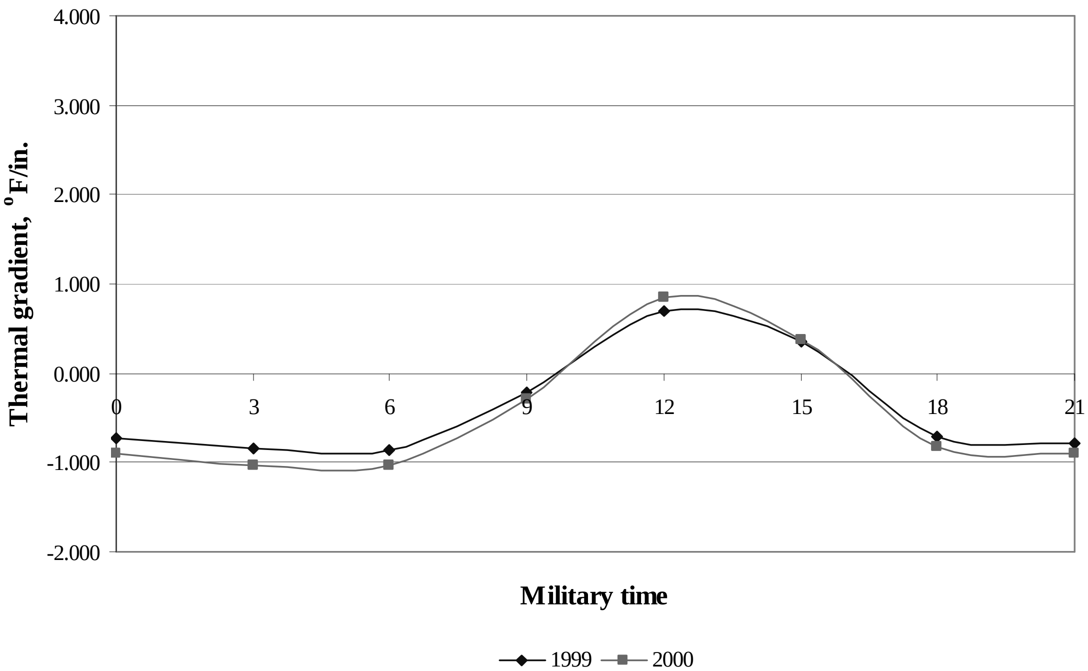


**Figure K-2: Hourly thermal gradients generated by EICM for 8-in. sections in January**

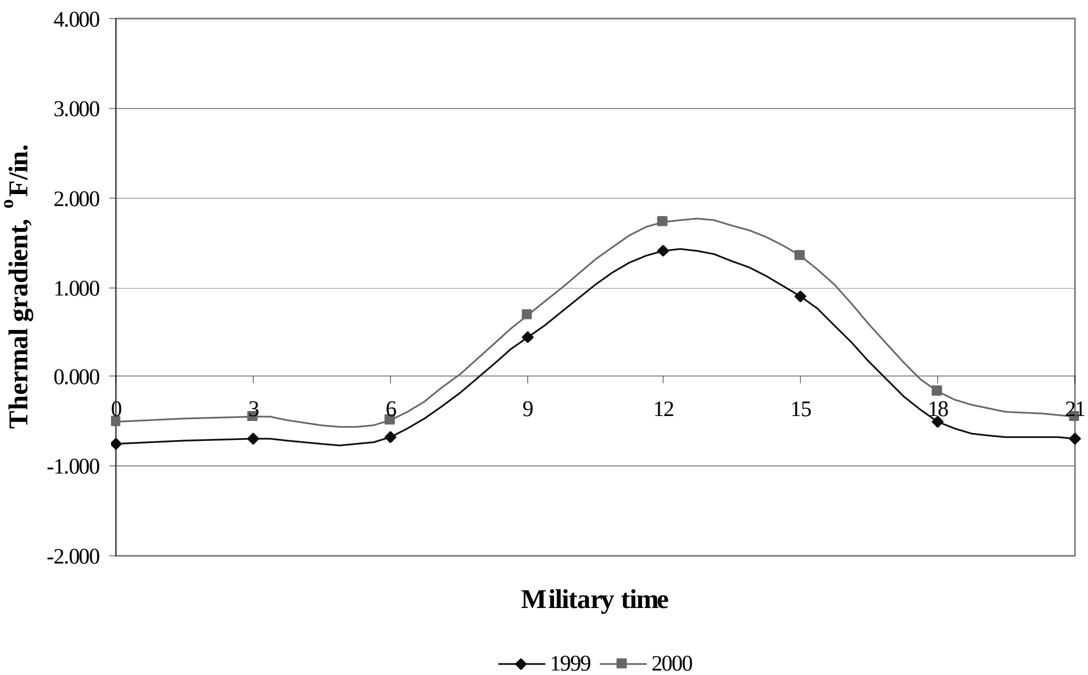


**Figure K-3: Hourly thermal gradients generated by EICM for 8-in. sections in February**

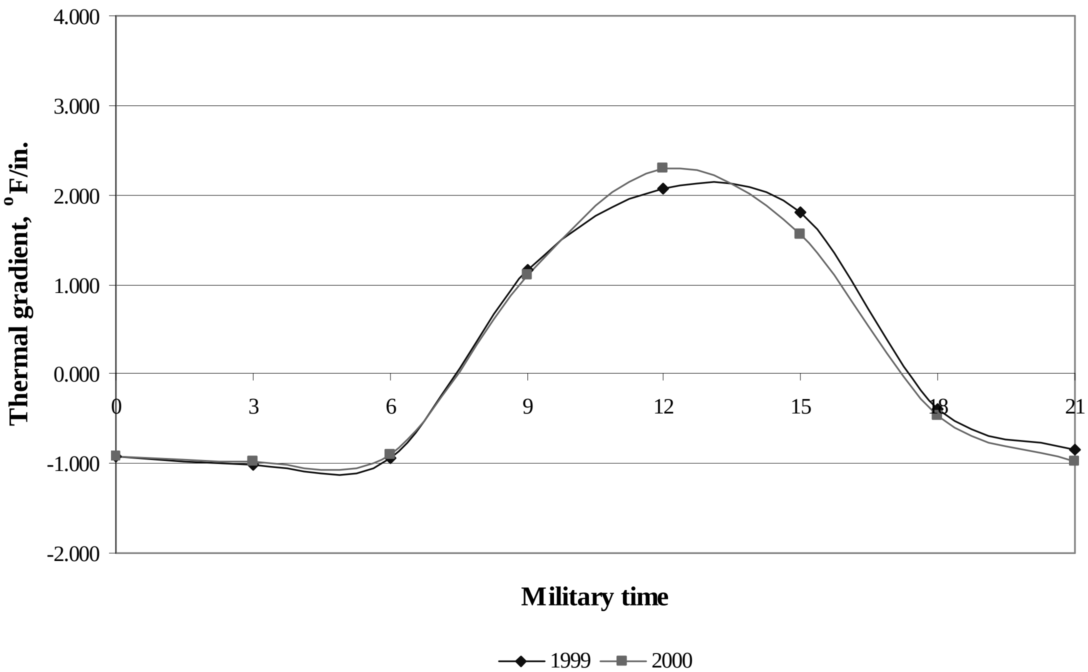


**Figure K-4: Hourly thermal gradients generated by EICM for 8-in. sections in March**

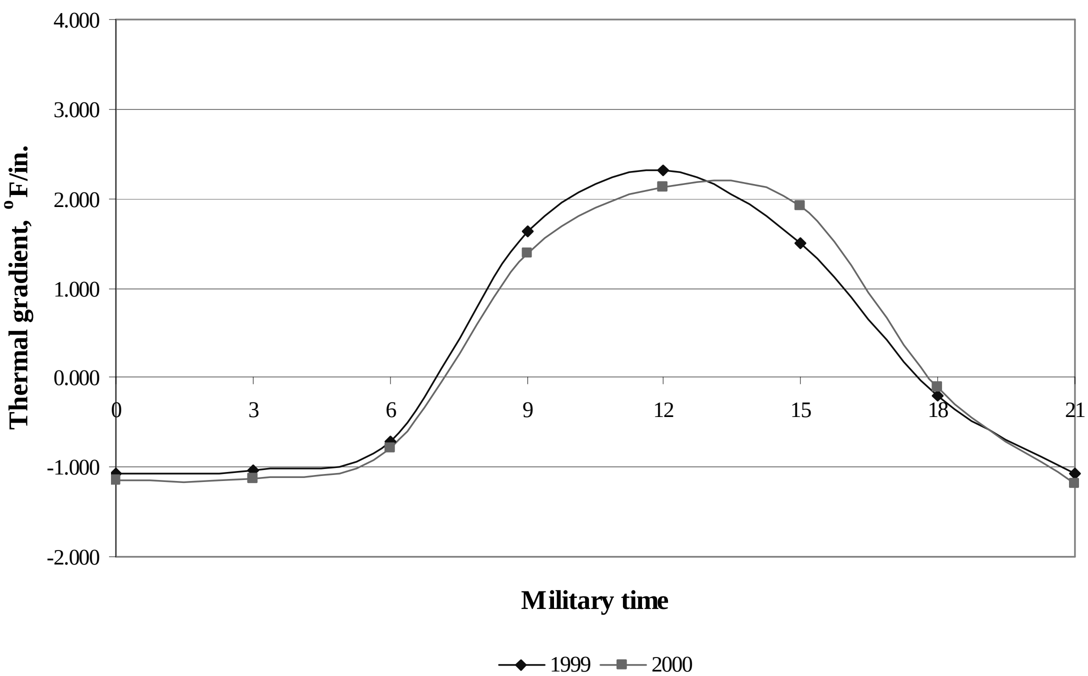


**Figure K-5: Hourly thermal gradients generated by EICM for 8-in. sections in April**

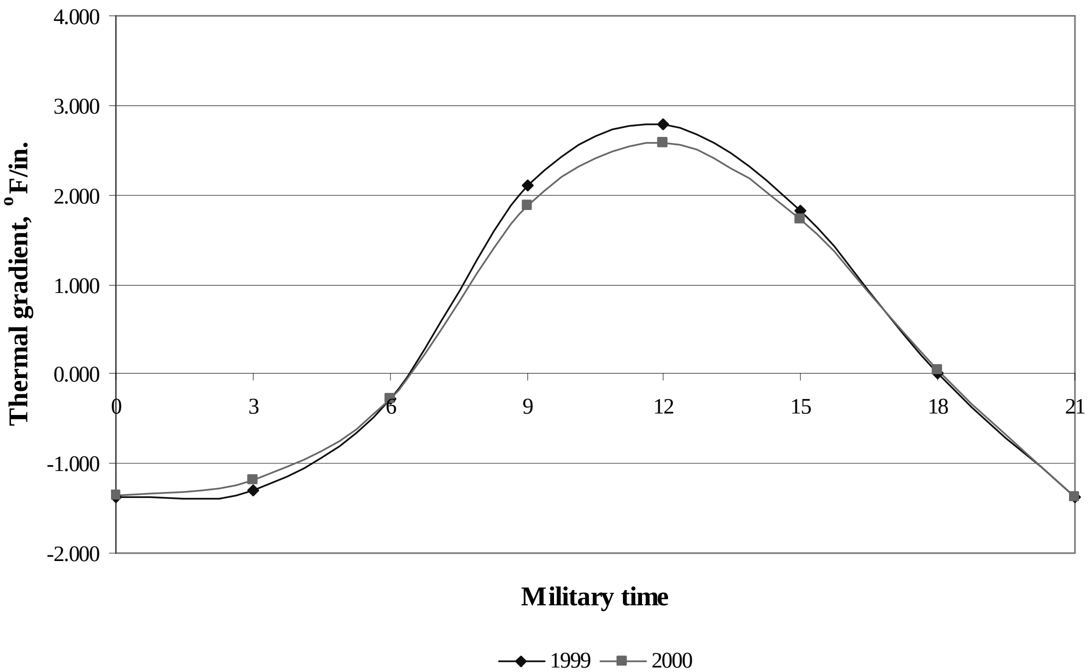


**Figure K-6: Hourly thermal gradients generated by EICM for 8-in. sections in May**

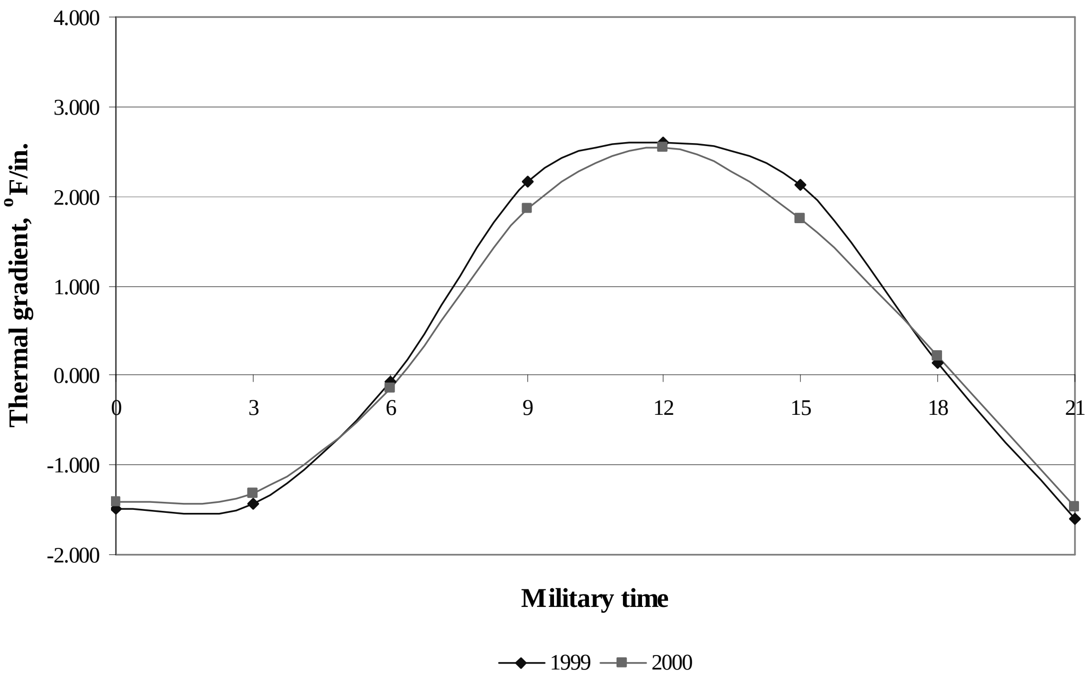


**Figure K-7: Hourly thermal gradients generated by EICM for 8-in. sections in June**

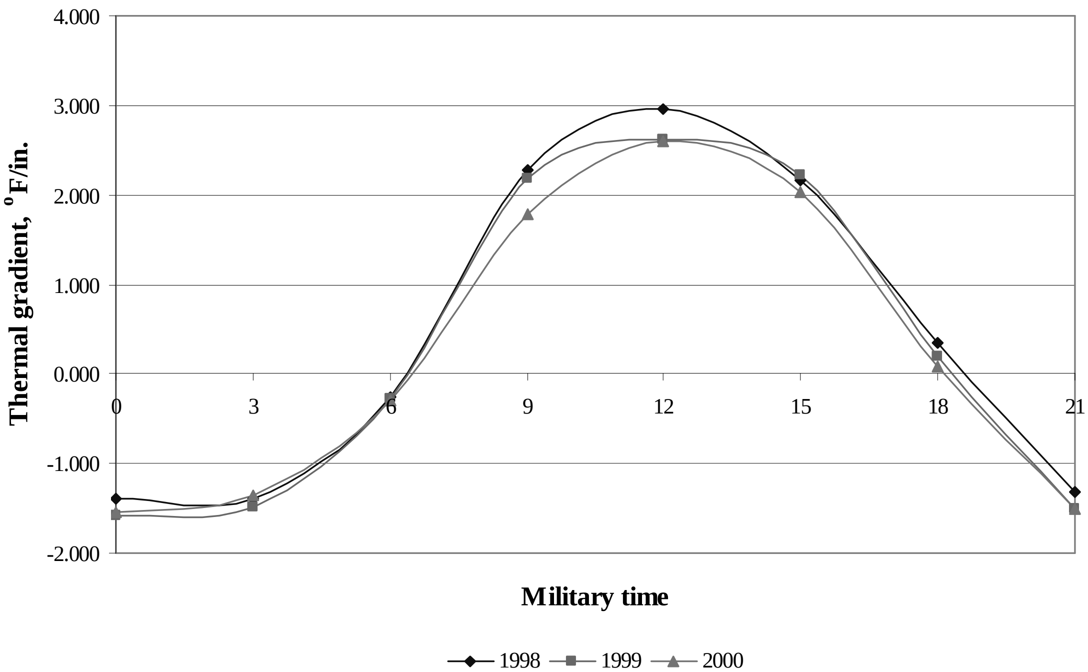


**Figure K-8: Hourly thermal gradients generated by EICM for 8-in. sections in July**

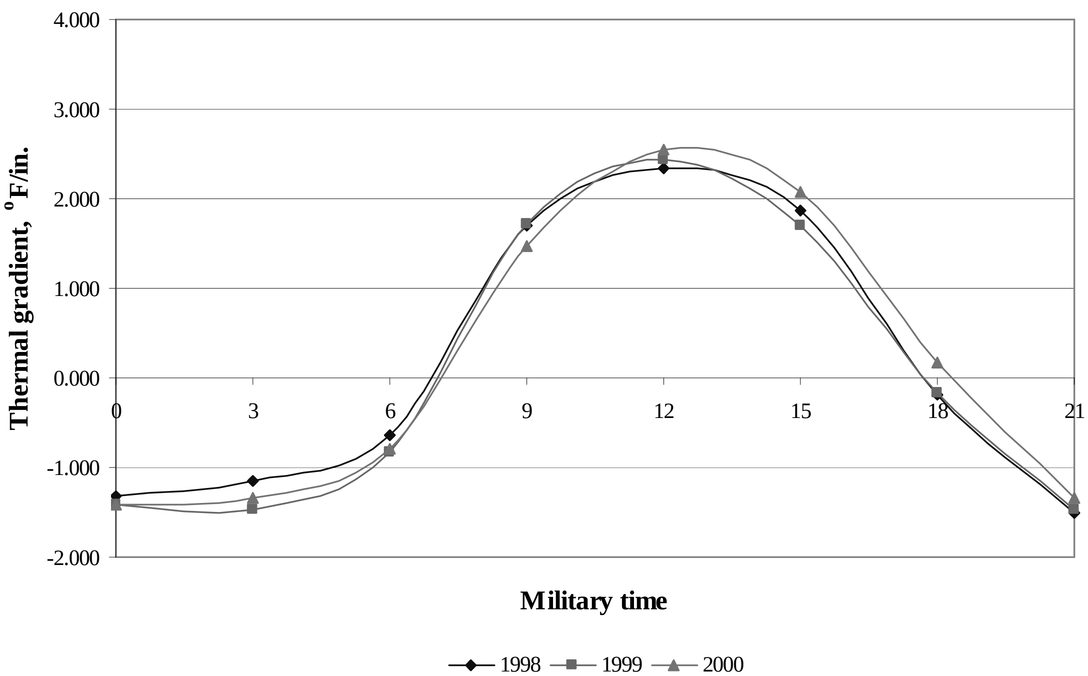


**Figure K-9: Hourly thermal gradients generated by EICM for 8-in. sections in August**

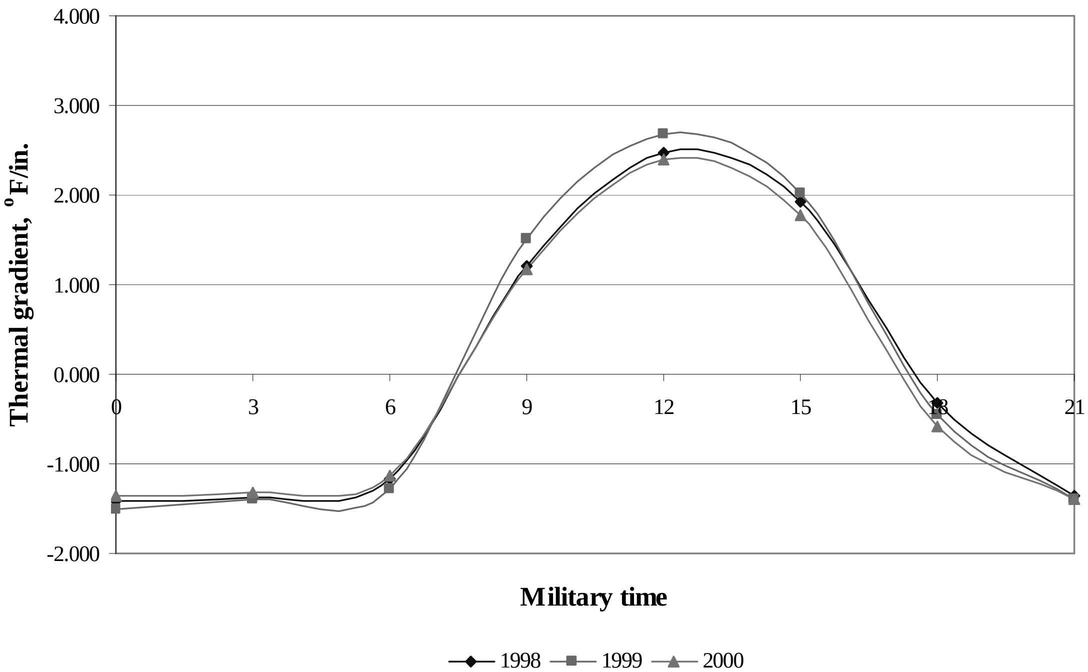


**Figure K-10: Hourly thermal gradients generated by EICM for 8-in. sections in September**

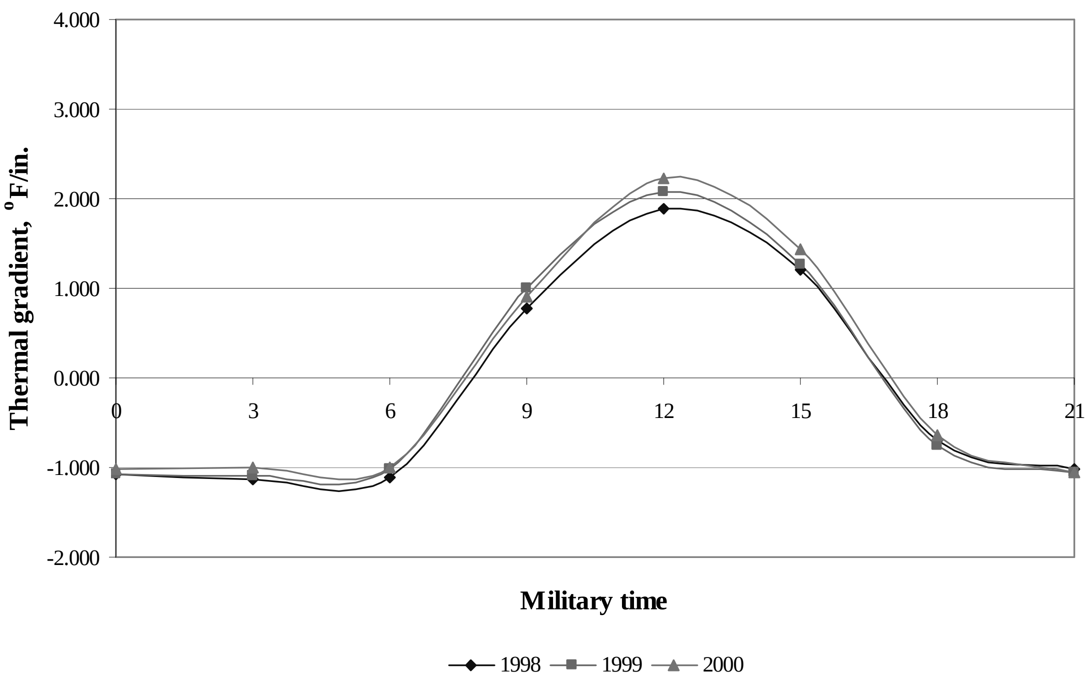


**Figure K-11: Hourly thermal gradients generated by EICM for 8-in. sections in October**

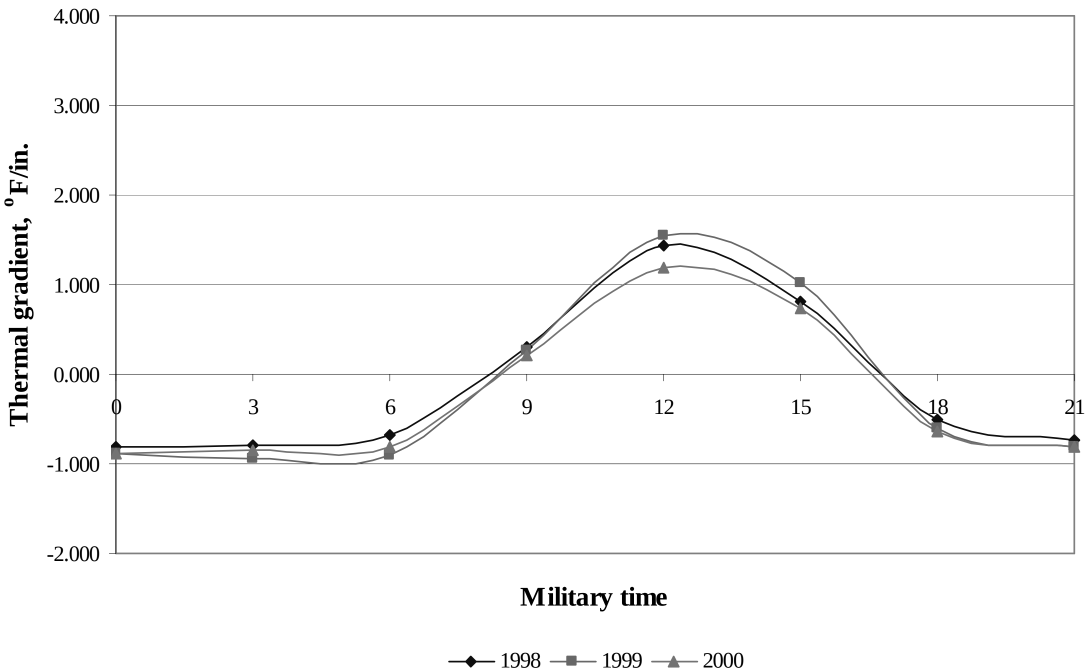


**Figure K-12: Hourly thermal gradients generated by EICM for 8-in. sections in November**

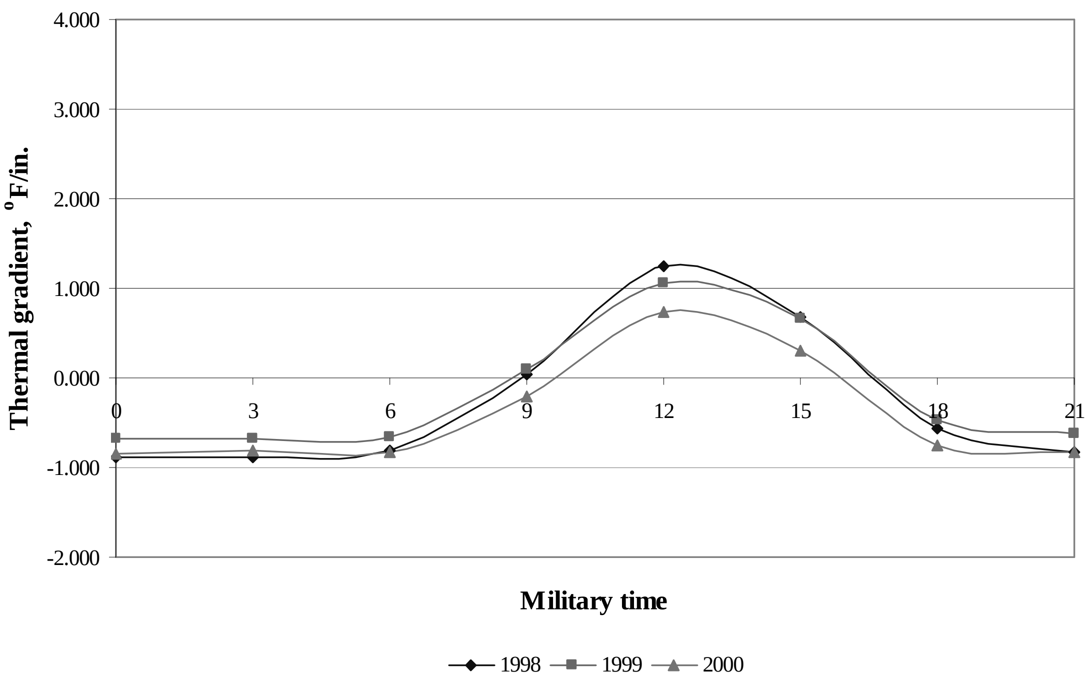


**Figure K-13: Hourly thermal gradients generated by EICM for 8-in. sections in December**

**Table K-2: Thermal gradients generated by EICM for 11-in. sections (sections 26-0215, 26-0216)**

| Year | Month | 12 am - 3 am | 3 am - 6 am | 6 am - 9 am | 9 am - 12 pm | 12 pm - 3 pm | 3 pm - 6 pm | 6 pm - 9 pm | 9 pm - 12 am |
|---|---|---|---|---|---|---|---|---|---|
| 1998 | July | -1.057 | -1.148 | -0.428 | 1.569 | 2.423 | 2.060 | 0.728 | -0.750 |
| 1998 | August | -1.070 | -1.001 | -0.699 | 1.085 | 1.853 | 1.702 | 0.230 | -0.994 |
| 1998 | September | -1.139 | -1.193 | -1.089 | 0.653 | 1.881 | 1.734 | 0.123 | -0.913 |
| 1998 | October | -0.909 | -1.000 | -1.025 | 0.319 | 1.380 | 1.082 | -0.314 | -0.763 |
| 1998 | November | -0.688 | -0.708 | -0.648 | 0.046 | 1.025 | 0.759 | -0.251 | -0.556 |
| 1998 | December | -0.766 | -0.787 | -0.750 | -0.158 | 0.852 | 0.571 | -0.372 | -0.659 |
| 1999 | January | -0.662 | -0.771 | -0.803 | -0.381 | 0.399 | 0.266 | -0.520 | -0.674 |
| 1999 | February | -0.616 | -0.627 | -0.621 | 0.166 | 1.042 | 0.839 | -0.212 | -0.498 |
| 1999 | March | -0.755 | -0.882 | -0.860 | 0.658 | 1.571 | 1.563 | -0.017 | -0.567 |
| 1999 | April | -0.862 | -0.897 | -0.719 | 1.050 | 1.835 | 1.426 | 0.161 | -0.710 |
| 1999 | May | -1.078 | -1.115 | -0.453 | 1.439 | 2.266 | 1.752 | 0.388 | -0.876 |
| 1999 | June | -1.166 | -1.219 | -0.340 | 1.465 | 2.116 | 1.971 | 0.537 | -1.003 |
| 1999 | July | -1.241 | -1.280 | -0.502 | 1.470 | 2.131 | 2.039 | 0.575 | -0.937 |
| 1999 | August | -1.157 | -1.282 | -0.900 | 1.050 | 1.884 | 1.563 | 0.209 | -0.994 |
| 1999 | September | -1.221 | -1.227 | -1.199 | 0.835 | 2.044 | 1.812 | 0.034 | -0.958 |
| 1999 | October | -0.908 | -0.972 | -0.949 | 0.499 | 1.561 | 1.174 | -0.323 | -0.775 |
| 1999 | November | -0.743 | -0.830 | -0.838 | -0.027 | 1.107 | 0.907 | -0.306 | -0.609 |
| 1999 | December | -0.582 | -0.601 | -0.601 | -0.075 | 0.738 | 0.559 | -0.304 | -0.498 |
| 2000 | January | -0.800 | -0.920 | -0.934 | -0.425 | 0.515 | 0.283 | -0.601 | -0.755 |
| 2000 | February | -0.406 | -0.407 | -0.447 | 0.375 | 1.273 | 1.123 | 0.031 | -0.285 |
| 2000 | March | -0.743 | -0.835 | -0.821 | 0.624 | 1.769 | 1.439 | -0.029 | -0.647 |
| 2000 | April | -0.918 | -0.971 | -0.796 | 0.864 | 1.671 | 1.726 | 0.274 | -0.772 |
| 2000 | May | -1.070 | -1.029 | -0.456 | 1.258 | 2.097 | 1.659 | 0.408 | -0.875 |
| 2000 | June | -1.107 | -1.128 | -0.374 | 1.272 | 2.056 | 1.674 | 0.536 | -0.926 |
| 2000 | July | -1.220 | -1.180 | -0.500 | 1.186 | 2.068 | 1.861 | 0.450 | -0.967 |
| 2000 | August | -1.118 | -1.149 | -0.832 | 0.908 | 1.985 | 1.868 | 0.500 | -0.838 |
| 2000 | September | -1.135 | -1.164 | -1.078 | 0.622 | 1.800 | 1.597 | -0.114 | -0.993 |
| 2000 | October | -0.845 | -0.885 | -0.923 | 0.430 | 1.647 | 1.322 | -0.211 | -0.748 |
| 2000 | November | -0.774 | -0.777 | -0.766 | -0.054 | 0.821 | 0.654 | -0.372 | -0.636 |
| 2000 | December | -0.740 | -0.733 | -0.746 | -0.322 | 0.439 | 0.236 | -0.565 | -0.697 |

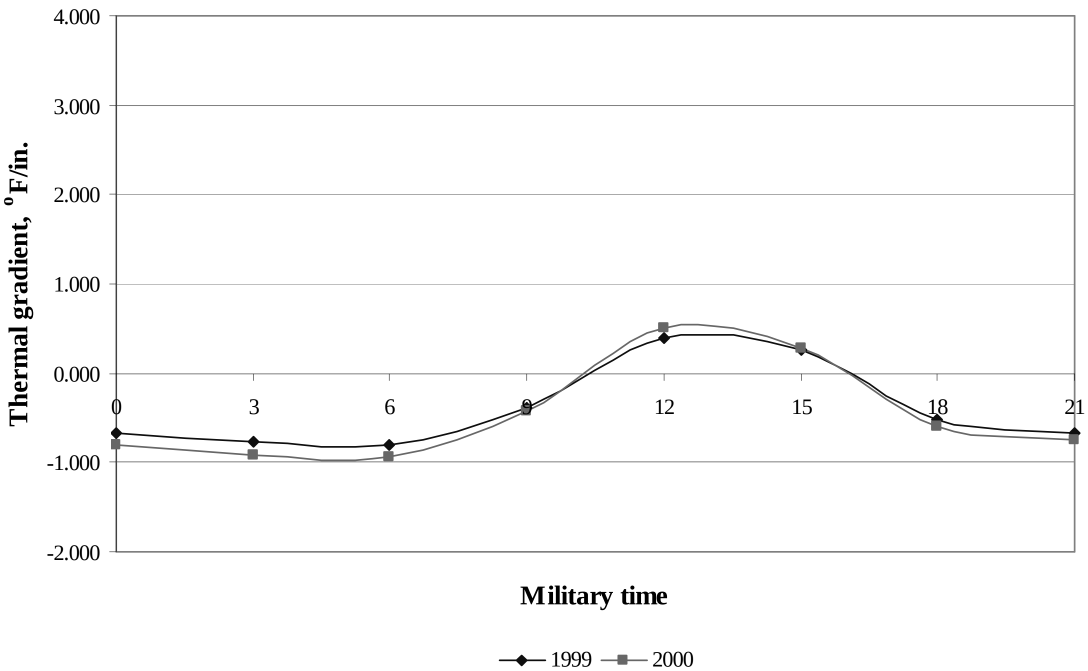


**Figure K-14: Hourly thermal gradients generated by EICM for 11-in. sections in January**

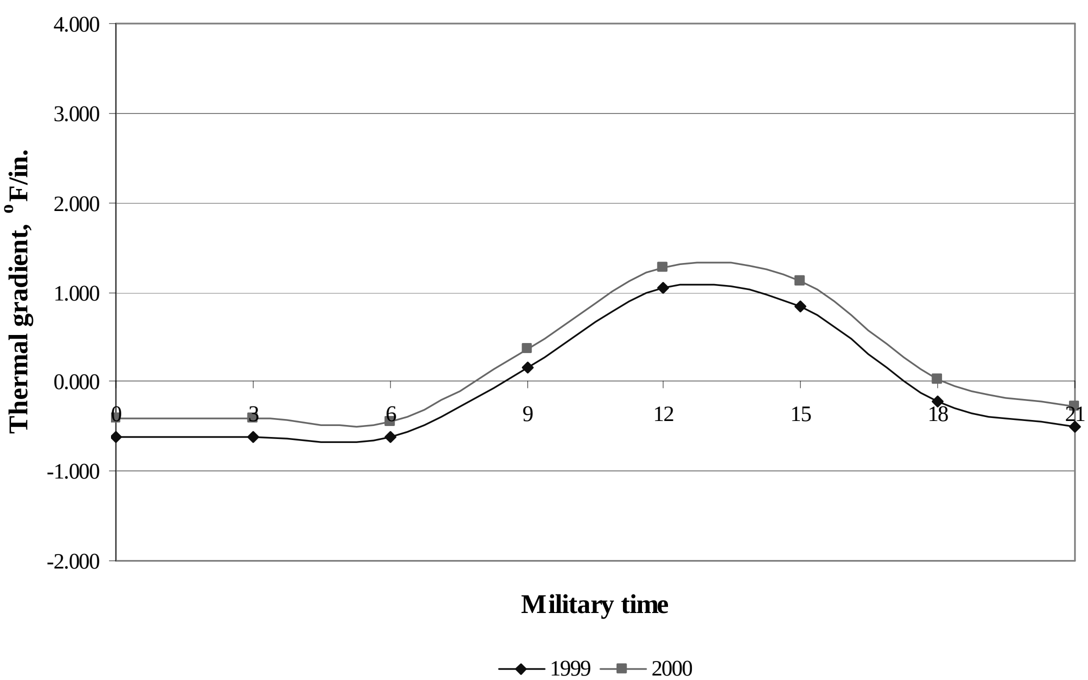


**Figure K-15: Hourly thermal gradients generated by EICM for 11-in. sections in February**

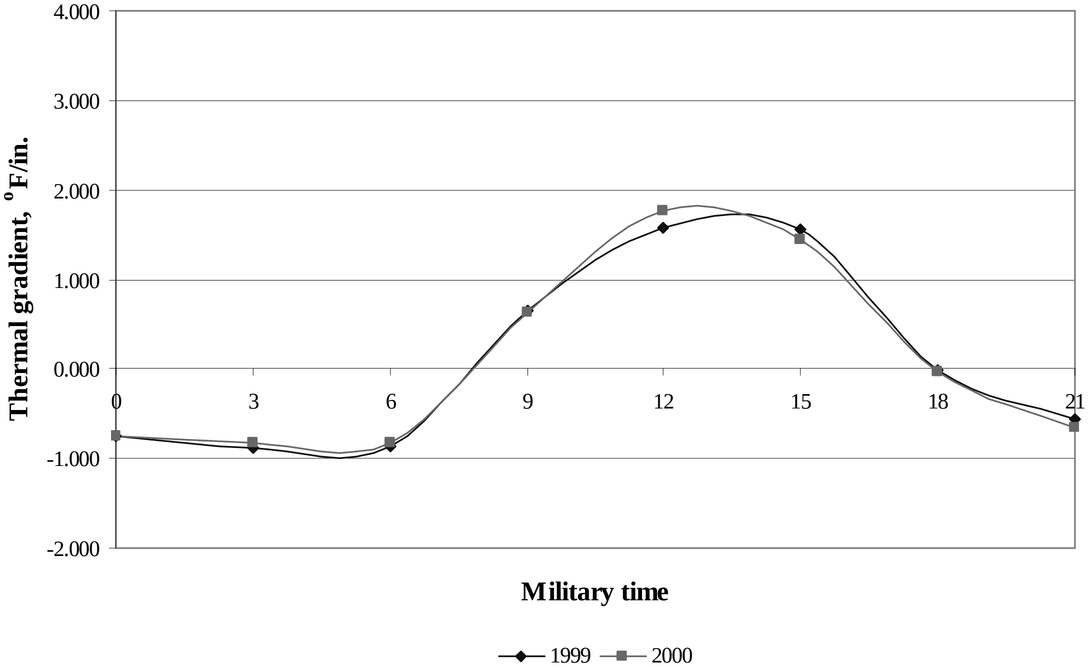


**Figure K-16: Hourly thermal gradients generated by EICM for 11-in. sections in March**

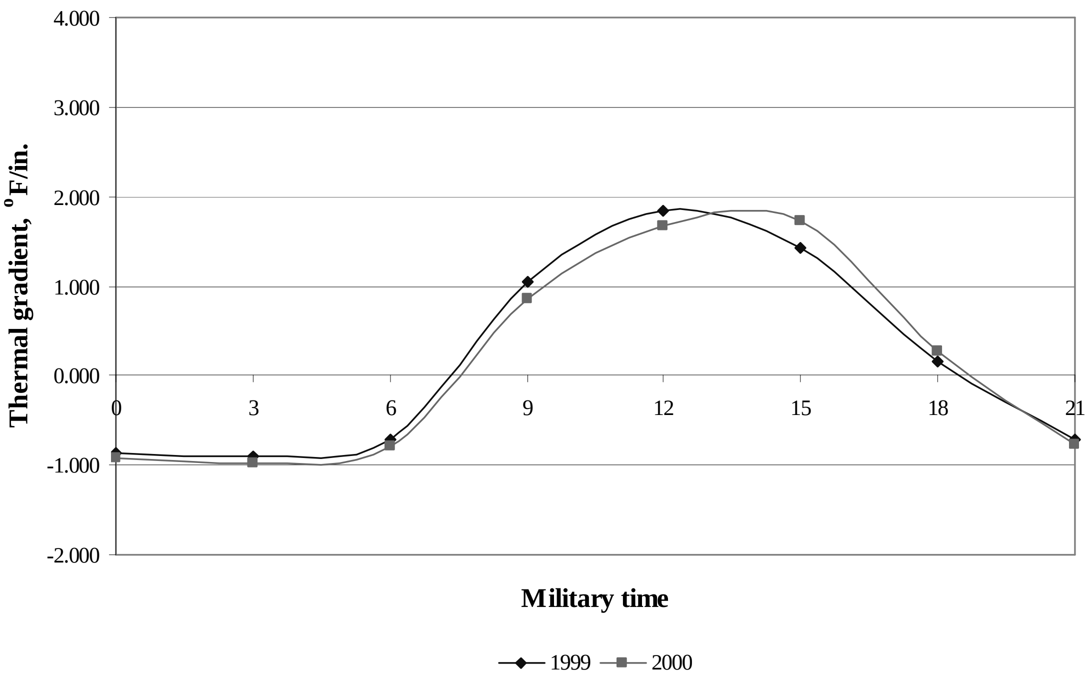


**Figure K-17: Hourly thermal gradients generated by EICM for 11-in. sections in April**

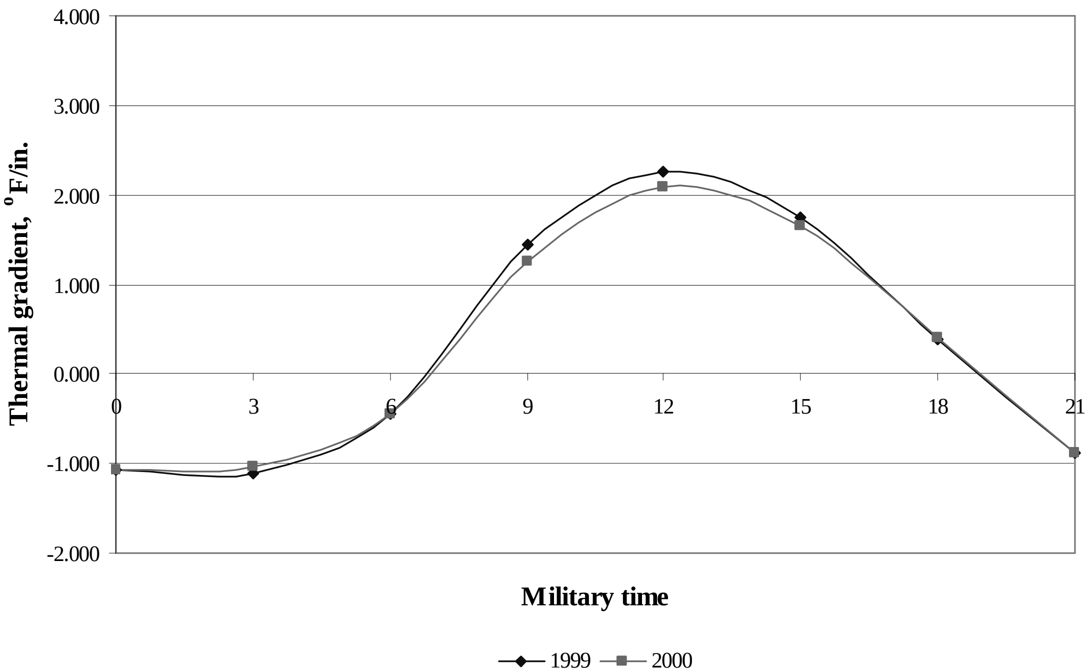


**Figure K-18: Hourly thermal gradients generated by EICM for 11-in. sections in May**

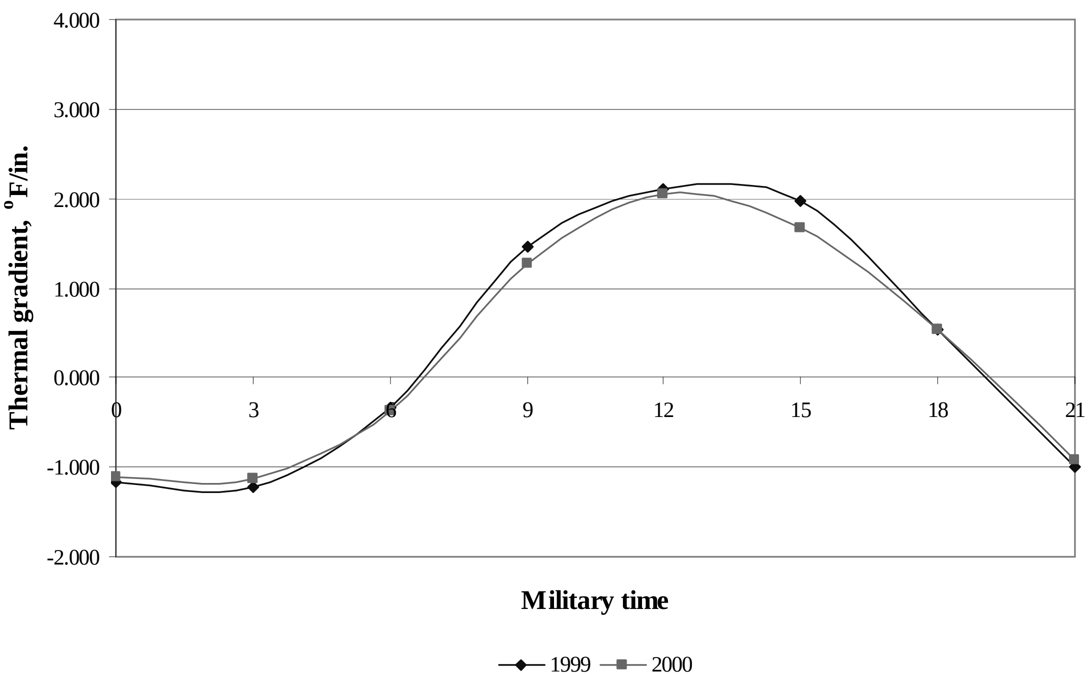


**Figure K-19: Hourly thermal gradients generated by EICM for 11-in. sections in June**

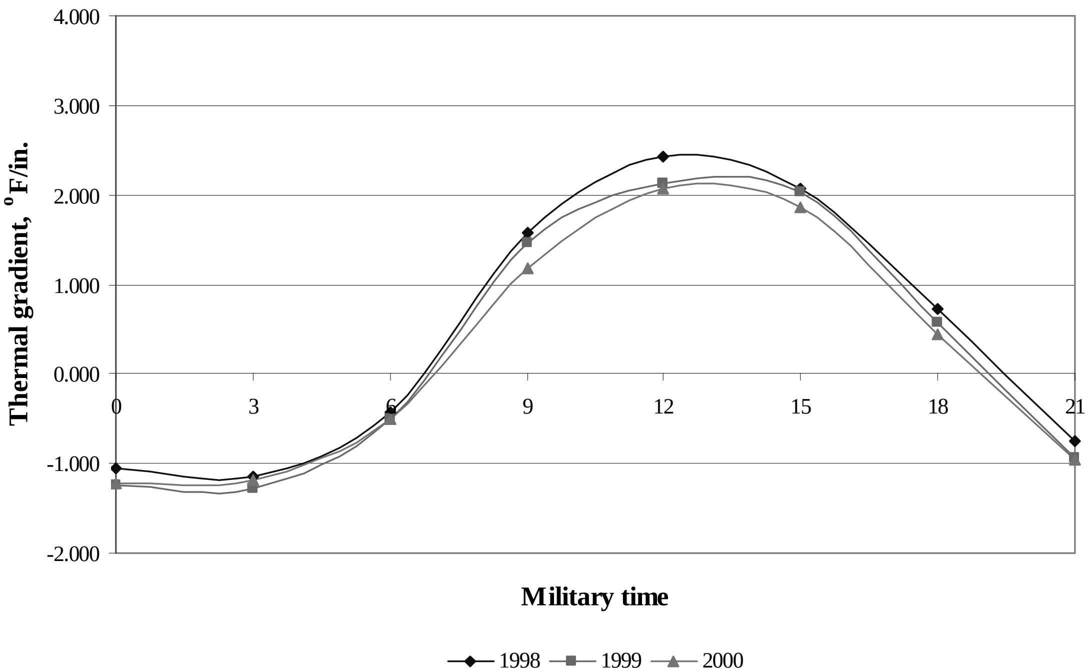


**Figure K-20: Hourly thermal gradients generated by EICM for 11-in. sections in July**

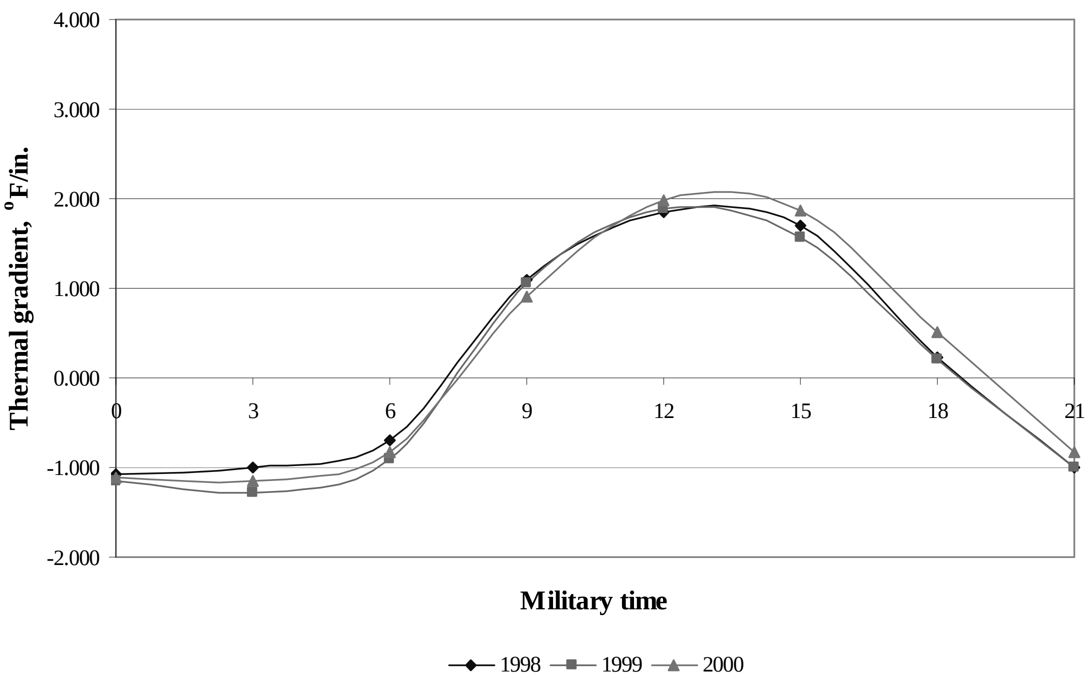


**Figure K-21: Hourly thermal gradients generated by EICM for 11-in. sections in August**

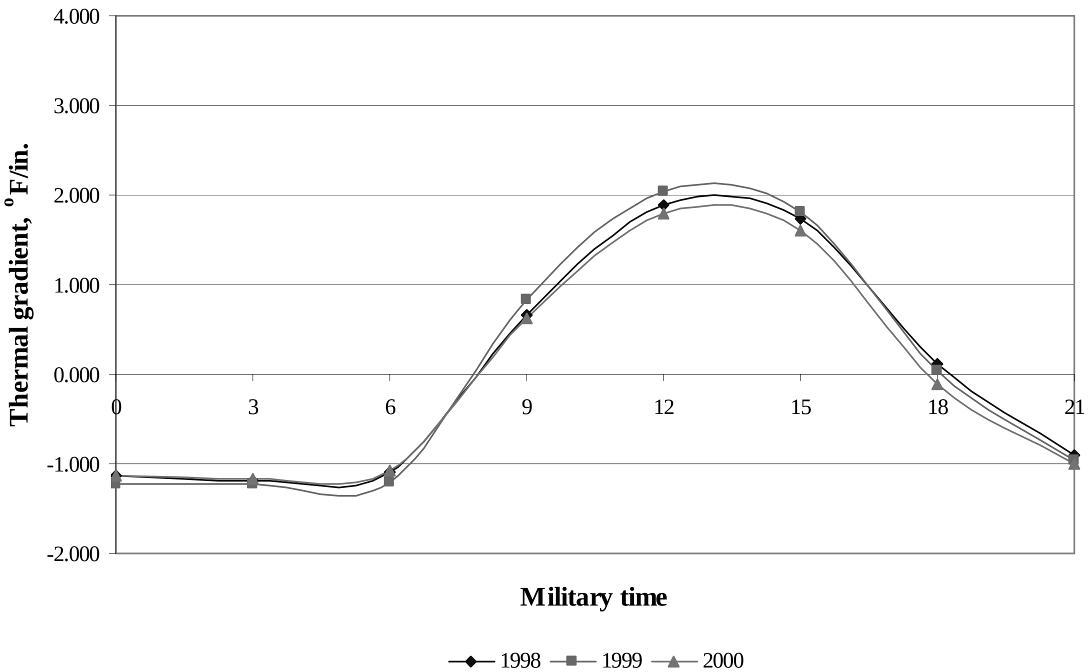


**Figure K-22: Hourly thermal gradients generated by EICM for 11-in. sections in September**

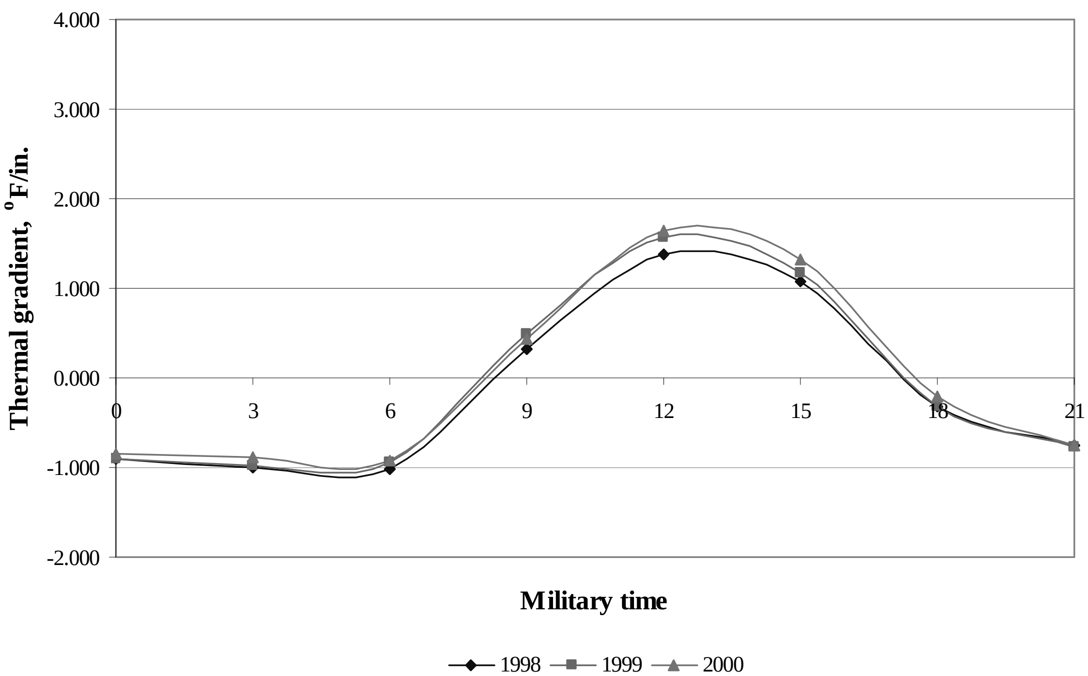


**Figure K-23: Hourly thermal gradients generated by EICM for 11-in. sections in October**

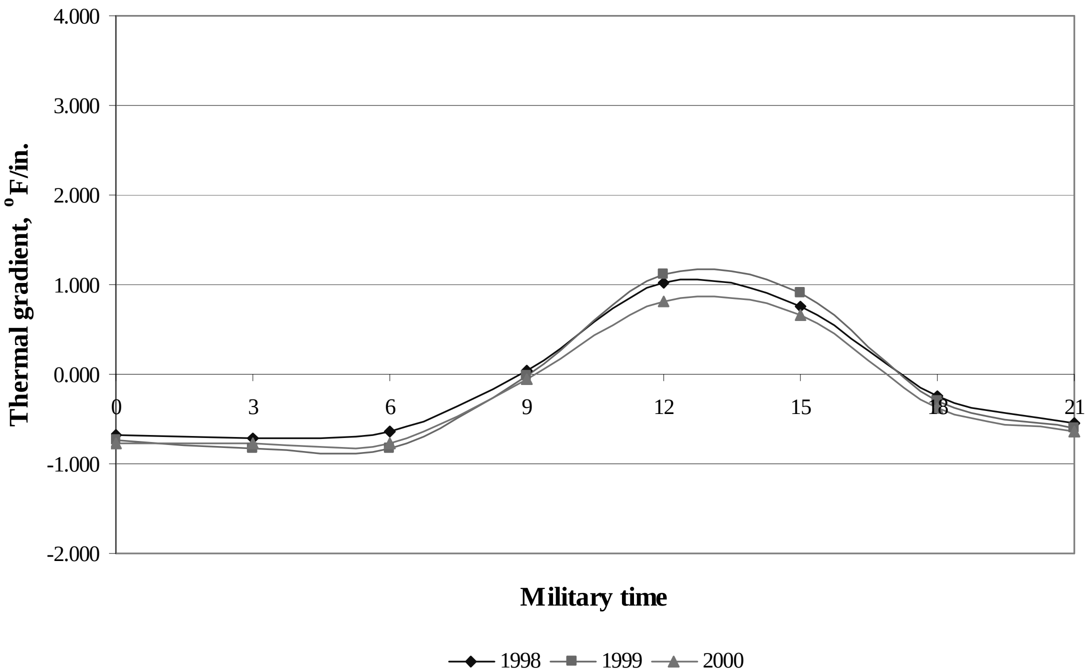


**Figure K-24: Hourly thermal gradients generated by EICM for 11-in. sections in November**

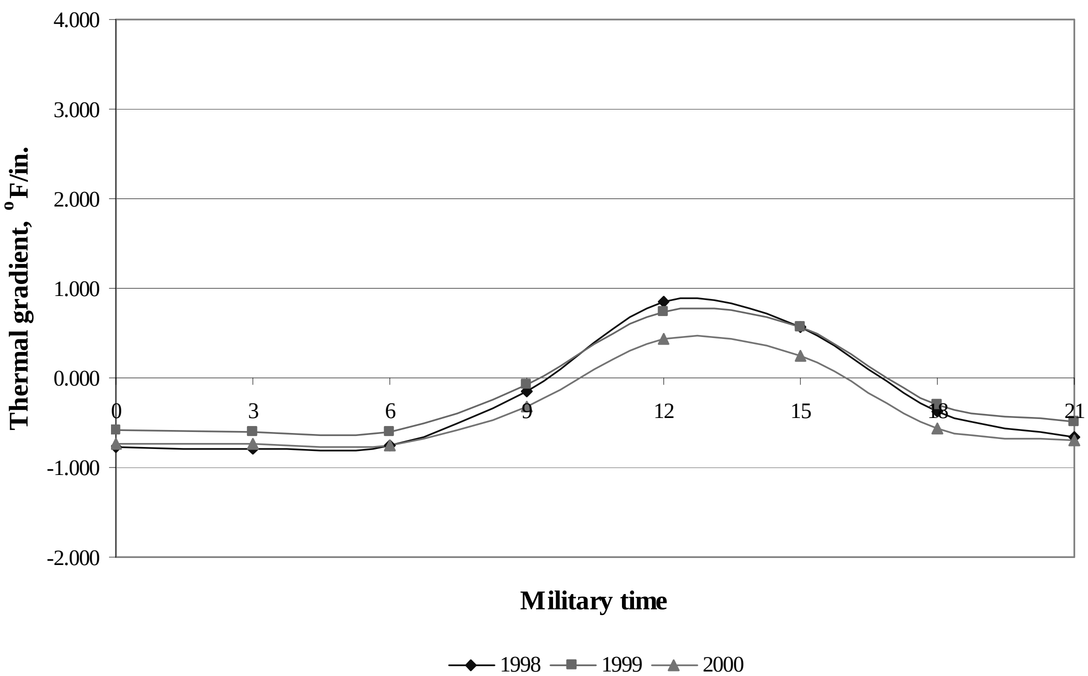


**Figure K-25: Hourly thermal gradients generated by EICM for 11-in. sections in December**

Table J-1: Summary of single axle load repetitions from SPS-2 section

| Load range, lbs | Time interval | | | | | | | | | |
|---|---|---|---|---|---|---|---|---|---|---|
| | 7/98-9/98 | 10/98-12/98 | 1/99-3/99 | 4/99-6/99 | 7/99-9/99 | 10/99-12/99 | 1/00-3/00 | 4/00-6/00 | 7/00-9/00 | 10/00-12/00 |
| 0-4999 | 73,897 | 32,139 | 34,057 | 66,686 | 64,857 | 49,400 | 34,017 | 52,423 | 68,877 | 58,896 |
| 5000-7999 | 60,122 | 30,905 | 34,364 | 58,049 | 58,986 | 52,168 | 46,874 | 42,322 | 58,098 | 55,975 |
| 8000-10999 | 214,552 | 127,964 | 141,516 | 225,246 | 208,159 | 206,808 | 142,597 | 153,711 | 219,733 | 208,158 |
| 11000-13999 | 99,780 | 55,168 | 65,935 | 106,207 | 100,406 | 91,723 | 69,660 | 72,201 | 93,886 | 94,095 |
| 14000-16999 | 44,970 | 27,668 | 30,027 | 48,737 | 43,026 | 38,696 | 38,084 | 29,325 | 38,642 | 34,699 |
| 17000-19999 | 30,322 | 16,948 | 19,744 | 32,313 | 31,365 | 30,560 | 29,086 | 23,056 | 32,010 | 26,885 |
| 20000-22999 | 9,427 | 4,683 | 6,560 | 9,720 | 9,756 | 9,254 | 6,412 | 6,144 | 9,188 | 7,113 |
| 23000-25999 | 2,018 | 1,100 | 1,467 | 2,264 | 2,334 | 1,744 | 1,106 | 991 | 1,471 | 1,172 |
| 26000-28999 | 594 | 307 | 488 | 561 | 628 | 496 | 276 | 221 | 300 | 275 |
| 29000-31999 | 133 | 68 | 149 | 158 | 148 | 116 | 73 | 53 | 60 | 54 |
| 32000-34999 | 36 | 20 | 46 | 34 | 29 | 26 | 18 | 12 | 20 | 11 |
| 35000-37999 | 5 | 4 | 16 | 9 | 13 | 5 | 4 | 4 | 10 | 3 |
| 38000-40999 | 4 | 1 | 4 | 2 | 2 | 3 | 0 | 1 | 0 | 0 |
| >41000 | 1 | 0 | 4 | 1 | 4 | 0 | 0 | 0 | 0 | 0 |

Table J-2: Summary of tandem axle load repetitions from SPS-2 section

| Load range, lbs | Time interval | | | | | | | | | |
|---|---|---|---|---|---|---|---|---|---|---|
| | 7/98-9/98 | 10/98-12/98 | 1/99-3/99 | 4/99-6/99 | 7/99-9/99 | 10/99-12/99 | 1/00-3/00 | 4/00-6/00 | 7/00-9/00 | 10/00-12/00 |
| 0-9999 | 65,457 | 55,233 | 39,411 | 52,386 | 54,205 | 53,444 | 31,429 | 24,211 | 44,844 | 38,954 |
| 10000-15999 | 113,470 | 97,841 | 62,729 | 100,599 | 99,644 | 98,989 | 79,753 | 70,261 | 101,550 | 102,054 |
| 16000-21999 | 81,779 | 72,875 | 50,835 | 82,935 | 75,736 | 74,204 | 67,743 | 61,949 | 81,472 | 83,218 |
| 22000-27999 | 73,319 | 64,717 | 47,237 | 74,352 | 64,502 | 60,455 | 53,444 | 49,981 | 64,713 | 65,338 |
| 28000-33999 | 98,301 | 91,484 | 65,400 | 105,950 | 95,230 | 89,498 | 77,218 | 73,024 | 96,309 | 91,395 |
| 34000-39999 | 41,867 | 35,275 | 27,330 | 44,421 | 48,277 | 48,201 | 41,889 | 33,371 | 49,251 | 43,921 |
| 40000-45999 | 7,619 | 4,633 | 3,391 | 5,619 | 6,485 | 4,388 | 2,907 | 2,161 | 3,776 | 3,129 |
| 46000-51999 | 695 | 399 | 377 | 505 | 626 | 399 | 287 | 210 | 330 | 339 |
| 52000-57999 | 105 | 64 | 83 | 78 | 95 | 62 | 53 | 35 | 55 | 52 |
| 58000-63999 | 27 | 22 | 14 | 19 | 18 | 17 | 16 | 8 | 11 | 5 |
| 64000-69999 | 6 | 4 | 4 | 8 | 2 | 5 | 2 | 2 | 1 | 1 |
| 70000-75999 | 1 | 0 | 1 | 0 | 1 | 0 | 0 | 0 | 0 | 0 |
| 76000-81999 | 1 | 0 | 0 | 0 | 0 | 0 | 0 | 0 | 0 | 0 |
| >82000 | 0 | 0 | 0 | 0 | 0 | 0 | 0 | 0 | 0 | 0 |

Table J-3: Summary of tridem axle load repetitions from SPS-2 section

| Load range, lbs | Time interval | | | | | | | | | |
|---|---|---|---|---|---|---|---|---|---|---|
| | 7/98-9/98 | 10/98-12/98 | 1/99-3/99 | 4/99-6/99 | 7/99-9/99 | 10/99-12/99 | 1/00-3/00 | 4/00-6/00 | 7/00-9/00 | 10/00-12/00 |
| 0-17999 | 7,305 | 4,891 | 1,547 | 3,049 | 3,495 | 4,312 | 2,237 | 2,188 | 2,906 | 3,486 |
| 18000-26999 | 1,340 | 727 | 475 | 799 | 798 | 684 | 654 | 610 | 686 | 631 |
| 27000-35999 | 1,507 | 1,394 | 992 | 1,438 | 1,059 | 1,317 | 1,074 | 1,200 | 1,374 | 1,596 |
| 36000-44999 | 4,833 | 5,160 | 2,889 | 6,679 | 5,588 | 5,483 | 3,817 | 5,352 | 7,466 | 7,245 |
| 45000-53999 | 4,194 | 4,160 | 1,924 | 3,894 | 4,224 | 3,469 | 1,605 | 1,735 | 3,662 | 2,825 |
| 54000-62999 | 695 | 587 | 244 | 465 | 487 | 443 | 206 | 251 | 439 | 343 |
| 63000-71999 | 84 | 53 | 38 | 57 | 72 | 53 | 28 | 32 | 92 | 47 |
| 72000-80999 | 10 | 8 | 5 | 8 | 11 | 12 | 1 | 7 | 10 | 4 |
| 81000-89999 | 1 | 2 | 5 | 3 | 4 | 2 | 1 | 1 | 3 | 2 |
| 90000-98999 | 3 | 0 | 0 | 0 | 0 | 0 | 0 | 4 | 3 | 0 |
| >99000 | 0 | 0 | 1 | 0 | 0 | 0 | 0 | 1 | 1 | 0 |

Table J-4: Summary of quad axle load repetitions from SPS-2 section

| Load range, lbs | Time interval | | | | | | | | | |
|---|---|---|---|---|---|---|---|---|---|---|
| | 7/98-9/98 | 10/98-12/98 | 1/99-3/99 | 4/99-6/99 | 7/99-9/99 | 10/99-12/99 | 1/00-3/00 | 4/00-6/00 | 7/00-9/00 | 10/00-12/00 |
| 0-23999 | 848 | 678 | 379 | 453 | 535 | 767 | 325 | 316 | 493 | 413 |
| 24000-35999 | 442 | 323 | 239 | 499 | 448 | 407 | 438 | 382 | 460 | 371 |
| 36000-47999 | 631 | 701 | 436 | 761 | 877 | 728 | 477 | 403 | 685 | 703 |
| 48000-59999 | 2,497 | 2,837 | 1,454 | 3,437 | 3,790 | 3,071 | 1,691 | 2,534 | 3,692 | 3,105 |
| 60000-71999 | 1,309 | 1,160 | 486 | 1,020 | 1,218 | 1,030 | 673 | 916 | 2,050 | 1,506 |
| 72000-83999 | 89 | 62 | 38 | 115 | 82 | 45 | 22 | 66 | 157 | 94 |
| 84000-95999 | 3 | 1 | 7 | 6 | 6 | 4 | 2 | 3 | 12 | 11 |
| 96000-107999 | 2 | 1 | 1 | 5 | 1 | 7 | 0 | 0 | 1 | 1 |
| 108000-119999 | 0 | 4 | 0 | 0 | 1 | 0 | 0 | 0 | 1 | 0 |
| 120000-131999 | 0 | 0 | 0 | 0 | 0 | 0 | 0 | 0 | 0 | 0 |
| >132000 | 0 | 0 | 0 | 0 | 0 | 0 | 0 | 0 | 0 | 0 |

Table J-5: Summary of multi-axle (5) load repetitions from SPS-2 section

| Load range, lbs | Time interval | | | | | | | | | |
|---|---|---|---|---|---|---|---|---|---|---|
| | 7/98-9/98 | 10/98-12/98 | 1/99-3/99 | 4/99-6/99 | 7/99-9/99 | 10/99-12/99 | 1/00-3/00 | 4/00-6/00 | 7/00-9/00 | 10/00-12/00 |
| 0-29999 | 634 | 316 | 221 | 306 | 337 | 473 | 237 | 238 | 283 | 273 |
| 30000-44999 | 62 | 19 | 45 | 41 | 39 | 71 | 41 | 23 | 40 | 23 |
| 45000-59999 | 73 | 79 | 68 | 158 | 99 | 160 | 75 | 97 | 96 | 135 |
| 60000-74999 | 686 | 779 | 386 | 1,142 | 1,207 | 983 | 513 | 710 | 1,053 | 1,018 |
| 75000-89999 | 267 | 199 | 137 | 242 | 409 | 175 | 86 | 123 | 223 | 113 |
| 90000-104999 | 17 | 18 | 16 | 14 | 12 | 11 | 5 | 3 | 7 | 8 |
| 105000-119999 | 3 | 3 | 4 | 8 | 2 | 1 | 0 | 1 | 2 | 0 |
| 120000-134999 | 0 | 0 | 0 | 0 | 0 | 0 | 0 | 0 | 0 | 0 |
| 135000-149999 | 0 | 0 | 0 | 0 | 0 | 0 | 0 | 0 | 0 | 0 |
| 150000-164999 | 0 | 0 | 0 | 0 | 0 | 0 | 0 | 0 | 0 | 0 |
| >165000 | 0 | 0 | 0 | 0 | 0 | 0 | 0 | 0 | 0 | 0 |

Table J-6: Summary of multi-axle (6) load repetitions from SPS-2 section

| Load range, lbs | Time interval | | | | | | | | | |
|---|---|---|---|---|---|---|---|---|---|---|
| | 7/98-9/98 | 10/98-12/98 | 1/99-3/99 | 4/99-6/99 | 7/99-9/99 | 10/99-12/99 | 1/00-3/00 | 4/00-6/00 | 7/00-9/00 | 10/00-12/00 |
| 0-35999 | 79 | 5 | 2 | 1 | 11 | 23 | 8 | 2 | 7 | 2 |
| 36000-53999 | 58 | 10 | 88 | 29 | 15 | 23 | 40 | 19 | 33 | 16 |
| 54000-71999 | 139 | 114 | 147 | 163 | 200 | 131 | 79 | 96 | 170 | 103 |
| 72000-89999 | 666 | 833 | 450 | 657 | 898 | 660 | 415 | 825 | 1,110 | 810 |
| 90000-107999 | 345 | 152 | 84 | 135 | 181 | 175 | 51 | 191 | 332 | 107 |
| 108000-125999 | 4 | 2 | 0 | 0 | 7 | 13 | 1 | 0 | 1 | 2 |
| 126000-143999 | 0 | 0 | 0 | 0 | 0 | 1 | 0 | 0 | 0 | 0 |
| 144000-161999 | 0 | 0 | 0 | 0 | 0 | 0 | 0 | 0 | 0 | 0 |
| 162000-179999 | 0 | 0 | 0 | 0 | 0 | 0 | 0 | 0 | 0 | 0 |
| 180000-197999 | 0 | 0 | 0 | 0 | 0 | 0 | 0 | 0 | 0 | 0 |
| >198000 | 0 | 0 | 0 | 0 | 0 | 0 | 0 | 0 | 0 | 0 |

Table J-7: Summary of multi-axle (7) load repetitions from SPS-2 section

| Load range, lbs | Time interval | | | | | | | | | |
|---|---|---|---|---|---|---|---|---|---|---|
| | 7/98-9/98 | 10/98-12/98 | 1/99-3/99 | 4/99-6/99 | 7/99-9/99 | 10/99-12/99 | 1/00-3/00 | 4/00-6/00 | 7/00-9/00 | 10/00-12/00 |
| 0-41999 | 4 | 6 | 2 | 4 | 4 | 6 | 6 | 1 | 4 | 4 |
| 42000-62999 | 23 | 6 | 9 | 21 | 29 | 18 | 23 | 13 | 31 | 21 |
| 63000-83999 | 128 | 104 | 62 | 115 | 77 | 81 | 93 | 118 | 197 | 155 |
| 84000-104999 | 249 | 100 | 46 | 147 | 211 | 168 | 140 | 139 | 308 | 394 |
| 105000-125999 | 25 | 21 | 6 | 5 | 15 | 9 | 6 | 6 | 16 | 20 |
| 126000-146999 | 0 | 0 | 0 | 0 | 1 | 0 | 0 | 0 | 1 | 0 |
| 147000-167999 | 0 | 0 | 0 | 0 | 0 | 0 | 0 | 0 | 0 | 0 |
| 168000-188999 | 0 | 0 | 0 | 0 | 0 | 0 | 0 | 0 | 0 | 0 |
| 189000-209999 | 0 | 0 | 0 | 0 | 0 | 0 | 0 | 0 | 0 | 0 |
| 210000-230999 | 0 | 0 | 0 | 0 | 0 | 0 | 0 | 0 | 0 | 0 |
| >231000 | 0 | 0 | 0 | 0 | 0 | 0 | 0 | 0 | 0 | 0 |

Table J-8: Summary of multi-axle (8) load repetitions from SPS-2 section

| Load range, lbs | Time interval | | | | | | | | | |
|---|---|---|---|---|---|---|---|---|---|---|
| | 7/98-9/98 | 10/98-12/98 | 1/99-3/99 | 4/99-6/99 | 7/99-9/99 | 10/99-12/99 | 1/00-3/00 | 4/00-6/00 | 7/00-9/00 | 10/00-12/00 |
| 0-47999 | 10 | 4 | 4 | 5 | 10 | 2 | 12 | 4 | 6 | 2 |
| 48000-71999 | 35 | 20 | 18 | 53 | 43 | 42 | 42 | 24 | 30 | 39 |
| 72000-95999 | 295 | 355 | 195 | 331 | 277 | 330 | 293 | 293 | 416 | 419 |
| 96000-119999 | 248 | 251 | 174 | 406 | 337 | 381 | 199 | 331 | 391 | 252 |
| 120000-143999 | 8 | 11 | 9 | 8 | 11 | 2 | 3 | 8 | 17 | 6 |
| 144000-167999 | 0 | 2 | 0 | 0 | 0 | 0 | 0 | 0 | 0 | 0 |
| 168000-191999 | 0 | 0 | 0 | 0 | 0 | 0 | 0 | 0 | 0 | 0 |
| 192000-215999 | 0 | 0 | 0 | 0 | 0 | 0 | 0 | 0 | 0 | 0 |
| 216000-239999 | 0 | 0 | 0 | 0 | 0 | 0 | 0 | 0 | 0 | 0 |
| 240000-263999 | 0 | 0 | 0 | 0 | 0 | 0 | 0 | 0 | 0 | 0 |
| >264000 | 0 | 0 | 0 | 0 | 0 | 0 | 0 | 0 | 0 | 0 |

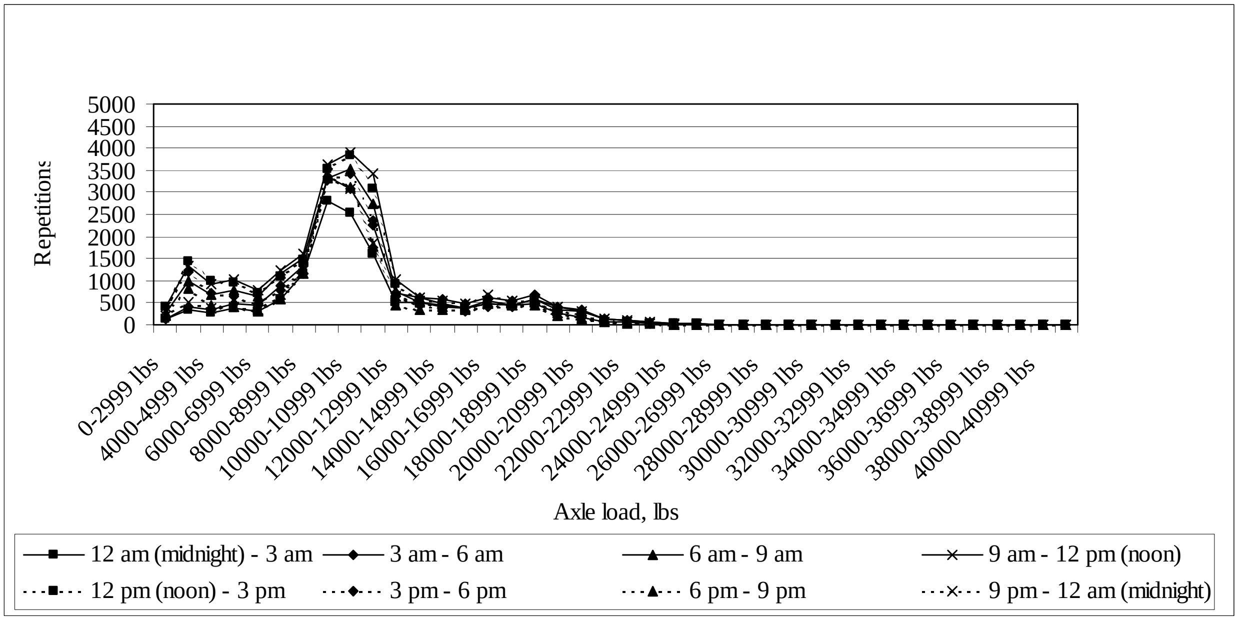


Figure J-1: Load spectrum from SPS2 sections for single axle in July, 1998

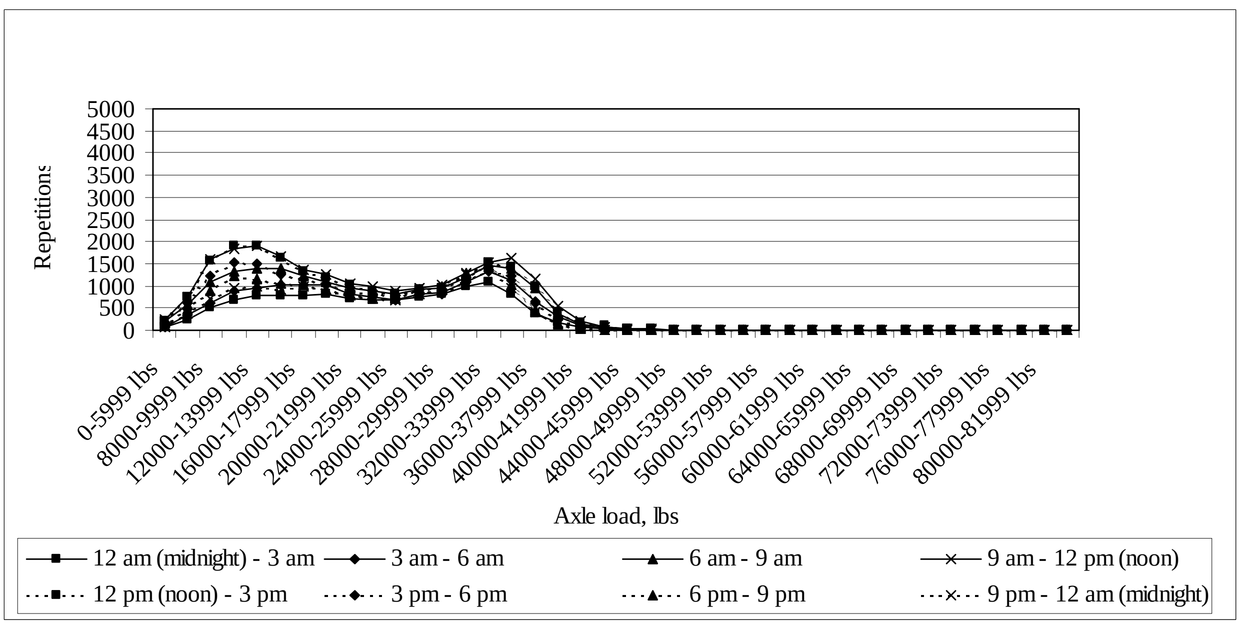


Figure J-2: Load spectrum from SPS2 sections for tandem axle in July, 1998

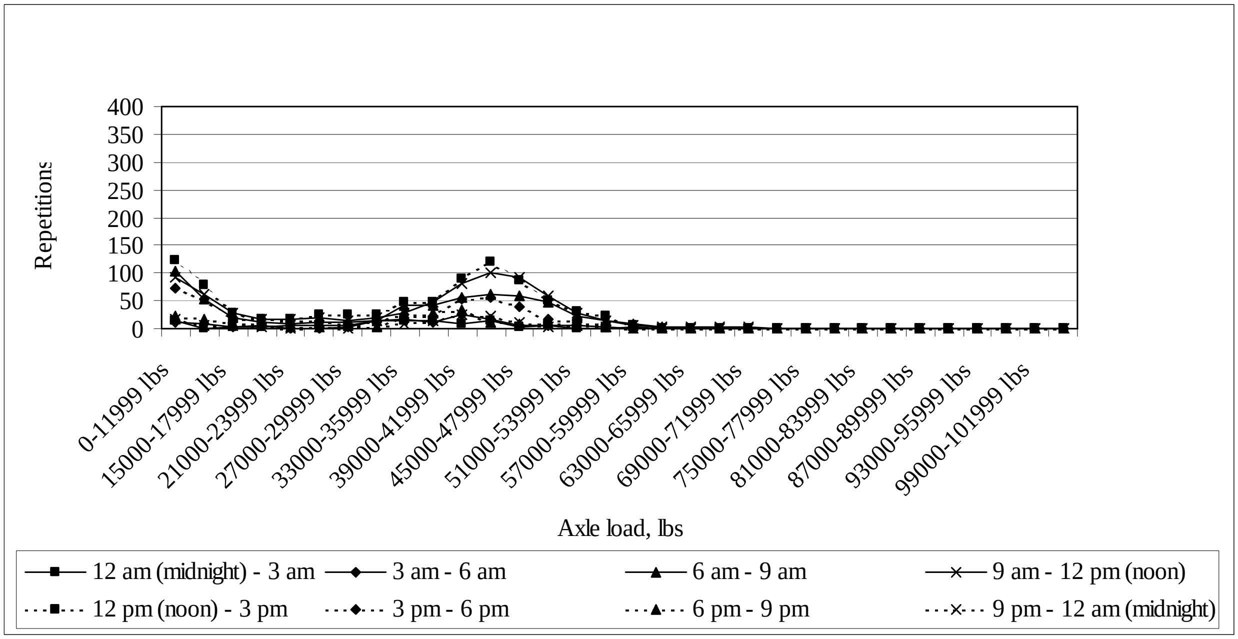


Figure J-3: Load spectrum from SPS2 sections for tridem axle in July, 1998

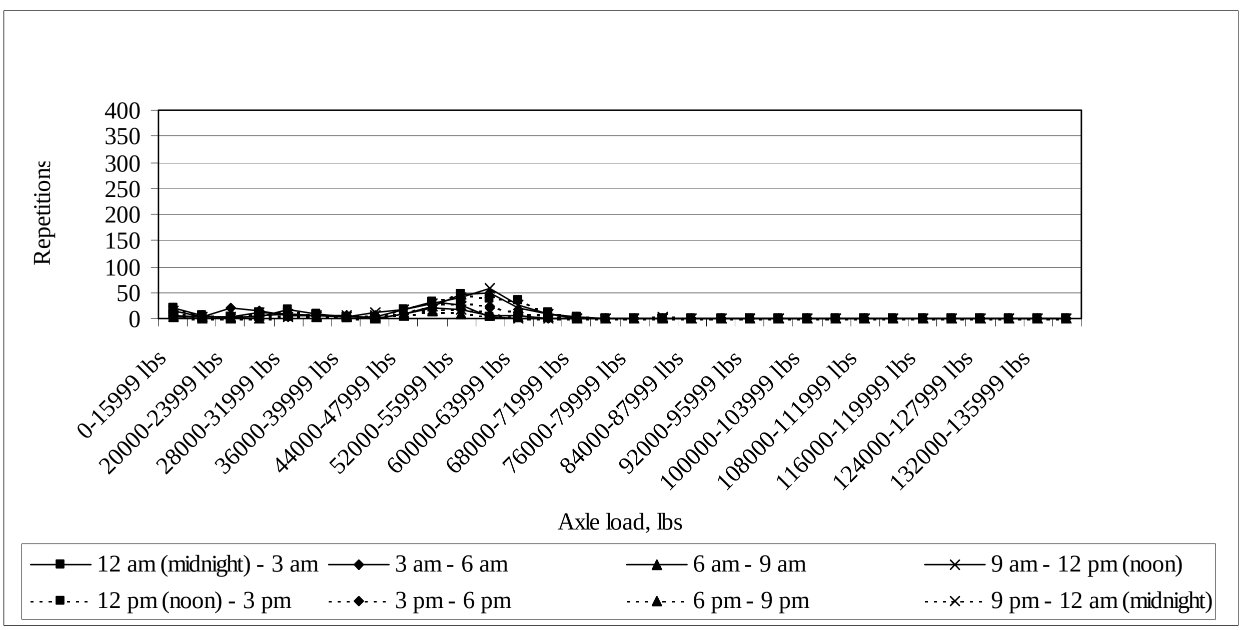


Figure J-4: Load spectrum from SPS2 sections for quad axle in July, 1998

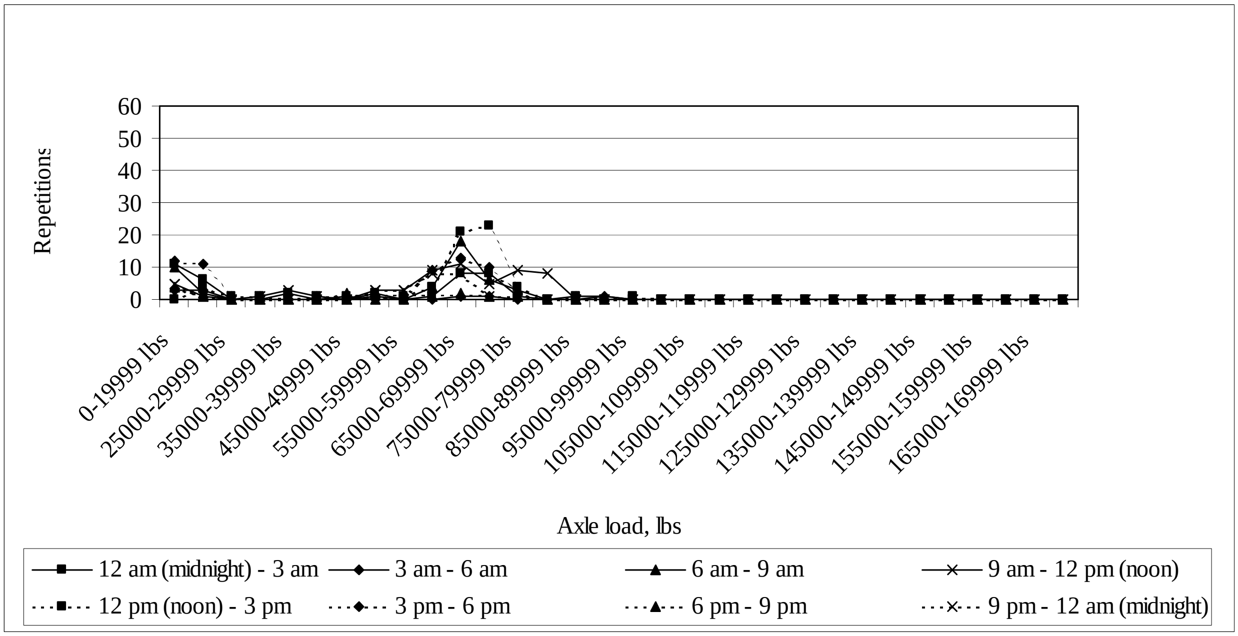


Figure J-5: Load spectrum from SPS2 sections for multi-axle (5) in July, 1998

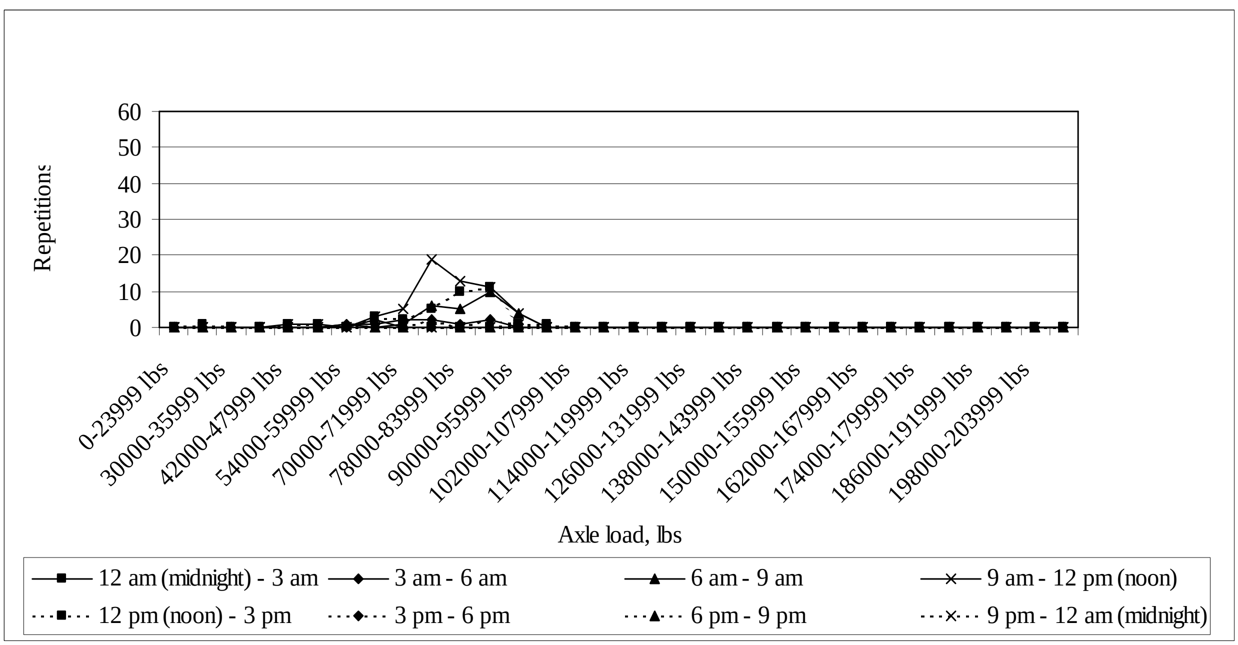


Figure J-6: Load spectrum from SPS2 sections for multi-axle (6) in July, 1998

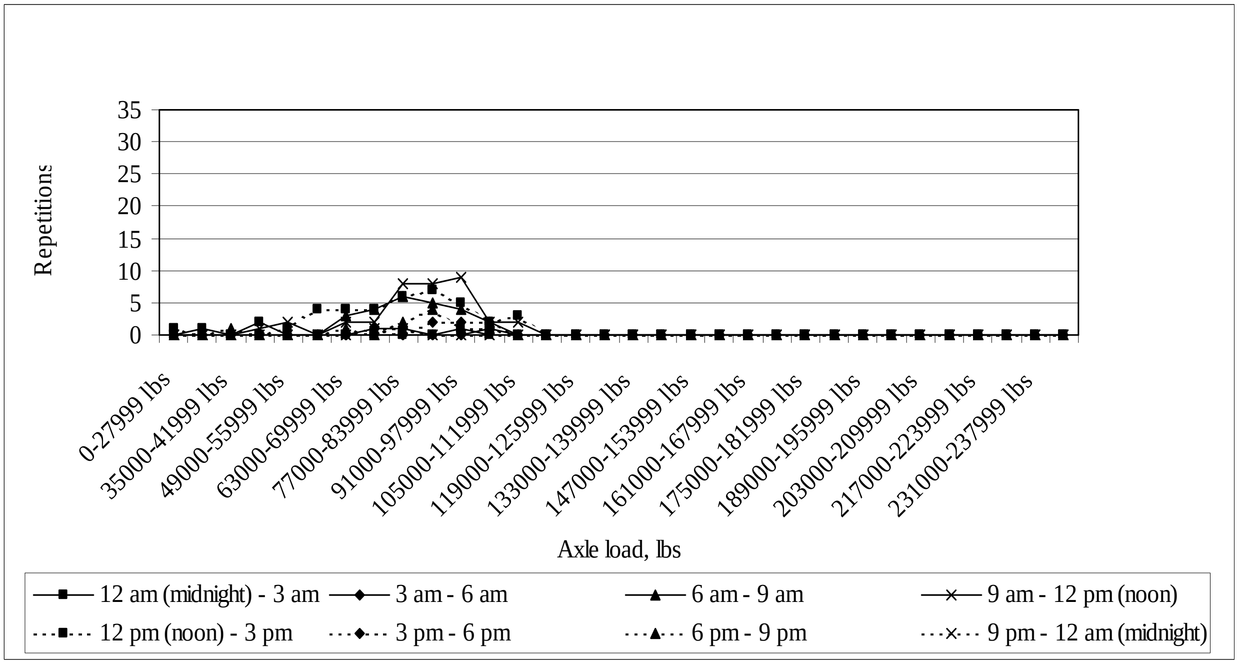


Figure J-7: Load spectrum from SPS2 sections for multi-axle (7) in July, 1998

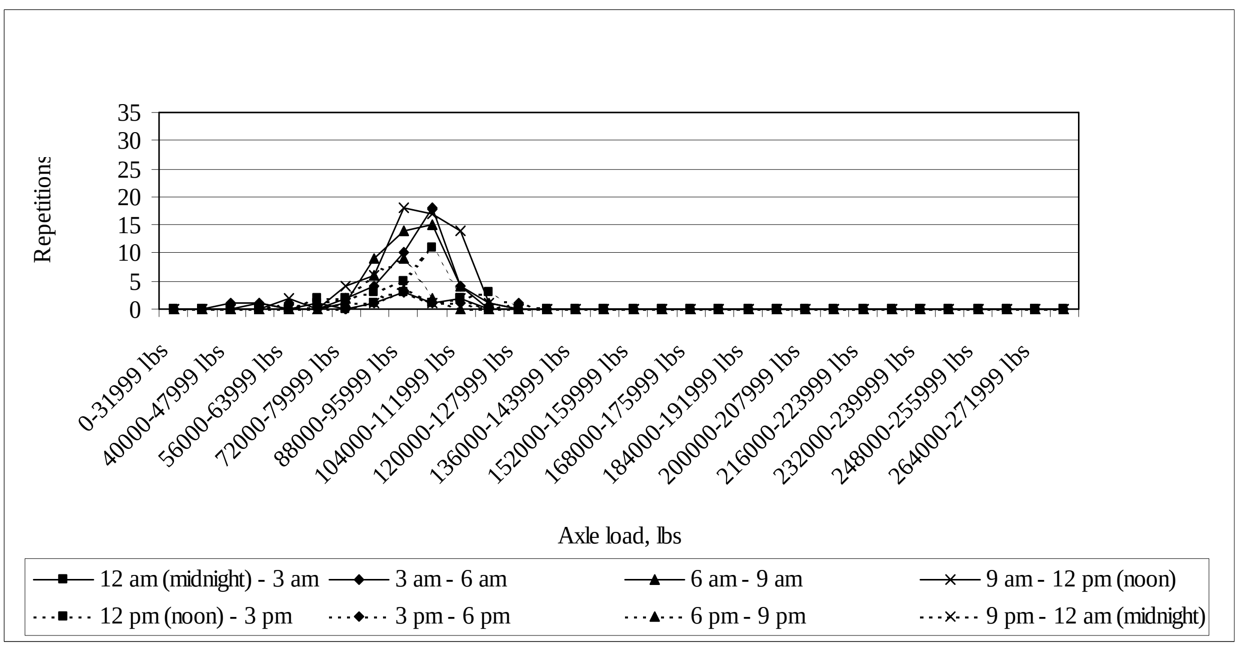


Figure J-8: Load spectrum from SPS2 sections for multi-axle (8) in July, 1998

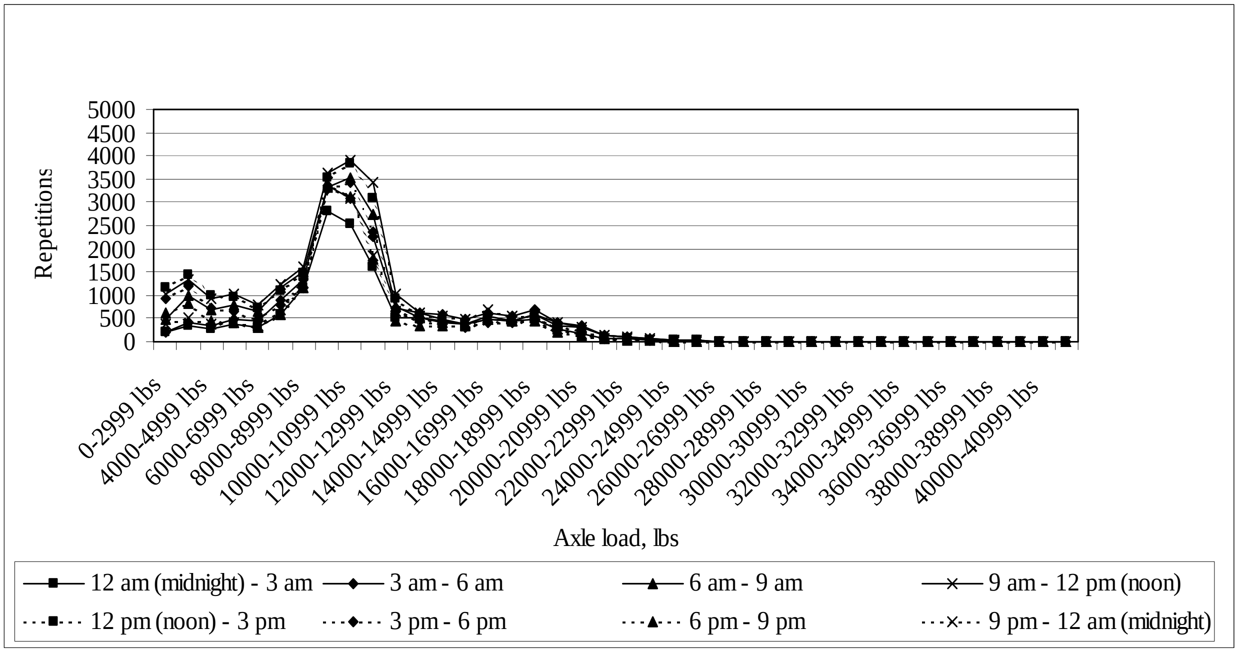


Figure J-9: Load spectrum from SPS2 sections for single axle in August, 1998

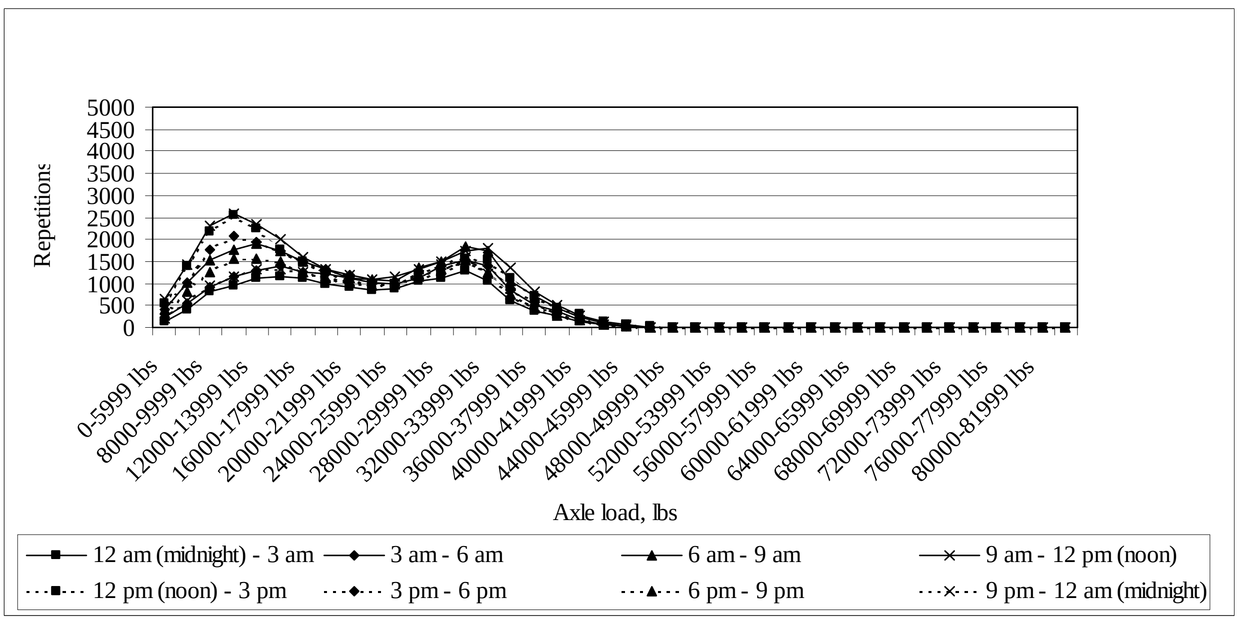


Figure J-10: Load spectrum from SPS2 sections for tandem axle in August, 1998

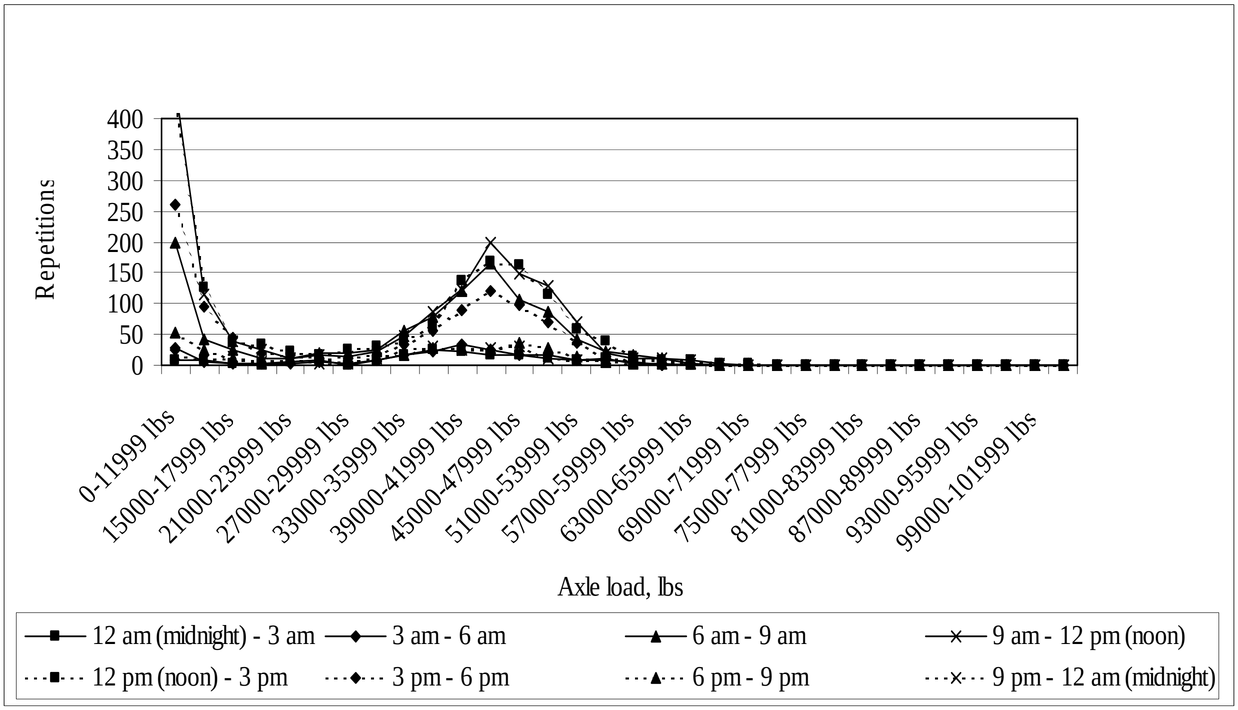


Figure J-11: Load spectrum from SPS2 sections for tridem axle in August, 1998

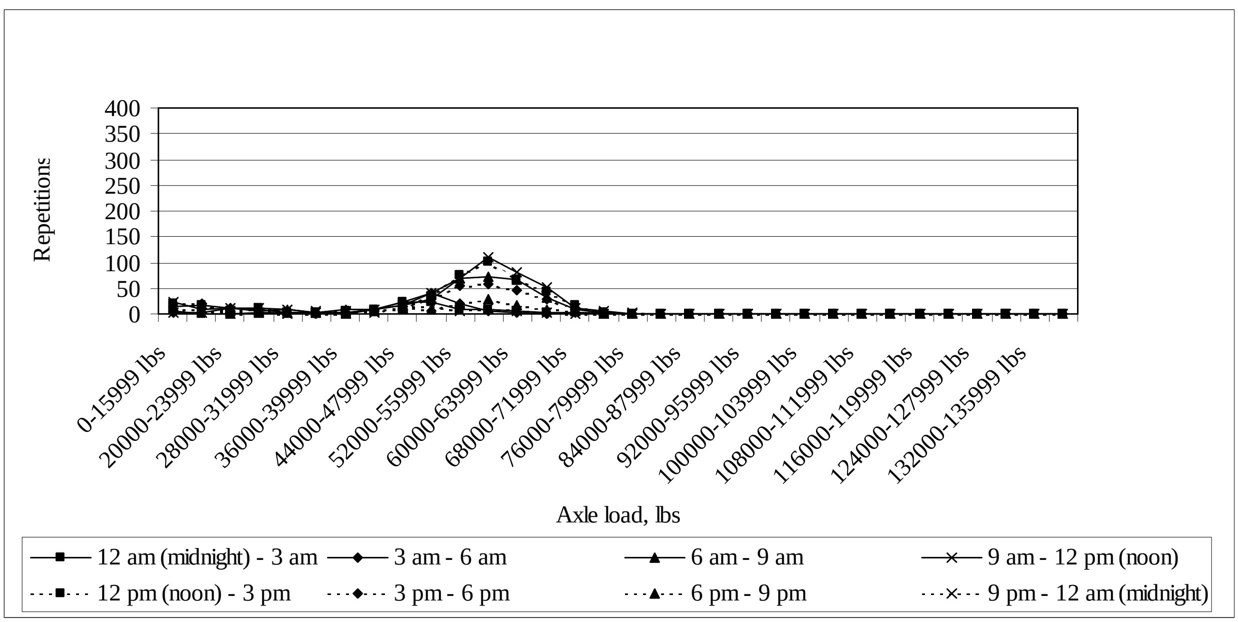


Figure J-12: Load spectrum from SPS2 sections for quad axle in August, 1998

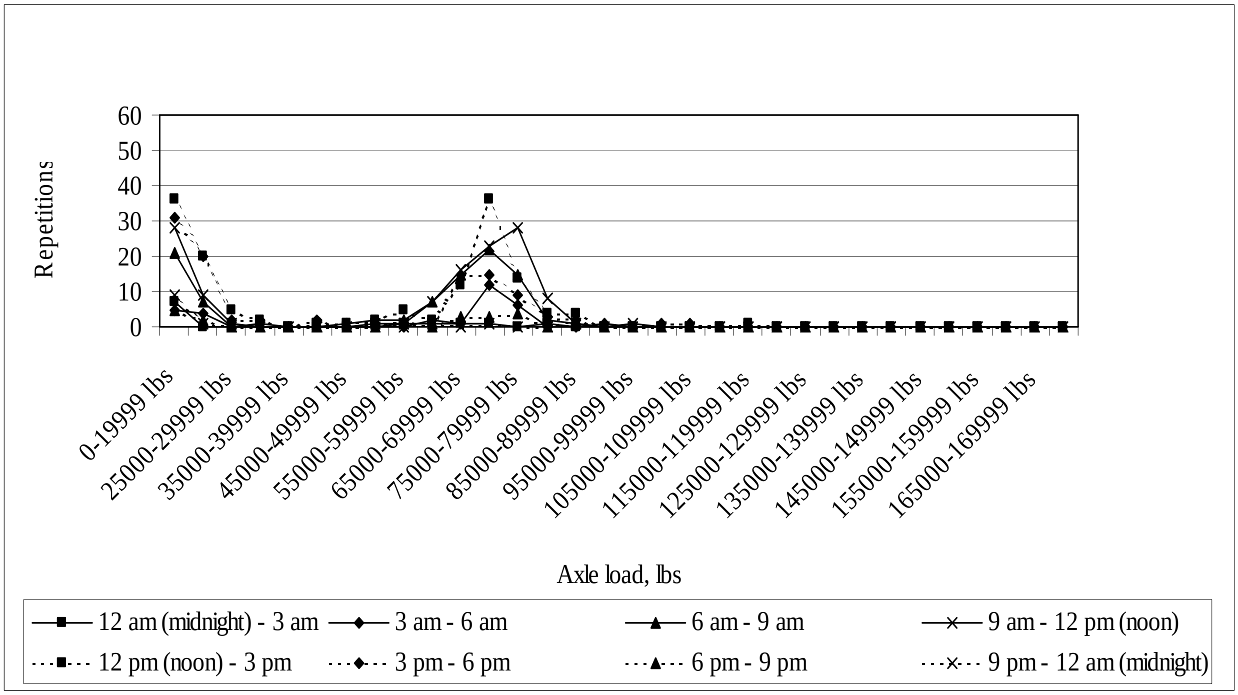


Figure J-13: Load spectrum from SPS2 sections for multi-axle (5) in August, 1998

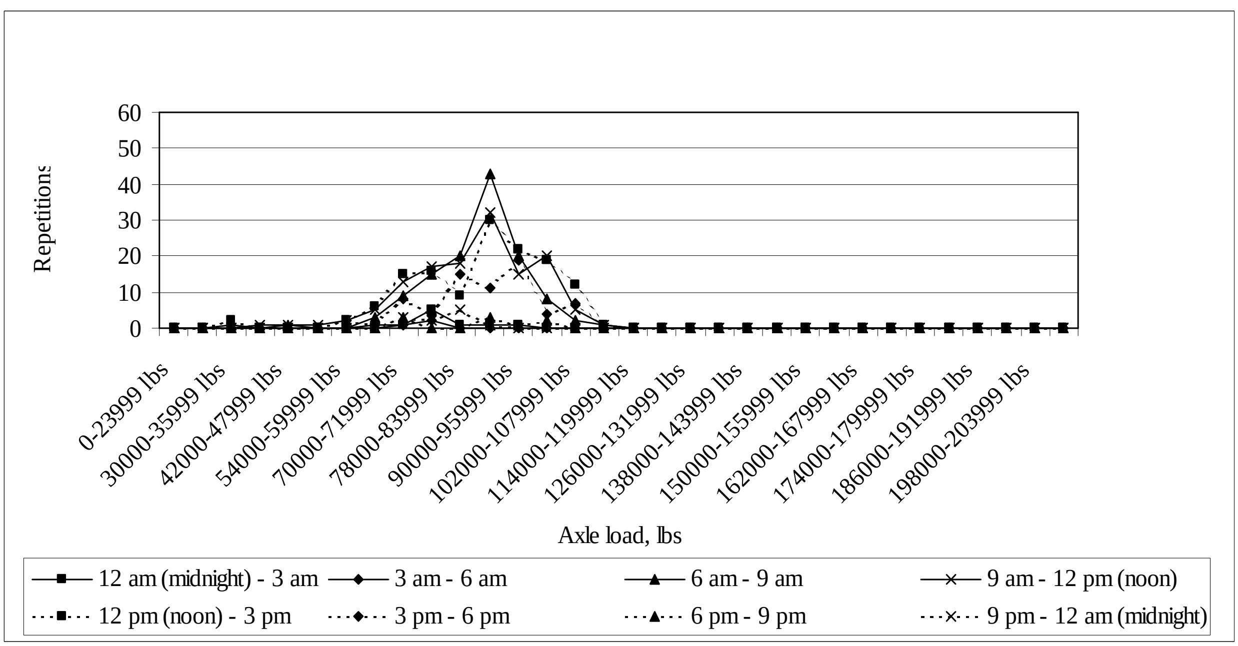


Figure J-14: Load spectrum from SPS2 sections for multi-axle (6) in August, 1998

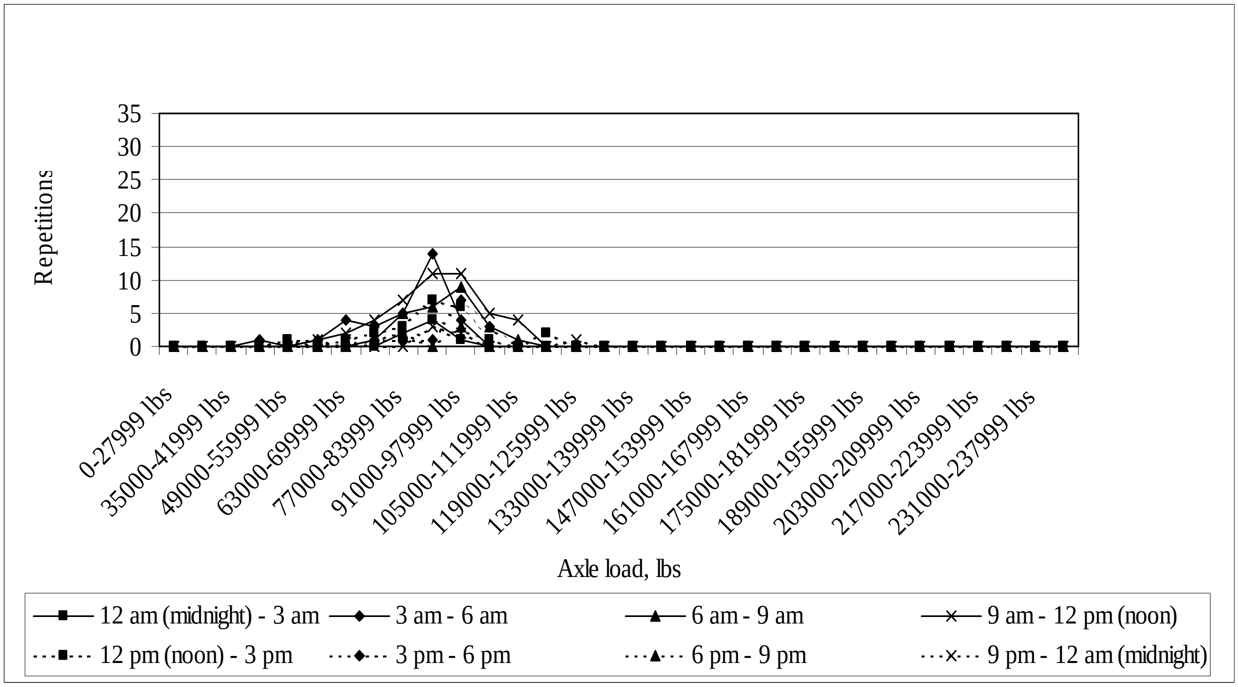


Figure J-15: Load spectrum from SPS2 sections for multi-axle (7) in August, 1998

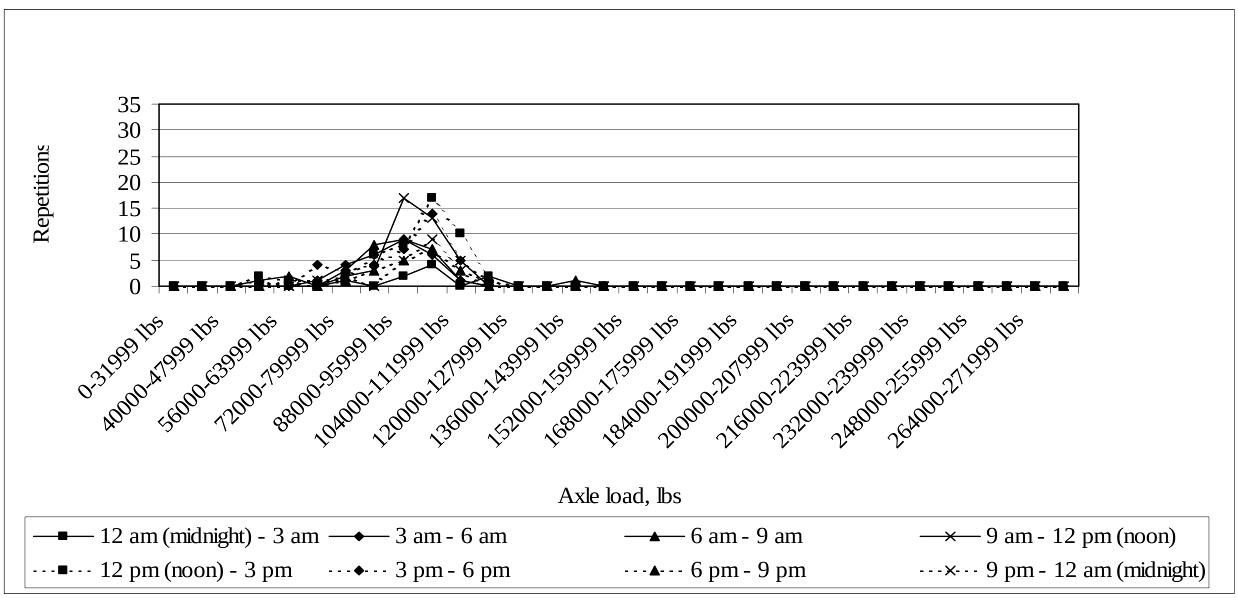


Figure J-16: Load spectrum from SPS2 sections for multi-axle (8) in August, 1998

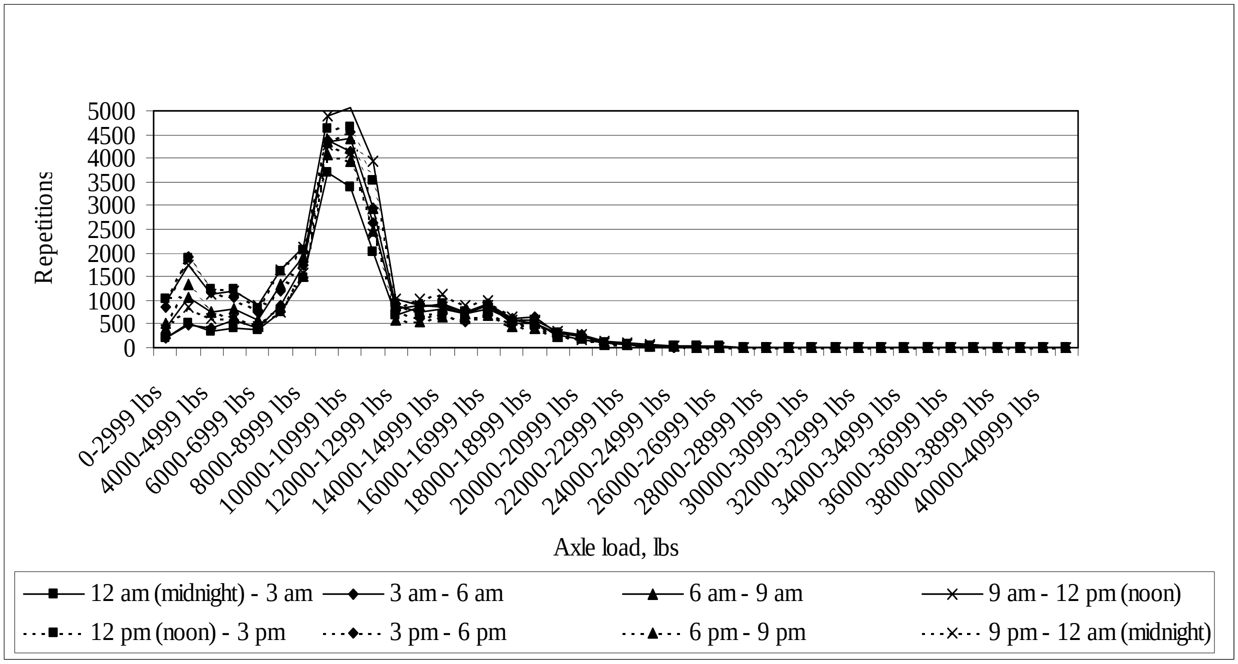


Figure J-17: Load spectrum from SPS2 sections for single axle in September, 1998

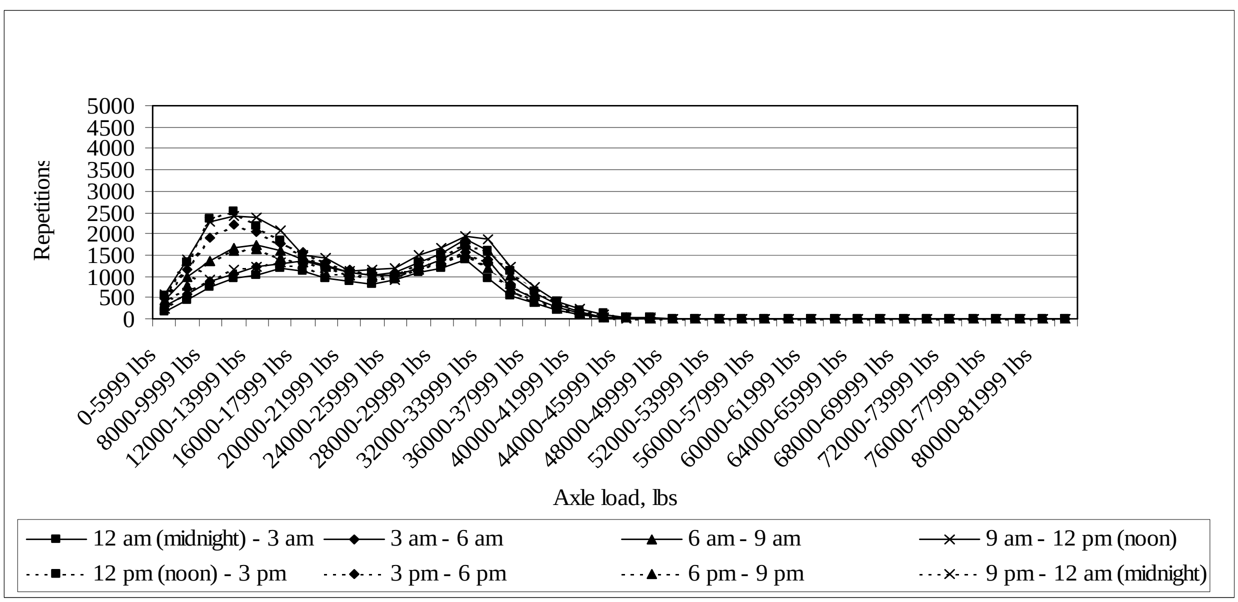


Figure J-18: Load spectrum from SPS2 sections for tandem axle in September, 1998

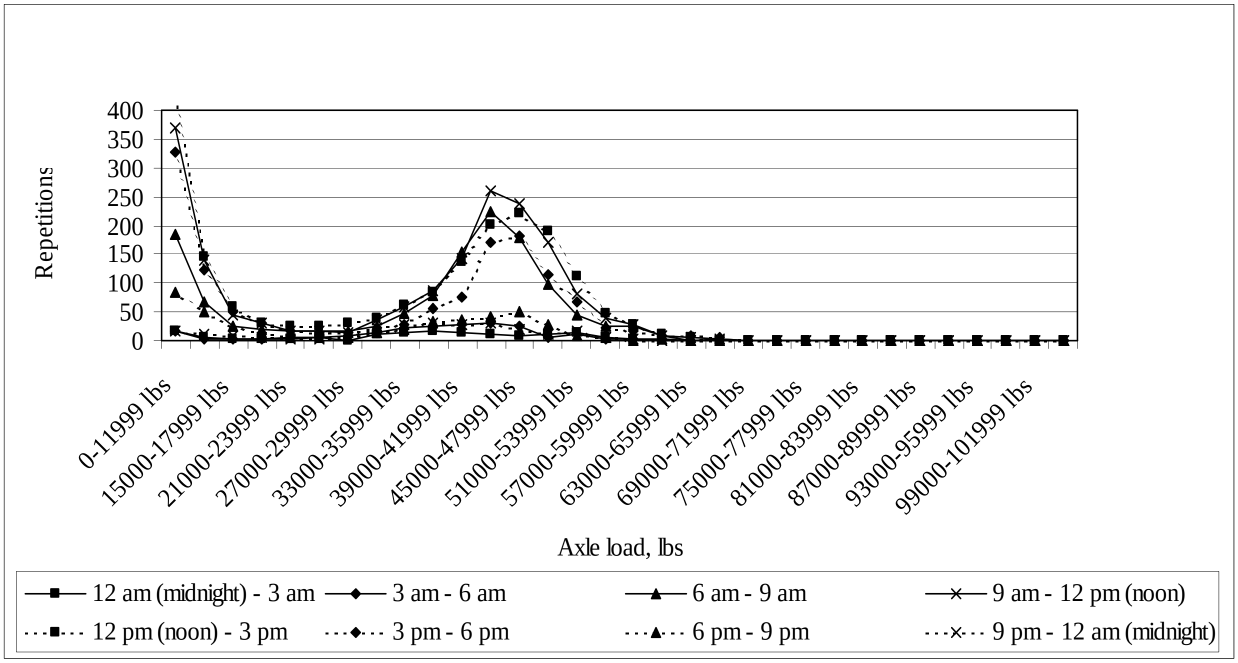


Figure J-19: Load spectrum from SPS2 sections for tridem axle in September, 1998

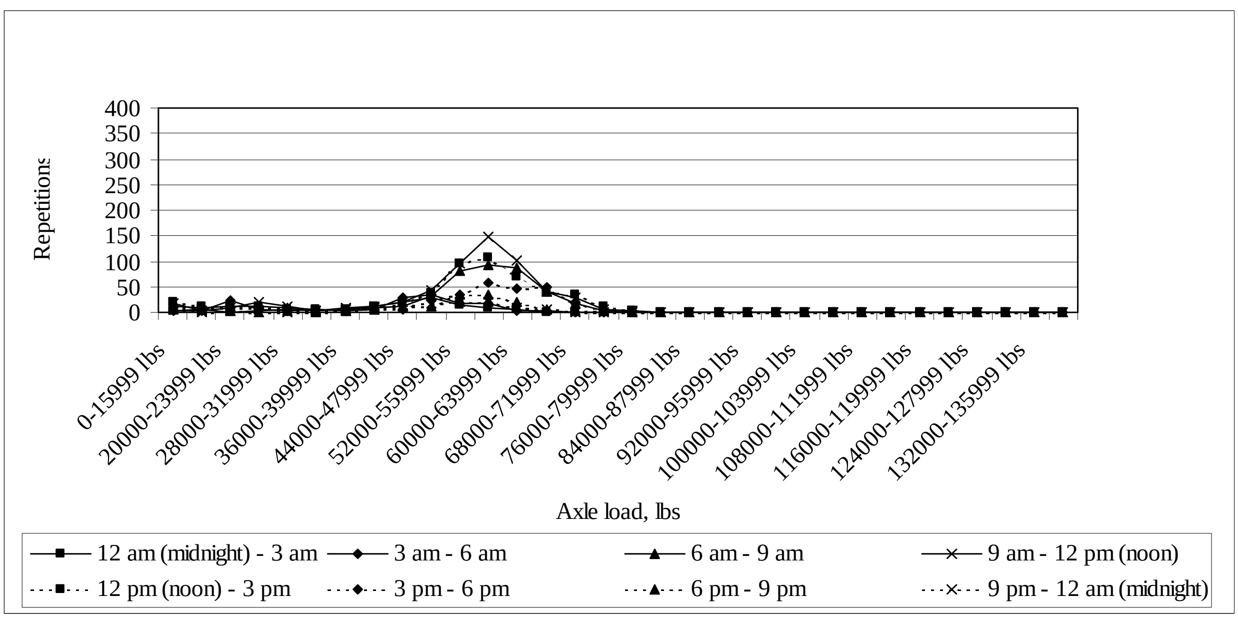


Figure J-20: Load spectrum from SPS2 sections for quad axle in September, 1998

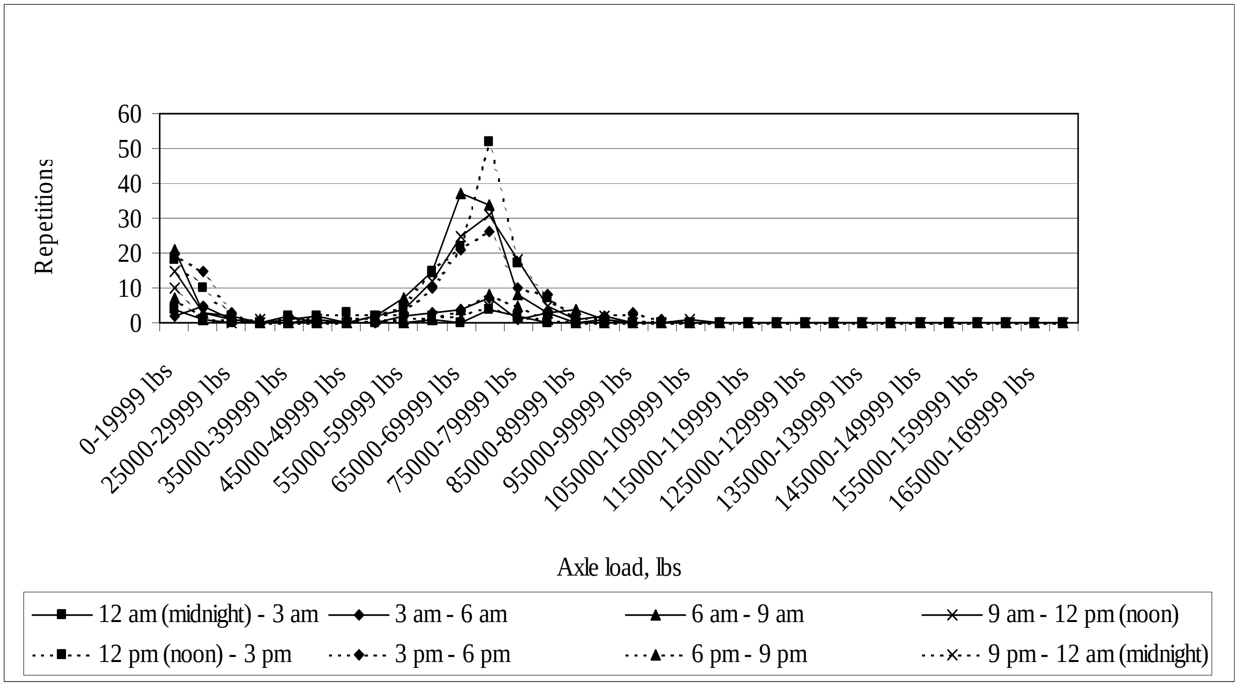


Figure J-21: Load spectrum from SPS2 sections for multi-axle (5) in September, 1998

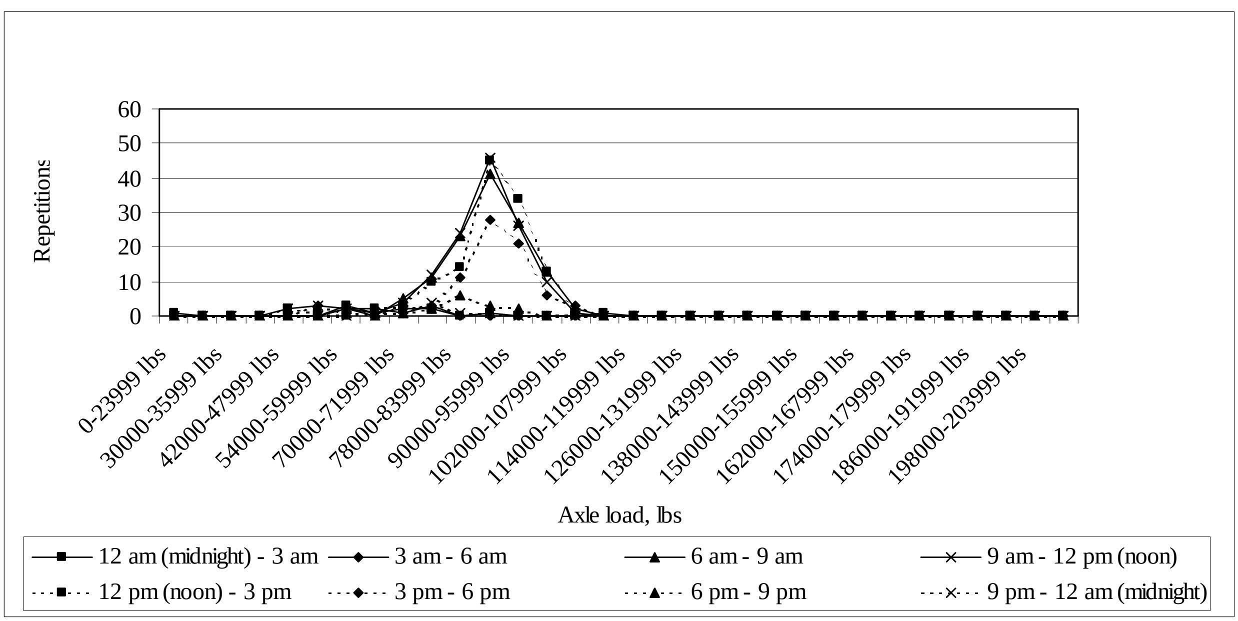


Figure J-22: Load spectrum from SPS2 sections for multi-axle (6) in September, 1998

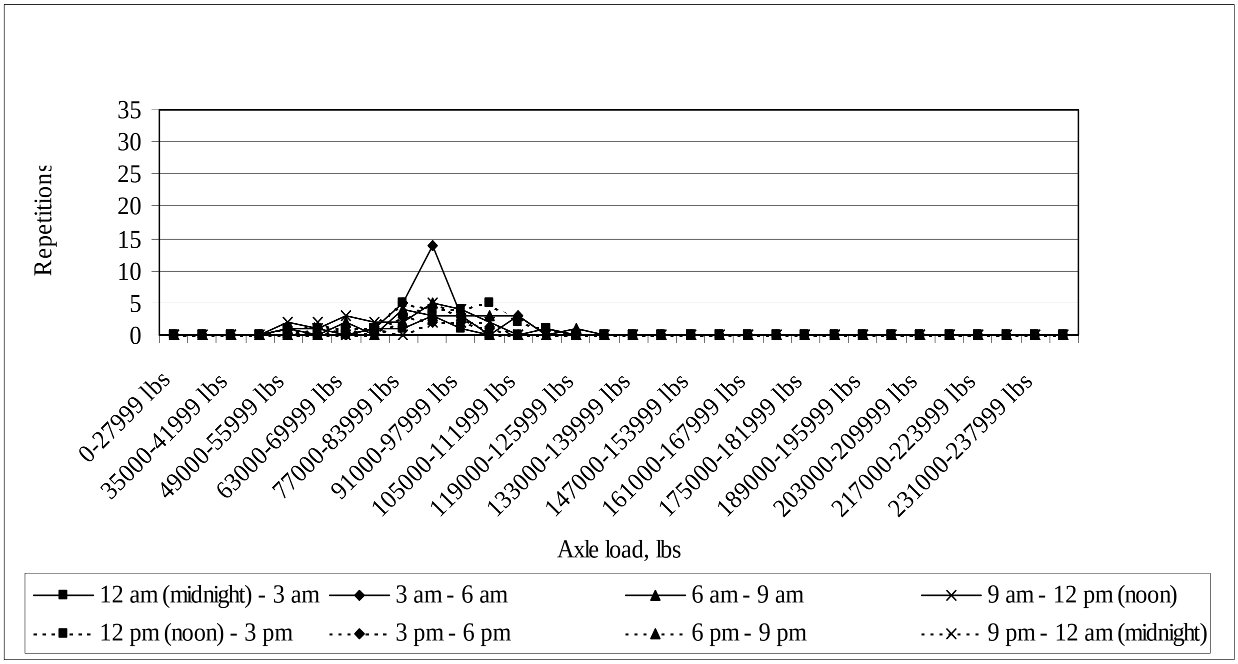


Figure J-23: Load spectrum from SPS2 sections for multi-axle (7) in September, 1998

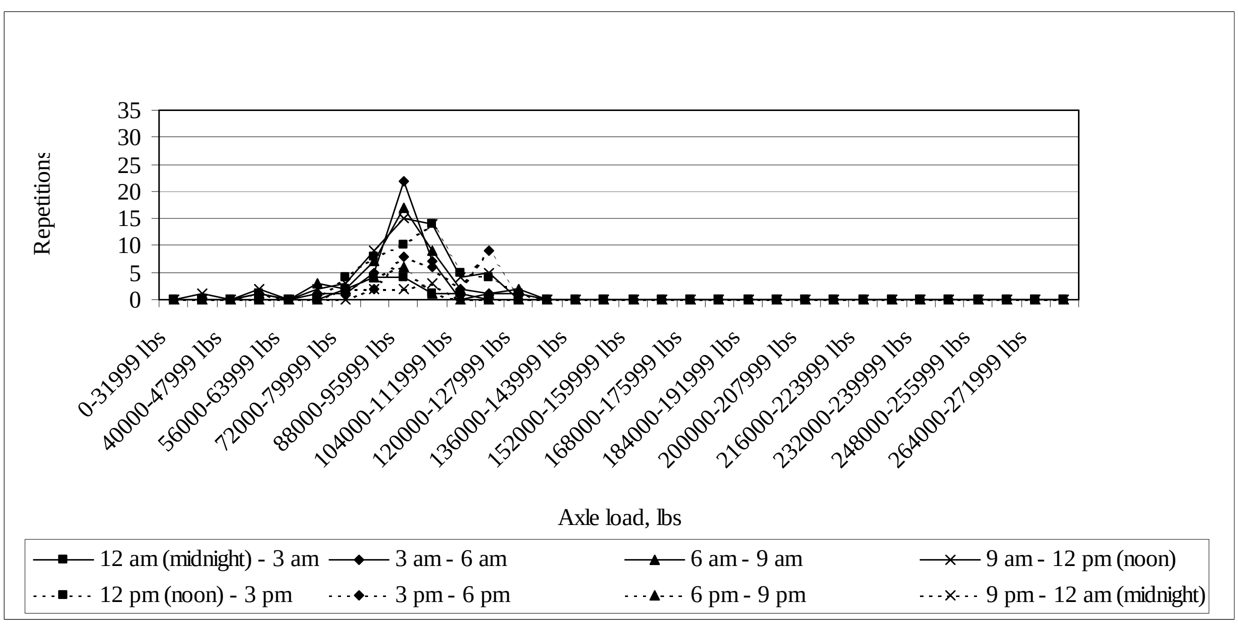


Figure J-24: Load spectrum from SPS2 sections for multi-axle (8) in September, 1998

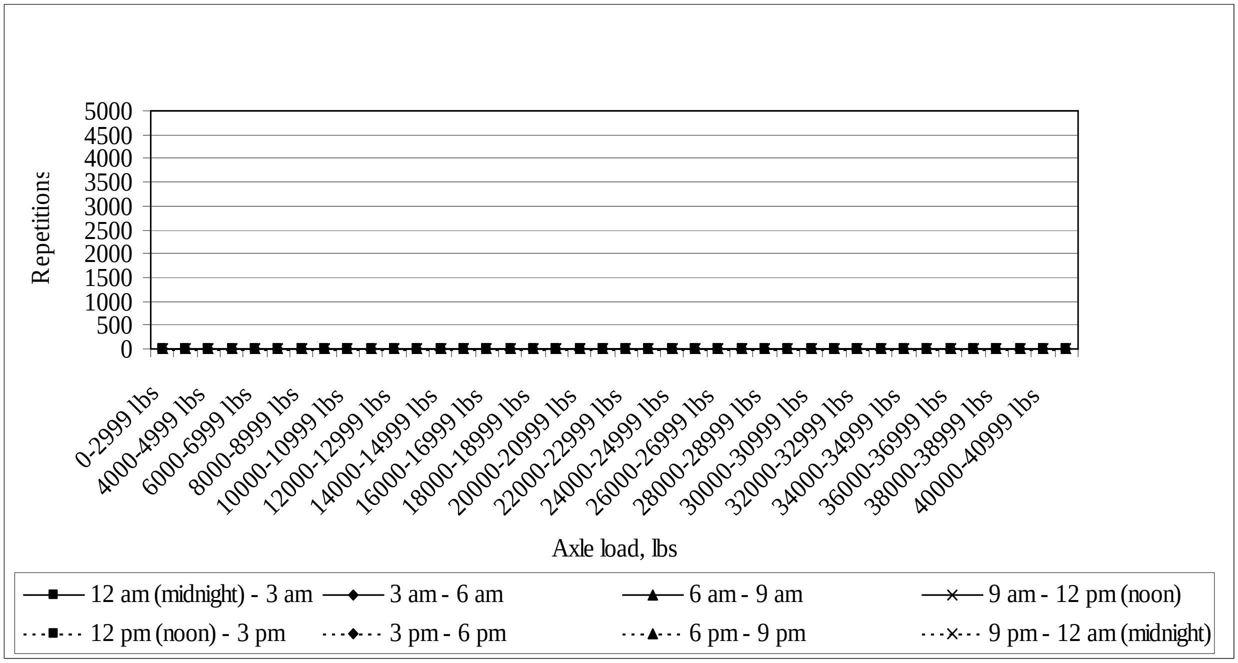


Figure J-25: Load spectrum from SPS2 sections for single axle in October, 1998

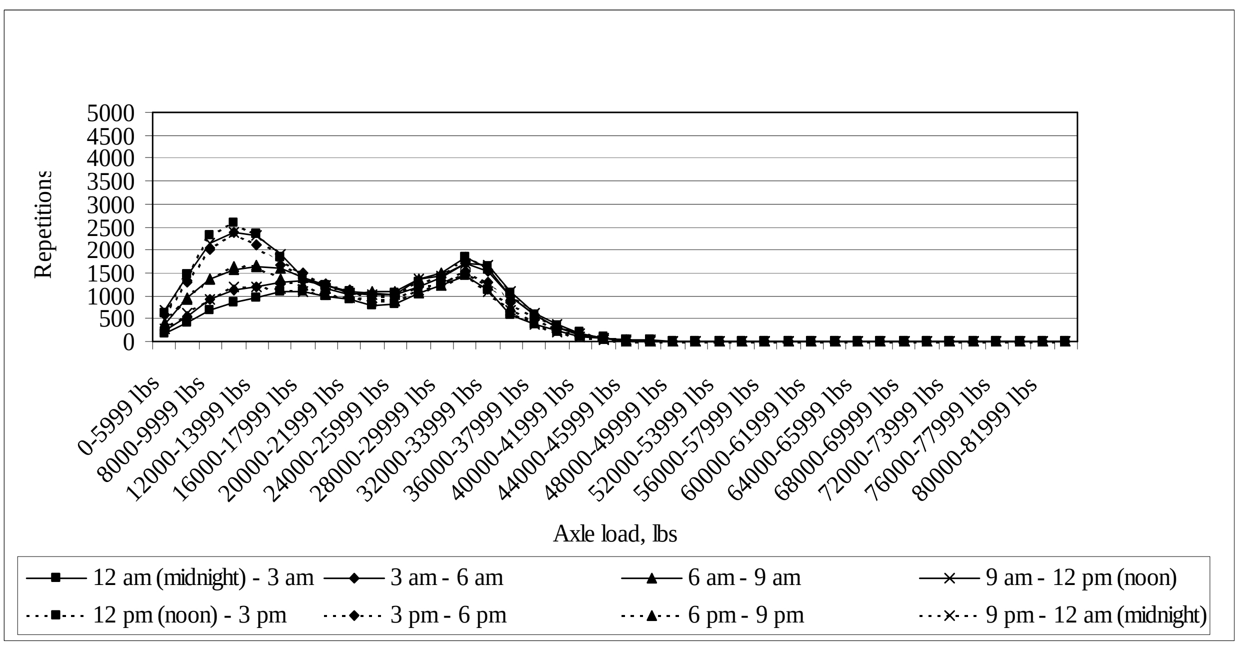


Figure J-26: Load spectrum from SPS2 sections for tandem axle in October, 1998

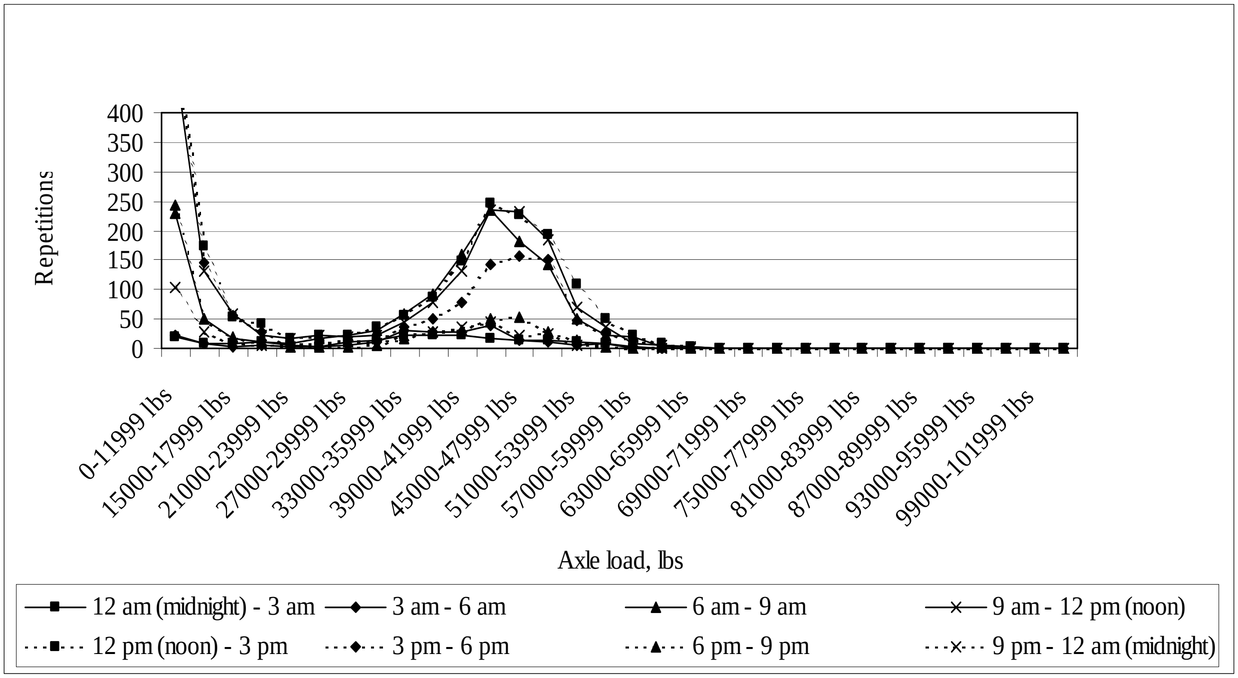


Figure J-27: Load spectrum from SPS2 sections for tridem axle in October, 1998

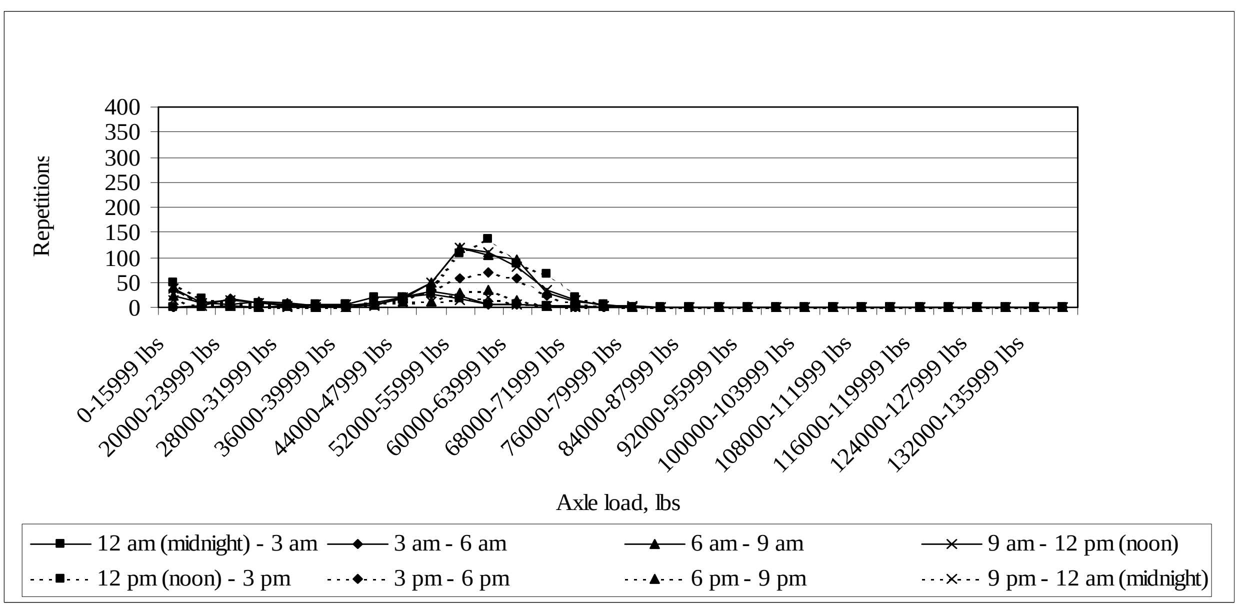


Figure J-28: Load spectrum from SPS2 sections for quad axle in October, 1998

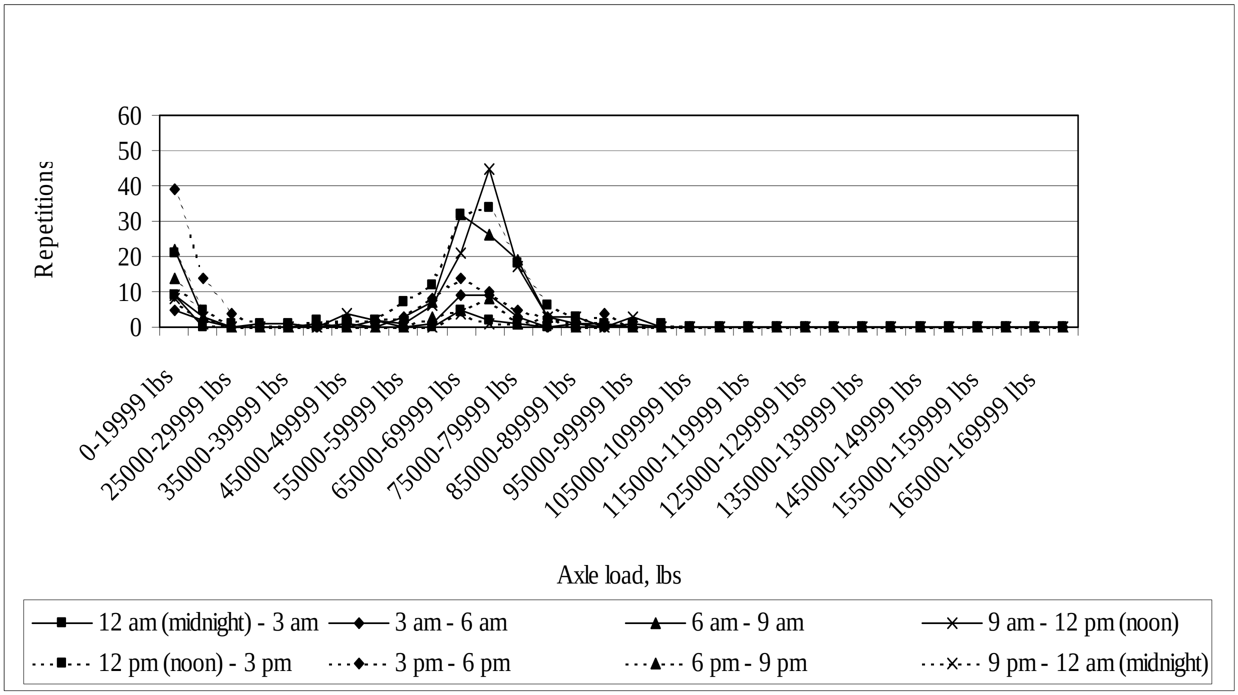


Figure J-29: Load spectrum from SPS2 sections for multi-axle (5) in October, 1998

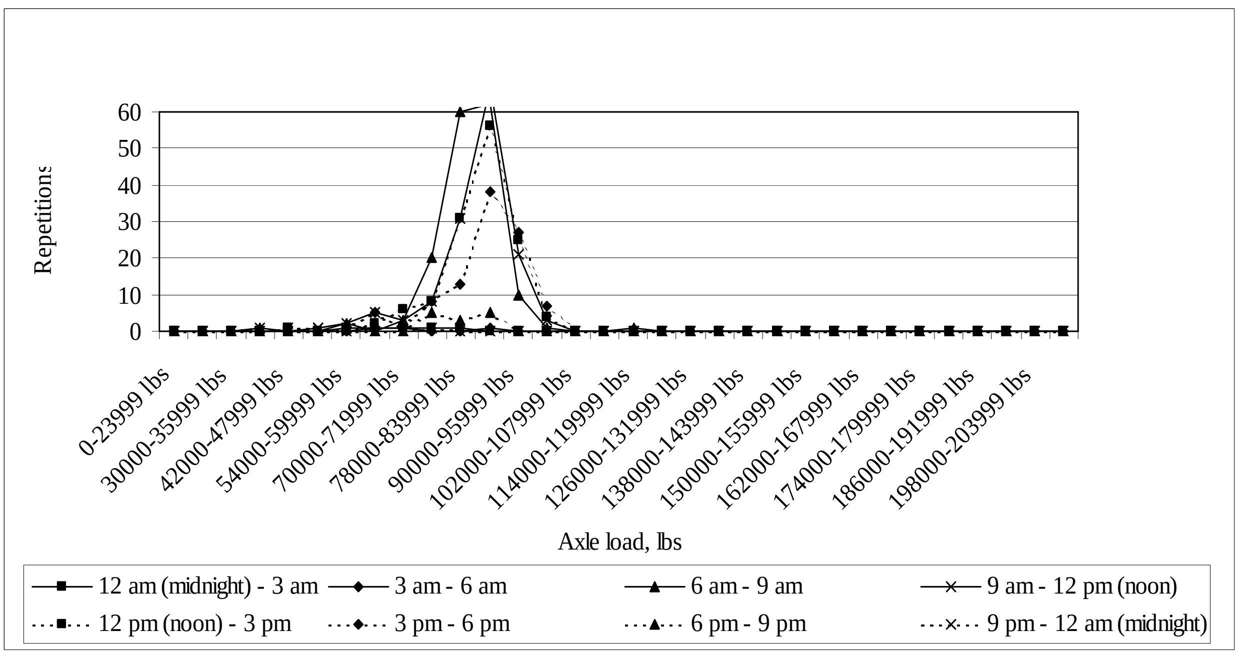


Figure J-30: Load spectrum from SPS2 sections for multi-axle (6) in October, 1998

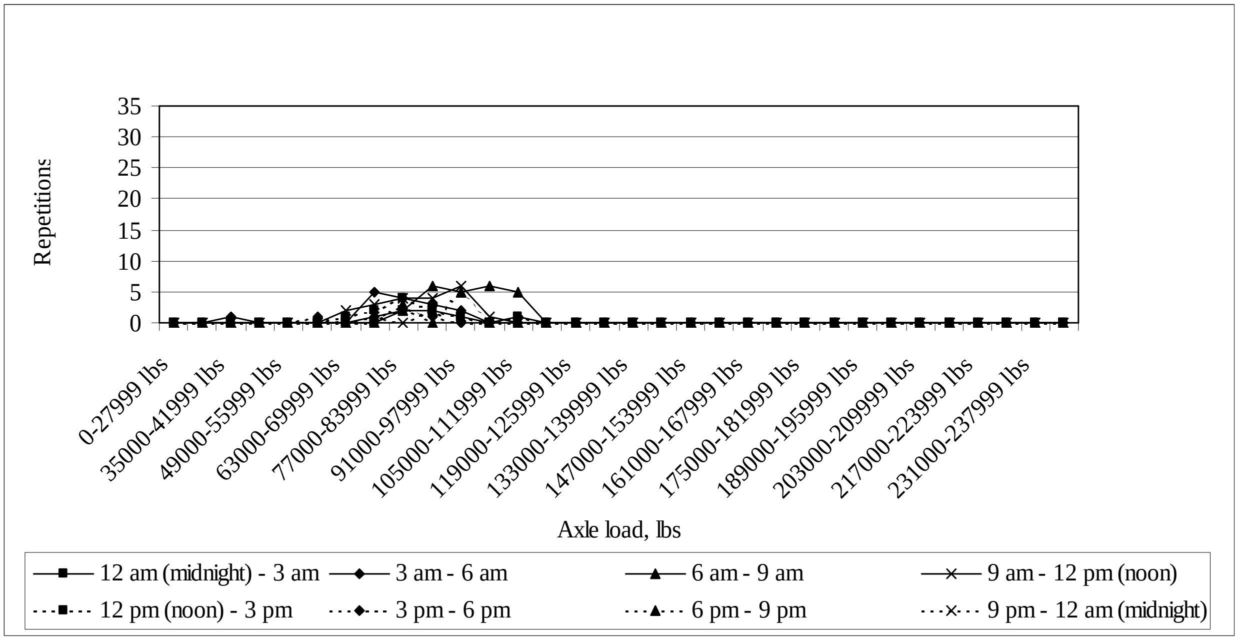


Figure J-31: Load spectrum from SPS2 sections for multi-axle (7) in October, 1998

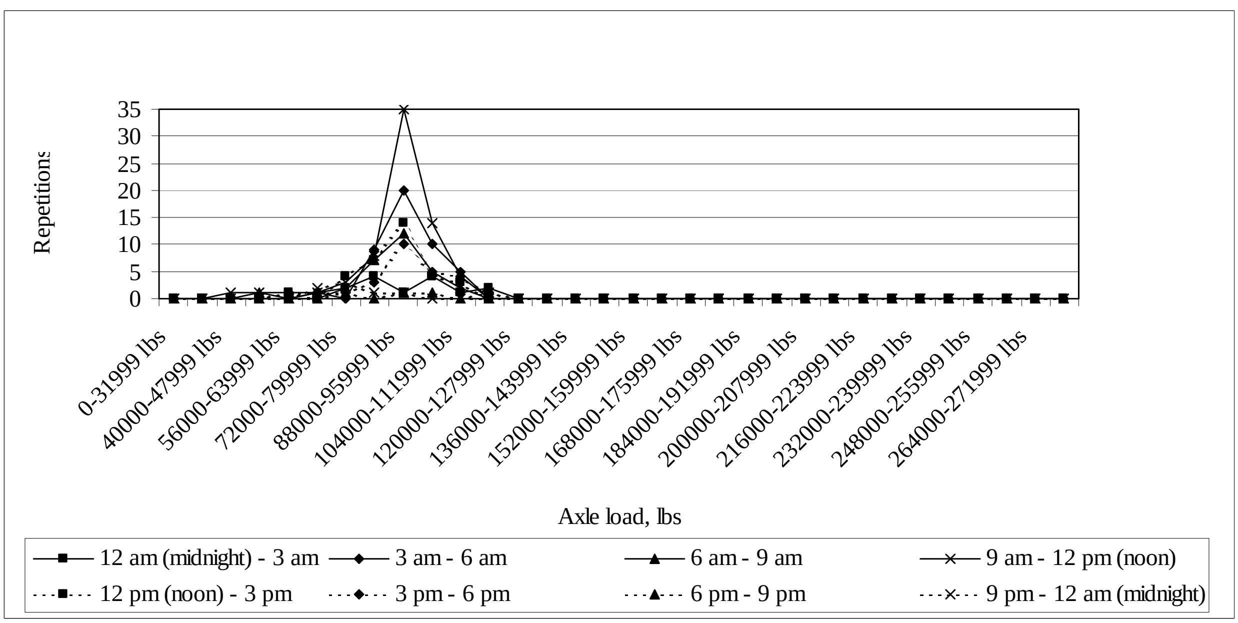


Figure J-32: Load spectrum from SPS2 sections for multi-axle (8) in October, 1998

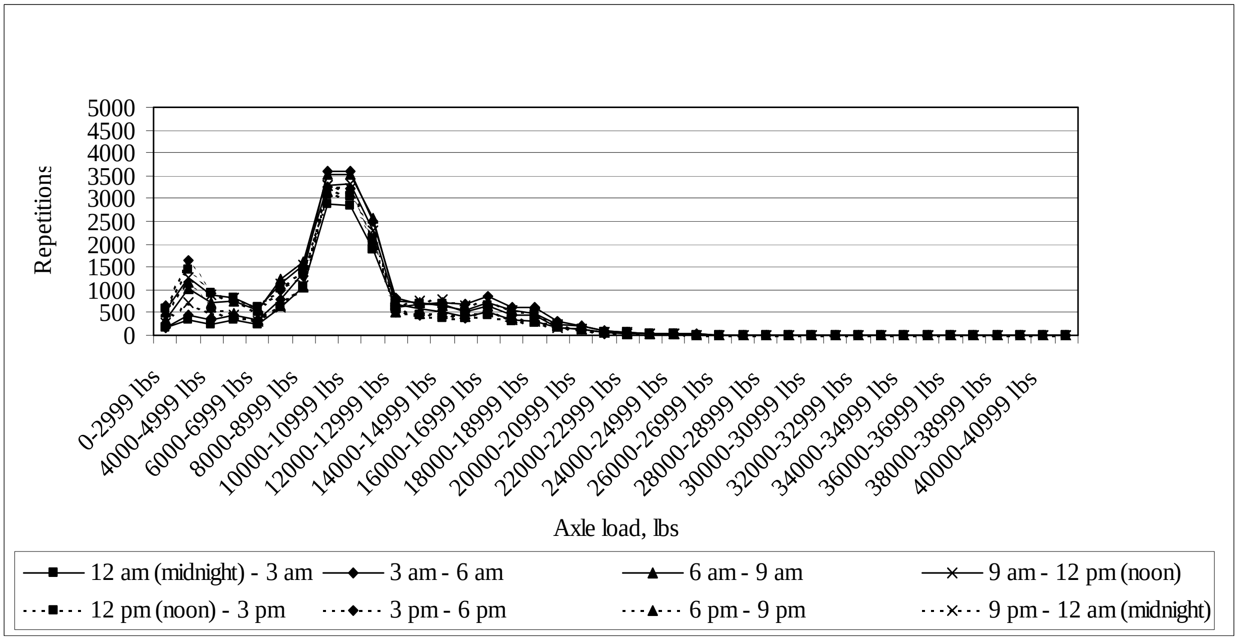


Figure J-33: Load spectrum from SPS2 sections for single axle in November, 1998

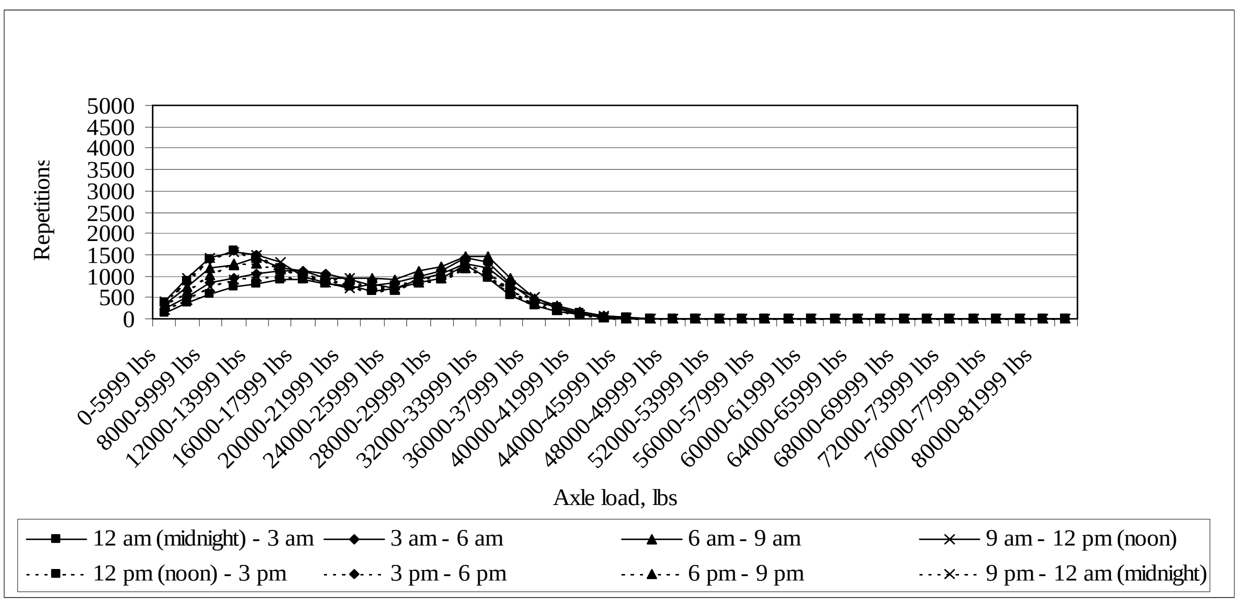


Figure J-34: Load spectrum from SPS2 sections for tandem axle in November, 1998

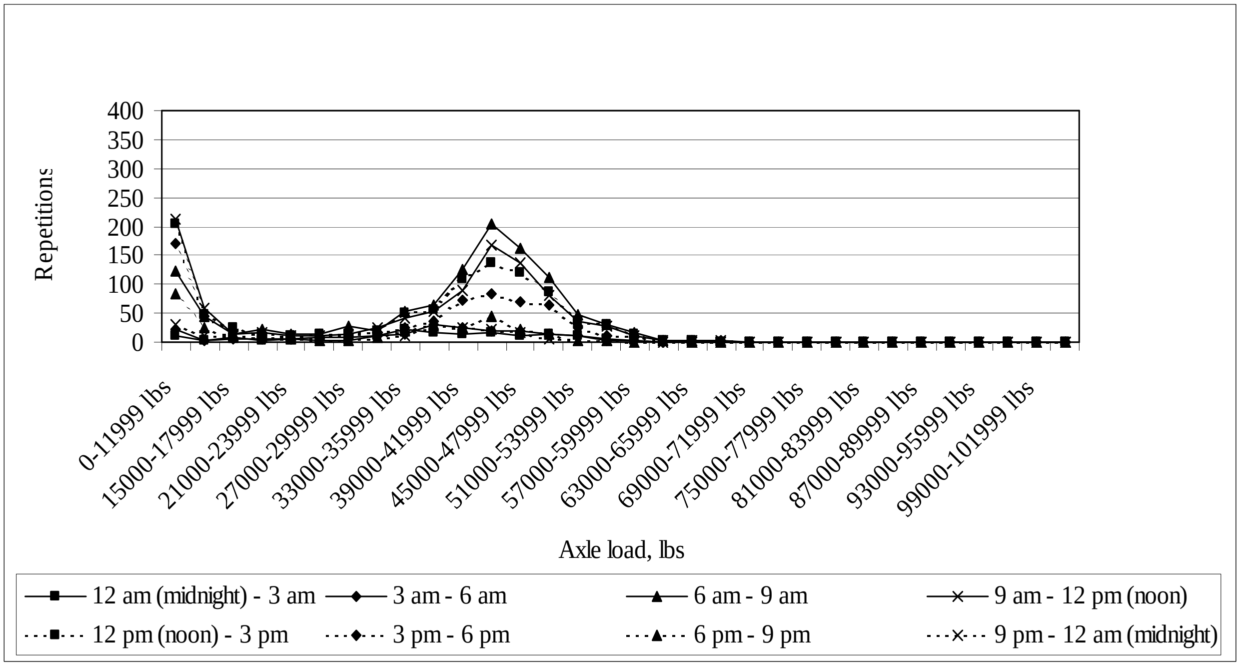


Figure J-35: Load spectrum from SPS2 sections for tridem axle in November, 1998

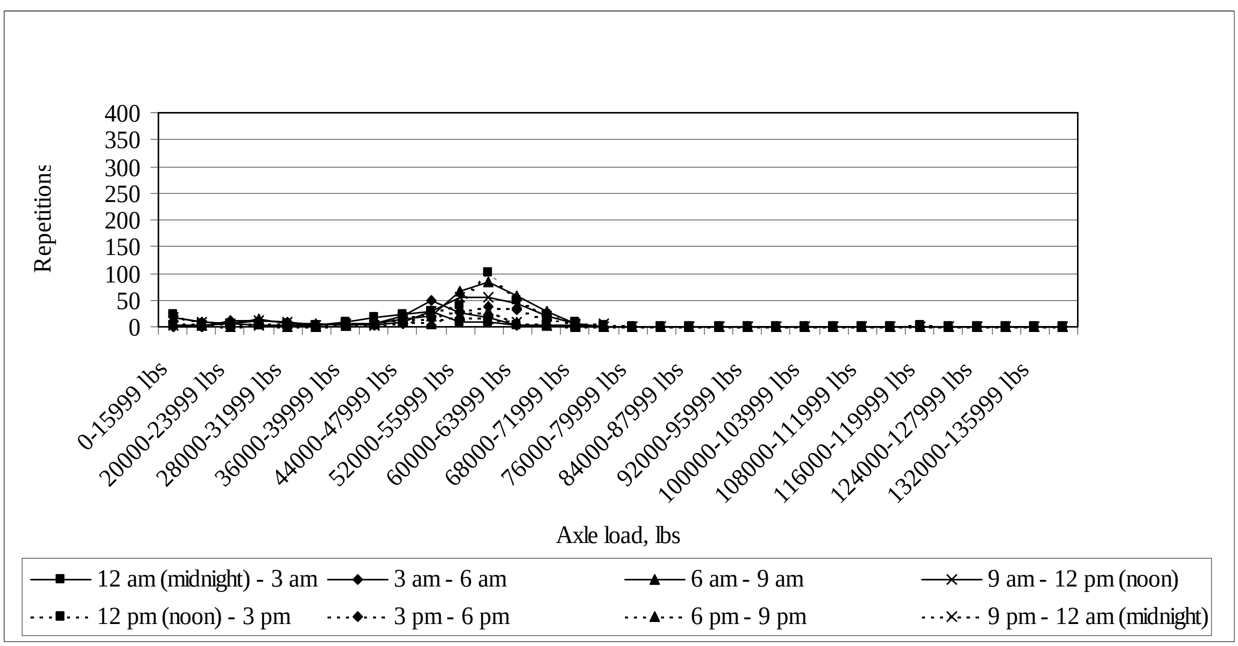


Figure J-36: Load spectrum from SPS2 sections for quad axle in November, 1998

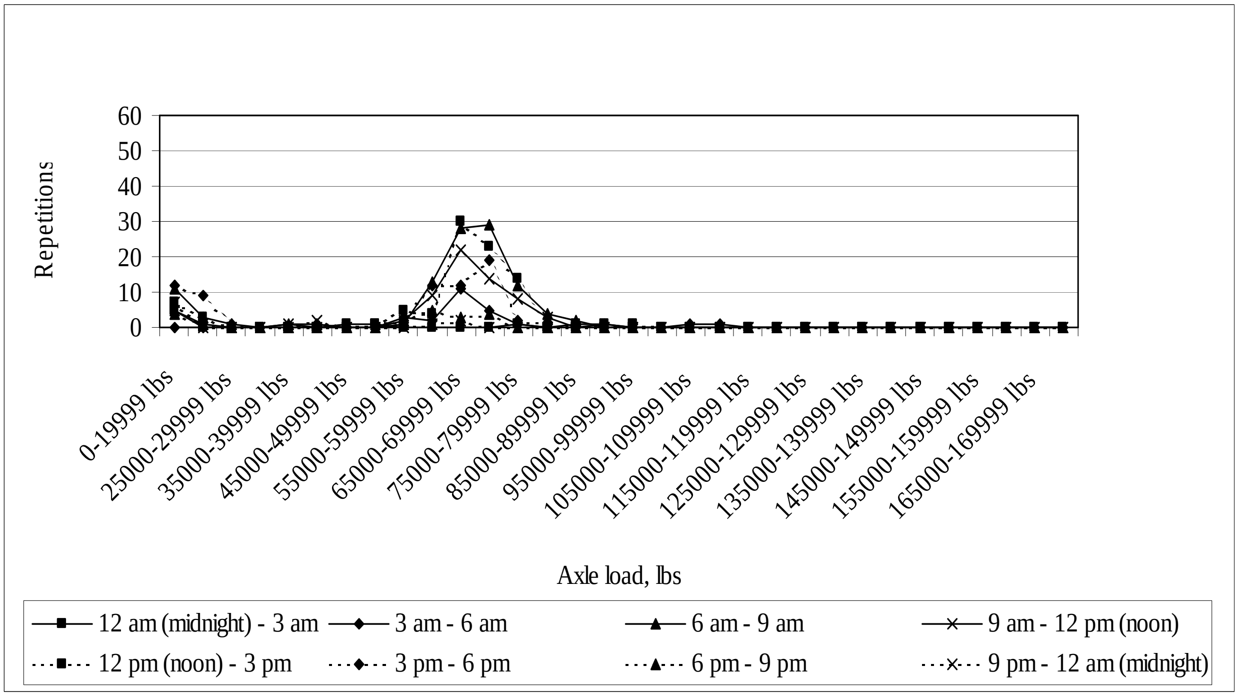


Figure J-37: Load spectrum from SPS2 sections for multi-axle (5) in November, 1998

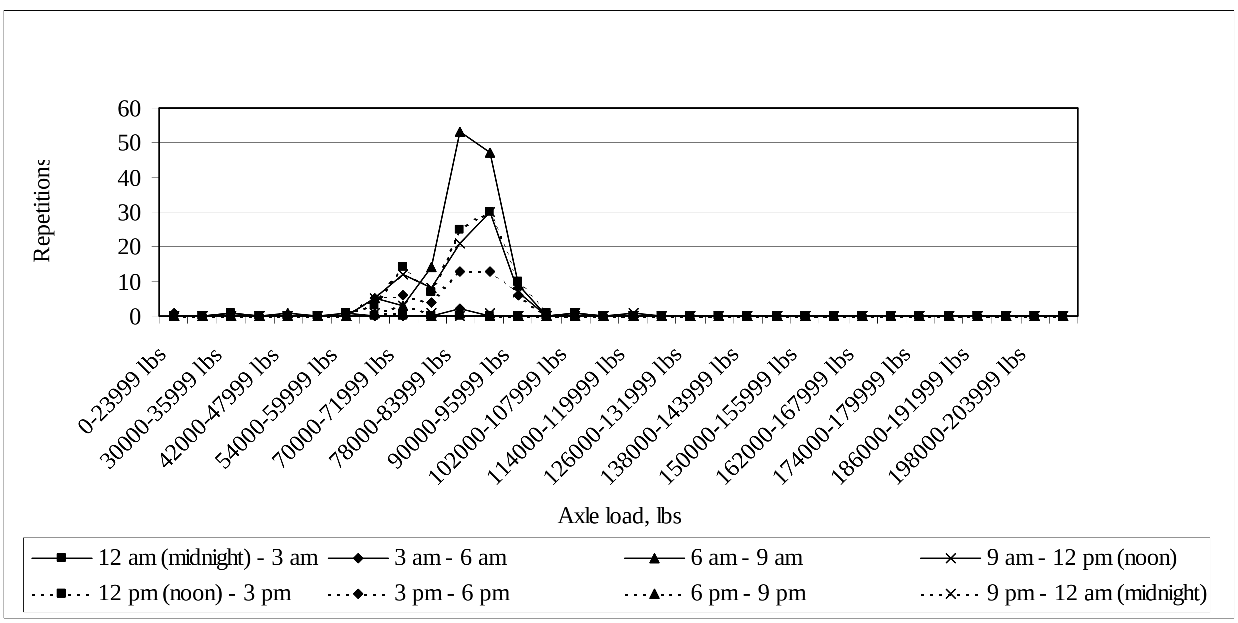


Figure J-38: Load spectrum from SPS2 sections for multi-axle (6) in November, 1998

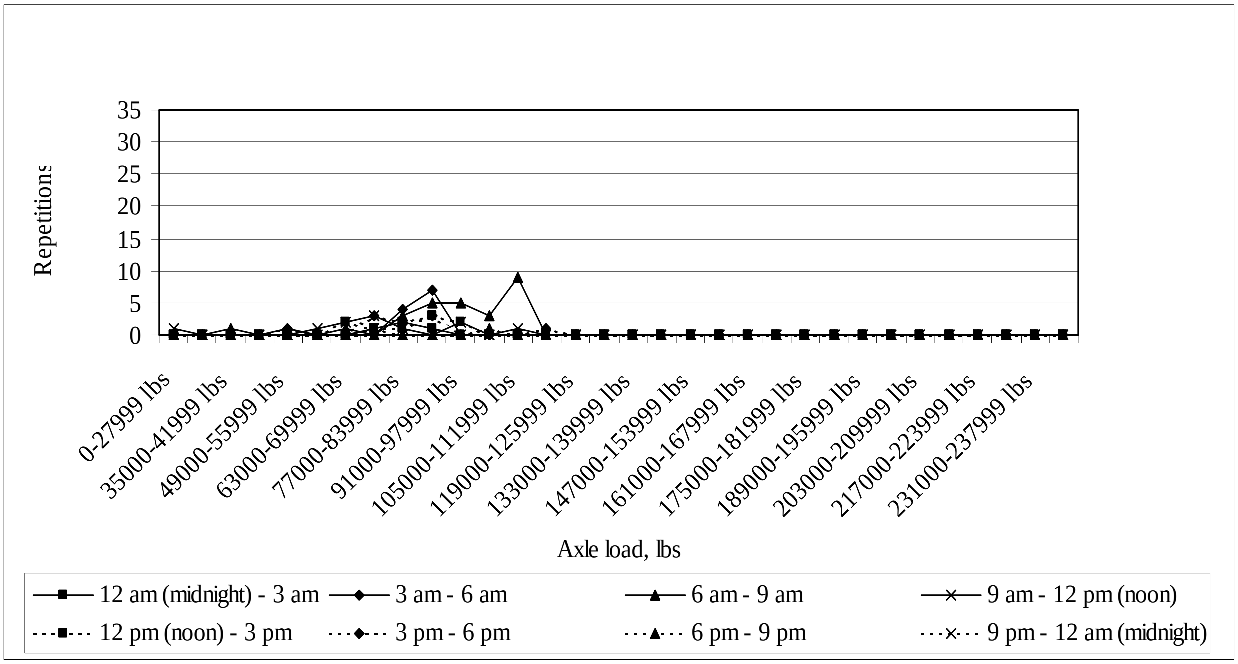


Figure J-39: Load spectrum from SPS2 sections for multi-axle (7) in November, 1998

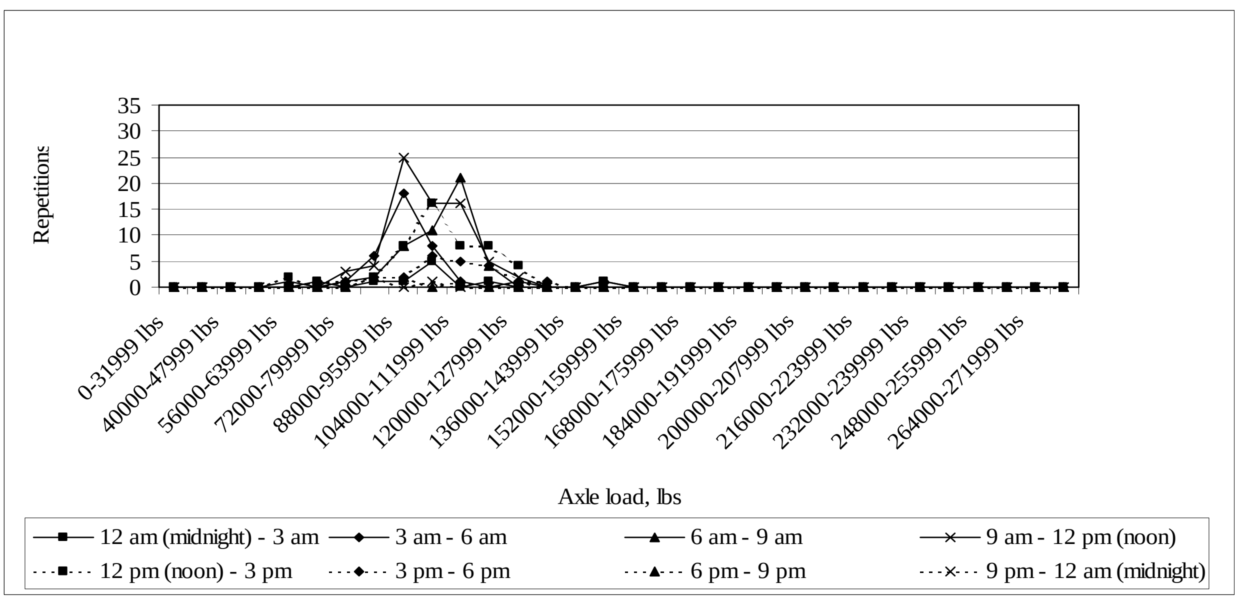


Figure J-40: Load spectrum from SPS2 sections for multi-axle (8) in November, 1998

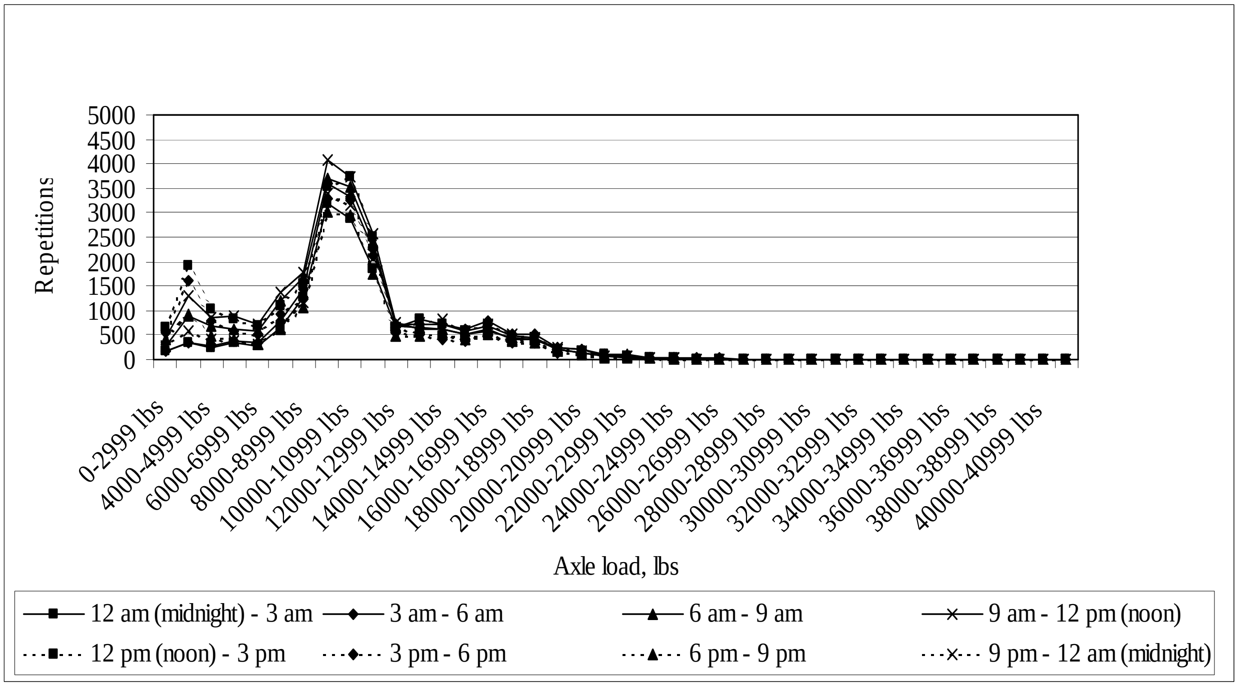


Figure J-41: Load spectrum from SPS2 sections for single axle in December, 1998

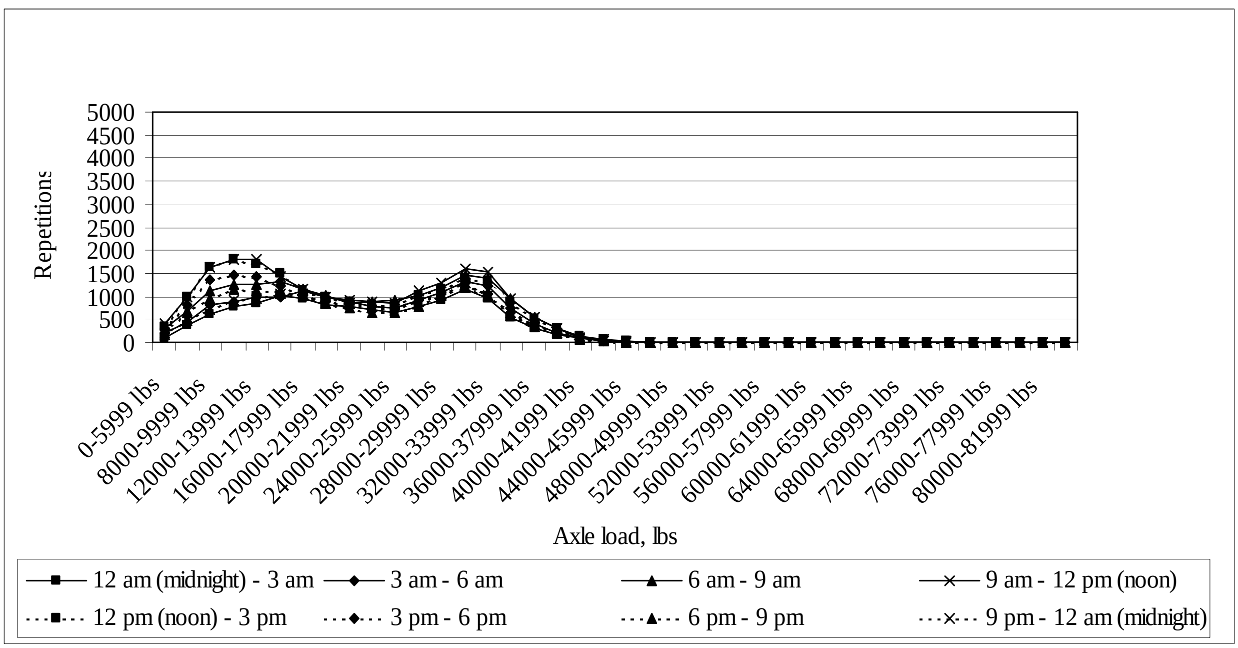


Figure J-42: Load spectrum from SPS2 sections for tandem axle in December, 1998

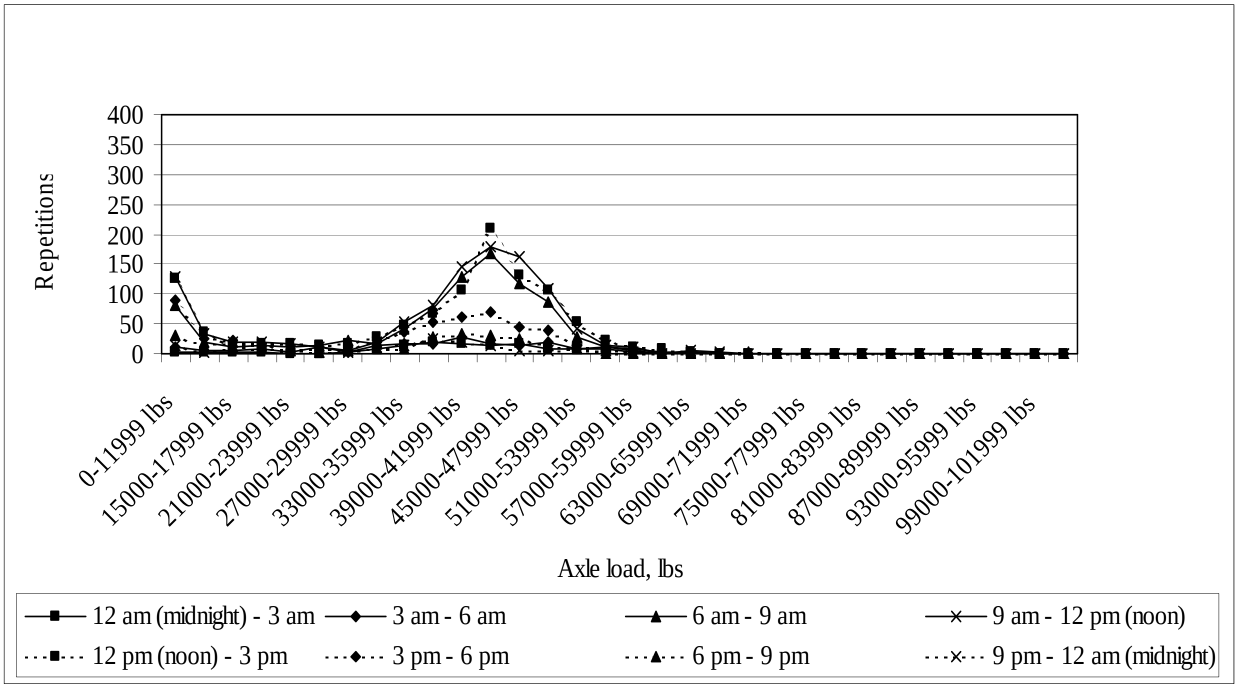


Figure J-43: Load spectrum from SPS2 sections for tridem axle in December, 1998

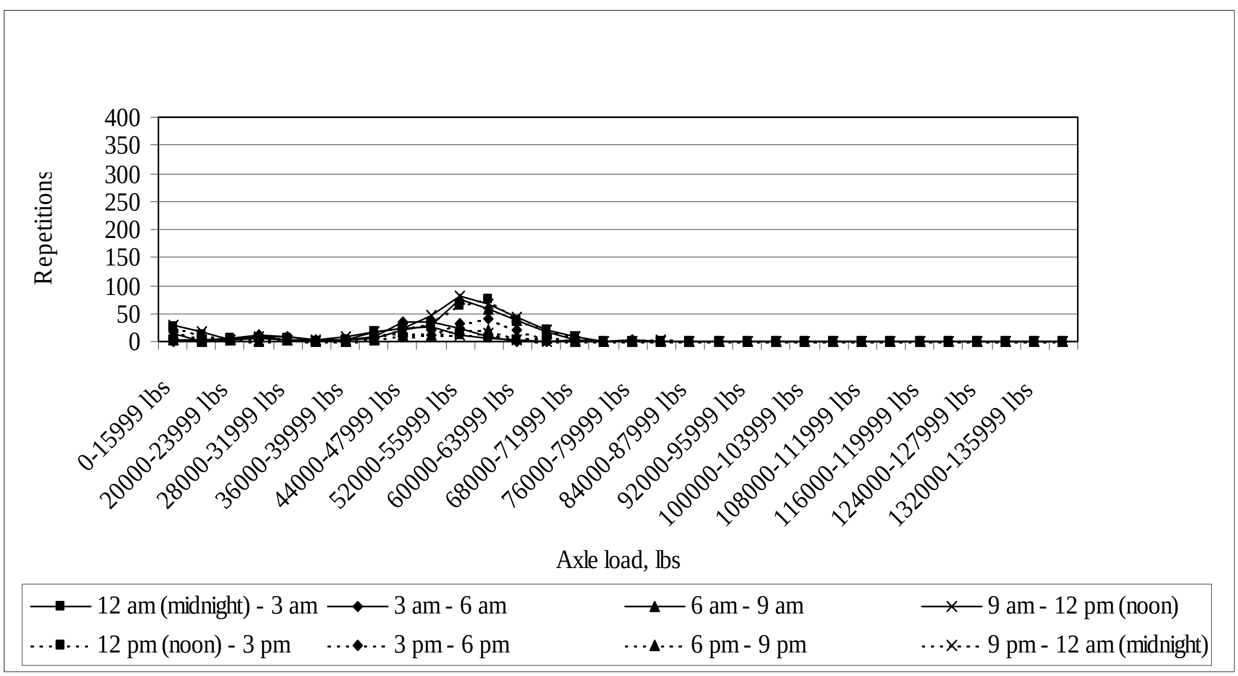


Figure J-44: Load spectrum from SPS2 sections for quad axle in December, 1998

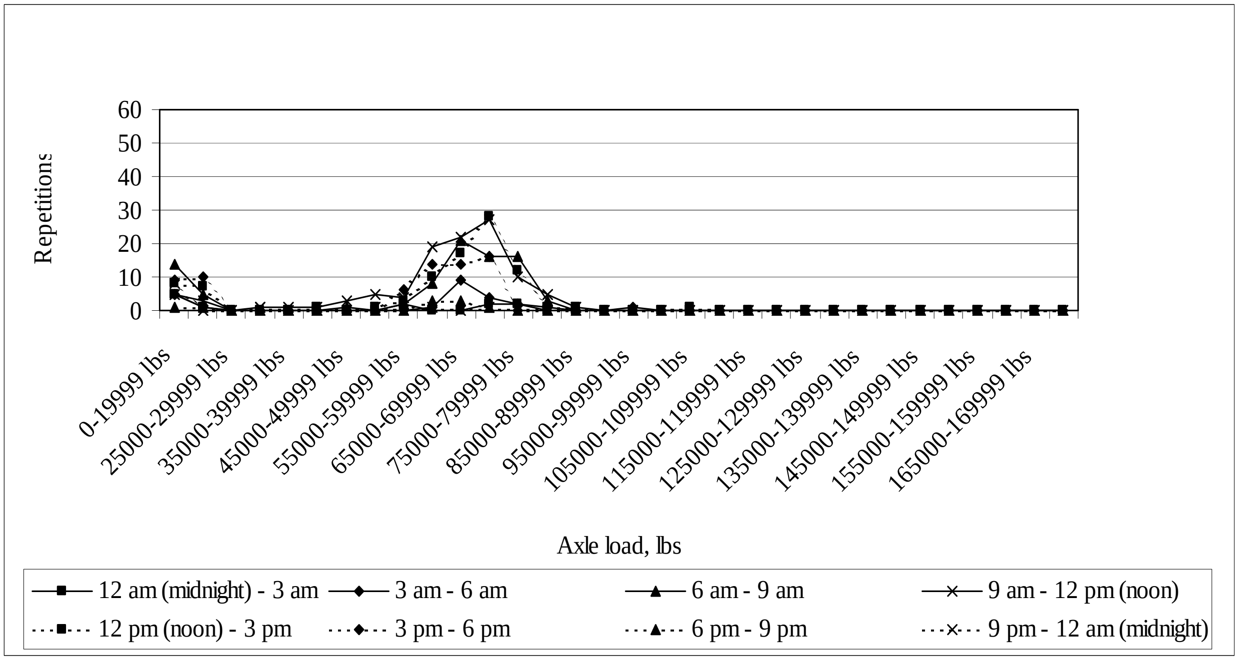


Figure J-45: Load spectrum from SPS2 sections for multi-axle (5) in December, 1998

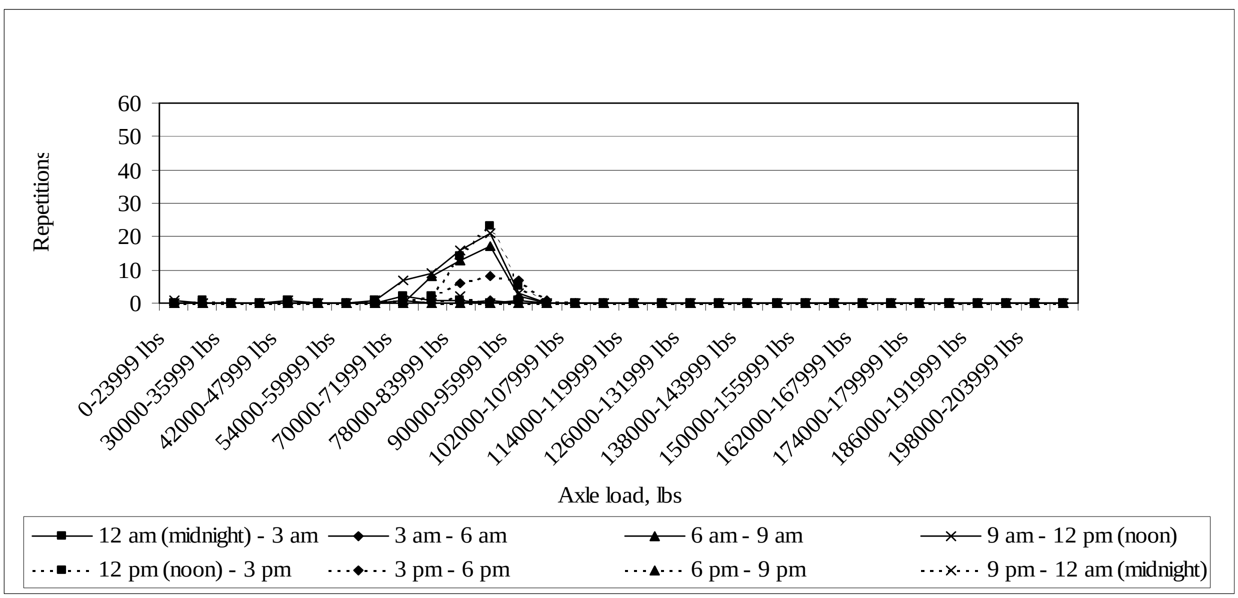


Figure J-46: Load spectrum from SPS2 sections for multi-axle (6) in December, 1998

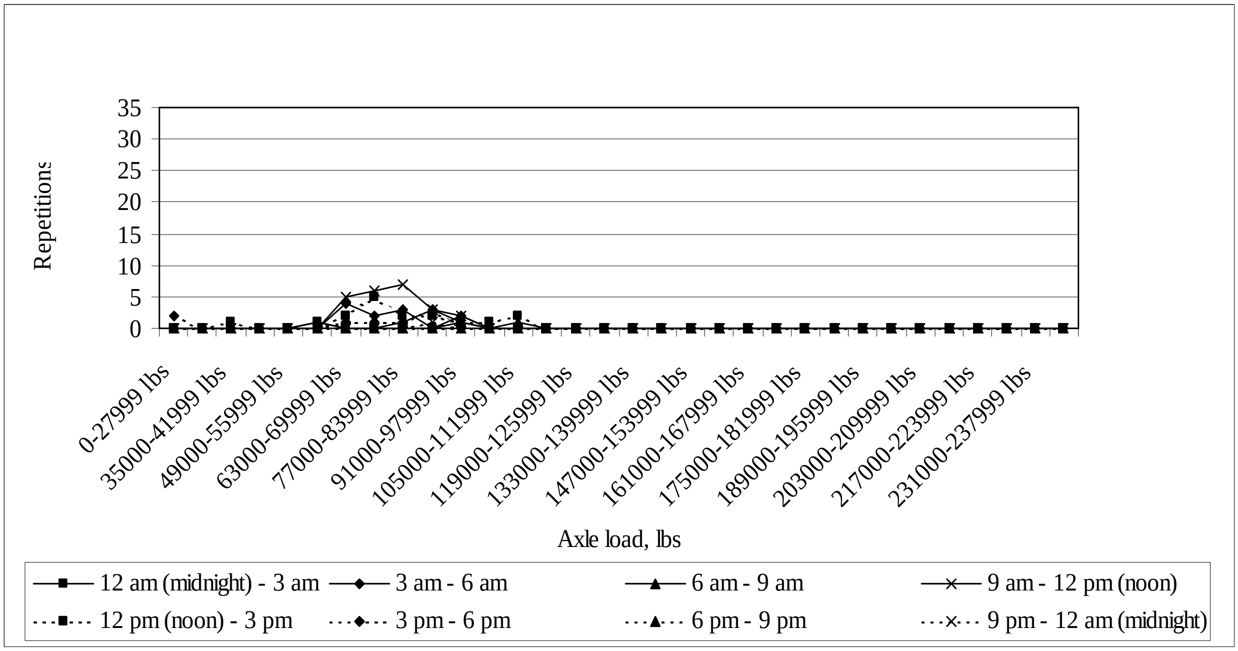


Figure J-47: Load spectrum from SPS2 sections for multi-axle (7) in December, 1998

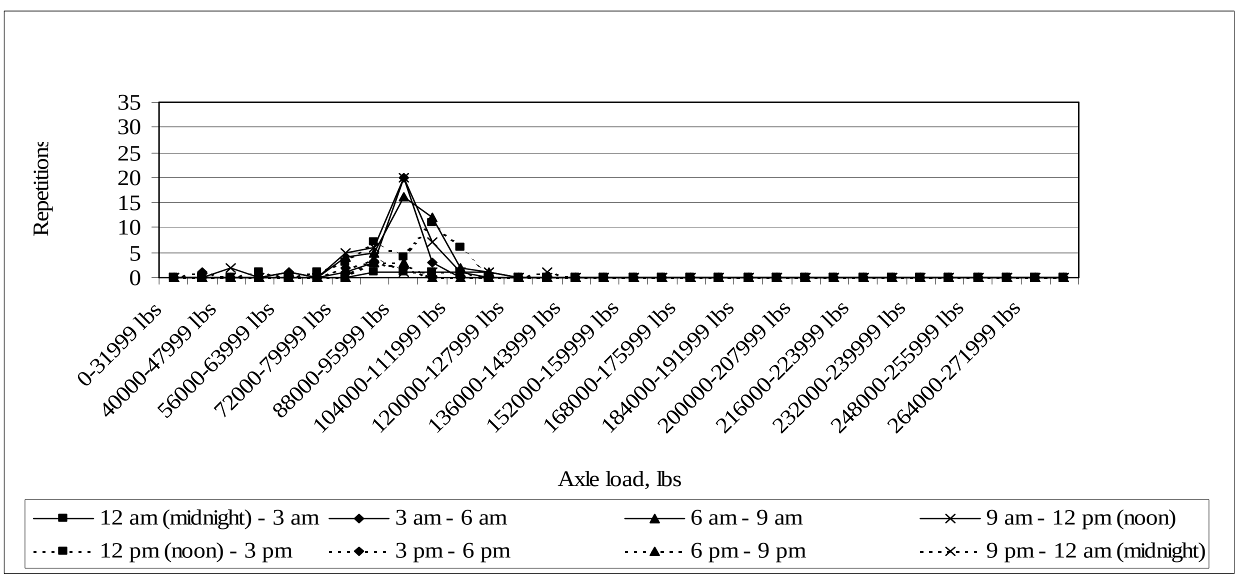


Figure J-48: Load spectrum from SPS2 sections for multi-axle (8) in December, 1998

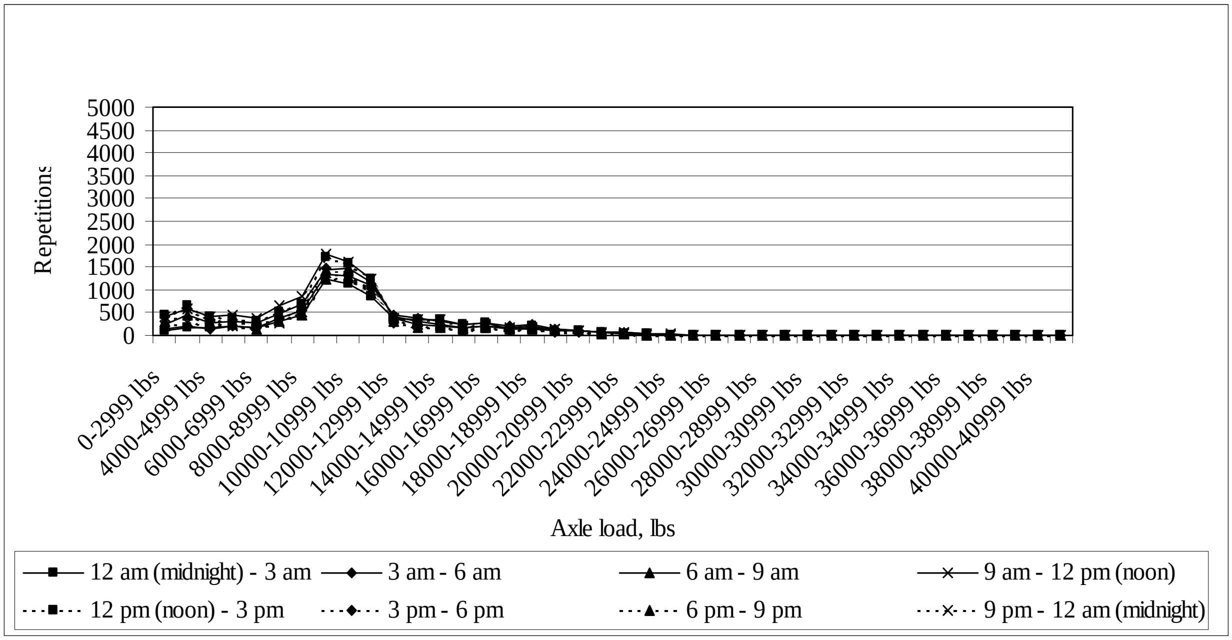


Figure J-49: Load spectrum from SPS2 sections for single axle in January, 1999

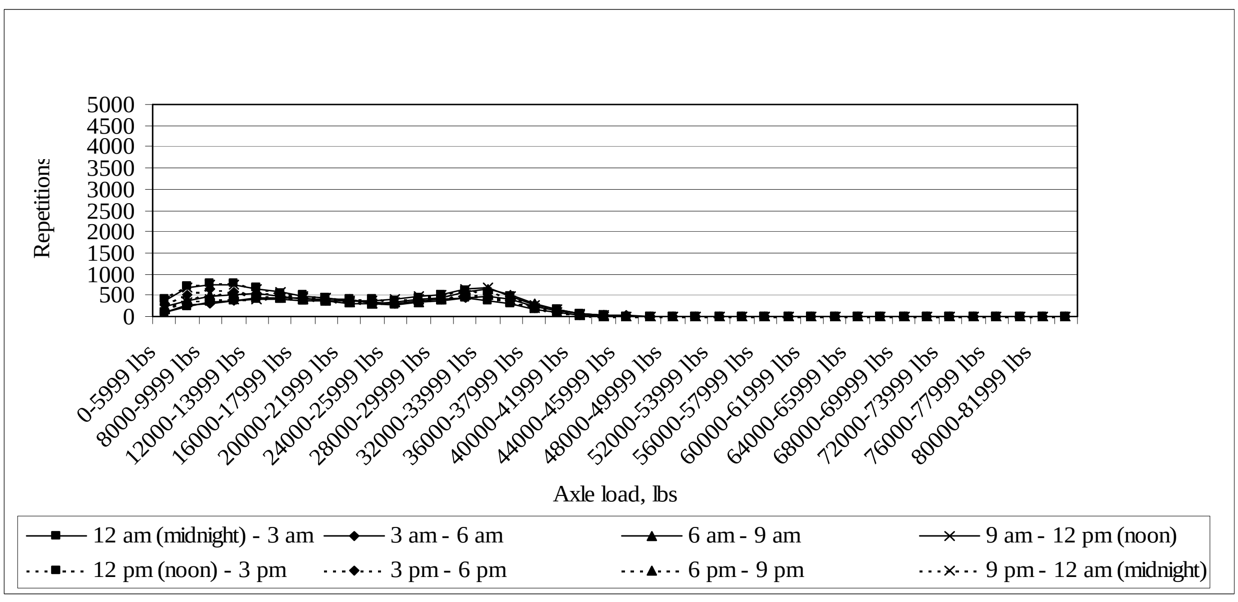


Figure J-50: Load spectrum from SPS2 sections for tandem axle in January, 1999

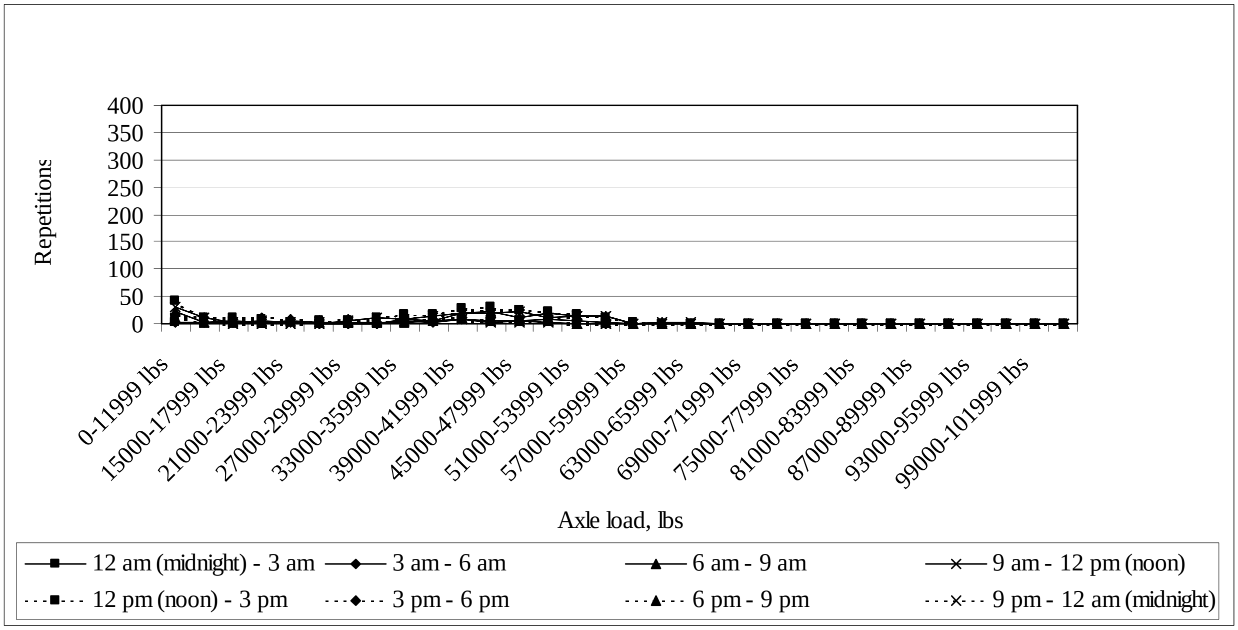


Figure J-51: Load spectrum from SPS2 sections for tridem axle in January, 1999

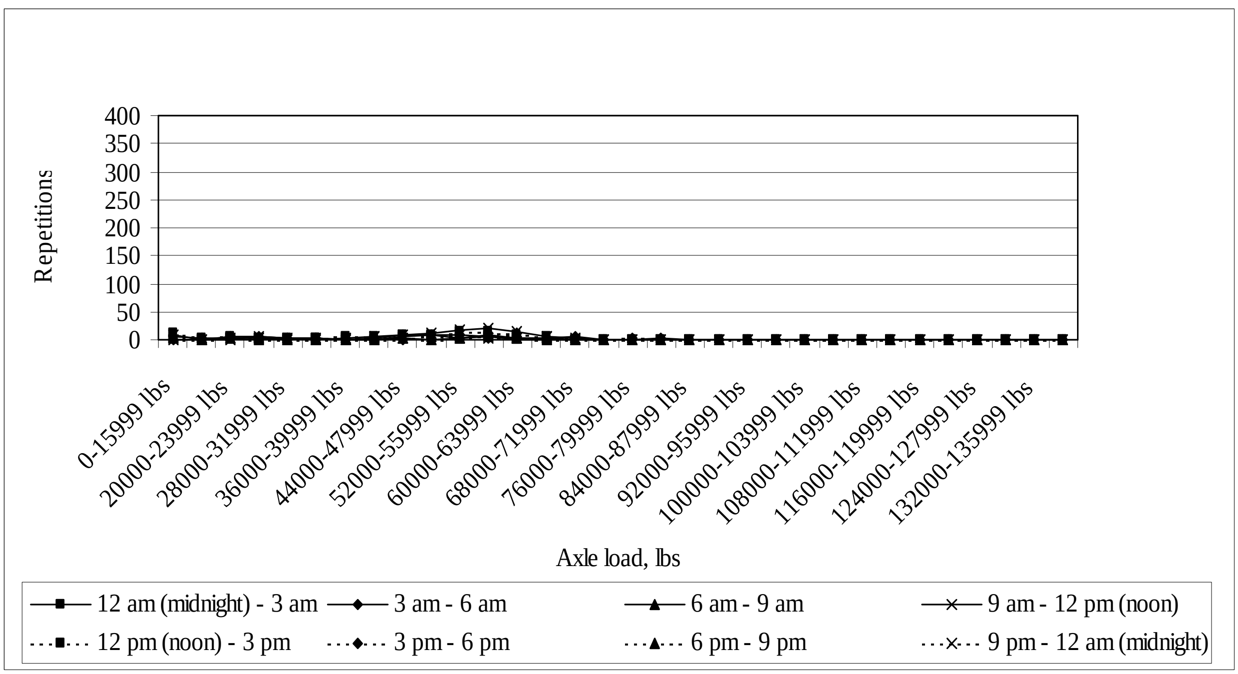


Figure J-52: Load spectrum from SPS2 sections for quad axle in January, 1999

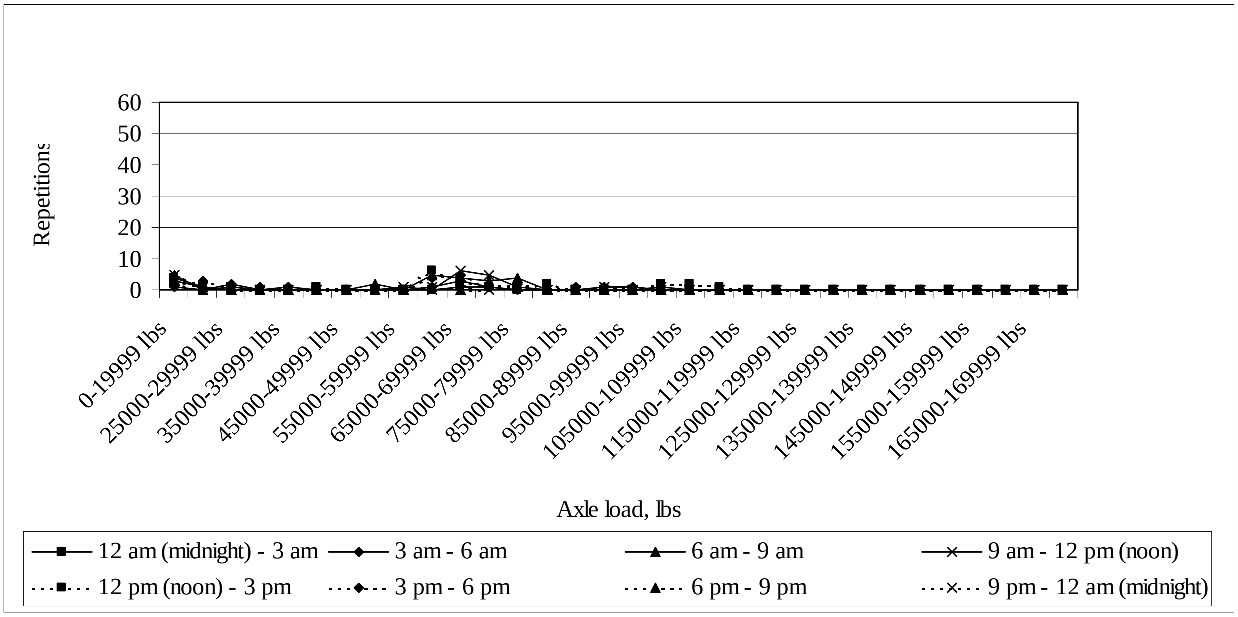


Figure J-53: Load spectrum from SPS2 sections for multi-axle (5) in January, 1999

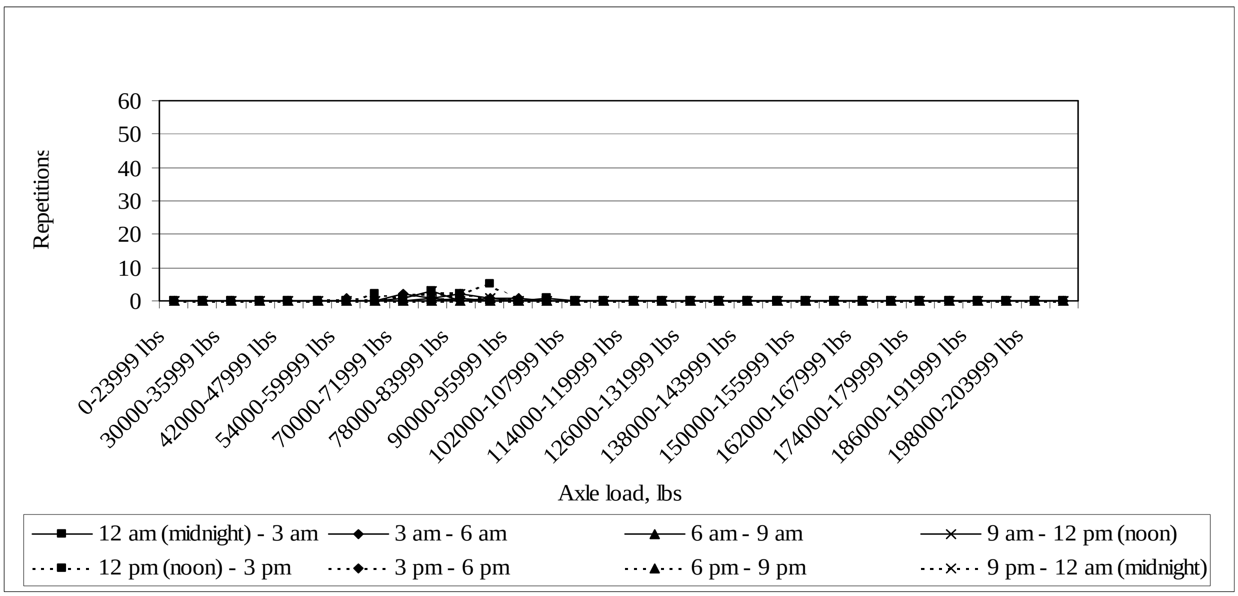


Figure J-54: Load spectrum from SPS2 sections for multi-axle (6) in January, 1999

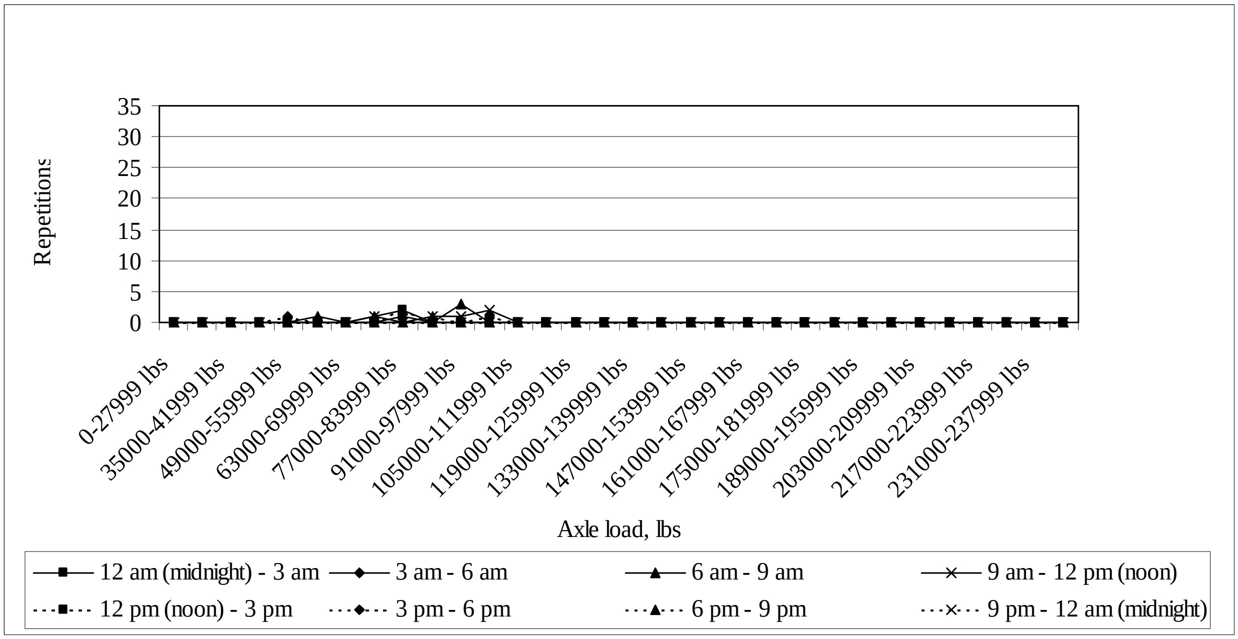


Figure J-55: Load spectrum from SPS2 sections for multi-axle (7) in January, 1999

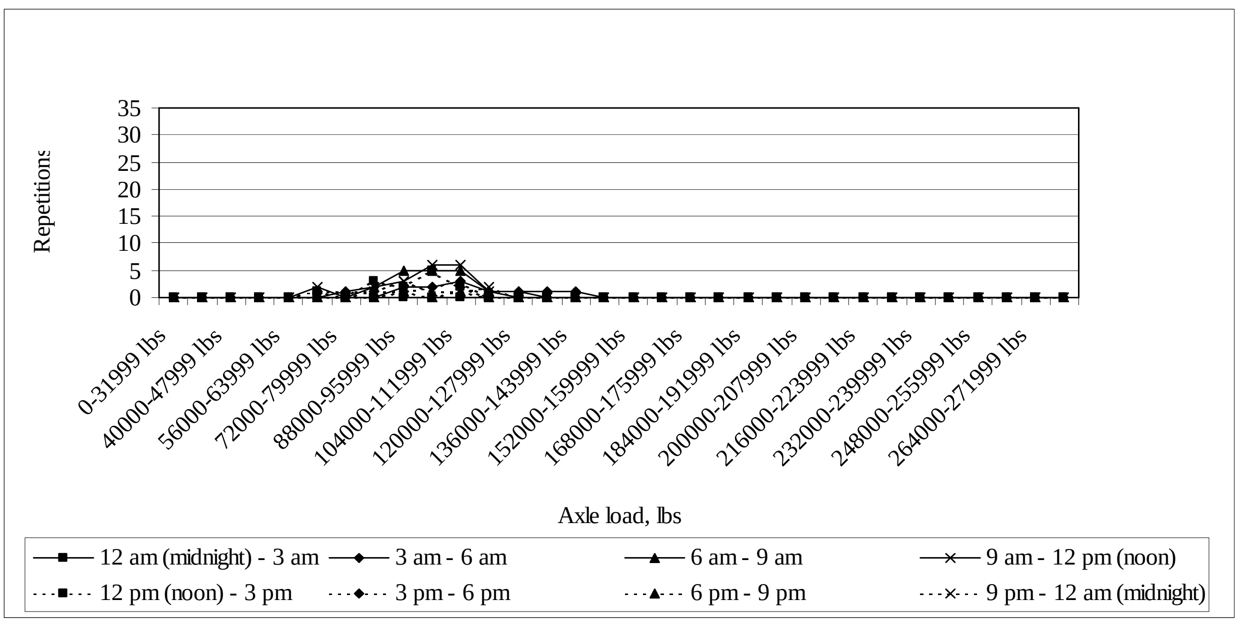


Figure J-56: Load spectrum from SPS2 sections for multi-axle (8) in January, 1999

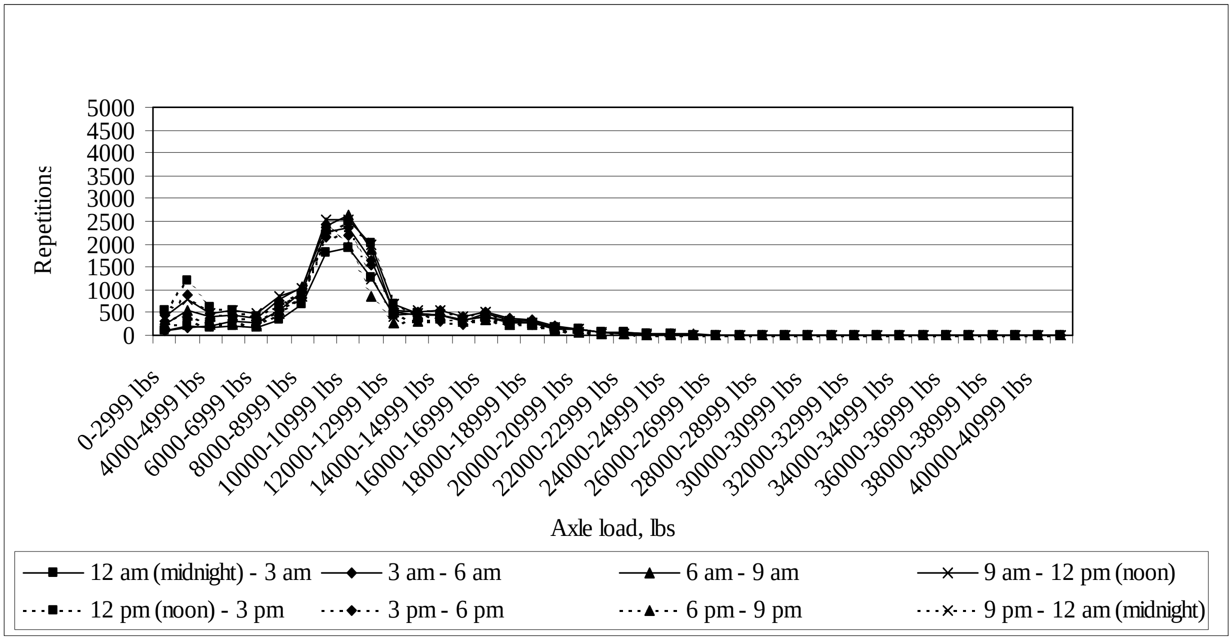


Figure J-57: Load spectrum from SPS2 sections for single axle in February, 1999

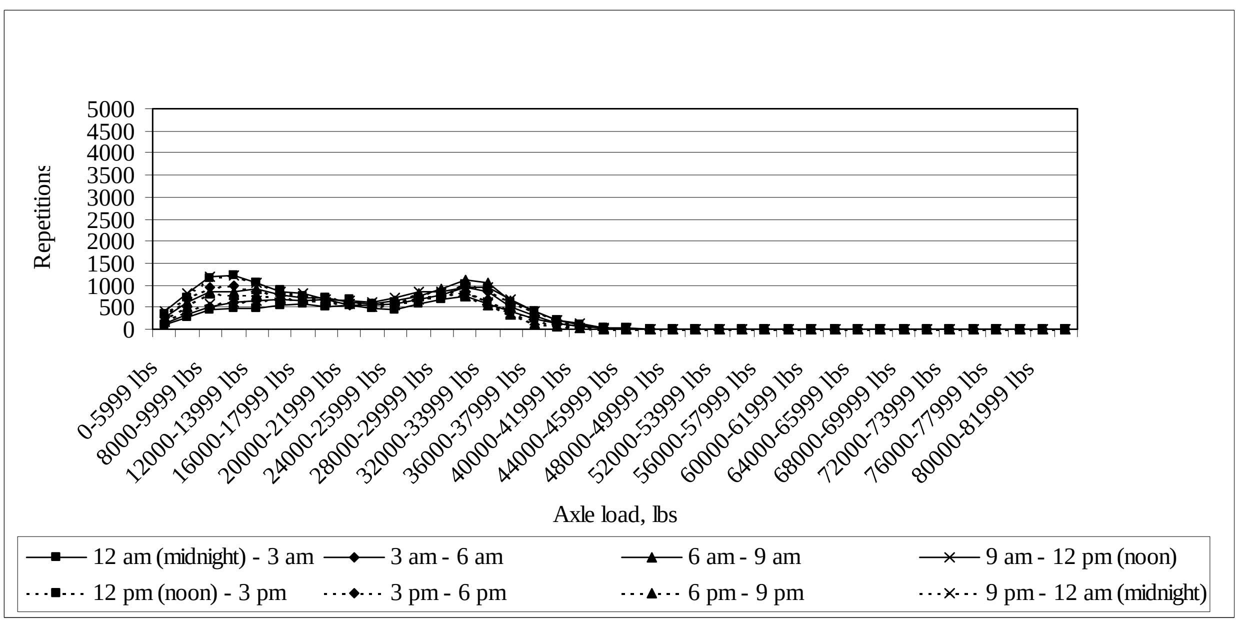


Figure J-58: Load spectrum from SPS2 sections for tandem axle in February, 1999

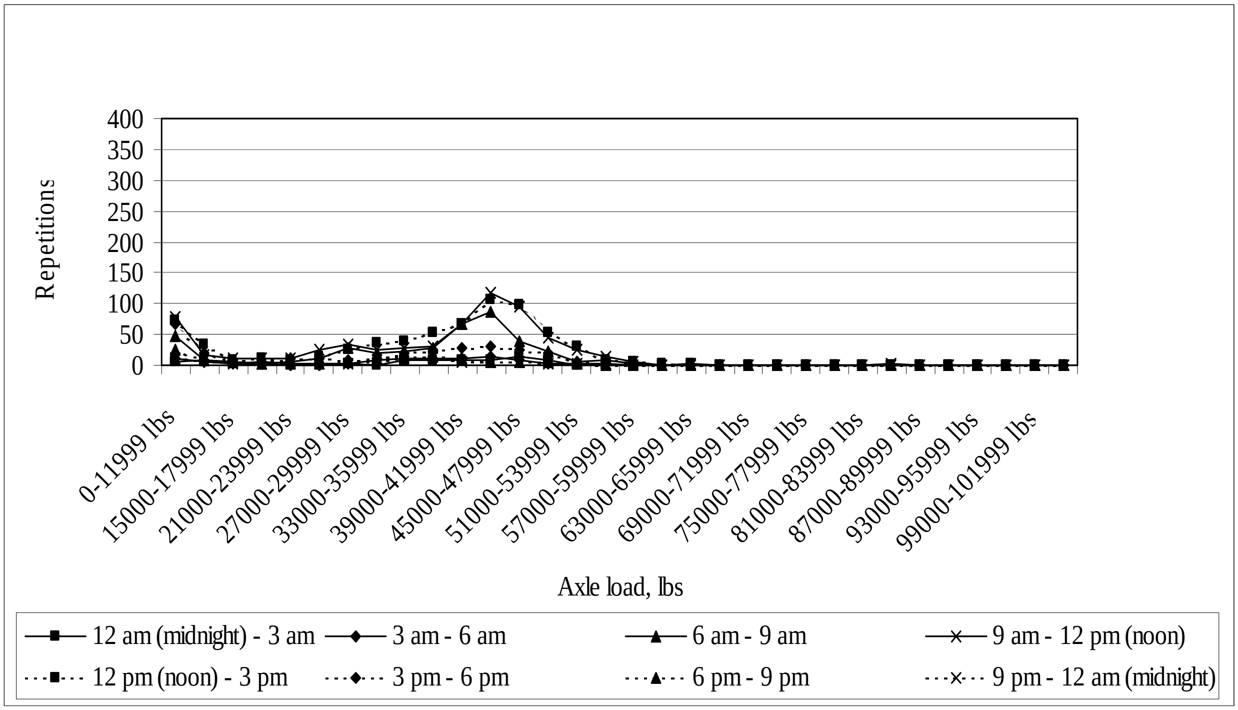


Figure J-59: Load spectrum from SPS2 sections for tridem axle in February, 1999

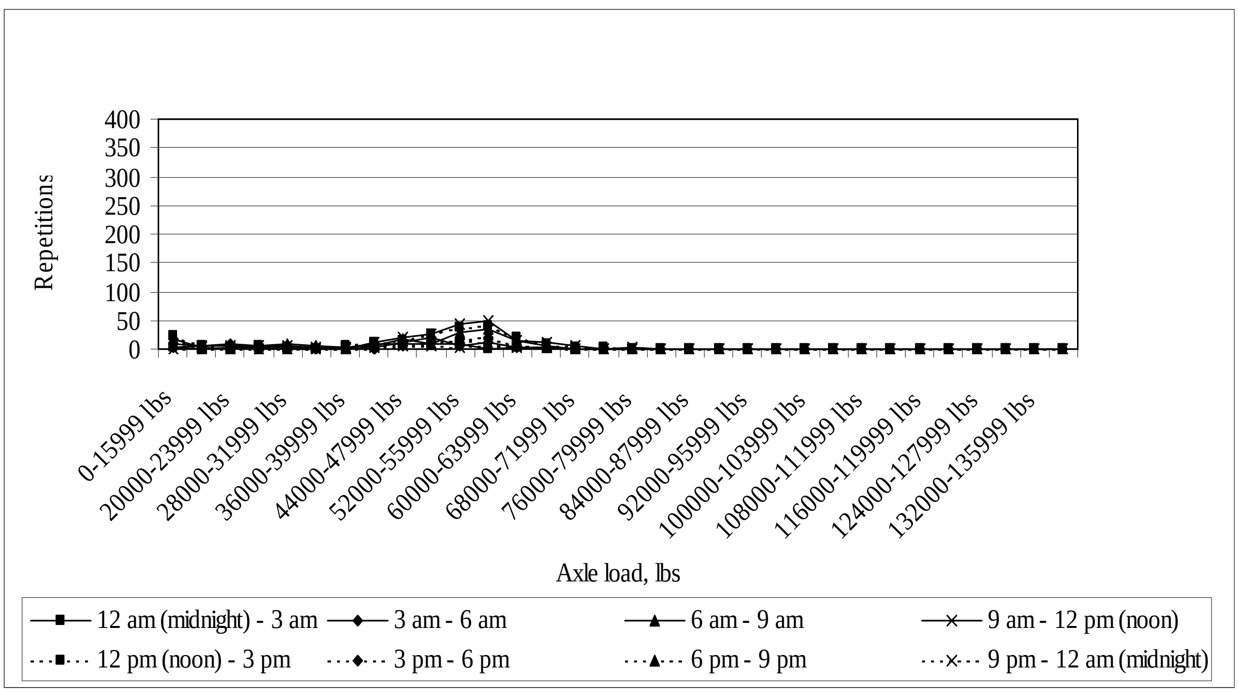


Figure J-60: Load spectrum from SPS2 sections for quad axle in February, 1999

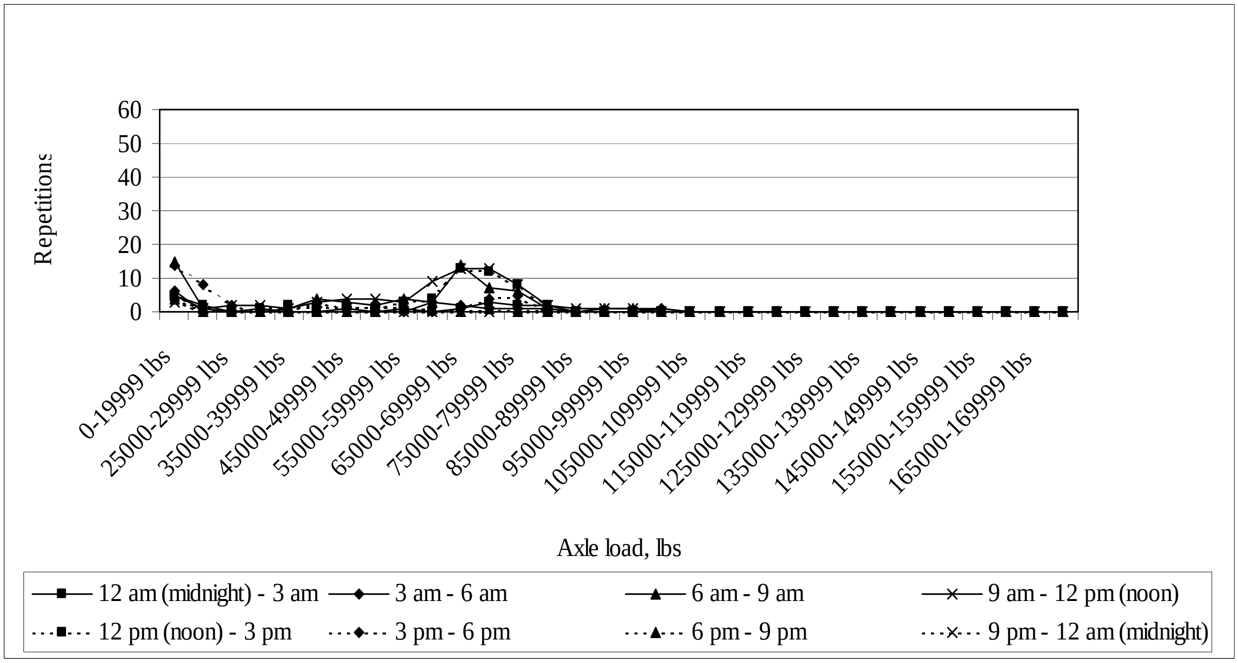


Figure J-61: Load spectrum from SPS2 sections for multi-axle (5) in February, 1999

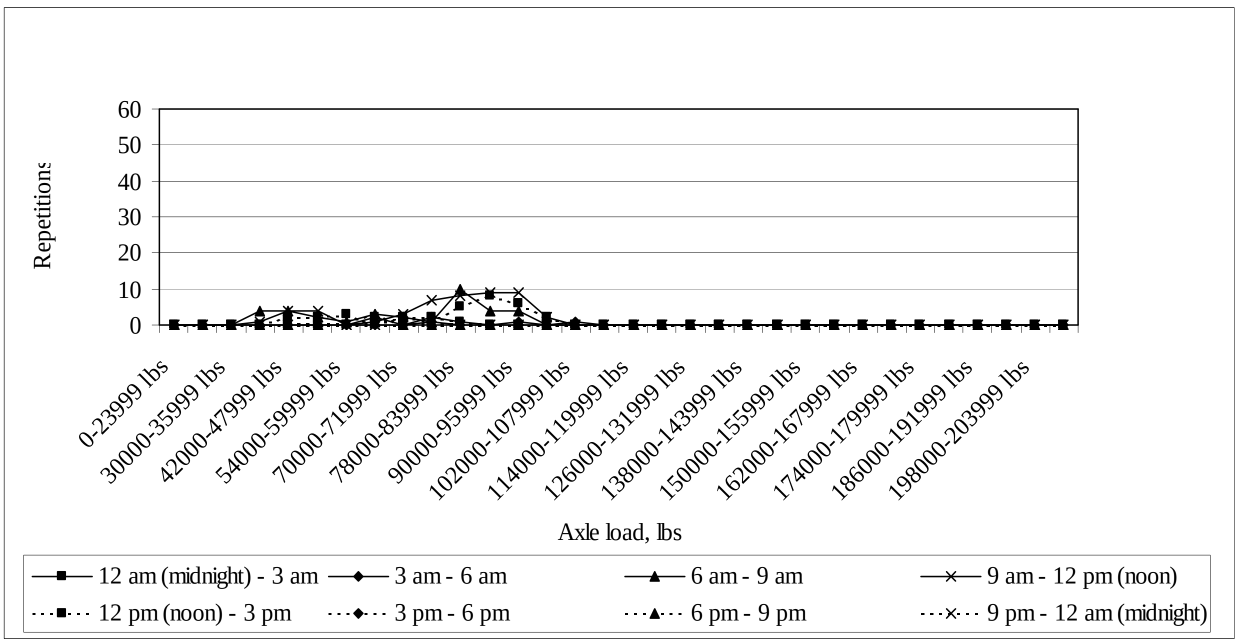


Figure J-62: Load spectrum from SPS2 sections for multi-axle (6) in February, 1999

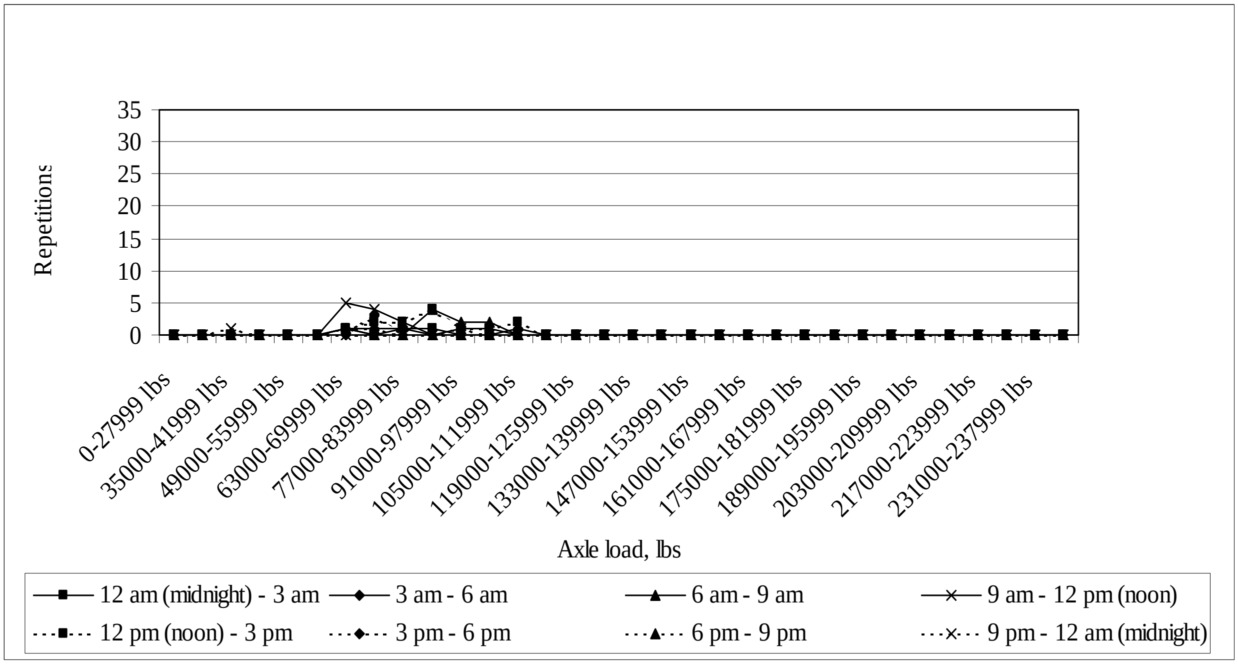


Figure J-63: Load spectrum from SPS2 sections for multi-axle (7) in February, 1999

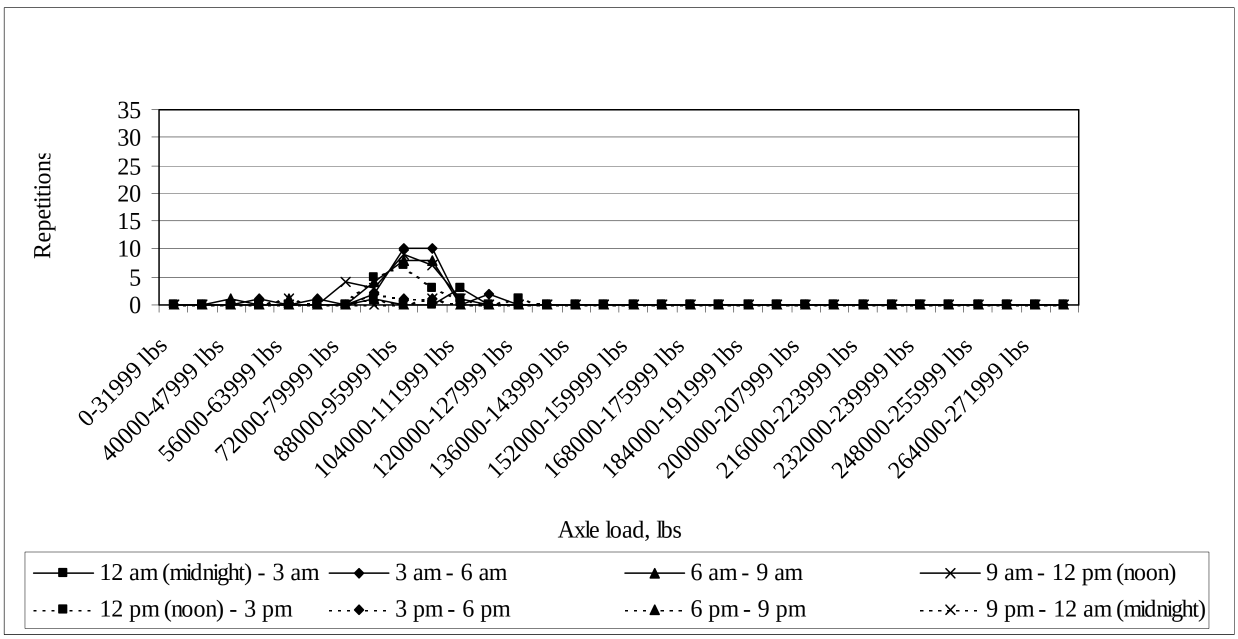


Figure J-64: Load spectrum from SPS2 sections for multi-axle (8) in February, 1999

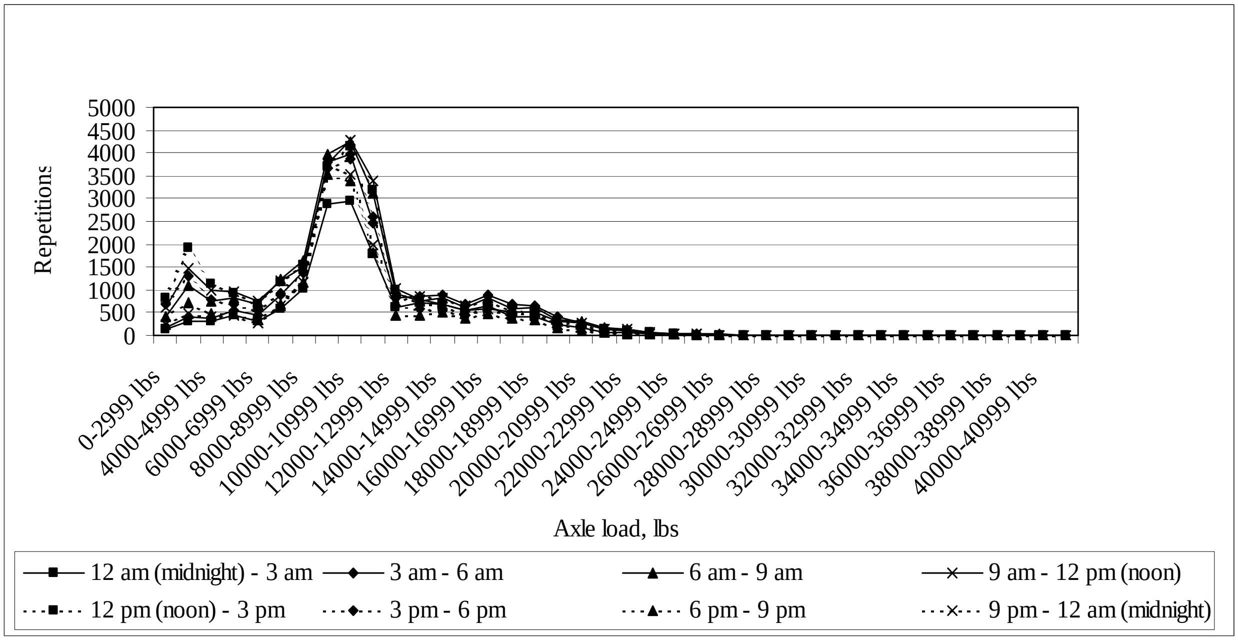


Figure J-65: Load spectrum from SPS2 sections for single axle in March, 1999

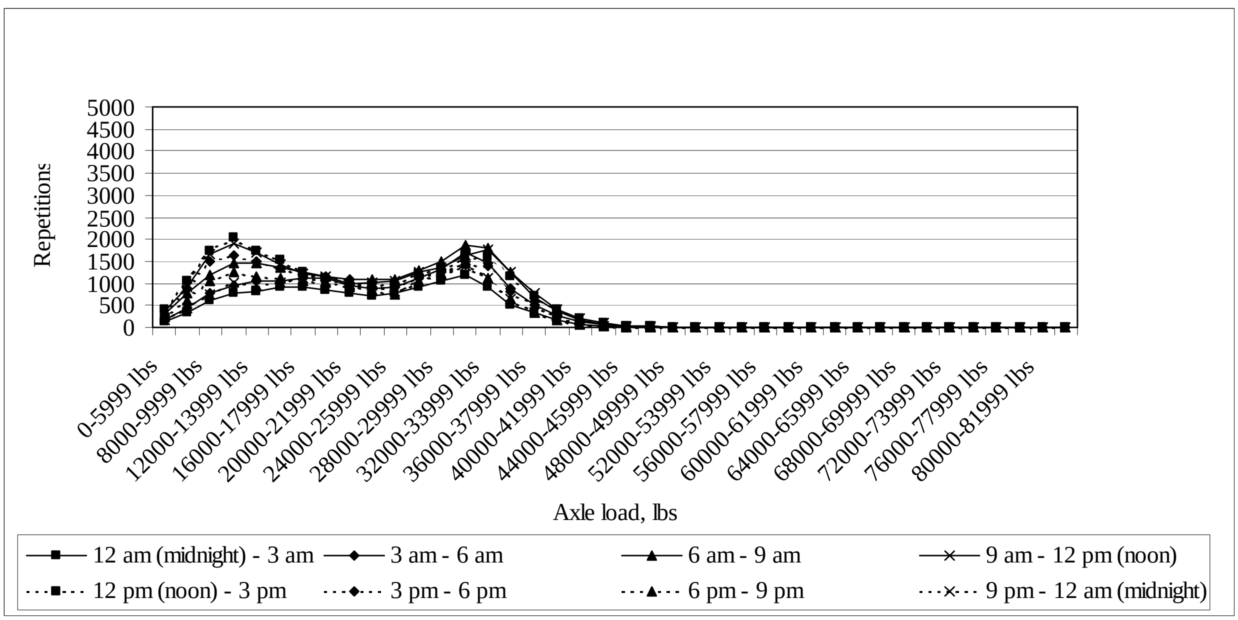


Figure J-66: Load spectrum from SPS2 sections for tandem axle in March, 1999

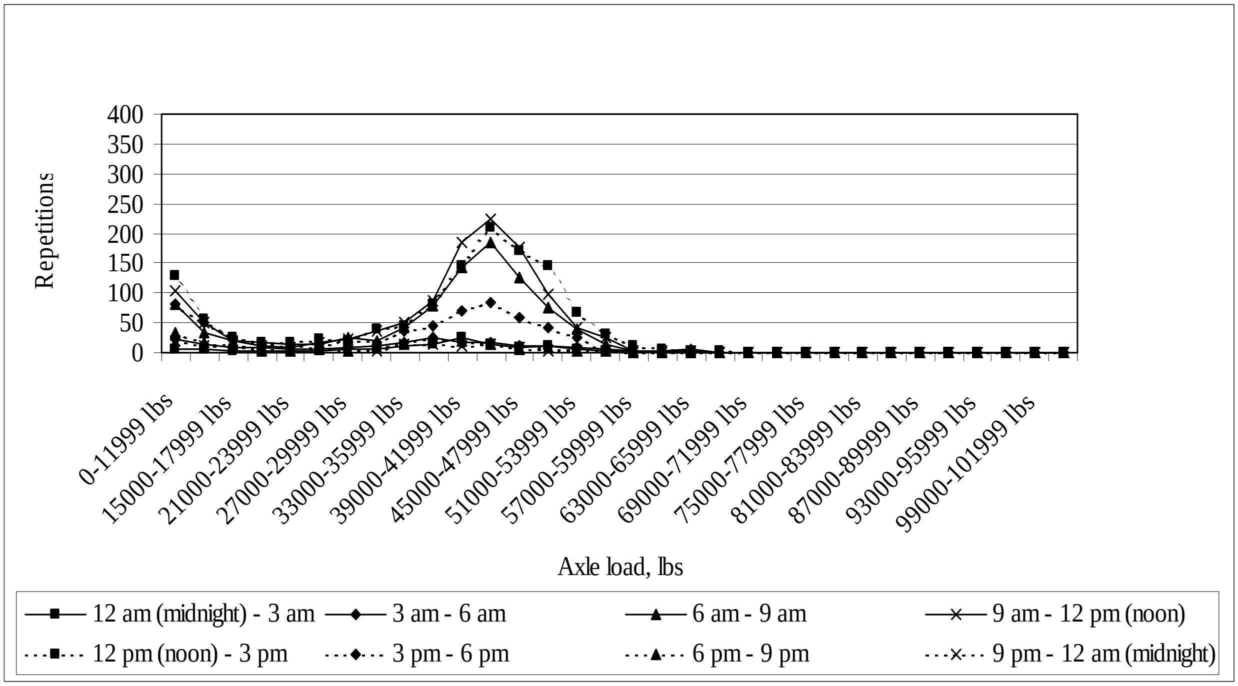


Figure J-67: Load spectrum from SPS2 sections for tridem axle in March, 1999

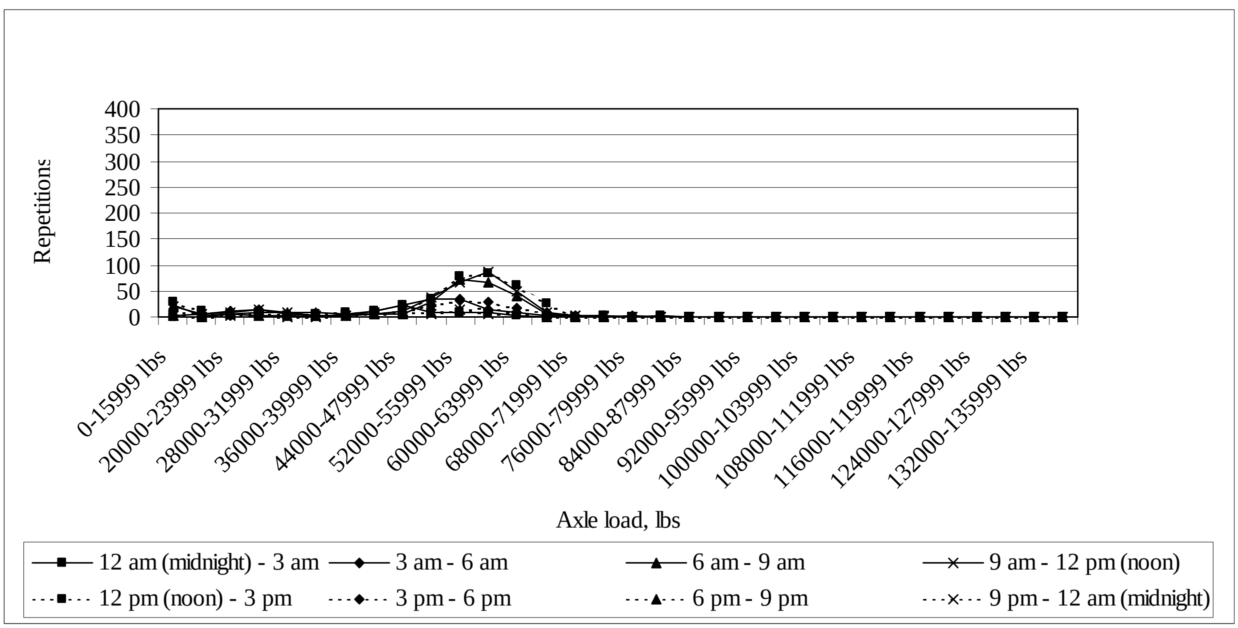


Figure J-68: Load spectrum from SPS2 sections for quad axle in March, 1999

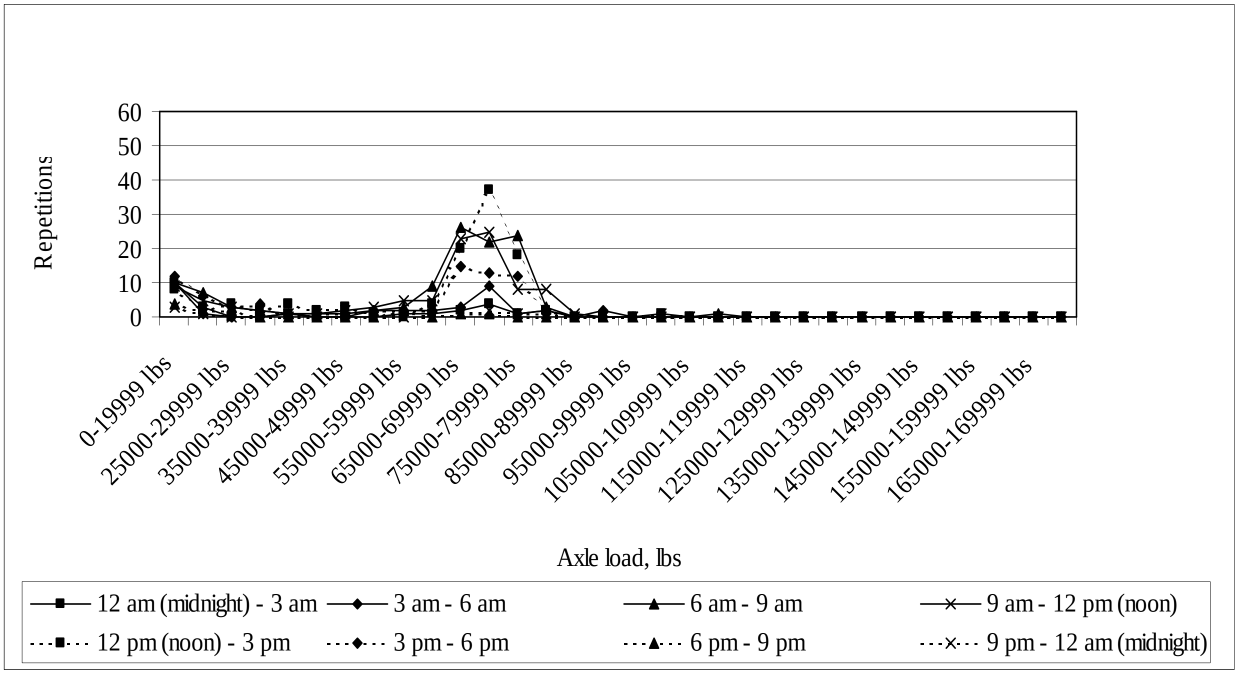


Figure J-69: Load spectrum from SPS2 sections for multi-axle (5) in March, 1999

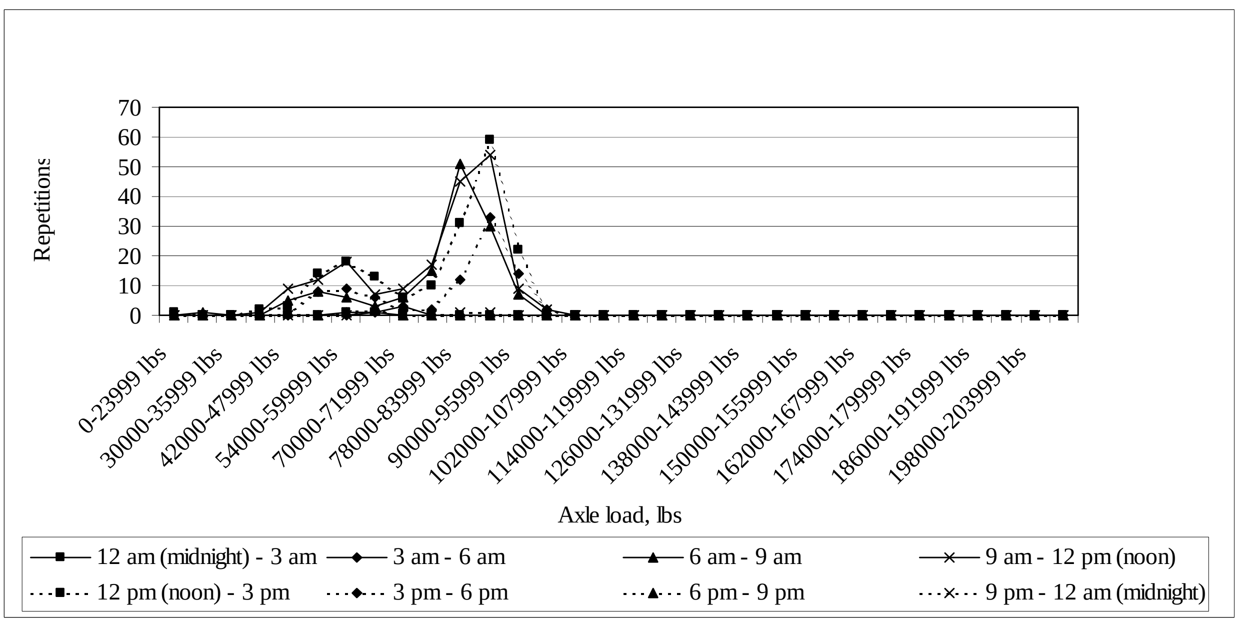


Figure J-70: Load spectrum from SPS2 sections for multi-axle (6) in March, 1999

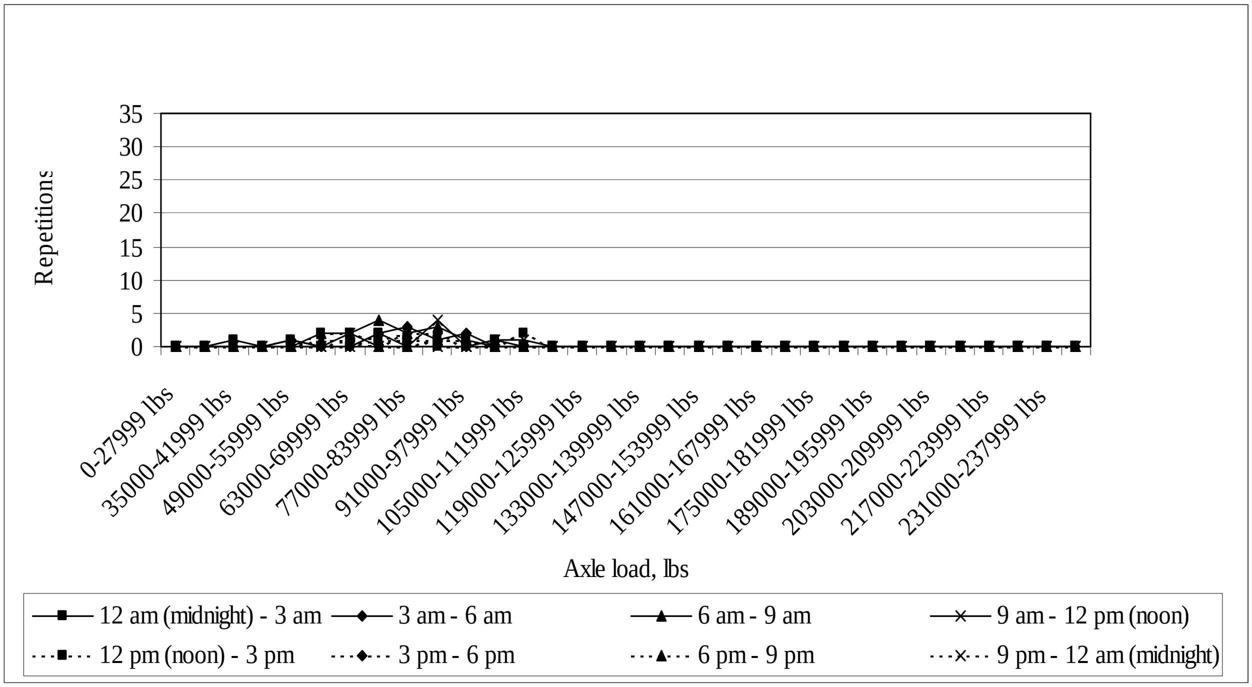


Figure J-71: Load spectrum from SPS2 sections for multi-axle (7) in March, 1999

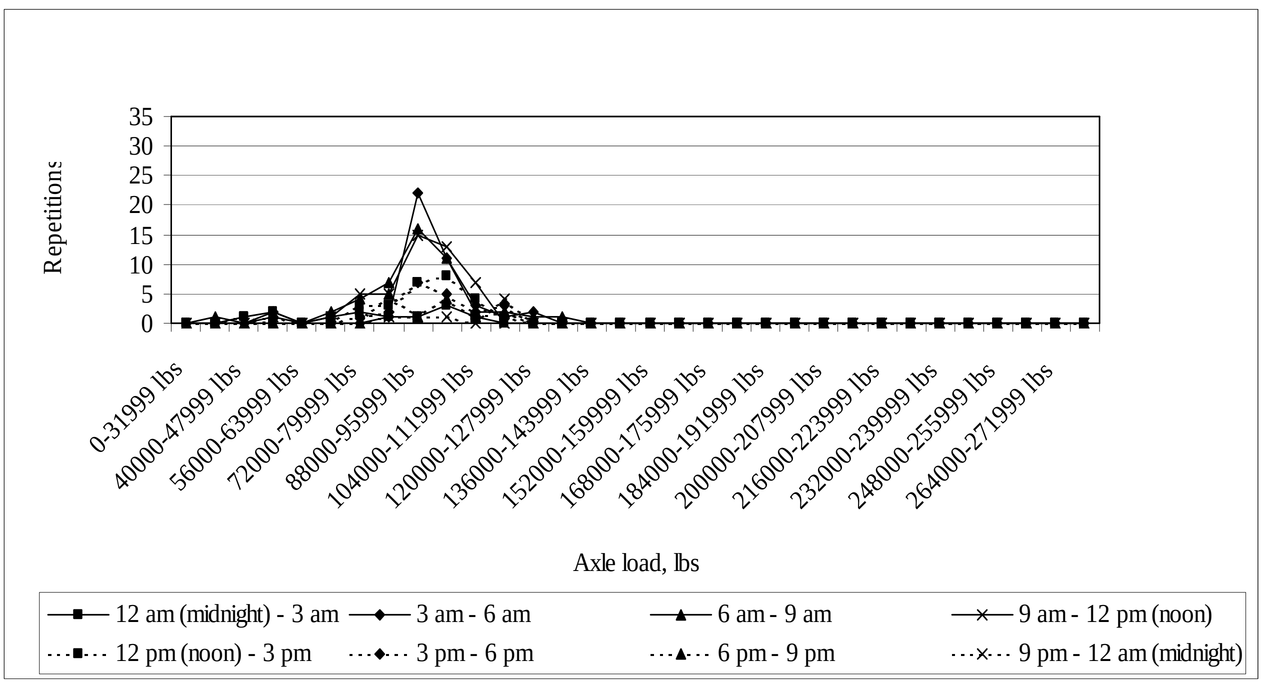


Figure J-72: Load spectrum from SPS2 sections for multi-axle (8) in March, 1999

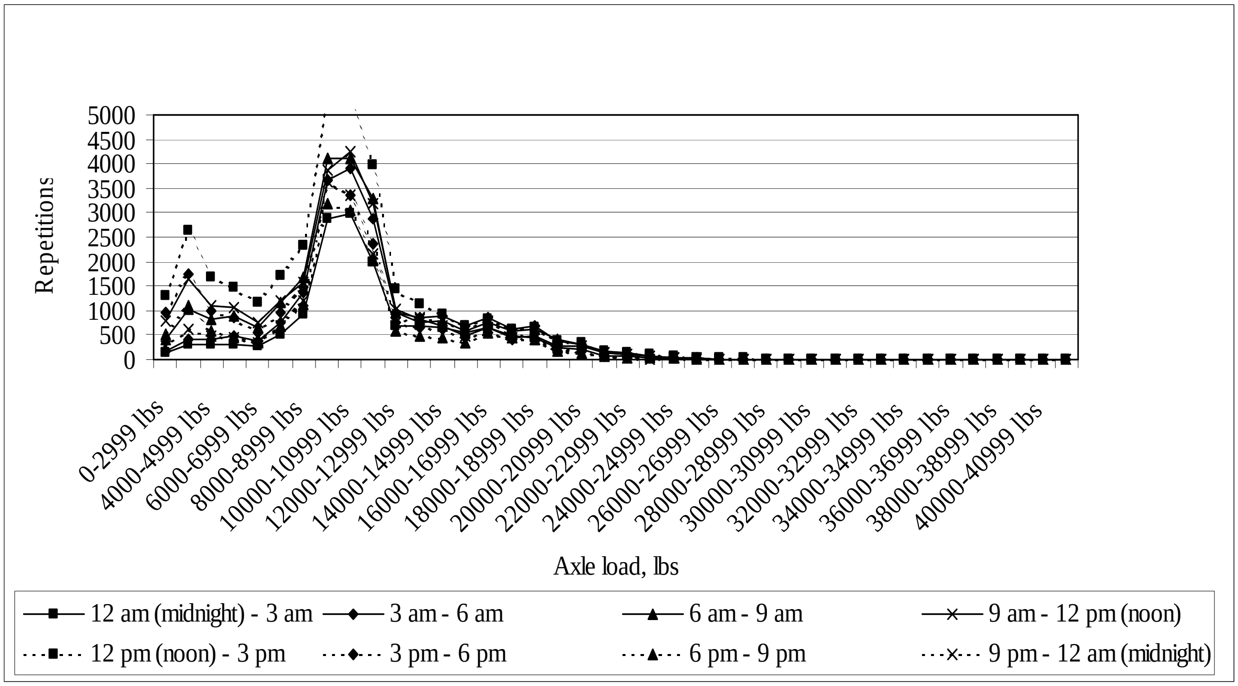


Figure J-73: Load spectrum from SPS2 sections for single axle in April, 1999

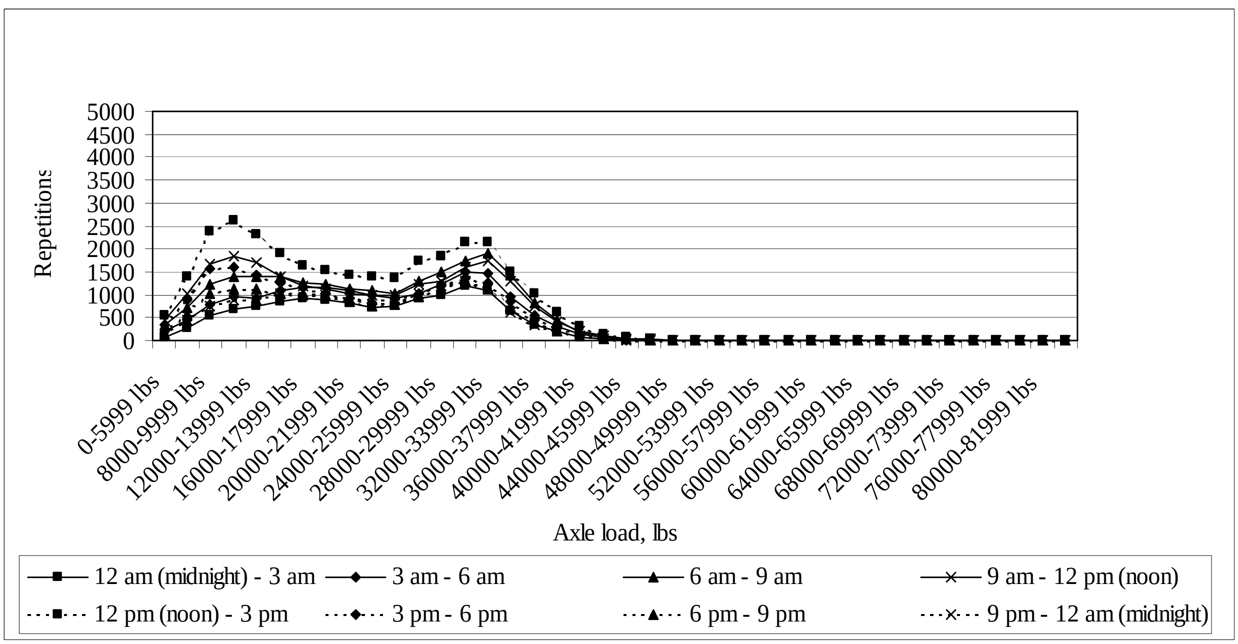


Figure J-74: Load spectrum from SPS2 sections for tandem axle in April, 1999

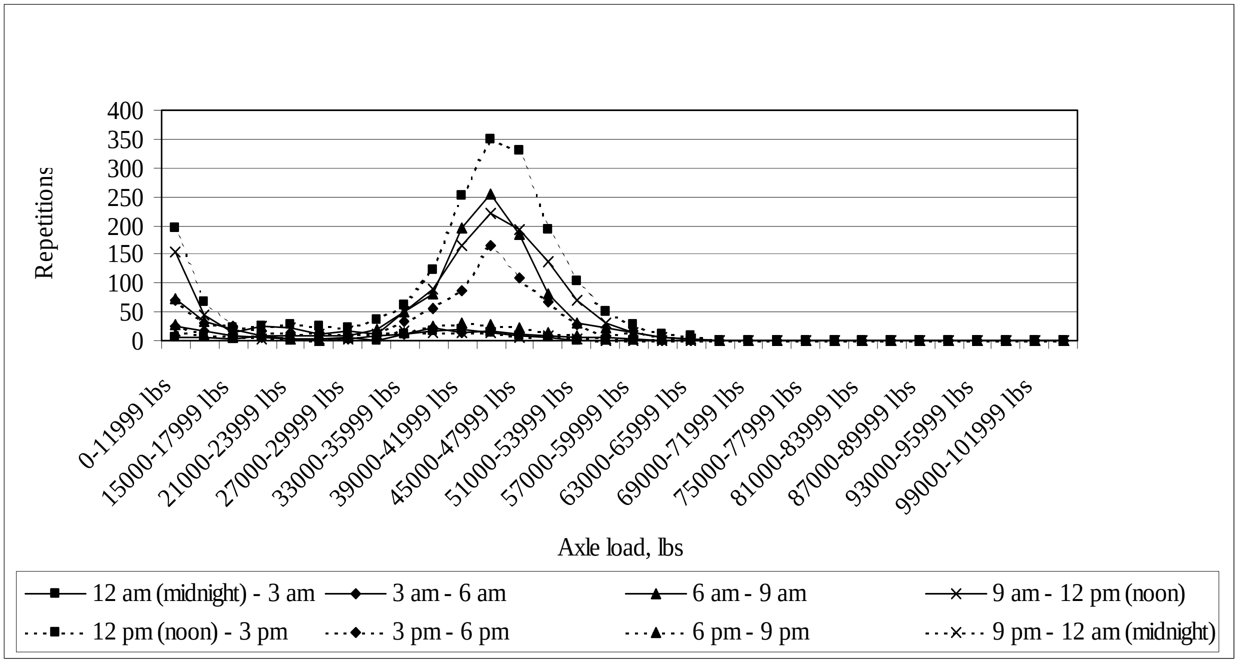


Figure J-75: Load spectrum from SPS2 sections for tridem axle in April, 1999

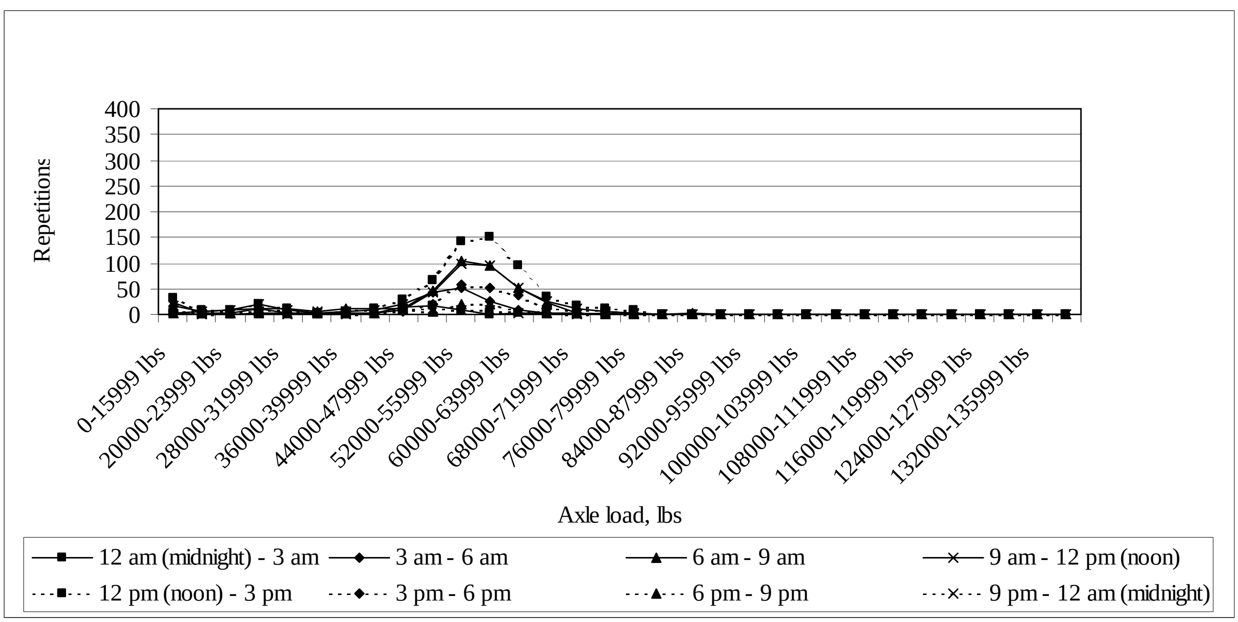


Figure J-76: Load spectrum from SPS2 sections for quad axle in April, 1999

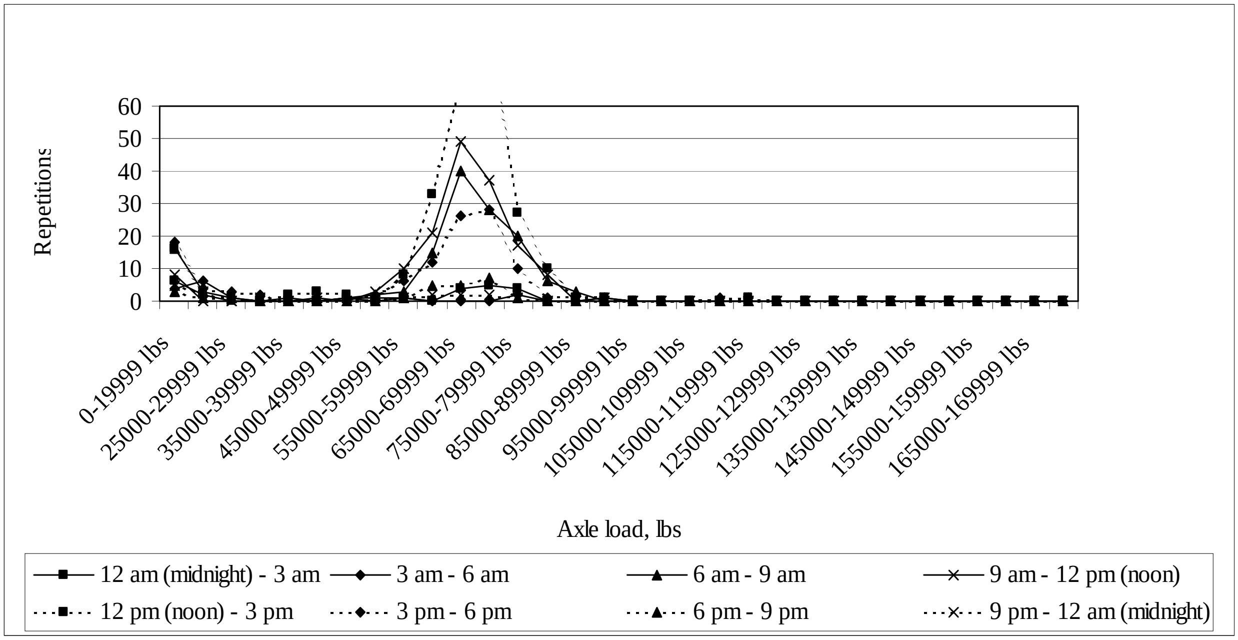


Figure J-77: Load spectrum from SPS2 sections for multi-axle (5) in April, 1999

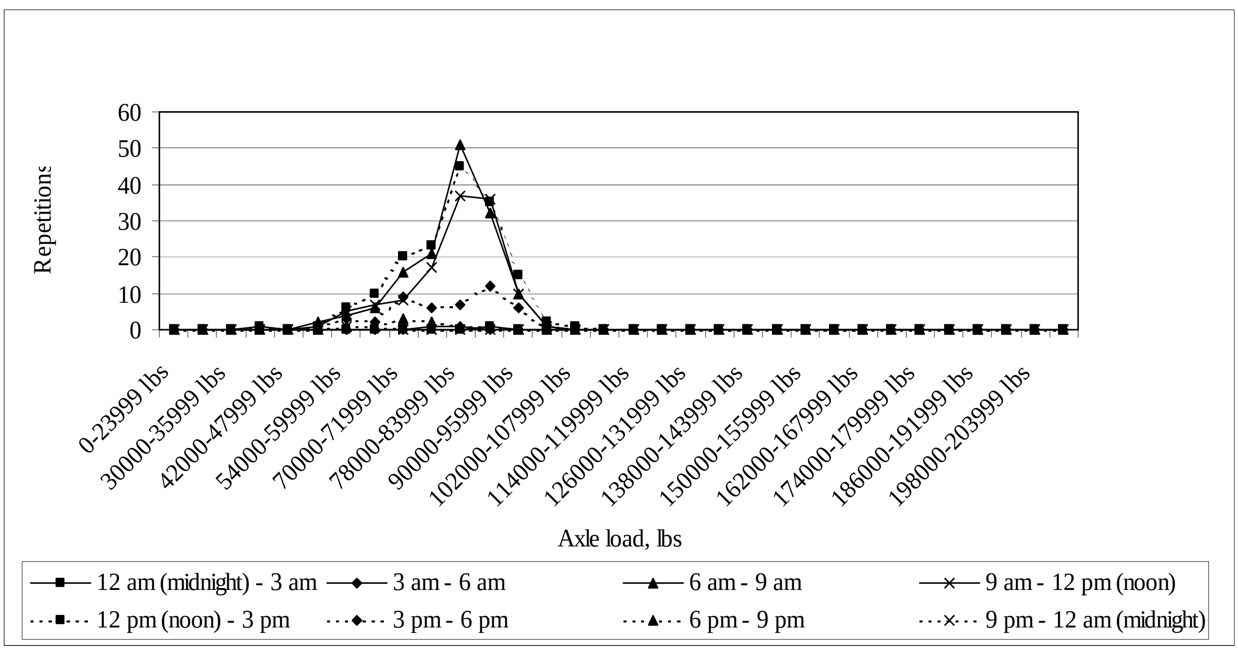


Figure J-78: Load spectrum from SPS2 sections for multi-axle (6) in April, 1999

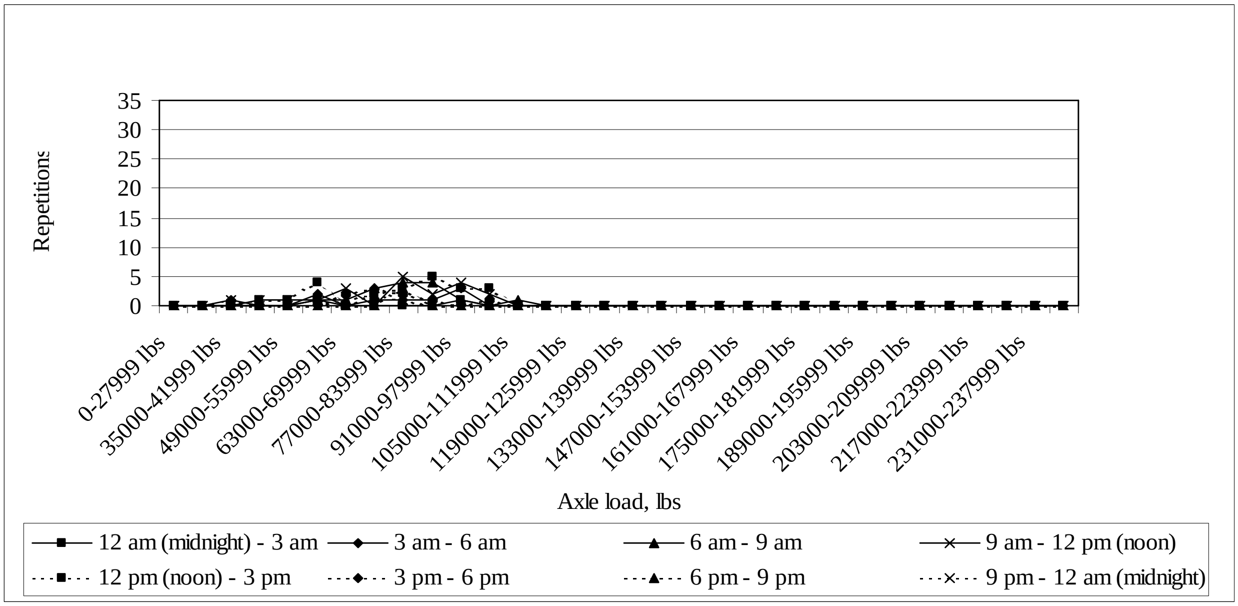


Figure J-79: Load spectrum from SPS2 sections for multi-axle (7) in April, 1999

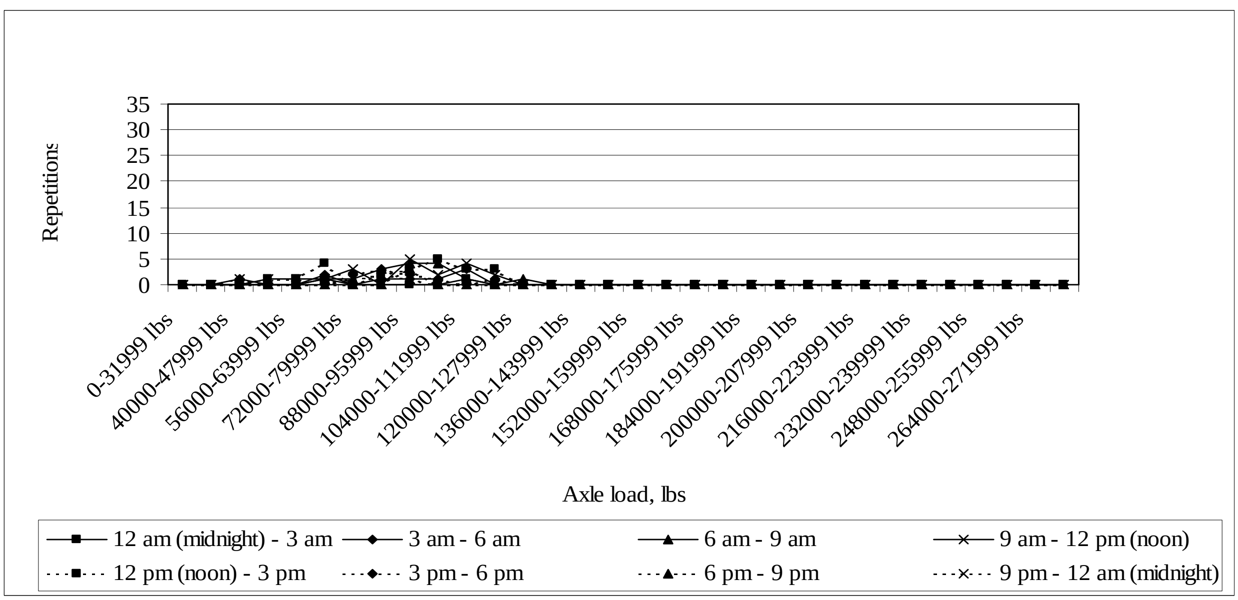


Figure J-80: Load spectrum from SPS2 sections for multi-axle (8) in April, 1999

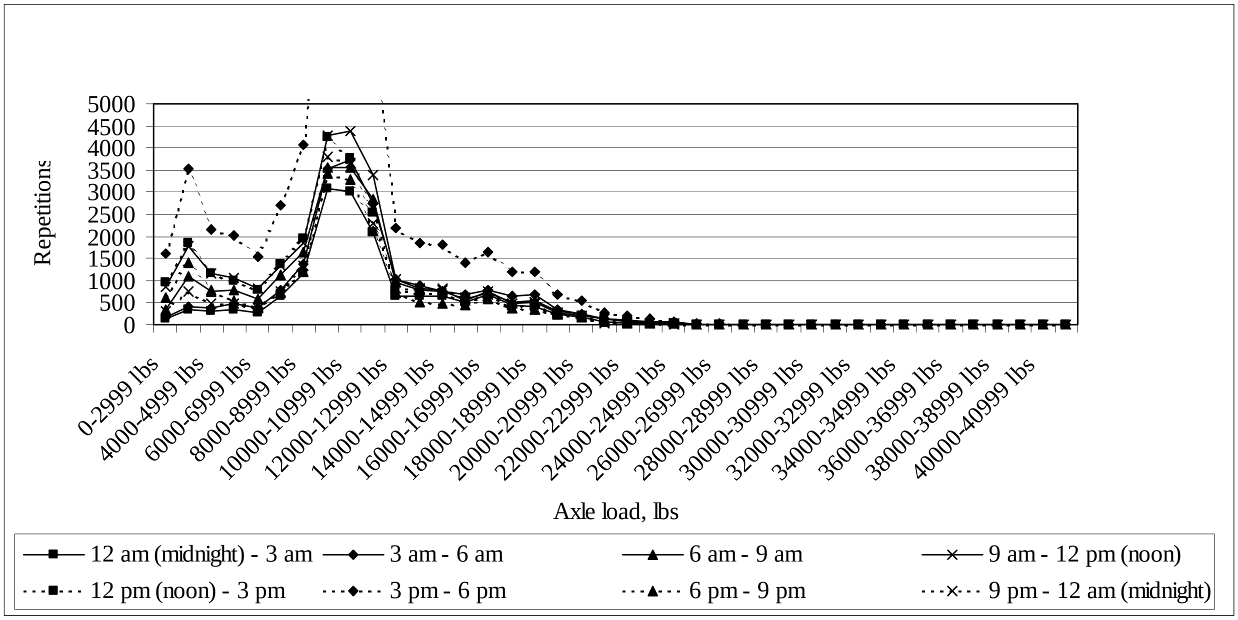


Figure J-81: Load spectrum from SPS2 sections for single axle in May, 1999

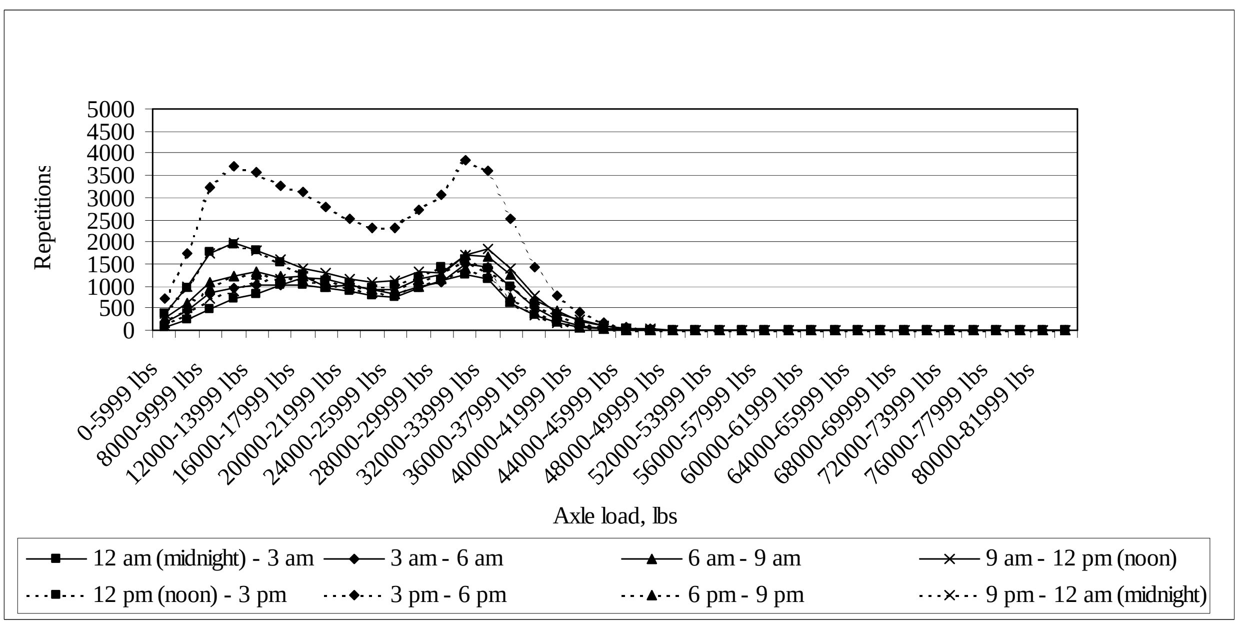


Figure J-82: Load spectrum from SPS2 sections for tandem axle in May, 1999

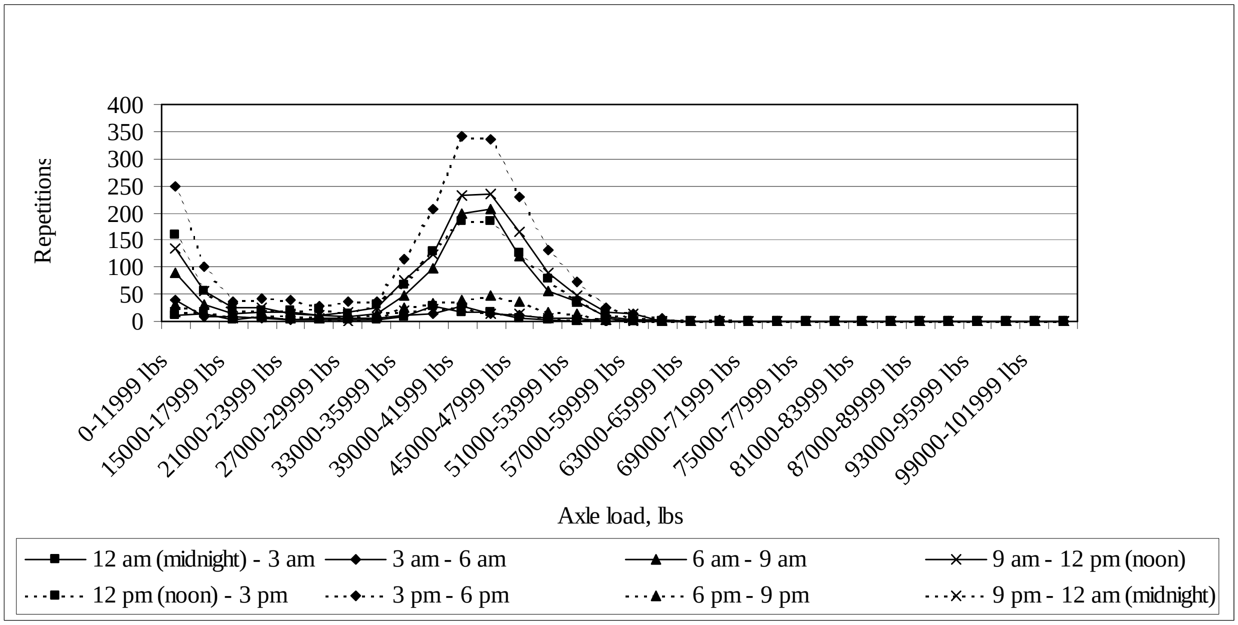


Figure J-83: Load spectrum from SPS2 sections for tridem axle in May, 1999

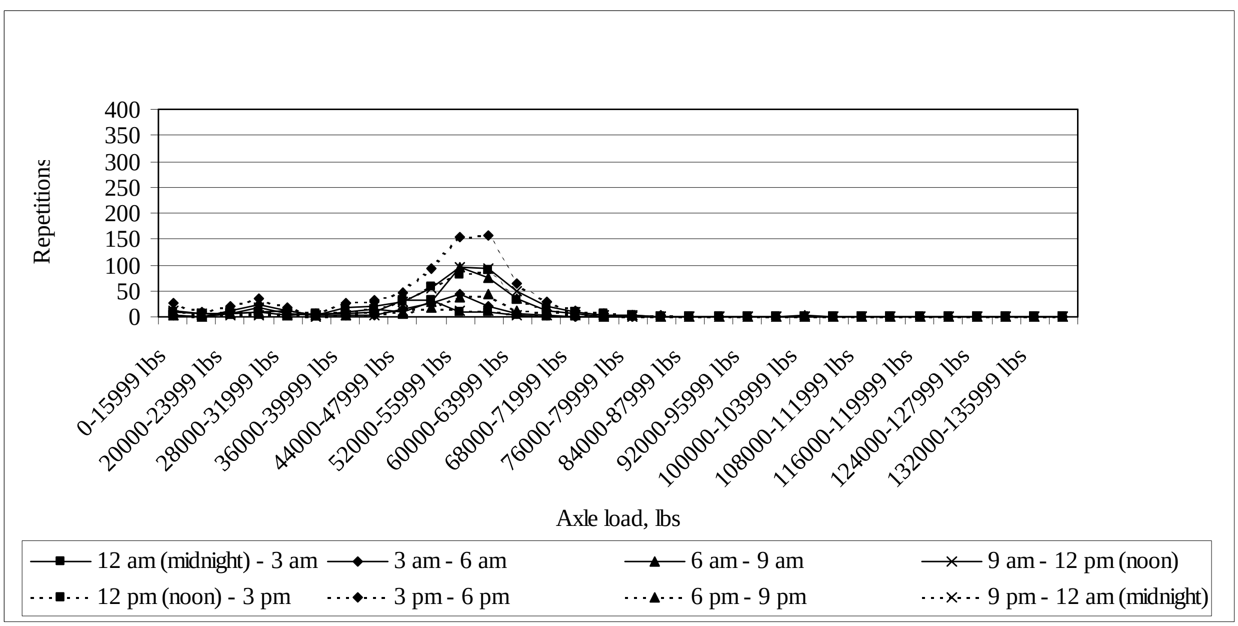


Figure J-84: Load spectrum from SPS2 sections for quad axle in May, 1999

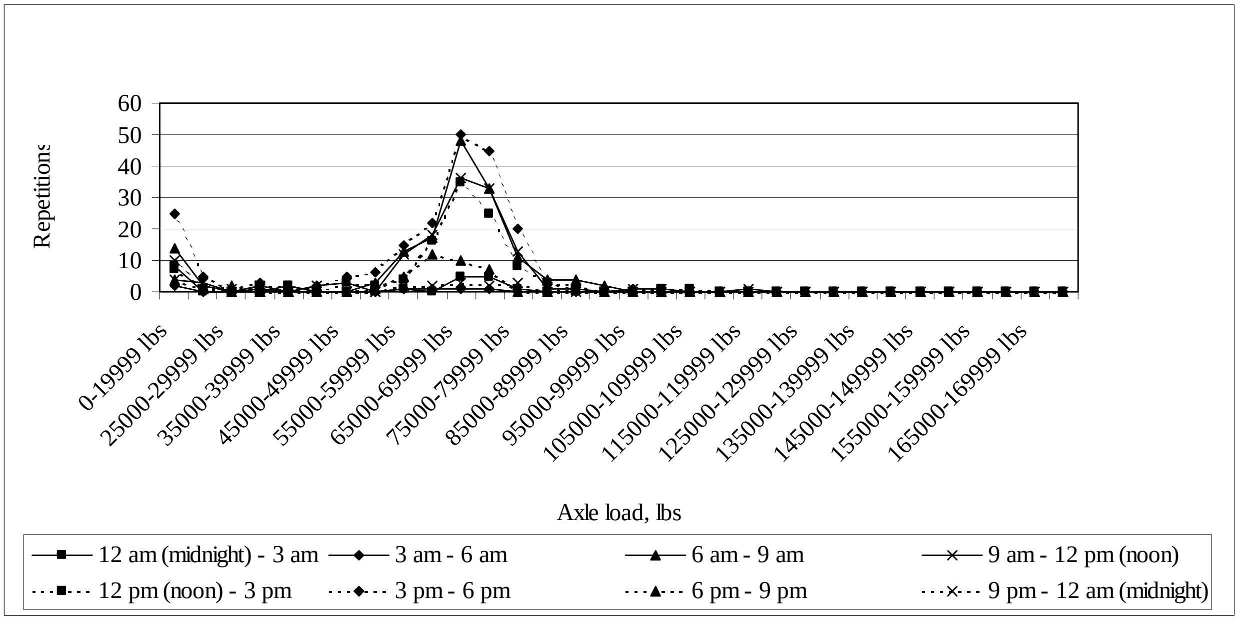


Figure J-85: Load spectrum from SPS2 sections for multi-axle (5) in May, 1999

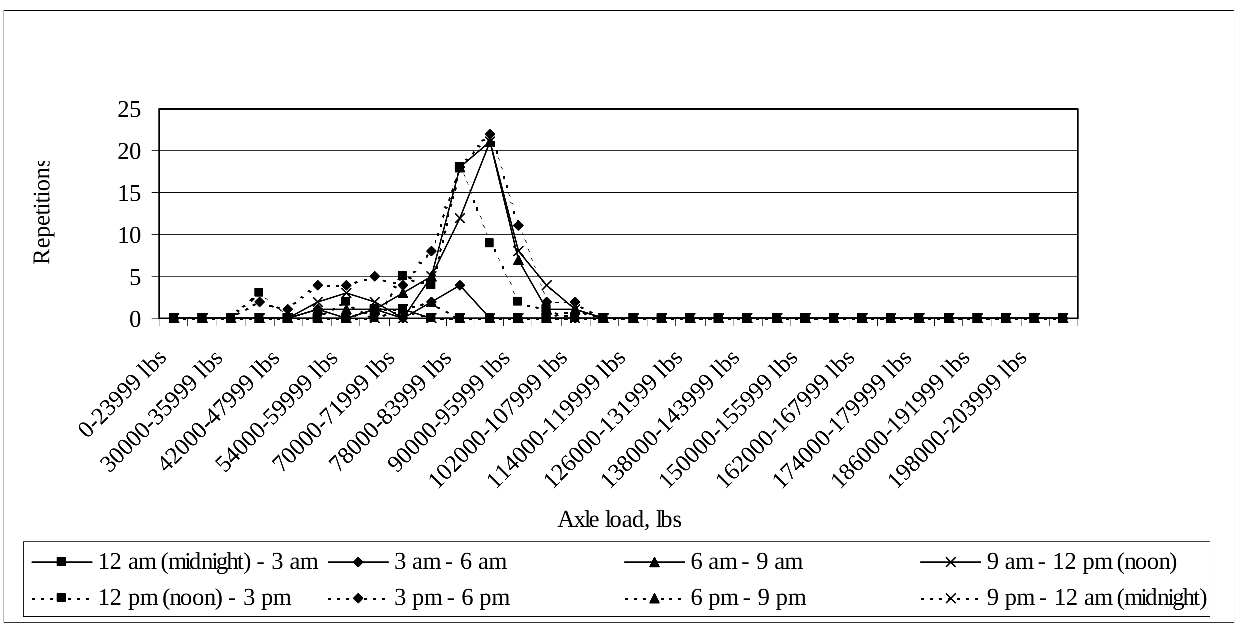


Figure J-86: Load spectrum from SPS2 sections for multi-axle (6) in May, 1999

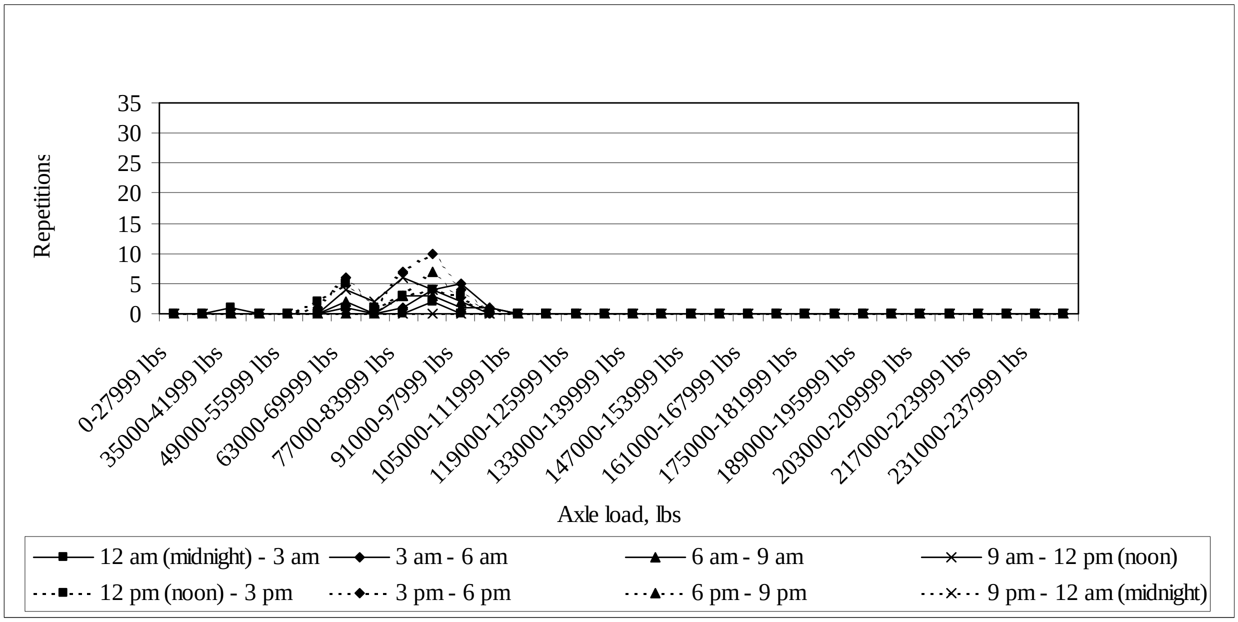


Figure J-87: Load spectrum from SPS2 sections for multi-axle (7) in May, 1999

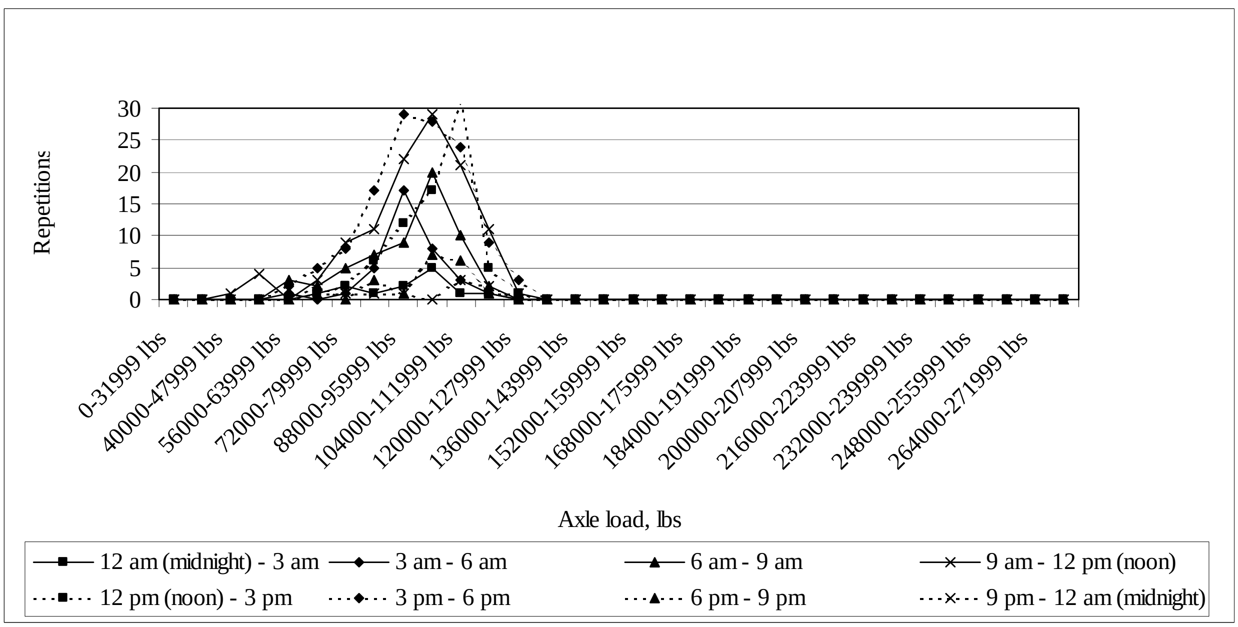


Figure J-88: Load spectrum from SPS2 sections for multi-axle (8) in May, 1999

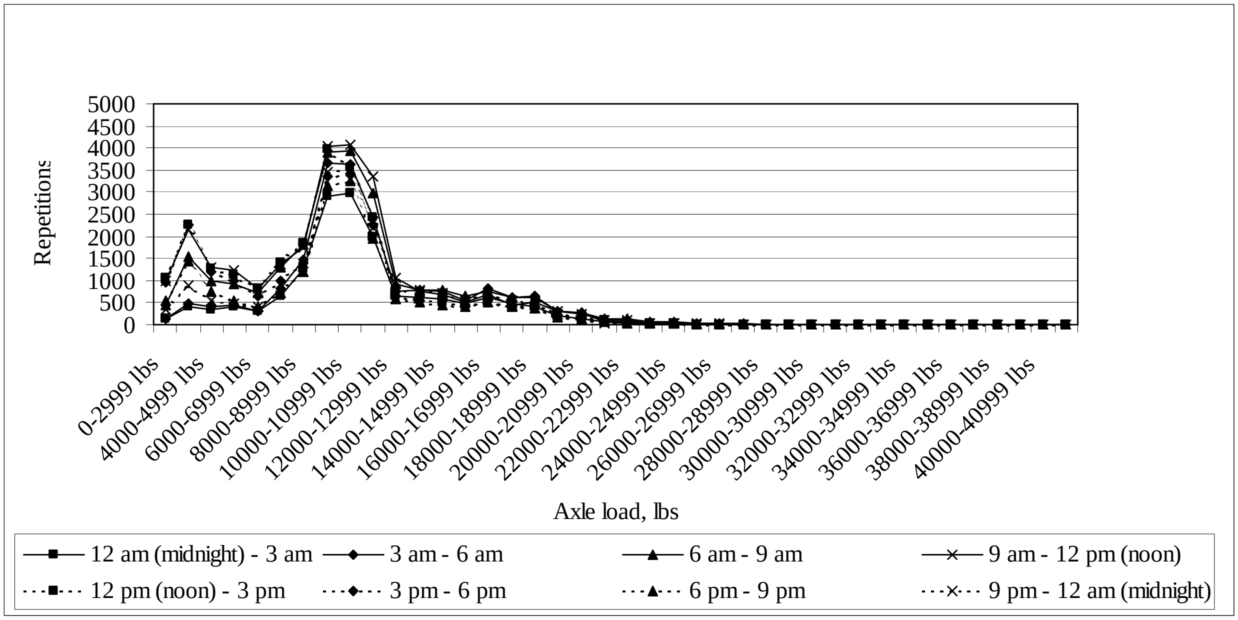


Figure J-89: Load spectrum from SPS2 sections for single axle in June, 1999

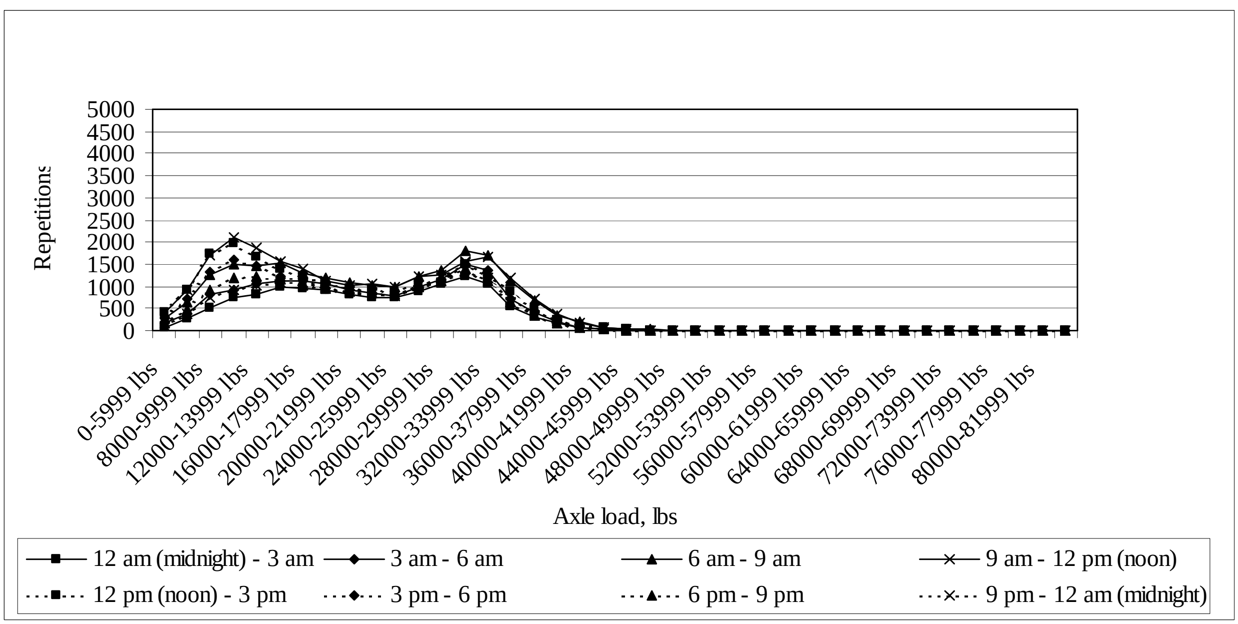


Figure J-90: Load spectrum from SPS2 sections for tandem axle in June, 1999

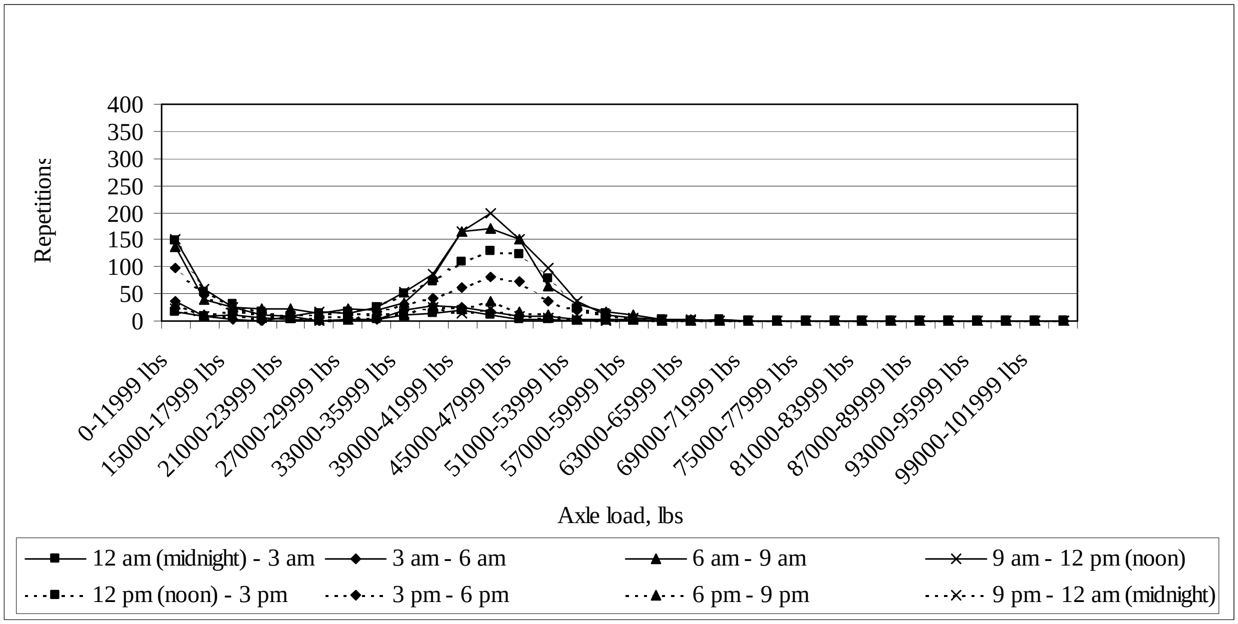


Figure J-91: Load spectrum from SPS2 sections for tridem axle in June, 1999

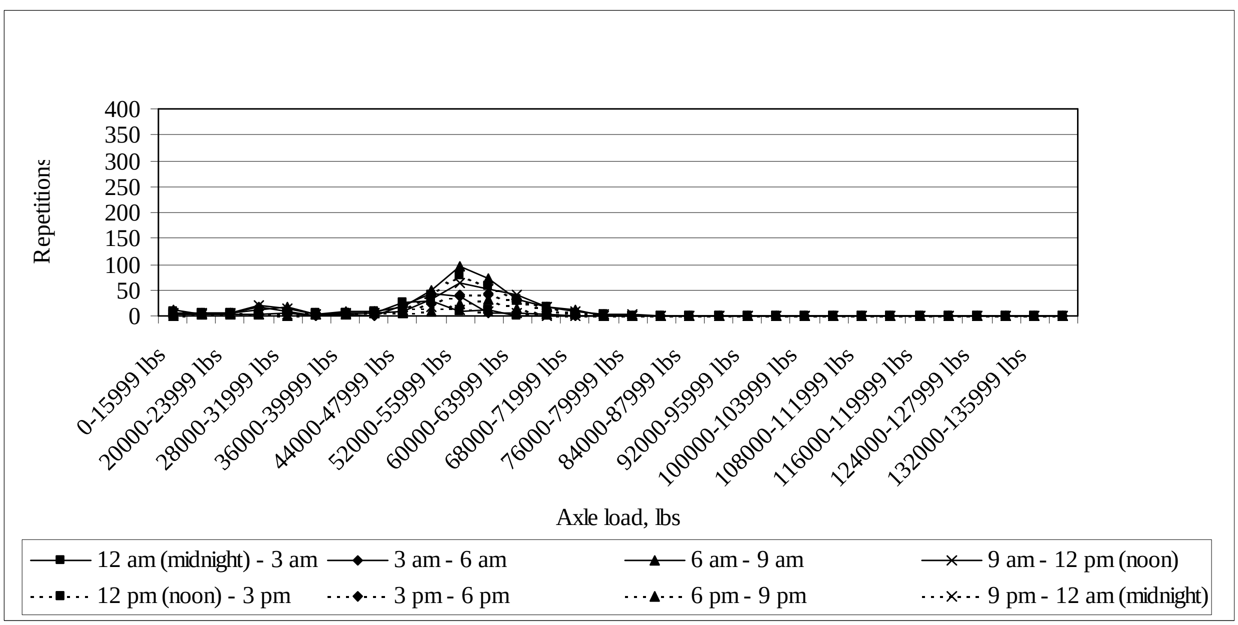


Figure J-92: Load spectrum from SPS2 sections for quad axle in June, 1999

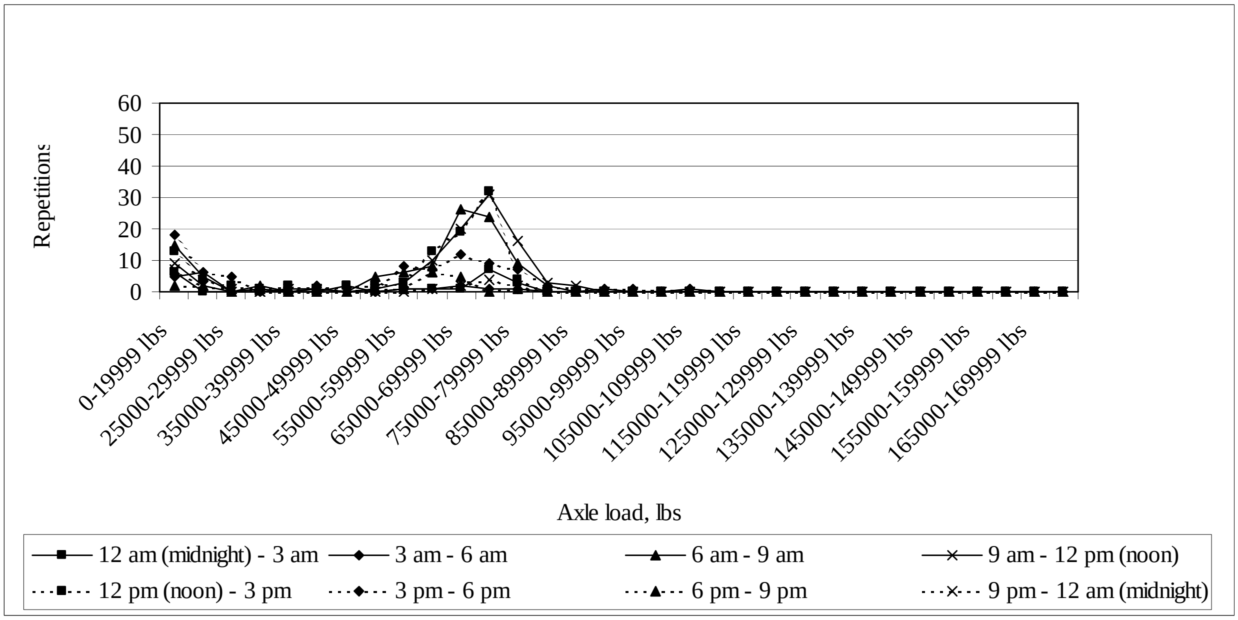


Figure J-93: Load spectrum from SPS2 sections for multi-axle (5) in June, 1999

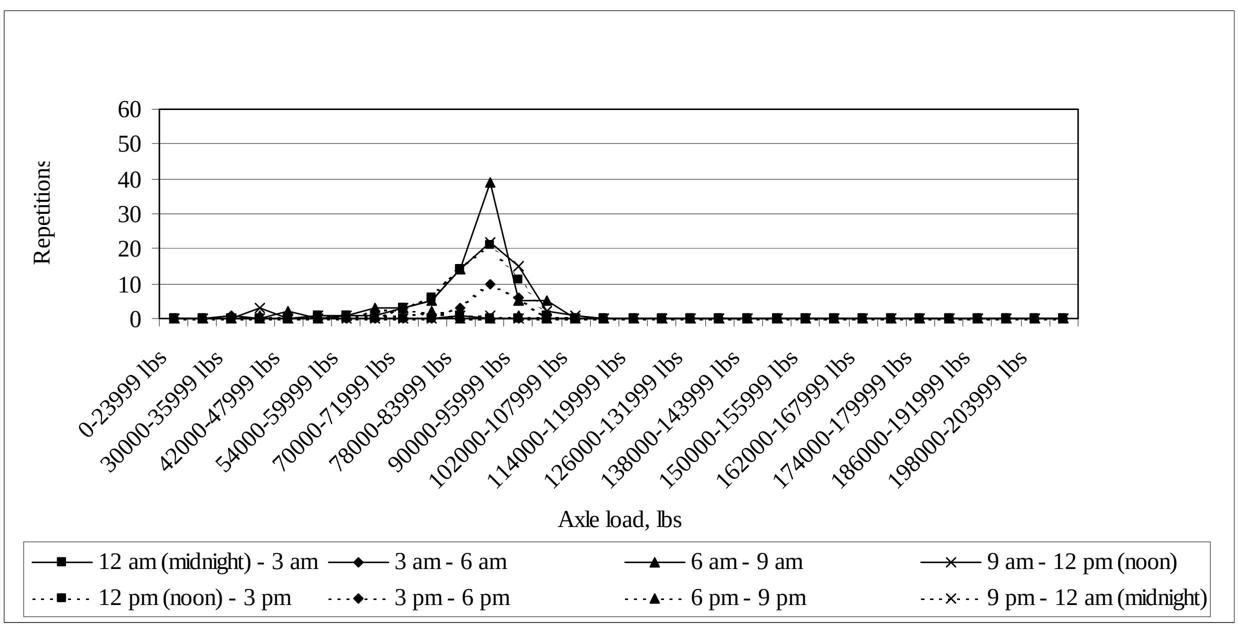


Figure J-94: Load spectrum from SPS2 sections for multi-axle (6) in June, 1999

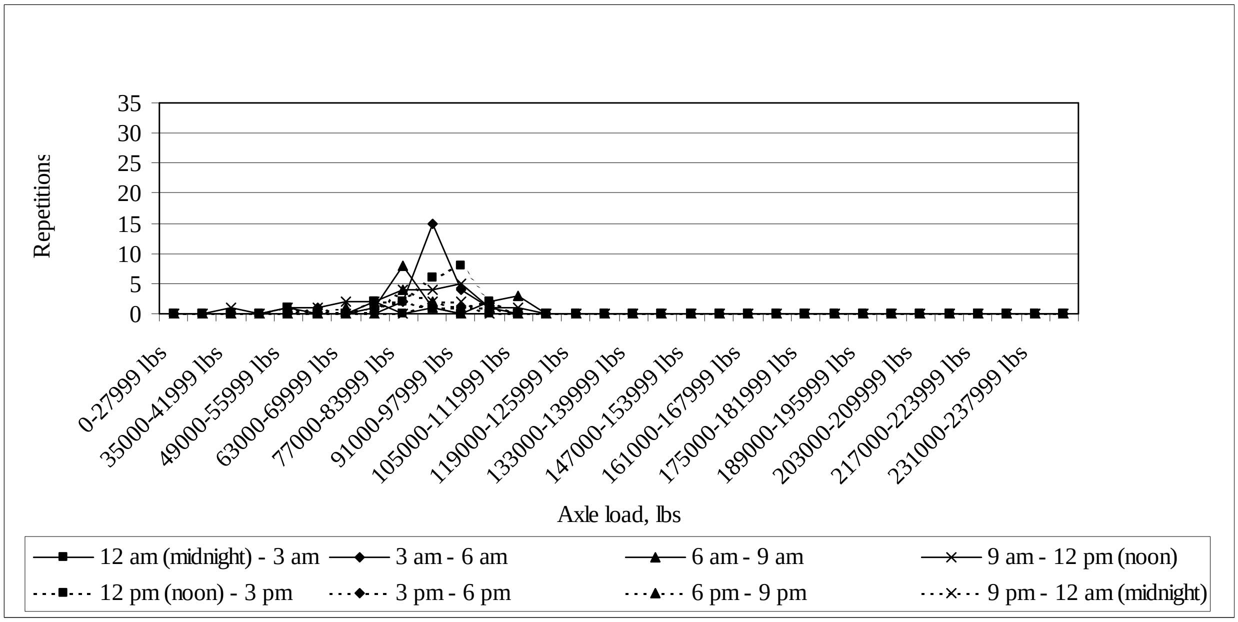


Figure J-95: Load spectrum from SPS2 sections for multi-axle (7) in June, 1999

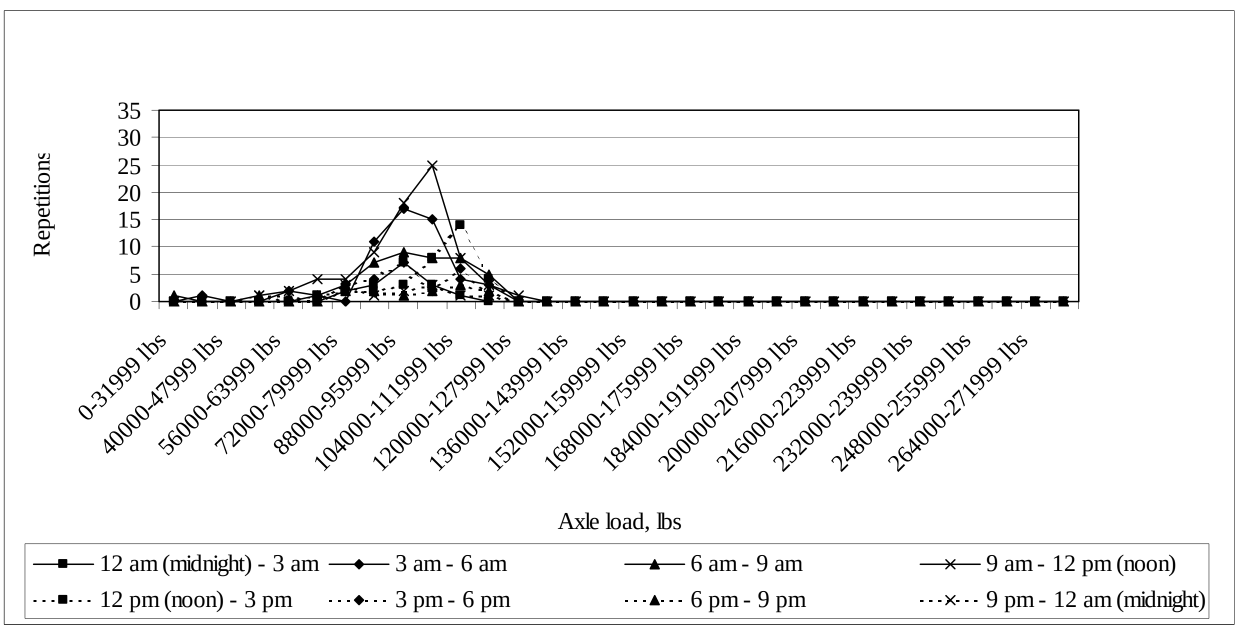


Figure J-96: Load spectrum from SPS2 sections for multi-axle (8) in June, 1999

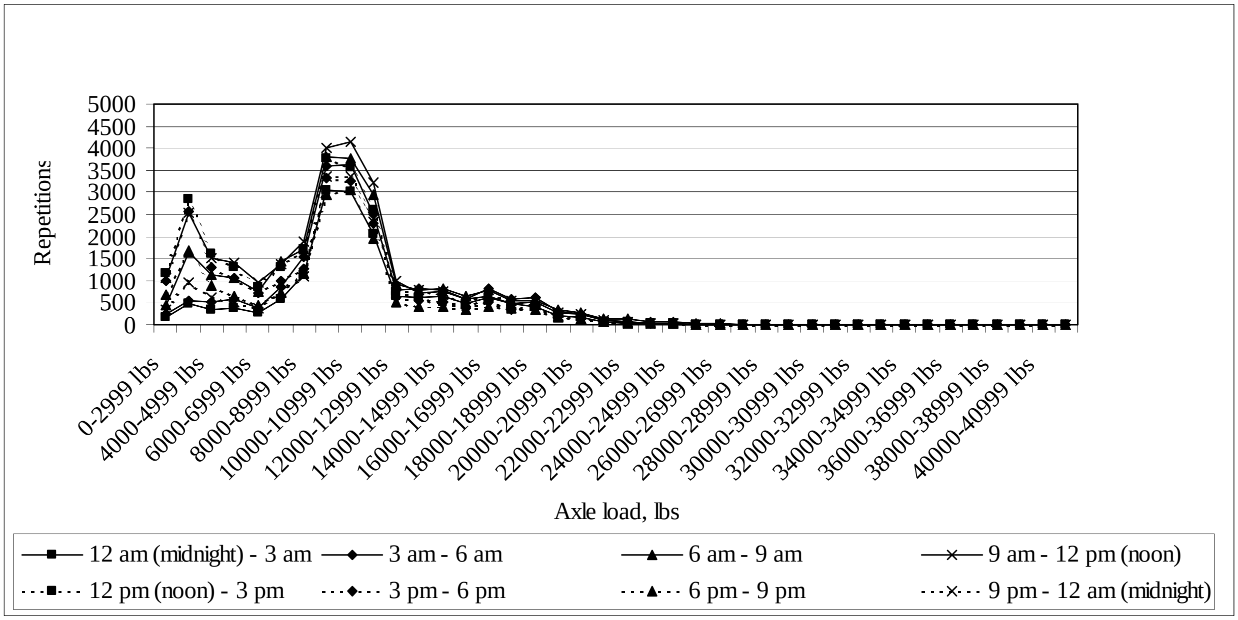


Figure J-97: Load spectrum from SPS2 sections for single axle in July, 1999

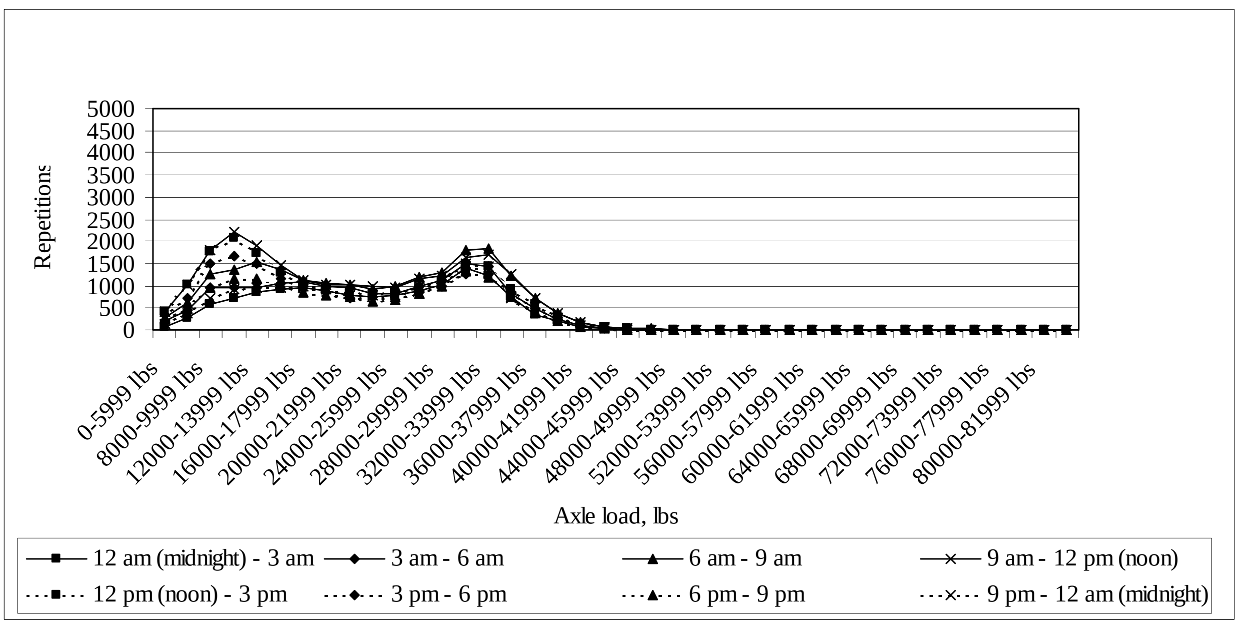


Figure J-98: Load spectrum from SPS2 sections for tandem axle in July, 1999

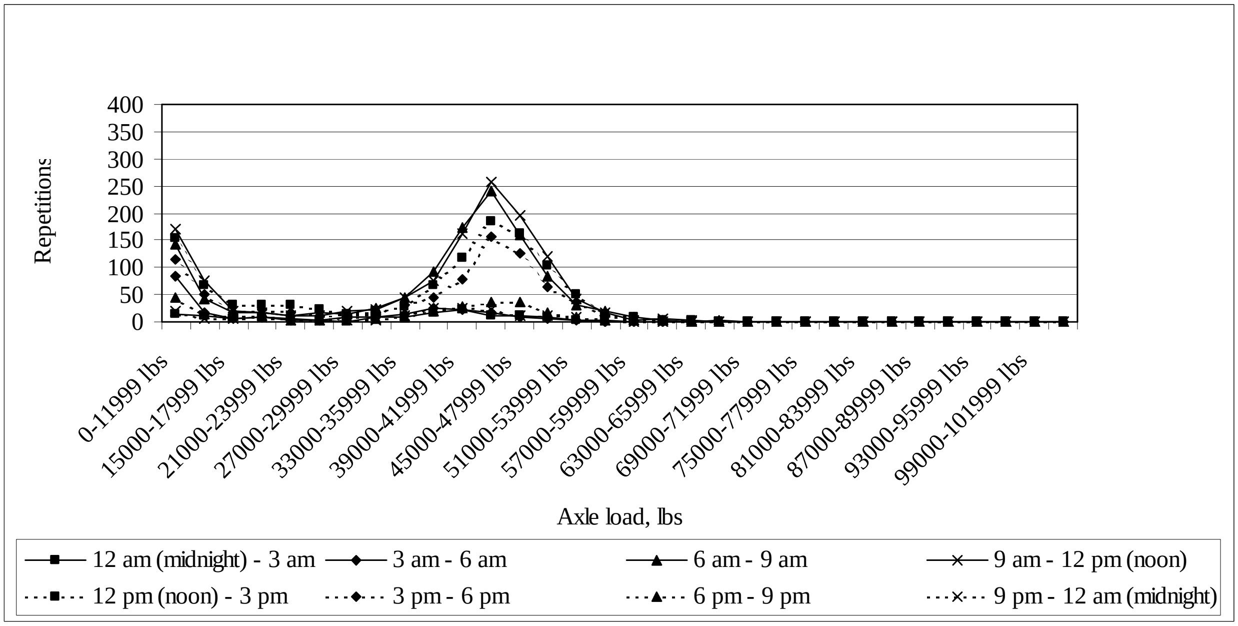


Figure J-99: Load spectrum from SPS2 sections for tridem axle in July, 1999

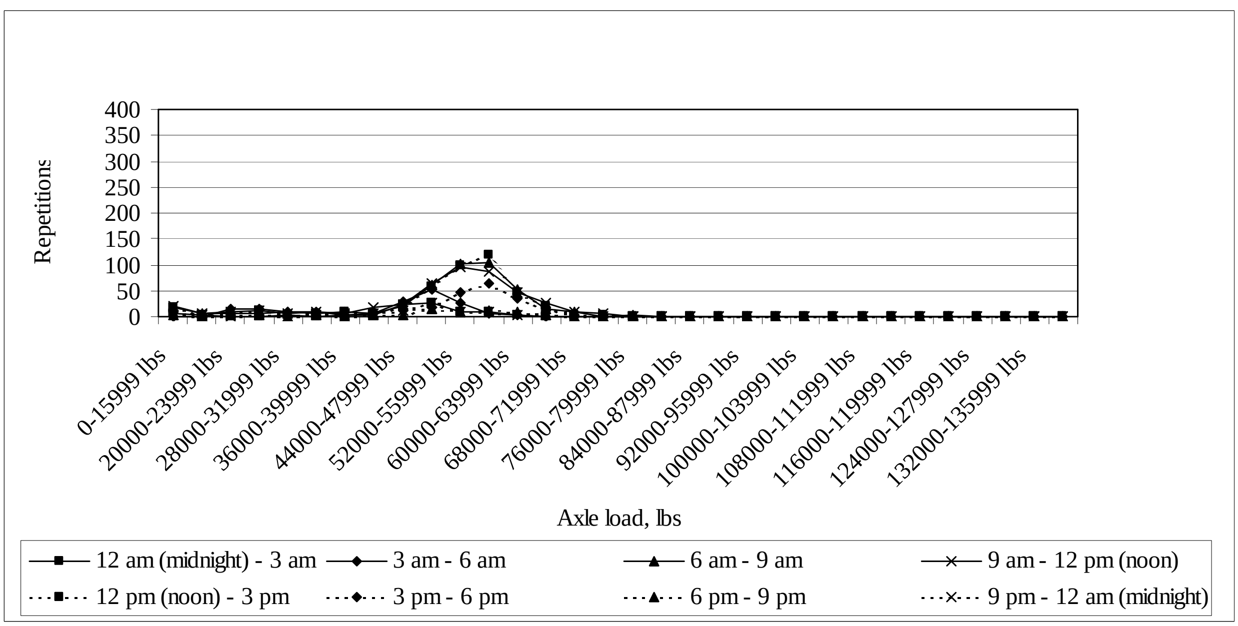


Figure J-100: Load spectrum from SPS2 sections for quad axle in July, 1999

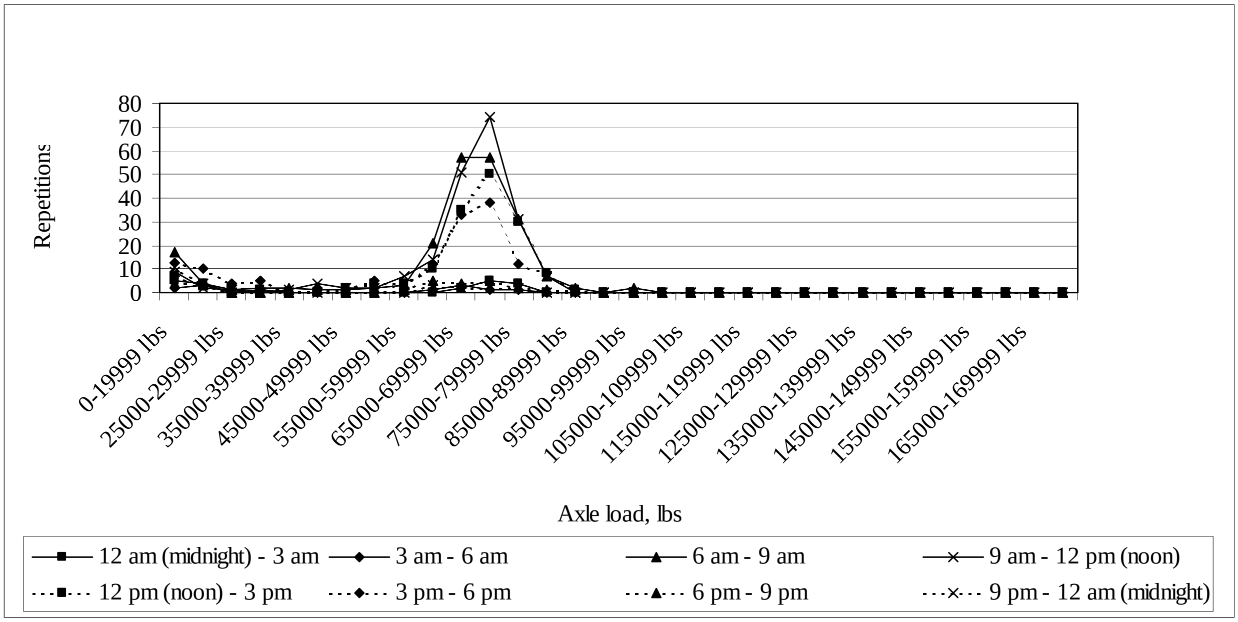


Figure J-101: Load spectrum from SPS2 sections for multi-axle (5) in July, 1999

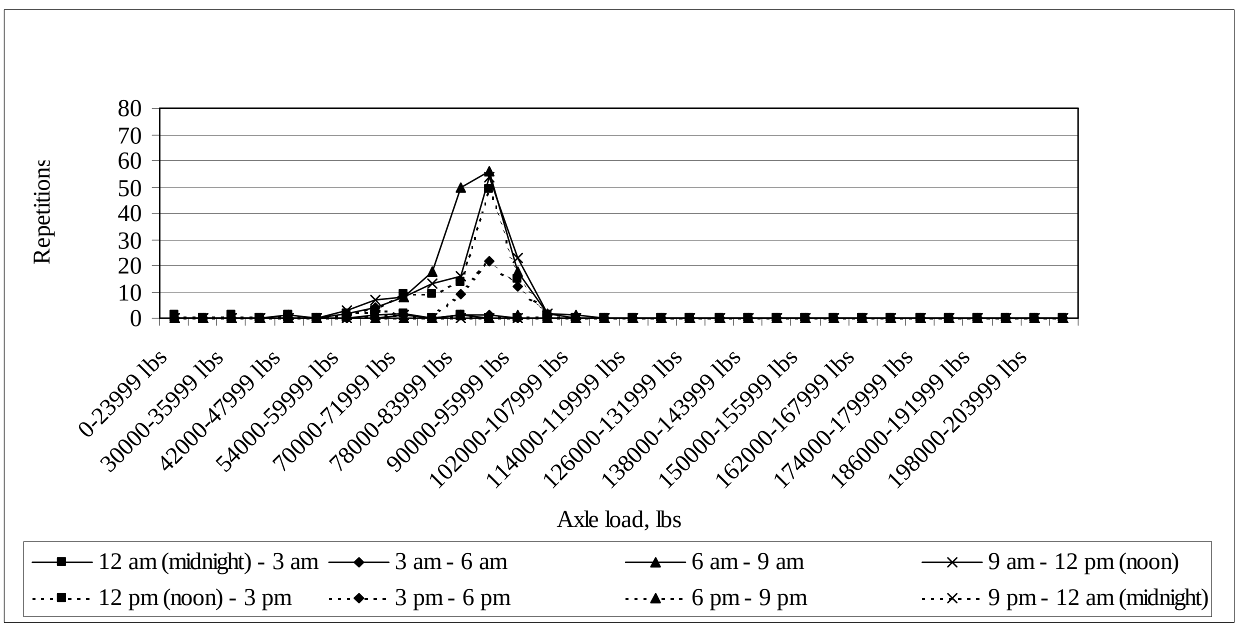


Figure J-102: Load spectrum from SPS2 sections for multi-axle (6) in July, 1999

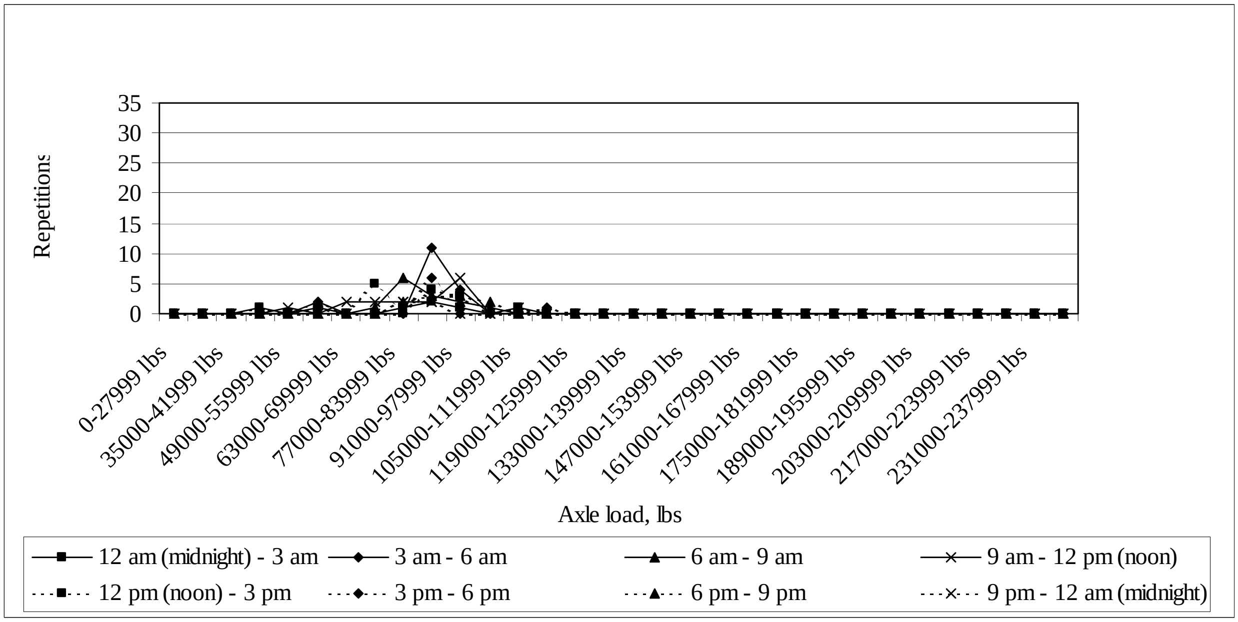


Figure J-103: Load spectrum from SPS2 sections for multi-axle (7) in July, 1999

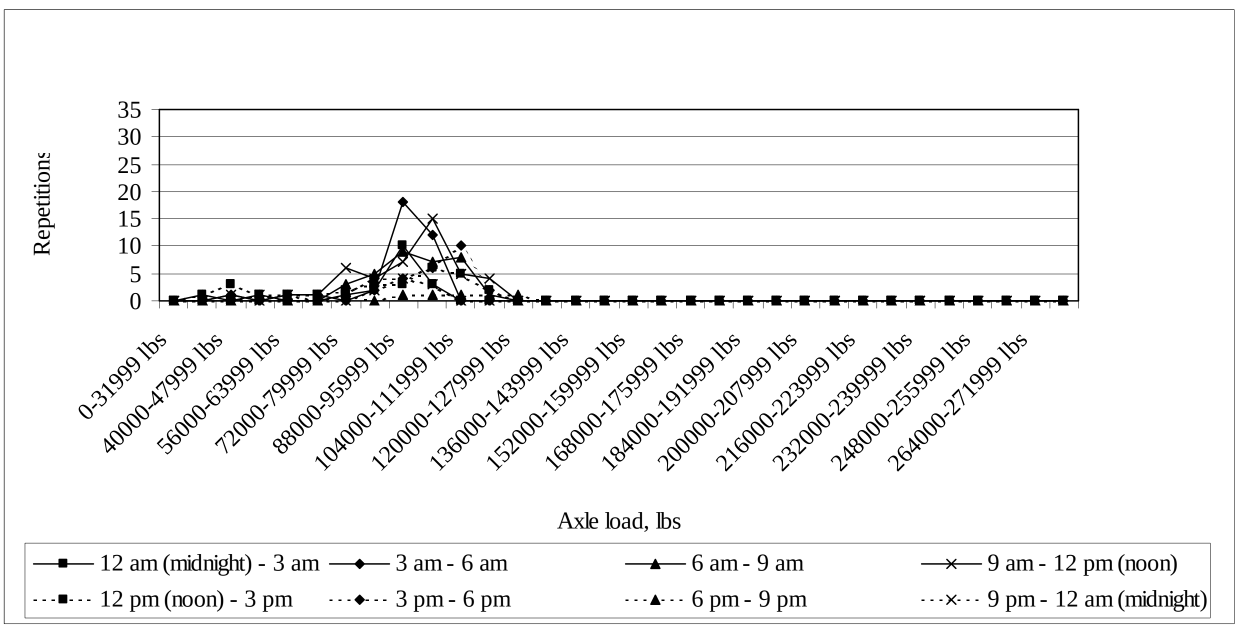


Figure J-104: Load spectrum from SPS2 sections for multi-axle (8) in July, 1999

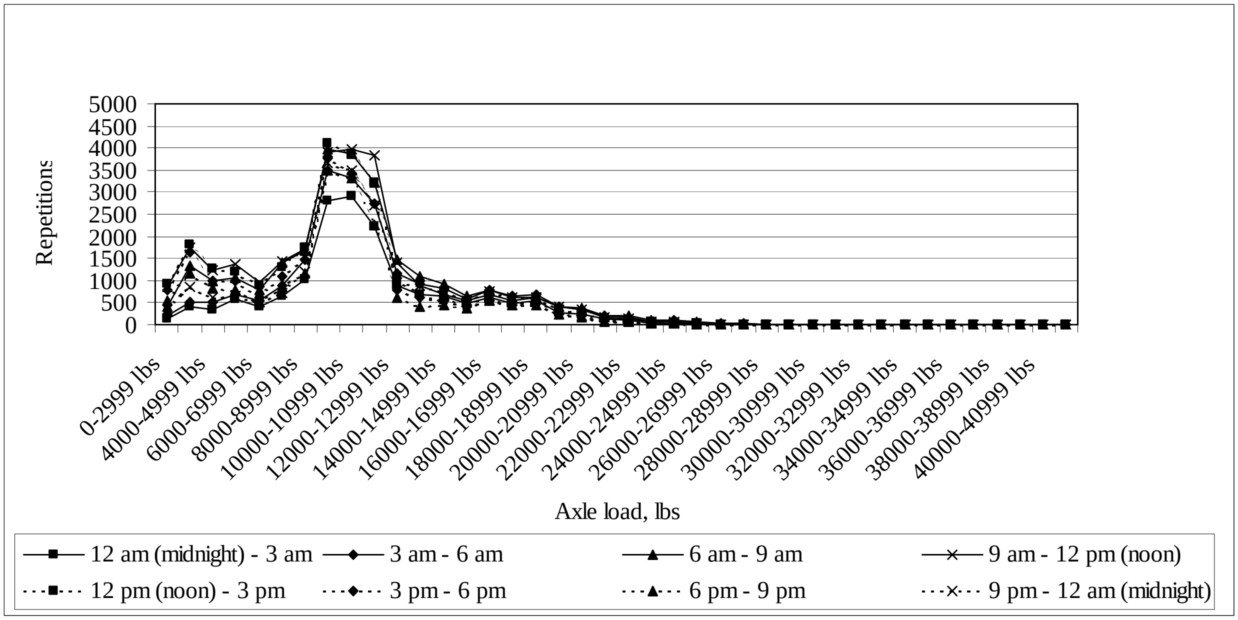


Figure J-105: Load spectrum from SPS2 sections for single axle in August, 1999

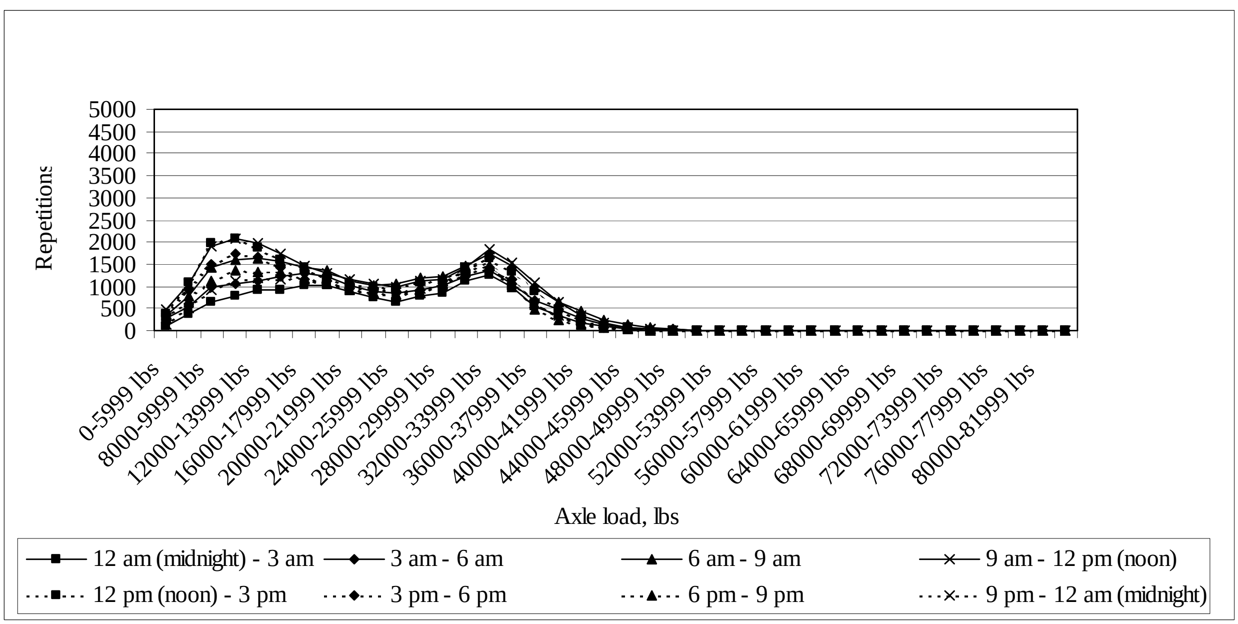


Figure J-106: Load spectrum from SPS2 sections for tandem axle in August, 1999

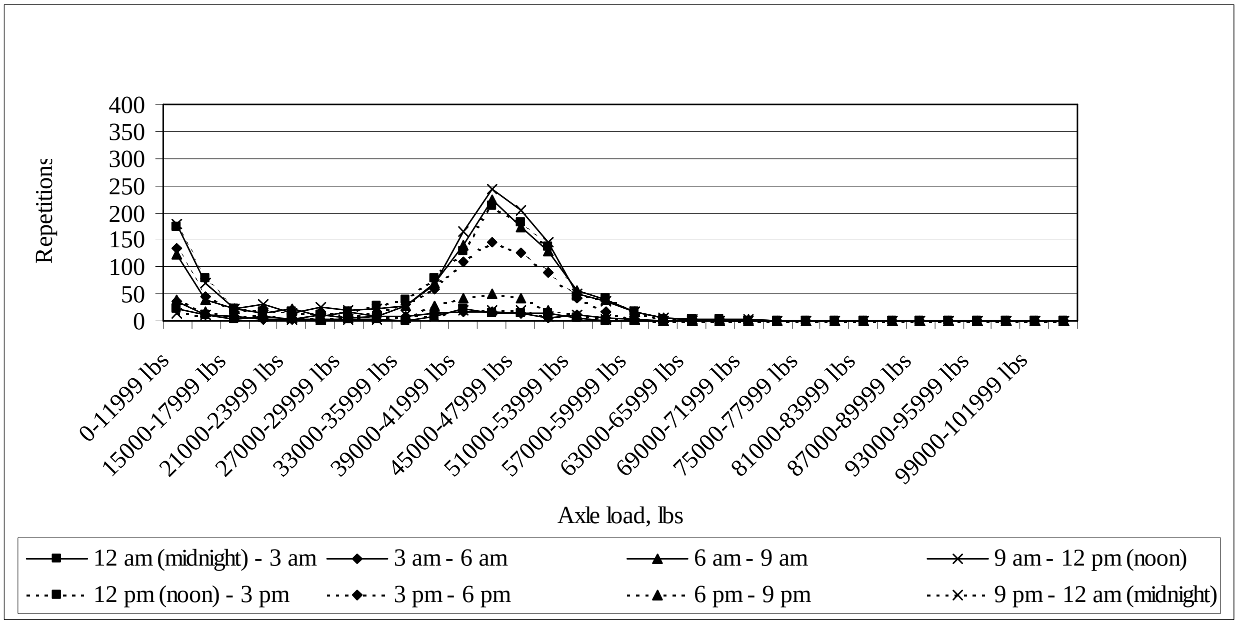


Figure J-107: Load spectrum from SPS2 sections for tridem axle in August, 1999

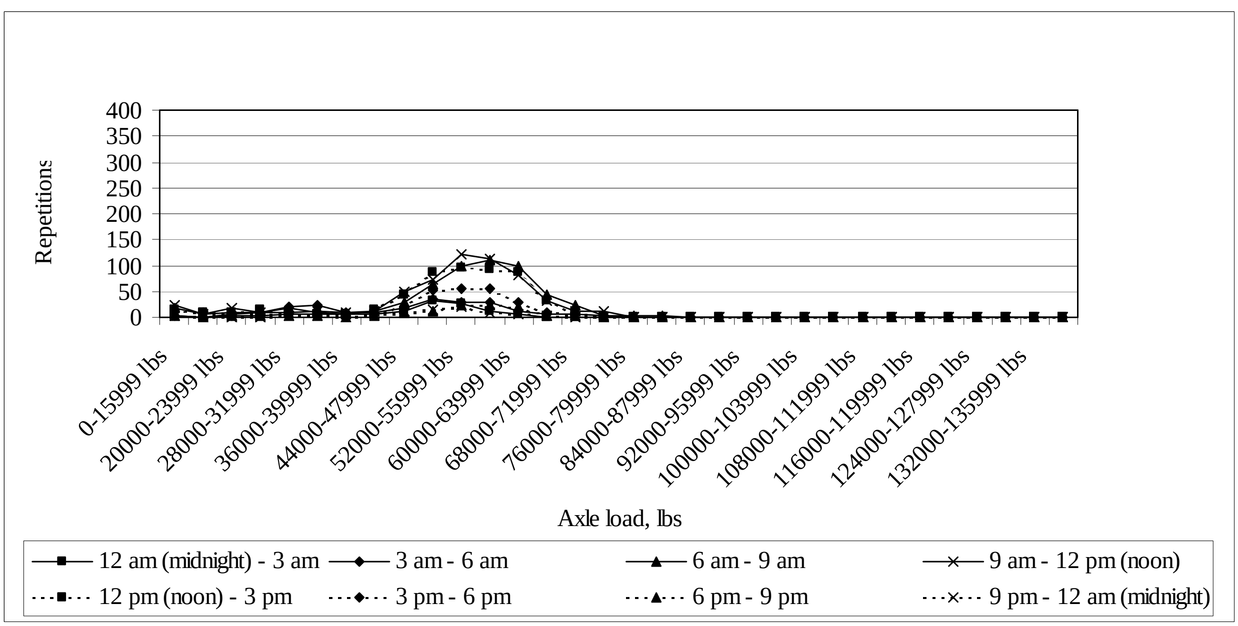


Figure J-108: Load spectrum from SPS2 sections for quad axle in August, 1999

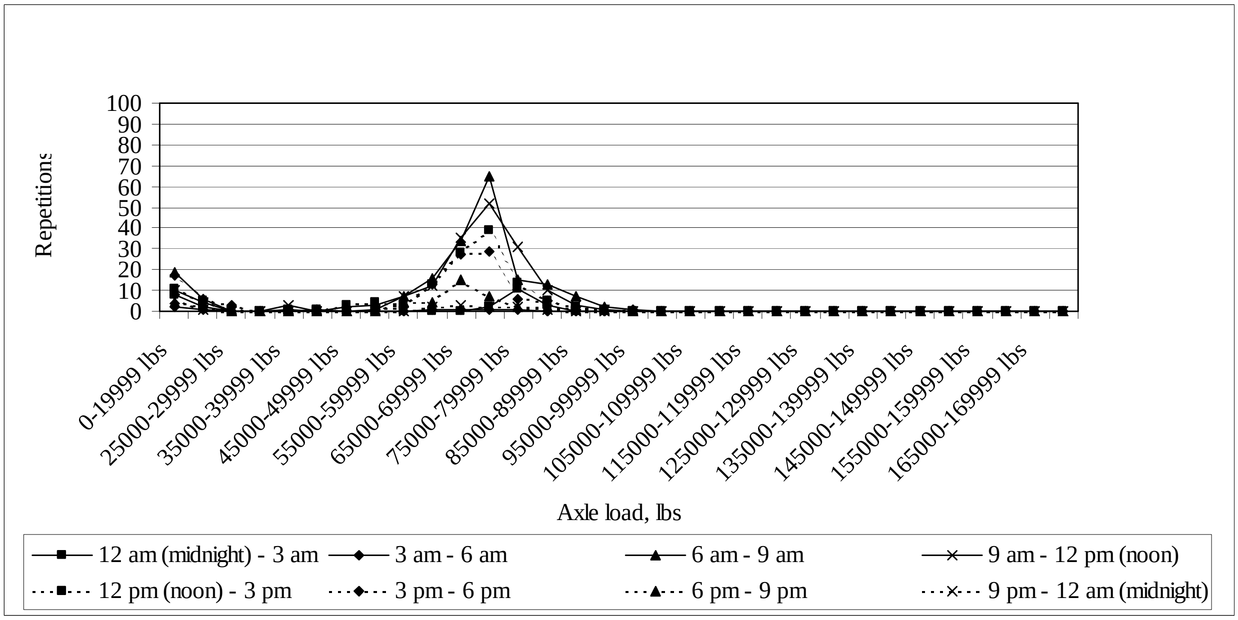


Figure J-109: Load spectrum from SPS2 sections for multi-axle (5) in August, 1999

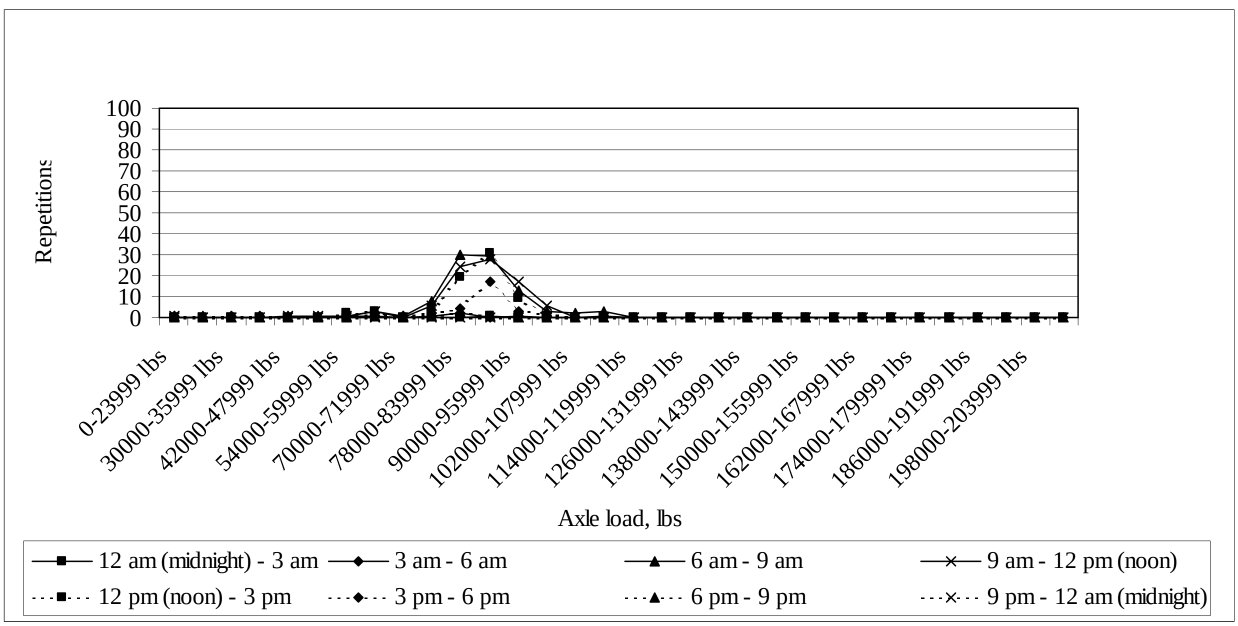


Figure J-110: Load spectrum from SPS2 sections for multi-axle (6) in August, 1999

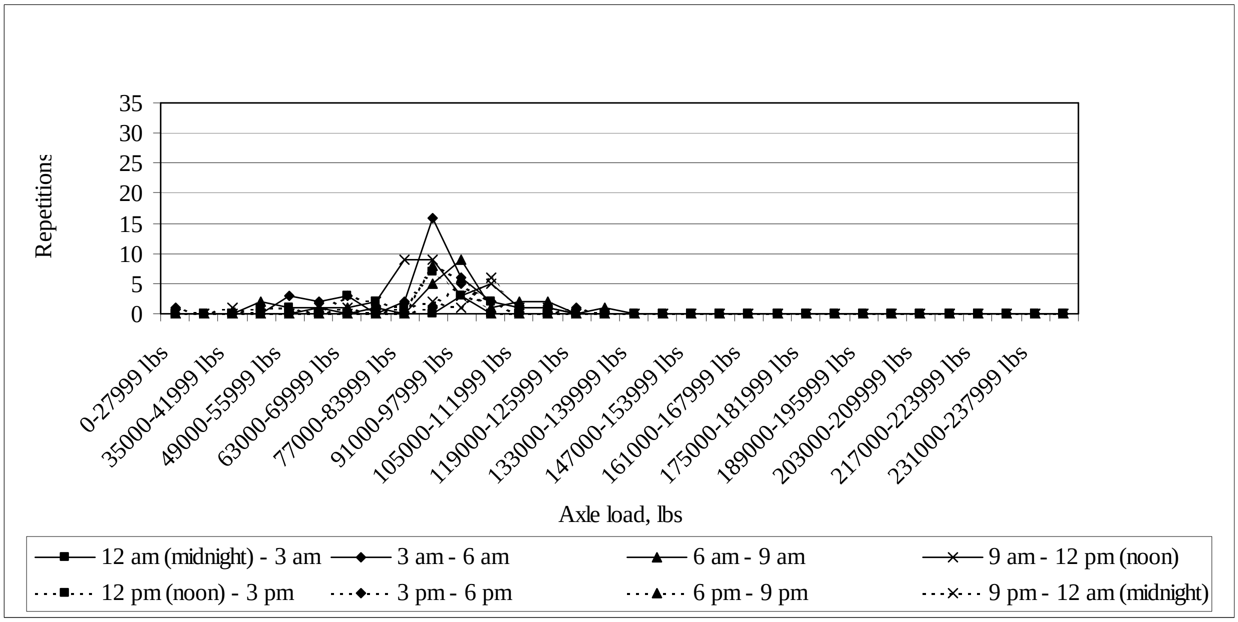


Figure J-111: Load spectrum from SPS2 sections for multi-axle (7) in August, 1999

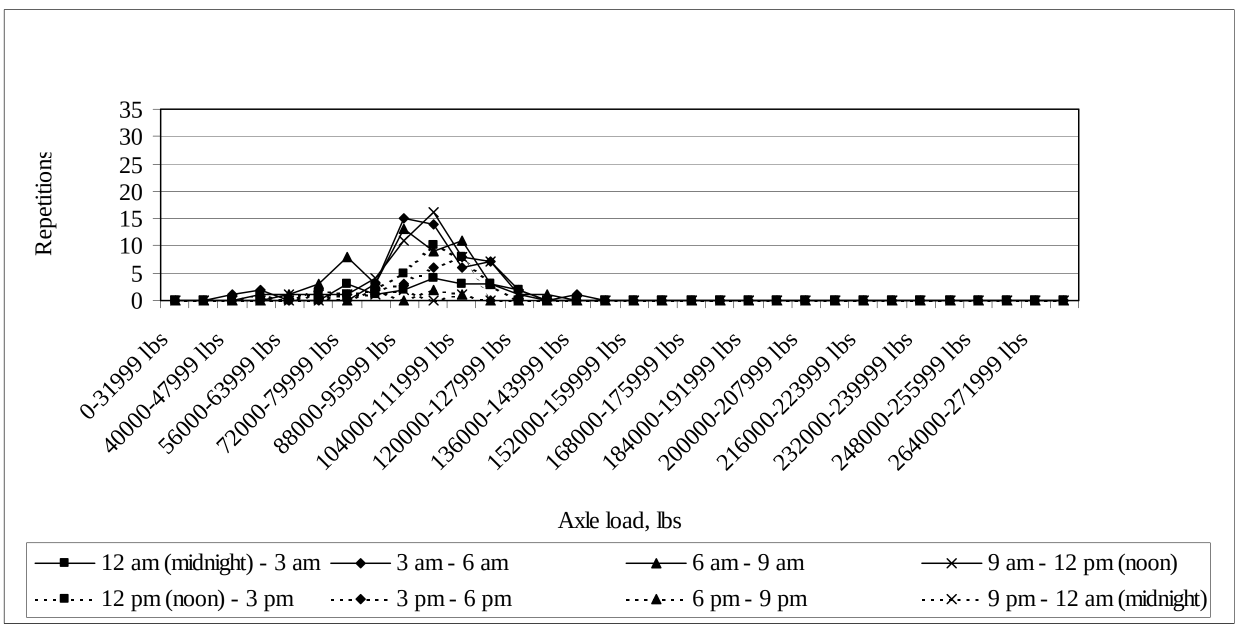


Figure J-112: Load spectrum from SPS2 sections for multi-axle (8) in August, 1999

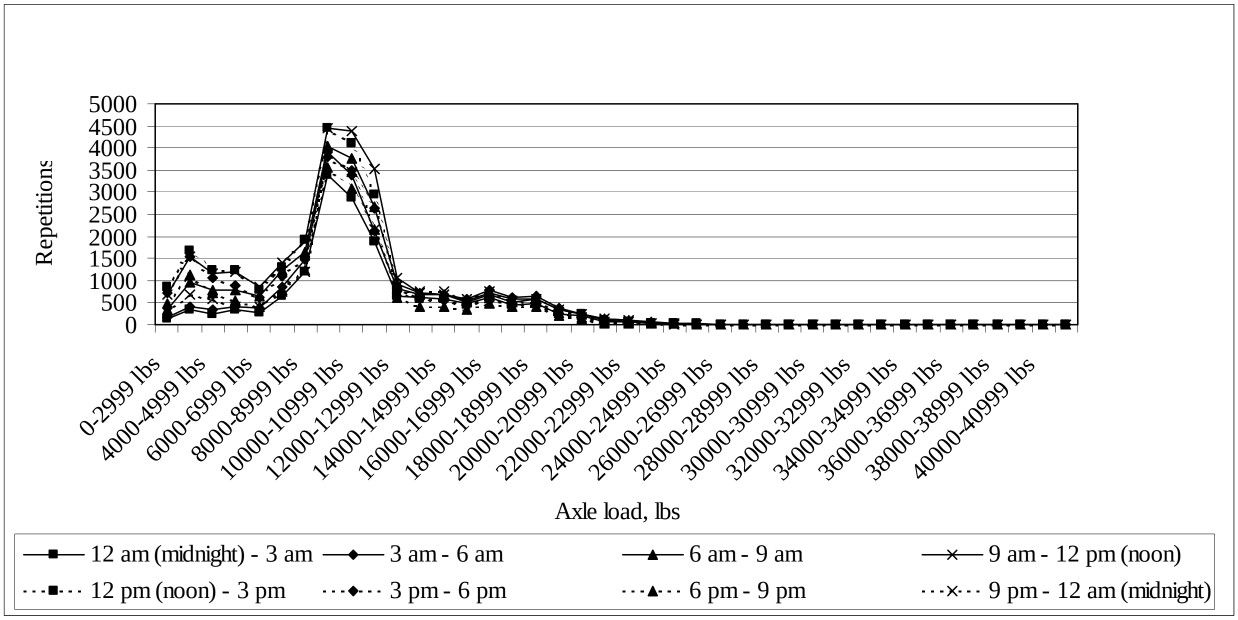


Figure J-113: Load spectrum from SPS2 sections for single axle in September, 1999

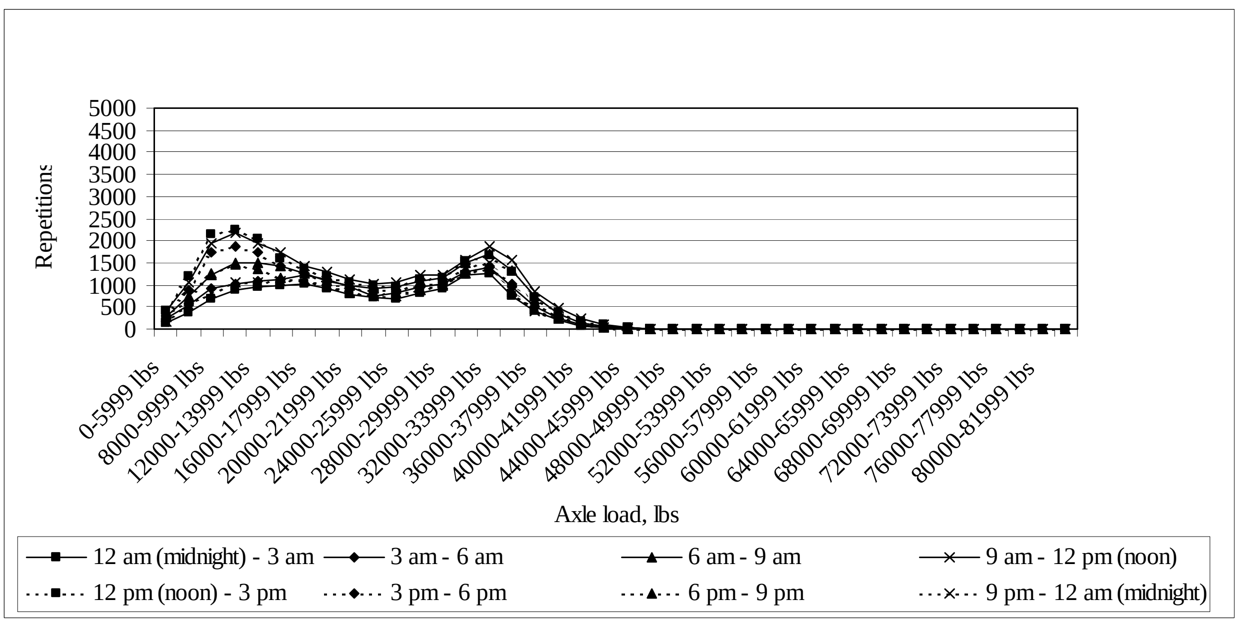


Figure J-114: Load spectrum from SPS2 sections for tandem axle in September, 1999

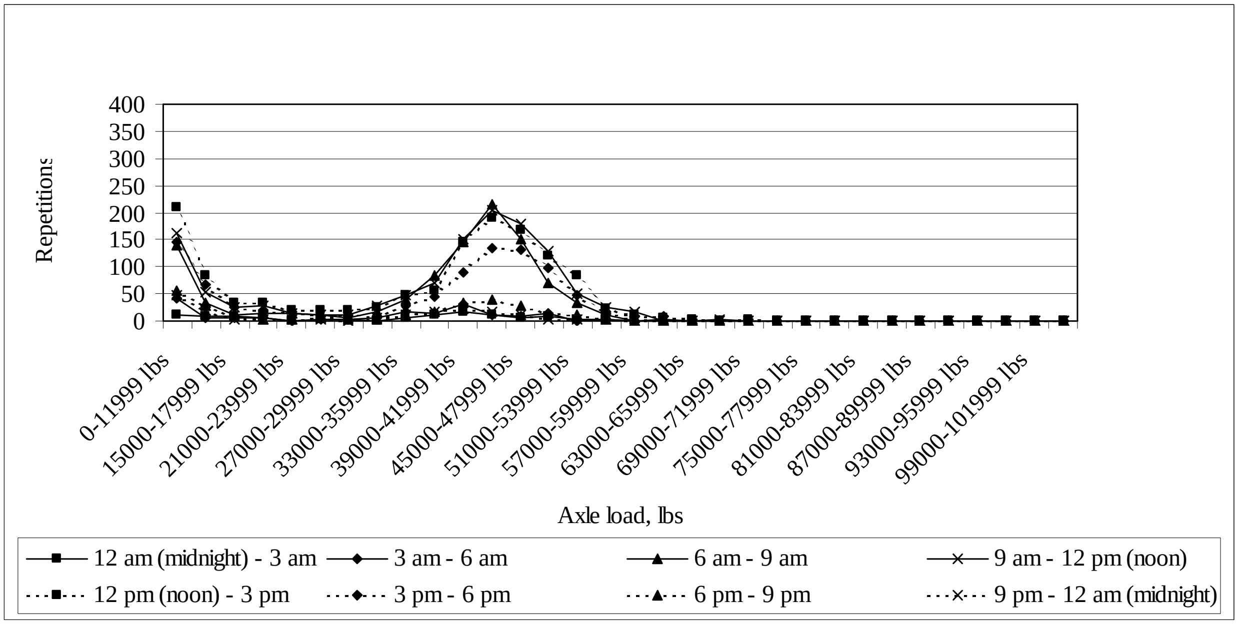


Figure J-115: Load spectrum from SPS2 sections for tridem axle in September, 1999

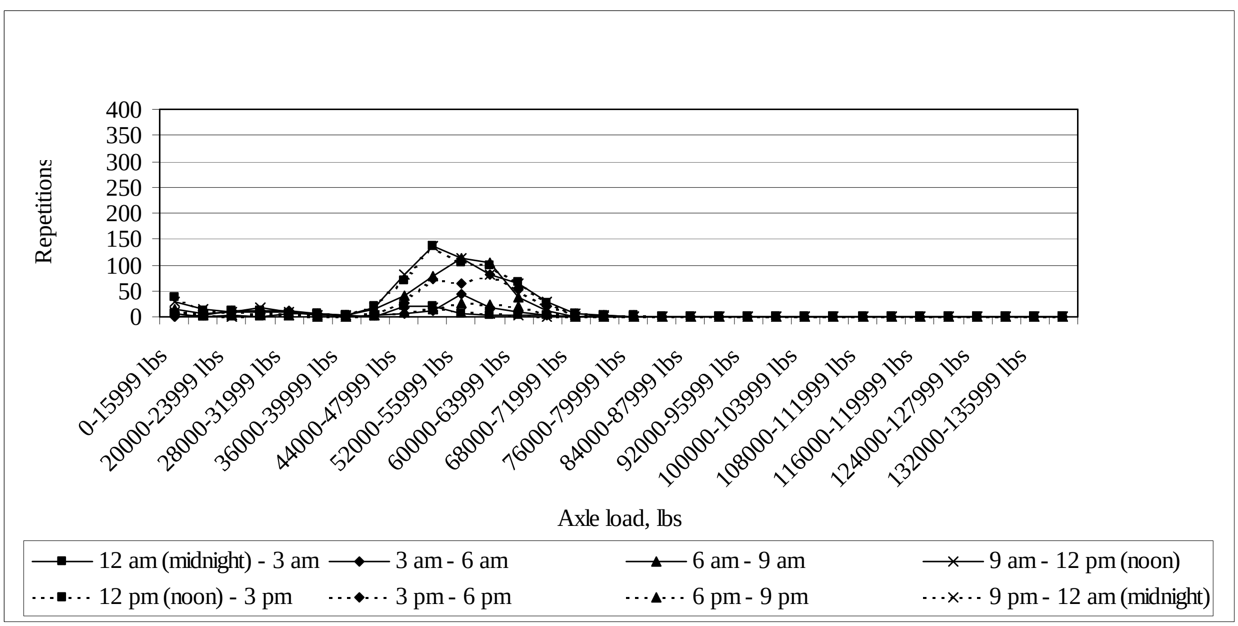


Figure J-116: Load spectrum from SPS2 sections for quad axle in September, 1999

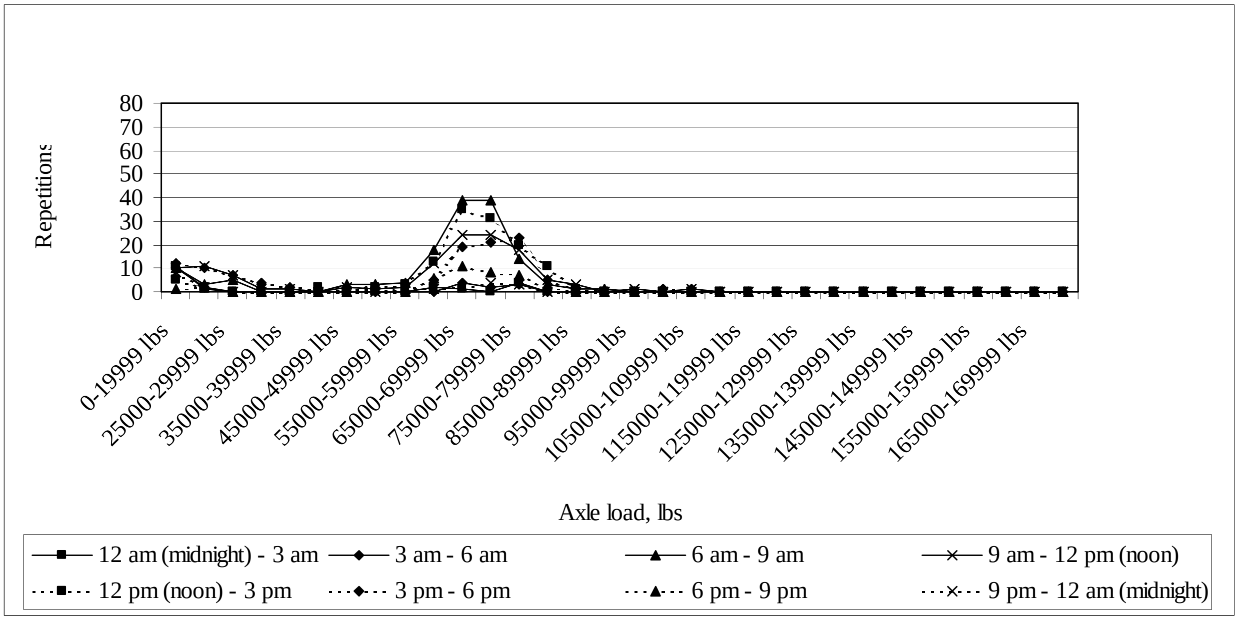


Figure J-117: Load spectrum from SPS2 sections for multi-axle (5) in September, 1999

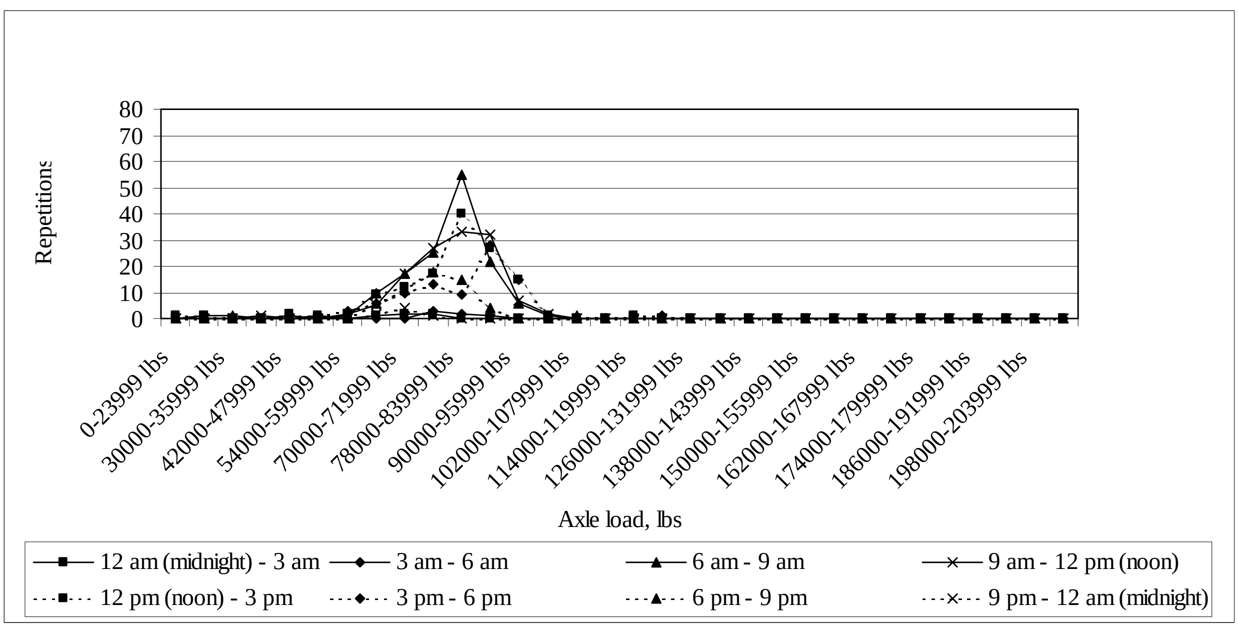


Figure J-118: Load spectrum from SPS2 sections for multi-axle (6) in September, 1999

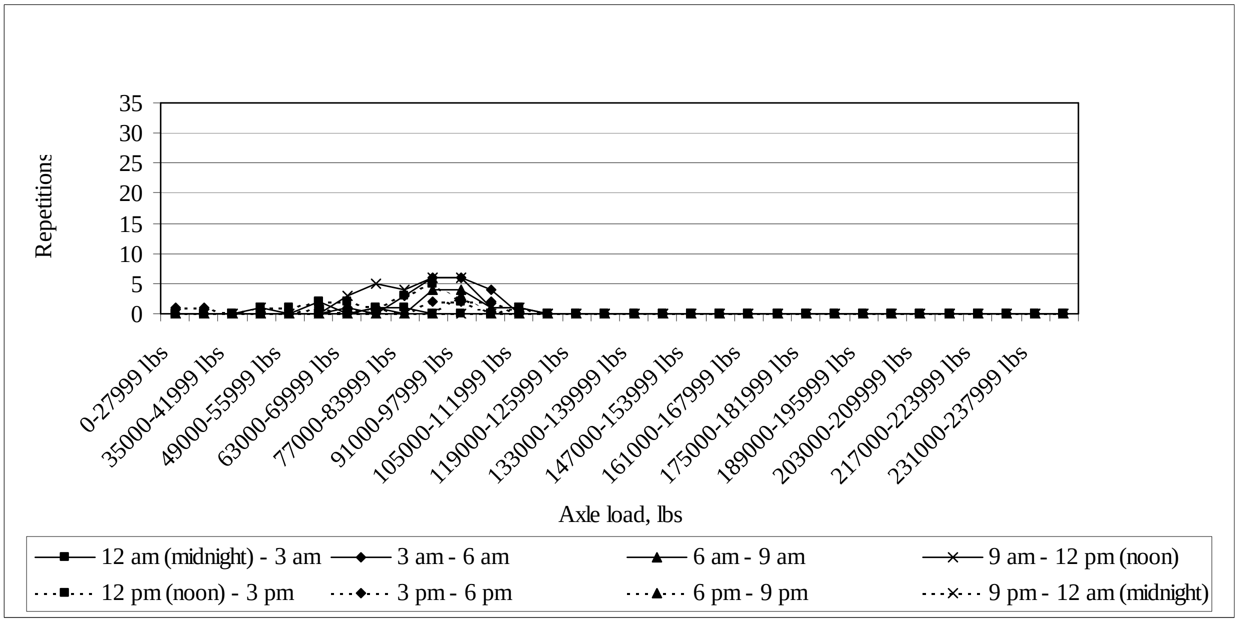


Figure J-119: Load spectrum from SPS2 sections for multi-axle (7) in September, 1999

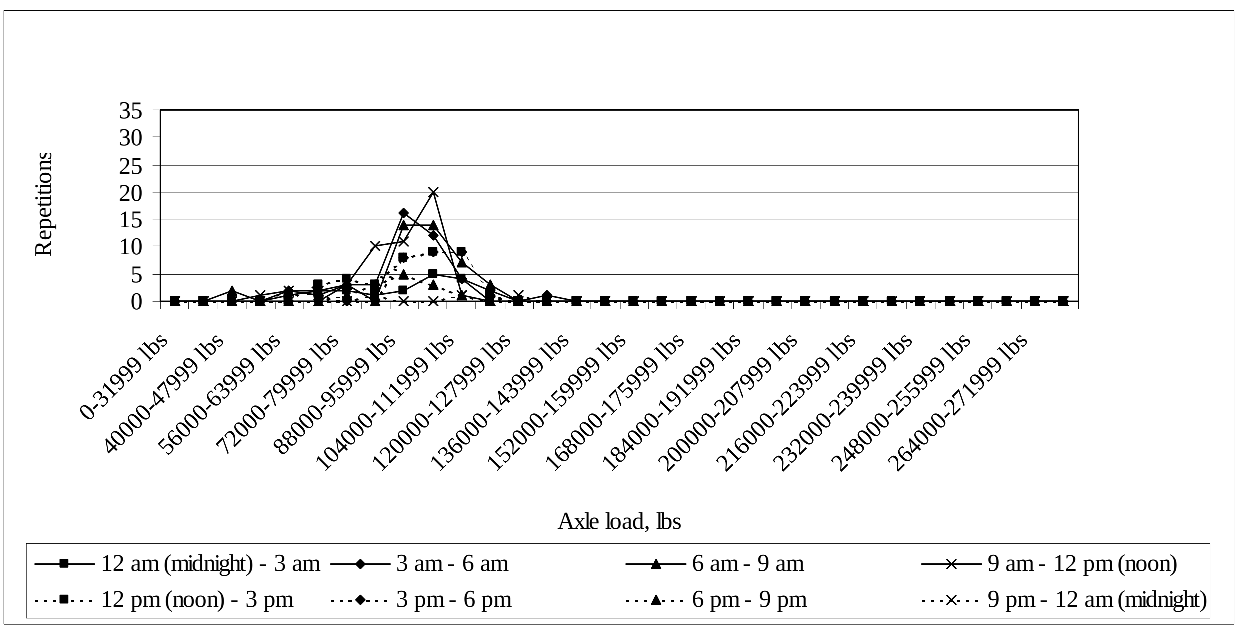


Figure J-120: Load spectrum from SPS2 sections for multi-axle (8) in September, 1999

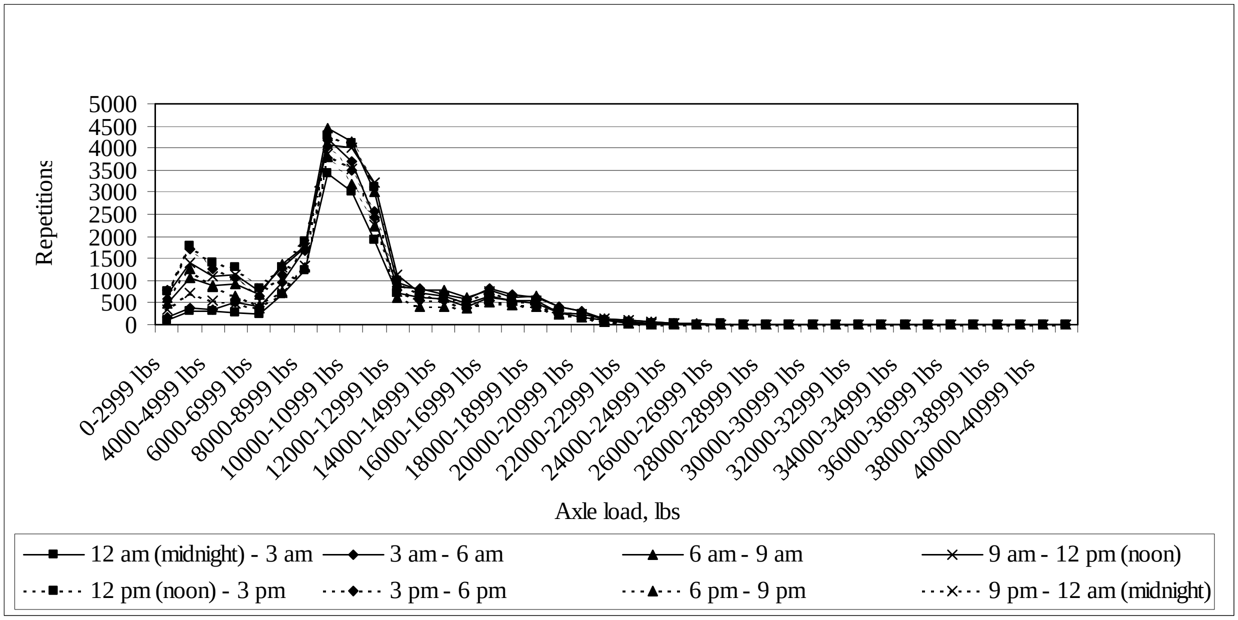


Figure J-121: Load spectrum from SPS2 sections for single axle in October, 1999

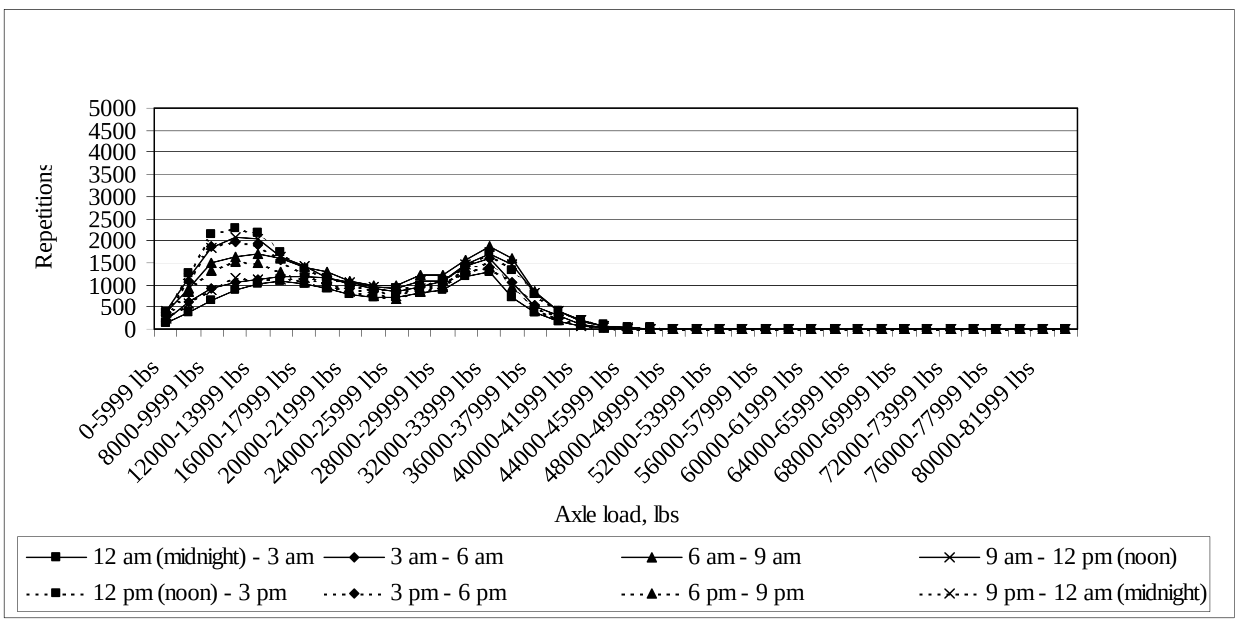


Figure J-122: Load spectrum from SPS2 sections for tandem axle in October, 1999

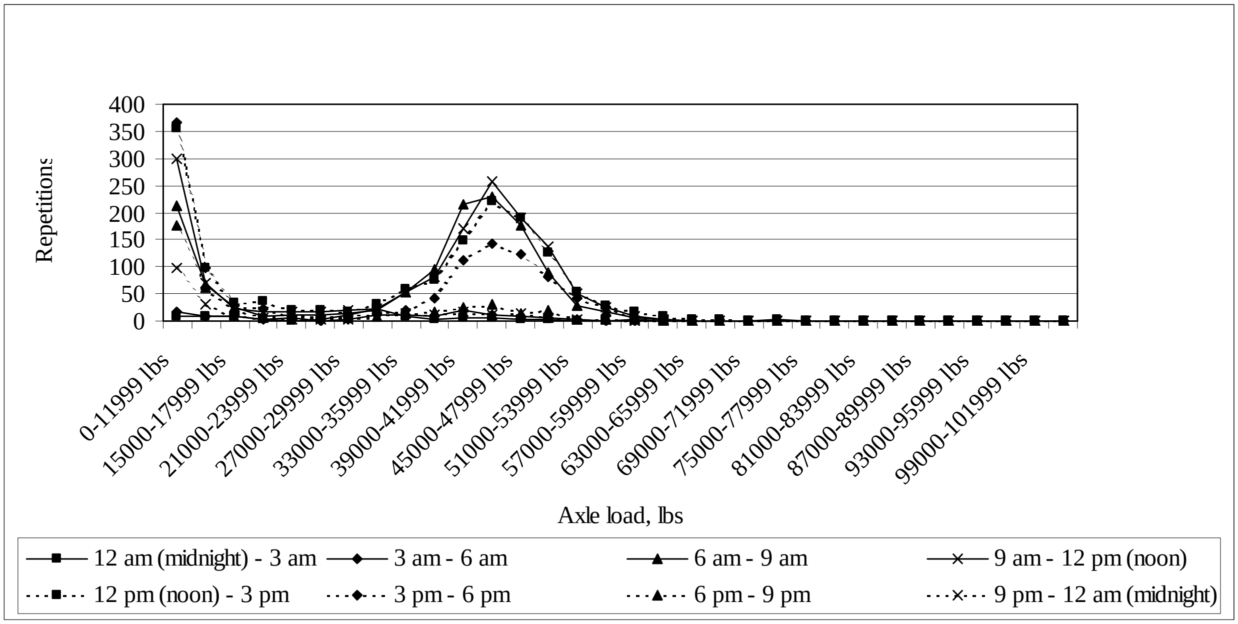


Figure J-123: Load spectrum from SPS2 sections for tridem axle in October, 1999

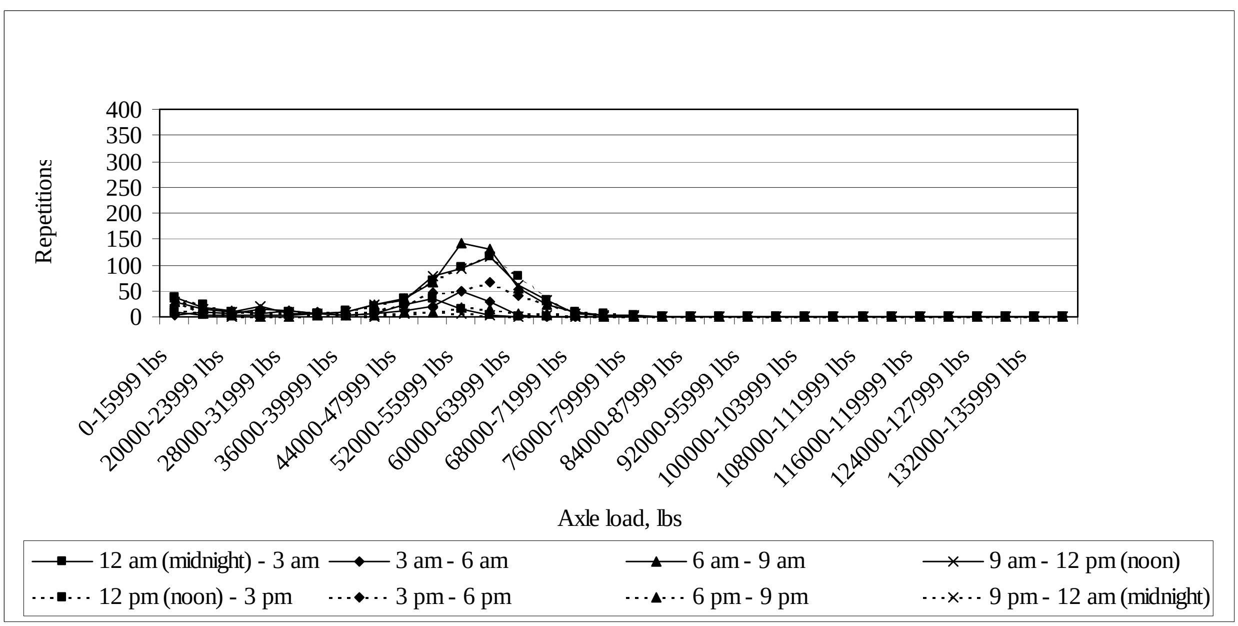


Figure J-124: Load spectrum from SPS2 sections for quad axle in October, 1999

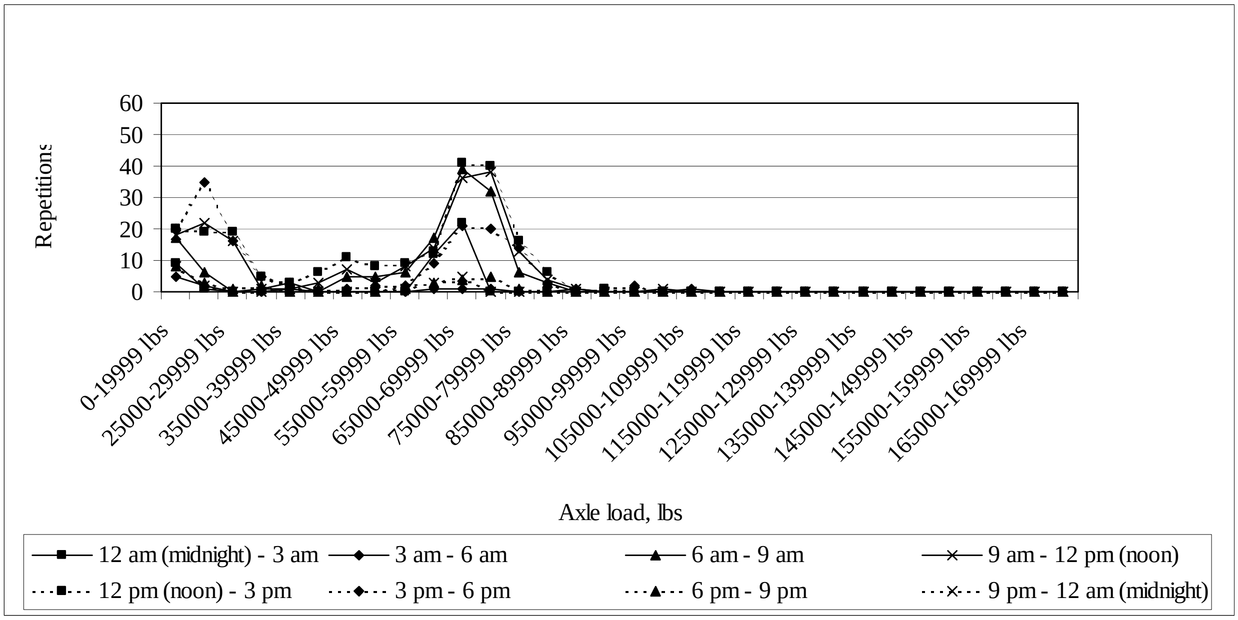


Figure J-125: Load spectrum from SPS2 sections for multi-axle (5) in October, 1999

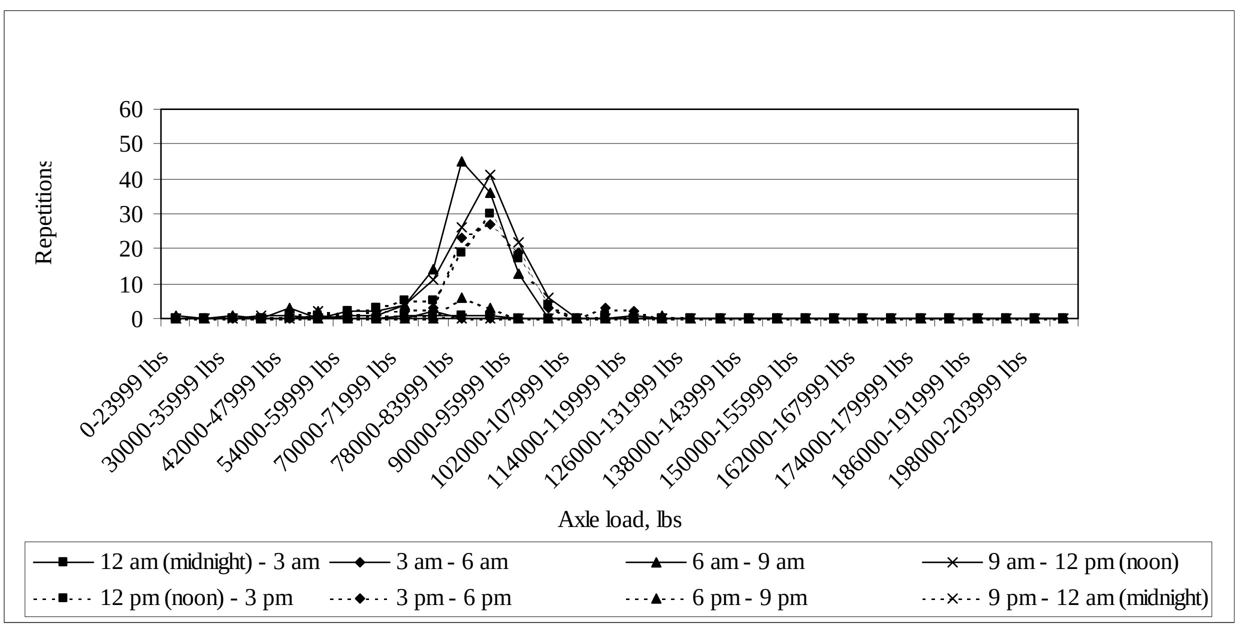


Figure J-126: Load spectrum from SPS2 sections for multi-axle (6) in October, 1999

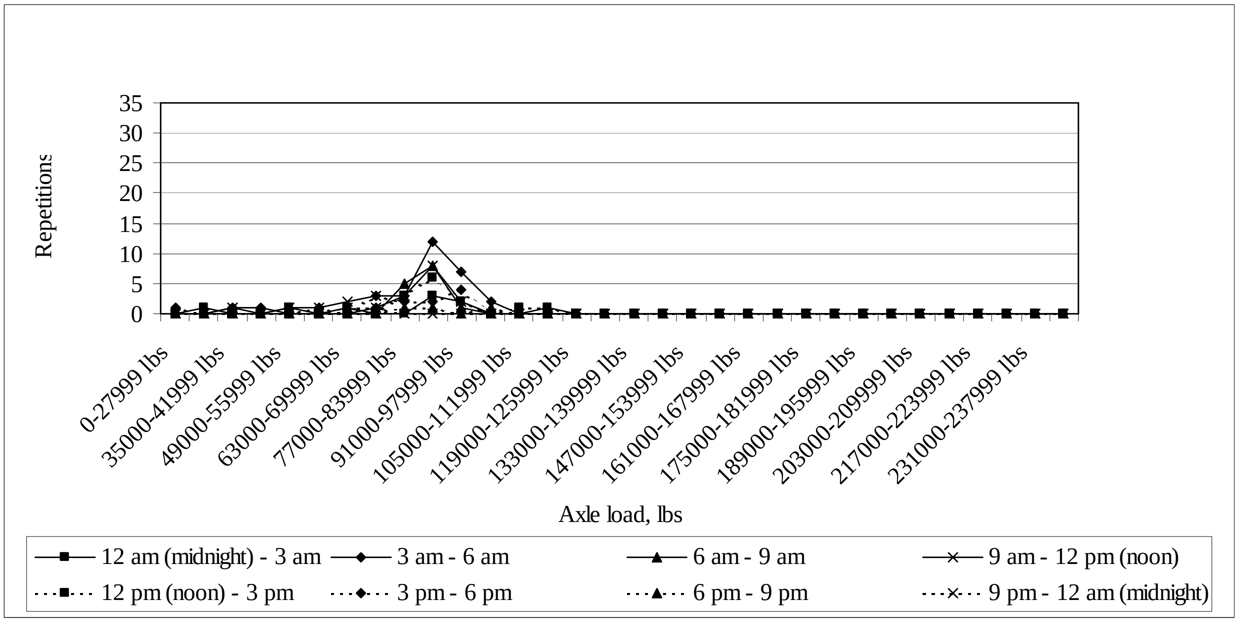


Figure J-127: Load spectrum from SPS2 sections for multi-axle (7) in October, 1999

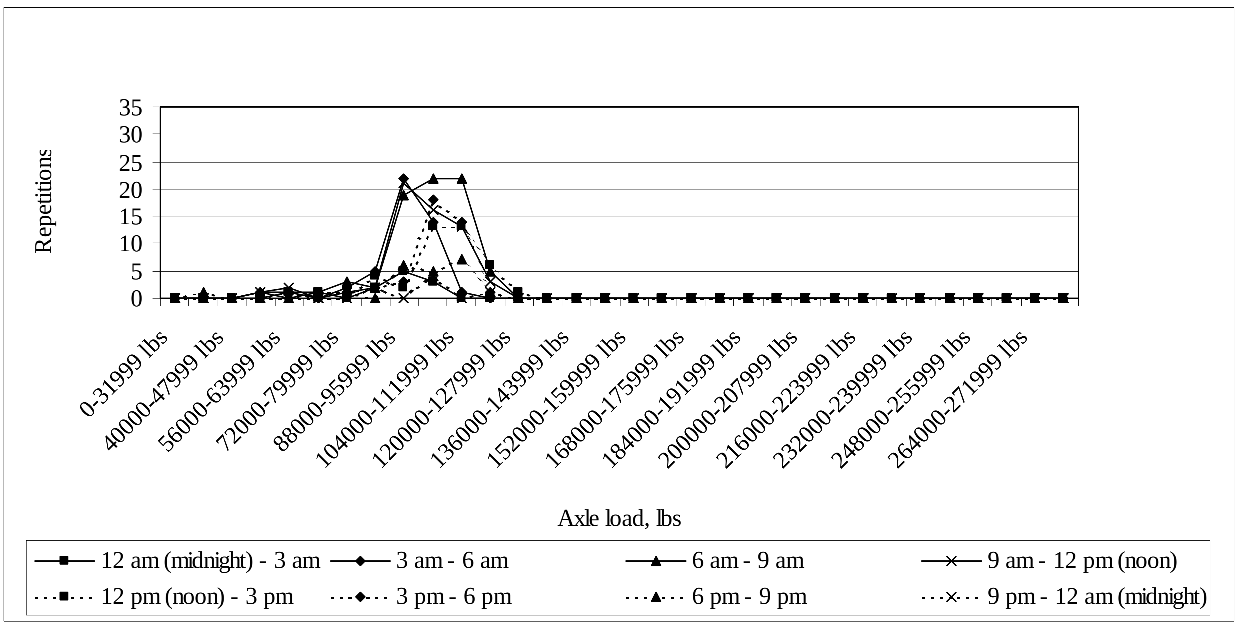


Figure J-128: Load spectrum from SPS2 sections for multi-axle (8) in October, 1999

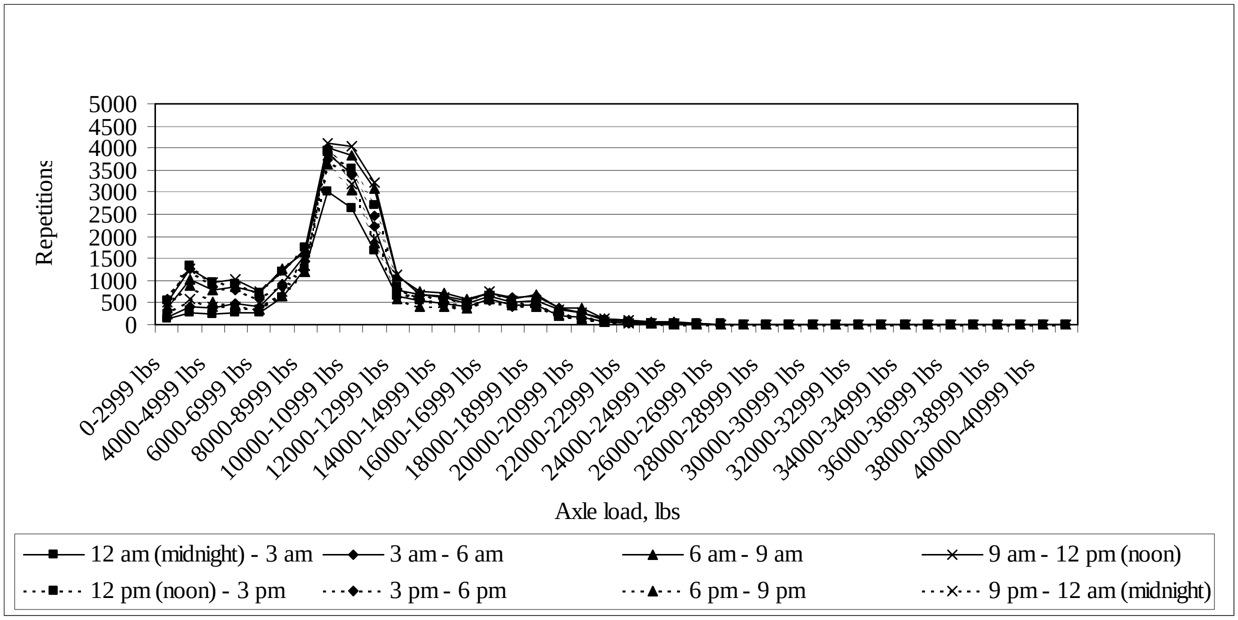


Figure J-129: Load spectrum from SPS2 sections for single axle in November, 1999

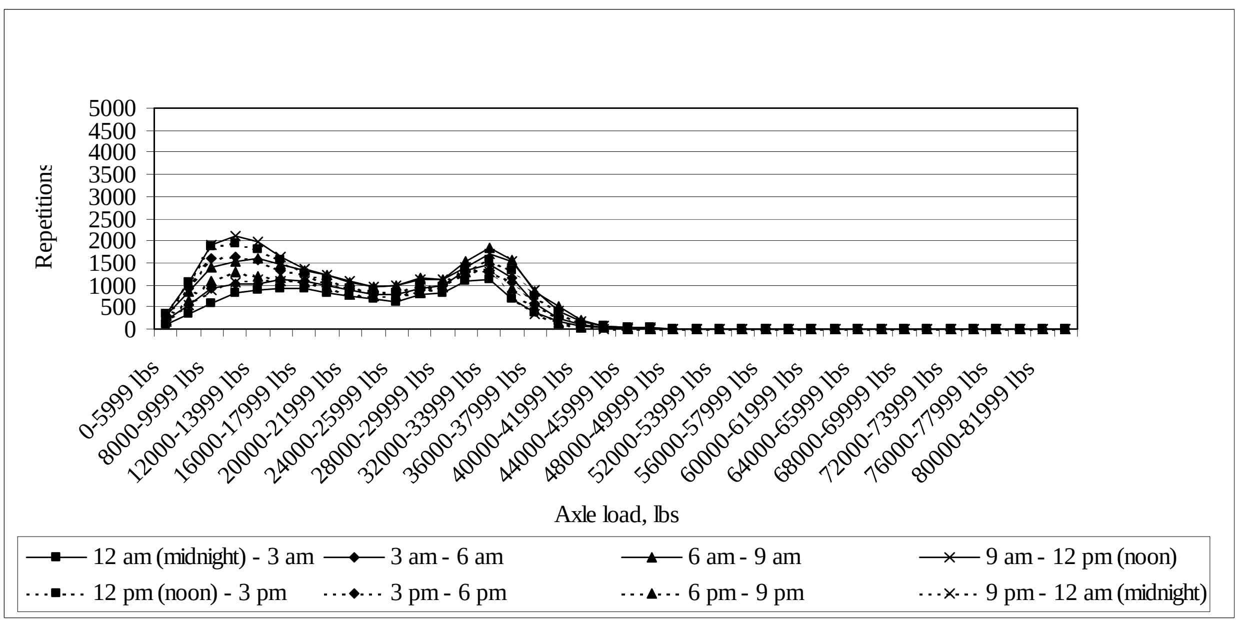


Figure J-130: Load spectrum from SPS2 sections for tandem axle in November, 1999

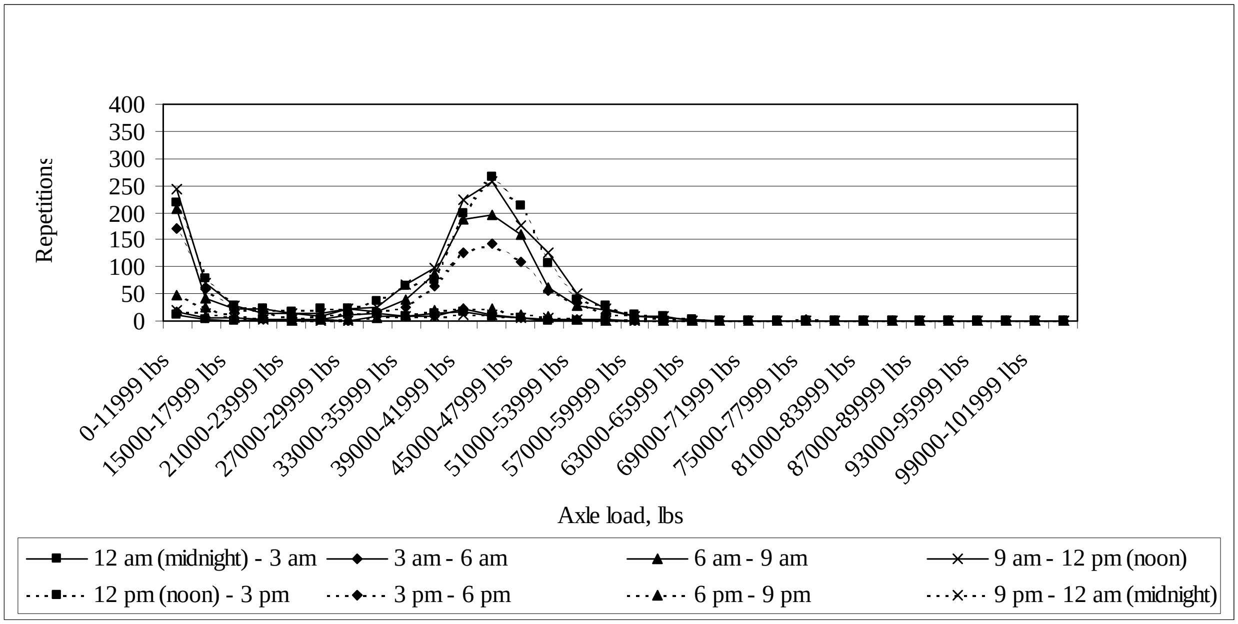


Figure J-131: Load spectrum from SPS2 sections for tridem axle in November, 1999

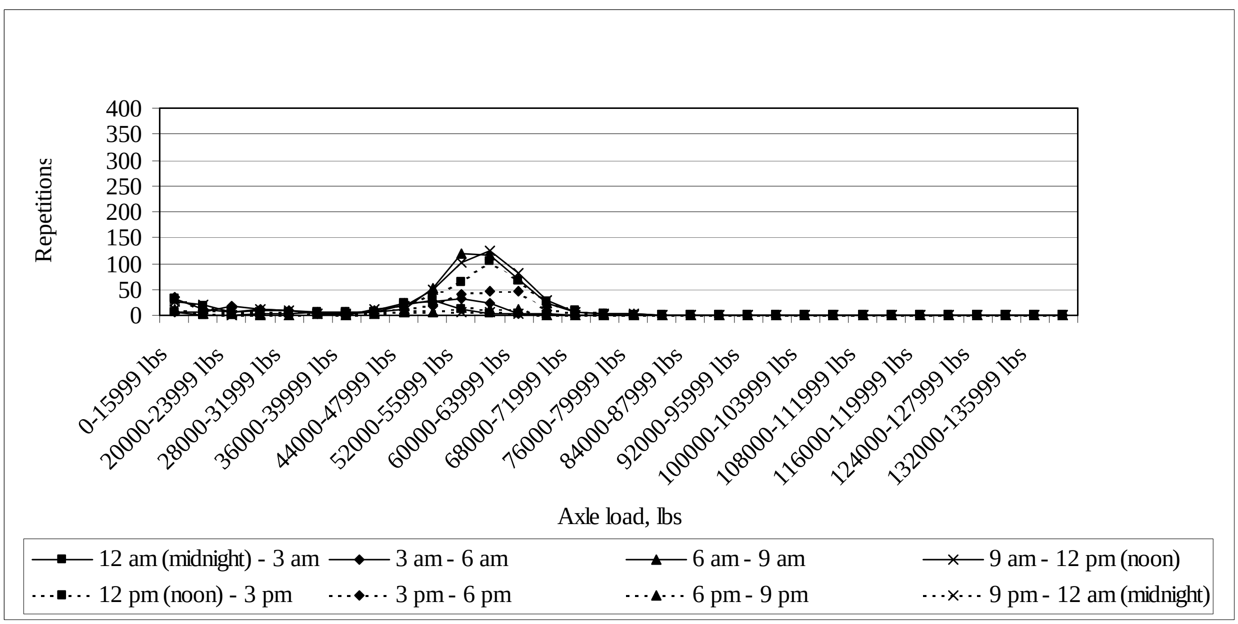


Figure J-132: Load spectrum from SPS2 sections for quad axle in November, 1999

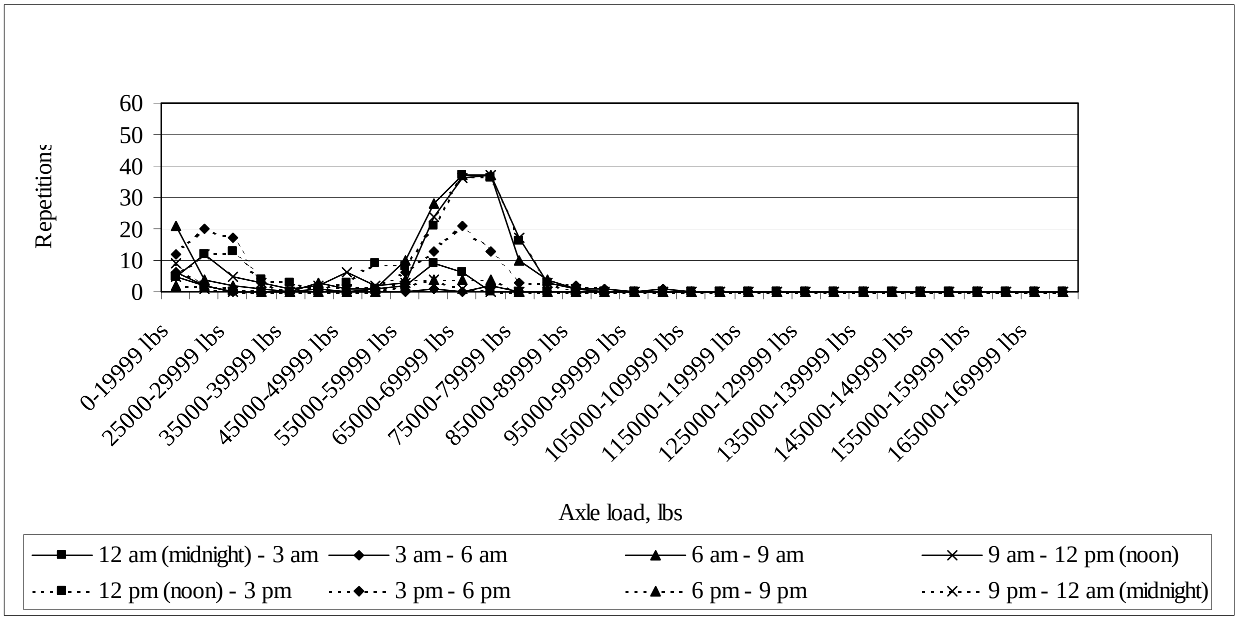


Figure J-133: Load spectrum from SPS2 sections for multi-axle (5) in November, 1999

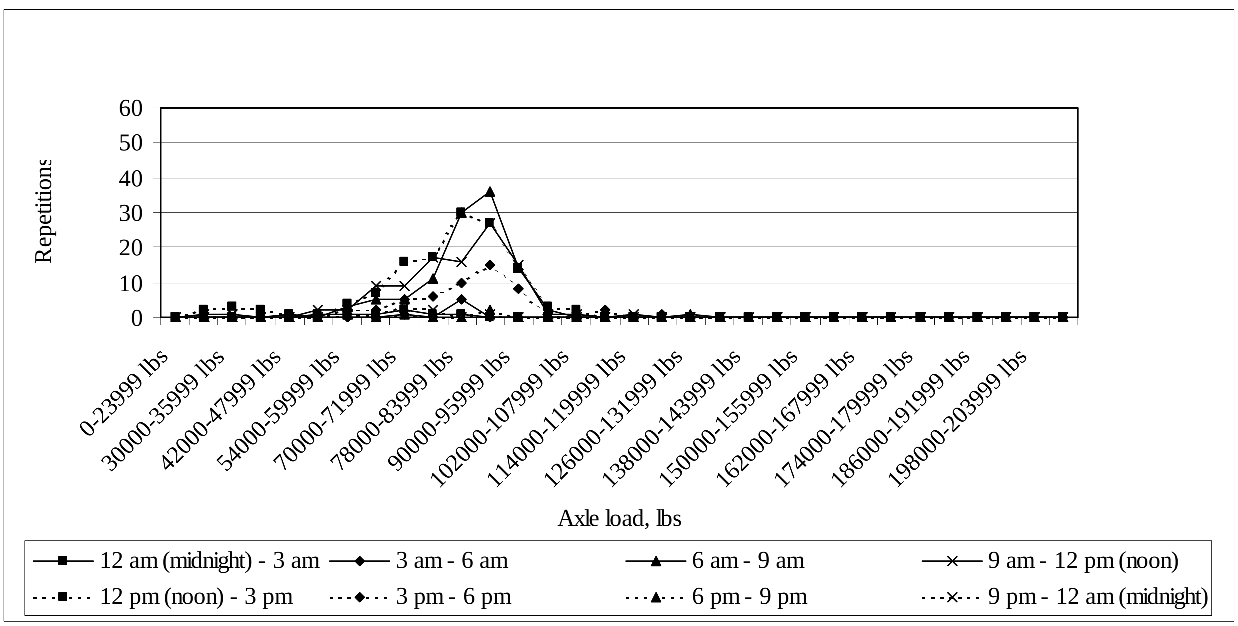


Figure J-134: Load spectrum from SPS2 sections for multi-axle (6) in November, 1999

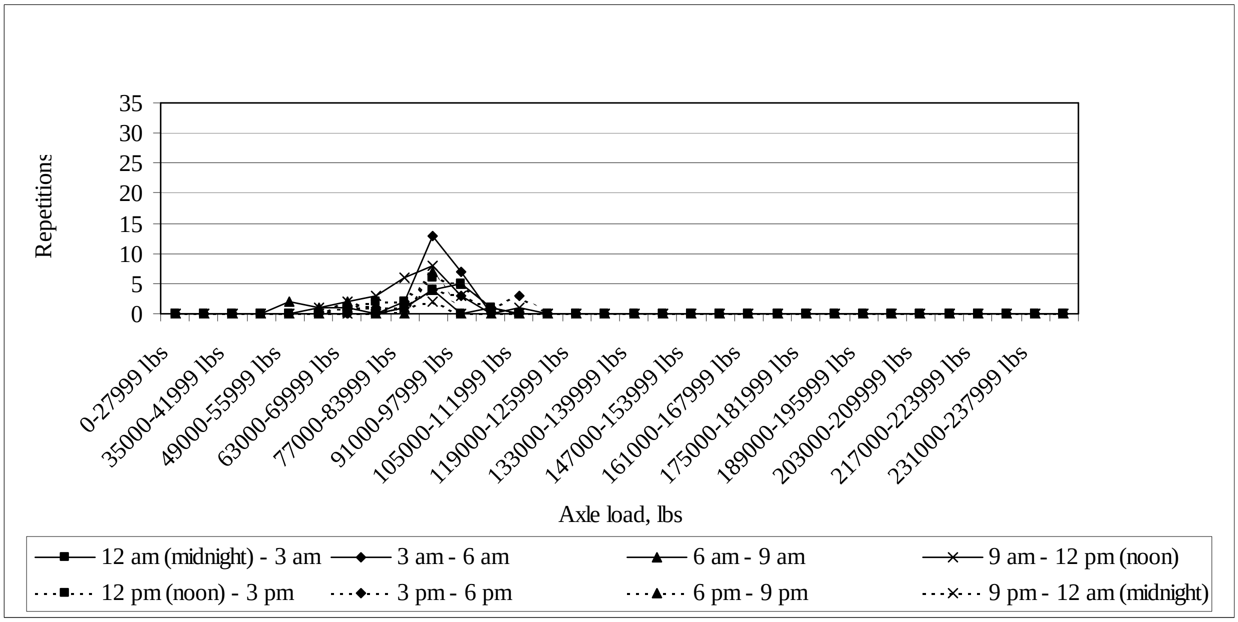


Figure J-135: Load spectrum from SPS2 sections for multi-axle (7) in November, 1999

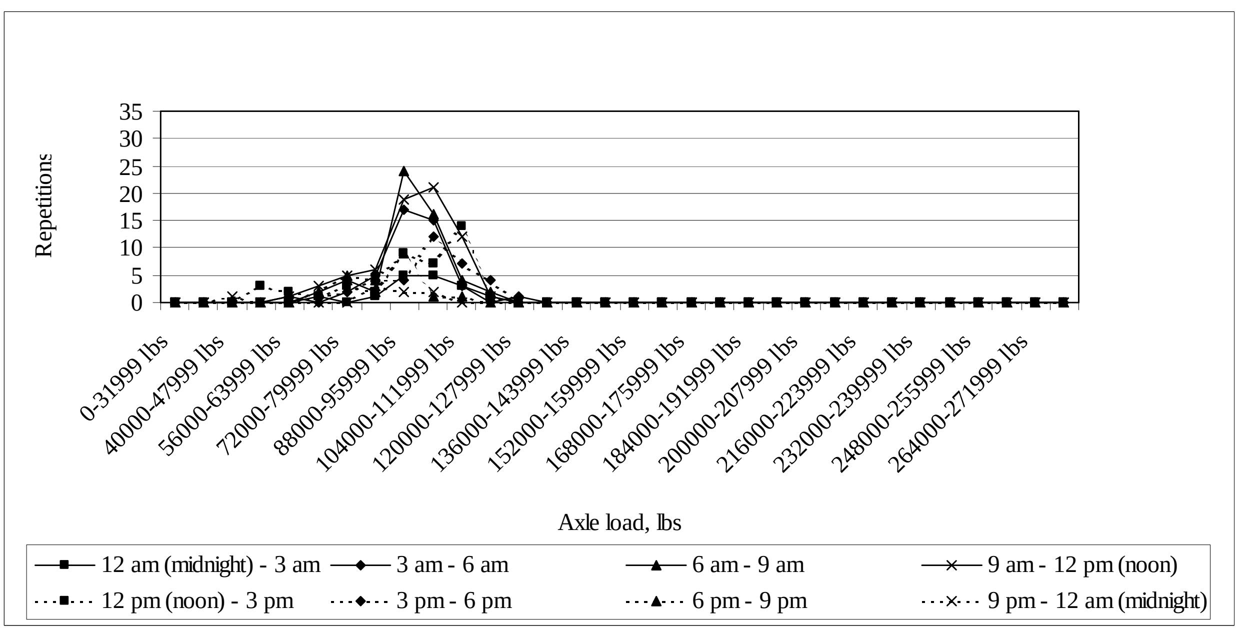


Figure J-136: Load spectrum from SPS2 sections for multi-axle (8) in November, 1999

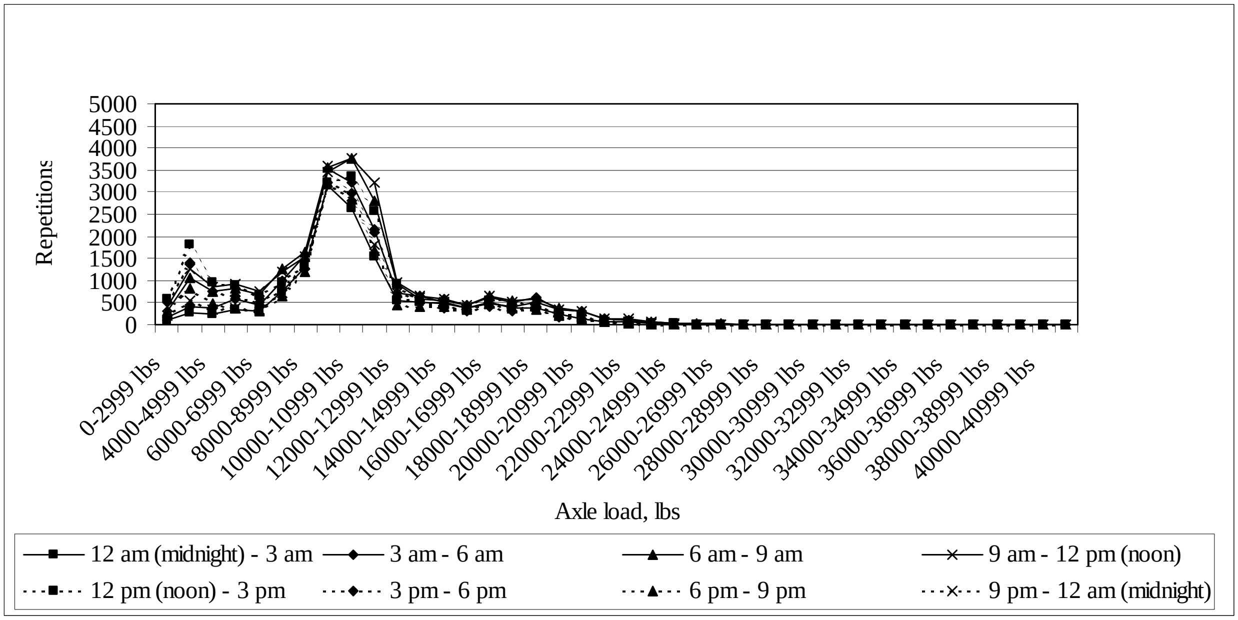


Figure J-137: Load spectrum from SPS2 sections for single axle in December, 1999

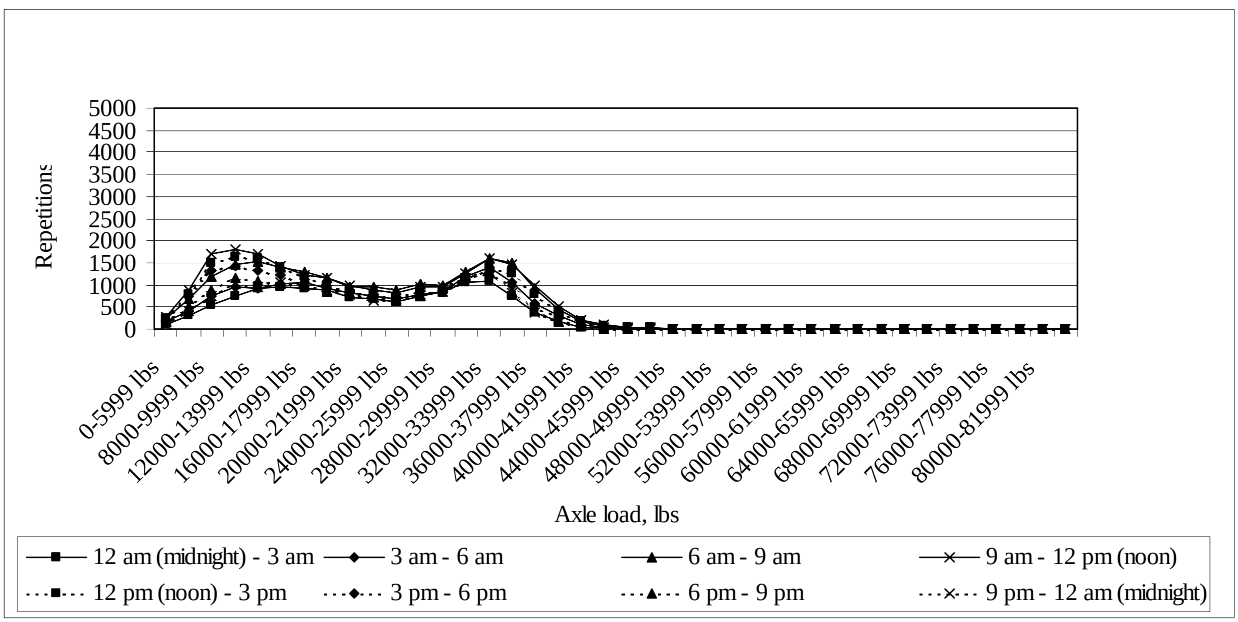


Figure J-138: Load spectrum from SPS2 sections for tandem axle in December, 1999

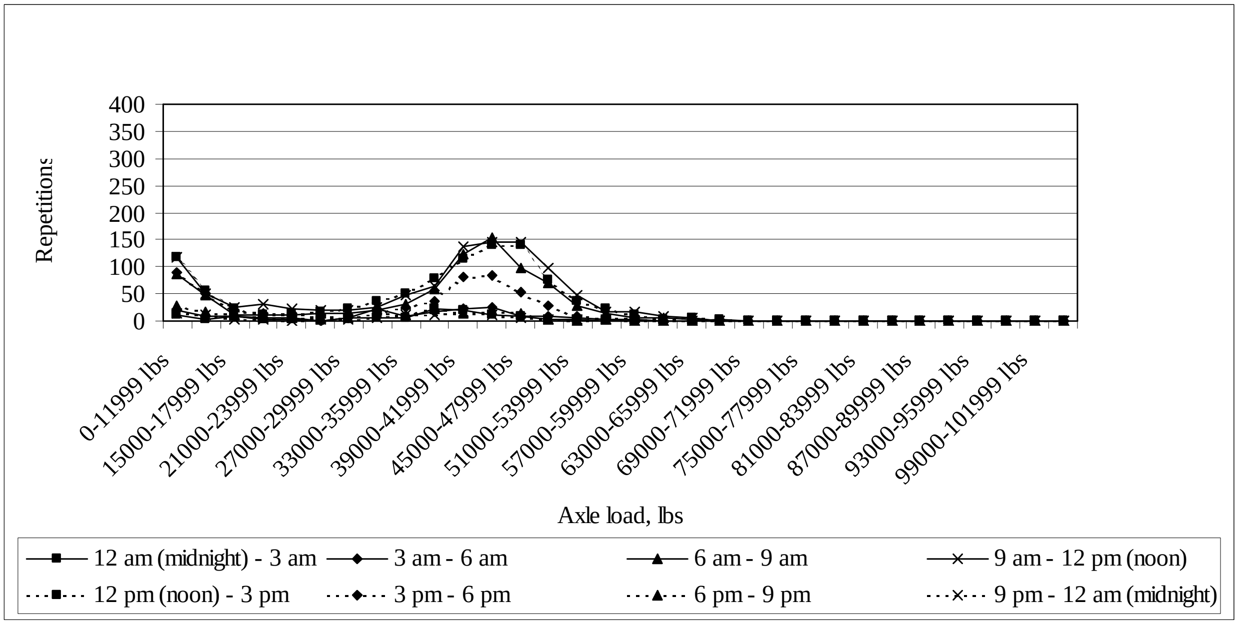


Figure J-139: Load spectrum from SPS2 sections for tridem axle in December, 1999

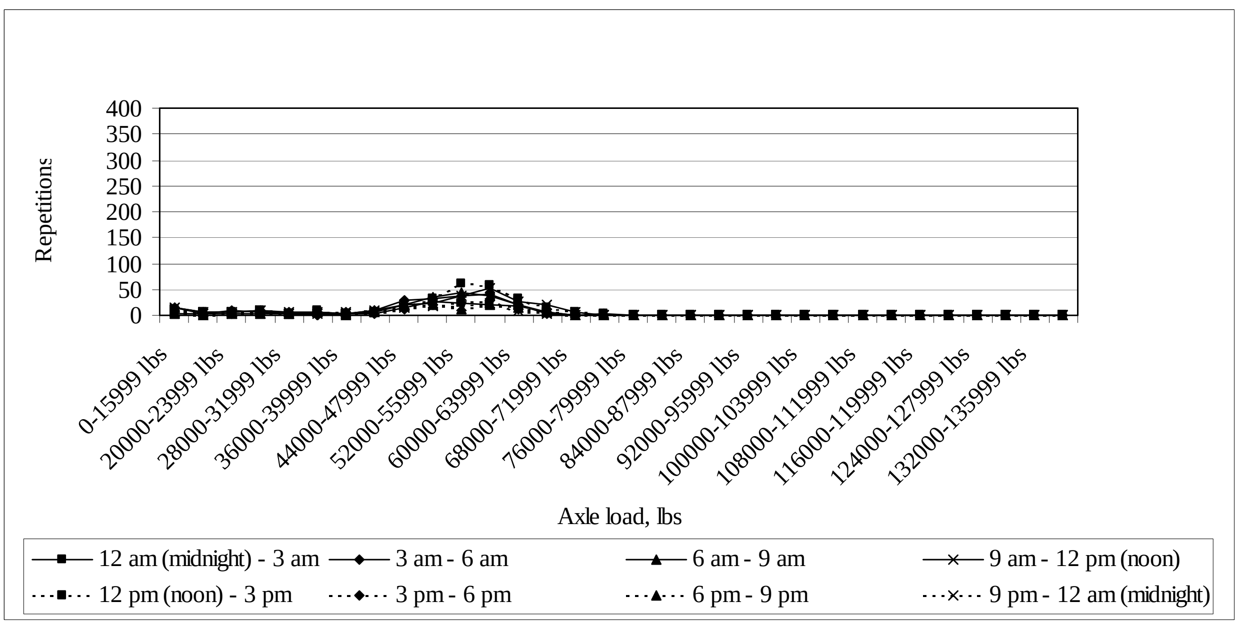


Figure J-140: Load spectrum from SPS2 sections for quad axle in December, 1999

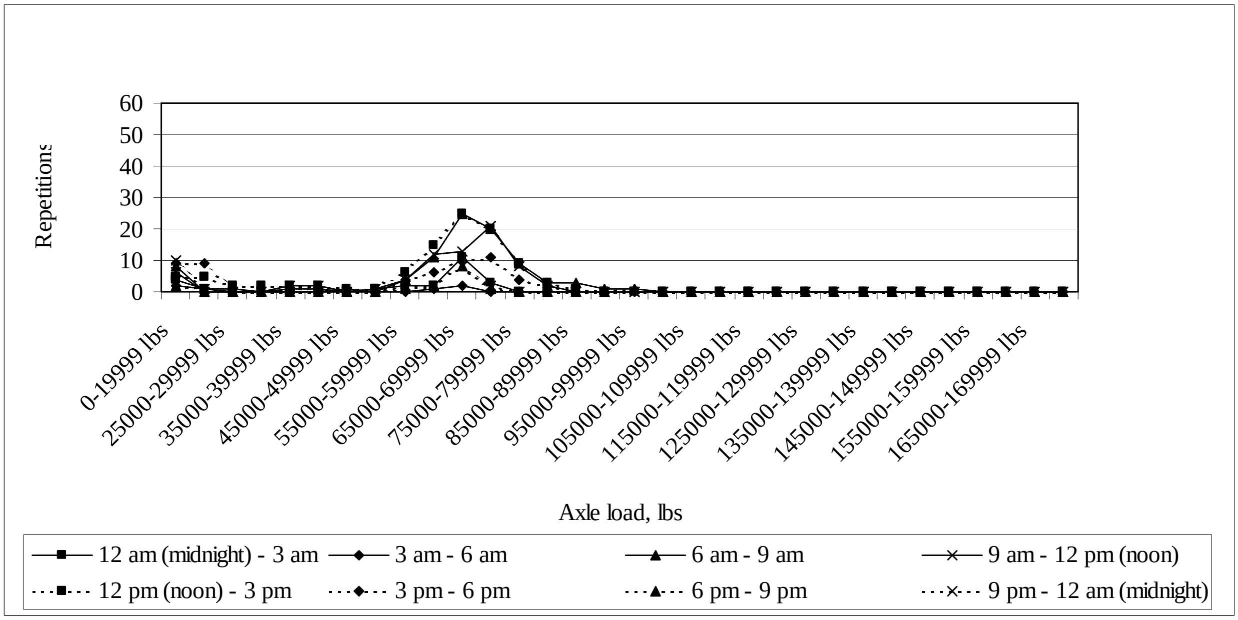


Figure J-141: Load spectrum from SPS2 sections for multi-axle (5) in December, 1999

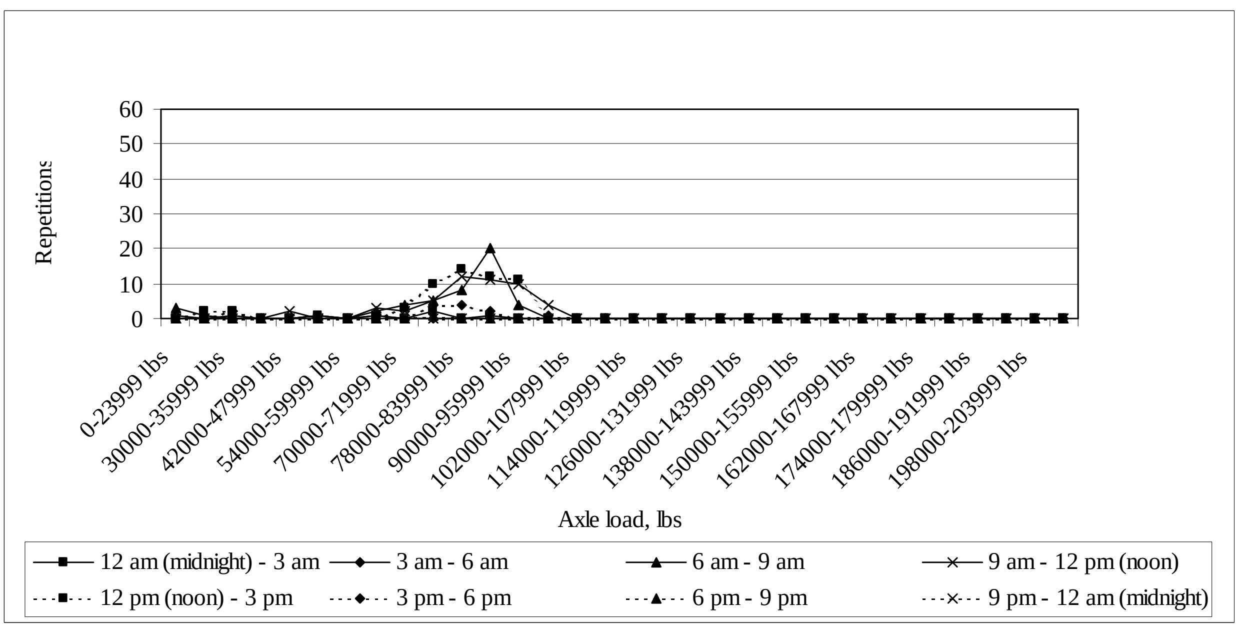


Figure J-142: Load spectrum from SPS2 sections for multi-axle (6) in December, 1999

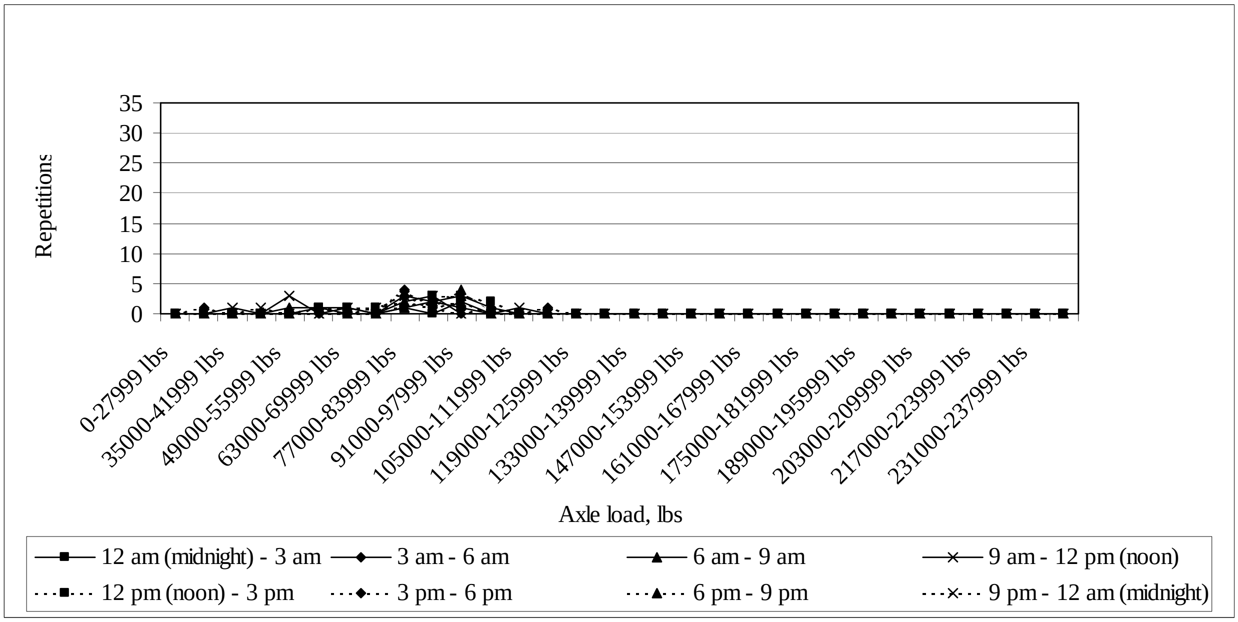


Figure J-143: Load spectrum from SPS2 sections for multi-axle (7) in December, 1999

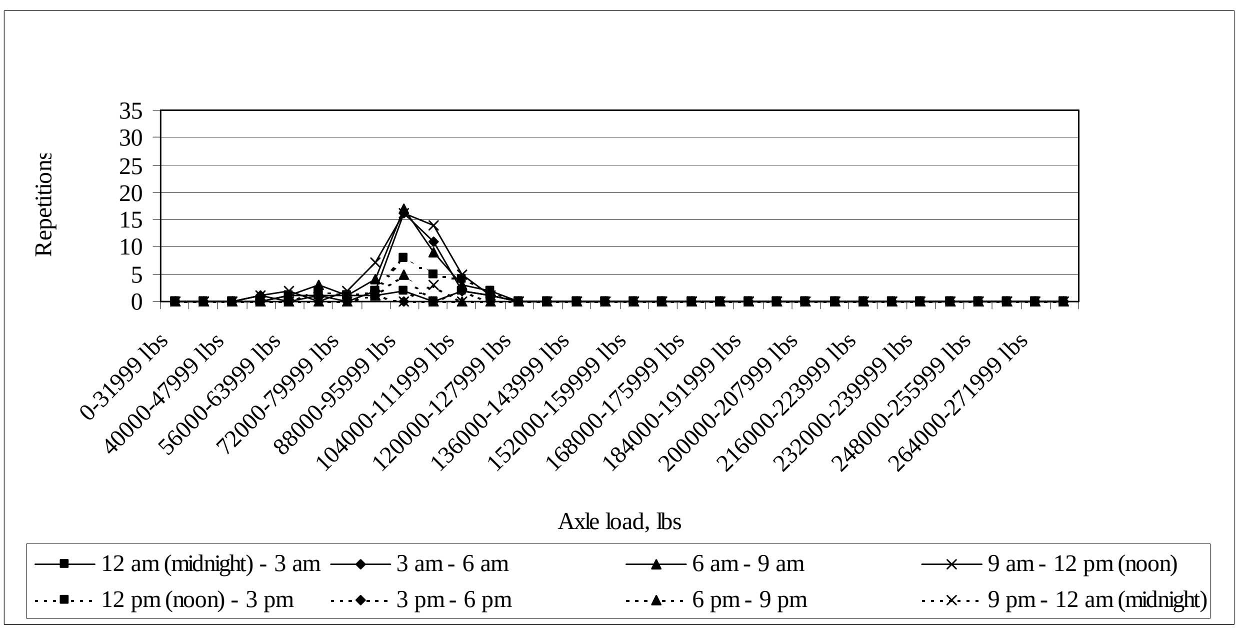


Figure J-144: Load spectrum from SPS2 sections for multi-axle (8) in December, 1999